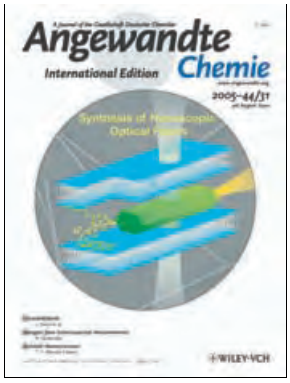
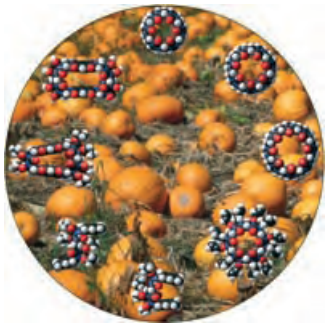
Cover Picture

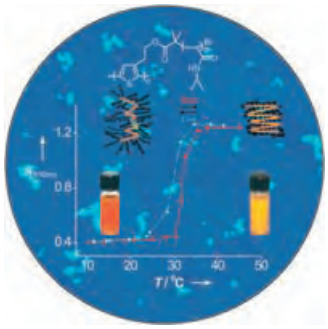


Gopakumar Gopalakrishnan, Jean-Manuel Segura, Dimitrios Stamou, Cédric Gaillard, Marinela Gjoni, Ruud Hovius, Kurt J. Schenk, Pierre A. Stadelmann, and Horst Vogel*

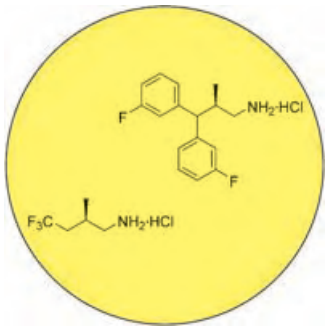
Nanoscopic optical fibers of $CdCl_2 \cdot 4H_2O$ have been synthesized using multilamellar lipid membranes as templates. The cover picture shows a scanning electron micrograph of the nanowires in the background and, from left to right, the synthetic route and the optical waveguiding properties of the nanowires. The center of the nanowire is excited at 488 nm (green laser), and orange light is emitted from the other end. For more details, see the Communication by H. Vogel and co-workers on page 4957 ff.



Cucurbit[n]urils
The Review by L. Isaacs and co-workers on page 4844 ff. introduces the synthesis and properties of the macrocyclic family of cucurbit[*n*]urils. The benchmark for possible applications in molecular recognition is the host–guest chemistry of cyclodextrins.



Thermochromic Polymers
The exceedingly high water-solubility and unique thermochromic behavior of a molecular brush copolymer composed of a polythiophene main chain and polyacrylamide side chains is described in the Communication by R. L. McCarley et al. on page 4872 ff.



Asymmetric Hydrogenation
A ruthenium–phosphate complex catalyzes the asymmetric hydrogenation of allylphthalimides. X. Zhang and co-workers describe on page 4933 ff. the efficient synthesis of β-methylamines.

Contents

The following Communications have been judged by at least two referees to be "very important papers" and will be published online at www.angewandte.org soon:

A. C. Filippou, G. Schnakenburg, A. I. Philippopoulos, N. Weidemann*
Bonding Analysis of the M≡Ge–Ge≡M Chain in the Germylidyne Complexes *trans,trans*-[Cl(depe)$_2$M≡Ge–Ge≡M(depe)$_2$Cl]

*M. Veith**
Cubane-Type Li_4H_4 and $Li_3H_3Li(OH)$: Stabilized in Molecular Adducts with Alane

S. Protti, M. Fagnoni, A. Albini**
Photochemical Cross-Coupling Reactions of Electron-Rich Aryl Chlorides and Aryl Esters with Alkynes: A Metal-Free Alkynylation

*V. Lavallo, Y. Canac, C. Präsang, B. Donnadieu, G. Bertrand**
Stable Cyclic (Alkyl)(amino)carbenes as Rigid or Flexible, Bulky, Electron-Rich Ligands for Transition-Metal Catalysts

H. Braunschweig, K. Radacki, D. Rais, D. Scheschkewitz*
A T-Shaped Platinum(II) Boryl Complex as the Precursor to a Base-Stabilized Borylene of Platinum

S. Aime, D. D. Castelli, E. Terreno*
Highly Sensitive MRI-CEST Agents using Liposomes (LIPOCEST)

Meeting Reviews

Metallomesogens — *S. J. Rowan** — **4830 – 4832**

Books

Biomineralization — Edmund Bäuerlein — *reviewed by S. Weiner* — **4833**

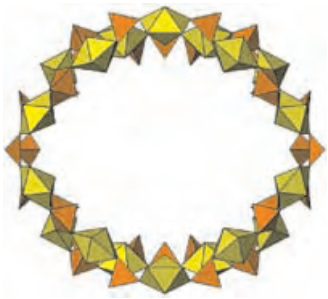
The Merck Druggernaut — Fran Hawthorne — *reviewed by A. Kleemann* — **4834**

Highlights

Actinide Nanostructures

T. E. Albrecht-Schmitt* — **4836 – 4838**

Actinide Materials Adopt Curvature: Nanotubules and Nanospheres

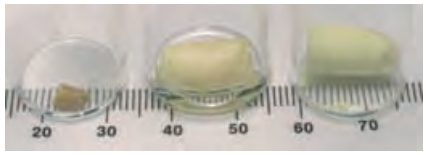


Actinides in action: The structural chemistry of the second-row f metals has received much attention over the past decade. Recently reported actinide-based nanotubules and nanospheres (see picture) offer prospective materials for ion transport and storage or as catalysts.

Semiconductor Nanocrystals

A. Eychmüller* — **4839 – 4841**

Aerogels from Semiconductor Nanomaterials



The door to a new class of materials has been opened through the combination of aerogels and semiconductor nanocrystals. Semiconductor nanoparticles are used as building blocks to give dry, mesoporous aerogels with large internal surface areas (see picture, center: wet CdS gel; left: unwashed CdS aerogel; right: monolithic CdS aerogel; scale in mm). These materials have many potential uses including in photovoltaic devices and sensors.

InterScience
© 2005 Wiley-VCH Verlag GmbH & Co. KGaA, Weinheim

Reviews

Is there anything cucurbituril can't do? With the cucurbit[*n*]uril family (see space-filling models of some examples) growing to include homologues, derivatives, congeners, and analogues, the tentative answer looks to be "No". The aim of the Review is to convince the reader of this optimistic assessment.



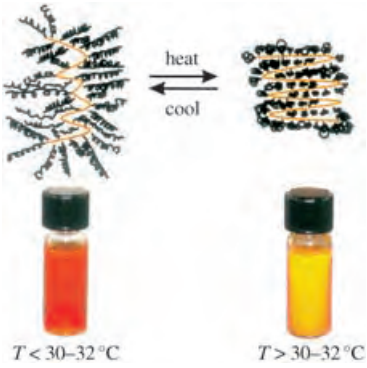
Host–Guest Systems

J. Lagona, P. Mukhopadhyay, S. Chakrabarti, L. Isaacs* — **4844 – 4870**

The Cucurbit[*n*]uril Family

Communications

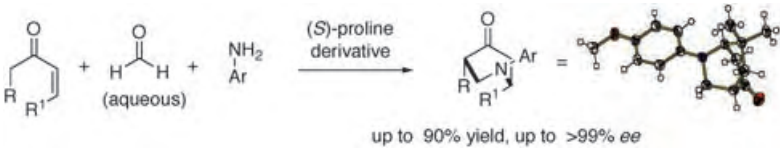
A brush with success: Responsive brushes composed of poly(*N*-isopropylacrylamide) grafted onto a poly(thiophene) backbone display the highest water solubility ever reported for a neutral poly(thiophene) as well as temperature-dependent optical properties and water solubilities (see picture). The graft polymer exhibits shifts in the π–π* transition of the poly(thiophene) backbone near the collapse temperature of the poly(*N*-isopropylacrylamide) chains.



Thermochromic Polymers

S. S. Balamurugan, G. B. Bantchev, Y. Yang, R. L. McCarley* — **4872 – 4876**

Highly Water-Soluble Thermally Responsive Poly(thiophene)-Based Brushes



Proline and its derivatives catalyze the asymmetric one-pot three-component aza-Diels–Alder reaction between unmodified α,β-unsaturated cyclic ketones, aqueous formaldehyde, and aryl amines with excellent chemo- and enantioselectivities (see scheme). Furthermore, this reaction provides a highly enantioselective entry to bicyclic non-proteogenic amino acid derivatives.

Asymmetric Catalysis

H. Sundén, I. Ibrahem, L. Eriksson, A. Córdova* — **4877 – 4880**

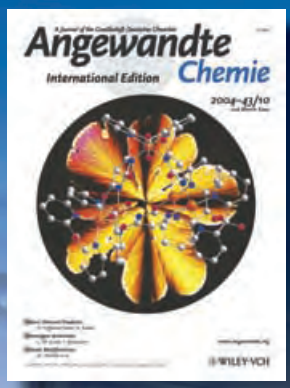
Direct Catalytic Enantioselective Aza-Diels–Alder Reactions

For the USA and Canada:
ANGEWANDTE CHEMIE International Edition (ISSN 1433-7851) is published weekly by Wiley-VCH PO Box 191161, D 69451 Weinheim, Germany. Air freight and mailing in the USA by Publications Expediting Inc. 200 Meacham Ave., Elmont, NY 11003. Periodicals postage paid at Jamaica NY 11431. US POSTMASTER: send address changes to *Angewandte Chemie*, Wiley-VCH, 111 River Street, Hoboken, NJ 07030. Annual subscription price for institutions: US$ 4948.00/4498.00 (valid for print and electronic / print or electronic delivery); for individuals who are personal members of a national chemical society, or whose institution already subscribes, or who are retired or self-employed consultants, print only: US$ 394.00. Postage and handling charges included. All Wiley-VCH prices are exclusive VAT.

© 2005 Wiley-VCH Verlag GmbH & Co. KGaA, Weinheim

The best in chemistry –

for more than a hundred years



A Journal of the Gesellschaft Deutscher Chemiker

Angewandte
International Edition **Chemie**

www.angewandte.org

1888: ***The beginning of a success story***

Constant Innovations

1962: *First issue of the International Edition*
1976: *Graphical abstracts*
1979: *Cover pictures*
1988: *Centenary of Angewandte*
1989: *Routine use of color*
1991: *New section: Highlights*
1992: *Computerized editorial tracking system*
1995: *Internet service for readers*
1998: *Regular press service; full-text online*
2000: *New section: Essays; EarlyView: Communications available online ahead of the printed version*
2001: *New section: Minireviews*
2002: *Online submission of manuscripts*
2003: *Weekly publication; new section: News; new layout*
2004: *Backfiles (1962-1997); ManuscriptXpress: Online system for authors and referees*



Angewandte's advisors...

Hartmut Wiezer
Clariant International AG, Sulzbach am Taunus

»**Angewandte Chemie** *is a highly acknowledged international chemical journal. Its attraction is based on excellence in content and presentation. It is a pleasure to commit myself to further the quality and success of* **Angewandte Chemie.**«

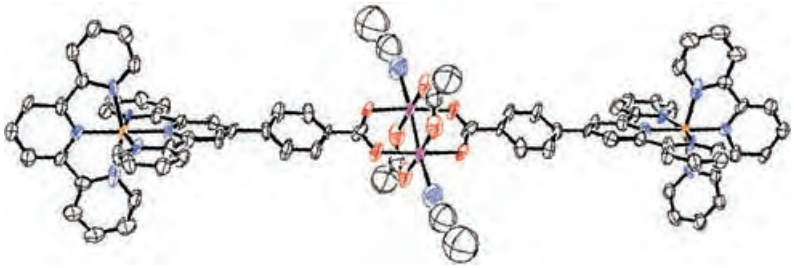
***Angewandte Chemie International Edition** is a journal of the German Chemical Society (GDCh)*

GDCh

WILEY InterScience® DISCOVER SOMETHING GREAT

WILEY-VCH

1191404_gu



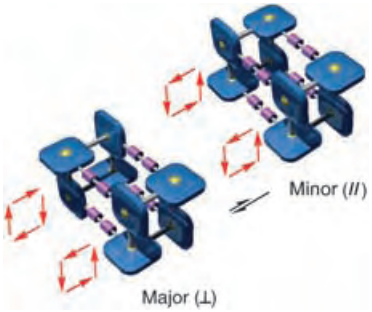
Giving in to templation: Coordination of acid-functionalized $\{Ru(tpy)_2\}^{2+}$ units (tpy = 2,2′:6′,2″-terpyridine) to a tetracarboxylato rhodium dimer leads to multinuclear polypyridylruthenium(II) complexes (see crystal structure, orange: Ru, purple: Rh, blue: N, red: O). Efficient energy transfer from the Ru-based MLCT levels to the lower-lying level involving the Rh dimer takes place at room temperature.

Energy Transfer

M. W. Cooke, G. S. Hanan,* F. Loiseau, S. Campagna,* M. Watanabe, Y. Tanaka* ——— **4881 – 4884**

The Structural and Functional Roles of Rhodium(II)–Rhodium(II) Dimers in Multinuclear Ruthenium(II) Complexes

A question of orientation: The self-assembly of a dialkynylene-bridged zinc pyridylporphyrin dimer with rotational freedom preferentially leads to a cyclic tetramer consisting of the perpendicular conformer (⊥), rather than the more usual planar conformer (//, see picture). This preference most likely arises from an efficient cancellation of dipole moments in the self-assembled structure.

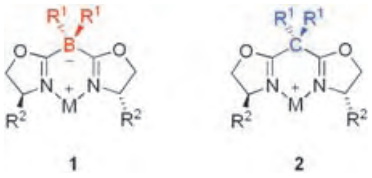


Supramolecular Chemistry

A. Tsuda,* H. Hu, R. Tanaka, T. Aida* ——— **4884 – 4888**

Planar or Perpendicular? Conformational Preferences of π-Conjugated Metalloporphyrin Dimers and Trimers in Supramolecular Tubular Arrays

Asymmetric cyclopropanation and monobenzoylation reactions of *meso* diols employing borabox catalysts **1** (M = Cu) result in high enantioselectivities. The borabox ligands are anionic analogues of the bisoxazolines **2** and are readily prepared by lithiation of oxazolines and subsequent trapping with boron halides.



The considerable potential of borabox ligands in asymmetric catalysis is shown.

N Ligands

C. Mazet, V. Köhler, A. Pfaltz* ——— **4888 – 4891**

Chiral Boron-Bridged Bisoxazolines: Readily Available Anionic Ligands for Asymmetric Catalysis



The anions went in two by two: Separate ion-pair binding of nano-sized α,ω-alkanediyldiammonium dichloride salts is achieved in organic media with high efficiency and selectivity by a heterotetratopic receptor that comprises two converging calix[5]arene units to tightly encapsulate the linear dication, as well as two ureido side functions to simultaneously bind the chloride counteranions through hydrogen bonding (see picture).

Host–Guest Chemistry

D. Garozzo, G. Gattuso, A. Notti, A. Pappalardo, S. Pappalardo,* M. F. Parisi,* M. Perez, I. Pisagatti ——— **4892 – 4896**

A Calix[5]arene-Based Heterotetratopic Host for Molecular Recognition of Long-Chain, Ion-Paired α,ω-Alkanediyldiammonium Salts

© 2005 Wiley-VCH Verlag GmbH & Co. KGaA, Weinheim

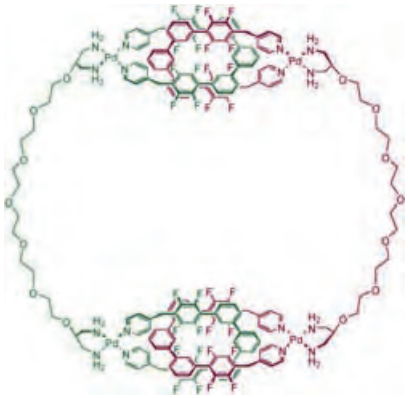
Contents

Supramolecular Chemistry

A. Hori, T. Sawada, K. Yamashita, M. Fujita* ——— **4896 – 4899**

Ultramacrocyclization through Reversible Catenation

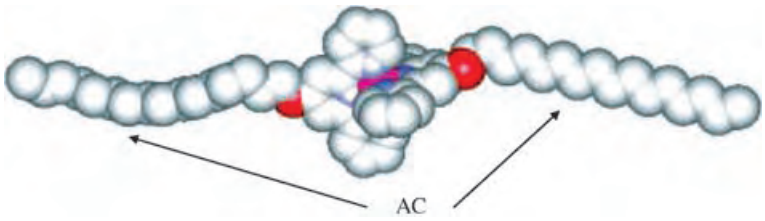
Extreme macrocyclization! An ultramacrocyclic structure with 238 non-hydrogen atoms in its backbone is obtained quantitatively through the reversible catenation of a double-loop compound that contains Pd^{II}-clipped coordination rings at both ends (see structure). The Pd^{II} ring can be regarded as a nanoscale reaction center that is available for connecting nanoscopic components without high entropy costs.



Switchable Molecules

S. Hayami,* Y. Shigeyoshi, M. Akita, K. Inoue, K. Kato, K. Osaka, M. Takata, R. Kawajiri, T. Mitani, Y. Maeda ——— **4899 – 4903**

Reverse Spin Transition Triggered by a Structural Phase Transition

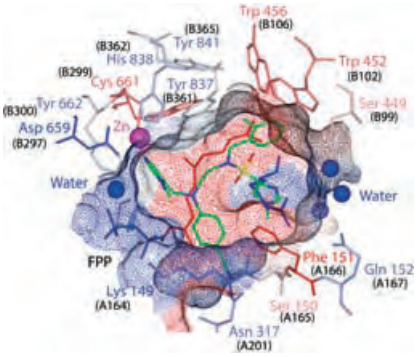


Reverse spin crossover (RSCO), the reversible spin transition from the high- to the low-spin state upon heating, was observed in $[Co(C_n\text{-terpy})_2](BF_4)_2$ (C_n-terpy = terpyridine) equipped with a long alkoxy chain (AC) of $n = 14$ or 16 methylene units (see picture). The wide thermal hysteresis of the RSCO around room temperature could allow such compounds to be used as molecular switches.

Medicinal Chemistry

M. P. Glenn, S.-Y. Chang, O. Hucke, C. L. M. J. Verlinde, K. Rivas, C. Horný, K. Yokoyama, F. S. Buckner, P. R. Pendyala, D. Chakrabarti, M. Gelb, W. C. Van Voorhis, S. M. Sebti, A. D. Hamilton* ——— **4903 – 4906**

Structurally Simple Farnesyltransferase Inhibitors Arrest the Growth of Malaria Parasites



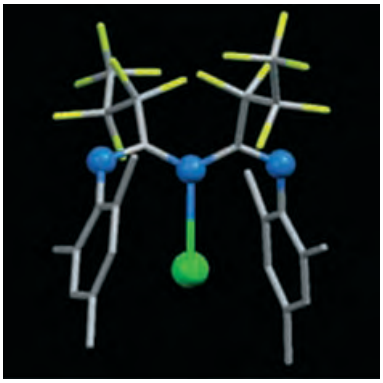
Antimalarial compounds: Structurally simple acyclic inhibitors of protein farnesyltransferase (active-site model shown) from the malaria parasite *Plasmodium falciparum* may allow third world countries access to an effective and inexpensive antimalarial therapy to counter the estimated half billion infections that occur annually.

Main Group Chemistry

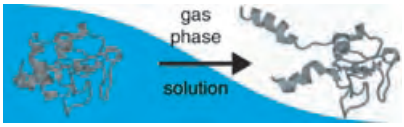
H. V. R. Dias,* S. Singh, T. R. Cundari ——— **4907 – 4910**

Monomeric Thallium(I) Complexes of Fluorinated Triazapentadienyl Ligands

Rare examples of thallium monocoordination? Polyfluorinated triazapentadienes $HN[C(C_3F_7)NAr]_2$ with bulky aryl substituents react with TlOEt to give rare, monomeric thallium(I) complexes in which the Tl^{I} center coordinates to the central nitrogen atom of the W-shaped triazapentadienyl ligand system (see figure; Ar = 2,4,6-trimethylphenyl; N: blue, F: yellow, Tl: green).



© 2005 Wiley-VCH Verlag GmbH & Co. KGaA, Weinheim

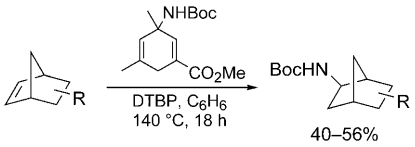


Unfolding upon dehydration:. What happens to the structure of a native protein that is suddenly exposed to vacuum? Native electron capture dissociation shows that dehydration turns the strongest intramolecular interactions in solution into the weakest in the gas phase.

Mass Spectrometry of Proteins

K. Breuker,*
F. W. McLafferty ——— **4911 – 4914**

The Thermal Unfolding of Native Cytochrome *c* in the Transition from Solution to Gas Phase Probed by Native Electron Capture Dissociation



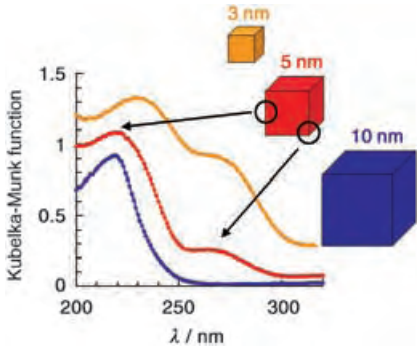
Radical transfer hydroaminations have been achieved with 3-aminated 1,4-cyclohexadienes rather than transition-metal reagents (see scheme; DTBP = di-*tert*-butylperoxide). These functionalized cyclohexadienes are efficient N-radical precursors. Moreover, they are stable and readily prepared, and radical generation occurs under neutral conditions.

Radical Chemistry

J. Kemper, A. Studer* ——— **4914 – 4917**

Stable Reagents for the Generation of N-Centered Radicals: Hydroamination of Norbornene

Meet on the edge: The relative concentration of corner and edge ions in a cubelike nanoparticle critically depends on the size of the nanoparticle. On MgO nanocubes this ratio is reflected by their optical properties (see picture).

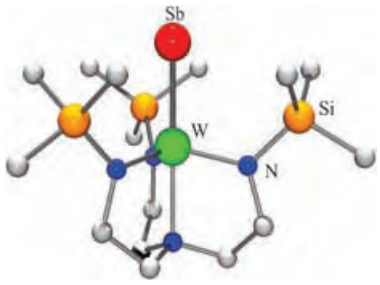


Nanostructures

S. Stankic, M. Müller, O. Diwald, M. Sterrer, E. Knözinger,* J. Bernardi ——— **4917 – 4920**

Size-Dependent Optical Properties of MgO Nanocubes

The intermediately generated Li[$(Me_3Si)_2CHSb(H)$] reacts with [$(N_3N)WCl$] to give the first complex with a terminal stibido ligand, [$(N_3N)W{\equiv}Sb$] (see structure). Spectroscopic features and the X-ray structure of this product clearly reveal the triple-bond character of the W≡Sb bond. A comparison of the bonding situations in the series [$(N_3N)W{\equiv}E$] (E = P, As, Sb, Bi) indicates only a weak polarization of the triple bond.



Pnicogen Complexes

G. Balázs, M. Sierka, M. Scheer* ——— **4920 – 4924**

Antimony–Tungsten Triple Bond: A Stable Complex with a Terminal Antimony Ligand

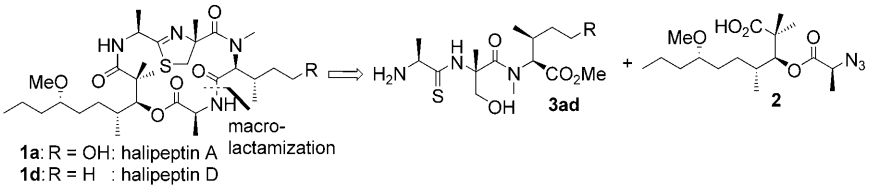
© 2005 Wiley-VCH Verlag GmbH & Co. KGaA, Weinheim

Contents

Natural Products Synthesis

K. C. Nicolaou,* D. W. Kim, D. Schlawe, D. E. Lizos, R. G. de Noronha, D. A. Longbottom _____ **4925 – 4929**

Total Synthesis of Halipeptins A and D and Analogues

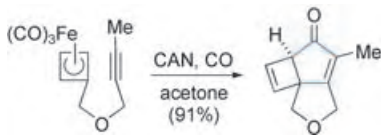


Deceptive rings: Halipeptins A (**1a**) and D (**1b**) and analogues thereof were synthesized from fragments **2** and **3a,b**, respectively. Key steps included peptide-bond formation, DAST-induced thiazoline construction, and macrolactamization. Unlike the naturally isolated (and possibly contaminated) material, synthetic **1b** exhibited only weak toxicity against tumor cells. DAST = (diethylamino)sulfur trifluoride.

Cycloaddition

B. A. Seigal, M. H. An, M. L. Snapper* _____ **4929 – 4932**

Intramolecular [2+2+1] Cycloadditions with (Cyclobutadiene)tricarbonyliron

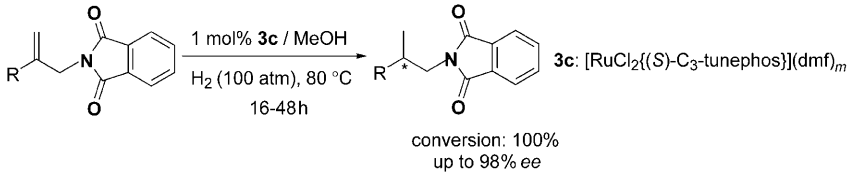


Highly functionalized strained rings are prepared through the cycloaddition of cyclobutadiene to alkynes. An intramolecular [2+2+1] cycloaddition is optimized for a variety of (cyclobutadiene)tricarbonyliron substrates with tethered alkynyl units (see scheme; CAN = cerium(IV) ammonium nitrate). The nature of the tether between the reactive functional groups in this transformation is found to have a significant influence on the outcome.

Asymmetric Catalysis

C.-J. Wang, X. Sun, X. Zhang* _____ **4933 – 4935**

Enantioselective Hydrogenation of Allylphthalimides: An Efficient Method for the Synthesis of β-Methyl Chiral Amines

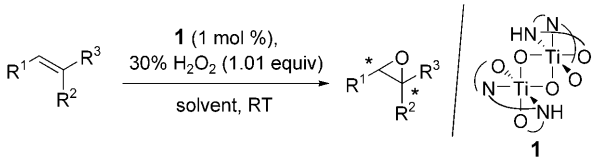


High yields and up to 98% *ee* have been achieved by asymmetric hydrogenation of allylphthalimides followed by hydrolysis to give β-methyl chiral amines by using a Ru–C_3-tunephos catalyst (see scheme). The synthetic utility of this procedure has been demonstrated through the synthesis of the key intermediate of the LTs receptor antagonist (Zeneca ZD3532).

Asymmetric Catalysis

K. Matsumoto, Y. Sawada, B. Saito, K. Sakai, T. Katsuki* _____ **4935 – 4939**

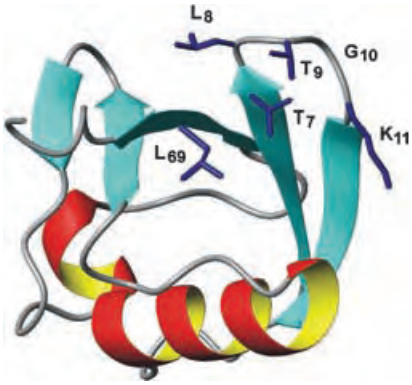
Construction of Pseudo-Heterochiral and Homochiral Di-μ-oxotitanium(Schiff base) Dimers and Enantioselective Epoxidation Using Aqueous Hydrogen Peroxide



Salen's lot: Meerwein–Ponndorf–Verley reduction of [Ti(salen)($OiPr$)$_2$] (salen = bis(salicylidene)ethylenediaminato) complexes followed by treatment with water leads to the synthesis of pseudo-heterochiral and homochiral di-μ-oxotitanium dimers. These dimers, in particular (a*R*,*S*,Δ, a*R*,*S*,Δ)-dimer **1**, efficiently catalyze the epoxidation of simple olefins using aqueous hydrogen peroxide (see scheme) with *ee* values up to 99% and turnover numbers up to 4600.

© 2005 Wiley-VCH Verlag GmbH & Co. KGaA, Weinheim

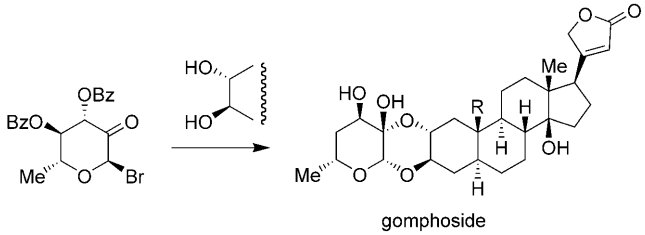
One good turn: β-Turns are an important component of protein structure and nucleation sites for β-hairpin folding. With ubiquitin as a "host" system (see structure), protein engineering methods have been used to determine the energetic contribution of type I′ β-turns to the stability of proteins, with a view to optimizing the rational design of model peptide systems.



Protein Models

E. R. Simpson, J. K. Meldrum, R. Bofill, M. D. Crespo, E. Holmes, M. S. Searle* ——— **4939 – 4944**

Engineering Enhanced Protein Stability through β-Turn Optimization: Insights for the Design of Stable Peptide β-Hairpin Systems

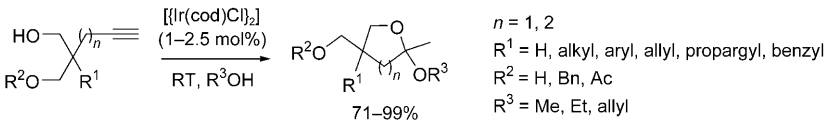


Spectinomycin and the gomphosides: Use of 6-deoxyhexulosyl derivatives of D-glucose in Ag_2CO_3-mediated glycosylation of gomphogenin and actinamine has allowed the first syntheses of cardiac glycosides with ring A-annulated sugar components (see picture; Bz = benzoyl) and an alternate synthesis of the antibiotic spectinomycin.

Natural Product Synthesis

F. W. Lichtenthaler,* E. Cuny, O. Sakanaka ——— **4944 – 4948**

A Concise and General Method for Doubly Attaching 2-Ketosugars to Aglycon Diols: Synthesis of the Gomphosides and Spectinomycin

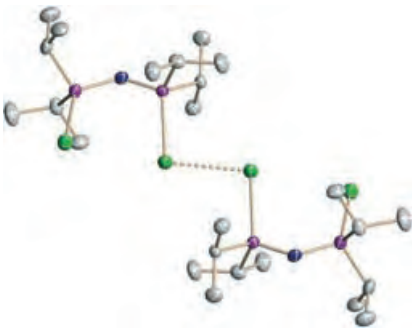


An efficient, selective, and atom-economical access to ketal building blocks is provided by the title reaction (see scheme). The entire process occurs smoothly in the presence of a catalytic amount of $[\{Ir(cod)Cl\}_2]$ at room temperature in methanol, ethanol, or allyl alcohol as solvents.

Catalytic Tandem Reactions

E. Genin, S. Antoniotti, V. Michelet,* J.-P. Genêt* ——— **4949 – 4953**

An Ir^I-Catalyzed *exo*-Selective Tandem Cycloisomerization/Hydroalkoxylation of Bis-Homopropargylic Alcohols at Room Temperature



Facile formation of the ditelluride $[(TeP\mathit{i}Pr_2N\mathit{i}Pr_2PTe\text{-})_2]$, which exists as a centrosymmetric dimer (see picture: Te green, P purple, N blue, C gray) with a weak Te—Te bond, embodies a new feature of the chemistry of dichalcogenoimidodiphosphinate ligands. The monotelluride $HP\mathit{i}Pr_2N\mathit{i}Pr_2PTe$ analogue is obtained as the P—H tautomer.

Main Group Chemistry

T. Chivers,* D. J. Eisler, J. S. Ritch, H. M. Tuononen ——— **4953 – 4956**

An Unusual Ditelluride: Synthesis and Molecular and Electronic Structures of the Dimer of the Tellurium-Centered Radical $[TeP\mathit{i}Pr_2N\mathit{i}Pr_2PTe]^{\bullet}$

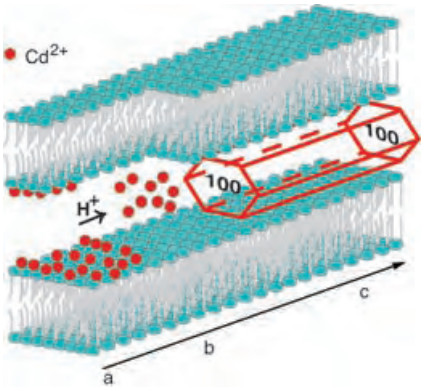
© 2005 Wiley-VCH Verlag GmbH & Co. KGaA, Weinheim

Contents

Nanostructures

G. Gopalakrishnan, J.-M. Segura, D. Stamou, C. Gaillard, M. Gjoni, R. Hovius, K. J. Schenk, P. A. Stadelmann, H. Vogel* ——— **4957 – 4960**

Synthesis of Nanoscopic Optical Fibers Using Lipid Membranes as Templates



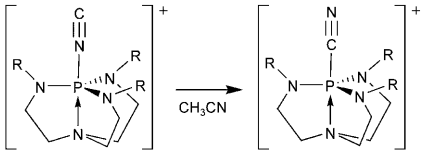
High-aspect-ratio, monocrystalline cadmium chloride nanowires doped with fluorescent CdS nanoparticles have been synthesized using planar lipid membranes as templates (see picture). Cd^{2+} ions bound to the lipid bilayers (a) are released at low pH to the nanometer-sized, interlamellar water films (b) where the sudden increase in concentration leads to the formation of nanowires (c) that show excellent light-waveguiding properties.

Coordination Modes

J. V. Kingston, A. Ellern, J. G. Verkade* ——— **4960 – 4963**

A Stable Structurally Characterized Phosphorus-Bound Isocyanide and Its Thermal and Catalyzed Isomerization to the Corresponding Cyanide

A P–NC linkage has been realized by the formation of a stable isocyano azaphosphatranium ion with a facile synthesis. Subsequent thermal or Lewis acid catalyzed isomerization of the isocyanide derivative to its cyanide isomer (see scheme) was carried out and followed by ^{31}P NMR spectroscopy. Both compounds



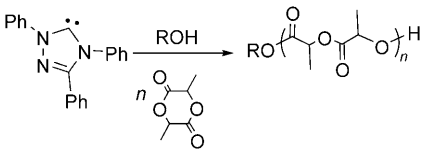
were characterized by X-ray crystallography.

Ring-Opening Polymerization

O. Coulembier, A. P. Dove, R. C. Pratt, A. C. Sentman, D. A. Culkin, L. Mespouille, P. Dubois,* R. M. Waymouth,* J. L. Hedrick* ——— **4964 – 4968**

Latent, Thermally Activated Organic Catalysts for the On-Demand Living Polymerization of Lactide

It's all about control: Alcohol adducts of stable N-heterocyclic carbenes function as excellent single-component catalysts/initiators for the ring-opening polymerization of lactide (see scheme). This polymerization can be reversibly terminated simply by modulating the temperature. The use of multifunctional macro-

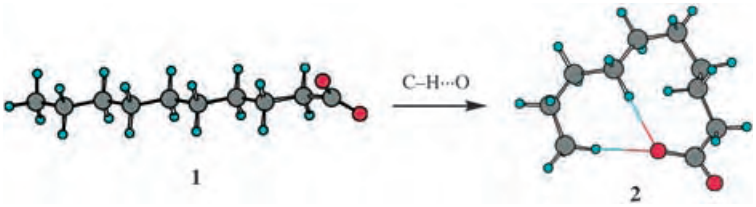


initiators enables the synthesis of more complex polymer architectures.

Hydrogen Bonding

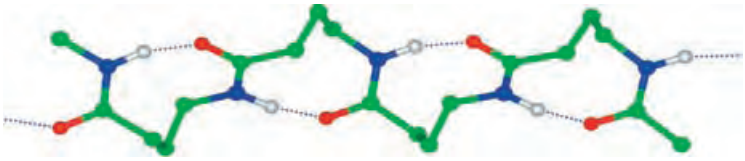
X.-B. Wang, H.-K. Woo, B. Kiran, L.-S. Wang* ——— **4968 – 4972**

Observation of Weak C–H···O Hydrogen Bonding to Unactivated Alkanes



From linear to folded simply by C–H···O bonding: A new low-temperature photoelectron spectroscopy apparatus is used to study hydrogen bonding between unactivated alkanes and a carboxylate group. Gaseous linear carboxylates **1**, $CH_3(CH_2)_nCO_2^-$, assume folded structures **2** at low temperatures by weak C–H···O hydrogen bonding between the terminal CH_3 and CO_2^- groups for $n \geq 5$.

© 2005 Wiley-VCH Verlag GmbH & Co. KGaA, Weinheim



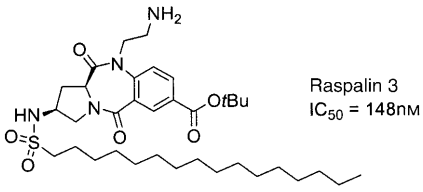
Nine is the number: Novel C_9-hydrogen-bonded structures (in which the hydrogen bonds enclose a ring of nine atoms) are observed in protected di- and tetrapeptides formed by the γ-amino acid residue gabapentin. The structures reveal new families of C_9 helices and ribbons (see structure) in γ-polypeptides.

γ-Peptide Structures

P. G. Vasudev, N. Shamala,* K. Ananda, P. Balaram* ——— **4972 – 4975**

C_9 Helices and Ribbons in γ-Peptides: Crystal Structures of Gabapentin Oligomers

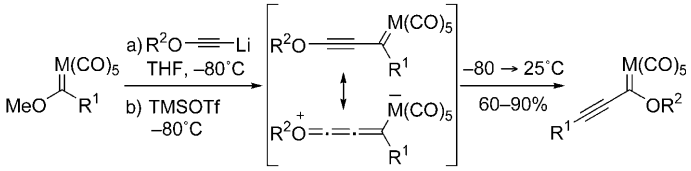
It works both ways: The development of potent peptidomimetic acyl protein thioesterase 1 (APT1) inhibitors, such as Raspalin 3 (see structure), and their use in biological and biochemical investigations are reported. The results show that the enzyme can deacylate and acylate Ras proteins.



Chemical Biology

P. Deck, D. Pendzialek, M. Biel, M. Wagner, B. Popkirova, B. Ludolph, G. Kragol, J. Kuhlmann,* A. Giannis,* H. Waldmann* ——— **4975 – 4980**

Development and Biological Evaluation of Acyl Protein Thioesterase 1 (APT1) Inhibitors



A single (or iterative) insertion of alkyne units into metal carbene complexes, accompanied by alkoxy exchange, occurs readily to give elusive alkynyl(alkoxy)carbenes (see scheme) as well as polyalkynyl(alkoxy)carbenes. M = W, Cr, Mo. TMSOTf = trimethylsilyl trifluoromethanesulfonate.

Carbene Complexes

J. Barluenga,* R. B. de la Rúa, D. de Sáa, A. Ballesteros, M. Tomás — **4981 – 4983**

Formal Alkyne Insertion into Alkoxycarbene Complexes: Simple Access to Enantiopure Group 6 Alkynyl(alkoxy)carbene Complexes

Sources

Product and Company Directory

You can start the entry for your company in "Sources" in any issue of *Angewandte Chemie*.

If you would like more information, please do not hesitate to contact us.

Wiley-VCH Verlag – Advertising Department
Tel.: 0 62 01 - 60 65 65
Fax: 0 62 01 - 60 65 50
E-Mail: MSchulz@wiley-vch.de

Service

Keywords ——— *4984*

Authors ——— *4985*

Preview ——— *4987*

© 2005 Wiley-VCH Verlag GmbH & Co. KGaA, Weinheim



Metallomesogens**

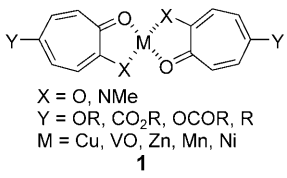
Stuart J. Rowan*

Over the past 25–30 years there has been significant growth in the area of metal-complex-containing liquid crystals (metallomesogens).[1] The incorporation of a metal ion into a mesogenic system offers the possibility of developing new materials with properties imparted by the metal component, such as magnetic, electrical, and optical properties. Furthermore, the wide range of coordination numbers and geometries that can be accessed through the metal component, along with the variety of known organic ligands offer a wealth of opportunities for the geometric design of new mesogenic materials. The design of liquid-crystalline materials which contain metal ions is not a facile process. Nonetheless, over the years a wide range of mesogenic systems that incorporate metal ions from all over the periodic table have been designed and developed. As a result, an assortment of liquid-crystalline phases (both thermotropic and lyotropic) can be accessed with metallomesogens.

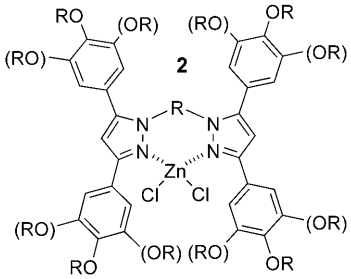
The last day of May 2005 saw the opening of the 9th International Symposium on Metallomesogens in Lake Arrowhead, California. The meeting was chaired by Gerald Van Hecke of Harvey Mudd College in California. In addition to Van Hecke, the organizing committee included Robert Bachman (The University of the South), Lee Park (Williams College), Eric Scharrer (University of Puget Sound), and Jodi Wesemann. This group put together an outstanding international program that included not only researchers working in the field of metallomesogens but scientists interested in a range of related topics as well. These areas included organic liquid crystals, organic–inorganic soft materials, and ordered inorganic networks and materials. As such, the four-day conference allowed scientists from a range of different disciplines to share their own perspectives in the development of new ordered organic–inorganic hybrid materials.

One of the themes discussed was the development of new classes of metallomesogens that expand on the type of ligands and/or metal ion combinations which allow access to such materials. Akira Mori (Kyushu University) outlined the potential of troponoid cores as ligands in the formation of metallomesogens **1**, and Emma Cavero (University of Zaragoza) discussed the investigation of a series of metal-bound pyrazole-based ligands such as **2**. Jadwiga Szydlowska (Warsaw University) showed that the tetradentate enaminoketone-based ligand could be used to form a variety of metallomesomorphic materials **3** upon binding to Ni^{II} or Cu^{II} metal ions. The incorporation of more-complex metal structures into liquid-crystalline materials was a challenge taken up by Eric Scharrer (University of Puget Sound). He showed that through the careful design of alkyne-based ligands, dicobalt hexacarbonyl complexes, such as **4**, do exhibit enantiotropic liquid-crystalline behavior.

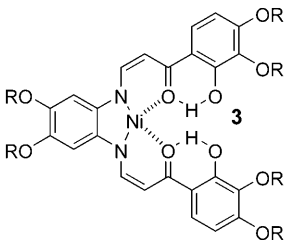
A number of research groups reported on the development of metallomesogens which contain lanthanide ions. The incorporation of such metal ions, which can exhibit interesting luminescent and/or paramagnetic properties, into liquid crystals opens the door to the development of new ordered materials with unique physical properties. For example, Koen Binnemans (Katholieke Universiteit Leuven) discussed the design, synthesis, and material properties of lanthanide ions bound to a series of imidazole[4,5-f]1,10-phenanthroline-based ligands such as **5**. These materials, in which the mesogenic 4-cyanobiphenyl unit is attached, not only exhibit a nematic phase but are also highly luminescent in the solid state as well as in a solution of a nematic liquid-crystal host. Claude Piguet (University of Geneva) discussed the effect lanthanide contraction has on the thermotropic liquid-crystalline behavior of a series of lanthanide metal ion complexes **6**, which consist of a rigid terdentate ligand based on the bis(1-ethylbenzimidazol-2-yl)pyridine moiety.[2] The larger lanthanide ions (Ce–Nd) allow the formation of 10-coordinate complexes that favor the formation of bimetallic rodlike nitrato-bridged dimers in the solid state; as a result, lamellar columnar phases are observed. However, upon heating, the formation of a cubic phase is observed in these systems,



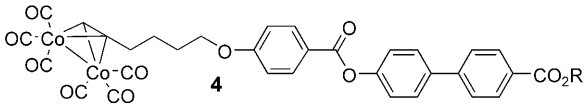
1



2



3

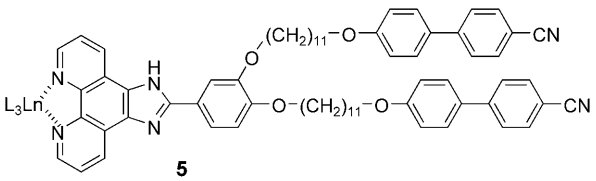


4

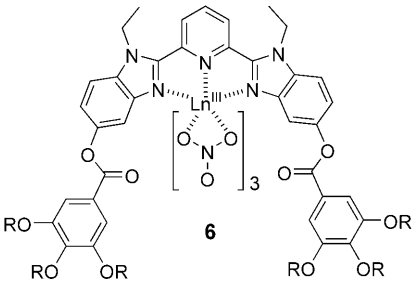
[*] Prof. S. J. Rowan
Department of Macromolecular Science and Engineering
Case Western Reserve University
2100 Adelbert Road, Cleveland, OH 44106-7202 (USA)
Fax (+1) 216-368-4202
E-mail: stuart.rowan@case.edu

[**] 9th International Symposium on Metallomesogens, May 31 to June 3, 2005, in Lake Arrowhead, California.

InterScience
© 2005 Wiley-VCH Verlag GmbH & Co. KGaA, Weinheim



5



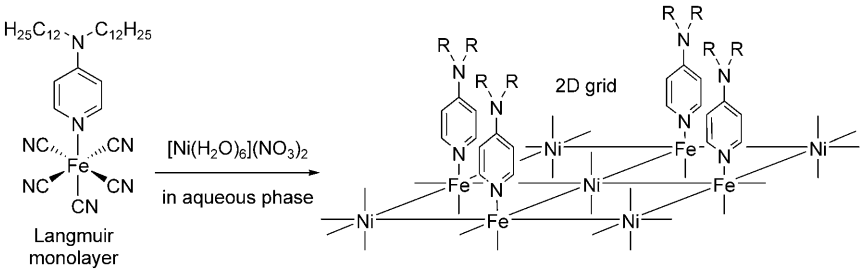
6

which is assigned to the formation of monometallic complexes. Across the lanthanide series, structural changes occur as a result of the contraction in ionic radius; a 9-coordinate system is favored with a smaller radius (Sm–Ho), and as a result, the formation of monometallic complexes is favored. Consistent with the previous system, these monometallic complexes form a body-centered cubic phase. A further decrease in radius (Er–Lu) yields hemi-disklike monometallic complexes, which are compact enough to result in the formation of a hexagonal columnar phase.

Metal–metal interactions in the formation of controlled structures and the alteration of functional properties (e.g. luminescence) was described in a number of talks. Mohammad Omary (University of North Texas) discussed the effect that aurophilic bonding (Au–Au) has on the structure and luminescent behavior of a series of isonitrile gold complexes (RNCAuX).[3] He described how different aggregated structures—from extended linear structures of Au atoms to simple dimers—could be obtained by changing the alkyl and/or halide groups attached to the Au^{I} metal ion. In general, compounds which form infinite chains of associated Au atoms exhibit low-energy emissions in the yellow-orange-red region, whereas compounds that associate as Au dimers exhibit higher-energy emissions in the blue-green region. Alice Bruce (University of Maine) discussed how initial investigations of these isonitrile gold complexes, in a collaboration with Omary, suggested that microcrystalline samples of cyclohexylgold(I) chloride exhibit liquid-crystalline behavior. Robert Bachman (The University of the South) discussed mesogenic materials in which Pt–Pt interactions play an important role in the functional properties of these systems. In particular, he focused on how such systems could be used in a diverse range of applications including LEDs and chemosensors.

A number of researchers discussed lyotropic organic–inorganic hybrid systems, with particular attention placed on the use of an organic surfactant to template the inorganic component. Sung Yeun Choi (University of Toronto) discussed the use of an amphiphilic triblock copolymer to template the formation of regular mesoporous thin films of titania that exhibit pore sizes of around 7–8 nm with narrow polydispersities. The electrochromic performance of such templated mesoporous titania that had been modified with viologen was also discussed. These materials showed electronic conductivity similar to that of viologen nanocrystalline titania, but with enhanced color contrast; this is at least partially due to the presence of the ordered mesoporous architecture.[4] John Seddon (Imperial College) discussed collaborative work with Duncan Bruce (University of Exeter) on the use of cationic ruthenium-based surfactants to template the formation of mesoporous silicates. Seddon reported recent work on the phase behavior of these lyotropic templates. After calcination the resulting mesoporous silicates contain RuO_2 particles and exhibit efficient heterogeneous catalytic behavior as a result.[5]

A number of talks focused on the formation of ordered materials with processes that either differ from or expand upon the more traditional liquid-crystalline approach. Dan Talham (University of Florida) discussed the use of supramolecular assembly at the air–water interface to form extended two-dimensional inorganic networks. For this, a Langmuir monolayer of the amphiphilic pentacyanoferrate(III) was allowed to react with appropriate metal ions such as nickel(II), present in the aqueous subphase (Scheme 1).[6] The resulting film consisted of an iron–nickel face-centered two-dimensional square grid network bridged by cyanide moieties, and could be transferred to solid supports by using conventional Langmuir–Blodgett film techniques. This allowed the systematic formation of multilayers of these interesting materials, and studies on how the magnetic behavior of these materials changes from monolayer through bilayer to multilayer were discussed. The formation of metal-containing organogels was described by A. J. Zucherro (The University of the South/Georgia Institute of Technology). The gel formation in these systems occurs through in situ complexation of a metal ion to a lipid of low molecular mass and which contains a Lewis base moiety. James Martin (North Carolina State University) discussed the formation of intermediate-range order in amorphous molten metal halide sys-



Scheme 1. Reaction of an amphiphilic pentacyanoferrate(III) at the air–water interface with aqueous nickel(II) ions results in the formation of mixed cyanide-bridged two-dimensional metal grids.

© 2005 Wiley-VCH Verlag GmbH & Co. KGaA, Weinheim

tems. To obtain such pseudo-structured materials, an approach analogous to that used for the templating of zeolites was investigated.[7] Structural networks can be obtained in metal halide melts such as $ZnCl_2$ through the addition of equimolar amounts of CuCl and a templating cation (A^+, for example, alkylammonium salts) designed to match the size of an integral number of chloride ions. Such halozeotypes, $A_n[Cu_nZn_{m-n}Cl_{2m}]^{n-}$ show the formation of organized network structures in the melt that persist over nanometer-length scales. The formation of controlled structures in other metal halide melts based on $GaCl_3$ and $GeCl_4$ were also discussed.

As can be seen from above, one of the goals of the organizing committee was to significantly broaden the scope of the symposium beyond its traditional focus on the synthesis and phase properties of thermotropic metal-containing materials. It was hoped by opening the meeting to a more diverse range of researchers with interests in metallosurfactants, metal-containing gels, and ordered liquids, that new synergisms and new research directions would be identified. The closing session of the meeting was a panel discussion designed to reflect on the relationship of some of these nontraditional topics to the core focus of the community and to identify some of the potential new directions for research. Wolfgang Haase (Darmstadt University of Technology) discussed the "four pillars" of the field—synthesis, properties, models, and applications—and noted that the first of these pillars is the most developed, while the second is rapidly growing. Some areas that he felt warrant significant study are the magnetic, electric, conductometric, and light-scattering properties of metallomesogens. He also noted the need for more deliberate feedback from the last two pillars in guiding future synthetic efforts. He specifically suggested that researchers in the field avoid thinking solely about nematics and display applications, for which organic materials are so well-developed; devices that take advantage of the color of metallomesogens or changes in physical properties in response to light should be promising future directions. Haase further noted that metals with their various oxidation states and positive or negative charges can be important components of polymers, supramolecular compounds, coordination compounds, catalysts, photonic devices using luminescence, nanomaterials, colloidal systems, and biological systems. All of these types of materials should fit within the scope of future meetings by using the broader context of soft materials with mesogenic-like properties.

[1] For some recent reviews, see: a) B. Donnio, D. Guillon, R. Deschenaux, D. W. Bruce, *Comp. Coord. Chem. II* **2004**, *7*, 357–627; b) R. Gimenez, D. P. Lydon, J. L. Serrano, *Curr. Opin. Solid State Mater. Sci.* **2003**, *6*, 527–535.

[2] E. Terazzi, S. Torelli, G. Bernardinelli, J.-P. Rivera, J.-M. Bénech, C. Bourgogne, B. Donnio, D. Imbert, J.-C. G. Bünzli, A. Pinto, D. Jeannerat, C. Piguet, *J. Am. Chem. Soc.* **2005**, *127*, 888–903.

[3] O. Elbjeirami, M. A. Omary, M. Stender, A. L. Balch, *Dalton Trans.* **2004**, *20*, 3173–3175.

[4] S. Y. Choi, M. Mamak, N. Coombs, N. Chopra, G. A. Ozin, *Nano Lett.* **2004**, *4*, 1231–1253.

[5] H. B. Jervis, M. E. Raimondi, R. Raja, T. Maschmeyer, J. M. Seddon, D. W. Bruce, *Chem. Commun.* **1999**, 2031–2032.

[6] J. T. Culp, J.-H. Park, D. Stratakis, M. W. Meisel, D. R. Talham, *J. Am. Chem. Soc.* **2002**, *124*, 10083–10090.

[7] J. D. Martin, S. J. Goettler, N. Fossé, L. Iton, *Nature* **2002**, *419*, 381–384.

DOI: 10.1002/anie.200502405

 © 2005 Wiley-VCH Verlag GmbH & Co. KGaA, Weinheim

Actinide Nanostructures

DOI: 10.1002/anie.200500936

Actinide Materials Adopt Curvature: Nanotubules and Nanospheres

*Thomas E. Albrecht-Schmitt**

Keywords:
actinides · cluster compounds · nanostructures · polyoxometalates · uranium

The structural chemistry of the actinides has undergone what can be described as nothing less than a revolution over the past decade. Indeed, the number of structurally characterized inorganic U^{VI} compounds reported has increased from approximately 180 examples in 1996 to over 355 in 2005.[1,2] The recent excitement over this rapidly expanding group of compounds might even be comparable to that felt during Zachariasen's early years of elucidating the structures of transuranium compounds.[3] One of the primary driving forces behind this transformation is the remarkable structural versatility of the actinides. In oxidation states of +III or +IV, the actinides are typically found in eight- or nine-coordinate environments, which are similar to those observed with lanthanide ions. However, when the oxidation state is raised to +V or +VI, the approximately linear triatomic actinyl unit AnO_2^{n+} (An = U, Np, Pu, Am; $n = 1$ or 2) is observed. This cation is bound by additional ligands that lie perpendicular to the actinyl axis to create six-, seven-, and eight-coordinate tetragonal, pentagonal, and hexagonal bipyramids, respectively. If sterically demanding ligands are introduced, the coordination number can be reduced to as low as three ligands in the equatorial plane to yield trigonal-bipyramidal complexes as found for $[Na(thf)_2][UO_2\{N(SiMe_3)_2\}_3]$.[4]

[*] Prof. T. E. Albrecht-Schmitt
Department of Chemistry and Biochemistry
Auburn University
179 Chemistry Building
Auburn, AL 36849 (USA)
Fax: (+1) 334-844-6959
E-mail: albreth@auburn.edu

There is a definite predisposition of An^V and An^{VI} compounds to adopt layered structures, as a direct consequence of the condensation of actinyl-containing polyhedra typically perpendicular to the terminal actinyl unit to form extended structures.[1,2] One of the trends in recent actinyl chemistry has been to move away from layered structures and instead prepare compounds with one-dimensional topologies such as in $A_2[(UO_2)_3(IO_3)_4O_2]$ (A = K, Rb, Tl)[5] and three-dimensional open-framework compounds such as $(C_6H_{14}N_2)_2[(UO_2)_6(H_2O)_2F_2(PO_4)_2(HPO_4)_4]\cdot 4H_2O$,[6] $K_2[(UO_2)_2(VO)_2(IO_6)_2O]\cdot H_2O$,[7] and $(C_6H_{16}N)_2[(UO_2)_6(MoO_4)_7(H_2O)_2(H_2O)_2]$.[8] Discrete cluster compounds have lagged behind their higher-dimensional counterparts, but rich examples of organometallic U^V clusters such as $[Cp^*_4(U_6O_{13})(bpy)_2]$ ($Cp^* = 1,2,4$-tris(*tert*-butyl)cyclopentadiene; bpy = 2,2′-bipyridine), which contain an isopolyoxometalate core, have been reported.[9]

The importance of nanoscale structural features in actinide chemistry has been known since it was first recognized that Pu^{IV} forms colloids that are important in its mobility in the environment.[10,11] Furthermore, pulsed laser ablation of hydrated plutonium oxalate has been shown to generate cluster ions that contain up to 18 Pu atoms.[12] What has been lacking from the literature regarding the actinides are examples of nanoscale features in well-defined compounds. This lacuna has now been partially filled with the recent discoveries of actinide-based nanotubules[13] and nanospheres.[14]

The finding by Krivovichev et al. that the organically templated uranyl selenate $(C_4H_{12}N)_{14}[(UO_2)_{10}(SeO_4)_{17}(H_2O)]$ contains $[(UO_2)_{10}(SeO_4)_{17}(H_2O)]^{14-}$ nanotubules is the first report of its kind in uranyl chemistry.[13] These nanotubules are constructed from $\{UO_7\}$ pentagonal bipyramids and $\{SeO_4\}$ tetrahedra and are shown in Figure 1. These tubules are somewhat elliptical and have outer dimensions of $2.5 \times 2.3\ nm^2$. They have a free crystallographic diameter of 12.6 Å, which is on the same scale as large-pore zeolites.[15] Note that tubular features have been observed in other uranyl phases such as in $K_2[(UO_2)_2(VO)_2(IO_6)_2O]\cdot H_2O$,[7] in which elliptical channels are formed from $\{UO_6\}$, $\{VO_6\}$, and $\{IO_6\}$ octahedra. However, in this latter structure the tubules are fused to form a three-dimensional structure. In $(C_4H_{12}N)_{14}[(UO_2)_{10}(SeO_4)_{17}(H_2O)]$, however, the tubules are isolated from one another. A further intriguing feature of this structure is found by displaying a nodal representation of the walls of the tubules. This graph provides a topology for the walls with a ratio of U/Se of 10:17, which is an entirely new pattern for inorganic compounds.

One of the key questions addressed by the authors is the mechanism by which these tubules form. It is proposed that the butylammonium templates form self-assembled cylindrical micelles in solution. The UO_2^{2+} cations and SeO_4^{2-} anions then assemble around these micelles to yield the final nanotubules. Some important questions remain unanswered regarding these uranyl nanotubules: First, will these compounds undergo ion-exchange reactions without collapsing? Do they display a selectivity for certain cations? Also, do these compounds have any other zeolitic

InterScience
© 2005 Wiley-VCH Verlag GmbH & Co. KGaA, Weinheim

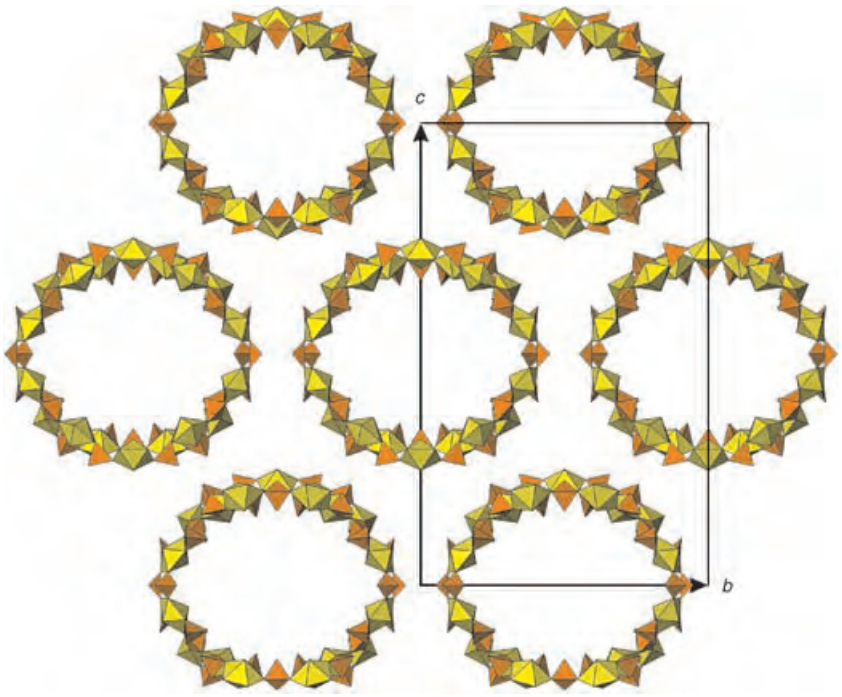


Figure 1. A view showing the packing of uranyl selenate nanotubules present in $[(C_4H_{12}N)_{14}\{(UO_2)_{10}(SeO_4)_{17}(H_2O)\}]$. UO_2^{2+} cations are bound by tetrahedral SeO_4^{2-} anions (shown in orange) to yield UO_7 pentagonal bipyramids (shown in yellow). The organic templates within the nanotubules are omitted for clarity.

properties? Can they be used to perform new (catalytic) chemistry?

Independent of the report by Krivovichev et al. on uranium-based nanotubules is an extremely important communication on the synthesis and structures of actinyl peroxide nanospheres by Burns et al.[14] It was observed that when alkaline peroxide solutions of U^{VI} and Np^{V} were allowed to stand in air for 7–14 days, crystals of actinyl peroxides formed. Single-crystal X-ray diffraction analyses of these crystals demonstrated that they contain actinyl peroxide nanospheres designated as U-24, U-28, U-32, and Np-24 according to the number of actinyl (U or Np) polyhedra in the clusters: example formulae for these compounds are $\{Li_6(H_2O)_8(NpO_2)(H_2O)_4[(NpO_2)(O_2)(OH)]_{24}\}^{20-}$ (Np-24) and $\{K_{16}(H_2O)_2(UO_2)(O_2)_2(H_2O)_2[(UO_2)(O_2)_{1.5}]_{28}\}^{14-}$ (U-28). The charges were balanced by additional alkali-metal cations. Interestingly with regards to these syntheses, the conditions described are relevant to those found in some nuclear waste tanks where basic conditions are prevalent and peroxide is generated by α radiolysis of water. It has already been demonstrated that natural radioactivity from uranium-bearing ores or nuclear waste may generate enough peroxide for the mineral studtite,[16] $[(UO_2)O_2(H_2O)_4]$, to form.[17] While the one-dimensional chain structure of studtite is of interest,[18] the structures of the actinyl nanospheres are simply astounding, being both aesthetically pleasing and nothing less than seminal (Figure 2).

These actinyl peroxide clusters have approximate diameters of 16.4 to 18.6 Å. The nanospheres are constructed from the edge-sharing of hexagonal-bipyramidal $\{AnO_8\}$ units. For U-24, U-32, and Np-24, the fundamental building unit is an actinyl cation bound by two edge-on peroxide groups and two hydroxide ligands, and can be formulated as $[(AnO_2)(O_2)_2(OH)_2]$. For the U-28 cluster, the UO_8 unit is formed from three edge-on peroxide anions and a uranyl cation to yield $[(UO_2)(O_2)_3]$. These clusters are hollow and may host both alkali-metal cations and partially occupied $[(UO_2)(O_2)_2(H_2O)_2]$ units. These nanospheres apparently form because of the short edge lengths on the hexagonal-bipyramidal units which are invoked by the O–O bond in the peroxide anions. While the U centers in U-24, U-28, and U-32 can be expected to contain U^{VI}, the same is not true for Np-24, which is apparently a mixed-valent species that contains both Np^{V} and Np^{VI}. Burns et al. utilized the Np=O bond lengths in the neptunyl units to assign the oxidation states on the Np centers. However, there was ambiguity concerning the Np center that occupies the center of the cluster. Of greater importance is the black coloration of Np-24 which indicates that the charges are not localized in the cluster; such charge-delocalization could lead to both interesting magnetic properties and electrochemical behavior.

A large number of prospects remain to be explored for these actinyl nanospheres. Small-angle X-ray scattering experiments demonstrate that these clusters are also present in solution; however, do they actually form in nuclear waste and how can they be detected? Can their hollow nature be exploit-

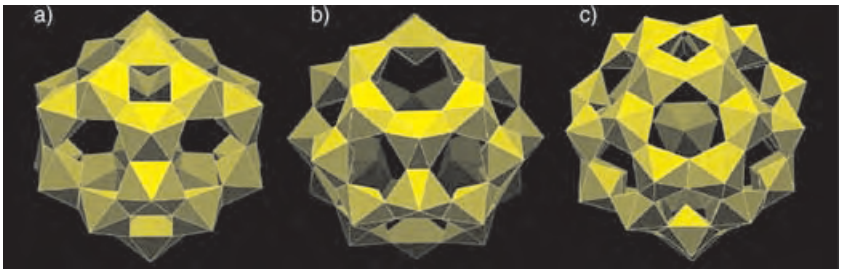


Figure 2. Polyhedral representations of actinyl peroxide nanospheres: a) U-24 and Np-24, b) U-28, and c) U-32. These nanospheres are constructed from UO_8 hexagonal bipyramids. For U-24, U-32, and Np-24, the fundamental building unit is an actinyl cation bound by two edge-on peroxide groups and two hydroxide ligands, and can be formulated as $[(AnO_2)(O_2)_2(OH)_2]$. For the U-28 cluster, the UO_8 unit is formed from three edge-on peroxide anions and a uranyl cation to yield $[(UO_2)(O_2)_3]$ units. Note the extremely short edges on these polyhedra invoked by the presence of O–O bonds.

© 2005 Wiley-VCH Verlag GmbH & Co. KGaA, Weinheim

ed for the transport and storage of other radionuclides, especially key fission products such as ^{90}Sr and ^{137}Cs? Do these compounds exhibit any of the important catalytic[19] and electrochemical[20] properties associated with polyoxometalates of Mo, W, and V? Answers to these questions will certainly underscore the importance of these actinyl nanospheres.

Published online: July 6, 2005

[1] P. C. Burns, M. L. Miller, R. C. Ewing, *Can. Mineral.* **1996**, *34*, 845 – 880.

[2] P. C. Burns, *Can. Mineral.* **2005**, in press.

[3] W. H. Zachariasen, *Acta Crystallogr.* **1948**, *1*, 265 – 268.

[4] C. J. Burns, D. L. Clark, R. J. Donohoe, P. B. Duval, B. L. Scott, C. D. Tait, *Inorg. Chem.* **2000**, *39*, 5464 – 5468.

[5] A. C. Bean, M. Ruf, T. E. Albrecht-Schmitt, *Inorg. Chem.* **2001**, *40*, 3959 – 3963.

[6] M. B. Doran, C. L. Stuart, A. J. Norquist, D. O'Hare, *Chem. Mater.* **2004**, *16*, 565 – 566.

[7] R. E. Sykora, T. E. Albrecht-Schmitt, *Inorg. Chem.* **2003**, *42*, 2179 – 2181.

[8] S. V. Krivovichev, T. Armbruster, D. Yu. Chernyshov, P. C. Burns, E. V. Nazarchuk, W. Depmeier, *Microporous Mesoporous Mater.* **2005**, *78*, 225 – 234.

[9] P. B. Duval, C. J. Burns, D. L. Clark, D. E. Morris, B. L. Scott, J. D. Thompson, E. L. Werkema, L. Jia, R. A. Andersen, *Angew. Chem.* **2001**, *113*, 3461 – 3465; *Angew. Chem. Int. Ed.* **2001**, *40*, 3357 – 3361.

[10] M. Kasha, *Natl. Nucl. Energy Ser. Manhattan Proj. Tech. Sect. Div. 4* **1949**, *14B*, 295 – 334.

[11] a) J. K. Bates, J. P. Bradley, A. Teetsov, C. R. Bradley, M. Buchholtz ten Brink, *Science* **1992**, *256*, 649 – 652; b) M. Dai, J. M. Kelley, K. O. Buesseler, *Environ. Sci. Technol.* **2002**, *36*, 3690 – 3699.

[12] J. K. Gibson, R. H. Haire, *J. Alloys Compd.* **2001**, *322*, 143 – 152.

[13] S. V. Krivovichev, V. Kahlenberg, I. G. Tananaev, R. Kaindl, E. Mersdorf, B. F. Myasoedov, *J. Am. Chem. Soc.* **2005**, *127*, 1072 – 1073.

[14] P. C. Burns, K.-A. Hughes Kubatko, G. Sigmon, B. J. Fryer, J. E. Gagnon, M. R. Antonio, L. Soderholm, *Angew. Chem.* **2005**, *117*, 2173 – 2177; *Angew. Chem. Int. Ed.* **2005**, *44*, 2135 – 2139.

[15] C. Baerlocher, W. M. Meier, D. H. Olson, *Atlas of Zeolite Structure Types*, Elsevier, London, **2001**.

[16] L. Berg, R. Keim, H. K. Kugler, P. Merlet, *Gmelin*, *Uran*, *Vol. C2*, Springer, Berlin, **1978**, pp. 293 – 321.

[17] K.-A. Hughes Kubatko, K. B. Helean, A. Navrotsky, P. C. Burns, *Science* **2003**, *302*, 1191 – 1194.

[18] P. C. Burns, K.-A. Hughes, *Am. Mineral.* **2003**, *88*, 1165 – 1168.

[19] For some recent examples, see: a) D. Sloboda-Rozner, P. Witte, P. L. Alsters, R. Neumann, *Adv. Synth. Catal.* **2004**, *346*, 339 – 345; b) I. A. Weinstock, E. M. G. Barbuzzl, M. W. Wemple, J. J. Cowan, R. S. Reiner, D. M. Sonnen, R. A. Heintz, J. S. Bond, C. L. Hill, *Nature* **2001**, *414*, 191 – 195.

[20] a) A. R. Howells, A. Sankarraj, C. Shannon, *J. Am. Chem. Soc.* **2004**, *126*, 12258 – 12259; b) M.-H. Chiang, J. A. Dzielawa, M. L. Dietz, M. R. Antonio, *J. Electroanal. Chem.* **2004**, *567*, 77 – 84; c) C. L. Hill, C. M. Prosser-McCartha, *Coord. Chem. Rev.* **1995**, *143*, 407 – 455.

 © 2005 Wiley-VCH Verlag GmbH & Co. KGaA, Weinheim

Semiconductor Nanocrystals

DOI: 10.1002/anie.200501052

Aerogels from Semiconductor Nanomaterials

*Alexander Eychmüller**

Keywords:
aerogels · materials science · mesoporous materials · semiconductors · sol–gel process

In a recently published paper in Science[1] a remarkable wedding has been announced which unites two very active fields of current materials research: semiconductor nanocrystals and aerogels. The Wayne State University team of Mohanan, Arachchige, and Brock employs colloidally prepared II–VI (CdS, ZnS, CdSe) or IV–VI (PbS) semiconductor nanoparticles as building blocks for dry, mesoporous, high surface area, and light weight aerogels which form after solvent removal under supercritical conditions from the gelated material.

Semiconductor nanocrystals[2] have been the focus of research for about 20 years and have encountered interest over the years from such diverse disciplines as solid-state physics, inorganic chemistry, physical chemistry, colloid chemistry, materials science, and recently even biological sciences, medical sciences, and engineering. Narrow and intensive emission spectra, continuous absorption bands, high chemical and photobleaching stability, processability, and surface functionality are among the most attractive properties of these materials. The breath-taking development of "nanochemistry" is reflected in an immense number of publications on the synthesis of semiconductor nanoparticles. Nearly all II–VI semiconductors and many of the IV–VI compounds have been prepared in colloidal form, some of them in a variety of different approaches. A great number of these developments have been summarized in surveys, in special issues of journals, and in books.[3] The ability to achieve desired particle sizes over the largest possible range, narrow size distributions, good crystallinity, desired surface properties and—should the occasion arise—high luminescence quantum yields as well as adjustable electronic properties, are all considered to be characteristics of a "good preparation".

The properties of the semiconductor nanocrystals also known as quantum dots depend strongly on the type of nanocrystal, the size (quantum-confinement) and the capping agent, thus they can be tuned by a proper choice of the synthetic conditions. There is a wide range of very efficient light-emitting semiconductor nanocrystals which can be synthesized both in organic media or as aqueous solutions. Worthy of mention are CdS, CdSe, and ZnSe[4] (UV spectral region) CdSe, InP, CdTe[5] (visible light region), PbSe, HgTe, and InAs[6] (near-infrared and infrared region). Furthermore, phase transition pressures, melting points, optical and optoelectronic, catalytic, magnetic, and electrical properties of nanomaterials differ from those of the bulk as well as from those of the molecular species they consist of, a situation which is appealing both scientifically and for applications. Assemblies of nanoparticles have been formed by coupling the particles by linker molecules. The formation of bioconjugates has been performed by connecting the nanoparticles to biological material, for example, for the use as fluorescent labels. The build-up of complex nanoparticle superstructures has been demonstrated with a very elaborate concept using highly specific interactions between bound biological functional groups such as complementary DNA strands.[7]

The other field of research touched by the work of Brock et al. is that of aerogels[8] which was opened by Kistler as early as in 1931.[9] Even in his first Nature article on this class of materials he reported the successful preparation of aerogels from "*silica, nickel tartarate, stannic oxide, tungstic oxide, gelatine, agar, nitrocellulose, cellulose, and egg albumin*" and he saw "*no reason why this list may not be extended indefinitely*"! A small constraint to this optimistic statement was added by Kistler in a follow-up publication in 1932:[10] "*Rubber offered difficulties not yet surmounted, but the way has been indicated.*" In the early 1940s he completed a license agreement with industry for the production of silica aerogel and the commercialization of his ideas began. In the 1960s scientists started to consider them as a medium for storing liquid rocket fuel. Silica aerogels are nonflammable, nontoxic, lightweight, transparent, and thermally stable to about 650 °C. Organic aerogels have been made for their thermal capabilities and they are stiffer and stronger than silica aerogels. For aerogels containing a conducting skeletal material such as carbon, electronic conductivity is introduced into the material. Aerogels have continuous porosity, nanosized pores, and an extremely high surface area of up to 1000 m^2 per gram of material. Very recently, Leventis et al. reported[11] that the strength of silica aerogel monoliths has been improved by a factor of over 100 through cross-linking the nanoparticle building blocks of preformed silica hydrogels with a polymer (Figure 1). Additionally they showed that composite monoliths are much less hygroscopic than native

[*] Priv.-Doz. Dr. A. Eychmüller
Institute for Physical Chemistry
University of Hamburg
Grindelallee 117
20146 Hamburg (Germany)
Fax: (+49) 40-42838-3452
E-mail: alexander.eychmueller@chemie.uni-hamburg.de

© 2005 Wiley-VCH Verlag GmbH & Co. KGaA, Weinheim



Figure 1. Strong silica aerogel resulting from cross-linking of the skeleton with a polymer.[11]

silica aerogels, and that they do not collapse when in contact with liquids.

Today, aerogels have broad applications in the commercial and military sectors, for example, as nanoporous thermal insulators, providing 3–10 times more thermal performance at a given thickness when compared to existing materials. Other reports stress the encapsulation capabilities of aerogels for bioactive molecules,[12] proteins, and even whole cells. Very promising is also the application of aerogels in the field of microphotonics.[13]

At this point it may have become more obvious why the paper from Brock and co-workers may be of such importance: by combining the properties of aerogels with those of semiconductor nanocrystals a new class of materials and new applications become accessible with possibly far reaching consequences. The monoliths prepared from CdS and ZnS have densities of between 0.07 and 0.35 $g\,cm^{-3}$ compared to the respective bulk values of 4.83 and 4.04 $g\,cm^{-3}$ and they contained mesopores of 2–50 nm in diameter. Most of the aerogels exhibit sharp absorption onsets at energies far above the respective bulk band gaps, thus, retaining their nanoparticle energetic features, namely the size quantization. This implies that the quantum dots remain electronically isolated which is attributed to the "fractal connectivity" of the network. This characteristic might be altered by post-preparative annealing of the structures which permits the absorption energy to be tuned to the red spectral region as the average crystallite size grows. The emission properties of the structures, however, are in need of considerable improvement: so far only weak and mainly trapped emission has been observed. In future efforts also pure band-to-band emission may be obtainable by using nanoparticles prepared by more elaborate synthetic routes such as, core–shell[14] or core–shell–shell[15] structures or nanocrystals with intrinsically stronger emission characteristics (Figure 2).[5d] Additionally, narrower distributions of nanocrystal sizes may be possible, which would lead to even sharper emission bands and consequently to purer colors.

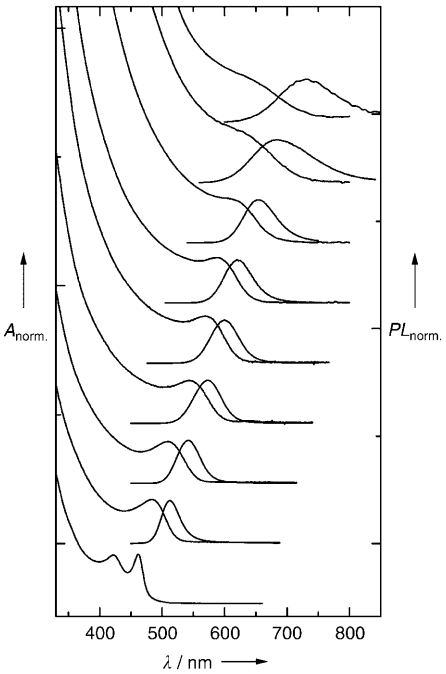


Figure 2. Absorption and emission spectra ($\lambda_{ex} = 400$ nm) of thiol-capped CdTe nanocrystals; *PL* = photoluminescence.[5d]

As optimistic as Kistler in his 1931 paper, Brock et al. state "*the generality of this method should lend itself to a number of new aerogel materials if the surface chemistry is appropriately tailored*". The latter can be agreed with completely and is largely based on the observations of Kotov, Peng, and others[16] that loss of particle-stabilizing molecules and/or photooxidation of surface ligands leads to aggregate formation in solution which is the basis of the production of robust gels.

Current efforts of the Wayne State team "*are devoted to preparing these materials in thin-film form and evaluating their potential for photovoltaic and sensing applications*". We are looking forward to many more papers on and possibly even applications of this door-opening synthetic route to materials combining two very topical areas of current materials research.

Published online: June 7, 2005

[1] J. L. Monahan, I. U. Arachchige, S. L. Brock, *Science* **2005**, *307*, 397.

[2] For reviews, see for example: a) H. Weller, *Angew. Chem.* **1993**, *105*, 43; *Angew. Chem. Int. Ed. Engl.* **1993**, *32*, 41; b) A. P. Alivisatos, *Science* **1996**, *271*, 933; c) C. B. Murray, C. R. Kagan, M. G. Bawendi, *Annu. Rev. Mater. Sci.* **2000**, *30*, 54; d) A. Eychmüller, A. L. Rogach, *Pure Appl. Chem.* **2000**, *72*, 179; e) A. Eychmüller, *J. Phys. Chem. B* **2000**, *104*, 6514; f) *Nanoparticles: From Theory to Application* (Ed.: G. Schmid), Wiley-VCH, Weinheim, **2004**.

[3] a) A. Henglein, *Top. Curr. Chem.* **1988**, *143*, 113; b) A. Henglein, *Chem. Rev.* **1989**, *89*, 1861; c) L. E. Brus, *J. Phys. Chem.* **1994**, *98*, 3575; d) A. Henglein, *Ber. Bunsen-Ges.* **1995**, *99*, 903; e) U. Woggon, S. V. Gaponenko, *Phys. Status Solidi B* **1995**, *189*, 285; f) A. P. Alivisatos, P. F. Barbara, A. W. Castleman, J. Chang, D. A. Dixon, D. M. L. Klein, G. L. McLendon, J. S. Miller, M. A. Ratner, P. J. Rossky, S. I. Stupp, M. E. Thompson, *Adv. Mater.* **1998**, *10*, 1297; g) N. Herron, D. L. Thorn, *Adv. Mater.* **1998**, *10*, 1173.

[4] a) L. Spanhel, M. Haase, H. Weller, A. Henglein, *J. Am. Chem. Soc.* **1987**, *109*, 5649; b) V. V. Nikesh, S. Mahamuni, *Semicond. Sci. Technol.* **2001**, *16*, 687; c) M. A. Hines, P. Guyot-Sionnest, *J. Phys. Chem. B* **1998**, *102*, 3655; d) A. Shavel, N. Gaponik, A. Eychmüller *J. Phys. Chem. B* **2004**, *108*, 5905.

[5] a) A. P. Alivisatos, *J. Phys. Chem.* **1996**, *100*, 13226; b) C. B. Murray, D. J. Norris, M. G. Bawendi, *J. Am. Chem. Soc.* **1993**, *115*, 8706; c) O. I. Mićić, J. Sprague, Z. Lu, A. J. Nozik, *Appl. Phys. Lett.* **1996**, *68*, 3150; d) N. Gaponik, D. V. Talapin, A. L. Rogach, K. Hoppe, E. V. Shevchenko, A. Kornowski, A. Eychmüller, H. Weller, *J. Phys. Chem. B* **2002**, *106*, 7177; e) D. V. Talapin, A. L. Rogach, I. Mekis, S. Haubold, A. Kornowski, M. Haase, H. Weller, *Colloids Surf. A* **2002**, *202*, 145.

[6] a) B. L. Wehrenberg, C. Wang, P. Guyot-Sionnest, *J. Phys. Chem. B* **2002**, *106*, 10634; b) H. Du, C. Chen, R. Krishnan, T. D. Krauss, J. M. Harbold, F. W. Wise, M. G. Thomas, J. Silcox, *Nano Lett.* **2002**, *2*, 1321; c) A. Rogach, S. Kershaw, M. Burt, M. Harrison, A. Kornowski, A. Eychmüller, H. Weller, *Adv. Mater.*

 © 2005 Wiley-VCH Verlag GmbH & Co. KGaA, Weinheim

1999, *11*, 552; d) Y.-W. Cao, U. Banin, *J. Am. Chem. Soc.* **2000**, *122*, 9692; e) S. Kudera, L. Carbone, M. F. Casula, R. Cingolani, A. Falqui, E. Snoeck, W. J. Parak, L. Manna, *Nano Lett.* **2005**, *5*, 445; f) E. Lifshitz, A. Sashchiuk, M. Brumer, A. Kigel, L. Amirav, *Phys. Status Solidi B*, in press; g) E. Lifshitz, A. Sashchiuk, M. Brumer, A. Kigel, L. Amirav, unpublished results.

[7] a) R. Elghanian, J. J. Storhoff, R. C. Mucic, R. L. Letsinger, C. A. Mirkin, *Science* **1997**, *277*, 1078; b) R. C. Mucic, J. J. Storhoff, C. A. Mirkin, R. L. Letsinger, *J. Am. Chem. Soc.* **1998**, *120*, 12674; c) M. Bruchez, Jr., M. Moronne, P. Gin, S. Weiss, A. P. Alivisatos, *Science* **1998**, *281*, 2013; d) W. C. W. Chan, S. Nie, *Science* **1998**, *281*, 2016; e) T. Torimoto, M. Yamashita, S. Kuwubata, T. Sakata, H. Mori, H. Yoneyama, *J. Phys. Chem. B* **1999**, *103*, 8799; f) G. P. Mitchell, C. A. Mirkin, R. L. Letsinger, *J. Am. Chem. Soc.* **1999**, *121*, 8122; g) S. Mann, W. Shenton, M. Li, S. Connolly, D. Fitzmaurice, *Adv. Mater.* **2000**, *12*, 147; h) C. M. Niemeyer, *Angew. Chem.* **2001**, *113*, 4254; *Angew. Chem. Int. Ed.* **2001**, *40*, 4128; i) A. N. Shipway, E. Katz, I. Willner, *ChemPhysChem* **2000**, *1*, 19; j) I. L. Medintz, A. R. Clapp, H. Mattoussi, E. R. Goldman, B. Fisher, J. M. Mauro, *Nat. Mater.* **2003**, *2*, 630; k) R. E. Bailey, A. M. Smith, S. Nie, *Phys. E* **2004**, *25*, 1; l) P. Alivisatos, *Nat. Biotechnol.* **2004**, *22*, 47; m) X. Michalet, F. F. Pinaud, L. A. Bentolila, J. M. Tsai, S. Doose, J. J. Li, G. Sundaresan, A. M. Wu, S. S. Gambhir, S. Weiss, *Science* **2005**, *307*, 538.

[8] For reviews, see for example: a) L. L. Hench, J. K. West, *Chem. Rev.* **1990**, *90*, 33; b) M. Schneider, A. Baiker, *Catal. Today* **1997**, *35*, 339; c) N. Hüsing, U. Schubert, *Angew. Chem.* **1998**, *110*, 22; *Angew. Chem. Int. Ed. Engl.* **1998**, *37*, 22.

[9] S. S. Kistler, *Nature* **1931**, *127*, 741.

[10] S. S. Kistler, *J. Phys. Chem.* **1932**, *36*, 52.

[11] a) N. Leventis, C. Sotiriou-Leventis, G. Zhang, A.-M. M. Rawashdeh, *Nano Lett.* **2002**, *2*, 957; b) M. A. B. Meador, E. F. Fabrizio, F. Ilhan, A. Dass, G. Zhang, P. Vassilaras, J. C. Johnston, N. Leventis, *Chem. Mater.* **2005**, *17*, 1085.

[12] J. M. Wallace, J. K. Rice, J. J. Oietron, R. M. Stroud, J. W. Long, D. R. Rolison, *Nano Lett.* **2003**, *3*, 1463.

[13] L. Tong, J. Lou, R. G. Gattass, S. He, X. Chen, L. Liu, E. Mazur, *Nano Lett.* **2005**, *5*, 259.

[14] M. A. Hines, P. Guyot-Sionnest, *J. Phys. Chem.* **1996**, *100*, 468.

[15] D. V. Talapin, I. Mekis, S. Götzinger, A. Kornowski, O. Benson, H. Weller, *J. Phys. Chem. B* **2004**, *108*, 18826.

[16] a) Z. Tang, N. A. Kotov, M. Giersig, *Science* **2002**, *297*, 237; b) J. Aldana, Y. A. Wang, X. Peng, *J. Am. Chem. Soc.* **2001**, *123*, 8844; c) H. Döllefeld, K. Hoppe, J. Kolny, K. Schilling, H. Weller, A. Eychmüller, *Phys. Chem. Chem. Phys.* **2002**, *4*, 4747.

 © 2005 Wiley-VCH Verlag GmbH & Co. KGaA, Weinheim

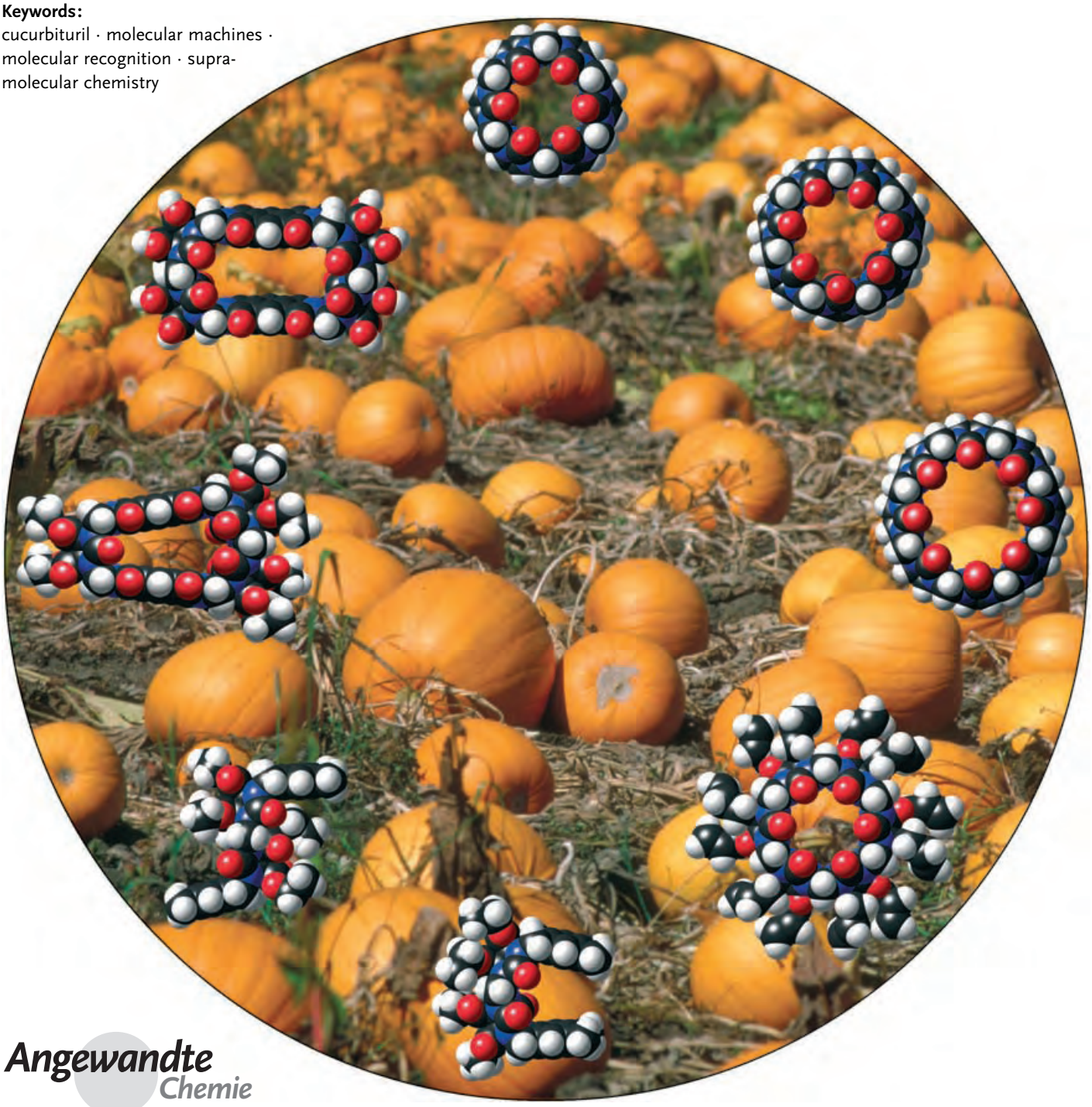
DOI: 10.1002/anie.200460675

Host–Guest Systems

The Cucurbit[*n*]uril Family

*Jason Lagona, Pritam Mukhopadhyay, Sriparna Chakrabarti, and Lyle Isaacs**

Keywords:
cucurbituril · molecular machines · molecular recognition · supramolecular chemistry



© 2005 Wiley-VCH Verlag GmbH & Co. KGaA, Weinheim

In 1981, the macrocyclic methylene-bridged glycoluril hexamer (CB[6]) was dubbed "cucurbituril" by Mock and co-workers because of its resemblance to the most prominent member of the cucurbitaceae *family of plants—the pumpkin. In the intervening years, the fundamental binding properties of CB[6]—high affinity, highly selective, and constrictive binding interactions—have been delineated by the pioneering work of the research groups of Mock, Kim, and Buschmann, and has led to their applications in wastewater remediation, as artificial enzymes, and as molecular switches. More recently, the cucurbit[n]uril family has grown to include homologues (CB[5]–CB[10]), derivatives, congeners, and analogues whose sizes span and exceed the range available with the α-, β-, and γ-cyclodextrins. Their shapes, solubility, and chemical functionality may now be tailored by synthetic chemistry to play a central role in molecular recognition, self-assembly, and nanotechnology. This Review focuses on the synthesis, recognition properties, and applications of these unique macrocycles.*

From the Contents

1. Introduction	4845
2. Synthesis of CB[n]	4847
3. Fundamental Properties of CB[n]	4847
4. Host–Guest Chemistry of CB[n]	4848
5. Control over the Recognition Processes	4853
6. Applications of the CB[n] Family	4855
7. Self-Assembly Processes Using CB[n]	4856
8. Derivatives, Analogues, and Congeners of the CB[n] Family	4859
9. Summary and Outlook	4864

1. Introduction

In 1905—contemporaneous with the pioneering work of Schardinger on the cyclodextrins—Behrend et al. reported that the condensation of glycoluril (acetyleneurea) and formaldehyde in concentrated HCl yields an insoluble polymeric substance now known as Behrend's polymer.[1] Behrend et al. were able to obtain a crystalline substance in good yield (40–70%) by recrystallization of the product from concentrated H_2SO_4 and demonstrated its ability to form cocrystals (complexes) with a variety of substances including $KMnO_4$, $AgNO_3$, H_2PtCl_6, $NaAuCl_4$, congo red, and methylene blue. The constitution of this substance remained unclear until 1981 when Mock reinvestigated the report by Behrend et al., and disclosed the remarkable macrocyclic structure comprising six glycoluril units and twelve methylene bridges; they dubbed the compound cucurbituril in recognition of its resemblance to a pumpkin, the most prominent member of the *cucurbitaceae* family (Figure 1).[2] In this Review we refer to cucurbituril as cucurbit[6]uril and abbreviate this as CB[6] to distinguish it from cucurbit[*n*]uril (CB[*n*]) homologues containing a different number of glycoluril units.

In contrast to the host–guest chemistry of α-, β-, and γ-cyclodextrin which has developed steadily over the past century, the supramolecular chemistry of CB[6] only began to develop in the 1980s and 1990s as a result of the pioneering work of Mock,[3] Buschmann and co-workers,[4] and Kim and co-workers.[5,6] Interest in the CB[*n*] family has increased dramatically in the new millennium following the preparation of four new CB[*n*] homologues (CB[5], CB[7], CB[8], and CB[10]·CB[5]) by the research groups of Kim and Day.[7–9] CB[5]–CB[8] are now even available commercially. This increase in interest in the CB[*n*] family correlates with the great advances in many areas of fundamental and applied science—chemistry, biology, materials science, and nanotechnology—that rely on the ability to employ and control noncovalent interactions between molecules. Consequently, CB[6] and the CB[*n*] family have been the focus of numerous reviews[3,5,6,10–30] and patents.[30–48]

The pioneering work of Lehn, Cram, and Pedersen brought host–guest and supramolecular chemistry to the forefront of contemporary science.[49] The scientific insights gained from fundamental studies of noncovalent interactions have been of practical value in a wide range of applications including chromatographic stationary phases, sequestration of contaminants from solution, and the development of catalysts, chemical sensors, and new drugs. All of these applications require the availability of low-molecular-weight receptors,[50–52] natural or non-natural oligomers and polymers,[53,54] or solid-state materials[55–57] that interact with their analytes in high affinity, highly selective binding processes. In response, supramolecular chemists have designed, synthesized, and evaluated the recognition properties of a wide variety of non-

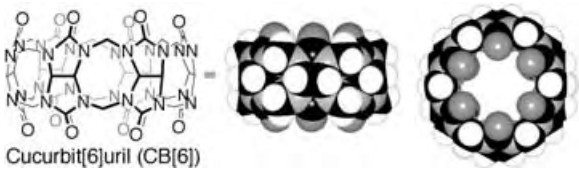


Figure 1. Structural formula of CB[6] as well as the side and top views of a space-filling model.

[*] J. Lagona, Dr. P. Mukhopadhyay, Dr. S. Chakrabarti, Prof. Dr. L. Isaacs
Department of Chemistry and Biochemistry
University of Maryland
College Park, MD 20742 (USA)
Fax: (+1) 301-314-9121
E-mail: LIsaacs@umd.edu

© 2005 Wiley-VCH Verlag GmbH & Co. KGaA, Weinheim

natural receptors—including cyclodextrins, calixarenes, cyclophanes, crown ethers, and many others—that display remarkable affinity and selectivity (Figure 2).[50–52] Amongst these non-natural receptors, α-, β-, and γ-cyclodextrin remain the

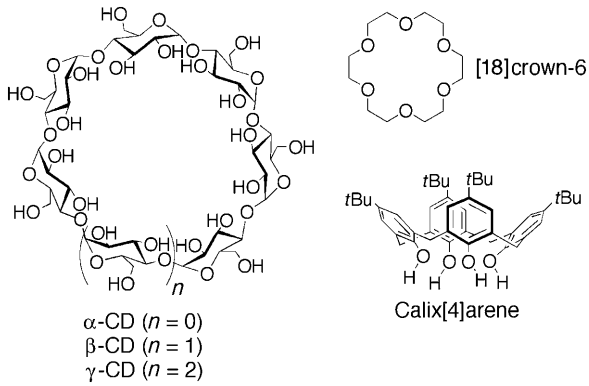


Figure 2. Structural formulas of α-, β-, and γ-cyclodextrin, [18]crown-6, and a calix[4]arene.

receptors of choice for industrial applications—despite a range of potential limitations which include low affinity, low selectivity, and challenges in their selective functionalization—because they are commercially available and inexpensive.

In this Review we trace the development of the supramolecular chemistry of CB[6] from its early days when it was plagued by issues—including poor solubility in aqueous and organic media, a lack of a homologous series of different sized hosts (for example, CB[*n*]), and an inability to access CB[*n*] derivatives and analogues by tailor-made synthetic procedures—to the present day when the CB[*n*] family is emerging as an outstanding platform for fundamental and applied molecular recognition and self-assembly studies. We, and others, believe that the CB[*n*] family is even poised to compete with the cyclodextrins as the platform of choice in industrial-scale applications. Today, the CB[*n*] family has overcome all of these early issues and currently possesses a confluence of properties that suggest their high potential in nanotechnology as components of molecular machines. These properties now include: 1) commercial availability in four different sizes, 2) binding interactions of high affinity, 3) high selectivity of binding, 4) synthetic control over size, shape, and functional-group placement, 5) high structural integrity, 6) solubility in both organic and aqueous solution, 7) association and dissociation with controlled kinetics, and 8) control of the molecular recognition processes by suitable electrochemical, photochemical, and chemical stimuli.

First, we begin with a discussion of the synthesis of CB[*n*] as well as their fundamental chemical and physical properties. Second, we present the recognition properties of the CB[*n*] family. In this section we emphasize the behavior of the most widely studied cucurbit[*n*]uril, CB[6], with an emphasis on those aspects of its recognition behavior—protonation, metal binding, selectivity based on size, shape, and charge, and the mechanism of binding—that are likely to apply universally to the CB[*n*] family. Third, we discuss the use of chemical, photochemical, and electrochemical stimuli to control recognition processes within CB[*n*]. Fourth, we discuss some applications of the CB[*n*] family in areas including catalysis,



Lyle Isaacs was born in New York City. After obtaining a BS from the University of Chicago (1991) he joined the group of Prof. François Diederich at the University of California, Los Angeles and then the ETH, Zürich. He was awarded the Silver Medallion of the ETH for his doctoral dissertation (1995). After a postdoctoral fellowship with Prof. George Whitesides at Harvard, he joined the faculty in the Department of Chemistry and Biochemistry at the University of Maryland, College Park in 1998 and was promoted to Associate Professor in 2004. His research interests focus on self-assembly, self-sorting, cucurbit[n]urils, and molecular clips.



Pritam Mukhopadhyay was born in Calcutta, India and obtained his BS and MS from the University of Calcutta and the University College of Science and Technology, respectively. He received his PhD from the Indian Institute of Technology, Kanpur in 2002 under the guidance of Professor Parimal K. Bharadwaj. He is currently a postdoctoral fellow with Professor Isaacs working on self-sorting systems involving cucurbit[n]urils.



Jason Lagona was born in Rochester, New York and earned his BS in Chemistry from the University of Maryland, College Park in 1999. He is currently pursuing his PhD with Professor Isaacs on the synthesis and applications of cucurbit[n]uril analogues.



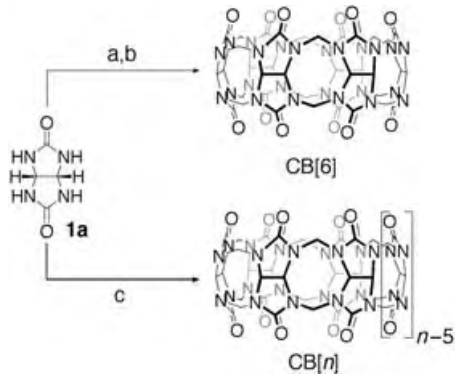
Sriparna Chakrabarti was born in Calcutta, India and obtained her BS and MS from the University of Calcutta and the University College of Science and Technology, respectively. She received her PhD from the Indian Institute of Technology, Kanpur under the guidance of Professor Hiriyakkanavar Ila. She is currently a postdoctoral fellow with Professor Isaacs working on cucurbit[n]urils.

 © 2005 Wiley-VCH Verlag GmbH & Co. KGaA, Weinheim

self-assembled monolayers, waste-stream remediation, DNA binding, gene transfection, and ion channels. Next, we discuss the use of the various CB[*n*] as components of molecular necklaces, rotaxanes and psuedorotaxanes, supramolecular amphiphiles, and self-sorting systems generated by self-assembly processes in solution and by crystal engineering in the solid state. Lastly, we discuss some mechanistic aspects of CB[*n*] synthesis based on our studies of the methylene-bridged glycoluril dimer as a model system and show how these insights lead to the synthesis of CB[*n*] derivatives, analogues, and congeners.

2. Synthesis of CB[n]

In the condensation of glycoluril (**1a**) and formaldehyde, neither Behrend et al. nor Mock detected any macrocyclic compounds (homologues) composed of a different number of glycoluril rings (for example, CB[5], CB[7], and CB[8]). It was not until nearly 20 years later when this reaction was conducted under milder, kinetically controlled conditions by the research groups of Kim and Day that CB[5]–CB[8] and CB[5]@CB[10] were detected and isolated (Scheme 1).[7–9,58]



Scheme 1. Synthesis of CB[6] from **1a** under forcing conditions and a mixture of CB[n] under milder conditions. a) CH_2O, HCl, heat; b) H_2SO_4; c) CH_2O, HCl, 100 °C, 18 h.

3. Fundamental Properties of CB[n]

3.1. Dimensions

CB[*n*] are cyclic methylene-bridged glycoluril oligomers whose shape resembles a pumpkin. Figure 3 shows the X-ray crystal structures for CB[5]–CB[8] and CB[5]@CB[10]. The cavity of CB[6] in the solid state contains three H-bonded H_2O molecules which can be released upon guest binding. The defining features of CB[5]–CB[10] are their two portals lined by ureido carbonyl groups that provide entry to their hydrophobic cavity.[59] Similar to the cyclodextrins, the various CB[*n*] have a common depth (9.1 Å), but their equatorial widths, annular widths *a*, and volumes vary systematically with ring size (Table 1). The portals guarding the entry to CB[*n*] are approximately 2 Å narrower than the cavity itself which results in constrictive binding that produces significant steric barriers to guest association and dissociation.[60] The cavity sizes available in the CB[*n*] family span and exceed those available with the cyclodextrins.

3.2. Solubility, Acidity, and Stability

One of the potential limitations of the CB[*n*] family is their relatively poor solubility in water: CB[6] and CB[8] are essentially insoluble, whereas CB[5] and CB[7] possess modest solubility in water (Table 1). The solubility of the CB[*n*] family is generally lower than the cyclodextrins. Like urea itself, however, the carbonyl groups lining the portals of CB[*n*] are weak bases: the pK_a value of the conjugate acid of CB[6] is 3.02. Although the pK_a values for CB[5], CB[7], and CB[8] have not been measured, they are likely to be similar to that of CB[6]. Accordingly, the solubility of CB[5]–CB[8] increase dramatically in concentrated aqueous acid (for example, 61 mM for CB[6] in HCO_2H/H_2O (1:1), about

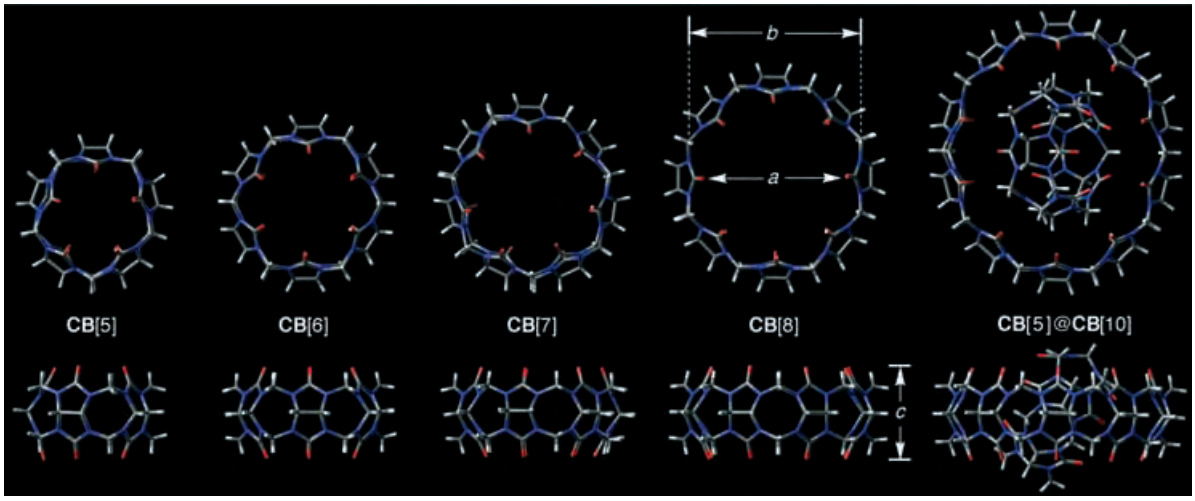


Figure 3. Top and side views of the X-ray crystal structures of CB[5],[7] CB[6],[2] CB[7],[7] CB[8],[7] and CB[5]@CB[10].[9] The various compounds are drawn to scale.

© 2005 Wiley-VCH Verlag GmbH & Co. KGaA, Weinheim

Table 1: Dimensions and physical properties of CB[*n*] and the cyclodextrins.

	M_r	a [Å][a]	b [Å][a]	c [Å][a]	V [Å^3]	s_{H_2O} [mM]	Stability [°C]	pK_a
CB[5]	830	2.4[5]	4.4[5]	9.1[5]	82[5]	20–30[5]	>420[5]	
CB[6]	996	3.9[5]	5.8[5]	9.1[5]	164[5]	0.018[61]	425[62]	3.02[63]
CB[7]	1163	5.4[5]	7.3[5]	9.1[5]	279[5]	20–30[5]	370[5]	
CB[8]	1329	6.9[5]	8.8[5]	9.1[5]	479[5]	<0.01[5]	>420[5]	
CB[10][b]	1661	9.0–11.0	10.7–12.6	9.1	–	–	–	–
α-CD	972	4.7[64]	5.3[64]	7.9[64]	174[64]	149[64]	297[65]	12.332[64]
β-CD	1135	6.0[64]	6.5[64]	7.9[64]	262[64]	16[64]	314[65]	12.202[64]
γ-CD	1297	7.5[64]	8.3[64]	7.9[64]	427[64]	178[64]	293[65]	12.081[64]

[a] The values quoted for a, b, and c for CB[*n*] take into account the van der Waals radii of the relevant atoms. [b] Determined from the X-ray structure of the CB[5]@CB[10] complex.[9]

60 mM for CB[5], about 700 mM for CB[7], and about 1.5 mM for CB[8] in 3 M HCl).[66–68] One of the outstanding features of CB[5]–CB[8] is their high thermal stability: thermal gravimetric analysis shows this to exceed 370 °C in all cases.

3.3. Electrostatic Potential

Electrostatic effects can play a crucial role in molecular recognition events in both aqueous and organic solution.[69] Figure 4 shows the electrostatic potentials of β-CD and CB[7]. Clearly, the electrostatic potential at the portals and within the cavity of CB[7] is significantly more negative than for β-CD. This difference in electrostatic potential has significant consequences for their recognition behavior: CB[*n*] exhibit a pronounced preference to interact with cationic guests whereas β-CD prefers to bind to neutral or anionic guests.

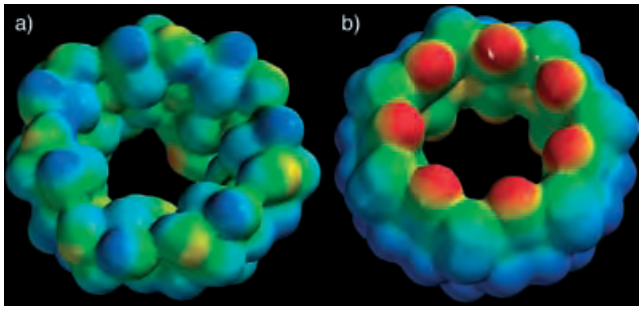


Figure 4. Electrostatic potential maps for a) β-CD and b) CB[7]. The red to blue color range spans −80 to 40 kcal mol^{-1}. Adapted from Kim and co-workers.[5]

4. Host–Guest Chemistry of CB[n]

The recognition properties of CB[6] are compared with those of α-CD and [18]crown-6 in this section. Many of the lessons learned from the chemistry of CB[6] can be generalized to the whole CB[*n*] family.

4.1 Comparison of the Thermodynamics of Complexation

Houk et al. recently reviewed the binding affinities for a wide variety of systems including synthetic host–guest, antibody–antigen, receptor–drug, and enzyme–substrate complexes.[70] The average binding affinity for 1257 α-, β-, and γ-CD complexes[71] ($K_a = 10^{2.5\pm1.1}$ M^{-1}) is an order of magnitude smaller and more narrowly distributed than the corresponding value for 973 synthetic host–guest pairs in water ($K_a = 10^{3.4\pm1.6}$ M^{-1}). A similar analysis using the 56 CB[6]·guest pairs reported by Mock and Shih[72] yields $K_a = 10^{3.8\pm1.5}$ M^{-1}. Table 2 compares the affinity of α-CD and CB[6] toward a series of alcohols, which are modest guests for both hosts. Despite its preference to interact with positively charged guests, CB[6] binds more tightly to the alcohols (except hexanol) than does α-CD although it does so in a nonselective manner. In general, CB[6] binds with higher affinity and higher selectivity toward its guest than do the cyclodextrins. A similar comparison between the affinity of CB[6] and [18]crown-6 toward several monovalent and divalent cations is given in Table 3. CB[6] shows higher affinity than [18]crown-6 toward all cations except Ba^{2+}, whose radius is a good match for the cavity of [18]crown-6. These examples are intended to illustrate that the binding ability of CB[6] generally equals or exceeds those of other well-known host molecules such as cyclodextrins and crown ethers.

Table 2: Calorimetrically determined log *K* values for the complexation of alcohols with CB[6] in HCO_2H/H_2O (1:1) at 25 °C and with α-CD in H_2O.[73,74]

	CH_3CH_2OH	$CH_3(CH_2)_2OH$	$CH_3(CH_2)_3OH$	$CH_3(CH_2)_4OH$	$CH_3(CH_2)_5OH$
CB[6]	2.64	2.61	2.53	2.73	2.71
α-CD	0.99	1.46	1.91	2.51	2.90

Table 3: Calorimetrically determined log *K* values for the complexation of monovalent and divalent cations with CB[6] in HCO_2H/H_2O (1:1) at 25 °C and with [18]crown-6 in water.[66,75]

	Li^+	Na^+	K^+	Rb^+	Ca^{2+}	Sr^{2+}	Ba^{2+}
CB[6]	2.38	3.23	2.79	2.68	2.80	3.18	2.83
[18]crown-6	–	0.80	2.03	1.56	<0.5	2.72	3.87

 © 2005 Wiley-VCH Verlag GmbH & Co. KGaA, Weinheim

4.2 Lessons Learned from CB[6]

Compared to CB[6], which recently celebrated its 100th birthday, the supramolecular chemistry of CB[5], CB[7], CB[8], and CB[10], which were isolated only 5 years ago, is relatively undeveloped. While these CB[*n*] homologues promise much new chemistry, many of the basic lessons learned from the studies of CB[6] can, we hypothesize, be transferred to CB[*n*]. This section presents those lessons from a largely mechanistic viewpoint: Scheme 2 depicts a comprehensive mechanism for the interaction of CB[6] with protons, metal ions, amines, and ammonium ions.

4.2.1. Protonation of CB[6] at the Carbonyl Groups Lining the Portals

CB[6] is a weak base ($pK_a = 3.02$) that can be protonated in moderately acidic media. Accordingly, when binding studies are conducted with CB[6] in strongly acidic media (for example, HCO_2H/H_2O (1:1)) H^+ competes with guest binding (Scheme 2, red equilibria). Comparisons between binding constants measured in different media must, therefore, be treated with caution.

4.2.2. Binding of Metal Ions by CB[6]

Given that CB[6] binds H^+ at the ureido carbonyl groups of the portals, it is perhaps unsurprising that CB[6] also binds alkali-metal, alkaline-earth, transition-metal, and lanthanide cations in homogenous solution (Scheme 2, blue equilibria).[4,63,66,67,76–79] Table 3 shows the binding constants determined by Buschmann et al. for CB[6] with a variety of monovalent and divalent cations. The selectivity between the different cations is less than tenfold. The low selectivity observed and the lack of a simple trend in $\log K$ values is attributed to a mismatch between the ionic radii of the cations and the annular radius of the relatively rigid CB[6] ionophore (1.95 Å). The metal-binding equilibria (Scheme 2, blue equilibria) are in competition with protonation (red equilibrium); thus, as the acidity of the solution is increased the observed $\log K$ values for metal binding should decrease. Table 4 documents the decrease in the $\log K$ value of 2.4 units observed for CB[6]·Ba^{2+} upon changing the medium from water to water/HCO_2H (1:1).

Table 4: Calorimetrically determined log *K* values for the complexation of Ba^{2+} with CB[6] in HCO_2H/H_2O mixtures at 25 °C.[66,75]

HCO_2H/H_2O	50:50	40:60	30:70	25:75	0:100
log *K*	2.83	3.50	4.13	4.39	5.23

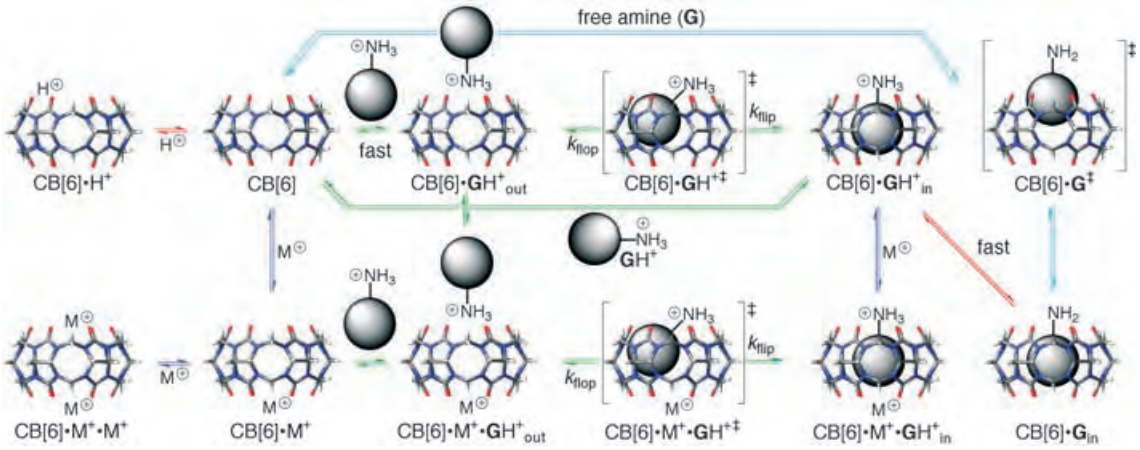
4.2.3. Preference of CB[6] for Positively Charged Organic Guests—Ion–Dipole Interactions

In their pioneering work, Mock and co-workers observed by a series of ^1H NMR competition experiments that alkylammonium ions bind tightly to CB[6] in HCO_2H/H_2O (1:1) and measured binding constants of 10^1–$10^7\ M^{-1}$. A selection of the results are given in Table 5.[2,72,80–82] Buschmann and coworkers have measured the corresponding thermodynamic parameters (ΔH and ΔS).[83] The experiments carried out by Mock and Shih were facilitated by two unusual characteristics

Table 5: Association constants measured for CB[6] with a variety of amines in H_2O/HCO_2H (1:1) at 40 °C.

Entry	Amine	K_a [M^{-1}]
1	NH_3	83
2	$H_2N(CH_2)_6H$ (**2**)	2300
3	$H_2N(CH_2)_6OH$ (**3**)	1200
4	$H_2N(CH_2)_6NH_2$ (**4**)	2800000
5	c-$(CH_2)_2CHCH_2NH_2$ (**5**)	15000
6	c-$(CH_2)_3CHCH_2NH_2$ (**6**)	370000
7	c-$(CH_2)_4CHCH_2NH_2$ (**7**)	330000
8	c-$(CH_2)_5CHCH_2NH_2$ (**8**)	80[a], 110000[b]
9	4-$MeC_6H_4CH_2NH_2$ (**9**)	320
10	3-$MeC_6H_4CH_2NH_2$ (**10**)	n.d.[c]
11	2-$MeC_6H_4CH_2NH_2$ (**11**)	n.d.[c]
12	$H_2N(CH_2)_5NH_2$ (**12**)	2400000
13	$H_2N(CH_2)_2S(CH_2)_2NH_2$ (**13**)	420000
14	$H_2N(CH_2)_2O(CH_2)_2NH_2$ (**14**)	5300

[a] Ref. [85]. [b] Measured for the hydrochloride salt in D_2O.[60] [c] n.d. = no binding detected.



Scheme 2. Comprehensive mechanistic scheme for molecular recognition by CB[6]. Red arrow: protonation; Blue arrow: cation binding, green arrow: ammonium ion binding, light blue arrow: amine binding.

© 2005 Wiley-VCH Verlag GmbH & Co. KGaA, Weinheim

of the host–guest complexes of CB[6]. First, the interior of CB[6] constitutes a ^{1}H NMR shielding region and upfield shifts of 1 ppm are common. The regions just outside the portals lined with carbonyl groups are weakly deshielding. Second, dynamic exchange processes between free and bound guest are often slow on the NMR time scale, thus allowing a direct observation of the free and bound guest simultaneously. To establish the importance of ion–dipole interactions relative to hydrogen bonds in the formation of CB[6] complexes (Figure 5), Mock and Shih considered the relative

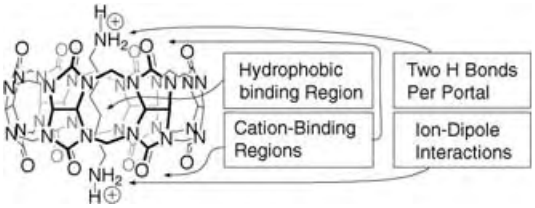


Figure 5. Representation of the different binding regions of CB[6] and the geometry of the complex between CB[6] and the hexanediammonium ion.

binding affinities of **2**–**4** (Table 4, entries 2–4). "Formal replacement of the terminal hydrogen of *n*-hexylamine with another amino group enhances binding 1200-fold. […] However, replacement of this hydrogen by a *hydroxyl* group contributes nothing to the stabilization of the complex. […] While the alcohol (and ammonium ions) may be hydrogen bonded in the complex, in the absence of CB[6] they would also be fully hydrogen bonded. […] The consequential feature of ammonium ions is that they are *charged*. […] Hence, it is our understanding that the high specificity for ammonium ions is largely an electrostatic *ion–dipole attraction*."[72] The preference of CB[6] for charged guests will transfer to the other members of the CB[*n*] family, but the relative importance of electrostatic interactions versus the hydrophobic effect may change as the cavity size increases. Blatov and coworkers recently developed a computational technique based on crystallographic data to identify suitable guests for each member of the CB[*n*] family.[84]

4.2.4. *Binding Selectivity of CB[6]*

The relative rigidity of CB[6] and the close juxtaposition of two binding regions that favor positively charged groups with one that favors hydrophobic residues imparts high selectivity to the binding of CB[6] (Figure 5). For example, Mock found that alkyl amines and alkane diamines exhibit length-dependent selectivity for CB[6]. Figure 6 shows a plot of the log K_a value versus chain length. CB[6] prefers butylamine relative to propylamine (8-fold) and pentylamine (4-fold) whereas pentanediamine and hexanediamine are preferentially bound relative to butanediamine (15-fold) and heptanediamine (64-fold). These high selectivities have been used to construct molecular switches (see Section 5.1). CB[6] is also size-selective: for example, it forms stable complexes with **6** and **7** whereas the three- and six-membered ring analogues **5** and **8** are rejected by CB[6] (Table 4, entries 5–8).

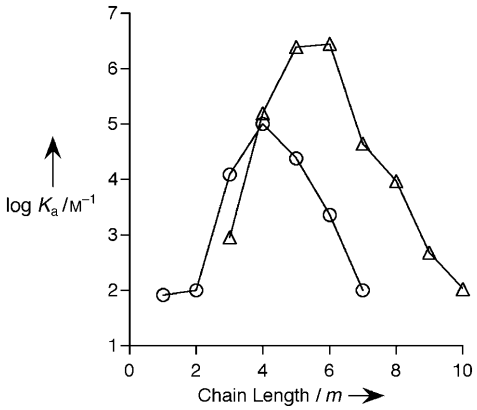


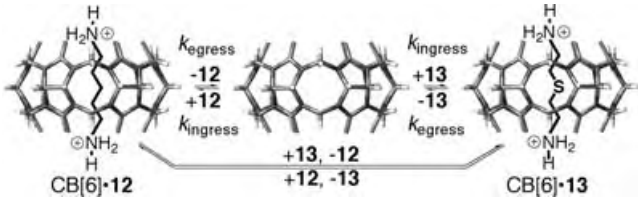
Figure 6. Relationship between the binding constant (log K_a) versus chain length m for $H(CH_2)_mNH_3^+$ (○) and $^+H_3N(CH_2)_mNH_3^+$ (△).

Similarly, CB[6] selects guests based on shape. For example, even though **7** and **9** have similar included volumes (86 versus 89 Å^3), the former binds 1000-fold more strongly (Table 4, entries 7 and 9).[60] Similarly, **9** is included within CB[6] whereas the *ortho* and *meta* isomers **10** and **11** are not bound (Table 4, entries 9–11). Lastly, CB[6] displays functional-group selectivity. For example, **12** binds 6-fold more tightly than **13**, which in turn binds 79-fold more tightly than **14** (Table 4, entries 12–14). Mock and Shih attribute this trend "to a solvation effect operating primarily on the uncomplexed guest; oxygen has greater intrinsic hydrophilicity than does sulfur, and a methylene group is more hydrophobic than is a thioether linkage."[72]

4.2.5. *Mechanistic Aspects of Association, Dissociation, and Exchange of Guests*

If CB[6] and other members of the CB[*n*] family are to become important components of molecular machines, it is critical that the factors controlling the kinetic and mechanistic aspects of their recognition behavior be thoroughly understood. In contrast to the behavior of most synthetic receptors in aqueous solution, CB[6] commonly displays slow kinetics of guest association, dissociation, and exchange on the NMR time scale. As discussed in Sections 4.2.1 and 4.2.2, CB[6] readily binds protons and metal ions at its portals that are lined with carbonyl groups. These equilibria compete with guest binding and lower the K_a value for guest binding accordingly (Scheme 2, red and blue equilibria).

Mock and Shih initially investigated the kinetics of guest exchange[72,82] according to the two limiting mechanisms shown in Scheme 3: 1) an associative mechanism that resem-



Scheme 3. Associative and dissociative mechanisms for guest exchange.

 © 2005 Wiley-VCH Verlag GmbH & Co. KGaA, Weinheim

bles an S_N2 reaction, and 2) a dissociative S_N1-like mechanism. The kinetics of displacement, which can be followed by ^{1}H NMR spectroscopy, are first order in the CB[6]·**12** complex and independent of the concentration of the displacing guest which implies that the dissociative S_N1-like mechanism is followed. Values of k_{egress} range from $1.6\times10^{-5}\ s^{-1}$ (CB[6]·**7**) to $>10^2\ s^{-1}$ (CB[6]·**5**), which allowed the calculation of $k_{ingress}$ values of CB[6]·**7**: $5.5\ M^{-1}\ s^{-1}$; CB[6]·**5**: $>10^6\ M^{-1}\ s^{-1}$ based on a knowledge of the K_a value ($K_a = k_{ingress}/k_{egress}$). Interestingly, the rates of ingression *do not* correlate with values of K_a. Instead, the rates of ingression are influenced by the width of the guest (**7**: 5.7 Å) when that width exceeds the diameter of the portal of CB[6] lined with carbonyl groups (3.9 Å). Accordingly, significant deformation of the portals of CB[6] must occur in the transition state for ingression to allow access to its interior which raises its free energy and reduces the $k_{ingress}$ value. Although CB[6] is commonly regarded as being a rigid host, it is subject to deformation in the transition states during ingression and egression of the guests and even in the ground state of its complexes. For example, the X-ray crystal structure of CB[6]·4-Me$C_5H_4NH^+$ shows an ellipsoidal-shaped macrocycle that is elongated by 1.31 Å along the plane defined by the guest molecule.[86] Even larger deformations can be observed during molecular mechanics calculations of larger CB[*n*] complexes and even in the X-ray crystal structure of CB[5]@CB[10] which shows an ellipsoidal deformation of 2.1 Å.[9]

4.2.6. *Association and Dissociation Proceed via a Transiently Formed Exclusion Complex*

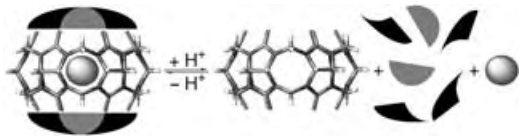
Mock and Shih recognized the possibility of two different modes of binding for an ammonium ion guest: the formation of an inclusion complex and an exclusion complex (for example, Scheme 2, CB[6]·**G**H^+_{in} and CB[6]·**G**H^+_{out}).[72] The equilibrium between those two isomeric complexes depends mainly on the size and shape of the attached alkyl groups. In a seminal study Knoche, Buschmann, and co-workers monitored the binding of **9**H^+ to CB[6] by UV/Vis measurements and found that the observed kinetic behavior could not be adequately explained by a simple equilibrium between CB[6], **9**H^+, and CB[6]·**9**H^+. Adequate modeling of the data requires the existence of two complexes: one in a fast pre-equilibrium with CB[6] and a second representing the spectroscopically observed inclusion complex CB[6]·**9**H^+_{in}.[4] Knoche, Buschmann, and co-workers proposed that the exclusion complex CB[6]·**9**H^+_{out} (shown in Scheme 2 as the general form CB[6]·**G**H^+_{out}) is the intermediate in fast pre-equilibrium. Nau and co-workers recently suggested that the transition state connecting the exclusion complex to the inclusion complex can be described by a flip-flop process (for example, Scheme 2, [CB[6]·**G**H^+]‡) in which the appended alkyl group pivots into the cavity without breaking its N-H···O hydrogen bonds.[60,85]

4.2.7. *pH-Dependency of the Transition States*

Although Mock and Shih showed early on that the rate of guest exchange does not respond to changes in pH in acidic solution (pH 1–4) they were unable to work at higher values of pH because of the limitations of the solvent mixture employed (HCO_2H/D_2O (1:1)). In important contributions, Nau and co-workers have studied the complexation of CB[6] with **8** as a function of pH (1–12), temperature (25–72 °C), cation identity, and cation concentration.[60,85] Most interestingly, the value of K_a is nearly constant in the region between the pK_a of CB[6] (3.02) and the pK_a of **8**H^+ (10.50); at lower and higher pH values, the value of K_a decreases as either H^+ competes with **8**H^+ for CB[6] (Scheme 2, red equilbria) or as the complex CB[6]·**8**H^+ is deprotonated to yield amine complex CB[6]·**8**. The rate constants for ingression and egression undergo dramatic increases near the pK_a of **8** and CB[6]·**8**H^+ (11.75), respectively. These dramatic changes can be explained by the involvement of the free amine **8** in the ingression and egression process (Scheme 2, **G**). Accordingly, Nau and co-workers included a new set of equilibria involving CB[6] and **8** into our general mechanistic understanding of CB[6] complexation (Scheme 2, light blue arrows). The free amine undergoes egression ($k_{egress}(\mathbf{8}) = 4.7\times10^{-6}\ s^{-1}$, $k_{egress}(\mathbf{8}H^+) = 1.45\times10^{-3}\ s^{-1}$) over 300-fold faster than its ammonium ion form. Similarly, the ingression rate constant ($k_{ingress}(\mathbf{8}) = 0.0145\ M^{-1}s^{-1}$, $k_{ingress}(\mathbf{8}H^+) = 8.0\times10^{-4}\ M^{-1}s^{-1}$) was 18-fold larger for the free amine. These results are extremely important for the development of molecular machines based on CB[*n*] since they indicate that not only can complexation be turned on and off by changes in pH, but also that the operational speed can be changed (up or down) by more than an order of magnitude.

4.2.8. *Studies on CB[6] in Saline Solution*

One of the major challenges that has faced the study of the CB[*n*] family is their poor solubility in aqueous and organic solution. For this reason, the majority of quantitative studies of binding with CB[6] have used HCO_2H/H_2O (1:1) as the solvent. It was known as early as 1992 that CB[6] binds to alkali and alkaline-earth cations in pure water and reaches a higher saturation concentration.[63] For example, the solubility of CB[6] increases dramatically in 0.2 M Na_2SO_4 (66 mM), LiCl (0.94 mM), KCl (37 mM), CsCl (59 mM), and $CaCl_2$ (70 mM). It was not until 1996, however, when Kim and co-workers reported that the solubilization of CB[6] in aqueous saline solution allows the study of guest binding in neutral water that the full importance of this discovery was realized.[87] The X-ray crystal structure of CB[6]·Na_4·$(H_2O)_{17}$·$(SO_4)_2$·THF revealed that the sodium ions act as lids that result in the encapsulation of THF (Scheme 4). Even more remarkably, the addition of CF_3CO_2H releases THF from this CB[6]·THF complex ($K_a = 510\ M^{-1}$) by competitive binding;[88] the process can be reversed by the addition of Na_2CO_3. In a related paper,



Scheme 4. Adding a lid to CB[6] and its removal. Sphere: THF, hemispheres: Na^+, wedges: H_2O.

© 2005 Wiley-VCH Verlag GmbH & Co. KGaA, Weinheim

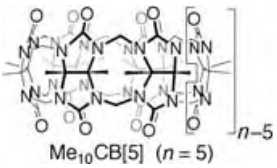
Kim and co-workers showed that the lids are not merely innocent by-standers, they actively participate in the binding of THF through formation of cesium–oxygen bonds.[89] Despite the reduced binding constants arising from competition with metal ions in solution, these pioneering studies showed that the supramolecular chemistry of CB[*n*] would not be limited to strongly acidic conditions. Currently, hydrochloride salts of suitable guests are often employed for the investigations since the resulting complexes are rendered water soluble in the absence of competing H^+ or M^+ ions.

4.3. Host–Guest Properties of the Homologues

We have focused on selected examples to illustrate the general principles and applications of CB[*n*] chemistry. There are, of course, a wealth of elegant contributions from numerous research groups that we have not been able to cover. This section highlights those examples that are not presented elsewhere in this Review.

4.3.1. CB[5] and Me_{10}CB[5]

The supramolecular chemistry of CB[5] and Me_{10}CB[5][90] (see Section 8.4) is controlled by the narrow portals lined with carbonyl groups which provide entry to a cavity of low



Me_{10}CB[5] ($n = 5$)

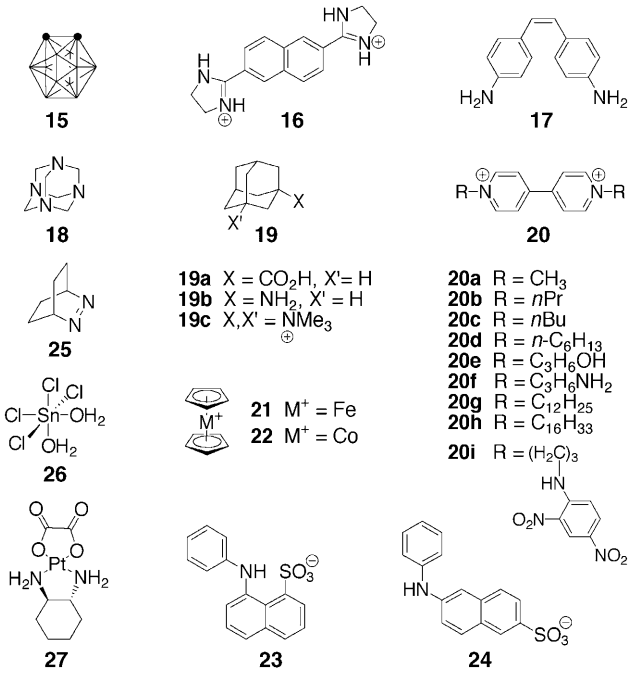
volume. Consequently, much of the supramolecular chemistry of CB[5] has been limited to the binding of protons as well as metal and ammonium ions at their portals.[67,68,76,77,79,91] Bradshaw, Izatt, and co-workers studied the ability of Me_{10}CB[5] to bind monovalent and divalent cations in HCO_2H/H_2O (1:1) and found a remarkably high selectivity toward Pb^{2+} ions ($> 10^{5.5}$ relative to alkali cations).[79] Somewhat surprisingly, CB[5] itself does not display a similar selectivity for Pb^{2+} ions.[76] CB[5] and Me_{10}CB[5] form weak host–guest complexes with α-, β-, and γ-cyclodextrins ($K_a \approx 10$).[61] Recently, Tao and co-workers reported that hexamethylenetetramine is capable of forming a lid on CB[5].[92] The most remarkable property of CB[5] and Me_{10}CB[5] is their ability to bind gases[93] (for example, Kr, Xe, N_2, O_2, Ar, N_2O, NO, CO, CO_2, and CH_4) and small solvents (for example, CH_3OH and CH_3CN). Such complexes were observed by Dearden and co-workers[91,94,95] by mass spectrometric investigations, by Miyahara et al.[96] in aqueous solution and the solid state, and discussed by Day[34,41] and Miyahara[45] in the patent literature. Miyahara demonstrated the reversible sorption and desorption of gas by solid Me_{10}CB[5], with capacities up to 40 mL g^{-1} (N_2O). These results suggest that Me_{10}CB[5] and CB[5] may be of practical utility in reducing the level of NO_x gases from air.

4.3.2. CB[6]

The pioneering work of Buschmann et al. has established equilibrium constants and in many cases the enthalpic (ΔH) and entropic (ΔS) contributions to ΔG for the binding of CB[6] to ω-amino acids and ω-amino alcohols,[97] aliphatic alcohols, acids, and nitriles,[73] bipyridine derivatives,[98] aromatic compounds,[99,100] non-ionic surfactants and poly(ethylene glycols),[101] cyclodextrins,[61] diamides,[102] and α-amino acids and dipeptides.[103] Analogous to CB[6]·M^+ complexes, the values of K_a measured for the complexation of organic guests with CB[6] increase as the percentage of HCO_2H decreases as a result of reduced competitive protonation of CB[6].[104] Knoche and co-workers studied the complexation of azobenzenes with CB[6],[4,105] Bartik and co-workers the binding of neutral guests such as Xe, THF, and CF_3CO_2H in CB[6] by ^{129}Xe, ^{19}F, and ^{1}H NMR spectroscopy,[88,106] and Dearden and co-workers the formation and dissociation of CB[6] pseudorotaxanes and the corresponding exclusion complexes in the gas phase.[91] The research groups of Wagner and Buschmann have shown that CB[6] enhances the fluorescence of 1,6- and 2,8-anilinonaphthalene sulfonates in solution and the solid state,[107–109] while Wu and co-workers shown recently that CB[6] also binds diazonium compounds.[110]

4.3.3. CB[7]

CB[7] is slightly more voluminous than β-CD (Table 1), and thus can bind a wider range of guests than CB[6] or CB[5]. CB[7] binds a variety of positively charged aromatic compounds including adamantanes and bicyclooctanes,[5,92,111,112] naphthalene,[7,113,114] stilbene,[115] viologen,[116–120] *o*-carborane,[121] ferrocene,[5,122] and cobaltocene[122] derivatives (**15**–**25**). CB[7] also binds the metal complexes



 © 2005 Wiley-VCH Verlag GmbH & Co. KGaA, Weinheim

26[123] and **27**[5,41] as well as related compounds[124,125] which suggests the use of CB[7] to reduce toxicity in cancer treatment.

A number of elegant studies by Kaifer and co-workers have demonstrated that many of the unusual properties of CB[6] are retained by CB[7]. For example, Ong and Kaifer determined the values of K_a for CB[7]·**20a** in 0–0.2 M NaCl and 0–0.2 M $CaCl_2$ and demonstrated that Na^+ and Ca^{2+} ions compete with **20a** for binding to CB[7] which reduces the K_a value by a factor of 9–40.[119] In two elegant studies, the research group of Kaifer showed that the CB[7] bead can reside in different locations along guests containing multiple binding sites (for examplw, CB[7]·**20a**–CB[7]·**20g**).[120,126] CB[7] resides on the longer butyl and hexyl chains of **20c** and **20d** whereas it resides on the viologen nucleus of derivatives that contain shorter (**20a** and **20b**) or hydrophilic residues (**20e** and **20f**). These results imply that CB[7] retains the highly selective binding properties noted above for CB[6]. CB[7] forms a pseudorotaxane with **20i**. Nau and co-workers have used CB[7]·2,3-diazabicyclo[2.2.2]oct-2-ene to show that the polarizability of the CB[7] cavity is extremely low[127,128] and to distinguish between alternative mechanisms in fluorescence-quenching studies.[58,129] Wagner et al. have studied the enhancement in fluorescence observed upon binding of anilinonaphthalene sulfonates by CB[7].[113] CB[7] was recently reported to form a weak 1:2 exclusion complex with C_{60} by high-speed vibration milling,[130] and more recently CB[7] has been used as an additive to separate positional isomers by capillary electrophoresis.[131]

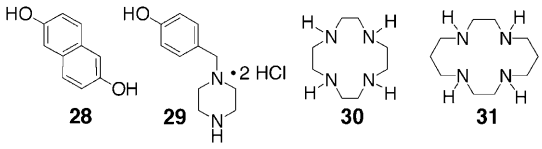
4.3.4. *CB[8]*

The cavity of CB[8] is similar in terms of volume to γ-CD, but is less conformationally flexible. CB[8] behaves like a larger version of CB[5]–CB[7] in many ways, but also exhibits more complex recognition behavior. Just like CB[5]–CB[7], CB[8] prefers to bind to positively charged guests by ion–dipole interactions.[7,132] CB[8] readily binds single guest molecules that partially (CB[8]·**20a**, $K_a = 1.1 \times 10^5\ M^{-1}$) or completely (CB[8]·**19b**) fill its cavity. In contrast to CB[5]–CB[7], the voluminous cavity of CB[8] is capable of simultaneously binding two aromatic rings (Figure 7), as shown by the ready formation of the termolecular complex CB[8]·**16**·**16**.[7,133] Even more strikingly, a mixture of CB[8] and CB[8]·$\mathbf{16}_2$ is formed when CB[8] and **16** are mixed in a 1:1 ratio. This result demonstrates there is cooperativity between the binding of the first and second aromatic rings. Kim and co-workers have also demonstrated the selective formation of a hetero-termolecular complex CB[8]·**20a**·**28** which results in



Figure 7. Schematic representations of the termolecular complexes CB[8]·**16**·**16** and CB[8]·**20a**·**28**.

enhanced charge-transfer interactions between **20a** and **28** in the complex.[134] This recognition motif has been used to



control intramolecular folding processes[135] and the formation of vesicles.[136] More recently, Tao and co-workers have shown that aromatic piperazine derivatives form a mixture of 1:1 and 1:2 complexes with CB[8] (for example, CB[8]·**29** and CB[8]·$\mathbf{29}_2$).[137] Similarly, Fedin and co-workers recently reported the crystal structure of the CB[8]·$PhPO(OH)_2$·$PhPO(OH)_2$ complex.[138] CB[8] is even capable of encapsulating cyclen (**30**) or cyclam (**31**). Even more remarkably, CB[8]·**30** and CB[8]·**31** can coordinate with Cu^{II} or Zn^{II} ions which results in macrocycle within macrocycle complexes that resemble the Russian Matrioshka dolls.[139]

4.3.5. *CB[10]*

Day et al. successfully isolated CB[10] as its CB[5]@CB[10] complex (Figure 3). The structure of this remarkable complex was established by X-ray crystallography to resemble a gyroscope.[9] Despite the fact that it was not possible to isolate free CB[10] by removal of CB[5], chemical exchange between free and bound CB[5] was demonstrated through the use of ^{13}C-labeled CB[5]. Such molecular gyroscopes and the related molecular ball bearing[121] CB[7]·**15** are potential components of future molecular machines.

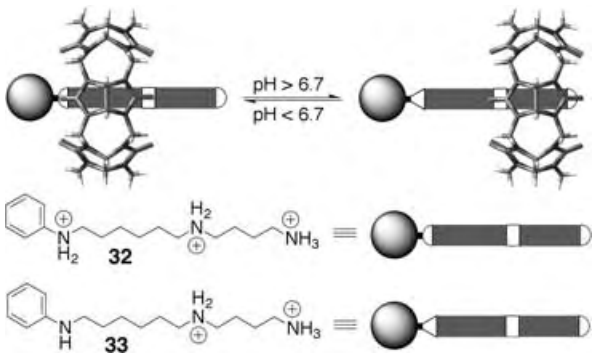
5. Control over the Recognition Processes

The creation of molecular machines[140] by self-assembly processes is currently of great interest. One of the most fundamental molecular machines is a molecular switch that can toggle between two different states by appropriate environmental stimuli (chemical, electrochemical, or photochemical). The CB[*n*] family is ideally suited for such applications because of the high affinity and high selectivity of their binding processes.

5.1. Chemical Control—Molecular Switches

An early example of a molecular switch was published by Mock and Pierpont in 1990. In this study, CB[6] was induced to shuttle along a triamine string by changing the pH value (which resulted in changes in the protonation state of the aniline N atom; Scheme 5).[141] At pH values below the pK_a value of the anilinium group (6.73), the CB[6] bead resides in the hexanediammonium region with its higher binding constant (CB[6]·**32**, left); above the pK_a value, the bead moves to the still fully protonated butanediammonium region (CB[6]·**33**, right). Kim and co-workers have reported

© 2005 Wiley-VCH Verlag GmbH & Co. KGaA, Weinheim



Scheme 5. CB[6]-based molecular switch.

molecular switches based on CB[6] rotaxanes with UV/Vis and fluorescence outputs[142] that can be actuated by changes in the pH value, but requires both the correct pH value and heat for the switch to be turned off,[143] and that a slow transformation occurs from the kinetic to the thermodynamically more-stable rotaxane.[144]

5.2. Photochemical Control

The ability of the two portals lined with carbonyl groups in the CB[*n*] family to orient two guests within their cavity (see Section 4.3.4) results in opportunities to accelerate and control chemical reactions. Kim and co-workers found that CB[8] binds two equivalents of (*E*)-**34** to form CB[8]·**34**·**34**.[145] Irradiation of this complex (300 nm, 30 min) results in the formation of CB[8]·*syn*-**35** and only a trace of CB[8]·*anti*-**35** (Scheme 6). Free **36** is released upon addition of base. The dimerization of (*E*)-**34** within γ-CD is slower (72 h) and less stereoselective (*syn*:*anti* = 80:20). CB[8] accelerates and controls the stereochemistry of the [2+2] photoreaction.

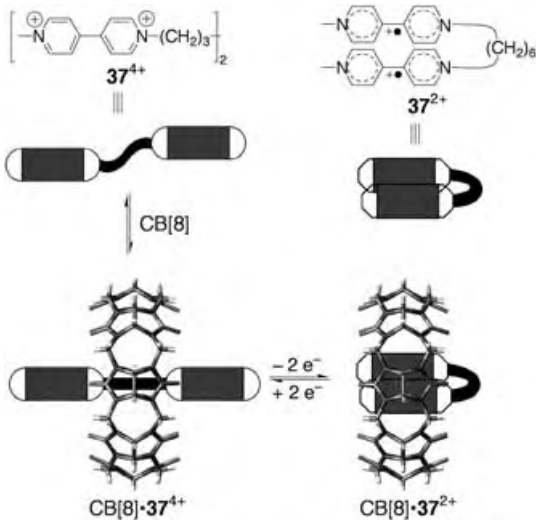
A solution of CB[7] and (*E*)-**34** forms the complex CB[7]·(*E*)-**34** which, upon irradiation (350 nm) converts nearly quantitatively into CB[7]·(*Z*)-**34**. Remarkably, CB[7]·(*Z*)-**34** is stable at room temperature for 30 days.[115] This result demonstrates that CB[7] is able to control the otherwise unfavorable equilibrium between CB[7]·(*E*)-**34** and CB[7]·(*Z*)-**34**.

5.3. Electrochemical Control

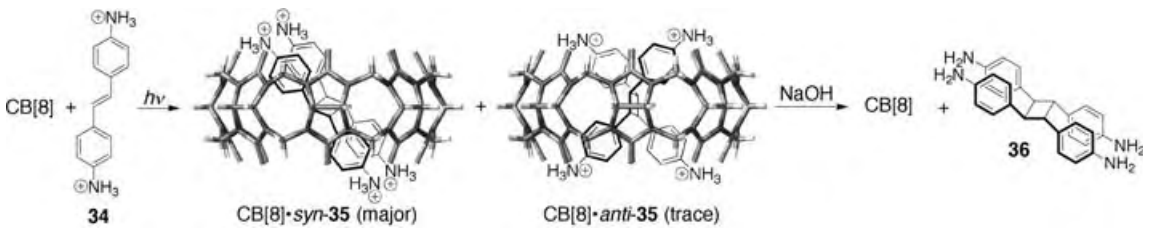
The CB[*n*] family displays a marked preference to interact with positively charged guest species. For example, the research groups of Kim[116] and Kaifer,[117] studied the interaction of CB[7] with $\mathbf{20a}^{2+}$ ($K_a = 2 \times 10^5\,\text{M}^{-1}$) and its reduced forms $\mathbf{20a}^{\bullet+}$ ($K_a = 8.5 \times 10^4\,\text{M}^{-1}$) and $\mathbf{20a}^{0}$ ($K_a = 2.5 \times 10^2\,\text{M}^{-1}$) by electrochemical measurements. Two unusual observations were made: 1) the presence of CB[7] prevents the dimerization of $\mathbf{20a}^{\bullet+}$ and 2) the reduction of $\mathbf{20a}^{\bullet+}$ occurs by a direct electron-transfer pathway. Related observations were made by Ong and Kaifer for the CB[7]·**21** and CB[7]·**22** complexes ($K \geq 10^6\,\text{M}^{-1}$).[122]

The cavity of CB[8] is large enough to accommodate two flat aromatic ring systems, provided they possess complementary electrostatic profiles (such as in the charge-transfer complex CB[8]·**20a**·**28**). Very interestingly, Kim and co-workers found that CB[8] binds a single molecule of $\mathbf{20a}^{2+}$ (CB[8]·$\mathbf{20a}^{2+}$, $K_a = 1.1 \times 10^5\,\text{M}^{-1}$); upon electrochemical reduction, however, the complex undergoes disproportionation to form a mixture of CB[8] and the termolecular complex CB[8]·$\mathbf{20a}^{\bullet+}$·$\mathbf{20a}^{\bullet+}$.[132a] The presence of CB[8] enhances the dimerization of $\mathbf{20a}^{\bullet+}$ by a factor of 10^5. Thus, electrochemistry allows quantitative control of the stoichiometry of the host–guest complex within CB[8]!

The dimerization of the tetrathiafulvalene radical cation is also promoted by CB[8].[146] Armed with this knowledge, Kim and co-workers prepared dimeric viologen $\mathbf{37}^{4+}$.[132b] This compound forms a stable 1:1 complex with CB[8] (CB[8]·$\mathbf{37}^{4+}$, $K_a = 2.3 \times 10^5\,\text{M}^{-1}$) where the CB[8] bead resides mainly on the hexamethylene spacer (Scheme 7). Electrochemical reduction (or light-induced chemical reduction with $[\text{Ru}^{\text{II}}(\text{bpy})_3]$) effects a folding process which results in the formation of molecular loop CB[8]·$\mathbf{37}^{2+}$ which displays dramatically reduced dimensions relative to CB[8]·$\mathbf{37}^{4+}$ (28 × 18 versus



Scheme 7. A [2]pseudorotaxane-based molecular machine.



Scheme 6. [2+2] photoaddition reaction mediated by CB[8].

 © 2005 Wiley-VCH Verlag GmbH & Co. KGaA, Weinheim

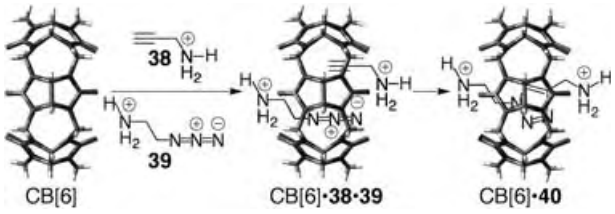
15 × 18 Å). The observed large changes in size and shape may be useful in the design of molecular actuators.[132c]

6. Applications of the CB[n] Family

The outstanding recognition properties of the CB[*n*] family have led to their use in numerous applications, some of which are highlighted in this section.

6.1. Catalysis

A long-standing challenge in supramolecular chemistry has been the design of catalysts. Mock et al. recognized that CB[6] was ideally suited for this purpose because of the presence of two portals lined with carbonyl groups that can potentially recognize two ammonium ions, thus forming a termolecular complex that orients and compresses those substrates for chemical reaction.[147,148] Mock et al. studied the dipolar cycloaddition between azide **38** and alkyne **39** catalyzed by CB[6] in an elegant example of click chemistry

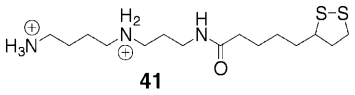


Scheme 8. Catalysis of a [3+2] dipolar cycloaddition inside CB[6].

(Scheme 8).[149] They found that the CB[6]-catalyzed reaction of **38** and **39** is a rare example of what is known as the Pauling principle of catalysis, which states that "the complementarity between an enzyme and the *transition state* for its conducted reaction ought to be greater than that between enzyme and the reactants".[147] Remarkably, CB[6] accelerates this reaction by a factor of 5.5×10^4 compared to the bimolecular reaction and renders it highly regioselective. The reaction also displays several features that are commonly observed in enzymatic reactions, namely: 1) reaching a limit in the reaction rate at high concentrations of **38** and **39**, 2) product release from CB[6]·**40** is rate-limiting, 3) inhibition of the substrate through formation of nonproductive termolecular complex CB[6]·**38**·**38**, and 4) competitive inhibition by nonreactive substrate analogues. Steinke's research group has used the CB[6]-promoted dipolar cycloadditon of azides and terminal acetylenes for the preparation of catalytically self-threading rotaxanes,[150,151] [2]-, [3]-, and [4]-rotaxanes and pseudorotaxanes,[152] as well as oligotriazoles.[153]

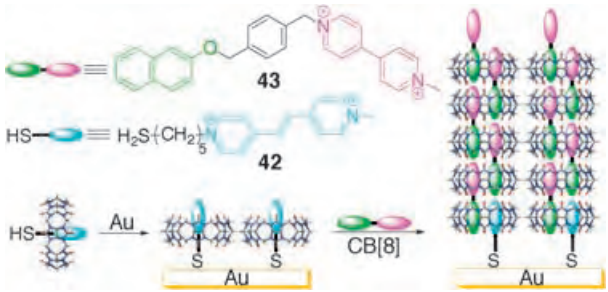
6.2. Self-Assembled Monolayers (SAMs)

To realize the full potential of pseudorotaxanes as components of molecular machines it is necessary to develop methods for their immobilization on solid substrates. Kim and co-workers have reported the functionalization of a gold surface with the pseudorotaxane CB[6]·**41**.[154] Surface plas-



mon resonance (SPR) studies have shown that SAMs comprising CB[6]·**41** undergo reversible dethreading and rethreading of the CB[6] beads upon treatment with 0.1 M NaOH followed by CB[6]. Cyclic voltametry measurements indicate that the SAM formed by pseudorotaxane CB[6]·**41** constitutes an effective barrier to redox processes involving $[Fe(CN)_6]^{3-}$: a quasireversible redox wave is observed after dethreading. This reversible gating behavior may have application in the design of surface-bound molecular machines.

More recently, Kim and co-workers have reported a surface-initiated supramolecular polymer based on CB[8]-stabilized charge-transfer interactions (Scheme 9). An aque-



Scheme 9. Formation of pseudorotaxane CB[8]·**42** on a gold substrate and formation of a surface-bound supramolecular polymer based on CB[8]-stabilized charge-transfer interactions.

ous solution containing CB[8] and thiol **42** results in the formation of pseudorotaxane CB[8]·**42**; dipping a gold substrate into this solution results in the formation of a self-assembled monolayer. Supramolecular polymerization from the CB[8]·**42** SAM was initiated by immersing the substrate in a solution containing CB[8] and **43**. The course of the reversible supramolecular polymerization could be monitored by FT-IR, SPR, and AFM and controlled by changing the conditions (time and concentration). The polymer consists of four CB[8] beads per chain on average.[155]

6.3. Waste-Stream Remediation of the Textile Industry

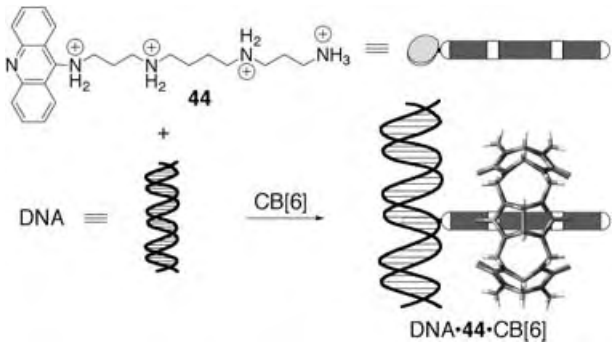
The application of CB[6] toward the complexation of indicator dyes such as congo red and methylene blue was published by Behrend et al. in 1905. Since then, the research groups of Buschmann[30,31,104,156–171] and Karcher[172–176] have studied the ability of CB[6] to effectively remove heavy metals, chromates and dichromate, aromatic substances, acid dyes, direct dyes, and reactive dyes from textile waste streams, quantified the influence of key parameters such as pH, temperature, salts, and surfactants on the process, and studied methods for regeneration of the solid phase. Taketsuji and

© 2005 Wiley-VCH Verlag GmbH & Co. KGaA, Weinheim

Tomioka found that Behrend's polymer was more efficient in these applications than CB[6].[35,177,178] Major issues that need to be resolved include loading levels, the covalent attachment of CB[6] to solid phases suitable for use in fixed-bed filters, and cost. The area has been reviewed previously.[14,19]

6.4. DNA Binding and Gene Transfection

Nakamura, Kim, and co-workers investigated a noncovalent approach to selectively deliver CB[6] to DNA.[179] The concept is illustrated in Scheme 10. Compound **44** contains



Scheme 10. Intercalation of acridine–spermine rotaxane CB[6]·**44** into DNA. The components are not drawn to scale.

acridine and tetramine regions which function as DNA intercalator and CB[6] binding elements, respectively. Mixing DNA, CB[6], and **44** results in formation of a termolecular complex (DNA·**44**·CB[6]) as monitored by gel electrophoresis. The DNA·**44**·CB[6] complex partially protects supercoiled DNA against cleavage by the restriction enzyme *Ban*II. In a complementary study, Kim and co-workers demonstrated that G3, G4, and G5 poly(propyleneimine) dendrimers bearing diaminobutane moieties (PPI-DAB) for binding CB[6] functions as a gene-delivery carrier.[180] The PPI-DAB·CB[6] conjugates have low cytotoxicity and successfully transfect Vero 76 and 293 cells with efficiencies only tenfold lower than poly(ethyleneimine), which is one of the most potent gene-transfer carriers.

7. Self-Assembly Processes Using CB[n]

This section describes the use of CB[*n*] in multicomponent self-assembly processes in solution and the solid state. The formation of CB[*n*] complexes with high affinity for binding a guest as well as their well-defined geometrical features make them particularly well-suited for these studies.

7.1. Molecular Necklaces

Interlocked structures such as rotaxanes and catenanes are the subject of intense investigation in supramolecular chemistry because of their potential use as molecular machines in nanotechnological applications.[140] Kim and co-workers have demonstrated the utility of the CB[*n*] family as a molecular bead in the formation of molecular necklaces ([*n*]MN) which contain $n-1$ rings threaded onto a single ring.[181–184] The members of the [*n*]MN family are topological isomers of the linear oligocatenanes exemplified by olympiadane (Figure 8).[185]

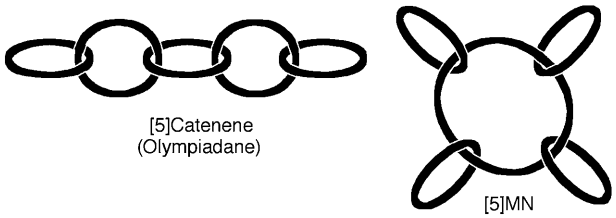
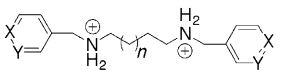
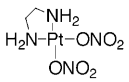


Figure 8. Oligocatenanes and molecular necklaces are topological isomers.

The interaction of **45** with CB[6] results in pseudorotaxane CB[6]·**45**. During this process the butanediammonium



45 $n = 1$, X = N, Y = CH
46 $n = 2$, X = CH, Y = N



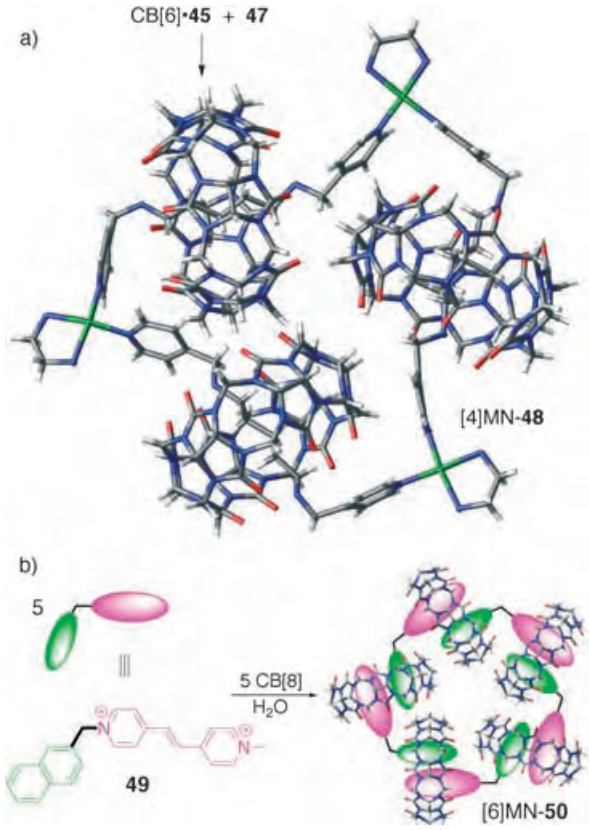
47

linker is rigidified in its all *trans* conformation, with the pyridyl groups displayed in roughly opposite directions. Heating CB[6]·**45** and **47** at reflux in water results in the formation of [4]MN-**48** through coordination of the pyridyl groups to the platinum centers (Scheme 11).[181] In a thorough study, the length of the alkanediammonium linker, the position of the pyridyl N atom (**45** versus **46**), and the temperature of the self-assembly process were found to control the equilibrium between [4]MN and [5]MN. Recently, Kim and co-workers demonstrated that their pseudorotaxane approach could be extended to different CB[*n*] and different noncovalent interactions. For example, **49** contains both electron-rich naphthalene rings and electron-poor dipyridylethylene units; these separate moieties are known to form a charge-transfer complex within CB[8]. To achieve formation of [6]MN, Kim and co-workers connected these two units by a methylene bridge whose angle of approximately 109° should favor the formation of a pentameric macrocycle. Indeed, the self-assembly process between CB[8] and **49** results in the formation of [6]MN-**50** as deduced by NMR spectroscopy, ESI mass spectrometry, and X-ray crystallographic analysis. Changing the length and angle of the linking groups should make it possible to synthesize molecular necklaces of different sizes, shapes, and number of CB[*n*] beads.

7.2. Pseudorotaxanes, Rotaxanes, and their Oligomeric Analogues

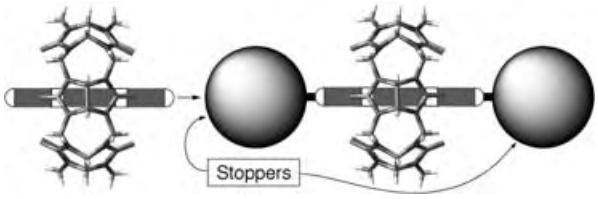
Rotaxanes—mechanically interlocked wheel and axle complexes—have assumed important roles in supramolecular

 © 2005 Wiley-VCH Verlag GmbH & Co. KGaA, Weinheim



Scheme 11. Formation of molecular necklaces using: a) CB[6] and b) CB[8] as beads.

chemistry and nanotechnology because of their ability to undergo controlled motions with respect to one another in response to environmental stimuli. Most commonly, rotaxanes are prepared from pseudorotaxanes—non-interlocked wheel and axle complexes—through the addition of bulky stoppers by reactions that result in the formation of covalent bonds (Scheme 12). The circular shape and outstanding



Scheme 12. The stoppering approach to rotaxane formation.

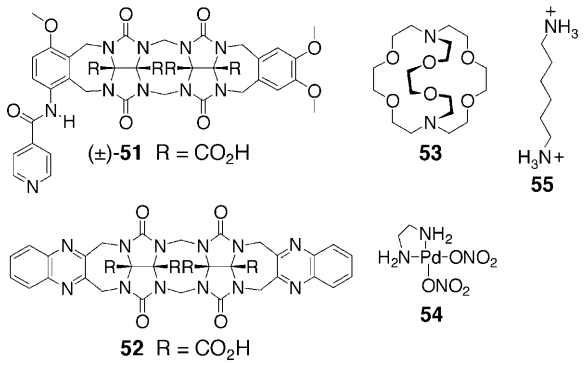
binding properties of CB[6] suggested its use as the wheel in rotaxane formation. Indeed, any CB[*n*] complex which extends past the rim of the cavity can be considered a pseudorotaxane starting material for reactions leading to the formation of rotaxane, polyrotaxane, and polypseudorotaxanes.[186] CB[6]-based rotaxanes have been prepared in solution by dipolar cycloadditions,[147,150–152,187] stoppering with dinitrophenyl groups,[188] amide-bond formation,[189–193] ionic interactions,[194] and coordination of alkylcobaloximes.[195,196] A variety of polymer backbones and side chains have been threaded with CB[6] beads including polyacrylamides and polystyrenes,[197] poly(hexamethyleneimine),[151,198] di- and polyviologen,[98,199] and poly(propyleneimine) dendrimers.[200] A rotaxane derived from Ph_2CB[6] (see Section 8.4) was stoppered with dinitrophenyl groups,[201] the CB[5]·spermine pseudorotaxane has been stoppered with benzoyl and furoyl groups,[202] and Newkome-type dendritic wedges containing viologen focal point functionality have been threaded with CB[7].[118]

7.3. Supramolecular Amphiphiles

Kim and co-workers reported the formation of a charge-transfer complex within CB[8] that triggered the assembly of vesicles.[136] Sonication of an equimolar mixture of CB[8], **28**, and **20g** or **20h** results in the formation of a turbid violet solution. Scanning electron microscopy (SEM), transmission electron microscopy (TEM), and dynamic light scattering measurements showed that the vesicles based on CB[8]·**20g**·**28** were nearly monodisperse with a diameter of 20 nm, whereas those based on CB[8]·**20h**·**28** had an average diameter of 870 nm. Remarkably, the vesicles are quite robust and retain their shape when allowed to dry on a substrate. Addition of cerium(IV) ammonium nitrate oxidizes **28** to the quinone which disrupts the charge-transfer complex and results in the collapse of the vesicles.

7.4. Self-Sorting Systems

Self-sorting—the ability to distinguish between identical and other molecules even within complex mixtures—is commonplace in natural and biological systems but is still rare in designed supramolecular systems.[203] The CB[*n*] family, with their high binding affinities, high selectivities, and reduced rates of chemical exchange are ideal components for self-sorting systems. Isaacs and co-workers demonstrated that a 12-component mixture comprising **51**$_2$·**54**$_2$, **52**$_2$, **53**·K^+, CB[6]·**55**, CB[8]·**20a**·**28**, and β-CD·**19a** undergoes a "social self-sorting" in aqueous solution.[111]



© 2005 Wiley-VCH Verlag GmbH & Co. KGaA, Weinheim

7.5. Crystal Engineering

The CB[*n*] family has been used extensively in crystal-engineering studies.

7.5.1. Polyrotaxanes

The use of CB[6] as a bead in the formation of polyrotaxanes in the solid state was the subject of an excellent review by Kim.[6] Kim's strategy uses the highly symmetrical CB[6] as a molecular bead to complex and conformationally order alkanediammonium ions containing pyridyl ligands at their termini. These pyridyl ligands subsequently coordinate to a variety of metal ions (for example, Cu^{II}, Co^{II}, Ni^{II}, Ag^{I}, and Cd^{II}). The X-ray structure of a polycatenated two-dimensional polyrotaxane net is illustrated in Figure 9.

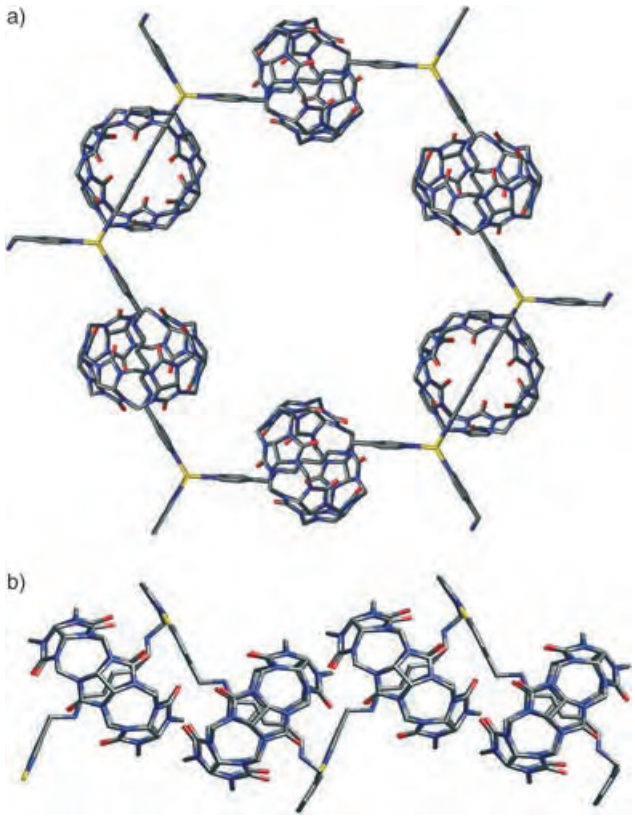


Figure 9. a) A portion of the polycatenated two-dimensional polyrotaxane network **56**, and b) the helical polyrotaxane **57** formed from CB[6], **46**, and $AgNO_3$. C: gray; N: blue; O: red; Ag: yellow.

Pseudorotaxane CB[6]·**45** is formed by threading CB[6] with **45**.[204] The CB[6] bead is held in position by ion–dipole interactions between the ammonium centers of the string (**45**) and the oxygen atoms of CB[6]. The addition of $AgNO_3$ results in a polyrotaxane (**56**) in which CB[6] is threaded on a 2D coordination polymer network (Figure 9a). The effects of structural variation of the components on the supramolecular structure are subtle: for example, the use of $Ag(O_3SC_6H_4CH_3)$ instead of $AgNO_3$ leads to the formation of a one-dimensional polyrotaxane coordination polymer whereas the use of **46** as the thread with $AgNO_3$ leads to helical polyrotaxane **57** (Figure 9b).[205] Other examples include zig-zag, square-wave, and linear one-dimensional polyrotaxanes, square-grid-shaped two-dimensional, and even three-dimensional polyrotaxane networks.[21,206–210]

7.5.2. CB[n] as a Ligand in Metal Complexes

The carbonyl groups lining the portals of CB[*n*] bind metal ions with high affinity and selectivity in solution and the solid state. Consequently, many X-ray crystal structures of CB[6] beads linked by various metal ions have been reported; we present three examples here that illustrate the approach. Fedin, Sykes, Clegg, and co-workers reported the crystal structure of an unusual trimetallic double cube cluster of $[Mo_6HgSe_8(H_2O)_{14}Cl_4]^{4+}$ which becomes sandwiched between adjacent CB[6] molecules and extends to form an infinite chain in the crystal (Figure 10a).[211,212] A triple-decker sandwich-type structure that forms upon crystallization of CB[6] and gadolinium bromide from water ($\{(CB[6])[Gd(H_2O)_4](CB[6])[Gd(H_2O)_4](CB[6])\}^{6+}$ Figure 10b) was reported by Fedin and co-workers.[213] An unusual aspect of this structure is that discrete structural units are formed containing only three CB[6] molecules connected by two Gd^{3+} ions and four hydrogen bonds. Such lanthanide-containing materials may be important in a variety of applications

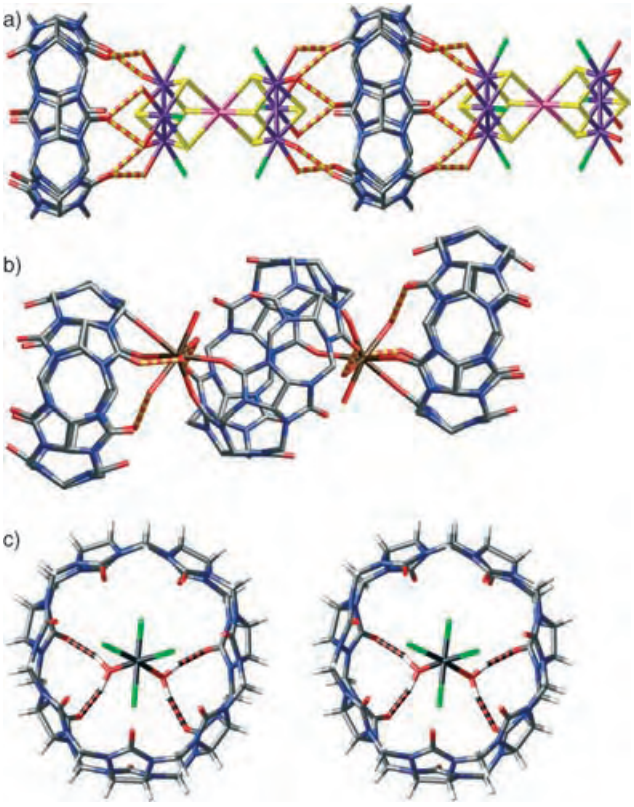


Figure 10. X-ray crystal structures of: a) $[Mo_6HgSe_8(H_2O)_{14}Cl_4]^{4+}$CB[6], b) $\{CB[6]\{Gd(H_2O)_4\}CB[6]\{Gd(H_2O)_4\}CB[6]\}^{6+}$, and c) a stereoview of *cis*-$[SnCl_4(OH_2)_2]$@CB[7]. C: gray; H: white; N: blue; O: red; Cl: green; Gd: brown; Se: yellow; Mo: purple; Hg: pink; Sn: gray; H bonds: striped.

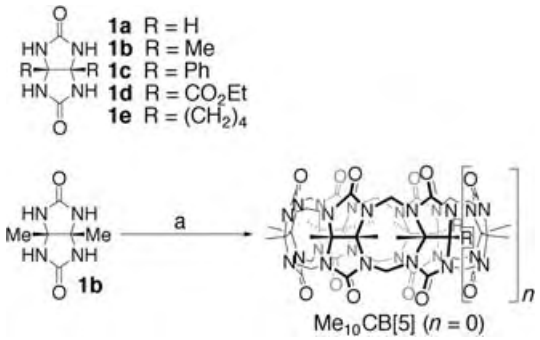
 © 2005 Wiley-VCH Verlag GmbH & Co. KGaA, Weinheim

including relaxation agents for magnetic resonance imaging, luminescent probes, and catalysts for the cleavage of DNA and RNA. The first endoannular metal halide complex of CB[7] was realized by Day and co-workers with the X-ray structure of *cis*-$[SnCl_4(OH_2)_2]$@CB[7] (**26**@CB[7], Figure 10c).[123] A CB[8] metal–aqua complex was recently realized by Fedin and co-workers with the structure of $Sr_2(H_2O)_{12}\cdot[Sr(H_2O)_3(NO_3)_2]_2CB[8]\cdot(NO_3)_4\cdot(H_2O)_8$ and a related complex.[214,215] Wu and co-workers recently reported a similar Cu(II) complex of CB[5].[216] Structures containing CB[6] complexed with a previously unknown tautomer of $HP(OH)_2$,[217] Rb^+,[218] Sm^{III},[219,220] Na^+,[87] Cs^+,[89] K^+,[221] Ca^{2+},[222,223] molybdenumselenide and tungstenselenide aqua complexes and related structures,[224–226] $[W_3S_4(H_2O)_9]^{4+}$ and related structures,[227–229] $[Nb_2(\mu\text{-}S_2)_2(H_2O)_8]^{4+}$,[230] $[ClPdMo_3Se_4(H_2O)_7Cl_2]^+$ and related structures,[231–233] $[W_3S_7Cl_6]_2$,[234] $[Mo_3S_4Ni(H_2O)_7Cl_3]^+$ and related structures,[235–237] *trans*-$[InCl_2(H_2O)_4]^+$ and *trans*-$[InCl_4(H_2O)_2]^-$,[238] $(H_7O_3)_4[FeCl_4]_2Cl_2(H_2O)_2$,[239] $(H_7O_3)_4[GaCl_4]_2Cl_2(H_2O)_2$,[240] $[(UO_2)_4O_2Cl_4(H_2O)_{11}]$,[241] $[Cl_3InW_3S_4(H_2O)_9]^{2+}$,[242] $[Cr(H_2O)_6(NO_3)_3(H_2O)_{13}]$,[243] and $[Zr_4(OH)_8(H_2O)_{16}]Cl_8\cdot(H_2O)_{16}$ are also known.[244]

8. Derivatives, Analogues, and Congeners of the CB[n] Family

The preceding sections have demonstrated the great potential of the CB[*n*] family in molecular recognition, self-assembly, and nanotechnology. Potential limitations of the CB[*n*] family include their poor solubility in water, which necessitates the use of high salt concentrations (for example, 0.2 M NaCl), and their insolubility in polar or nonpolar organic solvents. A second potential limitation of CB[*n*] when we began our research in this area in 1998 was an inability to modify the internal or external molecular surfaces of the CB[*n*] molecule. It seemed likely that if the CB[*n*] family could be modified to improve their solubility in organic media, to alter the size and shape of the cavity, and to provide different functional groups that interact directly with guests then the range of potential applications of the CB[*n*] family would be dramatically expanded. The following sections describe the approaches that we,[245–249] and others,[8,90,201,250–254] have taken toward alleviating these potential limitations.

Over the years there have been numerous attempts to prepare CB[*n*] derivatives by the use of substituted glycoluril derivatives in CB[*n*]-forming reactions. Nolte and co-workers were the first to pursue this line of inquiry, which led to the development of molecular clips based on diphenylglycoluril (**1c**).[255] The first fully characterized CB[*n*] derivative was reported by Stoddart and co-workers in 1992 with the synthesis of Me_{10}CB[5] from dimethylglycoluril (**1b**) and formaldehyde under acidic conditions (Scheme 13).[90,256] These studies led to more questions than they answered. Why was the CB[*n*]-forming reaction of **1b** successful whereas the corresponding reaction with **1c** failed? What is the scope of glycoluril monomers that can be used in CB[*n*]-forming reactions? Why did the original cyclization of **1a** lead



Scheme 13. Synthesis of Me_{10}CB[5]. a) Conc. HCl, CH_2O, reflux, 16% yield.

to CB[6] exclusively, whereas **1b** led to a pentameric macrocyclic Me_{10}CB[5] exclusively? What factors are responsible for the remarkably high yield observed for CB[6] formation given that the formation of a pair of methylene bridges between two glycoluril rings can result in either C- or S-shaped diastereomers (for example, **58C** and **58S**, respectively, Figure 11)?

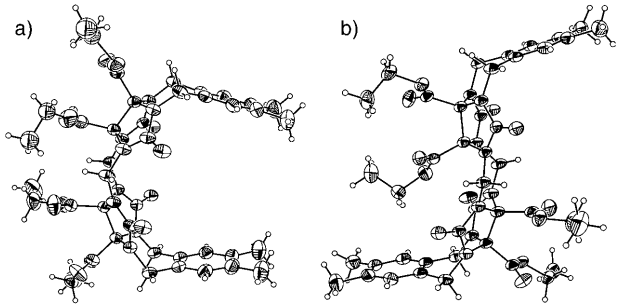
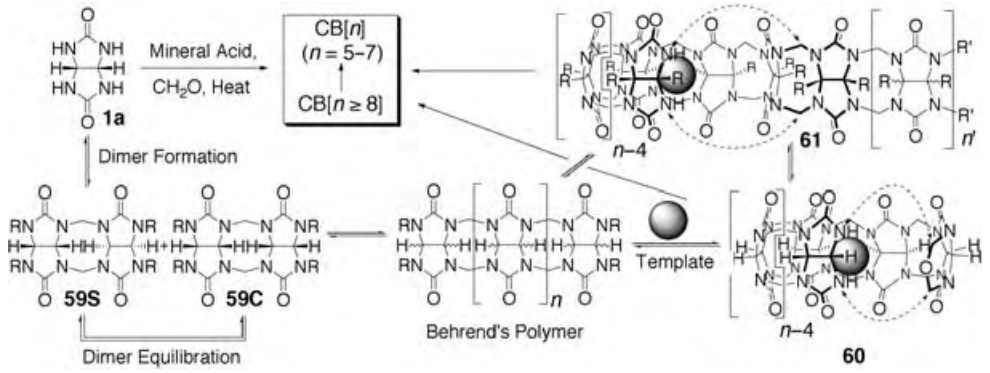


Figure 11. X-ray crystal structures of methylene-bridged glycoluril dimers: a) C-shaped **58C** and b) S-shaped **58S**.

8.1. Mechanistic Hypothesis for CB[n] Formation

Control over the tailor-made synthesis of CB[*n*] homologues, derivatives, and analogues was hampered by an inadequate understanding of the mechanism of CB[*n*] formation. A mechanistic framework advanced by Day et al.[8] and Isaacs and co-workers[247] is shown in Scheme 14. In brief, glycoluril (**1a**) undergoes condensation with H_2CO to yield a mixture of methylene-bridged glycoluril dimers **59C** and **59S** which can undergo further oligomerization to yield Behrend's polymer as a mixture of diastereomers. Further growth and isomerization of the S- to C-shaped structures in Behrend's polymer yields **60** and **61** under the potential control of suitable templating agents. Both **60** and **61** may undergo cyclization by end-to-end condensation (for example **60**→CB[*n*]) or by back-biting (for example, **61**→CB[*n*]) to enter the CB[*n*] manifold. Interconversions between the various CB[*n*] may then occur within the CB[*n*] manifold.

© 2005 Wiley-VCH Verlag GmbH & Co. KGaA, Weinheim



Scheme 14. Proposed mechanism for the formation of CB[*n*].

8.2. Effect of Acid, Salts, and Templates on the Product Distribution

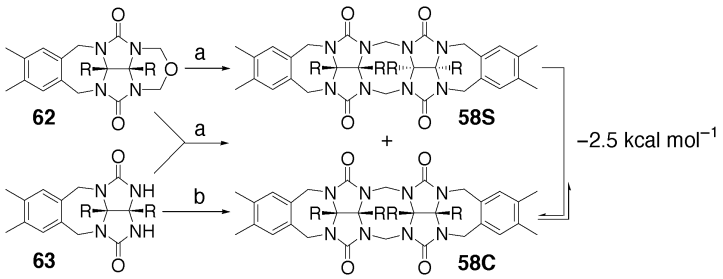
Day and co-workers performed a series of elegant experiments to determine the effect of acid type, acid and reactant concentration, salts, and templates on the distribution of CB[5]–CB[8] in the product mixture.[8,121,250] They surveyed a variety of acids for CB[*n*] formation (for example, HCl, H_2SO_4, HBF_4, CH_3SO_3H, PTSA, and trifluoroacetic acid (TFA)) and determined that a high concentration of strong acid, such as >5 M HCl, is necessary for conversion of oligomers **60** and **61** into CB[*n*]; weak acids such as TFA are insufficient. Decreasing the concentration of **1a** from 155 mg mL^{-1} to 0.125 mg mL^{-1} in concentrated HCl enhanced the combined yield of CB[5] and CB[6] from 67% to 100%, as would be predicted if the length of the oligomer **60** or **61** controls the size of the CB[*n*] formed. To address the fate of the formed CB[*n*] once it has entered the CB[*n*] manifold, Day and co-workers performed product resubmission experiments. CB[5], CB[6], and CB[7] are stable to the reaction conditions (conc. HCl, 100 °C, 24 h) whereas CB[8] contracted to give a mixture of CB[5]–CB[8] (4:13:38:45). These experiments suggest that the low abundance of the higher homologues ($n>8$) may be a consequence of their destruction under the reaction conditions. These experiments also suggest that fragmentation of the methylene-bridged glycoluril oligomers such as **61** to **60** are possible under aqueous acidic conditions.

Day et al. also found that salts such as LiCl, NaCl, KCl, RbCl, CsCl, and NH_4Cl have modest effects on the relative yields of CB[5]–CB[8].[250] For example, K^+ favors formation of CB[5] whereas Li^+ favors the formation of higher homologues; these salts are posited to exert their influence during the transformation of Behrend's polymer to **60** and **61**. Similarly, the addition of *o*-carborane as a potential template for the formation of CB[7] in CB[*n*]-forming reactions had a small but discernible effect on the CB[5]–CB[8] product distribution.[121] Theoretical studies suggest that H_3O^+ may act as a template during CB[*n*] synthesis.[257]

8.3. The Methylene-Bridged Glycoluril Dimer as a Model System

In contrast to the work of Day et al., which focused on the latter stages of the mechanism of CB[*n*] formation, we decided in 1998 to focus on the simplest building block of the CB[*n*] family, namely, the methylene-bridged glycoluril dimer substructure (**59C** and **59S**, Scheme 14). This section focuses on the insights that we gained from these model studies that led to the synthesis of CB[*n*] analogues.

We developed three related synthetic methods (two homodimerization and one heterodimerization) from **62** and **63** that provided efficient access to methylene-bridged glycoluril dimers, such as **58C** and **58S**, with *o*-xylylene "walls" and a variety of substituents (Scheme 15).[247,249] We found that substituted dimers bearing electron-withdrawing groups (for example, R = CO_2Et) form readily whereas those bearing groups such as R = Ph that stabilize adjacent positive charge form slowly and with significant formation of by-product. These experiments provide a rationale for the observed scope of CB[*n*]-forming reactions.[249] Since the equilibrium between **59S** and **59C** is of fundamental importance to CB[*n*] synthesis, we decided to investigate the equilibrium between the S-shaped and the C-shaped forms by following the separate isomerization of diasteromerically pure samples of **58S** and **58C** to yield equilibrium mixtures (**58C**:**58S** = 97:3, Scheme 15) of the two diastereomers.[247] The C-shaped form is about 2.5 kcal mol^{-1} more stable than

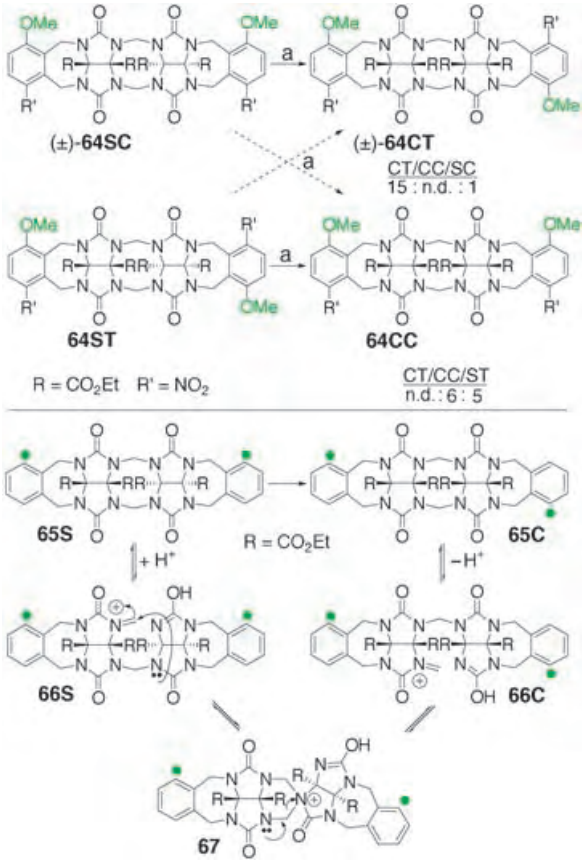


Scheme 15. Formation and isomerization of methylene-bridged glycoluril dimers. a) $ClCH_2CH_2Cl$, PTSA, reflux; b) $ClCH_2CH_2Cl$, CH_2O, PTSA, reflux. R = CO_2Et, PTSA = *para*-toluenesulfonic acid.

 © 2005 Wiley-VCH Verlag GmbH & Co. KGaA, Weinheim

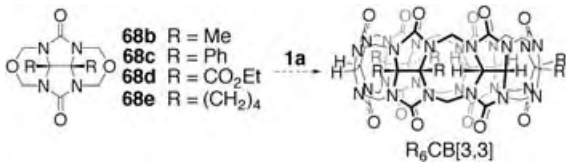
the S-shaped form, which provides a rationale for the high yields observed in the formation of the CB[*n*] family in which all the dimeric units adopt the C-shaped form.

During our studies of the model system with the methylene-bridged glycoluril dimer we also observed that the isomerization from the S-shaped to C-shaped dimer was highly diastereoselective. The isomerization of **64ST** (S-shaped, *trans*) and **64SC** (S-shaped, *cis*) under anhydrous acidic conditions ($ClCH_2CH_2Cl$, PTSA, reflux) gave **64CC** (C-shaped, *cis*) and **64CT** (C-shaped, *trans*), respectively (Scheme 16). In principle at least three different outcomes



Scheme 16. Isomerizations and a suggested mechanism.[258] a) PTSA, $ClCH_2CH_2Cl$, reflux. n.d. = not detected.

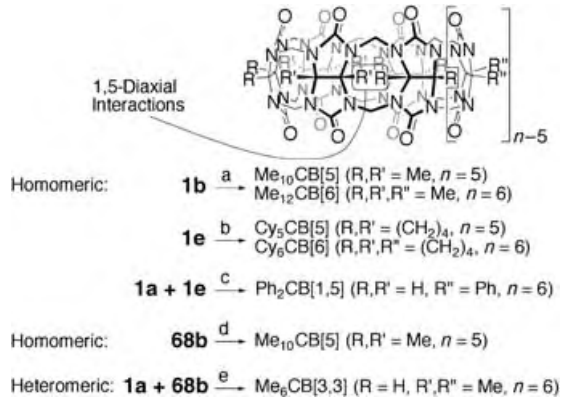
were conceivable: 1) scrambling, 2) retention, or 3) transposition of the relative position of the "methoxy labels" (green dots) as might occur during intermolecular (scrambling) or intramolecular (retention or trnscription) S- to C-shaped isomerization. Scheme 16 (bottom section) also shows our suggested mechanism for this *intramolecular* isomerization which proceeds by the intermediacy of a spirocyclic N-acylammonium intermediate (**67**). The implications of this result toward the synthesis of CB[*n*] derivatives and analogues are twofold: Under the anhydrous acidic conditions used, the methylene-bridged glycoluril dimer subunits do not undergo the fragmentation reactions observed during CB[*n*] synthesis (see Scheme 14, **61**→**60**). This result suggests that CB[8] and the higher homologues might display enhanced stability if synthesized under anhydrous acidic conditions. Since the methylene-bridged glycoluril dimer substructure does not become disconnected during isomerization, it should be possible to exploit the selective heterodimerization reactions between glycoluril NH compounds such as **1** and glycoluril cyclic ethers such as **68** to prepare CB[*n*] derivatives with control over their functionalization pattern and potentially their size. For example, we predicted that it might be possible to prepare CB[*n*] derivatives from two different glycoluril derivatives (for example, **1a** and **68**) and that those derivatives might alternate in the formed CB[*n*] derivative (for example, R_6CB[3,3]; Scheme 17).



Scheme 17. Proposed synthesis of CB[*n*] derivatives.

8.4. Preparation of CB[n] Derivatives

There are three potential pathways for the synthesis of CB[*n*] derivatives from glycolurils (**1**) and glycoluril cyclic ethers (**68**)—two homomeric cyclzations and one heteromeric cyclization. Examples of all three have now been demonstrated in the literature (Scheme 18). In 1992, Stoddart and



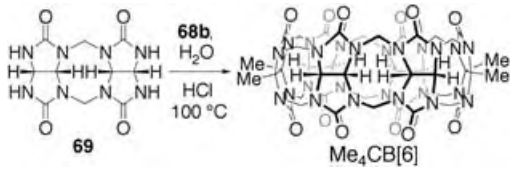
Scheme 18. Synthesis of CB[*n*] derivatives. a) CH_2O, HCl, heat; b) CH_2O, HCl, heat; then H_2SO_4, H_2O, heat; c) CH_2O, $(NH_4)_2SO_4$, H_2SO_4; then H_2O, 70–95 °C; d) HCl, H_2O, heat; e) HCl, LiCl, heat.

co-workers showed that the homomeric cyclization of **68b** yields the pentameric macrocycle Me_{10}CB[5] in low yield (Scheme 13).[90,256] Miyahara et al. reported an improved procedure to access Me_{10}CB[5] with a NH_4^+ lid (36%) and removal of the lid using Amberlite IRA410.[96] Keinan and co-workers recently reported a novel pentanediamine-derivatized polystyrene resin that allowed the isolation of Me_{12}CB[6].[259] Similarly, Kim and co-workers were able to isolate Cy_5CB[5] (16%) and Cy_6CB[6] (2%) by the cyclization of **1e**.[253] The distinguishing feature of Cy_5CB[5] and

© 2005 Wiley-VCH Verlag GmbH & Co. KGaA, Weinheim

$Cy_6CB[6]$ is their enhanced solubility in water (200 mM) and organic solvents (up to 30 mM in MeOH, DMSO, DMF, and CH_3CN). This enhanced solubility of $Cy_5CB[5]$ and $Cy_6CB[6]$ allowed the preparation of ion-selective electrodes which displayed a high selectivity for Pb^{2+} ions and acetylcholine, respectively, relative to potentially interfering cations (K^+, NH_4^+, Na^+, Cu^{2+}, and choline). Nakamura and co-workers demonstrated that mixtures of **1a** and **1c** gave a CB[6] derivative containing a single diphenylglycoluril unit ($Ph_2CB[1,5]$) in a remarkable 30% yield. $Ph_2CB[1,5]$ even forms a rotaxane with a spermine axle.[201] Day et al. showed that **68b** is transformed into $Me_{10}CB[5]$ in high yield (85%).[8]

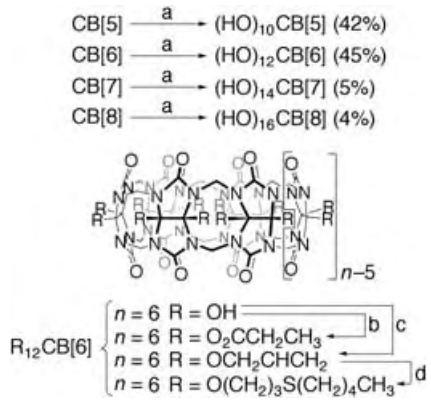
One potential drawback of the use of glycoluril derivatives in CB[*n*]-forming reactions is that derivatives of the smaller homologues CB[5] and CB[6] form preferentially. This result is attributed to 1,5-diaxial interactions between substituents on adjacent glycoluril rings that comprise the CH_2-bridged eight-membered rings; such interactions are postulated to increase as the size of the CB[*n*] increases.[33,34] To alleviate this problem, Day et al. studied CB[*n*]-forming reactions between substituted and unsubstituted glycoluril derivatives, with the reasoning that the presence of unsubstituted glycoluril would relieve the 1,5-diaxial interactions. The heteromeric cyclization reaction of **1a** and **68b** gave the D_{3h}-symmetrical $Me_6CB[3,3]$ in which substituted glycoluril units alternate with unsubstituted ones in 10% yield.[247,251] CB[5] and CB[7] derivatives were also present in the reaction mixture, but were not isolated in pure form. A related heteromeric cyclization reaction between **68b** and **69** delivers $Me_4CB[6]$ in 30% yield on multigram scale (Scheme 19).[260] Interestingly, the cavity of $Me_4CB[6]$ is ellipsoidal and binds 2,2′-bipyridine with its aromatic rings parallel to the long axis of the cavity.



Scheme 19. Synthesis of $Me_4CB[6]$.

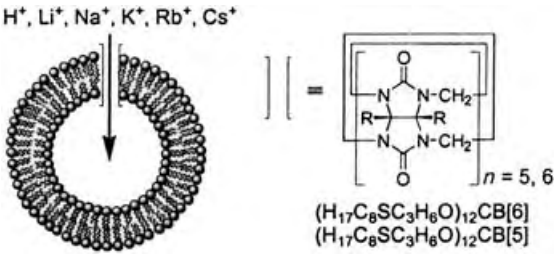
8.5. Direct Functionalization of CB[n]

Kim and co-workers recently made a major breakthrough in the synthesis of CB[*n*] derivatives by the direct functionalization of CB[5]–CB[8].[254] Scheme 20 shows the direct oxidation of CB[5]–CB[8] with $K_2S_2O_8$ in water to yield the perhydroxylated species $(HO)_{2n}CB[n]$. The reaction is efficient for CB[5] and CB[6] (yields of 42 and 45%, respectively); optimization of the reaction conditions is needed to improve the yields in the derivatization of CB[7] and CB[8] (ca. 5%). The cause of the low yields in these reactions is still unclear, but may be related to selective formation of CB[5] and CB[6] derivatives in the direct cyclization of glycoluril derivatives. $(HO)_{12}CB[6]$ has good solubility in DMSO and DMF which allows its subsequent derivatization. $(HO)_{2n}CB[6]$ can be acylated by treatment with propionic anhydride to yield $(CH_3CH_2CO_2)_{12}CB[6]$ and treated with allyl bromide to yield $(CH_2CHCH_2O)_{12}CB[6]$. The allylated compound $(CH_2CHCH_2O)_{12}CB[6]$ undergoes photochemical reaction with pentanethiol to afford $\{CH_3(CH_2)_4S(CH_2)_3O\}_{12}CB[6]$. These landmark reactions represent the first covalent derivatization reactions of CB[*n*] derivatives. $(CH_2CHCH_2O)_{12}CB[6]$ can even be covalently attached to slides derivatized with (3-sulfanylpropyl)triethoxysilane and can also be covalently attached to silica gel and used in chromatographic applications.[46,261]



Scheme 20. Direct functionalization of CB[*n*]. a) $K_2S_2O_8$, H_2O, 85 °C; b) Et_3N, $(CH_3CH_2CO)_2O$, DMSO; c) NaH, DMSO, allyl bromide; d) $CH_3(CH_2)_4SH$, *hν*.

Kim and co-workers have also demonstrated that these lipophilic CB[*n*] derivatives possess new properties. $\{CH_3(CH_2)_7S(CH_2)_3O\}_{12}CB[6]$ forms nanospheres with diameters of 50–150 nm when emulsified.[254] They also demonstrated recently that $\{CH_3(CH_2)_7S(CH_2)_3O\}_{12}CB[6]$ and $\{CH_3(CH_2)_7S(CH_2)_3O\}_{12}CB[5]$ become incorporated in large unilamellar vesicles and function as ion channels (Scheme 21).[262] The CB[6] derivative $(CH_3(CH_2)_7S(CH_2)_3O)_{12}CB[6]$ shows ion selectivity ($Li^+ > Cs^+ \approx Rb^+ > K^+ > Na^+$) which is opposite to the binding affinities of CB[6]. Remarkably, $\{CH_3(CH_2)_7S(CH_2)_3O\}_{12}CB[6]$ shows an ion flux of 5 pA (ca. 3×10^7 ions s^{-1}) which is comparable to that of gramicidin! In contrast, $\{CH_3(CH_2)_7S(CH_2)_3O\}_{10}CB[5]$ with its smaller portals (2.4 Å) only allows the smaller Li^+ and Na^+ ions to pass. Such lipophilic CB[*n*] derivatives show much promise for applications as sensors, in ion separations, and as components of molecular devices.

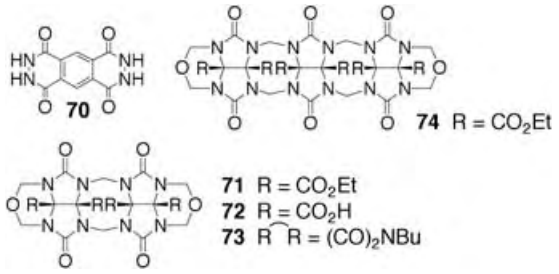


Scheme 21. Lipophilic CB[5] and CB[6] derivatives as ion channels.

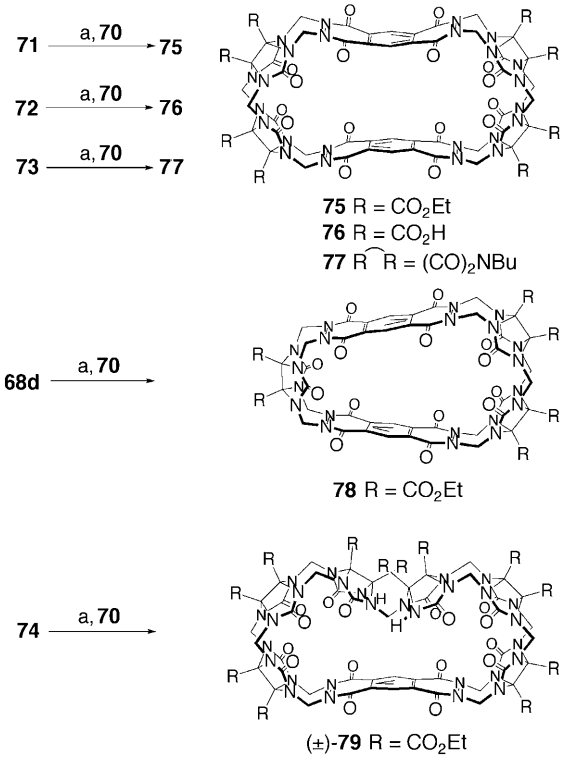
 © 2005 Wiley-VCH Verlag GmbH & Co. KGaA, Weinheim

8.6. Preparation of Cucurbit[n]uril Analogues

We discovered that phthalhydrazides function as nucleophilic glycoluril surrogates in typical methylene-bridge-forming reactions. On the basis of the mechanistic reasoning described above, we hypothesized that combinations of bis(phthalhydrazide) **70** and glycoluril ether building blocks **68**, **71**–**74** would yield CB[*n*] analogues with predetermined size, shape, and functionalization patterns.[246,248,263]



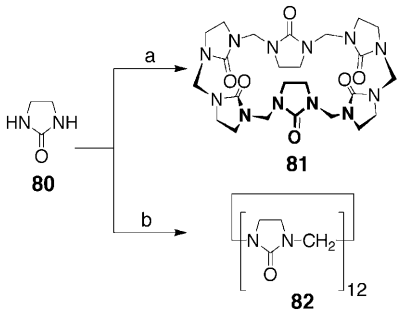
In accord with these expectations, cyclization reactions of **70** with **71**–**73** proceeded smoothly and delivered CB[6] analogues **75**–**77** in high yield (Scheme 22). Similarly, **70** reacts with **68d** to yield CB[5] analogue **78** in relatively low yield (6%). Remarkably, methylene-bridged glycoluril trimer **74** reacts with **70** to yield CB[7] analogue (±)-**79** incorporating a single bis(phthalhydrazide) unit rather than a CB[8] analogue with two such units. Several features of these cucurbit[*n*]uril analogues are noteworthy: 1) they contain electrochemically, UV/Vis, and fluorescently active "walls"; 2) their elongated shapes (**75**: 5.9 × 11.2 × 6.9 Å; **78**: 5.6 × 9.8 × 6.2 Å; (±)-**79**: 5.7 × 11.3 × 4.3 Å differ from those of the circular CB[*n*]; 3) the C_2-symmetric (±)-**79** is chiral and contains only a single bridging CH_2 group which points directly into the cavity; and 4) the analogues are soluble in both organic and aqueous media depending on the substituents. CB[6] analogue **77** retains the binding capacity of the parent macrocycles, as demonstrated by the complexation of the *p*-xylylenediammonium ion.[248]



Scheme 22. CB[*n*] analogues. a) $MeSO_3H$, 80°C.

8.7. Hemicucurbit[6]uril and Hemicucurbit[12]uril

Miyahara et al. recently further expanded the CB[*n*] family with the preparation of hemicucurbiturils by the acid-catalyzed condensation of ethyleneurea (**80**, Scheme 23).[264] Remarkably, hemicucurbit[6]uril (**81**) is



Scheme 23. Synthesis of **80** and **81**. a) CH_2O, 4 N HCl, RT; b) CH_2O, 1 N HCl, 55°C.

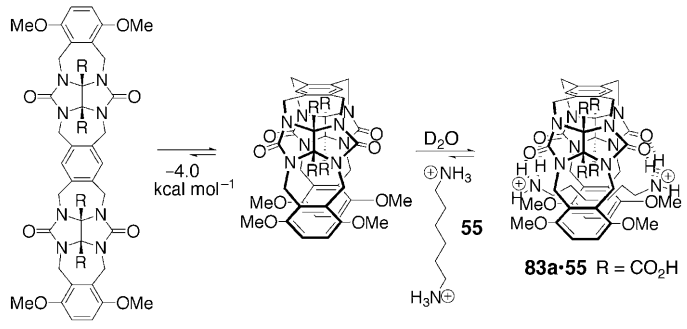
formed in 94% yield when the reaction is conducted at RT in 4 N HCl, whereas hemicucurbit[12]uril (**82**) is formed in 93% yield in 1 N HCl at 55°C. The X-ray crystal structure of **81** shows that it assumes the alternate conformation depicted in Scheme 23. Unlike CB[*n*], **81** does not bind metal cations, but does retain the ability to bind small organic molecules such as $HCONH_2$ and $HOCH_2CCH$. Interestingly, **82** gelates ethyleneglycol in the 0.5 to 5.0 wt% range. The detailed recognition properties and practical applications of **81** and **82** remain to be explored.

8.8. Preparation of Acyclic Cucurbit[n]uril Congeners

Issues associated with macrocyclization and stereochemistry (for example, S- versus C-shaped diastereomers) complicate the preparation of CB[*n*] derivatives and analogues that are poised to dramatically expand the scope of applications of the CB[*n*] family. Recently, we described an approach to acyclic CB[*n*] congeners (**83a**, Scheme 24) that circumvents these issues while maintaining the binding profile of CB[6] itself.[245,263b] Based on the precedent of Nolte,[265] we hypothesized that employing alternating glycoluril and aromatic rings would preorganize **83a** into the a,a,a,a conformation required

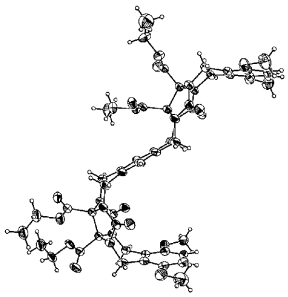
© 2005 Wiley-VCH Verlag GmbH & Co. KGaA, Weinheim

a)



83a R = CO_2H
83b R = CO_2Et

b)



Scheme 24. a) Structures of **83a** and **83b** as well as a schematic illustration of **83a·55**. b) X-ray crystal structure of the a,a,s,a conformer of **83b**.

to act as an acyclic CB[*n*] congener. Indeed, **83a** displays several of the features characteristic of the CB[*n*] family, namely: 1) high affinity and selectivity for positively charged guests, 2) length-dependent affinity for alkanediammonium ions, 3) guest discrimination on the basis of size and shape, and 4) competitive binding with alkali metals present in solution. The use of longer aromatic spacers may result in CB[*n*] congeners whose recognition properties parallel those of the higher homologues.

9. Summary and Outlook

Cucurbit[6]uril is celebrating its 100th birthday this year! It was only in 1981 at age 76, that the structure of this unusual macrocycle was elucidated by Mock and co-workers. In their early pioneering work they demonstrated that CB[6] displays: 1) remarkably high affinity for alkanediammonium ions as a consequence of ion–dipole and hydrophobic interactions, 2) size, shape, and functional-group selectivity, 3) unusually slow kinetics of association and dissociation, and 4) behavior of an enzyme mimic. CB[6] was clearly a talented host, but a series of perceived problems limited the scope of applications to which it could be applied. Compared to α-, β-, and γ-cyclodextrin with their good solubility in aqueous solution, their commercial availability in a variety of sizes, their well-known chemical functionalization, and their affinity toward a wide variety of species, CB[6] was not in a position to challenge the cyclodextrins as the recognition platform of choice for studies of molecular recognition in aqueous solution.

In the intervening time, all of these perceived issues have been either partially or fully resolved, which has dramatically expanded the range of applications to which the CB[*n*] family can be applied. The solubility of CB[6] increases dramatically in the presence of salts which allows their recognition and self-assembly processes to be studied in neutral aqueous solution. It was not until the turn of the millennium, however, that the CB[*n*] family expanded dramatically with the preparation of CB[5], CB[7], CB[8], and CB[10]·CB[5] by the research groups of Kim and Day. The recognition properties of these new CB[*n*] homologues—which are now commercially available—parallel and exceed those of CB[6]. Recognition processes within CB[6], CB[7], and CB[8] are subject to efficient chemical, electrochemical, and photochemical control. These attributes along with the detailed knowledge of the mechanism of formation and dissociation of CB[6] complexes has led to the application of the CB[*n*] family in areas as diverse as gas purification, catalysis, molecular machines, waste-stream remediation, supramolecular polymers, self-assembling and self-sorting systems, crystal engineering, self-assembled monolayers, and even gene transfection.

The remaining issue—the tailor-made preparation of CB[*n*] derivatives, analogues, and congeners—has been tackled by several research groups including ours. Fully and partially substituted CB[5] and CB[6] derivatives can be prepared by the use of substituted glycoluril derivatives in CB[*n*]-forming reactions. More recently, the direct perhydroxylation of CB[5]–CB[8] was achieved by Kim and co-workers. We have prepared CB[*n*] analogues and congeners by mechanistically guided building-block approaches. These CB[*n*] derivatives possess enhanced solubility in aqueous and organic media and largely retain the binding profile of the parent CB[*n*]. CB[*n*] derivatives have already been used as molecular "molecular sieves", in the preparation of ion-selective electrodes, as amphiphiles for vesicle formation, for the functionalization of glass substrates, and as artificial ion channels.

Many of the major issues confronting CB[*n*] supramolecular chemistry—enhanced aqueous and organic solubility, the (commercial) availability of a range of different-sized CB[*n*] homologues, and the development of tailor-made synthetic procedures for the synthesis of CB[*n*] derivatives, analogues, and congeners—have now been partially or fully addressed. We, and others, believe that the CB[*n*] family is now in a position to challenge the cyclodextrins as the recognition platform of choice for studies of molecular recognition in water. The unusual recognition properties of the CB[*n*] family—strong binding, high selectivity, tunable kinetics of association and dissociation, and efficient methods for chemical, electrochemical, and photochemical control of binding—suggest that the CB[*n*] family will become important components in molecular machines and nanotechnology. The groundwork has been laid for a second century of CB[*n*] chemistry that promises advances even more dramatic than the first!

 © 2005 Wiley-VCH Verlag GmbH & Co. KGaA, Weinheim

Addendum (6. July 2005)

Since submission of the final version of this review a number of papers,[266–299] reviews,[300–304] and patents[305–313] related to the CB[n] family have appeared in the literature.

We thank the talented and enthusiastic co-workers who have worked on the CB[n] project in our group: Dariusz Witt, Arindam Chakraborty, Anxin Wu, Avril Williams, Christopher Burnett, Daniel Coady, Katie Chiles, Marie Ofori, and Christian Ruspic. Our work in this area would not have been possible without the contributions of Dr. James C. Fettinger (X-ray analysis) and Dr. Yiu-Fai Lam (NMR spectroscopy) for which we are grateful. We thank the National Institutes of Health (GM61854) and the University of Maryland for financial support. L.I. is a Cottrell Scholar of Research Corporation.

Received: May 15, 2004
Revised: December 18, 2004

[1] R. Behrend, E. Meyer, F. Rusche, *Justus Liebigs Ann. Chem.* **1905**, *339*, 1 – 37.
[2] W. A. Freeman, W. L. Mock, N.-Y. Shih, *J. Am. Chem. Soc.* **1981**, *103*, 7367 – 7368.
[3] W. L. Mock, *Top. Curr. Chem.* **1995**, *175*, 1 – 24.
[4] R. Hoffmann, W. Knoche, C. Fenn, H.-J. Buschmann, *J. Chem. Soc. Faraday Trans.* **1994**, *90*, 1507 – 1511.
[5] J. W. Lee, S. Samal, N. Selvapalam, H.-J. Kim, K. Kim, *Acc. Chem. Res.* **2003**, *36*, 621 – 630.
[6] K. Kim, *Chem. Soc. Rev.* **2002**, *31*, 96 – 107.
[7] J. Kim, I.-S. Jung, S.-Y. Kim, E. Lee, J.-K. Kang, S. Sakamoto, K. Yamaguchi, K. Kim, *J. Am. Chem. Soc.* **2000**, *122*, 540 – 541.
[8] A. I. Day, A. P. Arnold, R. J. Blanch, B. Snushall, *J. Org. Chem.* **2001**, *66*, 8094 – 8100.
[9] A. I. Day, R. J. Blanch, A. P. Arnold, S. Lorenzo, G. R. Lewis, I. Dance, *Angew. Chem.* **2002**, *114*, 285 – 287; Angew. *Chem. Int. Ed.* **2002**, *41*, 275 – 277.
[10] T. J. Hubin, A. G. Kolchinski, A. L. Vance, D. H. Busch, *Adv. Supramol. Chem.* **1999**, *6*, 237 – 357.
[11] J. A. A. W. Elemans, A. E. Rowan, R. J. M. Nolte, *Ind. Eng. Chem. Res.* **2000**, *39*, 3419 – 3428.
[12] H.-J. Buschmann, L. Mutihac, K. Jansen, *J. Inclusion Phenom. Macrocyclic Chem.* **2001**, *39*, 1 – 11.
[13] N. Kihara, T. Takata, *Yuki Gosei Kagaku Kyokaishi* **2001**, *59*, 206 – 218.
[14] T. Robinson, G. McMullan, R. Marchant, P. Nigam, *Bioresour. Technol.* **2001**, *77*, 247 – 255.
[15] E. Schollmeyer, H.-J. Buschmann, K. Jansen, A. Wego, *Prog. Colloid Polym. Sci.* **2002**, *121*, 39 – 42.
[16] B. D. Wagner in *Handbook of Photochemistry and Photobiology, Vol. 3* (Ed.: H. S. Nalwa), American Scientific, California, **2003**, pp. 1 – 57.
[17] P. Cintas, *J. Inclusion Phenom. Mol. Recognit. Chem.* **1994**, *17*, 205 – 220.
[18] W. L. Mock in *Comprehensive Supramolecular Chemistry, Vol. 2* (Ed.: F. Vögtle), Pergamon, Oxford, **1996**, pp. 477 – 493.
[19] H.-J. Buschmann, *Biol. Abwasserreinig.* **1997**, *9*, 101 – 129.
[20] K. Kim, *Perspect. Supramol. Chem.* **1999**, *5*, 371 – 402.
[21] K.-M. Park, J. Heo, S.-G. Roh, Y.-M. Jeon, D. Whang, K. Kim, *Mol. Cryst. Liq. Cryst. Sci. Technol A* **1999**, *327*, 65 – 70.
[22] J. Heo, S.-Y. Kim, S.-G. Roh, K.-M. Park, G.-J. Park, D. Whang, K. Kim, *Mol. Cryst. Liq. Cryst. Sci. Technol A* **2000**, *342*, 29 – 38.
[23] V. P. Fedin, O. A. Geras'ko, *Priroda* **2002**, 3 – 8.
[24] O. A. Gerasko, D. G. Samsonenko, V. P. Fedin, *Russ. Chem. Rev.* **2002**, *71*, 741 – 760.
[25] B.-H. Han, Y. Liu, *Youji Huaxue* **2003**, *23*, 139 – 149.
[26] M. N. Sokolov, D. N. Dybtsev, V. P. Fedin, *Russ. Chem. Bull. Int. Ed.* **2003**, *52*, 1041 – 1060.
[27] M. J. Hardie, *Struct. Bonding (Berlin)* **2004**, *111*, 139 – 174.
[28] V. P. Fedin, *Russ. J. Coord. Chem.* **2004**, *30*, 151 – 158.
[29] K. Kim, N. Selvapalam, D. H. Oh, *J. Inclusion Phenom. Macrocyclic Chem.* **2004**, *50*, 31 – 36.
[30] K. Kim, H.-J. Kim in *Encyclopedia of Supramolecular Chemistry* (Ed.: L. J. Atwood), Dekker, New York, **2004**, pp. 390 – 397
[31] H.-J. Buschmann, H. Fink (Germany), DE 4001139, **1990** [*Chem. Abstr.* **1991**, *114*, 253475].
[32] H.-J. Buschmann, C. Jonas, W. Saus (Germany), DE 4412320, **1995** [*Chem. Abstr.* **1996**, *124*, 65677].
[33] H.-J. Buschmann, H. Fink, E. Schollmeyer (Germany), DE 19603377, **1997** [*Chem. Abstr.* **1997**, *127*, 205599].
[34] A. I. Day, A. P. Arnold, R. J. Blanch (Unisearch Limited, Australia), WO 2000068232, **2000** [*Chem. Abstr.* **2000**, *133*, 362775].
[35] K. Kim, J. Kim, I.-S. Jung, S.-Y. Kim, E. Lee, J.-K. Kang (Postech Foundation, South Korea), EP 1094065, **2001** [*Chem. Abstr.* **2001**, *134*, 326547].
[36] K. Kim, J. Kim, I.-S. Jung, S.-Y. Kim, E. Lee, J.-K. Kang (Postech Foundation, South Korea), US 6365734B1, **2002** [*Chem. Abstr.* **2001**, *134*, 326547z].
[37] K. Taketsuji, R. Ito (Hakuto Co., Ltd., Japan), JP 2001146690, **2001** [*Chem. Abstr.* **2001**, *135*, 6819].
[38] H. Blum, S. Sick, H. Salow, M. Kaussen (Germany), EP 1210966, **2002** [*Chem. Abstr.* **2002**, *137*, 21835].
[39] A. M. Richter, M. Felicetti (Germany), WO 2002096553, **2002** [*Chem. Abstr.* **2003**, *138*, 8757].
[40] A. M. Richter, M. Felicetti (Germany), DE 10040242, **2002** [*Chem. Abstr.* **2002**, *136*, 200050].
[41] A. I. Day, A. P. Arnold, R. J. Blanch (Australia), US 2003140787, **2003** [*Chem. Abstr.* **2003**, *139*, 135453].
[42] K. Kim, S.-Y. Jon, N. Selvapalam, D.-H. Oh (Postech Foundation, South Korea), WO 2003055888, **2003** [*Chem. Abstr.* **2003**, *139*, 101129].
[43] K. Kim, Y. J. Jeon, S.-Y. Kim, Y. H. Ko (Postech Foundation, South Korea), WO 2003024978, **2003** [*Chem. Abstr.* **2003**, *138*, 264767].
[44] K. Kim, J. Zhao, H.-J. Kim, S.-Y. Kim, J. Oh (Postech Foundation, South Korea), WO 2003004500, **2003** [*Chem. Abstr.* **2003**, *138*, 89832].
[45] Y. Miyahara (Sangaku Rentai Kiko Kyushu K. K., Japan), JP 2003212877, **2001** [*Chem. Abstr.* **2001**, *135*, 6819].
[46] S. Doering, S. Kainz, R. Roesmann (Henkel KGaA, Germany), WO 2004055258, **2004** [*Chem. Abstr.* **2004**, *141*, 90461].
[47] K. E. Geckeler, F. Constabel (South Korea), US 2004167328, **2004** [*Chem. Abstr.* **2004**, *141*, 207239].
[48] K. Kim, R. Balaji, D.-H. Oh, Y.-H. Ko, S.-Y. Jon (Postech Foundation, South Korea), WO 2004072151, **2004** [*Chem. Abstr.* **2004**, *141*, 207238].
[49] a) J.-M. Lehn, *Angew. Chem.* **1988**, *100*, 91 – 116; *Angew. Chem. Int. Ed. Engl.* **1988**, *27*, 89 – 112; b) D. J. Cram, *Angew. Chem.* **1988**, *100*, 1041 – 1052; *Angew. Chem. Int. Ed. Engl.* **1988**, *27*, 1009 – 1020; c) C. J. Pedersen, *Angew. Chem.* **1988**, *100*, 1053 – 1059; *Angew. Chem. Int. Ed. Engl.* **1988**, *27*, 1021 – 1027.
[50] *Comprehensive Supramolecular Chemistry, Vol. 1 Molecular Recognition: Receptors for Cationic Guests* (Ed.: G. W. Gokel), Pergamon, Oxford, **1996**.
[51] *Comprehensive Supramolecular Chemistry, Vol. 2 Molecular Recognition: Receptors for Molecular Guests* (Ed.: F. Vögtle), Pergamon, Oxford, **1996**.

 © 2005 Wiley-VCH Verlag GmbH & Co. KGaA, Weinheim

[52] *Comprehensive Supramolecular Chemistry*, *Vol. 3 Cyclodextrins* (Eds.: J. Szejtli, T. Osa), Pergamon, Oxford, **1996**.
[53] D. J. Hill, M. J. Mio, R. B. Prince, T. S. Hughes, J. S. Moore, *Chem. Rev.* **2001**, *101*, 3893 – 4011.
[54] R. P. Cheng, S. H. Gellman, W. F. DeGrado, *Chem. Rev.* **2001**, *101*, 3219 – 3232.
[55] G. Wulff, *Chem. Rev.* **2002**, *102*, 1 – 27.
[56] J. R. Epstein, D. R. Walt, *Chem. Soc. Rev.* **2003**, *32*, 203 – 214.
[57] J. J. Lavigne, E. V. Anslyn, *Angew. Chem.* **2001**, *113*, 3212 – 3225; *Angew. Chem. Int. Ed.* **2001**, *40*, 3118 – 3130.
[58] C. Marquez, F. Huang, W. M. Nau, *IEEE Trans. Nanobioscience* **2004**, *3*, 39 – 45.
[59] Thiocarbonyl analogues of cucurbiturils have been discussed in the patent literature. For DFT calculations, see: F. Pichierri, *Chem. Phys. Lett.* **2004**, *390*, 214 – 219.
[60] C. Márquez, R. R. Hudgins, W. M. Nau, *J. Am. Chem. Soc.* **2004**, *126*, 5806 – 5816.
[61] H.-J. Buschmann, E. Cleve, K. Jansen, A. Wego, E. Schollmeyer, *Mater. Sci. Eng. C* **2001**, *114*, 35 – 39.
[62] P. Germain, J. M. Letoffe, M. P. Merlin, H.-J. Buschmann, *Thermochim. Acta* **1998**, *315*, 87 – 92.
[63] H.-J. Buschmann, E. Cleve, E. Schollmeyer, *Inorg. Chim. Acta* **1992**, *193*, 93 – 97.
[64] J. Szejtli, *Chem. Rev.* **1998**, *98*, 1743 – 1753.
[65] F. Trotta, M. Zanetti, G. Camino, *Polym. Degrad. Stab.* **2000**, *69*, 373 – 379.
[66] H.-J. Buschmann, K. Jansen, C. Meschke, E. Schollmeyer, *J. Solution Chem.* **1998**, *27*, 135 – 140.
[67] G.-L. Zhang, Z.-Q. Xu, S.-F. Xue, Q.-J. Zhu, Z. Tao, *Wuji Huaxue Xuebao* **2003**, *19*, 655 – 659.
[68] K. Jansen, H.-J. Buschmann, A. Wego, D. Döpp, C. Mayer, H. J. Drexler, H. J. Holdt, E. Schollmeyer, *J. Inclusion Phenom. Macrocyclic Chem.* **2001**, *39*, 357 – 363.
[69] B. Honig, A. Nicholls, *Science* **1995**, *268*, 1144 – 1149.
[70] K. N. Houk, A. G. Leach, S. P. Kim, X. Zhang, *Angew. Chem.* **2003**, *115*, 5020 – 5046; *Angew. Chem. Int. Ed.* **2003**, *42*, 4872 – 4897.
[71] M. V. Rekharsky, Y. Inoue, *Chem. Rev.* **1998**, *98*, 1875 – 1917.
[72] W. L. Mock, N.-Y. Shih, *J. Org. Chem.* **1986**, *51*, 4440 – 4446.
[73] H.-J. Buschmann, K. Jansen, E. Schollmeyer, *Thermochim. Acta* **2000**, *346*, 33 – 36.
[74] H. Fujiwara, H. Arakawa, S. Murata, Y. Sasaki, *Bull. Chem. Soc. Jpn.* **1987**, *60*, 3891 – 3894.
[75] R. M. Izatt, R. E. Terry, B. L. Haymore, L. D. Hansen, N. K. Dalley, A. G. Avondet, J. J. Christensen, *J. Am. Chem. Soc.* **1976**, *98*, 7620 – 7626.
[76] H.-J. Buschmann, E. Cleve, K. Jansen, E. Schollmeyer, *Anal. Chim. Acta* **2001**, *437*, 157 – 163.
[77] H.-J. Buschmann, E. Cleve, K. Jansen, A. Wego, E. Schollmeyer, *J. Inclusion Phenom. Macrocyclic Chem.* **2001**, *40*, 117 – 120.
[78] H.-J. Buschmann, K. Jansen, E. Schollmeyer, *Inorg. Chem. Commun.* **2003**, *6*, 531 – 534.
[79] X. X. Zhang, K. E. Krakowiak, G. Xue, J. S. Bradshaw, R. M. Izatt, *Ind. Eng. Chem. Res.* **2000**, *39*, 3516 – 3520.
[80] W. L. Mock, N.-Y. Shih, *J. Org. Chem.* **1983**, *48*, 3618 – 3619.
[81] W. L. Mock, N.-Y. Shih, *J. Am. Chem. Soc.* **1988**, *110*, 4706 – 4710.
[82] W. L. Mock, N.-Y. Shih, *J. Am. Chem. Soc.* **1989**, *111*, 2697 – 2699.
[83] C. Meschke, H.-J. Buschmann, E. Schollmeyer, *Thermochim. Acta* **1997**, *297*, 43 – 48.
[84] A. V. Virovets, V. A. Blatov, A. P. Shevchenko, *Acta Crystallogr. B* **2004**, *60*, 350 – 357.
[85] C. Marquez, W. M. Nau, *Angew. Chem.* **2001**, *113*, 3248 – 3253; *Angew. Chem. Int. Ed.* **2001**, *40*, 3155 – 3160.
[86] D. G. Samsonenko, A. V. Virovets, J. Lipkowski, O. A. Geras'ko, V. P. Fedin, *J. Struct. Chem.* **2002**, *43*, 664 – 668.
[87] Y.-M. Jeon, J. Kim, D. Whang, K. Kim, *J. Am. Chem. Soc.* **1996**, *118*, 9790 – 9791.
[88] M. El Haouaj, Y. H. Ko, M. Luhmer, K. Kim, K. Bartik, *J. Chem. Soc. Perkin Trans. 2* **2001**, 2104 – 2107.
[89] D. Whang, J. Heo, J. H. Park, K. Kim, *Angew. Chem.* **1998**, *110*, 83 – 85; *Angew. Chem. Int. Ed.* **1998**, *37*, 78 – 80.
[90] A. Flinn, G. C. Hough, J. F. Stoddart, D. J. Williams, *Angew. Chem.* **1992**, *104*, 1550 – 1552; *Angew. Chem. Int. Ed.* **1992**, *31*, 1475 – 1477.
[91] H. Zhang, E. S. Paulsen, K. A. Walker, K. E. Krakowiak, D. V. Dearden, *J. Am. Chem. Soc.* **2003**, *125*, 9284 – 9285.
[92] Y. Shen, S. Xue, Y. Zhao, Q. Zhu, Z. Tao, *Chin. Sci. Bull.* **2003**, *48*, 2694 – 2697.
[93] D. M. Rudkevich, *Angew. Chem.* **2004**, *116*, 568 – 581; *Angew. Chem. Int. Ed.* **2004**, *43*, 558 – 571.
[94] K. A. Kellersberger, J. D. Anderson, S. M. Ward, K. E. Krakowiak, D. V. Dearden, *J. Am. Chem. Soc.* **2001**, *123*, 11316 – 11317.
[95] A. L. Rockwood, J. R. Van Orman, D. V. Dearden, *J. Am. Soc. Mass Spectrom.* **2004**, *15*, 12 – 21.
[96] Y. Miyahara, K. Abe, T. Inazu, *Angew. Chem.* **2002**, *114*, 3146 – 3149; *Angew. Chem. Int. Ed.* **2002**, *41*, 3020 – 3023.
[97] H.-J. Buschmann, K. Jansen, E. Schollmeyer, *Thermochim. Acta* **1998**, *317*, 95 – 98.
[98] H.-J. Buschmann, C. Meschke, E. Schollmeyer, *An. Quim. Int. Ed.* **1998**, *94*, 241 – 243.
[99] K. Jansen, A. Wego, H.-J. Buschmann, E. Schollmeyer, *Vom Wasser* **2000**, *94*, 177 – 190.
[100] K. Jansen, A. Wego, H.-J. Buschmann, E. Schollmeyer, *Vom Wasser* **2000**, *95*, 229 – 236.
[101] H.-J. Buschmann, K. Jansen, E. Schollmeyer, *J. Inclusion Phenom. Macrocyclic Chem.* **2000**, *37*, 231 – 236.
[102] K. Jansen, H.-J. Buschmann, E. Zliobaite, E. Schollmeyer, *Thermochim. Acta* **2002**, *385*, 177 – 184.
[103] H.-J. Buschmann, E. Schollmeyer, L. Mutihac, *Thermochim. Acta* **2003**, *399*, 203 – 208.
[104] H.-J. Buschmann, E. Schollmeyer, *J. Inclusion Phenom. Mol. Recognit. Chem.* **1997**, *29*, 167 – 174.
[105] R. Neugebauer, W. Knoche, *J. Chem. Soc. Perkin Trans. 2* **1998**, 529 – 534.
[106] M. El Haouaj, M. Luhmer, Y. H. Ko, K. Kim, K. Bartik, *J. Chem. Soc. Perkin Trans. 2* **2001**, 804 – 807.
[107] B. D. Wagner, A. I. MacRae, *J. Phys. Chem. B* **1999**, *103*, 10114 – 10119.
[108] B. D. Wagner, S. J. Fitzpatrick, M. A. Gill, A. I. MacRae, N. Stojanovic, *Can. J. Chem.* **2001**, *79*, 1101 – 1104.
[109] H.-J. Buschmann, T. Wolff, *J. Photochem. Photobiol. A* **1999**, *121*, 99 – 103.
[110] S.-M. Liu, X.-J. Wu, F. Liang, J.-H. Yao, C.-T. Wu, *Gaodeng Xuexiao Huaxue Xuebao* **2004**, *25*, 2038 – 2041.
[111] P. Mukhopadhyay, A. Wu, L. Isaacs, *J. Org. Chem.* **2004**, *69*, 6157 – 6164.
[112] P. Ma, J. Dong, S. Xiang, S. Xue, Q. Zhu, Z. Tao, J. Zhang, X. Zhou, *Sci. China Ser. B* **2004**, *47*, 301 – 310.
[113] B. D. Wagner, N. Stojanovic, A. I. Day, R. J. Blanch, *J. Phys. Chem. B* **2003**, *107*, 10741 – 10746.
[114] K.-C. Zhang, T.-W. Mu, L. Liu, Q.-X. Guo, *Chin. J. Chem.* **2001**, *19*, 558 – 561.
[115] S. Choi, S. H. Park, A. Y. Ziganshina, Y. H. Ko, J. W. Lee, K. Kim, *Chem. Commun.* **2003**, 2176 – 2177.
[116] H.-J. Kim, W. S. Jeon, Y. H. Ko, K. Kim, *Proc. Natl. Acad. Sci. USA* **2002**, *99*, 5007 – 5011.
[117] W. Ong, M. Gómez-Kaifer, A. E. Kaifer, *Org. Lett.* **2002**, *4*, 1791 – 1794.

 © 2005 Wiley-VCH Verlag GmbH & Co. KGaA, Weinheim

[118] W. Ong, A. E. Kaifer, *Angew. Chem.* **2003**, *115*, 2214 – 2217; *Angew. Chem. Int. Ed.* **2003**, *42*, 2164 – 2167.
[119] W. Ong, A. E. Kaifer, *J. Org. Chem.* **2004**, *69*, 1383 – 1385.
[120] K. Moon, A. E. Kaifer, *Org. Lett.* **2004**, *6*, 185 – 188.
[121] R. J. Blanch, A. J. Sleeman, T. J. White, A. P. Arnold, A. I. Day, *Nano Lett.* **2002**, *2*, 147 – 149.
[122] W. Ong, A. E. Kaifer, *Organometallics* **2003**, *22*, 4181 – 4183.
[123] S. Lorenzo, A. Day, D. Craig, R. Blanch, A. Arnold, I. Dance, *CrystEngComm* **2001**, *49*, 1 – 7.
[124] K. Yan, Z.-X. Huang, S.-M. Liu, L. Feng, C.-T. Wu, *Wuhan Univ. J. Nat. Sci.* **2004**, *9*, 99 – 101.
[125] N. J. Wheate, A. I. Day, R. J. Blanch, A. P. Arnold, C. Cullinane, J. G. Collins, *Chem. Commun.* **2004**, 1424 – 1425.
[126] V. Sindelar, K. Moon, A. E. Kaifer, *Org. Lett.* **2004**, *6*, 2665 – 2668.
[127] C. Marquez, W. M. Nau, *Angew. Chem.* **2001**, *113*, 4515 – 4518; *Angew. Chem. Int. Ed.* **2001**, *40*, 4387 – 4390.
[128] J. Mohanty, W. M. Nau, *Photochem. Photobiol. Sci.* **2004**, *3*, 1026 – 1031.
[129] C. Marquez, U. Pischel, W. M. Nau, *Org. Lett.* **2003**, *5*, 3911 – 3914.
[130] F. Constabel, K. E. Geckeler, *Tetrahedron Lett.* **2004**, *45*, 2071 – 2073.
[131] L. Xu, S.-M. Liu, C.-T. Wu, Y.-Q. Feng, *Electrophoresis* **2004**, *25*, 3300 – 3306.
[132] a) W. S. Jeon, H.-J. Kim, C. Lee, K. Kim, *Chem. Commun.* **2002**, 1828 – 1829; b) W. S. Jeon, A. Y. Ziganshina, J. W. Lee, Y. H. Ko, J. K. Kang, C. Lee, K. Kim, *Angew. Chem.* **2003**, *115*, 4231 – 4234; *Angew. Chem. Int. Ed.* **2003**, *42*, 4097 – 4100; c) W. S. Jeon, E. Kim, Y. H. Ko, I. Huang, J. W. Lee, S.-Y. Kim, H.-J. Kim, K. Kim, *Angew. Chem.* **2005**, *117*, 89 – 93; *Angew. Chem. Int. Ed.* **2005**, *44*, 87 – 91.
[133] T. W. Mu, L. Liu, K. C. Zhang, Q. X. Guo, *Chin. Chem. Lett.* **2001**, *12*, 783 – 786.
[134] H.-J. Kim, J. Heo, W. S. Jeon, E. Lee, J. Kim, S. Sakamoto, K. Yamaguchi, K. Kim, *Angew. Chem.* **2001**, *113*, 1574 – 1577; *Angew. Chem. Int. Ed.* **2001**, *40*, 1526 – 1529.
[135] J. W. Lee, K. Kim, S. Choi, Y. H. Ko, S. Sakamoto, K. Yamaguchi, K. Kim, *Chem. Commun.* **2002**, 2692 – 2693.
[136] Y. J. Jeon, P. K. Bharadwaj, S. W. Choi, J. W. Lee, K. Kim, *Angew. Chem.* **2002**, *114*, 4654 – 4656; *Angew. Chem. Int. Ed.* **2002**, *41*, 4474 – 4476.
[137] J.-X. Liu, Z. Tao, S.-F. Xue, Q.-J. Zhu, J.-X. Zhang, *Wuji Huaxue Xuebao* **2004**, *20*, 139 – 146.
[138] E. V. Chubarova, D. G. Samsonenko, M. N. Sokolov, O. A. Gerasko, V. P. Fedin, J. G. Platas, *J. Inclusion Phenom. Macrocyclic Chem.* **2004**, *48*, 31 – 35.
[139] S.-Y. Kim, I.-S. Jung, E. Lee, J. Kim, S. Sakamoto, K. Yamaguchi, K. Kim, *Angew. Chem.* **2001**, *113*, 2177 – 2179; *Angew. Chem. Int. Ed.* **2001**, *40*, 2119 – 2121.
[140] V. Balzani, A. Credi, F. M. Raymo, J. F. Stoddart, *Angew. Chem.* **2000**, *112*, 3484 – 3530; *Angew. Chem. Int. Ed.* **2000**, *39*, 3348 – 3391.
[141] W. L. Mock, J. Pierpont, *J. Chem. Soc. Chem. Commun.* **1990**, 1509 – 1511.
[142] S. I. Jun, J. W. Lee, S. Sakamoto, K. Yamaguchi, K. Kim, *Tetrahedron Lett.* **2000**, *41*, 471 – 475.
[143] J. W. Lee, K. Kim, K. Kim, *Chem. Commun.* **2001**, 1042 – 1043.
[144] J. W. Lee, S. Choi, Y. H. Ko, S.-Y. Kim, K. Kim, *Bull. Korean Chem. Soc.* **2002**, *23*, 1347 – 1350.
[145] S. Y. Jon, Y. H. Ko, S. H. Park, H.-J. Kim, K. Kim, *Chem. Commun.* **2001**, 1938 – 1939.
[146] A. Y. Ziganshina, Y. H. Ko, W. S. Jeon, K. Kim, *Chem. Commun.* **2004**, 806 – 807.
[147] W. L. Mock, T. A. Irra, J. P. Wepsiec, M. Adhya, *J. Org. Chem.* **1989**, *54*, 5302 – 5308.
[148] W. L. Mock, T. A. Irra, J. P. Wepsiec, T. L. Manimaran, *J. Org. Chem.* **1983**, *48*, 3619 – 3620.
[149] H. C. Kolb, M. G. Finn, K. B. Sharpless, *Angew. Chem.* **2001**, *113*, 2056 – 2075; *Angew. Chem. Int. Ed.* **2001**, *40*, 2004 – 2021.
[150] D. Tuncel, J. H. G. Steinke, *Chem. Commun.* **1999**, 1509 – 1510.
[151] D. Tuncel, J. H. G. Steinke, *Macromolecules* **2004**, *37*, 288 – 302.
[152] D. Tuncel, J. H. G. Steinke, *Chem. Commun.* **2002**, 496 – 497.
[153] T. C. Krasia, J. H. G. Steinke, *Chem. Commun.* **2002**, 22 – 23.
[154] K. Kim, W. S. Jeon, J.-K. Kang, J. W. Lee, S. Y. Jon, T. Kim, K. Kim, *Angew. Chem.* **2003**, *115*, 2395 – 2398; *Angew. Chem. Int. Ed.* **2003**, *42*, 2293 – 2296.
[155] K. Kim, D. Kim, J. W. Lee, Y. H. Ko, K. Kim, *Chem. Commun.* **2004**, 848 – 849.
[156] H.-J. Buschmann, A. Gardberg, E. Schollmeyer, *Textilveredlung* **1991**, *26*, 153 – 157.
[157] H.-J. Buschmann, D. Rader, E. Schollmeyer, *Textilveredlung* **1991**, *26*, 157 – 160.
[158] H.-J. Buschmann, A. Gardberg, D. Rader, E. Schollmeyer, *Textilveredlung* **1991**, *26*, 160 – 162.
[159] H.-J. Buschmann, C. Carvalho, U. Driessen, E. Schollmeyer, *Textilveredlung* **1993**, *28*, 176 – 179.
[160] H.-J. Buschmann, A. Gardberg, D. Rader, E. Schollmeyer, *Textilveredlung* **1993**, *28*, 179 – 182.
[161] H.-J. Buschmann, E. Schollmeyer, *Textilveredlung* **1994**, *29*, 58 – 60.
[162] H.-J. Buschmann, E. Schollmeyer, *Textilveredlung* **1997**, *32*, 249 – 252.
[163] H.-J. Buschmann, E. Schollmeyer, *Textilveredlung* **1998**, *33*, 44 – 47.
[164] H.-J. Buschmann, *Wiss. Ber. — Zentralinst. Festkoerperphys. Werkstoffforsch.* **1990**, *44*, 114 – 122.
[165] H.-J. Buschmann, E. Schollmeyer, *WLB Wasser Luft Boden* **1991**, *35*, 40 – 41.
[166] H.-J. Buschmann, E. Schollmeyer, *Textilveredlung* **1993**, *28*, 182 – 184.
[167] H.-J. Buschmann, E. Schollmeyer, *WLB Wasser Luft Boden* **1993**, *37*, 50 – 51.
[168] H.-J. Buschmann, *Vom Wasser* **1995**, *84*, 263 – 269.
[169] D. A. Dantz, Ö. Otyakmaz, H.-J. Buschmann, E. Schollmeyer, *Vom Wasser* **1998**, *91*, 305 – 314.
[170] H.-J. Buschmann, E. Schollmeyer, *J. Inclusion Phenom. Mol. Recognit. Chem.* **1992**, *14*, 91 – 99.
[171] D. A. Dantz, C. Meschke, H.-J. Buschmann, E. Schollmeyer, *Supramol. Chem.* **1998**, *9*, 79 – 83.
[172] S. Karcher, A. Kornmueller, M. Jekel, *Biol. Abwasserreinig.* **1997**, *9*, 131 – 152.
[173] S. Karcher, A. Kornmueller, M. Jekel, *Acta Hydrochim. Hydrobiol.* **1999**, *27*, 38 – 42.
[174] S. Karcher, A. Kornmüller, M. Jekel, *Water Sci. Technol.* **1999**, *40*, 425 – 433.
[175] S. Karcher, A. Kornmüller, M. Jekel, *Water Res.* **2001**, *35*, 3309 – 3316.
[176] A. Kornmüller, S. Karcher, M. Jekel, *Water Res.* **2001**, *35*, 3317 – 3324.
[177] K. Taketsuji, H. Tomioka, *Nippon Kagaku Kaishi* **1998**, 670 – 678.
[178] K. Taketsuji, *Res. Rep. Fac. Eng. Mie Univ.* **1999**, *24*, 119 – 120.
[179] H. Isobe, N. Tomita, J. W. Lee, H.-J. Kim, K. Kim, E. Nakamura, *Angew. Chem.* **2000**, *112*, 4424 – 4427; *Angew. Chem. Int. Ed.* **2000**, *39*, 4257 – 4260.
[180] Y.-B. Lim, T. Kim, J. W. Lee, S.-M. Kim, H.-J. Kim, K. Kim, J.-S. Park, *Bioconjugate Chem.* **2002**, *13*, 1181 – 1185.
[181] D. Whang, K.-M. Park, J. Heo, P. Ashton, K. Kim, *J. Am. Chem. Soc.* **1998**, *120*, 4899 – 4900.
[182] S.-G. Roh, K.-M. Park, G.-J. Park, S. Sakamoto, K. Yamaguchi, K. Kim, *Angew. Chem.* **1999**, *111*, 672 – 675; *Angew. Chem. Int. Ed.* **1999**, *38*, 638 – 641.

© 2005 Wiley-VCH Verlag GmbH & Co. KGaA, Weinheim

[183] K.-M. Park, S.-Y. Kim, J. Heo, D. Whang, S. Sakamoto, K. Yamaguchi, K. Kim, *J. Am. Chem. Soc.* **2002**, *124*, 2140 – 2147.
[184] Y. H. Ko, K. Kim, J.-K. Kang, H. Chun, J. W. Lee, S. Sakamoto, K. Yamaguchi, J. C. Fettinger, K. Kim, *J. Am. Chem. Soc.* **2004**, *126*, 1932 – 1933.
[185] D. B. Amabilino, P. R. Ashton, V. Balzani, S. E. Boyd, A. Credi, J. Y. Lee, S. Menzer, J. F. Stoddart, M. Venturi, D. J. Williams, *J. Am. Chem. Soc.* **1998**, *120*, 4295 – 4307.
[186] Z.-Q. Xu, X.-Q. Yao, S.-F. Xue, Q.-J. Zhu, Z. Tao, J.-X. Zhang, Z.-B. Wei, L.-S. Long, *Huaxue Xuebao* **2004**, *51*, 1927 – 1934.
[187] D. Tuncel, J. H. G. Steinke, *Polym. Prepr.* **1999**, *40*, 585 – 586.
[188] Y.-M. Jeon, D. Whang, J. Kim, K. Kim, *Chem. Lett.* **1996**, 503 – 504.
[189] C. Meschke, H.-J. Buschmann, E. Schollmeyer, *Macromol. Rapid Commun.* **1998**, *19*, 59 – 63.
[190] C. Meschke, H.-J. Buschmann, E. Schollmeyer, *Polymer* **1998**, *40*, 945 – 949.
[191] H.-J. Buschmann, E. Cleve, L. Mutihac, E. Schollmeyer, *Microchem. J.* **2000**, *64*, 99 – 103.
[192] H.-J. Buschmann, K. Jansen, E. Schollmeyer, *Acta Chim. Slov.* **1999**, *46*, 405 – 411.
[193] H.-J. Buschmann, A. Wego, E. Schollmeyer, D. Döpp, *Supramol. Chem.* **2000**, *11*, 225 – 231.
[194] S.-M. Liu, X. Wu, Z. Huang, J. Yao, F. Liang, C.-T. Wu, *J. Inclusion Phenom. Macrocyclic Chem.* **2004**, *50*, 203 – 207.
[195] X. He, G. Li, H. Chen, *Inorg. Chem. Commun.* **2002**, *5*, 633 – 636.
[196] X.-Y. He, J. Li, Y. Gao, H.-L. Chen, *Wuji Huaxue Xuebao* **2003**, *19*, 153 – 158.
[197] Y. Tan, S. Choi, J. W. Lee, Y. H. Ko, K. Kim, *Macromolecules* **2002**, *35*, 7161 – 7165.
[198] D. Tuncel, J. H. G. Steinke, *Chem. Commun.* **2001**, 253 – 254.
[199] S. Choi, J. W. Lee, Y. H. Ko, K. Kim, *Macromolecules* **2002**, *35*, 3526 – 3531.
[200] J. W. Lee, Y. H. Ko, S.-H. Park, K. Yamaguchi, K. Kim, *Angew. Chem.* **2001**, *113*, 768 – 771; *Angew. Chem. Int. Ed.* **2001**, *40*, 746 – 749.
[201] H. Isobe, S. Sato, E. Nakamura, *Org. Lett.* **2002**, *4*, 1287 – 1289.
[202] A. Wego, K. Jansen, H. J. Buschmann, E. Schollmeyer, D. Döpp, *J. Inclusion Phenom. Macrocyclic Chem.* **2002**, *43*, 201 – 205.
[203] A. Wu, L. Isaacs, *J. Am. Chem. Soc.* **2003**, *125*, 4831 – 4835.
[204] D. Whang, K. Kim, *J. Am. Chem. Soc.* **1997**, *119*, 451 – 452.
[205] D. Whang, J. Heo, C.-A. Kim, K. Kim, *Chem. Commun.* **1997**, 2361 – 2362.
[206] D. Whang, Y.-M. Jeon, J. Heo, K. Kim, *J. Am. Chem. Soc.* **1996**, *118*, 11333 – 11334.
[207] E. Lee, J. Heo, K. Kim, *Angew. Chem.* **2000**, *112*, 2811 – 2813; *Angew. Chem. Int. Ed.* **2000**, *39*, 2699 – 2701.
[208] E. Lee, J. Kim, J. Heo, D. Whang, K. Kim, *Angew. Chem.* **2001**, *113*, 413 – 416; *Angew. Chem. Int. Ed.* **2001**, *40*, 399 – 402.
[209] K.-M. Park, S.-G. Roh, E. Lee, J. Kim, H.-J. Kim, J. W. Lee, K. Kim, *Supramol. Chem.* **2002**, *14*, 153 – 158.
[210] K.-M. Park, D. Whang, E. Lee, J. Heo, K. Kim, *Chem. Eur. J.* **2002**, *8*, 498 – 508.
[211] M. N. Sokolov, A. V. Virovets, D. N. Dybtsev, O. A. Gerasko, V. P. Fedin, R. Hernandez-Molina, W. Clegg, A. G. Sykes, *Angew. Chem.* **2000**, *112*, 1725 – 1727; *Angew. Chem. Int. Ed.* **2000**, *39*, 1659 – 1661.
[212] V. P. Fedin, M. Sokolov, G. J. Lamprecht, R. Hernandez-Molina, M.-S. Seo, A. V. Virovets, W. Clegg, A. G. Sykes, *Inorg. Chem.* **2001**, *40*, 6598 – 6603.
[213] D. G. Samsonenko, J. Lipkowski, O. A. Gerasko, A. V. Virovets, M. N. Sokolov, V. P. Fedin, J. G. Platas, R. Hernandez-Molina, A. Mederos, *Eur. J. Inorg. Chem.* **2002**, 2380 – 2388.
[214] O. A. Gerasko, A. V. Virovets, D. G. Samsonenko, A. A. Tripol'skaya, V. P. Fedin, D. Fenske, *Russ. Chem. Bull. Int. Ed.* **2003**, *52*, 585 – 593.
[215] M. N. Sokolov, T. V. Mitkina, O. A. Gerasko, V. P. Fedin, A. V. Virovets, R. Llusar, *Z. Anorg. Allg. Chem.* **2003**, *629*, 2440 – 2442.
[216] S.-M. Liu, Z.-X. Huang, X.-J. Wu, F. Liang, C.-T. Wu, *Chin. J. Chem.* **2004**, *22*, 1208 – 1210.
[217] M. N. Sokolov, R. Hernández-Molina, W. Clegg, V. P. Fedin, A. Mederos, *Chem. Commun.* **2003**, 140 – 141.
[218] J. Heo, S.-Y. Kim, D. Whang, K. Kim, *Angew. Chem.* **1999**, *111*, 675 – 678; *Angew. Chem. Int. Ed.* **1999**, *38*, 641 – 643.
[219] D. G. Samsonenko, O. A. Gerasko, J. Lipkowski, A. V. Virovets, V. P. Fedin, *Russ. Chem. Bull. Int. Ed.* **2002**, *51*, 1915 – 1918.
[220] D. G. Samsonenko, M. N. Sokolov, O. A. Gerasko, A. V. Virovets, J. Lipkowski, D. Fenske, V. P. Fedin, *Russ. Chem. Bull. Int. Ed.* **2003**, *52*, 2132 – 2139.
[221] J. Heo, J. Kim, D. Whang, K. Kim, *Inorg. Chim. Acta* **2000**, *297*, 307 – 312.
[222] W. A. Freeman, *Acta Crystallogr. B* **1984**, *40*, 382 – 387.
[223] D. G. Samsonenko, A. A. Sharonova, M. N. Sokolov, A. V. Virovets, V. P. Fedin, *Russ. J. Coord. Chem.* **2001**, *27*, 10 – 15.
[224] O. A. Gerasko, A. V. Virovets, M. N. Sokolov, D. N. Dybtsev, A. V. Gerasimenko, D. Fenske, V. P. Fedin, *Russ. Chem. Bull. Int. Ed.* **2002**, *51*, 1800 – 1805.
[225] D. G. Samsonenko, A. V. Virovets, A. A. Sharonova, V. P. Fedin, D. Fenske, *Russ. Chem. Bull.* **2001**, *50*, 494 – 496.
[226] V. P. Fedin, M. N. Sokolov, D. N. Dybtsev, O. A. Gerasko, A. V. Virovets, D. Fenske, *Inorg. Chim. Acta* **2002**, *331*, 31 – 38.
[227] D. N. Dybtsev, O. A. Gerasko, A. V. Virovets, M. N. Sokolov, V. P. Fedin, *Inorg. Chem. Commun.* **2000**, *3*, 345 – 349.
[228] V. P. Fedin, A. V. Virovets, M. N. Sokolov, D. N. Dybtsev, O. A. Gerasko, W. Clegg, *Inorg. Chem.* **2000**, *39*, 2227 – 2230.
[229] M. N. Sokolov, O. A. Gerasko, D. N. Dybtsev, E. V. Chubarova, A. V. Virovets, C. Vicent, R. Llusar, D. Fenske, V. P. Fedin, *Eur. J. Inorg. Chem.* **2004**, 63 – 68.
[230] V. P. Fedin, A. V. Virovets, D. N. Dybtsev, O. A. Gerasko, K. Hegetschweiler, M. R. J. Elsegood, W. Clegg, *Inorg. Chim. Acta* **2000**, *304*, 301 – 304.
[231] M. N. Sokolov, D. N. Dybtsev, A. V. Virovets, K. Hegetschweiler, V. P. Fedin, *Russ. Chem. Bull. Int. Ed.* **2000**, *49*, 1877 – 1881.
[232] D. N. Dybtsev, O. A. Gerasko, A. V. Virovets, M. N. Sokolov, T. Weber, V. P. Fedin, *Zh. Neorg. Khim.* **2001**, *46*, 908 – 914.
[233] M. N. Sokolov, A. V. Virovets, D. N. Dybtsev, E. V. Chubarova, V. P. Fedin, D. Fenske, *Inorg. Chem.* **2001**, *40*, 4816 – 4817.
[234] O. A. Geras'ko, A. V. Virovets, D. N. Dybtsev, V. Klegg, V. P. Fedin, *Russ. J. Coord. Chem.* **2000**, *26*, 478 – 481.
[235] V. P. Fedin, V. Gramlich, M. Wörle, T. Weber, *Inorg. Chem.* **2001**, *40*, 1074 – 1077.
[236] M. N. Sokolov, R. Hernández-Molina, D. N. Dybtsev, E. V. Chubarova, S. F. Solodovnikov, N. V. Pervukhina, C. Vicent, R. Llusar, V. Fedin, *Z. Anorg. Allg. Chem.* **2002**, *628*, 2335 – 2339.
[237] R. Hernandez-Molina, M. Sokolov, P. Esparza, C. Vicent, R. Llusar, *Dalton Trans.* **2004**, 847 – 851.
[238] D. G. Samsonenko, M. N. Sokolov, A. V. Virovets, N. V. Pervukhina, V. P. Fedin, *Eur. J. Inorg. Chem.* **2001**, 167 – 172.
[239] A. V. Virovets, D. G. Samsonenko, D. N. Dybtsev, V. P. Fedin, W. Clegg, *J. Struct. Chem.* **2001**, *42*, 319 – 321.
[240] A. V. Virovets, D. G. Samsonenko, M. N. Sokolov, V. P. Fedin, *Acta Crystallogr. E* **2001**, *57*, 33 – 34.
[241] O. A. Gerasko, D. G. Samsonenko, A. A. Sharonova, A. V. Virovets, J. Lipkowski, V. P. Fedin, *Russ. Chem. Bull.* **2002**, *51*, 346 – 349.
[242] M. N. Sokolov, D. N. Dybtsev, A. V. Virovets, W. Clegg, V. P. Fedin, *Russ. Chem. Bull. Int. Ed.* **2001**, *50*, 1144 – 1147.

 © 2005 Wiley-VCH Verlag GmbH & Co. KGaA, Weinheim

[243] D. G. Samsonenko, O. A. Geras'ko, T. V. Mit'kina, J. Lipkowski, A. V. Virovets, D. Fenske, V. P. Fedin, *Russ. J. Coord. Chem.* **2003**, *29*, 166 – 174.
[244] T. V. Mit'kina, O. A. Gerasko, M. N. Sokolov, D. Y. Naumov, V. P. Fedin, *Russ. Chem. Bull. Int. Ed.* **2004**, *53*, 80 – 85.
[245] C. A. Burnett, D. Witt, J. C. Fettinger, L. Isaacs, *J. Org. Chem.* **2003**, *68*, 6184 – 6191.
[246] C. A. Burnett, J. Lagona, A. Wu, J. A. Shaw, D. Coady, J. C. Fettinger, A. I. Day, L. Isaacs, *Tetrahedron* **2003**, *59*, 1961 – 1970.
[247] A. Chakraborty, A. Wu, D. Witt, J. Lagona, J. C. Fettinger, L. Isaacs, *J. Am. Chem. Soc.* **2002**, *124*, 8297 – 8306.
[248] J. Lagona, J. C. Fettinger, L. Isaacs, *Org. Lett.* **2003**, *5*, 3745 – 3747.
[249] A. Wu, A. Chakraborty, D. Witt, J. Lagona, F. Damkaci, M. A. Ofori, J. K. Chiles, J. C. Fettinger, L. Isaacs, *J. Org. Chem.* **2002**, *67*, 5817 – 5830.
[250] A. I. Day, R. J. Blanch, A. Coe, A. P. Arnold, *J. Inclusion Phenom. Macrocyclic Chem.* **2002**, *43*, 247 – 250.
[251] A. I. Day, A. P. Arnold, R. J. Blanch, *Molecules* **2003**, *8*, 74 – 84.
[252] K. Jansen, A. Wego, H.-J. Buschmann, E. Schollmeyer, D. Döpp, *Des. Monomers Polym.* **2003**, *6*, 43 – 55.
[253] J. Zhao, H.-J. Kim, J. Oh, S.-Y. Kim, J. W. Lee, S. Sakamoto, K. Yamaguchi, K. Kim, *Angew. Chem.* **2001**, *113*, 4365 – 4367; *Angew. Chem. Int. Ed.* **2001**, *40*, 4233 – 4235.
[254] S. Y. Jon, N. Selvapalam, D. H. Oh, J.-K. Kang, S.-Y. Kim, Y. J. Jeon, J. W. Lee, K. Kim, *J. Am. Chem. Soc.* **2003**, *125*, 10186 – 10187.
[255] A. E. Rowan, J. A. A. W. Elemans, R. J. M. Nolte, *Acc. Chem. Res.* **1999**, *32*, 995 – 1006.
[256] N.-Y. Shih, Ph.D. thesis, University of Illinois at Chicago, **1981** [*Diss. Abst. Int.* **1982-B**, *42*, 4071].
[257] K. S. Oh, J. Yoon, K. S. Kim, *J. Phys. Chem. B* **2001**, *105*, 9726 – 9731.
[258] In the depicted mechanism the ureidyl N atom acts as a nucleophile to capture iminium ion **66S**. An alternative mechanism involves attack of the ureidyl O atom on **66S**, which obviates the intermediacy of *N*-acylammonium ion **67**. Both mechanisms are fully presented in Ref. [247].
[259] S. Sasmal, M. K. Sinha, E. Keinan, *Org. Lett.* **2004**, *6*, 1225 – 1228.
[260] Y. Zhao, S. Xue, Q. Zhu, Z. Tao, J. Zhang, Z. Wei, L. Long, M. Hu, H. Xiao, A. I. Day, *Chin. Sci. Bull.* **2004**, *49*, 1111 – 1116.
[261] S.-M. Liu, L. Xu, C.-T. Wu, Y.-Q. Feng, *Talanta* **2004**, *64*, 929 – 934.
[262] Y. J. Jeon, H. Kim, S. Jon, N. Selvapalam, D. H. Oh, I. Seo, C.-S. Park, S. R. Jung, D.-S. Koh, K. Kim, *J. Am. Chem. Soc.* **2004**, *126*, 15944 – 15945.
[263] For other glycoluril-based macrocycles containing alternating glycoluril and aromatic rings, see: a) J. W. M. Smeets, R. P. Sijbesma, F. G. M. Niele, A. L. Spek, W. J. J. Smeets, R. J. M. Nolte, *J. Am. Chem. Soc.* **1987**, *109*, 928 – 929; b) B. A. Murray, G. S. Whelan, *Pure Appl. Chem.* **1996**, *68*, 1561 – 1657.
[264] Y. Miyahara, K. Goto, M. Oka, T. Inazu, *Angew. Chem.* **2004**, *116*, 5129 – 5132; *Angew. Chem. Int. Ed.* **2004**, *43*, 5019 – 5022.
[265] R. P. Sijbesma, R. J. M. Nolte, *J. Am. Chem. Soc.* **1991**, *113*, 6695 – 6696.
[266] O. Braha, J. Webb, L.-Q. Gu, K. Kim, H. Bayley, *ChemPhysChem* **2005**, *6*, 889 – 892.
[267] H.-J. Buschmann, E. Cleve, E. Schollmeyer, *Inorg. Chem. Commun.* **2005**, *8*, 125 – 127.
[268] H.-J. Buschmann, L. Mutihac, R.-C. Mutihac, E. Schollmeyer, *Thermochim. Acta* **2005**, *430*, 79 – 82.
[269] E. V. Chubarova, D. G. Samsonenko, J. H. Platas, M. N. Sokolov, V. P. Fedin, *J. Struct. Chem.* **2004**, *45*, 906 – 911.
[270] H. Cong, F. Yang, Z. Tao, J.-X. Zhang, *Wuji Huaxue Xuebao* **2005**, *21*, 349 – 356.
[271] F. Constabel, K. E. Geckeler, *Fullerenes, Nanotubes, and Carbon Nanostruct.* **2004**, *12*, 811 – 818.
[272] L.-P. Dai, Z. Tao, Q.-J. Zhu, S.-F. Xue, J.-X. Zhang, X. Zhou, *Huaxue Xuebao* **2004**, *62*, 2431 – 2440.
[273] H. Fu, S. Xue, L. Mu, Y. Du, Q. Zhu, Z. Tao, J. Zhang, A. I. Day, *Sci. China Ser. B* **2004**, *34*, 517 – 525.
[274] H.-Y. Fu, S.-F. Xue, Q.-J. Zhu, Z. Tao, J.-X. Zhang, A. I. Day, *J. Inclusion Phenom. Macrocyclic Chem.* **2005**, *52*, 101 – 107.
[275] O. A. Gerasko, E. A. Mainicheva, D. Y. Naumov, N. V. Kuratieva, M. N. Sokolov, V. P. Fedin, *Inorg. Chem.* **2005**, *44*, 4133 – 4135.
[276] X.-Y. He, J. Li, Y. Gao, H. Chen, *Wuji Huaxue Xuebao* **2003**, *19*, 153 – 158.
[277] Z.-S. Hou, Y.-B. Tan, Y.-L. Huang, Q. F. Zhou, *Huaxue Xuebao* **2005**, *63*, 653 – 657.
[278] Z.-S. Hou, Y.-B. Tan, C.-W. Wang, Y.-L. Huang, Q.-F. Zhou, *Gaodeng Xuexiao Huaxue Xuebao* **2005**, *26*, 773 – 777.
[279] H. Isobe, S. Sota, J. W. Lee, H.-J. Kim, K. Kim, E. Nakamura, *Chem. Commun.* **2005**, 1549 – 1551.
[280] Y. J. Jeon, S.-Y. Kim, Y. H. Ko, S. Sakamoto, K. Yamaguchi, K. Kim, *Org. Biomol. Chem.* **2005**, *3*, 2122 – 2125.
[281] S. Liu, X. Wu, Z. Huang, J. Yao, F. Liang, C. Wu, *J. Inclusion Phenom. Macrocyclic Chem.* **2004**, *50*, 203 – 207.
[282] H.-K. Lee, K. M. Park, Y. J. Jeon, D. Kim, D. H. Oh, H. S. Kim, C. K. Park, K. Kim, *J. Am. Chem. Soc.* **2005**, *127*, 5006 – 5007.
[283] R. G. Lin, L. S. Long, R. B. Huang, L. S. Zheng, S. W. Ng, *Acta Crystallogr. E* **2005**, *61*, 885 – 888.
[284] T. V. Mitkina, D. Y. Naumov, O. A. Gerasko, F. M. Dolgushin, C. Vicent, R. Llusar, M. N. Sokolov, V. P. Fedin, *Russ. Chem. Bull.* **2004**, *53*, 2519 – 2524.
[285] J. Mohanty, W. M. Nau, *Angew. Chem.* **2005**, *117*, 3816 – 3820; *Angew. Chem. Int. Ed.* **2005**, *44*, 3750 – 3754.
[286] K. Moon, J. Grindstaff, D. Sobransingh, A. E. Kaifer, *Angew. Chem.* **2004**, *116*, 5612 – 5615; *Angew. Chem. Int. Ed.* **2004**, *43*, 5496 – 5499.
[287] L. Mu, X.-K. Chen, S.-F. Xue, X. Zeng, Q.-J. Zhu, Z. Tao, *Spectrosc. Spectral Anal.* **2004**, *24*, 231 – 232.
[288] K.-M. Park, E. Lee, S.-G. Roh, J. Kim, K. Kim, *Bull. Korean. Chem. Soc.* **2004**, *25*, 1711 – 1713.
[289] M. Pattabiraman, A. Natarajan, L. S. Kaanumalle, V. Ramamurthy, *Org. Lett.* **2005**, *7*, 529 – 532.
[290] F. Pichierri, *Chem. Phys. Lett.* **2005**, *403*, 252 – 256.
[291] M. A. Rankin, B. D. Wagner, *Supramol. Chem.* **2004**, *16*, 513 – 519.
[292] V. Sindelar, M. A. Cejas, F. M. Raymo, A. E. Kaifer, *New J. Chem.* **2005**, *29*, 280 – 282.
[293] A. A. Tripolskaya, O. A. Gerasko, D. Y. Naumov, J. Lipkowski, V. A. Logvinenko, V. P. Fedin, *J. Struct. Chem.* **2004**, *45*, 269 – 275.
[294] B. D. Wagner, P. G. Boland, J. Lagona, L. Isaacs, *J. Phys. Chem. B* **2005**, *109*, 7686 – 7691.
[295] F. Wei, S. Liu, L. Xu, C. Wu, Y. Feng, *Sepu* **2004**, 22, 476 – 478.
[296] F. Wei, S.-M. Liu, G.-Z. Cheng, C.-T. Wu, Y.-Q. Feng, *Electrophoresis* **2005**, *26*, 2214 – 2224.
[297] S.-L. Yang, S.-F. Xue, Q.-J. Zhu, Z. Tao, J.-X. Zhang, X. Zhou, *Youji Huaxue* **2005**, *25*, 427 – 431.
[298] F. Zhang, T. Yajima, Y.-Z. Li, G.-Z. Xu, H.-L. Chen, Q.-T. Liu, O. Yamauchi, *Angew. Chem.* **2005**, *117*, 3468 – 3473; *Angew. Chem. Int. Ed.* **2005**, *44*, 3402 – 3407.
[299] Y.-J. Zhao, S.-F. Xue, Y.-Q. Zhang, Q.-J. Zhu, Z. Tao, J.-X. Zhang, Z.-B. Wei, L.-S. Long, *Huaxue Xuebao* **2005**, *63*, 913 – 918.
[300] O. A. Gerasko, M. N. Sokolov, V. P. Fedin, *Pure Appl. Chem.* **2004**, *76*, 1633 – 1646.
[301] K. Kim, N. Selvapalam, D.-H. Oh, *J. Inclusion Phenom. Macrocyclic Chem.* **2004**, *50*, 31 – 36.
[302] G. Li, Y. Feng, *Huaxue Tongbao* **2005**, *68*, 1 – 8.

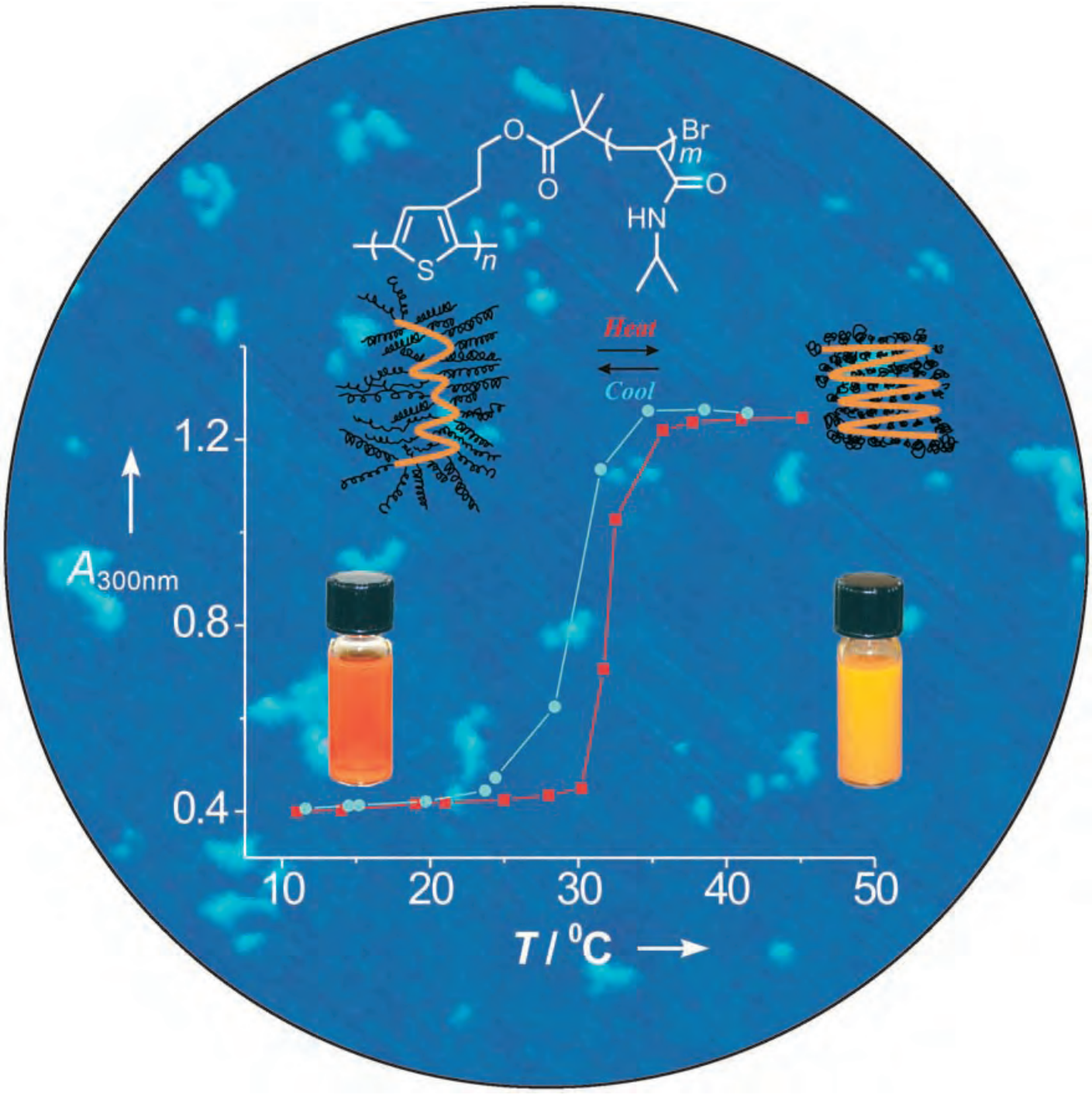
© 2005 Wiley-VCH Verlag GmbH & Co. KGaA, Weinheim

[303] S. Liu, C. Wu, *Huaxue Jinzhan* **2005**, *17*, 143 – 150.
[304] T. Krasia, S. Khodabakhsh, D. Tuncel, J. H. G. Steinke, *Springer Ser. Mater. Sci.* 2004, 78, 41 – 64.
[305] R. Bension (USA), US 2004214177, **2004** [*Chem. Abstr.* **2004**, *141*, 328101].
[306] A. I. Day, A. P. Arnold, R. J. Blanch (Unisearch Limited, Australia), WO 2005026168, **2005** [*Chem. Abstr.* **2005**, *142*, 336358]
[307] L. Isaacs, J. A. Lagona (USA), US 2005080068, **2005** [*Chem. Abstr.* **2005**, *142*, 392447].
[308] K. Kim, S.-Y. Jon, Y.-J. Jeon, D.-H. Oh, N. Selvapalam (Postech Foundation, South Korea), WO 2005010004, **2005** [*Chem. Abstr.* **2005**, *142*, 183488].
[309] K. Kim, D.-H. Oh, E. R. Nagarajan, Y.-H. Ko, S. Samal (Postech Foundation, South Korea), WO 2005010058, **2005** [*Chem. Abstr.* **2005**, *142*, 177710].
[310] E. Keinan (Technion Research and Development Foundation Ltd., Israel), WO 2005023816, **2005** [*Chem. Abstr.* **2005**, *142*, 316868].
[311] K. Kim, J.-K. Kang, W.-S. Jeon, M. Noh, D. Kim, (Postech Foundation, South Korea), WO 2005003136, **2005** [*Chem. Abstr.* **2005**, *142*, 110092].
[312] K. Kim, J.-K. Kang, W.-S. Jeon, S.-Y. Jon, S. Narayanan, D.-H. Oh (Postech Foundation, South Korea), WO 2005003391, **2005** [*Chem. Abstr.* **2005**, *142*, 110030].
[313] P. Wessig, U. Schedler (Germany), WO 2005016398, **2005** [*Chem. Abstr.* **2005**, *142*, 236090].

 © 2005 Wiley-VCH Verlag GmbH & Co. KGaA, Weinheim

Communications

DOI: 10.1002/anie.200500867



A molecular brush copolymer, composed of electrooptically active poly(3-substituted thiophene) and thermally responsive poly(*N*-isopropylacrylamide), displays an exceedingly high water-solubility and unique thermochromic behavior. For more information, see the Communication by R. L. McCarley et al. on the following pages.

InterScience
© 2005 Wiley-VCH Verlag GmbH & Co. KGaA, Weinheim

Thermochromic Polymers

DOI: 10.1002/anie.200500867

Highly Water-Soluble Thermally Responsive Poly(thiophene)-Based Brushes**

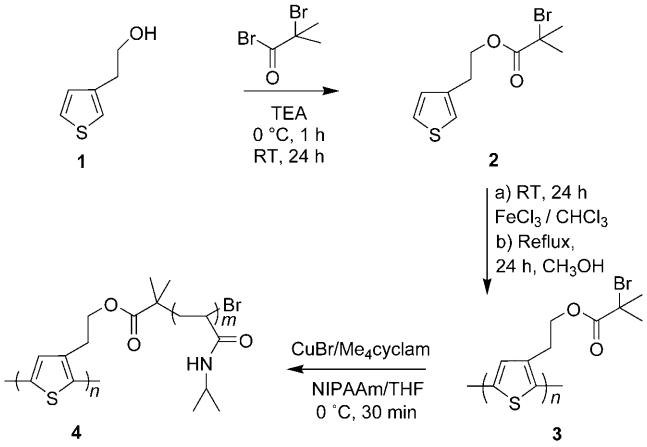
*Sreelatha S. Balamurugan, Grigor B. Bantchev, Yuming Yang, and Robin L. McCarley**

The need for highly water-soluble conducting polymers is great, particularly in applications that would benefit from environmentally friendly processing steps or those applications that center on use of conducting polymers in biological environments.[1] In addition, the chromic response of certain conducting polymers (due to changes in polymer conjugation length as a result of conformational changes of the polymer backbone)[2] should allow for development of sensing systems capable of detecting a multitude of analytes or stimuli, in a broad spectrum of environments, as long as conducting-polymer compatibility, solubility, and processability issues can be addressed. In particular, conducting polymers with a wide variety of solubilizing groups are needed, including those made soluble in aqueous media without the use of ionic solubilizing groups.

As the result of efforts to extend the unique optical and electrical properties of substituted poly(thiophene)s (PTs)[2–4] to aqueous media[5,6] and strategies for developing chromism-based PT materials that respond to biological analytes,[7–11] significant advances in the fabrication of water-soluble PTs have occurred. Water-soluble PTs possessing cationic side chains were recently used in the specific detection of DNA hybridization events,[10] nucleic acids,[12] and human thrombin.[11] Such aqueous-soluble PTs have been prepared by incorporating ionic groups into the side chains of the PT backbone[5,6,13–15] and by complexation of PT with cyclodextrins.[16] Recently, a low-molecular-weight oligo(thiophene) substituted with neutral oligo(ethylene oxide) groups at the 3-position ($M_n = 1400$) was shown to be water soluble to a level of approximately 1 g L^{-1}.[17,18]

Poly(*N*-isopropylacrylamide) (PNIPAAm) is an environmentally responsive polymer that has kindled interest in many researchers for a long time due to its unique lower critical solution temperature (LCST, 30–32 °C[19]) and its relative ease of synthesis. At its LCST, PNIPAAm undergoes a rapid and reversible conformational change from an extended hydrated coil to a collapsed hydrophobic globule that is insoluble in water;[19,20] the driving forces for this conformational change are associated with temperature-dependent hydrogen bonding and hydrophobic interactions. Substitution of responsive PNIPAAm units on PT at the 3-position should lead to a highly water-soluble conducting polymer possessing unique optical and electronic properties as the result of the extension and collapse of the PNIPAAm brushes toward the PT backbone; this system and its characteristics are the topic of the study reported here.

In general, the tethering of PNIPAAm brushes on PT (Scheme 1) involved functionalization of a thiophene monomer with an atom-transfer radical polymerization (ATRP) initiator to yield **2**, followed by its oxidative polymerization to afford a macro initiator **3**, and then growth of PNIPAAm chains from the PT macro initiator by ATRP.[21,22] Specifically, commercially available 2-(3-thienyl)ethanol (**1**) was esterified with 2-bromoisobutyryl bromide to yield 3-[1-ethyl-2-(2-bromoisobutyrate)]thiophene (**2**). Formation of **2** was confirmed by FTIR, GC-MS, and ^{1}H NMR analyses.[23] Compound **2** was polymerized by oxidative coupling[24] using $FeCl_3$ in chloroform to yield 2,5-poly(3-[1-ethyl-2-(2-bromoisobutyrate)]thiophene) **3** (83% yield). Because the initiator is anchored before polymerization, the presence of the grafting site at each repeat unit is ensured. The PT macroinitiator **3** is soluble in many organic solvents, such as tetrahydrofuran, dimethylformamide, chloroform, dichloromethane, and toluene, due to the presence of the bromoisobutyl initiator group at the 3-position. Formation of **3** was confirmed by ^{1}H NMR spectroscopy and gel permeation chromatography (GPC), the latter of which yielded $M_n = 1.09 \times 10^5$ and $M_w/M_n = 2.95$.[23] As expected owing to the $FeCl_3$-mediated polymerization, **3** was found to be regioirregular, as evident in its ^{1}H NMR spectrum; the protons on the 3-alkyl chain adjacent to the thiophene ring (65% head-to-tail coupling) give rise to a two-component signal at 3.24 ppm and 3.00 ppm.



Scheme 1. Synthesis of poly(thiophene-*g*-NIPAAm) **4**. TEA = triethylamine.

[*] Dr. S. S. Balamurugan, Dr. G. B. Bantchev, Y. Yang, Prof. Dr. R. L. McCarley
Department of Chemistry and
the Center for Biomodular Multi-Scale Systems
Louisiana State University
Baton Rouge, LA 70803-1804 (USA)
Fax: (+1) 225-578-3458
E-mail: tunnel@LSU.edu

[**] We acknowledge funding from NSF (CHE-0108961), NSF EPSCoR (EPS-0346411), and the State of Louisiana. We also thank Dr. Rafael Cueto, Prof. Ioan Negulescu, and Rebecca Brauch for GPC, DSC, and MALDI-MS analyses, respectively, and Prof. Paul S. Russo for helpful comments.

Supporting information for this article is available on the WWW under http://www.angewandte.org or from the author.

 © 2005 Wiley-VCH Verlag GmbH & Co. KGaA, Weinheim

PNIPAAm chains were grown from the PT macroinitiator **3** by the ATRP technique, using CuBr/1,4,8,11-tetramethyl-1,4,8,11-tetraazacyclotetradecane as the catalyst and THF as solvent (53% yield). This ATRP catalyst system has been used in the high-yield synthesis of PNIPAAm brushes having a polydispersity of ca. 1.4.[25–27] Formation of PNIPAAm grafts on the PT macroinitiator **3** to yield **4** was confirmed from ^{1}H NMR data, as indicated by the presence of a broad NH peak at $\delta = 6.59$ ppm and CH peak at $\delta = 3.98$ ppm, both associated with the PNIPAAm brushes.[23] Matrix-assisted laser desorption/ionization time-of-flight mass spectrometry evaluation of PNIPAAm chains cleaved from **4** (ester hydrolysis)[28] led to the routine observation of mass spectra characteristic of polymer molecules possessing the NIPAAm repeat unit and molecular weights between 1000 and 5000 amu. The molar mass of **4** was found by GPC to be roughly 2×10^6. It is interesting to note that the graft polymer is soluble in a wide spectrum of organic solvents, such as THF, acetone, chloroform, dichloromethane, and methanol. Importantly, poly(thiophene-*g*-PNIPAAm) **4** is soluble in room-temperature water up to 11 g L^{-1}! To date, this is the highest reported water solubility for a PT possessing neutral substituents, and only the second such PT described in the literature.

The individual poly(thiophene-*g*-NIPAAm) molecules were readily observed by scanning force microscopy (SFM; Figure 1). Images such as that in Figure 1 were routinely

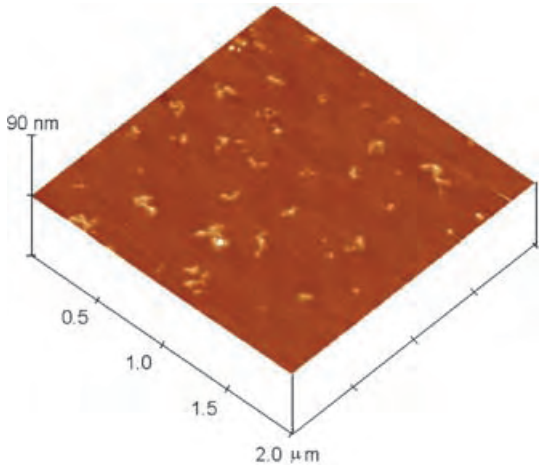


Figure 1. SFM image of poly(thiophene-*g*-NIPAAm) **4** on mica recorded in tapping mode.

obtained by imaging freshly cleaved mica that had a ≈ 1 mg L^{-1} solution of **4** (unfractionated) in acetone spin-coated on it. A broad distribution of random coiled structures for **4** on mica is noted in Figure 1, with lengths ranging from 30 to 260 nm and heights from 0.7 to 0.9 nm. This wide distribution in molecular size is in agreement with the GPC data for **4** and **3**, as well as that from MALDI-MS of the cleaved PNIPAAm.

The enthalpy of transition of the grafted polymer in water was monitored using differential scanning calorimetry (DSC) by repeatedly cycling the solution between 5 and 60 °C (four heating and three cooling cycles; Figure 2). Such temperature

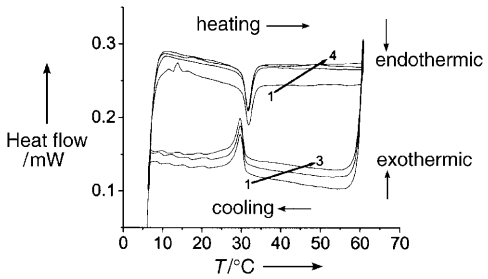


Figure 2. DSC data for 8.25 g L^{-1} poly(thiophene-*g*-NIPAAm) **4** in water; repeated cycles of heating (1–4) and cooling (1–3) between 5 and 60 °C.

excursions led to observation of an endothermic transition at 31.8 ± 0.2 °C and an associated exothermic peak at 29.6 ± 0.4 °C; these are assigned to the enthalpy change associated with the breaking/making of hydrogen bonds between PNIPAAm grafts and water.[20] These results are in agreement with previous studies of PNIPAAm and confirm that the stimuli-responsive conformational change of the poly(thiophene-*g*-NIPAAm) brushes is reversible and very sensitive to temperature variation.[19]

In Figure 3 are displayed the electronic absorption spectra of the PT macro initiator **3** and poly(thiophene-*g*-NIPAAm) **4**. In chloroform solution, **3** and **4** exhibit identical λ_{max} values (423 nm, 2.95 eV) for the absorption band associated with the $\pi \rightarrow \pi^*$ transition of the PT backbone. This indicates that PT

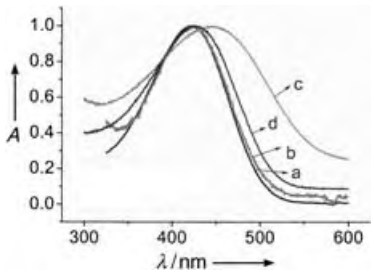


Figure 3. Electronic absorption spectra (normalized) of a) **3** and b) **4** in chloroform (0.01 g L^{-1}); films of c) **3** and d) **4** on quartz.

has a high degree of disorder in the main PT backbone. Thin films of **3** and **4** display bathochromic shifts of 21 nm and 8 nm, respectively, relative to their solution counterparts, indicating better structural ordering (increased conjugation length) of the PT backbone in the solid state.[28–30] The smaller increase in λ_{max} for the film of graft polymer **4** (8 nm) compared to that of the PT macroinitiator **3** (21 nm), versus the solution values, points to the fact that the PNIPAAm chains separate the PT backbones, preventing PT backbone–backbone interactions to some extent.[28] Aqueous solutions of the graft polymer **4** displayed a relatively low-energy λ_{max} at ca. 445 nm at room temperature (Figure 4) compared to that in chloroform solution ($\lambda_{max} = 423$ nm); this likely results from the nature of the solvent, for as the solvent quality decreases (becoming more polar), it is known for soluble PTs that the backbone units tend to adopt a more planar structure.[17]

 © 2005 Wiley-VCH Verlag GmbH & Co. KGaA, Weinheim

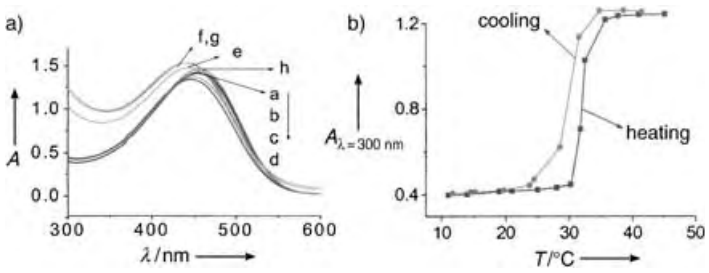


Figure 4. a) Electronic absorption spectra of 0.8 g L^{-1} poly(thiophene-*g*-NIPAAm) **4** in pure water at various temperatures: a) 11, b) 18, c) 28, d) 30, e) 32, f) 38, and g) 45 °C, all in the heating direction; h) at 11 °C after cooling from 45 to 11 °C. b) Absorbance intensity at 300 nm (heating and cooling).

Light-scattering studies of poly(thiophene-*g*-NIPAAm) **4** in water indicate that the polymer brush exhibits a change in molecular shape upon passing through the LCST of 32 °C.[23] Static light-scattering experiments of **4** in water demonstrate that at temperatures above the LCST, the scattering intensity is significantly greater than that below the LCST, and the radius of gyration of the poly(thiophene-*g*-NIPAAm) is approximately 50 % of that at temperatures below 32 °C ($\approx$70 nm vs. $\approx$150 nm). Confirming this decrease in molecular size on transition from below the LCST to above the LCST, analysis of low-angle (30°) dynamic light-scattering data leads to the observation of a roughly threefold increase in the apparent diffusion coefficient when the temperature is increased above the LCST (1.7×10^{-8} cm^2 s^{-1} vs. 5.2×10^{-8} cm^2 s^{-1}). Preliminary evaluation of the light-scattering data excludes the possibility for intermolecular aggregation of individual poly(thiophene-*g*-NIPAAm) molecules when the temperature is increased above the LCST and suggests that the shape of the molecules changes from a random coil to collapsed sphere when the LCST is traversed.[23] Finally, the light-scattering data points to a second, more subtle transition in the 25–28 °C temperature range that is associated with precollapse of the PNIPAAm chains; this is in agreement with theory and recent experimental work for surface-grafted PNIPAAm materials.[25,31] This precollapse is also noted in the electronic absorption spectra of **4** in water (see below). Extensive studies to more fully understand the temperature-induced changes in conformation of the poly(thiophene-*g*-NIPAAm) materials are planned.

In Figure 4a are displayed the electronic absorption spectra of poly(thiophene-*g*-NIPAAm) **4** in water as a function of temperature. As the temperature was increased from 11 °C to 30 °C, there was a small decrease in the intensity of the absorption band and a small blue-shift (456 to 446 nm). Above 30 °C, the solution became cloudy, and a significant increase in the absorption intensity, along with a 6-nm (from 446 to 440 nm) blue-shift of λ_{max} and a broadening of the absorption band, was noted. The temperature dependence of the absorption intensity at 300 nm for poly(thiophene-*g*-PNIPAAm) **4** in water upon heating and cooling is shown in Figure 4b; a very sharp change between 30 and 35 °C is evident. The data in Figure 4b demonstrate that this steep transition is reversible with some hysteresis, the latter which is most likely associated with PNIPAAm intrachain and interchain associations formed during collapse that require a significant amount of time to disentangle. Such hysteresis is observed in dilute solutions of PNIPAAm[32] and when the polymer is grafted on surfaces.[25] All of these observations reveal that the PT backbone responds to the temperature-induced conformational changes of the grafted PNIPAAm chains.

We propose that the temperature-dependent spectral shift and intensity change of the $\pi\rightarrow\pi^*$ transition of the poly(thiophene-*g*-NIPAAm) **4** in water are the result of changes in the effective conjugation length of the PT backbone caused by steric interactions between the collapsed PNIPAAm moieties and the PT backbone, as well as changes in the hydrophobicity of the environment near the PT main chain.[33] Furthermore, we conclude that the observed behavior is associated with the folding of a single chain (molecule) of poly(thiophene-*g*-NIPAAm). The spectroscopic changes are not due to the well-known thermochromic effect found in substituted regioregular and regioirregular PTs in solution[34] or in the solid state,[35–37] as the sensitivity of the changes in λ_{max} for the $\pi\rightarrow\pi^*$ transition for the poly(thiophene-*g*-NIPAAm) with temperature (21 °C increase yields a 16-nm blue-shift) is much higher than that previously reported for regioirregular poly(3-hexylthiophene) solutions in THF (100 °C increase yields a 20-nm blue-shift[34]). Instead, we propose that the collapse of the PNIPAAm chains toward the PT backbone causes an increase in the steric interactions between the PNIPAAm groups and the main PT chain, as well as an increase in the hydrophobicity of the PT backbone environment, the latter which would mimic an increase in the quality of the solvent. It is well known that upon its collapse above the LCST, PNIPAAm becomes quite hydrophobic due to expulsion of water from the polymer, loss of hydrogen bonding between amide groups, and substantially increased hydrophobic interactions between the isopropyl groups. The larger steric and environmental effects with increased solution temperature would result in a more twisted PT backbone (a lower conjugation length) for the poly(thiophene-*g*-NIPAAm) **4** in water. Also, the 10-nm blue-shift that occurs between 11 and 28 °C supports our conclusion and deserves further comment. It has been shown from theoretical[31,38] and experimental[25,39,40] points of view that tethered PNIPAAm brushes exhibit what is referred to as a continuous collapse before the precipitous collapse event at the LCST transition. That is to say, as the LCST is approached from lower temperatures, the solvent is expelled from the interfacial region from which the chains are grafted, and the interfacial PNIPAAm chains undergo precollapse. In our case, the interface is a poly(thiophene) backbone, and slow collapse toward it over the 11 °C to 28 °C range induces strain on the PT backbone and leads to an increase in the hydrophobicity of the interfacial region, both of which result in observation of the spectral changes. Finally, we found no effect of the concentration of the graft polymer (0.8–0.2 g L^{-1}) on the temperature-dependent spectral shift and intensity change for the $\pi\rightarrow\pi^*$ transition of the graft polymer in water, supporting a single-chain event for the temperature-dependent folding of poly(thiophene-*g*-NIPAAm) **4** in water.

 © 2005 Wiley-VCH Verlag GmbH & Co. KGaA, Weinheim

On the basis of the results obtained from light-scattering experiments, SFM, DSC, and electronic absorption spectroscopy, a proposal for the conformational transition of poly(thiophene-g-NIPAAm) **4** is schematically depicted in Figure 5. The highly water-soluble graft polymer possesses a

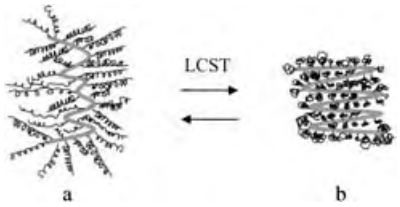


Figure 5. Conformational transition of poly(thiophene-*g*-NIPAAm) **4** at its LCST: a) extended random conformation of molecules that are soluble in water at $T < \text{LCST}$, and b) collapsed sphere conformation of molecules that are insoluble in water at $T > \text{LCST}$.

disordered backbone and adopts a roughly random-coiled structure at temperatures below the LCST. Once the solution temperature is above the LCST, **4** adopts a more globular structure, and the backbone is more ordered as a result of the combined steric interactions between the collapsed PNIPAAm and PT moieties and the hydrophobic environment afforded by the PNIPAAm.

In conclusion, the highly water-soluble, thermally responsive poly(thiophene-*g*-NIPAAm) was synthesized and characterized. The DSC, UV, and light-scattering measurements clearly show that between 28 and 35 °C in water this polymer undergoes a reversible phase transition from a coiled structure to a collapsed globule. By analyzing the optical properties of PT substituted with responsive PNIPAAm chains, we were able to gain insight into the mechanism for changes that happen to the PT backbone when transition of the PNIPAAm chains takes place. The unique optical and electronic properties that result from combining the PT with the water-soluble and temperature-responsive PNIPAAm side-chain groups promise important applications of this polymer brush system in responsive soft nanodevices, LEDs, bioelectronics, biosensors, actuators, fluorescent thermometers, and supramolecular materials. In particular, the use of regioregular PT materials will augment the capabilities of such applications.

Received: March 8, 2005
Published online: June 29, 2005

Keywords: microscopy · optical properties · polymers · semiconducting materials

[1] J. Jagur-Grodzinski, *Polym. Adv. Technol.* **2002**, *13*, 615 – 625.
[2] R. D. McCullough in *Handbook of Oligo- and Polythiophenes*, **1999**, pp. 1 – 44.
[3] T. A. Skotheim, R. L. Elsenbaumer, J. R. Reynolds, Editors, *Handbook of Conducting Polymers*, 2nd ed., Marcel Dekker, New York, **1997**.
[4] N. J. L. Guernion, W. Hayes, *Curr. Org. Chem.* **2004**, *8*, 637 – 651.
[5] A. O. Patil, Y. Ikenoue, F. Wudl, A. J. Heeger, *J. Am. Chem. Soc.* **1987**, *109*, 1858 – 1859.
[6] M. Andersson, P. O. Ekeblad, T. Hjertberg, O. Wennerstroem, O. Inganaes, *Polym. Commun.* **1991**, *32*, 546 – 548.
[7] B. Liu, G. C. Bazan, *Chem. Mater.* **2004**, *16*, 4467 – 4476.
[8] L. Chen, D. W. McBranch, H.-L. Wang, R. Helgeson, F. Wudl, D. G. Whitten, *Proc. Natl. Acad. Sci. USA* **1999**, *96*, 12287 – 12292.
[9] D. T. McQuade, A. E. Pullen, T. M. Swager, *Chem. Rev.* **2000**, *100*, 2537 – 2574.
[10] K. P. R. Nilsson, O. Inganas, *Nat. Mater.* **2003**, *2*, 419 – 424.
[11] H.-A. Ho, M. Leclerc, *J. Am. Chem. Soc.* **2004**, *126*, 1384 – 1387.
[12] H.-A. Ho, M. Boissinot, M. G. Bergeron, G. Corbeil, K. Dore, D. Boudreau, M. Leclerc, *Angew. Chem.* **2002**, *114*, 1618 – 1621; *Angew. Chem. Int. Ed.* **2002**, *41*, 1548 – 1551.
[13] B. Kim, L. Chen, J. Gong, Y. Osada, *Macromolecules* **1999**, *32*, 3964 – 3969.
[14] M. Chayer, K. Faied, M. Leclerc, *Chem. Mater.* **1997**, *9*, 2902 – 2905.
[15] J. Lukkari, M. Salomaeki, A. Viinikanoja, T. Aeaeritalo, J. Paukkunen, N. Kocharova, J. Kankare, *J. Am. Chem. Soc.* **2001**, *123*, 6083 – 6091.
[16] M. van den Boogaard, G. Bonnet, P. Van't Hof, Y. Wang, C. Brochon, P. van Hutten, A. Lapp, G. Hadziioannou, *Chem. Mater.* **2004**, *16*, 4383 – 4385.
[17] Y. Wang, W. B. Euler, B. L. Lucht, *Chem. Commun.* **2004**, 686 – 687.
[18] B. L. Lucht, personal communication, February 2005.
[19] H. G. Schild, *Prog. Polym. Sci.* **1992**, *17*, 163 – 249.
[20] M. Heskins, J. E. Guillet, *J. Macromol. Sci. Chem.* **1968**, *2*, 1441 – 1455.
[21] M. Kato, M. Kamigaito, M. Sawamoto, T. Higashimura, *Polym. Prepr. Jpn.* **1994**, *43*, 1792 – 1793.
[22] J.-S. Wang, K. Matyjaszewski, *J. Am. Chem. Soc.* **1995**, *117*, 5614 – 5615.
[23] See the Supporting Information.
[24] M. Leclerc, F. Martinez Diaz, G. Wegner, *Macromol. Chem.* **1989**, *190*, 3105 – 3116.
[25] S. Balamurugan, S. Mendez, S. S. Balamurugan, M. J. O'Brien, G. P. López, *Langmuir* **2003**, *19*, 2545 – 2549.
[26] H. Yim, M. S. Kent, S. Mendez, S. S. Balamurugan, S. Balamurugan, G. P. López, S. Satija, *Macromolecules* **2004**, *37*, 1994 – 1997.
[27] C. Li, N. Gunari, K. Fischer, A. Janshoff, M. Schmidt, *Angew. Chem.* **2004**, *116*, 1121 – 1124; *Angew. Chem. Int. Ed.* **2004**, *43*, 1101 – 1104.
[28] P. J. Costanzo, K. K. Stokes, *Macromolecules* **2002**, *35*, 6804 – 6810.
[29] T.-A. Chen, X. Wu, R. D. Rieke, *J. Am. Chem. Soc.* **1995**, *117*, 233 – 244.
[30] J. K. Politis, J. C. Nemes, M. D. Curtis, *J. Am. Chem. Soc.* **2001**, *123*, 2537 – 2547.
[31] V. A. Baulin, E. B. Zhulina, A. Halperin, *J. Chem. Phys.* **2003**, *119*, 10977 – 10988.
[32] X. Wang, X. Qiu, C. Wu, *Macromolecules* **1998**, *31*, 2972 – 2976.
[33] Calculations do not support scattering events as the cause of the observed changes in intensity and wavelength noted here.
[34] K. Faid, M. Frechette, M. Ranger, L. Mazerolle, I. Levesque, M. Leclerc, T.-A. Chen, R. D. Rieke, *Chem. Mater.* **1995**, *7*, 1390 – 1396.
[35] Y. Wang, N. Archambault, A. Marold, L. Weng, B. L. Lucht, W. B. Euler, *Macromolecules* **2004**, *37*, 5415 – 5422.
[36] C. Yang, F. P. Orfino, S. Holdcroft, *Macromolecules* **1996**, *29*, 6510 – 6517.
[37] M. Leclerc, *Adv. Mater.* **1999**, *11*, 1491 – 1498.
[38] E. B. Zhulina, O. V. Borisov, V. A. Pryamitsyn, T. M. Birshtein, *Macromolecules* **1991**, *24*, 140 – 149.
[39] P. W. Zhu, D. H. Napper, *Langmuir* **1996**, *12*, 5992 – 5998.
[40] W. Zhang, X. Zhou, H. Li, Y. Fang, G. Zhang, *Macromolecules* **2005**, *38*, 909 – 914.

 © 2005 Wiley-VCH Verlag GmbH & Co. KGaA, Weinheim

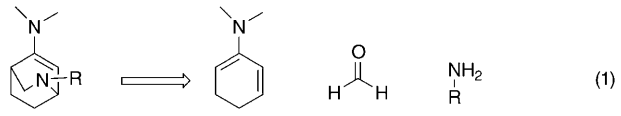
Asymmetric Catalysis

DOI: 10.1002/anie.200500811

Direct Catalytic Enantioselective Aza-Diels–Alder Reactions**

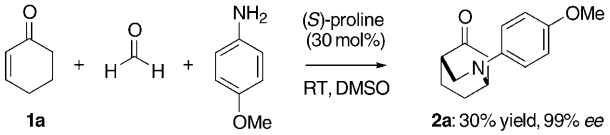
*Henrik Sundén, Ismail Ibrahem, Lars Eriksson, and Armando Córdova**

The synthesis of optically active nitrogen-containing compounds is a very important task in chemistry as they are key building blocks for the construction of valuable compounds such as amino acids, aza sugars, and alkaloids. The aza-Diels–Alder reaction is one of the most powerful C–C bond-forming reactions for the preparation of nitrogen-containing compounds such as piperidines and quinolidine derivatives,[1,2] and thus chemists have developed several diastereoselective aza-Diels–Alder reactions.[3,4] Despite the potential advantages of utilizing asymmetric catalysis, there are only a few examples of catalytic asymmetric indirect aza-Diels–Alder reactions between preformed imines and dienes or enolethers. For example, the research groups of Kobayashi and Jørgensen have successfully used chiral Lewis acid complexes as catalysts for these transformations.[5–7] However, there is to our knowledge no report of a direct catalytic enantioselective aza-Diels–Alder reaction. Organocatalysis is a rapidly growing research field and has been applied successfully to several different enantioselective reactions.[8] In particular, amino acid derivatives have been utilized as catalysts for enantioselective cycloadditions such as the Diels–Alder reaction.[9–13] This research and our interest in applying amino acids as catalysts in asymmetric synthesis[14] led to us becoming interested in whether an amino acid derivative would be able to mediate the classical aza-Diels–Alder reaction through a catalytic enamine mechanism. Retrosynthetic analyses suggested that an imine generated in situ would be able to react with a catalytically generated chiral diene and form an aza-Diels–Alder product [Eq. (1)].[15] Thus, we embarked on the quest to develop a one-pot three-component asymmetric aza-Diels–Alder reaction. Herein, we report the first direct catalytic enantioselective aza-Diels–Alder reaction that yields the corresponding products with excellent stereoselectivity.



(1)

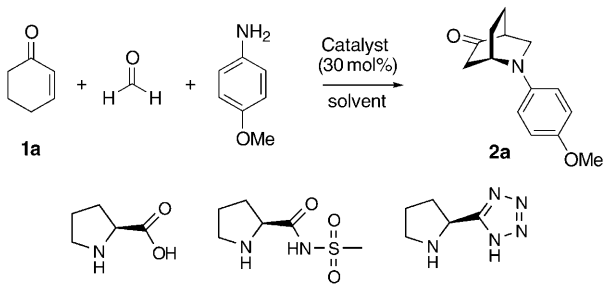
In an initial experiment, 2-cyclohexen-1-one (**1a**, 2 mmol), aqueous formaldehyde (1 mmol, 36 vol% aqueous solution), and *p*-anisidine (1.1 mmol) were mixed in the presence of a catalytic amount of (*S*)-proline (30 mol%). After vigorously stirring the mixture for 24 h, the reactions were quenched by extraction and the crude product purified by column chromatography on silica gel to furnish the desired aza-Diels–Alder product **2a** in 30% yield with excellent chemoselectivity and 99% *ee* [Eq. (2)]. Encouraged by this



(2)

experiment, we investigated different reaction conditions and the utilization of different proline derivatives as catalysts to increase the yield of the reaction (Table 1).

Table 1: Amine-catalyzed direct enantioselective aza-Diels–Alder reaction.[a]



Entry	Cat.	Solvent	*t* [h]	*T* [°C]	Yield [%][b]	*ee* [%][c]
1	**3**	DMSO	24	RT	30	99
2	**3**	DMSO	24	50	52	99
3	**3**	DMSO	24	50	82[d]	99
4	**3**	DMSO	24	75	45	99
5	**4**	DMSO	48	RT	31	94
6	**5**	DMSO	24	RT	61	99
7	**3**	DMF	24	50	35	98
8	**3**	NMP	24	50	10	97
9	**3**	toluene	24	50	< 5	n.d.

[a] Experimental conditions: A mixture of **1a** (2 mmol, 2 equiv), *p*-anisidine (1.1 mmol), aqueous formaldehyde (1 mmol), and catalyst (30 mol%) was stirred at the temperature and conditions displayed for 20–37 h. The crude product **2a** obtained after aqueous workup was purified by column chromatography. [b] Yield of the isolated pure products after column chromatography on silica gel. [c] Determined by chiral-phase HPLC analyses. [d] Yield of the corresponding alcohol (1:1 *cis*/*trans*) obtained by in situ reduction of **2a** with excess $NaBH_4$ after column chromatography on silica gel.

[*] H. Sundén, I. Ibrahem, Prof. Dr. A. Córdova
Department of Organic Chemistry
The Arrhenius Laboratory
Stockholm University
106 91 Stockholm (Sweden)
Fax: (+46) 815-4908
E-mail: acordova1a@netscape.net
E-mail: acordova@organ.su.se
Prof. Dr. L. Eriksson
Department of Structural Chemistry
The Arrhenius Laboratory
Stockholm University
106 91 Stockholm (Sweden)

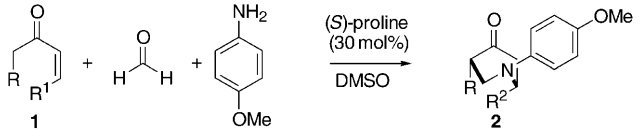
[**] We gratefully acknowledge the Swedish National Research council and the Wenner-Gren Foundation for financial support.

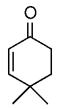
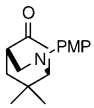
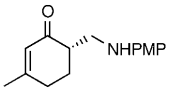
© 2005 Wiley-VCH Verlag GmbH & Co. KGaA, Weinheim

We found that the organocatalytic aza-Diels–Alder reaction was most efficient in DMSO and that the yield of **2a** could be increased from 30 to 52% by performing the reaction at 50°C without affecting the stereoselectivity of the reaction.[16] Furthermore, in situ reduction of **2a** with excess $NaBH_4$ furnished the corresponding bicyclic alcohol product in 82% yield and 99% *ee*. We also investigated the novel direct enantioselective aza-Diels–Alder reaction with amine catalysts **4** and **5**.[17,18] Both catalysts **4** and **5** were able to catalyze the direct three-component reaction with excellent regio- and enantioselectivity to furnish the corresponding aza-Diels–Alder adduct **2a** in 31 and 61% yields and 94 and 99% *ee*, respectively. Hence, of all the amino acid derivatives tested proline (**3**) and tetrazole **5** were the most efficient catalysts for the aza-Diels–Alder reaction. The amino acid derivatives also catalyzed the reaction in *N*-methylpyrrolidine (NMP) and DMF with high enantioselectivity.

We next investigated the one-pot three-component aza-Diels–Alder reaction for a set of different cyclic α,β-unsaturated ketones (Table 2). We found that α,β-unsaturated cyclohexenones and heptenones were excellent substrates for the direct catalytic enantioselective aza-Diels–Alder reactions with amino acids as the catalysts, and the corresponding bicyclic amines **2a**–**2c** protected with *p*-methoxyphenyl (PMP) groups were isolated in high yield with high *ee* values (up to >99% *ee*). For example, azabicyclooctanone **2b** was isolated in 72% yield with >99% *ee*. Thus, protected azabicycles can be assembled asymmetrically in one chemical manipulation from simple inexpensive readily available starting materials. Proline was the most efficient organic catalyst when unsaturated ketone **1c** was utilized as the donor and furnished the corresponding bicycle **2c** in high yield with 98% *ee*. Furthermore, the amino acid catalyzed aza-Diels–Alder reactions were operationally simple and performed in wet solvents. The proline-catalyzed one-pot three-component reaction with 3-substituted cyclohexanone **1d** only furnished the α,β-unsaturated Mannich adduct **2d** in 40% yield and 94% *ee* and not the aza-Diels–Alder product. The reaction with 2-cyclopentenone (**1e**) only furnished trace amounts of the desired aza-Diels–Alder adduct **2e**. Proline-catalyzed reactions between *trans*-4-phenyl-3-buten-2-one, formaldehyde, and *p*-anisidine did not provide any product under our reaction conditions. The PMP group of the aza-Diels–Alder adduct **2b** was removed with cerium ammonium nitrate (CAN) followed by treatment with $(Boc)_2O$

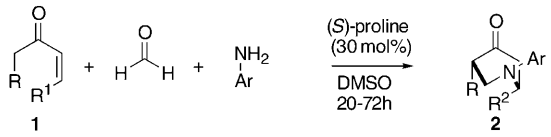
Table 2: Proline-catalyzed direct three-component enantioselective aza-Diels–Alder reaction.[a]

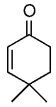
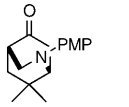
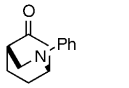
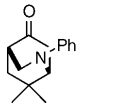
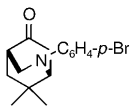
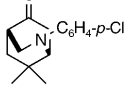


Entry	Ketone	Product		*t* [h]	*T* [°C]	Yield [%][b]	*ee* [%][c]
1		**1a**		**2a**	24	50	82[d]	99
2		**1b**		**2b**	48	50	72	>99
3					17	RT	70	>99
4		**1c**		**2c**	24	50	90[e]	98
5					24	RT	75	98
6					24	RT	20[f]	96[f]
7		**1d**		**2d**	24	RT	40	94
8		**1e**		**2e**	24	RT	10	n.d.[g]

[a] Experimental conditions: A mixture of **1** (2 mmol, 2 equiv), aniline (1.1 mmol), aqueous formaldehyde (1 mmol), and (*S*)-proline (30 mol%) was stirred at the temperature and conditions displayed for 20–72 h. The crude product **2** obtained after aqueous workup was purified by column chromatography. [b] Yield of the isolated pure products after column chromatography on silica gel. [c] Determined by chiral-phase HPLC analyses. [d] Yield of the corresponding alcohol (1:1 *cis*/*trans*) obtained by in situ reduction of **2a** with excess $NaBH_4$ after column chromatography on silica gel. [e] Combined yield of **2c** and the minor amount of the *retro*-Michael adduct, which was formed upon column chromatography. [f] Reaction performed with catalyst **5**. [g] Not determined.

Table 3: Proline-catalyzed direct three-component enantioselective aza-Diels–Alder reaction with different anilines.[a]



Entry	Ketone		Ar	Product		*T* [°C]	Yield [%][b]	*ee* [%][c]
1		**1b**	PMP		**2b**	RT	70	>99
2		**1a**	Ph		**2f**	RT	54	>96
3		**1b**	Ph		**2g**	RT	69	98
4		**1b**	4-BrC_6H_4		**2h**	RT	20	>99
5		**1b**	4-ClC_6H_4		**2i**	RT	32	>99

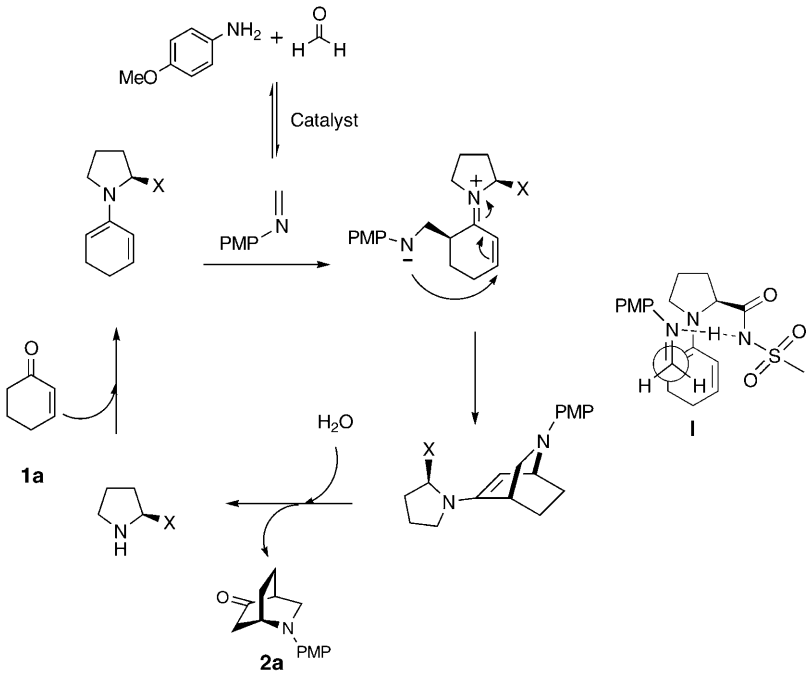
[a] Experimental conditions: A mixture of **1** (2 mmol, 2 equiv), aniline (1.1 mmol), aqueous formaldehyde (1 mmol), and (*S*)-proline (30 mol%) was stirred at the temperature and conditions displayed for 20–72 h. The crude product **2** obtained after aqueous work-up was purified by column chromatography. [b] Yield of the isolated pure products after column chromatography on silica gel. [c] Determined by chiral-phase HPLC analyses.

 © 2005 Wiley-VCH Verlag GmbH & Co. KGaA, Weinheim

(Boc = *tert*-butoxycarbonyl) to furnish the desired Boc-protected azabicycle.

We next investigated the effect of the amine component on the reaction catalyzed by an amino acid (Table 3). The reaction advanced with excellent chemo-, regio-, and stereoselectivity to yield the corresponding bicycles **2b** and **2f–2i** with up to >99% *ee*. In particular, the hetero-Diels–Alder reactions with anilines having an electron-donating substituent at the *para* position furnished the corresponding aza-Diels–Alder products with excellent stereocontrol. The yields of the products derived from the aza-Diels–Alder reactions with *p*-chloro- and *p*-bromoanilines were moderate in comparison to the reactions with aniline and *p*-anisidine.

The stereochemical outcome of the reaction was determined by X-ray structure analysis of **2b** (Figure 1), which revealed that bicycle (1*R*,4*S*)-**2b** was assembled asymmetrically when amino acid derivatives **3**, **4**, and **5** were used as catalysts.



Scheme 1. The plausible reaction pathway and transition state.

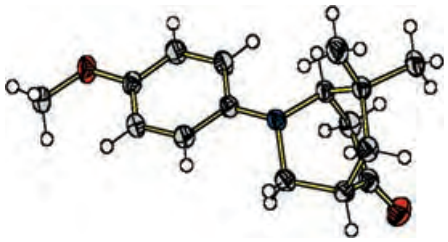
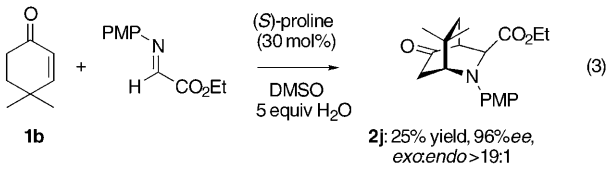


Figure 1. Structure of aza-Diels–Alder product **2b** (ORTEP picture).

On the basis of the absolute stereochemistry of the aza-Diels–Alder adducts and the isolation of Mannich adduct **2d**,[19] we propose the following reaction mechanism to account for the stereochemical outcome of the reaction (Scheme 1). The first step is that the proline-derived catalyst forms a chiral enamine with the α,β-unsaturated ketone **1**. Next, the in situ generated imine attacks the *si* face of the chiral diene via transition state **I**, and an activated iminium salt is formed. The secondary amine of the chiral iminium salt performs a subsequent selective 6-*endo-trig* cyclization to furnish the corresponding chiral azabicycle. Next, the amino acid derivative is released and the desired aza-Diels–Alder adduct **2** is obtained by hydrolysis and the catalytic cycle can be repeated. Thus, the reaction proceeds through a tandem one-pot three-component Mannich/Michael reaction pathway. The stepwise mechanism was further supported by the fact that in the aza-Diels–Alder reactions with *p*-chloroaniline and *p*-bromoaniline, minor amounts of the corresponding α,β-unsaturated Mannich bases were formed in addition to products **2h** and **2i**. This result is in accordance with the lower nucleophilicity of the secondary amine intermediate in the Michael step as compared to *p*-anisidine. Furthermore, the proline-catalyzed reaction with the substituted ketone **1d** failed to ring-close and provided the α,β-unsaturated Mannich base **2d** with excellent enantioselectivity.[16] Attempts to perform 6-*endo-trig* cyclizations of the unsaturated Mannich bases failed under our reaction conditions.

The proline derivatives also catalyzed the direct enantioselective aza-Diels–Alder reaction with preformed imines. For example, proline catalyzed the aza-Diels–Alder reaction between ketone **1b** and ethyl *N*-PMP-α-imino glyoxylate in wet DMSO, and the corresponding synthetically valuable bicyclic amino acid derivative **2j** was isolated exclusively as the *exo* adduct in moderate yield with 96% *ee* [Eq. (3)].



In summary, we have reported the first one-pot three-component direct catalytic enantioselective aza-Diels–Alder reaction. The reaction is catalyzed by proline and its derivatives with excellent chemo-, regio-, and stereoselectivity. For example, the amino acid catalyzed asymmetric aza-Diels–Alder reactions between aqueous formaldehyde, α,β-unsaturated cyclic ketones, and aromatic amines furnished the desired azabicyclic ketones with up to >99% *ee*. The reactions are operationally simple, performed in wet solvents, and environmentally friendly. Moreover, the reaction can be applied for the synthesis of protected azabicyclic amino acids with excellent *exo* and enantioselectivity. Further elaboration of this transformation and its synthetic application is ongoing.

 © 2005 Wiley-VCH Verlag GmbH & Co. KGaA, Weinheim

Experimental Section

Typical experimental procedure (Table 2, entry 2): Ketone **1b** (2 mmol) was added to a vial containing aqueous formaldehyde (1 mmol, 36% aqueous solution), *p*-anisidine (1.1 mmol), and a catalytic amount of (*S*)-proline (30 mol%) in DMSO (4 mL). After vigorously stirring the mixture for 24 h at 50 °C, the reaction was quenched by purifying the reaction mixture by column chromatography on silica gel (EtOAc/pentane 1:5) to afford **2b** in 72% yield as a slightly yellow solid. The *ee* value of **2b** was >99% as determined by HPLC analysis on a chiral stationary phase. ^{1}H NMR (400 MHz, $CDCl_3$): $\delta = 1.08$ (s, 3H), 1.10 (s, 3H), 1.77 (d, $J = 2.98$ Hz, 2H), 2.47 (dd, $J = 18.7$, 3.4 Hz 1H), 2.62 (m, 1H), 2.68 (dd, $J = 18.9$, 2.3 Hz 1H), 3.48, (d, $J = 2.5$ Hz, 2H), 3.75 (m, 1H), 3.76 (s, 3H), 6.61–6.63 (m, 2H), 6.84–6.86 ppm (m, 2H); ^{13}C NMR (100 MHz, $CDCl_3$): $\delta = 28.8$, 30.2, 36.1, 38.9, 41.3, 46.0, 47.9, 56.1, 58.5, 112.1, 115.54, 141.1, 151.4, 214.0 ppm; HPLC (Daicel Chiralpak AD, hexanes/*i*PrOH 99:1, flow rate 1.2 mL min^{-1}, $\lambda = 254$ nm): major isomer: $t_R = 24.94$ min; minor isomer: $t_R = 27.31$ min; $[\alpha]_D = -71.8$ ($c = 1.7$, $CHCl_3$); MALDI-TOF MS: 256.1689; $C_{16}H_{22}NO_2$ $[M+H]^+$: calcd 261.1683.

Received: March 4, 2005
Published online: June 23, 2005

Keywords: asymmetric catalysis · bicyclic amino acids · cycloaddition · enantioselectivity · ketones

[1] For reviews, see a) K. A. Jørgensen, *Angew. Chem.* **2000**, *112*, 3702; *Angew. Chem. Int. Ed.* **2000**, *39*, 3558; b) D. L. Boger, S. M. Weinreb, *Hetero Diels–Alder Methodology in Organic-Syntehsis*, Academic Press, San Diego. **1987**, chap. 2; c) H. Waldmann, *Synlett* **1995**, 133; d) L. F. Tietze, G. Kettschau, *Top. Curr. Chem.* **1997**, *190*, 1; e) S. M. Weinreb, *Top. Curr. Chem.* **1997**, *190*, 131; f) S. Kobayashi, H. Ishitani, *Chem. Rev.* **1999**, *99*, 1069.

[2] For examples of synthesis of complex compounds by an aza-Diels–Alder reaction, see a) R. T. Bailey, R. S. Garigipati, J. A. Morton, S. M. Weinreb, *J. Am. Chem. Soc.* **1984**, *106*, 3240; b) R. Lock, H. Waldmann, *Liebgs. Ann. Chem.* **1994**, 511; c) A. B. Holmes, A. Kee, T. Ladduwahetty, D. F. Smith, *J. Chem. Soc. Chem. Commun.* **1990**, 1412.

[3] For examples of diastereoselective aza-Diels–Alder reactions, see a) J. Barluenga, F. Aznar, C. Valdéz, A. Martín, S. García-Granada, E. Martín, *J. Am. Chem. Soc.* **1993**, *115*, 4403; b) A. S. Timen, A. Ficher, P. Somfai, *Chem. Commun.* **2003**, 1150; c) H. Waldmann, M. Braun, M. Dräger, *Angew. Chem.* **1990**, *102*, 1445; *Angew. Chem. Int. Ed. Engl.* **1990**, *29*, 1468; d) S. D. Larsen, P. A. Grieco, *J. Am. Chem. Soc.* **1985**, *107*, 1768.

[4] Stoichiometric amounts of chiral boron complexes have also been used to mediate enantiosalective aza-Diels–Alder reactions, see a) K. Hattori, H. Yamamoto, *J. Org. Chem.* **1992**, *57*, 3264; b) K. Ishihara, M. Miyata, K. Hattori, T. Tada, H. Yamamoto, *J. Am. Chem. Soc.* **1994**, *116*, 10520.

[5] a) H. Ishitani, S. Kobayashi, *Tetrahedron Lett.* **1996**, *37*, 7357; b) S. Kobayashi, S. Komiyama, H. Ishitani, *Angew. Chem.* **1998**, *110*, 1026; *Angew. Chem. Int. Ed.* **1998**, *37*, 979; c) S. Kobayashi, K. Kusakabe, S. Komiyama, H. Ishitani, *J. Org. Chem.* **1999**, *64*, 4220.

[6] a) S. Yao, M. Johannsen, R. G. Hazell, K. A. Jørgensen, *Angew. Chem.* **1998**, *110*, 3318; *Angew. Chem. Int. Ed.* **1998**, *37*, 3121; b) S. Yao, S. Saaby, R. G. Hazell, K. A. Jørgensen, *Chem. Eur. J.* **2000**, *6*, 2435.

[7] see also: a) N. S. Josephsohn, M. L. Snapper, A. H. Hoveyda, *J. Am. Chem. Soc.* **2003**, *125*, 4018; b) O. G. Mancheño, R. G. Arrayás, J. C. Carretero, *J. Am. Chem. Soc.* **2004**, *126*, 456.

[8] a) P. I. Dalko, L. Moisan, *Angew. Chem.* **2001**, *113*, 3840; *Angew. Chem. Int. Ed.* **2001**, *40*, 3726; b) B. List, *Tetrahedron* **2002**, *58*, 5573; c) R. O. Duthaler, *Angew. Chem.* **2003**, *115*, 1005; *Angew. Chem. Int. Ed.* **2003**, *42*, 975; d) P. I. Dalko, L. Moisan, *Angew. Chem.* **2004**, *116*, 5248; *Angew. Chem. Int. Ed.* **2004**, *43*, 5138.

[9] For organocatalytic Diels–Alder reactions, see a) A. B. Northrup, D. W. C. MacMillan, *J. Am. Chem. Soc.* **2002**, *124*, 2458; b) K. A. Ahrendt, C. J. Borths, D. W. C. MacMillan, *J. Am. Chem. Soc.* **2000**, *122*, 4243; c) D. B. Ramachary, N. S. Chowdari, C. F. Barbas III, *Angew. Chem.* **2003**, *115*, 4365; *Angew. Chem. Int. Ed.* **2003**, *42*, 4233.

[10] For reverse-electron-demand Diels–Alder reaction, see a) K. Juhl, K. A. Jørgensen, *Angew. Chem.* **2003**, *115*, 1536; *Angew. Chem. Int. Ed.* **2003**, *42*, 1498.

[11] For hetero-Diels–Alder reactions, see a) Y. Huang, K. Unni, A. N. Thadani, V. H. Rawal, *Nature* **2003**, *424*, 146; b) K. A. Unni, N. Tanaka, H. Yamamoto, V. H. Rawal, *J. Am. Chem. Soc.* **2005**, *127*, 1336.

[12] For nitroso-Diels–Alder reactions, see a) Y. Yamamoto, N. Momiyama, H. Yamamoto, *J. Am. Chem. Soc.* **2004**, *126*, 5962; b) Y. Hayashi, J. Yamaguchi, K. Hibino, T. Sumiya, T. Urushima, M. Shoji, D. Hashizume, H. Koshino, *Adv. Synth. Catal.* **2004**, *346*, 1435; c) H. Sundén, N. Dahlin, I. Ibrahem, H. Adolfsson, A. Córdova, *Tetrahedron Lett.* **2005**, *46*, 3385.

[13] For 1,3-dipolar cycloadditions, see a) W. S. Jen, J. J. M. Wiener, D. W. C. MacMillan, *J. Am. Chem. Soc.* **2000**, *122*, 9874; b) S. Karlsson, H. Högberg, *Tetrahedron: Asymmetry* **2002**, *13*, 923; for [4+3]cycloadditions, see c) M. Harmata, S. K. Ghosh, X. Hong, S. Wacharasindhu, P. Kirchhoefer, *J. Am. Chem. Soc.* **2003**, *125*, 2058.

[14] a) J. Casas, M. Engqvist, I. Ibrahem, B. Kaynak, A. Córdova, *Angew. Chem.* **2005**, *117*, 1367; *Angew. Chem. Int. Ed.* **2005**, *44*, 1343; b) A. Córdova, H. Sundén, M. Engqvist, I. Ibrahem, J. Casas, *J. Am. Chem. Soc.* **2004**, *126*, 8914; c) H. Sundén, M. Engqvist, J. Casas, I. Ibrahem, A. Córdova, *Angew. Chem.* **2004**, *116*, 6694; *Angew. Chem. Int. Ed.* **2004**, *43*, 6532; d) A. Córdova, *Acc. Chem. Res.* **2004**, *37*, 102; e) A. Bøgevig, H, Sundén, A. Córdova, *Angew. Chem.* **2004**, *116*, 1129; *Angew. Chem. Int. Ed.* **2004**, *43*, 1109; f) A. Córdova, H. Sundén, A. Bøgevig, M. Johansson, F. Himo, *Chem. Eur. J.* **2004**, *10*, 3673; g) A. Córdova, *Chem. Eur. J.* **2004**, *10*, 1987; h) A. Córdova, *Synlett* **2003**, 1651, and references therein.

[15] This strategy has been used successfully in a direct catalytic one-pot three-component Mannich reaction, see a) B. List, *J. Am. Chem. Soc.* **2000**, *122*, 9336; b) B. List, P. Porjaliev, W. T. Biller, H. J. Martin, *J. Am. Chem. Soc.* **2002**, *124*, 827; c) I. Ibrahem, J. Casas, A. Córdova, *Angew. Chem.* **2004**, *116*, 6690; *Angew. Chem. Int. Ed.* **2004**, *43*, 6528, and references therein.

[16] The aza-Diels–Alder products decomposed and underwent a *retro*-Michael reaction upon chromatography on silica gel, which decreased the yield.

[17] For the first use of catalyst **4**, see a) A. J. A. Cobb, D. M. Shaw, S. V. Ley, *Synlett* **2004**, 558; b) H. Torii, M. Nakadai, K. Ishihara, S. Saito, H. Yamamoto, *Angew. Chem.* **2004**, *116*, 2017; *Angew. Chem. Int. Ed.* **2004**, *43*, 1983; c) A. Hartikaa, P. I. Arvidsson, *Tetrahedron: Asymmetry* **2004**, *15*, 1831.

[18] Arylsulfonylcarboxamides have been used in aldol reactions, see a) A. Berkessel, B. Koch, J. Lex, *Adv. Synth. Catal.* **2004**, *346*, 1141; for the use of catalyst **5**, see reference [12c] and b) A. J. A. Cobb, D. M. Shaw, D. A. Longbottom, J. B. Gold, S. V. Ley, *Org. Biomol. Chem.* **2005**, *3*, 84.

[19] CCDC-265109 contains the supplementary crystallographic data for this paper. These data can be obtained free of charge from the Cambridge Crystallographic Data Centre via www.ccdc.cam.ac.uk/data_request/cif.

 © 2005 Wiley-VCH Verlag GmbH & Co. KGaA, Weinheim

Energy Transfer

DOI: 10.1002/anie.200500392

The Structural and Functional Roles of Rhodium(II)–Rhodium(II) Dimers in Multinuclear Ruthenium(II) Complexes**

*Michael W. Cooke, Garry S. Hanan,**
*Frédérique Loiseau, Sebastiano Campagna,**
*Masashi Watanabe, and Yasutaka Tanaka**

Polypyridylruthenium(II) complexes have received much attention as a result of their long-lived luminescent metal-to-ligand charge-transfer (MLCT) excited state, which is a useful property for intercomponent energy and electron-transfer processes in supramolecular systems.[1] In particular the characteristically rich electrochemistry of multinuclear Ru^{II}–polypyridyl assemblies make them excellent models for multicomponent systems capable of performing photo- and/or redox-active supramolecular functions, such as those occurring in light-harvesting antenna systems[2] and photo-activated molecular machines.[3]

Among the Ru^{II} chromophores employed in photoactive devices, particularly attractive are those based upon 2,2′:6′2″-terpyridine (tpy), as the $\{Ru(tpy)_2\}^{2+}$ unit is achiral when substituted in the 4′-position,[4] and appropriate substitution can render the complex emissive from an otherwise quasi-non-emissive excited state.[5,6] However, synthesis and purification becomes increasingly tedious as a function of the nuclearity of the photoactive complexes, particularly when the formation of covalent bonds and protection/deprotection sequences are relied upon to create the linkages.[7] As earlier work had shown that molecular squares and polymers can be built up using metal tetracarboxylato dimers,[8,9] we decided that a more facile strategy toward multinuclear systems could rely upon the coordination chemistry of metal dimers. Their well-known paddlewheel-like motif offers a robust template from which to attach appropriately functionalized Ru^{II}–polypyridyl units by using ligand exchange reactions. We selected the Rh^{II} dimer to assemble these chromophores as it is typically air stable, diamagnetic, and inert to scrambling of the carboxylate groups.[10]

The Ru^{II} chromophores are based on the readily available $[Ru(tpy)\{4'\text{-}(4\text{-carboxyphenyl})tpy\}]^{2+}$ complex (**4**).[11] The methanol adduct of (tetra-μ-acetato)dirhodium(II,II) (**5**) can be substituted under relatively mild conditions to yield substitution products **1**–**3** in 63% yield in refluxing acetonitrile (Scheme 1).[12] The product distribution can be shifted to the higher substituted Ru complexes by increasing the ratio of **4** to **5**, the reaction time, and the temperature. However, no tetra-substituted ($n = 4$) product was detected in any of the cases. The structural formulas of the new multinuclear complexes are shown in Scheme 2.

The substitution products, including the *cis/trans* isomers of **2**, can be separated by column chromatography. Crystals suitable for X-ray diffraction of *trans*-**2** were grown by vapor diffusion of diisopropyl ether into a dilute solution of *trans*-**2** in acetonitrile containing $NaBF_4$ and NH_4BPh_4 (Figure 1).[13] The solid-state structure shows a familiar paddlewheel motif about the rhodium(II) dimer, with a tip-to-tip distance of 36 Å and a nearly eclipsed relative disposition of the ligands. The metal–metal bond length of 2.367(2) Å is typical of dirhodium carboxylates,[10] as are the Rh–O(acetate) and Rh–N(CH_3CN) bond lengths of 1.936(11) and 2.200(15) Å, respectively. However, the Rh–O(carboxylate-tpy) bond length in *trans*-**2** is markedly elongated at 2.052(7) Å and is, to our knowledge, the longest such bond known for dirhodium(II,II) carboxylates.

Complex **4** and the products **1**–**3** have been characterized by ^{1}H NMR spectroscopic analysis in CD_3CN. All of the complexes display a marked electronic effect on the phenyl protons that is dependent on the number of substituted ruthenium units. The identity of each complex is readily verified through integration of the methyl singlets corresponding to equatorially coordinated acetate groups, and this is also supported by electrospray mass spectrometry data.

Although the absorption spectra of multinuclear species **1**–**3** (Figure 2) are the sum of the spectra of the individual components, their luminescence properties are significantly different from those of model species **4** (Table 1). Indeed, the MLCT emission of **4** is totally quenched at room temperature in **1**–**3**, and greatly reduced, as evidenced by lifetime measurements, in a rigid matrix at 77 K (see Table 1 and inset of Figure 2).

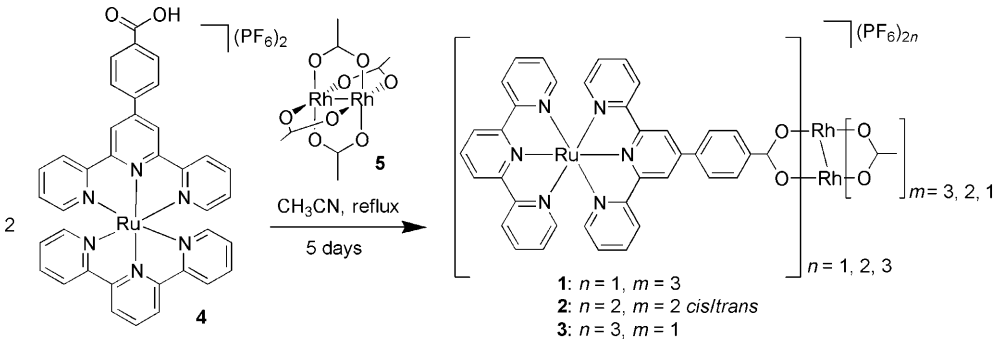
Cyclic and differential pulse voltammetry studies showed that the new compounds all exhibit a single reversible

[*] M. W. Cooke, Prof. G. S. Hanan
Département de Chimie
Université de Montréal
2900 Edouard-Montpetit, Montréal, QC, H3T1J4 (Canada)
Fax: (+1) 514-343-7586
E-mail: garry.hanan@umontreal.ca
Dr. F. Loiseau, Prof. S. Campagna
Dipartimento di Chimica Inorganica
Chimica Analitica e Chimica Fisica
Università di Messina
98166 Messina (Italy)
Fax: (+39) 090-393-756
E-mail: photochem@chem.unime.it
M. Watanabe, Prof. Y. Tanaka
Department of Materials Sciences
Faculty of Engineering
Shizuoka University
Hamamatsu, 432-8561 (Japan)
Fax: (+81) 53-478-1199
E-mail: tcytana@ipc.shizuoka.ac.jp

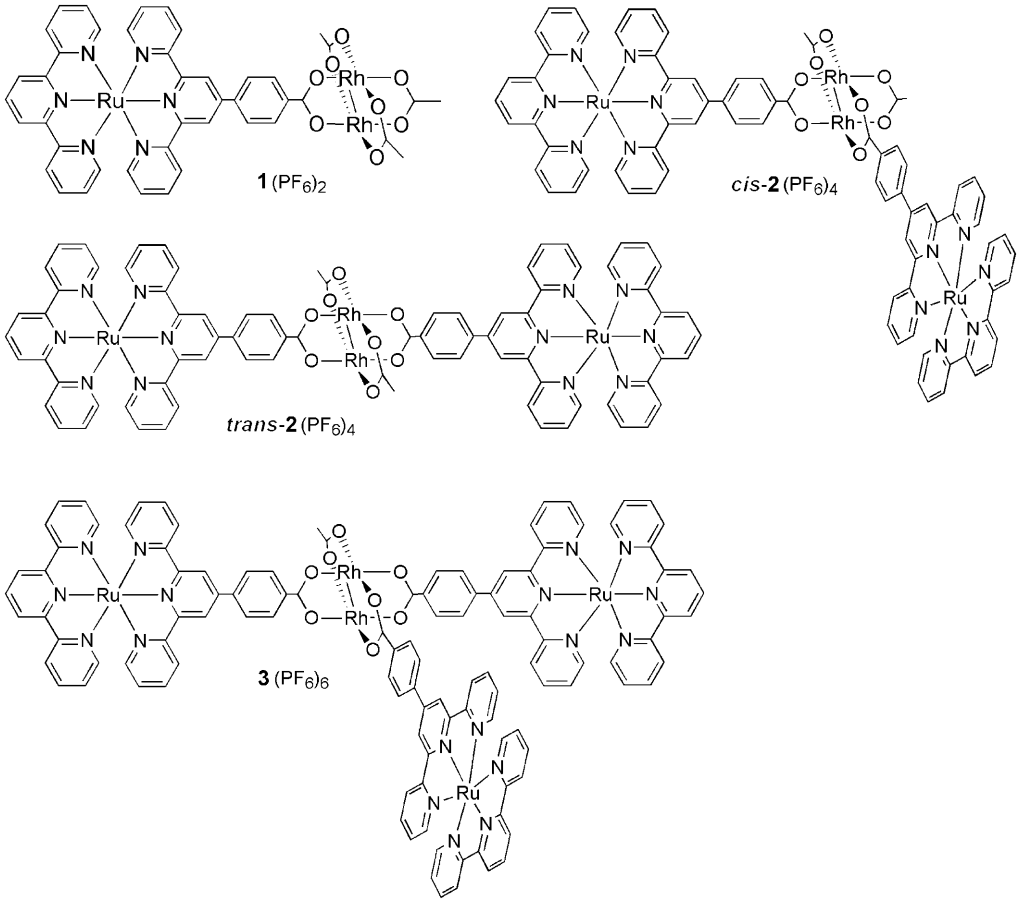
[**] Financial support from the Natural Sciences and Engineering Research Council of Canada, the Université de Montréal, Nissan Canada (M.W.C.), and MIUR (PRIN and FIRB projects) is acknowledged. Y.T. thanks PRESTO of the Japan Science and Technology Corporation. Francine Bélanger-Gariépy is thanked for the X-ray structural analysis of *trans*-**2**.

Supporting information for this article (^{1}H NMR spectra for complexes **1**–**3**, electrochemical studies of some representative compounds, details on the preparation and chromatographic separation of the compounds, elemental analysis, ESI-MS, and crystallographic data) is available on the WWW under http://www.angewandte.org or from the author.

 © 2005 Wiley-VCH Verlag GmbH & Co. KGaA, Weinheim



Scheme 1. Synthesis of mulitinuclear complexes **1**, *cis*-**2**, *trans*-**2**, and **3**.



Scheme 2. Multinuclear complexes **1**, *cis*-**2**, *trans*-**2**, and **3**. Charges are omitted for simplicity.

oxidation process in the potential window investigated (−1.70/+1.50 V versus the saturated calomel electrode (SCE)). The process is assigned to the oxidation of the Ru^{II} subunit(s) on the basis of the oxidation potential of **4** and of the constancy of the potential within the **1**–**3** series (Table 2). Oxidation of the Rh dimer apparently does not take place within the potential window, most likely because of the coordination of the positively charged Ru^{II} moieties. The new compounds all exhibit irreversible reduction processes, probably involving overlapping reduction of the Rh dimer and the Ru^{II} chromophores, namely the tpy ligands. The irreversibility of the reduction processes make their detailed discussion difficult.

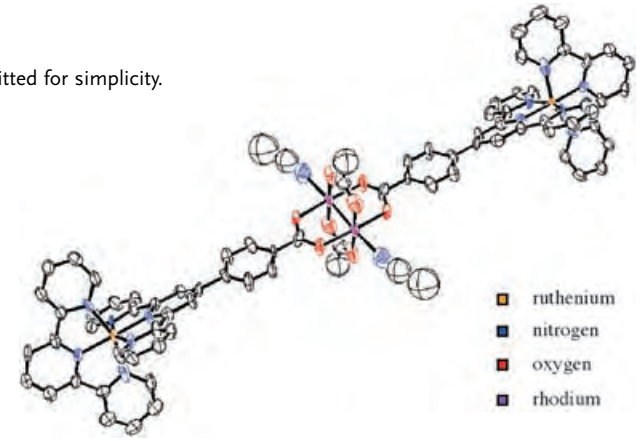


Figure 1. ORTEP diagram with 30% probability ellipsoids of *trans*-**2**. H atoms, solvent, and counterions have been omitted for clarity. The atoms are color coded as indicated.

 © 2005 Wiley-VCH Verlag GmbH & Co. KGaA, Weinheim

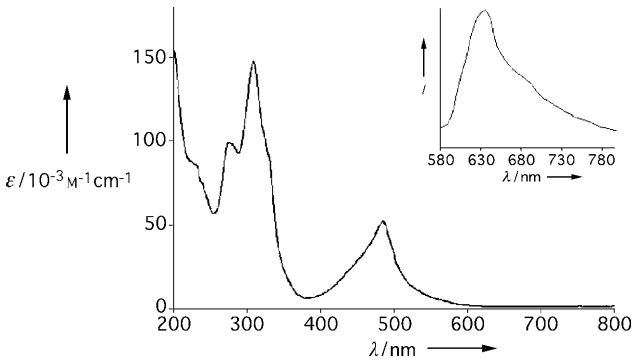


Figure 2. Absorption (298 K) and emission (inset, 77 K) spectra of *trans*-**2**.

Table 1: Luminescence data in a deoxygenated solution of acetonitrile (298 K) and in butyronitrile glass (77 K).

	298 K			77 K	
	λ_{max} [nm]	τ [ns]	Φ	λ_{max} [nm]	τ [μs]
1	–	–	–	639	2.5
cis-**2**	–	–	–	636	0.8
trans-**2**	–	–	–	634	1.2
3	–	–	–	635	0.8
4	666	9.5	8.4×10^{-5}	635	13.2

Table 2: Redox potentials for complexes **1**–**4** and models in argon-purged solutions of acetonitrile.[a]

	Potential [V] versus SCE			
	oxidation		reduction	
1	1.27		−1.21 (irr)	−1.55 (irr)
cis-**2**	1.29		−1.18 (irr)	−1.53 (irr)
trans-**2**	1.29		−1.20 (irr)	−1.48 (irr)
3	1.29		−1.18 (irr)	−1.53 (irr)
4	1.28		−1.24 (irr)	−1.49 (irr)
$Rh_2(OAc)_4$[b]	1.02	−1.08 (irr)		
$[Ru(tpy)_2]^{2+}$[c]	1.30		−1.24	−1.49

[a] $E_{1/2}$ values are given for reversible processes. The reported values for irreversible processes, labeled irr, are peak potentials. [b] Ref. [14]. [c] Ref. [15].

The redox data indicate that reductive electron transfer cannot be considered as a viable route for quenching. In fact, oxidation of the Rh dimer unit in **1**–**3** does not occur until above +1.5 V, and since the first reduction of the Ru moieties is about −1.2 V in all the new species, reductive electron transfer would be endoergonic and not efficient. Similar arguments also apply to oxidative electron transfer. However, the lowest-lying excited state of Rh dimers similar to those used here as templating units has been reported to lie between 1.30 and 1.70 eV, as characterized by relatively long lifetimes in solution (up to 5 μs, depending on the solvent and substituents), although they were found to be nonluminescent.[14a] Despite the large uncertainty concerning the exact energy level of the Rh dimer subunits, there is a substantial driving force in **1**–**3** for energy transfer from the (potentially emitting) Ru-based MLCT states (whose energy is around 1.95 eV) to the excited state based on the Rh dimer. Even if it is assumed that the limiting value of the excited-state energy of the acceptor Rh dimers is 1.70 eV, a ΔG value of −0.25 eV is found (the excited-state energy of the donor Ru chromophores is approximately the same as the maximum value of the emission of **4** at 77 K), which is large enough to make the energy-transfer process efficient. As a consequence, we attribute the quenching of the Ru-based MLCT luminescence in **1**–**3** to energy transfer from the MLCT state(s) to the lowest-lying Rh dimer based level, which would play the role of the energy trap in the multinuclear systems. Therefore, **1**–**3** behave as efficient light-harvesting antennae, where the light energy collected by the Ru^{II}-appended chromophore(s) is conveyed to the Rh dimer subunit. Interestingly, the energy-transfer process appears to be partial at 77 K, thus indicating the presence of significant energy barriers and suggesting that the dominating energy-transfer mechanism of the fast room temperature process could be electron exchange. Ultrafast experiments are in progress to fully characterize the photophysical properties of the new species.

In conclusion, we have developed a novel approach to build-up multinuclear polypyridylruthenium systems by relying upon coordination to a tetracarboxylato metal dimer. Multinuclear complexes are readily available by attaching mononuclear functional subunits (namely, Ru^{II} chromophores) to structural subunits (namely, metal dimers). This "chemistry-on-the-complex" approach simplifies the synthesis of multinuclear assemblies by allowing independent preparation of the different subunits.[8c,16] Intercomponent energy transfer between subunits is efficient, thus indicating that the metal dimers may play a functional role and not only act as a template. The rich chemistry of tetracarboxylato metal dimers and metal–polypyridine complexes with useful photophysical properties should provide ready access to diverse structures with different cores and/or peripheral chromophores and lead to a large library of novel and easily accessible multicomponent species with made-to-order properties. For example, replacement of the Ru chromophores employed here with Ru^{II}–polypyridine species having lower MLCT excited states would make the energy-transfer quenching inefficient and restore peripheral subunit luminescence, whereas the reaction of the partially "uncompleted" species bearing available coordinating units such as **1** and **2** with other metal chromophores (namely, Os^{II} species) should lead to more elaborated mixed-chromophore architectures.

Received: February 1, 2005
Revised: May 5, 2005
Published online: July 1, 2005

Keywords: energy transfer · luminescence · multinuclear complexes · rhodium · ruthenium

[1] a) V. Balzani, F. Scandola, *Supramolecular Photochemistry*, Horwood, Chichester, UK, **1991**; b) G. R. Newkome, K. S. Yoo, H. J. Kim, C. N. Moorefield, *Chem. Eur. J.* **2003**, *9*, 3367; c) H. Jiang, S. J. Lee, W. Lin, *J. Chem. Soc. Dalton Trans.* **2002**, 3429; d) V. Balzani, A. Credi, M. Venturi, *Molecular Devices and Machines. A Journey into the Nanoworld*, Wiley-VCH, Weinheim, **2003**.

 © 2005 Wiley-VCH Verlag GmbH & Co. KGaA, Weinheim

[2] a) V. Balzani, S. Campagna, G. Denti, A. Juris, S. Serroni, M. Venturi, *Acc. Chem. Res.* **1998**, *31*, 26; b) J. Andersson, F. Puntoriero, S. Serroni, A. Yartsev, T. Pascher, T. Polivka, S. Campagna, V. Sundström, *Faraday Discuss.* **2004**, *127*, 295; c) J. Andersson, F. Puntoriero, S. Serroni, A. Yartsev, T. Pascher, T. Polivka, S. Campagna, V. Sundström, *Chem. Phys. Lett.* **2004**, *386*, 336.

[3] J. D. Badjic, V. Balzani, A. Credi, S. Silvi, J. F. Stoddart, *Science* **2004**, *303*, 1845, and references therein.

[4] a) E. C. Constable, P. Harverson, C. E. Housecroft, *J. Chem. Soc. Dalton Trans.* **1999**, 3693; b) J.-P. Sauvage, J.-P. Collin, J. C. Chambron, S. Guillerez, C. Coudret, V. Balzani, F. Barigelletti, L. De Cola, L. Flamigni, *Chem. Rev.* **1994**, *94*, 993.

[5] a) R. Passalacqua, L. Loiseau, S. Campagna, Y.-Q. Fang, G. S. Hanan, *Angew. Chem.* **2003**, *115*, 1646; *Angew. Chem. Int. Ed.* **2003**, *42*, 1608; b) M. I. J. Polson, N. J. Taylor, G. S. Hanan, *Chem. Commun.* **2002**, 1356; c) Y. Q. Fang, N. J. Taylor, G. S. Hanan, F. Loiseau, R. Passalacqua, S. Campagna, H. Nierengarten, A. Van Dorsselaer, *J. Am. Chem. Soc.* **2002**, *124*, 7912; d) E. A. Medlycott, G. S. Hanan, *Chem. Soc. Rev.* **2005**, *34*, 133.

[6] The parent $[Ru(tpy)_2]^{2+}$ has an excited-state lifetime at RT on the order of 250 ps, see: a) J. R. Winkler, T. L. Netzel, C. Creutz, N. Sutin, *J. Am. Chem. Soc.* **1987**, *109*, 2381; b) M. Maestri, N. Armaroli, V. Balzani, E. C. Constable, A. M. W. Cargill Thompson, *Inorg. Chem.* **1995**, *34*, 2759.

[7] a) G. Denti, S. Campagna, L. Sabatino, S. Serroni, M. Ciano, V. Balzani, *Inorg. Chem.* **1990**, *29*, 4750; b) G. Denti, S. Campagna, S. Serroni, M. Ciano, V. Balzani, *J. Am. Chem. Soc.* **1992**, *114*, 2944.

[8] a) F. A. Cotton, C. Lin, C. A. Murillo, *Acc. Chem. Res.* **2001**, *34*, 759; b) M. H. Chisholm, *J. Organomet. Chem.* **2002**, *641*, 15; c) J. K. Bera, B. W. Smucker, R. A. Walton, K. R. Dunbar, *Chem. Commun.* **2001**, 2562.

[9] S. Lo Schiavo, S. Serroni, F. Puntoriero, G. Tresoldi, P. Piraino, *Eur. J. Inorg. Chem.* **2002**, 79, and references therein.

[10] a) F. A. Cotton, R. A. Walton, *Multiple Bonds Between Metal Atoms*, 3rd ed., Wiley, New York, **1994**; b) F. Basolo, R. G. Pearson, *Mechanisms of Inorganic Reactions: A Study of Metal Complexes in Solution*, 2nd ed., Wiley, New York, **1968**.

[11] E. Figgemeier, V. Aranyos, E. C. Constable, R. W. Handel, C. E. Housecroft, C. Risinger, A. Hagfeldt, E. Mukhtar, *Inorg. Chem. Commun.* **2004**, *7*, 117.

[12] Yield of 63% based on 11 mg of recovered **4**. In the reaction of two equivalents of **4** with **5**, the yield based on recovered **4** is **1**: 10%, *cis*-**2**:14%, *trans*-**2**: 18%, **3**: 21%.

[13] Crystal data for *trans*-**2**: $C_{82}H_{62}N_{14}O_8Rh_2Ru_2{\cdot}2(C_{24}H_{20}B){\cdot}2\,BF_4$ was collected on a Bruker APEX at 100 K using $Cu_{K\alpha}$ radiation ($\lambda = 1.54178$ Å). Full-matrix, least-squares refinements on F^2 using all data. 7673 reflections, $M_r = 2591.46$, triclinic, space group $P\bar{1}$, $a = 9.5166(7)$, $b = 13.4933(10)$, $c = 26.5103(17)$ Å, $\alpha = 89.659(4)$, $\beta = 82.213(4)$, $\gamma = 71.513(4)°$, $V = 3196.3(4)$ Å^3, $Z = 1$, $R1\ [I > 2\sigma(I)] = 0.0708$, $wR2 = 0.1905$.

[14] a) P. M. Bradley, B. E. Bursten, C. Turro, *Inorg. Chem.* **2001**, *40*, 1376; b) W. R. Tikkanen, E. Binamira-Soriaga, W. C. Kaska, P. C. Ford, *Inorg. Chem.* **1984**, *23*, 141.

[15] M. Beley, J.-P. Collin, J.-P. Sauvage, H. Sugihara, F. Heisel, A. Miehé, *J. Chem. Soc. Dalton Trans.* **1991**, 3157.

[16] a) F. M. MacDonnell, M.-J. Kim, K. L. Wouters, R. Konduri, *Coord. Chem. Rev.* **2003**, *242*, 47; b) Y.-Q. Fang, M. I. J. Polson, G. S. Hanan, *Inorg. Chem.* **2003**, *42*, 5; c) S.-S. Sun, A. J. Lees, *Coord. Chem. Rev.* **2002**, *230*, 171; d) S.-S. Sun, A. J. Lees, *Organometallics* **2002**, *21*, 39; e) S.-S. Sun, A. J. Lees, *Chem. Commun.* **2001**, 103; f) S.-S. Sun, A. J. Lees, *Inorg. Chem.* **2001**, *40*, 3154; g) O. Johansson, C. C. Tong, J. A. Lotoski, G. S. Hanan, *Chem. Commun.* **2000**, 819; h) S. Bodige, A. S. Torres, D. J. Maloney, D. Tate, G. Kinsel, A. Walker, F. M. MacDonnell, *J. Am. Chem. Soc.* **1997**, *119*, 10364.

 © 2005 Wiley-VCH Verlag GmbH & Co. KGaA, Weinheim

Supramolecular Chemistry

DOI: 10.1002/anie.200500887

Planar or Perpendicular? Conformational Preferences of π-Conjugated Metalloporphyrin Dimers and Trimers in Supramolecular Tubular Arrays**

Akihiko Tsuda, Haifeng Hu, Ryo Tanaka, and Takuzo Aida**

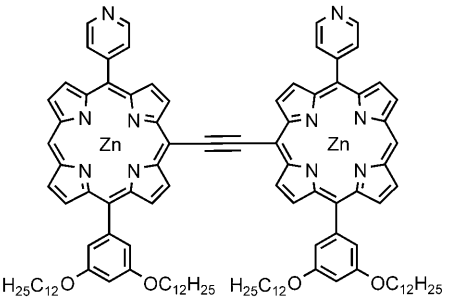
Conformational aspects of π-conjugated molecules are important not only for the basic understanding of their electronic properties but also for their practical application in molecular electronics and photonics.[1–3] The absorption and fluorescence properties of porphyrin pigments are highly sensitive to their π-electronic structures and so π-conjugated multiporphyrin arrays have been studied extensively.[4–10] Another advantage of π-conjugated multiporphyrin arrays is the possibility of controlling their conformation through supramolecular chemistry.[11–13] Studies on the conformational aspects of monoalkynylene-bridged bisporphyrins have suggested that these compounds, despite their rotational freedom around the triple bond, prefer to adopt a planar conformation since planar conformers are enthalpically more favorable than perpendicular conformers as a consequence of the extension of the π conjugation.[8] We have reported that the zinc complex of a monoalkynylene-bridged bisporphyrin with *meso*-pyridyl functionalities **2(≡)$_1$** forms a box-shaped cyclic tetramer, in which the dyad incorporated into the supramolecular box exclusively adopts the planar conformation **2(≡)$_1$//** (Figure 1).[13] Although bisporphyrins with a dialkynylene bridge have a much higher rotational freedom than the monoalkynylene-bridged versions, theory still suggests an energetic bias toward the planar conformation.[9] Anderson and co-workers have succeeded in fixing a dialkynylene-bridged zinc porphyrin oligomer in the planar conformation during the bipyridine-mediated formation of a supramolecular ladder.[11] In the present study we investigated cyclotetramerization[13–17] of zinc complex **2(≡)$_2$**, a dialkynylene-bridged analogue of **2(≡)$_1$**.[18] As with **2(≡)$_1$**, cyclotetramerization of **2(≡)$_2$** can possibly form two isomeric supramolecular boxes **[2(≡)$_2$//]$_4$** and **[2(≡)$_2$⊥]$_4$**, where **[2(≡)$_2$//]$_4$** consists

[*] Dr. A. Tsuda, Dr. H. Hu, R. Tanaka, Prof. T. Aida
Department of Chemistry and Biotechnology
School of Engineering
The University of Tokyo
7-3-1 Hongo, Bunkyo-ku, Tokyo 113-8656 (Japan)
Fax: (+81) 3-5841-7310
E-mail: tsuda@macro.t.u-tokyo.ac.jp
aida@macro.t.u-tokyo.ac.jp

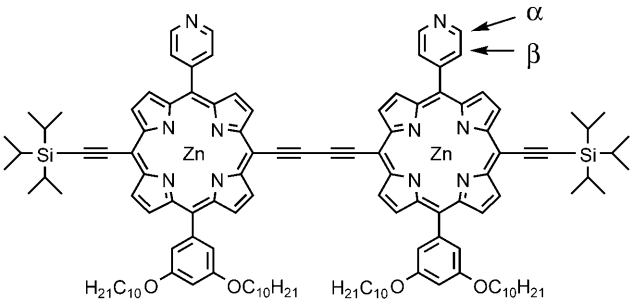
[**] This work was sponsored by a Grants-in-Aid for Scientific Research (No. 15350128) and Encouragement of Young Scientists (No. 15750028) from the Ministry of Education, Science, Sports, and Culture, Japan. A.T. thanks the Sumitomo Foundation.

Supporting information for this article is available on the WWW under http://www.angewandte.org or from the author.

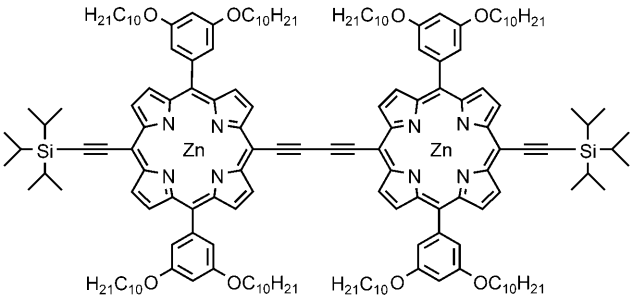
 InterScience © 2005 Wiley-VCH Verlag GmbH & Co. KGaA, Weinheim



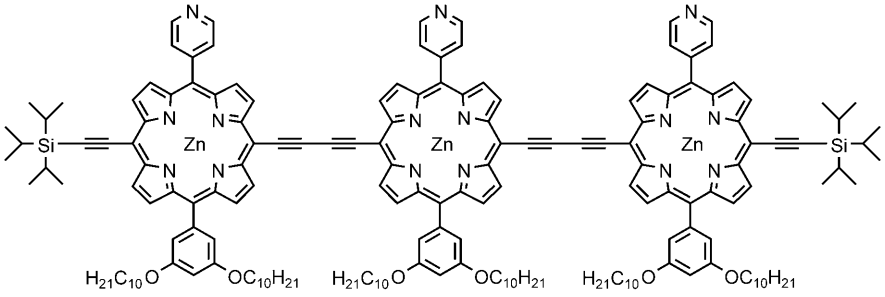
2(≡)$_1$



2(≡)$_2$



ref-**2(≡)$_2$**



3(≡)$_2$

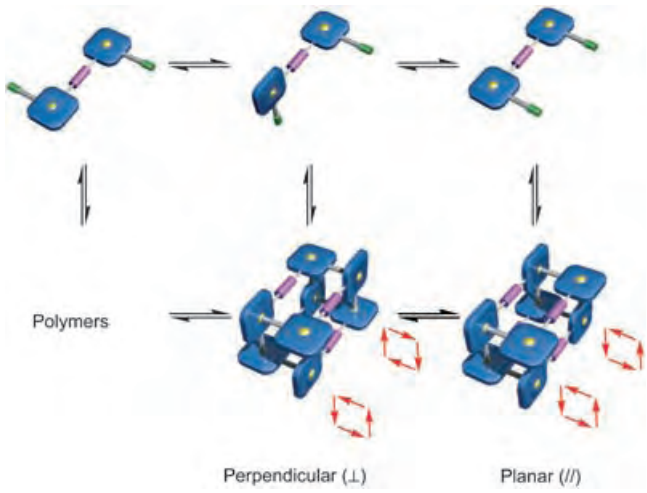


Figure 1. Schematic representation of the cyclotetramerization of alkynylene-bridged zinc pyridylporphyrin dimers. Pink cylinders represent either mono- or dialkynylene units. Red arrows indicate the direction of the Py→Zn coordination.

of the planar conformer of **2(≡)$_2$** (**2(≡)$_2$//**), while **[2(≡)$_2$⊥]$_4$** is composed of the perpendicular conformer (**2(≡)$_2$⊥**; Figure 1). To our surprise, detailed spectroscopic studies indicated that **2(≡)$_2$⊥** is favored over **2(≡)$_2$//** in the resulting supramolecular tubular array.

Compound **2(≡)$_2$** was prepared by treatment of the zinc complex of [5-(4-pyridyl)-10,20-bis(triisopropylsilylethynyl)-15-(3,5-didecyloxyphenyl)porphyrin (**1**) with 0.5 equivalents of tetrabutylammonium fluoride (TBAF), followed by Glaser–Hay coupling of the resulting mixture of derivatives in which the silyl group had been cleaved.[19] Demetalation under acidic conditions and subsequent preparative size-exclusion chromatography (SEC) allowed isolation of the free-base forms of **2(≡)$_2$** and **3(≡)$_2$** in 17 and 2% yields, respectively. Analytical SEC of zinc complex **2(≡)$_2$** with $CHCl_3$ as the eluent displayed a sharp elution peak with a shorter retention time (49.6 min) than that of a non-assembling reference compound without pyridyl groups (ref-**2(≡)$_2$**, 54.8 min).[19] Since the elution time of this chromatographic peak is shorter than that of the cyclic tetramer of the monoalkynylene-bridged analogue (**[2(≡)$_1$]$_4$**, 50.8 min) under identical SEC conditions, **2(≡)$_2$** most likely forms a cyclic oligomer with a larger hydrodynamic volume than **[2(≡)$_1$]$_4$** (Figure 1).[13]

^{1}H NMR spectroscopic analysis of **2(≡)$_2$** in $CDCl_3$ at 20°C provided two sets of characteristic signals corresponding to the porphyrin and pyridyl protons (Figure 2a). By analogy to the spectral patterns[19] of other box-shaped cyclic tetramers so far reported,[13,14] it is most likely that these two sets are both attributed to cyclotetrameric **[2(≡)$_2$]$_4$** (Figure 1). The most characteristic resonances are eight doublets a–d and e–h observed at $\delta = 2.4$–3.0 and 6.2–6.4 ppm, respectively. Addition of [D_5]pyridine (5%), a competitive ligand for the Zn-N coordination, to the system resulted in these characteristic signals disappearing completely, while new doublet signals appeared in the downfield region of $\delta = 8.05$ and 8.86 ppm. These new signals are

 © 2005 Wiley-VCH Verlag GmbH & Co. KGaA, Weinheim

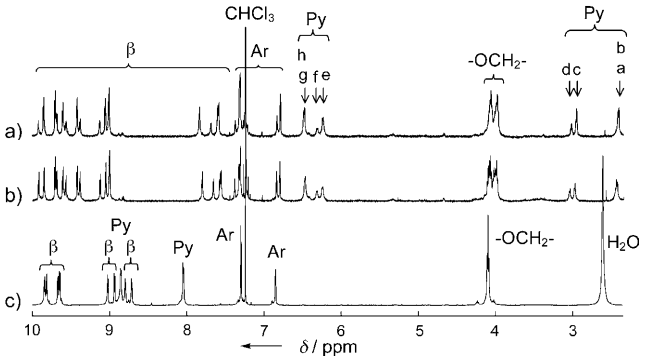


Figure 2. ^{1}H NMR spectra (500 MHz) of **2(≡)$_2$** at a) 20 °C, b) 50 °C in $CDCl_3$, and c) 20 °C in $CDCl_3$/[D_5]pyridine (0.95/0.05). β: β-Pyrrole, Ar: aryl, Py: pyridyl.

assigned to the *ortho* and *meta* protons of the pyridyl groups (Py), respectively, of non-associated **2(≡)$_2$** on the basis of the ^{1}H NMR spectral profile of the free-base form of **2(≡)$_2$** (δ = 8.10 and 9.01 ppm, respectively). Therefore, upfield-shifted signals a–d and e–h can be assigned to the Py groups of **2(≡)$_2$** coordinating to the metal centers. We have reported that the reference tetrameric complex **[2(≡)$_1$]$_4$**, which bears inner and outer Py protons as a result of its cyclic structure (Figure 1), shows a set of four upfield-shifted Py signals.[13] Together with the 2D {^{1}H-^{1}H} COSY spectrum of **2(≡)$_2$**,[19] the two sets of such unique multiple Py signals in Figure 2 can reasonably be assigned to cyclotetrameric **[2(≡)$_2$]$_4$**, provided that it is a mixture of two stereoisomers, namely, **[2(≡)$_2$⊥]$_4$** and **[2(≡)$_2$//]$_4$** which consist of the perpendicular and planar conformers of **2(≡)$_2$**, respectively (Figure 1). The ratio of the integrals of signals c and d, for example, indicates that the two stereoisomers exist in a ratio of 3:1 at 20 °C. We also found that the isomer ratio is temperature-dependent: raising the temperature from 20 to 50 °C results in the isomer ratio changing to 3:2 (Figure 2b).

Correlation of the ^{1}H NMR spectral profile of **2(≡)$_2$** with its absorption and emission spectral features allows the determination of which tetrameric stereoisomer is predominant in the self-assembly of **2(≡)$_2$** (Figure 3). A solution of **[2(≡)$_2$]$_4$** in $CHCl_3$ at 20 °C displayed Soret and Q-bands at 454 (A_I) and 657 nm (A_{III}), respectively. A pair of red-shifted minor bands were also observed at 490 (A_{II}) and 721 nm (A_{IV}). Photoexcitation of **[2(≡)$_2$]$_4$** at 450 nm (A_I) resulted in the appearance of a major fluorescence band at 663 nm (F_I), together with a minor emission at 735 nm (F_{II}; Figure 3b, black solid curve). However, photoexcitation at 500 nm (A_{II}) resulted in a notable enhancement of the minor emission F_{II} (Figure 3b, gray solid curve). A major band was observed at 454 nm (E_I) in the Soret-band region of the excitation spectrum monitored at 660 nm (F_I; Figure 3c, solid curve). Monitoring the fluorescence at 760 nm (F_{II}) provided an excitation spectrum with a split band at 464/494 nm (E_I/E_{II}) in the Soret-band region, along with two low-energy bands at 664 (E_{III}) and 720 nm (E_{IV}) in the Q-band region (Figure 3c, dashed curve). It is clear that the absorption profile of **[2(≡)$_2$]$_4$** (Figure 3a) can be represented by the summation of these two excitation spectra. Band-gap theory for π-conjugated molecules suggests that the higher-energy set of the Soret and Q-bands (A_I and A_{III}, respectively) most likely originates from **[2(≡)$_2$⊥]$_4$** containing the perpendicular conformer of **2(≡)$_2$**, while the lower-energy set (A_{II} and A_{IV}) can be assigned to the planar conformer of **2(≡)$_2$** in **[2(≡)$_2$//]$_4$**.[9] Non-associated **2(≡)$_2$**, generated upon addition of pyridine to **[2(≡)$_2$]$_4$**, showed a luminescence at 738 nm (Figure 3b, dashed curve) upon photoexcitation at 450 nm (A_I). Since alkynylene-bridged multiporphyrin arrays without any external conformational restriction have been reported to emit mainly from their planar conformers,[20] the fluorescence observed from **2(≡)$_2$** at 738 nm provides good experimental support for the assignment that the lower-energy F_{II} (735 nm) band in Figure 3b arises from **[2(≡)$_2$//]$_4$**. Heating the solution from 20 to 50 °C resulted in the latter set of signals arising from **[2(≡)$_2$//]$_4$** in the absorption spectrum intensifying at the expense of the former set assigned to **[2(≡)$_2$⊥]$_4$** (Figure 3a). The combination of this temperature dependency and the ^{1}H NMR spectral profile (see above) leads to the conclusion that **[2(≡)$_2$⊥]$_4$** is the major isomer, which exists in a ratio of 3:1 with the minor isomer **[2(≡)$_2$//]$_4$** at 20 °C and 3:2 at 50 °C. It should also be noted that the absorption and NMR spectral changes are both thermoreversible but extremely slow. As shown in Figure 4, the change in the absorption spectrum on

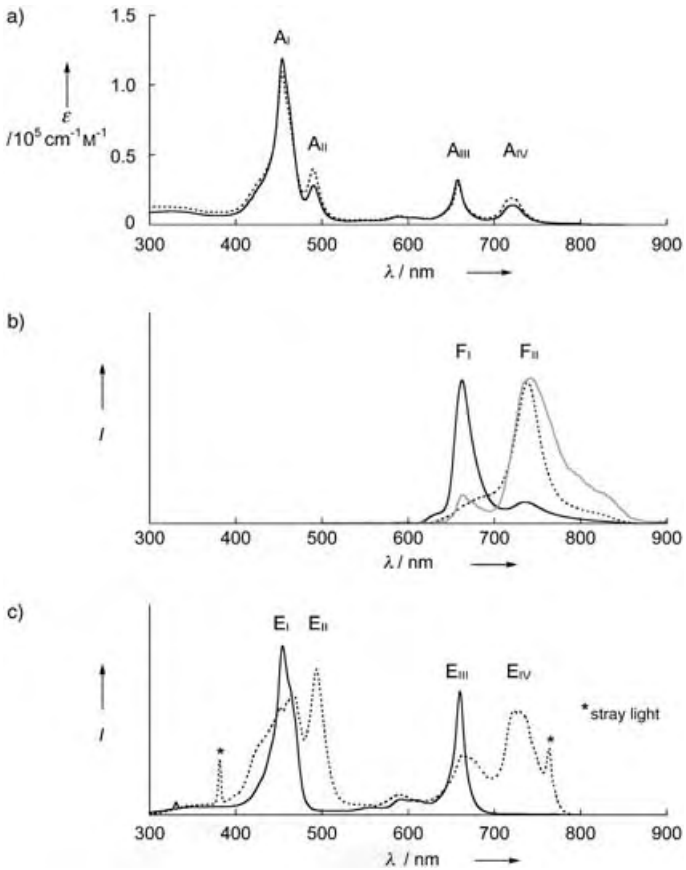


Figure 3. a) Absorption spectra of **2(≡)$_2$** at 20 °C (——) and 50 °C (----) in $CHCl_3$. b) Fluorescence spectra of **2(≡)$_2$** upon photoexcitation at 450 (——) and 500 nm (——) in $CHCl_3$, and 450 nm in $CHCl_3$/pyridine (9:1, ----) at 20 °C. c) Fluorescence excitation spectra of **2(≡)$_2$** monitored at 660 (——) and 760 nm (----) in $CHCl_3$ at 20 °C.

 © 2005 Wiley-VCH Verlag GmbH & Co. KGaA, Weinheim

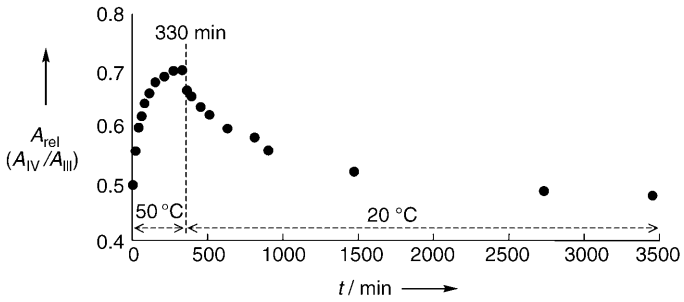


Figure 4. Changes in the relative absorbance (band A_{IV}/A_{III}) of **[2(≡)$_2$]$_4$** in $CHCl_3$ as a function of time upon heating from 20 to 50 °C and cooling from 50 to 20 °C.

heating from 20 to 50 °C subsided in 5 h. Subsequent cooling to 20 °C resulted in a complete recovery of the original spectrum in two days. Such a slow reorganization process indicates a very high thermodynamic stability of tetrameric **[2(≡)$_2$]$_4$**, most likely because of the presence of eight Zn–N coordination bonds.

As described earlier, it is considered that the perpendicular conformers of bis(porphyrins) with π-conjugated bridges are, in general, thermodynamically less stable than the planar conformers. However, the conformational preference toward **2(≡)$_2$**⊥ in the cyclotetramerization is opposite to this general consideration for monomeric **2(≡)$_2$**. We consider that this conformational preference may reflect the extent of the possible interaction of the dipole moments associated with the directions of the eight pyridyl groups in self-assembled **[2(≡)$_2$]$_4$**. Namely, cyclic tetramer **[2(≡)$_2$]$_4$** has two rotational arrays of pyridyl groups, whose directions are identical to one another in **[2(≡)$_2$//]$_4$** but opposite in **[2(≡)$_2$⊥]$_4$** (Figure 1). Since **[2(≡)$_2$⊥]$_4$** allows an efficient cancellation of the dipole moments of the pyridyl groups, **[2(≡)$_2$⊥]$_4$** is favored over **[2(≡)$_2$//]$_4$**.

With this assumption in mind, we investigated the self-assembling behavior of **3(≡)$_2$**, a trimeric version of **2(≡)$_2$**, which contains three dialkynylene-bridged zinc porphyrin units. Although the ^{1}H NMR spectral profile of **3(≡)$_2$** in $CDCl_3$ was less informative of its self-assembled structure, as a result of an enhanced complexity and considerable overlap of the signals, SEC of **3(≡)$_2$** with $CHCl_3$ as the eluent displayed a single, unimodal elution peak with a shorter retention time (47.6 min)[19] than **[2(≡)$_2$]$_4$** (49.6 min), thus suggesting that **3(≡)$_2$** also forms a cyclic oligomer (**[3(≡)$_2$]$_n$**), most likely a discrete cyclic tetramer ($n = 4$) analogous to **[2(≡)$_2$]$_4$**. The electronic absorption spectrum of **[3(≡)$_2$]$_n$** in $CHCl_3$ at 20 °C was very similar to that of **[2(≡)$_2$]$_4$** (Figure 5a). However, photoexcitation of **[3(≡)$_2$]$_n$** at its major absorption band (460 nm; A_I) resulted in a slightly different emission profile from that of **[2(≡)$_2$]$_4$** (Figure 5b, black solid curve). The fluorescence spectrum obtained consists of two distinct bands at 676 (F_I) and 746 nm (F_{II}), which are nearly identical in wavelength to those of **[2(≡)$_2$]$_4$** (Figure 3b). In addition to these major bands, a shoulder (F_{III}) appeared around 790 nm. However, the F_{II} and F_{III} bands were intensified relative to that of F_I when **[3(≡)$_2$]$_n$** was excited at a lower-energy minor absorption band (510 nm,

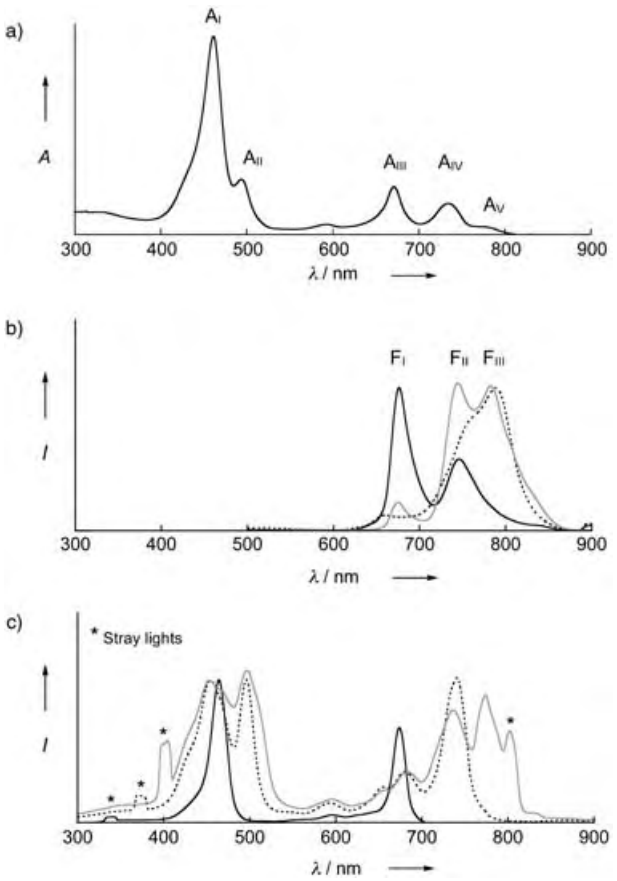


Figure 5. a) Absorption spectrum of **3(≡)$_2$** in $CHCl_3$ at 20 °C. b) Fluorescence spectra of **3(≡)$_2$** upon photoexcitation at 460 (——) and 510 nm (——) in $CHCl_3$, and 460 nm in $CHCl_3$/pyridine (9:1, -----) at 20 °C. c) Fluorescence excitation spectra of **3(≡)$_2$** monitored at 675 (——), 744 (-----), and 800 nm (——) in $CHCl_3$ at 20 °C.

A_{II}; Figure 5b, gray solid curve). From the HOMO–LUMO gap theory of π-conjugated molecules, along with the spectral analogy to **[2(≡)$_2$]$_4$**, the highest-energy F_I and lowest-energy F_{III} bands are assigned to isomers formed exclusively from the perpendicular and planar conformers **[3(≡)$_2$⊥]$_n$** and **[3(≡)$_2$//]$_n$**, respectively, while the middle band (F_{II}) is attributable to **[3(≡)$_2$⊥//]$_n$** consisting of both the planar and perpendicular conformers (Figure 6). Photoexcitation at 460 nm resulted in the non-associated **3(≡)$_2$**, formed by the addition of pyridine to **[3(≡)$_2$]$_n$**, displaying a luminescence centered at 789 nm (Figure 5b, dashed curve), which is close

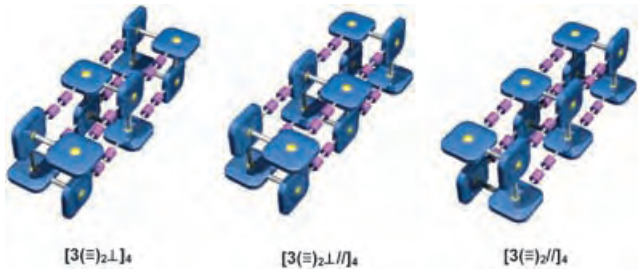


Figure 6. Schematic structures of three conformational isomers in the cyclotetramerization of **3(≡)$_2$**.

 © 2005 Wiley-VCH Verlag GmbH & Co. KGaA, Weinheim

to the F_{III} band assigned to $[3(\equiv)_2//]_n$ composed exclusively of the planar conformer of $3(\equiv)_2$. Examination of the excitation spectra of $[3(\equiv)_2]_n$ monitored at 675 (F_I), 744 (F_{II}), and 800 nm (F_{III}; Figure 5c) showed that the Q-bands observed at 671 (A_{III}), 735 (A_{IV}), and 780 nm (A_V) in the absorption spectrum (Figure 5a) originated mainly from $[3(\equiv)_2\perp]_n$, $[3(\equiv)_2\perp//]_n$, and $[3(\equiv)_2//]_n$, respectively. Provided that the molar absorption coefficients of the Q-bands of these three isomers are identical to one another, the relative intensity of A_{III}, A_{IV}, and A_V in Figure 5a may indicate that isomer $[3(\equiv)_2//]_n$ appears to be the least abundant among the three possible isomers. It should be noted that the dipole moments are cancelled to only a small extent in $[3(\equiv)_2\perp]_n$. Thus, similar to the case of $[2(\equiv)_2]_4$, a conformer that allows an efficient cancellation of the dipole moments in its supramolecular tubular array is preferred even if its enthalpic gain at the monomer level, associated with the π-electronic conjugation, is smaller than that of its counterpart. The trend observed for $[2(\equiv)_2]_4$ and $[3(\equiv)_2//]_n$ is in sharp contrast with that of $[2(\equiv)_1]_4$, which has only a single triple bond between the zinc porphyrin units, where the π-electronic conjugation at the monomer level is a dominant factor for determining the conformational aspect of $2(\equiv)_1$.[13]

In conclusion, we have reported the first supramolecular approach to the preferential fixation of the perpendicular conformers of dialkynylene-bridged zinc porphyrin dimer $2(\equiv)_2$ and trimer $3(\equiv)_2$ by coordinative cyclooligomerization. The contrasting conformational preferences of $2(\equiv)_2$ and $3(\equiv)_2$ with $2(\equiv)_1$[13] in cyclooligomerization are clearly the result of the lower enthalpic gains of the former two complexes upon planarization compared to the latter. Since cyclic tetramer $[2(\equiv)_2\perp]_4$ is chiral, and therefore has a variety of potential applications, structural optimization of $2(\equiv)_2$ to realize the perfect conformational selectivity toward $[2(\equiv)_2\perp]_4$ is one of the interesting subjects worthy of further investigations.

Received: March 9, 2005
Published online: July 1, 2005

Keywords: pi conjugation · porphyrinoids · self-assembly · supramolecular chemistry

[1] a) J. M. Tour, *Chem. Rev.* **1996**, *96*, 537; b) R. E. Martin, F. Diederich, *Angew. Chem.* **1999**, *111*, 1440; *Angew. Chem. Int. Ed.* **1999**, *38*, 1350.
[2] C. Joachim, J. K. Gimzewski, A. Aviram, *Nature* **2000**, *408*, 541.
[3] W.-S. Li, D.-L. Jiang, T. Aida, *Angew. Chem.* **2004**, *116*, 3003; *Angew. Chem. Int. Ed.* **2004**, *43*, 2943.
[4] M. J. Crossley, P. L. Burn, S. J. Langford, K. J. Prashar, *J. Chem. Soc. Chem. Commun.* **1995**, 1921.
[5] R. Paolesse, L. Jaquinod, F. D. Sala, D. J. Nurco, L. Prodi, M. Montalti, C. D. Natale, A. D'Amico, A. D. Carlo, P. Lugli, K. M. Smith, *J. Am. Chem. Soc.* **2000**, *122*, 11295.
[6] a) A. Tsuda, A. Osuka, *Science* **2001**, *293*, 79; b) A. Tsuda, H. Furuta, A. Osuka, *J. Am. Chem. Soc.* **2001**, *123*, 10304.
[7] a) D. P. Arnold, L. J. Nitschinsk, *Tetrahedron* **1992**, *48*, 8781; b) D. P. Arnold, D. A. James, *J. Org. Chem.* **1997**, *62*, 3460.
[8] V. S.-Y. Lin, S. G. DiMagno, M. J. Therien, *Science* **1994**, *264*, 1105.
[9] H. L. Anderson, *Chem. Commun.* **1999**, 2323.
[10] a) P. N. Taylor, J. Huuskonen, G. Rumbels, R. T. Aplin, E. Williams, H. L. Anderson, *Chem. Commun.* **1998**, 909; b) S. M. Kuebler, R. G. Denning, H. L. Anderson, *J. Am. Chem. Soc.* **2000**, *122*, 339.
[11] a) P. N. Taylor, H. L. Anderson, *J. Am. Chem. Soc.* **1999**, *121*, 11538; b) G. S. Wilson, H. L. Anderson, *Chem. Commun.* **1999**, 1539; c) T. E. O. Screen, J. R. G. Thome, R. G. Denning, D. G. Bucknall, H. L. Anderson, *J. Am. Chem. Soc.* **2002**, *124*, 9712.
[12] L. J. Twyman, A. S. H. King, *Chem. Commun.* **2002**, 910.
[13] A. Tsuda, H. Hu, R. Watanabe, T. Aida, *J. Porphyrins Phthalocyanines* **2003**, *7*, 388.
[14] a) A. Tsuda, T. Nakamura, S. Sakamoto, K. Yamaguchi, A. Osuka, *Angew. Chem.* **2002**, *114*, 2941; *Angew. Chem. Int. Ed.* **2002**, *41*, 2817; b) I.-W. Hwang, T. Kamada, T. K. Ahn, D. M. Ko, T. Nakamura, A. Tsuda, A. Osuka, D. Kim, *J. Am. Chem. Soc.* **2004**, *126*, 16187.
[15] X. Chi, A. J. Guerin, R. A. Haycock, C. A. Hunter, L. D. Sarson, *J. Chem. Soc. Chem. Commun.* **1995**, 2567.
[16] K. Funatsu, A. Kimura, T. Imamura, Y. Sasaki, *Chem. Lett.* **1995**, 765.
[17] J. Wojaczynski, L. L. Grazynski, *Coord. Chem. Rev.* **2000**, *204*, 113.
[18] The cyclic oligomers of $2(\equiv)_2$ and $3(\equiv)_2$ without terminal triisopropylsilyl (TIPS) groups both displayed slightly more complicated SEC profiles.
[19] See Supporting Information.
[20] J. J. Piet, P. N. Taylor, H. L. Anderson, A. Osuka, J. M. Warman, *J. Am. Chem. Soc.* **2000**, *122*, 1749.

 © 2005 Wiley-VCH Verlag GmbH & Co. KGaA, Weinheim

N Ligands

DOI: 10.1002/anie.200501111

Chiral Boron-Bridged Bisoxazolines: Readily Available Anionic Ligands for Asymmetric Catalysis**

*Clément Mazet, Valentin Köhler, and Andreas Pfaltz**

Dedicated to Professor Albert Eschenmoser on the occasion of his 80th birthday

The structural motif of the semicorrins **1**[1] has inspired the development of many related chiral ligands for asymmetric catalysis. The closest structural analogues are the bisoxazo-

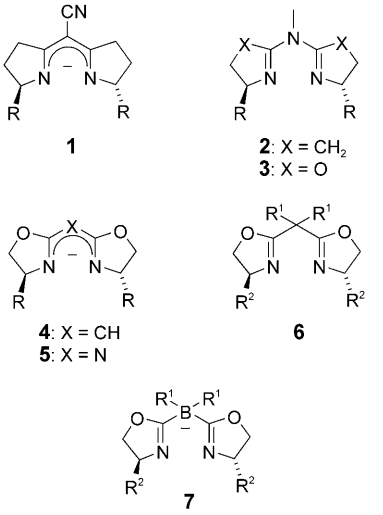
[*] Dr. C. Mazet, V. Köhler, Prof. A. Pfaltz
Department of Chemistry
University of Basel
St. Johanns Ring 19, 4056 Basel (Switzerland)
Fax: (+41) 61-267-1103
E-mail: andreas.pfaltz@unibas.ch

[**] Financial support from the Swiss National Science Foundation is gratefully acknowledged. We thank Markus Neuburger for the crystal-structure analyses.

Supporting information for this article is available on the WWW under http://www.angewandte.org or from the author.

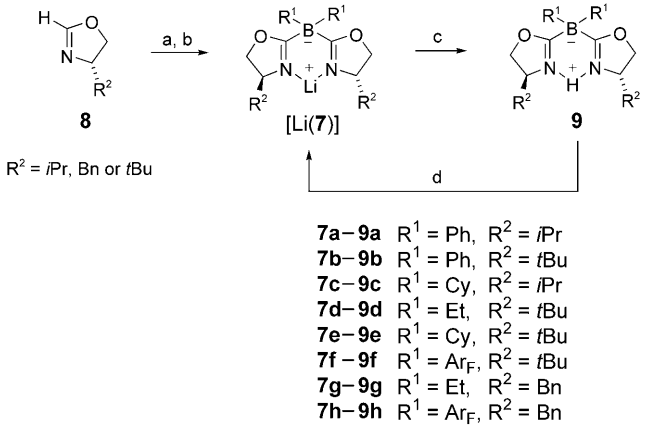
WILEY InterScience DISCOVER SOMETHING GREAT
© 2005 Wiley-VCH Verlag GmbH & Co. KGaA, Weinheim

lines **4**[1,2a,b] and the aza bisoxazolines **5**,[3] the backbone of which contains a planar, negatively charged π system. In



addition, neutral variants **2**[1] and **3**,[3] which contain a planar bridging N atom or a neutral dialkylated methylene bridge **6**, have been developed. The ligand charge, the geometry of the bridging atom, and the electronic properties of the coordinating N atoms all influence the reactivity and enantioselectivity of a metal catalyst.[1,3] Among the various semicorrin analogues reported to date, the bisoxazolines (box) **6** stand out as particularly versatile ligands that have been successfully applied in a wide range of metal-catalyzed reactions.[2] As a further variation of this structural motif, we report herein a class of readily available, anionic bisoxazoline ligands (borabox) **7** that contain a tetrasubstitued B atom that bridges the two oxazoline rings. In contrast to the known anionic ligands **1**, **4**, and **5**, the negative charge in the borabox structure is located in the backbone and the geometry of the bridging atom is tetrahedral as in the neutral box ligand **6**. Anionic ligands of this type that can form neutral zwitterionic complexes with metal cations have recently received increased attention, and a number of N, P, and S ligands which contain tetraorganoborate or indenyl anions as structural elements have been reported.[4–6]

The borabox ligand structure can be readily assembled by reaction of a metalated oxazoline with a dialkyl or diaryl haloborane (Scheme 1). This strategy, which differs from known synthetic approaches to bisoxazolines, is attractive because simple and readily accessible oxazolines **8** can be used as precursors. Lithiation of **8** following the procedure of Meyers and Novachek[7] and subsequent treatment with 0.5 equivalents of haloborane at low temperature led to the lithium salts of bora bisoxazolines **7a–f**. These compounds were isolated in analytically pure form as highly hygroscopic white powders in moderate to good yields, depending on the nature of the substituents at the B atom. The lithium salts could be converted into the protonated ligands **9a–f** by chromatographic workup on silica gel using hexanes/ethyl acetate/triethylamine as the eluent. Regeneration of the lithium salts of **7a–f** was readily accomplished by treatment of



Scheme 1. Synthesis of borabox ligands as the lithium salts of **7a–f** (34–98%) or in their protonated form **9a–f** (44–89%). a) *t*BuLi, −78°C, THF; b) $(R^1)_2BX$ (X = Cl, Br), toluene, −78°C; c) hexanes/EtOAc/Et_3N, SiO_2; d) *n*BuLi, THF, 0°C. Ar_F = 3,5-bis(trifluoromethyl)-phenyl, Cy = cyclohexyl, Bn = benzyl.

compounds **9a–f** with one molar equivalent of *n*-butyllithium in diethyl ether at room temperature.

A wide variety of sterically and electronically different ligands can be prepared by structural variation of the haloborane and the oxazoline **8**. The borabox ligands readily form stable complexes with transition-metal ions, such as Cu^{II}, Zn^{II}, Pd^{II}, Rh^{I}, and Ir^{I} ions, starting from the lithium salts [Li(**7**)] or the protonated precursors **9** in the presence of a base such as K_2CO_3. Figure 1 shows the crystal structure of the homoleptic Cu^{II} complex of **7a** alongside a Cu^{II} complex derived from the analogous diphenylmethyl-bridged box derivative **6a**.[8,9]

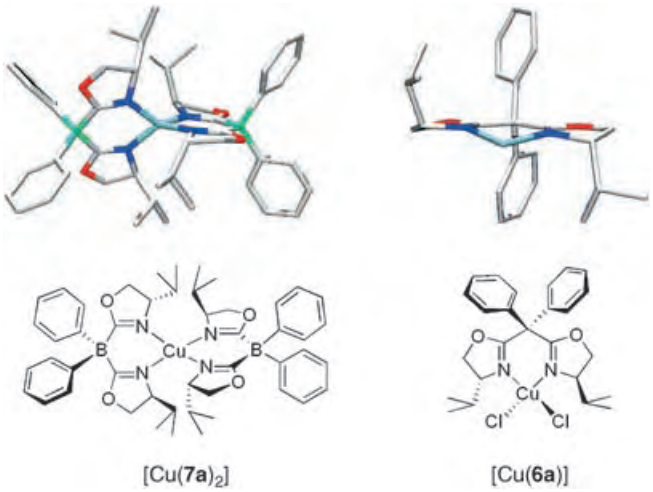


Figure 1. Crystal structures of complexes [Cu(**7a**)$_2$] and [$CuCl_2$(**6a**)]. Hydrogen and chlorine atoms have been omitted for clarity.

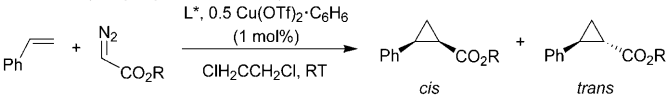
In contrast to the slightly distorted boatlike conformation of **6a**, the borabox ligand **7a** adopts an almost flat conformation. The average bond lengths between the bridging atom and the oxazoline rings, as well as the bite angle, are

 © 2005 Wiley-VCH Verlag GmbH & Co. KGaA, Weinheim

larger in complex [Cu(**7a**)$_2$] than in complex [$CuCl_2$(**6a**)] (B–C_{oxa} = 1.61 Å versus C–C_{oxa} = 1.50 Å (oxa = oxazoline), and N-Cu-N = 94.5° versus N-Cu-N = 89.9°). As a consequence, the substituents at the stereogenic centers in [Cu(**7a**)$_2$] are farther away from the metal ion than in [$CuCl_2$(**6a**)].

As a first test of the borabox ligands, we carried out a comparative study of the cyclopropanation of styrene with Cu^I catalysts prepared in situ from CuOTf (Tf = trifluoromethanesulfonyl), lithium salts of **7a–f**, and analogous box ligands **6a–b**, and **6d** (Table 1).[1,10] In this reaction, which

Table 1: Cyclopropanation of styrene.



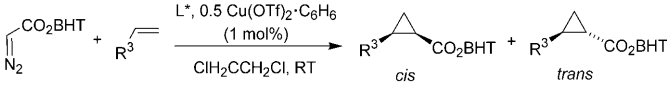
Entry	Ligand	R^1	R^2	Diazo ester (R)	*cis*/*trans*	*cis*[a] *ee* [%]	*trans*[a] *ee* [%]	Yield [%][b] (*cis*+*trans*)
1	**6a**[c]	Ph	*i*Pr	Et	36:64	54	51	85
2	**6b**[d]	Ph	*t*Bu	Et	33:67	91	89	72
3	**6d**[d]	Me	*t*Bu	Et	27:73	97	99	77
4	**7a**	Ph	*i*Pr	Et	29:71	58	65	77
5	**7b**	Ph	*t*Bu	Et	30:70	66	70	84
6	**7c**	Cy	*i*Pr	Et	32:68	24	33	68
7	**7d**	Et	*t*Bu	Et	28:72	59	72	75
8	**7e**	Cy	*t*Bu	Et	28:72	78	66	79
9	**7f**	Ar_F	*t*Bu	Et	32:68	68	77	89
10	**6b**	Ph	*t*Bu	*t*Bu	21:79	93	90	70
11	**6d**[e]	Me	*t*Bu	*t*Bu	19:81	93	96	75
12	**7b**	Ph	*t*Bu	*t*Bu	15:85	77	67	77
13	**7d**	Et	*t*Bu	*t*Bu	13:87	76	73	65
14	**7e**	Cy	*t*Bu	*t*Bu	9:91	82	73	63
15	**7f**	Ar_F	*t*Bu	*t*Bu	17:83	86	92	65
16	**6d**[d]	Me	*t*Bu	BHT	4:96[f]	–	99	85
17	**7f**	Ar_F	*t*Bu	BHT	1:99[f]	–	98	89

[a] Determined by GC or HPLC analysis (see the Supporting Information). [b] After chromatography. [c] Ligands **6a**, **b** were prepared from 2,2-diphenylmalonyl chloride (see the Supporting Information for detailed procedures). [d] In good agreement with reference [11b]. [e] Taken from reference [11b]. [f] Determined by ^{1}H NMR spectroscopic analysis. L* = ligand.

often serves as a benchmark for new ligands, the borabox complexes showed similar reactivities to the corresponding box complexes.[11] As observed for the box ligands, bulkier *tert*-butyl substituents at the stereogenic centers of the borabox ligands induced higher *ee* values than isopropyl groups. However, this effect was less pronounced than in the box series. In the reaction with ethyl diazoacetate, the borabox catalysts gave only moderate enantioselectivities. On the other hand, with *tert*-butyl diazoacetate and 2,6-di-*tert*-butyl-4-methylphenyl (BHT) diazoacetate, the performance of the borabox ligands was much better, with ligand **7f** rivaling the most efficient box derivative **6d**. Consistent with previous studies, the more bulky esters gave much higher ratios of *trans*/*cis* isomers. The best result, 98% *ee* and almost perfect diastereoselectivity, was obtained in the reaction of the BHT ester with borabox derivative **7f** (entry 17).

The borabox catalyst [Cu(**7f**)] also performed well with other alkenes (Table 2). Overall, the enantioselectivities were

Table 2: Cyclopropanation of different alkenes.



Entry	Ligand	R^1	R^2	R^3	*cis*/*trans*[a]	*trans*[b] *ee* [%]	Yield[c] [%] (*cis*+*trans*)
1	**6d**	Me	*t*Bu	Ph	4:96	99	85
2	**7f**	Ar_F	*t*Bu	Ph	1:99	98	89
3	**6d**	Me	*t*Bu	*p*-$MeOC_6H_4$	4:96	96	35[d]
4	**7f**	Ar_F	*t*Bu	*p*-$MeOC_6H_4$	4:96	97	65[d]
5	**6d**	Me	*t*Bu	*p*-FC_6H_4	4:96	99.4	89
6	**7f**	Ar_F	*t*Bu	*p*-FC_6H_4	1:99	99.5	91
7	**6d**	Me	*t*Bu	$PhCH_2$	7:93	99	ng[e]
8	**7f**	Ar_F	*t*Bu	$PhCH_2$	8:92	97	66
9	**6d**	Me	*t*Bu	*n*-hexyl	2:98	99	51[d]
10	**7f**	Ar_F	*t*Bu	*n*-hexyl	1:99	95	68[d]

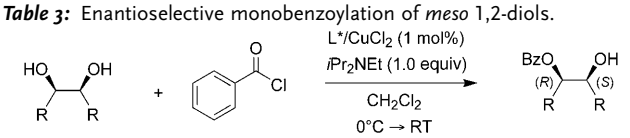
[a] Determined by ^{1}H NMR spectroscopic analysis. [b] Determined by HPLC (see the Supporting Information). [c] After chromatography; average of two runs. [d] Reaction time not optimized. [e] ng = not given; results taken from reference [11a].

similar to those obtained with box derivative **6d**, but in several cases the *trans* selectivitiy of the borabox catalyst was higher (compare entries 1, 5, and 9 with 2, 6, and 10, respectively).

To explore further the potential of the borabox ligands, we studied the Cu-catalyzed enantioselective monobenzoylation of *meso* 1,2-diols, a reaction recently reported by Matsumura et al. (Table 3).[12]

The monobenzoylated products were obtained in good yields (62–83%) under the optimized conditions. The borabox derivative **9h** proved to be the most effective ligand for all three substrates with *ee* values of 76, 90, and 94% being obtained. The corresponding benzyl-substituted bisoxazoline

Table 3: Enantioselective monobenzoylation of *meso* 1,2-diols.



Entry	Ligand	R^1	R^2	*meso* 1,2-diol	Yield [%][a]	*ee* [%][b]
1	**6c**	Me	Bn		70	33[c]
2	**6e**	Me	Ph		58	13
3	**9g**	Et	Bn		79	40
4	**9h**	Ar_F	Bn		73	76
5	**6c**	Me	Bn		74	85[c]
6	**6e**	Me	Ph		62	22
7	**9g**	Et	Bn		75	47
8	**9h**	Ar_F	Bn		83	90
9	**6c**	Me	Bn		68	84[c]
10	**6e**	Me	Ph		58	86
11	**9g**	Et	Bn		62	92
12	**9h**	Ar_F	Bn		65	94

[a] Average of two runs. [b] *ee* and absolute configuration values were determined by HPLC according to the literature data (see the Supporting Information). [c] The enantiomer of **6c** was used in this case and, therefore, a product of opposite configuration was obtained.

 © 2005 Wiley-VCH Verlag GmbH & Co. KGaA, Weinheim

6c and the diphenyl analogue **6e**, which in the study of Matsumura et al.[12a] had given the best results, induced distinctly lower enantioselectivities.

In summary, we have developed a new class of anionic, boron-bridged analogues of the box ligands. These ligands are of interest because they are anionic with the negative charge located in the backbone, but otherwise closely resemble the netural box ligands **6**. The results obtained in the asymmetric cyclopropanation and, especially, in the desymmetrization of *meso* diols point to a considerable potential for borabox ligands in asymmetric catalysis.

Received: March 29, 2005
Published online: July 11, 2005

Keywords: acylation · asymmetric catalysis · copper · diazo compounds · N ligands

[1] A. Pfaltz, *Acc. Chem. Res.* **1993**, *26*, 339 – 345.
[2] Reviews: a) A. K. Ghosh, P. Mathivanan, J. Cappiello, *Tetrahedron: Asymmetr.* **1998**, *9*, 1 – 45; b) H. A. McManus, P. J. Guiry, *Chem. Rev.* **2004**, *104*, 4151 – 4202; recent applications: c) D. A. Evans, C. W. Downey, J. L. Hubbs, *J. Am. Chem. Soc.* **2003**, *125*, 8706 – 8707; D. A. Evans, C. E. Masse, J. Wu, *Org. Lett.* **2002**, *4*, 3375 – 3378; d) C. Palomo, M. Oiarbide, B. G. Kardak, J. M. Garcia, A. Linden, *J. Am. Chem. Soc.* **2005**, *127*, 4154 – 4155; e) M. P. Sibi, K. Itoh, C. P. Jasperse, *J. Am. Chem. Soc.* **2004**, *126*, 5366 – 5367; f) A. S. Gothelf, K. V. Gothelf, R. G. Hazell, K. A. Jørgensen, *Angew. Chem.* **2002**, *114*, 4410 – 4412; *Angew. Chem. Int. Ed.* **2002**, *41*, 4236 – 4238.
[3] a) M. Glos, O. Reiser, *Org. Lett.* **2000**, *2*, 2045 – 2048; b) C. Geiger, P. Kreitmeier, O. Reiser, *Adv. Synth. Catal.* **2005**, *347*, 249 – 254; c) A. Gissibl, M. G. Finn, O. Reiser, *Org. Lett.* **2005**, 7, 2325 – 2328.
[4] a) C. Ohrenberg, P. Ge, P. Schebler, C. G. Riordan, G. P. A. Yap, A. L. Rheingold, *Inorg. Chem.* **1996**, *35*, 749 – 754; b) R. Krishnan, J. K. Voo, C. G. Riordan, L. Zahkarov, A. L. Rheingold, *J. Am. Chem. Soc.* **2003**, *125*, 442 – 4423.
[5] a) J. C. Thomas, J. C. Peters, *J. Am. Chem. Soc.* **2001**, *123*, 5100 – 5101; b) T. A. Betley, J. C. Peters, *Angew. Chem.* **2003**, *115*, 2487 – 2491; *Angew. Chem. Int. Ed.* **2003**, *42*, 2385 – 2389; c) J. C. Thomas, J. C. Peters, *Inorg. Chem.* **2003**, *42*, 5055 – 5073.
[6] M. Stradiotto, J. Cipot, R. McDonald, *J. Am. Chem. Soc.* **2003**, *125*, 5618 – 5619.
[7] A. I. Meyers, K. A. Novachek, *Tetrahedron Lett.* **1996**, *37*, 1747 – 1748.
[8] X-ray crystal-structure analysis of [Cu(**7a**)$_2$]: crystallized from CH_2Cl_2/Et_2O/hexane, $C_{48}H_{60}B_2Cu_1N_4O_4$, $M_r = 842.20$, $F(000) = 2684.448$, blue–green plates, $0.06 \times 0.28 \times 0.30$ mm^3, hexagonal, space group $P6_122$, $Z = 6$, $a = 10.9216(17)$, $b = 10.9216(17)$, $c = 65.042(9)$ Å, $\alpha = 90$, $\beta = 90$, $\gamma = 120°$, $V = 6718.9$ Å^3, $\rho_{calcd} = 1.249$ Mg m^{-3}. The crystal structure was measured on a Enraf Nonius Kappa CCD diffractometer at 173 K using graphite monochromated $Mo_{K\alpha}$ radiation with $\lambda = 0.71073$ Å, $\Theta_{max} = 27.47°$. Minimal/maximal transmission = 0.86/0.97, $\mu = 0.535$ mm^{-1}. The COLLECT suite has been used for data collection and integration. From a total of 28085 reflections, 5088 were independent (merging $r = 0.18$). From these, 2731 were considered as observed ($I > 2.00\sigma(I)$) and were used to refine 268 parameters. The structure was solved by direct methods by using the program SIR92. Least-squares refinement against F was carried out on all non-hydrogen atoms by using the program CRYSTALS. $R = 0.0469$ (observed data), $wR = 0.0413$ (all data), GOF = 1.0429. Minimal/maximal residual electron density = −0.62/0.58 e Å^{-3}. Chebychev polynomial weights were used to complete the refinement. Plots were produced using CAMERON.
[9] X-ray crystal-structure analysis of [$CuCl_2$(**6a**)]: crystallized from CH_2Cl_2/hexane, $C_{26}H_{32}Cl_4Cu_1N_2O_2$, $M_r = 609.91$, $F(000) = 1260$, blue blocks, $0.18 \times 0.21 \times 0.23$ mm^3, orthorhombic, space group $P2_12_12_1$, $Z = 4$, $a = 10.3143(6)$, $b = 15.0541(15)$, $c = 17.8386(11)$ Å, $\alpha = 90$, $\beta = 90$, $\gamma = 90°$, $V = 2769.8(4)$ Å^3, $\rho_{calcd} = 1.462$ Mg m^{-3}. The crystal was measured on a Nonius Kappa CCD diffractometer at 173 K using graphite monochromated $Mo_{K\alpha}$ radiation with $\lambda = 0.71073$ Å, $\Theta_{max} = 31.505°$. Minimal/maximal transmission = 0.78/0.81, $\mu = 1.201$ mm^{-1}. The COLLECT suite has been used for data collection and integration. From a total of 102125 reflections, 9224 were independent (merging $r = 0.07$). From these, 5664 were considered as observed ($I > 3.00\sigma(I)$) and were used to refine 446 parameters. The structure was solved by direct methods using the program SIR92. Least-squares refinement against F was carried out on all non-hydrogen atoms using the program CRYSTALS. $R = 0.0241$ (observed data), $wR = 0.0451$ (all data), GOF = 1.0959. Minimal/maximal residual electron density = −0.53/1.07 e Å^{-3}. Chebychev polynomial weights were used to complete the refinement. Plots were produced using ORTEP III for Windows. CCDC-267175 and -267176 contain the supplementary crystallographic data for this paper. These data can be obtained free of charge from the Cambridge Crystallographic Data Centre via www.ccdc.cam.ac.uk/data_request/cif. Programs used: structure solution: SIR92 A. Almatore, G. Cascarano, G. Giacovazzo, A. Guagliardi, M. C. Burla, G. Polidori, M. Camalli, *J. Appl. Crystallogr.* **1994**, *27*, 435 – 435; collect software: Nonius BV **1997–2001**; structure refinement: D. J. Watkin, C. K. Prout, J. R. Carruthers, P. W. Betteridge, R. I. Cooper, CRYSTALS *Issue 11.*, Chemical Crystallography Laboratory, Oxford, UK, **2001**.
[10] a) M. P. Doyle, D. C. Forbes, *Chem. Rev.* **1998**, *98*, 911 – 935; b) H. Lebel, J.-F. Marcoux, C. Molinaro, A. B. Charette, *Chem. Rev.* **2003**, *103*, 977 – 1050; c) A. Pfaltz in *Comprehensive Asymmetric Catalysis* (Eds.: A. Pfaltz, H. Yamamoto, E. N. Jacobsen), Springer, Heidelberg, **1999**, chap. 16, pp. 513 – 538.
[11] a) D. A. Evans, K. A. Woerpel, M. H. Hinman, M. M. Faul, *J. Am. Chem. Soc.* **1991**, *113*, 726 – 728; see, also: b) R. E. Lowenthal, A. Abiko, S. Masamune, *Tetrahedron Lett.* **1990**, *31*, 6005 – 6008; c) D. Müller, G. Umbricht, B. Weber, A. Pfaltz, C. Kratky, *Helv. Chim. Acta* **1991**, *74*, 232 – 240.
[12] a) Y. Matsumura, T. Maki, S. Murakami, O. Onomura, *J. Am. Chem. Soc.* **2003**, *125*, 2052 – 2053; b) S. Mizuta, M. Sadamori, T. Fujimoto, I. Yamamoto, *Angew. Chem.* **2003**, *115*, 3505 – 3507; *Angew. Chem. Int. Ed.* **2003**, *42*, 3383 – 3385.

 © 2005 Wiley-VCH Verlag GmbH & Co. KGaA, Weinheim

Host–Guest Chemistry

DOI: 10.1002/anie.200500985

A Calix[5]arene-Based Heterotetratopic Host for Molecular Recognition of Long-Chain, Ion-Paired α,ω-Alkanediyldiammonium Salts**

Domenico Garozzo, Giuseppe Gattuso, Anna Notti, Andrea Pappalardo, Sebastiano Pappalardo, Melchiorre F. Parisi,* Marta Perez, and Ilenia Pisagatti*

Ion-pair recognition, that is, the simultaneous complexation of cation and anion guest species by neutral hosts, is an emerging field of topical interest in supramolecular chemistry with great potential for biological, analytical, and environmental applications.[1] It is well known that the ion-binding process with neutral receptors is adversely affected by the ion-pairing of guest salts,[2] so that it is common practice to make use of salts with weakly coordinating counterions,[3] which result in enhanced host-guest associations. On the other hand, the ion-pairing interference can be circumvented either by using an appropriate combination of anion and cation receptors (binary host strategy)[4] or by designing specific heteroditopic receptors that take advantage of favorably positioned binding sites as well as induce positive cooperative and allosteric effects.[5] So far a plethora of heteroditopic receptors have been developed for inorganic ion pairs,[6] but much less has been reported for organic salts.[5c,7]

The molecular recognition of α,ω-alkanediyldiammonium salts has been actively investigated with different classes of artificial homo(poly)topic receptors. Among these, cylindrical macrotricyclic hosts,[8] cucurbiturils,[9] crown ether[10] and glycoluril derivatives,[11] bimetallic porphyrin dimers,[12] as well as *p-tert*-butylcalix[5]arenes[13] have been employed. However, none of the receptors used so far has been equipped with complementary counterion-binding sites.

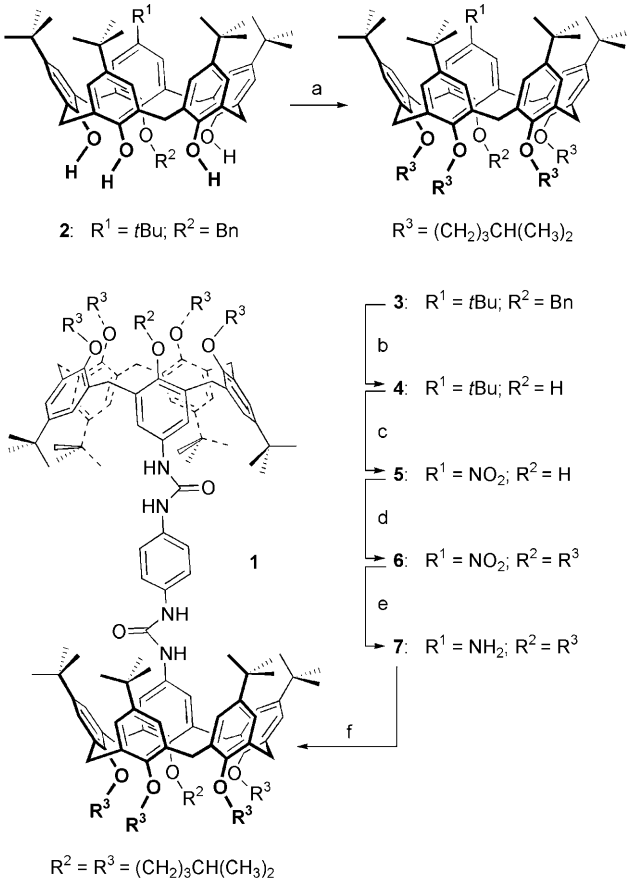
[*] Prof. S. Pappalardo
Dipartimento di Scienze Chimiche
Università di Catania
Viale A. Doria 6, 95125 Catania (Italy)
Fax: (+39) 095-580-138
E-mail: spappalardo@dipchi.unict.it
Dr. G. Gattuso, Dr. A. Notti, Dr. A. Pappalardo, Prof. M. F. Parisi, Dr. I. Pisagatti
Dipartimento di Chimica Organica e Biologica
Università di Messina
Salita Sperone 31, 98166 Messina (Italy)
Fax: (+39) 090-393-895
E-mail: mparisi@unime.it
Dr. D. Garozzo, Dr. M. Perez
CNR, ICTP Catania
Viale Regina Margherita 6, 95125 Catania (Italy)

[**] We thank the MIUR (PRIN 2003 project) for financial support, Prof. P. Finocchiaro for helpful discussions, and Prof. M. E. Amato for the acquisition of TROESY NMR spectra.

Supporting information for this article is available on the WWW under http://www.angewandte.org or from the author.

Following our specific interest in the development of neutral multisite receptors for biogenic (poly)ammonium salts,[14] we report herein the synthesis and unique molecular recognition abilities of the first heterotetratopic receptor, **1**, which consists of two convergent, conformationally fixed, cone calix[5]arene units (cation-binding sites) that are covalently linked at their upper rims by means of a 1,4-bis(ureido)phenylene spacer (anion-binding sites). Host **1** readily forms overall charge-neutral, unimolecular capsules (ligand-separated ion-pair complexes) of nanoscale dimensions by tight encapsulation[15] of linear α,ω-alkanediyldiammonium ions, which range from 1,12-dodecane- to 1,16-hexadecanediammonium, inside the inner space defined by the two converging calix[5]arene cavities by simultaneously binding each of the two counteranions to the peripheral ureido functions through hydrogen bonds.

The target biscalixarene **1** was synthesized in six steps from the known 31-benzyloxy-*p-tert*-butylcalix[5]arene (**2**)[16] according to the sequence illustrated in Scheme 1. The exhaustive *O*-alkylation of **2** with 4-methylpent-1-yl tosylate and K_2CO_3 in CH_3CN at reflux produced pentaether **3** in 77% yield which, upon Pd/C-catalyzed hydrogenolysis in EtOAc, gave monohydroxy intermediate **4** in 93% yield. The



Scheme 1. Synthesis of **1**: a) $TsO(CH_2)_3CH(CH_3)_2$, K_2CO_3, CH_3CN, reflux, 12 h, 77%; b) H_2, Pd/C, EtOAc, room temperature, 4 h, 93%; c) 68% HNO_3/AcOH, CH_2Cl_2, 0°C, 25 min, 77%; d) $TsO(CH_2)_3CH(CH_3)_2$, NaH, THF, reflux, 48 h, 70%; e) $SnCl_2 \cdot 2H_2O$, EtOAc/EtOH, reflux, 24 h, 68%; f) 1,4-C_6H_4-$(NCO)_2$, $CHCl_3$, room temperature, 6 h, 66%. Ts = *p*-toluenesulfonyl; Bn = benzyl.

InterScience © 2005 Wiley-VCH Verlag GmbH & Co. KGaA, Weinheim

subsequent selective *ipso*-nitration of **4** with 68% HNO_3 and acetic acid in CH_2Cl_2 afforded 5-nitro derivative **5** in 77% yield. Further *O*-alkylation of the residual hydroxy group with 4-methylpent-1-yl tosylate and NaH in dry THF furnished the 5-nitro pentaether **6** in 70% yield which was converted into 5-amino-calixarene **7** in 68% yield by reduction with $SnCl_2{\cdot}2H_2O$ in EtOH/EtOAc at reflux. Final coupling of two molecules of **7** with 1,4-phenylene diisocyanate in dry $CHCl_3$ led to biscalix[5]arene **1** in 66% yield.

The binding affinity of receptor **1** for linear, long-chain α,ω-alkanediyldiammonium ($\mathbf{C_8}$–$\mathbf{C_{16}}$) dichloride salts, as well as the host-guest architectures they form, were investigated by a combination of ^{1}H NMR spectroscopy and electrospray mass spectrometry (ESI-MS). The former method takes advantage of the large upfield shifts experienced by the methylene resonances of the guest upon encapsulation of the dication[4a,14] and the downfield shifts of the NH resonances of the host (in nonprotic media) which signal the simultaneous binding of the counteranions. ESI-MS exploits the remarkable tendency of the π-basic calix[5]arene cavity to include alkylammonium guests, thus providing ion labels for the detection of encapsulated complexes in the gas phase.[13,17,18]

H_3N^+—$(CH_2)_n$—$^+NH_3$

$\mathbf{C_8}$: n = 8
$\mathbf{C_{10}}$: n = 10
$\mathbf{C_{12}}$: n = 12
$\mathbf{C_{14}}$: n = 14
$\mathbf{C_{16}}$: n = 16

The affinity of **1** for α,ω-alkanediyldiammonium dichloride salts was initially investigated by ^{1}H NMR titration experiments in $(CDCl_2)_2/CD_3OD$ (2:1 *V*/*V*). Addition of the guest salt (up to 4 equivalents) to a solution of **1** (1.0×10^{-3} M) caused the formation of very strong inclusion complexes, whose host–guest stoichiometries (1:1 and/or 2:1) and geometries depend on the length of the diammonium ion and the [host]/[guest] ratio (see Figure 1). The ^{1}H NMR spectra of the inclusion complexes of calix[5]arenes with alkylammonium guest ions normally show distinct signals for the free and complexed host and guest species in slow exchange on the ^{1}H NMR timescale.[13,14,18] Here, signals corresponding to the free host and guests could barely be seen in the spectra of equimolar host–guest mixtures of **1** with the longer alkyldiammonium ($\mathbf{C_{12}}$–$\mathbf{C_{16}}$) dichloride salts, which suggests very high association constants ($K_a > 10^6\,M^{-1}$) for the formation of the capsular (C-shaped) 1:1 host–guest complexes with C_s symmetry. Similar results were observed using other solvent systems (including neat $(CDCl_2)_2$, $CDCl_3$, and CD_2Cl_2, or mixtures thereof with up to 50% content of CD_3OD), or on changing—in the case of $\mathbf{C_{12}}$—the nature of the counteranion (diacetate, dibromide, and dipicrate salts). Notably, the spectra did not change upon further addition of salt or on tenfold dilution of the solution.

In contrast, titration experiments of **1** with the shorter alkyldiammonium ($\mathbf{C_8}$ and $\mathbf{C_{10}}$) dichloride guest salts gave rise to changes in the ^{1}H NMR spectra that are consistent with the initial formation of the S-shaped (for $\mathbf{C_8}$) or C-shaped (for $\mathbf{C_{10}}$) 1:1 host–guest complexes for equimolar host–guest solutions and which eventually evolved toward the formation of the S-shaped 1:2 host–guest complexes (C_{2h} symmetry) after further addition of salt (Figure 1). This is clearly shown by the evolution of the ^{1}H NMR spectra in the titration experiment of **1** with $\mathbf{C_{10}}{\cdot}2\,Cl^-$ (Figure 2). Addition of one

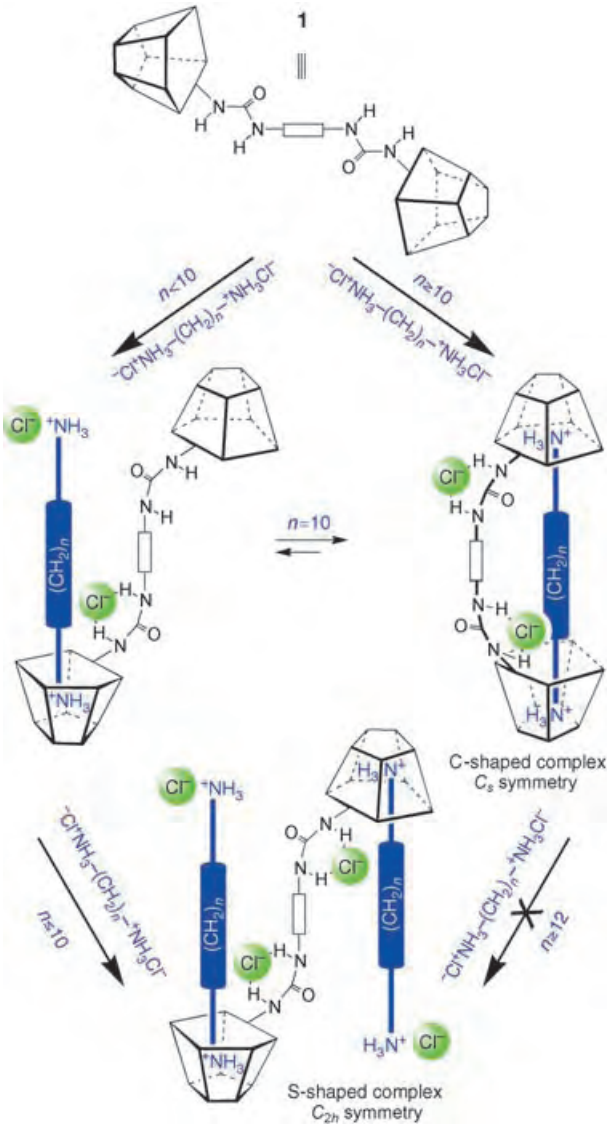


Figure 1. Schematic representation of the influence of the spanning of the guest α,ω-alkanediyldiammonium ions on the complexation pathways leading to C-shaped and/or S-shaped inclusion complexes with host **1**.

equivalent of salt caused the almost exclusive formation of the C-shaped 1:1 complex, as revealed by the presence of a set of five upfield methylene resonances for the included dication (Figure 2b).[19] Upon further addition of salt, a second more-spread set of signals for the included guest became evident in the highfield region of the spectra ($\delta = -1.9$ to 0.7 ppm) as a result of the incipient formation of the S-shaped 1:2 host–guest complex (Figure 2c and d). This conclusion is validated by the triplet detected at $\delta = 2.55$ ppm which is assigned to the α′-CH_2 protons of the guest and is judged of diagnostic value for the S-shaped complexes.[18] The latter architecture was the only host–guest species present in solution when a total of four equivalents of $\mathbf{C_{10}}{\cdot}2\,Cl^-$ had been added to **1** (Figure 2e).

The use of nonprotic solvents revealed the beneficial effect of the ureido functions of **1** which facilitate the loosening of the ion-paired salt and the association of the

 © 2005 Wiley-VCH Verlag GmbH & Co. KGaA, Weinheim

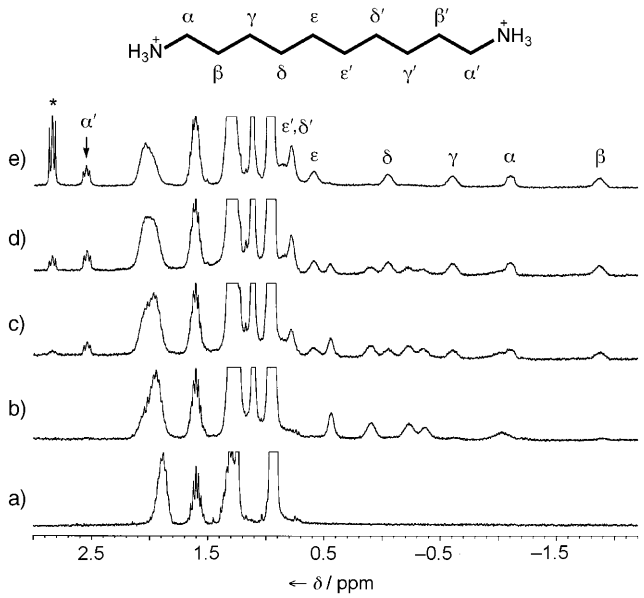


Figure 2. Highfield regions of the ^{1}H NMR spectra (300 MHz; 22 ± 1 °C; 2:1 $(CDCl_2)_2/CD_3OD$) recorded during the titration experiment of **1** (1.0×10^{-3} M) with $\mathbf{C_{10}}\cdot2Cl^-$: a) **1**; b) $\mathbf{1}/\mathbf{C_{10}}\cdot2Cl^-$ (1:1); c) $\mathbf{1}/\mathbf{C_{10}}\cdot2Cl^-$ (1:1.5); d) $\mathbf{1}/\mathbf{C_{10}}\cdot2Cl^-$ (1:2); e) $\mathbf{1}/\mathbf{C_{10}}\cdot2Cl^-$ (1:4). The triplet labeled with an asterisk refers to the α- and α′-CH_2 of uncomplexed $\mathbf{C_{10}}\cdot2Cl^-$, which is present in excess.

anion by formation of six-membered chelate rings with halide or picrate anions and eight-membered chelate rings with carboxylate anions.[20]

The shifts of the N-H resonances of **1** upon ligand-separated ion-pair complexation of the various $\mathbf{C_{12}}$ salts in $(CDCl_2)_2$ provide a qualitative picture of the strength of the anion-binding site (Table 1). Entries 3–6 suggest an anti-Hofmeister[21] trend in the complexation of the counteranion by heterotetratopic **1**, with the largest $\Delta\delta$ values being observed for the more densely charged Cl^- and $CH_3CO_2^-$ anions (in $(CDCl_2)_2$: $CH_3CO_2^- \approx Cl^- > Br^- > Pic^-$). A comparison between entries 2 and 4 shows also that the encapsulation of the dication enhances the acidity of the urea NH groups through an electron-withdrawing effect to result in a better uptake of chloride anions (positive allosteric effect).[5]

Table 1: Variation of the chemical shift of urea NH resonances of **1** (300 MHz, 1.0×10^{-3} M in $(CDCl_2)_2$) after the addition of one equivalent of guest salt.

Entry	Guest	δ [ppm]		Δδ [ppm]	
		NH_a[a]	NH_b[a]	NH_a[a]	NH_b[a]
1	none	6.44	5.88		
2	nBu$_4$N$^+$Cl$^-$	7.21[b]	6.63[b]	0.77	0.75
3	$\mathbf{C_{12}}\cdot2CH_3CO_2^-$	8.91	8.60	2.47	2.72
4	$\mathbf{C_{12}}\cdot2Cl^-$	8.81	8.51	2.37	2.63
5	$\mathbf{C_{12}}\cdot2Br^-$	8.28	8.08	1.84	2.20
6	$\mathbf{C_{12}}\cdot2Pic^-$	7.40[c]		1.24	

[a] NH_a and NH_b refer to the two groups close to the calixarene unit and the 1,4-phenylene moiety, respectively. [b] Fast complexation equilibrium on the NMR timescale; data refer to the addition of two equivalents of salt. [c] Broad signal, partly buried under the aromatic protons of the calixarene units. Pic = picrate.

The slow exchange in the capsular complexes of **1** with diammonium salts allowed TROESY (transverse rotating-frame Overhauser effect spectroscopy) NMR spectroscopy to be carried out at room temperature, and the spectra obtained were fully consistent with the expected structure and symmetry of the complexes. Most importantly, the TROESY spectra (Figure 3b) showed clear intermolecular NOE cross

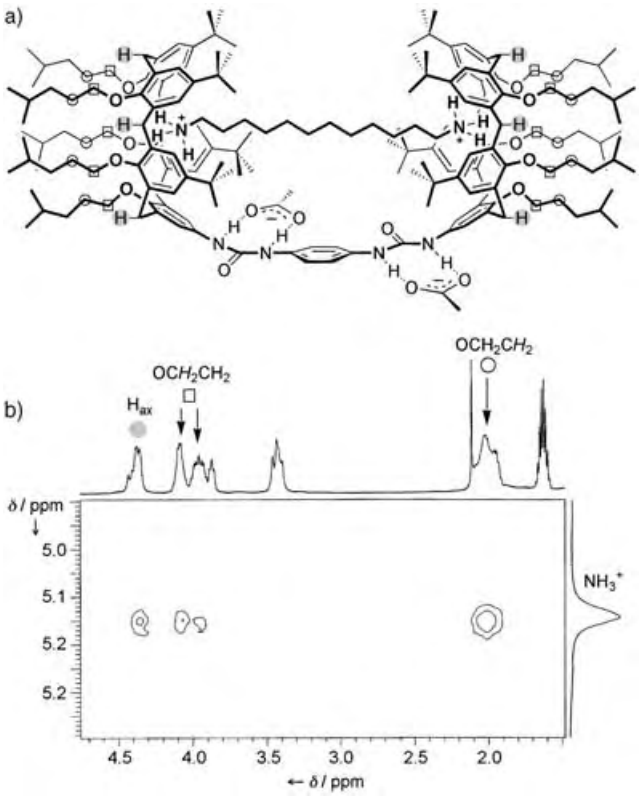


Figure 3. a) Structure of the C-shaped capsular $\mathbf{1}\cdot\mathbf{C_{12}}\cdot2CH_3CO_2^-$ complex with labeling of the relevant hydrogen atoms showing NOE interactions between the host and guest. b) Selected region of the TROESY NMR spectrum (500 MHz) of $\mathbf{1}\cdot\mathbf{C_{12}}\cdot2\ CH_3CO_2^-$ (5.0×10^{-3} M in $(CDCl_2)_2$). ax = axial.

peaks between the host and the guest. In particular, the NH_3^+ protons of the salt showed NOE peaks to the axial bridging methylene protons as well as to α- and β-oxymethylene protons of the lower rim substituents of the calix[5]arene moieties (Figure 3a), which provides evidence that the ammonium end group is held in position by hydrogen-bonding interactions with the ethereal oxygens. Moreover, the encapsulated ε-methylene protons of the $\mathbf{C_{12}}$ guest and the aromatic protons of the host gave rise to a cross peak.

The formation of capsular complexes between **1** and long-chain α,ω-alkanediyldiammmonium dichloride salts is further corroborated by the positive ESI mass spectra of equimolar host–guest mixtures which show prominent doubly-charged ions that correspond to $[\mathbf{1}\cdot\mathbf{C}_n]^{2+}$ (base peak) and low-intensity ion peaks for $[\mathbf{1}\cdot\mathbf{C}_n\mathrm{Cl}]^+$.[22]

The binding selectivity of **1** for the guest salts studied here was eventually determined by decreasing in highly coordinating solvents the cooperativity factors that arise from the

 © 2005 Wiley-VCH Verlag GmbH & Co. KGaA, Weinheim

anion-binding sites. Addition of dimethyl sulfoxide (DMSO) to a solution of **1** in chloroform led to a strong solvation of the hydrogen-bond donor sites of the ureido functions.[23,24] This solvation caused a weakening of the binding ability of **1** toward ion-paired salts[25] and allowed the determination of the association constants by ^{1}H NMR spectroscopy. Table 2 shows that among the substrates investigated the longer $\mathbf{C_{12}}$ and $\mathbf{C_{16}}$ guest salts are more tightly bound than $\mathbf{C_8}$ and $\mathbf{C_{10}}$ by **1** as the result of capsular complexation.

Table 2: Association constants (K_a) of α,ω-alkanediyldiammonium dichloride salts with receptor **1** in $CDCl_3$/[D_6]DMSO (3:2).[a]

$H_3N^+(CH_2)_n{}^+NH_3\cdot 2Cl^-$	K_a [M^{-1}]
$n=8$	212[b]
$n=10$	163[b]
$n=12$	2.4×10^3
$n=14$	–[c]
$n=16$	2.6×10^3

[a] Determined by ^{1}H NMR spectroscopy at 22 ± 1 °C using equimolar (1×10^{-3} M) host–guest mixtures. Values are derived from the average of at least three independent measurements (standard error ≤ 15%). [b] K_a values refer to the S-shaped 1:1 complex. [c] Measurements of K_a were precluded by the limited solubility of the salt.

The binding selectivity order of **1** toward $\mathbf{C_{12}}$, $\mathbf{C_{14}}$, and $\mathbf{C_{16}}$ as chloride salts was estimated from the ESI-MS distribution percentages[26] of the relevant capsular complexes ($[\mathbf{1}\cdot\mathbf{C}_n]^{2+}$ ions). A competitive complexation experiment of **1** with a mixture of the three salts ($\mathbf{1}/\mathbf{C_{12}}\cdot 2Cl^-/\mathbf{C_{14}}\cdot 2Cl^-/\mathbf{C_{16}}\cdot 2Cl^- = 1:1:1:1$; $c=1.0\times10^{-4}$ M in $CHCl_3/CH_3OH$ (1:1)) gave the order $\mathbf{C_{14}} > \mathbf{C_{16}} > \mathbf{C_{12}}$ (60.5, 24.6, and 14.9%, respectively).[27,28]

In conclusion, we have synthesized a novel heterotetratopic receptor, **1**, that efficiently and selectively forms ligand-separated ion-pair complexes with long-chain α,ω-alkanediyldiammonium dichloride salts by combining the cooperative action of two converging calix[5]arene cavities in the encapsulation of the dication with the ability of the two ureido functions to bind the relevant counteranions. Future work will be directed toward the design of new heteropolytopic systems with specific recognition patterns.

Received: March 17, 2005
Published online: July 6, 2005

Keywords: calixarenes · host–guest systems · inclusion compounds · ion pairs · molecular recognition

[1] Reviews: a) P. A. Gale, *Coord. Chem. Rev.* **2003**, *240*, 191–221; b) P. D. Beer, P. A. Gale, *Angew. Chem.* **2001**, *113*, 502–532; *Angew. Chem. Int. Ed.* **2001**, *40*, 486–516.

[2] a) A. Arduini, E. Brindani, G. Giorgi, A. Pochini, A. Secchi, *J. Org. Chem.* **2002**, *67*, 6188–6194; b) S. Bartoli, S. Roelens, *J. Am. Chem. Soc.* **2002**, *124*, 8307–8315; c) V. Böhmer, A. Dalla Cort, L. Mandolini, *J. Org. Chem.* **2001**, *66*, 1900–1902; d) R. Shukla, T. Kida, B. D. Smith, *Org. Lett.* **2000**, *2*, 3099–3102.

[3] a) I. Krossing, I. Raabe, *Angew. Chem.* **2004**, *116*, 2116–2142; *Angew. Chem. Int. Ed.* **2004**, *43*, 2066–2090; b) *The Supramolecular Chemistry of Anions* (Eds.: A. Bianchi, K. Bowman-James, E. Garcia-Espana), VCH, Weinheim, **1997**.

[4] a) G. Cafeo, G. Gattuso, F. H. Kohnke, A. Notti, S. Occhipinti, S. Pappalardo, M. F. Parisi, *Angew. Chem.* **2002**, *114*, 2226–2230; *Angew. Chem. Int. Ed.* **2002**, *41*, 2122–2126; b) K. Kavallieratos, B. A. Moyer, *Chem. Commun.* **2001**, 1620–1621.

[5] a) L. Kovbasyuk, R. Krämer, *Chem. Rev.* **2004**, *104*, 3163–3187; b) A. J. Evans, P. D. Beer, *Dalton Trans.* **2003**, 4451–4456; c) A. Arduini, G. Giorgi, A. Pochini, A. Secchi, F. Ugozzoli, *J. Org. Chem.* **2001**, *66*, 8302–8308.

[6] For representative examples, see: a) J. M. Mahoney, A. M. Beatty, B. D. Smith, *Inorg. Chem.* **2004**, *43*, 7617–7621, and references therein; b) M. Barboiu, G. Vaughan, A. van der Lee, *Org. Lett.* **2003**, *5*, 3073–3076; c) M.-L. Lehaire, R. Scopelliti, H. Piotrowski, K. Severin, *Angew. Chem.* **2002**, *114*, 1477–1480; *Angew. Chem. Int. Ed.* **2002**, *41*, 1419–1422; d) M. J. Deetz, M. Shang, B. D. Smith, *J. Am. Chem. Soc.* **2000**, *122*, 6201–6207; e) D. J. White, N. Laing, H. Miller, S. Parsone, S. Coles, P. A. Tasker, *Chem. Commun.* **1999**, 2077–2078; f) J. Scheerder, J. P. M. van Duynhoven, J. F. J. Engbersen, D. N. Reinhoudt, *Angew. Chem.* **1996**, *108*, 1172–1175; *Angew. Chem. Int. Ed. Engl.* **1996**, *35*, 1090–1093.

[7] a) T. Haino, M. Nakamura, N. Kato, M. Hiraoka, Y. Fukazawa, *Tetrahedron Lett.* **2004**, *45*, 2281–2284; b) G. Tumcharern, T. Tuntulani, S. J. Coles, M. B. Hursthouse, J. D. Kilburn, *Org. Lett.* **2003**, *5*, 4971–4974; c) J. M. Mahoney, J. P. Davis, A. M. Beatty, B. D. Smith, *J. Org. Chem.* **2003**, *68*, 9819–9820; d) J. L. Atwood, A. Szumna, *Chem. Commun.* **2003**, 940–941.

[8] F. Fages, J.-P. Desvergne, K. Kampke, H. Bouas-Laurent, J.-M. Lehn, M. Meyer, A.-M. Albrecht-Gary, *J. Am. Chem. Soc.* **1993**, *115*, 3658–3664.

[9] a) J. W. Lee, S. Samal, N. Selvapalam, H.-J. Kim, K. Kim, *Acc. Chem. Res.* **2003**, *36*, 621–630; b) W. L. Mock, N.-Y. Shih, *J. Org. Chem.* **1983**, *48*, 3618–3619.

[10] K. Tsubaki, H. Tanaka, T. Futura, K. Tanaka, T. Kinoshita, K. Fuji, *Tetrahedron* **2002**, *58*, 5611–5617.

[11] J. W. H. Smeets, R. P. Sijibesma, L. van Dalen, A. L. Spek, W. J. J. Smeets, R. J. M. Nolte, *J. Org. Chem.* **1989**, *54*, 3710–3717.

[12] a) M. J. Crossley, P. Thordarson, *Angew. Chem.* **2002**, *114*, 1785–1788; *Angew. Chem. Int. Ed.* **2002**, *41*, 1709–1712; b) Y. Kubo, Y. Murai, J.-i. Yamanaka, S. Tokita, Y. Ishimaru, *Tetrahedron Lett.* **1999**, *40*, 6019–6023.

[13] D. Garozzo, G. Gattuso, F. H. Kohnke, P. Malvagna, A. Notti, S. Occhipinti, S. Pappalardo, M. F. Parisi, I. Pisagatti, *Tetrahedron Lett.* **2002**, *43*, 7663–7667.

[14] a) F. P. Ballistreri, A. Notti, S. Pappalardo, M. F. Parisi, I. Pisagatti, *Org. Lett.* **2003**, *5*, 1071–1074; b) F. Arnaud-Neu, S. Fuangswasdi, A. Notti, S. Pappalardo, M. F. Parisi, *Angew. Chem.* **1998**, *110*, 120–122; *Angew. Chem. Int. Ed.* **1998**, *37*, 112–114.

[15] For a review on molecular encapsulation, see: F. Hof, S. L. Craig, C. Nuckolls, J. Rebek, Jr., *Angew. Chem.* **2002**, *114*, 1556–1578; *Angew. Chem. Int. Ed.* **2002**, *41*, 1488–1508.

[16] D. R. Stewart, M. Krawiec, R. M. Kashyap, W. H. Watson, C. D. Gutsche, *J. Am. Chem. Soc.* **1995**, *117*, 586–601.

[17] C. A. Schalley, R. K. Castellano, M. S. Brody, D. M. Rudkevich, G. Siuzdak, J. Rebek, Jr., *J. Am. Chem. Soc.* **1999**, *121*, 4568–4579.

[18] D. Garozzo, G. Gattuso, F. H. Kohnke, A. Notti, S. Pappalardo, M. F. Parisi, I. Pisagatti, A. J. P. White, D. J. Williams, *Org. Lett.* **2003**, *5*, 4025–4028.

[19] The guest is rather short to span the two calix[5]arene cavities, and the shielding experienced by the included chain is less effective than that observed with the longer, more tightly bound guest salts.

 © 2005 Wiley-VCH Verlag GmbH & Co. KGaA, Weinheim

[20] For a very recent report on the possible geometries of urea–anion complexes, see: B. P. Hay, T. K. Firman, B. A. Moyer, *J. Am. Chem. Soc.* **2005**, *127*, 1810–1819.
[21] F. Hofmeister, *Arch. Exp. Pathol. Pharmakol.* **1888**, *24*, 247–260.
[22] The ESI mass spectra recorded at higher concentrations (ca. 10^{-4} M) show additional peaks of low intensity that correspond to $[(\mathbf{1}\cdot\mathbf{C}_n)_m Cl_{(m-1)}]^{m+1}$ ($m \geq 2$), which may imply a chloride-driven self-assembly of the capsular complexes through an intercapsular 2:1 urea–chloride binding mode[20] in the gas phase.
[23] E. Fan, S. A. Van Arman, S. Kincaid, A. D. Hamilton, *J. Am. Chem. Soc.* **1993**, *115*, 369–370.
[24] Heteroditopic calix[4]arenes endowed with a ureido functionality have been reported to strongly coordinate thorugh hydrogen bonding to DMSO molecules; see: A. Arduini, E. Brindani, G. Giorgi, A. Pochini, A. Secchi, *Tetrahedron* **2003**, *59*, 7587–7594.
[25] The importance of the ureido functions on the host properties of **1** is demonstrated by the inability of the model *p-tert*-butyl-penta-*O*-isohexyl calix[5]arene, which lacks a ureido group at the upper rim, to form an inclusion complex with the ion-paired *n*-dodecylammonium chloride in 3:2 $CDCl_3$/[D_6]DMSO.
[26] G. Ferguson, A. J. Lough, A. Notti, S. Pappalardo, M. F. Parisi, G. Resnati, *Collect. Czech. Chem. Commun.* **2004**, *69*, 1109–1125, and references therein.
[27] Again, a possible chloride-driven self-assembly of the various capsular complexes is clearly indicated by the presence of mixed assemblies (see Supporting Information).
[28] ^{1}H NMR competitive complexation experiments under similar experimental conditions showed an analogous trend in the relative binding selectivities.

 © 2005 Wiley-VCH Verlag GmbH & Co. KGaA, Weinheim

Supramolecular Chemistry

DOI: 10.1002/anie.200501559

Ultramacrocyclization through Reversible Catenation**

*Akiko Hori, Tomohisa Sawada, Ken-ichi Yamashita, and Makoto Fujita**

Dedicated to Professor Iwao Ojima on the occasion of his 60th birthday

Whereas the cyclization of small (five- or six-membered) rings is a facile and high-yielding process in synthetic chemistry, that of larger rings becomes increasingly difficult with increasing number of ring members (n).[1–3] Macrocyclization with $n \approx 10$–30 is a difficult task, but is often achieved under high-dilution conditions. However, ultramacrocyclization[4] with $n > 100$ has scarcely been described because the entropy cost is too high in bringing the ends of a long acyclic compound together for cyclization to proceed (Figure 1 a). However, if the reaction sites are sufficiently large, the probability of the association of the both ends prior to cyclization should significantly increase and ultramacrocyclization should proceed efficiently. Such an idea prompted us to examine the reversible catenation[5,6] of coordination rings for ultramacrocyclization (Figure 1 b). Palladium(II)-clipped macrocycle **1** has a nanometer-sized framework and easily transforms into its catenated dimer in polar media through π–π aromatic interactions between the two rings.[7] In expectation of ultramacrocyclization through catenation, we designed the long acyclic compound **2**, which comprises Pd^{II}-clipped macrocyclic units at both ends. Accordingly, we found that compound **2** selectively catenates into ultramacrocyclic dimer **3**, which contains over 200 non-hydrogen atoms in its backbone.

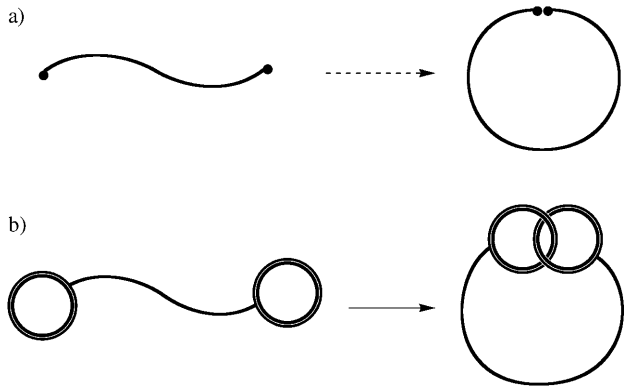


Figure 1. Cartoon representation for macrocyclization through a) the formation of a chemical bond and b) reversible catenation.

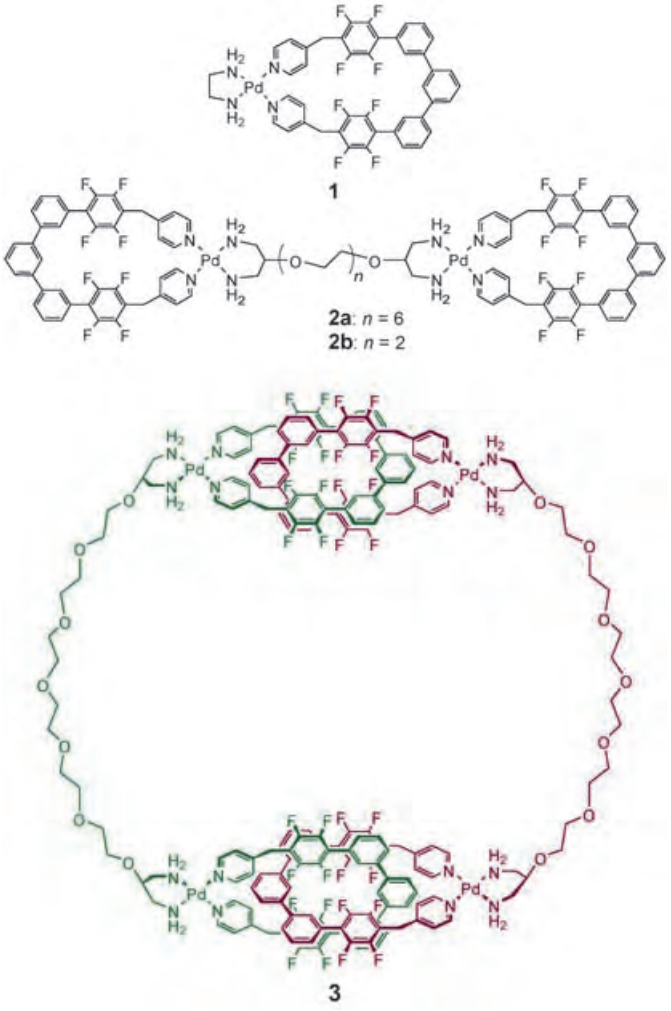
Double-loop compound **2a** was obtained by treating ligand **4** with bimetallic linker **5**[8] in dimethyl sulfoxide (DMSO; Scheme 1). Typically, ligand **4** (7.1 mg, 10 μmol) was treated with **5** (4.6 mg, 5.0 μmol) in DMSO (0.50 mL) for a few minutes at ambient temperature. The formation of **2a** as a single product was confirmed by ^{1}H NMR spectroscopy (Figure 2 a) and cold-spray ionization mass spectrometry (CSI-MS[9]).[10] Subsequently, we examined the catenation of **2a** at both loops by adding water to the solution in DMSO.[7] As revealed by ^{1}H NMR spectroscopy (Figure 2 b–g), peaks for the protons of the monomer **2a** decreased with increasing water content. Instead, significantly highfield-shifted aromatic protons appeared around $\delta = 8.20$–6.75 ppm, characteristic of the catenation of the Pd^{II}-clipped rings. CSI-MS clearly indicated that the newly formed product was cyclic dimer **3**, which contains two catenated frameworks. The spectrum from a solution in *N*,*N*-dimethylformamide (DMF) and H_2O (1:2) showed a series of peaks for $[\mathbf{3}-(NO_3)_n+(dmf)_m]^{n+}$: for example, $m/z = 669.7$ corresponds to $[\mathbf{3}-(NO_3)_7+(dmf)_7]^{7+}$;

[*] Dr. A. Hori, T. Sawada, K. Yamashita, Prof. Dr. M. Fujita
Department of Applied Chemistry
School of Engineering
The University of Tokyo
7-3-1 Hongo, Bunkyo-ku, Tokyo 113-8656 (Japan)
Fax: (+81) 3-5841-7257
E-mail: mfujita@appchem.t.u-tokyo.ac.jp

[**] This research was supported by the CREST project of the Japan Science and Technology Corporation (JST), for which M.F. is the principal investigator.

Supporting information for this article is available on the WWW under http://www.angewandte.org or from the author.

InterScience
© 2005 Wiley-VCH Verlag GmbH & Co. KGaA, Weinheim



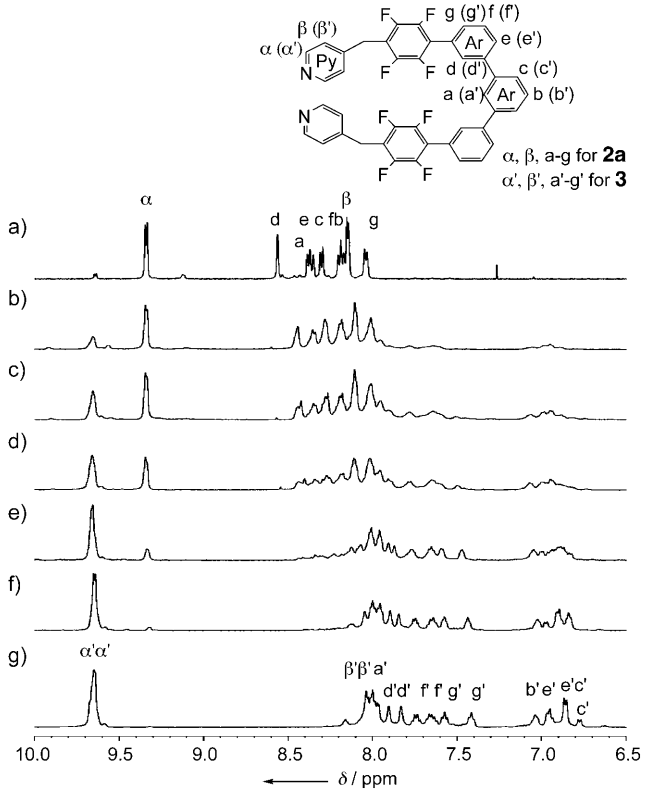
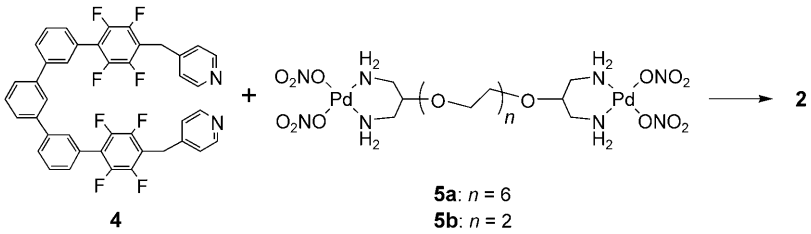


Figure 2. Observation by ^{1}H NMR spectroscopy (aromatic region, 500 MHz, 25 °C) of the ultramacrocyclization of monomer **2a** (5 mM) to dimer **3**. Spectra were obtained by treating the solution of **2a** in DMSO with water at room temperature. Solvent systems: a) [D$_6$]DMSO only, b) [D$_6$]DMSO/D$_2$O (3.5:1), c) [D$_6$]DMSO/D$_2$O (3:1), d) [D$_6$]DMSO/D$_2$O (2.5:1), e) [D$_6$]DMSO/D$_2$O (2:1), f) [D$_6$]DMSO/D$_2$O (1.5:1), and g) [D$_6$]DMSO/D$_2$O (1:1).



Scheme 1. Synthesis of double-loop compounds **2**.

$m/z = 767.5$ corresponds to $[\mathbf{3}-(NO_3)_6+(dmf)_5]^{6+}$; and $m/z = 874.7$ corresponds to $[\mathbf{3}-(NO_3)_5+dmf]^{5+}$ (Figure 3). Whereas the Pd^{II}-clipped ring is achiral, its catenated form is chiral. Therefore, equivalent proton pairs in each Pd^{II}-clipped ring become diastereotopic after catenation and are independently observed (see pairs for $H_{\alpha'}$, $H_{\beta'}$, and $H_{a'}$–$H_{g'}$ in Figure 2g).[11] Probably, **3** is a mixture of two diastereomers because of the chirality of the two catenated moieties, but the diastereomers are not clearly distinguishable.

The solution of catenated species in a mixture of [D$_6$]DMSO/D$_2$O (1:1) was subjected to a DOSY (diffusion-ordered NMR spectroscopy) study[12–14] to confirm the purity of the component (Figure 4). The spectrum clearly showed the appearance of all the signals at the same diffusion coefficient ($\log D = -10.35$) which indicates the selective formation of a single product.[15] It is remarkable that despite the flexible structure of the linker, no other products were formed. Presumably, a cyclic monomer derived from the intramolecular catenation of **2a** is less stable because of the unfavorable orientation of the two Pd^{II}-clip-

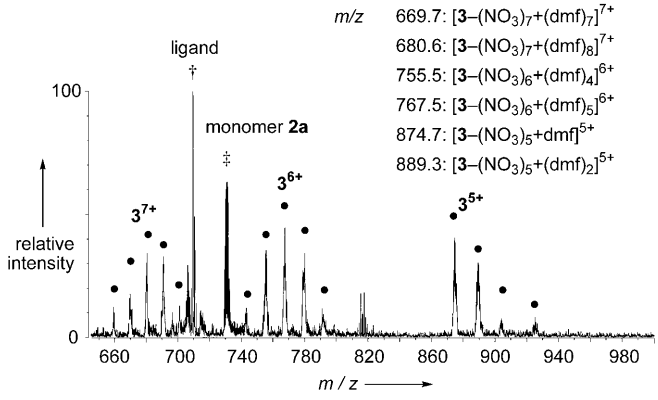


Figure 3. CSI mass spectrum of **3** as a solution in DMF/H$_2$O (1:2).

 © 2005 Wiley-VCH Verlag GmbH & Co. KGaA, Weinheim

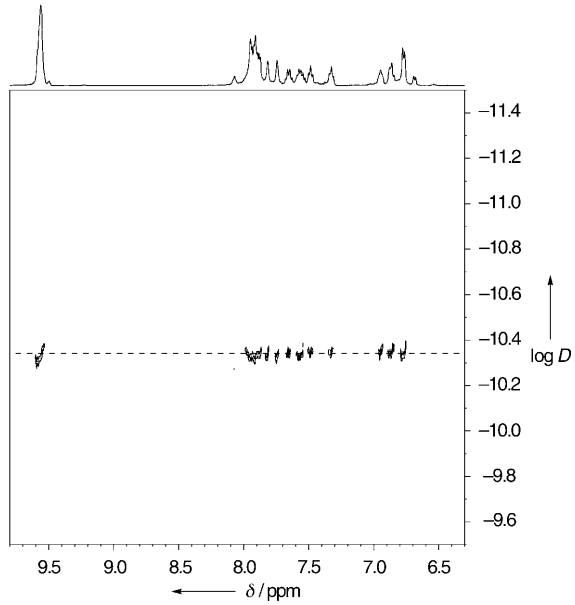


Figure 4. DOSY spectrum of **3** showing the formation of a single product. The spectrum was obtained after treatment of **4** (5 mM) with **5** (5 mM) for 5 minutes at room temperature in [D_6]DMSO/D_2O (1:1).

ped rings, whereas a cyclic trimer or higher oligomers are disfavored because of the higher entropy cost.

CPK modeling showed that an expanded conformation of **3** has an external diameter of approximately 4 nm (Figure 5). The backbone of **3** comprises 238 non-hydrogen atoms ($C_{204}N_{16}O_{14}Pd_4$), and it is one of the largest macrocyclic compounds to be synthesized in reasonable yields and characterized well.

Ultramacrocyclization through double catenation also proceeded smoothly when the length of the oligo(ethylene oxide) chain was limited.[8] The double catenation of **2b** ($n = 2$), which was also quantitatively prepared from **5b** in a polar solvent (Scheme 1), was examined. Upon addition of water, **2b** was efficiently transformed into an ultramacrocyclic dimer as indicated by ^{1}H NMR spectroscopy and CSI-MS studies.[16] Although conformational strain was anticipated to some extent, no other oligomers were detected. From a modeling study, the dimension of the dimer in its extended conformation is estimated to be 3.0 nm.

In the construction of nanoscopic assemblies from extraordinarily large components, close proximity of the reaction centers between the components is entropically unfavorable. As we have demonstrated here, the Pd^{II}-linked coordination ring can be regarded as a nanoscale reaction center. We suggest that the use of such large reaction centers may overcome the entropic disadvantage in nanoscopic molecular manufacturing. Accordingly, we expect that large nanoscopic objects, such as protein molecules or metal nanoparticles, can be easily linked together and aligned through reversible catenation.

Received: May 7, 2005
Published online: July 6, 2005

Keywords: catenanes · molecular recognition · palladium · self-assembly · supramolecular chemistry



Figure 5. A CPK (Corey–Pauling–Koltun) model for the expanded conformation of molecule **3**. Ar, Py black; O red; N blue; F green; Pd gray; H cream.

[1] For reviews, see: a) V. Prautzsch, S. Ibach, F. Vögtle, *J. Inclusion Phenom. Macrocyclic Chem.* **1999**, *33*, 427; b) C. Grave, A. D. Schlüter, *Eur. J. Org. Chem.* **2002**, 3075.

[2] For selected examples of very large covalent macrocycles, see: a) K. S. Lee, G. Wegner, *Makromol. Chem. Rapid Commun.* **1985**, *6*, 203(288-membered ring); b) M. Rothe, M. Lohmüller, U. Breuksch, G. Schmidtberg, *Angew. Chem.* **1994**, *106*, 2047; *Angew. Chem. Int. Ed. Engl.* **1994**, *33*, 1960 (280-membered ring); c) M. Mayor, C. Didschies, *Angew. Chem.* **2003**, *115*, 3284; *Angew. Chem. Int. Ed.* **2003**, *42*, 3176 (304-membered ring).

[3] For selected examples of very large noncovalent macrocycles, see: a) M. Mascal, N. M. Hext, R. Warmuth, M. H. Moore, J. P. Turkenburg, *Angew. Chem.* **1996**, *108*, 2347; *Angew. Chem. Int. Ed. Engl.* **1996**, *35*, 2204; b) Y. H. Ko, K. Kim, J.-K. Kang, H. Chun, J. W. Lee, S. Sakamoto, K. Yamaguchi, J. C. Fettinger, K. Kim, *J. Am. Chem. Soc.* **2004**, *126*, 1932; c) P. R. Andres, U. S. Schubert, *Macromol. Rapid Commun.* **2004**, *25*, 1371; d) M. Fujita, M. Tominaga, A. Hori, B. Therrien, *Acc. Chem. Res.* **2005**, *38*, 369.

[4] a) Large rings with 100 and more ring atoms have been described as "ultralarge rings"[4b] or "ultracycles".[1a] Herein, cyclization with $n > 100$ is termed ultramacrocyclization; b) M. Rothe, M. Lohmüller, U. Breuksch, G. Schmidtberg; *Angew. Chem.* **1994**, *106*, 2047; *Angew. Chem. Int. Ed. Engl.* **1994**, *33*, 1960.

[5] M. Fujita, F. Ibukuro, H. Hagihara, K. Ogura, *Nature* **1994**, *367*, 720.

[6] M. Fujita, *Acc. Chem. Res.* **1999**, *32*, 53.

 © 2005 Wiley-VCH Verlag GmbH & Co. KGaA, Weinheim

[7] A. Hori, A. Akasaka, K. Biradha, S. Sakamoto, K. Yamaguchi, M. Fujita, *Angew. Chem.* **2002**, *114*, 3403; *Angew. Chem. Int. Ed.* **2002**, *41*, 3269.
[8] The dinuclear Pd_2 linker, **5**, was prepared in five steps from commercially available 1,3-diaminopropan-2-ol and isolated as orange microcrystals in 19% overall yield. See Supporting Information for details of the synthesis and physical properties of **5**.
[9] S. Sakamoto, M. Fujita, K. Kim, K. Yamaguchi, *Tetrahedron* **2000**, *56*, 955.
[10] Compound **2a** was isolated as a white powder upon addition of a large amount of diethyl ether (68% yield). Selected data for **2a**: ^{1}H NMR (500 MHz, [D$_6$]DMSO, TMS): $\delta = 9.34$ (d, $J = 6.0$ Hz, 8H, PyH_α), 8.56 (s, 4H, H_d), 8.38 (d, $J = 8.0$ Hz, 4H, H_e), 8.35 (s, 2H, H_a), 8.30 (d, $J = 8.0$ Hz, 4H, H_c), 8.19 (t, $J = 8.0$ Hz, 4H, H_f), 8.17 (t, $J = 8.0$ Hz, 2H, H_b), 8.15 (d, $J = 6.0$ Hz, 8H, PyH_β), 8.04 (d, $J = 8.0$ Hz, 4H, H_g), 5.42 (br s, 4H, NH), 4.91 (br s, 4H, NH), 4.79 (s, 8H, CH_2), 4.40 (br s, 2H, CH), 4.15–4.03 (m, 24H, OCH_2), 3.14 ppm (br s, 8H, NCH_2); CSI-MS (3:1 DMF/CH_3OH) m/z: 605.6 $[\mathbf{2a}-(NO_3)_4+(dmf)_5]^{4+}$, 705.3 $[\mathbf{2a}-(NO_3)_3]^{3+}$, 1090.4 $[\mathbf{2a}-(NO_3)_2]^{2+}$.
[11] ^{1}H NMR data for **3** (500 MHz, 1:1 [D$_6$]DMSO/D_2O): $\delta = 9.66$ (br s, 16H, PyH_α), 8.05–7.97 (m, 20H, PyH_β, H_a), 7.92 (s, 4H, H_d), 7.85 (s, 4H, H_d), 7.77–7.75 (2t, $J = 8.5$ Hz, 4H, H_f), 7.68 −7.66 (2t, $J = 8.5$ Hz, 4H, H_f), 7.59–7.57 (2d, $J = 8.0$ Hz, 4H, H_g), 7.43–7.41 (2d, $J = 7.0$ Hz, 4H, H_g), 7.05 (br s, 4H, H_b), 6.97 (d, $J = 8.0$ Hz, 4H, H_e), 6.87 (d, $J = 8.0$ Hz, 4H, $H_{c,e}$), 6.79 (d, $J = 8.0$ Hz, 2H, H_c), 4.61 (br s, 4H, CH), 4.52–4.12 (m, 64H, OCH_2, CH_2), 3.39 ppm (br s, 16H, NCH_2). Addition of a large amount of water led to the precipitation of pure **3** in 48% isolated yield (see Supporting Information).
[12] A. Hori, K. Yamashita, T. Kusukawa, A. Akasaka, K. Biradha, M. Fujita, *Chem. Commun.* **2004**, 1798.
[13] A. Hori, K. Kumazawa, K. Kusukawa, D. K. Chand, M. Fujita, S. Sakamoto, K. Yamaguchi, *Chem. Eur. J.* **2001**, *7*, 4142.
[14] E. O. Stejskal, J. E. Tanner, *J. Chem. Phys.* **1965**, *42*, 288; C. S. Johnson, Jr., *Prog. Nucl. Magn. Reson. Spectrosc.* **1999**, *34*, 203.
[15] In the DOSY spectrum, the mixture of **2a** and **3** was clearly resolved. As expected, the diffusion coefficient (D) of **3** is smaller than that of **2a** ($\log D = -10.64$ for **3a** and −10.52 for **2a** in [D$_6$]DMSO/D_2O (2.3:1) mixed solvent).
[16] See Supporting Information for details about the syntheses and physical properties of **2b** and its double-catenated dimer.

 © 2005 Wiley-VCH Verlag GmbH & Co. KGaA, Weinheim

Switchable Molecules

DOI: 10.1002/anie.200500316

Reverse Spin Transition Triggered by a Structural Phase Transition**

Shinya Hayami, Yuji Shigeyoshi, Motoko Akita, Katsuya Inoue, Kenichi Kato, Keiichi Osaka, Masaki Takata, Ryo Kawajiri, Tadaoki Mitani, and Yonezo Maeda*

Designing molecules that could be used for information processing and information storage is one of the main challenges in molecular materials science. Molecules that are suitable for such applications must be bistable: a characteristic that allows the presence of two different stable electronic states over a certain range of external perturbation. Typical examples of molecular species that exhibit such bistability are the spin-crossover (SCO) compounds. Since the discovery of the first SCO compound,[1] a variety of d^n ($n = 4$–7) transition metal compounds exhibiting bistability between the high-spin (HS) and low-spin (LS) states have been reported.[2–4] Spin transition can be induced by variation of temperature, pressure, or illumination.[2–9] In general, temperature-dependent SCO behavior involves reversible spin transition from LS to HS upon heating and from HS to LS upon cooling.

Although the SCO transition is due to the electronic structure of the single molecule and can be observed even in

[*] Dr. S. Hayami, Y. Shigeyoshi, Prof. Dr. Y. Maeda
Department of Chemistry, Graduate School of Sciences
Kyushu University
6-10-1 Hakozaki, Higashi-ku, Fukuoka 812-8581 (Japan)
Fax: (+81) 92-642-2589
E-mail: hayascc@mbox.nc.kyushu-u.ac.jp

Dr. M. Akita
Institute for Molecular Science
Myodaiji, Okazaki 444-8585 (Japan)

Prof. Dr. K. Inoue
Department of Chemistry, Faculty of Science
Hiroshima University
1-3-1 Kagamiyama, Higashi-hiroshima 739-8526 (Japan)

Dr. K. Kato, Dr. K. Osaka, Prof. Dr. M. Takata
JASRI/SPring-8
1-1-1 Kouto, Mikazuki-cho, Sayo-gun, Hyogo 679-5198 (Japan)

R. Kawajiri, Prof. Dr. T. Mitani
Japan Advanced Institute of Science and Technology
Tatsunokuchi, Ishikawa 923-1292 (Japan)

[**] This work was supported by the Tokuyama Foundation, the Ogasawara Foundation, and the Research and Education Grant-in-Aid of IEI-J. The synchrotron radiation X-ray powder diffraction experiments were performed at the SPring-8 BL02B2 beam line with approval of the Japan Synchrotron Radiation Research Institute (JASRI). We thank Dr. Y. Kawashima and Dr. Y. Otsuka for their help in reviewing this contribution, as well as Prof. A. Mori and Prof. S. Ujiie for helpful suggestions for thermal analysis.

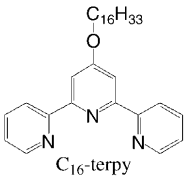
Supporting information for this article is available on the WWW under http://www.angewandte.org or from the author.

© 2005 Wiley-VCH Verlag GmbH & Co. KGaA, Weinheim

solutions or polymer matrices,[10,11] interaction between SCO molecules can dramatically influence the transition. Gradual or abrupt spin transitions may be observed in the solid state, depending on cooperativity.[12–14] The understanding of cooperative behavior in SCO transition can be a key to designing materials that are useful for information technology. In contrast, flexibility in the synthesis of molecular assemblies based on molecular units is also very important for synergy among the various interesting and novel physical properties of advanced materials.[15,16] The flexibility of ligands is one factor that can both directly and indirectly influence the cooperative interaction. The direct influence arises from the structural changes of the ligands, and the indirect influence comes from their random packing structure.

The SCO cobalt(II) compounds exhibit a 1/2↔3/2 spin change. The cobalt(II) compounds $[Co(terpy)_2]X_2 \cdot n\,H_2O$ (terpy = 2,2′:6′,2″-terpyridine; X = halide, pseudohalide, NO_3^-, ClO_4^-; $n = 0$–5) exhibit incomplete and gradual SCO behavior.[17,18] Not only liquid-crystal properties, but also unique physical properties can be expected for compounds with long alkyl chains because of the thermal motion of the alkyl chains. On the basis of these observations, we prepared cobalt(II) compounds with long alkyl chains and succeeded in observing "reverse spin transition" by using a major structural phase transition for the first time. Notably, reverse spin transition is unexpected because the driving force of the SCO phenomenon is entropy change, which is temperature-dependent.

The focus of the work reported herein was the cobalt(II) compound $[Co(C_{16}\text{-terpy})_2](BF_4)_2$ (**1**, in which C_{16}-terpy = 4′-hexadecyloxy-2,2′:6′,2″-terpyridine) having terpy ligands with long alkyl chains. Unsolvated **1** was obtained as a brown–orange powder by treating a solution of $Co^{II}(BF_4)_2$ in methanol with 2 equiv C_{16}-terpy. Single crystals of **1**·MeOH suitable for X-ray diffraction (XRD) studies were isolated by slow recrystallization from MeOH. The compound crystallizes in triclinic space group $P\bar{1}$. The cobalt(II) ion of **1**·MeOH is octahedrally coordinated by six nitrogen atoms of two C_{16}-terpy ligands (Figure 1). The bond lengths are intermediate between those of typical LS and HS cobalt(II) compounds.[19] The Co–N distances of the central pyridine ring of the terpyridine ligand (1.99 Å) are shorter than those of the peripheral pyridine rings (2.13 Å), and this induces a pronounced distortion of the CoN_6 octahedron. The three pyridine rings of the C_{16}-terpy ligand are coplanar, and the two tridentate C_{16}-terpy ligands are nearly perpendicular to one another. The long alkoxy chains $C_{16}H_{33}O$ form rodlike structures that protrude from the 4′-positions of the terpyridine moieties. The chain from O1 extends straight in zig-zag form, whereas the other is bent at C48–C49 and then extends straight in a zig-zag fashion. The thermal motions of the end carbon atoms C60, C61, and C62 of the long chain connected to O2 are larger than those of C29, C30, and C31 in the O1 chain. The two BF_4^- counteranions and one MeOH molecule are located in the intermolecular space, and there are short contacts between $[Co(C_{16}\text{-terpy})_2]^{2+}$ cations, BF_4^- anions, and MeOH molecules. The $[Co(C_{16}\text{-terpy})_2]^{2+}$ cations form short contacts (3.49 Å) between nearest-neighbor peripheral pyridine rings in the *ab* plane, and thus a 2D sheet is formed by π–π interactions. Furthermore, a fastener effect is present between the chains which face each other in the complexes. The very tight molecular packing of the compound suggests the presence of strong intermolecular interactions in the molecular assembly.



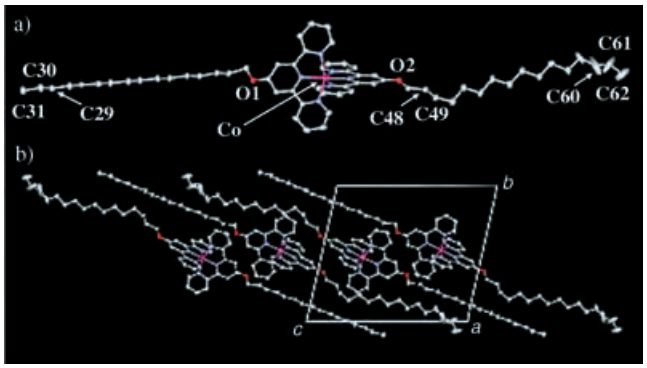


Figure 1. a) ORTEP plot of **1**·MeOH showing 50% probability displacement ellipsoids. b) Projection of the crystal structure of **1**·MeOH on the *bc* plane; BF_4^- ions, MeOH molecules, and H atoms are omitted for clarity.

The crystal structure of unsolvated **1** could not be determined, because the removal of MeOH induced cracks in the crystal that made single-crystal XRD studies impossible. However, powder XRD data suggested that the structure of unsolvated **1** is similar to that of **1**·MeOH (Supporting Information).

The temperature dependence of the molar magnetic susceptibility of unsolvated **1** is shown in Figure 2a. Solvated **1**·MeOH exhibited gradual SCO behavior in the temperature range of 5–360 K. The $\chi_m T$ value of **1**·MeOH gradually increases from 0.54 to 1.83 $cm^3 K mol^{-1}$ at 360 K, and then decreases to 1.58 $cm^3 K mol^{-1}$ at 400 K from the removal of MeOH. Unsolvated **1** was obtained by annealing **1**·MeOH at 400 K. The $\chi_m T$ value of **1** gradually decreases from 1.58 $cm^3 K mol^{-1}$ at 400 K to 0.41 $cm^3 K mol^{-1}$ at 226 K, and the gradual decrease in the $\chi_m T$ value shows normal thermal SCO behavior. Upon further cooling, the $\chi_m T$ value increases abruptly at around $T_{1/2}\downarrow = 217$ K to 2.01 $cm^3 K mol^{-1}$ at 206 K. The magnetic behavior shows that compound **1** exhibits reverse spin transition from the LS to the HS state upon cooling. Upon heating, $\chi_m T$ undulates between 1.70 and 2.15 $cm^3 K mol^{-1}$ in the temperature range of 5–251 K. Undulating magnetic behavior is also unusual and difficult to understand. It may be caused by structural changes. Powder XRD measurements showed that the structure at 50 K is different from that at 130 K ($2\theta = 8.8$, 11.9, 13.2, and 14.8°; Figure 3a). With further heating, the $\chi_m T$ value abruptly drops at around $T_{1/2}\uparrow = 260$ K with transition from the HS to the LS state. Then the $\chi_m T$ value gradually increases in the temperature range of 267–400 K. The wide thermal hysteresis loop ($\Delta T = 43$ K) remained unchanged in successive thermal cycles, and this confirms that compound **1** exhibits reverse spin transition. This is important because an abrupt transition

 © 2005 Wiley-VCH Verlag GmbH & Co. KGaA, Weinheim

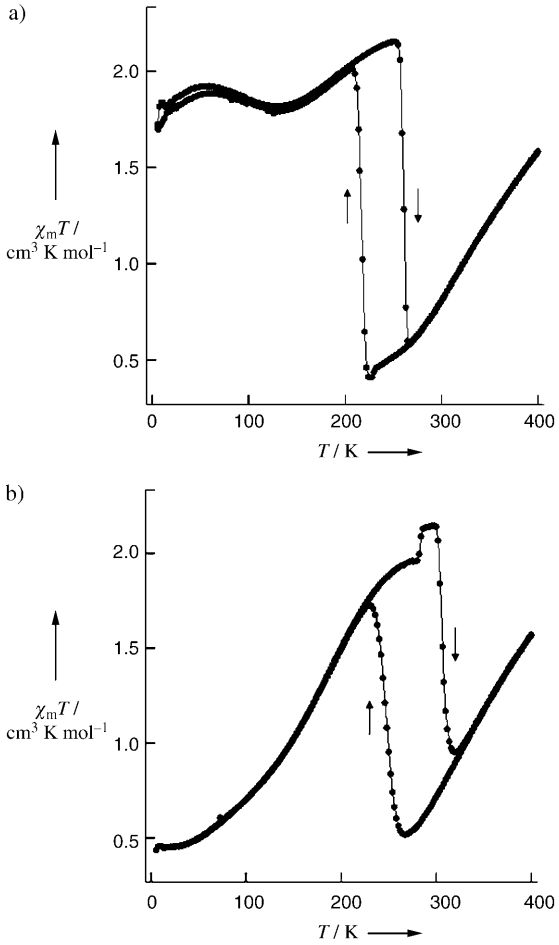


Figure 2. $\chi_m T$ versus T plots for a) **1** and b) **2**.

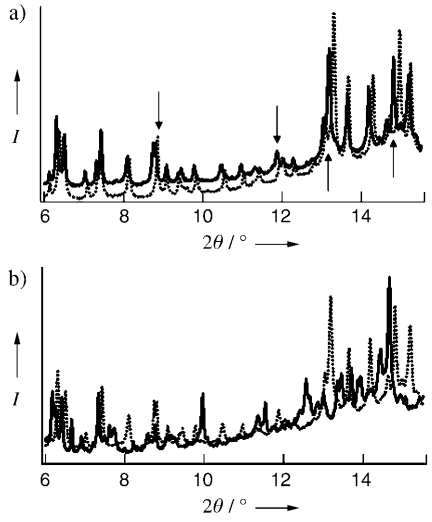


Figure 3. Temperature dependence of powder XRD patterns for **1** upon heating: a) (•••••): 50 K, (——): 130 K; b) (•••••): 130 K, (——): 270 K.

with a hysteresis loop appears only if the cooperative effect is strong enough. To confirm reverse spin transition, the variable-temperature ESR spectrum of **1** was measured. The spectrum shows a signal for the HS form at 3 K, and a signal for the LS form at 270 K. Powder XRD measurements show that the HS structure at 130 K differs greatly from the LS structure at 270 K, and a major structural phase transition is thought to occur in this temperature range (Figure 3b).

Upon warming, the reverse spin transition from the HS to the LS state ($T_{1/2}\uparrow = 260$ K) was found to be an endothermic phase transition ($\Delta H = 14.3$ kJ mol^{-1}, $\Delta S = 54.6$ J K^{-1} mol^{-1} at 262 K) by differential scanning calorimetry (DSC, Figure 4a).

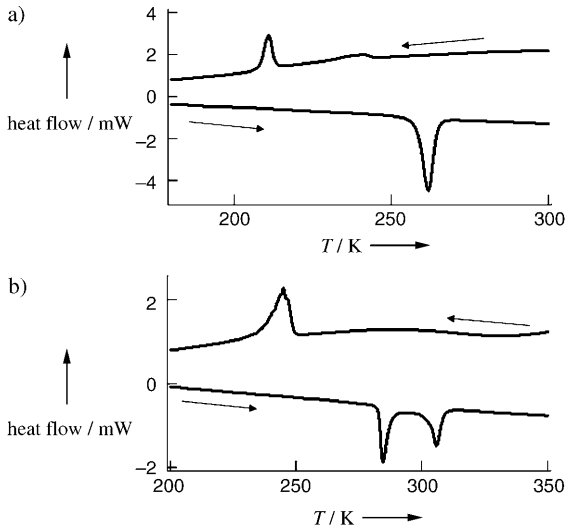


Figure 4. a) DSC curves of **1**. b) DSC of **2**.

Upon cooling, two peaks were observed, one at 211 K ($\Delta H = -6.1$ kJ mol^{-1}, $\Delta S = -28.6$ J K^{-1} mol^{-1}) and a broad peak at higher temperature. The exothermic peak at 211 K corresponds to the reverse spin transition temperature ($T_{1/2}\downarrow = 217$ K), and the broad peak can be assigned to another structural change. The sum of the two heat capacities upon cooling is equal to that of the peak at 262 K on heating. It has been reported that the change in entropy is 16–35 J mol^{-1} K^{-1} in SCO cobalt(II) compounds, and 40–65 J mol^{-1} K^{-1} in SCO iron(II) compounds.[7,18–21] The ΔS value for reverse spin transition ($\Delta S = 54.6$ J K^{-1} mol^{-1}) is larger than those previously reported for SCO cobalt(II) compounds, and is in the range of those observed in SCO iron(II) compounds ($\Delta S = 40$–65 J K^{-1} mol^{-1}). The ΔS value of **1** is much larger than the change in electronic spin expected for a cobalt(II) ion ($\Delta S_{spin} = R[\ln(2S+1)_{HS} - \ln(2S+1)_{LS}] = 5.8$ J K^{-1} mol^{-1}). The remaining entropy difference of 48.8 J K^{-1} mol^{-1} is mainly due to intramolecular vibrational changes. Furthermore, the iron(II) SCO compound $[Fe(ptz)_6](BF_4)_2$ (ptz = 1-propyltetrazole) undergoes spin transition with a structural phase transition from $R\bar{3}$ in the HS state to $P\bar{1}$ in the LS state, as deduced from powder diffraction experiments.[22] In such cases, the observed hysteresis is only the result of cooperative effects, as it is well-known that a first-order phase transition is generally accompanied by a hysteresis loop. We suggest that the major structural change in **1** is the origin of the reverse spin transition.

A similar compound, $[Co(C_{14}\text{-terpy})_2](BF_4)_2$ (**2**), which was synthesized by an analogous method, also exhibited reverse spin transition (Figure 2b). The $\chi_m T$ value of **2**

 © 2005 Wiley-VCH Verlag GmbH & Co. KGaA, Weinheim

gradually decreases from 1.57 $cm^3 K mol^{-1}$ at 400 K to 0.52 $cm^3 K mol^{-1}$ at 268 K, and then abruptly increases around $T_{1/2}\downarrow = 250$ K to 1.73 $cm^3 K mol^{-1}$ at 230 K. The magnetic behavior also shows that compound **2** exhibits reverse spin transition from the LS to the HS state upon cooling. With further cooling, the $\chi_m T$ value gradually decreases to 0.44 $cm^3 K mol^{-1}$ at 5 K which is normal SCO behavior. On heating, $\chi_m T$ value gradually increases to 1.96 $cm^3 K mol^{-1}$ at 280 K, and a jump in $\chi_m T$ from 1.96 $cm^3 K mol^{-1}$ to 2.15 $cm^3 K mol^{-1}$ was observed at 298 K. Upon further heating, $\chi_m T$ abruptly decreases, and shows the features of reverse spin transition from the HS to the LS state at $T_{1/2}\uparrow = 307$ K to 0.95 $cm^3 K mol^{-1}$ at 320 K. Then $\chi_m T$ gradually increases up to 400 K. The thermal hysteresis loop ($\Delta T = 57$ K) remained unchanged in successive thermal cycles, and thus confirmed that **2** exhibits reverse spin transition. An important characteristic of the present phenomenon is the wide hysteresis loop of 57 K. Furthermore, we emphasize that room temperature lies within the hysteresis loop.

Upon cooling, one peak was observed at 245 K ($\Delta H = -9.9$ kJ mol^{-1}, $\Delta S = -30.3$ J $K^{-1} mol^{-1}$), corresponding to a reverse spin transition from the LS to the HS state at $T_{1/2}\downarrow =$ 250 K. Upon warming, two peaks were observed for **2** up to 400 K, at 284 K ($\Delta H_1 = 3.3$ kJ mol^{-1}, $\Delta S_1 = 11.5$ J $K^{-1} mol^{-1}$), and 306 K ($\Delta H_2 = 3.3$ kJ mol^{-1}, $\Delta S_2 = 10.8$ J $K^{-1} mol^{-1}$) by DSC (Figure 4b). The peak at 284 K corresponds to the jump in $\chi_m T$ in the magnetic data. Powder XRD measurements showed that the pattern at 280 K differs greatly from that at 300 K, and it is thought that a major structural phase transition occurs in this temperature range (Figure 5a). The second peak at 306 K corresponds to reverse spin transition from the HS to the LS state at $T_{1/2}\uparrow = 306$ K. The ΔS value for reverse spin transition ($\Delta S = 30.3$ J $K^{-1} mol^{-1}$) is in the range of those observed in other SCO Co^{II} compounds.[18–21] The powder XRD pattern at 300 K differs greatly from that at 350 K (Figure 5b). The jump in $\chi_m T$ and the reverse spin transition are thought to be accompanied by a major structural change.

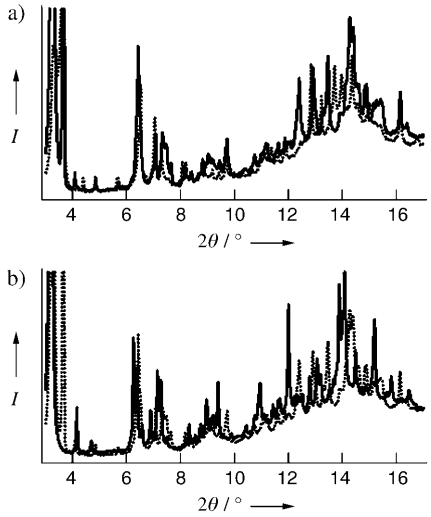


Figure 5. Temperature dependence of powder XRD patterns for **2** upon heating: a) (••••): 280 K, (——): 300 K; b) (••••):300 K, (——): 350 K.

Upon further heating, additional phase transitions due to the long alkyl chains were observed for **1** and **2** above 400 K by DSC (Supporting Information). Two peaks were observed for **1** at 437 and 512 K upon heating. The DSC peak at 437 K ($\Delta S = 33.9$ J $K^{-1} mol^{-1}$) can be assigned to a crystal–mesophase or crystal–crystal transition, and the peak at 512 K ($\Delta S = 17.7$ J $K^{-1} mol^{-1}$) can be assigned to the melting point. It is difficult to determine whether **1** exhibits mesophase transition. Two peaks were also observed for **2** at 443 K and 520 K upon heating. The DSC peak at 443 K ($\Delta S = 18.8$ J $K^{-1} mol^{-1}$) can be assigned to a crystal–crystal transition, and the peak at 520 K is assigned to the melting point.

Finally, we comment on the reverse spin transition observed in unsolvated compounds **1** and **2**. The molecular arrangement shows short contacts between $[Co(C_{16}\text{-terpy})_2]^{2+}$ cations, BF_4^- anions, and MeOH molecules, as well as between the long alkyl chains. The short contact distances are shorter than the sum of the van der Waals radius. Therefore, intermolecular interactions are strong and SCO behavior becomes cooperative. In such a case, the spin transitions between the HS and LS states are not only very abrupt, but also occur with hysteresis. The structural phase transitions that occur for **1** and **2** are likewise the result of strong intermolecular interactions. When one phase at low temperature prefers the HS state and another at high temperature prefers the LS state, reverse spin transition may be triggered by structural phase transitions.

In summary, we have synthesized $[Co(C_n\text{-terpy})_2](BF_4)_2$ ($n = 0$–22) with novel organic ligands based on a terpyridine frame. Compounds **1** and **2** with long alkyl chains exhibit reverse spin transition, which has been observed for compounds in which $n = 12$–16 so far. The reverse spin transitions have wide thermal hysteresis, which is important in switchable molecules. Thus, novel physical properties that could be important to the field of materials science may be discovered in compounds with long alkyl chains.

Experimental Section

1·MeOH: C_{16}-terpy (170 mg, 0.36 mmol) was dissolved in $CHCl_3$/MeOH (1:1, 20 mL) and added to a solution of $Co(BF_4)_2 \cdot 6H_2O$ (60 mg, 0.18 mmol) in MeOH (10 mL). The brown–orange solution was concentrated to ≈10 mL, and the resulting microcrystals were collected by filtration and recrystallized slowly from MeOH. Yield: 94 mg (43%); brown-orange crystals. Elemental analysis (%) calcd for $C_{63}H_{90}O_3N_6B_2F_8Co$: C 62.43, H 7.48, N 6.93, Co 4.86; found: C 62.48, H 7.53, N 6.98, Co 4.93. Elemental analysis (%) for **1** after removal of MeOH calcd for $C_{62}H_{86}O_2N_6B_2F_8Co$: C 63.11, H 7.35, N 7.12, Co 4.99; found: C 63.21, H 7.42, N 7.20, Co 4.83.

Crystallographic data for **1**·MeOH at 130 K ($C_{63}H_{90}O_3N_6B_2F_8Co_1$): $M_r = 1211.98$, brown–orange platelet ($0.35 \times 0.35 \times 0.15$ mm^3), triclinic, space group $P\bar{1}$, $a = 9.0412(6)$, $b = 17.598(1)$, $c = 20.684(2)$ Å, $\alpha = 102.545(3)$, $\beta = 101.622(3)$, $\gamma = 90.470(3)°$, $V = 3141.9(4)$ $Å^3$, $Z = 2$, $\rho_{calcd} = 1.281$ g cm^{-3}. Refinement by full-matrix least-squares methods gave an R factor of 0.08 from 9255 reflections with intensity $I > 3\sigma(I)$ for 748 variables; linear absorption coefficient $\mu(Mo_{K\alpha}) = 3.46$ cm^{-1}. Non-hydrogen atoms were refined anisotropically. Hydrogen atoms were included but not refined.

The magnetic susceptibilities $\chi(T)$ were measured between 5 and 300 K with a superconducting quantum interference device (SQUID) magnetometer (Quantum Design MPMS-5S) in an external field of 0.5 T. EPR spectra were recorded on a Bruker ESP 300 X-band (9.4 GHz) spectrometer equipped with a Hewlett-Packard 5350B

 © 2005 Wiley-VCH Verlag GmbH & Co. KGaA, Weinheim

microwave-frequency counter. Thermogravimetric data for **1** and **2** were collected on a Perkin-Elmer DSC-6 instrument over the temperature range of 290–450 K under an N_2 atmosphere.

To obtain X-ray powder diffraction data with good statistics and high angular resolution, XRD measurements were carried out at SPring-8, BL02B2 beam line (temperature dependence and illumination effect). The as-grown sample powders were sufficiently fine and gave a homogeneous intensity distribution in the Debye–Scherrer powder ring. At the BL02B2 beam line, the sample powders were sealed in glass capillaries in which the temperature was controlled in the range of 20–300 K. Reflections were collected on an imaging plate installed on a large Debye–Scherrer camera ($r = 286.5$ nm). The wavelength of the incident X-rays was ≈ 1.0 Å (slightly below the K edge of Rb), and typical exposure time was 15 min. The true wavelength was calibrated by using a standard CeO_2 powder obtained from NIST.

Received: January 27, 2005
Revised: March 5, 2005
Published online: July 11, 2005

Keywords: cobalt · magnetic properties · N ligands · spin crossover · tridentate ligands

[1] L. Cambi, A. Cagnasso, *Atti Accad. Naz. Lincei Cl. Sci. Fis. Mat. Nat. Re* **1931**, *53*, 809.
[2] P. Gütlich, Y. Garcia, H. A. Goodwin, *Chem. Soc. Rev.* **2000**, *29*, 419.
[3] J. A. Real, A. B. Gaspar, V. Niel, M. C. Munoz, *Coord. Chem. Rev.* **2003**, *236*, 121.
[4] J.-F. Letard, G. Chastanet, O. Nguyen, S. Marcen, M. Marchivie, P. Guionneau, D. Chasseau, P. Güetlich, *Monatsh. Chem.* **2003**, *134*, 165.
[5] W. S. Hammack, A. J. Conti, D. N. Hendrickson, H. G. Drickamer, *J. Am. Chem. Soc.* **1989**, *111*, 1738.
[6] S. Hayami, Y. Hosokoshi, K. Inoue, Y. Einaga, O. Sato, Y. Maeda, *Bull. Chem. Soc. Jpn.* **2001**, *74*, 2361.
[7] P. Gütlich, A. Hauser, H. Spiering, *Angew. Chem.* **1994**, *33*, 2109; *Angew. Chem. Int. Ed. Engl.* **1994**, *33*, 2024.
[8] S. Hayami, Z.-z. Gu, Y. Einaga, Y. Kobayasi, Y. Ishikawa, Y. Yamada, A. Fujishima, O. Sato, *Inorg. Chem.* **2001**, *40*, 3240.
[9] S. Hayami, Z.-z. Gu, M. Shiro, Y. Einaga, A. Fujishima, O. Sato, *J. Am. Chem. Soc.* **2000**, *122*, 7126.
[10] M. F. Tweedle, L. J. Wilson, *J. Am. Chem. Soc.* **1976**, *98*, 4824.
[11] A. Hauser, J. Adler, P. Gütlich, *Chem. Phys. Lett.* **1988**, *152*, 468.
[12] J.-F. Létard P. Guionneau, E. Codjovi, O. Lavastre, G. Bravic, D. Chasseau, O. Kahn, *J. Am. Chem. Soc.* **1997**, *119*, 10861.
[13] J. A. Real, E. Andrés, M. C. Muñoz, M. Julve, T. Granier, A. Bousseksou, F. Varret, *Science* **1995**, *268*, 265.
[14] A. J. Conti, C. L. Xie, D. N. Hendrickson, *J. Am. Chem. Soc.* **1989**, *111*, 1171.
[15] Y. Galyametdinov, V. Ksenofontov, A. Prosvirin, I. Ovchinnikov, G. Ivanova, P. Gütlich, W. Haase, *Angew. Chem.* **2001**, *113*, 4399; *Angew. Chem. Int. Ed.* **2001**, *40*, 4269.
[16] T. Fujigaya, D.-L. Jiang, T. Aida, *J. Am. Chem. Soc.* **2003**, *125*, 14690.
[17] J. S. Judge, W. A. Baker, Jr., *Inorg. Chim. Acta* **1967**, *1*, 68.
[18] S. Kremer, W. Henke, D. Reinen, *Inorg. Chem.* **1982**, *21*, 3013.
[19] A. B. Gaspar, M. C. Munoz, V. Niel, J. A. Real, *Inorg. Chem.* **2001**, *40*, 9.
[20] J. Zarembowitch, R. Claude, O. Kahn, *Inorg. Chem.* **1985**, *24*, 1576.
[21] J. Faus, M. Julve, F. Lloret, J. A. Real, J. Sletten, *Inorg. Chem.* **1994**, *33*, 5535.
[22] L. Wiehl, H. Spiering, P. Gütlich, K. Knorr, *J. Appl. Crystallogr.* **1990**, *23*, 151.

 © 2005 Wiley-VCH Verlag GmbH & Co. KGaA, Weinheim

Medicinal Chemistry

DOI: 10.1002/anie.200500674

Structurally Simple Farnesyltransferase Inhibitors Arrest the Growth of Malaria Parasites**

*Matthew P. Glenn, Sung-Youn Chang, Oliver Hucke, Christophe L. M. J. Verlinde, Kasey Rivas, Carrie Hornéy, Kohei Yokoyama, Frederick S. Buckner, Prakash R. Pendyala, Debopam Chakrabarti, Michael Gelb, Wesley C. Van Voorhis, Saïd M. Sebti, and Andrew D. Hamilton**

The development of antimalarial agents is not only constricted by the parameters common to the development of all new drugs (efficacy, toxicity, pharmacology), but importantly, must also recognize the economic reality of the countries most affected. It is estimated that there are 300–500 million acute cases of malaria each year, resulting in 1–3 million deaths, with 90% of the mortality occurring in Africa.[1] The severe poverty in the regions most affected by malaria and the staggering number of people infected necessitate very inexpensive treatment. In an effort to decrease the cost of developing new antimalarial drugs, recent attention has been

[*] Dr. M. P. Glenn, Dr. S.-Y. Chang, Prof. A. D. Hamilton
Department of Chemistry, Yale University
225 Prospect St., New Haven, CT 06511 (USA)
Fax: (+1) 203-432-3221
E-mail: andrew.hamilton@yale.edu

Dr. O. Hucke, Prof. C. L. M. J. Verlinde
Department of Biochemistry, University of Washington
Seattle, WA 98195 (USA)

K. Rivas, C. Hornéy, Prof. F. S. Buckner, Prof. W. C. Van Voorhis
Department of Medicine, University of Washington
Seattle, WA 98195 (USA)

Dr. K. Yokoyama, Prof. M. Gelb
Department of Chemistry and Biochemistry
University of Washington
Seattle, WA 98195 (USA)

Prof. S. M. Sebti
Drug Discovery Program, H. Lee Moffitt Cancer Center and Research Institute
Department of Oncology and Department of Biochemistry and Molecular Biology
University of South Florida
Tampa, FL 33612 (USA)

Dr. P. R. Pendyala, Prof. D. Chakrabarti
Department of Molecular Biology and Microbiology
University of Central Florida
Orlando, Fl 32826 (USA)

[**] This work was supported by the Medicines for Malaria Venture (MMV) and NIH grants CA67771 and AI054384. S.-Y.C. thanks the Postdoctoral Fellowship Program of Korea Science & Engineering Foundation (KOSEF). O.H. gratefully acknowledges a postdoctoral fellowship of the German Academy of Natural Scientists Leopoldina (BMBF-LPD 9901/8-77). We thank David Floyd, Lou Lombardo and David Williams from Bristol-Myers Squibb for helpful suggestions.

Supporting information for this article is available on the WWW under http://www.angewandte.org or from the author.

© 2005 Wiley-VCH Verlag GmbH & Co. KGaA, Weinheim

directed at investigating parasitic proteins that are validated therapeutic targets in other diseases, thereby accelerating access to new classes of inhibitors.[2,3]

Recently, prenylated proteins and associated prenyltransferases have been identified in the malarial protozoa *Plasmodium falciparum*.[2] Prenylation is a required modification for the function of a variety of cellular proteins, including small G proteins,[4] heterotrimeric G-protein γ subunits,[5] protein kinases,[6] and nuclear lamins.[7] Studies of the role of prenylation in modulating the function of the GTP-binding proteins Ras and Rho, which have oncogenic forms common to many human cancers (≈30%), have identified the ubiquitous eukaryotic enzyme protein farnesyltransferase (PFTase) as a key target for the interception of aberrant Ras activity.[8] Subsequent efforts to identify small-molecule inhibitors of PFTase have led to several potential anticancer agents currently in clinical trials.[9,10] The application of related PFTase inhibitors to cells infected with *P. falciparum* led to a decrease in farnesylated proteins and to the associated lysis of the parasites.[11] Importantly, the PFTase inhibitors studied were found to be significantly more toxic against the parasite than to mammalian cells. In this study, we developed a new series of PFTase inhibitors as novel antimalarial agents, emphasizing simple molecular architecture and straightforward chemical synthesis as a prerequisite for access to low-cost treatment.

PFTase is one of three closely related heterodimeric zinc metalloenzymes (protein farnesyltransferase and geranylgeranyltransferases I and II) that catalyze the transfer of prenyl groups from farnesyl or geranylgeranyl pyrophosphate to the free thiol group of a cysteine residue within the tetrapeptide recognition sequence CaaX (a = aliphatic amino acid, X is often M, S, A, or Q for PFTase) located at the carboxyl terminus of the substrate protein.[12] A homology model of malarial PFTase (*Pf*PFT) was generated with MODELLER,[13] by using the crystal structure of rat PFT complexed with the nonsubstrate tetrapeptide inhibitor CVFM, and farnesyl diphosphate (FPP) as the template structure (PDB entry 1JCR). The sequences of the two subunits (α and β) of *Pf*PFT were obtained from the PlasmoDB database (gene loci: PFL2050w, α and chr11.glm_528, β)[14,15] and aligned with the template with the program T-COFFEE.[16] Only regions with reasonable reliability in the alignment were included. The model of *Pf*PFT comprises the following sequence segments (the residue numbers of the corresponding segments of the rat PFT subunits are given in parentheses): α: 72–164 (87–179), 300–411 (184–283); β: 421–677 (71–315), 806–896 (330–417). *Pf*PFT and rat PFT share 23% identity and 53% similarity for the α subunit; the respective values for the β subunit are 37 and 56%. The catalytic zinc ion, six structurally conserved water molecules, and FPP were included in the model. The conformation of FPP was considered flexible during the model calculations. For this purpose, the force-field parameters for FPP were added to the MODELLER force field on the basis of the lipid parameters of the charmm27 force field.[17] The model with the lowest value of the objective function of MODELLER from twenty different calculations was used for docking studies.

The homology model indicates a large, open, and predominately hydrophobic cavity for the active site (≈20 × 20×20 Å^3), with the phospholipid binding partner (FPP) extending across the cavity base. The Zn ion coordinates to three residues (Cys661, Asp659, and His838) with a water molecule hydrogen bonded between the terminal phosphate of FPP and Asp659, defining the limit of the Zn binding domain (Figure 1). The remainder of the active-site cavity includes two well-defined hydrophobic pockets (Lys149, Asn317 Ser150, Phe150 and Trp456, Trp452, Tyr837), a larger hydrophilic domain formed by Arg564, and three water molecules participating in a hydrogen-bonded network between Ser449 and Gln152.

Flexible ligand-docking studies (GOLD)[18] indicate that the four pockets of the homology model active site can be efficiently accessed from a simple aliphatic tether, affording PFTase inhibitors with an acyclic scaffold that can be conveniently prepared through a short series of straightforward chemical transformations (Figure 1). One of the simplest scaffolds conceivable, ethylenediamine, provides an inexpensive and fourfold substitutable tether of appropriate size to project four different groups into the active site

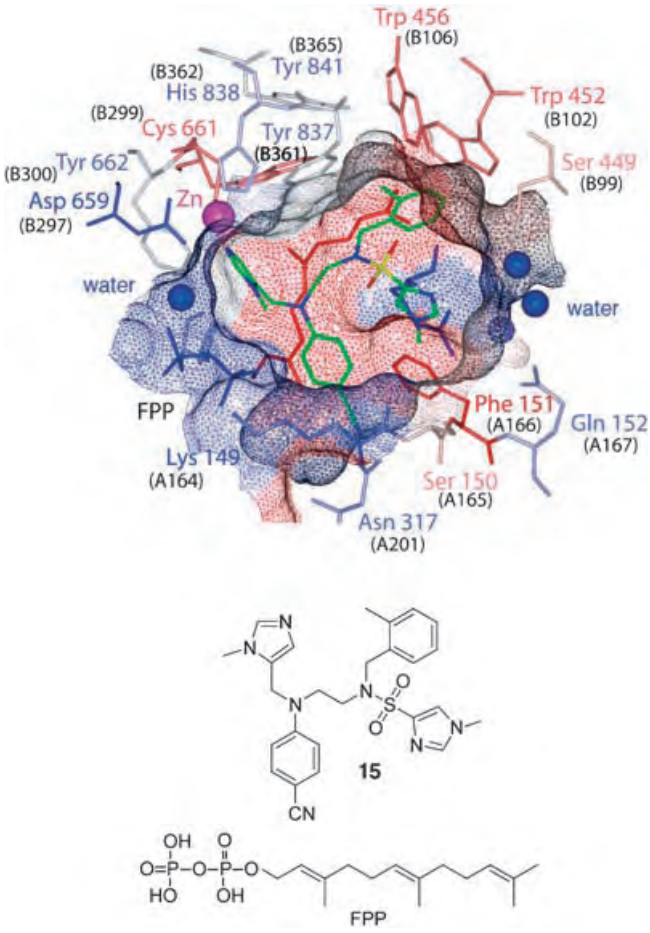


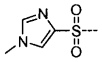
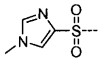
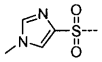
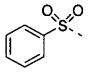
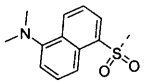
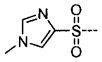
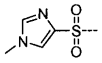
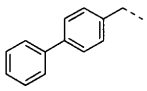
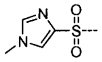
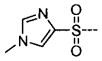
Figure 1. Active-site conformation of **15** (colored by atom type), as determined by flexible ligand docking[18] in the homology model of the active site of *Pf*PFT (red = hydrophobic, blue = hydrophilic residues). Values in parentheses refer to the corresponding positions in rat PFT (PDB entry 1JCR).

 © 2005 Wiley-VCH Verlag GmbH & Co. KGaA, Weinheim

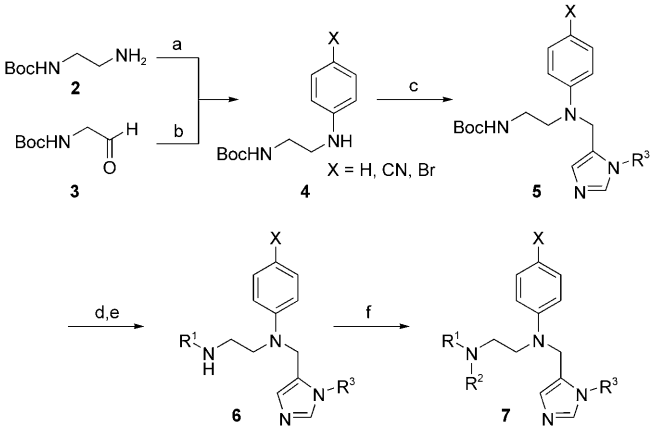
pockets. The incorporation of imidazole provides a zinc binding group that has been consistently demonstrated to confer activity in other series of inhibitors, whereas small hydrophobic (phenyl, benzyl) and simple sulfonamides (*N*-methylimidazole, phenyl) are predicted as suitable substitutions to access the remaining hydrophilic and hydrophobic pockets.

An initial series of PFTase inhibitors was prepared as outlined in Scheme 1. Substituted anilines **4** were formed either by the reductive amination of aniline (4-H, 4-Br), or by nucleophilic substitution of *para*-fluorobenzonitrile with monoprotected ethylenediamine. Chemoselective alkylation of aniline **4** through double deprotonation with LDA and subsequent alkylation at the anilide anion proceeds smoothly in THF with no evidence of alkylation of the carbamate. Some cyclic urea is observed, presumably generated through the elimination of *tert*-butoxide from the carbamate to provide the corresponding isocyanate and subsequent intramolecular cyclization to the anilide. Alkylation of carbamate **5**, deprotection, and coupling to sulfonyl chlorides furnishes the desired series of inhibitors (**1**, **8**–**15**, Table 1).

Table 1: Activity of acyclic ethylene diamine compounds against *Pf*PFT and parasite-infected cells.

Number	X	Compound R^1	R^2	R^3	IC_{50} [nM][a] *Pf*PFT	ED_{50} [nM][b] 3D7	K1
8	H			H	215	ND[c]	ND[c]
9	Br			CH_3	2.0	675	3200
1	CN			CH_3	0.5	349	375
10	CN			CH_3	8.9	2500	2250
11	CN			CH_3	55	300	388
12	CN			CH_3	4.5	220	850
13	CN			CH_3	>1000	2800	>5000
14	CN			CH_3	240	700	2500
15	CN			CH_3	0.6	93	150

[a] Inhibitor concentration required to decrease *Pf*PFT activity twofold. [b] Inhibitor concentration required to decrease hypoxanthine incorporation into parasites twofold. [c] Not determined.



Scheme 1. Conditions: a) 4-fluorobenzonitrile, TEA, DMSO, 120 °C; b) 4-bromoaniline, $NaCNBH_3$, acetic acid, molecular sieves (3 Å), MeOH; c) LDA, NaH, 5-chloromethyl-1-methyl-1*H*-imidazole·HCl (R^3), THF, −78 °C→RT; d) NaH, alkyl bromide (R^1), DMF, 0 °C; e) TFA; f) arylsulfonyl chloride (R^2), TEA, DMF. Boc = *tert*-butoxycarbonyl, DMF = *N*,*N*-dimethylformamide, LDA = lithium diisopropylamide, TEA = triethylamine, TFA = trifluoroacetic acid.

A focused set of diversity elements, predicted by docking studies (GOLD)[18] to efficiently occupy the four binding domains of the active site, were applied in the preparation of nine compounds, and their inhibition of *Pf*PFT was determined by using a scintillation proximity assay with partially purified *Pf*PFT (Table 1).[19] Eight of the nine compounds inhibit *Pf*PFT at concentrations of 50 nM or lower, with four compounds having IC_{50} values below 5 nM (**1**, **9**, **12**, and **15**). The growth of parasites in whole cells (3D7, K1) treated with inhibitors was monitored through the incorporation of tritium-labeled hypoxanthine. Six compounds displayed ED_{50} values below 1 μM, with compound **15** showing significant whole-cell activity (ED_{50}: 3D7, 93 nM; K1, 150 nM). The significantly improved activity of compounds **1** and **9**, relative to that of **8**, reflects docking solutions that suggest the *para* substituent of aniline (X) contacts a hydrophilic domain formed by Ser150, Asn317, and Lys149, whereas methylation of the zinc binding group complements a small adjacent hydrophobic pocket. Of the four substitutions investigated for the R^1 hydrophobic pocket, benzyl and cyclohexylmethyl groups afforded best activity, whereas *tert*-butylcarbamate and 4-phenylbenzyl groups are significantly less active. Three substitutions were assessed for the hydrophilic cavity formed predominately by Arg564. The small basic 1-methyl-1*H*-imidazole-4-sulfonamide conferred the best potency against both the enzyme and in whole-cell assays, whereas dansyl sulfonamide afforded significantly lower enzyme inhibition, but retained good potency (ED_{50} 300 nM) against whole cells.

Importantly, these early examples of a new series of simple acyclic *Pf*PFT inhibitors demonstrate their reasonable metabolic stability, and oral bioavailability. Treatment of **15** with rat liver microsomes resulted in a steady transformation of the inhibitor over one hour ($t_{1/2} = 20$ min), with principal metabolites observed by MS corresponding to oxidation of the inhibitor (+O), and loss of the aniline imidazole (R^3, data not shown). The promising metabolic stability of this series of inhibitors is further reflected by the reasonable plasma

 © 2005 Wiley-VCH Verlag GmbH & Co. KGaA, Weinheim

concentration of inhibitor observed after oral dosing. Oral gavage of rats with **15** induced peak plasma concentrations of inhibitor 10-fold above the ED_{50} value within 30–40 min. A plasma concentration at least fivefold above ED_{50} was maintained for approximately two hours, with inhibitor clearing observed ($t_{1/2} \approx 33$ min, Figure 2).

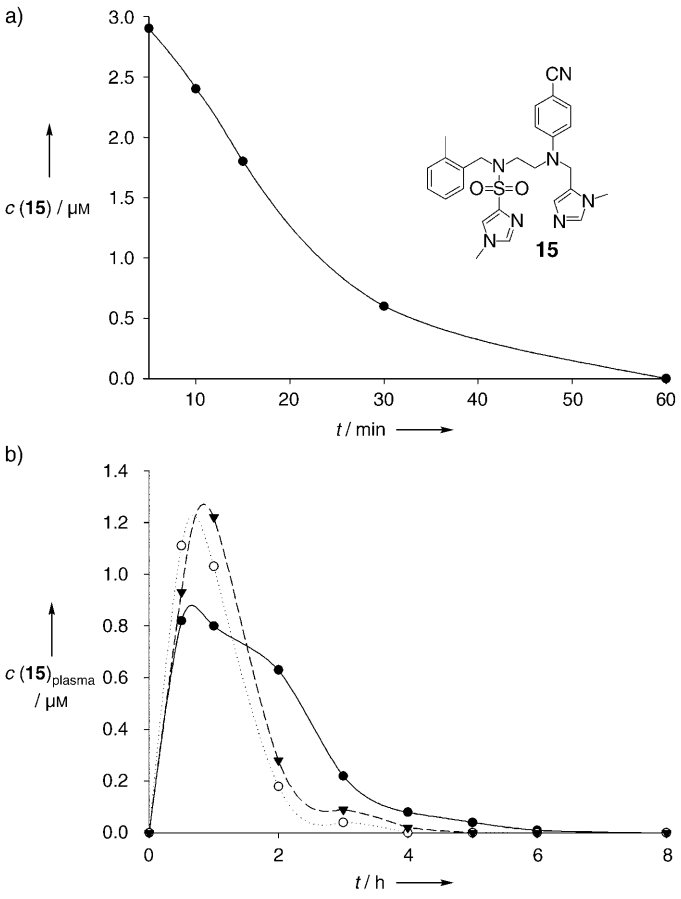


Figure 2. a) Metabolism of **15** by rat liver microsomes ($t_{1/2} = 20$ min); b) inhibitor concentration in plasma of **15** in three rats after oral garage (○ = rat 1, ▼ = rat 2, ● = rat 3; dose: 12.5 mg kg^{-1}, $t_{1/2} \approx 33$ min, $c_{max} = 1.05 \pm 0.21$ μM, $t_{max} = 40 \pm 17$ min).

In summary, a new series of simple acyclic *Pf*PFT inhibitors was developed, and their potency evaluated in enzyme and whole-cell assays. Compounds based on this readily accessible scaffold are highly active inhibitors of *Pf*PFT, with promising oral bioavailability. Expansion of this inhibitor series is expected to provide potent, orally available compounds as promising new low-cost drugs for the treatment of malaria.

Received: February 22, 2005
Published online: July 11, 2005

Keywords: drug design · enzymes · inhibitors · malaria · medicinal chemistry

[1] J. Sachs, P. Malaney, *Nature* **2002**, *415*, 680.
[2] D. Chakrabarti, T. Azam, C. DelVecchio, L. Qiu, Y.-i. Park, C. M. Allen, *Mol. Biochem. Parasitol.* **1998**, *94*, 175.
[3] J. Ohkanda, J. W. Lockman, K. Yokoyama, M. H. Gelb, S. L. Croft, H. Kendrick, M. I. Harrell, J. E. Feagin, M. A. Blaskovich, S. M. Sebti, A. D. Hamilton, *Bioorg. Med. Chem. Lett.* **2001**, *11*, 761.
[4] Y. Takai, K. Kaibuchi, A. Kikuchi, M. Kawata, *Int. Rev. Cytol.* **1992**, *133*, 187.
[5] H. K. Yamane, C. C. Farnsworth, H. Xie, W. Howald, B. K.-K. Fung, S. Clarke, M. H. Gelb, J. A. Glomset, *Proc. Natl. Acad. Sci. USA* **1990**, *87*, 5868.
[6] J. Inglese, W. J. Koch, M. G. Caron, R. J. Lefkowitz, *Nature* **1992**, *359*, 147.
[7] C. C. Farnsworth, S. L. Wolda, M. H. Gelb, J. A. Glomset, *J. Biol. Chem.* **1989**, *264*, 20422.
[8] S. M. Sebti, A. D. Hamilton, *Oncogene* **2000**, *19*, 6584.
[9] C. J. Dinsmore, I. M. Bell, *Curr. Top. Med. Chem.* **2003**, *3*, 1075.
[10] F. Caponigro, M. Casale, J. Bryce, *Expert Opin. Invest. Drugs* **2003**, *12*, 943.
[11] M. H. Gelb, W. C. Van Voorhis, F. S. Buckner, K. Yokoyama, R. Eastman, E. P. Carpenter, C. Panethymitaki, K. A. Brown, D. F. Smith, *Mol. Biochem. Parasitol.* **2003**, *126*, 155.
[12] C. L. Strickland, W. T. Windsor, R. Syto, L. Wang, R. Bond, Z. Wu, J. Schwartz, H. V. Le, L. S. Beese, P. C. Weber, *Biochemistry* **1998**, *37*, 16601.
[13] A. Sali, T. L. Blundell, *J. Mol. Biol.* **1993**, *234*, 779.
[14] A. Bahl, B. Brunk, R. L. Coppel, J. Crabtree, S. J. Diskin, M. J. Fraunholz, G. R. Grant, D. Gupta, R. L. Huestis, J. C. Kissinger, P. Labo, L. Li, S. K. McWeeney, A. J. Milgram, D. S. Roos, J. Schug, C. J. Stoeckert, Jr., *Nucleic Acids Res.* **2002**, *30*, 87.
[15] J. C. Kissinger, B. P. Brunk, J. Crabtree, M. J. Fraunholz, B. Gajria, A. J. Milgram, D. S. Pearson, J. Schug, A. Bahl, S. J. Diskin, H. Ginsburg, G. R. Grant, D. Gupta, P. Labo, L. Li, M. D. Mailman, S. K. McWeeney, P. Whetzel, C. J. Stoeckert, D. S. Roos, *Nature* **2002**, *419*, 490.
[16] C. Notredame, D. G. Higgins, J. Heringa, *J. Mol. Biol.* **2000**, *302*, 205.
[17] S. E. Feller, K. Gawrisch, A. D. MacKerell, Jr., *J. Am. Chem. Soc.* **2002**, *124*, 318.
[18] G. Jones, P. Willett, R. C. Glen, A. R. Leach, R. Taylor, *J. Mol. Biol.* **1997**, *267*, 727.
[19] D. Chakrabarti, T. Da Silva, J. Barger, S. Paquette, H. Patel, S. Patterson, C. M. Allen, *J. Biol. Chem.* **2002**, *277*, 42066.

 © 2005 Wiley-VCH Verlag GmbH & Co. KGaA, Weinheim

Main-Group Chemistry

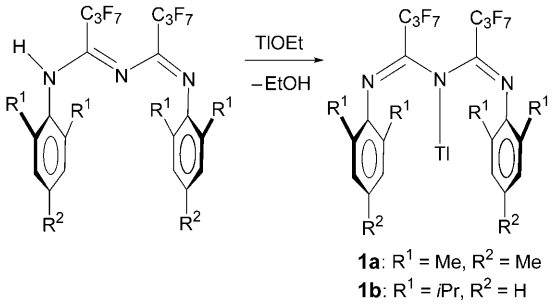
DOI: 10.1002/anie.200500401

Monomeric Thallium(I) Complexes of Fluorinated Triazapentadienyl Ligands**

H. V. Rasika Dias, Shreeyukta Singh, and Thomas R. Cundari*

Thallium(I) derivatives of monoanionic, nitrogen-based ligands show interesting structures and properties.[1–3] For example, $[\{Tl[(Me_3Si)_2N]\}_2]$ has a dimeric structure with a four-membered $\{[TlN]_2\}$ motif,[4] and these dimer units further aggregate to form Tl···Tl-linked extended chains. The related Tl^I amido derivative $[\{Tl[(dipp)(Me_3Si)N]\}_4]$ (dipp = 2,6-$iPr_2C_6H_3$) is also known,[5] but it is a tetramer in the solid state with weak Tl···arene interactions (mean Tl···Ct distance 3.11 Å; Ct = arene ring centroid) and long Tl···Tl contacts (average 4.06 Å). The pentaazapentadienylthallium(I) complex $[\{Tl\{[N(tol)N]_2\}\}_2]$ (tol = tolyl) has intermolecular Tl···Tl, Tl···N, and Tl···arene interactions,[6] and the tris(pyrazolyl)-borate complex $[\{Tl\{HB[3\text{-}(cyclopropyl)Pz]_3\}\}_4]$ (Pz = pyrazole) is a tetramer with a perfect tetrahedral Tl_4 core.[7] A rare, monomeric Tl^I species $[Tl\{HC[(Ph)C(Me_3Si)N]_2\}]$ involving a diazapentadienyl ligand was also reported recently.[8] In general, neutral thallium(I) compounds tend to aggregate into interesting structures with intermolecular Tl···Tl and/or Tl···donor-atom interactions.[1–3] Mononuclear complexes of Tl^I are relatively uncommon in the solid state, with most known examples, such as $[Tl\{MeB[3\text{-}(tBu)Pz]_3\}]$, being confined to sterically demanding poly(pyrazolyl)borate ligands.[1,3] It is also noteworthy that, in contrast to poly(pyrazolyl)borate complexes of Tl^I, thallium adducts of other monoanionic, nitrogen-based ligands are relatively less explored.[1–3]

We have recently investigated the chemistry of triazapentadienyl ligands[9,10] as these ligands show an interesting ability to vary their mode of coordination to fit the needs of the metal fragment.[9–12] Thallium(I) derivatives of triazapentadienyl ligands are of particular interest because they could serve as good ligand-transfer agents (like the commonly used thallium adducts of poly(pyrazolyl)borates and diazapentadienyl systems).[1,3,13–16] We discovered that it is possible to isolate mononuclear thallium(I) complexes containing fluorinated triazapentadienyl ligands. Specifically, $[Tl\{N[C(C_3F_7)N(Mes)]_2\}]$ (**1a**) and $[Tl\{N[C(C_3F_7)N(dipp)]_2\}]$ (**1b**; Mes = 2,4,6-$Me_3C_6H_2$) could be obtained in high yield by treating the parent ligands $HN[C(C_3F_7)N(Mes)]_2$ and $HN[C(C_3F_7)N(dipp)]_2$ with one equivalent of TlOEt in hexane (Scheme 1).[17] These thallium(I) complexes are colorless, crystalline solids that decompose slowly if exposed to air and light for prolonged periods. The ^1H and ^{19}F NMR spectra of **1a** and **1b** in $CDCl_3$ at room temperature are much simpler than the corresponding spectra of the related free ligands. For example, the ^1H NMR resonances of the *i*Pr protons of **1b** appear as four doublets (two of which are overlapping) and two septets, whereas in $HN[C(C_3F_7)N(dipp)]_2$ [10] these protons give rise to nine separate doublets and four separate septets. This is similar to changes observed during the formation of the silver adducts $[AgL\{N[C(C_3F_7)N(dipp)]_2\}]$ (L = MeCN, *t*BuNC) from the free ligand.[10,17]



Scheme 1. Synthesis of triazapentadienylthallium(I) complexes **1a** and **1b**.

The X-ray structures of **1a** and **1b** (Figure 1) reveal that the thallium ion coordinates to the triazapentadienyl ligand at the central nitrogen atom in both these systems.[18] The ligand backbones adopt a W-shaped configuration (an all-*trans* or zigzag arrangement of the N_3C_2 core) with the two aryl (Mes or dipp groups) moieties flanking the thallium atom. They show a short-long-long-short C–N bond distance pattern consistent with the resonance form illustrated in Scheme 1. The mesityl compound **1a** crystallizes in the *P*2/*n* space group with two molecular halves in the asymmetric unit, and is located on a crystallographic twofold rotation axis containing the Tl–N bond. It is monomeric, and has no close Tl···Tl contacts. The dipp analog **1b** crystallizes in the $P2_12_12_1$ space group with three molecules in the asymmetric unit. These molecules also do not show intermolecular Tl···Tl contacts: the closest contact involving the Tl^I ion and a neighboring molecule is of the Tl···F–CF type (3.21 Å), which is at the long end of weak thallium–fluorine interactions[19] and is probably a result of crystal packing. Furthermore, this interaction does not affect the C–F bond distance.

The Tl–N bond distances of **1a** are 2.608(3) and 2.675(4) Å. In **1b**, two molecules have similar Tl–N distances

[*] Prof. Dr. H. V. R. Dias, Dr. S. Singh
Department of Chemistry and Biochemistry
The University of Texas at Arlington
Arlington, TX 76019 (USA)
Fax: (+1) 817-272-3808
E-mail: dias@uta.edu
Prof. Dr. T. R. Cundari
Department of Chemistry
University of North Texas
Denton, TX 76203 (USA)

[**] H.V.R.D. thanks the Robert A. Welch Foundation (grant Y-1289) and the National Science Foundation (CHE-0314666) for financial support of this research, and 3M for providing a sample of $N(C_4F_9)_3$ for ligand synthesis. T.R.C. acknowledges the U.S. Department of Energy for support of this research through grant DOE-FG02-97ER14811.

Supporting information for this article is available on the WWW under http://www.angewandte.org or from the author.

 © 2005 Wiley-VCH Verlag GmbH & Co. KGaA, Weinheim

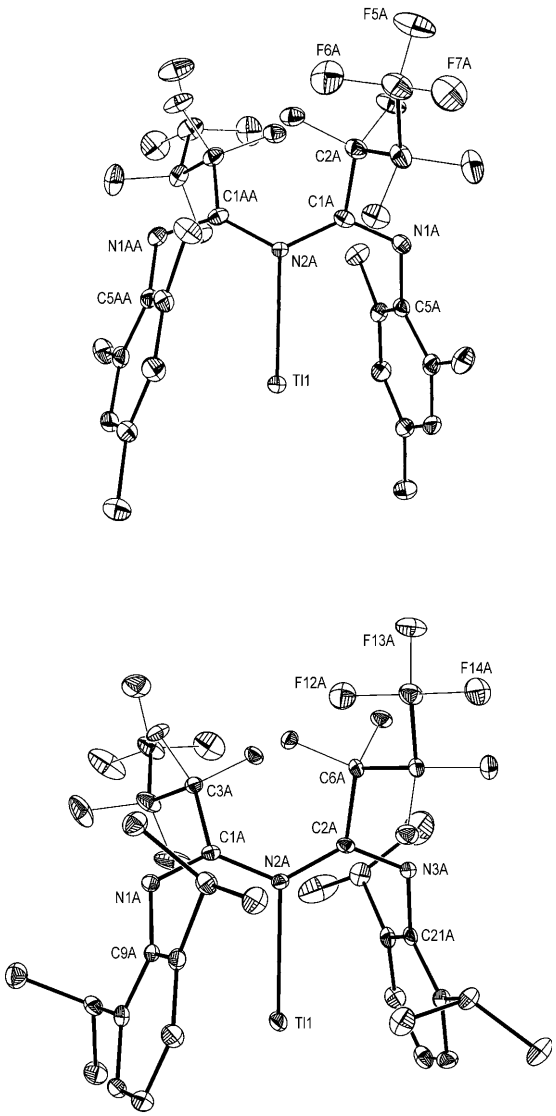


Figure 1. Molecular structures of $[Tl\{N[C(C_3F_7)N(Mes)]_2\}]$ (**1a**, above) and $[Tl\{N[C(C_3F_7)N(dipp)]_2\}]$ (**1b**, below). Only one molecule in the asymmetric unit is shown; hydrogen atoms have been omitted for clarity.

(2.672(2) and 2.666(2) Å) while the third molecule has a slightly longer Tl–N (2.732(2) Å) bond. These distances exceed the sum (2.30 Å) of the covalent radii of Tl (1.55 Å)[20] and N (0.75 Å). The Tl–N bonds in these adducts could therefore be considered as somewhat ionic. For comparison, the Tl–N bond distance in $[\{Tl[(dipp)(Me_3Si)N]\}_4]$ is 2.307(6) Å.[5] Further analysis of Tl–N distances for neutral complexes in the Cambridge Structural Database (CSD; the N center is restricted to three-coordination) yields a mean distance of 2.42 ± 0.20 Å (345 complexes),[21] thus the observed Tl–N distances in **1a** and **1b** are toward the long end of the range of reported Tl–N bonds, and most similar to Tl–N distances seen in tris(pyrazolyl)borate complexes of Tl^I. Indeed, restricting the search to bis- and tris(pyrazolyl)borate complexes yields a mean Tl–N distance of 2.63 ± 0.20 Å ($n = 107$).

The thallium(I) adducts **1a** and **1b** feature an intriguing structure. In addition to the Tl–N bond, as illustrated in Figure 1, each thallium center is flanked by two aryl moieties. Although the Tl–C distances are significantly longer than the typical Tl–C single bonds (e.g., 2.34(1) Å found in [(2,6-trip$_2$C$_6$H$_3$)Tl]; trip = 2,4,6-*i*Pr$_3$C$_6$H$_2$),[22] some separations are within the sum of the van der Waals radii of Tl and C (3.66 Å).[23] For example, the Tl–Ct distances (Ct = arene ring centroid) in the two molecules of **1a** and the three molecules of **1b** are 3.00, 3.00; 3.10, 3.10 (with shortest Tl–C separations of 3.02, 3.02; 3.04, 3.04) Å and 2.85, 3.44; 2.85, 3.56; 2.95, 3.08 (with closest Tl–C separations of 3.09, 2.94; 3.10, 2.92; 3.09, 3.08) Å, respectively. Furthermore, the Tl–carbon distances of structurally characterized Tl–arene π complexes are 3.29 ± 0.08 Å (72 complexes),[21] which corresponds to a mean Tl–Ct distance of around 3.00 Å, which is close to the shorter of the Tl–Ct values in the present crystal structures. On the other hand, the Tl···arene contacts in the complexes reported here do not seem to substantially modify the ligand parameters. For example, the C–N distance and C–N–C and N–C–N angles of the W-shaped ligand backbone are very similar in **1a** and **1b**, in the related anion $[N\{C(C_3F_7)NPh\}_2]^-$,[24] and in the κ^1N(central)-bonded metal adducts $[LM\{N[C(C_3F_7)N(dipp)]_2\}]$ (LM = MeCNAg, *t*BuNCAg, MeHg).[10,12,17]

To clarify whether Tl···arene contacts are "enforced" by the W-shape ligand conformation that places the aryl groups in a quasi-perpendicular arrangement (see Figure 1) or energetically driven, we undertook a computational study. A density functional (B3LYP/CEP-31G(d)) geometry optimization of D_6 $[Tl(\eta^6\text{-benzene})_2]^+$ yields a Tl–Ct distance of 2.92 Å,[15] in good agreement with the average values obtained from the CSD and the shorter distances measured here for **1a** and **1b**, thus indicating the potential for stabilization of the Tl by π-arene interactions. B3LYP/CEP-31G(d) calculation of the gas-phase dissociation energy of D_6 $[Tl(\eta^6\text{-benzene})_2]^+$ to Tl^+ and two benzene molecules shows the reaction to be exothermic by 42 kcal mol^{-1}, thus indicating an average Tl–π-arene interaction energy of 21 kcal mol^{-1}. Not surprisingly, neutral models such as $[Tl\{N[C(R')NR]_2\}]$ yield weaker, Tl–π-arene interaction energies of 11 (R′ = H, R = Ph) and 12 kcal mol^{-1} (R′ = F, R = Ph). These energies were estimated by taking the difference in the homolytic Tl–ligand bond energies for $[Tl\{N[C(R')NPh]_2\}]$ and $[Tl\{N[C(R')NH]_2\}]$, in which R′ = H or F.

Hybrid quantum/molecular mechanical calculations (see Figure 2 and the Supporting Information) on a full experimental model (geometries optimized starting from the three different molecules in the asymmetric unit of **1b**) yield commensurate Tl–π-arene interaction energies of 13 kcal mol^{-1}. The [Tl(2,6-trip$_2$C$_6$H$_3$)] complex reported by Niemeyer and Power, which to the best of our knowledge represents the most bona fide example of Tl^I monocoordination,[22] has arene interaction energies of around 3 kcal mol^{-1} between Tl and each aryl substituent. The Tl···arene interaction energies in the triazapentadienyl complexes can be compared to the Tl–N bond energies calculated from triazapentadienyl models without arene substituents—63 (R′ = R = H) and 64 kcal mol^{-1} (R′ = H, R = F)—at the same B3LYP/CEP-31G(d) level of theory. Therefore, computational estimates

 © 2005 Wiley-VCH Verlag GmbH & Co. KGaA, Weinheim

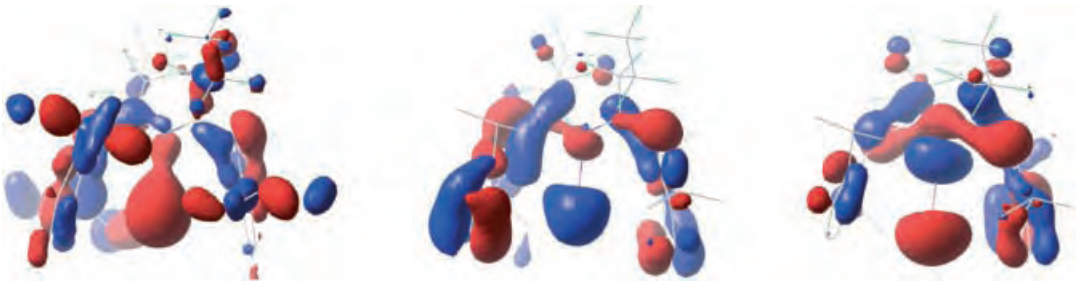


Figure 2. Orbitals derived from QM/MM (UFF force field for C_3F_7 and *i*Pr substituents; B3LYP/CEP-31G(d) for remainder of complex **1b**) geometry optimization that displays delocalization between the arene π-ring and the Tl 6s orbital.

imply an essentially monocoordinate Tl^I center in **1a** and **1b** whose stability is supplemented by Tl···arene interactions. A plot of the Kohn–Sham orbitals of **1b** shows three orbitals that display significant interactions; these correspond to the in-phase and out-of-phase combinations of the lowest energy arene π orbital and the Tl 6s orbital (Figure 2). Furthermore, the analogous orbitals (see the Supporting Information) for $[Tl(\eta^6\text{-benzene})_2]^+$ show greater Tl–π-arene delocalization for this cationic system, thus supporting the contention of weaker, albeit significant, Tl–π-arene interactions for the present neutral triazapentadienyl complexes.

The coordination properties of $[N\{C(C_3F_7)NR\}_2]^-$ also merit some comment as it binds to metal ions in several different fashions (e.g., κ^1N(central), κ^1N(terminal), or κ^2N-(terminal) with W- or U-shaped ligand conformers).[9–12] The two lowest energy conformations found for the full ligand models at the PM3 level of theory are U-shaped and W-shaped,[17] with the U-shaped conformer being only 0.1 kcal mol^{-1} lower in energy than the W-shaped conformer. Hence, these conformations are essentially degenerate. One may infer that the backbone conformation adopted upon ligation by a metal fragment will be primarily determined by the steric and electronic characteristics of the metal. The electronic properties for the two lowest energy conformations of $[N\{C(C_3F_7)NR\}_2]^-$ were thus calculated. A plot of the highest-unoccupied molecular orbital (HOMO) for $[N\{C(C_3F_7)NR\}_2]^-$ shows it to be the expected nonbonding π orbital of a conjugated five-atom entity. The HOMO for the W conformer is shown in Figure 3 (the HOMO of the U conformer is the same). Evidently, the HOMO is more or less evenly distributed among the three N atoms of the anionic ligand, which implies that in an orbitally controlled or covalent regime there will be little bias for ligation of the metal at either the terminal or central nitrogen atoms. Thus, it is plausible to infer that discrimination among different coordination modes will be made on the basis of charge considerations, the chelate effect, and/or steric effects. To probe the first of these inferences, the Mulliken charges of the U and W conformations were calculated. They are interesting in that they point to the central nitrogen atom of the N_3C_2 core being more nucleophilic/basic than the terminal nitrogen atoms. The calculated Mulliken charges are −0.2 for the terminal nitrogens and −0.4 for the central nitrogen. Hence, electrophiles/acids are expected to coordinate to the central nitrogen, as seen in the thallium(I) adducts described herein.

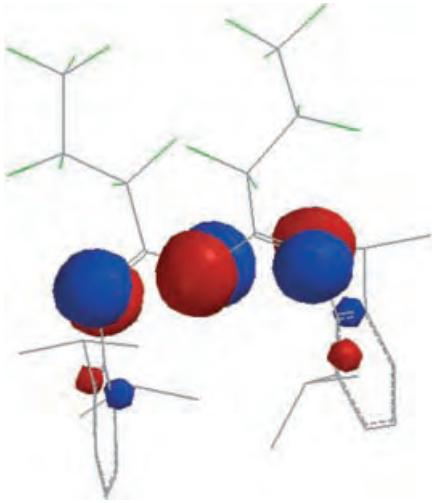


Figure 3. Highest energy molecular orbital (PM3 calculation) of $[N\{C(C_3F_7)N(dipp)\}_2]^-$.

Overall, we report here the isolation of the first monomeric, Tl–N-bonded complexes of triazapentadienyl ligands. Compounds **1a** and **1b** also feature weak Tl···arene contacts. The computational investigation has revealed that these interactions are energetically important, although secondary to Tl–N bond interactions. The thallium(I) ion coordinates to the more nucleophilic nitrogen site of the ligand anion. The triazapentadienyl ligands used in this study may be compared to the diazapentadienyl and pentaazapentadienyl systems. Few thallium(I) adducts of the latter two ligand types are known,[1] and only $[Tl\{PhC[C(H)N(dipp)]_2\}]$,[8] $[Tl\{HC[C(Ph)N(Me_3Si)]_2\}]$,[8] and $[\{Tl\{N[N(tol)N]_2\}\}_2]$[6] have been structurally characterized. Thus, the title compounds represent a rare addition to thallium derivatives of the azapentadienyl ligand family.[25]

Received: February 3, 2005
Revised: May 25, 2005
Published online: July 6, 2005

Keywords: amides · fluorinated ligands · main-group elements · N ligands · thallium

 © 2005 Wiley-VCH Verlag GmbH & Co. KGaA, Weinheim

[1] H. V. R. Dias, *Comprehensive Coordination Chemistry II*, *Vol. 3* **2004**, pp. 383 – 463.
[2] L. H. Gade, *Dalton Trans.* **2003**, 267 – 278.
[3] C. Janiak, *Coord. Chem. Rev.* **1997**, *163*, 107 – 215.
[4] K. W. Klinkhammer, S. Henkel, *J. Organomet. Chem.* **1994**, *480*, 167 – 171.
[5] S. D. Waezsada, T. Belgardt, M. Noltemeyer, H. W. Roesky, *Angew. Chem.* **1994**, *106*, 1413 – 1414; *Angew. Chem. Int. Ed. Engl.* **1994**, *33*, 1351 – 1352.
[6] J. Beck, J. Strähle, *Z. Naturforsch. B* **1986**, *41*, 1381 – 1386.
[7] A. L. Rheingold, L. M. Liable-Sands, S. Trofimenko, *Chem. Commun.* **1997**, 1691 – 1692.
[8] Y. Cheng, P. B. Hitchcock, M. F. Lappert, M. Zhou, *Chem. Commun.* **2005**, 752 – 754.
[9] H. V. R. Dias, S. Singh, *Inorg. Chem.* **2004**, *43*, 5786 – 5788.
[10] H. V. R. Dias, S. Singh, *Inorg. Chem.* **2004**, *43*, 7396 – 7402.
[11] A. R. Siedle, R. J. Webb, F. E. Behr, R. A. Newmark, D. A. Weil, K. Erickson, R. Naujok, M. Brostrom, M. Mueller, S.-H. Chou, V. G. Young, Jr., *Inorg. Chem.* **2003**, *42*, 932 – 934.
[12] A. R. Siedle, R. J. Webb, M. Brostrom, R. A. Newmark, F. E. Behr, V. G. Young, Jr., *Organometallics* **2004**, *23*, 2281 – 2286.
[13] L. D. Amisial, X. Dai, R. A. Kinney, A. Krishnaswamy, T. H. Warren, *Inorg. Chem.* **2004**, *43*, 6537 – 6539.
[14] X. Dai, P. Kapoor, T. H. Warren, *J. Am. Chem. Soc.* **2004**, *126*, 4798 – 4799.
[15] P. L. Holland, T. R. Cundari, L. L. Perez, N. A. Eckert, R. J. Lachicotte, *J. Am. Chem. Soc.* **2002**, *124*, 14416 – 14424.
[16] X. Dai, T. H. Warren, *Chem. Commun.* **2001**, 1998 – 1999.
[17] See Supporting Information for more details.
[18] X-ray quality crystals of **1a** and **1b** were obtained from hexane solutions at −5 °C. X-ray data for **1a**: $C_{26}H_{22}F_{14}N_3Tl$, monoclinic, space group $P2/n$; $a = 18.1041(7)$, $b = 8.8224(4)$, $c = 18.8037(8)$ Å, $\beta = 105.5130(10)°$, $V = 2900.5(2)$ Å^3, $Z = 4$, $\rho_{calcd} = 1.939$ Mg m^{-3}. Hydrogen atoms were placed in idealized positions and included as riding atoms. All non-hydrogen atoms were refined anisotropically. $R1$, $wR2$ $(I > 2\sigma(I)) = 0.0278$, $wR2 = 0.0653$. X-ray data for **1b**: $C_{32}H_{34}F_{14}N_3Tl$, orthorhombic, space group $P2_12_12_1$, $a = 17.1432(6)$, $b = 19.4275(7)$, $c = 30.7929(11)$ Å, $V = 10255.6(6)$ Å^3, $Z = 12$, $\rho_{calcd} = 1.809$ Mg m^{-3}. Hydrogen atoms were placed in idealized positions and included as riding atoms. All non-hydrogen atoms were refined anisotropically, $R1$, $wR2$ $(I > 2\sigma(I)) = 0.0217$, 0.0489. CCDC-262530 (**1a**) and -262531 (**1b**) contain the supplementary crystallographic data for this paper. These data can be obtained free of charge from the Cambridge Crystallographic Data Centre via www.ccdc.cam.ac.uk/data_request/cif.
[19] H. Plenio, *Chem. Rev.* **1997**, *97*, 3363 – 3384.
[20] L. Pauling, *The Nature of the Chemical Bond*, 3rd ed., Cornell University Press, Ithaca, NY, **1960**.
[21] *Cambridge Structural Database*, London, UK, **2004**.
[22] M. Niemeyer, P. P. Power, *Angew. Chem.* **1998**, *110*, 1291 – 1294; *Angew. Chem. Int. Ed.* **1998**, *37*, 1277 – 1279.
[23] A. Bondi, *J. Phys. Chem.* **1964**, *68*, 441 – 451.
[24] A. R. Siedle, R. J. Webb, M. Brostrom, S.-H. Chou, D. A. Weil, R. A. Newmark, F. E. Behr, V. G. Young, Jr., *Inorg. Chem.* **2003**, *42*, 2596 – 2601.
[25] Details of the synthesis, characterization, and computational study are given in the Supporting Information.

 © 2005 Wiley-VCH Verlag GmbH & Co. KGaA, Weinheim

Mass Spectrometry of Proteins

DOI: 10.1002/anie.200500668

The Thermal Unfolding of Native Cytochrome *c* in the Transition from Solution to Gas Phase Probed by Native Electron Capture Dissociation**

Kathrin Breuker and Fred W. McLafferty*

The effect of hydration on protein structure, dynamics, folding, and stability has been studied for decades and still is a topic of active research.[1–4] Removal of solvent results in the formation of stable gas-phase protein conformations that can be dramatically different from the original native state,[5–9] but so far nothing is known about the sequence of structural changes of a native protein that is suddenly exposed to vacuum. We address here the effect of hydration on structure and stability, and report for the first time site-specific data on the thermal unfolding of a native protein structure in the transition from solution to gas phase. Our data support a sequential unfolding mechanism dominated by the loss of hydrophobic bonding.

We have shown recently that electrospray ionization (ESI)[10] of aqueous solutions of ferric Cytochrome *c*, (Fe^{III})-Cyt *c*, in concentrations favorable for the formation of noncovalently bound homodimers (≈ 75 μM) produces unexpected backbone-cleavage products, a phenomenon we termed "native electron capture dissociation" (NECD).[11] Briefly, as an electrosprayed dimer ion is introduced into the Fourier transform mass spectrometer (FTMS) and passes the heated capillary for desolvation, one of its monomers partially unfolds. This causes proton transfer from the compact monomer **II** to the partially unfolded monomer **I**, and induces a substantial charge asymmetry.[12] In turn, this prompts intermolecular transfer of two electrons to the heme of monomer **I**, one reducing the heme iron and the other causing protein backbone cleavage (NECD) next to residues in contact with the heme.[11,13] Finally, the two cleavage products and monomer **II** separate and are detected in the trapped-ion cell of the FTMS.

Figure 1 shows the yield[14] of fragment ions from NECD of two aqueous solutions of horse heart (Fe^{III})Cyt *c* (75 μM, pH 5) versus backbone cleavage site; the capillary temperature was ≈ 31 °C.[15] Solutions A (for the experiment in Figure 1a) and B (for the experiment in Figure 1b) were prepared in the same way, except that A was stored overnight and B was stored for three months. In agreement with the proposed NECD mechanism,[11] protein backbone cleavage occurs next to residues with noncovalent bonding to the heme in the native structure. The NECD fragments from solution A result from cleavage next to K13, Y48/T49, L68, K79/M80, F82, and I85, while solution B gives additional products from cleavage next to L35, T40, F46, N52, and W59.

Thus the dimers in solutions A and B appear to represent different structures; that of solution B stabilizes more protein–heme bonds in monomer **I** so that they are still intact when NECD occurs.[16] The cleavage products from solution A are consistent with monomer **II** binding near K79/M80 of monomer **I**, and stabilization of its protein–heme interactions through the hydrogen-bond network that involves residues 49, 67, and 78–82 (Figure 2). The products from solution B indicate binding near Y48/T49 of monomer **I**, which in addition stabilizes its heme contacts of the residues associated with the extensive hydrogen-bond network of 37, 38, 40, 49, 50, 52–55, 57, and 59. This binding close to Y48/T49 actually corresponds to that found in the asymmetric dimer unit in crystals of (Fe^{III})Cyt *c* (horse heart) at low ionic strength in which T47 and D50 of monomer **I** bind to V11, Q12, and Q16 of monomer **II**.[17] Interestingly, the structure of the crystal monomer corresponding to our partially unfolded monomer **I** is somewhat more disordered than its counterpart.

Neither of the NECD spectra shows fragments from cleavage in the terminal regions, that is, next to F10, L94, and L98, or in the 18–34 segment. This suggests that the initial unfolding causing charge asymmetry in either dimer structure involves separation of the terminal helices, rupture of the H18–Fe coordinative bond,[18] and unfolding of the associated Ω-loop. Proton transfer to the newly exposed residues causes charge asymmetry, the extent of which can be calculated from the sum of the average charge values for the quasi-complementary fragment ions $\boldsymbol{c}_{48}$ and $\boldsymbol{y}_{56}$, +8.5 (Figure 3a), and the average monomer ion charge of +7.2 at 50% yield (representing all monomer **II**, as all monomer **I** ions are fragmented). Taking into account the two electrons for heme iron reduction and backbone cleavage, these +8.5 and +7.2 values correspond to +10.5 and +5.2 charges, respectively, prior to electron transfer. Thus a 2.0:1 charge asymmetry drives NECD for both of these solutions at pH 5, independent of temperature (Figure 3a), whereas the total NECD yield goes up from 4% at 28.5 °C to 23% at 42 °C and then down to 15% at 45.5 °C for solution A, and from 21% at 29 °C to 54% at 40 °C to 30% at 48 °C for solution B (Figure 3b).

A 75 μM solution at pH 4 gave cleavage products from the same sites as in Figure 1a, except none next to K13. The sums of the fragment-ion charges were $\approx +12.5$ at 27.5 and 29.5 °C, indicating the presence of more highly charged dimeric NECD precursors at pH 4. Although heating lowered the

[*] Dr. K. Breuker
Institute of Organic Chemistry and
Center for Molecular Biosciences Innsbruck (CMBI)
Innsbruck University
Innrain 52a, 6020 Innsbruck (Austria)
Fax: (+43) 512-507-2892
E-mail: kbreuker@gmx.net
Prof. Dr. F. W. McLafferty
Department of Chemistry and Chemical Biology
Baker Laboratory, Cornell University
Ithaca, NY 14853-1301 (USA)

[**] The authors thank the Austrian FWF and BMBWK (grants P15767, T229 to KB) and the NIH (grant GM16609 to FWM) for generous funding, and Huili Zhai, Cheng Lin, Xuemei Han, Robert Konrat, Harry B. Gray, Harold Hwang, and Mi Jin for stimulating discussions.

Supporting information for this article is available on the WWW under http://www.angewandte.org or from the author.

 © 2005 Wiley-VCH Verlag GmbH & Co. KGaA, Weinheim

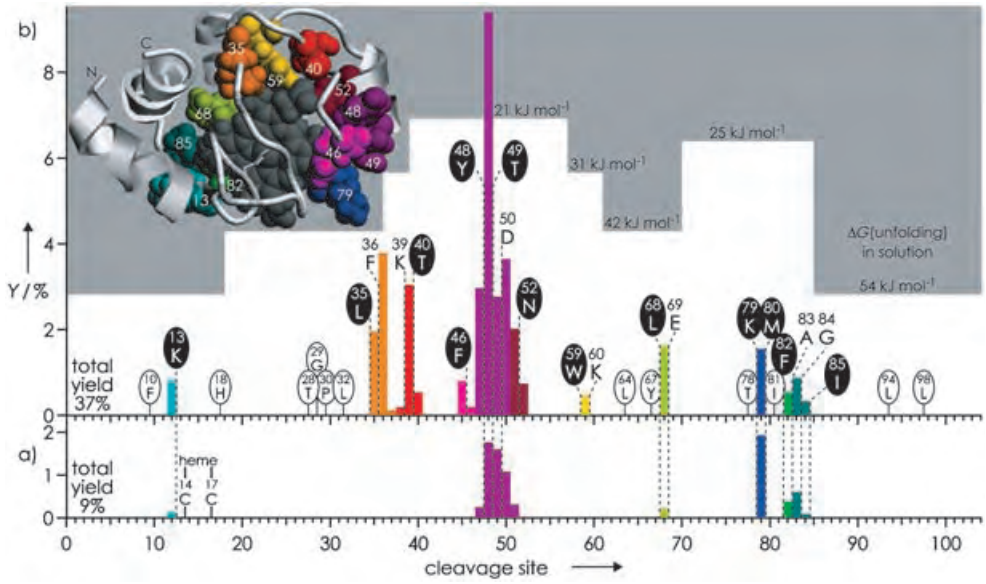


Figure 1. NECD fragment-ion yields (*Y*) versus backbone cleavage site from ESI of aqueous solutions of horse heart (Fe^{III})Cyt*c* (75 μM, pH 5). The samples were prepared by dissolving the lyophilized protein in pure water and storing a) overnight at 4 °C, b) at 4 °C for three months; capillary temperature ≈31 °C. Ellipses: residues with native heme contacts (filled black where NECD was observed). Upper left: Structure of native (Fe^{III})-Cyt*c* in solution;[23] heme: dark gray; contacting residues giving rise to NECD: same colors as in (a) and (b). Gray areas: unfolding free energies of (Fe^{III}) Cyt*c* in solution relative to the native state.[21,22]

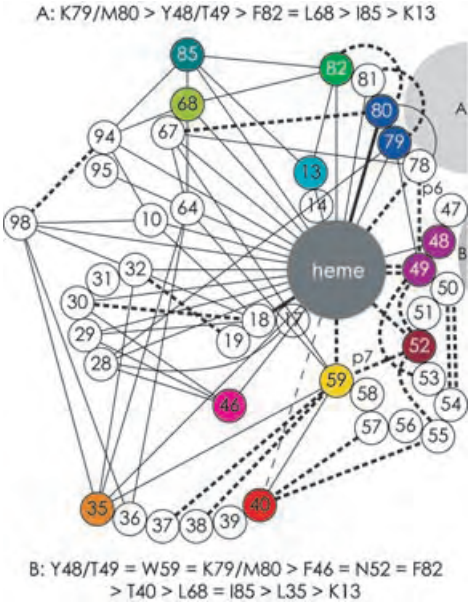


Figure 2. Schematic representation of hydrophobic (thin solid lines), hydrogen (thick dashed lines), and coordinative (thick solid lines) bonds (<3.5 Å) of heme-contacting residues in native horse heart (Fe^{III})Cyt*c*.[23] The T40–heme interaction (thin dashed line) is unspecific but within 2.9 Å. N52 and W59 are connected by hydrogen bonds to the same heme propionate 7 (p7) oxygen atom, and T49 and T78 are connected by hydrogen bonds to the same heme propionate 6 (p6) oxygen atom.

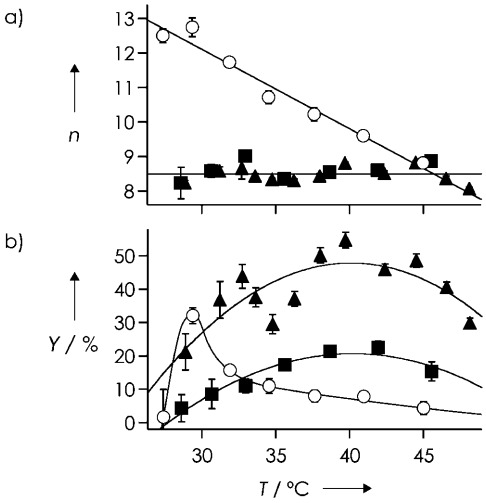


Figure 3. NECD of (Fe^{III})Cyt*c* solutions versus capillary temperature: a) summed average charge states (*n*) of c_{48} and y_{56}, b) total yields (*Y*). Solution A, pH 4 (○), pH 5 (■); solution B, pH 5 (▲).

fragment-ion charge of ≈+12.5 to the +8.5 value of the solutions at pH 5 (Figure 3a), the charge asymmetry before electron transfer changed little with temperature; the average value of +8.9 for monomers at 29.5 °C indicates a charge asymmetry of ≈14.5:6.9 (2.1:1) before electron transfer. Increasing temperature effects a dramatic yield increase from 2% at 27.5 °C to 32% at 29.5 °C, falling to 4% at 45 °C (Figure 3b).

This strong positive and negative effect of heating on NECD yields for both dimer solutions, one at both pH 4 and 5, without a change in the required charge asymmetry, indicates several competitive dissociations of the solution dimer structure. The lowest energy pathway must be the direct dissociation of the intermonomer bond, as no dimer ions were detected in the NECD spectra measured under any conditions. The increasing yield of NECD cleavage products

 © 2005 Wiley-VCH Verlag GmbH & Co. KGaA, Weinheim

with heating is then consistent with an increasingly competitive unfolding of monomer **I** and more dimer ions reaching the critical charge asymmetry for NECD before the intermonomer bond dissociates; NECD of solution B reaches a 50% fragment-ion yield at 40°C, corresponding to complete dissociation of all monomers **I**. Higher temperatures open up yet another pathway, the competitive unfolding of monomer **II**, which increases the proportion of dimer ions whose charge asymmetry stays below the critical level. Note that the less favored unfolding of monomer **II** is consistent with the asymmetric dimer structure of (Fe^{III})Cyt *c* crystals,[17] in which unfolding of the terminal helices of monomer **II** would be restricted by the V11, Q12, and Q16 binding in the dimer interface (Figure 1). However, an asymmetric dimer structure is not necessarily a requirement for asymmetric unfolding; many gas-phase dimer ions exhibit this phenomenon, although none as yet has shown NECD.[12,19,20]

The branching ratio of products from different cleavage sites can also be strongly affected by temperature, as illustrated for solution A in Figure 4. For example, the yield

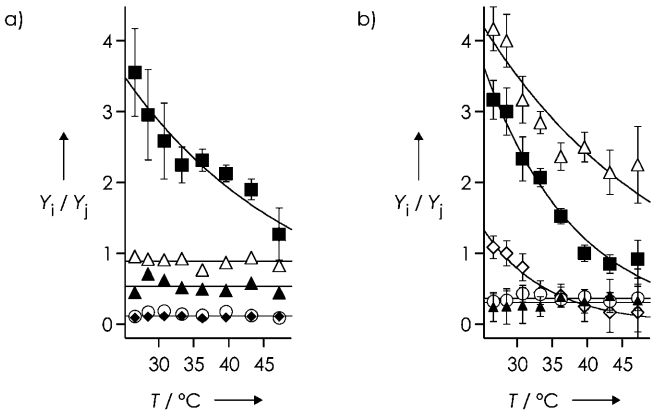


Figure 4. Branching ratio of NECD fragments from cleavage at sites i versus j, (Y_i/Y_j), for solution A, pH 5: a) Y_{47}/Y_{48} (◆), Y_{49}/Y_{48} (△), Y_{50}/Y_{48} (▲), Y_{51}/Y_{48} (○), $(Y_{47} + Y_{48} + Y_{49} + Y_{50} + Y_{51})/Y_{79}$ (■); b) Y_{82}/Y_{47} (■), Y_{83}/Y_{68} (△), Y_{84}/Y_{83} (▲), Y_{12}/Y_{84} (◇), Y_{68}/Y_{82} (○).

of fragments from cleavage at site 12, Y_{12}, versus that from cleavage at site 84, Y_{84}, decreases with increasing temperature, revealing that fewer dimers had retained the K13–heme interaction than the I85–heme interaction at higher temperatures. Y_{68}/Y_{82} does not change with temperature, suggesting a similar stability for the L68–heme and F82–heme interactions. The entire data set gives the order of stability, and the reverse order of unfolding: K79/M80 > Y48/T49 > F82 = L68 > I85 > K13; that for solution B is Y48/T49 = W59 = K79/M80 > F46 = N52 = F82 > T40 > L68 = I85 > L35 > K13 (see the Supporting Information).

From this order of unfolding, the most stable heme binding sites of monomer **I** for both the solution A and B dimers are those postulated to be close to the dimer binding interface (Figure 2). However, both dimers have initially unfolded in the same manner as indicated by the lack of fragments in the terminal and the 18–34 regions, and by the same charge asymmetry for both dimers. As shown in Figure 2 (solid lines), these initially unfolded regions are generally stabilized by hydrophobic bonding, in sharp contrast to the hydrogen-bond stabilization (dashed lines, Figure 2) of the least unfolded protein–heme bonding of monomer **I**. As previously postulated,[5–9] removal of water should weaken hydrophobic bonding (no solvent to avoid) but should also strengthen hydrogen bonding (no solvent to compete with).

Of further interest, this solution-to-gas phase stability order is essentially the reverse of the unfolding in solution. Englander and co-workers recently characterized five cooperative folding–unfolding units ("foldons") in native Cyt *c*, whose free energies of unfolding are shown in Figure 1 (K13 > L68 = L35 > W59 > K79/M80 = F82 = I85 > T40 = F46 = Y48/T49 = N52).[21,22] The most stable foldon in solution comprises the terminal helices that are held together by hydrophobic bonding; NECD found no bonding to the heme at F10, L94, and L98; bonding at K13 was found to be the next least stable. In solution, extensive hydrophobic bonding from the terminal helices (V20 with F10, Y97, L98, A101; L32 with L98) also stabilizes the 18–34 Ω-loop, as part of the second most stable foldon. In this region NECD finds L35 and L68 as the next weakest heme binding partners, with six other cleavage products missing. On the other hand, among the most stable interactions in the gas phase is the Y48/T49–heme contact, which is part of the least stable solution foldon. Dehydration of the native protein structure, plus the stabilization by monomer **II**, almost inverts the stabilities of the individual interactions in solution.

In conclusion, site ordering for the unfolding of a native protein in the transition from solution to gas phase greatly favors hydrophobic bonds, even those that are the last to unfold in solution. Surrounding such a bond by vacuum instead of water of course weakens it; intermediate effects of this type have been observed with protein conformations in nonpolar solutions.[24] The main requirement for NECD of the Cyt *c* dimers appears to be fast initial unfolding of a peripheral region, so that monomeric native proteins with peripheral hydrophobic bonding in extended structures should also be investigated for NECD. Although here NECD yields could be seriously reduced by heme absence or competitive unfolding of another part of the protein, competitive dissociation of intermolecular noncovalent bonds (e.g. dimer interface) would be no problem. The occurrence of NECD should also be sought in the dissociations of gaseous ion dimer structures that exhibit asymmetric charge partitioning.[12,19,20]

Experimental Section

This study utilized a 6-Tesla FTMS described previously.[25] Ions formed by ESI entered the instrument through a heated capillary where NECD occurs;[11] the products were transferred into the ion cell ($< 10^{-9}$ Torr) through quadrupole ion guides. ESI utilized homemade emitters with a tip inner diameter of ≈ 5 μm, flow rate of 200–500 nL min^{-1}, and spray potential of 1 kV. Horse heart Cyt *c* (Sigma, USA) was dissolved in pure water, with pH adjustment by addition of acetic acid.

Received: February 22, 2005
Published online: July 6, 2005

 © 2005 Wiley-VCH Verlag GmbH & Co. KGaA, Weinheim

Keywords: hydration · mass spectrometry · native electron capture dissociation · noncovalent interactions · protein structures

[1] M. F. Jarrold, *Annu. Rev. Phys. Chem.* **2000**, *51*, 179 – 207.
[2] J. Woenckhaus, *Int. J. Mass Spectrom.* **2002**, *213*, 9 – 24.
[3] F. Franks, *Biophys. Chem.* **2002**, *96*, 117 – 127.
[4] C. N. Pace, S. Trevino, E. Prabhakaran, J. M. Scholtz, *Philos. Trans. R. Soc. London Ser. B* **2004**, *359*, 1225 – 1235.
[5] F. W. McLafferty, Z. Q. Guan, U. Haupts, T. D. Wood, N. L. Kelleher, *J. Am. Chem. Soc.* **1998**, *120*, 4732 – 4740.
[6] C. S. Hoaglund-Hyzer, A. E. Counterman, D. E. Clemmer, *Chem. Rev.* **1999**, *99*, 3037 – 3079.
[7] D. M. Horn, K. Breuker, A. J. Frank, F. W. McLafferty, *J. Am. Chem. Soc.* **2001**, *123*, 9792 – 9799.
[8] K. Breuker, H.-B. Oh, D. M. Horn, B. A. Cerda, F. W. McLafferty, *J. Am. Chem. Soc.* **2002**, *124*, 6407 – 6420.
[9] H.-B. Oh, K. Breuker, S. K. Sze, Y. Ge, B. K. Carpenter, F. W. McLafferty, *Proc. Natl. Acad. Sci. USA* **2002**, *99*, 15863 – 15868.
[10] J. B. Fenn, M. Mann, C. K. Meng, S. F. Wong, C. M. Whitehouse, *Science* **1989**, *246*, 64 – 71.
[11] K. Breuker, F. W. McLafferty, *Angew. Chem.* **2003**, *115*, 5048 – 5052; *Angew. Chem. Int. Ed.* **2003**, *42*, 4900 – 4904.
[12] J. C. Jurchen, E. R. Williams, *J. Am. Chem. Soc.* **2003**, *125*, 2817 – 2826.
[13] NECD of (Fe^{II})Cyt*c* yields the same products but involves transfer of only a single electron.
[14] The yield was calculated as [fragments]/([fragments] + [molecular ions]); dimer ions were not detected in the mass spectra.
[15] Measured at the capillary orifice, the temperature inside is estimated to be two times this value.
[16] Many of the cleavage sites found for solution B are far apart on the monomer structure of Figure 1, so that it is only possible for a fraction of these sites to participate in the intermolecular bonding of a single dimer structure. Thus it is implausible that a direct electron transfer from monomer **II** to the cleavage site causes NECD. Multiple dimer structures are also less likely for solution B than for solution A, as the B dimers should have far more time to isomerize to a minimum-energy structure.
[17] R. Sanishvili, K. W. Volz, E. M. Westbrook, E. Margoliash, *Structure* **1995**, *3*, 707 – 716.
[18] Losing this coordination site will increase the electron affinity of the heme.
[19] C. Versluis, A. v. d. Staaij, E. Stokvis, A. J. R. Heck, *J. Am. Soc. Mass Spectrom.* **2001**, *12*, 329 – 336.
[20] N. Felitsyn, E. N. Kitova, J. S. Klassen, *J. Am. Soc. Mass Spectrom.* **2002**, *13*, 1432 – 1442.
[21] M. M. G. Krishna, Y. Lin, J. N. Rumbley, S. W. Englander, *J. Mol. Biol.* **2003**, *331*, 29 – 36.
[22] H. Maity, M. Maity, S. W. Englander, *J. Mol. Biol.* **2004**, *343*, 223 – 233.
[23] L. Banci, I. Bertini, H. B. Gray, C. Luchinat, T. Reddig, A. Rosato, P. Turano, *Biochemistry* **1997**, *36*, 9867 – 9877.
[24] T. Knubovets, J. J. Osterhout, A. M. Klibanov, *Biotechnol. Bioeng.* **1999**, *63*, 242 – 248.
[25] R. A. Zubarev, D. M. Horn, E. K. Fridriksson, N. L. Kelleher, N. A. Kruger, M. A. Lewis, B. K. Carpenter, F. W. McLafferty, *Anal. Chem.* **2000**, *72*, 563 – 573.

 © 2005 Wiley-VCH Verlag GmbH & Co. KGaA, Weinheim

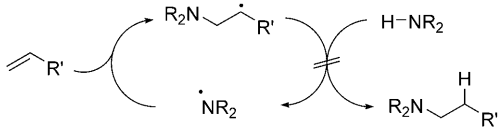
Radical Chemistry

DOI: 10.1002/anie.200463032

Stable Reagents for the Generation of N-Centered Radicals: Hydroamination of Norbornene**

*Jens Kemper and Armido Studer**

The transition-metal-mediated hydroamination of olefins has been investigated intensively during the last few years. Despite these efforts the methods developed so far are still limited to activated systems.[1] Radical chemistry may be an alternative. However, radical additions of amines or amine derivatives to olefins by H-transfer processes are not known to date. Whereas the addition of N radicals to alkenes is well established,[2,3] the H transfer from N to C radicals is not an efficient process [Eq. (1)]. In fact, the reverse reaction, H



(1)

transfer from C to N, has been successfully used. The well-known Hofmann–Löffler–Freytag reaction is an example.[4]

N radicals are generally generated via N–halogen, N-PTOC (PTOC = *N*-hydroxypyridine-2(1*H*)thione) and N-phenylthio derivatives either photochemically or by using an added reducing reagent.[2] However, most of these precursors are unstable and must be prepared in situ. Herein we present new stable N-radical precursors. Moreover, we show that these reagents can be applied for the intermolecular hydroamination of norbornene derivatives and electron-rich olefins.

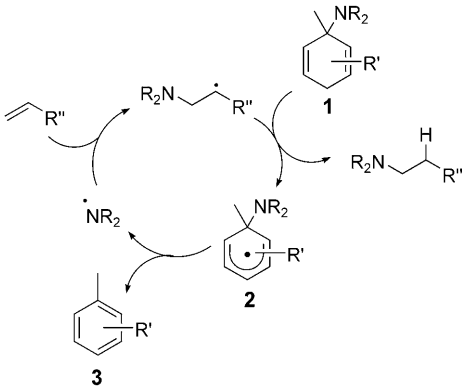
Walton et al. nicely demonstrated that substituted 1,4-cyclohexadienes can be used as precursors for C radicals.[5] We have further extended this concept to the generation of Si radicals.[6] Based on these results we assumed that 3-N-substituted 1,4-cyclohexadienes can be used as new stable N-radical precursors for the transition-metal-free transfer hydroamination of alkenes (Scheme 1). Addition of an N radical to an alkene will afford the corresponding C radical,

[*] Dr. J. Kemper, Prof. Dr. A. Studer
Westfälische-Wilhelms-Universität Münster
Organisch-Chemisches Institut
Corrensstrasse 40, 48149 Münster (Germany)
Fax: (+49) 251-833-6523
E-mail: studer@uni-muenster.de

[**] This research was supported by the Studienstiftung des deutschen Volkes (stipend for J.K). We thank J. Guin and F. Schleth for conducting some of the hydroamination experiments and K. Müller for preparing the norbornene derivatives.

Supporting information for this article is available on the WWW under http://www.angewandte.org or from the author.

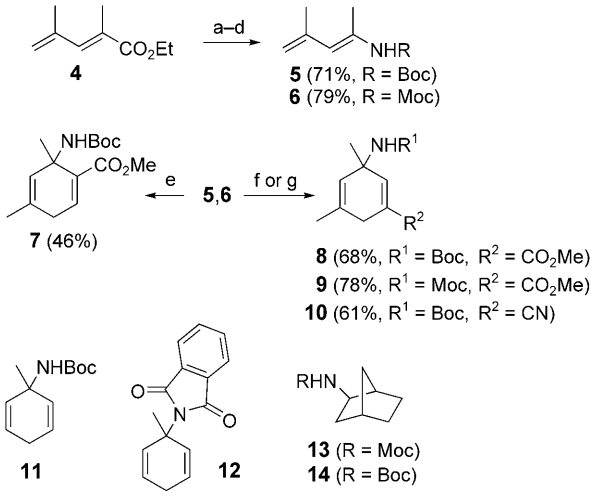
© 2005 Wiley-VCH Verlag GmbH & Co. KGaA, Weinheim



Scheme 1. Radical transfer hydroamination.

which should be reduced with **1** to provide **2** and the desired hydroamination product. Chain propagation should occur through aromatization of **2** to deliver an N-radical and **3**. The intrinsically difficult H transfer from N to C is replaced by a known H-transfer process. Since no additional reducing reagent is necessary, **1** can be regarded as a hydroamination reagent.

The syntheses of the reagents are depicted in Scheme 2. Ester **4** was readily prepared from commercially available materials by a Wittig reaction. Saponification and a Schmidt-



Scheme 2. a) NaOH, MeOH; b) Et_3N, ClC(O)OEt; c) NaN_3, H_2O; d) *t*BuOH or MeOH, toluene, reflux; e) methyl propiolate, dioxane, 110 °C; f) 1. 3-nitromethylacrylate, benzene; 2. DBU. g) 1. 3-nitroacrylonitrile, benzene; 2. DBU. Boc = *tert*-butoxycarbonyl, DBU = 1,8-diazabicyclo[5.4.0]undec-7-ene, Moc = methoxycarbonyl.

type rearrangement followed by alcoholysis of the intermediate isocyanate provided dienes **5** and **6**. Cyclohexadienes **8**–**10** were prepared by a Diels–Alder reaction using dienes **5** and **6**. The syntheses of cyclohexadienes **11** and **12** are described in the Supporting Information.

We first tested the stability of the reagents. To this end, dienes **7**–**12** were heated in C_6D_6 in sealed tubes at 140 °C (oil bath temperature) for 18 h. No decomposition was observed for compounds **8**–**10** as judged by ^{1}H NMR spectroscopy. For **11**, however, toluene (around 16 % yield) was identified as a product of aromatization. Compounds **7** and **12** turned out to be highly unstable: they underwent complete aromatization yielding methyl 2,4-dimethylbenzoate and toluene, respectively, in the stability test experiments. Hence, substituent at the 1-position of the cyclohexadiene that would destabilize a positive charge is important to suppress ionic decomposition.

The radical amination of norbornene using reagent **9** (→**13**) was studied next. Optimizations were conducted in benzene in sealed tubes at 140 °C using di-*tert*-butylperoxide (DTBP) as an initiator (Table 1). We were very pleased to

Table 1: Reaction of norbornene with **9** to give **13** under different conditions.

Run	**9** [equiv]	Norbornene [equiv]	DTBP [equiv]	*c* [M]	Yield [%][a]
1	1	1.0	0.3	0.25	30
2	1	1.1	0.4	0.25	36
3	1	1.1	0.6	0.25	30
4	1	1.1	0.8	0.25	30
5	1	1.1	1.0	0.25	28
6	1	2.0	0.4	0.25	44
7	1	3.0	0.4	0.25	45
8	1	4.3	0.4	0.25	39
9	1	5.3	0.4	0.25	39
10	1	7.0	0.4	0.25	37
11	2	1.0	0.4	0.18	41
12	4	1.0	0.4	0.18	42
13	5.7	1.0	0.4	0.18	57
14	1	2.9	0.4	0.5	41
15	1	3.1	0.4	0.76	37
16	1	3.0	0.5	1.0	38
17	1	2.9	0.4	–	38

[a] Determined by GC analysis with methyl benzoate as an internal standard.

observe that metal-free transfer hydroamination occurred. Variation of the initiator concentration revealed that the best results (36 % yield) for the reaction with 1 equiv of **9** and 1.1 equiv of norbornene at a concentration of 0.25 M were obtained with 0.4 equiv of peroxide (runs 1–5). Higher yields were obtained with 2 or 3 equivs of olefin (44 and 45 %, runs 6,7). However, a further increase of the norbornene concentration did not lead to better results (runs 8–10). The highest yield was obtained when **9** was used in a large excess: with a 5.7-fold excess a 57 % yield was obtained (run 13). Running the aminations at higher concentrations provided lower yields (runs 15,16). We found that the amination can be performed under solvent-free conditions (run 17). As a result of the optimization studies all subsequent experiments were performed with a threefold excess of olefin at a concentration of 0.25 M with 0.4 equiv of initiator.

The yield was improved further upon switching from the Moc derivative **9** to the Boc-protected reagent **8** (→**14**, 56 %). As expected from the stability tests, cyclohexadiene **7** is not an efficient hydroamination reagent (→**14**, 18 %). We also believe that the aromatization step delivering the carbamoyl radical is very slow for the cyclohexadienyl radical arising from **7**. Indeed, the methyl fragmentation product methyl 2-*tert*-butoxycarbonylaminyl-4-methyl benzoate was isolated as

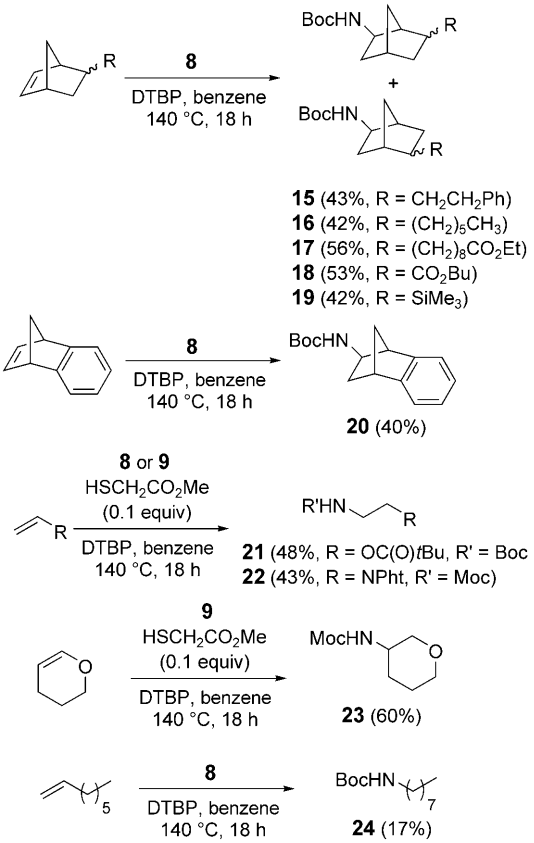
 © 2005 Wiley-VCH Verlag GmbH & Co. KGaA, Weinheim

the major product in 44% yield. The position of the electron-withdrawing group is obviously important. However, the methoxycarbonyl substituent can be replaced by a cyano group without affecting the yield greatly. Thus, the reaction with **10** afforded **14** in 45% yield. Substituents at the vinylic positions of our reagents are not mandatory. Amination using the unsubstituted diene **11** provided **14** in 47% yield. As expected, hydroamination of norbornene with phthaloyl-protected cyclohexadiene **12** did not work. The stability of **12** is a problem, as shown by the tests discussed above. Moreover, the addition of the sterically hindered *N*-phthaloyl radical is probably slow. Phthalimide was isolated in 61% yield. Our method delivers the amination products as Boc- or Moc-protected derivatives. This is highly desirable since most of the chemical manipulations on amine-functionalized molecules require N protection.

Finally, the most efficient reagents identified (**8**, **9**) were used to study other hydroaminations (Scheme 3). Products **15**–**19** were obtained in moderate-to-good yields as 1:1 mixtures of regioisomers. Hydroamination of benzannulated norbornene with **8** provided **20** in 40% yield. Hydroamination of vinyl pivalate under standard conditions afforded **21** along with telomers comprising two, three, and four monomer units, as identified by ESI-MS. Obviously, reduction of the α-oxy radical generated after N-radical addition onto vinyl pivalate cannot efficiently compete with telomerization. However, we found that this problem can be circumvented upon using polarity reversal catalysis.[7] Thus, hydroamination in the presence of methyl thioglycolate (10%) delivered the desired hydroamination product **21** in 48% yield.[8,9] Carbamoyl radical addition onto vinyl pivalate delivers a nucleophilic α-oxy radical, and a polar effect should favor H abstraction from the electronegative thiol. The electrophilic thiyl radical generated in this way will, in turn, abstract an H atom more readily from the cyclohexadienyl site of **8**, thus regenerating the thiol catalyst and continuing the chain (polymerization is suppressed).[8] Vinyl phthalimide was also successfully hydroaminated in the presence of 10% thiol catalyst (→**22**, 43%). The highest yield was obtained for the hydroamidation of dihydropyran (→**23**, 60%).[10]

As expected, addition of the electrophilic carbamoyl radicals derived from **8** or **9** onto electron-deficient olefins such as acrylonitrile and butyl acrylate did not occur. Pleasingly, we found that the highly challenging hydroamination of 1-octene could be accomplished (→**24**). Although the yield is currently not satisfactory (17%), manipulation of the electronic nature of the N-centered radical (varying the N-protecting group) should allow increasing the efficiency of the process. Work along this line is currently under way.

In conclusion we have presented a new method for the generation of N radicals under neutral conditions. In contrast to well-established procedures using N–halogen derivatives as N-radical precursors,[2] an additional stoichiometric reducing reagent such as the toxic tributyltin hydride is not necessary for N-radical generation. Moreover, the radical precursors are readily prepared and are stable compounds. To the best of our knowledge, this is the first report on a radical hydroamination reagent. Moreover, transition-metal-free transfer hydroaminations are unknown.[11]



Scheme 3. Hydroamination of various olefins. Pht = Phthaloyl.

Received: December 22, 2004
Revised: May 5, 2005
Published online: July 6, 2005

Keywords: hydroaminations · radical chemistry · synthetic methods

[1] T. E. Müller, M. Beller, *Chem. Rev.* **1998**, *98*, 675; M. Beller, C. Breindl, M. Eichberger, C. G. Hartung, J. Seayad, O. R. Thiel, A. Tillack, H. Trauthwein, *Synlett* **2002**, 1579; For a review in hydroaminations of alkynes, see: S. Doye, *Synlett* **2004**, 1653.

[2] L. Stella, *Angew. Chem.* **1983**, *95*, 368; *Angew. Chem. Int. Ed. Engl.* **1983**, *22*, 337; S. Z. Zard, *Synlett* **1996**, 1148; A. G. Fallis, I. M. Brinza, *Tetrahedron* **1997**, *53*, 17543; L. Stella in *Radicals in Organic Synthesis*, *Vol. 2* (Eds.: P. Renaud, M. P. Sibi), Wiley-VCH, Weinheim, **2001**, p. 407.

[3] Recent examples on intermolecular addition of N-centered radicals: T. Tsuritani, H. Shinokubo, K. Oshima, *J. Org. Chem.* **2003**, *68*, 3246; O. Kitagawa, S. Miyaji, Y. Yamada, H. Fujiwara, T. Taguchi, *J. Org. Chem.* **2003**, *68*, 3184; O. Kitagawa, Y. Yamada, H. Fujiwara, T. Taguchi, *Angew. Chem.* **2001**, *113*, 3983; *Angew. Chem. Int. Ed.* **2001**, *40*, 3865.

[4] P. Mackiewicz, R. Furstoss, *Tetrahedron* **1978**, *34*, 3241.

[5] G. Binmore, J. C. Walton, L. Cardellini, *J. Chem. Soc. Chem. Commun.* **1995**, 27; P. A. Baguley, G. Binmore, A. Mine, J. C. Walton, *Chem. Commun.* **1996**, 2199; P. A. Baguley, J. C. Walton, *J. Chem. Soc. Perkin Trans. 1* **1998**, 2073; L. V. Jackson, J. C. Walton, *Chem. Commun.* **2000**, 2327; L. V. Jackson, J. C. Walton, *J. Chem. Soc. Perkin Trans. 2* **2001**, 1758; A. F. Bella, L. V. Jackson, J. C. Walton, *J. Chem. Soc. Perkin Trans. 2* **2002**, 1839;

 © 2005 Wiley-VCH Verlag GmbH & Co. KGaA, Weinheim

A. F. Bella, A. M. Z. Slawin, J. C. Walton, *J. Org. Chem.* **2004**, *69*, 5926.
[6] A. Studer, S. Amrein, *Angew. Chem.* **2000**, *112*, 3196; *Angew. Chem. Int. Ed.* **2000**, *39*, 3080; S. Amrein, A. Timmermann, A. Studer, *Org. Lett.* **2001**, *3*, 2357; S. Amrein, A. Studer, *Chem. Commun.* **2002**, 1592; S. Amrein, A. Studer, *Helv. Chim. Acta* **2002**, *85*, 3559; A. Studer, S. Amrein, F. Schleth, T. Schulte, J. C. Walton, *J. Am. Chem. Soc.* **2003**, *125*, 5726.
[7] B. P. Roberts, *Chem. Soc. Rev.* **1999**, *28*, 25.
[8] A. F. Bella, L. V. Jackson, J. C. Walton, *Org. Biomol. Chem.* **2004**, *2*, 421.
[9] In the presence of 30% thiol catalyst the yield decreased (28%) and thiyl radical addition to vinyl pivalate was observed as a side reaction.
[10] The regioisomeric hydroamination product, the cyclic N,O acetal, was formed in 5% yield.
[11] For recent reports on transition-metal-free transfer hydrogenation see: J. W. Yang, M. T. Hechavarria Fonseca, B. List, *Angew. Chem.* **2004**, *116*, 6829; *Angew. Chem. Int. Ed.* **2004**, *43*, 6660; J. W. Yang, M. T. Hechavarria Fonseca, B. List, *Angew. Chem.* **2005**, *117*, 110; *Angew. Chem. Int. Ed.* **2005**, *44*, 108; S. G. Quellet, J. B. Tuttle, D. W. C. MacMillan, *J. Am. Chem. Soc.* **2005**, *127*, 32.

 © 2005 Wiley-VCH Verlag GmbH & Co. KGaA, Weinheim

Nanostructures

DOI: 10.1002/anie.200500663

Size-Dependent Optical Properties of MgO Nanocubes**

Slavica Stankic, Markus Müller, Oliver Diwald, Martin Sterrer, Erich Knözinger, and Johannes Bernardi*

Understanding the nature and chemical activity of well-defined surface structures on polycrystalline oxide systems requires atomic-scale characterization.[1,2] However, the properties of surface ions on polycrystals usually vary over a wide range, because different crystallographic faces are disposed to form edges, steps, and point defects. This situation leads to a substantial energetic heterogeneity in the surface properties. Consequently, it is one of the major challenges in current catalysis research to single out ions and point defects associated with specific surface structures and to characterize their role in the complex surface chemistry.[1–4] Magnesium oxide (MgO) is a particularly well-suited model system for such studies because of its straight-forward rock-salt crystal structure, the large abundance of thermodynamically stable (100) faces, and the purely ionic, nonconducting nature of the compound. Low-coordinate surface anions, which are considered to be chemically reactive sites, give rise to specific optical transitions in the UV light range, which can be assigned to the formation of surface excitons.[2,5] Their investigation provides an opportunity to establish a correlation between topological surface features such as corners, steps, and edges and the corresponding chemical and spectroscopic properties.[5–8] For the efficient investigation of surface sites, nanocrystalline model systems (where the number of surface ions is of the same order of magnitude as the number of bulk ions) are required.[9–11]

Herein we report the production of nanometer-sized MgO nanoparticles by chemical vapor deposition (CVD). They attain an almost perfect cubic shape after thermal activation at 1170 K under high-vacuum conditions ($p < 5 \times 10^{-6}$ mbar).[12] Depending on the CVD parameters they can adopt different average sizes between 3 nm and 10 nm. Preferential adjustment of the cube size is important since it sets the relative concentrations of corner and edge anions and thus determines the optical and chemical properties. Size-dependent trends in the relative intensities of absorption bands and photoluminescence emission bands were observed in the UV light range. A novel photoluminescence emission band was observed for nanocubes with edge lengths smaller than 9 nm and is attributed to the radiative deactivation of surface excitons at corner anions of the MgO nanocube.

The MgO nanoparticles are prepared by CVD in a flow-reactor system by the reaction of metal vapor with different gaseous oxidizing agents. At pressures under 20 mbar, metal atoms are evaporated from metal grains and transported by argon at a fixed flow rate to the downstream end of a quartz glass tube where the oxidant is introduced. There the metal vapor is combusted either with dry air (sample A), O_2 (sample B), or N_2O (sample C). The resulting metal oxide nanocrystals are then deposited downstream in a stainless steel net at room temperature.[13] Afterwards, the material is subjected to thermal activation at 1170 K. Figure 1 shows typical TEM images of MgO nanocube samples A, B, and C after such treatment. The nature and concentration of the oxidizing agent has a major influence on the nucleation process and consequently affects the average size of the particles after thermal activation. This feature is shown by the size distribution plots in Figure 2.[14] The particles of sample A are slightly less regular cubes and have an average edge length of 10 nm, whereas samples B and C consist of 5 and 3 nm sized nanocubes, respectively.

[*] Dipl.-Chem. S. Stankic, Dipl.-Ing. M. Müller, Dr. O. Diwald, Dr. M. Sterrer,[+] Prof. Dr. E. Knözinger
Institute of Materials Chemistry
Vienna University of Technology
Veterinärplatz 1/GA, 1210 Vienna (Austria)
Fax: (+43) 1-2507-73890
E-mail: knoe@imc.tuwien.ac.at
Dr. J. Bernardi
University Service Centre for Transmission Electron Microscopy
Vienna University of Technology
Wiedner Hauptstrasse 8–10/137, 1040 Vienna (Austria)
[+] Present address: Department of Chemical Physics
Fritz-Haber-Institute of the Max-Planck-Society
Faradayweg 4–6, 14195 Berlin (Germany)

[**] We thank T. Berger, K. Beck, P. V. Sushko, and A. L. Shluger for fruitful discussions and advice and gratefully acknowledge the financial support from the Austrian Fonds zur Förderung der wissenschaftlichen Forschung (FWF grants P14731-CHE and P14730-CHE) and the Hochschuljubiläumsstiftung der Stadt Wien (H-175/2001).

 © 2005 Wiley-VCH Verlag GmbH & Co. KGaA, Weinheim

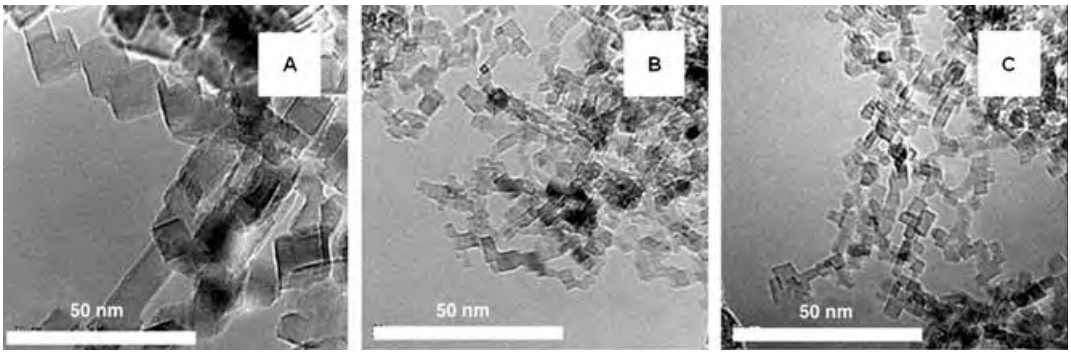


Figure 1. Typical TEM images of MgO nanocubes that result from CVD in conjunction with subsequent thermal activation at 1170 K and $p < 5\times10^{-6}$ mbar. For samples A, B, and C different oxidants were used at the same flow rates for the CVD process, as outlined in the text.

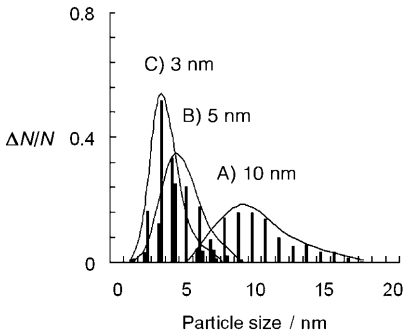


Figure 2. Size distribution plots of CVD MgO nanocubes. About 200 particles were observed to plot each distribution.

The optical properties of the nanocubes were measured by UV diffuse reflectance spectroscopy. The spectra, recorded in the presence of 10 mbar of O_2 to avoid photoluminescence (Figure 3),[15] reveal two clear trends with decreasing average cube size from sample A (10 nm) to sample C (3 nm):

1) The maximum of the high-energy absorption shifts from 220 nm (5.6 eV) to 230 nm (5.4 eV).
2) The absorption at 270 nm (4.6 eV), which is essentially absent on sample A (10 nm), gains relative intensity.

The second observation is perfectly in line with previous assignments of these optical features: with an energy of 5.4 eV ($\lambda = 230$ nm) four-coordinate anions in cube edges are excited whereas the 4.6 eV ($\lambda = 270$ nm) absorption band is attributed to the excitation of three-coordinate anions in corner positions.[2,5,8] Larger cube sizes imply lower relative concentrations of corner anions with respect to edge anions. This feature is exemplified in Table 1, where the calculated numbers of surface O^{2-} ions for the three particle sizes are listed. For the calculation we used an Mg^{2+}–O^{2-} distance of 2.1 Å and assumed a perfect cubic shape, where the particle is terminated by (100) planes, cube edges, and cube corners. For a constant quantity of 100 mg, the total number of corner anions ranges from 4×10^{16} for 10 nm cubes to 144×10^{16} ions for 3 nm cubes and the ratio of corner anions to edge anions increases from 0.01 to 0.04. This enhancement in the relative concentration of corner anions is qualitatively reflected in the relative growth of the 270 nm band (absorption on corners) compared to the one at 240 nm (absorption on edges) shown in Figure 3.

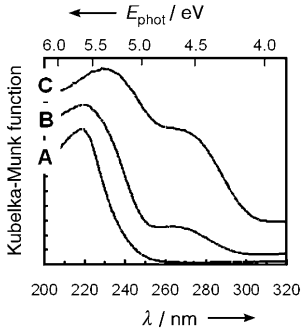


Figure 3. UV diffuse reflectance spectra of samples A, B, and C. For the sake of clarity, the curves were shifted on the ordinate scale.

Table 1: Calculated numbers of three- and four-coordinate surface anions located in ideal MgO nanocube edges and corners as a function of particle size.

Average edge length [nm]	Number of particles[a]	Number of corner O^{2-} ions[a]	Number of edge O^{2-} ions[a]	Ratio of corner to edge O^{2-} ions[a]
3	3.6×10^{17}	1.4×10^{18}	3.5×10^{19}	0.04
5	8.4×10^{16}	3.4×10^{17}	1.5×10^{19}	0.02
10	1.0×10^{16}	4×10^{16}	3.7×10^{18}	0.01

[a] In 100 mg of MgO powder.

Luminescence spectra of the three types of nanocube samples were recorded at 300 K and $p < 10^{-6}$ mbar (Figure 4). Depending on the excitation wavelength $\lambda = 240$ nm (5.2 eV) or $\lambda = 270$ nm (4.6 eV) the spectra are characterized by broad emission bands with maxima at $\lambda = 370$ nm (3.4 eV) and $\lambda = 380$ nm (3.3 eV), respectively. The full width at half maximum (FWHM) for both bands is 0.8 eV. The photoluminescence signal at 370 nm (excitation at 240 nm) is in general agreement with results from previous studies.[16–20] However, to our knowledge, the feature which is centered at slightly higher wavelength $\lambda = 380$ nm (excitation at $\lambda = 270$ nm) has not been reported as a distinct band to date.[21] The intensity of

 © 2005 Wiley-VCH Verlag GmbH & Co. KGaA, Weinheim

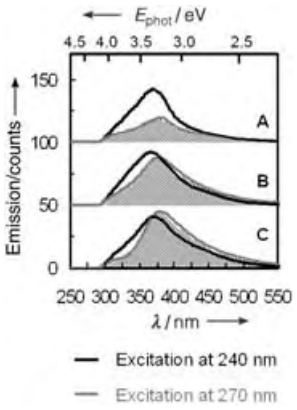


Figure 4. Photoluminescence emission spectra of samples A (10 nm), B (5 nm), and C (3 nm). For comparison, the emission signals excited at 240 nm (black curves) are set to the same nominal intensity as for the bands following excitation at 270 nm (gray curves).

this band is significantly higher for samples B and C with short cube edges than for sample A.[22] Excitation of corner anions produces surface excitons at these sites which then deactivate radiatively at 3.3 eV ($\lambda = 380$ nm). This photoluminescence effect is thus preferentially observed on small MgO cubes (samples B and C; Figure 4) and can only be understood in terms of the enhanced surface concentration of corner anions (Table 1). The higher Stokes shift of the emission band at 370 nm (5.4 to 3.4 eV compared to 4.6 to 3.3 eV) is explained by an energy transfer from the four-coordinate edge anion, where excitation initially occurs, to a three-coordinate corner anion acting as the emission site[6,8,16] On the basis of the demonstrated size-dependence, we attribute the novel band at 380 nm to a new electronic transition on MgO surfaces. This interpretation is in line with a recent electron paramagnetic resonance (EPR) study where the formation of two types of trapped hole centers, that is, O^- radicals on the MgO surface was reported.[23] The fact that the local crystal-field splittings of these two types of radicals are similar, connects well to the two emission bands of similar energy observed in this study. The linking of optical properties and the generation of surface radicals suggests that on MgO nanostructures the selective physical and chemical activation of well-defined surface structures is feasible. Further work is needed to understand the nature and mobility of surface excitons on MgO nanostructures and to investigate how changes in the concentration ratio of corner to edge ions affect surface reactivity.

In conclusion, size control over MgO nanocubes has been achieved through the CVD technique in conjunction with subsequent thermal activation steps at $p < 5 \times 10^{-6}$ mbar. The resulting adjustment of the ratio between corner and edge ions is clearly reflected in the optical properties of the MgO nanocubes as measured by UV diffuse reflectance and photoluminescence spectroscopy. Adjustment of the average particle size makes MgO nanocubes a powerful model system for surface-science studies on dispersed materials. In addition, it represents a promising building block element for the construction of functional nano- and mesostructures.

Experimental Section

The three types of MgO nanocube samples A, B, and C were obtained by using dry air ($N_2/O_2 = 4{:}1$ (A), O_2 (B), and N_2O (C) as the oxidizing agent in the CVD process.[13] Flow rates for Argon and the oxidizing agent were 1220 and 82 $s\,cm^3\,min^{-1}$, respectively. For UV Diffuse reflectance and photoluminescence measurements the sample material was transferred into a high-vacuum tight quartz cell providing pressures better than $p < 10^{-6}$ mbar. For each type of measurement, thermal treatment was carried out to remove hydroxy and carbonate groups from the surface (confirmed by IR spectroscopy). During this treatment the annealing rate was 5 $K\,min^{-1}$ and the pressure above the sample was $< 10^{-5}$ mbar. The sample was first heated to 873 K and treated with oxygen to remove organic contaminants. The final annealing temperature of 1173 K was kept for 3–10 h at pressures $< 5 \times 10^{-6}$ mbar. Photoluminescence measurements were carried out with a Perkin Elmer LS 50 B system equipped with a pulsed Xe discharge lamp as the excitation light source. The excitation light beam was passed through a UG 5 filter (Schott) in conjunction with a 295 nm long pass filter. UV diffuse reflectance measurements were performed on a Perkin Elmer Lambda 15 spectrometer with an integrating sphere. For TEM investigations a holey carbon grid was immersed into the metal oxide powder samples which had been previously investigated by spectroscopy. The TEM measurements were carried out with a TECNAI F20 analytical transmission electron microscope equipped with a field-emission electron source and a S-Twin objective lens. Images were recorded with a Gatan 794 MultiScan camera. No nitrogen impurities were detected on all samples as measured with electron energy loss spectrometry (EELS) using a Gatan Image Filter GIF 2001.

Received: February 22, 2005
Published online: July 6, 2005

Keywords: magnesium oxide · nanostructures · photoluminescence spectroscopy · transmission electron microscopy · UV diffuse reflectance

[1] a) V. E. Henrich, P. A. Cox, *The Surface Science of Metal Oxides*, Cambridge University Press, Cambridge, **1996**; b) G. Pacchioni, *ChemPhysChem* **2004**, *5*, 1041 – 1047; c) C. Barth, C. R. Henry, *Phys. Rev. Lett.* **2003**, *91*, 196102; d) M. Chiesa, M. C. Paganini, E. Giamello, C. Di Valentin, G. Pacchioni, *Angew. Chem.* **2003**, *115*, 1801 – 1803; *Angew. Chem. Int. Ed.* **2003**, *42*,1759 – 1761; e) Z. Yan, S. Chinta, A. A. Mohamed, J. P. Fackler, Jr., D. W. Goodman, *J. Am. Chem. Soc.* **2005**, *127*, 1604 – 1605.

[2] a) G. Spoto, E. N. Gribov, G. Ricchiardi, A. Damin, D. Scarano, S. Bordiga, C. Lamberti, A. Zecchina, *Prog. Surf. Sci.* **2004**, *76*, 71 – 146; b) E. Garrone, A. Zecchina, F. S. Stone, *Philos. Mag.* **1980**, *42*, 683 – 703.

[3] H. Knözinger, *Science* **2000**, *287*, 1407 – 1408.

[4] P. K. Stoimenov, V. Zaikovski, K. J. Klabunde, *J. Am. Chem. Soc.* **2003**, *125*, 12907 – 12913.

[5] P. V. Sushko, J. L. Gavartin, A. L. Shluger, *J. Phys. Chem. B* **2002**, *106*, 2269 – 2276.

[6] M. Sterrer, T. Berger, O. Diwald, E. Knözinger, *J. Am. Chem. Soc.* **2003**, *125*, 195 – 199.

[7] D. Ricci, C. Di Valentin, G. Pacchioni, P. V. Sushko, A. L. Shluger, E. Giamello, *J. Am. Chem. Soc.* **2003**, *125*, 738 – 747.

[8] a) A. L. Shluger, P. V. Sushko, L. N. Kantorovich, *Phys. Rev. B* **1999**, *59*, 2417 – 2430; b) P. V. Sushko, A. L. Shluger, *Surf. Sci.* **1999**, *421*, L157 – L165.

[9] R. Kakkar, P. N. Kapoor, K. J. Klabunde, *J. Phys. Chem. B* **2004**, *108*, 18140 – 18148.

[10] R. M. Richards, A. M. Volodin, A. F. Bedilo, K. J. Klabunde, *Phys. Chem. Chem. Phys.* **2003**, *5*, 4299 – 4305.

 © 2005 Wiley-VCH Verlag GmbH & Co. KGaA, Weinheim

[11] Z. Dohnalek, G. A. Kimmel, D. E. McCready, J. S. Young, A. Dohnalkova, R. S. Smith, B. D. Kay, *J. Phys. Chem. B* **2002**, *106*, 3526 – 3529.
[12] This treatment leads to entire sample dehydroxylation as judged by IR spectroscopy.
[13] Further details of this procedure are described in: E. Knözinger, K.-H. Jacob, S. Singh, P. Hofmann, *Surf. Sci.* **1993**, *290*, 388 – 402.
[14] The underlying differences in the process of nucleation and particle growth during CVD are not yet understood and in the process of investigation.
[15] Gaseous O_2 quenches luminescence and prevents artifacts that originate from light emission in the optical absorption spectra. This quenching effect, in turn, clearly demonstrates that UV-light absorption and emission exclusively stem from surface states.
[16] a) S. Coluccia, A. M. Deane, A. J. Tench, *J. Chem. Soc. Faraday Trans. 1* **1978**, *74*, 2913 – 2922; b) S. Coluccia in *Adsorption and Catalysis on Oxide Surfaces* (Eds.: M. Che, G. C. Bond), Elsevier, Amsterdam, **1985**, pp. 59 – 69.
[17] M. Anpo, M. Che, *Adv. Catal.* **2000**, *44*, 120 – 248.
[18] M. Anpo, Y. Yamada, Y. Kubokawa, S. Coluccia, A. Zecchina, M. Che, *J. Chem. Soc. Faraday Trans. 1* **1988**, *84*, 751 – 764.
[19] S. G. MacLean, W. W. Duley, *J. Phys. Chem. Solids* **1984**, *45*, 227 – 235.
[20] M. L. Bailly, G. Costentin, H. Lauron-Pernot, J. M. Krafft, M. Che, *J. Phys. Chem. B* **2005**, *109*, 2404 – 2413.
[21] Emission were also observed at higher wavelengths $\lambda > 450$ nm in the course of these studies on samples which had not been entirely dehydroxylated.
[22] Intensity trends of the absorptions bands at 240 nm and 270 nm in Figure 3 do not directly scale with those of the associated emission bands in Figure 4. This fact is attributed to one or the combination of the following reasons: a) the cross sections for absorption (measured in the presence of O_2) and emission (measured at $p < 10^{-6}$ mbar) are unknown and may be subject to particle size, b) Rayleigh scattering into the interior of the sample cell causes the loss of detectable light and has a distinct dependence on particle size ($\sim d^3$) and frequency ($\sim \nu^4$). The relative extent of scattering loss is expected to be different for both measurements owing to inherent differences in the optical set up. c) Photoluminescence spectroscopy is by far the more sensitive technique.
[23] O. Diwald, M. Sterrer, E. Knözinger, P. Sushko, A. Shluger, *J. Chem. Phys.* **2002**, *116*, 1707 – 1712.

 © 2005 Wiley-VCH Verlag GmbH & Co. KGaA, Weinheim

Pnicogen Complexes

DOI: 10.1002/anie.200500781

Antimony–Tungsten Triple Bond: A Stable Complex with a Terminal Antimony Ligand**

*Gábor Balázs, Marek Sierka, and Manfred Scheer**

Dedicated to Professor Wolf-Walther du Mont on the occasion of his 60th birthday

Complexes with transition-metal–element triple bonds of the heavier main-group elements constitute an exciting area in chemistry, since the investigation of the bonding situation as well as the reactivity potential open up a significant area of research. However, stability and reactivity are often opposing tendencies; thus existing complexes are often kinetically stabilized by bulky substituents to encumber the reactive triple bond. Exciting examples for this particular development in the chemistry of Group 14 elements are the recently synthesized complexes with a metal–lead triple bond.[1] Now, this series in Group 14 chemistry is almost complete.[2] For Group 15 elements however,[3] there still remains the challenge to synthesize stable complexes with terminal stibido as well as bismutido ligands. Indications of existing complexes with a terminal stibido ligand as intermediates were first reported by Rheingold et al. They were able to generate briefly existing complexes of the formulae $[(OC)_4MSb]^-$ (M = Cr, Mo, W) and $[(OC)_3FeSb]^-$ in the gas phase under the conditions of a Fourier transform cyclotron resonance spectrometer (FT-ICR).[4] The breakthrough for the synthesis of stable triply bonded terminal ligands of heavier[5] Group 15 elements occurred almost 10 years ago in 1995 when we were able to characterize spectroscopically the stable phosphido complex $[(t\mathrm{BuO})_3W{\equiv}P{\rightarrow}W(CO)_5]$ (**1**) [6] which was structurally characterized in 1999.[7] The difficulties in isolation arise from the high reactivity potential of this complex, since the

[*] Dr. G. Balázs, Prof. Dr. M. Scheer
Institut für Anorganische Chemie
Universität Regensburg
93040 Regensburg (Germany)
Fax: (+49) 941-943-4439
E-mail: mascheer@chemie.uni-regensburg.de
Dr. M. Sierka
Institut für Chemie
Humboldt-Universität zu Berlin
Unter den Linden 6, 10099 Berlin (Germany)

[**] This work was supported by the Deutsche Forschungsgemeinschaft and the Fonds der Chemischen Industrie. M. Sierka gratefully acknowledges Prof. Joachim Sauer and the Humboldt-Universität zu Berlin for providing computing facilities and Gregor Schnakenburg for helpful discussion. The recording of the Raman spectrum of the title complex by Dr. G. Stößer (University of Karlsruhe) is greatly appreciated.

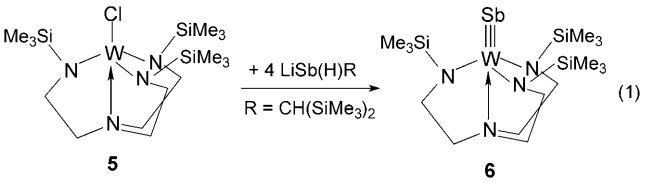
Supporting information for this article is available on the WWW under http://www.angewandte.org or from the author.

 InterScience © 2005 Wiley-VCH Verlag GmbH & Co. KGaA, Weinheim

*t*BuO groups only protect the triple bond in the solid state, whereas in solution the bond is still accessible.

Independently Cummins[8] and Schrock and co-workers[9] chose the steric protection of the M≡P triple bond by bulky substituents at the amido ligands, when they reported in 1995 the synthesis and the first structural characterization of terminal phosphido complexes $[(Ph''RN)_3Mo{\equiv}P]$ (**2**; Ph″ = 3,5-$Me_2C_6H_3$; R = $C(CD_3)_2CH_3$) and $[(N_3N)W{\equiv}P]$ (**3**; N_3N = tren = $N(CH_2CH_2NSiMe_3)_3$). Compound **3** was synthesized by treating $[(N_3N)WCl]$ (**5**)[10] with two equivalents of LiP(H)Ph. The use of $Li[E(SiMe_3)_2]$ (E = P, As) in reaction with **5** enabled us, in addition to an alternative route to **3**, the synthesis of $[(N_3N)W{\equiv}As]$ (**4**), the first terminal arsenido complex,[11] which was independently obtained by Schrock et al.[12] Our efforts to obtain the stibido complex $[(N_3N)W{\equiv}Sb]$ (**6**) in the same manner as the arsido and phosphido complexes **4** and **3** failed, probably because of the bulkiness of the $[(Me_3Si)_2Sb]^-$ fragment which did not fit into the cone formed by the three $SiMe_3$ groups of the tren ligand. Sterically less-demanding alkyl groups on the tris(amido)amine ligand such as isopropyl or neopentyl permitted the reaction of $[(Me_3Si)_2E]^-$ (E = Sb, Bi) with **5** but did not prevent further dimerization to form the heterocumulene complexes $[\{N(CH_2CH_2NR)_3W\}_2(\mu\text{-Sb})]$ (R = *i*Pr, Np).[13,14] Now we have finally succeeded in the synthesis and spectroscopic and structural characterization of the first isolable stibido complex $[(N_3N)W{\equiv}Sb]$ (**6**) which contains an antimony–tungsten triple bond.

For the synthesis of **6**, $(Me_3Si)_2CHSbH_2$ was lithiated at −60 °C with *n*BuLi in THF to generate $Li[(Me_3Si)_2CHSb(H)]$ as a reactive intermediate. The reaction of this solution with **5** leads to the formation of the stibido complex **6** [Eq. (1)].



5 **6** (1)

Owing to the instability of the lithiated stibane, it was necessary to use an excess of $RSbH_2$ and *n*BuLi to achieve total consumption of **5**. Thus, as side products the ethylidyne complex $[(N_3N)W{\equiv}CCH_3]$ and Sb_7^{3-} were formed as a result of the degradation of the tris(amido)amine ligand and the stibane, respectively. Furthermore, depending on the solvents used and the lithium base other side products could be identified.[15]

Decrease of the steric bulkiness of the antimony reactant was expected to increase the yield of **6**. Therefore we treated the comparatively slender $[Me_3SiCH_2(H)Sb]^-$ moiety with **5** under the conditions described above. Against our expectations the alkylidyne complex $[(N_3N)W{\equiv}CSiMe_3]$ (**7**) was obtained in about 50% yield. The low thermal stability of $Li[Me_3SiCH_2(H)Sb]$ gives rise to transmetalation reactions with the formation of $Li[Me_3SiCH_2]$, which reacts with **5** to give **7**. The characterization of **7** was achieved spectroscopically and by single-crystal X-ray diffraction (see Supporting Information).[16] The synthesis and spectroscopic data of **7** have been reported previously, as it is obtained in the reaction of **5** with $Li[CH_2SiMe_3]$.[17]

Complex **6** is a diamagnetic, air-sensitive, brown crystalline compound, which is readily soluble in hydrocarbons. In the mass spectra the molecular ion peak was observed. The relatively weak emission band at 240 cm^{-1} in the Raman spectra of **6** is in agreement with a tungsten–antimony triple bond. In comparison the stretching frequencies for the lighter W≡E homologues were found at 343 cm^{-1} (E = As) and 516 cm^{-1} (E = P).[18] The solution ^{1}H- and ^{13}C NMR spectra of **6** show the presence of a C_3 symmetric ligand system. The C_3 symmetry is also preserved in the solid state. Complex **6** crystallizes as brown cubes in the cubic space group $Pa\bar{3}$.[16]

The main feature of the structure of **6** (Figure 1) is a terminally coordinated antimony ligand. The observed W–Sb distance in **6** of 2.5255(17) Å is the shortest reported to date,

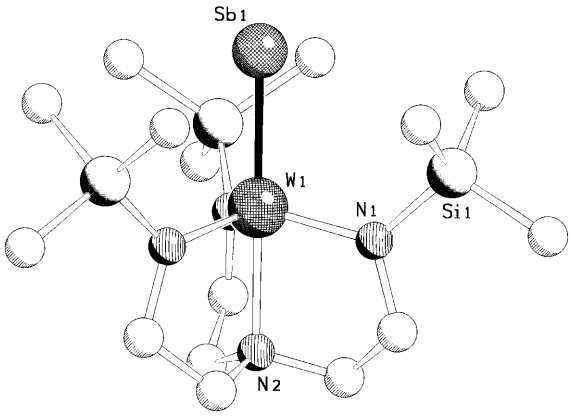


Figure 1. Crystal structure **6**. Hydrogen atoms are omitted for clarity. Selected bond lengths [Å] and angles [°]: W1-Sb1 2.5255(17), W1-N1 1.994(8), W1-N2 2.330(12), Si1-N1 1.759(8); N1-W1-N1′ 115.93(15), N1-W1-N2 78.2(2), N1-W1-Sb1 101.8(2), N2-W1-Sb1 180.0(4), Si1-N1-W1 125.8(4), C1-N1-W1 118.1(6), C1-N1-Si1 115.8(6).

consistent with the representation as a triple bond, and is comparable only with the W–Sb distances in the heterocumulene complexes $[\{N(CH_2CH_2NR)_3W\}_2Sb]$ (2.5275(5) Å R = *i*Pr;[13] 2.574(1) Å R = $CH_2C(CH_3)_3$[14]). Longer W–Sb bonds were observed in the stibinidene complexes $[\{(OC)_5W\}_2SbCl(thf)]$ (2.662(1) and 2.670(2) Å)[19] and $[\{(OC)_5W\}_2SbCH(SiMe_3)_2]$ (2.687(1) Å).[20] The tungsten atom has a distorted trigonal bipyramidal coordination geometry with three N atoms in equatorial and one N and a Sb atom in axial positions. The N_{eq}–W distance of 1.994(8) Å is comparable with the corresponding distances in $[(N_3N)WCl]$ (**5**) (1.985(11) Å),[10] $[(N_3N)W{\equiv}P]$ (**3**) (1.975(6) Å)[9] and $[(N_3N)W{\equiv}As]$ (**4**) (1.989(4) Å).[11] The N_{ax}–W distance (2.330(12) Å) is longer than in **5** (2.182(6) Å) but similar to those in **3** (2.343(4) Å) and **4** (2.336(6) Å). The N_{eq}-W-N_{eq} (115.9(2)°) and N_{eq}-W-N_{ax} (78.2(2)°) angles compare well with the equivalent angles in **5** and **3** (115.8(11), 78.1(2)°, and 115.69(8), 77.9(1)°, respectively). Along the series **3**, **4**, and **6** a very slight shortening of the N_{ax}–W distance is observed, reflecting the increase of the electropositive

 © 2005 Wiley-VCH Verlag GmbH & Co. KGaA, Weinheim

character of the terminal Group 15 ligand. None other structural parameters of the tren ligands is significantly influenced by the nature of the terminal ligand. As the size of the ligand E increases going from As to Sb, the cone formed from the three $SiMe_3$ groups is widened. This effect can be observed in the W-N_{eq}-Si angles (125.0(2) for **4** and 125.8(4)° for **6**). The wider angle for **3** (125.5(4)°) in comparison to **4** can be explained by the shorter W–P bond.

Density functional theory (DFT) calculations of complexes **3**, **4**, **6**, and a hypothetical complex [(N_3N)W≡Bi] (**8**) were performed to compare the [(N_3N)W≡E] (E = P, As, Sb, Bi) triple bonds of the Group 15 elements (Table 1 and Table 2). The calculated structural parameters of **3**, **4**, and **6** (Table 1) are similar to other reported values[11,21] and in a reasonable agreement with experimental data, except for the W–N2 distance. The experimental values are 0.16–0.19 Å shorter which may be due to solid-state effects.[21] As expected, the calculated W≡E bond lengths increase from E = P to E = Bi. This trend has also been found in similar metal–pnicogen complexes with alkoxy ligands.[22] The calculated W≡E harmonic stretching frequencies of 515 cm^{-1} (E = P) and 342 cm^{-1} (E = As) are in excellent agreement with observed data.[18] For E = Sb the calculated value of 264 cm^{-1} is slightly overestimated with respect to the experiment, probably due to the neglect of anharmonicity and approximate treatment of relativistic effects. Additionally, the W≡Sb stretching mode shows a strong coupling to other framework modes.

Analysis of the bonding situation using the natural bond orbital (NBO)[23] scheme and Wiberg bond indices (WBI)[24] strongly support the presence of W≡E triple bond in all calculated complexes (Table 2). Similar to other terminal pnicogen ligands in alkoxy substituted tungsten–pnicogen complexes[22] the σ and π components of the triple bonds obtained by the NBO analysis show only weak polarization. The W atom in the W–E σ bond is approximately sd hybridized, with a slight increase of s character for heavier pnicogen atoms. This situation is in disagreement with earlier published results using the PESHO method,[11] which indicate a largely d character of the tungsten contribution. The hybridization of the pnicogen atom in W≡E σ bond has a significant p character which increases from P to Bi and the two π components are composed mainly of d and p orbitals of the tungsten and pnicogen atoms, respectively.

Further support for the W≡E triple-bond character arise form the inspection of calculated molecular orbitals. The orbital picture of the W≡E is very similar for all investigated Group 15 elements and shows one σ and two degenerate π components. Figure 2 shows an example of the W≡Sb bond orbitals of **6**. The calculated NBO partial charges indicate that the tungsten atom carries significant positive charge while the pnicogen atoms are almost neutral or slightly positive charged (Sb, Bi). This result supports a strong covalent character of the tungsten–pnicogen triple bond. The calculated bond-dissociation energies decrease monotonically from P to Bi confirming that the heavier pnicogen atoms have significantly weaker W≡E bonds. Finally, the calculated [(N_3N)W≡E] complexes

Table 1: Comparison of selected experimental and calculated structural parameters [Å,°] of complexes **3**, **4**, **6**, and **8**.

	W–E[a]	W–N	W–N2	E-W-N1[a]	N1-W-N1	N1-W-N2
3 exp[9]	2.162(4)	1.975(6)	2.34(1)	101.9(2)	115.8(11)	78.1(2)
3 calcd	2.185	2.017	2.504	103.6	114.7	76.5
4 exp[11]	2.2903(11)	1.989(4)	2.336(6)	102.15(11)	115.69(8)	77.85(11)
4 calcd	2.294	2.017	2.499	103.6	114.7	76.4
6 exp	2.5255(17)	1.994(8)	2.330(12)	101.8(2)	115.93(15)	78.2(2)
6 calcd	2.514	2.015	2.516	104.1	114.3	75.9
8 calcd	2.590	2.016	2.507	103.9	114.4	76.1

[a] **3**: E = P, **4**: E = As, **6**: E = Sb, **8**: E = Bi.

Table 2: Results of the bonding analyses for compounds **3**, **4**, **6**, and **8**.[a]

Compound	Partial charge		NBO occ	% W	W hyb (% s)[b]	% E	E hyb (% s)[b]	WBI	D_e
3									
	W: 0.84	σ:	1.917	42.2	$sd^{1.30}$ (43.5)	57.8	$sp^{3.30}$ (23.2)	2.38	481.9
	P: −0.03	π:	1.652	46.9	d	53.1	p		
		π:	1.664	47.3	d	52.7	p		
4									
	W: 0.81	σ:	1.913	42.8	$sd^{1.24}$ (44.6)	57.2	$sp^{3.96}$ (20.1)	2.35	429.0
	As: 0.01	π:	1.636	47.3	d	52.7	p		
		π:	1.636	48.2	d	51.8	p		
6									
	W: 0.73	σ:	1.890	45.8	$sd^{1.10}$ (47.6)	54.2	$sp^{4.75}$ (17.4)	2.28	333.4
	Sb: 0.11	π:	1.591	47.3	d	52.7	p		
		π:	1.643	49.4	d	50.6	p		
8									
	W: 0.71	σ:	1.887	46.0	$sd^{1.09}$ (47.8)	54.0	$sp^{6.06}$ (14.2)	2.27	293.3
	Bi: 0.15	π:	1.664	51.4	d	48.6	p		
		π:	1.555	47.2	d	52.8	p		

[a] NBO partial charges, NBO occupancies (occ), bond polarizations in % W and % E (**3**: E = P, **4**: E = As, **6**: E = Sb, **8**: E = Bi), orbital hybridizations (hyb), Wiberg bond indices (WBI), and bond dissociation energies (D_e, kJ mol^{-1}). [b] Contribution of the s orbital [%].

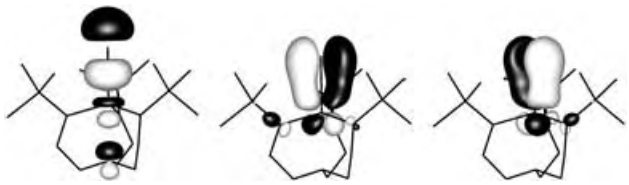


Figure 2. Kohn–Sham orbitals of the σ component (left) and two π components (middle and right) of the W≡Sb triple bond.

 © 2005 Wiley-VCH Verlag GmbH & Co. KGaA, Weinheim

show orbital and partial-charge patterns similar to those calculated for $[(MeO)_3W{\equiv}E]$ by Pandey and Frenking,[22] except for less positively charged tungsten atoms.

The results have shown the tris(amido)amine ligand complex of tungsten to be an excellent system for stabilization of terminal pnicogenido ligand complexes containing a W≡E triple bond. Now that the synthesis of the first stable terminal stibido ligand complex has been realized the path has been cleared for reactivity studies and the synthesis of the unknown bismutido complex.

Experimental Section

All manipulations were performed under an atmosphere of dry nitrogen using a glovebox and Schlenk techniques. Solvents were purified and degassed by standard procedures.

6: *n*BuLi in hexane (1.59 mL, 2.55 mmol, 1.6 M) was added to a stirred solution of $(Me_3Si)_2CHSbH_2$ (720 mg 2.55 mmol) in THF (5 mL), at −60 °C. The solution became dark red and gas evolution was observed. The reaction mixture was allowed to warm slowly to room temperature and a solution of $[N(CH_2CH_2NSiMe_3)_3WCl]$ (369 mg, 0.64 mmol) in toluene (12 mL) was added. The mixture was stirred for 20 h at 80 °C. All volatiles were removed in vacuum and the remaining black product was extracted with pentane (70 mL). Compound **6** was isolated from the orange-brown solution as brown cubes by fractionated crystallization at 5 °C. Yield: 37 mg (9 %). ^{1}H NMR (250 MHz, C_6D_6, 25 °C, TMS): $\delta = 0.847$ (s, ^2J(Si,H) = 5.85 Hz, 27 H; CH_3), 1.40 (t, ^3J (H,H) = 5.6 Hz, 6 H; CH_2), 3.58 ppm (t, ^3J(H,H) = 5.6 Hz, 6 H; CH_2); ^{13}C NMR (62.89 MHz, C_6D_6, 25 °C, TMS): $\delta = 7.70$ (s, CH_3), 51.66 (s, CH_2), 54.36 ppm (s, CH_2); EI-MS (70 eV): *m*/*z* (%): 666 (40) [M^+], 651 (100) [$M-CH_3$]$^+$, 636 (2) [$M-2CH_3$]$^+$, 621 (4) [$M-3CH_3$]$^+$, 593 (5) [$M-(CH_3)_3Si$]$^+$, 73 (95) [$(CH_3)_3Si$]$^+$. Raman (solid): $\tilde{\nu} = 240$ cm^{-1} (W≡Sb). Elemental analysis (%)calcd for $C_{15}H_{39}N_4Sb_1Si_3W_1$ (665.35): C 27.08, H 5.91, N 8.42; found: C 27.39, H 6.19, N 8.37.

The synthesis and X-ray structure of **7** is given in the Supporting Information

Structure optimizations and vibrational analyses at the DFT level were performed using the TURBOMOLE program package.[25] The BP86[26] exchange-correlation functional was used along with the triple zeta plus polarization (TZVP) basis set on all atoms.[27] To speed up calculations the Coulomb part was evaluated using the MARI-J method.[28] Quasi-relativistic pseudopotentials were used for the elements W, Sb, and Bi.[29] The NBO analysis was performed using the Gaussian03 program.[30] Calculations for **3**, **4**, **6**, and **8** were performed assuming C_3 symmetry and the nature of the stationary points was confirmed by vibrational analysis (no imaginary frequencies).

Received: March 3, 2005
Published online: July 6, 2005

Keywords: antimony · bond analysis · density functional calculations · pnicogen ligands · tungsten

[1] a) A. C. Filippou, N. Weidemann, G. Schnakenburg, H. Rohde, A. I. Philippopoulos, *Angew. Chem.* **2004**, *116*, 6674 – 6678; *Angew. Chem. Int. Ed.* **2004**, *43*, 6512 – 6516; b) A. C. Filippou, H. Rohde, G. Schnakenburg, *Angew. Chem.* **2004**, *116*, 2293 – 2297; *Angew. Chem. Int. Ed.* **2004**, *43*, 2243 – 2247; c) For a recent review in this field see: M. Weidenbruch, *Angew. Chem.* **2003**, *115*, 2322 – 2324; *Angew. Chem. Int. Ed.* **2003**, *42*, 2222 – 2224.

[2] For a discussion of the possible existence of the to date missing complex with a metal–silicon triple bond see: B. V. Mork, D. T. Tilley, *Angew. Chem.* **2003**, *115*, 371 – 374; *Angew. Chem. Int. Ed.* **2003**, *42*, 357 – 360.

[3] For a recent review in this field see: B. P. Johnson, G. Balázs, M. Scheer, *Top. Curr. Chem.* **2004**, *232*, 1 – 23, which continues the review: M. Scheer, *Coord. Chem. Rev.* **1997**, *163*, 271 – 286.

[4] F. P. Arnold, D. P. Ridge, A. L. Rheingold, *J. Am. Chem. Soc.* **1995**, *117*, 4427 – 4428.

[5] For reviews concerning the long-existing nitride complexes see: a) K. Dehnicke, J. Strähle, *Angew. Chem.* **1981**, *93*, 451 – 464; *Angew. Chem. Int. Ed. Engl.* **1981**, *20*, 413 – 426; b) W. A. Herrmann, *Angew. Chem.* **1986**, *98*, 57 – 77; *Angew. Chem. Int. Ed. Engl.* **1986**, *25*, 56 – 76; c) K. Dehnicke, J. Strähle, *Angew. Chem.* **1992**, *104*, 978 – 1000; *Angew. Chem. Int. Ed. Engl.* **1992**, *31*, 955 – 978; d) K. Dehnicke, F. Weller, J. Strähle, *Chem. Soc. Rev.* **2001**, *30*, 125 – 135.

[6] M. Scheer, K. Schuster T. A. Budzichowski, M. H. Chisholm, W. E. Streib, *J. Chem. Soc. Chem. Commun.* **1995**, 1671 – 1672.

[7] a) P. Kramkowski, G. Baum, U. Radius, M. Kaupp, M. Scheer, *Chem. Eur. J.* **1999**, *5*, 2890 – 2898; b) M. Scheer, P. Kramkowski, K. Schuster, *Organometallics* **1999**, *18*, 2874 – 2883.

[8] C. E. Laplaza, W. M. Davis, C. C. Cummins, *Angew. Chem.* **1995**, *107*, 2181 – 2183; *Angew. Chem. Int. Ed. Engl.* **1995**, *34*, 2042 – 2043.

[9] R. R. Schrock, N. C. Zanetti, W. N. Davis, *Angew. Chem.* **1995**, *107*, 2184 – 2186; *Angew. Chem. Int. Ed. Engl.* **1995**, *34*, 2044 – 2046.

[10] K.-Y. Shih, K. Totland, S. W. Seidel, R. R. Schrock, *J. Am. Chem. Soc.* **1994**, *116*, 12103 – 12104.

[11] M. Scheer, J. Müller, M. Häser, *Angew. Chem.* **1996**, *108*, 2637 – 2641; *Angew. Chem. Int. Ed. Engl.* **1996**, *35*, 2492 – 2494.

[12] N. C. Mösch-Zanetti, R. R. Schrock, W. M. Davis, K. Wanninger, S. W. Seidel, M. B. O'Donoghue, *J. Am. Chem. Soc.* **1997**, *119*, 11037 – 11048.

[13] M. Scheer, J. Müller, M. Schiffer, G. Baum, R. Winter, *Chem. Eur. J.* **2000**, *6*, 1252 – 1257.

[14] M. Scheer, J. Müller, G. Baum, M. Häser, *Chem. Commun.* **1998**, 2505 – 2506.

[15] A large number of reactions according to Eq. (1) were carried out to clarify the formation of the additional side-products (besides $[(N_3N)W{\equiv}CCH_3]$ and Sb_7^{3-}): for example, the reaction in toluene with *n*BuLi as metalation reagent leads to $[N_3NW{\equiv}CC_3H_7]$ as a result of the reaction of **5** with *n*BuLi, whereas with *t*BuLi in toluene, $[N_3NW{\equiv}CC_6H_5]$ was observed, formed as a result of the metalation of toluene and subsequent reaction with **5**. In contrast the use of THF or toluene as solvent with KH as metalation reagent as well as the reaction in benzene at 5 °C with *n*BuLi leads only to the "usual" side-products $[(N_3N)W{\equiv}CCH_3]$ and Sb_7^{3-}.

[16] Crystal-structure analyses of **6** and **7** were performed on a STOE IPDS diffractometer with $Ag_{K\alpha}$ radiation ($\lambda = 0.56087$ Å). The structures were solved by direct methods with the program SHELXS-97,[31a] and full-matrix least-squares refinement on F^2 in SHELXL-97[31b] was performed with anisotropic displacements for non-Hydrogen atoms. Hydrogen atoms were located in idealized positions and refined isotropically according to the riding model **6**: $C_{15}H_{39}N_4SbSi_3W$, $M_r = 665.37$, Crystal size $0.20 \times 0.15 \times 0.04$ mm^3, cubic space group $Pa\bar{3}$ (no. 205); $a = 17.297(2)$ Å, $T = 203(2)$ K, $Z = 8$, $V = 5174.8(10)$ Å^3, $\rho_{calcd} = 1.708$ Mg m^{-3}, $\mu(Ag_{K\alpha}) = 3.022$ mm^{-1}, 1640 unique reflections ($2\theta_{max} = 40°$), 79 parameters, $R_1 = 0.0527$, $wR_2 = 0.1565$. **7**: $C_{19}H_{48}N_4SbSi_4W$, $M_r = 628.82$, crystal size $0.50 \times 0.40 \times 0.20$ mm^3, monoclinic space group $P2_1$ (no. 4); $a = 10.266(2)$, $b = 11.711(2)$, $c = 12.290(3)$ Å, $\beta = 91.62°$, $T = 203(2)$ K, $Z = 2$, $V = 1477.0(5)$ Å^3, $\rho_{calcd} = 1.414$ Mg m^{-3}, $\mu(Ag_{K\alpha}) = 2.199$ mm^{-1}, 6620 unique reflections ($2\theta_{max} = 45°$), 267 parameters, $R_1 = 0.0217$, $wR_2 = 0.0554$, flack parameter −0.019(9). CCDC-263922 (**6**) and CCDC-263921 (**7**) contain the supplementary

 © 2005 Wiley-VCH Verlag GmbH & Co. KGaA, Weinheim

crystallographic data for this paper. These data can be obtained free of charge from the Cambridge Crystallographic Data Centre via www.ccdc.cam.ac.uk/data_request/cif.

[17] R. R. Schrock, S. W. Seidel, N. C. Mösch-Zanetti, D. A. Dobbs, K.-Y. Shih, W. M. Davis, *Organometallics* **1997**, *16*, 5195 – 5208.

[18] J. A. Johnson-Carr, N. C. Zanetti, R. R. Schrock, M. D. Hopkins, *J. Am. Chem. Soc.* **1996**, *118*, 11305 – 11306.

[19] M. Schiffer, diplom thesis, Karlsruhe, **1997**.

[20] A. M. Arif, A. H. Cowley, N. C. Norman, M. Pakulski, *Inorg. Chem.* **1986**, *25*, 4836 – 4840.

[21] T. Wagener, G. Frenking, *Inorg. Chem.* **1998**, *37*, 1805 – 1811.

[22] K. K. Pandey, G. Frenking, *Eur. J. Inorg. Chem.* **2004**, 4388 – 4395.

[23] a) J. P. Foster, F. Weinhold, *J. Am. Chem. Soc.* **1980**, *102*, 7211 – 7218; b) A. E. Reed, L. A. Curtiss, F. Weinhold, *Chem. Rev.* **1988**, *88*, 899 – 926.

[24] K. A. Wiberg, *Tetrahedron* **1968**, *24*, 1083 – 1096.

[25] a) R. Ahlrichs, M. Bär, M. Häser, H. Horn, C. Kölmel, *Chem. Phys. Lett.* **1989**, *162*, 165 – 169; b) O. Treutler, R. Ahlrichs, *J. Chem. Phys.* **1995**, *102*, 346 – 354.

[26] a) A. D. Becke, *Phys. Rev. A* **1988**, *38*, 3098 – 3100; b) S. H. Vosko, L. Wilk, M. Nusair, *Can. J. Phys.* **1980**, *58*, 1200 – 1211; c) J. P. Perdew, *Phys. Rev. B* **1986**, *33*, 8822 – 8824; erratum: J. P. Perdew, *Phys. Rev. B* **1986**, *34*, 7406.

[27] a) A. Schäfer, H. Horn, R. Ahlrichs, *J. Chem. Phys.* **1992**, *97*, 2571 – 2577; b) A. Schäfer, C. Huber, R. Ahlrich, *J. Chem. Phys.* **1994**, *100*, 5829 – 5835; c) K. Eichkorn, F. Weigend, O. Treutler, R. Ahlrichs, *Theor. Chem. Acc.* **1997**, *97*, 119 – 124.

[28] a) K. Eichkorn, O. Treutler, H. Öhm, M. Häser, R. Ahlrichs, *Chem. Phys. Lett.* **1995**, *242*, 652 – 660; b) M. Sierka, A. Hogekamp, R. Ahlrichs, *J. Chem. Phys.* **2003**, *118*, 9136 – 9148.

[29] a) D. Andrae, U. Häußermann, M. Dolg, H. Stoll, H. Preuss, *Theor. Chim. Acta* **1990**, *77*, 123 – 141; b) W. Küchle, M. Dolg, H. Stoll, H. Preuss, *Mol. Phys.* **1991**, *74*, 1245 – 1263; c) A. Bergner, M. Dolg, W. Küchle, H. Stoll, H. Preuss, *Mol. Phys.* **1993**, *80*, 1431 – 1441.

[30] Gaussian 03 (Revision B.04): M. J. Frisch, et al., see Supporting Information.

[31] a) G. M. Sheldrick, SHELXS-97, Universität Göttingen, **1996**; b) G. M. Sheldrick, SHELXL-97, Universität Göttingen, **1997**.

 © 2005 Wiley-VCH Verlag GmbH & Co. KGaA, Weinheim

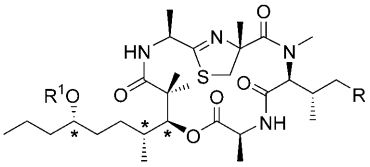
Natural Products Synthesis

DOI: 10.1002/anie.200500702

Total Synthesis of Halipeptins A and D and Analogues**

K. C. Nicolaou, David W. Kim, Daniel Schlawe, Dimitrios E. Lizos, Rita G. de Noronha, and Deborah A. Longbottom*

The halipeptins are a group of natural products whose structural identity and biological properties are still shrouded in mystery. In 2001 Gomez-Paloma et al. reported the isolation of halipeptins A and B from the marine sponge *Haliclona* sp. and showed that halipeptin A exhibits impressive antiinflammatory properties that exceed those of well-established drugs.[1] Their later isolation of halipeptin C prompted them to revise their structural assignment to that of thiazoline containing macrocycles as shown for halipeptins A–C (**1a–c**) in Scheme 1 leaving open the absolute configuration at the marked positions.[2] The isolation of a fourth member of this family of marine natural products, halipeptin D (**1d**, Scheme 1), by the group of Faulkner soon after,[3] did not reveal further stereochemical details but raised our interest in this class of natural products once halipeptin D (**1d**) was reported to exhibit strong inhibitory activity in vitro against different human cancer-cell lines.[4]

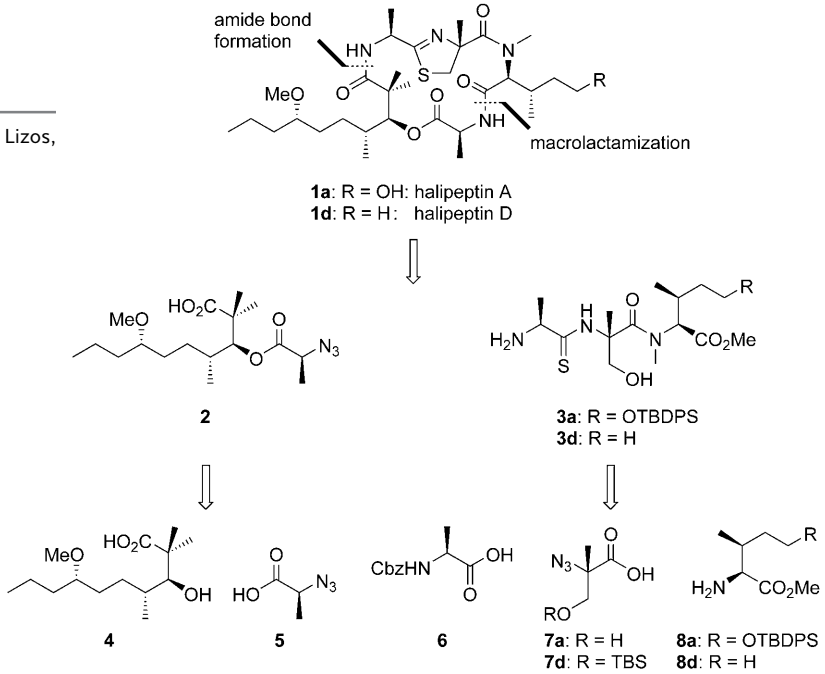


1a: R^1 = Me, R^2 = CH_2OH: halipeptin A
1b: R^1 = H, R^2 = CH_2OH: halipeptin B
1c: R^1 = H, R^2 = H : halipeptin C
1d: R^1 = Me, R^2 = Me : halipeptin D

Scheme 1. Structures of halipeptins A–D (**1a–d**). Positions of uncertain stereochemical assignment are marked *.

Determining their structural identity beyond any doubt[5] and rendering them available for further biological investigations were two reasons we undertook their total synthesis. There was a third motivation: their intriguing molecular architectures and the (subtle) challenge they posed for chemical synthesis. Indeed, these depsipeptides include in their molecular frameworks a novel, highly substituted peptide backbone connected to a hydroxylated carbon chain wrapped into a 16-membered macrolide ring. The entire C_{31} structure contains eight stereocenters (three of which are, in principle, epimerizable) and 11 methyl groups. The highly congested and conformationally rigid macrocyclic ring contains within its thread a Me-substituted thiazoline ring adjacent to an *N*-methyl-substituted amide, an arrangement that forces this linkage into a cisoid geometry, unlike the other two amide bonds that reside in their usual transoid forms. This highly substituted cisoid bond, postulated to persist even in open chain intermediates, is rare and was expected to present an unprecedented and adventurous challenge in the total synthesis of these molecules.

Our retrosynthetic analysis of halipeptins A (**1a**) and D (**1d**) (Scheme 2) relied on a retrolactamization to open the macrocycle and a subsequent retro amide-bond formation to dissect the generated chain into two key fragments, thioamides **3a** and **3d** as direct precursors for thiazoline formation, and alanine ester **2** within which are embedded both a 3-hydroxydecanoic acid domain and a masked L-alanine residue. This approach allows a late-stage construction of the thiazoline moiety, thus avoiding likely epimerization at its α position.[6] Further disconnection of these frag-

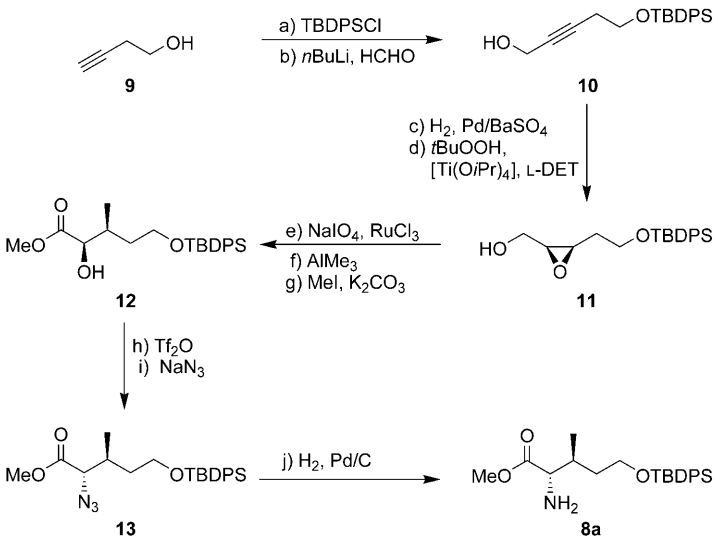


Scheme 2. Retrosynthetic analysis of halipeptins A (**1a**) and D (**1d**).

[*] Prof. Dr. K. C. Nicolaou, D. W. Kim, Dr. D. Schlawe, Dr. D. E. Lizos, R. G. de Noronha, Dr. D. A. Longbottom
Department of Chemistry and
The Skaggs Institute for Chemical Biology
The Scripps Research Institute
10550 North Torrey Pines Road, La Jolla, CA 92037 (USA)
Fax: (+1) 858-784-2469
E-mail: kcn@scripps.edu
and
Department of Chemistry and Biochemistry
University of California, San Diego
9500 Gilman Drive, La Jolla, CA 92093 (USA)

[**] We thank Dr. D. H. Huang and Dr. G. Siuzdak for NMR spectroscopic and mass spectrometric assistance, respectively. Financial support for this work was provided by the National Institutes of Health (USA), the CaPCURE Foundation, the Skaggs Institute for Chemical Biology, a predoctoral fellowship from the Foundation for Science and Technology, Portugal (grant SFRH/BD/5371/2001 to R.G.N.), and postdoctoral fellowships from the Ernst Schering Research Foundation (to D.S.) and the Royal Society Fulbright Commission (to D.A.L.).

 © 2005 Wiley-VCH Verlag GmbH & Co. KGaA, Weinheim

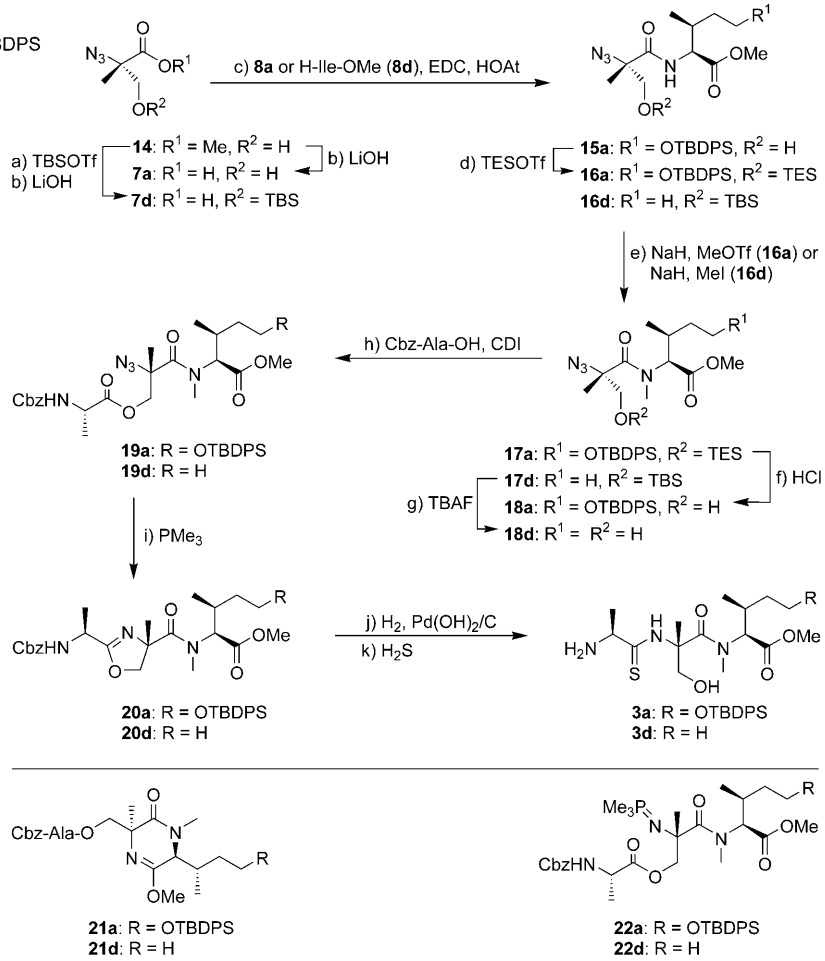


Scheme 3. Construction of TBDPS-protected δ-hydroxy-L-isoleucine methyl ester (**8a**). a) TBDPSCl (1.1 equiv), imidazole (2.2 equiv), CH_2Cl_2, 25 °C, 16 h, 99%; b) *n*BuLi (2.5 M in hexanes, 1.05 equiv), *p*-formaldehyde (1.1 equiv), Et_2O, −78→25 °C, 14 h, 72%; c) H_2 (1 atm), 5% Pd/$BaSO_4$ (7% by weight), quinoline (5% by weight), MeOH, 25 °C, 20 min, 98%; d) [Ti(O*i*Pr)$_4$] (0.3 equiv), L-DET (0.35 equiv), *t*BuOOH (2.0 equiv), M.S. (4 Å), CH_2Cl_2, −20 °C, 17 h, 99%; e) $NaIO_4$ (4.1 equiv), $RuCl_3 \cdot H_2O$ (2.2 mol%), $CCl_4/CH_3CN/H_2O$ (1:1:1.5), 25 °C, 2 h, 80%; f) $AlMe_3$ (3.0 equiv), hexanes, 25 °C, 30 h, 80%; g) MeI (1.3 equiv), K_2CO_3 (1.1 equiv), acetone, 25 °C, 18 h, 90%; h) Tf_2O (1.5 equiv), pyridine (10.0 equiv), CH_2Cl_2, 0 °C, 20 min; i) NaN_3 (1.5 equiv), DMF, 25 °C, 40 min, 75% (two steps); j) H_2 (1 atm), 10% Pd/C (30% by weight), EtOH, 25 °C, 2.5 h, 99%. DET = diethyl tartrate; DMF = *N*,*N*-dimethylformamide; M.S. = molecular sieves; TBDPS = *tert*-butyldiphenylsilyl; Tf = trifluoromethanesulfonyl.

ments led to the identification of building blocks **4**–**7** and **8a** for halipeptin A (**1a**), and **4**–**7** and **8d** for halipeptin D (**1d**), as shown in Scheme 2.

After having established[3] a stereochemically flexible route to hydroxydecanoic acid **4**,[5,7] our first objective towards the synthesis of halipeptin A (**1a**) was the construction of suitably protected δ-hydroxyisoleucine derivative[8] **8a** (Scheme 3). Silylation of homopropargylic alcohol **9** and trapping of the corresponding acetylide with formaldehyde gave propargylic alcohol **10** in 71% overall yield. Partial hydrogenation[9] of **10** with Lindlar catalyst gave the corresponding *Z* allylic alcohol (98% yield), which was subjected to Sharpless asymmetric epoxidation conditions to yield epoxy alcohol **11** in almost quantitative yield (99%). Compound **11** was then oxidized to the corresponding epoxy acid (80% yield), which was subsequently treated with $AlMe_3$[9] at ambient temperature to afford, upon methylation with MeI, hydroxyester **12** as a single isomer in 72% overall yield for the two steps. Treatment of **12** with triflic anhydride, followed by exposure of the resulting triflate to sodium azide furnished, with inversion of configuration, the orthogonally protected isoleucine derivative **13** in 75% overall yield. δ-Hydroxyisoleucine methyl ester **8a** was then obtained from **13** in quantitative yield by reduction of the azide group.

Initial attempts to obtain alanine–α-methylserine–*N*-methylisoleucine tripeptides as **3** (Scheme 2) by sequential peptide coupling failed as a result of cyclization of the dipeptide precursors upon activation (e.g. diketopiperazine formation upon reduction of azide **17d**). Instead, we devised a strategy to attach the N-terminal alanine unit that did not involve a free amino group as shown in Scheme 4. The *O*-silylated dipeptides **16a** and **16d** were obtained from α-methyl serine derivative **14**,[10] after suitable protection/deprotection steps and coupling to isoleucines **8a** and **8d**,

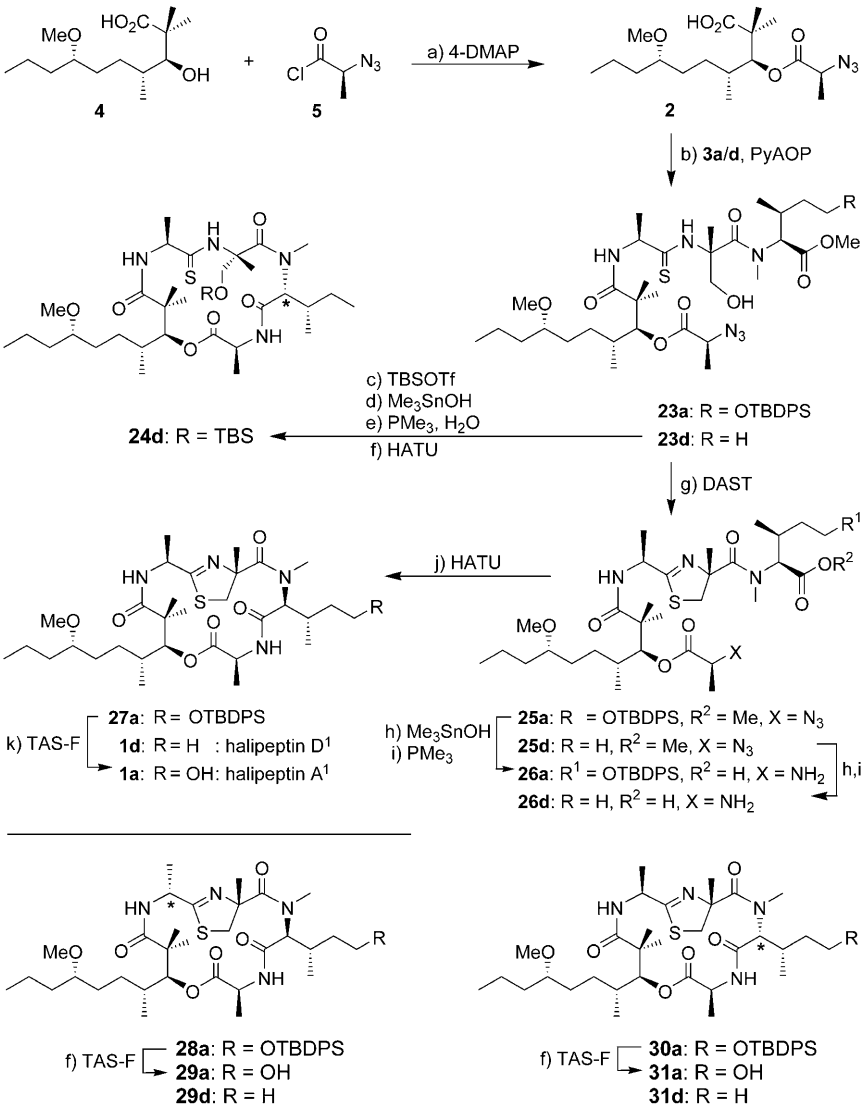


Scheme 4. Synthesis of thioamides **3a** and **3d**. a) TBSOTf (2.0 equiv), 2,6-lutidine (4.0 equiv), CH_2Cl_2, 0 °C, 1.5 h, 98%; b) LiOH·H_2O (3.0 equiv), MeOH/H_2O (4:1), 0→25 °C, 2 h, 100%; c) **8a** (1.0 equiv), EDC (1.2 equiv), HOAt (1.2 equiv), *i*Pr_2NEt (3.0 equiv), CH_2Cl_2, 25 °C, 17 h, 55% (**15a**); **8d** (2.0 equiv), EDC (2.0 equiv), HOAt (2.0 equiv), *i*Pr_2NEt (3.0 equiv), CH_2Cl_2, 25 °C, 17 h, 91% (**16d**); d) TESOTf (1.3 equiv), 2,6-lutidine (2.0 equiv), CH_2Cl_2, 0 °C, 20 min, 85%; e) NaH (4.0 equiv), MeOTf (2.5 equiv), THF, 0 °C, 1 h, 83% (**17a**); NaH (3.0 equiv), MeI (4.0 equiv), DMF, 0 °C, 1 h, 96% (**17d**); f) aqueous HCl (1 N; 20 equiv), THF, 25 °C, 1 h, 100%; g) TBAF (3.0 equiv), THF, 25 °C, 2 h, 98%; h) CDI (4.0 equiv), Cbz-Ala-OH (4.0 equiv), CH_2Cl_2, 25 °C, 0.5 h; then **18a** or **18d**, 18 h, **19a**: 88%, **19d**: 96%; i) PMe_3 (1.0 M in THF; 1.8 equiv), toluene, 25 °C, 2 h, **20a**: 79%, **20d**: 83%; j) H_2 (1 atm), 20% Pd(OH)$_2$/C (30% by weight), EtOH, 25 °C, 1 h, 100%; k) H_2S (excess), MeOH/Et_3N (2:1), 25 °C, 48–72 h, complete conversion, product not isolated. Cbz = benzyloxycarbonyl; CDI = carbonyldiimidazole; EDC = 1-(3-dimethylaminopropyl)-3-ethylcarbodiimide hydrochloride; HOAt = 1-hydroxy-7-azabenzotriazole; TBAF = tetra-*n*-butylammonium fluoride; TBS = *tert*-butyldimethylsilyl; TES = triethylsilyl.

 © 2005 Wiley-VCH Verlag GmbH & Co. KGaA, Weinheim

respectively. Deprotonation of the amide with NaH allowed selective methylation with MeOTf (→**17a**) or MeI (→**17d**), and selective desilylation with HCl or TBAF furnished the desired azide fragment **18a** (HCl) or **18d** (TBAF), respectively, which were converted into their alanine ester counterparts, **19a** (88% yield) and **19d** (96% yield), by CDI-mediated couplings with Cbz-Ala-OH in preparation for the impending tripeptide construction. It was postulated[11] that reaction of the azide group of **19a** and **19d** with a suitable phosphine reagent would generate the corresponding azaylide (**22a** and **22d**, respectively) which, upon intramolecular collapse onto the closest ester grouping, could furnish the desired oxazolines **20a** and **20d**, respectively. Indeed, this much-anticipated cascade proceeded smoothly upon exposure of **19a** and **19d** to PMe_3 in benzene or toluene at ambient temperature to furnish oxazolines **20a** (79% yield) and **20d** (83% yield) accompanied by only small amounts of the undesired six-membered rings (that is, dihydropyrazinones **21a** (17%) and **21d** (16%)). The chromatographically purified **20a** and **20d** were then converted into thioamides **3a** and **3d**, respectively, by hydrogenolytic cleavage of their Cbz group (100% yield) followed by thiolysis of the oxazoline rings with H_2S–Et_3N.[12] After evaporation of the solvents, the products **3a** and **3d** were used directly in the next step without further purification.

In our first attempt to synthesize halipeptin D (**1d**) from thioamide **5d** we improvised for a last-stage construction of the thiazoline moiety due to fears of epimerization[6] of the adjacent stereocenter (Scheme 5). The sterically congested ester **2** was prepared in 94% yield from hydroxydecanoic acid **4** and excess acid chloride **5** (10 equiv, prepared in situ from the corresponding carboxylic acid[13] and oxalyl choride in DMF) in the presence of Et_3N and 4-DMAP at 50°C. It is noteworthy that no epimerization at the azide-bearing center was observed in this step despite the basic conditions employed, as confirmed by the synthesis and characterization of the alanine epimer of **2** from **4** and *ent*-**5**. Coupling of carboxylic acid **2** with amino fragments **3a** and **3d** was best achieved by PyAOP activation in the presence of iPr$_2$NEt (92% yield). Protection of **23d** as a TBS ether (99%), selective hydrolysis of the methyl ester with Me_3SnOH[14] (52%), followed by Staudinger reduction of the azide group within the resulting carboxylic acid, and direct macrolactamization (HATU, HOAt, iPr$_2$NEt) yielded macrocycle **24d** as the only product (38%) with complete epimerization of the C-terminal isoleucine unit.



Scheme 5. Completion of the total synthesis of halipeptins A (**1a**) and D (**1d**) and their epimers **29a**, **29d**, **31a**, and **31d**. a) **5** (10.0 equiv), 4-DMAP (0.5 equiv), Et_3N (12 equiv), DMF, 50°C, 2 h, 94%; b) **3a** (1.0 equiv), PyAOP (1.5 equiv), iPr$_2$NEt (2.0 equiv), DMF, 25°C, 17 h, 71% (**23a**); **3d** (2.0 equiv), PyAOP (2.5 equiv), iPr$_2$NEt (2.5 equiv), DMF, 25°C, 17 h, 92% (**23d**); c) TBSOTf (1.2 equiv), 2,6-lutidine (1.5 equiv), CH_2Cl_2, 0°C, 0.5 h, 99%; d) Me_3SnOH (20 equiv), CH_2ClCH_2Cl, 80°C, 48 h, 52% at 79% conversion; e) PMe_3 (3.0 equiv), THF/H_2O (9:1), 25°C, 48 h; f) HATU (2.0 equiv), HOAt (2.0 equiv), iPr$_2$NEt (2.0 equiv), CH_2Cl_2 (0.5 mM), 25°C, 18 h, 38% (two steps); g) DAST (1.5 equiv), CH_2Cl_2, −78→−20°C, 1 h, **25a**: 85%; **25d**: 84%; h) Me_3SnOH (20 equiv), CH_2ClCH_2Cl, 90°C, 48–72 h, 82% from **25a**; 85% from **25d**; i) PMe_3 (2.5 equiv), THF/H_2O (9:1), 25°C, 2 h; j) HATU (2.0 equiv), HOAt (2.0 equiv), K_2CO_3 (10.0 equiv), CH_2Cl_2 (0.5 mM), 25°C, 24 h, **27a**: 31%, **28a**: 10%, **30a**: 14%; **1d**: 25%, **29d**: 5%, **31d**: 18%; k) TAS-F (5.0 equiv), DMF, 25°C, 24 h, **1a**: 85%; **29a**: 81%; **31a**: 85%. DAST = (diethylamino)sulfur trifluoride; 4-DMAP = 4-(dimethylamino)pyridine; HATU = *O*-(7-azabenzotriazol-1-yl)-*N*,*N*,*N*′,*N*′-tetramethyluronium hexafluorophosphate; PyAOP = (7-azabenzotriazol-1-yloxy)tripyrrolidinophosphonium hexafluorophosphate; TAS-F = tris(dimethylamino)-sulfur (trimethylsilyl)difluoride.

This problem was overcome by a detour, which adopted thiazoline formation prior to macrocyclization as shown in Scheme 5. Thus, exposure of thioamide intermediates **23a** and **23d** to DAST[15] in CH_2Cl_2 at −78°C led to thiazolines **25a** (85% yield) and **25d** (84% yield). Selective hydrolysis of the methyl esters of **25a** (82% yield) and **25d** (85% yield) was achieved by the mild action of Me_3SnOH,[14] delivering, upon Staudinger reduction with PMe_3/H_2O, amino acids **26a** and

 © 2005 Wiley-VCH Verlag GmbH & Co. KGaA, Weinheim

26d, respectively. The latter were utilized without isolation in the macrocyclization experiments.

Initial attempts to cyclize **26d** to halipeptin D (**1d**) under the influence of HATU in the presence of HOAt and *i*Pr_2NEt resulted in the predominant formation of, again, the isoleucine epimer **31d** (epimeric at the indicated (*) site, 17% yield from the corresponding azido carboxylic acid) which, however, this time was accompanied by the natural product, halipeptin D (**1d**, 13% from the corresponding azido carboxylic acid) and traces of **29d**, epimeric at the indicated (*) site adjacent to the thiazoline moiety. Changing the base to K_2CO_3 in the macrolactamization step increased both the yield and selectivity for the natural product (**1d**: 25% yield; **29d**: 5% yield; **31d**: 18% yield; Table 1). Owing to the profound differences in their R_f values, all isomers could be separated easily by preparative TLC (silica gel) by using hexane/EtOAc or CH_2Cl_2/acetone mixtures.

Under the HATU/HOAt/K_2CO_3 conditions for the macrolactamization step, amino acid **26a** was converted into halipeptin A TBDPS derivatives **27a** (31%; yield) and its epimers **28a** (10% yield) and **30a** (14% yield; Scheme 5). Exposure of these compounds to TAS-F liberated halipeptin A (**1a**, 86% yield) and its epimers **29a** (81% yield; Table 1) and **31a** (85% yield). Synthetic halipeptins A (**1a**) and D (**1d**) exhibited identical physical properties to those reported (**1a**,[1] **1d**[3]) for the natural products. Intriguingly, however, and despite previous reports regarding naturally derived halipeptin D,[4] synthetic halipeptin D (**1d**) and its synthesized epimers exhibited only weak toxicity against tumor cells (HCT-116 human colon carcinoma, IC_{50} values, **1d**: 32.5 μM; **29d**: 105.4 μM; **31d**: 111.4 μM).[16] Since natural halipeptin D (**1d**) was isolated from a marine species that contained several potent cytotoxic agents,[3] we attribute this discrepancy to contamination of the naturally derived material by one or more such contaminants.

The chemistry described herein confirmed the structures of halipeptins A (**1a**) and D (**1d**), highlighted their interesting chemical properties, and rendered them and their analogues readily available for further biological investigations.

Received: February 24, 2005
Revised: May 13, 2005
Published online: July 12, 2005

Keywords: macrocycles · natural products · oxazolines · thiazolines · total synthesis

[1] a) A. Randazzo, G. Bifulco, C. Giannini, M. Bucci, C. Debitus, G. Cirino, L. Gomez-Paloma, *J. Am. Chem. Soc.* **2001**, *123*, 10870–10876.

[2] C. Della Monica, A. Randazzo, G. Bifulco, P. Cimino, M. Aquino, I. Izzo, F. De Riccardis, L. Gomez-Paloma, *Tetrahedron Lett.* **2002**, *43*, 5707–5710.

[3] The isolation and characterization, the construction of certain fragments used in the present synthesis, and the total synthesis of a number of oxazoline analogues of the halipeptins are reported elsewhere: K. C. Nicolaou, D. Schlawe, D. W. Kim, D. A. Longbottom, R. G. de Noronha, D. E. Lizos, R. Rao Manam, D. J. Faulkner, *Chem. Eur. J.* **2005**, *11*, in press (DOI: 10.1002/chem.200500624).

Table 1: Selected physical properties of **1d**, **29a**, **29d**, and **31d**.

1d: colorless oil; $R_f = 0.36$ (silica, hexanes/EtOAc 1:1); $[\alpha]_D^{32} = -19.1$ ($c = 0.46$, $CHCl_3$); IR (thin film): $\tilde{\nu}_{max} = 3435, 3331, 2966, 2931, 2782, 1749, 1671, 1637, 1514, 1455, 1401, 1373, 1261, 1155, 1091, 1038, 973, 808, 756, 585\ cm^{-1}$; ^1H NMR (500 MHz, $CDCl_3$): $\delta = 7.20$ (d, $J = 7.7$ Hz, 1H), 7.01 (d, $J = 8.5$ Hz, 1H), 4.98 (d, $J = 10.3$ Hz, 1H), 4.84–4.74 (m, 2H), 4.68 (d, $J = 3.0$ Hz, 1H), 4.13 (d, $J = 12.1$ Hz, 1H), 3.28 (s, 3H), 3.27 (d, $J = 12.1$ Hz, 1H), 3.09–3.05 (m, 1H), 2.78 (s, 3H), 2.22–2.16 (m, 1H), 1.92–1.88 (m, 1H), 1.49 (d, $J = 7.4$ Hz, 3H), 1.44 (s, 3H), 1.39 (d, $J = 7.4$ Hz, 3H), 1.49–1.27 (m, 9H), 1.18 (s, 3H), 1.12 (s, 3H), 1.04–0.99 (m, 1H), 0.96–0.88 (m, 9H), 0.79 ppm (d, $J = 7.0$ Hz, 3H); ^{13}C NMR (150 MHz, $CDCl_3$): $\delta = 177.2, 173.6, 172.5, 169.6, 169.3, 83.9, 82.5, 80.6, 65.0, 56.5, 49.5, 48.5, 45.8, 44.3, 35.7, 34.2, 33.5, 31.9, 31.2, 30.7, 26.2, 25.0, 23.1, 22.3, 22.0, 18.5, 18.0, 17.7, 14.4, 14.3, 12.5$ ppm; HRMS (ESI TOF): calcd for $C_{31}H_{54}N_4O_6S$ [M+H^+]: 611.3837; found: 611.3836

29a: colorless oil; $R_f = 0.20$ (silica, EtOAc); $[\alpha]_D^{32} = -12.1$ ($c = 0.2$, $CHCl_3$); IR (thin film): $\tilde{\nu}_{max} = 3430, 2961, 2917, 2855, 1733, 1710, 1662, 1644, 1507, 1485, 1374, 1255, 1095\ cm^{-1}$; ^1H NMR (500 MHz, $CDCl_3$): $\delta = 6.79$ (d, $J = 5.5$ Hz, 1H), 6.58 (d, $J = 8.5$ Hz, 1H), 5.39 (d, $J = 10.0$ Hz, 1H), 4.87–4.84 (m, 1H), 4.78–4.75 (m, 1H), 4.74 (d, $J = 1.9$ Hz, 1H), 4.03 (d, $J = 12.0$ Hz, 1H), 3.82–3.79 (m, 1H), 3.72–3.67 (m, 1H), 3.33 (d, $J = 12.0$ Hz, 1H), 3.27 (s, 3H), 3.09–3.07 (m, 1H), 2.78 (s, 3H), 2.55–2.51 (m, 1H), 2.17–2.08 (m, 1H), 1.43 (d, $J = 6.4$ Hz, 3H), 1.41 (s, 3H), 1.31 (d, $J = 7.1$ Hz, 3H), 1.22 (s, 3H), 1.52–1.14 (m, 10H), 1.09 (s, 3H), 1.08–1.02 (m, 1H), 1.02–0.96 (m, 6H), 0.68 ppm (d, $J = 6.5$ Hz, 3H); ^{13}C NMR (125 MHz, $CDCl_3$): $\delta = 176.9, 173.6, 172.8, 170.3, 169.2, 84.7, 82.2, 80.5, 64.4, 60.9, 56.4, 49.2, 49.1, 45.1, 43.3, 35.7, 32.9, 32.3, 31.1, 30.7, 29.7, 28.3, 24.3, 23.2, 22.9, 21.5, 19.5, 18.4, 18.2, 14.3, 14.2$ ppm; HRMS (ESI TOF): calcd for $C_{31}H_{54}N_4O_7S$ [M+H^+]: 627.3786; found: 627.3790

29d: colorless oil; $R_f = 0.36$ (silica, hexanes/EtOAc 1:1); $[\alpha]_D^{32} = -13.8$ ($c = 0.45$, $CHCl_3$); IR (thin film): $\tilde{\nu}_{max} = 2965, 2924, 2874, 1749, 1673, 1638, 1613, 1507, 1452, 1397, 1371, 1261, 1095, 1035, 970, 804, 668\ cm^{-1}$; ^1H NMR (500 MHz, $CDCl_3$): $\delta = 6.79$ (d, $J = 5.5$ Hz, 1H), 6.58 (d, $J = 9.2$ Hz, 1H), 5.28 (d, $J = 10.3$ Hz, 1H), 4.87–4.81 (m, 1H), 4.77–4.72 (m, 1H), 4.71 (d, $J = 1.9$ Hz, 1H), 4.01 (d, $J = 12.2$ Hz, 1H), 3.32 (d, $J = 12.2$ Hz, 1H), 3.27 (s, 3H), 3.09–3.05 (m, 1H), 2.78 (s, 3H), 2.24–2.18 (m, 1H), 2.10–2.02 (m, 1H), 1.45 (d, $J = 6.6$ Hz, 3H), 1.43 (s, 3H), 1.32 (d, $J = 7.0$ Hz, 3H), 1.22 (s, 3H), 1.51–1.15 (m, 9H), 1.10 (s, 3H), 1.06–1.02 (m, 1H), 1.02–0.96 (m, 6H), 0.88 (t, $J = 7.1$ Hz, 3H), 0.66 ppm (d, $J = 6.6$ Hz, 3H); ^{13}C NMR (150 MHz, $CDCl_3$): $\delta = 176.9, 173.6, 172.7, 170.4, 169.3, 87.8, 82.1, 80.5, 64.8, 56.4, 49.1$ (2 peaks), $45.1, 43.4, 35.7, 33.4, 32.9, 32.3, 31.1, 30.6, 25.5, 24.3, 23.3, 22.8, 21.5, 19.5, 18.4, 17.5, 14.3, 14.1, 12.5$ ppm; HRMS (ESI TOF): calcd for $C_{31}H_{54}N_4O_6S$ [M+H^+]: 611.3837; found: 611.3833

31d: colorless oil; $R_f = 0.55$ (silica, hexanes/EtOAc 1:2); $[\alpha]_D^{32} = +6.0$ ($c = 0.15$, $CHCl_3$); IR (thin film): $\tilde{\nu}_{max} = 3413, 3342, 2966, 2932, 2861, 1743, 1667, 1637, 1514, 1455, 1373, 1261, 1096, 1032, 961, 797, 750, 585\ cm^{-1}$; ^1H NMR (500 MHz, $CDCl_3$, 3:1 ratio of conformers): $\delta = 7.17$ (d, $J = 5.3$ Hz, 1H), 7.11 (d, $J = 7.0$ Hz, 1H), 6.28 (minor d, $J = 6.5$ Hz), 6.02 (minor d, $J = 6.1$ Hz), 5.02 (d, $J = 1.7$ Hz, 1H), 4.93 (minor d, $J = 10.6$ Hz), 4.89 (minor d, $J = 2.2$ Hz), 4.84–4.83 (minor m), 4.74–4.70 (m, 1H), 4.62–4.56 (m, 1H), 4.53 (minor d, $J = 11.0$ Hz), 4.48 (d, $J = 10.9$ Hz, 1H), 3.50 (d, $J = 11.6$ Hz, 1H), 3.49 (d, $J = 11.6$ Hz, 1H), 3.27 (s, 3H), 3.24 (minor s), 3.09 (minor d, $J = 11.0$ Hz), 3.07–3.04 (m, 1H), 2.98 (s, 3H), 2.19–2.14 (m, 1H), 1.99–1.84 (m, 1H), 1.60 (d, $J = 7.0$ Hz, 3H), 1.50 (d, $J = 7.0$ Hz, 3H), 1.45 (s, 3H), 1.22 (s, 3H), 1.48–1.20 (m, 9H), 1.13 (s, 3H), 0.90–0.86 (m, 10H), 0.81–0.79 ppm (m, 3H); ^{13}C NMR (150 MHz, $CDCl_3$, 3:1 ratio of confomers, only major peaks are shown): $\delta = 174.7, 174.3, 172.4, 169.6, 169.6, 84.8, 82.8, 80.6, 63.6, 56.5, 51.6, 47.9, 45.4, 44.5, 35.6, 34.4, 33.9, 31.5, 31.2, 30.8, 26.9, 26.4, 25.7, 22.3, 20.3, 19.5, 18.4, 15.5, 14.4, 14.3, 11.6$ ppm; HRMS (ESI TOF): calcd for $C_{31}H_{54}N_4O_6S$ [M+H^+]: 611.3837; found: 611.3844

 © 2005 Wiley-VCH Verlag GmbH & Co. KGaA, Weinheim

[4] a) I. Izzo, E. Avallone, L. Della Corte, N. Maulucci, F. De Riccardis, *Tetrahedron: Asymmetry* **2004**, *15*, 1181 – 1186 (for some biological data of halippetin D, see footnote [3] in this publication); b) for data obtained by Faulkner and which appeared in a summary review, see: W. Fenical, P. R. Jensen, C. Kauffman, S. L. Mayhead, J. D. Faulkner, C. Sincich, R. M. Rao, E. J. Kantoroski, L. M. West, W. K. Strangman, Y. Shimizu, B. Li, S. Thammana, K. Drainville, M. T. Davies-Coleman, R. A. Kramer, C. R. Fairchild, W. C. Rose, R. C. Wild, G. D. Vite, R. W. Peterson, *Pharm. Biol.* **2003**, *41*, 6 – 14.

[5] In their total synthesis of halipeptin A, Ma and co-workers showed that the decanoic acid fragment had the configuration 3*S*,4*R*,7*S*: S. Yu, X. Pan, X. Lin, D. Ma, *Angew. Chem.* **2005**, *117*, 137 – 140; *Angew. Chem. Int. Ed.* **2005**, *44*, 135 – 138.

[6] a) Y. Hirotsu, T. Shiba, T. Kaneko, *Bull. Chem. Soc. Jpn.* **1970**, *43*, 1870 – 1873; b) P. Wipf, P. C. Fritch, *Tetrahedron Lett.* **1994**, *35*, 5397 – 5400.

[7] For alternative syntheses of this decanoic acid, see: a) C. Della Monica, N. Maulucci, F. De Riccardis, I. Izzo, *Tetrahedron: Asymmetry* **2003**, *14*, 3371 – 3378.

[8] For other syntheses of this building block, see: S. Hara, K. Makino, Y. Hamada, *Tetrahedron* **2004**, *60*, 8031 – 8035, and references [4a,5].

[9] For these steps, see: W. C. Still, H. Ohmizu, *J. Org. Chem.* **1981**, *46*, 5242 – 5244.

[10] a) A. Avenoza, C. Cativiela, F. Corzana, J. M. Peregrina, D. Sucunza, M. M. Zurbano, *Tetrahedron: Asymmetry* **2001**, *12*, 949 – 958; b) N. D. Smith, M. Goodman, *Org. Lett.* **2003**, *5*, 1035 – 1038.

[11] For previous examples of oxazoline construction through aza-Wittig cyclization, see: a) Yu. G. Gololobov, N. I. Gusar, M. P. Chaus, *Tetrahedron* **1985**, *41*, 793 – 799; b) J. Mulzer, A. Meier, J. Buschmann, P. Luger, *Synthesis* **1996**, 123 – 132; c) H. Kato, K. Ohmori, K. Suzuki, *Synlett* **2001**, 1003 – 1005. For thiazoline formations with triphenylphosphine see: d) G. B. Kok, M. Campbell, B. Mackey, M. von Itzstein, *J. Chem. Soc. Perkin Trans. 1* **1996**, *23*, 2811 – 2815; e) J. Chen, C. J. Forsyth, *Org. Lett.* **2003**, *5*, 1281 – 1284; f) J. Chen, C. J. Forsyth, *J. Am. Chem. Soc.* **2003**, *125*, 8734 – 8735.

[12] P. Wipf, C. P. Miller, S. Venkatraman, P. C. Fritch, *Tetrahedron Lett.* **1995**, *36*, 6395 – 6398.

[13] J. T. Lundquist, J. C. Pelletier, *Org. Lett.* **2001**, *3*, 781 – 783.

[14] a) K. C. Nicolaou, A. A. Estrada, M. Zak, S. H. Lee, B. S. Safina, *Angew. Chem.* **2005**, *117*, 1402 – 1406; *Angew. Chem. Int. Ed.* **2005**, *44*, 1378 – 1382; b) R. L. E. Furlan, E. G. Mata, O. A. Mascaretti, *J. Chem. Soc. Perkin Trans. 1* **1998**, 355 – 358; c) R. L. E. Furlan, E. G. Mata, O. A. Mascaretti, C. Pena, M. P. Coba, *Tetrahedron* **1998**, *54*, 13023 – 13034; d) R. L. E. Furlan, E. G. Mata, O. A. Mascaretti, *Tetrahedron Lett.* **1996**, *37*, 5229 – 5232.

[15] P. Lafargue, P. Guenot, J.-P. Lellouche, *Heterocycles* **1995**, *41*, 947 – 958.

[16] We thank Professor William Fenical for these biological data.

 © 2005 Wiley-VCH Verlag GmbH & Co. KGaA, Weinheim

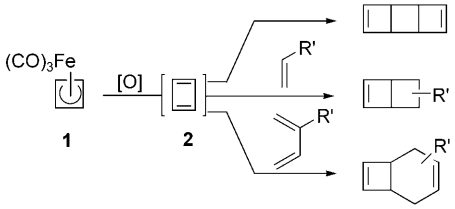
Cycloaddition

DOI: 10.1002/anie.200501100

Intramolecular [2+2+1] Cycloadditions with (Cyclobutadiene)tricarbonyliron**

*Benjamin A. Seigal, Mi Hyun An, and Marc L. Snapper**

Oxidative decomplexation of (cyclobutadiene)tricarbonyliron (**1**) is a convenient method for the generation of free cyclobutadiene (**2**).[1] Once released from the metal, this reactive, antiaromatic species can undergo rapid dimerization [Eq. (1)]. When cyclobutadiene is generated in the presence of olefins or dienes, intermolecular cycloadditions can occur which lead to various cyclobutene-containing adducts [Eqs. (2) and (3)].

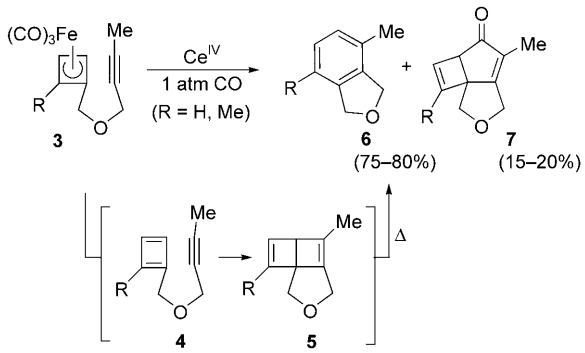


(1)

(2)

(3)

In 1974, Grubbs et al. studied intramolecular cycloadditions between cyclobutadiene and tethered alkynes [e.g., Eq. (4)].[2] The major product isolated from this reaction was compound **6**, which presumably was generated through rearrangement of the Dewar benzene cycloadduct **5**. In



(4)

[*] B. A. Seigal, M. H. An, Professor M. L. Snapper
Department of Chemistry
Merkert Chemistry Center, Boston College
Chestnut Hill, MA 02467 (USA)
Fax: (+1) 617-552-1442
E-mail: marc.snapper@bc.edu

[**] We thank the National Institute of General Medical Sciences (National Institutes of Health, GM62824) for financial support. We are grateful to Schering-Plough for support from their X-ray facility.

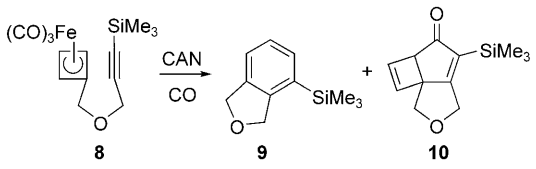
Supporting information for this article is available on the WWW under http://www.angewandte.org or from the author.

© 2005 Wiley-VCH Verlag GmbH & Co. KGaA, Weinheim

addition, a minor amount of ketone **7** was also obtained.[3] Elegant studies with chiral, nonracemic iron complexes (such as **3**, R = Me) suggested that **5** was formed through a [4+2] cycloaddition of a metal-free intermediate **4**, whereas the generation of cycloadduct **7** appeared to involve a more participative role for the ironcarbonyl component.

Given the synthetic utility of intramolecular cycloadditions of cyclobutadiene,[4] coupled with the established usefulness of the fused-ring system found in **7**,[5] we sought to develop this intramolecular cyclobutadiene [2+2+1] cycloaddition (the Pauson–Khand reaction) into an effective methodology.[6] Specifically, our goals were to improve the efficiency of the [2+2+1] cycloaddition and expand the substrate scope of the reaction.[7] Our preliminary steps towards these objectives are reported herein.

Our first aim was to improve the yield of the carbonylative cycloaddition process. We reasoned that a slower rate of oxidation of the iron complex in the presence of carbon monoxide would favor the iron-mediated Pauson–Khand reaction over the oxidative release of free cyclobutadiene required in the Diels–Alder reaction. Our initial efforts focused on the cycloaddition of alkyne **8** [Eq. (5)]. After



8 **9** **10** (5)

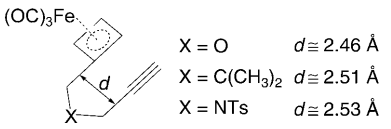
optimization of the reaction conditions (solvent, oxidant, reaction temperature, rate of addition of oxidant, CO pressure, and additives), we were able to improve the yield of adduct **10** obtained from the Pauson–Khand reaction from 15 to 60%, while minimizing the formation of the Diels–Alder product **9**. Further optimization of the workup, combined with the use of purified ammonium cerium(IV) nitrate (CAN),[8] increased the efficiency of the [2+2+1] cycloaddition to provide ketone **10** in 77% yield.[9]

The investigation of additional substrates is summarized in Table 1. Under the optimized Pauson–Khand conditions, the original Grubbs alkyne **11** afforded the [2+2+1] cycloadduct **12** in 91% yield (entry 2). Likewise, the sterically hindered *t*Bu alkyne **13** underwent [2+2+1] cyclization to provide **14** in 78% yield (entry 3). On the other hand, the cycloaddition of electron-deficient alkynes, such as **15**, did not undergo the desired [2+2+1] cycloaddition, but instead only generated the [4+2] cycloadduct **16** (entry 4).

On the basis of the emerging trend of electron-rich alkynes performing efficiently in this cycloaddition, we expected aryl alkynes to act similarly. In this regard, the oxidation of a *p*-methoxyphenyl alkyne **17** generated the desired [2+2+1] cycloadduct **18** in 71% yield as well as the [4+2] cycloadduct **19** in 20% yield (entry 5). Similar results were seen with a phenyl alkyne substrate **20**, which provided the [2+2+1] cycloadduct **21** in 69% yield, along with **22** in 24% yield (entry 6). Furthermore, it was demonstrated that terminal alkynes, such as **23**, will also take part in the Pauson–Khand reaction, as cycloadduct **24** was obtained in 60% yield (entry 7).

We next examined the influence of the tether functionality on the course of the cycloaddition. We replaced the oxygen atom in the tether with a *gem*-dimethyl group, thereby taking advantage of the reactive rotamer effect in the cycloaddition.[10] Oxidative carbonylation of the propargyl methyl ether **25** led to the desired [2+2+1] cycloadduct in 55% yield as a mixture of hydroxy diastereomers ($\beta/\alpha = 1.8{:}1$), with only a trace amount of the [4+2] cycloadduct (entry 8). In contrast, a phenyl alkyne **27** delivered a Pauson–Khand product **28** that favored the opposite diastereoselectivity ($\beta/\alpha = 1{:}3$) in 57% yield of combined product, as well as the Diels–Alder product **29** in 30% yield (entry 9). When the hydroxy group of **25** was protected as a MOM ether to generate **30**, oxidation resulted in the formation of the [2+2+1] cycloadduct **31** as a single diastereomer in 62% yield (entry 10). The sensitive role of the tether functionality in these cycloadditions was further demonstrated in entry 11 (compare with entries 6 and 9): oxidation of the *p*-toluenesulfonate-protected amine **33** favored the formation of the [4+2] cycloadduct **35** over the [2+2+1] cycloadduct **34**.

Previous studies have indicated that the intramolecular [4+2] cycloaddition of cyclobutadiene is sensitive to distortions imparted by the tether functionality on the transition-state geometries.[4c,d] The Pauson–Khand cycloadditions presented above also appear to be influenced by the geometry of the tether group. Although the transition state in the iron-mediated Pauson–Khand reaction is unclear at this time the span, or "bite size", of the tether group does correlate with the ratio of [2+2+1]/[4+2] cycloadducts obtained. The identity of the atoms used to connect the cyclobutadiene and the alkyne units can provide different idealized ground-state geometries (Scheme 1). Thus, the energetic cost of the distortion in each of these systems in their respective cycloaddition transition states may be different.

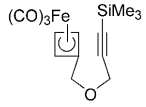
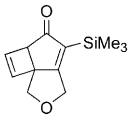
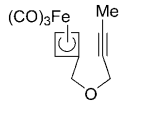
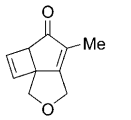
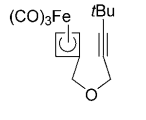
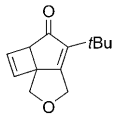
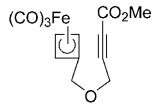
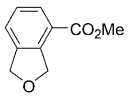
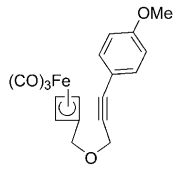
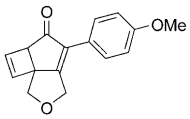
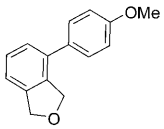
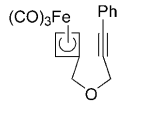
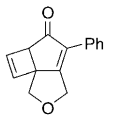
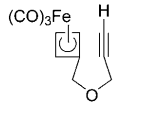
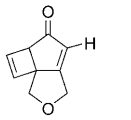
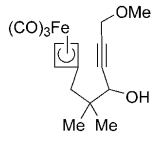
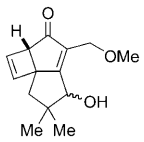
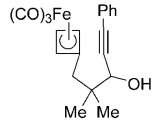
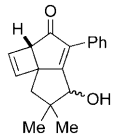
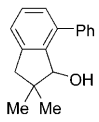
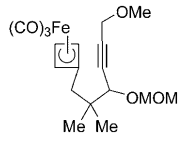
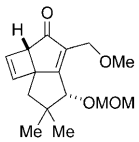
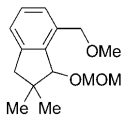
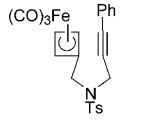
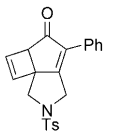
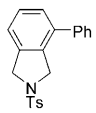


Scheme 1. Composition and geometry of the tether.

The results of the cyclization reactions for phenyl alkynes **20**, **27**, and **33** showed that an increase in the distance between the alkyne and the cyclobutadiene units disfavors the Pauson–Khand process relative to the Diels–Alder reaction. The cycloaddition of **20** (X = O), in which the ether tether allows a closer relationship between the reactive functionalities, provided the highest ratio of [2+2+1]/[4+2] cycloadducts (**21**/**22** = 2.9:1, entry 6). On the other hand, the *p*-toluenesulfonate amide linker in **33** (X = NTs) increases the distance between the alkyne and cycloabutadiene units, thus leading to an unfavorable ratio of [2+2+1]/[4+2] cycloadducts (**34**/**35** = 0.5:1, entry 11). Substrate **27**, with a *gem*-dimethyl linker (X = $C(CH_3)_2$), has a bite size between that of **20** and **33** and,

 © 2005 Wiley-VCH Verlag GmbH & Co. KGaA, Weinheim

Table 1: Intramolecular [2+2+1] cycloadditions.[a]

Entry	Alkyne	[2+2+1] Cycloadduct	Yield [%][a]	[4+2] Cycloadduct	Yield [%][a]
1			77	–	–
2			91	–	–
3			78	–	–
4		–	–		67
5			71		20
6			69		24
7			60	–	–
8			55[b]	–	–
9			57[c]		30
10			62		21
11			29		63

[a] An average of the two highest yields of isolated product. [b] $\beta/\alpha = 1.8{:}1$. [c] $\beta/\alpha = 1{:}3$. MOM = methoxymethyl. Ts = *p*-toluenesulfonate.

accordingly, provided an intermediate ratio of products (**28**/**29** = 1.9:1, entry 9).

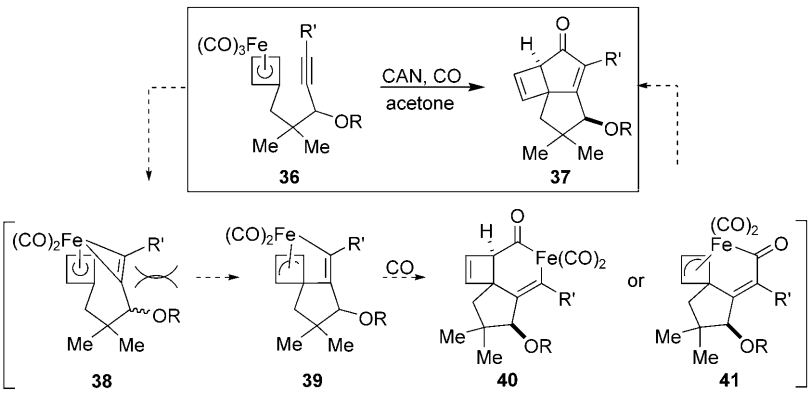
In addition to the influence of the tether geometry, there are also diastereoselectivity questions regarding the cycloaddition reactions of the hydroxy-substituted *gem*-dimethyl substrates **25**, **27**, and **30**. The mechanism of the [2+2+1] cycloaddition needs to be considered to gain insight into these trends (Scheme 2).[3] Conversion of alkyne **36** into the Pauson–Khand product **37** is likely to involve several steps. Depending on the reversibility of the steps, the diastereomeric control observed could result from favorable hydrogen-bonding interactions (entry 8) or unfavorable allylic strain (entries 9 and 10) in intermediates such as **38**. The importance of this latter interaction was particularly evident in the cyclization of the MOM-protected substrate **30**, where only diastereomer **31** was observed (entry 10).

In summary, we have developed a cyclobutadiene [2+2+1] cycloaddition that allows the efficient preparation of highly functionalized cyclobutene-containing systems in synthetically useful yields. In this process, the tricarbonyliron functionality, which usually serves to protect the cyclobutadiene against unwanted side reactions, also mediates a [2+2+1] cycloaddition with various alkynyl side chains. Both electronic and steric factors were found to influence the course of the reaction. Further studies will focus on expanding the scope of the cyclobutadiene [2+2+1] cycloaddition, as well as evaluating the transformation in the syntheses of targets of interest.

Received: March 28, 2005
Published online: July 11, 2005

Keywords: alkenes · alkynes · cycloaddition · cyclobutadiene · intramolecular reactions

 © 2005 Wiley-VCH Verlag GmbH & Co. KGaA, Weinheim



Scheme 2. Diastereoselectivity observed in the [2+2+1] cycloaddition.

[1] a) G. F. Emerson, L. Watts, R. Pettit, *J. Am. Chem. Soc.* **1965**, *87*, 131; b) M. Rosenblum, C. Gatsonis, *J. Am. Chem. Soc.* **1967**, *89*, 5074; c) L. A. Paquette, L. D. Wise, *J. Am. Chem. Soc.* **1967**, *89*, 6659; d) R. H. Grubbs, *J. Am. Chem. Soc.* **1970**, *92*, 6993; e) R. H. Grubbs, R. A. Grey, *J. Chem. Soc. Chem. Commun.* **1973**, 76; f) R. Pettit, *J. Organomet. Chem.* **1975**, *100*, 205; g) J. D. Fitzpatrick, L. Watts, G. F. Emerson, R. Pettit, *J. Am. Chem. Soc.* **1965**, *87*, 3254; h) G. Maier, *Angew. Chem.* **1974**, *86*, 491; *Angew. Chem. Int. Ed. Engl.* **1974**, *13*, 425; i) A. Efraty, *Chem. Rev.* **1977**, *77*, 691; j) A. A. Deniz, K. S. Peters, G. J. Snyder, *Science*, **1999**, *286*, 1119; k) T. Bally, S. Masamune, *Tetrahedron* **1980**, *36*, 343; l) Y. Li, K. N. Houk, *J. Am. Chem. Soc.* **1996**, *118*, 880, and references therein; m) L. Watts, J. D. Fitzpatrick, R. Pettit, *J. Am. Chem. Soc.* **1965**, *87*, 3253; n) R. H. Grubbs, R. A. Grey, *J. Am. Chem. Soc.* **1973**, *95*, 5765; o) E. K. G. Schmidt, *Angew. Chem.* **1973**, *85*, 820; *Angew. Chem. Int. Ed. Engl.* **1973**, *12*, 777; p) E. K. G. Schmidt, *Chem. Ber.* **1975**, *108*, 1599; q) for a discussion of cycloadditions between cyclobutadiene and unsaturated compounds coordinated to an iron center, see: J. S. Ward, R. Pettit, *J. Am. Chem. Soc.* **1971**, *93*, 262; r) L. Watt, J. D. Fitzpatrick, R. Pettit, *J. Am. Chem. Soc.* **1966**, *88*, 623.

[2] R. H. Grubbs, T. A. Pancoast, R. A. Grey, *Tetrahedron Lett.* **1974**, *15*, 2425.

[3] R. H. Grubbs, T. A. Pancoast, *J. Am. Chem. Soc.* **1977**, *99*, 2382.

[4] a) J. A. Tallarico, M. L. Randall, M. L. Snapper, *J. Am. Chem. Soc.* **1996**, *118*, 9196; b) J. Limanto, M. L. Snapper, *J. Org. Chem.* **1998**, *63*, 6440; c) J. Limanto, J. A. Tallarico, J. R. Porter, S. K. Khuong, K. N. Houk, M. L. Snapper, *J. Am. Chem. Soc.* **2002**, *124*, 14748; d) J. Limanto, S. K. Khuong, K. N. Houk, M. L. Snapper, *J. Am. Chem. Soc.* **2003**, *125*, 16310; e) M. L. Snapper, J. A. Tallarico, M. L. Randall, *J. Am. Chem. Soc.* **1997**, *119*, 1478; f) M. L. Randall, P. Lo, P. J. Bonitatebus, Jr., M. L. Snapper, *J. Am. Chem. Soc.* **1999**, *121*, 4534; g) J. Limanto, M. L. Snapper, *J. Am. Chem. Soc.* **2000**, *122*, 8071; h) H. L. Deak, S. S. Stokes, M. L. Snapper, *J. Am. Chem. Soc.* **2001**, *123*, 5152; i) P. C.-K. Lo, M. L. Snapper, *Org. Lett.* **2001**, *3*, 2819; j) S. J. Bader, M. L. Snapper, *J. Am. Chem. Soc.* **2005**, *127*, 1201.

[5] a) P. Magnus, L. M. Principe, M. J. Slater, *J. Org. Chem.* **1987**, *52*, 1483; b) N. H. Vo, B. B. Snider, *J. Org. Chem.* **1994**, *59*, 5419; c) Y. Tobe, T. Yamashita, K. Kakiuchi, Y. Odaira, *J. Chem. Soc. Chem. Commun.*, **1985**, 898; d) P. Magnus, M. J. Slater, L. M. Principe, *J. Org. Chem.* **1989**, *54*, 5148.

[6] For select reviews of the Pauson–Khand reaction, see: a) I. Ojima, M. Tzamarioudaki, Z. Li, R. J. Donovan, *Chem. Rev.* **1996**, *96*, 635; b) H. Frühauf, *Chem. Rev.* **1997**, *97*, 523; c) J. Blanco-Urgoiti, L. Añorbe, L. Pérez-Serrano, G. Domínguez, J. Pérez-Castells, *Chem. Soc. Rev.* **2004**, *33*, 32; d) S. E. Gibson, A. Stevenazzi, *Angew. Chem.* **2003**, *115*, 1844; *Angew. Chem. Int. Ed.* **2003**, *42*, 1800; e) K. M. Brummond, J. L. Kent, *Tetrahedron* **2000**, *56*, 3263; for examples of specific transformations, see: f) iron: H. Knölker, E. Baum, J. Heber, *Tetrahedron Lett.* **1995**, *36*, 7647; g) titanium: N. M. Kablaoui, F. A. Hicks, S. L. Buchwald, *J. Am. Chem. Soc.* **1997**, *119*, 4424; h) zirconium: T. Takahashi, S. Huo, R. Hara, Y. Noguchi, K. Nakajima, W. Sun, *J. Am. Chem. Soc.* **1999**, *121*, 1094; i) molybdenum: H. Xiong, R. P. Hsung, L. Wei, C. R. Berry, J. A. Mulder, B. Stockwell, *Org. Lett.* **2000**, *2*, 2869; j) ruthenium: T. Kondo, N. Suzuki, T. Okada, T. Mitsudo, *J. Am. Chem. Soc.* **1997**, *119*, 6187.

[7] For an example of a catalytic intermolecular Pauson–Khand cycloaddition with a cyclobutadiene surrogate, see: S. E. Gibson, N. Mainolfi, S. B. Kalindjian, P. T. Wright, *Angew. Chem.* **2004**, *116*, 5798; *Angew. Chem. Int. Ed.* **2004**, *43*, 5680.

[8] W. L. F. Armarego, D. D. Perrin, *Purification of Laboratory Chemicals*, Butterworth-Heinemann, Oxford, **2000**, p. 376.

[9] Representative cycloaddition procedure: Carbon monoxide was bubbled through a solution of (cyclobutadiene)tricarbonyliron in acetone for 20 min, and then the solution was stirred in an atmosphere of carbon monoxide at room temperature for the remainder of the reaction. A solution of CAN (5 equiv) in acetone was added over 3.0 h by syringe pump to the reaction mixture. At the conclusion of the slow addition, the reaction mixture was quenched with saturated aqueous $NaHCO_3$ and then concentrated under vacuum (to remove the acetone). The aqueous solution was extracted with CH_2Cl_2, the combined organic layers were washed with brine, dried over $MgSO_4$, and the organic solvent was removed under vacuum. The cycloaddition product was then purified by chromatography on silica gel.

[10] a) D. F. DeTar, N. P. Luthra, *J. Am. Chem. Soc.* **1980**, *102*, 4505; b) M. E. Jung, J. Gervay, *J. Am. Chem. Soc.* **1991**, *113*, 224.

 © 2005 Wiley-VCH Verlag GmbH & Co. KGaA, Weinheim

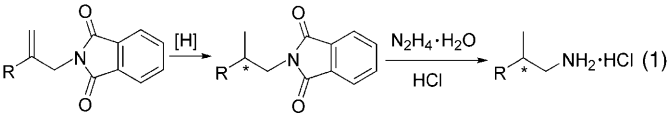
Asymmetric Catalysis

DOI: 10.1002/anie.200501332

Enantioselective Hydrogenation of Allylphthalimides: An Efficient Method for the Synthesis of β-Methyl Chiral Amines**

*Chun-Jiang Wang, Xianfeng Sun, and Xumu Zhang**

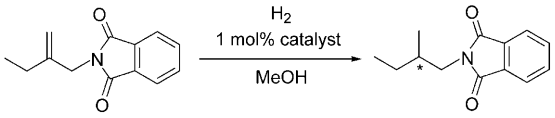
Chiral amines bearing a β-methyl group on the chiral center, and their derivatives, are key structural elements in natural products and pharmaceuticals.[1–3] For example, compound **A** is a key intermediate in the synthesis of the leukotrienes (LTs) receptor antagonist (Zeneca ZD 3532, a phase II drug candidate; Scheme 1). This compound is particularly useful for the treatment of asthma.[2] Compound **B** (NPS 1392) is a potent stereoselective antagonist of the NMDA receptor, which can be used for the control of ischemic strokes.[3] To our knowledge, there has been no successful catalytic method to make such important functional groups. Although some stoichiometric asymmetric synthesis or resolution routes have been reported for constructing this class of chiral amines,[2–4] the development of efficient and catalytic synthetic methods remains a significant challenge. Herein we report the first highly enantioselective catalytic asymmetric hydrogenation of disubstituted allylphthalimides[5] to form chiral phthalimides, which act as precursors to the β-methyl chiral amines [Eq. (1)].



(1)

We initiated our studies on the asymmetric hydrogenation of an *N*-2-ethylallylphthalimide (**6a**) by screening several known catalysts. Since the asymmetric hydrogenation of functionalized olefins using chiral phosphine/Rh complexes is well known,[6] a diverse array of bisphosphine/Rh complexes could be applied as catalyst precursors in this hydrogenation reaction. Some representative results are shown in Table 1.

Table 1: Asymmetric hydrogenation of **6a**.

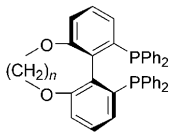


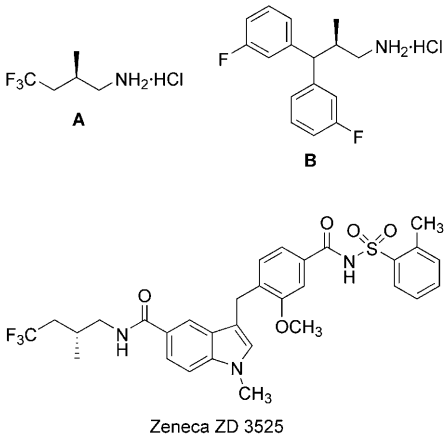
6a **7a**

Entry	Catalyst	*T* [°C]	$P(H_2)$ [atm]	Conv. [%]	*ee* [%][a]
1	**1**	RT	5	100	21
2	**2**	RT	5	100	15
3	**3c**	RT	5	0	NA
4	**3c**	80	100	100	96

[a] Determined by chiral-phase GC (see the Supporting Information).

[Rh(cod){(1*S*,1*S*′,2*R*,2*R*′)-tangphos}]BF_4 (**1**)
[Rh(cod)(*R*,*R*)-(Et-duphos)]BF_4 (**2**)
[$RuCl_2${(*S*)-C_n-tunephos}](dmf)$_m$ (**3a–f**)
$n=1$, **3a**; $n=2$, **3b**; $n=3$, **3c**
$n=4$, **3d**; $n=5$, **3e**; $n=6$, **3f**
(*S*)-C_n-tunephos, $n=1$–6





Scheme 1. Examples of β-methyl chiral amine hydrochlorides and Zeneca ZD 3525.

Although the complexes [Rh(cod){(1*S*,1*S*′,2*R*,2*R*′)-tangphos}]BF_4 (**1**)[7] (cod = cycloocta-1,5-diene, tangphos = 1,1′-di-*tert*-butyl-[2,2′]-diphosphanyl) and [Rh(cod){(*R*,*R*)-Et-duphos}]BF_4 (**2**)[8] (duphos = 1,2-bis(phospholanyl)benzene) were successful for the highly enantioselective hydrogenation of various substituted olefins, only low enantioselectivities were obtained at room temperature under low hydrogen pressure (Table 1, entries 1 and 2). However, Ru–diphosphine complexes have also been applied to asymmetric hydrogenation reactions. Catalyst **3c**[9] exhibited no reactivity under similar conditions (Table 1, entry 3). However, up to 96% *ee* and 100% conversion was observed when high hydrogen pressure (100 atm) and high temperature (80°C) were employed (Table 1, entry 4)

Encouraged by the results described above, we investigated the effects of solvents and catalyst precursors to enable the reaction conditions to be optimized (Table 2). A dramatic solvent effect was observed. Complex **3c** performs well in a number of alcohols to give **7a** with moderate to high enantioselectivities (Table 2, entries 1–4); an excellent level of enantioselectivity was observed when the reaction was carried out in methanol. Reaction in other solvents such as

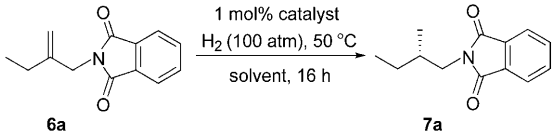
[*] Dr. C.-J. Wang, X. Sun, Prof. X. Zhang
Department of Chemistry
The Pennsylvania State University
University Park, PA, 16802 (USA)
Fax: (+1) 814-863-8403
E-mail: xumu@chem.psu.edu

[**] This work was supported by the National Institutes of Health. We acknowledge the generous gift of Ru complexes from Heraeus Inc.

Supporting information for this article is available on the WWW under http://www.angewandte.org or from the author.

© 2005 Wiley-VCH Verlag GmbH & Co. KGaA, Weinheim

Table 2: Effects of solvents and catalyst precursors on the asymmetric hydrogenantion of **6a**.



6a **7a**

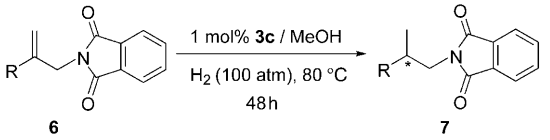
Entry	Catalyst	Solv.	Conv. [%]	*ee* [%][a]
1	**3c**	MeOH	100	96
2	**3c**	EtOH	100	76
3	**3c**	TFE[b]	100	37
4	**3c**	*i*PrOH	100	23
5	**3c**	CH_2Cl_2	0	NA
6	**3c**	EtOAc	100	19
7	**3c**	THF	100	12
8	**3a**	MeOH	100	88
9	**3b**	MeOH	100	91
10	**3d**	MeOH	100	94
11	**3e**	MeOH	100	92
12	**3f**	MeOH	100	92

[a] Determined by chiral-phase GC. [b] TFE = trifluoroethanol. NA = not available.

CH_2Cl_2, EtOAc, or THF led to lower enantioselectivities and reactivities (Table 2, entries 5–7). To test the effect of the dihedral angle of the chiral biaryl ligands on the enantioselectivity of the reaction, a set of tunephos[9] ligands with different dihedral angles were employed (Table 2, entries 1 and 8–12). The best result was observed when (*S*)-C_3-tunephos was used as the ligand (Table 1, entry 1).

The asymmetric hydrogenation reaction was carried out on a variety of substrates under the optimal reaction conditions (Table 3). Substrates with a primary *n*-alkyl substituent such as ethyl, *n*-butyl, or benzyl group at the 2-position of the allylphthalimides afforded products with high *ee* values (Table 3, entries 1–3). Several substrates with bulky substituents were also employed to probe the steric effects of the substituent on this hydrogenation system. The enantioselectivities decreased gradually along with increased steric hindrance of the substituents in the substrates (Table 3, entries 2 and 4–6). However, hydrogenation of cyclohexyl- and cyclopentyl-substituted substrates (**6g** and **6h**) still afforded products in 98 and 96% *ee*, respectively (Table 3, entries 7 and 8). The hydrogenation of the aromatic substrate **6i** proceeded smoothly with moderate enantioselectivity (Table 3, entry 9). To our surprise, 2-chloroallylphthalimide (**6j**) can also be hydrogenated and **7j** was obtained with up to 93% *ee* (Table 3, entry 10).

Table 3: Asymmetric hydrogenantion of *N*-2-substituted allylphthalimides.

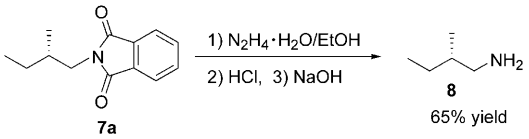


6 **7**

Entry	Substrate	R	Product	Yield [%][a]	*ee* [%]
1[b]	**6a**	Et	**7a**	98.5	96[c]
2	**6b**	*n*Bu	**7b**	98.0	96[c]
3	**6c**	Bn	**7c**	97.0	92[d]
4	**6d**	*i*Pu	**7d**	94.0	91[c]
5	**6e**	*i*Pr	**7e**	93.0	84[c]
6	**6f**	*t*Bu	**7f**	96.0	67[c]
7	**6g**	cyclohexyl	**7g**	95.0	98[c]
8	**6h**	cyclopentyl	**7h**	96.0	96[c]
9[b]	**6i**	Ph	**7i**	97.0	55[d]
10	**6j**	Cl	**7j**	97.0	93[c]

[a] Yield of isolated product. [b] The reaction was performed at 50 °C in 16 h. [c] Determined by chiral-phase GC. [d] Determined by chiral-phase HPLC.

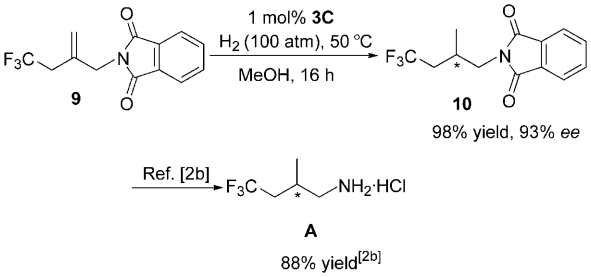
To determine the configuration of the hydrogenation product **7a** obtained with (*S*)-C_3-tunephos as a chiral ligand, phthalimide **7a** was hydrolyzed in refluxing ethanol in the presence of $NH_2NH_2{\cdot}H_2O$ followed by treatment with concentrated HCl according to a literature procedure to form the known compound **8** in 65% yield [Eq. (2)].[2b,10] The absolute



7a **8** 65% yield (2)

stereochemistry of **7a** was assigned as *S* by comparing the sign of the optical rotation of the obtained compound **8** with the reported data[4] (see the Supporting Information).

This asymmetric hydrogenation method can be applied to the preparation of the key intermediate **A** for the synthesis of the LTs receptor antagonist (Zeneca ZD3532;[2] Scheme 1). To the best of our knowledge, asymmetric hydrogenation provides the simplest method for the synthesis of this compound [Eq. (3)].



9 **10** **A** 88% yield[2b] (3)

In conclusion, we have developed the first highly enantioselective method for the synthesis of chiral phthalimides with a β-methyl group on the chiral center based on asymmetric hydrogenation, and up to 98% *ee* has been achieved with a Ru–C_3-tunephos catalyst. The synthetic utility has been demonstrated through the synthesis of the key intermediate **A** of the LTs receptor antagonist (Zeneca ZD3532). Since these hydrogenation substrates are easily obtainable, this methodology is potentially practical for the synthesis of such chiral amines, which are important pharmaceutical intermediates.

 © 2005 Wiley-VCH Verlag GmbH & Co. KGaA, Weinheim

Experimental Section

General hydrogenation procedure: $[RuCl_2(cymene)]_2$ (6.2 mg, 0.01 mmol) and (*S*)-C_3-tunephos (12.5 mg, 0.021 mmol) were dissolved in degassed DMF (3 mL) in a Schlenk tube under N_2. The solution was heated at 100 °C for 3.5 h. After the mixture had cooled to 50 °C, the solvent was removed under vacuum to give the catalyst as an orange-red solid. The catalyst was dissolved in degassed methanol (16 mL) in a glovebox and divided equally between eight vials. Substrate (0.25 mmol) was then added to the catalyst solution and the resulting mixture transferred to an autoclave and charged with H_2 (100 atm). The autoclave was stirred at 50 or 80 °C for 16–48 h, before cooling it to room temperature and carefully releasing the H_2. The solvent was then evaporated and the residue was purified by column chromatography to give the corresponding hydrogenation product, which was then analyzed directly by chiral-phase GC (gamma dex 225) or HPLC (Chiralpak AD) to determine the enantiomeric excess.

Received: April 17, 2005
Published online: June 27, 2005

Keywords: amines · asymmetric catalysis · enantioselectivity · hydrogenation · ruthenium

[1] a) S. Omura, *Macrolide Antibiotics*, Academic Press, Orlando, FL, **1984**; b) G. Lazarevski, G. Kobrehel, B. Metelko, H. Duddeck, *J. Antibiot.* **1996**, *49*, 1066; c) G. M. Nicholas, T. F Molinski, *Tetrahedron* **2000**, *56*, 2921.

[2] For the chemistry and biology of compound **A**, see: a) R. T. Jacobs, P. R. Bernstein, L. A. Cronk, E. P. Vacek, L. F. Newcomb, D. Aharony, C. K. Buckner, Kusner, E. J. *J. Med. Chem.* **1994**, *37*, 1282; b) R. T. Jacobs, Y. K. Yee, P. R. Bernstein, A. G. Brewster, G. J. Sependa, EP 489548A1, **1992**.

[3] For the chemistry and biology of compound **B**, see: S. T. Moe, S. M. Shimizu, D. L. Smith, B. C. Van Wagenen, E. G. DelMar, M. F. Balandrin, Y. Chien, J. L. Raszkiewicz, L. D. Artman, A. L Mueller, E. Lobkovsky, J. Clardy, *Bioorg. Med. Chem. Lett.* **1999**, *9*, 1915.

[4] T. Tachihara, S. Ishizaki, Y. Kurobayashi, H. Tamura, Y. Ikemoto, A. Onuma, K. Yoshikawa, T. Yanai, T. Kitahara, *Helv. Chim. Acta* **2003**, *86*, 274.

[5] a) Although the hydrogenation of some trisubstituted allylphthalimides can also form the desired products, the enantioselectivities were much lower than those reduced from disubstituted substrates (see the Supporting Information); b) A. Lei, S. Wu, M. He, X. Zhang, *J. Am. Chem. Soc.* **2004**, *126*, 1626.

[6] a) R. Noyori, *Asymmetric Catalysis in Organic Synthesis*, Wiley, New York, **1994**; b) I. Ojima, *Catalytic asymmetric synthesis*, Wiley-VCH, New York, **2000**; c) W. Tang, X. Zhang, *Chem. Rev.* **2003**, *103*, 3029.

[7] a) W. Tang, X. Zhang, *Angew. Chem.* **2002**, *114*, 1682; *Angew. Chem. Int. Ed.* **2002**, *41*, 1612; b) W. Tang, X. Zhang, *Org. Lett.* **2002**, *4*, 4159; c) W. Tang, D. Liu, X. Zhang, *Org. Lett.* **2003**, *5*, 205.

[8] M. J. Burk, J. E. Feaster, W. A. Nugent, R. L. Harlow, *J. Am. Chem. Soc.* **1993**, *115*, 10125.

[9] Z. Zhang, H. Qian, J. Longmire, X. Zhang, *J. Org. Chem.* **2000**, *65*, 6223.

[10] H. Brunner, J. Wachter, J. Schmidbauer, *Organometallics* **1986**, *5*, 2212.

 © 2005 Wiley-VCH Verlag GmbH & Co. KGaA, Weinheim

Asymmetric Catalysis

DOI: 10.1002/anie.200501318

Construction of Pseudo-Heterochiral and Homochiral Di-μ-oxotitanium(Schiff base) Dimers and Enantioselective Epoxidation Using Aqueous Hydrogen Peroxide

*Kazuhiro Matsumoto, Yuji Sawada, Bunnai Saito, Ken Sakai, and Tsutomu Katsuki**

Remarkable advances in asymmetric synthesis using optically active metal complexes as catalysts have been achieved in the last half century.[1] Monometallic complexes are used as the catalysts in most of the asymmetric reactions developed so far. Particularly in the last two decades, it has been revealed that chiral metallosalen complexes result in diverse and excellent asymmetric catalysis.[2] Chiral salen ligands can be synthesized in a single step from chiral diamine and chiral and/or appropriately substituted salicylaldehydes and form complexes with a variety of metal ions. Moreover, metallosalen complexes are conformationally flexible as a result of the presence of two methylene carbon atoms and they can adopt three different configurations (*trans*, *cis*-α, and *cis*-β). Metallosalen complexes usually adopt *trans* configurations, but they can be readily transformed in the presence of a bidentate ligand into the corresponding *cis*-β complexes.[2,3] Thus, various chiral metallosalen complexes have been synthesized and used as catalysts for a wide range of asymmetric reactions. Most of the metallosalen complexes used are monomeric, but for some reactions, depending on their mechanisms, dimeric or oligomeric metallosalen complexes have proven to be superior catalysts to the corresponding monomeric ones.[4] Nevertheless, the use of such dimeric or oligomeric metallosalen complexes as catalysts has been limited mainly because their synthesis involves laborious routes, except for metallosalen complexes prepared by self-assembly. Thus, di-μ-oxotitanium(salen) complexes that can be prepared spontaneously by treatment of monomeric [Ti(salen)] complexes with water,[5] attracted our attention.[6] Furthermore, in contrast to the usual monomeric [Ti(salen)] complexes that adopt *trans* configurations, each {Ti(salen)} unit of the di-μ-oxo complexes take a *cis*-β configuration. In contrast to the *trans* isomer, the *cis*-β isomer is chiral and exists in enantiomeric forms (Δ or Λ; Figure 1). Thus, there are six possible isomers for the di-μ-oxotitanium(salen) dimer

[*] K. Matsumoto, Y. Sawada, B. Saito, K. Sakai, T. Katsuki
Department of Chemistry
Faculty of Science
Graduate School
Kyushu University
33, Hakozaki, Higashi-ku, Fukuoka 812-8581 (Japan)
Fax: (+81) 92-642-2607
E-mail: katsuscc@mbox.nc.kyushu-u.ac.jp
K. Matsumoto, Y. Sawada, B. Saito, T. Katsuki
CREST
Japan Science and Technology Agency (JST) (Japan)

© 2005 Wiley-VCH Verlag GmbH & Co. KGaA, Weinheim

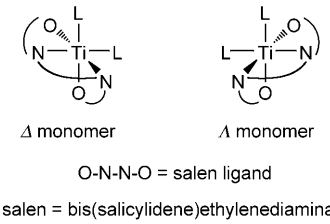


Figure 1. Enantiomeric isomers for the monomeric *cis*-β-titanium-(salen) complex.

(two enantiomeric pairs and two *meso* isomers).[5b] However, Belokon', North, et al. have reported that treatment of a *trans*-[$TiCl_2$(salen)] ([$TiCl_2$**A**]) complex with water in the presence of amine spontaneously gives homochiral dimer **1** as the sole product [(*RΔ*,*RΔ*)-*syn*-**1**] (Figure 2a).[5] This result indicated that the salen ligand **A** which included an (*R*,*R*)-cyclohexanediamine moiety as a constituent part forced the {Ti(salen)} unit to adopt the *Δ* configuration.

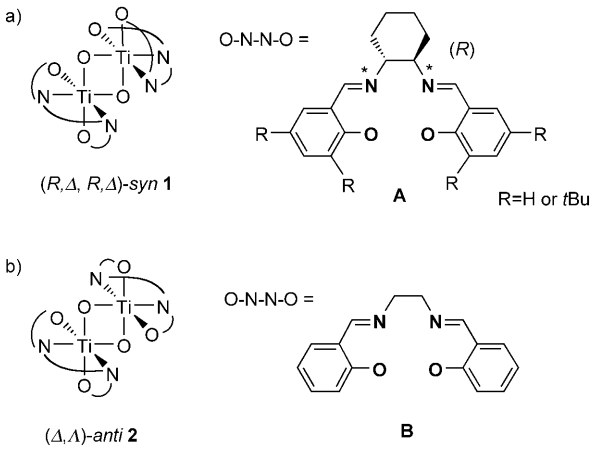
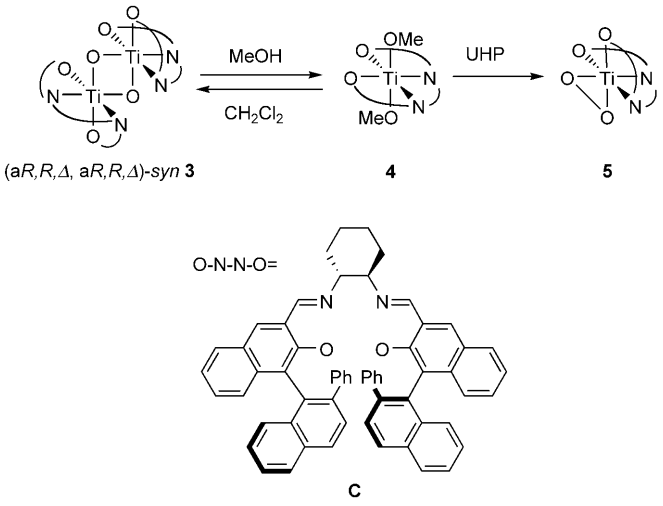


Figure 2. a) Structure of **1**. b) Structure of **2**.

In contrast to the report by Belokon', North, et al., Tsuchimoto has recently reported that di-μ-oxo dimer **2** bearing achiral ligand **B** is heterochiral: each {Ti(salen)} unit has opposite chirality (Figure 2b) and X-ray diffraction analysis has shown **2** to have a (*Δ*,*Λ*)-*anti* configuration.[7] This structure indicates that the interaction between the *Δ* and the *Λ* ligands is more favorable than the interaction between two *Δ* (or two *Λ*) ligands. This situation is reminiscent of asymmetric amplification (positive nonlinear effect) observed in asymmetric addition of diethylzinc to aldehydes using a chiral amino alcohol as the chiral auxiliary: the enantiomeric excess of the chiral auxiliary correlates nonlinearly with the enantioselectivity of the reaction, that is, carrying out the reaction even with a chiral auxiliary of low enantiomeric excess results in enantioselectivity similar to that obtained with the enantiopure auxiliary.[8] This unusual phenomenon has been rationally explained by self-recognition of the chirality of the complex upon its dimerization: the equilibrium between enantiomeric monomers, as well as homochiral and heterochiral dimers is weighted heavily towards the heterochiral dimer as a consequence of a favorable interaction between the enantiomeric monomers.

We also found that, in analogy with di-μ-oxo dimer **1**, complex **3** that was prepared from [$TiCl_2$**C**] also adopted a homochiral *aR*,*R*,*Δ*,a*R*,*R*,*Δ* configuration (Scheme 1) and it



Scheme 1. Structural change of di-μ-oxotitanium(salen) complex **3** bearing chiral salen ligand **C** as a result of the solvent or reagent.

served as an excellent catalyst for asymmetric sulfoxidation in the presence of urea·hydrogen peroxide (UHP).[9] However, complex **3** did not catalyze epoxidation. On the other hand, it was found that the asymmetric sulfoxidation with **3** showed a strong positive nonlinear effect and that di-μ-oxo-**3** and monomeric *trans*-**4** were readily interconverted by changing the solvent. This result indicated that the mixing of a*R*,*R*,*Δ* and the a*S*,*S*,*Λ* isomers made a heterochiral (a*R*,*R*,*Δ*,a*S*,*S*,*Λ*) dimer preferentially.[10] Taking into account Tuchimoto's and our own results, we expected that the pseudo-heterochiral (*aR*,*R*,*Δ*,a*R*,*R*,*Λ*)-**6**, in which each titanium ion carries the same but conformationally enantiomeric ligand, would be formed if the salen ligand became more flexible and if the a*R*,*R*,*Λ* configuration that is otherwise unstable is sufficiently stabilized by the interaction with the a*R*,*R*,*Δ* ligand. Furthermore, the unprecedented pseudo-heterochiral dimer might show unique asymmetric catalysis. Herein, we describe the construction of stable dimeric titanium/tetradentate Schiff base complexes that provide unique reaction sites as shown by in situ intramolecular Meerwein–Ponndorf–Verley (MPV) reduction in combination with self-assembly of the resulting titanium/tetradentate Schiff base complexes. We also describe their use as catalysts in the presence of hydrogen peroxide for asymmetric epoxidation.

We tried reducing one of the two imine bonds of a salen ligand to make it more flexible without losing its high asymmetry-inducing ability. Since titanium isopropoxide is known to undergo MPV reduction, we expected that the [Ti(salen)(O*i*Pr)$_2$] complex might undergo intramolecular MPV reduction of one or two of the imine bonds. Unfortunately, no reaction was observed for [Ti**A**(O*i*Pr)$_2$] (R = *t*Bu) that was prepared in situ and then left to stand. However, the

 © 2005 Wiley-VCH Verlag GmbH & Co. KGaA, Weinheim

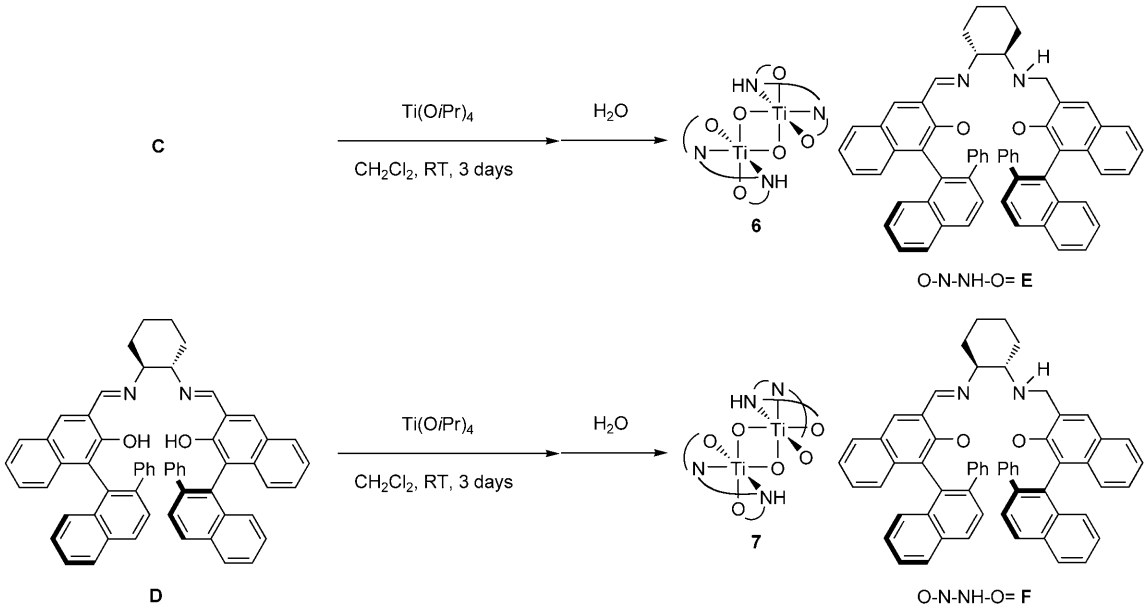
corresponding [Ti**C**(O*i*Pr)$_2$] complex prepared in situ from ligand **C** and Ti(O*i*Pr)$_4$ in dichloromethane was found to undergo the desired MPV reduction at room temperature, and the subsequent water treatment gave a new di-μ-oxo complex **6** that could be crystallized from heptane and dichloromethane (Scheme 2). X-ray diffraction analysis unambiguously demonstrated that the configuration of **6** was pseudo-heterochiral [(a*R*,*R*,*Δ*,a*R*,*R*,*Λ*)-*anti*].[11] Furthermore, the C–N bond lengths indicated that one of the two imine bonds of each salen ligand **C** was reduced to a single bond and the phenolic oxygen atom *ortho* to the reduced imine group occupied the apical position.[12] Encouraged by this result, we also synthesized the (a*RS*,a*RS*)-di-μ-oxotitanium complex **7**, bearing the corresponding half-reduced salen ligand **F**, according to the method described for the preparation of **6**. It is, however, noteworthy that complex **7** was found to adopt a homochiral configuration (a*R*,*S*,-*Δ*,a*R*,*S*,*Δ*) by X-ray diffraction analysis (Scheme 2).[11] These results suggested that the configuration of a di-μ-oxotitanium complex bearing a half-reduced salen ligand is determined by equilibrium involving ligand chirality, its structural flexibility, and weak intra- and interligand interactions such as CH–π interactions. To our delight, complexes **6** and **7** were much more stable than complex **3**: although complex **3** immediately dissociated into the corresponding monomeric {Ti(salen)} species **4** in methanol at room temperature (Scheme 1), complex **6** was stable in [D$_4$]MeOH for at least 5 h and complex **7** was stable even under aqueous epoxidation conditions for at least 24 h. On the basis of these findings, we examined epoxidation using hydrogen peroxide in the presence of complex **6** or **7**.[13]

The catalytic activities of **6** and **7** for epoxidation were examined with 1,2-dihydronaphthalene (**8**) as the test material (Table 1, entries 1–8). Epoxidation using **6** as the catalyst in the presence of the urea·hydrogen peroxide adduct proceeded with good enantioselectivity, but was slow and the turnover number (TON) of **6** was modest (TON = 14) (entry 1).[14] Epoxidation using **7** was performed in the presence of 1.01 equivalents of aqueous (30%) hydrogen peroxide at room temperature[15,16] and it was found that the epoxidation proceeded with excellent enantioselectivity as well as high yield (entry 2). The turnover number of **7** was 4600 when hydrogen peroxide was added slowly over a period of 8 h (entry 4).

Epoxidation of other conjugated olefins also proceeded smoothly with high enantioselectivity (entries 9–13). It is noteworthy that epoxidation of (*Z*)-5-phenylpent-2-en-3-yne (**11**) was stereospecific and gave the corresponding *cis*-epoxide as a single product, albeit with a slightly inferior enantioselectivity of 88% *ee* (entry 11). This result suggested that oxygen transfer proceeds in a concerted rather than a stepwise manner. This proposal was also supported by the fact that epoxidation of styrene (**12**) was highly enantioselective (entry 12). Moreover, the epoxidation of the nonconjugated olefin 1-octene (**14**) proceeded with slightly reduced but good enantioselectivity, albeit somewhat slowly (entry 14).

Although the reaction mechanism of the present epoxidation is unclear, a peroxotitanium species **15** or **16** is considered to act as the active species because the epoxidation is stereospecific (Figure 3).[17] Furthermore, we speculate that the peroxotitanium species may be activated by an intramolecular hydrogen bond with the amine proton. This speculation might explain why complex **3** that does not possess such an NH group cannot catalyze the epoxidation.

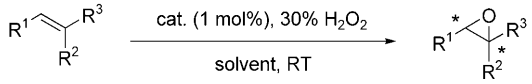
The oxidation of methyl phenyl sulfide was also examined in dichloromethane with **6** as the catalyst in the presence of UHP. The reaction smoothly proceeded but the enantioselectivity was moderate (67% *ee*), although the oxidation with **3** under the same conditions showed a high enantioselectivity of 95% *ee*. It is, however, noteworthy that the sense of asymmetric induction by **6** was opposite to that by **3**, thus suggesting that the structure of the active species derived from **6** was different from **5**.



Scheme 2. Syntheses of di-μ-oxotitanium complexes **6** and **7**.

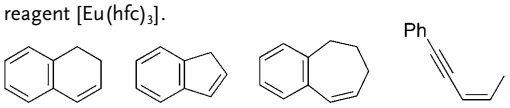
 © 2005 Wiley-VCH Verlag GmbH & Co. KGaA, Weinheim

Table 1: Asymmetric epoxidation using aqueous hydrogen peroxide as the terminal oxidant.[a]

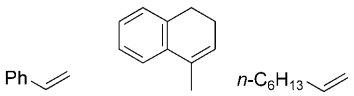


Entry	Substrate	Solvent	*t*	Yield [%][b]	*ee* [%]	Config.[c]
1	**8**	CH_2Cl_2	24	14	83[d,e]	1*S*,2*R*
2	**8**	CH_2Cl_2	12	>99	>99[d]	1*R*,2*S*
3	**8**	CH_2Cl_2	72	>99	>99[d,f]	1*R*,2*S*
4	**8**	CH_2Cl_2	48	92	>99[d,g]	1*R*,2*S*
5	**8**	toluene	18	>99	>99[d]	1*R*,2*S*
6	**8**	ethyl acetate	18	>99	>99[d]	1*R*,2*S*
7	**8**	THF	85	97	97[d]	1*R*,2*S*
8	**8**	MeOH	NR			
9	**9**	ethyl acetate	24	87	99	1*R*,2*S*
10	**10**	ethyl acetate	24	85	98[h]	5*R*,6*S*
11	**11**	ethyl acetate	24	64	88[i]	2*S*,3*R*
12	**12**	CH_2Cl_2	24	90	93[j]	*R*
13	**13**	CH_2Cl_2	24	75	95[k]	1*S*,2*R*
14	**14**	CH_2Cl_2	48	70	82[l,m]	*S*

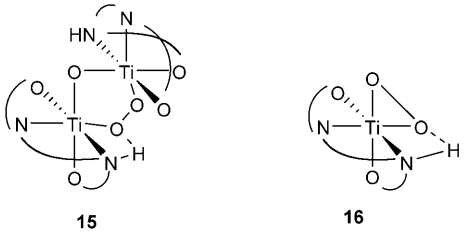
[a] Reactions were carried out at room temperature with a molar ratio of substrate/catalyst **7**/aq H_2O_2 = 1:0.01:1.01, unless otherwise stated. [b] Determined by ^{1}H NMR (400 MHz) spectroscopic analysis. [c] Determined by comparison of the elution order with that of the authentic sample in HPLC analysis and/or comparison of the chiroptical data with the literature value. [d] Determined by HPLC analysis on a chiral stationary phase (Daicel Chiralcel OB-H; hexane/*i*PrOH 99:1). [e] Reactions were carried out at room temperature with a molar ratio of substrate/catalyst **6**/UHP = 1:0.01:1. [f] 0.1 mol% of **7** was used. [g] 0.02 mol% of **7** was used and hydrogen peroxide was added over the period of 8 h. [h] Determined by HPLC analysis on a chiral stationary phase (Daicel Chiralpak AS-H; hexane/*i*PrOH 99.9:0.1). [i] Determined by HPLC analysis on a chiral stationary phase (Daicel Chiralcel OD-H; hexane/*i*PrOH = 99:1). [j] Determined by HPLC analysis on a chiral stationary phase (Daicel Chiralcel OD-H; hexane:*i*PrOH 99.9:0.1). [k] Determined by HPLC analysis on a chiral stationary phase (Daicel Chiralcel OB-H; hexane/*i*PrOH = 99:1). [l] 3 mol% of **7** was used. [m] Determined by ^{1}H NMR spectroscopic analysis using a chiral shift reagent [Eu(hfc)$_3$].



8 **9** **10** **11**



12 **13** **14**



15 **16**

Figure 3. Possible peroxo intermediates for the epoxidation.

In conclusion, we were able to synthesize stable di-μ-oxo dimers—not only a homochiral **7** but also an unprecedented pseudo-heterochiral di-μ-oxo dimer **6**—by using an in situ intramolecular Meerwein–Ponndorf–Verley reduction in combination with self-assembly of the resulting titanium/tetradentate Schiff base complexes. Furthermore, we were able to show that these stable di-μ-oxo dimers (**6** and **7**) catalyzed epoxidation with hydrogen peroxide; in particular, complex **7** efficiently catalyzed a highly enantioselective epoxidation using aqueous (30%) hydrogen peroxide as the oxidant. Other applications of the current oxidation are under investigation.

Experimental Section

7: Ti(O*i*Pr)$_4$ (2 equiv) was added to a solution of salen ligand **D** (1 equiv) in dry dichloromethane in a nitrogen atmosphere and the resultant solution was stirred at room temperature. After 3 days, water (4 equiv) was added and the reaction mixture was stirred for 2 h. The resulting yellow precipitate was collected by filtration and recrystallized from diethyl ether and dichloromethane to give crystalline complex **7** in 60% yield.

General procedure for epoxidation: Titanium complex **7** (1.8 mg, 1 μmol) and olefin (0.1 mmol) were dissolved in an appropriate solvent (1.0 mL) in a nitrogen atmosphere. After addition of 30% aqueous hydrogen peroxide (0.101 mmol), the resultant mixture was stirred at room temperature for the time indicated in Table 1. The solvent was removed in vacuo and the residue was purified by chromatography on silica gel (pentane/Et_2O 40:1) to give the corresponding epoxide. The *ee* values were determined by HPLC on a chiral stationary phase or by ^{1}H NMR analysis using [Eu(hfc)$_3$] (hfc = 3-(heptafluoropropylhydroxymethylene)-D-camphorate) under the conditions described in the footnotes to Table 1.

Received: April 15, 2005
Published online: July 6, 2005

Keywords: asymmetric catalysis · enantioselectivity · epoxidation · hydrogen peroxide · titanium

[1] a) *Comprehensive Asymmetric Catalysis* (Eds.: E. N. Jacobsen, A. Pfaltz, H. Yamamoto), Springer, Berlin, **1999**; b) *Catalytic Asymmetric Synthesis*, 2nd ed. (Ed.: I. Ojima), Wiley-VCH, New York, **2000**; c) *Transition Metals For Organic Synthesis: Building Blocks And Fine Chemicals* (Eds.: M. Beller, C. Bolm), Wiley-VCH, Weinheim, **2004**.

[2] a) L. Canali, D. C. Sherrington, *Chem. Soc. Rev.* **1999**, *28*, 85–93; b) T. Katsuki, *Synlett* **2003**, 281–297; c) T. Katsuki, *Chem. Soc. Rev.* **2004**, *33*, 437–444; d) J. F. Larrow, E. N. Jacobsen, *Top. Organomet. Chem.* **2004**, *6*, 123–152; e) P. G. Cozzi, *Chem. Soc. Rev.* **2004**, *33*, 410–421.

[3] A *cis*-α isomer is generally less stable than the corresponding *cis*-β isomer: see ref. [2c].

[4] a) J. M. Ready, E. N. Jacobsen, *J. Am. Chem. Soc.* **2001**, *123*, 2687–2688; b) Z. Luo, Q. Liu, L. Gong, X. Cui, A. Mi, Y. Jian, *Angew. Chem.* **2002**, *114*, 4714–4717; *Angew. Chem. Int. Ed.* **2002**, *41*, 4532–4535.

[5] a) Y. Belokon', S. Caveda-Cepas, B. Green, N. Ikonnikov, V. Khrustalev, V. Larichev, M. Moscalenko, M. North, C. Orizu, V. Tararov, M. Tasinazzo, G. Timofeeva, L. Yashkina, *J. Am. Chem. Soc.* **1999**, *121*, 3968–3973; b) V. Tararov, V. Larichev, M. Moscalenko, L. Yashkina, V. Khrustalev, M. Antipin, A. Borner, Y. Belokon', *Enantiomer* **2000**, *5*, 169–173.

 © 2005 Wiley-VCH Verlag GmbH & Co. KGaA, Weinheim

[6] Although the construction of a polymeric metallosalen complex by self-assembly has been reported, the catalysis of the polymeric complex is essentially the same as that of the parent monomeric complex: G. A. Morris, S. T. Nguyen, J. T. Hupp, *J. Mol. Catal. A* **2001**, *174*, 15 – 20.
[7] M. Tsuchimoto, *Bull. Chem. Soc. Jpn.* **2001**, *74*, 2101 – 2105.
[8] a) C. Puchot, O. Samuel, E. Dunach, S. Zhao, C. Agami, H. B. Kagan, *J. Am. Chem. Soc.* **1986**, *108*, 2353 – 2357; b) N. Oguni, Y. Matsuda, T. Kaneko, *J. Am. Chem. Soc.* **1988**, *110*, 7877 – 7878; c) M. Kitamura, S. Okada, S. Suga, R. Noyori, *J. Am. Chem. Soc.* **1989**, *111*, 4028 – 4036; d) C. Girard, H. B. Kagan, *Angew. Chem.* **1998**, *110*, 3088 – 3127; *Angew. Chem. Int. Ed.* **1998**, *37*, 2923 – 2959.
[9] B. Saito, T. Katsuki, *Tetrahedron Lett.* **2001**, *42*, 3873 – 3876.
[10] B. Saito, T. Katsuki, *Tetrahedron Lett.* **2001**, *42*, 8333 – 8336.
[11] CCDC-259826 (**6**) and CCDC-264266 (**7**) contain the supplementary crystallographic data for this paper. These data can be obtained free of charge from the Cambridge Crystallographic Data Centre via www.ccdc.cam.ac.uk/data_request/cif.
[12] This partially reduced structure was also supported by FABMS analysis ($[C_{120}H_{92}N_4O_6Ti_2]^+$: $m/z = 1780.6$): JEOL JMX-SX/SX 102A spectrometer by using *m*-nitrobenzyl alcohol as the matrix.
[13] For a review of asymmetric epoxidation, see: a) E. N. Jacobsen, M. H. Wu in *Comprehensive Asymmetric Catalysis*, *Vol. II* (Eds.: E. N. Jacobsen, A. Pfaltz, H. Yamamoto), Springer, Heidelberg, **1999**, chap. 21, pp. 649 – 677; b) T. Katsuki in *Comprehensive Coordination Chemistry II*, *Vol. 9* (Ed.: J. McCleverty), Elsevier Science, Oxford, **2003**, chap. 9.4, pp. 207 – 264; c) T. Katsuki, K. B. Sharpless, *J. Am. Chem. Soc.* **1980**, *102*, 5974 – 5976.
[14] Complex **6** was poorly soluble in methanol relative to complex **3**, and the reaction was carried out in dichloromethane at room temperature.
[15] For enantioselective epoxidation using hydrogen peroxide, see: a) M. K. Tse, C. Doebler, S. Bhor, M. Klawonn, W. Maegerlein, H. Hugl, M. Beller, *Angew. Chem.* **2004**, *116*, 5367 – 5372; *Angew. Chem. Int. Ed.* **2004**, *43*, 5255 – 5260; b) R. I. Kureshy, N. H. Khan, S. H. R. Abdi, S. Singh, I. Ahmed, R. S. Shukla, R. V. Jasra, *J. Catal.* **2003**, *219*, 1 – 7; c) L. Shu, Y. Shi, *Tetrahedron* **2001**, *57*, 5213 – 5218; d) S. Arai, H. Tsuge, T. Shioiri, *Tetrahedron Lett.* **1998**, *39*, 7563 – 7566; e) P. Pietkainen, *Tetrahedron* **1998**, *54*, 4319 – 4326; f) A. Berkessel, M. Frauenkron, T. Schwenkreis, A. Steinmetz, G. Baum, D. Fenske, *J. Mol. Catal. A* **1996**, *113*, 321 – 342; g) P. Pietkainen, *Tetrahedron Lett.* **1994**, *35*, 941 – 944; h) R. Irie, N. Hosoya, T. Katsuki, *Synlett* **1994**, 255 – 256; i) S. Juliá, J. Masana, J. C. Vega, *Angew. Chem.* **1980**, *92*, 968 – 969; *Angew. Chem. Int. Ed. Engl.* **1980**, *19*, 929 – 931; j) S. Colonna, H. Molinari, S. Banfi, S. Juliá, J. Masana, A. Alvalez, *Tetrahedron* **1983**, *39*, 1635 – 1641.
[16] For examples of nonstereoselective but highly efficient epoxidation using aqueous hydrogen peroxide as oxidant, see: a) D. E. De Vos, J. L. Meinershagen, T. Bein, *Angew. Chem.* **1996**, *108*, 2355 – 2357; *Angew. Chem. Int. Ed. Engl.* **1996**, *35*, 2211 – 2213; b) K. Sato, M. Aoki, M. Ogawa, T. Hashimoto, D. Panyella, R. Noyori, *Bull. Chem. Soc. Jpn.* **1997**, *70*, 905 – 915; c) J. Rudolph, K. L. Reddy, J. P. Chiang, K. B. Sharpless, *J. Am. Chem. Soc.* **1997**, *119*, 6189 – 6190; d) M. C. White, A. G. Doyle. E. N. Jacobsen, *J. Am. Chem. Soc.* **2001**, *123*, 7194 – 7195; e) K. Komatsu, K. Yonehara, Y. Sumida, K. Yamaguchi, S. Hikichi, N. Mizuno, *Science* **2003**, *300*, 964 – 966.
[17] At the moment, we cannot determine which titanium species, monomeric or dimeric, participates in activation of hydrogen peroxide. Study on the active species in this epoxidation is under way.

 © 2005 Wiley-VCH Verlag GmbH & Co. KGaA, Weinheim

Protein Models

DOI: 10.1002/anie.200500577

Engineering Enhanced Protein Stability through β-Turn Optimization: Insights for the Design of Stable Peptide β-Hairpin Systems**

*Emma R. Simpson, Jill K. Meldrum, Roger Bofill, Maria D. Crespo, Elizabeth Holmes, and Mark S. Searle**

β-Hairpins are a common component of protein structure and represent the smallest increments of protein β-sheets that are accessible through peptide model systems for studying sequence-dependent folding and stability.[1] A number of model hairpin systems are proving useful vehicles for quantitative studies of noncovalent interactions and for the analysis of the cooperative assembly of multistranded sheets. The choice of β-turn plays a key role in dictating β-strand alignment and stability, and these models have evolved around a few key turn sequences that are found to be statistically abundant in protein β-hairpins.[1] In more general terms, not only have β-turns and β-hairpins been implicated in nucleating protein folding and accelerating folding kinetics[2] but they also constitute binding epitopes in protein–protein and protein–nucleic acid recognition.[3,4] They have been used in the design of small peptide-based protease inhibitors, as recognition motifs in HIV therapeutics, as structured peptides that trigger a specific immune response as the basis for the design of vaccines,[5] and as novel minimalist peptide–DNA recognition scaffolds.[6] Protein engineering studies have shown that the rational redesign of, for example, protein secondary structure and surface charge distribution can lead to enhanced protein stability,[7] which may be a desirable feature for proteins of potential use in a range of biotechnological applications or in the large-scale use of enzymes in

[*] E. R. Simpson, J. K. Meldrum, Dr. R. Bofill,[+] Dr. M. D. Crespo,[++] E. Holmes, Prof. M. S. Searle
Centre for Biomolecular Sciences
University Park, University of Nottingham
Nottingham NG72RD (UK)
Fax: (+44) 115-951-3564
E-mail: mark.searle@nottingham.ac.uk

[+] Current address:
Unitat de Química Inorgànica
Departament de Química
Universitat Autònoma de Barcelona
08193 Bellaterra-Catalonia (Spain)

[++] Current address:
Biozentrum der Universitat Basel
Division of Biophysical Chemistry
Klingelbergstrasse 70, 4056 Basel (Switzerland)

[**] This work was supported by the Engineering and Physical Sciences Research Council (EPSRC) of the UK (studentships to E.R.S. and J.K.M.), the EU Marie Curie Individual Research Fellowship Scheme (R.B.), and the University of Nottingham (M.D.C.). We thank Dr. H. Williams and Mr. S. Simpson for assistance with NMR spectroscopy and modeling studies.

© 2005 Wiley-VCH Verlag GmbH & Co. KGaA, Weinheim

synthesis. Proteins have been shown to be tolerant to large sequence variability in turn regions, with stabilities modulated according to loop size and geometry.[8] Similarly, the population of folded β-hairpin peptides has been shown to be particularly sensitive to small changes in sequence, although quantitative analysis has proved more problematic.[1] With a view to improving the rational design of model peptide systems, we have determined the contribution to β-hairpin stability of the commonly occurring type I′ turn by using native ubiquitin as a "host" system. Herein, we present some energetic guidelines for the optimization of β-turn stability in peptide-based model systems.

High-resolution structures have shown that two-residue type I′ β-turns are particularly abundant in protein β-hairpins.[9] The turn geometry strongly complements the right-handed twist of the antiparallel β-sheet. Following the nomenclature of Sibanda and Thornton,[9] the turn is described by the sequence (−B1)-(L1)-(L2)-(+B1), where −B1 and +B1 are the β-strand residues preceding and following the turn, and L1 and L2 are the turn residues. The backbone ϕ and ψ angles of L1 and L2 both lie in the left-handed α-helical (L-α) region of the Ramachandran plot. In an analysis of 512 high-resolution structures we identified 408 two-residue type I′ turn sequences and were able to demonstrate clear residue preferences at the various sites,[10] in agreement with earlier studies that used a smaller database.[11] The data showed that Gly is by far the most abundant residue at position L2 (308 out of 408 cases) as the required backbone angles ($\phi \approx 90°$ and $\psi \approx 0°$) are disallowed for all residues other than Gly.[11] At position L1, the dihedral angles are accessible to other non-β-branched residues, with Asn, Asp, and Gly appearing in around 60% of cases, with Asn preferred. In contrast, Val, Ile, and Thr are rarely found in this position. On this basis the Asn-Gly type I′ turn has been widely used in model hairpin peptide systems for stability and folding studies and has proved highly effective at inducing folded structures.[1] In other cases, the use of D-Pro at position L1 to induce the correct L-α backbone geometry has also proved highly successful.[1]

To examine the influence of β-turn sequences on hairpin stability, we used the N-terminal 17-residue β-hairpin of native ubiquitin as a "host" for mutational studies (Figure 1a).[12–14] By using a fluorescent ubiquitin construct with a background F45W mutation (which we subsequently term wild-type ubiquitin, **WT***),[15–17] we engineered a series of turn mutations into the ubiquitin hairpin to examine quantitatively the effects on protein stability (Figure 1b). In the X-ray crystal structure of native ubiquitin,[12] the first and last of the five residues of the TLTGK loop close the native 3:5 type I G-bulged turn through cross-strand hydrogen bonding. We initially mutated the native turn sequence to the more flexible TGGGK loop (**G3** mutant) without affecting these closing residues. Protein stability was determined through fluorescence-detected chemical denaturation methods using guanidinium chloride (GdmCl). Sigmoidal unfolding curves were fitted to a two-state model from which transition midpoints (c_m), denaturant m values, and free energies of folding were determined (see Table 1).[18] Using this approach, **WT*** was observed to unfold with a transition midpoint (c_m) of 2.68 M GdmCl at pH 5.0 in acetate buffer (25 mM) at 298 K (Figure 2) from which we estimate a free energy of folding of $-27.3(\pm 0.6)$ kJ mol^{-1} (see Table 1). Strikingly, the **G3** mutant appears to be marginally more stable ($\Delta\Delta G \approx -1.6$ kJ mol^{-1}) despite the enhanced flexibility of the Gly-rich turn sequence and loss of side-chain interactions across the loop sequence.

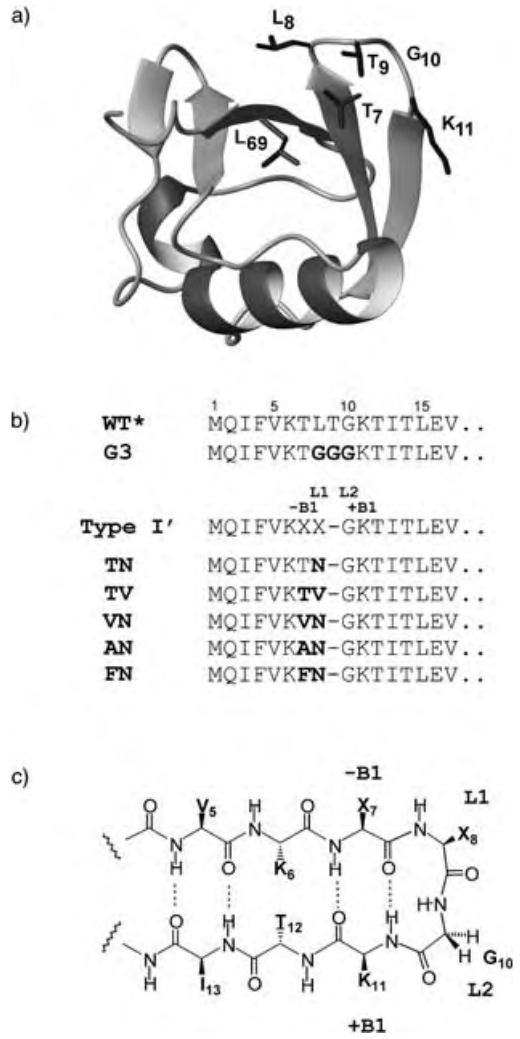


Figure 1. a) X-ray crystal structure of ubiquitin (1UBQ[12]) showing the solvent-exposed TLTGK type I G-bulged turn at the end of the N-terminal β-hairpin sequence. The position and orientation of the side chains of the β-turn residues T_7, L_8, T_9, and K_{11}, and also the L_{69} side chain on the C-terminal β-strand are also illustrated. b) Sequences of ubiquitin mutants containing type I′ β-turn substitutions. Only the N-terminal 17 residues that encompass the β-hairpin are illustrated. c) Two-residue type I′ β-turn conformation showing the mutated residues X_7 and X_8 and cross-strand hydrogen-bonding interactions. The residue numbering in (b) follows that in the **WT*** sequence (residue 9 has been deleted in the mutants). Residues X_7, X_8, G_{10}, and K_{11} represent turn residues −B1, L1, L2, and +B1, respectively, according to the nomenclature of Sibanda and Thornton (ref. [9]).

Subsequently, we replaced the native loop sequence (TLTGK) with the type I′ turn sequence (TXGK) by substituting LT with residue X at position L1 (Figure 1c).[9] We considered residues at position X which occur with either high frequency (X = Asn) or low frequency (X = Val) in protein β-

 © 2005 Wiley-VCH Verlag GmbH & Co. KGaA, Weinheim

Table 1: Thermodynamic data for the ubiquitin mutants derived from chemical denaturation experiments.

Mutant	Transition midpoint (c_m) [M][a]	ΔG_{eq} [kJ mol^{-1}][b]	$\Delta\Delta G$ (mut−WT*) [kJ mol^{-1}]
WT*	2.68	−27.3 ± 0.6	0
G3	2.84	−28.9 ± 0.7	−1.6 ± 0.9
TN	2.83	−28.8 ± 0.6	−1.5 ± 0.9
TV	2.54	−25.9 ± 0.6	+1.4 ± 0.9
VN	3.33	−33.9 ± 0.8	−6.6 ± 1.0
AN	2.58	−26.3 ± 0.6	+1.0 ± 0.9
FN	3.78	−38.5 ± 0.9	−11.2 ± 1.1

[a] Transition midpoints (c_m, 50% unfolded protein relative to [GdmCl]) were determined by fluorescence measurements at 298 K on 1.0 μM solutions of protein in acetate buffer (25 mM) at pH 5.0; fitting errors are typically less than 0.02 M. [b] Equilibrium stabilities calculated using $m = 10.18$ kJ mol^{-1} M^{-1} (with a standard error of ± 0.23 kJ mol^{-1} M^{-1}).

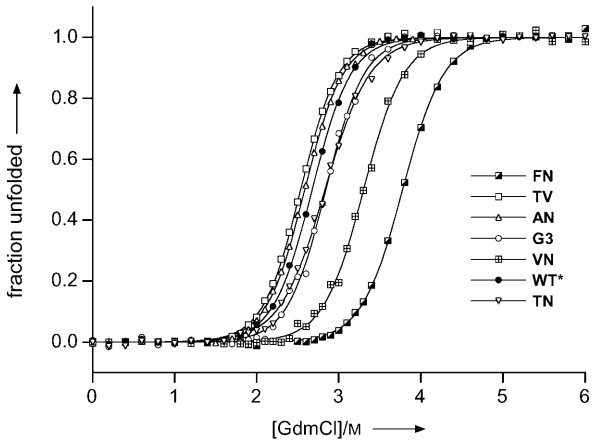


Figure 2. a) Guanidinium chloride (GdmCl) denaturation curves for the family of β-turn mutants measured at 298 K and pH 5.0 in acetate buffer (25 mM). Unfolding transitions were measured by fluorescence changes at $\lambda = 358$ nm, and the data were converted into the fraction unfolded versus the concentration of GdmCl. Stabilities were determined using the linear extrapolation method by fitting the curves to a two-state unfolding model to determine the midpoint denaturant concentration (c_m) and the slope (m value). Stability data are shown in Table 1.

hairpins (**TN** and **TV** mutants, respectively) while retaining the same β-strand residues present in the **WT*** sequence at positions −B1 and +B1.[10] The requirement for ϕ and ψ angles at position L1 which lie in the left-handed α-helical region highly disfavors Val at this position.[11] Despite the high abundance of type I′ turns in protein hairpins, the insertion of the Asn-Gly sequence produces only a small incremental increase in stability of −1.5 kJ mol^{-1} relative to that of the native G-bulged turn, suggesting that these are equally good turn sequences in this context. Substitution with the least favored L1 residue (TVGK) resulted in a modest reduction in stability of 2.9 kJ mol^{-1} relative to that of the most favored (TNGK) type I′ turn sequence. Although this is a relatively small overall effect on the stability of native ubiquitin, in the context of small hairpin peptides of only marginal stability ($\Delta G_{fold} \approx 0$), this equates to a significant change in the folded population (threefold change in equilibrium constant).[1]

To confirm that both the TNGK and TVGK turns are accommodated with the same turn conformation, rather than the stability difference reflecting grossly different backbone geometries, we examined in detail the **TN** and **TV** ubiquitin mutants by NMR spectroscopy. A complete assignment of the backbone NH and Hα protons enabled us to identify cross-strand NOEs and Hα chemical shift perturbations. By comparison with **WT***, Hα chemical shift perturbations from random coil values (ΔδHα [ppm]) for **TN** are shown in Figure 3a and demonstrate that the structural changes arising from the substitution of the turn sequence are largely confined to the region immediately adjacent to the mutated residues. Residues within the N and C termini of the β-strands (1–5 and 12–17) are perturbed by $\Delta\delta H\alpha < 0.1$ ppm. Intense cross-strand Hα–Hα NOEs, particularly between K_6 Hα and T_{12} Hα, confirm the nativelike strand alignment close to the type I′ turn. The ratio of NOE intensities at the T_7-N_8 step ($H\alpha_i$-NH_{i+1}/$H\alpha_i$-$NH_i \approx 1$) together with a small $^3J_{NH\text{-}H\alpha} < 5$ Hz for N_8 and a strong sequential NH_i-NH_{i+1} NOE between G_{10} and K_{11} identifies an abrupt change in direction of the peptide

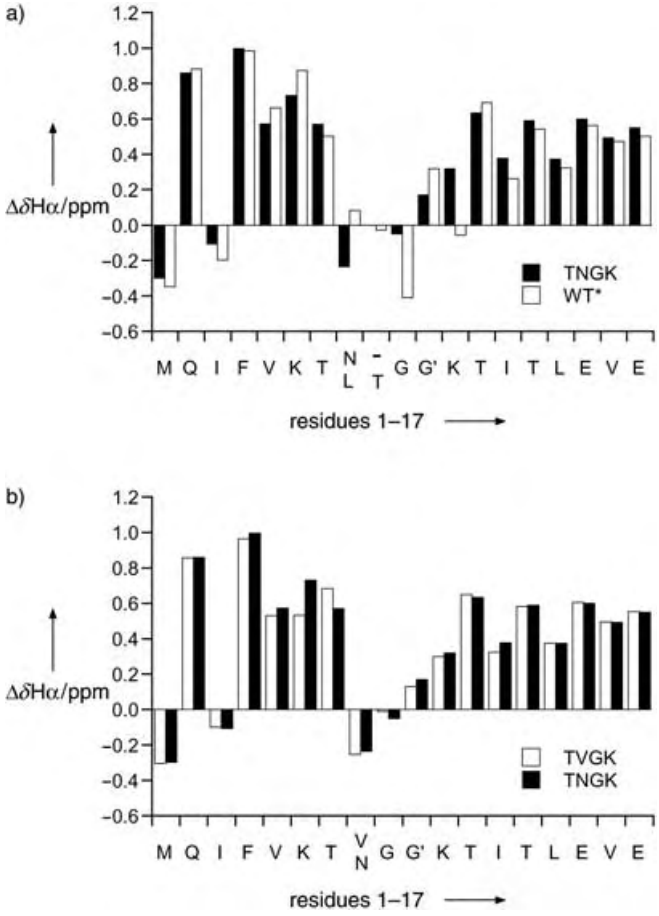


Figure 3. Perturbations to chemical shifts of Hα (measured values versus random coil values, ΔδHα [ppm]) of residues 1–17 in the N-terminal β-hairpin. NMR data were collected at 600 MHz at 298 K and pH 5.0. a) NMR data for **WT*** are compared to the **TN** mutant (TNGK turn sequence) and show that perturbations are largely confined to residues immediately adjacent to the mutated turn residues. b) Comparison of ΔδHα values for the **TN** and **TV** mutants, representing the most favored (Asn-Gly) and the least favored (Val-Gly) substitutions at position L1 in type I′ turns.

 © 2005 Wiley-VCH Verlag GmbH & Co. KGaA, Weinheim

chain at the T_7-N_8 and G_{10}-K_{11} steps which is consistent with N_8 and G_{10} occupying the L-α region of ϕ,ψ space. In Figure 3b, the Hα chemical shift data for mutants **TN** and **TV** show similar perturbations that are consistent with the two turns adopting the same conformation. Analogous patterns of NOEs and $^3J_{NH\text{-}H\alpha}$ values (not shown) confirm these conclusions. Thus, the two turns appear to be readily accommodated in the desired geometry with only modest local disruption to secondary structure, despite the differences in steric demand and frequency of occurrence of Val and Asn at the L1 position.

The earlier statistical analysis of type I′ turns also showed some preference for residues at the −B1 and +B1 positions flanking the turn sequence.[10] For example, Lys occurs with high frequency at position +B1 and, consequently, this residue has been retained in all constructs as well as being present in the native sequence. At position −B1 there is a clear preference for the β-branched residue Val,[10] however, there was little apparent discrimination between remaining side chains on the basis of size or hydrophobicity. Introduction of Val at this position (**VN** mutant) resulted in a noticeable increase in stability, with a shift in the denaturant-induced transition midpoint from 2.83 M GdmCl observed for **TN** to 3.33 M for **VN** ($\Delta\Delta G = -5.1$ kJ mol^{-1}). NMR data for the **TN** and **VN** mutants show that the isosteric Thr and Val residues at the −B1 position are accommodated with the same side-chain rotamer conformation. The substitution of the β-OH group of T_7 with the V_7 methyl affects the contacts largely within the β-turn, as evident from cross-strand NOEs from the V_7 CH_3 to protons of the aliphatic side-chain of K_{11} (β-CH_2/γ-CH_2). On the basis of intrinsic β-sheet-forming propensities, Thr and Val were anticipated to promote hairpin folding, whereas Ala has a high helical propensity and was expected to be destabilizing in the context of the β-hairpin. Accordingly, the ANGK turn (**AN** mutant) resulted in a loss of stability of +2.5 kJ mol^{-1} compared to TNGK (see Table 1). Overall, the relative turn stabilities appear to reflect the intrinsic β-sheet-forming propensity of the residue at the −B1 position at the end of the β-strand. We conclude that optimization of residues at positions −B1 and L1 in the context of the type I′ turn can lead to substantial net changes in protein stability in a manner that appears to correlate well with backbone ϕ,ψ structural propensities.[10]

We also modeled a number of other nonpolar residues at the −B1 position to investigate the possibility of engineering new stabilizing tertiary interactions at this site. The models suggested that the introduction of bulky aromatics such as Phe at the −B1 position should lead to very favorable context-dependent hydrophobic contacts with L_{69} and L_{71} on the adjacent C-terminal β-strand, even though Phe does not have a particularly high frequency of occurrence at position −B1 in type I′ turns.[10] As predicted from the model, the FNGK turn (**FN** mutant) showed a substantial further increase in stability over TNGK of −9.7 kJ mol^{-1}. As confirmation of the engineered F_7–L_{69}/L_{71} interactions, we observed significant upfield ring-current effects of between 0.6–0.9 ppm on the H_β, H_γ, and $C_\delta H_3$ resonances of L_{69}, placing the latter in a well-resolved region of the spectrum at $\delta = 0.03$ ppm. Upfield shifts (≈ 0.4 ppm) are observed for both $C_\delta H_3$ resonances of L_{71} (Figure 4a). We were readily able to identify NOEs from the side chain of F_7 to L_{69} and L_{71} which confirm the hydrophobic contacts. Local refinement of our structural model using the NOE data and restrained molecular dynamics enabled these local interactions to be visualized (Figure 4b). Thus, the high apparent β-sheet propensity of Phe at position −B1 appears to be rationalized largely on the basis of engineered tertiary interactions rather than intrinsic secondary structure propensity.

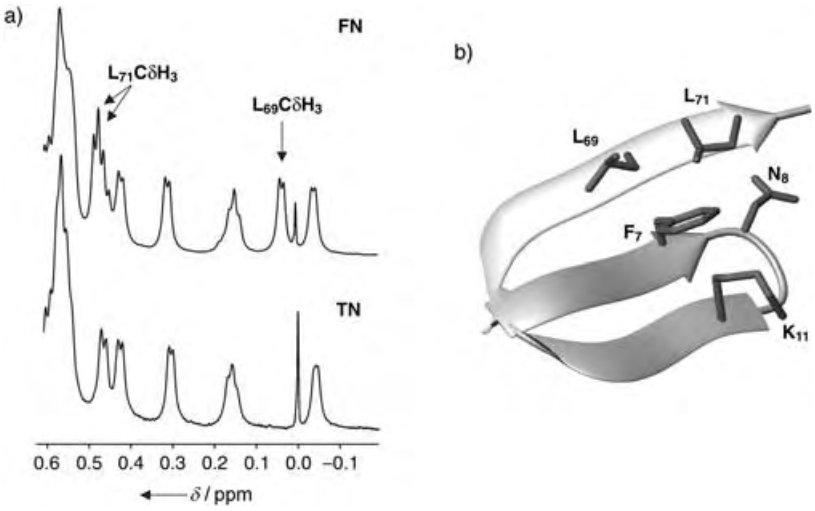


Figure 4. a) 1D ^{1}H NMR spectra of the **TN** and **FN** mutants showing the highfield-shifted methyl region ($\delta = -0.1$ to 0.6 ppm) at 298 K (pH 5.0). The spectra are similar except for the appearance of the two ring-current-shifted $C_\delta H_3$ resonances of L_{71} at $\delta = \approx 0.47$ ppm and that of L_{69} at $\delta = 0.03$ ppm owing to hydrophobic contacts with F_7 at position −B1 in the turn. b) Model of the **FN** mutant showing hydrophobic contacts between F_7 and L_{69}/L_{71} which account for the stability enhancement of the **FN** mutant and observed ring-current shifts to L_{69} and L_{71}. Other side chains of the turn residues N_8 and K_{11} are also shown.

In conclusion, we set out to examine quantitatively the effects of β-turn mutations on protein stability using the N-terminal hairpin sequence of ubiquitin as a "host" system. As demonstrated from a statistical analysis of β-hairpins in high-resolution protein structures and from work on model hairpin peptide systems, type I′ turns are effective promoters of hairpin folding, although the energetic contributions have not been systematically studied.[1,9–11,19] We have shown that optimization of residues at positions −B1 and L1 lead to substantial increases in stability that correlate well with backbone ϕ,ψ structural propensities. In the context of a weakly folded peptide model system of only marginal stability ($\Delta G \approx 0$), it is clear that the choice of type I′ turn sequence can be a critical factor in determining whether a significant population of the folded conformer can be detected.[1,11] The

 © 2005 Wiley-VCH Verlag GmbH & Co. KGaA, Weinheim

work of Gellman has shown that D-Pro at position L1 is also highly effective in nucleating hairpin folding in model peptide hairpin systems because the preferred ϕ,ψ backbone angles, together with the entropic constraints imposed by the backbone-to-side-chain cyclization, match the right-handed twist of the β-sheet.[1a–c] Substituting with the mirror image L-Pro switches the turn geometry from right-handed (type I′ or II′) to left-handed (type I or II) and makes the latter incompatible with the twisted alignment of the two β-strands which leads to a completely unfolded state.[20] However, to our knowledge a quantitative estimate of the difference in stability between the pair of diastereomeric hairpin peptides has not been reported.

We have presented some energetic guidelines for the stability contributions of type I′ turns to hairpin stability. These estimates probably represent an upper limit for model peptide systems because we have measured the incremental free energy contribution of the various turn sequences in the context of the cooperative folding transition of native ubiquitin. These limiting values may not be fully realized in the context of a more dynamic folded peptide system, although enthalpy/entropy compensations may play some part in achieving these stability differences.[21] Such compensatory effects may also be evident in the case of the TGGGK turn sequence for which intrinsic flexibility potentially compensates for any reduction in enthalpic benefits from poorer side-chain interactions or locally weaker hydrogen bonds. With regard to the design of model peptide systems that contain β-hairpin motifs, we have presented a quantitative analysis of the energetic contribution of the type I′ β-turn to β-hairpin stability in ubiquitin. The N-terminal β-hairpin sequence has previously been studied in isolation as a possible protein folding nucleation site and has been used as the basis of a number of other model systems for folding studies.[1a,14,22] However, the results presented here should be of more general use in peptide and protein design and in understanding aspects of the energetics of molecular recognition and self-assembly.

Experimental Section

A pKK223–3 plasmid construct containing the yeast ubiquitin gene was used to express the wildtype protein in *Escherichia coli* strain BL21(DE3) under the control of the IPTG-inducible *tac* promoter. The F45W mutant gene was cloned by overlap PCR methodology using the wild-type yeast ubiquitin gene in pKK223-3 (Pharmacia Biotech) as a template. Competent *Escherichia coli* cells were transformed with this construct. Expression and purification of **WT*** yielded typically 10–15 mg L^{-1} of ubiquitin. All other mutations using the **WT*** background were introduced using the QuikChange site-directed mutagenesis protocol (Stratagene, La Jolla, CA) and confirmed by DNA sequence analysis (School of Biomedical Sciences, Nottingham) and by NMR studies.

Protein stabilities were determined using methods previously described in references [15] and [17a] and by using established protocols.[18a,b] Protein stability was determined by fluorescence measurements on 1.0-μM solutions of protein in acetate buffer (25 mM) at pH 5.0 and 298 K. The change in fluorescence at $\lambda =$ 358 nm was monitored as a function of the concentration of guanidinium chloride (GdmCl). The linear extrapolation method was employed assuming that the stability varies with the concentration of denaturant, [D], according to the expression $\Delta G^{D} = \Delta G_{eq} + m[D]$, where ΔG^{D} is the stability at a given [D], m is the constant of proportionality, and ΔG_{eq} is the stability in water alone. The data were plotted as the fraction of unfolded protein versus [D]. The midpoint of the unfolding transition c_m for each mutant was determined by nonlinear least-squares fitting (see references [16] and [18a]). The equilibrium stability ΔG_{eq} was determined from the expression $\Delta G_{eq} = -m\,c_m$. For the mutants described we observed only a small variation in m values, 10.18 ± 0.23 kJ mol^{-1} M^{-1} (± standard error), and the expression $\Delta\Delta G_{eq} = -m(c_m^{mut} - c_m^{WT})$ was used to calculated changes in stability. This approach is justified by NMR spectroscopic analysis of all mutants which shows that they all fold to a nativelike structure with only minor localized chemical shift perturbations and changes in the hydrophobic surface area buried.[18c,d]

All NMR spectroscopy experiments were performed on a Bruker Avance600 spectrometer. Total correlation spectroscopy (TOCSY) and nuclear Overhauser effect spectroscopy (NOESY) experiments were used as previously described on 1-mM protein samples at pH 5.0.[15] Spectra were referenced internally to trimethylsilylpropionate (TSP), and random coil peptide shifts were used as reported.[23] Data were processed and assigned using Bruker XWINNMR and ANSIG software,[24] and structural models were visualized using MOLMOL.[25] The structure of the **FN** mutant was modeled from random unfolded starting structures using 345 NOE-derived distance restraints and 63 torsion angle restraints. 100 structures were refined using a combination of distance geometry and simulated annealing using the XPLOR-NIH program.[26] Acceptance criteria of no NOE violations greater than 0.5 Å and no angle restraint violations of greater than 5° were applied. Root-mean-square deviations for bonds and angles from ideality were less than 0.01 Å and 2°, respectively, for all structures. From this, 72 structures were accepted, the lowest energy of which is shown in Figure 4.

Received: February 16, 2005
Published online: July 6, 2005

Keywords: NMR spectroscopy · protein engineering · proteins · ubiquitin

[1] a) S. H. Gellman, *Curr. Opin. Chem. Biol.* **1998**, *2*, 717; b) M. S. Searle, *Biopolymers* **2004**, *76*, 185; c) M. S. Searle, B. Ciani, *Curr. Opin. Struct. Biol.* **2004**, *14*, 458; d) E. De Alba, M. A. Jimenez, M. Rico, *J. Am. Chem. Soc.* **1997**, *119*, 175.

[2] a) H. J. Dyson, M. Rance, R. A. Houghton, R. Lerner, *J. Mol. Biol.* **1988**, *201*, 161; b) D. K. Klimov, D. Thiumalai, *J. Mol. Biol.* **2002**, *315*, 721; c) J. Kim, S. R. Brych, J. Lee, T. M. Logan, M. Blaber, *J. Mol. Biol.* **2003**, *328*, 951; d) S. Nauli, B. Kuhlman, D. Baker, *Nat. Struct. Biol.* **2001**, *8*, 602; e) E. L. McCallister, E. Alm, D. Baker, *Nat. Struct. Biol.* **2000**, *7*, 669.

[3] a) M. A. Schumacher, B. K. Hurlburt, R. G. Brennan, *Nature* **2001**, *409*, 215; b) B. J. Hillier, K. S. Christopherson, K. E. Prehoda, D. S. Bredt, W. A. Lim, *Science* **1999**, *284*, 812; c) N. M. Stano, S. S. Patel, *J. Mol. Biol.* **2002**, *315*, 1009.

[4] a) H. C. Wong, J. H. Mao, J. T. Nguyen, S. Srinivas, W. X. Zhang, B. Liu, L. Li, D. Q. Wu, J. Zheng, *Nat. Struct. Biol.* **2000**, *7*, 1178; b) R. Berisio, F. Schluenzen, J. Harms, A. Bashan, T. Auerbach, D. Baram, A. Yonath, *Nat. Struct. Biol.* **2003**, *10*, 366; c) Z. Zavala-Ruiz, I. Strug, B. D. Walker, P. J. Norris, L. J. Stern, *Proc. Natl. Acad. Sci. USA* **2004**, *101*, 13279.

[5] a) M. L. J. Korsinczky, H. J. Schirra, K. J. Rosengren, J. West, B. A. Condie, M. A. Anderson, D. J. Craik, *J. Mol. Biol.* **2001**, *311*, 579; b) A. Descours, K. Moehle, A. Renard, J. A. Robinson, *ChemBioChem* **2002**, *3*, 318; c) J. A. Robinson, *Synlett* **2000**, *4*, 429; d) R. Fasan, R. L. A. Dias, K. Moehle, O. Zerbe, J. W. Vrijbloed, D. Obrecht, J. A. Robinson, *Angew. Chem.* **2004**, *116*, 2161; *Angew. Chem. Int. Ed.* **2004**, *43*, 2109; e) Z. Athanassiou, R. L. A. Dias, K. Moehle, N. Dobson, G. Varani, J. A. Robinson,

 © 2005 Wiley-VCH Verlag GmbH & Co. KGaA, Weinheim

J. Am. Chem. Soc. **2004**, *126*, 6906; f) R. L. Stanfield, M. K. Gorny, C. Williams, S. Zolla-Pazner, I. A. Wilson, *Structure* **2004**, *12*, 193; g) E. Drakopoulou, S. Zinn-Justin, M. Guenneuges, B. Gilquin, A. Menez, C. Vita, *J. Biol. Chem.* **1996**, *271*, 11979; h) C. E. Stotz, E. M. Topp, *J. Pharm. Sci.* **2004**, *93*, 2881.

[6] a) S. M. Butterfield, M. L. Waters, *J. Am. Chem. Soc.* **2003**, *125*, 9580; b) S. M. Butterfield, W. J. Cooper, M. L. Waters, *J. Am. Chem. Soc.* **2005**, *127*, 24.

[7] a) V. Villegas, A. R. Viguera, F. X. Aviles, L. Serrano, *Folding Des.* **1996**, *1*, 29; b) A. R. Viguera, V. Villegas, F. X. Aviles, L. Serrano, *Folding Des.* **1996**, *2*, 23; c) E. Lopez-Hernandez, P. Cronet, L. Serrano, V. Munoz, *J. Mol. Biol.* **1997**, *266*, 610; d) D. Perl, U. Mueller, U. Heineman, F. X. Schmid, *Nat. Struct. Biol.* **2000**, *7*, 380; e) A. Karshikoff, R. Ladenstein, *Trends Biochem. Sci.* **2001**, *26*, 550; f) S. Kumar, R. Nussinov, *Cell. Mol. Life Sci.* **2001**, *58*, 1216; g) C. Vetriani, D. L. Maeder, N. Tolliday, K. S. Yip, T. J. Stillman, K. L. Britton, D. W. Rice, H. H. Klump, F. T. Robb, *Proc. Natl. Acad. Sci. USA* **1998**, *95*, 12300; h) H. X. Zhou, R. H. Hoess, W. F. DeGrado, *Nat. Struct. Biol.* **1996**, *3*, 446.

[8] a) K. Takano, Y. Yamagata, K. Yutani, *Biochemistry* **2000**, *39*, 8655; b) T. R. Hynes, R. A. Krautz, Goodman, J. F. Gill, R. O. Fox, *Nature* **1989**, *339*, 73; c) P. F. Predki, V. Agrawal, A. T. Brunger, L. Regan, *Nat. Struct. Biol.* **1996**, *3*, 54; d) E. C. Ohage, W. Grami, M. M. Walter, S. Steinbacher, B. Steipe, *Protein Sci.* **1997**, *6*, 233; e) H. X. Zhou, R. H. Hoess, W. F. DeGrado, *Nat. Struct. Biol.* **1996**, *3*, 446.

[9] B. L. Sibanda, J. M. Thornton, *Nature* **1985**, *316*, 170.

[10] S. R. Griffiths-Jones, A. J. Maynard, M. S. Searle, *J. Mol. Biol.* **1999**, *292*, 1051.

[11] M. Ramirez-Alvarado, F. J. Blanco, H. Niemann, L. Serrano, *J. Mol. Biol.* **1997**, *273*, 898.

[12] S. Vijay-Kumar, C. E. Bugg, K. D. Wilkinson, R. D. Vierstra, P. M. Hatfield, W. J. Cook, *J. Biol. Chem.* **1987**, *262*, 6396.

[13] P.-Y. Chen, B. G. Gopalacushina, C.-C. Yang, S. I. Chan, P. A. Evans, *Protein Sci.* **2001**, *10*, 2063.

[14] a) M. S. Searle, D. H. Williams, L. C. Packman, *Nat. Struct. Biol.* **1995**, *2*, 999; b) M. Jourdan, S. R. Griffiths-Jones, M. S. Searle, *Eur. J. Biochem.* **2000**, *267*, 3539.

[15] G. W. Platt, S. A. Simpson, R. Layfield, M. S. Searle, *Biochemistry* **2003**, *42*, 13762.

[16] S. Khorasanizadeh, I. D. Peters, H. Roder, *Biochemistry* **1993**, *32*, 7054.

[17] a) M. D. Crespo, G. W. Platt, R. Bofill, M. S. Searle, *Eur. J. Biochem.* **2004**, *271*, 4474; b) H. Went, C. G. Benitez-Cardoza, S. E. Jackson, *FEBS Lett.* **2004**, *567*, 333; c) B. A. Krantz, T. R. Sosnick, *Biochemistry* **2000**, *39*, 11696.

[18] a) M. M. Santoro, D. W. Bolen, *Biochemistry* **1988**, *27*, 8063–8068; b) N. C. Pace, J. M. Scholtz, *Protein Structure—A Practical Approach* (Ed.: T. E. Creighton), *2nd ed.*, IRL, New York, **1997**; c) E. R. G. Main, S. E. Jackson, *J. Mol. Biol.* **1999**, *291*, 429; d) N. Ferguson, A. P. Capaldi, R. James, C. Kleanthous, S. E. Radford, *J. Mol. Biol.* **1999**, *286*, 1597.

[19] a) A. J. Maynard, G. J. Sharman, M. S. Searle, *J. Am. Chem. Soc.* **1998**, *120*, 1996; b) B. Ciani, M. Jourdan, M. S. Searle, *J. Am. Chem. Soc.* **2003**, *125*, 9038.

[20] a) T. S. Haque, S. H. Gellman, *J. Am. Chem. Soc.* **1997**, *119*, 2303; b) H. E. Stanger, S. H. Gellman, *J. Am. Chem. Soc.* **1998**, *120*, 4236; c) H. L. Schenck, S. H. Gellman, *J. Am. Chem. Soc.* **1998**, *120*, 4869.

[21] M. S. Searle, G. W. Platt, R. Bofill, S. A. Simpson, B. Ciani, *Angew. Chem.* **2004**, *116*, 2025; *Angew. Chem. Int. Ed.* **2004**, *43*, 1991.

[22] a) J. P. L. Cox, P. A. Evans, L. C. Packman, D. H. Williams, D. N. Woolfson, *J. Mol. Biol.* **1993**, *234*, 483; b) R. Zerella, P. A. Evans, J. M. C. Ionides, L. C. Packman, B. W. Trotter, J. P. Mackay, D. H. Williams, *Protein Sci.* **1999**, *8*, 1320; c) R. Zerella, P. Y. Chen, P. A. Evans, D. H. Williams, *Protein Sci.* **2000**, *9*, 2142.

[23] K. Wüthrich, *NMR of Proteins and Nucleic Acids*, Wiley, New York, **1986**.

[24] P. J. Kraulis, *J. Magn. Reson.* **1989**, *84*, 627.

[25] R. Koradi, M. Billeter, K. Wuthrich, *J. Mol. Graphics* **1996**, *14*, 51.

[26] C. D. Schwieters, J. J. Kuszewski, N. Tjandra, G. M. Clore, *J. Magn. Reson.* **2003**, *160*, 65.

 © 2005 Wiley-VCH Verlag GmbH & Co. KGaA, Weinheim

Natural Product Synthesis

DOI: 10.1002/anie.200500434

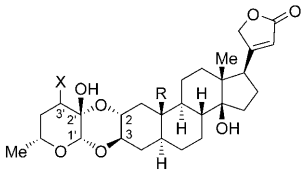
A Concise and General Method for Doubly Attaching 2-Ketosugars to Aglycon Diols: Synthesis of the Gomphosides and Spectinomycin**

Frieder W. Lichtenthaler, Eckehard Cuny, and Osamu Sakanaka*

Dedicated to Professor András Lipták on the occasion of his 70th birthday

Whereas the cardiac glycosides from *Digitalis* and *Strophantus* species carry one to five sugar units linked through the 3-OH of the steroid aglycon,[1] those produced by plants from the milkweed family *Asclepiadacea*, such as **1**–**6** (Table 1),[2–4]

Table 1: Cardenolide glycosides (**1**–**6**) isolated from the milkweed family *Asclepiadaceae*.



	Compound	3′-C–X	R	Reference
1	gomphoside	◄OH	Me	[2]
2	3′-*epi*-gomphoside	····OH	Me	[3]
3	3′-dehydrogomphoside	=O	Me	[3]
4	calactin	◄OH	CHO	[4]
5	calotrophin	····OH	CHO	[4]
6	usacharidin	=O	CHO	[4]

[*] Prof. F. W. Lichtenthaler, Dr. E. Cuny, Dr. O. Sakanaka
Clemens-Schöpf-Institut für Organische Chemie und Biochemie
Technische Universität Darmstadt
Petersenstrasse 22, 64287 Darmstadt (Germany)
Fax: (+49) 6151-166-674
E-mail: lichtenthaler@chemie.tu-darmstadt.de

[**] Funding by the Deutsche Forschungsgemeinschaft and the Fonds der Chemischen Industrie is gratefully acknowledged. O.S. thanks Meiji Seika Kaisha, Yokohama, for a postdoctoral fellowship.

Supporting information for this article is available on the WWW under http://www.angewandte.org or from the author.

InterScience
© 2005 Wiley-VCH Verlag GmbH & Co. KGaA, Weinheim

invariably contain a single sugar—the rare 4,6-dideoxy-D-hexos-2,3-diulose or its epimeric C-3 reduction products—in a unique "dioxanoid" attachment. The common β-glycosidic bond to the steroidal 3-OH is complemented by a hemiacetal linkage between the 2-carbonyl group of the sugar and the 2-OH group of the aglycone to result in a *cis,cisoid,trans*-fusion of pyran, dioxane, and cyclohexane rings. The antibiotic spectinomycin (**7**) and its dihydro derivative **8**, elaborated by *Streptomyces spectabilis*, contain the same 2-ketosugars in an analogous double attachment to actinamine, an *N*-methylated diaminoinositol (Figure 1).[5]

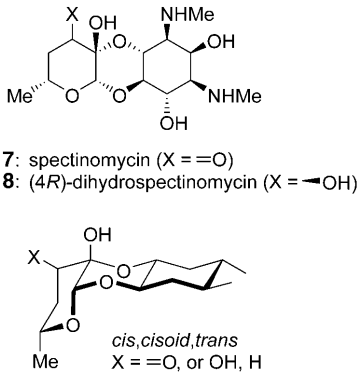
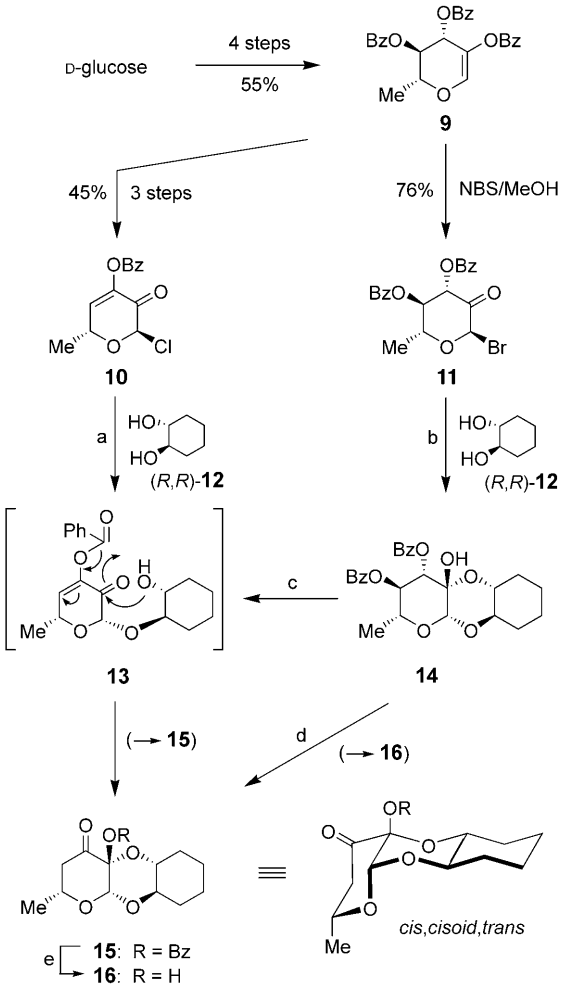


Figure 1. Two antibiotics (**7**, **8**) produced by *Streptomyces spectabilis*, each comprising a 4,6-dideoxy-2-ketohexose moiety doubly attached to a cyclohexanoid aglycone-diol in *cis,cisoid,trans* fusion.

Synthetically, the double attachment of a 2-ketosugar to a natural aglyconediol has only been addressed in the case of spectinomycin (**7**), for which two total syntheses (one in 9 steps from L-glucose,[6a] and the other in 23 steps from D-glucose[6b]) have been reported that comprise monoglycosylation of a readily accessible *N*-protected actinamine and subsequent gradual elaboration of the 2-carbonyl group of the sugar. In the case of cardenolide glycosides of type **1**–**6**, however, the aglycons are only laboriously available. Thus for annulation of their sugar portion, alternatives that are capable of reaching this objective more directly became imperative. On the basis of our previous studies on the extension of the "ulosyl donor approach"[7] to glycol and (*R*,*R*)-1,2-cyclohexanediol, which smoothly led to *cis*-fused pyranodioxanes[8] and to pyran-dioxane-cyclohexane tricycles[9] in *cis,cisoid,trans* fusion, we inferred that the D-glucose-derived 2-ketohexosyl donors **10** and **11** would be particularly well-adjusted for targeting natural products with annulated sugar components. The donors not only contain the 2-carbonyl function, which is essential for generation of the cyclohemiacetal linkage, but in the case of **10**, an enol-ester-protected carbonyl at C-3 is also present thereby closely matching the tricarbonyl sugar units in **3**, **6**, and **7**. Furthermore, these donors are fairly well accessible from D-glucose through the 6-deoxy-2-hydroxyglucal ester **9**:[10] ulosyl bromide **11** can be obtained in five, large-scale adaptable steps from D-glucose[11,12] versus seven steps for its unsaturated chloro analogue **10**,[12] with overall yields of 42 and 25%, respectively (Scheme 1).

The feasibility of advancing from donors **10** and **11** to cardenolides of type **1**–**6** was first probed with (*R*,*R*)-1,2-cyclohexanediol (**12**) as a model aglycon. On exposure of **12** to equimolar amounts of Ag_2CO_3 and donor **10**, a single product was obtained (TLC) and isolated in high yield (81%) which on the basis of cogent NMR evidence proved to be *cis,cisoid,trans*-fused pyran-dioxane-cyclohexane tricycle **15**. Thus, an essentially β-specific mono-*O*-glycosylation of diol **12** to glycosidulose **13** is spontaneously followed by a cascade reaction in which the second OH group engages in hemiacetal formation and the 3-*O*→2-*O*-benzoyl group (arrows in **13**) subsequently shifts, with seemingly exclusive preference for OH→C=O attack occurring from the lower (axial) face of the pyran ring.[13] Here, electronic interactions are minimized by *trans*-diaxial disposition of the oxygen of the pyran ring and the benzoyloxy acetal group—a consequence of the anomeric effect—and steric interactions are at a minimum due to chair conformations of the three rings.



Scheme 1. Synthesis of linear fused pyran-dioxane-cyclohexane tricycles that correspond to dioxanoid cardenolide glycosides in structure and linkage geometry. Reagents and conditions: a) **12** (1.0 equiv), Ag_2CO_3 (1.0 equiv), molecular sieves, CH_2Cl_2, 40°C, 8 h, 81%; b) **12** (1.0 equiv), Ag_2CO_3 (1.0 equiv), CH_2Cl_2, 25°C, 20 h, 87%; c) nBu_4NOAc, CH_2Cl_2, 25°C, 20 h, 85% (**15**); d) nBu_4NOAc, moist MeCN, 25°C, 6 h, 81% (**16**); e) K_2CO_3, MeOH, 25°C, 10 min, 87%. Bz = benzoyl; NBS = *N*-bromosuccinimide.

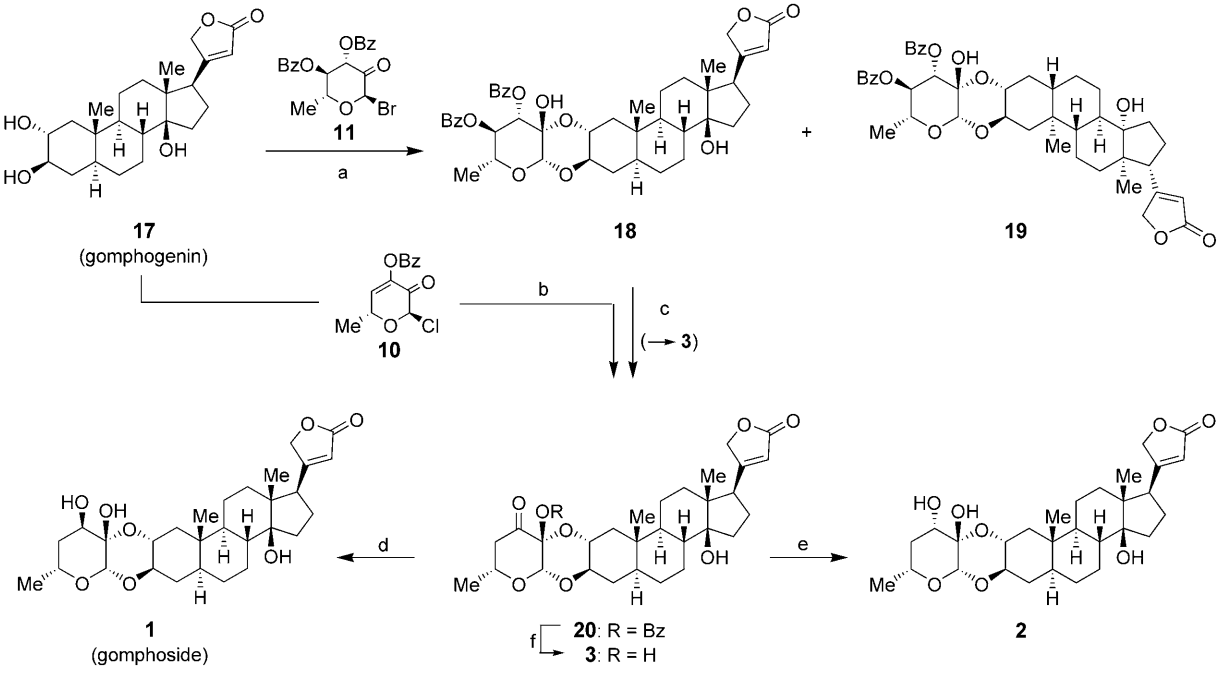
 © 2005 Wiley-VCH Verlag GmbH & Co. KGaA, Weinheim

In the case of the ulosyl bromide **11**, the Ag_2CO_3-mediated glycosylation of one OH group of diol **12** expectedly[7,12] proceeded in β-specific fashion and was similarly followed by sterically uniform hemiketalization with the other OH group to provide the *cis,cisoid,trans*-interconnected tricycle **14**, with the high yield (87%) emphasizing the extent of stereocontrol in the two reactions involved. Owing to its free ketalic OH group, **14** is prone to react in the ring-opened glycosidulose form, particularly under basic conditions. Thus, on stirring **14** with tetra-*n*-butylammonium acetate in CH_2Cl_2, 3,4-elimination of benzoic acid to the enolone ester **13** was induced; however, the ester was not isolable under these conditions, as hemiketalization and migration of the *O*-benzoyl group readily took place (arrows in **13**; see Scheme 1), thereby elaborating the tricyclic ketone **15** (85%). When β elimination of **14**→**13** was attempted with nBu$_4$NOAc in aqueous acetonitrile, the benzoyl migration step was intercepted by hydrolysis to afford instead the free hemiketal **16** in crystalline form[14] and 81% yield. Expectedly, **16** was also obtained on de-*O*-benzoylation of **15** (87%).

Thus, having established the utility of donors **10** and **11** for the dioxanoid annulation of 4,6-dideoxy-2-ketosugar units—the *cis,cisoid,trans*-fused **15** has all the structural and stereochemical essentials of the natural products—the methodology developed for (*R*,*R*)-1,2-cyclohexanediol was then applied to gomphogenin (**17**),[15] the steroid aglycone of gomphosides **1**–**3**. As **17** is an unsymmetric diol, it was expected to give two products as Ag_2CO_3-mediated *O*-glycosylation with donors **10** or **11** followed by folding of the hemiketal can occur on either of the OH groups. Fortunately, it appeared that the 3-OH group of gomphogenine is the more reactive of the two OH groups from the fact that the major components of the 3:1 mixtures obtained in each case proved to be the naturally fused products **18** (from ulosyl bromide **11**) and **20** (from donor **10**). These products were purified by preparative HPLC to afford **18** and **20** in yields of 61 and 54%, respectively (Scheme 2). De-*O*-benzoylation of **20** was readily effected by exposure to mild base to provide crystalline cardenolide **3** in excellent yield (95%). In analogy to the model conversion **14**→**16**, **3** could also be obtained from **18** by stirring with nBu$_4$NOAc in hydrous acetonitrile (81% yield). Compound **3** as synthesized here was identical in all respects with the 3′-dehydrogomphoside derived from *Asclepias fruticosa*[3] with respect to the melting point (300–301 °C; lit.: 302–304 °C[3]) and ^{1}H and ^{13}C NMR spectroscopic characteristics.

The integrity of synthetic **3** could further be verified through conversion into the epimeric 3′-hydroxy analogues. Hydrogenation over 5% Rh/C[16] led to a mixture of gomphoside (**1**) and its 3′-epimer **2**, from which **1** was secured in 80% yield and proved to be identical to the natural product[2b,17] with respect to melting point and spectral data. Reduction of **3** with $NaBH_4$ proceeded stereospecifically to afford 3′-*epi*-gomphoside (**2**) as a crystalline solid,[18] whose structure was analyzed by X-ray diffraction and clearly exposes the *cis,cisoid,trans* interconnection of the pyran, dioxane, and ring A cyclohexane rings (Figure 2).

The methodology developed so far for the dioxanoid annulation of sugars to cyclic 1,2-diols was also probed with *N*,*N*-bis(benzyloxycarbonyl)actinamine (**21**), the aglycon of spectinomycin in an accessible and suitably *N*,*N*-protected form.[19] As the bulky *N*-protecting groups impede glycosylation at the vicinal hydroxy groups through steric shielding,[6] a highly regioselective attack of donors **10** or **11** at 3-OH was anticipated. However, the acceptor reactivity of this 3-hydroxy group proved to be considerably lower than that in



Scheme 2. Reagents and conditions: a) **11** (2 equiv), Ag_2CO_3 (1 equiv), molecular sieves, CH_2Cl_2, 25 °C, 16 h, 61% (**18**), 14% (**19**); b) **10** (1.0 equiv), Ag_2CO_3 (1.0 equiv), molecular sieves, CH_2Cl_2, 40 °C, 2 h, 54% (**20**); c) nBu$_4$NOAc, MeCN/water 50:1, 25 °C, 15 h, 89% (**3**); d) 5% Rh/C, MeOH/water 9:1, 25 °C, 24 h, 80%; e) $NaBH_4$ (1.0 equiv), dry MeOH, 0 °C, 10 min, 81%; f) K_2CO_3, MeOH, 25 °C, 10 min, 95%.

 © 2005 Wiley-VCH Verlag GmbH & Co. KGaA, Weinheim

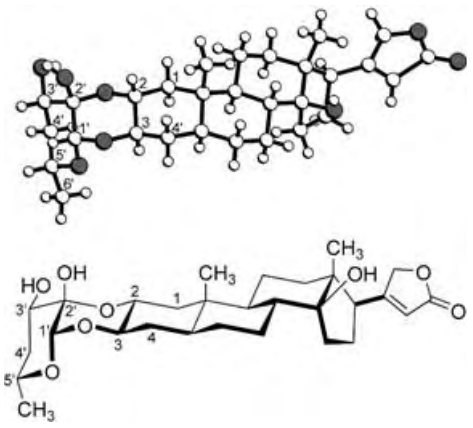
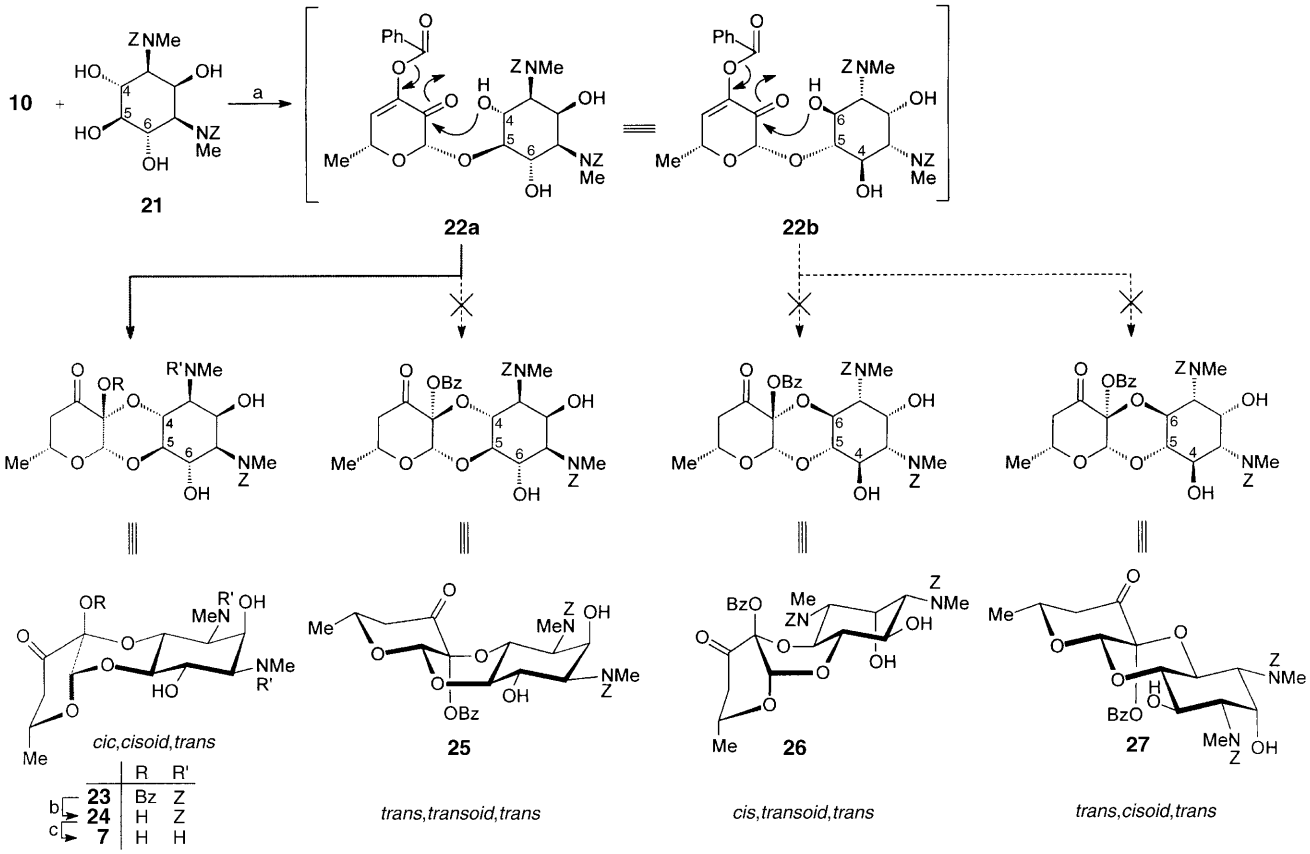


Figure 2. X-ray crystal structure of 3′-*epi*-gomphoside (**2**). The lactone ring is twofold disordered, as is the solvent molecule CH_2Cl_2 (omitted for clarity). The pyran, dioxane, and cyclohexane rings are all in near-perfect chair conformations. Dihedral angles [°] relevant to the dioxanoid attachment: C2-O2-C2′-C3′ −173.0, C3-O3-C1′-O5′ 64.7, O3-C1′-C2′-C3′ 172.7, O2′-C2′-C1′-O5′ 172.3.

diol **12** or in gomphogenine, seemingly due to the high oxygen substitution in its cyclohexane ring, and entailed sluggish glycosylations when promoted with Ag_2CO_3. After substantial experimentation with various insoluble silver catalysts—the more-reactive soluble promoters such as silver triflate were excluded as they entail α selectivity—silver aluminosilicate[20] in THF/CH_2Cl_2 or in toluene was found to effect β-selective *O*-glycosylation of **21** with donor **10**[21] to give **23** as the major product in 51 % isolated yield after removal of 4-*O*- and 6-*O*-glycosylated analogues (ca. 5 % each) by preparative HPLC (Scheme 3). The integrity of **23**, the 2′-*O*-benzoyl derivative of *N*,*N*-bis-(benzyloxycarbonyl)spectinomycin in its *cis,cisoid,trans*-fused tricyclic framework, was confirmed from its spectral data, its ready de-*O*-benzoylation to the known Boc-protected **24**,[6b,22] as well as from its hydrogenolysis to spectinomycin (**7**), which was found to be identical to the natural product in all respects.

The regioselectivity and β selectivity of the glycosylation reaction are remarkable, whereas the stereocontrol exercised in the hemiketal folding of the glycosidulose intermediate is even more so as it leads from a compound that contains two stereogenic centers to a product that contains nine! As a result of the thermodynamics derived from two anomeric effects and the propensity to form the sterically most favorable linear-fused tricycle, the glycosidulose C=O group in **22** is attacked with high and exclusive preference by the 4*R*-OH group from the axial (lower) face of the pyran ring to elaborate **23**, with the oxygen of the pyranoid ring and the ketalic OBz group positioned in the favorable *trans*-diaxial conformation, as well as chair conformations of the three rings. In contrast, the alternate possibilities—attack of 4*R*-OH from the β (equatorial) face (**22a**→**25**) or of 6*S*-OH in the two conceivable steric modes (**22b**→**26** or **27**)—invariably leads



Scheme 3. Unique stereocontrol in the intramolecular hemiketal folding of glycosidulose intermediate **22** towards the *cis*,*cisoid*,*trans*-fused framework of spectinomycin. Reagents and conditions: a) Ag aluminosilicate (1.2 equiv), toluene, 80 °C, 3 h, 51 %; b) K_2CO_3, MeOH, 25 °C, 10 min, 89 %; c) H_2, 5 % Pd/C, *i*PrOH, 25 °C, 12 h, 90 %. Z = benzyloxycarbonyl.

 © 2005 Wiley-VCH Verlag GmbH & Co. KGaA, Weinheim

to thermodynamically less stable products either because the central dioxane ring is forced into a boat conformation (**25** and **26**) or as unfavorable dipolar interactions are operative (**25**, **27**). The ease with which the glycosidulose intermediate spontaneously "folds" into the natural *cis,cisoid,trans* geometry may even be taken as evidence for such a process to be operative in non-enzyme-mediated fashion in the biosynthesis of spectinomycin from D-glucose,[23] with an unprotected form of glycosidulose **22** conceivably being the decisive intermediate.

In summary, the chemistry detailed herein defines a concise and general method for the construction of natural products with a *cis,cisoid,trans*-interconnected pyran-dioxane-cyclohexane framework and has enabled the first syntheses of cardiac glycosides with ring A annulated sugars and an alternate synthesis of the antibiotic spectinomycin. A key feature of the methodology is the monoglycosylation of the respective aglycon diols with 4,6-dideoxy-2-ketohexosyl donors, promoted by an insoluble silver salt, which thereby substantially extends the utility of the "ulosyl donor approach".[7]

Received: February 4, 2005
Published online: July 6, 2005

Keywords: fused-ring systems · glycosylation · gomphosides · natural products · spectinomycin

[1] a) T. Reichstein, E. Weiss, *Adv. Carbohydr. Chem.* **1962**, *17*, 65–120; b) P. M. Dewick, *Medicinal Natural Products*, Wiley, New York, **2002**, pp. 241.

[2] a) R. G. Coombe, T. R. Watson, *Aust. J. Chem.* **1964**, *17*, 92–100; b) H. T. A. Cheung, T. R. Watson, *J. Chem. Soc. Perkin Trans. 1* **1980**, 2162–2168; c) H. T. A. Cheung, R. G. Coombe, W. T. L. Sidwell, T. R. Watson, *J. Chem. Soc. Perkin Trans. 1* **1981**, 64–72.

[3] H. T. A. Cheung, F. C. K. Chiu, T. R. Watson, R. J. Wells, *J. Chem. Soc. Perkin Trans. 1* **1983**, 2827–2835.

[4] a) G. Hesse, F. Reicheneder, *Justus Liebigs Ann. Chem.* **1936**, *526*, 252–276; b) F. Brüschweiler, W. Stöcklin, K. Stöckel, T. Reichstein, *Helv. Chim. Acta* **1969**, *52*, 2086–2106; c) F. Brüschweiler, K. Stöckel, T. Reichstein, *Helv. Chim. Acta* **1969**, *52*, 2276–2302; d) P. Brown, J. von Euw, T. Reichstein, K. Stöckel, T. R. Watson, *Helv. Chim. Acta* **1979**, *62*, 412–441.

[5] For a pertinent review on spectinomycin, see: W. Rosenbrook, Jr., *J. Antibiot.* **1979**, *32*, S211–S227.

[6] a) D. R. White, R. D. Birkenmeyer, R. C. Thomas, S. A. Mizsak, V. H. Wiley, *Tetrahedron Lett.* **1979**, 2737–2740; b) S. Hanessian, R. Roy, *Can. J. Chem.* **1985**, *63*, 163–172.

[7] For reviews, see: a) E. Kaji, F. W. Lichtenthaler, *Trends Glycosci. Glycotechnol.* **1993**, *5*, 121–142; b) J. J. Gridley, H. M. I. Osborn, *J. Chem. Soc. Perkin Trans. 1* **2000**, 1471–1491; c) V. Pozgay in *Carbohydrates in Chemistry and Biology*, *Part I* (Eds.: B. Ernst, G. W. Hart, P. Sinaÿ), Wiley-VCH, Weinheim, **2000**, pp. 332–336. For recent applications towards β-D-mannosides, see: d) M. Nitz, D. R. Bundle, *J. Org. Chem.* **2001**, *66*, 8411–8423; e) F. W. Lichtenthaler, M. Lergenmüller, S. Peters, Z. Varga, *Tetrahedron: Asymmetry* **2003**, *14*, 727–736; f) F. W. Lichtenthaler, M. Lergenmüller, S. Schwidetzky, *Eur. J. Org. Chem.* **2003**, 3094–3103.

[8] E. Cuny, F. W. Lichtenthaler, H. J. Lindner, *Eur. J. Org. Chem.* **2004**, 4901–4910.

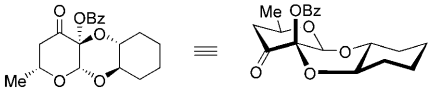
[9] F. W. Lichtenthaler, E. Cuny, *Eur. J. Org. Chem.* **2004**, 4911–4920.

[10] a) G. Ekborg, P. J. Garegg, S. Josephson, *Carbohydr. Res.* **1978**, *65*, 301–306; b) M. E. Evans, F. W. Parrish, *Methods Carbohydr. Chem.* **1972**, *6*, 177–179, M. E. Evans, F. W. Parrish, *Methods Carbohydr. Chem.* **1972**, *6*, 193–196; c) See ref. [9] (footnote 19 therein).

[11] F. W. Lichtenthaler, A. Löhe, E. Cuny, *Liebigs Ann. Chem.* **1983**, 1973–1985.

[12] F. W. Lichtenthaler, U. Kläres, M. Lergenmüller, S. Schwidetzky, *Synthesis* **1992**, 179–184.

[13] The alternative possibility, cyclo-hemiketalization of **13** by OH→C=O attack from the upper (equatorial) face would lead to the sterically and thermodynamically unfavorable *trans-transoid-trans*-fused product in which the central dioxane ring is forced into a boat (or twist-boat) conformation.



[14] Racemic **16**, in noncrystalline form, has previously been prepared through elaboration of the pyranoid portion through an aldehyde/diene cycloaddition approach: S. Danishefsky, J. Aubé, M. Bednarski, *J. Am. Chem. Soc.* **1986**, *108*, 4145–4149.

[15] Gomphogenin (**17**) was prepared from digitoxin by hydrolytic removal of the sugars and conversion of its aglycon, digitoxigenin, through a known seven-step procedure: Y. Kamano, G. R. Pettit, M. Tozawa, *J. Chem. Soc. Perkin Trans. 1* **1975**, 1972–1976; J. F. Templeton, H. T. A. Cheung, C. R. Sham, T. R. Watson, *J. Chem. Soc. Perkin Trans. 1* **1983**, 251–256.

[16] The catalyst was adapted from the Ru/C-mediated hydrogenation of spectinomycin (**7**), which provided an epimeric mixture mainly consisting of the (4*R*)-dihydro analogue **8**: W. Rosenbrook, Jr., R. E. Carney, *J. Antibiot.* **1975**, *28*, 953–959.

[17] T. R. Watson, S. E. Wright, *Chem. Ind. London* **1954**, 1178; T. R. Watson, S. E. Wright, *Aust. J. Chem.* **1957**, *10*, 79–84.

[18] Natural **2** derived from *Asclepias fruticosa* was isolated as a microcrystalline solid as its half-hydrate[3] with m.p. = 250–251 °C, whereas synthetic **2** with m.p. = 189–191 °C was found to crystallize with one mole of CH_2Cl_2, which accounts for the comparatively large difference in melting behavior.

[19] T. Suami, S. Nishiyama, H. Ishikawa, H. Okada, T. Kinoshita, *Bull. Chem. Soc. Jpn.* **1977**, *50*, 2754–2757.

[20] a) C. A. A. van Boeckel, T. Beetz, A. C. Kock-van Dalen, H. van Bekkum, *Recl. Trav. Chim. Pays-Bas* **1987**, *106*, 596–598; b) F. W. Lichtenthaler, T. Metz, *Eur. J. Org. Chem.* **2003**, 3081–3093.

[21] The less reactive ulosyl bromide (**11**) gave complex mixtures under these conditions which contained substantial amounts of **21**.

[22] P. M. Herrinton, K. L. Klotz, W. M. Hartley, *J. Org. Chem.* **1993**, *58*, 678–682.

[23] H. Otsuka, O. R. Mascaretti, L. H. Hurley, H. G. Floss, *J. Am. Chem. Soc.* **1980**, *102*, 6817–6820.

 © 2005 Wiley-VCH Verlag GmbH & Co. KGaA, Weinheim

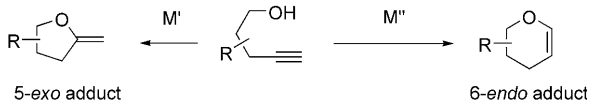
Catalytic Tandem Reactions

DOI: 10.1002/anie.200501150

An Ir^I-Catalyzed *exo*-Selective Tandem Cycloisomerization/Hydroalkoxylation of Bis-Homopropargylic Alcohols at Room Temperature**

Emilie Genin, Sylvain Antoniotti, Véronique Michelet, and Jean-Pierre Genêt**

Over the past few years, significant research has been directed toward the development of new methodologies that provide synthetic efficiency and atom economy.[1] Among them, tandem reactions, which allow the formation of several new bonds in a single step from readily available materials, are of particular interest.[2] Moreover, the potential of transition-metal-catalyzed heterocyclization reactions of unsaturated substrates has been regularly demonstrated, as they give a direct method for the synthesis of highly valuable nitrogen- and oxygen-containing heterocycles.[3] Palladium catalysis, in particular, has been the driving force behind many advances in the synthesis of heterocyclic derivatives.[4] However, cyclizations mainly occur at high temperature or in the presence of a base, copper co-catalysts, or other oxidants, and this has stimulated the search for alternative transition-metal catalysts.[3,4] In the course of our ongoing program concerning catalytic tandem reactions with functionalized enynes,[5] we became interested in the cyclization of bis-homopropargylic alcohols, which have shown challenging behaviors either in their *endo*- or *exo*-selective cyclizations in the presence of palladium, molybdenum, tungsten, ruthenium, and rhodium catalysts (Scheme 1).[1,3,4,6] We therefore turned our attention to iridium complexes, which have recently been reported to exhibit promising catalytic properties,[7,8] and we wish to report herein the first Ir^I-catalyzed *exo*-selective tandem cycloisomerization/hydroalkoxylation that proceeds exclusively and efficiently at room temperature and that involves inter- and intramolecular C–O bond formation.



Scheme 1. Metal-catalyzed cyclization of bis-homopropargylic alcohols. M′ = Pd; M″ = Mo, W, Ru, Rh, Pd.

Our initial experiments were performed with bis-homopropargylic alcohol **1a** as a model substrate, which is easily prepared by malonic addition to the corresponding halide and reduction of the resultant diester. Even though Ir^I catalysts have recently been shown to promote 1,6-enyne carbon–carbon cycloisomerization,[7j] the $[\{Ir(cod)Cl\}_2]$ dimer catalyst led to a completely different reaction in methanol at room temperature. The cyclization occurred very smoothly in the presence of 2.5 mol% of $[\{Ir(cod)Cl\}_2]$ at room temperature in a very short time with the concomitant addition of methanol to give the functionalized furanyl ketal **2a** in 99% yield (Table 1, entry 1). The use of an Ir^I catalyst is crucial as no reaction occurred either without catalyst or with $IrCl_3$. Interestingly, whereas the reaction of such bis-homopropargylic substrates catalyzed by transition metals such as Rh, Ru, W, and Mo usually leads to 6-*endo* cyclization products,[6] the cyclization was found to be 5-*exo*-selective, as no six-membered cyclic derivative was detected. The tandem addition of methanol was particularly intriguing as it has only rarely been reported in the literature: scarce examples are limited to the use of Pd catalysts and need a co-catalyst or other additive to be effective.[4e,9] We therefore embarked on a general study of this reaction in the presence of an Ir^I catalyst (Table 1). With the aim of examining the influence of the side chain R^1, we prepared several bis-homopropargylic alcohols by malonic addition of the corresponding alkyl bromide, reduction of the resultant diester functions, and, for some substrates, monoprotection of the diols.[10] The reactions were conducted in MeOH at room temperature in the presence of 1–2.5 mol% of $[\{Ir(cod)Cl\}_2]$.

The butyl-substituted alkyne **1b** was transformed into the ketal **2b** in a high 99% yield (Table 1, entry 2). Surprisingly, the addition of the remaining alcohol was not observed in these cases, presumably because MeOH, which is a potential ligand for the Ir complex, is present in excess close to the substrate.[11] The reaction conditions are compatible with other substitution patterns on alcohols **1**, such as a propargyl group (entry 3). Alcohols **1d–f** underwent smooth and rapid cyclization and functionalization (entries 4–6) to give the corresponding acetals **2d–f** in excellent yields (90–99%). Lowering the catalyst loading was possible (entry 6) with a slight enhancement of the reaction time. These derivatives constitute important building blocks for an easy access to natural product[12] and can be easily transformed into C1-substituted furans by treatment with functionalized silanes in the presence of a Lewis acid.[13]

To illustrate the synthetic utility of this tandem reaction, we envisaged the use of other alcohols for the intermolecular addition step. Other nucleophiles such as ethanol and allylic alcohol could be successfully used under the same reaction conditions at room temperature in the presence of 1–2.5 mol% of the $[\{Ir(cod)Cl\}_2]$ catalyst (Table 2).

Such a process offers a control of the R^1 and R^3 groups in the final furanyl product simply by varying the halide used in the preliminary malonate alkylation and the nature of the alcohol used as the solvent. This mode of functionalization also allows the introduction of structural diversity that cannot

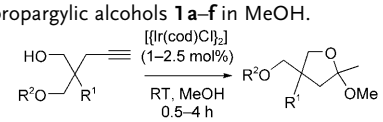
[*] E. Genin, Dr. S. Antoniotti, Dr. V. Michelet, Prof. J.-P. Genêt
Laboratoire de Synthèse Sélective Organique et Produits Naturels
E.N.S.C.P., UMR 7573
11 rue P. et M. Curie, 75231 Paris Cedex 05 (France)
Fax: (+33) 1-4407-1062
E-mail: veronique-michelet@enscp.fr
jean-pierre-genet@enscp.fr

[**] This work was supported by the Centre National de la Recherche Scientifique (CNRS). E.G. is grateful to the Ministère de l'Education et de la Recherche for financial support (2003–2006).

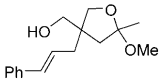
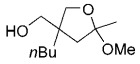
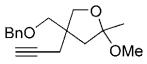
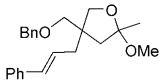
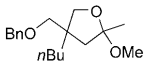
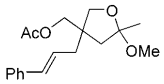
Supporting information for this article is available on the WWW under http://www.angewandte.org or from the author.

 © 2005 Wiley-VCH Verlag GmbH & Co. KGaA, Weinheim

Table 1: Cyclization/hydroalkoxylation of bis-homopropargylic alcohols **1a–f** in MeOH.



1a–f **2a–f**

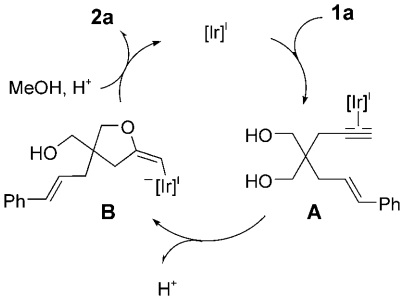
Entry		R^1	R^2	Product		*t* [h]	Yield [%][a]
1[b]	**1a**	(*E*)-cinnamyl	H		**2a**	0.5	99
2[b]	**1b**	*n*Bu	H		**2b**	0.5	99
3[b]	**1c**	propargyl	Bn[d]		**2c**	0.5	99
4[b]	**1d**	(*E*)-cinnamyl	Bn[d]		**2d**	0.5	91
5[b]	**1e**	*n*Bu	Bn[d]		**2e**	1.5	90
6[c]	**1f**	(*E*)-cinnamyl	Ac		**2f**	4	99

[a] Yield of isolated product; 1/1 mixture of diastereomers. [b] 2.5 mol% of catalyst. [c] 1 mol% of catalyst. [d] Bn = benzyl.

be achieved selectively by the functionalization of simple furanyl rings. Alcohols bearing either an unsaturated (entries 1, 2, and 4) or an alkyl (entry 3) side chain were cleanly, and in a very short time, cyclized with concomitant addition of EtOH to the ethoxy-substituted derivatives **3a**, **3c**, **3e**, and **3g** in good to excellent yields (78–99%). The cycloisomerization/hydroethoxylation was also effective with phenyl- (entry 5) and benzyl-substituted (entry 6) alcohols, as the substituted furans **3h**,**i** were obtained in 71% and 99% yields.

The addition of allyl alcohol was also very interesting as it could give an entry to further functionalization and other transition-metal-catalyzed reactions. Various substrates were efficiently converted into the corresponding allyloxy-substituted furans (entries 7–11). The reaction of diols **1a** and **1c**, which bear an (*E*)-cinnamyl and propargyl side chain, respectively, afforded the ketals **4a** and **4c** in high yields (entries 7 and 8). Benzyl-protected alcohols and allyl derivative **1g** (entries 9–11) could also be cyclized and functionalized to give furans **4e**, **4g**, and **4i** in 86–99% yield. These promising results prompted us to test the efficiency of our system for the formation of six-membered functionalized rings that are found as subunits of a number of cytotoxic natural products.[9d,12] Dimethyl 3-butynylmalonate[14] was alkylated in the presence of cinnamyl bromide to give the diester, which was subsequently reduced and monobenzylated to give the alcohol **1j**. Indeed, this cycloisomerization/hydroalkoxylation process is not limited to the synthesis of functionalized furans, as alcohol **1j** undergoes an equally facile and efficient Ir^I-catalyzed *exo*-selective tandem reaction to give, in 24 h, the functionalized pyrans **2j** and **3j** in high (99%) yield (Table 2, entries 12 and 13).

Next, we focused on the mechanism of the reaction. Two competitive mechanisms for this transformation may be envisioned, one based on a metal–vinylidene intermediate[6,8] and the other based on electrophilic alkyne activation.[3] Despite the fact that iridium catalysts can promote the formation of vinylidene intermediates from alkynes,[8] this mechanism was excluded owing to the *exo*-selective nature of the cyclization instead of the expected 6-*endo*-cyclization. A second mechanism based on the Lewis acidic character of the metal is much more probable (Scheme 2). The reaction may



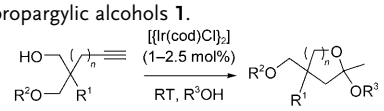
Scheme 2. Postulated mechanism for the formation of cyclic ketals from bis-homopropargylic alcohols.

be initiated by the formation of the π-alkynyl complex **A** by the complexation of the unsaturated triple bond to the Ir^I catalyst. Subsequent addition of the alcohol, which was supposed to occur *anti* to the π-complex **A**,[3a] would lead to a σ-complex **B**, which is favored in polar protic solvents such as MeOH, via a transient zwitterionic intermediate.[15] Proton transfer may then be followed by the intermolecular addition of MeOH to give the cyclic ketal **2a**.[16,17] An alternate pathway involving an Ir^{III} hydride species, and therefore a reductive elimination, cannot be ruled out.

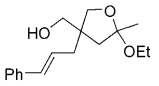
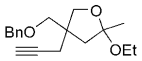
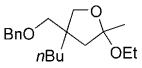
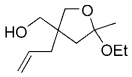
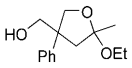
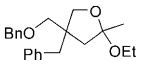
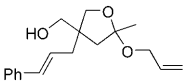
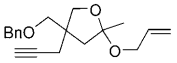
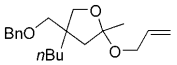
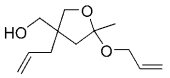
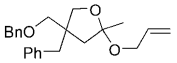
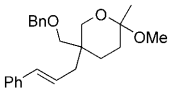
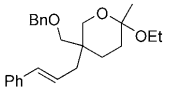
Labeling studies performed in the presence of 2.5 mol% of $[\{Ir(cod)Cl\}_2]$ either in CD_3OD for the cyclization of **1a** or in MeOH for the reaction of the deuterated alkyne $[D_1]$-**1a**

 © 2005 Wiley-VCH Verlag GmbH & Co. KGaA, Weinheim

Table 2: Cyclization/hydroalkoxylation of bis-homopropargylic alcohols **1**.



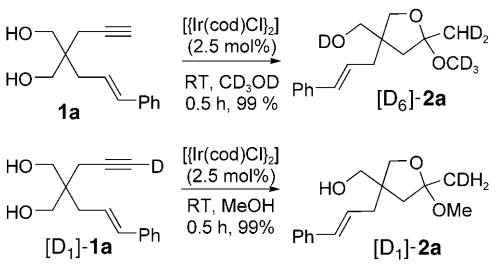
1a–j **2–4 a–j**

Entry		R^1	R^2	Product		t [h]	Yield [%][a]
1[b]	**1a**	(*E*)-cinnamyl	H		**3a**	0.5	99
2[b]	**1c**	propargyl	Bn		**3c**	2.5	99
3[b]	**1e**	*n*Bu	Bn		**3e**	0.5	99
4[c]	**1g**	allyl	H		**3g**	0.7	78
5[c]	**1h**	Ph	H		**3h**	0.7	71
6[c]	**1i**	Bn	Bn		**3i**	1.3	99
7[b]	**1a**	(*E*)-cinnamyl	H		**4a**	2.5	99
8[b]	**1c**	propargyl	Bn		**4c**	2.5	99
9[b]	**1e**	*n*Bu	Bn		**4e**	2.7	99
10[c]	**1g**	allyl	H		**4g**	2.5	86
11[c]	**1i**	Bn	Bn		**4i**	22	88
12[b]	**1j**	(*E*)-cinnamyl	Bn		**2j**	24	99
13[b]	**1j**	(*E*)-cinnamyl	Bn		**3j**	24	99

[a] Yield of isolated product; 1/1 mixture of diastereomers. [b] 2.5 mol% of catalyst. [c] 1 mol% of catalyst.

were in good agreement with the proposed mechanism, as the cycloisomerization/hydroalkoxylation reactions afforded the unique formation of the corresponding deuterated derivatives [D_6]-**2a** or [D_1]-**2a**, respectively (Scheme 3). No deuterium scrambling, which would result from insertion of iridium into a C–H(D) bond, was observed.

In summary, we have developed a general, efficient, and atom-economic method for the synthesis of cyclic ketals starting from easily accessible bis-homopropargylic alcohols. The [{Ir(cod)Cl}$_2$] dimer is used for the first time to promote a tandem cyclization/hydroalkoxylation reaction at room temperature in a very short time to give functionalized derivatives. The reaction conditions are compatible with various functional groups. Considering the ease of preparation of these substrates, this method provides a new route for constructing functionalized furanyl and pyranyl building blocks and is therefore a valuable tool for the synthesis of natural or biologically active products. The proposed reaction mechanism presumably involves a Lewis acid type activation, followed by an intramolecular cyclization, a protonolysis step, and the intermolecular addition of an alcohol molecule. The



Scheme 3. Labeling experiments for the cyclization reactions of **1a** and [D_1]-**1a**.

 © 2005 Wiley-VCH Verlag GmbH & Co. KGaA, Weinheim

high catalytic activity of [{Ir(cod)Cl}$_2$], along with the very mild reaction conditions, would probably allow the use of weaker nucleophiles, both as inter- and intramolecular partners.

Experimental Section

Representative standard procedure: A mixture of bis-homopropargylic alcohol **1a** (70 mg, 0.3 mmol) and [{Ir(cod)Cl}$_2$] (5.1 mg, 2.5 mol%) in degassed methanol (0.6 mL) was stirred under argon at room temperature for 30 min. After completion of the reaction, the mixture was filtered through a short pad of celite (eluent: EtOAc) and the solvents were evaporated under reduced pressure to give 79 mg of ketal **2a**. ^{1}H NMR (300 MHz, $CDCl_3$): $\delta = 1.43$ (s, 3H), 1.44 (s, 3H), 1.72 (d, $J = 13.3$ Hz, 1H), 1.84 (d, $J = 13.3$ Hz, 1H), 1.98 (d, $J = 13.3$ Hz, 1H), 2.00 (d, $J = 13.3$ Hz, 1H), 2.36–2.50 (m, 4H), 3.21 (s, 3H), 3.22 (s, 3H), 3.51–3.85 (m, 8H), 6.18 (dt, $J = 15.7$, 7.3 Hz, 2H), 6.47 (d, $J = 15.7$ Hz, 2H), 7.21–7.37 ppm (m, 10H). ^{13}C NMR (75 MHz, $CDCl_3$): $\delta = 21.0$, 21.8, 38.8, 41.8, 47.0, 47.7, 48.3, 48.6, 48.5, 48.7, 67.9, 68.0, 73.7, 73.9, 108.3, 108.5, 126.0, 126.4, 126.9, 127.5, 127.6, 128.8, 132.9, 133.7, 137.6 ppm. CI MS (NH_3): *m*/*z*: 248 $[M-MeOH+NH_4]^+$, 231 $[M-MeOH+H]^+$. HRMS calculated for $C_{15}H_{19}O_2$ $[M-MeOH+H]^+$: 231.1385; found 231.1389.

Received: March 31, 2005
Published online: July 11, 2005

Keywords: atom economy · cyclization · homogeneous catalysis · iridium · tandem reaction

[1] For recent reviews on atom-economical processes, see: a) B. M. Trost, *Acc. Chem. Res.* **2002**, *35*, 695–705; b) P. N. Anastas, M. M. Kirchhoff, *Acc. Chem. Res.* **2002**, *35*, 686–694; c) B. M. Trost, D. F. Toste, A. B. Pinkerton, *Chem. Rev.* **2001**, *101*, 2067–2096; d) B. M. Trost, M. J. Krische, *Synlett* **1998**, 1–16; e) B. M. Trost, *Science* **1991**, *254*, 1471–1477.

[2] For reviews on tandem reactions, see: a) L. F. Tietze, F. Haunert, *Stimulating Concepts in Chemistry* (Eds: F. Vögtle, J. F. Stoddart, M. Shibasaki), Wiley-VCH, Weinheim, **2000**, pp. 39–64; b) G. Poli, G. Giambastiani, A. Heumann, *Tetrahedron* **2000**, *56*, 5959–5989; c) L. F. Tietze, *Chem. Rev.* **1996**, *96*, 115–136; d) S. E. Denmark, A. Thorarensen, *Chem. Rev.* **1996**, *96*, 137–165; e) J. D. Winkler, *Chem. Rev.* **1996**, *96*, 167–176; f) M. Malacria, *Chem. Rev.* **1996**, *96*, 289–306.

[3] For representative examples, see: a) F. Alonso, I. P. Beletskaya, M. Yus, *Chem. Rev.* **2004**, *104*, 3079–3160; b) I. Nakamura, Y. Yamamoto, *Chem. Rev.* **2004**, *104*, 2127–2198; c) M. Beller, J. Seayad, A. Tillack, H. Jiao, *Angew. Chem.* **2004**, *116*, 3448–3479; *Angew. Chem. Int. Ed.* **2004**, *43*, 3368–3398.

[4] For representative examples, see: a) G. Zeni, R. C. Larock, *Chem. Rev.* **2004**, *104*, 2285–2310; b) G. Balme, N. Monteiro, D. Bouyssi, *Handbook of Organopalladium Chemistry for Organic Synthesis* (Ed.: E. I. Negishi), Wiley, New York, **2002**, pp. 2245–2265; c) T. Hosokawa, S.-I. Murahashi, *Handbook of Organopalladium Chemistry for Organic Synthesis* (Ed.: E. I. Negishi), Wiley, New York, **2002**, pp. 2169–2192; d) J. Tsuji, *Palladium Reagents and Catalysis*, Wiley-VCH, New York, **1996**; e) T. Hosokawa, S.-I. Murahashi, *Acc. Chem. Res.* **1990**, *23*, 49–54; f) K. Utimoto, *Pure Appl. Chem.* **1983**, *55*, 1845–1852.

[5] a) L. Charruault, V. Michelet, R. Taras, S. Gladiali, J.-P. Genêt, *Chem. Commun.* **2004**, 850–851; b) C. Nevado, L. Charruault, V. Michelet, C. Nieto-Oberhuber, M. P. Muñoz, M. Méndez, M.-N. Rager, J.-P. Genêt, A. M. Echavarren, *Eur. J. Org. Chem.* **2003**, 706–713; c) L. Charruault, V. Michelet, J.-P. Genêt, *Tetrahedron Lett.* **2002**, *43*, 4757–4760; d) J.-C. Galland, M. Savignac, J.-P. Genêt, *Tetrahedron Lett.* **1997**, *38*, 8695–8698. For recent reviews, see: e) A. M. Echavarren, C. Nevado, *Chem. Soc. Rev.* **2004**, *33*, 431–436; f) M. Méndez, V. Mamane, A. Fürstner, *Chemtracts* **2003**, *16*, 397–425; g) G. C. Lloyd-Jones, *Org. Biomol. Chem.* **2003**, *1*, 215–236; h) C. Aubert, O. Buisine, M. Malacria, *Chem. Rev.* **2002**, *102*, 813–834.

[6] For selected studies with W-based catalysts, see: a) E. Alcazar, J. M. Pletcher, F. E. McDonald, *Org. Lett.* **2004**, *6*, 3877–3880; b) F. E. McDonald, K. S. Reddy, *Angew. Chem.* **2001**, *113*, 3765–3767; *Angew. Chem. Int. Ed.* **2001**, *40*, 3653–3655; c) F. E. McDonald, *Chem. Eur. J.* **1999**, *5*, 3103–3106. For recent studies with Rh- and Ru-based catalysts, see: d) B. M. Trost, M. T. Rudd, *J. Am. Chem. Soc.* **2005**, *127*, 4763–4766; e) B. M. Trost, Y. H. Rhee, *Org. Lett.* **2004**, *6*, 4311–4313; f) B. M. Trost, M. T. Rudd, M. G. Costa, P. I. Lee, A. E. Pomerantz, *Org. Lett.* **2004**, *6*, 4235–4238; g) B. M. Trost, Y. H. Rhee, *J. Am. Chem. Soc.* **2003**, *125*, 7482–7483; h) B. M. Trost, Y. H. Rhee, *J. Am. Chem. Soc.* **2002**, *124*, 2528–2533.

[7] For selected Ir-catalyzed C–C bond-forming reactions, see: a) N. Kinoshita, K. H. Marx, K. Tanaka, K. Tsubaki, T. Kawabata, N. Yoshikai, E. Nakamura, K. Fuji, *J. Org. Chem.* **2004**, *69*, 7960–7964, and references cited therein; b) D. B. Grotjahn, J. M. Hoerter, J. L. Hubbard, *J. Am. Chem. Soc.* **2004**, *126*, 8866–8867; c) M. Janka, W. He, A. J. Frontier, R. Eisenberg, *J. Am. Chem. Soc.* **2004**, *126*, 6864–6865; d) G. Lipowsky, N. Miller, G. Helmchen, *Angew. Chem.* **2004**, *116*, 4695–4698; *Angew. Chem. Int. Ed.* **2004**, *43*, 4595–4597; e) R. Takeuchi, Y. Nakaya, *Org. Lett.* **2003**, *5*, 3659–3662; f) H. Takaya, K. Yoshida, K. Isozaki, H. Terai, S.-I. Murahashi, *Angew. Chem.* **2003**, *115*, 3424–3426; *Angew. Chem. Int. Ed.* **2003**, *42*, 3302–3304; g) T. Koike, X. Du, T. Sanada, Y. Danda, A. Mori, *Angew. Chem.* **2003**, *115*, 93–96; *Angew. Chem. Int. Ed.* **2003**, *42*, 89–92; h) T. Shibata, S. Kadowaki, M. Hirase, K. Takagi, *Synlett* **2003**, 573–575; i) S. Sakaguchi, T. Kubo, Y. Ishii, *Angew. Chem.* **2001**, *113*, 2602–2604; *Angew. Chem. Int. Ed.* **2001**, *40*, 2534–2536; j) N. Chatani, H. Inoue, T. Morimoto, T. Muto, S. Murai *J. Org. Chem.* **2001**, *66*, 4433–4436, and references cited therein; k) T. Shibata, K. Takagi, *J. Am. Chem. Soc.* **2000**, *122*, 9852–9853; l) R. Takeuchi, M. Kashio, *Angew. Chem.* **1997**, *109*, 268–270; *Angew. Chem. Int. Ed. Engl.* **1997**, *36*, 263–265; m) C.-H. Jun, Z. Lu, R. H. Crabtree, *Tetrahedron Lett.* **1992**, *33*, 7119–7120; n) N. Chatani, S. Ikeda, K. Ohe, S. Murai, *J. Am. Chem. Soc.* **1992**, *114*, 9710–9711.

[8] For references on iridium–vinylidene intermediates, see: a) C. S. Chin, G. Won, D. Chong, M. Kim, H. Lee, *Acc. Chem. Res.* **2002**, *35*, 218–225; b) S.-I. Murahashi, H. Takaya, *Acc. Chem. Res.* **2000**, *33*, 225–233; c) T. Ohmura, S. Yorozuya, Y. Yamamoto, N. Miyaura, *Organometallics* **2000**, *19*, 365–367. For reviews on other metal–vinylidene intermediates, see: d) [1a]; e) C. Bruneau, P. H. Dixneuf, *Acc. Chem. Res.* **1999**, *32*, 311–323; f) M. I. Bruce, *Chem. Rev.* **1991**, *91*, 197–257.

[9] For a reaction with alkenes, see: a) T. Hosokawa, F. Nakajima, A. Iwasa, S.-I. Murahashi, *Chem. Lett.* **1990**, 1387–1390. For a reaction with alkynes, see: b) B. Gabriele, G. Salerno, M. Costa, *Synlett* **2004**, 2468–2483, and references cited therein; c) B. Gabriele, G. Salerno, F. De Pascali, M. Costa, G. P. Chiusoli, *J. Organomet. Chem.* **2000**, *593–594*, 409–415; d) J. A. Marshall, M. M. Yanik, *Tetrahedron Lett.* **2000**, *41*, 4717–4721.

[10] T. W. Greene, P. G. M. Wuts, in *Protective Groups in Organic Synthesis*, Wiley, New York, **1999**. The alcohols were synthesized under conventional monoprotection conditions (NaH, BnBr, nBu$_4$NI, THF for the monobenzylation reaction and Ac_2O, DMAP, pyridine, CH_2Cl_2 for the monoacetylation reaction).

[11] In other solvents, such as acetone, acetonitrile, or toluene, the reaction is quite sluggish and involves the intramolecular addition of both hydroxy groups to give the bicyclic ketal.

 © 2005 Wiley-VCH Verlag GmbH & Co. KGaA, Weinheim

[12] a) C. Xu, E.-I. Negishi, *Handbook of Organopalladium Chemistry for Organic Synthesis* (Ed.: E. I. Negishi), Wiley, New York, **2002**, pp. 2289 – 2305; b) M. C. Elliot, E. Williams, *J. Chem. Soc. Perkin Trans. 1* **2001**, 2303 – 2340; c) M. C. Elliot, *J. Chem. Soc. Perkin Trans. 1* **2000**, 1291 – 1318; d) F. Q. Alali, X.-X. Liu, J. L. McLaughlin, *J. Nat. Prod.* **1999**, *62*, 504 – 540.

[13] M. D. Lewis, J. K. Cha, Y. Kishi, *J. Am. Chem. Soc.* **1982**, *104*, 4976 – 4977.

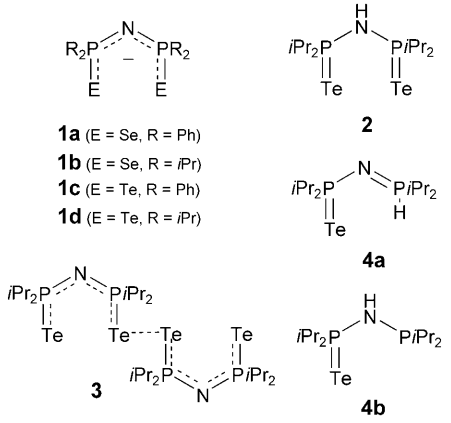
[14] For the preparation of **1j**, see: G. J. Laidig, L. S. Hegedus, *Synthesis* **1995**, 527 – 530.

[15] Isolation of the enol ether and detection of the σ-complex were unsuccessful. For Pt- and Pd-catalyzed hydroalkoxylation of alkenes, see: a) H. Qian, X. Han, R. A. Widenhoefer, *J. Am. Chem. Soc.* **2004**, *126*, 9536 – 9537; b) J. E. Bäckvall, B. Akermark, S. O. Ljunggren, *J. Am. Chem. Soc.* **1979**, *101*, 2411 – 2415.

[16] No traces of the dimethoxy ketal were detected when the dibenzylate of diol **1a** was treated with $[\{Ir(cod)Cl\}_2]$/MeOH, which excludes an intermolecular addition of MeOH prior to the intramolecular process. For recent syntheses of dimethoxy ketals from alkynes in the presence of Pd, Pt, Cu, Au, or Zn see: a) D. Masui, Y. Ishii, M. Hidai, *Chem. Lett.* **1998**, 717 – 718; b) J. W. Hartman, L. Sperry, *Tetrahedron Lett.* **2004**, *45*, 3787 – 3788; c) S. H. Bertz, G. Dabbagh, P. Cotte, *J. Org. Chem.* **1982**, *47*, 2216 – 2217; d) Y. Fukuda, K. Utimoto, *J. Org. Chem.* **1991**, *56*, 3729 – 3731; e) J. H. Teles, S. Brode, M. Chabanas, *Angew. Chem.* **1998**, *110*, 1475 – 1478; *Angew. Chem. Int. Ed.* **1998**, *37*, 1415 – 1418; f) K. Breuer, J. H. Teles, D. Demuth, H. Hibst, A. Schäfer, S. Brode, H. Domgörgen, *Angew. Chem.* **1999**, *111*, 1495 – 1502; *Angew. Chem. Int. Ed.* **1999**, *38*, 1401 – 1405.

[17] The addition of R^3OH may also be catalyzed by an $[Ir^I]$ complex.

 © 2005 Wiley-VCH Verlag GmbH & Co. KGaA, Weinheim



Main Group Chemistry

DOI: 10.1002/anie.200501138

An Unusual Ditelluride: Synthesis and Molecular and Electronic Structures of the Dimer of the Tellurium-Centered Radical [TeP*i*Pr$_2$N*i*Pr$_2$PTe]$^{\bullet}$**

Tristram Chivers, Dana J. Eisler, Jamie S. Ritch, and Heikki M. Tuononen*

The coordination chemistry of diselenoimidodiphosphinate ligands [SePR$_2$NR$_2$PSe]$^-$ (**1a** and **1b**)[1] has been extensively investigated.[2] In a series of recent articles, O'Brien and co-workers demonstrated that metal complexes of the isopropyl derivative **1b** are suitable single-source precursors for the generation of thin semiconducting films such as MSe (M = Zn, Cd),[3] HgSe,[4] M$_2$Se$_3$ (M = Ga, In),[5] PbSe,[6] Bi$_2$Se$_3$,[7] and CuInSe$_2$,[8] as well as CdSe quantum dots.[9] The analogous tellurium-containing ligands were not available until recently when we described a new synthetic methodology that facilitated the generation of the phenyl derivative **1c.**[10] Since a reasonably high volatility is needed for metal complexes in CVD applications, we turned our attention to the synthesis of the isopropyl analogue **1d**, and its protonated precursor, **2**. We report herein that the attempted synthesis of **2** unexpectedly produced the dimer **3**, which can be viewed to result from the association of two tellurium-centered radicals [TeP*i*Pr$_2$N*i*Pr$_2$PTe]$^{\bullet}$. The monotelluride **4** is obtained as the P–H tautomer HP*i*Pr$_2$N*i*Pr$_2$PTe (**4a**) rather than the N–H tautomer **4b**.

The reaction of P*i*Pr$_2$NH*i*Pr$_2$P with one equivalent of tellurium in *n*-hexane at 23 °C produced **4** in 81 % yield. Complex **4** was characterized in solution by NMR spectroscopy and in the solid state by IR spectroscopy and an X-ray structural determination.[11] The NMR spectra indicated the preferential formation of the P–H tautomer **4a**; there was no indication of the presence of the N–H tautomer **4b**. The resonance for the P–H proton in the ^{1}H NMR spectrum appears as a doublet of doublets of multiplets located at δ = 6.34 ppm, with a $^1J_{P,H}$ coupling of 443 Hz, which is consistent with values reported for related systems.[13–16] In the ^{31}P{^{1}H} NMR spectrum, two mutually coupled signals for phosphorus are observed, one of which exhibits ^{125}Te satellites ($^1J_{Te,P}$ = 1654 Hz). In the proton-coupled ^{31}P NMR spectrum the other signal appears as a doublet ($^1J_{P,H} \approx$ 445 Hz) of multiplets. The solid-state IR spectrum of **4a** exhibits a sharp band at 2329 cm^{-1}, which is in the middle of the range of values (2200–2460 cm^{-1}) reported for analogous compounds with a P^V–H functionality.[13–16]

The X-ray crystal structure (Figure 1) confirms the assignment of **4a** as the P–H tautomer. The P–H proton was located in the electron difference map and refined. The two P–N bond lengths are significantly different (P1–N1 1.622(2) versus P2–N1 1.589(2) Å). The phosphorus–tellurium bond length of 2.3798(8) Å is similar to that observed in related compounds that contain a terminal P=Te bond.[17] The preferential formation of the P–H tautomer, **4a**, may be contrasted with the series of monochalcogenides

[*] Prof. T. Chivers, Dr. D. J. Eisler, J. S. Ritch, H. M. Tuononen
Department of Chemistry
University of Calgary
Calgary, AB T2N 1N4 (Canada)
Fax: (+1) 403-289-9488
E-mail: chivers@ucalgary.ca

[**] The authors gratefully acknowledge financial support from the Natural Sciences and Engineering Research Council (Canada), the Alberta Ingenuity Fund (D.J.E.), Helsingin Sanomain 100-vuotis-säätiö (H.M.T.), and the University of Calgary for financial support.

 © 2005 Wiley-VCH Verlag GmbH & Co. KGaA, Weinheim

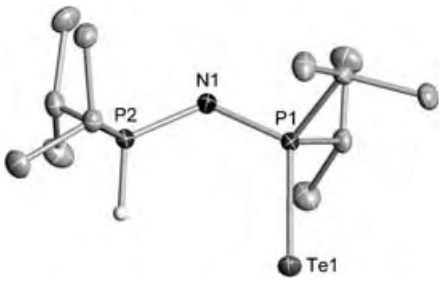


Figure 1. Molecular structure of **4** with hydrogen atoms on all carbon atoms omitted for clarity. Selected bond lengths [Å] and angles [°]: P1-Te1 2.3798(8), P1-N1 1.622(2), P2-N1 1.589(2), P1-N1-P2 127.3(1); τ P2-N1-P1-Te1 3.2(1), τ H2D-P2-P1-Te1 30.1(1).

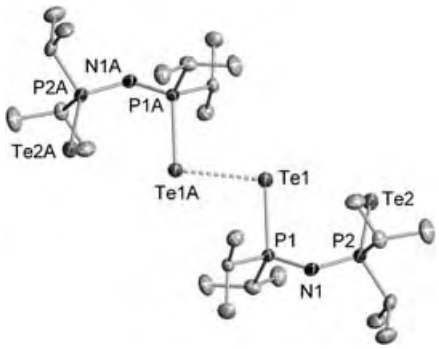


Figure 2. Molecular structure of **3** with hydrogen atoms omitted for clarity. Selected bond lengths [Å] and angles [°] [calculated values are given in brackets]: Te1–Te1A 2.946(1) [2.954], P1-Te1 2.489(2) [2.475], P2-Te2 2.394(2) [2.388], P1-N1 1.571(5) [1.610], P2-N1, 1.623(5) [1.642], P1-N1-P2 135.2(3) [124.5], τ P1-Te1-Te1A-P2 180.0 [180.0], τ Te1A-Te1-P1-N1 147.7 [135.1], τ Te1-P1-N1-P2 30.1 [37.7], τ P1-N1-P2-Te2 2.4 [10.0].

$PPh_2NHPh_2P(E)$ (E = O, S, Se), which all exist exclusively as the N–H tautomer, both in solution and in the solid state.[18,19] Consequently, we prepared the monoselenide by stoichiometric oxidation of $PiPr_2NHiPr_2P$ with selenium in *n*-hexane at 23 °C. This product also exhibits the characteristic spectroscopic signatures of a P^V–H functionality, namely, a signal centered at $\delta = 6.49$ ppm with $^1J_{PH} = 441$ Hz in the ^{1}H NMR spectrum and a strong band at 2342 cm^{-1} in the IR spectrum. Substituents that increase the basicity of the lone pair on the phosphorus atom are known to favor the formation of the P–H tautomer in related systems, for example, $HP(NMe_2)_2NPPh_2S$.[16] The present results show that a change in the substituent on the phosphorus atom from phenyl to isopropyl is sufficient to tip the balance in favor of the P–H tautomer.

Attempts to oxidize both phosphorus(III) centers in $PiPr_2NHiPr_2P$ by the direct reaction with tellurium to give **2** were unsuccessful under a variety of reaction conditions. During the course of these investigations, it was observed that direct exposure of pale-yellow solutions of **4a** to air resulted in the rapid formation of deep red solutions from which dark red, X-ray quality crystals of **3** could be grown. An X-ray crystal-structure determination revealed that **3** is the centrosymmetric dimer $[(TeP iPr_2NP iPr_2Te\text{-})_2]$ (Figure 2).[20]

The Te–Te interatomic distance of 2.946(1) Å in **3** indicates a significantly weaker bond than those in organic ditellurides (2.72–2.76 Å)[21] or that in the dianion $[Te–Te]^{2-}$ (2.79 Å).[22] The two P–Te bonds in **3** differ in length by about 0.1 Å, with the shorter separation indistinguishable from that observed for the terminal P=Te bond in **4a**. The metrical parameters of the P-N-P backbone in **3** and **4a** are also similar. In light of the structural determination, an alternative high-yield (87 %) synthesis of **3** was devised that involved the stoichiometric oxidation of the sodium salt of **1d** with iodine.

Complex **3** can be viewed as involving the association of two $[TeP iPr_2NHiPr_2PTe]^{\bullet}$ radicals through a Te···Te contact. To gain some insight into the nature of the bonding in **3**, we have carried out density functional theory (DFT) calculations for the model system $[(TePMe_2NPMe_2Te\text{-})_2]$ and the corresponding radical $[TePMe_2NPMe_2Te]^{\bullet}$.[23] The structure optimized with the PBE0/TZVP functions for the C_i symmetric dimer is in reasonable agreement with the X-ray crystal structure of **3** (Figure 2). Of particular note, the calculated Te–Te bond length is 2.954 Å, compared with 2.946(1) Å in **3**. The structure of $[TePMe_2NPMe_2Te]^{\bullet}$ is C_2 symmetric and the radical has a ^{2}B doublet ground state. The calculated Te–P and P–N bond lengths are 2.431 Å and 1.626 Å, respectively. The P-N-P and Te-P-N bond angles are 123.2° and 115.7°, respectively, and the dihedral angle τ Te-P-N-P is 23.8°. A comparison with the metrical parameters of the ditelluride shows the bond angles to be virtually identical and the bond lengths and the dihedral angle to be exactly averages of the bond parameters found for the monomeric unit in the dimer.

The bonding interaction between the singly occupied molecular orbitals (SOMOs) of two radicals is depicted in Figure 3. The SOMO is an almost pure linear combination of

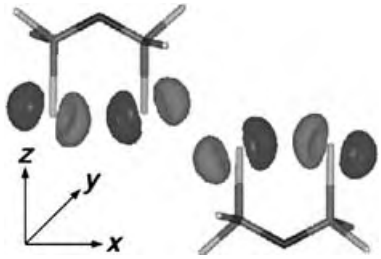


Figure 3. The bonding interaction between two $[TePMe_2NPMe_2Te]^{\bullet}$ SOMOs (±0.065 isosurface level). Hydrogen atoms are omitted for clarity.

tellurium p_x and p_y orbitals. Mulliken population analysis shows that the spin-density distribution mirrors the composition of the SOMO and is equally distributed among both tellurium centers. The spin densities on both nitrogen and phosphorus atoms are very small, 0.004 and 0.009, respectively. Consequently, the EPR spectrum of $[TePR_2NPR_2Te]^{\bullet}$ is expected to show large hyperfine couplings to two tellurium atoms and only very small couplings to nitrogen and two phosphorus centers. The calculated hyperfine coupling con-

 © 2005 Wiley-VCH Verlag GmbH & Co. KGaA, Weinheim

stants validate this hypothesis; hyperfine couplings of −68.1, 4.8, and −0.8 G were obtained for ^{125}Te, ^{31}P, and ^{14}N, respectively. Dissociation of the dimer, **3**, into the corresponding radical was not detectable by EPR spectroscopy in hexane, toluene, or THF solutions within the temperature range 20–90 °C.

In view of the modest steric protection around the radical centers in $[TePMe_2NPMe_2Te]^{\bullet}$ and the composition of the spin density in the SOMO, both the ease and the direction of the dimerization are apparent (see Figure 3). However, the spatial orientation of monomers in the dimer and the multicentered nature of the radical SOMO effectively weakens the Te–Te bonding interaction in $[(TePR_2NR_2Te\text{-})_2]$ compared with that in organic ditellurides, RTe–TeR. The calculated dimerization energy for the reaction $2\,[TePMe_2NPMe_2Te]^{\bullet} \rightarrow [(TePMe_2NMe_2Te\text{-})_2]$ is −80 kJ mol^{-1}, (Te–Te, D = 138 kJ mol^{-1}).[27] An electron localization function (ELF)-based[28] bonding analysis is in agreement with this result as it revealed that no pure disynaptic, bonding, valence basin can be found between Te1 and Te1A. This finding indicates a Te–Te covalent bond order of less than one for $[(TePMe_2NMe_2Te\text{-})_2]$. Calculations done for the R = H derivative $[(TePH_2NH_2Te\text{-})_2]$ show that the absence of organic R groups allows the dimeric structure to deform, and a twisted C_1 symmetric structure with a Te–Te bond length of 2.802 Å now becomes the global minima. However, the predicted Te–Te bond length for the *tert*-butyl derivative $[(TeP\textit{t}Bu_2N\textit{t}Bu_2Te\text{-})_2]$ is 3.010 Å, which implies that the use of very bulky substituents on the phosphorus atom may foster dissociation into the radical monomer $[TePR_2NPR_2Te]^{\bullet}$.

The NMR spectra of **3** exhibit broad signals at room temperature. The broad signal observed in the $^{31}P\{^1H\}$ NMR spectrum at 23 °C $[D_8]$THF resolves into two signals at 0 °C, which sharpen into mutually coupled doublets (δ = 45.8 and 42.2 ppm) at −60 °C. Each signal exhibits ^{125}Te satellites. The magnitude of the $^1J_{Te,P}$ coupling constants differs substantially (1500 versus 1026 Hz), which reflects the difference in the P–Te bond lengths. At +80 °C in $[D_8]$toluene, a relatively narrow signal at δ = 43 ppm ($\Delta\omega_{1/2} \approx 80$ Hz) with ^{125}Te tellurium satellites is observed. The value of the $^1J_{Te,P}$ (1290 Hz) is approximately the average of the two distinct coupling constants observed at −60 °C. Thus, the ^{31}P NMR spectroscopic data indicate that a rapid exchange process that leads to equivalent phosphorus environments on the NMR time scale occurs above 0 °C. Attempts to distinguish between an intermolecular and an intramolecular exchange process by variable-concentration ^{31}P NMR spectroscopy experiments were inconclusive as a result of the very low solubility of **3**.

In summary, the characterization of the novel ditelluride **3** represents a new aspect of the well-studied chemistry of dichalgenoimidodiphosphinate ligands. The facile formation of **3** suggests that the synthesis of potential single-source precursors of binary metal tellurides from reactions of the anionic ligand **1d** with metal halides may be accompanied by a redox transformation for certain p- or d-block metals. Compound **3** also exemplifies a new type of reagent for the direct synthesis of ditelluroimidodiphosphinate complexes by oxidative addition to electropositive metal centers, for example, upon photochemical activation.

Experimental Section

All reactions and the manipulations of products were performed under an argon atmosphere by using standard Schlenk techniques or an inert atmosphere glove box. Solvents were freshly distilled, dried, and degassed prior to use. NMR spectra were obtained by using a Bruker AMX 300 spectrometer. ^{125}Te NMR spectra were referenced to the external standard Te_2Ph_2. The reagent $[(tmeda)NaN(P\textit{i}Pr_2Te)_2]$ (tmeda = *N*,*N*,*N*′,*N*′-tetramethyl-1,2-ethanediamine)was prepared by modification of the procedure reported for the corresponding phenyl derivative.[10]

3: A solution of $[(tmeda)NaN(P\textit{i}Pr_2Te)_2]$ (0.204 g, 0.32 mmol) in THF (25 mL) was cooled to −78 °C and a cold (−78 °C) solution of I_2 (0.040 g, 0.16 mmol) in THF (25 mL) was added dropwise by cannula over 15 min. The resulting cherry red solution was stirred at −78 °C for 30 min and then warmed slowly to 23 °C to give a deep red solution, which was stirred for an additional 30 min. The solvent was removed in vacuo and the residue was dissolved in toluene then filtered to remove NaI. Toluene was then removed in vacuo to afford **3** as a dark red powder (0.138 mg, 87 %). Elemental analysis calcd (%) for $C_{24}H_{56}N_2P_4Te_4$: C 28.62, H 5.61, N 2.78; found: C 29.07, H 5.66, N 2.64; ^{1}H NMR ($[D_8]$THF, 23 °C): δ = 2.23 (br, 4H; C*H*-$(CH_3)_2$), 1.31 (d, ^3J(H,H) = 6 Hz, 6H; CH(C*H*$_3$)$_2$), 1.25 (d, ^3J(H,H) = 6 Hz, 12H; CH(C*H*$_3$)$_2$), 1.19 ppm (d, ^3J(H,H) = 6 Hz, 6H; CH-(C*H*$_3$)$_2$); $^{31}P\{^1H\}$ NMR: δ = 42.4 ppm (br); ^{1}H NMR (−60 °C): δ = 2.36 (m, 2H; C*H*$(CH_3)_2$), 1.95 (m, 2H; C*H*$(CH_3)_2$), 1.44, 1.39, 1.30, 1.24, 1.17, 1.15, 1.11, 1.08 ppm (eight doublets, ^3J(H,H) = 6 Hz, 3H each; CH(C*H*$_3$)$_2$); $^{31}P\{^1H\}$ NMR: δ = 45.8 (d, ^2J(P,P) = 26 Hz, ^1J-(^{125}Te,P) = 1026 Hz), 42.2 ppm (d, ^2J(P,P) = 26 Hz, ^1J(^{125}Te,P) = 1500 Hz). X-ray quality crystals of **3** were grown from a THF/*n*-hexane solution.

4: *n*-Hexane (120 mL) was added to a mixture of elemental tellurium (1.20 g, 9.40 mmol) and $P\textit{i}Pr_2NH\textit{i}Pr_2P$ (2.00 g, 8.02 mmol) and the mixture was stirred at 23 °C for 16 h. The resulting pale yellow solution was filtered and concentrated to about 10 mL, which caused **4** to precipitate as a pale yellow crystalline solid (2.45 g, 81 %). Elemental analysis calcd (%) for $C_{12}H_{29}NP_2Te$: C 38.24, H 7.76, N 3.72; found: C 38.59, H 7.73, N 3.76; ^{1}H NMR ($[D_8]$toluene, 23 °C): δ = 6.34 (ddm, ^1J(P,H) = 443 Hz, ^3J(P,H) = 10 Hz, 1H; PH), 1.86 (m, 4H; C*H*$(CH_3)_2$), 1.14, 1.10, 1.08, 1.04, 0.93, 0.90, 0.87, 0.84 ppm (eight doublets, ^3J(H,H) = 6 Hz, 3H each; CH(C*H*$_3$)$_2$); $^{31}P\{^1H\}$ NMR: δ = 48.2 (d, ^2J(P,P) = 18 Hz, ^1J(^{125}Te,P) = 1654 Hz; P(Te)), 44.0 ppm (d, ^2J(P,P) = 18 Hz; PH); $^{125}Te\{^1H\}$ NMR: δ = −846 ppm (dd, ^1J-(^{125}Te,P) = 1642 Hz, ^3J(^{125}Te,P) = 13 Hz).

Received: March 31, 2005
Published online: July 6, 2005

Keywords: dimerization · electronic structure · phosphorus · tautomerism · tellurium

[1] a) D. Cupertino, D. J. Birdsall, A. M. Z. Slawin, J. D. Woollins, *Inorg. Chim. Acta* **1999**, *290*, 1; b) P. Bhattacharyya, J. Novasad, J. Phillips, A. M. Z. Slawin, D. J. Williams, J. D. Woollins, *J. Chem. Soc. Dalton Trans.* **1995**, 1607.

[2] For a review, see: C. Silvestru, J. E. Drake, *Coord. Chem. Rev.* **2001**, *223*, 117.

[3] a) M. Afzall, D. Crouch, M. A. Malik, M. Motevalli, P. O'Brien, J.-H. Park, J. D. Woollins, *Eur. J. Inorg. Chem.* **2004**, 171; b) M. Afzall, D. Crouch, M. A. Malik, M. Motevalli, P. O'Brien, J.-H. Park, *J. Mater. Chem.* **2003**, *13*, 639.

 © 2005 Wiley-VCH Verlag GmbH & Co. KGaA, Weinheim

[4] D. J. Crouch, P. M. Hatton, M. Helliwell, P. O' Brien, J. Raftery, *Dalton Trans.* **2003**, 2761.
[5] J.-H. Park, M. Afzall, M. Helliwell, M. A. Malik, P. O'Brien, J. Raftery, *Chem. Mater.* **2003**, *15*, 4205.
[6] M. Afzall, K. Ellwood, N. l. Pickett, P. O'Brien, J. Raftrey, J. Waters, *J. Mater. Chem.* **2004**, *14*, 1310.
[7] a) J. Waters, D. Crouch, J. Raftery, P. O'Brien, *Chem. Mater.* **2004**, *16*, 3289; b) D. J. Crouch, M. Helliwell, P. O'Brien, J.-J. Park, J. Waters, D. J. Williams, *Dalton Trans.* **2003**, 1500.
[8] M. Afzaal, D. J. Crouch, P. O'Brien, J. Raftery, P. J. Skabara, A. J. P. White, D. J. Williams, *J. Mater. Chem.* **2004**, *14*, 233.
[9] D. J. Crouch, P. O'Brien, M. A. Malik, P. J. Skabara, S. P. Wright, *Chem. Commun.* **2003**, 1454.
[10] G. G. Briand, T. Chivers, M. Parvez, *Angew. Chem.* **2002**, *114*, 3618–3620; *Angew. Chem. Int. Ed.* **2002**, *41*, 3468.
[11] Crystal data for **3**: $C_{24}H_{56}N_2P_4Te_4$, $M_r = 1006.99$, triclinic, space group $P\bar{1}$, $a = 7.603(2)$, $b = 7.955(2)$, $c = 15.303(3)$ Å, $\alpha = 95.31(3)$, $\beta = 96.89(3)$, $\gamma = 92.90(3)°$, $V = 913.1(3)$ Å^3, $Z = 1$, $\rho_{calcd} = 1.831$ g cm^{-3}, $\mu = 3.354$ mm^{-1}, $T = 173(2)$ K. A dark red, blocklike crystal ($0.10 \times 0.10 \times 0.06$ mm^3) was coated with Paratone 8277 oil and mounted on a glass fiber. Data were collected on a Nonius Kappa CCD diffractometer with $Mo_{K\alpha}$ radiation ($\lambda = 0.71073$ Å) and with ω and ϕ scans and the data were scaled based on equivalent reflections by using SCALEPACK (Nonius, B.V. 1998). The structure was solved by direct methods by using the SHELX-TL V6.1 program and the model refined by using the SHELXL-97 program.[12] Of the 11150 reflections collected ($2\theta_{max} = 50.06°$), 3201 were unique ($R_{int} = 0.062$) and used to refine 154 parameters. The molecule was well-ordered and no special considerations for the refinement were necessary. All non-hydrogen atoms were refined with anisotropic thermal parameters. The hydrogen atoms were calculated geometrically and were riding on their respective carbon atoms. Refinement was carried out on F^2 against all independent reflections by the full-matrix least-squares method and converged at $R_1 = 0.0389$ (for 2475 reflections with $I > 2\sigma(I)$) and $wR_2 = 0.0851$ (for all data).
[12] G. M. Sheldrick, SHELXL-97, Program for refinement of crystal structures, University of Göttingen, Göttingen (Germany), **1997**.
[13] L. T. Burke, E. Hevia-Freire, R. Holland, J. C. Jeffery, A. P. Leedham, C. A. Russell, A. Steiner, A. Zagorski, *Chem. Commun.* **2000**, 1769.
[14] N. Burford, J. A. C. Clyburne, S. Mason, J. F. Richardson, *Inorg. Chem.* **1993**, *32*, 4988.
[15] H. R. O'Neal, R. H. Neilson, *Inorg. Chem.* **1984**, *23*, 1372.
[16] A. Schmidpeter, H. Rossknecht, *Angew. Chem.* **1969**, *81*, 572; *Angew. Chem. Int. Ed. Engl.* **1969**, *8*, 614.
[17] G. G. Briand, T. Chivers, M. Parvez, G. Schatte, *Inorg. Chem.* **2003**, *42*, 525.
[18] P. Bhattacharyya, A. M. Z. Slawin, D. J. Williams, J. D. Woollins, *J. Chem. Soc. Dalton Trans.* **1995**, 3189.
[19] P. Bhattacharyya, A. M. Z. Slawin, M. B. Smith, J. D. Woollins, *Inorg. Chem.* **1996**, *35*, 3675.
[20] Crystal data for **4**: $C_{12}H_{29}NP_2Te$, $M_r = 376.90$, triclinic, space group $P\bar{1}$, $a = 8.639(2)$, $b = 9.001(2)$, $c = 11.685(2)$ Å, $\alpha = 101.89(3)$, $\beta = 101.12(3)$, $\gamma = 91.43(3)°$, $V = 870.4(3)$ Å^3, $Z = 2$, $\rho_{calcd} = 1.438$ g cm^{-3}, $\mu = 1.874$ mm^{-1}, $T = 173(2)$ K. A pale yellow prismatic crystal ($0.10 \times 0.06 \times 0.03$ mm^3) was coated with Paratone 8277 oil and mounted on a glass fiber. Data collection, structure solution, and refinement followed the procedures outlined above for **3**. Of the 16995 reflections collected ($2\theta_{max} = 54.88°$), 3942 were unique ($R_{int} = 0.035$) and used to refine 149 parameters. The molecule was well ordered and no special considerations for the refinement were necessary. All non-hydrogen atoms were refined with anisotropic thermal parameters. The hydrogen atom on P2 was located and refined. All other hydrogen atoms were calculated geometrically and were riding on their respective atoms. Refinement converged at $R_1 = 0.0245$ (for 3411 reflections with $I > 2\sigma(I)$) and $wR_2 = 0.0552$ (for all data). CCDC-266932 and CCDC-266933 contain the supplementary crystallographic data for this paper. These data can be obtained free of charge from the Cambridge Crystallographic Data Centre via www.ccdc.cam.ac.uk/data_request/cif.
[21] S-P. Huang, M. G. Kantzidis, *J. Am. Chem. Soc.* **1992**, *114*, 5477.
[22] P. Böttcher, J. Getszchmann, R. Keller, *Z. Anorg. Allg. Chem.* **1993**, *619*, 476.
[23] Computational details: The structures of the diamagnetic dimer [$(TePMe_2NMe_2Te\text{-})_2$] and paramagnetic monomers [$TePMe_2NPMe_2Te$]$^\bullet$ were optimized in their ground states by using density functional theory and the hybrid PBE0 exchange-correlation functional.[24] The calculations used the Ahlrichs' triple-zeta valence basis set augmented by one set of polarization functions (TZVP); for tellurium, the corresponding effective core potential (ECP) basis set was used. Hyperfine coupling constants were calculated for the [$TePMe_2NPMe_2Te$]$^\bullet$ radical by a single-point calculation employing the optimized geometry, PBEPBE GGA functional,[24] QZ4P STO basis set and a fully relativistic ZORA spin–orbit formalism. All geometry optimizations were done with the Turbomole 5.71 program,[25] whereas ADF 2004.01 was used in the calculation of hyperfine couplings.[26]
[24] a) J. P. Perdew, K. Burke, M. Ernzerhof, *Phys. Rev. Lett.* **1996**, *77*, 3865; b) J. P. Perdew, K. Burke, M. Ernzerhof, *Phys. Rev. Lett.* **1997**, *78*, 1396; c) J. P. Perdew, M. Ernzerhof, K. Burke, *J. Chem. Phys.* **1996**, *105*, 9982.
[25] R. Ahlrichs, et al., TURBOMOLE, Program Package for ab initio Electronic Structure Calculations, Version 5.71, University of Karlsruhe, Karlsruhe (Germany), **2004**.
[26] ADF2004.01, SCM, Theoretical Chemistry, Vrije Universiteit, Amsterdam (The Netherlands), http://www.scm.com.
[27] L. Pauling, *The Nature of the Chemical Bond*, 3rd ed. Cornell University Press, Ithaca, NY, **1960**, p. 85.
[28] For a description of ELF see A. Savin, R. Nesper, S. Wengert, T. F. Fassler, *Angew. Chem.* **1997**, *109*, 1892; *Angew. Chem. Int. Ed. Engl.* **1997**, *36*, 1808.

 © 2005 Wiley-VCH Verlag GmbH & Co. KGaA, Weinheim

Nanostructures

DOI: 10.1002/anie.200500386

Synthesis of Nanoscopic Optical Fibers Using Lipid Membranes as Templates**

*Gopakumar Gopalakrishnan, Jean-Manuel Segura, Dimitrios Stamou, Cédric Gaillard, Marinela Gjoni, Ruud Hovius, Kurt J. Schenk, Pierre A. Stadelmann, and Horst Vogel**

Nanostructures of various materials with different sizes and shapes have been synthesized and studied in the past few years as a result of their high impact in optoelectronic applications. In particular, one-dimensional (1D) nanostructures (nanowires, nanorods, nanotubes, etc.) show optical and electronic properties[1] that are of importance to downsize optoelectronic components to the nanometer scale.[2] The development and integration of such 1D nanostructures relies on suitable synthetic procedures. Several methods have been designed such as template-directed synthesis,[3–6] solvothermal synthesis,[7] microfabrication,[8] metal-nanocluster-catalyzed growth,[1a] and surfactant-mediated self-assembly.[9] In particular, template-directed synthesis offers significant advantages: ease of performance, the possibility to work under mild reaction conditions, and above all the control over unique, well-defined morphologies of the resulting nanostructures. Various kinds of templates, such as porous alumina,[3] molecular sieves,[4] proteins,[5a] DNA,[5b] viruses,[5c] and self-assembled monolayers,[6] have been reported to guide the synthesis of 1D nanostructures. The critical issues in many template-directed syntheses are to obtain high yields and to achieve monocrystallinity.

Until now, lipid bilayers have not been used as templates for asymmetric synthesis although they are well-known self-organized nanostructures. The closed compartments of single phospholipid vesicles have already been used as nanoreactors to perform simple chemical reactions.[10,11] Upon drying from aqueous dispersions, many phospholipids spontaneously form well-organized periodic multilayers of lipid membranes separated by distinct nanometer-thick water films.[12] The rich variability of the lipid hydrocarbon chains and lipid polar head groups results in numerous lyotropic and thermotropic phases.[12] Of particular interest in the present context are lipid polar head groups that bind certain cations selectively and reversibly. This opens the possibility to modulate the concentration of precursor ions, for example, when a second reactant is added, and thus control the synthesis of nanomaterials in the confined, nanometer-sized water films of multilamellar lipid phases. Here, we have applied this strategy to synthesize high-aspect-ratio (≈ 1000) cadmium chloride nanowires, which exhibit interesting optical properties when doped in situ with fluorescent CdS quantum dots.

The nanowires were synthesized in hydrated, multilamellar stacks of lipid bilayers comprising lipid-bound Cd^{2+} ions. A proper design of the lipid template was crucial for the formation of nanowires. The lipid bilayers comprised 70 mol% of 1,2-dimyristoyl-*sn*-glycero-3-phosphocholine (DMPC), which acts as a stable matrix, and 30 mol% of a thiolipid, 1,2-dilauroyl-*sn*-glycero-3-phosphothioethanol (DLPSH), which was added for its strong ability to bind Cd^{2+} ions through the -SH groups (see Supporting Information). With a molar ratio of lipid/Cd^{2+} of about 2, large quantities of Cd^{2+} ions were complexed by the lipid head groups. Upon exposure to HCl vapor, Cd^{2+} ions were released as a result of competitive binding of protons to the polar lipid head groups,[13] leading to supersaturation of Cd^{2+} ions in the nanometer-sized water film and finally to the initiation of growth of nanowires. When either the concentration of Cd^{2+} was reduced by a factor of two or DLPSH was omitted, no nanowires were formed which shows that a critical concentration of Cd^{2+} is necessary (see Supporting Information).

The nanowires show high aspect ratios with a narrow distribution of diameters ranging from 80 to 200 nm and lengths extending up to 170 μm (Figure 1a). The lengths of the nanowires could be tuned by varying the duration of exposure to HCl while the diameters showed little variation. Transmission electron microscopy showed that the nanowires are monocrystalline along their entire lengths (Figure 1b). Selected-area electron diffraction patterns revealed that the nanowires are composed of orthorhombic $CdCl_2 \cdot 4H_2O$ crystals grown along the [100] direction (Figure 1c).

The synthesis of anisotropic structures requires that the template, here the lipid lamellar phase, restricts or promotes the growth in specific directions. Orthorhombic $CdCl_2 \cdot 4H_2O$ consists of [001] molecular chains formed by edge-sharing $[CdCl_4(H_2O)_2]^{2-}$ octahedrons (Figure 2a) that define a preferential growth direction along the octahedral chain axis to result in slightly elongated crystals of $CdCl_2 \cdot 4H_2O$ when

[*] G. Gopalakrishnan, Dr. J.-M. Segura, Dr. D. Stamou,[+] M. Gjoni, Dr. R. Hovius, Prof. H. Vogel
Laboratoire de Chimie Physique des Polymères et Membranes
Institut des Sciences et Ingénierie Chimiques
Ecole Polytechnique Fédérale de Lausanne (EPFL)
1015 Lausanne (Switzerland)
Fax: (+41) 21-693-61-90
E-mail: horst.vogel@epfl.ch
Dr. K. J. Schenk
Laboratoire de Cristallographie 1, EPFL
1015 Lausanne (Switzerland)
Dr. C. Gaillard,[++] Prof. P. A. Stadelmann
Centre Interdisciplinaire de Microscopie Electronique, EPFL
1015 Lausanne (Switzerland)
[+] Present Address:
Bio-Nanotechnology Laboratory
Nano-Science Center
University of Copenhagen (Denmark)
[++] Present Address:
INRA URPOI
Plate-forme RIO Microscopie
Nantes (France)

[**] This work was supported by a grant (No. 4047-057562) from the NRP-47 program of the Swiss National Science Foundation. Dr. A. Peer is acknowledged for help with the synthesis of lipids. Dr. W.-P. Ulrich is acknowledged for the treatment of data.

Supporting information for this article is available on the WWW under http://www.angewandte.org or from the author.

 © 2005 Wiley-VCH Verlag GmbH & Co. KGaA, Weinheim

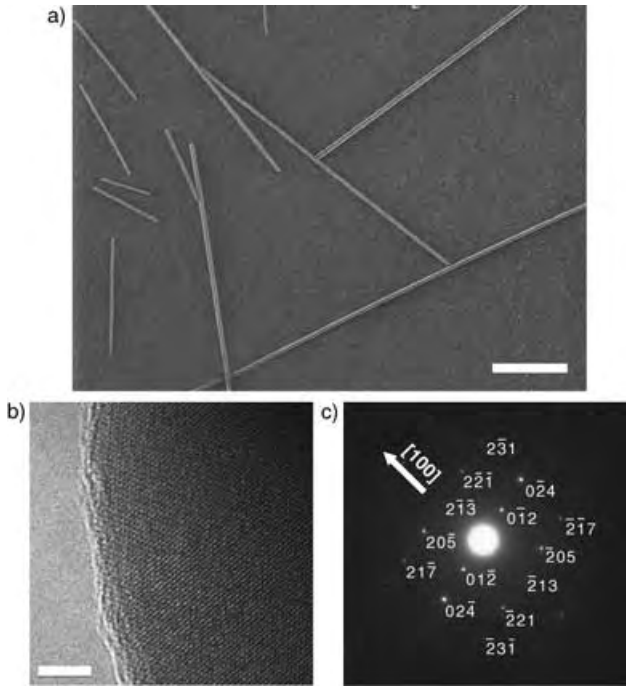


Figure 1. a) Scanning electron micrograph of typical $CdCl_2{\cdot}4\,H_2O$ nanowires illustrating the high aspect ratios. In this particular image, diameters of the nanowires are around 100 nm and lengths range from 1.5 μm up to more than 20 μm (scale bar = 2 μm). b) High-resolution transmission electron micrograph of the edge of a nanowire showing the regular atomic arrangement in the crystal lattice (scale bar = 5 nm). c) Selected-area electron diffraction pattern on a nanowire, with indexation corresponding to orthorhombic $CdCl_2{\cdot}4\,H_2O$. The arrow indicates the [100] direction, which is the long axis as well as the growth direction of the nanowires.

grown in aqueous solution.[14] It is remarkable that the growth direction of our nanowires is perpendicular to the preferential growth direction of bulk $CdCl_2$ crystals. Online monitoring of the synthesis of nanowires indicates that the initiation of growth critically depends on a rate-limiting step. Two sequential phases were observed with the rapid appearance of small nucleation points followed, after a certain delay, by the sudden and continuous, nonsynchronous 1D growth of the crystals (see Figure 2b and Supporting Information). By using fluorescent lipids, a close colocalization of lipids and nanowires was observed which demonstrates that the lipid membranes are intimately involved in the growth of the nanowires (Figure 2c). Taking these observations together, we propose a mechanistic model for the unusual, asymmetric growth of the nanowires. $CdCl_2{\cdot}4\,H_2O$ crystal nuclei grow unperturbed up to a critical size, at which point a collective binding of numerous protonated, positively charged head groups of the planar lipid membranes to the crystal planes that are rich in Cl^- (i.e. high negative-charge density) becomes favorable. This occurs for all crystal planes except the (100) plane, in which Cl^- ions are shielded by a layer of coordinated water molecules, thus inhibiting growth in these directions.

While $CdCl_2{\cdot}4\,H_2O$ crystals are nonfluorescent, CdS compounds and particularly their nanocrystals, show size-dependent fluorescence. To provide the nanowires with fluorescence properties, HCl vapor was supplemented with H_2S during the growth process. As a result, the nanowires became intensely fluorescent with high photostability as shown in the confocal image of Figure 3a, while a weak diffuse background fluorescence was observed within the lipid bilayer stacks. The diffuse fluorescence in the lipid stacks featured a broad emission band upon excitation at 458 nm, with a maximum at 522 nm typical for CdS nanoparticles (see Figure 3b and Supporting Information). TEM images revealed a heterogeneous mixture of crystallites of CdS nanoparticles (Figure 3c). Single nanoparticles were also detected by optical microscopy at high excitation intensities as diffraction-limited spots[15] in the middle of a fluorescent background (see Figure 3d and Supporting Information). The nanowires exhibited spectra that are identical to that of the diffuse background in the lipid stacks which shows that their fluorescence results from associated CdS nanoparticles. No nanoparticles could be observed by TEM on the surface of the nanowires which suggests that they intercalate in the $CdCl_2{\cdot}4\,H_2O$ lattice during crystal growth (see Supporting Information).

The extended length of the nanowires as well as their diameter, which is on the order of 100 nm, make them

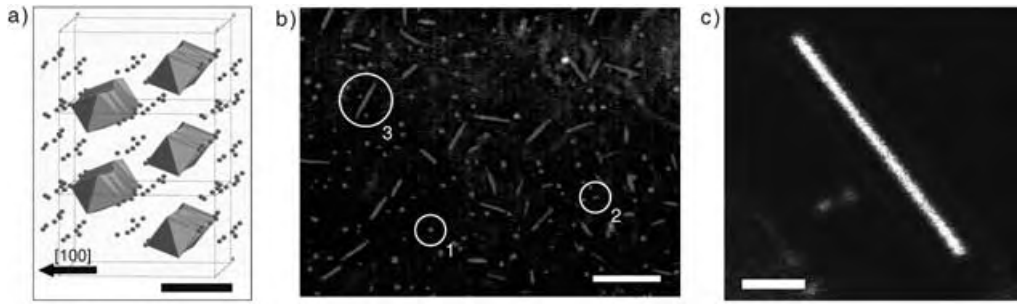


Figure 2. a) Crystal structure of orthorhombic $CdCl_2{\cdot}4\,H_2O$ showing the 1D molecular chains formed by edge-sharing $[CdCl_4(H_2O)_2]^{2-}$ octahedrons. The arrow indicates the [100] growth direction (scale bar = 6 Å; see Supporting Information for a more-detailed crystal structure). b) White-light transmission image of growing nanowires. As the initiation of growth is asynchronous, the various phases of the growth of the nanowires are present in a single image. Growth of nanowires occurs in two distinct steps: first, numerous nucleation points appear (1); after a while, some nucleation points grow into small nanowires (2); these latter continuously elongate upon addition of HCl vapor (3) without noticeable change in the diameter (scale bar = 60 μm). c) Fluorescence confocal image showing colocalization of a nanowire and rhodamine-labeled lipids (scale bar = 2 μm, λ_{ex} = 543 nm, λ_{em} = 560–610 nm).

 © 2005 Wiley-VCH Verlag GmbH & Co. KGaA, Weinheim

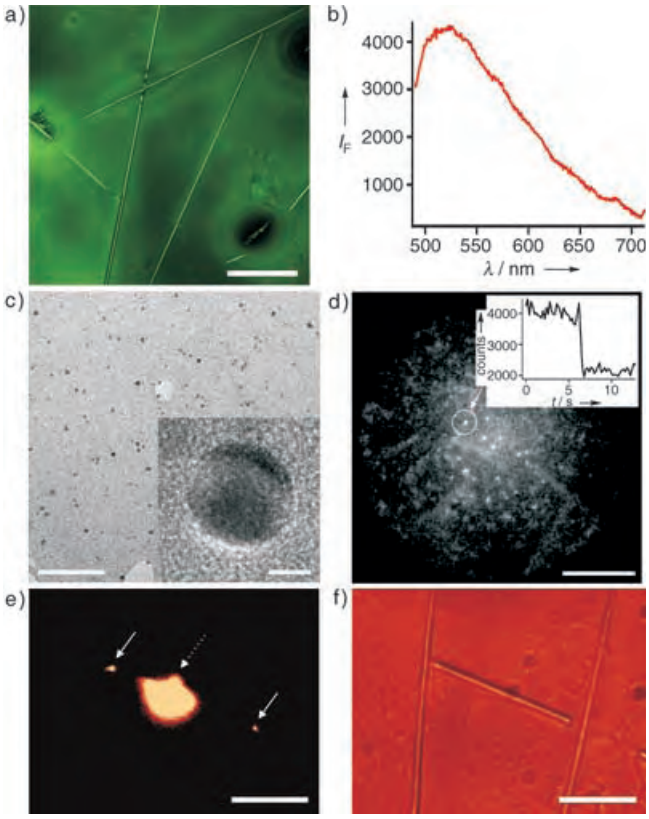


Figure 3. a) Fluorescence confocal image of nanowires (false color) grown in presence of H_2S showing that the as-prepared 100 μm-long nanowires are intensely fluorescent (scale bar = 20 μm, λ_{ex} = 488 nm, λ_{em} = 505–550 nm). b) Fluorescence emission spectrum of a single washed nanowire upon excitation at 457.9 nm. The emission maximum is at 522 nm with a full width at half-maximum larger than 100 nm. The spectrum of the fluorescent background is identical. c) Transmission electron micrograph of the background lipid multilayers showing the presence of a heterogeneous mixture of nanometer-sized CdS crystallites (scale bar = 200 nm). The inset shows the high-resolution transmission electron micrograph of a CdS nanoparticle (scale bar = 5 nm). d) Wide-field image showing single quantum dots, recognized as diffraction-limited spots, which appear in a structureless fluorescent background. Only a small fraction of the quantum dots is observed at the single-quantum-dot level owing to the stringent requirements for such observations, while the major fraction contributes to the structureless fluorescent background. The inset shows a time trace of the emission from the encircled quantum dot which features the characteristic single-step photobleaching (scale bar = 10 μm, λ_{ex} = 457.9 nm, integration time = 100 μs, measurement frequency = 5 Hz). e) False-color photoluminescence image of a nanowire upon local excitation at the middle (dotted arrow) with excitation at 488 nm. Luminescence is observed at the excitation location (dotted arrow) and from both ends (solid arrows) as result of optical waveguiding along the nanowire (scale bar = 10 μm). f) The corresponding false-color white-light transmission image of the nanowire (scale bar = 10 μm).

attractive candidates for optical waveguiding.[1a,16] When fluorescent nanowires were locally excited, fluorescence emission was detected not only at the excitation spot but also from the ends of the nanowires (Figure 3e and f). Nanowires waveguide light over tens of micrometers, thus acting as effective nanoscopic optical fibers. The ability to waveguide light is associated with the high refractive index of the nanowires, n_{nw}, which is expected to lie between the refractive indices of pure $CdCl_2 \cdot 2.5\,H_2O$ ($n = 1.65$) and CdS ($n = 2.5$). The corresponding minimal diameters, D, needed for the nanowire to act as a single-mode optical waveguide at the emission maximum at $\lambda = 520$ nm are thus between 80 and 190 nm by using the relationship, $D = (\lambda/\pi)(n_{nw}^2 - n_{medium}^2)$, where n_{medium}, the refractive index of the medium, is 1.4. The range of diameters found for the nanowires fall well within the theoretical sizes of the optical waveguides.

In conclusion, a novel synthetic route for state-of-the-art nanowires has been presented based on lipid membranes as an anisotropic template. This allows a straightforward, high-yield production of high-aspect-ratio monocrystalline nanowires under mild reaction conditions. The synthesized $CdCl_2 \cdot 4\,H_2O$ nanowires can be furthermore endowed with fluorescent properties by addition of H_2S. The appearance of highly fluorescent CdS quantum dots demonstrates that such nanoparticles can be synthesized in the confined interlamellar water film which might open novel synthetic routes for quantum dots. Our fluorescent nanowires could find a broad range of applications in optoelectronics, for instance in the development of nanolasers, as a complement to CdS nanowires.[1a] We furthermore speculate that this novel procedure using lipid membranes as templates may be extended to the synthesis of other materials by exchanging the thiolipid with other lipids that have suitable head groups which reversibly bind various ions. The possibility to manipulate the nanowires laterally, for instance by using laser tweezers (see Supporting Information) encourages the use of these nanowires for the nanofabrication of devices. In this respect, particularly attractive are the recent developments to form networks of lipid vesicles and lipid nanotubes,[11] which may be used as a template to build an array of connecting nanowires, opening a way to preassemble nanocomponents for future optoelectronics.

Experimental Section

Synthesis of nanowires: Solutions of DMPC (4 mM (Fluka); 100 μL) and DLPSH (16 mM (Avanti Polar Lipids); 10 μL) in chloroform were mixed and dried in vacuum, and the resulting lipid film was hydrated in deionized water (110 μL) at room temperature for 10 min. An aqueous solution of $CdCl_2$ (10 mM (Fluka); 30 μL) was added, then the mixture was dispersed for 5 min in a bath sonicator. A 15-μL aliquot of the obtained clear solution of vesicles was transferred onto a microscope glass coverslip and dried in vacuum. The resulting transparent lipid film was rehydrated in a 100 % humid atmosphere in a closed desiccator at 60 °C for 3 h. Then, a recipient containing 32 % hydrochloric acid (Merck) was inserted in the desiccator, and the lipid film was incubated for another 2 h with maintained humidity while the temperature was slowly decreased from 60 °C to room temperature. To produce fluorescent nanowires, the procedure was identical except that HCl was mixed with a small flake of FeS (Fluka, Germany) to produce H_2S while the dessicator was evacuated (400 mbar) to enhance the production of H_2S. A typical synthesis yielded around 1×10^6 nanowires of which 10–20 % showed lengths that exceeded 20 μm (see Supporting Information). Changing the ratio of DLPSH to DMPC reduced the yield and afforded shorter nanowires. Lipids could be removed from the produced nanowires by washing with toluene (Fluka). To observe colocalization of lipids and

 © 2005 Wiley-VCH Verlag GmbH & Co. KGaA, Weinheim

nanowires, 1% rhodamine-labeled lipids (TRITC-DHPE, Molecular Probes) was added. See Supporting Information for further experimental details.

Received: February 1, 2005
Revised: March 29, 2005
Published online: July 6, 2005

Keywords: crystal growth · lipids · nanostructures · quantum dots · template synthesis

[1] a) X. Duan, Y. Huang, R. Agarwal, C. M. Lieber, *Nature* **2003**, *421*, 241; b) X. Peng, L. Manna, W. Yang, J. Wickham, E. Scher, A. Kadavanich, A. P. Alivisatos, *Nature* **2000**, *404*, 59; c) Q. Wu, Z. Hu, X. Wang, Y. Lu, X. Chen, H. Xu, Y. Chen, *J. Am. Chem. Soc.* **2003**, *125*, 10176.
[2] J. Wang, M. S. Gudiksen, X. Duan, Y. Cui, C. M. Lieber, *Science* **2001**, *293*, 1455; H. Kind, H. Yan, B. Messer, M. Law, P. Yang, *Adv. Mater.* **2002**, *14*, 158.
[3] K. L. Hobbs, P. R. Larson, G. D. Lian, J. C. Keay, M. B. Johnson, *Nano Lett.* **2004**, *4*, 167.
[4] Z. M. Li, J. P. Zhai, H. J. Liu, I. L. Li, C. T. Chan, P. Sheng, Z. K. Tang, *Appl. Phys. Lett.* **2004**, *85*, 1253.
[5] a) H. Cölfen, S. Mann, *Angew. Chem.* **2003**, *115*, 2452; *Angew. Chem. Int. Ed.* **2003**, *42*, 2350; b) H. Liang, T. E. Angelini, J. Ho, P. V. Braun. G. C. L. Wong, *J. Am. Chem. Soc.* **2003**, *125*, 11786; c) C. Mao, D. J. Solis, B. D. Reiss, S. T. Kottmann, R. Y. Sweeney, A. Hayhurst, G. Georgiou, B. Iverson, A. M. Belcher, *Science* **2004**, *303*, 213.
[6] S. Hoeppener, R. Maoz, S. R. Cohen, L. Chi, H. Fuchs, J. Sagiv, *Adv. Mater.* **2002**, *14*, 1036.
[7] G. R. Patzke, F. Krumeich, R. Nesper, *Angew. Chem.* **2002**, *114*, 2554; *Angew. Chem. Int. Ed.* **2002**, *41*, 2446.
[8] B. Q. Wei, R. Vajtai, Y. Jung, J. Ward, R. Zhang, G. Ramanath, P. M. Ajayan, *Nature* **2002**, *416*, 495; L. Dai, *Polym. Adv. Technol.* **1999**, *10*, 357.
[9] M. Li, H. Schnablegger, S. Mann, *Nature* **1999**, *402*, 393.
[10] P.-Y. Bolinger, D. Stamou, H. Vogel, *J. Am. Chem. Soc.* **2004**, *126*, 8594; D. Stamou, C. Duschl, E. Delamarche, H. Vogel, *Angew. Chem.* **2003**, *115*, 5738; *Angew. Chem. Int. Ed.* **2003**, *42*, 5580.
[11] M. Karlsson, M. Davidson, R. Karlsson, A. Karlsson, J. Bergenholtz, Z. Konkoli, A. Jesorka, T. Lobovkina, J. Hurtig, M. Voinova, O. Orwar, *Annu. Rev. Phys. Chem.* **2004**, *55*, 613.
[12] G. Cevek, D. Marsh, *Phospholipid Bilayers: Physical Principles and Models*, Wiley, New York, **1987**.
[13] L. Girault, A. Boudou, E. J. Dufourc, *Biochim. Biophys. Acta* **1998**, *1414*, 140.
[14] H. Leligny, J. C. Monier, *Acta Crystallogr. Sect. B* **1979**, *35*, 569.
[15] M. Bäumle, D. Stamou, J.-M. Segura, R. Hovius, H. Vogel, *Langmuir* **2004**, *20*, 3828.
[16] M. Law, D. J. Sirbuly, J. C. Johnson, J. Goldberger, R. J. Saykally, P. Yang, *Science* **2004**, *305*, 1269.

 © 2005 Wiley-VCH Verlag GmbH & Co. KGaA, Weinheim

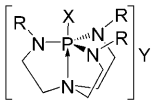
Coordination Modes

DOI: 10.1002/anie.200501401

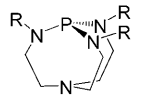
A Stable Structurally Characterized Phosphorus-Bound Isocyanide and Its Thermal and Catalyzed Isomerization to the Corresponding Cyanide**

*Jesudoss V. Kingston, Arkady Ellern, and John G. Verkade**

Although the chemistry and structural characteristics of carbon-bound isocyanides and cyanides have been well documented,[1] the relatively few examples of isocyanides that possess CN–heteroatom bonds are largely restricted to sulfur, nitrogen, oxygen, and phosphorus heteroatoms.[2–6] Isocyanides that are bound to heteroatoms are chemically reactive, thermally unstable, and, thus, are readily isomerizable to the corresponding cyanides, which are more stable. Indeed, these properties were reported for the first and only time 30 years ago by Stec et al. for a phosphorus-bound isocyanide.[7] The cationic halogen-bearing azaphosphatranes **1a** and **1b** are robust species stabilized by relatively short



	X	Y	R		X	Y	R
1a:	Cl	Cl	Me	**1g**:	–CN	Br	Me
1b:	F	Cl	Me	**1h**:	–CN	Br	*i*Bu
1c:	Br	Br	Me	**1i**:	Br	$AlCl_3Br$	*i*Bu
1d:	Br	Br	*i*Bu	**1j**:	–NC	$AlCl_3Br$	*i*Bu
1e:	–NC	Br	Me	**1k**:	–CN	$AlCl_3Br$	*i*Bu
1f:	–NC	Br	*i*Bu	**1l**:	Cl	Br	*i*Bu



2a: R = Me
2b: R = *i*Bu

$N_{ax}\rightarrow P$ transannular bonds (ax = axial).[8] It occurred to us that the pseudo-halogen character of the CN group might allow the formation of similarly stabilized isocyano analogues, which might isomerize to the cyano-bound species sufficiently slowly to be monitored by spectroscopic means. Herein, we report the facile synthesis of such analogues that were sufficiently stable to permit the structural parameters of a phosphorus-bound isocyano group and its cyano isomer to be determined for the first time and the thermal and Lewis acid catalyzed transformations of the P–NC species into the

[*] Dr. J. V. Kingston, Dr. A. Ellern, Prof. J. G. Verkade
Department of Chemistry
Iowa State University
Ames, IA 50011 (USA)
Fax: (+1) 515-294-0105
E-mail: jverkade@iastate.edu

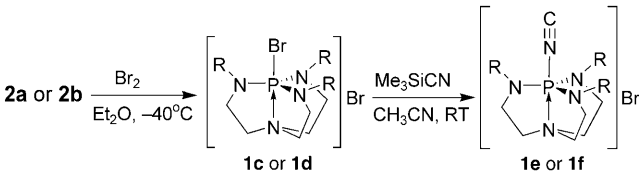
[**] We thank Aldrich Chemicals for their generous gift of proazaphosphatranes and the National Science Foundation for financial support. We also thank Jenny Schnobrich for experimental assistance.

Supporting information for this article is available on the WWW under http://www.angewandte.org or from the author.

© 2005 Wiley-VCH Verlag GmbH & Co. KGaA, Weinheim

isomeric P–CN species to be followed by ^{31}P NMR spectroscopic analysis.

The reaction of proazaphosphatranes **2a** and **2b** with bromine at room temperature resulted in the formation of **1c** and **1d**, respectively, in near quantitative yield (Scheme 1) as



Scheme 1. Synthesis of isocyano azaphosphatranes **1e** and **1f**.

pale yellow solids that are soluble in polar solvents. Trimethylsilyl cyanide reacted quickly with **1c** and **1d** at room temperature in dry acetonitrile (Scheme 1), and immediate removal of all volatiles at room temperature resulted in the formation of off-white solids. Characterization of the product from **2b** revealed the first example of a stable species **1f** that possesses a P–NC linkage, and the product from **2a** was found to be a mixture of **1e** and **1g**. The ^{31}P NMR spectrum of **1f** in solution showed a signal at $\delta = -40.3$ ppm (−40.8 ppm, solid-state ^{31}P MAS NMR spectroscopy). A strong isocyanide stretching vibration at 2088 cm^{-1} that is comparable with the N–C stretching frequencies reported for other known examples of heteroatom-bound isocyanides[6] was observed in the IR spectrum. The ^{13}C NMR spectrum of **1f** showed a doublet at $\delta = 173$ ppm with ^{2}J(P-C) = 26.4 Hz that is assignable to the isocyanide carbon atom. Compound **1f** is stable in the solid state and can be stored in an inert atmosphere at room temperature without observable decomposition or isomerization for at least one month. A single crystal of **1f**[9] suitable for X-ray crystallographic study was obtained by recrystallization from a cooled solution of acetonitrile/diethyl ether. Its molecular structure revealed a trigonal-bipyramidal geometry about the phosphorus center with a P–N_{ax} bond length of 1.9178(13) Å and an apical isocyano group with P–N and N–C bond lengths of 1.7814(14) and 1.154(2) Å, respectively (Figure 1; see also the Supporting Information). The stability of **1f** may, at least in part, be attributed to a linear delocalized

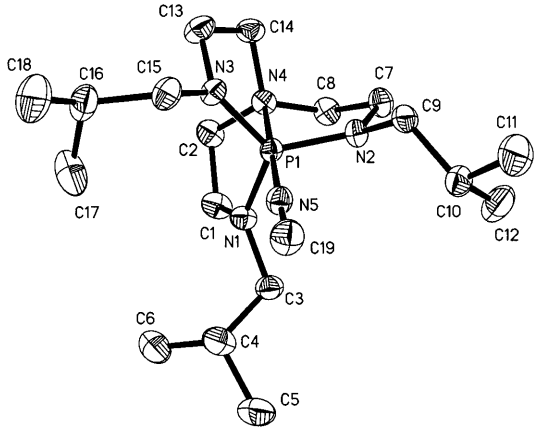
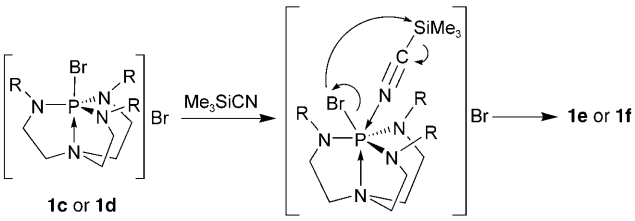


Figure 1. Molecular structure of isocyano azaphosphatrane **1f**.[9]

four-center six-electron σ-bonding framework along the pseudo-threefold axis of the cation. Interestingly, when the reaction of trimethylsilyl cyanide was attempted with the acyclic trisaminophosphine analogue (namely, $[(Me_2N)_3PBr]Br$),[10] no product formation was observed at room temperature over 16 h. At 80 °C, however, the cyanophosphonium salt $[(Me_2N)_3PCN]Br$ formed quantitatively in 48 h.

The initial formation of isocyanides **1e** and **1f** in the reaction of trimethylsilyl cyanide with **1c** and **1d**, respectively, is intriguing. Useful speculation on a reasonable pathway from **1c** and **1d** to **1e** and **1f**, respectively, is somewhat complicated by the assertion that Me_3SiCN exists in equilibrium with its more reactive isocyanide isomer.[11] However, the formation of Me_3SiNC is rather slow in solution (albeit in 1-chloronaphthalene rather than MeCN), thus taking approximately 10 minutes at 225 °C to reach an approximate concentration of 0.15 % relative to that of the cyano isomer.[12] It is therefore reasonable to conclude that this equilibrium would be reached even more slowly at room temperature, thus suggesting that the provenance of the isocyano isomers **1e** and **1f** and, through their isomerization, the cyano isomers **1g** and **1h**, respectively, is Me_3SiCN and not Me_3SiNC because of the almost instantaneous formation of **1e** and **1f** at room temperature.

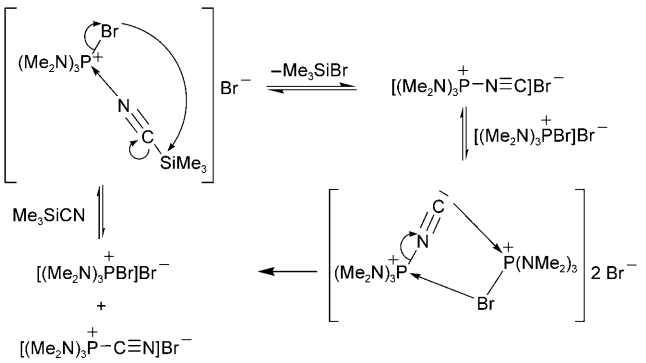
It has also been reported that the ability of Me_3SiCN to act as a source of either cyanide or isocyanide in reactions with ketones and epoxides is greatly affected by the presence of hard or soft Lewis acids that favor the formation of C–CN and C–NC linkages, respectively.[13] Compounds **1c** and **1d** could possess soft Lewis acid character, thus leading to the creation of the corresponding isocyanide isomers as the kinetically favored stable species **1e** and **1f** (Scheme 2). It is



Scheme 2. Possible mechanism for the formation of isocyanides **1e** and **1f**.

interesting in this regard that acyclic $[(Me_2N)_3PBr]Br$ does not form detectable amounts of $[(Me_2N)_3PNC]Br$ with Me_3SiCN but rather gives $[(Me_2N)_3PCN]Br$ (albeit only on heating). The preferential formation of the cyano isomer in the latter reaction may be associated with the harder Lewis acidity of the phosphorus center in the cation of $[(Me_2N)_3PBr]Br$ as a result of the greater concentration of positive charge at the phosphorus center than in **1d**, which delocalizes this charge more extensively over the nitrogen atoms. Therefore, it is possible that $[(Me_2N)_3PNC]Br$ is formed kinetically followed by rapid isomerization (Scheme 3). As the reaction proceeds, the Lewis acid catalyst, the $[(Me_2N)_3PBr]^+$ ion, in Scheme 3 would be replaced by Me_3SiBr (see later) or by the $[(Me_2N)_3PCN]^+$ ion as a Lewis

 © 2005 Wiley-VCH Verlag GmbH & Co. KGaA, Weinheim



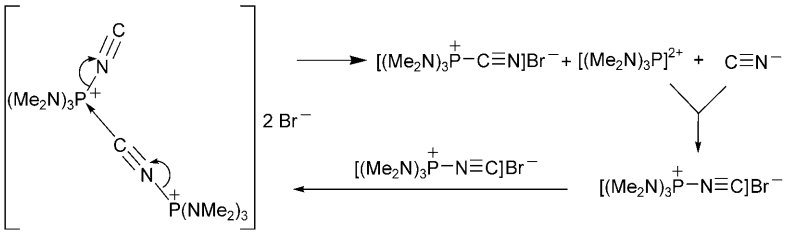
Scheme 3. Possible mechanism for the preferential formation of cyanide in the reaction of $[(Me_2N)_3PBr]Br$ with Me_3SiCN.

Table 1: Factors affecting the rate of isomerization of isocyanide **1f** to cyanide **1h**.

Entry	Solvent	Lewis acid	T [°C]	t	Isomerization [%]
1	MeCN		80	96 h	90
2	benzene		80	96 h	< 2
3	MeCN	Me_3SiCl	80	24 h	80
4	MeCN	Me_3SiBr[a]	80	30 min	98
5	MeCN	Me_3SiBr[a]	60	1 h	97
6	MeCN	Me_3SiBr[a]	25	16 h	97
7	MeCN	Me_3SiOTf	25	5 min	99
8	MeCN	$AlCl_3$	25	5 min	99

[a] One equivalent of Me_3SiBr was generated in situ by the reaction of **1d** with Me_3SiCN, as shown by ^1H NMR spectroscopic analysis. Tf = trifluoromethanesulfonyl.

acid isomerization catalyst (Scheme 4). However, the $[(Me_2N)_3PCN]^+$ ion in this role would form an unlikely dicationic intermediate. Such a mechanism might be contemplated, however, for the thermal isomerization of **1e** and **1f**

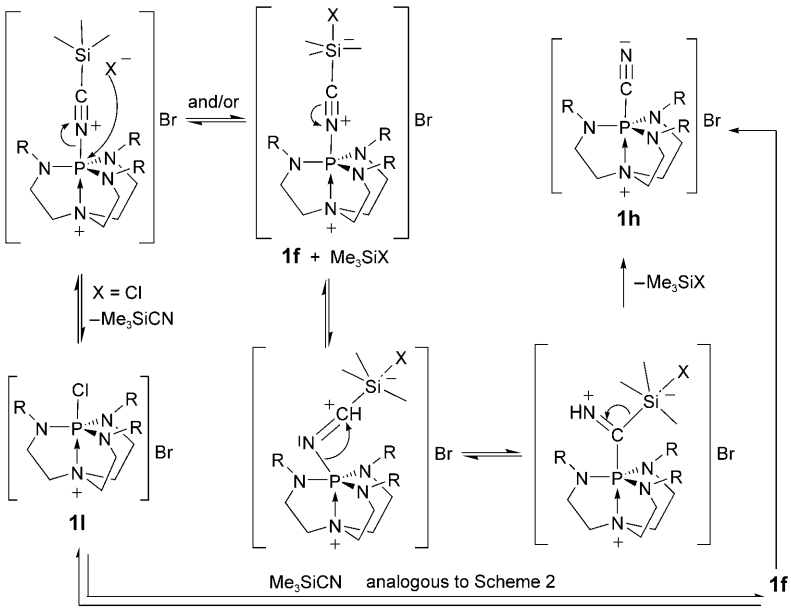


Scheme 4. Possible mechanism for the self-catalyzed isomerization of $[(Me_2N)_3PNC]Br$ to $[(Me_2N)_3PCN]Br$.

because the analogous intermediate $^+\overline{P(RNCH_2CH_2)_3N}^+$ is isoelectronic with boratrane ($\overline{B(OCH_2CH_2)_3N}$) (**4**), the structure of which has been determined by X-ray crystallographic studies.[14] Dipositive heterocyclic cations with charges on adjacent atoms are known, as in the cases of $^+\overline{S[(CH_2)_x]_2S}^+$ in which $x = 2$ or 3[15ab] and $^+\overline{P[(CH_2)_x]_3P}^+$ in which $x = 3$ or 4.[15c]

Heating a solution of **1f** in acetonitrile at 80 °C resulted in quantitative isomerization to **1h** in 120 h, as shown by ^{31}P NMR spectroscopic analysis. The rate of isomerization of **1f** was found to be dramatically influenced by the solvent polarity (Table 1, entries 1 and 2) and the presence of one equivalent of a Lewis acid (see Schemes 3–5 and the Supporting Information). Almost instantaneous isomerization occurred with the addition of one equivalent of $AlCl_3$ or Me_3SiOTf at room temperature. The trend $Me_3SiOTf > Me_3SiBr > Me_3SiCl$ in Table 1 parallels their decreasing Lewis acidity.[11] Interestingly, when the isomerization of **1f** promoted by Me_3SiCl was followed by ^{31}P NMR spectroscopic analysis, a transient signal at $\delta = -1.7$ ppm corresponding to **1l**, perhaps from an intermediate in a competing pathway, was observed (Scheme 5). It was expected that the addition of one equivalent of a Lewis acid (e.g., $AlCl_3$ or Me_3SiX) to the isomerization reaction of **1f** to **1h** would establish an equilibrium that involves the formation of the $[AlCl_3Br]^-$ ion or the pentavalent silicate $[Me_3Si(X)Br]^-$ ion (formed from $AlCl_3$ and Me_3SiX as the Lewis acids, respectively), which are both complex anions that would result from the addition of the bromide anion in **1f**. The presence of these anions containing coordinatively saturated central atoms was found to suppress the concentration of $[Me_3SiX]/[AlCl_3]$; consequently, the Lewis acid catalyzed izomerization of P–NC linkages to P–CN in **1f** was inhibited. It was interesting in this regard to observe that the conversion of **1i** into **1j** followed by the addition of a catalytic amount of $AlCl_3$ (10 mol %) resulted in the complete isomerization of **1j** to **1k** in CH_3CN in five minutes at room temperature.

Evidence to support an equilibrium process for the Lewis acid catalyzed isomerization of the phosphorus-bound isocyanides **1e** or **1f** was obtained as follows: Treatment of **1c** with one equivalent of Me_3SiCN at room temperature led to a



Scheme 5. Lewis acid promoted isomerization of isocyanide **1f** to cyanide **1h** by Me_3SiX.

 © 2005 Wiley-VCH Verlag GmbH & Co. KGaA, Weinheim

mixture of **1e** and **1g** in a ratio of 10:90 being obtained within five minutes. This ratio became 50:50 on addition of two equivalents of Me_3SiCN and 90:10 on addition of five equivalents of Me_3SiCN within the same time period. This observation suggests that a silicon-based Lewis acid catalyst does interact with the isocyano compound **1e** (or **1f**), perhaps as shown in Scheme 5, because in the presence of five equivalents of Me_3SiCN, which is a very weak Lewis acid relative to Me_3SiBr, it is more probable that Me_3SiCN will interact with **1e**, thus inhibiting the isomerization process.

Although an isomerization of tertiary alkyl isocyanides catalyzed by $BF_3{\cdot}Et_2O$ has been described,[16] neither $AlCl_3$ nor silicon-based Lewis acids have been reported to isomerize isocyanides of any type. Moreover, it is interesting that $AlCl_3$ and Me_3SiX (X = Cl, Br, OTf) are capable of converting **1f** into **1h**, even though **1f** bears a positive charge and might be expected to behave poorly as a Lewis base.

Although uni- and bimolecular mechanisms for the isomerization of carbon-bound isocyanide have been proposed, the available experimental and theoretical results suggest a unimolecular pathway that involves a three-membered-ring transition state.[17] Initial kinetic studies of the isomerization of **1f** to **1h** suggest that the mechanism for the uncatalyzed thermal isomerization involves a pathway more complicated than the uni- or bimolecular mechanisms.

A white solid was isolated after complete isomerization of **1f** in acetonitrile. The ^{31}P NMR spectrum of this compound showed a single resonance at $\delta = -35.3$ ppm with $^1J(P\text{-}C) = 122.4$ Hz consistent with **1h**, and the ^{13}C NMR spectrum revealed a doublet for the carbon atom of the cyano group at $\delta = 123$ ppm with $^1J(P\text{-}C) = 122.3$ Hz. IR spectroscopic analysis revealed a rather weak C–N stretching vibration at 2197 cm^{-1}, which is comparable with frequencies of other known examples of phosphorus-bound cyanides.[18] A single-crystal X-ray structural analysis of **1h**[9] supports its formation from the isomerization of **1f** (P–C: 1.854(2) Å; C–N: 1.148(3) Å) because the P–C bond is longer than the P–N bond in **1f**, which is as expected (see Figure 2 and the Supporting Information).

A detailed kinetic analysis of the isomerization of **1f** to **1h**, for example, and theoretical calculations aimed at a deeper understanding of the bonding and the isomerization pathways of these systems will be reported in due course.

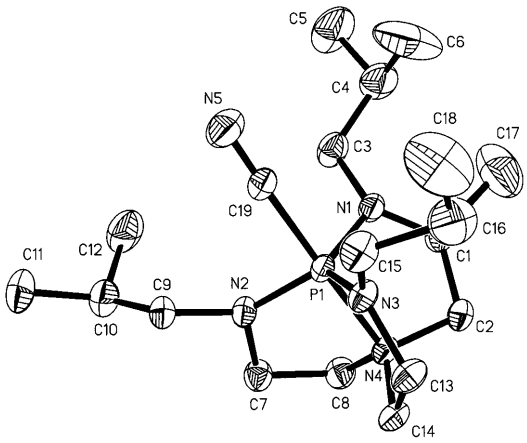


Figure 2. Molecular structure of cyano azaphosphatrane **1h**.[9]

Received: April 23, 2005
Published online: July 6, 2005

Keywords: coordination modes · cyanides · isocyanide ligands · isomerization · phosphorus

[1] a) Product class 7: isocyanides and related compounds, M. Suginome, Y. Ito, *Sci. Synth.* **2004**, *19*, 445–530; b) *Isonitrile chemistry* (Ed.: I. Ugi), Academic Press, New York, **1971**; c) F. Millich, *Chem. Rev.* **1972**, *72*, 101–113; d) F. Millich, *Macromol. Rev.* **1980**, *15*, 207–219.

[2] a) H. Bredereck, B. Folisch, K. Waltz, *Angew. Chem.* **1962**, *74*, 388–391; b) J. Buschmann, D. Lentz, P. Luger, G. Perpetuo, D. Preugschat, J. S. Thrasher, H. Willner, H.-J. Wölk, *Z. Anorg. Allg. Chem.* **2004**, *630*, 113–1142.

[3] a) C. Wentrup, H.-W. Winter, *J. Org. Chem.* **1981**, *46*, 1045–1046; b) C. Wentrup, B. Gerecht, D. Laqua, H. Briehl, H.-W. Winter, H. P. Reisenauer, M. Winnewisser, *J. Org. Chem.* **1981**, *46*, 1046–1048.

[4] a) I. Hagedorn, U. Eholzer, *Angew. Chem.* **1962**, *74*, 499–501; *Angew. Chem. Int. Ed. Engl.* **1962**, *1*, 514–; b) I. Hagedorn, K. E. Lichtel, H. D. Winklemann, *Angew. Chem.* **1965**, *77*, 726–728; *Angew. Chem. Int. Ed. Engl.* **1965**, *4*, 702–705; c) I. Hagedorn, H. Etling, K. E. Lichtel, *Chem. Ber.* **1966**, *99*, 520–524.

[5] a) T. Ignasiak, J. Suszko, B. Ignasiak, *J. Chem. Soc. Perkin Trans. 1* **1975**, 2122–2125; b) W. P. Fehlhammer, R. Metzner, R. Kunz, *Chem. Ber.* **1994**, *127*, 321–324; c) W. P. Fehlhammer, R. Metzner, W. Sperber, *Chem. Ber.* **1994**, *127*, 631–633; d) M. Lieb, M. Peach, V. Popov, *J. Fluorine Chem.* **1998**, *88*, 105–106.

[6] H. Briehl, A. Lukosch, C. Wentrup, *J. Org. Chem.* **1984**, *49*, 2772–2779.

[7] a) W. J. Stec, A. Konopka, B. Uznanski, *J. Chem. Soc. Chem. Commun.* **1974**, 923–924; b) W. J. Stec, T. Sudol, B. Uznanski, *J. Chem. Soc. Chem. Commun.* **1975**, 467–468.

[8] a) X. Liu, J. G. Verkade, *Inorg. Chem.* **1998**, *37*, 5189–5197; b) T. L. Windus, M. W. Schmidt, M. S. Gordon, *J. Am. Chem. Soc.* **1994**, *116*, 11449–11455.

[9] CCDC-271721 (**1f**) and -271723 (**1h**) contain the supplementary crystallographic data for this paper. These data can be obtained free of charge from The Cambridge Crystallographic Data Centre via www.ccdc.cam.ac.uk/data_request/cif.

[10] For the synthesis of $[(Me_2N)_3PBr]Br$; see, for example: a) B. Castro, J. R. Dormoy, *Tetrahedron Lett.* **1973**, *14*, 3243–3246; b) S. M. Godfrey, C. A. McAuliffe, I. Mushtaq, R. G. Pritchard, J. M. Sheffield, *J. Chem. Soc. Dalton Trans.* **1998**, 3815–3818.

[11] A. D. Dilman, S. L. Ioffe, *Chem. Rev.* **2003**, *103*, 733–772.

[12] J. A. Seckar, J. S. Thayer, *Inorg. Chem.* **1976**, *15*, 501–504.

[13] M. Onaka, A. Ohta, K. Sugita, Y. Izumi, *Appl. Catal. A* **1995**, *125*, 203–216.

[14] a) E. Mueller, H. B. Buergi, *Helv. Chim. Acta* **1984**, *67*, 399–405; b) Z. Taira, K. Osaki, *Inorg. Nucl. Chem. Lett.* **1971**, *7*, 509–512.

[15] a) W. K. Musker, P. B. Roush, *J. Am. Chem. Soc.* **1976**, *98*, 6745–6746; b) W. K. Musker, T. L. Wolford, P. B. Roush, *J. Am. Chem. Soc.* **1978**, *100*, 6416–6421; c) R. W. Alder, D. D. Ellis, R. Gleiter, C. J. Harris, H. Lange, G. A. Orpen, D. Read, P. N. Taylor, *J. Chem. Soc. Perkin Trans. 1*, **1998**, *10*, 1657–1668.

[16] T. Saegusa, N. T. Ishi, Y. Ito, *J. Org. Chem.* **1969**, *34*, 4040–4046.

[17] C. Ruchardt, M. Meier, K. Haaf, J. Pakusch, E. K. A. Wolber, B. Muller, *Angew. Chem.* **1991**, *103*, 907–915; *Angew. Chem. Int. Ed. Engl.* **1991**, *30*, 893–896.

[18] S. M. Godfrey, C. A. McAuliffe, R. G. Robin, J. M. Joanne, *J. Chem. Soc. Dalton Trans.* **1998**, *11*, 1919–1924.

 © 2005 Wiley-VCH Verlag GmbH & Co. KGaA, Weinheim

Ring-Opening Polymerization

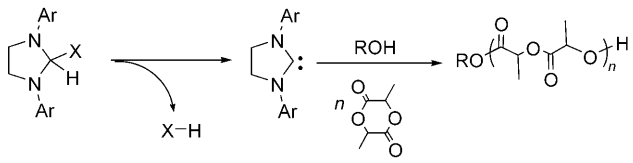
DOI: 10.1002/anie.200500723

Latent, Thermally Activated Organic Catalysts for the On-Demand Living Polymerization of Lactide**

Olivier Coulembier, Andrew P. Dove, Russell C. Pratt, Alan C. Sentman, Darcy A. Culkin, Laetitia Mespouille, Philippe Dubois, Robert M. Waymouth,* and James L. Hedrick**

The last decade has seen significant advances in carbene chemistry, including the isolation of the first heteroatom-subsituted singlet carbene and persistent triplet diarylcarbenes.[1,2] These advances have stimulated renewed interest and expanded the scope of possibilities engendered by these reactive species. Following the pioneering work by Wanzlick et al.,[3] the research groups of Bertrand[4] and Arduengo[5] isolated and characterized stable N-heterocyclic carbenes, and over the last decade the steric and electronic requirements for stable imidazolin-2-ylidene and imidazol-2-ylidene carbenes have been described.[6] Consequently, investigation into the properties and uses of N-heterocyclic carbenes (NHCs) has become a major area of research.[2,7] For example, the use of NHCs in place of phosphine ligands produces transition-metal complexes that exhibit enhanced catalytic performance and stability.[8] N-Heterocyclic carbenes have also proven to be effective organic catalysts for benzoin condensations, Stetter reactions, acylation/transesterification reactions, and the polymerization of cyclic esters.[9]

Despite advances in structural modifications to enhance the stability of N-heterocyclic carbenes[10] and the development of in situ methods for their generation,[11,12] the use of NHCs is complicated by their extreme air and moisture sensitivity, which necessitates the use of glove-box techniques. Our attention has been drawn towards the preparation and application of protected NHCs, particularly those that could be activated thermally. Many research groups realized in early studies that strongly nucleophilic carbenes underwent C–H insertion reactions with compounds containing acidic C–H bonds to form adducts in high yields.[13] Chloroform and pentafluorobenzene adducts of saturated carbenes[12] are useful precursors to transition-metal–carbene complexes; they also catalyze the ring-opening polymerization (ROP) of lactide (Scheme 1) at elevated temperatures.[12h] Grubbs



X = CCl_3, C_6F_5, etc.

Scheme 1. Polymerization of lactide with adducts of saturated N-heterocyclic carbenes.

and co-workers showed that imidazolium tetrafluoroborate salts could be treated with potassium *tert*-butoxide to reversibly generate 2-alkoxy-4,5-dihydroimidazoles.[14] Enders et al.[15] prepared alcohol adducts of the triazolylidene carbene; thermolysis of these adducts (80 °C) generated free carbene and alcohol. Our attention was drawn to alkoxytriazolines as possible unimolecular catalyst/initiator systems. Moreover, we anticipated that the hydroxy-terminated polymer and free carbene present in solution during the polymerization could react reversibly with each other to form an adduct after each propagation step,[14b] hence minimizing the concentration of the active species and possible adverse transesterification side reactions, which is a problem typical of other controlled/living polymerization procedures above 85 % conversion.[16] Herein, we describe the use of the commercially available 1,3,4-triphenyl-4,5-dihydro-1*H*-1,2-triazol-5-ylidene carbene (**1**) for the living ROP of lactide to generate functional, block, and dendritic star copolymers.

Polymerization of L-lactide (LA: 1–2 M solution in THF or toluene) by imidazolylidene carbenes in the presence of an initiator such as methanol (one equivalent of initiator to catalyst) is generally accomplished within a few minutes at 25 °C, depending on the targeted molecular weight.[14b] Only 16 % conversion was observed at 25 °C after 100 h for the polymerization of LA (1 M in toluene) with the triazolylidene carbene under similar conditions, whereas 40 % conversion was observed at 50 °C. Polymerization of LA at 90 °C proceeded with near quantitative monomer conversion in 50 h to give polylactide with a degree of polymerization (DP)

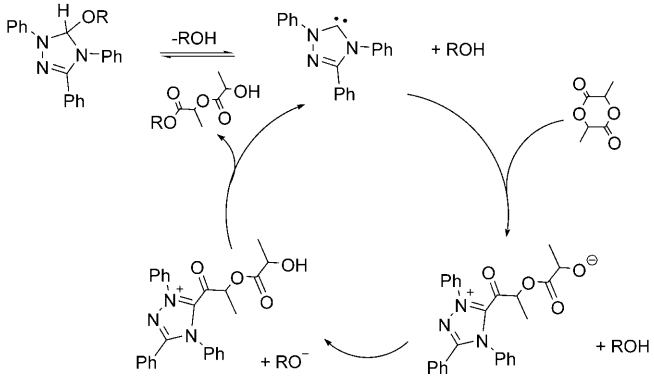
[*] O. Coulembier, L. Mespouille, Prof. P. Dubois
Laboratory of Polymeric and Composite Materials (LPCM)
University of Mons-Hainaut
Place du Parc 20, 7000 Mons (Belgium)
Fax: (+32) 65-373484
E-mail: philippe.dubois@umh.ac.bc
Dr. D. A. Culkin, Prof. R. M. Waymouth
Center for Polymeric Interfaces and Macromolecular Assemblies
Department of Chemistry
Stanford University
Stanford, CA 94305 (USA)
Fax: (+1) 650-736-2262
E-mail: waymouth@stanford.edu
Dr. A. P. Dove, Dr. R. C. Pratt, Dr. A. C. Sentman, Dr. J. L. Hedrick
IBM Almaden Research Center
650 Harry Road, San Jose, CA 95120 (USA)
Fax: (+1) 408-927-3310
E-mail: hedrick@almaden.ibm.com

[**] O.C. is grateful to the F.R.I.A. for financial support. This work was partially supported by the Belgian Federal Government Office of Science Policy (SSTC-PAI-5/3). A.P.D., R.C.P., and D.A.C. gratefully acknowledge support from the NSF Center on Polymeric Interfaces and Macromolecular Assemblies (CPIMA: NSF-DMR-0213618) and an NSF-GOALI grant (NSF-CHE-0313993). D.A.C. thanks the NIH for a postdoctoral fellowship (GM070181-01A1). Dolores Miller is gratefully thanked for the high-temperature NMR analysis. We thank Purac for the generous donation of L-lactide.

Supporting information for this article is available on the WWW under http://www.angewandte.org or from the author.

 InterScience © 2005 Wiley-VCH Verlag GmbH & Co. KGaA, Weinheim

of 70 ($M_n = 10000$) and a polydispersity (M_w/M_n) of 1.09. The diminished reactivity of the triazole carbenes for lactide polymerization compared to that observed with saturated imidazolin-2-ylidene or unsaturated imidazol-2-ylidene carbenes[9o,14b] suggested that some process was attenuating the reactivity of these carbenes towards polymerization. On the basis of the pioneering work by Enders et al. on the reactivity of triazolylidenes, we suspected that the reversible formation of alcohol adducts might be responsible for this behavior (Scheme 2).[15]



Scheme 2. Polymerization of lactide with triazole carbenes.

As reported by Enders et al.,[15] treatment of the triazolylidene with a slight excess of MeOH at room temperature readily generates the methoxytriazoline, as evidenced by resonances at $\delta = 46.8$, 101.0, and 142.9 ppm in the ^{13}C NMR (C_6D_6) spectrum. This alcohol adduct is stable at 50 °C, but dissociates at 90 °C into a mixture of the methoxytriazoline, free triazolylidene **1**, and free methanol, as evidenced by ^1H and ^{13}C NMR spectroscopic analysis. Spectroscopic analysis shows that cooling this mixture to room temperature regenerates the methoxytriazoline, thus revealing a temperature-dependent equilibrium between the triazolylidene carbene and methanol adduct: only the alcohol adduct is observed at room temperature in the presence of alcohols, and elevated temperatures are required to generate the free carbene and the alcohol.

The reversible formation of alcohol adducts provides an explanation for the low reactivity of the triazole carbenes in the polymerization of LA at room temperature. Therefore, the polymerization of LA with a variety of initiating alcohols was carried out at 90 °C (1 M in toluene). The molecular weights obtained under these conditions correlated with those predicted with monomer to initiator ratios ranging from 25:1 to 350:1 and yielded polymers with narrow dispersities (Table 1). A plot of the molecular weight and polydispersity versus conversion for the ROP catalyzed by **1** was linear (Figure 1) and the gel permeation chromatography (GPC) traces of polylactide generated with a 4-pyrene-1-butanol initiator and using both refractive index and UV detectors (410 and 350 nm, respectively) clearly show pyrene is distributed throughout the sample (Figure 1). This was corroborated by ^1H NMR analysis of the polymer end-groups which indicated the presence of one initiator per polymer chain, thus confirming the end-group fidelity.

Table 1: Selected polymerization data of L-lactide using triazolium carbene as a catalyst.

Entry	I (cat./I)[a]	M/I[b]	Time of polym. [h]	Conv.[c]	DP[d]	PDI[e]
1	MeOH (2:1)	25:1	19	72	18	
2	MeOH (4:1)	50:1	[f]	94	50	1.36
3	MeOH (4:1)	100:1	[f]	97	84	1.34
4	pyrenebutanol (1:1)	100:1	95	85	72	1.09
5	pyrenebutanol (1:1)	150:1	113	90	130	1.06
6	pyrenebutanol (1:1)	350:1	96	35		
7	PEO-OH (1:1)	100:1	63	88	90	1.17
8	bis-MPA (24:1)	40:1	42	96	38[g]	1.14

[a] Initiator (catalyst:initiator ratio). [b] Monomer:initiator ratio. [c] Conversion as measured by ^1H NMR spectroscopy. [d] Degree of polymerization determined by gel permeation chromatography using Mark–Houwink parameters from a polystrene calibration. [e] Polydispersity index, measured by gel permeation chromatography. [f] See Figure 2. [g] DP obtained for each arm of the star polymer.

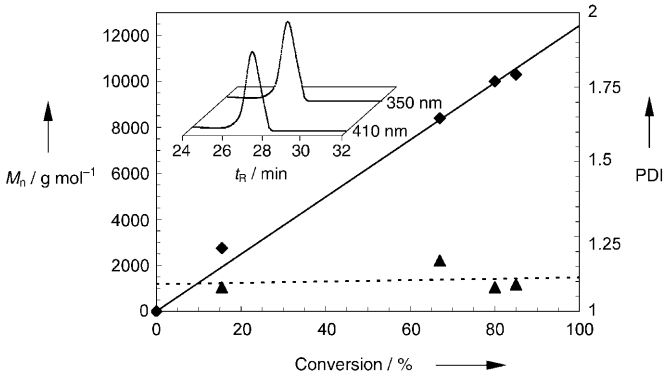


Figure 1. Evolution of molecular weight (◆), as determined by GPC, and PDI (▲) versus conversion for the polymerization of LA (Table 1, entry 4) together with GPC scans using both RI (410 nm) and UV (350 nm) detectors.

A chain-extension experiment with an initial polymerization ($[LA]_0 = 1$ M; $[\text{pyrenebutanol}]_0 = 0.04$ M; $[\text{catalyst}]_0 = 0.02$ M) was performed at 90 °C for 19 h to give polylactide of $M_n = 2500\ g\,mol^{-1}$, as determined by ^1H NMR spectroscopic analysis. L-lactide (3.47×10^{-4} mol) and **1** (2.36×10^{-5} mol) were added to this solution and the solution heated to 90 °C for an additional 7 h. The molecular weight of the sample increased to $9000\ g\,mol^{-1}$ as deduced by ^1H NMR spectroscopic analysis. GPC analysis of the sample revealed an absolute molecular weight of $7300\ g\,mol^{-1}$ and a PDI of 1.36. This solution was charged again with 3.47×10^{-4} mol of L-lactide without any further catalyst and heated to 90 °C for 7 h. The final molecular weight increased to $14000\ g\,mol^{-1}$, as determined by ^1H NMR spectroscopic analysis ($M_n(GPC) = 12000\ g\,mol^{-1}$), with no change in the polydispersity (1.34). Thus, this system exhibits the characteristics of a living polymerization.[16a]

A unique feature of this particular system is that polymerization can be reversibly terminated simply by modulating the temperature. Heating a 1 M solution of LA

 © 2005 Wiley-VCH Verlag GmbH & Co. KGaA, Weinheim

to 90 °C in the presence of **1** and 4-pyrene-1-butanol results in the conversion of LA, which stops upon rapid cooling of the solution to 20 °C (Figure 2; 4-pyrene-1-butanol/catalyst = 3:1, L-lactide/4-pyrene-1-butanol = 50:1). Re-initiation of the polymerization occurs upon re-heating at 90 °C, with deactivation occurring upon cooling again to 20 °C. This process was repeated four times. Figure 2 demonstrates clearly that the polymerization can be activated/deactivated with temperature on demand. Significantly, analysis of the polymer after four successive heating and cooling cycles revealed quantitative conversion of the monomer to give polylactide with M_n = 5900 (DP = 41) and M_w/M_n = 1.13:1. Further heating of this sample at 90 °C for 720 minutes revealed little discernable change in the molecular weight or polydispersity (M_n(GPC) = 5400; PDI = 1.29), thus suggesting that the polylactides prepared under these conditions are resistant to further transesterification reactions.

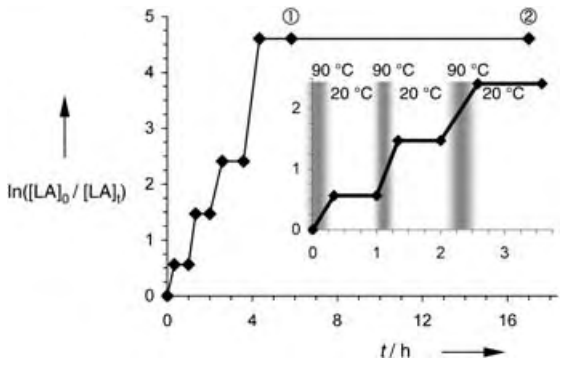
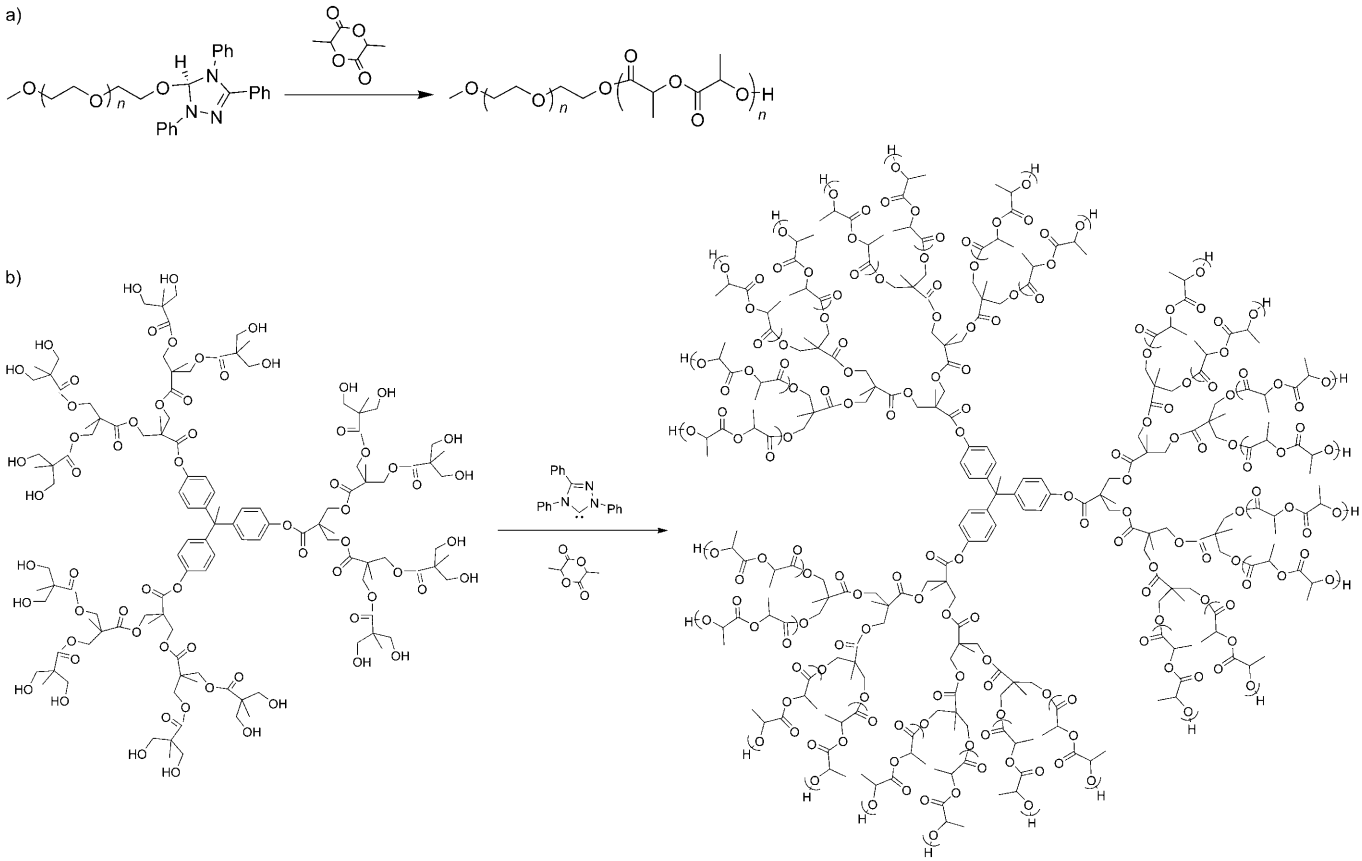


Figure 2. Time dependence of ln([LA]$_0$/[LA]) as a function of time ([LA]$_0$ = 1 M; [alcohol]$_0$ = 0.02 M; [alcohol]$_0$/[catalyst]$_0$ = 1:3) with alternation of high (90 °C) and low (20 °C) temperature. The molecular weights and polydispersity index for ① and ② are 5900 (1.13) and 5400 (1.29), respectively, as determined by GPC. Inset: the first 4 h of the reaction.

A kinetic study of the polymerization of L-lactide (LA) initiated by 4-pyrene-1-butanol (ROH) and catalyzed by **1** was performed at 90 °C using an initial monomer concentration [LA]$_0$ of 1 M. The dependence of ln([LA]$_0$/[LA]) on time at constant triazole concentration ([triaz]$_0$ = 0.02 M) was linear with an intercept at zero, which indicates that the polymerization is first order in monomer and that the number of growing species does not change during the polymerization. Plots of k_{obs} versus [triaz] or [ROH] reveal that the rate is first order both in triazole and alcohol for [triaz]/[ROH] = 1:1. These results demonstrate that the polymerization is first order with respect to catalyst, alcohol, and monomer, according to the rate law given in Equation (1), where [ROH] = [ROH]$_0$, [triaz] = [triaz]$_0$, and k_p = 530 $L^2 mol^{-2} s^{-1}$.

$$-\frac{d[LA]}{dt} = k_p[LA][ROH][triaz] \quad (1)$$



Scheme 3. Generation of block and star copolymers from triazolium alcohol adducts.

 © 2005 Wiley-VCH Verlag GmbH & Co. KGaA, Weinheim

The well-defined polymerization behavior of the alkoxytriazoline catalyst systems is ideally suited for the preparation of block copolymers and complex macromolecular architectures. Several adducts of hydroxy-functionalized oligomers and multifunctional alcohols were synthesized either in situ, or isolated and used as thermally stable macroinitiators for the ring-opening polymerization of lactide at 90 °C. A monohydroxypoly(ethylene oxide) oligomer (PEO-OH) ($M_W = 2000\ g\,mol^{-1}$, PDI = 1.05) was treated with **1** in toluene at RT for 12 h to give quantitative conversion of the corresponding alkoxytriazoline. The oligo-alkoxytriazoline is stable at room temperature, but readily polymerizes LA at 90 °C to yield a narrowly dispersed diblock copolymer in near quantitative yields (ca. 90 %; Table 1, entry 7; Scheme 3 a). Dendritic star-shaped polymers were prepared from a hydroxy-functionalized third generation dendrimer derived from 2,2′-(bishydroxymethyl)propionic acid (bis-MPA).[17,18] The dendrimer, 24 equivalents of **1**, and lactide were suspended in toluene and after approximately two hours at room temperature, the solution became homogeneous. The temperature was then increased to 90 °C to yield a narrowly dispersed, 24-arm star polymer (Table 1, entry 8; Scheme 3 b, 40 h, ca. 96 % conversion). The functional groups of the bis-MPA repeating units provide sensitive markers for the spectroscopic analysis of the polymers, since the quartenary carbon atom and the protons on the methylene group are very sensitive to the substitution of the neighboring hydroxy groups.[19] ^1H and ^{13}C NMR spectroscopic analyses showed that the efficiency of the initiation was quantitative and afforded a well-defined 24-arm star polymer (Table 1, entry 8; Scheme 3 b). Significantly, the ester functionality of the dendritic core was retained, thus indicating that the catalyst polymerizes lactide without degrading the polyester-derived dendritic core under these conditions.

In summary, alkoxytriazolines were shown to reversibly dissociate at 90 °C to generate an initiating/propagating alcohol and triazolium carbene for the on-demand living polymerization of lactide. The kinetic results demonstrate that the polymerization is first order with respect to catalyst, alcohol, and monomer, thus suggesting that all the components have an equal role in the propagation step of the mechanism. We have also demonstrated that **1** reversibly forms alcohol adducts that result in an active and dormant form of the catalyst. We postulate that dissociation of the carbene and alcohol from the adduct results in activation of the monomer by the nucleophilic carbene, with propagation occurring through a step involving the activated monomer–carbene adduct and the alcohol. The recombination of the carbene with the new alcohol species results in the formation of the dormant carbene–alcohol adduct. This reversible dissociation is believed to be responsible for the exquisite control of molecular weight, narrow polydispersities, and end-group fidelity, analogous to modern controlled radical procedures.[20]

Received: February 25, 2005
Revised: April 15, 2005
Published online: July 11, 2005

Keywords: homogeneous catalysis · lactide · N-heterocyclic carbenes · ring-opening polymerization

[1] *Carbenes*, *Vol. 1* (Eds.: M. Jones, R. A. Moss), Wiley, New York, **1973**; *Carbenes*, *Vol. 2* (Eds.: M. Jones, R. A. Moss), Wiley, New York, **1975**.

[2] For general reviews, see a) D. Bourissou, O. Guerret, F. P. Gabbai, G. Bertrand, *Chem. Rev.* **2000**, *100*, 39; b) H. Tomioka, *Acc. Chem. Res.* **1997**, *30*, 315; c) W. A. Herrmann, C. Kocher, *Angew. Chem.* **1997**, *109*, 2256; *Angew. Chem. Int. Ed. Engl.* **1997**, *36*, 2162.

[3] a) H. W. Wanzlick, H. J. Kleiner, *Angew. Chem.* **1961**, *73*, 493; b) H. W. Wanzlick, *Angew. Chem.* **1962**, *74*, 129; *Angew. Chem. Int. Ed. Engl.* **1962**, *1*, 75; c) H. W. Wanzlick, T. Esser, H. J. Kleiner, *Chem. Ber.* **1963**, *96*, 1208.

[4] a) A. Igau, A. Baceiredo, G. Trinquier, G. Bertrand, *Angew. Chem.* **1989**, *101*, 617; *Angew. Chem. Int. Ed. Engl.* **1989**, *28*, 621; b) A. Igau, A. Baceiredo, H. Gruetzmacher, G. Bertrand, *J. Am. Chem. Soc.* **1988**, *110*, 6463.

[5] a) A. J. Arduengo, R. L. Dais, R. Harlow, M. Kline, *J. Am. Chem. Soc.* **1991**, *113*, 361; b) A. Arduengo, R. L. Dias, R. Harlow, M. Kline, *J. Am. Chem. Soc.* **1992**, *114*, 5530.

[6] a) A. J. Arduengo, *Acc. Chem. Res.* **1999**, *32*, 913; b) A. J. Arduengo, R. Krfczyk, *Chem. Ztg.* **1998**, *32*, 6; c) M. K. Denk, A. Thadani, K. Hatano, A. J. Lough, *Angew. Chem.* **1997**, *109*, 2719; *Angew. Chem. Int. Ed. Engl.* **1997**, *36*, 2607.

[7] See, for example: a) D. Bourissou, O. Guerret, F. P. Gabbai, G. Bertrand, *Chem. Rev.* **2000**, *100*, 39; b) W. Herrmann, C. Kocher, *Angew. Chem.* **1997**, *109*, 2256; *Angew. Chem. Int. Ed. Engl.* **1997**, *36*, 2162; c) M. Scholl, T. M. Trnka, J. P. Morgan, R. H. Grubbs, *Tetrahedron Lett.* **1999**, *40*, 2247; d) J. Huang, E. D. Stevens, S. P. Nolan, J. L. Petersen, *J. Am. Chem. Soc.* **1999**, *121*, 2674; e) T. Weskamp, W. C. Schattenmann, M. Spiegler, W. A. Herrmann, *Angew. Chem.* **1998**, *110*, 2631; *Angew. Chem. Int. Ed. Engl.* **1998**, *37*, 2490; f) W. A. Herrmann, M. Elison, J. Fisher, C. Kocher, G. J. Artus, *Angew. Chem.* **1995**, *107*, 2602; *Angew. Chem. Int. Ed. Engl.* **1995**, *34*, 2371; g) W. A. Herrmann, L. Goossen, C. Kocher, G. Artus, *Angew. Chem.* **1996**, *108*, 2980; *Angew. Chem. Int. Ed. Engl.* **1996**, *35*, 2805; h) M. J. Lappert, *J. Organomet. Chem.* **1988**, *358*, 185; i) D. Enders, K. Breuer, G. Raabe, J. Runsink, T. Henrique, J.-P. Melder, K. Ebel, S. Brode, *Angew. Chem.* **1995**, *107*, 1119; *Angew. Chem. Int. Ed. Engl.* **1995**, *34*, 1021; j) M. C. Perry, K. Burgess, *Tetrahedron: Asymmetry* **2003**, *14*, 951; k) L. Jafarpour, S. P. Nolan, *Adv. Organomet. Chem.* **2001**, *46*, 181.

[8] See, for example: a) W. A. Herrmann, *Angew. Chem.* **2002**, *114*, 1342; *Angew. Chem. Int. Ed.* **2002**, *41*, 1290; b) M. S. Stanford, M. Ulman, R. H. Grubbs, *J. Am. Chem. Soc.* **2001**, *123*, 749; c) W. A. Herrman, L. J. Goossen, M. Spiegler, *Organometallics* **1998**, *17*, 2162; d) T.-L. Choi, R. H. Grubbs, *Chem. Commun.* **2001**, 2648; e) J. Haung, H.-J. Schanz, E. D. Stevens, S. P. Nolan, *Organometallics* **1998**, *17*, 2370; f) M. M. McCormick, H. A. Duong, G. Zuo, J. Louie, *J. Am. Chem. Soc.* **2005**, submitted; g) H. A. Duong, H. A. M. J. Cross, J. Louie, *J. Am. Chem. Soc.* **2004**, *126*, 11438; h) G. Zuo, J. Louie, *Angew. Chem.* **2004**, *116*, 2327; *Angew. Chem. Int. Ed.* **2004**, *43*, 2277.

[9] See, for example: a) R. Breslow, *J. Am. Chem. Soc.* **1958**, *80*, 3719; b) H. Stetter, *Angew. Chem.* **1976**, *88*, 695; *Angew. Chem. Int. Ed. Engl.* **1976**, *15*, 639; c) D. Enders, J. H. Breuer, *Helv. Chim. Acta* **1996**, *79*, 1217; d) J. Teles, J. Melder, K. Ebel, D. Enders, J. H. Breuer, *Helv. Chim. Acta* **1996**, *79*, 61; e) M. S. Kerr, J. R. De Alaniz, T. Rovis, *J. Am. Chem. Soc.* **2002**, *124*, 10298; f) D. Enders, U. Kallfass, *Angew. Chem.* **2002**, *114*, 1822; *Angew. Chem. Int. Ed.* **2002**, *41*, 1743; g) G. A. Grasa, R. M. Kissling, S. P. Nolan, *Org. Lett.* **2002**, *4*, 3583; h) G. W. Nyce, J. A. Lamboy, E. F. Connor, R. M. Waymouth, J. L. Hedrick, *Org.*

 © 2005 Wiley-VCH Verlag GmbH & Co. KGaA, Weinheim

Lett. **2002**, *4*, 3587; i) D. Enders, T. Balensiefer, *Acc. Chem. Res.* **2004**, *37*, 534; j) N. T. Reynolds, J. Read de Alaniz, T. Rovis, *J. Am. Chem. Soc.* **2004**, *126*, 9518; k) S. S. Sohn, E. L. Rosen, W. J. Bode, *J. Am. Chem. Soc.* **2004**, *126*, 14370; l) H. A. Duong, M. J. Cross, J. Louie, *Org. Lett.* **2004**, *6*, 4679; m) G. A. Grasa, T. Guveli, R. Singh, S. P. Nolan, *J. Org. Chem.* **2003**, *68*, 2812; n) N. T. Reynolds, J. R. De Alaniz, T. Rovis, *J. Am. Chem. Soc.* **2004**, *126*, 9518; o) G. W. Nyce, T. Glauser, E. F. Connor, A. Mock, R. M. Waymouth, J. L. Hedrick, *J. Am. Chem. Soc.* **2003**, *125*, 3046.

[10] A. J. Arduengo, F. Davidson, H. V. R. Dias, J. R. Goerlich, D. Khasnis, W. J. Marshall, T. K. Prakasha, *J. Am. Chem. Soc.* **1997**, *119*, 12742.

[11] See, for example: a) J. P. Morgan, R. H. Grubbs, *Org. Lett.* **2000**, *2*, 3153; b) L. S. Jafarpour, S. P. Nolan, *Organometallics* **2000**, *19*, 2055.

[12] a) H.-W. Wanzlick, F. Esser, H.-J. Kleiner, *Chem. Ber.* **1963**, *96*, 1208; b) B. Cetinkaya, E. Cetinkaya, J. A. Chamizo, P. B. Hitchcock, H. A. Jasim, H. Kücükbay, M. F. Lappert, *J. Chem. Soc. Perkin Trans. 1* **1998**, 2047; c) T. M. Trnka, J. P. Morgan, M. S. Sanford, T. E. Wilhelm, M. Scholl, T.-L. Choi, S. Ding, M. W. Day, R. H. Grubbs, *J. Am. Chem. Soc.* **2003**, *125*, 2546; d) D. Enders, K. Breuer, G. Raabe, J. Runsink, J. H. Teles, J. P. Melder, K. Ebel, S. Brode, *Angew. Chem.* **1995**, *107*, 1119; *Angew. Chem. Int. Ed. Engl.* **1995**, *34*, 1021; e) D. Enders, K. Breuer, J. Runsink, J. H. Teles, *Liebigs Ann.* **1996**, 2019; f) J. P. Morgan, R. H. Grubbs, *Org. Lett.* **2000**, *2*, 3153; g) B. Lachmann, H. W. Wanzlick, *Liebigs Ann. Chem.* **1969**, *729*, 27; h) G. W. Nyce, S. Csihony, R. M. Waymouth, J. L. Hedrick, *Chem. Eur. J.* **2004**, *10*, 4073.

[13] See, for example: a) A. J. Arduengo, J. C. Calabrese, F. Davidson, H. V. R. Dias, J. R. Goerlich, R. Krafczyk, W. J. Marshall, M. Tamm, R. Schmutzler, *Helv. Chim. Acta* **1999**, *82*, 2348; b) H. W. Wanzlick, H. Ahrens, *Chem. Ber.* **1966**, *99*, 1580; c) Wanzlick, H. W. Kleiner, *Chem. Ber.* **1963**, *96*, 3024; d) D. Enders, K. Breuer, J. Runsink, J. H. Teles, *Liebigs Ann.* **1996**, 2019; e) J. A. Cowan, J. A. C. Clyburne, M. G. Davidson, R. L. W. Harris, J. A. K. Howard, P. Kupper, M. A. Leech, S. P. Richards, *Angew. Chem.* **2002**, *114*, 1490; *Angew. Chem. Int. Ed.* **2002**, *41*, 1432; f) L. McKenzie, J. C. Brodovitch, P. W. Percival, T. Ramnial, J. A. C. Clyburne, *J. Am. Chem. Soc.* **2003**, *125*, 11565.

[14] M. Scholl, S. Ding, C. W. Lee, R. H. Grubbs, *Org. Lett.* **1999**, *1*, 953.

[15] D. Enders, K. Breuer, G. Raabe, J. Runsink, J. H. Teles, J. P. Melder, K. Ebel, S. Brode, *Angew. Chem.* **1995**, *107*, 1119; *Angew. Chem. Int. Ed. Engl.* **1995**, *34*, 1021.

[16] a) S. Penczek, T. Biela, A. Duda, *Macromol. Rapid Commun.* **2000**, *21*, 941; b) A. Lofgren, A. C. Albertsson, P. Dubois, R. Jerome, *J. Macromol. Sci. Rev. Macromol. Chem. Phys.* **1995**, *35*, 379.

[17] a) H. Ihre, A. Hult, *Polym. Mater. Sci. Eng.* **1997**, *77*, 71; b) H. Ihre, A. Hult, E. Soderlind, *J. Am. Chem. Soc.* **1996**, *118*, 6388.

[18] H. Ihre, O. L. Padilla De Jesu, J. M. J. Frechet, *J. Am. Chem. Soc.* **2001**, *123*, 5908.

[19] E. Malmstrom, M. Johansson, A. Hult, *Macromolecules* **1995**, *28*, 1698.

[20] a) K. Matyjaszewski, T. P. Davis, *Handbook of Radical Polymerization*, Wiley-Interscience, New York, **2002**; b) C. J. Hawker, A. W. Bosman, E. Harth, *Chem. Rev.* **2001**, *101*, 3661.

 © 2005 Wiley-VCH Verlag GmbH & Co. KGaA, Weinheim

Hydrogen Bonding

DOI: 10.1002/anie.200501349

Observation of Weak C–H···O Hydrogen Bonding to Unactivated Alkanes**

*Xue-Bin Wang, Hin-Koon Woo, Boggavarapu Kiran, and Lai-Sheng Wang**

The hydrogen bond plays an essential role in chemistry and biochemistry.[1] It generally has the form X–H···Y, where X and Y are highly electronegative atoms such as O or N. The fact that a relatively less electronegative carbon can also behave as a proton donor to form C–H···O-type hydrogen bonds has been the subject of controversy for many years.[2–4] However, it is now well accepted and has been identified in many biological systems[5–13] and crystal engineering.[14–18] Most C–H···O hydrogen bonds have been observed for the so-called activated C, where the hydrogen-donor C atom is attached to electronegative groups such as halogen atoms or NH groups in the protein backbone. In biological systems or molecular crystals, C–H···O hydrogen bonds are usually accompanied by other stronger molecular interactions that make it difficult to evaluate their relative contributions. Despite the importance of the C–H···O hydrogen bond and extensive theoretical studies,[19–25] its nature is still being debated,[26–29] and there have been no experimental characterizations of its strength to date. We report here the first direct experimental observation of conformation changes induced solely by C–H···O hydrogen bonding in a series of unactivated aliphatic carboxylate molecules, $CH_3(CH_2)_nCO_2^-$, in the gas phase, where the C–H···O hydrogen bonding is the only molecular interaction driving the conformational changes.

Photoelectron spectra of $CH_3(CH_2)_nCO_2^-$ ($n = 0$–8) were measured at both room and low temperatures, as shown in Figure 1. We observed very similar spectra at room temperature for all the species, which all have adiabatic detachment energies (ADEs) of around 3.4 eV because the aliphatic chain

[*] Dr. X.-B. Wang, Dr. H.-K. Woo, Dr. B. Kiran, Prof. Dr. L.-S. Wang
Department of Physics, Washington State University
2710 University Drive, Richland, WA 99352 (USA)
and
W. R. Wiley Environmental Molecular Sciences Laboratory and Chemical Sciences Division
Pacific Northwest National Laboratory
MS 8-88, P.O. Box 999, Richland, WA 99352 (USA)
Fax: (+1) 509-376-6066
E-mail: ls.wang@pnl.gov

[**] We thank Dr. S. E. Barlow for valuable discussions. This work was supported by the U.S. Department of Energy (DOE), Office of Basic Energy Sciences, Chemical Science Division. The experiment and calculations were performed at the W. R. Wiley Environmental Molecular Sciences Laboratory, a national scientific user facility sponsored by the DOE Office of Biological and Environmental Research and located at Pacific Northwest National Laboratory, which is operated for the DOE by Battelle.

Supporting information for this article is available on the WWW under http://www.angewandte.org or from the author.

© 2005 Wiley-VCH Verlag GmbH & Co. KGaA, Weinheim

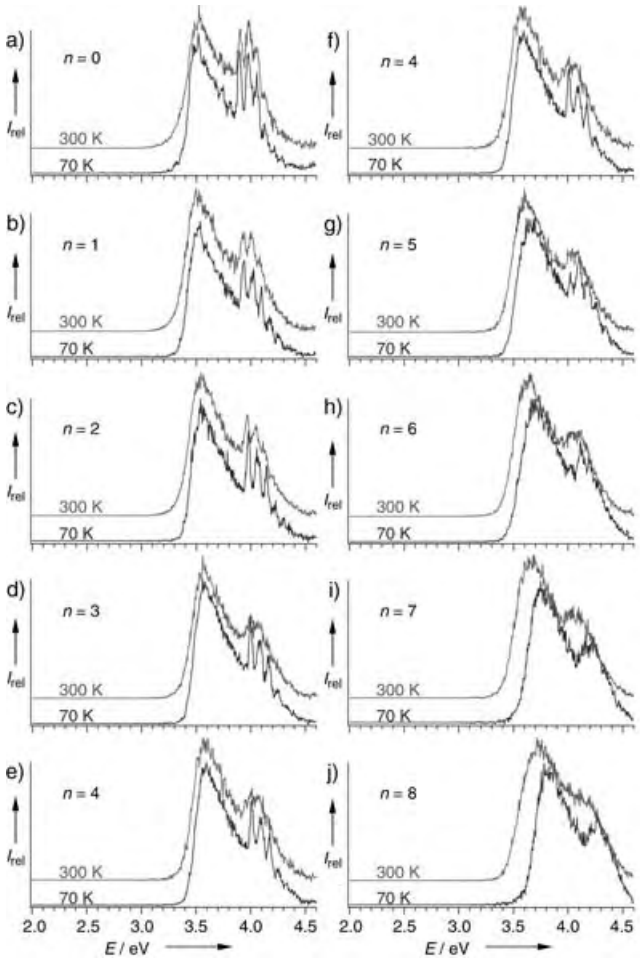


Figure 1. Photoelectron spectra of $CH_3(CH_2)_nCO_2^-$ ($n = 0$–8) measured at 266 nm (4.661 eV) and at two different ion-trap temperatures. Note the blue shift of the 70 K spectra starting from $n = 5$.

has very little effect on the electron binding energies of the carboxylate group. The two observed bands in all the spectra are due to detachment from three oxygen lone-pair orbitals on the carboxylate, and the first broad band actually contains two detachment channels.[30,31] The second spectral band was vibrationally resolved for $n = 0$–2, with a vibrational frequency of about 640 cm^{-1} that is characteristic of the CO_2 bending motion.[32] The vibrational structure is smeared out in the larger systems in the room temperature spectra. Significant changes were observed in the PES spectra at a trapping temperature of 70 K. For $n = 0$–4 (Figure 1, left column), the low-temperature spectra are much sharper and the CO_2 bending vibrational progression in the second band is much better resolved in all the spectra. The reduction of the vibrational hot band can clearly be observed by comparing the threshold regions of the spectra taken at 70 and at 300 K. For $n = 5$–8, in addition to the spectral sharpening, the 70 K spectra surprisingly exhibit a systematic blue shift, which ranges from 50 meV for $n = 5$ to 150 meV for $n = 8$. Vibrational structures in the second band were also resolved for these larger species, more clearly for $n = 5$ and 6, but the Franck–Condon envelope is quite different in the larger systems than in the smaller species.

The blue shift observed for $n = 5$–8 in the low-temperature spectra suggests a conformational change in which the negative charge on the carboxylate is stabilized, most likely resulting from the formation of C–H···O hydrogen bonds between the terminal CH_3 group and the -CO_2^- group to form a folded structure.[32,33] Because of the anticipated weakness of this C–H···O hydrogen bonding, the folded conformation can only be observed at lower temperatures owing to the large entropy contributions at higher temperatures for the linear structure. To obtain further insight into the folding transition, we performed temperature-dependent studies for $n = 6$ and 8 at trapping temperatures from 300 to 18 K (Figure 2). For

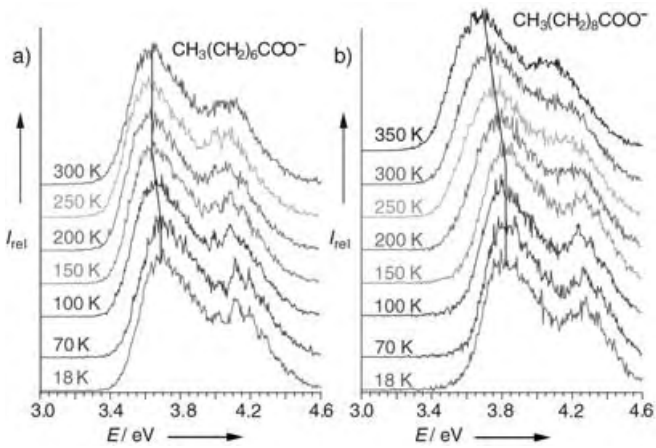


Figure 2. Temperature-dependent photoelectron spectra of $CH_3(CH_2)_6CO_2^-$ and $CH_3(CH_2)_8CO_2^-$. The lines drawn are intended to guide the eyes and have no other significance.

$CH_3(CH_2)_6CO_2^-$ there was no observable blue shift from 300 K to 200 K, but at 150, 100, and 70 K the PES spectra exhibit successive blue shifts of about 10, 10, and 40 meV, respectively. The spectrum shows no blue shift upon further cooling the trap to 18 K. These observations suggest that the folding transition starts at around 150 K for $CH_3(CH_2)_6CO_2^-$, and at around 70 K all the anions are already in the folded conformation due to the C–H···O hydrogen bonding. For $CH_3(CH_2)_8CO_2^-$, a blue shift of about 30 meV was already observed upon cooling the trap from 300 K to 250 K. Further blue shifts of about 45 and 65 meV were observed at 200 and 150 K, respectively. No measurable shift was observed upon further cooling, which suggests that at 150 K all the $CH_3(CH_2)_8CO_2^-$ anions are already in the folded conformation. The blue shift observed immediately upon cooling from 300 K indicates that there might already be folded conformations present at room temperature for $CH_3(CH_2)_8CO_2^-$. We therefore made one more measurement by heating the ion trap to 350 K, and indeed observed a red shift relative to the 300 K spectrum by about 50 meV. The 300 K spectrum seems to be slightly broader than the 350 K spectrum, which is consistent with the fact that both linear and folded conformations coexist at room temperature. The ADE of $CH_3(CH_2)_8CO_2^-$ at 350 K is now about 3.47 eV, similar to those of the smaller species, thus indicating that the linear structure dominates for $CH_3(CH_2)_8CO_2^-$ only at 350 K.

 © 2005 Wiley-VCH Verlag GmbH & Co. KGaA, Weinheim

Our temperature-dependent PES data yielded the following blue shifts between the folded and linear structures: 50, 60, 130, and 190 meV for $n = 5$–8, respectively. These shifts reflect the stabilization of the negative charge on the -CO_2^- group by the C–H···O hydrogen bonding, as illustrated in Figure 3. As the strength of the C–H···O hydrogen bonding in the neutral $CH_3(CH_2)_nCO_2^{\bullet}$ radical is expected to be small (0.5 kcal mol^{-1} or less),[20] the observed blue shifts provide lower limits for the C–H···O hydrogen bonding strength in the $CH_3(CH_2)_nCO_2^-$ anions (1.2, 1.4, 3.0, and 4.4 kcal mol^{-1} for $n = 5$–8, respectively).

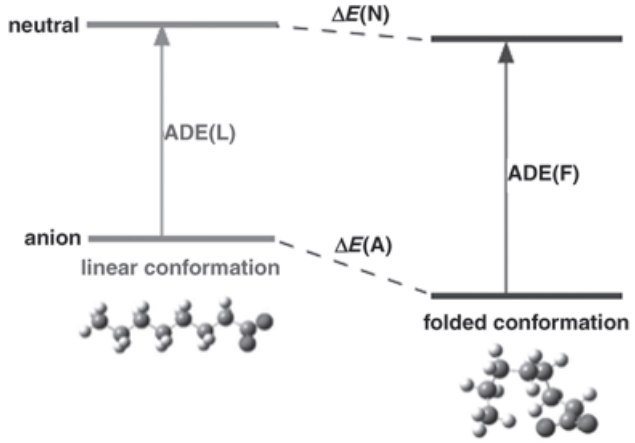


Figure 3. The energetic relationships between the anions and the neutral species and between the linear and folded configurations. ADE(L) and ADE(F) are the adiabatic detachment energies of the linear and folded conformations, respectively. ΔE(A) and ΔE(N) are the stabilization energies of the folded relative to the linear conformations for the anions and neutrals, respectively. The stabilization energies have two components, the C–H···O hydrogen-bonding energies in the folded conformations (E_H(A) and E_H(N) for the anions and neutrals, respectively) and the strain energies in the folded backbones (E_s(A) and E_s(N) for the anions and neutrals, respectively). The strain energies in the anions and neutrals are expected to be similar for a given chain length. Thus, the measured spectral shift (ΔADE) between the folded and linear conformations is equivalent to the difference of the C–H···O hydrogen-bond strength in the anions and neutrals: ΔADE = -ADE(F) − ADE(L) = ΔE(A) − ΔE(N) = E_H(A) − E_H(N).

To obtain further insight into the nature of the C–H···O hydrogen bonding in the $CH_3(CH_2)_nCO_2^-$ anions, we performed theoretical calculations on the linear and folded conformations for $n = 3$–8 (Figure 4). We found that the folded conformations are more stable than the linear structures in all cases. However, we also observed that there is no C–H···O hydrogen-bonding interaction in the cases of $n = 3$ and 4 because either the CH···O distances or the ∢C-H-O angles are outside the normal ranges expected for such interactions. One C–H···O hydrogen bond was observed for $n = 5$ and 6, whereas for $n = 7$ and 8 two C–H···O hydrogen bonds are formed, consistent with the large ADE shifts observed for these two species in the PES spectra at low temperature. The calculations also revealed that the two C–O bond lengths become different upon hydrogen-bond formation as a result of the charge localization onto the hydrogen-bonded O atom. The abrupt change in the CO_2 bending vibrational progression in the second PES band for $n = 5$–8 is consistent with the subtle geometric changes as a result of the C–H···O hydrogen-bond formation. The C–H···O hydrogen-bond strengths are different in each system owing to the different steric effects that lead to different C–H···O hydrogen-bonding geometries. The strengths of the two C–H···O hydrogen bonds in the $n = 7$ and 8 species are also not equivalent. However, an average bond strength for each C–H···O hydrogen bond in $n = 7$ and 8 can be obtained from the PES spectral shifts. Thus, we obtained the following lower limits of the bond strength for a single C–H···O hydrogen bond in $CH_3(CH_2)_nCO_2^-$: 1.2, 1.4, 1.5, and 2.2 kcal mol^{-1} for $n = 5$–8, respectively.

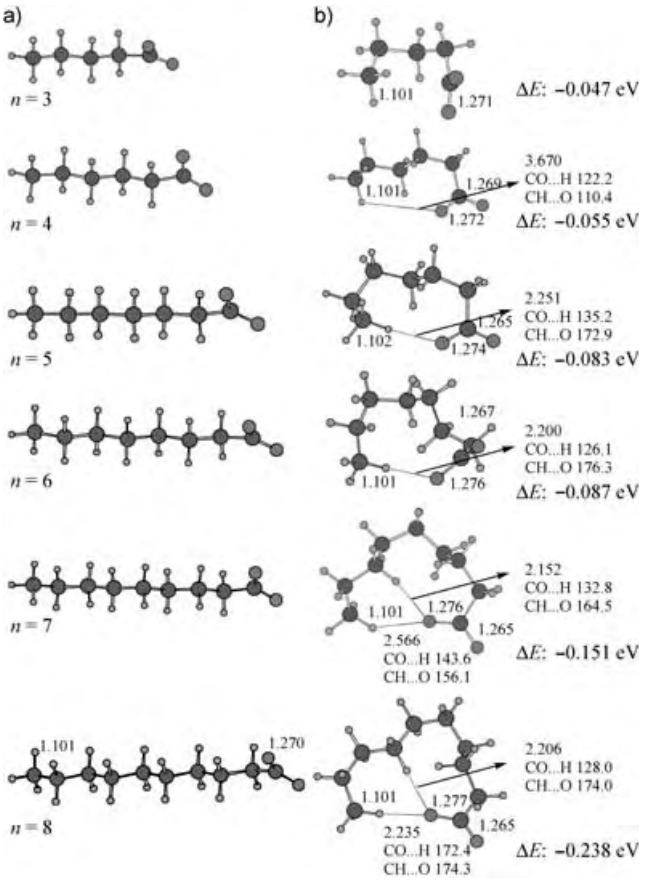


Figure 4. Optimized structures for the a) linear and b) folded conformations of $CH_3(CH_2)_nCO_2^-$ ($n = 3$–8) at the MP2/aug-cc-pVDZ level of theory. Selected C–H, C–O, and H···O bond distances are indicated in Å. The CO···H and CH···O bond angles are given in degrees. ΔE: the stabilization energies of the folded relative to the linear conformation.

Unactivated alkanes form the weakest C–H···O hydrogen bonds.[20] For example, the calculated C–H···O hydrogen-bond strength in the $H_2C{=}O/CH_4$ complex is only 0.46 kcal mol^{-1} which increases to 1.2 kcal mol^{-1} in $H_2C{=}O/CH_3F$.[20] The relatively large C–H···O hydrogen-bond strength in $CH_3(CH_2)_nCO_2^-$ is due to the negative charge on the carboxylate group, which usually forms a strong ionic hydrogen bond.[34] Thus, even unactivated alkanes can form relatively strong C–H···O hydrogen bonds to strong acceptors. The current work provides the first examples that pure C–

 © 2005 Wiley-VCH Verlag GmbH & Co. KGaA, Weinheim

H···O hydrogen bonding can play a significant structural role in determining molecular conformations. These results should have major implications to assess the role of C–H···O hydrogen bonding in biological structures and reactivities. The quantitative experimental data can also be used to verify theoretical calculations and help evaluate the dependence of the C–H···O hydrogen-bond strength on its geometry. We have also demonstrated that the low-temperature capability is not only valuable to remove vibrational hot bands and enhance photoelectron spectral resolution, but also opens up new research opportunities and allows weak molecular interactions to be isolated and investigated.

Experimental Section

Low-temperature photoelectron spectroscopy with electrospray: The experiments were carried out with a brand new home-built instrument that couples electrospray ionization with a magnetic-bottle time-of-flight photoelectron spectrometer, with a new capability of being able to control the ion temperatures. The electrospray source and the magnetic-bottle photoelectron spectrometer are similar to those described previously.[35] Briefly, the anions of interest, $CH_3(CH_2)_nCO_2^-$ ($n = 0$–8), were produced from solutions of the corresponding acids under slightly basic conditions in a mixed methanol/water solvent (3/1 volume ratio). Anions from the source were guided by a RF-only octopole device into a quadrupole mass filter, which was operated in the RF-only mode in the current experiment. Following the mass filter, the ion beam was guided by a 90 degree ion bender into a 3D Paul trap, which was attached to the cold head of a closed-cycle helium refrigerator. The temperature of the cold head can be controlled between 10–350 K. A portion of the incoming ions was trapped and collisionally cooled with a background gas (≈ 1 mTorr N_2 in most cases for temperatures between 350–70 K, or 5% H_2 in helium for lower-temperature operations). The ions were trapped for a period of 20–100 ms and cooled by translational and rovibrational energy transfers to the background gas (the number of collisions was estimated to be about 2000–10000). The trap was operated at low q values (< 0.3) to avoid RF heating.[36,37] The trapped ions were pulsed out into the extraction zone of a time-of-flight mass spectrometer at a 10 Hz repetition rate.

The ions of interest were mass-selected and decelerated before being intercepted with a 266-nm laser beam in the interaction zone of the magnetic-bottle photoelectron analyzer. The laser was operated at a 20 Hz repetition rate with the ion beam off at alternate shots for background subtraction. The photodetached electrons were collected with nearly 100% efficiency by the magnetic-bottle and analyzed in a 5-meter-long electron flight tube. The electron energy resolution was $\Delta E/E \approx 2\%$, i.e., 20 meV for 1 eV electrons. Photoelectron time-of-flight spectra were collected and then converted into kinetic energy spectra, calibrated by the known spectra of ClO_2^- [33] and I^-. The electron binding energy spectra presented were obtained by subtracting the kinetic energy spectra from the detachment photon energies.

Two known anions,[38,39] ClO_2^- and C_{60}^-, were used to test the effectiveness of the ion cooling. At a trap temperature of 70 K, vibrational hot bands in the photoelectron spectrum of ClO_2^- were completely removed. At the same trap temperature, vibrational hot bands were still detectable in the photoelectron spectrum of the relatively large C_{60}^- anion, whose vibrational temperature was estimated to be about 100 K, which yields a difference of around 30 K between the trapping temperature and the C_{60}^- vibrational temperature. We expected that this difference would be smaller for the $CH_3(CH_2)_nCO_2^-$ anions because of their relatively smaller size.

Theoretical methods: All calculations were performed with the programs Gaussian 03[40] and NWChem.[41] An initial search of the stable conformers was done with local density functional theory (LSDA) with an augmented correlation consistent polarized valence double-ζ basis set (aug-cc-pVDZ). The lowest energy geometries were used for geometry optimization at the second-order Moller–Plesset Perturbation Theory (MP2) level with the same basis set. Frequencies and other thermodynamic values were calculated at the LSDA level. All DFT calculations were performed with Gaussian 03 and MP2 optimizations with NWChem.

Received: April 19, 2005
Published online: July 8, 2005

Keywords: alkanes · conformation analysis · density functional calculations · hydrogen bonds · photoelectron spectroscopy

[1] G. A. Jeffrey, W. Saenger, in *Hydrogen Bonding in Biological Structures*, Springer, Berlin, **1991**.
[2] D. J. Sutor, *Nature* **1962**, *195*, 68–69.
[3] R. Taylor, O. Kennard, *J. Am. Chem. Soc.* **1982**, *104*, 5063–5070.
[4] G. R. Desiraju, *Acc. Chem. Res.* **1991**, *24*, 290–296.
[5] T. Steiner, W. Saenger, *J. Am. Chem. Soc.* **1992**, *114*, 10146–10154.
[6] Z. S. Derewenda, L. Lee, U. Derewenda, *J. Mol. Biol.* **1995**, *252*, 248–262.
[7] J. Bella, H. M. Berman, *J. Mol. Biol.* **1996**, *264*, 734–742.
[8] M. C. Wahl, S. T. Rao, M. Sundaralingam, *Nat. Struct. Biol.* **1996**, *3*, 24–31.
[9] I. Berger, M. Egli, A. Rich, *Proc. Natl. Acad. Sci. USA* **1996**, *93*, 12116–12121.
[10] M. C. Wahl, M. Sundaralingam, *Trends Biochem. Sci.* **1997**, *22*, 97–101.
[11] E. L. Ash, J. L. Sudmeier, R. M. Day, M. Vincent, E. V. Torchilin, K. C. Haddad, E. M. Bradshaw, D. G. Sanford, W. W. Bachovchin, *Proc. Natl. Acad. Sci. USA* **2000**, *97*, 10371–10376.
[12] K. M. Lee, H.-C. Chang, J.-C. Jiang, J. C. C. Chen, H.-E. Kao, S. H. Lin, I. J. B Lin, *J. Am. Chem. Soc.* **2003**, *125*, 12358–12364.
[13] M. Motamal, T. Lazaridis, *Biochemistry* **2005**, *44*, 1607–1613.
[14] G. R. Desiraju, *Acc. Chem. Res.* **1996**, *29*, 441–449.
[15] K. N. Houk, S. Menger, S. P. Newton, F, M. Raymo, J. F. Stoddart, D. J. Williams, *J. Am. Chem. Soc.* **1999**, *121*, 1479–1487.
[16] E. May, R. Destro, C. Gatti, *J. Am. Chem. Soc.* **2001**, *123*, 12248–12254.
[17] C. K. Broder, M. G. Davidson, V. T. Forsyth, J. A. K. Howard, S. Lamb, S. A. Mason, *Cryst. Growth Des.* **2002**, *2*, 163–169.
[18] J. A. van der Berg, K. R. Seddon, *Cryst. Growth Des.* **2003**, *3*, 643–661.
[19] Y. Gu, T. Kar, S. Scheiner, *J. Am. Chem. Soc.* **1999**, *121*, 9411–9422.
[20] R. Vargas, J. Garza, D. A. Dixon, B. P. Hay, *J. Am. Chem. Soc.* **2000**, *122*, 4750–4755.
[21] M. Hartmann, S. D. Wetmore, L. Radom, *J. Phys. Chem. A* **2001**, *105*, 4470–4479.
[22] S. Scheiner, S. J. Grabowski, T. Kar, *J. Phys. Chem. A* **2001**, *105*, 10607–10612.
[23] Y. Tatamitani, B. Liu, J. Shimada, T. Ogata, P. Ottaviani, A. Maris, W. Caminati, J. S. Alanso, *J. Am. Chem. Soc.* **2002**, *124*, 2739–2743.
[24] A. Kovacs, A. Szabo, D. Nemcsok, S. Hargittai, *J. Phys. Chem. A* **2002**, *106*, 5671–5678.
[25] H. B. Guo, R. F. Beahm, H. Guo, *J. Phys. Chem. B* **2004**, *108*, 18065–18072.
[26] P. Hobza, Z. Havlas, *Chem. Rev.* **2000**, *100*, 4253–4264.
[27] S. Scheiner, T. Kar, *J. Phys. Chem. A* **2002**, *106*, 1784–1789.
[28] X. Li, L. Liu, H. B. Schlegel, *J. Am. Chem. Soc.* **2002**, *124*, 9639–9647.

 © 2005 Wiley-VCH Verlag GmbH & Co. KGaA, Weinheim

[29] W. Qian, S. Krimm, *J. Phys. Chem. A* **2002**, *106*, 6628 – 6636.
[30] E. H. Kim, S. E. Bradforth, D. W. Arnold, R. B. Metz, D. M. Neumark, *J. Chem. Phys.* **1995**, *103*, 7801 – 7814.
[31] Z. Lu, R. E. Continetti, *J. Phys. Chem. A* **2004**, *108*, 9962 – 9969.
[32] K. Norrman, T. B. McMahon, *J. Phys. Chem. A* **1999**, *103*, 7008 – 7016.
[33] J. Catalan, *Chem. Phys. Lett.* **1994**, *221*, 68 – 70.
[34] M. Meot-Ner, *Chem. Rev.* **2005**, *105*, 213 – 284.
[35] L. S. Wang, C. F. Ding, X. B. Wang, S. E. Barlow, *Rev. Sci. Instrum.* **1999**, *70*, 1957 – 1966.
[36] J. F. J Todd, *Mass Spectrom. Rev.* **1991**, *10*, 3 – 52.
[37] E. R. Lovejoy, R. Bianco, *J. Phys. Chem. A* **2000**, *104*, 10280 – 10287.
[38] M. K. Gilles, M. L. Polak, W. C. Lineberger, *J. Chem. Phys.* **1992**, *96*, 8012 – 8020.
[39] X. B. Wang, C. F. Ding, L. S. Wang, *J. Chem. Phys.* **1999**, *110*, 8217 – 8220.
[40] Gaussian 03 (Revision B.04): M. J. Frisch et al., see Supporting Information.
[41] High Performance Computational Chemistry Group NWChem (Version 4.5), A Computational Chemistry Package for Parallel Computers, Pacific Northwest National Laboratory, Richland, WA, **2002**.

 © 2005 Wiley-VCH Verlag GmbH & Co. KGaA, Weinheim

γ-Peptide Structures

DOI: 10.1002/anie.200501055

C_9 Helices and Ribbons in γ-Peptides: Crystal Structures of Gabapentin Oligomers**

Prema G. Vasudev, Narayanaswamy Shamala, Kuppanna Ananda, and Padmanabhan Balaram**

The insertion of additional atoms into α-polypeptide backbones by the introduction of β-, γ-, and higher ω-amino acid residues expands the range of polypeptide secondary structures.[1] Two new helices, the 2.5_{12} ((*P*)-2.5_1) helix and the 3_{14} ((*M*)-3_1) helix, were first identified in studies of oligopeptides containing β-amino residues.[2] Several recent studies have focused on the conformations of peptides containing β- and γ-amino acids.[3] The symmetrically β,β-disubstituted γ-amino acid gabapentin (Gpn, Figure 1a) is a readily available

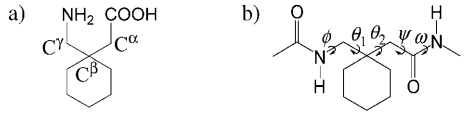


Figure 1. a) The amino acid gabapentin (Gpn); b) parameters used to define the backbone dihedral angles of the Gpn residue.

stereochemically constrained γ-amino acid residue.[4] Four degrees of torsional freedom, ϕ, θ_1, θ_2, and ψ (Figure 1b), are available for the Gpn residue. The presence of geminal substituents at the central C^β atom limits the range of conformations about the C^γ–C^β (θ_1) and C^β–C^α (θ_2) bonds to the two possible *gauche* conformations ($\theta_1 \approx \theta_2 \approx \pm 60°$).[4a,5] Herein, we describe the crystal structures of the peptides Boc-Gpn-Gpn-NHMe and Boc-Gpn-Gpn-Gpn-Gpn-NHMe (Boc = *tert*-butoxycarbonyl), which provide examples of C_9-hydrogen-bond-stabilized, folded conformations (in which the hydrogen bonds enclose a ring of nine assorted atoms). Repetition of this hydrogen-bonded motif reveals new families of C_9 ribbons and C_9 helices.

Figure 2 shows the molecular conformations determined in crystals by X-ray diffraction for Boc-Gpn-Gpn-NHMe and

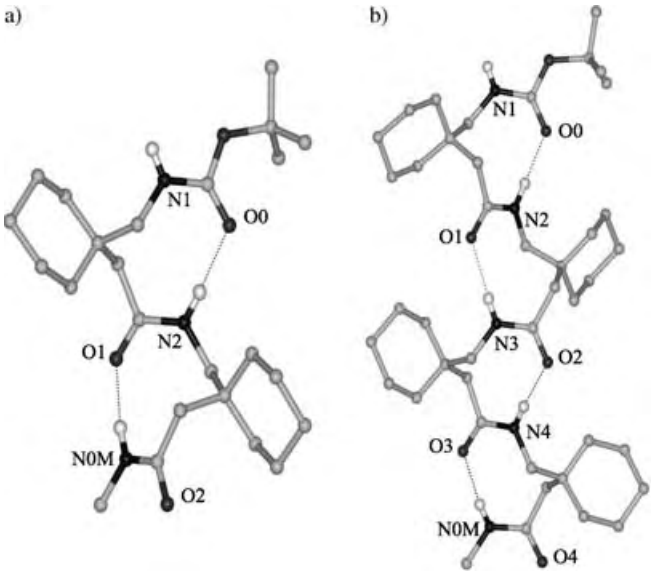


Figure 2. Molecular conformation of a) Boc-Gpn-Gpn-NHMe and b) Boc-Gpn-Gpn-Gpn-Gpn-NHMe in crystals; the intramolecular hydrogen bonds are represented as dotted lines.

Boc-Gpn-Gpn-Gpn-Gpn-NHMe. The observed backbone torsion angles and hydrogen-bond parameters are summarized in Table 1 and Table 2. In all six independent Gpn residues in these two structures, a C_9 hydrogen bond between the C=O moiety of the preceding residue (i–1) and the N–H group of the succeeding residue (i+1) is observed. The

[*] P. G. Vasudev, Prof. N. Shamala
Department of Physics, Indian Institute of Science
Bangalore—560 012 (India)
Fax: (+91) 80-2360-2602/-0683
E-mail: shamala@physics.iisc.ernet.in
Dr. K. Ananda, Prof. P. Balaram
Molecular Biophysics Unit, Indian Institute of Science
Bangalore—560 012 (India)
Fax: (+91) 80-2360-0683/-0535
E-mail: pb@mbu.iisc.ernet.in

[**] This research was supported by a grant from the Council of Scientific and Industrial Research (CSIR) and Program Support in the area of Molecular Diversity and Design, Department of Biotechnology, India. We thank Dr. K. Nagarajan of Hikal R&D Centre, Bangalore (India), for the sample of gabapentin. P.G.V. and K.A. thank the CSIR for a senior research fellowship and research associateship, respectively. X-ray diffraction data were collected on the CCD facility funded under the IRHPA program of the Department of Science and Technology, India.

InterScience
© 2005 Wiley-VCH Verlag GmbH & Co. KGaA, Weinheim

Table 1: Backbone torsion angles [°] for Boc-Gpn-Gpn-NHMe and Boc-Gpn-Gpn-Gpn-Gpn-NHMe.[a]

	ϕ	θ_1	θ_2	ψ	ω	Orientation of aminomethyl group
Boc-Gpn-Gpn-NHMe						
Gpn (1)	108.9	−63.2	−76.6	87.2	−174.9	axial
Gpn (2)	108.2	−61.9	−78.2	88.0	−178.1	equatorial
Boc-Gpn-Gpn-Gpn-Gpn-NHMe						
Gpn (1)	100.5	−69.6	−72.8	84.5	−171.6	equatorial
Gpn (2)	−103.8	69.9	73.4	−90.5	−174.5	axial
Gpn (3)	−112.2	66.8	72.6	−88.4	174.8	axial
Gpn (4)	104.6	−70.7	−71.5	97.2	179.0	equatorial

[a] Estimated standard deviation for the dihedral angles is approximately 0.4°.

Table 2: Intramolecular hydrogen bonds in Boc-Gpn-Gpn-NHMe and Boc-Gpn-Gpn-Gpn-Gpn-NHMe.[a]

Donor	Acceptor	N···O [Å]	H···O [Å]	∢ N–H···O [°]
Boc-Gpn-Gpn-NHMe				
N2	O0	2.90	2.00	172.5
N0M	O1	2.86	2.00	170.8
Boc-Gpn-Gpn-Gpn-Gpn-NHMe				
N2	O0	2.82	1.90	176.3
N3	O1	2.89	2.05	173.6
N4	O2	2.87	2.03	169.9
N0M	O3	2.90	2.05	168.4

[a] Estimated standard deviations in the hydrogen-bond lengths N···O and H···O and angles are approximately 0.01 Å, 0.02 Å, and 2.5°, respectively.

backbone torsion angles for all six residues reveal that they adopt very similar *gauche*,*gauche* conformations. Interestingly, three of the observed cyclohexane rings have the amino methyl group in an axial orientation, whereas in the other three this group adopts an equatorial orientation. A comparison of the di- and tetrapeptide structures, however, reveals an important difference. In the protected dipeptide the two Gpn residues adopt the same combination of signs for the four backbone torsion angles. In sharp contrast, in the protected tetrapeptide the combination of signs for the torsion angles for residues 1 and 4 is opposite to that of residues 2 and 3. Notably, as both structures are of achiral peptides crystallizing in centrosymmetric space groups, the choice of sign reported in Table 1 is arbitrary. However, differences in the handedness of conformations between residues in the same structure can be observed.

The repetitive C_9-hydrogen-bonded structures determined in the two peptides can be viewed as analogues of the corresponding C_7-hydrogen-bonded structures described for polypeptides composed of α-amino acids. The isolated γ turn stabilized by a 3→1 hydrogen bond between C=O ($i-1$) and N–H ($i+1$) has been observed in the structure of proteins and peptides.[6] The repetitive C_7 structure, the 2.2_7 helix, was first proposed for α polypeptides by Donohue.[7] Subsequently, two structures were theoretically considered, the 2_7 ribbon ($\phi = -70°$, $\psi = 70°$) and the 2.2_7 helix ($\phi = -78.1°$, $\psi = 59.2°$).[8] However, these structures have not been experimentally observed in the crystal structures of polypeptides and proteins. A recent report describes two consecutive γ-turn conformations in a synthetic dipeptide.[9] Ab initio molecular orbital calculations have been used to examine all possible periodic structures of γ-peptides. These studies suggest that helical structures with hydrogen bonds enclosing 14- and 9-membered rings are most stable.[10] An isolated C_9 hydrogen bond has been described in the crystal structure of a γ-dipeptide.[11] A C_9-ribbon structure has also been postulated on the basis of NMR spectroscopy data for γ-peptide oligomers of *cis*-γ-amino-L-proline.[12] The C_9 structures described above constitute an expansion of the C_7 structures by the insertion of two additional backbone atoms.

Figure 3 shows views of three possible repetitive polypeptide structures generated by using the C_9-repeat motif. Figure 3b shows the C_9 helix generated by repeating the structure determined for the dipeptide Boc-Gpn-Gpn-NHMe. In this case, the monomeric unit is a single Gpn residue and the combination of signs for the torsion angles is the same for all residues in the helical structure. The number of residues/turn (n) value in this C_9 helix is 2.67 and the height/residue (h) value is 3.40 Å. The view down the axis of this 2.7_9 helix is shown in Figure 3c. A projection of the analogous C_7-helical structure of α polypeptides (2.2_7 helix) is also shown for comparison (Figure 3a).

Inspection of the torsion angles in Table 1 for the tetrapeptide Boc-Gpn-Gpn-Gpn-Gpn-NHMe reveals that the signs of the four torsion angles between adjacent Gpn residues can also be inverted. It is thus possible to consider a range of repetitive C_9 structures employing different handedness at adjacent residues. The helical structure pictured in Figure 3b may be represented by the notation ++++, which indicates that the handedness of all residues along the polymeric chain is identical. Two alternative structures, +−+− and ++−−++−−, are illustrated in Figure 3d–g. The regular alternation of sign in the +−+− structure leads to a C_9 ribbon with a significant degree of curvature, which can result in cyclization after 79 residues (Figure 4). Figure 3f and g illustrates two views of the ++−−++−− structure, where the repeating unit consists of four Gpn residues. This structure can be obtained by repeating the backbone torsion angles determined in the structure of Boc-Gpn-Gpn-Gpn-Gpn-NHMe. Once again, the structure can be viewed as a ribbon but one with a much smaller degree of curvature than the C_9 ribbon obtained from the regular +−+− combination (Figure 3d).

The structures described herein for Gpn oligomers reveal a new family of polypeptide structures which are C_9 ribbons and helices. The C_9-hydrogen-bond structure is determined by a specific combination of the four degrees of torsional freedom at the Gpn residue and is independent of the flanking residues. In Gpn homooligomers, C_9 helices and ribbons will undoubtedly be the energetically favored structures. In mixed sequences, where Gpn is inserted into polypeptides containing α- and β-amino acids, alternative hydrogen-bonding patterns may be anticipated.[1b]

 © 2005 Wiley-VCH Verlag GmbH & Co. KGaA, Weinheim

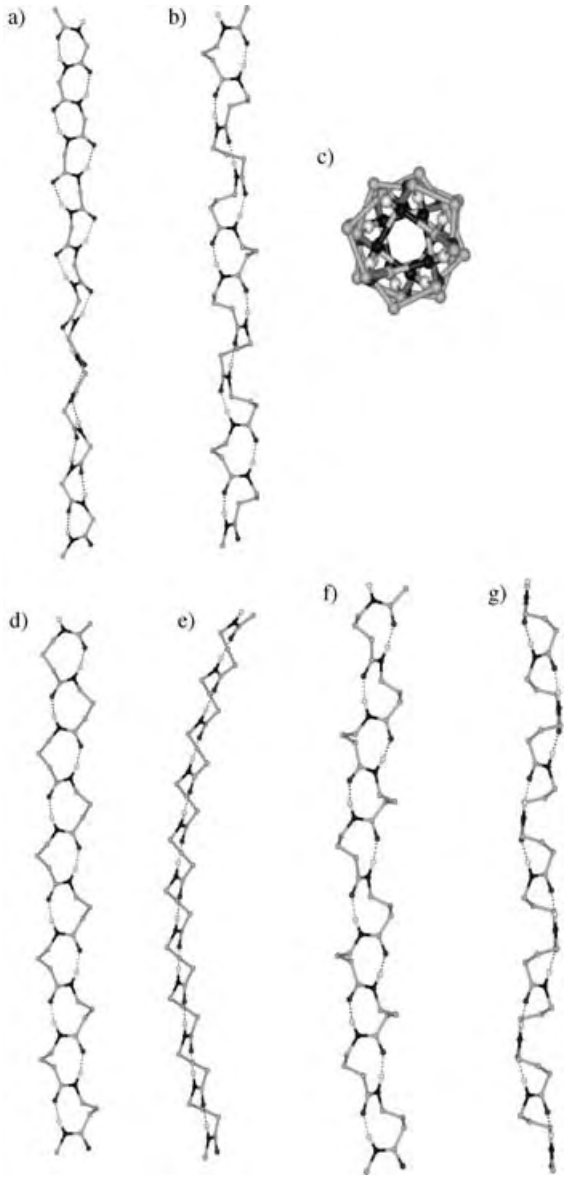


Figure 3. a) 2.2_7 helix formed by α-amino acids; b) 2.7_9 (C_9) helix formed by the Gpn ++++ repeat motif; c) view down the helix axis of the 2.7_9 (C_9) helix; d) C_9 ribbon formed by the Gpn +−+− repeat motif; e) side view of the C_9 ribbon formed by the Gpn +−+− repeat motif; f) C_9 ribbon formed by the Gpn ++−−++−− repeat motif; g) side view of the ribbon formed by the Gpn ++−−++−− repeat motif. (Signs + and − denote the handedness of the Gpn residues.)

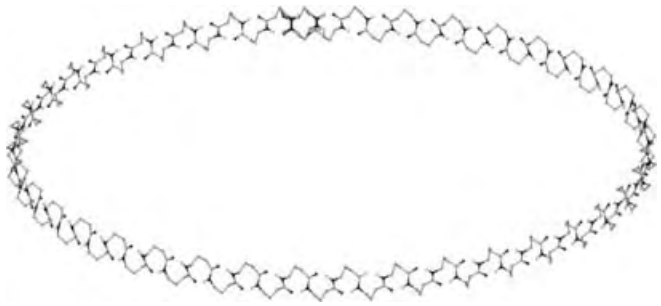


Figure 4. Cyclic structure generated by the repetition of the Gpn +−+− motif.

Experimental Section

Peptides Boc-Gpn-Gpn-NHMe (peptide 1) and Boc-Gpn-Gpn-Gpn-Gpn-NHMe (peptide 2) were synthesized by conventional solution-phase procedures. Coupling was mediated by *N*,*N*′-dicyclohexylcarbodiimide (DCC) and *N*-hydroxysuccinimide (HOSu) in tetrahydrofuran (THF). Boc-Gpn-NHMe was synthesized from Boc-Gpn-OH by using a mixed anhydride strategy and employing methylamine as the amino compound. Subsequent elongation of the chain was carried out by formic acid mediated deprotection of the Boc group, followed by coupling to Boc-Gpn-OH. Stepwise elongation was used up to the tetrapeptide structure. The peptides, which were obtained as crystalline solids, were further purified by medium-pressure liquid chromatography over a reversed-phase C_{18} column (40–60 μm) and characterized by 500 MHz ^{1}H NMR spectroscopy; m.p.: 96–97 °C for peptide 1; 162–163 °C for peptide 2.

Single crystals suitable for X-ray diffraction were grown by slow evaporation from mixtures of ethyl acetate/petroleum ether (peptide 1) and methanol/chloroform (peptide 2). X-ray intensity data were collected at room temperature on a Bruker AXS SMART APEX CCD diffractometer, by using $Mo_{K\alpha}$ radiation ($\lambda = 0.71073$ Å). The ω scan type was used. In total, 37219 reflections were measured (5232 independent reflections) with $2\theta_{max} = 53.6°$ and $R_{int} = 0.06$ for peptide 1 ($C_{24}H_{43}N_3O_4$, $M_w = 437.6$). The data were collected from a crystal of dimensions $0.14 \times 0.10 \times 0.03$ mm. The space group is *Pbca* with unit cell dimensions and parameters of $a = 11.771(6)$, $b = 20.724(11)$, and $c = 22.206(12)$ Å, $V = 5233(5)$ Å^3, $Z = 8$, $\rho_{calcd} = 1.11$ g cm^{-3}, $\mu = 0.07$ mm^{-1}, and $F(000) = 1920$. For peptide 2 ($C_{42}H_{73}N_5O_6$, $M_w = 744.0$) 31521 reflections were measured (8500 independent reflections) with $2\theta_{max} = 53.4°$ and $R_{int} = 0.03$. The crystal dimensions are $0.22 \times 0.14 \times 0.10$ mm. The space group is $P2_1/c$ with unit cell dimensions and parameters of $a = 10.004(7)$, $b = 12.648(8)$, and $c = 35.240(2)$ Å, $\beta = 92.632°$ (12), $V = 4454.0(5)$ Å^3, $Z = 4$, $\rho_{calcd} = 1.11$ g cm^{-3}, $\mu = 0.07$ mm^{-1}, and $F(000) = 1632$. Both the structures were solved by direct methods by using SHELXS-97[13a] and refined against F^2, with full-matrix least squares methods, by using SHELXL-97.[13b] All the hydrogen atoms were located from the difference Fourier map. The final R value for peptide 1 was $R_1 = 0.0616$ ($wR_2 = 0.1461$) for 3134 observed reflections with $F_o \geq 4\sigma|F_o|$ and for 452 parameters. The data to parameter ratio is 6.9:1.0 and the goodness of fit $S = 0.99$. The largest difference peak was 0.18 e Å^{-3} and the largest difference hole was −0.15 e Å^{-3}. The final R value for peptide 2 was $R_1 = 0.0655$ ($wR_2 = 0.1782$) for 5474 observed reflections with $F_o \geq 4\sigma|F_o|$ and for 758 parameters. The data to parameter ratio is 7.2:1.0 and the goodness of fit $S = 1.16$. The largest difference peak was 0.27 e Å^{-3} and the largest difference hole was −0.16 e Å^{-3}. CCDC 266651 (Boc-Gpn-Gpn-NHMe) and CCDC 266652 (Boc-Gpn-Gpn-Gpn-Gpn-NHMe) contain the supplementary crystallographic data for this paper. These data can be obtained free of charge from the Cambridge Crystallographic Data Centre via www.ccdc.cam.ac.uk/data_request/cif.

Received: March 23, 2005
Published online: July 8, 2005

Keywords: helical structures · hydrogen bonds · peptide conformation · ribbon structures

[1] a) S. Aravinda, N. Shamala, R. S. Roy, P. Balaram, *Proc. Indian Acad. Sci. Chem. Sci.* **2003**, *115*, 373–400; b) R. S. Roy, P. Balaram, *J. Pept. Res.* **2004**, *63*, 279–289.

[2] a) D. Seebach, M. Overhand, F. N. M. Kühnle, B. Martinoni, *Helv. Chim. Acta* **1996**, *79*, 913–941; b) D. H. Appella, L. A. Christianson, I. L. Karle, D. R. Powell, S. H. Gellman, *J. Am. Chem. Soc.* **1996**, *118*, 13071–13072; c) D. H. Appella, L. A.

 © 2005 Wiley-VCH Verlag GmbH & Co. KGaA, Weinheim

Christianson, D. A. Klein, M. R. Richards, D. R. Powell, S. H. Gellman, *J. Am. Chem. Soc.* **1999**, *121*, 7574 – 7581.
[3] a) D. Seebach, A. K. Beck, D. J. Bierbaum, *Chem. Biodiversity* **2004**, *1*, 1111 – 1239; b) R. P. Cheng, S. H. Gellman, F. DeGrado, *Chem. Rev.* **2001**, *101*, 3219 – 3232; c) S. Hanessian, X. Luo, R. Schaum, *Tetrahedron Lett.* **1999**, *40*, 4925 – 4929; d) S. Hanessian, X. Luo, R. Schaum, S. Michnick, *J. Am. Chem. Soc.* **1998**, *120*, 8569 – 8570; e) D. J. Hill, M. J. Mio, R. B. Prince, T. S. Hughes, J. S. Moore, *Chem. Rev.* **2001**, *101*, 3893 – 4011; f) I. L. Karle, A. Pramanik, A. Banerjee, S. Bhattacharjya, P. Balaram, *J. Am. Chem. Soc.* **1997**, *119*, 9087 – 9095; g) A. Banerjee, P. Balaram, *Curr. Sci.* **1997**, *73*, 1067 – 1077.
[4] a) K. Ananda, S. Aravinda, P. G. Vasudev, K. M. P. Raja, H. Sivaramakrishnan, K. Nagarajan, N. Shamala, P. Balaram, *Curr. Sci.* **2003**, *85*, 1002 – 1011; b) J. S. Bryans, D. C. Horwell, G. S. Ratcliffe, J.-M. Receveur, J. R. Rubin, *Bioorg. Med. Chem.* **1999**, *7*, 715 – 721.
[5] S. Aravinda, K. Ananda, N. Shamala, P. Balaram, *Chem. Eur. J.* **2003**, *9*, 4789 – 4795.
[6] a) G. Némethy, M. P. Printz, *Macromolecules* **1972**, *5*, 755 – 758; b) B. W. Matthews, *Macromolecules* **1972**, *5*, 818 – 819.
[7] J. Donohue, *Proc. Natl. Acad. Sci. USA* **1953**, *39*, 470 – 478.
[8] a) G. N. Ramachandran, V. Sasisekharan in *Advances in Protein Chemistry*, *Vol. 23* (Eds.: C. B. Anfinsen, Jr., M. L. Anson, J. T. Edsall, F. M. Richards), Academic Press, New York, **1968**, pp. 283 – 437; b) R. E. Dickerson, I. Geis, *The Structure and Action of Proteins*, Harper & Row, New York, **1969**, Chap. 2.
[9] A. I. Jiménez, G. Ballano, C. Cativiela, *Angew. Chem.* **2005**, *117*, 400 – 403; *Angew. Chem. Int. Ed.* **2005**, *44*, 396 – 399.
[10] C. Baldauf, R. Günther, H.-J. Hofmann, *Helv. Chim. Acta* **2003**, *86*, 2573 – 2588.
[11] D. Seebach, M. Brenner, M. Rueping, B. Jaun, *Chem. Eur. J.* **2002**, *8*, 573 – 584.
[12] J. Farrera-Sinfreu, L. Zaccaro, D. Vidal, X. Salvatella, E. Giralt, M. Pons, F. Albericio, M. Royo, *J. Am. Chem. Soc.* **2004**, *126*, 6048 – 6057.
[13] a) G. M. Sheldrick, SHELXS-97, A program for automatic solution of crystal structures, University of Göttingen, Göttingen, **1997**; b) G. M. Sheldrick, SHELXL-97, A program for crystal structure refinement, University of Göttingen, Göttingen, **1997**.

 © 2005 Wiley-VCH Verlag GmbH & Co. KGaA, Weinheim

Chemical Biology

DOI: 10.1002/anie.200462625

Development and Biological Evaluation of Acyl Protein Thioesterase 1 (APT1) Inhibitors**

Patrick Deck, Dirk Pendzialek, Markus Biel, Melanie Wagner, Boriana Popkirova, Björn Ludolph, Goran Kragol, Jürgen Kuhlmann, Athanassios Giannis,* and Herbert Waldmann**

Lipidation of proteins is often an unalterable prerequisite for correct biological function. Prime examples are the N and H isoforms of the signal transducing Ras protein, which in the normal and oncogenic state are anchored to the plasma membrane by means of *S*-farnesylation and *S*-palmitoylation at their C terminus and which have to be palmitoylated to exert their full biological activity.[1,2] Inhibition of the enzyme protein farnesyltransferase has opened up an unprecedented opportunity for the treatment of tumors carrying a mutation in the Ras oncogene.[3] However, the enzyme responsible for palmitoylation of H- and N-Ras and other proteins crucial to biological signaling, like heterotrimeric G proteins, G-protein-coupled receptors, and nonreceptor tyrosine kinases, has not been identified so far. Clearly the development of potent inhibitors for this biocatalyst might open up new opportuni-

[*] Dr. M. Wagner, Dr. B. Popkirova, Priv.-Doz. Dr. J. Kuhlmann
Department of Structural Biology
Max Planck Institute of Molecular Physiology
Otto-Hahn-Strasse 11, 44227 Dortmund (Germany)
Fax: (+49) 231-133 2699
E-mail: juergen.kuhlmann@mpi-dortmund.mpg.de

Dipl.-Chem. M. Biel, Prof. Dr. A. Giannis
Institute of Organic Chemistry
University of Leipzig
Johannisallee 29, 04103 Leipzig (Germany)
Fax: (+49) 341-973 6599
E-mail: giannis@chemie.uni-leipzig.de

Dr. P. Deck, Dipl.-Biol. D. Pendzialek, Dr. B. Ludolph, Dr. G. Kragol, Prof. Dr. H. Waldmann
Department of Chemical Biology
Max Planck Institute of Molecular Physiology
Otto-Hahn-Strasse 11, 44227 Dortmund (Germany)
Fax: (+49) 231-133 2499
E-mail: herbert.waldmann@mpi-dortmund.mpg.de
and
Fachbereich Chemie, Universität Dortmund

[**] This research was supported by the Max-Planck-Gesellschaft, the Fonds der Chemischen Industrie, and the Deutsche Forschungsgemeinschaft. The authors are grateful to Prof. K. Sandhoff (Kekulé-Institut für Organische Chemie und Biochemie der Rheinischen Friedrich-Wilhelms-Universität Bonn) and Prof. F. Bordusa (Max-Planck-Forschungsstelle für Enzymologie der Proteinfaltung Halle/Saale) for helpful discussions, and to Prof. E. A. Dennis (University of California) for providing a pET vector with the APT1 coding sequence.

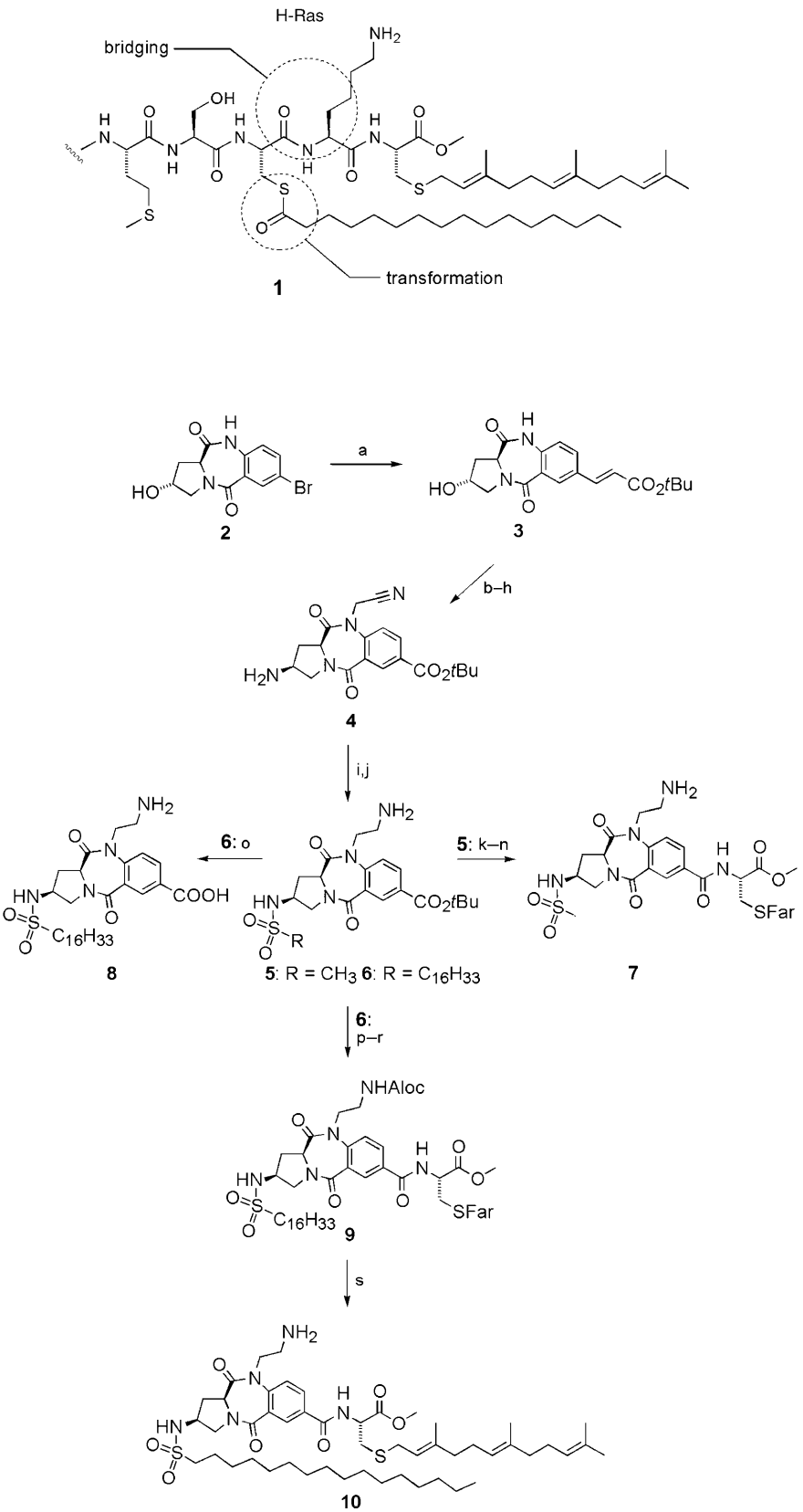
Supporting information for this article is available on the WWW under http://www.angewandte.org or from the author.

© 2005 Wiley-VCH Verlag GmbH & Co. KGaA, Weinheim

ties for the treatment of cancers with a mutation in the H- and N-Ras oncogenes.

In yeast, the Erf2 and Erf4 proteins were found to palmitoylate the yeast Ras oncogene homologues.[4,5] While orthologues of the Erf2 gene can be found in the genomes of various eukaryotes including *Homo sapiens*, proteins with the corresponding *S*-palmitoylating activity have not been identified to date.[6] Erf4 homologues have only been identified in closely related yeasts. Instead, acyl protein thioesterase 1 (APT1) was described as "the first bona fide player" in the regulated thioacylation of intracellular proteins.[7] APT1 was found to depalmitoylate the H-Ras protein and the α subunits of heterotrimeric G proteins. Herein we report a chemical biology approach aimed at determination of the involvement of APT1 in H-Ras palmitoylation in vitro and possibly in vivo.

For a reverse chemical genetics approach,[8] inhibitors to antagonize the biological function of the enzyme were designed based on the structure of the H-Ras C terminus **1** (Scheme 1). To this end, a peptide-imitating benzodia-



Scheme 1. Structure of the lipidated C terminus **1** of the H-Ras protein and synthesis of the corresponding benzodiazepinediones **5**–**10**. a) *tert*-Butyl acrylate, $Pd(OAc)_2$, $P(oTol)_3$, NEt_3, CH_3CN, 100 °C, sealed tube, 97%; b) MsCl, pyridine, 0 °C→RT; c) NaN_3, DMF, 45 °C, 89% over two steps; d) NaH, THF, −40 °C; e) $BrCH_2CN$, −40 °C→RT, 95% over two steps; f) $RuCl_3$, $NaIO_4$, $H_2O/CH_3CN/CCl_4$ (2:1:1); g) Me_3CBr, K_2CO_3, $Et_3(PhCH_2)NCl$, DMA, 55 °C, 90% over two steps; h) H_2, $Pd/BaSO_4$, MeOH, $CHCl_3$, quantitative; i) MsCl, $NEtiPr_2$, DMF, 0 °C→RT, 92%; or $C_{16}H_{33}SO_2Cl$, $NEtiPr_2$, DMF, 0 °C→RT, 82%; j) H_2, $PtO_2{\cdot}H_2O$, EtOH, $CHCl_3$, 85% (**5**); or H_2, $PtO_2{\cdot}H_2O$, EtOH, $CHCl_3$, 81% (**6**); k) AlocCl, NEt_3, CH_2Cl_2, 83%; l) TFA/CH_2Cl_2 (1:1); m) H-Cys(Far)-OMe, EDC, HOBt, CH_2Cl_2, 0 °C→RT, 89% over two steps; n) $[Pd(PPh_3)_4]$, DMB, THF, 65%; o) HCl/Et_2O, quantitative; p) AlocCl, NEt_3, CH_2Cl_2, 84%; q) TFA/CH_2Cl_2 (1:1), quantitative; r) H-Cys(Far)-OMe, EDC, HOBt, CH_2Cl_2, 0 °C→RT, 89%; s) $[Pd(PPh_3)_4]$, DMB, THF, 80%. Tol = tolyl, Ms = mesyl = methane sulfonyl, DMF = *N*,*N*-dimethylformamide, THF = tetrahydrofuran, DMA = *N*,*N*-dimethylacetamide, Aloc = allyloxycarbonyl, TFA = trifluoroacetic acid, Far = farnesyl, EDC = 3-(3-dimethylaminopropyl)-1-ethylcarbodiimide, HOBt = 1-hydroxy-1*H*-benzotriazole, DMB = dimethylbarbituric acid.

 © 2005 Wiley-VCH Verlag GmbH & Co. KGaA, Weinheim

zepinedione core[9] was chosen as the underlying scaffold and equipped with a hydrolysis-stable sulfonamide to mimic the tetrahedral intermediate passed in the hydrolysis of the thioester (see **10**, Scheme 1).

For the synthesis of the desired compounds, 4-(*R*)-hydroxyproline and 5-bromoisatoic acid anhydride were condensed to give the benzodiazepinedione framework **2**, which was subjected to a ten-step synthesis sequence yielding central intermediates **5** and **6**. Methanesulfonamide **5** was converted into *N*-acylated and *S*-farnesylated cysteine methyl ester **7**. The *tert*-butyl ester was cleaved from hexadecylsulfonamide **6**, thereby giving rise to acid **8**. Alternatively, the amino group was masked and *S*-farnesylated cysteine methyl ester was attached to the C terminus to yield **9**, which was selectively *N*-deprotected to give benzodiazepinedione **10**, a mimic of the C terminus of fully processed H-Ras.

For determining the APT1-inhibiting potency of the synthetic benzodiazepinediones, a fluorescence-based biochemical assay was developed by employing the acrylodated intestinal fatty acid binding protein (ADIFAB) as the detecting system.[10]

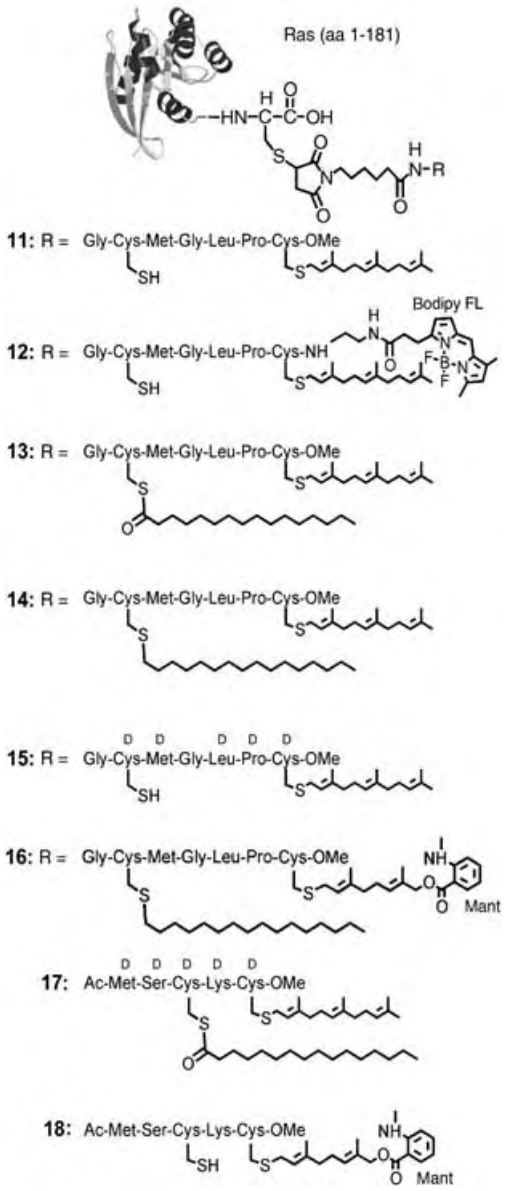
The results of the biochemical assay are shown in Table 1 (for additional data, see the Supporting Information). Compound **10** proved to be the most potent APT1 inhibitor with

Table 1: Inhibition of APT1 by benzodiazepinediones **5**–**10**.

Compound	IC_{50} [nM]
10	27 ± 5
9	149 ± 30
6	148 ± 6
8	97 ± 8
7	27 000 ± 17 000
5	250 000 ± 160 000

an IC_{50} value of 27 nM. The data indicate that a hexadecylsulfonamide moiety mimicking the palmitic acid thioester is required for high inhibitory activity (compare **7** and **10** or **5** and **6**). The primary amine moiety representing the ε-amino group of the lysine residue found at the C terminus of H-Ras should be liberated to obtain full inhibitory activity (compare **9** and **10**). An *S*-farnesylated cysteine methyl ester at the C terminus is beneficial for activity but not as essential as the palmitic acid mimic (compare **7**, **8**, and **10**). If both lipid residues are lacking, inhibitory activity is lost, that is, the benzodiazepinedione core is not sufficient for activity. The investigated compounds were not inhibitors of the enzyme protein farnesyltransferase (data not shown).

The biological activity of the APT1 inhibitors was investigated by employing the rat pheochromocytoma cell line PC-12. Under normal growth conditions, this cell line has a chromaffin-cell-like morphology. Upon microinjection of full-length recombinant oncogenic RasG12V proteins, these cells differentiate into nonreplicating sympathetic neuron-like cells.[11] The same morphological change is observed upon microinjection of semisynthetic oncogenic Ras protein **11** (Scheme 2), which carries an *S*-farnesylated cysteine methyl ester and a second unmasked, and therefore palmitoylatable,



Scheme 2. Structures of the semisynthetic Ras proteins **11**–**16** and the synthetic lipopeptides **17** and **18**; bodipy FL = 4,4-difluoro-5,7-dimethyl-4-bora-3a,4a-diaza-*s*-indacene-3-propionyl, mant = *N*-methylanthranilate.

cysteine residue at the C terminus.[12–14] In both cases lipidation of Ras is completed by *S*-palmitoylation in the cell, that is, protein **11** is converted into protein **13**, thereby resulting in plasma-membrane localization of and active signaling by the Ras proteins,[14] which is quantifiable by determining the frequency of neurite outgrowth in PC-12 cells. Microinjection of farnesylated but not *S*-palmitoylatable synthetic Ras (because of omission of a second cysteine in the synthesis) does not lead to neurite outgrowth. Consequently, a change in neurite outgrowth correlates directly with the degree of Ras palmitoylation.

Microinjection of synthetic, palmitoylatable N-Ras protein **11** was adjusted to give a neurite outgrowth rate of approximately 50% (see Figure 1). Depalmitoylation of Ras

 © 2005 Wiley-VCH Verlag GmbH & Co. KGaA, Weinheim

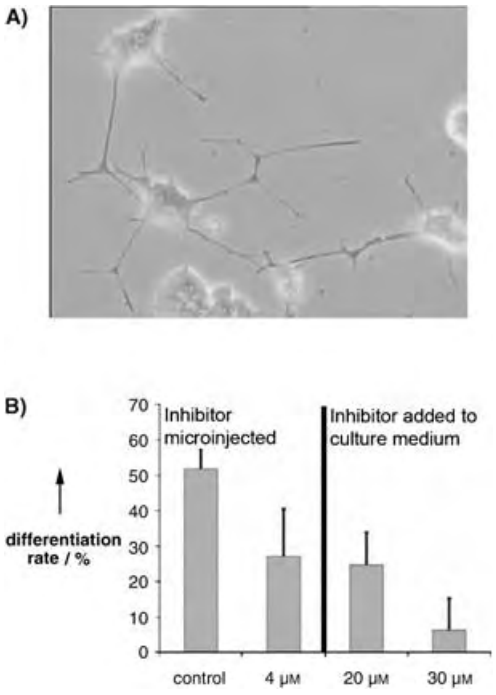


Figure 1. Reduction of PC-12 cell differentiation rate by APT1 inhibitor **6**. PC-12 differentiation assays were performed according to the procedure of Bader et al.[12] A 50 μM solution of the palmitoylatable lipopeptide coupling product of N-RasG12V(1–181) and **11** was microinjected into cells, thereby inducing a neurite outgrowth in approximately 50% of the injected cells (A). If APT1 inhibitor **6** was either coinjected (4 μM stock solution) with the Ras lipoprotein or added to the medium 1 h before microinjection (20 and 30 μM), the differentiation rate decreased significantly (B). For each experiment, an average of 100 cells were treated.

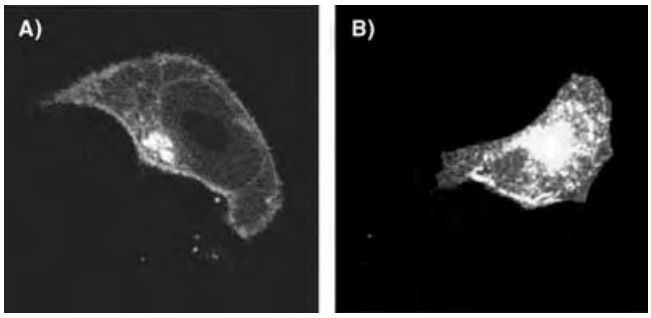


Figure 2. Inhibition of plasma-membrane localization of fluorescently labeled Ras protein **12** by APT1 inhibitor **6**. A 40 μM solution of the coupling product of N-RasG12V(1–181) and lipopeptide **12** was microinjected into MDCK cells. Localization of the fluorescent lipoprotein was monitored 7 h after microinjection by confocal microscopy. Although Ras protein alone shows a distinct staining of the plasma membrane (A), coinjection of 2 μM inhibitor **6** results in an accumulation of the lipoprotein in cytoplasmic structures, which is typical for nonpalmitoylatable Ras constructs (B).

by APT1 should result in reduced membrane binding of the oncogenic proteins[12,14] and in a reduction of neurite outgrowth. Therefore, upon inhibition of this process, an increased differentiation rate was to be expected.

Surprisingly, however, coinjection of a 4 μM solution or addition of APT1 inhibitor **6** to the culture medium (final concentration 20 μM) 1 h before microinjection of the Ras protein resulted in a *decrease* in the neurite outgrowth rate from above 50 to below 30%. An increase in the inhibitor concentration in the medium to 30 μM reduced the neurite outgrowth rate to a value below 10% (Figure 1).

To ascertain that the reduction in proliferation rate correlates with a lack of localization of Ras at the plasma membrane and consequently with inhibition of *S*-palmitoylation, synthetic fluorescent *S*-farnesylated and *S*-palmitoylatable N-Ras protein **12** was coinjected with compound **6** into MDCK cells. Confocal fluorescence microscopy revealed that the fluorescent protein had accumulated in cytoplasmic structures and the Golgi (Figure 2). In the absence of inhibitor, localization of the protein to the plasma membrane was clearly observed. When the corresponding fluorescent Ras protein in which the palmitoylatable cysteine residue was replaced by a nonpalmitoylatable serine residue was microinjected into Madin–Darby Canine Kidney (MDCK) cells, the protein was also localized in the cytoplasm and the Golgi (not shown).

When Ras protein **14**, which incorporates a hydrolysis-resistant hexadecyl thioether, was coinjected with inhibitor **6** at the same concentration as the palmitoylatable Ras protein had been, no reduction in neurite outgrowth was observed, as compared to the results after microinjection of lipidated protein **14** alone (not shown).

Microinjection of protein **15**, which carries only D-amino acids at the C terminus, into PC-12 cells surprisingly induced a differentiation rate that was comparable to the rate induced by the protein containing the natural L-amino acids.[14] This result indicates that the enzyme catalyzing the *S*-palmitoylation reaction must be fairly stereotolerant. To determine whether APT1 fulfills this criterion, the H-Ras-derived D-peptide **17** and the corresponding L-peptide were synthesized and subjected to depalmitoylation by APT1. The enzyme depalmitoylates both compounds with nearly identical rates (for the corresponding data, see the Supporting Information).

These results indicate that benzodiazepinedione **6** specifically inhibits Ras localization to the plasma membrane in the cells and, consequently, inhibits Ras palmitoylation rather than depalmitoylation. The fact that compound **6** displays an IC_{50} value for APT1 in the nanomolar range and that in the cells that were used for the microinjection experiments only *S*-palmitoylation remained to complete all the steps of posttranslational Ras modification required for plasma-membrane localization and induction of neurite outgrowth suggested that the observed effect might be linked to the inhibition of processes mediated by APT1. This includes the possibility that APT1 might be involved directly in Ras palmitoylation and in further downstream events that lead to Ras acylation by a different mechanism. We also cannot exclude the possibility that the effects described above are due to inhibition of other enzymes by benzodiazepinedione **6**.

To investigate whether APT1, in principle, can function as an *S*-palmitoylating enzyme in vitro, fluorescent palmitoylable peptide **18**, which represents the characteristic C termi-

 © 2005 Wiley-VCH Verlag GmbH & Co. KGaA, Weinheim

nus of the H-Ras protein and incorporates a geranyl-*N*-mant function as a fluorescent substitute for the farnesyl group,[13] was treated with APT1 in the presence of palmitic acid. The palmitoylation reaction was monitored spectroscopically since conversion of the substrate **18** into the palmitic acid thioester results in a diagnostic shift of the fluorescence emission maximum from 440 to 410 nm, as determined by employing synthesized reference compounds (Figure 3).

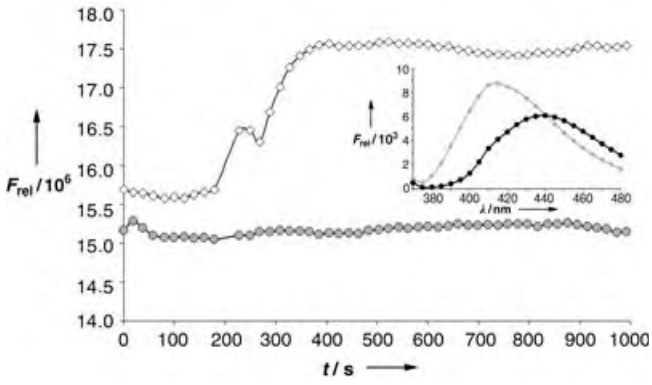


Figure 3. Palmitoylating activity of APT1 indicated by the change in relative fluorescence units (F_{rel}; measured at 410 nm) over time. Gray circles: control, that is, H-Ras peptide **18** and palmitic acid without APT1; white diamonds: H-Ras peptide **18**, palmitic acid, and added APT1. Conditions were as described in the Supporting Information). For better solubility of the palmitic acid, 10% dimethylsulfoxide (DMSO) was added to the reaction mixture. The concentrations for substrate **18**, APT1, and palmitic acid were 1, 1, and 100 μM, respectively. After the reaction mixture was incubated for 13 min, the reaction was started by addition of APT1. The result of a representative experiment is shown. Each data point represents the average of two independent measurements. The experiment was repeated six times with similar results (not shown). Small inset: emission spectra (370–480 nm) of palmitoylated (gray diamonds) and depalmitoylated (black circles) substrate peptide upon excitation at 360 nm.

Addition of APT1 to the reaction mixture led to a significant increase in fluorescence at 410 nm, thereby indicating *S*-palmitoylation of the substrate. The formation of the *S*-palmitoylated peptide was additionally confirmed by HPLC analysis of the reaction mixture and MALDI mass spectrometry (data not shown).[15]

A similar shift in fluorescence emission maximum was also observed when APT1 and palmitoyl coenzyme A were incubated with the synthetic, palmitoylatable N-Ras lipoprotein **16**, which again incorporates a fluorescent geranyl-mant instead of the farnesyl group.[13] Ras lipoprotein and palmitoyl donor or enzyme alone did not result in a shift of the emission maximum (see the Supporting Information). We utilized the hypsochromic effect to test whether inhibitors of APT1 were capable of preventing the enzyme-catalyzed palmitoylation of the Ras lipoprotein. Indeed, addition of compound **8** resulted in a clear blocking of the APT1-mediated shift in the fluorescence emission of the N-Ras construct (Figure 4).

To further determine whether APT1 does palmitoylate N-Ras in vitro, the protein was incubated with APT1 and [9, 10-^{3}H]-palmitic acid and the incorporation of radioactivity was

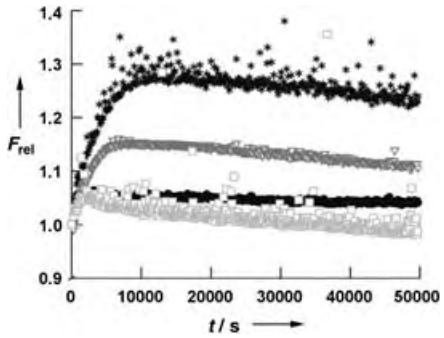


Figure 4. The APT1-mediated *S*-palmitoylation of N-Ras lipoprotein **16** employing palmitoyl coenzyme A (CoA) is inhibited by compound **8.** The change in relative fluorescence emission at 400 nm (F_{rel}) was measured under continuous stirring as a function of time. The concentrations of substrate **16**, APT1, and palmitoyl CoA were 500 nM, 50 nM, and 50 μM, respectively. After the reaction mixture was incubated for 15 min in the presence of different inhibitor concentrations, the reaction was started by addition of the enzyme. The result of one representative set of experiments (out of three) is shown. The palmitoylating reaction was studied in the absence of inhibitor (stars) or upon addition of compound **8** to the reaction mixture (triangles: 20 μM; circles: 40 μM; squares: 60 μM). The excitation wavelength was 360 nm. Measurements were performed at 20°C in 20 mM Hepes buffer (pH 7.4), 150 mM NaCl, 5 mM KCl, and 1 mM Na_2HPO_4. Palmitoyl CoA was stored at −20°C in aqueous solution containing 5 mM Na_2HPO_4. In each reaction mixture, the content of DMSO used as a solvent for compound **8** was adjusted to 0.3%.

determined by scintillation counting. In three separate experiments, the activity determined for the bands corresponding to the Ras protein in sodium dodecylsulfate PAGE was approximately 100% above the background value, thereby proving that N-Ras was palmitoylated (see the Supporting Information).

These results demonstrate that APT1 cannot only mediate Ras depalmitoylation but also Ras palmitoylation in vitro. Since the compounds shown in Table 1 may therefore be regarded as Ras-palmitoylation inhibitors we would like to refer to them as Raspalins 1–6 (according to the entries in the table, that is, compound **6** is termed Raspalin 3).

Enzymatic acylation by hydrolase-catalyzed reversal of the hydrolysis reaction, including that for plasma-membrane constituents,[16] is well-known[17] and incorporation of [^{3}H]-palmitic acid into N-Ras-derived farnesylated peptides in CV-1 cells has been noticed before.[18] In particular, Schuchman, Sandhoff, and co-workers convincingly demonstrated that acid ceramidase can catalyze ceramide synthesis in vitro and in vivo from free fatty acids and sphingosine by reverse hydrolysis, thereby providing a "salvage" pathway for ceramide biosynthesis.[16]

In addition, very recently Rando and co-workers reported that the enzyme lecithin retinal acyl transferase (LRAT) catalyzes the reversible interconversion of all-*trans*-retinal, *trans*-retinyl palmitate, and the triply *S*-palmitoylated membrane-associated protein mRPE65.[19]

The notion that APT1 may not only function as a thioesterase but also as an acyltransferase is furthermore supported by the fact that the nucleophilic serine residue 114

 © 2005 Wiley-VCH Verlag GmbH & Co. KGaA, Weinheim

that forms part of the catalytic Ser-His-Asp triad of the protein is located within a Gly-Xaa-Ser-Xaa-Gly motif (Gly112-Phe113-Ser114-Glu115-Gly116). This motif has previously been identified as typical for enzymes with acyltransferase and thioesterase activity[20] and proven to be of diagnostic and predictive value.[21] Finally, we note that the broad substrate tolerance displayed by APT1 would also explain the finding that a consensus palmitoylation peptide sequence motif does not seem to exist.[4]

Our results demonstrate that the thioesterase APT1 can depalmitoylate and palmitoylate the Ras protein in vitro. From these observations a direct involvement of APT1 in Ras palmitoylation in vivo cannot be conclusively delineated. However, this possibility exists. Future in-depth evaluation of the biological role of APT1 by biology and chemical biology techniques is required to prove such a hypothesis.

Received: November 16, 2004
Revised: April 20, 2005
Published online: July 8, 2005

Keywords: biological activity · enzyme inhibitors · esterases · peptidomimetics · proteins

[1] P. J. Casey, *Science* **1995**, *268*, 221 – 225.
[2] J. F. Hancock, *Nat. Rev. Mol. Cell Biol.* **2003**, *4*, 373 – 384.
[3] H. Waldmann, A. Wittinghofer, *Angew. Chem.* **2000**, *112*, 4360 – 4383; *Angew. Chem. Int. Ed.* **2000**, *39*, 4192 – 4214.
[4] D. J. Bartels, D. A. Mitchell, X. Dong, R. J. Deschenes, *Mol. Cell. Biol.* **1995**, *15*, 6775 – 6787.
[5] S. Lobo, W. K. Greentrees, M. E. Linders, R. Deschenes, *J. Biol. Chem.* **2002**, *277*, 41268 – 41273.
[6] M. E. Linder, R. J. Deschenes, *Biochemistry* **2003**, *42*, 4311 – 4320.
[7] J. A. Duncan, A. G. Gilman, *J. Biol. Chem.* **1998**, *273*, 15830 – 15837.
[8] S. L. Schreiber, *Bioorg. Med. Chem.* **1998**, *6*, 1127 – 1152.
[9] E. Addicks, R. Mazitschek, A. Giannis, *ChemBioChem* **2002**, *3*, 1078 – 1088.
[10] G. V. Richieri, R. T. Ogata, A. M. Kleinfeld, *Mol. Cell. Biochem.* **1999**, *192*, 87 – 94.
[11] D. Vaudry, P. J. S. Stork, P. Lazarovici, L. E. Eiden, *Science* **2002**, *296*, 1648 – 1649.
[12] B. Bader, K. Kuhn, D. J. Owen, H. Waldmann, A. Wittinghofer, J. Kuhlmann, *Nature* **2000**, *403*, 223 – 222.
[13] K. Kuhn, D. J. Owen, B. Bader, A. Wittinghofer, J. Kuhlmann, H. Waldmann, *J. Am. Chem. Soc.* **2001**, *123*, 1023 – 1035.
[14] M. Wagner, R. Reents, M. Völkert, P. P. Mruthunjaya, M. H. Gelb, H. Waldmann, J. Kuhlmann, unpublished results.
[15] The enzymatic synthesis of a thioester from a carboxylic acid and a thiol a priori is an energetically uphill process; in this respect, it is comparable to the enzymatic synthesis of a peptide from the thermodynamically more favorable amine. The principle by which a thioesterase can catalyze the formation of a thioester from a thiol and an acid can therefore be regarded as analogous to peptide synthesis by proteases if both enzyme types employ the same mechanism. APT1 is a cysteine hydrolase displaying the same catalytically active triad as cysteine and serine proteases; the enzymes chymotrypsin (serine protease) and papain (cysteine protease) can serve as analogous cases. For these enzymes, it has been demonstrated that catalysis of the synthesis reaction is achieved by lowering the transition state of the transformation through entropic and enthalpic contributions. Thus, the enzymes concentrate and correctly orientate the substrate and restrict the mobility of the groups concerned with the transition state, thereby causing changes in activation entropy. In addition, charge distinction in the active site and the geometry of substrate binding are changed, which affects the activation enthalpy. Furthermore, in the presence of solvents other than water and in the presence of a second phase, criteria that both are fulfilled in a membraneous environment, the hydration of ionic groups, most notably carboxy functions, is diminished, thereby making them more prone to nucleophilic attack. Also, the formed product, which is more hydrophilic than the starting materials, is sequestered away under these conditions, particularly in a two-phase system, for example, at a water/membrane interface. The free-energy change of this transfer also provides a driving force for synthesis. In addition, the decision between deacylation of an intermediary acyl–enzyme complex by water (that is, hydrolysis) and acyl transfer to a different nucleophile like an amine or a thiol (that is, synthesis) is strongly influenced by the nucleophilic strength of the competitors. In this respect, amines and, even more so, thiols have an unequivocal advantage over water. For instance, leucine amide (0.25 M) deacylates an acyl–chymotrypsin complex 20 times faster than water (55 M); see: K. Morihara, T. Oka, *Biochem. J.* **1977**, *163*, 531.
[16] N. Okino, X. He, S. Gatt, K. Sandhoff, M. Ito, E. H. Schuchman, *J. Biol. Chem.* **2003**, *278*, 29948 – 29953.
[17] *Enzyme Catalysis in Organic Synthesis: A Comprehensive Handbook*, *Vol. I–III*, 2nd ed. (Eds.: K. Drauz, H. Waldmann), Wiley-VCH, Weinheim, **2002**.
[18] H. Schroeder, R. Leventis, S. Rex, M. Schelhaas, E. Nägele, H. Waldmann, J. Silvius, *Biochemistry* **1997**, *36*, 13102 – 13109.
[19] L. Xue, D. R. Gollapalli, P. Maiti, W. J. Jahng, R. R. Rando, *Cell* **2004**, *117*, 761 – 771.
[20] Y. Lemoine, A. Wach, M. Geltsch, *Mol. Microbiol.* **1996**, *19*, 645 – 647.
[21] R. Sanishvili, A. F. Yakunin, R. A. Laskowski, T. Sfarina, E. Evdokimova, A. Doherty-Kirby, G. A. Lajoie, J. M. Thornton, C. H. Arrowsmith, A. Savchenko, A. Joachimiak, A. M. Edwards, *J. Biol. Chem.* **2003**, *278*, 26039 – 26045.

 © 2005 Wiley-VCH Verlag GmbH & Co. KGaA, Weinheim

Carbene Complexes

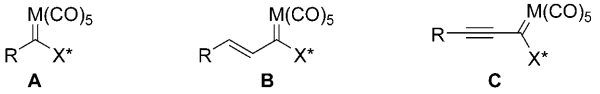
DOI: 10.1002/anie.200501400

Formal Alkyne Insertion into Alkoxycarbene Complexes: Simple Access to Enantiopure Group 6 Alkynyl(alkoxy)carbene Complexes**

José Barluenga, Ramón Bernardo de la Rúa, Diana de Sáa, Alfredo Ballesteros, and Miguel Tomás*

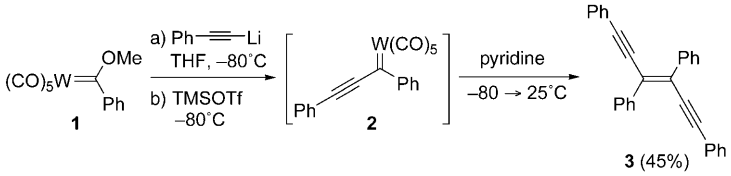
Dedicated to Professor Heinz Hoberg on the occasion of his 80th birthday

Since their discovery in 1964, Fischer carbene complexes have been developed into efficient carbene-transfer agents.[1] The successful implementation of enantioselective processes through chiral nonracemic carbene complexes of chromium and tungsten has greatly increased their potential in selective synthesis.[2] In particular, chiral alkoxy carbenes **A** and **B**



derived from enantiopure alcohols (X* = OR) are efficient systems in a wide array of reactions,[3] while the less reactive chiral amino carbene complexes **A** and **B** (X* = NR_2) have proved to be useful when the metal carbene function is not involved, for example, in aldol, Michael, and Diels–Alder reactions.[4] It is remarkable that there was previously no methodology to access chiral alkynyl(alkoxy)carbenes of type **C** (X* = OR).[5]

We report herein that group 6 enantiopure alkynylcarbene complexes derived from chiral alcohols, as well as related polyalkynyl(alkoxy)carbenes, can be readily prepared from ordinary alkoxy carbenes via non-heteroatom-stabilized carbene complexes. First, the tungsten phenyl(methoxy)carbene complex **1** was treated in THF at −80 °C with lithium phenylacetylide (Scheme 1). Once the addition was completed the color of the solution changed from orange to yellow. Trimethylsilyl triflate (TMSOTf) was added, and the mixture was stirred for a few minutes until the solution

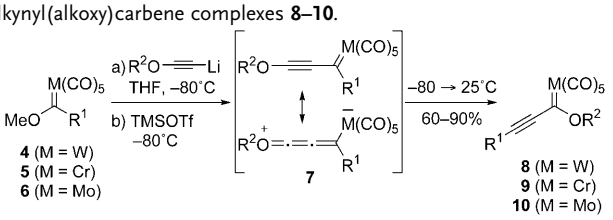


Scheme 1. Generation and dimerization of non-heteroatom-stabilized alkynyl carbene complex **2**.

became deep blue. The nonstabilized carbene complex **2**, which is presumed to be formed by elimination of methyl trimethylsilyl ether from the tetrahedral addition species,[6] were not isolated, but allowed to dimerize in the presence of pyridine (5 equiv) to (*E*)-1,3,4,6-tetraphenyl-3-hexen-1,5-diyne (**3**; 45 % yield).[7]

Unlike some previous reports regarding alkynylcarbene complexes of rhodium,[8] rhenium,[9] and manganese,[10] neither 1,3-migration of the metal center nor products derived thereof were observed in the case of intermediates of type **2**. Focused on this point, we checked whether the rearrangement is an electronically controlled process by using appropriate lithium reagents such as alkoxyacetylides. Gratifyingly, phenylethynyl(ethoxy)carbene complex **8a** was obtained in 90 % yield from carbene complex **4a** and ethoxyethynyl lithium (Table 1, entry 1). We observed that the initially formed nonstabilized carbene **7** undergoes rapid rearrangement, even at low temperatures (below −50 °C), to the more stable alkoxy carbene **8a**. Since alkynyl carbenes were also found to react readily, the reaction was extended to the preparation of elusive Fischer carbene complexes such as

Table 1: Synthesis of achiral (1–3) and enantiopure (4–8) Group 6 alkynyl(alkoxy)carbene complexes **8–10**.



Entry	R^1	R^2	**8** [%][a]	**9** [%][a]	**10** [%][a]
1	Ph	Et	**8a** (90)		
2	PhC≡C	Et	**8b** (81)	**9b** (89)	
3	Ph(C≡C)$_2$[b]	Et	**8c** (60)		
4	Ph	menthyl[c]	**8d** (90)	**9d** (77)	**10d** (85)
5	Ph	8-PhMenth[d]	**8e** (90)	**9e** (85)	**10e** (85)
6	Ph	2-PhCy[e]	**8f** (87)	**9f** (84)	
7	PhC≡C	8-PhMenth[d]	**8g** (75)	**9g** (80)	
8	*i*Pr	2-PhCy[e]	**8h** (65)		

[a] Yields of pure, isolated products. [b] Complex **8b** is used as starting carbene. [c] Menthyl = (1*R*,2*S*,5*R*)-5-methyl-2-(1-methylethyl)cyclohexyloxy. [d] 8-PhMenth = (1*R*,2*S*,5*R*)-5-methyl-2-(1-methyl-1-phenylethyl)-cyclohexyloxy. [e] 2-PhCy = (1*R*,2*S*/1*S*,2*R*)-2-phenylcyclohexyloxy.

[*] Prof. Dr. J. Barluenga, Dr. R. B. de la Rúa, D. de Sáa, Dr. A. Ballesteros, Prof. Dr. M. Tomás
Instituto Universitario de Química Organometálica "Enrique Moles"
Unidad Asociada al C.S.I.C., Universidad de Oviedo
33006 Oviedo (Spain)
Fax: (+34) 98-510-3450
E-mail: barluenga@uniovi.es

[**] This research was partially supported by the Spain and Principado de Asturias Governments (BQU-2001-3853 and GE-EXP01-11; fellowships to D.S. and R.B.R.). We are also grateful to Dr. A. Soldevilla (Universidad de la Rioja), Dr. A. L. Suárez-Sobrino (Universidad de Oviedo), and Dr. J. Borge (Universidad de Oviedo) for their assistance in the X-ray crystallographic analysis. Generous support from Merck Sharp & Dohme (UK) is gratefully acknowledged.

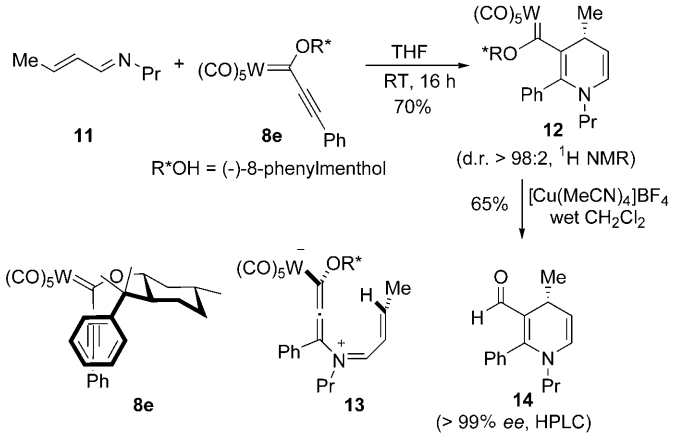
Supporting information for this article (characterization data and ^{13}C NMR spectra of **8, 9, 10, 12**, **14**) is available on the WWW under http://www.angewandte.org or from the author.

 © 2005 Wiley-VCH Verlag GmbH & Co. KGaA, Weinheim

diynyl(alkoxy)carbenes.[11] This is exemplified for 4-phenyl-1,3-butadiynyl carbenes of tungsten **8b** (81%) and chromium **9b** (89%) (Table 1, entry 2). Moreover, (6-phenyl-1,3,5-hexatriynyl)carbene complex **8c** (Table 1, entry 3) was synthesized in 60% yield from the tungsten diynylcarbene complex **8b** as starting material.

This finding prompted us to investigate whether it was feasible to access group 6 alkynylcarbenes with a chiral alkoxy group, as the preparation of such compounds had hitherto been unsuccessful. Importantly, a number of alkynyl carbenes derived from chiral alcohols were readily synthesized in high yields by following the routine protocol (Table 1, entries 4–8). The process seems to be of wide scope on the basis of the following observations: 1) common chiral bulky alkoxy groups are efficiently assembled into the carbene structure (menthyloxy, 8-phenylmenthyloxy, *trans*-2-phenylcyclohexyloxy); 2) the process is applicable not only to tungsten and chromium metals (compounds **8** and **9**), but also to the much more elusive molybdenum metal (compounds **10**);[12] 3) besides aryl-substituted complexes, enolizable carbenes ($R^1 = i$Pr; Table 1, entry 8) can also be employed successfully.

As enantioselective cycloaddtition reactions with chiral alkynes are very rare,[13–15] the chiral induction by the alkoxy group was then examined in the [4+2]-cycloaddition with 1-azadienes (Scheme 2).[16] Thus, the reaction of 1-azadiene **11**



Scheme 2. Diastereoselective [4+2] cycloaddition of 1-azadiene **11** and carbene **8e**. Synthesis of enantiopure 1,4-dihydropyridine **14**.

with phenylethynyl(8-phenylmenthyloxy)carbene complex **8e** in THF at room temperature furnished, after chromatographic purification, the dihydropyridine complex **12** in 70% yield as a sole regio- and diastereoisomer (by NMR spectroscopic analyis). The structure of the cycloadduct was determined by a X-ray crystallographic analysis.[16] According to our previous reports[17,18] we propose a working model that involves, 1) diastereoselective conjugate addition of the nitrogen atom of **11** to the more accessible face of alkyne (probably due to a π-stacking effect as shown) to form the intermediate **13** with central and axial chirality; and 2) cyclization of **13** through the *Re* face of the C=C bond to afford the observed cycloadduct **12**.[19] The latter was demetalated, and the chiral auxiliary removed by treatment with $[Cu(MeCN)_4]BF_4$ in wet CH_2Cl_2 to provide the aldehyde **14** (65%, >99.5% *ee*).[20]

In conclusion, new aspects that enhance the synthetic utility of Fischer carbene complexes are featured in this report: 1) 1,3-alkynyl carbene ligand rearrangement is a very easy process for non-heteroatom-stabilized alkynyl carbenes and seems to be thermodynamically controlled; 2) based on this finding a facile and general access to novel chiral alkynyl(alkoxy)carbene complexes was undertaken; 3) their efficient chiral induction was proved and allowed the first enantioselective synthesis of 1,4-dihydropyridines through [4+2]-cycloaddition;[21] 4) this procedure should find application in the extensive chemistry already reported for achiral alkynyl(alkoxy)carbene complexes of various transition metals;[1c] 5) this methodology might provide access to different achiral and chiral heteroatom-susbstituted carbene complexes of metals and heteroatom substituents other than Group 6 and alkoxy or amino groups.

Experimental Section

General procedure (**8**, **9**, **10**): The appropriate Fischer carbene complex **4**–**6** (1 mmol) was added to a solution of lithium alkoxyacetylide (1.5 mmol) in THF (10 mL) at −80 °C. After stirring for 15 minutes at this temperature, the mixture was transferred with a cannula into a solution of trimethylsilyl triflate (1.6 mmol, 290 μL) in THF (5 mL) at −80 °C. The deep coloured solution was allowed to reach room temperature. Removal of the solvents and chromatographic purification of the residue on silica gel (hexanes) gave the corresponding Fischer carbene complexes **8**–**10**.

12 and **14**: 1-Azadiene **11** (0.122 g, 1.1 mmol) was added to a solution of the complex **8e** (0.484 g, 1 mmol) in THF (20 mL), and the mixture was stirred at room temperature for 16 h. Removal of solvents followed by chromatographic purification on silica gel (10% ethyl acetate in hexanes, $R_f = 0.55$) yielded pure dihydropyridine complex **12** as a sole regio- and diastereoisomer (0.55 g, 70%). Further crystallization from pentane gave crystals suitable for X-ray crystallographic analysis. A solution of cycloadduct **12** (0.4 g, 0.5 mmol) in CH_2Cl_2/H_2O (49:1 v/v; 50 mL) was stirred at room temperature with $[Cu(CH_3CN)_4]BF_4$ (0.15 g,0,5 mmol) for 48 h. The mixture was quenched with water (10 mL) and extracted with dichloromethane (3 × 20 mL). The organic layer was washed with water (2 × 20 mL) and dried over Na_2SO_4. The solvents were removed, and the residue purified by chromatography on silica gel (hexanes/EtOAc/Et_3N 5:1:1; $R_f = 0.45$) to afford the metal-free cycloadduct **14** (79 mg, 65%).

Received: April 22, 2005
Published online: July 11, 2005

Keywords: acetylides · asymmetric synthesis · carbene complexes · cycloaddition · rearrangements

[1] a) E. O. Fischer, A. Maäsbol, *Angew. Chem.* **1964**, *76*, 645; b) F. Z. Dörwal, *Metal Carbenes in Organic Synthesis*, Wiley-VCH, New York, **1999**; c) A. de Meijere, H. Schirmer, M. Duetsch, *Angew. Chem.* **2000**, *112*, 4124; *Angew. Chem. Int. Ed.* **2000**, *39*, 3964.

[2] a) W. D. Wulff, *Organometallics* **1998**, *17*, 3116; b) K. H. Dötz, P. Tomuschat, *Chem. Soc. Rev.* **1999**, *28*, 187.

 © 2005 Wiley-VCH Verlag GmbH & Co. KGaA, Weinheim

[3] For recent papers, see: a) H. Kagoshima, T. Okamura, T. Akiyama, *J. Am. Chem. Soc.* **2001**, *123*, 7182; b) J. Barluenga, S. K. Nandy, Y. R. S. Laxmi, J. R. Suárez, I. Merino, J. Flórez, S. García-Granda, J. Montejo-Bernardo, *Chem. Eur. J.* **2003**, *9*, 5725.

[4] Aldol: a) T. S. Powers, Y. Shi, K. J. Wilson, W. D. Wulff, A. L. Rheingold, *J. Org. Chem.* **1994**, *59*, 6882; for [4+2] cycloaddition, see: b) T. S. Powers, W. Jiang, J. Su, W. D. Wulff, B. E. Waltermire, A. L. Rheingold, *J. Am. Chem. Soc.* **1997**, *119*, 6438; for Michael addition to nitroolefins, see: c) E. Licandro, S. Maiorana, L. Capella, R. Manzotti, A. Papagni, B. Vandoni, A. Albinati, S. H. Chuang, J.-R. Hwu, *Organometallics* **2001**, *20*, 485.

[5] The methoxy-amine exchange reaction has occasionally served in the preparation of amino carbenes **C** (X* = (*S*)-methoxymethylpyrrolidines): A. Rahm, A. L. Rheingold, W. D. Wulff, *Tetrahedron* **2000**, *56*, 4951.

[6] J. Barluenga, A. Ballesteros, R. Bernardo de la Rúa, J. Santamaría, E. Rubio, M. Tomás, *J. Am. Chem. Soc.* **2003**, *125*, 1834.

[7] a) T. Shimizu, D. Miyasaka, N. Kamigata, *Org. Lett.* **2000**, *2*, 1923; b) further chemical characterization of **2** can be undertaken by oxidation with pyridine oxide to 1,3-diphenyl-1-propynone.

[8] A. Padwa, D. J. Austin, Y. Gareau, J. M. Kassir, S. L. Xu, *J. Am. Chem. Soc.* **1993**, *115*, 2637.

[9] C. P. Casey, S. Kraft, D. R. Powell, *J. Am. Chem. Soc.* **2003**, *125*, 2584.

[10] a) C. P. Casey, T. L. Dzwiniel, S. Kraft, I. A. Guzei, *Organometallics* **2003**, *22*, 3915; b) C. P. Casey, T. L. Dzwiniel, *Organometallics* **2003**, *22*, 5285; c) Y. Ortin, A. Sournia-Saquet, N. Lugan, R. Mathieu, *Chem. Commun.* **2003**, 1060.

[11] The formation of diynyl(amino)carbene complexes by copper-catalyzed coupling of pentacarbonyl[ethynyl(amino)carbene]-tungsten(0) with bromoalkynes is known: C. Hartbaum, H. Fischer, *Chem. Ber.* **1997**, *130*, 1063.

[12] a) The pentacarbonyl[phenylethynyl(ethoxy)carbene]molybdenum(0) complex has been used for kinetic studies, but details on its preparation and spectral data are not given: R. Pipoh, R. van Eldik, G. Henkel, *Organometallics* **1993**, *12*, 2236; b) Carbonylcyclopentadienyl [methoxy(4-methylphenyl)ethynylcarbene]nitrosylmolybdenum has been obtained in 12% yield: K. H. Dötz, C. Christoffers, J. Christoffers, D. Böttcher, M. Nieger, S. Kotila, *Chem. Ber.* **1995**, *128*, 645.

[13] The cycloaddition of carbodienes to chiral ethynyl(amino)-carbenes of chromium and tungsten derived from *(S)*-methoxymethyl- and *(S)*-methoxy(dimethyl)methylpyrrolidine occurs with moderate selectivity (d.r. 60:40–86:14).[5]

[14] a) For [4+2] cycloaddition of chiral acetylenic diesters, see: R. N. Buckle, D. J. Burnell, *Tetrahedron* **1999**, *55*, 14829; b) for [2+2] cycloaddition of chiral acetylenic acyl sultam, see: K. Villeneuve, W. Tam, *Angew. Chem.* **2004**, *116*, 620; *Angew. Chem. Int. Ed.* **2004**, *43*, 610.

[15] For leading papers on asymmetric, catalyzed reactions involving alkynes, see: a) E. J. Corey, T. W. Lee, *Tetrahedron Lett.* **1997**, *38*, 5755; b) K. Ishihara, S. Kondo, H. Kurihara, H. Yamamoto, S. Ohashi, S. Inagaki, *J. Org. Chem.* **1997**, *62*, 3026; c) R. Shintani, G. C. Fu, *J. Am. Chem. Soc.* **2003**, *125*, 10778; R. Shintani, G. C. Fu, *Angew. Chem.* **2003**, *115*, 4216; *Angew. Chem. Int. Ed.* **2003**, *42*, 4082.

[16] The model reaction with achiral carbenes was reported: J. Barluenga, M. Tomás, J. A. López-Pelegrín, E. Rubio, *Tetrahedron Lett.* **1997**, *38*, 3981.

[17] CCDC-268919 contains the supplementary crystallographic data for this paper. These data can be obtained free of charge from the Cambridge Crystallographic Data Centre via www.ccdc.cam.ac.uk/data_request/cif.

[18] J. Barluenga, J. M. Monserrat, J. Flórez, S. García-Granda, E. Martín, *Chem. Eur. J.* **1995**, *1*, 236.

[19] A reviewer pointed out that the cyclization of **13** into **12** could be seen, not only as an intramolecular Michael-type addition, but alternatively as an electrocyclization reaction. a) for pseudopericyclic cyclizations of (*Z*)-1,2,4,6-heptatetraene derivatives, see: J. Rodríguez-Otero, E. M. Cabaleiro-Lago, *Chem. Eur. J.* **2003**, *9*, 1837; b) for torquoselectivity in electrocyclic reactions of 1-aza-1,3,5-trienes, see: M. J. Walker, B. N. Hietbrink, B. E. Thomas, IV, K. Nakamura, E. A. Kallel, K. N. Houk, *J. Org. Chem.* **2001**, *66*, 6669; c) for a preliminary communication on torquoselectivity in electrocyclic reactions of (*Z*)-1,2,4,6-heptatetraenes, see: B. N. Hietbrink, C. A. Merlic, K. N. Houk, *Abstract of Papers*, 221st ACS National Meeting, San Diego (CA), **2001**, ORGN-354.

[20] This demetalation procedure will be optimized and the details publish elsewhere.

[21] For efficient access through 1,4-nucleophilic addition of ketene silyl acetals to chiral pyridinium salts, see: S. Yamada, C. Morita, *J. Am. Chem. Soc.* **2002**, *124*, 8184.

 © 2005 Wiley-VCH Verlag GmbH & Co. KGaA, Weinheim

Cover Picture

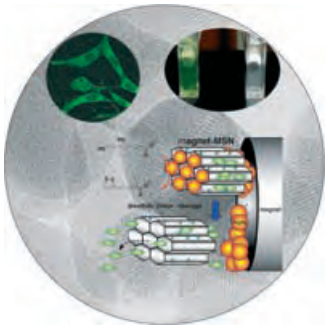


Haikuo Li, Jiehuan Huang, Junhong Lv, Hongjie An, Xiaodong Zhang, Zhizhou Zhang,* Chunhai Fan,* and Jun Hu*

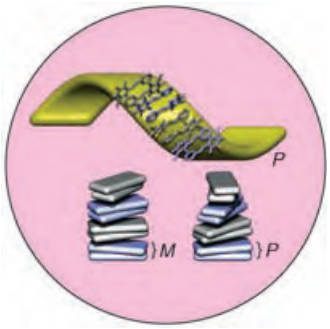
Favorable binding of gold nanoparticles to single-stranded DNA decreases the likelihood of mispair formation during annealing and clearly increases the specificity and yield of PCR, one of the most important standard methods of molecular biology. In their Communication on pp. 5100 ff., Z. Zhang, C. Fan, J. Hu, and co-workers report on this promising field of biotechnology. (Xiaobin Wang assisted in the production of this image.)



Cationic Boron Compounds
The possible synthetic uses of boronium, borenium, and borinium ions are increasing rapidly. W. E. Piers et al. explore the chemistry of these reactive electrophiles in their Review on page 5016 ff.



Drug-Delivery Systems
In their Communication on pp. 5038 ff., V. S.-Y. Lin et al. introduce a model system for the site-specific delivery of drugs. For this purpose, mesoporous MCM-41-type silica nanorods (MSNs) covered with superparamagnetic iron oxide nanoparticles were used.



Self-Assembly
Helical bis(merocyanin)dye nanorods organize themselves through an inversion of the exciton chirality as well as through structural changes that occur in the transition from kinetic to thermodynamic self-assembly. For more information, see the Communication by F. Würthner et al. on pp. 5071 ff.

Contents

VIP *The following Communications have been judged by at least two referees to be "very important papers" and will be published online at www.angewandte.org soon:*

A. C. Filippou, G. Schnakenburg, A. I. Philippopoulos, N. Weidemann*
Bonding Analysis of the M≡Ge–Ge≡M Chain in the Germylidyne Complexes *trans,trans*-[Cl(depe)$_2$M≡Ge–Ge≡M(depe)$_2$Cl]

*M. Veith**
Cubane-Type Li_4H_4 and $Li_3H_3Li(OH)$: Stabilized in Molecular Adducts with Alane

S. Protti, M. Fagnoni, A. Albini**
Photochemical Cross-Coupling Reactions of Electron-Rich Aryl Chlorides and Aryl Esters with Alkynes: A Metal-Free Alkynylation

*V. Lavallo, Y. Canac, C. Präsang, B. Donnadieu, G. Bertrand**
Stable Cyclic (Alkyl)(amino)carbenes as Rigid or Flexible, Bulky, Electron-Rich Ligands for Transition-Metal Catalysts

H. Braunschweig, K. Radacki, D. Rais, D. Scheschkewitz*
A T-Shaped Platinum(II) Boryl Complex as the Precursor to a Base-Stabilized Borylene of Platinum

S. Aime, D. D. Castelli, E. Terreno*
Highly Sensitive MRI-CEST Agents using Liposomes (LIPOCEST)

News

F. D. Toste Receives Pfizer Award — **5004**

A. Zumbusch Receives Sommerfeld Prize and Goes to London — **5004**

Several Awards for A. Müller — **5004**

Books

Modern Cyclophane Chemistry — Rolf Gleiter, Henning Hopf — *reviewed by U. H. Bunz* — **5005**

Strategic Applications of Named Reactions in Organic Synthesis — Laszlo Kürti, Barbara Czako — *reviewed by S. R. Waldvogel* — **5005**

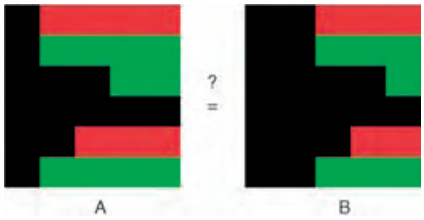
Highlights

Drug Research

T. Berg* — **5008 – 5011**

Cellular Profiling of Small-Molecule Bioactivities: an Alternative Tool for Chemical Biology

Are they a good match? Target identification is critical to the success of chemical genetics projects that start with phenotypic screens. The method highlighted herein is a novel way to decrease the number of potential biological targets of compounds identified in phenotypic screens by comparison of their cellular activity profiles with those obtained with reference compounds. Activity profiles for hypothetical compounds A and B are shown.

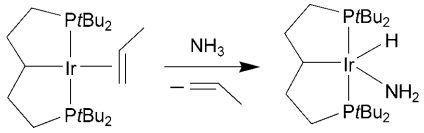


Ammonia Activation

T. Braun* — **5012 – 5014**

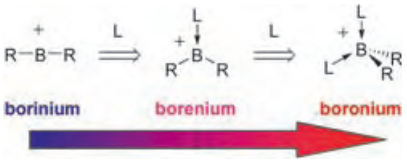
Oxidative Addition of NH_3 to a Transition-Metal Complex: A Key Step for the Metal-Mediated Derivatization of Ammonia?

Bond cleavage with model character? The oxidative addition of ammonia to a transition-metal complex to yield a terminal amido complex was achieved for the first time recently (see scheme). This model reaction might provide new pathways to use ammonia as a feedstock in catalytic reactions.



InterScience
© 2005 Wiley-VCH Verlag GmbH & Co. KGaA, Weinheim

Reviews



Any old ion? The title boron cations (see scheme) are elusive and have largely been regarded as chemical curiosities. However, as potent electrophiles the enormous potential of these species is beginning to be recognized. Advances in mass spectrometry have made a systematic investigation of the gas-phase chemistry of these ions possible and have facilitated predictions of practical relevance to their reactivity in the condensed phase.

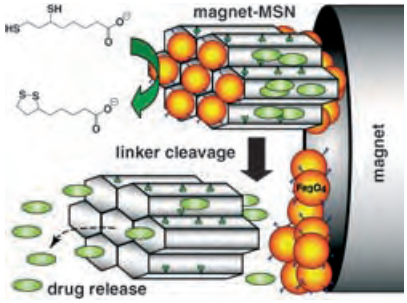
Cationic Boron Compounds

W. E. Piers,* S. C. Bourke, K. D. Conroy ——— **5016 – 5036**

Borinium, Borenium, and Boronium Ions: Synthesis, Reactivity, and Applications

Communications

Stand and deliver! The release of pore-encapsulated fluorescein molecules from a core/shell mesoporous silica nanorod/superparamagnetic iron oxide nanoparticle carrier in the presence of an external magnetic field and only in response to cell-produced antioxidants indicates promise for such systems in controlled-release drug delivery.

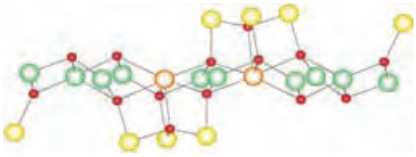


Nanodevices

S. Giri, B. G. Trewyn, M. P. Stellmaker, V. S.-Y. Lin* ——— **5038 – 5044**

Stimuli-Responsive Controlled-Release Delivery System Based on Mesoporous Silica Nanorods Capped with Magnetic Nanoparticles

In a spin: The mixed-valent $\{Mn^{III}_{20-x}Mn^{II}_{x}\}$ cage complexes ($x = 2$–6) have structures corresponding to a fragment of a cubic close-packed lattice (see picture, Mn large sphere, O small sphere). Magnetic studies show for the cage with $x = 2$ that the ground state has a spin (S) of 19 ± 1 in low field, which increases to about $S = 30$ at higher fields. The cage is a "single molecule magnet" with a high energy barrier (43 K) to reorientation of the magnetization.

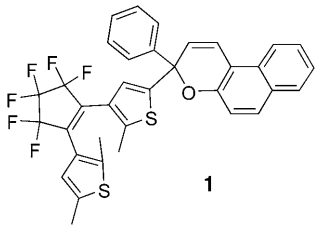


Molecular Magnets

S. Maheswaran, G. Chastanet, S. J. Teat, T. Mallah, R. Sessoli,* W. Wernsdorfer, R. E. P. Winpenny* ——— **5044 – 5048**

Phosphonate Ligands Stabilize Mixed-Valent $\{Mn^{III}_{20-x}Mn^{II}_{x}\}$ Clusters with Large Spin and Coercivity

Affairs of state: Investigation of the photochromic properties of a combined naphthopyran and diarylethene biphotochromic system (**1**) has revealed that four different states with entirely different absorption behaviors are formed. Opening of the naphthopyran ring leads to conjugation and electronic connection of both photochromes, while closure of the open diarylethene system extends the π-electron system over the whole molecule.



1

Photochemistry

M. Frigoli, G. H. Mehl* ——— **5048 – 5052**

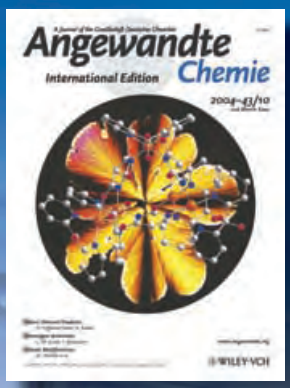
Multiple Addressing in a Hybrid Biphotochromic System

For the USA and Canada:
ANGEWANDTE CHEMIE International Edition (ISSN 1433-7851) is published weekly by Wiley-VCH PO Box 191161, D 69451 Weinheim, Germany. Air freight and mailing in the USA by Publications Expediting Inc. 200 Meacham Ave., Elmont, NY 11003. Periodicals postage paid at Jamaica NY 11431. US POSTMASTER: send address changes to *Angewandte Chemie*, Wiley-VCH, 111 River Street, Hoboken, NJ 07030. Annual subscription price for institutions: US$ 4948.00/4498.00 (valid for print and electronic / print or electronic delivery); for individuals who are personal members of a national chemical society, or whose institution already subscribes, or who are retired or self-employed consultants, print only: US$ 394.00. Postage and handling charges included. All Wiley-VCH prices are exclusive VAT.

© 2005 Wiley-VCH Verlag GmbH & Co. KGaA, Weinheim

The best in chemistry –

for more than a hundred years



A Journal of the Gesellschaft Deutscher Chemiker

Angewandte International Edition **Chemie**

www.angewandte.org

1888: ***The beginning of a success story***

Constant Innovations

1962: *First issue of the International Edition*
1976: *Graphical abstracts*
1979: *Cover pictures*
1988: *Centenary of Angewandte*
1989: *Routine use of color*
1991: *New section: Highlights*
1992: *Computerized editorial tracking system*
1995: *Internet service for readers*
1998: *Regular press service; full-text online*
2000: *New section: Essays; EarlyView: Communications available online ahead of the printed version*
2001: *New section: Minireviews*
2002: *Online submission of manuscripts*
2003: *Weekly publication; new section: News; new layout*
2004: *Backfiles (1962-1997); ManuscriptXpress: Online system for authors and referees*



Angewandte's advisors...

Richard N. Zare
Stanford University

» *Size does matter, as well as shape, motion, composition, and chemical complexity. I read* ***Angewandte Chemie*** *each week to learn about the latest, most exciting developments in the world of chemistry.* «

Angewandte Chemie International Edition *is a journal of the German Chemical Society (GDCh)*

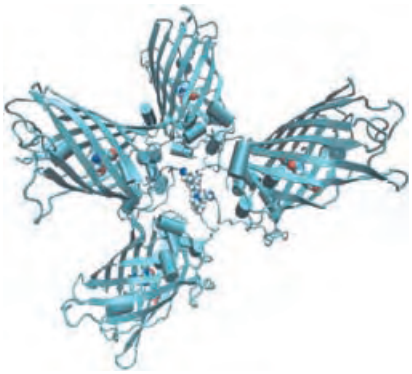
GDCh

WILEY InterScience® DISCOVER SOMETHING GREAT

WILEY-VCH

11921404_gu

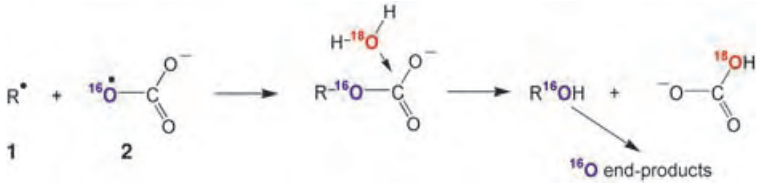
A wide variety of well-defined multivalent peptides and proteins can be made by conjugating synthetic peptides and recombinantly expressed proteins to cysteine-functionalized dendrimers using native chemical ligation (see picture). This modular approach provides access to dendrimers that are attractive both for understanding fundamental issues of multivalency in biological interactions as well as for biomedical applications.



Bioorganic Chemistry

I. van Baal, H. Malda, S. A. Synowsky, J. L. J. van Dongen, T. M. Hackeng, M. Merkx,* E. W. Meijer* — **5052 – 5057**

Multivalent Peptide and Protein Dendrimers Using Native Chemical Ligation

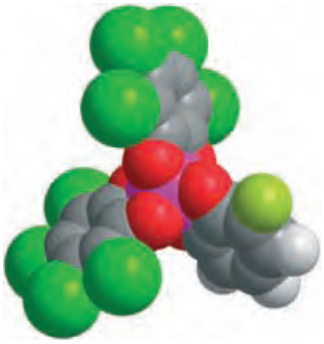


Under oxidative stress: The oxidation of guanine and 8-oxo-7,8-dihydroguanine has been monitored by ^{18}O-labeling methods. The combination of nucleobase radicals **1** with the carbonate radical anion **2** results in the net transfer of O^- from $CO_3^{\bullet-}$ to the end products (see scheme).

Guanine Oxidation

C. Crean, N. E. Geacintov, V. Shafirovich* — **5057 – 5060**

Oxidation of Guanine and 8-oxo-7,8-Dihydroguanine by Carbonate Radical Anions: Insight from Oxygen-18 Labeling Experiments

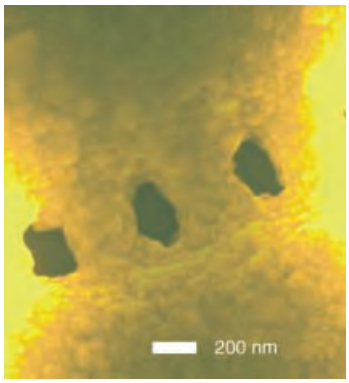


Placing fluorine atoms at selected positions allows enantiopure hexacoordinate phosphate anions to behave as effective chiral solvating and resolving agents for Ru^{II} complexes (the structure of one of the anions is shown: F: yellow; O: red; Cl: green; P: purple). The structural features of the asymmetric ion pairing can be determined by NMR spectroscopy owing to the presence of the fluorine atoms.

Chiral Resolution

R. Frantz, A. Pinto, S. Constant, G. Bernardinelli, J. Lacour* **5060 – 5064**

Fluorinated TRISPHAT Anions: Spectroscopic Probes for Detailed Asymmetric Ion Pairing Studies



Biological templates: Diatom cell walls were coated with metallic films and then subsequently dissolved to yield nanostructured metallic microshells that exhibit the structural characteristics of the diatom templates. The unique nanostructural details of the microshells (see image) make them useful as substrates for surface-enhanced Raman scattering.

Nanostructure Synthesis

E. K. Payne, N. L. Rosi, C. Xue, C. A. Mirkin* — **5064 – 5067**

Sacrificial Biological Templates for the Formation of Nanostructured Metallic Microshells

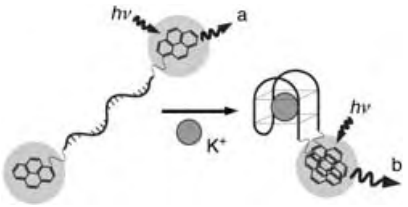
© 2005 Wiley-VCH Verlag GmbH & Co. KGaA, Weinheim

Contents

Fluorescent Probes

S. Nagatoishi, T. Nojima, B. Juskowiak, S. Takenaka* ——— **5067 – 5070**

A Pyrene-Labeled G-Quadruplex Oligonucleotide as a Fluorescent Probe for Potassium Ion Detection in Biological Applications

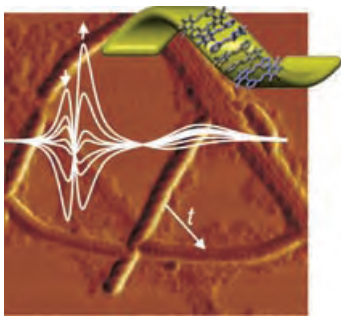


Ion probes: A potassium-sensing oligonucleotide with terminal pyrene moieties can be used as a fluorescent probe for the real-time monitoring of the extracellular concentration of K^+ ions under physiological conditions. The excimer emission intensity (b) of the chair-type quadruplex structure formed depends on the K^+ ion concentration (0–200 mM), and differs significantly from that in the absence of potassium (a).

Self-Assembled Nanostructures

A. Lohr, M. Lysetska, F. Würthner* ——— **5071 – 5074**

Supramolecular Stereomutation in Kinetic and Thermodynamic Self-Assembly of Helical Merocyanine Dye Nanorods



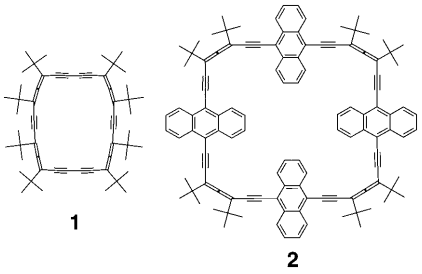
An inversion of the exciton chirality and structural changes upon transformation from kinetic to thermodynamic assembly are features of helical bis(merocyanine) dye nanorods (see picture), as elucidated by time-dependent circular dichroism (CD) spectroscopy and atomic force microscopy.

Macrocycles

S. Odermatt, J. L. Alonso-Gómez, P. Seiler, M. M. Cid,* F. Diederich* ——— **5074 – 5078**

Shape-Persistent Chiral Alleno-Acetylenic Macrocycles and Cyclophanes by Acetylenic Scaffolding with 1,3-Diethynylallenes

Rings on her fingers: The chiral alleno-acetylenic macrocycle **1** and the related cyclophane **2** with intriguing three-dimensional shapes were prepared and isolated in diastereoisomerically pure form. The symmetries and structures of these novel unsaturated hydrocarbons were elucidated by ^{1}H NMR spectroscopy and X-ray crystallography. The isolated stereoisomeric cyclophanes undergo photoisomerization; presumably the anthracene moieties serve as intramolecular sensitizers.

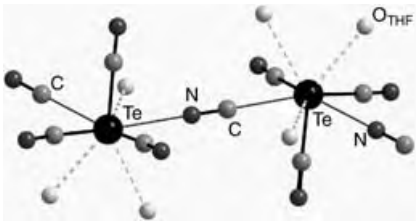


1 **2**

Pseudopolymorphism

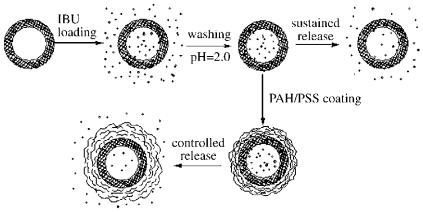
D. Lentz,* M. Szwak ——— **5079 – 5082**

Synthesis and Structure Determination of Tellurium Tetracyanide Solvates: Pseudopolymorphism of $Te(CN)_4$ and TeF_4



The pseudopolymorphic solvates $[\{Te(CN)_4(CH_3CN)_2\}_n]$ and $[\{Te(CN)_4(thf)_3\}_n]$ form coordination polymers in the solid state in which $Te(CN)_3$ units are connected by CN groups in *cis* position to form infinite chains. The picture shows a section of $[\{Te(CN)_4(thf)_3\}_n]$. In contrast, the tellurium tetrafluoride solvate $[TeF_4(thf)_2]$ contains monomeric ψ-trigonal-bipyramidal TeF_4 units.

© 2005 Wiley-VCH Verlag GmbH & Co. KGaA, Weinheim



Keeping drugs under control: Hydrothermally stable, hollow mesoporous silica spheres have a high drug storage capacity, and polyelectrolyte multilayers coated on the spheres act as a switch for drug release which is controlled by the pH or ionic strength of the release medium. The picture shows the release of ibuprofen (IBU) from spheres with and without coatings of sodium polystyrene sulfonate (PSS) and poly(allylamine hydrochloride) (PAH).

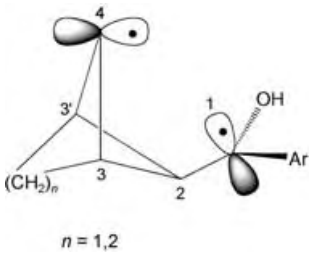
Drug Delivery

Y. Zhu, J. Shi,* W. Shen, X. Dong, J. Feng, M. Ruan, Y. Li ——— **5083 – 5087**

Stimuli-Responsive Controlled Drug Release from a Hollow Mesoporous Silica Sphere/Polyelectrolyte Multilayer Core–Shell Structure

---

Radical reform: Cleavage of the enantiotopic C2–C3 or C2–C3′ bonds in bicyclic 1-hydroxy-1,4-biradicals (see structure) leads to enantiomeric products. Absolute configuration correlations demonstrate that, in the crystalline state, cleavage occurs mainly in one direction and is controlled by the orientation of the cleaving bonds with respect to the p orbital at the C1 position.



$n = 1,2$

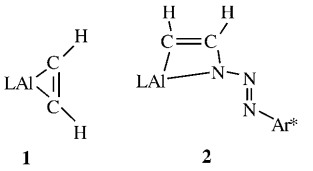
Biradicals

C. Yang, W. Xia, J. R. Scheffer,* M. Botoshansky, M. Kaftory **5087 – 5089**

Orbital-Overlap Control of the Reactivity of a Bicyclic 1-Hydroxy-1,4-Biradical

---

Not all down-to-Earth: A stable aluminacyclopropene LAl(η^2-C_2H_2) **1** was isolated from the reaction of LAl with C_2H_2. Further reaction of **1** with C_2H_2 results in terminal C≡CH and CH=CH_2 groups at the Al center. The end-on insertion of an azide into one Al–C bond in **1** leads to the first aluminaazacyclobutene **2**. These reactions can be considered prebiotic, as Al^I species and acetylene are found in outer space.



1 **2**

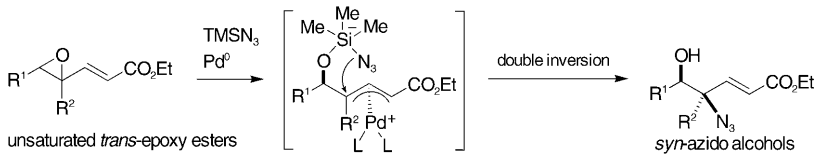
L = $HC[(CMe)(NAr)]_2$, Ar = 2,6-*i*$Pr_2C_6H_3$
Ar* = 2,6-$Ar'_2C_6H_3$, Ar' = 2,4,6-$Me_3C_6H_2$

Metallacycles

H. Zhu, J. Chai, H. Fan, H. W. Roesky,* C. He, V. Jancik, H.-G. Schmidt, M. Noltemeyer, W. A. Merrill, P. P. Power ——— **5090 – 5093**

A Stable Aluminacyclopropene LAl(η^2-C_2H_2) and Its End-On Azide Insertion to an Aluminaazacyclobutene

---



Acyclic, cyclic, and optically active unsaturated γ,δ-epoxy esters are employed in a highly stereoselective synthesis of functionalized amino alcohols, amino acids, and α,α-disubstituted amino acids. The key step of the reaction sequence is a double inversion of configuration (see scheme).

Synthetic Methods

M. Miyashita,* T. Mizutani, G. Tadano, Y. Iwata, M. Miyazawa, K. Tanino ——— **5094 – 5097**

Pd-Catalyzed Stereospecific Azide Substitution of α,β-Unsaturated γ,δ-Epoxy Esters with Double Inversion of Configuration

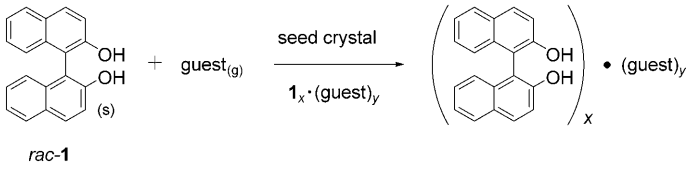
© 2005 Wiley-VCH Verlag GmbH & Co. KGaA, Weinheim

Contents

Host–Guest Chemistry

K. Yoshizawa, S. Toyota, F. Toda,*
S. Chatziefthimiou, P. Giastas,
I. M. Mavridis, M. Kato ____ **5097 – 5100**

Control of Differential Inclusion Complexation in the Solid State by Seed Crystals



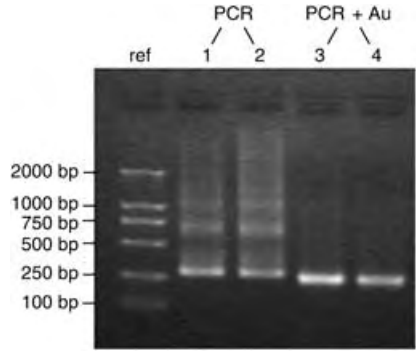
Sowing the seeds: Complexation of *rac*-**1** in the solid state with a guest such as Et_2O in the gas phase proceeds in the presence of a seed crystal of the inclusion complex (see scheme). For example, passing Et_2O over a mixture of **1** and a seed of **1**·$(Et_2O)_3$ gives rise to exclusive formation of the 1:3 complex.

Nanobiotechnology

H. Li, J. Huang, J. Lv, H. An, X. Zhang,
Z. Zhang,* C. Fan,* J. Hu* **5100 – 5103**

Nanoparticle PCR: Nanogold-Assisted PCR with Enhanced Specificity

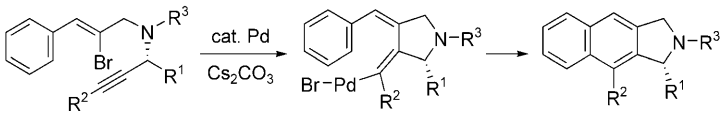
Nanogold may not glitter, but its presence significantly improves the specificity and yield of PCR reactions owing to the greater affinity of gold nanoparticles to single-stranded DNA than to double-stranded DNA which helps to reduce mispairing. Indeed, gel electrophoresis shows a single predominant band for the target DNA obtained by this method, in contrast to streaking bands for products obtained by conventional PCR (lanes 1 and 2; see image).



Synthetic Methods

H. Ohno,* M. Yamamoto, M. Iuchi,
T. Tanaka* ____ **5103 – 5106**

Palladium-Catalyzed Tandem Cyclization of Bromoenynes through Aromatic C–H Bond Functionalization



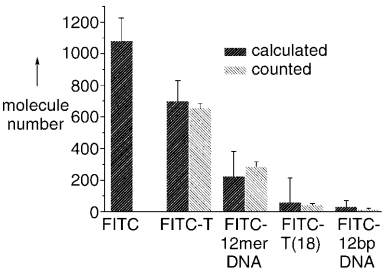
The direct approach: Tandem cyclization of 1-aryl-4-aza-2-bromo-1-alken-6-ynes with catalytic $Pd(OAc)_2$ and cesium carbonate in EtOH led to direct construction of tri- or tetracyclic heterocycles, through intramolecular carbopalladation and aromatic C–H bond functionalization (see scheme). This route in which two C–C bonds are formed enables the construction of complex heterocyclic skeletons directly from readily prepared enynes.

Fluorescence Imaging

H. Gai, Q. Wang, Y. Ma,*
B. Lin* ____ **5107 – 5110**

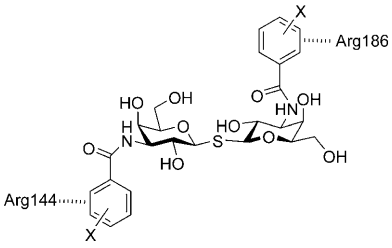
Correlations between Molecular Numbers and Molecular Masses in an Evanescent Field and Their Applications in Probing Molecular Interactions

Complex numbers: The number of molecules detected in the evanescent field during single-molecule fluorescence imaging decreases with increasing molecular weight in free solution (see graphic; FITC = fluorescein isothiocyanate). This technique could be useful for screening undefined molecular interactions at extremely low concentrations without separation.



© 2005 Wiley-VCH Verlag GmbH & Co. KGaA, Weinheim

Inhibitors of galectin-3, which has been implicated in cancer- and immunity-related processes, can be synthesized from thiodigalactoside derivatives with aromatic amide substituents at both C3 positions (see structure). Dissociation constant (K_d) values as low as 33 nM have been obtained. Computer modeling suggests that such high affinity stems from double arginine–arene stacking interactions.

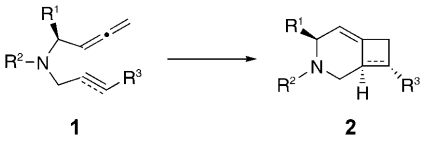


Lectin Inhibitors

I. Cumpstey, A. Sundin, H. Leffler, U. J. Nilsson* ——— 5110 – 5112

C_2-Symmetrical Thiodigalactoside Bis-Benzamido Derivatives as High-Affinity Inhibitors of Galectin-3: Efficient Lectin Inhibition through Double Arginine–Arene Interactions

Squaring the circle: A route to bicyclo[4.2.0]octane derivatives has been developed by the [2+2] cycloaddition of allenenes or allenynes. The thermal intramolecular [2+2] cycloaddition of simple allenes **1** with an additional multiple bond leads to direct and regioselective formation of the distal adducts **2** in good to excellent yields.



Synthetic Methods

H. Ohno,* T. Mizutani, Y. Kadoh, K. Miyamura, T. Tanaka* — 5113 – 5115

Thermal Intramolecular [2+2] Cycloaddition of Allenenes and Allenynes: Diastereoselective Access to Bicyclic Nitrogen Heterocycles

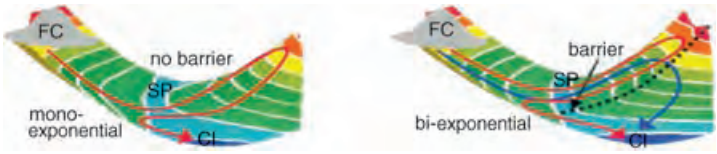


Wet and dry: Titanium dioxide nanorod films with micro- and nanoscale hierarchical surface structures have been successfully prepared (left). The nanorod films, which show superhydrophobicity (middle), reversibly become superhydrophilic (right) when exposed to UV light. The mechanism involves the cooperation of the special surface structures, the orientation of crystal planes, and the surface photosensitivity.

Materials Science

X. Feng, J. Zhai, L. Jiang* — 5115 – 5118

The Fabrication and Switchable Superhydrophobicity of TiO_2 Nanorod Films



Excitement over something small: The protonated Schiff base of retinal photoisomerizes on an excited-state hypersurface (S_1) that connects the Franck–Condon (FC) point via a flat valley centered on a planar structure (SP) to a conical intersection (CI; see picture). Wave-packet (gray hat) quantum dynamics shows that the depletion of the S_1 population switches from mono- to biexponential when a small ridge (dotted line) between SP and CI is present.

Computer Chemistry

M. Olivucci, A. Lami, F. Santoro* ——— 5118 – 5121

A Tiny Excited-State Barrier Can Induce a Multiexponential Decay of the Retinal Chromophore: A Quantum Dynamics Investigation

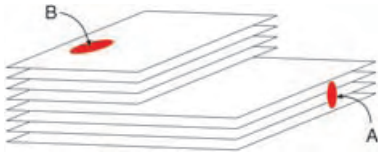
© 2005 Wiley-VCH Verlag GmbH & Co. KGaA, Weinheim

Contents

Surface Electrochemistry

T. J. Davies, M. E. Hyde, R. G. Compton* ——— 5121 – 5126

Nanotrench Arrays Reveal Insight into Graphite Electrochemistry

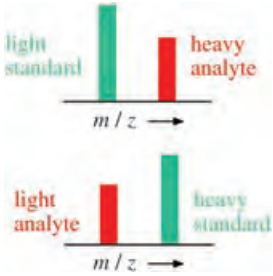


Watch your step! Decoupling the individual contributions of edge-plane steps (A) and basal-plane terraces (B) to the voltammetry of graphite electrodes can provide information of fundamental importance. This was done by selectively blocking the basal-plane terraces with insulating material to form nanotrench arrays of edge-plane graphite.

Food Chemistry

S. Sforza,* C. Dall'Asta, A. Moseriti, G. Galaverna, A. Dossena, R. Marchelli ——— 5126 – 5130

Alternate Isotope-Coded Derivatization Assay: An Isotope Dilution Method Applied to the Quantification of Zearalenone in Maize Flour



Low-cost isotope dilution made easy: An alternate reaction of an analyte in a matrix and in a standard solution with isotope-labeled or unlabeled derivatizing reagents allows quantification of zearalenone in maize flour without the need for a calibration curve. This is possible by direct calculation of the relative response factor for the analyte/internal standard ratio of the sample (see picture).

Cycloaddition

S. Carret, A. Blanc, Y. Coquerel, M. Berthod, A. E. Greene, J.-P. Deprés* ——— 5130 – 5133

Approach to the Blues: A Highly Flexible Route to the Azulenes

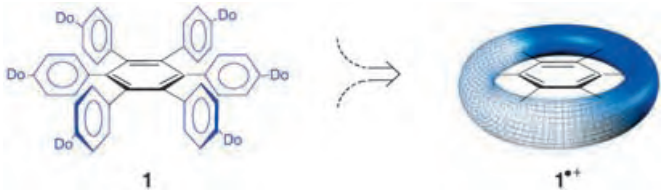


A palette of blues: Chlorobicyclo-[5.3.0]decatrienones are readily prepared from cycloheptatrienes by cycloaddition of dichloroketene, ring expansion with a diazoalkane, and dehydrochlorination in dimethylformamide. These compounds are used as intermediates in the regiocontrolled synthesis of a wide variety of natural and nonnatural azulenes (see scheme).

Conjugation

D. Sun, S. V. Rosokha, J. K. Kochi* ——— 5133 – 5136

Through-Space (Cofacial) π-Delocalization among Multiple Aromatic Centers: Toroidal Conjugation in Hexaphenylbenzene-like Radical Cations



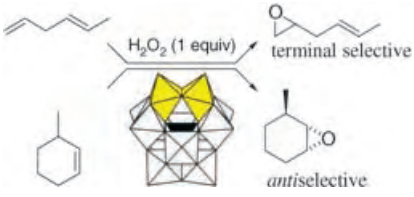
Pi and doughnuts: Highly effective through-space conjugation among cofacial (aromatic) redox centers is established in stable hexaanilinylbenzene radical cations (**1**$^{\bullet+}$; π conjugation shown by toroid). The radical cations show unusual intervalence absorption bands and are quantitatively analyzed by Mulliken–Hush formulation.

Catalytic Epoxidation

Y. Nakagawa, K. Kamata, M. Kotani, K. Yamaguchi, N. Mizuno* 5136 – 5141

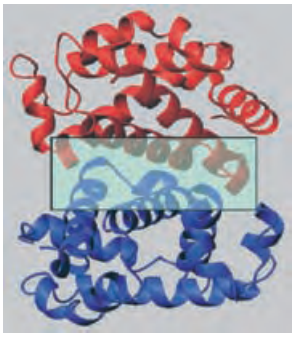
Polyoxovanadometalate-Catalyzed Selective Epoxidation of Alkenes with Hydrogen Peroxide

The bis(μ-hydroxo)-bridged dioxovanadium site in [γ-1,2-$H_2SiV_2W_{10}O_{40}$]$^{4-}$ catalyzes the epoxidation of alkenes in the presence of only one equivalent of H_2O_2 with a high yield of epoxide, high efficiency of H_2O_2 utilization, unusual regioselectivity, and unprecedented diastereoselectivity (see picture).



© 2005 Wiley-VCH Verlag GmbH & Co. KGaA, Weinheim

Making contact: A protein–protein interface (see structure) can be identified unambiguously from the dependence of amide-proton relaxation on proton density, as demonstrated by the identification of subunit contacts in hemoglobin. The information on upper limits for effective distances thus obtained allows the protein complex structure to be modeled more accurately with docking techniques.



Protein–Protein Interactions

X. G. Sui, Y. Q. Xu, J. L. Giovannelli, N. T. Ho, C. Ho, D. W. Yang* ——— **5141 – 5144**

Mapping Protein–Protein Interfaces on the Basis of Proton Density Difference

Looking for outstanding employees?

Do you need another expert for your excellent team?
... Chemists, PhD Students, Managers, Professors, Sales Representatives...

Place an advert in the printed version and have it made available online for 1 month, free of charge!

Angewandte Chemie International Edition
Advertising Sales Department: Marion Schulz
Phone: 0 62 01 - 60 65 65
Fax: 0 62 01 - 60 65 50
E-Mail: MSchulz@wiley-vch.de

Service

Keywords ——— *5146*

Authors ——— *5147*

Vacancies ——— *A45*

Preview ——— *5149*



© 2005 Wiley-VCH Verlag GmbH & Co. KGaA, Weinheim



Awarded...

F. D. Toste Receives Pfizer Award

F. Dean Toste (University of California, Berkeley) is the recipient of the 2005 Pfizer Award for Creativity in Organic Chemistry. Toste was awarded for his contributions to the development of catalysts and catalytic methods for organic synthesis, particularly gold(I)-catalyzed propargyl Claisen rearrangements, Conia-ene reactions, 1,5-enyne isomerizations and 5-*endo-dig* cyclizations of acetylenic β-keto esters.[1] The goal of his work is to facilitate the synthesis of complex molecules with interesting structural, biological, and physical properties. Toste's research group is also involved in the development of new methods for the addition of water and alcohols to enones, providing an alternative access to aldol adducts.



F. D. Toste

Toste studied at the University of Toronto and received his PhD for work with B. M. Trost at Stanford University in 2000. He carried out his postdoctoral research in the group of R. H. Grubbs at the California Institute of Technology (Pasadena) between 2001 and 2002. Since that time, he has been an assistant professor at the University of California in Berkeley.

A. Zumbusch Receives Sommerfeld Prize and Goes to London

Andreas Zumbusch (University College London) received the Arnhold Sommerfeld Prize of the Bavarian Academy of Sciences for his contributions to biophysical chemistry. He was awarded for the development of coherent anti-Stokes Raman scattering (CARS) microscopy, which permits the examination of living cells in high three-dimensional resolution without the need for staining. Moreover, he was honored for his contributions to single-molecule spectroscopy, for example, in the use of green fluorescent protein as a biological probe. His research group recently reported in *ChemPhysChem* on the vibronic excitation of single molecules as a new technique for the study of low-temperature dynamics.[2]

Zumbusch studied Chemistry in Munich and Bordeaux. He received his PhD in 1996 under the direction of H. Schnöckel at the University of Karlsruhe (Germany). From 1997 to 1998 he worked as a postdoc in the research group of X. S. Xie at the Pacific Northwest National Laboratory in Richland, Washington. Starting in 1999, he led a research group in the chemistry department at the University of Munich (C. Bräuchle), where he was promoted to professor for his work in high-sensitivity optical microscopy and its application in biophysics. Since February of 2005 he has been working as a Reader at University College London.



A. Zumbusch

Several Awards for A. Müller

Achim Müller (University of Bielefeld, Germany), whose large metal clusters continue to gather attention, received three additional distinctions. The Université Pierre et Marie Curie (Paris) awarded him an honorary doctorate. The title was conferred during a colloquium about the frontiers of inorganic chemistry, at which Müller discussed perspectives in nanotechnology, including porous capsules, artificial cells, sphere surfaces, and "super-supramolecular" chemistry. Furthermore, he was accorded with the Premio Elhuyar Goldschmidt of the Real Sociedad Española de Química (RSEQ, Spanish Chemical Society), and he also delivered this year's annual Lewis Lecture at the University of Cambridge. He recently reported on uniquely linked triangular motifs and their magnetic properties at the surfaces of spherical capsules composed of molybdenum and vanadium or iron in *Angewandte Chemie*.[3]



A. Müller

Müller received his PhD in 1965 from the University of Göttingen (Germany) under the direction of O. Glemser in work on thermochemistry and completed a habilitation there in the field of vibrational spectroscopy. In 1971, he accepted a professorship at the University of Dortmund (Germany), and has been working at the University of Bielefeld since 1977. His research involves the chemistry of transition metals, particularly inorganic supramolecular chemistry and bioinorganic chemistry in synthesis, spectroscopy, and theory. "The Chemistry of Nanomaterials", edited by A. Müller, C. N. R. Rao, and A. K. Cheetham, and published by Wiley-VCH appeared at the beginning of 2004.

[1] S. T. Staben, J. J. Kennedy-Smith, F. D. Toste, *Angew. Chem.* **2004**, *116*, 5464; *Angew. Chem. Int. Ed.* **2004**, *43*, 5350.

[2] A. Kiraz, M. Ehrl, C. Hellriegel, C. Bräuchle, A. Zumbusch, *ChemPhysChem* **2005**, *6*, 919.

[3] A. Müller, A. M. Todea, J. van Slageren, M. Dressel, H. Bögge, M. Schmidtmann, M. Luban, L. Engelhardt, M. Rusu, *Angew. Chem.* **2005**, *117*, 3925; *Angew. Chem. Int. Ed.* **2005**, *44*, 3857.

DOI: 10.1002/anie.200502385

InterScience
© 2005 Wiley-VCH Verlag GmbH & Co. KGaA, Weinheim

Drug Research

DOI: 10.1002/anie.200500721

Cellular Profiling of Small-Molecule Bioactivities: an Alternative Tool for Chemical Biology**

*Thorsten Berg**

Keywords:
fluorescent probes · inhibitors · phenotypic screening · proteins · signal transduction

One of the main goals of chemical biology is to identify cell-permeable organic molecules that interfere with protein function to provide the scientific community with novel research tools for the investigation of biological questions.[1] There are currently two major approaches for the primary screening of chemical libraries to identify such bioactive organic molecules. In the first approach, inhibitors or activators of purified proteins or reconstituted, narrowly defined signaling pathways are sought in vitro. In the second approach, cells or organisms are treated with small molecules; those compounds which cause a desired phenotype are selected. The success of research projects that begin with such a phenotypic screen is dependent on the subsequent identification of the molecular target(s) of the identified compounds that elicit the phenotype, as a meaningful analysis of the biological profiles of the hit compound can only be performed when the cellular target is known. Most of the current methods used to pinpoint the molecular target(s) of compounds identified in phenotypic screens can be classified into two subgroups: 1) affinity-based biochemical methods based on small-molecule binding to target proteins and the subsequent identification of the protein bound and 2) genetic approaches that monitor cellular changes in response to treatment with the compound. As discussed at the end of this Highlight, neither approach is generally applicable; alternative approaches aimed at the identification of molecular targets of bioactive compounds from phenotypic screens would therefore be highly welcome.

The research groups of Altschuler, Wu, and Mitchison recently reported a method which can be used to profile the effects of interfering agents on cells by the analysis of multiple parameters related to the expression, post-translational modification, and localization of preselected proteins.[2] This approach registers the biological effects of a compound with an unknown mode of action on a defined set of biological markers and then compares them with the effects observed with a set of reference compounds with known activities.[3] If the biological effects of a compound with unknown target(s) resemble one of more of the biological profiles of the reference compounds, a potential mechanism of action for the new inhibitor can be proposed. This could provide valuable information for decreasing the number of potential targets for subsequent investigation.

To demonstrate the principle of this method, cells grown in microtiter plates were treated with 100 different chemical substances at a range of concentrations. 90 of the 100 compounds had a known mechanism of action, and thereby served as references for the classification of the remaining 10 test compounds. Six of these 10 were simply blinded references, three had an unknown biological mechanism, and one compound was known to have multiple effects. Treated cells were then stained with fluorescently labeled antibodies raised against a small number of proteins involved in a range of cell signaling pathways. In this way, a very broad overview of the effects of compounds on the cells was obtained. The wells were photographed with an automated microscope, and special software was employed to convert the large amount of data obtained into interpretable information. Changes in various parameters related to the fluorescence of the antibodies in response to various compound concentrations were analyzed; these changes were subsequently expressed as color codes, as shown in the example case of the topoisomerase inhibitor camptothecin (Figure 1a).

For a meaningful comparison of the biological effects of two compounds, it is necessary to depict the compound profiles in a manner that is independent of the absolute concentration at which an effect is initially observed. Otherwise, two compounds with identical biological mechanisms yet different potencies would be erroneously regarded as having different biological effects, as the observation of any effect would occur at different concentration thresholds. Therefore, the authors devised a method to analyze the similarity of the compound effects in a concentration-independent manner and used this information for the unsupervised clustering of the compounds depicted in Figure 1b. The names of the compounds and their mode of action as described in the

[*] Dr. T. Berg
Max Planck Institute of Biochemistry
Department of Molecular Biology
Am Klopferspitz 18, 82152 Martinsried (Germany)
Fax: (+49) 89-8578-2454
E-mail: berg@biochem.mpg.de

[**] I extend my thanks to Professor Dr. Axel Ullrich for his support of my research. I also thank Angela Hollis for critical reading of the manuscript.

Supporting information for this article (complete citations) is available on the WWW under http://www.angewandte.org or from the author.

InterScience
© 2005 Wiley-VCH Verlag GmbH & Co. KGaA, Weinheim

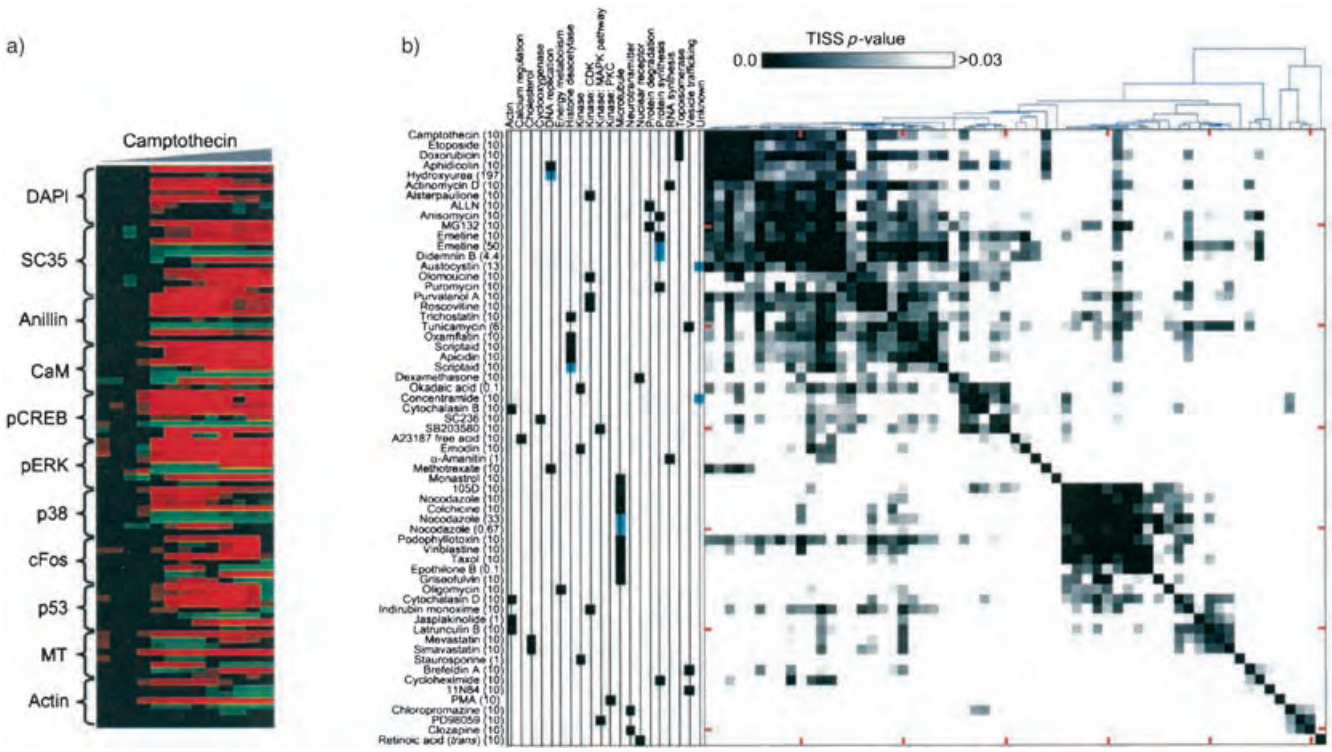


Figure 1. a) Cellular responses to different concentrations of the topoisomerase inhibitor camptothecin. The response of each parameter to a given concentration of the drug is expressed as a colored rectangle. The vertical axis depicts 93 biological parameters. b) Clustering analysis of drug effects; excerpted from Ref. [2] (Copyright 2004, AAAS).

literature are given in the left, and on the right, the similarities between compound pairs are given: high similarities are indicated by dark squares; lower degrees of similarity are represented with lighter squares. (The list of compounds as given on the left side of Figure 1b is omitted from top of the right part of the figure.) Naturally, the biological profiles of each compound match perfectly in self-comparison, which explains the diagonal line of black squares.

Successful clustering analysis lists compounds with similar modes of action adjacent to each other, as observed by adjacent black squares in the left part of Figure 1b, and leads to an accumulation of dark squares around the diagonal line in the right portion. Good clustering is indeed observed for histone deacetylase inhibitors, topoisomerase inhibitors, and microtubule poisons. However, for other compound classes such as protein synthesis inhibitors, clustering was not ideal.

Another criterion for success was to determine if the 10 test compounds mentioned above could be properly classified. Five of the six blinded alternate titrations of known drugs showed usable activity profiles and clustered well with their unmasked counterparts, or at least with drugs of similar mechanism, as indicated by the blue squares in the left part of Figure 1b. The single compound with many cellular functions clustered correctly with others known to have one of its functions.[4] Of the three remaining compounds with uncharacterized mechanisms, only one could be grouped with a certain inhibitor class (it would have been helpful to see the independent experimental data supporting the correct classification of the compound).

Whereas the success rate of the current study is not optimal, it is the principle of the approach which deserves credit. About 60 of the 100 compounds showed a meaningful response in the experiment, and it is possible that the other 40 compounds either acted on proteins or pathways not represented by the relatively small set of antibodies used in this study, or that their biological targets were not expressed in the chosen cell line. A larger set of reference compounds would also improve the chances of pinpointing the biological functions of novel compounds identified in phenotypic screens. Therefore, the power of this method is likely to be improved with the use of larger sets of antibodies and reference compounds, and by extending the experiments to additional cell lines. The antibodies and reference compounds could be adapted to the specific needs of the researcher. A distinctly positive aspect of the method is that it permits the analysis of compound concentrations at which various cellular parameters change. Such information could be useful for the identification of an optimal dose below the threshold of undesirable (toxic) effects. One severe limitation of the approach, however, is that the hardware and software necessary for these experiments are not currently in place at most academic settings; acquisition of these resources may require an industrial-level budget. The expansion of the set of reference compounds, anti-

© 2005 Wiley-VCH Verlag GmbH & Co. KGaA, Weinheim

body probes, and cell lines might require even more investment in screening infrastructure and computing power.

The cellular targets of most chemical genetic screens have been identified through biochemical affinity-based techniques.[5–8] Such approaches require the attachment of a tag that facilitates immobilization of the bioactive molecule. The resulting hybrid molecule is then attached to a solid support by the tag and then incubated with cell lysates. Proteins successfully immobilized through specific interactions with the compound are subsequently analyzed by protein microsequencing, MS-based methods, or immunoblotting. Examples of successful applications of this approach include the discovery of the molecular targets of the natural product FK506[9] and of several kinase inhibitors.[10–13] One general concern is that compound-binding proteins identified by this method may not be the physiologically relevant binding partners in vivo. In this respect, irreversible inhibitors with reactive functional groups are advantageous, in that intact cells, instead of cell lysates, can be treated with the tagged inhibitor. Therefore, it can be assumed that only the physiologically relevant proteins will bind to the inhibitor. Examples of the successful discovery of cellular targets of irreversible inhibitors include the natural products fumagillin,[14] parthenolide,[15] epoxomicin,[16] and lactacystin.[17]

In a variation of the approach referred to as "photoaffinity labeling", a reversible inhibitor is tagged with a photolabile group, which inserts itself into chemical bonds in close proximity upon irradiation, thereby forming covalent bonds with its protein-binding partners.[18,19] Despite the success of affinity-based purification approaches, they suffer from the following limitations: 1) the approach requires a tight interaction between the small molecule and its protein target, 2) the protein target must be abundant in the cell, and 3) the addition of a tag without significant loss of biological activity requires precise knowledge of structure–activity relationships, and there is no guarantee that a tagged inhibitor with sufficient biological potency can be identified and synthesized. Several modified approaches have been suggested to overcome these hurdles, for example: 1) the alignment of proteins on solid supports (protein arrays)[20] or their display on the surface of phages[21] to artificially increase the local concentration of potential target proteins, 2) the yeast three-hybrid system,[22] and 3) the screening of small-molecule libraries pre-equipped with a linker that allows rapid immobilization without the need for structural modification of the inhibitor.[23] Future research will assess the power of these modified approaches.

Most genetic approaches for target identification have been developed in yeast, and make use of the availability of complete sets of viable homozygous and heterozygous gene-deletion mutants. The most obvious approach is to compare the effect of an interfering agent on the gene expression profile of a wild-type yeast strain with that of yeast strains in which single genes have been deleted.[24–27] Another experimental approach exploits the phenomenon that heterozygous deletion mutants (yeast strains in which only one of the two alleles of the respective gene is deleted) are more susceptible to inhibition by compounds which act on the gene product encoded by the remaining undeleted gene.[28–30] Genetic approaches with yeast as a model system may be an interesting alternative for cases in which the affinity purification approach cannot be applied; perhaps the main drawback is that a homologue of the gene product targeted in human cells (30000–40000 genes) may not be present in yeast ($\approx$6000 genes).

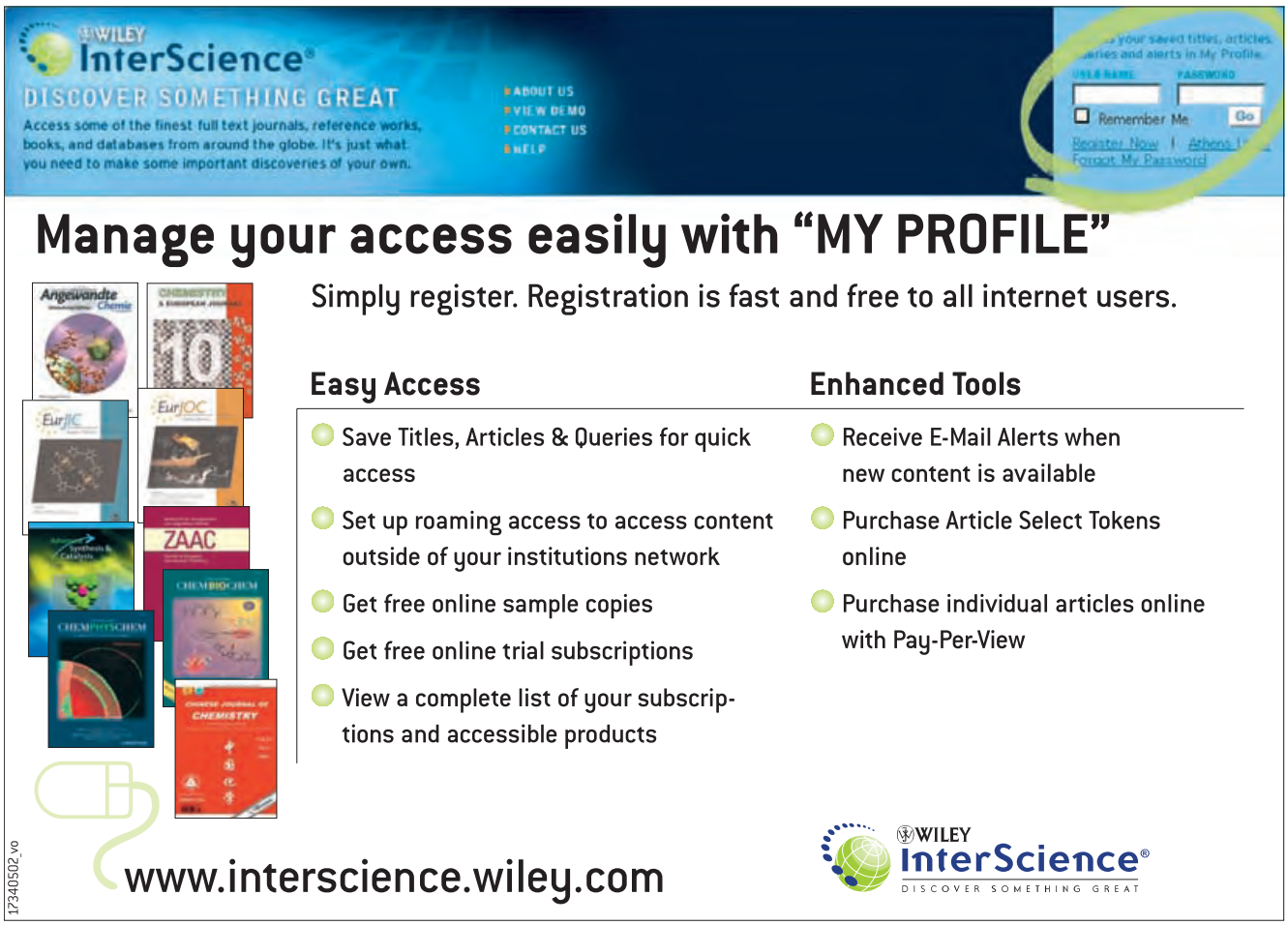
The cellular profiling of small-molecule bioactivities highlighted herein represents a significant advantage over most methods in current use, as it does not require a tag and is not restricted to yeast. However, it appears unlikely that this method will permit the definition of the target of an interfering agent down to a single protein, as the information provided is of a more general nature. Therefore, this novel method may represent a useful supplement to the toolbox of chemical geneticists in cases in which 1) the affinity purification approach fails, 2) the aim is to decrease the mode of action of a compound to a pathway or a group of proteins, or 3) cellular systems other than yeast are necessary. It will be interesting to witness the results obtained with this method in its future applications.

Published online: June 23, 2005

[1] T. U. Mayer, *Trends Cell Biol.* **2003**, *13*, 270–277.
[2] Z. E. Perlman, M. D. Slack, Y. Feng, T. J. Mitchison, L. F. Wu, S. J. Altschuler, *Science* **2004**, *306*, 1194–1198.
[3] T. J. Mitchison, *ChemBioChem* **2005**, *6*, 33–39.
[4] M. D. Vera, M. M. Joullie, *Med. Res. Rev.* **2002**, *22*, 102–145.
[5] L. Burdine, T. Kodadek, *Chem. Biol.* **2004**, *11*, 593–597.
[6] S. Wang, T. B. Sim, Y.-S. Kim, Y.-T. Chang, *Curr. Opin. Chem. Biol.* **2004**, *8*, 371–377.
[7] G. P. Tochtrop, R. W. King, *Comb. Chem. High Throughput Screening* **2004**, *7*, 677–688.
[8] S. Ding, T. Y. H. Wu, A. Brinker, E. C. Peters, W. Hur, N. S. Gray, P. G. Schultz, *Proc. Natl. Acad. Sci. USA* **2003**, *100*, 7632–7637.
[9] M. W. Harding, A. Galat, D. E. Uehling, S. L. Schreiber, *Nature* **1989**, *341*, 758–760.
[10] C. Kung, K. M. Shokat, *ChemBioChem* **2005**, *6*, 523–526.
[11] K. Godl et al., *Proc. Natl. Acad. Sci. USA* **2003**, *100*, 15434–15439.
[12] G. R. Rosania, J. Merlie, Jr., N. Gray, Y.-T. Chang, P. G. Schultz, R. Heald, *Proc. Natl. Acad. Sci. USA* **1999**, *96*, 4797–4802.
[13] M. Knockaert, P. Lenormand, N. Gray, P. Schultz, J. Pouysségur, L. Meijer, *Oncogene* **2002**, *21*, 6413–6424.
[14] N. Sin, L. Meng, M. Q. W. Wang, J. J. Wen, W. G. Bornmann, C. M. Crews, *Proc. Natl. Acad. Sci. USA* **1997**, *94*, 6099–6103.
[15] B. H. B. Kwok, B. Koh, M. I. Ndubuisi, M. Elofsson, C. M. Crews, *Chem. Biol.* **2001**, *8*, 759–766.
[16] L. Meng, R. Mohan, B. H. B. Kwok, M. Elofsson, N. Sin, C. M. Crews, *Proc. Natl. Acad. Sci. USA* **1999**, *96*, 10403–10408.
[17] G. Fenteany, R. F. Standaert, W. S. Lane, S. Choi, E. J. Corey, S. L. Schreiber, *Science* **1995**, *268*, 726–731.
[18] J. R. Colca, G. G. Harrigan, *Comb. Chem. High Throughput Screening* **2004**, *7*, 699–704.
[19] G. Dormán, G. D. Prestwich, *Trends Biotechnol.* **2000**, *18*, 64–77.
[20] J. Huang, H. Zhu, S. J. Haggarty, D. R. Spring, H. Hwang, F. Jin, M. Snyder, S. L. Schreiber, *Proc. Natl. Acad. Sci. USA* **2004**, *101*, 16594–16599.
[21] P. P. Sche, K. M. McKenzie, J. D. White, D. J. Austin, *Chem. Biol.* **1999**, *6*, 707–716.

 © 2005 Wiley-VCH Verlag GmbH & Co. KGaA, Weinheim

[22] E. J. Licitra, J. O. Liu, *Proc. Natl. Acad. Sci. USA* **1996**, *93*, 12817–12821.
[23] S. M. Khersonsky et al., *J. Am. Chem. Soc.* **2003**, *125*, 11804–11805.
[24] M. J. Marton et al. , *Nat. Med.* **1998**, *4*, 1293–1301.
[25] T. R. Hughes et al., *Cell* **2000**, *102*, 109–126.
[26] T.-F. Chan, J. Carvalho, L. Riles, X. F. S. Zheng, *Proc. Natl. Acad. Sci. USA* **2000**, *97*, 13227–13232.
[27] A. B. Parsons et al., *Nat. Biotechnol.* **2004**, *22*, 62–69.
[28] P. Y. Lum et al., *Cell* **2004**, *116*, 121–137.
[29] K. Baetz et al., *Proc. Natl. Acad. Sci. USA* **2004**, *101*, 4525–4530.
[30] G. Giaever et al., *Proc. Natl. Acad. Sci. USA* **2004**, *101*, 793–798.



 © 2005 Wiley-VCH Verlag GmbH & Co. KGaA, Weinheim

Ammonia Activation

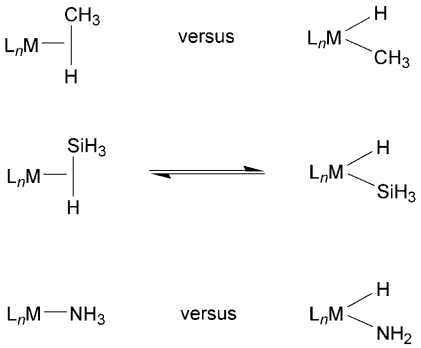
DOI: 10.1002/anie.200501505

Oxidative Addition of NH_3 to a Transition-Metal Complex: A Key Step for the Metal-Mediated Derivatization of Ammonia?

*Thomas Braun**

Keywords:
N–H activation · amido complexes · hydroamination · iridium · oxidative addition

The oxidative addition of element–hydrogen bonds, which have been considered to be "unreactive" at transition-metal centers, has been a long-standing challenge.[1] One major focus of the investigations has been the C–H activation of alkanes by insertion of a transition-metal center into the carbon–hydrogen bond.[2] Matrix isolation techniques, laser flash photolysis, isotope labeling techniques, and NMR spectroscopic studies provide considerable evidence that an alkane σ complex is formed prior to the oxidative addition of the C–H bond.[2–4] In principle, several coordination modes for an alkane are conceivable, but an η^2-C,H interaction is thought to precede the oxidative addition step (Scheme 1).[1–3] Low-temperature IR spectroscopy in liquid xenon or krypton provides evidence for complexes with an alkane coordinated to a $\{(\eta^5\text{-}C_5Me_5)Rh(CO)\}$ moiety, which subsequently undergoes C–H bond cleavage.[5] The coordination of methane—as the simplest alkane—*and* its C–H activation reaction have not been observed to date, although the oxidative addition of methane is well known.[1–4] For SiH_4 a tautomeric equilibrium between an η^2-Si,H silane species and the oxidative addition product has been detected in solution by NMR spectroscopy (Scheme 1).[6]



Scheme 1. Coordination and activation of CH_4, SiH_4, and NH_3; an equilibrium has been observed for SiH_4 only.[6]

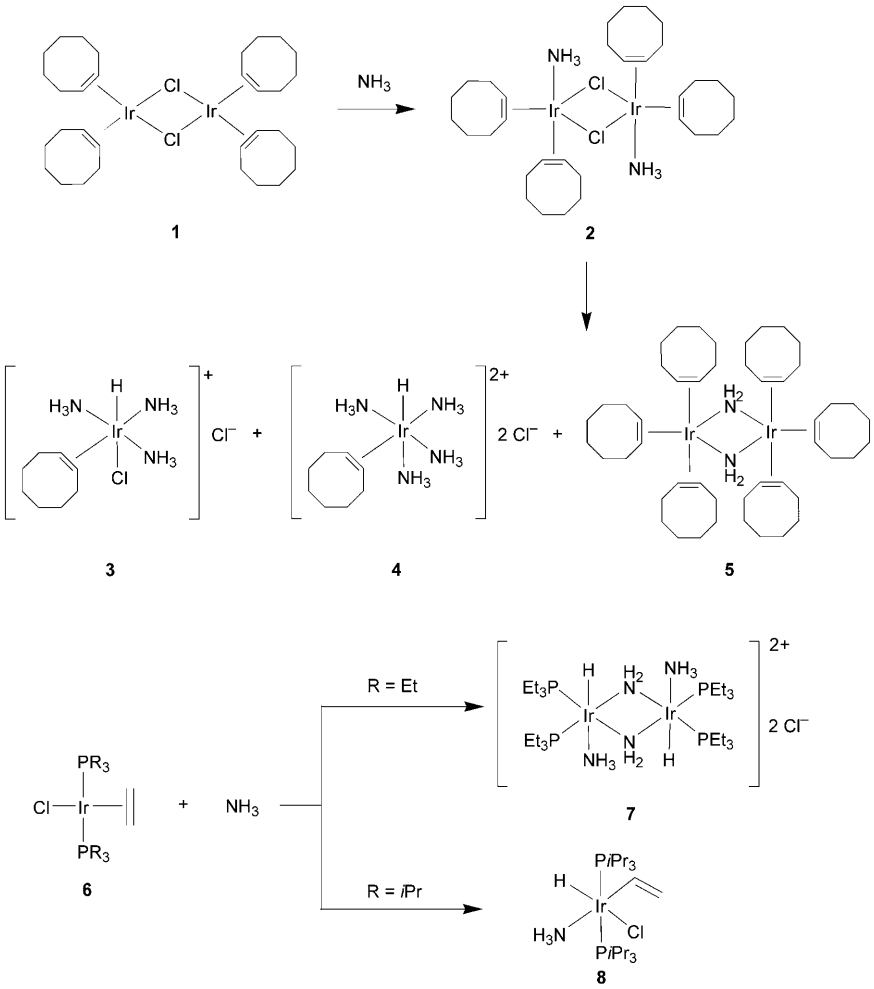
In contrast, reactions of ammonia with transition-metal complexes usually generate simple Lewis acid–base adducts, although there is some precedent for the activation of ammonia by transition-metal complexes.[7] It is known that aromatic amines are reactive towards N–H bond cleavage by oxidative addition,[8] but very little has been reported on the oxidative addition reaction of an N–H bond in ammonia itself (Scheme 1).[9,10] Early work reveals that such a reaction is feasible at cluster compounds.[9] Binuclear oxidative additions to give μ-amido complexes have also been demonstrated.[10] Milstein and Koelliker described the stepwise coordination and activation of ammonia at the iridium complex **1**.[10c] The ammonia complex **2** was obtained as the initial product, which then reacts further at room temperature to give **3**, **4**, and the amido compound **5** (Scheme 2). In another example ammonia was activated by binuclear oxidative addition at the ethylene iridium complex **6** to give the hydrido compound **7**, which also exhibits bridging amido ligands (Scheme 2).[10a,b] Interestingly, if $PiPr_3$ is used instead of PEt_3, C–H activation of the olefin yields complex **8**.

Another significant development in this field was made recently by Zhao, Goldman, and Hartwig, who reported on the insertion of an iridium center in one of the N–H bonds of NH_3 to give the mononuclear iridium hydrido amido complex **10**.[11] The iridium complex **9a** bearing a tridentate pincer ligand reacts at room temperature with NH_3 to generate the oxidative addition product **10** (Scheme 3). Complex **10** can also be prepared independently by an alternative route on treatment of the chloro complex **11** with NH_3 followed by deprotonation with $K[N(SiMe_3)_2]$ (Scheme 3). The oxidative addition of 3,5-dimethylaniline to **9a** or **9b** to yield the amido compound **12** is thermodynamically less favored than the reaction with ammonia. This has been shown by the determination of equilibrium constants for **9b**⇄**10** and **9b**⇄**12** (Scheme 3). The iridium complex **13** bearing an aromatic pincer ligand shows a different reactivity: the oxidative addition of aniline to **13** gives **14**, whereas in the reaction of **13** with ammonia no insertion into the N–H bond occurs;[8d] instead, the ammonia complex **15** is formed.

Mechanistic investigations on the formation of **10** from **9b** have been performed.[11] Isotope labeling studies using $[D_3]$ammonia showed no incorporation of deuterium into the pincer ligand. This suggests that no C–H acti-

[*] Priv.-Doz. Dr. T. Braun
Fakultät für Chemie
Universität Bielefeld
Postfach 100131, 33501 Bielefeld
(Germany)
Fax: (+49) 521-106-6026
E-mail: thomas.braun@uni-bielefeld.de

InterScience
© 2005 Wiley-VCH Verlag GmbH & Co. KGaA, Weinheim



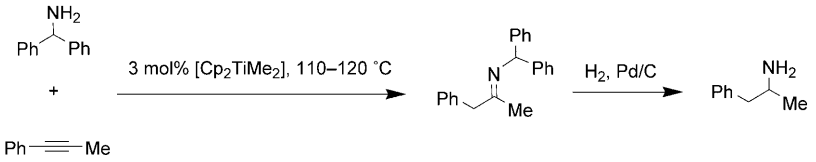
Scheme 2. Oxidative addition of ammonia at transition-metal complexes.

vation of the pincer ligand occurs prior to the oxidative addition of ammonia.[11] In addition, kinetic studies reveal that the activation proceeds by a dissociative reaction pathway, in which ammonia reacts with a 14-electron complex generated after dissociation of the olefin in **9b**.

Considering the importance of oxidative addition reactions of H–H, Si–H, C–H, or B–H bonds in various catalytic processes,[1,3,12] comparable N–H bond cleavage reactions of amines or ammonia at transition-metal centers can be regarded as model reactions for the development of new catalytic reaction cycles. To date, only a few catalytic conversions are known that proceed by the insertion of a late transition metal into an N–H bond, such as some homogeneously catalyzed hydroaminations.[12a,13–15] In an early report Milstein et al. described the iridium-catalyzed hydroamination of norbornene with aniline;[8a] model reactions provide strong evidence for an oxidative N–H addition pathway. Togni and co-workers investigated the same reaction with various iridium complexes bearing chiral diphosphane ligands as catalysts and a source for "naked fluoride" as cocatalyst.[14] Other recently developed transformations include the rhodium-catalyzed oxidative amination of vinylarenes

Scheme 3. Coordination and activation of ammonia and aniline derivatives by iridium complexes with pincer ligands.

 © 2005 Wiley-VCH Verlag GmbH & Co. KGaA, Weinheim



Scheme 4. Dimethyltitanocene-catalyzed hydroamination of alkynes using aminodiphenylmethane as ammonia equivalent.

and their hydroamination with unusual anti-Markovnikow selectivity as well as the palladium-catalyzed oxidative amination of alkenes.[15] The activation of amines by oxidative N–H addition followed by the insertion of an olefin into the metal–nitrogen bond are considered to be key steps in these conversions.

It has been shown that aminodiphenylmethane can serve as an ammonia equivalent in the dimethyltitanocene-catalyzed intermolecular hydroamination of alkynes to give primary amines after hydrogenation of an intermediate imine (Scheme 4).[16] The homogeneously catalyzed hydroamination of olefins with ammonia has so far remained elusive.[7g,12a,13a] The studies by Zhao, Goldman, and Hartwig on the insertion of a transition-metal center into an N–H bond of NH_3 to give a mononuclear amido hydrido complex might provide a new pathway to use ammonia itself as a feedstock in catalytic reactions. This discovery is therefore an important step forward for the development of new N–C coupling reactions based on the oxidative addition of an N–H bond in ammonia.

Published online: July 12, 2005

[1] a) "Activation of Unreactive Bonds and Organic Synthesis": S. Murai, *Top. Organomet. Chem.* **1999**, 3; b) C. Elschenbroich, *Organometallchemie*, Teubner, Wiesbaden, **2003**, p. 276–292.

[2] a) W. D. Jones, *Top. Organomet. Chem.* **1999**, *3*, 9–46; b) W. D. Jones, F. J. Feher, *Acc. Chem. Res.* **1989**, *22*, 91–100; c) J. A. Labinger, J. E. Bercaw, *Nature* **2002**, *417*, 507–510; d) R. H. Crabtree, *J. Chem. Soc. Dalton Trans.* **2001**, 2437–2450; e) A. E. Shilov, G. B. Shul'pin, *Chem. Rev.* **1997**, *97*, 2879–2932; f) R. H. Crabtree, *J. Organomet. Chem.* **2004**, *689*, 4083–4091.

[3] C. Hall, R. N. Perutz, *Chem. Rev.* **1996**, *96*, 3125–3146.

[4] a) W. D. Jones, *Acc. Chem. Res.* **2003**, *36*, 140–146; b) M. W. Holtcamp, J. A. Labinger, J. E. Bercaw, *J. Am. Chem. Soc.* **1997**, *119*, 848–849.

[5] a) B. H. Weiler, E. P. Wasserman, R. G. Bergman, C. B. Moore, G. C. Pimentel, *J. Am. Chem. Soc.* **1989**, *111*, 8288–8290; b) A. A. Bengali, R. H. Schultz, C. B. Moore, R. G. Bergman, *J. Am. Chem. Soc.* **1994**, *116*, 9585–9589; c) R. H. Schultz, A. A. Bengali, M. J. Tauber, B. H. Weiler, E. P. Wasserman, K. R. Kyle, C. B. Moore, R. G. Bergman, *J. Am. Chem. Soc.* **1994**, *116*, 7369–7377.

[6] X.-L. Luo, G. J. Kubas, C. J. Burns, J. C. Bryan, C. J. Unkefer, *J. Am. Chem. Soc.* **1995**, *117*, 1159–1160.

[7] a) M. M. B. Holl, P. T. Wolczanski, G. D. Van Duyne, *J. Am. Chem. Soc.* **1990**, *112*, 7989–7994; b) J. E. Bercaw, D. L. Davies, P. T. Wolczanski, *Organometallics* **1986**, *5*, 443–450; c) H. W. Roesky, Y. Bai, M. Noltemeyer, *Angew. Chem.* **1989**, *101*, 788–789; *Angew. Chem. Int. Ed. Engl.* **1989**, *28*, 754–755; d) J. N. Armor, *Inorg. Chem.* **1978**, *17*, 203–213; e) G. L. Hillhouse, J. E. Bercaw, *J. Am. Chem. Soc.* **1984** *106*, 5472–5478; f) D. Connor, K. N. Jayaprakash, T. R. Cundari, T. B. Gunnoe, *Organometallics* **2004**, *23*, 2724–2733; g) D. M. Roundhill, *Chem. Rev.* **1992**, *92*, 1–27; h) M. V. Ovchinnikov, E. LeBlanc, I. A. Gutzei, R. J. Anglici, *J. Am. Chem. Soc.* **2001**, *123*, 11494–11495.

[8] a) A. L. Casalnuovo, J. C. Calabrese, D. Milstein, *J. Am. Chem. Soc.* **1988**, *110*, 6738–6744; b) J. Fornies, M. Green, J. L. Spencer, F. G. A. Stone, *J. Chem. Soc. Dalton Trans.* **1977**, 1006–1009; c) S. Park, D. Hedden, D. M. Roundhill, *Organometallics* **1986**, *5*, 2151–2152; d) M. Kanzelberger, X. Zhang, T. J. Emge, A. S. Goldman, J. Zhao, C. Incarvito, J. F. Hartwig, *J. Am. Chem. Soc.* **2003**, *125*, 13644–13645.

[9] a) G. Süß-Fink, *Z. Naturforsch. B.* **1980**, *35*, 454–457; b) E. G. Bryan, B. F. G. Johnson, J. Lewis, *J. Chem. Soc. Dalton Trans.* **1977**, 1328–1330.

[10] a) A. L. Casalnuovo, J. C. Calabrese, D. Milstein, *Inorg. Chem.* **1987**, *26*, 971–973; b) M. Schulz, D. Milstein, *J. Chem. Soc. Chem. Commun.* **1993**, 318–319; c) R. Koelliker, D. Milstein, *Angew. Chem.* **1991**, *103*, 724–726; *Angew. Chem. Int. Ed. Engl.* **1991**, *30*, 707–709.

[11] J. Zhao, A. S. Goldman, J. F. Hartwig, *Science* **2005**, *307*, 1080–1082.

[12] a) *Catalytic Heterofunctionalization from Hydroamination to Hydrozirconation* (Eds.: A. Togni, H. Grützmacher), Wiley-VCH, Weinheim, **2001**; b) S. S. Stahl, J. A. Labinger, J. E. Bercaw, *Angew. Chem.* **1998**, *110*, 2298–2311; *Angew. Chem. Int. Ed.* **1998**, *37*, 2180–2192; c) H. Chen, S. Schlecht, T. C. Semple, J. F. Hartwig, *Science* **2000**, *287*, 1995–1997; d) W. D. Jones, *Science* **2000**, *287*, 1942–1943; e) S. Shimada, A. S. Batsanov, J. A. K. Howard, T. B. Marder, *Angew. Chem.* **2001**, *113*, 2226–2229; *Angew. Chem. Int. Ed.* **2001**, *40*, 2168–2171.

[13] Recent reviews on hydroaminations: a) C. Hultzsch, *Adv. Synth. Catal.* **2005**, *347*, 367–391; b) P. W. Roesky, T. E. Müller, *Angew. Chem.* **2003**, *115*, 2812–2814; *Angew. Chem. Int. Ed.* **2003**, *42*, 2708–2710; c) J. Seayad, A. Tillack, G. C. Hartung, M. Beller, *Adv. Synth. Catal.* **2002**, *344*, 795–813; d) I. Bytschkov, S. Doye, *Eur. J. Org. Chem.* **2003**, 935–946; e) F. Pohlki, S. Doye, *Chem. Soc. Rev.* **2003**, *32*, 104–114; f) S. Doye, *Synlett* **2004**, 1653–1672.

[14] a) R. Dorta, P. Egli, F. Zürcher, A. Togni, *J. Am. Chem. Soc.* **1997**, *119*, 10857–10858; b) D. Vasen, A. Salzer, F. Gerhards, H.-J. Gais, R. Stürmer, N. H. Bieler, A. Togni, *Organometallics* **2000**, *19*, 539–546.

[15] a) M. Utsunomiya, R. Kuwano, M. Kawatsura, J. F. Hartwig, *J. Am. Chem. Soc.* **2003**, *125*, 5608–5609; b) M. Beller, H. Trauthwein, M. Eichberger, C. Breindl, J. Herwig, T. E. Müller, O. R. Thiel, *Chem. Eur. J.* **1999**, *5*, 1306–1318; c) M. Beller, M. Eichberger, H. Trauthwein, *Angew. Chem.* **1997**, *109*, 2306–2308; *Angew. Chem. Int. Ed. Engl.* **1997**, *36*, 2225–2227; d) M. Beller, H. Trauthwein, M. Eichberger, C. Breindl, T. E. Müller, *Eur. J. Inorg. Chem.* **1999**, 1121–1132; e) J. L. Brice, J. E. Harang, V. I. Timokhin, N. R. Anastasi, S. S. Stahl, *J. Am. Chem. Soc.* **2005**, *127*, 2868–2869.

[16] E. Haak, H. Siebeneicher, S. Doye, *Org. Lett.* **2000**, *2*, 1935–1937.

 © 2005 Wiley-VCH Verlag GmbH & Co. KGaA, Weinheim

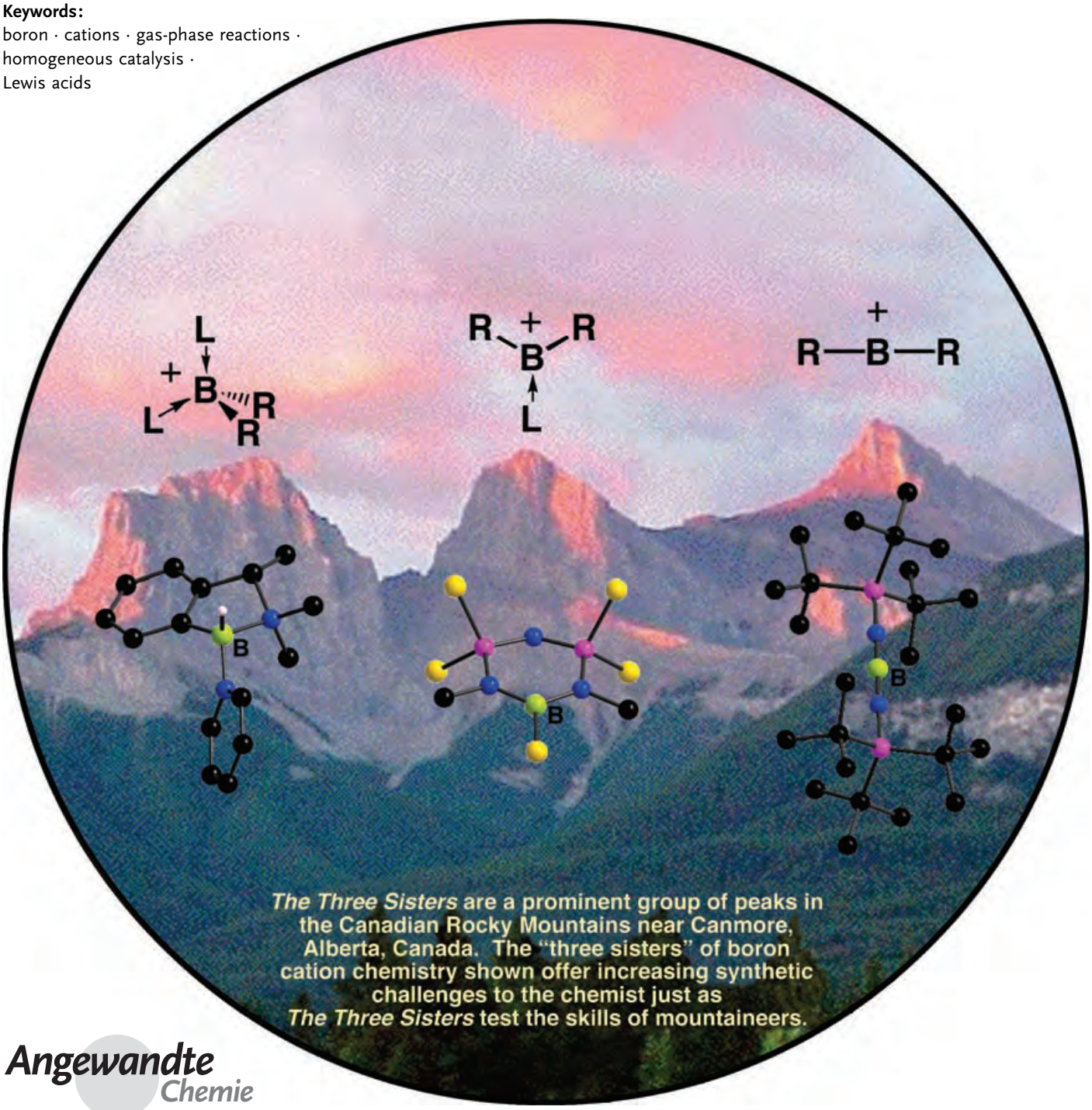
DOI: 10.1002/anie.200500402

Cationic Boron Compounds

Borinium, Borenium, and Boronium Ions: Synthesis, Reactivity, and Applications

Warren E. Piers, Sara C. Bourke, and Korey D. Conroy*

Keywords:
boron · cations · gas-phase reactions · homogeneous catalysis · Lewis acids



The Three Sisters are a prominent group of peaks in the Canadian Rocky Mountains near Canmore, Alberta, Canada. The "three sisters" of boron cation chemistry shown offer increasing synthetic challenges to the chemist just as *The Three Sisters* test the skills of mountaineers.

© 2005 Wiley-VCH Verlag GmbH & Co. KGaA, Weinheim

Boron cations are elusive and highly electrophilic species that play a key role in the chemistry of boron. Despite early interest in the chemistry of boron cations, until recently they have largely remained chemical curiosities. However, hints at harnessing their potential as potent electrophiles have begun to appear and developments in weakly coordinating anion technology suggest that this is an area of research that is ripe for exploration. It has been nearly 20 years since the last major review on boron cations; herein we summarize the progress in the area since that time.

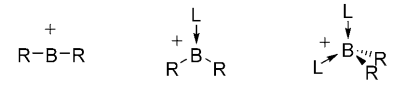
From the Contents

1. Introduction 5017
2. Syntheses and Structures of Borocations 5018
3. Reactivity of Borocations 5029
4. Summary and Outlook 5034

1. Introduction

The chemistry of the boron-group elements is defined by their exceptional Lewis acidity, which is induced by their intrinsic electron deficiency. The observed bonding motifs of these elements, as well as their propensity to undergo reactions that serve to saturate their coordination sphere and/or fill their valence shell, are largely dictated by this deficiency. For example, neutral three-coordinate boron-group species, which can readily abstract hydride, halide, alkyl, and aryl functional groups to give anionic four-coordinate products, have been exploited in the field of olefin polymerization as Lewis acid co-catalysts.[1] Inasmuch as neutral boron-group compounds exhibit significant electrophilic character, the corresponding cationic species have been found to be even more reactive owing to their even greater electronic deficiency and their (sometimes) coordinative unsaturation. The chemistry of the heavier boron-group-element cations (Al, Ga, In, and Tl) has been recently reviewed.[2] However, low-coordinate cationic boron compounds have not been thoroughly examined since 1985,[3] and their four-coordinate analogues since 1975[4,5] despite the attention being paid to main-group Lewis acid catalysts and an ever-increasing search for the limit at which Lewis acidity is maximized without there being a decrease in synthetic utility.[6]

Boron cations can be classified into three distinct structural classes based on the coordination number at boron. Borinium cations (**I**) are two-coordinate and typically bound by two substituents that can relieve the electron



borinium (I) borenium (II) boronium (III)

deficiency at boron through π donation of lone pairs. Borinium compounds are notoriously reactive, and condensed-phase analysis is often hampered by significant interactions with solvent and/or counterions. Conversely, gas-phase studies of these species have proven to be powerful in the elucidation of their intrinsic reactivity. Borenium cations (**II**) are three-coordinate species that comprise two σ-bound substituents (R) and one dative interaction with a ligand (L) that serves to occupy a third coordination site as well as to reduce some of the electron deficiency at boron. Although the valence shell of boron in such species is not full, the added stability imparted by the donor ligand (L) renders borenium cations notably more amenable to solution studies than their two-coordinate counterparts. The third, and most common, class of boron cations is that of the tetrahedral, four-coordinate boronium cations (**III**), with two coordination sites occupied by σ-bound substituents and the other two populated by neutral donor ligands. The stability gained by the filled coordination sphere and the electron density provided by the donor ligands is reflected in the prevalence of reports that describe the generation of these species or invoke them as intermediates in various chemical transformations.

The donor ligands in **II** and **III** serve to partially quench the positive charge at boron and, indeed, are often depicted with the charge formally localized on the ligand L (or on the donating atom of L e.g. N or O). Given that 1) B is more electropositive than most of the donor elements in L, 2) computations indicate significant positive charge on boron, and 3) these compounds generally react as though they were boron cations, we prefer to represent these compounds with the positive charge on boron and the bonds between L and B as being dative in nature and do so throughout this review. While some contribution from a resonance structure in which charge resides on L and the bond is more covalent in nature must be present, the "cationic boron" view of these compounds emphasizes their potential reactivity as boron Lewis acids.

The innate reactivity of borocations,[+] particularly in the condensed phase, has made their characterization rather difficult. The majority have been characterized by NMR and IR spectroscopy, some by mass spectrometry, and a few examples by X-ray diffraction. The chemical shifts observed for these cations in ^{11}B NMR spectra are diagnostic and are typically found significantly downfield of neutral tricoordinate borane precursors or analogues. The $\delta = 30$–38 ppm range is typical for resonance signals from ion-separated bis(dialkylamido)borinium cations, while slightly lower

[*] Prof. W. E. Piers, Dr. S. C. Bourke, K. D. Conroy
Department of Chemistry
University of Calgary
2500 University Drive NW, Calgary, AB, T2N 1N4 (Canada)
E-mail: wpiers@ucalgary.ca

[+] For simplicity, in this review cationic boron species will be denoted "borocations".

 © 2005 Wiley-VCH Verlag GmbH & Co. KGaA, Weinheim

values ($\delta = 25$–30 ppm) are observed for the analogous amine-ligated borenium salts. A much larger range is observed for boronium species, although signals between 0 and 15 ppm are typical. In general, more cationic charge density on the boron center and a lower degree of electronic stabilization results in a more downfield-shifted resonance signal; for example, the presence of alkyl substituents in **I** can yield ^{11}B shifts of close to $\delta = 60$ ppm,[7] whereas the corresponding signals for alkoxy derivatives of **I** have been measured at $\delta \approx 23$ ppm.[8] Isolated cases that involve a boron atom coordinated in an η^5 fashion by a cyclopentadienyl ring display anomalously upfield-shifted resonances in the ^{11}B NMR spectrum (at ca. $\delta = -40$ ppm) which is a result of the unique electronic properties of such ligands (see Section 2.2.4). An increased line width associated with an increase in field gradient and resultant rapid relaxation, is also typical in the ^{11}B NMR spectrum of borinium ions.[3]

As nitrogen-based substituents are prevalent for boron complexes, the B–N stretching modes, in the infrared spectrum, are often cited. However, they are not always apparent and may be absent as a result of molecular symmetry. Perhaps more diagnostic is a hypsochromic trend, in the UV/Vis spectrum, upon going from a parent borane to the corresponding borocation.

Although powerful, mass spectrometry is not a routinely employed form of characterization, except in the case of gas-phase studies, where it dominates. And, while crystal structures are extremely informative with regards to condensed-phase conformations, their availability is largely dependant on the crystalline integrity and condensed-phase stability of the species in question. Indeed, only five examples of crystallographically characterized borinium and borenium ions were reported prior to Nöth's review of the field in 1985.[3,7,9,10]

Previous reviews on the topic of boron cations[3–5,11] have focused largely on their synthesis and characterization. However, although there have been synthetic advances over the past 20 years, often involving unique routes to highly stabilized species, much of the interim work in the area has focused on the gas-phase reactivity of borinium ions. The development of condensed-phase applications has, however, been initiated with promising results. Thus, advances in the syntheses of novel condensed-phase borocations as well as reactivity studies, both in the gas and condensed phases, will be detailed herein, thus emphasizing activity over the last two decades. The emergence of new applications for borocations is growing and the area is poised for rapid development.

2. Syntheses and Structures of Borocations

In all three classes of boron cations, the unfilled p orbitals of the boron atom in the parent borinium cation can become partially occupied as a result of either π donation from covalently bound substituents (e.g. **I**) or the donation of singlet lone pairs from donor ligands (e.g. **II** and **III**). The progression from **I**–**III** is characterized by a steady increase in the p character in the hybridized σ-bonding orbitals at boron, this increase is directly induced by the incoming ligands. Calculations[7,12] as well as the few structurally characterized examples of borinium cations **I**[7,9,13] give an R-B-R angle at boron that is nearly linear and indicative of sp hybridization, while bond angles for **III** that approach 109.5° (tetrahedral, sp^3 hybridized) are expected and observed (see Section 2.2.3).

The linearity observed for structures in class **I** is representative of an energetic minimum that allows for optimal orbital overlap between the empty p orbitals on boron and lone-pair-containing orbitals of π-donor substituents. Thus, these species adopt structures analogous to that observed for allene (Figure 1 a), with the substituents oriented 90° out of phase to one another to facilitate stabilization by means of π backbonding and reduce the interligand steric repulsions. This situation is particularly true for condensed-phase examples of **I**, for which dual-purpose ligands that include both a sterically bulky periphery and a functional group capable of π bonding to boron, are usually required. The steric bulk is

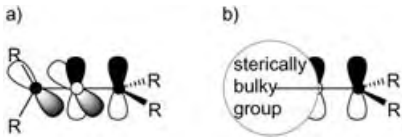


Figure 1. Schematic representations of the geometries required for stabilization of coordinatively unsaturated borinium cations (**I**) by a) two π-donating/sterically bulky substituents and b) one π-donating/sterically bulky substituent and one highly sterically demanding substituent (○ boron atom, ● π-donor atom (e.g. nitrogen), R = large alkyl or aryl groups).



Warren Piers obtained his B.Sc. (1984) and Ph.D. (1988) from the University of British Columbia. He then went to the California Institute of Technology as an NSERC and Killam Postdoctoral Fellow with Prof. John Bercaw. From 1990–1995, he was an Assistant Professor at the University of Guelph before moving to the Chemistry Department at the University of Calgary as an Associate Professor. In July 2000, he was appointed to the S. Robert Blair Chair in Polymerization Catalysis and Polymer Synthesis, a research chair sponsored by Nova Chemicals. His research interests include the chemistry of perfluoroaryl diboranes, catalysis, and the development of boron-based organometallic materials.



Korey Conroy was born in New Brunswick, Canada in 1980 and received his B.Sc. in 2002 from Dalhousie University under the supervision of Prof. Neil Burford. Since September 2002 he has been pursuing his Ph.D. as an NSERC and AIF scholar under the supervision of Prof. Warren Piers at the University of Calgary. His current research is focused on catalysis and the organometallic chemistry of neutral and cationic scandium-group compounds.

 © 2005 Wiley-VCH Verlag GmbH & Co. KGaA, Weinheim

generally achieved by the inclusion of large alkyl and aryl groups, while the π-donation character is usually provided by a nitrogen or oxygen atom that can offer electron density from nonbonding lone pairs into the vacant p orbitals on boron. Alternatively, condensed-phase examples of **I** in which only one substituent is capable of π backdonation generally require an extremely bulky group to afford added protection of the electron-deficient boron center (Figure 1b).

Although these specific ligand properties enable the isolation and characterization of condensed-phase borinium ions, the steric restriction and lessened effective nuclear charge at boron hamper nucleophilic attack and dampen reactivity. Thus, gas-phase experiments that allow the study of reactive borinium ions (**I**) in the absence of the influences of solvation and ion pairing have been developed (see Section 3.1).

The stabilization provided by π-backdonating substituents is less critical for the higher coordinate borocations (**II** and **III**) in condensed phases, primarily because of the additional σ-electron density offered to the electrophilic boron center by the donor lone pairs of the ligand(s). Three-coordinate borenium ions ($R_2B{\leftarrow}L^+$, **II**) can be considered as neutrally ligated analogues of anionically ligated boranes (R_2BR'). As such, they are sp^2-hybridized and trigonal planar in geometry. Because of the reduced electronic demand of the boron center, the need for strong σ- and π-donor substituents R is lessened.[12] The electrostatic and steric properties of the neutral donor ligands L determine the strength of their interactions with the borinium fragment $\{R_2B\}^+$, with nitrogen- and oxygen-based σ-donors, particularly aromatic amines, being most effective.[12] Three-coordinate borenium ions **II** can be formed when sufficient steric stabilization is achieved.

In the case of boronium ions **III**, stabilization of the four-coordinate cations becomes increasingly dominated by steric factors because of the small size of boron.[4] With two neutral σ-donor species (e.g. amines) that can satisfy boron's demands for electronic stabilization, steric congestion around the boron atom can readily reach a critical limit. Small donors are more readily accommodated and larger donors are more prone to displacement from the coordination sphere, often by the anion. Thus, the size of the covalently bound substituents and the size and nucleophilicity of the anion play a significant role. The majority of isolable boronium salts are air and water stable, which makes them much more stable than their low-coordinate counterparts. Thus, in terms of applications, access to borenium ions (**II**) and to a lesser extent borinium ions (**I**) is desirable. This access is potentially provided by boronium ions (**III**) through dissociation equilibria.



Sara Bourke was born in Ottawa, Canada. She obtained her B.Sc. at Queen's University in 1997 after completing her honours project with Prof. Michael C. Baird in the area of the metal-derivatizion of C_{60}. She subsequently completed her M.Sc. (2000) and Ph.D. (2004) degrees under the supervision of Prof. Ian Manners at the University of Toronto where her studies focused on the fundamental reactivity of strained inorganic silicon-containing rings. She is currently pursuing interests in science writing and post-secondary education at the University of Calgary.

2.1 Synthesis of Gas-Phase Borinium Ions

Early mass spectrometric studies made it clear that electron ionization (EI) of a wide variety of boranes (BR_3) can yield the corresponding disubstituted borinium cations (BR_2^+; e.g. R = H, Me, Et, F, Cl, OR′, SMe),[14,15] often among the most abundant cationic products. As early as 1948, Dibeler and Mohler described the generation of BH_2^+ ions by means of EI of diborane (B_2H_6).[14] Many of these studies focused on identifying and/or determining relative abundances and appearance potentials for the ionic products. More recently, studies have moved on to explore, in conjunction with computational investigations, the nature of these ions as well as their gas-phase reactivities (see Section 3.1).

To facilitate reactivity studies, some research into alternative strategies for the generation of borinium ions (**I**) have been investigated. Murphy and Beauchamp determined that, in addition to generation by EI, BMe_2^+ ions could be generated through gas-phase reactions of BMe_3 with self-protonating gases G (G = CH_4, H_2S, and CH_2O), with the concomitant release of methane [Eq. (1)].[16] The generation

$$GH^+ + BMe_3 \rightarrow BMe_2^+ + CH_4 + G \qquad (1)$$

of the BMe_2^+ ion was indicative of the ease of heterolytic cleavage of one B–Me bond in BMe_3, as well as stability of this cationic fragment in the gas-phase under low-pressure conditions. Staley and co-workers took advantage of this inherent stability to minimize the generation of ions other than BMe_2^+ under EI conditions; by lowering the ionization voltage (from the typical values of 50–70 eV to 15 eV) they were able to generate ionization products that consisted of only BMe_3^+ and BMe_2^+.[17]

The use of alternative precursors has improved the accessibility of particular species. For example, methyl boronic acid ($MeB(OH)_2$) has been shown to be an effective precursor for the generation of $B(OH)_2^+$ ions under fairly standard EI conditions (70 eV), whereas the previously employed precursor, orthoboric acid, is problematic owing to a tendency to decompose in the ion source.[18,19] Calculations at the G2 level of theory have revealed an almost linear O-B-O geometry (172°) for this ion, consistent with the expected π-type interactions for this borinium ion.[18]

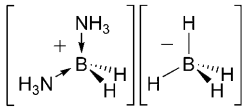
Advances in mass spectrometric methods have also allowed for the generation of previously inaccessible borinium ions. Despite the simplicity of the system, the gas phase ion chemistry of the BH_2^+ ion was not looked at in detail until 1998. The use of a flowing afterglow-selected ion flow tube (FA-SIFT) instrument for ionization of diborane (low flow), allowed a collisionally cooling flow of helium to minimize the

© 2005 Wiley-VCH Verlag GmbH & Co. KGaA, Weinheim

production of higher cluster ions that result from the reaction of the parent BH_2^+ ion with excess diborane;[20] normally EI spectra are typically dominated by the B_2H^{5+} ion.[21]

2.2 Synthesis in the Condensed-Phase and Structural Characterization

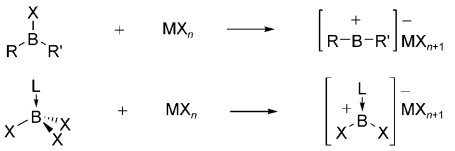
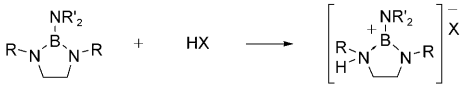
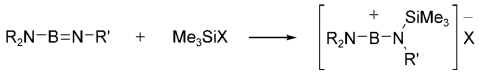
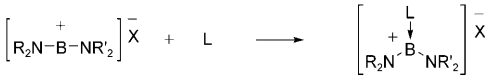
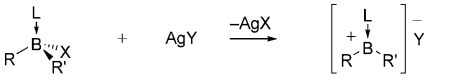
The first condensed-phase borocation, discovered in 1955, was originally misconstrued as a "diammoniate of diborane" and later found to be a boronium salt **1** that consists of two



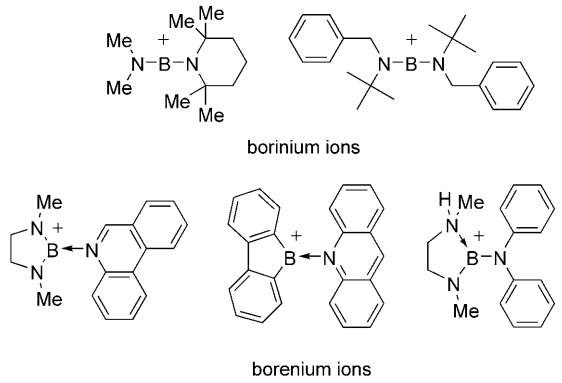
1

tetracoordinate boron centers.[22,23] Since then various synthetic routes to borocations have been described,[3] the most common of which is boron–halogen (B–X) bond heterolysis. Heterolysis can be employed to generate borinium ions (Table 1, entry 1) and, in the presence of auxiliary donors, borenium ions (Table 1, entry 1). Other methods, summarized in Table 1, include protic attack of the boron–nitrogen bond (Table 1, entry 2), electrophilic attack at boron–nitrogen bonds (entry 3), nucleophilic substitution (entry 4), base addition to borinium ions (entry 5), and metathesis (entry 6). As a generalization, boronium ions can be generated by any of these methods in the presence of another equivalent of an appropriate donor molecule.

Table 1: Common routes to condensed-phase low-coordinate borocations.

Entry	Preparation Method	Equation
1	B–X bond heterolysis	
2	Protic attack of B–N bond	
3	Electrophilic attack at B–N bond	
4	Nucleophilic displacement	
5	Base addition to borinium ions	
6	Metathesis	

Although these diverse preparative techniques summarized in Table 1 allow for facile generation of borocations in situ, isolation of crystals suitable for X-ray analysis has been considerably more challenging, particularly for the low-coordinate borinium and borenium cations, for which only five structures were reported prior to 1985 (Scheme 1).[3,7,9,10]



Scheme 1. Borinium and borenium ions that had been characterized by X-ray crystallography by 1985.

Furthermore, since then, there has been only one additional crystal structure of a borinium cation reported (see Section 2.2.1),[13] a handful of structures of borenium cations (Section 2.2.2), and fewer than ten structures of boronium cations (Section 2.2.3) have been published. It is also noteworthy that the discovery of novel borocations has often been serendipitous, rather than by rational design.

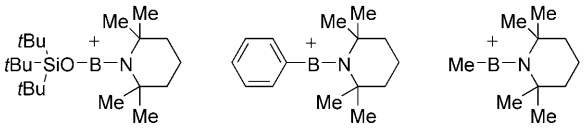
2.2.1 Borinium Cations

It was not until 1982 that the first report of a stable condensed-phase borinium cation, bis(diisopropylamido)borinium, appeared.[24] The first crystallographically characterized species, an $[AlBr_4]^-$ salt in which the electrophilic boron center is stabilized by the tetramethylpiperidino ligand, was reported later that year (Scheme 1).[7] These results prompted the generation and characterization of a number of bis(amido)borinium ions with varied amido substituents and/or counterions,[7,9,25,26] although only one other compound, with very bulky benzyl-*tert*-butylamido substituents,[9] has been successfully characterized by X-ray crystallography.

The prevalence of reports of such species is consistent with quantum mechanical calculations (MP2 and CCSD(T) levels of theory) which indicate the effective stabilization of Group 4 cations (C and Si) by amido substituents.[27] These studies showed that the stabilization energies of carbenium and silylium ions decreased with the increasing electronegativity of the π-donor substituents in the order: pnictogens >

 © 2005 Wiley-VCH Verlag GmbH & Co. KGaA, Weinheim

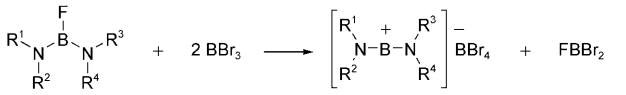
chalcogens > halogens. A similar ligand–cation interaction is likely for borinium ions. This assumption is supported by the paucity of reports of stable oxy-substituted borinium ions, although the larger relative steric shielding capacity of amido ligands also plays a role. Reports of condensed-phase alkyl- and aryl-substituted borinium cations are equally scarce, as accessible stabilization mechanisms (e.g. hyperconjugation) are not as effective. Indeed, none of the three reported species (Scheme 2) are stable at room temperature, and all have required the extremely bulky tetramethylpiperidino group as the second substituent.[7,8]



Scheme 2. Known borinium cations (that are unstable at room temperature) with aryl or alkyl substituents

Among the strategies employed to generate solution-stable species is the placement of sterically cumbersome trimethylsilyl (TMS) groups on the nitrogen atom of the donor ligand.[26] A series of reactions between an assortment of fluoro(trimethylsilyl)aminoboranes and excess boron tribromide resulted in preparation of a new family of borinium cations (**2**) that are stabilized by very bulky amino groups (Table 2). In the absence of X-ray data, extensive spectroscopic studies were performed to confirm the identity of the salts (see Table 2 for ^{11}B NMR spectroscopy data). Each salt **2** consisted of both a borinium cation and a borate anion; these resonate in distinctly different regions of the ^{11}B NMR spectrum. In all cases the borinium resonance lies in the expected range $\delta = 32$–36 ppm, while the borate signal appears significantly upfield ($\delta = -24.5$ ppm). The IR spectra of these compounds provide diagnostic bands near 1800 cm^{-1} for the B–N stretch and the N-B-N bend.

Table 2: Synthesis of trimethylsilyl-substituted bis(amido)borinium ions **2** by means of halide abstraction.

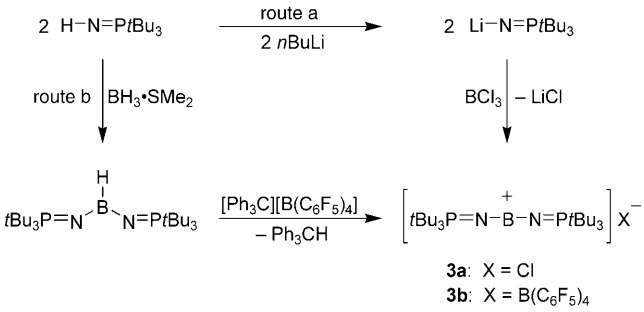


2

Product	R^1	R^2	R^3	R^4	$\delta(^{11}B)$ [ppm][a]
2a	*t*Bu	Bz[b]	*t*Bu	$SiMe_3$	35.8
2b	*t*Bu	$SiMe_3$	*t*Bu	$SiMe_3$	35.2
2c	*t*Bu	*t*Bu	$SiMe_3$	$SiMe_3$	32.8
2d	*t*Bu	$SiMe_3$	$SiMe_3$	$SiMe_3$	33.3
2e	$SiMe_3$	$SiMe_3$	$SiMe_3$	$SiMe_3$	32.8

[a] The chemical shift of the signal of the BBr_4^- ion is $\delta = -24.5$ ppm. [b] Bz = Benzoyl.

Despite a multitude of reports of borinium ions in the mid-1980s, research in the area of condensed-phase borinium ions had been somewhat neglected until a recent report by Stephan and co-workers that described an "extended borinium cation" **3**.[13] This bis(tri-*tert*-butylphosphinimide)borinium cation was prepared by two routes a) by the reaction of two equivalents of the lithium salt of the phosphinimide ligand with boron trichloride to yield the chloride salt **3a**-Cl (Scheme 3 route a), and b) by the reaction of two equivalents of phosphinimide ligand with $BH_3{\cdot}SMe_2$ to generate the disubstituted borane and subsequent trityl salt-induced hydride abstraction to yield the analogous borate salt **3b**-$B(C_6F_5)_4$ (Scheme 3, route b). This B–H heterolysis is analogous to the previous examples of BX heterolysis (Table 1, entry 1).



Scheme 3. Synthetic routes (a and b) to the bis(tri-*tert*-butylphosphinimide)boronium cation **3**.

These borinium salts contain two very sterically demanding tri-*tert*-butylphosphinimide ligands that serve to dictate both the geometry and electronic properties of the borinium center. The phosphinimide ligands sterically protect the highly Lewis acidic boron atom and allow for delocalization of the positive charge onto the four adjacent pnictogen centers. The generation of **3a** in the absence of a halide-abstraction agent suggests that, upon addition of two phosphinimide ligands, the boron center becomes so sterically congested that it can no longer accommodate the chloride ion in a covalent bond. This sterically induced halide dissociation marked a new synthetic approach to borocations.

The ^{11}B NMR spectrum of the parent borane shows a single broad resonance at $\delta = 24.6$ ppm, which is considerably downfield shifted from those seen for **3a** and **3b** ($\delta = -6.1$ and 11.1 ppm, respectively). The chemical shifts of the boron resonances demonstrate the π-donation ability of the phosphinimide ligands and their ability to relieve electron deficiency at the boron center. However, the chemical shift differences observed for **3a** and **3b** (despite their similar solid-state conformations) demonstrate that tight ion pairing between the Cl^- ion and **3a** is likely in nonpolar (C_6D_6) solutions, a proposal that is supported calculations. In **3a**-Cl the boron–anion separation is 7.30 and **3b**-$B(C_6F_5)_4$) it is 10.43 Å. The crystal structures of **3a** and **3b** (Figure 2), both reveal a linear geometry at boron (**3a**: N-B-N 180.0(4)°; **3b**: N-B-N 180.0(3)°). Although the linearity is imposed by the cell symmetry, the B–N bonds (1.258(5) and 1.236(3) Å, respectively) are considerably shorter than those of B-$(NPPh_3)_3$[28] or for the bis(dialkylamido)boron cations,[7] and thus indicate strong donation from the phosphinimide ligand.

© 2005 Wiley-VCH Verlag GmbH & Co. KGaA, Weinheim

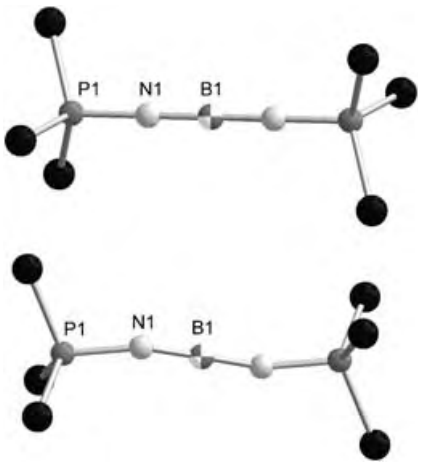


Figure 2. Molecular structures of the cations **3a** (top) and **3b** (bottom), the *tert*-butyl methyl groups and counterions are omitted for clarity.

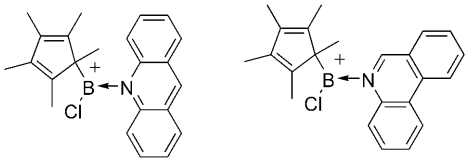
The N–P bond lengths are within the range of typical phosphinimide derivatives.

A final family of two-coordinate boron compounds worthy of mention are the cationic terminal borylenes $[Cp^*Fe(CO)_2{=}BAr]^+[BAr^F_4]^-$ ($Ar = 2,4,6\text{-}Me_3C_6H_2$; $Ar^F = 3,5\text{-}(CF_3)_2C_6H_3$) studied in detail by Aldridge et al.[29] In these compounds, density functional theory (DFT) calculations and metrical parameters point to a bonding description which involves an Fe–B double bond and charge localization on the electropositive iron center. Strictly speaking, then, these interesting compounds may not qualify as borinium ions, although reactions with small, hard nucleophiles (e.g. halide ions) result in addition to the boron center. Reactions with softer nucleophiles (e.g. olefins, CO), however, results in borylene ligand displacement.

2.2.2 *Borenium Cations*

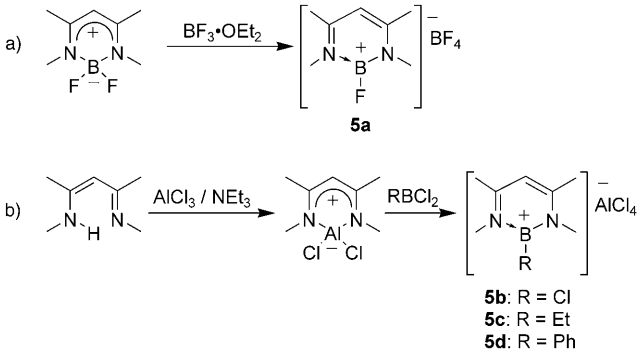
Reports for well defined three-coordinate borenium cations have been almost as elusive as for their borinium counterparts. Only three structural reports were made prior to 1985 (Scheme 1),[10] and in each case a bulky auxiliary base capable of electronic stabilization was required and a five-membered borocyle was formed that is incapable of achieving the linear geometry necessary for electronic stabilization of a borinium cation. Since then, there have been only a handful of reports on tricoordinate borenium cations.

Jutzi and co-workers reported synthesis and characterization of two novel borenium cations, **4a** and **4b**, from reactions of dichloro(η^1-pentamethylcyclopentadienyl)borane with the bulky nitrogen-based donors acridine and phenanthridine, respectively.[30] These salts were characterized by ^{11}B NMR spectroscopy, they gave broad downfield resonances for the boronium center of **4a** at $\delta = 32.8$ ppm (full width at half height (FWHH) 158 Hz) and that of **4b** at $\delta =$ 30.9 ppm (FWHH 155 Hz). Crystallographic characterizations were impeded by the solvolysis of these species in polar aprotic solvents.



4a **4b**

A series of 1,3,2-diazaborenium cations, which are isoelectronic with benzene, have been reported by Kuhn and coworkers.[31] Fluoride abstraction from a zwitterionic six-membered β-diketiminato ("nacnac") boron chelate by the strong Lewis acid $BF_3{\cdot}OEt_2$ resulted in the generation of a 1,3,2-diazaborenium heterocycle **5a**-BF_4 that has a formal positive charge (Scheme 4a). The ^{11}B NMR spectrum



Scheme 4. Syntheses of 1,3,2-diazaborenium cations **5** by means of a) fluoride abstraction and b) an aluminocycle intermediate.

revealed a doublet ($^1J_{F\text{-}B} = 12.3$ Hz) at $\delta = 23.05$ ppm and AM1 calculations predicted a planar geometry for the six-membered ring with B–N bond lengths of 1.468 Å, a N-B-N angle of 118.6°, and π interactions of boron with both of the nitrogen atoms. Other cations of this type were prepared by initial deprotonation of the "nacnac" ligand, subsequent aluminum insertion, and treatment with $RBCl_2$ (R = Cl, Et, Ph) to afford the 1,3,2-diazaborenium cations **5b–d**-$AlCl_4$ (Scheme 4b).

By replacing the methyl substituents on nitrogen with bulky aryl groups, Cowley and co-workers were able to synthesize an analogue that was suitable for X-ray characterization (Figure 3).[32] A metathesis reaction of the potassium

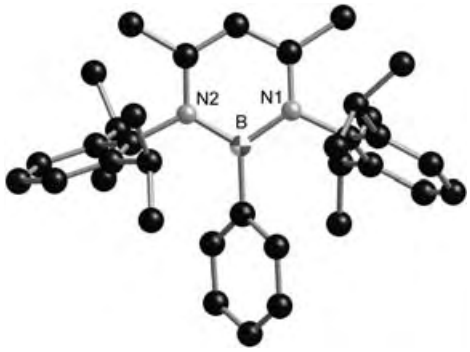
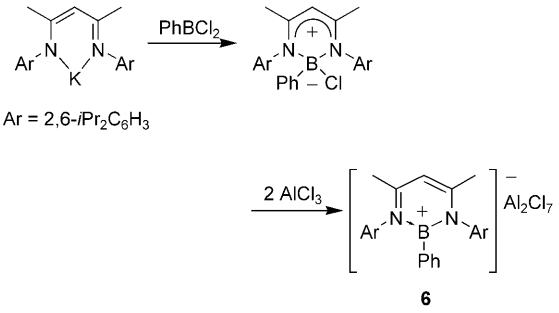


Figure 3. Molecular Structure of **6**, hydrogen atoms are omitted for clarity.

 © 2005 Wiley-VCH Verlag GmbH & Co. KGaA, Weinheim

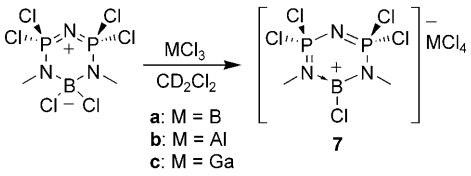
salt of the β-diketiminate ligand $K[HC(CMe)_2(NAr)_2]$ (Ar = 2,6-*i*$Pr_2C_6H_3$) with $PhBCl_2$, and subsequent treatment with $AlCl_3$ yielded the salt **6**-Al_2Cl_7 [Eq. (2)] which was characterized by a chemical shift in the ^{11}B NMR spectrum of $\delta =$ 72 ppm. Structural characterization showed the BN_2C_3 ring to



(2)

be planar and DFT calculations at the B3LYP level produced data for HOMO-6 and HOMO-7 that demonstrated BN_2C_3 π-bonding character.

Manners and co-workers showed that halide could be abstracted from a boratophosphazene to yield the borazine–phosphazine hybrid cation **7**, which has a PNP fragment in place of the ring carbons of **5b** [Eq. (3)].[33] The borenium



(3)

cations of **7**-MCl_4 (M = B, Al, Ga; e.g. Figure 4) show only slight deviations from planarity as well as shortened B–N bonds (1.43–1.45 Å) that are indicative of increased π character relative to the boratophosphazene. In the ^{11}B NMR

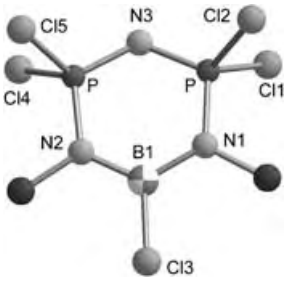
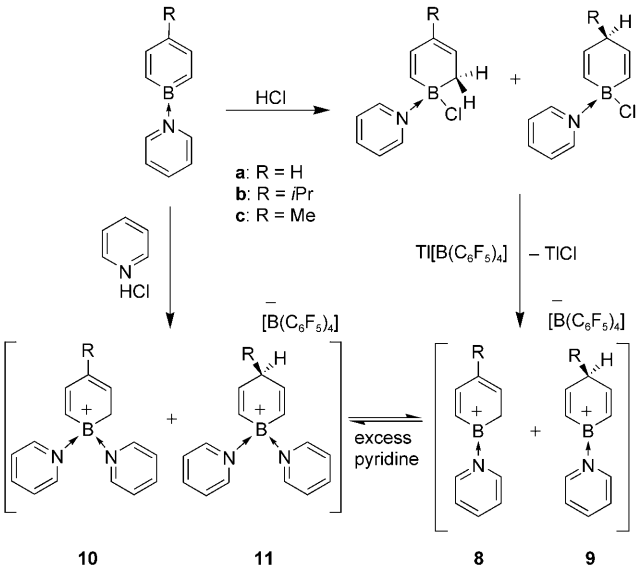


Figure 4. Molecular structure of the borazine–phosphazene hybrid cation **7a**, hydrogen atoms and counterion are omitted for clarity.

spectrum, the signals for **7b** (M = Al) and **7c** (M = Ga), at $\delta =$ 29.6 ppm and 30.2 ppm, respectively, are consistent with the tricoordinate planar environment around boron and are downfield shifted from that of the boratophosphazene precursor ($\delta = 5.4$ ppm), however, the solution spectrum of **7a**-BCl_4 showed evidence for an exchange process between free **7a** and a chloride-bridged species.

We have recently shown that the presence of nitrogen atoms in the boracyclic unit of such species are not necessary for the generation of borocations. Thus, the pyridine-stabilized borenium ions **8** (R = H, *i*Pr, or Me) and **9** (R = H) have been generated by chloride abstraction from the corresponding pyridine–borane adducts (Scheme 5).[34] ^{11}B NMR spectroscopic characterization of these species revealed signals at $\delta \approx 56$ (**8**) and 46 ppm (**9**). Interestingly, in the presence of

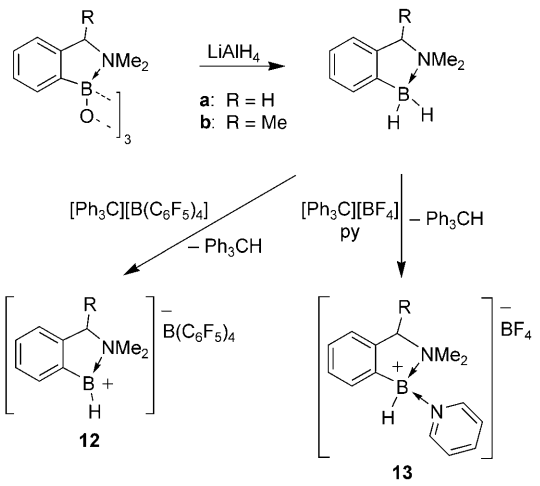


Scheme 5. Synthetic routes to the isomeric borenium ions **8** and **9** and their boronium analogues **10** and **11**.

excess pyridine, the chloroborane precursor adducts appear to be in equilibrium with the boronium chloride species **10** and **11**, which have also proven accessible by electrophilic attack of pyridinium chloride on the neutral borabenzene–pyridine adducts (see Section 2.2.3).

Vedejs and co-workers generated two borenium ions **12a** and **12b** by reduction of arylboronic anhydrides with lithium aluminum hydride (Scheme 6).[35] Initially the corresponding 2,3-benzazaborolidines are formed which then undergo hydride abstraction with trityl tetrakis(pentafluorophenyl)-borate (trityl = triphenylmethyl). The low-temperature ^{11}B NMR spectrum of **12a** revealed a singlet at $\delta -17.2$ ppm for the borate counterion and a broad resonance at $\delta \approx 38$ ppm (FWHH 460 Hz). However, this species is transient and the signal disappears as the solution is warmed to room temperature. Compounds **12** are interesting since the majority of borenium cations reported have strong π-donating ligands that provide crucial stabilization to the electropositive boron center. In species **12**, however, the boron center is bound by a phenyl substituent of almost negligible π-donating ability as well as an electronically benign hydride ligand. These results show that boron cations without π stabilizing ligands are viable intermediates. Interestingly, hydride abstraction from the 2,3-benzazaborolidine (R = Me) with trityl tetrafluoroborate in pyridine did not yield the anticipated borenium species

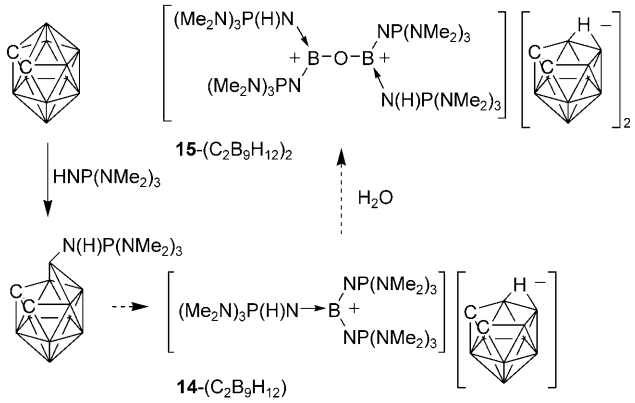
© 2005 Wiley-VCH Verlag GmbH & Co. KGaA, Weinheim



Scheme 6. 2,3-benzazaborolidines as precursors to the corresponding borenium (**12**) and boronium (**13**) ions.

but, rather, the corresponding pyridine-coordinated boronium cation **13b** which was crystallographically characterized (see Section 2.2.3).

With the deboronation of *ortho*-carborane by iminotris (dimethylamino)phosphorane, Fox and co-workers discovered a novel route to borenium ions (Scheme 7).[36] The



Scheme 7. Generation of the protonated tris(imino)borane cation **14** and its conversion into the diborenium dication **15** by adventitious water.

phosphorane effectively converts *closo*-$C_2B_{10}H_{12}$ into *nido*-$C_2B_9H_{12}^-$ through formal loss of a B^{3+} unit. Among the counterions detected in solution was the protonated tris(imino)borane cation **14**, with a ^{11}B NMR resonance at $\delta =$ 22.3 ppm. Attempts to isolate crystals of **14**-$C_2B_9H_{12}$ led to X-ray crystallographic characterization of the first reported diborenium dication **15** (Figure 5), which is presumably the product of reaction of **14** with adventitious water.

There are distinct differences in the B–O bond lengths (B1–O 1.373(5) vs. B2–O 1.416(5) Å), which may indicate a greater π donation to one boron atom (B1) to form a pseudo B=O structure in the solid state. Bond order calculations carried out on the structure indicate strong B–N π bonding to the imino residue (NR) of each BN_2 unit and enough

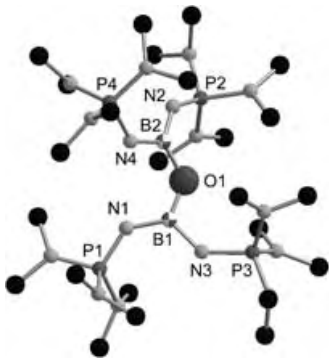


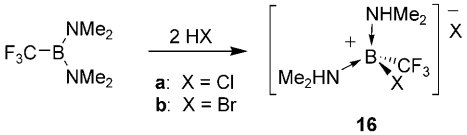
Figure 5. Molecular structure of dication **15**, hydrogen atoms are omitted for clarity.

π bonding to the amino residue (RNH) to maintain the planarity of each $(PN)_2BO$ unit. Unfortunately, no ^{11}B NMR data was reported for **15**.

2.2.3 *Boronium Cations*

Tetracoordinate borocations have received the most attention, undoubtedly because of their relative stability, which arises from a filled octet and a complete coordination sphere. In almost all cases, boronium cations consist of two covalently bound ligands and two σ-donating ligands that serve to partially occupy the unfilled orbitals on boron and thus facilitate a depression of the ground-state energy of these species. This area has been thoroughly reviewed[4,5] and, owing to the volume of reports of these species and their more common nature, only a selection of recent synthetic results are highlighted herein.

The reaction of trifluoromethylbis(dimethylamido)borane with excess HCl and HBr, to yield, in situ, the trifluoromethylhalide boronium salts **16a** (X = Cl) and **16b** (X = Br), respectively [Eq. (4)], was reported in 1987.[37] These salts are



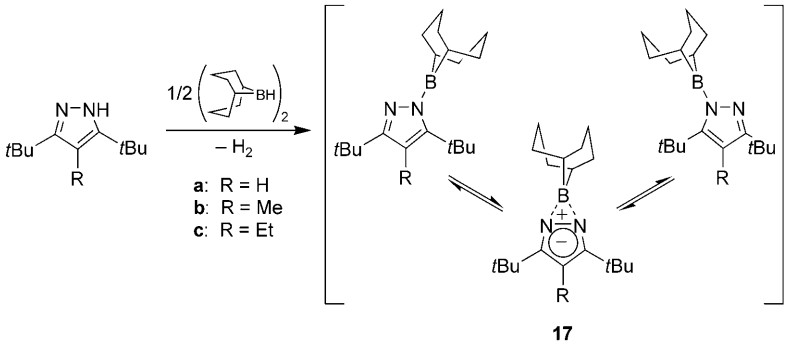
(4)

colorless, nonvolatile solids and are insoluble in nonpolar solvents. The ^{11}B NMR spectrum in acetonitrile of the more soluble **16a** provided a single signal at $\delta = 1.5$ ppm. This reaction represents protic attack on each of the B–N bonds in the precursor, in a manner similar to that described for the generation of borenium ions (Table 1, entry 2)

Although aminoboranes are susceptible to self-association (e.g. dimerization), the equilibria can be pushed towards the monomer through the incorporation of very bulky substituents. For example, the reaction between sterically restricted trisubstituted pyrazoles with 9-BBN (BBN = borabicyclononane), a bulky and rigid borane[38] led to the facile generation of a series of diorgano(pyrazolyl)boranes (R = H,

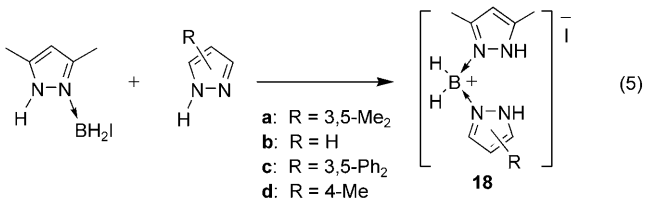
 © 2005 Wiley-VCH Verlag GmbH & Co. KGaA, Weinheim

Me, Et; Scheme 8). X-ray analysis and low-temperature studies of one of these species (R = Et) reveal a very constrained geometry with the boron bound to only one of the two nitrogen centers. However, room-temperature analysis indicates a rapid exchange of the borane moiety between the two nitrogen centers, a process that may be facilitated by a symmetrical zwitterionic boronium intermediate **17**. Evidence for this structure has been abstracted from UV/Vis spectroscopic data, which reveals a hypsochromic shift indicative of an increased dipole character. In addition, MNDO (modulated neglect of diatomic overlap approximation) calculations performed on the three boranes indicate a progressive decrease in the enthalpy of formation of **17** as the pyrazole becomes more sterically crowded, to the extent that for R = Et, formation of the cyclic boronium is only endothermic by 14.4 kJ mol^{-1}.



Scheme 8. Equilibrium generation of the zwitterionic boronium intermediate **17** from organopyrazolylboranes.

Pyrazoles have also been involved in the production of boronium-salt intermediates in the synthesis of polypyrazolylborate ligands. A series of boronium cations **18a–d** has been prepared from the reaction of the 3,5-dimethylpyrazole·iodoborane with one equivalent of another functionalized pyrazole [Eq. (5)].[39] Unfortunately, characterization of the proposed cations was limited to IR and ^{1}H NMR spectroscopy and elemental analysis.



(5)

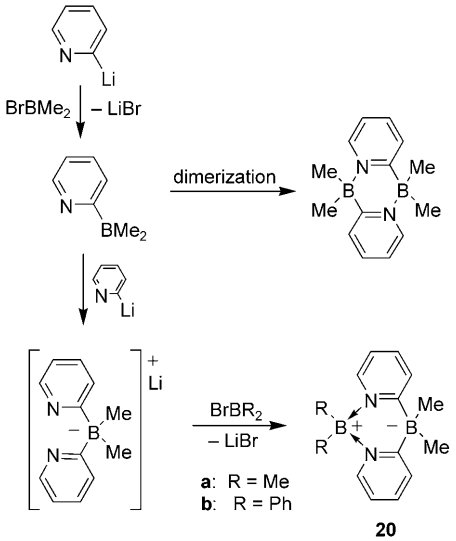
The isosteric relationship between boronium ions and secondary ammonium ions prompted Davis and Madura to prepare a boronium analogue of the conjugate acid of the biologically active bicyclic tropane ring 8-azabicyclo[3.2.1]octane (a structural element of several neuroactive compounds; for example, atropine).[40] The boronium cation **19** was prepared in a one-step, one-pot synthesis from equimolar quantities of homopiperazine and bromoborane·dimethylsulfoxide. The white solid was characterized by multinuclear NMR spectroscopy and the ^{11}B NMR spectrum revealed an overlapping doublet of doublets with chemical shift of $\delta = -3.87$ ppm (D_2O).



8-azabicyclo[3.2.1]octane **19**

While not tested for biological activity, computational studies at the DFT/6-31G* level illustrated a remarkable structural similarity between the two bicyclic species, with the major discrepancy originating in the longer bridgehead bonds in **19** (B–N 1.624 Å vs. N–C 1.556 Å) which fall in the range between dative and non-π-bonding covalent B–N bond lengths. While the positive charge in 8-azabicyclo[3.2.1]octane is associated with the apical nitrogen atom the charge in **19** is distributed along the sides of the molecule (N→B) and not completely at the apical boronium site, although the hydrogen atoms on boron do remain slightly hydridic (charge −0.05).

In a previous report by Hodgkins and co-workers[41] it was noted that slow addition of bromodimethylborane and 2-lithiopyridine, to form novel pyrazabole ligands, did not exclusively produce the anticipated dimeric dimethyl(2-pyridyl)borate; the dimethylboronium dimethylbis(2-pyridyl) borate zwitterion **20a** was also formed, with the two products observed in a 15:85 ratio (Scheme 9). Initial reaction between the lithiated pyridine and bromodimethylborane is believed to form the monomeric borane which can either dimerize in a head-to-tail fashion or react with unconsumed 2-lithiopyridine to form a dimethyl borate intermediate which can



Scheme 9. Generation of the zwitterionic diboracycle **20**.

 © 2005 Wiley-VCH Verlag GmbH & Co. KGaA, Weinheim

further react with borane to generate the boronium–borate complex **20**.

In addition to boronium **20a**, the diphenyl analogue (**20b**) was prepared through addition of bromodiphenylborane to the isolated borate precursor. Zwitterion **20b** was isolated as a crystalline solid and its ^{11}B NMR spectrum showed a resonance at $\delta = 4.0$ ppm for the boronium center and at $\delta = -17.6$ ppm for the borate moiety. Crystallographic data were collected for both **20a** and **20b**, however only **20b** presented a $C_2B_2N_2$ ring that was not disordered (Figure 6). The equivalent B–N bond lengths of 1.59 Å are indicative of the σ-donating nature of these stabilizing interactions.

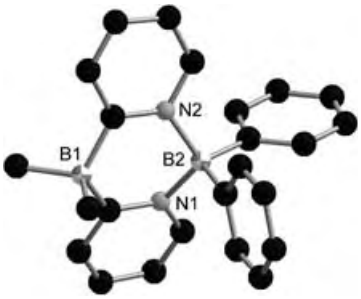


Figure 6. Molecular structure of zwitterion **20b**, hydrogen atoms are omitted for clarity.

As already mentioned, during the preparation of various borenium compounds, Vedejs and co-workers were able to isolate and structurally characterize a boronium cation (**13b**) of the 2,3-benzazaborolidine series (Section 2.2.2, Scheme 6).[35] The boronium cation was characterized by multinuclear NMR spectroscopy, however, no ^{11}B chemical shift was reported and the B–H coupling in the ^{1}H NMR spectrum is not observed owing to quadrupolar line broadening. The crystal structure of **13b** revealed a distorted tetrahedral geometry around boron with the most constrained angle (C-B1-N1 99.5°) resulting from the location of the boron atom within a 5-membered ring (Figure 7). A related boronium ion partnered by a dinuclear manganese counterion was reported by Braunschweig and Ganter.[42]

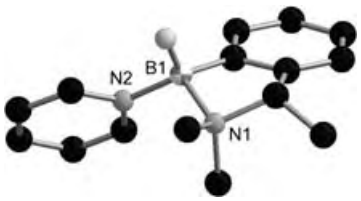
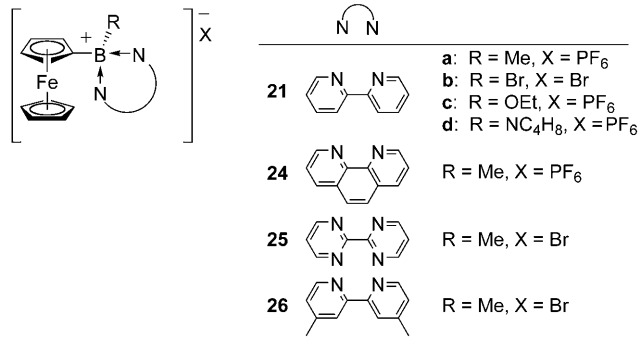
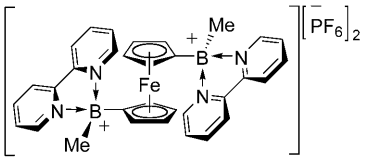


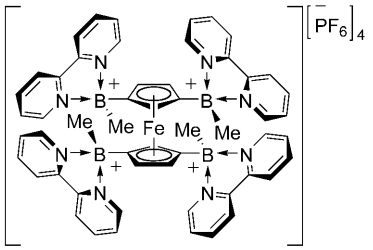
Figure 7. Molecular structure of **13b**, the BF_4^- counterion and protons are omitted for clarity.

Wagner and co-workers have prepared series of ferrocene-based 2,2′-bipyridylboronium salts to investigate their utility as novel electron acceptors in charge-transfer complexes. The first family prepared consisted of ferrocene cores functionalized by one (**21a–d**), two (**22**), and four (**23**) boron substituents and were synthesized from their correspondingly





22



23

substituted ferrocenylborane precursors.[43] Boronium salts analogous to **21**, with differing N-donor ligands, were also prepared (**24**–**26**). All of the compounds were characterized by multinuclear NMR spectroscopy studies as well as elemental analysis. Broad singlets were observed in the ^{11}B NMR spectrum for each salt and ranged from $\delta = 6$–11 ppm (FWHH 140–500 Hz).

In all cases, the boronium cations were isolated from the reaction mixtures as solid precipitates and crystal structures of the 2,2′-dipyridyl salts were obtained (e.g. Figure 8). Crystals of **21a** and **22** were deep purple in color while **23** was isolated as a black solid. The electrochemistry of these

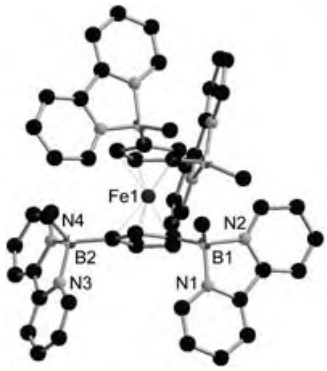
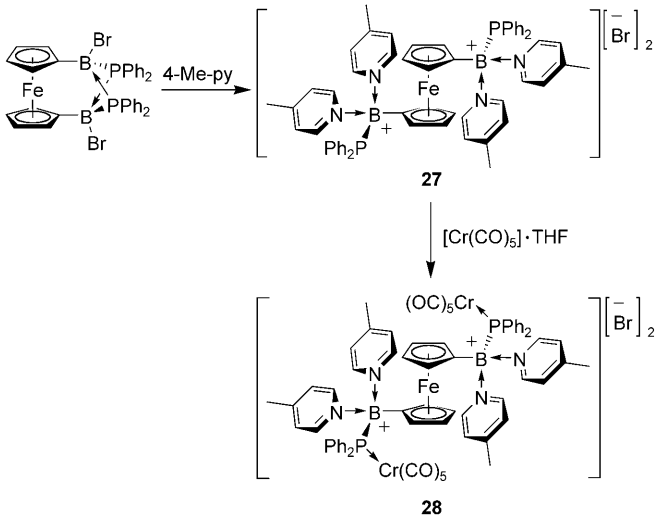


Figure 8. Molecular structure of **23**, the hydrogen atoms and Br^- counterions are omitted for clarity. The PF_6^- salt can be obtained by precipitation of the Br^- salt from aqueous solution by using NH_4PF_6.

 © 2005 Wiley-VCH Verlag GmbH & Co. KGaA, Weinheim

boronium salts was evaluated and they were found to display one chemically reversible oxidation and two consecutive chemically reversible reductions in DMF. This data suggest the possibility to develop these species and their derivatives as redox catalysts, nonlinear optical materials, or as components of electronic devices (e.g. amperometric biosensors and modified electrodes).

Wagner and co-workers have also reported the preparation of a tetrapyridyl diboronium dication **27** analogous to **22** from an interesting *ansa*-bridged ferrocene as well as the preparation of an analogous trinuclear complex (**28**) linked through the two phosphido moieties (Scheme 10).[44] Complex



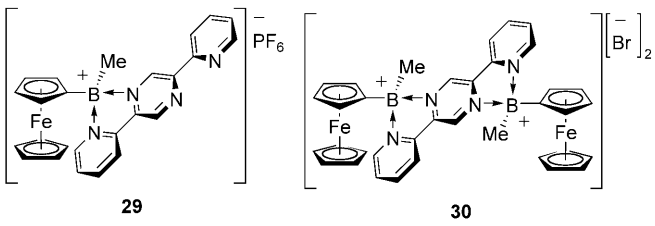
27

28

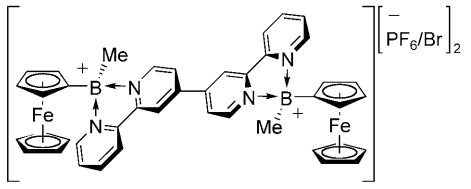
Scheme 10. Generation of the cation **27** and its reaction with $[Cr(CO)_5]$·THF to produce the trinuclear metal complex **28**.

28 was prepared in an effort to confirm the presence of three-coordinate phosphorus centers in the noncomplexed boronium salt **27**. The ^{11}B NMR spectra of both **27** and **28** show resonances at $\delta = 7.3$ ppm (FWHH 500 Hz) and 8.4 ppm (FWHH 500 Hz), respectively, which are downfield relative to that of the precursor ferrocenophane. A similar downfield shift in the ^{31}P NMR spectrum is noted between the precursor ferrocenophane and the boronium complex **27** ($\Delta\delta_P = 9$ ppm).

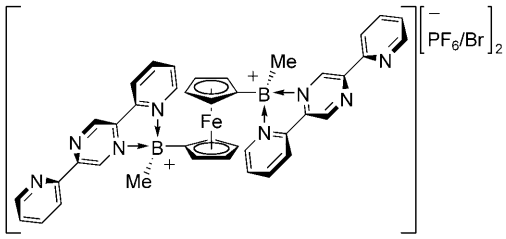
Further exploration of dichelating nitrogen-based ligands has demonstrated the potential for forming oligomeric and macrocyclic ferrocene-based boronium cation complexes.[45] The bases 2,5-bis(pyridyl)pyrazine (bppz) and 2,2′:4′,4″:2″,2‴-quaterpyridine (qpy) were used to generate linear chains and macrocycles, respectively. After reactions of the ligands in appropriate stoichiometries with ferrocenyl-based boron precursors, ^{11}B and ^{1}H NMR spectroscopy and, importantly, FAB-MS spectrometry, provided evidence of formation of novel mono- (**29**) and dicationic (**30**–**32**) boronium compounds. Furthermore, reactions of equimolar amounts of qpy with a disubstituted ferrocene precursor yielded a mixture of macrocyclic stereoisomers, **33a** and **33b**. Although, X-ray quality crystals were elusive, analyses of related structures present suitable evidence to suggest that isomer **33a** is the more favorable.[46] The ^{11}B NMR spectrum of **33** exhibited a



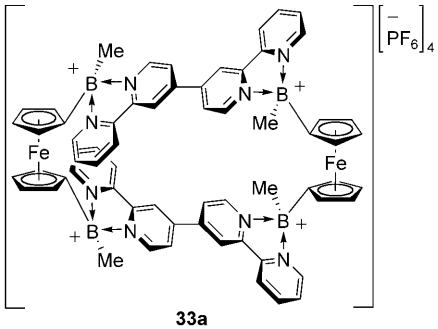
29 30



31



32

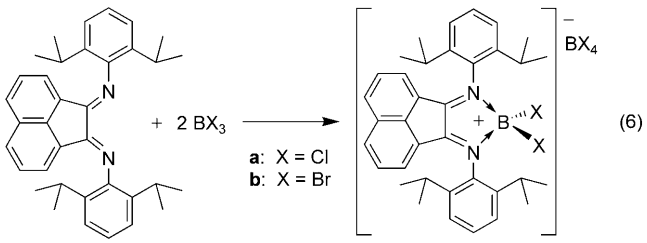


33a

broad signal at $\delta = 12.4$ ppm characteristic of tetracoordinate boronium center while ESI-MS of **33** yielded two prominent peaks at m/z 691 and 412 corresponding to $[\mathbf{33}\text{-}(PF_6)_2]^{2+}$ and $[\mathbf{33}\text{-}PF_6]^{3+}$, respectively.

Recent reports of chloroboration reactions analogous to hydroborations prompted Clyburne and co-workers to prepare a series of cationic complexes capable of undergoing facile addition across a C=O or C=N bond, for example.[47] The very bulky bis(2,6-diisopropylphenylimino)acenapthene ligand was used which was expected to provide π stabilization as well as steric bulk. Reactions with two equivalents of BCl_3 or BBr_3 yielded red crystals of the boronium ions **34a** and **34b**, respectively [Eq. (6)]. NMR spectroscopic studies were hampered by the insolubility of these species as well as their propensity to decompose in CD_2Cl_2. X-ray quality crystals of **34a** (albeit with an *R* factor of only 12%) showed the two dative B–N bonds (1.57(2) and 1.54(2) Å) to be in the range typical for nitrogen-based ligands bound to tetracoordinate borocations.

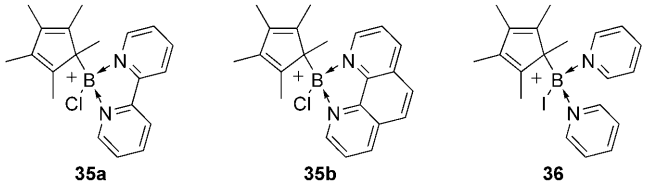
 © 2005 Wiley-VCH Verlag GmbH & Co. KGaA, Weinheim



(6)

As mentioned in section 2.2.2 our group has synthesized the boronium ions **10** (R = H, *i*Pr) and **11** (R = H) in which the cationic boron center is part of a BC_5 ring and stabilized by two equivalents of pyridine (Scheme 5).[34] Crystallographic characterization of **11a** showed a roughly tetrahedral coordination environment around the boron atom with similar B–C bonds (1.582 and 1.588 Å) and more disparate B–N bond lengths (1.622 and 1.608 Å).

Jutzi and co-workers have demonstrated that the η^1-Cp* (Cp* = pentamethylcyclopentadienyl) coordinated boronium cations **35** and **36** could be prepared by reaction of equimolar



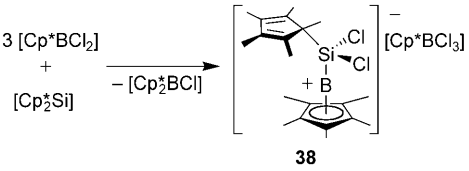
quantities of η^1-Cp*BCl_2 and a bidentate nitrogen donor (bipyridine or phenanthrene) or reaction of [Cp*BI][BI_4] with excess pyridine (compare with **4**, Section 2.2.2).[30] While ^{11}B and ^{1}H NMR spectroscopic analyses of these salts confirmed their identity in solution (^{11}B NMR spectrum $\delta = 7.0$ (**35a**), 6.5 (**35b**), and −19.1 ppm (**36**)) none of the compounds were sufficiently crystalline to allow for X-ray structural analysis.

2.2.4 Borocations with Nonclassical Coordination Environments

Jutzi[30,48,49] and Cowley[50] have developed a number of η^5-Cp*-substituted borocations that can be viewed as dicoordinate borinium ions; alternatively, as the boron atom is closely associated with six other atoms it could be viewed as being hypercoordinate. However, the η^5-coordinated ligands formally act as six-electron donors. Therefore, although these compounds display some of the structural and reactivity features of borinium ions, they can also be viewed electronically as boronium ions and should thus be considered independently as hybrids of these two types of boracations.

As early as 1979 Jutzi demonstrated that the η^5-coordinated borocations [Cp*BX]$^+$ (X = Cl, Br, I) (**37**) could be formed by reaction of η^1-coordinated Cp*BX_2 (generated in situ for X = I) with an appropriate trihaloborane (or $AlCl_3$) in a classical halide elimination reaction.[48] In their ^{11}B NMR spectra these species have highly upfield-shifted resonances ($\delta = -39$ to -51 ppm) relative to the precursor dihalides ($\Delta\delta = 100$–110 ppm) and most other borocations. This is similar to the situation observed in hypercoordinate *nido*-boranes[48b] and is indicative of the change in coordination of the Cp* ring relative to the boron atom and the efficient transfer of charge to the cationic boron center of the product. Notably, interaction between the Cp* methyl groups and the boron center was demonstrated by coupling observed by multinuclear NMR spectroscopy.

A recent report by Jutzi and co-workers demonstrated that the reaction of three equivalents of Cp*BCl_2 with Cp^*_2Si can yield the novel η^5-Cp* boronium cation **38** as a borate salt [Eq. (7)].[49]



(7)

The salt of **38** with a $[Cp^*BCl_3]^-$ ion is rather insoluble in common hydrocarbon solvents and thus the analogous tetrachloroborate salt was generated and subsequently characterized by multinuclear NMR spectroscopy. The ^{11}B NMR spectrum of **38**-BCl_4 has signals at $\delta = 6.1$ and -54.6 ppm that corresponded to the borate and boronium centers, respectively. The upfield boronium resonance agrees with the range characteristic for the previously discussed [Cp*BX]$^+$ ions **37**.[51]

In the crystal structure of **38**, boron is bound to a Cp* ring in a η^5 fashion with an average B–C bond length of 1.75 Å (Figure 9). The slight deviation from linearity for the Si-B-$Cp^*_{cent.}$ angle (170.8°) was attributed to crystal packing forces.

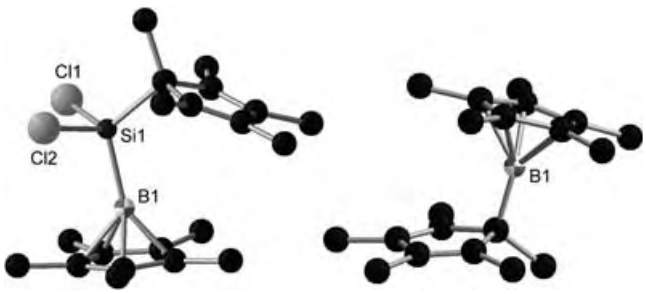


Figure 9. Molecular structures of **38** (left) and one of the two independent cations of **39** (right), the hydrogen atoms are omitted for clarity.

The electrophilic nature of the boronium center is exemplified by the bending of the Cp* methyl groups out of the plane of the ligand (angle of 4.2°) towards the Lewis acidic center.

Further studies involving Cp*-ligated boranes have resulted in the formation of the decamethylborocenium cation (**39**), which is described by Cowley and co-workers as "the most tightly-squeezed metallocene", because of its short intramolecular contacts.[50] X-ray quality crystals of **39** were isolated upon reaction of a chloride-abstraction reagent ($AlCl_3$ was most effective) with Cp^*_2BCl (Figure 9). A

 © 2005 Wiley-VCH Verlag GmbH & Co. KGaA, Weinheim

single resonance at $\delta = -41.5$ ppm was found in the solution ^{11}B NMR spectrum, however, in the solid state the cation was found to have both η^1- and η^5-bound Cp* rings, with the η^1-bound Cp* B–C bond considerably longer than that to the centroid of the η^5-bound Cp* ring ($\Delta_{B-C} = 0.313$ Å). The structure has a near linear arrangement (avg. of 177.6°) along the C-B-centroid axis. Calculations on this structure, as well as the hypothetical nonmethylated analogue $[Cp_2B]^+$ ($Cp = C_5H_5$) at the BP86/A level were carried out to determine the reason for the highly constrained geometry. Geometry optimization studies, in agreement with the experimental results, showed that the η^1–η^5 geometry lies in a global minimum, with a predicted ring tip of 123°, similar to the experimentally observed 113.4° (avg.). The η^5–η^5 configuration resides almost 50 kcal mol^{-1} higher in energy than the observed geometry. It is believed that the small size and the increased effective nuclear charge of the boronium center is responsible for the tightly bound Cp* rings.

Further theoretical studies concerning the ring exchange of the borocenium cation were performed by Kwon and McKee and supported the findings of Cowley et al.[52] The small size of the degenerate p_x and p_y orbitals at boron prohibit effective π-type interactions with the appropriate orbitals on the Cp rings and make the η^5–η^5-Cp structure unfavorable relative to the η^1–η^5 structure. This situation is in contrast with metallocene complexes of heavier elements which have sufficiently diffuse orbitals to undergo π bonding. In addition, a series of relative energies was computed at the B3LYP/6-311 + G(2d,p) level for the exchange of the two Cp rings in $[Cp_2B]^+$ (Figure 10). The data depicts a significant barrier to exchange (approximately 15 kcal mol^{-1}). Similar results were found for $[Cp^*_2B]^+$.

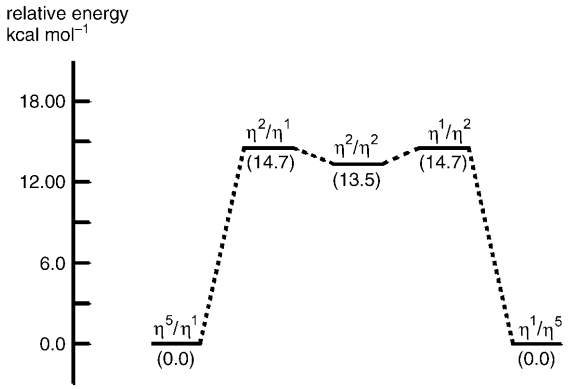
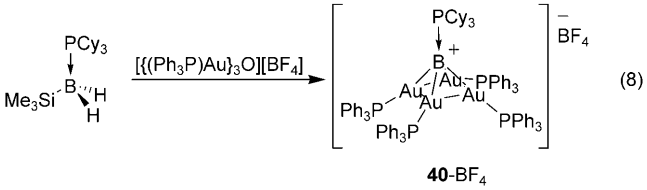


Figure 10. Relative energies for the exchange of η^1- and η^5-bound rings of $[Cp_2B]^+$.

A second type of "hypercoordinate" borocation has been prepared by Schmidbaur and co-workers, in this case the borocation is part of a gold cluster.[53] Reaction of tricyclohexylphosphine(trimethylsilyl)borane with tris[(triphenylphosphine)gold(I)] oxonium tetrafluoroborate provided the formally pentacoordinate boronium cation **40** [Eq. (8)]. The yellow crystalline material is air stable and, upon recrystallization from CH_2Cl_2, yielded crystals suitable for X-ray analysis. The FAB-MS and exhibits a molecular cation signal



40-BF_4

at m/z 2127.5 as well as diagnostic lower m/z signals. The ^{11}B NMR spectrum reveals a broad resonance at $\delta = 12.2$ ppm for the cluster-centered borocation and a sharp resonance at $\delta = -4$ ppm for the borate counterion. The crystal structure reveals an asymmetric square-based-pyramid core with the apical boron atom bridging the four gold atoms. The B-Au-P angles are near to linear and the B–Au bonds are relatively short compared with those of other boron-centered bimetallic clusters.[54]

While significant steps forward have been made in terms of the determination of the types of substitution and conditions necessary for the production of relatively stable borocations, much less has been elucidated with regards to the reactivity of the less-stable congeners and the potential applications of their enhanced reactivity. This situation is due in part to the difficulty involved in the design of experiments that can probe this behavior in a discernable manner (e.g. in the gas phase) and in part to the required development of metastable species that incorporate fewer stabilizing features (especially in the condensed phase). However, progress is being made in these areas and the results show promise for the development of both fundamental structure–reactivity relationships and catalytic applications for borocations.

3. Reactivity of Borocations

3.1 Gas-Phase Reactivity

As the gas phase eliminates the perturbing influences of solvation and ion pairing it can facilitate the study of chemical and physical properties of highly reactive ions and molecules. Thus, mass spectrometric studies of highly electron-deficient borocations, particularly borinium cations, have been used extensively to probe their stabilities and reactivities. Avenues of interest currently include the determination of fundamental physical constants, such as binding affinities, and the potential use of borinium ions as chemical ionization agents. Adducts with organic molecules tend to display highly diagnostic fragmentation patterns which may be useful for structure determination when used in conjunction with a knowledge of reactivity patterns and spectral libraries.[55]

Although electron ionization (EI) mass spectrometry has been used since the middle of the 20th century to detect borinium ions in the gas phase (Section 2.1) more sophisticated experimental techniques needed to be developed to effectively study the gas-phase chemistry of these highly electrophilic species. Specifically, isolation strategies and the ability to study the interactions of specific ions with various substrates were necessary.

© 2005 Wiley-VCH Verlag GmbH & Co. KGaA, Weinheim

Kenttämaa and co-workers performed pioneering work in the field of gas-phase borinium ion (BR_2^+) chemistry in the 1990s with a dual cell Fourier-transform ion cyclotron mass spectrometer,[56,57] an effective instrument for the isolation and examination of ions of specific m/z ratios in an environment devoid of solvent molecules. Ionic fragments other than those of the desired borinium ions that are present following ionization of neutral borane precursors can be expelled from the cell by precise voltage sweeps and quenching pulses.[57] Upon isolation of the desired borinium cation, introduction of neutral substrates can yield explicit data regarding the reactivity of these ions in the vapor phase. Cooks and co-workers have developed the use of quadrupole ion trap tandem mass spectrometry[59] and pentaquadrupole mass spectrometry[60] to investigate reactions of organic substrates with borinium cations.[61–63] These MS^2 and MS^3 experiments also allow for isolation of the borinium cation and subsequent reactions with neutral substrates. The use of a flowing afterglow-selected ion flow tube (FA-SIFT), as already mentioned (Section 2.1), has allowed for the moderate-pressure generation of BH_2^+ ions. The additional capability of this instrument to select for a single m/z ratio has facilitated the study of the reactivity of these ions.[20]

Chemical ionization mass spectrometry (CI-MS) has also been employed by both Yaozu[64] and Brodbelt.[55] However, this technique differs principally from the previous two in that the borinium cation is often not isolated prior to reactions with neutral reagents. This approach makes the assignment of the fragment ions more arduous and isotopic-labeling studies are often essential to verify the molecular formula of the fragment ions.

Both ^{10}B and ^{2}D (deuterium) labeling of reactants have proven useful in the confirmation of product-ion identities. Reactions performed with ^{10}B-doped borinium ions provide diagnostic signals for the boron-containing product ions one m/z value lower than the analogous nonlabeled ions; the reaction of ions with deuterated substrates gives the expected perturbations to the m/z ratios.

3.1.1 Gas-Phase Affinities for Donor Molecules

Thermochemical information can play an important role in the development of ion-molecule chemistry, the elucidation of product-ion structures, and the prediction of mechanisms.[65] Thus, in addition to serving as potent electrophiles for various organic conversions (Section 3.1.2), borinium cations have also been utilized as reagents for the determination of relative gas-phase binding affinities. Many such studies have used the readily generated $B(OMe)_2^+$ and BMe_2^+ ions.

Prior to the development of more advanced MS technology Staley and co-workers looked at the reactivity of the BMe_2^+ ion by ICR-MS and determined binding affinities for several species, both anionic and neutral. By studying the transfer of anionic groups to and/or from the BMe_2^+ ion in exchange reactions with species of known affinities for these groups they were able to determine the chloride (192.5 ± 3 kcal mol^{-1}), fluoride (238.5 ± 3 kcal mol^{-1}), and methide (250 ± 15 kcal mol^{-1}) anion affinities for the BMe_2^+ ion. Relative affinities for a variety of neutral donors L that form monoadducts $[BMe_2(L)]^+$ with BMe_2^+ were determined, by the preferred direction of displacement reactions, to be: $Me_2S < MeCN < C_6H_5OMe < Me_2O < C_6H_5CN <$ pyridine, in keeping with previously described preferences for stabilization by nitrogen-based donors, particularly aromatic amines.[17]

Brodbelt and co-workers have used an equilibrium method, which looks at the position of equilibrium or the rate of cation transfer between two bases, to determine gas-phase affinities of several substituted pyridines for B(OMe) BMe_2^+.[66] Results showed a general correlation with gas-phase basicities, with the differences in binding affinities for dimethyl- and methyl-substituted pyridines consistent with the differences in the analogous gas-phase basicities upon comparison of species with either no *ortho*-substitution (e.g. 3,5-dimethylpyridine vs. 3-methylpyridine) or a consistent degree of *ortho*-substitution (e.g. 2,4-dimethylpyridine vs. 2-methylpyridine). However, comparison of an *ortho*-substituted pyridine such as 2,3-dimethylpyridine with *meta*-methylated 3-methylpyridine showed deviation from this trend and indicated that different steric effects near the site of cation attachment can have a significant effect on binding affinities for the anisotropic borinium ions, when compared with the small spherically symmetric proton.

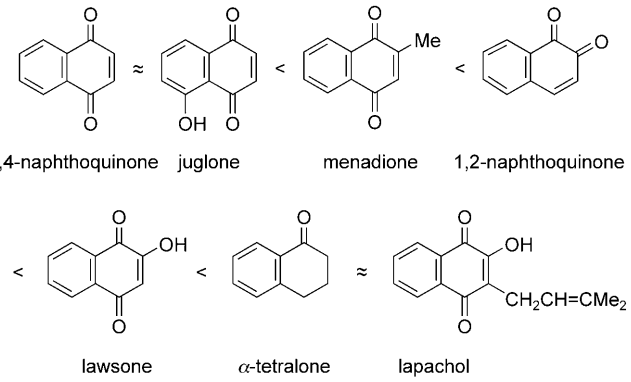
In an effort to obtain more systematic and reliable thermochemical data on borinium ions Cooks and co-workers carried out similar studies on the gas-phase affinities of the borinium ions B(OMe) BMe_2^+ and $HBOMe^+$ for a large set of pyridines. The investigation was by means of kinetic methods that involve the competitive dissociation of mass-selected cluster ions under collision-induced dissociation (CID) or metastable ion conditions.[65] In such studies, the ratio of rates of competitive dissociations of cation-bound diadducts (A-M^+-B) can be used to estimate the difference in affinity ($\Delta M^+_{affinity}$) of the cation for two substrates (A and B), based upon the relative abundances of the monoadduct products ($[AM^+]/[BM^+]$) of dissociation [Eq. (9)]. This method is sensitive to small thermochemical differences and has been widely used to measure proton affinities of various compounds. In addition, the method has been extended towards the measurements of electron and small-ion affinities (e.g. NH_4^+, NO_2^+, $OCNCO^+$, $SiCl^+$, $SiCl_3^+$, SF_3^+).[65,67] The relative affinities of $B(OMe)_2^+$ or $HBOMe^+$ for a variety of pyridines were also determined via on-molecule reactions using similar methods.[65]

$$\ln \frac{[AM^+]}{[BM^+]} = \frac{\Delta M^+_{affinity}}{R T_{eff}} \quad (9)$$

Brodbelt and co-workers have also used the $B(OMe)_2^+$ ion to assess the relative basicities and binding affinities of a number of classes of bioactive molecules.[55,68,69] Ion trap mass spectrometry,[59] was used to monitor the reactions of isolated $B(OMe)_2^+$ ions with various quinones (Q).[69] The initial product in most cases was the quinone–borinium adduct $(Q1)\cdot B(OMe)_2^+$ which could be isolated. Addition of a second quinone (Q2) and analysis of the relative intensities of the $(Q1)\cdot B(OMe)_2^+$ and $(Q2)\cdot B(OMe)_2^+$ signals yielded the

 © 2005 Wiley-VCH Verlag GmbH & Co. KGaA, Weinheim

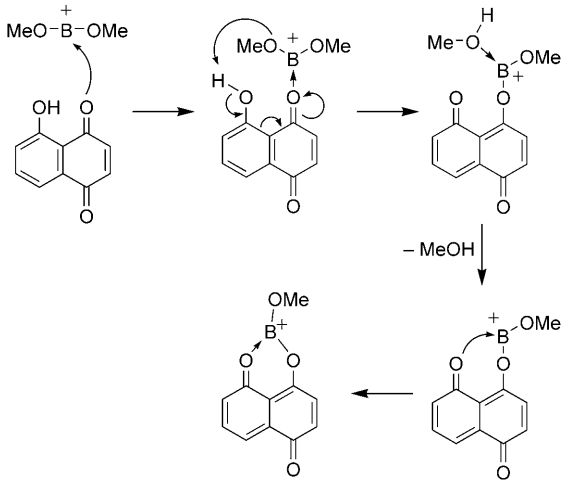
relative binding affinities of the two substrates. The relative scale of binding affinities shown in Scheme 11 closely parallels the gas-phase basicities, the exception being the inversion of the relative affinities for 1,2-naphthoquinone and lawsone which is due an interaction between a secondary hydroxy group proton and the borinium methoxide.



Scheme 11. Relative $B(OMe)_2^+$-ion affinity for a series of quinones (Q).

Although many of these adducts are relatively stable, upon collisional activation the presence of a proximal hydroxy substituent can lead to further reactions. It has been proposed that this reaction occurs first by internal proton transfer of the acidic hydroxy proton to one of the Q·$B(OMe)_2^+$ methoxy oxygen atoms and subsequent collapse of the complex with the concomitant loss of methanol. In the case of juglone this reaction leads to the generation of a tricyclic borenium ion (Scheme 12, which poses a potentially interesting synthetic target for the solution chemist.

Complex organic substrates that have multiple functional groups have also been adopted for the evaluation of the reactivity of gas-phase borinium cations. Barbiturates are a common family of pharmaceutical reagents based primarily on derivatized (e.g. with carbonyl and amine substituents)



Scheme 12. Proposed mechanism for the cyclization of juglone in the presence of $B(OMe)_2^+$.

pyrimidine rings. Studies of reactions between barbiturates and the $B(OMe)_2^+$ ion have provided valuable information about the binding affinities of these highly Lewis acidic reagents for various functional groups.[68] A test reaction performed with barbital revealed a signal in the CI-MS that corresponds to the borinium–barbital adduct less methanol. This result offered little evidence for the site of nucleophilic attack as possible mechanisms can implicate either oxygen or nitrogen binding. Other competition studies between piperidine, cyclohexanone, and glutarimide indicated that, although carbonyl groups are characteristically stronger Lewis bases than amidic nitrogen atoms, nitrogen in the barbital ring is the thermodynamically favored binding site for such rings. This observation is consistent with the vast number of stable condensed-phase borocations bearing nitrogen-containing ligands and the dearth of analogous alkoxy-based cations.[3] The observed affinities also imply that adjacent carbonyl groups can reduce the binding affinity of the amidic site.

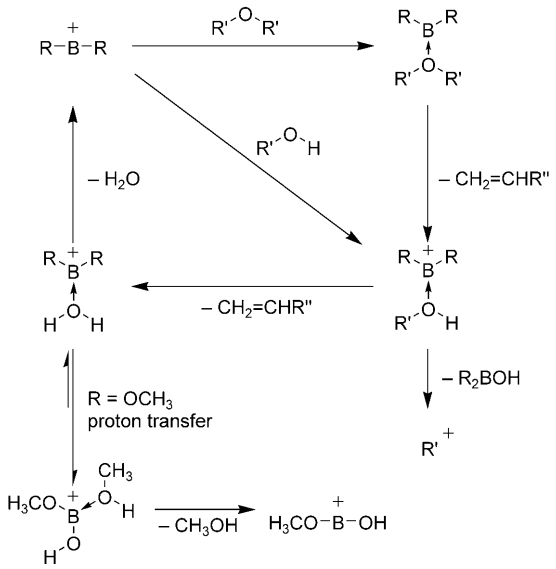
3.1.2 ***Gas-Phase Reactions***

In many cases borinium ions generated upon electron ionization of borane or borate precursors have been found to react strongly and relatively selectively with organic substrates. These reactions give only a few ionic products that yield valuable structural information about the substrates (e.g. with quinines, Section 3.1.1). Thus, borinium ions can act as efficient chemical ionization reagents for the mass spectrometric analysis of a variety of organic molecules. It must be noted that the reactivity seen in the gas phase is under highly idealized nonsolvated conditions and is probably not directly transferable to condensed phases. Therefore, although these studies are collectively fairly comprehensive and offer insights into the kinds of rearrangements triggered by borinium ions, they will not be treated in detail herein.

However, to exemplify the character of these reactions, we will discuss some of the first investigations to evaluate the reactivity of borinium cations with neutral organic molecules, namely the reactivity of BMe_2^+ and $B(OMe)_2^+$ towards a series of ethers (R′OR′)[56] and alcohols (R′OH).[70] Generation, collisional cooling, and isolation of the borinium ion BR_2^+ (R = Me or OMe), introduction of a R′OR′ or R′OH, and subsequent monitoring of the ionic reaction products by mass spectrometry led to a proposal for the mechanism of the observed dehydration of the ROH and ROR substrates (Scheme 13).

The first step of the proposed mechanism necessarily involves nucleophilic attack at the borinium center, by oxygen, to form a borenium ion (R_2B-OR'_2^+ or R_2B-$O(H)R'^+$). This type of interaction is supported by analogous results obtained for ethers in the presence of other electrophilic species; ethers in acidic media become protonated to form the analogous oxonium ion before proceeding to form an alcohol through counterion-induced loss of an alkyl or aryl function.[71] Under gas-phase conditions interaction of the borenium ion with a counterion is unlikely and the ionic products support the proposed C–O cleavage and loss of a neutral alkene, by way of a proton-bound adduct. While

© 2005 Wiley-VCH Verlag GmbH & Co. KGaA, Weinheim



Scheme 13. Proposed mechanism for the gas-phase dehydration of alcohols and ethers by borinium ions R_2B^+ (R = Me or OMe).[56,70]

ethers must undergo two stepwise alkene eliminations, alcohols need only undergo one to give the ionic dehydration product $R_2B\text{-}OH_2^+$, and/or its more stable rearrangement product $(HO)RB\text{-}RH^+$. The prevalence of alkyl elimination versus alkyl cation formation (hydroxy abstraction) is dependent upon the instability of the proposed alkyl cation. Thus alkyl elimination dominates for short-chain alcohols and ethers capable of alkene elimination. As inferred by the mechanism proposed in Scheme 13, and later confirmed by experiment, compounds unable to eliminate an alkene (i.e. methanol or alkylmethyl ethers) do not undergo dehydration, and collisional activation leads only to methanol dissociation from the borenium ion. Although gas-phase proton-catalyzed dehydration of alcohols is well known, the facile ionic dehydration of alcohol and ether functional groups by borinium ions is notable.

Using these methods and techniques, the reactions of borinium ions, such as $B(OMe)_2^+$, with a variety of organic functional groups have led to the identification of reactivity patterns expected upon complexation of the organic function to the boron cation. The *cis* and *trans* isomers of 1,2-cyclopentane diols have different reactivities[64,72] because of their different geometries. Five-membered acetals and ketals react with the $B(OMe)_2^+$ ion[61] and with the much more electron-rich bis(dimethylamino)borinium cation $(B(NMe_2)_2^+)$[62] to effect *trans*-acetalization by the elimination of, for example, acetone. Similar reactivity patterns have been observed in the reactions of these substrates with phosphonium ions such as $OP^+(OMe)_2$.[73] Kenttämaa and co-workers have also examined the reactivity of borinium ions with carbonyl-containing species such as aldehydes and ketones,[74] Small compounds, such as acetaldehyde, propanal, acetone, and 2-butanone, tend to form stable adducts, while aldehydes and ketones that contain alkyl chains of three or more carbon atoms are subject to abstraction of a smaller aldehydes and/or hydroxy groups by way of C–C bond cleavage. FTICR-MS was also utilized in the study of the reactions of borinium cations with a series of methyl and ethyl carboxylate esters[70,75] and organic amides.[63,76]

The above studies all utilize relatively stable borinium ions containing electron-rich substituents (Me, OMe, NMe_2). The gas-phase behavior of the simplest borinium ion BH_2^+ has long been of interest, but, as previously mentioned, the ability to study the chemistry of the BH_2^+ ion has only recently become possible through the use of new MS techniques. Studies into its reactivity with simple molecules such as H_2 and CH_4 have revealed it to react generally by a mechanism of addition followed by H_2 elimination.[20] Reactions with D_2 revealed an isotope exchange which was calculated to proceed by association of H_2 to boron through a three-center-two-electron (3c–2e) bond to form planar BH_4^+, followed by subsequent rearrangement and dissociation. Similar calculations on the structure of the BH_4^+ ion performed by Olah and co-workers revealed that, although the bulk of the charge remains on boron, a significant amount resides on the 3c–2e H_2 fragment (2×0.19).[77] Existence of the $[BH_2(H_2)]^+$ intermediate, which may be viewed as a borenium ion, was confirmed by experiments run at higher H_2 pressures, the presence of the diadduct boronium ion, $[BH_2(H_2)_2]^+$, was also revealed.

Reactions with methane parallel those of the CH_3^+ ion. However, in contrast, deuterium labeling studies (BD_2^+) have revealed greater selectivity for methane, with the exclusive elimination of HD, rather than the statistical mixture of products observed for CH_3^+ reactions. Reactions with ethane are rapid and involve addition followed by elimination of either H_2 or CH_4. The mechanism of addition followed by H_2 elimination was also observed for other small reagents such as H_2O, H_2S, and NH_3.

Olah and co-workers have further explored the reactivity of the ions BH_2^+ and BCl_2^+ with simple aldehydes and alkenes by means of DFT calculations at the B3LYP/6-311G** level.[78] Aldehydes were found to associate with the borinium ions to form an oxygen-coordinated nonplanar allylic species. While the BH_2^+ adduct can subsequently undergo a hydride shift from the BH_2 group to the carbonyl carbon an analogous chloride shift was calculated to be endothermic. In contrast, association of the borinium ions with ethene was by means of a 3c–2e bond involving the boron atom and two carbon atoms (unsymmetrical for BCl_2^+). Hydride transfer from the BH_2 unit to one of the carbon atoms was less exothermic than that calculated in the case of the homologous aldehydes while calculations of the chloride transfer from the BCl_2 unit were not feasible owing to facile rearrangement to a stable cyclic chloronium structure. Interestingly, reactions of the BH_2^+ and BCl_2^+ ions with propene were found to give unbridged structures and hydride and chloride transfers to the resulting carbocations were endothermic or not found, respectively.

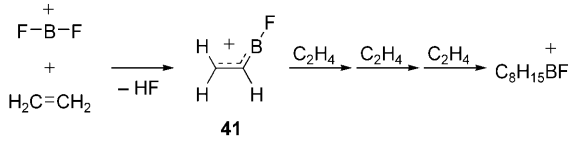
3.1.3 Initiation of Oligomerization of Olefinic Monomers by Gaseous BF_2^+

For olefin polymerization, catalysts that exhibit both coordinative and electronic unsaturation are preferred, as the former provides a binding site for the monomer while the latter is often necessary to support monomer coupling. Two-

 © 2005 Wiley-VCH Verlag GmbH & Co. KGaA, Weinheim

coordinate borinium cations fulfill these requirements and were the first borocations to be tested as olefin polymerization catalysts. Bohme and co-workers were able to observe gas-phase oligomerization of olefinic monomers by BF_2^+.[79,80] These researchers utilized the selected-ion flow tube (SIFT)[81] technique to study the reactions of BF_2^+ (generated by electron impact at 55 to 80 eV from pure BF_3) with ethylene, propylene, isobutene, *cis*-2-butene, and styrene.

Upon introduction of ethylene into the flow-tube, reaction with the borinium ion by means of HF elimination is evidenced by the appearance of a signal that corresponds to a new borinium cation **41** (Scheme 14). As the parent BF_2^+



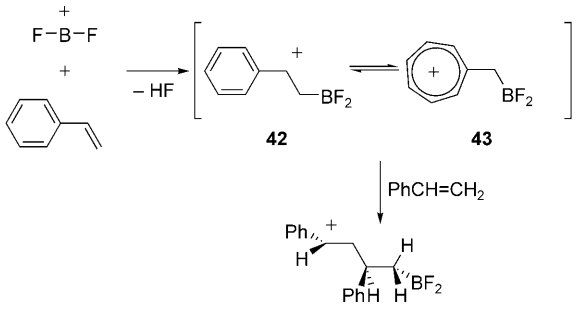
41

Scheme 14. Initiation of the oligomerization of ethylene by BF_2^+.

ion is consumed the sequential addition of up to three ethylene units to **41** can be detected, although experimentally calculated rate constants indicate that ethylene addition becomes progressively less efficient as the reaction proceeds.

Calculations at the 6-31G*/6-31G* level of theory predict ethylene addition to BF_2^+ to be exothermic by -58 kcal mol^{-1}. A Mullikan population analysis of the two possible resonance structures (boro- and carbocations) indicate an energetic preference for localization of the cationic charge on boron. This result is further supported by STO-3G level calculations on the subsequent attack of ethylene by **41**, which showed that attack at the boron was 38 kcal mol^{-1} lower in energy than attack at a terminal carbenium center. However, all additional polymerization steps would proceed through terminal carbenium ions. Similar reactivity was observed for the oligomerization of acetylene,[80] while parallel studies with *cis*-2-butene and isobutene were more complex owing to isomerization side reactions.

In contrast to the multiple products obtained from the isomeric butene reagents, the addition of styrene to gaseous BF_2^+ ions yielded only one primary product, believed to be the adduct ion **42**, which may also be in equilibrium with a tropylium-type ring **43**. Experiments only provided evidence for the addition of one further styrene unit (Scheme 15). However, it has been proposed that further polymerization



42 43

Scheme 15. Proposed reaction of BF_2^+ with two equivalents of styrene.

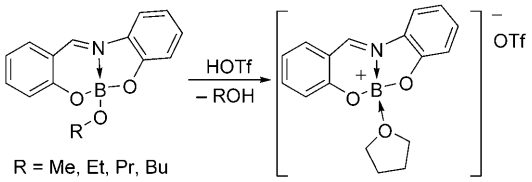
may occur under optimized conditions. Propylene does not exhibit the same reactivity owing to rapid formation of $C_3H_5^+$ followed by termination.

3.2 Synthesis with Condensed-Phase Boron Cations

Since the early studies into condensed-phase cationic boron compounds in 1955,[22] the thrust has been the development of novel structure and bonding motifs for these notoriously unstable species. However, the accumulated data concerning borocations as well as their heavier Group 13 analogues[2] has encouraged investigations into potential applications of these inherently electrophilic species. Recent reports have exploited the properties that make these species so reactive, particularly in condensed phases, in the development of new applications. Thus far, studies in this nascent area have shown borocations to behave as catalysts in polymerization studies (see also section 3.1.3 for gas-phase polymerization studies), as well as enantioselective Lewis acid activators in Diels–Alder reactions.

3.2.1 Polymerization of Propylene Oxide by a Boronium Catalyst

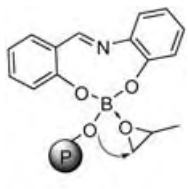
Studies that have shown the successful polymerization of propylene oxide (PO) by aluminum cations[82] have led to the development of analogous borocation systems. Atwood and Wei have used a tridentate O-N-O ligand to prepare a base-coordinated boronium cation and evaluated its capacity to polymerize PO.[83] The boronium salt was prepared by treatment of the parent boronic acid derivative with a strong protic acid to form the corresponding boronium species **44**-OTf, with concomitant loss of alcohol [Eq. (10)].



44 (10)

The signal at $\delta = 3.91$ ppm in the ^{11}B NMR spectrum confirms the presence of a four-coordinate borocation center with a THF donor ligand, the coordination environment about the boron center is believed to be tetrahedral.

Cation **44** was found to polymerize PO at similar rates at room temperature and slightly elevated temperatures, which indicated a moderate efficiency for this reaction. In the proposed mechanism, coordinated PO is activated towards nucleophilic attack by the triflate anion. Subsequent cleavage of the dative B–N bond to provide a vacant coordination site for the incoming PO unit (as in **45**) is implicated. An alternative mechanism would require cleavage of the B–O covalent bond of the polymeric chain, which is substan-



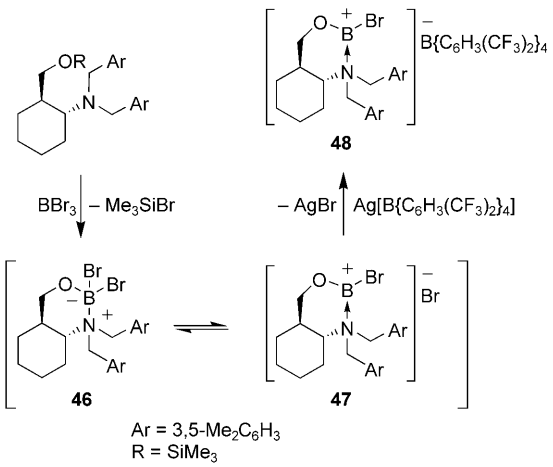
45

© 2005 Wiley-VCH Verlag GmbH & Co. KGaA, Weinheim

tially stronger than the B–N coordinative bond, and is therefore unlikely.

3.2.2 Borocation-Mediated Enantioselective Diels–Alder Reactions

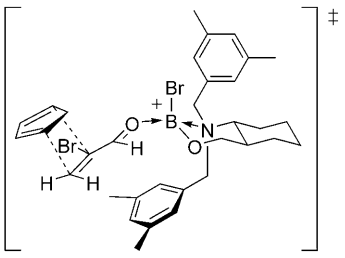
The introduction of Lewis acids, particularly chiral analogues, as catalysts has made Diels–Alder transformations a very powerful tool in organic synthesis. Corey and co-workers[84] designed an enantiopure borenium cation **46** (Scheme 16) and examined its utility for the coupling of



Scheme 16. Synthesis of the borenium-cation catalyst **48**.

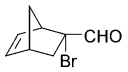
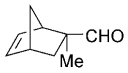
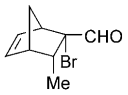
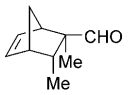
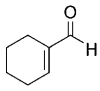
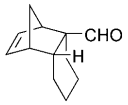
cyclopentadiene with α,β-unsaturated aldehydes. The catalyst exists in equilibrium with the ammonium-borate ylid **47**. The equilibrium can be shifted towards the fully ionic form (**48**) when the reaction of the precursor ligand with BBr_3 is conducted in the presence of $Ag[B\{C_6H_3\text{-}3,5\text{-}(CF_3)_2\}_4]$. Although complete conversion into **48** is never achieved, the activity of the equilibrium mixture is still reasonably good.

A summary of the results obtained from the couplings a series of α,β-unsaturated aldehydes with cyclopentadiene in the presence of 10 mol% of **46**/**47** is outlined in Table 3. *Exo*/*endo* ratios were determined by ^{1}H NMR spectroscopy. The enantioselectivities were extrapolated by a) reduction of the products to the corresponding primary alcohols using $NaBH_4$, b) conversion into the Mosher ester, and c) ^{1}H NMR spectroscopic analysis. A transition state (**49**), in which the bottom face is sterically obstructed by one aryl ring while the other



49

Table 3: Enantioselective Diels–Alder reactions of various α,β-unsaturated aldehydes with cyclopentadiene.[a]

Dienophile	*Exo*:*endo*	Yield [%]	*ee* [%] (config)	Product
	94:6	99	95 (2*R*)	
	88:12	99	90 (2*S*)	
	>98:2	99	91	
	>98:2	88	89	
	>98:2	99	96	

[a] Reactions in CH_2Cl_2 at −94 °C for 2 h.

ring limits the rotational freedom of the incoming cyclopentadiene, was proposed based on these results. An X-ray structure of the hydrochloride salt of the ligand precursor depicts a similar arrangement of the aromatic substituents and supports this proposal.

Since this initial work, Corey and co-workers have reported several similar catalysts that are based on oxaazaborolidines and also function as highly enantioselective catalysts for Diels–Alder condensations.[85] These results indicate the general applicability of such borenium catalysts for enantioselective Diels–Alder condensations and highlight the potential for such species as catalysts for other organic transformations.[86]

4. Summary and Outlook

Cationic boron species were discovered half a century ago, and although activity in the area has been steady, their high Lewis acidity and reactivity has only just begun to be harnessed in useful ways. Advances in ligand design and weakly coordinating anion technology has enhanced our ability to generate and study these elusive species in the condensed phase, while gas-phase experiments using sophisticated mass spectrometric techniques have provided a useful reactivity map to act as a guide for developing applications of these species. As the discussion above indicates, these applications are beginning to appear. Particularly exciting are the potential of well-designed boron cations as Lewis acid catalysts in polymerization reactions and organic transformations. The incorporation of cationic boron centers in organic heterocycles or transition-metal metallocenes is also providing opportunities for the development of new redox active and optical materials. Furthermore, the strategy of preparing cationic compounds based on boron that are isoelectronic with, for example, ammonium-based cations potentially opens up new areas in bioorganic chemistry. These emerging studies indicate that the chemistry of cationic boron com-

 © 2005 Wiley-VCH Verlag GmbH & Co. KGaA, Weinheim

pounds is on the cusp of a quantum leap in activity; it is our hope that this review will stimulate further activity in this exciting area of research.

Received: February 3, 2005

[1] a) E. Y.-X. Chen, T. J. Marks, *Chem. Rev.* **2000**, *100*, 1391 – 1434, and references therein; b) W. E. Piers, *Adv. Organomet. Chem.* **2005**, *52*, 1 – 77.
[2] D. A. Atwood, *Coord. Chem. Rev.* **1998**, *176*, 407 – 430.
[3] P. Kölle, H. Nöth, *Chem. Rev.* **1985**, *85*, 399 – 418, and references therein.
[4] O. P. Shitov, S. L. Ioffe, V. A. Tartakovskii, S. S. Novikov, *Russ. Chem. Rev.* **1970**, *39*, 905 – 922.
[5] G. E. Ryschkewitsch in *Boron Hydride Chemistry* (Ed.: E. L. Muetterties), Academic Press, New York, **1975**, pp. 223 – 239.
[6] A. D. Dilman, S. L. Ioffe, *Chem. Rev.* **2003**, *103*, 733 – 772.
[7] H. Nöth, R. Staudigl, H.-U. Wagner, *Inorg. Chem.* **1982**, *21*, 706 – 716.
[8] B. Rasthofer, Ph.D. thesis, University of Munich **1984**. Some details of this work are reported in ref. [3].
[9] P. Kölle, H. Nöth, *Chem. Ber.* **1986**, *119*, 313 – 324.
[10] a) C. K. Narula, H. Nöth, *J. Chem. Soc. Chem. Commun.* **1984**, 1023 – 1024; b) C. K. Narula, H. Nöth, *Inorg. Chem.* **1984**, *23*, 4147 – 4152; c) C. K. Narula, H. Nöth, *Inorg. Chem.* **1985**, *24*, 2532 – 2539.
[11] R. Köster in *Methoden Org. Chem. (Houben-Weyl)*, *4th ed.*, Vol. *13/3a*, **1984**, p. 1, 12.
[12] W. F. Schneider, C. K. Narula, H. Nöth, B. E. Bursten, *Inorg. Chem.* **1991**, *30*, 3919 – 3927.
[13] S. Courtenay, J. Y. Mutus, R. W. Schurko, D. W. Stephan, *Angew. Chem.* **2002**, *114*, 516 – 519; *Angew. Chem. Int. Ed.* **2002**, *41*, 498 – 501.
[14] V. H. Dibeler, F. L. Mohler, *J. Am. Chem. Soc.* **1948**, *70*, 987 – 989.
[15] a) R. W. Law, J. L. Margrave, *J. Chem. Phys.* **1956**, *25*, 1086 – 1087; b) B. C. Tollin, R. Schaeffer, H. J. Svec, *J. Inorg. Nucl. Chem.* **1957**, *4*, 273 – 278; c) O. Osberghaus, *Z. Phys.* **1950**, *128*, 366 – 377; d) Y. Wada, R. W. Kiser, *J. Phys. Chem.* **1964**, *68*, 1588 – 1590; e) P. J. Fallon, P. Kelly, J. C. Lockhart, *Int. J. Mass Spectrom. Ion Phys.* **1968**, *1*, 133 – 139; f) R. H. Cragg, J. F. J. Todd, A. F. Weston, *J. Chem. Soc. Dalton Trans.* **1972**, 1373 – 1375; g) R. L. Hettich, T. Cole, B. S. Freiser, *Int. J. Mass Spectrom. Ion Processes* **1987**, *81*, 203 – 215.
[16] M. K. Murphy, J. L. Beauchamp, *J. Am. Chem. Soc.* **1976**, *98*, 1433 – 1440.
[17] M. M. Kappes, J. S. Uppal, R. H. Staley, *Organometallics* **1982**, *1*, 1303 – 1307.
[18] R. Srinivas, S. Vivekananda, S. J. Blanksby, D. Schröder, H. Schwarz, L. M. Fell, J. K. Terlouw, *Int. J. Mass Spectrom.* **2000**, *197*, 105 – 111.
[19] a) M. Attinà, F. Cacace, A. Ricci, F. Grandinetti, G. Occhiucci, *J. Chem. Soc. Chem. Commun.* **1991**, 66 – 68; b) J. S. Ogden, N. A. Young, *J. Chem. Soc. Dalton Trans.* **1988**, 1645 – 1652.
[20] C. H. DePuy, R. Garayev, J. Hankin, G. E. Davico, M. Krempp, R. Damrauer, *J. Am. Chem. Soc.* **1998**, *120*, 5086 – 5092.
[21] R. C. Dunbar, *J. Am. Chem. Soc.* **1968**, *90*, 5676 – 5682.
[22] S. G. Shore, R. W. Parry, *J. Am. Chem. Soc.* **1955**, *77*, 6084 – 6085.
[23] a) D. R. Schultz, R. W. Parry, *J. Am. Chem. Soc.* **1958**, *80*, 4 – 8; b) S. G. Shore, R. W. Parry, *J. Am. Chem. Soc.* **1958**, *80*, 8 – 12; c) S. G. Shore, R. W. Parry, *J. Am. Chem. Soc.* **1958**, *80*, 12 – 15; d) R. W. Parry, S. G. Shore, *J. Am. Chem. Soc.* **1958**, *80*, 15 – 20; e) S. G. Shore, P. R. Girardot, R. W. Parry, *J. Am. Chem. Soc.* **1958**, *80*, 20 – 24.
[24] J. Higashi, A. D. Eastman, R. W. Parry, *Inorg. Chem.* **1982**, *21*, 716 – 720.
[25] a) H. Nöth, B. Rasthofer, S. Weber, *Z. Naturforsch. B* **1984**, *39*, 1058 – 1068; b) S. Weber, Ph.D. thesis, University of Munich **1984**; c) H. Nöth, S. Weber, *Chem. Ber.* **1985**, *118*, 2144 – 2146; d) H. Nöth, B. Rasthofer, *Chem. Ber.* **1986**, *119*, 2075 – 2079.
[26] P. Kölle, H. Nöth, *Chem. Ber.* **1986**, *119*, 3849 – 3855.
[27] J. Rissler, M. Hartmann, C. M. Marchand, H. Grützmacher, G. Frenking, *Chem. Eur. J.* **2001**, *7*, 2834 – 2841.
[28] M. Möhlen, B. Neumüller, K. Dehnicke, *Z. Anorg. Allg. Chem.* **1998**, *624*, 177 – 178.
[29] a) D. L. Coombs, S. Aldridge, C. Jones, D. J. Willock, *J. Am. Chem. Soc.* **2003**, *125*, 6356 – 6357; b) D. L. Coombs, S. Aldridge, S. J. Coles, M. B. Hursthouse, *Organometallics* **2003**, *22*, 4213 – 4217; c) D. L. Coombs, S. Aldridge, A. Rossin, C. Jones, D. J. Willock, *Organometallics* **2004**, *23*, 2911 – 2926.
[30] P. Jutzi, B. Krato, M. Hursthouse, A. J. Howes, *Chem. Ber.* **1987**, *120*, 1091 – 1098.
[31] N. Kuhn, A. Kuhn, J. Lewandowski, M. Speis, *Chem. Ber.* **1991**, *124*, 2197 – 2201.
[32] A. H. Cowley, Z. Lu, J. N. Jones, J. A. Moore, *J. Organomet. Chem.* **2004**, *689*, 2562 – 2564.
[33] a) D. P. Gates, A. R. McWilliams, R. Ziembinski, L. M. Liable-Sands, I. A. Guzei, G. P. A. Yap, A. L. Rheingold, I. Manners, *Chem. Eur. J.* **1998**, *4*, 1489 – 1503; b) D. P. Gates, R. Ziembinski, A. L. Rheingold, B. S. Haggerty, I. Manners, *Angew. Chem.* **1994**, *106*, 2367 – 2369; *Angew. Chem. Int. Ed. Engl.* **1994**, *33*, 2277 – 2279.
[34] I. Ghesner, W. E. Piers, R. McDonald, *Chem. Commun.* **2005**, 2480 – 2482.
[35] E. Vedejs, T. Nguyen, D. R. Powell, M. R. Schrimpf, *Chem. Commun.* **1996**, 2721 – 2722.
[36] M. G. Davidson, M. A. Fox, T. G. Hibbert, J. A. K. Howard, A. Mackinnon, I. S. Neretin, K. Wade, *Chem. Commun.* **1999**, 1649 – 1650.
[37] D. J. Brauer, H. Bürger, G. Pawelke, W. Weuter, J. Wilke, *J. Organomet. Chem.* **1987**, *329*, 293 – 304.
[38] M. Yalpani, R. Köster, R. Boese, W. A. Brett, *Angew. Chem.* **1990**, *102*, 318 – 320; *Angew. Chem. Int. Ed. Engl.* **1990**, *29*, 302 – 304.
[39] G. Agrifoglio, *Inorg. Chim. Acta* **1992**, *197*, 159 – 162.
[40] J. H. Davis, Jr., J. D. Madura, *Tetrahedron Lett.* **1996**, *37*, 2729 – 2730.
[41] T. G. Hodgkins, D. R. Powell, *Inorg. Chem.* **1996**, *35*, 2140 – 2148.
[42] H. Braunschweig, B. Ganter, *J. Organomet. Chem.* **1997**, *545*, 163 – 167.
[43] F. F. de Biani, T. Gmeinwieser, E. Herdtweck, F. Jäkle, F. Laschi, M. Wagner, P. Zanello, *Organometallics* **1997**, *16*, 4776 – 4787.
[44] E. Herdtweck, F. Jäkle, M. Wagner, *Organometallics* **1997**, *16*, 4737 – 4745.
[45] L. Ding, K. Ma, G. Dürner, M. Bolte, F. F. de Biani, P. Zanello, M. Wagner, *J. Chem. Soc. Dalton Trans.* **2002**, 1566 – 1573.
[46] R. E. Dinnebier, L. Ding, K. Ma, M. A. Neumann, N. Tanpipat, F. J. J. Leusen, P. W. Stephens, M. Wagner, *Organometallics* **2001**, *20*, 5642 – 5647.
[47] H. A. Jenkins, C. L. Dumaresque, D. Vidovic, J. A. C. Clyburne, *Can. J. Chem.* **2002**, *80*, 1398 – 1403.
[48] a) P. Jutzi, A. Seufert, W. Buchner, *Chem. Ber.* **1979**, *112*, 2488 – 2493; b) P. Greiwe, A. Bethäuser, H. Pritzkow, T. Kühler, P. Jutzi, W. Siebert, *Eur. J. Inorg. Chem.* **2000**, 1927 – 1929.
[49] U. Holtmann, P. Jutzi, T. Kühler, B. Neumann, H.-G. Stammler, *Organometallics* **1999**, *18*, 5531 – 5538.
[50] A. Voigt, S. Filipponi, C. L. B. Macdonald, J. D. Gorden, A. H. Cowley, *Chem. Commun.* **2002**, 911 – 912.
[51] P. Jutzi, A. Seufert, *Angew. Chem.* **1977**, *89*, 339 – 340; *Angew. Chem. Int. Ed. Engl.* **1977**, *16*, 330 – 331.
[52] O. Kwon, M. L. McKee, *J. Phys. Chem. A* **2001**, *105*, 10133 – 10138.

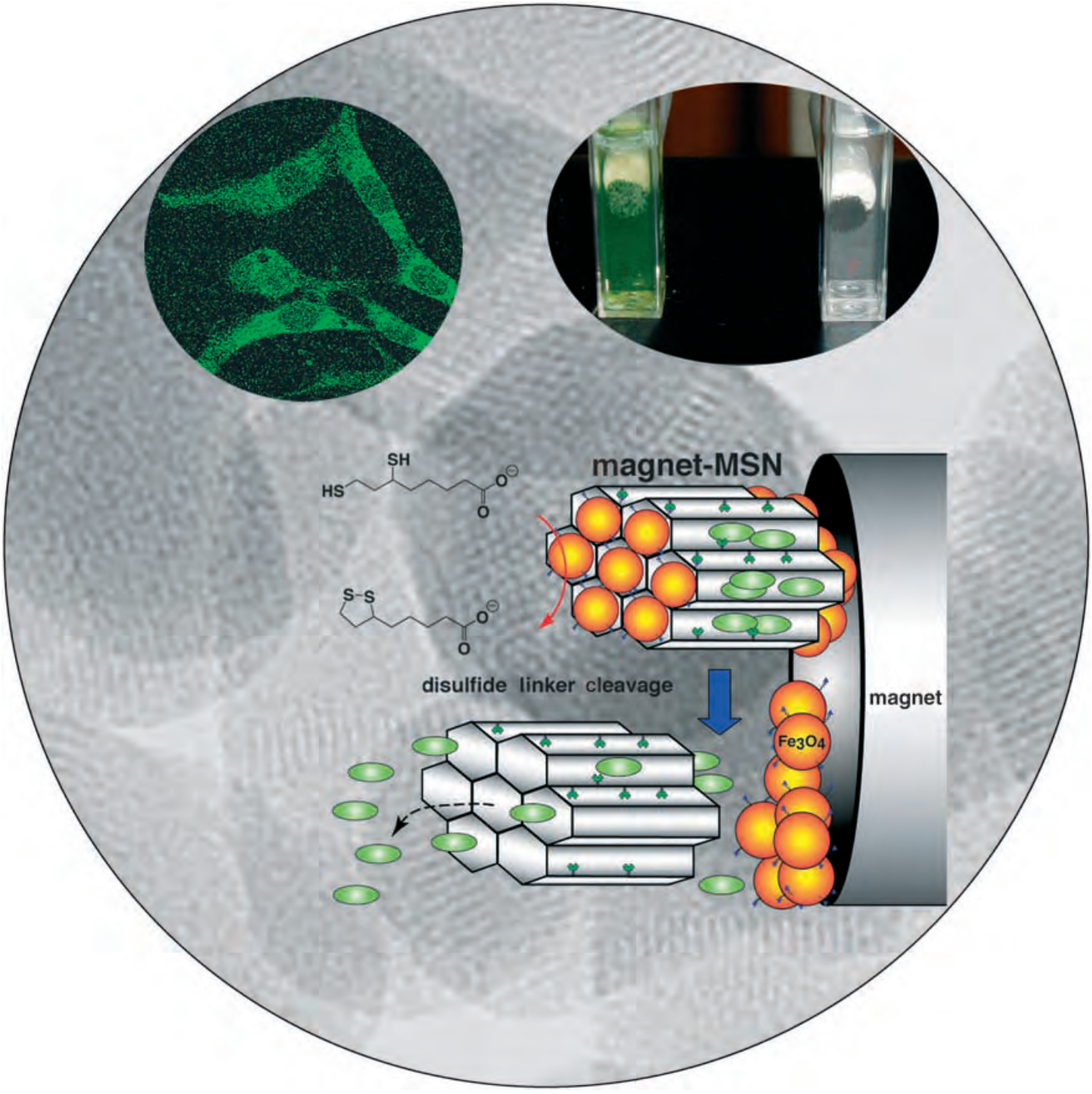
 © 2005 Wiley-VCH Verlag GmbH & Co. KGaA, Weinheim

[53] A. Blumenthal, H. Beruda, H. Schmidbaur, *J. Chem. Soc. Chem. Commun.* **1993**, 1005 – 1006.
[54] S. M. Draper, C. E. Housecroft, J. E. Rees, M. S. Shongwe, B. S. Haggerty, A. L. Rheingold, *Organometallics* **1992**, *11*, 2356 – 2367.
[55] E. C. Kempen, J. S. Brodbelt, *J. Mass Spectrom.* **1997**, *32*, 846 – 854.
[56] T. D. Ranatunga, H. I. Kenttämaa, *J. Am. Chem. Soc.* **1992**, *114*, 8600 – 8604.
[57] a) M. B. Comisarow, A. G. Marshall, *Chem. Phys. Lett.* **1974**, *25*, 282 – 283; b) J. T. Farrell, Jr., P. Lin, H. I. Kenttämaa, *Anal. Chim. Acta* **1991**, *246*, 227 – 232.
[58] J. R. de Laeter, *Applications of Inorganic Mass Spectrometry*, Wiley, Toronto, **2001**.
[59] J. N. Louris, R. G. Cooks, J. E. P. Syka, P. E. Kelley, G. C. Stafford, Jr., J. F. J. Todd, *Anal. Chem.* **1987**, *59*, 1677 – 1685.
[60] J. C. Schwartz, K. L. Schey, R. G. Cooks, *Int. J. Mass Spectrom. Ion Process* **1990**, *101*, 1 – 20.
[61] F. Wang, W. A. Tao, F. C. Gozzo, M. N. Eberlin, R. G. Cooks, *J. Org. Chem.* **1999**, *64*, 3213 – 3223.
[62] W. A. Tao, X. Zheng, R. G. Cooks, *J. Mass Spectrom.* **2000**, *35*, 1215 – 1221.
[63] X. Zheng, W. A. Tao, R. G. Cooks, *J. Am. Soc. Mass Spectrom.* **2001**, *12*, 948 – 955.
[64] H. Suming, C. Yaozu, J. Longfei, X. Shuman, *Org. Mass Spectrom.* **1985**, *20*, 719 – 723.
[65] S. Ma, P. Wong, R. G. Cooks, *J. Mass Spectrom.* **1997**, *32*, 159 – 166.
[66] J. J. Isbell, J. S. Brodbelt, *Rapid Commun. Mass Spectrom.* **1996**, *10*, 1418 – 1420.
[67] a) R. G. Cooks, T. L. Kruger, *J. Am. Chem. Soc.* **1977**, *99*, 1279 – 1281; b) S. A. McLuckey, D. Cameron, R. G. Cooks, *J. Am. Chem. Soc.* **1981**, *103*, 1313 – 1317.
[68] A. Colorado, J. Brodbelt, *J. Mass Spectrom.* **1996**, *31*, 403 – 410.
[69] B. J. Hall, J. S. Brodbelt, *Int. J. Mass Spectrom. Ion Processes* **1996**, *155*, 123 – 131.
[70] T. D. Ranatunga, H. I. Kenttämaa, *Inorg. Chem.* **1995**, *34*, 18 – 27.
[71] G. Bouchoux, Y. Hoppilliard, *J. Am. Chem. Soc.* **1990**, *112*, 9110 – 9115.
[72] D. T. Leeck, T. D. Ranatunga, R. L. Smith, T. Partanen, P. Vainiotalo, H. I. Kenttämaa, *Int. J. Mass Spectrom. Ion Processes* **1995**, *141*, 229 – 240.
[73] a) S. Kobayashi, R. Tokunoh, M. Shibasaki, R. Shinagawa, K. Murakami-Murofushi, *Tetrahedron Lett.* **1993**, *34*, 4047 – 4050; b) F. Wang, S. Ma, W. A. Tao, R. G. Cooks, *Angew. Chem.* **1999**, *111*, 399 – 401; *Angew. Chem. Int. Ed.* **1999**, *38*, 386 – 389.
[74] T. D. Ranatunga, J. M. Kennady, H. I. Kenttämaa, *J. Am. Chem. Soc.* **1997**, *119*, 5200 – 5207.
[75] K. K. Thoen, D. Tutko, T. D. Ranatunga, H. I. Kenttämaa, *J. Am. Soc. Mass Spectrom.* **1996**, *7*, 1138 – 1143.
[76] E. Uggerud, L. Bache-Andreassen, *Chem. Eur. J.* **1999**, *5*, 1917 – 1930.
[77] G. Rasul, G. A. Olah, *Inorg. Chem.* **1997**, *36*, 1278 – 1281.
[78] G. A. Olah, G. K. S. Prakash, G. Rasul, *ARKIVOC* **2002**, 7 – 18.
[79] a) L. Forte, M. H. Lien, A. C. Hopkinson, D. K. Bohme, *Makromol. Chem. Rapid Commun.* **1987**, *8*, 87 – 92; b) L. Forte, M. H. Lien, A. C. Hopkinson, D. K. Bohme, *Can. J. Chem.* **1989**, *67*, 1576 – 1583.
[80] L. Forte, M. H. Lien, A. C. Hopkinson, D. K. Bohme, *Can. J. Chem.* **1990**, *68*, 1629 – 1635.
[81] D. W. Grattan, P. H. Plesch, *J. Chem. Soc. Dalton Trans.* **1977**, 1734 – 1744.
[82] D. A. Atwood, J. A. Jegier, D. Rutherford, *Inorg. Chem.* **1996**, *35*, 63 – 70.
[83] P. Wei, D. A. Atwood, *Inorg. Chem.* **1998**, *37*, 4934 – 4938.
[84] Y. Hayashi, J. J. Rohde, E. J. Corey, *J. Am. Chem. Soc.* **1996**, *118*, 5502 – 5503.
[85] a) E. J. Corey, T. Shibata, T. W. Lee, *J. Am. Chem. Soc.* **2002**, *124*, 3808 – 3809; b) D. H. Ryu, T. W. Lee, E. J. Corey, *J. Am. Chem. Soc.* **2002**, *124*, 9992 – 9993; c) Q.-Y. Hu, G. Zhou, E. J. Corey, *J. Am. Chem. Soc.* **2004**, *126*, 13708 – 13713.
[86] For example, enantioselective cyanosilation of aldehydes and ketones: a) D. H. Ryu, E. J. Corey, *J. Am. Chem. Soc.* **2004**, *126*, 8106 – 8107; b) D. H. Ryu, E. J. Corey, *J. Am. Chem. Soc.* **2005**, *127*, 5384 – 5387.

 © 2005 Wiley-VCH Verlag GmbH & Co. KGaA, Weinheim

Communications

DOI: 10.1002/anie.200501819



The controlled release of fluorescein from a mesoporous silica/superparamagnetic iron oxide core/shell nanodevice in the presence of an external magnetic field takes place by using cell-produced antioxidants as stimuli. For more information on this promising approach to drug-delivery systems, see the Communication by V. S.-Y. Lin and co-workers on the following pages.

InterScience
© 2005 Wiley-VCH Verlag GmbH & Co. KGaA, Weinheim

Nanodevices

DOI: 10.1002/anie.200501819

Stimuli-Responsive Controlled-Release Delivery System Based on Mesoporous Silica Nanorods Capped with Magnetic Nanoparticles**

*Supratim Giri, Brian G. Trewyn, Michael P. Stellmaker, and Victor S.-Y. Lin**

Recent reports on surface-functionalized, superparamagnetic iron oxide nanoparticles have demonstrated their feasibility for use in a variety of biological applications such as drug/gene delivery,[1–5] magnetic resonance imaging,[6–9] bioseparation,[10–13] tissue repairing,[14] and thermal tumor therapy.[15–18] In contrast, only a few examples of controlled-release drug-delivery systems based on magnetic nanoparticles have been reported.[19,20] Most of these systems comprise magnetic nanoparticle "cores" coated with organic or inorganic "shell" constituents, and encapsulated within the layers of shells are the pharmaceutical drugs. In the presence of an external magnetic field, these core–shell materials are attracted toward the magnet. This magnetic motor effect is indeed attractive for the development of site-specific drug-delivery systems. However, many important site-selective delivery systems, such as those for highly toxic antitumor drugs, require "zero release" before reaching the targeted cells or tissues. To the best of our knowledge, no controlled-release delivery systems based on magnetic nanoparticles that are stimuli-responsive and capable of "zero premature release" have been reported.

Surface-functionalized mesoporous silica materials have been demonstrated to be excellent hosts of molecules of various sizes, shapes, and functionalities.[21–28] Recent reports[29–33] on the design of capped and gated mesoporous silica derivatives have shown promise in the generation of controlled-release nanodevices. Herein, we report the synthesis of a controlled-release delivery system that is based on MCM-41-type mesoporous silica nanorods (MSNs) capped with superparamagnetic iron oxide nanoparticles and is stimuli-responsive and chemically inert to guest molecules entrapped in the matrix.

The system consists of MSNs functionalized with 3-(propyldisulfanyl)propionic acid to give "linker-MSNs", which have an average particle size of 200 nm × 80 nm (length × width) and an average pore diameter of around 3.0 nm. As a proof of principle, fluorescein was used as the guest molecule to be encapsulated inside the linker-MSN material. By introducing dry linker-MSNs to an aqueous solution of fluorescein, the mesopores of the MSNs behaved like sponges by soaking up fluorescein molecules (Figure 1). Next, the openings of the mesopores of the fluorescein-loaded linker-MSN were covalently capped in situ through amidation[34] of the 3-(propyldisulfanyl)propionic acid functional groups bound at the pore surface with 3-aminopropyltriethoxysilyl-functionalized superparamagnetic iron oxide (APTS-Fe_3O_4) nanoparticles.[35] The disulfide linkages between the MSNs and the Fe_3O_4 nanoparticles are chemically labile and can be cleaved with various cell-produced antioxidants and disulfide reducing agents such as dihydrolipoic acid (DHLA) and dithiothreitol (DTT), respectively. The release of the magnetic nanoparticle caps from the fluorescein-loaded MSNs can be regulated by the concentration of trigger molecules (Figure 1).

The mercaptopropyl-derivatized mesoporous silica nanorods (thiol-MSNs) were initially prepared according to our previously reported co-condensation method.[31,33,36–41] After removal of the surfactant, thiol-MSNs were treated with 2-carboxyethyl-2-pyridyl disulfide to yield the acid-functionalized linker-MSNs. The rod shape, the average particle size, and the MCM-41-type mesoporous structure of the linker-MSNs were confirmed by transmission electron microscopy (TEM). The mesopores (porous channels) are represented by the alternating black and white stripes as shown in Figure 2a. The N_2 sorption isotherms of the material further revealed a BET isotherm typical of an MCM-41 structure (type IV), with a surface area of 1018.0 $m^2 g^{-1}$ and a narrow BJH pore-size distribution (average pore diameter: 3.0 nm).[42]

The superparamagnetic Fe_3O_4 nanoparticles coated with 3-aminopropylsiloxy groups (APTS-Fe_3O_4) were prepared according to a reported procedure.[34] The TEM micrograph (Figure 2b) of the resultant APTS-Fe_3O_4 particles revealed an average diameter of 10 nm for the particles. APTS-Fe_3O_4 nanoparticles (960.00 mg) were treated with the linker-MSNs (80.00 mg) in a solution of fluorescein (3.60 μM) in PBS medium (100.0 mM, pH 7.4). The resulting suspensions were centrifuged, and the Fe_3O_4–MSN-fluorescein material (magnet-MSNs) along with the unreacted APTS-Fe_3O_4 nanoparticles were isolated by filtration. The concentration of fluorescein in the filtrate was determined by UV/Vis spectroscopy to be 1.50 μM. The decrease in the concentration of fluorescein in solution ($\approx$2.10 μM) was attributed to the uptake of 1.68×10^{-8} moles of fluorescein by the MSNs which corresponds to a loading efficiency of approximately 58.3 mol%.

The successful incorporation of APTS-Fe_3O_4 nanoparticles in the MSN matrix was confirmed by various spectroscopic methods. The covalent immobilization of the surface-functionalized Fe_3O_4 nanoparticles to the linker-MSN led to a decrease in intensity of the powder X-ray diffraction (XRD) peaks (Figure 3a). Such a decrease in scattering contrast between the pores and the framework of the MCM-41 materials as a result of pore-filling has been reported previously.[43–46] Furthermore, a small increase was observed in the d_{100} (spacing) value of the Fe_3O_4-capped magnet-MSNs

[*] S. Giri, B. G. Trewyn, M. P. Stellmaker, Prof. Dr. V. S.-Y. Lin
Department of Chemistry and U.S. DOE Ames Laboratory
Iowa State University
Ames, Iowa 50011 (USA)
Fax: (+1) 515-294-0105
E-mail: vsylin@iastate.edu

[**] We thank the U.S. National Science Foundation (grant nos. CHE-0239570 and CMS-0409625) for financial support of this research.

Supporting information for this article is available on the WWW under http://www.angewandte.org or from the author.

 © 2005 Wiley-VCH Verlag GmbH & Co. KGaA, Weinheim

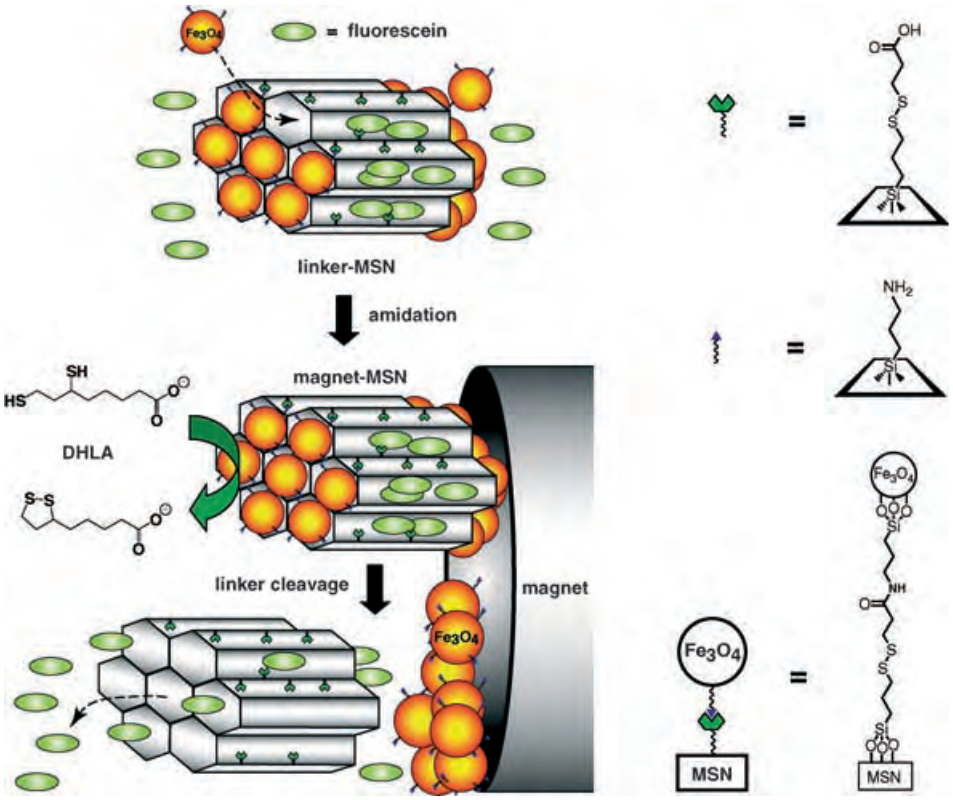


Figure 1. Schematic of the stimuli-responsive delivery system (magnet-MSN) based on mesoporous silica nanorods capped with superparamagnetic iron oxide nanoparticles. The controlled-release mechanism of the system is based on reduction of the disulfide linkage between the Fe_3O_4 nanoparticle caps and the linker-MSN hosts by reducing agents such as DHLA.

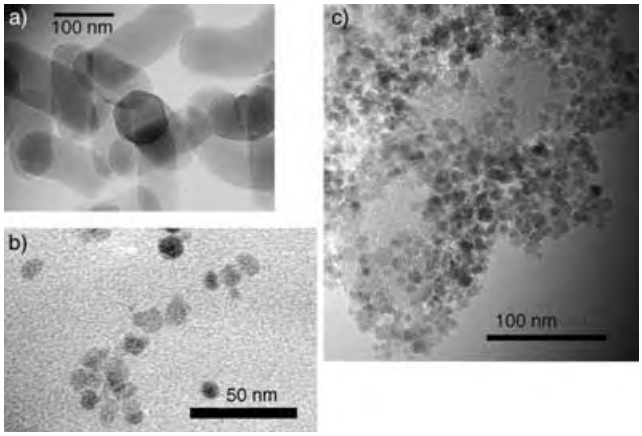


Figure 2. TEM images of a) linker-MSNs, b) APTS-coated Fe_3O_4 nanoparticles, and c) Fe_3O_4-capped magnet-MSNs.

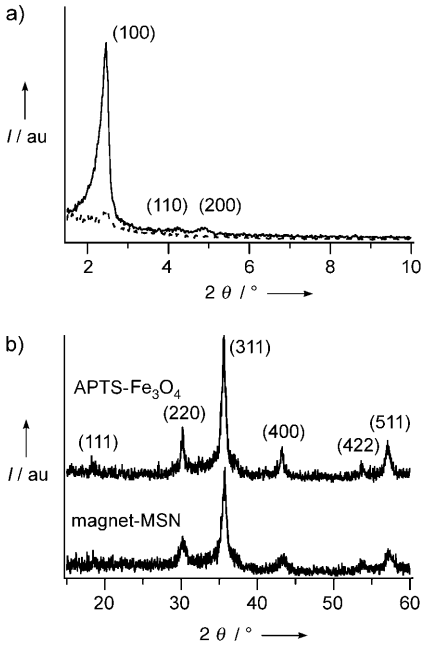


Figure 3. a) Low-angle X-ray diffraction (XRD) patterns of linker-MSN (——) and magnet-MSN (-----) powders. b) High-angle XRD patterns of APTS-coated Fe_3O_4 nanoparticles (top) and magnet-MSN (below).

relative to that of linker-MSN and could also be attributed to the covalent-bond-induced pore-filling effect between the Fe_3O_4 nanoparticles and the mesoporous silica matrix. The high-angle powder XRD patterns of magnet-MSNs matched exactly that of the APTS-Fe_3O_4 nanoparticles (Figure 3b) and confirmed the presence of APTS-Fe_3O_4 on the surface of the linker-MSNs. The pore-filling effect was also confirmed by the N_2 adsorption/desorption isotherms of the Fe_3O_4-capped magnet-MSNs. In contrast to the high surface area ($1018.0\ m^2 g^{-1}$) of linker-MSNs, magnet-MSNs showed a type I BET isotherm typical of nonporous materials, with a surface area of $296.0\ m^2 g^{-1}$.[42] The results indicated that most of the pore openings of the linker-MSN precursor were

 © 2005 Wiley-VCH Verlag GmbH & Co. KGaA, Weinheim

indeed blocked by Fe_3O_4 nanoparticles. TEM investigations of magnet-MSN also provided direct evidence of the distribution of Fe_3O_4 nanoparticles on the organically functionalized linker-MSN material. The Fe_3O_4 nanoparticles are clearly visible as dark areas on the outside edge of the mesopores (Figure 2c). In contrast to the features observed for Fe_3O_4-capped MSNs, the TEM micrograph of the linker-MSNs (Figure 2a) prior to capping with Fe_3O_4 nanoparticles showed smooth edges and a good contrast between the mesoporous channels and the silica matrix.

As mentioned earlier, the disulfide bonds between the MSNs and the Fe_3O_4 nanoparticles in the magnet-MSNs are labile and can be cleaved with disulfide reducing agents to release the trapped guest molecules from the mesopores. As the entire Fe_3O_4-capped MSN carrier system is magnetic, the system can be magnetically directed to a site of interest from where the release can take place. To demonstrate the release of a drug with the magnet-MSNs under a magnetic field, two cuvettes were charged with fluorescein-loaded magnet-MSNs (50.0 mg each) dispersed in 3.00 mL of PBS solution (100.0 mM, pH 7.4). Both cuvettes were held against the tips of two magnets (magnetic stirrer-bar retrievers). As illustrated in Figure 4a, the magnet-MSNs were attracted to the walls of the cuvettes closest to the tips of the external magnets. Dithiothreitol (DTT, 48.5 mg, 3.15×10^{-4} mol) was added to one of the two cuvettes (left) for the release experiment, while the other cuvette (right) served as a control. After 2 days (Figure 4b), green fluorescence was clearly observed in the solution to which DTT was added whereas no fluorescence could be observed from the control solution. As fluorescein-loaded magnet-MSNs do not fluoresce—Fe_3O_4 nanoparticles quench the fluorescence of fluorescein, as recently described[47]—the result indicates that fluorescein molecules were indeed released from the magnet-MSNs by the introduction of the disulfide-reducing trigger DTT. Note, the color of the accumulated magnet-MSNs near the external magnet changed from black to gray after 4 days following the addition of DTT (Figure 4c). A white precipitate of MSNs was also observed at the bottom of the cuvette. As the black Fe_3O_4 nanoparticles are attracted to the external magnetic field whereas the MSNs are not, it is plausible that the Fe_3O_4 nanoparticle caps from the Fe_3O_4–MSN ensembles were pulled in toward the magnet while the MSNs diffused away from the magnetic field as the disulfide linkage was cleaved by DTT.

Magnet-MSNs exhibited less than 1.0% release of fluorescein in PBS solutions (100.0 mM, pH 7.4) over a period of 132 h in the absence of trigger molecules (Figure 4d). This result suggested a good efficiency of the Fe_3O_4 nanoparticles to retain fluorescein molecules and prevent undesired leaching by capping the mesopores. Addition of 0.1 mM of disulfide reducing agents such as DHLA and DTT to a suspension of magnet-MSNs (13.0 mg) in PBS solution (3.00 mL, 100.0 mM, pH 7.4) triggered a rapid release of the mesopore-entrapped fluorescein. Within 48 h, 85% of the total release of fluorescein (40% of total loading) was attained; the maximum extent of release was achieved after 5 days (Figure 4d). With lipoic acid DHLA, the maximum percentage of

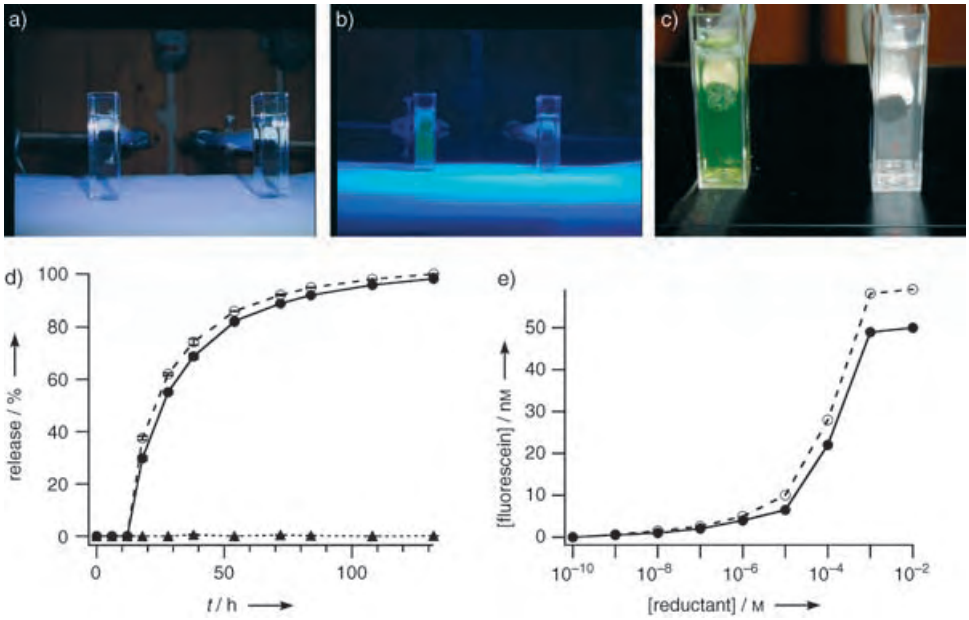


Figure 4. Photographs of two cuvettes charged with fluorescein-loaded magnet-MSNs (50.0 mg each) dispersed in 3.00 mL of PBS solution (100.0 mM, pH 7.4): a) Accumulation of magnet-MSNs on the walls of the cuvettes closest to the tips of the external magnets (magnetic stirrer-bar retrievers shown behind the cuvettes); b) 2 days after the addition of DTT (48.5 mg) to the solution contained in the cuvette on the left, green fluorescence was observed from the sample which signalled the release of encapsulated fluorescein from the matrix; c) 4 days after the addition of DTT, the color of the accumulated magnet-MSNs changed from black to gray. d) Controlled release of fluorescein from magnet-MSNs (13.0 mg) in 3.00 mL of PBS solution (100.0 mM, pH 7.4) triggered by 0.1 mM DHLA (●) or DTT (○). No noticeable release was observed in the absence of a reductant (▲). e) The dependence of the release of fluorescein from magnet-MSNs on the concentration of the reductant, measured 72 h after the addition of DHLA (●) or DTT (○).

 © 2005 Wiley-VCH Verlag GmbH & Co. KGaA, Weinheim

fluorescein released was 31.4 % of the total loading. Interestingly, the rates of release of fluorescein by the two different triggers showed similar diffusional kinetic profiles which indicates that the reducing powers of DHLA and DTT are similar. The similarity could be attributed to the fact that DHLA self-oxidizes into a disulfanyl-linked five-membered ring upon reducing the targeted disulfide bond, whereas DTT self-oxidizes into a disulfanyl-linked six-membered ring. The thermodynamic considerations of cyclizations into five- and six-membered rings should be similar. Furthermore, the amount of fluorescein released after 72 h following the addition of DHLA and DTT showed similar dependencies on the concentration of the trigger (Figure 4e) which indicates that the rate of release was dictated by the rate at which the Fe_3O_4 nanoparticle caps were removed.

To investigate the endocytosis and biocompatibility of our system, HeLa (human cervical cancer) cells ($\approx 10^5$ cells mL^{-1}) were incubated overnight with magnet-MSNs (0.2 mg mL^{-1}) to allow the endocytosis of magnet-MSNs.[40] The cells that took up magnet-MSNs were magnetically separated from those that did not. The isolated cells were treated with 0.001 % of 4′,6-diamidino-2-phenylindole (DAPI) dye in PBS solution (100.0 mM, pH 7.4) and placed in a cuvette. DAPI is known to form blue-fluorescent complexes with natural double-stranded DNA and has been widely used as a fluorescent dye for nucleus staining. These DAPI-stained, fluorescent cells were first accumulated to the right side wall of the cuvette by applying an external magnetic field—a commercially available grade N45 neodymium iron boron magnet. When the magnet was moved to the left side of the cuvette, the blue-fluorescent HeLa cells were clearly seen to move across the cuvette toward the magnet (Figure 5a–c) indicating that the magnet-MSNs were indeed endocytosed by HeLa cells. To further confirm the endocytosis of magnet-MSNs, these HeLa cells were examined by confocal fluorescence microscopy. A series of fluorescence images of different cross-sections of magnet-MSN-containing HeLa cells were obtained by changing the focal depth every 1.2 μm vertically (see Supporting Information). Green fluorescence was clearly observed within the cell bodies of these HeLa cells upon excitation at 494 nm (Figure 5d) which strongly indicates that the mesopore-encapsulated fluorescein molecules were released inside the cells. As previously reported by Biaglow et al., cancer cell lines express significant amounts of DHLA.[48] We believe that the efficient intracellular release of fluorescein was triggered by the high intracellular concentration of DHLA. To visualize the locations of the nuclei, the cells were excited at 358 nm (Figure 5e). The appearance of healthy intact nuclei and the visibility of fully grown cells by transmission (Figure 5f) suggested that the magnet-MSNs are biocompatible with HeLa cells in vitro under these experimental conditions.

In conclusion, we have demonstrated that mesoporous silica nanorods capped with superparamagnetic iron oxide nanoparticles—so-called magnet-MSNs— can be used as a stimuli-responsive controlled-release delivery carrier. Guest molecules that are smaller than 3 nm, such as fluorescein, could be encapsulated and released from the magnet-MSN delivery system by using cell-produced antioxidants (e.g. dihydrolipoic acid) as triggers in the presence of an external magnetic field. Furthermore, the biocompatibility and efficiency of intracellular delivery of the magnet-MSN system with human cervical cancer cells offer promising potential in utilization of this system to investigate various inter- and

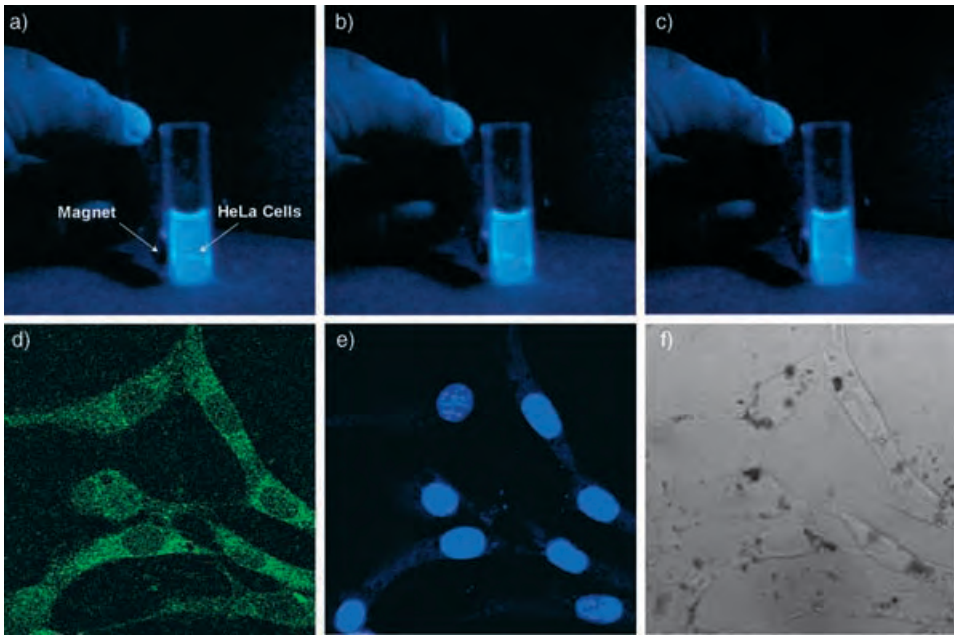


Figure 5. a–c) Single frames of photographs of HeLa cells with Fe_3O_4-capped fluorescein-loaded MSNs traveling across the cuvette, propelled by magnetic force. d–f) Fluorescence confocal micrographs of HeLa cells after 10 h incubation with Fe_3O_4-capped fluorescein-loaded MSNs: d) cells excited at 494 nm; e) cells excited in the UV region; f) a pseudo-brightfield image, where dark aggregations of magnet-MSNs can be clearly observed.

 © 2005 Wiley-VCH Verlag GmbH & Co. KGaA, Weinheim

intracellular chemical/neurochemical communications in vitro. We envision that these magnet-MSNs could play a significant role in the development of new generations of site-selective controlled-release delivery devices and interactive sensory nanodevices.

Experimental Section

$FeCl_2 \cdot 4H_2O$, $FeCl_3 \cdot 6H_2O$, 3-aminopropyltriethoxysilane (APTS), 3-mercaptopropionic acid, 2-aldrithiol, 3-mercaptopropyltrimethoxysilane (MPTMS), tetraethylorthosilicate (TEOS), *n*-cetyltrimethylammonium bromide (CTAB), 1-(3-(dimethylamino)propyl)-3-ethylcarbodiimide hydrochloride (EDC), fluorescein, and dithiothreitol (DTT) were purchased from Aldrich and used as received. Dihydrolipoic acid (DHLA) was obtained from Sigma and used without further purification. Nanopure water (18.1 MHz) prepared from a Barnstead E-pure water-purification system was employed throughout. PBS (phosphate-buffered saline) solution (100.0 mM, pH 7.4) was used as the solvent for the loading experiments.

APTS-coated magnetite (Fe_3O_4) nanoparticles: Magnetic nanoparticles were prepared and coated with APTS according to a slightly modified reported procedure[34] (see Supporting Information).

MCM-41-type mesoporous silica nanoparticles functionalized with 3-(propyldisulfanyl)propionic acid (linker-MSN): The thiol-MSN material was prepared according to a slightly modified version of our previously reported procedure[31] (see Supporting Information). The purified thiol-MSNs (1.000 g) were treated with a solution of 2-carboxyethyl-2-pyridyl disulfide (1.340 g, 6.23×10^{-3} mol; prepared according to a reported procedure[49]) in ethanol (80.00 mL) at room temperature for 24 h under vigorous stirring (vortex stirrer) to obtain the desired disulfide bond-exchange reaction. The resulting acid-functionalized MSN was filtered, washed with ethanol, and dried in air. The surface coverage of chemically accessible thiol groups was quantified at 7.01×10^{-4} mol g^{-1}.[38]

Loading of fluorescein into the mesoporous framework of linker-MSN and the capping of the mesopores with APTS coated Fe_3O_4 nanoparticles: The purified linker-MSNs (80.0 mg) was stirred vigorously (vortex stirrer) in a solution of fluorescein (3.6×10^{-6} M) in PBS solution (8.00 mL, 100.0 mM, pH 7.4) for 24 h. Then, APTS-coated Fe_3O_4 nanoparticles (960.0 mg) were added to the suspension followed by 1-(3-(dimethylamino)propyl)-3-ethylcarbodiimide hydrochloride (EDC) (60.0 mg, 3.13×10^{-4} mol). The mixture was stirred vigorously (vortex stirrer) for another 48 h before the precipitate was filtered, washed extensively with buffer, and dried under vacuum. The precipitate (480.0 mg) was stirred vigorously again in PBS solution (10.00 mL, 100.0 mM, pH 7.4) for 48 h, followed by filtration and washing (×7) with PBS solution to remove physisorbed, uncapped fluorescein molecules from the exterior surface of the material. The purification procedure was repeated once more to further remove any physisorbed fluorescein, and the solid material was finally dried into a powder. All the washings were collected, and the loading of fluorescein (2.1×10^{-10} mol mg^{-1} linker-MSN) was calculated from the difference in the concentration of the initial solution of fluorescein and that of the reaction medium combined with the subsequent washings.

Endocytosis of Fe_3O_4-capped MSNs in HeLa cells: Human cervical cancer (HeLa) cell lines were obtained from the American Tissue Culture Collection (ATCC) and were maintained using DMEM (Dulbecco's modified Eagle's medium) supplemented with horse serum (10%), L-glutamine (2.00 mM), penicillin (100 U mL^{-1}), streptomycin (100.0 mg mL^{-1}), and gentamicin (1.0 mg mL^{-1}). HeLa cells were seeded onto 6-well plates (1×10^5 cells in 3.00 mL of growth medium per well) 24 h prior to the experiment. After 24 h, the wells were seeded with Fe_3O_4-capped MSNs (0.2 mg mL^{-1}) in growth medium. After 10 h, the medium was removed and the cells were washed with fresh growth medium. Then, the cells were trypsinized with 0.25% trypsin. A magnet was used to keep the cells associated with the magnetic nanoparticles stationary while the remaining (nonmagnetic) cells were removed. The cells that took up the Fe_3O_4-capped MSNs were centrifuged and resuspended in a solution of 4′,6-diamidino-2-phenylindole (DAPI, 100.0 μg mL^{-1}) in PBS (100.0 mM, pH 7.4).

Received: May 26, 2005
Published online: July 22, 2005

Keywords: drug delivery · fluorescence · magnetic properties · mesoporous materials · nanostructures

[1] A. K. Gupta, A. S. G. Curtis, *J. Mater. Sci. Mater. Med.* **2004**, *15*, 493.
[2] T. Neuberger, B. Schoepf, H. Hofmann, M. Hofmann, B. von Rechenberg, *J. Magn. Magn. Mater.* **2005**, *293*, 483.
[3] A. S. Lubbe, C. Bergemann, J. Brock, D. G. McClure, *J. Magn. Magn. Mater.* **1999**, *194*, 149.
[4] U. Schillinger, T. Brill, C. Rudolph, S. Huth, S. Gersting, F. Kroetz, J. Hirschberger, C. Bergemann, C. Plank, *J. Magn. Magn. Mater.* **2005**, *293*, 501.
[5] F. Scherer, M. Anton, U. Schillinger, J. Henke, C. Bergemann, A. Kruger, B. Gansbacher, C. Plank, *Gene Ther.* **2002**, *9*, 102.
[6] J. M. Perez, L. Josephson, T. O'Loughlin, D. Hoegemann, R. Weissleder, *Nat. Biotechnol.* **2002**, *20*, 816.
[7] J. M. Perez, T. O'Loughin, F. J. Simeone, R. Weissleder, L. Josephson, *J. Am. Chem. Soc.* **2002**, *124*, 2856.
[8] J. W. M. Bulte, T. Douglas, B. Witwer, S.-C. Zhang, E. Strable, B. K. Lewis, H. Zywicke, B. Miller, P. van Gelderen, B. M. Moskowitz, L. D. Duncan, J. A. Frank, *Nat. Biotechnol.* **2001**, *19*, 1141.
[9] J. Gellissen, C. Axmann, A. Prescher, K. Bohndorf, K. P. Lodemann, *Magn. Reson. Imaging* **1999**, *17*, 557.
[10] P. S. Doyle, J. Bibette, A. Bancaud, J.-L. Viovy, *Science* **2002**, *295*, 2237.
[11] D. Wang, J. He, N. Rosenzweig, Z. Rosenzweig, *Nano Lett.* **2004**, *4*, 409.
[12] C. Xu, K. Xu, H. Gu, R. Zheng, H. Liu, X. Zhang, Z. Guo, B. Xu, *J. Am. Chem. Soc.* **2004**, *126*, 9938.
[13] H. Gu, P.-L. Ho, K. W. T. Tsang, L. Wang, B. Xu, *J. Am. Chem. Soc.* **2003**, *125*, 15702.
[14] A. K. Gupta, M. Gupta, *Biomaterials* **2005**, *26*, 3995.
[15] A. Jordan, R. Scholz, P. Wust, H. Schirra, T. Schiestel, H. Schmidt, R. Felix, *J. Magn. Magn. Mater.* **1999**, *194*, 185.
[16] I. Hilger, W. Andra, R. Hergt, R. Hiergeist, H. Schubert, W. A. Kaiser, *Radiology* **2001**, *218*, 570.
[17] D. C. F. Chan, D. B. Kirpotin, P. A. Bunn, Jr., *J. Magn. Magn. Mater.* **1993**, *122*, 374.
[18] L. R. Hirsch, R. J. Stafford, J. A. Bankson, S. R. Sershen, B. Rivera, R. E. Price, J. D. Hazle, N. J. Halas, J. L. West, *Proc. Natl. Acad. Sci. USA* **2003**, *100*, 13549.
[19] T.-J. Yoon, J. S. Kim, B. G. Kim, K. N. Yu, M.-H. Cho, J.-K. Lee, *Angew. Chem.* **2005**, *117*, 1092; *Angew. Chem. Int. Ed.* **2005**, *44*, 1068.
[20] P. Chattopadhyay, R. B. Gupta, *Ind. Eng. Chem. Res.* **2002**, *41*, 6049.
[21] J. F. Diaz, K. J. Balkus, Jr., *J. Mol. Catal. B* **1996**, *2*, 115.
[22] Y.-J. Han, G. D. Stucky, A. Butler, *J. Am. Chem. Soc.* **1999**, *121*, 9897.
[23] H. Takahashi, B. Li, T. Sasaki, C. Miyazaki, T. Kajino, S. Inagaki, *Microporous Mesoporous Mater.* **2001**, *44–45*, 755.
[24] M. Vallet-Regi, A. Ramila, R. P. del Real, J. Perez-Pariente, *Chem. Mater.* **2001**, *13*, 308.
[25] B. Munoz, A. Ramila, J. Perez-Pariente, I. Diaz, M. Vallet-Regi, *Chem. Mater.* **2003**, *15*, 500.

 © 2005 Wiley-VCH Verlag GmbH & Co. KGaA, Weinheim

[26] A. Ramila, B. Munoz, J. Perez-Pariente, M. Vallet-Regi, *J. Sol-Gel Sci. Technol.* **2003**, *26*, 1199.
[27] C. Tourne-Peteilh, D. Brunel, S. Begu, B. Chiche, F. Fajula, D. A. Lerner, J.-M. Devoisselle, *New J. Chem.* **2003**, *27*, 1415.
[28] M. Vallet-Regi, J. C. Doadrio, A. L. Doadrio, I. Izquierdo-Barba, J. Perez-Pariente, *Solid State Ionics* **2004**, *172*, 435.
[29] N. K. Mal, M. Fujiwara, Y. Tanaka, *Nature* **2003**, *421*, 350.
[30] R. Hernandez, H.-R. Tseng, J. W. Wong, J. F. Stoddart, J. I. Zink, *J. Am. Chem. Soc.* **2004**, *126*, 3370.
[31] C.-Y. Lai, B. G. Trewyn, D. M. Jeftinija, K. Jeftinija, S. Xu, S. Jeftinija, V. S. Y. Lin, *J. Am. Chem. Soc.* **2003**, *125*, 4451.
[32] J. A. Gruenhagen, C.-Y. Lai, D. R. Radu, V. S. Y. Lin, E. S. Yeung, *Appl. Spectrosc.* **2005**, *59*, 424.
[33] D. R. Radu, C.-Y. Lai, W. Wiench Jerzy, M. Pruski, V. S. Y. Lin, *J. Am. Chem. Soc.* **2004**, *126*, 1640.
[34] W. C. W. Chan, S. Nie, *Science* **1998**, *281*, 2016.
[35] M. Ma, Y. Zhang, W. Yu, H.-Y. Shen, H.-Q. Zhang, N. Gu, *Colloids Surf. A* **2003**, *212*, 219.
[36] S. Huh, W. Wiench Jerzy, B. G. Trewyn, S. Song, M. Pruski, V. S. Y. Lin, *Chem. Commun.* **2003**, 2364.
[37] S. Huh, J. W. Wiench, J.-C. Yoo, M. Pruski, V. S. Y. Lin, *Chem. Mater.* **2003**, *15*, 4247.
[38] V. S. Y. Lin, C.-Y. Lai, J. Huang, S.-A. Song, S. Xu, *J. Am. Chem. Soc.* **2001**, *123*, 11510.
[39] D. R. Radu, C.-Y. Lai, J. Huang, X. Shu, V. S. Y. Lin, *Chem. Commun.* **2005**, 1264.
[40] D. R. Radu, C.-Y. Lai, K. Jeftinija, E. W. Rowe, S. Jeftinija, V. S. Y. Lin, *J. Am. Chem. Soc.* **2004**, *126*, 13216.
[41] B. G. Trewyn, C. M. Whitman, V. S. Y. Lin, *Nano Lett.* **2004**, *4*, 2139.
[42] See Supporting Information for details.
[43] B. Marler, U. Oberhagemann, S. Vortmann, H. Gies, *Microporous Mater.* **1996**, *6*, 375.
[44] H. Winkler, A. Birkner, V. Hagen, I. Wolf, R. Schmechel, H. Von Seggern, R. A. Fischer, *Adv. Mater.* **1999**, *11*, 1444.
[45] W.-H. Zhang, J.-L. Shi, L.-Z. Wang, D.-S. Yan, *Chem. Mater.* **2000**, *12*, 1408.
[46] W.-H. Zhang, J.-L. Shi, H.-R. Chen, Z.-L. Hua, D.-S. Yan, *Chem. Mater.* **2001**, *13*, 648.
[47] L. Josephson, M. F. Kircher, U. Mahmood, Y. Tang, R. Weissleder, *Bioconjugate Chem.* **2002**, *13*, 554.
[48] J. E. Biaglow, J. Donahue, S. Tuttle, K. Held, C. Chrestensen, J. Mieyal, *Anal. Biochem.* **2000**, *281*, 77.
[49] J. Carlsson, H. Drevin, R. Axen, *Biochem. J.* **1978**, *173*, 723.

 © 2005 Wiley-VCH Verlag GmbH & Co. KGaA, Weinheim

Molecular Magnets

DOI: 10.1002/anie.200501265

Phosphonate Ligands Stabilize Mixed-Valent $\{Mn^{III}_{20-x}Mn^{II}_{x}\}$ Clusters with Large Spin and Coercivity**

Shanmugam Maheswaran, Guillaume Chastanet, Simon J. Teat, Talal Mallah, Roberta Sessoli, Wolfgang Wernsdorfer, and Richard E. P. Winpenny**

The discovery that some molecules show a slow relaxation of magnetization below a critical temperature has prompted a large interest in the materials now generally known as "single molecule magnets" (SMMs).[1,2] Investigations have been inspired partly by the idea that SMMs could be used as molecular magnetic storage devices but also because they show unusual phenomena such as quantum-tunneling of magnetization,[3] which can be exchange-biased.[4] The majority of SMMs have been made by Christou and co-workers, and contain Mn^{III} ions;[5–7] the use of Mn^{III} ions has significant advantages as cages containing this ion often have ground states with large spin values and considerable anisotropy derived from the Jahn–Teller distortion common to a d^4 ion.

Phosphonates, such as benzylphosphonate ($PhCH_2PO_3^{2-}$), have only rarely been employed in making transition-metal cages, probably because of the insolubility of metal phosphonates. Recently we showed that the reaction of phosphonates

[*] Dr. G. Chastanet, Prof. R. Sessoli
Laboratorio di Magnetismo Molecolare
Dipartimento di Chimica
Università degli Studi di Firenze & INSTM
Via della Lastruccia n. 3, 50019 Sesto Fiorentino (Italy)
Fax: (+39) 055-457-3372
E-mail: roberta.sessoli@unifi.it

S. Maheswaran, Prof. R. E. P. Winpenny
University of Manchester
School of Chemistry
Oxford Road, Manchester, M13 9PL (UK)
Fax: (+44) 161-275-4616
E-mail: richard.winpenny@manchester.ac.uk

Dr. S. J. Teat
CCLRC Daresbury Laboratory
Warrington, Cheshire, WA4 4AD (UK)

Prof. T. Mallah
Laboratoire de Chimie Inorganique
UMR CNRS 8613, Université Paris Sud
91405 Orsay (France)

Dr. W. Wernsdorfer
Laboratoire Louis Néel–CNRS, BP 166
25 Avenue des Martyrs, 38042 GRENOBLE Cedex 9 (France)

[**] This work was supported by the EC-TMR Network "QuEMolNa" (MRTN-CT-2003-504880), the ORS (UK), the University of Manchester, the "Deutsche Forschungsgemeinschaft" (SPP1137), and Italian MIUR (for FIRB and PRIN funding). S.M. thanks EST, FP6-504204: MOLMAG for supporting a study period in Florence.

Supporting information for this article is available on the WWW under http://www.angewandte.org or from the author.

 InterScience © 2005 Wiley-VCH Verlag GmbH & Co. KGaA, Weinheim

with preformed trinuclear iron–carboxylate clusters generates a range of new polymetallic complexes.[8] In our search for new SMMs we have extended this work to mixed-valent basic manganese carboxylates such as $[Mn_3O(O_2CR)_6(py)_3]$ (py = pyridyl).

Reaction of equimolar amounts of $H_2O_3PCH_2Ph$ and $[Mn_3O(O_2CCMe_3)_6(py)_3]$ in CH_3CN in the presence of Et_3N gave a dark brown solution from which $[Et_3NH]_2[Mn^{III}_{18}Mn^{II}_2(\mu_4\text{-}O)_8(\mu_3\text{-}O)_4(\mu_3\text{-}OH)_2(O_3PCH_2Ph)_{12}(O_2CCMe_3)_{10}(py)_2]$ (**1**) crystallizes in 40% yield after two days. Structural analysis[9] shows that the μ_3-oxo-centered triangular array of manganese centers in the precursor cage is maintained in the product (for example: Mn1, Mn2, Mn3, and symmetry equivalents; Figure 1); however, **1** is best described as a centrosymmetric cubic-close packed array of Mn sites. Twelve of the manganese centers lie in one plane, which includes the two Mn^{II} sites (Mn6 and Mn6a in Figure 1). Two Mn^{III} triangles (Mn5, Mn8, and Mn10, and the symmetry related ions) lie above and below hexagons of Mn in the central plane and bridged to the central layer by a μ_4-oxide group (Figure 1b). The relative orientation of the two triangles makes the packing ABC, not ABA, hence this is a fragment of a cubic close-packed (ccp) lattice (see Figure 1b). Mn1 lies in the outer plane containing the triangle formed by Mn5, Mn8, and Mn10, and forms a μ_3-oxo-centered triangle with two ions of the central plane (Mn2 and Mn3). The Mn^{II} site is seven-coordinate, while all the Mn^{III} sites are six-coordinate with Jahn–Teller elongations. Valence bond sum analysis confirms the oxidation states, as well as the assignment of two hydroxide and twelve oxide bridges. The Et_3NH cations hydrogen bond to O atoms from phosphonate groups (N–H···O(phos) 2.78 Å). The twelve phosphonate ligands in **1** show three bonding modes: 3.111, 4.211, and 5.221 (Harris notation[8]), with four examples of each mode in the structure.

Two related clusters can be made from mixed-valent $[Mn_3O(O_2CPh)_6(py)_2(H_2O)]$ and homovalent $[Mn_3O(O_2CPh)_6(py)_3]ClO_4$ benzoate triangles: $K_4[Mn^{III}_{16}Mn^{II}_4(\mu_4\text{-}O)_4(\mu_3\text{-}O)_6(PhCH_2PO_3)_{14}(PhCO_2)_{12}(PhCO_2H)_{0.5}(CH_3CN)_2]$ (**2**) and $Na_6[Mn^{III}_{14}Mn^{II}_6(\mu_4\text{-}O)_4(\mu_3\text{-}O)_4(OH)_4(PhCH_2PO_3)_{14}(PhCO_2)_{12}(PhCO_2H)_2(H_2O)_4(CH_3CN)_4]$ (**3**) can be formed, depending on whether K^I or Na^I ions are present. The manganese cores are similar to that in **1**, and the center of symmetry is retained; however, additional Mn^{II} sites are found within the central layer. Mn4 in **2** has been assigned as being in the Mn^{II} oxidation state because of an increase in the average bond length to 2.163 Å (from 2.011 Å in **1**), while the other Mn–O bond lengths remain virtually unchanged. The average bond length to Mn4 in **3** remains long (2.184 Å), but a significant increase is also observed around Mn7 (2.140 Å compared to 2.023 Å for **1** and 2.022 Å for **2**). Mn4 and Mn7 in **3** are thus assigned as Mn^{II} sites. The alkali-metal cations are attached to the periphery of the cages and have no structure-directing role. This result allows us to isolate three different redox states of mixed-valent cages with the same high nuclearity.

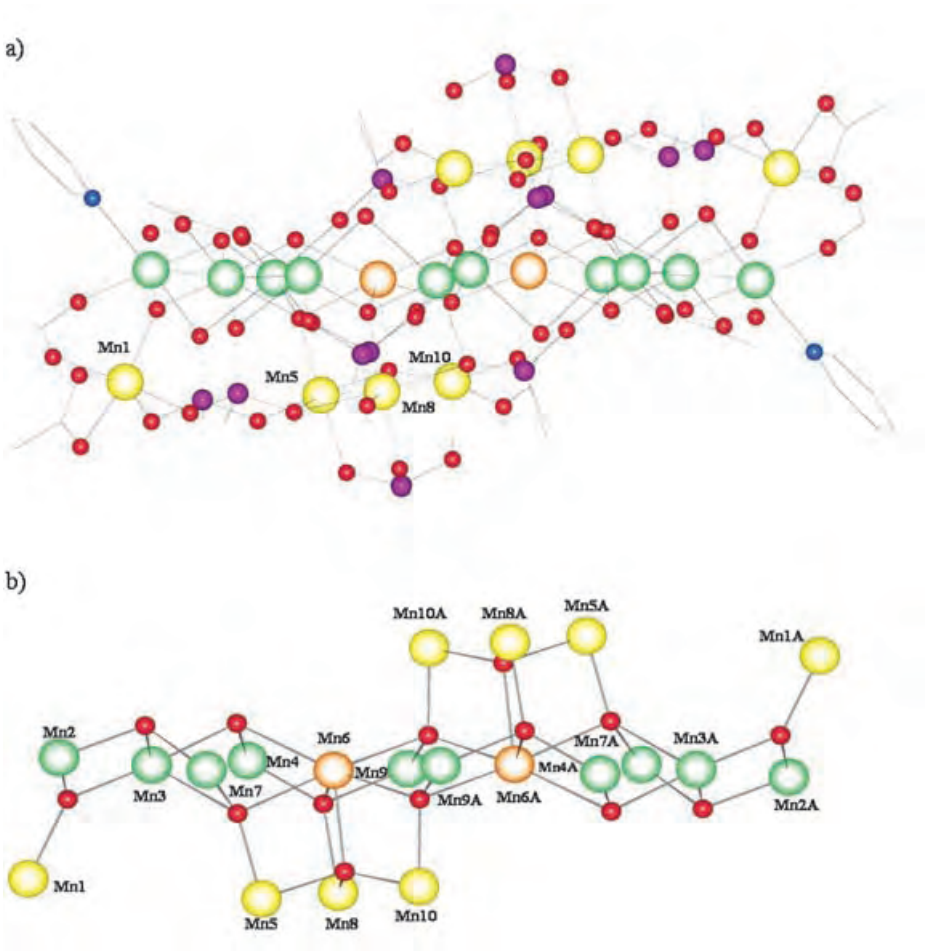


Figure 1. The structure of **1** in the crystal: a) viewed parallel to the central Mn plane (the H and C atoms of the organic side-chains are omitted for clarity), color code: green and yellow, Mn^{III}; orange, Mn^{II}; magenta, P; red, O; blue, N; b) view parallel to the central plane showing the ABC packing of the Mn ions and the bridging oxygen atoms.

The variable-temperature direct current (dc) magnetic susceptibilities measured for the three compounds are shown in Figure 2a. All three compounds show the same type of behavior: the χT value increases from nearly 60 (**1**) and 68 emu K mol^{-1} (**2** and **3**) at room temperature to reach maxima of 210 (**1**), 115 (**2**), and 74 emu K mol^{-1} (**3**). A rapid decrease is observed around 10 K which probably results from zero-field splitting or intermolecular interactions. These curves suggest the three cages have a high-spin ground state: $S = 19 \pm 1$ for **1**, $S =$

 © 2005 Wiley-VCH Verlag GmbH & Co. KGaA, Weinheim

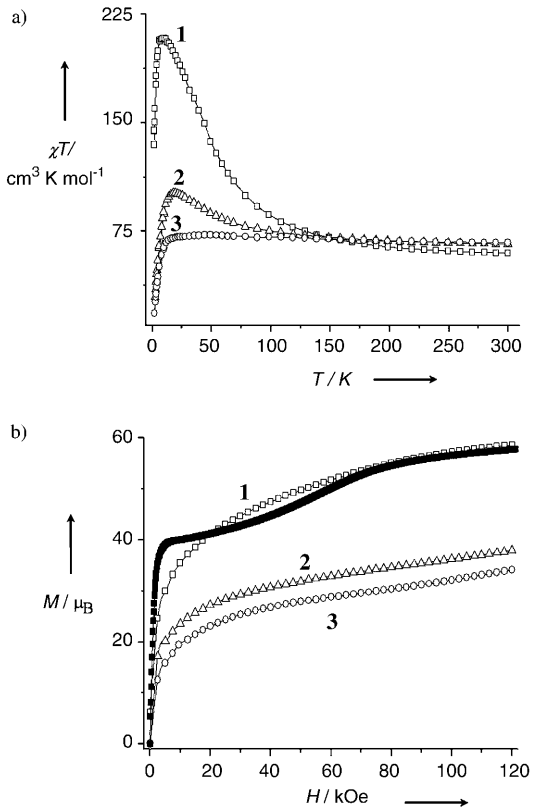


Figure 2. a) Temperature-dependence of the χT value for a polycrystalline sample of **1**, **2**, and **3**; b) magnetization versus field data for **1**, **2**, and **3** recorded at 1.55 K. The filled squares represent the single-crystal magnetization of **1** along the easy axis.

14 ± 1 for **2**, and $S = 11 \pm 1$ for **3**. The magnetization (M) versus magnetic field (H) data are in agreement with the χT plots, and further confirm the large spin values of the ground states. Magnetization measurements were performed on polycrystalline samples at 1.55 K to determine the ground state more accurately (Figure 2b). A two-step curve is obtained for all three compounds, with first a rapid saturation around 40 μ_B (**1**), 30 μ_B (**2**), and 25 μ_B (**3**), followed by a slow increase in the value of M. Single-crystal magnetization measurements performed along the easy axis of the cluster **1** show a pronounced saturation around 40 μ_B at low field, followed by a broad step (Figure 2b).

The further increase in the magnetization is consistent with the presence of excited states close in energy that have a larger spin value. This observation is not surprising when Mn^{II} ions are present as they often lead to weak antiferromagnetic exchange interactions, which can easily be overcome by an external magnetic field. The observed difference in the single-crystal and powder data for **1** suggests that it has a significant magnetic anisotropy which when associated with the large S value ($S = 19 \pm 1$) could lead to slow relaxation of the magnetization.

Alternating current (ac) susceptibility measurements in zero field allows estimation of the energy barrier for the reorientation of the magnetization of superparamagnetic particles or molecules functioning as SMMs.[2] The applied oscillating field probes the dynamics of this reorientation, as the out-of-phase signal (χ'') is maximal when the frequency of the ac field equals the relaxation rate of the magnetization. We monitored the value of χ'' from 1.5 to 10 K at several frequencies between 100 to 20000 Hz. Maxima were observed for compounds **1** and **2** (the data for **1** are shown in Figure 3).

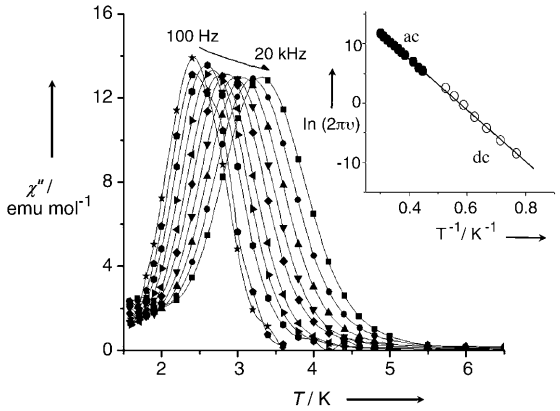


Figure 3. Temperature-dependence of the out-of-phase susceptibility of **1** measured from 100 to 20000 Hz. Inset: the temperature-dependence of the relaxation time extracted from ac measurements and time decay of the magnetization.

In contrast, only a frequency-dependent increase in the value of χ", with no maxima down to 1.5 K, has been observed for **3**. The energy barrier for the relaxation can be derived from the Arrhenius plot[2c] as 43 K ($\tau_0 = 2 \times 10^{-11}$ s) for **1** and 17 K ($\tau_0 = 2 \times 10^{-10}$ s) for **2**, with a moderate distribution of relaxation times. All three compounds are therefore new SMMs, and **1** possesses one of the highest energy barriers known after $\{Mn_{12}\}$ clusters.[2a] It is also one of the highest spin SMMs known.[6,10] It is worth noting that the energy barrier increases from **3** to **1** as the content of anisotropic Mn^{III} ions and the ground spin state of the cluster increases.

The decay of remnant magnetization (see Supporting Information) has been followed on a microcrystal of **1** with a micro-Squid[11] and the relaxation time—extracted as the time delay at which M/M_0 equals $1/e$—is in good agreement with the values extracted from ac measurements (see inset of Figure 3). A square hysteresis loop has been measured that widens on lowering the temperature, with a remarkably high coercive field of 10 kOe below 0.4 K (Figure 4). Previously reported large Mn cages have much narrower hysteresis loops.[6,7] No sudden jumps at $H = 0$ are observed here, which suggests resonant quantum tunneling is not particularly efficient. This proposal is confirmed by the unchanged value of the relaxation time τ extracted from ac susceptibility measurements in zero and under moderate static fields. The shape of the hysteresis is unusual, as it shows small steps around 4 and 9 kOe on the descending field branch. A detailed analysis of the hysteretic behavior of these steps shows that they are not related to dynamic properties but rather that they correspond to a cross-over to a magnetic ground state of higher S value that is induced by the applied field.[12]

The $S = 19 \pm 1$ ground state of **1** in low field can be tentatively rationalized as follows. The strongest antiferro-

 © 2005 Wiley-VCH Verlag GmbH & Co. KGaA, Weinheim

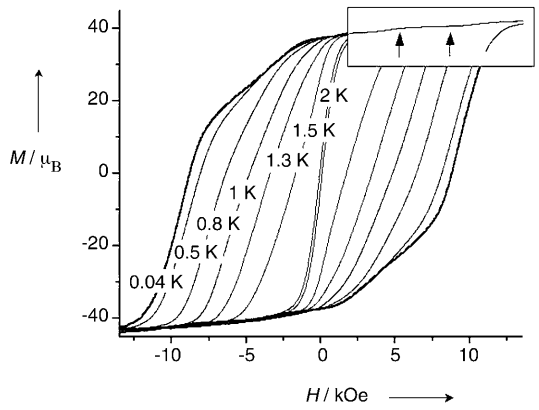


Figure 4. Hysteresis loops measured at a sweep rate of 350 Oe s^{-1} on a crystal of **1** at different temperatures. Steps at 4 and 9 kOe are indicated by arrows.

magnetic interactions are likely to result from μ_3-oxides which are all associated with the triangle Mn1-Mn2-Mn3 and its symmetry equivalent. We assume that these triangles are spin-frustrated and have a low resulting spin.[13]

We can then consider the remaining twelve Mn^{III} and two Mn^{II} sites in the structure; the Mn^{III} sites are bridged by μ_4-oxide and μ_3-hydroxide groups, which can often create ferromagnetic exchange. In contrast, exchange between Mn^{II} and Mn^{III} sites in similar structures is often weak and antiferromagnetic. We can thus propose that the spin of the ground state at low field arises as a consequence of the spin of the twelve Mn^{III} ions ($S = 24$) opposed to the spin of the two Mn^{II} ions ($S = 5$) plus the contribution from the two frustrated triangles. The large change in the ground state S value would then result from the field overcoming the antiferromagnetic exchange between the Mn^{III} and Mn^{II} ions, thus leading to an increase in the S value of 10 and in the M value of 20 μ_B. The observed decrease in the value of S on reduction of Mn^{III} to Mn^{II} confirms the proposed picture, in which the antiparallel aligned spins are associated with Mn^{II} sites. This oversimplified model would, however, predict changes in S of 9 and 18 in going from **1** to **2** and **3**, respectively. The smaller difference observed suggests a more complicated scenario where intermediate spin states are stabilized by competing antiferromagnetic interactions. X-ray magnetic circular dichroism, which is able to distinguish how the two oxidation states contribute to the magnetic moment, thus seems the appropriate technique to investigate the spin structure of these compounds.

The three compounds are therefore very unusual SMMs as shown by the very high spin and high coercivity of **1**, in the immediate availability of three redox forms of the cluster, and finally the observation of a dramatic change in the spin of the ground state.

Experimental Section

All reagents were used as received from Aldrich. $[Mn_3O(O_2CCMe_3)_6(py)_3]$, $[Mn_3O(PhCO_2)_6(py)_2(H_2O)]$, and $[Mn_3O(PhCO_2)_6(py)_3]$ ClO_4 were made by literature procedures.[14]

1: A brown solution of $[Mn_3O(O_2CCMe_3)_6(py)_3]$ (0.58 g, 0.56 mmol) in MeCN (10 mL) was treated with $PhCH_2PO_3H_2$ (0.096 g, 0.56 mmol) and triethylamine (0.14 mL). The resulting solution was stirred for 15 h and then filtered. Very large crystals grew from the filtrate after two days. The crystals were suitable for X-ray studies. Yield: 0.24 g (40 %). Elemental analysis calcd (%) for $C_{156}H_{218}Mn_{20}N_4O_{70}P_{12}\cdot 2\,CH_3CN$: C 39.85, H 4.68, N 1.74, P 7.71; found: C 39.12, H 4.75, N 2.09, 7.73.

2: $[Mn_3O(PhCO_2)_6(py)_2(H_2O)]$ (0.54 g, 0.5 mmol) and $PhCH_2PO_3$ (0.086 g, 0.5 mmol) were mixed in a CH_3CN/EtOH (5:1) mixture (12 mL), and KOMe (0.035 g, 0.5 mmol) was added. The solution was stirred overnight and filtered. Crystals of **2** grew from the filtrate after three days. Yield: 0.21 g (60 %). Elemental analysis (%) calcd for $C_{189.5}H_{167}Mn_{20}N_2K_4O_{77}P_{14}$ (dried): C 42.50, H 3.12, N 0.51, P 8.04; found: C 42.63, H 3.41, N 0.22, P 7.76.

3: $[Mn_3O(PhCO_2)_6(py)_3]ClO_4$ (0.59 g, 0.5 mmol), $PhCH_2PO_3H_2$ (0.086 g, 0.5 mmol), and Et_3N (0.14 mL) were mixed in CH_3CN (10 mL) and the solution stirred for 15 h before being filtered. A solution of $NaClO_4$ (0.24 g) in CH_3CN (2–3 mL) was added to the filtrate and the mixture again filtered before keeping the filtrate for crystallization. After two days dark brown single crystals of **3** grew that were suitable for X-ray analysis. Yield: 0.15 g (30 %). Elemental analysis calcd (%) for $C_{204}H_{194}Mn_{20}N_4Na_6O_{86}P_{14}$ (dried) : C 42.61, H 3.40, N 0.98, P 7.54; found: C 42.98, H 3.81, N 0.98, P 7.72.

Magnetic measurements: The temperature-dependence of the magnetization was measured on polycrystalline powder samples with a Cryogenic S600 SQUID magnetometer at 10 kOe and below 50 K at 1 kOe to avoid saturation. Data have been corrected for the diamagnetic contribution according to Pascal tables. Magnetization curves up to 120 kOe have been obtained by using an Oxford Instruments Vibrating Sample Magnetometer (VSM). Alternating current susceptibility data were obtained by using a home-made probe[15] with an oscillating field of 0.8 Oe. A home-made μ-SQUID magnetometer[11] was used for low-temperature magnetic measurements on single microcrystals of **1**.

Received: April 11, 2005
Published online: July 20, 2005

Keywords: cluster compounds · magnetic properties · manganese · molecular magnets · spin crossover

[1] A. Caneschi, D. Gatteschi, R. Sessoli, A. L. Barra, L. C. Brunel, M. Guillot, *J. Am. Chem. Soc.* **1991**, *113*, 5873 – 5874.
[2] a) R. Sessoli, H.-L. Tsai, A. R. Schake, S. Wang, J. B. Vincent, K. Folting, D. Gatteschi, G. Christou, D. N. Hendrickson, *J. Am. Chem. Soc.* **1993**, *115*, 1804 – 1816; b) R. Sessoli, D. Gatteschi, A. Caneschi, M. A. Novak, *Nature* **1993**, *365*, 141 – 143; c) D. Gatteschi, R. Sessoli, *Angew. Chem.* **2003**, *115*, 278 – 309; *Angew. Chem. Int. Ed.* **2003**, *42*, 268 – 297, and references therein.
[3] a) J. R. Friedman, M. P. Sarachik, J. Tejada, R. Ziolo, *Phys. Rev. Lett.* **1996**, *76*, 3830 – 3833; b) L. Thomas, F. Lionti, R. Ballou, D. Gatteschi, R. Sessoli, B. Barbara, *Nature* **1996**, *383*, 145 – 147.
[4] W. Wernsdorfer, N. Aliaga-Acaldse, D. N. Hendrickson, G. Christou, *Nature* **2002**, *416*, 406 – 409.
[5] E. K. Brechin, C. Boskovic, W. Wernsdorfer, J. Yoo, A. Yamaguchi, E. C. Sanudo, T. R. Concolino, A. Rheingold, H. Ishimoto, D. N. Hendrickson, G. Christou, *J. Am. Chem. Soc.* **2002**, *124*, 9710 – 9711, and references therein.
[6] M. Murugesu, M. Habrych, W. Wernsdorfer, K. A. Abboud, G. Christou, *J. Am. Chem. Soc.* **2004**, *126*, 4766 – 4767.
[7] A. Tasiopoulos, A. Vinslava, W. Wernsdorfer, K. A. Abboud, G. Christou, *Angew. Chem.* **2004**, *116*, 2169 – 2173; *Angew. Chem. Int. Ed.* **2004**, *43*, 2117 – 2121.

 © 2005 Wiley-VCH Verlag GmbH & Co. KGaA, Weinheim

[8] E. I. Tolis, M. Helliwell, S. Langley, J. Raftery, R. E. P. Winpenny, *Angew. Chem.* **2003**, *115*, 3934 – 3938; *Angew. Chem. Int. Ed.* **2003**, *42*, 3804 – 3808.

[9] Crystal data for **1**·10 MeCN: $C_{176}H_{240}Mn_{20}N_{14}O_{70}P_{12}$, $M_r = 5142.26\ g\,mol^{-1}$, small brown block, monoclinic, space group $P2_1/c$, $a = 15.9789(15)$, $b = 26.171(2)$, $c = 29.955(3)$ Å, $\beta = 121.131(6)°$, $V = 10722.9(17)$ Å^3, $Z = 2$ (the molecule lies on an inversion centre), $T = 100(2)$ K, $\rho_{calcd} = 1.593\ g\,cm^{-1}$, $F(000) = 5268$, $\mu(Mo_{K\alpha}) = 1.306\ mm^{-1}$. Crystal data for **2**: $C_{189.5}H_{167}Mn_{20}N_2K_4O_{77}P_{14}$, dark brown block, triclinic, space group $P\bar{1}$, $a = 17.3198(13)$, $b = 18.7550(14)$, $c = 20.4374(15)$ Å, $\alpha = 80.494(10)$, $\beta = 82.255(10)$, $\gamma = 81.169(10)°$, $V = 6429.1(8)$ Å^3, $Z = 1$ (the molecule lies on an inversion centre), $T = 100.0(2)$ K, $\rho_{calcd} = 1.447\ g\,cm^{-1}$, $F(000) = 2828$, $\mu(MoK_\alpha) = 1.174\ mm^{-1}$. Crystal data for **3**: $C_{204}H_{194}Mn_{20}N_4Na_6O_{86}P_{14}$, dark brown plate, triclinic, space group $P\bar{1}$, $a = 16.166(3)$, $b = 20.360(4)$ $c = 22.781(5)$ Å, $\alpha = 68.97(19)°$, $\beta = 71.69(2)°$, $\gamma = 77.051(16)°$, $V = 6592(2)$ Å^3, $Z = 1$ (the molecule lies on an inversion centre), $T = 100.0(2)$ K, $\rho_{calcd} = 1.577\ g\,cm^{-1}$, $F(000) = 3178$, $\mu(Mo_{K\alpha}) = 1.104\ mm^{-1}$. Data were collected on a Bruker SMART CCD diffractometer ($Mo_{K\alpha}$, $\lambda = 0.71073$). In all cases the selected crystals were mounted on the tip of a glass pin using paratone-N oil and placed in the cold flow (100 K) produced with an Oxford cryocooling device. Complete hemispheres of data were collected using ω scans (0.3°, 30 seconds per frame). Integrated intensities were obtained with SAINT+ [16] and they were corrected for absorption using SADABS.[16] Structure solution and refinement was performed with the SHELX package.[16] The structures were solved by direct methods and completed by iterative cycles of ΔF syntheses and full-matrix least-squares refinement against F^2 to give: for **1**: using 1321 parameters and 98 restraints, $wR_2 = 0.2260$ (12935 unique reflections), $R_1 = 0.1033$ (11281 reflections with $I > 2\sigma(I)$); for **2:** using 1397 parameters and 478 restraints, $wR_2 = 0.2206$ (20413 unique reflections), $R_1 = 0.0611$ (17353 reflections with $I > 2\sigma(I)$); for **3**: using 1608 parameters without restraints, $wR_2 = 0.2626$ (7978 unique reflections), $R_1 = 0.0893$ (7306 reflections with $I > 2\sigma(I)$). CCDC-268450–268452 contain the supplementary crystallographic data for this paper. These data can be obtained free of charge from the Cambridge Crystallographic Data Centre via www.ccdc.cam.ac.uk/data_request/cif.

[10] J. Lorionova, M. Gross, M. Pilkington, H. Andres, H. S. Evans, H. U. Gudel, S. Decurtins, *Angew. Chem.* **2000**, *112*, 1667 – 1672; *Angew. Chem. Int. Ed.* **2000**, *39*, 1605 – 1609.

[11] W. Wernsdorfer, *Adv. Chem. Phys.* **2001**, *118*, 99 – 192.

[12] K. L. Taft, C. D. Delfs, G. C. Papaefthymiou, S. Foner, D. Gatteschi, S. J. Lippard, *J. Am. Chem. Soc.* **1994**, *116*, 823 – 832.

[13] An isosceles triangle of antiferromagnetically coupled $S = 2$ spins described by the spin Hamiltonian $\mathscr{H} = J(\mathbf{S_1S_2}+\mathbf{S_1S_3}) + J'(\mathbf{S_2S_3})$ has $S = 0$ ground state if J'/J is between 2/3 and 3/2. The reduction in the symmetry and the introduction of a third coupling constant does not significantly alter this picture.

[14] J. B. Vincent, H. Chang, K. Folting, J. C. Huffman, G. Christou, D. N. Hendrickson, *J. Am. Chem. Soc.* **1987**, *109*, 5703 – 5711.

[15] S. Midollini, A. Orlandini, P. Rosa, L. Sorace, *Inorg. Chem.* **2005**, *44*, 2060 – 2066.

[16] SHELX-PC Package: Bruker Analytical X-ray Systems, Madison, WI, **1998**.

 © 2005 Wiley-VCH Verlag GmbH & Co. KGaA, Weinheim

Photochemistry

DOI: 10.1002/anie.200462575

Multiple Addressing in a Hybrid Biphotochromic System

*Michel Frigoli and Georg H. Mehl**

Addressing the optical and electronic properties of organic materials by light is currently a very active research area and such systems are expected to be of great importance for optical computing—as logic gates, as the optical equivalent of field-effect transistors, as high density (3D) data storage systems, as well as for light rectification and harvesting.[1–3] The goal is a miniaturization of functional elements down to the molecular level, or at least close to that, which could result in a markedly increased performance as a consequence of the higher volume density of the functional elements compared to that of current devices.

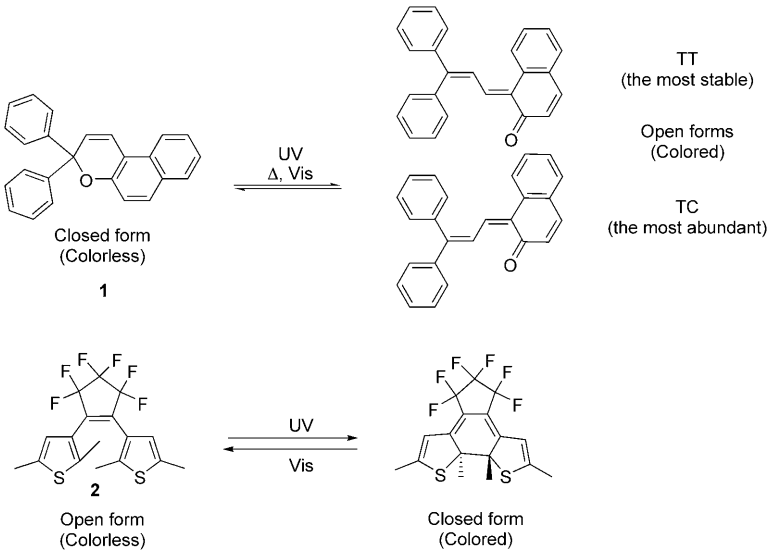
Irradiation of photochromic systems at selected wavelengths leads to the reversible formation of colored forms as a result of a change of the structure of conjugated π systems. Bistable materials or systems that are dependent on continuous irradiation to maintain the colored (high-energy) form are suitable candidates for such applications. Nanostructured crystalline systems, high-density photochromic polymers, and a range of systems which form anisotropic fluids either as mixtures or as molecular materials in the condensed state, have been reported recently.[4,5]

In this context, biphotochromic systems are particularly attractive, as the controlled sequential interaction of photons in one molecular system promises synergies in the design and electronic properties (for example, a sequential change of the electronic properties would be a precondition for a fully photonic molecular logic gate).[2a,g,3g] Investigations on biphotochromes based on naphthacene–diarylethene, interconnected diarylethenes, and diarylethene–dihydroazulene systems have been reported recently.[6–8] The challenge with biphotochromic systems is both the selective and controlled addressing of individual photochromic units and the conversion of the combined system. In this context, the combination of naphthopyrans and photochemically bistable and very fatigue resistant diarylethene groups (Scheme 1) are particularly interesting, and as yet not investigated.[2b]

Naphthopyrans are currently the most important class of photochromes commercially as a result of their high stability, fatigue resistance, and addressable bleaching kinetics.[9] Herein we report the synthesis and investigation of the photochromic properties of a combined system consisting of a

[*] Dr. M. Frigoli, Dr. G. H. Mehl
University of Hull
Department of Chemistry
Cottingham Road
Hull, HU6 7RX (UK)
Fax: (+44) 1482-466-411
E-mail: g.h.mehl@hull.ac.uk

 InterScience © 2005 Wiley-VCH Verlag GmbH & Co. KGaA, Weinheim

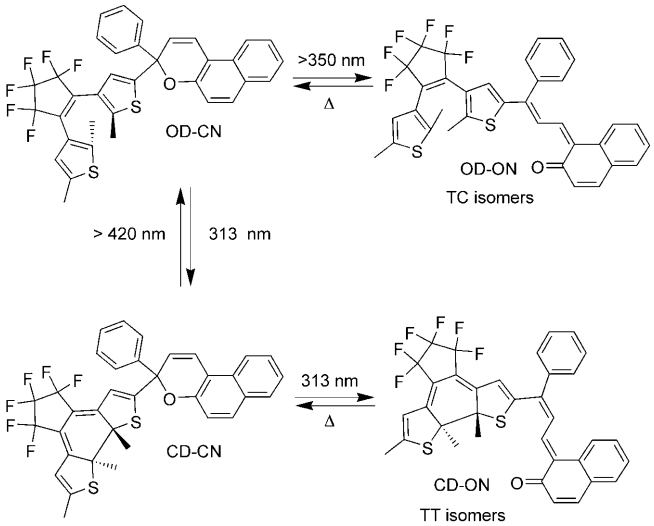


Scheme 1. Photochemical interconversion in the [3*H*]-naphthopyran and dithienylethene series; TT = transoid,*trans*; TC = transoid,*cis*.

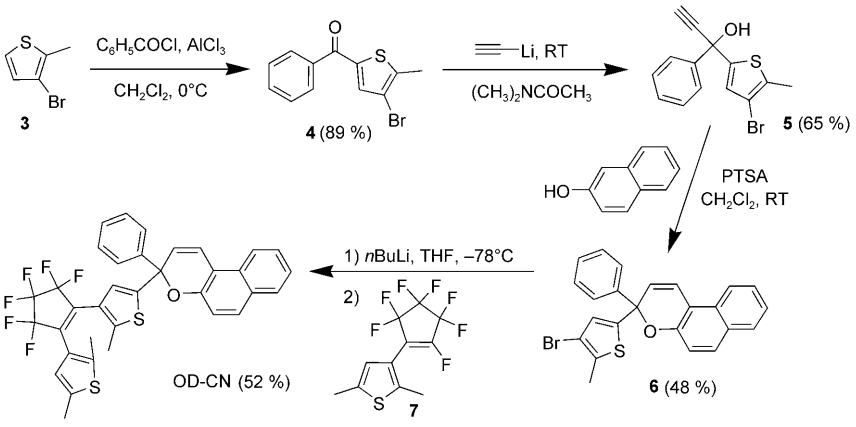
naphthopyran unit and a diarylethene group. An important feature in the design of this system is the different absorption behaviors of the naphthopyran (CN) and the diarylethene (OD) groups which are connected through a sp^3-hybrdized carbon center. Only the conversion of the closed naphthopyran (CN) into the open form (ON) leads to conjugation and an electronic connection. Closure of the open diarylethene system (OD to CD) extends the π-electron system over the whole molecule. The different behavior of these two photochromes—diarylethenes are essentially bistable and naphthopyrans open on irradiation to a number of isomers, most of which revert back thermally to the closed forms in the dark—results in a multiaddressable hybrid photochrome.

The synthesis of OD-CN (Scheme 2) starts with the preparation of ketone **4**, which was obtained (89% yield) from the reaction of 2-methyl-3-bromothiophene with benzoyl chloride in the presence of $AlCl_3$. The subsequent condensation of the lithium acetylide diamine complex with **4** resulted in the corresponding propargylic alcohol **5** (65% yield).[10] The intermediate chromene **6** was obtained by a "one-pot reaction" of **5** and 2-naphthol in the presence of a catalytic amount of *para*-toluenesulfonic acid (PTSA; yield 48%).[11] Lithiation of the chromene **6** by bromine/lithium exchange using *n*BuLi in THF at −78°C, followed by quenching of the reaction mixture with **7** afforded the hybrid biphotochrome OD-CN (52% yield).[12a]

The mode of action of the multiaddressable photochromic system OD-CN is illustrated in Scheme 3. The path from OD-CN to CD-ON requires the interaction of OD-CN with two photons. The photochromic properties were investigated by a series of steady-state experiments in which light was either switched on or off (input: 0,1) and spectra were recorded until a photostationary state (PS) was obtained. This sequential approach revealed the formation of four different states with entirely different absorption behaviors, and five addressing modes were investigated.[12b]



Scheme 3. Photochemical reactions of the hybrid OD-CN showing all four photochromic states.



Scheme 2. Synthesis of the biphotochromic hybrid OD-CN.

The associated investigated reaction pathways are: 1) OD-CN→OD-ON, 2) OD-CN→CD-ON (via CD-CN), 3) CD-ON→CD-CN, 4) CD-CN→CD-ON, 5) CD-CN→OD-CN. Our experimental set-up did not allow for the investigation of the potential direct path from OD-ON to CD-ON. Two of the states, OD-CN and CD-CN, are bistable, while OD-ON and CD-ON have to be triggered by irradiation. The absorption spectra of all four forms are shown in Figure 1 and the colored solutions are shown in Figure 2.

 © 2005 Wiley-VCH Verlag GmbH & Co. KGaA, Weinheim

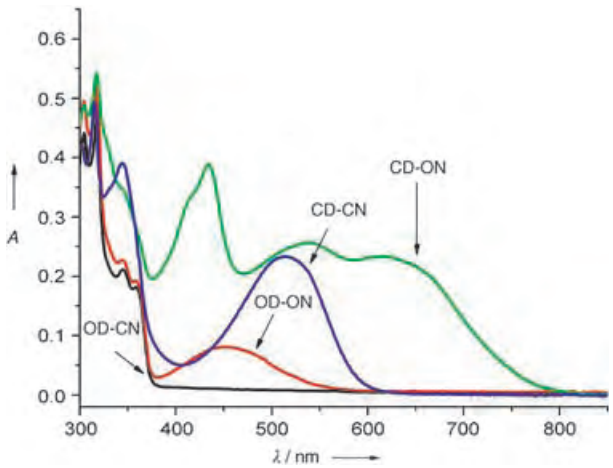


Figure 1. UV/Vis absorption spectra (cylohexane solution, 3.33×10^{-5} M) of the four photochromic states of the system OD-CN, before irradiation (OD-CN), with irradiation at 366 nm (OD-ON), with irradiation at 313 nm (CD-ON), after irradiation at 313 nm then left in the dark (CD-CN).

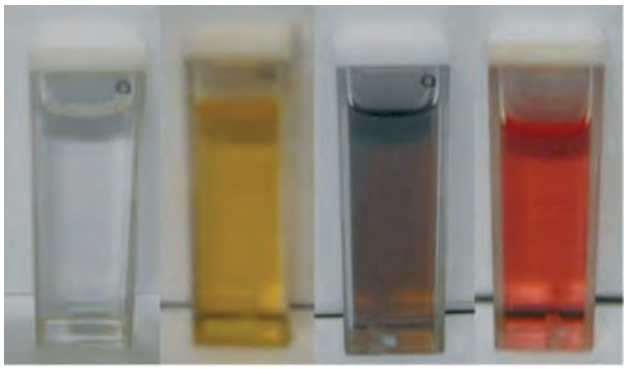


Figure 2. Colors obtained for each stationary state: OD-CN (initial state, colorless), OD-ON (after irradiation at 366 nm, yellow), CD-ON (after irradiation of OD-CN or CD-CN at 313 nm, brown), and CD-CN (from thermal bleaching of OD-ON in the dark, red/pink).

An interesting feature of the OD-CN system is the electronic decoupling of the two photochromic groups connected through a sp^3-hybridized carbon atom. Irradiation above 350 nm transforms the naphthopyran group selectively from the closed (colorless) form of OD-CN to the open form (orange, $\lambda_{max}=456$ nm) of OD-ON (path 1; Figure 1). The thermal bleaching kinetics of the majority of the photoproducts (ca. 81 %) can be described with a monoexponential function ($k_{\Delta}=0.055\ s^{-1}$; Figure 3), with a value for the closure rate similar to that observed for other chromene systems.[13] The residual absorption (ca. 19 %) in the visible region is typical for 2*H*-chromenes and is attributed to the presence of stable isomers; such isomers have been observed with other naphthopyrans.[14] These forms can be converted fully into the closed form by irradiation above 400 nm. In other words, this system has a read-out window between 350 and 380 nm, where the naphthopyran group can be switched selectively without affecting the diarylethene moiety.

Irradiation of OD-CN at 313 nm triggers both the ring-opening reaction of the naphthopyran and also the ring-closing reaction of the diarylethene, as the electronic properties of the ground states of the two photochromic moieties overlap between 300 and 350 nm, which leads initially to the formation of OD-ON and CD-CN. After irradiation for one minute the absorption is centered at 539 nm with a shoulder at 434 nm and also with absorption above 600 nm (Figure 4a). This is, however, not an equilibrium, CD-CN is bistable while OD-ON is not and reverts to OD-CN. Continuing the irradiation leads to an enrichment of CD-CN in the mixture, which is subsequently converted into CD-ON on further irradiation (path 2). The initially colorless solution turns brown, and the UV/Vis spectrum shows absorption up to 800 nm with three absorption maxima at 434, 539, and 618 nm.

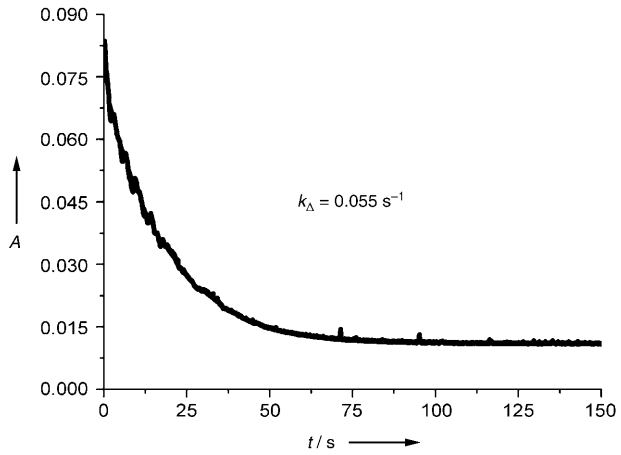


Figure 3. Thermal bleaching of OD-ON monitored at 456 nm.

When the irradiation is stopped, the open forms of the naphthopyran revert back to the closed form CD-CN (see Figure 4b) and the solution turns slowly from brown to pink (the maxima at 434 and 618 nm decrease and a new maximum at 516 nm is observed; path 3). Monitoring the kinetics of the conversion of CD-ON into CD-CN at 680 nm, where only the fully conjugated system absorbs, gives a bleaching rate constant of $1.95\times10^{-3}\ s^{-1}$ (monoexponential; Figure 4d). This comparatively high value indicates that the extension of the π conjugation in the CD-ON isomer stabilizes the open naphthopyran moiety to a large extent.[15]

Two photopathways are possible from the stationary state of CD-CN. Ring opening of the diarylethene to recover the OD-CN starting material (path 4) can be effected quantitatively from CD-CN with visible light (> 420 nm), a behavior typical of dithienylethenes. Irradiation of CD-CN (path 5) at 313 nm (OD-CN and CD-CN have a similar absorption at 313 nm; see Figure 1) induces the formation of CD-ON. The photostationary state (CD-ON) is reached faster from CD-CN than starting from OD-CN (Figure 4c).

The absorption characteristics of CD-ON are the same, regardless of whether the conversion is from OD-CN or CD-CN, which indicates that the naphthopyran group can be selectively opened and closed using UV light without affecting the diarylethene moiety.

In summary, we have investigated a hybrid biphotochromic system based on the thermally reversible naphthopyran

 © 2005 Wiley-VCH Verlag GmbH & Co. KGaA, Weinheim

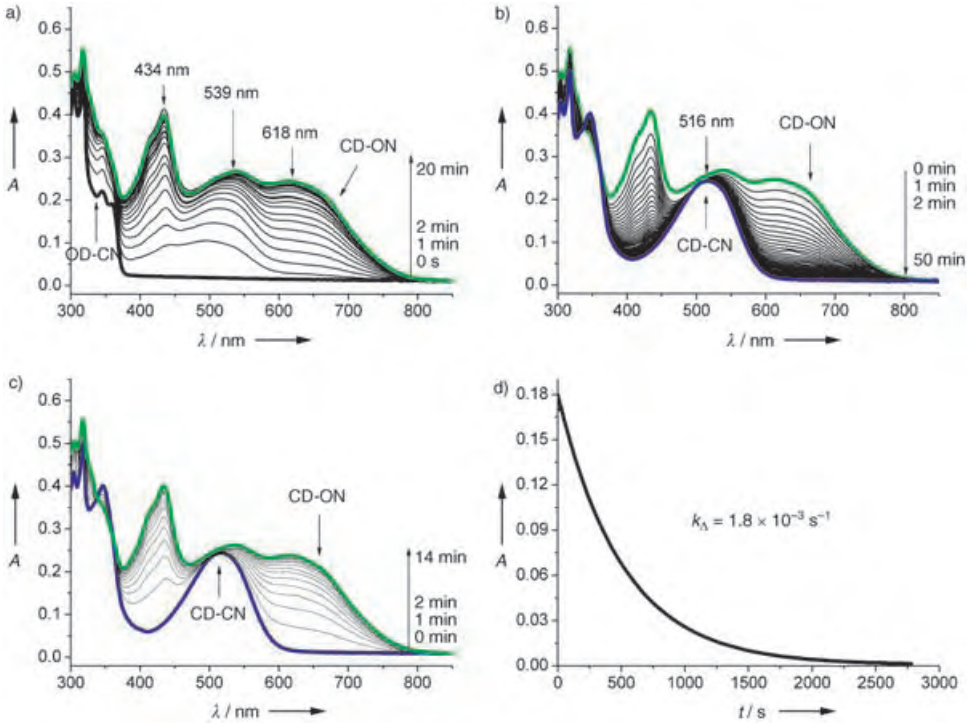


Figure 4. a) Time-dependent absorption spectra of a solution of OD-CN in cyclohexane (3.33×10^{-5} M) upon irradiation at 313 nm; b) fading of CD-ON after irradiation at 313 nm; c) time-dependent absorption spectra of CD-CN upon irradiation at 313 nm; d) thermal bleaching of CD-ON monitored at 680 nm.

and photochemically bistable dithienyl groups. Four different states were detected in this system, which are characterized by very different absorption properties and which can be addressed in the photon mode.

Received: November 10, 2004
Revised: March 23, 2005
Published online: July 20, 2005

Keywords: conjugation · molecular devices · photochemistry · photochromism · UV/Vis spectroscopy

[1] a) For a ecent review, see: *Electron Transfer in Chemistry*, *Vol. 1–5* (Ed.: V. Balzani), Wiley-VCH, Weinheim, **2001**, particularly Vols. 3 and 5; b) V. Balzani, A. Credi, M. Venturi, *Chem. Eur. J.* **2002**, *8*, 5525; c) G. J. Brown, A. P. de Silva, S. Pagliari, *Chem. Commun.* **2002**, 2461; d) V. Balzani, A. Credi, M. Venturi, *ChemPhysChem* **2003**, *3*, 49.

[2] For recent reviews, see: a) *Molecular Switches* (Ed.: B. L. Feringa), Wiley-VCH, Weinheim, **2001**; b) M. Irie, *Chem. Rev.* **2000**, *100*, 1685; c) B. L. Feringa, R. A. van Delden, Konimura, E. M. Geertsma, *Chem. Rev.* **2000**, *100*, 1789; d) A. P. de Silva, N. S. McClenaghan, *Chem. Eur. J.* **2004**, *10*, 574; e) B. L. Feringa, *Acc. Chem. Res.* **2001**, *34*, 504; f) H. Dürr in *Organic Photochromic and Thermochromic Compounds* (Eds.: J. C. Crano, R. J. Guglielmetti), Plenum, New York, **1999**; g) *Photochromism* (Eds.: H. Dürr, H. Buoas-Laurent), Elsevier, Amsterdam, **2003**.

[3] a) C. J. Brabec, A. Cravino, D. Meisner, N. S. Sariciftci, T. Fromherz, M. T. Rispens, L. Sanchez, J. C. Hummelen, *Adv. Funct. Mater.* **2001**, *11*, 134; b) A. Cravino, N. S. Sariciftci, *Nat. Mater.* **2003**, *2*, 360; C. Winder, N. S. Sariciftci, *J. Mater. Chem.* **2004**, *14*, 1077; c) I. M. Bennett, H. M. V. Farfano, F. Bogani, A. Primak, P. A. Lidell, L. Otero, L. Sereno, J. J. Silber, A. L. Moore, T. A. Moore, D. Gust, *Nature* **2002**, *420*, 398; d) P. A. Lidell, G. Kodis, J. Andreasson, L. de la Garza, S. Banduopadhyay, R. H. Mitchell, A. L. Moore, T. A. Moore, D. Gust, *J. Am. Chem. Soc.* **2004**, *126*, 4803; e) F. Pina, J. C. Lima, A. J. Parola, C. A. M. Afonso, *Angew. Chem.* **2004**, *116*, 1551; *Angew. Chem. Int. Ed.* **2004**, *43*, 1525; f) M. K. J. ter Wiel, R. A. van Delden, A. Meetsma, B. L. Feringa, *J. Am. Chem. Soc.* **2003**, *125*, 15076; g) K. L. Kompa, R. D. Levine, *Proc. Natl. Acad. Sci. USA* **2001**, *98*, 410; h) S. A. Ahmed, X. Sallenave, F. Fages, G. Mieden-Gudert, W. M. Müller, U. Müller, F. Vögtle, J. L. Pozzo, *Langmuir* **2002**, *18*, 7096; i) F. M. Raymo, S. Giordani, *Proc. Natl. Acad. Sci. USA* **2002**, *99*, 4941.

[4] a) K. E. Maly, M. D. Wand, R. P. Lemieux, *J. Am. Chem. Soc.* **2002**, *124*, 7898; b) M. Frigoli, G. H. Mehl, *ChemPhysChem* **2003**, *4*, 101; c) S. H. Chen, H. M. P. Chen, Y. Geng, S. D. Jacobs, K. L. Marshall, *Adv. Mater.* **2003**, *15*, 1061; d) M. Frigoli, G. H. Mehl, *Eur. J. Org. Chem.* **2004**, 636; e) R. A. van Delden, T. Mecca, C. Rosini, B. L. Feringa, *Chem. Eur. J.* **2004**, *10*, 61; f) M. Frigoli, G. H. Mehl, *Chem. Commun.* **2004**, 818; g) M. Frigoli, G. H. Mehl, *Chem. Eur. J.* **2004**, *10*, 5243; h) M. Frigoli, C. Welch, G. H. Mehl, *J. Am. Chem. Soc.* **2004**, *126*, 15382.

[5] a) M. Marimoto, S. Kobatake, M. Irie, *J. Am. Chem. Soc.* **2003**, *125*, 11080; b) M. Marimoto, S. Kobatake, M. Irie, *Photochem. Photobiol. Sci.* **2003**, *2*, 1088; c) M. Marimoto, S. Kobatake, M. Irie, *Chem. Rec.* **2004**, *4*, 23.

[6] a) A. J. Myles, T. J. Wigglesworth, N. R. Branda, *Adv. Mater.* **2003**, *15*, 745; b) A. J. Miles, B Gorodetsky, N. R. Branda, *Adv. Mater.* **2004**, *16*, 922; c) A. Peters, R. McDonald, N. R. Branda, *Chem. Commun.* **2002**, 2275.

[7] a) T. Mrozek, H. Görner, J. Daub, *Chem. Commun.* **1999**, 1487; b) T. Mrozek, H. Görner, J. Daub, *Chem. Eur. J.* **2001**, *7*, 1028; c) L. Gobbi, P. Seiler, F. Diederich, V. Gramlich, C. Boudon, J.-P. Giisselbrecht, M. Gross, *Helv. Chim. Acta* **2001**, *84*, 743; d) V.

 © 2005 Wiley-VCH Verlag GmbH & Co. KGaA, Weinheim

De Waele, U. Schmidhammer, T. Mrozek, E Riedle, J. Daub, R. T. Eberhard, *J. Am. Chem. Soc.* **2002**, *124*, 2438.
[8] T. Kawai, T. Iseda, M. Irie, *Chem. Commun.* **2004**, 72.
[9] Selected examples are: a) C. D. Gabutt, J. D. Hepworth, B. M. Heron, S. M. Partington, D. A. Thomas, *Dyes Pigm.* **2001**, *49*, 65; b) D. A. Clarke, B. M. Heron, C. D. Gabutt, J. D. Hepworth, S. M. Partington, S. N. Corns, PCT WO 98/45281, **1998** [*Chem. Abstr.* **1998**, *128*, 317585]; c) B. Van Gemmert, M. B. Bergomi, US Pat. No. 5066818, **1998** [*Chem. Abstr.* **1998**, *129*, 317585].
[10] O. F. Beumel, Jr., R. F. Harris, *J. Org. Chem.* **1964**, *29*, 1872.
[11] M. Frigoli, C. Moustrou, A. Samat, R. Guglielmetti, *Eur. J. Org. Chem.* **2003**, 2799.
[12] a) A solution of *n*BuLi in hexane (2.5 M, 0.53 mL) was added dropwise to a solution of **6** (0.52 g, 1.20 mmol) in dry THF (20 mL) at −78 °C. After the mixture had been stirred for 1 h at this temperature, a solution of **7** (0.36 g, 1.20 mmol) in dry THF (5 mL) was added dropwise. The reaction mixture was allowed to warm up to room temperature and then an aqueous solution of NH_4Cl was added. The resulting mixture was extracted twice with diethyl ether, washed with water, dried over magnesium sulfate, then concentrated under vacuum. Column chromatography (silica, hexane/CH_2Cl_2, 70/30) gave OD-CN as a slightly orange pure product (0.4 g, 52%). M.p. 67.5–68.5 °C; ^{1}H NMR (400 MHz, $CDCl_3$): $\delta = 1.38$ (s, 3H), 1.84 (s, 3H), 2.33 (s, 3H), 6.17 (d, $J = 9.8$ Hz, 1H,), 6.60 (s, 1H), 6.85 (s, 1H), 7.16 (d, $J = 9.0$ Hz, 1H), 7.29–7.58 (m, 8H), 7.68 (d, $J = 9.0$ Hz, 1H), 7.73 (d, $J = 8.2$ Hz, 1H), 7.96 ppm (d, $J = 8.4$ Hz, 1H). Elemental analysis calcd (%) for $C_{35}H_{24}F_6OS_2$: C 65.82, H 3.79; found: C 65.98, H 3.67; b) the experimental set-up for the photochemical measurements is described in ref. [4d,g].
[13] a) M. Frigoli, C. Moustrou, A. Samat, R. Guglielmetti, *Helv. Chim. Acta* **2000**, *83*, 3043; b) M. Frigoli, PhD thesis, Marseille, **2000**.
[14] a) F. Ortica, P. Smimmo, G. Favaro, U. Mazzucato, S. Delbaere, D. Venec, G. Vermeersch, M. Frigoli, C. Moustrou, A. Samat, *Photochem. Photobiol. Sci.* **2004**, *3*, 878; b) S. Delbaere, J.-C. Micheau, G. Vermeersch, *J. Org. Chem.* **2003**, *68*, 8968; c) note: this is typical for 2*H*-chromenes and indicates, in principle, the presence of four photoproducts (CTC, TTC, TTT, and CTC). The isomers differ only in the configuration at the double bond attached to the naphthalene ring and at the position of the aryl group at the terminal double bond. The isomers CTC and TTC are thermoreversible whereas the other two are thermally stable and bleach on exposure to visible light. (TTT = *trans*,transoid, *trans*, CTT = *cis*,transoid,*trans*).
[15] Note: The thermal stability of CD-ON increased about 28 times relative to OD-ON. This result, together with monoexponential bleaching kinetics, might indicate that TT isomers, whose formation is selectively photoinduced by the extended π conjugation throughout the molecule, are formed preferentially.

 © 2005 Wiley-VCH Verlag GmbH & Co. KGaA, Weinheim

Bioorganic Chemistry

DOI: 10.1002/anie.200500635

Multivalent Peptide and Protein Dendrimers Using Native Chemical Ligation**

Ingrid van Baal, Hinke Malda, Silvia A. Synowsky, Joost L. J. van Dongen, Tilman M. Hackeng, Maarten Merkx, and E. W. Meijer**

Multiple, simultaneous interactions are often used in biology to enhance the affinity and specificity of binding, an effect that is known as multivalency.[1] The principle of multivalency has been recognized as an important strategy for the development of (semi)synthetic ligands with high affinity and specificity for biological targets.[1–6] Dendrimers are well-defined, hyperbranched polymers with a high density of functional groups and are therefore attractive scaffolds for multivalent display of natural ligands.[7–9] Dendrimers have been successfully applied in the design of multivalent sugar ligands,[10–12] but much less work has been reported on multivalent peptide and protein dendrimers. Solid-phase peptide synthesis has been used to construct dendritic peptide wedges by condensation of successive generations of lysine residues followed by functionalization of the α and ε amine groups with peptides.[13,14] These so-called multiple antigen peptides (MAPs) typically contain two to eight peptide chains and have been found to be more immunogenic than single

[*] I. van Baal, H. Malda, J. L. J. van Dongen, Dr. M. Merkx, Prof. E. W. Meijer
Laboratory of Macromolecular and Organic Chemistry
Eindhoven University of Technology
P.O. Box 513, 5600 MB, Eindhoven (The Netherlands)
Fax: (+31) 40-245-1036
E-mail: m.merkx@tue.nl
e.w.meijer@tue.nl

S. A. Synowsky
Department of Biomolecular Mass Spectrometry
Bijvoet Center for Biomolecular Research and
Utrecht Institute for Pharmaceutical Sciences
Utrecht University
Sorbonnelaan 16, 3584 CA Utrecht (The Netherlands)

Dr. T. M. Hackeng
Department of Biochemistry
Cardiovascular Research Institute Maastricht
University Maastricht
P.O. Box 616, 6200 MD Maastricht (The Netherlands)

[**] I. van Baal and H. Malda contributed equally to this work. We acknowledge grants from the department of Biomedical Engineering of the Eindhoven University of Technology and the NRSC Catalysis. We thank Robert H. H. van den Heuvel and Albert J. R. Heck (Utrecht University, The Netherlands) for useful discussions and mass spectrometry equipment, Alex Faesen for preparation of illustrations, and Marcel van Genderen and Anouk Dirksen for helpful discussions.

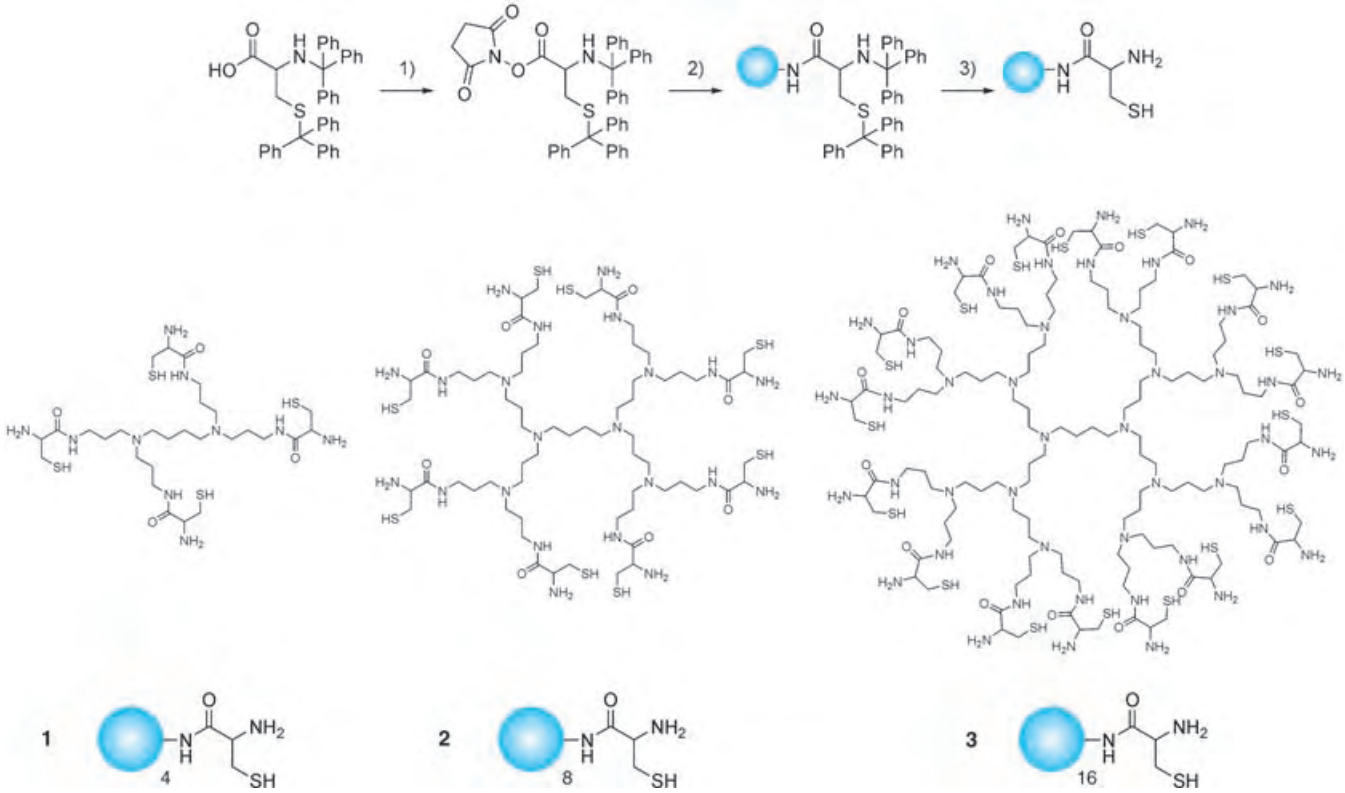
Supporting information (synthesis and characterization of the dendrimers, including mass spectra for all the peptide and protein dendrimers) for this article is available on the WWW under http://www.angewandte.org or from the author.

InterScience
© 2005 Wiley-VCH Verlag GmbH & Co. KGaA, Weinheim

peptides. Dendrimers functionalized with cysteine-reactive chloroacetyl[15] and maleimide[16] groups have been used to conjugate cysteine-containing peptides, but this strategy cannot be applied to peptides and proteins containing functionally important native cysteine residues. Convergent synthesis of peptide dendrimers has also been reported by condensation of ketone-functionalized polyamidoamine (PAMAM) dendrimers with aminooxy-functionalized peptides, but this method is unsuitable for native proteins.[9] The few reports of protein ligation to dendrimers typically involve the coupling of a single protein (for example, an antibody) using nonspecific conjugation chemistry that results in conjugation at multiple sites on the protein. Recently, the preparation of multivalent hemoglobin dendrimers was reported that involved specific conjugation of a fourth generation PAMAM dendrimer to hemoglobin using a hemoglobin-specific cross-linking agent.[17] However, no general synthetic strategy is currently available that allows conjugation of dendrimers with both oligopeptides and recombinant proteins in a chemoselective manner.

Native chemical ligation was first reported by Dawson et al. as a unique method to ligate two unprotected peptide fragments to form a native peptide bond.[18] This chemoselective reaction occurs spontaneously between a peptide with a C-terminal thioester and a peptide with an N-terminal cysteine residue under aqueous conditions at neutral pH. Native chemical ligation has allowed the chemical synthesis of large proteins (by multistep ligation of several peptide fragments), the synthesis of proteins with synthetic moieties such as fluorescent dyes and biotin tags, and the immobilization of peptides and proteins on surfaces.[19–23] The application of native chemical ligation was recently extended to recombinantly expressed proteins by the development of expression systems based on self-cleavable intein domains that generate proteins containing N-terminal cysteine or C-terminal thioester groups.[24,25] Herein we report the application of native chemical ligation as an attractive and general synthetic strategy to conjugate both oligopeptides and recombinantly expressed proteins to dendrimers, thus resulting in multivalent peptide and protein dendrimers.

Dendrimers can either be functionalized with thioester groups or with cysteine residues to allow native chemical ligation. We chose the latter strategy because the synthesis of these cysteine dendrimers is more straightforward. Cysteine dendrimers generations 1–3 (Scheme 1)were synthesized by reaction of the amine end groups of poly(propyleneimine) dendrimers with succinimide-activated and trityl-protected cysteine residues (Scheme 1). Deprotection of the trityl-protected amine and thiol groups using trifluoroacetic acid (TFA) yielded the cysteine-functionalized dendrimers **1**–**3** in good yields. Analysis of **1**–**3** by electrospray ionization mass spectrometry (ESI-MS) showed that the cysteine residues were reduced in the presence of the mild reductant β-mercaptoethanol. Removal of the reductant and addition of



Scheme 1. Top: synthesis of cysteine-functionalized poly(propyleneimine) dendrimers: activation of trityl-protected cysteine with disuccinimidylcarbonate in acetonitrile (1), coupling of activated cysteine to poly(propyleneimine) dendrimer using triethylamine in dichloromethane (2), and deprotection of cysteine end groups using trifluoroacetic acid, 2.5% triisopropylsilane, and 2.5% water (3). Bottom: schematic structures of cysteine dendrimers **1**, **2**, and **3**.

 © 2005 Wiley-VCH Verlag GmbH & Co. KGaA, Weinheim

hydrogen peroxide resulted in the immediate formation of dendrimers with two, four, or eight intramolecular disulfide bonds, respectively (see Supporting Information). To assess the reactivity of the cysteine dendrimers in native chemical ligation reactions we performed ligation reactions with several peptides functionalized with an MPAL thioester at their C-terminus.[19] Ligation of **1** with four equivalents of LYRAG, a peptide previously used in studies on native chemical ligation,[19] resulted in the formation of the peptide tetramer **1**-(LYRAG)$_4$ (Figure 1 a). Analysis by liquid chromatography/mass spectrometry (LC-MS) showed that the reaction went to completion as no **1**-(LYRAG)$_{1-3}$ were detected (not shown). Ligation reactions were also performed between LYRAG and dendrimers **2** and **3** to test the efficiency of the ligation reaction for higher generations of cysteine dendrimers. Ligation of **2** with LYRAG again went to completion and yielded the peptide octamer **2**-(LYRAG)$_8$ exclusively (Figure 1 b). The MALDI-TOF spectrum obtained after ligation of **3** with LYRAG showed a signal consistent with the formation of **3**-(LYRAG)$_{16}$, but also contained signals attributable to **3**-(LYRAG)$_{12-15}$. Similar results were obtained for other oligopeptides such as GRGDSGG (Table 1). The RGD sequence present in this peptide is known to bind to various extracellular integrin receptors and can thus be used to attach dendrimers to cell surfaces.

Table 1: Overview of peptide and protein dendrimers obtained by native chemical ligation.

Dendrimer	Observed mass [Da]	Calculated average mass [Da][a]
1-(LYRAG)$_4$	3139.7	3139.8
2-(LYRAG)$_8$	6419.7	6419.9
3-(LYRAG)$_{16}$	12262[b]	12307.6
1-(GRGDSGG)$_4$	3243.2	3243.5
2-(GRGDSGG)$_8$	6627.1	6627.1
1-(GFP)$_1$	28288.6 (0.5)[c]	28291
1-(GFP)$_1$(GRGDSGG)$_3$	30172.5 (0.7)[c]	30177
1-(GFP)$_4$	110971.1 (4.7)[c]	110976

[a] Average masses were calculated assuming the complete reduction of the cysteine groups. [b] In addition to the signal of **3**-(LYRAG)$_{16}$, the MALDI-TOF spectrum showed signals consistent with **3**-(LYRAG)$_{12-15}$. [c] The number between brackets is the experimental error as determined using the program MaxEnt 1.

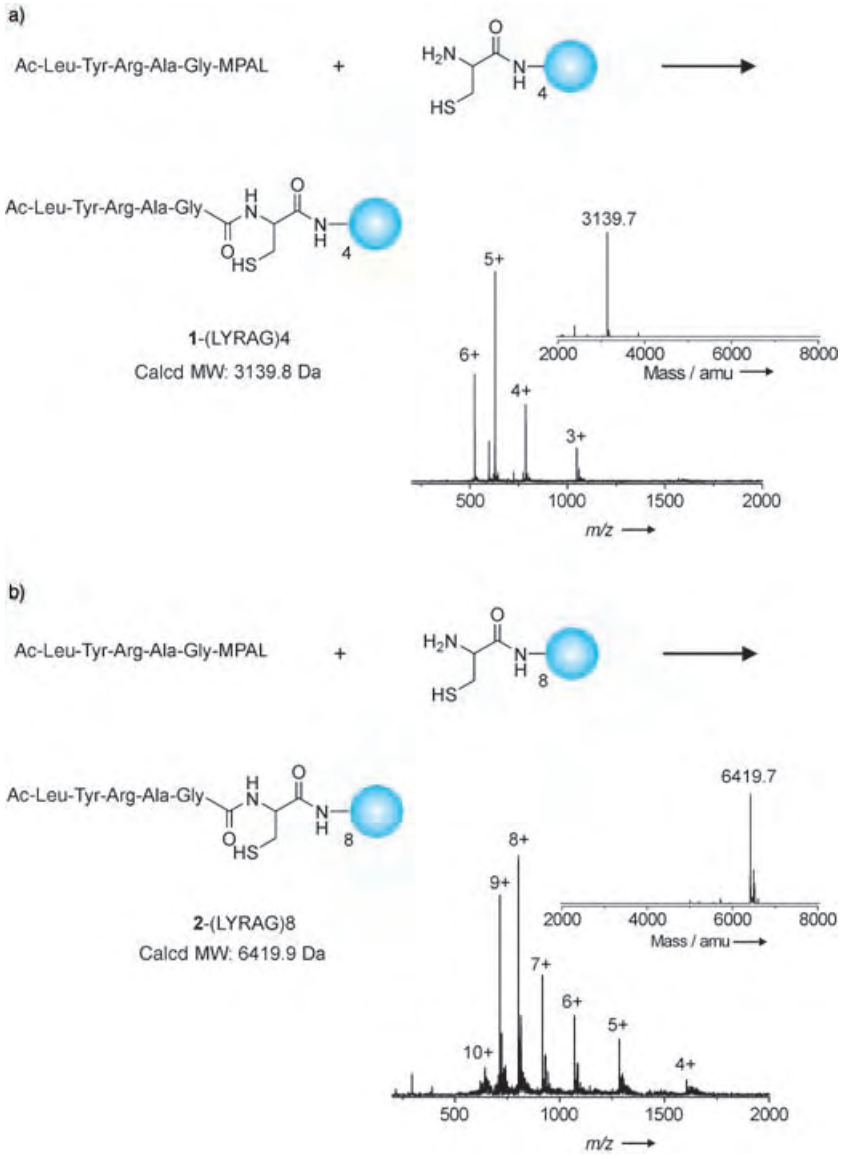


Figure 1. Native chemical ligation of the MPAL-thioester of LYRAG to first (a) and second (b) generation cysteine dendrimers **1** and **2**. Dendrimer was dissolved in 0.1 M Tris, 6 M guanidine, 2% (v/v) thiophenol, and 2% (v/v) benzyl mercaptan pH 7.0–7.5 and treated with four (**1**) or eight equivalents (**2**) of MPAL-peptide for 1 h at 37 °C. The mass spectra were obtained by ESI-MS after removal of the buffer components by RP-HPLC.

Green fluorescent protein (GFP) was chosen as a model protein to study the ligation of folded proteins to cysteine dendrimers. GFP was cloned into the IMPACT vector pTXB1 to yield an *E. coli* expression vector for a fusion protein of GFP with an intein domain and a chitin-binding domain (CBD). The cloning strategy used here meant that the GFP contained eight additional residues at the C-terminus of GFP, that is, NEFLEGSS. Overnight incubation of the GFP-intein-CBD protein bound to the chitin column with MESNA resulted in cleavage of the peptide bond to the GFP and the formation of GFP thioester. ESI-MS analysis showed the presence of a single protein signal with a mass of 27705 Da that is consistent with the MESNA thioester of GFP (theoretical mass: 27703.9 Da). The GFP thioester was first ligated to dendrimer **1** using a large excess of the dendrimer. ESI-MS of the reaction mixture after incubation for 20 h at room temperature showed the clean conversion of GFP thioester to **1**-(GFP)$_1$, with no indication of the presence of the initial GFP thioester or dendrimer with more than one GFP (Figure 2). The large difference in molecular weight between **1**-(GFP)$_1$ and **1** allowed the easy removal of excess of **1** from the ligation mixture by repeated concentration/dilution steps using a centrifugal filter with a 10-kDa molecular-weight cutoff. Subsequently, **1**-(GFP)$_1$ was treated with an

 © 2005 Wiley-VCH Verlag GmbH & Co. KGaA, Weinheim

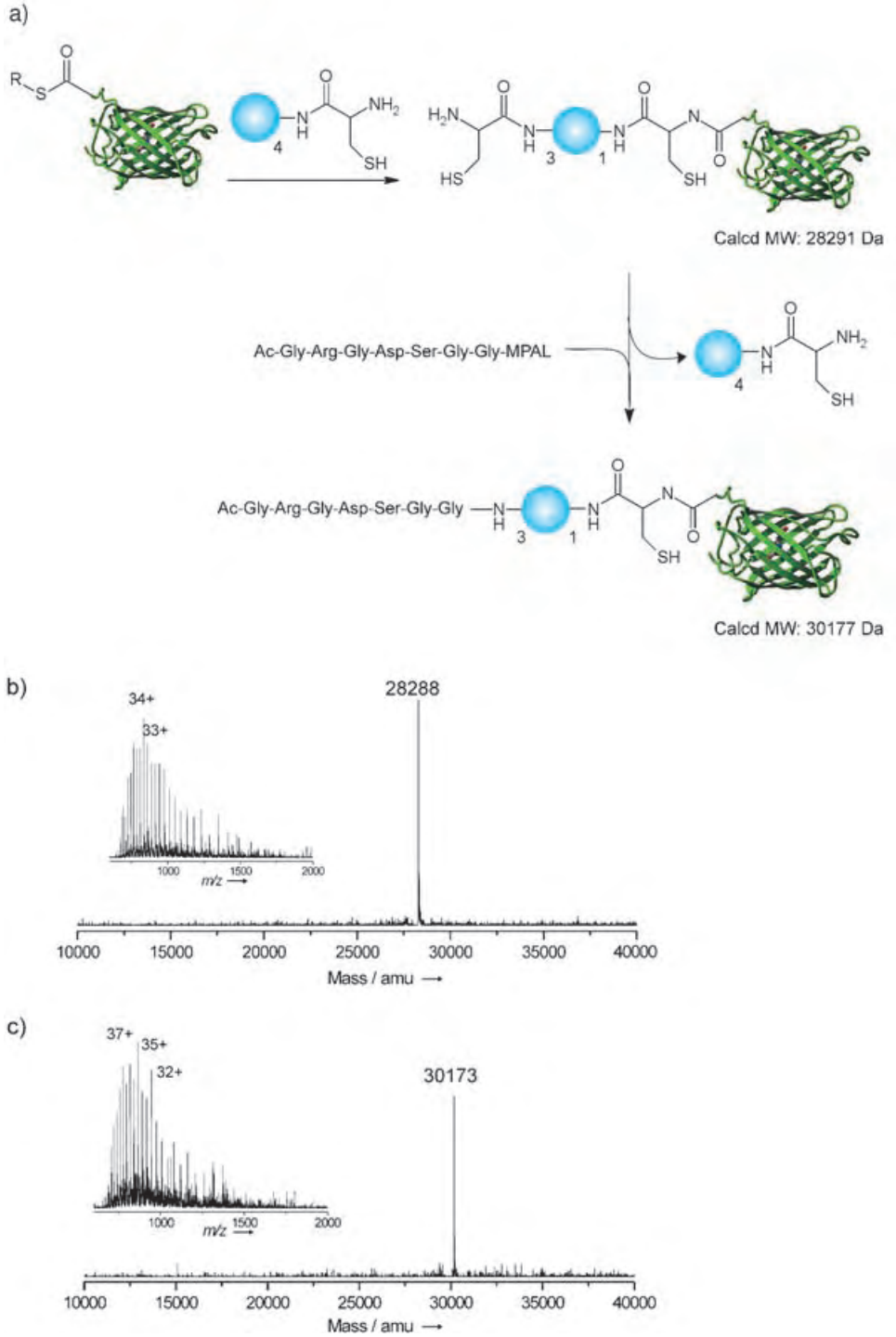


Figure 2. a) Synthesis of a dendrimer containing both protein and peptide end groups. GFP thioester (75 μM) was treated with a large excess of dendrimer **1** (2 mM) for 20 h at 20 °C to yield the monofunctionalized **1**-$(GFP)_1$ exclusively. After removal of remaining dendrimer **1**, **1**-$(GFP)_1$ was treated with excess GRGDSGG-MPAL peptide (375 μM) for 4 h at 20 °C to yield **1**-$(GFP)_1(GRGDSGG)_3$ exclusively. b) Experimental (inset) and deconvoluted ESI-MS of **1**-$(GFP)_1$. c) Experimental (inset) and deconvoluted ESI-MS of **1**-$(GFP)_1(GRGDSGG)_3$.

excess of the MPAL thioester of GRGDSGG. ESI-MS showed the presence of a single, high-molecular-weight signal at 30173 Da, which is exactly the mass expected for **1**-$(GFP)_1(GRGDSGG)_3$ assuming formation of two intramolecular disulfide bonds. This synthetic methodology should be generally applicable to prepare dendrimers with (exactly) one copy of any recombinant protein and multiple copies of any peptide or other synthetic ligand with a thioester functionality.

To test whether our synthetic strategy can be used to obtain multivalent protein dendrimers, a 25 μM solution of dendrimer **1** was incubated with four or eight equivalents of

 © 2005 Wiley-VCH Verlag GmbH & Co. KGaA, Weinheim

GFP thioester and the ligation reaction was monitored using sodium dodecyl sulfate polyacrylamide gel electrophoresis (SDS-PAGE) (Figure 3a). Analysis of the reaction after 20 h showed the presence of four distinct bands at 27, 55, about 120, and about 170 kDa that we attribute, respectively, to GFP thioester and **1**-$(GFP)_1$, **1**-$(GFP)_2$, **1**-$(GFP)_3$, and **1**-$(GFP)_4$. The bands of **1**-$(GFP)_3$ and **1**-$(GFP)_4$ appear at a higher apparent molecular weight than expected, which is probably a consequence of the branched structure of these multivalent proteins. A similar effect of branching on the apparent molecular weight has been reported for ubiquitinated proteins, which are a natural form of branched proteins.[26] The limited solubility of GFP under the conditions suitable for native chemical ligation (100–200 μM GFP thioester) probably makes the ligation of GFP slower than the peptide-ligation reactions that are typically performed at 2–10 mM.[27] A second factor that may prevent the full conversion into **1**-$(GFP)_4$ is increased steric crowding that occurs when attaching four 27-kDa proteins around a 0.7-kDa dendritic core.

The ligation product was further purified using size-exclusion chromatography and analyzed using electrospray ionization time-of-flight mass spectrometry under native conditions to provide definitive evidence for the formation of the GFP tetramer (Figure 3b, c). The spectrum of the first species that elutes from the column shows a limited number of signals that can be deconvoluted to a single mass of 110971 Da. This mass corresponds almost exactly to the average mass calculated for **1**-$(GFP)_4$ with two disulfide bonds (110972 Da). The other detected ions originated from GFP, **1**-$(GFP)_1$, **1**-$(GFP)_2$, and **1**-$(GFP)_3$ and clearly reveal that size-exclusion liquid chromatography coupled to mass spectrometry under native conditions is an ideal analytical tool to separate and analyze these protein mixtures. Moreover, the high m/z values and the narrow charge distribution indicate that the proteins may still be properly folded in **1**-$(GFP)_4$.[28,29]

In summary, we have demonstrated that native chemical ligation is an attractive ligation reaction to functionalize dendrimers with both oligopeptides and recombinantly expressed proteins. Furthermore, dendrimers can be derivatized with exactly one copy of a recombinant protein, and the remaining cysteine residues can then be further functionalized with oligopeptides. Our approach allows chemoselective dendrimer conjugation to the C-terminus of a protein, which is much less likely to interfere with protein function than other less-specific protein-ligation strategies. The modular approach presented here provides access to a wide variety of well-defined multivalent peptides and proteins that are attractive both for understanding the fundamental mecha-

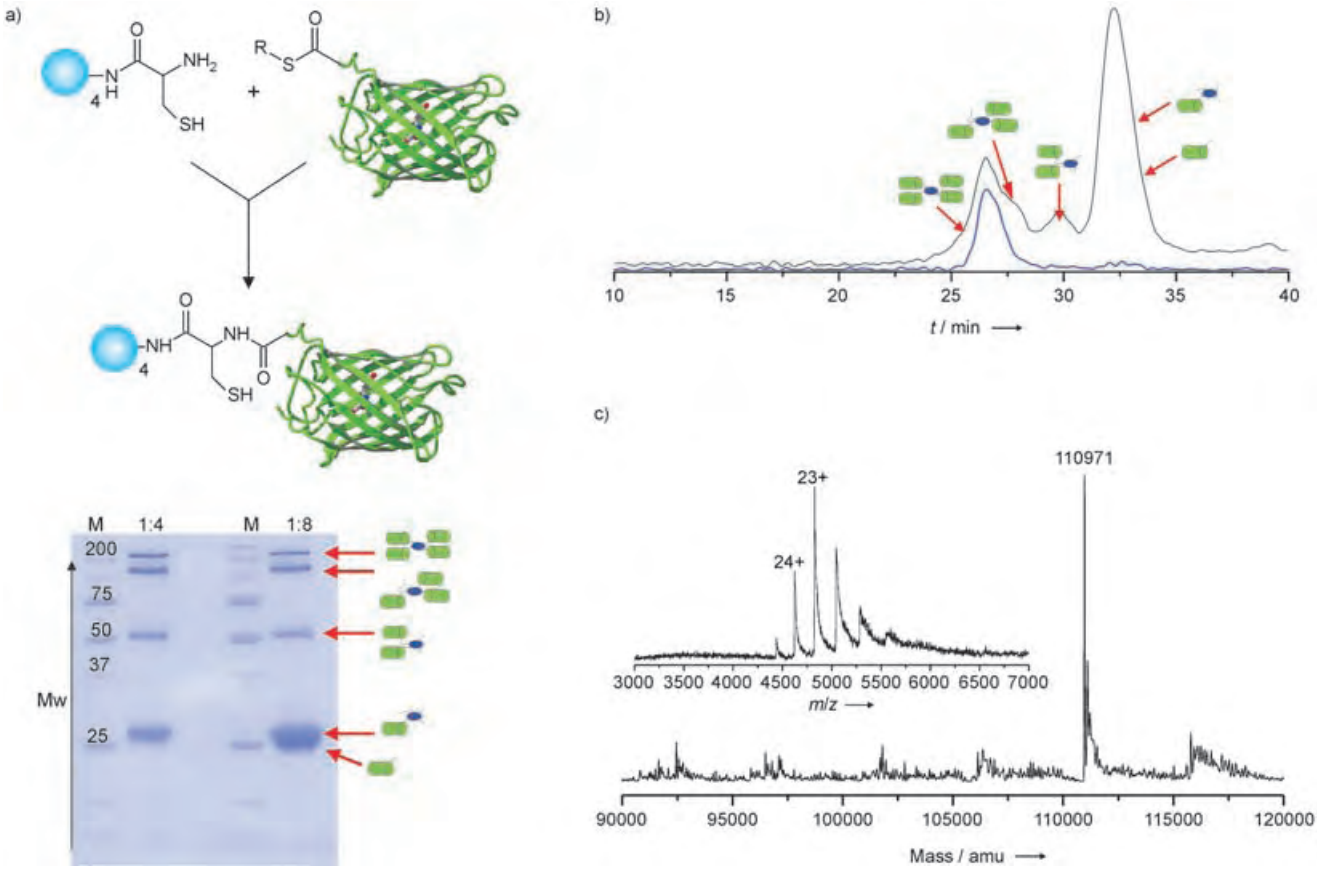


Figure 3. a) Native chemical ligation of dendrimer **1** (25 μM) with four (reaction 1) or eight equivalents (reaction 2) of GFP thioester in 0.1 M sodium phosphate, 2% (v/v) thiophenol, and 2% (v/v) benzyl mercaptan pH 7–7.5 for 20 h at 20°C. b) Size-exclusion chromatogram of the ligation reaction mixture on an analytical Superdex 200 PC 3.2/30 column showing the total ion current (black trace) and the selected ion current for **1**-$(GFP)_4$ (blue trace). c) Experimental (inset) and deconvoluted ESI-MS of **1**-$(GFP)_4$ (fraction that eluted between 25.7 and 27.6 min).

 © 2005 Wiley-VCH Verlag GmbH & Co. KGaA, Weinheim

nisms of multivalency in biological interactions and for biomedical applications in targeted drug delivery, molecular imaging, and immunology.

Experimental Section

All peptide ligation experiments were performed in a buffer containing 0.1M tris(hydroxymethyl)aminomethane (tris), 6M guanidine, 2% (v/v) thiophenol, and 2% (v/v) α-toluenethiol (benzyl mercaptan) pH 7.0–7.5. One equivalent of dendrimers **1**, **2**, or **3** was treated with 4, 8, or 16 equivalents of peptide thioester (ca. 10 mg mL^{-1}), respectively, with stirring for 1 h at 37 °C. The ligation products were analyzed by LC-MS. All protein-ligation experiments were performed at 20 °C in a buffer containing 0.1M sodium phosphate, 2% (v/v) thiophenol, and 2% (v/v) benzyl mercaptan pH 7–7.5. Precipitates were removed after the reaction by centrifugation. **1**-$(GFP)_1$ was obtained by ligation of 75 μM GFP thioester with 2 mM dendrimer **1** for 20 h at 20 °C. Remaining dendrimer was removed by repeated concentration and dilution of the reaction mixture using an Amicon Ultra-4 centrifugal concentrator with a 10-kDa cut-off. **1**-$(GFP)_1(GRGDSGG)_3$ was obtained by subsequent ligation with 375 μM GRGDSGG-MPAL for 4 h at 20 °C, followed by analysis using LC-MS.

Received: February 21, 2005
Published online: July 11, 2005

Keywords: bioorganic chemistry · dendrimers · multivalency · peptides · proteins

[1] M. Mammen, S.-K. Choi, G. M. Whitesides, *Angew. Chem.* **1998**, *110*, 2908; *Angew. Chem. Int. Ed.* **1998**, *37*, 2754.
[2] L. L. Kiessling, L. E. Strong, J. E. Gestwicki, *Curr. Opin. Chem. Biol.* **2000**, *4*, 696.
[3] L. L. Kiessling, L. E. Strong, J. E. Gestwicki, *Annu. Rev. Med. Chem.* **2000**, *35*, 321.
[4] E. Fan, Z. Zhang, W. E. Minke, Z. Hou, C. L. M. J. Verlinde, W. G. J. Hol, *J. Am. Chem. Soc.* **2000**, *122*, 2663.
[5] P. L. Kitov, J. M. Sadowska, G. Mulvey, G. D. Amstrong, H. Ling, N. S. Pannu, R. J. Read, D. R. Bundle, *Nature* **2000**, *403*, 669.
[6] J. Rao, J. Lahiri, L. Isaacs, R. M. Weis, G. M. Whitesides, *Science* **1998**, *280*, 708.
[7] A. W. Bosman, H. M. Janssen, E. W. Meijer, *Chem. Rev.* **1999**, *99*, 1665.
[8] U. Boas, P. M. H. Heegard, *Chem. Soc. Rev.* **2004**, *33*, 43.
[9] J. P. Mitchell, K. D. Roberts, J. Langley, F. Koentgen, J. N. Lambert, *Bioorg. Med. Chem. Lett.* **1999**, *9*, 2785.
[10] J. D. Reuter, A. Myc, M. M. Hayes, Z. Gan, R. Roy, D. Qin, R. Yin, L. T. Piehler, R. Esfand, D. A. Tomalia, J. R. J. R. Baker, *Bioconjugate Chem.* **1999**, *10*, 271.
[11] I. Vrasidas, N. J. de Mol, R. M. J. Liskamp, R. J. Pieters, *Eur. J. Org. Chem.* **2001**, *24*, 4685.
[12] W. B. Turnbull, J. F. Stoddart, *Rev. Mol. Biotechnol.* **2002**, *90*, 231.
[13] C. Rao, J. P. Tam, *J. Am. Chem. Soc.* **1994**, *116*, 6975.
[14] K. Sadler, J. P. Tam, *Rev. Mol. Biotechnol.* **2002**, *90*, 195.
[15] M. Sakamoto, A. Ueno, H. Mihara, *Chem. Commun.* **2000**, *2000*, 1741.
[16] M. Zhou, D. Bentley, I. Ghosh, *J. Am. Chem. Soc.* **2004**, *126*, 734.
[17] R. Kluger, J. Zhang, *J. Am. Chem. Soc.* **2003**, *125*, 6070.
[18] P. E. Dawson, T. W. Muir, I. Clark-Lewis, S. B. Kent, *Science* **1994**, *266*, 776.
[19] T. M. Hackeng, J. H. Griffin, P. E. Dawson, *Proc. Natl. Acad. Sci. USA* **1999**, *96*, 10068.
[20] T. J. Tolbert, C.-H. Wong, *J. Am. Chem. Soc.* **2000**, *122*, 5421.
[21] R. Y. P. Lue, G. Y. J. Chen, Y. Hu, Q. Zhu, S. Q. Yao, *J. Am. Chem. Soc.* **2004**, *126*, 1055.
[22] D. S. Y. Yeo, R. Srinivasan, G. Y. J. Chen, S. Q. Yao, *Chem. Eur. J.* **2004**, *10*, 4664.
[23] J. A. Camarero, Y. Kwon, M. A. Coleman, *J. Am. Chem. Soc.* **2004**, *126*, 14730.
[24] T. W. Muir, D. Sondhi, P. A. Cole, *Proc. Natl. Acad. Sci. USA* **1998**, *95*, 6705.
[25] R. David, M. P. O. Richter, A. G. Beck-Sickinger, *Eur. J. Biochem.* **2004**, *271*, 663.
[26] A. Borodovsky, H. Ovaa, N. Kolli, T. Gan-Erdene, K. D. Wilkinson, H. L. Ploegh, B. M. Kessler, *Chem. Biol.* **2002**, *9*, 1149.
[27] We have observed similar noncomplete ligation reactions for small, hydrophobic peptides with limited solubility.
[28] A. J. R. Heck, R. H. H. van den Heuvel, *Mass Spectrom. Rev.* **2004**, *23*, 368.
[29] R. H. H. van den Heuvel, A. J. R. Heck, *Curr. Opin. Chem. Biol.* **2004**, *8*, 519.

 © 2005 Wiley-VCH Verlag GmbH & Co. KGaA, Weinheim

Guanine Oxidation

DOI: 10.1002/anie.200500991

Oxidation of Guanine and 8-oxo-7,8-Dihydroguanine by Carbonate Radical Anions: Insight from Oxygen-18 Labeling Experiments**

*Conor Crean, Nicholas E. Geacintov, and Vladimir Shafirovich**

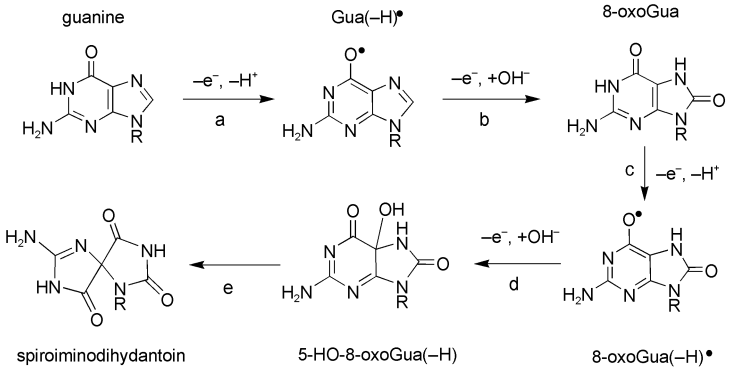
The carbonate radical anion ($CO_3^{\bullet-}$) is of significant current interest, as it plays an important oxidative role in biological systems.[1] These radical anions arise during the inflammatory response in tissues[2] by the one-electron oxidation of bicarbonate anions in the active site of copper–zinc superoxide dismutase,[3] and the reaction of peroxynitrite with carbon dioxide.[4,5] The $CO_3^{\bullet-}$ radical is a strong one-electron oxidant ($E° = 1.59$ V versus normal hydrogen electrode)[6] which gives rise to the post-translational modification of proteins[7,8] and causes oxidative DNA damage.[2] Guanine is the most susceptible base in DNA toward oxidative damage,[9] and is oxidized by $CO_3^{\bullet-}$ radicals[10,11] predominantly to oxidative end-products such as spiroiminodihydantoin (Sp) lesions,[12] which are highly mutagenic.[13,14] We have shown earlier that 8-oxo-7,8-dihydroguanine, itself the product of a two-electron oxidation of guanine, is an intermediate in the

[*] Dr. C. Crean, Prof. Dr. N. E. Geacintov, Prof. Dr. V. Shafirovich
Chemistry Department and Radiation and Solid State Laboratory
New York University
31 Washington Place, New York, NY 10003-5180 (USA)
Fax: (+1) 212-998-8421
E-mail: vs5@nyu.edu

[**] This work was supported by the National Institutes of Health Grant 5-R01-ES11589, and by a grant from the Kresge Foundation.

© 2005 Wiley-VCH Verlag GmbH & Co. KGaA, Weinheim

complex series of reactions that ultimately results in the formation of Sp.[11] The generation of Sp formally requires four electron-transfer steps[12] (Scheme 1) and the transfer of oxygen atoms from either the $CO_3^{\bullet-}$ radical species or water.



Scheme 1. Formation of spiroiminodihydantoin by the consecutive abstraction of four electrons from guanine (a–d) followed by an acyl shift (e) in the 5-HO-8-oxoGua(-H) intermediate.[12]

However, the critical mechanistic aspects of the consecutive four-electron oxidation of G by $CO_3^{\bullet-}$ radicals that culminate in the formation of Sp are still obscure.

Herein, we report the use of a combination of ^{18}O labeling and mass spectrometry to address these questions with 2′,3′,5′-tri-*O*-acetylguanosine (tri-*O*-Ac-Guo) or 2′,3′,5′-tri-*O*-acetyl-8-oxo-7,8-dihydroguanosine (tri-*O*-Ac-8-oxoGuo) derivatives as standard model systems.[12,15] We show that the oxygen atoms incorporated into the Sp end-products formed by the oxidation of either tri-*O*-Ac-Guo or tri-*O*-Ac-8-oxoGuo originate from $CO_3^{\bullet-}$ radicals and not from H_2O. These observations indicate that the intermediate steps occur by the radical–radical combination of $CO_3^{\bullet-}$ with Gua(-H)• and 8-oxoGua(-H)•, and that these reactions can be formally viewed as O^--transfer mechanisms.

The $CO_3^{\bullet-}$ radicals were generated by the laser photolysis method used in our previously reported experiments.[10,11] This method involves the photodissociation of persulfate to sulfate radical anions followed by one-electron oxidation of HCO_3^- anions by $SO_4^{\bullet-}$ radicals. Solutions of tri-*O*-Ac-Guo or tri-*O*-Ac-8-oxoGuo (30 μM), $NaHCO_3$ (0.3 M), and $Na_2S_2O_8$ (0.01 M) containing ≈43% $H_2{}^{18}O$ were equilibrated in air, adjusted to pH 7.5 by NaH_2PO_4 (1 M), and excited by excimer laser pulse train ($\lambda = 308$ nm, 15 mJ pulse^{-1} cm^{-2}, 10 pulse s^{-1}) for ≈10 s. After irradiation, the $Na_2S_2O_8$ was reduced by the addition of a solution of $Na_2S_2O_4$ to quench any further potential oxidation reactions. The Sp nucleoside products, in agreement with our previous experiments,[11] were formed in high yield (40–60%). The Sp products were isolated by reversed-phase HPLC and subjected to ESI MS–MS analysis. The major signals from the Sp molecular ions $[M+H]^+$ were observed at $m/z = 442$; the two additional O atoms in Sp (relative to the parent guanine) are ^{16}O (Figure 1a and c, black traces). The presence of lower-intensity peaks at $m/z =$ 444 in these spectra suggests that some ^{18}O atoms are incorporated into Sp nucleosides. These incorporation pathways could include hydration[12,16–21] of the Gua and 8-oxoGua

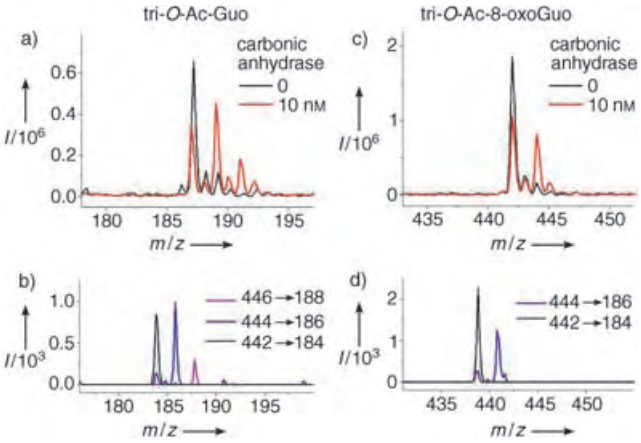


Figure 1. Positive ion spectra of the spiroiminodihydantoin nucleosides prepared by the oxidation of a) tri-*O*-Ac-Guo and c) tri-*O*-Ac-8-oxoGuo by $CO_3^{\bullet-}$ radicals in buffer solutions (pH 7.5) containing $H_2{}^{18}O$ (fraction of ^{18}O atoms $\alpha = 0.43 \pm 0.03$). The reaction mixtures contained either no carbonic anhydrase (black) or carbonic anhydrase at 10 nM to provide a complete exchange of ^{18}O between $HC^{16}O_3^-$ and $H_2{}^{18}O$ (red); Mass spectra obtained by fragmentation of the molecular ion ($[M+H]^+$) at $m/z = 442$ (black), 444 (blue), and 446 (magenta) from b) Sp nucleosides prepared by the oxidation of tri-*O*-Ac-Guo and the oxidation of d) tri-*O*-Ac-8-oxoGuo. In the presence of carbonic anhydrase, the experimentally observed fractions of isotope-labeled Sp nucleosides are 0.37 ± 0.04 for the m/z 442→184 ions, 0.46 ± 0.02 in the case of the m/z 444→186 ions, and 0.17 ± 0.03 for the m/z 446→188 ions. These fractions are close to the expected values of $(1-\alpha)^2 = 0.33 \pm 0.04$ ($^{16}O^{16}O$), $2(1-\alpha)\alpha = 0.49 \pm 0.01$ ($^{16}O^{18}O$), and $\alpha^2 = 0.19 \pm 0.03$ ($^{18}O^{18}O$) for a random transfer of two oxygen atoms from the carbonate radical anions to the Sp products.

radicals or isotope exchange[22] of $HC^{16}O_3^-$ with $H_2{}^{18}O$ that occurs slowly in the absence of the carbonic anhydrase catalyst[23]. Hence, the O atoms in the Sp nucleosides could have been transferred either from molecular oxygen ($^{16}O_2$) or from $C^{16}O_3^{\bullet-}$ radicals, but not from $H_2{}^{18}O$. In contrast, generation of Sp by the oxidation of tri-*O*-Ac-8-oxoGuo by $IrCl_6^{2-}$ in $H_2{}^{18}O$ solution results in the incorporation of an ^{18}O atom from the heavy water molecules.[12] As Sp can be formed in the absence of oxygen,[11] O_2 can be ruled out as the source of the additional oxygen atoms in Sp, and the $C^{16}O_3^{\bullet-}$ radical can be concluded as the source of ^{16}O.

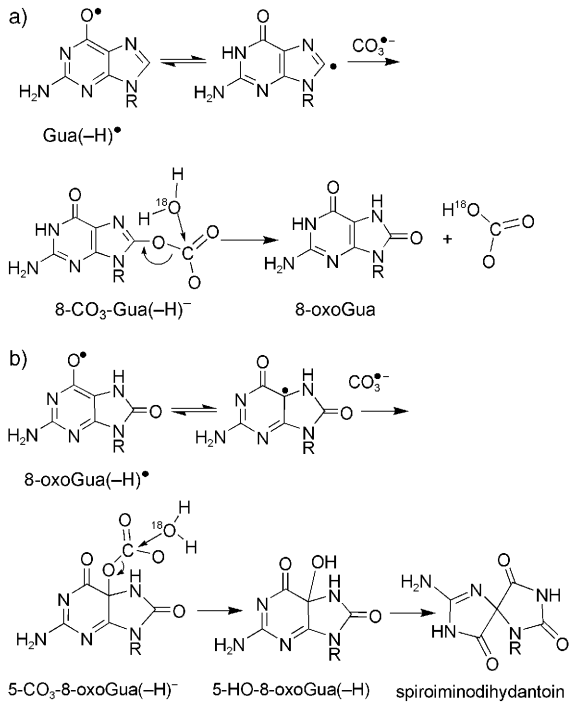
Normally, isotope exchange between $HC^{16}O_3^-$ and $H_2{}^{18}O$ is slow because it occurs only through the hydration of carbon dioxide in equilibrium with bicarbonate.[22] Therefore, even if the reactions are carried out in heavy water, the isotopic composition of the $CO_3^{\bullet-}$ radicals will be close to that of the parent $HC^{16}O_3^-$ anions, and Sp will contain only ^{16}O. To confirm that the source of the O atoms in Sp are transferred from the carbonate radical anions, the oxidation reactions were conducted in the presence of carbonic anhydrase (Figure 1). This enzyme catalyzes the oxygen isotope exchange between $HC^{16}O_3^-$ and $H_2{}^{18}O$[23] and thus the ^{18}O isotope content in the carbonate radical anions is expected to be the same as that of the water at equilibrium. Indeed, the MS data of the Sp samples prepared by the oxidation of tri-*O*-Ac-Guo in $H_2{}^{18}O/H_2{}^{16}O$ solutions incubated with carbonic anhydrase (≈10 nM) for ≈2 h, are characterized by molecular ions at $m/z = 442$, 444 and 446 (Figure 1a, red trace). The

 © 2005 Wiley-VCH Verlag GmbH & Co. KGaA, Weinheim

assignment of these molecular ions as the Sp nucleosides was confirmed by monitoring the 442→184, 444→186, and 446→188 transitions (Figure 1b), which correspond to the abstraction of the sugar residues (258 au) from the $^{16}O^{16}O$-, $^{16}O^{18}O$-, and $^{18}O^{18}O$-containing Sp molecular ions.[12] Therefore, these results confirm that both O atoms in the Sp nucleoside derived from the oxidation of tri-*O*-Ac-Guo originate from the $CO_3^{\bullet-}$ radicals.

The MS data of the Sp samples prepared by the oxidation of tri-*O*-Ac-8-oxoGuo in $H_2{}^{18}O/H_2{}^{16}O$ solutions incubated with carbonic anhydrase are characterized by molecular ions at $m/z = 442$ and 444 (Figure 1c, red trace) and their fragmentation patterns at $m/z = 184$ and 186 (Figure 1d). In these spectra, the signals at $m/z = 446$ and 188 were not detected because the first O atom in the Sp nucleoside is derived from a tri-*O*-Ac-8-oxoGuo molecule, and only the second originates from $CO_3^{\bullet-}$ labeled with ^{18}O.

The results of this work suggest that the reaction mechanisms leading to Sp oxidation products involve bimolecular combinations of the $CO_3^{\bullet-}$ radicals with Gua(-H)$^{\bullet}$ or 8-oxoGua(-H)$^{\bullet}$ radicals (Scheme 2). The primary products of



Scheme 2. The O^- transfer mechanism of the combination of $CO_3^{\bullet-}$ radicals with a) Gua(-H)$^{\bullet}$ and b) 8-oxoGua(-H)$^{\bullet}$ radicals.

radical addition can be considered as monoesters of carbonic acid (H_2CO_3). The seminal works of Polanyi,[24] Ingold[25] and co-workers showed that, in the acid–base hydrolysis of esters, the ^{18}O atoms from water are transferred to the acid component and not to the alcohol product. In agreement with this mechanism of ester hydrolysis, the O atoms in Sp originate from the $CO_3^{\bullet-}$ radicals and not from H_2O (Figure 1). Therefore, the combination reactions of $CO_3^{\bullet-}$ radicals with Gua(-H)$^{\bullet}$ and 8-oxoGua(-H)$^{\bullet}$ radicals can be formally considered as a transfer of O^- from $CO_3^{\bullet-}$ to these radicals. The O^--transfer mechanism has been proposed earlier on the basis of the results of pulse radiolysis experiments for the reactions of $CO_3^{\bullet-}$ radicals with inorganic radicals $^{\bullet}NO_2$, $SO_3^{\bullet-}$, and $^{\bullet}NO$, resulting in the formation of CO_2 and the anions NO_3^-, SO_4^{2-}, and NO_2^-.[26,27] In contrast, metal complexes such as $IrCl_6^{2-}$ induce consecutive abstraction of two electrons from 8-oxoGua followed by the addition of water to the carbocation intermediate, and the O atom in the Sp residue originates from water.[12]

These results constitute the first experimental evidence that the combination of carbonate radical anions with organic radicals occurs through the transfer of oxygen atoms from $CO_3^{\bullet-}$ to the target nucleobase radicals, formally corresponding to the transfer of an O^- anion.

Received: March 18, 2005
Published online: July 13, 2005

Keywords: DNA damage · isotopic labeling · oxidation · radical reactions · reaction mechanisms

[1] O. Augusto, M. G. Bonini, A. M. Amanso, E. Linares, C. C. Santos, S. L. De Menezes, *Free Radical Biol. Med.* **2002**, *32*, 841–859.
[2] P. C. Dedon, S. R. Tannenbaum, *Arch. Biochem. Biophys.* **2004**, *423*, 12–22.
[3] H. Zhang, J. Joseph, M. Gurney, D. Becker, B. Kalyanaraman, *J. Biol. Chem.* **2002**, *277*, 1013–1020.
[4] S. V. Lymar, J. K. Hurst, *J. Am. Chem. Soc.* **1995**, *117*, 8867–8868.
[5] M. G. Bonini, R. Radi, G. Ferrer-Sueta, A. M. Ferreira, O. Augusto, *J. Biol. Chem.* **1999**, *274*, 10802–10806.
[6] R. E. Huie, C. L. Clifton, P. Neta, *Radiat. Phys. Chem.* **1991**, *38*, 477–481.
[7] M. Tien, B. S. Berlett, R. L. Levine, P. B. Chock, E. R. Stadtman, *Proc. Natl. Acad. Sci. USA* **1999**, *96*, 7809–7814.
[8] H. Ischiropoulos, J. S. Beckman, *J. Clin. Invest.* **2003**, *111*, 163–169.
[9] J. Cadet, S. Bellon, M. Berger, A. G. Bourdat, T. Douki, V. Duarte, S. Frelon, D. Gasparutto, E. Muller, J. L. Ravanat, S. Sauvaigo, *Biol. Chem.* **2002**, *383*, 933–943.
[10] V. Shafirovich, A. Dourandin, W. Huang, N. E. Geacintov, *J. Biol. Chem.* **2001**, *276*, 24621–24626.
[11] A. Joffe, N. E. Geacintov, V. Shafirovich, *Chem. Res. Toxicol.* **2003**, *16*, 1528–1538.
[12] W. Luo, J. G. Muller, E. M. Rachlin, C. J. Burrows, *Org. Lett.* **2000**, *2*, 613–616.
[13] O. Kornyushyna, A. M. Berges, J. G. Muller, C. J. Burrows, *Biochemistry* **2002**, *41*, 15304–15314.
[14] P. T. Henderson, J. C. Delaney, J. G. Muller, W. L. Neeley, S. R. Tannenbaum, C. J. Burrows, J. M. Essigmann, *Biochemistry* **2003**, *42*, 9257–9262.
[15] J. L. Ravanat, J. Cadet, *Chem. Res. Toxicol.* **1995**, *8*, 379–388.
[16] H. Kasai, Z. Yamaizumi, M. Berger, J. Cadet, *J. Am. Chem. Soc.* **1992**, *114*, 9692–9694.
[17] W. Luo, J. G. Muller, C. J. Burrows, *Org. Lett.* **2001**, *3*, 2801–2804.
[18] J. L. Ravanat, C. Saint-Pierre, J. Cadet, *J. Am. Chem. Soc.* **2003**, *125*, 2030–2031.
[19] Y. Ye, J. G. Muller, W. Luo, C. L. Mayne, A. J. Shallop, R. A. Jones, C. J. Burrows, *J. Am. Chem. Soc.* **2003**, *125*, 13926–13927.
[20] R. Misiaszek, C. Crean, A. Joffe, N. E. Geacintov, V. Shafirovich, *J. Biol. Chem.* **2004**, *279*, 32106–32115.

 © 2005 Wiley-VCH Verlag GmbH & Co. KGaA, Weinheim

[21] R. Misiaszek, Y. Uvaydov, C. Crean, N. E. Geacintov, V. Shafirovich, *J. Biol. Chem.* **2005**, *280*, 6293 – 6300.
[22] G. A. Mills, H. C. Urey, *J. Am. Chem. Soc.* **1940**, *62*, 1019 – 1026.
[23] D. N. Silverman, C. K. Tu, *J. Am. Chem. Soc.* **1976**, *98*, 978 – 984.
[24] M. Polanyi, C. Szabo, *Trans. Faraday Soc.* **1934**, *30*, 508 – 512.
[25] S. C. Datta, J. N. E. Day, C. K. Ingold, *J. Chem. Soc.* **1939**, 838 – 840.
[26] J. Lilie, R. J. Hanrahan, A. Henglein, *Radiat. Phys. Chem.* **1978**, *11*, 225 – 227.
[27] G. Czapski, J. Holcman, B. H. J. Bielski, *J. Am. Chem. Soc.* **1994**, *116*, 11 465 – 11 469.

 © 2005 Wiley-VCH Verlag GmbH & Co. KGaA, Weinheim

Chiral Resolution

DOI: 10.1002/anie.200500862

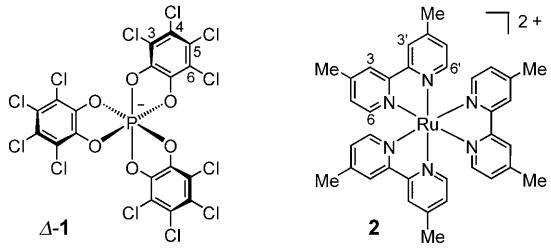
Fluorinated TRISPHAT Anions: Spectroscopic Probes for Detailed Asymmetric Ion Pairing Studies**

*Richard Frantz, André Pinto, Samuel Constant, Gérald Bernardinelli, and Jérôme Lacour**

Ion pairing is an important phenomenon, which strongly affects the chemistry of organic, metallo-organic, and organometallic compounds.[1] Many reactions performed with homogeneous cationic transition-metal catalysts are directly influenced by the negative counterion, as the anion plays a critical role for the reaction rate and (enantio)selectivity.[2,3] Recently, detailed structural analyses of ion pairs, experimental[4] and theoretical,[5] have shed new light on the precise nature of salt effects. Much progress has been made using NMR spectroscopy: Homonuclear $^{1}H,^{1}H$-NOESY and heteronuclear $^{1}H,^{19}F$-HOESY experiments have allowed qualitative and quantitative structural investigations on the interactions of cationic moieties and their counterions,[6] and diffusion data from pulse-field gradient spin echo (PGSE) experiments have provided useful information on the average dimensions of salt aggregates in solution.[7]

Many different cationic moieties have been analyzed. In comparison, a relatively limited number of anionic substances have been studied. Only a dozen derivatives possess both NMR-sensitive atoms in their core or periphery as well as the requisite reactivity when associated to a given cation. Typical examples are BF_4^-, BPh_4^-, $BArF^-$,[8] and PF_6^-; this collection of anions is varied enough to allow most ion pairing studies. However, many of the cationic moieties that were studied are chiral and little information regarding asymmetry has been obtained from their interactions with the above-mentioned achiral anions. Here we report on the synthesis and resolution of two novel fluorine-containing, enantiopure, hexacoordinate phosphate anions, named TRISPHAT-F3 and TRISPHAT-F4, which can be used to demonstrate the exact geometry within ion pairs of chiral cations and anions.

Recently, the chemistry of chiral hexacoordinate phosphate anions has been rejuvenated,[9] as anions such as tris(tetrachlorobenzenediolato)phosphate(v) (**1**, TRISPHAT, *Λ* or *Δ* enantiomers) have been shown to be valuable chiral NMR solvating, resolving, and asymmetry-inducing reagents.[10] Effective resolution protocols involving configurationally stable Ru^{II} complexes, in particular $[Ru(4,4'\text{-}Me_2bpy)_3]^{2+}$ (**2**, bpy = 2,2′-bipyridine), have been developed using anion **1**.[9]



Although a high level of chiral recognition was achieved with salts of **1** and **2**, the exact topography within the preferred ion pairs remained uncertain. Monitoring of the addition of enantiopure TRISPHAT salts to racemic D_3-symmetric $[Ru(LL)_3]^{2+}$ complexes by ^{1}H NMR spectroscopy has shown the following: 1) Anions *Δ*-**1** have a stronger influence on homochiral cationic moieties (*ΔΔ* versus *ΔΛ*), and 2) the protons of the cation along the C_3 axis are more strongly perturbed, indicating a preferred approach of the anion in that direction.[11] However, no such qualitative information has been gathered for the chiral anion since the chlorine atoms at the periphery of phosphate **1** are "silent" in NMR spectroscopy. The precise structural geometry within the ion pairs in solution was, overall, a mystery.

To obtain a complete and conclusive image of the situation, we decided to replace the chlorine by fluorine atoms, as these NMR-sensitive atoms are possible probes for selective approaches within the ion pairs. If one considers the D_3 symmetry of **1**, halogen atoms positioned at C3 and C6 ought to be sensitive to approaches along the C_3 axis of the anion, and those at the C4 and C5 positions to the approach of cations along the three C_2 axes (Figure 1). Selective replace-

[*] Dr. R. Frantz, A. Pinto, S. Constant, Prof. J. Lacour
Department of Organic Chemistry
University of Geneva
quai Ernest Ansermet 30, 1211 Genève 4 (Switzerland)
Fax: (+41) 22-379-3215
E-mail: jerome.lacour@chiorg.unige.ch
Dr. G. Bernardinelli
Laboratory of Crystallography
University of Geneva
quai Ernest Ansermet 24, 1211 Genève 4 (Switzerland)

[**] We thank Prof. Ian Dance for helpful discussions and preliminary calculations and Prof. Alceo Macchioni for his expert advice on HOESY NMR experiments. We are grateful for financial support of this work by the Swiss National Science Foundation, the Federal Office for Education and Science, and the Sandoz Family Foundation (R.F., J.L.).

Supporting information for this article is available on the WWW under http://www.angewandte.org or from the author.

InterScience © 2005 Wiley-VCH Verlag GmbH & Co. KGaA, Weinheim

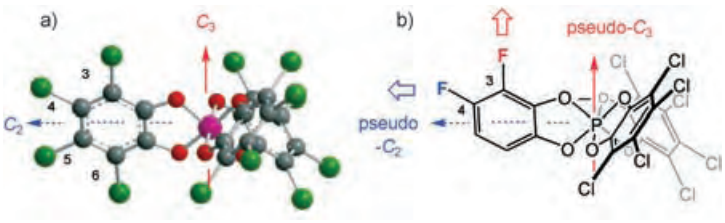
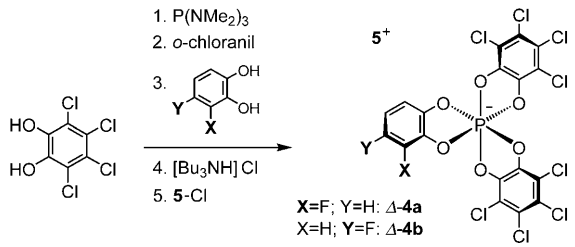


Figure 1. a) Lateral view of *Δ*-**1** and the axes of symmetry. b) Sensing of pseudo-C_3 or pseudo-C_2 approaches by selective positioning of fluorine atoms.

ment of chlorine by fluorine at the C3 and C4 positions would thus generate anions biased towards recognition along the pseudo-C_3 and pseudo-C_2 axes of the derived phosphates, respectively.

To minimize the structural modifications of TRISPHAT, only one of the three tetrachlorocatecholate ligands was exchanged by a fluorine-containing diol. 3-Fluorocatechol (**3a**) and 4-fluorocatechol (**3b**) were selected for their commercial availability. The phosphate anions **4a** and **4b**, namely TRISPHAT-F3 and TRISPHAT-F4, were prepared on a 5-g scale following reported guidelines (Scheme 1):[12]



Scheme 1. Synthesis of phosphate anions **4a** and **4b** and their subsequent resolution using **5**-Cl.

Anhydrous tetrachlorocatechol and $P(NMe_2)_3$ were allowed to react in toluene at reflux. After concentration in vacuo, successive addition in CH_2Cl_2 of *o*-chloranil (3,4,5,6-tetrachloro-3,5-cyclohexadiene-1,2-dione), **3a** or **3b**, and then $[Bu_3NH]Cl$ yielded the desired tri-*n*-butylammonium salts of racemic phosphates **4a** and **4b**. Analytically pure compounds $[Bu_3NH][$**4a**$]$ or $[Bu_3NH][$**4b**$]$ were obtained after chromatography (yield 85%, four consecutive steps).

The resolution of the anions was achieved by the addition of *N*-benzyl-cinchonidinium chloride salt (**5**-Cl, 1.0 equiv) to solutions of $[Bu_3NH][$*rac*-**4a**$]$ or $[Bu_3NH][$*rac*-**4b**$]$ in $CHCl_3$. The diastereomerically pure (−)-[**5**][*Δ*-**4a**] and (−)-[**5**][*Δ*-**4b**] salts were selectively precipitated with good yields (> 45%). X-ray structure determination with the cinchonidinium derivatives (e.g. (−)-[**5**][*Δ*-**4a**], Figure 2) showed an absolute *Δ* configuration for **4a** and **4b**.[13,14] The P–O bond lengths and O-P-O bond angles are virtually identical to those measured for TRISPHAT **1**. The nonracemic anions **4a** and **4b** displayed good chemical and configurational stability, as no evidence of a racemization could be found, for instance, during the ion-exchange metathesis of cation **5** by Bu_4N^+.

The ability of anions **4a** and **4b** to behave as effective chiral auxiliaries for cation **2** was first tested in ^{1}H NMR titration experiments. Various amounts of (−)-$[Bu_4N][$*Δ*-**4a**$]$ or (−)-$[Bu_4N][$*Δ*-**4b**$]$ (0.5–10 equiv) were added to solutions of $[$*rac*-**2**$](PF_6)_2$ in CD_2Cl_2 (see the Supporting Information). In all these experiments, a strong NMR enantiodifferentiation was observed upon addition of the anions (Figure 3a,b);

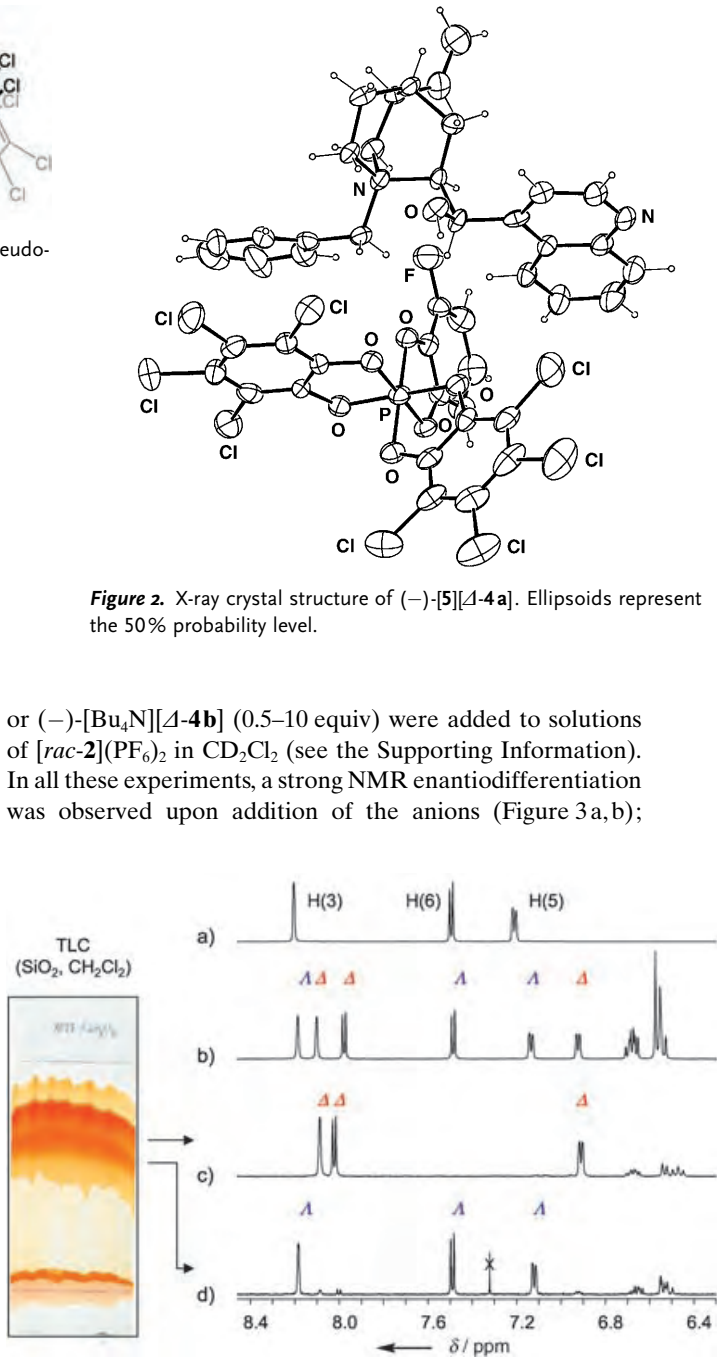


Figure 2. X-ray crystal structure of (−)-[**5**][*Δ*-**4a**]. Ellipsoids represent the 50% probability level.

Figure 3. Left: View of the TLC plate in the separation of the complexes. Right: The corresponding ^{1}H NMR spectra (400 MHz, CD_2Cl_2): a) $[$*rac*-**2**$](PF_6)_2$; b) $[$*rac*-**2**$](PF_6)_2$ + 5.0 equiv of $[Bu_4N][$*Δ*-**4a**$]$; c) [*Δ*-**2**][*Δ*-**4a**]$_2$, d.r. > 48:1; d) [*Λ*-**2**][*Δ*-**4a**]$_2$, d.r. 13.5:1. X = trace of $CHCl_3$.

TRISPHAT-F3 and TRISPHAT-F4 behaved similarly to the original anion **1**. To determine precisely 1) the nature of the preferred association, 2) the effect of the position of the fluorine atom, and 3) the exact topography within the preferred ion pairs, we decided to obtain the enantio- and diastereomerically pure salts [*Δ*-**2**][*Δ*-**4a**]$_2$, [*Λ*-**2**][*Δ*-**4a**]$_2$, [*Δ*-**2**][*Δ*-**4b**]$_2$, and [*Λ*-**2**][*Δ*-**4b**]$_2$.

Chromatographic separation of these complexes was therefore performed.[10c,15] The salts $[$*rac*-**2**$](PF_6)_2$ and [**5**][*Δ*-

 © 2005 Wiley-VCH Verlag GmbH & Co. KGaA, Weinheim

4a] or [**5**][*Δ*-**4b**] (2.2 equiv) were mixed, dissolved, and adsorbed on preparative thin-layer chromatographic plates. In each case, elution with CH_2Cl_2 resulted in two well-separated bands (Figure 3, left), which were scraped off the glass surface and stirred in CH_2Cl_2. The resulting suspensions were filtered and concentrated in vacuo. ^{1}H NMR spectroscopy revealed sets of signals corresponding to the separated *Δ* and *Λ* enantiomers of cation **2** (Figure 3 c,d). The circular dichroism analysis indicated that the first and second eluted fractions contained predominantly the cationic complex with absolute *Δ* and *Λ* configurations, respectively (see the Supporting Information).[16] The diastereomeric salts [*Δ*-**2**][*Δ*-**4a**]$_2$/[*Λ*-**2**][*Δ*-**4a**]$_2$ and [*Δ*-**2**][*Δ*-**4b**]$_2$/[*Λ*-**2**][*Δ*-**4b**]$_2$ were thus obtained in decent chemical yields (30–40%, Table 1).

The NMR spectra of the homochiral and heterochiral salts [*Δ*-**2**][*Δ*-**4**]$_2$ and [*Λ*-**2**][*Δ*-**4**]$_2$, respectively, were then compared with those of the PF_6^- and *Δ*-**1** salts. The chemical shifts for the cationic protons of all these compounds are reported in Table 1. Several trends can be observed. Only the *Δ* enantiomer of **2** is strongly perturbed by the presence of the homochiral anions *Δ*-**4a** and *Δ*-**4b**; the *Λ* enantiomer shows a much smaller influence of the anions ($\Delta\delta_{max} = -0.14$ versus 0.53). In the homochiral series, protons H(6,6′) along the C_3 axis are the most efficiently split with a drift towards higher frequencies. For all other signals, upfield shifts result with a decreased influence along the C_2 axes. It had previously been shown that classical anions have preferred contacts with methyl and H(3,3′) protons of cationic 4,4′-Me_2bpy transition-metal complexes.[17] Interestingly, this is not the case with the TRISPHAT family. Anions *Δ*-**4a**, *Δ*-**4b**, and *Δ*-**1** all behave in favor of homochiral associations along the C_3 axis of the cation (Table 1, entries 3, 5, and 7).[11,18]

Nonetheless, detailed quantitative analysis revealed some nuances. Anion *Δ*-**4b** induces weaker variations of proton chemical shifts than do anions *Δ*-**1** and *Δ*-**4a** (e.g., protons H(6,6′): $\Delta\delta = 0.32$, 0.51 and 0.53, respectively). The chemical shifts of the fluorine atom of anion *Δ*-**4b** within its *Δ*-**2** and *Λ*-**2** salts are identical, whereas a difference can be noted for *Δ*-**4a**. Anion *Δ*-**4b** also displays a reduced chromatographic separation of the enantiomers of **2** as compared to *Δ*-**1** and *Δ*-**4a** ($\Delta R_f = 0.19$, 0.27, and 0.30, respectively). The lack of halogen substituent at the C3 or C6 positions of one of the

Table 1: Data on the diastereomeric ion pairs [*Δ*$^+$][*Δ*$^-$]$_2$ and [*Λ*$^+$][*Δ*$^-$]$_2$ of cation **2** and anions **4a**, **4b**, and **1**. The solvent for ^{1}H NMR spectroscopy was CD_2Cl_2.

Entry	Compound	Yield [%]	R_f[a]	d.r.[b]	$[\alpha]_D^{20}$	H(6)		H(5)		CH_3		H(3)		F	
						δ	$\Delta\delta$[c]	δ	$\Delta\delta$[c]	δ	$\Delta\delta$[c]	δ	$\Delta\delta$[c]	δ	$\Delta\delta$[d]
1	[*rac*-**2**]$(PF_6)_2$	–	0	–	–	7.50	–	7.21	–	2.57	–	8.20	–	−72.90	–
2	[*Λ*-**2**][*Δ*-**4b**]$_2$	40	0.36	15:1	+17	7.42	−0.08	7.15	−0.06	2.45	−0.12	8.17	−0.03	−122.90	−0.50
3	[*Δ*-**2**][*Δ*-**4b**]$_2$	36	0.55	>48:1	−839	7.82	+0.32	6.97	−0.24	2.34	−0.23	8.12	−0.08	−122.90	−0.50
4	[*Λ*-**2**][*Δ*-**4a**]$_2$	30	0.31	13.5:1	+46	7.56	+0.06	7.11	−0.10	2.43	−0.14	8.19	−0.01	−139.40	−1.17
5	[*Δ*-**2**][*Δ*-**4a**]$_2$	30	0.61	>48:1	−734	8.03	+0.53	6.92	−0.29	2.27	−0.30	8.09	−0.11	−139.65	−1.42
6	[*Λ*-**2**][*Δ*-**1**]$_2$	30	0.55	26:1	+36	7.46	−0.04	7.18	−0.03	2.48	−0.09	8.18	−0.02	–	–
7	[*Δ*-**2**][*Δ*-**1**]$_2$	35	0.82	>48:1	−882	8.01	+0.51	6.95	−0.26	2.31	−0.24	8.11	−0.09	–	–

[a] CH_2Cl_2 was used as eluent. [b] The diastereomeric purity was determined by ^{1}H NMR spectroscopy. [c] The difference in chemical shift for the protons of **2** as compared to those of the [*rac*-**2**]$(PF_6)_2$ salts. [d] The difference in chemical shift for the fluorine atom as compared to those of the [Bu_4N][*Δ*-**4**] salts.

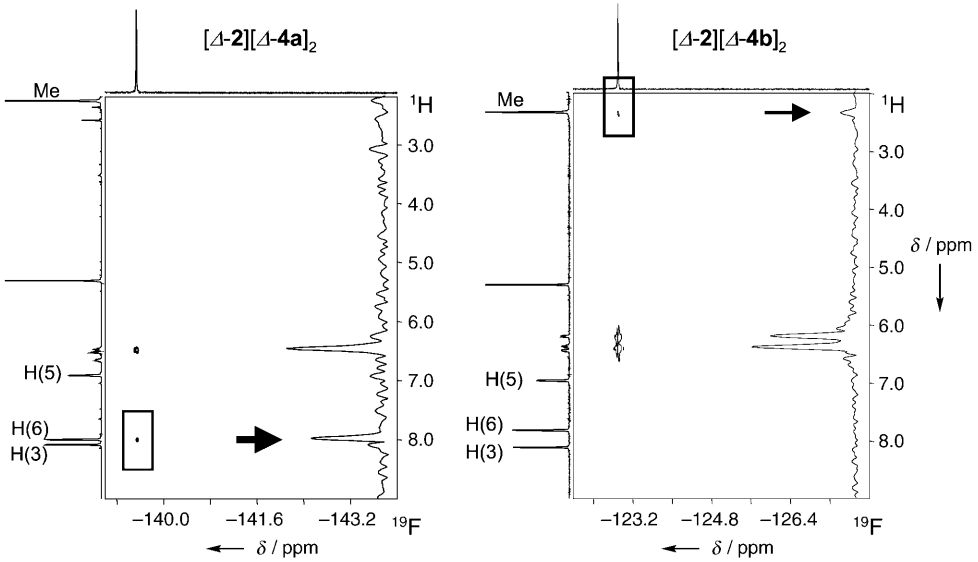


Figure 4. The ^{1}H,^{19}F-HOESY NMR spectra (470.59 MHz, CD_2Cl_2, $\tau_m = 0.7$ s) of [*Δ*-**2**][*Δ*-**4a**]$_2$ and [*Δ*-**2**][*Δ*-**4b**]$_2$ showing the "heteronuclear interionic contacts". The F1 trace (indirect dimension) relative to one component of the fluorine is shown on the right.

 © 2005 Wiley-VCH Verlag GmbH & Co. KGaA, Weinheim

catecholate ligands apparently has a negative effect (anion **4b**). The presence of Cl or F atoms at the C4 positions cannot compensate the disappearance at C3 and C6.

The positioning of electronegative elements (Cl, F) along the C_3 axis of the anion is thus crucial for both NMR enantiodifferentiation and chiral recognition among the propellers. Only an approach of the cation along this axis can explain the results. As electronegative halogen atoms can participate in charge-assisted C–H···X hydrogen bonds,[19] one can propose that such intermolecular interactions occur upon the alignment of the C_3 axes of the homochiral complexes. The downfield shifts of the H(6,6′) protons is a good indication of the hydrogen-bonding situation with chlorine or fluorine at the C3 positions.

Final and conclusive evidence for this preferred geometry was gathered through $^{1}H,^{19}F$-HOESY NMR experiments (CD_2Cl_2) of salts [*Δ*-**2**][*Δ*-**4a**]$_2$ and [*Δ*-**2**][*Δ*-**4b**]$_2$. In both cases, strong intramolecular interactions between the protons of the anions and the neighboring fluorine atoms were observed. More importantly, selective cross-peaks showing interionic contacts could be determined, from the fluorines at the C3 and C4 positions of *Δ*-**4a** and *Δ*-**4b** towards the H(6,6′) and the methyl protons of cation *Δ*-**2**, respectively (Figure 4).[20,21] These interactions can only be rationalized through an alignment of the propeller ions along their C_3 axes.[22,23]

In conclusion, enantiopure anions **4a** and **4b** can be readily synthesized in two steps from commercially available materials. They display effective NMR discriminating abilities useful for structural determinations of asymmetric ion pairing geometries. Their application in the context of enantioselective homogeneous catalysis is currently in progress.

Received: March 8, 2005
Published online: July 12, 2005

Keywords: chiral resolution · ion pairs · NMR spectroscopy · phosphates · ruthenium

[1] M. Szwarc, *Ions and ion pairs in Organic Reactions*, Krieger, New York, **1972**; A. Loupy, B. Tchoubar, *Salt Effects in Organic and Organometallic Chemistry*, VCH, Weinheim, **1992**; S. H. Strauss, *Chem. Rev.* **1993**, *93*, 927–942; C. A. Reed, *Acc. Chem. Res.* **1998**, *31*, 133–139.

[2] A. Macchioni, *Chem. Rev.* **2005**, *105*, 2039–2073.

[3] D. A. Evans, J. A. Murry, P. von Matt, R. D. Norcross, S. J. Miller, *Angew. Chem.* **1995**, *107*, 864–866; *Angew. Chem. Int. Ed. Engl.* **1995**, *34*, 798–800; R. Romeo, G. Arena, L. Monsu Scolaro, M. R. Plutino, *Inorg. Chim. Acta* **1995**, *240*, 81–92; D. Carmona, C. Cativiela, R. Garcia-Correas, F. J. Lahoz, M. P. Lamata, J. A. Lopez, M. P. Lopez-Ram de Viu, L. A. Oro, E. San Jose, F. Viguri, *Chem. Commun.* **1996**, 1247–1248; A. Lightfoot, P. Schnider, A. Pfaltz, *Angew. Chem.* **1998**, *110*, 3047–3050; *Angew. Chem. Int. Ed.* **1998**, *37*, 2897–2899; E. P. Kündig, C. M. Saudan, G. Bernardinelli, *Angew. Chem.* **1999**, *111*, 1298–1301; *Angew. Chem. Int. Ed.* **1999**, *38*, 1220–1223; S. P. Smidt, N. Zimmermann, M. Studer, A. Pfaltz, *Chem. Eur. J.* **2004**, *10*, 4685–4693; R. Chinchilla, P. Mazon, C. Najera, F. J. Ortega, *Tetrahedron: Asymmetry* **2004**, *15*, 2603–2607; P. G. A. Kumar, P. S. Pregosin, M. Vallet, G. Bernardinelli, R. F. Jazzar, F. Viton, E. P. Kündig, *Organometallics* **2004**, *23*, 5410–5418.

[4] T. C. Pochapsky, A. P. Wang, P. M. Stone, *J. Am. Chem. Soc.* **1993**, *115*, 11084–11091; X. Song, M. Thornton-Pett, M. Bochmann, *Organometallics* **1998**, *17*, 1004–1006; C. L. Beswick, T. J. Marks, *J. Am. Chem. Soc.* **2000**, *122*, 10358–10370.

[5] K. Vanka, M. S. W. Chan, C. C. Pye, T. Ziegler, *Organometallics* **2000**, *19*, 1841–1849; G. Lanza, I. L. Fragala, T. J. Marks, *J. Am. Chem. Soc.* **2000**, *122*, 12764–12777.

[6] Recent articles: C. Hofstetter, T. C. Pochapsky, *Magn. Reson. Chem.* **2000**, *38*, 90–94; A. Macchioni, A. Magistrato, I. Orabona, F. Ruffo, U. Rothlisberger, C. Zuccaccia, *New J. Chem.* **2003**, *27*, 455–458; A. Macchioni, *Eur. J. Inorg. Chem.* **2003**, 195–205, and references therein; P. G. A. Kumar, P. S. Pregosin, T. M. Schmid, G. Consiglio, *Magn. Reson. Chem.* **2004**, *42*, 795–800; R. P. Hughes, D. Zhang, A. J. Ward, L. N. Zakharov, A. L. Rheingold, *J. Am. Chem. Soc.* **2004**, *126*, 6169–6178; M. Aresta, A. Dibenedetto, I. Papai, G. Schubert, A. Macchioni, D. Zuccaccia, *Chem. Eur. J.* **2004**, *10*, 3708–3716; F. Song, S. J. Lancaster, R. D. Cannon, M. Schormann, S. M. Humphrey, C. Zuccaccia, A. Macchioni, M. Bochmann, *Organometallics* **2005**, in press; T. Beringhelli, G. D'Alfonso, D. Maggioni, P. Mercandelli, A. Sironi, *Chem. Eur. J.* **2005**, *11*, 650–661; D. Maggioni, T. Beringhelli, G. D'Alfonso, L. Resconi, *J. Organomet. Chem.* **2005**, *690*, 640–646.

[7] For recent articles see: M. Valentini, P. S. Pregosin, H. Ruegger, *Organometallics* **2000**, *19*, 2551–2555; B. Binotti, A. Macchioni, C. Zuccaccia, D. Zuccaccia, *Comments Inorg. Chem.* **2002**, *23*, 417–450; P. S. Pregosin, E. Martinez-Viviente, P. G. A. Kumar, *Dalton Trans.* **2003**, 4007–4014; B. Binotti, C. Carfagna, E. Foresti, A. Macchioni, P. Sabatino, C. Zuccaccia, D. Zuccaccia, *J. Organomet. Chem.* **2004**, *689*, 647–661; E. Martinez-Viviente, P. S. Pregosin, L. Vial, C. Herse, J. Lacour, *Chem. Eur. J.* **2004**, *10*, 2912–2918; C. Zuccaccia, N. G. Stahl, A. Macchioni, M. C. Chen, J. A. Roberts, T. J. Marks, *J. Am. Chem. Soc.* **2004**, *126*, 1448–1464; J. M. Goicoechea, M. F. Mahon, M. K. Whittlesey, P. G. A. Kumar, P. S. Pregosin, *Dalton Trans.* **2005**, 588–597.

[8] BArF = tetrakis(3,5-bistrifluoromethylphenyl)borate.

[9] a) J. Lacour, C. Ginglinger, C. Grivet, G. Bernardinelli, *Angew. Chem.* **1997**, *109*, 660–662; *Angew. Chem. Int. Ed. Engl.* **1997**, *36*, 608–609; b) J. Lacour, V. Hebbe-Viton, *Chem. Soc. Rev.* **2003**, *32*, 373–382; c) J. Lacour, R. Frantz, *Org. Biomol. Chem.* **2005**, *3*, 15–19.

[10] a) J. Lacour, J. J. Jodry, C. Ginglinger, S. Torche-Haldimann, *Angew. Chem.* **1998**, *110*, 2522–2524; *Angew. Chem. Int. Ed.* **1998**, *37*, 2379–2380; b) J. Lacour, C. Goujon-Ginglinger, S. Torche-Haldimann, J. J. Jodry, *Angew. Chem.* **2000**, *112*, 3830–3832; *Angew. Chem. Int. Ed.* **2000**, *39*, 3695–3697; c) D. Monchaud, J. J. Jodry, D. Pomeranc, V. Heitz, J. C. Chambron, J. P. Sauvage, J. Lacour, D. Monchaud, *Angew. Chem.* **2002**, *114*, 2423–2425; *Angew. Chem. Int. Ed.* **2002**, *41*, 2317–2319; d) C. Herse, D. Bas, F. C. Krebs, T. Bürgi, J. Weber, T. Wesolowski, B. W. Laursen, J. Lacour, *Angew. Chem.* **2003**, *115*, 3270–3274; *Angew. Chem. Int. Ed.* **2003**, *42*, 3162–3166.

[11] O. Maury, J. Lacour, H. Le Bozec, *Eur. J. Inorg. Chem.* **2001**, 201–204.

[12] C. Pérollier, S. Constant, J. J. Jodry, G. Bernardinelli, J. Lacour, *Chem. Commun.* **2003**, 2014–2015.

[13] Crystal data: The cell dimensions and intensities were measured at 200 K on a Stoe IPDS diffractometer with graphite-monochromated $Mo_{K\alpha}$ radiation ($\lambda = 0.71073$ Å). (−)-[**5**][*Δ*-**4a**] $(C_{18}H_3O_6FPCl_8)^-(C_{26}H_{29}N_2O)^+(C_3H_6O)$: $M_r = 1092.4$; orthorhombic space group, $P2_12_12_1$, $a = 11.5311(5)$, $b = 19.2565(10)$, $c = 22.6497(13)$ Å; $V = 5029.3(4)$ Å^3, $Z = 4$, $\mu = 0.537$ mm^{-1}, $\rho_{calcd} = 1.443$ g cm^{-3}. Of 70173 measured reflections, 10859 were unique and 4837 were observed ($|F_o| > 4\sigma(F_o)$); $R = 0.039$, $\omega R = 0.035$, Flack parameter x = −0.03(8). (−)-[**5**][*Δ*-**4b**] $(C_{18}H_3O_6FPCl_8)^-(C_{26}H_{29}N_2O)^+(C_3H_6O)$: $M_r = 1092.4$; orthorhombic space group, $P2_12_12_1$, $a = 11.3676(5)$, $b = 19.0586(11)$,

 © 2005 Wiley-VCH Verlag GmbH & Co. KGaA, Weinheim

$c = 22.9182(12)$ Å; $V = 4965.2(4)$ Å^3, $Z = 4$, $\mu = 0.544$ mm^{-1}, $\rho_{calcd} = 1.461$ g cm^{-3}. Of 69474 measured reflections, 10668 were unique and 5449 were observed ($|F_o| > 4\sigma(F_o)$); $R = 0.036$, $\omega R = 0.035$, Flack parameter $x = -0.03(8)$, the fluorine atom is disordered on the C4 and C5 positions with refined population parameters of 0.70(1) and 0.30(1) respectively. CCDC-265389 and CCDC-265390 contain the supplementary crystallographic data for this paper. These data can be obtained free of charge from the Cambridge Crystallographic Data Centre via www.ccdc.cam.ac.uk/data_request/cif.

[14] Circular dichroism analysis of salts (−)-[**5**][*Δ*-**4a**] and (−)-[**5**][*Δ*-**4b**] (MeOH, $\approx 10^{-6}$ M) revealed strong exciton coupling in the π–π* region with positive and negative Cotton effects at lowest and highest wavelengths, confirming the *Δ* configuration: D. Bas, T. Bürgi, J. Lacour, J. Vachon, J. Weber, *Chirality* **2005**, 15, S143 – S145.

[15] D. Monchaud, J. Lacour, C. Coudret, S. Fraysse, *J. Organomet. Chem.* **2001**, *624*, 388 – 391.

[16] A. J. McCaffery, S. F. Mason, J. Norman, *J. Chem. Soc. A* **1969**, 1428 – 1441; R. Kuroda, Y. Saito in *Circular Dichroism: Principles and Applications* (Eds.: K. Nakanishi, N. Berova, R. W. Woody), Wiley, New York, **1994**, pp. 217 – 258; M. Ziegler, A. von Zelewsky, *Coord. Chem. Rev.* **1998**, *177*, 257 – 300.

[17] D. Drago, P. S. Pregosin, A. Pfaltz, *Chem. Commun.* **2002**, 286 – 287; N. C. Fletcher, F. R. Keene, *J. Chem. Soc. Dalton Trans.* **1999**, 683 – 689; A. Macchioni, G. Bellachioma, G. Cardaci, M. Travaglia, C. Zuccaccia, B. Milani, G. Corso, E. Zangrando, G. Mestroni, C. Carfagna, M. Formica, *Organometallics* **1999**, *18*, 3061 – 3069.

[18] I. Dance, *CrystEngComm* **2003**, *5*, 208 – 221.

[19] T. Steiner, G. R. Desiraju, *Chem. Commun.* **1998**, 891 – 892; F. Grepioni, G. Cojazzi, S. M. Draper, N. Scully, D. Braga, *Organometallics* **1998**, *17*, 296 – 307.

[20] The ^{1}H,^{19}F-HOESY measurements were carried out on a 500-MHz Bruker DRX spectrometer equipped with a QNP probe; mixing time 700 ms, sample concentration 5 mM, number of scans 96, number of increments in the F1 dimension 256.

[21] The ^{1}H,^{19}F-HOESY NMR experiment on salt [*rac*-**2**](PF$_6$)$_2$ shows cross-peaks of the achiral anions with all the protons of the coordination complex (see the Supporting Information).

[22] The DFT calculations on the preferred geometry of interaction between ions *Δ*-**1** and *Δ*-**2** clearly showed this preferred topography. I. Dance, unpublished results.

[23] Anions **4a** and **4b** also possess H nuclei on the fluorine-containing ligands, which can be equally used for detecting interionic contacts. The results of the ^{1}H,^{1}H-NOESY experiments on salts [*Δ*-**2**][*Δ*-**4a**]$_2$ and [*Δ*-**2**][*Δ*-**4b**]$_2$ are reported in the Supporting Information and confirm the data from the HOESY experiments. These experiments further show that the preferred interaction of the anion with the cation comes indeed from the face containing the fluorine substituent.

 © 2005 Wiley-VCH Verlag GmbH & Co. KGaA, Weinheim

Nanostructure Synthesis

DOI: 10.1002/anie.200500988

Sacrificial Biological Templates for the Formation of Nanostructured Metallic Microshells**

*Emma Kathryn Payne, Nathaniel L. Rosi, Can Xue, and Chad A. Mirkin**

One of the challenges facing chemists and materials scientists is the fabrication of metallic micro- and macroscale materials that exhibit well-defined and controllable nanometer-scale features. Such materials are generally fabricated by using either lithographic or template-mediated approaches and are potentially useful for micro- and nanoelectronics, plasmon optics, and catalysis. In particular, lithographic techniques have proven useful in the generation of surface-confined nanostructured metallic materials.[1] However, fabrication of similarly structured free-standing and isolable metallic materials has proven more difficult. To create these structures, man-made templates have been used,[2] but they generally lack the structural sophistication necessary to yield the intricate details that lithographic methods routinely provide. Microorganism templates such as viruses,[3] bacteria,[4] diatoms,[5] and fungi,[6] on the other hand, offer unique organism- and species-specific details not provided by man-made templates. In this work, diatoms, a form of unicellular algae, were used as sacrificial templates for the formation of 3D metal-coated diatoms and free-standing nanostructured metallic microshells. Herein, we describe their structures and investigate their potential as substrates for surface-enhanced Raman scattering.

Several reports have described and characterized the nanostructure of diatom cell walls (frustules) and the proteins that direct their formation.[7] Of particular interest is the observation that diatom frustules (typically 1–100 μm in size) appear to be composed of fused or aggregated silica nanoparticles[7b] arranged in a manner that imparts species-specific nanometer-scale features including pores and grooves. These unique topological properties are difficult to generate with conventional materials fabrication techniques, which renders diatoms as attractive templates for the formation of new nanostructured metallic materials having potentially interesting optical and catalytic properties.

To produce metal-coated diatom frustules, pure diatom cultures (*Synedra* spp. and *Thalassiosira* spp.), grown in either

[*] E. K. Payne,[+] N. L. Rosi,[+] C. Xue, Prof. C. A. Mirkin
Department of Chemistry and Institute for Nanotechnology
Northwestern University
2145 Sheridan Road, Evanston, IL 60208-3113 (USA)
Fax: (+1) 847-467-5123
E-mail: chadnano@northwestern.edu

[+] These authors contributed equally to this work.

[**] CAM acknowledges the AFOSR for support of this research.

Supporting information for this article is available on the WWW under http://www.angewandte.org or from the author.

InterScience
© 2005 Wiley-VCH Verlag GmbH & Co. KGaA, Weinheim

freshwater (*Synedra*) or seawater (*Thalassiosira*) silicate-rich growth medium, were first subjected to piranha digestion to remove their organic components (Figure 1). The remaining silica frustules were washed with water and then suspended in ethanol and deposited as a non-overlapping monolayer onto a piranha-cleaned glass substrate. Ti metal (5 nm) and Ag metal (30 nm) were evaporated onto the diatom-coated substrate. Following evaporation, the resulting metal-coated diatoms were isolated by brief sonication in EtOH (Figure 1). SEM images of the 3D products reveal that the silver coating is deposited homogeneously across the diatom surfaces and maintains the morphology and intricate nanometer-scale features of the diatom templates (Figure 2).

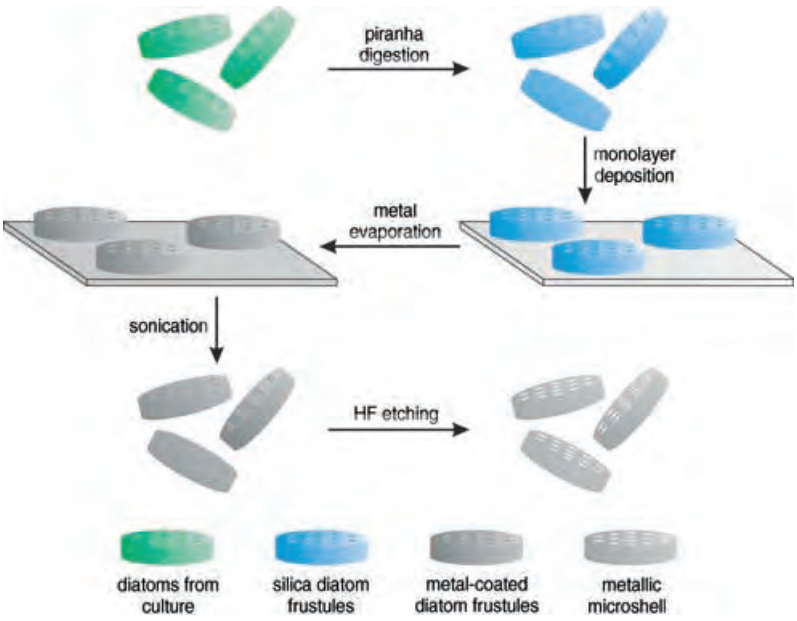


Figure 1. The preparation of metal-coated diatom frustules and the isolation of diatom-templated metallic microshells.

To isolate metallic microshell replicas of the diatoms, the metal-coated diatoms were subjected to HF (1%) etching solutions for 12–15 h which removed the silica shell and the 5-nm Ti layer (Figure 1 and Supporting Information). The resulting metallic materials (Figure 3) are structurally identical to their respective diatom templates in that they retain all of the nanostructural detail present on the diatom surfaces. Moreover, the 30-nm thick silver microshell is robust and remains intact throughout the etching process. This fabrication process is important for a number of reasons. First, thousands of structurally unique diatoms can be chosen as templates,[8] which allows one to choose particular species with topological patterns that best suit their interests. Second, the process is straightforward, high-yielding, easily reproducible, and can be performed with a variety of metals and metal compositions, depending on the desired application. Finally, the resulting 3D free-standing products exhibit nanostructural detail, including regularly patterned sub-200-nm pore sizes (Figure 3b,d). Thus, the diatoms act as sacrificial templates for the formation of 3D nanostructured metallic microshells.

Both the silver-coated diatoms and silver microshell diatom replicas (Figure 2b,d and Figure 3b,d) display pronounced sub-100-nm topological features. Similar features were not observed upon the evaporation of 30 nm Ag onto a glass microscope cover slip, showing that the fused silica particles that constitute the underlying structure of the diatom frustules are responsible for the observed roughness of the resulting metallic materials. As roughened metal surfaces and silver colloids have proven effective as surface-enhanced Raman scattering (SERS) substrates, we hypothesized that the diatom-templated metallic materials could potentially be used as substrates for the optical detection of analytes by using SERS.[9]

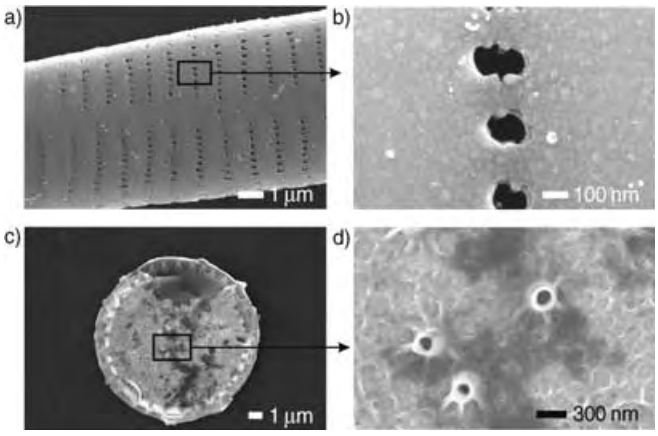


Figure 2. SEM images of the a) and b) *Synedra*, and c) and d) *Thalassiosira* frustules coated with silver (30 nm). The nanometer-scale features of the diatoms are preserved during the coating process.

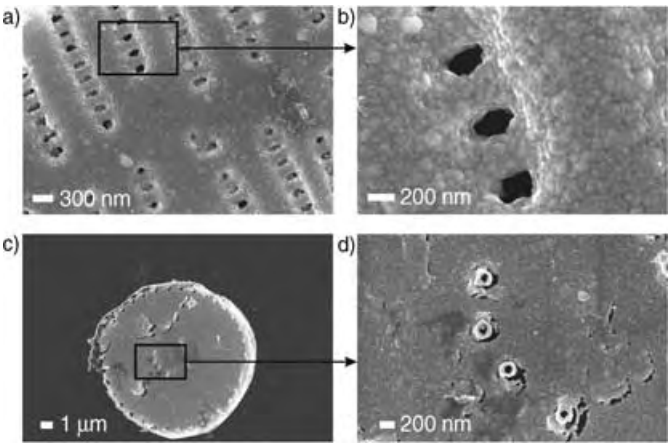


Figure 3. SEM images of silver metallic microshells after HF (1%) etching. The microshells exhibit the nanostructural detail present on the diatom templates.

© 2005 Wiley-VCH Verlag GmbH & Co. KGaA, Weinheim

As a first step in this direction, we began by investigating the SERS activity of the silver-coated diatom frustules. After soaking for four hours in aqueous solutions of rhodamine 6G (R6G) of varying concentration (1 mM, 1 μM, 100 nM), the diatom-templated materials were dispersed onto a piranha-cleaned glass slide and the dye solution was left to evaporate. SERS spectra were collected with a He/Ne laser (633 nm) excitation source with a power of 30 mW. For both *Synedra* and *Thalassiosira*, only the highest R6G concentration (1 mM) resulted in detectable SERS signal (Figure 4). Assuming

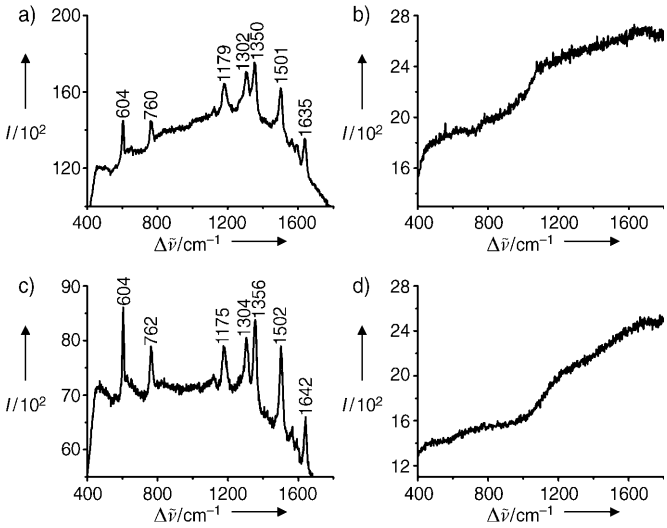


Figure 4. SERS spectra of a) 1-mM R6G and b) 1-μM R6G dye concentrations adsorbed on the silver-coated *Synedra* diatom frustules; c) and d) SERS spectra for 1-mM and 1-μM R6G, respectively, on silver-coated *Thalassiosira* frustules.

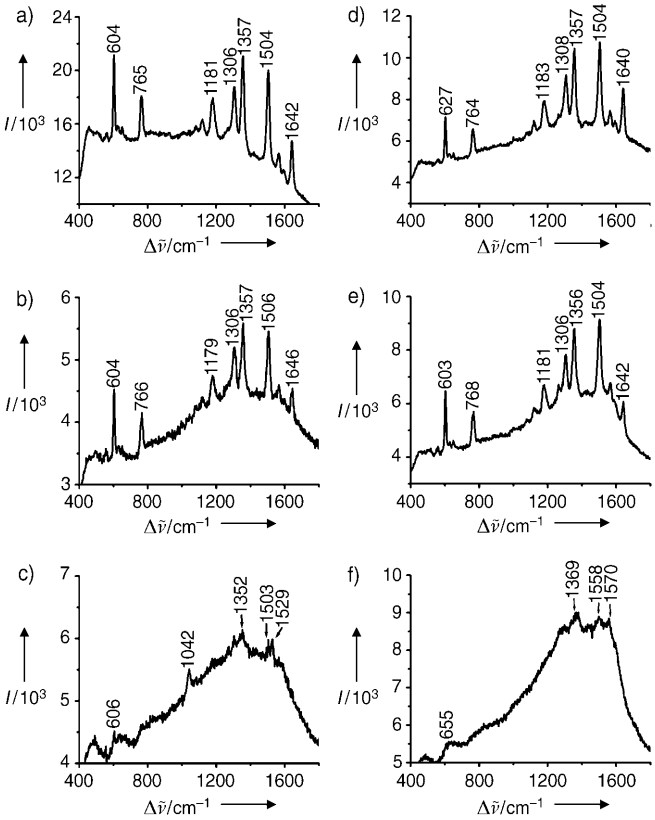


Figure 5. SERS spectra of a) 1-mM R6G, b) 1-μM R6G, and c) 100-nM R6G dye concentrations adsorbed on the silver microshell replicas of the *Synedra* frustules; d), e), and f) SERS spectra for 1-mM, 1-μM, and 100-nM R6G, respectively, on the silver microshell replicas of the *Thalassiosira* frustules.

100% coverage of the dye on the silver-coated diatom substrate, the enhancement factor was calculated to be approximately 4×10^5 for the *Synedra* and 2×10^5 for the *Thalassiosira*.[10]

The SERS signal intensity for the 1-mM solution increased dramatically in identical SERS experiments that were performed on the isolated silver microshells, and significant signal was recorded for both the 1-μM and 100-nM dye solutions (Figure 5). In this case, the enhancement factor was calculated to be 1×10^6 for the *Synedra* and 7×10^5 for *Thalassiosira*. The striking increase in SERS intensity upon template removal can be partially attributed to an increase in the exposed metal surface area onto which the Raman dye can associate, but this does not entirely explain the observed change. It is possible that HF treatment could also impact the SERS signal, as others have reported that mineral acids and anions can result in chemical enhancement of a SERS substrate.[11]

In conclusion, we report a straightforward fabrication method that employs diatoms as templates for the formation of 3D microscale metallic materials that exhibit elaborately detailed and patterned nanometer-scale features. The procedure is general and can be used with a variety of metals and any diatom species to produce a library of structurally unique materials. An important aspect of this work involves the selection of microorganism templates based on specific structural features that may benefit targeted applications. In this regard, we have shown that the nanostructured surfaces of diatom-templated metallic materials, which are inherent to the chosen diatom template, render them useful as SERS substrates.

Received: March 17, 2005
Revised: May 9, 2005
Published online: July 15, 2005

Keywords: biomaterials · diatoms · nanostructures · Raman spectroscopy · template synthesis

[1] a) D. S. Ginger, H. Zhang, C. A. Mirkin, *Angew. Chem.* **2004**, *116*, 30–46; *Angew. Chem. Int. Ed.* **2004**, *43*, 30–45; b) C. R. K. Marrian, D. M. Tennant, *J. Vac. Sci. Technol. A* **2003**, *21*, S207–S215; c) M. M. Alkaisi, R. J. Blaikie, S. J. McNab, *Adv. Mater.* **2001**, *13*, 877–887.

[2] a) W. T. S. Huck, J. Ten, G. M. Whitesides, *J. Am. Chem. Soc.* **1998**, *120*, 8267–8268; b) F. Caruso, R. A. Caruso, H. Mohwald, *Science* **1998**, *282*, 1111–1114; c) J. C. Love, B. D. Gates, D. B. Wolfe, K. E. Paul, G. M. Whitesides, *Nano Lett.* **2002**, *2*, 891–894; d) V. N. Paunov, O. J. Cayre, *Adv. Mater.* **2004**, *16*, 788–791; e) Y. Lu, G. L. Liu, J. Kim, Y. X. Mejia, L. P. Lee, *Nano Lett.* **2005**, *5*, 119–124.

 © 2005 Wiley-VCH Verlag GmbH & Co. KGaA, Weinheim

[3] a) W. Shenton, T. Douglas, M. Young, G. Stubbs, S. Mann, *Adv. Mater.* **1999**, *11*, 253 – 256; b) E. Dujardin, C. Peet, G. Stubbs, J. N. Culver, S. Mann, *Nano Lett.* **2003**, *3*, 413 – 417; c) M. Knez, A. M. Bittner, F. Boes, C. Wege, H. Jeske, E. Maiß, K. Kern, *Nano Lett.* **2003**, *3*, 1079 – 1082; d) A. S. Blum, C. M. Soto, C. D. Wilson, J. D. Cole, M. Kim, B. Gnade, A. Chatterji, W. F. Ochoa, T. Lin, J. E. Johnson, B. R. Ratna, *Nano Lett.* **2004**, *4*, 867 – 870; e) C. Mao, C. E. Flynn, A. Hayhurst, R. Sweeney, J. Qi, G. Georgiou, B. Iverson, A. M. Belcher, *Proc. Natl. Acad. Sci. USA* **2003**, *100*, 6946 – 6951; f) C. Mao, D. J. Solis, B. D. Reiss, S. T. Kottmann, R. Y. Sweeney, A. Hahurst, G. Georgiou, B. Iverson, A. M. Belcher, *Science* **2004**, *303*, 213 – 217.

[4] V. Berry, S. Rangaswamy, R. F. Saraf, *Nano Lett.* **2004**, *4*, 939 – 942.

[5] a) N. L. Rosi, C. S. Thaxton, C. A. Mirkin, *Angew. Chem.* **2004**, *116*, 5616 – 5619; *Angew. Chem. Int. Ed.* **2004**, *43*, 5500 – 5503; b) M. W. Anderson, S. M. Holmes, N. Hanif, C. S. Cundy, *Angew. Chem.* **2000**, *112*, 2819 – 2822; *Angew. Chem. Int. Ed.* **2000**, *39*, 2707 – 2710; c) Y. J. Wang, Y. Tang, X. D. Wang, A. G. Dong, W. Shan, Z. Gao, *Chem. Lett.* **2001**, *30*, 1118 – 1119; d) Y. Wang, Y. Tang, A. Dong, X. Wang, N. Ren, Z. Gao, *J. Mater. Chem.* **2002**, *12*, 1812 – 1818; e) F. Xu, Y. Wang, X. Wang, Y. Zhang, Y. Tang, P. Yang, *Adv. Mater.* **2003**, *15*, 1751 – 1753; f) K. H. Sandhage, M. B. Dickerson, P. M. Huseman, M. A. Caranna, J. D. Clifton, T. A. Bull, T. J. Heibel, W. R. Overton, M. E. A. Schoenwaelder, *Adv. Mater.* **2002**, *14*, 429 – 433; g) V. Sanhueza, U. Kelm, R. Cid, *J. Chem. Technol. Biotechnol.* **2003**, *78*, 485 – 488; h) R. R. Unocic, F. M. Zalar, P. M. Sarosi, Y. Cai, K. H. Sandhage, *Chem. Commun.* **2004**, 796 – 797.

[6] Z. Li, S.-W. Chung, J.-M. Nam, D. S. Ginger, C. A. Mirkin, *Angew. Chem.* **2003**, *115*, 2408 – 2411; *Angew. Chem. Int. Ed.* **2003**, *42*, 2306 – 2309.

[7] a) M. Sumper, *Science* **2002**, *295*, 2430 – 2433; b) F. Noll, M. Sumper, N. Hampp, *Nano Lett.* **2002**, *2*, 91 – 95; c) R. W. Drum, R. Gordon, *Trends Biotechnol.* **2003**, *21*, 325 – 328; d) G. A. Ozin, *Acc. Chem. Res.* **1997**, *30*, 17 – 27; e) H. R. Luckarift, J. C. Spain, R. R. Naik, M. O. Stone, *Nat. Biotechnol.* **2004**, *22*, 211 – 213.

[8] J. J. Dodd, *Diatoms*, Southern Illinois University Press, Carbondale, **1987**.

[9] a) D. L. Jeanmarie, R. P. Van Duyne, *J. Electroanal. Chem.* **1977**, *84*, 1 – 20; b) M. G. Albrecht, J. A. Creighton, *J. Am. Chem. Soc.* **1977**, *99*, 5215 – 5217; c) Z.-Q. Tian, B. Den, D.-Y. Wu, *J. Phys. Chem. B* **2002**, *106*, 9463 – 9483; d) K. Kneipp, H. Kneipp, I. Itzkan, R. R. Dasari, M. S. Feld, *Chem. Rev.* **1999**, *99*, 2957 – 2975; e) A. Campion, P. Kambhampati, *Chem. Soc. Rev.* **1998**, *27*, 241 – 250; f) S. R. Emory, S. Nie, *Science* **1997**, *275*, 1102 – 1106; g) A. Otto, *J. Raman Spectrosc.* **1991**, *22*, 743 – 752; h) Z.-Q. Tian, B. Ren, D.-Y. Wu, *J. Phys. Chem. B* **2002**, *106*, 9463 – 9483.

[10] a) R. P. Van Duyne, J. C. Hulteen, D. A. Treichel, *J. Chem. Phys.* **1993**, *99*, 2101 – 2115; b) B. Nikoobakht, J. Wang, M. A. El-Sayed, *Chem. Phys. Lett.* **2002**, *366*, 17 – 23.

[11] a) P. Hildebrandt, M. Stockburger, *J. Phys. Chem.* **1984**, *88*, 5935 – 5944; b) K. Kneipp, E. Roth, C. Engert, W. Kiefer, *Chem. Phys. Lett.* **1993**, *207*, 450 – 454; c) H. Lin, J. Mock, D. Smith, T. Gao, M. J. Sailor, *J. Phys. Chem. B* **2004**, *108*, 11654 – 11659.

 © 2005 Wiley-VCH Verlag GmbH & Co. KGaA, Weinheim

Fluorescent Probes

DOI: 10.1002/anie.200501506

A Pyrene-Labeled G-Quadruplex Oligonucleotide as a Fluorescent Probe for Potassium Ion Detection in Biological Applications**

*Satoru Nagatoishi, Takahiko Nojima, Bernard Juskowiak, and Shigeori Takenaka**

Alkali metal ions contribute to several physiological functions in living organisms.[1] Fluorescent indicators, particularly for Na^+ and K^+ ions, should permit the continuous or intermittent optical determination of these ions and visualization of their dynamic changes in living cells, extracellular spaces, vesicles, vascular tissue of plants and animals, biological fluids, and environmental samples.[2]

We have focused on fluorescent probes for the potassium ion, which plays a significant role as a transmitter in cells and in the regulation of membrane potential, nerve stimulation, and hormone secretion.[3] Potassium-binding benzofuran isophthalate (PBFI)[4] and coumarin diacid cryptand [2.2.2] (CD222)[5] have been recommended for the fluorimetric detection of K^+ ions in biological fluids, although these indicators show rather poor selectivity against sodium (a 1.5- and 3.4-fold excess of Na^+ ions is tolerated in each case, respectively).[4,5] Therefore, they can only be used for intracellular applications at sufficiently high K^+ concentrations. Other fluorescent probes for K^+ ions have recently been reported,[6] but only some of them are suitable for real-time monitoring applications at high Na^+ concentrations.[6c] Recently, we reported the potassium-sensing oligonucleotide (PSO)[7] as a FRET (fluorescence resonance energy transfer) probe for K^+ ions. It consists of two fluorophores (*N*,*N*,*N*′,*N*′-tetramethyl-6-carboxyrhodamine (TAMRA) and 6-carboxyfluorescein (FAM)) that are attached to the termini of a 21-mer oligonucleotide (human telomeric DNA sequence), which can form stable G-quadruplex complexes with metal cations.[8] Although PSO has been suggested to be useful for the monitoring of K^+ in an excess of Na^+ ions, its application

[*] Prof. S. Takenaka
Department of Materials Science, Faculty of Engineering
Kyushu Institute of Technology
Kitakyushu-shi 804-8550 (Japan)
Fax: (+81) 93-884-3333
E-mail: shige@che.kyutech.ac.jp
S. Nagatoishi, Dr. T. Nojima
Department of Applied Chemistry, Faculty of Engineering
Kyushu University, Fukuoka 812-858 (Japan)
Prof. B. Juskowiak
Faculty of Chemistry, A. Mickiewicz University
Poznan 60-780 (Poland)

[**] This work was supported in part by a Grant-in-Aid for Scientific Research from the Ministry of Education, Culture, Sports, Science, and Technology (MEXT), Japan.

Supporting information for this article is available on the WWW under http://www.angewandte.org or from the author.

© 2005 Wiley-VCH Verlag GmbH & Co. KGaA, Weinheim

for real-time K^+ ion monitoring under physiological conditions was rather difficult. Two factors hampered such an application: 1) the binding constant of the potassium complex was too high, resulting in saturation of the probe at a submillimolar concentration of K^+ and 2) FRET for the PSO complex was more efficient with Na^+ than that with PSO/K^+ (apparent quenching).

Herein, we report a novel PSO probe for the facile detection of potassium in the presence of an excess of Na^+ ions, in which these disadvantages are circumvented. The idea behind this new fluorescent probe (termed PSO-py) is to exploit the pyrene excimer emission for the transduction of a cation-binding event. Unlike the FRET system, in which stacking interactions between FRET partners resulted in unwanted quenching phenomena,[7] the pyrene moieties are expected to produce efficient excimer emission when stacked by π interactions.[9] However, potassium and sodium binding preferences were carefully tuned by selection of a quadruplex-forming oligonucleotide. The 15-mer oligonucleotide with the sequence d(GGTTGGTGTGGTTGG), known as a thrombin-binding aptamer (TBA),[10] was chosen for this purpose. TBA forms a chair-type quadruplex structure upon binding to thrombin protein, and this quadruplex incorporates K^+ ions with a 1:1 stoichiometry.[11] Therefore, binding of potassium ions should organize the 5′ and 3′ termini of TBA so that the two attached pyrene moieties are arranged face-to-face (Figure 1). As a result of this spatial orientation

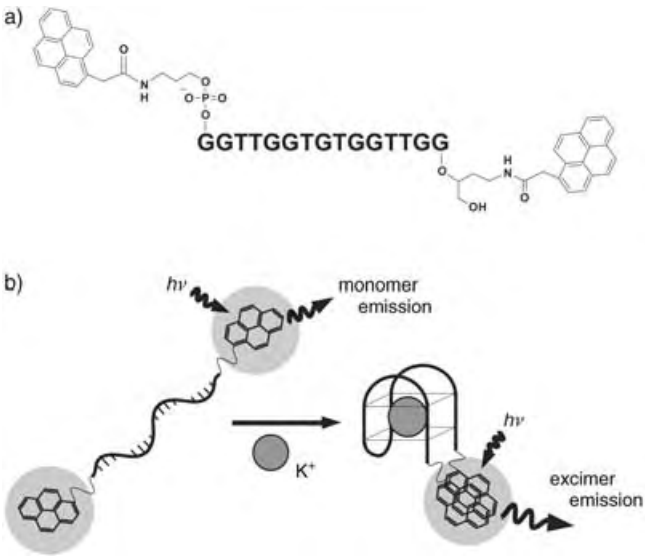


Figure 1. a) Chemical structure of PSO-py and b) the expected quadruplex formation induced by K^+ ions.

of the pyrene rings, the PSO-py/K^+ complex emits only excimer fluorescence, whereas the random-coil structure of PSO-py in the absence of K^+ ions gives only monomer emission. Consequently, PSO-py is expected to exhibit an excimer-emission intensity that depends on the K^+ concentration.[12] The presence of other metal cations is expected to cause minor interferences, as TBA forms weak complexes with Na^+, Mg^{2+}, and Ca^{2+} ions.[11c,13] PSO-py was obtained by modification of the synthetic TBA oligonucleotide termini with the appropriate derivatives of 1-pyrenylacetic acid: the phosphoramidite form for the 5′ end and the succinimidyl ester for the 3′ end. Modification and purification procedures were similar to those described by Fujimoto et al.[9d]

The suitability of PSO-py for the detection of K^+ ions was tested by fluorimetric titration with KCl (Figure 2). The

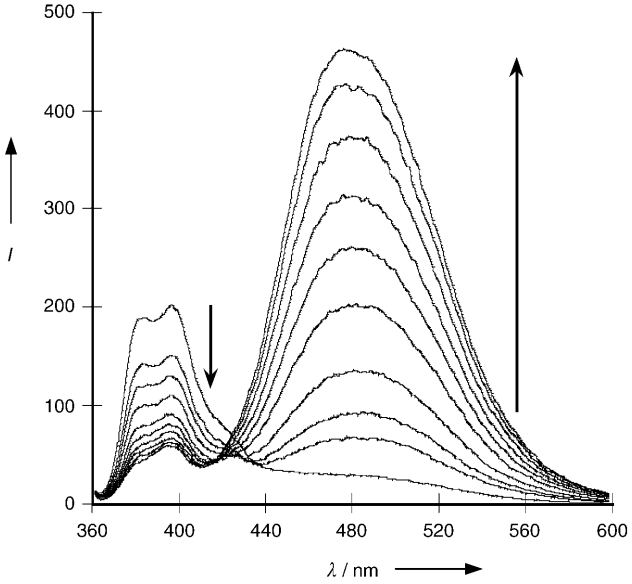


Figure 2. Fluorescence titration spectra of PSO-py (0.2 μM) with KCl (0–200 mM) in Tris·HCl solution (5 mM, pH 7.2) at 25 °C; $\lambda_{ex} = 347$ nm. Tris = tris(hydroxymethyl)aminomethane.

fluorescence spectrum of PSO-py in the absence of K^+ exhibits only a weak monomer band at 390 nm. The addition of K^+ ions results in the appearance of a new broad excimer band around 480 nm,[9] accompanied by quenching of the monomer emission. Interestingly, the weak monomer band at 390 nm lacks the vibronic structure that is probably connected with stacking interactions of the pyrene fluorophore with nucleobases.[9e,f] Notably, there is no clear isoemissive point in the system, which suggests a more complex situation than the simple two-component excimer–monomer equilibrium. Besides excimer emission, an additional fluorescence is most likely present from the excited dimer, for example. Contrary to the classic "dynamic excimer" observed in nonrestricted systems, some pyrene-bridged structures were reported to exhibit a "static excimer" or "fluorescent dimer" emission.[14] Circular dichroism (CD) recorded for PSO-py upon the addition of K^+ ions showed that the excimer fluorescence resulted from a structural change from a random coil to a chair-type quadruplex structure (the negative band near 265 nm and the positive band at 290 nm with an isoelliptic point at 280 nm).[8,13c]

Changes in the excimer fluorescence of PSO-py were also monitored in the presence of Na^+, Mg^{2+}, and Ca^{2+} ions. Excimer emission intensities were plotted against concentration of the tested ions (Figure 3). Only the potassium ion gave a positive response, but excimer emission was detectable for concentrations of Na^+ ions exceeding 100 mM. The small

 © 2005 Wiley-VCH Verlag GmbH & Co. KGaA, Weinheim

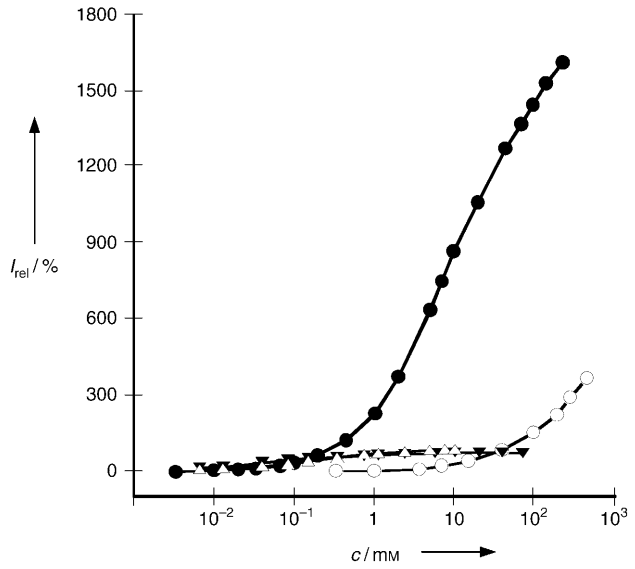


Figure 3. Plots of the relative fluorescence intensity of PSO-py (0.2 μM) against the concentration of KCl (●), NaCl (○), $CaCl_2$ (△), and $MgCl_2$ (▼).

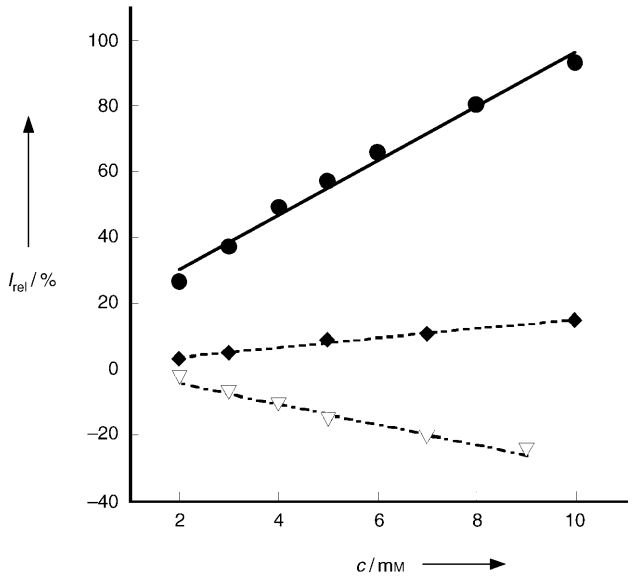


Figure 4. Comparison of the sensitivity of potassium detection for PSO-py (0.2 μM, ●), PBFI (0.2 μM, ◆), and PSO (0.2 μM, ▽) in Tris·HCl (5 mM, pH 7.2) containing 145-mM Na^+, 1.5-mM Mg^{2+}, and 2.5-mM Ca^{2+}.

changes observed in the CD spectra of PSO-py in the presence of Na^+ and Ca^{2+} ions confirmed the low binding affinity of PSO-py toward these cations. The dissociation constants (K_d) of PSO-py complexes were calculated from the plots shown in Figure 3 by fitting experimental data to an equation derived as before,[7] but for a complex with 1:1 stoichiometry. Values of 7.33 and 272 mM were determined for the K^+ and Na^+ complexes, respectively. The selectivity coefficient of 37, obtained from the ratio of sodium and potassium dissociation constants, is much higher than those for PBFI and CD222 (1.5 and 3.4, respectively).[4,5]

Real-time monitoring of the extracellular concentration of K^+ ions (2–10 mM) requires the PSO-py probe to exhibit a sufficiently high response in the presence of a complex matrix containing several ions (Na^+, Mg^{2+}, Ca^{2+}, and Cl^-) at millimolar concentrations. Therefore, the performance of PSO-py was studied by examining the K^+ calibration graph in the presence of a synthetic mixture containing 145-mM Na^+, 1.5-mM Mg^{2+}, and 2.5-mM Ca^{2+}. The increase in excimer emission of PSO-py was observed upon the addition of K^+ ions in the concentration range of 0–200 mM with linear dependence up to 10 mM K^+. The slope of the linear plot was +8.3% per 1 mM K^+, which is an excellent result given the typical physiological level of extracellular potassium. Similar calibration graphs with PBFI and PSO probes were determined for comparison (Figure 4), and these plots exhibit much lower sensitivities of +1.5 and −3.1% per 1 mM K^+, respectively. Undoubtedly, the PSO-py probe exhibits the highest sensitivity for K^+ ions relative to other probes reported so far. The dynamics of the fluorescence response and the reproducibility of excimer emission were also tested for the PSO-py/K^+ system by monitoring fluorescence changes upon subsequent alteration of the K^+ concentration between 5 and 6 mM (sequential dilution of solution and addition of concentrated KCl). The results of this experiment (Figure 5) indicate that the response time to the millimolar

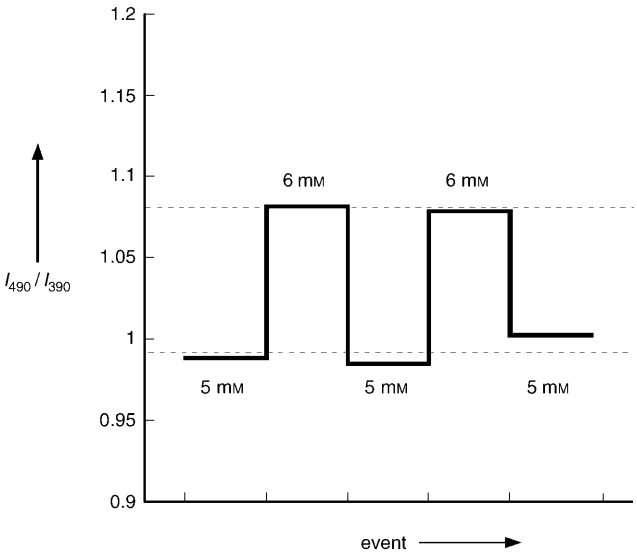


Figure 5. Fluorescence changes of PSO-py (0.2 μM) registered upon the subsequent variation of K^+ concentration between 5 and 6 mM in Tris·HCl (5 mM, pH 7.2).

variation in K^+ concentration is very short (within a few seconds), the excimer fluorescence of PSO-py/K^+ is reversible, and the probe shows reproducibility of the fluorescence signal within 5%.

In conclusion, we have designed the fluorescent probe PSO-py, which can be potentially exploited for the real-time monitoring of K^+ ions under extracellular conditions. The PSO-py ligand possesses the following advantages: 1) it binds potassium with a dissociation constant (K_d) of 7.33 mM, which perfectly matches the expected concentration range for K^+ ions and maximizes sensitivity; 2) it has sufficient discrimination against other ions, especially Na^+ (37-fold, K_d =

 © 2005 Wiley-VCH Verlag GmbH & Co. KGaA, Weinheim

272 mM), so that variations in the physiological concentration of sodium and other ions have little effect; 3) it shows reasonably good sensitivity (ΔF of +8.3% per 1 mM K^+); 4) its excitation wavelength (>350 nm) avoids the need for expensive quartz optics (microscope) and minimizes light absorption by nucleic acids and aromatic amino acids; and 5) the long wavelength of excimer emission (>450 nm) decreases overlap with tissue autofluorescence. Further studies, including application of the PSO-py probe for K^+ monitoring in biological systems, are in progress.

Received: May 2, 2005
Published online: July 20, 2005

Keywords: alkali metals · DNA structures · excimer emission · fluorescent probes · potassium

[1] S. J. Lippard, J. M. Berg, *Principles of Bioinorganic Chemistry*, University Science Books, Mill Valley, CA, **1994**.
[2] R. P. Haugland, *Handbook of Fluorescent Probes and Research Products*, 9th ed., Molecular Probes, Eugene, OR, **2002**.
[3] B. Alberts, A. Johnson, J. Lewis, M. Raff, K. Roberts, P. Walter, *Molecular Biology of the Cell*, 4th ed., Garland, New York, **2002**.
[4] a) D. J. Cram, *Science* **1988**, *240*, 760–767; b) K. Meuwis, N. Boens, F. C. De Schryver, J. Gallay, M. Vincent, *Biophys. J.* **1995**, *68*, 2469–2473.
[5] a) R. Crossley, Z. Goolamali, P. G. Sammes, *J. Chem. Soc. Perkin Trans. 2* **1994**, 1615–1623; b) P. Buet, B. Gersch, E. Grell, *J. Fluoresc.* **2001**, *11*, 79–87.
[6] a) A. Yamauchi, T. Hayashita, S. Nishizawa, M. Watanabe, N. Teramae, *J. Am. Chem. Soc.* **1999**, *121*, 2319–2320; b) W. Xia, R. H. Schmehl, C. Li, *Eur. J. Org. Chem.* **2000**, *3*, 387–389; c) H. He, M. A. Mortellaro, M. J. Leiner, R. J. Fraatz, J. K. Tusa, *J. Am. Chem. Soc.* **2003**, *125*, 1468–1469; d) C. Li, G. Law, W. Wong, *Org. Lett.* **2004**, *6*, 4841–4844.
[7] H. Ueyama, M. Takagi, S. Takenaka, *J. Am. Chem. Soc.* **2002**, *124*, 14286–14287.
[8] P. Balagurumoorthy, S. K. Brahmachari, *J. Biol. Chem.* **1994**, *269*, 21858–21869.
[9] a) F. D. Lewis, Y. Zhang, R. L. Letsinger, *J. Am. Chem. Soc.* **1997**, *119*, 5451–5452; b) E. Kostenko, M. Dobrikov, D. Pyshnyi, V. Petyuk, N. Komarova, V. Vlassov, M. Zenkova, *Nucleic Acids Res.* **2001**, *29*, 3611–3620; c) K. Yamana, T. Iwai, Y. Ohtani, S. Sato, M. Nakamura, H. Nakano, *Bioconjugate Chem.* **2002**, *13*, 1266–1273; d) K. Fujimoto, H. Shimizu, M. Inouye, *J. Org. Chem.* **2004**, *69*, 3271–3275; e) A. Okamoto, T. Ichba, I. Saito, *J. Am. Chem. Soc.* **2004**, *126*, 8364–8365; f) M. Kosuge, M. Kubota, A. Ono, *Tetrahedron Lett.* **2004**, *45*, 3945–3947.
[10] L. C. Bock, L. C. Griffin, J. A. Latham, E. H. Vermaas, J. J. Toole, *Nature* **1992**, *355*, 564–566.
[11] a) R. F. Macaya, P. Schultze, F. W. Smith, J. A. Roe, J. Feigon, *Proc. Natl. Acad. Sci. USA* **1993**, *90*, 3745–3749; b) P. Schultze, R. F. Macaya, J. Feigon, *J. Mol. Biol.* **1994**, *235*, 1532–1547; c) V. M. Marathias, P. H. Bolton, *Biochemistry* **1999**, *38*, 4355–4364 .
[12] First, we studied the FRET system containing the TBA sequence with FAM and TAMRA at both termini. However, we did not observe any FRET signal after quadruplex formation with K^+ ions. This effect was probably caused by quenching between dyes, which were prone to direct π-stacking interactions (data not shown). Furthermore, the TBA oligonucleotide carrying FAM and TAMRA showed residual FRET in the absence of K^+ ions.
[13] a) J. L. Mergny, A. T. Phan, L. Lacroix, *FEBS Lett.* **1998**, *435*, 74–78; b) B. I. Kankia, L. A. Marky, *J. Am. Chem. Soc.* **2001**, *123*, 10799–10804; c) N. Kumar, S. Maiti, *Biochem. Biophys. Res. Commun.* **2004**, *319*, 759–767.
[14] F. M. Winnik, *Chem. Rev.* **1993**, *93*, 587–614.

 © 2005 Wiley-VCH Verlag GmbH & Co. KGaA, Weinheim

Self-Assembled Nanostructures

DOI: 10.1002/anie.200500640

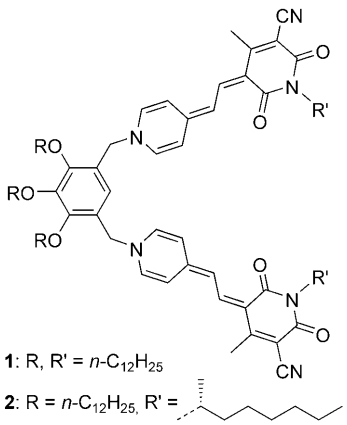
Supramolecular Stereomutation in Kinetic and Thermodynamic Self-Assembly of Helical Merocyanine Dye Nanorods**

*Andreas Lohr, Marina Lysetska, and Frank Würthner**

In memoriam Rüdiger Wortmann

Self-organization of natural nanostructures controlled by noncovalent interactions is an important topic in biophysics. In most cases, such as protein folding, biological self-assembly is considered to be a kinetically controlled process.[1] On the contrary, most self-assembled artificial systems are formed under thermodynamic control,[2] and only few kinetically controlled processes have been reported, especially for polymeric or metallosupramolecular assemblies.[3–5] Besides self-assembly another key feature of natural structures is the chirality, which is expressed at every level of organization. Hence, it is not surprising that artificial systems with molecular and supramolecular chirality have received increasing attention recently.[6,7]

We are particularly interested in the self-assembly of merocyanine dyes,[8,9] a class of chromophores that is of interest for nonlinear optical and photorefractive applications owing to their outstanding dipolar and polarizability properties.[10] In our earlier work we showed that aggregation of merocyanine dyes into centrosymmetric dimers arises predominantly from dipolar interactions with dimerization constants of $K_{dim} > 10^6\,M^{-1}$ in low-polar solvents.[8a] By utilizing this dipolar aggregation we achieved the self-assembly of the achiral bis(merocyanine) dye **1** into highly defined nanorods through supramolecular polymerization and hierarchical self-organization.[9] Forcefield calculations suggested that these nanorods are formed from six helically intertwined supramolecular single-stranded polymers. The chromophores are organized in a card-pack fashion and helically wound around the long axis of the rods; however, no direct evidence for the helicity of these supramolecular assemblies could be provided by the previously applied methods. Since achiral monomers were used, it was assumed that helices of opposite handedness were formed in equal amounts, that is, a racemic mixture was obtained. To provide evidence for the helicity, we decided to investigate the self-assembly of a chiral bis(merocyanine) derivative **2** bearing two (*R*)-2-octyl side chains at the imide positions. This should lead to the preferential formation of right-handed or left-handed helices. Indeed, pronounced supramolecular and macroscopic chirality effects were observed upon self-assembly of dye **2**, indicating a highly stereoselective self-assembly process. Moreover, a novel phenomenon was observed in the self-assembly of these dyes. Accordingly, herein we report the kinetically controlled self-assembly of merocyanine **2** into helical nanorods that exhibit a supramolecular stereomutation upon subsequent transformation into the thermodynamically stable nanorods, as elucidated by circular dichroism (CD) spectroscopy and atomic force microscopy (AFM).



1: R, R' = *n*-$C_{12}H_{25}$

2: R = *n*-$C_{12}H_{25}$, R' =

The time course of the self-assembly of **2** was studied by UV/Vis and CD spectroscopy, methods that are particularly suited to gain insight into the formation and packing properties of dye aggregates. The starting point for the self-assembly was defined by the addition of methylcyclohexane (MCH) to a stock solution of monomer **2** ($c = 3.33 \times 10^{-5}$ M) in tetrahydrofuran (THF) to provide a 1×10^{-5} M solution in THF/MCH = 30:70 vol%. In the stock solution, bis(merocyanine) **2** is present predominantly in the monomeric form owing to the high polarity of THF ($\varepsilon_r = 7.52$). Upon addition of unpolar MCH ($\varepsilon_r = 2.02$) the monomers instantaneously aggregate into supramolecular polymers and further into H-aggregated species owing to the increased Coulomb forces between the dipolar dyes. The THF/MCH ratio and, thus, the polarity of the solvent affects not only the thermodynamic equilibrium between different self-assembled species,[9b] but also the kinetic rates of the observed self-assembly processes. A 30:70 ratio of THF/MCH was established as the best-suited solvent system for the study of both the kinetic and thermodynamic processes at room temperature on convenient time scales.

Time-dependent UV/Vis spectra (Figure 1, bottom) show the transition from instantaneously formed D-aggregated species to H-aggregated species.[11] The decrease of the D band at 486 nm (assigned to the dimerized chromophores)[8a] and the increase of the hypsochromically shifted sharp H band at 444 nm with increasing time, and the occurrence of a well-defined isosbestic point at 462 nm suggest the conversion between two structurally defined species, which in the following we will refer to as **D** and **H1**, respectively. As the

[*] A. Lohr, Dr. M. Lysetska, Prof. Dr. F. Würthner
Institut für Organische Chemie
Universität Würzburg
Am Hubland, 97074 Würzburg (Germany)
Fax: (+49) 931-888-4756
E-mail: wuerthner@chemie.uni-wuerzburg.de

[**] This work was supported by the Deutsche Forschungsgemeinschaft (Wu 317/1-5) and the Fonds der Chemischen Industrie.

Supporting information for this article is available on the WWW under http://www.angewandte.org or from the author.

© 2005 Wiley-VCH Verlag GmbH & Co. KGaA, Weinheim

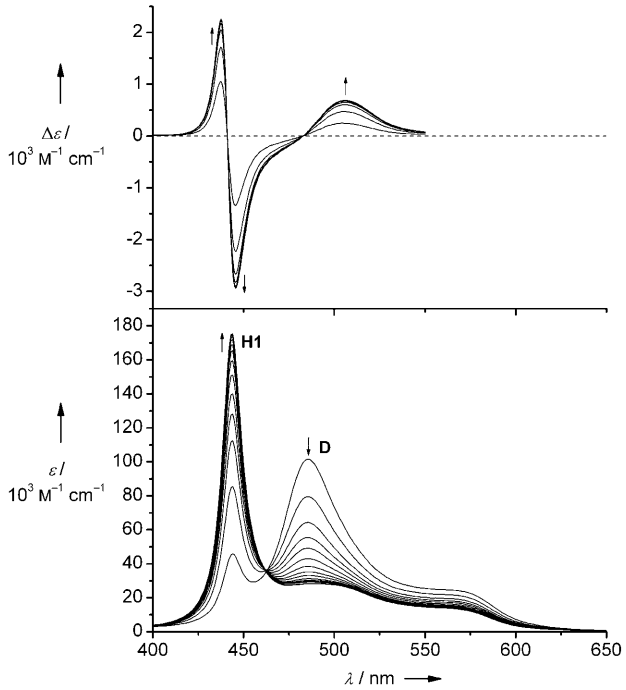


Figure 1. Time-dependent CD (top) and UV/Vis spectra (bottom) showing the transition from the D-aggregated species **D** into the kinetically formed H-aggregated species **H1** for dye **2** in a mixture of THF/MCH = 30:70 vol% at 20°C ($c = 1 \times 10^{-5}$ M). Arrows indicate changes with time (1–53 min).

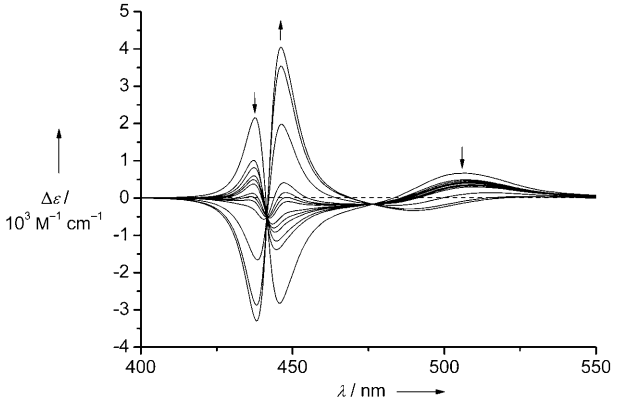


Figure 2. Time-dependent CD spectra showing the transition from the initially formed H-aggregated species **H1** into the thermodynamically more stable H-aggregated species **H2** for dye **2** in a mixture of THF/MCH = 30:70 vol% at 20°C ($c = 1 \times 10^{-5}$ M). Arrows indicate changes with time (96–7050 min).

concentration of **H1** rises, strong induced Cotton effects appear in the CD spectra (Figure 1, top), indicating chiral excitonic coupling of the chromophores in the self-assembled helical nanorods.[12] The CD spectra feature a strong negative bisignate exciton couplet located at the short wavelength absorption band of **H1**. The long wavelength shoulder at around 470 nm (negative) and the band at 506 nm (positive) may be attributed to a second bisignate CD signal with a positive sign, which originates from partly forbidden low-energy transitions of **H1**-aggregated dyes. The formation of the **H1**-aggregated species obeys first-order kinetics with a rate constant of $k = 0.42\ \text{min}^{-1}$ (Supporting Information).

To our surprise we observed a total inversion of this CD spectrum (Figure 2) as the time course of self-assembly progressed, while the UV/Vis spectra remained almost unchanged (Supporting Information). Since the formation of the initial **H1** aggregate is fast and the subsequent inversion is very slow, both processes can be studied independently with good approximation. Two well-defined isodichroic points at 441 nm and 476 nm reveal a transition between **H1** and another H-aggregated species with opposite exciton chirality, which in the following we denote as **H2**.

The UV/Vis and CD spectroscopic data of species **D**, **H1**, and **H2** are summarized in Table 1. The observed spectral changes can be explained in terms of kinetically and thermodynamically controlled self-assembly into two H-aggregated species **H1** and **H2** with opposite exciton chirality.[3a,b] First, the species **H1** is formed in a rapid process by kinetic self-assembly. Subsequently, **H1** is transformed in a much more slower process into the thermodynamic self-assembly product **H2**. It is remarkable that at higher MCH contents (i.e. lower solvent permittivity) this process becomes such slow that the kinetic product (species **H1**) can be trapped for weeks. On the other hand, the self-assembly processes are strongly accelerated at higher temperature.

To gain more insight into the **D**→**H1**→**H2** self-assembly process, we carried out atomic force microscopy (AFM) investigations. Figure 3 illustrates tapping mode AFM images of samples prepared by spin-coating of solutions of monomer **2** ($c = 1 \times 10^{-5}$ M, THF/MCH = 30:70 vol%) onto highly ordered pyrolytic graphite (HOPG) at different time intervals after initiation of the self-assembly process (i.e. addition of MCH into the stock solution in THF). After 1 min (Figure 3a) the height image shows wide disordered "grainy" regions that can be assigned to less structured supramolecular

Table 1: UV/Vis and CD spectroscopic data of species **D**, **H1**, and **H2**, and structural data determined by AFM in tapping mode.

Species	UV/Vis λ [nm]		CD λ [nm] (Δε [M⁻¹cm⁻¹])					AFM[a]		
	$\lambda_{max.}$	isosb. point	peak			isodichr. point		helicity	pitch [nm]	height [nm]
			1	2	3	1	2			
D	486									
		462				441 (0)	483 (0)			
H1	444		437 (2156)	445 (−2823)	506 (670)			*P*	10.4 ± 0.60	3.34 ± 0.40
						441 (−509)	476 (−164)			
H2	445		438 (−3297)	446 (4049)	490 (−337)			*P*	4.9 ± 0.60	3.16 ± 0.25

[a] Helicity and helical pitch of observed morphology.

 © 2005 Wiley-VCH Verlag GmbH & Co. KGaA, Weinheim

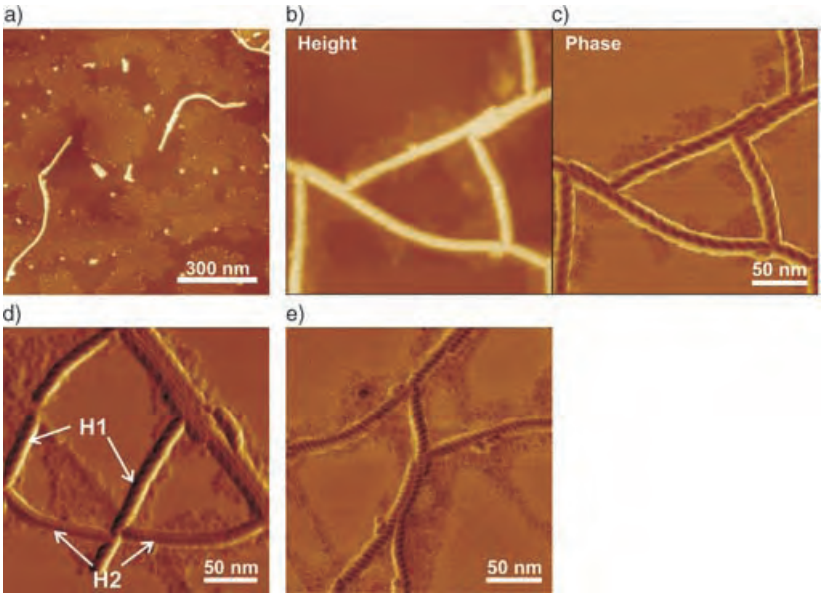


Figure 3. AFM height (a, b) and phase (c–e) images of samples prepared by spin-coating of solutions of bis(merocyanine) dye **2** ($c = 1 \times 10^{-5}$ M, THF/MCH = 30:70 vol%, 20 °C) onto HOPG at different times after initiation of self-assembly: a) 1 min; b,c) 14 min; d) 11 h; e) 22 h. In a and b the *z* scale is 10 nm and in c–e the *z* scale is 30°.

polymers (**D** species), and some short **H1** rods in the initial stage of their formation. After 14 min, when the bisignate CD signal has reached its maximum negative amplitude, the disordered regions have mostly disappeared and much longer **H1** rods are formed. Figure 3b and Figure 3c show the height and the corresponding phase image of the **H1** rods after 14 min in higher resolution. A pronounced right-handed helical (*P*) structure with a pitch of 10.4 ± 0.6 nm can be observed in the phase image (Figure 3c). The **H1** rods have a height of 3.34 ± 0.40 nm. After 11 h the coexistence of the **H2** species is evident (Figure 3d and Supporting Information). The **H2** rods have also right-handed helicity, but now with a helical pitch of only 4.9 ± 0.6 nm, and a height of 3.16 ± 0.25 nm (see Table 1). Subsequently, after 22 h merely the **H2** rods can be observed (Figure 3e). In contrast to the phase images, the corresponding height images do not show the helical morphology, which suggests that regions of different "hardness" render the helical contrast in the phase images. Artefacts caused by sample preparation or measurements can surely be excluded as rods assembled out of the enantiomeric (*S*,*S*)-monomers show opposite left-handed helicity (not shown).

A structural model for the spatial arrangement of the chromophores in the **H1** and **H2** rods is proposed in Figure 4. During the conversion process from **H1** into **H2**, the chromophores are rearranged only slightly as both species are very similar nanorods that contain the chromophores in helically wound stacks (CD, AFM). On the basis of the rod diameter (height values of AFM), a more compact structure is assigned to the thermodynamic **H2** assembly. The induced Cotton effects can be attributed to the H-type interaction of tightly stacked dyes in a slightly twisted antiparallel arrangement. Similar (−/+/−)-shaped CD spectra were observed for natural chlorin dye and artificial cyanine dye J-aggregates and theoretical calculations have revealed that such a spectral shape is a common feature of helical cylindrical dye aggregates.[7h,13] Although we would like to point out that the current model is only preliminary in the absence of theoretical calculations, the CD data strongly suggest a $M \rightarrow P$ change of the helical twist between the closest neighboring chromophores in the helically wound stacks at the **H1**→**H2** transition (Figure 4). Furthermore, our model accounts for the preservation of the right-handed (*P*) macroscopic helical twist in both dye stacks, which is more pronounced in **H2** than in **H1**. This could explain the right-handed helicity of both **H2** and **H1** rods and the smaller helical pitch of **H2** compared to **H1** as observed by AFM. The antiparallel stacking of these dye dipoles with a next closest and a second more distant neighboring dye unit has been established by several crystal structures of dipolar merocyanine dyes.[8a]

To summarize, this work confirms unequivocally the helical nature of self-assembled bis(merocyanine) nanorods and discloses a rare example of a supramolecular stereomutation as visualized spectroscopically by time-dependent CD spectroscopy and, to the best of our knowledge, for the first time microscopically by atomic force microscopy. Our studies reveal a complex transition from an initial kinetic self-assembly into a more stable thermodynamic structure, which is almost undetectable by conventional methods such as UV/Vis spectroscopy. Further investigations on other features of these chiral

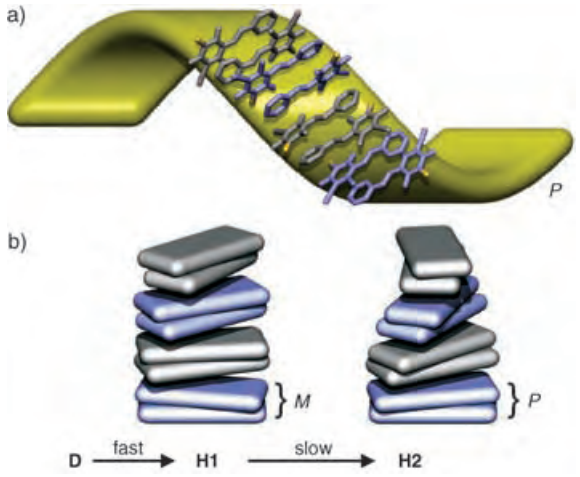


Figure 4. a) Model for right-handed (*P*) helically wound arrangement of the stacked chromophores in the rod aggregates. For the sake of clarity only a section of eight chromophores is shown. For more information on our model see reference [9b]. b) Schematic illustration of the left- to right-handed ($M \rightarrow P$) rearrangement between closest neighboring dyes during the **H1**→**H2** transition. The overall helical twist remains right-handed (*P*) for both **H1** and **H2**, but is more pronounced for **H2** than for **H1**.

 © 2005 Wiley-VCH Verlag GmbH & Co. KGaA, Weinheim

merocyanine dye aggregates, for example the "sergeant-and-soldiers" principle and self-assembly behavior of (*R*,*R*)-**2**/(*S*,*S*)-**2** mixtures are underway. Furthermore, such densely packed homochiral assemblies of highly polarizable merocyanine dyes might exhibit pronounced $\chi^{(2)}$ nonlinear optical properties even without electric-field-induced symmetry breaking.[14]

Received: February 21, 2005
Published online: July 13, 2005

Keywords: atomic force microscopy · circular dichroism · dyes/pigments · merocyanine · self-assembly

[1] C. M. Dobson, A. Šali, M. Karplus, *Angew. Chem.* **1998**, *110*, 908 – 935; *Angew. Chem. Int. Ed.* **1998**, *37*, 868 – 893.
[2] J. M. Lehn, *Supramolecular Chemistry: Concepts and Perspectives*, VCH, Weinheim, **1995**.
[3] For polymeric assemblies see, for example: a) P. Jonkheijm, A. Miura, M. Zdanowska, F. J. M. Hoeben, S. De Feyter, A. P. H. J. Schenning, F. C. De Schryver, E. W. Meijer, *Angew. Chem.* **2004**, *116*, 76 – 80; *Angew. Chem. Int. Ed.* **2004**, *43*, 74 – 78; b) M. Simonyi, Z. Bikádi, F. Zsila, J. Deli, *Chirality* **2003**, *15*, 680 – 698.
[4] For metallosupramolecular architectures see, for example: a) A. Hori, K. Yamashita, M. Fujita, *Angew. Chem.* **2004**, *116*, 5126 – 5129; *Angew. Chem. Int. Ed.* **2004**, *43*, 5016 – 5019; b) B. J. Holliday, Y.-M. Jeon, C. A. Mirkin, C. L. Stern, C. D. Incarvito, L. N. Zakharov, R. D. Sommer, A. L. Rheingold, *Organometallics* **2002**, *21*, 5713 – 5725; c) B. Hasenknopf, J. M. Lehn, N. Boumediene, E. Leize, A. Van Dorsselaer, *Angew. Chem.* **1998**, *110*, 3458 – 3460; *Angew. Chem. Int. Ed.* **1998**, *37*, 3265 – 3268.
[5] For hydrogen-bonded supramolecular architectures see, for example: a) J. D. Badjić, S. J. Cantrill, J. F. Stoddart, *J. Am. Chem. Soc.* **2004**, *126*, 2288 – 2289; b) V. Paraschiv, M. Crego-Calama, T. Ishi-i, C. J. Padberg, P. Timmerman, D. N. Reinhoudt, *J. Am. Chem. Soc.* **2002**, *124*, 7638 – 7639.
[6] For general reviews on helical structures see: a) E. Yashima, K. Maeda, T. Nishimura, *Chem. Eur. J.* **2004**, *10*, 43 – 51; b) C. Schmuck, *Angew. Chem.* **2003**, *115*, 2552 – 2556; *Angew. Chem. Int. Ed.* **2003**, *42*, 2448 – 2452; c) L. Brunsveld, B. J. B. Folmer, E. W. Meijer, R. P. Sijbesma, *Chem. Rev.* **2001**, *101*, 4071 – 4097; d) D. J. Hill, M. J. Mio, R. B. Prince, T. S. Hughes, J. S. Moore, *Chem. Rev.* **2001**, *101*, 3893 – 4011; e) A. E. Rowan, R. J. M. Nolte, *Angew. Chem.* **1998**, *110*, 65 – 71; *Angew. Chem. Int. Ed.* **1998**, *37*, 63 – 68.
[7] a) J. J. D. de Jong, L. N. Lucas, R. M. Kellogg, J. H. van Esch, B. L. Feringa, *Science* **2004**, *304*, 278 – 281; b) S. J. George, A. Ajayaghosh, P. Jonkheijm, A. P. H. J. Schenning, E. W. Meijer, *Angew. Chem.* **2004**, *116*, 3504 – 3507; *Angew. Chem. Int. Ed.* **2004**, *43*, 3422 – 3425; c) C. Keith, R. A. Reddy, U. Baumeister, C. Tschierske, *J. Am. Chem. Soc.* **2004**, *126*, 14312 – 14313; d) T. S. Balaban, A. D. Bhise, M. Fischer, M. Linke-Schaetzel, C. Roussel, N. Vanthuyne, *Angew. Chem.* **2003**, *115*, 2190 – 2194; *Angew. Chem. Int. Ed.* **2003**, *42*, 2140 – 2144; e) J. M. Ribo, J. Crusats, F. Sagues, J. Claret, R. Rubires, *Science* **2001**, *292*, 2063 – 2066; f) L. J. Prins, F. De Jong, P. Timmerman, D. N. Reinhoudt, *Nature* **2000**, *408*, 181 – 184; g) R. Oda, I. Huc, M. Schmutz, S. J. Candau, F. C. MacKintosh, *Nature* **1999**, *399*, 566 – 569; h) A. Pawlik, S. Kirstein, U. De Rossi, S. Daehne, *J. Phys. Chem. B* **1997**, *101*, 5646 – 5651.
[8] a) F. Würthner, S. Yao, T. Debaerdemaeker, R. Wortmann, *J. Am. Chem. Soc.* **2002**, *124*, 9431 – 9447; b) F. Würthner, S. Yao, B. Heise, C. Tschierske, *Chem. Commun.* **2001**, 2260 – 2261; c) F. Würthner, S. Yao, *J. Org. Chem.* **2003**, *68*, 8943 – 8949.
[9] a) F. Würthner, S. Yao, U. Beginn, *Angew. Chem.* **2003**, *115*, 3247 – 3250; *Angew. Chem. Int. Ed.* **2003**, *42*, 3247 – 3250; b) S. Yao, U. Beginn, T. Gress, M. Lysetska, F. Würthner, *J. Am. Chem. Soc.* **2004**, *126*, 8336 – 8348.
[10] F. Würthner, R. Wortmann, K. Meerholz, *ChemPhysChem* **2002**, *3*, 17 – 31.
[11] The D-aggregated state is inherently a polymeric strand or cyclic oligomer due to the existence of two receptor sites at each molecule (see ref. [9]).
[12] a) N. Berova, K. Nakanishi in *Circular Dichroism. Principles and Applications*, *2nd ed.* (Eds.: N. Berova, K. Nakanishi, R. W. Woody), Wiley, New York, **2000**, pp. 337 – 382; b) V. Buß, C. Reichardt, *J. Chem. Soc. Chem. Commun.* **1992**, 1636 – 1638.
[13] a) V. I. Prokhorenko, D. B. Steensgaard, A. R. Holzwarth, *Biophys. J.* **2003**, *85*, 3173 – 3186; b) C. Didraga, J. A. Klugkist, J. Knoester, *J. Phys. Chem. B* **2002**, *106*, 11474 – 11486.
[14] a) G. J. Simpson, *ChemPhysChem* **2004**, *5*, 1301 – 1310; b) T. Verbiest, S. Van Elshocht, M. Kauranen, L. Hellemans, J. Snauwaert, C. Nuckolls, T. J. Katz, A. Persoons, *Science* **1998**, *282*, 913 – 915.

 © 2005 Wiley-VCH Verlag GmbH & Co. KGaA, Weinheim

Macrocycles

DOI: 10.1002/anie.200501621

Shape-Persistent Chiral Alleno-Acetylenic Macrocycles and Cyclophanes by Acetylenic Scaffolding with 1,3-Diethynylallenes**

Severin Odermatt, J. Lorenzo Alonso-Gómez, Paul Seiler, M. Magdalena Cid, and François Diederich**

The chemistry of chiral allenes has attracted increasing interest in recent years due to the development of improved syntheses and their emerging use in pharmaceuticals.[1] While strained small-ring allenes have been investigated in greater detail for their theoretical properties and their limits of

[*] J. L. Alonso-Gómez, Prof. Dr. M. M. Cid
Facultade de Química, Universidade de Vigo
Lagoas-Marcosende, 36310 Vigo (Spain)
Fax: (+34) 986812262
E-mail: mcid@uvigo.es
S. Odermatt, P. Seiler, Prof. Dr. F. Diederich
Laboratorium für Organische Chemie
ETH Hönggerberg
HCI, 8093 Zürich (Switzerland)
Fax: (+41) 1-632-1109
E-mail: diederich@org.chem.ethz.ch

[**] This work was supported by a grant from the ETH Research Council, the Fonds der Chemischen Industrie, MCYT, Spain (SAF2001-3288), and the Ministerio de Educación y Ciencia (PhD fellowship to J.L.A.-G.). We thank Dr. C. Thilgen for his help with the stereochemical assignments.

Supporting information for this article is available on the WWW under http://www.angewandte.org or from the author.

 © 2005 Wiley-VCH Verlag GmbH & Co. KGaA, Weinheim

stability and isolability,[2] macrocyclic allenes, in particular shape-persistent ones,[3] are nearly unknown.[4] The only such macrocycle known is a [3$_4$]cyclophane, reported by Krause and co-workers,[5] in which four *para*-phenylene moieties are bridged by four 1,3-dimethylallene-1,3-diyl linkers and which was isolated as a mixture of several stereoisomers. This absence of allenic macrocycles is rather surprising in view of the opportunities for creating new nonplanar, chiral topologies and for developing new chiral host molecules.

The recently described synthesis of the first stable 1,3-diethynylallenes[6] now opens up the way for acetylenic scaffolding, and here we report the preparation of the new chiral, unsaturated macrocycles **1** and **2** (Figure 1). Compound **1** is the first alleno-acetylenic macrocycle without aromatic rings in the backbone. It exists as seven stereoisomers, two pairs of enantiomers and three achiral diastereoisomers, which could be isolated as pure compounds. For one of the enantiomeric pairs, the relative configuration could be assigned unambiguously. Cyclophane **2** was prepared as a mixture of six stereoisomers, two pairs of enantiomers and two achiral diastereoisomers; remarkably, both racemates and the two achiral isomers could all be isolated and their relative configurations assigned.

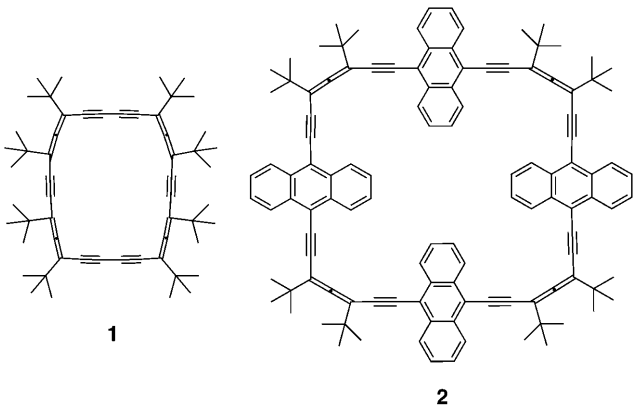
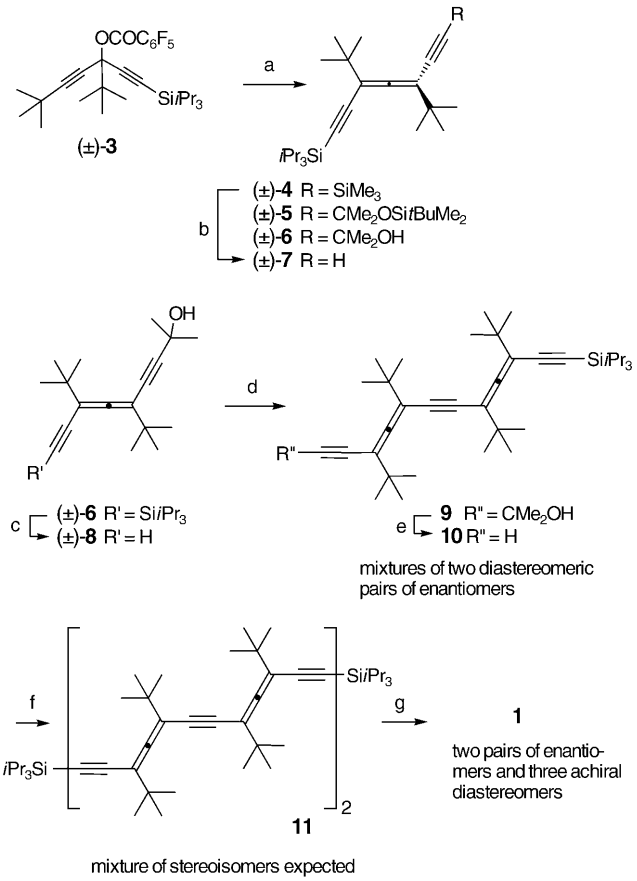


Figure 1. Two pairs of enantiomers and three achiral diastereoisomers are expected for macrocycle **1**; two pairs of enantiomers and two achiral diastereoisomer are expected for cyclophane **2**.

The synthesis of allenes (±)-**4** through (±)-**6** (Scheme 1) by Pd-catalyzed cross-coupling of ester (±)-**3** with the corresponding alkynes followed the previously described protocol;[6] however, a considerable improvement in reaction yields was obtained by using pentafluorobenzoate as the leaving group.[7] Removal of the silyl groups from (±)-**4** and (±)-**6** afforded the free terminal alkynes (±)-**7** and (±)-**8**, respectively. A second cross-coupling of (±)-**3** with (±)-**8** provided diallene **9** in 71% yield as a mixture of two diastereoisomeric pairs of enantiomers as evident from the ^{13}C NMR spectrum (125 MHz, C_6D_6). All attempts to separate the two diastereoisomeric pairs by HPLC failed.[8] The acetonide protecting group in **9** was removed with KOH in hot benzene to give the free alkyne **10**. Subsequent oxidative homocoupling under Hay conditions[17] yielded tetraallene **11** in high yield (91%). The formation of different stereoisomers



Scheme 1. Synthesis of the allene–alkyne macrocycle **1**. Reagents and conditions: a) R-C≡CH, [Pd(PPh$_3$)$_4$], CuI, *i*Pr$_2$NEt, (CH$_2$Cl)$_2$, 50°C; 74% ((±)-**4**), 53% ((±)-**5**), 69% ((±)-**6**); b) K$_2$CO$_3$, MeOH/THF, 20°C; 90%; c) *n*Bu$_4$NF, THF, 0°C; 67%; d) (±)-**3**, [Pd(PPh$_3$)$_4$], CuI, (CH$_2$Cl)$_2$, Cy$_2$NMe, 60°C; 71%; e) KOH, C$_6$H$_6$, 80°C; 65%; f) CuCl, TMEDA, (CH$_2$Cl)$_2$, 50°C; 91%; g) 1. *n*Bu$_4$NF, *ortho*-nitrophenol, THF, 20°C; 2. CuCl, CuCl$_2$, pyridine, [**11**] ≈ 10^{-4} M; 80% total yield of seven stereoisomers. Cy = cyclohexyl, TMEDA = *N*,*N*,*N*′,*N*′-tetramethylethylenediamine.

was expected, but the spectroscopic data did not give precise information on the composition of the mixture and HPLC analyses showed mainly one peak. Deprotection of **11** with *n*Bu$_4$NF in THF in the presence of *ortho*-nitrophenol provided the crude free terminal bis(alkyne) which, after a filtration through SiO$_2$, was subjected directly to the final ring closure under high dilution (10^{-4} M). The Eglinton–Galbraith conditions[9] proved to be the most effective, providing a total yield of 80% of the macrocyclic tetraallene **1**: higher molecular weight products were not detected by analytical gel permeation chromatography (GPC) after filtration through SiO$_2$ (for experimental details see the Supporting Information).

The individual detection of the expected stereoisomers (two racemates and three achiral diastereoisomers) was possible by analytical HPLC on SiO$_2$ (see the Supporting Information).[10] The increased rigidity of the formed macrocycles **1**, compared to the flexible acyclic precursors **11**, most likely had beneficial effects on the separation. Preparative separation was hampered by the highly apolar nature and the

 © 2005 Wiley-VCH Verlag GmbH & Co. KGaA, Weinheim

reduced solubility (despite the *tert*-butyl groups) of the compounds. The five stereoisomeric products were finally isolated with the aid of two different preparative HPLC separations on "Buckyclutcher 1" and Kromasil columns.[11] The detected ratio of the stereoisomers roughly corresponded to the values of 1:1:4:1:1 expected for an unselective ring closure. The formation of racemic, C_1-symmetric (*M*,*P*,*P*,*P*)/(*P*,*M*,*M*,*M*)-**1** (Figure 2)[12] is statistically favored over the formation of the other isomers.

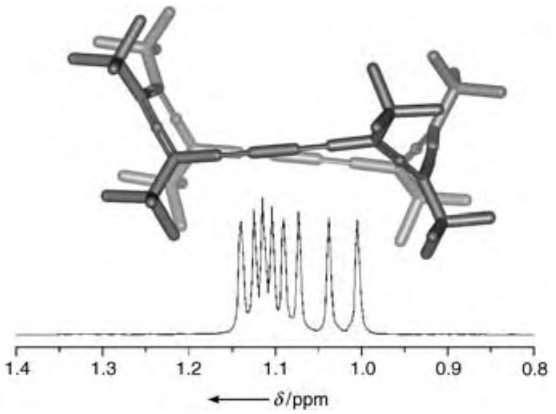
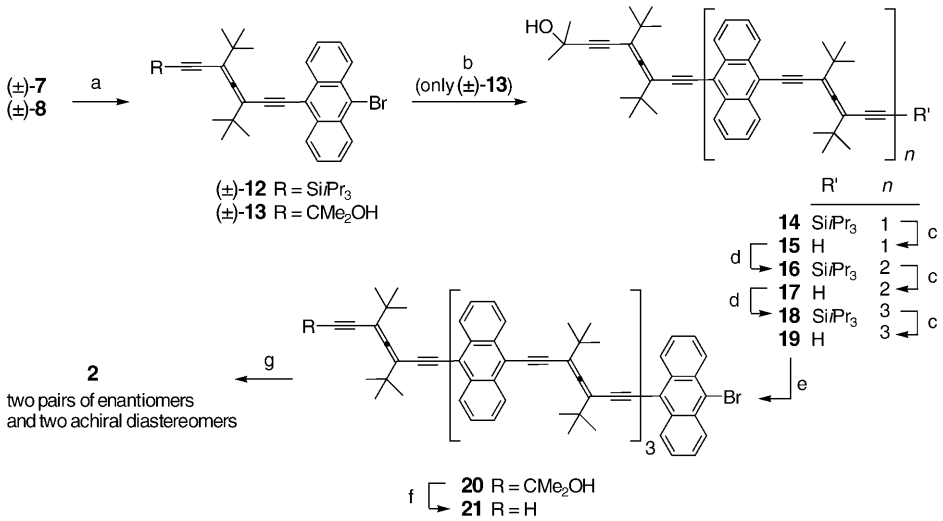


Figure 2. Tube model and ^{1}H NMR spectrum (300 MHz, $C_6D_5CD_3$) of twisted, C_1-symmetric (*M*,*P*,*P*,*P*)/(*P*,*M*,*M*,*M*)-**1**. The conformation of the (*M*,*P*,*P*,*P*) isomer was optimized by AM1 calculations using Spartan Pro.[12]

The assigned relative configuration of (*M*,*P*,*P*,*P*)/(*P*,*M*,*M*,*M*)-**1** was clearly proven spectroscopically. In the ^{1}H NMR spectrum in deuterated benzene or toluene, all eight expected resonances of the eight nonequivalent *tert*-butyl groups were clearly separated (Figure 2). Furthermore, the ^{13}C NMR spectrum showed four signals for the four nonequivalent cumulenic C atoms of the four allene moieties. The relative configuration of the other isolated stereoisomers could not be assigned based on symmetry considerations. For the second racemate, D_2-symmetric (*M*,*M*,*M*,*M*)/(*P*,*P*,*P*,*P*)-**1**, and the three achiral isomers, C_{2h}-symmetric (*M*,*M*,*P*,*P*)-**1** and (*M*,*P*,*P*,*M*)-**1**, and C_{2v}-symmetric (*M*,*P*,*M*,*P*)-**1**, two magnetically different *tert*-butyl groups and one signal for the central C atom of the four allene moieties was expected and observed in the ^{13}C NMR spectra (see the Supporting Information).

The synthesis of anthracenophane **2** started with the Sonogashira cross-coupling[13] of (±)-**7** and (±)-**8** with 9,10-dibromoanthracene to give (±)-**12** and (±)-**13**, respectively (Scheme 2). A series of four Sonogashira cross-couplings alternating with three deprotection steps afforded, after acetonide cleavage, the linear tetraallene , the precursor to cyclophane **2**, as a mixture of stereoisomers (15% overall yield starting from (±)-**13**), which were not separated. Macrocyclization with one equivalent of [Pd(PPh$_3$)$_4$] and CuI provided **2** in 60% yield as a mixture of two racemates and two achiral diastereoisomers, which were separated by preparative HPLC ("Buckyclutcher 1"; for experimental details see the Supporting Information).[11]

In the case of cyclophane **2**, the relative configuration of all the stereoisomers could be assigned. Thanks to its symmetry the major product was identified by ^{1}H NMR spectroscopy (300 MHz, $CDCl_3$) as C_2-symmetric (*M*,*P*,*P*,*P*)/(*P*,*M*,*M*,*M*)-**2** with four magnetically different *tert*-butyl groups (Figure 3a). On the other hand, the spectrum of the achiral C_{2h}-symmetric (*M*,*M*,*P*,*P*)-**2** features only two different *tert*-butyl resonances (Figure 3b). The ^{1}H NMR spectra of the other two products display only one *tert*-butyl signal as expected as a result of their higher symmetry (D_4 and D_{2d}, respectively). Fortunately, the structure of D_4-symmetric (*P*,*P*,*P*,*P*)/(*M*,*M*,*M*,*M*)-**2** could be assigned unambiguously by an X-ray crystal structure analysis of moderate resolution (Figure 3c; for further details of the crystal structure see the



Scheme 2. Synthesis of anthracenophane **2**. Reagents and conditions: a) 9,10-dibromoanthracene, [PdCl$_2$(PPh$_3$)$_2$], CuI, TMEDA, toluene, 110°C; 56% ((±)-**12**), 73% ((±)-**13**); b) (±)-**7**, [PdCl$_2$(PPh$_3$)$_2$], CuI, TMEDA, toluene, 110°C; 83%; c) *n*Bu$_4$NF, THF, 20°C; 95% (**15**); 96% (**17**); 86% (**19**); d) (±)-**12**, [PdCl$_2$(PPh$_3$)$_2$], CuI, TMEDA, toluene, 110°C; 63% (**16**); 65% (**18**); e) 9,10-dibromoanthracene, [PdCl$_2$(PPh$_3$)$_2$], CuI, TMEDA, toluene, 110°C; 64%; f) NaOH, C_6H_6, 90°C, 85%; g) [Pd(PPh$_3$)$_4$], CuI, *i*Pr$_2$NEt, toluene, 110°C, 2 h, then air, CH_2Cl_2, 20°C, 24 h; 60%.

 © 2005 Wiley-VCH Verlag GmbH & Co. KGaA, Weinheim

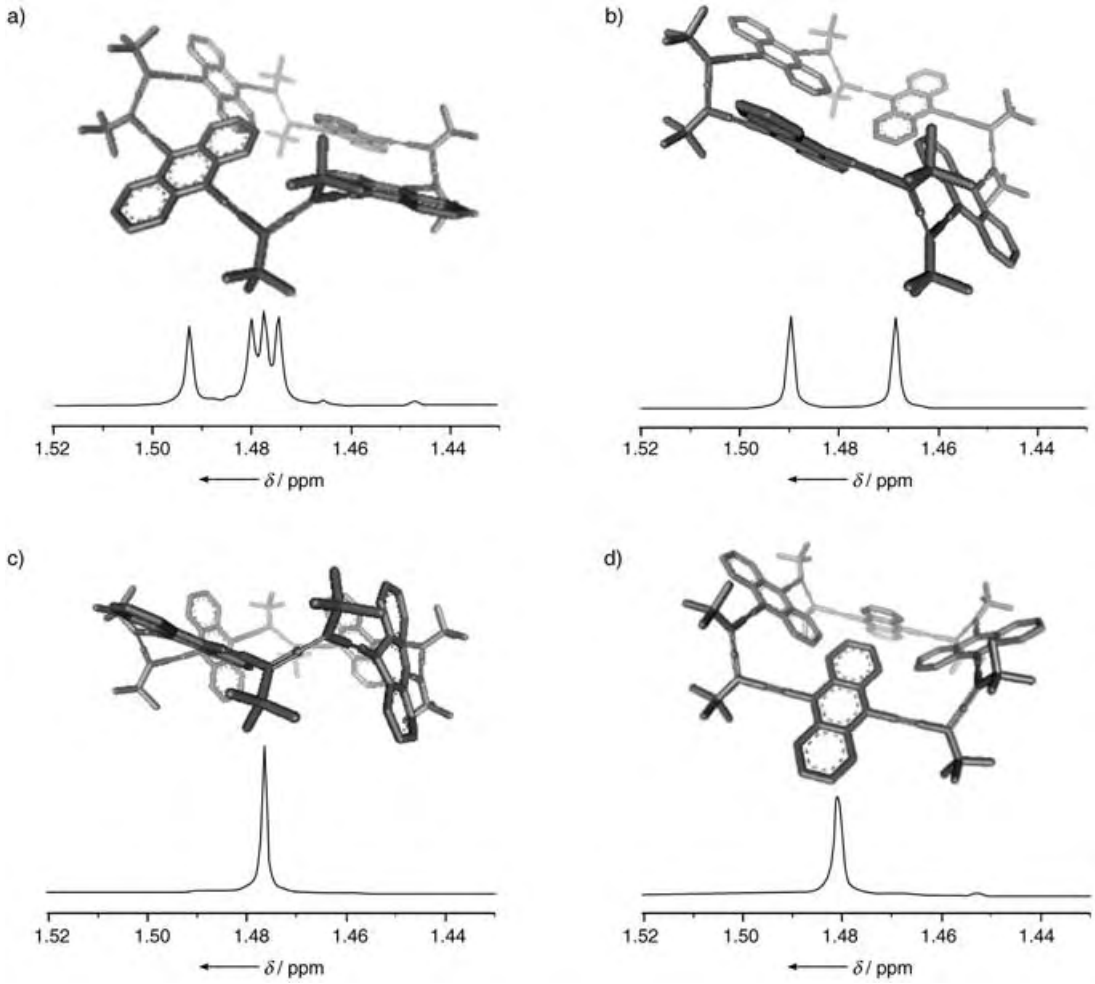


Figure 3. Tube models and ^{1}H NMR spectra of a) C_2-symmetric (*M*,*P*,*P*,*P*)/(*P*,*M*,*M*,*M*)-**2**, ((*P*,*M*,*M*,*M*) isomer shown), b) C_{2h}-symmetric (*M*,*M*,*P*,*P*)-**2**, c) (*P*,*P*,*P*,*P*)/(*M*,*M*,*M*,*M*)-**2**, and d) D_{2d}-symmetric (*M*,*P*,*M*,*P*)-**2**. ^{1}H NMR spectra in $CDCl_3$. The models in (a), (b), and (d) show conformations optimized by AM1 calculations.[12] The X-ray crystal structure of (*M*,*M*,*M*,*M*)-**2** is shown in (c). (Note that in the crystal structure the actual symmetry is C_1 in contrast to the observation from NMR spectroscopy; for further details see the Supporting Information.)

Supporting Information and ref. [14]). Finally, the structure of the last isomer, D_{2d}-symmetric (*M*,*P*,*M*,*P*)-**2**, was assigned by exclusion (Figure 3d).

Macrocycle **1** and cyclophane **2** differ substantially in their properties. While the isomers of **1** are colorless solids, those of **2** are brown-colored. All compounds are stable for weeks upon storage in the air at ambient conditions, when protected from light. The characteristic anthracene bands in the visible region of the electronic absorption spectra of the isomers of **2** are retained but red-shifted by nearly 100 nm (see the Supporting Information). Similar to anthracene, the macrocycles show fluorescence ($\Phi = 0.2$; $\lambda_{max} = 478$–481 and 510–515 nm at $\lambda_{exc} = 315$ nm). The isomers of **2** undergo two reversible $2e^-$ oxidation and one reversible $4e^-$ reduction steps under cyclovoltametric conditions.[15] Whereas the isomers of **1** are stable upon irradiation, photoisomerization of the allene moieties in **2** occurs. The different stereoisomers interconvert slowly upon irradiation (within days under sunlight or within hours under xenon-lamp irradiation, 450 W; $\lambda_{exc} = 300$ nm or 463 nm) to finally reach the photostationary state with an isomeric ratio of 10:5:1:5 (C_2/C_{2h}/D_4/D_{2d}). This ratio differs slightly from the statistically expected ratio of 4:2:1:2. Photoisomerization of **2** but not of **1** is probably a result of the anthracene moieties, which can act as intramolecular sensitizers.[16]

In summary, we have prepared, separated, and characterized the first members of a new class of unsaturated allenoacetylenic macrocycles as well as four new cyclophanes which undergo photoisomerization. The three-dimensional shapes and symmetries of these novel hydrocarbons are intriguing, and the preparation of optically pure derivatives with potentially promising chiroptical properties is being pursued. Furthermore, the host–guest complexation properties of **2** and related macrocycles, which are obtained by Diels–Alder reaction of the anthracene moieties, are now under investigation.

Experimental Section

(*M*,*P*,*P*,*P*)/(*P*,*M*,*M*,*M*)-**1**: A solution of **11** (216 mg, 0.203 mmol) and *ortho*-nitrophenol (43 mg, 0.31 mmol) in THF (100 mL) was treated with nBu$_4$NF (0.30 mL of a 1M solution in THF, 0.30 mmol). After the

 © 2005 Wiley-VCH Verlag GmbH & Co. KGaA, Weinheim

reaction mixture had been stirred for 1 h at 20 °C, the solvent was removed under reduced pressure. The orange oil was taken up in cyclohexane/CH_2Cl_2 and filtered through a plug of SiO_2 (eluent: cyclohexane/EtOAc 20:1). After concentration, the residue was dissolved in pyridine (0.30 L) and added to a degassed solution of CuCl (1.50 g, 15.1 mmol) and $CuCl_2$ (0.20 g, 1.51 mmol) in pyridine (1.20 L). The green mixture was degassed with Ar and stirred for 3 d at 20 °C. Pyridine was removed under vacuum until a volume of about 100 mL remained, and cyclohexane and toluene were added. The Cu salts were extracted with aq NH_4Cl solution (3×) and aq EDTA (0.2 M) solution. The organic layer was dried over $MgSO_4$ and concentrated. The residual brown solid was filtered twice through SiO_2 and eluted with toluene and cyclohexane successively to give a light brown solid (160 mg). Analytical HPLC analysis (Kromasil, hexane, 1 mL min^{-1}) showed roughly a 1:1:4:1:1 mixture of stereoisomers. Isolation of the most abundant C_1-symmetric isomer (≈60 mg) on preparative scale was successful on a "Buckyclutcher 1" column (eluent: hexane, 10 mL min^{-1}). White solid. M.p. >290 °C (decomp); ^{1}H NMR (300 MHz, $C_6D_5CD_3$): $\delta = 1.007$ (s, 9H), 1.040 (s, 9H), 1.075 (s, 9H), 1.093 (s, 9H), 1.106 (s, 9H), 1.116 (s, 9H), 1.127 (s, 9H), 1.142 ppm (s, 9H); ^{13}C NMR (75 MHz, $C_6D_5CD_3$): $\delta = 29.51$, 29.54, 29.56, 29.62, 29.73, 29.75, 29.80, 29.84, 36.01 (2×), 36.06 (2×), 36.18, 36.21, 36.34, 36.43, 76.43, 76.49 (3×), 78.86, 78.93, 79.11, 79.21, 87.52, 87.64, 88.06, 88.16, 104.04, 104.13, 104.24, 104.44, 105.43, 105.47, 105.60 (2×), 214.56, 215.07, 215.20, 215.46 ppm; UV/Vis (hexane): λ_{max} (ε) = 237 (126700), 266 (sh, 48800), 281 (sh, 32500), 295 (sh, 21300), 321 nm (12800); MALDI-MS (%): $m/z = 783.53$ (19, $[M+K]^+$), 767.55 (34, $[M+Na]^+$), 745.57 (100, $[M+H]^+$), 689.50 (22, $[M+H-t\mathrm{Bu}]^+$); HR-MALDI-MS: $m/z = 745.5694$ ($[M+H]^+$, $C_{56}H_{73}^+$; calcd 745.5707).

Received: May 11, 2005
Published online: July 20, 2005

Keywords: allenes · chirality · cross-coupling · macrocycles · photoisomerization

[1] a) *Modern Allene Chemistry*, *Vols. 1 and 2* (Eds.: N. Krause, A. S. K. Hashmi), Wiley-VCH, Weinheim, **2004**; b) A. Hoffmann-Röder, N. Krause, *Angew. Chem.* **2002**, *114*, 3057–3059; *Angew. Chem. Int. Ed.* **2002**, *41*, 2933–2935; c) A. Hoffmann-Röder, N. Krause, *Angew. Chem.* **2004**, *116*, 1216–1236; *Angew. Chem. Int. Ed.* **2004**, *43*, 1196–1216.

[2] H. Hopf, *Classics in Hydrocarbon Chemistry*, Wiley-VCH, Weinheim, **2000**, chap. 9, pp. 171–196.

[3] a) C. S. Jones, M. J. O'Connor, M. M. Haley in *Acetylene Chemistry: Chemistry, Biology, and Material Science* (Eds.: F. Diederich, P. J. Stang, R. R. Tykwinski), Wiley-VCH, Weinheim, **2005**, pp. 303–385; b) S. Höger in *Acetylene Chemistry: Chemistry, Biology, and Material Science* (Eds.: F. Diederich, P. J. Stang, R. R. Tykwinski), Wiley-VCH, Weinheim, **2005**, pp. 427–452; c) for a recent report: W. Zhang, J. S. Moore, *J. Am. Chem. Soc.* **2004**, *126*, 12796.

[4] In contrast to allenes, [3]- and [5]cumulenes are found more frequently in macrocyclic structures, such as planar dehydroannulenes; see: a) ref. [2]; b) M. Nakagawa, *Angew. Chem.* **1979**, *91*, 215–226; *Angew. Chem. Int. Ed. Engl* **1979**, *18*, 202–214.

[5] a) S. Thorant, F. Vögtle, N. Krause, *Angew. Chem.* **1999**, *111*, 3929–3931; *Angew. Chem. Int. Ed.* **1999**, *38*, 3721–3723; b) C. Kind, M. Reiher, J. Röder, B. A. Hess, *Phys. Chem. Chem. Phys.* **2000**, *2*, 2205–2210.

[6] a) R. C. Livingston, L. R. Cox, V. Gramlich, F. Diederich, *Angew. Chem.* **2001**, *113*, 2396–2399; *Angew. Chem. Int. Ed.* **2001**, *40*, 2334–2337; b) R. Livingston, L. R. Cox, S. Odermatt, F. Diederich, *Helv. Chim. Acta* **2002**, *85*, 3052–3065.

[7] a) M. I. Calaza, E. Hupe, P. Knochel, *Org. Lett.* **2003**, *5*, 1059–1061; b) N. Harrington-Frost, H. Leuser, M. I. Calaza, F. Kneisel, P. Knochel, *Org. Lett.* **2003**, *5*, 2111–2114.

[8] R. W. Saalfrank, M. Haubner, C. Deutscher, W. Bauer, *Eur. J. Org. Chem.* **1999**, 2367–2372.

[9] G. Eglinton, A. R. Galbraith, *Chem. Ind.* **1956**, 737–738.

[10] For good separations, the HPLC columns should be very well conditioned. Best analytical results were obtained with a Kromasil 100 Si column (5 μm) and pure hexane as the eluent.

[11] Rexchrom "Buckyclutcher 1" Prep, 10 μm 100 Å Trident-Tri-DNP, 50 cm × 21.1 mm ID and Spherical Silica Kromasil Prep, 5 μm, 100 Å, 30 cm × 21.1 mm ID.

[12] Spartan 02, Wavefunction, Inc. Irvine, CA **2002**.

[13] J. A. Marsden, M. M. Haley in *Metal-Catalyzed Cross-Coupling Reactions*, *Vol. 1* (Eds.: A. de Meijere, F. Diederich), Wiley-VCH, Weinheim, **2004**, pp. 317–394.

[14] X-ray crystal structure of (*P,P,P,P*)/(*M,M,M,M*)-**2**: Crystal data at 220(2) K for $C_{116}H_{104} \times 4\,CH_3OH \times 4\,H_2O$. $M_r = 1698.22$. Triclinic, space group $P\bar{1}$ (no. 2), $\rho_{calcd} = 0.997$ g cm^{-3}, $Z = 2$, $a = 11.2927(2)$, $b = 13.4550(3)$, $c = 37.9436(8)$ Å, $\alpha = 83.672(1)$, $\beta = 89.873(1)$, $\gamma = 80.841(1)°$, $V = 5656.4(2)$ Å^3. Bruker-Nonius Kappa-CCD diffractometer, $Mo_{K\alpha}$ radiation, $\lambda = 0.7107$ Å, $\mu = 0.061$ mm^{-1}. A yellow crystal of (*P,P,P,P*)/(*M,M,M,M*)-**2** (linear dimensions ca. 0.25 × 0.15 × 0.13 mm) was obtained by slow evaporation of a CH_2Cl_2/CH_3OH solution. It was mounted at low temperature to prevent evaporation of enclosed solvent. The numbers of measured and unique reflections are 15697 and 11184, respectively ($R_{int} = 0.030$). The structure was solved by direct methods (SHELXS-97; G. M. Sheldrick, SHELXS-97 Program for the Solution of Crystal Structures, University of Göttingen, Germany, **1997**) and refined by full-matrix least-squares analysis (SHELXL-97; G. M. Sheldrick, SHELXL-97 Program for the Refinement of Crystal Structures, University of Göttingen, Germany, **1997**), using an isotropic extinction correction. The subunit C(88)–C(102) is disordered over two orientations (for arbitrary atom numbering, see the Supporting Information). For C(91)–C(98), C(100), and C(101), two sets of atomic parameters with population parameters of 0.5 were refined. The derived solvents exhibit static and dynamic disorder. All heavy atoms were refined anisotropically, H atoms of the ordered part isotropically, whereby H-atom positions are based on stereochemical considerations. Final $R(F) = 0.138$, $wR(F^2) = 0.325$ for 1277 parameters and 7418 reflections with $I > 2\sigma(I)$ and $2.93 < \theta < 21.01°$ (corresponding *R*-values based on all 11184 reflections are 0.185 and 0.347 respectively). CCDC-271068 contains the supplementary crystallographic data for this paper. These data can be obtained free of charge from the Cambridge Crystallographic Data Centre via www.ccdc.cam.ac.uk/data_request/cif.

[15] M. Gross, J.-P. Gisselbrecht, C. Boudon, F. Diederich, J. L. Alonso-Gómez, S. Odermatt, unpublished results.

[16] O. Rodriguez, H. Morrison, *J. Chem. Soc. Chem. Commun.* **1971**, 679.

[17] A. S. Hay, *J. Org. Chem.* **1962**, *27*, 3320–3321.

 © 2005 Wiley-VCH Verlag GmbH & Co. KGaA, Weinheim

Pseudopolymorphism

DOI: 10.1002/anie.200500168

Synthesis and Structure Determination of Tellurium Tetracyanide Solvates: Pseudopolymorphism of $Te(CN)_4$ and TeF_4**

Dieter Lentz and Małgorzata Szwak*

Until recently, tellurium dicyanide (**1**), known since 1908,[1] was the only binary cyano compound of tellurium. Its chemistry has remained almost unexplored, and only a few spectroscopic data have been published so far.[2] Very recently, Klapötke et al. reported the crystal structure determination of **1** and the synthesis of an extremely unstable tellurium tetracyanide, which was characterized on the basis of a Raman spectrum and its decomposition into **1** and cyanogens.[3] Extremely explosive tellurium tetraazide was obtained by Klapötke et al.[4] and Christe et al.;[5] again structural data are missing. To the best of our knowledge further homoleptic tellurium(IV) pseudohalides are unknown.

In the course of our studies of pseudohalogen compounds of the chalcogens we have investigated the reaction of tellurium tetrafluoride with trimethylsilyl cyanide in acetonitrile and THF, and have isolated the crystalline solvates of tellurium tetracyanide $[\{Te(CN)_4(CH_3CN)_2\}_n]$ (**2a**) and $[\{Te(CN)_4(thf)_3\}_n]$ (**2b**) [Eq. (1)]. The compounds easily lose

$$n\mathrm{TeF_4} + 4n\ \mathrm{Me_3SiCN} \xrightarrow{\mathrm{CH_3CN}} [\{\mathrm{Te(CN)_4\,(CH_3CN)_2}\}_n] + 4n\ \mathrm{Me_3SiF} \quad \mathbf{2a}$$

$$n\mathrm{TeF_4} + 4n\ \mathrm{Me_3SiCN} \xrightarrow{\mathrm{THF}} [\{\mathrm{Te(CN)_4\,(thf)_3}\}_n] + 4n\ \mathrm{Me_3SiF} \quad \mathbf{2b} \qquad (1)$$

the solvate molecules and decompose readily both as solids and in solution to give **1** ($\delta(^{125}\mathrm{Te}, \mathrm{THF}) = 547$ ppm, $\delta(^{13}\mathrm{C}, \mathrm{THF}) = 86.6$ ppm) and cyanogen ($\nu(\mathrm{CN}, \mathrm{gas}) = 2157\ \mathrm{cm}^{-1}$). Nevertheless, we succeeded in characterizing **2b** and the mixed substituted compounds $TeF_x(CN)_{4-x}$ ($x = 4, 2, 1$) by ^{125}Te, ^{19}F, and ^{13}C NMR spectroscopy at low temperature and in eludicating the structures of **2a** and **2b** by single-crystal X-ray diffraction (Figures 2–4).[6]

The ^{125}Te NMR spectrum (Figure 1) of a mixture of TeF_4 and less than four equivalents of TMSCN at −100 °C exhibits

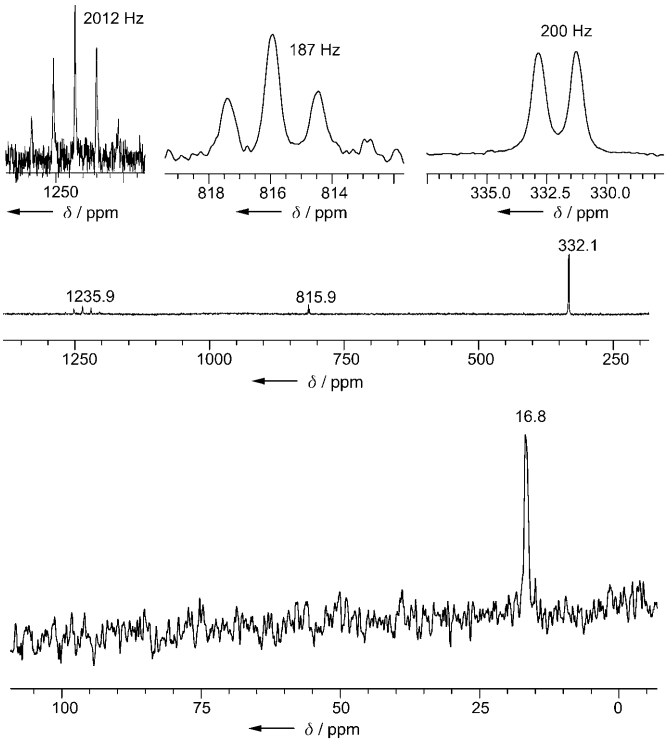


Figure 1. ^{125}Te NMR spectrum of $TeF_x(CN)_{4-x}$ ($x = 4, 2, 1$) at −100 °C (top) and **2b** at −80 °C (bottom) in [D$_8$]THF; dimethyl telluride was used as an external reference.

a quintet at $\delta = 1235.9$ ppm ($^1J(^{125}\mathrm{Te}\text{-}^{19}\mathrm{F}) \approx 2012$ Hz) for TeF_4, a triplet at $\delta = 815.9$ ppm ($^1J(^{125}\mathrm{Te}\text{-}^{19}\mathrm{F}) \approx 187$ Hz) for $TeF_2(CN)_2$, and a doublet at $\delta = 332.1$ ppm ($^1J(^{125}\mathrm{Te}\text{-}^{19}\mathrm{F}) \approx 200$ Hz) for $TeF(CN)_3$. Correspondingly, the ^{19}F NMR spectrum exhibits three resonances with ^{125}Te satellites at $\delta = -45.1$ ppm ($^1J(^{125}\mathrm{Te}\text{-}^{19}\mathrm{F}) \approx 2000$ Hz) for TeF_4, $\delta = -12.8$ ppm ($^1J(^{125}\mathrm{Te}\text{-}^{19}\mathrm{F}) \approx 196$ Hz) for $TeF(CN)_3$, and $\delta = -80.3$ ($^1J(^{125}\mathrm{Te}\text{-}^{19}\mathrm{F}) \approx 182$ Hz) for $TeF_2(CN)_2$, respectively, besides the signal of Me_3SiF. Thus no intermolecular fluoride exchange occurs on the NMR time scale at −100 °C. The small ^{19}F-^{125}Te coupling constants of $TeF_x(CN)_{4-x}$ ($x = 1, 2$) in comparison with those of TeF_4 and $TeF_2(OTeF_5)_2$ ($^1J(^{125}\mathrm{Te^{IV}}\text{-}^{19}\mathrm{F}) = 2812$ Hz)[7] indicate that in these compounds the fluorine atoms occupy the axial positions of the ψ-trigonal-bipyramidal structure as predicted by the VSPER model and as already been observed for $TeF_2(CF_3)_2$[8] ($^1J(^{125}\mathrm{Te}\text{-}^{19}\mathrm{F}) = 234$ Hz). In the case of TeF_4, rapid intramolecular exchange of the fluorine substituents takes place even at −100 °C. On warming, the ^{125}Te-^{19}F scalar coupling disappears as a result of fast intermolecular fluoride exchange. Because of the low solubility of **2b** at −80 °C—a saturated solution contains approximately 25–50 μmol **2b** in 0.7–1.0 mL [D$_8$]THF—it was difficult to obtain the ^{125}Te and ^{13}C NMR spectra. The ^{125}Te NMR spectrum of **2b** at −80 °C exhibits a single resonance at $\delta = 16.8$ ppm which is shifted to $\delta = 45.0$ ppm on warming to −30 °C. The ^{13}C NMR spectrum at −80 °C exhibits two signals at $\delta = 111.6$ and 114.2 ppm, which can be assigned to the CN substituents, besides the resonances of the solvent and trimethylsilyl fluoride. No ^{125}Te satellites could be detected due to the bad signal-to-noise ratio. The low-temperature

[*] Priv.-Doz. Dr. D. Lentz, M. Szwak
Fachbereich Biologie, Chemie, Pharmazie
Institut für Chemie – Anorganische und Analytische Chemie
Freie Universität Berlin
Fabeckstrasse 34–36, 14195 Berlin (Germany)
Fax: (+49) 30-8385-2424
E-mail: lentz@chemie.fu-berlin.de

[**] This work was supported by the Deutsche Forschungsgemeinschaft.

Supporting information for this article is available on the WWW under http://www.angewandte.org or from the author.

 © 2005 Wiley-VCH Verlag GmbH & Co. KGaA, Weinheim

Raman spectrum (−80 °C) of **2b** exhibits three bands for the CN stretching modes at 2153 (m), 2178 (w), and 2185 cm^{-1} (w).

In the solid state the structures of **2a** and **2b** are very different from the structure of an isolated $Te(CN)_4$ molecule calculated by ab initio methods[3] which has C_{2v} symmetry (ψ-trigonal-bipyramidal structure including the electron lone pair). Both **2a** and **2b** form a coordination polymer in the shape of bent chains (Figures 2–4). Both compounds have trigonal-pyramidal $\{Te(CN)_3\}$ units as building blocks, which are connected by unsymmetrical CN bridges (TeC < TeN) to form chains and expanding the coordination sphere of tellurium. The Te–C distances to the terminal CN groups range from 2.086 to 2.217 Å. In **2a** two short and one long distance were found, whereas in **2b** one short and two slightly longer distances were observed. The C-Te-C bond angles are between 78 and 87 ° (one small and two larger angles).

The structures of **2a** and **2b** differ in the connection of the $\{Te(CN)_3\}$ units and the coordination of the solvate molecules.

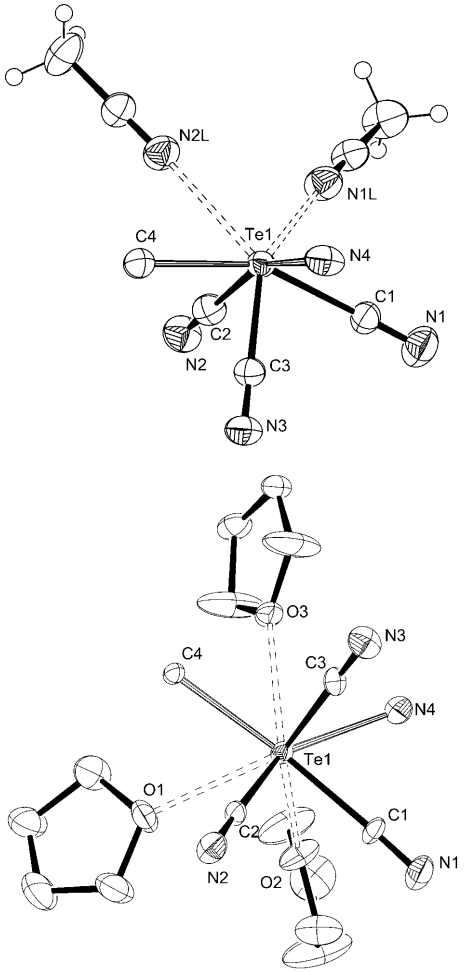


Figure 2. Structure of one monomeric unit of **2a** (ORTEP,[15] 50% ellipsoids, top) and **2b** (ORTEP,[15] 30% ellipsoids, H atoms omitted, bottom). Selected distances [Å] and angles [°] in **2a**/**2b**: Te1–C1 2.217(4)/2.166(7), Te1–C2 2.102(4)/2.157(7), Te1–C3 2.116(4)/2.086(7), Te1–C4 2.397(3)/2.482(7), Te1–N4 2.601(4)/2.567(8); C4-Te1-N4 91.0(1)/128.1(2), C1-Te1-C2 86.9(1)/78.2(3), C1-Te1-C3 79.1(1)/84.4(3), C2-Te1-C3 86.0(1)/86.6(3), C1-Te1-C4 154.3(1)/148.2(3), C2-Te1-N4 158.5(1)/149.1(3).

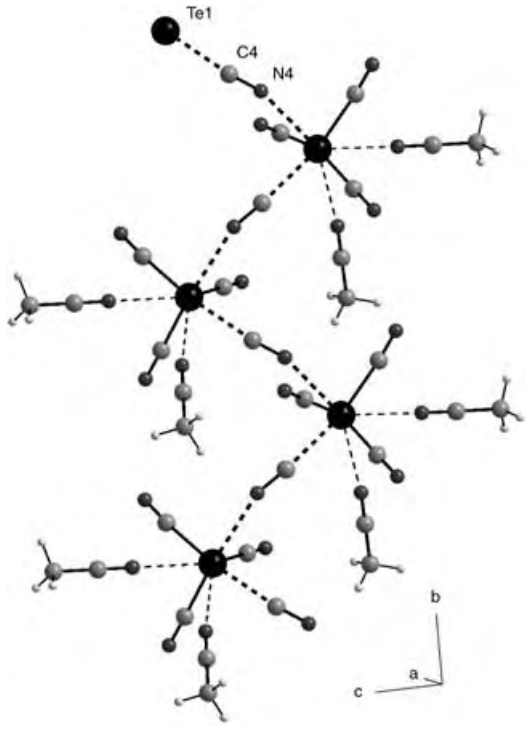


Figure 3. Polymer chain of **2a** (DIAMOND[16]).

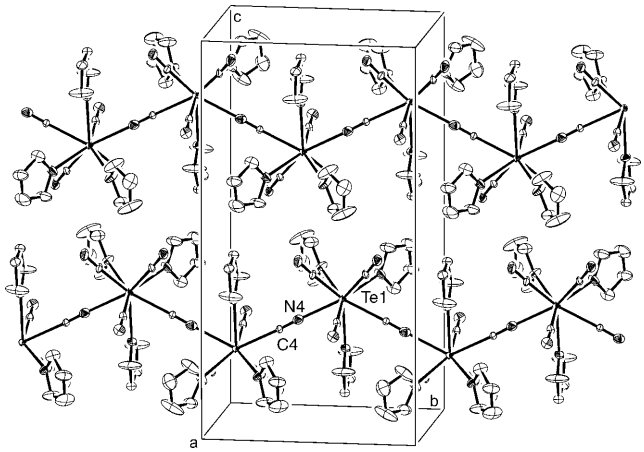


Figure 4. Unit cell of **2b** (ORTEP,[15] 30% ellipsoids, H atoms omitted).

In **2a** the trigonal $[Te(CN)_3]$-pyramid is completed by the bridging ligand atoms C4 ($d_{Te1\text{-}C4} = 2.397(3)$ Å) und N4 ($d_{Te1\text{-}N4} = 2.601(4)$ Å) forming a strongly distorted square pyramid as the coordination polyhedron. Both distances are significantly larger than the sum of covalency radii.[9] The bond angle to the bridging atoms ($\sphericalangle_{C4\text{-}Te1\text{-}N4}$) is 91.0(1)°. Finally the coordination sphere is completed by two acetonitrile molecules which have very large Te–N distances (2.728(4), 2.866(4) Å). The principal coordination in **2b** is rather similar; however, the square pyramid is even more distorted, and the $d_{Te1\text{-}C4}$ (2.482(7) Å) is larger. Furthermore the angle C4-Te1-N4 of 128.1(2) ° is much larger. Three THF molecules are coordinated to the tellurium atom over very large distances (2.700(7)–2.774(7) Å) by dipole interactions.

 © 2005 Wiley-VCH Verlag GmbH & Co. KGaA, Weinheim

In both structures the volume attributed to the lone pair is unoccupied by solvate molecules and ligands. Both compounds **2a** and **2b** can be described as $[Te(CN)_3]CN$ with the ionic character being more pronounced in **2b**.

For comparison, the structures of the previously not characterized solvates $[TeF_4(thf)_2]$ (**3a**)[6] (Figure 5) and

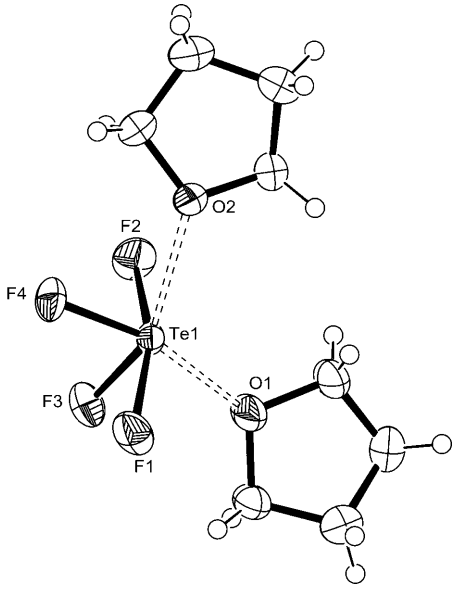


Figure 5. Crystal structure of **3a** (ORTEP,[15] 50% ellipsoids). Selected distances [Å] and angles [°]: Te1–F1 1.966(2), Te1–F2 1.941(2), Te1–F3 1.862(2), Te1–F4 1.867(2), Te1–O1 2.448(2), Te1–O2 2.697; F1-Te1-F2 161.33(7), F3-Te1-F4 86.98(6), F1-Te-F3 80.97(6), F1-Te1-F4 84.74(7), F2-Te1-F3 82.15(7), F2-Te1-F4 86.45, F3-Te1-O2 155.89, F4-Fe1-O1 160.89(7), O1-T1-O2 122.95.

$[\{TeF_4(toluene)\}_n]$ (**3b**)[6] (Figure 6) were elucidated by X-ray crystallography. Unexpectedly, **3a** consists of monomeric C_{2v}-symmetric TeF_4 units in accordance to the ψ-trigonal-bipyramidal geometry expected by the VSEPR model and in contrast to **2a**, **2b**, and **3b**. As expected, the distances to the axial fluorine atoms are about 0.1 Å longer than those to the equatorial ones. Due to the steric influence of the electron lone pair, the angles $\sphericalangle_{F1\text{-}Te1\text{-}F2}$ and $\sphericalangle_{F3\text{-}Te1\text{-}F4}$ are significantly smaller than 180 and 120°, respectively. The distance $d_{Te1\text{-}O1}$, (2.448(2) Å) is shorter than the distance $d_{Te1\text{-}O2}$ (2.697(2) Å) and the comparable Te–O distances in **2b**.

The structures of **2a** and **2b** can be compared to those of **3b** (Figure 6) and tellurium tetrafluoride,[10] in which trigonal-pyramidal TeF_3 units are completed by two bridging fluorine atoms in *cis* position forming a square pyramid. The nearest distances of the aromatic carbon atoms to the tellurium atom range from 3.151(7) to 3.449(7) Å. Thus these distances are shorter than the sum of van der Waals radii (3.8 Å).[11] Tellurium tetrachloride forms a tetramer with a heterocubane structure which is formed by connecting four $TeCl_3$ units with bridging chlorine atoms.[12]

It is surprising that with the same solvate molecule, tetrahydofuran, TeF_4 forms a pseudopolymorphic structure with isolated TeF_4 units, whereas $Te(CN)_4$ forms a coordination polymer that can be better described as $[\{Te(CN)_3(thf)_3\text{-}(\mu\text{-}CN)\}_n]$. Further studies on the influence of solvate molecules on the pseudopolymorphic structures[13] of tellurium halides and pseudohalides are underway in our group.

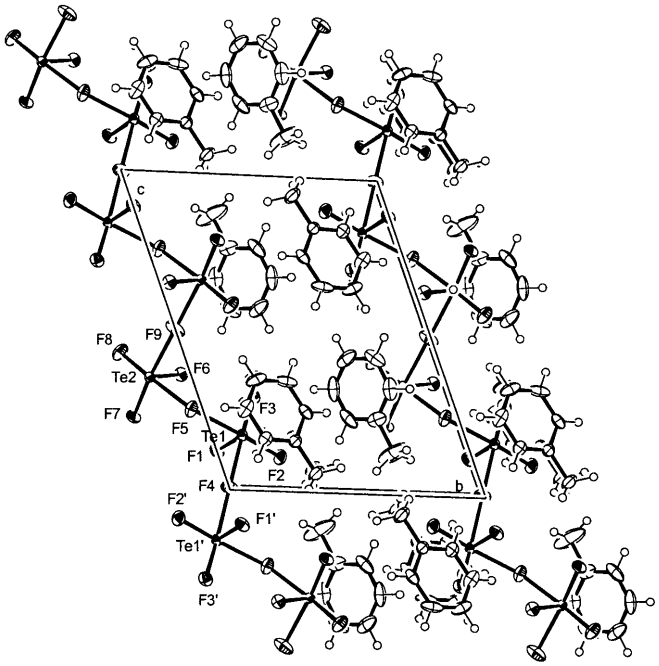


Figure 6. Unit cell of **3b** (ORTEP,[15] 50% ellipsoids, view along $\bar{1}00$). Selected distances [Å] and angles [°]: Te–F(apical) 1.846(3)–1.847(4), Te–F(basal) 1.873(4)–1.886(4), Te–F(Brücke) 2.171(4)–2.23(4), Te1–C-(arom.) 3.151(7)–3.449(7), Te2–C(arom.) 3.202(7)–3.356(7); F5-Te2-F9 95.33(9), F4-Te1-F5 100.39(9).

Experimental Section

All reactions were carried out in carefully dried apparatus under an atmosphere of dry argon or under vacuum. TeF_4 was handled in an automatic drybox. Volatile solvents were carefully dried and condensed into the reaction vessel using a glass vacuum line system.

2a: Acetonitrile (5 mL) was condensed into a 50-mL Schlenk flask containing TeF_4 (0.2 g, 1 mmol), which was dissolved by warming the mixture to ambient temperature. Acetonitrile (4 mL) was condensed into a 50-mL Schlenk flask containing TMSCN (0.45 g, 4.5 mmol). After warming to ambient temperature both solutions were cooled again to −35 °C. After flushing with argon the TeF_4 solution was added to the TMSCN solution by a Teflon tube. The reaction mixture was allowed to warm slowly to −6 °C with stirring. The colorless solution was placed in a refrigerator (−30 °C). After 12 h **2a** was obtained as colorless platelets.

2b: THF (15 mL) was condensed into a 50-mL Schlenk flask containing TeF_4 (0.1 g, 0.5 mmol), which was dissolved by warming the mixture to ambient temperature. THF (20 mL) was condensed into a 100-mL Schlenk flask containing TMSCN (0.25 g, 2.5 mmol), which was dissolved at ambient temperature, and the mixture was cooled to −68 °C. After flushing with argon the TeF_4 solution (−40 °C) was added within 5 min to the stirred TMSCN solution using a Teflon tube. The reaction mixture was warmed slowly to −6 °C (30 min between −10 and −6 °C). Most of the solvent and the trimethylsilyl fluoride (^{19}F NMR, decett at $\delta = -157$ ppm) formed were removed under vacuum at −68 °C. After warming to −8 °C to form a colorless solution, the flask and the cold bath were placed in a refrigerator (−84 °C). Colorless needle-shaped crystals of **2b** formed overnight.

 © 2005 Wiley-VCH Verlag GmbH & Co. KGaA, Weinheim

3a: Crystals of **3a** were first obtained from the attempted reaction of TeF_4 with one equivalent of TMSCN in toluene after crystallization of the nonvolatile residue from THF at −80 °C. The compound can be obtained directly by crystallization of TeF_4 from THF.

3b: Crystals of **3b** were obtained by slowly cooling a solution of TeF_4 (0.1 g, 0.5 mmol) in 1.5 mL of toluene to −84 °C.

NMR spectra: Approximately 5 to 10 mg of TeF_4 was filled into 5-mm NMR tube equipped with a magnetic stirring bar. Using a glass vacuum line 0.5 mL of [D_8]THF was condensed into the tube by cooling with liquid nitrogen. After warming to ambient temperature, the TeF_4 dissolved completely. A further 0.3 mL of THF and approximately 25 mg of TMSCN were condensed by cooling with liquid nitrogen. The reaction mixture was warmed slowly to −6 °C with stirring. The stirring bar was removed from the solution using a magnet; the sample was cooled with liquid nitrogen and sealed under vacuum. The samples were stored at −84 °C before the measurement. NMR spectra were recorded using a JEOL Lambda 400 multinuclear NMR spectrometer at temperatures between −100 and −20 °C.

Received: January 17, 2005
Revised: April 7, 2005
Published online: July 20, 2005

Keywords: cyanides · pseudohalogens · pseudopolymorphism · solid-state structures · tellurium

[1] H. E. Cocksedge, *J. Chem. Soc.* **1908**, *93*, 2175 – 2177.
[2] H. P. Fritz, H. Keller, *Chem. Ber.* **1961**, *94*, 1524 – 1533.
[3] T. M. Klapötke, B. Krumm, J. C. Gálvez-Ruiz, H. Nöth, I. Schwab, *Eur. J. Inorg. Chem.* **2004**, 4764 – 4769.
[4] T. Klapötke, B. Krumm, P. Mayer, I. Schwab, *Angew. Chem.* **2003**, *115*, 6024 – 6026; *Angew. Chem. Int. Ed.* **2003**, *42*, 5843 – 5846.
[5] R. Haiges, J. A. Boatz, A. Vij, M. Gerken, S. Schneider, T. Schroer, K. O. Christe, *Angew. Chem.* **2003**, *115*, 6027 – 6030; *Angew. Chem. Int. Ed.* **2003**, *42*, 5847 – 5851.
[6] Crystal structure analysis: Colorless crystals of **2a**, **2b**, **3a**, and **3b** were obtained as described above. A few crystals were transferred with a pipette onto a piece of filter paper, which was mounted in a stream of cold nitrogen onto an apparatus described in the literature.[14] A suitable crystal was selected using a microscope, mounted onto a glass fiber using silicon grease, and transferred into the cold gas stream of a diffractometer without interrupting the cooling. BRUKER-AXS, SMART CCD, $Mo_{K\alpha}$, $\lambda = 0.71073$ Å, $T = 173$ K. **2a**: $C_8H_6N_6Te$, $M_w = 313.79$, monoclinic, $P2_1$, $a = 6.006(1)$, $b = 8.328(2)$, $c = 11.976(2)$ Å, $\beta = 92.097(8)°$, $V = 598.6(2)$ Å^3, $Z = 2$, $\rho_{calcd} = 1.741$ Mg m^{-3}, $\mu(Mo_{K\alpha}) = 2.464$ mm^{-1}, 7471 measured reflections, 3597 [R(int) = 0.014] crystallographically independent reflections, empirical absorption correction (SADABS[17]), least squares refinement (SHELXL-97[18]), anisotropic temperature factors, H atoms isotropic on calculated positions (riding model), 138 refined parameters, GOOF = 1.083, $R_1 = 0.0188$ [$I > 2\sigma(I)$], w$R_2 = 0.0488$ (all data), ρ(max./min) = 0.996 and −0.383 e Å^{-3}, Flack parameter 0.00(2); a displacement of C4 and N4 converges at $R_1 = 0.0200$, therefore the assignment of the nitrogen and carbon atoms is unambiguous. **2b**: $C_{16}H_{24}N_4O_3Te$, $M_w = 447.99$, monoclinic, $P2_1/c$, $a = 8.473(2)$, $b = 11.030(3)$, $c = 20.505(6)$ Å, $\beta = 92.627(7)°$, $V = 1914.3(9)$ Å^3, $Z = 4$, $\rho_{calcd} = 1.554$ Mg m^{-3}, $\mu(Mo_{K\alpha}) = 1.574$ mm^{-1}, 17163 measured reflections, 3927 [R(int) = 0.113] crystallographically independent reflections, least squares refinement (SHELXL-97[18]), anisotropic temperature factors, H atoms isotropic on calculated positions (riding model), 217 refined parameters, GOOF = 1.035, $R_1 = 0.0566$ [$I > 2\sigma(I)$], w$R_2 = 0.1474$ (all data), ρ(max./min) = 1.416 and −0.851 e Å^{-3}, no attempt was made to refine the disorder of some of the C atoms of the THF molecules which resulted in very large anisotropic displacement parameters on split-atom positions. **3a**: $C_8H_{16}F_4O_2Te$, $M_w = 347.81$, triclinic, $P\bar{1}$, $a = 6.816(2)$, $b = 9.390(2)$, $c = 10.465(2)$ Å, $\alpha = 109.140(4)$, $\beta = 101.744(6)$, $\gamma = 100.421(5)°$, $V = 596.9(2)$ Å^3, $Z = 2$, $\rho_{calcd} = 1.935$ Mg m^{-3}, $\mu(Mo_{K\alpha}) = 2.524$ mm^{-1}, 7429 measured reflections, 3579 [R(int) = 0.0134] crystallographically independent reflections, empirical absorption correction (SADABS[17]), least squares refinement (SHELXL-97[18]), anisotropic temperature factors, H atoms isotropic on calculated positions (riding model), 137 refined parameters, GOOF = 1.059, $R_1 = 0.0191$ [$I > 2\sigma(I)$], w$R_2 = 0.0475$ (all data), ρ(max./min) = 0.984 and −0.501 e Å^{-3}. **3b**: $C_7H_8F_4O_2Te$, $M_w = 295.73$, triclinic, $P\bar{1}$, $a = 7.583(2)$, $b = 10.446(2)$, $c = 13.131(3)$ Å, $\alpha = 107.632(4)$, $\beta = 96.929(4)$, $\gamma = 108.243(4)°$, $V = 914.4(3)$ Å^3, $Z = 4$, $\rho_{calcd} = 2.148$ Mg m^{-3}, $\mu(Mo_{K\alpha}) = 3.260$ mm^{-1}, 11412 measured reflections, [R(int) = 0.0239] crystallographically independent reflections, empirical absorption correction (SADABS[17]), least squares refinement (SHELXL-97[18]), anisotropic temperature factors, H atoms isotropic on calculated positions (riding model), 222 refined parameters, GOOF = 1.166, $R_1 = 0.0384$ [$I > 2\sigma(I)$], w$R_2 = 0.0735$ (all data), ρ(max./min) = 1.437 and −0.903 e Å^{-3}. CCDC-259967 (**2a**), CCDC-259968 (**2b**), CCDC-259969 (**3a**), and CCDC-260727 (**3b**) contain the supplementary crystallographic data for this paper. These data can be obtained free of charge from the Cambridge Crystallographic Data Centre via www.ccdc.cam.ac.uk/data_request/cif.
[7] R. Damerius, P. Huppmann, D. Lentz, K. Seppelt, *J. Chem. Soc. Dalton Trans.* **1984**, 2821 – 2826; M. J. Collins, G. Schrobilgen, *Inorg. Chem.* **1985**, *24*, 2608 – 2614.
[8] D. Naumann, S. Herberg, *J. Fluorine Chem.* **1982**, *19*, 205 – 212; H. Breut, B. Wilkes, D. Naumann, *Acta Crystallogr. Sect. C* **1990**, *46*, 1113 – 1115.
[9] L. Pauling, *The Nature of the Chemical Bond*, 3rd ed., Cornell University Press, Ithaca, NY, **1960**; *Tables of Interatomic Distances and Configuration in Molecules and Ions* (Ed.: L. Sutton) Spec. Publ. 11 and 18, The Chemical Society London, **1958** and **1965**; C. H. Suresh, N. Koga, *J. Phys. Chem. A* **2001**, *105*, 5940 – 5944; P. Politzer, J. S. Murray, P. Lane, *J. Comput. Chem.* **2003**, *24*, 505 – 511. The covalent radii of tellurium atoms range from 1.35 to 1.40 Å, those of sp^3-hybridized carbon atoms are close to 0.77 Å, and of nitrogen atoms are from 0.70 to 0.75 Å.
[10] R. Kniep, L. Korte, R. Kryschie, W. Poll, *Angew. Chem.* **1984**, *96*, 351; *Angew. Chem. Int. Ed. Engl.* **1984**, *23*, 388 – 389; A. J. Edwards, F. E. Hewaidy, *J. Chem. Soc.* **1968**, 2977 – 2980.
[11] A. Bondi, *J. Phys. Chem.* **1964**, *68*, 441 – 451.
[12] A. Alemi, E. Soleimani, Z. A. Starikova, *Acta Chim. Slov.* **2000**, *47*, 89 – 98; B. Buss, B. Krebs, *Inorg. Chem.* **1971**, *10*, 2795 – 2800.
[13] J. Ulrich, M. J. Jones, *Nachr. Chem.* **2005**, *53*, 19 – 23.
[14] M. Veith, H. Bärnighausen, *Acta Crystallogr. Sect. B* **1974**, *30*, 1806 – 1813.
[15] ORTEP3 for Windows—L. J. Farrugia, *J. Appl. Crystallogr.* **1997**, *30*, 565.
[16] DIAMOND Version 2.1d, K. Brandenburg, Crystal Impact GbR **1996**.
[17] SADABS: Area-Detector Absorption Correction; Siemens Industrial Automation, Inc., Madison, WI, **1996**; R. H. Blessing, *Acta Crystallogr. Sect. A* **1995**, *51*, 33 – 38.
[18] SHELX97—*Programs for Crystal Structure Analysis* (Release 97-2). G. M. Sheldrick, Universität Göttingen, Germany, **1998**.

 © 2005 Wiley-VCH Verlag GmbH & Co. KGaA, Weinheim

Drug Delivery

DOI: 10.1002/anie.200501500

Stimuli-Responsive Controlled Drug Release from a Hollow Mesoporous Silica Sphere/Polyelectrolyte Multilayer Core–Shell Structure**

Yufang Zhu, Jianlin Shi, Weihua Shen, Xiaoping Dong, Jingwei Feng, Meilin Ruan, and Yongsheng Li*

Recently, there has been increased interest in mesoporous silica materials for use as carriers in controlled drug release, to meet the need for prolonged and better control of drug administration. Amorphous mesoporous silica materials have been investigated as drug supports because of their nontoxic nature, adjustable pore diameter, and very high specific surface area with abundant Si–OH bonds on the pore surface.[1–10] Several research groups have investigated the conventional mesoporous silica materials (such as MCM-41 and SBA-15) used as drug-delivery systems.[1–8] These systems exhibit sustained-release properties, but their drug storage capacity is relatively low, and also the irregular bulk morphology is not perfect for drug delivery. To overcome these disadvantages, one strategy is to synthesize hollow mesoporous silica (HMS) spheres on the nanoscale with pore channels penetrating from the outside to the inner hollow core. Recently, our group has successfully synthesized HMS spheres with a 3D pore-network shell.[11,12] We also investigated the aspirin storage capacity and release properties of these spheres,[13] which indicated that they could store significantly more aspirin molecules than the conventional mesoporous silicas MCM-41 and MCM-48, and also have sustained-release properties.

Compared to the sustained-release system, the stimuli-responsive controlled-release system can achieve a site-selective, controlled-release pattern, which can improve the therapeutic efficacy. Up to now, only two reports have been published about stimuli-responsive controlled drug release from mesoporous silica MCM-41.[9,10] Lin and co-workers reported the stimuli-responsive controlled release of water-soluble drugs from MCM-41 by using chemically removable CdS nanoparticles as caps for mesoporous channels and disulfide bond-reducing molecules as release triggers.[9] Fujiwara and co-workers accomplished, for the first time, the photocontrolled reversible release of drug molecules from coumarin-modified MCM-41.[10] Therefore, it is still a challenge to find more convenient ways to achieve a fully controllable drug-release system under normal physiological pH and NaCl concentrations.

The properties and structure of polyelectrolyte multilayers (PEM) are sensitive to the various physical and chemical conditions of the surrounding medium. The polyelectrolyte pair, which comprises sodium polystyrene sulfonate (PSS) and the polycation poly(allylamine hydrochloride) (PAH), has been widely investigated for hollow microcapsules.[14–24] Möhwald and co-workers prepared hollow PAH/PSS capsules by colloid-templated assembly of polyelectrolytes (layer-by-layer technique),[15] and confirmed the controlled encapsulation and release of several kinds of molecules (such as dyes, enzymes, dextran, and DNA) from the capsules by changing the pH value (or ionic strength) of the release medium.[16–20] However, these hollow capsules are not mechanically strong and about 10% of them easily break in the course of drying and the removal of the colloid templates. In addition, reports on the storage and controlled release of drugs with the freestanding capsules are not found, probably as a result of the relatively low molecular weight of most drugs. Researchers have also tried to directly coat the polyelectrolyte multilayers onto certain drug microcrystals of low molecular weight.[22–24] These systems could prolong the release time to some extent, but unfortunately they did not show the stimuli-responsive controlled release of drug molecules.

It is known that the surface of mesoporous silica is negatively charged above the isoelectric point (pH 2–3),[25] which favors a first-layer coating of the positively charged polycation PAH, followed by the negatively charged PSS. Thus, polyelectrolyte multilayer coatings on mesoporous silica spheres can be prepared. The HMS spheres can be used as a container for drug molecules and the polyelectrolyte multilayer coatings as a stimuli-responsive switch. It is encouraging that with this system one can not only increase the drug-storage capacity, but also achieve stimuli-responsive controlled release of drug molecules and enhance the mechanical strength of the polyelectrolyte multilayers to prevent them from breaking.

Herein, we propose a strategy to combine the advantages of HMS spheres with a 3D pore network and polyelectrolyte multilayers with a stimuli-responsive property. We also report a stimuli-responsive controlled drug-delivery system, which consists of HMS spheres with an average sphere diameter of 300–400 nm and polyelectrolyte multilayer coatings (PAH/PSS) with an average thickness of 14 nm. Prior reports on such a controlled-release system have not been found. In addition, the uncoated HMS sphere drug-release system was used for comparison to investigate the release property.

Figure 1 schematically illustrates two drug-delivery systems, which were designed to demonstrate the stimuli-responsive controlled drug release from PAH/PSS polyelectrolyte multilayer coatings on HMS loaded with ibuprofen (IBU-HMS@PEM) or a simplex sustained-release pattern from the IBU-HMS system. In the former system, the key is to coat the PAH/PSS multilayers on IBU-HMS spheres, which could cap the mesopore channels. During the release process,

[*] Y. Zhu, Prof. J. Shi, W. Shen, X. Dong, J. Feng, M. Ruan, Y. Li
State Key Laboratory of High-Performance Ceramics and Superfine Microstructures
Shanghai Institute of Ceramics, Chinese Academy of Sciences
1295 Ding-xi Road, Shanghai 200050 (P.R. China)
Fax: (+86) 21-5241-3122
E-mail: jlshi@sunm.shcnc.ac.cn

[**] The authors gratefully acknowledge the support of this research by the National Science Foundation of China (Nos. 20341002, 50232050) and Shanghai Nanoscience Program (No. 0352nm101).

Supporting information for this article is available on the WWW under http://www.angewandte.org or from the author.

 © 2005 Wiley-VCH Verlag GmbH & Co. KGaA, Weinheim

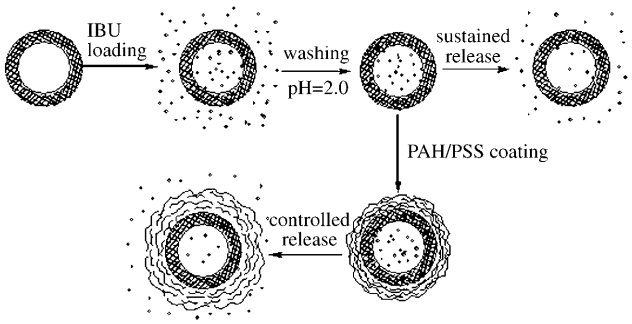


Figure 1. Schematic illustration of two drug-delivery systems which give the different controlled-release patterns.

the loaded drugs need to diffuse subsequently through the mesoporous shell and the PAH/PSS multilayers into the release medium. That is, drug release is doubly controlled by the mesoporous shell and the PAH/PSS multilayers sequentially. The stimuli-responsive controlled drug-release pattern of this system is possible as a consequence of the pH sensitivity and salt-induced responsive property of the PAH/PSS multilayers. For the IBU-HMS system, only the mesoporous shells control drug diffusion, which results in the sustained-release behavior alone.

The detailed synthesis, characterization, and formation mechanism of HMS spheres with a 3D pore network can be found in our recent report.[11] Figure 2a and b show TEM micrographs of spherical mesoporous silica particles with an average diameter of 300–400 nm. The noticeable contrast between the core and the shell of the sphere implies a hollow-core structure. The highly ordered lattice array over the shell suggests that HMS products have a uniform, well-defined mesostructure. Figure 2c shows a TEM micrograph of the HMS sphere after adsorption of IBU molecules (IBU-HMS).

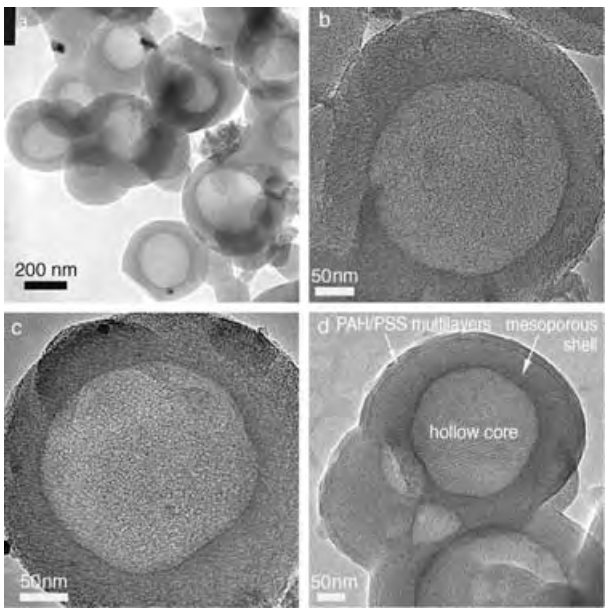


Figure 2. TEM micrographs of HMS (a and b), the IBU-HMS system (c), and the IBU-HMS@PEM system (d).

No apparent difference can be observed compared to HMS, although IBU-HMS contains a large number of IBU molecules. One reason might be that the scattering effects of IBU molecules (which contain carbon, hydrogen, and oxygen) in the hollow core and the pore channels are not strong enough to show the contrast. Figure 2d shows a TEM micrograph of IBU-HMS after being coated with PAH/PSS multilayers (IBU-HMS@PEM). A uniform thin layer with a thickness of around 14 nm exists on the outer surface of the HMS sphere, and the thin layer has coated the whole sphere. Furthermore, the hollow core–mesoporous shell structure still remains intact. Therefore, two controlling layers (mesoporous shell and PAH/PSS multilayers) have been formed in the IBU-HMS@PEM system.

Thermogravimetric analysis (TGA) curves of the IBU-HMS and IBU-HMS@PEM systems are shown in Figure 3,

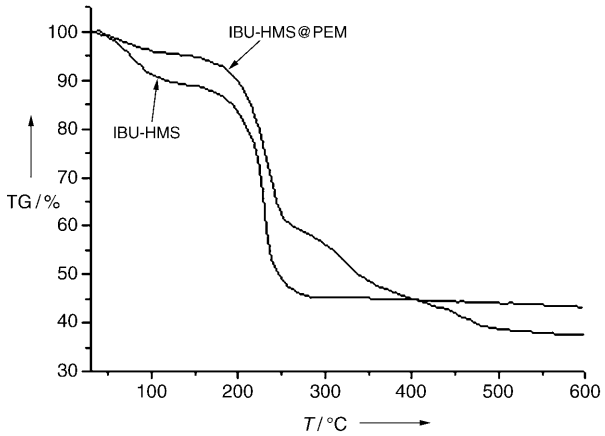


Figure 3. TGA curves of the IBU-HMS and IBU-HMS@PEM systems.

and the results are summarized in Table 1. Both systems showed weight losses below 180 °C that resulted from the physical loss of water. For the IBU-HMS system, another

Table 1: TGA results for the two drug-delivery systems.

	30–180 °C (wt %)	180–280 °C (wt %)	280–500 °C (wt %)	SiO_2 [wt %]	Storage capacity [mg_{IBU}/g_{SiO_2}]
IBU-HMS	13.03	41.64	–	45.33	918.6
IBU-HMS@PEM	7.1	34.60	19.65	39.65	872.6

weight loss (about 41.64 %) occurred between 180 and 280 °C, which demonstrates that the IBU storage capacity of the IBU-HMS system is 41.64 % (918.6 mg_{IBU}/g_{SiO_2}). In the IBU-HMS@PEM system, three weight losses were detected from 180 to 600 °C. The loss of 34.60 % (872.6 mg_{IBU}/g_{SiO_2}) between 180 and 280 °C is attributed to the removal of IBU from the IBU-HMS@PEM system, while the other two weight losses occur by the removal of the PAH/PSS multilayers. Here, the IBU storage capacity in the IBU-HMS@PEM system is a little

 © 2005 Wiley-VCH Verlag GmbH & Co. KGaA, Weinheim

lower than that in the IBU-HMS system, which may have resulted from the loss of some IBU molecules during the PAH/PSS multilayer coating process. However, this drug storage capacity is almost three times higher than that of the conventional mesoporous material MCM-41.[1–4]

Figure 4 shows the cumulative drug release from the two systems in release media of pH 1.4 (a simulated gastric fluid)

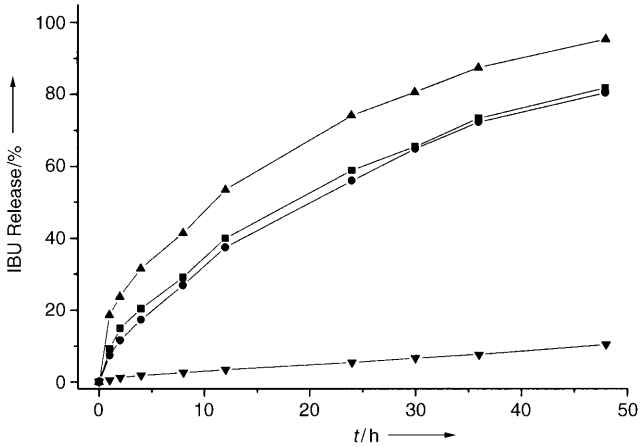


Figure 4. Cumulative drug release from the two systems in release media of different pH values. ■: pH 1.4 from IBU-HMS, ●: pH 1.4 from IBU-HMS@PEM, ▲: pH 8.0 from IBU-HMS, ▼: pH 8.0 from IBU-HMS@PEM.

and pH 8.0 (a simulated intestinal fluid). This diagram clearly proves that both systems exhibit sustained-release properties and that the drug release rates from both systems are very close to each other in the medium of pH 1.4. The amounts released from the two systems reach about 80% in 48 h. This result implies that the PAH/PSS multilayers are incompact and have open pathways in the release medium of pH 1.4, and the incompact wall of the PAH/PSS multilayers could not cap the openings of the mesoporous channels. Therefore, the drug molecules can easily diffuse into the release medium through the mesoporous channels and PAH/PSS multilayers, that is, this system only exhibits the sustained-release property with the IBU-HMS system in acid media. When the pH value of the release medium increases to 8.0, the drug release rates from both systems become apparently different. The IBU-HMS system also exhibits the sustained-release property and the amount released reaches 95% in 48 h; the release rate in the pH 8.0 release medium is higher than that in the pH 1.4 medium. This difference in release rates should mainly be attributed to the different solubility of IBU in release media of different pH values. IBU has limited solubility in low-pH (<7) solutions but is readily soluble in high-pH (>7) solutions. For the IBU-HMS@PEM system the release rate is very low, and the released amount only reaches 10% over a period of 48 h. This finding indicates the good storage and sealing effect of the PAH/PSS multilayer coating on HMS spheres in pH 8.0 solution; that is, the PAH/PSS multilayers are compact and have decreased permeability at the increased pH value, and the compact multilayers could easily cap the openings of the mesoporous channels. It can be concluded that the IBU-HMS@PEM system has a much better controlled drug-release property than the IBU-HMS system and the reported polyelectrolyte multilayer capsule system.[22–24] That is, the IBU-HMS@PEM system can achieve a pH-responsive controlled drug-release pattern by changing the pH value of the release medium.

As we know, the structure and properties of PAH/PSS multilayers are sensitive to the NaCl concentration.[17,26] Therefore, we investigated drug release from the two systems in release media of different NaCl concentration. Sustained releases from both systems are obtained in 10 mM NaCl media (Figure 5) and the release rates are very close to each other,

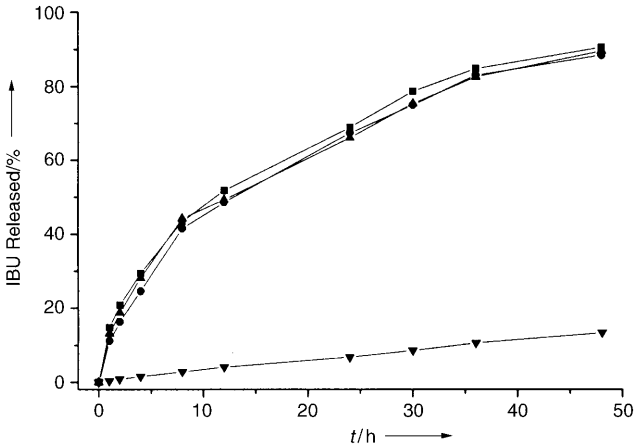


Figure 5. Cumulative drug release from the two systems in release media of different NaCl concentration. ■: 10 mM NaCl from IBU-HMS, ●: 10 mM NaCl from IBU-HMS@PEM, ▲: 0.5 mM NaCl from IBU-HMS, ▼: 0.5 mM NaCl from IBU-HMS@PEM.

which is similar to the result in release media of pH 1.4. In 0.5 mM NaCl media, the amount of drug released from the IBU-HMS system reaches about 90% in 48 h, which is also close to the release rate in 10 mM NaCl media. However, the amount released from the IBU-HMS@PEM system only reaches 13% in 48 h. Therefore, a salt-induced controlled drug-release pattern can be achieved from the IBU-HMS@PEM system. The PAH/PSS multilayers play an important role during the controlled-release process. At the higher salt concentration, the high ionic strength weakens the electrostatic binding between the oppositely charged layers, which results in incompact PAH/PSS multilayers. The multilayers can no longer cap the openings of the mesoporous channels and provide the pathways for drug molecules to diffuse into the release medium. At the lower salt concentration, the electrostatic binding between the oppositely charged layers becomes stronger and the openings of the mesoporous channels are more easily capped by the compact PAH/PSS multilayers. Therefore, the multilayers can play a switch role between the lower and the higher salt concentrations.

In addition, the drug storage and release process does not damage the pore structure (see the Supporting Information). The low-angle XRD patterns show a diffraction peak at $2\theta = 2.2$–$2.5°$ (θ is the Bragg angle) which is unaffected by the drug

 © 2005 Wiley-VCH Verlag GmbH & Co. KGaA, Weinheim

loading and release. The pore size becomes smaller after drug loading; however, the size distribution and pore volume can mostly recover after drug release from the two systems (see the Supporting Information). Therefore, the two controlled drug-release systems show good stability.

In summary, we have demonstrated a concept to design a novel stimuli-responsive controlled drug-release system by using PAH/PSS multilayers as a coating to cap the mesopore openings of drug-loaded hollow mesoporous silica spheres. The drug storage capacity of this system is three times higher than that of the reported MCM-41 system. Compared with the system without a polyelectrolyte multilayer coating, the reported system can give stimuli-responsive controlled release; for example, it can be designed to release into the stomach instead of the intestine. The drug release rate from the IBU-HMS@PEM system can be well-controlled by changing the pH value (or the salt concentration) of the release medium. Therefore, this system combines the advantages of both high drug storage capacity and the property of stimuli-responsive controlled release, and has potential for applications in drug delivery.

Experimental Section

Materials: Tetrapropylammonium hydroxide (TPAOH, 25% in water) was from Acros. Poly(allylamine hydrochloride) (PAH, $M_w = 15000$) and sodium polystyrene sulfonate (PSS, $M_w = 70000$) were from Aldrich and used without further purification. Ibuprofen (IBU, 99%) was from Shanghai Yuanji Chem. Co. and used as received. Cetyltrimethylammonium bromide (CTAB, 99%), tetraethyl orthosilicate (TEOS, 98%), hydrogen chloride (36–38%), hexane, sodium hydroxide, and aluminum sulfate ($Al_2(SO_4)_3{\cdot}18H_2O$) were purchased from Shanghai Chem. Agents Co. and used without further purification.

Preparation of hollow mesoporous silica spheres and drug-delivery system: HMS spheres were prepared by our method as described in the literature.[11] The drug-storage profile was taken as previously reported.[1–4] IBU was dissolved in hexane at a concentration of 60 mg mL^{-1}. HMS (1.0 g) was added to this solution (50 mL) at room temperature. The vials were sealed to prevent the evaporation of hexane, then the mixture was stirred for 24 h. The HMS with adsorbed IBU was separated by centrifugation and washed several times with a solution of pH 1.4. Finally, the sample was dried under vacuum at 60 °C. This sample is denoted as IBU-HMS.

Preparation of polyelectrolyte multilayer coating: PAH (5 mL) with a monomer concentration of 5 mg mL^{-1} in 0.5 M NaCl was added to a suspension of IBU-HMS (1.0 wt%, 20 mL, pH 6.0). After stirring for 20 min, the suspension was centrifuged three times in water. Gentle shaking followed by ultrasonic treatment for 1 min was used to disperse the particles after centrifugation. Then, oppositely charged PSS (5 mg mL^{-1} in 0.5 M NaCl) was coated on the particles. This coating process was repeated for eight layers and finally a composite of IBU-HMS coated with PAH/PSS multilayers was obtained. This sample is denoted as IBU-HMS@PEM.

In vitro drug-release study: The IBU-HMS (or IBU-HMS@PEM) sample was immersed in release media of different pH values (pH 1.4 and 8.0) or different ionic strength (0.5 and 10 mM NaCl solution) at room temperature, with stirring at a rate of 100 rpm. The release medium (2.0 mL) was removed for analysis at given time intervals with a syringe, and replaced with the same volume of fresh release medium. The extracted medium was diluted to a desired concentration (0.01–0.5 mg mL^{-1}) with release medium, and analyzed by UV/Vis spectroscopy at a wavelength of 264 nm. The samples with released IBU are denoted as IBU-HMS$_R$ and IBU-HMS@PEM$_R$.

Characterization methods: Powder XRD patterns were obtained on a Rigaku D/MAX-2550V diffractometer at 40 kV and 40 mA ($Cu_{K\alpha}$ radiation). TEM analysis was performed using a JEOL 2100F electron microscope operated at 200 kV. The UV/Vis absorbance spectra were measured with a Shimadzu UV-3101PC spectrophotometer. N_2 adsorption–desorption isotherms were obtained on a Micromeritics Tristar 3000 pore analyzer at 77 K under continuous adsorption conditions. Brunauer, Emmett, and Teller (BET) and Barrett, Joyner, and Halenda (BJH) analyses were used to determine the surface area, pore size, and pore volume. Thermogravimetric analysis (TGA) was recorded on an STA-449C thermal analyzer at 10 °C min^{-1} in an N_2 atmosphere.

Received: May 1, 2005
Published online: July 14, 2005

Keywords: drug delivery · mesoporous materials · multilayers · nanostructures · polyelectrolytes

[1] M. Vallet-Regí, A. Rámila, R. P. del Real, J. Pérez-Pariente, *Chem. Mater.* **2001**, *13*, 308 – 311.
[2] A. Rámila, B. Muñoz, J. Pérez-Pariente, M. Vallet-Regíi, *J. Sol–Gel Sci. Technol.* **2003**, *26*, 1199 – 1202.
[3] B. Muñoz, A. Rámila, J. Pérez-Pariente, I. Díaz, M. Vallet-Regí, *Chem. Mater.* **2003**, *15*, 500 – 503.
[4] P. Horcajada, A. Rámila, J. Pérez-Pariente, M. Vallet-Regí, *Microporous Mesoporous Mater.* **2004**, *68*, 105 – 109.
[5] A. L. Doadrio, E. M. B. Sousa, J. C. Doadrio, J. Pérez-Pariente, I. Izquierdo-Barba, M. Vallet-Regí, *J. Controlled Release* **2004**, *97*, 125 – 132.
[6] C. Tourné-Péteilh, D. A. Lerner, C. Charnay, L. Nicole, S. Bégu, J. M. Devoisselle, *ChemPhysChem* **2003**, *4*, 281 – 286.
[7] K. A. Fisher, K. D. Huddersman, M. J. Taylor, *Chem. Eur. J.* **2003**, *9*, 5873 – 5878.
[8] H. Hata, S. Saeki, T. Kimura, Y. Sugahara, K. Kuroda, *Chem. Mater.* **1999**, *11*, 1110 – 1119.
[9] C.-Y. Lai, B. G. Trewyn, D. M. Jeftinija, K. Jeftinija, S. Xu, S. Jeftinija, V. S.-Y. Lin, *J. Am. Chem. Soc.* **2003**, *125*, 4451 – 4459.
[10] N. K. Mal, M. Fujiwara, Y. Tanaka, *Nature* **2003**, *421*, 350 – 353.
[11] Y. Li, J. Shi, Z. Hua, H. Chen, M. Ruan, D. Yan, *Nano Lett.* **2003**, *3*, 609 – 612.
[12] Y. Li, J. Shi, H. Chen, Z. Hua, L. Zhang, M. Ruan, J. Yan, D. Yan, *Microporous Mesoporous Mater.* **2003**, *60*, 51 – 56.
[13] Y. Zhu, J. Shi, Y. Li, H. Chen, W. Shen, X. Dong, *J. Mater. Res.* **2005**, *20*, 54 – 61.
[14] C. S. Peyratout, L. Dähne, *Angew. Chem.* **2004**, *116*, 3850 – 3872; *Angew. Chem. Int. Ed.* **2004**, *43*, 3762 – 3783.
[15] E. Donath, G. B. Sukhoruko, F. Caruso, S. A. Davis, H. Möhwald, *Angew. Chem.* **1998**, *110*, 2324 – 2327; *Angew. Chem. Int. Ed.* **1998**, *37*, 2202 – 2205.
[16] D. C. Shchukin, G. B. Sukhoruko, H. Möhwald, *Angew. Chem.* **2003**, *115*, 4610 – 4613; *Angew. Chem. Int. Ed.* **2003**, *42*, 4472 – 4475.
[17] G. Sukhorukov, L. Dähne, J. Hartmann, E. Donath, H. Möhwald, *Adv. Mater.* **2000**, *12*, 112 – 115.
[18] G. Ibarz, L. Dähne, E. Donath, H. Möhwald, *Adv. Mater.* **2001**, *13*, 1324 – 1327.
[19] G. B. Sukhoruko, A. A. Antipov, A. Voigt, E. Donath, H. Möhwald, *Macromol. Rapid Commun.* **2001**, *22*, 44 – 46.
[20] Y. Wang, F. Caruso, *Chem. Commun.* **2004**, 1528 – 1529.
[21] A. A. Antipov, G. B. Sukhoruko, S. Leporatti, I. L. Radtchenko, E. Donath, H. Möhwald, *Colloids Surf. A* **2002**, *198–200*, 535 – 541.
[22] X. Qiu, S. Leporatti, E. Donath, H. Möhwald, *Langmuir* **2001**, *17*, 5375 – 5380.

 © 2005 Wiley-VCH Verlag GmbH & Co. KGaA, Weinheim

[23] A. A. Antipov, G. B. Sukhoruko, E. Donath, H. Möhwald, *J. Phys. Chem. B* **2001**, *105*, 2281 – 2284.
[24] H. Ai, S. A. Jones, M. M. de Villiers, Y. M. Lvov, *J. Controlled Release* **2003**, *86*, 59 – 68.
[25] M. Kosmilski, *J. Colloid Interface Sci.* **2004**, *275*, 214 – 224.
[26] A. A. Antipov, G. B. Sukhoruko, H. Möhwald, *Langmuir* **2003**, *19*, 2444 – 2448.

 © 2005 Wiley-VCH Verlag GmbH & Co. KGaA, Weinheim

Biradicals

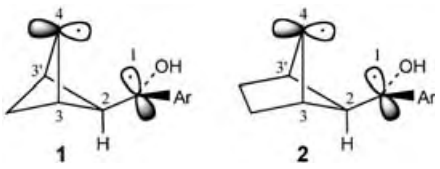
DOI: 10.1002/anie.200500983

Orbital-Overlap Control of the Reactivity of a Bicyclic 1-Hydroxy-1,4-Biradical**

Chao Yang, Wujiong Xia, John R. Scheffer, Mark Botoshansky, and Menahem Kaftory*

1,4-Biradicals are among the most ubiquitous reactive intermediates in organic chemistry, and are formed or implicated in a variety of reactions including [2+2] photocycloaddition,[1] the Paterno–Büchi reaction (oxetane formation),[2] the Norrish–Yang type II reaction,[3] and the elimination of nitrogen from cyclic azo compounds.[4] Once formed, 1,4-biradicals suffer two main fates: closure to form compounds containing a four-membered ring, and cleavage of the central bond to produce a pair of double-bond-containing fragments.[5] Based on organic intuition backed by semiempirical calculations,[6] and supported by a wide variety of product studies,[1–4] the generally accepted qualitative picture of biradical reactivity is that cleavage is favored when the conformation allows the radical-containing orbitals at positions 1 and 4 to overlap with the sigma bond between positions 2 and 3. Increasing amounts of cyclization are observed as this overlap diminishes, provided that the radical termini are within reasonable bonding distance of one another.

However, quantitative experimental tests of this hypothesis are rare, in part as a result of the difficulty of establishing structure–reactivity relationships for conformationally mobile systems in fluid media. In the case of triplet 1,4-biradicals, the picture is complicated by the likelihood that biradical behavior reflects the geometry in which the singlet biradical is formed by intersystem crossing (isc) from the triplet, which may differ significantly from the geometry of the conformationally equilibrated species.[7] For these reasons, we have elected to work with compounds in the crystalline state, where molecular conformation is fixed and determinable by X-ray crystallography, and where the singlet biradical formed by isc has the same geometry as its triplet precursor. We have shown that 1-hydroxy-1,4-biradicals can be generated conveniently in the solid state by the Norrish–Yang type II reaction, and that because hydrogen-atom transfer occurs with very little movement of the associated heavy atoms, the structure and conformation of the biradicals can be inferred directly from the X-ray crystal structures of their ground-state precursors.[8] Herein, we compare and contrast the behavior of 1-hydroxy-1,4-biradicals of general structures **1** and **2**. These biradicals are interesting because,



unlike the majority of biradicals studied previously, they have only one significant degree of conformational freedom, namely, rotation about the C1–C2 bond. Among the questions we wished to answer about these biradicals were: 1) how does the orientation of the p orbital at the C1 position affect the ratio of cyclization to cleavage; and 2) can we correlate the orientation of the p orbital at C1 with preferential cleavage of either the C2–C3 or C2–C3′ bond? As described below, satisfactory answers to these questions were obtained by generating biradicals **1** and **2** in the crystalline state and correlating their behavior in this medium with their conformations as determined by X-ray crystallography.

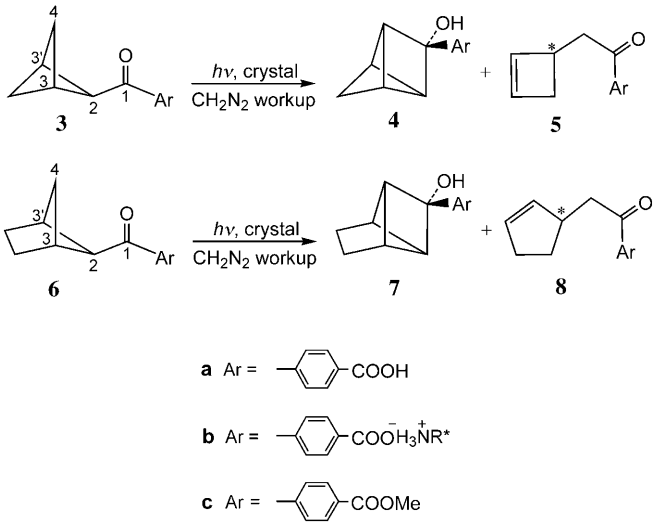
We are not the first to study biradicals of types **1** and **2**. The solution-phase behavior of biradical **2** (Ar = Ph) was reported in 1972 by Padwa and Eisenberg and shown to consist of 66% cleavage and 30% cyclization.[9] Similarly, Alexander and Uliana showed in 1976 that, in solution, biradical **1** (Ar = Ph) bearing a phenyl substituent at the C2 position undergoes 100% cyclization.[10] In both cases, the biradicals were formed by a Norrish–Yang type II photoreaction of the corresponding ketone. In the present work, we chose to investigate ketones in which the aryl group bears a carboxylic acid substituent in the *para* position, that is, ketones of general structures **3** and **6** (Scheme 1). This choice was based on the following considerations: previous work from our group had shown that when achiral keto acids such as **3a** and **6a** are treated with optically pure amines, the resulting salts (**3b** and **6b**) crystallize with the carboxylate anions in homochiral conformations.[11] In principle, these salts could react when photolyzed in the solid state to produce, after diazomethane workup, the achiral Yang cyclization products **4c**/**7c** along with the chiral Norrish type II cleavage products **5c**/**8c** (Scheme 1). Cleavage of the

[*] Dr. C. Yang, Dr. W. Xia, Prof. Dr. J. R. Scheffer
Department of Chemistry, University of British Columbia
2036 Main Mall, Vancouver, B.C. V6T1Z1 (Canada)
Fax: (+1) 604-822-3496
E-mail: scheffer@chem.ubc.ca
Dr. M. Botoshansky, Prof. Dr. M. Kaftory
Department of Chemistry, Technion
Haifa 32000 (Israel)

[**] We thank the Natural Sciences and Engineering Research Council of Canada for financial support. J.R.S. is grateful to the Rockefeller Foundation for a one-month residency at their Bellagio Study Center, where this paper was written.

Supporting information for this article is available on the WWW under http://www.angewandte.org or from the author.

 © 2005 Wiley-VCH Verlag GmbH & Co. KGaA, Weinheim



Scheme 1. Ketone reactants and their cyclization/cleavage photoproducts.

C2–C3 bond leads to (*R*)-**5c**/**8c** and cleavage of the C2–C3′ bond leads to (*S*)-**5c**/**8c**. Thus, by determining the absolute configuration of the cleavage product in each case and correlating this information with the absolute conformation of the carboxylate anion obtained by X-ray crystallography, we were able to establish which bond was cleaved and its degree of overlap with the p orbital on C1.

Although a number of different salts were prepared and their solid-state photochemistry investigated, we limit the present discussion to the two salts whose X-ray crystal structures were successfully determined, namely, the (*S*)-(−)-1-phenylethylamine salts of keto acids **3a** and **6a**.[12] Polycrystalline samples of these salts (2–5 mg) were crushed between pyrex microscope slides and the resulting sandwiches taped together, sealed under nitrogen in polyethylene bags, and irradiated (450-W medium-pressure mercury lamp) on both sides at various temperatures for different lengths of time. Even at high conversions, no melting could be detected. After photolysis, the crystals were treated with diazomethane in ether to remove the ionic chiral auxiliaries and form the corresponding methyl esters. The reaction mixtures were then subjected to GC analysis to determine the cyclization-to-cleavage ratios, and to chiral HPLC analysis to measure the enantiomeric excess (*ee*) in which photoproducts **5c** and **8c** were formed. The results are summarized in Table 1.[13]

Table 1: Solid-state photochemistry of (*S*)-(−)-1-phenylethylamine salts of keto acids **3a** and **6a**.

Acid	*T* [°C]	Conversion [%][a]	CY/CL[b]	*ee* [%][c]	α[d]
3a	−20	45	88:10	90	(−)
3a	20	38	87:11	87	(−)
3a	20	72	87:11	70	(−)
6a	−20	85	21:75	98	(−)
6a	20	21	20:79	>98	(−)
6a	20	53	21:77	98	(−)

[a] Determined by GC. [b] Ratio of cyclization (CY) to cleavage (CL). [c] Determined by chiral HPLC. [d] Sign of rotation of major enantiomer at sodium D line.

An independent, enantioselective synthesis of photoproduct **8c** was carried out to determine whether the major enantiomer produced in these photolysis reactions was of *R* or *S* configuration. Optically pure (*S*)-2-cyclopentene-1-acetic acid was prepared by resolution of the racemate with brucine according to the procedure of Mislow and Steinberg.[14] This material was then converted by reduction with lithium aluminum hydride, oxidation with pyridinium chlorochromate (PCC), addition of *p*-carbomethoxyphenylmagnesium iodide, and oxidation with PCC to (*S*)-**8c**, which proved to be dextrorotatory ($[\alpha]_D^{22} = +98.0°$, $c = 0.45$, MeOH). According to the sign of rotation shown in Table 1, this means that compound **8c** formed in the photolysis of the (*S*)-(−)-1-phenylethylamine salt of keto acid **6a** has the *R* absolute configuration. On the basis of the very close structural similarity between photoproducts **8c** and **5c**, we assume that the latter also has the *R*-(−) absolute configuration.

Concomitant with the photochemical and synthetic studies, the X-ray crystal structures of the (*S*)-(−)-1-phenylethylamine salts of keto acids **3a** and **6a** were determined (see Figure 1). A number of important geometric parameters were

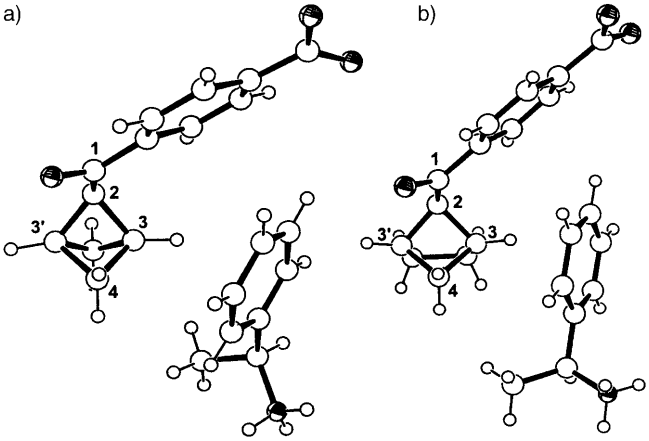


Figure 1. X-ray crystal structures of (*S*)-(−)-1-phenylethylamine salts of keto acids a) **3a** and b) **6a**.

calculated from the crystal structures, including the γ-hydrogen-atom abstraction geometries as well as the geometric relationships relevant to the cyclization and cleavage of the 1-hydroxy-1,4-biradical intermediates (see Table 2).

To begin our discussion of the geometric parameters, we note that the value of d_{O-H4}, the distance between the carbonyl oxygen atom and the γ-hydrogen atom on C4, is similar for both salts and well within the guidelines established by us for

Table 2: Geometric data derived from the X-ray crystal structures of the (*S*)-(−)-1-phenylethylamine salts of keto acids **3a** and **6a**.

Acid	d_{O-H4} [Å][a]	d_{C1-C4} [Å][b]	β [°][c]	φ_1 [°][d]	φ_4 [°][e]
3a	2.67	2.81	22	22 (67)	43 (43)
6a	2.62	2.82	32	16 (78)	35 (35)

[a] C=O···H4 distance. [b] C1–C4 distance. [c] Angle between p orbital on C1 and the C2–C4 vector. [d] Angle between p orbital on C1 and C2–C3 (C2–C3′). [e] Angle between p orbital on C4 and C2–C3 (C2–C3′).

 © 2005 Wiley-VCH Verlag GmbH & Co. KGaA, Weinheim

successful Norrish type II hydrogen abstraction in the crystalline state ($d = 2.7 \pm 0.2$ Å).[15] Similarly, the value of d_{C1-C4}, the distance between atoms C1 and C4 in the biradical produced by hydrogen abstraction, is the same for both salts. As a result, distance factors can be excluded as the source of the cyclization-to-cleavage ratio differences. The parameter β, defined as the angle between the p orbital on C1 and the C2–C4 vector, is ideal for cyclization when $\beta = 0°$, that is, when the p orbitals are pointing directly at one another. The values of β in Table 2 indicate that the **3a**-derived biradical is better arranged for cyclization than the **6a**-derived species.

The parameters φ_1 and φ_4 represent the angles formed between the p orbitals on atoms C1 and C4 and the C2–C3 and C2–C3′ bonds (the values of φ_1 and φ_4 for the C2–C3′ bond are shown in parentheses). The best arrangement for cleavage is expected when φ_1 and $\varphi_4 = 0°$, and the data indicate that cleavage of the C2–C3 bond is favored over cleavage of the C2–C3′ bond for both salts. This finding predicts that cleavage photoproducts **5c** and **8c** should have the *R* absolute configuration, a prediction that agrees with the configurational assignment made by independent synthesis of optically pure (*S*)-(+)-**8c**. It is interesting to speculate that the *ee* for **5c** is lower (70–90%) than that for **8c** (98%), because the difference in φ_1 for the former is less ($67-22 = 45°$) than that for the latter ($78-16 = 62°$). Of course, supramolecular factors[16] could contribute to the difference in *ee*, but the fact that the (*S*)-1-phenylethylammonium ion is common to both salts supports the notion that the major determinant of solid-state biradical behavior in these systems is the structure and conformation of the carboxylate anion.

The values of φ_1 and φ_4 also show that the biradical derived from **6a** has a better geometry for cleavage ($\varphi_1 = 16°$, $\varphi_4 = 35°$) than that from **3a** ($\varphi_1 = 22°$, $\varphi_4 = 43°$). Taken together with the earlier conclusion that the biradical from **3a** has a better geometry for cyclization than that from **6a**, the data clearly predict that salts derived from keto acid **3a** should have a higher Norrish–Yang cyclization-to-cleavage ratio than those derived from keto acid **6a**. This prediction is in accordance with the counterintuitive result that Yang photocyclization predominates in the bicyclo[1.1.1]pentane system **3a**, even though the cyclobutanol product in this case is more strained than that formed from the bicyclo-[2.1.1]hexane reactant **6a**.

The work reported herein complements our previous research in this area[8] and highlights, in a quantitative fashion, the fact that relatively small differences in geometry can have a profound effect on 1-hydroxy-1,4-biradical behavior. Furthermore, it demonstrates once again the efficacy of the solid-state ionic chiral auxiliary approach to asymmetric synthesis in organic photochemistry.[17]

Experimental Section

Full experimental details on the synthesis of the starting materials, photolysis of the salts in the crystalline state, the diazomethane workup procedure, and the characterization of the photoproducts are available in the Supporting Information. CCDC 265554 and 265555 contain the supplementary crystallographic data for this paper. These data can be obtained free of charge from the Cambridge Crystallographic Data Centre via www.ccdc.cam.ac.uk/data_request/cif.

Received: March 17, 2005
Published online: July 20, 2005

Keywords: asymmetric synthesis · photochemistry · radicals · solid-state reactions · structure–activity relationships

[1] D. Andrew, A. C. Weedon, *J. Am. Chem. Soc.* **1995**, *117*, 5647, and references therein.
[2] a) A. G. Griesbeck, H. Mauder, S. Stadtmüller, *Acc. Chem. Res.* **1994**, *27*, 70; b) A. G. Griesbeck, S. Buhr, M. Fiege, H. Schmickler, J. Lex, *J. Org. Chem.* **1998**, *63*, 3847.
[3] a) P. J. Wagner, P. Klán in *CRC Handbook of Organic Photochemistry and Photobiology*, 2nd ed. (Eds.: W. Horspool, F. Lenci), CRC, Boca Raton, **2004**, chap. 52; b) P. J. Wagner in *CRC Handbook of Organic Photochemistry and Photobiology*, 2nd ed. (Eds.: W. Horspool, F. Lenci), CRC, Boca Raton, **2004**, chap. 58.
[4] a) W. Adam, C. Sabin in *CRC Handbook of Organic Photochemistry and Photobiology* (Eds.: W. M. Horspool, P.-S. Song), CRC, Boca Raton, **1995**, p. 937; b) W. Adam, A. V. Trofimov in *CRC Handbook of Organic Photochemistry and Photobiology*, 2nd ed. (Eds.: W. Horspool, F. Lenci), CRC, Boca Raton, **2004**, chap. 93.
[5] In the case of 1-hydroxy-1,4-biradicals generated in the photochemical Norrish–Yang type II reaction, a third possibility is reverse hydrogen transfer to regenerate the ground-state ketone, a quantum yield-lowering process.
[6] a) P. J. Wagner, A. E. Kemppainen, *J. Am. Chem. Soc.* **1968**, *90*, 5896; b) R. Hoffmann, S. Swaminathan, B. G. Odell, R. Gleiter, *J. Am. Chem. Soc.* **1970**, *92*, 7091.
[7] a) J. C. Scaiano, *Tetrahedron* **1982**, *38*, 819; b) A. G. Griesbeck, H. Heckroth, *J. Am. Chem. Soc.* **2002**, *124*, 396; c) A. G. Griesbeck, *Synlett* **2003**, 451.
[8] D. Braga, S. Chen, H. Filson, L. Maini, M. R. Netherton, B. O. Patrick, J. R. Scheffer, C. Scott, W. Xia, *J. Am. Chem. Soc.* **2004**, *126*, 3511.
[9] A. Padwa, W. Eisenberg, *J. Am. Chem. Soc.* **1972**, *94*, 5852.
[10] E. C. Alexander, J. Uliana, *J. Am. Chem. Soc.* **1976**, *98*, 4324.
[11] B. O. Patrick, J. R. Scheffer, C. Scott, *Angew. Chem.* **2003**, *115*, 3905; *Angew. Chem. Int. Ed.* **2003**, *42*, 3775.
[12] See the Supporting Information for a description of the preparation and solid-state photochemistry of the salts whose structures were not determined by X-ray crystallography.
[13] The photoreactions were significantly less selective in solution. The cyclization-to-cleavage ratio resulting from irradiation of keto ester **3c** in acetonitrile was 77:23 and that from **6c** was 30:66; in both cases, the cleavage products were racemic.
[14] K. Mislow, I. V. Steinberg, *J. Am. Chem. Soc.* **1955**, *77*, 3807.
[15] J. R. Scheffer in *Molecular and Supramolecular Photochemistry: Chiral Photochemistry, Vol. 11* (Eds.: V. Ramamurthy, Y. Inoue), Marcel Dekker, New York, **2004**, p. 463.
[16] By supramolecular factors, we refer to the interaction of the reactant with the surrounding crystal lattice during reaction. For a qualitative treatment of this aspect of solid-state photochemistry, see: R. G. Weiss, V. Ramamurthy, G. S. Hammond, *Acc. Chem. Res.* **1993**, *26*, 530; for a quantitative treatment, see: H. E. Zimmerman, E. E. Nesterov, *Acc. Chem. Res.* **2002**, *35*, 77.
[17] For reviews, see: a) J. R. Scheffer, *Can. J. Chem.* **2001**, *79*, 349; b) "Organic Solid State Reactions": J. R. Scheffer, W. Xia, *Top. Curr. Chem.* **2005**, *254*, 233.

 © 2005 Wiley-VCH Verlag GmbH & Co. KGaA, Weinheim

Metallacycle

DOI: 10.1002/anie.200500899

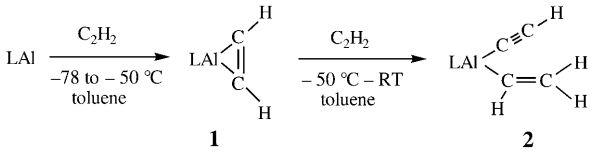
A Stable Aluminacyclopropene LAl(η^2-C_2H_2) and Its End-On Azide Insertion to an Aluminaazacyclobutene**

Hongping Zhu, Jianfang Chai, Hongjun Fan, Herbert W. Roesky, Cheng He, Vojtech Jancik, Hans-Georg Schmidt, Mathias Noltemeyer, William A. Merrill, and Philip P. Power*

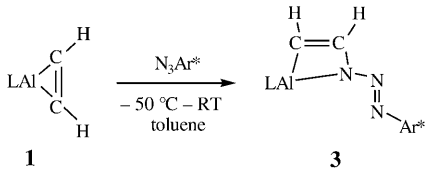
Dedicated to Kit Cummins

The MC_2 rings of cyclopropene derivatives substituted with heavier main-group elements have a highly strained structure and indicate a remarkable reactivity. They are often involved in such reactions as ring opening, insertion, substitution, dimerization, and hydrogen [1,2] sigmatropic shifts.[1] Therefore, they are of great interest in syntheses, especially in the preparation of larger heterocycles that contain main-group elements and C–C unsaturated bonds.

Such three-membered heterocyclic compounds with organic substituents at the two olefinic carbon atoms have been reported previously.[1–4] However, species with the simplest M(η^2-C_2H_2) moiety are either discussed on the basis of theoretical calculations,[5] or observed in metal-vapor deposition reactions at 12 K.[6] Among the AlC_2 ring compounds, Et(solvent)Al(η^2-C_2Ph_2) (solvent = Et_2O, THF) and ClAl(η^2-C_2R_2) (R = Me, Et) were assumed to be the respective intermediates in the formation of 1,4-(dialumina)cyclohexadiene and $(ClAl{\cdot}RC{\equiv}CR)_4$.[7] The bulky β-diketiminato ligand L (L = HC(C(Me)NAr)$_2$; Ar = 2,6-*i*Pr$_2$C$_6$H$_3$) was subsequently found to stabilize the ring of the Al(η^2-$C_2R^1R^2$) species (R^1, R^2: $SiMe_3$, Ph). Such compounds have been prepared by the reductive coupling of $LAlI_2$ and potassium in the presence of $R^1C{\equiv}CR^2$.[3] Species with the formula XAl(η^2-C_2H_2) (X = H, Cl) are supported in calculations, yet are considered unstable in comparison with the acyclic isomers.[5d–e] The IR and ESR spectroscopic data on matrix-isolated products from the reaction of AlCl with C_2H_2 confirm the results.[5e] Herein, we show the reaction of the aluminum(I) monomer LAl[8] directly with C_2H_2 in the temperature range from low to room temperature and the successful isolation of the first stable aluminacyclopropene LAl(η^2-C_2H_2) **1**. The subsequent reaction of **1** with C_2H_2 results in the product **2**: LAl(C≡CH)(CH=CH$_2$) (Scheme 1). The reaction of **1** with a large bulky organic azide leads to the unusual aluminaazacyclobutene insertion product **3**: LAl(CH=CHN(N=NAr*)) (Ar* = 2,6-Ar′$_2$C$_6$H$_3$, Ar′ = 2,4,6-Me$_3$C$_6$H$_2$) (Scheme 2).



Scheme 1. The stepwise reaction of LAl with C_2H_2 to **1** and **2**; L = HC(C(Me)NAr)$_2$; Ar = 2,6-*i*Pr$_2$C$_6$H$_3$



Scheme 2. The end-on insertion of N_3Ar* into **1** to form **3**; L = HC(C(Me)NAr)$_2$; Ar = 2,6-*i*Pr$_2$C$_6$H$_3$; Ar* = 2,6-Ar′$_2$C$_6$H$_3$; Ar′ = 2,4,6-Me$_3$C$_6$H$_2$

The reaction of LAl with an excess of carefully dried C_2H_2 in toluene was initially carried out in the temperature range of −78 °C to room temperature. The instant color change of the solution from red to orange and then the slow change to almost colorless was easily observed, and compound **2** was formed. Clearly, the formation of **2** indicates that LAl reacted with two molecules of C_2H_2. When this reaction was controlled in the temperature range between −78 and −50 °C, the red solution only changed to orange (this color change occurred even if the reaction was performed at ≈ −100 °C). By removal of unreacted C_2H_2, the 1:1 adduct LAl(η^2-C_2H_2) **1** was isolated. Notably, when this reaction was continued without the removal of excess C_2H_2, the corresponding ^{1}H NMR spectrum showed the formation of small amounts of **2**, whereas the reaction solution remained orange in color.

Compound **1** was obtained as an orange crystalline solid in quantitative yield and is extremely air-sensitive. Upon exposure to air, the orange color of the solution of **1** immediately becomes colorless. However, **1** is stable in an inert gas atmosphere. It is readily soluble in aromatic solvents and sparingly soluble in nonbranched hydrocarbons. Compound **2** is a colorless crystalline solid and is highly soluble in hydrocarbons. Compounds **1** and **2** were characterized by MS, ^{1}H and ^{13}C NMR spectroscopy, and by X-ray crystallography.[9a–b]

The structural analyses clearly reveal that compound **1** contains the simple Al(η^2-C_2H_2) moiety (Figure 1), whereas **2** contains terminal C≡CH and CH=CH$_2$ groups at the Al cen-

[*] Dipl.-Chem. H. Zhu, Dr. J. Chai, Prof. Dr. H. W. Roesky, Dr. C. He, Dr. V. Jancik, H.-G. Schmidt, Dr. M. Noltemeyer
Institut für Anorganische Chemie
Georg-August Universität Göttingen
Tammannstrasse 4, 37077 Göttingen (Germany)
Fax: (+49) 551-39-3373
E-mail: hroesky@gwdg.de
Dr. H. Fan
Labor für Physikalische und Theoretische Chemie
Universität Siegen
57068 Siegen (Germany)
W. A. Merrill, Prof. P. P. Power
Department of Chemistry
University of California, Davis
One Shields Avenue, Davis, CA 95616 (USA)

[**] This work was supported by the Göttinger Akademie der Wissenschaften. C.H. thanks the Alexander von Humboldt Foundation for a fellowship.

 InterScience © 2005 Wiley-VCH Verlag GmbH & Co. KGaA, Weinheim

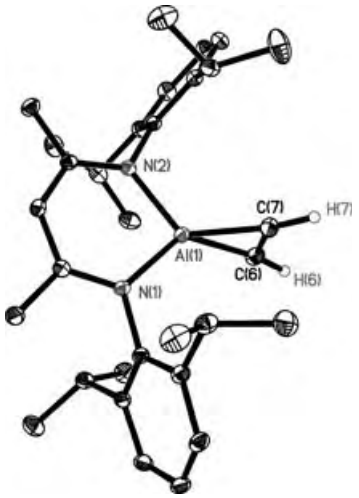


Figure 1. Molecular structure of LAl(η^2-C_2H_2) **1**. Protons in L are omitted for clarity. Selected bond lengths [Å] and angles [°]: Al(1)–N(1) 1.875(1), Al(1)–N(2) 1.884(1), Al(1)–C(6) 1.885(2), Al(1)–C(7) 1.878(2), C(6)–C(7) 1.358(2), C(6)–H(6) 1.000, C(7)–H(7) 1.021; N(1)-Al(1)-N(2) 97.98(5), C(6)-Al(1)-C(7) 42.30(7), Al(1)-C(6)-C(7) 68.57(10), Al(1)-C(7)-C(6) 69.13(10), H(6)-C(6)-C(7) 126.4, H(7)-C(7)-C(6) 127.1.

ter (Figure 2). The latter is the first crystallographically authenticated example of terminal C≡CH and CH=CH_2 groups attached to the same Al center. In **2**, the X-ray reflection data indicate that both CH=CH_2 and C≡CH groups are disordered in two positions (C(6)H(6)C(7)H(7)H(8), C(8)C(9)H(9), 62.2%; C(6A)H(6A)C(7A)H(7A)H(8A), C(8A)C(9A)H(9A), 37.8%). Thus, the central Al ion appears to have a disordered tetrahedral geometry with $\sphericalangle = 96.99(6)°$ for N–Al–N, and $\sphericalangle = 111.6(5)°$ for C–Al–C bond angles (av). The Al–N bond lengths in **1** (1.875(1), 1.884(1) Å) are close to those in **2** (1.895(1), 1.910(2) Å), and are similar to those observed in compounds with four-coordinate β-diketiminato aluminum(III) (1.888(2)–1.935(2) Å).[10] However, they are shorter than the Al–N bonds in LAl (1.957(2) Å) as a result of the Al^I center[8] having a larger radius than that of Al^{III}.

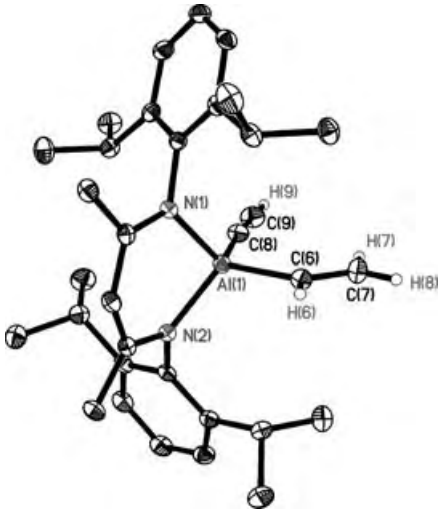


Figure 2. Molecular structure of LAl(C≡CH)(CH=CH_2) **2**, with both C≡CH and CH=CH_2 groups in 62.2% occupation. Protons in L are omitted for clarity. Selected bond lengths [Å] and angles [°]: Al(1)–N(1) 1.910(2), Al(1)–N(2) 1.895(1), Al(1)–C(6) 1.944(11), Al(1)–C(8) 1.962(11), C(6)–C(7) 1.325(17), C(8)–C(9) 1.173(11); N(1)-Al(1)-N(2) 96.99(6), C(6)-Al(1)-C(8) 110.8(4), Al(1)-C(6)-C(7) 124.6(12), Al(1)-C(8)-C(9) 173.9(13).

In **2**, the Al–C bond lengths (Al–$C_{C\equiv C}$ = 1.941(14) Å (av); Al–$C_{C=C}$ = 1.954(14) Å (av)) are similar to those in related compounds $LAlMe_2$ (1.955(4)–1.961(3) Å) and L′$AlMe_2$ (1.958(3)-1.970(3) Å, in which L′ = HC(C(Me)N-*p*-toluene)$_2$).[11] The C≡C (1.170(14) Å (av)) and C=C bond lengths (1.323(18) Å (av)) are indicative of characteristic C-C triple and double bonds, whereas the Al–C≡C (175.4(19)° (av)) and Al–C=C (124.6(14)° (av)) bond angles deviate from the ideal 180° and 120°, respectively.[12] The ^{1}H and ^{13}C NMR spectra of **2** confirm the functional CH=CH_2 and C≡CH groups at the Al center. In the Al–CH=CH_2 moiety, the corresponding protons resonate at $\delta = 5.70$–6.20 ppm; carbon resonances are at $\delta = 125.4$ (=CH_2) and 138.0 ppm (br, Al–*C*H=); both ^{1}H and ^{13}C NMR resonances are within the typical range for alkenyl groups. Furthermore, three groups of double doublets are observed and are indicative for these three protons in a nonequivalent steric environment. The Al–C≡CH group exhibits proton resonance at $\delta = 1.55$ ppm (s) and carbon resonances at $\delta = 94.6$ (br, ≡CH) and 137.3 ppm (br, Al–C≡). The absorptions at 1996 and 3270 cm^{-1} in the IR spectrum of **2** are tentatively assigned to the stretching frequencies of C≡C and ≡C–H bonds.

In **1**, the parameters within the Al(η^2-C_2H_2) moiety (Al–C 1.882(2) Å (av), C–C 1.358(2) Å, C–H 1.010 Å (av); $\sphericalangle$ C–Al–C 42.30(7)°, $\sphericalangle$ Al–C–C 68.85(10)° (av), $\sphericalangle$ H–C–C 126.6° (av)) fit well in comparison with those of Al(η^2-C_2) in LAl(η^2-$C_2R^1R^2$) (R^1 = $SiMe_3$, R^2 = Ph) (Al–C 1.889(2)–1.899(3) Å, C–C 1.356(5)–1.382(4) Å; C–Al–C $\sphericalangle$ 42.02(14)–42.57(11)°, Al–C–C $\sphericalangle$ 68.39(15)–68.80(19)°),[3] and are also much closer to those of the calculated HAl(η^2-C_2H_2) (Al–C 1.844–1.852 Å, C–C 1.362–1.384 Å, C–H 1.076–1.089 Å; H–C–C $\sphericalangle$ 126.8–127.3°).[5d] Notably, in the AlC_2 ring of **1** the average Al–C bond length is shorter than that of **2**, whereas the C–C bond length is longer (standard deviations of 0.072 and 0.036 Å, respectively). This may indicate a conjugated ring system in AlC_2. Furthermore, the ^{1}H and ^{13}C NMR spectra recorded in C_6D_6 show that the proton ($\delta = 8.82$ ppm (s)) and carbon resonances (177.2 ppm (br)) of the Al(η^2-C_2H_2) moiety are in the low-field region characteristic for the alkenyl system. These results indicate a certain aromatic character of the AlC_2 ring in **1**.

The reaction of **1** with a large bulky azide N_3Ar* shows an end-on azide insertion, resulting in the four-membered aluminaazacyclobutene LAl(CH=CHN(N=NAr*)) **3** (Scheme 2). A handful of reactions between monovalent Group 13 compounds and organic azides have been reported.[13] The initial N_2 elimination is generally accepted, and supported by experimental observations.[13e–f] The formation of a five-membered AlN_4 ring in LAl($(NSiMe_3)_2N_2$) was suggested to proceed through a [2+3] cycloaddition of an Al=N intermediate and N_3SiMe_3,[13d] whereas the disubstituted aluminacyclopropene LAl(η^2-$C_2(SiMe_3)_2$) reacted under disassociation and N_2 elimination with a similar bulky

 © 2005 Wiley-VCH Verlag GmbH & Co. KGaA, Weinheim

azide to an Al=N compound.[3] Accordingly, the end-on N_3Ar^* insertion into the Al–C bond unambiguously reveals the initial interaction between an Al center and the terminal N atom of the azide group. This type of reaction is, to the best of our knowledge, so far unknown. Compound **3** has been well-characterized by spectroscopic, analytical, and X-ray crystallographic measurements.[9c] The molecular structure of **3** is shown in Figure 3.

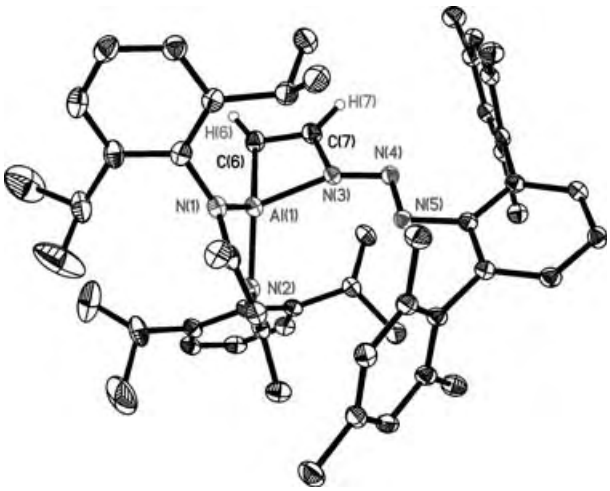


Figure 3. Molecular structure of LAl(CH=CHN(N=NAr*)) (**3**). Protons in L are omitted for clarity. Selected bond lengths [Å] and angles [°]: Al(1)–N(1) 1.866(2), Al(1)–N(2) 1.867(2), Al(1)–N(3) 1.892(2), Al(1)–C(6) 1.932(3), C(6)–C(7) 1.342(4), C(7)–N(3) 1.410(3), N(3)–N(4) 1.320(3), N(4)–N(5) 1.284(3); N(1)-Al(1)-N(2) 99.8(1), C(6)-Al(1)-N(3) 72.6(1), Al(1)-N(3)-C(7) 88.2(2), Al(1)-C(6)-C(7) 88.5(2), C(6)-C(7)-N(3) 110.7(2), N(3)-N(4)-N(5) 112.4(2).

In summary, we have isolated the stable aluminacyclopropene LAl(η^2-C_2H_2) **1** from the reaction of LAl with one equivalent C_2H_2. Further reaction of **1** with another equivalent of C_2H_2 yields LAl(C≡CH)(CH=CH_2) **2**. This may be considered as a prebiotic reaction owing to Al^I species (AlF) and acetylene having been detected spectroscopically in dense interstellar clouds.[14] The crystallographic and NMR spectral data of **1** indicate an electron-delocalized AlC_2 heterocycle, which can be described as a Hückel 2π aromatic system. The Schmidt degradation and Curtius rearrangement of $RC(O)N_3$ to RN=C=O with the elimination of N_2 was described 105 years ago,[15] and the Staudinger reaction in which R_3P interacts with N_3R' via the R_3PNNNR' intermediate to form R_3P=NR′ with the elimination of N_2 was reported in 1919.[16] The reaction of **1** with N_3Ar^* results in an end-on azide insertion to yield an aluminaazacyclobutene LAl(CH=CHN(N=NAr*)) **3**: a novel finding in which degradation or rearrangement of the N_3 moiety is not observed. This reflects the unusual trapping ability of **1**. Current work is focused on experimental confirmation by using **1** to trap small molecules such as NO, N_2O, and CO.

Experimental Section

All manipulations were carried out under a purified nitrogen atmosphere using Schlenk techniques or inside a glove box filled with dry nitrogen in which the calibrated values of O_2 and H_2O were strictly controlled to below 1 ppm.

1: A toluene solution (30 mL) of LAl (0.22 g, 0.5 mmol) at decreased pressure was cooled to −78 °C and exposed to dried C_2H_2. This mixture was kept in the temperature range of −78 °C to −50 °C for 2 h. An instant color change of the solution from red to orange was observed. All volatiles were removed, and an orange crystalline solid of **1** was afforded (> 95 %); m.p. 219 °C; IR (Nujol): $\tilde{\nu}$ = 442.7(w), 529.1(w), 589.8(m), 613.5(w), 647.4(w), 712.7(m), 748.3(w), 758.5(w), 778.2(w), 801.0(s), 867.7(w), 893.9(w), 936.7(w), 1026.0(m), 1055.6(w), 1100.6(m), 1177.4(w), 1260.7(m), 1304.9(w), 1318.7(w), 1410.5(s), 1485.6(s), 1532.8(m), 1653.7(w) cm^{-1}; ^1H NMR (500.13 MHz, [D_6]benzene, 25 °C, TMS): δ = 1.12 (d, ^3J = 6.9 Hz, 4 × 3 H, $CH(CH_3)_2$), 1.46 (d, ^3J = 6.9 Hz, 4 × 3 H, $CH(CH_3)_2$), 1.53 (s, 2 × 3 H, β-CH_3), 3.33 (sept, ^3J = 6.9 Hz, 4 × 1 H, $CH(CH_3)_2$), 4.89 (s, 1 H, γ-CH), 7.02–7.12 (m, 6 H, Ar-*H*), 8.82 ppm (s, 2 × 1 H, Al-η^2-C_2H_2); ^{13}C NMR (125.77 MHz, C_6D_6, 25 °C, TMS): δ = 23.4, 24.4, 24.6, 28.9 ($CH(CH_3)_2$, β-CH_3), 96.5 (γ-*C*), 124.4, 138.8, 143.9 (Ar-*C*), 172.8 (*C*N), 177.2 ppm (broad, Al-η^2-C_2); ^{27}Al NMR (77.13 MHz, C_6D_6, 25 °C, $AlCl_3$): signal too broad to be observed. ^{27}Al NMR (77.13 MHz, [D_8]toluene, −70 °C, $AlCl_3$): signal too broad to be observed. MS: *m*/*z* (%): 469.3 (20) [M^+−1], 455.3 (30) [M^+−Me], 429.3 (100) [M^+−Me−C_2H_2]; elemental analysis (%) calcd for $C_{31}H_{43}AlN_2$ (470.68): C 79.10, H 9.21, N 5.95; found: C 79.43, H 9.18, N 6.03. Single crystals of **1** were obtained by keeping the *n*-hexane/toluene solution of **1** at −26 °C for one week. TMS = tetramethylsilane.

2: The initial procedure (LAl (0.22 g, 0.5 mmol), C_2H_2 (excess), and toluene (30 mL)) is the same as the synthesis of **1**. At −50 °C, the mixture was stirred and warmed to ambient temperature within 48 h, the color of the solution slowly turned to almost colorless. All volatiles were removed in vacuum and the residue was washed with *n*-hexane (2 mL) to afford a colorless crystalline solid of **2** (0.22 g, 90 %); m.p. 163 °C; IR (Nujol): $\tilde{\nu}$ = 1992 (C≡C), 3277 cm^{-1} (≡CH); ^1H NMR (500.13 MHz, [D_8]toluene, 25 °C, TMS): δ = 1.08 (d, ^3J = 6.8 Hz, 2 × 3 H, $CH(CH_3)_2$), 1.25 (d, ^3J = 6.8 Hz, 2 × 3 H, $CH(CH_3)_2$), 1.28 (d, ^3J = 6.8 Hz, 2 × 3 H, $CH(CH_3)_2$), 1.44 (d, ^3J = 6.8 Hz, 2 × 3 H, $CH(CH_3)_2$), 1.55 (s, 2 × 3 H, β-CH_3), 1.73 (s, 1 H, C≡C*H*), 3.23 (sept, ^3J = 6.8 Hz, 2 × 1 H, $CH(CH_3)_2$), 3.81 (sept, ^3J = 6.8 Hz, 2 × 1 H, $CH(CH_3)_2$), 4.91 (s, 1 H, γ-CH), 5.79 (dd, $^3J_{(trans)}$ = 20.9 Hz, ^2J = 6.4 Hz, 1 H), 6.04 (dd, $^3J_{(cis)}$ = 16.5 Hz, ^2J = 6.4 Hz, 1 H), 6.12 (dd, $^3J_{(trans)}$ = 20.9 Hz, $^3J_{(cis)}$ = 16.5 Hz, 1 H), (*CH*=CH_2), 6.97–7.12 ppm (m, 6 H, Ar-*H*); ^{13}C NMR (125.76 MHz, [D_8]toluene, 25 °C, TMS): δ = 23.4, 24.5, 24.7, 24.8, 27.2, 28.2, 28.6 ($CH(CH_3)_2$, β-CH_3), 94.6 (broad, ≡CH), 98.4 (γ-*C*), 124.1, 124.8, 127.5, 128.8, 129.2, 137.1, 140.3, 143.7, 145.4 (Ar-*C*), 125.4, (=CH_2), 137.3 (broad, Al-*C*≡), 138.0 (broad, Al-*C*=), 170.6 ppm (*C*N); MS: *m*/*z* (%): 496.4 (15) [M^+], 469.4 (100) [M^+−CH=CH_2]; elemental analysis (%) calcd for $C_{33}H_{45}AlN_2$ (496.72): C 79.80, H 9.13, N 5.64; found: C 79.26, H 9.18, N 5.56. Single crystals of **2** were grown from the *n*-hexane solution of **2** at 4 °C within one week.

3: Toluene (25 mL) was added to a mixture of **1** (0.24 g, 0.5 mmol) and N_3Ar^* (0.18 g, 0.5 mmol) at −50 °C. The suspension was stirred and allowed to warm to room temperature. After stirring for 12 h, removal of the solvent and washing with *n*-hexane (2 mL) afforded **3** as an orange crystalline solid (0.37 g, 90 %); m.p. 215 °C; ^1H NMR (300.13 MHz, [D_6]benzene, 25 °C, TMS): δ = 1.02 (d, ^3J = 6.8 Hz, 2 × 3 H, $CH(CH_3)_2$), 1.05 (d, ^3J = 6.8 Hz, 2 × 3 H, $CH(CH_3)_2$), 1.16 (d, ^3J = 6.8 Hz, 4 × 3 H, $CH(CH_3)_2$), 1.50 (s, 2 × 3 H, β-CH_3), 2.23 (s, 2 × 3 H), 2.27 (s, 4 × 3 H, *Me*(in Ar′)), 2.83 (sept, ^3J = 6.8 Hz, 2 × 1 H, $CH(CH_3)_2$), 3.03 (sept, ^3J = 6.8 Hz, 2 × 1 H, $CH(CH_3)_2$), 4.92 (s, 1 H, γ-CH), 5.03 (d, $^3J_{(cis)}$ = 7.6 Hz, 1 H), 7.51 (d, $^3J_{(cis)}$ = 7.6 Hz, 1 H), (*HC*=C*H*), 6.83, 6.97–7.12 (m), 7.15 ppm (14 H, Ar-*H*, Ar*-*H*, Ar′-*H*); ^{13}C NMR (75.47 MHz, [D_6]benzene, 25 °C, TMS): δ = 21.3, 22.3, 23.0, 23.2, 24.4, 24.7, 25.0, 25.8, 26.7, 29.1, 31.9 ($CH(CH_3)_2$, β-CH_3, *Me*(Ar′)), 100.5 (γ-*C*), 114.8 (broad, Al-*C*=), 123.5, 123.8, 125.1, 130.9, 134.2, 136.0, 138.5, 141.6, 146.2, 147.3 (Ar-*C*, Ar*-*C*, Ar′-*C*), 162.4 (N-*C*(H)=), 171.9 ppm (*C*N); MS: *m*/*z* (%): 825 (5) [M^+−1], 417 (100) [M^+−N_3Ar^*−C_2H_2−Al]; elemental analysis (%) calcd for $C_{55}H_{68}AlN_5$ (826.17): C 79.96, H 8.30, N 8.48; found: C 79.28,

 © 2005 Wiley-VCH Verlag GmbH & Co. KGaA, Weinheim

H 8.38, N 8.42. Single crystals of **3**·0.5 *n*-hexane were grown from the *n*-hexane/toluene solution of **3** at 4 °C within 5 days.

Received: March 10, 2005
Published online: July 14, 2005

Keywords: alkenes · alkynes · aluminum · azides · metallacycles

[1] E. Roskamp, C. Roskamp in *Comprehensive Heterocyclic Chemistry II*, *Vol. 2* (Eds.: A. R. Katritzky, C. W. Rees, E. F. V. Scriven), Pergamon, Oxford, **1996**, pp. 305–332.

[2] a) A. Krebs, J. Berndt, *Tetrahedron Lett.* **1983**, *24*, 4083–4086; b) M. P. Egorov, S. P. Kolesnikov, Y. T. Struchkov, Y. M. Antipin, S. V. Sereda, O. M. Nefedov, *J. Organomet. Chem.* **1985**, *290*, C27-C30; c) L. R. Sita, R. D. Bicherstaff, *J. Am. Chem. Soc.* **1988**, *110*, 5208–5209; d) W. Ando, H. Ohgaki, Y. Kabe, *Angew. Chem.* **1994**, *106*, 723–725; *Angew. Chem. Int. Ed. Engl.* **1994**, *33*, 659–661.

[3] C. Cui, S. Köpke, R. Herbst-Irmer, H. W. Roesky, M. Noltemeyer, H.-G. Schmidt, B. Wrackmeyer, *J. Am. Chem. Soc.* **2001**, *123*, 9091–9098.

[4] W. Uhl, T. Spies, R. Koch, W. Saak, *Organometallics* **1999**, *18*, 4598–4602.

[5] a) M. H. Lien, A. C. Hopkinson, *Chem. Phys. Lett.* **1981**, *80*, 114–118; b) M. S. Gordan, R. D. Koob, *J. Am. Chem. Soc.* **1981**, *103*, 2939–2944; c) J. A. Boatz, M. S. Gordan, L. D. Sita, *J. Phys. Chem.* **1990**, *94*, 5488–5493; d) Y. Xie, H. F. Schaefer III, *J. Am. Chem. Soc.* **1990**, *112*, 5393–5400; e) H.-G. Himmel, *Organometallics* **2003**, *22*, 2679–2687.

[6] T. R. Burkholder, L. Andrews, *Inorg. Chem.* **1993**, *32*, 2491–2496.

[7] a) H. Hoberg, V. Gotor, A. Milchereit, C. Krüger, J. C. Sekutowski, *Angew. Chem.* **1977**, *89*, 563–564; *Angew. Chem. Int. Ed. Engl.* **1977**, *16*, 539–540; b) H. Hoberg, F. Aznar, *J. Organomet. Chem.* **1979**, *164*, C13-C15; c) H. Schnöckel, M. Leimkühler, R. Lotz, R. Mattes, *Angew. Chem.* **1986**, *98*, 929–930; *Angew. Chem. Int. Ed. Engl.* **1986**, *25*, 921–922; d) C. Üffing, A. Ecker, R. Köppe, K. Merzweiler, H. Schnöckel, *Chem. Eur. J.* **1998**, *4*, 2142–2147.

[8] C. Cui, H. W. Roesky, H.-G. Schmidt, M. Noltemeyer, H. Hao, F. Cimpoesu, *Angew. Chem.* **2000**, *112*, 4444–4446; *Angew. Chem. Int. Ed.* **2000**, *39*, 4274–4276.

[9] a) Crystal data for **1**: $C_{31}H_{43}AlN_2$, $M_r = 470.65$, monoclinic, space group $P2_1/n$, $a = 12.199(1)$, $b = 16.932(1)$, $c = 13.974(1)$ Å, $\beta = 103.87(1)°$, $V = 2802(1)$ Å^3, $Z = 4$, $\rho_{calcd} = 1.116$ Mg m^{-3}, $F(000) = 1024$, $\lambda = 0.71073$ Å, $T = 133(2)$ K, $\mu(Mo_{K\alpha}) = 0.093$ mm^{-1}; 29105 measured reflections, 4818 independent ($R_{int} = 0.0486$). The final refinements converged at $R1 = 0.0349$ and $wR2 = 0.0867$ for $I > 2\sigma(I)$ and $R1 = 0.0502$ and $wR2 = 0.0916$ for all data. Fourier synthesis gave a min/max residual electron density $-0.255/+0.263$ e Å^3; b) crystal data for **2**: $C_{33}H_{45}AlN_2$, $M_r = 496.69$, monoclinic, space group $P2_1/n$, $a = 18.844(4)$, $b = 8.732(2)$, $c = 20.080(4)$ Å, $\beta = 112.61(1)°$, $V = 3050(1)$ Å^3, $Z = 4$, $\rho_{calcd} = 1.082$ Mg m^{-3}, $F(000) = 1080$, $\lambda = 0.71073$ Å, $T = 133(2)$ K, $\mu(Mo_{K\alpha}) = 0.089$ mm^{-1}; 14544 measured reflections, 5145 independent ($R_{int} = 0.0394$). The final refinements converged at $R1 = 0.0364$ and $wR2 = 0.0820$ for $I > 2\sigma(I)$ and $R1 = 0.0582$ and $wR2 = 0.0877$ for all data. Fourier synthesis gave a min/max residual electron density $-0.208/+0.163$ e Å^3; c) crystal data for **3**: $C_{58}H_{75}AlN_5$, $M_r = 869.21$, monoclinic, space group $P2_1/c$, $a = 22.289(5)$, $b = 13.057(3)$, $c = 18.765(4)$ Å, $\beta = 109.71(3)°$, $V = 5141(2)$ Å^3, $Z = 4$, $\rho_{calcd} = 1.123$ Mg m^{-3}, $F(000) = 1884$, $\lambda = 0.71073$ Å, $T = 133(2)$ K, $\mu(Mo_{K\alpha}) = 0.081$ mm^{-1}; 53490 measured reflections, 8850 independent ($R_{int} = 0.0825$). The final refinements converged at $R1 = 0.0560$ and $wR2 = 0.1371$ for $I > 2\sigma(I)$ and $R1 = 0.0933$ and $wR2 = 0.1508$ for all data. Fourier synthesis gave a min/max residual electron density $-0.437/+0.589$ e Å^3. The crystallographic data for **1**–**3** were collected on a Stoe IPDS II-array detector system using graphite-monochromated $Mo_{K\alpha}$ radiation ($\lambda = 0.71073$ Å). Intensity measurements were performed on a rapidly cooled crystal with dimensions $0.40 \times 0.40 \times 0.30$ mm^3 in the range $1.92 \le \theta \le 24.83°$ for **1**, with $0.30 \times 0.30 \times 0.30$ mm^3 in $1.89 \le \theta \le 24.82°$ for **2**, and with $0.20 \times 0.10 \times 0.10$ mm^3 in $1.84 \le \theta \le 24.87°$ for **3**. The structures were solved by direct methods (SHELXS-97)[17] and refined with all data by full-least-squares against F^2.[18] The non-hydrogen atoms were located by difference Fourier synthesis and refined anisotropically, in which the C≡CH and CH=CH_2 groups in **2** are both disordered and located in two positions with the same occupation ratio of 0.622/0.378. The hydrogen atoms except for H(6) and H(7) in **1** and **3** were included in geometrically idealized positions with the *U*iso tied to that of the parent atoms and were refined with the riding model. H(6) and H(7) in **1** and **3** were located by difference Fourier synthesis and refined isotropically. CCDC-265784 (**1**), 265785 (**2**), and 265786 (**3**) contain the supplementary crystallographic data for this paper. These data can be obtained free of charge from the Cambridge Crystallographic Data Centre via www.ccdc.cam.ac.uk/data_request/cif.

[10] a) C. Cui, H. W. Roesky, H. Hao, H.-G. Schmidt, M. Noltemeyer, *Angew. Chem.* **2000**, *112*, 1885–1887; *Angew. Chem. Int. Ed.* **2000**, *39*, 1815–1817; b) V. Jancik, Y. Peng, H. W. Roesky, J. Li, D. Neculai, A. M. Neculai, R. Herbst-Irmer, *J. Am. Chem. Soc.* **2003**, *125*, 1452–1453; c) G. Bai, H. W. Roesky, J. Li, M. Noltemeyer, H.-G. Schmidt, *Angew. Chem.* **2003**, *115*, 5660–5664; *Angew. Chem. Int. Ed.* **2003**, *42*, 5502–5506; d) V. Jancik, L. W. Pineda, J. Pinkas, H. W. Roesky, D. Neculai, A. M. Neculai, R. Herbst-Irmer, *Angew. Chem.* **2004**, *116*, 2194–2197; *Angew. Chem. Int. Ed.* **2004**, *43*, 2142–2145.

[11] B. Qian, D. L. Ward, M. R. Smith III, *Organometallics* **1998**, *17*, 3070–3076.

[12] Structural parameters for C_2H_4 in gas phase: C–C 1.330 Å, C–H, 1.076 Å, C–C–H 121.7°, H–C–H 116.6°; for C_2H_2: C–C 1.203 Å, C–H 1.061 Å, C–C–H 180°: K. P. C. Vollhardt, N. E. Schore in *Organic Chemistry (3rd ed.)*, W. H. Freeman and Company (New York), **1998**, p. 438, 543.

[13] a) S. Schulz, L. Häming, R. Herbst-Irmer, H. W. Roesky, G. M. Sheldrick, *Angew. Chem.* **1994**, *106*, 1052–1054; *Angew. Chem. Int. Ed. Engl.* **1994**, *33*, 969–971; b) S. Schulz, A. Voigt, H. W. Roesky, L. Häming, R. Herbst-Irmer, *Organometallics* **1996**, *15*, 5252–5253; c) P. Jutzi, B. Neumann, G. Reumann, H.-G. Stammler, *Organometallics* **1999**, *18*, 2037–2040; d) C. Cui, H. W. Roesky, H.-G. Schmidt, M. Noltemeyer, *Angew. Chem.* **2000**, *112*, 4705–4707; *Angew. Chem. Int. Ed.* **2000**, *39*, 4531–4533; e) N. J. Hardman, C. Cui, H. W. Roesky, W. H. Fink, P. P. Power, *Angew. Chem.* **2001**, *113*, 2230–2232; *Angew. Chem. Int. Ed.* **2001**, *40*, 2172–2174; f) R. J Wright, A. D. Phillips, T. L. Allen, W. H. Fink, P. P. Power, *J. Am. Chem. Soc.* **2003**, *125*, 1694–1695; g) H. Zhu, J. Chai, V. Chandrasekhar, H. W. Roesky, J. Magull, D. Vidovic, H.-G. Schmidt, M. Noltemeyer, P. P. Power, W. A. Merrill, *J. Am. Chem. Soc.* **2004**, *126*, 9472–9473.

[14] a) I. W. M. Smith, *Chem. Soc. Rev.* **2002**, *31*, 137–146; b) H.-P. Gail, E. Sedlmayr, *Faraday Discuss.* **1998**, *109*, 303–319.

[15] J. D. Roberts, M. C. Caserio in *Basic Principles of Organic Chemistry*, W. A. Benjamin, New York, **1964**, p. 656.

[16] D. E. C. Corbridge in *Phosphorus (An Outline of Its Chemistry, Biochemistry and Technology)*, 3rd ed., Elsevier Science Publishers, Dordrecht, **1985**, p. 335.

[17] SHELXS-90, *Program for Structure Solution* G. M. Sheldrick, *Acta Crystallogr. Sect. A* **1990**, *46*, 467–473.

[18] SHELXL-97, *Program for Crystal Structure Refinement* G. M. Sheldrick, University of Göttingen, Germany, **1997**.

 © 2005 Wiley-VCH Verlag GmbH & Co. KGaA, Weinheim

Synthetic Methods

DOI: 10.1002/anie.200500838

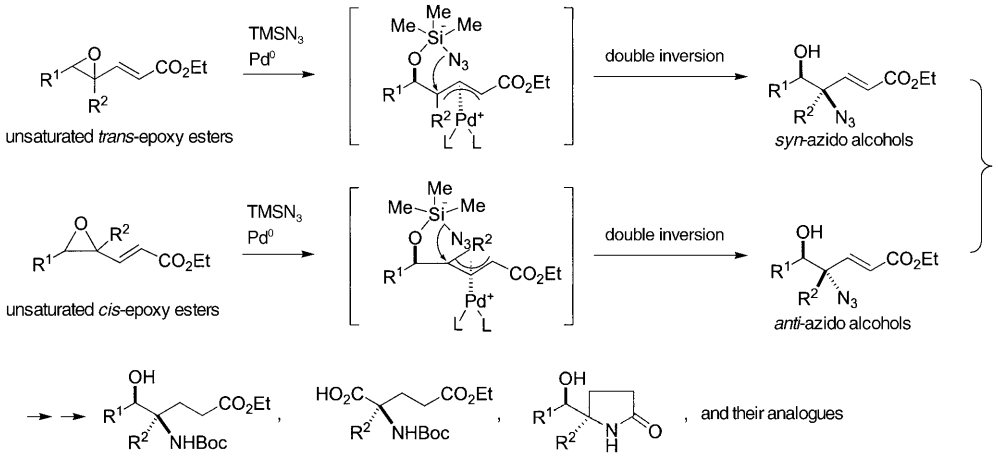
Pd-Catalyzed Stereospecific Azide Substitution of α,β-Unsaturated γ,δ-Epoxy Esters with Double Inversion of Configuration**

Masaaki Miyashita, Taiku Mizutani, Genta Tadano, Yasuhiro Iwata, Masahiro Miyazawa, and Keiji Tanino*

Over recent years, much interest has been focused on the development of not only a stereoselective but also a practical methodology for the synthesis of chiral β-amino alcohols,[1] α-amino acids,[2] and α,α-disubstituted amino acids[2–4] (including natural and unnatural congeners) in the context of medicinal chemistry. Although many synthetic approaches to these biologically important compounds have been reported,[1–4] there is still a need for a new type of methodology that allows the stereospecific synthesis of functionalized amino alcohols and amino acids that bear contiguous chiral centers. We report herein an approach that permits the highly stereoselective synthesis of a variety of amino alcohols, amino acids, and quaternary amino acids, including acyclic and cyclic congeners. This methodology involves the palladium-catalyzed stereospecific azide substitution reaction of α,β-unsaturated γ,δ-epoxy esters with a double inversion of configuration as the key step.

In connection with our recent studies on the palladium-catalyzed stereospecific hydroxy substitution reactions of unsaturated γ,δ-epoxy esters with phenylboronic acid[5] and boric acid[6] with a double inversion of configuration, we anticipated that the palladium-catalyzed azide substitution reaction of α,β-unsaturated γ,δ-epoxy esters with an appropriate azide reagent might occur by a similar π-allyl palladium species to afford an azide substitution product with double inversion of configuration, as shown in Scheme 1. Namely, this new method involves two consecutive S_N2 processes to afford a substitution product with double inversion of configuration in contrast with the normal S_N2 epoxide-opening reactions.[7]

Initially, we chose ethyl *trans*-4,5-epoxy-(2*E*)-octenoate (**1**)[5] as a model substrate and examined its palladium-catalyzed reaction with $TMSN_3$ to confirm whether such a reaction indeed takes place. Thus, first $TMSN_3$ (2 equiv) then



Scheme 1. Pd^0-catalyzed stereospecific azide substitution reaction of unsaturated γ,δ-epoxy esters with double inversion of configuration. TMS = trimethylsilyl, Boc = *tert*-butoxycarbonyl, L = ligand.

a palladium catalyst ($[Pd(PPh_3)_4]$ (10 mol %)) was added to a solution of **1** in THF and the mixture was stirred at room temperature for 20 minutes. The reaction was then quenched with a solution of citric acid in MeOH. The azide substitution reaction of **1** with double inversion of configuration did occur at the γ-position to afford a single *syn* azido alcohol **2** in 90 % yield of the isolated product after purification by chromatography on silica gel (Scheme 2). The configuration of the product was unambiguously determined by NOE interaction studies of its δ-lactone derivative **3**, which was readily derived from **2** by catalytic hydrogenation in the presence of di-*tert*-butyl dicarbonate (Boc_2O)[8] followed by lactonization with PPTS in dichloroethane (Scheme 2). It should be noted that the present palladium-catalyzed azide substitution reaction took place not only in high yield but also with complete stereoselectivity, thus giving rise to the single product with a double inversion of configuration.

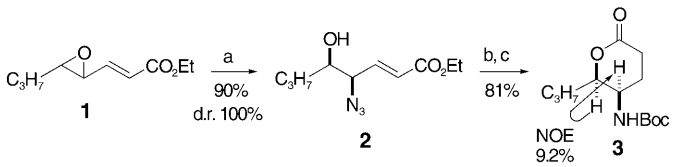
[*] Prof. Dr. M. Miyashita, T. Mizutani, G. Tadano, Dr. Y. Iwata, Dr. M. Miyazawa,[+] Dr. K. Tanino
Division of Chemistry
Graduate School of Science, Hokkaido University
060-0810 Sapporo (Japan)
Fax: (+81) 11-706-4920
E-mail: miyasita@sci.hokudai.ac.jp

[+] Present Address:
Department of Chemistry
Faculty of Science, Toyama University
930-8555 Toyama (Japan)

[**] Financial support from the Ministry of Education, Culture, Sports, Science, and Technology, Japan (a Grant-in-Aid for Scientific Research (A) (No. 12304042), a Grant-in-Aid for Scientific Research (B) (No. 16350049), and a Grant-in-Aid for Scientific Research on Priority Areas (A) "Exploitation of Multielement Cyclic Molecules" (No. 13029003)) is gratefully acknowledged.

Supporting information for this article is available on the WWW under http://www.angewandte.org or from the author.

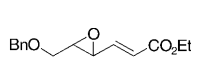
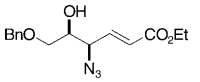
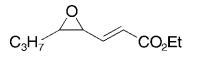
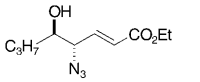
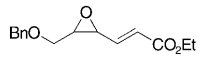
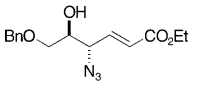
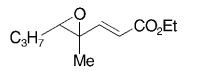
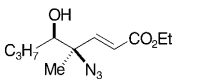
InterScience
© 2005 Wiley-VCH Verlag GmbH & Co. KGaA, Weinheim



Scheme 2. Pd^0-catalyzed azide substitution reaction of ethyl *trans*-4,5-epoxy-(2*E*)-octenoate (**1**): a) $TMSN_3$ (2 equiv), $[Pd(PPh_3)_4]$ (10 mol%), THF, RT, 20 min (90%); b) H_2, PtO_2, Boc_2O, EtOAc, RT, 5 h (84%); c) PPTS, $ClCH_2CH_2Cl$, 90°C, 3 h (96%). Ac = acetate, PPTS = pyridinium *para*-toluenesulfonate, Boc = *tert*-butoxycarbonyl.

These excellent preliminary results led us to examine the scope of the new synthetic methodology with various substrates (Table 1). Thus, the reaction of ethyl 6-benzyloxy-*trans*-4,5-epoxy-(2*E*)-hexenoate (**4**) proceeded cleanly to furnish the *syn* azido alcohol **5** as a single product in 97% yield (Table 1, entry 1). On the other hand, the reaction of a unsaturated *cis* epoxy ester **6** afforded an *anti* azido alcohol **7** in 95% yield (Table 1, entry 2), and a benzyloxy-substituted substrate **8** similarly produced the *anti* isomer **9** in 93% yield with complete stereoselectivity (Table 1, entry 3). Furthermore, a trisubstituted unsaturated epoxy ester **10** containing a methyl group at the γ-position reacted smoothly to produce a *syn tert*-azido alcohol **11** in 93% yield. It is critical to add $TMSN_3$ first to the substrate in solution then the palladium catalyst for a successful reaction. Thus, the palladium-catalyzed azide substitution reaction of acyclic unsaturated γ,δ-epoxy esters was shown to occur stereospecifically at the γ-position with complete stereoselectivity, namely, with double inversion of configuration, regardless of the configuration and substitution pattern of the epoxide substrates.

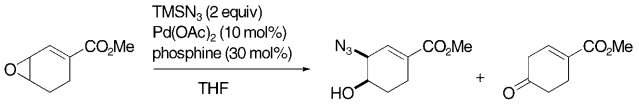
Table 1: Pd^0-catalyzed azide substitution reactions of acyclic α,β-unsaturated γ,δ-epoxy esters with $TMSN_3$ in THF.[a]

Entry	Substrate		*t*	Product		Yield [%][b]	*syn*/*anti*
1		**4**	20 min		**5**	97	>99:1
2		**6**	1 h		**7**	95	>1:99
3		**8**	2 h		**9**	93	>1:99
4		**10**	8 h		**11**	93	>99:1

[a] The reaction was carried out with $TMSN_3$ (2 equiv) and $[Pd(PPh_3)_4]$ (10 mol%) in THF at room temperature. [b] Yield of isolated product. Bn = benzyl.

Next, we focused on the azide substitution reaction of cyclic unsaturated epoxy esters, since Tsuda, Saegusa, and coworkers reported that the Pd^0-catalyzed reaction of an α,β-unsaturated γ,δ-epoxy ester containing a cyclohexane ring with nitrogen nucleophiles did not produce the corresponding substitution products at all.[9] To probe the behavior of cyclic substrates, we initially examined the reaction of methyl 3,4-epoxy-1-cylochexenecarboxylate (**12**).[10] Contrary to our expectations, however, the reaction of **12** under the same conditions as those for acyclic substrates was fruitless. Namely, the reaction of **12** with $TMSN_3$ (2 equiv), $Pd(OAc)_2$ (10 mol%), and PPh_3 (30 mol%) in THF afforded ketone **14** as the unexpected major product (61% yield), along with a smaller amount of the desired product **13** (37% yield; Table 2, entry 1). Therefore, we examined in detail the effect of a phosphine ligand on the reaction, and it was found that the azide substitution reaction of **12** was critically dependent on the nature of the phosphine ligand: The use of $PnBu_3$ was totally ineffective, and a large amount of the starting material was recovered (Table 2, entry 2). Similarly, the reaction with a bulky phosphine, such as $P(C_6H_{11})_3$, $P(tolyl)_3$, or $PtBu_3$, merely resulted in the recovery of the starting material. However, the use of $P(OiPr)_3$ gave a similar result to that of PPh_3 (Table 2, entry 3). In contrast to these ligands, P(2-furyl)$_3$ was found to improve this particular reaction dramatically. Thus, the reaction of **12** with $TMSN_3$ (2 equiv), $Pd(OAc)_2$ (10 mol%), and P(2-furyl)$_3$ (30 mol%) in THF produced the desired product **13** in 87% yield along with 13% yield of **14** (Table 2, entry 4). It is noteworthy that the reaction with P(2-furyl)$_3$ was very fast and was completed in 5 minutes at 0°C, thus producing **13** in high yield. The configuration of **13** was determined unambiguously by X-ray crystallographic analysis of its *para*-bromobenzoate derivative. In turn, we examined the stoichiometry in which P(2-furyl)$_3$ was added and the effect of the solvent on the reaction, and it was found eventually that the use of 25 mol% of P(2-furyl)$_3$ in THF gave the best result. Under these conditions, the desired product **13** was obtained in 96% yield of isolated product and the formation of **14** was suppressed to less than 4% (Table 2, entry 5).[11]

Table 2: Pd^0-catalyzed azide substitution reactions of cyclic unsaturated γ,δ-epoxy ester **12** with $TMSN_3$ in THF.[a]



12 **13** **14**

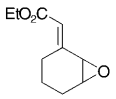
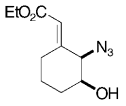
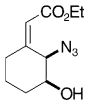
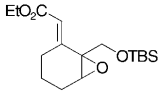
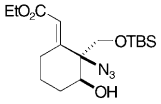
Entry	Phosphine	*T* [°C]	*t*	Yield [%] **13**	**14**
1	PPh_3	RT	5 min	37	61
2	$PnBu_3$	0→50	4 h	<2	10
3	$P(OiPr)_3$	0	5 min	39	57
4	P(2-furyl)$_3$	0	5 min	87	13
5[b]	P(2-furyl)$_3$	0	5 min	96	4

[a] The reaction was carried out by adding a premixed solution of $Pd(OAc)_2$ (5 mol%) and P(2-furyl)$_3$ (30 mol%) in THF. [b] The reaction was carried out with 25 mol% of P(2-furyl)$_3$.

 © 2005 Wiley-VCH Verlag GmbH & Co. KGaA, Weinheim

We then applied these optimized conditions to various cyclic substrates (Table 3). Both the *Z*-unsaturated ester **17**[12] and the cyclic *E*-unsaturated γ,δ-epoxy ester **15**[12] (as seen previously) were found to react smoothly under these conditions (Table 3, entries 2 and 1, respectively), thus furnishing the corresponding azide substitution products **18** and **16**, respectively. It should be noted that products **16** and **18** were obtained in remarkably high yields, whereas they had been inaccessible using the previously reported method.[9] Contrary to our expectations, a trisubstituted unsaturated epoxy ester **19**[13] did not react at all under similar conditions and the starting material was recovered (Table 3, entry 3). Fortunately, we found that the reaction of **19** with $TMSN_3$ and $[Pd(PPh_3)_4]$ in *N*,*N*-dimethylformamide (DMF) proceeded smoothly at 50 °C and gave rise to the desired product **20** in 92% yield (Table 3, entry 4).[14] These results demonstrate unambiguously that the palladium-catalyzed azide substitution reaction of unsaturated γ,δ-epoxy esters with acyclic and cyclic substrates occurs stereospecifically at the γ-position with double inversion of configuration, thus producing azido alcohols in high yields regardless of the stereochemistry of the epoxide and unsaturated ester moieties.

Table 3: Pd^0-catalyzed azide substitution reactions of cyclic unsaturated epoxy esters with $TMSN_3$.[a]

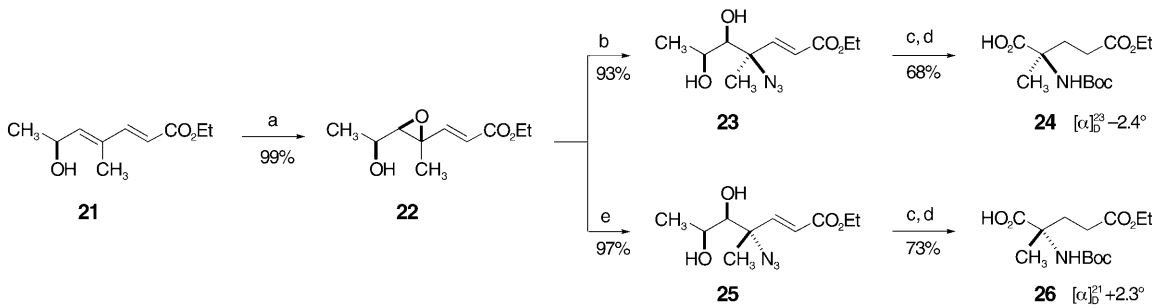
Entry	Substrate		Ligand	Solvent	*t* [h]	Product		Yield [%]
1[b]		**15**	$P(2\text{-furyl})_3$	THF	1		**16**	98
2		**17**	$P(2\text{-furyl})_3$	THF	1		**18**	quant.
3		**19**	$P(2\text{-furyl})_3$	THF	4		**20**	trace
4[c]		**19**	PPh_3	DMF	6		**20**	92

[a] The reaction was carried out by adding a mixture of $Pd(OAc)_2$ (5 mol%) and the phosphine (25 mol%) in THF to a solution of each substrate and $TMSN_3$ (2 equiv) in THF at room temperature. [b] After the reaction mixture had been stirred for 50 min at room temperature, $Pd(OAc)_2$ (5 mol%) and the phosphine (25 mol%) were added and then the mixture was stirred for an additional 10 min at room temperature. [c] The reaction was carried out in DMF at 50 °C using $TMSN_3$ (2 equiv) and $[Pd(PPh_3)_4]$ (10 mol%); $[Pd(PPh_3)_4]$ (10 mol%) was added after 2.5 and 4.5 h, respectively. TBS = *tert*-butyldimethylsilyl, quant. = quantitative yield.

To demonstrate the synthetic potential of the current method, we performed a stereospecific synthesis of both (*R*)- and (*S*)-*N*-*tert*-butoxycarbonyl-α-methylglutamic acid γ-ethyl ester (**24** and **26**, respectively; Scheme 3). Thus, treatment of the diene ester **21**, which is readily derived from ethyl (*S*)-lactate, with *meta*-chloroperoxybenzoic acid (*m*CPBA) in CH_2Cl_2 led to unsaturated β-epoxy ester **22** being obtained as a single product in quantitative yield. When the unsaturated epoxy ester **22** was subjected to the palladium-catalyzed azide substitution reaction under the conditions employed for acyclic substrates, azido alcohol **23** was produced exclusively in 93% yield with double inversion of configuration. In contrast, the reaction of **22** with NaN_3 and $[Ti(OEt)_4]$ in DMF under modified Sharpless conditions[15] proceeded through an S_N2 process to afford the single azido alcohol **25** in 97% yield. These products were efficiently transformed into **24** and **26** by the two-step reaction sequence of 1) concomitant hydrogenation of the double bond and the azido group over the Adams catalyst in EtOAc in the presence of Boc_2O[8] and 2) oxidative cleavage of the diol moiety with $RuCl_3$ and $NaIO_4$ in $CCl_4/H_2O/CH_3CN$.[16] The two enantiomers **24** and **26** were efficiently and highly stereoselectively prepared starting from the same compound **21** by applying two contrasting azide substitution reactions.

In summary, we have developed a palladium-catalyzed azide substitution reaction of α,β-unsaturated γ,δ-epoxy esters with $TMSN_3$ that occurs stereospecifically at the γ-position to produce azido alcohols in excellent yields with double inversion of configuration. This new method is widely applicable to various acyclic and cyclic substrates and provides a powerful tool in the synthesis of functionalized β-amino alcohols and α-amino acids, including α,α-disubstituted amino acids. Further investigations into the synthetic applications of this methodology are ongoing.

Received: March 7, 2005
Published online: July 15, 2005



Scheme 3. Stereospecific synthesis of both enantiomers of *N*-*tert*-butoxycarbonyl-α-methylglutamic acid γ-ethyl ester: a) *m*CPBA (1.5 equiv), CH_2Cl_2, 0 °C, 1 h (99%); b) $TMSN_3$ (2 equiv), $[Pd(PPh_3)_4]$ (5 mol%), THF, RT, 1 h (93%); c) H_2, PtO_2, Boc_2O (4 equiv), AcOEt, RT, 4 h; d) $RuCl_3$ (cat.), $NaIO_4$ (6 equiv), CCl_4, aq. CH_3CN, RT, 2 h; e) NaN_3 (4 equiv), $[Ti(OEt)_4]$ (2 equiv), DMF, RT, 1 h.

 © 2005 Wiley-VCH Verlag GmbH & Co. KGaA, Weinheim

Keywords: amino acids · asymmetric synthesis · azides · epoxides · palladium

[1] a) D. J. Ager, I. Prakash, D. R. Schaad, *Chem. Rev.* **1996**, *96*, 835; b) N. A. Petasis, I. A. Zavialov, *J. Am. Chem. Soc.* **1998**, *120*, 11798; c) B. List, P. Pojarliev, W. T. Biller, H. J. Martin, *J. Am. Chem. Soc.* **2002**, *124*, 827; d) B. Olofsson, P. Somfai, *J. Org. Chem.* **2002**, *67*, 8574; e) B. M. Trost, L. R. Terrell, *J. Am. Chem. Soc.* **2003**, *125*, 338; f) N. J. Adderley, D. J. Buchanan, D. J. Dixon, D. I. Laine, *Angew. Chem.* **2003**, *115*, 4373; *Angew. Chem. Int. Ed.* **2003**, *42*, 4241.

[2] For representative reviews on the preparation of optically active α-amino acids, see: a) R. M. Williams, *Synthesis of Optically Active α-Amino Acids* (Ed.: J. E. Baldwin), Pergamon, Oxford, **1989**; b) R. M. Williams, J. A. Hendrix, *Chem. Rev.* **1992**, *92*, 889; c) R. O. Duthaler, *Tetrahedron* **1994**, *50*, 1539; d) D. Seebach, A. R. Sting, M. Hoffmann, *Angew. Chem.* **1996**, *108*, 2880; *Angew. Chem. Int. Ed. Engl.* **1996**, *35*, 2708; e) C. Cativiela, M. D. Diaz-de-Villegas, *Tetrahedron: Asymmetr.* **1998**, *9*, 3517; f) J.-A. Ma, *Angew. Chem.* **2003**, *115*, 4426; *Angew. Chem. Int. Ed.* **2003**, *42*, 4290; g) K. Maruoka, T. Ooi, *Chem. Rev.* **2003**, *103*, 3013; h) J. M. O'Donnel, *Acc. Chem. Res.* **2004**, *37*, 506.

[3] a) B. G. M. Burgaud, D. C. Horwell, A. Padova, M. C. Pritchard, *Tetrahedron* **1996**, *52*, 13050; b) T. Wirth, *Angew. Chem.* **1997**, *109*, 235; *Angew. Chem. Int. Ed. Engl.* **1997**, *36*, 225; c) S. Hatakeyama, H. Matsumoto, H. Fukuyama, Y. Mukugi, H. Irie, *J. Org. Chem.* **1997**, *62*, 2275; d) D. Obrecht, M. Altorfer, U. Bohdal, J. Daly, W. Huber, A. Labhardt, C. Lehmann, K. Müller, R. Ruffieux, P. Schönholzer, C. Spiegler, C. Zumbrunn, *Biopolymers* **1997**, *42*, 575; e) T. Ooi, M. Takeuchi, M. Kameda, K. Maruoka, *J. Am. Chem. Soc.* **2000**, *122*, 5228; f) T. Ooi, E. Tayama, K. Maruoka, *Angew. Chem.* **2003**, *115*, 599; *Angew. Chem. Int. Ed.* **2003**, *42*, 579.

[4] For the synthesis of chiral α,α-disubstituted α-amino acids by enzymatic resolution, see: a) V. S. Parmar, A. Singh, K. S. Sisht, N. Kumar, Y. N. Belokon, K. A. Kocketkov, N. S. Ikonnikiv, S. A. Orlova, V. I. Taranov, T. F. Saveleva, *J. Org. Chem.* **1996**, *61*, 1223, and references therein; b) D. M. Spero, S. J. Kapadia, *J. Org. Chem.* **1996**, *61*, 7398; c) S. Sano, K. Hayashi, T. Miwa, T. Ishii, M. Fujii, H. Mima, Y. Nagao. Y. *Tetrahedron* **1998**, *39*, 5571.

[5] A. Hirai, X.-Qiang Yu, T. Tonooka, M. Miyashita, *Chem. Commun.* **2003**, 2482.

[6] X.-Qiang Yu, A. Hirai, M. Miyashita, *Chem. Lett.* **2004**, *33*, 764.

[7] For epoxide-opening reactions with azides, see: a) K. Maruoka, H. Sano, H. Yamamoto, *Chem. Lett.* **1985**, 599; b) C. H. Behrens, K. B. Sharpless, *J. Org. Chem.* **1985**, *50*, 5696; c) M. Onaka, K. Sugita, Y. Izumi, *Chem. Lett.* **1986**, 1327; d) M. Caron, P. R. Carlier, K. B. Sharpless, *J. Org. Chem.* **1988**, *53*, 5185; e) S. Saito, S. Yamashita, T. Nishikawa, Y. Yokoyama, M. Inaba, T. Moriwake, *Tetrahedron Lett.* **1989**, *30*, 4153; f) K. I. Sutowardoyo, M. Emziane, P. Lhoste, D. Sinou, *Tetrahedron* **1991**, *47*, 1435; g) F. Benedetti, F. Berti, S. Norbedo, *Tetrahedron Lett.* **1998**, *39*, 7971; h) H. Hayakawa, N. Okada, M. Miyazawa, M. Miyashita, *Tetrahedron Lett.* **1999**, *40*, 4589; i) C. Schneider, *Synlett* **2000**, *12*, 1840; j) R. Martin, G. Islas, A. Moyano, M. A. Pericas, A. Riera, *Tetrahedron* **2001**, *57*, 6367; k) G. Sabitha, R. S. Babu, M. S. K. Reddy, J. S. Yadav, *Synthesis* **2002**, *15*, 2254; l) M. Sasaki, K. Tanino, A. Hirai, M. Miyashita, *Org. Lett.* **2003**, *5*, 1789.

[8] a) H. Kotsuki, A. Miyazaki, M. Ochi, *Tetrahedron Lett.* **1991**, *32*, 4503; b) M. Miyashita, T. Yamasaki, T. Shiratani, S. Hatakeyama, M. Miyazawa, H. Irie, *Chem. Commun.* **1997**, 1787.

[9] T. Tsuda, Y. Horii, Y. Nakagawa, T. Ishida, T. Saegusa, *J. Org. Chem.* **1989**, *54*, 977.

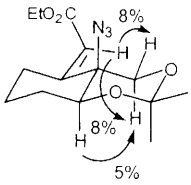
[10] E. Wolfgang, C. J. Claude, *Chem. Ber.* **1981**, *114*, 1027.

[11] The use of P(2-furyl)$_3$ in the reaction of acyclic substrates also gave excellent results with even better yields of isolated product than with the use of [Pd(PPh$_3$)$_4$].

[12] B. Norbert, H. Juergen, M. Helga, W. Peter, *Chem. Ber.* **1979**, *112*, 2256.

[13] The substrate **19** was prepared from 2-hydroxymethyl-2-cyclohexenone in five steps.

[14] The configuration of **20** was confirmed unambiguously by NOE interaction studies of its acetonide derivative, which was



obtained by the removal of the TBS protecting group with HF in CH_3CN (90%) and subsequent treatment of the resulting 1,3-diol with *para*-toluenesulfonic acid and 2,2-dimethoxypropane in CH_2Cl_2 (99%).

[15] M. Carron, K. B. Sharpless, *J. Org. Chem.* **1985**, *50*, 1557.

[16] P. H. J. Carlsen, T. Katsuki, V. S. Martin, K. B. Sharpless, *J. Org. Chem.* **1981**, *46*, 3936.

 © 2005 Wiley-VCH Verlag GmbH & Co. KGaA, Weinheim

Host–Guest Chemistry

DOI: 10.1002/anie.200501364

Control of Differential Inclusion Complexation in the Solid State by Seed Crystals**

Kazuhiro Yoshizawa, Shinji Toyota, Fumio Toda, Spyros Chatziefthimiou, Petros Giastas, Irene M. Mavridis, and Masako Kato*

Simple phenol and naphthol derivatives include various guest compounds through host–guest hydrogen bonds to produce crystalline inclusion complexes.[1] As these inclusion complexation processes occur selectively, separation of isomers and enantiomers can be carried out upon complexation.[2] Of these phenol and naphthol derivatives, 2,2′-dihydroxy-1,1′-binaphthyl (**1**) is the most interesting host compound because of its axel-asymmetric structure. As optically active **1** precisely recognizes the chirality of the guest molecule it includes, enantiomeric separation of the guest can be

[*] Dr. K. Yoshizawa, Prof. Dr. S. Toyota, Prof. Dr. F. Toda, S. Chatziefthimiou, P. Giastas, Prof. Dr. I. M. Mavridis, Prof. Dr. M. Kato
Department of Chemistry
Okayama University of Science
Ridaicho 1-1, Okayama 700-0005 (Japan)
Fax: (+81) 86-256-9604
E-mail: toda@chem.ous.ac.jp

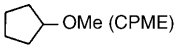
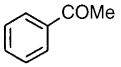
[**] We thank Mr. Tomikatu Kubo and Mitsuhiro Hamada of Rigaku Ltd. for their measurements of XRD spectra. This work was supported financially by MEXT HAITEKU (2001–2005).

 © 2005 Wiley-VCH Verlag GmbH & Co. KGaA, Weinheim InterScience

performed easily.[3] However, inclusion complexation of guest compounds with racemic **1** has not been extensively studied to date. Herein, we report that differential inclusion complexation between racemic host **1** and simple gaseous guests in the solid state can be controlled by a seed crystal. We also report that inclusion complexation of **1** with gaseous guests in the solid state occurs only in the presence of a seed crystal.

First, inclusion complexes were prepared by recrystallization of **1** from the liquid guests indicated in Table 1. Four types of inclusion patterns are possible according to the host/guest ratio, namely, with 1:2, 1:1, 2:3, and 3:1 stoichiometries. Interestingly, Et_2O formed two types of inclusion complexes with host/guest ratios of 1:2 and 3:1. The 1:2 complex, **2**, loses Et_2O at a relatively lower temperature (40–61 °C) than the 3:1 complex **3** does (87–108 °C). X-ray crystal structural studies showed that **2** has a loose structure (Figure 1), whereas **3** has a more compact and rigid structure (Figure 2). In complex **2**, Et_2O probably evaporates easily through the channel shown in Figure 1. In complex **3**, however, the molecule of Et_2O is trapped tightly, surrounded by three host molecules.

Table 1: Properties of inclusion complexes of **1** with various liquid guests.

Guest	Host/guest ratio[a]	Decomposition temperature [°C]	$\tilde{\nu}$OH [cm^{-1}][b]
Et_2O	3:1	87–108	3419, 3459, 3489
Et_2O	1:2	40–61	3198
	1:2	37–74	3198
THF	2:3	48–106	3173, 3519
	2:3	61–116	3248
MeOAc	3:1	83–108	3403, 3463, 3491
EtOAc	3:1	75–105	3413, 3464, 3490
	1:2	87–128	3366
$Me_2C=O$	1:1	70–98	3036, 3404
	1:1	79–107	3321, 3419
	1:1	87–117	3264, 3417
	1:2	94–121	3199
	1:2	97–141	3198

[a] The ratio was determined by ^1H NMR spectroscopy and thermogravimetric analysis. [b] IR spectra were measured using the ATR (attenuated total reflectance) method.

Interestingly, **2** and **3** could also be prepared by recrystallization of **1** (0.2 g) from 3 and 5 mL of Et_2O to give **3** and **2**, respectively (Scheme 1). The more stable complex **3** ($(\mathbf{1})_3{\cdot}Et_2O$) formed preferentially when the complexation was performed rapidly from a concentrated solution. When the complexation was performed slowly from a diluted solution, the less stable **2** ($\mathbf{1}{\cdot}(Et_2O)_2$) crystallized out. This is the first example of differential inclusion complexation by controlling the concentration of the solution, although differential complexations by controlling the temperature[3] or the type of solvent used for crystallization[4] have also been reported. However, when **1** (0.2 g) was recrystallized from an intermediate volume of Et_2O (4 mL), either **2** or **3** formed

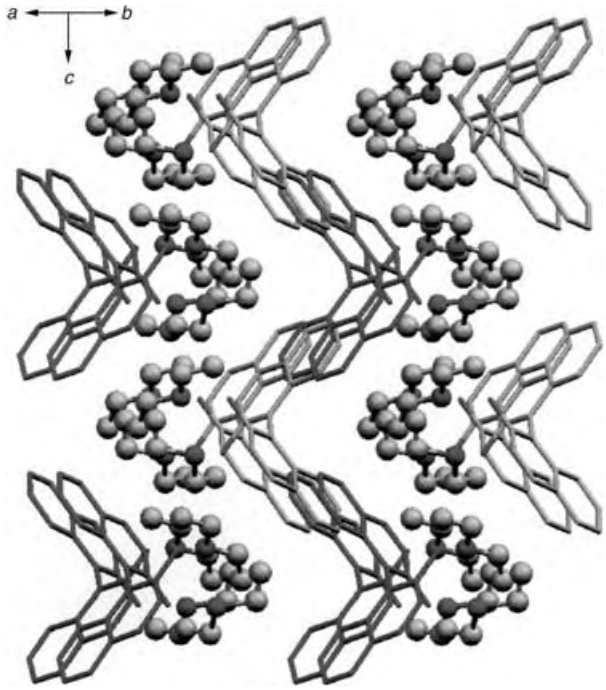


Figure 1. Crystal structure of **2** ($\mathbf{1}{\cdot}(Et_2O)_2$).

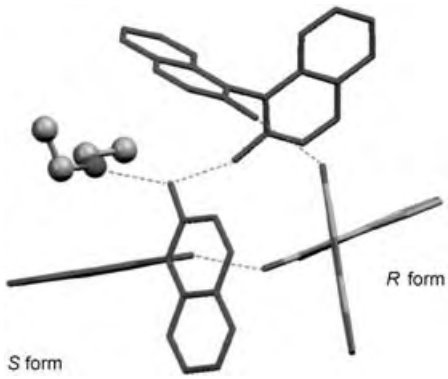
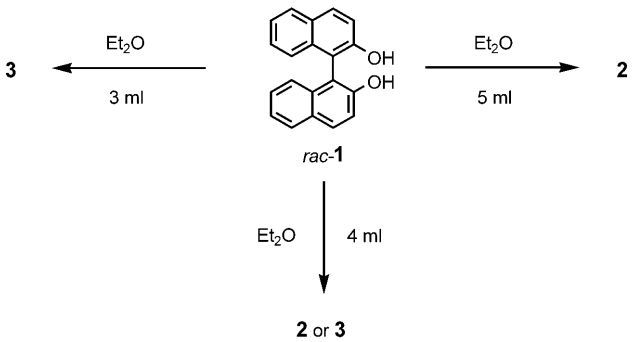


Figure 2. Crystal structure of **3** ($(\mathbf{1})_3{\cdot}Et_2O$).

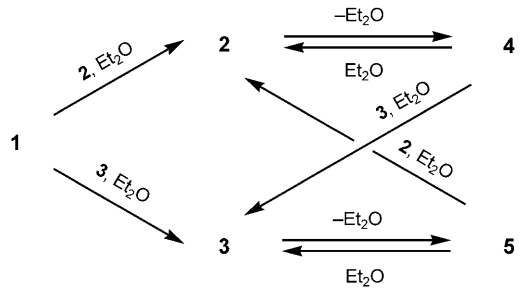


Scheme 1. Inclusion complexation of host **1** and guest Et_2O by recrystallization of **1** from solutions in Et_2O at different concentrations.

 © 2005 Wiley-VCH Verlag GmbH & Co. KGaA, Weinheim

depending on the specific conditions. The pattern of the complexation could be controlled by the seed crystal which formed initially, and this was confirmed by the following seed crystal experiments: Recrystallization of **1** (0.2 g) from 3 and 4 mL of Et_2O by adding one seed crystal of **2** led to formation of **2**; similar recrystallization of **1** (0.2 g) from 3 and 4 mL of Et_2O by adding one seed crystal of **3** led to formation of **3**.

Surprisingly, these seed crystal experiments could also be carried out in the solid state. First, Et_2O (guest)-free hosts **4** and **5** were prepared by evaporation of the guest from **2** and **3**, respectively, by heating at 50 °C under 20 mmHg. Contact of **4** and **5** with Et_2O vapor at room temperature for 12 and 3 h, respectively, gave **2** and **3**, respectively (Scheme 2). These



Scheme 2. Seed crystal experiments in the inclusion complexation between solid host **1** and gaseous guest Et_2O.

data strongly suggest that **4** and **5** "remember" the original inclusion pattern of **2** and **3**, respectively. Nevertheless, no structural differences between **4** and **5** could be observed by IR spectroscopy or X-ray powder diffraction studies. There is a possibility that **4** and **5** still keep a small amount of Et_2O guest molecules in their inclusion cavities and that these inclusion complex lattices play a role as the seed crystal during complexation in the solid state. When a mixture of powdered **4** and a seed crystal of **3** (2 wt %) was exposed to Et_2O vapor for 3 h, **4** was converted into **3** ($(\mathbf{1})_3{\cdot}Et_2O$) in quantitative yield. By similar contact of a powdered mixture of **5** and a seed crystal of **2** (2 wt %) for 12 h, **5** was converted into **2** ($\mathbf{1}{\cdot}(Et_2O)_2$). Furthermore, contact of a powdered mixture of **1** (98 mg, 0.34 mmol) and **2** (2 mg, 4.6 μmol; 2 wt %, 1.35 mol %) with Et_2O vapor for 12 h gave **2** in quantitative yield (Scheme 2). Similar contact of a powdered mixture of **1** (98 mg, 0.34 mmol) and **3** (2 mg, 2.1 μmol; 2 wt %, 0.62 mol %) with Et_2O vapor for 3 h gave **3** in quantitative yield. However, contact of powdered **1** with Et_2O vapor in the absence of a seed crystal for 72 h did not lead to the formation of any inclusion complexes.

Seed crystals were also effective for the inclusion complexation of **1** with some other guests. Contact of powdered **1** with gaseous MeOAc and EtOAc for 3 h in the presence of seed crystals of inclusion complexes $(\mathbf{1})_3{\cdot}$MeOAc and $(\mathbf{1})_3{\cdot}$EtOAc, respectively, led to the corresponding inclusion complexes in quantitative yields. Inclusion complexation of **1** and gaseous cyclopentyl methyl ether (CPME) in the presence of a seed crystal of the 1:2 complex $\mathbf{1}{\cdot}(CPME)_2$ for 12 h gave the same inclusion complex as the complex of the seed crystal in quantitative yield. In all of the cases studied, inclusion complexation did not occur in the absence of the seed crystal.

IR spectral data of inclusion complexes of **1** with different guests but at the same host/guest ratio were similar to each other, and the complexes decomposed at similar temperatures (Table 1). The complexes at the same host/guest ratio also have similar solid-state structures. For example, the crystal structures of **2** ($\mathbf{1}{\cdot}(Et_2O)_2$) and the 1:2 complex of **1** with CPME ($\mathbf{1}{\cdot}(CPME)_2$) are very similar, while the crystal structures of **3** ($(\mathbf{1})_3{\cdot}Et_2O$) and the 3:1 complex of **1** with EtOAc[6] ($(\mathbf{1})_3{\cdot}$EtOAc) are also very similar. However, the crystal structure of a 1:2 complex of **1** with 2-cyclohexenone is completely different to that of **2**, and the structures of 2:3 complexes of **1** with THF and 1,4-dioxane are also different.[7]

These data suggest that a crystal of an inclusion complex is effective as a pseudo seed crystal for the formation of a complex at the same host/guest ratio but with a different guest compound (Table 2). For example, contact of powdered **1**

Table 2: Inclusion complexation of powdered **1** and gaseous guests in the presence of a pseudo seed crystal.

Guest in seed crystal (**1**/guest ratio)	Gaseous guest	Reaction time [h]	Guest in product (**1**/guest ratio)
MeOAc (3:1)	EtOAc	3	EtOAc (3:1)
MeOAc (3:1)	Et_2O	3	Et_2O (3:1)
EtOAc (3:1)	MeOAc	3	MeOAc (3:1)
EtOAc (3:1)	Et_2O	3	Et_2O (3:1)
Et_2O (3:1)	MeOAc	3	MeOAc (3:1)
Et_2O (1:2)	CPME	12	CPME (1:2)
CPME (1:2)	Et_2O	12	Et_2O (1:2)
MeOAc (3:1)	CPME	12	–
Et_2O (3:1)	CPME	12	–

with gaseous EtOAc for 3 h in the presence of seed crystal $(\mathbf{1})_3{\cdot}$MeOAc gave the complex $(\mathbf{1})_3{\cdot}$EtOAc, also in a 3:1 host/guest ratio. Similar contact of **1** with gaseous guests in the presence of seed crystals of complexes with host/guest ratios as anticipated in the products indeed gave quantitative yields of inclusion complexes with the same host/guest ratio as those of the seed. These data clearly show the high efficiency of the pseudo seed crystal. However, contact of **1** with gaseous guests in the presence of seed crystals that have a different host/guest ratio from those of the expected product did not afford any inclusion complexes. In the last two examples shown in Table 2, seed crystals $(\mathbf{1})_3{\cdot}$MeOAc and $(\mathbf{1})_3{\cdot}Et_2O$ did not work as seed crystals for the complexation of **1** with CPME, which forms only the 1:2 host/guest complex. In all the cases studied, 3:1 host/guest complexes were formed more easily than those at a 1:2 ratio.

The efficient role of the seed crystal for inclusion complexation in the solid state is fascinating and has not been reported until now. As far as we are aware, only one report of a seed crystal experiment has been described in which the transformation among three polymorphs of chloramphenicol palmitate in the solid state proceeded two times faster in the presence of a seed crystal.[8] The present findings on the role of seed crystals will become useful in many

 © 2005 Wiley-VCH Verlag GmbH & Co. KGaA, Weinheim

scientific fields and will give various hints to develop new technologies.

Although the mechanism of the role of seed crystals is interesting, it is not easy to clarify. However, as it has been established that molecules in a crystal move quite easily in the solid state,[9] easy movement of gaseous molecules into the crystal is understandable. Surprisingly, host **1** which has a helical structure with a twofold symmetry axis[10] is converted efficiently into a sheet structure in **2** and a cyclic structure in **3** in the solid state upon contact with Et_2O vapor in the presence of a seed crystal.

Experimental Section

Crystal data for **1**·$(Et_2O)_2$ (**2**): $C_{28}H_{34}O_4$, $M_r = 434.55$, monoclinic, $\beta = 108.86(2)°$, $a = 11.659(7)$, $b = 9.757(6)$, $c = 11.886(7)$ Å, $V = 1279.4(13)$ Å^3, $T = 293$ K, space group Pn, $Z = 2$, $\lambda(Cu_{K\alpha}) = 1.54$ Å; for 1835 observed reflections, the final R (on F) = 0.0798 and wR (on F^2) = 0.2306 for $I > 2\sigma(I)$.

Crystal data for $(\mathbf{1})_3$·Et_2O (**3**): $C_{64}H_{52}O_7$, $M_r = 933.11$, triclinic, $\alpha = 83.395(5)$, $\beta = 80.977(5)$, $\gamma = 77.516(5)°$, $a = 10.403(2)$, $b = 10.790(2)$, $c = 22.282(4)$ Å, $V = 2403.1(8)$ Å^3, $T = 173.1$ K, space group $P\bar{1}$, $Z = 2$, $\lambda(Mo_{K\alpha}) = 0.71$ Å; for 7107 observed reflections, the final R (on F) = 0.0510 and wR (on F^2) = 0.1250 for $I > 2\sigma(I)$.

Crystal data for **1**·$(CPME)_2$: $C_{16}H_{19}O_2$, $M_r = 243.31$, monoclinic, $\beta = 118.84(2)°$, $a = 22.957(15)$, $b = 9.811(7)$, $c = 13.998(9)$ Å, $V = 2762(3)$ Å^3, $T = 293$ K, space group $C2/c$, $Z = 8$, $\lambda(Cu_{K\alpha}) = 1.54$ Å; for 1960 observed reflections, the final R (on F) = 0.0767 and wR (on F^2) = 0.2065 for $I > 2\sigma(I)$.

Crystal data for **1**·(2-cyclohexen-1-one)$_2$: $C_{26}H_{22}O_3$, $M_r = 382.44$, monoclinic, $\beta = 91.371(16)°$, $a = 13.598(9)$, $b = 10.488(6)$, $c = 17.895(11)$ Å, $V = 2551(3)$ Å^3, $T = 293$ K, space group $P2_1/n$, $Z = 4$, $\lambda(Cu_{K\alpha}) = 1.54$ Å; for 3605 observed reflections the final R (on F) = 0.1130 and wR (on F^2) = 0.2123 for $I > 2\sigma(I)$.

Received: April 20, 2005
Published online: July 11, 2005

Keywords: crystal growth · host–guest systems · inclusion compounds · solid-state reactions

[1] *Separation and Reactions in Organic Supramolecular Chemistry* (Eds.: F. Toda, R. Bishop), Wiley, New York, **2004**.
[2] F. Toda, *Top. Curr. Chem.* **1987**, *140*, 43; F. Toda, K. Tanaka, S. Nagamatsu, *Tetrahedron Lett.* **1984**, *25*, 4929.
[3] F. Toda, K. Yoshizawa, S. Hyoda, S. Toyota, S. Chatziefthimiou, I. M. Mavridis, *Org. Biomol. Chem.* **2004**, *2*, 449; K. Yoshizawa, S. Toyota, F. Toda, *Tetrahedron* **2004**, *60*, 7767.
[4] K. Bekotov, E. Weber, J. Seidel, K. Köhnke, K. Makhkamov, B. Ibragimov, *Chem. Commun.* **1999**, 91.
[5] N. Tanifuji , K. Kobayashi, *CrystEngComm* **2001**, *3*, 1; S. B. Raj, P. T. Muthiah, U. Rychlewska, B. Warzajtis, *CrystEngComm* **2003**, *5*, 48.
[6] K. Wen-Jun, L. Yang, Z. Qi-Tai, G. Wen-Sheng, X. Feng, W. De-Dong, T. C. Mak, *Chin. J. Struct. Chem.* **1997**, *16*, 97.
[7] L. R. Nassimbeni, H. Su, *J. Phys. Org. Chem.* **2000**, *13*, 368; L. R. Nassimbeni, H. Su, *New J. Chem.* **2002**, *26*, 989.
[8] M. Otsuka, N. Kaneniwa, *J. Pharm. Sci.* **1986**, *75*, 506.
[9] F. Toda, K. Tanaka, A. Sekikawa, *J. Chem. Soc. Chem. Commun.* **1987**, 279; D. Braga, F. Grepioni, *Angew. Chem.* **2004**, *116*, 4092; *Angew. Chem. Int. Ed.* **2004**, *43*, 4002.
[10] F. Toda, K. Tanaka, H. Miyamoto, H. Koshima, I. Miyahara, K. Hirotsu, *J. Chem. Soc. Perkin Trans. 2* **1997**, 1877.

 © 2005 Wiley-VCH Verlag GmbH & Co. KGaA, Weinheim

Nanobiotechnology

DOI: 10.1002/anie.200500403

Nanoparticle PCR: Nanogold-Assisted PCR with Enhanced Specificity**

Haikuo Li, Jiehuan Huang, Junhong Lv, Hongjie An, Xiaodong Zhang, Zhizhou Zhang, Chunhai Fan,* and Jun Hu**

The polymerase chain reaction (PCR) revolutionized molecular genetics and has become one of the most popular techniques in modern biological and medical sciences.[1] Owing to the exponential amplification ability of PCR, one could start from even a single copy of target DNA to produce large amounts of DNA copies for sequencing, molecular diagnosis, or genetic analysis.[2–4] This remarkable amplification ability is critical in many circumstances, such as early-stage diagnosis of HIV or cancers. Given the rapidly increasing interest in optoelectronic DNA biosensors, the extremely high detection sensitivity of PCR has not been surpassed until now.[5–9] However, the specificity of PCR does not match its unparalleled sensitivity.[10] It is well known that even with sophisticated optimization, PCR specificity is not always satisfactory (e.g. in multiple-round PCR or multiplex PCR).[10] Herein, we report a novel PCR method that employs inexpensive gold nanoparticles to effectively avoid nonspecific PCR reactions.

Gold nanoparticles have found broad and important applications in biology; for example, a variety of ultrasensitive biosensor strategies have been reported which take

[*] H. Li, J. Huang, H. An, Dr. X. Zhang, Prof. Dr. Z. Zhang, Prof. Dr. C. Fan, Prof. Dr. J. Hu
Bio-X DNA Computer Consortium
Shanghai Jiao Tong University
Shanghai 200030 (China)
Fax: (+86) 21-6407-7361
E-mail: zhangzz@sjtu.edu.cn
fchh@sinap.ac.cn
jhu@sjtu.edu.cn

H. Li, J. Huang, H. An, Dr. X. Zhang, Prof. Dr. Z. Zhang, Prof. Dr. J. Hu
Bio-X Life Science Research Center
Shanghai Jiao Tong University
Shanghai 200030 (China)
Fax: (+86) 21-6407-7361

Dr. J. Lv, Prof. Dr. C. Fan, Prof. Dr. J. Hu
Shanghai Institute of Applied Physics
Chinese Academy of Sciences
Shanghai 201800 (China)
Fax: (+86) 21-5955-6902

[**] This work was supported by the Chinese Academy of Sciences, the National Natural Science Foundation (10335070 and 20404016), the Ministry of Science and Technology of China (2002CCA00600, 2003A310A02, and 2003AA226011), the Shanghai Municipal Commission for Science and Technology (0452M068, 03DZ14025, and 02JC14029), and the Ministry of Personnel. We also thank Prof. Kevin Plaxco (UCSB) for helpful comments.

InterScience
© 2005 Wiley-VCH Verlag GmbH & Co. KGaA, Weinheim

advantage of gold nanoparticles.[8,9,11–14] Gold nanoparticles are nontoxic, biocompatible nanomaterials that can be either obtained from commercial sources or conveniently produced in laboratories,[15] and owing to the availability of versatile chemistry for functionalization at their surface as well as their unique optoelectronic properties[9,11] gold nanoparticles provide a particularly useful platform for attachment of biomolecules.[15] However, to the best of our knowledge, the use of gold nanoparticles to improve the performance of PCR has not been reported.

Herein, we employed an error-prone two-round PCR as our model system. Amplification of very low quantities of copies of target genes usually increases the possibility of amplifying nonspecific sequences.[16] In the first round, we amplified a 283-bp sequence using a λ-DNA template with 35 PCR cycles; in the second round PCR, this 283-bp DNA was employed as the template for the other 35-cycle PCR amplification sequence. Nonspecific PCR products tend to accumulate after two rounds of PCR, as manifest by a broad molecular size distribution of amplified products in agarose gel electrophoresis (Figure 1). Strikingly, in the presence of

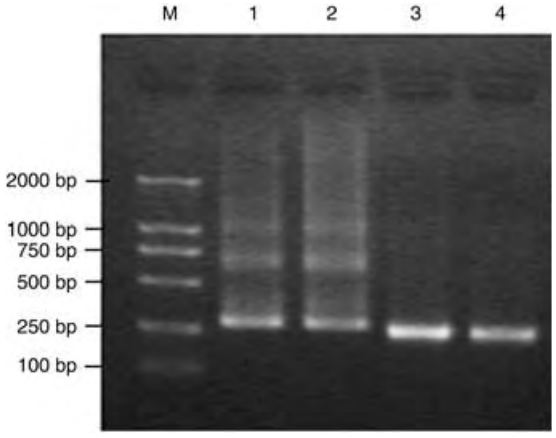


Figure 1. The effect of gold nanoparticles on the specificity of PCR. PCR was performed by employing a 283-bp target sequence from a λ-DNA template, and PCR products were analyzed by agarose gel electrophoresis (1.5%). Lane M is for markers; lanes 1 and 2 show the results of PCR performed in the absence of gold nanoparticles; lanes 3 and 4 show the results of PCR performed with gold nanoparticles (0.4 nM of 10-nm gold nanoparticles). bp = base pair.

0.4-nM gold nanoparticles (10 nm, Sigma) we only observed a single predominant band corresponding to the 283-bp target, and the yield of this target was also much higher in this case (Figure 1). Control experiments show that the high specificity of gold-nanoparticle-assisted PCR (nanoparticle PCR) arises solely because of the effect of gold nanoparticles. We performed nanoparticle PCR by using freshly prepared gold nanoparticles that were free of additives such as tannic acid and sodium azide[17] and observed similar electrophoresis patterns (data not shown). In contrast, we did not observe any improvement by using solely the medium in which the gold nanoparticles were provided (the gold nanoparticles were removed by centrifugation).[18] The concentration of gold nanoparticles is critical for obtaining optimal PCR results. We observed that nonspecific "tailing" bands gradually diminished by increasing the concentration of gold nanoparticles in the range of 0.2–0.8 nM. However, the presence of excess gold nanoparticles (1.0 nM) effectively inhibited the PCR reaction, as manifest by the significantly lowered yield of PCR (Figure 2). This inhibition effect is discussed later.

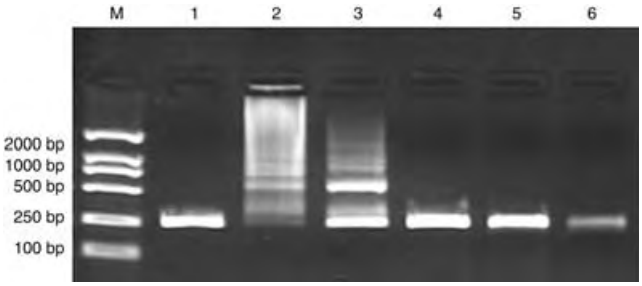


Figure 2. The effect of the concentration of gold nanoparticles on the specificity of PCR: lane M: (markers) 0; lane 1: 0.6 nM; lane 2: 0; lane 3: 0.2 nM; lane 4: 0.4 nM; lane 5: 0.8 nM; lane 6: 1.0 nM.

In conventional PCR, it is essential to find the optimal annealing temperature by the so-called "touchdown" PCR[19] to obtain optimal yields (which requires a lower annealing temperature) and specificity (which requires a higher annealing temperature) of the target. Our nanoparticle PCR strategy allows reliable PCR amplification even at lowered annealing temperatures, obviating time-consuming "touchdown" PCR. As demonstrated in Figure 3, in the presence of 0.4-nM gold nanoparticles we could obtain a single product band at a nonoptimal annealing temperature of 40 °C. We even observed a product band with minor tailing bands at an annealing temperature as low as 25 °C, in sharp contrast to normal PCR in the absence of gold nanoparticles which produces negligible amplified target DNA at this temperature. This specificity could be further improved by using 0.6-nM gold nanoparticles, which produced a single product band at the annealing temperature of 25 °C (Figure 3). Therefore, it is possible to 1) employ gold nanoparticles to perform PCR without the need for sophisticated optimization of annealing temperature and/or 2) to increase PCR yields at lowered annealing temperatures without compromising PCR specificity.

The problems associated with specificity of PCR possibly arise owing to performance of the procedure in vitro. During DNA replication in vivo, DNA polymerase is assisted by a variety of proteins/enzymes, which ensure the specificity of DNA replication.[20] For example, single-stranded DNA-binding protein SSB selectively binds to single-stranded DNA (ssDNA) and not to double-stranded DNA (dsDNA). This selectivity largely minimizes mispairing between primers and templates during DNA replications.[20] Indeed, mimicking Nature's strategy, Nielson et al., among others, successfully employed a thermostable SSB to increase PCR specificity and fidelity.[21–23] Note that the use of thermostable SSB from the *T. thermophilus* strain is critical to withstand the temperature cycles (up to 94 °C) involved in PCR.[23] Here, similarly enhanced PCR specificity is observed for our nanoparticle

 © 2005 Wiley-VCH Verlag GmbH & Co. KGaA, Weinheim

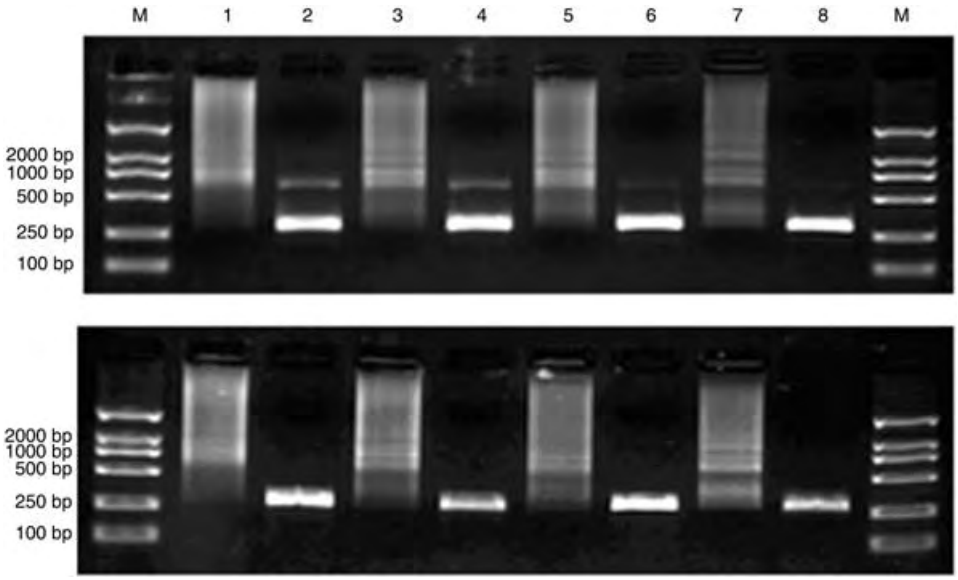


Figure 3. The effect of the annealing temperature on the specificity of PCR: lanes 1, 2: 25 °C; lanes 3, 4: 30 °C; lanes 5, 6: 35 °C; lanes 7, 8: 40 °C; lane M is for markers; lanes 1, 3, 5, and 7 show the results of PCR performed in the absence of gold nanoparticles; lanes 2, 4, 6, and 8 show the results of nanoparticle PCR (the concentration of gold nanoparticles is 0.4 and 0.6 nM in the upper and lower panels, respectively).

PCR system. We reason that this enhancement arises also as a result of a similar mechanism to SSB-assisted PCRs. Indeed, both gold nanoparticles and SSB significantly enhance the specificity of this error-prone two-round PCR (see the Supporting Information). However, in this case, the enhancing effect of gold nanoparticles exceeds that of the commercially available SSB.

Analogous to SSB, gold nanoparticles bind to ssDNA much more strongly than to dsDNA.[8] While not yet fully understood, it is generally recognized that the selectivity of gold nanoparticles for binding to ssDNA arises for various reasons. First, for electrostatic reasons the binding of anionic DNA strands to negatively charged surfaces of citrate-stabilized gold nanoparticles is not favored. Note that dsDNA has a higher surface charge density and thus experiences more repulsion than ssDNA.[6] Second, the four bases—adenine, guanine, thymine, and cytosine (A, G, T, and C)—contain nitrogen atoms that display high affinities to gold.[24,25] Formation of a DNA duplex prevents the exposure of the bases to gold surfaces and thus reduces interactions between the two.[7] Third, the rigidity of dsDNA does not favor the wrapping of dsDNA around gold surfaces, while ssDNA is a "soft", flexible polymer that has a much higher freedom to wrap around gold nanoparticles. (Note that the persistence lengths of ssDNA and dsDNA are approximately 1 and 50 nm, respectively.[26]) However, an excess of gold nanoparticles can significantly reduce PCR yields which suggests that even correctly matched DNA may be adsorbed during PCR amplification (Figure 2). This effect is not unexpected as dsDNA may still bind to gold nanoparticles, although with a much lower affinity relative to ssDNA–gold binding.[27]

An approximate concentration of 10 μM of 1,6-dithiothreitol (DTT) is present in PCR solutions and is required for storage of Taq polymerase, the enzyme that is used to copy DNA. This thiol could self-assemble on gold nanoparticles through Au–S bonds and possibly cross-link them. As DTT-free Taq is not active, we cannot exclude the effect of DTT at present; however, we suggest that its effect is relatively small for the following reasons. First, the concentration of DTT is fairly low. Usually millimolar or higher concentrations of thiols are required for the preparation of densely packed monolayers on gold surfaces.[28] Second, Au–S bonds are labile at elevated temperatures.[29,30] PCR reactions were carried out at a high temperature at which Au–DTT complexes are unstable. Third, the PCR reaction was largely inhibited in the presence of 1.0 nM of gold nanoparticles (Figure 2). If the presence of 10 μM of DTT is enough to cross-link all gold nanoparticles, this inhibition effect could not have occurred. It was mentioned earlier that PCR specificity was enhanced by increasing the concentration of gold nanoparticles in the range of 0.2–0.8 nM. This observation suggests that DTT may cross-link some gold nanoparticles, while the excess gold nanoparticles ensure the enhancing effect. However, the mechanism of nanogold-assisted PCR remains to be explored.

In conclusion, we have developed a highly selective nanoparticle PCR strategy by employing gold nanoparticles. We have demonstrated that in the presence of appropriate concentrations of gold nanoparticles, PCR amplification can be optimized with respect to both yields and specificity. Thus the use of these highly stable, commercially available, and inexpensive inorganic nanomaterials open new opportunities for improving PCR, which is the most important standard method in molecular biology. Besides the two-round PCR employed here, gold nanoparticles may also be applied to many other PCR reactions that require either high specificity or high yields, such as single-molecular, multiplex, and long-distance PCRs. Further investigation into the effect of gold nanoparticles on these PCR reactions is required.

 © 2005 Wiley-VCH Verlag GmbH & Co. KGaA, Weinheim

Experimental Section

λ-DNA templates and Ex Taq DNA polymerase were obtained from TaKaRa Bio. Inc. Colloidal gold nanoparticles (10 nm, 0.01% $HAuCl_4$) were either purchased from Sigma or freshly produced in our laboratory following the reported procedure.[31] (Gold nanoparticles from Sigma contain $< 0.01\%$ tannic acid, 0.04% trisodium citrate, 0.26 mM potassium carbonate, and 0.02% sodium azide.) For PCR reactions, final concentrations of primers = 0.1 μM, template = 20 $\mu g L^{-1}$, and deoxynucleotide triphosphates (dNTPs) = 0.5 mM; reaction conditions: 2 min at 94°C for denaturation, followed by 35 cycles of a–c: a) 45 s at 94°C (denaturation), b) 1 min at 50°C (annealing), and c) 1 min at 72°C (elongation). Then after an additional extension step of 72°C for 5 min, PCR tubes were mainatined at 4°C. PCR products were analyzed by agarose gel electrophoresis (1.5%). Aliquots of the solution of gold nanoparticles were added to the PCR reaction system to an appropriate concentration.

Received: February 3, 2005
Revised: April 4, 2005
Published online: June 8, 2005

Keywords: DNA replication · gold · nanotechnology · polymerase chain reaction

[1] K. B. Mullis, F. A. Faloona, *Methods Enzymol.* **1987**, *155*, 335.
[2] R. K. Saiki, D. H. Gelfand, S. Stoffel, S. J. Scharf, R. Higuchi, G. T. Horn, K. B. Mullis, H. A. Erlich, *Science* **1988**, *239*, 487.
[3] J. Lu, H. Li, H. An, G. Wang, Y. Wang, M. Li, Y. Zhang, J. Hu, *J. Am. Chem. Soc.* **2004**, *126*, 11136.
[4] C. Ding, C. R. Cantor, *Proc. Natl. Acad. Sci. USA* **2003**, *100*, 7449.
[5] C. Fan, K. W. Plaxco, A. J. Heeger, *Proc. Natl. Acad. Sci. USA* **2003**, *100*, 9134.
[6] B. S. Gaylord, A. J. Heeger, G. C. Bazan, *Proc. Natl. Acad. Sci. USA* **2002**, *99*, 10954.
[7] E. M. Boon, D. M. Ceres, T. G. Drummond, M. G. Hill, J. K. Barton, *Nat. Biotechnol.* **2000**, *18*, 1096.
[8] H. Li, L. Rothberg, *Proc. Natl. Acad. Sci. USA* **2004**, *101*, 14036.
[9] T. A. Taton, C. A. Mirkin, R. L. Letsinger, *Science* **2000**, *289*, 1757.
[10] J. Sambrook, D. W. Russell, *Molecular Cloning: A Laboratory Manual*, *3rd ed.*, Cold Spring Harbor Laboratory Press, Cold Spring Harbor, **2001**.
[11] S. J. Park, T. A. Taton, C. A. Mirkin, *Science* **2002**, *295*, 1503.
[12] C. Fan, S. Wang, J. W. Hong, G. C. Bazan, K. W. Plaxco, A. J. Heeger, *Proc. Natl. Acad. Sci. USA* **2003**, *100*, 6297.
[13] Y. Xiao, F. Patolsky, E. Katz, J. F. Hainfeld, I. Willner, *Science* **2003**, *299*, 1877.
[14] B. Dubertret, M. Calame, A. J. Libchaber, *Nat. Biotechnol.* **2001**, *19*, 365.
[15] J. Gu, G. W. Hacker, *Gold and Silver Straining: Techniques in Molecular Morphology*, CRC, Boca Raton, FL, **2002**.
[16] K. Porter-Jordan, E. I. Rosenberg, J. F. Keiser, J. D. Gross, A. M. Ross, S. Nasim, C. T. Garrett, *J. Med. Virol.* **1990**, *30*, 85.
[17] Solutions of gold nanoparticles purchased from Sigma contain $< 0.01\%$ tannic acid and 0.02% sodium azide.
[18] Solutions of gold colloids (Sigma) were centrifuged at 13500 rpm for 30 min to remove gold nanoparticles.
[19] R. H. Don, P. T. Cox, B. J. Wainwright, K. Baker, J. S. Mattick, *Nucleic Acids Res.* **1991**, *19*, 4008.
[20] J. W. Chase, K. R. Williams, *Annu. Rev. Biochem.* **1986**, *55*, 103.
[21] K. Nielson, A. Wilbanks, C. Hansen, E. J. Mathur, *Strategies* **1991**, *4*, 38.
[22] Q. Chou, *Nucleic Acids Res.* **1992**, *20*, 4371.
[23] C. Perales, F. Cava, W. J. J. Meijer, J. Berenguer, *Nucleic Acids Res.* **2003**, *31*, 6473.
[24] L. M. Demers, M. Ostblom, H. Zhang, N.-H. Jang, B. Liedberg, C. A. Mirkin, *J. Am. Chem. Soc.* **2002**, *124*, 11248.
[25] J. J. Storhoff, R. Elghanian, C. A. Mirkin, R. L. Letsinger, *Langmuir* **2002**, *18*, 6666.
[26] V. A. Bloomfield, D. M. Crothers, I. Tinoco, Jr., *Nucleic Acids: Structures, Properties, and Functions*, University Science Books, Herndon, VA, **2000**.
[27] P. Sandstrom, M. Boncheva, B. Akerman, *Langmuir* **2003**, *19*, 7537.
[28] *Self-Assembled Monolayers on Electrodes*, H. O. Finklea in *Encyclopedia of Analytical Chemistry*, *Vol. 11* (Ed.: R. A. Meyers), Wiley, New York, **2000**.
[29] C. D. Bain, E. B. Troughton, Y. Tao, J. Evall, G. M. Whitesides, R. G. Nuzzo, *J. Am. Chem. Soc.* **1989**, *111*, 321.
[30] J. B. Schlenoff, M. Li, H. Ly, *J. Am. Chem. Soc.* **1995**, *117*, 12528.
[31] K. C. Grabar, R. G. Freeman, M. B. Hommer, M. J. Natan, *Anal. Chem.* **1995**, *67*, 735.

 © 2005 Wiley-VCH Verlag GmbH & Co. KGaA, Weinheim

Synthetic Methods

DOI: 10.1002/anie.200500159

Palladium-Catalyzed Tandem Cyclization of Bromoenynes through Aromatic C–H Bond Functionalization**

Hiroaki Ohno, Mio Yamamoto, Mutsumi Iuchi, and Tetsuaki Tanaka**

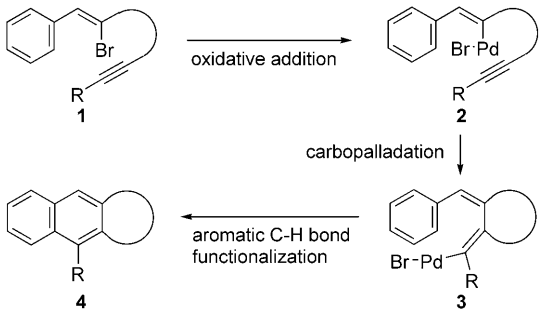
Transition-metal-catalyzed cyclization of dienes, diynes, and enynes has received considerable attention in recent years.[1] In contrast, cyclization of this class of compounds through functionalization of a C–H bond of an aromatic ring has scarcely been investigated. We anticipated that tandem cyclization of enynes of type **1** (Scheme 1) could serve as a useful synthetic method for direct construction of tricyclic products such as **4** through the use of a nonfunctionalized aryl group.

Recent investigations in palladium chemistry has revealed that functionalization of a C–H bond of an aromatic group is highly effective for the construction of fused aromatic rings.[2–6] Although tandem cyclization involving C–H bond functionalization that generates two,[7] three,[8] or four carbon–carbon bonds[9] in a one-pot manner and leads to

[*] Dr. H. Ohno, M. Yamamoto, M. Iuchi, Prof. Dr. T. Tanaka
Graduate School of Pharmaceutical Sciences
Osaka University
1–6 Yamadaoka, Suita, Osaka 565-0871 (Japan)
Fax: (+81) 6-6879-8214
E-mail: hohno@phs.osaka-u.ac.jp
t-tanaka@phs.osaka-u.ac.jp

[**] This work was supported by a Grant-in-Aid for Scientific Research from the Ministry of Education, Culture, Sports, Science, and Technology of Japan.

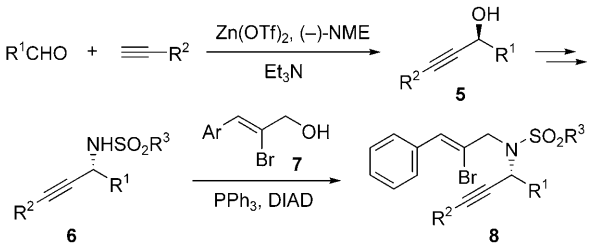
© 2005 Wiley-VCH Verlag GmbH & Co. KGaA, Weinheim



Scheme 1. Palladium-catalyzed tandem cyclization of bromoenynes.

monocyclized products is well documented, the tandem reaction involving a biscyclization process is extremely rare. Grigg et al. reported that an aryl halide bearing a carbon–carbon multiple bond and an additional aryl group undergoes bis- or triscyclization on treatment with a palladium(0) catalyst.[10] More recently, the palladium(0)-catalyzed tandem cyclization of alkyne-substituted phenyl iodide to form condensed aromatic rings[11] and the tandem biscyclization of allenenes with aryl halides[12] were also reported. However, to the best of our knowledge, there has been no report on the successful C–H functionalization of halogenated enynes. Herein we describe a tandem biscyclization of bromoenynes through intramolecular carbopalladation and functionalization of an aromatic C–H bond in the presence of a palladium catalyst.

Benzoisoindole is an important structural motif in medicinal chemistry and exists in many pharmaceutically useful compounds.[13] With a view to synthesizing nitrogen heterocycles, including benzoisoindole derivatives, we prepared enynes **8** as shown in Scheme 2. The chiral propargyl amine

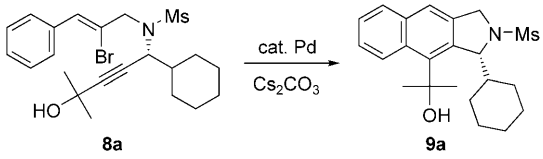


Scheme 2. Synthesis of bromoenynes through the procedure developed by Carreira and co-workers.

derivatives **6** could be prepared with high enantiomeric excess through the asymmetric alkynylation of aldehydes in the presence of zinc triflate and *N*-methylephedrine (NME) developed by Carreira and co-workers,[14] followed by amination of the resulting propargyl alcohols. In some cases, racemic propargylamines which were readily prepared by the reaction of lithium acetylide with aldehydes followed by amination, were used. Condensation of propargyl amines **6** with 3-aryl-2-bromoprop-2-en-1-ols **7** under Mitsunobu conditions gave the desired brominated enynes **8**.

With the requisite brominated enynes in hand, we next investigated the tandem cyclization of bromoenynes under various reaction conditions. After considerable experimentation, we found that bromoenyne **8a** yielded the desired cyclized product **9a** in the presence of a palladium catalyst and Cs_2CO_3 in EtOH (Table 1).[15] Other bases such as

Table 1: Optimization of reaction conditions using bromoenyne **8a**.[a]



8a **9a**

Entry	Catalyst (mol%)	Solvent	*T*	*t* [h]	Yield [%][b]
1	$[Pd(PPh_3)_4]$ (6)	EtOH	reflux	1	26
2	$[Pd_2(dba)_3]\cdot CHCl_3$ (2)	EtOH	reflux	5	59
3	$[Pd(dppf)_2Cl_2]$ (2)	EtOH	reflux	3.5	38
4	$Pd(OAc)_2$ (6)	EtOH	reflux	2.5	74
5	$Pd(OAc)_2$ (2)	EtOH	reflux	7	64
6	$Pd(OAc)_2$ (2)	DMF	100 °C	21	35
7	$Pd(OAc)_2$ (2)	dioxane	reflux	21	27

[a] Reactions were carried out with Cs_2CO_3 (2 equiv). [b] Yields of isolated products. dba = dibenzylideneacetone, dppf = 1,1′-bis(diphenylphosphanyl)ferrocene, Ms = methylsulfonyl.

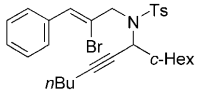
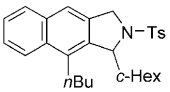
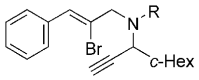
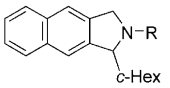
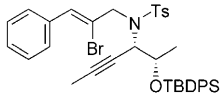
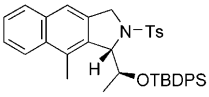
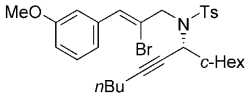
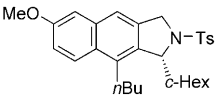
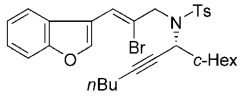
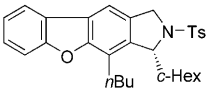
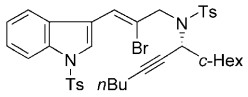
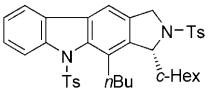
NaOAc were ineffective. Of the palladium catalysts investigated (entries 1–4), palladium acetate most effectively catalyzed the desired conversion (74%, entry 4). Decreased loading of the catalyst (2 mol%) slightly lowered the yield of the tricyclic product **9a** (64%, entry 5). EtOH proved to be a better solvent than DMF or dioxane for the tandem cyclization (entries 6 and 7).

Next we investigated the tandem cyclization of various bromoenynes in the presence of palladium acetate and cesium carbonate in EtOH (Table 2). The cyclization of tosylamide **8b** having an *n*-butyl group on the alkyne terminus gave the desired benzoisoindole **9b** in 79% yield (entry 1). Bromoenyne **8c** (entry 2) and **8d** (entry 3), each with a terminal alkyne, yielded **9c** and **9d**, respectively, in moderate yields (46 and 56%, respectively). The reaction of lactate-derived enyne **8e** with a protected hydroxy group led to functionalized benzoisoindole **9e** (entry 4), although the yield was relatively low. It is noteworthy that bromoenynes having a heteroaromatic ring can also be used for the tandem cyclization involving the functionalization of the aromatic C–H bond. For example, treatment of enyne **8g** bearing a benzofuranyl group with a catalytic amount of palladium acetate and cesium carbonate yielded tetracyclic product **9g** in a shorter reaction time (1 h, entry 6). A similar result was obtained with *N*-tosylindole derivative **8h** in DMF (entry 7).[16]

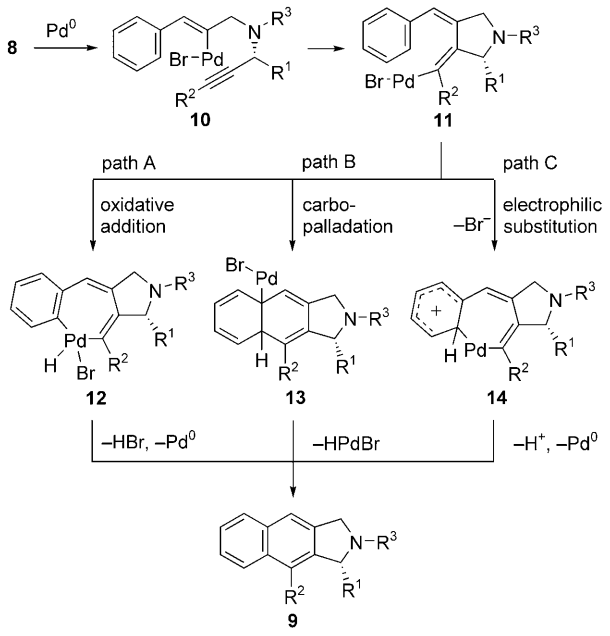
As shown in Scheme 3, this tandem cyclization could proceed through the oxidative addition of bromoenyne **8** to palladium(0), carbopalladation onto the carbon–carbon triple bond of the intermediate **10**, and functionalization of an aromatic C–H bond of **11**. The final arylation step would be promoted through 1) intramolecular oxidative addition of an aromatic C–H bond to palladium(II) (path A),[2] 2) carbopalladation onto the aryl group in **11** and the subsequent β-hydride elimination (path B),[3] or 3) electrophilic attack by the palladium(II) intermediate **11** to the aromatic carbon atom

 © 2005 Wiley-VCH Verlag GmbH & Co. KGaA, Weinheim

Table 2: Tandem cyclization of bromoenynes **8**.[a]

Entry	Substrate		*t* [h]	Product		Yield [%][b]
1		**8b**	6		**9b**	79
						
2		**8c** (R = Ms)	6		**9c** (R = Ms)	46
3		**8d** (R = Ts)	2		**9d** (R = Ts)	56
4[c]		**8e**	24		**9e**	39
5		**8f**	5		**9f**	57
6		**8g**	1		**9g**	59
7[d]		**8h**	18		**9h**	51

[a] Reactions were carried out with $Pd(OAc)_2$ (2 mol%) and Cs_2CO_3 (2 equiv) in EtOH. [b] Yields of isolated products. [c] An increased amount of $Pd(OAc)_2$ (4 mol%) was used. [d] DMF was used as the solvent. Ts = toluene-4-sulfonnyl, *c*-Hex = cyclohexyl.



Scheme 3. Possible reaction pathways for functionalization of the C–H bond.

followed by deprotonation and reductive elimination (path C).[4] It is difficult to say at present which is the most favorable reaction course, as is also the case in related palladium-catalyzed functionalizations of aromatic C–H bonds.[5]

In conclusion, we have developed a novel tandem cyclization of bromoenynes for the synthesis of tri- and tetracyclic heterocycles. This study has demonstrated for the first time that enynes can undergo a tandem cyclization involving functionalization of C–H bonds of benzene or heteroaromatic rings, such as benzofuran and indole, in the presence of a palladium catalyst. This tandem cyclization in which two carbon–carbon bonds are formed is synthetically useful since complex heterocyclic skeletons can be constructed directly from readily prepared enynes.

Experimental Section

General procedure for condensation of propargylamine derivatives **6** with 3-aryl-2-bromoprop-2-en-1-ols **7**: Diisopropyl azodicarboxylate (DIAD; 2.2 equiv) was added dropwise to a stirred mixture of **6** (1 equiv), **7** (2.2 equiv), and PPh_3 (2.2 equiv) in THF at 0 °C. The mixture was stirred for 4 h at room temperature and concentrated under reduced pressure. The residue was purified by column chromatography on silica gel with an eluent of *n*-hexane/EtOAc to give **8**.

General procedure for the palladium-catalyzed cyclization of bromoenynes **8** (Table 1, entry 5): A mixture of **8a** (124 mg, 0.265 mmol), Cs_2CO_3 (173 mg, 0.531 mmol), and $Pd(OAc)_2$ (1.2 mg, 0.0531 mmol; 2 mol%) in EtOH (1.5 mL) was heated under reflux for 7 h. After cooling the mixture, saturated NH_4Cl was added. The mixture was then extracted with EtOAc and dried over $MgSO_4$. Concentration under reduced pressure gave an oily residue, which was purified by column chromatography on silica gel with *n*-hexane/EtOAc (10:1) to give **9a** (65.7 mg, 64% yield) along with an unidentified minor product (2.5 mg, 3% yield). **9a**: colorless oil; $[\alpha]_D^{28} = +31.4$ ($c = 0.62$, $CHCl_3$); IR (KBr): $\tilde{\nu} = 3545$ (OH), 1336

 © 2005 Wiley-VCH Verlag GmbH & Co. KGaA, Weinheim

(NSO_2), 1153 cm^{-1} (NSO_2); ^1H NMR (300 MHz, $CDCl_3$): $\delta = 0.90$–1.28 (m, 5H), 1.58–1.85 (m, 6H), 1.96 (s, 3H; CMe), 2.03 (s, 3H; CMe), 2.55 (s, 3H; SO_2Me), 4.65 (dd, $J = 16.8$, 1.2 Hz, 1H; NCH_aH_b), 4.80 (dd, $J = 16.8$, 1.2 Hz, 1H; NCH_aH_b), 5.97 (d, $J = 1.2$ Hz, 1H; 1-H), 7.42–7.50 (m, 2H; Ar), 7.61 (s, 1H; Ar), 7.79–7.82 (m, 1H; Ar), 8.25 ppm (dd, $J = 9.9$, 2.7 Hz, 1H; Ar); ^{13}C NMR (67.5 MHz, $CDCl_3$): $\delta = 26.2$, 26.3, 26.7 (2C), 31.4, 32.6, 34.2 (2C), 47.0, 53.4, 71.9, 75.2, 120.8, 125.0, 125.1, 126.5, 129.0, 130.3, 134.6, 136.4, 137.3, 139.0 ppm; MS (FAB): *m/z* (%): 388 [$M+H^+$] (53), 154 (100); HRMS (FAB): calcd for $C_{22}H_{30}NO_3S$ [$M+H^+$]: 388.1946; found: 388.1948.

Received: January 15, 2005
Revised: May 11, 2005
Published online: July 13, 2005

Keywords: C–H activation · cyclization · enynes · heterocycles · palladium

[1] For recent reviews, see: a) K. Tamao, K. Kobayashi, Y. Ito, *Synlett* **1991**, 539–546; b) I. Ojima, M. Tzamarioudaki, Z. Li, R. J. Donovan, *Chem. Rev.* **1996**, *96*, 635–662; c) E. Negishi, C. Coperet, S. Ma, S.-Y. Liou, F. Liu, *Chem. Rev.* **1996**, *96*, 365–393; d) B. M. Trost, M. J. Krische, *Synlett* **1998**, 1–16; e) F. Sato, H. Urabe, S. Okamoto, *Chem. Rev.* **2000**, *100*, 2835–2886; see also: f) W. Oppolzer, *Angew. Chem.* **1989**, *101*, 39–53; *Angew. Chem. Int. Ed. Engl.* **1989**, *28*, 38–52.

[2] a) M. Catellani, G. P. Chiusoli, C. Castagnoli, *J. Organomet. Chem.* **1991**, *407*, C30–C33; b) M. Burwood, B. Davies, I. Díaz, R. Grigg, P. Molina, V. Sridharan, M. Hughes, *Tetrahedron Lett.* **1995**, *36*, 9053–9056; c) M. A. Campo, R. C. Larock, *J. Am. Chem. Soc.* **2002**, *124*, 14326–14327; for a review on organopalladium(IV) chemistry, see: d) A. J. Canty, *Acc. Chem. Res.* **1992**, *25*, 83–90.

[3] a) M. Toyota, A. Ilangovan, R. Okamoto, T. Masaki, M. Arakawa, M. Ihara, *Org. Lett.* **2002**, *4*, 4293–4296; b) B. Glover, K. A. Harvey, B. Liu, M. J. Sharp, M. F. Tymoschenko, *Org. Lett.* **2003**, *5*, 301–304; c) B. Sezen, D. Sames, *J. Am. Chem. Soc.* **2003**, *125*, 5274–5275.

[4] a) D. E. Ames, D. Bull, *Tetrahedron* **1982**, *38*, 383–387; b) J. J. González, N. García, B. Gómez-Lor, A. M. Echavarren, *J. Org. Chem.* **1997**, *62*, 1286–1291; c) S. Pivsa-Art, T. Satoh, Y. Kawamura, M. Miura, M. Nomura, *Bull. Chem. Soc. Jpn.* **1998**, *71*, 467–473; d) C.-H. Park, V. Ryabova, I. V. Seregin, A. W. Sromek, V. Gevorgyan, *Org. Lett.* **2004**, *6*, 1159–1162.

[5] a) R. Grigg, V. Savic, V. Tambyrajah, *Tetrahedron Lett.* **2000**, *41*, 3003–3006; b) C. C. Hughes, D. Trauner, *Angew. Chem.* **2002**, *114*, 1639–1642; *Angew. Chem. Int. Ed.* **2002**, *41*, 1569–1572; c) E. J. Hennessy, S. L. Buchwald, *J. Am. Chem. Soc.* **2003**, *125*, 12084–12085; d) B. Sezen, D. Sames, *J. Am. Chem. Soc.* **2003**, *125*, 10580–10585; e) B. S. Lane, D. Sames, *Org. Lett.* **2004**, *6*, 2897–2900.

[6] a) D. E. Ames, A. Opalko, *Tetrahedron* **1984**, *40*, 1919–1925; b) J. E. Rice, Z.-W. Cai, *J. Org. Chem.* **1993**, *58*, 1415–1424; c) S. Pogodin, P. U. Biedermann, I. Agranat, *J. Org. Chem.* **1997**, *62*, 2285–2287; d) T. Iwaki, A. Yasuhara, T. Sakamoto, *J. Chem. Soc. Perkin Trans. 1* **1999**, 1505–1510; e) T. Harayama, H. Yasuda, T. Akiyama, Y. Takeuchi, H. Abe, *Chem. Pharm. Bull.* **2000**, *48*, 861–864; f) L.-C. Campeau, M. Parisien, M. Leblanc, K. Fagnou, *J. Am. Chem. Soc.* **2004**, *126*, 9186–9187.

[7] a) R. C. Larock, Q. Tian, *J. Org. Chem.* **1998**, *63*, 2002–2009; b) Q. Tian, R. C. Larock, *Org. Lett.* **2000**, *2*, 3329–3332.

[8] a) M. Catellani, G. P. Chiusoli, *J. Organomet. Chem.* **1985**, *286*, C13–C6; b) G. Dyker, *Angew. Chem.* **1992**, *104*, 1079–1081; *Angew. Chem. Int. Ed. Engl.* **1992**, *31*, 1023–1025; c) M. Catellani, F. Frignani, A. Rangoni, *Angew. Chem.* **1997**, *109*, 142–145; *Angew. Chem. Int. Ed. Engl.* **1997**, *36*, 119–122.

[9] a) O. Reiser, M. Weber, A. de Meijere, *Angew. Chem.* **1989**, *101*, 1071–1072; *Angew. Chem. Int. Ed. Engl.* **1989**, *28*, 1037–1038; b) P. Mauleón, A. A. Núñez, I. Alonso, J. C. Carretero, *Chem. Eur. J.* **2003**, *9*, 1511–1520.

[10] a) R. Grigg, P. Fretwell, C. Meerholtz, V. Sridharan, *Tetrahedron* **1994**, *50*, 359–370; b) D. Brown, R. Grigg, V. Sridharan, V. Tambyrajah, *Tetrahedron Lett.* **1995**, *36*, 8137–8140; c) R. Grigg, V. Loganathan, V. Sridharan, *Tetrahedron Lett.* **1996**, *37*, 3399–3402; tandem carbon–carbon bond formation between aryl halides and enynes has also been reported, see: d) S. Brown, S. Clarkson, R. Grigg, V. Sridharan, *Tetrahedron Lett.* **1993**, *34*, 157–160.

[11] a) F. Teply, I. G. Stará, I. Stary, A. Kollárovic, D. Saman, P. Fiedler, *Tetrahedron* **2002**, *58*, 9007–9018; b) M. A. Campo, Q. Huang, T. Yao, Q. Tian, R. C. Larock, *J. Am. Chem. Soc.* **2003**, *125*, 11506–11507.

[12] a) H. Ohno, K. Miyamura, Y. Takeoka, T. Tanaka, *Angew. Chem.* **2003**, *115*, 2751–2754; *Angew. Chem. Int. Ed.* **2003**, *42*, 2647–2650; b) H. Ohno, K. Miyamura, T. Mizutani, Y. Kadoh, Y. Takeoka, H. Hamaguchi, T. Tanaka, *Chem. Eur. J.* **2005**, DOI: 10.1002/chem.200500050.

[13] For some recent examples, see: a) A. Mertens, H. Zilch, B. Koenig, W. Schaefer, T. Poll, W. Kampe, H. Seidel, U. Leser, H. Leinert, *J. Med. Chem.* **1993**, *36*, 2526–2535; b) G. W. Muller, L. G. Corral, M. G. Shire, H. Wang, A. Moreira, G. Kaplan, D. I. Stirling, *J. Med. Chem.* **1996**, *39*, 3238–3240; c) A. Cappelli, M. Anzini, S. Vomero, L. Mennuni, F. Makovec, E. Doucet, M. Hamon, M. C. Menziani, P. G. De Benedetti, G. Giorgi, C. Ghelardini, S. Collina, *Bioorg. Med. Chem.* **2002**, *10*, 779–801; d) A. Cappelli, A. Gallelli, C. Braile, M. Anzini, S. Vomero, L. Mennuni, F. Makovec, M. C. Menziani, P. G. De Benedetti, A. Donati, G. Giorgi, *Bioorg. Med. Chem.* **2002**, *10*, 2681–2691.

[14] a) D. E. Frantz, R. Fässler, E. M. Carreira, *J. Am. Chem. Soc.* **2000**, *122*, 1806–1807; b) N. K. Anand, E. M. Carreira, *J. Am. Chem. Soc.* **2001**, *123*, 9687–9688.

[15] Cesium carbonate in EtOH is a good combination for a cascade palladium-catalyzed cyclization–Suzuki coupling reaction of 2-bromo-1,6-enynes, see: C. H. Oh, Y. M. Lim, *Tetrahedron Lett.* **2003**, *44*, 267–270.

[16] The reaction in EtOH led to cleavage of the tosyl group on the nitrogen atom without formation of the desired tetracyclic product **9h**.

 © 2005 Wiley-VCH Verlag GmbH & Co. KGaA, Weinheim

Fluorescence Imaging

DOI: 10.1002/anie.200500461

Correlations between Molecular Numbers and Molecular Masses in an Evanescent Field and Their Applications in Probing Molecular Interactions**

Hongwei Gai, Qi Wang, Yinfa Ma, and Bingcheng Lin**

Single-molecule detection (SMD) technology has made remarkable progress within this decade.[1] It has been demonstrated that it is a unique technique for exploiting the fundamental physical and chemical principles of molecules, down to the single-molecule level, and that it could lead to significant biological and medical applications in the near future. A small probe volume to minimize the background effect is a critical factor for detecting individual molecules in solution. Confocal microscopy[2] or evanescent-wave excitation[3] are two valid techniques to optically confine the excitation volume. An evanescent wave is generated by total internal reflection (TIR) of the light at the interface between two media of different refractive indices, when a parallel beam of light propagates to the interface from a dense medium with a refractive index n_2 to a less dense medium with a refractive index n_1, and the incident angle θ exceeds the critical angle $\theta_c = \arcsin(n_2/n_1)$. The penetration distance z_p away from the interface, located at $z = 0$, is calculated by Equation (1):[4]

$$z_p = \frac{\lambda_0}{4\pi\sqrt{n_2^2 \sin^2\theta - n_1^2}} \quad (1)$$

in which λ_0 is the wavelength of the light. In our experiments, a laser at $\lambda_0 = 488$ nm was focused at an angle of incidence of 40–45° onto a fused silica prism ($n_2 = 1.46$). The laser beam was refracted through the prism at an angle of incidence $\theta =$ 71–74° at the fused silica/water ($n_1 = 1.33$, $\theta_c = 66°$) interface. The penetration distance z_p was 107–89 nm. The scheme for exciting a single fluorophore in an evanescent field has been employed by several research groups. Funatsu et al.[5] used refined TIR fluorescence microscopy to visualize a single fluorophore in a solution and observed adenosine triphosphate turnover reactions. Evanescent-wave excitation[6] was also adopted at the boundary of a cover slip and a polyacrylamide gel for the detection of fluorophores diffusing in and out of the gel. Yeung and co-workers[3] measured the diffusion and photodecomposition of single molecules in solution, and studied the electrostatic trapping and absorption/desorption of protein molecules at a solid/liquid interface. Fang and Tan[7] demonstrated a new fluorescence method for SMD and imaging by using an optical-fiber probe. The fluorophores were excited by the evanescent-wave field that was produced on the core surface of an optical fiber. Gai et al.[8] simultaneously determined the velocities of single molecules flowing near the channel wall and at the center of the channel by using the evanescent-field excitation mode combined with the traditional wide-field microscope.

Heparin consists of repeating disaccharide units of hexuronic acids linked to either N-sulfated or N-acetylated glucosamine units by a (1→4) bond. Both units can be sulfated to a different extent, the hexuronic acid at the C2 carbon atom and the glucosamine at C6.[9] Heparin is known for its interaction with many biologically important proteins such as proinflammatory chemokines, growth factors, extracellular matrix proteins, leukocyte proteinases, and cytokines.[10] The biological activity of heparin is strongly affected by binding to target proteins. Strong binding of heparin to the granulocyte–macrophage colony-stimulating factor (GM-CSF) and fibroblast growth factor (FGF) has been reported in the literature.[11] The granulocyte colony-stimulating factor (G-CSF) is a glycoprotein that can stimulate the proliferation and differentiation of hematopoietic progenitor cells of the neutrophil lineage and also increase the functional activity of fully differentiated neutrophils. The interaction between standard heparin, low-molecular-weight heparin (LMWH), and G-CSF has been studied by Liang et al.[12] with capillary zone electrophoresis.

We designed an experiment to detect fluorescein isothiocyanate (FITC, $M_w = 398$), FITC-deoxythymidine monophosphate (FITC-T, $M_w = 701$), FITC-12-mer oligonucleotides ($M_w = 4358$), FITC-18-mer oligonucleotides ($M_w = 6338$), and FITC-12 bp DNA ($M_w = 8318$) independently in an evanescent field at the single-molecule level and counted their molecular numbers. The numbers of molecules decreased with increasing molecular weight. We then tested a series of single fluorophores of 2-aminoacridone (2-AMAC), oligochitosan labeled with 2-AMAC, and heparin labeled with 2-AMAC, and similar results were obtained. We therefore established, on the basis of these experimental results, a new method for detecting the molecular interactions of heparin and G-CSF as model compounds in a free solution by using a single-molecule fluorescence imaging system.

The imaging system was similar to that used in previous studies,[3] except that an electron-multiplier charge coupled

[*] H. Gai, Dr. Q. Wang, Prof. Y. Ma, Prof. B. Lin
Dalian Institute of Chemical Physics
Chinese Academy of Sciences
457 Zhongshan Road, Dalian, 116023 (China)
Fax: (+86) 411-8437-9065
E-mail: yinfa@umr.edu
bclin@dicp.ac.cn
Prof. Y. Ma
Department of Chemistry
University of Missouri, Rolla
Rolla, MO 65409 (USA)
Fax: (+01) 573-341-6033
Dr. Q. Wang
The Second Affiliated Hospital of
Dalian Medical University (China)

[**] We appreciate the financial support from the National Natural Science Foundation of China (20275039, 20299035, 30470464), the "Hundred Talents Fund" of the Chinese Academy Sciences, and the project of Olympic (2002BA904B04-04). We also thank Mr. Junguang Xu of DICP for preparation of 2-AMAC-oligochitosan and 2-AMAC-heparin.

 © 2005 Wiley-VCH Verlag GmbH & Co. KGaA, Weinheim

device (EMCCD) was used instead of an intensified CCD. The detection of single Rhodamine 6G molecules was used to calibrate the system and the results were the same as those in previous reports.[3,7] A series of oligonucleotides of different lengths and labeled with FITC at the 5′ end were used as a model system. A small detection volume and low fluorophore concentration were employed in SMD,[3,7] which was mainly a statistical argument for high confidence in the results. Our experimental data demonstrated that there were excellent linear relationships between the molecular concentrations and the numbers of molecules observed in the images. As shown in Figure 1, the numbers of bright spots were proportional to the concentrations of FITC, FITC-T, FITC-12-mer oligonucleotides, FITC-18-mer oligonucleotides, and FITC-12 bp DNA. Based on these five linear fits, we quantitatively calculated the molecular numbers in the evanescent field for each individual solution at a concentration of 1000 nM (Figure 2). The expected numbers of molecules of the test compounds detected in the evanescent field should be undifferentiated, with the same concentration of fluorophores under the same fluorescence imaging conditions. The experimental results, however, indicated that the numbers of molecules that were detected in the evanescent field decreased with increasing molecular weight. We also counted the molecule numbers of real samples (at 1000 nM) and compared them with the calculated values (Figure 2); the two groups of molecule numbers are almost the same. This unexpected result indicates that, as a consequence of steric hindrance, larger molecules labeled with a single fluorophore cannot be completely immersed in the 100-nm-deep evanescent field near the surface. Although the number of molecules detected in the evanescent field was constant for each specified molecule at a given concentration, the numbers of molecules detected under the same conditions can be different for different molecules because of the variations in molecular masses and/or structures.

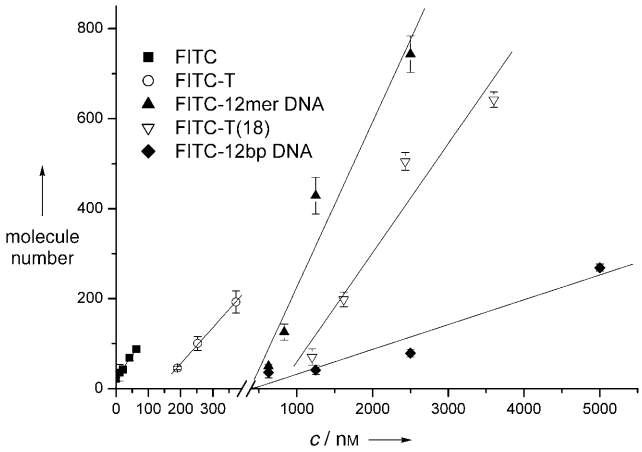


Figure 1. The linear relationships between the numbers of molecules of FITC, FITC-T, FITC-12-mer oligonucleotides, FITC-18-mer oligonucleotides, and FITC-12 bp DNA and different concentrations of each type of molecule. Samples (3 μL) were placed on the surface of the prism. The results were obtained from 128×128 pixel subframe images that were acquired by excitation with a 488-nm Ar^+ laser (100× NA 1.3 objective). The laser power was measured at about 25 mW before reaching the prism. Each pixel represents a square with 0.16-μm edges, as calibrated by the microscope stage micrometer. The excitation depth was about 100 nm (see text) and the volume of each pixel was 2.56×10^{-18} L. The EMCCD was maintained at −60 °C; the gain and exposure time were set at 255 and 100 ms, respectively. A mechanical shutter with 3-s closure was used to minimize photobleaching by blocking the laser beam when data were not being collected.

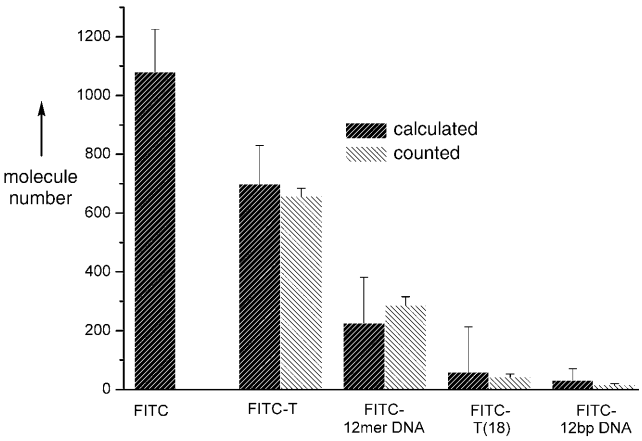


Figure 2. Comparison of the experimental and calculated numbers of individual molecules of FITC, FITC-T, FITC-12-mer oligonucleotides, FITC-18-mer oligonucleotides, and FITC-12 bp DNA at the same fluorophore concentration (1000 nM). All other experimental conditions were the same as those in Figure 1.

Oligochitosan and heparin molecules were derivatized with 2-AMAC according to the literature.[13] The 2-AMAC-glycan derivatives were produced by a "one-pot" Schiff reaction at the reducing end (the *N*-acetylglucosamine residues) followed by reduction, and one carbohydrate molecule was labeled with one fluorophore. After four extraction steps with tetrahydrofuran, free 2-AMAC dye was totally removed from the 2-AMAC-labeled oligochitosan and heparin solution. The fluorescence concentration and purity of the derivatives were determined by fluorescence spectrometry and high-performance thin-layer chromatography.

As shown in Figure 3a, the numbers of molecules were proportional to the concentrations of 2-AMAC, 2-AMAC-oligochitosan, and 2-AMAC-heparin. Similarly, the calculated molecular numbers for each individual solution (Figure 3b) decreased with an increase in molecular weight.

Oligochitosan is a mixture of chitosan oligomers with a degree of polymerization of 3–10,[14] obtained by the enzymatic hydrolysis of chitosan. Its average molecular weight was about 1800 according to mass spectrometry (data not shown). Heparin is a glycosaminoglycan with an average molecular mass of about 14000. Oligochitosan and heparin molecules were both derivatized with 2-AMAC. All of the bright spots in the fluorescence images corresponded to the 2-AMAC-derivatized molecules.

The two series of correlated experimental data allow us to hypothesize that the interaction of molecules can be probed in a mixture without separation, based on the decreased numbers of product molecules in the probed area after

 © 2005 Wiley-VCH Verlag GmbH & Co. KGaA, Weinheim

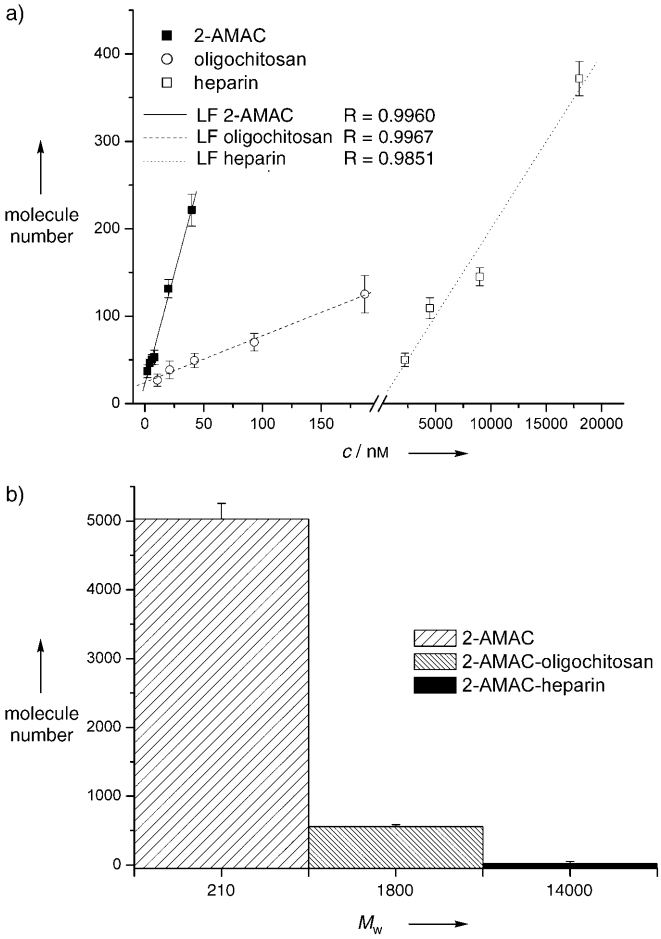


Figure 3. a) The linear relationships between the numbers of molecules of 2-AMAC (■), 2-AMAC-oligochitosan (○), and 2-AMAC-heparin (□) and different concentrations of each type of molecule. LF = linear fit. b) Comparison of the numbers of individual molecules of 2-AMAC, 2-AMAC-oligochitosan, and 2-AMAC-heparin at the same fluorophore concentration (1000 nM). All other experimental conditions were the same as those in Figure 1.

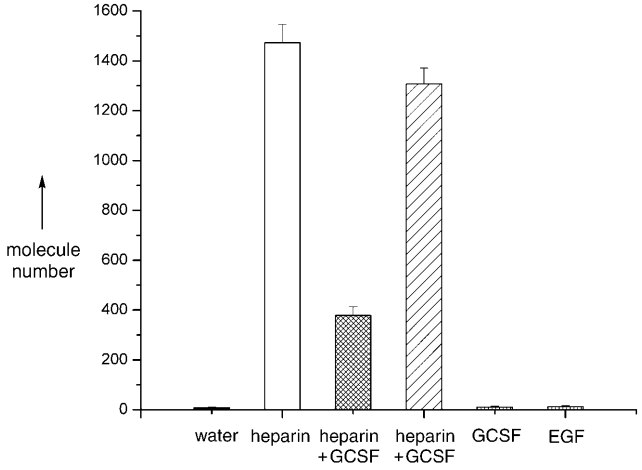


Figure 4. The numbers of molecules counted in purified water, heparin (73 μM), a mixture of heparin (73 μM) with G-CSF (6.5 μM), a mixture of heparin (73 μM) with EGF (34.72 μM), G-CSF (6.5 μM), and EGF (34.72 μM). The experimental conditions were the same as those indicated in Figure 1.

reaction relative to the numbers of reactant molecules. To test this hypothesis, the complex of heparin with G-CSF was studied as a model.

The binding of heparin with G-CSF was demonstrated by Liang et al.[12] with capillary zone electrophoresis. The heparin-G-CSF complex has a higher molecular mass (M_w = 14000 + 18987) than heparin itself (M_w = 14000), and therefore the number of heparin-G-CSF complex molecules observed in the evanescent field should be less than that of the heparin molecules. The imaging results fully supported our hypothesis (see Figure 4). Furthermore, we imaged a mixture of heparin and epidermal growth factor (EGF) to confirm that the decrease in the number of heparin-G-CSF complex molecules was not a result of the co-existing protein molecules. EGF is an ideal negative control for the formation of heparin-G-CSF complex because EGF molecules do not bind to heparin at all.[15] At EGF concentrations up to 34.72 μM, the number of heparin molecules counted in the evanescent field was about the same as the number counted for the solution that did not contain EGF. The G-CSF and EGF molecules were also counted separately to determine whether their fluorescence backgrounds were comparable with that of water, as both of these proteins had no fluorescence. This step was to ensure that the numbers of extra G-CSF molecules in solution did not contribute to the count of the heparin-G-CSF complexes when using this technique. The results in Figure 4 confirm that the existence of G-CSF and EGF molecules at this concentration level does not significantly increase the background signal. The findings support our hypothesis that the formation of a macromolecular complex changes the number of molecules detected in the evanescent field, which means that the interaction of macromolecules can be probed with this technique. Conversely, the data prove that the number of molecules decreases with an increase of molecular weight in the evanescent field.

In summary, with our single-molecule fluorescence imaging technique we discovered that the numbers of molecules probed in the evanescent field decreased with an increase of molecular weight as a consequence of steric hindrance. Our results suggest that this technique and phenomenon could be potentially useful for screening undefined molecular interactions at extremely low concentrations without any separation, for which other methods may not be applicable. This finding could be especially useful for studying the interactions of biological molecules. Future investigations will focus on quantitative measurements of the relationship between molecule numbers and molecular mass, quantitative determination of binding constants, and exploration of the effects of binding constants on the numbers of molecules detected in a probed area.

Received: February 7, 2005
Revised: March 8, 2005
Published online: July 12, 2005

 © 2005 Wiley-VCH Verlag GmbH & Co. KGaA, Weinheim

Keywords: evanescent field · fluorescence · molecule counting · oligonucleotides · single-molecule studies

[1] a) S. M. Nie, R. N. Zare, *Annu. Rev. Biophys. Biomol. Struct.* **1997**, *26*, 567–596; b) S. Weiss, *Science* **1999**, *283*, 1676–1683; c) W. P. Ambrose, P. M. Goodwin, J. H. Jett, A. Van Orden, J. H. Werner, R. A. Keller, *Chem. Rev.* **1999**, *99*, 2929–2956.
[2] a) A. Castro, F. R. Fairfield, E. B. Shera, *Anal. Chem.* **1993**, *65*, 849–852; b) S. M. Nie, D. T. Chiu, R. N. Zare, *Science* **1994**, *266*, 1018–1021.
[3] a) X. H. Xu, E. S. Yeung, *Science* **1997**, *275*, 1106–1109; b) X. H. N. Xu, E. S. Yeung, *Science* **1998**, *281*, 1650–1653; c) S. H. Kang, E. S. Yeung, *Anal. Chem.* **2002**, *74*, 6334–6339.
[4] D. Axelrod, T. P. Burghardt, N. L. Thompson, *Annu. Rev. Biophys. Bioeng.* **1984**, *13*, 247–268.
[5] T. Funatsu, Y. Harada, M. Tokunaga, K. Saito, T. Yanagida, *Nature* **1995**, *374*, 555–559.
[6] R. M. Dickson, D. J. Norris, Y. L. Tzeng, W. E. Moerner, *Science* **1996**, *274*, 966–969.
[7] X. H. Fang, W. H. Tan, *Anal. Chem.* **1999**, *71*, 3101–3105.
[8] H. W. Gai, Y. Li, Z. Silber-Li, Y. F. Ma, B. C. Lin, *Lab Chip* **2005**, *5*, 443–449.
[9] V. Ruiz-Calero, E. Moyano, L. Puignou, M. T. Galceran, *J. Chromatogr. A* **2001**, *914*, 277–291.
[10] Q. C. Jiao, Q. Liu, C. Sun, H. He, *Talanta* **1999**, *48*, 1095–1101.
[11] a) P. Jaakkola, V. Kainulainen, M. T. Jalkanen in *Proteoglycans (Structure, Biology, and Molecular Interaction)* (Ed.: R. V. Lozzo), Marcel Dekker, New York, **2000**, pp. 115–145; b) J. T. Gallagher, M. Lyon in *Proteoglycans (Structure, Biology, and Molecular Interaction)* (Ed.: R. V. Lozzo), Marcel Dekker, New York, **2000**, pp. 27–61.
[12] A. Y. Liang, X. Y. He, Y. G. Du, K. Y. Wang, Y. S. Fung, B. C. Lin, *Electrophoresis* **2004**, *25*, 870–875.
[13] a) G. Okafo, J. Langridge, S. North, A. Organ, A. West, M. Morris, P. Camilleri, *Anal. Chem.* **1997**, *69*, 4985–4993; b) P. Jackson, *Anal. Biochem.* **1991**, *196*, 238–244.
[14] a) H. Zhang, Y. G. Du, X. J. Yu, *Chin. J. Biochem. Pharm.* **1999**, *20*, 99–101; b) H. Zhang, Y. G. Du, X. J. Yu, M. Mitsutomi, S. Aiba, *Carbohydr. Res.* **1999**, *320*, 257–260.
[15] Y. Shing, J. Folkman, R. Sullivan, C. Butterfield, J. Murray, M. Klagsbrun, *Science* **1984**, *223*, 1296–1299.

 © 2005 Wiley-VCH Verlag GmbH & Co. KGaA, Weinheim

Lectin Inhibitors

DOI: 10.1002/anie.200500627

C_2-Symmetrical Thiodigalactoside Bis-Benzamido Derivatives as High-Affinity Inhibitors of Galectin-3: Efficient Lectin Inhibition through Double Arginine–Arene Interactions**

*Ian Cumpstey, Anders Sundin, Hakon Leffler, and Ulf J. Nilsson**

Galectin-3 is a β-galactoside-binding protein[1] that has been implicated as playing an important role in cancer and inflammation processes.[2] Recently, a dominant negative C-terminal fragment of galectin-3 was shown to slow the growth of breast cancer in mice by blocking galectin-3 endogenous ligands.[3] Although many intriguing biological activities have been demonstrated,[2] the precise mode of action of galectin-3 remains unknown. The synthesis of potent, low-molecular-weight inhibitors of galectin-3 is therefore an important goal, as such molecules could be used both as tools to investigate the molecular biology of the protein and as lead compounds for drugs.

The β-galactoside binding site (termed subsite C in Ref. [1b]) is highly conserved across the galectins, whereas the neighboring sites on either side of the Gal group (B, toward the nonreducing terminus; D, toward the reducing terminus) are more variable, albeit important, contributors to the interaction. *N*-Acetyllactosamine (LacNAc, **1**), which binds in subsites C and D, is the best natural disaccharide ligand for galectin-3 (Figure 1a). We have previously reported the synthesis of potent inhibitors of galectin-3 based on modification of LacNAc at C3 of galactose to target subsite B.[5] The best inhibitors were aromatic amides of general structure **2** (Figure 1c) and according to the crystal structure of an inhibitor–galectin-3 complex, the increase in binding affinity results from particularly favorable interactions of the aromatic amide moiety with an arginine side chain (Arg 144).[5b] Arene–guanidinium interactions[6] have attracted considerable interest in recent years, as they can be as strong as cation–anion interactions[6c] and up to 70% of all arginine side chains are involved in such interactions.[6b]

[*] Dr. I. Cumpstey, A. Sundin, Dr. U. J. Nilsson
Organic Chemistry, Lund University
Box 124, 221 00 Lund (Sweden)
Fax: (+46) 46-222-8209
E-mail: ulf.nilsson@organic.lu.se
Dr. H. Leffler
Section MIG, Department of Laboratory Medicine
Lund University
Solvegatan 23, 223 62 Lund (Sweden)

[**] This work was supported by the Swedish Research Council and the programs "Chemistry for the Life Sciences" and "Glycoconjugates in Biological Systems" sponsored by the Swedish Foundation for Strategic Research.

Supporting information for this article is available on the WWW under http://www.angewandte.org or from the author.

InterScience
© 2005 Wiley-VCH Verlag GmbH & Co. KGaA, Weinheim

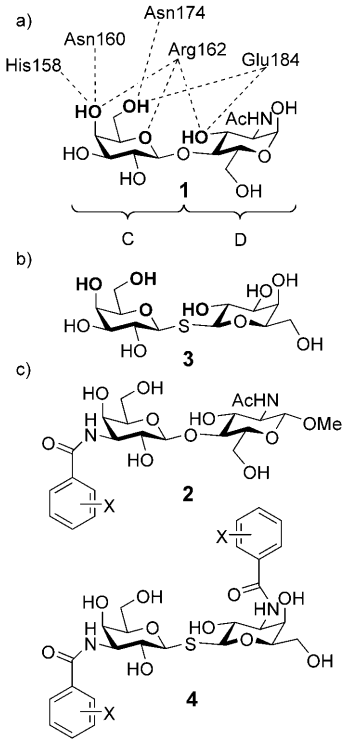


Figure 1. a) Representation of the complex of *N*-acetyllactosamine **1** with galectin-3 in which dashed lines represent hydrogen bonds.[4] The areas known as subsites C and D are indicated, and the key polar interacting groups on the saccharide are shown in bold.[1b] b) Thiodigalactoside **3** with key polar groups for interaction with galectin-1 shown in bold.[8b] c) Lactosamine-based galectin inhibitors **2** and proposed thiodigalactoside-based inhibitors **4**, showing the similarity in structure and conformation.

The guanidinium ion is positively charged, has a π system, and is poorly solvated in water,[7] which makes it ideal for interactions with aromatic π systems. Consequently, the targeting of protein arginine residues with aromatic structures is emerging as an attractive strategy for protein inhibitor development.

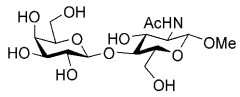
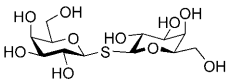
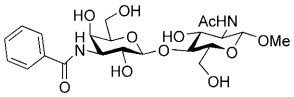
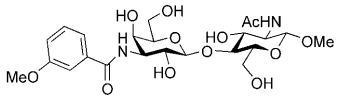
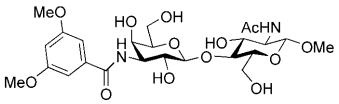
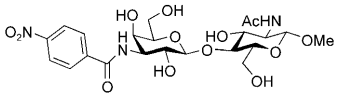
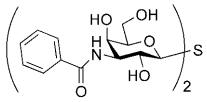
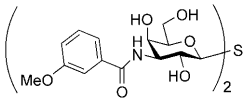
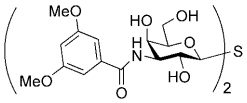
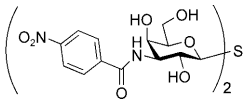
Thiodigalactoside **3** has been shown to bind to galectins with about the same affinity as LacNAc,[8] and it was hypothesized that it bound in a mode similar to that of LacNAc,[8a] that is, in subsites C and D, with a similar conformation and hydrogen-bonding network (Figure 1b). This notion has recently been confirmed for galectin-1, for which X-ray structures have been solved both with LacNAc **1** and with thiodigalactoside **3** as ligands.[8b] The galactose residues bind identically in subsite C for the two disaccharides, and in subsite D, the Gal of thiodigalactoside and GlcNAc of LacNAc show identical patterns of interaction with the protein.

We reasoned that derivatization with aromatic amides at C3 of galactose in thiodigalactoside, as for **2**, could increase the affinity for galectin-3 through favorable interactions with Arg144 in subsite B. Furthermore, similar derivatization at the second galactose C3 of **2** would give an amide that could interact with an arginine residue (Arg186) in subsite D (Figure 1c). The resulting molecules **4** are C_2-symmetrical, which simplifies the synthesis and could also lead to interesting thermodynamic properties as there are two degenerate binding modes.

Computer modeling[9] of the complex of galectin-3 with a thiodigalactoside bis-benzamido derivative **4a** (Table 1), which was performed by starting from the reported crystal structure of galectin-3 complexed with a C3-benzamido LacNAc-based inhibitor,[5b] gave an energy minimum with the two galactose units bound in subsites C and D (Figure 2). Moreover, the two aromatic rings of the benzamides were involved in stacking interactions with the two arginine residues, Arg144 and Arg186.

To test the potential of 3,3′-bis-amide-derivatized thiodigalactosides as inhibitors of galectin-3, we synthesized a selection of these compounds. The amide structures were

Table 1: K_d values for the inhibitors **4a–d** established by fluorescence polarization.[11]

	Compound	K_d [nM]	Relative activity[a]
9		69000[5b]	1
3		43000	1.6
2a		6700[5b]	10
2b		2500[5b]	28
2c		1100[5b]	63
2d		950[5b]	73
4a		3000	23
4b		61	1130
4c		50	1380
4d		33	2090

[a] Compounds **9**, **2a–d**, and **3** are included for reference.

 © 2005 Wiley-VCH Verlag GmbH & Co. KGaA, Weinheim

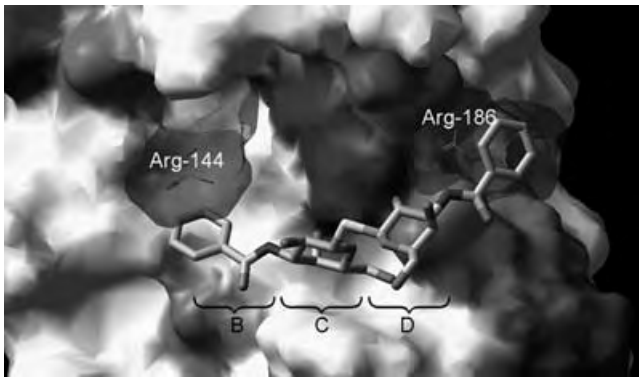


Figure 2. Molecular model of **4a** bound in the galectin-3 active site, energy-minimized by using MacroModel MMFF/water. The two arginine residues, Arg144 and Arg186, in subsites B and D, respectively, are stacked against the two aromatic rings of the amide groups.

chosen based on the best results from our investigation into C3-benzamido LacNAc derivatives **2**.[5] Consequently, the bis-amide structures **4a–d** were synthesized starting from the known 1,2,4,6-tetra-*O*-acetyl-3-azido-3-deoxy-D-galactopyranose[10] (Supporting Information).

Bis-amides **4a–d** were tested for binding to galectin-3 with a fluorescence polarization assay[11] (Table 1). Pleasingly, our strategy was successful; bis-amides **4a–d** all have dissociation constant values ($K_d = 33$–3000 nM) significantly better than those of nonderivatized thiodigalactoside **3** and the methyl β-glycoside of *N*-acetyllactosamine **9**, both of which were included in the test as reference compounds. The substituted benzamides **4b–d** bind much better than the unsubstituted benzamide **4a**, as would be expected if the thiodigalactoside derivatives **4** bound in the galactose binding site of galectin-3 (subsite C) similarly to the LacNAc-derived amides **2**.[5b] Furthermore, these thiodigalactosides **4** have much higher affinities than the corresponding LacNAc derivatives **2** (compare **2a–d** and **4a–d**), and it is logical to conclude that this finding is the consequence of a favorable interaction between the second aromatic amide and Arg186, as suggested by our docking experiments (Figure 2). An alternative interpretation would be that compounds **4a–d** cross-link by binding to subsites B and C of two galectin-3 molecules. However, such a binding mode is unlikely as, for steric reasons, it would require a much longer galactose–galactose distance than that present in **4a–d**.

In conclusion, the targeting of arginine side chains with aromatic structures has been demonstrated as an efficient approach toward the discovery of monovalent high-affinity lectin inhibitors. The 3,3′-bis-benzamido-thiodigalactosides **4a–d** are the best monovalent galectin-3 inhibitors reported to date and, as such, constitute promising lead structures for the development of galectin-targeting drugs. In general, the targeting of arginine–arene interactions may be underexploited in drug design relative to targeting, for example, hydrogen-bonding and ionic interactions. Our observation that both of the arginine–arene interactions between galectin-3 and the inhibitors **4a–d** provide substantial affinity enhancements implies that systematic targeting of such interactions could find wider use in drug design.

Received: February 21, 2005
Published online: July 11, 2005

Keywords: arenes · drug design · inhibitors · proteins · stacking interactions

[1] a) D. Houzelstein, I. R. Gonçalves, A. J. Fadden, S. S. Sidhu, D. N. Cooper, K. Drickamer, H. Leffler, F. Poirier, *Mol. Biol. Evol.* **2004**, *21*, 1177; b) H. Leffler, S. Carlsson, M. Hedlund, Y. Qian, F. Poirier, *Glycoconjugate J.* **2002**, *19*, 433.
[2] a) H. Leffler, *Glycoconjugate J.* **2002**, *19*, 433; b) F.-T. Liu, G. A. Rabinovich, *Nat. Rev. Cancer* **2005**, *5*, 29.
[3] C. M. John, H. Leffler, B. Kahl-Knutson, I. Svensson, G. A. Jarvis, *Clin. Cancer Res.* **2003**, *9*, 2374.
[4] J. Seetharaman, A. Kanigsberg, R. Slaaby, H. Leffler, S. H. Barondes, J. Rini, *J. Biol. Chem.* **1998**, *273*, 13047.
[5] a) P. Sörme, Y. Qian, P.-G. Nyholm, H. Leffler, U. J. Nilsson, *ChemBioChem* **2002**, *3*, 183; b) P. Sörme, P. Arnoux, B. Kahl-Knutsson, J. M. Rini, H. Leffler, U. J. Nilsson, *J. Am. Chem. Soc.* **2005**, *127*, 1737.
[6] a) J. C. Ma, D. A. Dougherty, *Chem. Rev.* **1997**, *97*, 1303; b) J. P. Gallivan, D. A. Dougherty, *Proc. Natl. Acad. Sci. USA* **1999**, *96*, 9459; c) J. P. Gallivan, D. A. Dougherty, *J. Am. Chem. Soc.* **2000**, *122*, 870; d) N. Zacharias, D. A. Dougherty, *Trends Pharmacol. Sci.* **2002**, *23*, 281.
[7] P. E. Mason, G. W. Neilson, C. E. Dempsey, A. C. Barnes, J. M. Cruickshank, *Proc. Natl. Acad. Sci. USA* **2003**, *100*, 4557.
[8] a) H. Leffler, S. Barondes, *J. Biol. Chem.* **1986**, *261*, 10119; b) M. A. Bianchet, H. Ahmed, G. R. Vasta, L. M. Amzel, *Proteins* **2002**, *40*, 378; c) C. F. Brewer, *Glycoconjugate J.* **2002**, *19*, 459.
[9] MacroModel version 8.6: http://www.schrodinger.com/ See: F. Mohamadi, N. G. J. Richards, W. C. Guida, R. Liscamp, M. Lipton, C. Caufield, G. Chang, T. Hendrickson, W. C. Still, *J. Comput. Chem.* **1990**, *11*, 440.
[10] T. L. Lowary, O. Hindsgaul, *Carbohydr. Res.* **1994**, *251*, 33.
[11] P. Sörme, B. Kahl-Knutson, M. Huflejt, U. J. Nilsson, H. Leffler, *Anal. Biochem.* **2004**, *334*, 36.

 © 2005 Wiley-VCH Verlag GmbH & Co. KGaA, Weinheim

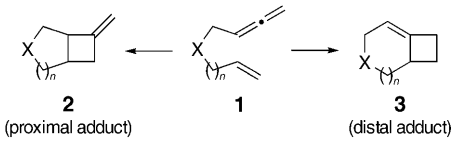
Synthetic Methods

DOI: 10.1002/anie.200501413

Thermal Intramolecular [2+2] Cycloaddition of Allenenes and Allenynes: Diastereoselective Access to Bicyclic Nitrogen Heterocycles**

Hiroaki Ohno, Tsuyoshi Mizutani, Yoichi Kadoh, Kumiko Miyamura, and Tetsuaki Tanaka**

Cycloaddition reactions that occur without the use of reagents or catalysts and without creating any waste have attracted much attention in recent years as an ideal process in terms of atom economy.[1] Considerable research efforts have been particularly focused on the development of cycloaddition of allenes,[2] on account of the current interest in the reactions of allenes with an additional multiple bond, including transition-metal-catalyzed carbocyclizations.[3,4] The [2+2] cycloaddition reactions[5] between allenes and alkenes are extremely useful for the synthesis of methylenecyclobutane derivatives.[6] Especially, intramolecular cycloaddition constitutes a versatile method for the stereoselective synthesis of a variety of bicyclic compounds having a strained bicyclo[*n*.2.0] framework (Scheme 1).[7] In most reported intramolecular [2+2]



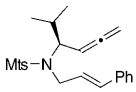
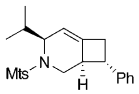
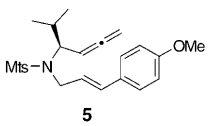
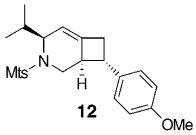
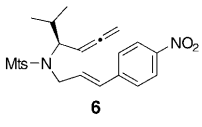
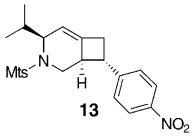
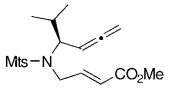
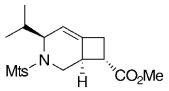
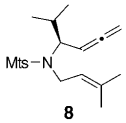
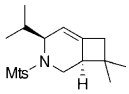
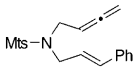
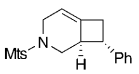
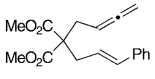
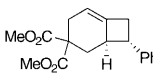
Scheme 1. Intramolecular [2+2] cycloaddition of allenenes.

cycloaddition reactions of simple unactivated allenes, the proximal 2π component of the allene moiety participates in the cycloaddition to form bicyclic products **2**.[2] Only limited examples of the intramolecular [2+2] reaction of the distal allenic double bond to give **3** have been reported to date, which used a special class of allenes such as allene carboxylates,[8] allenyl sulfones,[9] difluoroallenes,[10] β-lactam-tethered allenes,[11] or diyne-diallenes.[12]

In the course of our efforts toward the development of a new methodology for the synthesis of heterocyclic compounds by the transition-metal-catalyzed cyclization of allenes,[4,13] we found that the thermal cycloaddition of simple allenes with an additional multiple bond proceeds by simply heating the allenenes or allenynes in the absence of any catalyst. Herein, we present an intramolecular [2+2] cycloaddition of unactivated allenes to form distal adducts of type **3**, which constitute an important class of compounds in synthetic[14] and natural product chemistry.[15]

Various allenenes **4**–**10** (Table 1) were prepared according to the reported procedure[4d] and their thermal cycloaddition reaction was investigated. First, the [2+2] cycloaddition of

Table 1: Thermal [2+2] cycloaddition of allenenes.[a]

Entry	Substrate	*t* [h]	Product	Yield [%][b]
1	 **4**	65[c]	 **11**	89
2		3		96
3	 **5**	3	 **12**	71
4	 **6**	1	 **13**	93
5	 **7**	2	 **14**	73
6	 **8**	24[d]	 **15**	82
7	 **9**	19[d]	 (±)-**16**	68
8	 **10**	30	 (±)-**17**	69

[a] Unless otherwise stated, reactions were carried out in DMF at 150 °C. [b] Yields of isolated products. [c] Reaction was carried out in dioxane under reflux conditions. [d] Reaction was carried out in DMF under reflux conditions. Mts = 2,4,6-trimethylphenylsulfonyl.

allenene **4** was examined under various reaction conditions. Among the solvents employed, dioxane and dimethylformamide (DMF) were the solvents of choice leading to 3-azabicyclo[4.2.0]oct-5-ene derivative **11** in 89 and 96 % yields, respectively, as the sole isolable isomer (Table 1, entries 1 and 2). The structure and configuration of **11** were confirmed by

[*] Dr. H. Ohno
Graduate School of Pharmaceutical Sciences
Kyoto University
Sakyo-ku, Kyoto 606-8501 (Japan)
Fax: (+81) 7-5753-4570
E-mail: hohno@pharm.kyoto-u.ac.jp
T. Mizutani, Y. Kadoh, K. Miyamura, Prof. Dr. T. Tanaka
Graduate School of Pharmaceutical Sciences
Osaka University
1-6 Yamadaoka, Suita, Osaka 565-0871 (Japan)
Fax: (+81) 6-6879-8214
E-mail: t-tanaka@phs.osaka-u.ac.jp

[**] We thank Dr. S. Aoki, Graduate School of Pharmaceutical Sciences, Osaka University, for NMR spectroscopic analyses. This work was supported by a Grant-in-Aid for Encouragement of Young Scientists from the Ministry of Education, Culture, Sports, Science, and Technology of Japan and Mitsubishi Chemical Corporation Fund, which are gratefully acknowledged.

 © 2005 Wiley-VCH Verlag GmbH & Co. KGaA, Weinheim

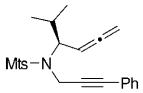
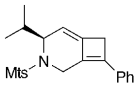
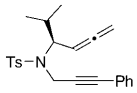
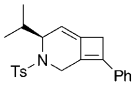
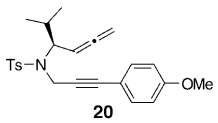
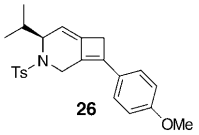
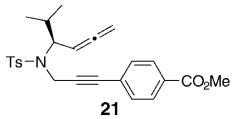
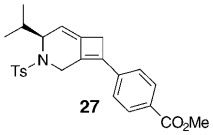
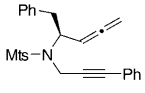
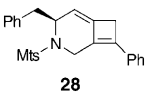
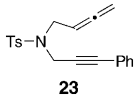
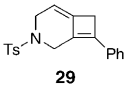
heteronuclear multiple quantum correlation (HMQC) and NOESY analysis of the corresponding hydrogenated derivatives. The reaction in dioxane under reflux was rather slow (Table 1, entry 1), and therefore the cycloaddition of the other allenenes **5**–**10** was conducted in DMF. All the allenenes were successfully converted into the corresponding bicyclic products in good to excellent yields, with complete regioselectivity. The reaction of the allenene **5** bearing an electron-donating aryl group gave **12** in relatively low yield (71%, Table 1, entry 3), whereas the allenene **6** with an electron-withdrawing group afforded **13** in 93% yield within a shorter reaction time (1 h, Table 1, entry 4). Allene **7** with an α,β-unsaturated ester group showed sufficient reactivity to give the cycloadduct **14** in 73% yield. Allenene **8** with a geminal dimethyl group on the olefinic carbon atom (Table 1, entry 6), α-unsubstituted allene derived substrate **9** (Table 1, entry 7), and dimethyl malonate derived allenene **10** (Table 1, entry 8) gave the distal cycloadducts **15**–**17** in 68–82% yields, although prolonged reaction times were required.

Next, the thermal cycloaddition of allenynes **18**–**23** (Table 2) was investigated, which were easily prepared by the N-arylpropargylation of known amino allenes. In contrast to the cycloaddition of allenenes **4** (Table 1, entries 1 and 2), the reaction of the allenyne **18** was complete within 2 h in dioxane under reflux conditions to give 3-azabicyclo-[4.2.0]octa-1(8),5-diene derivative **24** in 92% yield (Table 2, entry 1). In the reaction of N-tosylated allenyne derivatives **19**–**21**, the effect of the electron-donating and -withdrawing aryl group on the reactivity was not dramatic (Table 2, entries 2–4). More important is the α substituent of the allene: the reaction of the allenyne **22** bearing a smaller substituent at the α position was complete in 8 h, whereas the cycloaddition of α-unsubstituted allene derivative **23** required a prolonged reaction time (117 h) to give **29** in 94% yield.

The related [2+2] thermal reactions of allenes are thought to proceed by a two-step mechanism, that is, via a diradical intermediate.[2, 9b,c, 16] In the present [2+2] cyclization of simple allenenes and allenynes, the substituent on the double or triple bond, which effectively stabilizes the radical intermediate, is essential for successful conversion: the corresponding allenenes or allenynes without the radical-stabilizing group were completely inert to the thermal [2+2] cycloaddition. This experimental result supports the diradical mechanism; however, further study is necessary to elucidate the reaction mechanism.

In conclusion, a stereoselective route to bicyclo-[4.2.0]octane derivatives has been developed by using thermal [2+2] cycloaddition of allenes with an additional multiple bond. This study first demonstrated that unactivated allenenes and allenynes can regioselectively undergo intramolecular [2+2] cycloaddition of the distal double bond of the allene moiety. This simple and environmentally benign process would extend the potential application of fused bicyclic cyclobutane derivatives in synthetic and medicinal chemistry.

Table 2: Thermal [2+2] cycloaddition of allenynes.[a]

Entry	Substrate	*t* [h]	Product	Yield [%][b]
1	 **18**	2	 **24**	92
2	 **19**	3	 **25**	70
3	 **20**	2	 **26**	61
4	 **21**	2	 **27**	67
5	 **22**	8	 **28**	91
6	 **23**	117	 **29**	94

[a] All reactions were carried out in dioxane under reflux conditions. [b] Yields of isolated products. Mts = 2,4,6-trimethylphenylsulfonyl; Ts = *p*-toluenesulfonyl.

Received: April 25, 2005
Published online: July 20, 2005

Keywords: allenes · bicyclic compounds · cycloaddition · nitrogen heterocycles · regioselectivity

[1] a) B. M. Trost, *Acc. Chem. Res.* **2002**, *35*, 695–705; see also, b) B. M. Trost, *Science* **1991**, *254*, 1471–1477.

[2] For excellent reviews, see: a) D. J. Pasto, *Tetrahedron* **1984**, *40*, 2805–2827; b) M. Murakami, T. Matsuda in *Modern Allene Chemistry*, *Vol. 2* (Eds.: N. Krause, A. S. K. Hashmi), Wiley-VCH, Weinheim, **2004**, pp. 727–815.

[3] a) S. Shin, T. V. RajanBabu, *J. Am. Chem. Soc.* **2001**, *123*, 8416–8417; b) C. H. Oh, S. H. Jung, C. Y. Rhim, *Tetrahedron Lett.* **2001**, *42*, 8669–8671; c) J. Franzén, J. Löfstedt, I. Dorange, J.-E. Bäckvall, *J. Am. Chem. Soc.* **2002**, *124*, 11246–11247; d) J. Franzén, J.-E. Bäckvall, *J. Am. Chem. Soc.* **2003**, *125*, 6056–6057; e) C. H. Oh, S. H. Jung, D. I. Park, J. H. Choi, *Tetrahedron Lett.* **2004**, *45*, 2499–2502.

[4] a) H. Ohno, K. Miyamura, Y. Takeoka, T. Tanaka, *Angew. Chem.* **2003**, *115*, 2751–2754; *Angew. Chem. Int. Ed.* **2003**, *42*, 2647–2650; b) H. Ohno, Y. Takeoka, K. Miyamura, Y. Kadoh, T. Tanaka, *Org. Lett.* **2003**, *5*, 4763–4766; c) H. Ohno, Y. Takeoka, Y. Kadoh, K. Miyamura, T. Tanaka, *J. Org. Chem.* **2004**, *69*, 4541–4544; d) H. Ohno, K. Miyamura, T. Mizutani, Y. Kadoh, Y. Takeoka, H. Hamaguchi, T. Tanaka, *Chem. Eur. J.* **2005**, *11*, 3728–3741.

[5] For some recent examples of [2+2] cycloaddition, see: a) B. M. Trost, M. Yanai, K. Hoogsteen, *J. Am. Chem. Soc.* **1993**, *115*, 5294–5295; b) F. Marion, J. Coulomn, C. Courillon, L. Fensterbank, M. Malacria, *Org. Lett.* **2004**, *6*, 1509–1511; c) K. Villeneuve, W. Tam, *Angew. Chem.* **2004**, *116*, 620–623; *Angew. Chem. Int. Ed.* **2004**, *43*, 610–613; d) R. F. Sweis, M. P. Schramm, S. A. Kozmin, *J. Am. Chem. Soc.* **2004**, *126*, 7442–7443; e) K.

 © 2005 Wiley-VCH Verlag GmbH & Co. KGaA, Weinheim

Inanaga, K. Takasu, M. Ihara, *J. Am. Chem. Soc.* **2005**, *127*, 3668 – 3669; f) J. D. Winkler, E. C. McLaughlin, *Org. Lett.* **2005**, *7*, 227 – 229.

[6] For some recent examples, see: a) Y. Gu, T. Hama, G. B. Hammond, *Chem. Commun.* **2000**, 395 – 396; b) T. Akiyama, K. Daidouji, K. Fuchibe, *Org. Lett.* **2003**, *5*, 3691 – 3693; c) Y. Horino, M. Kimura, S. Tanaka, T. Okajima, Y. Tamaru, *Chem. Eur. J.* **2003**, *9*, 2419 – 2439.

[7] For recent examples, see: a) M. S. Shepard, E. M. Carreira, *J. Am. Chem. Soc.* **1997**, *119*, 2597 – 2605; b) T. Tsuno, K. Sugiyama, *Bull. Chem. Soc. Jpn.* **1999**, *72*, 519 – 531; for transition-metal-catalyzed [2+2] cycloadditions, see: c) S.-K. Kang, T.-G. Baik, A. N. Kulak, Y.-H. Ha, Y. Lim, J. Park, *J. Am. Chem. Soc.* **2000**, *122*, 11529 – 11530; d) M. Murakami, S. Ashida, T. Matsuda, *J. Am. Chem. Soc.* **2004**, *126*, 10838 – 10839.

[8] a) M. Yoshida, M. Hiromatsu, K. Kanematsu, *Heterocycles* **1986**, *24*, 881 – 884; b) M. Yoshida, Y. Hidaka, Y. Nawata, J. M. Rudziñski, E. Õsawa, K. Kanematsu, *J. Am. Chem. Soc.* **1988**, *110*, 1232 – 1238; for a related reaction of cumulenes, see: c) J. G. Garcia, B. Ramos, L. M. Pratt, A. Rodríguez, *Tetrahedron Lett.* **1995**, *36*, 7391 – 7394.

[9] a) K. Kanematsu, N. Sugimoto, M. Kawaoka, S. Yeo, M. Shiro, *Tetrahedron Lett.* **1991**, *32*, 1351 – 1354; b) A. Padwa, M. A. Filipkowski, M. Meske, S. H. Watterson, Z. Ni, *J. Am. Chem. Soc.* **1993**, *115*, 3776 – 3777; c) A. Padwa, M. Meske, S. S. Murphree, S. H. Watterson, Z. Ni, *J. Am. Chem. Soc.* **1995**, *117*, 7071 – 7080; d) A. Padwa, H. Lipka, S. H. Watterson, S. S. Murphree, *J. Org. Chem.* **2003**, *68*, 6238 – 6250.

[10] Q. Shen, G. B. Hammond, *J. Am. Chem. Soc.* **2002**, *124*, 6534 – 6535.

[11] B. Alcaide, P. Almendros, C. Aragoncillo, *Org. Lett.* **2003**, *5*, 3795 – 3798.

[12] Recently, in their study of the molybdenum-mediated allenic Pauson–Khand reaction, Cook and co-workers observed the formation of distal adducts in 30–40% yield, by heating of conformationally restricted diyne-allenes in toluene at 100 °C in the absence of any catalyst. As far as we are aware, this is the first example of thermal [2+2] cycloaddition between unactivated allenes and alkynes. See: a) H. Cao, J. Flippen-Anderson, J. M. Cook, *J. Am. Chem. Soc.* **2003**, *125*, 3230 – 3231; b) H. Cao, S. G. Van Ornum, J. Deschamps, J. Flippen-Anderson, F. Laib, J. M. Cook, *J. Am. Chem. Soc.* **2005**, *127*, 933 – 943.

[13] a) H. Ohno, A. Toda, Y. Miwa, T. Taga, E. Osawa, Y. Yamaoka, N. Fujii, T. Ibuka, *J. Org. Chem.* **1999**, *64*, 2992 – 2993; b) H. Ohno, M. Anzai, A. Toda, S. Ohishi, N. Fujii, T. Tanaka, Y. Takemoto, T. Ibuka, *J. Org. Chem.* **2001**, *66*, 4904 – 4914; c) H. Ohno, *Yakugaku Zasshi* **2001**, *121*, 733 – 741; d) H. Ohno, H. Hamaguchi, M. Ohata, T. Tanaka, *Angew. Chem.* **2003**, *115*, 1791 – 1795; *Angew. Chem. Int. Ed.* **2003**, *42*, 1749 – 1753; e) H. Ohno, H. Hamaguchi, M. Ohata, S. Kosaka, T. Tanaka, *J. Am. Chem. Soc.* **2004**, *126*, 8744 – 8754; f) H. Hamaguchi, S. Kosaka, H. Ohno, T. Tanaka, *Angew. Chem.* **2005**, *117*, 1537 – 1541; *Angew. Chem. Int. Ed.* **2005**, *44*, 1513 – 1517.

[14] For example, see: a) E. Piers, Y.-F. Lu, *J. Org. Chem.* **1989**, *54*, 2267 – 2268; b) H. Suginome, T. Takeda, M. Itoh, Y. Nakayama, K. Kobayashi, *J. Chem. Soc. Perkin Trans. 1* **1995**, 49 – 61; c) M. T. Crimmins, S. Huang, L. E. Guise-Zawacki, *Tetrahedron Lett.* **1996**, *37*, 6519 – 6522.

[15] a) J. T. Naik, P. G. Mantle, R. N. Sheppard, E. S. Waight, *J. Chem. Soc. Perkin Trans. 1* **1995**, 1121 – 1125; b) A. Carotenuto, M. R. Conte, E. Fattorusso, V. Lanzotti, S. Magno, *Tetrahedron* **1995**, *51*, 10751 – 10758; c) K. Kurata, K. Taniguchi, Y. Agatsuma, M. Suzuki, *Phytochemistry* **1998**, *47*, 363 – 369; d) Y. Kashiwada, K. Yamazaki, Y. Ikeshiro, T. Yamagishi, T. Fujioka, K. Mihashi, K. Mizuki, L. M. Cosentino, K. Fowke, S. L. Morris-Natschke, K.-H. Lee, *Tetrahedron* **2001**, *57*, 1559 – 1563.

[16] a) S.-H. Dai, W. R. Dolbier, Jr., *J. Am. Chem. Soc.* **1972**, *94*, 3946 – 3952; b) R. D. Froese, G. L. Lange, J. D. Goddard, *J. Org. Chem.* **1996**, *61*, 952 – 961; c) M. Schmittel, M. Maywald, M. Strittmatter, *Synlett* **1997**, 165 – 166; d) Y. Yang, J. L. Petersen, K. K. Wang, *J. Org. Chem.* **2003**, *68*, 8545 – 8549.

 © 2005 Wiley-VCH Verlag GmbH & Co. KGaA, Weinheim

Materials Science

DOI: 10.1002/anie.200501337

The Fabrication and Switchable Superhydrophobicity of TiO_2 Nanorod Films**

*Xinjian Feng, Jin Zhai, and Lei Jiang**

Titanium dioxide (TiO_2) is an important material that is used in many industrial applications related to photo-splitting of water,[1] photocatalysis,[2] photovoltaic devices,[3] etc. Since the discovery[4] of photoinduced superhydrophilicity (water contact angle (CA) $< 10°$) on a hydrophilic TiO_2 surface in 1997, many research efforts[5–8] have been devoted to exploring this photosensitive mechanism with the aim of manipulating the surface wettability to a larger extent in virtue of the good light, thermal, and chemical stability and better biocompatibility of TiO_2 than of other organic or inorganic materials. However, its wettability has only been tuned in a limited region thus far.

In the past several years, inspired by the surface-topography-induced superhydrophobicity of lotus leaves[9,10] and water striders' legs,[11] various films that exhibit superhydrophobic properties have been fabricated.[12–19] On the other hand, superhydrophilic surfaces have been realized by taking advantage of a 2D[4] or 3D[20] capillary effect. Very recently, several stimuli-responsive, smart, interfacial materials that can be switched between superhydrophilicity and superhydrophobicity by combining the geometrical morphology of

[*] Dr. X. Feng, Prof. J. Zhai, Prof. L. Jiang
Center for Molecular Science
Institute of Chemistry
Chinese Academy of Sciences
Beijing 100080 (China)
Fax: (+86) 10-8262-7566
E-mail: jianglei@iccas.ac.cn
Prof. L. Jiang
National Center for Nanoscience and Nanotechnology
Beijing 100080 (China)
Dr. X. Feng
Graduate School of the Chinese Academy of Science
Beijing 100080 (China)

[**] We thank the State Key Project for Fundamental Research and the Special Research Foundation of the National Natural Science Foundation of China for continuing financial support.

Supporting information for this article is available on the WWW under http://www.angewandte.org or from the author.

© 2005 Wiley-VCH Verlag GmbH & Co. KGaA, Weinheim

the surface with a change of surface chemistry have been reported.[21–23] Herein, we report on the creation of superhydrophobic surfaces consisting of inorganic nanorods fabricated from hydrophilic TiO_2, and further demonstrate that their wettability can be reversibly switched between superhydrophobicity and superhydrophilicity. The mechanism involves the cooperation of the micro- and nanoscale hierarchical surface structures, the orientation of the crystal planes, and the surface photosensitivity.

The TiO_2 nanorod films were deposited on glass substrates by a low-temperature hydrothermal approach. Typically, aqueous solutions of titanium trichloride supersaturated with NaCl were heated to 160 °C for 2 h. The films deposited on glass wafers used as substrate were rinsed thoroughly with deionized water and ethanol, dried at room temperature, and stored in the dark for two weeks. Figure 1 a shows a typical

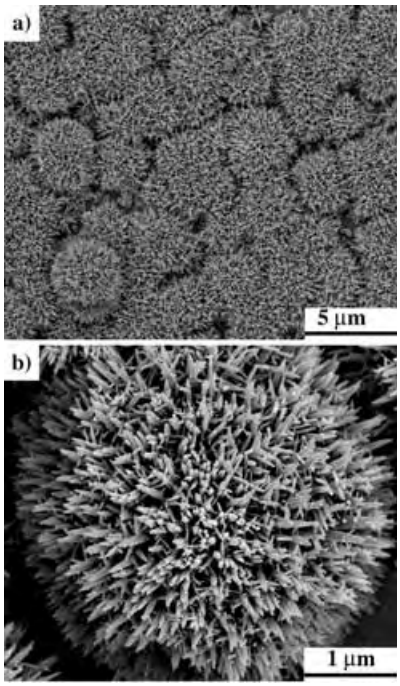


Figure 1. a) Low-magnification FE-SEM image of a TiO_2 nanorod film deposited on a glass wafer; b) morphology of a single papilla at high magnification.

field emission scanning electron microscopy (FE-SEM) image of the as-synthesized nanorod films. Many papillae can be found on the surface in a random pattern with diameters ranging from 2 to 6 μm. Each of these papillae is composed of nanorods with uniform diameters of 30 to 60 nm. As can be seen from the magnified image of a single papilla (Figure 1 b), the nanorods grow radial to the substrate and are self-assembled into micro- and nanoscale hierarchical structures.

According to the X-ray diffraction (XRD) pattern of the as-prepared TiO_2 films, the nanorods can be classified as having a standard tetragonal rutile structure (space group $P4_2/mnm$; JCPDS file no. 21-1276). The peaks are relatively broad compared with those of the bulk material, thus corroborating the small crystal size. In contrast to the standard pattern, the XRD profiles clearly exhibit an enhanced peak for the (110) reflection and a comparatively low diffraction intensity for (101) and (111) (see Supporting Information), which indicates that the growth of the nanorods has a preferred orientation. The samples were then dispersed onto a transmission electron microscopy (TEM) grid for further detailed structure analysis. Figures 2 b and c show the high-resolution TEM images of the

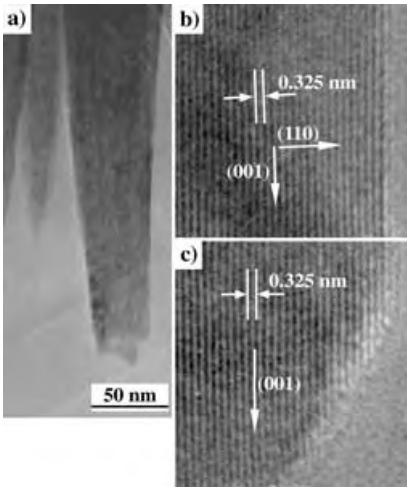


Figure 2. TEM image of a single TiO_2 nanorod (a). High-resolution TEM images of a nanorod wall at the side surface (b) and at the top surface (c) of the nanorod.

side and top surfaces, respectively, of the nanorod wall shown in Figure 2 a at low magnification. It can be seen that the nanorod is well crystallized with clear lattice fringes parallel to the wall. The inter-plane distance of 0.325 nm for the (110) planes perpendicular to the rod axis can be readily resolved. Combined with the XRD data and SEM images, such features imply that the nanorods grow along the (110) crystal plane with a preferred orientation in the (001) direction.

The wettability of the films was evaluated by contact angle (CA) measurements. The rutile form of TiO_2 is a hydrophilic material with a water CA of 72 and 74° on smooth single crystal (110) and (001) surfaces, respectively.[6] As shown in Figure 3 a (left), the water CA of the as-prepared rough TiO_2 nanorod films is large ($(154 \pm 1.3)°$), that is, the as-prepared films show superhydrophobicity. This result indicates that the surface structure strongly affects the wetting behavior. There are two equations in the literature that describe the water CA on rough surfaces. One is Wenzel's law,[24] $cos\theta_f = r\cos\theta_w$, where θ_f and θ_w are, respectively, the water CA on a rough and smooth surface and r is the surface roughness. For $\theta_w < 90°$, it can be seen that an increase of r will result in a smaller CA, and water will fill the grooves below the droplet. However, the high water CA of the as-prepared films indicates that the water droplet does not penetrate the trough but is suspended on the sharp nanorod films, and that an air pocket might be formed on the surface.

The apparent contact angle θ_f can be described by another equation, first formulated by Cassie and Baxter,[25] which is generally valid for heterogeneous surfaces composed of air and a solid with superhydrophobicity, $\cos\theta_f = f_s\cos\theta_w - f_v$,

 © 2005 Wiley-VCH Verlag GmbH & Co. KGaA, Weinheim

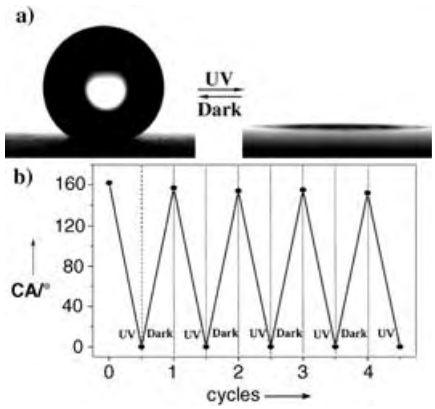


Figure 3. a) Photographs of a spherical water droplet with a CA of (154 ± 1.3)° (left) and a flat water film with a CA of 0° (right) before and after the films were exposed to UV illumination, respectively; b) reversible superhydrophobicity/superhydrophilicity transition of the as-prepared films by alternating UV irradiation and storage in the dark.

where f_s and f_v are the area fractions of the projecting solid and air on the surface, respectively ($f_s + f_v = 1$). The large fraction of air trapped in the films forms a cushion at the film–water interface that prevents the penetration of the water droplet into the grooves. All these results indicate that the preferred orientation of the (001) crystal plane of TiO_2 nanorods and the micro- and nanoscale hierarchical surface structures result in a significant change of the wetting behavior from hydrophilic to superhydrophobic.

When the as-prepared films were exposed to UV light, their surface superhydrophobicity transformed into superhydrophilicity; this remarkable surface wettability transition can be tuned reversibly. Figure 3a shows the change of the water CA when the films are irradiated with UV light (obtained from a 500-W high-pressure Hg lamp with a filter centered at (365 ± 10) nm) for 2 h. The spherical water droplet spreads out on the film with a CA of about 0°. After the UV-irradiated films were placed in the dark for two weeks, their superhydrophobicity was obtained again. This process was repeated for several cycles; a good reversibility of the surface wettability was observed (Figure 3b). TiO_2 is a photosensitive material,[5] and when the film is irradiated with UV light the photogenerated hole reacts with lattice oxygen to form surface oxygen vacancies, to which water molecules kinetically coordinate. This improves the surface hydrophilicity greatly. For the as-prepared multiscale rough surface, the water droplet will fill the grooves along the nanorods and replace the trapped air. This results in a water CA of about 0°. After the hydroxy group adsorption, the surface transforms into an energetically metastable state, and the adsorbed hydroxy groups can gradually be replaced by atmospheric oxygen[6] when the films are placed in the dark. Subsequently, the surface evolves back to its original state, and the surface wettability converts from superhydrophilic to superhydrophobic again.

In conclusion, TiO_2 nanorod films with special micro- and nanoscale hierarchical surface structures have been prepared. A remarkable, controllable surface wettability that shows reversible superhydrophobicity/superhydrophilicity, which is a challenge in surface chemistry, is observed on this inorganic oxide nanorod film. The cooperation of the hierarchical surface microstructures, the orientation of the crystal planes, and the surface photosensitivity are considered to be responsible for this behavior.

Experimental Section

The films were synthesized by hydrothermal treatment of an aqueous titanium trichloride (0.15 M) solution supersaturated with NaCl. The solution was placed in a Teflon-lined autoclave. Thoroughly cleaned glass wafers were used as substrates and immersed in the solution. The mixture was then heated to (160 ± 2) °C for 2 h. The as-deposited films were rinsed with deionized water and ethanol, dried at room temperature, and stored in the dark. The structure and morphology of the product was investigated by FE-SEM (JSM-6700F, Japan), HRTEM (Tecnai F30, Japan), and powder XRD (diffractometer D/max2500 using $Cu_{K\alpha}$ radiation). Water CAs were measured with an OCA20 (DataPhysics, Germany) at ambient temperature.

Received: April 18, 2005
Published online: July 15, 2005

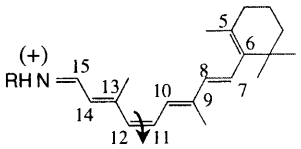
Keywords: hydrophilicity · hydrophobicity · nanostructures · surface chemistry · titanium

[1] A. Fujishima, K. Honda, *Nature* **1972**, *238*, 37.
[2] B. O'Regan, M. Grätzel, *Nature* **1991**, *353*, 737.
[3] A. L. Linsebigler, G. Lu, J. T. Yates, *Chem. Rev.* **1995**, *95*, 735.
[4] R. Wang, K. Hashimoto, A. Fujishima, M. Chikuni, E. Kojima, A. Kitamura, M. Shimohigoshi, T. Watanabe, *Nature* **1997**, *388*, 431.
[5] R. Wang, K. Hashimoto, A. Fujishima, M. Chikuni, E. Kojima, A. Kitamura, M. Shimohigoshi, T. Watanabe, *Adv. Mater.* **1998**, *10*, 135.
[6] R. Wang, N. Sakai, A. Fujishima, T. Watanabe, K. Hashimoto, *J. Phys. Chem. B* **1999**, *103*, 2188.
[7] N. Stevens, C. L. Priest, R. Sedev, J. Ralston, *Langmuir* **2003**, *19*, 3272.
[8] X. S. Peng, A. C. Chen, *J. Mater. Chem.* **2004**, *14*, 2542.
[9] W. Barthlott, C. Neinhuis, *Planta* **1997**, *202*, 1.
[10] L. Feng, S. Li, Y. Li, H. Li, L. Zhang, J. Zhai, Y. Song, B. Liu, L. Jiang, D. Zhu, *Adv. Mater.* **2002**, *14*, 1857.
[11] X. F. Gao, L. Jiang, *Nature* **2004**, *432*, 36.
[12] a) T. Onda, S. Shibuichi, N. Satoh, K. Tsujii, *Langmuir* **1996**, *12*, 2125; b) S. Shibuichi, T. Onda, N. Satoh, K. Tsujii, *J. Phys. Chem.* **1996**, *100*, 19512.
[13] a) W. Chen, A. Y. Fadeev, M. C. Hsieh, D. Öner, J. Youngblood, T. J. McCarthy, *Langmuir* **1999**, *15*, 3395; b) D. Öner, T. J. McCarthy, *Langmuir* **2000**, *16*, 7777–7782.
[14] S. Herminghaus, *Europhys. Lett.* **2000**, *52*, 165.
[15] I. Woodward, W. C. E. Schofield, V. Roucoules, J. P. S. Badyal, *Langmuir* **2003**, *19*, 3432.
[16] B. Blossey, *Nat. Mater.* **2003**, *2*, 301.
[17] H. Y. Erbil, A. L. Demirel, Y. Avcý, O. Mert, *Science* **2003**, *299*, 1377.
[18] F. Shi, Z. Q. Wang, X. Zhang, *Adv. Mater.* **2005**, *17*, 1005.
[19] a) H. Li, X. Wang, Y. Song, Y. Liu, Q. Li, L. Jiang, D. Zhu, *Angew. Chem.* **2001**, *113*, 1790; *Angew. Chem. Int. Ed.* **2001**, *40*, 1743; b) L. Feng, S. Li, H. Li, J. Zhai, Y. Song, L. Jiang, D. Zhu, *Angew. Chem.* **2002**, *114*, 1269; *Angew. Chem. Int. Ed.* **2002**, *41*, 1221.
[20] a) J. Bico, C. Tordeux, D. Quéré, *Europhys. Lett.* **2001**, *55*, 214; b) J. Bico, C. Tordeux, D. Quéré, *Colloids Surf. A* **2002**, *206*, 41.

 © 2005 Wiley-VCH Verlag GmbH & Co. KGaA, Weinheim

[21] S. Minko, M. Müller, M. Motornov, M. Nitschke, K. Grundke, M. Stamm, *J. Am. Chem. Soc.* **2003**, *125*, 3896.
[22] T. Sun, G. Wang, L. Feng, B. Liu, Y. Ma, L. Jiang, D. Zhu, *Angew. Chem.* **2004**, *116*, 361; *Angew. Chem. Int. Ed.* **2004**, *43*, 357.
[23] X. J. Feng, L. Feng, M. H. Jin, J. Zhai, L. Jiang, D. B. Zhu, *J. Am. Chem. Soc.* **2004**, *126*, 62.
[24] R. N. Wenzel, *Ind. Eng. Chem.* **1936**, *28*, 988.
[25] A. B. D. Cassie, S. Baxter, *Trans. Faraday Soc.* **1944**, *40*, 546.

 © 2005 Wiley-VCH Verlag GmbH & Co. KGaA, Weinheim



Scheme 1. The *N*-alkyl-protonated Schiff base of retinal (PSBR).

Computer Chemistry

DOI: 10.1002/anie.200501236

A Tiny Excited-State Barrier Can Induce a Multiexponential Decay of the Retinal Chromophore: A Quantum Dynamics Investigation**

Massimo Olivucci, Alessandro Lami, and Fabrizio Santoro**

The *N*-alkyl protonated Schiff base of retinal (PSBR) is the chromophore of rhodopsin proteins,[1–3] a large class of transmembrane photoreceptors comprising the human retina visual pigment rhodopsin (Rh) and the bacterial proton pump bacteriorhodopsin (bR). In these receptors, PSBR undergoes an efficient *cis–trans* photoisomerization (e.g., the 11-*cis* to all-*trans* isomerization marked with a curved arrow in Scheme 1) which, ultimately, triggers a conformational change of the protein. It has been established that in solution the excited-state decay of PSBR is multiexponential and shows a fast (subpicosecond to picosecond) and a slow (picosecond) component, whose values depend on the type of signal recorded, the probing wavelength, and the nature of the solvent.[4–7] More recently, evidence for multiexponential excited-state decay has also been reported for Rh[8,9] and bR.[10]

The precise origin of the observed PSBR multiexponential decay is unknown. Several models have been proposed such as the existence of competing excited-state isomerization paths[7] (for example, one reactive and one nonreactive path as demonstrated in ref. [9]) or the occurrence of an isomerization path splitting,[8] or the generation of a vibrationally hot photoproduct followed by cooling.[11] The possibility that a multiexponential decay arises from dynamics along a single coordinate has also been discussed.[12] Herein, we present an investigation on a different origin of multiexponential decay: the dynamics prompted by the specific shape of the excited-state potential-energy surface.

Ab initio CASPT2//CASSCF calculations on the reaction path of different isolated PSBR models,[13–16] and more recently on Rh,[17] have invariably shown that the isomerization path on the excited state (S_1) involves mainly two nuclear modes. The process begins with the relaxation of the Franck–Condon (FC) structure along a collective C–C stretching (double-bond expansion and single-bond contraction) mode of the chromophore backbone. It then proceeds along the torsion corresponding to the change from *cis* to *trans*; this torsion leads to a conical intersection (CI) between the S_1 and the ground-state (S_0) potential-energy surfaces. The essential features of the calculated surface, which are in line with the indication of time-resolved experiments,[18–24] are reproduced by the simple analytical potential V^C [Eq. (1)]

$$V^C(x_s,y_t) = a_s x_s^2 - b_t(x_s/x_{seq})y_t^2 \qquad (1)$$

with $b_t > 0$.[25] As illustrated in Figure 1a, a vibrational wave packet released at FC initially evolves along the stretching coordinate x_s. V^C is bound along y_t when $x_s < 0$, but it is unbound (i.e., gives the wave packet an acceleration towards large y_t values) when $x_s > 0$ (Figure 1b). This anharmonic feature creates a shallow valley around the origin (SP) and, for $x_s > 0$, a decay channel along y_t, whose existence has been documented by mapping the minimum-energy path for realistic PSBR models.[16] V^C does not describe the region of the conical intersection, which must be thought somewhere along the channels. Below, we assume that once the wave packet is entered into the decay channels, it will irreversibly proceed towards the CI and decay to S_0.

Because of its low dimensionality V^C provides an attractive model for the study of the quantum dynamics of the photoinduced wave packet. While we do not try to reproduce experimental data, we show that the peculiar topology of the S_1 energy surface of PSBR may be responsible for biexponential decay. In particular, we show that such a decay regime

[*] Prof. Dr. M. Olivucci
Dipartimento di Chimica
Università degli Studi di Siena
via Aldo Moro, 53100 Siena (Italy)
Fax: (+39) 577-234-278
and Centro Studio Sistemi Complessi
via Tommaso Pendola 37, 53100 Siena (Italy)
E-mail: olivucci@unisi.it
Prof. Dr. M. Olivucci, Dr. A. Lami, Dr. F. Santoro
Istituto per i Processi Chimico-Fisici
Area della Ricerca del CNR di Pisa
via Moruzzi 1, 56124 Pisa (Italy)
Fax: (+39) 50-315-2442
E-mail: f.santoro@ipcf.cnr.it

[**] We thank Dr. G. Granucci of Università di Pisa for valuable discussion on classical simulation of wave-packet dynamics. M.O. acknowledges the Università di Siena (Progetto di Ateneo 02/04), HFSP (RG 0229/2000M), and FIRB (project No. RBAU01EPMR) for providing the funds.

Supporting information for this article is available on the WWW under http://www.angewandte.org or from the author.

InterScience
© 2005 Wiley-VCH Verlag GmbH & Co. KGaA, Weinheim

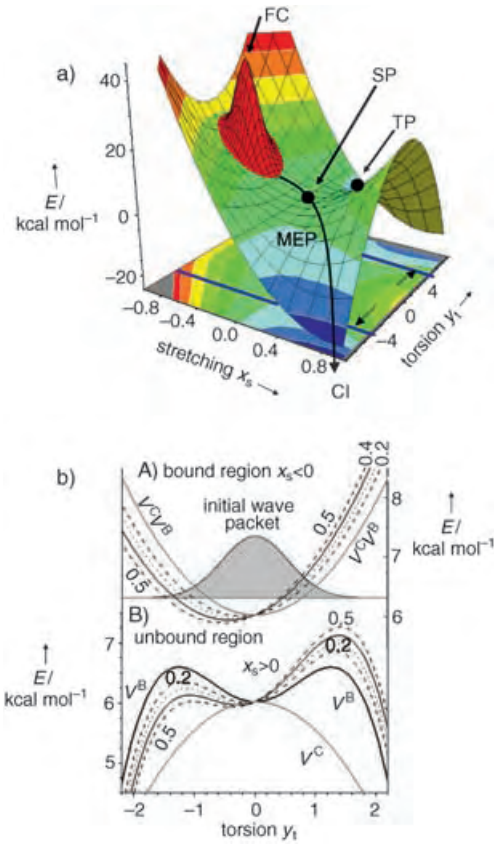


Figure 1. a) 3D plot of the potential V^C; the initial wave packet at $t=0$ is superimposed. x_s and y_t are given in atomic units. Two lines on the $x_s y_t$ plane mark the borders of the NR region (-4 au $\le y_t \le 4$ au). The curved arrow indicates the minimum-energy path (labeled MEP) towards negative values of y_t (an equivalent MEP develops towards positive values of y_t). b) Profiles of the potential with no barrier (V^C), with a symmetric barrier (V^B), and with an asymmetric barrier (asymmetry parameter c_t: 0.2, 0.3, 0.4, 0.5 kcal mol^{-1} bohr^{-1}). A) $x_s = -0.475$ au (FC); the larger c_t the more shifted the minimum is towards negative y_t values. The cross section of the initial wave packet is given as a gray Gaussian. B) $x_s = 0.475$ au (TP); the larger c_t the higher the barrier for positive y_t and the lower the barrier for negative y_t.

is induced by the presence of a flat energy ridge located between the SP and CI regions.

We begin by looking at a barrierless potential. The parameters of Equation (1) are fixed by assuming typical values for pure stretching ($\omega_s = 1500$ cm^{-1}, $a_s = 1/2\, m_s \omega_s^2$, $m_s = 1$ u; u = atomic mass unit, $\omega = \tilde{\nu}$) and torsional frequencies ($\omega_t = 200$ cm^{-1}, $b_t = 1/2\, m_t \omega_t^2$, $m_t = 1$ u). The FC point is located at $x_s(0) = x_{seq} = -0.475$ au by imposing an energy gap of 6 kcal mol^{-1} between the points FC and SP, which is consistent with the results of ab initio calculations.[15] To study how the wave packet moves along the SP→CI channel, we monitor $P_{NR}(t)$, which describes the population in the nonreactive (NR) region comprising FC and SP (see Figure 1a) or, in other words, the transient S_1 population of PSBR. The results (see the thick gray line in Figure 2a, b) demonstrate that after an induction time of about 50 fs there is a substantial monoexponential decay of $P_{NR}(t)$ with a time constant of about 150 fs (see the Supporting Information for a table with the exponential fits of $P_{NR}(t)$ for the S_1 potential).

The presence of a barrier < 1 kcal mol^{-1} on the S_1 surface has been detected experimentally[6] and is consistent with CASPT2//CASSCF calculations on a realistic PSBR model.[16] We now show that energy ridges (Figure 2c, dotted lines)—which start at $x_s = 0$ and $y_t = \pm 1.26$ au, increase linearly for $x_s > 0$ (along the stretching), and impose a tiny torsional barrier (B^{max} of 0.6 kcal mol^{-1} at the turning-point (TP) level (see V^B Figure 1b, plot B)—have a drastic effect on the decay dynamics. Naming V^B the potential with a barrier (see the Supporting Information for mathematical details), we report in Figures 2a and b the $P_{NR}(t)$ function. As apparent from an inspection of the graphs, the barrier switches the S_1 population decay from monoexponential to biexponential with time constants of 257 fs (19% of the population) and 2110 fs (81% of the population). The appearance of the biexponential decay does not depend on a specific choice of the V^B parameters; for example, the biexponential decay persists if the barrier is moved along y_t between 0.8 and 1.5 au and its height is fixed to the value of 0.6 kcal mol^{-1} (the time constants and the populations of the fast and slow components vary significantly). Furthermore, the extension of the ridge to negative x_s values, which creates a barrier along the MEP, should prompt the biexponential regime more readily.

Figure 2c provides a mechanistic interpretation of the biexponential regime. The tiny barrier in the region of the

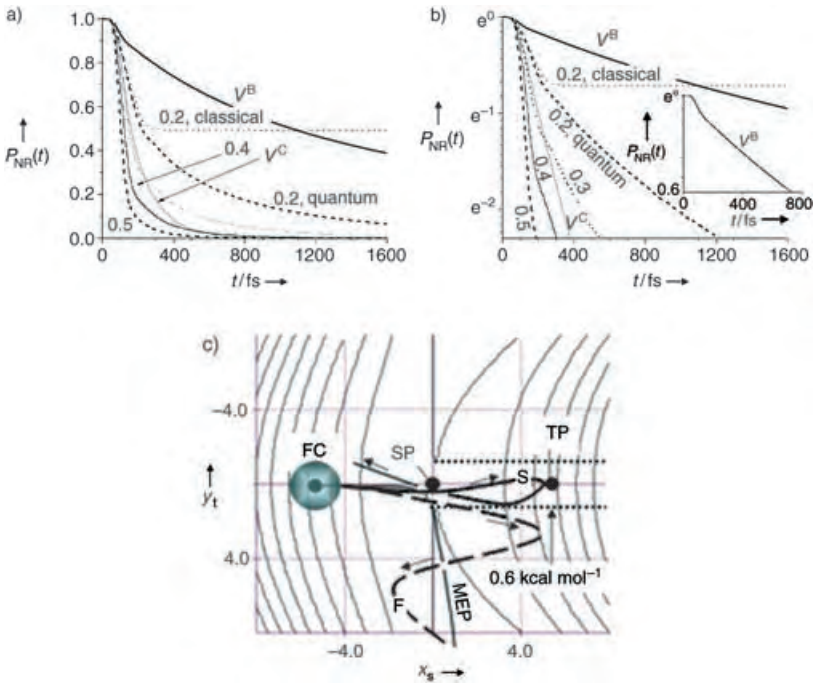


Figure 2. Decay of the quantum NR population, $P_{NR}(t)$: a) linear scale; b) semilogarithmic scale. Potentials V^C (thick gray line), V^B (solid line), and $V^B + c_t y_t$ (curves marked by the c_t values 0.2, 0.3, 0.4, 0.5 kcal mol^{-1} bohr^{-1}; for $c_t = 0.2$ the classical result is also given). Notice that the larger c_t the faster the decay. Inset: detail of the decay for V^B. c) Schematic representation of a fast (F) and slow (S) trajectory on a contour plot of V^C. The positions of the V^B energy ridges are marked by two dotted lines.

 © 2005 Wiley-VCH Verlag GmbH & Co. KGaA, Weinheim

turning point restrains the decay of a large subset of trajectories that temporarily remain in the NR region (S trajectory) rather than evolve immediately along the SP→CI channel (F trajectory). However, the introduction of a barrier does not cause an "isomerization path splitting". In fact, the wave packet oscillates along the stretching mode in the SP region without splitting. What actually happens is a progressive loss of population of the NR region that enters the SP→CI channel of no return (for an analysis of the flow of the population in the SP→CI channel as a function of the stretching x_s see the Supporting Information).

The investigation of the origin of the biexponential decay in the protein environment (e.g., in Rh[8,9] or bR[10]) requires the detailed understanding of the PSBR V^B topology in these systems. While this is outside the scope of the present work, we can easily introduce in V^B the zero-order effect of the chiral protein cavity, that is, the breaking of the mirror symmetry of the torsional potential. This is done through an additional term, $c_t y_t$, which shifts the equilibrium position along y_t, removes the symmetry of the barriers for positive torsion values (B_+^{max}) and for negative torsion values (B_-^{max}), and decreases the size of the SP valley (see Figure 1b and the Supporting Information).

In Figure 2a,b, we report the changes of $P_{NR}(t)$ as a function of the increase of the asymmetry parameter c_t. It is apparent that even when c_t induces a limited symmetry breaking (see Figure 1b and the Supporting Information), both time constants of the biexponential fit decrease (i.e., the overall decay is faster) and more remarkably the population decay with the faster kinetic increases while the population decay with the slower kinetic decreases (for $c_t = 0.2$ kcal mol^{-1} bohr^{-1} these are 62% for the fast decay and 38% for the slow decay). When $c_t = 0.5$ kcal mol^{-1} bohr^{-1} the slow component disappears and the biexponential fit collapses into the monoexponential one with a time constant of 72 fs. These results show that, according to our basic model, the symmetry breaking induced by the protein cavity would decrease the multiexponential character of the decay, which would ultimately lead to a monoexponential behavior due to the removal of the plateau around SP and the decrease of the barrier along one sense of rotation ($B_-^{max} < B_+^{max}$ in Figure 1b).

The comparison between quantum and classical $P_{NR}(t)$ for the case $c_t = 0.2$ kcal mol^{-1} bohr^{-1} (see Figures 2a,b) demonstrates that quantum effects, like tunneling, are essential for the correct description of the slower decay of the NR population. In fact, classical trajectories (see the Supporting Information) do not reproduce the behavior described above but predict that after the fast decay, a part of the wave packet remains unreactive and is permanently trapped on the SP valley.

In conclusion, exploratory quantum dynamics on a two-dimensional analytical potential that mimics the PSBR S_1 potential derived through ab initio quantum chemical calculations provides a novel explanation for the observed biexponential decay of the excited-state population. Such an explanation may be proposed for other systems featuring a biexponential decay with a fast component in the subpicosecond regime. The motion of the wave packet is strongly affected by the existence of a tiny barrier along the channel leading to the conical intersection. This phenomenon is general (as an example it still survives for $\omega_s \approx 700$ cm^{-1} and $\omega_s \approx 500$ cm^{-1}) and depends on the topology of the S_1 surface. The sensitivity of the quantum dynamics of the wave packet to the precise features of the potential is also reflected by the chaotic behavior found for classical trajectories released on V^C. This fact and other details of the investigation reported above will be documented in a forthcoming publication.

Experimental Procedure

Quantum dynamical calculations were performed assuming the simple kinetic operator $T = (2m_s)^{-1}\partial^2/\partial x_s^2 + (2m_t)^{-1}\partial^2/\partial y_t^2$ ($m_s = m_t = 1$ u) by adopting the Fourier method,[26] and propagating the wave packet through an orthogonalized Lanczos algorithm.[27,28] We assume an FC excitation from the ground (harmonic) vibrational state of the S_0 surface to S_1 and equal frequencies on the S_0 (ω_s', ω_t'') and S_1(ω_s, ω_t) surfaces ($\omega_s' = \omega_s$, $\omega_t' = \omega_t$). An initial thermal distribution of the torsional states increases, moderately, the population of the fast component of the biexponential decay.

Supporting Information includes: Computational details; a mathematical expression for the V^B potential; a table of the exponential fits of quantum $P_{NR}(t)$ for different values of the S_1 potential; a table reporting the positions and heights of the barriers for the different potentials considered and the comparison between mono- and biexponential fits; further discussion of the reaction mechanism through the analysis of snapshots of the wave packet and through the study of the $P_{NR}(t)$ decay as a function of x_s.

Received: April 8, 2005
Published online: July 20, 2005

Keywords: ab initio calculations · isomerization · photochemistry · Schiff bases

[1] R. A. Mathies, J. Lutehnburg in *Handbook of Biological Physics*, *Vol. 3* (Eds.: D. G. Stavenga, W. J. De Grip, E. N. Pugh), Elsevier Science, New York, **2000**.
[2] R. Needlman in *CRC Handbook of Organic Photochemistry and Photobiology* (Eds.: W. M. Horspool, P.-S. Song), CRC, Boca Raton, FL, **1995**.
[3] M. Ottolenghi, M. Sheves, *Isr. J. Chem.* **1995**, *35*,193.
[4] H. Kandori, H. Sasabe, *Chem. Phys. Lett.* **1993**, *216*, 126.
[5] P. Hamm, M. Zurek, T. Röschinger, H. Patzelt, D. Oesterhelt, W. Zinth, *Chem. Phys. Lett.* **1996**, *263*, 613.
[6] S. L. Logunov, L. Song, M. A. El-Sayed, *J. Phys. Chem.* **1996**, *100*, 18586.
[7] G. Zgrablic, K. Voïtchovsky, M. Kindermann, M. Chergui, S. Haacke in *Femtochemistry and Femtobiology: Ultrafast Events in Molecular Science* (Eds.: M. Martin, J. T. Hynes), Elsevier Science, New York, **2004**, pp. 457–460.
[8] M. Yan, L. Rothberg, R. Callender, *J. Phys. Chem. B* **2001**, *105*, 856–859.
[9] H. Kandori, Y. Furutani, S. Nishimura, Y. Shichida, H. Chosrowjan, Y. Shibata, N. Mataga, *Chem. Phys. Lett.* **2001**, *334*, 271–276.
[10] S. Schenkl, E. Portuondo, G. Zgrablic, M. Chergui, S. Haacke, N. Friedman, M. Sheves, *Phys. Chem. Chem. Phys.* **2002**, *4*, 5020–5024.
[11] J. E. Kim, D. W. McCamant, L. Zhu, R. A. Mathies, *J. Phys. Chem. B* **2001**, *105*, 1240–1249.
[12] M. Du, G. R. Fleming, *Biophys. Chem.* **1993**, *48*, 101.
[13] L. De Vico, C. S. Page, M. Garavelli, F. Bernardi, R. Basosi, M. Olivucci, *J. Am. Chem. Soc.* **2002**, *124*, 4124–4134.

 © 2005 Wiley-VCH Verlag GmbH & Co. KGaA, Weinheim

[14] M. Garavelli, P. Celani, F. Bernardi, M. A. Robb, M. Olivucci, *J. Am. Chem. Soc.* **1997**, *119*, 6891 – 6901.
[15] M. Garavelli, T. Vreven, P. Celani, F. Bernardi, M. A. Robb, M. Olivucci, *J. Am. Chem. Soc.* **1998**, *120*, 1285 – 1288.
[16] R. Gonzalez-Luque, M. Garavelli, F. Bernardi, M. Merchan, M. A. Robb, M. Olivucci, *Proc. Natl. Acad. Sci. USA* **2000**, *97*, 9379 – 9384.
[17] T. Andruniów, N. Ferré, M. Olivucci, *Proc. Natl. Acad. Sci. USA* **2004**, *101*, 17908 – 17913.
[18] a) Q. Zhong, S. Ruhman, M. Ottolenghi, *J. Am. Chem. Soc.* **1996**, *118*, 12828 – 12829; b) B. Hou, N. Friedman, S. Ruhman, M. Sheves, M. Ottolenghi, *J. Phys. Chem. B* **2001**, *105*, 7042 – 7048.
[19] G. Haran, K. Wynne, A. Xie, Q. He, M. Chance, R. M. Hochstrasser, *Chem. Phys. Lett.* **1996**, *261*, 389 – 395.
[20] L. Song, M. A. El-Sayed, *J. Am. Chem. Soc.* **1998**, *120*, 8889 – 8890.
[21] T. Kakitani, R. Akiyama, Y. Hatano, Y. Imamoto, Y. Shichida, P. Verdegem, J. Lugtenburg, *J. Phys. Chem. B* **1998**, *102*, 1334 – 1339.
[22] G. Haran, E. A. Morlino, J. Matthes, R. H. Callander, R. M. Hochstrasser, *J. Phys. Chem. A* **1999**, *103*, 2202 – 2207.
[23] S. Haacke, S. Vinzani, S. Schenkl, M. Chergui, *ChemPhysChem* **2001**, *2*, 310 – 315.
[24] T. Kobayashi, T. Saito, H. Ohtani, *Nature* **2001**, *414*, 531 – 534.
[25] A. Cembran, F. Bernardi, M. Olivucci, M. Garavelli, *J. Am. Chem. Soc.* **2003**, *125*, 12509.
[26] R. Kosloff in *Dynamics of Molecules and Chemical Reactions* (Eds.: R. E. Wyatt, J. Z. H. Zhang), Marcel Dekker, New York, **1996**.
[27] C. Lanczos, *Natl. Bur. Stand. Circ.* **1950**, *45*, 225.
[28] A. Ferretti, G. Granucci, A. Lami, M. Persico, G. Villani, *J. Chem. Phys.* **1996**, *104*, 5517.

 © 2005 Wiley-VCH Verlag GmbH & Co. KGaA, Weinheim

Surface Electrochemistry

DOI: 10.1002/anie.200462750

Nanotrench Arrays Reveal Insight into Graphite Electrochemistry**

*Trevor J. Davies, Michael E. Hyde, and Richard G. Compton**

Over the past few decades the popularity of carbon as an electrode material has increased dramatically. The fact that so many different types of carbon materials are commercially available has led to their use in a wide range of applications.[1] However, despite the large amount of research conducted with carbon electrodes, there still remains uncertainty about the individual roles of the edge-plane and basal-plane regions in the electrochemical response of a graphite surface. Herein, we address this fundamental problem and introduce a novel approach to investigate the source of the electrochemical reactivity of graphite.

A good way to understand the electrochemical properties of graphite electrodes is to study the voltammetry of well-defined graphite surfaces. For this reason, basal-plane highly ordered pyrolytic graphite (HOPG) is an attractive material; the surface consists of atomically flat basal-plane graphite terraces separated by steps and defects which expose extremely thin bands (multiples of 0.335 nm) of edge-plane graphite.[1,2] Accordingly, the voltammetric characteristics of basal-plane HOPG electrodes in simple redox couples are well-documented.[1,3,4] HOPG cyclic voltammograms provide relatively poor fits to linear diffusion simulations and display an increased peak-to-peak separation, indicative of slow electron-transfer kinetics relative to other electrode materials.[1,3–5] These characteristics become more pronounced if fewer defects are present on the surface.[6–8]

With the aid of a 2D simulation approach that allowed us to take the actual size and separation of surface defects into account, we recently demonstrated that the characteristics of HOPG cyclic voltammograms are consistent with the voltammetry of a macroarray of nanobands (edge-plane steps).[9,10] In other words, for the range of redox couples considered, the basal plane was effectively inert (Supporting Information). Given that edge-plane steps can make up less than 0.5% of the total electrode area, and heterogeneous electron-transfer electrons are known to occur at basal-plane terraces as well as edge-plane steps,[11,15] the suggestion that basal-plane graphite makes no contribution to HOPG voltammograms is quite controversial.

For the work reported herein, we sought to prove beyond any doubt that the cyclic voltammetry response of basal-plane HOPG is solely due to the edge-plane steps present as defects on the electrode surface by selectively blocking the basal-plane terraces to leave only the edge-plane defects uncovered; covering the basal-plane terraces with inert material should make no difference to the observed voltammetry. Although heterogeneous electron-transfer reactions occur at basal-plane terraces, a combination of nonlinear diffusion and the large difference in reactivity between basal- and edge-plane graphite gives cyclic voltammograms in which the basal-plane terraces appear to be inert. For example, a previous study in which we compared experimental and simulated cyclic voltammograms for the oxidation of ferrocyanide at an HOPG electrode produced results suggesting that the electron-transfer rate constant for the edge-plane oxidation was $0.022\ cm\,s^{-1}$, whereas that for the basal-plane reaction was less than $10^{-9}\ cm\,s^{-1}$. Furthermore, as all graphite electrodes are made from essentially the same building blocks (graphene sheets) we can expand our conclusions to other carbon materials such as pyrolytic graphite, carbon fibers, and even carbon nanotubes.[10]

[*] T. J. Davies, M. E. Hyde, Prof. R. G. Compton
Physical and Theoretical Chemistry Laboratory
Oxford University
South Parks Road, Oxford OX1 3QZ (UK)
Fax: (+44) 1865-275-410
E-mail: richard.compton@chemistry.ox.ac.uk

[**] The authors thank the EPSRC for studentships for T.J.D. and M.E.H. We further thank Roger Bowler for his expertise in making the HOPG electrode housing. T.J.D. thanks Lincoln College and the Lord Crewe's Society for a scholarship 2004–2005, and Abi Smith for all her support.

Supporting information for this article is available on the WWW under http://www.angewandte.org or from the author.

 © 2005 Wiley-VCH Verlag GmbH & Co. KGaA, Weinheim

To generate an HOPG surface upon which the basal plane is selectively covered, we employ a three-stage method that involves the initial "protection" of the edge-plane steps, followed by "passivation" of the remaining carbon, and then the re-exposure of the edge-plane sites. This results in the formation of "nanotrenches" (relatively long grooves in the electrode surface with nanometer-scale dimensions in width and depth) which we identify by using AFM. The contribution of edge-plane steps to basal-plane HOPG voltammograms can then be assessed by comparing the cyclic voltammetry of the nanotrench arrays with that of the freshly cleaved basal-plane HOPG.

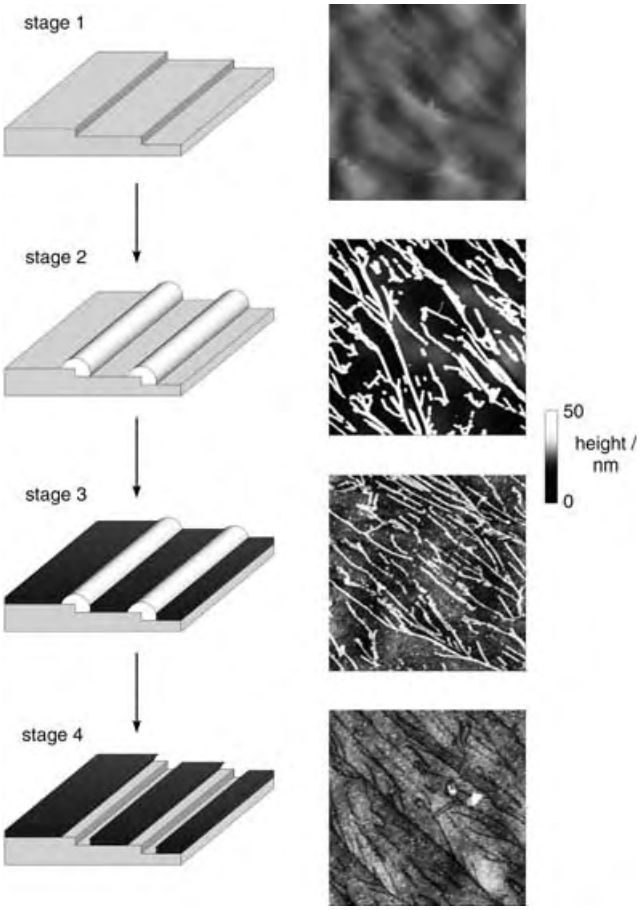


Figure 1. Schematic diagram and corresponding AFM images ($5 \times 5 \mu m^2$ each) of the four stages involved in nanotrench fabrication.

Figure 1 outlines the stages involved in nanotrench formation, along with the corresponding AFM images ($5 \times 5\ \mu m^2$ each). Initially, a HOPG slab of the highest quality ($10 \times 10 \times 2\ mm^3$, SPI 1 grade, equivalent to ZYA grade of Union Carbide[12]) was adhesively cleaved to produce a fresh surface, as illustrated in Figure 1, stage 1 (only relatively large edge-plane steps are resolved owing to the resolution limits of the AFM scanner used). The following electrochemical experiments with the HOPG slab were conducted with the HOPG housing previously described, which resulted in an exposed electrode area of 0.32 cm^2.[13]

Recently, Penner and co-workers reported that the electrodeposition of MoO_2 (by Equation (1)) at a basal-

$$MoO_4^{2-} + 2\,H_2O + 2\,e^- \rightarrow MoO_2 + 4\,OH^- \quad (1)$$

plane HOPG surface occurs exclusively at edge-plane sites (at the appropriate deposition potential) resulting in the formation of MoO_2 nanowires along the edge-plane steps.[14–16]

Following the procedure of Penner and co-workers, MoO_2 nanowires were electrodeposited on HOPG from a solution of sodium molybdate (1.1 mM) in sodium chloride (1M) and ammonium hydroxide (1M) adjusted to pH 8.5 with sodium hydroxide. The AFM image in Figure 1 for stage 2 was recorded immediately after nanowire deposition at −1.0 V versus standard calomel electrode (SCE) for 130 s, and illustrates an ensemble of nanowires $\approx$50 nm in diameter (the average thickness has been shown to depend on the deposition time, which permits the preparation of specific diameters[15]). Further experiments confirmed that the wires were indeed on edge-plane steps. Experiments at short deposition times produced incomplete nanowires for which it was possible to see the edge-plane steps emerging from the ends of the nanowires (that is, these further experiments confirmed the wires had been formed along the edge-plane steps).

With the edge-plane sites covered, the HOPG surface was effectively passivated by nitrophenyl radicals, formed from the electrochemical reduction of 4-nitrobenzenediazonium cations. Savéant and co-workers demonstrated that the reduction of diazonium salts yields N_2 and a radical, which aggressively chemisorbs to both the edge and basal planes of graphite.[17–18] Stage 3 in Figure 1 illustrates the HOPG surface after electroreduction at −0.5 V versus SCE for 30 s in a stirred solution containing 4-nitrobenzenediazonium tetrafluoroborate (1.2 mM) and tetrabutylammonium perchlorate (0.1M) in acetonitrile. The AFM image displays a clear change in texture of the material surrounding the nanowires (the basal-plane terraces) consistent with the formation of a thin film. Because the nanowires are composed of MoO_2 (an electrically conductive metal oxide), chemisorption of the nitrophenyl radicals to the nanowire surface should not be possible. Furthermore, comparison of the images for stages 2 and 3 in Figure 1 reveals that the surface surrounding the nanowires is relatively higher after treatment with diazonium salt. Thus the nanowires are not as prominent after the modification which also suggests the presence of a thin film formed over the basal-plane terraces.

In the final stage, the nanowires are removed by placing the HOPG surface in a stirred solution of hydrochloric acid (1M) for 300 s.[19] As observed for stage 4 in Figure 1, this results in the formation of nanotrenches along which the edge-plane steps reside. Figure 2 illustrates more AFM images of these nanotrenches at various scan ranges. Similar nanotrenches were observed on a large number of different sections of the HOPG surface which confirms that the acid treatment only removed the nanowires and not the basal-plane coating. As observed from the inset section analysis, the depth of the nanotrenches is $\approx$8 nm, which is significantly deeper than expected from a monolayer coverage. Given that

 © 2005 Wiley-VCH Verlag GmbH & Co. KGaA, Weinheim

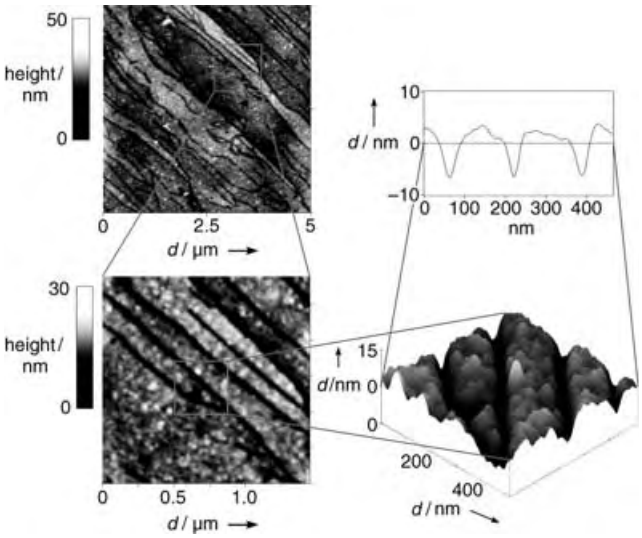


Figure 2. AFM images of nanotrenches at various scan ranges and perspectives.

the length of a nitrophenyl group is ≈5 Å,[20] the walls of the nanotrenches correspond to approximately 15 monolayers. Previous work by more than one research group has concluded that a monolayer is formed when diazonium salts are reduced at carbon electrodes.[17,18,21,22] However, our system is slightly different in that the nitrophenyl radicals should not chemisorb to the MoO_2 nanowires. This allows more nitrophenyl radicals to be generated than would be on a pure graphite surface. The AFM images provide clear evidence of a "multilayer" film which could be caused by the attack of nitrophenyl radicals on an already modified surface. Indeed, for experiments in which no MoO_2 was present, no evidence was found of a multilayer film after reduction of the diazonium salt. Alternatively, the nitrophenyl radicals could induce a polymerization reaction that forms a thin polymer film over the electrode surface rather than a chemisorbed multilayer.

Having developed an experimental method that selectively blocks the basal-plane terraces, we were next able to turn our attention to identifying the role of edge-plane defects in HOPG cyclic voltammetry. Figure 3 illustrates four cyclic voltammograms taken with an HOPG electrode in $[Ru(NH_3)_6]^{3+}$ (1.1 mM) at each of the four stages of nanotrench synthesis. Figure 3a illustrates a cyclic voltammogram with a freshly cleaved HOPG electrode taken at $2.0\,V\,s^{-1}$. Overlaid as a dashed curve is the corresponding response from an edge-plane pyrolytic graphite electrode 5 mm in diameter (in this case, the difference in surface area between the two electrodes required that the y axis be represented by I/I_p instead of I). Analysis of the edge-plane experimental data with DigiSim gave $D_{[Ru(NH_3)_6]^{3+}} = 8.0\times10^{-6}\,cm^2\,s^{-1}$ and $k^\circ_{edge} = 0.4\,cm\,s^{-1}$ for the $[Ru(NH_3)_6]^{3+}/[Ru(NH_3)_6]^{2+}$ system. The corresponding fit of the HOPG voltammogram to DigiSim gives the effective electron transfer rate constant: $k^\circ_{eff} = 0.018\,cm\,s^{-1}$. The term "effective electron transfer rate constant" is used rather than k°_{basal} because the surface is electrochemically heterogeneous, and its response is clearly dependent on the population of defects.[9] If our previous conclusion is correct, then the HOPG voltammogram in Figure 3a is solely the result of the tiny amount of edge-plane defects on the HOPG surface.[9] By using the method outlined in reference [9], the coverage of edge-plane defects can be approximated as: $\Theta_{edge} = \frac{k^\circ_{eff}}{k^\circ_{edge}} = 0.045$. Thus, 4.5 % of the surface is edge-plane graphite, which agrees well with the appropriate STM studies of Bard and Chang.[2] It follows that selective blockage of the basal-plane terraces should have no effect on the voltammetry.

Figure 3b illustrates the voltammogram recorded at $0.2\,V\,s^{-1}$ immediately after stage 2 of the nanotrench fabrication process, in which MoO_2 was deposited along edge-plane steps. Overlaid is the corresponding voltammogram from stage 1, that is, the freshly cleaved HOPG surface at $0.2\,V\,s^{-1}$. As observed, the HOPG with MoO_2 nanowires instead of edge-plane steps gives a response with a larger peak-to-peak separation (ΔE_p) than the freshly cleaved HOPG. This indicates slower electrode kinetics and agrees with the hypothesis that the HOPG response is that of a nanoband array.[9] Although MoO_2 is electrically conductive, one might

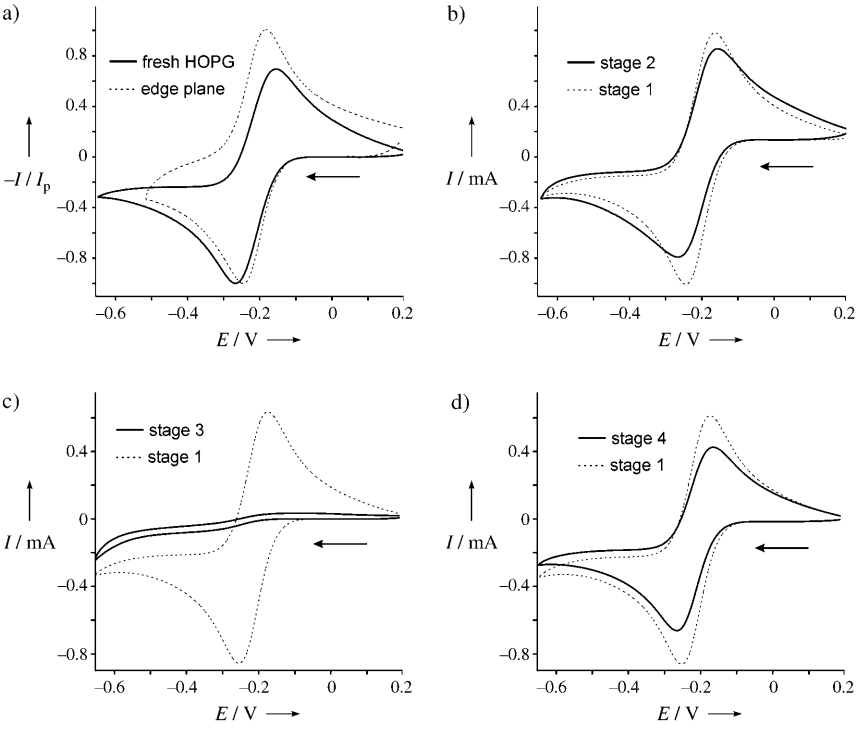


Figure 3. Cyclic voltammograms for the reduction of 1.1 mM $[Ru(NH_3)_6]^{3+}$ at a HOPG electrode (versus SCE) after each stage of nanotrench fabrication (——): a) stage 1, b) stage 2, c) stage 3, d) stage 4. The voltammogram ----- in a) was obtained from the same experiment with an edge-plane pyrolytic graphite electrode. Voltammograms ----- in b)–d) were obtained after stage 1 of nanotrench fabrication; experimental details are given in the text.

 © 2005 Wiley-VCH Verlag GmbH & Co. KGaA, Weinheim

expect an MoO_2 electrode to display slower electrode kinetics than that of a noble metal, for example. For a random array of nano- or microbands in which the surface coverage is Θ, the peak-to-peak separation is approximately that expected for a cyclic voltammogram in the same system at a macroelectrode with an electron transfer rate constant of Θk°_{mat}, in which k°_{mat} is the electron transfer rate constant of the nano- or microband material.[9,23] Therefore, as k°_{edge} is expected to be greater than $k^{\circ}_{MoO_2}$, the increased ΔE_p is easily explained. The decrease in peak current was a general characteristic observed after each stage of the process and is probably due to relatively large defects created as a result of adhesive cleaving,[2] and thus becoming inactive or separated from the surface.

Figure 3c illustrates the cyclic voltammogram recorded immediately after stage 3, in which the scan rate is $0.2\ V\,s^{-1}$. As before, the corresponding voltammogram obtained from a freshly cleaved HOPG surface is overlaid (-----). The reduction of the diazonium salt appears to have passivated the entire surface (both the MoO_2 nanowires and basal-plane terraces), with only a tiny response from the modified electrode. As discussed above, nitrophenyl radicals are not expected to chemisorb to MoO_2. This suggests a more plausible result of generating nitrophenyl radicals in the absence of edge-plane graphite through a polymerization reaction which effectively blocks the entire surface. Although this may be unexpected, it does show that the surface is sufficiently blocked by the generation of nitrophenyl radicals.

Figure 3d shows the cyclic voltammogram obtained immediately after the final stage, along with the corresponding response obtained at stage 1 (freshly cleaved HOPG). As observed, the two voltammograms are almost identical, with the small difference in ΔE_p probably the result of a slight loss in activity of the edge-plane sites caused by the preceding treatments. In the case of the modified electrode, only the edge-plane steps located along the bottom of the nanotrenches are exposed to the solution (that is, we have effectively created an array of nanobands).[24] Thus, as predicted for a simple redox couple, the cyclic voltammetric response of a basal-plane HOPG electrode is solely due to the edge-plane defects, no matter how small their coverage may be (which can be as low as 0.2%[11]). The basal-plane graphite terraces have no influence on the voltammetry and are effectively inert; blocking the basal-plane sites results in no overall change to the observed voltammetry.

Cyclic voltammetry with the nanotrench arrays was performed in other redox couples and gave exactly the same results. Figure 4 shows the voltammetric response at $200\ mV\,s^{-1}$ taken at stage 1 (-----) and stage 4 (——) for the oxidation of a) 2,3,5,6-tetramethyl-1,4-phenylenediamine (TMPD, 1.1 mM) and b) ferrocyanide (1.1 mM) for which the background electrolyte is KCl (0.1M) in both cases. Figures 4a and b clearly show that the ensemble of nanotrenches gives almost identical *I*-*E* signals to the freshly cleaved HOPG.

In conclusion, performing cyclic voltammetry with our nanotrench arrays has answered and raised some fundamental questions. For example, we now know categorically that edge-plane sites are responsible for the cyclic voltammetric response of a basal-plane HOPG electrode; there is no reason

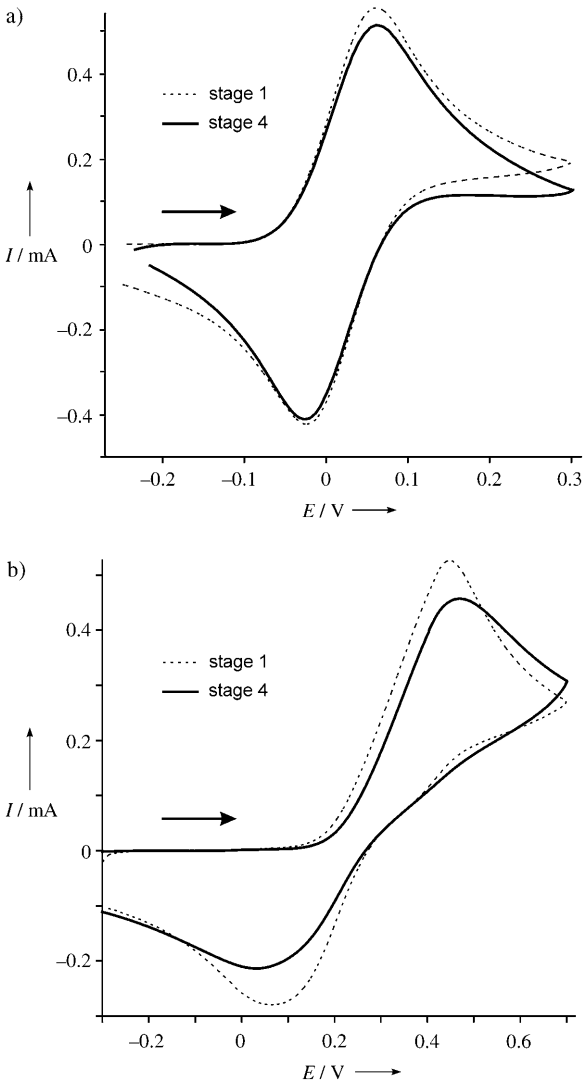


Figure 4. Cyclic voltammograms (versus SCE) taken at stage 1 (-----) and stage 4 (——) of nanotrench fabrication for the oxidation of a) TMPD (1.1 mM) and b) ferrocyanide (1.1 mM); experimental details are given in the text.

why these findings cannot be applied to other carbon materials such as carbon nanotubes (which are effectively rolled-up graphene sheets).[10,25] Furthermore, our nanotrenches could have major applications for the synthesis of nanowires, which is currently under investigation. What, however, are the implications for basal-plane graphite? The results of electrodeposition experiments demonstrate that basal-plane graphite cannot be electrochemically inert.[15] Conversely, our simulations show that k°_{basal} is significantly smaller than k°_{edge}. Otherwise, we would observe strange voltammetric characteristics.[9] The value of k°_{basal} could be determined by performing the inverse of this experiment and selectively blocking the edge-plane steps. This is currently under investigation. However, an important question to consider is why there is such a large difference in electrochemical reactivity between basal and edge-plane graphite.

To answer this question one must attempt to link electrochemical activity with electronic structure.[4] Theoretical

 © 2005 Wiley-VCH Verlag GmbH & Co. KGaA, Weinheim

calculations predict graphite to have both semiconductor and metallic properties, in that the density of states (DOS) at the Fermi Level, E_f, is smaller than that of a metal, but there is no band gap.[26,27] The problem to consider is how the 3D pristine graphite DOS relates to our HOPG electrode surface.

In a differential capacitance study on basal-plane HOPG, Gerischer and co-workers determined the DOS around E_f to be both qualitatively and quantitatively similar to the most popular theoretical models for graphite.[28] It can therefore be inferred that the theoretical calculations for graphite are relevant to basal-plane terraces. This is not surprising; the major contribution to the DOS diagram for graphite comes from orbital overlap in the planes of individual graphene sheets, so exposing the basal plane should not have a significant effect. (Indeed, the DOS diagrams for a 2D graphene sheet and 3D graphite are similar.[27]) In addition to well-established parameters such as reorganization energy, the rate of electron transfer (reflected in the value of $k°$) also depends on the surface concentration of electrons. The electron-transfer reaction proceeds by electron tunneling; the more electrons present, the more likely it is that a tunneling event will occur.[4,29]

For metals such as gold, the DOS at E_f is relatively large, and the rates of electron transfer depend on the properties of the redox system with the electrode band structure having no limiting effect.[4,30] However, redox reactions for which the DOS at E_f is much smaller (or even zero) are limited by the low surface concentrations of electrons.[4,29] Basal-plane graphite appears to fall into this category, effectively behaving like a semiconductor with zero band gap, in agreement with the DOS diagram for graphite.

McCreery and co-workers have shown edge-plane graphite to have a capacitance over 30-fold that of basal-plane graphite.[7] Furthermore, electrochemical reactions at edge-plane pyrolytic graphite electrodes for a wide range of redox couples possess similar $k°$ values to those conducted at metal electrodes. Therefore, electron surface concentration is not a limiting factor for edge-plane graphite, and the theoretical calculations for pristine graphite are clearly not relevant. Indeed, exposed edge-plane graphite is expected to have a far different electronic structure than 3D pristine graphite, with the "cut-off" along the surface severely disrupting the main orbital interactions.

There is notable overlap between the conclusions reported herein and those of Gerischer et al.[28] In a differential capacitance study, the experimentally observed capacitance (C_{obs}) for the HOPG surface is expected to scale with the relative areas of edge-plane and basal-plane graphite, as expressed in Equation (2) in which C_i is the capacitance of the

$$C_{obs} = \frac{A_{basal}}{A_{HOPG}} C_{basal} + \frac{A_{edge}}{A_{HOPG}} C_{edge} \quad (2)$$

given electrode material, A_{HOPG} is the total area of the HOPG electrode, and A_i is the total surface area of the given electrode material. Therefore, by using high quality basal-plane HOPG, Gerischer and co-workers were able to minimize the contribution of edge-plane graphite and obtain experimental data attributable to basal-plane graphite.

In the case of cyclic voltammetry, the experimental observation is an $I-E$ response, $I-E$(HOPG). Owing to the depleting effects of nonlinear diffusion, the individual contributions of edge and basal-plane graphite do not scale with relative areas; Equation (3) is thus a more appropriate description in which

$$I-E_{HOPG} = \beta[I-E_{basal}] + \varepsilon[I-E_{edge}] \quad (3)$$

$I-E_i$ is the cyclic voltammetry response for the given electrode material and β and ε are complicated functions that take into account the relative areas and sizes of the two electrode materials as well as nonlinear diffusion. For HOPG cyclic voltammetry at scan rates of $\approx 1\ V s^{-1}$ and diffusion coefficients greater than $\approx 10^{-6}\ cm^2 s^{-1}$, $\beta = 0$, so there is no contribution from the basal-plane terraces as evidenced by the work reported herein. This means that unlike the results of Gerischer et al.,[28] the use of HOPG in cyclic voltammetry experiments (with the aforementioned parameters) will not provide experimental results that are attributable to basal-plane graphite. The same can be said for all other types of graphite electrodes. Therefore, to obtain a response from which kinetic parameters for basal-plane graphite could be determined would require setting ε to zero (by selectively blocking edge-plane sites) or by making $\beta > 0$. This approach is currently under investigation.

Previously, researchers described anomalously slow kinetics for basal-plane HOPG electrodes relative to their edge-plane counterparts. Our work herein shows that edge-plane defects are responsible for the voltammetric response at basal-plane HOPG electrodes, with the basal plane being effectively inert. A $k°_{basal}$ value significantly less than that of a metal (that is, $k°_{edge}$) agrees with the extensive amount of theoretical work on the electronic structure of graphite.[26,31–33] Therefore, we suggest the more appropriate perception that *electrochemical reactions at edge-plane graphite are anomalously fast*. Whatever the reason for this, the fact that massive changes in electronic structure occur over the traverse of a basal-plane HOPG surface is quite fascinating.

Received: November 29, 2004
Revised: February 10, 2005
Published online: July 15, 2005

Keywords: carbon · electrochemistry · materials science · nanostructures · scanning probe microscopy

[1] R. L. McCreery in *Electroanalytical Chemistry, Vol. 17* (Ed.: A. J. Bard), Marcel Decker, New York, **1990**, p. 221.
[2] H. Chang, A. J. Bard, *Langmuir* **1991**, *7*, 1143.
[3] K. R. Kneton, R. L. McCreery, *Anal. Chem.* **1992**, *64*, 2518.
[4] K. K. Cline, M. T. McDermott, R. L. McCreery, *J. Phys. Chem.* **1994**, *98*, 5314.
[5] M. T. McDermott, K. Kneten, R. L. McCreery, *J. Phys. Chem.* **1992**, *96*, 3124.
[6] C. A. Goss, J. C. Brumfield, E. A. Irene, R. W. Murray, *Anal. Chem.* **1993**, *65*, 1378.
[7] R. J. Rice, R. L. McCreery, *Anal. Chem.* **1989**, *61*, 1637.
[8] R. J. Bowling, R. T. Packard, R. L. McCreery, *J. Am. Chem. Soc.* **1989**, *111*, 1217.

 © 2005 Wiley-VCH Verlag GmbH & Co. KGaA, Weinheim

[9] T. J. Davies, R. R. Moore, C. E. Banks, R. G. Compton, *J. Electroanal. Chem.* **2004**, *574*, 123.
[10] C. E. Banks, T. J. Davies, G. G. Wildgoose, R. G. Compton, *Chem. Commun.* **2005**, 813.
[11] M. T. McDermott, R. L. McCreery, *Langmuir* **1994**, *10*, 4307.
[12] http://www.2spi.com/catalog/new/hopgsub.shtml.
[13] R. Bowler, T. J. Davies, M. E. Hyde, R. G. Compton, *Anal. Chem.* **2005**, *77*, 1916.
[14] M. P. Zach, K. H. Ng, R. M. Penner, *Science* **2000**, *290*, 2120.
[15] M. P. Zach, K. Inazu, K. H. Ng, J. C. Hemminger, R. M. Penner, *Chem. Mater.* **2002**, *14*, 3206.
[16] E. C. Walter, M. P. Zach, F. Favier, B. J. Murray, K. Inazu, J. C. Hemminger, R. M. Penner, *ChemPhysChem* **2003**, *4*, 131.
[17] M. Delamar, R. Hitmi, J. Pinson, J. M. Savéant, *J. Am. Chem. Soc.* **1992**, *114*, 5883.
[18] P. Allongue, M. Delamar, B. Desbat, O. Fagebaume, R. Hitmi, J. Pinson, J. M. Savéant, *J. Am. Chem. Soc.* **1997**, *119*, 201.
[19] M. Pourbaix, J. A. Franklin, *Atlas of Electrochemical Equilibria in Aqueous Solutions*, NACE International Cebelcor, Houston, TX, **1974**.
[20] J. Trotter, *Acta Crystallogr.* **1959**, *12*, 884.
[21] K. Ray III, R. L. McCreery, *Anal. Chem.* **1997**, *69*, 4680.
[22] Y.-C. Liu, R. L. McCreery, *J. Am. Chem. Soc.* **1995**, *117*, 11254.
[23] C. Amatore, J.-M. Savéant, D. Tessier, *J. Electroanal. Chem.* **1983**, *147*, 39.
[24] This could be misleading. The bottom of the nanotrenches consist of the surface originally covered by nanowires which includes the basal-plane sites adjacent to the edge-plane steps, as well as the edge-plane sites themselves.
[25] C. E. Banks, R. R. Moore, T. J. Davies, R. G. Compton, *Chem. Commun.* **2004**, *16*, 1804.
[26] I. L. Spain, *Chemistry and Physics of Carbon*, *Vol. 16* (Ed.: P. L. Thrower), Marcel Dekker, New York, **1980**.
[27] P. J. F. Harris, *Carbon Nanotubes and Related Structures: New Materials for the Twenty-First Century*, Cambridge University Press, **1999**.
[28] H. Gerischer, R. McIntyre, D. Scherson, W. Storck, *J. Phys. Chem.* **1987**, *91*, 1930.
[29] H. Gerischer, *J. Phys. Chem.* **1991**, *95*, 1356.
[30] T. Iwasita, W. Schmickler, J. W. Schultze, *Ber. Bunsen-Ges.* **1985**, *86*, 138.
[31] I. L. Spain, *Chemistry and Physics of Carbon*, *Vol. 8* (Ed.: P. L. Thrower), Marcel Dekker, New York, **1973**.
[32] R. C. Tatar, S. Rabii, *Phys. Rev. B* **1982**, *25*, 4126.
[33] E. J. Duplock, M. Scheffler, P. J. D. Lindan, *Phys. Rev. Lett.* **2004**, *92*, 225502/1.

 © 2005 Wiley-VCH Verlag GmbH & Co. KGaA, Weinheim

Food Chemistry

DOI: 10.1002/anie.200500148

Alternate Isotope-Coded Derivatization Assay: An Isotope Dilution Method Applied to the Quantification of Zearalenone in Maize Flour**

Stefano Sforza, Chiara Dall'Asta, Alessandra Moseriti, Gianni Galaverna, Arnaldo Dossena, and Rosangela Marchelli*

The chromatographic quantification of analytes in complex matrices such as food or feed can be problematic as a result of the possible presence of interfering agents. The application of liquid chromatography coupled to mass spectrometric detection (LC–MS) is particularly helpful in these cases given the high selectivity of mass detectors. However, the response of a given amount of analyte at atmospheric pressure interfaces is quite variable, as ionization and evaporation depend on the different eluent mixtures used and small instrumental variations. They are also affected by the co-elution of interfering agents, which may result in ion-suppressive effects.[1] Moreover, serious recovery problems may arise from the extraction procedures performed to concentrate the analytes. The best way to handle these problems, given the ability of MS to detect simultaneously different isotopes of the same molecule, is to use the isotope dilution approach, in which the same analyte containing with stable isotopes is used as an internal standard.[2] The evident drawback, however, is that stable, isotope-labeled analogues of most analytes are either not available, not completely labeled, or are very costly.

Herein, we present an innovative approach for the application of isotope dilution methods to the quantification of analytes for which stable isotope-labeled analogues are not available. We were inspired by the isotope-coded affinity tagging (ICAT) method, which is widely used for the detection of differential protein expression in living systems:[3] isotope-labeled molecules can be obtained by using isotope-labeled derivatizing reagents starting either from standards or samples. The purpose of this method is to determine a suitable derivative of the analyte that is obtained by derivatization with reagents that are available in two pure isotopic forms, "light" and "heavy" (for example, protonated or deuterated). In the approach proposed herein, two standard analyte solutions containing the same amount of standard are used in two derivatization reactions, one with the "light" derivatizing reagent and the other with the "heavy"

[*] Dr. S. Sforza, Dr. C. Dall'Asta, A. Moseriti, Prof. G. Galaverna, Prof. A. Dossena, Prof. R. Marchelli
Department of Organic and Industrial Chemistry
University of Parma
Parco Area delle Scienze 17/A
43100 Parma (Italy)
Fax: (+39) 0521-905-472
E-mail: stefano.sforza@unipr.it

[**] The Italian Ministry of Health is gratefully acknowledged for financial support.

InterScience
© 2005 Wiley-VCH Verlag GmbH & Co. KGaA, Weinheim

reagent. The derivatized products are added to the matrix in two portions, with the "light" derivatized standard added to one half and the "heavy" derivatized standard to the other half. The derivatization procedure is then repeated on both matrices, thereby derivatizing the part containing the "heavy" derivatized standard with the "light" derivatizing reagent and the part containing the "light" derivatized standard with the "heavy" derivatizing reagent. Both mixtures are then extracted by conventional methods and analyzed by LC–MS, monitoring the "light"- and the "heavy"-derivatized analytes with the former as standard for the latter in one case, and vice versa in the other (Figure 1).

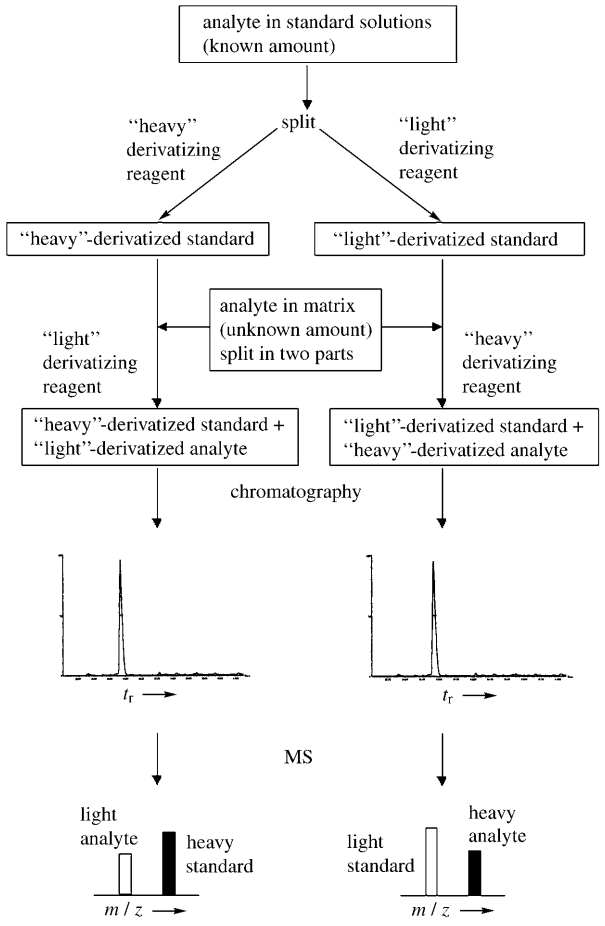


Figure 1. Procedure for the application of the AIDA method.

In this way, two independent quantifications can be carried out on the same sample. We therefore termed this method the alternate isotope-coded derivatization assay (AIDA). The addition of the derivatized internal standard before the extraction procedure permits corrections for the recovery. In the LC–MS analysis, both derivatives, which are isotopomers are expected to have almost the same retention times. They will therefore experience the same instrumental and matrix conditions, thus allowing accurate results. This procedure may allow the adoption of a fast and simplified sample preparation technique that avoids loss of analytes, as any matrix interference during LC analysis will be corrected by the use of the isotopic internal standard. Indeed, the most important self-correction of the analytical data obtained in this way comes from the use of a double determination ("light" standard and "heavy" analyte and vice versa), which allows the determination of the relative response factor (the ratio of the response factor of the analyte to that of the standard) directly on the sample analyzed, without the need to calculate it from a calibration curve or by checking the linearity range.

The theoretical background is derived directly from the following simple calculations: for the analysis of molecule **A** in the presence of an internal standard **B**, quantitative data are given by Equation (1):

$$q_A = (R_{fA}/R_{fB}) \times (A_A/A_B^S) \times q_B^S \quad (1)$$

(q : quantity; R_f : response factor; A : area; the superscript S indicates the use as internal standard)

The relative response factor $R_r = (R_{fA}/R_{fB})$ usually must be calculated previously from a calibration curve. According to our AIDA method, **A** and **B** are isotopomers, and **B** is used as a standard for **A** in one case, and **A** as a standard for **B** in the other. In the latter case, Equation (1) can be written as Equation (2):

$$q_B = (R_{fB}/R_{fA}) \times (A_B/A_A^S) \times q_A^S \quad (2)$$

Dividing the two equations gives Equation (3):

$$q_A/q_{B=}(R_{fA}/R_{fB})^2 \times (A_A/A_B^S) \times (A_A^S/A_B) \times (q_B^S/q_A^S) \quad (3)$$

Clearly, $q_A/q_B = 1$, as this value should always be the same regardless of whether the analyte has been treated with the "heavy" or the "light" derivatizing reagent. Moreover, also $q_B^S/q_A^S = 1$ if the "light" and "heavy" derivatized standards are used in the same amounts. Accordingly, Equation (4) can be derived from Equation (3), thus allowing the calculation of R_r.

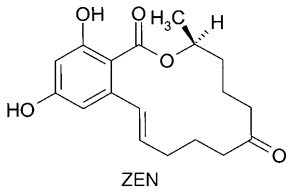
$$(R_{fA}/R_{fB})^2 = (A_B^S/A_A) \times (A_B/A_A^S) \quad (4)$$

It is therefore possible to calculate the relative response factor directly from the area ratios **A**/**B** obtained from the two different determinations, in which **A** and **B** are alternatively used as analyte and internal standard. The quantitative data obtained can then be corrected according to the relative response factors ($R_{fA}/R_{fB} = R_r$ and $R_{fB}/R_{fA} = 1/R_r$). It is very important to ensure that the reaction gives the same conversion both for the matrix and the standard solution to avoid inaccurate results. Moreover, for the same reasons, both "light" and "heavy" derivatizing agents should also give the same conversion. Both these conditions appear to be easily achievable.

To test the applicability of the method, we addressed the quantification of the mycotoxin Zearalenone (ZEN) in food and feed. ZEN is a fungal toxin that is mainly produced by several *Fusarium* species, such as *F. culmorum, F. graminearum*, and *F. sporotrichioides*, which are known to colonize maize, barley, wheat, oats, and sorghum in both warm and temperate climates.[4] ZEN consists of a resorcinol moiety

 © 2005 Wiley-VCH Verlag GmbH & Co. KGaA, Weinheim

fused to a 14-membered macrocyclic lactone ring that includes a *trans* double bond, a ketone, and a methyl substituent on a stereogenic center. The structure is flexible



ZEN

enough to allow ZEN to adopt a conformation that is able to bind to the mammalian estrogen receptor; ZEN can therefore act as an endocrine disrupter.[5] The analysis of ZEN is commonly performed by applying a clean-up step with immunoaffinity chromatography (IAC) after extraction, followed by HPLC with fluorescence detection that takes advantage of the native fluorescence of this mycotoxin.[6] As an alternative to fluorescence detection, several LC–MS methods have been developed with various interfaces.[7] In all cases, however, quantification was hampered by the choice of an appropriate standard.

To apply the AIDA method to the ZEN molecule, we chose as derivatizing reagent a compound that can easily react with the hydroxy functional groups, and which is commonly available in two isotopic forms: acetic anhydride and its deuterated [D_6] analogue. A standard solution of ZEN was derivatized either with [H_6]- or [D_6]acetic anhydride,[8] and LC–MS analysis[9] revealed only the presence of the [H_6]- or [D_6]bisacetylated compound, respectively, with no chromatographic peaks attributable to nonderivatized or monoacetylated toxin (Figure 2). NaCl was added to the eluent to enhance detection of the sodiated compounds according to a method recently published by our research group[10]: infusion experiments of ZEN and bisacetylated ZEN performed by adding NaCl to the solvent confirmed that, under these conditions, only the sodiated molecular ion is present; LC–MS experiments performed with and without NaCl added to the eluent showed an average 20-fold increase of the chromatographic peak intensity for the former relative to the latter case (data not shown).

The derivatization reaction was also repeated in food matrices by spiking several toxin-free maize flour samples with ZEN. The samples were blended and the toxins extracted in a 1:4 water/acetonitrile mixture, filtered, evaporated to dryness, and derivatized with acetic anhydride.[11] Again, only the bisacetylated compounds were observed by LC–MS both with [H_6]- and [D_6]acetic anhydride (Figure 2). To ensure that the AIDA method gives no artifacts, some important controls were performed. The most important was the stability of the acetyl groups during the derivatization reaction. As after the addition of the [D_6]bisacetylated standard to the food matrix, a second acetylation with [H_6]acetic anhydride is carried out (or vice versa), it is essential that the acetyl groups do not undergo exchange with each other. This control can be done rapidly in the case of ZEN: if an exchange does occur, it would be possible to detect bisacetylated molecules that bear one [H_3]acetyl group and one [D_3]acetyl group. As shown in

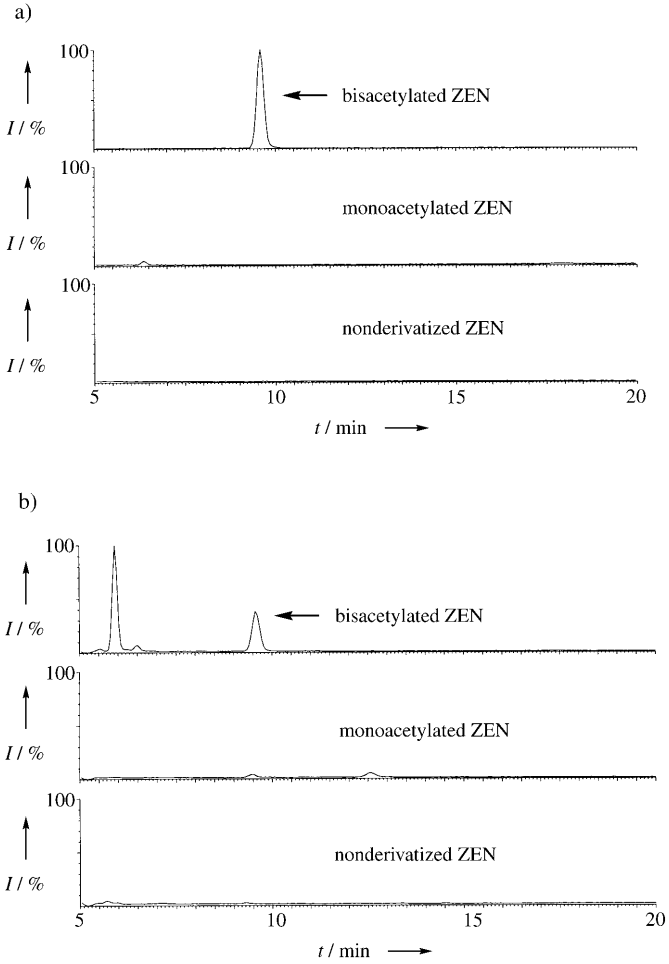


Figure 2. LC–MS chromatograms (single-ion mode acquisition of sodiated molecular ions) of the acetylation reaction in a) standard solution and b) with spiked flour. Bisacetylated, monoacetylated, and nonderivatized ZEN were monitored, thus confirming that in both cases only the bisacetylated compound was present.

Figure 3, no species of this type were detected after the derivatization reaction. Full-scan MS data of the [D_6]bisacetylated ZEN also confirmed that the protons on the acetyl groups do not exchange with the solvent, as the molecule shows only minimal traces of a [D_5H]compound that was already present in the starting [D_6]acetic anhydride preparation and no sign of other [$D_{6-x}H_x$]derivatives.

The above method was then applied to the determination of ZEN in several spiked maize flours by LC–MS.[11] The limits of detection (S/N = 3:1) and quantification (S/N = 10:1) of the method were determined by spiking toxin-free flour samples at the appropriate level and were found to be 5 ppb (absolute amount injected: 100 pg) and 10 ppb (absolute amount injected: 200 pg), respectively. Notably, a calibration curve was not calculated before the analyses, and six independent determinations (three with the deuterated standard and three with the protonated standard) were run for every sample. The chromatographic peak areas were then measured for both isotopes by extracting the chromatograms given by the corresponding sodiated ions. The response-factor ratios were calculated from Equation (4) and the amounts

 © 2005 Wiley-VCH Verlag GmbH & Co. KGaA, Weinheim

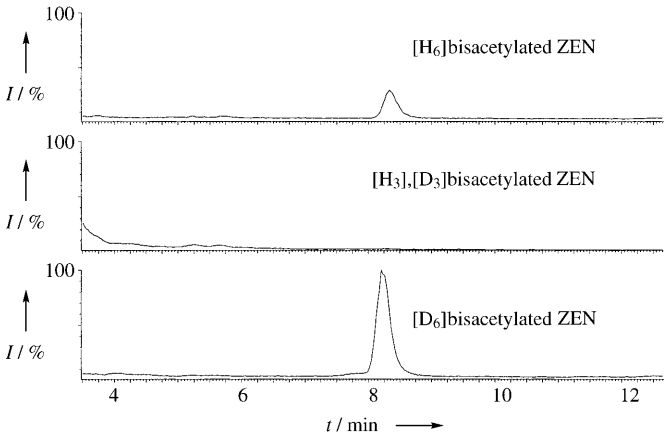


Figure 3. LC–MS chromatograms (single-ion mode acquisition of sodiated molecular ions) of a flour preparation spiked with [D_6]bisacetylated ZEN and derivatized with [H_6]acetic anhydride. [D_3],[H_3]bisacetylated ZEN was not detected, thus indicating the absence of acetyl group exchange.

were then calculated from Equations (1) and (2). The true results were taken as the average of these six determinations. The data are reported in Table 1, together with the results for

Table 1: Determination of ZEN in spiked samples and in a FAPAS-certified reference material.

Quantity spiked [ppb]	Quantity detected [ppb]	Average response factor ratio [H_6]Ac_2-ZEN/ [D_6]Ac_2-ZEN
10	13 ± 3	1.20 ± 0.14
50	48 ± 7	1.20 ± 0.17
100	104 ± 5	1.26 ± 0.05
500	516 ± 58	1.34 ± 0.05
1000	1039 ± 72	1.41 ± 0.02
certified flour (648 ± 140)	709 ± 24	1.07 ± 0.04

a FAPAS-certified reference material (FAPAS = food analysis performance assessment scheme). The results are quite outstanding, considering that no calibration curve or linearity tests were performed. The response ratio between protonated and deuterated compounds was calculated in every sample analyzed and are also reported in Table 1. These ratios always appear to be slightly, yet significantly, different from unity, which implies that the methodology proposed herein must be followed with the subsequent response-factor correction for the results to be accurate. These data constitute definitive proof of the validity of the AIDA concept. The chromatograms of the FAPAS-certified reference material corresponding to the two cases ([H_6]acetylated ZEN as standard with [D_6]acetylated ZEN as analyte and [D_6]acetylated ZEN as standard with [H_6]acetylated ZEN as analyte) are shown in Figure 4. Notably, in all these cases, no IAC purification was carried out before the LC–MS analyses, which is usually performed before ZEN analysis by LC-FLD (FLD = fluorescence detection), which demonstrates that the acetylation procedure used is also suitable for the detection of ZEN in

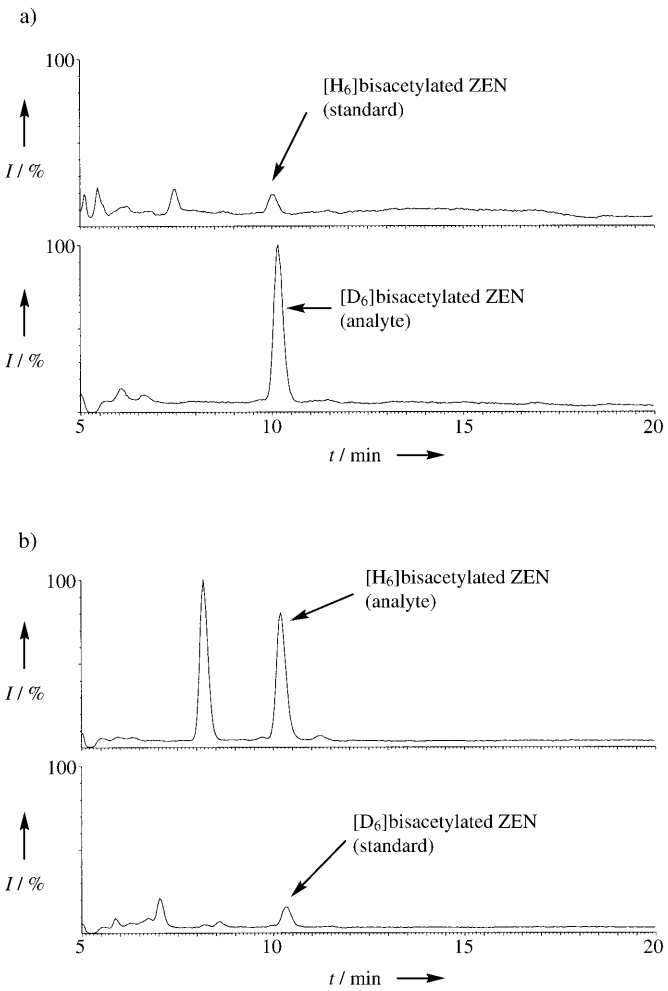


Figure 4. LC–MS chromatograms (single-ion mode acquisition of sodiated molecular ions) of a) the FAPAS-certified flour with added [H_6]bisacetylated ZEN (standard, 100 ppb) and derivatized with [D_6]acetic anhydride and b) the same sample with added [D_6]bisacetylated ZEN (standard, 100 ppb) and derivatized with [H_6]acetic anhydride.

natural samples by using raw extracts. This allows one to avoid the cumbersome and expensive IAC clean-up procedure that can also prevent a full recovery of the analyte.

The data presented herein on the quantification of ZEN in flour samples demonstrate how the AIDA method may be applied for the accurate quantification of analytes in complex matrices, such as food or feed, by LC–MS. This method avoids errors due to instrumental and matrix effects, yields accurate results with minimal sample preparation, and exploits all the advantages of isotope dilution methods in a low-cost, easy-to-perform procedure, although two independent experiments have to be performed for each sample analyzed. This procedure is currently being extended to the detection of other mycotoxins in food samples.

Received: January 14, 2005
Published online: July 13, 2005

 © 2005 Wiley-VCH Verlag GmbH & Co. KGaA, Weinheim

Keywords: analytical methods · isotopic labeling · liquid chromatography · mass spectrometry · zearalenone

[1] C. R. Mallet, Z. L. Lu, J. R. Mazzeo, *Rapid Commun. Mass Spectrom.* **2004**, *18*, 49–58.
[2] M. Lindenmeier, P. Schieberle, M. Rychlik, *J. Chromatogr. A* **2004**, *1023*, 57–66.
[3] D. K. Han, J. Eng, H. L. Zhou, R. Aebersold, *Nat. Biotechnol.* **2001**, *19*, 946–951.
[4] V. Betina, *Bioactive Molecules*, *Vol. 9*: *Mycotoxins*, Elsevier, Amsterdam, **1989**, p. 271.
[5] E. E. Creppy, *Toxicol. Lett.* **2002**, *127*, 19–28.
[6] a) A. Visconti, M. Pascale, *J. Chromatogr. A* **1998**, *815*, 133–140; b) S. C. Kruger, B. Kohn, C. S. Ramsey, R. Prioli, *J. AOAC Int.* **1999**, *82*, 1364–1368; c) B. Fazekas, A. Tar, *J. AOAC Int.* **2001**, *84*, 1453–1459; d) S. De Saeger, L. Sibanda, C. Van Peteghem, *Anal. Chim. Acta* **2003**, *487*, 137–143; e) G. K. Mortensen, B. W. Strobel, H. C. B. Hansen, *Anal. Bioanal. Chem.* **2003**, *376*, 98–101.
[7] a) E. Rosenberg, R. Krska, R. Wissiak, V. Kmetov, R. Josephs, E. Razzazi, M. Grassbauer, *J. Chromatogr. A* **1998**, *819*, 277–288; b) P. Zollner, J. Jodlbauer, W. Lindner, *J. Chromatogr. A* **1999**, *858*, 167–174; c) P. Zoellner, D. Berner, J. Jodlbauer, W. Lindner, *J. Chromatogr. B* **2000**, *738*, 233–241; d) P. Zoellner, J. Jodlbauer, M. Kleinova, H. Kahlbacher, T. Kuhn, W. Hochsteiner, W. Lindner, *J. Agric. Food Chem.* **2002**, *50*, 2494–2501; e) E. O. van Bennekom, L. Brouwer, E. H. M. Laurant, H. Hooijerink, M. W. F. Nielen, *Anal. Chim. Acta* **2002**, *473*, 151–160; f) L. Pallaroni, C. von Holst, *J. Chromatogr. A* **2003**, *993*, 39–45.
[8] Procedure for the preparation of derivatized standards: 100 μL of a 10-ppm standard solution of ZEN in dry acetonitrile was added to 35 μL triethylamine, 270 μL dry acetonitrile, and 95 μL either [H_6]- or [D_6]acetic anhydride. The mixture was left at room temperature for 60 min, then evaporated to dryness and redissolved in 1 mL water/acetonitrile (1:4) to be added to the food/feed samples or directly analyzed by LC–MS.
[9] LC–MS conditions: C18 column (Waters, 250 × 4.6, 5 μm) on a Waters Alliance 2695 separation module, isocratic elution with 0.2 mM aqueous NaCl/CH_3OH (35:65); flow: 1 mL min^{-1}. Injected volume: 10 μL. A Micromass ZMD mass spectrometer equipped with an ESI interface was used as MS detector by splitting 90% of the flow with a T-valve before the probe. Acquisition in positive ion mode; capillary voltage: 3.5 kV (pos); cone voltage: 30 V (pos); source temperature: 80 °C; desolvation temperature: 150 °C; cone gas (N_2): 100 L h^{-1}; desolvation gas (N_2): 400 L h^{-1}. Acquisition in single-ion monitoring: $m/z = 425.3$ for sodiated [H_6]bisacetylated ZEN and 431.3 for sodiated [D_6]bisacetylated ZEN; dwell time: 0.5 s; span: 0.2. Acquisition in full scan: range: 150–1000; scan time: 3 s; inter-scan delay: 0.1 s.
[10] C. Dall'Asta, S. Sforza, G. Galaverna, A. Dossena, R. Marchelli, *J. Chromatogr. A* **2004**, *1054*, 389–395.
[11] Sample preparation: 10 g flour was mixed with 39 mL water/acetonitrile (1:4) and 1 mL of a water/acetonitrile (1:4) solution containing 1 μg of [H_6]- or [D_6]bisacetylated ZEN, prepared as reported in Ref. [8]. The mixture was blended for 2 min in a high-speed blender. After filtration through paper filters, the filtrate (4 mL) was dried under a nitrogen stream. The residue was redissolved in 35 μL triethylamine, 370 μL dry acetonitrile, and 95 μL [H_6]acetic anhydride (in the case of [D_6]bisacetylated standard) or [D_6]acetic anhydride (in the case of [H_6]bisacetylated standard). For acidic food matrices, which may give incomplete derivatization, the amount of triethylamine was doubled. The mixture was left at room temperature for 60 min, then evaporated to dryness and redissolved in 500 μL water/acetonitrile (1:4) to be analyzed by LC–MS.

 © 2005 Wiley-VCH Verlag GmbH & Co. KGaA, Weinheim

Cycloaddition

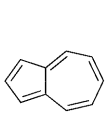
DOI: 10.1002/anie.200501276

Approach to the Blues: A Highly Flexible Route to the Azulenes**

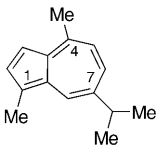
*Sébastien Carret, Aurélien Blanc, Yoann Coquerel, Mikaël Berthod, Andrew E. Greene, and Jean-Pierre Deprés**

Dedicated to Dr. Jean-Louis Luche on the occasion of his retirement

Nearly a century and a half ago, Septimus Piesse applied the descriptive name azulene to azure-blue distillates from various sources, such as chamomile, yarrow, and wormwood.[1] However, it was only in 1937 that Placidus Plattner and Alexander Pfau successfully carried out the first synthesis of azulene (**1**),[2] the appellation given to the parent compound



Azulene (**1**)



Guaiazulene (**2**)

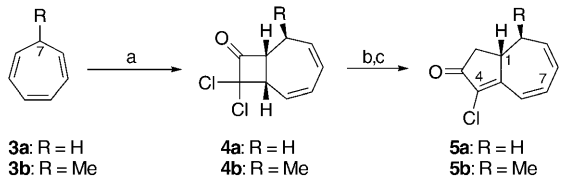
of the family of bicyclo[5.3.0]decapentaenes, which are now collectively referred to as the azulenes. Since this historical event, additional syntheses of the parent azulene and preparations of various other azulenes, such as guaiazulene (**2**), which is the archetype of the major azulene class, have been reported.[3] Although the approaches to these fascinating and electronically unique compounds are often ingenious, they suffer for the most part from being excessively long, low yielding, or lacking in generality. Many substitution patterns of the azulenes are still difficult to access, if they can be accessed at all.[3]

We have found that chlorotrienones **5a** and **5b** are readily prepared from cycloheptatriene and 7-methylcycloheptatriene, respectively, through a doubly regioselective cycloaddition of dichloroketene, a regioselective ring expansion with ethereal diazomethane, and dehydrochlorination in dimethylformamide (DMF; Scheme 1).[4]

[*] S. Carret, A. Blanc, Y. Coquerel, M. Berthod, Dr. A. E. Greene, Prof. J.-P. Deprés
Chimie Recherche (LEDSS)
Université Joseph Fourier
B.P. 53X, 38041 Grenoble, Cedex 9 (France)
Fax: (+33) 4-7651-4494
E-mail: jean-pierre.depres@ujf-grenoble.fr

[**] We thank Prof. P. Dumy for his interest in our research, the Research Ministry for fellowship awards to S.C. and Y.C., and the Université Joseph Fourier and the CNRS (UMR 5616, FR 2607) for financial support.

InterScience
© 2005 Wiley-VCH Verlag GmbH & Co. KGaA, Weinheim

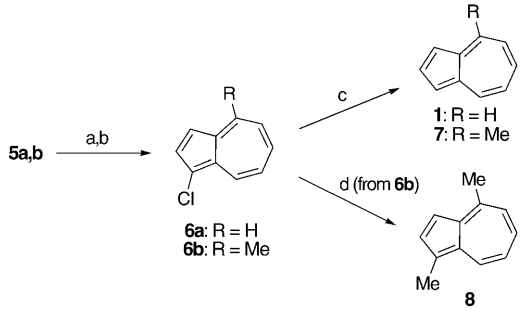


Scheme 1. Preparation of chlorotrienones **5a** and **5b**: a) Zn/Cu, $POCl_3$, CCl_3COCl, Et_2O, 20 °C, 20 h; b) CH_2N_2, MeOH/Et_2O (5:95), 0→20 °C, 35 min; c) DMF, 20 °C, 12 h (44–45 % yield, 3 steps).

As other C7-substituted cycloheptatrienes and diazoalkane reagents are also readily available[4a,5] for use in this sequence, it appeared to us that a broad approach to the azulenes might now be possible if 1) the oxygen atom at C3 could be excised, 2) the fused rings could be dehydrogenated to aromaticity, 3) the chlorine atom at C4 could be replaced, and 4) additional substituents could be regioselectively introduced into the trienones, particularly at C7. Herein, we disclose an efficient and exceptionally versatile preparation of azulenes, which are compounds of considerable interest for use in cosmetics,[6a] pharmaceutical preparations,[6b] and new molecular materials,[6c] through effective resolution of these concerns.

Azulene itself was targeted initially so that the first three critical points could be addressed at the outset. It was pleasing to find, after a number of failed attempts, that sequential treatment of **5a** with $NaBH_4/CeCl_3$, the Burgess reagent,[7] and *p*-chloranil could transform **5a** into chloroazulene **6a** in 45 % overall yield (Scheme 2).[8] Azulene could then be obtained from **6a** in 92 % yield through modification of the reduction recently described by Rahaim and Maleczkza.[9] Analogously, 4-methylazulene (**7**)[2,10] was readily prepared from **5b** in a slightly higher overall yield.

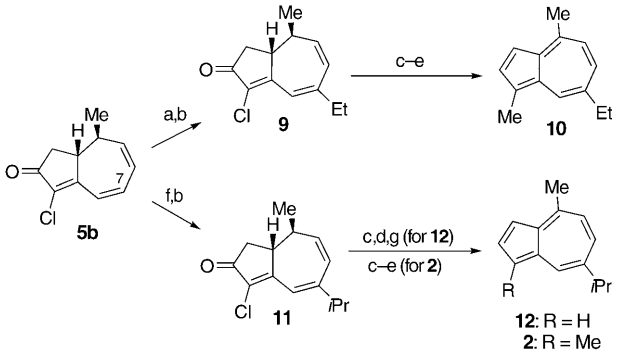
As most naturally occurring azulenes have methyl groups at C1 and C4, the discovery that **6b** could also be methylated by reaction with methylboronic acid, dpdb, and K_3PO_4[11] to give 1,4-dimethylazulene (**8**)[12a] in 98 % yield was welcomed



Scheme 2. Preparation of azulene (**1**), 4-methylazulene (**7**), and 1,4-dimethylazulene (**8**): a) $NaBH_4$, MeOH/$CeCl_3$, 0 °C, 1.5 h (from **5a**: 96 %; from **5b**: 98 %); b) the Burgess reagent, THF, 0→20 °C, 1 h; *p*-chloranil, 20 °C, 24 h (from **6a**: 47 %; from **6b**: 52 %); c) PMHS, $Pd(OAc)_2$, dpdb, K_3PO_4, THF, 80 °C, 12 h (**1**: 92 %; **7**: 91 %); d) $MeB(OH)_2$, $Pd(OAc)_2$, dpdb, K_3PO_4, PhMe, 100 °C, 24 h (98 %). Burgess reagent = (methoxycarbonylsulfamoyl)triethylammonium hydroxide inner salt, *p*-chloranil = tetrachloro-1,4-benzoquinone, PMHS = poly(methylhydrosiloxane), dpdb = dicyclohexylphosphano-2′,6′-dimethoxybiphenyl.

and augured well for the application of this approach to many other naturally occurring azulenes.[12b]

Considerable study was required to resolve point (4) satisfactorily. Although several different types of organometallic reagents did indeed add regio- (and stereo-)selectively to **5b** at C7, the yields were modest and, furthermore, aromatization of the resultant dienones proved difficult to achieve efficiently. We were, therefore, pleased to find that organozinc reagents, in the presence of CuOTf (cat.) and TMSCl,[13] were highly effective in transforming **5b** into the corresponding 1,6-conjugate addition products: Me, 91 %; Et, 98 %; *i*Pr, 71 %. Even better, it was discovered that simply by adding PhSeCl to the reaction mixture and then effecting oxidative (H_2O_2) elimination, the chlorotrienone system could be smoothly regenerated (Scheme 3).[14] Thus, chloro-



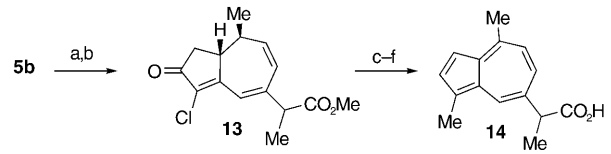
Scheme 3. Preparation of chamazulene (**10**), 7-isopropyl-4-methylazulene (**12**), and guaiazulene (**2**): a) 1. Et_2Zn, CuOTf, HMPA, TMSCl, −50 °C, 6 h; 2. PhSeCl, −50→0 °C, 2 h; b) H_2O_2, pyridine, 0 °C, 1 h (**9**: 71 %, 2 steps; **11**: 62 %, 2 steps); c) $NaBH_4$, MeOH/$CeCl_3$, 0 °C, 1.5 h (97 %); d) 1. Burgess reagent, THF, 0 °C, 1 h; 2. *p*-chloranil, 20 °C, 24 h (58–59 %); e) $MeB(OH)_2$, $Pd(OAc)_2$, dpdb, K_3PO_4, PhMe, 100 °C, 24 h (**10**: 89 %; **2**: 94 %); f) 1. iPr_2Zn, CuOTf, HMPA, TMSCl, −100 °C, 6 h; 2. PhSeCl, −50→0 °C, 2 h; g) PMHS, $Pd(OAc)_2$, dpdb, K_3PO_4, THF, 80 °C, 12 h (95 %). Tf = trifluoromethanesulfonyl, HMPA = hexamethylphosphoramide, TMSCl = trimethylsilyl chloride.

trienones **9** and **11** were prepared in 71 and 62 % yields, respectively. The former, through application of the above chemistry, provided chamazulene (**10**), and the latter, 7-isopropyl-4-methylazulene (**12**) and guaiazulene (**2**).[15]

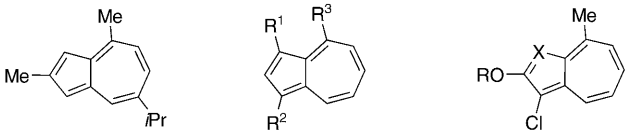
Ketene acetals can also be employed for 1,6-conjugate addition, thus adding to the synthetic possibilities: the treatment of **5b** with the *tert*-butyldimethylsilyl (TBDMS) ketene acetal, derived from methyl propionate, in the presence of lithium perchlorate[16] readily generated the 1,6-conjugate addition product, which on successive treatment with PhSeCl and H_2O_2 afforded chlorotrienone **13** (Scheme 4). Aromatization, methylation, and saponification then provided chamazulenecarboxylic acid (**14**).[17]

The attractiveness of the present approach resides, in part, in the diversity of structures that can readily be accessed with total regiocontrol, a feature that few other approaches enjoy. To further illustrate this point, regiochemically pure 7-isopropyl-2,4-dimethylazulene (**15**)[18a] (a naturally occurring isomer of guaiazulene (**2**)),[15b] 1-chloro-3-methylazulene (**16a**),[18b] and the phenylazulenes **16b**[18c] and **16c**[18d] have

 © 2005 Wiley-VCH Verlag GmbH & Co. KGaA, Weinheim



Scheme 4. Preparation of (±)-chamazulenecarboxylic acid (**14**): a) 1. MeCH=C(OMe)OTBDMS, $LiClO_4$, CH_2Cl_2, 20 °C, 12 h; 2. PhSeCl, −50→0 °C, 2 h; b) H_2O_2, pyridine, 0 °C, 1 h (46%, 2 steps); c) $NaBH_4$, MeOH/$CeCl_3$, 0 °C, 1.5 h (92%); d) 1. Burgess reagent, THF, 0 °C, 1 h; 2. *p*-chloranil, 20 °C, 24 h (55%); e) $MeB(OH)_2$, $Pd(OAc)_2$, dpdb, K_3PO_4, PhMe, 100 °C, 24 h (99%); f) LiOH, THF, H_2O, 20 °C, 12 h (94%).



15

16a: R^1 = Me, R^2 = Cl, R^3 = H
16b: R^1 = H, R^2 = Cl, R^3 = Ph
16c: R^1 = H, R^2 = Ph, R^3 = Me

17a: R = Ac, X = CH
17b: R = Me, X = N

also been efficiently prepared, thereby demonstrating four distinctly different substitution options as well. Finally, acetoxy and aza derivatives **17a**[18e] and **17b**[18f] are examples of novel azulenes that are readily prepared with this methodology.

In conclusion, modern chemistry has been applied to the long-standing problem of azulene synthesis and an efficient, highly flexible approach has resulted. Our approach allows controlled access to a wide variety of substituents and substitution arrays and should prove to be among the most broadly useful methods to prepare these important compounds.

Experimental Section

Experimental procedure for the preparation of **6b** from **5b**: $NaBH_4$ (43 mg, 1.13 mmol) was added to a stirred solution of **5b** (200 mg, 1.03 mmol) in MeOH/$CeCl_3$ (2.80 mL, 0.40 M, 1.12 mmol) at 0 °C. The reaction mixture was stirred for 1.5 h at 0 °C and then treated with a saturated solution of aqueous NaH_2PO_4. The crude product was isolated with EtOAc/pentane (1:1) in the usual manner and purified by column chromatography on dry silica gel with diethyl ether/pentane (40:60) to afford 198 mg (98%) of the *trans* alcohol as a white solid. M.p. 67–68 °C; ^{1}H NMR (300 MHz, $CDCl_3$): δ = 1.17 (d, J = 7.1 Hz, 3H), 1.38–1.48 (m, 1H), 2.16–2.24 (m, 2H), 2.33 (pseudo q, $J\cong$7.3 Hz, 1H), 2.68–2.77 (m, 1H), 4.57 (pseudo t, $J\cong$7.2 Hz, 1H), 5.66 (dd, J = 11.4, 3.3 Hz, 1H), 5.85–5.94 (m, 1H), 6.01 (dd, J = 11.5, 6.9 Hz, 1H), 6.51 ppm (d, J = 11.5 Hz, 1H); ^{13}C NMR (75.5 MHz, $CDCl_3$): δ = 19.2, 38.9, 40.3, 46.6, 74.6, 123.7, 125.3, 127.7, 133.6, 139.6, 141.5 ppm; FTIR: $\tilde{\nu}$ = 3360, 3016, 1700 cm^{-1}. A solution of the Burgess reagent (347 mg, 1.46 mmol) in dry THF (5 mL) was added to a stirred solution of the above alcohol (198 mg, 1.01 mmol) in dry THF (6.0 mL) at 0 °C. The reaction mixture was allowed to warm to 20 °C and stirred for 1 h, whereupon *p*-chloranil (745 mg, 3.03 mmol) was added and the resulting mixture was stirred for a further 24 h. The crude product was isolated with pentane in the usual way and purified by column chromatography on dry silica gel with pentane to give 92 mg (52%) of chloroazulene **6b** as a blue solid. M.p. 36 °C; ^{1}H NMR (300 MHz, $CDCl_3$): δ = 2.86 (s, 3H), 7.13 (d, J = 10.3 Hz, 1H), 7.14 (pseudo t (dd), $J\cong$9.5 Hz, 1H), 7.30 (d, J = 4.2 Hz, 1H), 7.53 (pseudo t (dd), $J\cong$10.3 Hz, 1H), 7.67 (d, J = 4.2, 1H), 8.40 ppm (d, J = 9.5 Hz, 1H); ^{13}C NMR (75.5 MHz, $CDCl_3$): δ = 24.1, 113.4, 117.1, 122.0, 127.2, 133.3, 133.5, 134.8, 136.7, 137.8, 148.0 ppm; FTIR: $\tilde{\nu}$ = 3085, 3021, 2957, 2923, 2853, 1591, 1560, 1487, 1419, 1389, 1358, 906, 772, 743 cm^{-1}; MS (DCI): m/z: 177 $[M+H]^+$; HRMS calcd for $[C_{11}H_9Cl+H]^+$: 177.0471; found: 177.0484; elemental analysis (%) calcd for $C_{11}H_9Cl$: C 74.79, H 5.14; found: C 74.84, H 5.18.

Data for selected compounds: **2**: M.p. 31–32 °C; ^{1}H NMR (300 MHz, $CDCl_3$): δ = 1.36 (d, J = 6.9 Hz, 6H), 2.66 (s, 3H), 2.83 (s, 3H), 3.08 (sept, J = 6.9 Hz, 1H), 7.01 (d, J = 10.7 Hz, 1H), 7.22 (d, J = 3.7 Hz, 1H), 7.42 (dd, J = 10.7, 1.8 Hz, 1H), 7.62 (d, J = 3.7 Hz, 1H), 8.19 ppm (d, J = 1.8 Hz, 1H); ^{13}C NMR (75.5 MHz, $CDCl_3$): δ = 13.0, 24.2, 24.9, 38.4, 112.9, 125.2, 125.3, 133.5, 135.0, 136.2, 136.4, 137.4, 140.0, 144.4 ppm; FTIR: $\tilde{\nu}$ = 3095, 3064, 2958, 2924, 2854, 1554, 1527, 1462, 1420, 1387, 1367, 772 cm^{-1}; MS (DCI): m/z: 199 $[M+H]^+$; HRMS calcd for $[C_{15}H_{19}+H]^+$: 199.1487; found: 199.1482.

10: ^{1}H NMR (300 MHz, $CDCl_3$): δ = 1.34 (t, J = 7.6 Hz, 3H), 2.65 (s, 3H), 2.82 (s, 3H), 2.83 (q, J = 7.6 Hz, 2H), 6.98 (d, J = 10.5 Hz, 1H), 7.21 (br s, 1H), 7.38 (dd, J = 10.5, 1.9 Hz, 1H), 7.61 (br s, 1H), 8.15 ppm (d, J = 1.9 Hz, 1H); ^{13}C NMR (75.5 MHz, $CDCl_3$): δ = 13.0, 17.5, 24.2, 34.0, 112.9, 125.1, 125.2, 134.8, 135.9, 136.3, 136.4, 136.5, 137.5, 144.4 ppm; FTIR: $\tilde{\nu}$ = 3098, 3063, 2960, 2926, 2866, 1555, 1561, 1526, 1452, 1422, 1364, 772 cm^{-1}; MS (DCI): m/z: 185 $[M+H]^+$; HRMS calcd for $[C_{14}H_{16}+H]^+$: 185.1330; found: 185.1334; elemental analysis (%) calcd for $C_{14}H_{16}$: C 91.25, H 8.75; found: C 91.44, H 8.86.

12: ^{1}H NMR (300 MHz, $CDCl_3$): δ = 1.35 (d, J = 6.8 Hz, 6H), 2.88 (s, 3H), 3.07 (sept, J = 6.8 Hz, 1H), 7.11 (d, J = 10.6 Hz, 1H), 7.29 (d, J = 3.8 Hz, 1H), 7.31 (d, J = 3.8 Hz, 1H), 7.46 (dd, J = 10.6, 2.0 Hz, 1H), 7.80 (pseudo t (dd), $J\cong$3.8 Hz, 1H), 8.31 ppm (d, J = 2.0 Hz, 1H); ^{13}C NMR (75.5 MHz, $CDCl_3$): δ = 24.3, 24.7, 38.2, 114.7, 118.0, 126.0, 135.3, 135.4, 136.6, 137.4, 140.2, 141.8, 145.2 ppm; FTIR: $\tilde{\nu}$ = 3093, 3064, 2958, 2924, 1556, 1529, 1461, 1422, 1389, 1362, 749 cm^{-1}; MS (DCI): m/z: 185 $[M+H]^+$; HRMS calcd for $[C_{14}H_{16}]^+$: 184.1252; found: 184.1259.

14: M.p. 86–87 °C; ^{1}H NMR (300 MHz, $CDCl_3$): δ = 1.61 (d, J = 7.2 Hz, 3H), 2.65 (s, 3H), 2.83 (s, 3H), 3.88 (q, J = 7.2 Hz, 1H), 7.00 (d, J = 10.7 Hz, 1H), 7.28 (d, J = 3.8 Hz, 1H), 7.44 (dd, J = 10.7, 1.9 Hz, 1H), 7.64 (d, J = 3.8 Hz, 1H), 8.22 ppm (d, J = 1.9 Hz, 1H); ^{13}C NMR (75.5 MHz, $CDCl_3$): δ = 13.0, 19.2, 24.2, 48.8, 114.3, 125.1, 127.1, 130.9, 133.9, 135.7, 135.8, 136.9, 137.6, 145.6 ppm; FTIR: $\tilde{\nu}$ = 3585, 3103, 3065, 2961, 2923, 2853, 1704, 1556, 1454, 1261, 1023, 774 cm^{-1}; MS (DCI): m/z: 229 $[M+H]^+$.

Received: April 12, 2005
Published online: July 13, 2005

Keywords: aromatic compounds · azulenes · cycloaddition · natural products · synthesis design

[1] S. Piesse, *C. R. Hebd. Seances Acad. Sci.* **1863**, *57*, 1016.
[2] P. A. Plattner, A. S. Pfau, *Helv. Chim. Acta* **1937**, *20*, 224–232; see, also: H.-J. Hansen, *Chimia* **1996**, *50*, 489–496.
[3] For reviews on the azulenes, see: a) M. Gordon, *Chem. Rev.* **1952**, *52*, 127–200; b) V. B. Mochalin, Y. N. Porshnev, *Russ. Chem. Rev.* **1977**, *46*, 530–547; c) K.-P. Zeller in *Methoden der Organischen Chemie (Houben-Weyl)*, *Vol. V/2c* (Ed.: H. Kropf), Georg Thieme, Stuttgart, **1985**, pp. 127–418; for a recent synthetic approach, see: d) A. L. Crombie, J. L. Kane, Jr., K. M. Shea, R. L. Danheiser, *J. Org. Chem.* **2004**, *69*, 8652–8667.
[4] a) Y. Coquerel, PhD Thesis, University of Grenoble, **2001**; b) Y. Coquerel, A. Blanc, J.-P. Deprés, A. E. Greene, M.-T. Averbuch-Pouchot, C. Philouze, A. Durif, *Acta Crystallogr. Sect. C* **2000**, *56*, 1480–1481; c) Y. Coquerel, A. E. Greene, J.-P. Deprés, *Org. Lett.* **2003**, *5*, 4453–4455; see, also: d) R. Yokoyama, S. Ito, M.

 © 2005 Wiley-VCH Verlag GmbH & Co. KGaA, Weinheim

Watanabe, N. Harada, C. Kabuto, N. Morita, *J. Chem. Soc. Perkin Trans. 1* **2001**, 2257 – 2261.

[5] H. Günther, M. Görlitz, H. H. Hinrichs, *Tetrahedron* **1968**, *24*, 5665 – 5676; tropylium tetrafluoroborate is now commercially available.

[6] a) C. S. Slavtcheff, S. R. Barrow, V. D. Kanga, M. C. Cheney, A. Znaiden (Unilever PLC, UK) WO9503779, **1995** [*Chem. Abstr.* **1995**, *123*, 17488w]; b) T. Yanagisawa, S. Wakabayashi, T. Tomiyama, M. Yasunami, K. Takase, *Chem. Pharm. Bull.* **1988**, *36*, 641 – 647; A. E. Asato, A. Peng, M. Z. Hossain, T. Mirzadegan, J. S. Bertram, *J. Med. Chem.* **1993**, *36*, 3137 – 3147; W.-G. Friebe, J. Dickhaut, R. Haag, H. Leinert, F. Grams (Roche Diagnostics GmbH, Germany), EP922702, **1999** [*Chem. Abstr.* **1999**, *131*, 58665k]; T. Toyama, I. Toyama, M. Yokota (Kotobuki Seiyaku Co. Ltd., Japan), JP2000007611, **2000** [*Chem. Abstr.* **2000**, *132*, 64075e]; B.-C. Hong, Y.-F. Jiang, E. S. Kumar, *Bioorg. Med. Chem. Lett.* **2001**, *11*, 1981 – 1984; D. A. Becker, J. J. Ley, L. Echegoyen, R. Alvarado, *J. Am. Chem. Soc.* **2002**, *124*, 4678 – 4684; H. Wakabayashi, K. Hashiba, K. Yokoyama, K. Hashimoto, H. Kikuchi, H. Nishikawa, T. Kurihara, K. Satoh, S. Shioda, S. Sato, S. Kusano, H. Nakashima, N. Motohashi, H. Sakagami, *Anticancer Res.* **2003**, *23*, 4747 – 4755; c) L. Cristian, I. Sasaki, P. G. Lacroix, B. Donnadieu, I. Asselberghs, K. Clays, A. C. Razus, *Chem. Mater.* **2004**, *16*, 3543 – 3551, and references therein.

[7] E. M. Burgess, H. R. Penton, Jr., E. A. Taylor, *J. Org. Chem.* **1973**, *38*, 26 – 31.

[8] Application of the Shapiro reaction, a) chlorotrienone, $TsNHNH_2$; b) MeLi, failed to produce the expected dihydroazulene; alternative allylic alcohol treatments, Al_2O_3, Pd/C; *p*-chloranil, Δ; HCl, Δ; Martin sulfurane reagent, were not fruitful.

[9] R. J. Rahaim, Jr., R. E. Maleczka, Jr., *Tetrahedron Lett.* **2002**, *43*, 8823 – 8826; the reported conditions gave **1** in only 54% yield.

[10] P. A. Plattner, E. Heilbronnzer, A. Fürst, *Helv. Chim. Acta* **1947**, *30*, 1100 – 1105.

[11] S. D. Walker, T. E. Barder, J. R. Martinelli, S. L. Buchwald, *Angew. Chem.* **2004**, *116*, 1907 – 1912; *Angew. Chem. Int. Ed.* **2004**, *43*, 1871 – 1876.

[12] a) P. A. Plattner, J. Wyss, *Helv. Chim. Acta* **1940**, *23*, 907 – 911; b) 1,4-dimethylazulene is naturally occurring, see: D. Meuche, S. Huneck, *Chem. Ber.* **1966**, *99*, 2669 – 2674; U. Siegel, R. Mues, R. Dönig, T. Eicher, M. Blechschmidt, H. Becker, *Phytochemistry* **1992**, *31*, 1671 – 1678.

[13] M. Kitamura, T. Miki, K. Nakano, R. Noyori, *Bull. Chem. Soc. Jpn.* **2000**, *73*, 999 – 1014.

[14] It should be noted that the aromatization of the azulenes, not unexpectedly, is directly dependent on the degree of unsaturation in the substrates; see reference [3b].

[15] Chamazulene is an artifact from various sesquiterpene oils; 7-isopropyl-4-methylazulene and guaiazulene are found naturally in different sources, see: a) T. K. Devon, A. I. Scott *in Handbook of Naturally Occurring Compounds*, *Vol. 2*, Academic Press, New York, **1972**; b) *Dictionary of Terpenoids*, *Vol. 2* (Eds.: J. D. Connolly, R. A. Hill), Chapman and Hall, New York, **1991**, and references therein.

[16] C. S. Wilcox, R. E. Babston, *J. Org. Chem.* **1984**, *49*, 1451 – 1453; M. T. Reetz, D. D. A. Fox, *Tetrahedron Lett.* **1993**, *34*, 1119 – 1122.

[17] E. Stahl, *Naturwissenschaften* **1954**, *41*, 257; E. Stahl, *Chem. Ber.* **1954**, *87*, 505 – 507; an earlier synthesis has been reported in a patent, see: Robugen GmbH Pharmazeutische Fabrik Esslingen A.N. , Germany DE 10065683, **2001** [*Chem. Abstr.* **2001**, *135*, 76647t].

[18] a) Prepared by sequential treatment of **11** with MeMgBr, the Burgess reagent, *p*-chloranil, and PMHS/$Pd(OAc)_2$; b) synthesized by treatment of **4a** with $MeCHN_2$ rather than CH_2N_2, followed by DMF, $NaBH_4/CeCl_3$, the Burgess reagent, and *p*-chloranil; c) obtained from 7-phenylcycloheptatriene; see references [4a,5]; d) prepared from **6b** by using phenylboronic acid rather than methylboronic acid (98% yield); e) obtained by heating **5b** with Ac_2O and Pd/C in toluene (50% yield), for several related examples, see reference [4a]; f) synthesized from cyclobutanone **4b** by sequential treatment with *O*-mesitylenesulfonylhydroxylamine, $[Me_3O][BF_4]$, and DMF; for other examples of aza azulenes, see: M. Kitamura, S. Chiba, O. Saku, K. Narasaka, *Chem. Lett.* **2002**, 606 – 607.

 © 2005 Wiley-VCH Verlag GmbH & Co. KGaA, Weinheim

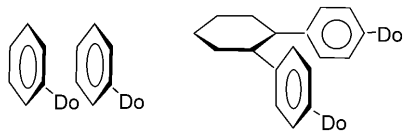
Conjugation

DOI: 10.1002/anie.200501005

Through-Space (Cofacial) π-Delocalization among Multiple Aromatic Centers: Toroidal Conjugation in Hexaphenylbenzene-like Radical Cations**

*Duoli Sun, Sergiy V. Rosokha, and Jay K. Kochi**

Strong (nonbonded) π-to-π interactions were first recognized by the appearance of characteristic near-IR absorption bands and doubled hyperfine lines in the electronic and ESR spectra of various intermolecular dimer cations formed upon electron ejection from stacked aromatic donors, as in $\mathbf{I} \rightarrow \mathbf{I}^{+\cdot} + e^-$.[1,2] Equivalent spectral changes are also observed in the corresponding intramolecular assembly derived from tethering the same aromatic dyad, as in **II** (Do = electron donating functional group).[3,4] Indeed, such a spectral (NIR, ESR) equivalence relates to the common π-electronic transition from the filled HOMO to the singly occupied LUMO that are



I **II**

[*] Dr. D. Sun, Dr. S. V. Rosokha, Prof. Dr. J. K. Kochi
Chemistry Department
University of Houston
Houston, TX 77204 (USA)
Fax: (+1) 713-743-2709
E-mail: jkochi@uh.edu

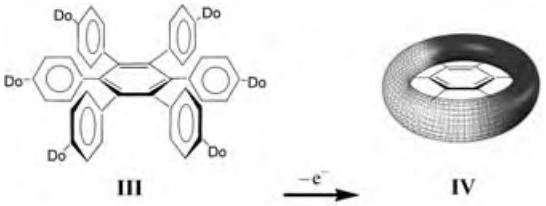
[**] We thank I. S. Neretin for computational assistance and the R. A. Welch Foundation for financial support.

Supporting information for this article (synthesis, characterization, and X-ray data for the hexaarylbenzene donors **1**–**3**, spectral (Vis-NIR) characterization of their radical cations, and Mulliken–Hush (six-state) analysis of the radical cation of **1**) is available on the WWW under http://www.angewandte.org or from the author.

© 2005 Wiley-VCH Verlag GmbH & Co. KGaA, Weinheim

more or less equally disposed in **I** and **II**. This HOMO–LUMO or charge-transfer (intervalence) transition is well accommodated by Mulliken–Hush theory to provide the important connection between the experimental NIR spectrum and the electronic coupling energy (H_{DA}) that binds such cofacial moieties.[5]

In broader context, the further applicability of Mulliken–Hush theory to extended aromatic (stacking) arrays that are inherent to molecular conductors and wires for organic materials science,[6] depends first on the stepwise extension of the dyad structure **II** to the closed-loop hexad structure **III**,[7] in which extensive π-electron delocalization would result in complete toroidal conjugation **IV** in the limit of



strong interactions among the six (Do-phenyl) centers.[8] To this end, we now report the synthesis and structural characterization of the hexadonor **1** (see the Supporting Information for structure) which is an analogue of **III** containing six electron-rich anilinyl groups with the six donor groups Do being *N*,*N*-diethylamino or *N*-methyl-*N*-ethylamino. Compound **1** has highly unusual redox properties in two important ways: First, the linear-sweep voltammogram of the hexaanilinylbenzene **1** (Figure 1 A) shows a reversible one-electron-

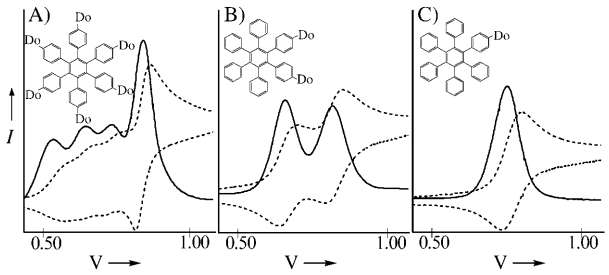


Figure 1. CV (dotted line) and Osteryoung square-wave voltammetry (OSWV; solid line) in V versus SCE of A) hexadonor **1**, B) bidonor **2**, and C) monodonor **3**.

oxidation wave at $E_{1/2} = 0.51$ V (versus saturated calomel electrode (SCE)) which is strongly (negative) shifted relative to those of the bis and monoanilinyl analogues **2** and **3** (Figure 1 B and C). Indeed, the voltammetry of **1** shows four separate anodic waves at 0.51, 0.64, 0.74, and 0.86 V; and controlled-potential coulommetry reveals each of the first three waves to correspond to reversible one-electron changes and the fourth a composite three-electron process.

The wide separation of the potentials of the redox events in **1** allow the radical cation (**1**$^{\bullet+}$) to be quantitatively prepared either by controlled-potential anodic oxidation or by chemical oxidation with dodecamethylcarboranyl (B$^{\bullet}$).[3b] In the latter case, the blue polycrystalline solid is isolated in excellent yields and quantitatively analyzed as **1**$^{\bullet+}$B$^-$.

The second unusual redox property of **1** is detected in the electronic spectrum of **1**$^{\bullet+}$, generated by either method. This spectrum shows the highly distinctive low-energy absorption (Figure 2) that stretches continuously from the visible (red)

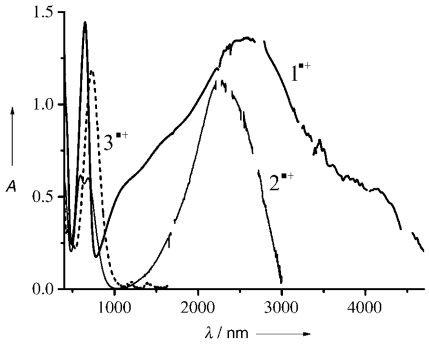
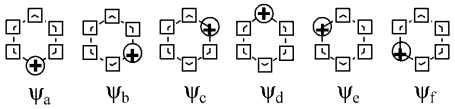


Figure 2. Electronic spectrum of hexadonor radical cation **1**$^{\bullet+}$ in comparison with its bidonor **2**$^{\bullet+}$ and monodonor **3**$^{\bullet+}$ models.

region all the way to the infrared region beyond 4000 nm (with $\lambda_{max} = 2570$ nm, $\varepsilon = 3300\ M^{-1}cm^{-1}$). By comparison, the bidonor analogue **2**$^{\bullet+}$ merely exhibits a single near-Gaussian[9] band in the NIR region with $\lambda_{max} = 2300$ nm ($\varepsilon = 2800\ M^{-1}cm^{-1}$); and the monodonor **3**$^{\bullet+}$ is completely transparent in the region beyond 1000 nm. Indeed, such characteristic low-energy optical behaviors in **1**$^{\bullet+}$ and **2**$^{\bullet+}$ are diagnostic of intervalence transitions as observed in both organic and inorganic mixed-valence systems.[3,5,10]

To account for the spectral and electrochemical properties of the radical cation **1**$^{\bullet+}$, we extend the Mulliken–Hush (two-state) model to the redox system with six equivalent (anilinyl) centers. The diabatic (non-interacting) states $\psi_a - \psi_f$ with the hole localized on different centers in the hexagonal array are presented pictorially in Scheme 1 (hole = ⊕) and the adiabatic wave functions ($\Psi_1 - \Psi_6$) of **1**$^{\bullet+}$ are given in Equation (1).

$$\Psi_i = a_i\,\psi_a + b_i\,\psi_a + c_i\,\psi_c + d_i\,\psi_d + e_i\,\psi_e + f_i\,\psi_f \qquad (1)$$



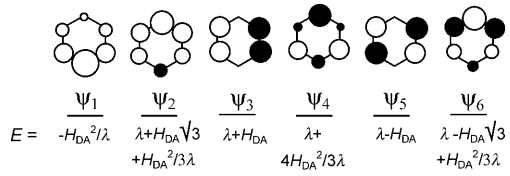
Scheme 1.

To evaluate the adiabatic states, we follow Lambert–Noll[7b] and take into account only equivalent interactions (H_{DA}) between neighboring groups (neglecting other interactions), and set the diabatic state ψ_a with relaxed nuclear geometry of all six centers as the zero point of reaction coordinate (i.e., $H_{aa} = 0$ at $X = 0$). As such, the energy of the other diabatic states at the same point on the nuclear reaction coordinate (Franck–Condon excitation) are equal to the reorganization energy λ; and the secular determinant is expressed as Equation (2).

 © 2005 Wiley-VCH Verlag GmbH & Co. KGaA, Weinheim

$$\begin{vmatrix} -E & H_{DA} & 0 & 0 & 0 & H_{DA} \\ H_{DA} & \lambda-E & H_{DA} & 0 & 0 & 0 \\ 0 & H_{DA} & \lambda-E & H_{DA} & 0 & 0 \\ 0 & 0 & H_{DA} & \lambda-E & H_{DA} & 0 \\ 0 & 0 & 0 & H_{DA} & \lambda-E & H_{DA} \\ H_{DA} & 0 & 0 & 0 & H_{DA} & \lambda-E \end{vmatrix} = 0 \quad (2)$$

The resulting energy levels of the adiabatic states (truncated to the second order) and their pictorial representations are shown in Scheme 2 (exact eigenvalues and



Scheme 2.

coefficients a_i–f_i in terms of H_{DA} and λ are given in the Supporting Information). In contrast to bidonor **2**$^{\bullet+}$ with one intervalence transition (i.e., $\nu_{IV}=\lambda$), the absorption band of **1**$^{\bullet+}$ contains five optical transitions with energies determined as differences between ground state Ψ_1 and excited states Ψ_2 to Ψ_6. The intensities of the transitions are related to the corresponding transition moments which can be expressed (according to Mulliken–Hush theory[5]) as Equation (3), in which $i=2$ to 6, and μ_a to μ_f are moments of diabatic states a to f within the arbitrarily chosen coordinate system.

$$\mu_{oi} = \int \Psi_1 \mu \Psi_i = \int (a_1\psi_a + \ldots + f_1\psi_f)\mu(a_i\psi_a + \ldots + f_i\psi_f) \approx (a_1 a_i \mu_a + \ldots + f_1 f_i \mu_f) \quad (3)$$

When the coupling element is small ($H_{DA}\approx 0$), all optical transitions ($\Psi_1 \rightarrow \Psi_i$, $i=2$–6) are essentially degenerate (i.e., $\nu_{IV}\approx\lambda$), however significant electronic coupling between the redox sites leads to broadening of the intervalence absorption and splitting into individual components with the energy difference between the highest and lowest transition given by $\nu_5-\nu_1=2H_{DA}\sqrt{3}$. Indeed, the broad intervalence NIR absorption of **1**$^{\bullet+}$ in Figure 2 (with several partially resolved components) points to a significant value of H_{DA}, and digital deconvolution into Gaussian bands (see Supporting Information Figure S2) leads to $\lambda = 5400\pm600\ cm^{-1}$ and $H_{DA}=1600\pm400\ cm^{-1}$ (see Supporting Information for details). The coefficients (a_1 to f_6) and transition moments are calculated from λ and H_{DA} (see Supporting Information Table S2), and the results in Table 1 demonstrate how the energies and intensities of the optical transitions based on the Mulliken–Hush (six-state) model agree with those obtained by deconvolution of the experimental (intervalence transfer) spectrum.

In conclusion, the compounds **1**–**3**, which are closely related to **III**, have been prepared and studied. The Mulliken–Hush (MH) quantification of λ and H_{DA} confirms for the first time the substantial stabilization allowed in the one-electron oxidized hexadonor system **III** since the resonance energy of $\Delta G_r = -2H_{DA}^2/\lambda \approx -3.5\ kcal\,mol^{-1}$ shows the extensive intra-annular (electron) delocalization in **1**$^{\bullet+}$ relative to the localized **3**$^{\bullet+}$. Furthermore, the MH treatment of the experimental spectral behavior correctly predicts the potential shift of $\Delta E_{ox}=0.21$ V (for the first anodic wave of **1** relative to **3**) which is close to the experimental value of $\Delta E_{ox}=0.23$ V when the entropy contribution is taken into account. Finally, the attractive interaction in **1**$^{\bullet+}$ with $H_{DA}=5.3\ kcal\,mol^{-1}$ is almost sufficient to offset the reorganization penalty of $\lambda/2=8.0\ kcal\,mol^{-1}$ and predicts a low barrier for hole (electron) hopping between six (contiguous) anilinyl sites (Scheme 1). Indeed, the value of $\Delta G^{\ddagger}=0.5\ kcal\,mol^{-1}$ evaluated from H_{DA} and λ[11] is at the threshold of the thermal barrier, and implies that **1**$^{\bullet+}$ has borderline Robin–Day Class II/III behavior.[9,10] As such, we hope that our search for other redox systems will reveal complete toroidal delocalization (i.e., Robin–Day Class III behavior) as in **IV**—of practical interest for the new design of molecular "motors."

Table 1: Energies[a] and relative intensities[b] of intervalence optical transitions in radical cation **1**$^{\bullet+}$.

	$\Psi_1\rightarrow\Psi_2$	$\Psi_1\rightarrow\Psi_3$	$\Psi_1\rightarrow\Psi_4$	$\Psi_1\rightarrow\Psi_5$	$\Psi_1\rightarrow\Psi_6$
Theoretical (MH)[c]	3.7(0.30)	4.8(0.50)	7.5(0.07)	8.6(0.12)	10.2(≈0)
Spectral[d]	3.7(0.25)	4.8(0.52)	7.4(0.10)	8.6(0.13)	10.1(0.01)

[a] In $10^3\ cm^{-1}$. [b] In parenthesis, normalized intensities. [c] MH = Mulliken–Hush model. Calculated according to MH with $\lambda=5500\ cm^{-1}$ and $H_{DA}=1900\ cm^{-1}$. [d] From Gaussian deconvolution of the intervalence absorption.

Experimental Section

Solvents and chemicals were prepared and handled as described earlier.[3] Hexaanilinylbenzene donors (**1**) were obtained by trimerization of bis(*N*,*N*-diethyl or methylethylanilinyl)acetylene with dicobalt octacarbonyl catalyst.[7b,12a] Bidonor (**2**) and monodonor (**3**) models were synthesized by Diels–Alder addition of tetraphenylcyclopentadienone to the appropriate anilinylacetylene and subsequent decarbonylation.[12b] Electronic spectra were measured on Varian Cary 5 spectrometer, IR spectra measured with a Nexus 470 FT-IR (Thermo Nicolet), and structural studies were carried out with Siemens SMART APEX diffractometer. Cyclic voltammetry (CV) and Osteryoung square wave voltammetry (OSWV) were performed on BAS 100A Electrochemical Analyzer, as described previously.[3] For full experimental and analytical details see the Supporting Information.

Received: March 18, 2005
Published online: July 12, 2005

Keywords: arenes · charge transfer · conjugation · Mulliken–Hush theory · radical ions

[1] a) B. Badger, B. Brocklehurst, *Nature* **1968**, *219*, 263; b) B. Badger, B. Brocklehurst, *Trans. Faraday Soc.* **1969**, *65*, 2582; B. Badger, B. Brocklehurst, *Trans. Faraday Soc.* **1970**, *66*, 2939; c) I. C. Lewis, L. S. Singer, *Chem. Phys.* **1965**, *43*, 2712; d) O. W. Howarth, G. K. Fraenkel, *J. Am. Chem. Soc.* **1966**, *88*, 4514.

[2] See also: a) C. Kröhnke, V. Enkelmann, G. Wegner, *Angew. Chem.* **1980**, *92*, 941; *Angew. Chem. Int. Ed. Engl.* **1980**, *19*, 912; b) J. D.

 © 2005 Wiley-VCH Verlag GmbH & Co. KGaA, Weinheim

Stenger-Smith, R. W. Lenz, V. Enkelmann, G. Wegner, *Makromol. Chem.* **1992**, *193*, 575; c) W. Lau, J. K. Kochi, *J. Org. Chem.* **1986**, *51*, 326; d) J. K. Kochi, R. Rathore, P. LeMagueres, *J. Org. Chem.* **2000**, *65*, 6826; Compare also: e) D. Small, V. Zaitsev, Y. Jung, S. V. Rosokha, M. Head-Gordon, J. K. Kochi, *J. Am. Chem. Soc.* **2004**, *126*, 13850.

[3] a) D. Sun, S. V. Rosokha, S. V. Lindeman, J. K Kochi, *J. Am. Chem. Soc.* **2003**, *125*, 15950; b) D. Sun, S. V. Rosokha, J. K. Kochi, *J. Am. Chem. Soc.* **2004**, *126*, 1388.

[4] a) For a few examples of multiple aromatic π-stacking with some evidence of delocalized radical cations, see b) P. LeMagueres, S. V. Lindeman, J. K. Kochi, *Org. Lett.* **2000**, *2*, 3562; c) R. Rathore, S. H. Albelwahed, I. A. Guzei, *J. Am. Chem. Soc.* **2003**, *125*, 9712.

[5] a) R. S. Mulliken, W. B. Person, *Molecular Complexes*, Wiley, New York, **1969**; b) N. S. Hush, *Prog. Inorg. Chem.* **1967**, *8*, 391; c) For recent review, see: M. D. Newton, *Electron Transfer in Chemistry*, *Vol. 1* (Ed.: V. Balzani), Wiley-VCH, New York, **2001**, p. 3.

[6] a) J. M. Williams, *Organic Superconductors: Synthesis, Structure, Properties and Theory*, Prentice Hall, Englewood Cliffs, **1992**; b) *Organic Conductors: Fundamentals and Applications* (Ed.: J.-P. Farges), Marcel Dekker, New York, **1994**; c) *Magnetism: Molecules to Materials* (Eds.: J. S. Miller, M. Drillon), Wiley-VCH, Weinheim, **2001**; d) See also: Thematic Issue Ed.: P., Batai, *Chem. Rev.* **2004**, *104*, 4887.

[7] For some previous studies of hexaarylbenzenes, see: a) C. Lambert, G. Nöll, *Angew. Chem.* **1998**, *110*, 2239; *Angew. Chem. Int. Ed.* **1998**, *37*, 2107; b) C. Lambert, G. Nöll, *Chem. Eur. J.* **2002**, *8*, 3467; c) R. E. Bauer, V. Enkelmann, U. M. Wiesler, A. J. Berresheim, K. Müllen, *Chem. Eur. J.* **2002**, *8*, 3858; d) H. P. Dijkstra, P. Steenwinkel, D. M. Grove, M. Lutz, A. L. Spek, G. van Koten, *Angew. Chem.* **1999**, *111*, 2321; *Angew. Chem. Int. Ed.* **1999**, *38*, 2186; e) K. Kobayashi, T. Shirasaka, A. Sato, E. Horn, N. Furukawa, *Angew. Chem.* **1999**, *111*, 3692; *Angew. Chem. Int. Ed.* **1999**, *38*, 3483; f) K. Kobayashi, A. Sato, S. Sakamoto, K. Yamaguchi, *J. Am. Chem. Soc.* **2003**, *125*, 3035; g) B. Traber, J. J. Wolff, F. Rominger, T. Oeser, R. Gleiter, M. Goebel, R. Wortmann, *Chem. Eur. J.* **2004**, *10*, 1227; h) X. Shen, D. M. Ho, R. A. Pascal, Jr., *J. Am. Chem. Soc.* **2004**, *126*, 5798; i) R. Rathore, C. L. Burns, M. I. Deselnicu, *Org. Lett.* **2001**, *3*, 2887; j) G. Bottari, T. Torres, *Chem. Commun.* **2004**, 2668.

[8] a) Toroidal conjugation occurring through π-faces is to be distinguished from the usual planar conjugation occurring at π-edges of aromatic moieties; b) A reviewer has kindly pointed out an earlier study[8c] of hexaiodobenzene dication as a stable σ-delocalized or (Hückel) σ-aromatic species. Such extensive conjugation is essentially circular since it occurs among six iodo atoms in a single plane. This contrasts with electron delocalization among six anilinyl faces (each involving multiple π-centers), which is thus enveloped by a toroid-shaped surface. As such, the concept of toroidal conjugation also extends to enlarged systems including perarylnaphthalenes, anthracenes, and to various other polyacenes (in general), as well as to more flexible perarylated polyacetylenes; c) D. J. Sagl, J. C. Martin, *J. Am. Chem. Soc.* **1988**, *110*, 5820.

[9] For analogous distortions of intervalence absorption bands in mixed-valence radical cations, see: a) C. Lambert, G. Nöll, *J. Am. Chem. Soc.* **1999**, *121*, 8434; b) S. F. Nelsen, *Chem. Eur. J.* **2000**, *6*, 581.

[10] a) C. Creutz, *Prog. Inorg. Chem.* **1983**, *30*, 1; b) K. D. Demadis, C. M. Hartshorn, T. J. Meyer, *Chem. Rev.* **2001**, *101*, 2655; c) T. Nishiumi, Y. Nomura, Y. Chimoto, M. Higuchi, K. Yamamoto, *J. Phys. Chem.* **2004**, *108*, 7992.

[11] a) Calculated as $\Delta G^{\neq} = (\lambda - 2H_{DA})^2/(4\lambda)$ based on two-state model.[11b] Preliminary results indicate that the six-state model predicts even lower energies; b) B. S. Brunschwig, N. Sutin, *Coord. Chem. Rev.* **1999**, 187, 233.

[12] a) K. P. C. Vollhardt, *Acc. Chem. Res.* **1977**, *10*, 1; b) N. Tugcu, S. K. Park, J. A. Moore, S. M. Cramer, *Ind. Eng. Chem. Res.* **2002**, *41*, 6482.

 © 2005 Wiley-VCH Verlag GmbH & Co. KGaA, Weinheim

Catalytic Epoxidation

DOI: 10.1002/anie.200500491

Polyoxovanadometalate-Catalyzed Selective Epoxidation of Alkenes with Hydrogen Peroxide**

*Yoshinao Nakagawa, Keigo Kamata, Miyuki Kotani, Kazuya Yamaguchi, and Noritaka Mizuno**

Vanadium is an important element in biology, inorganic chemistry, and organic syntheses,[1–8] and can heterogeneously or homogenously catalyze selective oxidation reactions of alkanes, alkenes, aromatic compounds, alcohols, halides, etc.[1–4,7–14] While homogenous oxidation catalysis by mono- and divanadium complexes has extensively been studied, the oxidation catalysis by bis(μ-hydroxo)-bridged divanadium compounds is scarcely known.[1–8,15,16] In addition, even monovanadium complexes cannot efficiently catalyze the epoxidation of alkenes by a green oxidant such as H_2O_2 because of a contribution from the radical mechanism; for example, the oxidation of cyclohexene by H_2O_2 in the presence of vanadium-based catalysts proceeds mainly at the allylic position.[9–14] Moreover, the efficiency of H_2O_2 utilization is intrinsically low.[9–14] Therefore the vanadium-catalyzed, H_2O_2-based epoxidation of alkenes with high selectivity to the epoxide and high efficiency of H_2O_2 utilization is currently not possible, although it is well known that other transition metals such as tungsten, manganese, and iron show high activity and selectivity.[17–20]

[*] Dr. Y. Nakagawa, Dr. K. Yamaguchi, Prof. Dr. N. Mizuno
Department of Applied Chemistry
School of Engineering
The University of Tokyo
7-3-1 Hongo, Bunkyo-ku, Tokyo 113-8656 (Japan)
Fax: (+81) 3-5841-7220
E-mail: tmizuno@mail.ecc.u-tokyo.ac.jp
K. Kamata, M. Kotani, Dr. K. Yamaguchi, Prof. Dr. N. Mizuno
Core Research for Evolutional Science and Technology (CREST)
Japan Science and Technology Agency (JST)
4-1-8 Honcho, Kawaguchi, Saitama 332-0012 (Japan)

[**] This work was supported by the CREST program of JST and a Grant-in-Aid for Scientific Research from the Ministry of Education, Culture, Science, Sports, and Technology of Japan.

Supporting information for this article is available on the WWW under http://www.angewandte.org or from the author.

InterScience
© 2005 Wiley-VCH Verlag GmbH & Co. KGaA, Weinheim

The catalytic function of polyoxometalates has attracted much attention because the ability to design catalytically active sites means that their redox and acidic properties can be controlled at the atomic or molecular levels.[21–28] Recently, various efficient catalytic systems for H_2O_2-based epoxidation by polyoxometalates have been developed with peroxotungstates or -molybdates as catalyst precursors or with transition-metal-substituted polyoxometalates. However, these require either an excess of H_2O_2 with respect to the alkene or an excess of alkene with respect to H_2O_2 to attain a high yield of epoxide or high efficiency of H_2O_2 utilization.[29] Herein, we report that $[\gamma\text{-}1,2\text{-}H_2SiV_2W_{10}O_{40}]^{4-}$ (**1**), which has a {VO-(μ-$OH)_2$-VO} core, can catalyze the epoxidation of alkenes in the presence of only one equivalent of H_2O_2 with a high yield of epoxide and high efficiency of H_2O_2 use. Notably, this system shows unique stereospecificity, diastereoselectivity, and regioselectivity that are quite different from those reported for the epoxidation systems based on $[\gamma\text{-}SiW_{10}O_{34}(H_2O)_2]^{4-}$.[30,31] Furthermore, we have investigated the active site of **1** and the active species for the present epoxidation on the basis of various physicochemical characterizations.

First, we examined the scope of the present epoxidation with the tetra-*n*-butylammonium salt of **1** (TBA-**1**), various kinds of alkenes, and with only one equivalent of H_2O_2 (except for gaseous alkenes; Table 1). Under the present reaction conditions, the amounts of allylic oxidation products and glycols produced by hydrolysis were negligible in all cases. The epoxidation did not proceed at all in the absence of catalyst, and no epoxidation was observed with *tert*-butylhydroperoxide (TBHP) as the oxidant. Nonactivated aliphatic terminal C_3–C_{10} alkenes, including propene, could be transformed into the corresponding epoxides with $\geq 99\,\%$ selectivity and $\geq 87\,\%$ efficiency of H_2O_2 utilization. A larger-scale reaction (50-fold scale-up) for 1-octene showed the same results as the small-scale experiments (99 % selectivity to 1,2-epoxyoctane, 93 % yield determined by GC, and 86 % yield of isolated product). The reaction rate increased with an increase in the reaction temperature, and the TOF reached as high as 38 h^{-1} at 313 K whilst maintaining the selectivity for 1,2-epoxyoctane as high as $> 99\,\%$, although the efficiency of H_2O_2 utilization decreased slightly from 93 % (293 K) to 85 % (313 K). Acid-sensitive styrene was epoxidized to give styrene oxide as the sole product. Also, the catalytic epoxidation of cyclic alkenes such as cyclohexene and cyclooctene proceeded efficiently to afford the corresponding epoxides in high yields.

Table 1: Epoxidation of various monoalkenes catalyzed by TBA-**1**.[a]

Substrate	Product	Yield [%]	Selectivity [%]	E_{ox} [%][b]
[c]		87	99	87
[d]		91	99	91
		92	99	92
		93	99	93
		90	99 (only *cis*)	90
		88	98	90
		93	99	93
		88	99	88
		90	99	92
		93	99	93
		91	97 (*syn*/*anti* = 5/95)	91
OH	OH	87	95 (*syn*/*anti* = 12/88)	91

[a] Reaction conditions: alkene (33.3 mM), TBA-**1** (1.67 mM), H_2O_2 (30 % aq., 33.3 mM), and CH_3CN/*t*BuOH (1.5/1.5 mL) at 293 K for 24 h. Yields and selectivities were determined by gas chromatography or ^{1}H NMR spectroscopy using an internal standard technique and are based on alkenes. [b] E_{ox}(H_2O_2 efficiency) = [products (mol)/consumed H_2O_2-(mol)] × 100. [c] Propene pressure 6 atm. [d] 1-Butene pressure 3 atm.

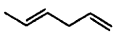
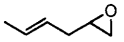
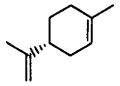
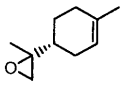
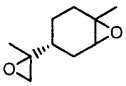
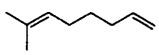
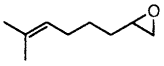
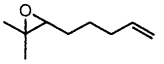
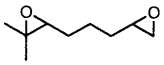
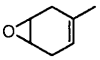
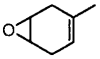
The epoxidation of *cis*- and *trans*-2-octene gave *cis*-2,3-epoxyoctane (90 % yield; Table 1) and *trans*-2,3-epoxyoctane (6 % yield), respectively; the configuration around the C=C moieties is retained in these epoxides. Moreover, for the competitive epoxidation of *cis*- and *trans*-2-octenes (100 μmol each, the other conditions were the same as in Table 1), the initial rates for the epoxidation were 0.32 and 0.001 mM min^{-1}, respectively. The ratio of the formation rate of *cis*-2,3-epoxyoctane to that of the *trans* isomer is more than 3×10^2, which is much larger than the ratios (1.3–11.5) reported for other stereospecific epoxidation systems (see Supporting Information). For competitive epoxidation of *cis*- and *trans*-2-octenes, the yields of *cis*-2,3-epoxyoctane and the *trans* isomer (based on H_2O_2), even after 24 h, were 91 and 2 %, respectively. The epoxidation of 3-substituted cyclohexenes, such as 3-methyl-1-cyclohexene and 2-cyclohexen-1-ol, showed an unusual diastereoselectivity: the corresponding epoxides are formed highly diastereoselectively with the oxirane ring *trans* to the substituents (*anti* configuration; Table 1 and Tables S2 and S3 in the Supporting Information).

Further, the more accessible, but less nucleophilic double bonds in nonconjugated dienes such as *trans*-1,4-hexadiene, (*R*)-(+)-limonene, 7-methyl-1,6-octadiene, and 1-methyl-1,4-cyclohexadiene were epoxidized in high yields in a highly regioselective manner, as shown in Table 2. The values of [less-substituted epoxide]/[total epoxides] (≥ 0.88) are much higher than those reported for the other epoxidation systems (Tables S4–S7 in the Supporting Information). As far as we know, such unique stereospecificity, diastereoselectivity, and regioselectivity have never been reported for **1**.

The relative reactivity (rate) of a series of C_8 alkenes decreased in the order of 2-methyl-1-heptene (1.1) > 1-octene (1.0 taken as unity) > *cis*-2-octene (0.87) > 2-methyl-2-heptene (0.03) > *trans*-2-octene (< 0.01) (see Table S8 in the Supporting Information). This order is not consistent with that of the π(C=C) HOMO energies of C_8 alkenes because they decrease with an increase in the number of alkyl substituents in alkenes, as reported previously.[30] Therefore, the inconsistency between the ordering of the π(C=C)

 © 2005 Wiley-VCH Verlag GmbH & Co. KGaA, Weinheim

Table 2: Epoxidation of various nonconjugated dienes catalyzed by TBA-**1**.[a]

Substrate	Product	Yield [%]	[less-substituted epoxide]/[total epoxides]	E_{ox} [%][b]
		91	> 0.99	91
		89	0.99	91
		1		
		77	0.93	87
		5		
		4		
		71	0.88	81
		5		

[a], [b] See footnotes to Table 1.

HOMO energies and the reactivities should be caused by the steric constraints of the active site of **1**, that is, an active oxygen species formed by the reaction of **1** with H_2O_2 is embedded in the polyoxometalate framework and thus a sterically hindered C=C double bond cannot easily approach the site.

The mono- and trivanadium-substituted compounds [α-$SiVW_{11}O_{40}]^{5-}$ and [α-1,2,3-$SiV_3W_9O_{40}]^{7-}$ are inactive for the epoxidation under the present conditions, which suggests that the V–O–W and V=O centers are not the active sites. The fully occupied silicotungstate [γ-$SiW_{12}O_{40}]^{4-}$, which has the same structure as **1**, is also inactive, which suggests that the tungsten atoms in **1** are not the active sites. The regioselectivity of the catalytic epoxidation of nonconjugated dienes by **1** is quite different from that by [γ-$SiW_{10}O_{34}(H_2O)_2]^{4-}$ (Tables S4–S7 in the Supporting Information), which shows that the catalytically active site (species) of **1** is different from that of [γ-$SiW_{10}O_{34}(H_2O)_2]^{4-}$.

In addition, we confirmed by in situ IR and NMR measurements that tungstate compounds such as [γ-$SiW_{10}O_{34}(H_2O)_2]^{4-}$ and $[W_2O_3(O_2)_4(H_2O)_2]^{2-}$ are not formed during the catalysis. The ^{51}V NMR spectrum of the recovered catalyst in CD_3CN shows a line at $\delta = -564$ ppm ($\Delta\nu_{1/2} = 125$ Hz) and the ^{183}W NMR spectrum in CD_3CN shows three lines at $\delta = -84$ ($\Delta\nu_{1/2} = 9.9$ Hz), -97 ($\Delta\nu_{1/2} = 2.3$ Hz), and -131 ppm ($\Delta\nu_{1/2} = 1.6$ Hz) with an integrated intensity ratio of 2:1:2, in agreement with the γ-Keggin framework. Signals due to tungstate compounds such as [α-$SiW_{12}O_{40}]^{4-}$, [γ-$SiW_{10}O_{34}(H_2O)_2]^{4-}$, $[W_2O_3(O_2)_4(H_2O)_2]^{2-}$, and $[H_nWO_2(O_2)_2]^{(2-n)-}$ were not observed. The IR and UV/Vis spectra of the catalyst recovered after the completion of the epoxidation were the same as those of the fresh one, which also suggests the maintenance of the γ-Keggin framework of **1**.

All these facts strongly indicate that the {VO-(μ-$OH)_2$-VO} core is preserved in the cluster framework of **1** during the catalytic process and that tungstate compounds are not the true catalytically active species in the present epoxidation. The fact that the regioselectivities for nonconjugated dienes with **1** are different from those with [γ-$SiW_{10}O_{34}(H_2O)_2]^{4-}$ and $[W_2O_3(O_2)_4(H_2O)_2]^{2-}$ also support this idea.

Next, the reactivity of **1** with H_2O_2 was investigated. The cold-spray ionization mass spectrum (CSI-MS) of TBA-**1** in 1,2-$C_2H_4Cl_2$ shows the most intense parent-ion peak (centered at m/z 3337.9) with an isotopic distribution (Figure 1a and Supporting Information) that agrees with the pattern calculated for $[(TBA)_3H_2SiV_2W_{10}O_{40}]^-$ (Figure 1b and Supporting Information). Upon the addition of 350 equiv of H_2O_2, a new peak centered at m/z (3337.9 + 16) appeared (Figure 1c) which agrees with the pattern calculated for $[(TBA)_3HSiV_2W_{10}O_{39}(OOH)]^-$ (Figure 1d).

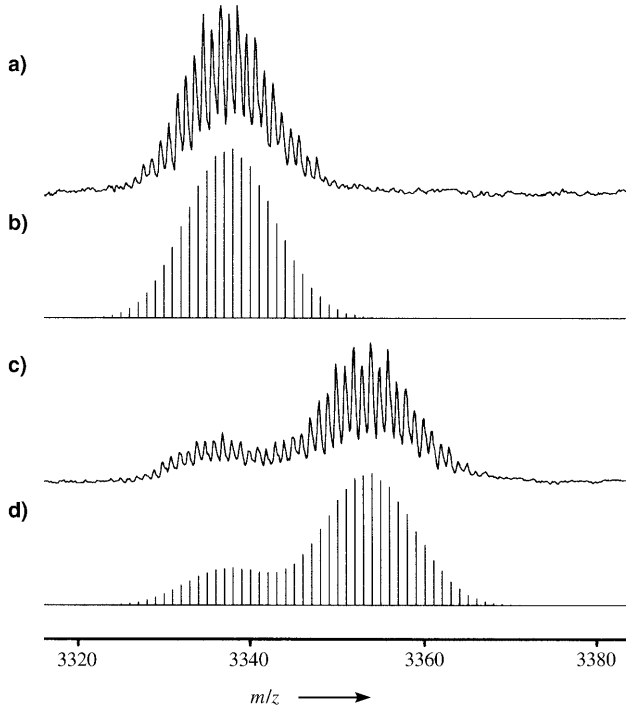


Figure 1. CSI-MS (anion mode, m/z 3300–3400) of a) TBA-**1** (0.14 mM) in 1,2-$C_2H_4Cl_2$ and c) TBA-**1** (0.14 mM) in 1,2-$C_2H_4Cl_2$ treated with 350 equiv of H_2O_2 (96% aqueous solution) with respect to TBA-**1** (253 K, 2 h). The lines in (b) are the pattern calculated for $[(TBA)_3H_2SiV_2W_{10}O_{40}]^-$ and the lines in (d) are the pattern calculated for a mixture of $[(TBA)_3H_2SiV_2W_{10}O_{40}]^-$ (22%) and $[(TBA)_3HSiV_2W_{10}O_{39}(OOH)]^-$ (78%). The small increase in the content of $[(TBA)_3H_2SiV_2W_{10}O_{40}]^-$ in comparison with those of Figures 2–4 is probably caused by a slight increase in the temperature at the inlet of the injection port of the spectrometer.

The ^{1}H NMR spectrum of **1** (2.5 mM) in 1,2-$C_2D_4Cl_2$ at 253 K shows a signal at $\delta = 4.80$ ppm due to the hydroxy proton of the {VO-(μ-$OH)_2$-VO} core in **1**. Upon the addition of 20 equiv of H_2O_2, two signals appear at $\delta = 5.10$ and

 © 2005 Wiley-VCH Verlag GmbH & Co. KGaA, Weinheim

9.45 ppm with an intensity ratio of 1:1, and the intensity of the signal at $\delta = 4.80$ ppm has greatly decreased (by $(93 \pm 1)\%$) after 2 h, although the sum of the three signal intensities remains almost constant (Figure 2). A similar lower-field shift

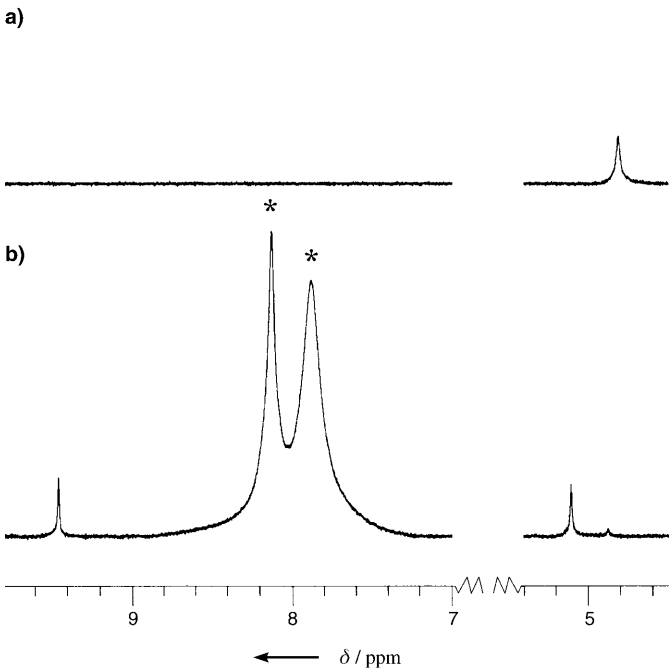


Figure 2. ^{1}H NMR spectra of a) TBA-**1** (2.5 mM) in 1,2-$C_2D_4Cl_2$ and b) TBA-**1** (2.5 mM) in 1,2-$C_2D_4Cl_2$ treated with 20 equiv of H_2O_2 (95% aqueous solution) with respect to TBA-**1** at 253 K for 2 h. The asterisks indicate the signals of H_2O_2 in the organic and aqueous phases.

of the hydroxy proton signal from $\delta = 5.10$ to $\delta = 5.18$ ppm has been observed upon the formation of $[\gamma\text{-}1,2\text{-}SiV_2W_{10}O_{38}(\mu\text{-}OH)(\mu\text{-}OCH_3)]^{4-}$ in CD_3CN.[32] The chemical shift of $\delta = 9.45$ ppm is close to those of other hydroperoxide species such as H_2O_2 ($\delta = 8.74$ ppm), *t*BuOOH ($\delta = 8.84$ ppm), and $PhC(CH_3)_2OOH$ ($\delta = 8.95$ ppm).

One new ^{51}V NMR signal appears at $\delta = -530$ ppm in 1,2-$C_2D_4Cl_2$ upon the addition of H_2O_2, and the intensity of the signal of **1** at $\delta = -562$ ppm has greatly decreased (by $(93 \pm 1)\%$) after 2 h, although, again, the sum of the two signal intensities remains almost constant (Figure 3). Six new ^{183}W NMR signals appear at $\delta = -79$, -83, -92, -104, -127, and -132 ppm with an intensity ratio of 2:2:1:1:2:2, in 1,2-$C_2D_4Cl_2$ upon the addition of 15 equiv of H_2O_2, and the signals at $\delta = -81$, -95, and -128 ppm due to **1** have almost completely disappeared after 2 h, although the sum of the nine signal intensities remains almost constant (Figure 4). A quantitative analysis of the ^{1}H, ^{51}V, and ^{183}W NMR data gives an atomic ratio of H(δ=5.10 ppm):H(9.45):V(-530):W(-79):W(-83):W(-92):W(-104):W(-127):W(-132) of 1:1:2:2:2:1:1:2:2.

The ^{183}W NMR spectral pattern depends on the structure and symmetry of the anion. The anion **1** has C_{2v} symmetry and shows three signals with intensities of 2:1:2. The reaction of **1** with H_2O_2 lowers or does not change the symmetry of the anion, and there are five possibilities for the symmetry of the resulting compound: 1) C_2, 2) C_s with a symmetry plane containing two vanadium atoms, 3) C_s with a symmetry plane

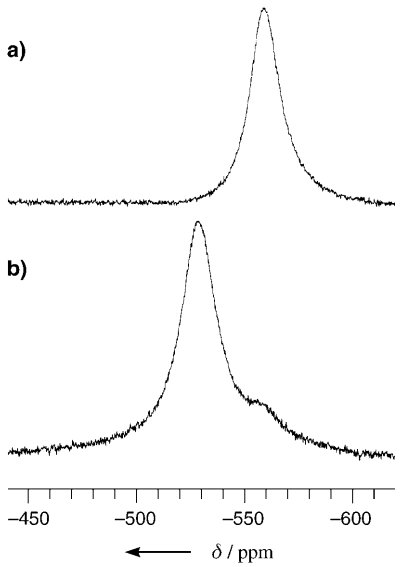


Figure 3. ^{51}V NMR spectra of the same samples as for Figure 2.

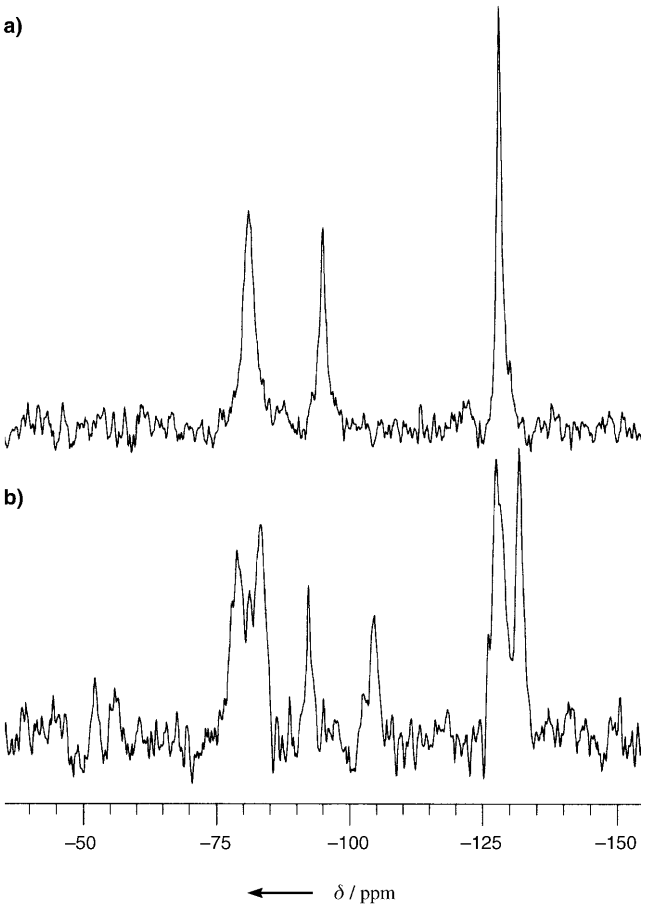


Figure 4. ^{183}W NMR spectra of a) TDA-**1** (0.1 M) in 1,2-$C_2D_4Cl_2$ and (b) TDA-**1** (0.1 M) in 1,2-$C_2D_4Cl_2$ treated with 15 equiv of H_2O_2 (95% aqueous solution) with respect to TDA-**1** at 253 K for 2 h. TDA = *n*-decylammonium.

 © 2005 Wiley-VCH Verlag GmbH & Co. KGaA, Weinheim

containing two V–O–V bridging oxygen atoms, 4) C_1, and 5) C_{2v}. After the treatment of **1** with H_2O_2, six ^{183}W NMR signals are observed with an intensity ratio of 2:2:1:1:2:2; only case (3) can explain the observed ^{183}W NMR spectrum.[33] The ^1H NMR spectrum shows two signals at $\delta = 5.14$ (1H) and 9.45 ppm (1H). These two protons must exist in the symmetry plane, which favors the C_s symmetry. The ^{51}V NMR spectrum shows one signal. Therefore, the NMR data indicate the formation of a {VO-(μ-OH)(μ-OOH)-VO} species.

The chemical shifts of the ^{51}V and ^{183}W NMR signals are also in agreement with this idea: the oxo→peroxo transformation for complexes of ^{51}V, ^{95}Mo, and ^{183}W leads to significant upfield shifts in the NMR signals (see Table S11 in the Supporting Information). On the other hand, the oxo→hydroperoxo transformation from $H_xMoO_2(O_2)_2^{(2-x)-}$ ($0 \le x \le 1$) to $[MoO(O_2)_2OOH]_2^{2-}$ produces a 15–30 ppm downfield shift in the ^{95}Mo signals;[34] no ^{51}V NMR data have been reported for the oxo→hydroperoxo transformation as far as we know. In the present case, a downfield shift of 32 ppm is observed for the ^{51}V NMR signal after the treatment of **1** with H_2O_2. Such a downfield shift is in accordance with the oxo→hydroperoxo transformation. These NMR and CSI-MS data strongly suggest that the {VO-(μ-OH)$_2$-VO} core in **1** reacts with H_2O_2 to form a {VO-(μ-OH)(μ-OOH)-VO} species.

The methanol monoester of **1** (**2**) was easily formed by the dehydrative condensation between the hydroxy group in **1** and methanol (equilibrium constant 75).[32] No diester was formed even in the presence of an excess of methanol. The anionic cluster **2** retains the γ-Keggin structure with the two vanadium atoms bridged by one protonated oxygen atom and one methoxy group.[32] Therefore, the dehydrative condensation between **1** and H_2O_2 to form the hydroperoxo complex should proceed as reported for bis(μ-hydroxo) complexes of the first row transition metals.[35] When one proton in the {VO-(μ-OH)$_2$-VO} site in **1** was removed by titration with 1 equivalent of nBu_4NOH with respect to **1**, neither esterification of **1** with methanol nor its epoxidation with H_2O_2 proceeded. All these results indicate that the {VO-(μ-OH)$_2$-VO} core in **1** is the active site that forms {VO-(μ-OH)(μ-OOH)-VO} species for the epoxidation of olefins with H_2O_2, according to Equation (1) with R = OH, CH_3.

$$[\gamma\text{-}1,2\text{-}H_2SiV_2W_{10}O_{40}]^{4-} + ROH \rightarrow [\gamma\text{-}1,2\text{-}SiV_2W_{10}O_{38}(\mu\text{-}OH)(\mu\text{-}OR)]^{4-} + H_2O \quad (1)$$

As has been reported previously,[32] the esterification of the {VO-(μ-OH)$_2$-VO} core in **1** with alcohols is sterically controlled: the esters of primary alcohols with a bulky substituent, such as neopentyl alcohol, or of secondary and tertiary alcohols are hardly formed (equilibrium constant < 0.02) because of the steric repulsion from the polyoxometalate framework. For the same reason, no reaction of **1** with TBHP occurs. Thus, the hydroperoxo group in the possible intermediate $[\gamma\text{-}1,2\text{-}SiV_2W_{10}O_{38}(\mu\text{-}OH)(\mu\text{-}OOH)]^{4-}$ may also be sterically hindered, which could explain the unique stereospecificity, diastereoselectivity, and regioselectivity in the epoxidation catalysis (Figure S3 in the Supporting Information).

Experimental Section

An aqueous solution of $[\gamma\text{-}1,2\text{-}H_2SiV_2W_{10}O_{40}]^{4-}$ was prepared according to reference [36], and the anion was isolated as the tetra-*n*-butylammonium salt (TBA-**1**): $K_8[\gamma\text{-}SiW_{10}O_{36}]\cdot 12H_2O$[37] (8 g, 2.7 mmol) was quickly dissolved in 1M HCl (28 mL), $NaVO_3$ (0.5M, 11 mL, 5.5 mmol) was added, and the mixture was gently stirred for 5 min. The solution was filtered and $[(n\text{-}C_4H_9)_4N]Br$ (8 g, 25 mmol) added in a single step. The resulting yellow precipitate was collected by filtration and then washed with a large amount of water (300 mL). The crude product was purified twice by precipitation (addition of 1 L of H_2O to an acetonitrile solution of TBA-**1** (50 mL)). Analytically pure TBA-**1** was obtained as a pale-yellow powder. Yield: 7.43 g (76%). Anal. calcd. for $[(C_4H_9)_4N]_4[\gamma\text{-}1,2\text{-}H_2SiV_2W_{10}O_{40}]\cdot H_2O$: C 21.4, H 4.15, N 1.56, Si 0.78, V 2.83, W 51.1, H_2O 0.50; found: C 21.4, H 3.91, N 1.59, Si 0.79, V 2.88, W 51.2, H_2O 0.50. ^{51}V NMR (CD_3CN): An intense signal at $\delta = -563.6$ ppm ($\Delta\nu_{1/2} = 133$ Hz) attributed to two equivalent vanadium atoms is observed. ^{183}W NMR (CD_3CN): $\delta = -82.2$ ($\Delta\nu_{1/2} = 9.6$ Hz), -95.6 ($\Delta\nu_{1/2} = 2.5$ Hz), and -129.7 ppm ($\Delta\nu_{1/2} = 2.9$ Hz) with an integrated intensity ratio of 2:1:2. ^{29}Si NMR (CD_3CN): $\delta = -84.0$ ppm ($\Delta\nu_{1/2} = 2.0$ Hz). The UV/Vis spectrum (in CH_3CN) shows shoulder bands at 240 ($\varepsilon = 36000\ M^{-1}cm^{-1}$), 285 (24000), and 350 nm (5900), characteristic of the γ-Keggin structure.[38,39] IR (KBr): $\tilde{\nu} = 1151, 1106, 1057, 1004, 995, 966, 915, 904, 875, 840, 790, 691, 550, 519, 482, 457, 405\ cm^{-1}$.

The epoxidation of gaseous substrates (propene and 1-butene) was carried out in a Teflon-coated autoclave; a glass-tube reactor was used for the other substrates. The epoxidation was carried out as follows: catalyst (1.67 mM), CH_3CN/*t*BuOH (1.5/1.5 mL), H_2O_2 (30% aq., 33.3 mM), and substrate (propene, 6 atm; 1-butene, 1 atm; others, 33.3 mM) were charged in the reaction vessel. The reaction was carried out at (293 ± 0.2) K. The reaction solution was sampled periodically and analyzed by GC in combination with mass spectrometry. The products were identified by comparing their mass and NMR spectra with those of authentic samples. The carbon balance in each experiment was in the range of 95–100%. The amount of H_2O_2 remaining after the reaction was analyzed by Ce^{4+}/Ce^{3+} titration.[40] After the reaction, the catalyst was recovered by evaporating the reaction mixture to dryness, followed by washing with *t*BuOH and *n*-hexane. TOF values were estimated from the initial rates below 10% conversion of H_2O_2.

Received: February 9, 2005
Revised: May 24, 2005
Published online: July 11, 2005

Keywords: alkenes · epoxidation · hydrogen peroxide · polyoxometalates · vanadium

[1] T. Hirao, *Coord. Chem. Rev.* **2003**, *237*, 1.
[2] T. Hirao, *Chem. Rev.* **1997**, *97*, 2707.
[3] A. E. Shilov, G. B. Shul'pin, *Chem. Rev.* **1997**, *97*, 2879.
[4] Thematic issue on vanadium-based catalysts for the selective oxidation of hydrocarbons and their derivatives: *Appl. Catal. A* **1997**, *157*, 1–425.
[5] H. Sigel, A. Sigel, *Vanadium and Its Role in Life*, Marcel Dekker, New York, **1995**.
[6] F. Jiang, O. P. Anderson, S. M. Miller, J. Chen, M. Mahroof-Tahir, D. C. Crans, *Inorg. Chem.* **1998**, *37*, 5439.
[7] A. Butler, M. J. Clague, G. E. Meister, *Chem. Rev.* **1994**, *94*, 625.
[8] A. G. J. Ligtenbarg, R. Hage, B. L. Feringa, *Coord. Chem. Rev.* **2003**, *237*, 89.
[9] U. Schuchardt, M. C. Guerreiro, G. B. Shul'pin, *Russ. Chem. Bull.* **1998**, *107*, 247.
[10] O. Bortolini, F. Di Furia, P. Scrimin, G. Modena, *J. Mol. Catal.* **1980**, *7*, 59.

 © 2005 Wiley-VCH Verlag GmbH & Co. KGaA, Weinheim

[11] E. J. Eisenbraun, A. R. Bader, J. W. Polacheck, E. Reif, *J. Org. Chem.* **1963**, *28*, 2057.
[12] R. Neumann, M. Levin-Elad, *Appl. Catal. A* **1995**, *122*, 85.
[13] D. Wei, W. Chuei, G. L. Haller, *Catal. Today* **1999**, *51*, 501.
[14] G. Bellussi, M. S. Rigutto, *Stud. Surf. Sci. Catal.* **1994**, *85*, 177.
[15] A. M. Khenkin, L. Weiner, Y. Wang, R. Neumann, *J. Am. Chem. Soc.* **2001**, *123*, 8531.
[16] R. D. Gall, M. Faraj, C. L. Hill, *Inorg. Chem.* **1994**, *33*, 5015.
[17] B. S. Lane, K. Burgess, *Chem. Rev.* **2003**, *103*, 2457.
[18] G. Grigoropoulou, J. H. Clark, J. A. Elings, *Green Chem.* **2003**, *5*, 1.
[19] R. Noyori, M. Aoki, K. Sato, *Chem. Commun.* **2003**, 1977.
[20] I. W. C. E. Arends, R. A. Sheldon, *Top. Catal.* **2002**, *19*, 133.
[21] M. T. Pope in *Comprehensive Coordination Chemistry II*, *Vol. 4* (Eds.: J. A. McCleverty, T. J. Meyer), Elsevier, Amsterdam, **2003**, p. 635–678.
[22] C. L. Hill in *Comprehensive Coordination Chemistry II*, *Vol. 4* (Eds.: J. A. McCleverty, T. J. Meyer), Elsevier, Amsterdam, **2003**, p. 679–759.
[23] I. V. Kozhevnikov, *Catalysis by Polyoxometalates*, Wiley, Chichester, UK, **2002**.
[24] I. V. Kozhevnikov, *Chem. Rev.* **1998**, *98*, 171.
[25] N. Mizuno, M. Misono, *Chem. Rev.* **1998**, *98*, 199.
[26] R. Neumann, *Prog. Inorg. Chem.* **1998**, *47*, 317.
[27] T. Okuhara, N. Mizuno, M. Misono, *Adv. Catal.* **1996**, *41*, 113.
[28] C. L. Hill, C. M. Prosser-McCartha, *Coord. Chem. Rev.* **1995**, *143*, 407.
[29] See Table S10 in the Supporting Information.
[30] K. Kamata, Y. Nakagawa, K. Yamaguchi, N. Mizuno, *J. Catal.* **2004**, *224*, 224.
[31] K. Kamata, K. Yonehara, Y. Sumida, K. Yamaguchi, S. Hikichi, N. Mizuno, *Science* **2003**, *300*, 964.
[32] Y. Nakagawa, K. Uehara, N. Mizuno, *Inorg. Chem.* **2005**, *44*, 14.
[33] In the cases (1), (2), (4), and (5), the ^{183}W NMR spectra should show five lines (intensity ratio 1:1:1:1:1), five lines (1:1:1:1:1), ten lines (1:1:1:1:1:1:1:1:1:1), and three lines (2:2:1), respectively.
[34] V. Nardello, J. Marko, G. Vermeersch, J. M. Aubry, *Inorg. Chem.* **1995**, *34*, 4950.
[35] M. Akita, S. Hikichi, *Bull. Chem. Soc. Jpn.* **2002**, *75*, 1657.
[36] J. Canny, R. Thouvenot, A. Tézé, G. Hervé, M. Leparulo-Loftus, M. T. Pope, *Inorg. Chem.* **1991**, *30*, 976.
[37] A. Tézé, G. Hervé, *Inorg. Synth.* **1990**, *27*, 85.
[38] A. Tézé, J. Canny, L. Gurdan, R. Thouvenot, G. Hervé, *Inorg. Chem.* **1996**, *25*, 1001.
[39] N. Mizuno, C. Nozaki, I. Kiyoto, M. Misono, *J. Am. Chem. Soc.* **1998**, *120*, 9267.
[40] A. I. Vogel, *A Textbook of Quantitative Inorganic Analysis Including Elementary Instrumental Analysis*, Longman, New York, **1978**.

 © 2005 Wiley-VCH Verlag GmbH & Co. KGaA, Weinheim

DOI: 10.1002/anie.200501209

Mapping Protein–Protein Interfaces on the Basis of Proton Density Difference**

*Xiaogang Sui, Yingqi Xu, Janel L. Giovannelli, Nancy T. Ho, Chien Ho, and Daiwen Yang**

A protein normally functions through interacting with its partners. In order to understand the molecular basis for biochemical and biological processes, it is important to identify the contact surfaces of interacting molecules or even to characterize the structures of protein complexes. Since it is much easier and faster to define interacting surfaces by NMR spectroscopy than to determine the full structures, a number of methods have been developed to map protein interactions.[1] The traditional approach based on chemical-shift perturbation is easy to do,[2] but its precision is low. In cases where the entire protein changes conformation, this approach fails as a mapping device but can indicate the presence of allosteric processes.[3] It cannot be applied to map the intersubunit interface of oligomeric proteins in which the monomeric form is unstable. There exist methods based on the paramagnetic line-broadening effect with the use of site-specific spin labeling[4] or paramagnetic ions,[5] but they are applicable only to systems in which spin labeling is available or conformation change upon forming a complex does not increase relaxation protection from paramagnetic ions.

Amide-proton exchange has also been used to map protein interfaces,[6] but it is not a reliable tool because the change of exchange rates depends on local and global structural changes upon the formation of the complexes. Intermolecular NOESY analysis can be used to map the interactions, but it is difficult to completely suppress intra-moleuclar NOEs.[7] A more sophisticated method based on saturation transfer from an acceptor to a reporting protein, called cross-saturation,[8] has been proposed. It provides more reliable information about the binding interface, but highly

[*] X. G. Sui, Dr. Y. Q. Xu, Prof. D. W. Yang
Department of Biological Sciences
Department of Chemistry
National University of Singapore
14 Science Drive 4, Singapore 117543 (Singapore)
Fax: (+65) 6779-2486
E-mail: dbsydw@nus.edu.sg
J. L. Giovannelli, N. T. Ho, Prof. C. Ho
Department of Biological Sciences
Carnegie Mellon University
Pittsburgh, PA 15213 (USA)

[**] This research was supported by a Young Investigator Award from the Biomedical Research Council (BMRC) and the Agency for Science, Technology and Research A*Star of Singapore to D.W.Y. and by a grant from the National Institutes of Health (R01HL-24525) to C.H.

Supporting information for this article is available on the WWW under http://www.angewandte.org or from the author.

 © 2005 Wiley-VCH Verlag GmbH & Co. KGaA, Weinheim InterScience

deuterated ^{15}N-labeled protein is required for the suppression of spin diffusion in the reporting protein. Incomplete deuteration of the reporting protein may result in the identification of false interaction sites. In addition, to reduce spin diffusion among amide protons, especially for α-helical proteins, it is necessary to do experiments in a solvent mixture of $H_2O/^2H_2O$ with $<30\%$ H_2O. This is equivalent to lowering the effective sample concentration by a factor of about three or more. Thus, this technique may not work for proteins with moderate solubility or that are difficult to obtain fully deuterated.

Herein, we propose a novel strategy to map amino acid residues involved in protein–protein interactions at interfaces on the basis of the dependence of NMR relaxation on proton density, by using two moderately deuterated samples in which the reporting protein in a protein–protein complex is ^{2}H,^{15}N-labeled while the acceptor protein is either unlabeled or ^{2}H-labeled. Figure 1 shows the pulse scheme used to measure

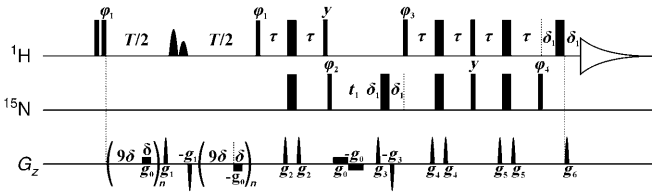


Figure 1. Pulse scheme used; all narrow (wide) bars represent 90° (180°) rectangular pulses. The first shaped 180° pulse (1 ms, REBURP, centered at 9.1 ppm) selectively inverts the signals of amide protons, the second shaped 180° pulse (2 ms, rectangle) that of H_2O (G_z represents pulsed field z gradients). The delays used are: $\tau = 2.3$ ms, $\delta = 0.5$ ms, and $\delta_1 = 1.1$ ms. Radiation damping during the relaxation delay T is suppressed by gradient g_0. The phase cycling employed is: $\varphi_1 = x,x,-x,-x$; $\varphi_2 = x,-x$; $\varphi_3 = y$; $\varphi_4 = x$; rec $= x,-x$. The durations and strengths of the sine-shaped gradients are: $g_1 = 2$ ms, 20 G cm^{-1}; $g_2 = 1$ ms, 17.5 G cm^{-1}; $g_3 = 1$ ms, 40 G cm^{-1}; $g_4 = 1$ ms, 22.5 G cm^{-1}; $g_5 = 1$ ms, 35 G cm^{-1}; and $g_6 = 1$ ms, 8 G cm^{-1}. The strength of g_0 is 1.5 G cm^{-1}. Quadrature detection in F_1 uses the enhanced sensitivity pulse gradient method, where for each t_1 separate data sets are recorded for (g_6, φ_3, φ_4) and ($-g_6$, φ_3+180°, φ_4+180.

selective longitudinal relaxation rates of amide protons in a deuterated reporting protein A, which binds to its acceptor protein B. The effect of phase alternation of φ_1 is to alternately store magnetization along the $-Z$ axis and the $+Z$ axis at the very beginning of the relaxation period so that the longitudinal magnetization relaxes as $\exp(-RT)$.[9] In this way, the measurement of relaxation rates will be independent of the interscan delay. Suppression of cross-relaxation between amide and aliphatic protons is achieved by selective inversion of only amide and aromatic protons, while reduction of amide magnetization loss due to exchange with H_2O is achieved by maintaining the proton magnetization of the amide and H_2O along the same direction during the entire relaxation period. A single scan TROSY scheme[10] is used to obtain TROSY-HSQC data.

The initial relaxation rate of an amide proton ($R^1(H_Z^N)$) under selective inversion is dominated by dipolar interactions with its surrounding aliphatic protons and it can be approximated as shown in Equation (1), where τ_c is the molecular

$$R^1(H_Z^N) \approx 0.1\,\tau_c \left(\frac{\mu_0 \hbar \gamma_H^2}{4\pi}\right)^2 \left\{ \sum_{j=1}^{m} \frac{S_j^2}{r_{HHAj}^6} + \sum_{k=1}^{n} \frac{S_k^2}{r_{HHBk}^6} \right\} + R_{ex} \qquad (1)$$

tumbling time; μ_0 is the permeability in vacuum; $\hbar = h/2\pi$ and h is Planck's constant; γ_H is the proton gyromagnetic ratio; r_{HHAj} is the distance between the amide proton and the jth residual aliphatic proton in protein A; r_{HHBk} is the distance between the amide proton and the kth residual aliphatic proton in protein B; S_j^2 and S_k^2 are the order parameters describing the motional amplitude of an H–H$_j$ and an H–H$_k$ vector, respectively; m and n are the total numbers of the respective aliphatic protons in proteins A and B interacting with the amide proton; and R_{ex} is the relaxation contribution from the unsuppressed NH–H_2O exchange effect, which is minimized by preventing radiation damping and keeping H_Z^N and H_2O magnetization parallel.

If protein A is perdeuterated (that is, $m = 0$), amide protons located at the binding interface have larger R^1 values than other amide protons since they are much closer to the protons in protein B. In principle, amino acid residues in the interacting region can be identified based on R^1 values by using a single sample consisting of a perdeuterated reporting protein and an unlabeled acceptor. However, incomplete deuteration in aliphatic protons and the unsuppressed NH–H_2O exchange effect (R_{ex}) can lead to the incorrect identification of interacting sites. In order to overcome this drawback, we propose herein the use of two samples in $H_2O/^2H_2O$ (95:5) solution: 1) ^{15}N,^{2}H-labeled protein A complexed with unlabeled protein B and 2) ^{15}N,^{2}H-labeled protein A complexed with ^{2}H-labeled protein B. The difference of R^1 values for a given amide proton in the two samples [Eq. (2), in which n_1 and n_2 are the numbers of aliphatic

$$\Delta R^1 \propto \sum_{k=1}^{n_1} S_k^2 r_{HHBk}^{-6} - \sum_{j=1}^{n_2} S_j^2 r_{HHBj}^{-6} \qquad (2)$$

protons in protein B in samples 1 and 2, respectively] is mainly determined by the location of the amide (that is, r_{HHBk}) but is independent of the deuteration percentage of protein A (m) and the R_{ex} value. Although incomplete deuteration of protein B in the second sample affects the amplitude of ΔR^1, it cannot result in false binding sites. With the assumption that $S^2 = 1$ and of perdeuteration of protein B in sample 2 (that is, $n_2 = 0$), the ΔR^1 value can be used to estimate an upper limit of the effective distance between an amide proton in protein A and its proximal protons in protein B (r_{eff}) [Eq. (3)]. Even in the case of 85% deuteration of protein B

$$r_{eff} = [\sum r_{HHBk}^{-6}]^{-1/6} \qquad (3)$$

and $S^2 = 0.3$, the actual r_{eff} is $\approx 25\%$ shorter than its upper limit, a fact implying that effects of the local dynamics and deuteration rate of protein B can be neglected (see Figure S1 in the Supporting Information). On the basis of r_{eff} values, one can model the structure of a protein complex, provided that individual structures are known.

We have applied the above-mentioned strategy to map the intersubunit interface of recombinant human adult hemoglobin in the carbonmonoxide form (rHbCO A, 1 mM, pH 7.0)

 © 2005 Wiley-VCH Verlag GmbH & Co. KGaA, Weinheim

on an 800 MHz NMR spectrometer. Here, proteins A and B correspond to the α and β chains, respectively, and the α chain is ^{15}N,^{2}H-labeled. The average deuteration percentage was ≈85% for both chains. As expected, the decay of H_Z^N often follows a multiexponential form due to strong cross-relaxation among amide protons.[11] Nevertheless, it is possible to obtain initial relaxation rates for both samples and then to calculate ΔR^1 values. Since we are interested in only the ΔR^1 value, an alternative way to obtain it is from the dependence of the intensity ratio of a given proton in two samples ($I_1(t)$/$I_2(t)$) on the relaxation delay (which is shown by numerical simulations; see Figure S1 in the Supporting Information), for which $I_1(t)$ ($I_2(t)$) is the relative intensity at time t with respect to that at the first delay for sample 1 with unlabeled β chains (sample 2 with ^{2}H-labeled β chains).

Figure 2 shows the decays of a number of representative amide protons. Amides not involved in subunit contacts have shown no dependence of I_1/I_2 on the relaxation delay. Amides involved in weak contacts display nearly monoexponential profiles during a period of 500 ms, while those located in close-contact regions show nearly monoexponential profiles within the first 150 ms. Amide protons that involve weak or no direct subunit contact but that are close to the amides with strong subunit interactions display slower decay or no decay in the initial period and then faster decay in the later stage (F36 in Figure 2). This is due to the two-step "spin-diffusion" process. Fortunately, the spin-diffusion effect decreases dramatically with the steps and it has been found to be negligible for multistep processes for rHbCO A within a relaxation delay of up to 400 ms.

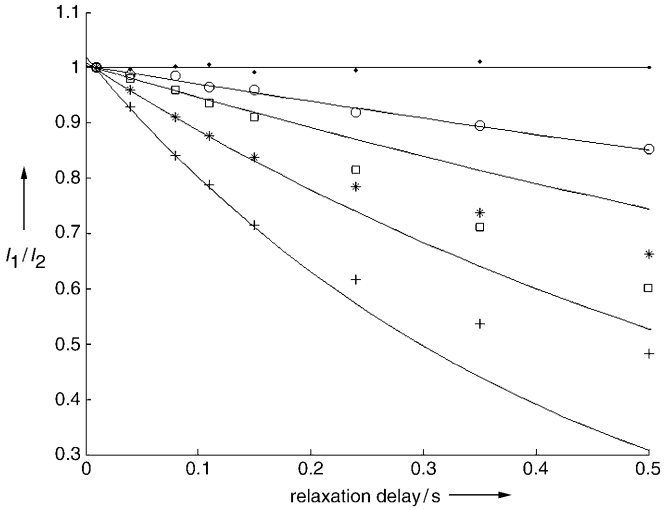


Figure 2. The dependence of the intensity ratio of normalized peak intensities in two samples (I_1/I_2) on the relaxation delay for a number of representative residues of rHbCO A (K60, ◆; V96, ○; F36, □; R31, *; A123, +). The normalized intensity for a given amide in one sample ($I(t)$) was obtained by taking the ratio of the peak intensities at delay t and the first delay (10 ms). Experimental data and initial decay profiles are indicated by symbols and solid lines, respectively. The total experimental time was ≈22 h.

Amino acid residues involved in subunit contacts can be simply identified from the ratios of normalized peak intensities (I_1/I_2) at one desired delay (for example, 250 ms; Figure 3a). Alternatively, they can be identified more confidently from ΔR^1 values (Figure 3b). The difference in the initial rate (ΔR^1) of an amide proton was estimated by fitting I_1/I_2 to a monoexponential equation in three steps: 1) calculation of the relaxation rate with all data points; 2) removal of the point with the longest delay in the existing data; and 3) repetition of step 2 until the absolute difference of the relaxation rates obtained with m+1 and m data points is smaller than the sum of the fitting errors of these two fittings, where m is the number of data points and $m > 3$. The fitting error was determined by using the Jackknife method.[12] The relaxation rate and fitting error obtained with m+1 points were reported. Amide protons in the α chain with a ΔR^1 value smaller than 0.7 times the average ΔR^1 value (≈0.1 s^{-1}, the noise level) are considered to have no interaction with the β chain. The results are consistent with the contact sites derived from the crystal structure of the R2 state of human normal adult hemoglobin (PDB entry 1BBB). With the use of a cross-saturation experiment on sample 1 in H_2O/$^{2}H_2O$ (30:70) solution, many residues in the contact region were also identified.

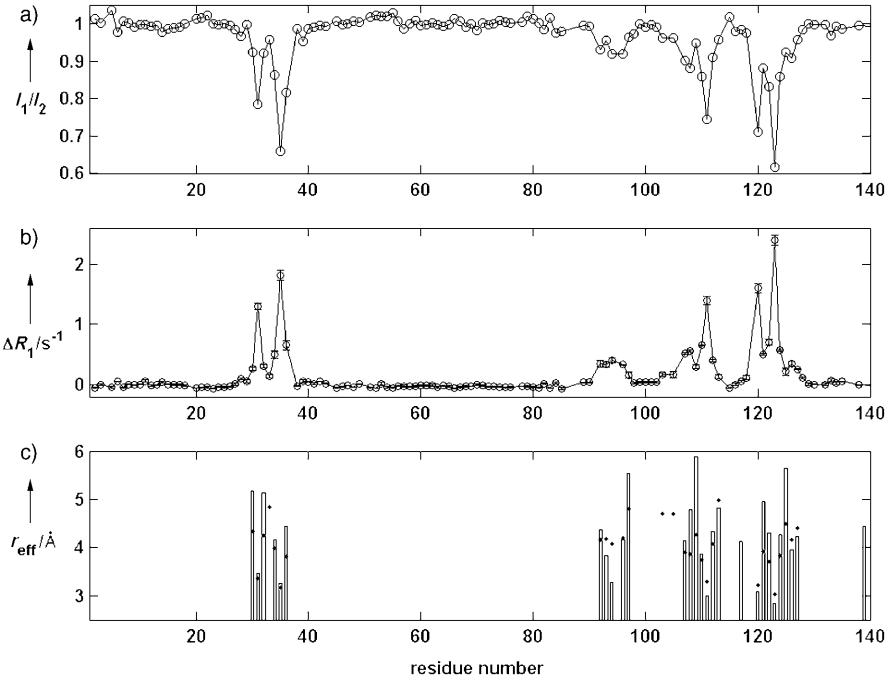


Figure 3. a) Peak intensity ratios of amides in two samples (I_1/I_2) against the residue number of the α chain of human normal adult hemoglobin; desired delay: 250 ms; first delay: 10 ms. b) Difference of initial relaxation rates (ΔR^1) between samples 1 and 2. Errors are indicated with vertical bars. c) Comparison of effective distances derived from the ΔR^1 values (◆) and from the crystal structure of the R2 state of rHbCO A (bar). The r_{eff} value is set to zero when it is larger than 5 and 6 Å for the NMR-derived data and the crystal-structure-based data, respectively.

 © 2005 Wiley-VCH Verlag GmbH & Co. KGaA, Weinheim

However, the $\alpha_1\beta_2$ interface (residues 92–97) cannot be identified because of the strong noise level caused by spin diffusion among many residual protons in the α chain (see Figure S2 in the Supporting Information).

Figure 3c shows the upper limits of effective distances (r_{eff}) estimated from the ΔR^1 values and a τ_c value of 32 ns (τ_c was established from ^{15}N relaxation times). The distances agree well with those calculated from the R2 structure except for a few residues (see Table S1 in the Supporting Information). The r_{eff} value for α94D estimated from the ΔR^1 value (4.07 Å) is significantly larger than that from the R2 crystal structure (3.28 Å) because the $\alpha_1\beta_2$ interface is more dynamic in solution than in the crystal state. The dynamics of this region has been shown previously by a relaxation study of β37W which is in contact with α94D.[13] The discrepancy for α117F (in a loop) and α139K (in the C terminus) is also due to different mobility in the solution and crystal states. The effective distances for α33F, α103H, and α105L are significantly shorter from the present method than from the crystal structure. This can be explained by a slight difference in subunit arrangement and side-chain packing in the solution and crystal states. The slight difference of the $\alpha_1\beta_1$ interface in solution and in the crystal state has previously been evidenced by the different solvent exchange rates of side-chain protons of α103H and α122H in the T and R states.[14]

Although the experiment proposed here requires deuteration of both the reporting protein and its binding partner, only moderate deuteration that is easily achievable is required. Residues located in the protein–protein interface can be mapped out simply from the ratios of normalized amide peak intensities at one desired delay in two samples. The effect of protein-concentration difference in the two samples is removed by normalizing the peak intensities of each sample at the desired delay with respect to those at a very short delay (for example, 10 ms). In order to obtain upper limits of effective distances for the amides at contact sites, one can measure the initial relaxation rate differences (ΔR^1) in the two samples. The distance information together with other experimental data such as residual dipolar couplings can be used to model protein complex structures with docking techniques.[2,15]

Received: April 6, 2005
Revised: June 2, 2005
Published online: July 20, 2005

Keywords: heme proteins · interfaces · NMR spectroscopy · protein–protein interactions · structure elucidation

[1] E. R. P. Zuiderweg, *Biochemistry* **2002**, *41*, 1.
[2] G. M. Clore, C. D. Schwieters, *J. Am. Chem. Soc.* **2003**, *125*, 2902.
[3] Y. Chen, J. Reizer, M. H. Saier, W. J. Fairbrother, P. E. Wright, *Biochemistry* **1993**, *32*, 32.
[4] T. Scherf, R. Hiller, J. Anglister, *FASEB J.* **1995**, *9*, 120.
[5] S. Arumugam, C. L. Hemme, N. Yoshida, K. Suzuki, H. Nagase, M. Berjanskii, B. Wu, S. R. Van Doren, *Biochemistry* **1998**, *37*, 9650.
[6] G. A. Mueller, A. M. Smith, M. D. Chapman, G. S. Rule, D. C. Benjamin, *J. Biol. Chem.* **2001**, *276*, 9359.
[7] a) C. Zwahlen, P. Legault, S. J. F. Vincent, J. Greenblatt, R. Konrat, L. E. Kay, *J. Am. Chem. Soc.* **1997**, *119*, 6711; b) C. Eichmüller, W. Schüler, R. Konrat, B. Kräutler, *J. Biomol. NMR* **2001**, *21*, 107.
[8] H. Takahashi, T. Nakanishi, K. Kami, Y. Arata, I. Shimada, *Nat. Struct. Biol.* **2000**, *7*, 220.
[9] L. K. Nicholson, L. E. Kay, D. M. Baldisseri, J. Arango, P. E. Young, A. Bax, D. A. Torchia, *Biochemistry* **1992**, *31*, 5253.
[10] J. Weigelt, *J. Am. Chem. Soc.* **1998**, *120*, 10778.
[11] R. L. Vold, R. R. Vold, *Prog. Nucl. Magn. Reson. Spectrosc.* **1978**, *12*, 79.
[12] A. F. Bissell, R. A. Ferguson, J. Roy. , *Stat. Soc. D-Sta.* **1975**, *24*, 79.
[13] Y. Yuan, V. Simplaceanu, J. A. Lukin, C. Ho, *J. Mol. Biol.* **2002**, *321*, 863.
[14] M. R. Mihailescu, I. M. Russu, *Proc. Natl. Acad. Sci. USA* **2001**, *98*, 3773.
[15] C. Dominguez, R. Boelens, A. M. J. J. Bonvin, *J. Am. Chem. Soc.* **2003**, *125*, 1731.

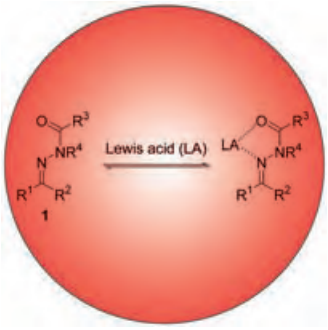
 © 2005 Wiley-VCH Verlag GmbH & Co. KGaA, Weinheim

Cover Picture



David Loffreda,* Françoise Delbecq, Fabienne Vigné, and Philippe Sautet

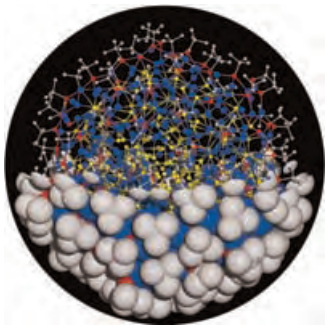
The selective hydrogenation of unsaturated aldehydes such as propenal on a Pt(111) surface, as shown in the cover picture, is an example of a heterogeneous catalysis reaction that yields two competitive products: propenol and propanal. The selectivity of this reaction is controlled by the balance between the surface hydrogenation steps and the desorption of the product. D. Loffreda et al. describe on page 5279 ff. the use of density functional theory and a microkinetic model to investigate the reaction pathways.



Electrophilic Reagents
N-Acylhydrazones are stable imine equivalents that can combine with a variety of nucleophiles to yield many useful synthetic building blocks. S. Kobayashi and M. Sugiura present the latest developments in this area in their Minireview on page 5176 ff.



Organic Azides
Despite the fact that they are often difficult to handle, organic azides have established a niche in organic synthesis. In their Review on page 5188 ff., S. Bräse and co-workers discuss fundamental reactions and new developments in organoazide chemistry.



Cluster Chemistry
In their Communication on page 5242 ff., D. Fenske et al. detail the synthesis and structural characterization of spherical cluster complexes that comprise an ordered shell of {AgS*t*Bu} groups and a disordered $\{(Ag_2S)_n\}$ core.

Contents

The following Communications have been judged by at least two referees to be "very important papers" and will be published online at www.angewandte.org soon:

K. Haraguchi, H.-J. Li*
Control of the Coil-to-Globule Transition of Poly(*N*-isopropylacrylamide) and Ultrahigh Mechanical Properties in Nanocomposite Hydrogels

*T. Buskas, S. Ingale, G.-J. Boons**
Towards a Fully Synthetic Carbohydrate-Based Anticancer Vaccine: Synthesis and Immunological Evaluation of a Lipidated Glycopeptide Containing the Tumor-Associated Tn Antigen

A. C. Filippou, G. Schnakenburg, A. I. Philippopoulos, N. Weidemann*
Bonding Analysis of the M≡Ge–Ge≡M Chain in the Germylidyne Complexes *trans*,*trans*-[Cl(depe)$_2$M≡Ge–Ge≡M(depe)$_2$Cl]

*M. Veith**
Cubane-Type Li_4H_4 and $Li_3H_3Li(OH)$: Stabilized in Molecular Adducts with Alane

S. Protti, M. Fagnoni, A. Albini**
Photochemical Cross-Coupling Reactions of Electron-Rich Aryl Chlorides and Aryl Esters with Alkynes: A Metal-Free Alkynylation

*V. Lavallo, Y. Canac, C. Präsang, B. Donnadieu, G. Bertrand**
Stable Cyclic (Alkyl)(amino)carbenes as Rigid or Flexible, Bulky, Electron-Rich Ligands for Transition-Metal Catalysts

Meeting Review

Kaleidoscope of Catalysis: Heidelberg Forum of Molecular Catalysis 2005 — M. Oestreich — **5166**

Books

The Life and Work of Friedrich Wöhler (1800–1882) — Johannes Büttner — *reviewed by H. Hopf* — **5168**

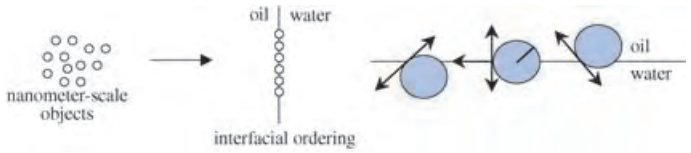
Our Lives — István Hargittai — *reviewed by W. Schroth* — **5169**

Highlights

Self-Assembly

W. H. Binder* — **5172 – 5175**

Supramolecular Assembly of Nanoparticles at Liquid–Liquid Interfaces



At the interface: The supramolecular organization of nanometer-scale objects is of great interest in the field of applied nanotechnology. Liquid–liquid interfaces can provide an alternative to current methods for the formation of highly ordered structures through the self-assembly of nanoparticles, nanocrystals, and even viruses (see picture). The concept is generally applicable and can be transferred to other interfaces, such as those of polymers.

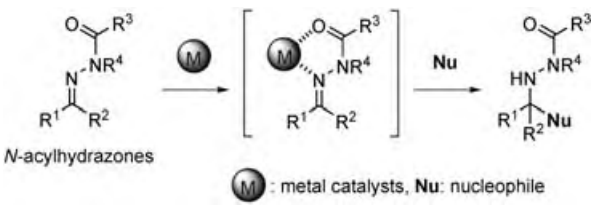
InterScience
© 2005 Wiley-VCH Verlag GmbH & Co. KGaA, Weinheim

Minireviews

Electrophilic Reagents

M. Sugiura, S. Kobayashi* _ **5176 – 5186**

N-Acylhydrazones as Versatile Electrophiles for the Synthesis of Nitrogen-Containing Compounds



Stable imine surrogates: *N*-Acylhydrazones are readily prepared from aldehydes and ketones with *N*-acylhydrazines. As imine equivalents in the presence of metal catalysts, they effectively promote reactions with a variety of nucleophiles (see scheme). Substrate *N*-acyl groups chelate the metal catalyst, which increases substrate electrophilicity and stereochemical control. The hydrazide products of *N*-acylhydrazones are useful chiral building blocks for various nitrogen-containing compounds.

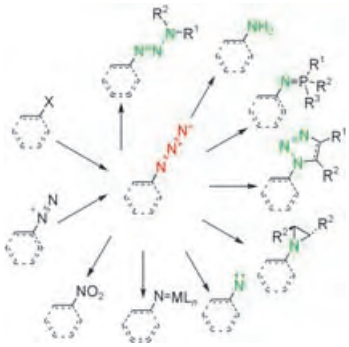
Reviews

Azides

S. Bräse,* C. Gil, K. Knepper, V. Zimmermann _____ **5188 – 5240**

Organic Azides: An Exploding Diversity of a Unique Class of Compounds

Tricky reagents: Besides their special thermal properties, organic azides also have unique reactivities (see scheme). This Review covers the use of organic azides in fundamental reactions as well as more recent developments in the Staudinger ligation, in copper-catalyzed dipolar cycloadditions, and in heterocyclic synthesis.

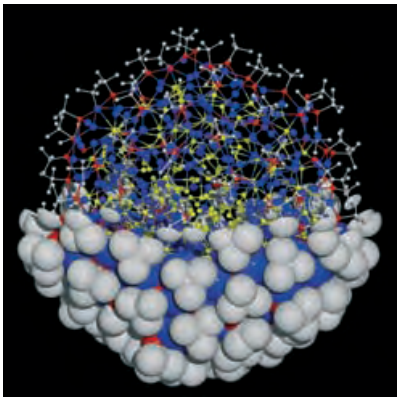


Communications

Cluster Compounds

D. Fenske,* C. E. Anson, A. Eichhöfer, O. Fuhr, A. Ingendoh, C. Persau, C. Richert _____ **5242 – 5246**

Syntheses and Crystal Structures of $[Ag_{123}S_{35}(StBu)_{50}]$ and $[Ag_{344}S_{124}(StBu)_{96}]$



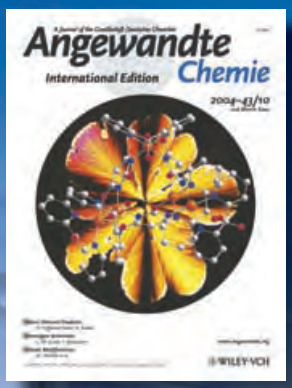
On cores: Silver carboxylates react with a mixture of $S(tBu)SiMe_3$ and $S(SiMe_3)_2$ (in the presence of a bidentate phosphine ligand) to yield $[Ag_{123}S_{35}(StBu)_{50}]$ (**1**) or $[Ag_{344}S_{124}(StBu)_{96}]$ (**2**, see picture: blue Ag^+, red S atoms of the *S*t*B*u groups, yellow S^{2-}, gray C) with maximum diameters of 2.5 (**1**) or 3.7 nm (**2**). These clusters can be described as core–shell particles with the $\{(Ag_2S)_{35}Ag_3\}$ (**1**) and the $\{(Ag_2S)_{124}\}$ (**2**) cores surrounded by shells of AgS*t*Bu units.

For the USA and Canada:
ANGEWANDTE CHEMIE International Edition (ISSN 1433-7851) is published weekly by Wiley-VCH PO Box 191161, D 69451 Weinheim, Germany. Air freight and mailing in the USA by Publications Expediting Inc. 200 Meacham Ave., Elmont, NY 11003. Periodicals postage paid at Jamaica NY 11431. US POSTMASTER: send address changes to *Angewandte Chemie*, Wiley-VCH, 111 River Street, Hoboken, NJ 07030. Annual subscription price for institutions: US$ 4948.00/4498.00 (valid for print and electronic / print or electronic delivery); for individuals who are personal members of a national chemical society, or whose institution already subscribes, or who are retired or self-employed consultants, print only: US$ 394.00. Postage and handling charges included. All Wiley-VCH prices are exclusive VAT.

© 2005 Wiley-VCH Verlag GmbH & Co. KGaA, Weinheim

The best in chemistry –

for more than a hundred years



A Journal of the Gesellschaft Deutscher Chemiker

Angewandte
International Edition **Chemie**

www.angewandte.org

1888: ***The beginning of a success story***

Constant Innovations

1962: *First issue of the International Edition*
1976: *Graphical abstracts*
1979: *Cover pictures*
1988: *Centenary of Angewandte*
1989: *Routine use of color*
1991: *New section: Highlights*
1992: *Computerized editorial tracking system*
1995: *Internet service for readers*
1998: *Regular press service; full-text online*
2000: *New section: Essays; EarlyView: Communications available online ahead of the printed version*
2001: *New section: Minireviews*
2002: *Online submission of manuscripts*
2003: *Weekly publication; new section: News; new layout*
2004: *Backfiles (1962-1997); ManuscriptXpress: Online system for authors and referees*



Angewandte's advisors...

Daniel Bellus
Ciba Specialty Chemicals, Basel

» For the past thirty years ***Angewandte Chemie*** *has continued to be my primary source of inspiration and self-education. In each new issue I find a real gem of chemistry, capable of further nurturing the innovation process. It is my pleasure to inject my industrial R&D experience into the International Advisory Board.«*

Angewandte Chemie International Edition *is a journal of the German Chemical Society (GDCh)*

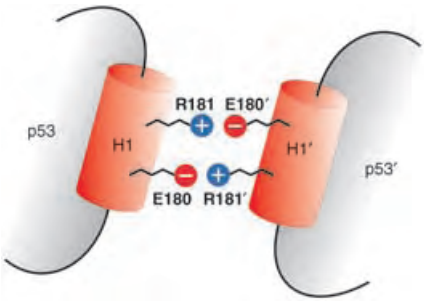
GDCh

WILEY InterScience® DISCOVER SOMETHING GREAT

WILEY-VCH

1180104_gu

Mutations in the transcription factor p53 enhance one's predisposition to cancer. Mutational studies show that double salt bridges are key elements for the dimerization of p53, its cooperative binding to DNA, and thus its proper function as a tumor suppressor (see picture). This might explain certain germ-line mutations found in patients with Li–Fraumeni syndrome.

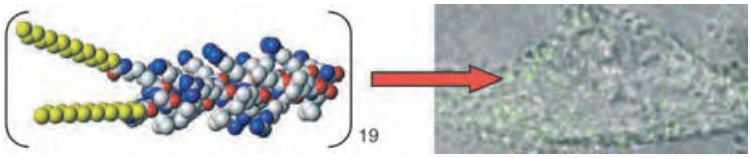


Protein Structures

A. Dehner, C. Klein, S. Hansen, L. Müller, J. Buchner, M. Schwaiger, H. Kessler* ——— **5247 – 5251**

Cooperative Binding of p53 to DNA: Regulation by Protein–Protein Interactions through a Double Salt Bridge

---



Detergent activity is conferred upon a cell-penetrating peptide by dipalmitoylation, and the peptide can incorporate large amounts of phospholipid into supramolecular particles with unique physicochemical properties. These nanocarriers combine the advantages of both liposomes and micelles as they offer a membrane-like environment in spite of their small size, thus preserving the biofunctionality of the vector peptide and affording efficient internalization into live cells.

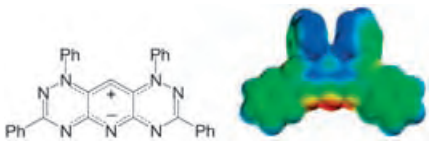
Drug Delivery

S. Keller,* I. Sauer, H. Strauss, K. Gast, M. Dathe, M. Bienert ——— **5252 – 5255**

Membrane-Mimetic Nanocarriers Formed by a Dipalmitoylated Cell-Penetrating Peptide

---

Zwitterionic structures with very low lying triplet states are the dominant characteristics of the first hexaazaacridine, 3,5,7,9-tetraphenylhexaazaacridine (TPH-acridine, see picture), and the analogous TPH-anthracene. The structure and spectroscopic properties were studied experimentally and by DFT calculations and analysis of nucleus-independent chemical shifts.



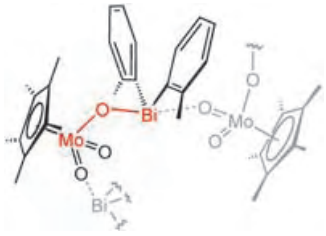
Antiaromatic Species

P. Langer,* A. Bodtke, N. N. R. Saleh, H. Görls, P. R. Schreiner* ——— **5255 – 5259**

3,5,7,9-Tetraphenylhexaazaacridine: A Highly Stable, Weakly Antiaromatic Species with 16 π Electrons

---

Bridging the gap: Encapsulation by "soft" organic ligands is the key to the isolation of complexes containing "hard" Mo^{VI}-O-Bi^{V} and Mo^{VI}-O-Bi^{III} units (see example), which might be regarded as molecular models for pivotal species on the surfaces of heterogeneous catalysts.



Coordination Chemistry

S. Roggan, C. Limberg,* B. Ziemer ——— **5259 – 5262**

Molecular Compounds with Mo-O-Bi Moieties

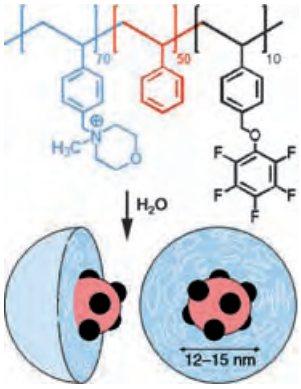
© 2005 Wiley-VCH Verlag GmbH & Co. KGaA, Weinheim

Contents

Multicomponent Micelles

S. Kubowicz, J.-F. Baussard, J.-F. Lutz, A. F. Thünemann, H. von Berlepsch, A. Laschewsky* ——— **5262 – 5265**

Multicompartment Micelles Formed by Self-Assembly of Linear ABC Triblock Copolymers in Aqueous Medium

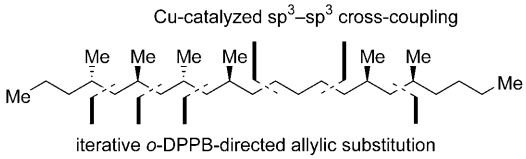


Like a doughnut with a raspberry filling: ABC triblock copolymers, composed of a hydrophilic block with morpholinium units (blue in the picture), a hydrophobic hydrocarbon block (red), and a hydrophobic fluorocarbon-rich block (black), self-assemble in water to form multicompartment micelles with a hydrophilic corona and a hydrophobic core with nanometer-scale subdomains.

Asymmetric Synthesis

C. Herber, B. Breit* ——— **5267 – 5269**

Enantioselective Total Synthesis and Determination of the Absolute Configuration of the 4,6,8,10,16,18-Hexamethyldocosane from *Antitrogus parvulus*

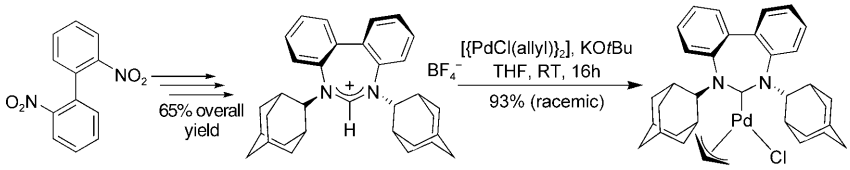


A copper-catalyzed sp^3–sp^3 cross-coupling for fragment coupling in a total synthesis is demonstrated. The diastereo- and enantioselective total synthesis of the 4,6,8,10,16,18-hexamethyldocosanes highlights the synthetic power of deoxypropionate construction based on an *ortho*-diphenylphosphanylbenzoyl (*o*-DPPB)-directed and copper-mediated allylic substitution with Grignard reagents (see scheme).

Organometallic Chemistry

C. C. Scarborough, M. J. W. Grady, I. A. Guzei, B. A. Gandhi, E. E. Bunel, S. S. Stahl* ——— **5269 – 5272**

Pd^{II} Complexes Possessing a Seven-Membered N-Heterocyclic Carbene Ligand

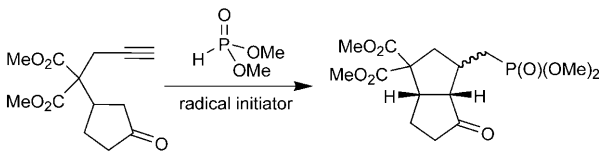


Carbenes with a twist: A seven-membered N-heterocyclic carbene (NHC) ligand is prepared from an amidinium precursor, derived from 2,2′-dinitrobiphenyl, and yields the NHC–Pd^{II} complex [PdCl(allyl)(NHC)] (see scheme). This carbene framework exhibits a tortional twist that results in axial symmetry. This ligand class can be readily modified and is attractive for future application in asymmetric catalysis.

Radical Reactions

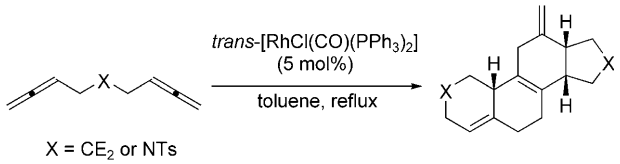
F. Beaufils, F. Dénès, P. Renaud* ——— **5273 – 5275**

Dimethyl Phosphite Mediated Hydrogen Atom Abstraction: A Tin-Free Procedure for the Preparation of Cyclopentane Derivatives



A radical transformation! An efficient radical cascade reaction leads to functionalized five-membered rings. Alkenyl radicals are generated from readily available terminal alkynes and a dialkyl phosphite. This tin-free procedure can be run under one-pot conditions (no slow addition), is high yielding, and can be applied to the assembly of fused bicyclic compounds (see scheme).

© 2005 Wiley-VCH Verlag GmbH & Co. KGaA, Weinheim

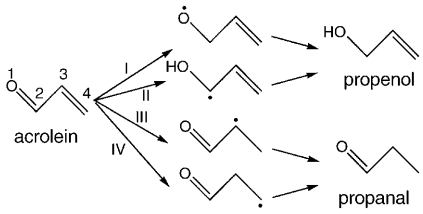


Homogeneous Catalysis

S. Ma,* P. Lu, L. Lu, H. Hou, J. Wei, Q. He, Z. Gu, X. Jiang, X. Jin ——— **5275 – 5278**

What Can a Metal Catalyst Do with Allenes? One-Step Formation of Steroid Scaffolds from Readily Available Starting Materials

The beauty and power of transition-metal-catalyzed reactions has been demonstrated by the one-step synthesis of steroid scaffolds from readily available allenes. The best results (57–73% yield) were obtained using *trans*-[RhCl(CO)(PPh$_3$)$_2$] as the catalyst in toluene (see scheme; E = CN, CO$_2$Me, SO$_2$Ph, Ts = toluene-4-sulfonyl).

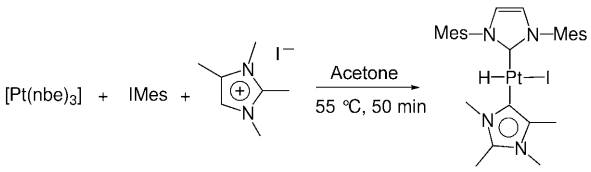


Heterogeneous Catalysis

D. Loffreda,* F. Delbecq, F. Vigné, P. Sautet ——— **5279 – 5282**

Catalytic Hydrogenation of Unsaturated Aldehydes on Pt(111): Understanding the Selectivity from First-Principles Calculations

Coordinating the attack: A theoretical approach based on first-principles calculations and a kinetic model has shown that the partial hydrogenation of the C=O or C=C bonds in acrolein on a Pt(111) catalyst is controlled by the balance between the hydrogenation steps on the surface and the desorption of the partially hydrogenated products. The scheme shows the four possible surface intermediates and the two products.

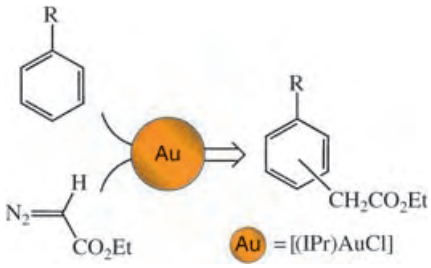


Carbene Ligands

D. Bacciu, K. J. Cavell,* I. A. Fallis, L.-l. Ooi ——— **5282 – 5284**

Platinum-Mediated Oxidative Addition and Reductive Elimination of Imidazolium Salts at C4 and C5

Wrong way round: Imidazolium salts blocked at C2 undergo oxidative addition to a Pt^0 center at C4/C5 (see scheme; nbe = norbornene, IMes = 1,3-bis(2,4,6-trimethylphenyl)imidazolin-2-ylidene). The resulting carbene ligands, which are bound the "wrong way" are susceptible, in common with their "normal" counterparts, to reductive elimination reactions to regenerate Pt^0 complexes and imidazolium salts.



Carbene Chemistry

M. R. Fructos, T. R. Belderrain, P. de Frémont, N. M. Scott, S. P. Nolan,* M. M. Díaz-Requejo,* P. J. Pérez* ——— **5284 – 5288**

A Gold Catalyst for Carbene-Transfer Reactions from Ethyl Diazoacetate

Approaching El Dorado: A gold catalyst has been discovered that transfers a carbene unit from ethyl diazoacetate to aromatic substrates (see scheme) as well as olefins, amines, and alcohols. The insertion of carbene units into the C–H bonds of the aromatic ring of benzene, toluene, and styrene is a novel reaction. R = H, CH$_3$, CH=CH$_2$; IPr = 1,3-bis(diisopropylphenyl)imidazol-2-ylidene.

 © 2005 Wiley-VCH Verlag GmbH & Co. KGaA, Weinheim

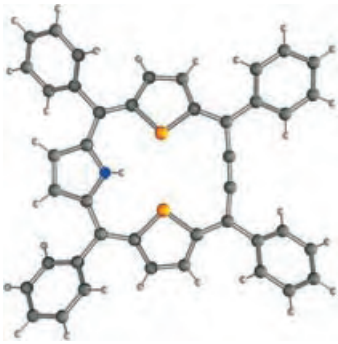
Contents

Porphyrinoids

A. Berlicka, L. Latos-Grażyński,* T. Lis ——— **5288 – 5291**

Dithiaethyneporphyrin: An Atypical [18]Triphyrin(4.1.1) Frame for Contracted Porphyrins

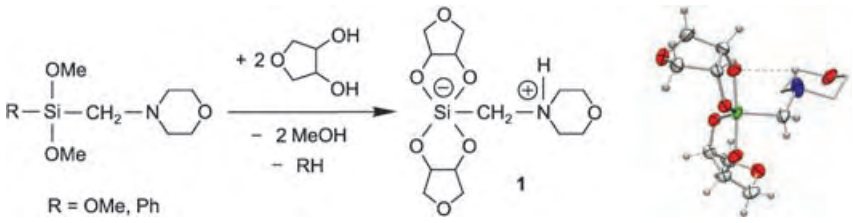
Fusion of the structural motifs 21,23-dithiaporphyrin and acetylene yields the 18-π-aromatic [18]triphyrin(4.1.1) framework (see structure; C gray, N blue, S yellow). The butyne moiety that joins the two thiophene rings reveals a slight distortion from linearity, showing a bowlike deformation directed out of the macrocycle.



Higher-Coordinate Si Compounds

R. Tacke,* R. Bertermann, C. Burschka, S. Dragota ——— **5292 – 5295**

A Zwitterionic Spirocyclic Pentacoordinate Silicon Compound Synthesized in Water by Si–O and Si–C Bond Cleavage



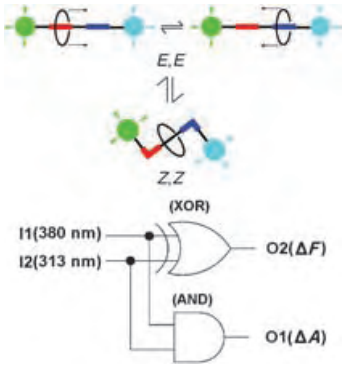
Remarkable hydrolytic stability in the range pH 7.0–8.0 is exhibited by the zwitterionic λ^5*Si*-silicate **1**, which can even be prepared in water and forms a stable hydrate **1**·H_2O. The synthetic route to **1** and the structure of the zwitterion in the crystal (O red; N blue; Si green; C gray) are shown in the picture.

Molecular Devices

D.-H. Qu, Q.-C. Wang, H. Tian* ——— **5296 – 5299**

A Half Adder Based on a Photochemically Driven [2]Rotaxane

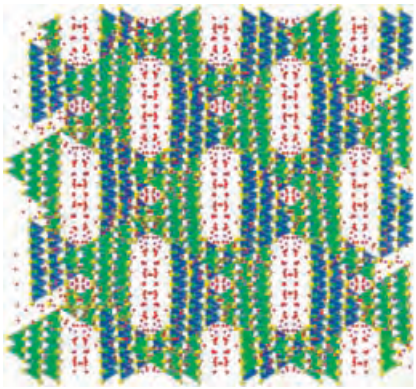
A molecular abacus: In a [2]rotaxane that mimicks a half adder with distinct AND and XOR logic gates, all the inputs (I) and outputs (O) are photochemical (see scheme; *F* = fluorescence, *A* = absorbance). Reversible *E*→*Z* photoisomerization about two double bonds (shown in red and dark blue) in the thread molecule leads to four conformers that have different spectral properties.



Green Chemisty

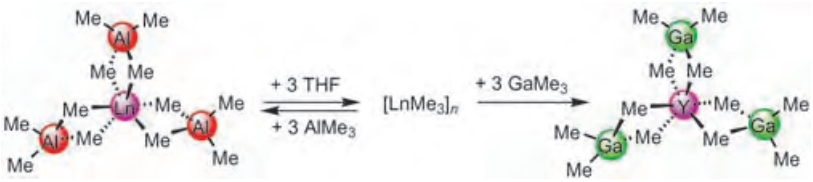
N. Zheng, X. Bu, H. Vu, P. Feng* ——— **5299 – 5303**

Open-Framework Chalcogenides as Visible-Light Photocatalysts for Hydrogen Generation from Water



Light work: Open-framework chalcogenides are efficient visible-light photocatalysts for the reduction of water to hydrogen. These materials contain 3D covalent superlattices built from nanosized supertetrahedral clusters (see picture). Unlike dense semiconductors, they allow the easy incorporation of dye sensitizers within their channels, which can further enhance their photocatalytic response in the visible-light region.

© 2005 Wiley-VCH Verlag GmbH & Co. KGaA, Weinheim

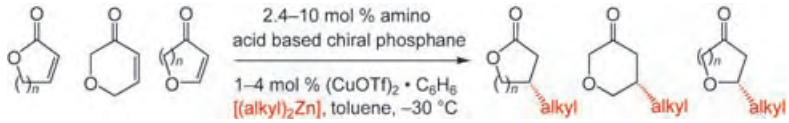


Complexes in disguise: Homoleptic $[Ln(AlMe_4)_3]$ (Ln = Y, Lu) complexes are effectively masked $[LnMe_3]_n$ species, which are produced reversibly upon equimolar addition of a Lewis base to the former. Compounds $[LnMe_3]_n$ are thermally stable and readily form peralkylated heterobimetallic complexes with alkylaluminum, -gallium, and -magnesium reagents (see scheme).

Organolanthanides

H. M. Dietrich, G. Raudaschl-Sieber, R. Anwander* ——— 5303 – 5306

Trimethylyttrium and Trimethyllutetium

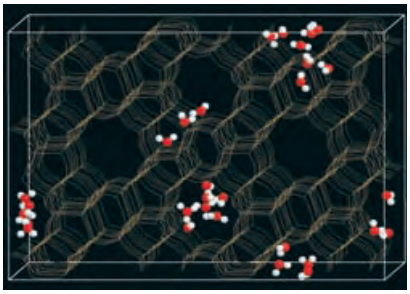


The first generally effective method for catalytic asymmetric conjugate addition (ACA) of dialkylzinc reagents to unsaturated furanones and pyranones (see scheme) with different steric and electronic properties is reported. Synthesis, isolation, and characterization of catalytically active and air-stable chiral Cu–peptide complexes are also described.

Asymmetric Catalysis

M. K. Brown, S. J. Degrado, A. H. Hoveyda* ——— 5306 – 5310

Highly Enantioselective Cu-Catalyzed Conjugate Additions of Dialkylzinc Reagents to Unsaturated Furanones and Pyranones: Preparation of Air-Stable and Catalytically Active Cu–Peptide Complexes

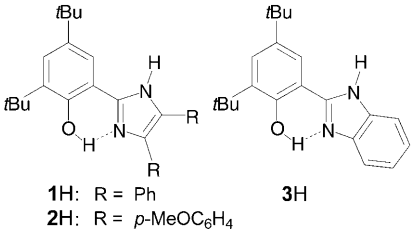


Simple but effective: The intrusion/extrusion cycle of a nonwetting fluid in a hydrophobic solid can be described by simple models and simulation methods found useful for studying gas adsorption in nanoporous materials. The water confined to hydrophobic spaces of nanoscopic dimensions in the zeolite silicalite-1 is shown to be a strongly depleted and highly inhomogeneous fluid (see picture).

Zeolites

N. Desbiens, I. Demachy, A. H. Fuchs,* H. Kirsch-Rodeschini, M. Soulard, J. Patarin ——— 5310 – 5313

Water Condensation in Hydrophobic Nanopores



The one-electron oxidation of compounds 1H–3H occurs by a proton-coupled electron-transfer mechanism to produce a phenoxyl radical hydrogen-bonded to an imidazolium carbon atom. Thus, these compounds serve as analogues for tyrosyl D• in photosystem II. This insight was obtained from a combination of W-band EPR spectroscopy and DFT calculations.

Radical Cations

L. Benisvy,* R. Bittl, E. Bothe, C. D. Garner, J. McMaster, S. Ross, C. Teutloff, F. Neese* ——— 5314 – 5317

Phenoxyl Radicals Hydrogen-Bonded to Imidazolium: Analogues of Tyrosyl D• of Photosystem II: High-Field EPR and DFT Studies

© 2005 Wiley-VCH Verlag GmbH & Co. KGaA, Weinheim

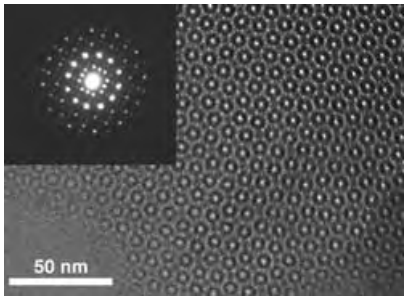
Contents

Mesoporous Silicates

A. E. Garcia-Bennett,* N. Kupferschmidt, Y. Sakamoto, S. Che, O. Terasaki _____ **5317 – 5322**

Synthesis of Mesocage Structures by Kinetic Control of Self-Assembly in Anionic Surfactants

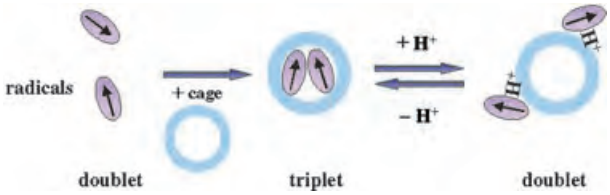
Varying the time between adding a co-structure-directing agent and a silica source to an anionic surfactant template results in either well-ordered cubic or a novel tetragonal ($P4_2/mnm$) mesocage material by arrangement of micellar spheres of various sizes. The image shows the high-resolution transmission electron micrograph of the tetragonal structure and the corresponding electron diffraction pattern (inset).



Host–Guest Systems

K. Nakabayashi, M. Kawano,* M. Fujita* _____ **5322 – 5325**

pH-Switchable Through-Space Interaction of Organic Radicals within a Self-Assembled Coordination Cage



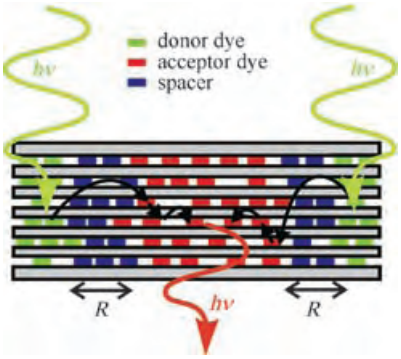
Twinned spins yield triplets: The through-space interaction of non-associative stable organic radicals within a self-assembled coordination cage (see scheme) is controlled by pH. The amino group of the radical can be protonated, and the affinity of the radicals for the host consequently decreases at low pH owing to coulombic repulsion. This leads to their release, as observed by ESR spectroscopy.

Zeolites

C. Minkowski, G. Calzaferri* _____ **5325 – 5329**

Förster-Type Energy Transfer along a Specified Axis

Quasi-1D transport of electronic excitation energy in dye-loaded zeolite L was observed when a spacer molecule was introduced between the donor and the acceptor dyes to separate them locally (see picture). In the system shown, the donor–spacer and spacer–acceptor phase boundaries are both diffuse. Alternatively, all the donors can be fixed at the same position and only the spacer–acceptor phase boundary is diffuse.

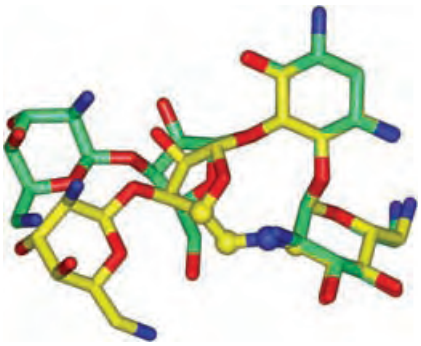


Structural Biochemistry

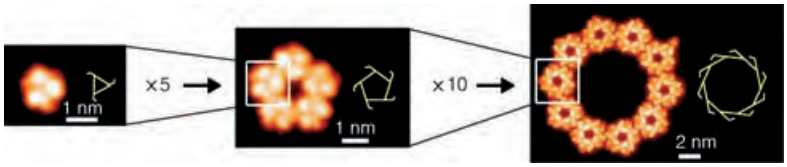
F. Zhao, Q. Zhao, K. F. Blount, Q. Han, Y. Tor, T. Hermann* _____ **5329 – 5334**

Molecular Recognition of RNA by Neomycin and a Restricted Neomycin Derivative

The preorganized presentation of functional groups in the antibiotic neomycin (green) is exploited to obtain a conformationally restricted aminoglycoside (yellow) by regioselective intramolecular cyclization. X-ray crystallography data show how the natural product and the derivative recognize the RNA target motif that is the binding site of aminoglycoside antibiotics.



© 2005 Wiley-VCH Verlag GmbH & Co. KGaA, Weinheim

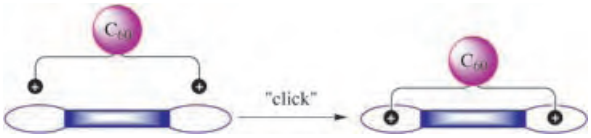


Nested assembly: Chiral molecules of 5,6,11,12-tetraphenylnaphthacene (rubrene) organize spontaneously into homochiral supramolecular architectures of increasing complexity. Adsorbed individual molecules self-assemble enantioselectively into chiral pentagonal supermolecules, which act as building blocks for the formation of chiral supramolecular decagons (see STM images).

Supramolecular Chemistry

M.-C. Blüm,* E. Ćavar, M. Pivetta, F. Patthey, W.-D. Schneider **5334 – 5337**

Conservation of Chirality in a Hierarchical Supramolecular Self-Assembled Structure with Pentagonal Symmetry



All clicking into place: Self-complementarity between a bis(crown ether) derivative and a bisammonium fullerene leads to the formation of a stable noncovalent macrocyclic 1:1 complex (see schematic representation). The binding constant for this complex is three orders of magnitude larger than that for other closely related systems as a result of the two-center host–guest topography.

Host–Guest Chemistry

U. Hahn, M. Elhabiri, A. Trabolsi, H. Herschbach, E. Leize, A. Van Dorsselaer,* A.-M. Albrecht-Gary,* J.-F. Nierengarten* **5338 – 5341**

Supramolecular Click Chemistry with a Bisammonium-C_{60} Substrate and a Ditopic Crown Ether Host

The issues for August 2005 appeared online on the following dates
Issue 29: July 8 · Issue 30: July 18 · Issue 31: July 29 · Issue 32: August 8.

Looking for outstanding employees?

Do you need another expert for your excellent team?
... Chemists, PhD Students, Managers, Professors, Sales Representatives...

Place an advert in the printed version and have it made available online for 1 month, free of charge!

Angewandte Chemie International Edition
Advertising Sales Department: Marion Schulz
Phone: 0 62 01 - 60 65 65
Fax: 0 62 01 - 60 65 50
E-Mail: MSchulz@wiley-vch.de

Service

Keywords **5342**

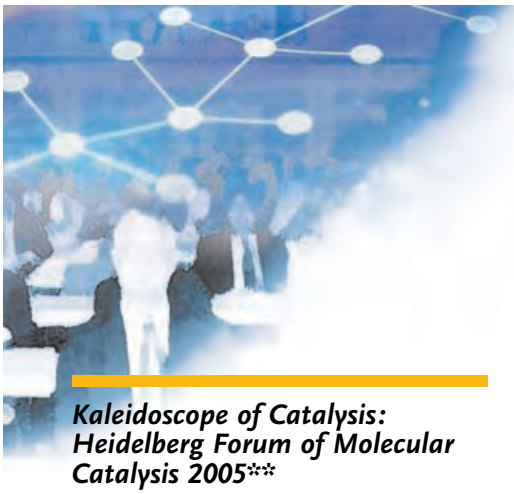
Authors **5343**

Angewandte's Sister Journals **5344 – 5345**

Preview **5347**



© 2005 Wiley-VCH Verlag GmbH & Co. KGaA, Weinheim



Kaleidoscope of Catalysis: Heidelberg Forum of Molecular Catalysis 2005**

Martin Oestreich*

The Heidelberg Forum of Molecular Catalysis (HFMC) originated from the Georg Wittig Lectureship in 1999 and continues as a one-day symposium that has been held biennially ever since. The event is sponsored by the BASF corporation which reflects the considerable importance this company sees in academic research and innovation. In the tradition of the forum, the BASF Catalysis Award is presented to an outstanding young researcher in recognition of her or his significant contributions to the thriving field of molecular catalysis. Frank Glorius (University of Marburg, Germany) is the recipient of this year's award, which includes prize money of €10000.

As in preceding years, the program attracted well over 500 junior and senior scientists from academia and industry. In addition to four plenary lectures (three invited and one by the prize winner), a strong poster session with more than 100 contributions rounded off the scientific program. The chairman of the local collaborative research center, Peter Hofmann (University of Heidelberg, Germany), moderated the symposium.

The scientific program commenced with a talk by David W. C. MacMillan (California Institute of Technology) on state-of-the-art asymmetric organocatalysis, which is hinged on two distinct strategies for the reversible activation of carbonyl groups by amines: activation through lowering the lowest unoccupied molecular orbital (iminium catalysis) and activation through raising the highest occupied molecular orbital (enamine catalysis). Starting with a brief outline of the evolution of suitable chiral catalysts based on the imidazolidinone framework, MacMillan presented an impressive number of applications, sometimes outshining classic asymmetric Lewis acid catalysis. Some of the recent accomplishments of his research group include heteroconjugate addition reactions with one amine as the catalyst and a second amine as the reactant, unusual *exo*-selective Diels–Alder reactions, aldehyde–aldehyde direct aldol reactions (enabling rapid access to orthogonally protected carbohydrates), and α-halogenations of carbonyl compounds. Another part of his talk was devoted to a formidable challenge in organic synthesis: the asymmetric construction of quaternary carbons. The core architecture ("the heart of the beast") of diazonamide A (and likewise, of pyrroloindoline alkaloids) was elegantly assembled by Friedel–Crafts-type conjugate additions of indoles to α,β-unsaturated aldehydes coupled with the cyclization of a pendant heteroatom donor. The fireworks ended with an alternative organocatalytic concept for complex molecule synthesis. The efficiency of a synthetic process decreases exponentially with an increase in the number of sequential operations; tandem catalysis provides a strategic foundation to bypass this disadvantage. A highly stereoselective tandem iminium–enamine–enamine one-pot process carried out for the first time has already demonstrated promise for facilitating asymmetric syntheses.

In his ceremonial address, Stefan Marcinowski (BASF) introduced the prizewinner, Frank Glorius, to the audience with a comprehensive summary of his academic background and a list of his significant scientific achievements. This was followed by a lecture given by the prizewinner himself. Glorius presented a blend of novel homogeneous and heterogeneous catalytic processes. Within the theme of homogeneous catalysis, part of his research program is directed toward the synthesis and application of N-heterocyclic carbenes. His research group devised a new family of sterically demanding carbene ligands (IBiox) with restricted flexibility and applied them in transition-metal catalysis. The unique feature of flexible steric constraints enables these ligands to adapt to the changing requirements of the catalytic cycle, thereby allowing the intricate preparation of tetra-*ortho*-substituted biaryl compounds by Suzuki–Miyaura cross-coupling of aryl chlorides. An additional research area for Glorius is the use of carbenes in organocatalysis; thus α,β-unsaturated aldehydes can be transformed into homoenolate equivalents upon reaction with N-heterocyclic carbenes. Through this organocatalytic conjugate Umpolung and the subsequent reaction with an aldehyde, several γ-butyrolactones were made accessible in one step. Within the theme of heterogeneous catalysis, Glorius reported on a highly diastereoselective hydrogenation of oxazolidinone-substituted pyridines accompanied by the "traceless" cleavage of the chiral auxiliary. This single synthetic operation affords highly enantiomerically enriched piperidine derivatives with up to three stereocenters!

The afternoon session opened with a talk by Amir H. Hoveyda (Boston College) about the quest for ligand–metal combinations of broad utility in asymmetric synthesis. With a catalyst system for the asymmetric alkylation of alkenes as a starting point, Hoveyda nicely delineated the subtle and unforeseeable influences of incidental additives ("impurities") as well as the substrate itself on reaction efficiency and selectivity. The targeted design of general chiral ligands is an attractive alternative to the painstaking search for the right substrate for a given ligand, and Hoveyda has addressed this challenge by using peptide-based ligands. These ligands provide multiple sites for steric and electronic alterations, and libraries of considerable size are easily accessible by

[*] Dr. M. Oestreich
Institut für Organische Chemie und Biochemie
Albert-Ludwigs-Universität Freiburg
Albertstrasse 21, 79104 Freiburg (Germany)
Fax: (+49) 761-203-6100
E-mail: martin.oestreich@orgmail.chemie.uni-freiburg.de

[**] The 3rd Heidelberg Forum of Molecular Catalysis (July 8, 2005) was jointly organized by the University of Heidelberg, BASF AG, and the Collaborative Research Center (SFB 623) "Molecular Catalysts: Structure and Functional Design" of the German Research Foundation (DFG).

InterScience
© 2005 Wiley-VCH Verlag GmbH & Co. KGaA, Weinheim

parallel synthesis on solid support. With a plethora of ligands and reasonable mechanistic models at hand, several transformations, such as titanium-catalyzed Strecker reactions, copper-catalyzed conjugate addition and allylic substitution reactions, and aluminum-catalyzed alkylation reactions, were carried out with excellent enantioselectivity. Application of the asymmetric Strecker reaction to the synthesis of non-natural α-amino acids led to the total synthesis and stereochemical assignment of members of the complestatin family of natural products. Hoveyda closed his lecture with the presentation of a novel silver-based chiral N-heterocyclic carbene complex that has already been successfully applied toward enantioselective ruthenium-catalyzed alkene metatheses and copper-catalyzed allylic substitutions.

The scientific program ended with a guided tour by Gregory C. Fu (Massachusetts Institute of Technology) through palladium- and nickel-catalyzed coupling reactions. Equipped with a profound understanding of the importance of electron-rich (facilitating oxidative addition) and sterically demanding (facilitating reductive elimination) ligands at the transition-metal center, Fu introduced broadly applicable tricyclohexylphosphine and tri-*tert*-butylphosphine ligands. These afford unusually active catalysts, which assist in a number of cross-coupling reactions (Suzuki, Stille, Negishi, and Heck reactions) of aryl and vinyl chlorides under exceptionally mild reaction conditions ($C(sp^2)$–Cl bonds appeared to be more reactive than $C(sp^2)$–OSO_2CF_3 bonds). Careful mechanistic investigations revealed the pivotal influence of the base in the resting state of the catalytic cycle. Another focus of his research is the development of capricious $C(sp^3)$–$C(sp^3)$ cross-coupling reactions, which are often thwarted by facile β-hydride elimination. Nevertheless, Fu reported powerful reaction protocols including elucidation of the stereochemical course of the oxidative addition at $C(sp^3)$–$OSO_2C_6H_4CH_3$. This final part culminated in the development of catalytic enantioselective Negishi couplings of racemic secondary benzylic bromides and alkyl zinc reagents.

The well-balanced content of these four plenary lectures provided an excellent up-to-date overview of some first-rate facets of modern molecular catalysis. Interlacing the talks with poster sessions created a relaxed atmosphere in which there was ample time for mutual scientific and personal exchange. The afternoon session ended with a social get-together including complimentary dinner for all participants. All those infected with the "catalysis virus" will have the opportunity to meet again in two years at the 4th Heidelberg Forum of Molecular Catalysis!

DOI: 10.1002/anie.200502426

 © 2005 Wiley-VCH Verlag GmbH & Co. KGaA, Weinheim

Self-Assembly

DOI: 10.1002/anie.200501220

Supramolecular Assembly of Nanoparticles at Liquid–Liquid Interfaces**

*Wolfgang H. Binder**

Keywords:
interfaces · nanoparticles · polymers · self-assembly · supramolecular chemistry

The supramolecular organization of nanoparticles, nanocrystals and other nanometer-sized objects (NPs) is an important prerequisite for permanent applications in the field of nano-(bio)technology.[1] There is an intense search for a simple and general strategy to organize NPs on interfaces through self-assembly processes, as NPs exhibit a wide range of size-dependent physical effects (optical, electrical, magnetic, etc.).[2] Such processes require adequate stabilization of the NP at interfaces with a high degree of organizational selectivity. Sufficient dynamic freedom is necessary in the course of the ordering process and once completed, the assembly must be stabilized. Three different approaches are currently explored to effect ordering of NPs by the self-assembly processes (Figure 1):

a) Crystallization of nanoparticles[1a,2a,2b,3] leads to a 3D ordering to produce so-called "colloidal crystals", in which high levels of order are possible through sedimentation and precipitation processes. An advantage of this process is the high level of order within the materials obtained. A main disadvantage lies in the low rate of sedimentation, which may require weeks to generate the ordered materials.

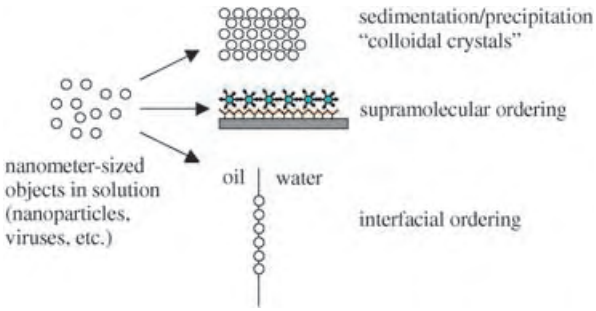


Figure 1. Strategies for the self-assembly of nanoparticles.

b) Another type of self-assembly process uses directed supramolecular interactions between a surface and the NP (for example: electrostatic interactions,[4] oligonucleotides,[5] metal complexes,[6] directed hydrogen bonds,[7] and hydrophobic forces[8]). This technique is usually carried out by a wet-deposition processes. A general disadvantage of using direct supramolecular interactions for assembly lies in the formation of irregular arrays that result from initially strong attachments, which usually do not allow the correction of errors or mismatches during the assembly process.

c) Liquid–liquid interfaces offer an important alternative scaffold for the organization of nanometer-sized objects. For example, interfacial ordering effects[9] can be used for the self-assembly of NPs and viruses. Of key importance is the assembly of NPs at an oil–water interface where the interfacial tension is high. In this process, the assembly is highly dynamic, which enables errors to be corrected rapidly. At the macroscopic level, such processes have been known for over 100 years as "Pickering emulsions",[10] in which large particles ($d > 1$ μm) stabilize emulsions efficiently by adsorption to the liquid–liquid interface.

The theory of the self-assembly of NPs and other nanometer-sized objects at liquid–liquid interfaces was developed initially by Binks et al.[11] (Figure 2). The high interfacial energy between oil and water can be decreased by the assembly of the NPs at the interface. This decrease in surface energy favors the formation of a monolayer of NPs located at the interface. Clearly this process is counterbalanced by the kinetic energy of the NPs in solution. The energetics of the assembly process can be calculated from several parameters according to the equation outlined in Figure 2. The placement of one NP at the interface leads to a decrease in the interfacial energy, which

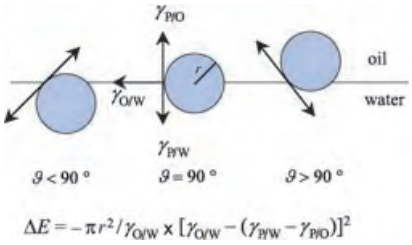


Figure 2. Energy balance (ΔE) of particle assembly at interfaces; adapted from ref. [9a]; γ: interfacial energy, P: particle, W: water, O: oil, r: effective NP radius.

[*] Prof. Dr. W. H. Binder
Institute of Applied Synthetic Chemistry
Division of Macromolecular Chemistry
Getreidemarkt 9/163/MC
1060 Vienna (Austria)
Fax: (+43) 1-58801-16299
E-mail: wbinder@mail.zserv.tuwien.ac.at

[**] The author thanks the Austrian Science Foundation for financial support through project FWF 14844 CHE.

InterScience
© 2005 Wiley-VCH Verlag GmbH & Co. KGaA, Weinheim

is expressed as the difference between the energies of the oil–water ($\gamma_{O/W}$), the particle–water ($\gamma_{P/W}$), and the particle–oil ($\gamma_{P/O}$) interfaces, in which R is the effective radius of the nanoparticle. Three parameters influence the energy of the assembly process:

a) Simple surface modification of the NPs can be used to modulate the interfacial energies $\gamma_{P/O}$ and $\gamma_{P/W}$; either covalently bound or adsorbed ligands may be used for this. An important aspect of NP surface modification is the influence of the ligand on the properties of the NP core which may limit the range of feasible surface modifications.
b) The nature of the oil–water interface (modification of $\gamma_{O/W}$).
c) The effective radius (R) of the nanoparticles. According to this theory, smaller NPs should adsorb more weakly to the interface than larger NPs.

All three parameters can be used to control the exact location of the NPs; only if the contact angle is exactly 90° will the particle be located exactly at the middle of the oil–water interface (that is, positioned equally between the oil and water phases). In all other cases, the oil or the water will be favored as an adsorption site. The energy of the adsorption process can be determined in the following way: based on known values[12b] ($\gamma_{O/W} = 35.7\ mN\,m^{-1}$; $\gamma_{P/O} = 15\ mN\,m^{-1}$; $\gamma_{P/W} = 40\ mN\,m^{-1}$) the energy is strongly dependent on NP size. A particle with $d \approx 1\ \mu m$ yields a stabilizing interfacial energy of $\Delta E \approx 10^7\ k_B T$, which leads to an almost irreversible adsorption at this interface. Particles with smaller radii adsorb with smaller energy values, as ΔE is proportional to r^2 (for $d = 100$ nm, $\Delta E \approx 10^5\ k_B T$; $d = 10$ nm, $\Delta E \approx 10^3\ k_B T$, $d = 1$ nm, $\Delta E \approx 10^1\ k_B T$).

So much for theory—but what is theory without proof? Russell and co-workers[12] (Figure 3a) recently investigated the assembly of CdSe nanoparticles of two different radii (2.7 nm and 4.6 nm) by competitive adsorption, stabilized with phosphinoxide ligands. Discrimination in adsorption can be followed by taking advantage of the size-dependent fluorescence (F) of the CdSe NPs: the initial fluorescence of adsorption of the smaller particles ($r = 2.7$ nm, $\lambda_F = 525$ nm) at a toluene–water interface was followed by a change at $\lambda = 610$ nm, which indicates the interfacial adsorption of the larger particles added subsequently. This not only gives proof to the theory that larger particles may win the adsorption process in competition with smaller NPs, but also allows determination of the time constant of the selective adsorption process. The particles are mobile (in a fluid phase) at the interface without the formation of ordered arrays. Extending this concept yields isolable films after evaporation of the solvent. Furthermore, charged gold NPs[9c] and voltage-induced processes[13] effect the same type of assembly at interfaces. A related concept developed by Möhwald and co-workers[9a] (Figure 3b) uses Au, Ag or γ-Fe_2O_3 NPs that have been surface-modified with a 2-bromo-2-methylpropionate ligand. The contact angle of these particles has a value close to 90°, resulting in the assembly of the particles exactly in the middle of a toluene–water interface. The formation of a thin film (transferable by Langmuir–Blodgett techniques) with metallic gold reflectance and blue transmittance demonstrates the formation of closely packed NP layers. "Nanoalloys", controlled mixtures of different nanoparticles (assemblies of Ag and Au NPs, for example), can also be formed at the interface given that the NP size and packing permits the formation of matching lattices.

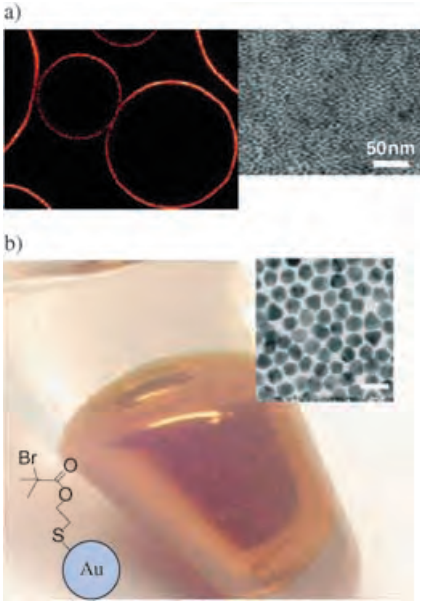


Figure 3. a) Left: fluorescence confocal microscope image of CdSe-particle-coated water droplets dispersed in toluene; right: TEM image of a dried film; from ref. [12a]. b) Photograph of self-assembled Au nanoparticles ($d = 12$ nm) covered with 2,2′-dithiobis(1-(2-bromo-2-methylpropionyloxy)ethane) at a toluene–water interface. Inset: HRTEM image of the film (scale bar = 25 nm); from ref. [9a].

The method is not restricted to metallic, siliceous or semiconductive NPs.[14] Regular biological objects are as important for the formation of thin films and nanometer-sized membranes as are NPs. A recent example of viral assembly (with $r = 33$ nm) was demonstrated by Russell and co-workers[15] with Cowpea Mosaic Virus (CPMV) at a perfluorodecaline–water interface. The virus offers an excellent system, as it is stable in organic solvents and is easily isolated in large quantities from infected black-eyed pea plants. Detection was assisted by chemical labeling with a fluorescent dye (rhodamine). Cross-linking of the CPMV particles at the interface was carried out with glutaraldehyde or biotin groups (Figure 4). Noncovalent cross-linking with the biotin–avidin interaction was superior to chemical cross-linking with glutaraldehyde, as stable and ultrathin membranes consisting of the assembled viruses were obtained. This proves the assembly concept proposed by Whitesides and Boncheva,[16] that a self-assembling system needs a sufficient degree of reversibility to form highly ordered arrays. Otherwise, disordered (glassy) arrays are produced. Thus interfaces not only provide a scaffold for the facile assembly of NPs, but also retain sufficient flexibility to rapidly correct errors during the assembly process, leading to a high degree of order with a rapid process.

The assembly of NPs at polymeric surfaces[17] demonstrates the broad applicability of the interfacial assembly concept. The interface of immiscible block-copolymer micelles provide an environment in which the surface energy in a nonaqueous system (block-copolymer micelles formed in a selective solvent for one block) is comparable to the interfacial energy of oil–water interfaces. Thus Au NPs (with $r = 5.4$ nm) can be assembled within micelles composed of polystyrene-*block*-poly(4-vinylpyridine) (PS-PVP) in toluene—a selective

© 2005 Wiley-VCH Verlag GmbH & Co. KGaA, Weinheim

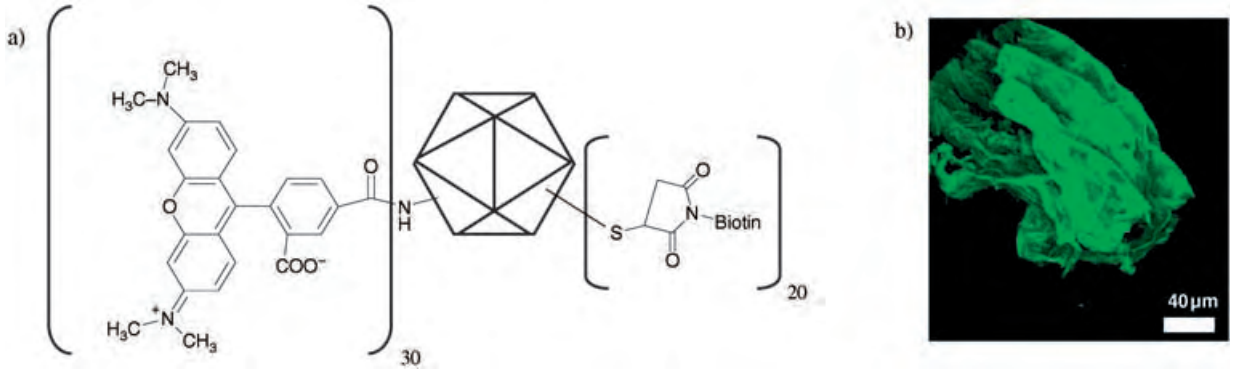


Figure 4. a) CPMV particles modified with rhodamine and biotin. b) Optical micrograph of a CPMV membrane after self-assembly and cross-linking; from ref. [15a].

solvent for the PS block (Figure 5a). Subsequent spin coating leads to an ultrathin film that concentrates the nanoparticles at the interface between the micellar core and corona in a hexagonal pattern ($d \approx 40$ nm per hexagon).[18] An extension of this concept relies on the formation of "honeycomb-patterns"[19] from a homopolymer (polystyrene) under humid conditions from a solution containing CdSe nanoparticles (Figure 5b,c).[20] During evaporation, the CdSe NPs assemble at the interface between $CHCl_3$ and water, leaving behind the micrometer-sized honeycomb pattern of the polymer with the CdSe NPs concentrated at the former location of the evaporated water droplet.

The interfaces can also be used as a medium for chemical reactions in the synthesis of heterodimeric nanoparticles.[21] For example, preassembled Fe_3O_4 nanoparticles ($d = 8$ nm) can be assembled at the interface of a dichloromethane droplet and water (Figure 6). Owing to the high density and stability of the assembly, these particles can act as seeds for the subsequent nucleation of Ag NPs ($d = 5.5$ nm) only on the outside of the Fe_3O_4 assemblies. This is an elegant approach to heterodimeric nanoparticles, consisting of two different materials.

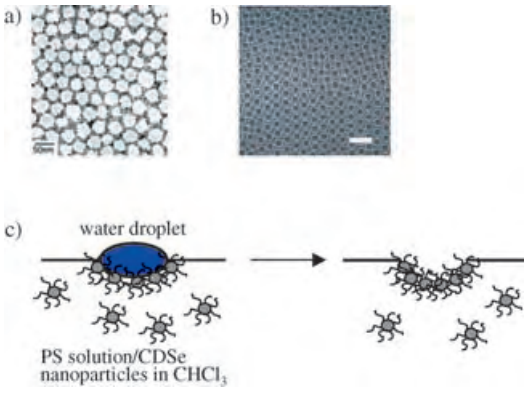


Figure 5. a) Assembly of Au nanoparticles at a polymer interface (*block*-copolymer micelles); from ref. [18a]. b) Optical fluorescence image of CdSe nanoparticles ($d = 4$ nm) of a sample obtained from solvent casting a polystyrene film from chloroform with CdSe nanoparticles under humid conditions (scale bar = 16 µm); from ref. [20]. c) Mechanism of pattern formation and concomitant particle assembly at the water–chloroform interface; from ref. [20].

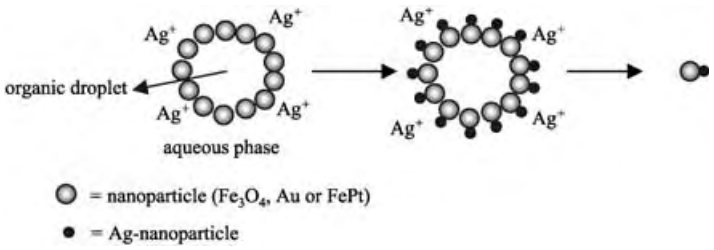


Figure 6. Formation of heterodimeric nanoparticles through the assembly of Fe_3O_4 nanoparticles on a liquid–liquid interface and subsequent seeding of Ag nanoparticles on the outside of the Fe_3O_4 nanoparticles; adapted from ref. [21].

In summary, interfaces are ubiquitous in nature and can be used broadly as ideal means for the self-assembly of nanoparticles. The ease and speed of this approach make it an excellent method for large-scale use and potentially valuable for industrial application. Especially in the area of thin-membrane generation, the functionalization and modification of nanometer-scale objects at specific positions, the size selection of nanometer-sized objects, and the controlled mixing of nanoparticles all give this method great potential for future applications in the field of nanotechnology.

Published online: July 20, 2005

[1] a) E. Katz, I. Willner, *Angew. Chem.* **2004**, *116*, 6166–6235; *Angew. Chem. Int. Ed.* **2004**, *43*, 6048–6108; b) *Nanobiotechnology* (Eds.: C. M. Niemeyer, C. A. Mirkin), Wiley-VCH, **2004**; c) *Nanoparticles* (Ed.: G. Schmid), Wiley-VCH, **2004**; d) E. Katz, A. N. Shipway, I. Willner in *Nanoscale Materials* (Eds.: L. M. Liz-Marzan, V. P. Kamat), Kluwer, Norwell, **2003**, pp. 317–343; e) C. Niemeyer, *Angew. Chem.* **2001**, *113*, 4254–4287; *Angew. Chem. Int. Ed.* **2001**, *40*, 4128–4158.

[2] a) C. P. Collier, T. Vossmeyer, J. R. Heath, *Annu. Rev. Phys. Chem.* **1998**, *49*, 371–404; b) C. B. Murray, C. R. Kagan, M. G. Bawendi, *Annu. Rev. Mater. Sci.* **2000**, *30*, 545–610; c) P. Alivisatos, *Science* **1996**, *271*, 933–937; d) E. Granot, P. Fernando, I. Willner, *J. Phys. Chem. B* **2004**, *108*, 5875–5881; e) B. B. Yellen, G. Friedman, *Adv. Mater.* **2004**, *16*, 111–115; f) H. Weller, *Angew. Chem.* **1998**, *110*, 1748–1750;

 © 2005 Wiley-VCH Verlag GmbH & Co. KGaA, Weinheim

Angew. Chem. Int. Ed. **1998**, *37*, 1658 – 1659.

[3] Representative reviews: a) A. L. Rogach, D. V. Talapin, E. V. Shevchenko, A. Kornowski, M. Haase, H. Weller, *Adv. Funct. Mater.* **2002**, *12*, 653 – 664; b) E. V. Shevchenko, D. V. Talapin, A. L. Rogach, A. Kronowski, M. Haase, H. Weller, *J. Am. Chem. Soc.* **2002**, *124*, 11480 – 11485; c) E. Shevchenko, D. Talapin, A. Kronowski, F. Wiekhorst, J. Kötzler, M. Haase, A. Rogach, H. Weller, *Adv. Mater.* **2002**, *14*, 287 – 290; an example of convective self-assembly: d) S. Vengallatore, Y. Peles, L. R. Arana, S. M. Spearing, *Sens. Actuators A* **2004**, *113*, 124 – 131.

[4] Two representative reviews: a) M.-C. Daniel, D. Astruc, *Chem. Rev.* **2004**, *104*, 293 – 346; b) S. Maenosono, T. Okubo, Y. Yamaguchi, *J. Nanopart. Res.* **2003**, *5*, 5 – 15; see also: c) M. Mizuno, Y. Sasaki, A. C. C. Yu, M. Inoue, *Langmuir* **2004**, *20*, 11305 – 11307; d) A. Gole, C. J. Orendorff, C. J. Murphy, *Langmuir* **2004**, *20*, 7117 – 7122; e) Z. Zhong, S. Patskovsky, P. Bouvrette, J. H. T. Luong, A. Gedanken, *J. Phys. Chem. B* **2004**, *108*, 4046 – 4052; f) X.-M. Li, V. Paraschiv, J. Huskens, D. N. Reinhoudt, *J. Am. Chem. Soc.* **2003**, *125*, 4279 – 4284; g) K. Lee, F. Pang, G. T. Carroll, N. J. Turro, J. T. Koberstein, *Langmuir* **2004**, *20*, 1812 – 1818; h) H. Tanaka, M. Mituishi, T. Miyashita, *Langmuir* **2003**, *19*, 3103 – 3105; i) S. Maenosono, T. Okubo, Y. Yamaguchi, *J. Nanopart. Res.* **2003**, *5*, 5 – 15; j) L. Sheeney-Hai-Ichida, B. Basnar, I. Willner, *Angew. Chem.* **2004**, *116*, 80 – 85; *Angew. Chem. Int. Ed.* **2004**, *43*, 78 – 83; k) A. N. Shipway, M. Lahav, R. Gabai, I. Willner, *Langmuir* **2000**, *16*, 8789 – 8795; l) J. B. Carroll, B. L. Frankamp, S. Srivastava, V. M. Rotello, *J. Mater. Chem.* **2004**, *14*, 690 – 694; an example of nanoparticle binding onto polymeric surfaces: m) I. Tokareva, S. Minko, J. H. Fendler, E. Hutter, *J. Am. Chem. Soc.* **2004**, *126*, 15950 – 15951; n) M. Carrara, J. J. Kakkassery, J.-P. Abid, D. J. Fermin, *ChemPhysChem* **2004**, *5*, 571 – 575; o) R. Bhat, J. Genzer, B. N. Chaney, H. W. Sugg, A. Liebmann-Vinson, *Nanotechnology* **2003**, *14*, 1145 – 1152.

[5] a) M. Andersson, K. Elihn, K. Fromel, K. D. Caldwell, *Coll. Surf. B: Biointerfaces* **2004**, *34*, 165 – 171; b) L. M. Demer, D. S. Ginger, S.-J. Park, Z. Li, S.-W. Chung, C. A. Mirkin, *Science* **2002**, *296*, 1836 – 1838; c) Y. Cao, R. Jin, C. A. Mirkin, *J. Am. Chem. Soc.* **2001**, *123*, 7961 – 7962; d) S. Park, A. A. Lazarides, C. A. Mirkin, P. W. Brazis, C. R. Kannewurf, R. L. Letsinger, *Angew. Chem.* **2000**, *112*, 4003 – 4006; *Angew. Chem. Int. Ed.* **2000**, *39*, 3845 – 3848; e) N. L. Rosi, C. S. Thaxton, C. A. Mirkin, *Angew. Chem.* **2004**, *116*, 5616 – 5619; *Angew. Chem. Int. Ed.* **2004**, *43*, 5500 – 5503; f) J. J. Storhoff, C. A. Mirkin, *Chem. Rev.* **1999**, *99*, 1849 – 1862, and references therein; g) L. M. Demers, C. A. Mirkin, *Angew. Chem.* **2001**, *113*, 3159 – 3161; *Angew. Chem. Int. Ed.* **2001**, *40*, 3069 – 3071.

[6] A. Mulder, J. Huskens, D. N. Reinhoudt, *Org. Biomol. Chem.* **2004**, *2*, 3409 – 3424, and references therein.

[7] a) A. K. Boal, F. Ilhan, J. E. DeRouchey, T. Thurn-Albrecht, V. M. Rotello, *Nature* **2000**, *404*, 476 – 478; b) A. K. Boal, V. M. Rotello, *Langmuir* **2000**, *16*, 9527 – 9532; c) R. Zirbs, F. Kienberger, P. Hinterdorfer, W. H. Binder, *Langmuir* **2005**, in press.

[8] a) V. Mahalingam, S. Onclin, M. Peter, B. J. Ravoo, J. Huskens, D. B. Reinhoudt, *Langmuir* **2004**, *20*, 11756 – 11762; b) A. Mulder, S. Onclin, M. Peter, J. P. Hoogenboom, H. Beijleveld, J. ter Maar, M. F. Garcia-Parajo, B. Ravoo, J. Huskens, N. F. van Hulst, D. N. Reinhoudt, *Small* **2005**, *1*, 242 – 253; c) A. Sanyal, T. B. Norsten, O. Uzun, V. M. Rotello, *Langmuir* **2004**, *20*, 5958 – 5964.

[9] a) H. Duan, D. Wang, D. G. Kurth, H. Möhwald, *Angew. Chem.* **2004**, *116*, 5757 – 5760; *Angew. Chem. Int. Ed.* **2004**, *43*, 5639 – 5642; b) Y. Lin, H. Skaff, T. Emrick, A. D. Dinsmore, T. P. Russell, *Science* **2003**, *299*, 226 – 229; c) F. Reincke, S. G. Hickey, W. K. Kegel, D. Vanmaekelbergh, *Angew. Chem.* **2004**, *116*, 464 – 468; *Angew. Chem. Int. Ed.* **2004**, *43*, 458 – 462.

[10] a) R. Aveyard, B. P. Binks, J. H. Clint, *Adv. Coll. Interfac. Sci.* **2003**, *100–102*, 503 – 546; a theoretical description: b) P. P. Kralchevski, I. B. Ivanov, K. P. Ananthapadmanabhan, A. Lips, *Langmuir* **2005**, *21*, 50 – 63.

[11] a) B. Binks, J. H. Clint, *Langmuir* **2002**, *18*, 1270 – 1273, and references therein; b) B. P. Binks, S. O. Lumsdon, *Langmuir* **2000**, *16*, 8622 – 8631.

[12] a) Y. Lin, A. Böker, H. Skaff, D. Cookson, A. D. Dinsmore, T. Emrick, T. P. Russell, *Langmuir* **2005**, *21*, 191 – 194; b) Y. Lin, H. Skaff, T. Ermick, A. D. Dinsmore, T. P. Russell, *Science* **2003**, *299*, 226 – 229.

[13] B. Su, J.-P. Abid, D. J. Fermin, H. H. Girault, H. Hoffmannova, P. Krtil, Z. Samec, *J. Am. Chem. Soc.* **2004**, *126*, 915 – 919.

[14] a) J.-W. Hu, G.-B. Han, S.-G. Sun, Z.-Q. Tian, *Langmuir* **2004**, *20*, 8831 – 8838; b) S. Chen, H. Yao, K. Kimura, *Langmuir* **2001**, *17*, 733 – 739; J. K. Sakata, A. Dwoskin, J. L. Vigorita, E. M. Spain, *J. Phys. Chem. B* **2005**, *109*, 138 – 141; U. K. Gautam, M. Gosh, C. N. R. Rao, *Langmuir* **2004**, *20*, 10775 – 10778; c) H. Schwartz, Y. Harel, S. Efrima, *Langmuir* **2001**, *17*, 3884 – 3892; d) D. Rautaray, R. Kavathekar, M. Sastry, *Faraday Discuss.* **2005**, *129*, 205 – 217; e) M. Platt, R. A. W. Dryfe, E. P. L. Roberts, *Electrochim. Acta* **2004**, *49*, 3937 – 3945.

[15] a) J. T. Russell, Y. Lin, A. Böker, L. Su, P. Carl, H. Zettl, J. He, K. Still, R. Tangirala, T. Emrick, K. Littrell, P. Thiyagarajan, D. Cookson, A. Frey, Q. Wang, T. P. Russell, *Angew. Chem.* **2005**, *117*, 2472 – 2478; *Angew. Chem. Int. Ed.* **2005**, *44*, 2420 – 2426; b) Y. Lin, H. Skaff, A. Böker, A. D. Dinsmore, T. Emrick, T. P. Russell, *J. Am. Chem. Soc.* **2003**, *125*, 12690 – 12691.

[16] G. M. Whitesides, M. Boncheva, *Proc. Natl. Acad. Sci. USA* **2002**, *99*, 4769 – 4774.

[17] For a review, see: a) I. W. Hamley, *Nanotechnology* **2003**, *14*, R39 – R54; b) R. Glass, M. Möller, J. Spatz, *Nanotechnology* **2003**, *14*, 1153 – 1160; c) S.-W. Yeh, Y.-T. Chang, C.-H. Chou, K.-H. Wie, *Macromol. Rapid Commun.* **2004**, *25*, 1679 – 1686, and references therein.

[18] a) B.-H. Sohn, J.-M. Choi, S. I. Yoo, S.-H. Yun, W.-C. Zin, J. C. Jung, M. Kanehara, T. Hirata, T. Teranishi, *J. Am. Chem. Soc.* **2003**, *125*, 6368 – 6369; b) J. J. Chiu, B. J. Kim, E. J. Kramer, D. J. Pine, *J. Am. Chem. Soc.* **2005**, *127*, 5036 – 5037.

[19] G. Widawski, M. Rawiso, B. Francois, *Nature* **1994**, *369*, 387 – 389.

[20] A. Böker, Y. Lin, K. Chiapperin, R. Horowitz, M. Thompson, V. Careon, T. Xu, C. Abetz, H. Skaff, A. D. Dinsmore, T. Emrick, T. P. Russell, *Nat. Mater.* **2004**, *3*, 302 – 306.

[21] H. Gu, Z. Yang, J. Gao, C. K. Chang, B. Xu, *J. Am. Chem. Soc.* **2005**, *127*, 34 – 35.

 © 2005 Wiley-VCH Verlag GmbH & Co. KGaA, Weinheim

DOI: 10.1002/anie.200500691

Electrophilic Reagents

N-Acylhydrazones as Versatile Electrophiles for the Synthesis of Nitrogen-Containing Compounds

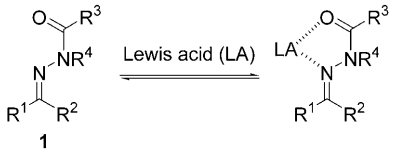
*Masaharu Sugiura and Shū Kobayashi**

Keywords:
allylation · cyanation · cycloaddition · Mannich reaction · *N*-acylhydrazones

The use of N-acylhydrazones as electrophiles in reactions with nucleophiles has recently made some important advances. N-Acylhydrazones, which can be readily prepared and stored, act as stable imine surrogates in these reactions. The hydrazide products are useful, often chiral building blocks which can be transformed into various nitrogen-containing compounds by cleavage of the N–N bond. The N-acyl groups often play important roles as templates for metal catalysis in controlling stereochemistry. This Minireview summarizes the most recent results of N-acylhydrazone chemistry, and provides an overview of current developments in this field.

1. Introduction

N-Acylhydrazones **1**, which are readily obtained by the condensation of aldehydes or ketones and acylhydrazines[1] in the presence of an acid catalyst, represent a class of azomethine compounds (Scheme 1). They are often crystalline, can be purified by simple recrystallization, and have



1

Scheme 1. The chelation effect of *N*-acylhydrazones toward metal catalysts.

therefore been used for the identification and purification of carbonyl compounds.[2] However, organic chemists have only quite recently focused on their utility as electrophiles for the synthesis of nitrogen-containing compounds. *N*-Acylhydrazones serve as storable, stable imine equivalents which can react with various nucleophiles. A variety of *N*-acylhydrazones can be prepared from enolizable, sterically hindered (α- or β-branched), water-soluble, and/or chiral α-substituted aldehydes or ketones (Scheme 2). Even aqueous solutions of aldehydes or ketones such as glyceraldehyde and chloral can be used. Various *N*-acyl groups ($-COR^3$) can be installed and often play an important role in the control of reactivity and selectivity. The *N*-acylhydrazone structure provides a suitable template for the chelation of Lewis acids, which activate the imino carbon atom as a target for nucleophilic attack (Scheme 1). This Minireview summarizes recent developments in the chemistry of *N*-acylhydrazones as electrophiles (Scheme 2).

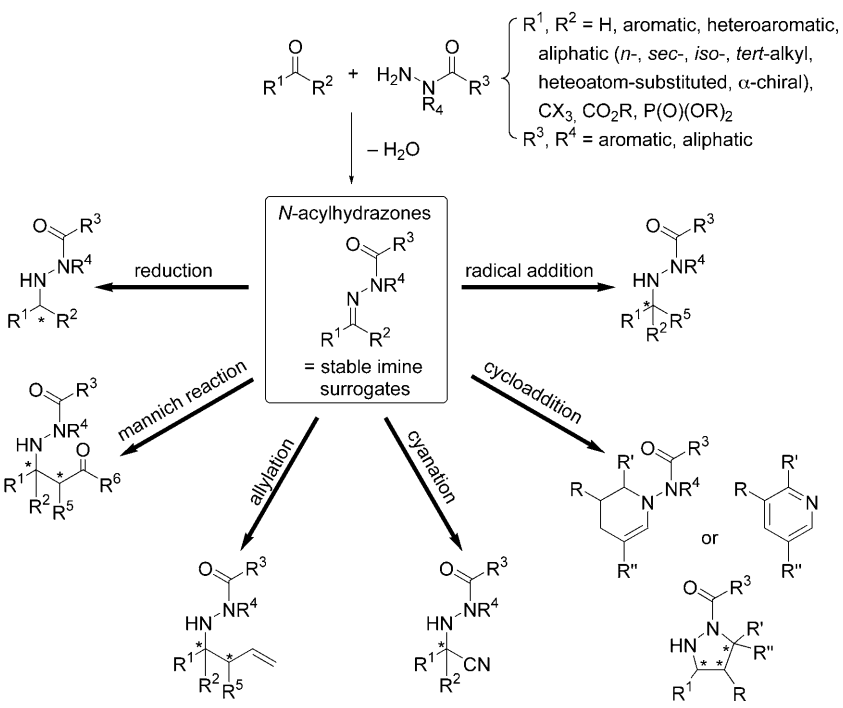
[*] Dr. M. Sugiura, Prof. S. Kobayashi
Graduate School of Pharmaceutical Sciences
The University of Tokyo
Hongo, Bunkyo-ku, Tokyo 113-0033 (Japan)
Fax: (+81) 3-5684-0634
E-mail: skobayas@mol.f.u-tokyo.ac.jp

2. Reductions

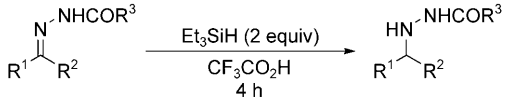
Reductions of *N*-acylhydrazones to *N*′-alkyl-*N*-acylhydrazines have been accomplished with catalytic hydrogenation,[3] reducing metals,[4] and boron,[5] silicon,[6] or tin[7] reagents. For example, triethylsilane reduces aldehyde- or ketone-derived *N*-acylhydrazones in trifluoroacetic acid (Scheme 3).[6] Whereas aldehyde-derived *N*-acylhydrazones are readily reduced at 0 °C, higher temperatures are needed for the ketone derivatives.

Recently, Qin and Friestad reported that *N*-acylhydrazones **1** derived from ketones and a chiral *N*-aminooxazolidinone were diastereoselectively reduced by tributyltin hydride in the presence of boron trifluoride etherate, whereas the use of triethylsilane as reducing agent resulted only in recovery of the starting material (Scheme 4).[7] Diastereomeric ratios of the products corresponded to the *E*/*Z* ratios of

InterScience
© 2005 Wiley-VCH Verlag GmbH & Co. KGaA, Weinheim



Scheme 2. The formation and reactions of *N*-acylhydrazones.



R^1 = Ar or alkyl, R^2 = H, R^3 = Me or Ph (0 °C): 74-95%
R^1 = R^2 = Me, R^3 = Me or Ph (50 °C): 86% each
R^1 = Ph, R^2 = Me, R^3 = Me or Ph (50 °C): 56% or 46%

Scheme 3. Reduction of *N*-acylhydrazones by triethylsilane.

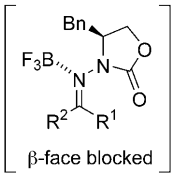
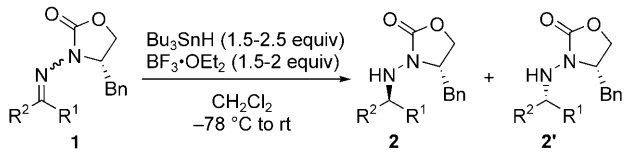


Figure 1. Proposed intermediate of the diastereoselective reduction shown in Scheme 4.

compound **1**. The observed stereochemistry was explained through a nonchelation model in which the *N*-acyl oxygen lies *anti* with respect to the BF_3 group coordinated to the imino nitrogen atom (Figure 1).

In 1992, Burk and co-workers reported pioneering work on catalytic asymmetric hydrogenation of *N*-acylhydrazones (Scheme 5).[3] The concept of substrate chelation in the highly enantioselective hydrogenation of enamides or enol acetates led them to apply hydrazones with *N*-acyl groups as secondary donors. The best results were obtained with cationic rhodium-DuPhos complexes as catalysts, an alcohol as solvent, conjugatively electron-donating *N*-acyl groups (R^3: 4-$Me_2NC_6H_4$ > 4-$MeOC_6H_4$ > Ph > 2-furyl > 2-$MeOC_6H_4$ > Me > 4-$O_2NC_6H_4$), and electron-withdrawing groups on R^1 ($R^1 = p$-XC_6H_4, X = $NO_2 \approx CO_2Et$ > Br > H > $SiMe_3$ > OMe; R^2 = Me). The high electron-donating ability of the *N*-acyl group and strong π-backbonding from the metal to the electron-deficient C=N bonds have been suggested to be responsible for the decrease in conformational mobility of the substrate in the transition state, leading to high enantioselectivity. Notably, high chemoselectivity was observed in this hydrogenation; only the C=N bonds of hydrazones were reduced in the presence of other functional groups (ketones, aldehydes, esters, nitriles, imines, halogens, nitro groups, alkenes and alkynes). Even chalcon-derived *N*-benzoylhydrazone showed complete chemoselectivity in the same molecule to afford homoallylic hydrazide, although enantio-



R^1 = Et, R^2 = *i*Pr (89%, 80:20), *c*C_5H_9 (82%, 76:24), *c*C_6H_{11} (76%, 85:15) or *t*Bu (94%, 89:11)
R^1 = Ph, R^2 = *i*Pr (92%, 19:81), *c*C_5H_9 (78%, 26:74), *c*C_6H_{11} (94%, 18:82) or *t*Bu (94%, 12:88)

Scheme 4. Diastereoselective reduction of *N*-acylhydrazones by tributyltin hydride. Yields and diastereomeric ratios (**2**/**2'**) are given in parentheses. Bn = benzyl.

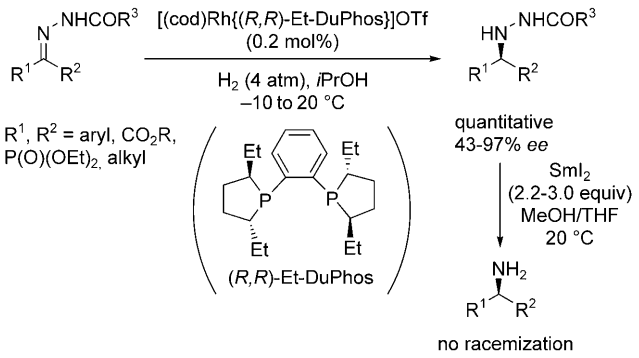


Masaharu Sugiura was born in 1970 in Tokyo and received his PhD at the Tokyo Institute of Technology in 1997 under the supervision of Professor Takeshi Nakai. After postdoctoral work at Sagami Chemical Research Center (Dr. Shiro Terashima) and at Florida State University (Professor Marie E. Krafft), he joined the research group of Professor Kobayashi as a JST postdoctoral fellow in 2000. He was appointed assistant professor in 2004, and lecturer in 2005 at the Graduate School of Pharmaceutical Sciences of the University of Tokyo. His research interests include the development of new synthetic methods and novel catalysts.



Shū Kobayashi was born in Tokyo in 1959. He received his PhD in 1988 under the direction of Professor T. Mukaiyama at the University of Tokyo. After eleven years at Science University of Tokyo, he moved to the Graduate School of Pharmaceutical Sciences of the University of Tokyo in 1998. His research interests include development of new synthetic methods and novel catalysts, organic reactions in water, solid-phase synthesis, total synthesis of biologically interesting compounds, and organometallic chemistry. His honors include the Springer Award in Organometallic Chemistry (1997), the IBM Science Award (2001), and the Organic Reactions Lecturer Award (2002).

© 2005 Wiley-VCH Verlag GmbH & Co. KGaA, Weinheim



Scheme 5. Asymmetric catalytic hydrogenation of *N*-acylhydrazones.

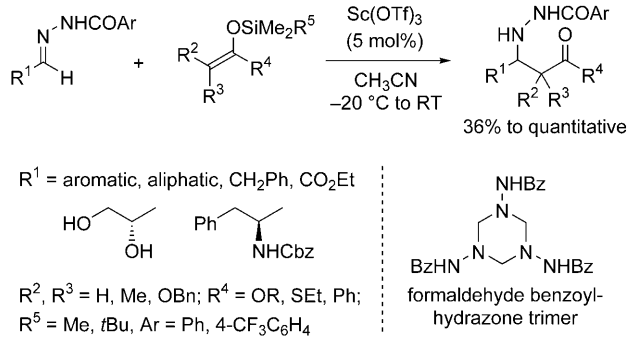
selectivity in this case was low. High chemoselectivity can be attributed to two effects: 1) capture of the catalyst by substrate chelation by the *N*-acyl group; 2) product inhibition by *N*-acylhydrazine (Scheme 5). With regards to the second effect, it has been established that the Rh-DuPhos catalyst can reduce aldehydes, alkenes, and alkynes, but the presence of *N*-acylhydrazine inhibits the reduction of these functional groups. Furthermore, *N*-acylhydrazone coordinates to the catalyst with higher affinity than does *N*-acylhydrazine, allowing catalytic turnover.

Burk and co-workers also developed a new method for the cleavage of the N–N bond in *N*-acylhydrazine. Treatment with samarium(II) iodide (2.2–3.0 equiv) at 20 °C in MeOH/THF gave primary amines almost instantaneously without loss of enantiomeric purity.

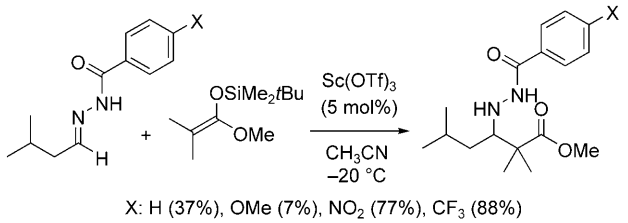
3. Mannich Reactions

Mannich reactions are among the most powerful tools for the preparation of β-amino carbonyl compounds. In particular, the last two decades have witnessed significant developments, including asymmetric catalytic Mannich reactions with preformed imines and/or enolates.[8]

In 1998, our research group found that *N*-acylhydrazones can be efficiently activated by a catalytic amount of a Lewis acid such as $Sc(OTf)_3$ or $Yb(OTf)_3$ to react with silicon enolates (Scheme 6).[9] Various types of *N*-acylhydrazones (aromatic, aliphatic, α,β-unsaturated, α-oxy and α-aza aldehydes, as well as glyoxylate and formaldehyde) and silicon enolates (ester, thioester, and ketone derivatives) readily gave rise to β-*N*′-acylhydrazinocarbonyl compounds in high yield. In contrast to $Sc(OTf)_3$ and $Yb(OTf)_3$, typical Lewis acids such as titanium tetrachloride, tin tetrachloride, and boron trifluoride were not effective. The effect of *N*-acyl groups on reactivity was examined in the $Sc(OTf)_3$-catalyzed reaction of isovaleraldehyde-derived *N*-aroylhydrazones with a silicon enolate (Scheme 7). Among the *para*-substituted

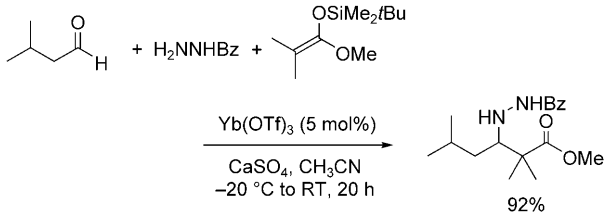


Scheme 6. Lewis acid catalyzed Mannich reactions with *N*-acylhydrazones. Cbz = benzyloxycarbonyl, Bz = benzoyl.



Scheme 7. Effect of *N*-acyl groups on Lewis acid catalyzed Mannich reactions.

benzoyl groups tested, electron-withdrawing groups such as CF_3 were found to be the most reactive. A three-component reaction of isovaleraldehyde, benzhydrazide and the silicon enolate shown in Scheme 7 was also found to proceed smoothly with high yield in the presence of $Yb(OTf)_3$ and $CaSO_4$ (Scheme 8).

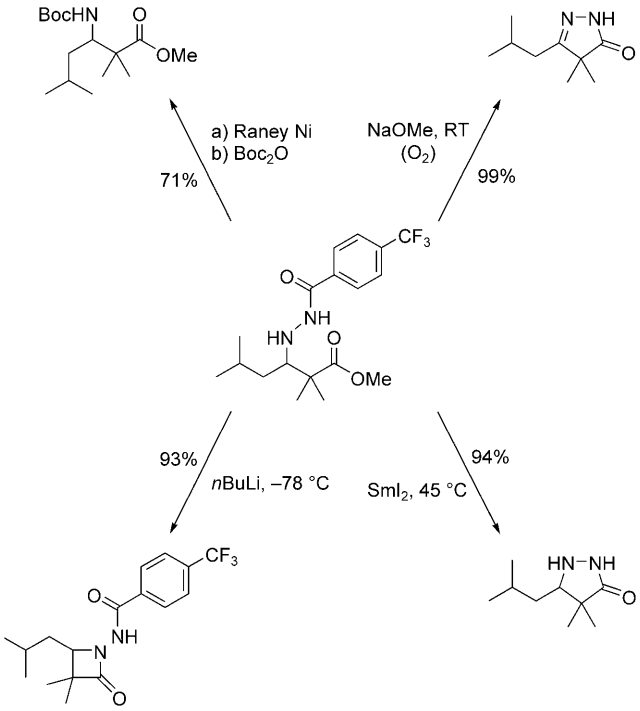


Scheme 8. Three-component Mannich reaction.

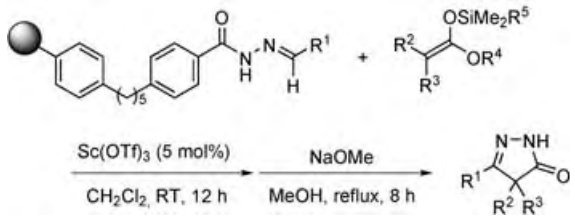
β-*N*′-Acylhydrazinocarbonyl compounds produced by Mannich reaction can undergo further transformations as shown in Scheme 9. Reductive cleavage of the N–N-bond with Raney nickel under a hydrogen atmosphere provided β-amino esters, whereas reactions with *n*-butyl lithium, sodium methoxide, and samarium (II) iodide, gave β-lactam, pyrazolone, and pyrazolidinone derivatives, respectively. Polymer-supported *N*-acylhydrazones were also developed, and their reactions with silicon enolates in the presence of $Sc(OTf)_3$ followed by treatment of sodium methoxide gave various pyrazolone derivatives (Scheme 10).[9c]

Catalytic asymmetric Mannich reactions of *N*-acylhydrazones have also been performed with a chiral zirconium catalyst prepared from zirconium(IV) *tert*-butoxide and (*R*)-3,3′-dibromo-2,2′-dihydroxy-1,1′-dinaphthyl (Scheme 11).[10] 4-Trifluoromethylbenzoyl hydrazones reacted with silicon enolates to afford the corresponding adducts in good yield and with high enantiomeric excess. The products were

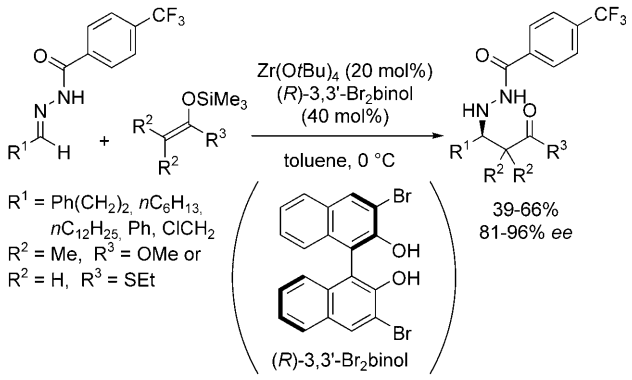
© 2005 Wiley-VCH Verlag GmbH & Co. KGaA, Weinheim



Scheme 9. Transformation of β-*N*′-acylhydrazinocarbonyl products of Mannich reactions.



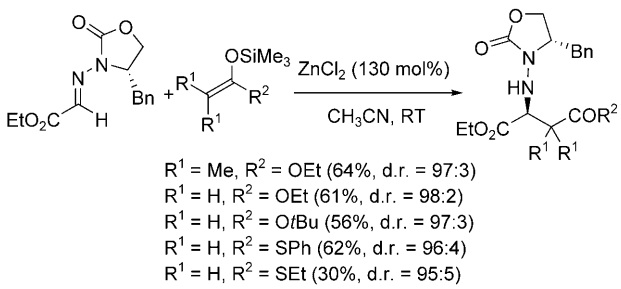
Scheme 10. Solid-phase synthesis of pyrazolone.



Scheme 11. Asymmetric catalytic Mannich reaction.

transformed into β-amino esters, β-lactams or pyrazolidinones without loss of enantiomeric purity.

Mannich reactions of chiral *N*-aminooxazolidinone-derived acylhydrazones with silicon enolates proceeded in the presence of zinc(II) chloride (130 mol%) with high diastereofacial selectivity (Scheme 12).[11] A catalytic amount of $Sc(OTf)_3$ was also effective in some cases, whereas an attack of the nucleophile on the ester group to some extent was observed in other cases. The diastereofacial selectivity can be explained by a selective chelation of Zn^{II} between the imino nitrogen atom and the *N*-acyl oxygen atom. The nucleophile attacks from the *Si* face, as the *Re* face is blocked by the benzyl group (Figure 2).



Scheme 12. Diastereoselective Mannich reaction.

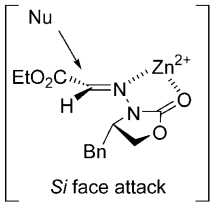
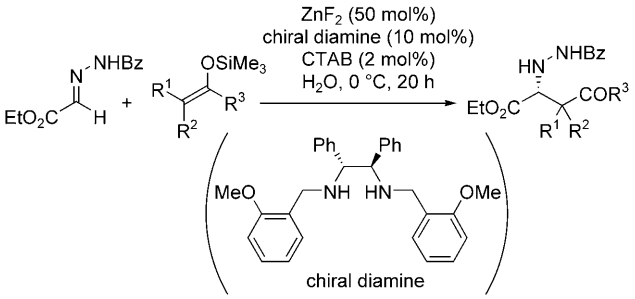


Figure 2. Proposed transition state of the diastereofacial Mannich reaction shown in Scheme 12.

Catalytic asymmetric Mannich reactions in aqueous media were carried out for the first time by the use of *N*-acylhydrazono esters, taking advantage of the tolerance *N*-acylhydrazines have toward water (Scheme 13).[12] It was found that a complex of zinc(II) fluoride with chiral 1,2-phenylethylene diamine effectively catalyzed the reactions of hydrazono esters with silicon enolates to afford Mannich adducts with high enantio- and diastereoselectivity. Reactions proceeded smoothly in water as the sole solvent (mostly in the presence of cetyltrimethylammonium bromide (CTAB), a cationic surfactant). Both diastereomers were obtained with high selectivity by choosing geometrical isomers of silicon enolates. Notably, the use of water as a solvent is a key to obtain high yields and selectivities.



$R^1 = R^2 = H$, $R^3 = p\text{-}XC_6H_4$ (X = H, Me, OMe, Cl): 91-94%, 91-95% *ee*[a]
R^1 = Me, R^2 = H, R^3 = Ph (>99% *Z*): 93%, 94% *syn*, 96% *ee* (*syn*)
R^1 = Et, R^2 = H, R^3 = Ph (>99% *Z*): 76%, 96% *syn*, 96% *ee* (*syn*)
R^1 = Me, R^2 = H, R^3 = Et (98% *Z*): 57%, 86% *syn*, 97% *ee* (*syn*)
R^1 = H, R^2 = Me, R^3 = Et (76% *E*): 94%, 88% *anti*, 94% *ee* (*anti*)
R^1 = Me, R^2 = H, R^3 = S*t*Bu (98% *E*): 39%, 92% *anti*, 94% *ee* (*anti*)
R^1 = H, R^2 = Me, R^3 = S*t*Bu (97% *Z*): 51%, 86% *syn*, 67% *ee* (*syn*)

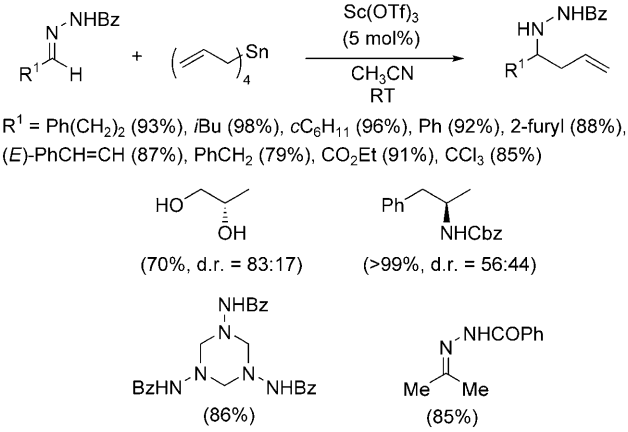
Scheme 13. Catalytic enantioselective Mannich reaction in an aqueous medium. [a] Without CTAB.

© 2005 Wiley-VCH Verlag GmbH & Co. KGaA, Weinheim

4. Allylation

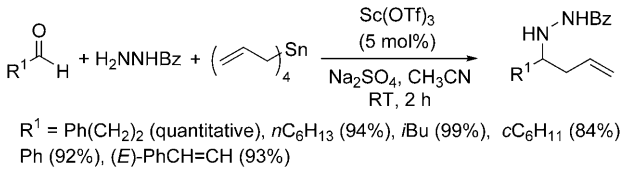
The addition of allyl metal compounds to azomethines provides synthetically useful homoallylic amine derivatives.[13] In contrast to the allylation of carbonyl compounds, the stereoselective allylation of azomethines has undergone very little study.

A variety of *N*-acylhydrazones can be allylated by tetraallyltin in the presence of a Lewis acid catalyst (Scheme 14).[9b,14] The reaction is tolerant to many functional



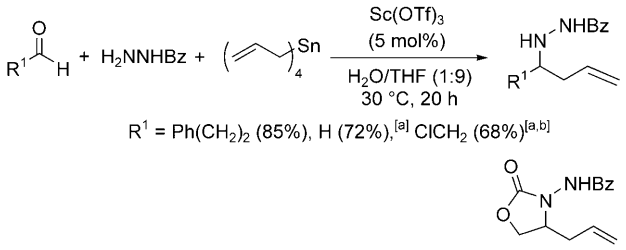
Scheme 14. Lewis acid catalyzed allylation of *N*-acylhydrazones.

groups, and homoallylic hydrazides were obtained in high yield. Furthermore, it was possible to use *N*-acylhydrazones prepared in situ without isolation (Scheme 15). It was re-



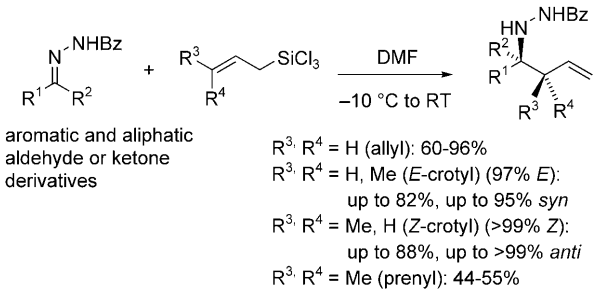
Scheme 15. Three-component allylation with in situ formation of *N*-acylhydrazones.

vealed in a subsequent study that three-component reactions of aldehydes, *N*-acylhydrazines, and tetraallyltin also proceeds well in an aqueous medium (Scheme 16).[14b]



Scheme 16. Allylation in an aqueous medium. [a] A commercial aqueous solution of the aldehyde was used. [b] The oxazolidin-2-one shown at right was obtained in 75% yield if the reaction was treated directly with saturated aqueous $NaHCO_3$.

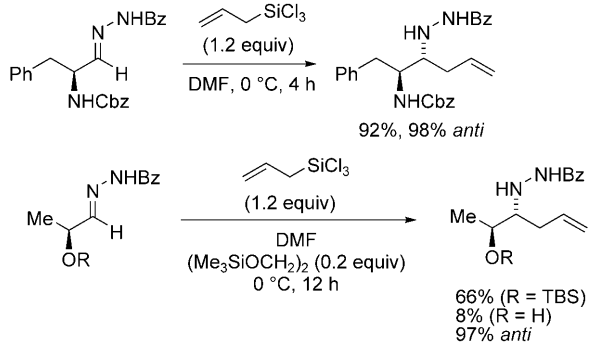
The stereospecific allylation of *N*-acylhydrazones with allyltrichlorosilanes as allylation agents is possible upon the use of *N*,*N*-dimethylformamide (DMF) as a solvent (Scheme 17).[15] *Syn*-crotylated products were obtained from



Scheme 17. Stereoselective allylation of *N*-acylhydrazones with allyltrichlorosilanes in DMF.

(*E*)-crotyltrichlorosilane with high diastereoselectivity, whereas (*Z*)-crotyltrichlorosilane stereoselectively afforded *anti*-crotylated products. *N*,*N*-Dimethylformamide is proposed to coordinate allyltrichlorosilanes to form hypervalent silicon species, which then undergo nucleophilic attack to afford *N*-acylhydrazone products *via* six-membered chair-like transition states. We defined such Lewis base catalysts as neutral coordinate organocatalysts (NCOs). Notably, even sterically demanding ketone-derived *N*-acylhydrazones underwent highly diastereoselective crotylation.[15c]

Reactions of α-chiral *N*-acylhydrazones with allyltrichlorosilane in DMF showed high diastereofacial selectivity (Scheme 18). The Felkin–Anh model could explain

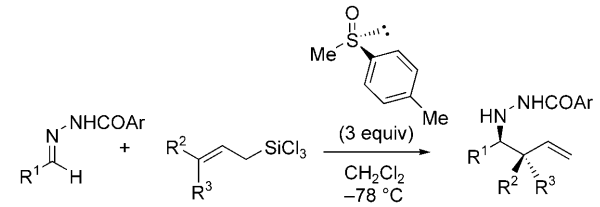


Scheme 18. Diastereofacial selective allylation of chiral *N*-acylhydrazones. TBS = *tert*-butyldimethylsilyl.

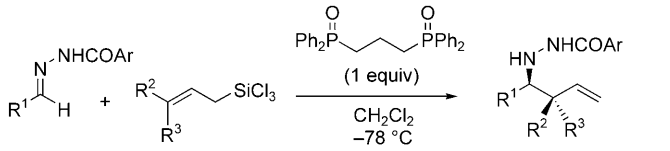
the observed *anti*-selectivity.[15b] A search for further effective NCOs revealed that a stoichiometric amount of a sulfoxide species promoted the reaction (Scheme 19).[16] Importantly, enantioselective allylation was accomplished for the first time by the use of simple, optically active (*R*)-methyl *p*-tolylsulfoxide. High stereoselectivity was observed not only in allylation but also in crotylation.

In an effort to decrease the amount of NCOs needed, a bidentate propylene-tethered bis(phosphine) dioxide emerged as a more efficient catalyst (Scheme 20),[17] with

© 2005 Wiley-VCH Verlag GmbH & Co. KGaA, Weinheim

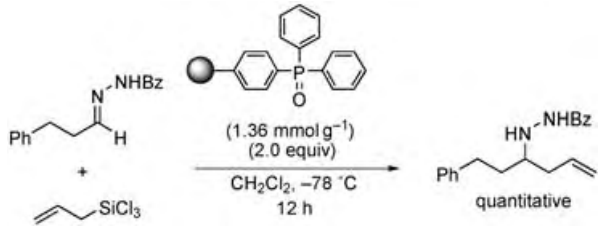


Scheme 19. Enantioselective allylation with a chiral sulfoxide.



Scheme 20. A bis(phosphine) dioxide as an NCO for allylation.

which the less-reactive aromatic *N*-acylhydrazones were found to react well. Furthermore, a polymer-supported phosphine oxide was also developed as a recoverable and

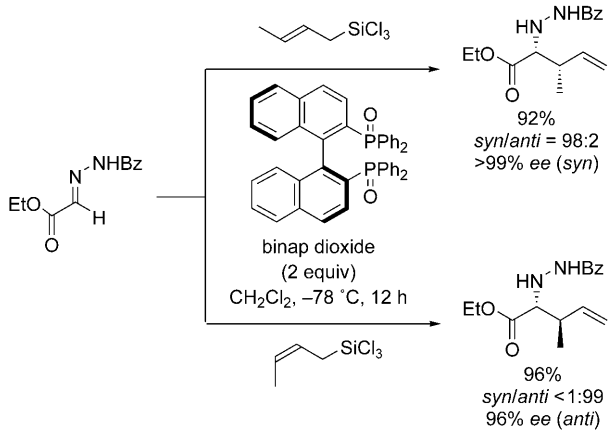


Scheme 21. A polymer-supported phosphine oxide as an NCO for allylation.

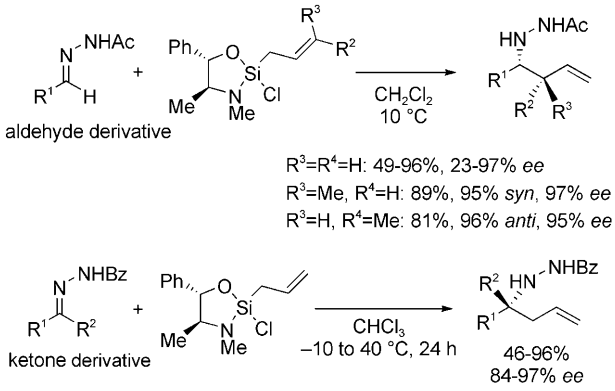
reusable NCO (Scheme 21). This polymer-bound catalyst exhibited a higher activity than a polymer-supported formamide, which was effective for the allylation of aldehydes with allyltrichlorosilane.

Meanwhile, the highly stereoselective asymmetric allylation of a hydrazino ester was carried out with (*S*)-binap dioxide as a chiral NCO (Scheme 22).[17b] The synthetic utility of this system was demonstrated by the highly enantio- and diastereoselective syntheses of α- and β-chiral amino acid derivatives, such as D-alloisoleucine.

Leighton and co-workers reported related reactions with ephedrine-derived chiral allylchlorosilanes (Scheme 23).[18] It is significant that even sterically encumbered ketone-derived *N*-acylhydrazones underwent highly enantioselective allylation. The chlorine atom of the allylsilane is important for reactivity, and *N*-methylated *N*-acylhydrazone is unreactive;



Scheme 22. Enantioselective allylation of an *N*-acylhydrazono ester with binap dioxide; binap = 2,2′-bis(diphenylphosphino)-1,1′-binaphthyl.



Scheme 23. Enantioselective allylation with a chiral allylsilane.

these two points suggest that the reaction proceeds by the formation of a covalent Si–O bond between the silane reactant and the acyl oxygen atom of the *N*-acylhydrazone with the liberation of hydrogen chloride (Figure 3).

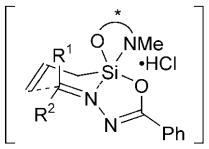
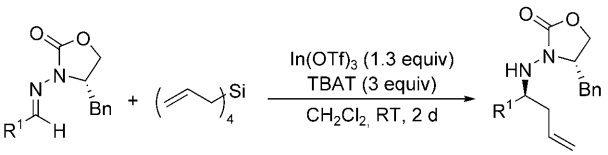


Figure 3. Proposed transition state of the allylation shown in Scheme 23.

Friestad and Ding reported the diastereoselective reaction of *N*-acylhydrazones derived from a chiral *N*-aminooxazolidinone with allylsilanes in the presence of a stoichiometric amount of indium triflate and tetrabutylammonium triphenyldifluorosilicate (TBAT) (Scheme 24).[19] Among the allylsilanes tested, allyltrimethylsilane, allyl(diisopropylamino)dimethylsilane, and tetraallylsilane (in increasing order of reactivity) were found to be effective as



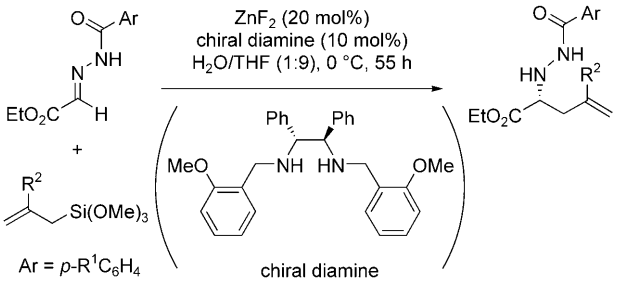
R1 = Ph (78%, d.r. > 99:1), *p*-MeC6H4 (94%, d.r. = 98:2), *m*-O2NC6H4 (71%, d.r. > 99:1), 2-naphthyl (82%, d.r. = 98:2), 2-furyl (58%, d.r. = 96:4), (*E*)-PhCH=CH (60%, d.r. = 95:5), Et (51%, d.r. = 82:18)

Scheme 24. Diastereoselective allylation with allylsilanes.

 © 2005 Wiley-VCH Verlag GmbH & Co. KGaA, Weinheim

allylating agents, whereas triphenyl-, trimethoxy-, and chlorinated allylsilanes were ineffective. It was suggested that the reaction proceeded through the addition of a hypervalent silicate to the Lewis acid complexed hydrazone.

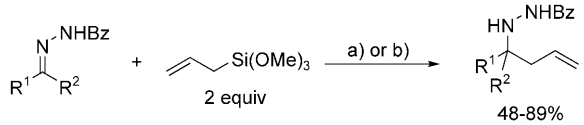
The first catalytic asymmetric allylation of *N*-acylhydrazono esters in an aqueous medium was performed with allyltrimethoxysilanes as allylating agents and zinc(II) fluoride in combination with a chiral 1,2-phenylethylenediamine



R^1 = H, R^2 = H (77%, 75% *ee*[a]), R^1 = OMe, R^2 = H (84%, 81% *ee*),
R^1 = OEt, R^2 = H (92%, 81% *ee*), R^1 = OEt, R^2 = Me (88%, 65% *ee*),
R^1 = OEt, R^2 = Ph (62%, 78% *ee*)

Scheme 25. Catalytic enantioselective allylation in an aqueous medium. [a] 90 h.

derivative as catalyst (Scheme 25).[20] The Zn(OH)F/chiral diamine was catalytically inactive, yet following the addition of $(EtO)_3SiF$ to this system, similar yield and selectivity to those of the reaction with ZnF_2/chiral diamine were observed. This is indicative of the regeneration of ZnF_2 from Zn(OH)F and the fluorosilane by-product, leading to catalytic turnover of the fluoride anion. The methoxy groups of the chiral diamine ligand play an essential role in attaining high yields and selectivities. Improvement of the yield was also observed upon the use of 4-alkoxybenzoylhydrazones. Importantly, water was indispensable for the promotion of this reaction.



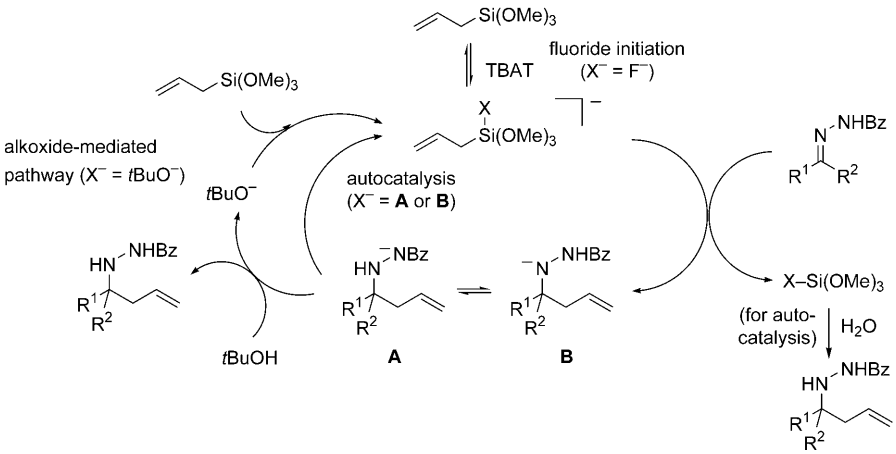
R^1 = Ph, nC_5H_{11}, (*E*)-PhCH=CH, *p*-$NO_2C_6H_4$, 3,4-$(MeO)_2C_6H_4$, R^2 = H;
R^1 = R^2 = Me; R^1 = Me, R^2 = CO_2Et
a) CuCl, TBAT, dppe (20 mol% each), *t*BuOH (2 equiv), DMF, 80 °C, 1-2 h
b) TBAT (20 mol%), *t*BuOH (2 equiv), DMF, RT, 17-72 h

Scheme 26. Catalytic allylation under various reaction conditions; dppe = 1,2-bis(diphenylphosphino)ethane

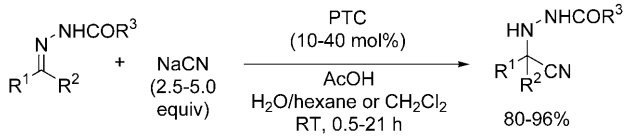
More recently, Ding and Friestad reported the reaction of *N*-acylhydrazones with allyltrimethoxysilane under two possible conditions (Scheme 26).[21] One case is closely related to the conditions reported by Shibasaki and co-workers,[22] in which CuCl, TBAT, and a phosphorous ligand are used in the presence of *t*BuOH as a proton source. The other set of conditions involves a catalytic amount of TBAT and two equivalents of *t*BuOH. Control experiments supported the hypothesis that reactions under these conditions proceed through distinctly different mechanisms. A Cu-containing allyl nucleophile was suggested for the former case, whereas an autocatalytic and/or alkoxide-catalytic mechanism was proposed for the latter (Scheme 27).

5. Cyanation

The hydrocyanation of *N*-acylhydrazones enables a practical access to α-hyrazino acids and related chiral building blocks.[23] It was reported in 1990 that the addition of hydrogen cyanide generated in situ to *N*-acyl or *N*-tosylhydrazones in a biphasic system takes place efficiently in the presence of a phase-transfer catalyst (Scheme 28).[24] More recently, the Lewis acid hafnium(IV) triflate was found to



Scheme 27. Proposed mechanism of the allylation shown in Scheme 26b.



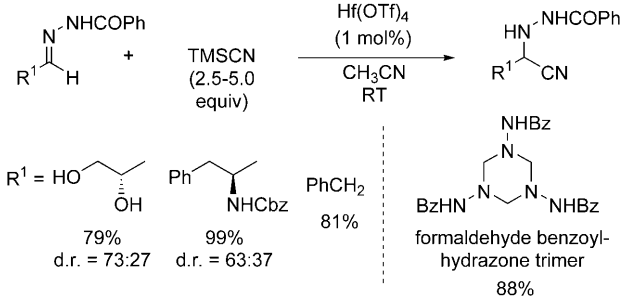
R^1 = R^2 = *n*- or *i*-alkyl, -$(CH_2)_n$- etc.
R^1 = Ph, R^2 = Me
R^3 = Ph or OMe
(PTC: *n*Oct_3MeNCl or *n*Bu_4NBr)

Scheme 28. Biphasic hydrocyanation in the presence of a phase-transfer catalyst.

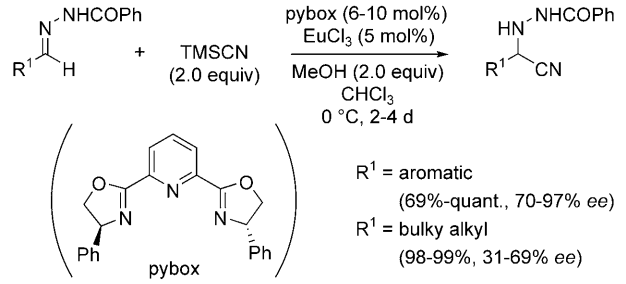
catalyze the addition of trimethylsilyl cyanide to functionalized *N*-acylhydrazones in acetonitrile (Scheme 29).[9b]

Keith and Jacobsen reported the first asymmetric catalytic hydrocyanation of *N*-acylhydrazones (Scheme 30),[25] in which

© 2005 Wiley-VCH Verlag GmbH & Co. KGaA, Weinheim



Scheme 29. Lewis acid catalyzed cyanation.

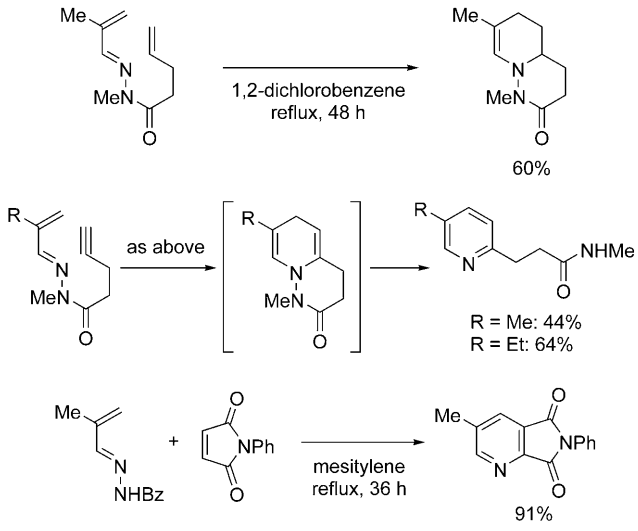


Scheme 30. Asymmetric Lewis acid catalyzed hydrocyanation.

a $EuCl_3$/pybox complex was found to be an efficient enantioselective catalyst. Although long reaction times were required, high enantioselectivities were observed. The best results were obtained with aromatic hydrazones bearing electron-rich substituents; electron-deficient substrates gave very poor reactivity. This suggests that the formation of a complex between the hydrazone and the Lewis acid catalyst may be the rate-limiting step in this process.

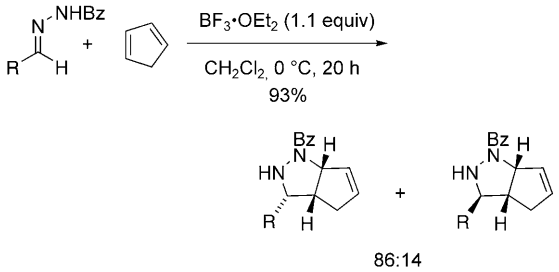
6. Cycloaddition

N-Acylhydrazones can serve as azadienes in aza-Diels–Alder reactions (Scheme 31).[26] Methacrolein or ethylacrolein-derived hydrazones can undergo both intra- and intermolecular [4+2] cycloadditions at high temperatures (> 140 °C) to afford pyridopyridazines or pyridines. Pyridines were formed by the elimination of the carbamoyl groups (followed by air oxidation in the case of reactions with *N*-phenylmaleimide). The reaction of phenylhydrazone with *N*-phenylmaleimide is appreciably faster than that of *N*-acyl or *N*-tosylhydrazones.



Scheme 31. Aza-Diels–Alder reactions with *N*-acylhydrazones.

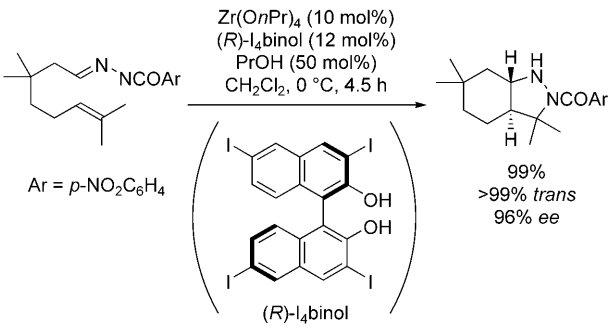
It is also known that hydrazones can serve as 1,3-dipolar agents in [3+2] cycloadditions with olefins. Hesse first reported in 1971 that three-component reactions of *N*-phenyl or *N*-acetylhydrazine, aldehydes, and olefins in acetic acid in the presence of a stoichiometric amount of sulfuric acid can provide pyrazolines in good yield.[27] Protonated hydrazones were suggested to be the active species. Since that time, several examples of [3+2] cycloadditions of *N*-acylhydrazones and alkenes under thermal conditions have been reported.[28] We recently found that Lewis acids also promote this transformation (Scheme 32).[29] *N*-Benzoylhydrazones



Scheme 32. Lewis acid catalyzed [3+2] cycloaddition.

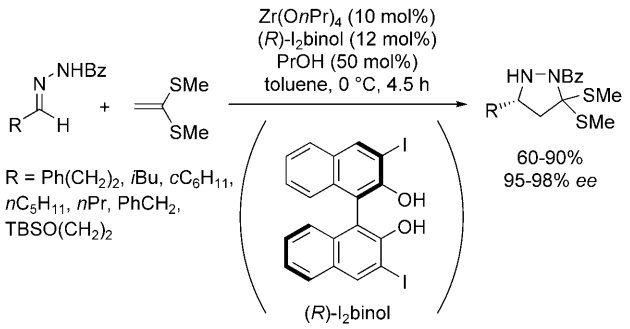
derived from 3-phenylpropanal, benzaldehyde, and ethyl glyoxylate in reaction with conjugated dienes in the presence of a stoichiometric amount of $BF_3{\cdot}OEt_2$ or a catalytic amount of $Zr(OTf)_4$ and $Hf(OTf)_4$ afford the corresponding pyrazolidine derivatives.

Asymmetric cycloadditions of this type have also been carried out in our research group. Both intra- and intermolecular [3+2] cycloaddition reactions proceeded smoothly in the presence of a catalytic amount of $Zr(OPr)_4$/binol derivatives to afford pyrazolidine products in high yield with high enantioselectivity (example reactions shown in Schemes 33 and 34).[30] In the case of intermolecular reaction

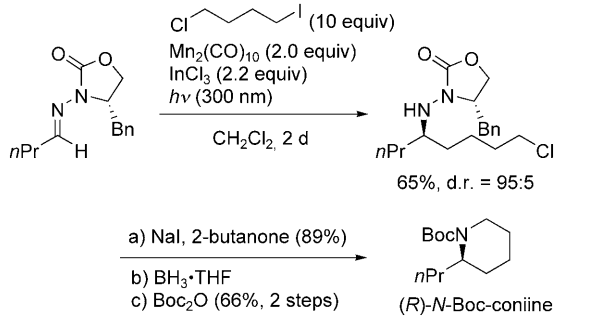


Scheme 33. Asymmetric catalytic intramolecular [3+2] cycloaddition.

© 2005 Wiley-VCH Verlag GmbH & Co. KGaA, Weinheim



Scheme 34. Asymmetric catalytic intermolecular [3+2] cycloaddition.



Scheme 36. Diastereoselective addition of a primary alkyl radical to an *N*-acylhydrazone.

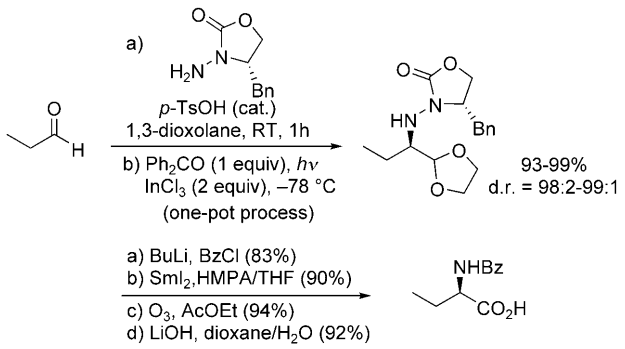
(Scheme 34), vinyl ethers such as propyl vinyl ether can be used. Enantiomeric excess of the major and minor diastereomers were different in this case, although no epimerization between the diastereomers occurred during the course of the reaction. If the reaction were to proceed by a stepwise mechanism, the enantioselectivity of both diastereomers would be expected to be the same; this suggests that the reaction proceeds by a concerted mechanism.

7. Radical Addition

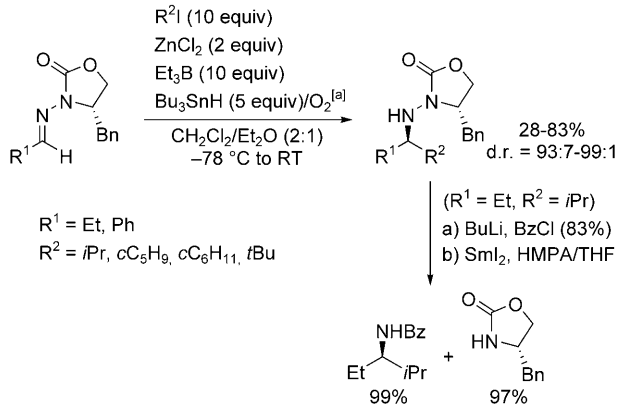
As a result of the lower electron density of their C=N bonds, hydrazones are better radical acceptors than imines.[31] Three-electron π-bond interactions could also stabilize a transition state leading to an aminyl radical adduct.

Friestad and Qin reported the diastereoselective reaction of chiral *N*-acylhydrazones with secondary and tertiary alkyl radicals in the presence of a stoichiometric amount of zinc chloride as an activator and tributylstannane as a radical mediator (Scheme 35).[32] Adducts were obtained with high diastereoselectivity and could be transformed into optically active benzamides without epimerization through treatment with BuLi/benzoyl chloride and SmI_2. It was also discovered that primary alkyl radicals react with chiral *N*-acylhydrazones if $InCl_3$ is employed as a Lewis acid with $[Mn_2(CO)_{10}]$ as a radical mediator under irradiation (Scheme 36).[33] In these reactions, high diastereofacial selectivity similar to that of the previous system was observed. Photolytic Mn–Mn homolysis facilitated formation of primary alkyl radicals, thus allowing the use of toxic tin reagents to be avoided. Reaction of the radical species [·Mn(CO)$_5$] with primary halides was more efficient than that with secondary and tertiary halides.

More recently, Fernández and Alonso discovered that α-oxygenated carbon radicals, generated from methanol, 2-propanol, or 1,3-dioxolane under irradiation in the presence of benzophenone, can react with the chiral hydrazones reported by Friestad (Scheme 37).[34] In this case as well,



Scheme 37. Diastereoselective addition of a 1,3-dioxolanyl radical.

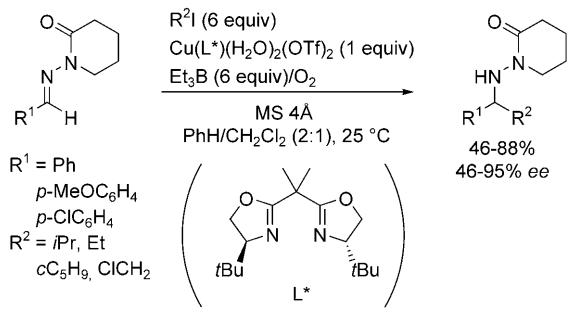


Scheme 35. Diastereoselective addition of secondary and tertiary alkyl radicals to *N*-acylhydrazones; HMPA = hexamethylphosphoramide. [a] Added by syringe pump.

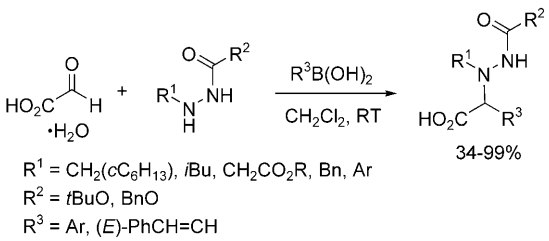
$InCl_3$ was effective for the control of diastereofacial selectivity; the selectivity was also largely dependent on the aldehyde source for the formation of hydrazones. Hydrazone formation and radical addition could be performed in a one-pot process to improve yield and selectivity, and in one case, the product was transformed into an α-amino acid derivative.

Friestad et al. also reported enantioselective radical addition (Scheme 38).[35] Although their initial attempts with prochiral oxazolidione-derived *N*-acylhydrazones resulted in insignificant enantioselectivity, dramatic improvement was observed with valerolactam-derived *N*-acylhydrazones. Further optimization of Lewis acids and chiral ligands revealed that a combination of $Cu(OTf)_2$ and a chiral *tert*-leucinol-derived bis(oxazoline) ligand gave high enantioselectivity in a less-polar reaction medium (benzene/CH_2Cl_2). Notably, with the catalyst present at 10 mol% (R^1 = Ph, R^2 = *i*Pr), the product was obtained in 74% yield with 46% *ee*, whereas

 © 2005 Wiley-VCH Verlag GmbH & Co. KGaA, Weinheim



Scheme 38. Enantioselective addition of alkyl radicals to *N*-acylhydrazones.



Scheme 39. Three-component reaction of glyoxylic acid, hydrazides and boronic acids.

slightly lower yield (66%) and much higher enantiomeric excess (95% *ee*) were observed with the catalyst at 100 mol%.

8. Transformation of Products

A valuable range of nitrogen-containing compounds with N–N bonds, for example *N*-carbamoyl-β-lactam, pyrazolidinone, pyrazolone, and pyrazolidine derivatives (see Schemes 9, 10, 31–34)[9,10,27–30] are available from *N*-acylhydrazine products. Cleavage of the N–N bond can convert *N*-acylhydrazines into further interesting derivatives. This transformation is enabled by hydrogenolysis (with palladium, platinum or Raney nickel), reduction with dissolved metals, and hydroboration.[36] Reductive cleavage with samarium(II) iodide,[3] has gained increased attention in recent studies.[9d,10,11,12a,14a,15,18b,19,20,30a,32,34] Indeed, Friestad and Ding recently reported a dramatic improvement of SmI_2-mediated N–N bond cleavage by the *N*′-benzoylation or *N*′-trifluoroacetylation of *N*-acylhydrazines.[37] Benzoyl groups have been suggested to decrease the reducing potential of the N–N bond, while chelation of SmI_2 between the amide oxygen atom and the fluorine atom of the trifluoroacetyl group (Figure 4) is proposed to enhance the rate of reduction.



Figure 4. Proposed transition state that explains the rate enhancement of SmI_2-mediated N–N-bond cleavage by the trifluoroacetyl group.

9. Other Reactions

The addition of an ethyl Grignard reagent to an *N*-formylhydrazone[38] and Friedel–Crafts reactions of *N*-acylhydrazonium ions[39] have also been reported. Furthermore, it has been found that Petasis three-component reactions of glyoxylic acid, *N*-(alkoxycarbonyl)hydrazines, and aryl or styryl boronic acids afford α-hydrazinocarboxylic acids efficiently (Scheme 39).[40] Interestingly, the reaction of an unsubstituted hydrazine ($R^1 = H$, $R^2 = t$BuO) with pMeO$C_6H_4B(OH)_2$ gave a complex mixture, whereas reactions of the preformed *N*-acylhydrazone BocNHN=$CHCO_2H$ provided the adduct in 71% yield. However, other reactions with substituted hydrazones ($R^1 \neq H$) cannot involve *N*-acylhydrazones, but presumably *N*-acylhydrazonium ions.

10. Summary and Outlook

N-Acylhydrazones as versatile electrophiles have attracted increasing attention not only because they are readily prepared, storable, and stable imine surrogates, but also because the *N*-acyl groups act as good templates for metal catalysts which facilitate stereochemical control. Chiral hydrazide products can be used as chiral building blocks and can also be transformed into a variety of nitrogen-containing compounds through cleavage of the N–N bond. It is expected that new stereoselective reactions that take advantage of *N*-acylhydrazones will be developed, and that the use of *N*-acylhydrazones as imine equivalents will be expanded to the chemical and pharmaceutical industries.[41]

Received: February 24, 2005
Published online: August 1, 2005

[1] For a recent review of the chemistry of *N*-acylhydrazines, see: E. Licandro, D. Perdicchia, *Eur. J. Org. Chem.* **2004**, 665.
[2] *The Chemistry of Amides* (Eds.: S. Patai, J. Zabicky), Wiley, New York, **1970**, pp. 515–600, and references therein.
[3] a) M. J. Burk, J. E. Feaster, *J. Am. Chem. Soc.* **1992**, *114*, 6266; b) M. J. Burk, J. P. Martinez, J. E. Feaster, N. Cosford, *Tetrahedron* **1994**, *50*, 4399.
[4] F. E. Henoch, C. R. Hauser, *Can. J. Chem.* **1969**, *47*, 157.
[5] a) F. E. Condon, *J. Org. Chem.* **1972**, *37*, 3615; b) R. Calabretta, C. Gallina, C. Giordano, *Synthesis* **1991**, 536; c) N. I. Ghali, D. L. Venton, S. C. Hung, G. C. Breton, *J. Org. Chem.* **1981**, *46*, 5413; d) Y. Kikugawa, M. Kawase, *Synth. Commun.* **1979**, *9*, 49.
[6] P.-L. Wu, S. Y. Peng, J. Magrath, *Synthesis* **1995**, 435.
[7] J. Qin, G. K. Friestad, *Tetrahedron* **2003**, *59*, 6393.
[8] a) E. F. Kleinman in *Comprehensive Organic Synthesis*, *Vol. 2* (Ed.: B. M. Trost), Pergamon, Oxford, **1991**, p. 893; b) M. Arend, B. Westermann, N. Risch, *Angew. Chem.* **1998**, *110*, 1096; *Angew. Chem. Int. Ed.* **1998**, *37*, 1044.
[9] a) S. Kobayashi, T. Furuta, K. Sugita, H. Oyamada, *Synlett* **1998**, 1019; b) K. Manabe, H. Oyamada, K. Sugita, S. Kobayashi, *J. Org. Chem.* **1999**, *64*, 8054; c) S. Kobayashi, T. Furuta, K. Sugita, O. Okitsu, H. Oyamada, *Tetrahedron Lett.* **1999**, *40*, 1019; d) O. Okitsu, H. Oyamada, T. Furuta, S. Kobayashi, *Heterocycles* **2000**, *52*, 1143.
[10] S. Kobayashi, Y. Hasegawa, H. Ishitani, *Chem. Lett.* **1998**, 1131.
[11] M. F. Jacobsen, L. Ionita, T. Skrydstrup, *J. Org. Chem.* **2004**, *69*, 4792.

© 2005 Wiley-VCH Verlag GmbH & Co. KGaA, Weinheim

[12] a) S. Kobayashi, T. Hamada, K. Manabe, *J. Am. Chem. Soc.* **2002**, *124*, 5640; b) T. Hamada, K. Manabe, S. Kobayashi, *J. Am. Chem. Soc.* **2004**, *126*, 7768.
[13] For reviews of the addition of allylmetals to C=O and C=N bonds, see: a) Y. Yamamoto, N. Asano, *Chem. Rev.* **1993**, *93*, 2207; b) S. E. Denmark, N. G. Almstead in *Modern Carbonyl Chemistry* (Ed.: J. Otera), Wiley-VCH, Weinheim, **2000**, chap. 10; c) C. O. Puentes, V. Kouznetsov, *J. Heterocycl. Chem.* **2002**, *39*, 595; d) D. Enders, U. Reinhold, *Tetrahedron: Asymmetry* **1997**, *8*, 1895; e) E. F. Kleinman, R. A. Volkmann, in *Comprehensive Organic Chemistry*, *Vol. 2* (Eds.: B. M. Trost, I. Fleming), Pergamon, Oxford, pp. 975–1006.
[14] a) S. Kobayashi, K. Sugita, H. Oyamda, *Synlett* **1999**, 138; b) S. Kobayashi, H. Hamada, K. Manabe, *Synlett* **2001**, 1140.
[15] a) S. Kobayashi, R. Hirabayashi, *J. Am. Chem. Soc.* **1999**, *121*, 6942; b) R. Hirabayashi, C. Ogawa, M. Sugiura, S. Kobayashi, *J. Am. Chem. Soc.* **2001**, *123*, 9493; c) C. Ogawa, M. Sugiura, S. Kobayashi, *J. Org. Chem.* **2002**, *67*, 5359; For a review, see: d) S. Kobayashi, M. Sugiura, C. Ogawa, *Adv. Synth. Catal.* **2004**, *346*, 1023.
[16] S. Kobayashi, C. Ogawa, H. Konishi, M. Sugiura, *J. Am. Chem. Soc.* **2003**, *125*, 6610.
[17] a) C. Ogawa, H. Konishi, M. Sugiura, S. Kobayashi, *Org. Biomol. Chem.* **2004**, 446; b) C. Ogawa, H. Sugiura, S. Kobayashi, *Angew. Chem.* **2004**, *116*, 6653; *Angew. Chem. Int. Ed.* **2004**, *43*, 6491.
[18] a) R. Berger, P. M. A. Rabbat, J. L. Leighton, *J. Am. Chem. Soc.* **2003**, *125*, 9596; b) R. Berger, K. Duff, J. L. Leighton, *J. Am. Chem. Soc.* **2004**, *126*, 5686.
[19] G. K. Friestad, H. Ding, *Angew. Chem.* **2001**, *113*, 4623; *Angew. Chem. Int. Ed.* **2001**, *40*, 4491.
[20] T. Hamada, K. Manabe, S. Kobayashi, *Angew. Chem.* **2003**, *115*, 4057; *Angew. Chem. Int. Ed.* **2003**, *42*, 3927.
[21] H. Ding, G. K. Friestad, *Synthesis* **2004**, 2216.
[22] S. Yamasaki, K. Fujii, R. Wada, M. Kanai, M. Shibasaki, *J. Am. Chem. Soc.* **2002**, *124*, 6536.
[23] a) R. L. Munier, G. C. R. Bompeix, *Acad. Sci. Ser.* **1985**, *300*, 203; b) L. M. Brand, A. E. Harper, *Biochemistry* **1976**, *15*, 1814; c) S. Tanase, B. M. Guirard, E. E. Snell, *J. Biol. Chem.* **1985**, *260*, 6738; d) R.-H. Yamada, Y. Wakabayashi, A. Iwashima, T. Hasegawa, *Biochim. Biophys. Acta* **1985**, *831*, 82.
[24] T. Chiba, M. Okimoto, *Synthesis* **1990**, 209.
[25] J. M. Keith, E. N. Jacobsen, *Org. Lett.* **2004**, *6*, 153.
[26] a) S. J. Allocock, T. L. Gilchrist, F. D. King, *Tetrahedron Lett.* **1991**, *32*, 125; b) S. J. Allocock, T. L. Gilchrist, S. J. Shuttleworth, *Tetrahedron* **1991**, *47*, 10053.
[27] K.-D. Hesse, *Justus Liebigs Ann. Chem.* **1971**, *743*, 50.
[28] a) M. A. Badawy, S. A. El-Bahaie, A. M. Kadry, Y. A. Ibrahim, *Heterocycles* **1988**, *27*, 7; b) V. V. Khau, M. J. Martinelli, *Tetrahedron Lett.* **1996**, *37*, 4323.
[29] S. Kobayashi, R. Hirabayashi, H. Shimizu, H. Ishitani, Y. Yamashita, *Tetrahedron Lett.* **2003**, *44*, 3351.
[30] a) S. Kobayashi, H. Shimizu, Y. Yamashita, H. Ishitani, J. Kobayashi, *J. Am. Chem. Soc.* **2002**, *124*, 13678; b) Y. Yamashita, S. Kobayashi, *J. Am. Chem. Soc.* **2004**, *126*, 11279.
[31] For a review: G. K. Friestad, *Tetrahedron* **2001**, *57*, 5461.
[32] G. K. Friestad, J. Qin, *J. Am. Chem. Soc.* **2000**, *122*, 8329.
[33] a) G. K. Friestad, J. Qin, *J. Am. Chem. Soc.* **2001**, *123*, 9922; b) G. K. Friestad, J.-C. Marié, A. M. Deveau, *Org. Lett.* **2004**, *6*, 3249.
[34] M. Fernández, R. Alonso, *Org. Lett.* **2003**, *5*, 2461.
[35] G. K. Friestad, Y. Shen, E. L. Ruggles, *Angew. Chem.* **2003**, *115*, 5215; *Angew. Chem. Int. Ed.* **2003**, *42*, 5061.
[36] See Ref. [2], and references cited in Ref. [37].
[37] H. Ding, G. K. Friestad, *Org. Lett.* **2004**, *6*, 637.
[38] A. K. Saksena, V. M. Girijavallabhan, H. Wang, R. G. Lovey, F. Guenter, I. Mergelsberg, M. S. Puar, *Tetrahedron Lett.* **2004**, *45*, 8249.
[39] a) F. P. J. T. Rutjes, H. Hiemstra, H. H. Mooiweer, W. N. Speckamp, *Tetrahedron Lett.* **1988**, *29*, 6975; b) F. P. J. T. Rutjes, N. M. Teerhuis, H. Hiemstra, W. N. Speckamp, *Tetrahedron* **1993**, *49*, 8605; c) F. P. J. T. Rutjes, H. Hiemstra, F. O. H. Pirrung, W. N. Speckamp, *Tetrahedron* **1993**, *49*, 10027; d) N. M. Teerhuis, H. Hiemstra, W. N. Speckamp, *Tetrahedron Lett.* **1997**, *38*, 159; e) N. M. Teerhuis, H. Hiemstra, W. N. Speckamp, *Tetrahedron Lett.* **1997**, *38*, 155; f) H. Suzuki, S. Aoyagi, C. Kibayashi, *J. Org. Chem.* **1995**, *60*, 6114; g) A. Fogain-Ninkam, A. Daïch, B. Decroix, P. Netchitaïlo, *Eur. J. Org. Chem.* **2003**, *68*, 4273.
[40] D. E. Portlock, D. Naskar, L. West, M. Li, *Tetrahedron Lett.* **2002**, *43*, 6845.
[41] For a review on *N*-acylhydrazones: G. K. Friestad, *Eur. J. Org. Chem.* **2005**, 3157.

 © 2005 Wiley-VCH Verlag GmbH & Co. KGaA, Weinheim

Azides

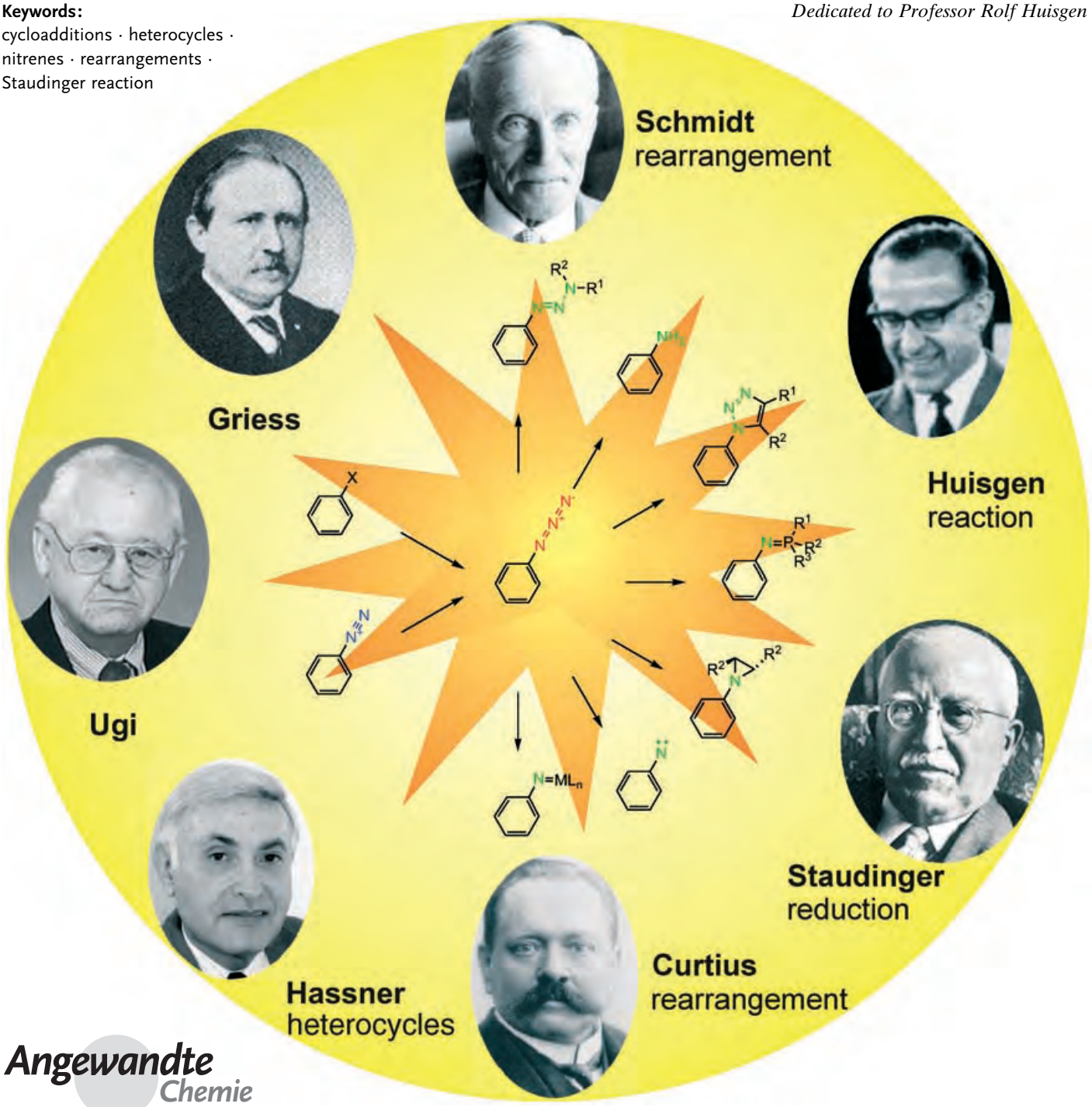
DOI: 10.1002/anie.200400657

Organic Azides: An Exploding Diversity of a Unique Class of Compounds

Stefan Bräse, Carmen Gil, Kerstin Knepper, and Viktor Zimmermann*

Keywords:
cycloadditions · heterocycles · nitrenes · rearrangements · Staudinger reaction

Dedicated to Professor Rolf Huisgen



© 2005 Wiley-VCH Verlag GmbH & Co. KGaA, Weinheim

Since the discovery of organic azides by Peter Grieß more than 140 years ago, numerous syntheses of these energy-rich molecules have been developed. In more recent times in particular, completely new perspectives have been developed for their use in peptide chemistry, combinatorial chemistry, and heterocyclic synthesis. Organic azides have assumed an important position at the interface between chemistry, biology, medicine, and materials science. In this Review, the fundamental characteristics of azide chemistry and current developments are presented. The focus will be placed on cycloadditions (Huisgen reaction), aza ylide chemistry, and the synthesis of heterocycles. Further reactions such as the aza-Wittig reaction, the Sundberg rearrangement, the Staudinger ligation, the Boyer and Boyer–Aubé rearrangements, the Curtius rearrangement, the Schmidt rearrangement, and the Hemetsberger rearrangement bear witness to the versatility of modern azide chemistry.

From the Contents

1. Introduction 5189

2. Physicochemical Properties of Organic Azides 5189

3. Synthesis of Organic Azides 5191

4. Reactions of Organic Azides 5202

5. Applications of Azides 5226

6. Summary and Outlook 5227

1. Introduction

Since the preparation of the first organic azide, phenyl azide, by Peter Grieß in 1864 these energy-rich and flexible intermediates have enjoyed considerable interest.[1,2] A few years later Curtius developed hydrogen azide and discovered the rearrangement of acyl azides to the corresponding isocyanates (Curtius rearrangement).[3] The organic azides received considerable attention in the 1950s and 1960s[4,5] with new applications in the chemistry of the acyl, aryl, and alkyl azides. Industrial interest in organic azide compounds began with the use of azides for the synthesis of heterocycles such as triazoles and tetrazoles as well as with their use as blowing agents and as functional groups in pharmaceuticals. Thus, for example, azidonucleosides attract international interest in the treatment of AIDS.[6]

Like hydrogen azide most other azides are also explosive substances that decompose with the release of nitrogen through the slightest input of external energy, for example pressure, impact, or heat. The heavy-metal azides are used, for example, in explosives technology, in which they serve as detonators. Sodium azide is applied in airbags. The organic azides, particularly methyl azide, often decompose explosively.

However, in spite of their explosive properties, organic azides are valuable intermediates in organic synthesis.[7,8] Thus they are used in cycloadditions, the synthesis of anilines and *N*-alkyl-substituted anilines,[9] as well as precursors for nitrenes. In this Review, which is not meant to be a comprehensive overview,[10] the fundamental characteristics of organoazide chemistry with its "explosive" diversity in modern synthetic chemistry will be illustrated. In this context, inorganic azides, purely main-group azides (such as $Te(N_3)_5$[11]), and purely structural-chemical aspects will not be discussed. After the section on their properties, the synthetic opportunities and applications of organoazides will be illustrated.

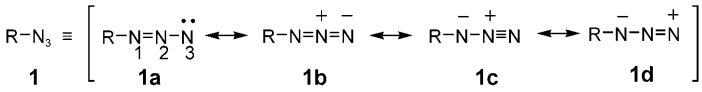
2. Physicochemical Properties of Organic Azides

The structural determination of azides originates from the initial postulation of Curtius and Hantzsch, who had suggested a cyclic 1*H*-triazirine structure [3,12,13], that was, however, rapidly revised in favor of the linear structure.



1-phenyl-1*H*-triazirine

A basis for the chemical diversity of azides comes from the physicochemical properties of azides. Some of the physicochemical properties of the organic azides can be explained by a consideration of polar mesomeric structures.[1] Aromatic azides are stabilized by



conjugation with the aromatic system. The dipolar structures of type **1c**,**d** (proposed by Pauling[14]) also compellingly explained the facile decomposition into the corresponding nitrene and dinitrogen (see Section 4.2) as well as the reactivity as a 1,3-dipole. The regioselectivity of their reactions with electrophiles and nucleophiles is explained

[*] Prof. Dr. S. Bräse
Institut für Organische Chemie
Universität Karlsruhe (TH)
Fritz-Haber-Weg 6, 76131 Karlsruhe (Germany)
Fax: (+49) 0721-608-8581
E-mail: braese@ioc.uka.de
Dr. C. Gil, Dr. K. Knepper, Dipl.-Chem. V. Zimmermann
Kekulé-Institut für Organische Chemie und Biochemie
Rheinischen Friedrich-Wilhelms-Universität Bonn
Gerhard-Domagk-Strasse 1, 53121 Bonn (Germany)

© 2005 Wiley-VCH Verlag GmbH & Co. KGaA, Weinheim

on the basis of the mesomeric structure **1d** (attack on N^3 by nucleophiles, whereas electrophiles are attacked by N^1).

The angles $R–N^1–N^2N^3$ and $RN^1–N^2–N^3$ are approximately 115.2° and 172.5°, respectively (calculated for methyl azide, $R = CH_3$[15]). The bond lengths in methyl azide were determined as $d(R–N^1) = 1.472$, $d(N^1–N^2) = 1.244$, and $d(N^2–N^3) = 1.162$ Å; slightly shorter $N^2–N^3$ bond lengths are observed with aromatic azides. Thus an almost linear azide structure is present, with sp^2 hybridization at N^1 and a bond order of ≈ 2.5 between N^3 and N^2 and ≈ 1.5 between N^2 and N^1. Figure 1 is an example of the molecular structure of an aromatic azide.

The polar resonance structures **1b**,**c** explain the strong IR absorption at $\approx 2114\ cm^{-1}$ (for phenyl azide),[17] the UV absorption (287 nm and 216 nm for alkyl azides), the weak dipole moment (1.44 D for phenyl azide), and the acidity of aliphatic azides (e.g. see Scheme 12).[18] The azide ion is regarded as a pseudohalide[19] and organic azides are similar in certain respects to organic halogen compounds. The Hammett parameters for arenes with azide groups in the *meta* and *para* positions are 0.35 and 0.10, respectively, which are comparable with those of fluoroarenes. In aromatic substitution reactions the azide group acts as an *ortho*- and *para*-directing substituent.

Whereas ionic azides such as sodium azide are relatively stable (see box), covalently bound and heavy-metal azides are thermally decomposable and in part explosive classes of compounds. For organic azides to be manipulable or non-explosive, the rule is that the number of nitrogen atoms must not exceed that of carbon and that $(N_C + N_O)/N_N \geq 3$ ($N =$ number of atoms; Smith[20]). Synthesized but potentially explosive compounds include hexakis(azidomethyl)benzene (**2**),[16] triazidotrinitrobenzene (**3**),[21] azidotetrazole (**4**) (88 %

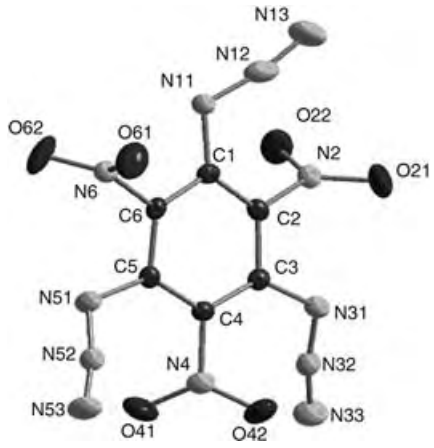
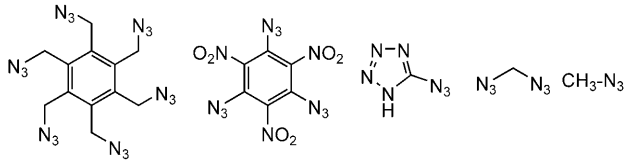


Figure 1. ORTEP representation of 1,3,5-triazido-2,4,6-trinitrobenzene with the ellipsoids of the C, N, and O atoms drawn at the 50% probability level.[16b]





Stefan Bräse was born in Kiel in 1967 and studied at Göttingen, Marseille (France), and Bangor (Wales) (PhD: Prof. Armin de Meijere). After periods of research in Uppsala (Sweden) and La Jolla (USA) he completed his Habilitation at the RWTH Aachen (Prof. Dieter Enders). In the same year he was appointed C3 professor at Bonn University. He was guest professor in Madison (USA) before taking up his current professorship at the Universität Karlsruhe (TH) in 2003. His research interests combine asymmetric catalysis, the synthesis of natural products, combinatorial chemistry, and medicinal chemistry.



Carmen Gil was born in Talavera de la Reina, Spain in 1972. She studied at the Complutense University of Madrid and received her PhD in 2001 at the Medicinal Chemistry Institute in Madrid (Prof. Ana Martínez). After a postdoctoral appointment at Bonn University (Prof. Stefan Bräse) as a Marie-Curie fellow, she joined the Medicinal Chemistry Institute in Madrid in 2004. Her research interests includes combinatorial chemistry applied to the synthesis of bioactive molecules.



Viktor Zimmermann studied chemistry at the universities of Nowosibirsk, Göttingen, and the RWTH Aachen. He completed his Diploma at the RWTH Aachen in 2002. Since then he has been working for his PhD at Bonn University (Prof. Stefan Bräse). The main topic of his research is carrier-supported combinatorial synthesis of benzotriazoles and azides.



Kerstin Knepper was born in Dortmund, Germany in 1976 and studied chemistry at the University of Dortmund. In 2001, she obtained her Diploma in chemistry (Prof. Norbert Krause). She received her PhD in 2004 at the University of Bonn (Prof. Stefan Bräse). She is currently a postdoctoral fellow with Prof. N. Winssinger (Université Louis Pasteur, Strasbourg, France). Her research interests include the solid-phase synthesis of benzannelated heterocycles, methods of organometallic chemistry, and the combinatorial synthesis of natural product analogues.

 © 2005 Wiley-VCH Verlag GmbH & Co. KGaA, Weinheim

nitrogen!),[22] and azidomethane (**6**). Diazidomethane (**5**) is prepared from sodium azide and dichloromethane.[23] Certain low-molecular-weight azides, which in practice have proved to be nonreactive, can still decompose under unexplained circumstances so that special care is needed.

Safety in the Handling of Sodium Azide and other Azides

Sodium azide is toxic (LD_{50} oral (rats) = 27 mg kg^{-1}) and can be absorbed through the skin. It decomposes explosively upon heating to above 275 °C; hence its use in airbags in the automotive industry).

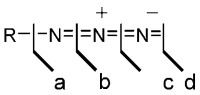
Sodium azide reacts vigorously with CS_2, bromine, nitric acid, dimethyl sulfate, and a series of heavy metals, including copper and lead. In reaction with water or Brønsted acids the highly toxic and explosive hydrogen azide is released. It has been reported that sodium azide and polymer-bound azide reagents form explosive di- and triazidomethane with CH_2Cl_2 and $CHCl_3$, respectively.[23a]

Heavy-metal azides that are highly explosive under pressure or shock are formed when solutions of NaN_3 or HN_3 vapors come into contact with heavy metals or their salts. Heavy-metal azides can accumulate under certain circumstances, for example, in metal pipelines and on the metal components of diverse equipment (rotary evaporators, freeze-drying equipment, cooling traps, water baths, waste pipes), and thus lead to violent explosions.

Some organic and other covalent azides are classified as toxic[24] and highly explosive[25], and appropriate safety measures must be taken at all times.

3. Synthesis of Organic Azides

In principle, organic azides may be prepared through five different methods: a) insertion of the N_3 group (substitution or addition), b) insertion of an N_2 group (diazo transfer), c) insertion of a nitrogen atom (diazotization), d) cleavage of triazines and analogous compounds, and e) rearrangement of azides. As the properties and the synthesis of aromatic and aliphatic azides vary considerably, the two classes of compounds will be discussed separately.[26]



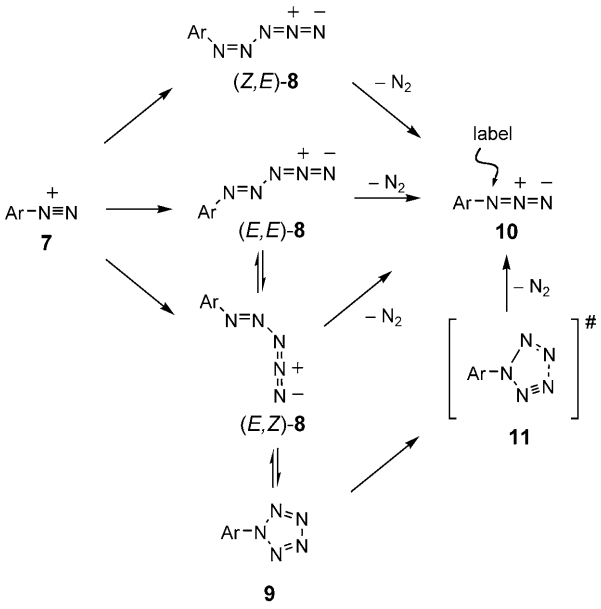
3.1. Aryl Azides

Because of their relatively high stability, aryl azides[27,28] have found biological and industrial use as photoaffinity labels,[29] as cross-linkers in photoresistors,[30] for conducting polymers,[31] and for light-induced activation of polymer surfaces[32] and are important intermediates in organic chemistry. Classic aromatic chemistry is usually the access of choice.

3.1.1. Aryl Azides from Diazonium Compounds

The older preparative methods for aryl azides are based on the reaction of diazonium salts with hydrazine[33] or *O*-benzylhydroxylamine hydrochloride.[34] The reaction of arene diazonium perbromides with ammonia also leads to aryl azides and is the oldest method for the preparation of azides.[2,34,35]

In the meantime, however, more convenient conversions of diazonium salts into aryl azides are known. Thus, aryl diazonium salts react directly with azide ions without catalysts directly to the corresponding aryl azides.[36] Alkali azides or trimethylsilyl azide act as source.[37] The latter compound is especially suitable because of its solubility in organic solvents (see Section 3.5.1). Unlike the Sandmeyer reaction, this reaction does not take place with cleavage of the C–heteroatom bond but occurs with attack of the azide on the diazonium ion with formation of aryl pentazoles and its subsequent products.[38] This reaction is sufficiently rapid even at low temperatures; *p*-chlorophenyldiazonium chloride reacts with azide ion even at −80 °C. The mechanism of this reaction (whether it occurs through a concerted [3+2] mechanism or takes place stepwise) and the nature of the intermediates have been the subject of controversial discussions since its discovery. There is a general consensus that the intermediate pentazenes and pentazoles lose dinitrogen. The corresponding azides are obtained at low reaction temperatures.[39] A pentazole structure was established for the first time by X-ray crystal-structure analysis in 1983.[40a] A British group investigated this reaction spectroscopically by ^{1}H and ^{15}N NMR spectroscopy (Scheme 1)[39] and established that



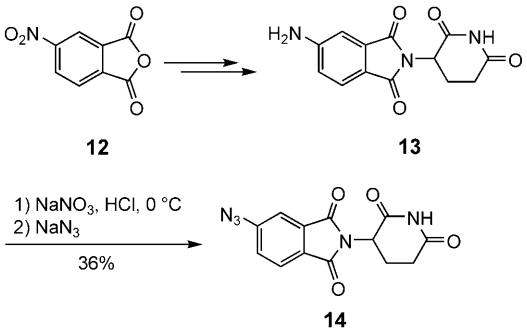
Scheme 1. Mechanism of the conversion of diazonium ions into azides.[39]

three isomeric aryl pentazenes **8**, namely the (*Z*,*E*), (*E*,*E*), and (*E*,*Z*) isomers, were formed by the attack of the azide ion at the β nitrogen atom of the diazonium ion **7**, as already postulated by Huisgen.[41] Whereas (*E*,*Z*)-**8** produces the 1-aryl pentazole **9**, (*Z*,*E*)-**8** forms the aryl azide directly by cleavage and does not rearrange to the *E* isomer. The *Z*,*E*-**8** isomer is considered to be the stereoelectronically favored product. This mechanism also explains the isotope labeling of the aryl azides found during the decomposition of labeled

 © 2005 Wiley-VCH Verlag GmbH & Co. KGaA, Weinheim

diazonium ions.[39c] Besides the isolated diazonium salts, other precursors such as benzotriazinones[42] may be used for the synthesis of aryl azides according to this scheme.

A more recent example of the decomposition of diazonium salts into the corresponding aryl azides is illustrated by the synthesis of azidothalidomide (**14**; Scheme 2).[43] The

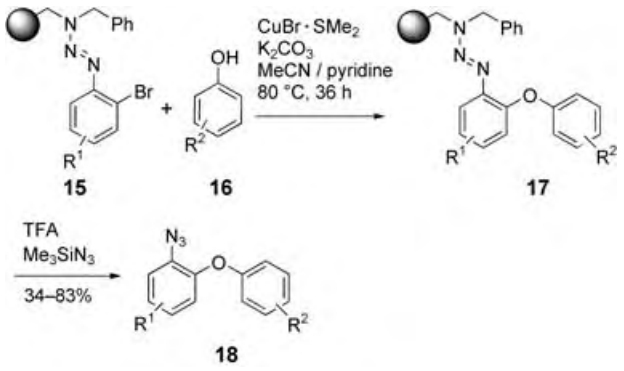


Scheme 2. Synthesis of azido-thalidomide (**14**).[43]

heterocycle was formed from nitrophthalic anhydride (**12**) by classic procedures, and the amino group in **13** was obtained by reduction. Diazotization and its subsequent reaction with sodium azide gave **14**. This compound is more active than thalidomide in the inhibition of the proliferation of human microvascular endothelial cells (HMEC) both in the presence and absence of vascular endothelial growth factors (VEGF). It was possible to demonstrate that the effect on endothelial cell growth by introduction of the azide group did not influence the affinity for the thalidomide-binding domains negatively.

A combinatorial access to aryl azides **18** is provided by the cleavage of polymer-bound aryl triazenes **15**. These aryl triazenes can be modified on the polymer support in a number of different reactions, for example, the Ullmann–Nicolaou reaction (Scheme 3). The cleavage of the resulting aryl triazenes **17** to azides **18** is then carried out in good yields in the presence of trimethylsilyl azide.[44,45]

Although the conversion of diazonium salts into aryl azides represents one of the most important reactions of this class of compounds, the need to prepare the diazonium salts is

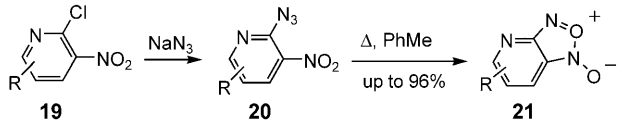


Scheme 3. Solid-phase synthesis of aryl azides **18** after a successful Ullmann–Nicolaou reaction.[44]

a severe limitation, so that in a few cases they may be synthesized only with difficulty if at all.

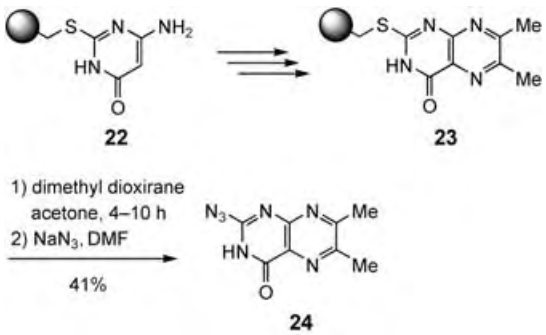
3.1.2. *Nucleophilic Aromatic Substitution: S_NAr Reactions*

Activated aromatic systems such as fluoro- and chloronitro arenes[46a] and a few heteroaromatic systems[46b] can undergo nucleophilic substitution by azide ions. They are generally sufficiently nucleophilic to produce aryl azides in good yields. The *ortho*-nitroazidoarenes formed react further at elevated temperatures with loss of nitrogen and formation of benzofurozane derivatives. Analogous reactivity is exhibited by the corresponding azidonitropyridine **20**, which may be prepared from chloronitropyridine **19** and sodium azide. (Scheme 4).[47]



Scheme 4. Aromatic substitution to give aryl azides.[47]

Heteroaryl sulfones are also cleaved regioselectively by azide ions. They can be used for the functionalizing cleavage of heteroaryl azides from polymeric supports, in which case the sulfur linker is first activated by oxidation to the sulfone with dimethyldioxirane (Scheme 5).[48]



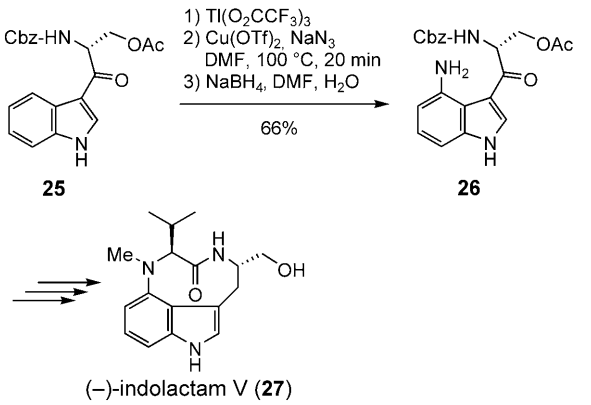
Scheme 5. Functionalizing cleavage to give heteroaryl azides.[48]

If aromatic systems are provided with appropriate leaving groups, such as thallium substituents, the nucleophilic substitution can be carried out with electron-rich arenes. This aromatic substitution has been used in the total synthesis of indolactam V (**27**; Scheme 6),[49a] an indole alkaloid isolated from *Streptomyces blasmyceticum*. Alternatively, activated and deactivated aryl iodides can be converted into aryl azides under mild conditions with sodium azide in the presence of proline and copper(I) iodide.[49b]

3.1.3. *Aryl Azides from Organometallic Reagents*

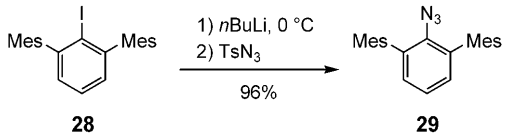
Over the last decades, numerous methods for the preparation of aryl azides with organometallic reagents have been developed. For example, tosyl azide reacts with Grignard or

 © 2005 Wiley-VCH Verlag GmbH & Co. KGaA, Weinheim



Scheme 6. Total synthesis of indolactam according to Kogan et al.[49a] Cbz = benzyloxycarbonyl; Tf = trifluoromethanesulfonyl.

lithium reagents—depending on the corresponding aryl halide—to form novel aryl azides (see also Section 3.5.2).[50] One example is the preparation of aryl azide **29** (Scheme 7).

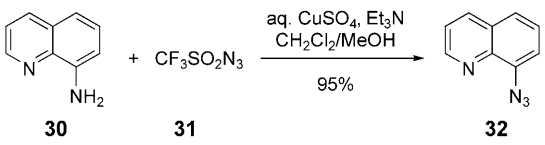


Scheme 7. Aryl azides according to Tilley and co-workers.[51] Mes = mesityl; Ts = *para*-toluenesulfonyl.

2,6-Dimesitylphenyl iodide (**28**) was initially treated with *n*-butyllithium at 0°C, and the resulting lithium salt reacted with *p*-toluenesulfonyl azide to form **29** in 96% yield.[51] Similarly, aryl amide salts (generated from the corresponding anilines and strong bases) react with tosyl azide to form the desired aryl azides.[52]

3.1.4. Aryl Azides by Diazo Transfer

In analogy to aliphatic amines (see Section 3.3.6), aryl azides and heteroaryl azides may be prepared by the reaction of anilines with triflyl azide (**31**).[53] The mild reaction conditions and very high yields make these transformations the method of choice for the preparation of numerous aromatic azides. In the typical reaction (Scheme 8) freshly prepared **31** is treated with 8-aminoquinoline (**30**) at room temperature in a mixture of dichloromethane and methanol in the presence of triethylamine and copper sulfate. The reaction produces 8-azidoquinoline (**32**) in almost quantitative yield.



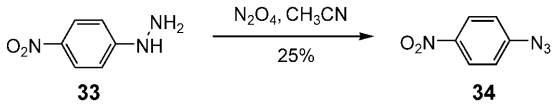
Scheme 8. Conversion of aromatic amines **30** into aryl azides **32** according to Tor and co-workers.[53]

3.1.5. Aryl Azides from Nitrosoarenes

The reaction of nitrosoarenes with hydrogen azide leads to aryl azides in good yields.[54] However, the diazonium ions must first be formed and then treated with azide ions as the second step: Thus, 2 equivalents of the explosive acid are required.

3.1.6. Diazotization of Hydrazines

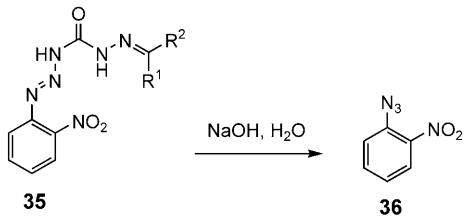
A well-established procedure that is equally suitable for the preparation of different classes of compounds such as aromatic and aliphatic azides, acyl azides, and sulfonyl azides is the reaction of hydrazines with nitrosyl ions or their precursors. N_2O_4,[55] mixtures of nitrogen oxide/oxygen,[56] nitrosyl salts,[57] and sodium nitrite[58] are particularly suitable (Scheme 9). The use of hydrazones[59] or 1-*tert*-butyl-1-aryl hydrazines,[60] which are cleaved under the reaction conditions used, is also a possibility.



Scheme 9. Conversion of the aromatic hydrazine **33** into aryl azide **34** according to Kim et al.[55,57]

3.1.7. Modification of Triazenes and Related Compounds

An older method for the preparation of azides is based on the rearrangement of triazenes into azides.[61] In particular, the base-induced cleavage of semicarbazones **35** can be used for the preparation of azides **36** (Scheme 10).[61a]



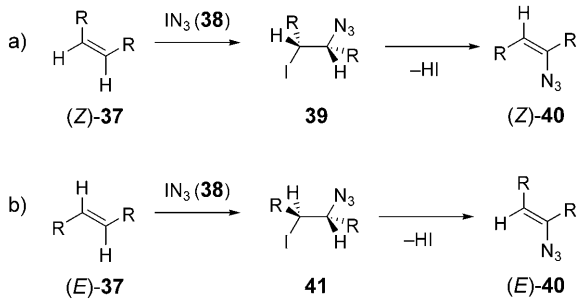
Scheme 10. Synthesis of the aryl azide **36** from the semicarbazone **35**.[61a]

3.2. Alkenyl Azides

Alkenyl azides are important as precursors for alkenyl nitrenes[62,63] and hence for the rearrangement to 2*H*-azirines.[64] A general synthetic route for alkenyl azides was developed by Hassner and co-workers.[63] In this method, the addition of iodine azide (**38**) to the double bond and the subsequent elimination of hydrogen iodide (base induced) occurs with a high degree of stereospecificity. On the one hand, exclusively vinyl azides and no allyl azides are formed from the 2-azido-3-iodoalkanes **39** and **41** formed as intermediates (with the exception of cyclopentene and cyclo-

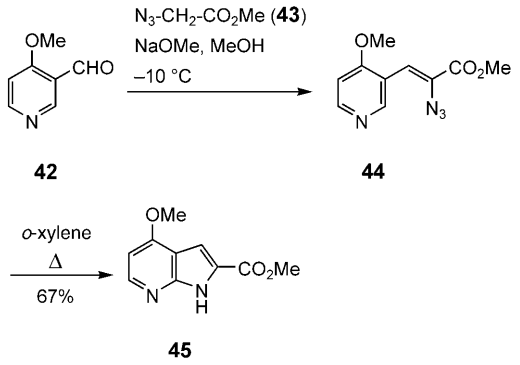
 © 2005 Wiley-VCH Verlag GmbH & Co. KGaA, Weinheim

hexene adducts). On the other, the product configuration is determined by that of the starting material (Scheme 11).



Scheme 11. General synthesis of alkenyl azides **40** according to Hassner et al.[63]

An interesting access to 3-aryl-2-azidopropenoates is provided by the Knoevenagel reaction of aldehydes (e.g. **42**) and azidoacetate (e.g. **43**; Scheme 12, see also Scheme 77).[65] The subsequent thermolysis then gives the corresponding indoles or pyrroles. This reaction sequence was first described by Hemetsberger and co-workers.[66]

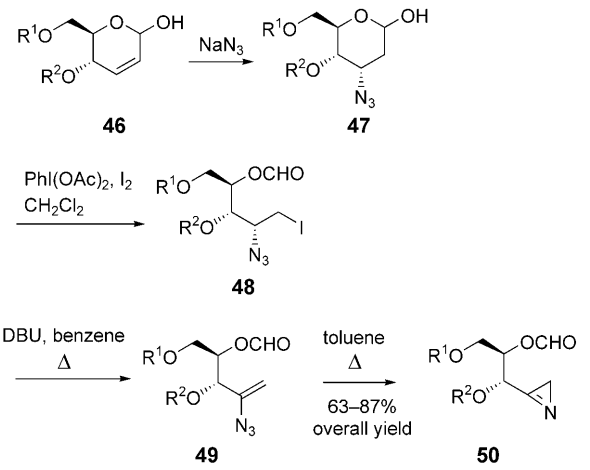


Scheme 12. Synthetic steps in the synthesis of the alkaloid varioline (**45**) and its analogues according to Molina et al.[65]

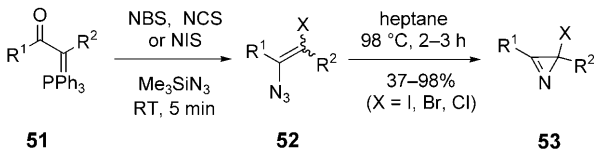
A new possibility for the synthesis of vinyl azides lies in the fragmentation of azide-substituted alkoxy radicals,[67] which are readily available from 3-azido-2,3-didesoxyhexopyranoses[68] **47** and consequently from glycals **46** and sodium azide. In the presence of an iodine source; the fragmentation initially results in vicinal iodoazides **48**, which then undergo elimination under mild conditions to the azidoalkenes **49**. This reaction sequence was used for the synthesis of 2*H*-azirines **50** (Scheme 13).

Alkenyl azides may also be prepared by conjugative addition of azide ions to activated alkynes or allenes.[69] A very convenient synthesis of 2-azidoacrylates is provided by the reaction of α,β-dibromopropanoic acid derivatives with sodium azide (see Scheme 64).[70,71]

Halogenated alkenyl azides can be formed from, among others, α-oxophosphonium ylides by reaction with *N*-halosuccinimides and trimethylsilyl azide. These haloalkenyl azides can be transformed into the corresponding 2-halo-2*H*-azirines **53** by heating to 98 °C (Scheme 14).[72]

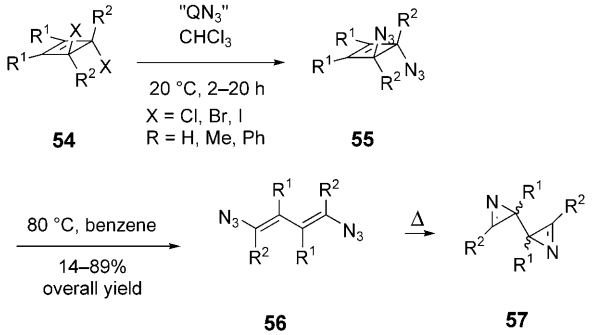


Scheme 13. Fragmentation of alkoxy radicals in the synthesis of alkenyl azides **49**.[67] DBU = 1,8-diazabicyclo[5.4.0]undec-7-ene.



Scheme 14. Synthesis of 2-halo-2*H*-azirines **53** via haloalkenyl azides **52**.[72] NBS = *N*-bromosuccinimide, NCS = *N*-chlorosuccinimide, NIS = *N*-iodosuccinimide.

1,4-Diazido-1,§-dienes **56** serve as precursors for biazirinyls **57** (see Scheme 65). They may be prepared in acceptable yields only by conrotatory opening of *trans*-diazidocyclobutanes **55** (Scheme 15). The latter are accessible by reaction of the *trans*-dihalocyclobutanes **54** with tributylhexadecylphosphonium azide ("QN_3").[73]



Scheme 15. Synthesis of 1,4-diazido-1,3-dienes **56** and biazirinyls **57**.[73]

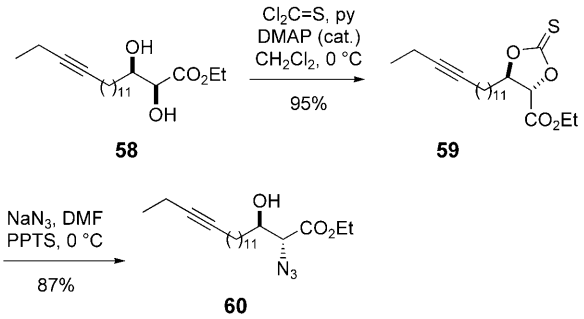
3.3. Alkyl Azides

Alkyl azides were first discovered by Curtius and, after aryl azides, represent the second most important class of azide compounds. In most cases, classic nucleophilic substitution is the method of choice.

 © 2005 Wiley-VCH Verlag GmbH & Co. KGaA, Weinheim

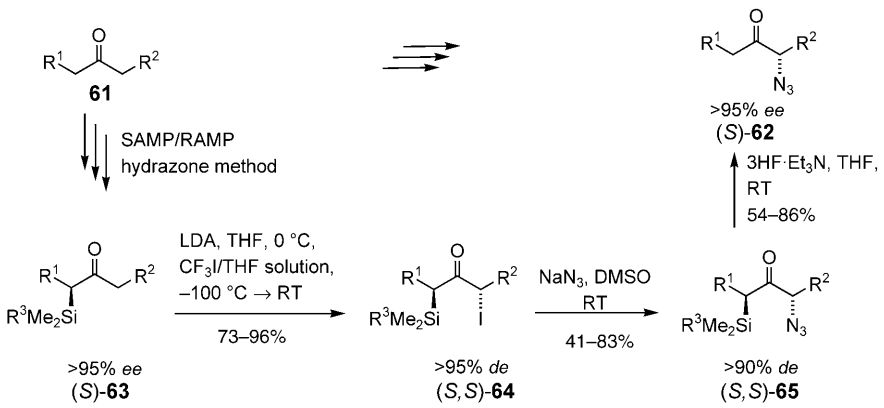
3.3.1. Classic Nucleophilic Substitution

Aliphatic azides are compounds readily accessible by nucleophilic substitution (S_N2 type) with the highly nucleophilic azide ion. Sodium azide is most commonly used as the azide source, although other alkali azides, tetraalkylammonium azides, polymer-bound azides,[74] or (as in the classic variant) the highly explosive silver azide[3] are also used. In most cases halides,[75] carboxylates,[76] and (cyclic) sulfonates[77] as well as mesylates,[78] nosylates,[79a] and triflates[79b,80] are chosen as leaving groups,[81,82] although sulfonium salts are possible substrates.[83] Besides the classic variants with DMF as solvent under thermal conditions, ionic liquids,[84] supercritical carbon dioxide,[85] or microwave radiation[86] can be used. A regioselective azide substitution at the α position of α,β-dihydroxy ester **58** via a cyclic thiocarbonate intermediate **59** was described by Bittman and co-workers in 2000 (Scheme 16).[87]



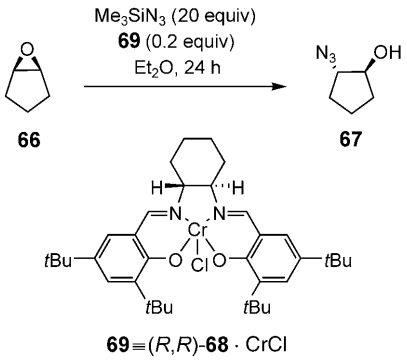
Scheme 16. Synthesis of α-azido-β-hydroxy ester **60** via a cyclic thiocarbonate intermediate **59**[87] DMAP = 4-dimethylaminopyridine, py = pyridine, PPTS = pyridinium *para*-toluenesulfonate.

The asymmetric synthesis of α-azidoketones **62** was described by Enders and Klein in 1999.[88] The key step in this reaction is a diastereoselective nucleophilic substitution of the iodine substituent in α-silylated-α′-iodoketones **64** with sodium azide. The necessary iodoketones **64** were prepared by the well-established SAMP technique. The α-azidoketones **62** are useful intermediates in the synthesis of protected and unprotected α-aminoketones (Scheme 17).



Scheme 17. Asymmetric synthesis of α-azidoketones **62** according to Enders et al.[88]

A further possibility for the synthesis of organic azides is the ring opening of epoxides by azide ions.[18] This useful reaction, which leads to α-azidoalcohols **67** and thus potentially to α-aminoalcohols and aziridines,[18] can also be carried out enantioselectively on the corresponding *meso*-epoxides **66** (Scheme 18).[89,90] A kinetic racemate separation is also possible.[91] Catalysts of choice are salen complexes **69** (salen = *N*,*N*′-bis(salicylidene)ethylenediamine, **68**)[92] with chromium as the central metal.[93] A monomeric salen structure is the reactive species with the participation of a bimetallic intermediate,[94] although macrocyclic and linear oligomer variants are significantly more active then their monomeric analogues.[95] The tolerance of biological systems towards azides also allows kinetic racemate separation of styrene epoxides with halohydrin dehalogenase from *Agrobacterium radiobacter*. The products (the *S* epoxide and the *R* azidoalcohol) were formed with excellent enantiomeric excesses.[96]



Scheme 18. Asymmetric synthesis of α-azidoalcohols **67** according to Jacobsen and co-workers.[89]

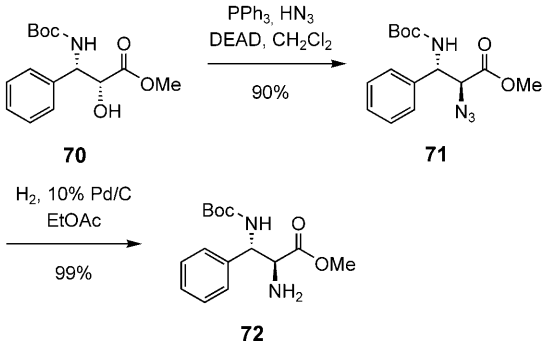
Sodium azide, either zeolite-bound[97a] or in the presence of molecular sieves,[97b] has also been used for the organic transformation of epoxides into organic azides. Glycidols, which can be readily obtained by the Sharpless epoxidation of allyl alcohols, can be opened regioselectively with titanium reagents such as $Ti(OiPr)_2(N_3)_2$.[98] In contrast, a reverse regioselectivity to Markovnikow products is achieved with aluminum reagents such as diethylaluminum azide.[99] The analogous ring opening of aziridines[100]—preferably in the presence of cerium[101] or copper[102] ions—leads to valuable 1,2-diaminoalkanes.[103–105]

S_N1 reactions are also frequently observed. Azide ions react especially readily with oxonium cations, such as are formed in the reaction of glycosyl cations. In this way thioacetals and other precursors can be transformed with azide ions in the presence of Lewis acids.[106] A stereoselective synthesis of anomeric organic azides involves the opening of oxazolines by trimethylsilyl azide and a fluoride source as described by DeShong and co-workers.[107a]

 © 2005 Wiley-VCH Verlag GmbH & Co. KGaA, Weinheim

3.3.2. The Mitsunobu Reaction

A derivation of the Mitsunobu reaction published in 1967[108] provides a simple access to organic azides from alcohols.[109,110] Primary and secondary alcohols react with hydrogen azide, triphenylphosphane, and diethyl azodicarboxylate (DEAD). Secondary alcohols are of considerable interest as substrates because they react with inversion of stereochemistry. Lee et al. used this reaction as the key step in the synthesis of 2,3-diamino-3-phenylpropanoic acid derivatives **72** (Scheme 19), which are important structural elements of many biologically active compounds such as antibiotics.[111]

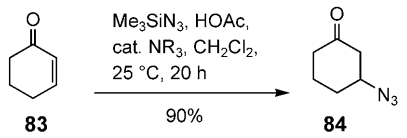


Scheme 19. Application of the Mitsunobu reaction to the asymmetric synthesis of 2,3-diamino-3-phenylpropanoic acid derivates.[111] Boc = *tert*-butoxycarbonyl.

Diphenylphosphoryl azide (DPPA) in the liquid phase[112–115] or immobilized on polymeric supports (see Scheme 125)[116] can also be used successfully in place of the explosive hydrogen azide. In 2002, Jiang et al. published the enantioselective total synthesis of hamacanthine B (**82**) in which this variant of the Mitsunobu reaction was a key reaction (Scheme 20).[117] The central chiral pyrazinone ring was formed in a Staudinger/aza-Wittig sequence (Section 4.3.3). Another Mitsunobu azide source is zinc azide.[118]Alkyl azides can also be prepared by the reaction of alcohols with a reagent combination of tetrabromomethane, triphenylphosphane, and sodium azide—comparable with the classic Appel reaction—as shown in a formal synthesis of mappicin.[119] Homada and co-workers used the Mitsunobu reaction for the preparation of biologically active peptides.[120] The substitution of hydroxy groups under Mitsunobu conditions has been carried out in the solid phase with DPPA.[121,122] In Scheme 32 (Section 3.3.8), the key step of the preparation of a sarcodictyin library by Nicolaou and coworkers is illustrated as an example.[122]

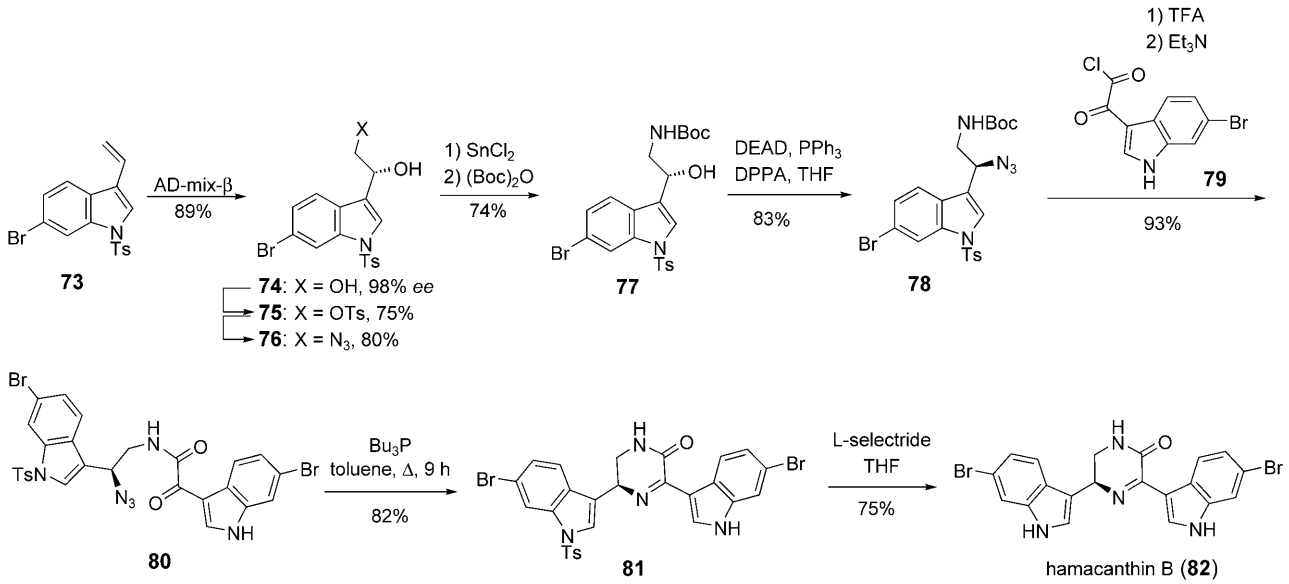
3.3.3. Polar 1,2- and 1,4-Addition Reactions

α,β-Unsaturated carbonyl compounds react with azide ions in 1,4-additions—unlike organic azides, which form triazoles. One example of this valuable method for the synthesis of alkyl azides was described by Miller and coworkers in 1999 for 2-cyclohexenone (**83**).[123,124] The source for the azide ion in this Michael-like reaction is an equimolecular mixture of trimethylsilyl azide and acetic acid, while tertiary amines as Lewis bases catalyze the reaction (Scheme 21). Other suitable Michael acceptors are glycals



Scheme 21. Conjugate addition of azide ions to cyclohexenone **83**.[123]

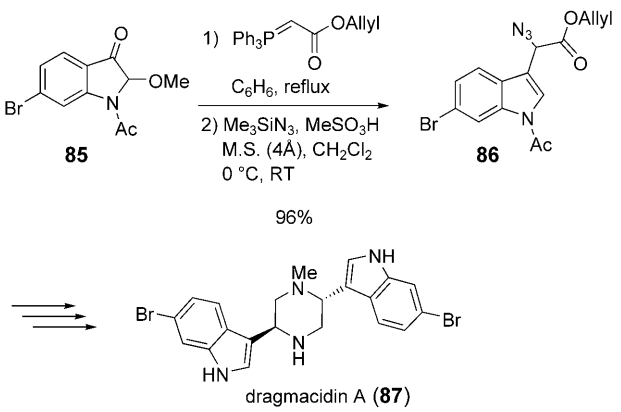
(Scheme 13) or quinones.[125] However, in the presence of Lewis acids (aluminum), azide ions react differently with α,β-unsaturated ketones: triazoles are formed after a hydride



Scheme 20. Enantioselective synthesis of the marine indole alkaloid hamacanthin B (**82**).[117] L-Selectride = lithium tri(*sec*-butyl)borohydride.

 © 2005 Wiley-VCH Verlag GmbH & Co. KGaA, Weinheim

shift.[126] Kawasaki et al. used the 1,4-addition of azides to an indolenium intermediate as key step in the total synthesis of dragmacidin A (**87**; Scheme 22).[127]

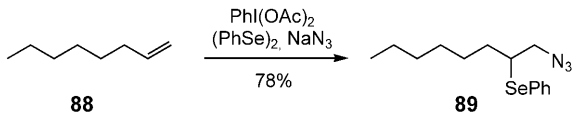


Scheme 22. Synthesis of dragmacidin A according to Kawasaki and co-workers.[127]

3.3.4. 1,2-Addition to Non-Activated Double Bonds

The addition of halogen azides to olefins was first described by Hassner and Levy in 1965.[63] This reaction eventually permitted wide access to vinyl azides (see Section 3.2).

In recent years, single- and multistep radical syntheses have become increasingly important.[128] 1,2-Addition to non-activated double bonds with azide sources can involve a radical reaction since the azidyl radical behaves as a pseudohalogen radical. The reaction of olefins with diphenyldiselenium, diacetoxyiodobenzene, and sodium azide is a radical azidoselenation (Scheme 23).[129,130b] The unusual

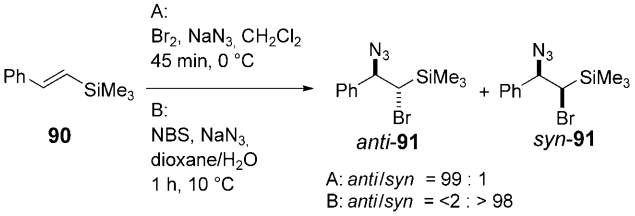


Scheme 23. Radical 1,2-addition to non-activated double bonds.[130b]

regiochemistry—the azide group is inserted at the least-substituted position—is an indication of the radical nature of this reaction. Recently Klapötke and co-workers isolated a stabilized aryl selenium azide,[131] a member of the class of selenium azides whose existence had been postulated in a number of reactions.[132] The radical azidoselenation has found interesting applications in sugar chemistry.[133]

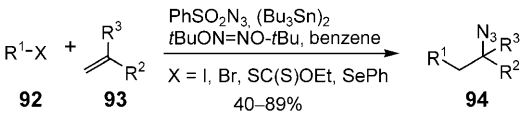
In contrast, the addition of bromoazide to alkenes by pre-electrophiles (Br_2, NBS) and azide ions is mostly polar in nature. The choice of the pre-electrophile and the substrate allows control of the stereochemistry, as shown in Scheme 24 (see also Scheme 11).[134,135]

In 2001, Renaud and co-workers described an efficient carbon–nitrogen bond formation in the reaction of radicals with sulfonyl azides.[136] In 2002, they extended this to the intermolecular addition of radicals to non-activated alkenes



Scheme 24. Polar 1,2-addition to non-activated double bonds.[134,135]

with subsequent azidation. This reaction sequence formally represents a carboazidation of alkenes and is a key step in the three-component syntheses of pyrrolidone, pyrrolizidinone, and indolizinone derivatives.[137] One example is the reaction of the terminal alkenes **93** with different radical precursors (Scheme 25).

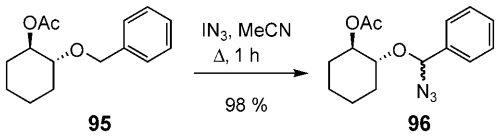


Scheme 25. Radical azide insertion according to Renaud et al.[137]

Kirschning and co-workers elegantly showed that iodoazide can be used as a polymer-bound reagent and in this way were able to convert a series of alkenes into vicinal iodoazides.[138–140] Furthermore, alkenes can be converted into β-azido alkyl mercury compounds by hydrogen azide in the presence of azide ions.[141a] Glycals can be converted into 2-desoxyglycosyl azides by the action of trimethylsilyl azide in the presence of catalytic amounts of trimethylsilyl nitrate.[141b]

3.3.5. C–H Activation

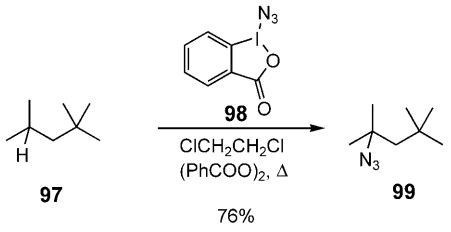
The activation of C–H bonds can also be carried out with azides. The radical azidation in the benzyl position of benzyl ethers **95** with iodoazide[25] was recently described by Viuf and Bols.[142] This reaction takes place in very good yields (74–98%) and relatively short reaction times with a number of substrates (Scheme 26). Related to this reaction is the open-



Scheme 26. Radical azidation of the benzyl position with iodoazide.[142]

ing of benzal acetals with the formation of β-azidobenzoates (azido-Hanessian reaction).[143] A domino radical iodoazide cyclization strategy was used as a key step in the formal total synthesis of (±)-aspidospermidine.[144] Hydrocarbons can also undergo radical azidation at high temperatures with the somewhat more stable hypervalent iodo reagent **98** (Scheme 27).[145]

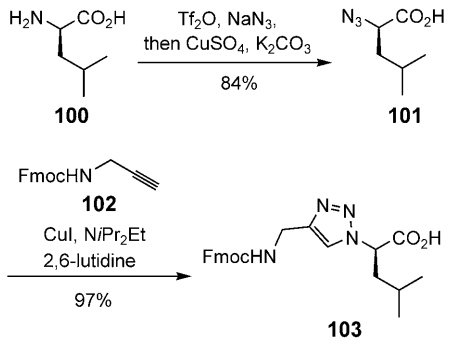
 © 2005 Wiley-VCH Verlag GmbH & Co. KGaA, Weinheim



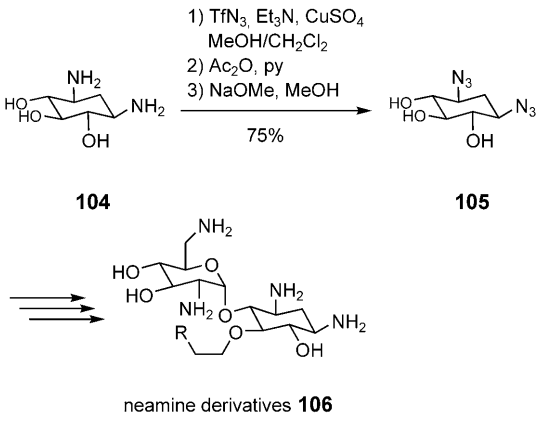
Scheme 27. Activation of the C–H bond by azidoiodinane **98** according to Zhdankin et al.[145]

3.3.6. *Diazo Transfer: A Simple Synthesis of Alkyl Azides from Amines*

Primary aliphatic amines may be converted into the corresponding azides by diazo transfer. In this way, the step involving sensitive aliphatic diazonium ions can be circumvented.[146,147] The reagent of choice for this transformation is triflyl azide (**31**), which can be prepared from trifluoromethanesulfonic anhydride and sodium azide. Aliphatic primary amines **100** give the azides **101** in the presence of a copper catalyst in exceptionally good yields.[148–150] The azides can then be converted, for example, into 1,2,3-triazoles **103** with different alkynes (Scheme 28; see Section 4.1.1). These methods were also used in the syntheses of aminoglycosides, an important group of antibiotics.[151,152] The synthesis of neamine derivatives **106** by Wong and co-workers is shown here as an example (Scheme 29).[152]



Scheme 28. Diazo transfer to primary amines and subsequent triazole synthesis according to Ghadiri and co-workers.[150] Fmoc = fluorenylmethoxycarbonyl.

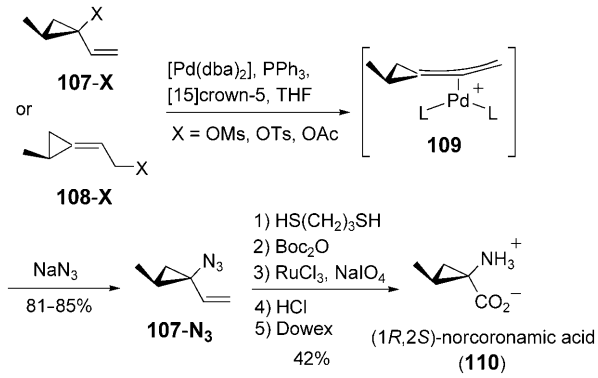


neamine derivates **106**

Scheme 29. Synthesis of neamine derivates **106** according to Wong and co-workers.[152]

3.3.7. *Azide Addition to Palladium Complexes: Synthesis of Allyl Azides*

The addition of azide ions to 1,1-substituted π-allylpalladium complexes has been used by de Meijere, Salaün, and coworkers in the synthesis of aminocyclopropanoic acids. π-Allyl palladium compounds are formed from allyl acetates **107**-OAc, **108**-OAc, or similar compounds in the presence of palladium(0) complexes and are then treated with sodium azide.[153–155] Whereas normally the addition of nucleophiles occurs at the unsubstituted end with formation of the thermodynamically less stable methylenecyclopropanes, in the case of 1,1-ethanoallylpalladium complexes **109**, azide ions give the corresponding alkenylcyclopropanes. A subsequent [3,3] rearrangement may also have occurred (Section 4.8) after the initial formation of methylenecyclopropane derivatives. The azidocyclopropane **107**-N_3 formed stereoselectively could then be transformed into (−)-(1*R*,2*S*)-norcoronamic acid (**110**) in a sequence comprising a reduction (Section 4.4.2) and an oxidative cleavage of the double bond (Scheme 30).[156] 1-Aminocyclopropanecarboxylic acid was also prepared in this way.[157] Structurally demanding π-allyl palladium complexes, which are formed according to Grigg and co-workers [158] in a cascade cyclization or by arylation of allenes,[159] could also be converted regioselectively into the corresponding allyl azides. A special feature is the fact that π-allyl complexes can also be transformed into enantiomerically pure allyl azides by the action of chiral ligands.



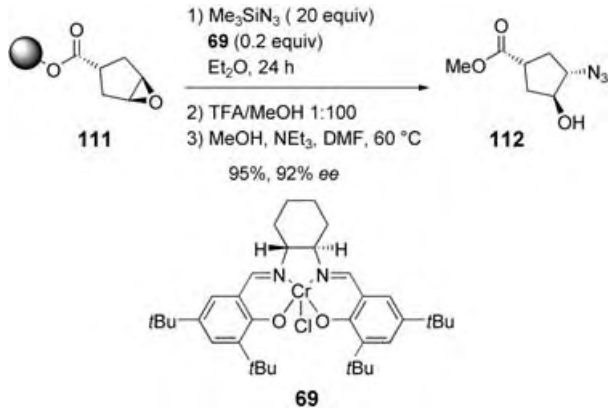
Scheme 30. Synthesis of (−)-(1*R*,2*S*)-norcoronamic acid (**110**) according to de Meijere, Salaün, and co-workers.[156] dba = Dibenzylideneacetone.

According to Yamamoto and co-workers π-allyl palladium complexes also play a role in the reaction of allyl carbonates, trimethylsilyl azide, and alkynyl aryl isocyanides to give indoles.[160] Allyl azides that bear a leaving group such as nitrite in the 1-position can readily fragment with the loss of this leaving group to form α,β-unsaturated nitriles.[161]

 © 2005 Wiley-VCH Verlag GmbH & Co. KGaA, Weinheim

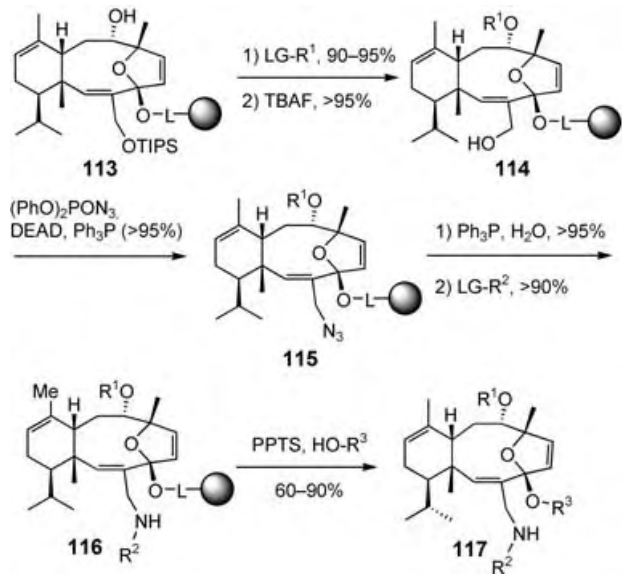
3.3.8. Solid-Phase Synthesis of Aliphatic Azides

Aliphatic azides have already been frequently synthesized on solid supports. In each case a start was made from a polymer-bound electrophile, which reacted with the corresponding azide-transfer reagent. The substitution of alkyl halides and alkyl alcohols was carried out with sodium azide[162,163] or tetra-*N*-butylammonium azide.[164] The ring opening of epoxides was carried out with sodium azide.[165,166] Jacobsen and co-workers used trimethylsilyl azide for the asymmetric ring opening of *meso*-epoxides in the solid-phase synthesis of cyclic azidoalcohols (Scheme 31).[167]

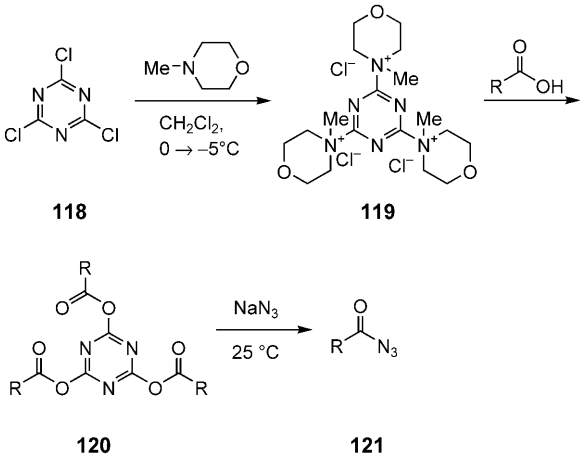


Scheme 31. Asymmetric epoxide opening on solid supports.[167] TFA = trifluoroacetic acid.

The substitution of hydroxy groups on solid-supports can be carried out under Mitsunobu conditions with DPPA[121,122,168] or under classic conditions.[169] In 1998, Nicolaou and co-workers reported the solid-phase synthesis of a sarcodictyin library with three points of diversity (Scheme 32) in which the Mitsunobu reaction played an important role.[122]



Scheme 32. Solid-phase synthesis of sarcodictyin analogues by Nicolaou and co-workers.[122] L = linker, TIPS = triisopropylsilyl, LG = leaving group, TBAF = tetrabutylammonium fluoride.



Scheme 33. Synthesis of acyl azides **121** from cyanurtrichloride **118**.[171]

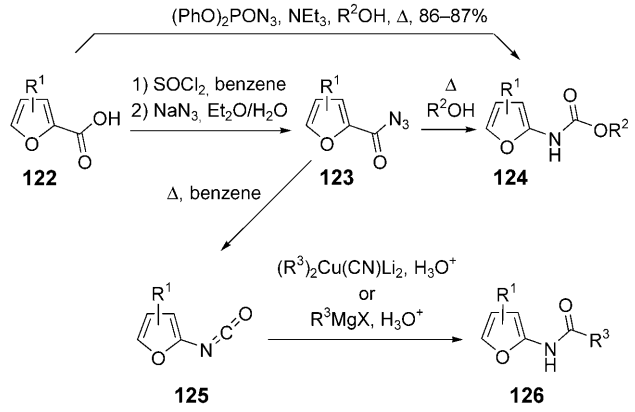
3.4. Acyl Azides

Acyl azides are widespread, highly reactive reagents in organic chemistry and are used for the preparation of amides and heterocycles. Acyl azides are normally prepared from acid derivatives such as acyl chlorides or mixed anhydrides[170] with azide ions or by reaction of acyl hydrazines with nitrosyl precursors. A very mild and efficient method for the preparation of acyl azides without subsequent Curtius rearrangement (see Section 4.5.1), which would lead to the isocyanate, was described by Banddgar and Pandit in 2002 (Scheme 33).[171] In this case, different aryl, heteroaryl, alkyl aryl, and alkyl carboxylic acids are converted into the respective acyl azides **121** under mild conditions with cyanurtrichloride (**118**) in the presence of sodium azide and *N*-methylmorpholine.

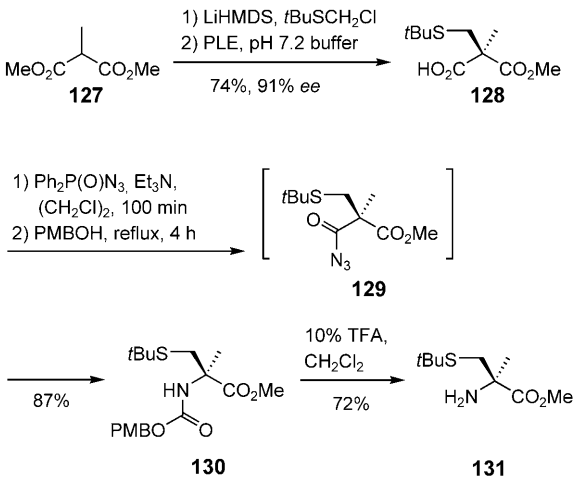
Padwa et al. used the synthesis of acyl azides **123** in the preparation of substituted furans.[172] The free acids **122** are first converted into the corresponding acid chloride with thionyl chloride and then into the corresponding acyl azide **123** with sodium azide. Formation of the isocyanates **125** under Curtius conditions and subsequent reaction leads to amidofurans **126**. If the acyl azides **123** are heated in the presence of alcohols, furanamino carboxylates **124** are formed. The latter can also be prepared directly from the carboxylic acids by reaction with DPPA and alcohols in the presence of triethylamine (Scheme 34). The reaction of carboxylic acids with DPPA and subsequent Curtius rearrangement can also be used for the conversion of malonic ester derivatives **127** into α-amino acid esters **131**. In particular, the enantioselective, enzymatic desymmetrization with pig liver esterases (PLE) leads to the enantiomerically pure amino acids (Scheme 35).[173]

Enamides were prepared by Kitahara and co-workers by rearrangement of α,β-unsaturated acyl azides to alkenyl isocyanates **133** and subsequent addition of nucleo-

 © 2005 Wiley-VCH Verlag GmbH & Co. KGaA, Weinheim



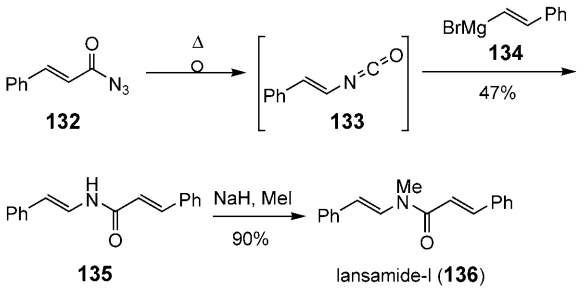
Scheme 34. Derivatization of furoic acids **122** according to Padwa et al.[172]



Scheme 35. Asymmetric conversion of the dimethyl malonate derivate **127** into α-amino acid ester **131**.[173] LiHMDS = lithium hexamethyldisilazide; PMB = *para*-methoxybenzyl.

philes.[174,175] The reaction sequence was used for the preparation of a series of natural products such as the lansiumamides A–C and lansamide-I (**136**; Scheme 36),[176] coscinamide, chondriamide, igziamide,[174] salicylihalamide,[177] apicularen A,[178] and others.[179]

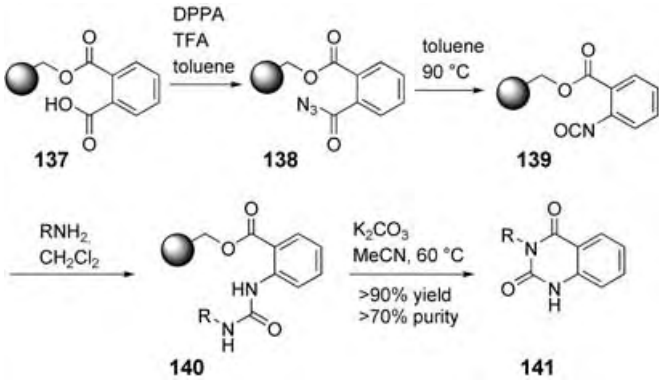
The synthesis of (poly)peptides can also be carried out with the highly reactive acyl azides[180] that are formed



Scheme 36. Total synthesis of lansamide-I (**136**) according to Taylor and co-workers.[176]

directly, for example, from DPPA and carboxylic acids. The azide unit with its ability to activate the acid group can then be replaced by nucleophiles—as already found by Curtius. Lucente and co-workers used the synthesis of acyl azides for the preparation of ergopeptides,[181] while Larsen and co-workers prepared β-1,3-glycosidically bound aminomonocarbodisaccharides.[182]

One application was described by Castelhano and co-workers in 1998 with the solid-phase synthesis of quinazoline-2,4-diones **141**.[183] Phthalic acid was first immobilized on a PEG4-PS resin and then converted into the acyl azide with DPPA in the presence of trifluoroacetic acid in toluene. Rearrangement to the isocyanate followed by reaction with a primary amine and subsequent base-catalyzed cleavage with ring closure gave the heterocycles in good yields with excellent purity (Scheme 37).



Scheme 37. Solid-phase synthesis of quinazoline-2,4-diones **141** with the generation of an acyl azide synthesis as a key step.[183]

A new variant for the preparation of acyl azides was described by Bols and co-workers. Aldehydes react with iodoazide[25] at room temperature, presumably in a radical mechanism.[184] If this reaction is carried out at elevated temperatures the acyl azides rearrange and the resulting isocyanates are captured with the formation of carbamoyl azides. Unlike acyl azides, *C*-azidoimines rearrange to tetrazoles (Scheme 145).

3.5. Heteroazides and Azide Reagents

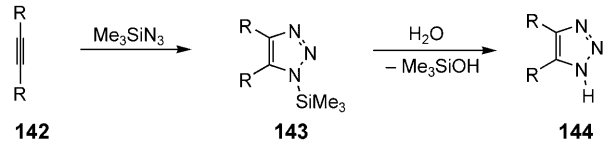
Besides organoazides, in which the azide function is connected directly to the carbon atom, different heteroazides are of importance in organic synthesis and are briefly mentioned here.

3.5.1. Silyl azides

Silyl azides are valuable reagents in organic synthesis,[185,186] because, unlike sodium azide and hydrogen azide, they have no immediate explosive properties.[187] However, they hydrolyze in the long term to the volatile, toxic, and explosive hydrogen azide and therefore must be stored in the absence of moisture and acids. Trimethylsilyl azide (bp.

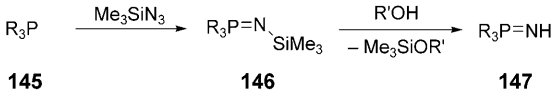
 © 2005 Wiley-VCH Verlag GmbH & Co. KGaA, Weinheim

95 °C), which is also commercially available, can be prepared by photolysis of tetrakis(trimethylsilyl)-2-tetrazene[188] or by reaction of tris(trimethylsilyl)phosphate with sodium azide.[189] Most conveniently, however, it is formed from trimethylsilyl chloride by reaction with sodium azide in diglyme.[190] The higher thermal stability of trimethylsilyl azide relative to hydrazoic acid[191] can be used in the preparation of 1,2,3-triazoles from trimethylsilyl azide and acetylenes (Scheme 38).[192]



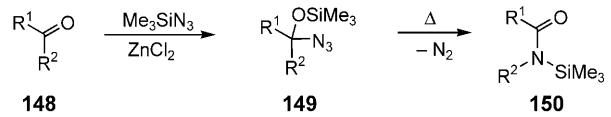
Scheme 38. Cycloadditions with trimethylsilyl azide.[192]

The facile cleavage of the Si–N bond governed the success of the synthesis of trialkyl- and triarylphosphinimines **147** from the corresponding phosphines **145** and trimethylsilyl azide (Scheme 39).[193] This reaction is significantly simpler than the reaction of phosphines with chloramine.[194]



Scheme 39. Synthesis of triaryl phosphinimines.[194]

Trimethylsilyl azide reacts with aldehydes or ketones **148** and their enol ethers with the formation of trimethylsilyloxy azides **149**, which can be transformed thermally[195a] or photochemically[195b] in a Schmidt rearrangement into *N*-trimethylsilyl amides **150** (Scheme 40) or the respective protiodesilylated amides. This reaction sequence is superior to the Schmidt reaction at least for a few derivatives because of the higher yields.[195b]



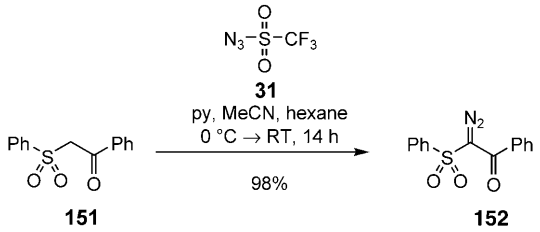
Scheme 40. Conversion of ketones into *N*-trimethylsilylamides.[195]

It was reported recently that trimethylsilyl azide can be immobilized in the solid phase as a reagent.[196]

3.5.2. *Sulfonyl Azides*

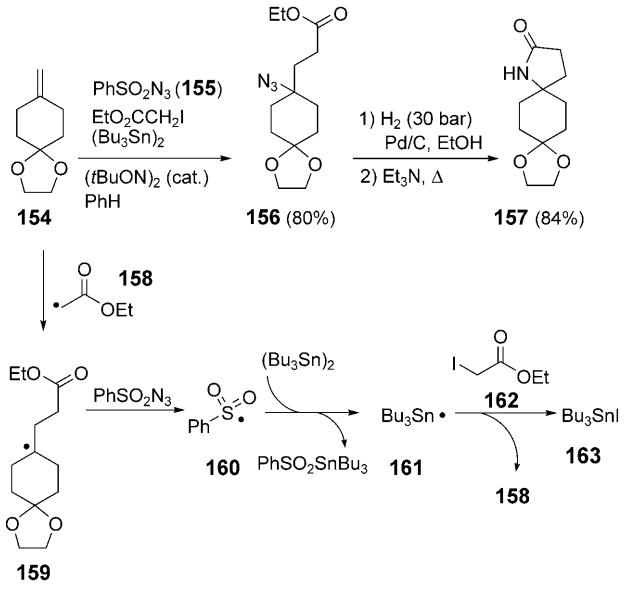
Sulfonyl azides[197] can be prepared from the corresponding sulfonyl chlorides by reaction with sodium azide in acetone.[198] These useful but sensitive[199] reagents are also available as shock-resistant solid-phase variants.[200]

The sulfonyl azides are used for diazo transfer[201] to CH-acid compounds, especially activated esters, β-ketoesters, and ketosulfones.[198,202] The enolate or enol attacks the organoazide with formation of a triazene, which after tautomerization reacts to form the diazo compound and the sulfonamide. Trifluoromethanesulfonyl azide (triflyl azide, **31**) was proposed by Charette and co-workers as a highly electrophilic diazo-transfer reagent that gives good results with activated acetic acid esters and ketones, particularly with pyridine as base (Scheme 41).[203,204]



Scheme 41. Diazo transfer with sulfonyl azide **153**.[203]

An interesting application of *p*-toluenesulfonyl azide (tosyl azide, **153**) is the proline-mediated enantioselective α-amination of aldehydes (see Scheme 46).[226] Recently sulfonyl azides, including pyridine-3-sulfonyl azide,[205] were successfully used in the azidation of nucleophilic radicals.[206] This reaction can also be used for intra- or intermolecular carboazidation of olefins. Renaud and co-workers demonstrated the use of this method in the synthesis of the spirolactam **157** (Scheme 42). The radical **158**, produced from ethyl iodoacetate, reacts with the olefin **154**, and the newly generated (nucleophilic) tertiary radical **159** extracts the azide group from phenylsulfonyl azide (**155**). The electrophilic radical **158** is, in contrast, unable to react with the sulfonyl azide. Tin-free methods are being intensively investigated, and triethyl borane appears to be a useful alternative.[207]



Scheme 42. Synthesis of spirolactam **157** by radical-induced carboazidation of olefins according to Renaud et al.[206]

 © 2005 Wiley-VCH Verlag GmbH & Co. KGaA, Weinheim

Furthermore, sulfonyl azides (especially triisopropylbenzenesulfonyl azide)[208] have been used in the electrophilic (diastereoselective) α azidation[208b] of the harder amide enolates of the Evans type[208] and ester enolates (Scheme 146)[134] for the synthesis of α-amino acid derivatives (Section 3.1.3, Scheme 7, Section 3.3.4, Scheme 25, Section 3.3.6).

Other important azides are iodoazide,[25,63,138–140,209] phosphoryl azides such as DPPA,[210] tributylhexadecylphosphonium azide ("QN_3"),[211] and *tert*-butoxycarbonyl azide (Boc azide), a transfer reagent for the *tert*-butoxycarbonyl group onto amines. The Zhdankin reagent (a stable azidoiodinone) was used for the direct azidation of hydrocarbons (see Scheme 27).[145] An important reagent is tetramethylguanidinium azide introduced by Papa[212] which has been used for the synthesis of vinyl azides,[69] among others (Section 3.2) and is advantageous for safety reasons.[213]

4. Reactions of Organic Azides

Azides can react very differently under different reaction conditions. In principle, they react with electron-deficient compounds (electrophiles) at N^1 (Section 4.6; Figure 2) and

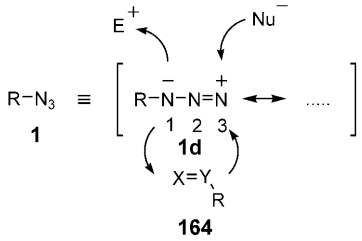


Figure 2. Reactivity of organic azides.[1]

electron-rich compounds (nucleophiles) at N^3 (Sections 4.3 and 4.4; Figure 2). There can be retention of the azide unit, but also cleavage of the nitrogen–nitrogen single bond, as in the case of nitrene chemistry. The simplest case mechanistically—an addition—has been used extensively in cycloaddition reactions.

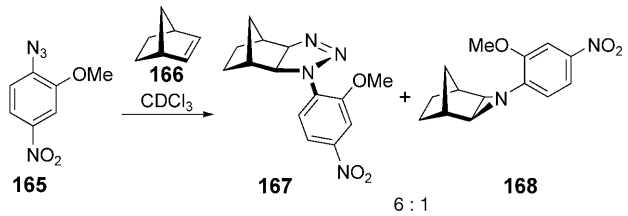
4.1. "Clicked": Cycloadditions Newly Discovered

The Huisgen reaction[214]—the cycloaddition of dipoles to dipolarophiles—also succeeds with azides as dipoles,[215] and selected dipolarophiles can be used.

4.1.1. 1H-Trazoles and Δ^2-1,2,3-Triazolines Made Simple

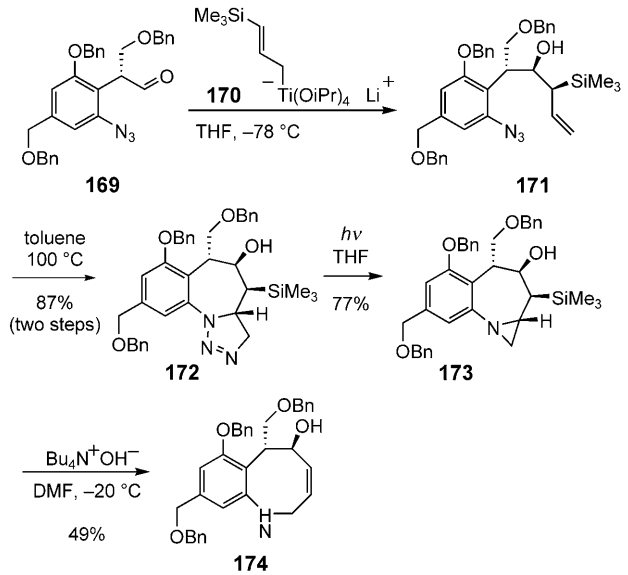
The uncatalyzed thermal cycloaddition of organic azides to alkynes and olefins allows the synthesis of 1*H*-triazoles and Δ^2-1,2,3-triazolines.[74,216,217] The addition takes place at different rates depending on the dipolarophile. Whereas strained olefins or alkynes such as norbornene and cyclooctyne[218] react readily, terminal alkenes react extremely slowly.[217b] In principle, suitable dipolarophiles include both electron-deficient and electron-rich alkenes (enol ethers such as glycans,[216f] enamines,[219a,b]; see Scheme 45) as well as magnesium acetylides.[216e] Many olefins are so unreactive, however, that intramolecular reaction control or the use of microwaves is necessary.[220]

The reaction of organoazides with alkenes is illustrated with a number of examples.[221,222] The aryl azide **165**, prepared as part of a combinatorial approach, reacted with norbornene **166** at 40 °C within 18 h and a conversion of ≈75 % with the formation of the Δ^2-1,2,3-triazoline **167** and the aziridine derivative **168** in a ratio of 6:1.[45] This ratio is temperature-dependent as the primarily formed Δ^2-1,2,3-triazoline **167** can react further to furnish the aziridine derivative **168** (Scheme 43).



Scheme 43. Cycloaddition of aryl azide **165** to norbornene.[45]

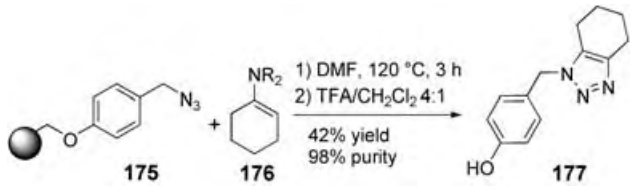
Ciufolini and co-workers demonstrated the use of intramolecular cycloadditions in their total synthesis of FR66979. After a selective Cram allylmetal addition of the titanium allyl compound **170** to an aldehyde **169** with an azide moiety through a Zimmerman–Traxler transition state, diastereoselective 1,3-dipolar cycloaddition gave the tricycle **172**. After photochemical nitrogen extrusion from the Δ^2-1,2,3-triazoline **172** and ring contraction to the aziridine **173**, an anionically induced azacyclopropylmethyl-azahomoallyl rearrangement took place (Scheme 44).[223]



Scheme 44. Part of the total synthesis of FR66979 according to Ciufolini and co-workers.[223] Bn = benzyl.

 © 2005 Wiley-VCH Verlag GmbH & Co. KGaA, Weinheim

If the alkene bears a suitable leaving group, the initially formed Δ^2-1,2,3-trazoline aromatizes to the 1*H*-triazole.[224] In the case of enamines **176**, cycloaddition with organoazides **175** is usually followed by elimination of the amine group so that 1,2,3-triazoles **177** are formed (Scheme 45).[219] In a few cases, these and the analogous enol ether adducts rearrange to form β-lactams.[225]

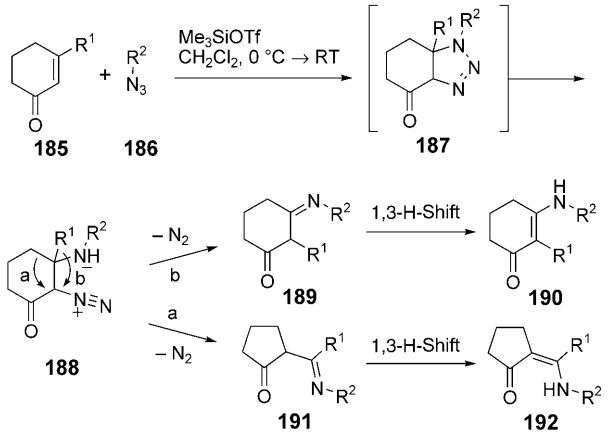


Scheme 45. Synthesis of 1,2,3-triazoles on a polymer support according to Harju et al.[219]

The enamine **180**, which is formed in a proline-mediated enantioselective α sulfamidation of 2-phenylpropanal (**178**), reacts with nosyl azide in moderate yield via the triazoline **181** to give *N*-nosyl-2-amino-2-phenylpropanal (**179**) with 89% *ee* (Scheme 46).[226] Compound **182** and the aziridine **183** are presumed to be intermediates; the latter undergoes ring opening to **184** by participation of the proline nitrogen atom to form **179** after hydrolysis.

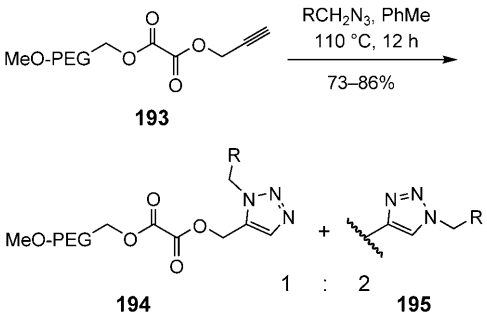
The assumed reaction mechanism is supported by work from Benati et al.[227] and Zhu et al.[228]

A series of α,β-unsaturated ketones **185** react with alkyl azides **186** under Lewis acid catalysis in a similar mechanism, as determined by Aubé and co-workers (Scheme 47).[229] Unlike the known rearrangements of this type,[230] the Lewis acid catalyzed variant takes place at low temperatures. The Δ^2-1,2,3-triazolines **187** are indeed first formed. However, they are not stable under the prevailing reaction conditions. It is a case of nonstabilized triazenes.[231] In the presence of Lewis acids, they open to amidodiazonium betaines **188**, which according to the structure of the addition product either rearrange with migration of the substituents (path b) or ring contraction occurs (path a). Endo- or exocyclic enaminones **190**/**192** are formed. Cyclohexenones usually form the (*Z*)-configured ring contraction product **192**. Cyclopentenones, in contrast, usually give aminocyclopentenones. Aziridines can also be formed.

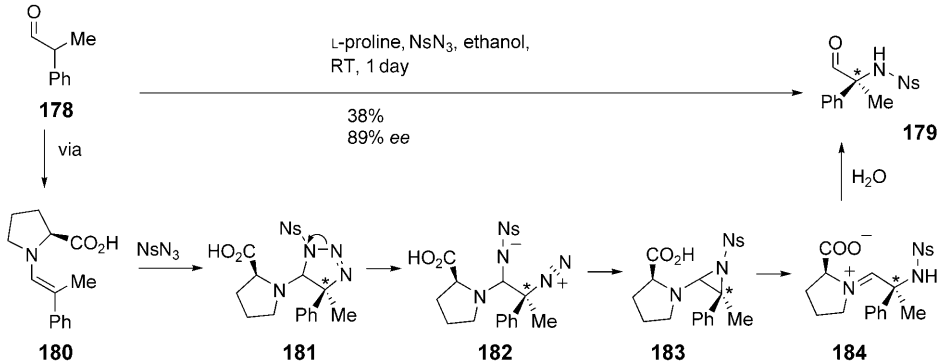


Scheme 47. Cycloaddition of alkyl azides to α,β-unsaturated ketones according to Aubé et al.[229]

Related to this reaction are the additions of arynes to azides, which lead to benzotriazoles, as Huisgen and co-workers were able to show quite early.[215,232,233] Trimethylsilylacetylene[234] and a number of strained or electronically activated alkynes react with organoazides at room temperature or below, whereas with many other alkynes the reaction must be carried out at elevated temperatures in the absence of catalysts. The cycloaddition of immobilized alkynes with organic azides has also been carried out on soluble polymers[235] (Scheme 48) and on polystyrene resins.[236,237] Furthermore, other solid-phase variants of this reaction with immobilized azide have been used for the preparation of



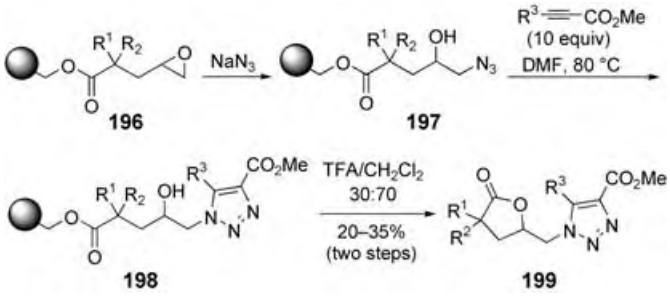
Scheme 48. Synthesis of 1,2,3-triazoles on a soluble polymer according to Norris et al.[235]



Scheme 46. Enantioselective α sulfamidation of 2-phenylpropanal (**178**) with tosyl azide.[226]

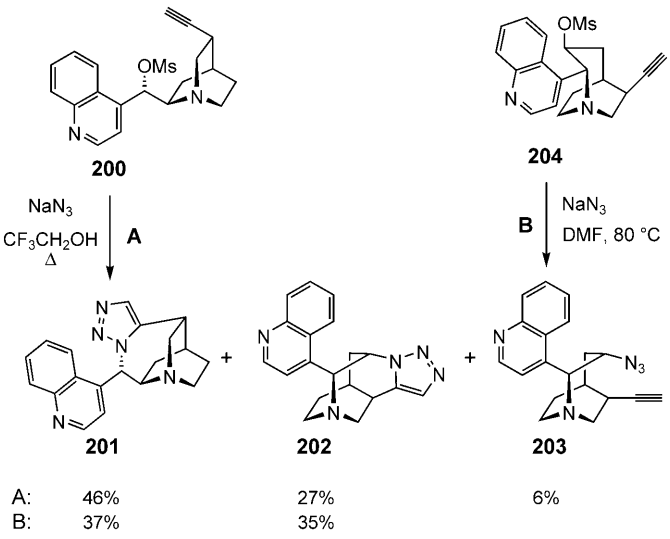
 © 2005 Wiley-VCH Verlag GmbH & Co. KGaA, Weinheim

substituted 1,2,3-triazoles.[237,238] In the example shown in Scheme 49, the final product **199** is obtained by subsequent cleavage and cyclization.



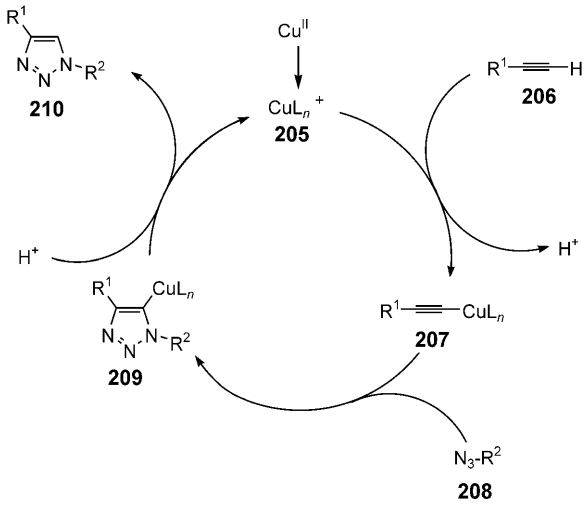
Scheme 49. Synthesis of 1,2,3-triazoles **199** on a polystyrene support according to David and co-workers.[237]

The intramolecular 1,3-dipolar cycloaddition[239] of cinchona azides to a C10–C11 alkyne and a C10–C11 alkene was demonstrated recently by Hoffmann and co-workers (Scheme 50).[240] Thus, *O*-mesylcinchonidine **200** and NaN_3 reacted to form the triazole **201** and the ring-expanded derivative **202**. Both triazoles **201** and **202** were formed with retention of configuration at C9 and C3. The 1-azabicyclo[3.2.2] rearrangement is clearly reversible.



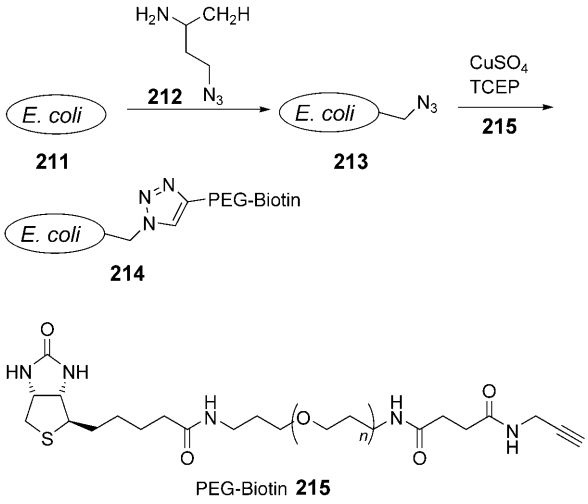
Scheme 50. Substitution, rearrangement, and cycloadditions to cinchona alkaloids according to Hoffmann and co-workers.[240] Ms = methanesulfonyl.

A breakthrough in triazole chemistry occurred with the independent observations by the groups of Meldal[241] and Sharpless[242] that the reaction of aliphatic azides **208** with terminal alkynes **206** is accelerated by copper ions, and their regioselectivity is improved (Scheme 51).[243–247] These reactions have been used frequently in recent years[248] and are also considered as a contribution to "click chemistry"[249]



Scheme 51. Possible catalytic cycle for the copper-catalyzed triazole synthesis.

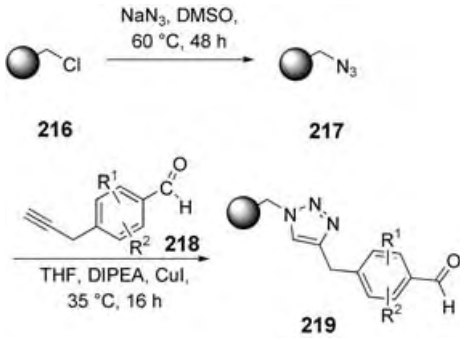
because they take place under mild conditions and form complex structures. The special feature of this reaction is that it is biocompatible[250,251] and takes place particularly well in aqueous media. They can also be carried out very efficiently in organic solvents in the presence of a copper complex with appropriate ligands.[247] The sensitivity of the reaction towards copper catalysts is so high that even copper wire is sufficient to maintain the corresponding copper ion concentration. Thus it was possible, for example, to label the surface of *Escherichia coli* cells. Azidohomoalanine (**212**) was incorporated metabolically into the outer membrane protein C (OmpC), one of the most common membrane porines of *Escherichia coli*. Selective modification of the azide functionality was possible by copper-mediated [3+2] azide–alkyne cycloaddition with an alkyne **215** that carries a biotin marker (Scheme 52). The specificity of this reaction was demonstrated by Western blotting and continuous-flow cytometry.[252]



Scheme 52. Labeling of bacteria by cycloadditions.[252] TCEP = tris(2-carboxyethyl)phosphane.

 © 2005 Wiley-VCH Verlag GmbH & Co. KGaA, Weinheim

A copper-catalyzed 1,3-dipolar cycloaddition with an alkyl azide **217** in the solid phase that was synthesized starting with Merrifield resin was reported recently by Gmeiner and co-workers.[253] Based on this concept, aldehydes **218** can be immobilized to generate amides in subsequent steps (Scheme 53).



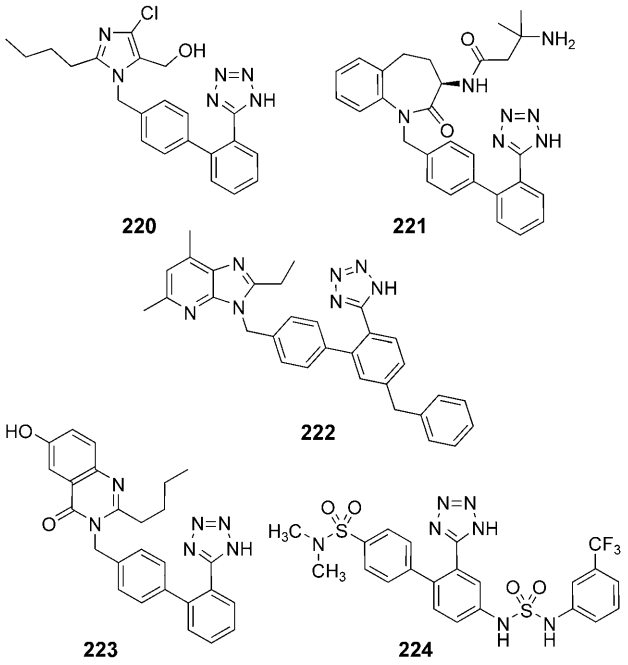
Scheme 53. Synthesis of a new family of SPOS resins by 1,3-dipolar cycloaddition through a click linker.[253] SPOS = solid-phase organic synthesis, DIPEA = diisopropylethylamine.

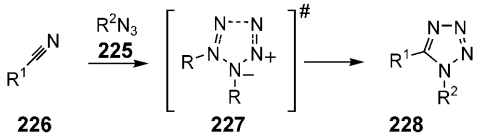
A new three-component reaction of azides, alkynes, and allyl carbonates leads to 2-allyl-1,2,3-triazoles.[254] A more recent and preparatively interesting preparation of 1,2,3-triazoles takes place through the less stable allenyl azides **586** formed from propargyl azides **585** in a [3,3] sigmatropic shift of the azide group (see Section 4.8, Scheme 144).[255]

4.1.2. *Tetrazoles*

Because of their stability towards acids and bases and oxidative and reducing conditions[256] tetrazoles are interesting building blocks and target structures in organic synthesis.[257] They are lipophilic, metabolically stable compounds,[257] carboxylic acid bioisosteres[258] and *cis*-amide isosteres in peptide chemistry,[259] and are used frequently in different pharmaceuticals such as losartan[260] and in materials science.[261] Suitably substituted biphenyltetrazoles, in particular, are potent and selective ligands for different proteins such as G protein-coupled receptors, enzymes, and ion channels. Besides their well-known antihypertensive property in pharmaceuticals such as losartan (**220**),[260] biphenyltetrazoles stimulate the release of growth hormones (e.g. **221**).[262] Furthermore, they inhibit metalloproteases (e.g. **222**, **223**)[263,264] and are chloride-channel effectors (e.g. **224**).[265]

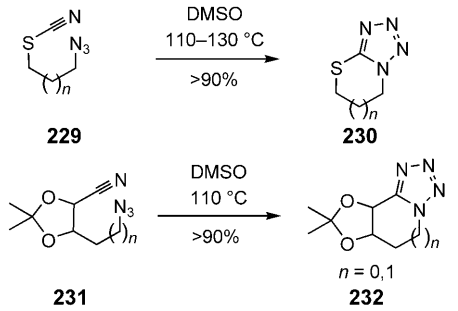
Tetrazoles **227** can be synthesized directly by a [3+2] dipolar cycloaddition between an organoazide **225** and a nitrile **226** (Scheme 54).[266] This reaction occurs through a concerted[266] and regioselective[267] [3+2] cycloaddition between an organic azide and an organic nitrile with formation of the 1,5-disubstituted product.[268] However, it only takes place sufficiently rapidly if electron-withdrawing groups are present on the nitrile,[269] or the reaction is intramolecular.[268,270] Polycyclic tetrazoles are formed in very good yields. This reaction could be improved further by the introduction of further heteroatoms such as oxygen, nitrogen, and sulfur at the nitrile terminal (thiocyanate,





Scheme 54. [3+2] Cycloaddition of nitriles **226** and organoazides **225** to give tetrazoles **228**.[266]

cyanate) (Scheme 55).[271] The spectrum of suitable azidonitriles for these intramolecular [3+2] cycloadditions is considerable, the second ring thus formed can be unsaturated or



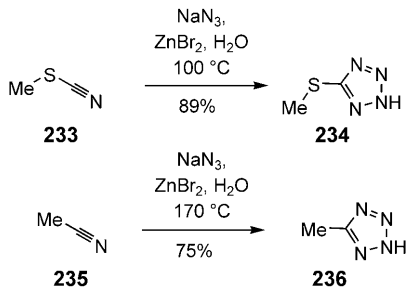
Scheme 55. Intramolecular synthesis of tetrazoles.[271,273]

contain heteroatoms. If the necessary reaction temperature is taken as a measure of the reactivity, cyanates are more reactive in zinc-catalyzed reactions than simple nitriles. In the absence of the catalyst, however, this reactivity is reversed.[272]

If azide ions or hydrogen cyanide are used as dipoles, 1*H*-tetrazoles are formed in high yields,[274] as demonstrated by Hantzsch and Vagt more than 100 years ago.[275] The addition

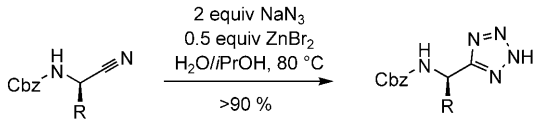
 © 2005 Wiley-VCH Verlag GmbH & Co. KGaA, Weinheim

of azide ions to nitriles is accelerated by microwaves[276] or by catalysis with zinc salts (Scheme 56).[277,278] This latter discovery was used for the synthesis of, among others, chiral, enantiomerically pure tetrazoles **238** under relatively mild conditions (Scheme 57).[279]



233 **234** **235** **236**

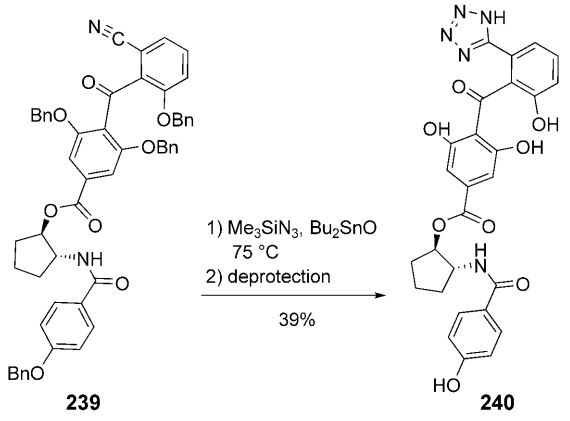
Scheme 56. [3+2] Cycloaddition of thiocyanates **233** and nitriles **235** with azide ions.[278]



237 **238**

Scheme 57. Synthesis of tetrazoles **238** according to Sharpless et al.[279]

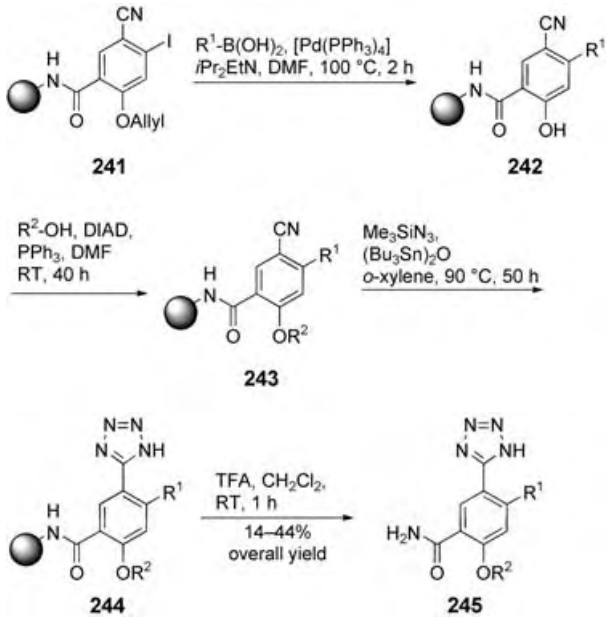
Trimethysilyl azide (in the presence of catalytic amounts of tin oxides,[280a,b] or tetrabutylammonium fluoride)[280c] and trialkyl stannyl azides[258] can act as surrogates for azide ions. They are not only more soluble in organic solvents but are probably less toxic. The tetrazoles obtained may be readily deprotected. The synthesis of the balanol analogue **240**, which has a high affinity for protein kinases A and C, is shown as an example (Scheme 58).[281]



239 **240**

Scheme 58. Synthesis of tetrazoles **240** according to Lampe et al.[281]

A solid-phase synthesis of biphenyltetrazoles was described recently.[282a] The formation of the tetrazole ring from polymer-bound nitriles **243** (which were prepared in two stages on the support from the iodides **241**) was achieved with Me_3SiN_3 and catalytic amounts of n-Bu_2SnO within 50 h at 90 °C in o-xylene and gave the solid-phase-bound biphenyltetrazoles **244**. Cleavage from the support with TFA/CH_2Cl_2 gave the tetrazoles **245** in good purity (Scheme 59).

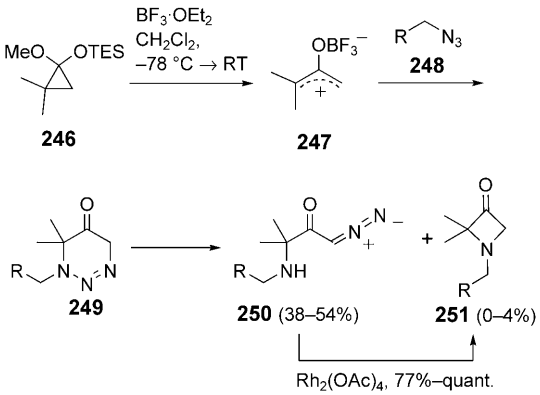


241 **242** **243** **244** **245**

Scheme 59. Synthesis of tetrazoles **245** on a polystyrene support according to Kivrakidou et al.[282] DIAD = azodicarboxylic acid diisopropyl ester.

4.1.3. Reactions of Organoazides with Other Dipolarophiles

Other π systems such as allyl cations also react with organoazides, as demonstrated by the Lewis acid induced intramolecular reaction of hydroxyazidoalkenes.[283] Thus far, however, this reaction has found little use in the synthesis of dihydrotriazines. One interesting application is the cycloaddition of aliphatic azides **248** to 2-oxyallyl systems **247** that were prepared from cyclopropanone derivatives **246** (Scheme 60).[284] The regioselective dihydrotriazines **249** formed initially fragment to give α-diazoketones **250**. The



246 **247** **248** **249** **250** (38–54%) **251** (0–4%)

Scheme 60. Synthesis of α-diazoketones according to Desai and Aubé.[284] TES = triethylsilyl.

 © 2005 Wiley-VCH Verlag GmbH & Co. KGaA, Weinheim

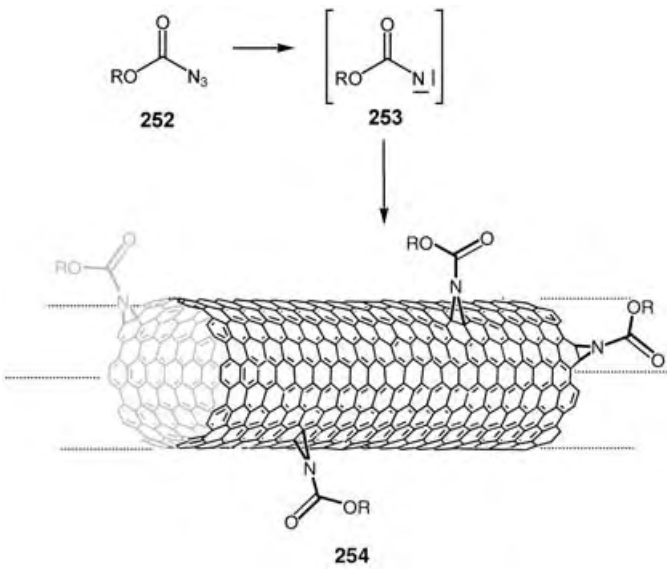
latter can be transformed into the azetidinones **251**, which otherwise only occur as by-products, in very good yields with catalytic amounts of rhodium acetate.

4.2. Nitrene Chemistry

The chemistry of aryl azides (and the postulate by Tiemann[285] of nitrenes during the decomposition of azides) has a long history that stretches back to the 19th century. However, targeted photochemical rearrangements with aryl nitrenes is a relatively new area of research. Both the complexity of the possible products and the diverse applications makes this area of research of special interest. In general, nitrenes are formed either thermally or photochemically.[27d,286,287] Nitrenes are related to carbenes but have different properties.[28] A difference is drawn between singlet and triplet nitrenes, and it has been possible to detect the latter by matrix isolation experiments.[288,289] The reactions of nitrenes stretch from cycloaddition, to rearrangements, to insertion reactions. Reference is made here to the cited review articles[1] and monographs[7] for an exhaustive treatment of the very broad spectrum.

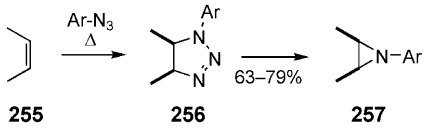
4.2.1. Intermolecular Cycloadditions of Nitrenes

The intermolecular cycloaddition of thermochemically or photolytically generated nitrenes to alkenes gives aziridines. This reaction is stereospecific as long as it occurs through singlet nitrene and can be catalyzed by metal ions. In this context, enantioselective variants have been developed which use the photolysis of aryl sulfonyl azides in the presence of copper ions.[290] Whereas acylnitrenes react in a secondary reaction to form isocyanates through a Curtius rearrangement (Section 4.5.1),[291] ethyl azidoformate usually gives the corresponding aziridines in good yields.[222] This reaction can also be used, for example, for the functionalization of carbon nanotubes (Scheme 61)[292,293]



Scheme 61. Functionalization of carbon nanotubes according to Holzinger et al.[293]

However, the cycloaddition of organoazides to alkenes is not necessarily a direct nitrene addition, as Δ^2-1,2,3-triazolines **256** can be formed which then react in a further step to aziridines **257** (Scheme 62). Both (strained) alkyl-substituted alkenes and electron-deficient or -rich alkenes such as fullerenes[294] can act as dipolarophiles.[295]



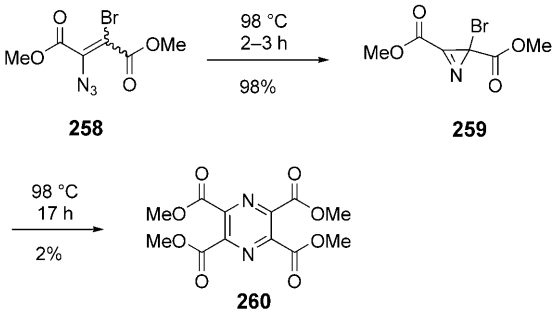
Scheme 62. Intermolecular synthesis of aziridines **257** via Δ^2-1,2,3-triazolines **256**.[295]

4.2.2. Intramolecular Cycloadditions of Nitrenes

4.2.2.1. Intramolecular Cycloadditions of Alkenyl Nitrenes

The (reversible) transformation of alkenyl nitrenes, which are formed by thermal or photolytic decomposition of alkenyl azides into the corresponding 2*H*-azirines,[62c,296] is a very frequently used reaction.[62,64] Recently, further reaction of the photolabile azirines has been suppressed by the use of microwaves[297] or brief heating at 150 °C in closed vessels.[70] The preparation of 2-halo-2*H*-azirines **53** was carried out with the method of Pinho e Melo et al. by heating haloazidoalkenes **52** to 100 °C (Scheme 14).[72] According to Hassner et al., 2*H*-azirines are formed from 3-monoalkylalkenylazides under thermolysis conditions.[298] The 2*H*-azirines formed react further, sometimes rapidly, with the formation of, for example, indoles (Scheme 76). Frequently found by-products are the corresponding nitriles (Scheme 93, Scheme 95)[299] or occasionally isonitriles.[300] 2-Halo-2*H*-azirines **259** with electron-withdrawing groups at C3 decompose after a few days at room temperature. Heating to ≈100 °C leads to the formation of small amounts of substituted pyrazines **260** (Scheme 63).

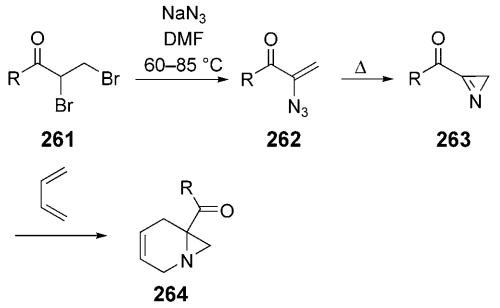
Recently, activated 2*H*-azirines **263** with electron-withdrawing substituents have proved to be particularly good dienophiles in *endo*-selective Diels–Alder reactions with electron-rich dienes. This was demonstrated recently in



Scheme 63. Synthesis and decomposition of 2-halo-2*H*-azirines.[72]

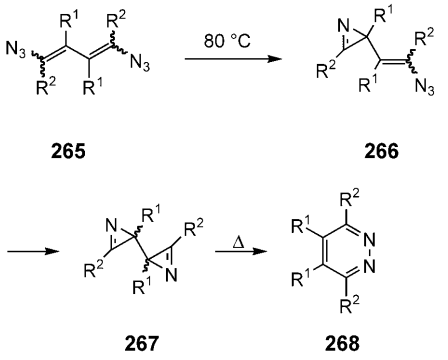
© 2005 Wiley-VCH Verlag GmbH & Co. KGaA, Weinheim

particular by Gilchrist and co-workers[301] and by Somfai and Timen[302] in the synthesis of bridged aziridines **264** (Scheme 64). The use of chiral 2*H*-azirines, chiral dienophiles, or chiral Lewis acids allows the asymmetric synthesis of such ring systems.



Scheme 64. Synthesis and Diels–Alder reactions of 2*H*-azirines.[301,302]

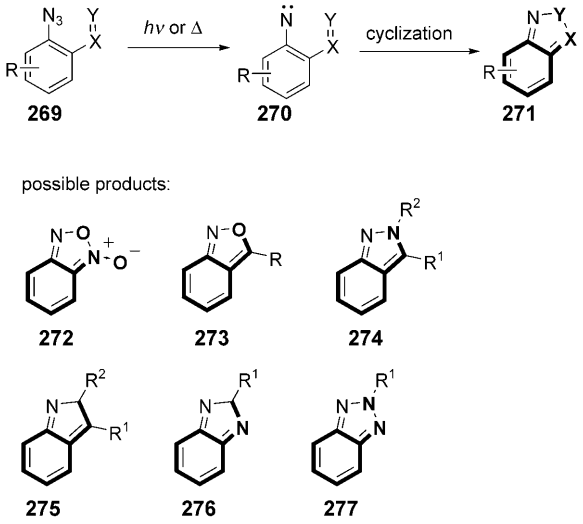
Interesting biazirinyls **267** were synthesized from 1,4-diazido-1,3-dienes **265** via 2-alkenyl-2*H*-azirines **266** intermediates (see Scheme 15). The pyridazines **268** are formed as by-products into which the biazirinyls **267** can also be converted upon heating for longer periods of time (Scheme 65).[73]



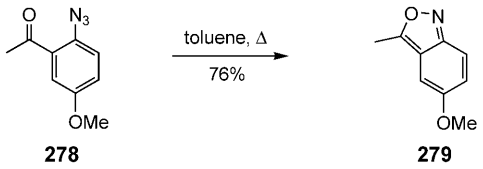
Scheme 65. Synthesis of biazirinyls.[73]

4.2.2.2. *Intramolecular Cycloadditions of Alkyl, Acyl, and Aryl Nitrenes to C=X Double Bonds*

Aryl azides with a suitable double bond in the *ortho* position decompose photochemically or thermally to form the corresponding heterocycle with loss of dinitrogen. Indazoles **274**,[303,304] benzofuroxanes **272**,[305,306] benzisoxazoles **273**,[307–311] and other heterocycles (Schemes 66 and 67) are formed amongst others. This reaction sequence was demonstrated nearly 100 years ago.[309] An electrocyclic mechanism is assumed[306b,308] in which, in a few cases, subsequent aromatization occurs through an H or alkyl shift. This applies especially to the 2*H*-indoles and 2*H*-benzimidazoles. As this latter reaction represents a formal insertion into a C–H bond, it is discussed in more detail in Section 4.2.3.1.



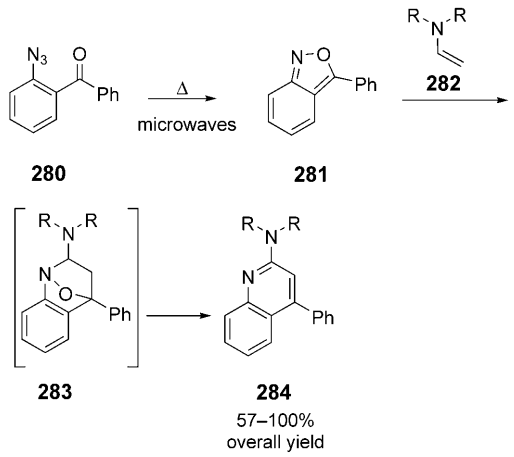
Scheme 66. Cyclization of substituted aryl azides.



Scheme 67. Thermal cyclization of *ortho*-acylaryl azides.[310]

These cycloaddition-derived heterocycles can in turn also react as reactive intermediates with further substrates, as shown in the microwave-induced synthesis of 2-aminoquinolines **284**.[312] In this synthesis, 3-aryl benzo[*c*]isoxazoles **281** react with enamines **282** to form the tricycles **283**, which then lose water. The quinolines **284** formed were isolated in good yields and with high purity after solid-phase extraction (Scheme 68).

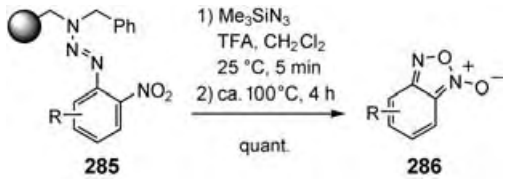
One application, the synthesis of benzofuroxanes **286**, could be demonstrated with *ortho*-nitro resins **285**. The azides formed after displacement cyclize at approximately 70 °C to



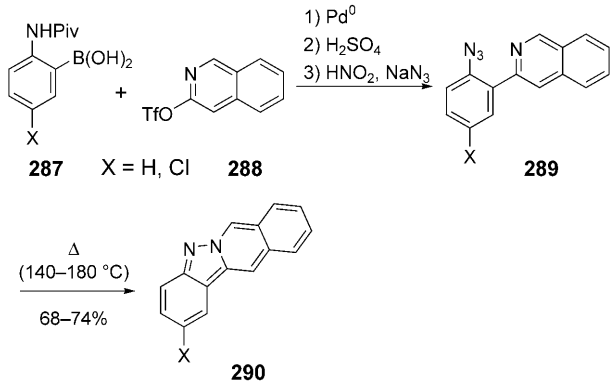
Scheme 68. Synthesis of aminoquinolines **284** by cycloaddition of intermediate benzoisoxazoles **281**.[312]

 © 2005 Wiley-VCH Verlag GmbH & Co. KGaA, Weinheim

give the benzofuroxanes **286** (Scheme 69).[45a] Benzofuroxanes are biologically active compounds with considerable synthetic potential.[313] Complex heterocyclic structures can also be prepared in this way, as shown by the synthesis of indazolo[2,3-b]isoquinolines **290** (Scheme 70).[314]



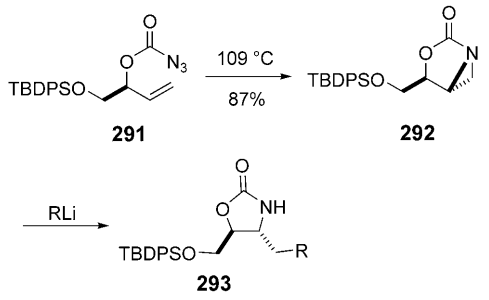
Scheme 69. Preparation of benzofuroxans **286** according to Bräse et al.[45a]



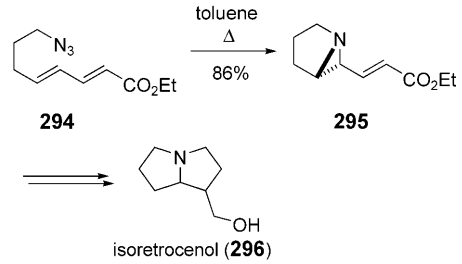
Scheme 70. Synthesis of indazolo[2,3-*b*]isoquinolines **290** according to Hajós and co-workers.[314] Piv = pivaloyl.

4.2.2.3. *Intramolecular Cycloaddition of Nitrenes to C=X Double Bonds*

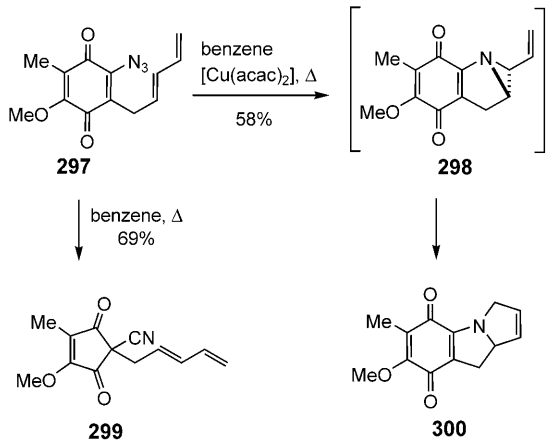
In the presence of a double bond in the nitrene precursor, which allows the formation of a relatively unstrained bicyclic system, intramolecular cycloaddition occurs with the formation of aziridine systems. This is particularly the case with the azabicyclo[3.1.0]hexane systems **292**, which can be opened regioselectively by nucleophiles (Scheme 71).[315] This reaction finds further application in the synthesis of pyrrolizidines, which can then react further to give isoretrocenol (**296**) as described by Hudlicky et al. (Scheme 72).[316] This formal nitrene–diene cycloaddition can also be carried out directly, as demonstrated in the synthesis of the tricyclic system **300** (Scheme 73).[317] In the absence of copper ions, the quinoyl nitrene rearranges to form a nitrilocyclopentenedione **299** (see also Scheme 95).



Scheme 71. Intramolecular aziridines synthesis and subsequent nucleophilic ring opening.[315] TBDPS = *tert*-butyldiphenylsilyl.



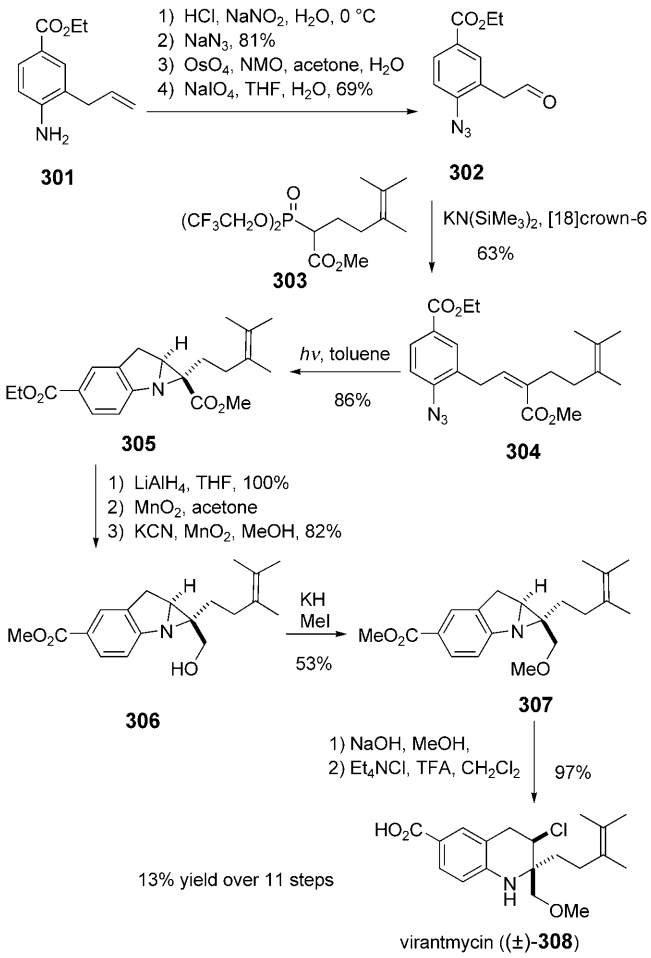
Scheme 72. Synthetic pathway for the preparation of isoretrocenol (**296**).[316]



Scheme 73. Intramolecular [4+1] cycloaddition.[317] acac = acetylacetonate.

An application of intramolecular cycloadditions of nitrenes to alkenes was demonstrated by the total synthesis of the natural product (−)-virantmycin (**308**), which was first isolated in 1981 by Ōmura and co-workers in the fermentation broth of the bacterial culture *Streptomyces nitrosporeus*, strain AM-2722.[318] This tetrahydroquinoline derivative is characterized by extremely high antiviral action against a series of different RNA and DNA viruses, although its antifungal activity is much weaker. In the 11-step total synthesis optimized by Morimoto et al.,[319c,d] the aryl azide **304** was obtained from ethyl 3-allyl-4-aminobenzoate (**301**) in a stereoselective *trans* olefination by reaction with the Still–Gennari phosphonate **303** (Scheme 74). Subsequent stereospecific photochemical nitrene addition gave the tricyclic aziridine derivative **305**, which was transformed into the methyl benzoate derivative **306** by reduction of the ester group and subsequent chemoselective oxidation to the benzaldehyde derivative. In subsequent synthetic steps, the primary alcohol **306** was converted into the corresponding methyl ether **307**. This aziridine derivative **307** was trans-

 © 2005 Wiley-VCH Verlag GmbH & Co. KGaA, Weinheim



Scheme 74. Total synthesis of (±)-virantmycin (**308**) according to Morimoto et al.[319] NMO = *N*-methylmorpholine-*N*-oxide.

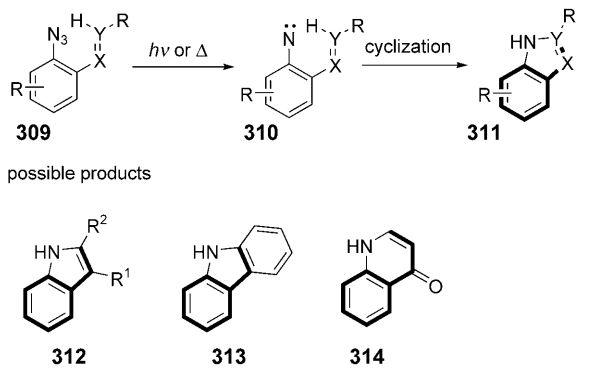
formed regioselectively and stereoselectively into (±)-virantmycin (**308**) under basic conditions. The overall yield in this total synthesis was 13% over 11 steps.

4.2.3. Insertion into C–H Bonds

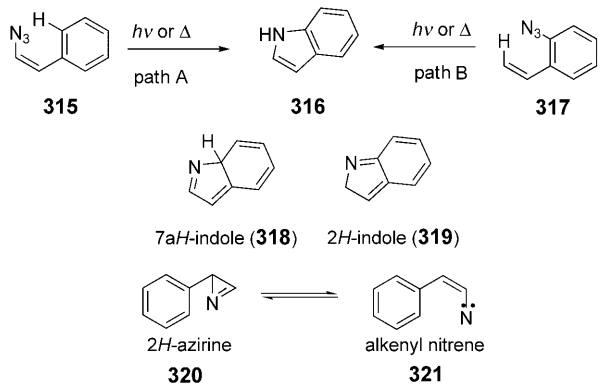
4.2.3.1. Insertion into C(sp^2)–H Bonds

The cycloadditions of nitrenes described earlier are related to insertion reactions. In particular, the formal insertion into C(sp^2)–H bonds is a frequently used reaction, which in part also follows the cycloaddition principle (Section 4.2.2.2). Thus indoles **312**,[303] carbazoles **313**,[268] and other heterocycles can be formed (Scheme 75). Early mechanistic investigations showed that the nitrogen atom in the product originates from the probable nitrene precursor.[320]

Indoles in particular are readily accessible by this reaction, and two strategies are conceivable. Either the cyclization of (*Z*)-2-aryl alkenyl nitrenes (path A) (Scheme 76) or the cyclization of 2-alkenyl aryl nitrenes (path B) can be used. 7a*H*-Indoles (path A) or 2*H*-indoles (path B) may be formulated as reactive intermediates. Viewed mechanistically, the cyclization of (*Z*)-2-aryl alkenyl nitrenes (path A) presumably involves prior intramolecular 2*H*-azirine formation, which follows reversible alkenyl



Scheme 75. Cyclization possibilities of substituted aryl azides: insertion reactions.

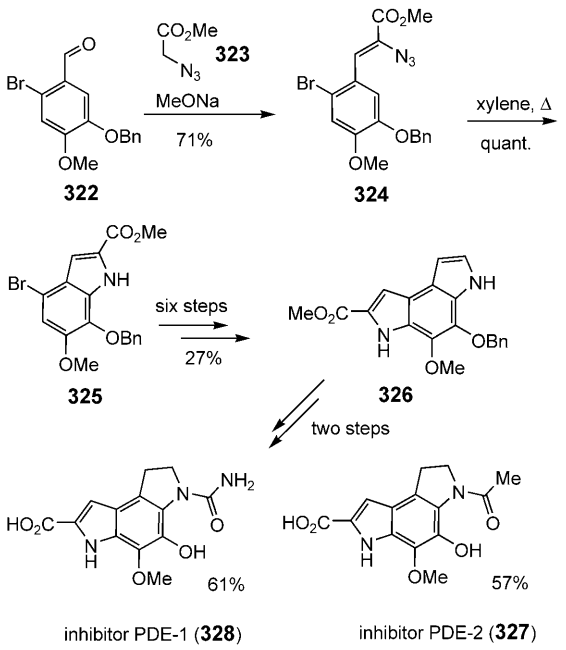


Scheme 76. Syntheses of indoles from organoazides.

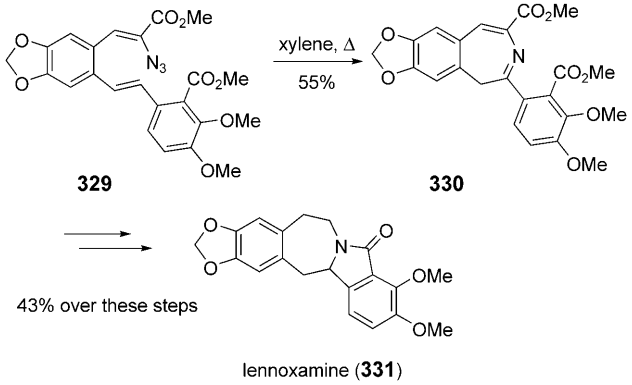
nitrene formation and determines the necessary stereochemistry. The required azidocinnamic esters are readily formed by condensation of azidoacetic esters and aryl aldehydes (Scheme 12). This reaction, named after Isomura, Hemetsberger, and Rees,[321–323] is one of the most important indole syntheses[324,325] and was used with success in a number of natural products syntheses such as murrayquinone,[326] discorhabdin C, makaluvamine D,[327] and varioline (**45**)[65] (Scheme 12). Furthermore, this reaction is used in the synthesis of phosphodiesterase inhibitors PDE-1 (**328**) and PDE-2 (**327**), which are related to the antibiotic CC-1065 (Scheme 77).[328] The choice of the correct solvent, which also influences the thermolysis temperature, is pivotal for success. 2*H*-Azirines can otherwise occur as by-products. Dimerization can also give pyrazines.[329] The Hemetsberger reaction can also be used for the synthesis of pyrroles from αβ-unsaturated aldehydes.[330] If another accessible double bond is present in the molecule, a competitive addition to this double bond can occur which can even be the main reaction. This was used by Moody and co-workers in their total synthesis of lennoxamine (**331**) (Scheme 78).[349]

Ortho-alkenyl aryl azides also rearrange to indoles upon heating. This reaction, known as the Sundberg cyclization,[331,332] takes place by direct attack at the β-carbon atom and not after insertion into the C–H bond.[332] This reaction was recently applied to the synthesis of complex indoles

 © 2005 Wiley-VCH Verlag GmbH & Co. KGaA, Weinheim



Scheme 77. Synthesis and conversion of the alkenyl azide **324** into indoles **327** and **328**.[328]



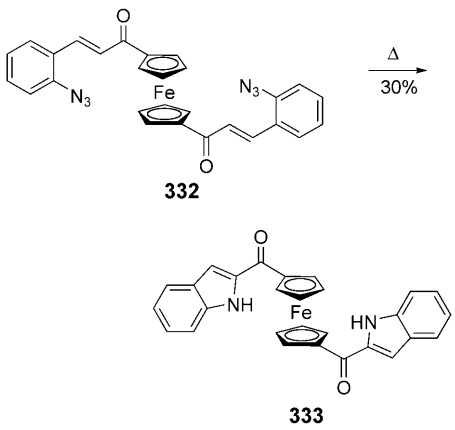
Scheme 78. Synthesis of lennoxamine (**331**) according to Moody et al.[349]

(Scheme 79).[333–335] As an alternative to thermolysis or photolysis this cyclization can also be carried out by protonation or by the action of Lewis acids with the formation of electrophilic nitrenium ions (see also Section 4.6.3).[336]

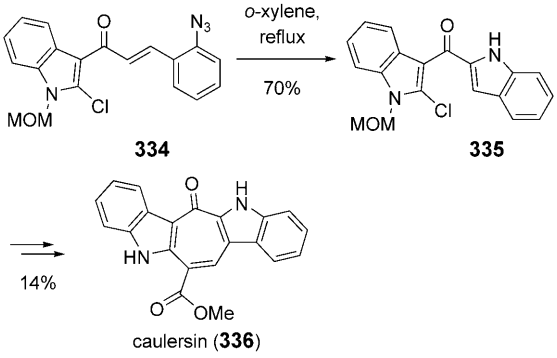
The first synthesis of the marine bisindole alkaloid caulersin (**336**) in seven steps was reported by Molina and co-workers in 1999 (Scheme 80).[337] The key step is the conversion of the azide **334** into the bisindole ketone **335** upon heating.

Other recent natural products syntheses that use this reaction pathway have been published, for example, those of the indole alkaloid meridianine from the fungus *Aplidium meridianum*,[338] novel indolecarboxylic acids related to the plant hormone indolylacetic acid,[325] and (±)-*cis*- and (±)-*trans*-trikentrin A.[339]

2-Biaryl azides decompose photochemically or thermally to carbazoles. The photolysis of azidobiaryls such as **337** with

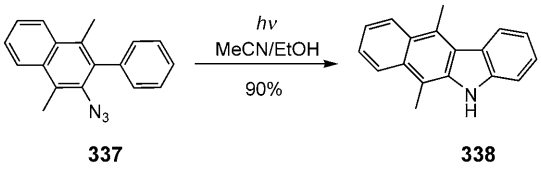


Scheme 79. Synthesis of bisindolylferrocene **333**.[333]



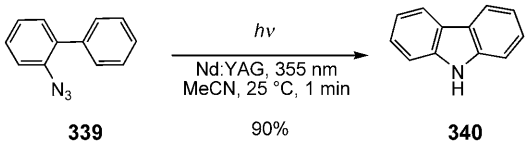
Scheme 80. Total synthesis of the marine bisindole alkaloid caulersin (**336**) according Molina et al.[337] MOM = methoxymethyl.

conventional UV lamps has been known for some time in the synthesis of carbazoles such as **338**, but this reaction has been carried out with only a few examples of substituted compounds and yields different by-products, such as the corresponding azo compounds (Scheme 81).[28,340] The use of laser



Scheme 81. Synthesis of carbazoles **338** by photolysis.[340]

light not only significantly accelerates the reaction, but also improves the selectivity of this preparatively important and extensively investigated process (Scheme 82). A further



Scheme 82. Laser-induced preparation of carbazoles **340** according to Bremus-Köbberling et al.[341]

 © 2005 Wiley-VCH Verlag GmbH & Co. KGaA, Weinheim

improvement is its execution in miniaturized photoreactors (Figure 3) which gave a greater turnover of photolysis products.[341]

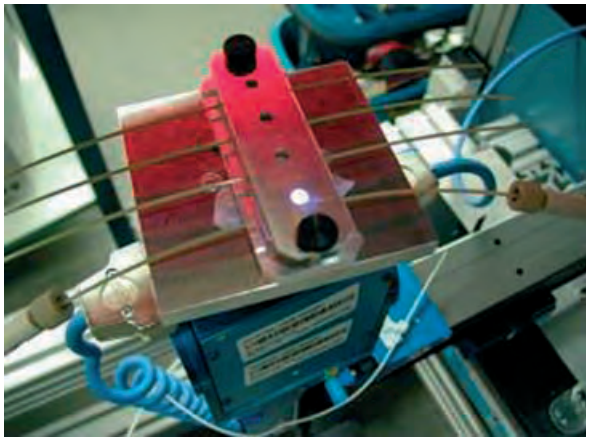
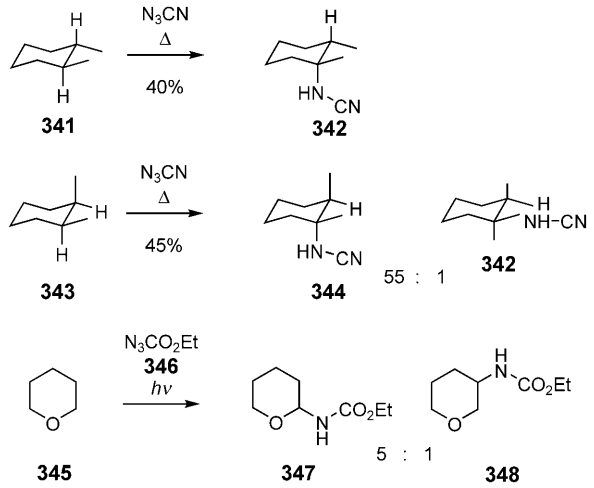


Figure 3. A miniphotoreactor for the photolysis of aryl azides. Picture reprinted with kind permission from the Fraunhofer-ILT, Aachen (Germany).[341]

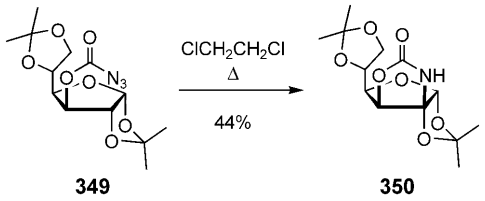
4.2.3.2. *Insertion into sp^3 C–H Bonds*

Nitrenes also undergo insertion into sp^3 C–H bonds. The selectivity of the insertion decreases from tertiary and finally to secondary to primary species. Thus statistically corrected reactivities of 25:10:1 were determined for the insertion of ethoxycarbonyl nitrene into the C–H bonds of 2-methylbutane.[342] This reaction can be both intramolecular[343] and intermolecular. These insertions usually take place with retention of configuration and regioselectively α to the oxygen atoms (Scheme 83).[345] In a few cases suitable metal catalysts have been found, although metal–nitrene complexes are not necessarily formed because these species undergo intermolecular reactions to form azoarenes.[344] An example of an intramolecular insertion of an acyl azide is the functionalization of furanose derivatives **349**

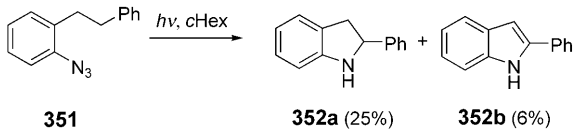


Scheme 83. Stereoselective and regioselective azide addition.[345]

(Scheme 84).[346] The newly formed rings are mostly five- or six-membered, of which the smaller rings are formed more readily. In 1995 Tomioka and co-workers synthesized 2-phenylindoline (**352a**) in this way (Scheme 85).[347] The

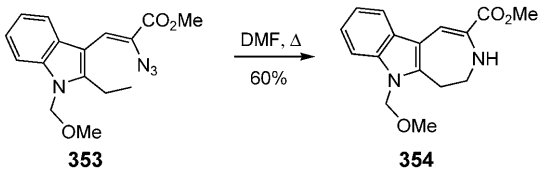


Scheme 84. Functionalization of furanose derivates.[346]



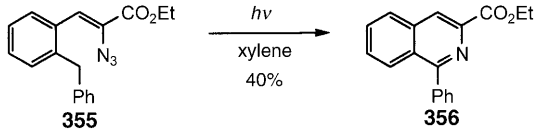
Scheme 85. Synthesis of 2-phenylindoline (**352a**) according to Tomioka et al.[347] *c*Hex = cyclohexane.

thermal decomposition of azidoacrylates **353** in refluxing DMF produces the pharmacologically important azepino[4,5-*b*]indoles **354** (Scheme 86).[348] The synthesis of isoquinolines



Scheme 86. Synthesis of azepino-[4,5-*b*]indole **354** according to Moody et al.[348]

by insertion into sp^3 C–H bonds has also been extensively investigated by Moody and co-workers.[349] In this case, the nitrene inserts into the benzhydrylic C–H bond, and the isoquinoline **356** is formed after aromatization (Scheme 87)[350]. In the case of *ortho* substituents (methyl or similar), a hydrogen atom is extracted and an imidoquinone methide is formed.[287,350]



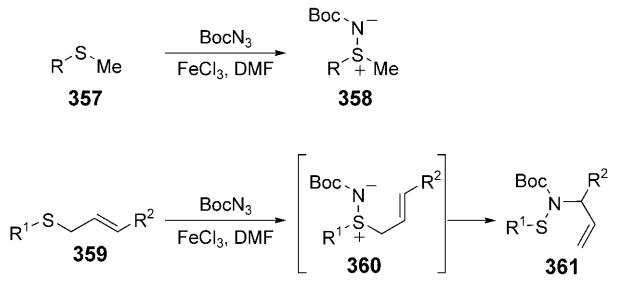
Scheme 87. Synthesis of isoquinoline **356** according to Moody et al.[350]

4.2.4. *Addition of Nitrenes to Heteroatoms*

Nitrenes that are formed from azides react with electron-rich heteroatoms (nitrogen,[27c,351,352] sulfur, phosphorus) to form the corresponding ylides. The reaction of phosphorus compounds to form aza ylides is discussed in Section 4.3.

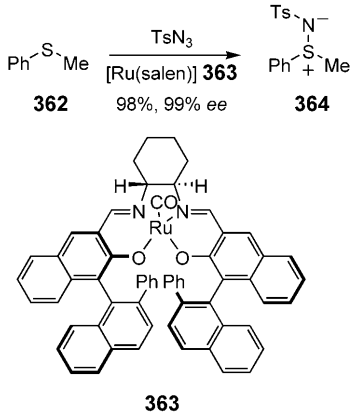
 © 2005 Wiley-VCH Verlag GmbH & Co. KGaA, Weinheim

Different organoazides can be converted into sulfur ylides **358** by reaction with sulfides **357**. Bach and co-workers reported an iron-catalyzed reaction of Boc azide with organic methyl sulfides (Scheme 88).[353] These authors also showed that allyl thioethers **359** undergo a [2,3] sigmatropic shift to give α-branched allylamines **361**.[354] This reaction was extended by Van Vranken and co-workers to propargyl thioethers, which form *N*-allenylsulfenimides.[355]



Scheme 88. Azide additions according to Bach and Körber.[353,354]

A ruthenium–salen-catalyzed, highly enantioselective variant of this reaction of alkyl aryl sulfides with arylsulfonyl azides and alkoxycarbonyl azides was reported recently by Katsuki and co-workers (Scheme 89).[356] The electron-deficient and sterically demanding reagent $Cl_3C(tBu)_2COCON_3$ proved to be especially useful in the case of alkoxycarbonyl azides, which produce somewhat more readily deprotected alkoxycarbonyl aziridines. This asymmetric synthesis can be carried out with allyl sulfides in the synthesis of chiral allylamines.[357]



Scheme 89. Synthesis of enantiomerically pure sulfur ylides.[356]

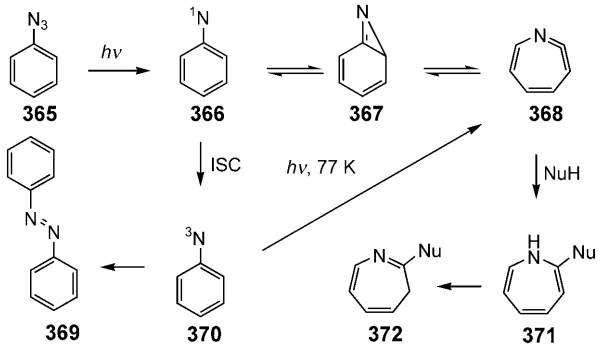
4.2.5. *Rearrangement of Nitrenes*

4.2.5.1. *Rearrangement of Acyl Nitrenes and Alkyl Nitrenes*

The rearrangement of acyl azide to isocyanates through the corresponding nitrene is well known as the Curtius rearrangement (see Section 4.5.1), whereas the general rearrangement of alkyl nitrenes is usually known as the Schmidt rearrangement (see Section 4.5.2). In the case of methyl azide (**6**) photolysis leads to methanimine, which is formed by simultaneous cleavage of dinitrogen and a 1,2-H shift.[15]

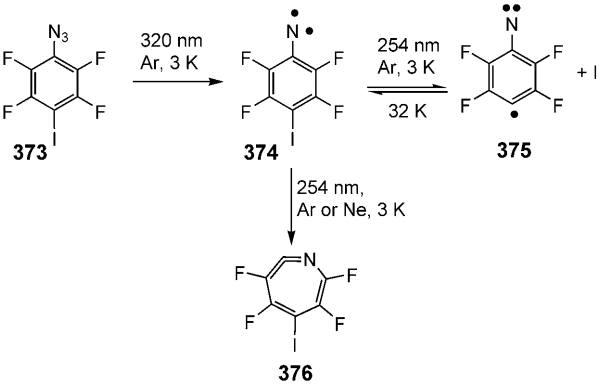
4.2.5.2. *Rearrangement of Aryl Nitrenes*

The rearrangement of aryl nitrenes by the photolysis of aryl azides leads to a broad spectrum of possible products.[358–363] As the large number of published examples would extend beyond the scope of this article, this section will be restricted to current examples. The work of Platz and co-workers in particular has helped greatly to explain the complex mechanism. In-depth analysis of reaction mixtures with matrix-isolation spectroscopy, laser flash photolysis (LFP), and modern molecular-orbital theory (MO) have all contributed to this understanding. In the photolysis of phenyl azide, various reactive intermediates are formed, of which the singlet phenyl nitrene **366** is the key molecule (Scheme 90). Intersystem crossing next gives the triplet nitrene **370**, which dimerizes to **369**. A special feature is the ring expansion of the benzazirine **367** to form the highly strained azepine derivative **368** and its subsequent products.[364] In a few cases, ring contraction to form cyanocyclopentadienes is observed.



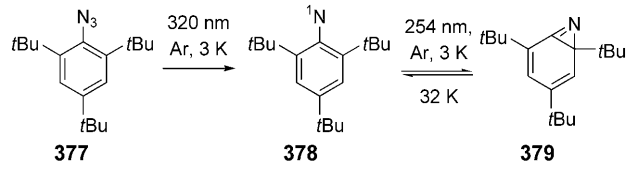
Scheme 90. Rearrangement of aryl nitrenes.[364]

An application example was provided by Wenk and Sander in 2002 with the synthesis of 2,3,5,6-tetrafluorophenylnitren-4-yl (**375**). The intermediate **374** can also undergo iodine transfer to give dehydro-2,3,5,6-tetrafluoro-4-iodo-1*H*-azepine (**376**; Scheme 91).[365] Aryl azides with bulky *ortho* substituents react somewhat slower; the resulting benzazirines are stable for a few nanoseconds and can be detected spectroscopically (Scheme 92).[366]

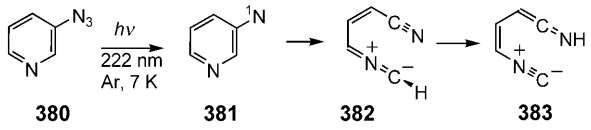


Scheme 91. Synthesis of **375** according to Wenk und Sander.[365]

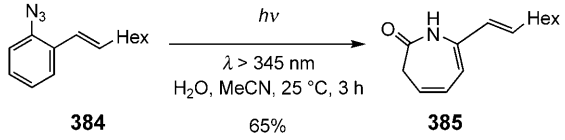
 © 2005 Wiley-VCH Verlag GmbH & Co. KGaA, Weinheim



Scheme 92. Synthesis of stabilized benzazirines according to Platz et al.[366]



Scheme 93. Rearrangement of pyridylnitrenes **381**.[372]



Scheme 94. Synthesis of azepinones **385** according to Knepper and Bräse.[373a]

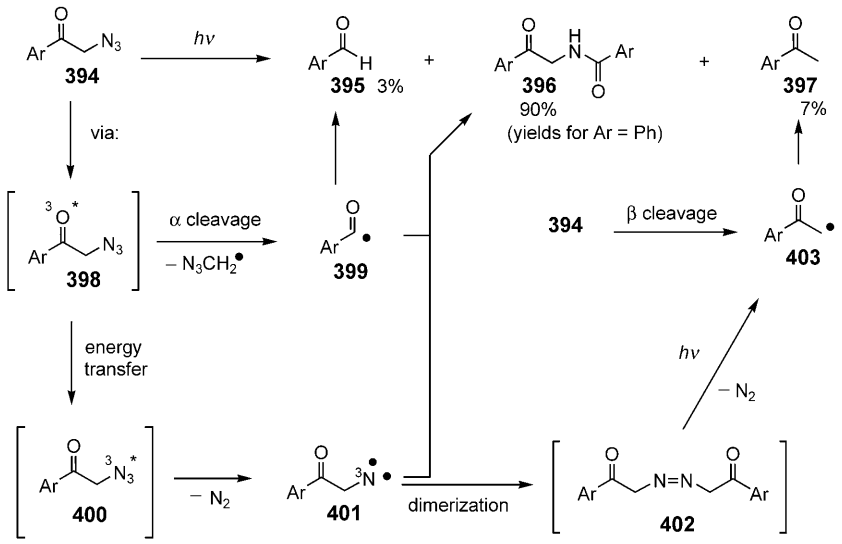
Functionalized aryl azides[367] and a few other azidopyridines[368] (see reference [369]) also rearrange under photolytic conditions in accord with this scheme. Another feature of aryl nitrenes is a reversible rearrangement between phenylnitrene and 2-pyridyl carbene, and 3-pyridyl carbene and 4-pyridyl carbene.[28,370] Furthermore, a coarctate ring opening[371] of 3-pyridyl nitrene with formation of a cyanovinylnitrile ylide complicates the reaction (Scheme 93).[372]

In the presence of water, alkenylaryl azides **384** provide access to substituted azepinones **385** by ring expansion (Scheme 94), as previously demonstrated by Scriven and co-workers.[373]

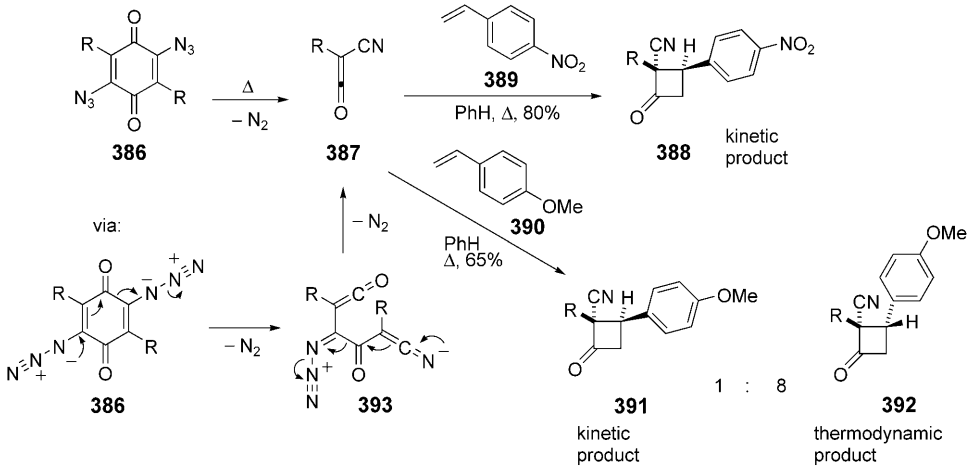
As a special case, azidoquinones usually rearrange to form nitriles (see also Scheme 73). However, 2,5-diazidoquinone (**386**) gives rise to the Moore ketene **387**, which reacts stereoselectively, for example, with styrenes **389** and **390** in intermolecular [2+2] cycloadditions to cyclobutanones **388** and **391**/**392**, respectively. Different reaction control is observed with the electron-rich styrene **390**, which gives predominantly **392** (Scheme 95).[374]

4.2.5.3. ***Fragmentation of Nitrenes***

Besides nitrene formation, alkyl azides with a photosensitive group in the α position (e.g. phenacyl azides **394**) can also react by α cleavage under radiation (Scheme 96).[375] This arises from the fact that with the supply of light the carbonyl group is first excited to the triplet state **398**. This can react either through the excited azide triplet state **400** to the triplet nitrenes **401**, or directly (by α cleavage)



Scheme 96. Fragmentation of phenacyl azides **394**.[375]



Scheme 95. Fragmentation of 2,6-diazidoquinones **386** according to Moore and synthesis of the corresponding cyclobutanone.[374]

 © 2005 Wiley-VCH Verlag GmbH & Co. KGaA, Weinheim

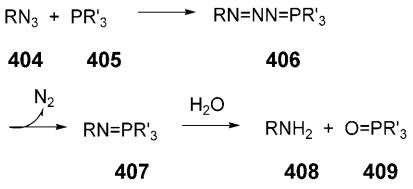
to the benzoyl radicals **399**. The benzoyl radicals **399** react predominantly with the triplet nitrenes **401** to give ketoamides **396**. Benzaldehydes **395** are formed to a small extent by H extraction. Acetophenones **397** also occur as by-products and are presumably formed by dimerization of the nitrene **401** to the azo compound **402**; direct β cleavage of **394** is also conceivable.

4.3. Nucleophilic Addition to Organoazides: Aza Ylides

As already discussed, organoazides react readily with nucleophiles. One of the most frequent applications is the attack by phosphorus nucleophiles.

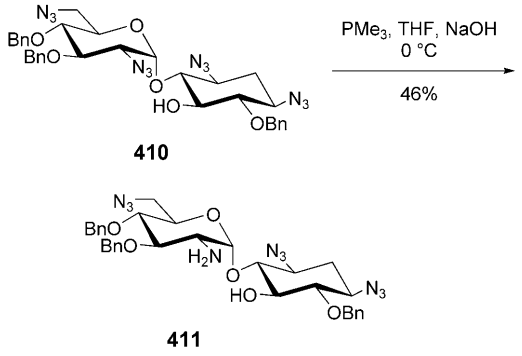
4.3.1. Azides as Amine Surrogates: The Staudinger Reduction

The Staudinger reduction was developed in 1919 by Staudinger and Meyer[376,377] as a procedure for the reduction of organoazides. This reaction involves the formation of a phosphazine intermediate **406** by nucleophilic attack of the phosphorus atom of a trialkyl or triaryl phosphine at the terminal nitrogen atom of the organoazide, which immediately loses nitrogen to form the iminophosphorane **407**.[378,379] These iminophosphoranes **407** are important reagents and intermediates in organic synthesis.[380,381] In the presence of water, the iminophosphorane **407** is spontaneously hydrolyzed to a primary amine **408** and to the corresponding phosphine oxide **409** (Staudinger reduction; Scheme 97).



Scheme 97. The Staudinger reduction.

If trimethylphosphane is used at low temperature, the organoazide—depending on its electronic properties—can be reduced chemoselectively in moderate yields in a modification of the Staudinger reaction (Scheme 98).[382]



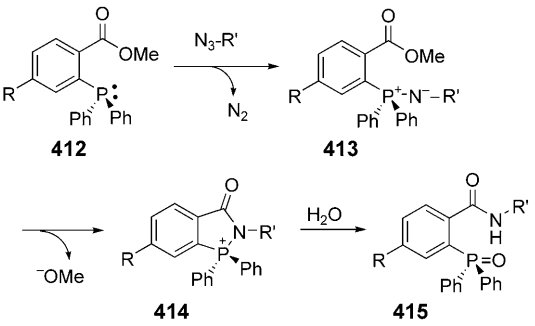
Scheme 98. Chemoselective reduction of organoazides.[382]

The Staudinger reaction between phosphines and organoazides has been used recently in the synthesis of dendrimers,[383] long-chain acyclic phosphazenes,[384] P-stereogenic phosphine oxides,[385] amides, [386] and glycosidated peptides,[387] as well as in the solid-phase synthesis of 3,5-disubstituted oxazolidine-2-ones.[388] A general Staudinger protocol has been developed for the liquid-phase parallel synthesis with fluoroalkyl-chain-modified triphenylphosphines which permits an extraction of the otherwise relatively poorly separable triphenylphosphane oxide into an organofluorous phase.[389]

4.3.2. The Staudinger Ligation

The intermediate in the Staudinger reaction is an iminophosphorane with a nucleophilic nitrogen atom. Vilarrasa and co-workers showed that this nitrogen atom can attack an acyl donor in an intermolecular or intramolecular reaction.[390] The amide is obtained as the final product after hydrolysis of the amidophosphonium salt. Thioamides can also be prepared by a coupling of thiocarboxylic acids and alkyl azides with triarylphosphines.[391]

Saxon and Bertozzi reported a modification of the Staudinger reaction for the first time in 2000—the intramolecular Staudinger ligation.[392,393] This generates an amide bond starting from organoazides and specifically functionalized phosphines.[393] This reaction takes place by nucleophilic attack at the organoazide to form an aza-ylide intermediate. A methoxycarbonyl group on one of the aryl rings of the phosphine traps the aza-ylide **413** to yield, after hydrolysis, an amidic phosphine oxide **415** (Scheme 99).[394] The reaction is



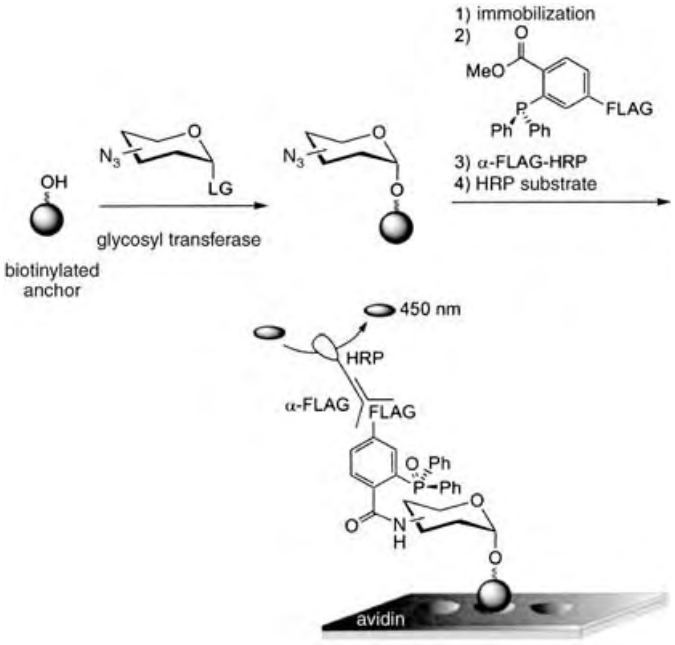
Scheme 99. The Staudinger ligation according to Saxon and Bertozzi.[393]

compatible with a large number of functional groups and therefore has various uses in organic synthesis and biological chemistry. The reaction has already been used in the investigation of cellular metabolism of synthetic azidosugars,[395] for biological labeling,[396,397] and for immobilization of substrates to surfaces.[398,399] The Staudinger ligation has been used successfully by Bertozzi and co-workers even on living organisms such as a mouse.[396b]

Bertozzi and co-workers recently reported an ELISA (enzyme-coupled immunosorbent assay) based on the Staudinger ligation (azido-ELISA).[398] A potential substrate, in this case a sugar, is equipped with an azide functionality and a

 © 2005 Wiley-VCH Verlag GmbH & Co. KGaA, Weinheim

biotin anchor by an enzyme-induced coupling. This allows binding to an avidine-coated surface. The Staudinger reaction with a α-phosphinylbenzoic acid ester that bears a short peptide chain forms a conjugate. The short peptide chain (FLAG) can then be recognized by a specific monoclonal antibody (α-FLAG) to which a horseradish peroxidase is attached (α-FLAG-HRP). A substrate for this peroxidase then gives a signal at 450 nm. This system allows rapid screening of different glycosyl transferases, but should also be transferable to other systems (Scheme 100).

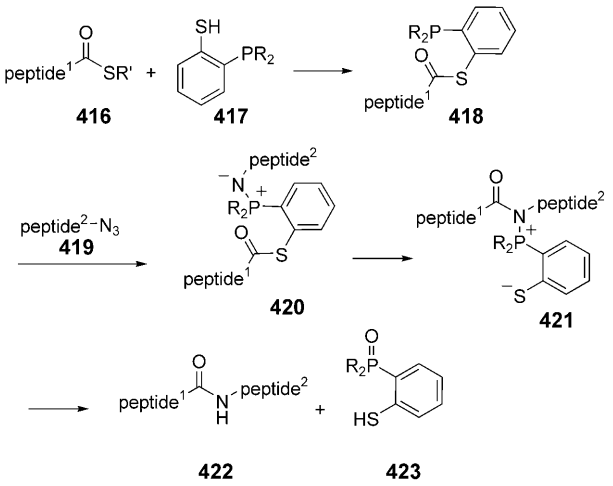


Scheme 100. Azido-ELISA according to Bertozzi and co-workers.[398]

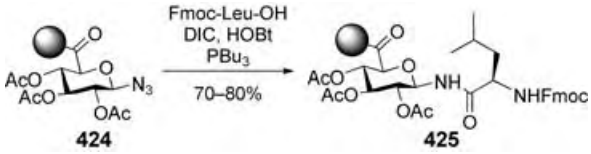
The Staudinger ligation was applied to peptide synthesis by Raines, Kiessling, and co-workers. In this case, an amide bond is formed between a peptide fragment with a C-terminal phosphinylthioester **418** and a further peptide fragment **419** with N-terminal azide functionality (Scheme 101).[400] The reaction can be used to obtain dipeptides in high yields with retention at the α carbon atom[401,402] and is useful for the preparation of tetra- and pentapeptides.[403] The solid-phase synthesis of peptides and proteins under the conditions depicted was recently described in detail.[404]

Modified Staudinger reactions with activated carboxylic acids are applied in the liquid- and solid-phase synthesis of glycosyl amides **425** (Scheme 102);[405a] stereoselective methods are also known.[405b] The reaction conditions are compatible with Boc and Fmoc protecting-group strategies, which are common in solid-phase synthesis and may be used in the synthesis of glycopeptides.

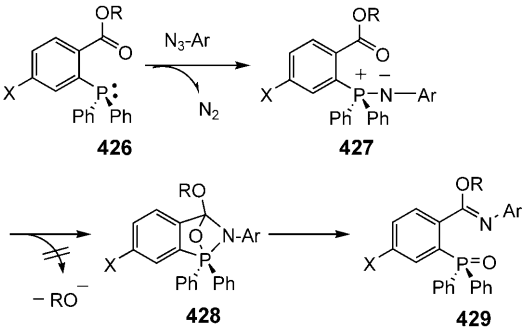
This reaction can also be applied to aryl azides and, in particular, to purinyl azides to obtain ligated material. The main product from this ligation contains a relatively stable imidate compound. *O*-Alkoxycarbonyltriaryl phosphines react somewhat differently with aryl azides. After Staudinger ligation, they form *O*-alkyl imidates **429** (Scheme 103).[406]



Scheme 101. Peptide synthesis by Staudinger ligation.[400]



Scheme 102. Coupling of amino acids to glycosyl azides **424** by Staudinger ligation for the preparation of glycoamino acids **425**.[405] DIC = diisopropylcarbodiimide, HOBt = 1-hydroxy-1*H*-benzotriazole.



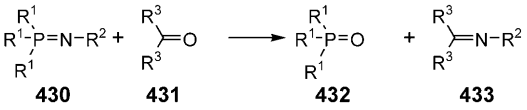
Scheme 103. Staudinger ligation with aryl azides.[406]

The intramolecular Staudinger ligation is a particularly efficient ring-closing reaction for the formation of medium-sized lactams that are difficult to prepare by other methods.[407]

4.3.3. The Aza-Wittig Reaction in a New Light

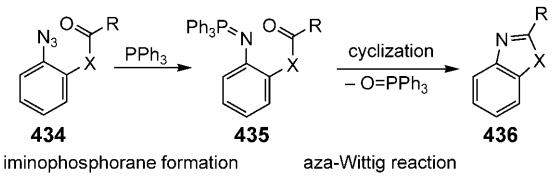
As described, the azide functionality is very useful for the synthesis of other nitrogen compounds. The reaction of iminophosphoranes **430**[381]—obtainable by Staudinger reaction from organic azides and phosphorus(III) reagents—with carbonyl compounds **431** has frequently been used for the synthesis of imines **433** by the aza-Wittig reaction (Scheme 104).[76,380,381,408–410]

 © 2005 Wiley-VCH Verlag GmbH & Co. KGaA, Weinheim



Scheme 104. Aza-Wittig reaction.

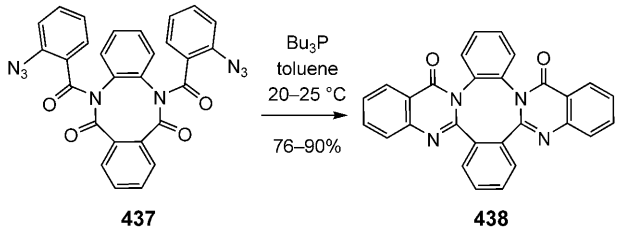
Because of its high synthetic potential, the intramolecular version of this reaction[408] is often the method of choice for the preparation of nitrogen heterocycles[411] such as isoxazolines[412] and for the synthesis of five-,[411] six-, and seven-membered nitrogen heterocycles, among others (Scheme 105).[411,413–416] A series of natural products syntheses



Scheme 105. Intramolecular aza-Wittig reaction.

uses precisely this reaction as the key step. The reactivity of the precursors is controlled by several factors: chain length, substituents at the phosphorus and nitrogen atoms of the iminophosphorane, and the chemical nature of the carbonyl group. Ester carbonyl groups are normally unreactive in the intermolecular aza-Wittig reaction, but they react in intramolecular versions and form the corresponding imino cyclization products.[76]

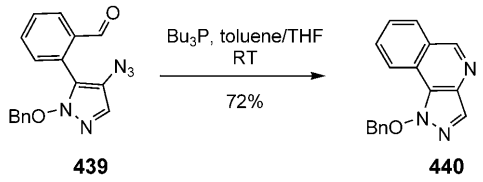
According to Eguchi et al. the reactivity of amidic carbonyl groups in intramolecular aza-Wittig reactions gives access to iminolactams.[417] Lactams can also act as substrates and give the corresponding annelated quinazolinones (for an alternative, see Section 4.6.2, Scheme 134).[413,415] This reaction can also be carried out twice, as demonstrated in the synthesis of the polyazamacrocycle **438** (Scheme 106).[418]



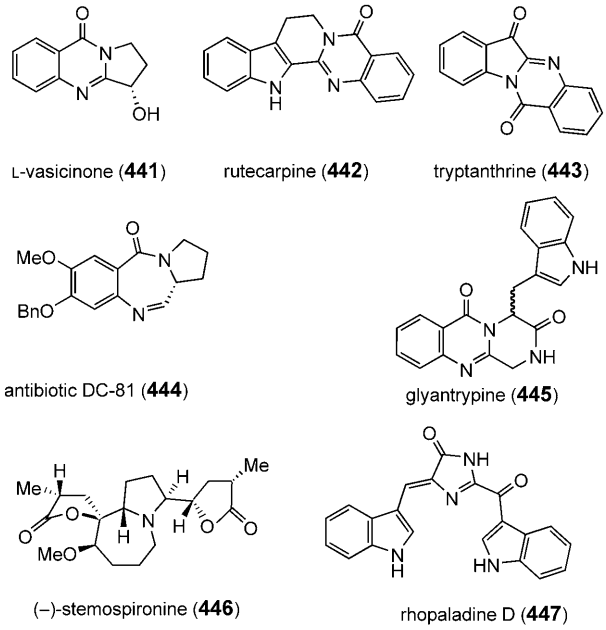
Scheme 106. Synthesis of the benzanellated polyazamacrocycle **438**.[418]

The pyridine ring of pyrazoloisoquinoline **440** was formed by a Staudinger/aza-Wittig cyclization of a formyl group with the azide group of a 4-azido-1-(benzyloxy)-5-(2-formylphenyl)pyrazole (**439**; Scheme 107).[419] Oxazoles are available from β-(acyloxy)vinyl azides and triethylphosphane.[420]

Efficient access to quinazolines by Eguchi et al. allows the synthesis of natural products in a domino Staudinger–intramolecular aza-Wittig reaction, for example, vasicinon (**441**),[421] desoxyvasicinon,[414] rutecarpin (**442**),[422] and tryp-



Scheme 107. Preparation of pyrazoloisoquinoline **440** by aza-Wittig reaction.[419]



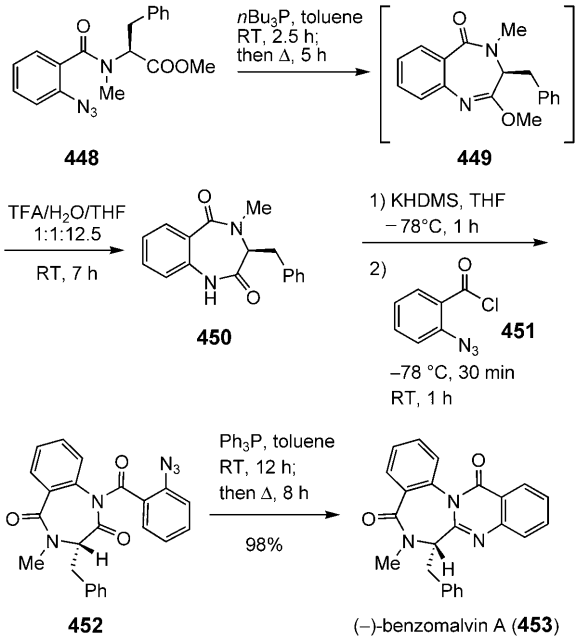
tanthrin (**443**).[422] This methodology is particularly suitable for the synthesis of seven-membered nitrogen heterocycles such as the antitumor antibiotic DC-81 (**444**),[423–425] and for the synthesis of trifluoromethylated nitrogen heterocycles.[426] Furthermore, studies on the total synthesis of the marine alkaloids of the chartellamide group[427] and pinnatoxin A[428] by aza-Wittig reactions have been reported. Other successful examples are glyantrypine (**445**),[429] (−)-stemospironine (**446**),[430] rhopaladine (**447**),[431] ardeemin,[432] and hamacanthin A[433] and B (**82**; Scheme 20).[117]

The first total synthesis of (−)-benzomalvin A (**453**), which bears both a quinazoline-4(3*H*)-one and a 1,4-benzodiazepine-5-one unit, was reported by Eguchi and co-workers.[434,435] Both heterocycle frameworks were prepared by an aza-Wittig reaction as the key step (Scheme 108).

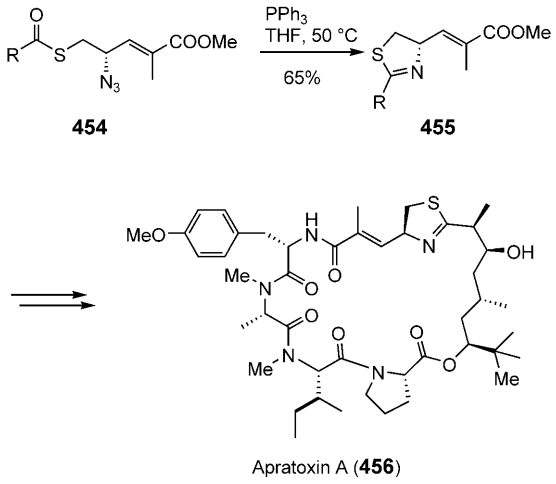
Enantiomerically pure 2,4-disubstituted thiazolines **455** can also be prepared efficiently from thioesters **454** in a mild Staudinger/aza-Wittig process,[436] as demonstrated in the total synthesis of apratoxin (**456**) (Scheme 109).[437]

The intramolecular aza-Wittig reaction can also be used in the synthesis of nonnatural products, as demonstrated by the synthesis of novel heterocycles based on ferrocenophanes that are used as ligands for metal ions (Scheme 110).[438] A new class of orthoacylimine-derived chiral auxiliaries have been synthesized by the reaction of the corresponding

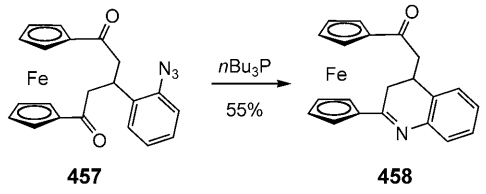
 © 2005 Wiley-VCH Verlag GmbH & Co. KGaA, Weinheim



Scheme 108. Synthesis of (−)-benzomalvin A (**453**).[435]



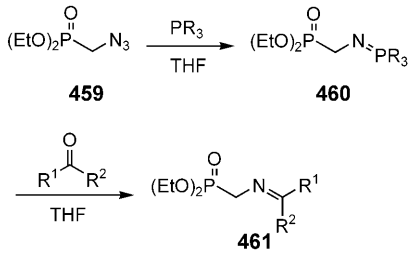
Scheme 109. Thiazole synthesis by aza-Wittig reactions in the total synthesis of apratoxin A.[437]



Scheme 110. Conversion of a ferrocenophane into the ligand **458**.[438]

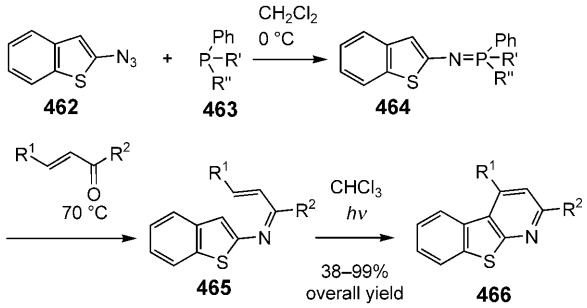
orthoacyl azides and a series of aldehydes in the presence of trialkylphosphines.[408]

The aza-Wittig reaction can thus be used for the introduction of imine units, for example, to prepare iminophosphonates **461** (Scheme 111),[439] or in keto acids for the preparation of imino acids.[440]



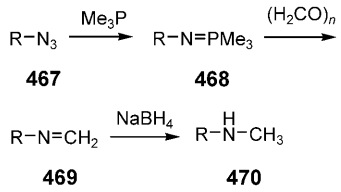
Scheme 111. Synthesis of functionalized imines **461**.[439]

The preparation of pharmacologically important benzothieno[2,3-*b*]pyridines **466** takes place by an intermolecular aza-Wittig reaction of iminophosphoranes **464** with various unsaturated aldehydes and ketones and subsequent photocyclization (Scheme 112).[441]



Scheme 112. Synthesis of benzothienopyridines **466**.[441]

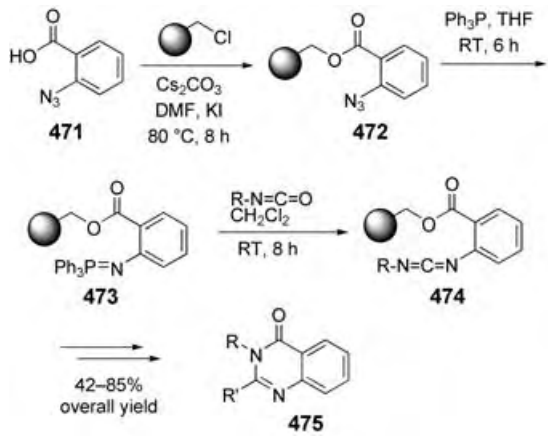
A one-pot synthesis of *N*-monomethylamines **470** from organoazides **467** by Suzuki and co-workers[442] uses an aza-Wittig reaction with paraformaldehyde. The resulting imine **469** is then reduced with $NaBH_4$ to give the corresponding *N*-monomethylamine **470** (Scheme 113). Although a frequent structural motif in natural products, the *N*-monomethylamine group is at times difficult to insert without the formation of by-products.



Scheme 113. Synthesis of *N*-monomethylamines from organoazides.[442]

Owing to the potential of iminophosphoranes in the mild and neutral synthesis of nitrogen heterocycles, different solid-phase variants have been developed. Either the triarylphosphine in the aza-Wittig reaction or the substrate is immobilized on the support. The solid-phase synthesis of 1,4-benzodiazepine-2,5-diones,[443] trisubstituted guanidines,[162] oligomeric guanidines,[444] and 3*H*-quinazolin-4-ones (**475**; Scheme 114)[445] has been carried out with aza-Wittig reac-

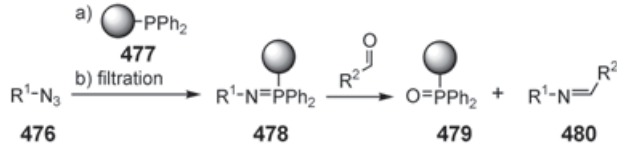
 © 2005 Wiley-VCH Verlag GmbH & Co. KGaA, Weinheim



Scheme 114. Solid-phase synthesis of 3*H*-quinazolin-4-ones **475**.[445]

tions and permitted the synthesis of libraries of these classes of compounds.

The use of the commercially available, polymer-bound diphenylphosphine (**477**) combines the advantages of solid phase synthesis with the use of polymer-bound reagents. The usual Wittig by-product triphenylphosphane oxide is normally difficult to separate from polar products, but in this way it can be readily removed as the polymer-bound diphenylphosphane oxide (**479**) by filtration (Scheme 115).[446] Owing to the high cost of the reagent **477**, it is occasionally

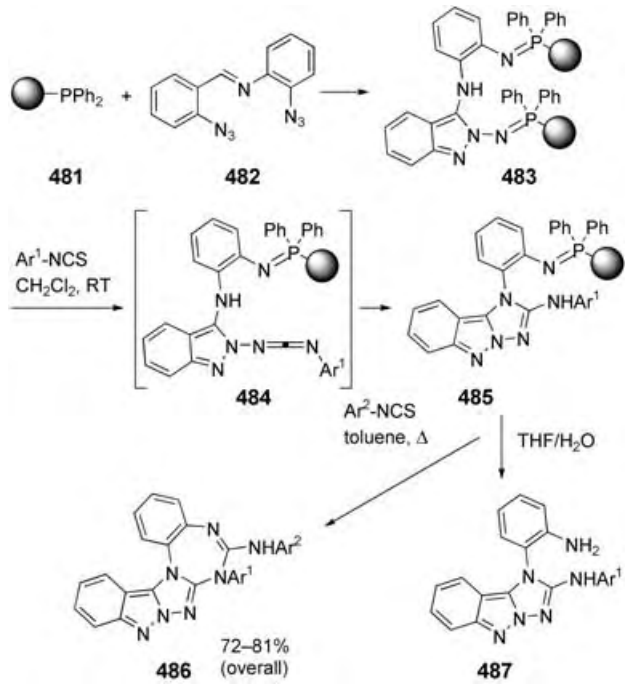


Scheme 115. Aza-Wittig reaction with polymer-bound diphenylphosphane.

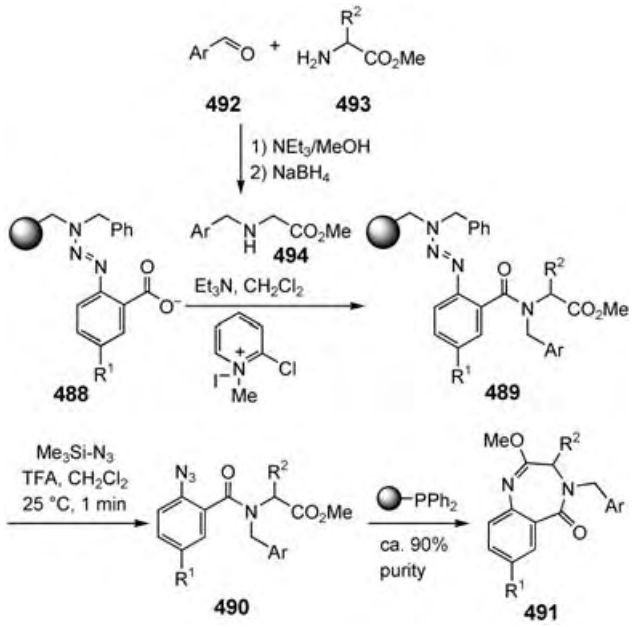
recovered, usually by reduction with trichlorosilane. In particular, the fact that the iminophosphorane **478** is polymer-bound in the first step the purification of the final product is simplified, as excess organoazide **476** can be removed before the aza-Wittig reaction.

This strategy has been used in the synthesis of condensed indazolobis(guanidines) **486** (Scheme 116),[447] amines,[448] pyrrolo[2,1-*c*][1,4]benzodiazepines such as the natural product DC-81 (**444**),[424b] pyrido[1,2-*c*]pyrimidines,[449] non-anomeric glycosidyl isothiocyanates,[450] the antitumor-active phloeodictin A1,[451] and libraries of benzodiazepine–quinaxolinone alkaloids of the circumdatin type.[452]

A combined solid-phase strategy for the synthesis of benzodiazepinones **491** starts from substituted triazene resins **488**, which were first treated with a series of *N*-benzyl amino acid esters. The latter are readily prepared by reductive amination of aryl aldehydes **492** with amino acid esters **493**. The cleavage of the resulting amide **489** in the presence of trimethylsilyl azide gave the highly functionalized aryl azides **490**. The intramolecular aza-Wittig reaction with polymer-bound triphenylphosphane then gave **491** in good yields (Scheme 117).[453]



Scheme 116. Solid-phase synthesis of condensed indazolo-bis(guanidines) **486**.[447]



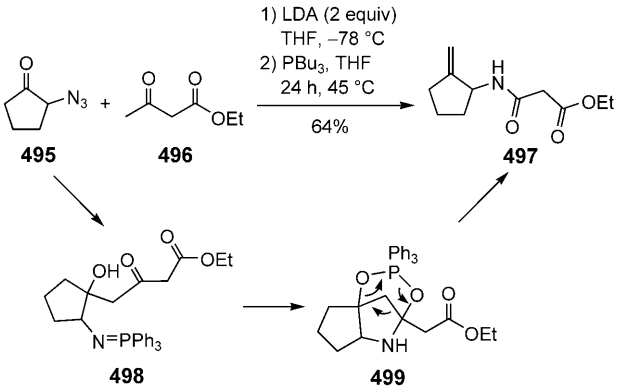
Scheme 117. Solid-phase synthesis of benzodiazepinones **491**.[453]

Soluble and easily separable triphenylphosphane reagents have been prepared from noncrosslinked polystyrene (NCPS)[454] or through perfluoroalkyl-substituted triphenylphosphane[455] and are also used in the Staudinger/aza-Wittig reaction.

A new reaction sequence that includes iminophosphoranes was recently reported by Langer and co-workers. α-Azidoketones **495** are converted into allyl amides **497** with enolizable β-carbonyl compounds in a sequence of Stau-

 © 2005 Wiley-VCH Verlag GmbH & Co. KGaA, Weinheim

dinger–aza-Wittig–1,5-phosphonium rearrangement–fragmentation sequence (Scheme 118).[456] This reaction differs from a related reaction,[457] such that the iminophosphorane does not cyclize to the pyrrole under aza-Wittig conditions,



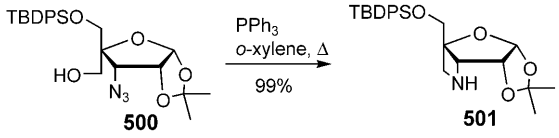
Scheme 118. A rearrangement cascade for the synthesis of allyl amides **497**.[456]

but first attacks the ketone and forms compound **499**. Ring opening of intermediate **499** and fragmentation of the resulting phosphonium oxide gives the allyl amide in a retro-Prins reaction with elimination of triphenylphosphane oxide.

At this point it must not be overlooked that alternative substrates and reagents for imine syntheses from organoazides and carbonyl compounds or their derivatives have recently been published (Section 4.6.2).

4.3.4. Reaction of Iminophosphoranes with other Electrophiles

Iminophosphoranes also react with other electrophiles, for example, epoxides or activated carbon electrophiles.[458] These intramolecular reactions take place with the formation of aziridines.[18,381] Recently, a new bridged nucleic acid monomer **501** was successfully synthesized by azetidine formation under Staudinger conditions (Scheme 119).[458a]

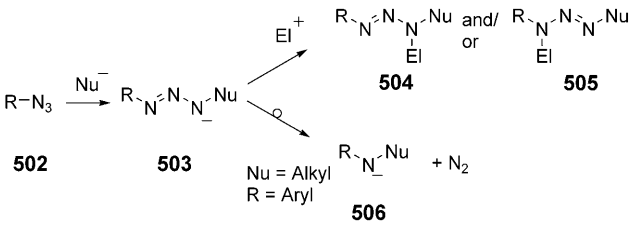


Scheme 119. Synthesis of azetidine-condensed nucleoside analogues.[458a]

4.4. Other Reactions of Organoazides with Nucleophiles

4.4.1. Reactions of Carbanions: Synthesis of Triazenes

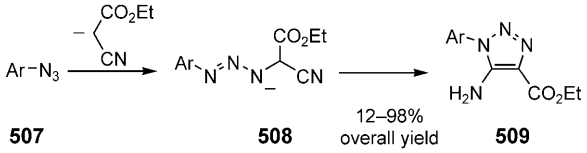
Stabilized and nonstabilized carbanions react with organoazides **502** (Scheme 120) to form triazenyl anions **503**, which can then be trapped with electrophiles—under certain circumstances regioselectively. (For the reaction with sulfonyl azides see Section 3.1.3.) This reaction is particularly useful for the preparation of the corresponding aliphatic triazenes,



Scheme 120. Synthesis of triazenes and secondary amides **506** from organoazides **502**.[9,460]

as other possible precursors (aliphatic diazonium ions) are not stable. The addition of nucleophiles to organoazides can also be used for diazo transfer[459] or for electrophilic amination of carbanions as found by Trost, Kabalka, and others,[460] because the triazenes cleave under mildly acidic conditions. However, triazenyl anions **503** that are formed by attack of aliphatic Grignard reagents on aromatic azides, are in a few cases not stable and lead to formal *N*-alkylation (Scheme 120).[9]The recently reported indium-induced Barbier synthesis of *N*-allylamines from allyl bromides and azides also probably follows a similar pattern.[461]

More than 100 years ago it was shown that in the presence of an internal electrophile the triazenyl anions **508** cyclize, for example, to triazoles **509** (Dimroth cyclization; Scheme 121).[58] Malonic, cyanoacetic, and related esters can be used.



Scheme 121. Synthesis of triazoles **509** from azides **507**.[58a]

4.4.2. Reduction of Azides to Amines

The reduction of azides[462] to the corresponding amines has been carried out with hydrogen in the presence of catalysts such as Lindlar catalyst,[78] with thiols,[463,464] complex hydrides, boranes, and phosphanes (see Section 4.3.1, Staudinger reduction).[122,409a,465–467]

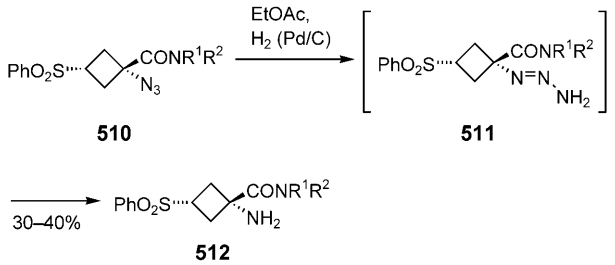
Thioethers R_2S are often used in catalytic amounts; different boranes[468,469] or borohydrides[470] function as stoichiometric reducing agents. The high reactivity of the reducing agent $BHCl_2{\cdot}SMe_2$ is exploited in the selective reduction of azides in the presence of double bonds. With $BH_3{\cdot}SMe_2$, hydroboration is preferred to reduction.[469] The reduction also takes place in good yields with various metals in the presence of Lewis[471] or Brønsted acids.[472] Acyl azides can be reduced to the corresponding primary amines with lithium/DTBB (di-*tert*-butylbiphenyl) at room temperature.[473] One mild reducing agent is *N*,*N*-dimethylhydrazine, which requires the presence of catalytic amounts of iron(III) chloride.[474] A further reducing agent is SmI_2, which transforms aliphatic, aromatic, and benzoyl azides smoothly into the corresponding amines under mild conditions.[475] Analo-

 © 2005 Wiley-VCH Verlag GmbH & Co. KGaA, Weinheim

gously, the reduction also takes place with zinc borohydride,[476] sodium borohydride under Cu(II) or Co(II) catalysis,[477] sulfur-modified calcium or barium borohydrides $M^{II}(BH_2S_3)$,[478] lithium aminoborohydrides (aliphatic and benzylic azides),[479] as well as classically with lithium aluminum hydride.[480]

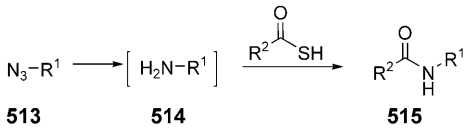
Iron(II) salts under basic conditions are also suitable reducing agents,[481] as are tetrathiomolybdates.[482] Very powerful yet selective reducing agents are the thioaryl-substituted Sn(II) complexes $Sn(SAr)_3^-$ (Bartra reagent).[483–485] Bu_3SnH is also used as reducing agent, sometimes with Ni(II) catalysis,[486,487] although a radical mechanism is assumed here.[486] Aliphatic, aromatic, and benzoyl azides can be reduced to the corresponding amines or amides by the action of trimethylchlorosilane.[488] The direct conversion of organazides into Boc-protected amines,[465,489] which provides elegant access to orthogonally protected diamines, is very attractive. The selective reduction of an azide group on an anomeric carbon atom of a saccharide by tetrathiomolybdates has also been reported, while the azide groups at other sites of the sugar were not attacked.[490] Enzymatic reductions of azides with baker's yeast[491] and lipases[491d] are also known.

The classic heterogeneous catalytic hydrogenation of aliphatic, aromatic, and sulfonyl azides with palladium on charcoal[492] as catalyst can also be carried out with other supports such as molecular sieves.[493] An interesting reduction of tertiary azides **510** to stable, monosubstituted triazenes **511** has been reported by Gaoni (Scheme 122).[494] At this point it has to be speculated whether most of the aforementioned reductions occur through triazenes.



Scheme 122. Reduction of organoazides **510** via triazene intermediate **511** according to Gaoni.[494]

A highly promising reaction is the transformation of thioacids with azides **513**, which leads directly to amides **515** (Scheme 123). Since this reaction takes place in water, it is suitable for aqueous peptide syntheses. Alkyl, acyl, and sulfonyl azides react equally well, and the amine **514** is formed in situ.[495,496]

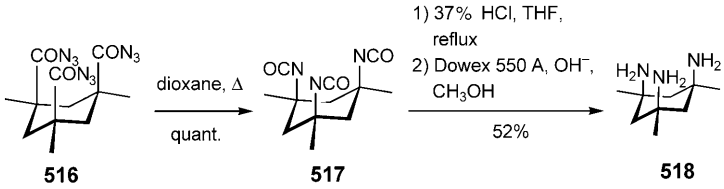


Scheme 123. Acylation of azides **513** with thiocarboxylic acids.[495]

4.5. The Curtius Rearrangement and Related Reactions

4.5.1. Curtius Rearrangement

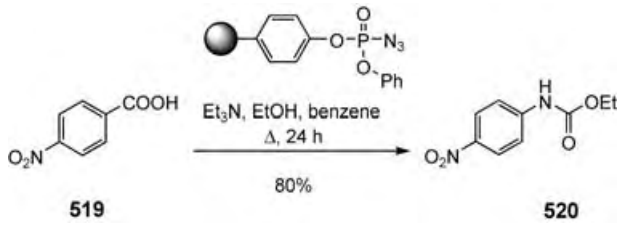
The Curtius rearrangement is a widely applicable reaction for the preparation of isocyanates and their secondary products.[497] Acid azides are photolytically decomposed to nitrenes, which in a further reaction at room temperature are converted into the isocyanates.[498] In principle, this reaction can be regarded as an aminating decarboxylation. The potential was demonstrated in a series of syntheses of complex natural products.[174,499,500] Owing to the widespread use of this reaction,[170,173,184,501,502] only a few selected examples are described here. Menger and co-workers recently reported the synthesis of 1,3,5-triaminocyclohexane **518** (in which the three amino groups adopt an axial disposition) from the Kemp triacid (Scheme 124).[503] The stereospecific triple



Scheme 124. Preparation of 1,3,5-triaminocyclohexane **518** according to Menger et al.[503]

Curtius rearrangement occurs with complete conversion in refluxing dioxane or toluene. The subsequent hydrolysis gave the triamine **518** in good yield.

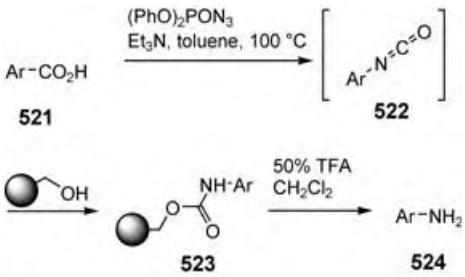
Carboxylic acids and their derivatives can also be transformed directly into the corresponding amines through a Curtius rearrangement. Thus monoesters of dicarboxylic acids can be converted into amino acids.[170] Usually diphenylphosphoryl azide (DPPA) is used as the reagent; however, its use is severely restricted owing to its high toxicity. Recently Taylor prepared and successfully used a solid-phase-bound phosphoryl azide in a Curtius rearrangement (Scheme 125).[116]



Scheme 125. Curtius rearrangement with immobilized phosphoryl azide according Taylor and Lu.[116]

The Curtius rearrangement is a key step in the total synthesis of (+)-zamoanolide, a tumor-growth inhibitor.[500] Solid-phase Curtius rearrangements have also been described for the amine[504] or carboxylic acid[505] immobilized on the solid phase. The isocyanate **522** is first formed as an intermediate in a Curtius rearrangement before further transformation (Scheme 126).

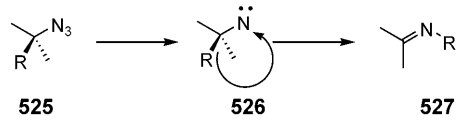
© 2005 Wiley-VCH Verlag GmbH & Co. KGaA, Weinheim



Scheme 126. Solid-phase synthesis of amines **524** according to Morishima and co-workers.[505]

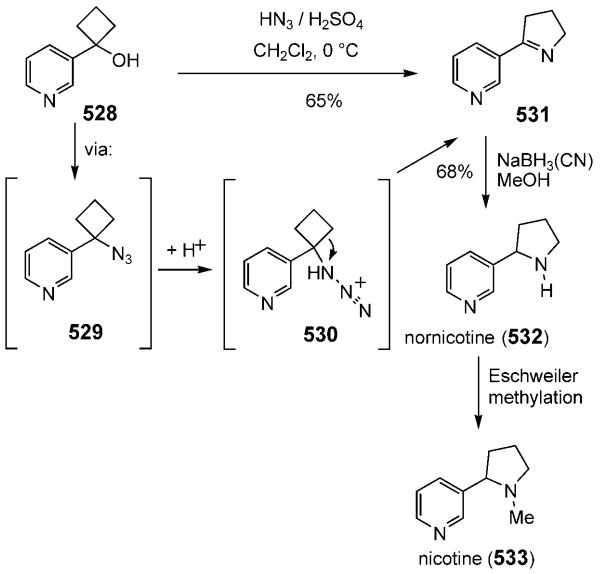
4.5.2. *The Schmidt Rearrangement*

The Schmidt rearrangement has been somewhat less extensively investigated than the Curtius rearrangement and usually takes place under pyrolysis or thermolysis conditions (Scheme 127).[506] An alkyl azide is either converted into a nitrene and further rearranges into an imine, or the rearrangement and loss of nitrogen takes place in a concerted manner.



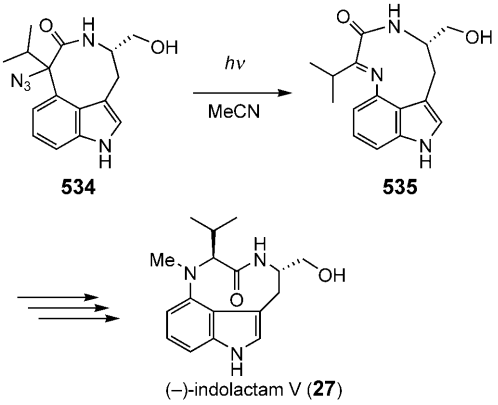
Scheme 127. Gas-phase pyrolysis of alkyl azides according to Bock et al.[506]

Andrieux and co-workers prepared tobacco alkaloids such as nicotine (**533**) with a Schmidt reaction as a key step. The intermediate in the nicotine synthesis is a cyclobutyl azide **529** (Scheme 128).[507]



Scheme 128. Synthesis of tobacco alkaloids according to Andrieux and co-workers.[507]

Another application of this rearrangement is the total synthesis of indolactam V (**27**) reported by Moody and Mascal in 1988 (Scheme 129).[508] The preparation is based on a photocyclization reaction of *N*-haloacetyltryptophan, also described by Moody and co-workers[509] and uses the α,α-dichloroisovaleryl amide of tryptophanol as starting material.



Scheme 129. Total synthesis of indolactam **27**.[508]

Further applications are found in the rearrangement of azidocubanes[147] and the synthesis of tetrazoles from fatty acids,[510] and the total synthesis of stenine.[511] In a series of examples, the Schmidt reaction takes place in the presence of Brønsted or Lewis acids. In a few of these cases, for example, in the reaction with aldehydes or ketones, the intermediate imine reacts either in an intermolecular or intramolecular fashion with a further equivalent of azide to form tetrazoles.[512]

4.6. *Reactions of Azides with Electrophiles*

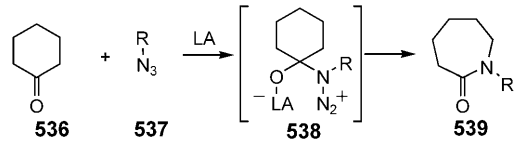
Suitable electrophiles (carbon electrophiles, protons, boranes) normally react with organoazides at N^1, mostly to form initially an amine-substituted diazonium ion, which loses nitrogen. The electron-deficient nitrenium ion usually rearranges or reacts with nucleophiles.

4.6.1. *Boyer Reaction*

In the presence of Lewis acids, organoazides react with carbon electrophiles with framework expansion in analogy to the Schmidt reaction. Suitable (pre)electrophiles include ketones (Aubé[513]), epoxides, or carbenium ions, which can be obtained from alkenes or alcohols through protonation (Pearson[514]) or mercuration.[515] The aminodiazonium ion formed initially loses dinitrogen with simultaneous migration of the alkyl residue to the electron-deficient nitrogen atom. The reaction of aliphatic azides with ketones in the presence of Brønsted acids—the Boyer reaction[516]—occurs in good yields to form *N*-alkylated amides or lactams,[517] but is limited to aliphatic ketones. An improvement was brought about by the observation by Aubé and co-workers that Lewis acids can

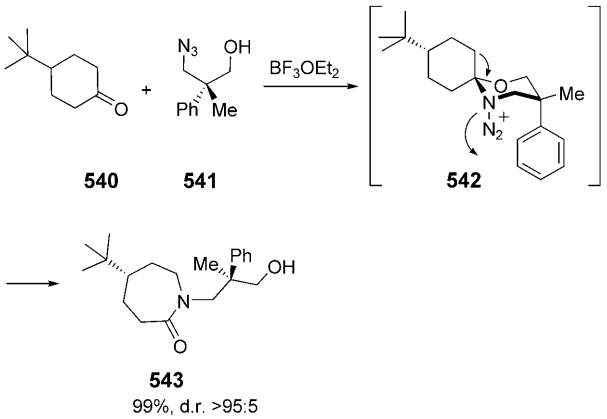
 © 2005 Wiley-VCH Verlag GmbH & Co. KGaA, Weinheim

also accelerate this reaction (Scheme 130). α,β-Unsaturated ketones react through another reaction pathway (Scheme 47).



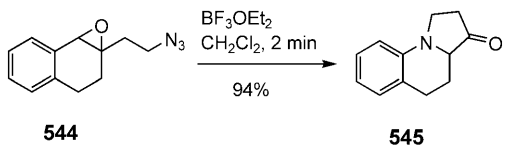
Scheme 130. Boyer reaction according to Aubé and co-workers.[513] LA = Lewis acid.

The asymmetric variant of this Boyer rearrangement was also developed by Aubé and co-workers.[518,519] Prochiral cycloalkanones **540** react with chiral 3-hydroxyalkyl azides **541** in the presence of Lewis acids and yield ring-expanded *N*-alkyl lactams **543** with high diastereoselectivity. Prior to the antiperiplanar migration, the phenyl ring in the intermediate **542** adopts an axial disposition, and the methyl group is arranged equatorially (Scheme 131). The cause of this otherwise unusual behavior lies in the interaction of the phenyl group with the electron-deficient diazonium unit.[519,520]



Scheme 131. The asymmetric Boyer reaction according to Aubé and co-workers.[518]

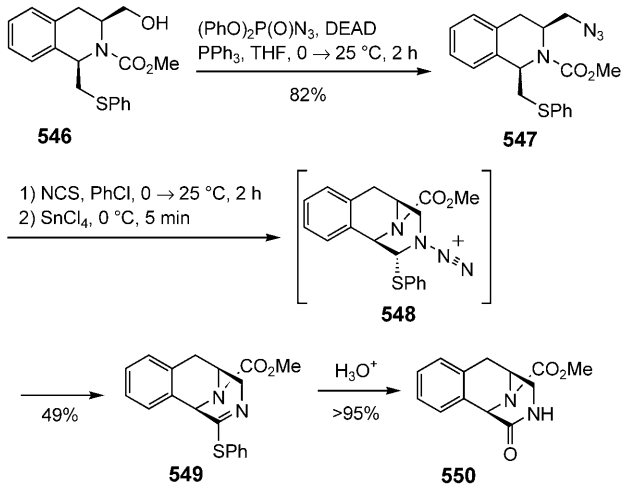
Alternatively, besides ketones, azidoalkyl-substituted epoxides such as **544** can be transformed in an intramolecular reaction (Scheme 132).[521,522] The benzylic nature of the nitrenium ion formed allows the migration of the aromatic residue, and an amino-substituted aromatic system is formed (see Scheme 136).



Scheme 132. The azido-Schmidt reaction with epoxides **544**.[522]

4.6.2. *New Electrophiles for the Synthesis of Imines from Azides: Alternatives to the Aza-Wittig Reaction*

A reaction sequence, the first stage of which is related to the organoazide Schmidt reaction, was reported by Magnus and co-workers in 2003.[523] An α-chlorinated thioether acts as the electrophile, which undergoes intramolecular attack by an alkyl azide with loss of a chloride ion. Unlike the Schmidt reaction, however, both a proton and dinitrogen are lost. The resulting thioimine **549** then releases an amide functionality under hydrolytic conditions. The overall reaction sequence thus corresponds to an aza-Wittig reaction (Scheme 133).



Scheme 133. Intramolecular alkylation of azides according to Magnus and co-workers.[523]

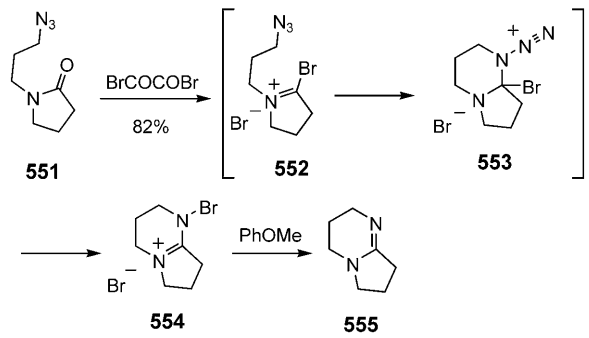
A related reaction sequence for the preparation of imines from azides was reported recently by Shibasaki and co-workers.[524] They observed that a number of azidoalkyl lactams **551** reacted only slowly, if at all, under Staudinger–aza-Wittig conditions with formation of the corresponding amidines. A search for suitable reagents led to oxalyl bromide/anisole as an efficient reagent combination. A bromoaminium ion is probably formed which acts as an electrophile and attacks the azide group. The resulting aminodiazonium ion **553** loses dinitrogen with migration of the bromine atom to the nitrogen atom. A dipolar mechanism has been proposed as an alternative. In any case, anisole then removes the electrophilic bromine, leading finally to the amidine **555** (Scheme 134).

4.6.3. *Nitrenium Ions by Protonation of Organoazides*

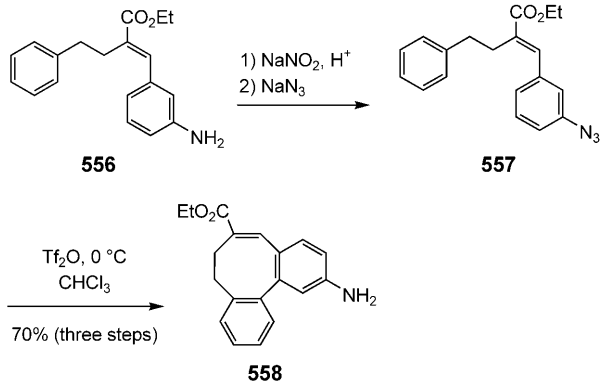
According to Bamberger, the protonation of organoazides with strong acids (e.g. TFA) gives aryl or alkyl nitrenium ions that are analogous to carbocations.[525–527] Aryl nitrenium ions are highly reactive intermediates, which react as electrophiles in either inter- or intramolecular[336] reactions with aromatic groups (Scheme 135).[526,528] The high reactivity is an argument for the carcinogenicity of such compounds.[529]

The acid-catalyzed rearrangement of azidobenzyl compounds to anilines,[530,531] which are accessible by conjugate

 © 2005 Wiley-VCH Verlag GmbH & Co. KGaA, Weinheim

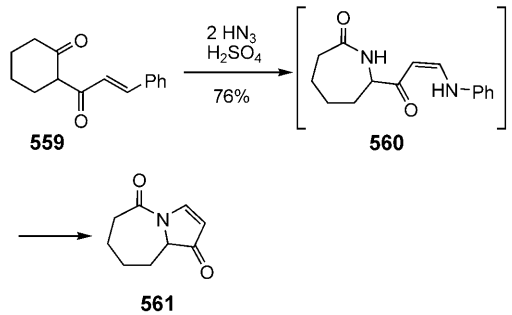


Scheme 134. Intramolecular synthesis of amidine **555** according to Shibasaki and co-workers.[524]



Scheme 135. Intramolecular cyclization of aryl nitrenium ions.[526]

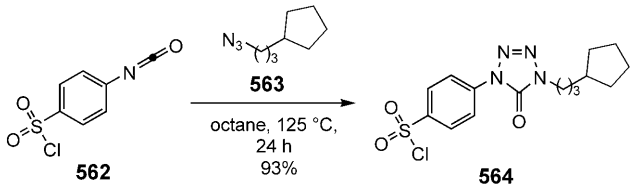
Boyer addition, also involves the participation of nitrenium ions.[532] This rearrangement takes place through an intramolecular electrophilic substitution and subsequent ring opening of the resulting aziridine to form an iminium ion. Hydrolysis then gives the aniline derivative. In the case of cyclohexanone-substituted ketones of type **559**, insertion of nitrogen atoms from 2 equivalents of HN_3 leads to the enamine **560**, and cyclization produces the unsaturated lactams **561** (Scheme 136).[533]



Scheme 136. Double rearrangement of the Schmidt type according to Casey et al.[533]

4.6.4. ***Reaction of Organoazides with Heterocumulenes***

The reaction of organic azides with aryl isocyanates takes place rapidly and in the presence of excess azide gives 1,4-disubstituted Δ^2-tetrazoline-5-ones in very good yields.[534,186] The addition is largely chemoselective, so that even sensitive functions such as the sulfonyl chloride group are not attacked (Scheme 137).[535] Alkoxycarbonyl isocyanates, sulfonyl isocyanates, and isothiocyanates react with organic azides in the same manner to form Δ^2-tetrazoline-5-ones.[536]

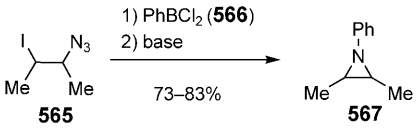


Scheme 137. Selective addition of alkyl azide **563** to 4-isocyanatobenzenesulfonyl chloride (**562**).[535]

4.6.5. ***Reaction of Organoazides with Boron Compounds***

According to an early observation by Brown et al., trialkyl boranes react with aromatic and aliphatic azides to form secondary amines.[537] The formation of nitrogen follows second-order kinetics so that a mechanism that proceeds via a nitrene intermediate is excluded. The organoboranes react reversibly with the organoazides, which subsequently react further with loss of nitrogen and simultaneous migration of the alkyl groups from the boron to the nitrogen. This reaction follows a similar but relatively older observation of Paetzold and Habereder on the decomposition of azidoboranes.[538]

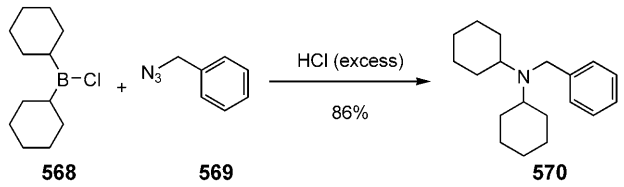
As the steric demand of the alkyl residue increases, the reaction slows down significantly, and the yields decrease. Haloboranes such as monochloro-,[539] dichloro-,[540,541] and difluoroboranes[542] or their precursors such as aminoboranes in the presence of anhydrous HCl[543] can be used likewise and even advantageously[469,539] because they are more reactive. Only dibromoboranes react differently, with simultaneous formation of tetraazaborolines.[544] In the presence of alkylating agents, subsequent alkylation occurs, as in the synthesis of the aziridines **567** (Scheme 138).[539]



Scheme 138. Arylation of organoazides with boranes and subsequent intramolecular alkylation.[539]

As dichloroboranes can be prepared readily in enantiomerically pure form by diastereoselective hydroboration and subsequent transformation, α-chiral amines are readily accessible.[545] This reaction sequence also proceeds in an intramolecular fashion with the synthesis of chiral cyclic amines.[542] Under certain conditions, two alkyl groups can be transferred (Scheme 139).[543]

 © 2005 Wiley-VCH Verlag GmbH & Co. KGaA, Weinheim



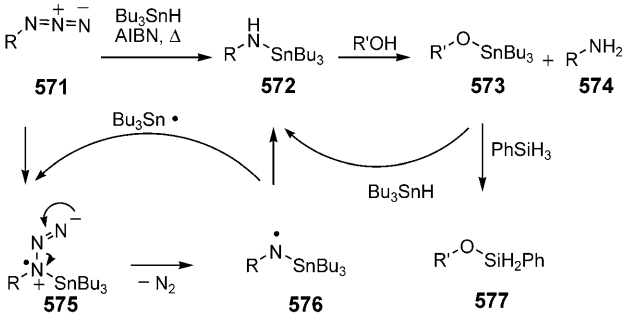
Scheme 139. Alkylation of organoazides with boranes.[543]

4.6.6. Reaction of Organoazides with Heteroelectrophiles

The reaction of aliphatic and aromatic azides with HOF/CH_3CN leads to an immediate oxidation with formation of nitro compounds. Initially, the electrophilic oxygen atom in HOF is attacked with concomitant loss of HF and dinitrogen. The nitroso compound is thus formed and reacts further to form the nitro compound. This single-step reaction is simpler than other variants.[546]

4.7. Radical Additions to Organoazides

The addition of tributyltin radicals to organoazides **571** leads initially to triazenyl radicals **575**. Loss of nitrogen leads to amine radicals **576**, which finally react with tributyltin hydride to give **572** (Scheme 140).[486a] The latter are transformed into the amines **574** with phenylsilyl hydride in the presence of alcohols. Tributyltin hydride is regenerated so that only catalytic amounts are needed.

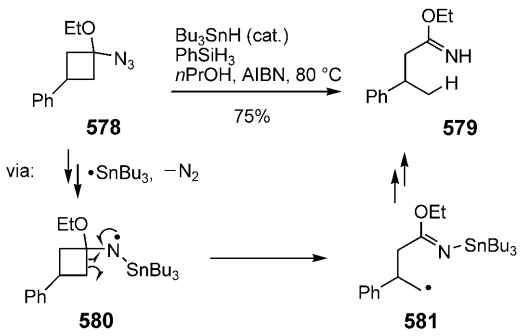


Scheme 140. Reduction of organoazides with phenylsilyl hydride under tributyltin hydride catalysis.[486] AIBN = 2,2′-azobis(isobutyronitrile).

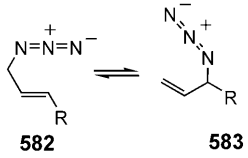
The radical reaction mechanism is confirmed by the conversion of cyclobutane azide **578** which proceeds through ring opening (Scheme 141). A few synthetically very useful azide-transfer reactions also proceed through a radical mechanism (see Scheme 27, Scheme 42).[145,206]

4.8. [3,3] Sigmatropic Rearrangements and Electrocyclizations of Organoazides

The rearrangement of allyl azides (Scheme 142) was first reported by Gagneux, Winstein, and Young in 1960, and has since then been observed with different substrates, including



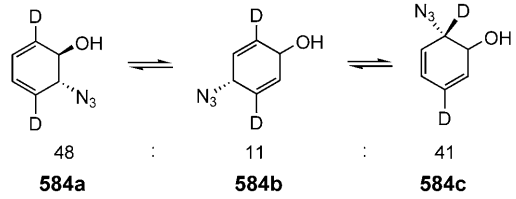
Scheme 141. Ring opening of azidocyclobutanes **578**.[486,547]



Scheme 142. Sigmatropic rearrangement of allyl azides.[549]

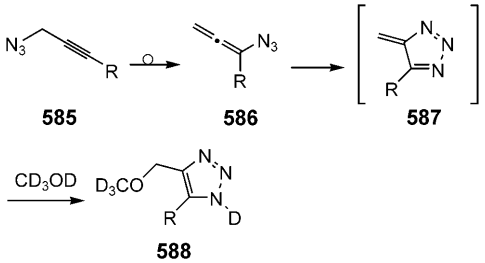
substituted cyclopropene azides.[548–551] This [3,3] sigmatropic rearrangement takes place even at low temperatures.

In the case of azidocyclohexadienes, all possible products are in thermal equilibrium (Scheme 143).[548] In some cases, a mixture of all possible products is also formed in the synthesis of allyl azides.[552]



Scheme 143. Consecutive sigmatropic rearrangements of cyclohexadienyl azides **584**.[548]

The propargyl azides **585** rearrange to the less stable allenyl azides **586** (Banert cascade, Scheme 144).[255] The short-lived allenyl azides **586** cyclize rapidly to the triazafulvenes **587**, which in the presence of a nucleophilic trapping reagent (e.g. $[D_4]$MeOH) form the corresponding 1,2,3-triazoles **588** quantitatively. In the absence of a nucleophilic trapping reagent, the allenyl azides polymerize.



Scheme 144. Preparation of 1,2,3-triazoles from allenyl azides.[255]

 © 2005 Wiley-VCH Verlag GmbH & Co. KGaA, Weinheim

C-Azidoimines **589** can form tetrazoles **590** in a reversible electrocyclic reaction (Scheme 145).[553] These *C*-azidoimines **589** are formed, for example, in a Mitsunobu reaction of amides with trimethylsilyl azide and in most cases, rearrange directly to the tetrazoles **590**. This reaction is complementary to the cycloaddition of organoazides with nitriles.[554]

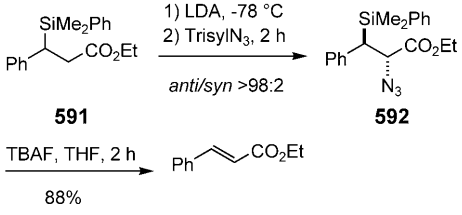


589 **590**

Scheme 145. Electrocyclization of *C*-azidoimines **589** to tetrazoles **590**.[553]

4.9. Azide Ions as Leaving Groups

Aliphatic azides can be either eliminated or substituted by suitable organic bases or nucleophiles. In this case, the property of the azide as pseudohalogen comes to the fore. Thus β-silyl azides **592** undergo *anti* elimination stereoselectively in the presence of fluoride ions to give the olefins **593**.[134] The corresponding silanes **591** are readily accessible either through haloazidation of silylalkanes (Scheme 24) or by electrophilic azidation of enolates (Scheme 146). Whereas sterically unhindered aliphatic azides are reduced smoothly to amines with Ni(II)/Bu_3SnH (see Section 4.4.2), this reagent effects substitution of the azide group by hydride with benzylic azides.[486a]



591 **592** **593**

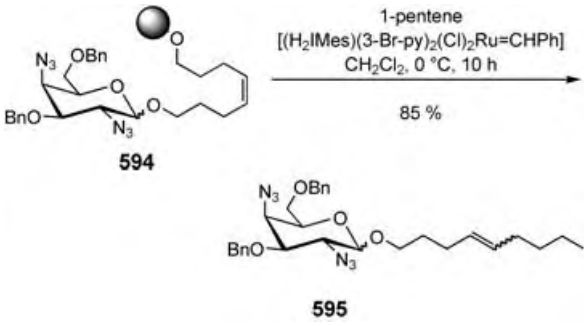
Scheme 146. Synthesis and elimination of β-silyl azides **592**.[134] Trisyl = 2,4,6-triisopropylbenzenesulfonyl.

5. Applications of Azides

5.1. Use as Protecting Groups

The azide function provides a good possibility to protect coordinating primary amines, especially in sensitive substrates such as oligosaccharides, aminoglycoside antibiotics,[152,155] glycosoaminoglycans such as heparin[556] and peptidonucleic acids (PNA).[557] Furthermore, the azide group is stable in osmium-[558] and ruthenium-induced[559] dihydroxylations or alkylations (see Scheme 44).

The protection of the amino function is carried out with, for example, triflyl azide (see Schemes 28 and 29). A more recent example of the stability of alkyl azides towards organometallic catalysts in this context was provided by Seeberger and co-workers, who demonstrated the compatibility of the azido group in cleaving alkene metathesis of saccharides (Scheme 147).[560]



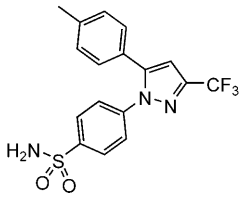
594 **595**

Scheme 147. Cleavage metathesis of organoazides.[560]

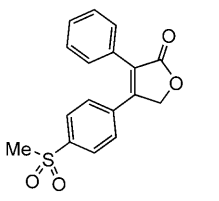
In addition to its use as a protecting group, the azide function provides other creative possibilities, for example, in the aza-Wittig reaction.

5.2. Azides as Biologically Active Compounds and in Natural Products Synthesis

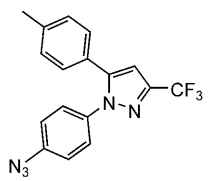
A number of syntheses for the preparation of natural products have been described in the text,[78,80,114b,386,514f,517,561] (see Schemes 6, 20, 22, 30, 36, 44, 74, 78, and 108). Although no natural products are (yet) known with an azide functionality, there is a series of potentially active compounds with this functionality. The high activity can be seen in bioisosteric comparisons of the azide group with other functional groups (see also Section 4.1.2).[562] Parallels have been drawn between the methylsulfonyl and aminosulfonyl groups. The relatively smaller azide group is slightly more lipophilic than these two groups, and, for example, interacts better with arginine units than with sulfonyl functions. Azide derivatives (such as **598**) of the COX-2 inhibitors colecoxib (**596**) and rofecoxib (**597**) are also more potent than the corresponding sulfone derivatives.[563] Comparisons between a 1,1-dichloroethyl group (as in chloramphenicol) and the azidomethyl group have shown that they exhibit similar behavior. A well-



celecoxib (**596**)

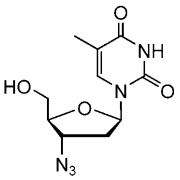


rofecoxib (**597**)



598

 © 2005 Wiley-VCH Verlag GmbH & Co. KGaA, Weinheim



599

known example is the anti-HIV medication AZT (**599**; 3′-azido-2′,3′-didesoxythymidine).[564,565]

5.3. *Photoaffinity Labeling*

The labeling of receptor compounds and ligands with the azide functionality is used in photoaffinity labeling.[566,567] The ligand is equipped with this nitrene precursor at a position (for thalidomide see Scheme 2) that does not distort its affinity for the receptor, but yet is close enough to its target protein. The azide group is particularly suitable for this labeling since after photolysis the organoazide can be inserted into many carbon, nitrogen, oxygen, or sulfur compounds by the formation of nitrenes. An additional radioactive label can also be used to identify the ligand–protein complex (Figure 4).

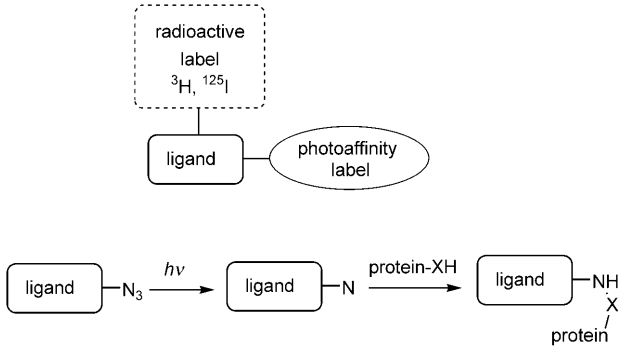
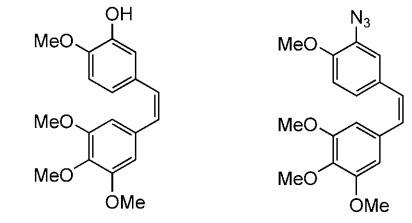


Figure 4. The principle of photoaffinity labeling.

This principle was used, for example, in the synthesis of combrestatin analogues as molecular probes for tubulin polymerization (Figure 5).[568] Furthermore, there have recently been a number of applications in medicinal chemistry.[569]

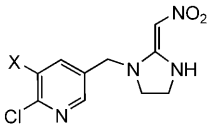


combrestatin A-4 (**600**)

azide-analogous combrestatin A-4 (**601**)

Figure 5. Aryl azides as molecular probes according to Pinney et al.[568]

This process has also been used in modern plant protection research to analyze, for example, the interaction of proteins with insecticides, as in the neonicotinoids (e.g. imidacloprid (**607**), Figure 6).[570] In this connection it was important that the biological properties of the labeled compounds differ only little from the starting compound. The lipophilicity of organic azides has a direct advantage here.



X = H: imidacloprid (**602**)
X = N_3: 5-azidoimidacloprid (**603**)

Figure 6. Heteroaryl azides as molecular probes according to Zhang and co-workers.[570]

Not only can the interaction of small molecules with proteins[571] be investigated by photolabeling with organoazides but also protein–protein [572] and protein–nucleic acid interactions.[573]

The photoaffinity labeling can also be carried out in an intramolecular fashion, which leads to crosslinking. One current example is the covalent bonding of an RNA duplex strand with an internally attached aryl azide (**606**) by photolysis. It was crucial that a hydroxy group occupied the 3-position of the aryl azide **606**, for in this way the evidence was obtained that a ketene imine or a corresponding sequential product as active species leads to the crosslink under nucleophilic attack by the antisense strand (Figure 7).[574]

6. Summary and Outlook

Organic azides have in recent times enjoyed much popularity in synthetic organic chemistry. In spite of—or perhaps because of—their partly less attractive properties (explosiveness, toxicity), a plethora of new applications has been published. In the area of cycloadditions, in particular, the discovery of new reaction conditions has led to a true "explosion" of new applications. It remains to be seen how organic azides will find use in chemical biology or in materials science.

Addendum (April 7, 2005)

Since the submission of this Review, the number of articles on organic azides has continued to increase tremendously—on average, there are more than 1000 publications a year. We refer to some of the excellent papers that have appeared most recently.[575]

Organic azides were used as flexible building blocks in the partial synthesis of some very complex natural products;[576] modern techniques in gene technology have even allowed the incorporation of biochemically modified amino acids as "proteogenes" in peptides.[577]

The 1,3-dipolar cycloaddition of alkynes with azides, an application of the Huisgen reaction in the field of "click chemistry", was discussed several times in review articles.[578] The number of applications of this useful reaction is steadily increasing.[579] The reaction has been optimized considerably, especially in biochemical applications,[580] such that larger biomolecules can also participate in this type of reaction.

 © 2005 Wiley-VCH Verlag GmbH & Co. KGaA, Weinheim

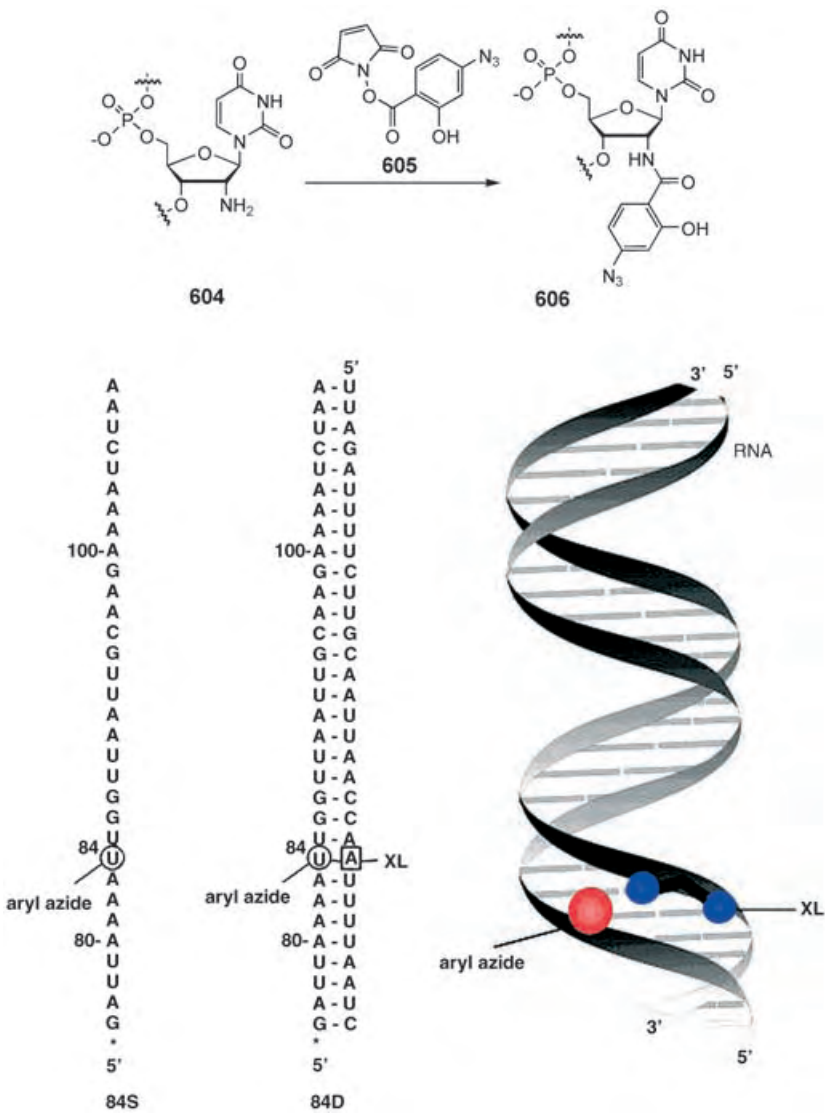


Figure 7. 3-Hydroxyaryl azides as crosslinkers according to Platz, Weeks et al.[574] *: Position of a radioactive ^{32}P label, XL = crosslinking.

Furthermore, this reaction can even take place in enzyme pockets.[581] Consequently, the mechanism of the 1,3-dipolar cycloaddition of alkynes with azides has been investigated in depth.[582] Moreover, polymers can also be prepared in this manner.[583] Azides have also been employed in other cycloadditions.[584]

The Staudinger reaction[585,586] and its application as a ligation method for the conjugation of biomolecules has been widely popular among bioorganic chemists[587] and was used in the synthesis of complex structures.[588] Investigations into the mechanism of this reaction have also been carried out.[589]

Further applications include radical reactions,[590] multicomponent reactions,[591] rearrangements,[592] and several well-known reactions such as the Curtius,[593] Hemetsberger–Knittel,[594] Schmidt,[595] Mitsunobu,[596] and Wittig (aza-Wittig)[597] reactions. Diazido iodinate (formed in situ or polymer-bound) was used in a safe azidation of aldehydes and benzyl ethers.[598] Organic azides are also important structural motifs in the field of high-energy materials, for example, in the synthesis of tetrazolylazide[599] and as precursors in materials research.[600] The rearrangement of organic azides has been investigated within organic cavitands[601] as well as spectroscopically.[602]

We thank G. Bucher, R. Breinbauer, A. Hirsch, T. M. Klapötke, J. Podlech, and J. L. Radkiewicz for the availability of preprints, schemes, and comments, and B. Lesch and S. Vanderheiden for their critical reading of the manuscript. We thank the referees for critical suggestions for improvement. Our work was supported by the Fonds der Chemischen Industrie, the Deutsche Forschungsgemeinschaft, and the European Union (Marie-Curie-Fellowship (Program "Improving Human Research Potential and the Socio-Economic Knowledge Base) to C.G.).

Received: February 16, 2004
Revised: December 13, 2004

[1] For previous reviews on this topic, see: a) E. F. V. Scriven, K. Turnbull, *Chem. Rev.* **1988**, *88*, 297–368; b) G. L'Abbé, *Chem. Rev.* **1969**, *69*, 345–363.
[2] a) P. Grieß, *Philos. Trans. R. Soc. London* **1864**, *13*, 377; b) P. Grieß, *Justus Liebigs Ann. Chem.* **1865**, *135*, 131.
[3] a) T. Curtius, *Ber. Dtsch. Chem. Ges.* **1890**, *23*, 3023–3033; b) T. Curtius, *J. Prakt. Chem.* **1894**, *50*, 275.
[4] P. A. S. Smith, *Org. React.* **1946**, *3*, 337–349.
[5] J. H. Boyer, F. C. Canter, *Chem. Rev.* **1954**, *54*, 1–57.
[6] T. S. Lin, W. H. Prusoff, *J. Med. Chem.* **1978**, *21*, 109–112.
[7] a) *The Chemistry of the Azido Group* (Ed.: S. Patai), Wiley, New York, **1971**; b) *The Chemistry of Halides, Pseudo-halides and Azides*, Supplement D, (Eds.: S. Patai, Z. Rappoport), Wiley, Chichester **1983**; c) *Chemistry of Halides, Pseudo-Halides and Azides, Part 1* (Ed.: S. Patai), Wiley, Chichester, **1995**; d) *Chemistry of Halides, Pseudo-Halides and Azides, Part 2* (Ed.: S. Patai), Wiley, Chichester, **1995**.
[8] Monograph: *Azides and Nitrenes—Reactivity and Utility* (Ed.: E. F. V. Scriven), Academic Press, New York, **1984**.
[9] H. M. S. Kumar, B. V. S. Reddy, S. Anjaneyulu, J. S. Yadav, *Tetrahedron Lett.* **1999**, *40*, 8305–8306.
[10] According to a Chemical Abstracts search, an average of over 1000 publications a year have been published on the topic of azides over the last few years.
[11] a) T. M. Klapötke, B. Krumm, P. Mayer, I. Schwab, *Angew. Chem.* **2003**, *115*, 6024–6026; *Angew. Chem. Int. Ed.* **2003**, *42*, 5843–5846; b) R. Haiges, J. A. Boatz, A. Vij, M. Gerken, S. Schneider, T. Schroer, K. O. Christe, *Angew. Chem.* **2003**, *115*, 6027–6031; *Angew. Chem. Int. Ed.* **2003**, *42*, 5847–5851.
[12] 1*H*-Triazirines have not been observed previously,[13] but N_3H should have less strain energy (198.3 kJ mol^{-1}) than the homologous cyclopropenes: M. N. Glukhovtsev, R. D. Bach, L. Laiter, *Int. J. Quantum Chem.* **1997**, *62*, 373–384. A CAS search also gave no results; in a few publications the saturated heterocycle (triaziridine) has been called triazirine.
[13] A. Hantzsch, *Ber. Dtsch. Chem. Ges.* **1933**, *66*, 1349–1354.
[14] a) L. Pauling, L. O. Brockway, *J. Am. Chem. Soc.* **1937**, *59*, 13–20; b) L. O. Brockway, L. Pauling, *Proc. Natl. Acad. Sci. USA* **1933**, *19*, 860–867.
[15] M. T. Nguyen, D. Sengupta, T.-K. Ha, *J. Phys. Chem.* **1996**, *100*, 6499–6503.

 © 2005 Wiley-VCH Verlag GmbH & Co. KGaA, Weinheim

[16] a) T. M. Klapötke, D. Adam, unpublished results; b) D. Adam, PhD Thesis, Ludwigs-Maximillians-Universität München (Germany), **2001**.
[17] Further vibrations lie at 1340–1180 cm^{-1} and 680 cm^{-1}.
[18] A. Breuning, R. Vicik, T. Schirmeister, *Tetrahedron: Asymmetry* **2003**, *14*, 3301 – 3312, and references therein.
[19] Mulliken electronegativities: Cl (8.3 eV), Br (7.5 eV), N_3 (7.7 eV). I. C. Tornieporth-Oetting, T. M. Klapötke, *Angew. Chem.* **1995**, *107*, 559 – 568; *Angew. Chem. Int. Ed. Engl.* **1995**, *34*, 511 – 520.
[20] a) P. A. S. Smith, *Open-Chain Nitrogen Compounds*, *vol. 2*, Benjamin, New York, **1966**, 211 – 256; b) J. H. Boyer, R. Moriarty, B. de Darwent, P. A. S. Smith, *Chem. Eng. News* **1964**, *42*, 6.
[21] D. Adam, K. Karaghiosoff, T. M. Klapötke, G. Holl, M. Kaiser, *Propellants Explos. Pyrotech.* **2003**, *27*, 7 – 11.
[22] A. Hammerl, T. M. Klapötke, H. Nöth, M. Warchhold, G. Holl, *Propellants Explos. Pyrotech.* **2003**, *28*, 165 – 173.
[23] a) A. Hassner, M. Stern, H. E. Gottlieb, F. Frolow, *J. Org. Chem.* **1990**, *55*, 2304 – 2306; b) Aliphatic azides can be detected colorimetrically: S. Punna, M. G. Finn, *Synlett* **2004**, 99 – 100.
[24] These include, in particular, inorganic azides as neurotoxins; azide ions as cytochrome c oxidase (COX) inhibitors. See also: http://pubs.acs.org/cen/safety/.
[25] Solid iodoazide is explosive and should not be prepared in the absence of solvent.[184]
[26] a) A. Hassner in *Organic Nitrogen Compounds I*, *Vol. E16a* (Ed.: D. Klamann), Thieme, Stuttgart, **1990**, pp. 1243 – 1290; b) A. Hassner, *Acc. Chem. Res.* **1971**, *4*, 9 – 16.
[27] a) R. A. Abramovitch, B. A. Davis, *Chem. Rev.* **1964**, *64*, 149 – 185; b) E. F. V. Scriven in *Reactive Intermediates*, *Vol. 2* (Ed.: R. A. Abramovitch), Plenum, New York, **1982**, Chapter 1, pp. 1 – 54; c) P. A. S. Smith in *Azides and Nitrenes—Reactivity and Utility* (Ed.: E. F. V. Scriven), Academic Press, New York, **1984**, Chapter 3, pp. 95 – 204; d) G. B. Schuster, M. S. Platz, *Adv. Photochem.* **1992**, *18*, 69 – 143; e) W. T. Borden, N. P. Gritsan, C. M. Hadad, W. L. Karney, C. R. Kemnitz, M. S. Platz, *Acc. Chem. Res.* **2000**, *33*, 765 – 771; f) N. P. Gritsan, M. S. Platz, *Adv. Phys. Org. Chem.* **2001**, *36*, 255 – 304.
[28] M. S. Platz, *Acc. Chem. Res.* **1995**, *28*, 487 – 492.
[29] a) S. X. Cai, D. J. Glenn, K. R. Gee, M. D. Yan, R. E. Cotter, N. L. Reddy, E. Weber, J. F. W. Keana, *Bioconjugate Chem.* **1993**, *4*, 545 – 548; b) M. S. Platz, *Photochem. Photobiol.* **1997**, *65*, 193 – 194; c) H. Bayley, J. V. Staros in *Azides and Nitrenes—Reactivity and Utility* (Ed.: E. F. V. Scriven), Academic Press, New York, **1984**, Chapter 9, pp. 433 – 490; for overviews on aryl azides as photoaffinity labels, see: d) *Applications of Photochemistry in Probing Biological Targets*, *Vol. 346* (Eds: A. M. Tometsko, F. M. Richards), Annals of the New York Academy of Sciences, New York, **1980**; e) A. Radominska, R. R. Drake, *Methods Enzymol.* **1994**, *230*, 330 – 339; f) J. S. Fedan, G. K. Hogaboom, J. P. O'Donnell, *Biochemical Pharmacology* **1984**, *33*, 1167 – 1180.
[30] S. X. Cai, D. J. Glenn, M. Kanskar, M. N. Wybourne, J. F. W. Keana, *Chem. Mater.* **1994**, *6*, 1822 – 1829.
[31] E. W. Meijer, S. Nijhuis, F. C. B. M. Vroonhoven, *J. Am. Chem. Soc.* **1988**, *110*, 7209 – 7210.
[32] a) P. Nahar, N. M. Wali, R. P. Gandhi, *Anal. Biochem.* **2001**, *294*, 148 – 153; b) S. X. Cai, D. J. Glenn, J. F. W. Keana, *J. Org. Chem.* **1992**, *57*, 1299 – 1304.
[33] a) E. Noelting, O. Michel, *Ber. Dtsch. Chem. Ges.* **1893**, *26*, 86 – 87; b) E. Noelting, O. Michel, *Ber. Dtsch. Chem. Ges.* **1893**, *26*, 88 – 92.
[34] E. Noelting, E. Grandmougin, O. Michel, *Ber. Dtsch. Chem. Ges.* **1892**, *25*, 3328 – 3342.
[35] T. Zincke, P. Schwarz, *Ann.* **1899**, *307*, 28 – 49.
[36] For a review, see: a) M. E. C. Biffin, J. Miller, D. B. Paul in *The Chemistry of the Azido* Group (Ed.: S. Patai), Wiley, New York, **1971**, pp. 147 – 176; b) J. C. Kauer, R. A. Carboni, *J. Am. Chem. Soc.* **1967**, *89*, 2633 – 2637; c) M. Takahashi, D. Suga, *Synthesis* **1998**, 986 – 990.
[37] T. Keumi, T. Umeda, Y. Inoue, H. Kitajima, *Bull. Chem. Soc. Jpn.* **1989**, *62*, 89 – 95.
[38] For reviews, see: a) I. Ugi in *Comprehensive Heterocyclic Chemistry* (Eds.: A. R. Katritzky, C. W. Rees), Pergamon, Oxford, **1984**, vol. 5, pp. 839 – 845; b) R. N. Butler in *Comprehensive Heterocyclic Chemistry 11*, *vol. 4* (Ed.: R. C. Storr), Pergamon, Oxford, **1996**, pp. 897 – 904; R. N. Butler in *Comprehensive Heterocyclic Chemistry II*, *Vol. 4* (Ed.: R. C. Storr), Pergamon, Oxford, **1996**, pp. 905 – 1006; c) R. Huisgen I. Ugi, *Angew. Chem.* **1956**, *68*, 705 – 706; d) R. Huisgen, I. Ugi, *Chem. Ber.* **1957**, *90*, 2914 – 2925; e) R. Huisgen, I. Ugi, *Chem. Ber.* **1958**, *91*, 531 – 537; f) I. Ugi, R. Huisgen, K. Clusius, M. Vecchi, *Angew. Chem.* **1956**, *68*, 753 – 754.
[39] R. N. Butler, A. Fox, S. Collier, L. A. Burke, *J. Chem. Soc. Perkin Trans. 2* **1998**, 2243 – 2247.
[40] a) J. D. Wallis, J. D. Dunitz, *J. Chem. Soc. Chem. Commun.* **1983**, 910 – 911; b) F. Biesemeier, U. Müller, W. Massa, *Z. Anorg. Allg. Chem.* **2002**, *628*, 1933 – 1934.
[41] R. Huisgen, *The Adventure Playground of Mechanisms and Novel Reactions*, American Chemical Society, Washington, **1994**, pp. 79 – 82.
[42] A. Gescher, M. F. Stevens, C. P. Turnbull, P. Colin, *J. Chem. Soc. Perkin Trans. 1* **1977**, 103 – 106.
[43] S. M. Capitosti, T. P. Hansen, M. L. Brown, *Org. Lett.* **2003**, *5*, 2865 – 2867.
[44] K. Knepper, M. E. P. Lormann, S. Bräse, *J. Comb. Chem.* **2004**, *6*, 460 – 463.
[45] a) F. Avemaria, V. Zimmermann, S. Bräse, *Synlett* **2004**, 1163 – 1166; b) M. E. P. Lormann, C. H. Walker, M. Es-Sayed, S. Bräse, *Chem. Commun.* **2002**, 1296 – 1297; c) S. Bräse, *Acc. Chem. Res.* **2004**, *37*, 804 – 815.
[46] a) K. A. H. Chehade, H. P. Spielmann, *J. Org. Chem.* **2000**, *65*, 4949 – 4953; b) D. R. Miller, D. C. Svenson, E. G. Gillan, *J. Am. Chem. Soc.* **2004**, *126*, 5372 – 5373.
[47] a) C. K. Lowe-Ma, R. A. Nissan, W. S. Wilson, *J. Org. Chem.* **1990**, *55*, 3755 – 3761; b) W. Stadlbauer, W. Fiala, M. Fischer, G. Hojas, *J. Heterocycl. Chem.* **2000**, *37*, 1253 – 1256.
[48] C. L. Gibson, S. La Rosa, C. J. Suckling, *Tetrahedron Lett.* **2003**, *44*, 1267 – 1270.
[49] a) T. P. Kogan, T. C. Somers, M. C. Venuti, *Tetrahedron* **1990**, *46*, 6623 – 6632; b) W. Zhu, D. Ma, *Chem. Commun.* **2004**, 888 – 889.
[50] a) P. A. S. Smith, C. D. Rowe, L. B. Bruner, *J. Org. Chem.* **1969**, *34*, 3430 – 3433; b) P. A. S. Smith, G. F. Budde, S.-S. P. Chou, *J. Org. Chem.* **1985**, *50*, 2062 – 2064.
[51] J. Gavenonis, T. D. Tilley, *Organometallics* **2002**, *21*, 5549 – 5563.
[52] W. Fisher, J.-P. Anselme, *J. Am. Chem. Soc.* **1967**, *89*, 5284 – 5285.
[53] Q. Liu, Y. Tor, *Org. Lett.* **2003**, *5*, 2571 – 2572.
[54] S. Maffei, A. M. Rivolta, *Gazz. Chim. Ital.* **1954**, *84*, 750 – 752.
[55] Y. H. Kim, K. Kim, S. B. Shim, *Tetrahedron Lett.* **1986**, *27*, 4749 – 4752.
[56] Y. I. T. Matsuya, K. Nagata, A. Ohsawa, *Tetrahedron* **1997**, *53*, 15701 – 15710.
[57] V. Pozsgay, H. Jennings, *Tetrahedron Lett.* **1987**, *28*, 5091 – 5092.
[58] a) H. Wamhoff, W. Wambach, *Chem.-Ztg.* **1989**, *113*, 11 – 15; b) O. Dimroth, *Ann.* **1909**, *364*, 183 – 226.
[59] L. Caglioti, F. Gasparrini, D. Misiti, G. Palmieri, *Synthesis* **1979**, 207 – 208.
[60] M. de Rosa, P. Haberfield, *J. Org. Chem.* **1981**, *46*, 2639 – 2643.

 © 2005 Wiley-VCH Verlag GmbH & Co. KGaA, Weinheim

[61] a) M. O. Forster, *J. Chem. Soc.* **1906**, 233; b) R. Kühein, H. Jensen, *Justus Liebigs Ann. Chem.* **1974**, 869.
[62] a) G. L'Abbé, A. Hassner, *Angew. Chem.* **1971**, *83*, 103 – 109; *Angew. Chem. Int. Ed. Engl.* **1971**, *10*, 98 – 104; b) G. L'Abbé, *Angew. Chem.* **1975**, *87*, 831 – 838; *Angew. Chem. Int. Ed. Engl.* **1975**, *14*, 775 – 782; c) T. L. Gilchrist, *Aldrichimica Acta* **2001**, *34*, 51 – 55; d) B. C. G. Soderberg, *Curr. Org. Chem.* **2000**, *4*, 727 – 764; e) K. Banert, *Liebigs Ann.* **1997**, 2005 – 2018.
[63] a) A. Hassner, L. A. Levy, *J. Am. Chem. Soc.* **1965**, *87*, 4203 – 4204; b) F. W. Fowler, A. Hassner, L. A. Levy, *J. Am. Chem. Soc.* **1967**, *89*, 2077 – 2082; c) A. Hassner, F. W. Fowler, *J. Org. Chem.* **1968**, *33*, 2686 – 2691; d) A. Hassner, F. P. Boerwinkle, A. B. Levy, *J. Am. Chem. Soc.* **1972**, *94*, 4879 – 4883.
[64] G. Smolinsky, *J. Org. Chem.* **1962**, *27*, 3557 – 3559.
[65] P. Molina, P. M. Fresneda, S. Delgado, *J. Org. Chem.* **2003**, *68*, 489 – 499.
[66] H. Hemetsberger, D. Knittel, *Monatsh. Chem.* **1972**, *103*, 194 – 204.
[67] C. R. Alonso-Cruz, A. R. Kennedy, M. S. Rodriguez, E. Suarez, *Org. Lett.* **2003**, *5*, 3729 – 3732.
[68] a) J.-C. Florent, C. Monneret, *J. Chem. Soc. Chem. Commun.* **1987**, 1171 – 1172; b) J. Wengel, J. Lau, E. B. Pedersen, C. M. Nielsen, *J. Org. Chem.* **1991**, *56*, 3591 – 3594; c) B. Liberek, A. Sikorski, A. Melcer, K. Konitz, *Carbohydr. Res.* **2003**, *338*, 795 – 799.
[69] F. Palacios, D. Aparicio, J. M. de los Santos, J. Perez de Heredia, G. Rubialas, *Org. Prep. Proced. Int.* **1995**, *27*, 171 – 178.
[70] A. Sjöholm Timén, E. Risberg, P. Somfai, *Tetrahedron Lett.* **2003**, *44*, 5339 – 5341.
[71] T. L. Gilchrist, R. Mendonca, *Synlett* **2000**, 1843 – 1845.
[72] T. M. V. D. Pinho e Melo, C. S. J. Lopes, A. L. Cardoso, A. M. d'A. Rocha Gonsalves, *Tetrahedron* **2001**, *57*, 6203 – 6208.
[73] K. Banert, F. Köhler, *Angew. Chem.* **2001**, *113*, 173 – 176; *Angew. Chem. Int. Ed.* **2001**, *40*, 174 – 177.
[74] B. E. Blass, K. R. Coburn, A. L. Faulkner, W. L. Seibela, A. Srivastava, *Tetrahedron Lett.* **2003**, *44*, 2153 – 2155.
[75] a) G. Righi, C. D'Achille, G. Pescatore, C. Bonini, *Tetrahedron Lett.* **2003**, *44*, 6999 – 7002; b) N. Halland, A. Braunton, S. Bachmann, M. Marigo, K. A. Jørgensen, *J. Am. Chem. Soc.* **2004**, *126*, 4790 – 4791; c) G. P. Miller, E. T. Kool, *J. Org. Chem.* **2004**, *69*, 2404 – 2410.
[76] W. Kurosawa, T. Kan, T. Fukuyama, *J. Am. Chem. Soc.* **2003**, *125*, 8112 – 8113.
[77] a) A. Avenoza, J. H. Busto, F. Corzana, J. I. Garcia, J. M. Peregrina, *J. Org. Chem.* **2003**, *68*, 4506 – 4513; b) I. A. Sayyed, A. Sudali, *Tetrahedron: Asymmetry* **2004**, *15*, 3111 – 3116.
[78] For a total synthesis of *rac*-sceptrin, see: P. S. Bara, A. L. Zografos, D. O'Malley, *J. Am. Chem. Soc.* **2004**, *126*, 3726 – 3727.
[79] a) K. S. Feldmann, A. G. Karatjas, *Org. Lett.* **2004**, *6*, 2849 – 2852; b) G. J. Sanjayan, A. Stewart, S. Hachisu, R. Gonzalez, M. P. Watterson, G. W. J. Fleet, *Tetrahedron Lett.* **2003**, *44*, 5847 – 5851.
[80] Ustiloxin D: H. Tanaka, A. M. Sawayama, T. J. Wandless, *J. Am. Chem. Soc.* **2003**, *125*, 6864 – 6865.
[81] C. Mazzini, L. Sambri, H. Regeling, B. Zwanenburg, G. J. F. Chittenden, *J. Chem. Soc. Perkin Trans. 1* **1997**, 3351 – 3356.
[82] O. N. Yuadina, A. A. Sherman, N. E. Nifantiev, *Carbohydr. Res.* **2001**, *332*, 363 – 371.
[83] M. Gibson, J. M. Goodman, L. J. Farrugia, R. C. Hartley, *Tetrahedron Lett.* **2003**, *44*, 2841 – 2844.
[84] C. Chiappe, D. Pieraccini, P. Saullo, *J. Org. Chem.* **2003**, *68*, 6710 – 6715.
[85] A. Loris, A. Perosa, M. Selva, P. Tundo, *J. Org. Chem.* **2003**, *68*, 4046 – 4051.
[86] For a microwave-assisted synthesis of alkyl azides, see: P. N. D. Singh, S. Muthukrishnan, R. S. Murthy, R. F. Klima, S. M. Mandel, M. Hawk, N. Yarbrough, A. D. Gudmundsdóttir, *Tetrahedron Lett.* **2003**, *44*, 9169 – 9171.
[87] a) L. He, H. S. Byun, R. Bittman, *J. Org. Chem.* **2000**, *65*, 7627 – 7633; b) L. Alvarez de Cienfuegos, C. Rodriguez, A. J. Mota, R. Robles, *Org. Lett.* **2003**, *5*, 2743 – 2745.
[88] D. Enders, D. Klein, *Synlett* **1999**, 719 – 720.
[89] L. E. Martínez, J. L. Leighton, D. H. Carsten, E. N. Jacobsen, *J. Am. Chem. Soc.* **1995**, *117*, 5897 – 5898.
[90] a) D. M. Hodgson, A. R. Gibbs, G. P. Lee, *Tetrahedron* **1996**, *52*, 14361 – 14384; b) A. C. Rondon, J. S. Panek, *Chemtracts* **1997**, *10*, 1058 – 1061; c) N. C. Gianneschi, P. A. Bertin, S. T. Nguyen, C. A. Mirkin, L. N. Zakharov, A. L. Rheingold, *J. Am. Chem. Soc.* **2003**, *125*, 10508 – 10509.
[91] B. M. L. Dioos, P. A. Jacobs, *Tetrahedron Lett.* **2003**, *44*, 4715 – 4717, and references therein.
[92] For immobilized variants, see: B. M. L. Dioos, P. A. Jacobs, *Tetrahedron Lett.* **2003**, *44*, 8815 – 8817.
[93] E. N. Jacobsen, *Acc. Chem. Res.* **2000**, *33*, 421 – 431.
[94] K. B. Hansen, J. L. Leighton, E. N. Jacobsen, *J. Am. Chem. Soc.* **1996**, *118*, 10924 – 10925.
[95] a) R. G. Konsler, J. Karl, E. N. Jacobsen, *J. Am. Chem. Soc.* **1998**, *120*, 10780 – 10781; b) J. M. Ready, E. N. Jacobsen, *J. Am. Chem. Soc.* **2001**, *123*, 2687 – 2688; c) J. M. Ready, E. N. Jacobsen, *Angew. Chem.* **2002**, *114*, 1432 – 1435; *Angew. Chem. Int. Ed.* **2002**, *41*, 1374 – 1377.
[96] J. H. Spelberg, J. E. T. van Hylckama Vlieg, L. Tang, D. B. Janssen, R. M. Kellog, *Org. Lett.* **2001**, *3*, 41 – 43.
[97] a) S. E. Sen, S. M. Smith, K. A. Sullivan, *Tetrahedron* **1999**, *55*, 12657 – 12698; b) J. Boruwa, J. C. Borah, B. Kalita, N. C. Barua, *Tetrahedron Lett.* **2004**, *45*, 7355 – 7358.
[98] a) M. Caron, P. R. Carlier, K. B. Sharpless, *J. Org. Chem.* **1988**, *53*, 5185 – 5187; b) X. Ginesta, M. Pastó, M. A. Pericàs, A. Riera, *Org. Lett.* **2003**, *5*, 3001 – 3004.
[99] C. E. Davis, J. L. Bailey, J. W. Lockner, R. M. Coates, *J. Org. Chem.* **2003**, *68*, 75 – 82.
[100] Review: X. E. Hu, *Tetrahedron* **2004**, *60*, 2701 – 2743.
[101] G. Sabitha, R. S. Babu, M. Rajkumar, J. S. Yadav, *Org. Lett.* **2002**, *4*, 343 – 345.
[102] A. Bisai, G. Pandey, M. K. Pandey, V. K. Singh, *Tetrahedron Lett.* **2003**, *44*, 5839 – 5841
[103] a) D. Lucet, T. Le Gall, C. Mioskowski, *Angew. Chem.* **1998**, *110*, 2724 – 2772; *Angew. Chem. Int. Ed.* **1998**, *37*, 2580 – 2627; b) M. Sasaki, A. Yudin, *J. Am. Chem. Soc.* **2003**, *125*, 14242 – 14243.
[104] K. J. Hale, M. M. Domostoj, D. A. Tocher, E. Irving, F. Scheinmann, *Org. Lett.* **2003**, *5*, 2927 – 2930.
[105] C. U. Kim, W. Lew, M. A. Williams, H. Liu, L. Zhang, S. Swaminathan, N. Bischofberger, M. S. Chen, D. B. Mendel, C. Y. Tai, W. G. Laver, R. C. Stevens, *J. Am. Chem. Soc.* **1997**, *119*, 681 – 690.
[106] H. Tsukamoto, Y. Kondo, *Tetrahedron Lett.* **2003**, *44*, 5247 – 5249.
[107] a) E. D. Soli, A. S. Manoso, M. C. Patterson, P. DeShong, *J. Org. Chem.* **1999**, *64*, 3171 – 3177; b) For an application, see: V. Y. Dudkin, D. Crich, *Tetrahedron Lett.* **2003**, *44*, 1787 – 1789.
[108] O. Mitsunobu, *Bull. Chem. Soc. Jpn.* **1967**, *40*, 4235 – 4238.
[109] D. L. Hughes, *Org. React.* **1992**, *42*, 335 – 656.
[110] H. Loibner, E. Zibral, *Helv. Chim. Acta* **1976**, *59*, 2100 – 2113.
[111] S.-H. Lee, J. Yoon, S.-H. Chung, Y.-S. Lee, *Tetrahedron* **2001**, *57*, 2139 – 2145.
[112] C. Simon, S. Hosztafi, S. Makleit, *Tetrahedron Lett.* **1993**, *34*, 6475 – 6478.
[113] Y. Yoshimura, K. Kitano, K. Yamada, H. Satoh, M. Watanabe, S. Miura, S. Sakata, T. Sasaki, A. Matsuda, *J. Org. Chem.* **1997**, *62*, 3140 – 3152.

 © 2005 Wiley-VCH Verlag GmbH & Co. KGaA, Weinheim

[114] a) M. E. Maier, C. Hermann, *Tetrahedron* **2000**, *56*, 557 – 561; b) T. Watanabe, Y. Tanaka, R. Shoda, R. Sakamoto, K. Kamikawa, M. Uemura, *J. Org. Chem.* **2004**, *69*, 4152 – 4158.
[115] J. A. Gómez-Vidal, R. B. Silverman, *Org. Lett.* **2001**, *3*, 2481 – 2484.
[116] a) Y. Lu, R. T. Taylor, *Tetrahedron Lett.* **2003**, *44*, 9267 – 9269; b) Y. Lu, R. T. Taylor, *Heterocycles* **2004**, *62*, 869 – 876.
[117] B. Jiang, C.-G. Yang, J. Wang, *J. Org. Chem.* **2002**, *67*, 1396 – 1398.
[118] a) S. Czernecki, S. Horms, J. M. Valery, *J. Org. Chem.* **1995**, *60*, 650 – 655; b) A. S. Thompson, G. R. Humphrey, A. M. DeMarco, D. J. Mathre, E. J. J. Grabowski, *J. Org. Chem.* **1993**, *58*, 5886 – 5888; c) S.-I. Murahashi, Y. Taniguchi, Y. Imada, Y. Tanigawa, *J. Org. Chem.* **1989**, *54*, 3292 – 3303; d) M. C. Viaud, P. Rollin, *Synthesis* **1990**, 130 – 133; e) M. Safi, R. Fahrang, D. Sinou, *Tetrahedron Lett.* **1990**, *31*, 527 – 530; f) B. M. Trost, S. R. Pulley, *Tetrahedron Lett.* **1995**, *36*, 8737 – 8740.
[119] M. Toyota, C. Komori, M. Ihara, *J. Org. Chem.* **2000**, *65*, 7110 – 7113.
[120] a) T. Shioiri, Y. Hamada, *Synlett* **2001**, 184 – 201; b) M. D. Fletcher, M. M. Campbell, *Chem. Rev.* **1998**, *98*, 763 – 795.
[121] S. Hanessian, F. Xie, *Tetrahedron Lett.* **1998**, *39*, 737 – 740.
[122] K. C. Nicolaou, N. Winssinger, D. Vourloumis, T. Ohshima, S. Kim, J. Pfefferkorn, J. Y. Xu, T. Li, *J. Am. Chem. Soc.* **1998**, *120*, 10814 – 10826.
[123] D. J. Guerin, T. E. Horstmann, S. J. Miller, *Org. Lett.* **1999**, *1*, 1107 – 1109.
[124] L.-W. Xu, X.-G. Xia, J.-W. Li, S.-L. Xhou, *Synlett* **2003**, 2246 – 2248.
[125] E. A. Couladouros, Z. F. Plyta, S. A. Haroutounian, V. P. Papageorgiou, *J. Org. Chem.* **1997**, *62*, 6 – 10.
[126] I. Adamo, F. Benedetti, F. Berti, G. Nardin, S. Norbedo, *Tetrahedron Lett.* **2003**, *44*, 9095 – 9097.
[127] T. Kawasaki, H. Enoki, K. Matsumura, M. Ohyama, M. Inagawa, M. Sakamoto, *Org. Lett.* **2000**, *2*, 3027 – 3029.
[128] For the use of cerium ammonium nitrate, see: V. Nair, L. Balagopal, R. Rojan, J. Mathew, *Acc. Chem. Res.* **2004**, *37*, 21 – 30, and references therein.
[129] P. Renaud, *Top. Curr. Chem.* **2000**, *208*, 81 – 112.
[130] a) A. Hassner, A. S. Amarasekara, *Tetrahedron Lett.* **1987**, *28*, 5185 – 5188; b) M. Tingoli, M. Tiecco, D. Chianelli, R. Balducci, A. Temperini, *J. Org. Chem.* **1991**, *56*, 6809 – 6813; c) Y. V. Mironov, A. A. Sherman, N. E. Nifantiev, *Tetrahedron Lett.* **2004**, *45*, 9107 – 9110; d) For the diazidation of olefins, see: W. E. Fristad, T. A. Brandvold, J. R. Peterson, S. R. Thompson, *J. Org. Chem.* **1985**, *50*, 3647 – 3649; e) B. B. Snider, J. R. Duvall, *Org. Lett.* **2004**, *6*, 1265 – 1268.
[131] T. M. Klapötke, B. Krumm, K. Polborn, *J. Am. Chem. Soc.* **2004**, *126*, 710 – 711.
[132] M. Tiecco, L. Testaferri, C. Santi, C. Tomassini, F. Marini, L. Bagnoli, A. Temperini, *Angew. Chem.* **2003**, *115*, 3239 – 3241; *Angew. Chem. Int. Ed.* **2003**, *42*, 3131 – 3133.
[133] S. Czernecki, E. Ayadi, D. Randriamandimby, *J. Org. Chem.* **1994**, *59*, 8256 – 8260.
[134] L. Chabaud, Y. Landais, *Tetrahedron Lett.* **2003**, *44*, 6995 – 6998.
[135] A. R. Bassindale, P. A. Kyle, M. Soobramanien, P. G. Taylor, *J. Chem. Soc. Perkin Trans. 1* **2000**, 1173 – 1180.
[136] C. Ollivier, P. Renaud, *J. Am. Chem. Soc.* **2001**, *123*, 4717 – 4727.
[137] a) P. Renaud, C. Ollivier, P. Panchaud, *Angew. Chem.* **2002**, *114*, 3610 – 3612; *Angew. Chem. Int. Ed.* **2002**, *41*, 3460 – 3462; b) P. Panchaud, C. Ollivier, P. Renaud, S. Zigmantas, *J. Org. Chem.* **2004**, *69*, 2755 – 2759.
[138] H. Monenschein, G. Sourkouni-Argirusi, K. M. Schubothe, T. O'Hare, A. Kirschning, *Org. Lett.* **1999**, *1*, 2101 – 2104.
[139] A. Kirschning, H. Monenschein, C. Schmeck, *Angew. Chem.* **1999**, *111*, 2720 – 2722; *Angew. Chem. Int. Ed.* **1999**, *38*, 2594 – 2596.
[140] A. Kirschning, M. Jesberger, H. Monenschein, *Tetrahedron Lett.* **1999**, *40*, 8999 – 9002.
[141] a) A. P. Marchand, V. D. Sorokin, S. D. Rajagopal, S. G. Bott, *Synth. Commun.* **1994**, *24*, 3141 – 3147, and references therein; b) B. G. Reddy, K. P. Madhusudanan, Y. D. Vankar, *J. Org. Chem.* **2004**, *69*, 2630 – 2633.
[142] C. Viuf, M. Bols, *Angew. Chem.* **2001**, *113*, 643 – 645; *Angew. Chem. Int. Ed.* **2001**, *40*, 623 – 625.
[143] M. Baruah, M. Bols, *Synlett* **2002**, 1111 – 1112.
[144] B. Patro, J. A. Murphy, *Org Lett.* **2000**, *2*, 3599 – 3601.
[145] V. V. Zhdankin, A. P. Krasutsky, C. J. Kuehl, A. J. Simonsen, J. K. Woodward, B. Mismash, J. T. Bolz, *J. Am. Chem. Soc.* **1996**, *118*, 5192 – 5197.
[146] a) C. J. Caveander, V. J. Shiner, *J. Org. Chem.* **1972**, *37*, 3567 – 3569; b) J. R. Zaloom, C. David, *J. Org. Chem.* **1981**, *46*, 5173 – 5176; c) P. E. Eaton, A. M. Fisher, R. E. Hormann, *Synlett* **1990**, 737 – 738.
[147] P. E. Eaton, R. E. Hormann, *J. Am. Chem. Soc.* **1987**, *109*, 1268 – 1269.
[148] P. B. Alper, S.-C. Hung, C.-H. Wong, *Tetrahedron Lett.* **1996**, *37*, 6029 – 6032.
[149] J. T. Lundquist, J. C. Pelletier, *Org. Lett.* **2001**, *3*, 781 – 783.
[150] W. S. Horne, C. S. Stout, M. R. Ghadiri, *J. Am. Chem. Soc.* **2003**, *125*, 9372 – 9376.
[151] Y. Ding, E. E. Swayze, S. A. Hofstadler, R. H. Griffey, *Tetrahedron Lett.* **2000**, *41*, 4049 – 4052.
[152] W. A. Greenberg, E. S. Priestley, P. S. Sears, P. B. Alper, C. Rosenbohm, M. Hendrix, S.-C. Hung, C.-H. Wong, *J. Am. Chem. Soc.* **1999**, *121*, 6527 – 6541.
[153] G. Shapiro, D. Büchler, *Tetrahedron Lett.* **1994**, *35*, 5421 – 5424.
[154] G. Shapiro, D. Büchler, C. Dalvit, P. Frey, M. del Carmen Fernandez, B. Gomez-Lor, E. Pombo-Villar, U. Stauss, R. Swoboda, C. Waridel, *Bioorg. Med. Chem.* **1997**, *5*, 147 – 156.
[155] D. Maclean, J. R. Schullek, M. M. Murphy, Z. J. Ni, E. M. Gordon, M. A. Gallop, *Proc. Natl. Acad. Sci. USA* **1997**, *94*, 2805 – 2810.
[156] V. Atlan, S. Racouchot, M. Rubin, C. Bremer, J. Ollivier, A. de Meijere, J. Salaün, *Tetrahedron: Asymmetry* **1998**, *9*, 1131 – 1135.
[157] A. Stolle, J. Ollivier, P. P. Piras, J. Salaün, A. de Meijere, *J. Am. Chem. Soc.* **1992**, *114*, 4051 – 4067.
[158] M. Gardiner, R. Grigg, M. Kordes, V. Sridharan, N. Vicker, *Tetrahedron* **2001**, *57*, 7729 – 7735.
[159] H. M. Chang, C. H. Cheng, *J. Chem. Soc. Perkin Trans. 1* **2000**, 3799 – 3807.
[160] a) S. Kamijo, Y. Yamamoto, *J. Am. Chem. Soc.* **2002**, *124*, 11940 – 11945; b) S. Kamijo, T. Jin, Y. Yamamoto, *J. Am. Chem. Soc.* **2001**, *123*, 9453 – 9454; c) S. Kamijo, T. Jin, Z. Huo, Y. Yamamoto, *J. Org. Chem.* **2002**, *67*, 2386 – 2393.
[161] K. Jayakanthan, K. P. Madhusudanan, Y. D. Vankar, *Tetrahedron* **2004**, *60*, 397 – 403.
[162] D. H. Drewry, S. W. Gerritz, J. A. Linn, *Tetrahedron Lett.* **1997**, *38*, 3377 – 3380.
[163] C. E. Lee, E. K. Kick, J. A. Ellman, *J. Am. Chem. Soc.* **1998**, *120*, 9735 – 9747.
[164] D. R. Tortolani, S. A. Biller, *Tetrahedron Lett.* **1996**, *37*, 5687 – 5690.
[165] C. Le Hetet, M. David, F. Carreaux, B. Carboni, A. Sauleau, *Tetrahedron Lett.* **1997**, *38*, 5153 – 5156.
[166] H. S. Oh, H. G. Hahn, S. H. Cheon, D. C. Ha, *Tetrahedron Lett.* **2000**, *41*, 5069 – 5072.
[167] D. A. Annis, O. Helluin, E. N. Jacobsen, *Angew. Chem.* **1998**, *110*, 2010 – 2012; *Angew. Chem. Int. Ed.* **1998**, *37*, 1907 – 1909.

 © 2005 Wiley-VCH Verlag GmbH & Co. KGaA, Weinheim

[168] A. Graven, M. Meldal, *J. Chem. Soc. Perkin Trans. 1* **2001**, 3198 – 3203.
[169] S.-J. Ryoo, J. Kim, J.-S. Kim, Y.-S. Lee, *J. Comb. Chem.* **2002**, *4*, 187 – 190.
[170] a) C. Bolm, I. Schiffers, I. Atodiresei, C. Hackenberger, *Tetrahedron: Asymmetry* **2003**, *14*, 3455 – 3467; b) C. Bolm, I. Schiffers, C. L. Dinter, L. Defrère, A. Gerlach, G. Raabe, *Synthesis* **2001**, 1719 – 1730; c) C. Bolm, C. L. Dinter, I. Schiffers, L. Defrère, *Synlett* **2001**, 1875 – 1877.
[171] B. P. Banddgar, S. S. Pandit, *Tetrahedron Lett.* **2002**, *43*, 3413 – 3414.
[172] A. Padwa, M. A. Brodney, B. Liu, K. Satake, T. Wu, *J. Org. Chem.* **1999**, *64*, 3595 – 3607.
[173] B. L. Kedrowski, *J. Org. Chem.* **2003**, *68*, 5403 – 5406.
[174] K. Kuramochi, Y. Osada, T. Kitahara, *Tetrahedron* **2003**, *59*, 9447 – 9454.
[175] K. Kuramochi, H. Watanabe, T. Kitahara, *Synlett* **2000**, 397 – 399.
[176] I. Stefanuti, S. A. Smith, R. J. K. Taylor, *Tetrahedron Lett.* **2000**, *41*, 3735 – 3738.
[177] a) Y. Wu, O. R. Seguil, J. K. De Brabander, *Org. Lett.* **2000**, *2*, 4241 – 4244; b) Y. Wu, X. Liao, R. Wang, X.-S. Xie, J. K. De Brabander, *J. Am. Chem. Soc.* **2002**, *124*, 3245 – 3253.
[178] A. Bhattacharjee, O. R. Seguil, J. K. De Brabander, *Tetrahedron Lett.* **2001**, *42*, 1217 – 1220.
[179] Y. Wu, L. Esser, J. K. De Brabander, *Angew. Chem.* **2000**, *112*, 4478 – 4480; *Angew. Chem. Int. Ed.* **2000**, *39*, 4308 – 4310.
[180] a) J. Lutz, H.-J. Musiol, L. Moroder in *Houben-Weyl Methods of Organic Chemistry. Synthesis of Peptides and Peptidomimetics*, vol. E22a (Ed.: M. Goodman, A. Felix, L. Moroder, C. Toniolo), Thieme, Stuttgart, **2001**, pp. 427 – 442; b) Y. S. Klausner, M. Bodanshky, *Synthesis* **1974**, 549 – 559; c) S.-Y. Han, Y.-A. Kim, *Tetrahedron* **2004**, *60*, 2447 – 2467.
[181] A. Calcagni, G. Lucente, G. Luisi, F. Pinnen, D. Rossi, E. Gavuzzo, *J. Chem. Soc. Perkin Trans. 1* **1997**, 2223 – 2227.
[182] D. S. Larsen, R. J. Lins, R. J. Stoodley, N. S. Trotter, *J. Chem. Soc. Perkin Trans. 1* **2001**, 2204 – 2212.
[183] H. Shao, M. Colucci, S. J. Tong, H. S. Zhang, A. L. Castelhano, *Tetrahedron Lett.* **1998**, *39*, 7235 – 7238.
[184] L. Marinescu, J. Thinggaard, I. B. Thomsen, M. Bols, *J. Org. Chem.* **2003**, *68*, 9453 – 9455.
[185] a) R. M. Pike, N. Sobinski, P. J. McManus, *J. Organomet. Chem.* **1983**, *253*, 183 – 216; b) C. Moberg, H. Adolfsson in *Organometallics: Compounds of Group 15 (As, Sb, Bi) and Silicon Compounds, Vol. 4* (Ed.: I. Fleming), Thieme, Stuttgart, **2002**, pp. 435 – 449.
[186] O. Tsuge, S. Urano, K. Oe, *J. Org. Chem.* **1980**, *45*, 5130 – 5136.
[187] W. C. Groutas, D. Felker, *Synthesis* **1980**, 861 – 868.
[188] N. Wiberg, S. K. Vasisht, H. Bayer, R. Meyers, *Chem. Ber.* **1979**, *112*, 2718 – 2729.
[189] L. A. Lazukina, V. P. Kukhar, *Zh. Obshch. Khim.* **1990**, *60*, 693 – 694.
[190] a) L. Birkofer, P. Wegner, *Org. Synth.* **1970**, *50*, 107 – 110; b) L. Birkofer, A. Ritter, P. Richter, *Chem. Ber.* **1963**, *96*, 2750 – 2756.
[191] O. Dimroth, G. Fester, *Ber. Dtsch. Chem. Ges.* **1910**, *43*, 2219 – 2223.
[192] L. Birkofer, P. Wegner, *Chem. Ber.* **1966**, *99*, 2512 – 2517.
[193] a) L. Birkofer, A. Ritter, S. M. Kim, *Chem. Ber.* **1963**, *96*, 3099 – 3100; b) L. Birkofer, S. M. Kim, *Chem. Ber.* **1964**, *97*, 2100 – 2101; c) H. Vogt, A. Fischer, P. G. Jones, *Z. Naturforsch. B* **1996**, *51*, 865 – 868.
[194] R. Appel, A. Hauss, *Chem. Ber.* **1960**, *93*, 405 – 411.
[195] a) L. Birkofer, F. Müller, W. Kaiser, *Tetrahedron Lett.* **1967**, *8*, 2781 – 2783; b) P. A. Evans, D. P. Modi, *J. Org. Chem.* **1995**, *60*, 6662 – 6663.
[196] A. Missio, C. Marchioro, T. Rossi, M. Panunzio, S. Selva, P. Seneci, *Biotechnol. Bioeng.* **2000**, *71*, 38 – 43.
[197] For information on the explosiveness of sulfonyl azides, see: a) H. Spencer, *Chem. Br.* **1981**, *17*, 106; b) D. Rewicki, C. Tuchscherer, *Angew. Chem.* **1972**, *84*, 31 – 32; *Angew. Chem. Int. Ed. Engl.* **1972**, *11*, 44 – 45.
[198] H. M. L. Davies, W. R. Cantrell, Jr., K. R. Romines, J. S. Baum, *Org. Synth.* **1992**, *70*, 93 – 100.
[199] a) Dodecylbenzenesulfonyl azide is the least sensitive compound in this series: R. G. Bistline, Jr., W. R. Noble, W. M. Linfield, *J. Am. Oil Chem. Soc.* **1974**, *51*, 126 – 132; b) for the preparation, see: G. G. Hazen, F. W. Bollinger, F. E. Roberts, W. K. Russ, J. J. Seman, S. Staskiewicz, *Org. Synth.* **1996**, *73*, 144 – 151.
[200] G. M. Green, N. P. Peet, W. A. Metz, *J. Org. Chem.* **2001**, *66*, 2509 – 2511.
[201] For a review, see: T. Ye, M. A. McKervey, *Chem. Rev.* **1994**, *94*, 1091 – 1160.
[202] For a recent example, see: C. C. Hughes, J. J. Kennedy-Smith, D. Trauner, *Org. Lett.* **2003**, *5*, 4113 – 4115.
[203] a) A. B. Charette, R. P. Wurz, T. Ollevier, *J. Org. Chem.* **2000**, *65*, 9252 – 9254; b) A. B. Charette, R. P. Wurz, T. Ollevier, *Helv. Chim. Acta* **2002**, *85*, 4468 – 4484; c) R. P. Wurz, W. Lin, A. B. Charette, *Tetrahedron Lett.* **2003**, *44*, 8845 – 8848, and references therein.
[204] N. A. Swain, R. C. D. Brown, G. Bruton, *Chem. Commun.* **2002**, 2042 – 2043.
[205] P. Panchaud, P. Renaud, *Adv. Synth. Catal.* **2004**, *346*, 925 – 928.
[206] P. Panchaud, L. Chabaud, Y. Landais, C. Ollivier, P. Renaud, S. Zigmantas, *Chem. Eur. J.* **2004**, *10*, 3606 – 3614.
[207] P. Panchaud, P. Renaud, *J. Org. Chem.* **2004**, *69*, 3205 – 3207.
[208] a) D. A. Evans, T. C. Britton, J. A. Ellman, R. L. Dorow, *J. Am. Chem. Soc.* **1990**, *112*, 4011 – 4030; b) For a review on amination, see: E. Erdik, *Tetrahedron* **2004**, *60*, 8747 – 8762.
[209] a) K. Dehnicke, *Angew. Chem.* **1979**, *91*, 527 – 534; *Angew. Chem. Int. Ed. Engl.* **1979**, *18*, 507 – 514; b) V. V. Zhdankin, P. J. Stang, *Chem. Rev.* **2002**, *102*, 2523 – 2584; c) T. Wirth, U. H. Hirt, *Synthesis* **1999**, 1271 – 1287; d) T. Muraki, H. Togo, M. Yokoyama, *Rev. Heteroat. Chem.* **1997**, *17*, 213 – 243; e) V. V. Zhdankin, *Rev. Heteroat. Chem.* **1997**, *17*, 133 – 151.
[210] O. Wolff, S. R. Waldvogel, *Synthesis* **2004**, 1303 – 1305.
[211] a) D. Landini, A. Maia, F. Montanari, *J. Am. Chem. Soc.* **1978**, *100*, 2796 – 2801; b) K. Banert, *Chem. Ber.* **1985**, *118*, 1564 – 1574; c) W. Kirmse, K. H. Kampmann, V. Zellmer, *Chem. Ber.* **1987**, *120*, 1301 – 1306; d) T. Ando, T. Kimura, H. Yamataka, *Adv. Chem. Ser.* **1987**, *215*, 103 – 114.
[212] A. J. Papa, *J. Org. Chem.* **1966**, *31*, 1426 – 1430.
[213] C. Li, T.-L. Shih, J. U. Jeong, A. Arasappan, P. L. Fuchs, *Tetrahedron Lett.* **1994**, *35*, 2645 – 2646.
[214] R. Huisgen, *Angew. Chem.* **1963**, *75*, 604 – 637; *Angew. Chem. Int. Ed. Engl.* **1963**, *2*, 565 – 598.
[215] R. Huisgen, R. Knorr, L. Möbius, G. Szeimies, *Chem. Ber.* **1965**, *98*, 4014 – 4021.
[216] a) V. Melai, A. Brillante, P. Zanirato, *J. Chem. Soc. Perkin Trans. 2* **1998**, 2447 – 2449; b) A. R. Katritzky, Y. Zhang, S. K. Singh, *Heterocycles* **2003**, *60*, 1225 – 1239; c) G. Molteni, A. Ponti, *Chem. Eur. J.* **2003**, *9*, 2770 – 2774; d) J. S. Tullis, J. C. VanRens, M. G. Natchus, M. P. Clark, B. De, L. C. Hsieh, M. J. Janusz, *Bioorg. Med. Chem. Lett.* **2003**, *13*, 1665 – 1668; e) A. Krasiński, V. V. Fokin, K. B. Sharpless, *Org. Lett.* **2004**, *6*, 1237 – 1240; f) R. S. Dahl, N. S. Finney, *J. Am. Chem. Soc.* **2004**, *126*, 8356 – 8357.
[217] For a review, see: a) C.-K. Sha, A. K. Mohanakrishnan in *Synthetic Application of 1,3-Dipolar Cycloaddition Chemistry toward Heterocycles and Natural Products* (Eds.: A. Padwa, W. H. Pearson), Wiley, New York, **2003**, pp. 623 – 679; b) R. Huisgen, R. Grashey, J. Sauer in *Chemistry of Alkenes* (Ed.: S. Patai), Wiley-Interscience, New York, **1964**, pp. 806 – 877.

 © 2005 Wiley-VCH Verlag GmbH & Co. KGaA, Weinheim

[218] N. J. Agard, J. A. Prescher, C. R. Bertozzi, *J. Am. Chem. Soc.* **2004**, *126*, 15046 – 15047, and references therein.
[219] a) K. Harju, M. Vahermo, I. Mutikainen, J. Yli-Kauhaluoma, *J. Comb. Chem.* **2003**, *5*, 826 – 833; b) F. Z. Dörwald (Nova Nordisk), WO 9740025 [*Chem. Abstr.* **1997**, *128*, 13278].
[220] A. R. Katritzky, S. K. Singh, *J. Org. Chem.* **2002**, *67*, 9077 – 9079.
[221] P. Schneider, J. H. Schomaker, S. Deming, W. J. Libbey, G. P. Nowack, *J. Am. Chem. Soc.* **1965**, *87*, 306 – 311.
[222] P. P. Nicholas, *J. Org. Chem.* **1975**, *40*, 3396 – 3398.
[223] R. Ducray, M. A. Ciufolini, *Angew. Chem.* **2002**, *114*, 4882 – 4885; *Angew. Chem. Int. Ed.* **2002**, *41*, 4688 – 4691.
[224] a) W. Peng, S. Zhu, *Tetrahedron* **2003**, *59*, 4395 – 4404, cit. lit; b) P. Zanirato, *J. Chem. Soc. Perkin Trans. 1* **2002**, 1420 – 1425.
[225] a) R. A. Wohl, *Helv. Chim. Acta* **1973**, *56*, 1826 – 1828; b) R. A. Wohl, *Tetrahedron Lett.* **1973**, *14*, 3111 – 3114; c) V. P. Semenov, T. D. Andreeva, K. A. Ogloblin, *Zh. Org. Khim.* **1988**, *24*, 217 – 220; d) V. P. Semenov, M. A. Mishin, K. A. Ogloblin, *Zh. Org. Khim.* **1988**, *24*, 2384 – 2388; e) V. P. Semenov, K. A. Ogloblin, *Zh. Org. Khim.* **1987**, *23*, 898 – 899; f) V. P. Semenov, K. A. Ogloblin, *Zh. Org. Khim.* **1988**, *24*, 2389 – 2397; g) Y. Xu, Y. Wang, S. Zhu, *Synthesis* **2000**, 513 – 516.
[226] H. Vogt, S. Bräse, unpublished results.
[227] a) L. Benati, D. Nanni, P. Spagnolo, *J. Chem. Soc. Perkin Trans. 1* **1997**, 457 – 461; b) L. Benati, G. Calestani, D. Nanni, P. Spagnolo, *J. Org. Chem.* **1998**, *63*, 4679 – 4684; c) L. Benati, D. Nanni, P. Spagnolo, *J. Org. Chem.* **1999**, *64*, 5132 – 5138.
[228] S. Zhu, G. Jin, Y. Xu, *Tetrahedron* **2003**, *59*, 4389 – 4394.
[229] D. S. Reddy, W. R. Judd, J. Aubé, *Org. Lett.* **2003**, *5*, 3899 – 3902.
[230] a) A. G. Schultz, W. G. McMahon, *J. Org. Chem.* **1984**, *49*, 1676 – 1678; b) A. G. Schultz, R. Ravichandran, *J. Org. Chem.* **1980**, *45*, 5008 – 5009; c) C.-K. Sha, S.-L. Ouyang, D.-Y. Hsieh, T.-H. Hseu, *J. Chem. Soc. Chem. Commun.* **1984**, 492 – 494; d) C.-K. Sha, S.-L. Ouyang, D.-Y. Hsieh, R.-C. Chang, S.-C. Chang, *J. Org. Chem.* **1986**, *51*, 1490 – 1494; e) L. Benati, G. Calestani, P. C. Montevecchi, P. Spagnolo, *J. Chem. Soc. Perkin Trans. 1* **1995**, 1381 – 1385; f) P. E. Hansen, K. Undheim, *J. Chem. Soc. Perkin Trans. 1* **1975**, 305 – 308; g) L. Benati, P. C. Montevecchi, P. Spagnolo, *J. Chem. Soc. Perkin Trans. 1* **1991**, 71 – 77; h) L. Benati, P. C. Montevecchi, P. Spagnolo, E. Foresti, *J. Chem. Soc. Perkin Trans. 1* **1992**, 2845 – 2850; i) G. A. Molander, C. T. Bibeau, *Tetrahedron Lett.* **2002**, *43*, 5385 – 5388.
[231] For a Review on the chemistry of the triazenes, see: D. B. Kimball, M. M. Haley, *Angew. Chem.* **2002**, *114*, 3484 – 3498; *Angew. Chem. Int. Ed.* **2002**, *41*, 3338 – 3351.
[232] R. Huisgen, R. Knorr, *Naturwissenschaften* **1962**, *48*, 716.
[233] T. Kitamura, M. Todaka, I. Shin-machi, Y. Fujiwara, *Heterocycl. Commun.* **1998**, *4*, 205 – 208.
[234] S. Businelli, E. Di Martino, P. Zanirato, *ARKIVOC* **2001**, *2*, 1027 – 1035.
[235] a) S. Freeze, P. Norris, *Heterocycles* **1999**, *51*, 1807 – 1817; b) M. Moore, P. Norris, *Tetrahedron Lett.* **1998**, *39*, 7027 – 7030.
[236] a) F. Zaragoza, S. V. Petersen, *Tetrahedron* **1996**, *52*, 10823 – 10826; b) M. W. Wilson, A. S. Hernández, A. P. Calvet, J. C. Hodges, *Mol. Diversity* **1998**, *3*, 95 – 112; c) K. Hojo, M. Maeda, S. Iguchi, T. Smith, H. Okamoto, K. Kawasaki, *Chem. Pharm. Bull.* **2000**, *48*, 1740 – 1744.
[237] N. Gouault, J.-F. Cupif, A. Sauleau, M. David, *Tetrahedron Lett.* **2000**, *41*, 7293 – 7297.
[238] a) B. E. Blass, K. R. Coburn, A. L. Faulkner, C. L. Hunn, M. G. Natchus, M. S. Parker, D. E. Portlock, J. S. Tullis, R. Wood, *Tetrahedron Lett.* **2002**, *43*, 4059 – 4061; b) L. Garanti, G. Molteni, *Tetrahedron Lett.* **2003**, *44*, 1133 – 1135
[239] For intramolecular dipolar cycloadditions, see: I. N. N. Namboothiri, A. Hassner, *Top. Curr. Chem.* **2001**, *216*, 1 – 49.
[240] S. Röper, M. H. Franz, R. Wartchow, H. M. R. Hoffmann, *Org. Lett.* **2003**, *5*, 2773 – 2776.
[241] C. W. Tornoe, C. Christensen, M. Meldal, *J. Org. Chem.* **2002**, *67*, 3057 – 3064.
[242] V. V. Rostovtsev, L. G. Freen, V. V. Fokin, K. B. Sharpless, *Angew. Chem.* **2002**, *114*, 2708 – 2711; *Angew. Chem. Int. Ed.* **2002**, *41*, 2596 – 2599.
[243] a) Q. Wang, T. Chan, R. Hilgraf, V. V. Fokin, K. B. Sharpless, M. G. Finn, *J. Am. Chem. Soc.* **2003**, *125*, 3192 – 3193; b) dendrimer synthesis: P. Wu, A. K. Feldman, A. K. Nugent, C. J. Hawker, A. Scheel, B. Voit, J. Pyun, J. M. J. Fréchet, K. N. Sharpless, V. V. Vokin, *Angew. Chem.* **2004**, *116*, 4018 – 4022; *Angew. Chem. Int. Ed.* **2004**, *43*, 3928 – 3932; c) dendronized linear polymers: B. Helms, J. L. Mynar, C. J. Hawker, J. M. J. Fréchet, *J. Am. Chem. Soc.* **2004**, *126*, 15020 – 15021; d) fluorophosphorus synthesis: Z. Zhou, C. J. Fahrni, *J. Am. Chem. Soc.* **2004**, *126*, 8862 – 8863; e) D. B. Ramachary, C. F. Barbas III, *Chem. Eur. J.* **2004**, *10*, 5323 – 5331.
[244] For applications, see: a) F. Fazio, M. C. Bryan, O. Blixt, J. C. Paulson, C.-H. Wong, *J. Am. Chem. Soc.* **2002**, *124*, 14397 – 14402; b) A. Dondoni, P. P. Giovannini, A. Massi, *Org. Lett.* **2004**, *6*, 2929 – 2932.
[245] L. V. Lee, M. L. Mitchell, S.-J. Huang, V. V. Fokin, K. B. Sharpless, C.-H. Wong, *J. Am. Chem. Soc.* **2003**, *125*, 9588 – 9589.
[246] A. E. Speers, G. C. Adam, B. F. Cravatt, *J. Am. Chem. Soc.* **2003**, *125*, 4686 – 4687.
[247] F. Pérez-Balderas, M. Ortega-Muñoz, J. Morales-Sanfrutos, F. Hernández-Mateo, F. G. Calvo-Flores, J. A. Calvo-Asín, J. Isac-García, F. Santoyo-González, *Org. Lett.* **2003**, *5*, 1951 – 1954.
[248] For examples, see: a) K. D. Bodine, D. Y. Gin, M. S. Gin, *J. Am. Chem. Soc.* **2004**, *126*, 1638 – 1639; b) for new catalysts, see: W. G. Lewis, F. G. Magallon, V. V. Fokin, M. G. Finn, *J. Am. Chem. Soc.* **2004**, *126*, 9152 – 9153; c) T. R. Chan, R. Hilgraf, K. B. Sharpless, V. V. Fokin, *Org. Lett.* **2004**, *6*, 2853 – 2855; d) B. Khanetskyy, D. Dallinger, C. O. Kappe, *J. Comb. Chem.* **2004**, *6*, 884 – 892.
[249] For a Review of click chemistry, see: H. C. Kolb, M. G. Finn, K. B. Sharpless, *Angew. Chem.* **2001**, *113*, 2056 – 2075; *Angew. Chem. Int. Ed.* **2001**, *40*, 2004 – 2021.
[250] For reviews, see: a) R. Breinbauer, M. Köhn, *ChemBioChem* **2003**, *4*, 1147 – 1149; b) R. Breinbauer, M. Köhn, *Angew. Chem.* **2004**, *116*, 3168 – 3178; *Angew. Chem. Int. Ed.* **2004**, *43*, 3106 – 3116.
[251] a) W. G. Lewis, L. G. Green, F. Grynszpan, Z. Radić, P. R. Carlier, P. Taylor, M. G. Finn, K. B. Sharpless, *Angew. Chem.* **2002**, *114*, 1095 – 1098; *Angew. Chem. Int. Ed.* **2002**, *41*, 1053 – 1057; b) F. Tian, M.-L. Tsao, P. G. Schultz, *J. Am. Chem. Soc.* **2004**, *126*, 15962 – 15963.
[252] a) A. J. Link, D. A. Tirrell, *J. Am. Chem. Soc.* **2003**, *125*, 11164 – 11165; b) A. J. Link, M. K. S. Vink, D. A. Tirrell, *J. Am. Chem. Soc.* **2003**, *125*, 11164 – 11165;
[253] S. Loeber, P. Rodriguez-Loaiza, P. Gmeiner, *Org. Lett.* **2003**, *5*, 1753 – 1755.
[254] S. Kamijo, T. Jin, Z. Huo, Y. Yamamoto, *J. Am. Chem. Soc.* **2003**, *125*, 7786 – 7787.
[255] K. Banert, M. Hagedorn, *Angew. Chem.* **1989**, *101*, 1710 – 1711; *Angew. Chem. Int. Ed. Engl.* **1989**, *28*, 1675 – 1676.
[256] F. R. Benson in *Heterocyclic Compounds*, *Vol. 8* (Ed.: R. C. Elderfield), Wiley, New York, **1966**.
[257] R. N. Butler in *Comprehensive Heterocyclic Chemistry II*, *Vol. 4* (Ed.: R. C. Storr), Pergamon, Oxford, **1996**, pp. 621 – 678, 905 – 1006.
[258] a) For a review, see: R. J. Herr, *Bioorg. Med. Chem.* **2002**, *10*, 3379 – 3393; b) A. J. A. Cobb, D. A. Longbottom, D. M. Shaw, S. V. Ley, *Chem. Commun.* **2004**, 1808 – 1809.
[259] a) K.-L. Yu, R. L. Johnson, *J. Org. Chem.* **1987**, *52*, 1051 – 1056; b) J. Zabrocki, G. D. Smith, J. B. Dunbar, Jr., H. Iijima, G. R.

 © 2005 Wiley-VCH Verlag GmbH & Co. KGaA, Weinheim

Marshall, *J. Am. Chem. Soc.* **1988**, *110*, 5875 – 5880; c) P. A. Bartlett, F. Acher, *Bull. Soc. Chim. Fr.* **1986**, 771 – 775.
[260] a) R. D. Smith, C. S. Sweet, A. Goldberg, P. B. M. W. M. Timmermans, *Drugs Today* **1996**, *32*, 1 – 42; b) K. Dickstein, P. B. M. W. M. Timmermans, R. Segal, *Expert Opin. Invest. Drugs* **1998**, *7*, 1897 – 1914.
[261] a) V. A. Ostrovskii, M. S. Pevzner, T. P. Kofmna, M. B. Shcherbinin, I. V. Tselinskii, *Targets Heterocycl. Syst.* **1999**, *3*, 467 – 526; b) M. Hiskey, D. E. Chavez, D. L. Naud, S. F. Son, H. L. Berghout, C. A. Bome, *Proc. Int. Pyrotech. Semin.* **2000**, *27*, 3 – 14; c) G. I. Koldobskii, V. A. Ostrovskii, *Usp. Khim.* **1994**, *63*, 847 – 865.
[262] R. G. Smith, K. Cheng, W. R. Schoen, S. S. Pong, G. Hickey, T. Jacks, B. Butler, W. W.-S. Chan, L. Y.-P. Chaung, F. Judith, J. Taylor, M. J. Wyvratt, M. H. Fisher, *Science* **1993**, *260*, 1640 – 1643.
[263] G. B. Green, J. H. Toney, J. W. Kozarich, S. K. Grant, *Arch. Biochem. Biophys.* **2000**, *375*, 355 – 358.
[264] a) J. H. Toney, P. M. D. Fitzgerald, N. Grover-Sharma, S. H. Olson, W. J. May, J. G. Sundelof, D. E. Vanderwall, K. A. Cleary, S. K. Grant, J. K. Wu, J. W. Kozarich, L. Pompliano, G. G. Hammond, *Chem. Biol.* **1998**, *5*, 185 – 196; b) J. H. Toney, K. A. Cleary, G. G. Hammond, X. Yuan, W. J. May, S. M. Hutchins, W. T. Ashton, D. E. Vanderwall, *Bioorg. Med. Chem. Lett.* **1999**, *9*, 2741 – 2746.
[265] P. Christophersen, B. H. Dahl (Neurosearch, DK), WO Patent 002470,7, **2000** [*Chem. Abstr.* **2000**, *132*, 308142].
[266] R. Huisgen, *J. Org. Chem.* **1968**, *33*, 2291 – 2297.
[267] W. R. Carpenter, *J. Org. Chem.* **1962**, *27*, 2085 – 2088.
[268] P. A. S. Smith, J. M. Clegg, J. H. Hall, *J. Org. Chem.* **1958**, *23*, 524 – 529.
[269] a) H. Quast, L. Bieber, *Tetrahedron Lett.* **1976**, *17*, 1485 – 1488; b) M. M. Krayushkin, A. M. Beskopyl'nyi, S. G. Zlotin, O. A. Luk'yanov, V. M. Zhulin, *Izv. Akad. Nauk SSSR Ser. Khim.* **1980**, *11*, 2668; c) A. S. Katner (Lilly, USA), US Patent 3,962,272, **1974** [*Chem. Abstr.* **1976**, *85*, 123929]; e) Z. P. Demko, K. B. Sharpless, *Angew. Chem.* **2002**, *114*, 2214 – 2217; *Angew. Chem. Int. Ed.* **2002**, *41*, 2110 – 2113; d) Z. P. Demko, K. B. Sharpless, *Angew. Chem.* **2002**, *114*, 2217 – 2220; *Angew. Chem. Int. Ed.* **2002**, *41*, 2113 – 2116.
[270] a) *The Chemistry of the Cyano Group* (Ed.: Z. Rappoport), Interscience, London, **1970**, p. 351; b) Z. Foldi, W. Kereszty (Gyogyszer), US Patent 2,020,937, **1935** [*Chem. Abstr.* **1935**, *30*, 4174]; c) R. Fusco, L. Garanti, G. Zecchi, *J. Org. Chem.* **1975**, *40*, 1906 – 1909; d) L. Garanti, G. Zecchi, *J. Org. Chem.* **1980**, *45*, 4767 – 4769; e) B. Davis, T. W. Brandstetter, C. Smith, L. Hackett, B. G. Winchester, G. W. J. Fleet, *Tetrahedron Lett.* **1995**, *36*, 7507 – 7510; f) T. C. Porter, R. K. Smalley, M. Teguiche, B. Purwono, *Synthesis* **1997**, 773 – 777.
[271] Z. P. Demko, K. B. Sharpless, *Org. Lett.* **2001**, *3*, 4091 – 4094.
[272] F. Himo, Z. P. Demko, L. Noodleman, *J. Org. Chem.* **2003**, *68*, 9076 – 9080.
[273] a) T. W. Brandstetter, B. Davis, D. Hyett, C. Smith, L. Hackett, B. G. Winchester, G. W. J. Fleet, *Tetrahedron Lett.* **1995**, *36*, 7511 – 7514; b) B. G. Davis, R. J. Nash, A. A. Watson, C. Smith, G. W. J. Fleet, *Tetrahedron Lett.* **1999**, *40*, 4501 – 4520; c) B. G. Davis, A. Hull, C. Smith, R. J. Nash, A. A. Watson, D. A. Winkler, R. C. Griffiths, G. W. J. Fleet, *Tetrahedron: Asymmetry* **1998**, *9*, 2947 – 2960; d) B. G. Davis, T. W. Brandstetter, L. Hackett, B. G. Winchester, R. J. Nash, A. A. Watson, R. C. Griffiths, C. Smith, G. W. J. Fleet, *Tetrahedron* **1999**, *55*, 4489 – 4500.
[274] a) J. S. Mihina, R. M. Herbst, *J. Org. Chem.* **1950**, *15*, 1082 – 1092; b) W. G. Finnegan, R. A. Henry, R. Lofquist, *J. Am. Chem. Soc.* **1958**, *80*, 3908 – 3911; c) V. E. Wiberg, H. Michaud, *Z. Naturforsch. B* **1954**, *9*, 496 – 497; d) J. V. Dunica, M. E. Pierce, J. B. Santella III, *J. Org. Chem.* **1991**, *56*, 2395 – 2400; e) S. J. Wittenberger, *Org. Prep. Proced. Int.* **1994**, *26*, 499 – 531.
[275] A. Hantzsch, A. Vagt, *Ann.* **1901**, 314 – 339.
[276] M. Alterman, A. Hallberg, *J. Org. Chem.* **2000**, *65*, 7984 – 7989.
[277] F. Himo, Z. P. Demko, L. Noodleman, K. B. Sharpless, *J. Am. Chem. Soc.* **2003**, *125*, 9983 – 9987.
[278] Z. P. Demko, K. B. Sharpless, *J. Org. Chem.* **2001**, *66*, 7945 – 7950.
[279] Z. P. Demko, K. B. Sharpless, *Org. Lett.* **2002**, *4*, 2525 – 2527.
[280] a) S. J. Wittenberger, B. G. Donner, *J. Org. Chem.* **1993**, *58*, 4139 – 4141; b) F. A. J. Kerdesky, A. Haight, B. A. Narayanan, C. W. Nordeen, D. Scarpetti, L. S. Seif, S. J. Wittenberger, H. E. Morton, *Synth. Commun.* **1993**, *23*, 2027 – 2039; c) D. Amantini, R. Beleggia, F. Fringuelli, F. Pizzo, L. Vaccaro, *J. Org. Chem.* **2004**, *69*, 2896 – 2898.
[281] J. W. Lampe, C. K. Biggers, J. M. Defauw, R. J. Foglesong, S. E. Hall, J. M. Heerding, S. P. Hollinshead, H. Hu, P. F. Hughes, G. E. Jagdmann, Jr., M. G. Johnson, Y.-S. Lai, C. T. Lowden, M. P. Lynch, J. S. Mendoza, M. M. Murphy, J. W. Wilson, L. M. Ballas, K. Carter, J. W. Darges, J. E. Davis, F. R. Hubbard, M. L. Stamper, *J. Med. Chem.* **2002**, *45*, 2624 – 2643.
[282] a) O. Kivrakidou, S. Bräse, F. Hülshorst, N. Griebenow, *Org. Lett.* **2004**, *6*, 1143 – 1146; b) for the synthesis of 5-aminiotetrazoles from azides, see: A. R. Katritzky, B. V. Rogovoy, K. V. Kovalenko, *J. Org. Chem.* **2003**, *68*, 4941 – 4943; c) for further solid-phase syntheses, see: Y. Yu, J. M. Ostresh, R. A. Houghten, *Tetrahedron Lett.* **2004**, *45*, 7787 – 7789.
[283] W. H. Pearson, W.-k. Fang, J. W. Kampf, *J. Org. Chem.* **1994**, *59*, 2682 – 2684.
[284] P. Desai, J. Aubé, *Org. Lett.* **2000**, *2*, 1657 – 1659.
[285] F. Tiemann, *Ber. Dtsch. Chem. Ges.* **1891**, *24*, 4162 – 4167.
[286] a) N. P. Gritsan, E. A. Pritchina, *Russ. Chem. Rev.* **1992**, *61*, 500 – 516; b) M. F. Budyka, M. M. Kantor, M. V. Alfimov, *Russ. Chem. Rev.* **1992**, *61*, 25 – 39.
[287] G. Bucher in *CRC Handbook of Organic Photochemistry and Photobiology* (Eds.: W. Horspool, F. Lenci), 2nd ed., CRC, Boca Raton, **2004**, pp. 44/1 – 44/31.
[288] N. P. Gritsan, I. Likhotvorik, Z. Zhu, M. S. Platz, *J. Phys. Chem. A* **2001**, *105*, 3039 – 3041.
[289] For the photolysis of diazides, see: R. S. Kalgutkar, P. M. Lahti, *J. Am. Chem. Soc.* **1997**, *119*, 4771 – 4772.
[290] Z. Li, R. W. Quan, E. N. Jacobsen, *J. Am. Chem. Soc.* **1995**, *117*, 5889 – 5890.
[291] For a Review, see: W. Lwowski, *Angew. Chem.* **1967**, *79*, 922 – 931; *Angew. Chem. Int. Ed. Engl.* **1967**, *6*, 897 – 906.
[292] Theoretical consideration: X. Lu, F. Tian, X. Xu, N. Wang, Q. Zhang, *J. Am. Chem. Soc.* **2003**, *125*, 10459 – 10464.
[293] M. Holzinger, J. Abraham, P. Whelan, R. Graupner, L. Ley, F. Hennrich, M. Kappes, A. Hirsch, *J. Am. Chem. Soc.* **2003**, *125*, 8566 – 8580.
[294] J. Averdung, J. Mattay, D. Jacobi, W. Abraham, *Tetrahedron* **1995**, *51*, 2543 – 2552.
[295] K. R. Henery-Logan, R. A. Clark, *Tetrahedron Lett.* **1968**, *9*, 801 – 806.
[296] For reviews on this class of compounds, see: a) F. Palacios, A. M. Ochoa de Retana, E. Martínez de Marigorta, J. Manuel - de los Santos, *Eur. J. Org. Chem.* **2001**, 2401 – 2414; b) H. Heimgartner, *Angew. Chem.* **1991**, *103*, 271 – 297; *Angew. Chem. Int. Ed. Engl.* **1991**, *30*, 238 – 264; c) K. L. M. Rai, A. Hassner, *Adv. Strained Interesting Org. Mol.* **2000**, *8*, 187 – 257; d) F. Palacios, A. M. Ochoa de Retana, E. Martínez de Marigorta, J. Manuel de los Santos, *Org. Prep. Proced. Int.* **2002**, *34*, 219 – 269.
[297] For the microwave-assisted decomposition of alkenyl azides, see: N. D. P. Singh, C. L. Carter, A. D. Gudmundsdóttir, *Tetrahedron Lett.* **2003**, *44*, 6763 – 6765.

 © 2005 Wiley-VCH Verlag GmbH & Co. KGaA, Weinheim

[298] A. Hassner, N. H. Wiegand, H. E. Gottlieb, *J. Org. Chem.* **1986**, *51*, 3176 – 3180.
[299] B. A. Belinka, A. Hassner, J. M. Hendler, *J. Org. Chem.* **1981**, *46*, 631 – 632.
[300] K. Banert, F. Köhler, B. Meier, *Tetrahedron Lett.* **2003**, *44*, 3781 – 3783.
[301] Y. S. P. Álvarez, M. J. Alves, N. Z. Azoia, J. F. Bickley, T. L. Gilchrist, *J. Chem. Soc. Perkin Trans. 1* **2002**, 1911 – 1919.
[302] A. S. Timen, P. Somfai, *J. Org. Chem.* **2003**, *68*, 9958 – 9963.
[303] a) V. V. Rozhkov, A. M. Kuvshinov, S. A. Shevelev, *Org. Prep. Proced. Int.* **2000**, *32*, 94 – 96; b) V. V. Rozhkov, A. M. Kuvshinov, V. I. Gulevskaya, I. I. Chervin, S. A. Shevelev, *Synthesis* **1999**, 2065 – 2070.
[304] B. J. Clark, R. J. Grayshan, *J. Chem. Res. Miniprint* **1981**, 3786 – 3795.
[305] a) E. Noelting, O. Kohn, *Chem.-Ztg.* **1894**, *18*, 1095; b) P. A. S. Smith, J. H. Boyer, *Org. Synth.* **1951**, *31*, 14 – 16.
[306] a) M. Chaykovsky, H. G. Adolph, *J. Heterocycl. Chem.* **1991**, *28*, 1491 – 1495; b) G. Rauhut, F. Eckert, *J. Phys. Chem. A* **1999**, *103*, 9086 – 9092; c) M. R. Kamal, M. M. El-Abadelah, A. A. Mohammad, *Heterocycles* **1999**, *50*, 819 – 832.
[307] R. K. Smalley, *Sci. Synth.* **2002**, *11*, 337 – 382.
[308] L. K. Dyall, G. J. Karpa, *Aust. J. Chem.* **1988**, *41*, 1231 – 1241.
[309] a) A. Schaarschmidt, *Ber. Dtsch. Chem. Ges.* **1916**, *49*, 1635 – 1636; b) S. L. Klimenko, E. A. Pritchina, N. P. Gritsan, *Chem. Eur. J.* **2003**, *9*, 1639 – 1644.
[310] L. K. Dyall, J. A. Ferguson, T. B. Jarman, *Aust. J. Chem.* **1996**, *49*, 1197 – 1202.
[311] P. Molina, A. Tárraga, J. L. López, J. C. Martinez, *J. Organomet. Chem.* **1999**, *584*, 147 – 158.
[312] N. S. Wilson, C. R. Sarko, G. P. Roth, *Tetrahedron Lett.* **2002**, *43*, 581 – 583.
[313] a) P. B. Ghosh, M. W. Whitehouse, *J. Med. Chem.* **1968**, *11*, 305 – 311; b) H. Cerecetto, R. Di Maio, M. Gonzalez, M. Risso, P. Saenz, G. Seoane, A. Denicola, G. Peluffo, C. Quijano, C. Olea-Azar, *J. Med. Chem.* **1999**, *42*, 1941 – 1950.
[314] G. Timári, T. Soós, G. Hajós, A. Messmer, J. Nacsa, J. Molnár, *Bioorg. Med. Chem. Lett.* **1996**, *6*, 2831 – 2836.
[315] S. C. Bergmeier, D. M. Stanchina, *J. Org. Chem.* **1999**, *64*, 2852 – 2859.
[316] T. Hudlicky, J. O. Frazier, G. Seoane, M. Tiedje, A. Seoane, L. W. Kwart, C. Beal, *J. Am. Chem. Soc.* **1986**, *108*, 3755 – 3762.
[317] Y. Naruta, N. Nagai, K. Maruyama, *J. Chem. Soc. Perkin Trans. 1* **1988**, 1143 – 1148.
[318] a) A. Nakagawa, Y. Iwai, H. Hashimoto, N. Miyazaki, R. Oiwa, Y. Takahashi, A. Hirano, N. Shibukawa, Y. Kojima, S. Ōmura, *J. Antibiot.* **1981**, *34*, 1408 – 1415; b) S. Ōmura, A. Nakagawa, H. Hashimoto, R. Oiwa, Y. Iwai, A. Hirano, N. Shibukawa, Y. Kojima, *J. Antibiot.* **1980**, *33*, 1395 – 1396.
[319] a) S. Ōmura, A. Nakagawa, *Tetrahedron Lett.* **1981**, *22*, 2199 – 2202; b) Y. Morimoto, F. Matsuda, H. Shirahama, *Tetrahedron Lett.* **1990**, *31*, 6031 – 6034; c) Y. Morimoto, H. Shirahama, *Tetrahedron* **1996**, *52*, 10631 – 10652; d) Y. Morimoto, F. Matsuda, H. Shirahama, *Tetrahedron* **1996**, *52*, 10609 – 10630; e) Y. Morimoto, F. Matsuda, H. Shirahama, *Synlett* **1991**, 201 – 203.
[320] M.-L. Tsao, N. Gritsan, T. R. James, M. S. Platz, D. A. Hrovat, W. T. Borden, *J. Am. Chem. Soc.* **2003**, *125*, 9343 – 9358.
[321] K. Isomura, S. Kobayashi, H. Taniguchi, *Tetrahedron Lett.* **1968**, *9*, 3499 – 3502.
[322] a) H. Hemetsberger, D. Knittel, H. Weidmann, *Monatsh. Chem.* **1970**, *101*, 161 – 165; b) H. Hemetsberger, D. Knittel, H. Weidmann, *Monatsh. Chem.* **1969**, *100*, 1599 – 1603.
[323] A. R. MacKenzie, C. J. Moody, C. W. Rees, *J. Chem. Soc. Chem. Commun.* **1983**, *22*, 1372 – 1373.
[324] For recent examples, see: a) I. Borza, S. Kolok, A. Gere, E. Agai-Csongor, B. Agai, G. Tarkanyi, C. Horvath, G. Barta-Szalai, E. Bozo, C. Kiss, A. Bielik, J. Nagy, S. Farkas, G. Domany, *Bioorg. Med. Chem. Lett.* **2003**, *13*, 3859 – 3861; b) F. Hong, J. Zaidi, B. Cusack, E. Richelson, *Bioorg. Med. Chem. Lett.* **2002**, *12*, 3849 – 3858; c) K. L. Milkiewicz, D. J. Parks, T. Lu, *Tetrahedron Lett.* **2003**, *44*, 4257 – 4260.
[325] F. A. F. da Rosa, R. A. Rebelo, M. G. Nascimento, *J. Braz. Chem. Soc.* **2003**, *14*, 11 – 15.
[326] a) T. Martin, C. J. Moody, *J. Chem. Soc. Chem. Commun.* **1985**, 1391 – 1392; b) T. Martin, C. J. Moody, *J. Chem. Soc. Perkin Trans. 1* **1988**, 241 – 246.
[327] E. V. Sadanandan, S. K. Pillai, M. V. Lakshmikantham, A. D. Billimoria, J. S. Culpepper, M. P. Cava, *J. Org. Chem.* **1995**, *60*, 1800 – 1805.
[328] a) D. L. Boger, R. S. Coleman, *J. Am. Chem. Soc.* **1987**, *109*, 2717 – 2727; b) R. E. Bolton, C. J. Moody, C. W. Rees, G. Tojo, *J. Chem. Soc. Perkin Trans. 1* **1987**, 931 – 936.
[329] D. Knittel, *Synthesis* **1985**, 186 – 188.
[330] H. Hemetsberger, I. Spira, W. Schoenfelder, *J. Chem. Res. Synop.* **1977**, 247.
[331] R. J. Sundberg, H. F. Russell, W. V. Ligon, Jr., L.-S. Lin, *J. Org. Chem.* **1972**, *37*, 719 – 724.
[332] P. A. S. Smith, C. D. Rowe, D. W. Hansen, *Tetrahedron Lett.* **1983**, *24*, 5169 – 5172.
[333] A. Tárraga, P. Molina, J. L. López, M. D. Velasco, D. Bautista, P. G. Jones, *Organometallics* **2002**, *21*, 2055 – 2065.
[334] S. Kar, S. Lahiri, *J. Indian Chem. Soc.* **1999**, *76*, 607 – 610.
[335] E. T. Pelkey, G. W. Gribble, *Tetrahedron Lett.* **1997**, *38*, 5603 – 5606.
[336] M. De Carvalho, A. E. P. M. Sorrilha, J. A. R. Rodrigues, *J. Braz. Chem. Soc.* **1999**, *10*, 415 – 420.
[337] P. M. Fresneda, P. Molina, S. M. Angeles Saez, *Synlett* **1999**, 1651 – 1653.
[338] P. M. Fresneda, P. Molina, J. A. Bleda, *Tetrahedron* **2001**, *57*, 2355 – 2363.
[339] J. K. MacLeod, L. C. Monahan, *Aust. J. Chem.* **1990**, *43*, 329 – 337.
[340] a) E. J. Forbes, J. C. Tatlow, R. T. Wragg, *Tetrahedron* **1960**, *16*, 73 – 78; b) J. S. Swenton, T. J. Ikeler, B. H. Williams, *J. Am. Chem. Soc.* **1970**, *92*, 3103 – 3109; c) O. Meth-Cohn, *Heterocycles* **1980**, *14*, 1497 – 1516; d) D. G. Hawkins, O. Meth-Cohn, *J. Chem. Res. Miniprint* **1982**, 1218 – 1225; e) A. Albini, G. Bettinetti, G. Minoli, *J. Chem. Soc. Perkin Trans. 2* **1999**, 2803 – 2808.
[341] E. Bremus-Köbberling, A. Gillner, R. Poprawe, F. Avemaria, S. Bräse, unpublished results.
[342] W. Lwowski, T. W. Maricich, *J. Am. Chem. Soc.* **1964**, *86*, 3164 – 3165.
[343] S. C. Ghosh, A. De, *Chem. Commun.* **2000**, 979 – 980.
[344] F. Ragaini, A. Penoni, E. Gallo, S. Tollari, C. Li Gotti, M. Lapadula, E. Mangioni, S. Sergio, *Chem. Eur. J.* **2003**, *9*, 249 – 259.
[345] a) H. Nozaki, S. Fujita, H. Takaya, R. Noyori, *Tetrahedron* **1967**, *23*, 45 – 49; b) N. Torimoto, T. Shingaki, T. Nagai, *Bull. Chem. Soc. Jpn.* **1976**, *49*, 2572 – 2578; c) A. G. Anastassiou, H. E. Simmons, F. D. Marsh, *J. Am. Chem. Soc.* **1965**, *87*, 2296 – 2297.
[346] D. F. Berndt, P. Norris, *Tetrahedron Lett.* **2002**, *43*, 3961 – 3962.
[347] S. Murata, R. Yoshidome, Y. Satoh, N. Kato, H. Tomioka, *J. Org. Chem.* **1995**, *60*, 1428 – 1434.
[348] C. J. Moody, J. G. Ward, *J. Chem. Soc. Perkin Trans. 1* **1984**, 2895 – 2901.
[349] C. J. Moody, G. J. Warrellow, *J. Chem. Soc. Perkin Trans. 1* **1990**, 2929 – 2936.
[350] D. M. B. Hickey, C. J. Moody, C. W. Rees, *J. Chem. Soc. Chem. Commun.* **1982**, 3 – 4.
[351] L. Henn, D. M. B. Hickey, C. J. Moody, C. W. Rees, *J. Chem. Soc. Perkin Trans. 1* **1984**, 2189 – 2197.

 © 2005 Wiley-VCH Verlag GmbH & Co. KGaA, Weinheim

[352] S. Z. Zhu, Y. Xu, *Tetrahedron* **1999**, *55*, 13725 – 13734.
[353] T. Bach, C. Körber, *Tetrahedron Lett.* **1998**, *39*, 5015 – 5016.
[354] T. Bach, C. Körber, *J. Org. Chem.* **2000**, *65*, 2358 – 2367.
[355] J. P. Bacci, K. L. Greenman, D. L. van Vranken, *J. Org. Chem.* **2003**, *68*, 4955 – 4958.
[356] a) M. Murakami, T. Uchida, T. Katsuki, *Tetrahedron Lett.* **2001**, *42*, 7071 – 7074; b) Y. Tamura, T. Uchida, T. Katsuki, *Tetrahedron Lett.* **2003**, *44*, 3301 – 3303; mechanism: c) T. Uchida, Y. Tamura, M. Ohba, T. Katsuki, *Tetrahedron Lett.* **2003**, *44*, 7965 – 7968.
[357] M. Murakami, T. Katsuki, *Tetrahedron Lett.* **2002**, *43*, 3947 – 3949.
[358] E. Leyva, M. S. Platz, G. Persy, J. Wirz, *J. Am. Chem. Soc.* **1986**, *108*, 3783 – 3790.
[359] J. C. Hayes, R. S. Sheridan, *J. Am. Chem. Soc.* **1990**, *112*, 5879 – 5881.
[360] L. Yu-Zhou, J. P. Kirby, M. W. George, M. Pollakoff, G. B. Schuster, *J. Am. Chem. Soc.* **1988**, *110*, 8092 – 8098.
[361] A. K. Schrock, G. B. Schuster, *J. Am. Chem. Soc.* **1984**, *106*, 5228 – 5234.
[362] R. Born, C. Burda, P. Senn, J. Wirz, *J. Am. Chem. Soc.* **1997**, *119*, 5061 – 5062.
[363] N. P. Gritsan, Z. Zhu, C. M. Hadad, M. S. Platz, *J. Am. Chem. Soc.* **1999**, *121*, 1202 – 1207.
[364] W. L. Karney, W. T. Borden, *J. Am. Chem. Soc.* **1997**, *119*, 1378 – 1387.
[365] H. H. Wenk, W. Sander, *Angew. Chem.* **2002**, *114*, 2873 – 2876; *Angew. Chem. Int. Ed.* **2002**, *41*, 2742 – 2745.
[366] M.-L. Tsao, M. S. Platz, *J. Am. Chem. Soc.* **2003**, *125*, 12014 – 12025.
[367] A. Maltsev, T. Bally, M.-L. Tsao, M. S. Platz, A. Kuhn, M. Vosswinkel, C. Wentrup, *J. Am. Chem. Soc.* **2004**, *126*, 237 – 249, and references therein.
[368] R. A. Evans, C. Wentrup, *J. Chem. Soc. Chem. Commun.* **1992**, 1062 – 1064.
[369] S. V. Chapyshev, A. Kuhn, M. W. Wong, C. Wentrup, *J. Am. Chem. Soc.* **2000**, *122*, 1572 – 1579.
[370] W. L. Karney, W. T. Borden, *Adv. Carbene Chem.* **2001**, *3*, 205 – 251.
[371] a) R. Herges, *Angew. Chem.* **1994**, *106*, 261 – 283; *Angew. Chem. Int. Ed. Engl.* **1994**, *33*, 255 – 276, and references therein; b) R. Herges, D. Geuenich, G. Bucher, C. Tonsdorff, *Chem. Eur. J.* **2000**, *6*, 1224 – 1228.
[372] P. Bednarek, C. Wentrup, *J. Am. Chem. Soc.* **2003**, *125*, 9083 – 9089.
[373] a) K. Knepper, S. Bräse, unpublished results; b) R. Colman, E. F. V. Scriven, H. Suschitzky, D. R. Thomas, *Chem. Ind.* **1981**, 249 – 250.
[374] a) H. W. Moore, *Chem. Soc. Rev.* **1973**, *2*, 415 – 455; b) H. W. Moore, W. Weyler, Jr., *J. Am. Chem. Soc.* **1970**, *92*, 4132 – 4133; c) H. W. Moore, L. Hernandez, A. Sing, *J. Am. Chem. Soc.* **1976**, *98*, 3728 – 3730; d) M. D. Gheorghiu, L. Parvulescu, C. Draghici, M. Mihai, A. Popescu, *Rev. Roum. Chim.* **1996**, *41*, 283 – 289.
[375] P. N. D. Singh, S. M. Mandel, R. M. Robinson, Z. Zhu, R. Franz, B. S. Ault, A. D. Gudmundsdóttir, *J. Org. Chem.* **2003**, *68*, 7951 – 7960
[376] H. Staudinger, J. Meyer, *Helv. Chim. Acta* **1919**, *2*, 635 – 646.
[377] a) Review: Y. G. Gololobov, L. F. Kasukhin, *Tetrahedron* **1992**, *48*, 1353 – 1406; b) for more-recent examples, see: B. Chen, A. K. Mapp, *J. Am. Chem. Soc.* **2004**, *126*, 5364 – 5365.
[378] M. Alajarín, C. Conesa, H. S. Rzepa, *J. Chem. Soc. Perkin Trans. 2* **1999**, 1811 – 1814.
[379] D. E. Shalev, S. M. Chiacchiera, A. E. Radkowsky, E. M. Kosower, *J. Org. Chem.* **1996**, *61*, 1689 – 1701.
[380] For a review of the aza-Wittig reaction, see: P. Molina, M. J. Vilaplana, *Synthesis* **1994**, 1197 – 1218.
[381] For excellent reviews on the chemistry of iminophosphoranes, see: a) H. Wamhoff, G. Richardt, S. Stölben, *Adv. Heterocycl. Chem.* **1995**, *33*, 159 – 249; b) P. M. Fresneda, P. Molina, *Synlett* **2004**, 1 – 17.
[382] P. T. Nyffeler, C.-H. Liang, K. M. Koeller, C.-H. Wong, *J. Am. Chem. Soc.* **2002**, *124*, 10773 – 10778.
[383] V. Maraval, R. Laurent, B. Donnadieu, M. Mauzac, A.-M. Caminade, J.-P. Majoral, *J. Am. Chem. Soc.* **2000**, *122*, 2499 – 2511.
[384] M. S. Balakrishna, R. M. Abhyankar, M. G. Walawalker, *Tetrahedron Lett.* **2001**, *42*, 2733 – 2734.
[385] N. G. Andersen, P. D. Ramsden, D. Che, M. Parvez, B. A. Keay, *J. Org. Chem.* **2001**, *66*, 7478 – 7486.
[386] a) *rac*-Perphoramidines: J. R. Fuchs, R. L. Funk, *J. Am. Chem. Soc.* **2004**, *126*, 5068 – 5069; b) F. Palacios, A. M. Ochoa de Retana, J. Pagalday, *Eur. J. Org. Chem.* **2003**, 913 – 919.
[387] Y. He, R. J. Hinklin, J. Chang, L. L. Kiessling, *Org. Lett.* **2004**, *6*, 4479 – 4482.
[388] S. K. Rastogi, G. K. Srivastava, S. K. Singh, R. K. Grover, R. Roy, B. Kundu. *Tetrahedron Lett.* **2002**, *43*, 8327 – 8330.
[389] C. W. Lindsley, Z. Zhao, R. C. Newton, W. H. Leister, K. A. Strauss, *Tetrahedron Lett.* **2002**, *43*, 4467 – 4470.
[390] I. Bosch, A. Gonzalez, F. Urpi, J. Vilarrasa, *J. Org. Chem.* **1996**, *61*, 5638 – 5643.
[391] S.-D. Park, J.-H. Oh, D. Lim, *Tetrahedron Lett.* **2002**, *43*, 6309 – 6311.
[392] J. M. Humphrey, R. Chamberlin, *Chem. Rev.* **1997**, *97*, 2243 – 2266.
[393] a) E. Saxon, C. R. Bertozzi, *Science* **2000**, *287*, 2007 – 2010; b) see also: S. Gilbertson, *Chemtracts* **2001**, *14*, 524 – 528; c) K. L. Kiick, E. Saxon, D. A. Tirrell, C. R. Bertozzi, *Proc. Natl. Acad. Sci. USA* **2002**, *99*, 19 – 24.
[394] E. Saxon, J. I. Armstrong, C. R. Bertozzi, *Org. Lett.* **2000**, *2*, 2141 – 2143.
[395] E. Saxon, S. J. Luchansky, H. C. Hang, C. Yu, S. C. Lee, C. R. Bertozzi, *J. Am. Chem. Soc.* **2002**, *124*, 14893 – 14902.
[396] a) G. A. Lemieux, C. L. Granffenried, C. R. Bertozzi, *J. Am. Chem. Soc.* **2003**, *125*, 4708 – 4709; b) J. A. Prescher, D. H. Dube, C. R. Bertozzi, *Nature* **2004**, *430*, 873 – 877.
[397] C. C.-Y. Wang, T. S. Seo, Z. Li, H. Ruparel, J. Ju, *Bioconjugate Chem.* **2003**, *14*, 697 – 701.
[398] a) H. C. Hang, C. Yu, M. R. Pratt, C. R. Bertozzi, *J. Am. Chem. Soc.* **2004**, *126*, 6 – 7; b) D. J. Vocadlo, C. R. Bertozzi, *Angew. Chem.* **2004**, *116*, 5452 – 5456; *Angew. Chem. Int. Ed.* **2004**, *43*, 5338 – 5342.
[399] a) M. Köhn, R. Wacker, C. Peters, H. Schröder, L. Soulère, R. Breinbauer, C. M. Niemeyer, H. Waldmann, *Angew. Chem.* **2003**, *115*, 6010 – 6014; *Angew. Chem. Int. Ed.* **2003**, *42*, 5830 – 5834; b) M. C. Bryan, F. Fazio, H.-K. Lee, C.-Y. Huang, A. Chang, M. D. Best, D. A. Calarese, O. Blixt, J. C. Paulson, D. Burton, I. A. Wilson, C.-H. Wong, *J. Am. Chem. Soc.* **2004**, *126*, 8640 – 8641.
[400] a) B. L. Nilsson, L. L. Kiessling, R. T. Raines, *Org. Lett.* **2000**, *2*, 1939 – 1941; b) for a review on chemical ligation, see: D. Y. Yeo, R. Srinivasan, G. Y. J. Chen, S. Q. Yao, *Chem. Eur. J.* **2004**, *10*, 4664 – 4672.
[401] B. L. Nilsson, L. L. Kiessling, R. T. Raines, *Org. Lett.* **2001**, *3*, 9 – 12.
[402] M. B. Soellner, B. L. Nilsson, R. T. Raines, *J. Org. Chem.* **2002**, *67*, 4993 – 4996.
[403] R. Merkx, D. T. S. Rijkers, J. Kemmink, R. M. J. Liskamp, *Tetrahedron Lett.* **2003**, *44*, 4515 – 4518.
[404] B. L. Nilsson, R. J. Hondal, M. B. Soellner, R. T. Raines, *J. Am. Chem. Soc.* **2003**, *125*, 5268 – 5269.
[405] a) J. P. Malkinson, R. A. Falconer, I. Toth, *J. Org. Chem.* **2000**, *65*, 5249 – 5252; b) Y. He, R. J. Hinklin, J. Chang, L. L. Kiessling, *Org. Lett.* **2004**, *6*, 4479 – 4482.

 © 2005 Wiley-VCH Verlag GmbH & Co. KGaA, Weinheim

[406] J. A. Restituyo, L. R. Comstock, S. G. Petersen, T. Stringfellow, S. R. Rajski, *Org. Lett.* **2003**, *5*, 4357 – 4360.
[407] O. David, W. J. N. Messter, H. Bieraeugel, H. E. Schoemaker, H. Hiemstra, J. H. van Maarseveen, *Angew. Chem.* **2003**, *115*, 4509 – 4511; *Angew. Chem. Int. Ed.* **2003**, *42*, 4373 – 4375.
[408] For reviews on the aza-Wittig reaction in heterocyclic syntheses, see: S. Eguchi, Y. Matsushita, K. Yamashita, *Org. Prep. Proced. Int.* **1992**, *24*, 209 – 243.
[409] a) D. H. Valentine, Jr., J. H. Hillhouse, *Synthesis* **2003**, 317 – 334; b) M. W. Ding, Z. J. Liu, *Chin. J. Org. Chem.* **2001**, *21*, 1 – 7.
[410] For more-recent examples, see: A. A. Boezio, G. Solberghe, C. Lauzon, A. B. Charette, *J. Org. Chem.* **2003**, *68*, 3241 – 3245.
[411] A.-B. N. Luheshi, S. M. Salem, R. K. Smalley, P. D. Kennewell, R. Westwood, *Tetrahedron Lett.* **1990**, *31*, 6561 – 6564.
[412] F. Damkaci, P. DeShong, *J. Am. Chem. Soc.* **2003**, *125*, 4408 – 4409.
[413] H. Takeuchi, Y. Matsushita, S. Eguchi, *Tetrahedron* **1991**, *47*, 1535 – 1537.
[414] H. Takeuchi, S. Hagiwara, S. Eguchi, *Tetrahedron* **1989**, *45*, 6375 – 6386.
[415] M. Alajarín, P. Molina, A. Vidal, F. Tovar, *Synlett* **1998**, 1288 – 1290.
[416] P. Cledera, C. Avendaño, J. C. Menéndez, *Tetrahedron* **1998**, *54*, 12349 – 12360.
[417] S. Eguchi, H. Takeuchi, *J. Chem. Soc. Chem. Commun.* **1989**, 602 – 603.
[418] S. Eguchi, Y. Matsushita, H. Takeuchi, *J. Org. Chem.* **1992**, *57*, 6975 – 6979.
[419] J. Pawlas, P. Vedsø, P. Jakobsen, P. O. Huusfeldt, M. Begtrup, *J. Org. Chem.* **2000**, *65*, 9001 – 9006.
[420] H. Takeuchi, S. Yanagida, T. Ozaki, S. Hagiwara, S. Eguchi, *J. Org. Chem.* **1989**, *54*, 431 – 434.
[421] S. Eguchi, T. Suzuki, T. Okawa, Y. Matsushita, E. Yashima, Y. Okamoto, *J. Org. Chem.* **1996**, *61*, 7316 – 7319.
[422] S. Eguchi, H. Takeuchi, Y. Matsushita, *Heterocycles* **1992**, *33*, 153 – 156.
[423] S. Eguchi, K. Yamashita, Y. Matsushita, A. Kakehi, *J. Org. Chem.* **1995**, *60*, 4006 – 4012.
[424] P. Molina, I. Díaz, A. Tárraga, *Tetrahedron* **1995**, *51*, 5617 – 5630.
[425] A. Kamal, K. Laxma Reddy, V. Devaiah, N. Shankaraiah, *Synlett* **2004**, 2533 – 2536.
[426] T. Okano, T. Sakaida, S. Eguchi, *J. Org. Chem.* **1996**, *61*, 8826 – 8830.
[427] J. L. Pinder, S. M. Weinreb, *Tetrahedron Lett.* **2003**, *44*, 4141 – 4143.
[428] J. Wang, S. Sakamoto, K. Kamada, A. Nitta, T. Noda, H. Oguri, M. Hirama, *Synlett* **2003**, 891 – 893.
[429] P. Cledera, C. Avendaño, J. C. Menéndez, *J. Org. Chem.* **2000**, *65*, 1743 – 1749.
[430] D. R. Williams, M. G. Fromhold, J. D. Earley, *Org. Lett.* **2001**, *3*, 2721 – 2724.
[431] P. M. Fresneda, P. Molina, M. A. Sanz, *Synlett* **2000**, 1190 – 1192.
[432] K. M. Depew, S. P. Marsden, D. Zatorska, A. Zatorski, W. G. Bornmann, S. J. Danishefsky, *J. Am. Chem. Soc.* **1999**, *121*, 11953 – 11963.
[433] B. Jiang, C.-G. Yang, J. Wang, *J. Org. Chem.* **2001**, *66*, 4865 – 4869.
[434] T. Sugimori, T. Okawa, S. Eguchi, E. Yashima, Y. Okamoto, *Chem. Lett.* **1997**, 869 – 870.
[435] T. Sugimori, T. Okawa, S. Eguchi, A. Kakehi, E. Yashima, Y. Okamoto, *Tetrahedron* **1998**, *54*, 7997 – 8008.
[436] J. Chen, C. J. Forsyth, *Org. Lett.* **2003**, *5*, 1281 – 1283.
[437] J. Chen, C. J. Forsyth, *J. Am. Chem. Soc.* **2003**, *125*, 8734 – 8735.
[438] A. Tárraga, P. Molina, J. L. López, *Tetrahedron Lett.* **2000**, *41*, 2479 – 2482.
[439] F. Palacios, A. M. Ochoa de Retana, E. Martínez de Marigorta, M. Rodríguez, J. Pagalday, *Tetrahedron* **2003**, *59*, 2617 – 2623.
[440] W. C. Lu, R. Q. Zhang, Q. J. Zang, N. B. Wong, *J. Phys. Chem. B* **2003**, *107*, 2061 – 2067.
[441] C. Bonini, M. D'Auria, M. Funicello, G. Romaniello, *Tetrahedron* **2002**, *58*, 3507 – 3512.
[442] H. Kato, K. Ohmori, K. Suzuki, *Synlett* **2001**, 1003 – 1005.
[443] D. A. Goff, R. N. Zuckermann, *J. Org. Chem.* **1995**, *60*, 5744 – 5745.
[444] S. E. Schneider, P. A. Bishop, M. A. Salazar, O. A. Bishop, E. V. Anslyn, *Tetrahedron* **1998**, *54*, 15063 – 15086.
[445] J. M. Villalgordo, D. Obrecht, A. Chucholowsky, *Synlett* **1998**, 1405 – 1407.
[446] M. Bernard, W. T. Ford, *J. Org. Chem.* **1983**, *48*, 326 – 332.
[447] P. López-Cremades, P. Molina, E. Aller, A. Lorenzo, *Synlett* **2000**, 1411 – 1414.
[448] K. Hemming, M. J. Bevan, C. Loukou, S. D. Patel, D. Renaudeau, *Synlett* **2000**, 1565 – 1568.
[449] P. Molina, E. Aller, A. Lorenzo, P. López-Cremades, I. Rioja, A. Ubeda, M. C. Terencio, M. J. Alcaraz, *J. Med. Chem.* **2001**, *44*, 1011 – 1014.
[450] M. I. García-Moreno, P. Díaz-Pérez, J. M. Benito, C. Ortiz-Mellet, J. Defaye, J. M. García Fernández, *Carbohydr. Res.* **2002**, *337*, 2329 – 2334.
[451] B. J. Neubert, B. B. Snider, *Org. Lett.* **2003**, *5*, 765 – 768.
[452] A. Grieder, A. W. Thomas, *Synthesis* **2003**, 1707 – 1711.
[453] C. Gil, S. Bräse, *Chem. Eur. J.* **2005**, *11*, 2680 – 2688.
[454] A. B. Charette, A. A. Boezio, M. K. Janes, *Org. Lett.* **2000**, *2*, 3777 – 3779.
[455] S. Barthélémy, S. Schneider, W. Bannwarth, *Tetrahedron Lett.* **2002**, *43*, 807 – 810.
[456] P. Langer, I. Freifeld, H. Shojaei, *Chem. Commun.* **2003**, 3044 – 3045.
[457] P. Langer, I. Freifeld, *Chem. Commun.* **2002**, 2668 – 2669.
[458] a) S. Obika, J.-i. Andoh, M. Onoda, O. Nakagawa, A. Hiroto, T. Sugimoto, T. Imanishi, *Tetrahedron Lett.* **2003**, *44*, 5267 – 5270; b) for use of the sulfoxy group as an electrophile, see: K. Hemming, C. Loukou, S. Elkatip, R. K. Smalley, *Synlett* **2004**, 101 – 105; c) for the formation of aziridines from α-azidoalcohols, see: D. Paumier, M. Garcia, M. Shipman, J. C. Muir, *Synlett* **2004**, 2212 – 2214.
[459] F. W. Bollinger, L. D. Tuma, *Synlett* **1996**, 407 – 413.
[460] a) P. Dembech, G. Seconi, A. Ricci, *Chem. Eur. J.* **2000**, *6*, 1281 – 1286; b) B. M. Trost, W. H. Pearson, *J. Am. Chem. Soc.* **1983**, *105*, 1054 – 1056; c) G. W. Kabalka, G. Li, *Tetrahedron Lett.* **1997**, *38*, 5777 – 5778.
[461] J. S. Yadav, C. Madhuri, B. V. S. Reddy, G. S. Kiran Kumar-Reddy, G. Sabitha, *Synth. Commun.* **2002**, *32*, 2771 – 2777.
[462] D. Amantini, F. Fringuelli, F. Pizzo, L. Vaccaro, *Org. Prep. Proced. Int.* **2002**, *34*, 111 – 147.
[463] A. Capperucci, A. Deglinnocenti, M. Funicello, G. Mauriello, P. Scafato, P. Spagnolo, *J. Org. Chem.* **1995**, *60*, 2254 – 2256.
[464] a) M. Meldal, M. A. Juliano, A. M. Jansson, *Tetrahedron Lett.* **1997**, *38*, 2531 – 2534; b) D. D. Long, M. D. Smith, D. G. Marquess, T. D. W. Claridge, G. W. J. Fleet, *Tetrahedron Lett.* **1998**, *39*, 9293 – 9296; c) J. M. Kim, Y. Z. Bi, S. J. Paikoff, P. G. Schultz, *Tetrahedron Lett.* **1996**, *37*, 5305 – 5308; d) K. A. Savin, J. C. G. Woo, S. J. Danishefsky, *J. Org. Chem.* **1999**, *64*, 4183 – 4186.
[465] C. A. M. Afonso, *Tetrahedron Lett.* **1995**, *36*, 8857 – 8858.
[466] A. R. Hajipour, S. E. Mallakpour, *Synth. Commun.* **2001**, *31*, 1177 – 1185.
[467] a) Z. L. Tang, J. C. Pelletier, *Tetrahedron Lett.* **1998**, *39*, 4773 – 4776; b) M. R. Tremblay, D. Poirier, *Tetrahedron Lett.* **1999**, *40*, 1277 – 1280; c) N. J. Osborn, J. A. Robinson, *Tetrahedron* **1993**, *49*, 2873 – 2884; d) R. Liang, L. Yan, J. Loebach, M. Ge, Y. Uozumi, K. Sekanina, N. Horan, J. Gildersleeve, C. Thompson,

 © 2005 Wiley-VCH Verlag GmbH & Co. KGaA, Weinheim

A. Smith, K. Biswas, W. C. Still, D. Kahne, *Science* **1996**, *274*, 1520 – 1522.
[468] a) A. M. Salunkhe, H. C. Brown, *Tetrahedron Lett.* **1995**, *36*, 7987 – 7990; b) Y. Z. Pei, B. O. S. Wickham, *Tetrahedron Lett.* **1993**, *34*, 7509 – 7512.
[469] A. M. Salunkhe, P. V. Ramachandran, H. C. Brown, *Tetrahedron* **2002**, *58*, 10059 – 10064.
[470] a) I. Bosch, A. M. Costa, M. Martin, F. Urpi, J. Vilarrasa, *Org. Lett.* **2000**, *2*, 397 – 399; b) H. Firouzabadi, M. Adibi, B. Zeynizadeh, *Synth. Commun.* **1998**, *28*, 1257 – 1273.
[471] a) C. B. Li, P. W. Zheng, Z. X. Zhao, W. Q. Zhang, M. B. Li, Q. C. Yang, Y. Cui, Y. L. Xu, *Chin. Chem. Lett.* **2003**, *14*, 773 – 775; b) M. Baruah, A. Boruah, D. Prajapati, J. S. Sandhu, A. C. Ghosh, *Tetrahedron Lett.* **1996**, *37*, 4559 – 4560; c) D. Pathak, D. D. Laskar, D. Prajapati, J. S. Sandhu, *Chem. Lett.* **2000**, 816 – 817; d) A. Boruah, M. Boruah, D. Prajapati, J. S. Sandhu, *Synlett* **1997**, 1253 – 1254; e) H. Y. Wu, R. Chen, Y. M. Zhang, *J. Chem. Res. Synop.* **2000**, *5*, 248 – 249.
[472] a) G. V. Reddy, G. V. Rao, D. S. Iyengar, *Tetrahedron Lett.* **1999**, *40*, 3937 – 3938; b) J. G. Lee, K. I. Choi, H. Y. Koh, Y. Kim, Y. Kang, Y. S. Cho, *Synthesis* **2001**, 81 – 84.
[473] M. Yus, G. Radivoy, F. Alonso, *Synthesis* **2001**, 914 – 918.
[474] A. Kamal, B. S. N. Reddy, *Chem. Lett.* **1998**, 593 – 594.
[475] a) Y. Huang, Y. M. Zhang, Y. L. Wang, *Synth. Commun.* **1996**, *26*, 2911 – 2915; b) C. Goulaouic-Dubois, M. Hesse, *Tetrahedron Lett.* **1995**, *36*, 7427 – 7430; c) L. Benati, P. C. Montevecchi, D. Nanni, P. Spagnolo, M. Volta, *Tetrahedron Lett.* **1995**, *36*, 7313 – 7314; d) Y. Huang, Y. M. Zhang, Y. L. Wang, *Tetrahedron Lett.* **1997**, *38*, 1065 – 1066.
[476] B. C. Ranu, A. Sarkar, R. Chakraborty, *J. Org. Chem.* **1994**, *59*, 4114 – 4116.
[477] a) H. S. P. Rao, P. Siva, *Synth. Commun.* **1994**, *24*, 549 – 555; b) F. Fringuelli, F. Pizzo, L. Vaccaro, *Synthesis* **2000**, 646 – 650.
[478] a) H. Firouzabadi, B. Tamami, A. R. Kiasat, *Synth. Commun.* **2000**, *30*, 587 – 596; b) H. Firouzabadi, M. Ghadami, *Phosphorus Sulfur Silicon Relat. Elem.* **2000**, *166*, 83 – 98.
[479] S. G. Alvarez, G. B. Fischer, B. Singaram, *Tetrahedron Lett.* **1995**, *36*, 2567 – 2570.
[480] T. K. Chakraborty, P. Laxman, *Tetrahedron Lett.* **2003**, *44*, 4989 – 4992.
[481] A. Kamal, E. Laxman, M. Arifuddin, *Tetrahedron Lett.* **2000**, *41*, 7743 – 7746.
[482] A. R. Ramesha, S. Bhat, S. Chandrasekaran, *J. Org. Chem.* **1995**, *60*, 7682 – 7683.
[483] M. Bartra, P. Romea, F. Urpí, J. Vilarassa, *Tetrahedron* **1990**, *46*, 587 – 594.
[484] Z. Zhang, T. Carter, E. Fan, *Tetrahedron Lett.* **2003**, *44*, 3063 – 3066
[485] M. Jost, J.-C. Greie, N. Stemmer, S. D. Wilking, K. Altendorf, N. Sewald, *Angew. Chem.* **2002**, *114*, 4438 – 4440; *Angew. Chem. Int. Ed.* **2002**, *41*, 4267 – 4269; .
[486] a) D. S. Hays, G. C. Fu, *J. Org. Chem.* **1998**, *63*, 2796 – 2797; b) L. Benati, G. Bencivienni, R. Leardini, M. Minozzi, D. Nanni, R. Sciapi, P. Spagnolo, G. Zanardi, C. Rizzi, *Org. Lett.* **2004**, *6*, 417 – 420, and references therein.
[487] C. Malanga, S. Mannucci, L. Lardicci, *J. Chem. Res. Synop.* **2000**, *6*, 256 – 257.
[488] A. Kamal, N. V. Rao, E. Laxman, *Tetrahedron Lett.* **1997**, *38*, 6945 – 6948.
[489] a) P. G. Reddy, T. V. Pratap, G. D. K. Kumar, S. K. Mohanty, S. Baskaran, *Eur. J. Org. Chem.* **2002**, 3740 – 3743; b) S. Saito, H. Nakajima, M. Inaba, T. Moriwaki, *Tetrahedron Lett.* **1989**, *30*, 837 – 838.
[490] P. R. Sridhar, K. R. Prabhu, S. Chandrasekaran, *J. Org. Chem.* **2003**, *68*, 5261 – 5264.
[491] a) M. Baruah, A. Boruah, D. Prajapati, J. S. Sandhu, *Synlett* **1996**, 1193 – 1194; b) A. Kamal, B. Laxminarayana, N. L. Gayatri, *Tetrahedron Lett.* **1997**, *38*, 6871 – 6874; c) A. Kamal, Y. Damayanthi, B. S. N. Reddy, B. Lakminarayana, B. S. P. Reddy, *Chem. Commun.* **1997**, 1015 – 1016; d) S. Mazumder, D. D. Laskar, D. Prajapati, M. K. Roy, *Chem. Biodiversity* **2004**, *1*, 925 – 929.
[492] J. Ohlsson, U. J. Nilsson, *Tetrahedron Lett.* **2003**, *44*, 2785 – 2787.
[493] M. L. Kantam, N. S. Chowdari, A. Rahman, B. M. Choudary, *Synlett* **1999**, 1413 – 1414.
[494] Y. Gaoni, *J. Org. Chem.* **1994**, *59*, 6853 – 6855.
[495] a) T. Rosen, I. M. Lico, D. T. W. Chu, *J. Org. Chem.* **1988**, *53*, 1580 – 1582; b) T. Bielfeldt, S. Peters, M. Meldal, K. Bock, H. Paulsen, *Angew. Chem.* **1992**, *104*, 881 – 883; *Angew. Chem. Int. Ed. Engl.* **1992**, *3*, 857 – 859; c) Y. Nakahara, Y. Nakahara, T. Ogawa, *Carbohydr. Res.* **1996**, *292*, 71 – 81; d) X.-T. Chen, D. Sames, S. J. Danishefsky, *J. Am. Chem. Soc.* **1998**, *120*, 7760 – 7769; e) K. Matsuoka, T. Ohtawa, H. Hinou, T. Koyama, Y. Esumi, S.-I. Nishimura, K. Hatanoa, D. Terunuma, *Tetrahedron Lett.* **2003**, *44*, 3617 – 3620.
[496] N. Shangguan, S. Katukojvala, R. Greenberg, L. J. Williams, *J. Am. Chem. Soc.* **2003**, *125*, 7754 – 7755.
[497] N. A. LeBel, R. M. Cherluck, E. A. Curtis, *Synthesis* **1973**, 678 – 679.
[498] A. Rauk, P. Alewood, *Can. J. Chem.* **1977**, *55*, 1498 – 1510.
[499] For some examples, see: a) J. B. Hendrickson, T. L. Bogard, M. E. Fisch, S. Grossert, N. Yoshimura, *J. Am. Chem. Soc.* **1974**, *96*, 7781 – 7789; b) F. Z. Basha, S. Hibino, D. Kim, W. E. Pye, T.-T. Wu, S. M. Weinreb, *J. Am. Chem. Soc.* **1980**, *102*, 3962 – 3964; c) E. E. Van Tamelen, J. P. Demers, E. G. Taylor, K. Koller, *J. Am. Chem. Soc.* **1980**, *102*, 5424 – 5425; d) A. S. Kende, D. P. Lorah, R. J. Boatman, *J. Am. Chem. Soc.* **1981**, *103*, 1271 – 1273; e) R. A. Earl, K. P. C. Vollhardt, *J. Am. Chem. Soc.* **1983**, *105*, 6991 – 6993; f) Y. Xia, A. P. Kozikowski, *J. Am. Chem. Soc.* **1989**, *111*, 4116 – 4117; g) D. L. Boger, K. C. Cassidy, S. Nakahara, *J. Am. Chem. Soc.* **1993**, *115*, 10733 – 10741; h) A. B. Charette, B. Cote, Bernard, *J. Am. Chem. Soc.* **1995**, *117*, 12721 – 12732.
[500] A. B. Smith, I. G. Safonov, R. M. Corbett, *J. Am. Chem. Soc.* **2002**, *124*, 11102 – 11113.
[501] L. M. Yagupolskii, S. V. Shelyazhenko, I. I. Maletina, V. N. Petrik, E. B. Rusanov, A. N. Chermega, *Eur. J. Org. Chem.* **2001**, 1225 – 1233.
[502] For recent examplese, see: a) B. S. Patil, G.-R. Vasanthakumar, V. V. S. Babu, *J. Org. Chem.* **2003**, *68*, 7274 – 7280; b) G. M. Sammis, E. N. Jacobsen, *J. Am. Chem. Soc.* **2003**, *125*, 4442 – 4443; c) J. H. Rigby, C.-S. Lee, *Org. Lett.* **2003**, *5*, 1151 – 1153; d) A. Padwa, K. R. Crawford, P. Rashatasakhon, M. Rose, *J. Org. Chem.* **2003**, *68*, 2609 – 2617.
[503] F. M. Menger, J. Bian, V. A. Azov, *Angew. Chem.* **2002**, *114*, 2693 – 2696; *Angew. Chem. Int. Ed.* **2002**, *41*, 2581 – 2584.
[504] M. T. Migawa, E. E. Swayze, *Org. Lett.* **2000**, *2*, 3309 – 3311.
[505] S. Sunami, T. Sagara, M. Ohkubo, H. Morishima, *Tetrahedron Lett.* **1999**, *40*, 1721 – 1724.
[506] H. Bock, R. Dammel, *J. Am. Chem. Soc.* **1988**, *110*, 5261 – 5269.
[507] G. F. Alberici, J. Andrieux, G. Adam, M. M. Plat, *Tetrahedron Lett.* **1983**, *24*, 1937 – 1940.
[508] M. Mascal, C. J. Moody, *J. Chem. Soc. Chem. Commun.* **1988**, 589 – 590.
[509] M. Mascal, C. J. Moody, A. M. Z. Slawin, D. J. Williams, *J. Chem. Soc. Perkin Trans. 1* **1992**, 823 – 830.
[510] S. Furmeier, J. O. Metzger, *Eur. J. Org. Chem.* **2003**, 885 – 893.
[511] J. E. Golden, J. Aubé, *Angew. Chem.* **2002**, *114*, 4492 – 4494; *Angew. Chem. Int. Ed.* **2002**, *41*, 4316 – 4318.
[512] H.-J. Cristau, X. Marat, J.-P. Vorsb, J.-L. Pirata, *Tetrahedron Lett.* **2003**, *44*, 3179 – 3181.
[513] a) J. Aubé, G. L. Milligan, *J. Am. Chem. Soc.* **1991**, *113*, 8965 – 8966; b) J. Aubé, G. L. Milligan, C. J. Mossman, *J. Org. Chem.* **1992**, *57*, 1635 – 1637; c) A.-L. Dhimane, L. Fensterbank, M.

 © 2005 Wiley-VCH Verlag GmbH & Co. KGaA, Weinheim

Malacria, V. Gracias, G. L. Milligan, J. Aubé, *J. Am. Chem. Soc.* **1995**, *117*, 8047 – 8048; d) G. L. Milligan, C. J. Mossman, J. Aubé, *J. Am. Chem. Soc.* **1995**, *117*, 10449 – 10459; e) J. A. Wendt, J. Aubé, *Tetrahedron Lett.* **1996**, *37*, 1531 – 1534; f) J. E. Forsee, J. Aubé, *J. Org. Chem.* **1999**, *64*, 4381 – 4385; g) P. Desai, K. Schildknegt, K. A. Agrios, C. Mossman, G. L. Milligan, J. Aubé, *J. Am. Chem. Soc.* **2000**, *122*, 7226 – 7232; h) R. Iyengar, K. Schildknegt, J. Aubé, *Org. Lett.* **2000**, *2*, 1625 – 1627; i) A. Wrobleski, J. Aubé, *J. Org. Chem.* **2001**, *66*, 886 – 889.

[514] a) W. H. Pearson, J. M. Schkeryantz, *Tetrahedron Lett.* **1992**, *33*, 5291 – 5294; b) W. H. Pearson, R. Walavalkar, J. M. Schkeryantz, W.-K. Fang, J. D. Blickensdorf, *J. Am. Chem. Soc.* **1993**, *115*, 10183 – 10194; c) W. H. Pearson, W.-K. Fang, *J. Org. Chem.* **1995**, *60*, 4960 – 4961; d) W. H. Pearson, B. M. Gallagher, *Tetrahedron* **1996**, *52*, 12039 – 12048; e) W. H. Pearson, *J. Heterocycl. Chem.* **1996**, *33*, 1489 – 1496; f) Gephrotoxin synthesis: W. H. Pearson, W.-K. Fang, *J. Org. Chem.* **2000**, *65*, 7158 – 7174; g) erratum: W. H. Pearson, W.-K. Fang, *J. Org. Chem.* **2001**, *66*, 6838; h) W. H. Pearson, R. Walavalkar, *Tetrahedron* **2001**, *57*, 5081 – 5089.

[515] W. H. Pearson, D. A. Hutta, W.-K. Fang, *J. Org. Chem.* **2000**, *65*, 8326 – 8332.

[516] J. H. Boyer, *J. Am. Chem. Soc.* **1955**, *77*, 951 – 954.

[517] Indolizidin 251F: A. Wrobleski, K. Sahasrabudhe, J. Aubé, *J. Am. Chem. Soc.* **2004**, *126*, 5475 – 5481.

[518] K. Sahasrabudhe, V. Gracias, K. Furness, B. T. Smith, C. E. Katz, S. D. Reddy, J. Aubé, *J. Am. Chem. Soc.* **2003**, *125*, 7914 – 7922.

[519] C. E. Katz, J. Aubé, *J. Am. Chem. Soc.* **2003**, *125*, 13948 – 13949.

[520] N. D. Hewlett, J. Aubé, J. L. Radkiewicz-Poutsma, *J. Org. Chem.* **2004**, *69*, 3439 – 3446.

[521] P. Reddy, B. Varghese, S. Baskaran, *Org. Lett.* **2003**, *5*, 583 – 585.

[522] S. Lang, A. R. Kennedy, J. A. Murphy, A. H. Payne, *Org. Lett.* **2003**, *5*, 3655 – 3658.

[523] P. Magnus, K. S. Matthews, V. Lynch, *Org. Lett.* **2003**, *5*, 2181 – 2184.

[524] N. Kumagai, S. Matsunaga, M. Shibasaki, *Angew Chem.* **2004**, *116*, 484 – 488; *Angew Chem. Int. Ed.* **2004**, *43*, 478 – 482.

[525] a) R. A. Abramovitch, M. Cooper, S. Iyer, R. Jeyaraman, J. A. Rosario Rodríguez, *J. Org. Chem.* **1982**, *47*, 4819 – 4820; b) for a overview, see: M. Novak, S. Rajagopal, *Adv. Phys. Org. Chem.* **2001**, *36*, 167 – 254.

[526] R. A. Abramovitch, J. Miller, A. J. C. de Souza, *Tetrahedron Lett.* **2003**, *44*, 6965 – 6967.

[527] P. Ramlall, R. A. McClelland, *J. Chem. Soc. Perkin Trans. 2* **1999**, 225 – 232.

[528] a) H. Takeuchi, K. Takano, K. Koyama, *J. Chem. Soc. Chem. Commun.* **1982**, 1254 – 1256; b) H. Takeuchi, K. Takano, *J. Chem. Soc. Chem. Commun.* **1983**, 447 – 449; c) R. A. Abramovitch, R. Jeyaraman, K. Yannakopoulou, *J. Chem. Soc. Chem. Commun.* **1985**, 1107 – 1108; d) H. Takeuchi, K. Takano, *J. Chem. Soc. Perkin Trans. 1* **1986**, 611 – 618; e) R. Abramovitch, M. M. Cooper, R. Jeyaraman, G. Rusek, *Tetrahedron Lett.* **1986**, *27*, 3705 – 3708; f) H. Takeuchi, S. Hirayama, M. Mitani, K. Koyama, *J. Chem. Soc. Perkin Trans. 1* **1988**, 521 – 527; g) R. A. Abramovitch, P. Chinnasamy, K. Evertz, G. Huttner, *J. Chem. Soc. Chem. Commun.* **1989**, 3 – 5; h) A. M. Almerico, G. Cirrincione, G. Dattolo, E. Aiello, F. Mingoia, *J. Heterocycl. Chem.* **1994**, *31*, 193 – 198; i) A. M. Almerico, G. Cirrincione, P. Diana, S. Grimaudo, G. Dattolo, E. Aiello, F. Mingoia, P. Barraja, *Heterocycles* **1994**, *37*, 1549 – 1559; j) J. J. Kulagowski, C. J. Moody, C. W. Rees, *J. Chem. Soc. Perkin Trans. 1* **1985**, 2725 – 2732; k) J. D. F. De Sousa, J. A. R. Rodrigues, *J. Am. Chem. Soc.* **1994**, *116*, 9745 – 9746.

[529] R. A. McClelland, A. Ahmad, A. P. Dicks, V. E. Licence, *J. Am. Chem. Soc.* **1999**, *121*, 3303 – 3310.

[530] A. S. R. Donald, R. E. Marks, *J. Chem. Soc. C* **1967**, 1188 – 1189.

[531] S. Arseniyadis, A. Wagner, C. Mioskowski, *Tetrahedron Lett.* **2002**, *43*, 9717 – 9719.

[532] J. H. Boyer, *J. Am. Chem. Soc.* **1951**, *73*, 5248 – 5252.

[533] M. Casey, J. A. Donnelly, J. C. Ryan, S. Ushioda, *ARKIVOC* **2003**, *7*, 310 – 327.

[534] G. Denecker, G. Smets, G. L'Abbé, *Tetrahedron* **1975**, *31*, 765 – 775.

[535] G. J. Ho (Merck, USA), US Patent 13595P, **1996** [*Chem. Astr.* **1996**, *128*, 114952].

[536] J.-M. Vandensavel, G. Smets, G. L'Abbé, *J. Org. Chem.* **1973**, *38*, 675 – 678.

[537] H. C. Brown, A. Suzuki, S. Sono, M. Itoh, M. M. Midland, *J. Am. Chem. Soc.* **1971**, *93*, 4329 – 4330.

[538] P. Paetzold, P. P. Habereder, *J. Organomet. Chem.* **1967**, *7*, 61 – 70.

[539] H. C. Brown, M. M. Midland, A. B. Levy, A. Suzuki, S. Sono, M. Itoh, *Tetrahedron* **1987**, *43*, 4079 – 4088.

[540] H. C. Brown, M. M. Midland, A. B. Levy, *J. Am. Chem. Soc.* **1973**, *95*, 2394 – 2396.

[541] B. Koroskenyi, R. Faust, *Polymer Prepr. (ACS)* **1998**, *39*, 492 – 493.

[542] D. S. Matteson, G. Y. Kim, *Org. Lett.* **2002**, *4*, 2153 – 2155.

[543] P. Y. Chavant, F. Lhermitte, M. Vaultier, *Synlett* **1993**, 519 – 521.

[544] B. Carboni, M. Vaultier, T. Courgeon, R. Carrie, *Bull. Soc. Chim. Fr.* **1989**, 844 – 849.

[545] H. C. Brown, A. M. Salunkhe, B. Singaram, *J. Org. Chem.* **1991**, *56*, 1170 – 1175.

[546] a) S. Rozen, M. Carmeli, *J. Am. Chem. Soc.* **2003**, *125*, 8118 – 8119; b) G. K. S. Prakash, M. Etzorn, *Angew. Chem.* **2004**, *116*, 26 – 28; *Angew. Chem. Int. Ed.* **2004**, *43*, 26 – 28.

[547] S. Kim, G. H. Joe, J. Y. Do, *J. Am. Chem. Soc.* **1993**, *115*, 3328 – 3329.

[548] M. J. McManus, G. A. Berchtold, D. M. Jerina, *J. Am. Chem. Soc.* **1985**, *107*, 2977 – 2978.

[549] A. Gagneux, S. Winstein, W. G. Young, *J. Am. Chem. Soc.* **1960**, *82*, 5956 – 5957.

[550] K. Schulze, F. Richter, *Z. Chem.* **1983**, *23*, 96.

[551] G. L. Closs, A. M. Harrison, *J. Org. Chem.* **1972**, *37*, 1051 – 1052.

[552] T. A. Kale, M. D. Distefano, *Org. Lett.* **2003**, *5*, 609 – 612.

[553] a) E. Cubero, M. Orozco, F. J. Luque, *J. Am. Chem. Soc.* **1998**, *120*, 4723 – 4731; b) E. Kessenich, K. Polborn, S. Schulz, *Inorg. Chem.* **2001**, *40*, 1102 – 1109; c) A. H. Dabbagh, A. R. Modarresi-Alam, *J. Chem. Res.* **2000**, 44 – 45; d) D. Kurz, J. Reinhold, *J. Mol. Struct.: Theochem.* **1999**, *492*, 187 – 196; e) P. Cmoch, H. Korczak, L. Stefaniak, G. A. Webb, *J. Phys. Org. Chem.* **1999**, *12*, 470 – 478; f) T. Lioux, G. Gosselin, C. Mathe, *Eur. J. Org. Chem.* **2003**, 3997 – 4002.

[554] M. G. Yang, D. P. Modi, R. R. Wexler, R. E. Olson, *Tetrahedron Lett.* **2004**, *45*, 111 – 112, and references therein.

[555] a) P. B. Alper, M. Hendrix, P. Sears, C.-H. Wong, *J. Am. Chem. Soc.* **1998**, *120*, 1965 – 1978; b) C.-H. Wong, M. Hendrix, D. D. Manning, C. Rosenbohm, W. A. Greenberg, *J. Am. Chem. Soc.* **1998**, *120*, 8319 – 8327.

[556] a) For a Review, see: C. A. A. van Boeckel, M. Petitou, *Angew. Chem.* **1993**, *105*, 1741 – 1761; *Angew. Chem. Int. Ed. Engl.* **1993**, *32*, 1671 – 1690; b) H. A. Orgueira, A. Bartolozzi, P. Schell, P. H. Seeberger, *Angew. Chem.* **2002**, *114*, 2232 – 2235; *Angew. Chem. Int. Ed.* **2002**, *41*, 2128 – 2131.

[557] F. Debaene, N. Winssinger, *Org. Lett.* **2003**, *5*, 4445 – 4447

[558] T. Ainai, Y.-G. Wang, Y. Tokoro, Y. Kobayashi, *J. Org. Chem.* **2004**, *69*, 655 – 659.

[559] B. Plietker, M. Niggemann, *Org. Lett.* **2003**, *5*, 3353 – 3356.

[560] T. Kanemitsu, P. H. Seeberger, *Org. Lett.* **2003**, *5*, 4541 – 4544.

[561] For further classic examples, see: a) pantetheins: E. L. Wittle, J. A. Moore, R. W. Stipek, F. E. Peterson, V. M. McGlohon,

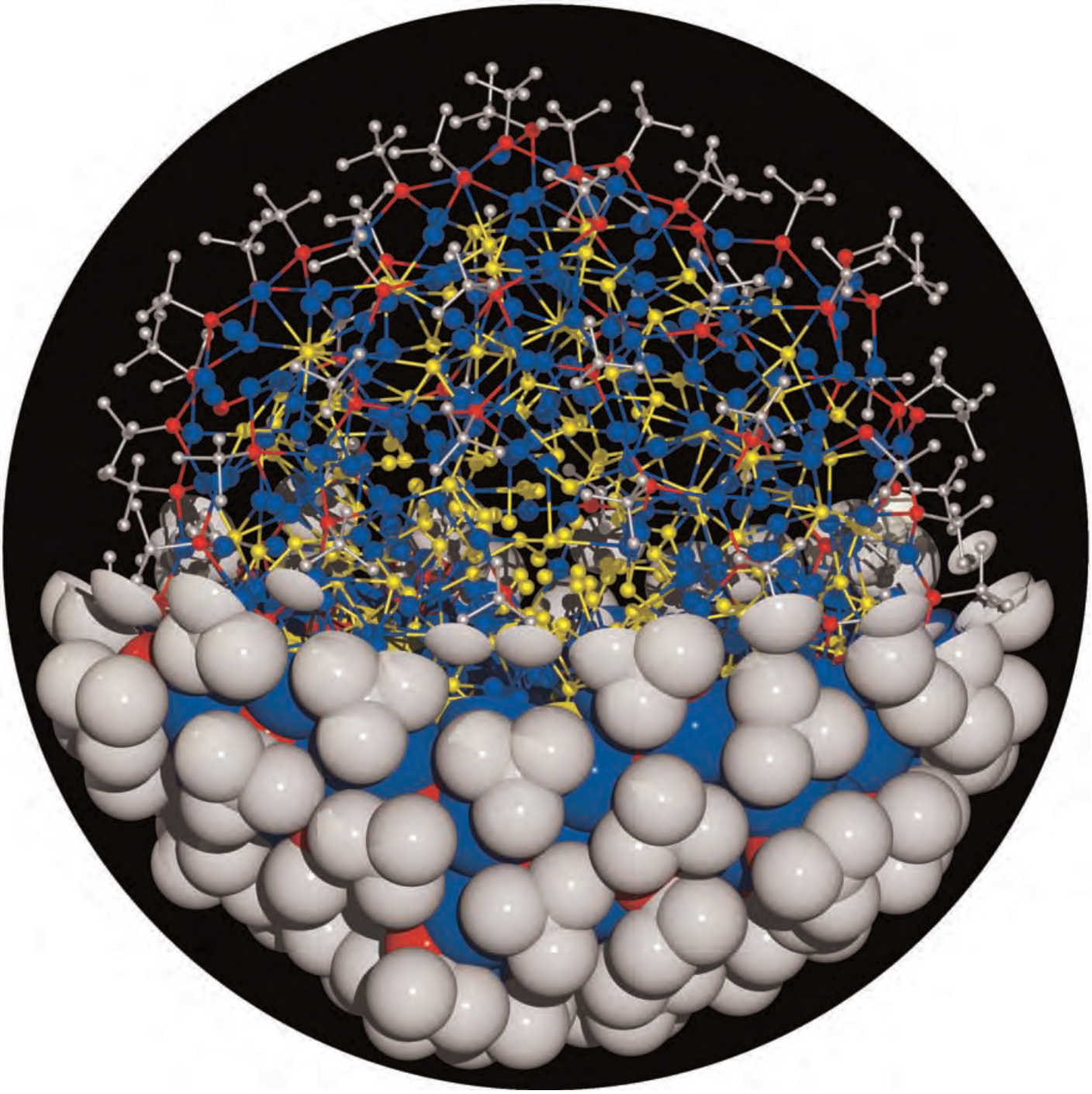
 © 2005 Wiley-VCH Verlag GmbH & Co. KGaA, Weinheim

O. D. Bird, G. M. Brown, E. E. Snell, *J. Am. Chem. Soc.* **1953**, *75*, 1694 – 1700; b) conessin: D. H. Barton, L. R. Morgan, *J. Chem. Soc.* **1962**, 622 – 631.
[562] Physicochemically, the azide ion is indeed isosteric with the isocyanate ion, but because of the sensitivity of isocyanates towards hydrolysis this is not consequential for the following considerations;
[563] A. G. Habeeb, P. N. P. Rao, E. E. Knaus, *J. Med. Chem.* **2001**, *44*, 3039 – 3042.
[564] S. Piantadosi, C. J. Marasco, E. J. Modest, *J. Med. Chem.* **1991**, *34*, 1408 – 1414.
[565] T. Pathak, *Chem. Rev.* **2002**, *102*, 1623 – 1667.
[566] C. A. Gartner, *Curr. Med. Chem.* **2003**, *10*, 671 – 689.
[567] a) S. A. Fleming, *Tetrahedron* **1995**, *51*, 12479 – 12520; b) for examples (fullerenes), see: E. Okada, Y. Komazawa, M. Kuriwara, H. Inoue, N. Miyata, H. Okada, T. Tsuchiya, Y. Yamakochi, *Tetrahedron Lett.* **2004**, *45*, 527 – 529.
[568] K. G. Pinney, M. P. Mejia, V. M. Villalobos, B. E. Rosenquist, G. R. Pettit, P. Verdier-Pinard, E. Hamel, *Bioorg. Med. Chem. Lett.* **2000**, *10*, 2417 – 2425.
[569] a) K. A. H. Chehade, K. Kiegiel, R. J. Isaacs, J. S. Pickett, K. E. Bowers, C. A. Fierke, D. A. Andres, H. P. Spielmann, *J. Am. Chem. Soc.* **2002**, *124*, 8206 – 8219; b) F. Mesange, M. Sebbar, J. Capdevielle, J.-C. Guillemot, P. Ferrara, F. Bayard, M. Poirot, J.-C. Faye, *Bioconjugate Chem.* **2002**, *13*, 766 – 772.
[570] a) P. Maienfisch, J. Haettenschwiler, A. Rindlisbacher, A. Decock, H. Wellmann, H. Kayser, *Chimia* **2003**, *57*, 710 – 714; b) S. Kagabu, P. Maienfisch, A. Zhang, J. Granda-Minones, J. Haettenschwiler, H. Kayser, T. Maetzke, J. E. Casida, *J. Med. Chem.* **2000**, *43*, 5003 – 5009.
[571] a) E. Mappus, C. Chambon, B. Fenet, M. Rolland de Ravel, C. Grenot, C. Y. Cuilleron, *Steroids* **2000**, *65*, 459 – 481; b) photochemical knock-out in vivo: J. J. Chambers, H. Gouda, D. M. Young, I. D. Kuntz, P. M. England, *J. Am. Chem. Soc.* **2004**, *126*, 13886 – 13887.
[572] a) F. Teixeira-Clerc, S. Michalet, A. Menez, P. Kessler, *Bioconjugate Chem.* **2003**, *14*, 554 – 562; b) S. C. Alley, F. T. Ishmael, A. D. Jones, S. J. Benkovic, *J. Am. Chem. Soc.* **2000**, *122*, 6126 – 6127.
[573] D. Hu, M. Crist, X. Duan, F. A. Quiocho, F. S. Gimble, *J. Biol. Chem.* **2000**, *275*, 2705 – 2712.
[574] K. L. Buchmueller, B. T. Hill, M. S. Platz, K. M. Weeks, *J. Am. Chem. Soc.* **2003**, *125*, 10850 – 10861.
[575] For a large number of current publications on organic azides, see: http://www.azides.org.
[576] a) B. B. Snider, J. Zhou, *J. Org. Chem.* **2005**, *70*, 1087 – 1088; b) V. Mascitti, E. J. Corey, *J. Am. Chem. Soc.* **2004**, *126*, 15664 – 15665; c) M. P. Cassidy, A. D. Oezdemir, A. Padwa, *Org. Lett.* **2005**, *7*, 1339 – 1342.
[577] L. Wang, P. G. Schultz, *Angew. Chem.* **2005**, *117*, 34 – 68; *Angew. Chem. Int. Ed.* **2005**, *44*, 34 – 66.
[578] a) P. F. van Swieten, M. A. Leeuwenburgh, B. M. Kessler, H. S. Overkleeft, *Org. Biomol. Chem.* ***2005***, *3*, 20 – 27; b) L. Ballell, K. J. Alink, M. Slijper, C. Versluis, R. M. J. Liskamp, R. J. Pieters, *ChemBioChem* **2005**, *6*, 291 – 295.
[579] a) D. Ermolat'ev, W. Dehaen, E. van der Eycken, *QSAR Comb. Sci.* **2004**, *23*, 915 – 918; b) Y.-M. Wu, J. Deng, X. Fang, Q.-Y. Chen, *J. Fluorine Chem.* **2004**, *125*, 1415 – 1423; c) L. Zhu, V. M. Lynch, E. V. Anslyn, *Tetrahedron* **2004**, *60*, 7267 – 7275.
[580] S. Punna, J. Kuzelka, Q. Wang, M. G. Finn, *Angew. Chem.* **2005**, *117*, 2255 – 2260; Angew. Chem. Int. Ed. **2005**, 44, 2215 – 2220.
[581] a) V. P. Mocharla, B. Colasson, L. V. Lee, S. Roeper, K. B. Sharpless, C. H. Wong, H. C. Kolb, *Angew. Chem.* **2005**, *117*, 118 – 122; *Angew. Chem. Int. Ed.* **2005**, *44*, 116 – 120; b) Y. Bourne, H. C. Kolb, Z. Radic, K. B. Sharpless, P. Taylor, P. Marchot, *Proc. Natl. Acad. Sci. USA* **2004**, *101*, 1449 – 1454; c) R. Manetsch, A. Krasinski, Z. Radic, J. Raushel, P. Taylor, K. B. Sharpless, H. C. Kolb, *J. Am. Chem. Soc.* **2004**, *126*, 12809 – 12818.
[582] a) V. O. Rodionov, V. V. Fokin, M. G. Finn, *Angew. Chem.* **2005**, *117*, 2250 – 2255; *Angew. Chem. Int. Ed.* **2005**, *44*, 2210 – 2215; b) F. Himo, T. Lovell, R. Hilgraf, V. V. Rostovtsev, L. Noodleman, K. B. Sharpless, V. V. Fokin, *J. Am. Chem. Soc.* **2005**, *127*, 210 – 216.
[583] J. A. Opsteen, C. M. van Hest, *Chem. Commun.* **2005**, 57 – 59.
[584] J. M. Mahoney, C. R. Smith, J. N. Johnston, *J. Am. Chem. Soc.* **2005**, *127*, 1354 – 1355.
[585] For a paper on the phosphine effect, see: D. P. Curran, X. Wang, Q. Zhang, *J. Org. Chem.* **2005**, *70*, 3716 – 3719.
[586] M. S. M. Timmer, M. D. P. Mattie, M. Verdoes, D. V. Filippov, J. R. Plaisier, G. A. van der Marel, H. S. Overkleeft, J. H. van Boom, *Tetrahedron: Asymmetry* **2005**, *16*, 177 – 185.
[587] a) L. R. Comstock, S. R. Rajski, *Nucleic Acids Res.* **2005**, *33*, 1644 – 1652; b) A. Bianchi, A. Russo, A. Bernardi, *Tetrahedron: Asymmetry* **2005**, *16*, 381 – 386; c) J. Cai, X. Li, X. Yue, J. S. Taylor, *J. Am. Chem. Soc.* **2004**, *126*, 16324 – 16325.
[588] R. Merkx, A. J. Brouwer, D. T. S. Rijkers, R. M. J. Liskamp, *Org. Lett.* **2005**, *7*, 1125 – 1128.
[589] F. L. Lin, H. M. Hoyt, H. van Halbeek, R. G. Bergman, C. R. Bertozzi, *J. Am. Chem. Soc.* **2005**, *127*, 2686 – 2695.
[590] H. Pedersen, S. Sinning, A. Buelow, O. Wiborg, L. Falborg, M. Bols, *Org. Biomol. Chem.* **2004**, *2*, 2861 – 2869.
[591] a) I. Bae, H. Han, S. Chang, *J. Am. Chem. Soc.* **2005**, *127*, 2038 – 2039; b) J. Waser, H. Nambu, E. M. Carreira, *J. Am. Chem. Soc.* **2005**, *127*, 8294–8295.
[592] a) G. Cardillo, S. Fabbroni, L. Gentilucci, R. Perciaccante, F. Piccinelli, A. Tolomelli, *Org. Lett.* **2005**, *7*, 533 – 536; b) K. S. Feldman, M. R. Iyer, *J. Am. Chem. Soc.* **2005**, *127*, 4590 – 4591.
[593] a) O. V. Larionov, S. I. Kozhushkov, A. de Meijere, *Synthesis* **2005**, 158 – 160; b) G. Ricci, R. Ruzziconi, *J. Org. Chem.* **2005**, *70*, 1011 – 1018; c) A. Basso, L. Banfi, R. Riva, G. Guanti, *J. Org. Chem.* **2005**, *70*, 575 – 579.
[594] P. Roy, C. Dufresne, N. Lachance, J.-P. Leclerc, M. Boisvert, Z. Wang, Y. Leblanc, Abstr. Pap., 229th ACS National Meeting, San Diego, CA, USA, March 13 – 17, **2005**, ORGN-141.
[595] a) S. K. Ramanathan, J. Keeler, H.-L. Lee, D. S. Reddy, G. Lushington, J. Aubé, *Org. Lett.* **2005**, *7*, 1059 – 1062; b) S. Baskaran, P. G. Reddy, M. G. Sankar, M. Gomathi; Abstr. Pap., 229th ACS National Meeting, San Diego, CA, USA, March 13 – 17, 2005, ORGN-663; c) Y. Zeng, D. S. Srinivasa, E. Hirt, J. Aubé, *Org. Lett.* **2004**, *6*, 4993 – 4995.
[596] G. Papeo, H. Posteri, P. Vianello, M. Paola, M. Varasi, *Synthesis* **2004**, 2886 – 2892.
[597] a) For an overview, see: R. Hartung, L. Paquette, *Chemtracts* **2004**, *17*, 72 – 82; see also: b) G. Cami-Kobeci, J. M. J. Williams, *Chem. Commun.* **2004**, 1072 – 1073; c) L. Tafesse, D. J. Kyle, *Comb. Chem. High Throughput Screening* **2004**, *7*, 153 – 161.
[598] a) L. G. Marinescu, C. Pedersen, M. Bols, *Tetrahedron* **2005**, *61*, 123 – 127; b) C. M. Pedersen, L. G. Marinescu, M. Bols, *Org. Biomol. Chem.* **2005**, *3*, 816 – 822.
[599] A. Hammerl, T. M. Klapötke, P. Mayer, J. J. Weigand, *Propellants Explos. Pyrotech.* **2005**, *30*, 17 – 26.
[600] M. H. V. Huynh, M. A. Hiskey, J. G. Archuleta, E. L. Roemer, *Angew. Chem.* **2005**, *117*, 747 – 749; *Angew. Chem. Int. Ed.* **2005**, *44*, 737 – 739.
[601] R. Warmuth, S. Makowiec, *J. Am. Chem. Soc.* **2005**, *127*, 1084 – 1085.
[602] a) S. Mandel, J. Liu, C. M. Hadad, M. S. Platz, *J. Phys. Chem.* **2005**, *109*, 2816 – 2821; b) C. Carra, T. Bally, A. Albini, *J. Am. Chem. Soc.* **2005**, *127*, 5552 – 5562.

 © 2005 Wiley-VCH Verlag GmbH & Co. KGaA, Weinheim

Communications

DOI: 10.1002/anie.200501414



Silver carboxylates react with silylated sulfur compounds to yield the cluster complexes $[Ag_{123}S_{35}(StBu)_{50}]$ and $[Ag_{344}S_{124}(StBu)_{96}]$. The nanoscopic clusters have an ordered outer shell that comprises {AgS*t*Bu} groups, while the $\{(Ag_2S)_n\}$ core is disordered. For more information, see the Communication by D. Fenske et al. on the following pages.

WILEY InterScience DISCOVER SOMETHING GREAT
© 2005 Wiley-VCH Verlag GmbH & Co. KGaA, Weinheim

Cluster Compounds

DOI: 10.1002/anie.200501414

Syntheses and Crystal Structures of $[Ag_{123}S_{35}(StBu)_{50}]$ and $[Ag_{344}S_{124}(StBu)_{96}]$**

Dieter Fenske, Christopher E. Anson, Andreas Eichhöfer, Olaf Fuhr, Arnd Ingendoh, Claudia Persau, and Clemens Richert*

Dedicated to Professor Malcolm H. Chisholm on the occasion of his 60th birthday

We have recently reported the syntheses of metal-rich silver chalcogenide clusters.[1] Examples of these are $[Ag_{70}S_{16}(SPh)_{34}(PhCO_2)_4(triphos)_4]$, $[Ag_{70}S_{20}(SPh)_{28}(dppm)_{20}](CF_3CO_2)_2$, $[Ag_{188}S_{94}(PnPr_3)_{20}]$, and $[Ag_{262}S_{100}(StBu)_{62}(dppb)_6]$ (triphos = 1,1,1-tris(diphenylphosphinomethyl)-ethane, dppm = bis(diphenylphosphino)methane, dppb = 1,4-bis(diphenylphosphino)butane). These compounds are formed in high yield by the reaction of silylated sulfur compounds with silver salts. The reaction of $AgCF_3CO_2$ with $PnPr_3$ and $S(SiMe_3)_2$ yields $[Ag_{188}S_{94}(PnPr_3)_{20}]$, whereas $[Ag_{262}S_{100}(StBu)_{62}(dppb)_6]$ is formed from the reaction of $AgPhCO_2$ and dppb with a mixture of $S(tBu)SiMe_3$ and $S(SiMe_3)_2$ in THF.[1] Both compounds contain unusual sections of the structure of binary silver sulfide;[2–4] these Ag–S cluster cores are surrounded by tertiary phosphines or S*t*Bu groups. Such compounds can be regarded as intermediary stages in the formation of Ag_2S, in which phosphine and S*t*Bu ligands have inhibited further growth of the cluster core towards crystalline Ag_2S. A striking feature of these structures is the tendency to disorder shown by the anions and cations. In this respect the molecules already possess to a large extent the properties of the binary Ag_2S phase.[2–4] $[Ag_{188}S_{94}(PnPr_3)_{20}]$ is a spheroidal molecule which has a Ag_2S core with a diameter of 1.9 nm. In $[Ag_{262}S_{100}(StBu)_{62}(dppb)_6]$ the molecules have the form of oblate ellipsoids, in which the Ag–S cluster has a maximum diameter of 2.6 nm. In the course of studying size-dependent properties, such as the conductivity of electrons and Ag^+ ions, which could also possibly be studied in single molecules, we have attempted to synthesize further examples of this class of molecules.

To prepare $[Ag_{123}S_{35}(StBu)_{50}]$ (**1**), a suspension of $AgCH_3CO_2$ and 1,4-bis(diphenylphosphinomethyl)benzene (dppxy) in toluene is treated with a mixture of $S(tBu)SiMe_3$ and $S(SiMe_3)_2$. A red solution results, from which, over a few days, dark brown crystals of **1** are formed [Eq. (1)].

$$AgCH_3CO_2 + 0.9\,S(tBu)SiMe_3 + 0.5\,S(SiMe_3)_2 \xrightarrow[\text{toluene}]{0.25\,\text{dppxy}} \mathbf{1} \quad (1)$$

$[Ag_{344}S_{124}(StBu)_{96}]$ (**2**) is formed by the analogous reaction of $AgPhCO_2$, dppxy, $S(tBu)SiMe_3$, and $S(SiMe_3)_2$ in toluene [Eq. (2)]. It can also be prepared by treating AgS*t*Bu with $S(SiMe_3)_2$ in toluene [Eq. (3)]. In both cases, a red solution forms initially, which darkens after a few days. After several weeks, black crystals of **2** form. The formation of **1** and **2** apparently occur via an intermediate, as red crystals appear in the red solution and later dissolve. However, the structures of these red compounds have so far not been determined.

$$AgPhCO_2 + S(tBu)SiMe_3 + 0.5\,S(SiMe_3)_2 \xrightarrow[\text{toluene}]{0.25\,\text{dppxy}} \mathbf{2} \quad (2)$$

$$AgStBu + 0.5\,S(SiMe_3)_2 \xrightarrow[\text{toluene}]{0.25\,\text{dppxy}} \mathbf{2} \quad (3)$$

In contrast to the above-mentioned Ag_{188} and Ag_{262} clusters, which are formed under similar conditions, **1** and **2** do not contain phosphine ligands. Apparently dppxy is necessary for the formation of these compounds, because otherwise a mixture of Ag_2S and AgS*t*Bu is obtained. The formation of **2** from the reaction of AgS*t*Bu with $S(SiMe_3)_2$ in the presence of dppxy is not understood; possibly $S(tBu)SiMe_3$ is formed as a leaving group.

A crystal structure analysis[5] shows that **1** crystallizes in the space group $R\bar{3}c$ with six molecules per unit cell and 15 toluene molecules per formula unit. Assuming the presence of a cluster molecule with the formula $[Ag_{123}S_{35}(StBu)_{50}]$, then cluster should be a cation with a charge of 3+. However, a close inspection of the structure did not reveal the presence of $CH_3CO_2^-$ counterions. It is therefore assumed that there is a nonstoichiometric Ag:S ratio, as has been found in other metal chalcogenide clusters.[1,11] This situation is not surprising, because this effect is also observed in solid Ag_2S.[3]

From Figure 1, it can be seen that the sulfur atoms of the S*t*Bu groups act either as μ_2- or μ_3-ligands (μ_2: Ag–S (S1, S2, S4): 2.400–2.439(5) Å; μ_3 Ag–S: (S3, S5–S9): 2.211–2.686(4) Å).[5] The S^{2-} ions show a range of bonding modes. S11 is a μ_4-ligand with Ag–S distances of 2.392–2.576(3) Å. In contrast, S10 and S12–S14 are bonded as μ_5-ligands and S15 and S16 as μ_7-ligands ((μ_5-S)-Ag: 2.346–2.953(3) Å; (μ_7-S)-Ag: 2.585–2.937(5) Å).

The silver atoms Ag2, Ag5, Ag8–Ag10, Ag12, Ag13, Ag16, and Ag18–Ag20 are coordinated by two sulfur atoms in a nearly linear arrangement (Ag–S: 2.387–2.594(5) Å; S-Ag-S: 131.2–172.5(1)°). The Ag atoms Ag1, Ag4, Ag5, Ag7, Ag11, Ag14, Ag17, Ag21, and Ag23 (Ag–S: 2.211–2.960(4) Å) are each linked to three sulfur atoms in a quasiplanar environment. Ag6 has a distorted tetrahedral coordination of four sulfur atoms (Ag–S: 2.529–2.687(3) Å),

[*] Prof. Dr. D. Fenske, Dr. C. E. Anson, Dr. A. Eichhöfer, Dr. O. Fuhr, Dr. C. Persau
Institut für Anorganische Chemie der Universität Karlsruhe
Engesserstrasse 15, Geb. 30.45, 76131 Karlsruhe (Germany)
and
Institut für Nanotechnologie, Forschungszentrum Karlsruhe
Fax: (+49) 721-608-8440
E-mail: dieter.fenske@aoc1.uni-karlsruhe.de
Dr. A. Ingendoh
Bruker Daltronik GmbH
Fahrenheitstrasse 4, 28359 Bremen (Germany)
Prof. Dr. C. Richert
Institut für Organische Chemie der Universität Karlsruhe
Fritz-Haber-Weg 6, Geb. 30.42, 76131 Karlsruhe (Germany)

[**] This work was supported by the Deutsche Forschungsgemeinschaft (Center for Functional Nanostructures) and the Fonds der Chemischen Industrie.

 © 2005 Wiley-VCH Verlag GmbH & Co. KGaA, Weinheim

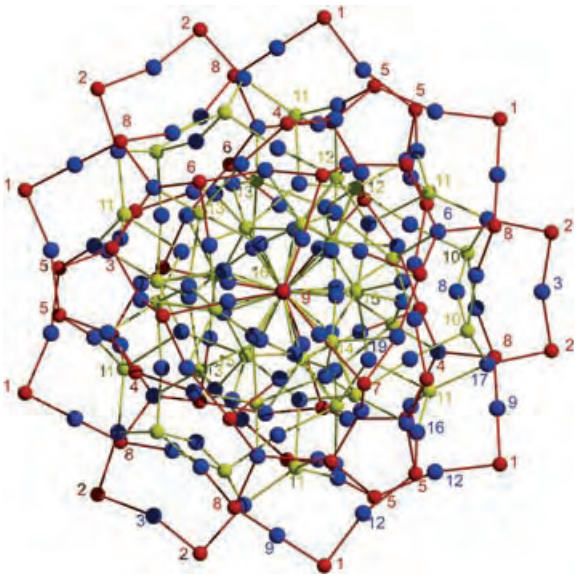


Figure 1. Molecular structure of **1** with *t*Bu groups omitted. For clarity the atoms are only numbered: blue: Ag^+; red: S atoms of the S*t*Bu groups; yellow: S^{2-} atoms.

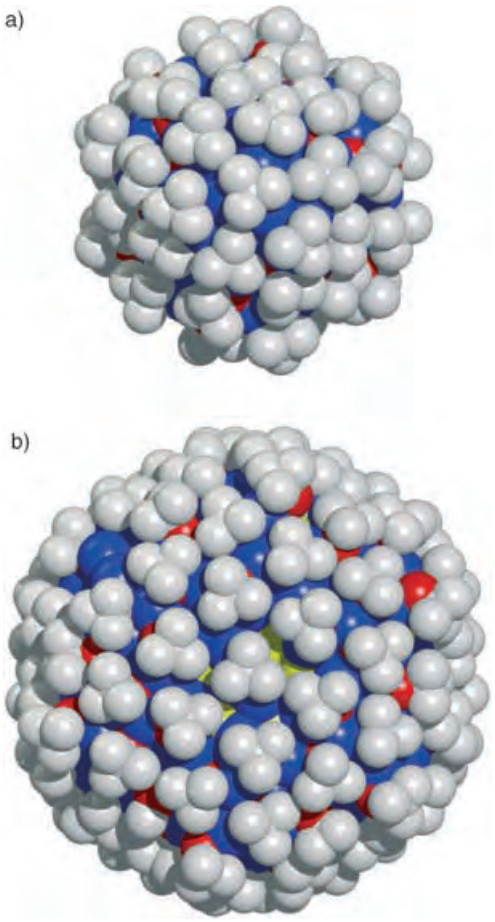


Figure 2. Space-filling models of a) **1** and b) **2** to the same scale. Gray: C; blue: Ag^+; red: S atoms of the S*t*Bu groups; yellow: S^{2-}.

and Ag22, which is at the center of the cluster, has a trigonal-bipyramidal coordination sphere (Ag–S: 2.692–2.937(5) Å).

The space-filling model of **1** in Figure 2a shows that the Ag-S-core, which has a maximum diameter of 1.7–2.0 nm, is completely shielded by the *t*Bu groups of the S*t*Bu ligands in the oblate-spheroidal cluster. Further cluster growth is thus not possible. The maximum diameter of the molecule including the *t*Bu groups is 2.0–2.5 nm.

Surprisingly, the use of another silver salt ($AgPhCO_2$ or Ag*S*t*Bu instead of $AgCH_3CO_2$) leads to the formation of the metal-rich cluster **2**. Crystal-structure analysis[5] shows that **2** crystallizes in the space group *C*2/*c* with four molecules per unit cell. The cluster molecules form a quasi cubic close packing in the lattice, with the 12 disordered toluene molecules per formula unit situated in the holes.

In Figure 2b a space-filling diagram of **2** is shown. As in **1**, the cluster surface is covered exclusively by *t*Bu groups. The maximum total diameter of the molecule is 3.7 nm. The molecular shape is similar to am ellipsoid, which has a minor diameter of 2.6 nm (see Figure 4b). The dimensions of the Ag–S core are 3.2 and 2.2 nm. A precise description of the formula of **2** is, however, not possible from the structural analysis alone. The molecules are clearly not well ordered in the lattice. This is apparent since when using $Mo_{K\alpha}$ radiation there are almost no reflections above $2\theta = 36°$ with significant intensity.

Disorder in the cluster renders a full discussion of the molecular structure impossible. We have measured 20 data sets from different crystals at different temperatures. None of these led to an improved interpretation of the structure. It is of note, however, that the outermost cluster layer of 96 Ag*S*t*Bu groups is ordered. The nearer the Ag and S atoms lie to the center of the cluster, the higher the degree of disorder. This situation is revealed in the higher temperature factors of the inner Ag and S layers. In this sense **2** is comparable with the structure of $[Ag_{262}S_{100}(StBu)_{62}]$, although the degree of disorder is clearly higher in **2**. In both cases an there is an ordered layer surrounding a solid solution of Ag_2S. Assuming that nonbonding Ag–Ag distances are greater than 2.80 Å, and bonding Ag–S interactions are in the range 2.40–2.90 Å, the formula $[Ag_{344}S_{124}(StBu)_{96}]$ can be obtained. The elemental analysis of **2** is in excellent agreement with this formula.[6] The experimental density of the crystal is also consistent with the density calculated from the X-ray crystal structure. The MALDI-TOF mass spectrum of **2**[7] shows broad mass distribution with maxima at *m*/*z* 49446, 93104, 135586, 176572, and 216487 (Figure 3). At higher resolution, molecular ions with *m*/*z* 258028 and 298149 can be assigned. The molecular weight of **2** (49.645 kDa) is, allowing for the errors in the determination of the peak maxima, in good agreement with the signal at *m*/*z* 49446. Note, however, that the fragmentation of the molecule is such that it leads to a very broad size distribution. Between the individual maxima a difference of approximately 41.5 kDa is found. This mass could be assigned to $[Ag_{344}S_{124}]^+$ (41.046 kDa), the molecule fragment of **2** from which all the S*t*Bu groups have been lost. The higher masses are likely to result from aggregates with unknown composition, which are formed from these molecular ions under the conditions of the MALDI-TOF experiment.[7]

 © 2005 Wiley-VCH Verlag GmbH & Co. KGaA, Weinheim

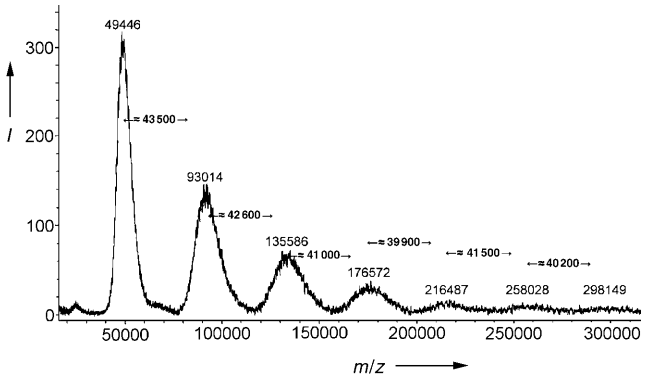


Figure 3. MALDI-TOF spectrum of **2**.

MALDI-TOF mass spectrometry has only recently been shown to be a significant technique for the characterization of ZnS nanoparticles. It is clear that it offers the possibility to characterize related materials.[8]

Additional evidence for the proposed formula of **2** is obtained through transmission electron microscopy (TEM) investigations of the reaction solutions from the synthesis of **2**. Such TEM images,[9] shows particles with a monodisperse size distribution and a diameter of approximately 3 nm (Figure 4).

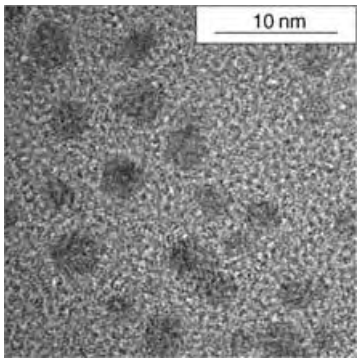


Figure 4. Electron microscope image of cluster **2**.

This diameter corresponds to the size of the Ag-S-core in **2**. Further elucidation of the structure of the cluster is however not possible, since upon irradiation of the cluster for a long time the Ag–S cluster is converted into silver. This change is to be expected since Ag_2S decomposes at temperatures above 200 °C. Further discussion of the structure of **2** is therefore not realistic. Figure 5 illustrates the molecular structure from two directions, with the disorder omitted for clarity. The sulfur atoms of the S*t*Bu groups act as μ_2- and μ_3-bridging ligands. The Ag–S distances are similar to those found in **1**.

It is possible that the observed disorder is an intrinsic problem of nanoscopic Ag–S clusters. The surface tension of these particles gives rise to a Laplace pressure which in turn leads to a pressure within the particles, which is dependent upon particle radius.[13] This pressure can result in disorder or a phase change. The transition of crystalline *a*-Ag_2S into the tetragonal high-pressure phase has been reported.[12] Another explanation is that interactions between defects in the cluster

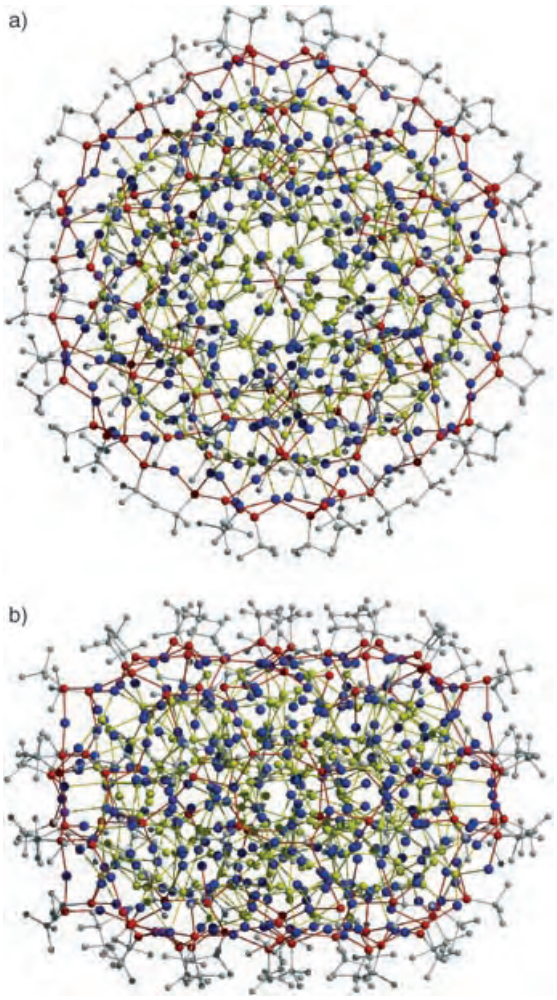


Figure 5. a) and b) Molecular structure of **2** viewed from two directions. For clarity, the disorder is omitted. Image (b) is rotated by 90° relative to image (a). Color code as for Figure 2.

can lead to a rise in the concentration of defects. This defect concentration is temperature dependent.[10] To test this idea we have collected X-ray data sets over the temperature range 100–200 K. Measurement at higher temperatures is not possible because the crystals lose solvent of crystallization and become amorphous. Over this temperature range, however, no increase in the disorder could be determined.

In conclusion, **1** and **2** can be described as core–shell particles. In **1** the core is $\{(Ag_2S)_{35}Ag_3\}^-$, and in **2** $\{(AgS)_{124}\}$, the core in **1** is surrounded by a shell of 50 S*t*Bu units and in **2** by 96 S*t*Bu units. We believe that clusters that are metal-richer and have larger particle diameters can be synthesized. These may, as a consequence of the lower Laplace pressure, have an ordered $\{(Ag_2S)_n\}$ core.

It is emphasized that the syntheses of **1** and **2** are reproducible under the described conditions. Small changes, such as the choice of solvent or the ratio of the amounts of starting materials, however lead to the formation of cubic or needle-like crystals, the structures of which we have not yet determined. The unit cell volumes of these crystals are however significantly larger than those of **1** and **2**. It is likely that current analytical techniques will reach the limits of their

 © 2005 Wiley-VCH Verlag GmbH & Co. KGaA, Weinheim

ability to characterize these compounds, and precise formulations and crystal-structure determinations may at present not be possible.

Experimental Section

All processes were carried out with the exclusion of water and oxygen in an atmosphere of purified N_2.

1: $AgCH_3CO_2$ (0.167 g, 1 mmol) and dppxy (0.119 g, 0.25 mmol) were suspended in toluene (20 mL), and S(*t*Bu)SSiMe$_3$ (0.16 mL, 0.9 mmol) was added at room temperature. The solution became yellow, then orange. After the mixture had been stirred for 5 min, $S(SiMe_3)_2$ (0.08 mL, 0.5 mmol) was added at room temperature. After a few hours the solution became deep red, and undissolved starting material was slowly consumed. The solution was stirred for a further 2 h and then allowed to rest. After four to six weeks dark brown rhombic crystals of **1** formed with a yield of 40 %.

2: $AgPhCO_2$ (0.23 g, 1 mmol) and dppxy (0.119 g, 0.25 mmol) were suspended in toluene (25 mL), and S(*t*Bu)SiMe$_3$ (0.18 mL, 1 mmol) was added at room temperature. The mixture became orange-red and contained residual starting material. After the mixture had been stirred for 5 min, $S(SiMe_3)_2$ (0.08 mL, 0.5 mmol) was added and after a further 30 min the mixture was heated to reflux. The solution became clear and deep red. After the solution was allowed to cool to room temperature, red crystals formed and then dissolved, and after 3–5 weeks black crystals of **2** were formed in 60 % yield.

In the alternative synthesis of **2** a suspension of AgS*t*Bu (0.1 g, 0.5 mmol) with dppxy (0.06 g, 0.125 mmol) in toluene (25 mL) was mixed with $S(SiMe_3)_2$ (0.04 mL, 0.25 mmol). The solution, cloudy from undissolved starting material, initially turned red. Brief heating to reflux yielded a clear deep red solution, which then rapidly became dark brown. After the solution was allowed to cool to room temperature, black crystals of **2** formed in 30–50 % yield over several weeks.

Received: April 25, 2005
Published online: July 29, 2005

Keywords: cluster compounds · mass spectrometry · silver · structure elucidation · sulfur

[1] a) X. J. Wang, T. Langetepe, C. Persau, B. S. Kang, G. S. Sheldrick, D. Fenske, *Angew. Chem.* **2002**, *114*, 3972 – 3977; *Angew. Chem. Int. Ed.* **2002**, *41*, 3818 – 3822; b) D. Fenske, C. Persau, S. Dehnen, C. E. Anson, *Angew. Chem.* **2004**, *116*, 309 – 313; *Angew. Chem. Int. Ed.* **2004**, *43*, 305 – 309.

[2] a) G. A. Wiggers, *Am. Mineral.* **1971**, *56*, 1882 – 1888; b) Z. G. Pinsker, C. Chiang Ling, R. M. Imamov, E. L. Lapidus, *Sov. Phys. Cristallogr. (Engl. Transl.)* **1965**, *7*, 225 – 233.

[3] a) F. C. Kracek, *Trans. Am. Geophys. Union* **1946**, *27*, 364; b) S. Djurle, *Acta Chem. Scand.* **1958**, *12*, 1427; c) P. Rahlfs, *Z. Phys. Chem. Abt. B* **1936**, *31*, 157 – 194; d) E. Rickert, *Z. Phys. Chem.* **1960**, *24*, 418 – 421; e) A. Böttcher, G. Haase, H. Treupel, *Z. Angew. Phys.* **1955**, *7*, 478 – 487; f) P. Junod, *Helv. Phys. Acta* **1959**, *32*, 567 – 600.

[4] A. J. Früh, *Z. Kristallogr.* **1958**, *110*, 136 – 144.

[5] Crystal structure analyses: Data were collected on a Stoe-IPDS2 diffractometer using $Mo_{K\alpha}$ radiation, corrected numerically for absorption, and refined using SHELX97 and SHELXD.[14] CCDC-269220 and CCDC-269221 contain the supplementary crystallographic data for this paper. These data can be obtained free of charge from The Cambridge Crystallographic Data Centre via www.ccdc.cam.ac.uk/data_request/cif. **1**: $C_{200}H_{450}Ag_{123}S_{85}\cdot 15\,C_7H_8$, $T = 123$ K, trigonal, space group $R\bar{3}c$ (No. 167), $Z = 6$, $a = 37.572(5)$, $c = 59.473(11)$ Å, $V = 72708.9$ Å^3, $\mu(Mo_{K\alpha}) = 5.24$ mm^{-1}; $2\theta_{max} = 50.2°$, 117415 data measured, of which 14158 were independent and 12430 with $I > 2\sigma(I)$, $R_{int} = 0.082$, $R_\sigma = 0.11$. 717 parameters (Ag, S: anisotropic, C: isotropic), max. final difference peak = 1.8 e Å^{-3}, $R_1 = 0.078$, $wR_2 = 0.23$. The Ag atoms were refined with full occupancy. Near Ag1 and Ag2 residual electron density of up to 10 e Å^{-3} was refined as partial-occupancy Ag atoms (X1–X7). Some *t*Bu groups were refined as disordered. **2**: $C_{384}H_{864}S_{220}Ag_{344}\cdot 12\,C_7H_8$, $T = 100$ K, monoclinic, space group $C2/c$ (No. 15), $Z = 4$, $a = 64.648(4)$, $b = 36.269(2)$, $c = 54.320(4)$ Å, $\beta = 118.14(1)°$, $V = 111444$ Å^3, $\mu(Mo_{K\alpha}) = 6.31$ mm^{-1}; $2\theta_{max} = 42°$; 182746 data measured, of which 80376 were independent and 39632 with $I > 2\sigma(I)$, $R_{int} = 0.053$, $R_\sigma = 0.086$; 3171 parameters (Ag, S: anisotropic; C: isotropic), max. final difference peak 6.3 e Å^{-3}, $R_1 = 0.137$; $wR_2 = 0.34$. Some Ag atoms within the cluster were refined with partial occupancies. Large ghost peaks were found up to 0.1 Å from these atoms and these were refined as partial-occupancy atoms (X1–X77). The silver atoms are labeled A1–A175; S1–S48 are the remaining S atoms, some of which are disordered. The C atoms of the 96 *t*Bu groups could be assigned from the Fourier difference maps. These were included in the final refinement as rigid groups (S–C 1.84 Å, C–C 1.54 Å, C···C 2.51 Å). Without modeling of the disorder, R_1 remained above 0.19.

[6] The toluene of crystallization was removed by heating the crystals to 40 °C in vacuo. Elemental analysis for the solvent-free crystals: (%) calcd for $C_{384}H_{864}S_{220}Ag_{344}$: C 9.29, H 1.75, S 14.21, Ag 74.75; found: C 9.62, H 1.66, S 13.88, Ag 74.40.

[7] a) We thank Dr. V. Sauerland (Bruker Daltronik GmbH, Fahrenheitstrasse 4, D-28359 Bremen) for help with measuring the MALDI-TOF spectra, using an Ultraflex MALDI-TOF mass spectrometer; b) Similar results were obtained using an Applied Biosystems Voyager System 6059 MALDI-TOF spectrometer. With nitroanthracene as matrix, the most intense peaks were distributed between *m*/*z* 48467 and 49901. By adjusting the instrumental parameters, the formation of higher molecular masses could be completely suppressed.

[8] G. A. Khitrov, G. F. Strouse, *J. Am. Chem. Soc.* **2003**, *125*, 10465 – 10469.

[9] Very dilute toluene solutions of **2** were used, which were dropped onto a graphite grid. We thank Dr. M. Wanner, Labor für Elektronenmikroskopie, Universität Karlsruhe, for his help in recording the TEM images.

[10] J. Maier, *Solid State Ionics* **2002**, *154–155*, 291 – 301; J. Maier, *Solid State Ionics* **2002**, *148*, 367 – 374; J. Maier, W. Münch, *Z. Anorg. Allg. Chem.* **2000**, *626*, 264 – 269.

[11] S. Dehnen, A. Eichhöfer, D. Fenske, *Eur. J. Inorg. Chem.* **2002**, 279 – 317, and references therein.

[12] L. H. Adams, B. L. Davis, *Am. J. Sci.* **1965**, *263*, 359 – 383.

[13] The Laplace pressure is the additional pressure which is operative under a curved liquid surface. This pressure is caused by the surface tension attempting to reduce the size of the droplet.

[14] G. M. Sheldrick, SHELX-97, Program for the Solution of Crystal Structures, Universität Göttingen, **1997**.

 © 2005 Wiley-VCH Verlag GmbH & Co. KGaA, Weinheim

Protein Structures

DOI: 10.1002/anie.200501887

Cooperative Binding of p53 to DNA: Regulation by Protein–Protein Interactions through a Double Salt Bridge**

*Alexander Dehner, Christian Klein, Silke Hansen, Lin Müller, Johannes Buchner, Manfred Schwaiger, and Horst Kessler**

The p53 protein is a transcription factor that regulates many cellular processes and acts as major tumor suppressor.[1–5] It is mutated to a loss of function in 50% of all human tumors, and the majority of these mutations occur in the DNA-binding domain (DBD).[6,7] So far, two main functional classes of p53 mutations have been identified: 1) mutations that affect direct contact with DNA and 2) mutations that destabilize the structural integrity of p53 (R249S, G245S, R175H, C242S, V143A).[8,9] They cause the Li–Fraumeni syndrome (LFS), which is based in germ-line mutations in the p53 gene. LFS is a familial, dominantly inherited cancer characterized by a wide range of neoplasms occurring in children and young adults.[10] Some Li–Fraumeni syndrome mutations such as E180X, localized in the proposed dimerization interface of the H1 helix region, do not fall into either of the above classes, and the reasons behind the observed cancer illness phenotypes were previously unknown.[11] Herein, we present a mutational study of solvent-exposed residues within the H1 helix region of p53. The results provide evidence for the presence of two intermolecular salt bridges, which are essential for cooperative DNA binding. Moreover, the absence of cooperativity observed[12] in the p53 family members[13] p63DBD and p73DBD can now be understood on a structural basis.

The complete p53 molecule contains 393 amino acids. It recognizes and binds a consensus sequence of promoter DNA in tetrameric, octameric, and higher oligomeric forms. There is currently no structural information about full-length p53 and its tetrameric organization bound to DNA, yet several reports discuss modeling of the interdomain contacts in p53[8,14–18] based on individual structures of p53DBD[14,17] and the tetramerization domain.[19–21] We have shown previously[22,23] that the DBD binds cooperatively to small (2×16 nucleotide) DNA sequences as dimers. Titrations of this oligonucleotide into ^{15}N-labeled p53DBD (monitored by NMR spectroscopy) allowed us to identify the protein–protein contact interface, and to postulate an essential role for the short H1 helix (P177–C182) in mediating intermolecular p53DBD dimerization. Furthermore, symmetry considerations led us to propose a model in which two antiparallel DNA strands bind p53 in its tetrameric state, whereby the tetramerization domain in the C-terminal fragment of p53 is in the center of this model complex.[22] However, no direct experimental proof has been presented for the participation of the H1 helix in protein–protein interactions upon p53 binding to DNA.

Herein, we report investigations of the possible role of H1 helix residues through site-directed mutagenesis and analysis of the ability of p53DBD mutants to bind to p53 consensus DNA by using electrophoretic mobility shift assays (EMSAs), NMR spectroscopic diffusion measurements, and fluorescence anisotropy measurements. The following dimerization mutations were introduced by site-directed mutagenesis: H178A, R181A, C182A, E180R, R181E, and one double-site mutation: E180R/R181E. Additionally, three alanine mutations H178A, R181A, and C182A and the R181E mutation were introduced into a GST fusion plasmid (GST = glutathione S transferase) yielding GST–mutant p53DBD fusion proteins. As the GST domain acts as an artificial dimerization domain, such constructs are expected to enhance the cooperative DNA binding affinity, as previously observed for p63DBD.[12]

Besides the structurally important residues that coordinate the zinc atom such as H179,[14] even the solvent-exposed residues of the H1 helix are highly conserved and mostly identical across various species, as illustrated by the sequence alignment of this region (Figure 1). An overlay of the ^{15}N HSQC spectra of all six mutants and the wild-type p53DBD is shown in Figure 2. Major differences in chemical shifts are only observed for signals of residues within the H1 helix or near the specifically mutated residues. Residues further away are only slightly affected by these mutations or not affected at all, which affords the conclusion that all dimerization mutants are folded in the native conformation. Addition of 0.5 equivalent of a decamer consensus DNA oligonucleotide (CON2x5; 5′-CCTAGACATGCCTAAT-3′, elongated by three nucleotides on each side) to the U-^{15}N-labeled p53DBD dimerization mutants resulted in changes in chemical shift and a strong line-broadening in the ^{15}N,^{1}H correlation spectrum of the protein. This is the result of a slow exchange process in the micro- to millisecond range, as has been observed for the wild-type p53DBD–DNA complex.[22,23] Addition of DNase II to the DNA–p53DBD dimerization mutant complexes restored the original spectrum of the respective p53DBD mutant, excluding protein degradation.

The translational diffusion coefficient of a molecule is proportional to its effective molecular weight and shape[24]

[*] Dr. A. Dehner, Dr. L. Müller, Prof. Dr. J. Buchner, Prof. Dr. Dr. H. Kessler
Department Chemie, Technische Universität München
Lichtenbergstrasse 4, 85747 Garching (Germany)
Fax: (+49) 89-289-13210
E-mail: Horst.Kessler@ch.tum.de
Dr. C. Klein, Dr. S. Hansen, Dr. M. Schwaiger
Roche Diagnostics GmbH, Pharma Research
Nonnenwald 2, 82372 Penzberg (Germany)

[**] We thank K. Bauer, R.-M. Busl-Schuller, and R. Schmitt (all Roche Diagnostics GmbH) and G. Gemmecker (TUM) for discussions, and A. Mertens, J. P. Hoelck, and M. Weidner (all Roche Diagnostics GmbH) for their support. Financial support by the Deutsche Forschungsgemeinschaft and the Fond der Chemischen Industrie is acknowledged.

Supporting information for this article is available on the WWW under http://www.angewandte.org or from the author.

 © 2005 Wiley-VCH Verlag GmbH & Co. KGaA, Weinheim

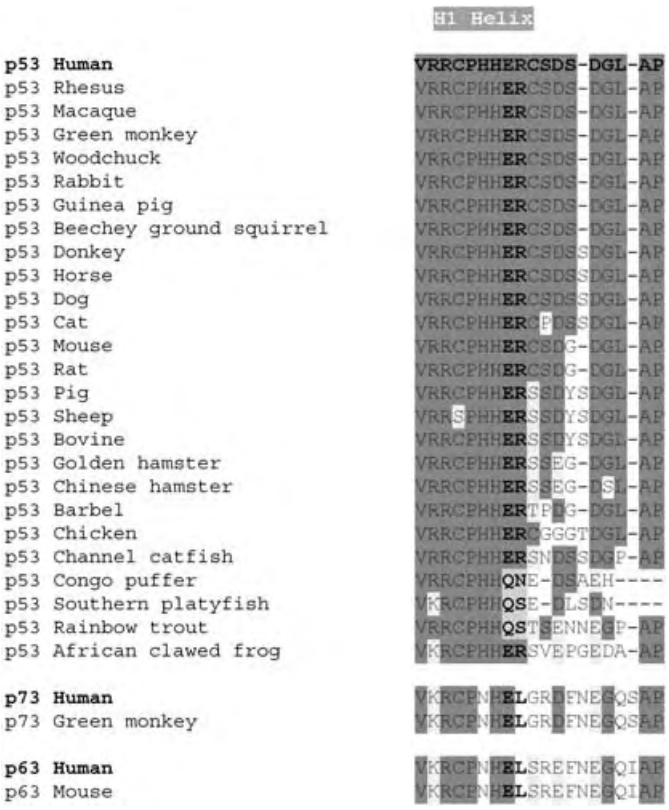


Figure 1. Primary structure alignment of the H1 helix regions of p53DBD and the homologous p63- and p73DBDs. Residues identical or similar to human p53 are shown in gray.

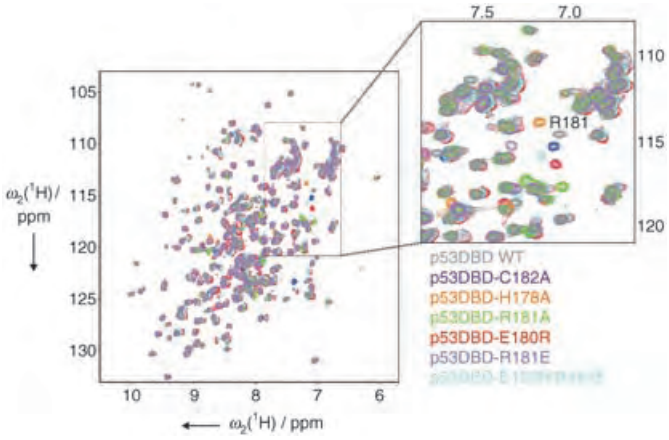


Figure 2. Superposition of the ^{15}N HSQC spectra of wild-type p53DBD (gray) and the six mutated p53DBD forms. The enlarged section shows residue R181 within the H1 helix.

and is therefore a sensitive gauge of changes in the overall molecule. Thus, measuring the diffusion rate is an independent way to study intermolecular interactions.[25–28] We analyzed the hydrodynamic properties of p53DBD dimerization mutants and their DNA binding by pulsed field gradient diffusion experiments.[29] The addition of the consensus oligonucleotide to wild-type p53DBD causes the diffusion coefficient of p53DBD to decrease by 27.1% (Figure 3). This

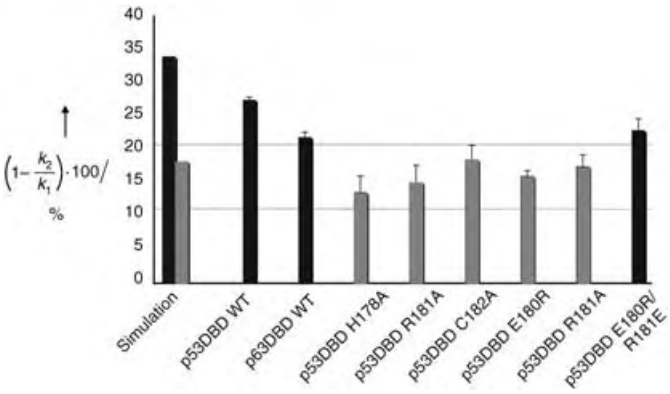


Figure 3. Decrease in the diffusion coefficients of p53DBD, p63DBD and the p53DBD dimerization mutants upon complex formation (k_2) with consensus DNA (CON2x5) as measured by pulsed field gradient NMR spectroscopy; black: cooperative DNA binding, gray: nonspecific DNA binding. A hydrodynamic simulation with a cooperative model complex with p53DBD/DNA = 2:1 yields a theoretical decrease of 33%, whereas a single-site binding of DNA (PDB code 1TSR, chain B, including DNA) results in a decrease of 18%.

is due to the cooperative binding of two p53DBDs to one decamer half-site consensus oligonucleotide. The measured value is in good agreement with hydrodynamic calculations performed with the shell model of HYDRONMR[30] and a dimeric p53DBD–DNA model complex as described by Klein et al.[22] This results in a theoretical decrease in the diffusion coefficient of about 33%. The monomeric p53DBD–DNA complex (PDB code 1TSR; chain B including the DNA) was also used for hydrodynamic calculations, and gave a decrease of 18% upon binding DNA relative to the coefficient of free p53DBD. These two theoretical values represent the expected range for an equilibrium between monomeric and fully cooperative DNA-bound forms. Deviations from theoretical and experimental data reflect an averaging of higher and lower oligomeric states.

Figure 3 illustrates the decrease in diffusion coefficient upon addition of 0.6 equivalent CON2x5 half-site oligonucleotide to obtain a stoichiometric DNA/p53DBD ratio of 1:2 for the wild-type DBD forms of p53 and p63 and the p53DBD dimerization mutants. As already indicated by ^{15}N HSQC titration experiments, all mutants bind to DNA, resulting in a decrease in diffusion rate of at least 13%. NMR spectroscopic experiments were performed in the absence of nonspecific competitor DNA; therefore, it cannot be concluded whether this overall decrease results from nonspecific or specific cooperative DNA binding. However, with experimental errors taken into consideration, two classes of p53 can be distinguished: p53DBD wild-type and the p53DBD E180R/R181E double-site mutant have a significantly higher population of oligomeric states upon DNA binding than all other p53DBD dimerization mutants (Figure 3). Therefore, p53DBD wild-type and the E180R/R181E double-site mutant share a similar tendency to bind DNA cooperatively, whereas this tendency is less pronounced in the single-site mutants p53DBD-H178A, p53DBD-R181A, p53DBD-C 182A, p53DBD-E180R, and p53DBD-R181E.

 © 2005 Wiley-VCH Verlag GmbH & Co. KGaA, Weinheim

EMSAs were performed to clarify whether the dimerization mutants bind DNA specifically or nonspecifically. After incubation with fluorescently labeled double-stranded consensus oligonucleotide (CON4x5; 5′-CCTAGACATGCCTAGACATGCCTAAT-3′) in the presence of nonspecific and unlabeled competitor DNA, p53DBD wild-type dimerizes and binds specifically to labeled consensus DNA (Figure 4a, lane 1). As a negative control, we analyzed the p53DBD mutant R248W. Arg248 interacts directly with bound DNA; mutations of this residue result in p53 forms that belong to the class of mutants with impaired DNA binding;[9] indeed, this is reflected in lane 2 of Figure 4a. p63DBD was unable to bind labeled consensus DNA significantly (Figure 4a, lane 3), whereas an artificial dimerization of p63DBD through the GST–p63DBD fusion protein restores a DNA binding affinity similar to that of p53DBD (Figure 4c, lane 2).[12] Lanes 4–6 of Figure 4a show that p53 alanine mutations of solvent-exposed residues H178A, R181A, and C182A have decreased specific DNA-binding affinity relative to that of wild-type p53DBD.

The single-site mutants p53DBD-E180R and p53DBD-R181E, in which two consecutive Arg and two consecutive Glu residues are respectively present, do not bind DNA (Figure 4a, lanes 7 and 8). However, an exchange of the wild-type position of these two residues reflected in the double-site mutant p53DBD-E180R/R181E restores DNA binding affinity to nearly that of wild-type p53DBD (Figure 4a, lane 9). As a cross-check to determine whether two identically charged sequential residues in mutants p53DBD-E180R and p53DBD-R181E have an impact on the structural integrity of the H1 helix (which would preclude DNA binding), we co-incubated both mutants with consensus DNA and competitor DNA, which restored DNA-binding affinity through heterodimerization of each mutant (Figure 4b). Thus these EMSAs corroborate the pulsed field gradient diffusion measurements in which both the p53DBD wild-type and the p53DBD-E 180R/R181E mutant bind specifically and cooperatively to fluorescently labeled consensus DNA in the presence of competitor DNA. In contrast, the single-site mutants p53DBD-E180R and p53DBD-R181E, which both display two identically charged sequential residues within the designated dimerization interface, do not show any specific binding of consensus DNA (Figure 4a, lanes 7 and 8).

Additional EMSAs were performed under the same conditions, but with a selection of mutant p53DBD–GST fusion proteins: the three alanine mutants p53DBD-H178A,

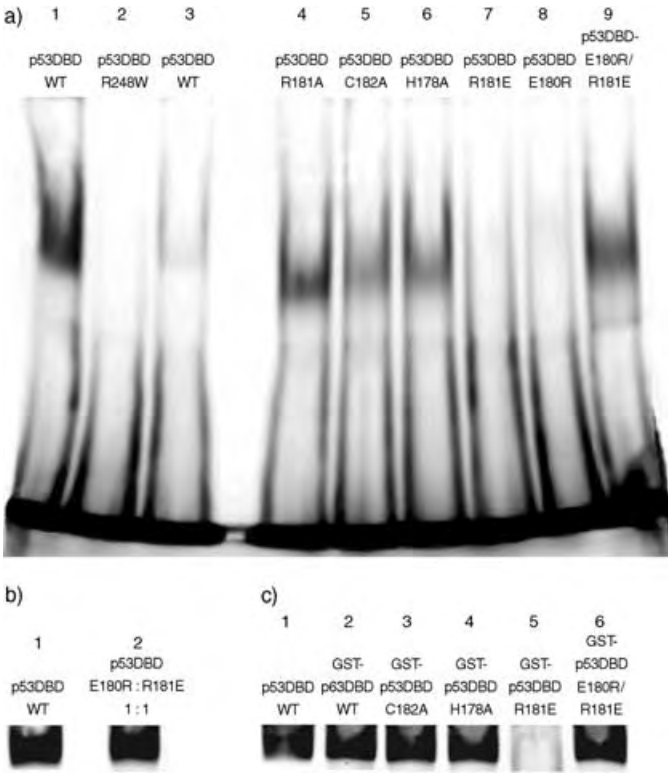


Figure 4. a) EMSAs of wild-type p53DBD, p53DBD-R248W, wild-type p63DBD, and p53DBD dimerization mutants in the presence of nonspecific unlabeled pBluescriptII SK$^+$ competitor DNA. b) A 1:1 mixture of p53DBD-R181E and p53DBD-E180R. c) EMSAs for wild-type p53DBD and the GST fusion proteins.

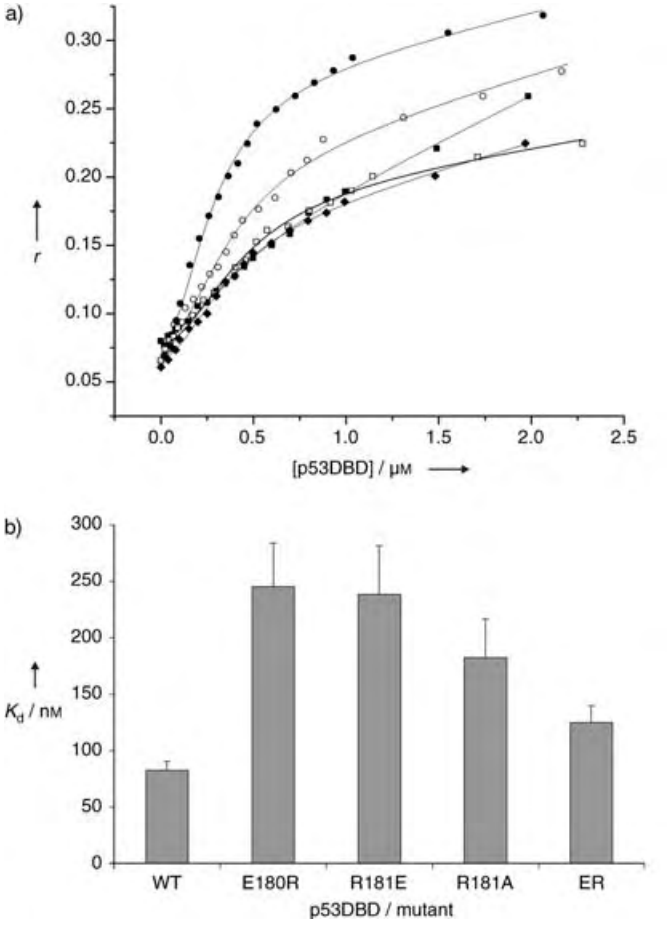


Figure 5. a) Binding of double-stranded CON4x5 DNA to wild-type p53DBD and the dimerization mutants detected by fluorescence anisotropy *r*: ● wild-type p53DBD, ○ p53DBD-R181A, □ p53DBD-R181E, ■ p53DBD-E180R, ◆ p53DBD-E180R/R181E. Data were fitted according to a cooperative model. b) Dissociation constants K_d of p53DBD and the dimerization mutants as determined by fluorescence anisotropy data. ER = p53DBD-E180R/R181E.

 © 2005 Wiley-VCH Verlag GmbH & Co. KGaA, Weinheim

p53DBD-R181A, p53DBD-C182A, as well as p53DBD-R 181E, which contains two consecutive, negatively charged (Glu) residues at positions 180 and 181. The GST portion of these mutants serves as an artificial dimerization domain in an analogous manner to the tetramerization domain of full-length wild-type p53; it enhances cooperativity and therefore specific DNA binding. As a positive control, lanes 1 and 2 in Figure 4c contain p53DBD and p63DBD–GST, respectively, which bind consensus DNA with similar affinity, whereas free p63DBD without the GST domain lacks this cooperativity (Figure 4a, lane 2).[12] Analogous to p63DBD, the three alanine mutations of p53DBD exhibit enhanced cooperativity in DNA binding with the dimeric GST fusion domain and show an affinity similar to that of wild-type p53DBD. Therefore, the alanine mutations p53DBD-H178A, p53DBD-R181A, and p53DBD-C182A do not actively prevent possible dimerization upon binding of DNA, as demonstrated by 1) residual DNA binding and 2) such DNA binding can be enhanced by GST-mediated dimerization. The p53DBD-R181E–GST mutant, however, does not exhibit specific DNA binding; the induced cooperative effect of GST-mediated dimerization is not strong enough to overcome the repulsive charge–charge interactions which would occur at the dimerization interface. From this we can conclude that there is no other dimerization interface within p53DBD that could substitute for the E180–R181 intermolecular salt bridges.

The GST-mediated enhancement of cooperative DNA binding was already observed for p63DBD.[12] It was deduced that conformational differences within the H1 helix might be responsible for the different dimerization behavior. However, from our results it is clear that the aliphatic leucine group present at the homologous p53DBD codon position 180 (Figure 1) is not able to form an intermolecular salt bridge, which explains the previously observed absence of selective and cooperative DNA binding with free p63DBD (Figure 6a).[12]

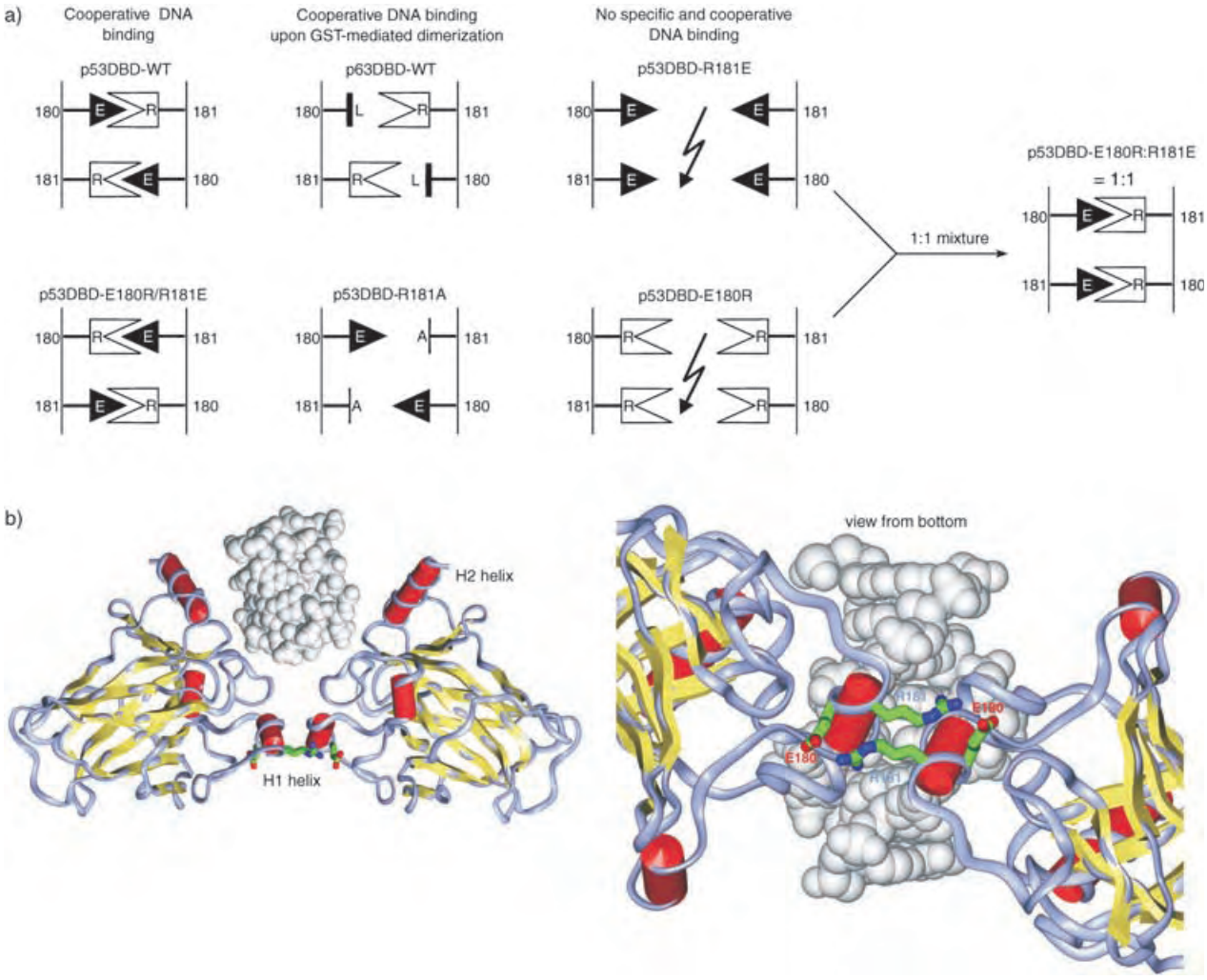


Figure 6. a) Schematic representation of dimerization patterns. Cooperative DNA binding is observed with wild-type p53DBD, the double-site mutant p53DBD-E180R/R181E, and a 1:1 mixture of p53DBD-E180R and p53DBD-R181E. Cooperative DNA binding by wild-type p63DBD and the alanine dimerization mutants of p53DBD can be enhanced by GST-mediated dimerization. Repulsive charge–charge interactions prevent cooperative DNA binding for the p53DBD-E180R and p53DBD-R181E mutants. b) C_2-symmetric model complex for the identified dimerization interface of p53DBD upon cooperative DNA binding. The dimerization interface is stabilized by a double intermolecular salt bridge between residues E180 and R181 of each monomer.

 © 2005 Wiley-VCH Verlag GmbH & Co. KGaA, Weinheim

These results were further corroborated by fluorescence anisotropy measurements.[31] Figure 5a shows the specific affinity of wild-type p53DBD and the dimerization mutants toward consensus DNA. Increasing concentrations of wild-type p53DBD and mutant forms were added to fluorescently labeled CON4x5 oligonucleotide (25 nM) in potassium phosphate (50 mM), KCl (50 mM), and dithiothreitol (DTT, 5 mM). For a low concentration of p53DBD or the mutants, a single cooperative binding to CON4x5 can be assumed (Figure 5a). The details of curve fitting are described in the Supporting Information. Wild-type p53DBD gives a dissociation constant of 82 ± 8 nM, whereas the binding affinities of the p53DBD mutants are about threefold less (p53DBD-E180R: 245 ± 38 nM; p53DBD-R181E: 238 ± 43 nM). The value for the alanine mutant p53DBD-R181A ($K_d = 182 \pm 34$ nM) lies halfway between those of the wild-type and the p53DBD-E180R and p53DBD-R181E mutants, which may explain the slightly higher binding affinity observed in the EMSAs (Figure 4a, lane 4). The double mutant p53DBD-E180R/R181E ($K_d = 124 \pm 15$ nM) has a dissociation constant similar to that of wild-type p53DBD (Figure 5b).

Taken together, our results prove that the proposed additional p53DBD dimerization interface, which stabilizes cooperative and selective DNA binding events, consists mainly of two intermolecular Glu180–Arg181 salt bridges from each monomer to the other (Figure 6a). These salt bridges are in agreement with a C_2-symmetric model complex (Figure 6b) as proposed by Lebrun, Klein, and co-workers.[15,22] The formation of salt bridges also rationalizes the difference in DNA-binding behavior between p53DBD and p63DBD. Moreover, the results provide new insight into the oncogenic mutations E180X and R181X in Li–Fraumeni syndrome, as they decrease the cooperativity in DNA binding.

Received: May 31, 2005
Published online: July 20, 2005

Keywords: DNA · mutagenesis · NMR spectroscopy · p53 · protein structures

[1] A. J. Levine, *Cell* **1997**, *88*, 323 – 331.
[2] P. May, E. May, *Oncogene* **1999**, *18*, 7621 – 7636.
[3] B. Vogelstein, D. Lane, A. J. Levine, *Nature* **2000**, *408*, 307 – 310.
[4] K. Vousden, *Br. J. Cancer* **2003**, *88*, S7.
[5] K. H. Vousden, *Cell* **2000**, *103*, 691 – 694.
[6] M. Hollstein, D. Sidransky, B. Vogelstein, C. C. Harris, *Science* **1991**, *253*, 49 – 53.
[7] D. R. Walker, J. P. Bond, R. E. Tarone, C. C. Harris, W. Makalowski, M. S. Boguski, M. S. Greenblatt, *Oncogene* **1999**, *18*, 211 – 218.
[8] C. H. Arrowsmith, P. Morin, *Oncogene* **1996**, *12*, 1379 – 1385.
[9] A. N. Bullock, A. R. Fersht, *Nat. Rev. Cancer* **2001**, *1*, 68 – 76.
[10] A. Chompret, *Biochimie* **2002**, *84*, 75 – 82.
[11] J. M. Varley, *Hum. Mutat.* **2003**, *21*, 313 – 320.
[12] C. Klein, G. Georges, A. P. Künkele, R. Huber, R. A. Engh, S. Hansen, *J. Biol. Chem.* **2001**, *276*, 37390 – 37401.
[13] C. Maisse, P. Guerrieri, G. Melino, *Biochem. Pharmacol.* **2003**, *66*, 1555 – 1561.
[14] Y. Cho, S. Gorina, P. D. Jeffrey, N. P. Pavletich, *Science* **1994**, *265*, 346 – 355.
[15] A. Lebrun, R. Lavery, H. Weinstein, *Protein Eng.* **2001**, *14*, 233 – 243.
[16] C. Prives, *Cell* **1994**, *78*, 543 – 546.
[17] K. H. Zhao, X. M. Chai, K. Johnston, A. Clements, R. Marmorstein, *J. Biol. Chem.* **2001**, *276*, 12120 – 12127.
[18] A. K. Nagaich, V. B. Zhurkin, S. R. Durell, R. L. Jernigan, E. Appella, R. E. Harrington, *Proc. Natl. Acad. Sci. USA* **1999**, *96*, 1875 – 1880.
[19] W. T. Lee, T. S. Harvey, Y. Yin, P. Yau, D. Litchfield, C. H. Arrowsmith, *Nat. Struct. Biol.* **1994**, *1*, 877 – 890.
[20] P. D. Jeffrey, S. Gorina, N. P. Pavletich, *Science* **1995**, *267*, 1498 – 1502.
[21] G. M. Clore, J. Ernst, R. Clubb, J. G. Omichinski, W. M. Kennedy, K. Sakaguchi, E. Appella, A. M. Gronenborn, *Nat. Struct. Biol.* **1995**, *2*, 321 – 333.
[22] C. Klein, E. Planker, T. Diercks, H. Kessler, K. P. Künkele, K. Lang, S. Hansen, M. Schwaiger, *J. Biol. Chem.* **2001**, *276*, 49020 – 49027.
[23] T. M. Rippin, S. M. V. Freund, D. B. Veprintsev, A. R. Fersht, *J. Mol. Biol.* **2002**, *319*, 351 – 358.
[24] C. R. Cantor, P. R. Schimmel in *Biophysical Chemistry, Part II: Techniques for the Study of Biological Structure and Function*, *Vol. II* (Ed.: W. H. Freeman), New York, **1980**, pp. 570 – 590; Y. Cohen, L. Avram, L. Frish, *Angew. Chem.* **2005**, *117*, 524; *Angew. Chem. Int. Ed.* **2005**, *44*, 520.
[25] A. Dehner, E. Planker, G. Gemmecker, Q. B. Broxterman, W. Bisson, F. Formaggio, M. Crisma, C. Toniolo, H. Kessler, *J. Am. Chem. Soc.* **2001**, *123*, 6678 – 6686.
[26] T. S. Derrick, E. F. McCord, C. K. Larive, *J. Magn. Reson.* **2002**, *155*, 217 – 225.
[27] A. J. Dingley, J. P. Mackay, B. E. Chapman, M. B. Morris, P. W. Kuchel, B. D. Hambly, G. F. King, *J. Biomol. NMR* **1995**, *6*, 321 – 328.
[28] A. Dehner, H. Kessler, *ChemBioChem* **2005**, accepted.
[29] W. S. Price, *Concepts Magn. Reson.* **1997**, *9*, 299 – 336.
[30] J. Garcia de la Torre, M. L. Huertas, B. Carrasco, *J. Magn. Reson.* **2000**, *147*, 138 – 146.
[31] V. LeTilly, C. A. Royer, *Biochemistry* **1993**, *32*, 7753 – 7758.

 © 2005 Wiley-VCH Verlag GmbH & Co. KGaA, Weinheim

Drug Delivery

DOI: 10.1002/anie.200500519

Membrane-Mimetic Nanocarriers Formed by a Dipalmitoylated Cell-Penetrating Peptide**

Sandro Keller, Ines Sauer, Holger Strauss, Klaus Gast, Margitta Dathe, and Michael Bienert*

Molecular and supramolecular drug-delivery systems have attracted great attention as pharmaceutical formulations for the administration of otherwise only poorly soluble, rapidly degradable, or even toxic molecules.[1] Within the multitude of colloidal vehicles developed to date, micelles belong to the most useful tools for the delivery of hydrophobic compounds.[2] However, some serious disadvantages of micellar carriers remain, among which the problem that some normally membrane-located biomolecular devices like vector peptides lose their native conformation and are severely compromised in their activity when removed from the lipid bilayer.[3,4] Here we introduce a dipalmitoylated cell-penetrating peptide that is superior to previously described biofunctional colloids in its ability to incorporate large amounts of lipid in mixed micelles. Hence this peptide constitutes a potent lead for the intracellular delivery of hydrophobic drugs using bilayer-mimetic nanocarriers.

Ideally, such vehicles would meet a number of criteria. First, a customizable peptide sequence designed to trigger a specific response upon interaction with biological targets has to be exposed on the micellar surface.[5] Second, the nanocarriers should contain an excess of lipid and thus offer a bilayer-like environment in order to preserve the functionality of the surface-bound peptide. Third, as such a compound will unavoidably be a strong detergent, its aggregational state must be easily controllable, and the kinetics of membrane solubilization should be slow.

In our search for a peptidic vector promoting internalization into a broad range of different cells, we chose a 20-residue tandem dimer [A2, $(LRKLRKRLLR)_2$] comprising binding sites for the low-density lipoprotein receptor and for cell-surface heparan sulfate proteoglycans, two ubiquitous mammalian membrane constituents able to mediate uptake of their ligands.[6] A2 has recently been demonstrated to induce internalization of liposomes into primary rat brain capillary endothelial cells when covalently linked to the vesicle surface,[7] and the presence of lipids is known to be crucial for receptor binding by its parent apolipoprotein E.[3] As fatty acid modified peptides have turned out to be extraordinarily powerful detergents for suspending membrane proteins in mixed micelles providing a bilayer-mimetic environment,[8,9] we opted for dipalmitoylation (P2) of two neighboring amino acids in a 3-residue sequence linked to the N terminus of A2 as a means of hydrophobization. The lipopeptide P2A2 was prepared with high yields and in quantities of several hundred milligrams in a simple and effective procedure. A standard solid-phase protocol based on N^{α}-9-fluorenylmethoxycarbonyl(Fmoc)-protected amino acids was used to synthesize A2 extended N-terminally with the sequence Fmoc-WK(Dde)G containing an N^{ε}-1-(4,4-dimethyl-2,6-dioxocyclohex-1-ylidene)ethyl(Dde)-protected lysine residue. After hydrazine cleavage of the Dde and the amino-terminal Fmoc moieties, the two amino groups in the lysine side chain and at the N terminus were acylated simultaneously with palmitic acid.[10]

The resulting chimera P2A2 (Figure 1) with a molar mass of 3.53 kg mol^{-1} has an amphipathic structure in which the two acyl chains form a very hydrophobic tail attached to the charged peptide, but it is nevertheless well-soluble (> 5 mM)

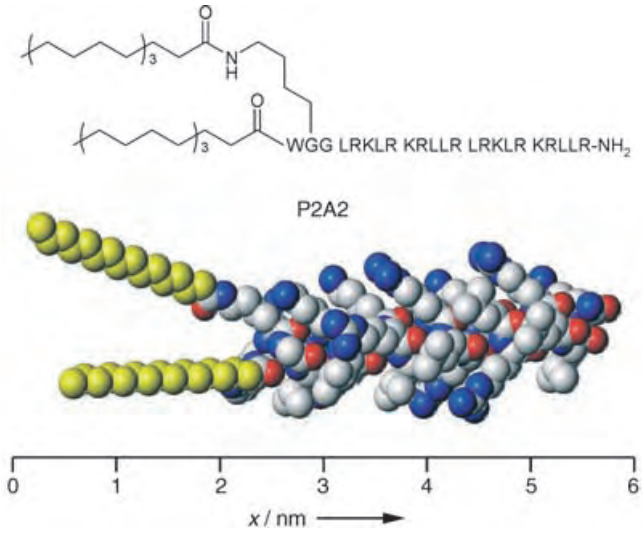


Figure 1. Structure of P2A2. The two palmitoyl chains are linked through amide groups to the N-terminal tryptophan and to the side chain of the neighboring lysine (one-letter amino acid code, formal valence $z = 12$ at pH 7.4). The hydrophobic methylene and methyl groups of the palmitoyl residues are highlighted in yellow in the space-filling model.[11]

[*] S. Keller, Dr. I. Sauer, H. Strauss, Dr. M. Dathe, Prof. Dr. M. Bienert
Research Institute of Molecular Pharmacology FMP
Robert-Rössle-Strasse 10, 13125 Berlin (Germany)
Fax: (+49) 30-94793-159
E-mail: mail@sandrokeller.com
Dr. K. Gast
Physical Biochemistry
Institute of Biochemistry and Biology
University of Potsdam
Karl-Liebknecht-Strasse 24–25, Haus 25
14467 Potsdam-Golm (Germany)

[**] This work was supported by the European Commission (grant no. QLK3-CT-2002-01989 to SK) and by the Deutsche Forschungsgemeinschaft (grant no. DA 324/4-1/2 to IS and SFB 498 to HS). We thank Prof. Hartmut Oschkinat and Prof. Peter Pohl for helpful comments on the manuscript and Dr. Annette Meister, Dr. Michael Schümann, Dr. Michael Beyermann, and Dr. Heiko Heerklotz for fruitful discussions. We are indebted to Heidemarie Lerch for mass-spectrometric measurements, to Bernhard Schmikale for peptide synthesis, and to Heike Nikolenko, Carolyn Vargas, Seong-Ji Han, Jens H. Laettig, and Stephan Pritz for excellent technical assistance.

Supporting information for this article is available on the WWW under http://www.angewandte.org or from the author.

InterScience
© 2005 Wiley-VCH Verlag GmbH & Co. KGaA, Weinheim

in aqueous solution (10 mM 2-amino-2-(hydroxymethyl)propane-1,3-diol (Tris), 154 mM NaCl, 0.1 mM ethylenediaminetetraacetate (EDTA), pH 7.4).[12] Unlike double-chained phospholipids possessing relatively small headgroups, the bulky peptide of P2A2 does not appear to allow self-association into bilayers but rather implies detergent-like micellization.

Analytical ultracentrifugation revealed indeed that P2A2 assembles into well-defined aggregates with a molar mass of $M = 68\ \mathrm{kg\,mol^{-1}}$ corresponding to 19 monomers (Figure 2a).

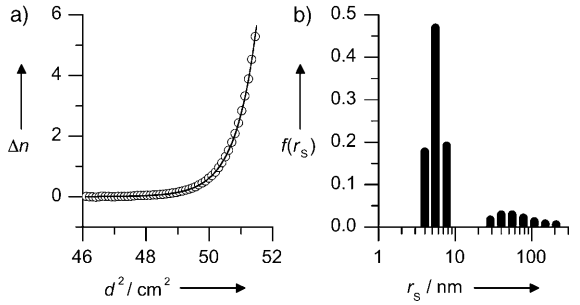


Figure 2. Mass and size characterization of P2A2 micelles. a) Analytical ultracentrifugation at $c_{P2A2} = 96\ \mu M$ and 20 krpm gave the local refractive index difference, Δn, (open circles) as a function of the squared distance from the rotor axis, d^2, at sedimentation equilibrium. The best single-species fit (solid line) was obtained for a molar mass of $M = (67.7 \pm 0.3)\ \mathrm{kg\,mol^{-1}}$. b) Dynamic light scattering at $c_{P2A2} = 244\ \mu M$ yielded the distribution function, $f(r_S)$, of the Stokes radius, r_S. The stronger peaks at small radii observed at four different concentrations were used to extrapolate $r_S^{expt} = (5.25 \pm 0.30)$ nm.[10]

Static light scattering (LS) confirmed this result;[10] however, dynamic LS yielded a Stokes radius of $r_S^{expt} = 5.3$ nm (Figure 2b), which is distinctly larger than the value of $r_S^{calcd} = 3.4$ nm calculated for a spherical particle of this mass.[10] This discrepancy and the small aggregation number most likely arise from a nonspherical micellar geometry as invoked for other lipopeptides[8] and are also reminiscent of bile salts.[13]

However, as a practical advantage over bile salts, the critical micellar concentration (CMC) of P2A2 is expected to be considerably lower owing to the pronounced hydrophobicity conferred by the two palmitoyl chains, which should thus preserve the colloidal state also upon extreme dilution. In fact, the subnanomolar CMC of the lipopeptide is below the ranges experimentally accessible by fluorescence spectroscopy (nanomolar) and calorimetry (micromolar),[12,14] suggesting that the concentration of monomeric P2A2 is always negligible.

The efficacy of P2A2 in forming lipid-rich micelles was monitored on the basis of the light scattering intensity, I, of its mixtures with the zwitterionic phospholipid 1-palmitoyl-2-oleoyl-*sn*-glycero-3-phosphocholine (POPC). To this end, dry lipid films were suspended in buffer containing various concentrations of P2A2, and standard procedures for preparing unilamellar vesicles were then applied.[10] For a series of samples with identical lipid concentration, the I values rose only slightly with the P2A2 concentration up to a saturating detergent/lipid mole ratio, $R_e^{sat.}$, at which membrane solubilization began (Figure 3a). A further increase in c_{P2A2} led to a drastic drop in I until solubilization was completed at $R_e^{sol.}$. This was in excellent agreement with a second type of

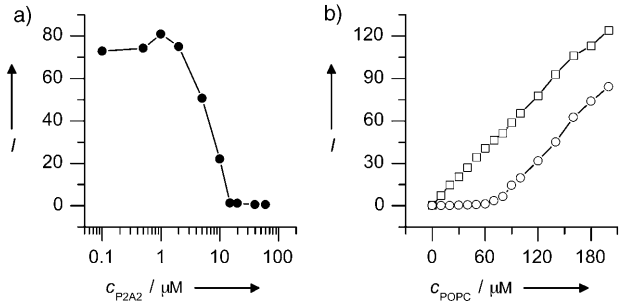


Figure 3. Detergent activity of P2A2 on 100-nm POPC vesicles as monitored by right-angle light scattering. a) Scattering intensity, I, obtained from 100 μM POPC extruded along with increasing P2A2 concentrations, c_{P2A2}. b) I values for various lipid concentrations, c_{POPC}, prepared in the presence (circles) or absence (squares) of 10 μM P2A2.

scattering experiment employing a constant lipopeptide concentration but different amounts of lipid (Figure 3b).

Plotting the characteristic P2A2 concentrations at the break points in the curves obtained with LS and calorimetry[10,15] versus the lipid concentration yields a simple phase diagram (Figure 4).[16,17] The two straight lines with slopes of

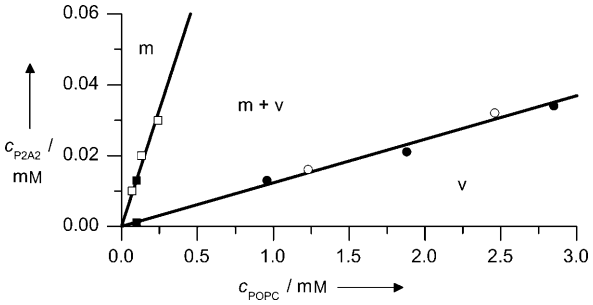


Figure 4. Phase diagram of dilute aqueous P2A2/POPC mixtures. Data are taken from solubilization (filled symbols) and reconstitution (open symbols) experiments conducted with light scattering (squares) and titration calorimetry (circles), [10] respectively. The linear regression lines separate the micellar (m) and the vesicular (v) areas from the transition range (m + v).[17]

$R_e^{sat.} = 0.012$ and $R_e^{sol.} = 0.13$ delimit three areas ascribed to the micellar, the transitional, and the vesicular range, respectively.[18] Thus, to our knowledge P2A2 is by far the most efficient detergent in that it can solubilize about seven lipid molecules per lipopeptide, that is, 50 times more than other peptides with two fatty acyl chains.[8] The partition coefficient of P2A2 from vesicles (v) to micelles (m) amounts to $P_{P2A2}^{m/v} = 10$ and reflects the preference of the lipopeptide for the micellar state. In contrast, POPC reveals only a slight penchant for membranes with $P_{POPC}^{m/v} = 0.9$, indicating that

 © 2005 Wiley-VCH Verlag GmbH & Co. KGaA, Weinheim

the lipid can be accommodated in the micelle almost as well as in the liposome and underpinning the suitability of P2A2 for micellar vehicles offering a bilayer-mimetic environment.

Most importantly, the clearcut boundaries in the phase diagram (Figure 4) permit direct control of the aggregational state of P2A2/POPC mixtures by adjusting the concentrations of the components. Hence, in addition to micellar also liposomal structures are available as supramolecular carriers, and vesicles doped with P2A2 reveal superior properties in terms of high lipid affinity, stable bilayer anchorage, and low membrane permeabilization when compared with the properties of other hydrophobized A2 derivatives.[19] Preliminary studies with confocal laser scanning microscopy revealed the efficient internalization of micelles composed of a fluorescently labeled P2A2 derivative (P2fA2) into mouse brain capillary endothelial cells (Figure 5). Moreover, the slow kinetics of solubilization[10] even suggests application of nonequilibrium formulations in which P2A2-oversaturated vesicles gradually rearrange into mixed micelles. This is particularly intriguing in light of the increasing importance of delayed and sustained release of drugs from delivery systems.[20]

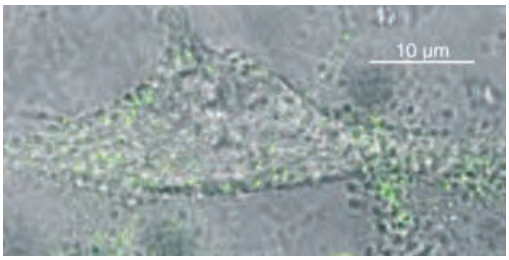


Figure 5. Internalization of a carboxyfluorescein-labeled P2A2 derivative (P2fA2) into immortalized b.End3 mouse brain capillary endothelial cells as visualized by confocal laser scanning microscopy. After exposure to 1 µM P2fA2 for 30 min at 37 °C, this representative cell displayed a punctuate intracellular fluorescence pattern pointing to a predominantly endocytotic mode of uptake. Membrane integrity and cell viability were confirmed by staining with trypan blue.[12]

We have shown that a novel lipopeptide composed of a target-specific peptidic vector and two adjacent fatty acyl chains is a highly promising candidate for solubilizing hydrophobic drugs in lipid-rich, membrane-mimetic nanocarriers. Owing to their small size, these supramolecular vehicles share many advantages with other micelles,[2] while the bioactivity of the peptide moiety is maintained thanks to the bilayer-like environment offered by the palmitoyl tails. These unique properties and the sound physicochemical characterization make the colloidal state of P2A2/lipid systems readily manageable and provide versatile formulations for in vitro experiments, which have indeed demonstrated rapid cellular internalization. The straightforward synthesis and good solubility should render P2A2 amenable to a more detailed structure elucidation and might also prove useful for other fields, such as membrane protein reconstitution.[8,9] Finally, the peptide sequence need not be restricted to the cell-penetrating A2 but may be adaptable to a broad spectrum of ligands destined to diverse biological targets. We are conducting further studies to shed light on the mechanism of uptake and to extend the approach presented in this work to similar chimerical lipopeptides.

Received: February 10, 2005
Revised: April 12, 2005
Published online: July 20, 2005

Keywords: drug delivery · lipopeptides · membranes · micelles · self-assembly

[1] D. E. Discher, A. Eisenberg, *Science* **2002**, *297*, 967–973; H. Dou, M. Jiang, H. Peng, D. Chen, Y. Hong, *Angew. Chem.* **2003**, *115*, 1554–1557; *Angew. Chem. Int. Ed.* **2003**, *42*, 1516–1519; R. Duncan, *Nat. Rev. Drug Discovery* **2003**, *2*, 347–360; J. Kreuter, *Colloidal Drug Delivery Systems*, Marcel Dekker, New York, **1994**; R. Langer, *Science* **2001**, *293*, 58–59; D. D. Lasic, D. Papahadjopoulos, *Science* **1995**, *267*, 1275–1276; M. A. Moses, H. Brem, R. Langer, *Cancer Cell* **2003**, *4*, 337–341; P. C. Rensen, R. L. de Vrueh, J. Kuiper, M. K. Bijsterbosch, E. A. Biessen, T. J. van Berkel, *Adv. Drug Delivery Rev.* **2001**, *47*, 251–276.

[2] Y. Bae, S. Fukushima, A. Harada, K. Kataoka, *Angew. Chem.* **2003**, *115*, 4788–4791; *Angew. Chem. Int. Ed.* **2003**, *42*, 4640–4643; R. Haag, *Angew. Chem.* **2004**, *116*, 280–284; *Angew. Chem. Int. Ed.* **2004**, *43*, 278–282; Y. Kakizawa, K. Kataoka, *Adv. Drug Delivery Rev.* **2002**, *54*, 203–222; K. Kataoka, T. Matsumoto, M. Yokoyama, T. Okano, Y. Sakurai, S. Fukushima, K. Okamoto, G. S. Kwon, *J. Controlled Release* **2000**, *64*, 143–153; K. Kataoka, A. Harada, Y. Nagasaki, *Adv. Drug Delivery Rev.* **2001**, *47*, 113–131; M. Krämer, J. F. Stumbé, H. Türk, S. Krause, A. Komp, L. Delineau, S. Prokhorova, H. Kautz, R. Haag, *Angew. Chem.* **2002**, *114*, 4426–4431; *Angew. Chem. Int. Ed.* **2002**, *41*, 4252–4256; N. Nasongkla, X. Shuai, H. Ai, B. D. Weinberg, J. Pink, D. A. Boothman, J. Gao, *Angew. Chem.* **2004**, *116*, 6483–6487; *Angew. Chem. Int. Ed.* **2004**, *43*, 6323–6327; R. Savic, L. Luo, A. Eisenberg, D. Maysinger, *Science* **2003**, *300*, 615–618; V. P. Torchilin, *Cell. Mol. Life Sci.* **2004**, *61*, 2549–2559; J. V. Weaver, Y. Tang, S. Liu, P. D. Iddon, R. Grigg, N. C. Billingham, S. P. Armes, R. Hunter, S. P. Rannard, *Angew. Chem.* **2004**, *116*, 1413–1416; *Angew. Chem. Int. Ed.* **2004**, *43*, 1389–1392.

[3] T. L. Innerarity, R. E. Pitas, R. W. Mahley, *J. Biol. Chem.* **1979**, *254*, 4186–4190; K. H. Weisgraber, *Adv. Protein Chem.* **1994**, *45*, 249–302.

[4] L. Nobs, F. Buchegger, R. Gurny, E. Allemann, *J. Pharm. Sci.* **2004**, *93*, 1980–1992; M. Zaiou, K. S. Arnold, Y. M. Newhouse, T. L. Innerarity, K. H. Weisgraber, M. L. Segall, M. C. Phillips, S. Lund-Katz, *J. Lipid Res.* **2000**, *41*, 1087–1095.

[5] Throughout the text, the term "micelle" is used to denote aggregates of colloidal size, without making any assumptions regarding their shape or composition.

[6] C. A. Dyer, L. K. Curtiss, *J. Biol. Chem.* **1991**, *266*, 22803–22806; C. A. Dyer, R. S. Smith, L. K. Curtiss, *J. Biol. Chem.* **1991**, *266*, 15009–15015; C. A. Dyer, D. P. Cistola, G. C. Parry, L. K. Curtiss, *J. Lipid Res.* **1995**, *36*, 80–88; M. P. Mims, A. T. Darnule, R. W. Tovar, H. J. Pownall, D. A. Sparrow, J. T. Sparrow, D. P. Via, L. C. Smith, *J. Biol. Chem.* **1994**, *269*, 20539–20547.

[7] I. Sauer, I. R. Dunay, K. Weisgraber, M. Bienert, M. Dathe, *Biochemistry* **2005**, *44*, 2021–2029.

[8] C. L. McGregor, L. Chen, N. C. Pomroy, P. Hwang, S. Go, A. Chakrabartty, G. G. Privé, *Nat. Biotechnol.* **2003**, *21*, 171–176.

 © 2005 Wiley-VCH Verlag GmbH & Co. KGaA, Weinheim

[9] C. R. Sanders, A. K. Hoffmann, D. N. Grayn, M. H. Keyes, C. D. Ellis, *ChemBioChem* **2004**, *5*, 423 – 426.
[10] See the Supporting Information for details.
[11] For simplicity, the peptide moiety is depicted as an ideal α helix even though circular dichroism spectroscopy has shown that the helicity depends on the aggregational state and never exceeds 50 %.
[12] Data not shown.
[13] M. Almgren, *Biochim. Biophys. Acta* **2000**, *1508*, 146 – 163; P. Garidel, A. Hildebrand, R. Neubert, A. Blume, *Langmuir* **2000**, *16*, 5267 – 5275; M. Janich, J. Lange, H. Graener, R. Neubert, *J. Phys. Chem. B* **1998**, *102*, 5957 – 5962; A. Jover, F. Meijide, E. R. Núñez, J. V. Tato, M. Mosquera, *Langmuir* **1997**, *13*, 161–164.
[14] S. Paula, W. Süs, J. Tuchtenhagen, A. Blume, *J. Phys. Chem.* **1995**, *99*, 11742 – 11751.
[15] H. Heerklotz, J. Seelig, *Biochim. Biophys. Acta* **2000**, *1508*, 69 – 85; H. Heerklotz, G. Lantzsch, H. Binder, G. Klose, A. Blume, *Chem. Phys. Lett.* **1995**, *235*, 517 – 520.
[16] H. Heerklotz, G. Lantzsch, H. Binder, G. Klose, A. Blume, *J. Phys. Chem.* **1996**, *100*, 6764 – 6774.
[17] Vesicle–micelle coexistence is the simplest but not the only model providing a consistent interpretation, and other scenarios might be envisaged, for example, a transition from vesicles to disk-shaped bilayers or bicelles at $R_e^{sat.}$ followed by a gradual shrinking caused by a further increase in c_{P2A2}. Rather than a thermodynamically meaningful parameter, $R_e^{sol.}$ would then be an arbitrarily defined threshold at which the bilayer disks become hardly distinguishable in size from pure P2A2 micelles as judged from the *I* values.
[18] D. Lichtenberg, *Biochim. Biophys. Acta* **1985**, *821*, 470 – 478.
[19] I. Sauer, H. Nikolenko, S. Keller, M. Bienert, M. Dathe, K. Abu Ajaj, submitted .
[20] S. Mantripragada, *Prog. Lipid Res.* **2002**, *41*, 392 – 406; M. P. Ramprasad, G. M. Anantharamaiah, D. W. Garber, N. V. Katre, *J. Controlled Release* **2002**, *79*, 207 – 218.

 © 2005 Wiley-VCH Verlag GmbH & Co. KGaA, Weinheim

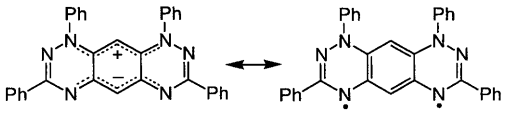
Antiaromatic Species

DOI: 10.1002/anie.200500831

3,5,7,9-Tetraphenylhexaazaacridine: A Highly Stable, Weakly Antiaromatic Species with 16 π Electrons**

Peter Langer, Anja Bodtke, Nehad N. R. Saleh, Helmar Görls, and Peter R. Schreiner**

The efficiency of electrical, magnetic, and optical devices based on organic materials is closely related to their HOMO–LUMO energy gap.[1] The structure of tetraphenylhexaazaanthracene (TPH-anthracene, **1**), first prepared in 1908 as a



1a (TPH-anthracene) **1b**

stable, highly fluorescent compound,[2] was recently studied by Wudl and Houk et al.; **1** exists as a zwitterionic cyanine (resonance structure **1a**) that undergoes photoinduced intramolecular electron transfer to give a radical pair.[3,4] Wudl and

[*] Prof. Dr. P. Langer
Institut für Chemie, Universität Rostock
Albert-Einstein-Strasse 3a, 18059 Rostock (Germany)
Fax: (+49) 381-498-6412
E-mail: peter.langer@uni-rostock.de
and
Leibniz-Institut für Organische Katalyse (IfOK)
an der Universität Rostock e.V.
Albert-Einstein-Strasse 29a, 18059 Rostock (Germany)

Prof. Dr. P. R. Schreiner
Institut für Organische Chemie, Justus-Liebig-Universität
Heinrich-Buff-Ring 58, 35392 Giessen (Germany)
Fax: (+49) 641-99-34309
E-mail: prs@chem.uga.edu
and
The University of Georgia, Department of Chemistry
Athens, GA (USA)
E-mail: prs@chem.uga.edu

Dr. A. Bodtke, Dr. N. N. R. Saleh
Institut für Chemie und Biochemie
Ernst-Moritz-Arndt Universität Greifswald
Soldmannstrasse 16, 17487 Greifswald (Germany)

Dr. H. Görls
Institut für Anorganische und Analytische Chemie
Universität Jena
August-Bebel-Strasse 2, 07740 Jena (Germany)

[**] This work was supported by the German state of Mecklenburg-Western Pomerania (scholarship for A.B.), the Dr. Dr. Gerda-von-Mach Gedächtnisstiftung (scholarship for N.N.R.S.), and the Deutsche Forschungsgemeinschaft. P.R.S. was supported at UGA through the National Science Foundation (CHE-0209827).

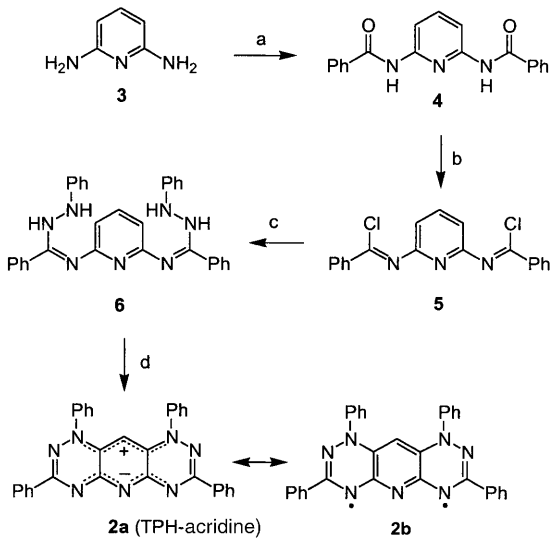
Supporting information for this article is available on the WWW under http://www.angewandte.org or from the author.

 © 2005 Wiley-VCH Verlag GmbH & Co. KGaA, Weinheim

Houk et al. concluded that the apparent antiaromaticity of **1** is overwhelmed by the dominance of cyanine ion stabilization. However, the aromatic properties, which can be assessed in a straightforward manner by, for instance, nucleus-independent chemical shifts (NICS),[5] were not analyzed further.

Herein, we report the synthesis of what is, to the best of our knowledge, the first example of a hexaazaacridine, namely 3,5,7,9-tetraphenylhexaazaacridine (TPH-acridine, **2**). By means of a combination of experimental and computational results, we show that **1** and **2** can be viewed as stable, 16-π-electron, weakly antiaromatic highly zwitterionic structures with very low lying triplet states. As neutral molecules are usually less polarized than their excited states, **2**, along with its carbon analogue **1**, is the exception where the state polarity is reversed so that photoexcitation leads to a less polarized excited state. As a consequence, normally much higher lying triplet and singlet states are much closer in energy. It is conceivable that appropriately substituted acridines can have open-shell ground states and would be excellent candidates for organic magnets and data storage.[1]

The synthesis of TPH-acridine (**2**) essentially follows the strategy reported for the synthesis of **1** (Scheme 1).[2,3]



Scheme 1. Synthesis of TPH-acridine (**2a**): a) PhCOCl (2 equiv), NEt_3 (2 equiv), CH_2Cl_2, 14 h, 0–20 °C, 48%; b) PCl_5 (2.9 equiv), toluene, 1.5 h, 20 °C, then 2 h, reflux, 88%; c) $PhNHNH_2$ (2.7 equiv), *n*-hexane, 14 h, 0–20 °C, 90%; d) air, DBU (2.8 equiv), MeOH, 4 d, 20 °C, 10%. DBU = diazabicyclo[5.4.0]undec-7-ene.

However, the oxidative cyclization of **6** as the key step proved to be very sluggish and afforded **2** in only 3% yield. After much experimentation, we found that **2** can be obtained reproducibly in 10% yield. Both the workup of the final product and the quality of **6** proved to be important parameters. In this context, the preparation of (rather unstable) bis(imidoyl) dichloride **5** in high purity was crucial and required careful handling.

The deep purple hexaazaacridine **2** is air stable, thermally stable up to 400 °C, and poorly soluble in most organic solvents. Particularly noteworthy is its strong solvatochromic character (Table 1): a solution of **2** in DMF is orange colored ($\lambda_{max} = 547$ nm) and, despite the low solubility of **2**, highly fluorescent at $F(\lambda_{max}) = 585$ nm. In TFA (CF_3CO_2H), however, the solubility of **2** is higher owing to protonation to give

Table 1: Solvatochromic properties of **2**.

Solvent	λ_{max} [nm] ($\log\varepsilon$)	Color of solution
DMF	547 (4.51)	orange, strongly fluorescent, poorly soluble
CH_3CO_2H	535 (4.57)	orange, fluorescent, poorly soluble
conc. HNO_3	–	red, very poorly soluble
conc. H_3PO_4	540 (4.29)	bluish purple, poorly soluble
conc. $HClO_4$	–	green, very poorly soluble
CF_3CO_2H	–	deep purple, reasonably soluble
conc. H_2SO_4	662 (4.34)	deep green, highly soluble

cationic **2**-H^+ (deep purple solution). Therefore, most NMR spectra were recorded in [D_1]TFA. Compound **2** is somewhat soluble in glacial acetic acid, concentrated nitric acid, phosphoric acid, and perchloric acid to give orange, red, bluish purple, and green solutions, respectively. Excellent solubility and strong bathochromism were observed in concentrated sulfuric acid ($\lambda_{max} = 662$ nm, deep green solution). Successive dilution of this solution with water or acetone changes the color from green to blue and purple and finally to pink and orange (see Supporting Information for quantitative measurements); this process is reversible. In addition to the acidity and concentration, the counterion also affects the absorption of the solution, which suggests the formation of aggregates.

The structure of TPH-acridine (**2**) was independently confirmed through a crystal structure analysis of the cation **2**-H^+, which was prepared by protonation of **2** with hydrochloric and glacial acetic acids (Figures 1 and 2). Protonated TPH-

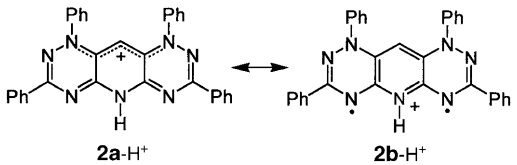


Figure 1. Resonance structures of protonated TPH-acridine, **2**-H^+.

acridine is a symmetric molecule that is protonated at the central nitrogen atom. Analysis of the bond lengths of THP-acridine indicates that the ionic resonance structure **2a**-H^+ is more important than the diradical contributor **2b**-H^+; this compares well with **1**.

For a better understanding of the electronic nature of **2**, we also computed its properties and compared those to **1**. As Wudl and Houk et al. successfully employed density functional theory (DFT) to examine the structures and energies of **1**, we adopted the same approach (B3LYP)[6] but expanded the basis set from 6-31G* to 6-311 + G** for the energies on the B3LYP/6-31G*-optimized geometries because we noted a marked basis set dependence of the singlet–triplet energy separation (ΔE_{ST}); this is not unexpected for species with

 © 2005 Wiley-VCH Verlag GmbH & Co. KGaA, Weinheim

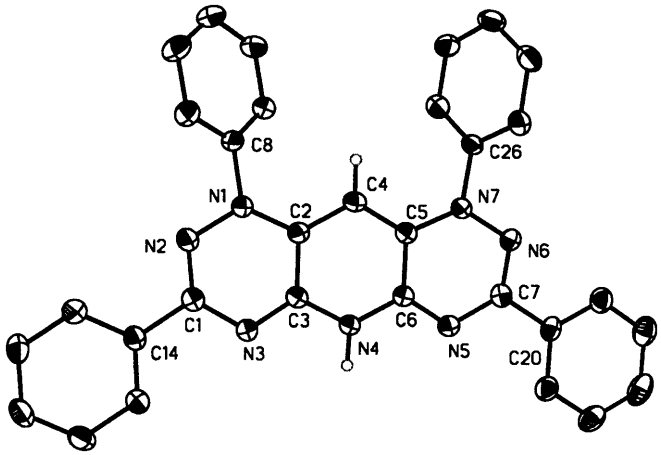


Figure 2. ORTEP plot of protonated TPH-acridine, **2**-H$^+$. Bond lengths [Å] and angles [°]: N1-C2 1.353(3), N1-N2 1.368(3), N2-C1 1.307(3), N3-C3 1.304(3), N3-C1 1.368(3), N4-C3 1.359(3), N4-C6 1.359(3), C2-C4 1.390(3), C2-C3 1.441(3); C2-N1-N2 123.28(19), C1-N2-N1 116.34(19), C3-N3-C1 115.8(2), C3-N4-C6 123.7(2), N2-C1-N3 126.2(2), N1-C2-C4 125.4(2), N1-C2-C3 114.46(19), C4-C2-C3 120.2(2), N3-C3-C2 123.3(2). CCDC 255822 contains the supplementary crystallographic data for this paper. These data can be obtained free of charge from the Cambridge Crystallographic Data Centre via www.ccdc.cam.ac.uk/data_request/cif.

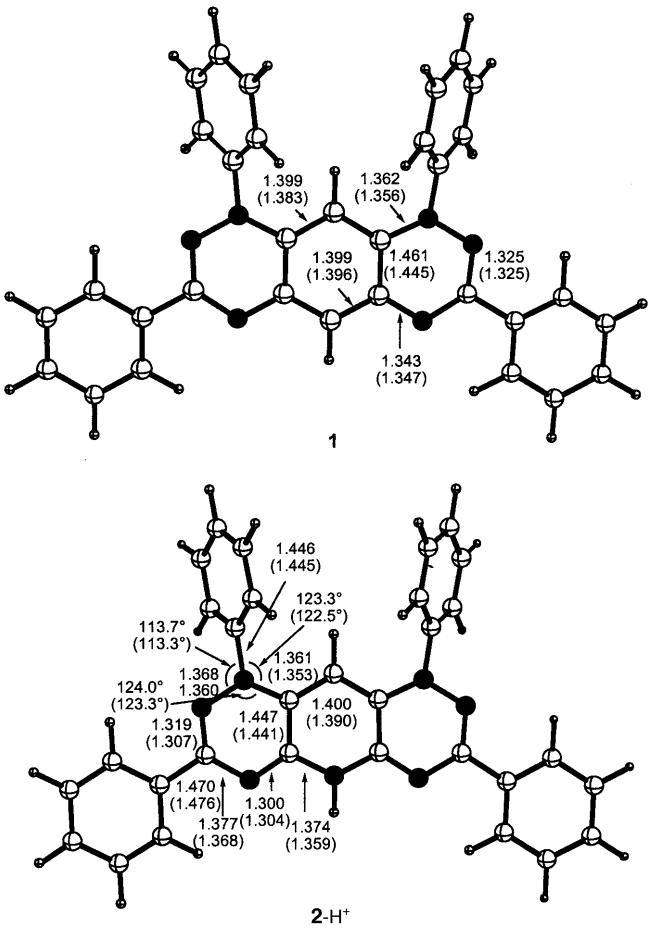


Figure 3. TPH-anthracene (**1**) and protonated TPH-acridine, **2**-H$^+$: comparison of selected bond lengths [Å] of the computed structure (B3LYP/6-31G*) and the crystal structure (in parentheses).

highly polarized ground and close-lying excited states. Our final level is therefore B3LYP/6-311+G**//B3LYP/6-31G*; zero-point vibrational energy (ZPVE) differences are marginal and are therefore not applied (the ZPVEs are reported in the Supporting Information). For the computation of UV spectra, we utilized time-dependent DFT (TD-B3LYP/6-311+G**), which is capable of describing vertical excited states more reliably than, for example, configuration interaction with single excitations (CIS).[7]

Since the crystal structure of TPH-anthracene (**1**) is known and the structure of the complete molecule had not been computed (the phenyl groups had been replaced by hydrogen atoms in the original publication),[3] we first optimized the structure of **1** to establish whether our computational approach would reproduce the structural details within acceptable errors. We computed **1** in C_s and C_2 symmetry (rotation of one of the *N*-phenyl groups relates these two structures) and found the C_s form to be very slightly preferred (0.3 kcal mol^{-1}); the X-ray crystal structure is asymmetric (C_1) as a result of packing effects. The key structural parameters agree quite well (Figure 3), and we expect our approach also to give good structural data for TPH-acridine (**2**). The phenyl groups in **1** lower ΔE_{ST} by 2.4 kcal mol^{-1} (at B3LYP/6-31G*), but this separation (16.3 kcal mol^{-1} for the preferred C_s structure) increases to 17.1 kcal mol^{-1} when we employ a more polarizable and diffuse basis set at our reference level. For proper comparison, we also computed protonated TPH-acridine, **2**-H$^+$, at B3LYP/6-31G*; the key structural parameters are in excellent agreement with the crystal structure data (Figure 3).

A comparison of the measured and computed ^{13}C NMR data of protonated **2** (the spectrum was recorded in [D$_1$]TFA) also is favorable (Table 2); the average deviation of the computed data to lower fields is only about 5 ppm and can be explained by neglect of solvent effects.

The UV/Vis spectrum is also well reproduced computationally with a maximum absorption at 506 nm (experimentally at 535 nm in AcOH), which is assigned to an excited state that corresponds qualitatively to the lowest triplet state (as in **1**).[3] By analogy to **1**, the fluorescence spectrum is not a mirror image of the UV/Vis absorption spectrum; the Stoke's

Table 2: Experimental and computed (B3LYP/6-311+G**//B3LYP/6-31G*) ^{13}C NMR chemical shifts (δ [ppm], relative to TMS as internal standard) for **2**-H$^+$.

Type	CH	CH	CH	CH	C	CH	CH	CH	C	C	C	C
exptl	91.1	126.3	129.4	131.2	132.1	132.5	134.0	135.4	141.2	141.5	158.3	158.6
theor	89.2	133.5	134.8	136.7	136.2	139.0	139.8	143.1	143.0	147.3	159.1	166.0
$\Delta\delta$	1.9	7.2	5.4	5.5	4.1	6.5	5.8	7.7	1.8	5.8	0.8	7.4

 © 2005 Wiley-VCH Verlag GmbH & Co. KGaA, Weinheim

shift of **2** is about 26000 cm^{-1}, even larger than that of **1** (15000 cm^{-1}) and hence about 5 to 40 times the typical Stoke's shift of typical laser dyes.[8]

Azaacridine **2** also has a C_s singlet ground state with a ΔE_{ST} of 15.1 kcal mol^{-1}; note that this gap is significantly larger at B3LYP/6-31G* (21.1 kcal mol^{-1}). The C_2 singlet state lies 7.9 kcal mol^{-1} higher in energy and displays an even larger basis set effect on the ΔE_{ST} (20.8 at B3LYP/6-31G* and only 6.2 kcal mol^{-1} at our reference level). Stability tests showed no instabilities in the wavefunctions of the singlet states; in other words, the small ΔE_{ST} can be interpreted on the basis of aromaticity/antiaromaticity (see below). Like anthracene **1**, acridine **2** is highly polar (dipole moment: 8.2 D) and displays pronounced charge separation. The nitrogen atom in the central ring is the most negatively polarized (−0.53 according to a natural bond orbital (NBO) analysis) and is also the preferred site of protonation (in either the C_s or C_2 form); protonation at N3 and N2 is 3.8 and 18.4 kcal mol^{-1} less favorable, respectively. This is nicely confirmed by the crystal structure of **2**-H^+.

The computed NICS values in the ring centers (Table 3) reveal that all three rings of acridine **2** are antiaromatic. The same is true for **1** although the degree of antiaromaticity varies more strongly. As NICS values in the ring centers often are affected by the σ electrons of neighboring bonds, we also computed the NICS values above the ring centers and compare these with the extreme case of an antiaromatic species, namely D_{4h} cyclobutadiene.[9] This analysis shows that the outer rings of **1**, **2**, and **2**-H^+ at 0.5 Å above the ring of the plane are, with the exception of the inner ring of **1**, weakly antiaromatic. NICS points that are further away from the ring centers demonstrate that the antiaromatic character decreases rapidly, in particular for the inner rings; these NICS values are typical for nonaromatic structures. The decrease in antiaromaticity, which is much more pronounced than for cyclobutadiene, can be rationalized by differences in the ring size and the high polarity of the heterocycles in **1** and **2**.

Table 3: NICS values (B3LYP/6-311+G**//B3LYP/6-31G*) of **1**, **2**, and **2**-H^+.

NICS value relative to ring center	**1**		**2**		**2**-H^+		Cyclobutadiene (D_{4h})
	inner	outer	inner	outer	inner	outer	
0.0	+0.6	+7.9	+3.5	+6.3	+3.1	+4.1	+27.1
0.5	−1.1	+5.6	+0.9	+4.0	+1.5	+1.9	+27.9
1.0	−2.0	+2.6	−1.1	+1.4	+0.3	−0.1	+19.0
2.0	−0.2	+0.7	−0.5	+0.1	+0.2	−0.3	+4.5
3.0	+0.2	+0.2	−0.2	−0.1	0.0	−0.2	+1.2
4.0	+0.2	+0.1	−0.2	−0.2	−0.1	−0.2	+0.4

Hence, **1** and **2** must be considered to be stable, weakly antiaromatic molecules with highly polar singlet ground states. Our conclusions are further supported by visual inspection of the HOMO of **2** (C_s; Figure 4), which is symmetrically π-antibonding. This is in analogy to the simplest neutral antiaromatic singlet, the highly unstable D_{4h}-symmetric cyclobutadiene (it is common knowledge that it has a triplet ground state). Remarkably, the ΔE_{ST} for cyclobutadiene is in the same range (5.9 kcal mol^{-1} at B3LYP/6-311+G** and 11.5 kcal mol^{-1} at CCSD(T)/cc-pVDZ//B3LYP/6-311+G**)[10] as that of **1** and **2**, which lends further support to the proposal that these polycyclic structures are indeed stable antiaromatic entities. Although this formally contradicts the conclusions of Wudl und Houk et al.[3] for TPH-anthracene that double cyanine ion stabilization of zwitterion **1a** is preferred over the formal 16-π antiaromaticity (**1b**),[11] we remark that the earlier study computationally examined a smaller model system with a smaller basis set, which has a large effect on the energies (see above). However, the two conclusions are not necessarily mutually exclusive because the systems under consideration are only weakly antiaromatic and partially avoid this unfavorable situation through strong polarization.

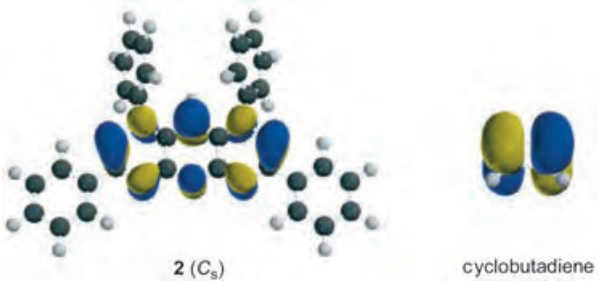


Figure 4. HOMOs of **2** and cyclobutadiene (only one of the two degenerate HOMOs is shown).

In conclusion, TPH-acridine, which we have synthesized and characterized, represents the first hexaazaacridine. The structure and spectroscopic properties of TPH-acridine and TPH-anthracene were studied by DFT computations and NICS analysis. TPH-acridine and TPH-anthracene represent highly zwitterionic structures with very low-lying triplet states. Both polycyclic structures can be considered to be stable 16-π-electron, weakly antiaromatic entities. TPH-acridine and TPH-anthracene are of great theoretical and structural interest and exhibit exciting physical properties that may be utilized in organomagnetic applications.

Received: March 6, 2005
Published online: July 20, 2005

Keywords: antiaromaticity · aromaticity · density functional theory · hexaazaacridine · hexaazaanthracene

[1] For oligothiophenes with low-lying triplet states see: a) F. Garnier, *Angew. Chem.* **1989**, *101*, 529; *Angew. Chem. Int. Ed. Engl.* **1989**, *28*, 513; b) F. Garnier, A. Yassar, R. Hajlaoui, G. Horowitz, F. Deloffre, B. Servet, S. Ries, P. Alnot, *J. Am. Chem. Soc.* **1993**, *115*, 8716; c) F. Garnier, R. Hajlaoui, A. Yassar, P. Srivastava, *Science* **1994**, *265*, 1684; d) A. Dodabalapur, L. Torsi, H. E. Katz, *Science* **1995**, *268*, 270; e) A. Dodabalapur, L. J. Rothberg, A. W. P. Fung, H. E. Katz, *Science* **1996**, *272*, 1462; a low-lying triplet state was predicted for the not-yet-synthesized

 © 2005 Wiley-VCH Verlag GmbH & Co. KGaA, Weinheim

cyclohepta[*def*]fluorene: f) U. Grieser, K. Hafner, *Chem. Ber.* **1994**, *127*, 2307, and references therein.
[2] P. Pierron, *Ann. Chim. Phys.* **1908**, *15*, 269.
[3] K. A. Hutchison, G. Srdanov, R. Hicks, H. Yu, F. Wudl, T. Strassner, M. Nendel, K. N. Houk, *J. Am. Chem. Soc.* **1998**, *120*, 2989.
[4] K. A. Hutchison, K. Hasharoni, F. Wudl, A. Berg, Z. Shuali, H. Levanon, *J. Am. Chem. Soc.* **1998**, *120*, 6362.
[5] a) P. v. R. Schleyer, C. Maerker, A. Dransfeld, H. Jiao, N. J. R. van Eikema Hommes, *J. Am. Chem. Soc.* **1996**, *118*, 6317.
[6] a) A. D. Becke, *J. Chem. Phys.* **1993**, *98*, 5648; b) C. Lee, W. Yang, R. G. Parr, *Phys. Rev. B* **1988**, *37*, 785.
[7] R. Singh, B. M. Deb, *Phys. Rep.* **1999**, *311*, 48.
[8] T. Clark, J. Chandrasekhar, *Isr. J. Chem.* **1993**, *33*, 435.
[9] P. v. R. Schleyer, M. Manoharan, Z.-X. Wang, B. Kiran, H. Jiao, R. Puchta, N. J. R. van Eikema Hommes, *Org. Lett.* **2001**, *3*, 2465.
[10] V. Gogonea, P. v. R. Schleyer, P. R. Schreiner, *Angew. Chem.* **1998**, *110*, 2045; *Angew. Chem. Int. Ed.* **1998**, *37*, 1945.
[11] Whereas a variety of cationic cyanine dyes are known, stable anionic cyanines are rare. TPH-acridine (**2**) represents, with the exception of **1**, the first molecule with a nitrogen-based anionic cyanine moiety: a) P. F. Gordon, P. Gregory, *Organic Chemistry in Colour*, Springer, Berlin, **1983**; b) D. R. Waring, G. Hallas, *The Chemistry and Application of Dyes* (Eds.: D. R. Waring, G. Hallas), Plenum, New York, **1990**.

 © 2005 Wiley-VCH Verlag GmbH & Co. KGaA, Weinheim

Coordination Chemistry

DOI: 10.1002/anie.200500375

Molecular Compounds with Mo-O-Bi Moieties**

Stefan Roggan, Christian Limberg, and Burkhard Ziemer*

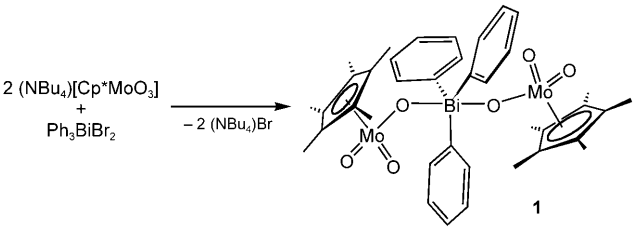
Dedicated to Professor Manfred Meisel on the occasion of his 65th birthday

The unique property of $n MoO_3/Bi_2O_3$ phases to act as catalysts for the allylic oxidation of propene (SOHIO process) remains a subject of intense discussion.[1] It might be related inter alia to the presence of surface species containing Mo-O-Bi linkages, assuming that these possess favorable hydrogen-atom abstraction or radical trapping properties. At present, there are no structurally characterized molecular complexes known that contain Mo-O-Bi moieties,[2] and the hypothesis that such units might play key roles in heterogeneous catalysis[1] stimulates attempts to create them at the molecular level.

We initially pursued the synthesis of Mo-O-Bi compounds by salt metathesis by employing seemingly suitable starting materials. However, these reactions all led only to insoluble, intractable solids, so we turned our attention to Mo-Bi-alkoxide chemistry. Alkoxidic systems are often related to oxides but exhibit certain advantages in practical terms, and it was hoped that the access to Mo/Bi alkoxides would lead to an understanding of principal problems and to new strategies for the development of oxidic structures. By employing starting materials in which part of the coordination sphere at the Mo centers was shielded by tightly bound organic ligands, we finally achieved the synthesis of the first Mo/Bi alkoxides.[3] These proved to be suitable single-source precursors for the creation of novel types of molybdenumoxo/bismuthoxo composites on inert supports.[4] However, as all attempts to prepare Mo-O-Bi complexes starting from these compounds failed, we decided to follow an alternative strategy: new complexes containing Mo–Bi metal bonds were prepared, which appeared to be appropriate to be treated with oxygenating reagents;[5] the latter were envisioned to insert oxo atoms into the metal–metal bonds. Even though this approach led to an interesting C–H activation chemistry,[6] Mo-O-Bi compounds still remained elusive.

In 1980 Klemperer and Liu communicated[7] that the reaction between Ph_3BiBr_2 and water-containing $(NBu_4)_2[MoO_4]$ leads to a white solid that analyses as $(NBu_4)_2[BiPh_3(MoO_4)_2]\cdot 3H_2O$. A structure with a Bi^V ion surrounded by three phenyl substituents and two molybdate units was suggested, and the water molecules were proposed to act only as solvate molecules. However, X-ray quality crystals could not be obtained; these would have allowed the confirmation of that idea and the clarification of whether the interaction between the Bi center and the molybdate anions has a covalent or more ionic character.

Having experienced that Mo/Bi alkoxides became accessible when organomolybdenum starting materials were employed,[3] we performed the reaction reported by Klemperer by replacing the molybdate $[MoO_4]^{2-}$ by an organomolybdenum(VI)oxo anion, namely $[Cp^*MoO_3]^-$ ($Cp^* = \eta^5$-C_5Me_5). Treatment of Ph_3BiBr_2[8] with two equivalents of $(NBu_4)[Cp^*MoO_3]$[9] in dichloromethane leads to a yellow solution containing $[(Cp^*MoO_3)_2BiPh_3]$ (**1**; Scheme 1). Workup and recrystallization from diethyl ether yielded single crystals, which were examined by X-ray diffraction. The structure analysis revealed, to our knowledge, the first structurally authenticated Mo-O-Bi linkages in a molecular compound (Figure 1).[10]



Scheme 1. The synthesis of **1**.

[*] S. Roggan, Prof. Dr. C. Limberg, Dr. B. Ziemer
Humboldt-Universität zu Berlin
Institut für Chemie
Brook-Taylor-Strasse 2, 12489 Berlin (Germany)
Fax: (+49) 30-2093-6966
E-mail: christian.limberg@chemie.hu-berlin.de

[**] We are grateful to the Deutsche Forschungsgemeinschaft, the Fonds der Chemischen Industrie, the BMBF, and the Dr. Otto Röhm Gedächtnisstiftung for financial support. We also thank P. Neubauer for crystal structure analyses as well as C. Jankowski for the preparation of starting materials.

 © 2005 Wiley-VCH Verlag GmbH & Co. KGaA, Weinheim

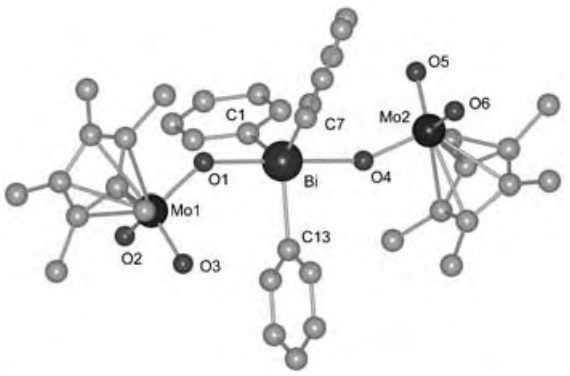
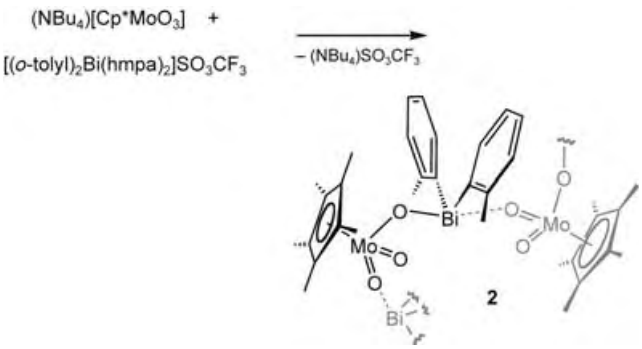


Figure 1. Molecular structure of **1**; all hydrogen atoms as well as a co-crystallized molecule of diethyl ether were omitted for clarity. Selected bond lengths [Å] and angles [°]: Bi-O1 2.198(6), Bi-O4 2.204(6), Bi-C1 2.187(9), Bi-C7 2.211(7), Bi-C13 2.195(7), Mo1-O1 1.835(5), Mo1-O2 1.725(6), Mo1-O3 1.706(6), Mo2-O4 1.822(5), Mo2-O5 1.728(6), Mo2-O6 1.718(6); O1-Bi-O4 176.7(2), C1-Bi-C13 114.3(3), C1-Bi-C7 122.0(3), C13-Bi-C7 123.7(3), C1-Bi-O1 92.9(3), C13-Bi-O1 91.0(3), C7-Bi-O1 88.0(3), C1-Bi-O4 90.3(3), C7-Bi-O4 89.6(3), C13-Bi-O4 88.4(3), Mo1-O1-Bi 139.5(3), Mo2-O4-Bi 152.8(3), O3-Mo1-O2 105.9(3), O3-Mo1-O1 106.9(3), O2-Mo1-O1 106.3(3), O6-Mo2-O5 106.1(3), O6-Mo2-O4 107.4(3), O5-Mo2-O4 105.4(3).

The Bi atom is located at the center of a slightly distorted trigonal bipyramid, in which the oxygen atoms occur at the apical sites. The phenyl rings occupy the equatorial positions in a typical manner for Ph_3BiX_2 structures.[11a] The Mo-O-Bi moieties are bent (Mo1-O1-Bi 139.5(3)°, Mo2-O4-Bi 152.8(3)°) and the Bi–O distances of 2.198(6) (Bi–O1) and 2.204(6) (Bi–O4) Å are somewhat longer than those reported for the known μ-oxo-bridged dinuclear organobismuth(V) compounds of the type $[(Ar_3BiY)_2O]$ ($Y = ClO_4^-$, $CF_3SO_3^-$, $Ar = Ph$; $Y = Cl^-$, $Ar = 4\text{-}(Me_2N)C_6H_4$), which cover a range from 2.02 to 2.12 Å.[11b–d] This is probably due to the fact that the two oxo ligands in **1** are located *trans* to each other and compete as strong π acceptors for the same orbitals (thereby mutually weakening their bonds), whereas in the other compounds mentioned the oxo ligands are positioned *trans* to weakly coordinating ligands; they can thus form stronger bonds. The Mo–O single-bond lengths of 1.835(5) (Mo1–O1) and 1.822(5) Å (Mo2–O4) in **1** appear quite short compared to those in the polymorphs of $[(Cp^*MoO_2)_2O]$ (1.855(6)–1.894(4) Å).[12] The latter exhibit a wide range of distances for the Mo=O double bonds (1.667(8)–1.721(5) Å),[12] and those in **1** (1.706(6)–1.728(6) Å) are more similar to the longer ones.

As the strategy of combining a hard {(O_2Mo)-O-Bi} metal-oxo core with soft ligands proved appropriate for the preparation of a Mo^{VI}-O-Bi^{V} compound, it should now be applied to the next synthetic target: Although some authors have assigned an active role[13] to Bi^V ions during the SOHIO process, Bi^{III} species are thought to be more relevant by the majority.[1] We thus pursued the synthesis of Mo^{VI}-O-Bi^{III} complexes in the next step, and the route to success seemed to be straightforward: the reaction of Ph_2BiBr[8] with $(NBu_4)[Cp^*MoO_3]$. However, Bi^{III} compounds such as Ph_2BiBr are Lewis acidic and show a strong tendency to accept an additional anionic ligand to form a hypervalent compound. Hence, many attempts to react the above-mentioned compounds ultimately led to the isolation of the well-crystallizing $(NBu_4)[Ph_2BiBr_2]$.[14] This finding certainly indicates that the intended metathesis under elimination of $[NBu_4]Br$ must have proceeded at least to some extent, but trapping of the $[NBu_4]Br$ by unconsumed starting material led to a non-uniform course of the reaction, which prohibited the isolation of the second bismuth-containing product. We therefore decided to employ $[(o\text{-tolyl})_2Bi(hmpa)_2]SO_3CF_3$ (o-tolyl = 2-$(Me)C_6H_4$; hmpa = hexamethylphosphoric acid triamide)[15] instead of Ph_2BiBr as the starting material, as it seemed to offer several advantages with respect to the above-mentioned problems: The *o*-tolyl groups are sterically somewhat more demanding than phenyl groups are, the hmpa ligands can occupy vacant coordination sites where necessary, and moreover, in contrast to halide ions, triflate anions are very weak ligands.

The reaction of $[(o\text{-tolyl})_2Bi(hmpa)_2]SO_3CF_3$ with $(NBu_4)[Cp^*MoO_3]$ proceeds smoothly in THF and yields a yellow solid that can be recrystallized from a mixture of diethyl ether and dichloromethane. A single-crystal X-ray structure analysis[10] confirmed the successful synthesis of the first Mo^{VI}-O-Bi^{III} complex, namely $[(Cp^*MoO_2)$-μ-O-{$Bi(o\text{-tolyl})_2$}$]_n$ (**2**; Scheme 2, Figure 2).



Scheme 2. The synthesis of **2**.

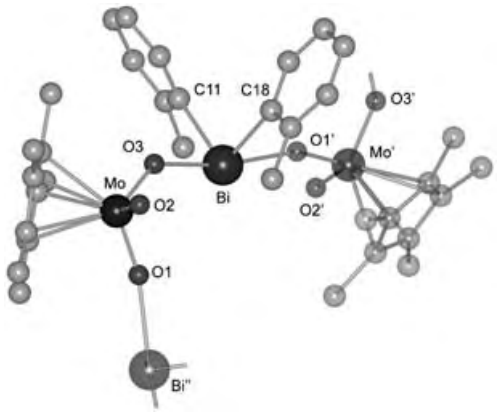


Figure 2. Molecular structure of **2**; all hydrogen atoms as well as the cocrystallized molecules of dichloromethane were omitted for clarity. Selected bond lengths [Å] and angles [°]: Bi-O3 2.310(2), Bi-O1′ 2.385(2), Bi-C18 2.237(3), Bi-C11 2.240(3), Mo-O1 1.768(2), Mo-O2 1.720(2), Mo-O3 1.786(2); O3-Bi-O1′ 170.46(9), O2-Mo-O1 105.5(2), O2-Mo-O3 105.9(2), O1-Mo-O3 105.4(2), Mo-O1-Bi′′ 160.6(2), Mo-O3-Bi 138.0(2), C18-Bi-C11 94.6(2), C18-Bi-O3 89.7(2), C11-Bi-O3 86.6(2), C18-Bi-O1′ 82.1(2), C11-Bi-O1′ 89.12(2).

 © 2005 Wiley-VCH Verlag GmbH & Co. KGaA, Weinheim

In **2** a $[Cp^*MoO_3]^-$ moiety is covalently bonded through an oxygen atom to a $[(o\text{-tolyl})_2Bi]^+$ ion. The resulting hypothetical molecule $[(Cp^*MoO_2)\text{-}(\mu\text{-}O)\text{-}\{Bi(o\text{-tolyl})_2\}]$ features a still Lewis acidic Bi^{III} center on one side and basic Mo=O oxygen atoms on the other side. Consequently, Lewis acid/base Mo=O···Bi interactions occur leading to a chainlike coordination polymer with pseudo-trigonal bipyramidal or seesaw ligand geometries around the Bi atoms: the C atoms of the *o*-tolyl ligands occupy equatorial positions, the oxygen atoms the apical sites. The angle between the oxygen atoms (O1′-Bi-O3 170.46(9)°) is close to the ideal value of 180°. In contrast, the angle between the *ipso*-carbon atoms (C11-Bi-C18) of only 94.6(2)° is much smaller than expected for a trigonal bipyramid (120°). Such acute angles are not uncommon in the structural chemistry of heavy main group elements and can be explained in two ways: if the ligand sphere is described as pseudo-trigonal bipyramidal, a strong stereochemical effect of the bismuth lone pair on the C-Bi-C angle is implied. Alternatively, a bonding model based on unhybridized 6p orbitals with the lone pair of electrons at the bismuth center in a 6s orbital appears equally appropriate.[11a,e,f,g]

The Mo-O-Bi moieties are bent with angles (Mo-O1-Bi″ 160.6(2)°, Mo-O3-Bi 138.0(2)°) similar to those in **1**. Surprisingly, the Bi–O1′ bond in the Bi···O=Mo moiety (2.385(2) Å) is only slightly longer than the Bi–O bond in the covalent Mo-O-Bi unit (Bi–O3 2.310(2) Å). This might be understood if the Mo=O···Bi interaction is accomplished with a strong involvement of the Bi–O3 σ* orbital. A strong coordinative O···Bi interaction would then weaken the covalent Bi–O bond, and indeed the Bi···O=Mo interaction has to be considered as strong: the situation is comparable to the one in the complex $[\{Cl_3Bi\cdots O{=}V(OC_2H_4OCH_3)_3\}_2]$[16] in which, however, the distance between the Bi center and the vanadyl O atom is 2.703(!) Å. Naturally, both Bi–O bonds in **2** are significantly longer than those in **1**, but they are comparable to the bonds in the $\{Bi_3(\mu_3\text{-}O)\}$ units (2.037(8)–2.665(8) Å) of the recently communicated bismuth-oxo cluster cation $[Bi_{22}O_{26}]^{14+}$.[17] The Bi–O bond lengths found for Mo-O-Bi units in β-bismuth molybdate, $Bi_2Mo_2O_9$,[18] lie between 2.34(3) and 2.79(3) Å, and are thus longer than those in **2**. The Mo–O3 distance in the Mo-O-Bi unit in **2** is 1.786(2) Å and is thus significantly shorter than the Mo–O bond lengths in $[\{Cp^*MoO_2\}_2O]$[12] (1.855(6)–1.894(4) Å). At the same time it is at the upper end of the corresponding range determined for Mo–O bonds in the $Bi_2Mo_2O_9$ phase (1.71(3)–1.78(3) Å).[18] The two Mo=O distances in **2** differ significantly from each other. Whereas the Mo=O2 bond length (1.720(2) Å) is comparable to those found for the $[\{Cp^*MoO_2\}_2O]$ system (1.667(8)–1.721(5) Å), the Mo=O1 double bond (1.768(2) Å) is only slightly shorter than the Mo–O3 single bond. This significant elongation must be the consequence of the strong coordination of O1 to the Lewis acidic bismuth center.

In conclusion we have managed to access to Mo-O-Bi complexes—a previously unknown and long-sought class of compounds. Currently we are investigating their chemical properties, that is, their behavior in the presence of hydrocarbons such as olefins, substrates with weak C–H bonds, and as organic radicals, to establish their potential as functional models for Mo-O-Bi units on bismuth molybdate surfaces.

Experimental Section

All manipulations were carried out in an argon atmosphere using dried solvents.

1: A solution of Ph_3BiBr_2 (0.115 g, 0.19 mmol)[8] in CH_2Cl_2 (10 mL) was added slowly at −78 °C to a stirred solution of $(Bu_4N)[Cp^*MoO_3]$ (0.200 g, 0.38 mmol)[9] in CH_2Cl_2 (10 mL). The reaction mixture slowly turned yellow, and after stirring at −78 °C for 1 h and for a further 4 h at room temperature, the solvent was evaporated under reduced pressure. The resulting yellow residue was extracted with toluene leading to a yellow solution which was separated from undissolved $(NBu_4)Br$ by filtration. Evaporation of the solvent yielded crude **1** (160 mg; 83 %), which according to ^{1}H NMR spectroscopy was still contaminated by some ammonium salt as well as by the known compound $[(Cp^*MoO_2)_2O]$.[19] Repeated recrystallization from diethyl ether finally yielded pure **1** (30 mg; 16 %). C,H analysis calcd (%) for $C_{38}H_{45}BiMo_2O_6$: C 45.70, H 4.54; found: C 45.47, H 4.87; ^{1}H NMR (400.1 MHz, CD_2Cl_2): $\delta = 8.04$ (d, 6H, $^3J_{H,H} = 8.19$ Hz; *o*-phenyl), 7.71 (m, 6H; *m*-phenyl), 7.57 (m, 3H; *p*-phenyl), 1.69 ppm (s, 30H; Me_{Cp^*}); ^{13}C NMR (100.6 MHz, CD_2Cl_2): $\delta = 10.3$ ($Cp^*\text{-}CH_3$), 118.0 ($Me\text{-}C_{Cp^*}$), 131.3 (*m*-phenyl), 131.8 (*p*-phenyl), 134.5 (*o*-phenyl); signals for the *ipso*-carbon atoms were not detected; IR (KBr): $\tilde{\nu} = 3050$w, 2964w, 2916w, 2857w, 1637b, 1561w, 1469w, 1437m, 1377w, 1262w, 1162w, 1096w, 1024w, 1013w, 989m, 897s, 865s, 817m, 805m, 800m, 736s, 697vs, 621m, 447m, 423w cm^{-1}.

2: A colorless solution of $(Bu_4N)[Cp^*MoO_3]$ (0.200 g, 0.38 mmol) in THF (10 mL) was added over 10 min to a stirred light yellow solution of $[(o\text{-tolyl})_2Bi(hmpa)_2]SO_3CF_3$ (0.345 g, 0.38 mmol)[16] in THF (10 mL) held at −78 °C. The solution turned yellow immediately. After the addition was complete, the solution was stirred for a further 45 min at −78 °C and then for 2 h at room temperature. The solution was then reduced to a volume of 10 mL and cooled to −30 °C. A yellow solid precipitated overnight which was still contaminated by small amounts of $(NBu_4)SO_3CF_3$ and hmpa. An analytically pure sample (170 mg; 67 % yield) was obtained by washing the precipitate repeatedly with cold CH_2Cl_2. Single crystals suitable for X-ray analysis were grown by overlaying a solution of **2** in CH_2Cl_2 with diethyl ether. C, H analysis calcd (%) for $C_{24}H_{29}BiMoO_3$: C 43.00, H 4.36; found: C 43.02, H 4.68. ^{1}H NMR (400.1 MHz, CD_2Cl_2): $\delta = 8.25$ (dd, 2H, $^3J_{H,H} = 7.63$ Hz, $^4J_{H,H} = 1.55$ Hz; *o*-tolyl), 7.51 (m, 4H; *m*-tolyl), 7.32 (m, 2H; *p*-tolyl), 2.45 (s, 6H; CH_3), 1.72 ppm (s, 15H; Me_{Cp^*}); ^{13}C NMR (100.6 MHz, CD_2Cl_2): $\delta = 144.5/137.4/132.2/129.6/128.5$ (aryl C), 118.9 ($Me\text{-}C_{Cp^*}$), 24.0 ($tolyl\text{-}CH_3$), 10.31 ppm ($Cp^*\text{-}CH_3$); the signals for the *ipso*-carbon atoms were not detected; IR (KBr): $\tilde{\nu} = 3048$w, 2995w, 2961w, 2913m, 2857w, 1448m, 1379w, 1272w, 1203w, 1157w, 1116w, 1069w, 1031w, 1019w, 988w, 8921s, 863w, 819s, 802s, 783s, 744vs, 719vs, 703s, 621m, 472m cm^{-1}.

Received: February 1, 2005
Published online: July 20, 2005

Keywords: bismuth · cyclopentadienyl ligands · molybdenum · organometallic compounds · oxides

[1] Recent reviews: C. Limberg, *Angew. Chem.* **2003**, *115*, 6112; *Angew. Chem. Int. Ed.* **2003**, *42*, 5932; T. A. Hanna, *Coord. Chem. Rev.* **2004**, *248*, 429, and references therein.

[2] One compound has been described in the literature, which contains a hybrid between Mo-O-Bi and Mo=O···Bi moieties: R. Villanneau, A. Proust, F. Robert, P. Gouzerh, *J. Chem. Soc. Dalton Trans.* **1999**, 421.

 © 2005 Wiley-VCH Verlag GmbH & Co. KGaA, Weinheim

[3] M. Hunger, C. Limberg, P. Kircher, *Angew. Chem.* **1999**, *111*, 1171; *Angew. Chem. Int. Ed.* **1999**, *38*, 1105; M. Hunger, C. Limberg, P. Kircher, *Organometallics* **2000**, *19*, 1044.

[4] C. Limberg, M. Hunger, W. Habicht, E. Kaifer, *Inorg. Chem.* **2002**, *41*, 3359.

[5] M. Hunger, C. Limberg, E. Kaifer, P. Rutsch, *J. Organomet. Chem.* **2002**, *641*, 9.

[6] S. Roggan, C. Limberg, B. Ziemer, M. Brandt, *Angew. Chem.* **2004**, *116*, 2906; *Angew. Chem. Int. Ed.* **2004**, *43*, 2846; S. Roggan, G. Schnakenburg, C. Limberg, S. Sandhöfner, H. Pritzkow, B. Ziemer, *Chem. Eur. J.* **2005**, *11*, 225.

[7] W. G. Klemperer, R.-S. Liu, *Inorg. Chem.* **1980**, *19*, 3863.

[8] A. Michaelis, A. Marquardt, *Justus Liebigs Ann. Chem.* **1889**, *251*, 323.

[9] J. Sundermeyer, U. Radius, C. Burschka, *Chem. Ber.* **1992**, *125*, 2379.

[10] Data for the X-ray structure analyses: **1**·Et_2O: $C_{42}H_{55}BiMo_2O_7$, $M_r = 1072.72$, monoclinic, space group $P2_1/n$, $a = 13.809(2)$, $b = 10.319(1)$, $c = 30.728(4)$ Å, $\beta = 101.26(2)°$, $V = 4294.4(9)$ Å^3, $Z = 4$, $T = 180(2)$ K, $F_{000} = 2120$, $\mu = 4.708$ mm^{-1}, $\Theta = 2.09$–$24.09°$, reflections collected 28609, independent reflections 6397 ($R_{int} = 0.0874$), GoF = 1.101, $R = 0.0574$, $wR_2 = 0.0939$, largest diffraction peak and hole 1.814/−1.388 e Å^{-3}; **2**·CH_2Cl_2: $C_{25}H_{31}BiCl_2MoO_3$, $M_r = 755.32$, monoclinic, space group $P2_1/n$, $a = 12.1123(6)$, $b = 11.2738(3)$, $c = 20.3994(9)$ Å, $\beta = 104.319(4)°$, $V = 2699.0(3)$ Å^3, $Z = 4$, $T = 100(2)$ K, $F_{000} = 1456$, $\mu = 7.197$ mm^{-1}, $\Theta = 4.94$–$27.99°$, reflections collected 42504, independent reflections 6471 ($R_{int} = 0.0481$), GoF = 1.183, $R = 0.0258$, $wR_2 = 0.0515$, largest diffraction peak and hole 1.091/−0.897 e Å^{-3}. The data for **1** were collected on a STOE IPDS I, those for **2** on a STOE IDPS2T using $Mo_{K\alpha}$ radiation, $\lambda = 0.71073$ Å, and the structures were solved by direct methods (SHELXS-97), refined versus F^2 (SHELXL-97),[20] with anisotropic temperature factors for all non-hydrogen atoms. All hydrogen atoms were added geometrically and refined by using a riding model. CCDC-261495 (**1**) and CCDC-261496 (**2**) contain the supplementary crystallographic data for this paper. These data can be obtained free of charge from the Cambridge Crystallographic Data Centre via www.ccdc.cam.ac.uk/data_request/cif.

[11] a) C. Silvestru, H. J. Breunig, H. Althaus, *Chem. Rev.* **1999**, *99*, 3277; b) F. C. March, G. J. Ferguson, *J. Chem. Soc. Dalton Trans.* **1975**, 1291; c) Y. Matano, N. Azuma, H. Suzuki, *J. Chem. Soc. Perkin Trans. 1* **1994**, 1739; d) A. Hassan, S. R. Breeze, S. Courtenary, C. Deslippe, S. Wang, *Organometallics* **1996**, *15*, 5613; e) W. Clegg, R. J. Errington, G. A. Fisher, D. C. R. Hockless, N. C. Norman, A. G. Orpen, S. E. Stratford, *J. Chem. Soc. Dalton Trans.* **1992**, 1967; f) W. Clegg, R. J. Errington, G. A. Fisher, R. J. Flynn, N. C. Norman, *J. Chem. Soc. Dalton Trans.* **1993**, 637; g) B. M. Gimarc, S. A. Khan, *J. Am. Chem. Soc.* **1978**, *100*, 2340.

[12] A. L Rheingold, J. R. Harper, *J. Organomet. Chem.* **1991**, *403*, 335.

[13] Y. H. Jang, W. A. Goddard III, *J. Phys. Chem. B* **2002**, *106*, 5997; Y. H. Jang, W. A. Goddard III, *Top. Catal.* **2001**, *15*, 273.

[14] Whereas the structure of $(NBu_4)[Ph_2BiBr_2]$ is yet unpublished, the one of $(PPh_4)[Ph_2BiBr_2]$ has been reported: W. Clegg, R. J. Errington, G. A. Fisher, D. C. R. Hockless, N. C. Norman, A. G. Orpen, S. E. Stratford, *J. Chem. Soc. Dalton Trans.* **1992**, 1967.

[15] Y. Matano, T. Miyamatsu, H. Suzuki, *Organometallics* **1996**, *15*, 1951.

[16] J. W. Pell, W. C. Davis, H. C. zur Loye, *Inorg. Chem.* **1996**, *35*, 5754.

[17] D. Mansfeld, M. Mehring, M. Schürmann, *Angew. Chem.* **2005**, *117*, 250; *Angew. Chem. Int. Ed.* **2005**, *44*, 245.

[18] H.-Y. Chen, A. W. Sleight, *J. Solid State Chem.* **1986**, *63*, 70.

[19] M. Herberhold, W. Kremnitz, A. Razavi, H. Schöllhorn, U. Thewalt, *Angew. Chem.* **1985**, *97*, 603; *Angew. Chem. Int. Ed. Engl.* **1985**, *24*, 601.

[20] G. M. Sheldrick, SHELXS-97, Program for Crystal Structure Solution, University of Göttingen, **1997**; G. M. Sheldrick, SHELXL-97, Program for Crystal Structure Refinement, University of Göttingen, **1997**.

 © 2005 Wiley-VCH Verlag GmbH & Co. KGaA, Weinheim

Multicomponent Micelles

DOI: 10.1002/anie.200500584

Multicompartment Micelles Formed by Self-Assembly of Linear ABC Triblock Copolymers in Aqueous Medium**

*Stephan Kubowicz, Jean-François Baussard, Jean-François Lutz, Andreas F. Thünemann, Hans von Berlepsch, and André Laschewsky**

Multicompartment micelles composed of a water-soluble shell and a segregated hydrophobic core are novel, most interesting morphologies for nanotechnology, in particular for

[*] Dipl.-Phys. S. Kubowicz, J.-F. Baussard, Dr. J.-F. Lutz, Prof. Dr. A. Laschewsky
Fraunhofer Institute for Applied Polymer Research
Geiselbergstrasse 69, 14476 Potsdam (Germany)
Fax: (+49) 331-977-5054
E-mail: andre.laschewsky@rz.uni-potsdam.de

Dipl.-Phys. S. Kubowicz
Max Planck Institute of Colloids and Interfaces
Am Mühlenberg 1, 14476 Potsdam (Germany)

J.-F. Baussard
Department of Chemistry
Université catholique de Louvain
1 Place Louis Pasteur, 1348 Louvain-la-Neuve (Belgium)

Prof. A. F. Thünemann
Federal Institute for Materials Research and Testing
Richard-Willstätter-Strasse 11, 12489 Berlin (Germany)

Dr. H. von Berlepsch
Research Center for Electron Microscopy
Free University of Berlin
Fabeckstrasse 36a, 14195 Berlin (Germany)

Prof. Dr. A. Laschewsky
Department of Chemistry
University of Potsdam
Karl-Liebknecht-Strasse 24–25, 14476 Potsdam (Germany)

[**] This research was supported by the Fonds der Chemischen Industrie, the Fraunhofer Society, the Max-Planck Society, and the French Community of Belgium (Action de Recherche Concertée, convention n° 00/05-2619). The authors thank H. Ringsdorf (Universität Mainz), A. Jonas, B. Nysten, and A. Pallandre (Université catholique de Louvain) for stimulating discussions, and C. Böttcher (FU Berlin) for his help with the cryo-TEM experiments.

Supporting information for this article is available on the WWW under http://www.angewandte.org or from the author.

InterScience
© 2005 Wiley-VCH Verlag GmbH & Co. KGaA, Weinheim

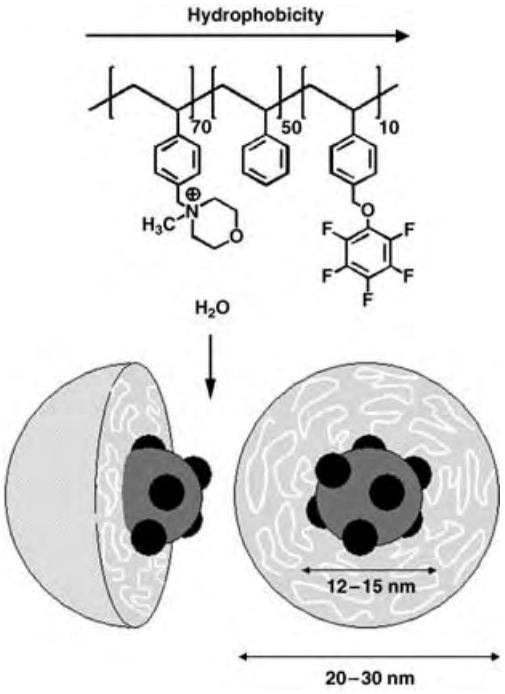
nanobiotechnology.[1,2] For example, for drug-delivery applications the separated incompatible compartments of the hydrophobic core could enable the selective entrapment and release of various hydrophobic drugs, while the hydrophilic shell stabilizes these nanostructures in physiological media. Thus, several strategies for preparing multicompartment micelles have been proposed recently.[1,3–8] However, so far, the number of morphological studies concerning such micelles is rather low and therefore little is known about their exact internal structure.[2]

The most straightforward pathway for preparing multicompartment micelles is the direct aqueous self-assembly of synthetic polymeric amphiphiles possessing one hydrophilic segment and two incompatible hydrophobic segments. Copolymers made of different segments covalently bonded together such as block, graft, star-block, and miktoarm star copolymers can often spontaneously self-assemble into various organized superstructures.[9] Such self-assembly processes are driven by diverse repulsion forces between the segments. In a bulk material, the thermodynamic incompatibility between various connected results in ordered segregated nanophases.[10] In liquid media, the differences in affinity of the various segments for the solvent lead to dispersed organized objects. Either in bulk or in solution, the morphology of the self-assembled structures depends on the molecular shape of the polymeric building blocks (number of segments, segment lengths, block sequence, architecture, and composition).[9] Naturally, the more complex the starting copolymers, the more complicated and difficult to analyze the resulting superstructures are. The latter is particularly true in solution because of the dynamic behavior of most self-assemblies.

For copolymers composed of only two different segments (AB), the factors governing self-assembly in solution are now well-understood, and the main morphologies such as spherical micelles,[11] wormlike micelles,[12] and vesicles[13] have been described. However, for more complex macromolecules such as ABC triblock copolymers, the possibilities of self-assembly in solution remain quite unexplored, although some morphologies have been characterized in either aqueous or organic media. In the simplest case, two of the three ABC segments are soluble in the solvent, resulting in micelles with an insoluble inner core and a mixed-arm soluble shell.[14–16] But, if two of the three ABC segments are insoluble in the solvent, the precise morphology of the self-assemblies is usually more difficult to describe. Concerning the general shape of the superstructure: spherical micelles[15–23] and vesicles[19,24] have been prepared from ABC copolymers having two insoluble segments. However, the morphology of the inner core is usually hard to elucidate.

If the two blocks composing the core are large enough and thermodynamically incompatible, they should most likely segregate into different phases, forming two or more separated compartments in the core of the micelle. Nevertheless, depending on the molecular structure of the segments, diverse morphologies can be expected for the multicompartment core, for example, "spheres in spheres" (core–shell model, onionlike) or "spheres on spheres" (raspberrylike). Up to now, the core structures were often presumed (in most cases, core–shell construction was proposed) but were not characterized or observed by microscopy. Most recently, Lodge et al. reported a first convincing visualization by cryo-transmission electron microscopy (cryo-TEM) of multicompartment micelles prepared in aqueous medium by self-assembly of miktoarm star copolymers;[25] they described the coexistence of segregated domains in the hydrophobic core of the formed nanostructures. However, the precise morphology of this inner core was not assessed.

In the present work, the aqueous self-assembly of an ABC linear triblock copolymer, poly(4-methyl-4-(4-vinylbenzyl)morpholin-4-ium chloride)-*block*-polystyrene-*block*-poly(pentafluorophenyl 4-vinylbenzyl ether) (PVBM-*b*-PS-*b*-PVBFP) was studied (Scheme 1). The copolymer



Scheme 1. Molecular structure of the triblock copolymer PVBM-*b*-PS-*b*-PVBFP and possible morphology of the multicompartment micelles observed in aqueous medium. Light gray: hydrophilic block with morpholinium units; dark gray: hydrophobic hydrocarbon block; black: hydrophobic fluorocarbon-rich block.

building blocks consist of a long cationic hydrophilic block, PVBM, and two short consecutive hydrophobic blocks: a hydrocarbon one (PS) and a mixed hydrocarbon/fluorocarbon one (PVBFP). Hydrocarbon and fluorocarbon blocks were selected since such segments tend to be strongly incompatible and should thus favor the segregation into distinct domains.[1] Moreover, such a choice should lead to compartments of markedly differing properties,[1,3,5,6] as desirable, for example, for drug-delivery applications.

The copolymer PVBM-*b*-PS-*b*-PVBFP was obtained by quaternization of a poly(vinylbenzyl chloride)-*b*-PS-*b*-PVBFP precursor with *N*-methylmorpholine. The triblock precursor was prepared by a three-step reversible addition fragmentation transfer (RAFT) polymerization process using

 © 2005 Wiley-VCH Verlag GmbH & Co. KGaA, Weinheim

benzyl dithiobenzoate as a chain-transfer agent. To prepare the multicompartment micelles, the triblock PVBM-*b*-PS-*b*-PVBFP was initially dispersed in a dioxane/water mixture and subsequently dialyzed stepwise against pure water. Indeed, the choice of the organic solvent and of the mode of its removal is crucial for the outcome of the self-assembly.[26]

Figure 1 shows typical cryo-TEM images of the aqueous solution obtained. The images reveal uniformly dispersed dark gray spherical objects with an average diameter of 12–15 nm. These correspond to the formed micelles' hydrophobic core, which is composed of segregated domains: inside the sphere of the micellar core, dark spheres with an average diameter of about 3.4 ± 0.2 nm can be distinguished. The strong contrast in the images can be attributed to the presence of electron-rich fluorine atoms.[25] In average, four to ten segregated dark domains are observed for each micellar core. The hydrosoluble PVBM corona of the micelles is not directly observable but can be estimated from the objects interdistance to be around 20–30 nm in diameter.

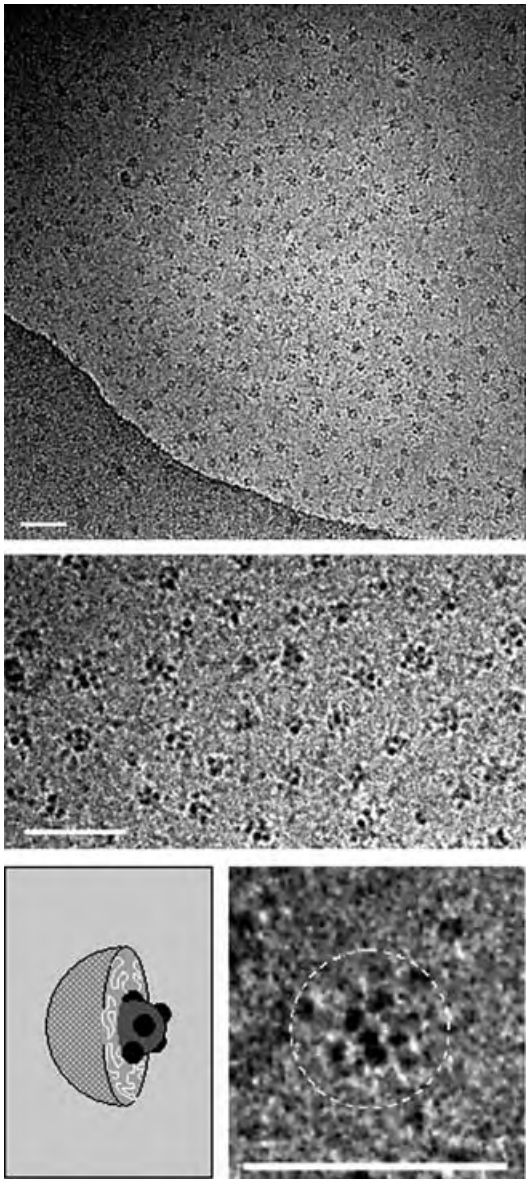


Figure 1. Cryo-TEM images and a schematic representation of the structure of multicompartment micelles obtained by self-assembly of the triblock copolymer PVBM-*b*-PS-*b*-PVBFP in aqueous medium. The corona of the micelles is not visible. The scale bars correspond to 50 nm.

The observed core morphology resembles a raspberrylike morphology, as first described by Stadler et al. for the bulk self-assembly of polystyrene-*b*-polybutadiene-*b*-poly(methyl methacrylate) (SBM) triblock copolymers.[27] Pascault et al. demonstrated that the raspberrylike morphology can also be observed in a micellar structure.[28,29] In their study, micelles of SBM were initially dispersed in a reactive epoxy–amine mixture, which was subsequently polymerized. Their work indicated that the initial micelle morphology was fixed in the polymer matrix by polymerization and therefore could be studied by TEM. Figure 1 shows a first example of a similar morphology for micelles prepared in aqueous medium. However, the cryo-TEM images cannot distinguish whether the dark fluorocarbon domains are covering the surface of a central hydrocarbon core (spheres-on-spheres, raspberrylike morphology) as shown in Scheme 1 and as described by Stadler et al.,[27] or whether the dark domains are embedded in the hydrocarbon core (spheres-in-spheres morphology). The latter structure might be expected intuitively since the fluorinated block is the C block of the ABC sequence.

Another question arises concerning the observed morphology: are the segregated dark domains made of the complete PVBFP blocks or only of the fluorocarbon moieties of PVBFP? Only if the latter scenario is true can the size measured by cryo-TEM be correlated to the molecular volumes of the copolymers (see the Supporting Information). For this scenario, the calculations give a global theoretical diameter of 20.5 nm for the whole micelle (swelling of the corona with water is not taken into account), and a diameter of 13.8 nm for the whole hydrophobic core, values in good agreement with the numbers obtained from the cryo-TEM images. In contrast, when we assume that the dark regions are due to the whole PVBFP blocks (hydrocarbon and fluorocarbon parts), the calculated diameters for the whole micelle and for the hydrophobic core are too small. Therefore, we conclude that the dark spheres comprise only the fluorocarbon moieties of PVBFP, whereas the dark gray region contains both the hydrocarbon domains of PS and PVBFP.

The overall dimension of the micelle was also confirmed by static light scattering (see the Supporting Information). The scattering curve corresponds to the scattering of spherical particles with a radius of gyration R_g of 14.5 nm. This number is in good agreement with theoretical calculations and size estimated from cryo-TEM. Also in agreement with the micrographs, the scattering curve indicates that the size distribution of these objects is relatively broad, as may be expected from the polydispersity of the polymers ($M_w/M_n = 1.7$).

In conclusion, multicompartment micelles having a diameter of 20–30 nm were prepared by the self-assembly in aqueous medium of the amphiphilic triblock copolymer PVBM-*b*-PS-*b*-PVBFP. As evidenced by cryo-TEM, the core is segregated into nanometer-sized compartments in which many small, fluorocarbon-rich domains coexist with a

 © 2005 Wiley-VCH Verlag GmbH & Co. KGaA, Weinheim

continuous hydrocarbon-rich region. These novel nanostructured colloids may serve as models as well as mimics for biological structures such as globular proteins, and may open up interesting opportunities for nanotechnology applications.

Received: February 16, 2005
Revised: March 29, 2005
Published online: July 20, 2005

Keywords: amphiphiles · block copolymers · colloids · micelles · self-assembly

[1] A. Laschewsky, *Curr. Opin. Colloid Interface Sci.* **2003**, *8*, 274.
[2] J.-F. Lutz, A. Laschewsky, *Macromol. Chem. Phys.* **2005**, *206*, 813.
[3] K. Stähler, J. Selb, F. Candau, *Langmuir* **1999**, *15*, 7565.
[4] R. Weberskirch, J. Preuschen, H. W. Spiess, O. Nuyken, *Macromol. Chem. Phys.* **2000**, *201*, 995.
[5] A. Kotzev, A. Laschewsky, R. H. Rakotoaly, *Macromol. Chem. Phys.* **2001**, *202*, 3257.
[6] A. Kotzev, A. Laschewsky, P. Adriaensens, J. Gelan, *Macromolecules* **2002**, *35*, 1091.
[7] Z. Li, M. A. Hillmyer, T. P. Lodge, *Macromolecules* **2004**, *37*, 8933.
[8] F. Boschet, C. Branger, A. Margaillan, T. E. Hogen-Esch, *Polym. Int.* **2005**, *54*, 90.
[9] S. Förster, T. Plantenberg, *Angew. Chem.* **2002**, *114*, 712; *Angew. Chem. Int. Ed.* **2002**, *41*, 688.
[10] F. S. Bates, *Science* **1991**, *251*, 898.
[11] G. Riess, *Prog. Polym. Sci.* **2003**, *28*, 1107.
[12] Y. Y. Won, H. T. Davis, F. S. Bates, *Science* **1999**, *283*, 960.
[13] D. E. Discher, A. Eisenberg, *Science* **2002**, *297*, 967.
[14] C. S. Patrickios, A. B. Lowe, S. P. Armes, N. C. Billingham, *J. Polym. Sci. Part A* **1998**, *36*, 617.
[15] Y. Cai, S. P. Armes, *Macromolecules* **2004**, *37*, 7116.
[16] V. Sfika, C. Tsitsilianis, A. Kiriy, G. Gorodyska, M. Stamm, *Macromolecules* **2004**, *37*, 9551.
[17] W. Y. Chen, P. Alexandridis, C. K. Su, C. S. Patrickios, W. R. Hertler, T. A. Hatton, *Macromolecules* **1995**, *28*, 8604.
[18] J. Kriz, B. Masar, J. Plestil, Z. Tuzar, H. Pospisil, D. Doskocilova, *Macromolecules* **1998**, *31*, 41.
[19] G.-E. Yu, A. Eisenberg, *Macromolecules* **1998**, *31*, 5546.
[20] Q. Ma, K. L. Wooley, *J. Polym. Sci. Part A* **2000**, *38*, 4805.
[21] J.-F. Gohy, N. Willet, S. K. Varshney, J.-X. Zhang, R. Jérôme, *Angew. Chem.* **2001**, *113*, 3314; *Angew. Chem. Int. Ed.* **2001**, *40*, 3214.
[22] J.-F. Gohy, B. G. G. Lohmeijer, S. K. Varshney, B. Decamps, E. Leroy, S. Boileau, U. S. Schubert, *Macromolecules* **2002**, *35*, 9748.
[23] J.-F. Gohy, E. Khousakoun, N. Willet, S. K. Varshney, R. Jérôme, *Macromol. Rapid Commun.* **2004**, *25*, 1536.
[24] A. K. Brannan, F. S. Bates, *Macromolecules* **2004**, *37*, 8816.
[25] Z. Li, E. Kesselman, Y. Talmon, M. Hillmyer, T. Lodge, *Science* **2004**, *306*, 98.
[26] N. S. Cameron, M. K. Corbierre, A. Eisenberg, *Can. J. Chem.* **1999**, *77*, 1311.
[27] U. Breiner, U. Krappe, T. Jakob, V. Abetz, R. Stadler, *Polym. Bull.* **1998**, *40*, 219.
[28] S. Ritzenthaler, F. Court, L. David, E. Girard-Reydet, L. Leibler, J. P. Pascault, *Macromolecules* **2002**, *35*, 6245.
[29] S. Ritzenthaler, F. Court, E. Girard-Reydet, L. Leibler, J. P. Pascault, *Macromolecules* **2003**, *36*, 118.

 © 2005 Wiley-VCH Verlag GmbH & Co. KGaA, Weinheim

Asymmetric Synthesis

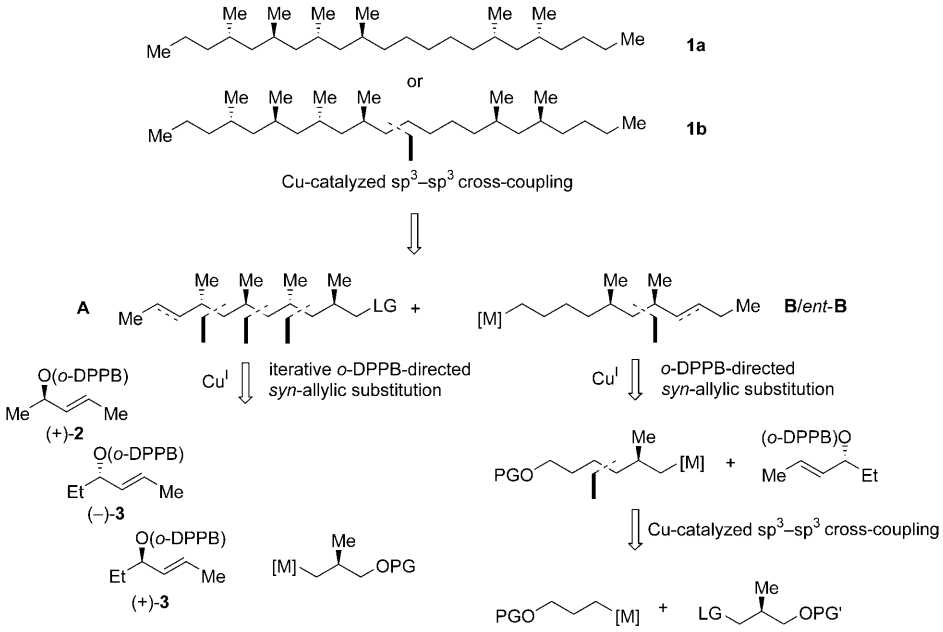
DOI: 10.1002/anie.200501612

Enantioselective Total Synthesis and Determination of the Absolute Configuration of the 4,6,8,10,16,18-Hexamethyldocosane from *Antitrogus parvulus***

*Christian Herber and Bernhard Breit**

The larvae of the cane beetle *Antitrogus parvulus* (known as cane grubs) are a source of major damage in sugar-cane crops in Australia.[1] On searching for an environmentally benign plant-protection strategy, recent research has focused on the identification of sex pheromones of the cane beetle. As a result hydrocarbons, such as 4,6,8,10,16-penta- and 4,6,8,10,16,18-hexamethyldocosanes (**1**), that feature an unprecedented *anti-anti-anti* stereochemistry in the 4,6,8,10-methyl tetrad have been discovered.[2] However, the small amount of material isolated from the natural source has not yet allowed the determination of their biological role. Combined spectroscopic and synthetic efforts have elucidated the relative *anti* configuration of the four methyl-bearing stereocenters in the tetrad unit of **1** and the relative *syn* configuration within the methyl diad region. However, so far the stereochemical relation between the all-*anti* tetrad and the *syn* diad remains unknown (**1a** or **1b**), as does the absolute configuration (Scheme 1).[2]

We herein report on the total synthesis of both diastereomers **1a** and **1b** in enantiomerically pure form, thus enabling the determination of the relative and absolute configurations of the natural product. The synthesis relies heavily on our recently developed copper-mediated and *ortho*-diphenylphosphanylbenzoyl (*o*-DPPB)-directed *syn*-allylic substitution with Grignard reagents for iterative deoxypropionate synthesis.[3] Additionally, we demonstrate the power of copper-catalyzed sp^3–sp^3 cross coupling by employing it for building-block construction and as the fragment-coupling step in a convergent total synthesis.



Scheme 1. Retrosynthesis for **1a** and **1b**. PG = protecting group, LG = leaving group, M = metal.

Our synthetic plan is outlined in Scheme 1. Fragment coupling of the methyl tetrad and the methyl diad by employing a catalytic sp^3–sp^3 cross-coupling reaction[4] was envisioned as an attractive final step of the synthesis to allow the flexible construction of both diastereomers **1a** and **1b**.

The corresponding tetradeoxypropionate building block should be assembled by our iterative deoxypropionate synthetic strategy employing enantiomerically pure allylic *o*-DPPB building blocks **2** and **3** as propionate acetate and propionate units, respectively.[3] The two optical antipodes of the methyl diad building block should be readily accessible by similar chemistry.

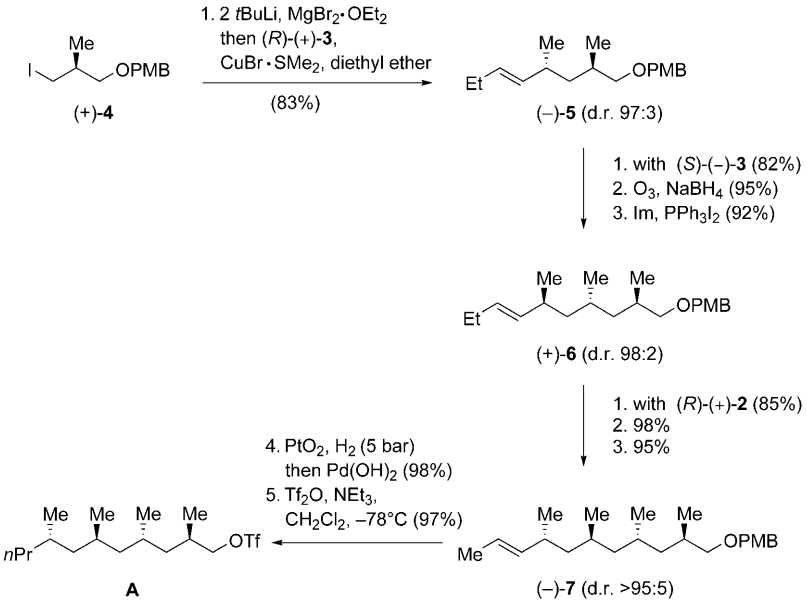
The synthesis began with construction of the tetrad building block **A** (Scheme 2). Thus, iodide (+)-**4** (available

[*] Dipl.-Chem. C. Herber, Prof. Dr. B. Breit
Institut für Organische Chemie und Biochemie
Albert-Ludwigs-Universität Freiburg
Albertstrasse 21, 79104 Freiburg (Germany)
Fax: (+49) 761-203-8715
E-mail: bernhard.breit@organik.chemie.uni-freiburg.de

[**] This work was supported by the Fonds der Chemischen Industrie, the Deutsche Forschungsgemeinschaft, and the Alfried Krupp Award for young university teachers of the Krupp foundation (to B.B.). We thank Y. Schmidt for preliminary experiments, C. Steinger for technical assistance, and Novartis AG and BASF AG for generous gifts of chemicals. We particularly thank Prof. W. Kitching (University of Queensland, Brisbane, Australia) for providing a sample of the natural product.

Supporting information for this article is available on the WWW under http://www.angewandte.org or from the author.

 © 2005 Wiley-VCH Verlag GmbH & Co. KGaA, Weinheim

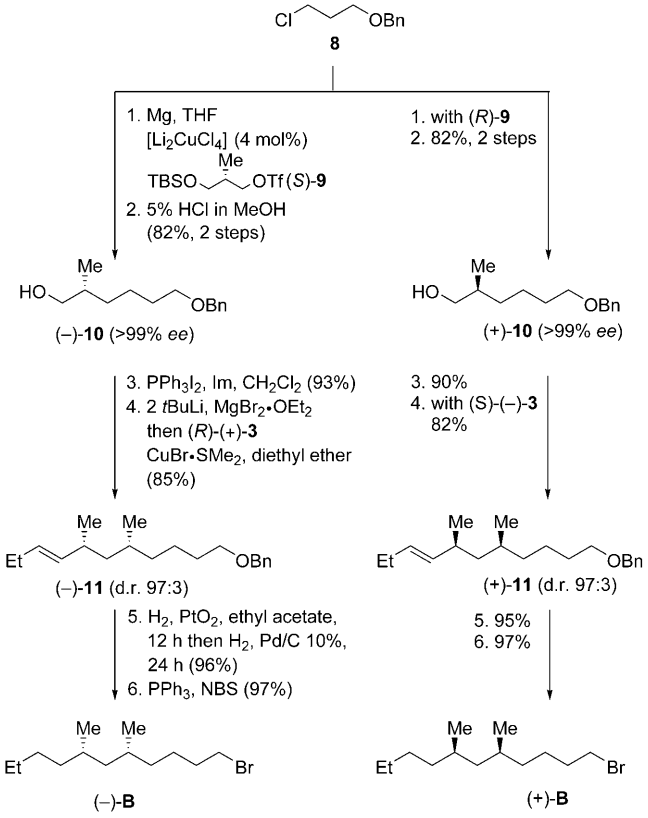


Scheme 2. Synthesis of tetradeoxypropionate building block **A**. Im = imidazole, Tf = trifluoromethanesulfonyl.

in three steps from the Roche ester)[5] was transformed into a Grignard reagent and subjected to *o*-DPPB-directed *syn*-allylic substitution with allylic *o*-DPPB ester (*R*)-(+)-**3** in the presence of 0.5 equivalents of copper bromide·dimethyl sulfide to give the dideoxypropionate (−)-**5** with a complete 1,3-chirality transfer.[3] Two separate iterations consisting of three steps (alkene ozonolysis with a reductive workup ($NaBH_4$), transformation to the iodide, and directed *syn*-allylic substitution with (*S*)-(−)-**3** and (*R*)-(+)-**2**, respectively) furnished the tetradeoxypropionate (−)-**7** with all the carbon atoms and stereocenters in place. Alkene hydrogenation and reductive cleavage of the *para*-methoxybenzyl (PMB) ether group occurred upon heterogenous catalytic hydrogenation. The thus-derived building block **A** was stored as the alcohol and activated prior to fragment coupling as the corresponding triflate.

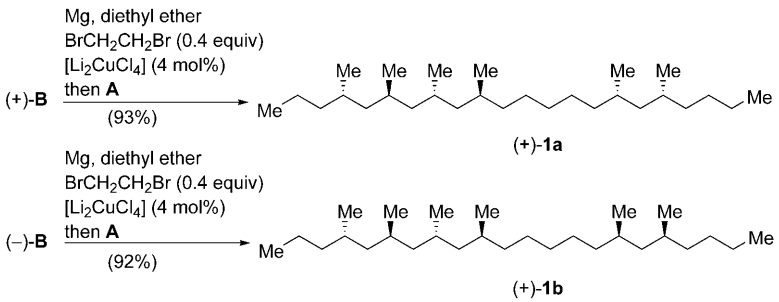
Synthesis of the dideoxypropionate building blocks **B** commenced from chloride **8** (Scheme 3).[6] For the expansion of the carbon skeleton, we chose a copper-catalyzed sp^3–sp^3 cross-coupling reaction with a three-carbon electrophile of type **9** derived from the Roche ester.[7] Orientating experiments with the corresponding bromide and iodide derivatives, however, showed that significant chemoselectivity problems occurred because of elimination and reduction processes. These problems could be circumvented by employing the triflates (+)-**9** and (−)-**9** at −20 °C. In these cases, clean cross coupling in the presence of 4 mol % of $[Li_2CuCl_4]$ was observed. Exposure of the crude coupling product to methanolic hydrogen chloride gave the primary alcohols (−)-**10** and (+)-**10** in 82 % yield (two steps). The Mukaiyama redox condensation furnished the corresponding iodides, which were subjected to the above protocol for the directed *syn*-allylic substitution with (*R*)-(+)-**3** and (*S*)-(−)-**3**, respectively, to furnish the dideoxypropionates (−)-**11** and (+)-**11** in excellent yield and complete diastereoselectivity. Minimal, standard functional-group manipulation led to building blocks (−)-**B** and (+)-**B**.

The final fragment-coupling step (Scheme 4) employing a copper-catalyzed sp^3–sp^3 cross coupling of the Grignard reagent derived from (−)/(+)-**B** with triflate **A** required some optimization because of problems that arose from the small scale of the reaction (0.1 mmol). It was found that generation of a Grignard reagent on this small scale was successful in the presence of an excess of dibromoethane. However, the thus-formed excess of magnesium bromide also reacted with the triflate electrophile to yield the corresponding bromide as a by-product (which unfortunately did not undergo further cross coupling). This problem could be circumvented by the addition of an ethereal solution of triflate **A** together with 4 mol % of the catalyst $[Li_2CuCl_4]$ to an ethereal solution of the Grignard-reagent-derived form of **B**. Excellent yields of both diastereomers **1a** and **1b** were obtained under these conditions. Purification of the final product was achieved through kugelrohr distillation, which, as an additional benefit, allowed the boiling points of **1a** and **1b** (210 °C/20 mbar) to be determined.



Scheme 3. Synthesis of the enantiomeric dideoxypropionate building blocks (−)-**B**/(+)-**B**. Bn = benzyl, TBS = *tert*-butyldimethylsilyl, NBS = *N*-bromosuccinimide.

 © 2005 Wiley-VCH Verlag GmbH & Co. KGaA, Weinheim



Scheme 4. Fragment coupling through Cu-catalyzed sp^3–sp^3 cross coupling. Synthesis of (+)-**1a** and (+)-**1b**.

To prove the identity of the natural and synthetic material ^{13}C NMR spectra of **1a** and **1b** were recorded in the presence of an internal glass-capillary tube containing a solution of the natural product in $CDCl_3$.[8] Comparison of these spectra showed a perfect match for diastereomer **1b**. Finally, comparison of the optical-rotation studies of the natural material ($[\alpha]_D^{20}$ +10.7 ($c = 0.44$, $CHCl_3$)) and the synthetic product **1b** ($[\alpha]_D^{20}$ +8.5 ($c = 1.21$, $CHCl_3$)) determined the absolute configuration of the natural product as that depicted in Scheme 4.

In conclusion, the enantioselective total synthesis of the (4*S*,6*R*,8*R*,10*S*,16*R*,18*S*)-hexamethyldocosane from *Antitrogus parvulus* has been accomplished, thus enabling the relative and the absolute configuration of the natural product to be determined. The successful enantioselective synthesis of **1b** (and its diastereomer **1a**) highlights the synthetic power of our recent methodology for deoxypropionate construction, which relies on an *o*-DPPB-directed and copper-mediated allylic substitution by Grignard reagents. Furthermore, the synthetic utility of copper-catalyzed sp^3–sp^3 cross-coupling for fragment coupling in a total synthesis has been demonstrated.

Received: May 11, 2005
Published online: July 20, 2005

Keywords: asymmetric synthesis · C—C coupling · Grignard reaction · organocopper reagents · total synthesis

[1] P. G. Allsopp, K. J. Chandler, *Proc. Int. Soc. Sugar-Cane Technol.* **1989**, *20*, 810–816.
[2] a) M. T. Fletcher, S. Chow, L. K. Lambert, O. P. Gallagher, B. W. Cribb, P. G. Allsopp, C. J. Moore, W. Kitching, *Org. Lett.* **2003**, *5*, 5083–5086; b) S. Chow, M. T. Fletcher, L. K. Lambert, O. P. Gallagher, C. J. Moore, B. W. Cribb, P. G. Allsopp, W. Kitching, *J. Org. Chem.* **2005**, *70*, 1808–1827.
[3] B. Breit, C. Herber, *Angew. Chem.* **2004**, *116*, 3878–3880; *Angew. Chem. Int. Ed.* **2004**, *43*, 3790–3792.
[4] For previous reports on copper-catalyzed sp^3–sp^3 cross-coupling reactions, see: a) M. Tamura, J. Kochi, *Synthesis* **1971**, 303–305; b) G. Fouquet, M. Schlosser, *Angew. Chem.* **1974**, *86*, 82–83; *Angew. Chem. Int. Ed. Engl.* **1974**, *13*, 701–702; c) H. Kotsuki, I. Kadota, M. Ochi, *J. Org. Chem.* **1990**, *55*, 4417–4422; d) T. Netscher, *Chimia* **1996**, *50*, 563–567; e) G. Cahiez, C. Chaboche, M. Jezequel, *Tetrahedron* **2000**, *56*, 2733–2737.
[5] Prepared analogously to (*R*)-**3**, see: T. J. Heckrodt, J. Mulzer, *Synthesis* **2002**, 1857–1866.
[6] E. Dimitriadis, R. A. Massy-Westropp, *Aust. J. Chem.* **1984**, *37*, 619–627.
[7] G. F. Solberghe, I. E. Marko, *Tetrahedron Lett.* **2002**, *43*, 5061–5066.
[8] A comparison of the analytical data of the natural material and synthetic compounds **1a** and **1b** can be found in the Supporting Information.

 © 2005 Wiley-VCH Verlag GmbH & Co. KGaA, Weinheim

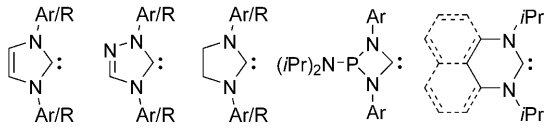
Organometallic Chemistry

DOI: 10.1002/anie.200501522

Pd^{II} Complexes Possessing a Seven-Membered N-Heterocyclic Carbene Ligand**

*Christopher C. Scarborough, Michael J. W. Grady, Ilia A. Guzei, Bhavesh A. Gandhi, Emilio E. Bunel, and Shannon S. Stahl**

Since the discovery of stable N-heterocyclic carbenes (NHCs),[1] these complexes have found widespread use in catalysis, in which they serve both as nucleophilic catalysts[2] and as ligands in metal-mediated reactions.[3] Carbenes derived from five-membered heterocycles represent the most common class of these molecules (**1**–**3**, Scheme 1);[1–3] however, four-[4] and six-membered[5] analogues have also been reported (**4** and **5**). Most of these structures possess a



Scheme 1. Typical heterocyclic frameworks of NHCs.

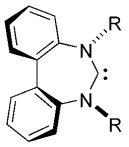
[*] C. C. Scarborough, M. J. W. Grady, Dr. I. A. Guzei, B. A. Gandhi, Prof. S. S. Stahl
Department of Chemistry
University of Wisconsin—Madison
1101 University Avenue, Madison, WI 53706 (USA)
Fax: (+1) 608-262-6143
E-mail: stahl@chem.wisc.edu
Dr. E. E. Bunel
Amgen Inc.
1 Amgen Center Drive
Thousand Oaks, CA 91320 (USA)

[**] This work was supported by the National Institutes of Health (RO1 GM67173-01) and the Dreyfus Foundation (Teacher–Scholar Award).

Supporting information for this article is available on the WWW under http://www.angewandte.org or from the author.

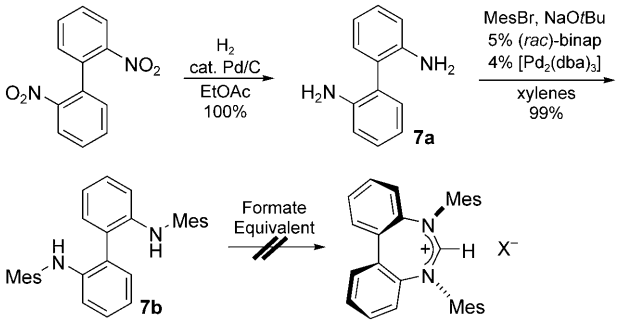
© 2005 Wiley-VCH Verlag GmbH & Co. KGaA, Weinheim

nearly planar heterocyclic framework, and this feature places constraints on the spatial arrangement of the NHC substituents. To relax this constraint, we targeted a new class of NHCs with a seven-membered heterocyclic framework **6** that would undergo a torsional twist to alleviate ring strain. Structures of this type have been analyzed previously by computational methods,[6] but synthetic examples have not been prepared. We describe herein the facile synthesis of two Pd^{II} complexes that possess the first member of this new class of carbene ligands, in which R = 2-adamantyl (2-ad).



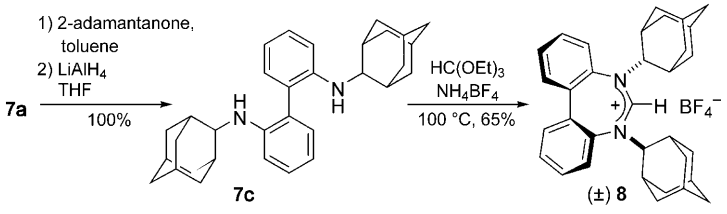
6

Our initial synthetic efforts targeted analogues of **6** with bulky aryl substituents (e.g., R = mesityl, 2,6-diisopropylphenyl), which are commonly found in stable NHCs. 2,2′-Diaminobiphenyl (**7a**) was obtained in quantitative yield by reduction of 2,2′-dinitrobiphenyl, and mesitylation of **7a** proceeded effectively under previously reported conditions (Scheme 2).[7] Subsequent condensation to afford the amidinium salt, however, was unsuccessful when a variety of known protocols was used. The origin of this failure is not certain, but we reasoned that it may result from the weak basicity of the diaryl amines, and therefore *N*-alkylated derivatives might be more successful.



Scheme 2. Attempted synthesis of an arylated seven-membered NHC. Mes = mesitylene, binap = 1,1′-binaphthalene-2,2′-diylbis(diphenylphosphine).

Preparation of *N*-substituted derivatives of **7a** with sterically encumbered primary and secondary alkyl groups proceeds smoothly (R = neopentyl, 2-adamantyl; Scheme 3).[8] For example, condensation of **7a** with 2-adamantanone followed by reduction of the imine with lithium aluminum hydride produces **7c** in quantitative yield.[9] Heating **7c** in neat triethylorthoformate with NH_4BF_4[10] produces the C_2-symmetric amidinium tetrafluoroborate salt **8**, which was characterized by single-crystal X-ray diffraction analysis (Figure 1).[11]



Scheme 3. Synthesis of a seven-membered biphenyl amidinium salt.

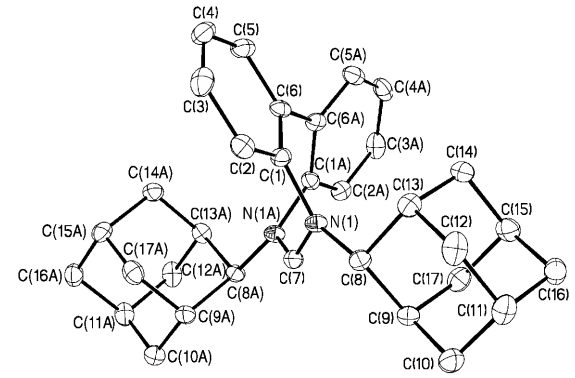
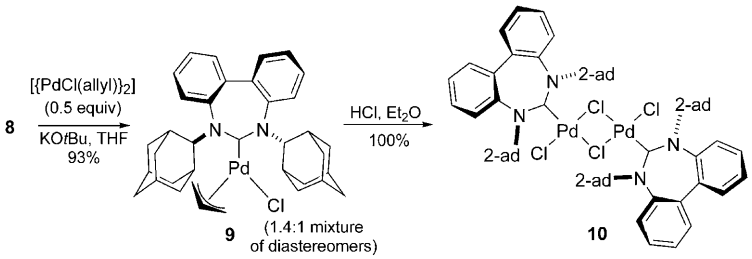


Figure 1. Molecular structure of the amidinium salt **8**. Hydrogen atoms and the BF_4^- counterion are omitted for clarity. Thermal ellipsoids are shown at 50% probability. Selected bond lengths [Å] and angles [°]: C(7)-N(1) 1.319(2), N(1)-C(1) 1.456(3), C(1)–C(6) 1.393(3), C(6)-C(6A) 1.472(4), C(1)-C(2) 1.388(3), C(2)-C(3) 1.385(3), C(3)-C(4) 1.384(3), C(4)-C(5) 1.401(3), C(55)-C(6) 1.401(3); N(1)-C(7)-N(1A) 124.2(3), C(7)-N(1)-C(8) 118.52(19), C(7)-N(1)-C(1) 117.21(18), C(1)-N(1)-C(8) 120.89(16).

The amidinium salt **8** represents an attractive NHC precursor, and our initial studies focused on the preparation of NHC-coordinated Pd^{II} complexes. Deprotonation of **8** with potassium *tert*-butoxide in a THF solution of [{PdCl(allyl)}$_2$][12–14] generated the NHC–PdCl(allyl) complex **9** in high yield (Scheme 4). This complex is air stable and can be purified by flash column chromatography on silica gel under ambient conditions. The ^{1}H NMR spectrum of **9** reveals the presence of two diastereomeric allyl rotamers in solution in a 1.4:1 ratio.[15] Single-crystal X-ray diffraction studies[11] confirmed the identity of **9** (Figure 2); a mixture of diastereomers is also present in the solid state, with the allyl group disordered over two positions in a 2.7:1 ratio.



Scheme 4. Synthesis of NHC-coordinated Pd^{II} complexes.

Protonolysis of the allyl ligand[12] of **9** with HCl produces [{$PdCl_2$(NHC)}$_2$] (**10**) in quantitative yield (Scheme 4). Only one isomer of this dimeric compound is detected in solution by ^{1}H NMR spectroscopic analysis. Single-crystal X-ray diffraction studies reveal the presence of a heterochiral dimer (Figure 3).[11]

 © 2005 Wiley-VCH Verlag GmbH & Co. KGaA, Weinheim

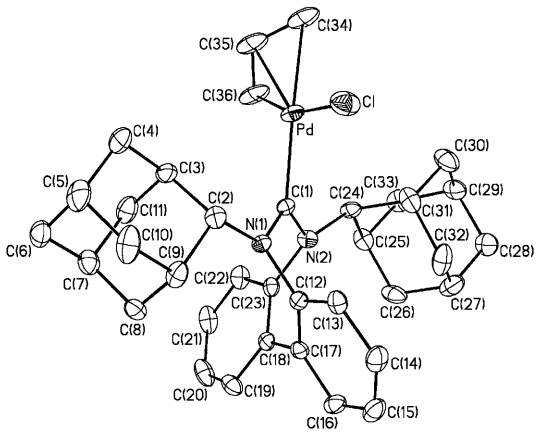


Figure 2. Solid-state molecular structure of **9**. Only the preferred orientation of the allyl group is shown. Hydrogen atoms and the solvent are omitted for clarity. Thermal ellipsoids are shown at 30% probability.

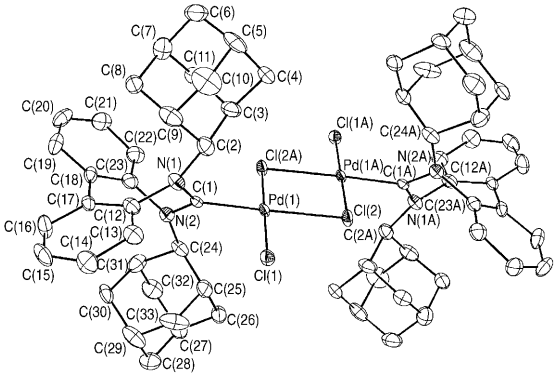
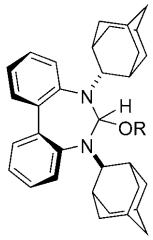


Figure 3. Molecular structure of **10**. Hydrogen atoms and solvent molecules are omitted for clarity. Thermal ellipsoids are shown at 30% probability.

The amidinium salt **8** and the NHC ligands in **9** and **10** exhibit axial symmetry arising from the torsional twist of the seven-membered ring. The torsional angle α between the two phenyl rings in **8** (C(1)-C(6)-C(6A)-C(1A)) is 46.1(4)°, which is similar to this angle in **9** and **10** (41.9(5) and 46.4(8)°, respectively). Another relevant metric is the torsional angle between the two N–C(2-ad) bonds, which reflects the spacial disposition of the adamantyl groups directed into the metal coordination sphere. This angle β in **8** (namely, $M = H^+$) is 56.2(5)° and expands to 72.3(8) and 79.7(1.3)° in the Pd^{II} complexes **9** and **10**, respectively. The larger size of the Pd^{II} center relative to a proton probably accounts for this increase. Overall, these torsional parameters highlight the utility of the seven-membered heterocycle to induce out-of-plane deviations in the orientation of the NHC substituents. Moreover, the C_2 symmetry of these structures supports their potential utility as templates for the preparation of non-fluxional, enantiomerically resolved analogues for use in asymmetric catalysis.

Thus far, attempts to isolate and characterize the free carbene have been unsuccessful. Numerous bases have been applied in these studies, including mesityl lithium, potassium hexamethyldisilazide, potassium *tert*-butoxide, sodium methoxide, and sodium hydride. ^{1}H NMR spectroscopic data reveals that alkoxide bases, which are the most effective reagents for the in situ preparation of NHC–Pd complexes form NHC–alcohol adducts **11a** and **11b**. Attempts to isolate the free carbene from such compounds by vacuum thermolysis[16] or trapping the released alcohol (in the case of the methanol adduct) in a Dean–Stark apparatus equipped with 4-Å molecular sieves and benzene at reflux were unsuccessful and only yielded slightly decomposed starting material in each case. These adducts do not react further in the presence of $[\{PdCl(allyl)\}_2]$ to form the NHC–PdCl(allyl) complex **9**. These results suggest that the preparation of **9** occurs by an in situ deprotonation of **8** by KO*t*Bu and competitive trapping of the free carbene by $[\{PdCl(allyl)\}_2]$ in solution.



11a: R = Me
11b: R = *t*Bu

Rzepa and co-workers analyzed a series of 8π-electron heterocycles, including seven-membered NHCs, by DFT computational methods.[6] These studies highlight the attenuation of antiaromatic character when such heterocyclic rings undergo a torsional twist. This conformational change enables partial Möbius aromatic stabilization[17] in addition to relief of the ring strain intrinsic to seven-membered rings. These calculations also suggest that coordination of these ligands to metal complexes results in higher inversion barriers between the two enantiomeric conformations.

In conclusion, we have prepared the first examples of metal complexes with a seven-membered N-heterocyclic carbene ligand that exhibits a tortional twist resulting in C_2 symmetry. This architecture can be readily altered with different substituents at the nitrogen atom and modifications to the biaryl backbone. Future studies will focus on the preparation of conformationally stable and enantiomerically resolved analogues, and their utility in asymmetric catalysis will be investigated.

Experimental Section

All manipulations were performed in an inert nitrogen atmosphere unless otherwise specified. Dry, oxygen-free solvents were employed. ^{1}H and ^{13}C NMR spectra were recorded on either a Bruker Homer-300, Bruker Athena-300, Varian Mercury-300, or Varian Inova-500 NMR spectrometer. ^{1}H NMR chemical shifts are reported in ppm relative to Me_4Si as the external standard, and the ^{13}C NMR chemical shifts are reported in ppm relative to $CHCl_3$. Please refer to the Supporting Information for the spectral data of all the compounds.

7a: Compound **7a** was synthesized by the adaptation of a literature procedure:[18] 2,2′-Dinitrobiphenyl (102.0 g, 417.5 mmol) and 10% Pd/C (16.4 g) were combined with EtOAc (300 mL) in a hydrogenation vessel. The vessel was pressurized to 40 psi H_2 for 3.5 h (when H_2 was no longer being consumed). The slurry was filtered through a plug of celite. Rotary evaporation followed by drying on a vacuum line gave the pure product as a light yellow–orange powder in 100% yield.

7c: 2,2′-Diaminobiphenyl (**7a**; 614 mg, 3.33 mmol) and 2-adamantanone (1 g, 6.65 mmol) were combined with *para*-toluenesulfonic acid (1% (per amine functionality)) in a Dean–Stark apparatus. The reagents were dissolved in toluene (ca. 200 mL) and refluxed for

 © 2005 Wiley-VCH Verlag GmbH & Co. KGaA, Weinheim

72 h. The solvent was removed, and lithium aluminum hydride (122 mg, 3.22 mmol) was added followed by THF (ca. 200 mL). The reaction flask was heated to 50 °C for 2 h followed by a careful quenching with water (ca. 100 mL) and sat. NH_4BF_4 (10 mL). The resulting slurry was filtered through a plug of celite, and the plug washed with CH_2Cl_2. The aqueous layer was washed once with CH_2Cl_2 (ca. 100 mL). The organic layers were combined, dried over $MgSO_4$, filtered, and the solvent was removed, thus yielding pure **7c** in 100% yield.

(±)-**8**: 2,2′-Bis(2-adamantylamino)biphenyl (**7c**; 5.76 g, 12.7 mmol) and NH_4BF_4 (1.3 g, 12.7 mmol) were combined under nitrogen in a 500-mL round-bottomed flask and triethyl orthoformate (c.a. 200 mL) was added. The reaction was heated to 100 °C for 16 h, after which time the product precipitated as a white powder. The reaction mixture was allowed to cool to room temperature and filtered. The solid was washed with diethyl ether followed by pentane to give the amidinium salt (±)-**8** in 65% yield as a light fluffy white powder without further purification. Crystals suitable for X-ray analysis were achieved by vapor diffusion of *n*-pentane onto a solution of (±)-**8** in $CHCl_3$.

(±)-**9**: Aminidinium salt (±)-**8** (200 mg, 0.363 mmol) and [{PdCl(allyl)}$_2$] (78 mg, 0.213 mmol) were combined with KO*t*Bu (1.2 equiv) under nitrogen. The reaction mixture was stirred in THF for 12 h, filtered through celite, and purified by column chromatography under ambient conditions (SiO_2, diethyl ether/hexanes 1:1) to give the NHC–PdCl(allyl) complex (±)-**9** in 93% yield as a light yellow–tan solid. Crystals suitable for X-ray analysis were obtained by layering *n*-heptane onto a −20 °C ethereal solution of (±)-**9** followed by diffusion overnight at −20 °C. (±)-**9** crystallized as a mixture of diastereomers in a ratio of 73:27.

10: A 50-mL round-bottomed flask was charged with (±)-**9** (100 mg, 0.16 mmol) and ethereal HCl (2.0 mL, 2.0 M). The color of the reaction mixture instantly changed to bright yellow–orange. Diethyl ether (8.0 mL) was added, and the resultant suspension was stirred for 1 h. Volatiles were removed in vacuo, which left pure **10** as a bright yellow–orange powder in quantitative yield. Recrystallization was carried out by dissolving **10** in a small amount of toluene and adding excess *n*-pentane to cause precipitation (87% yield). Crystals suitable for X-ray analysis were achieved by vapor diffusion of *n*-pentane onto a solution of **10** in CH_2Cl_2.

Received: May 3, 2005
Published online: July 20, 2005

Keywords: carbene ligands · N-heterocyclic carbenes · organometallic chemistry · palladium

[1] a) A. J. Arduengo III, R. L. Harlow, M. Kline, *J. Am. Chem. Soc.* **1991**, *113*, 361–363; b) A. J. Arduengo III, *Acc. Chem. Res.* **1999**, *32*, 913–921; c) D. Bourissou, O. Guerret, F. P. Gabbaï, G. Bertrand, *Chem. Rev.* **2000**, *100*, 39–91; d) W. A. Herrmann, C. Köcher, *Angew. Chem.* **1997**, *109*, 2256–2282; *Angew. Chem. Int. Ed. Engl.* **1997**, *36*, 2162–2187.

[2] D. Enders, T. Balensiefer, *Acc. Chem. Res.* **2004**, *37*, 534–541.

[3] a) W. A. Herrmann, T. Weskamp, V. P. W. Böhm, *Adv. Organomet. Chem.* **2002**, *48*, 1–69; b) W. A. Herrmann, *Angew. Chem.* **2002**, *114*, 1342–1363; *Angew. Chem. Int. Ed.* **2002**, *41*, 1290–1309; c) M. C. Perry, K. Burgess, *Tetrahedron: Asymmetry* **2003**, *14*, 951–961.

[4] a) E. Despagnet-Ayoub, R. H. Grubbs, *J. Am. Chem. Soc.* **2004**, *126*, 10198–10199; b) E. Despagnet-Ayoub, R. H. Grubbs, *Organometallics* **2005**, *24*, 338–340.

[5] a) R. W. Alder, M. E. Blake, C. Bortolotti, S. Bufali, C. P. Butts, E. Linehan, J. M. Oliva, A. G. Orpen, M. J. Quayle, *Chem. Commun.* **1999**, 241–242; b) F. Guillen, C. L. Winn, A. Alexakis, *Tetrahedron: Asymmetry* **2001**, *12*, 2083–2086; c) P. Bazinet, G. P. A. Yap, D. S. Richeson, *J. Am. Chem. Soc.* **2003**, *125*, 13314–13315.

[6] a) C. J. Kastrup, S. V. Oldfield, H. S. Rzepa, *J. Chem. Soc. Dalton Trans.* **2002**, 2421–2422; b) C. J. Kastrup, S. P. Oldfield, H. S. Rzepa, *Chem. Commun.* **2002**, 642–643.

[7] M. T. Reetz, H. Oka, R. Goddard, *Synthesis* **2003**, 1809–1814.

[8] The neopentyl-substituted derivative of NHC **6** is less stable than the 2-adamantyl derivative; full presentation of the synthesis and properties of this carbene and its metal complexes will be described in a forthcoming full paper.

[9] Full characterization data of the reported compounds are provided in the Supporting Information.

[10] a) S. Saba, A. Brescia, M. K. Kaloustian, *Tetrahedron Lett.* **1991**, *32*, 5031–5034; b) R. W. Alder, M. E. Blake, S. Bufali, C. P. Butts, A. G. Orpen, J. Schütz, S. J. Williams, *J. Chem. Soc. Perkin Trans. 1* **2001**, 1586–1593.

[11] CCDC-272584–272586 (**8**–**10**, respectively) contain the supplementary crystallographic data for this paper. These data can be obtained free of charge from the Cambridge Crystallographic Data Centre via www.ccdc.cam.ac.uk/data_request/cif.

[12] D. R. Jensen, M. S. Sigman, *Org. Lett.* **2003**, *5*, 63–65.

[13] NHC–PdCl(allyl) complexes were first synthesized by Nolan and co-workers by combination of free carbene and [{PdCl(allyl)}$_2$]; see: a) M. S. Viciu, R. F. Germaneau, O. Navarro-Fernandez, E. D. Stevens, S. P. Nolan, *Organometallics* **2002**, *21*, 5470–5472; b) M. S. Viciu, O. Navarro, R. F. Germaneau, R. A. Kelly III, W. Sommer, N. Marion, E. D. Stevens, L. Cavallo, S. P. Nolan, *Organometallics* **2004**, *23*, 1629–1635.

[14] Nolan and co-workers have shown that such complexes are able to function as cross-coupling catalysts; for the first example, see: M. S. Viciu, R. F. Germaneau, S. P. Nolan, *Org. Lett.* **2002**, *4*, 4053–4056.

[15] Similar observations have been made for other chiral NHC–PdCl(allyl) complexes: S. Roland, M. Audouin, P. Mangeney, *Organometallics* **2004**, *23*, 3075–3078.

[16] D. Enders, K. Breuer, G. Raabe, J. Runsink, J. H. Teles, J.-P. Melder, K. Ebel, S. Brode, *Angew. Chem.* **1995**, *107*, 1119–1121; *Angew. Chem. Int. Ed. Engl.* **1995**, *34*, 1021–1023.

[17] a) E. Heilbronner, *Tetrahedron Lett.* **1964**, *5*, 1923–1928; b) H. E. Zimmerman, *Acc. Chem. Res.* **1971**, *4*, 272–280.

[18] K. M. Gillespie, C. J. Sanders, P. O'Shaughnessy, I. Westmoreland, C. P. Thickitt, P. Scott, *J. Org. Chem.* **2002**, *67*, 3450–3458.

 © 2005 Wiley-VCH Verlag GmbH & Co. KGaA, Weinheim

Radical Reactions

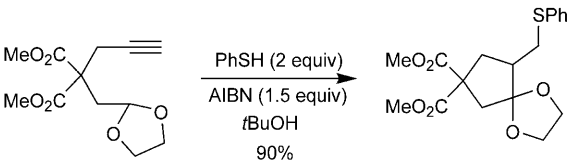
DOI: 10.1002/anie.200501309

Dimethyl Phosphite Mediated Hydrogen Atom Abstraction: A Tin-Free Procedure for the Preparation of Cyclopentane Derivatives**

*Florent Beaufils, Fabrice Dénès, and Philippe Renaud**

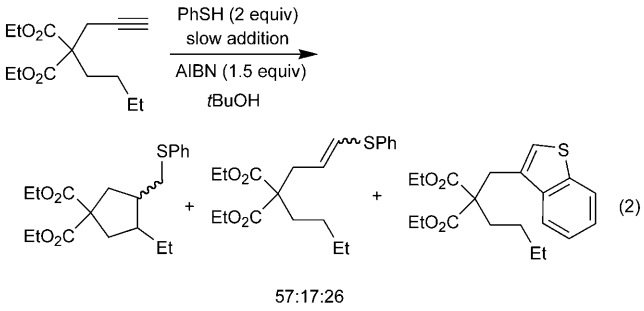
Radical reactions have been investigated intensively over the last two decades.[1] The new synthetic methods that have emerged from this work are complementary to ionic processes and are characterized by mild reaction conditions and broad functional-group tolerance. The potential of these reactions is immense, as demonstrated by their recent use in the synthesis of complex natural products. However, several aspects of this chemistry merit further investigation to increase the synthetic efficiency of the radical approach. Among these objectives, the development of nontoxic and environmentally friendly reagents to perform efficient radical reactions represents a challenging target.

The tin hydride mediated alkenyl radical translocation/cyclization process developed by Curran et al. represents a powerful procedure for the preparation of functionalized five-membered rings by selective activation of a C–H bond.[2,3] Recently, we reported an efficient tin-free version of this reaction involving thiophenol for the preparation of cyclopentane derivatives through a 1,5-hydrogen transfer/cyclization sequence [Eq. (1); AIBN = azobisisobutyronitrile].[4]



(1)

This method using thiophenol proved to be very efficient with a wide range of substrates but required high dilution (10^{-2} M of substrate) and the slow addition of thiophenol with a syringe pump [Eq. (1)]. Some limitations were also noticed, with some substrates undergoing slow hydrogen transfers. For example, the generation of a nonstabilized acyclic secondary alkyl radical proved to be difficult because of the reduction of the alkenyl radical and its cyclization onto the phenylthio group, thus leading to benzothiophene derivatives [Eq. (2)].[5]

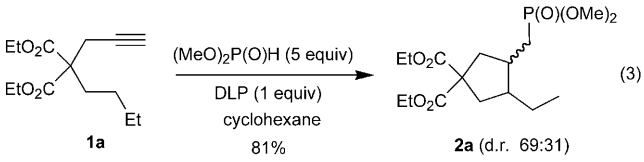


(2)

Recent developments in radical reactions involving phosphorus reagents have attracted our attention. Hypophosphorous acid and its corresponding 1-ethylpiperidine salt have been used to mediate radical cyclization reactions as an alternative to tributyltin hydride.[6,7] Diethyl phosphine oxide (DEPO)[8] and diethyl phosphite[9,10] were also recently used in radical processes.[11,12]

As diethyl phosphite is known to be a slower reducing agent than tributyltin hydride and thiophenol,[13] we were motivated to test the use of a phosphorus reagent in a radical cascade involving the addition of a P radical onto a triple bond followed by 1,5-hydrogen abstraction. To the best of our knowledge, only one radical addition of a dialkyl phosphite to a terminal triple bond has been reported, which was by Ishii and co-workers using $Mn(OAc)_2$ as a radical initiator in the presence of air.[14] Parsons and co-workers reported the failure of such a radical addition but presented one example of a clean addition of a thiophosphite to a terminal alkyne.[15] Herein, we report that dimethyl phosphite is a particularly efficient reagent for radical additions to terminal alkynes followed by 1,5-hydrogen transfer/cyclization processes.

Optimization of the reaction conditions were conducted on substrate **1a** [Eq. (3); DLP = dilauroyl peroxide]. Highly



(3)

reproducible results and excellent yields were obtained by treating a 0.1 M solution of the alkyne **1a** with five equivalents of dimethyl phosphite and one equivalent of DLP[16] in cyclohexane at reflux for 6 h. The desired cyclized product **2a** was obtained in 81 % yield, and no trace of the product from direct reduction was observed. In this particular example, neither the procedure using tin hydride developed by Curran and Shen[3] nor our procedure using thiophenol[4] [see Eq. (2)] gave satisfactory results because of the slow rate of the hydrogen-abstraction step.

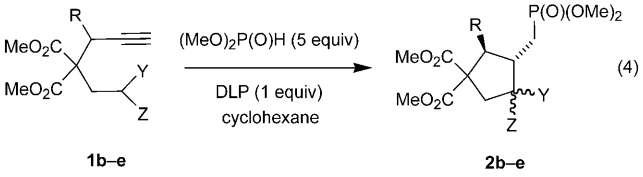
Propargylmalonates **1b**–**e** were then tested according to Equation (4). The generation of a tertiary alkyl radical from **1b** is very efficient with dimethyl phosphite (Table 1, entry 1),

[*] F. Beaufils, Dr. F. Dénès, Prof. P. Renaud
University of Berne
Department of Chemistry and Biochemistry
Freiestrasse 3, 3000 Bern 9 (Switzerland)
Fax: (+41) 316-313-426
E-mail: philippe.renaud@ioc.unibe.ch

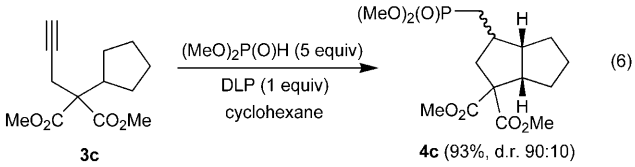
[**] We thank the Swiss National Science Foundation (Grant 20-103627), the Roche Foundation (postdoctoral fellowship to F.D.), and the University of Berne for support of this study.

Supporting information for this article is available on the WWW under http://www.angewandte.org or from the author.

© 2005 Wiley-VCH Verlag GmbH & Co. KGaA, Weinheim



(4)



(6)

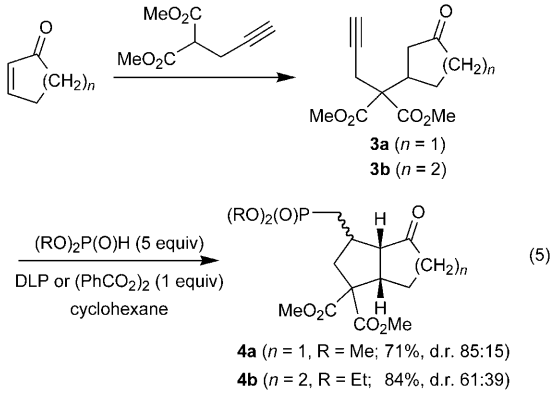
Table 1: Dimethyl phosphite mediated hydrogen abstraction [cyclization according to Eq. (4)].

Entry	Substrate	R	Y	Z	Product	d.r.[a]	Yield [%][b]
1	**1b**	H	Me	Me	**2b**	–	91
2	**1c**	*i*Pr	CO_2Et	H	**2c**	82:18	91
3	**1d**	H	Ph	H	**2d**	92:8	55
4	**1e**	H	OTBS	H	**2e**	73:27	79

[a] Determined by GC or NMR analysis of the crude reaction mixture. [b] Yield of isolated product. TBS = *tert*-butyldimethylsilyl.

and the cyclic product **2b** is obtained in 91% yield. Substrates **1c** and **1d**, which bear an ester and a phenyl substituent, respectively, undergo a radical translocation/cyclization process to the desired substituted cyclopentanes **2c** and **2d** in 91 and 55% yield (entries 2 and 3), respectively. Finally, a radical reaction with substrate **1e** gave the cyclopentane derivative in 79% yield[17] (entry 4).

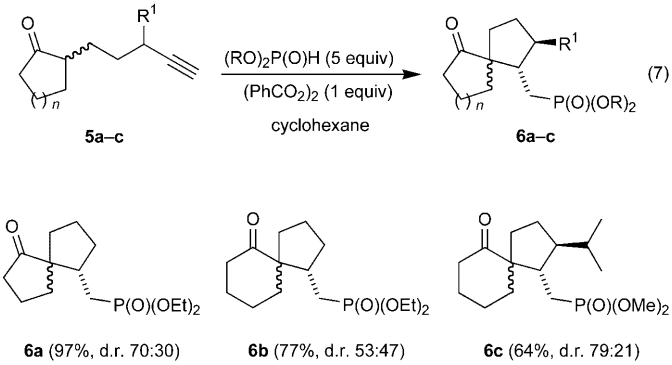
On the basis of these initial results, a method for the rapid assembly of fused bicyclic compounds was investigated [Eq. (5)]. Conjugate addition of dimethyl propargylmalonate



(5)

to cyclopentenone and cyclohexenone affords the radical precursors **3a** and **3b**, respectively. Reaction of **3a** and **3b** with dimethyl phosphite and diethyl phosphite proceeds [Eq. (5)] with complete regioselectivity and affords the fused bicycles **4a** and **4b** in 71 and 84% yield as a mixture of two diastereomers (d.r. 85:15 and 61:39, respectively). Radical stabilization by the ketone explains the regioselectivity. Interestingly, the deoxygenated compound **3c** gives the expected bicycloalkanes **4c** in 93% yield (d.r. 90:10) under similar reaction conditions, thus demonstrating that stabilization of the translocated radical is not a prerequisite for the formation of fused bicyclic systems [Eq. (6)].

The synthesis of spiro compounds through 1,5-hydrogen transfer has been reported recently employing an iodoalkenyl derivative.[18] However, this method suffers from the use of tin hydride and the difficulty of preparing the starting alkenyl iodides. On the other hand, substrates **5a–c** are readily prepared by alkylation of the corresponding β-keto ester followed by decarboxylation and are efficiently converted [Eq. (7)] into the spiro ketone **6a** (97%, d.r. 70:30), **6b** (77%, d.r. 53:47), and **6c** (64%, d.r. 79:21).



(7)

In conclusion, we have reported herein that dialkyl phosphites are powerful reagents for radical translocation/cyclization reactions that start from readily available terminal alkynes. A simple one-pot procedure has been developed. The excess reagent is easily removed by evaporation, and filtration through a short pad of silica gel affords a clean reaction product. The cyclic phosphonates produced by this reaction cascade are particularly attractive for further transformations.[11,19,20] Application of this process to the synthesis of natural products is currently underway.

Experimental Section

A mixture of **1b** (1.0 mmol, 226 mg), DLP (1.0 mmol, 398 mg), and dimethyl phosphite (5 mmol, 550 mg) in cyclohexane (10 mL) was heated at 80 °C for 6 h. After completion (monitoring by GC), the solution was cooled and the cyclohexane evaporated under reduced pressure. CH_3CN (10 mL) was added to precipitate the by-products derived from DLP. After filtration and evaporation, the residue was purified by flash chromatography (EtOAc/cyclohexane, 80:20) to afford the phosphonate **2b** (306 mg, 91%).

Received: April 14, 2005
Published online: July 20, 2005

Keywords: alkynes · cyclopentanes · fused-ring systems · hydrogen transfer · radical reactions

 © 2005 Wiley-VCH Verlag GmbH & Co. KGaA, Weinheim

[1] For general reviews on radical reactions, see: B. Giese, *Radicals in Organic Synthesis: Formation of Carbon–Carbon Bonds*, Pergamon, Oxford, **1988**; D. P. Curran in *Comprehensive Organic Synthesis*, *Vol. 4* (Eds.: B. M. Trost, I. Fleming, M. F. Semmelhack), Pergamon, Oxford, **1991**, p. 715 and 779; W. B. Motherwell, D. Crich, *Free Radical Chain Reactions in Organic Synthesis*, Academic Press, London, **1992**; J. Fossey, D. Lefort, J. Sorba, *Free Radicals in Organic Synthesis*, Wiley, Chichester, **1995**; *Radicals in Organic Synthesis* (Eds.: P. Renaud, M. P. Sibi), Wiley-VCH, Weinheim, **2001**; S. Zard, *Radical Reaction in Organic Synthesis*, Oxford University Press, Oxford, **2003**.

[2] D. P. Curran, D. Kim, C. Ziegler, *Tetrahedron* **1991**, *47*, 6189.

[3] D. P. Curran, W. Shen, *J. Am. Chem. Soc.* **1993**, *115*, 6051.

[4] F. Beaufils, F. Dénès, P. Renaud, *Org. Lett.* **2004**, *6*, 2563.

[5] L. Capella, P. C. Montevecci, M. L. Navacchia, *J. Org. Chem.* **1996**, *61*, 6783.

[6] D. H. R. Barton, D. O. Jang, J. C. Jaszerberenyi, *J. Org. Chem.* **1993**, *58*, 6838.

[7] M. T. Reding, T. Fukuyama, *Org. Lett.* **1999**, *1*, 7, 973; S. R. Graham, J. A. Murphy, A. R. Kennedy, *J. Chem. Soc. Perkin Trans. 1* **1999**, 3071; S. R. Graham, J. A. Murphy, D. Coates, *Tetrahedron Lett.* **1999**, *40*, 2415; H. Yorimitsu, H. Shinokubo, K. Oshima, *Chem. Lett.* **2000**, 104; H. Yorimitsu, H. Shinokubo, K. Oshima, *Bull. Chem. Soc. Jpn.* **2001**, *74*, 225; Y. Kita, H. Nambu, N. G. Ramesh, G. Anilkumar, M. Matsugi, *Org. Lett.* **2001**, *3*, 8, 1157; H. Yorimitsu, H. Shinokubo, K. Oshima, *Synlett* **2002**, *5*, 674; S. C. Roy, C. Guin, K. K. Rana, G. Maiti, *Tetrahedron* **2002**, *58*, 2435; N. G. Nambu, G. Anilkumar, M. Matsugi, Y. Kita *Tetrahedron* **2003**, *59*, 77.

[8] T. A. Khan, R. Tripoli, J. J. Crawford, C. G. Martin, J. A. Murphy, *Org. Lett.* **2003**, *5*, 2971.

[9] R. L. Kenney, G. S. Fisher, *J. Org. Chem.* **1974**, *39*, 682.

[10] J. M. Barks, B. C. Gilbert, A. F. Parsons, B. Upeandran, *Tetrahedron Lett.* **2001**, *42*, 3137; C. M. Jessop, A. F. Parsons, A. Routledge, D. Irvine, *Tetrahedron Lett.* **2003**, *44*, 479; C. M. Jessop, A. F. Parsons, A. Routledge, D. Irvine, *Tetrahedron Lett.* **2004**, *45*, 5095.

[11] For other radical phosphorus reagents, see: C. Lopin, G. Gouhier, A. Gautier, S. R. Piettre, *J. Org. Chem.* **2003**, *68*, 9916; A. Robertson, C. Bradaric, C. S. Frampton, J. McNulty, A. Capretta, *Tetrahedron Lett.* **2001**, *42*, 2609; J. E. Brumwell, N. S. Simpkins, N. K. Terret, *Tetrahedron Lett.* **1993**, *34*, 1215; J. E. Brumwell, N. S. Simpkins, *Tetrahedron* **1994**, *50*, 13533; A. Sato, H. Yorimitsu, K. Oshima, *Angew. Chem.* **2005**, *117*, 1722; *Angew. Chem. Int. Ed.* **2005**, *44*, 1694; R. A. Stockland, R. I. Taylor, L. E. Thompson, P. B. Patel, *Org. Lett.* **2005**, *7*, 851.

[12] For examples of the transition-metal-catalyzed addition of dialkyl phosphites to alkynes, see: D. K. Wicht, D. S. Glück in *Catalytic Heterofunctionalization* (Eds.: A. Togni, H. Grützmacher), Wiley-VCH, Weinheim, **2001**, p. 143.

[13] The rate of hydrogen abstraction from diethyl phosphite by a primary radical has been shown to be $1.2 \times 10^5\,\text{M}^{-1}\text{s}^{-1}$ at 130 °C: C. Chatgilialoglu, V. I. Timokhin, M. Ballestri, *J. Org. Chem.* **1998**, *63*, 1327; a rate constant for the reduction of alkyl radicals by thiophenol of $1.3 \times 10^8\,\text{M}^{-1}\text{s}^{-1}$ has been reported: J. A. Franz, B. A. Bushaw, M. S. Alnajjar, *J. Am. Chem. Soc.* **1989**, *111*, 268; finally, a rate constant for the reduction of primary alkyl radicals by Bu_3SnH of $2.3 \times 10^6\,\text{M}^{-1}\text{s}^{-1}$ has been measured: C. Chatgilialoglu, M. Newcomb, *Adv. Organomet. Chem.* **1999**, *44*, 67.

[14] O. Tamaya, A. Nakano, T. Iwahama, S. Sakaguchi, Y. Ishii, *J. Org. Chem.* **2004**, *69*, 5494.

[15] C. M. Jessop, A. F. Parsons, A. Routledge, D. Irvine, *Tetrahedron: Asymmetry* **2003**, *14*, 2849.

[16] Benzoyl peroxide can also be used as initiator; no reaction was observed with AIBN.

[17] Cleavage of the silylated alcohol was observed when benzoyl peroxide was used as initiator.

[18] C. K. Sha, C. W. Hsu, Y. T. Cheng, S. Y. Cheng, *Tetrahedron Lett.* **2000**, *41*, 9865.

[19] J. F. Reichwein, B. L. Pagenkopf, *J. Am. Chem. Soc.* **2003**, *125*, 1821.

[20] M. P. Healy, A. F. Parsons, J. G. T. Rawlinson, *Org. Lett.* **2005**, *7*, 1597.

 © 2005 Wiley-VCH Verlag GmbH & Co. KGaA, Weinheim

Homogeneous Catalysis

DOI: 10.1002/anie.200501350

What Can a Metal Catalyst Do with Allenes? One-Step Formation of Steroid Scaffolds from Readily Available Starting Materials**

Shengming Ma, Ping Lu, Lianghua Lu, Hairong Hou, Jiemin Wei, Qiwen He, Zhenhua Gu, Xuefeng Jiang, and Xing Jin*

The diversity of available transition metals and organic ligands for the formation of organometallic catalysts offers the possibility of excellent selectivity and tunability in homogeneous transformations.[1–4] Alkynes and alkenes are two classes of well-studied compounds in organic chemistry that have formed the basis of the petroleum industry and modern organic chemistry.[5] It should be noted that 1–1.5 % of allene exists in propylene produced by the cracking of hydrocarbons in petroleum.[6] The large amount of propylene consumed means that the production of propadiene in considerable quantities is thus possible. Although van't Hoff predicted the correct structures of allenes and higher cumulenes as early as 1874,[7] for a long period of time allenes were considered to be highly unstable, which retarded the demonstration of their synthetic potential. However, the situation has changed dramatically during the last 8 to 10 years, and many new reactions have been developed based on the chemistry of allenes.[8–13] Steroids are characterized by a carbon skeleton with four fused rings, and their presence in plants and animals illustrates their immense biological importance.[14–17] Steroids are used for the treatment of cancer, arthritis, allergies, and in birth control. Thus,

[*] Prof. S. Ma, P. Lu, L. Lu, H. Hou, J. Wei, Q. He, Z. Gu, X. Jiang, X. Jin
State Key Laboratory of Organometallic Chemistry
Shanghai Institute of Organic Chemistry
Chinese Academy of Sciences
354 Fenglin Lu, Shanghai 200032 (P.R. China)
Fax: (+86) 21-6416-7510
E-mail: masm@mail.sioc.ac.cn

[**] Financial support from the National Natural Science Foundation of China and the Major State Basic Research Development Program (grant no. G2000077500) is greatly appreciated.

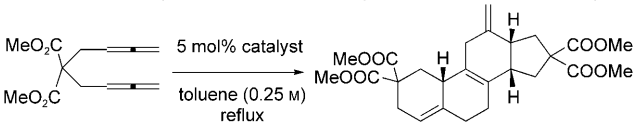
Supporting information for this article is available on the WWW under http://www.angewandte.org or from the author.

© 2005 Wiley-VCH Verlag GmbH & Co. KGaA, Weinheim

efficient catalytic approaches to new steroid derivatives are still of current interest.[18–25] Recently, during our study of allene chemistry,[26] we identified a very efficient one-step transition-metal-catalyzed transformation of simple 1,5-bisallenes to steroid skeletons.

We prepared 5,5-bis(methoxycarbonyl)-1,2,7,8-nonatetraene (**1a**)[27] from the bisallenylation of diethyl malonate with 2,3-butadienyl bromide.[28] The reaction of **1a** in the presence of a catalyst of 5 mol% $[RhCl(PPh_3)_3]$ and 10 mol% $AgSbF_6$[29] afforded a product with a complicated ^1H NMR spectrum (entry 1, Table 1). The structure of this product was unambiguously established by X-ray diffraction studies to be the 18,19-norsteroid derivative **2a** (Figure 1).[30]

Table 1: Dimeric cyclization of **1a** in the presence of different catalysts.



1a **2a**

Entry	Catalyst	*t* [h]	Yield of **2a** [%]
1	$[RhCl(PPh_3)_3] + AgSbF_4$[a]	3	10
2	$[\{RhCl(cod)\}_2] + P(OPh)_3$[b]	12.5	15
3[c]	$[RhH(CO)(PPh_3)_2]$	2.5	31
4	$[\{RhCl(cod)\}_2] + PPh_3$[d]	12	38
5	$[RhCl(PPh_3)_3]$	2	38
6	*trans*-$[RhCl(CO)(PPh_3)_2]$	2	42
7	$[Rh(cod)_2]BF_4$	12	–
8	$PtCl_2$	4	–

[a] 10 mol% $AgSbF_4$ was added. [b] 10 mol% $P(OPh)_3$ was added. [c] The reaction was conducted at 0.125 M **1a** in toluene. [d] 10 mol% PPh_3 was added.

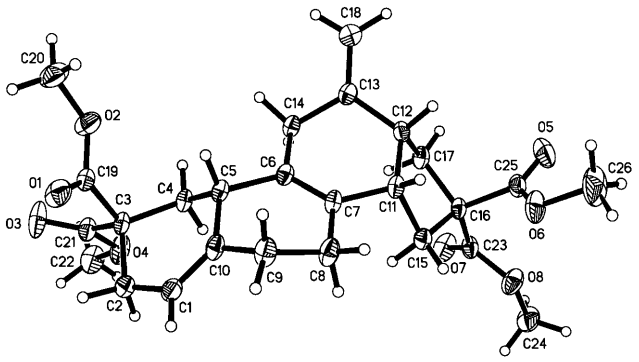
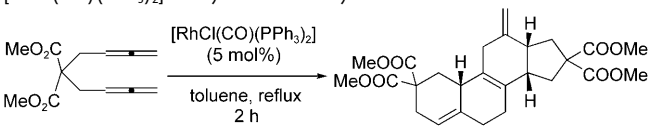


Figure 1. ORTEP representation of **2a**.

We screened a variety of catalysts using compound **1a** as the model, and some typical results are summarized in Table 1. The yields were improved when we used $[RhH(CO)(PPh_3)_2]$, $[RhCl(cod)]_2 + PPh_3$ (cod = cycloocta-1,5-diene), and $[RhCl(PPh_3)_3]$ without an Ag^+ salt (entries 3–5, Table 1). Further research showed that *trans*-$[RhCl(CO)(PPh_3)_2]$ was the best catalyst (entry 6, Table 1) while neither $[Rh(cod)_2]BF_4$ nor $PtCl_2$ showed any activity in this transformation (entries 7 and 8, Table 1).

Furthermore, a clear relationship between yields and concentrations was observed for this reaction (Table 2). It should be noted that the yield was greatly improved when a lower substrate concentration was used. We found that the reaction of **1a** at a concentration of 0.0417 M in toluene in the presence of 5 mol% *trans*-$[RhCl(CO)(PPh_3)_2]$ as the catalyst under reflux was very clean and afforded **2a** with a *cis* conjunction at the C/D rings in 73% yield as the only stereoisomer. It should be noted that no intermediate product was observed during the reaction process and no other stereoisomers were detected in the crude product by ^1H NMR spectroscopic analysis.

Table 2: Effect of the concentration of **1a** in toluene on the *trans*-$[RhCl(CO)(PPh_3)_2]$-catalyzed dimeric cycloisomerization of **1a**.[a]



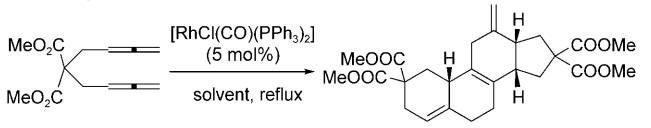
1a **2a**

Entry	Concentration of **1a** [M]	Yield of **2a** [%]
1	0.25	42
2	0.125	55
3	0.0625	69
4	0.0417	73
5	0.0313	72

[a] The reaction was carried out using **1a** (0.25 mmol) and *trans*-$[RhCl(CO)(PPh_3)_2]$ (5 mol%) in toluene under reflux.

The effect of the solvent on this reaction are summarized in Table 3. Among the solvents tested, the best results were obtained in toluene (entry 1, Table 3). Furthermore, the yield and reaction rate both dropped when the reaction was carried out at a lower temperature (compare entries 2 and 1, Table 3).

Table 3: Effect of the solvent on the *trans*-$[RhCl(CO)(PPh_3)_2]$-catalyzed dimeric cycloisomerization of **1a**.[a]



1a **2a**

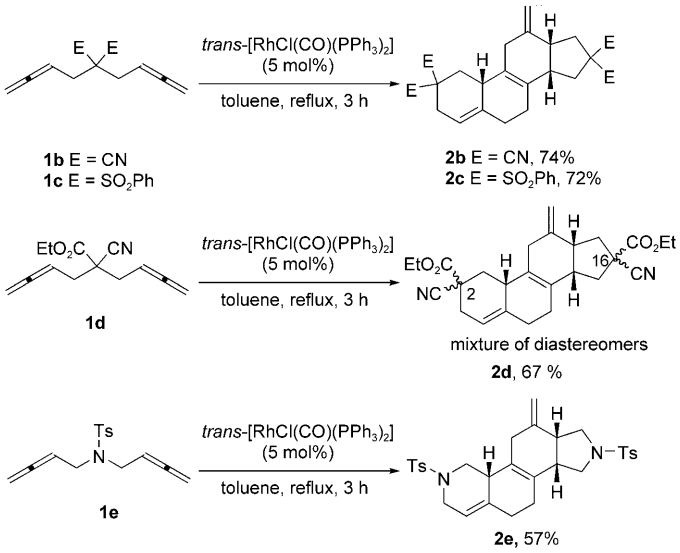
Entry	Solvent	*t* [h]	Yield of **2a** [%][b]
1	toluene	2	73
2[c]	toluene	57	43
3	CH_3CN	9.6	17
4	THF	6	36
5[d]	DMF	2.5	28
6	dioxane	2.5	41
7	benzene	7	54
8	xylene	2	41

[a] The reaction was carried out using **1a** (0.0417 M, 0.25 mmol) and *trans*-$[RhCl(CO)(PPh_3)_2]$ (5 mol%) in the specified solvent under reflux. [b] Yields determined by NMR spectroscopy by using 1,3,5-trimethyl benzene as the internal standard. [c] The reaction was conducted at 60 °C. [d] The reaction was conducted at 110 °C.

 © 2005 Wiley-VCH Verlag GmbH & Co. KGaA, Weinheim

The reaction was also slow and the yield was quite low when CH_3CN was used as the solvent (entry 3, Table 3), while the use of benzene, xylene, and dioxane led to the formation of **2a** in yields of 41–54% (entries 6–8, Table 3). It should be noted that the ^1H NMR spectrum of the crude products indicated that only one stereoisomer was observed in all these cases.

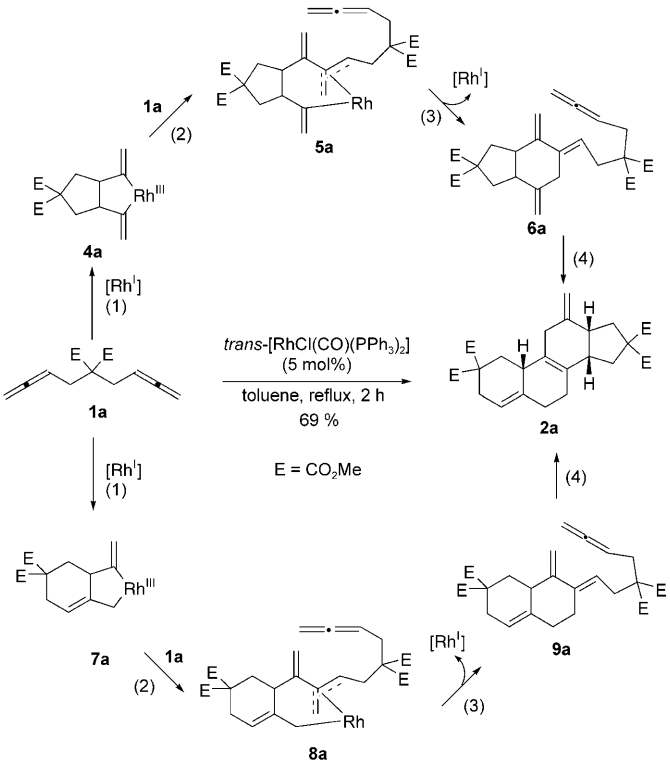
With the optimized conditions in hand, we studied the scope of this reaction, and found that it is general for differently substituted bisallenes. 18,19-Norsteroid derivative **2c** was readily prepared (1.086 g, 72%) from 1.5 g of bisallene **1c**, which was prepared from $CH_2(SO_2Ph)_2$, 2,3-butandienyl bromide,[28] and NaH in quantitative yield. The nitrogen analogue **2e** can be prepared from the bis(2,3-allenyl)amine **1e**. The dimeric cyclization of **1d** resulted in a mixture of 2,16 epimers **2d** in 67% yield (Scheme 1).



Scheme 1. Dimeric cyclization of bisallenes **1** with a *trans*-[RhCl(CO)-$(PPh_3)_2$] catalyst. Ts = toluene-4-sulfonyl.

A possible mechanism was postulated on the basis of the above results (Scheme 2). The reaction may proceed through the cyclometalation[31] of **1a** to afford **4a** or **7a**, which may then undergo carbometalation with one of the two allene moieties in **1a** to afford **5a** or **8a**, respectively. Subsequent reductive elimination would afford **6a** or **9a**, which could then undergo a Diels–Alder reaction to form the 18,19-norsteroid **2a** (Scheme 2). The results obtained illustrate that the intramolecular Diels–Alder reaction between an allene moiety and an alkene partner can proceed either in the presence[31a] or absence[32] of a metal catalyst. The reaction was conducted at a low temperature in an attempt to capture any possible intermediate(s), but the reaction was very fast and no intermediate product was detected.

In conclusion, we have reported an efficient route to 18,19-norsteroid derivatives from bisallenes by using a catalytic amount of *trans*-[RhCl(CO)$(PPh_3)_2$]. Although some steroids have been prepared from acyclic precursors by long synthetic routes,[18–25] the availability of the starting materials and the catalyst as well as the simplicity of the current procedure makes this methodology a very efficient route to steroids with new structural and steric features. Thus, this route may open up a new direction in steroid-related science.



Scheme 2. A possible mechanism for the transition-metal-catalyzed transformation of simple 1,5-bisallenes to steroid skeletons. (1) Cyclometalation, (2) carbometalation, (3) reductive elimination, (4) Diels–Alder reaction.

Experimental Section

Typical procedure: A solution of **1c** (1.509 g, 3.76 mmol) and *trans*-[RhCl(CO)$(PPh_3)_2$] (130 mg, 0.19 mmol, 5 mol%) in dry toluene (90 mL) was heated at reflux under Ar for 3 h. After the reaction was complete, as monitored by TLC (eluent: CH_2Cl_2/MeOH 40:1), removal of the solvent by rotary evaporation and flash chromatography of the product on silica gel (eluent: CH_2Cl_2/MeOH 100:1) afforded 1.086 g (72%) of **2c**. M.p. 143–145°C (dichloromethane/diethyl ether); ^1H NMR (300 MHz, $CDCl_3$): $\delta = 8.18$–7.86 (m, 8H), 7.72–7.35 (m, 12H), 4.91 (br s, 1H), 4.75 (s, 1H), 4.71 (s, 1H), 3.02–2.50 (m, 9H), 2.42–2.20 (m, 3H), 2.15–1.90 (m, 4H), 1.70–1.62 ppm (m, 1H); ^{13}C NMR (75.4 MHz, $CDCl_3$): $\delta = 26.1$, 28.5, 30.2, 30.5, 31.9, 34.3, 36.1, 37.5, 46.4, 47.4, 87.9, 93.5, 110.7, 114.1, 126.9, 128.6(×2), 128.7, 128.8, 131.0, 131.2, 131.4(×3), 131.5, 134.3, 134.5, 134.6, 135.8, 136.0, 136.4, 136.7, 139.8, 142.3 ppm; IR (KBr): $\tilde{\nu} = 3066$, 2906, 1447, 1328, 1309, 1144 cm^{-1}; MALDI: m/z: 839 $[M+K]^+$, 823 $[M^+ + Na]$; HRMS calcd for $C_{42}H_{40}O_8S_4Na$ $[M+Na]^+$: 823.1498; found: 823.1497. Elemental analysis calcd for $C_{42}H_{40}O_8S_4$: C 62.98, H 5.03; found: C 62.96, H 5.47%.

Received: April 19, 2005
Published online: July 20, 2005

Keywords: allenes · cyclization · homogeneous catalysis · rhodium · steroids

 © 2005 Wiley-VCH Verlag GmbH & Co. KGaA, Weinheim

[1] *Applied Homogeneous Catalysis with Organometallic Compounds* (Ed.: B. Cornils, W. A. Herrmann), Wiley-VCH, Weinheim, **2002**.

[2] A. Mortreux, F. Petit, *Industrial Applications of Homogeneus Catalysis*, D. Reidel, Dordrecht, **1988**.

[3] J. Tsuji, *Transition Metal Reagents and Catalysts*, Wiley, Cichester, **2000**.

[4] S. Bhaduri, D. Mukesh, *Homogeneous Catalysis*, Wiley-Interscience, New York, **2000**.

[5] M. M. Green, H. A. Wittcoff, *Organic Chemistry Principles and Industrial Practice*, Wiley-VCH, Weinheim, **2003**.

[6] For a review, see: K. Griesbaum, *Angew. Chem.* **1966**, *78*, 953; *Angew. Chem. Int. Ed. Engl.* **1966**, *5*, 933.

[7] For a review, see: A. Hoffmann-Röder, N. Krause, *Angew. Chem.* **2004**, *116*, 1216; *Angew. Chem. Int. Ed.* **2004**, *43*, 1196.

[8] S. Patai, *The Chemistry of Ketenes, Allenes, and Related Compounds*, *Part 1*, Wiley, New York, **1980**.

[9] S. R. Landor, *The Chemistry of Allenes*, *Vols. 1–3*, Academic Press, New York, **1982**.

[10] H. F. Schuster, G. M. Coppola, *Allenes in Organic Synthesis*, Wiley, New York, **1984**.

[11] S. Ma in *Handbook of Organopalladium Chemistry for Organic Synthesis* (Eds.: E. Negishi, A. de Meijer), Wiley, New York, **2002**, p. 1491.

[12] *Modern Allene Chemistry* (Eds.: N. Krause, A. S. K. Hashmi), Wiley-VCH, Weinheim, **2004**.

[13] For reviews, see: a) Y. Yamamoto, U. Radhakrishnan, *Chem. Soc. Rev.* **1999**, *28*, 199; b) R. C. Larock, *J. Organomet. Chem.* **1999**, *576*, 111; c) R. Grigg, V. Sridharan, *J. Organomet. Chem.* **1999**, *576*, 65; d) R. Zimmer, C. U. Dinesh, E. Nandanan, F. A. Khan, *Chem. Rev.* **2000**, *100*, 3067; e) A. S. K. Hashmi, *Angew. Chem.* **2000**, *112*, 3737; *Angew. Chem. Int. Ed.* **2000**, *39*, 3590; f) H. U. Reissig, S. Hormuth, W. Schade, M. O. Amombo, T. Watanabe, R. Pulz, A. Hausherr, R. Zimmer, *J. Heterocycl. Chem.* **2000**, *37*, 597; g) S. Ma, L. Li, *Synlett* **2001**, 1206; h) H. U. Reissig, W. Schade, M. O. Amombo, R. Pulz, A. Hausherr, *Pure Appl. Chem.* **2002**, *74*, 175.

[14] K. Nakanishi in *Natural Products Chemistry*, *Vol. 1* (Eds.: K. Nakanishi, T. Goto, S. Ito, S. Nastori, S. Nozoe), Kodansha, Tokyo, **1974**, chap. 6.

[15] J. B. Dence, *Steroids and Peptides*, Wiley, New York, **1980**.

[16] J. R. Sabine, *Cholesterol*, Marcel Dekker, New York, **1977**.

[17] *Steroid-biochemistry* (Ed.: R. Hobkirk), CRC, Boca Raton, FL, **1979**.

[18] A. A. Akhrem, Y. A. Tltov, *Total Steroid Synthesis*, Plenum, New York, **1970**.

[19] W. S. Johnson, M. F. Semmelhack, M. U. S. Sultanbawa, L. A. Dolak, *J. Am. Chem. Soc.* **1968**, *90*, 2994.

[20] R. L. Funk, K. P. C. Vollhardt, *J. Am. Chem. Soc.* **1977**, *99*, 5483.

[21] E. E. van Tamelen, J. R. Hwu, *J. Am. Chem. Soc.* **1983**, *105*, 2490.

[22] Y. Zhang, G. Wu, G. Angel, E. Negishi, *J. Am. Chem. Soc.* **1990**, *112*, 8590.

[23] E. J. Corey, H. B. Wood, *J. Am. Chem. Soc.* **1996**, *118*, 11982.

[24] a) L. F. Tietze, T. Nöbel, M. Spescha, *J. Am. Chem. Soc.* **1998**, *120*, 8971; b) L. F. Tietze, G. Schneider, J. Wölfling, A. Fecher, T. Nöbel, S. Petersen, I. Schuberth, C. Wulff, *Chem. Eur. J.* **2000**, *6*, 3755; c) L. F. Tietze, J. Matthias, C. Vock, *J. Organomet. Chem.* **2003**, *687*, 346.

[25] R. Thoma, T. Schulz-Gasch, B. D'Arcy, J. Benz, J. Aebi, H. Dehmlow, M. Hennig, M. Stihle, A. Ruf, *Nature* **2004**, *432*, 118.

[26] S. Ma, *Acc. Chem. Res.* **2003**, *36*, 701.

[27] For some typical reports on the reactions between two allenes, see: a) A. S. K. Hashmi, *Angew. Chem.* **1995**, *107*, 1749; *Angew. Chem. Int. Ed. Engl.* **1995**, *34*, 1581; b) A. S. K. Hashmi, T. L. Ruppert, T. Knöfel, J. W. Bats, *J. Org. Chem.* **1997**, *62*, 7295; c) A. S. K. Hashmi, L. Schwarz, J.-H. Choi, T. M. Frost, *Angew. Chem.* **2000**, *112*, 2382; *Angew. Chem. Int. Ed.* **2000**, *39*, 2285; d) C. H. Oh, H. S. Yoo, S. H. Jung, *Chem. Lett.* **2001**, 1288; e) R. Grigg, N. Kongathip, B. Kongathip, S. Luangkamin, H. A. Dondas, *Tetrahedron* **2001**, *57*, 9187; f) D. Hideura, H. Urabe, F. Sato, *Chem. Commun.* **1998**, 271; g) M. Arisawa, T. Sugihara, M. Yamaguchi, *Chem. Commun.* **1998**, 2615; h) M. Yoshida, T. Gotou, M. Ihara, *Tetrahedron Lett.* **2003**, *44*, 7151; i) M. Takimoto, M. Kawamura, M. Mori, *Org. Lett.* **2003**, *5*, 2599.

[28] 2,3-Butadienyl bromide was prepared from the bromination of 2,3-butadienol, see: J. Pornet, M. L. B. Randrianoelina, *J. Organomet. Chem.* **1979**, *174*, 1.

[29] a) P. A. Evans, J. E. Robinson, E. W. Baum, A. N. Fazal, *J. Am. Chem. Soc.* **2002**, *124*, 8782; b) S. R. Gilbertson, B. DeBoef, *J. Am. Chem. Soc.* **2002**, *124*, 8784.

[30] Crystal data for compound **2a**: $C_{26}H_{32}O_8$, $M_r = 472.52$, orthorhombic, space group $P2(1)2(1)2(1)$, 293 K, $Mo_{K\alpha}$, $a = 8.6778(12)$, $b = 9.7305(13)$, $c = 28.671(4)$ Å, $V = 2421.0(6)$ Å^3, $Z = 4$, final R indices $[I > 2\sigma(I)]$, $R1$ 0.0507, $wR2 = 0.1035$, no. of reflection measured/unique 14786/5647 ($R_{int} = 0.1486$). No. observations ($I > 2.00\sigma(I)$) 4180, no. variable 190, GOF = 0.898. Absolute structure parameter 0.1(10). CCDC-262016 contains the supplementary crystallographic data for this paper. These data can be obtained free of charge from The Cambridge Crystallographic Data Centre via www.ccdc.cam.ac.uk/data_request/cif.

[31] a) P. A. Wender, T. E. Jenkins, S. Suzuki, *J. Am. Chem. Soc.* **1995**, *117*, 1843; b) B. M. Trost, J. M. Tour, *J. Am. Chem. Soc.* **1988**, *110*, 5231; c) P. A. Wender, F. Glorius, C. O. Husfeld, E. Langkopf, J. A. Love, *J. Am. Chem. Soc.* **1999**, *121*, 5348; d) K. M. Brummond, H. Chen, P. Sill, L. You, *J. Am. Chem. Soc.* **2002**, *124*, 15186; e) T. Shibata, Y. Takesue, S. Kadowaki, K. Takagi, *Synlett* **2003**, 268; f) T. Makino, K. Itoh, *Tetrahedron Lett.* **2003**, *44*, 6335; g) T. Makino, K. Itoh, *J. Org. Chem.* **2004**, *69*, 395.

[32] a) M. E. Jung, N. Nishimura, *J. Am. Chem. Soc.* **1999**, *121*, 3529; b) C. Spino, S. Fréchette, *Tetrahedron Lett.* **2000**, *41*, 8033; c) M. E. Jung, N. Nishimura, *Org. Lett.* **2001**, *3*, 2113; d) D. Regás, J. M. Ruiz, M. M. Afonso, A. Galindo, J. A. Palenzuela, *Tetrahedron Lett.* **2003**, *44*, 8471; e) J. D. Winkler, K. J. Quinn, C. H. MacKinnon, S. D. Hiscock, E. C. McLaughlin, *Org. Lett.* **2003**, *5*, 1805.

 © 2005 Wiley-VCH Verlag GmbH & Co. KGaA, Weinheim

Heterogeneous Catalysis

DOI: 10.1002/anie.200500913

Catalytic Hydrogenation of Unsaturated Aldehydes on Pt(111): Understanding the Selectivity from First-Principles Calculations**

David Loffreda, Françoise Delbecq, Fabienne Vigné, and Philippe Sautet*

Selectivity is an essential aspect of chemistry in general and of heterogeneous catalysis in particular. It is commonly acknowledged that the C=C bond is more reactive than the C=O bond in the hydrogenation on metal surfaces of molecules with a vinyl or carbonyl bond.[1,2] Hence, according to this statement, the partial hydrogenation of α,β-unsaturated aldehydes containing conjugated C=C and C=O bonds should selectively produce the saturated aldehyde (SAL), which is the thermodynamic product, instead of the unsaturated alcohol (UOL), which is in practice the desired product in the pharmaceutical and fragrance industries. Although this rule is respected for the hydrogenation of acrolein (propenal) on Pt(111), which yields almost exclusively the SAL (93% of propanal versus only 2% of propenol), it is violated for prenal (methylbutenal), for which the selectivity is reversed in favor of the UOL.[2,3] Thus, understanding the selectivity requires a thorough knowledge of all the competitive steps involved in the reaction mechanism.

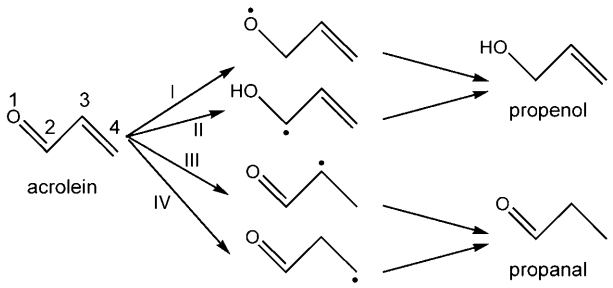
In this study we combine first-principles calculations for the exploration of elementary reaction steps and a kinetic model to understand how selectivity is controlled for a chemo-regioselective reaction occurring on a metallic surface. The simplest system chosen for illustration is the hydrogenation of acrolein (CH_2=CH−HC=O) on a Pt(111) catalyst which leads to the competitive formation of propanal (CH_3−CH_2−HC=O) and propenol (CH_2=CH−CH_2−OH).

The adsorption of acrolein has been previously studied on Pt(111)[4] and on Pt/Sn alloys.[5] Reaction barriers on Pt(111) and on Ag(111) have recently been proposed from an empirical approach with no connection with a kinetic model.[6] Our calculations are performed in the density-functional theory (DFT) periodic formalism. Only the hydrogenation pathways starting from the most stable adsorbed structure (the planar η^4-*trans* geometry where both C=C and C=O bonds interact with the surface) are considered here. This is not an important limitation since the molecule can easily adapt its geometry prior to hydrogenation in the approach used for calculating the reaction pathways.

[*] Dr. D. Loffreda, Dr. F. Delbecq, Dr. F. Vigné, Dr. P. Sautet
Laboratoire de Chimie, UMR CNRS 5182
Ecole Normale Supérieure de Lyon
46 Allée d'Italie, 69364 Lyon, Cedex 07 (France)
Fax: (+33) 4-7272-8860
E-mail: david.loffreda@ens-lyon.fr

[**] The authors acknowledge IDRIS at Orsay and CINES at Montpellier, France, for CPU time and assistance.

Exploring the hydrogenation of such a molecule remains a complex task. There are four possibilities for the attack of the first H atom that give four surface intermediates adsorbed on the surface (Scheme 1). For each of them, there are three



Scheme 1. Competitive hydrogenation routes of an acrolein molecule (propenal). The first hydrogenation intermediates (allyloxy, hydroxyallyl, 1-formylethyl, and 2-formylethyl for pathways I, II, III, and IV, respectively) and the products in competition (propenol (UOL) and propanal (SAL)) are shown.

possibilities to add a second H atom, but the present study is limited to the formation of the unsaturated closed-shell species through further hydrogenation of the previously attacked double bond. The adsorbed propenol and propanal can then desorb, or be further hydrogenated (an event which will not be considered here).

First, the four surface intermediates are optimized on the Pt surface. In all cases, both the remaining double bond and the non-hydrogenated site interact with the surface to give structures bound by three atoms (η^3,μ_3). The adsorbed hydroxyallyl intermediate is much more stable than the other ones (Figure 1). As in the final products, propenol adsorbs through the C=C bond (η^2,μ_2) without participation of the O atom, and with an adsorption energy (104 kJ mol^{-1}) similar to that of η^4-*trans*-acrolein (102 kJ mol^{-1}). In contrast, the adsorption of propanal is weaker (22 kJ mol^{-1}) and can occur either through the C=O bond (η^2,μ_2) or through the O atom (η^1,μ_1).[7]

Several coadsorption geometries have been tested for a hydrogen atom and the adsorbate to be hydrogenated—either acrolein or the surface intermediates. The coadsorption states are 4 to 10 kJ mol^{-1} less stable than the reference state (adsorbate and H atom at an infinite distance on the surface). Generally, the H atom is in a ternary site, and less commonly in a bridging or a top position. For each reaction step, one coadsorption geometry is selected as the precursor state of the reaction, depending on the considered reactant.

The first hydrogenation on a C atom of the C=C bond has an energy barrier of 91 and 89 kJ mol^{-1} (see pathways III and IV, respectively, in Figure 1). This barrier is lowered to 60 kJ mol^{-1} for the attack on the C=O bond (see pathway I in Figure 1). The hydrogenation on the O atom (pathway II) occurs in three steps. First, the H atom migrates from one ternary site to another one closer to the molecule while the C=O bond decoordinates from the surface to give a (η^2,μ_2) precursor state (not shown in Figure 1). Then the H atom migrates again to a top position from which the hydrogenation occurs. The overall barrier associated with pathway II is 40 kJ mol^{-1}, hence the lowest one.

 © 2005 Wiley-VCH Verlag GmbH & Co. KGaA, Weinheim

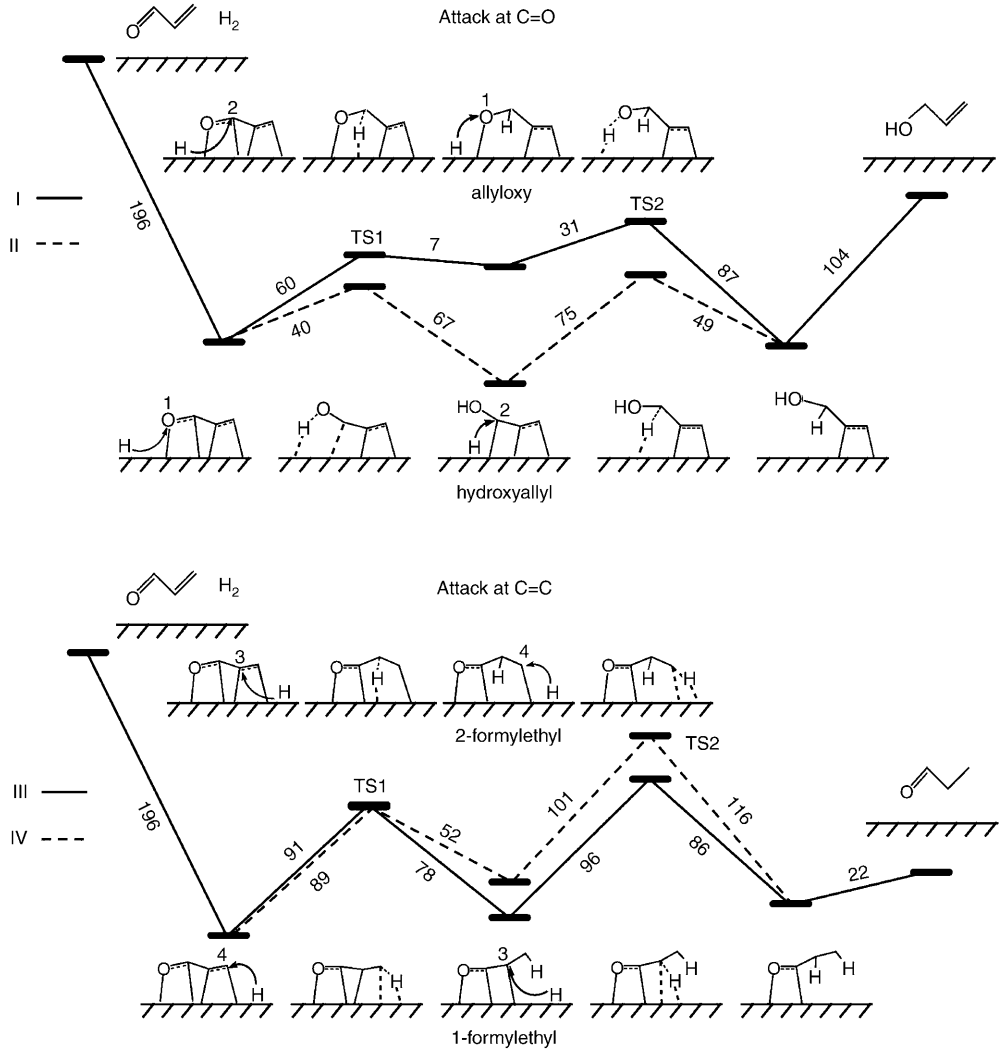


Figure 1. Energy profiles of hydrogenation pathways for acrolein on Pt(111): attack on the C=O bond (pathways I and II) and on the C=C bond (pathways III and IV). The energies (kJ mol^{-1}) refer to the initial state (H_2 + acrolein, gas phase). The adsorption energies of acrolein and two hydrogen atoms are summed in the initial coadsorption state. The transition states are labeled TS1 and TS2 for the first and the second hydrogenation, respectively.

The second hydrogenation takes place at a C atom for pathways II–IV. There is again a high barrier to the second attack at the C=C bond (96 and 101 kJ mol^{-1} for pathways III and IV, respectively) while the final saturation of the C=O bond is easier (75 kJ mol^{-1}, pathway II). The barrier for the attack at the O atom (pathway I) is again the lowest one (31 kJ mol^{-1}), with a mechanism similar to the one calculated for the first hydrogenation step. One important comment is that the barriers calculated by DFT differ significantly from the empirical results reported previously, with a maximum deviation of 100 kJ mol^{-1}.[6]

In agreement with the Hammond principle, the activation energy is small when the step is exothermic. This is the case for the hydrogenation on oxygen where the transition states are similar to the initial states with long OH bonds (1.60–1.63 Å, see Figure 2). In contrast, attack on the C=C

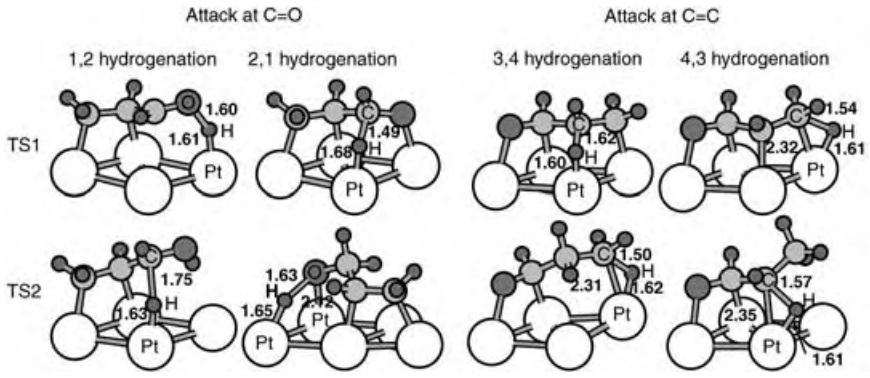


Figure 2. Geometries of the transition states for the first (TS1) and second (TS2) hydrogenation steps of acrolein on a Pt(111) catalyst. In each case, the lengths of the formed C–H or O–H bonds and the broken Pt–H bonds are given in Å.

 © 2005 Wiley-VCH Verlag GmbH & Co. KGaA, Weinheim

bond is mainly endothermic and the CH bonds formed are short (1.50–1.62 Å) in the corresponding transition states.

In summary, all the surface reaction barriers for hydrogenation of the C=O bond (pathways I and II) are smaller than those for hydrogenation of the C=C bond (pathways III and IV), which is opposite to the generally assumed hypothesis. These low energy barriers might suggest that the formation of propenol on the surface is a facile process, which is in apparent disagreement with the selective formation of propanal found experimentally. However, desorption of the product from the surface is a necessary last step. This step, which is found to be non-activated, is much easier for propanal (22 kJ mol^{-1}) than for propenol (104 kJ mol^{-1}). The key of the selectivity therefore resides in the competition between the surface reaction barriers and the desorption endothermicity.

The determination of the final balance between these two effects and of the product mixture thus requires a kinetic treatment. The fundamental assumptions of our model have been developed in the literature previously.[8] The elementary steps considered in the model are depicted in steps 1–7.

$$\text{(l)}\quad H_{2(gas)} \Leftrightarrow 2H_{(ads)}$$

$$\text{(2)}\quad \text{propenal}_{(gas)} \Leftrightarrow \text{propenal}_{(ads)}$$

$$\text{(3)}\quad \text{propenal}_{(ads)} + H_{(ads)} \Leftrightarrow \begin{cases} \text{allyloxy}_{(ads)} \\ \text{hydroxyallyl}_{(ads)} \\ \text{1-formylethyl}_{(ads)} \\ \text{2-formylethyl}_{(ads)} \end{cases}$$

$$\text{(4)}\quad \left.\begin{matrix} \text{allyloxy}_{(ads)} + H_{(ads)} \\ \text{hydroxyallyl}_{(ads)} + H_{(ads)} \end{matrix}\right\} \Leftrightarrow \text{propenol}_{(ads)}$$

$$\text{(5)}\quad \left.\begin{matrix} \text{1-formylethyl}_{(ads)} + H_{(ads)} \\ \text{2-formylethyl}_{(ads)} + H_{(ads)} \end{matrix}\right\} \Leftrightarrow \text{propanal}_{(ads)}$$

$$\text{(6)}\quad \text{propenol}_{(ads)} \Leftrightarrow \text{propenol}_{(gas)}$$

$$\text{(7)}\quad \text{propanal}_{(ads)} \Leftrightarrow \text{propanal}_{(gas)}$$

Steps 1 and 2 correspond to the adsorption of the two reactants, H_2 and propenal, respectively. Step 3 corresponds to the competitive first hydrogenation steps on the surface that lead to the four partially hydrogenated intermediates. In steps 4 and 5, a second H atom further hydrogenates the intermediates on the surface to yield the products (propenol and propanal); these steps are in competition. Steps 6 and 7 are the desorption steps of the products.

The partial pressures of the gas reactants are kept constant in our kinetic model. The adsorption (acrolein and H_2) and the desorption (propenol and propanal) steps are considered to be equilibrated, so the initial coverages of the reactants are imposed by the temperature and the partial pressures. The rate constants are calculated from our DFT activation barriers by using the transition-state theory,[9] and no empirical data are used. All the surface intermediate coverages are obtained by integration of the set of nonlinear differential equations with time. The selectivity is defined from the partial pressures of the desorbed products. An almost 100% selectivity to propanal is obtained from a mixture of acrolein (30 Torr) and hydrogen (900 Torr) at 350 K, a result which is in close agreement with experiments and which can be qualitatively related to the energy profiles. The rate-limiting step in the hydrogenation of the C=O bond is the product desorption, with a barrier of 104 kJ mol^{-1}, whereas for the hydrogenation of the C=C bond, it is the formation of the second C–H bond (101 kJ mol^{-1}). This second pathway is thus favored and propanal is selectively formed. The hydroxyallyl intermediate and hydrogen are the main species adsorbed during the reaction. The coverage of propenol increases on the surface, while propanal rapidly desorbs without accumulation. Hence, the species which is present to the greatest extent on the surface is not associated with the most abundant gas-phase product. As a result, product desorption appears to be a key factor in determining the reaction selectivity and can be used as a tuning parameter. If the energy for the desorption of propenol is numerically decreased by 30 kJ mol^{-1} without changing the other barriers, the calculated selectivity is reversed in favor of the unsaturated alcohol. This could explain qualitatively the change of selectivity observed experimentally for other reactants such as prenal on Pt(111), for which the desorption barriers of the corresponding UOL are decreased by this amount. Clearly, the determination of the other barriers are required to provide fully reliable conclusions in these other cases.

In this study, the partial hydrogenation of the C=C or the C=O bonds of acrolein on a Pt(111) catalyst has been studied by a theoretical approach based on first-principles calculations and a kinetic model. Total energy calculations have shown that the selectivity between the two competing products is controlled by the balance between the hydrogenation steps on the surface and the desorption of the partially hydrogenated products. The surface steps favor the attack at the C=O moiety to yield propenol, whereas desorption is easier for the product arising from the attack at the C=C bond (propanal). The kinetic model shows that the desorption step controls the selectivity in this case and almost 100% of propanal is obtained for a simulation under catalytic conditions (350 K and respective partial pressures of 30 and 900 Torr for acrolein and hydrogen reactants, respectively). Hence, the desorption energy of the product appears to be the critical tuning parameter for the selectivity.

Experimental Section

All the calculations were performed with the DFT formalism with the plane wave based VASP code.[10] The projector-augmented wave method[11] and the Perdew Wang 91 generalized gradient approximation[12] were used. The plane wave cutoff was set to 400 eV. The Pt(111) surface was modeled by a periodic four-layer slab with a vacuum region equivalent to five Pt layers. Adsorption took place on one side of the slab. A 3×3 unit cell was considered and gave a coverage of 1/9 monolayer. The Brillouin zone integration was performed on a $3 \times 3 \times 1$ grid. For the stationary points, the positions of the adsorbate and of the two uppermost layers were optimized. There are two main sources of error in the DFT adsorption energy: the systematic error arising from the limited thickness of the metallic slab, which is the largest one (10 kJ mol^{-1}), and the numerical error arising from the choice of the basis set and the k-point mesh, which is smaller (5 kJ mol^{-1}). The search for the transition states (TS) was performed with the climbing-image nudged elastic band method (CI-NEB).[13] The considered reaction surface intermediates did not show a spin-polarized electronic structure after adsorption. The transition-state structures were characterized by a vibrational analysis which showed one pure imaginary frequency.

Received: March 11, 2005
Published online: June 16, 2005

 © 2005 Wiley-VCH Verlag GmbH & Co. KGaA, Weinheim

Keywords: density functional calculations · heterogeneous catalysis · hydrogenation · reaction mechanisms · surface chemistry

[1] P. N. Rylander, *Hydrogenation Methods*, Academic Press, London, **1985**.
[2] T. B. L. W. Marinelli, S. Nabuurs, V. Ponec, *J. Catal.* **1995**, *151*, 431.
[3] T. Birchem, C. M. Pradier, Y. Berthier, G. Cordier, *J. Catal.* **1994**, *146*, 503.
[4] F. Delbecq, P. Sautet, *J. Catal.* **2002**, *211*, 398.
[5] F. Delbecq, P. Sautet, *J. Catal.* **2003**, *220*, 115.
[6] B. C. Khanra, Y. Jugnet, J. C. Bertolini, *J. Mol. Catal. A* **2004**, *208*, 167.
[7] R. Alcala, J. Greeley, M. Mavrikakis, J. A. Dumesic, *J. Chem. Phys.* **2002**, *116*, 8973.
[8] H. Lynggaard, A. Andreasen, C. Stegelmann, P. Stoltze, *Prog. Surf. Sci.* **2004**, *77*, 71.
[9] R. A. van Santen, J. W. Niemantsverdriet, *Chemical Kinetics and Catalysis*, Plenum, New York, **1995**.
[10] G. Kresse, J. Hafner, *Phys. Rev. B* **1993**, *47*, 558.
[11] G. Kresse, D. Joubert, *Phys. Rev. B* **1999**, *59*, 1758.
[12] J. P. Perdew, Y. Wang, *Phys. Rev. B* **1992**, *45*, 13244.
[13] G. Henkelman, B. P. Uberuaga, H. Jonsson, *J. Chem. Phys.* **2000**, *113*, 9901.

 © 2005 Wiley-VCH Verlag GmbH & Co. KGaA, Weinheim

Carbene Ligands

DOI: 10.1002/anie.200500884

Platinum-Mediated Oxidative Addition and Reductive Elimination of Imidazolium Salts at C4 and C5**

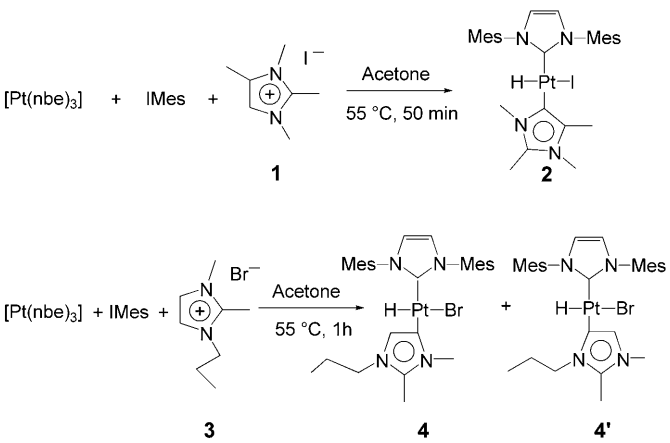
Deborha Bacciu, Kingsley J. Cavell, Ian A. Fallis, and Li-ling Ooi*

Nucleophilic N-heterocyclic carbenes (NHCs) have attracted considerable interest as ligands in organometallic chemistry and catalysis.[1] This attention is largely because of the unique combination of strong σ-donor, poor π-acceptor, and steric properties.[2] Typical transition-metal NHC complexes show "normal" binding at C2 because of the acidity of the C2 proton in the precursor azolium salt.[3] "Abnormal" metalation at C5 of the NHC ring was first reported in elegant studies by Crabtree and co-workers for pyridyl- and picolyl-NHC dihydride complexes of Ir^{III};[4] blocking C2 with a substituent, such as Me or Ph groups, will also encourage binding at C5.[5] Nolan and co-workers have recently reported the structure and interesting catalytic reactivity of $[PdCl_2(NHC)_2]$ complexes containing NHC ligands bound the "wrong way" that are derived from imidazolium salts.[6] In both these studies, the carbene bound at C4/5 was generated through deprotonation by the addition of a base or use of basic ligands on the metal.

In previous studies on metal–carbene complexes, we identified a facile reductive-elimination process, in which the carbene is lost as an imidazolium salt.[7] Conversely, it was found that imidazolium salts (ionic liquids) add oxidatively to low-valent metal centers through C2 activation.[7–9] The combination of these two redox steps lead to a new atom-efficient catalytic reaction for the substitution of azolium salts at C2.[10] The nature of this reaction and its wider implications is of major interest; for example, ionic liquids may add oxidatively to metal complexes dissolved within them, which generates catalytically active (hydrido)metal(carbene) complexes, and ionic liquids may also be incorporated into the reaction products, thus both problems and opportunities are presented.[11]

Herein, we report a novel extension to our investigations on this redox behavior. Platinum hydride complexes have been synthesized that bear NHC ligands in an abnormal binding mode through the oxidative addition of imidazolium salts with the C2 position blocked by a methyl group.

Complexes **2**, **4**, and **4′** were prepared in one-pot reactions by mixing $[Pt(norbornene)_3]$,[12] 1,3-bis(2,4,6-trimethylphenyl)imidazolin-2-ylidene (IMes), and either 1,2,3,4-tetramethylimidazolium iodide (**1**), in the case of **2**, or 1,2-dimethyl-3-propylimidazolium bromide (**3**), in the case of **4** and **4′**, in a molar ratio of 1:1:1.8 (Scheme 1). The reactions yielded the desired products after washing the crude residues with *n*-hexane and extraction with THF. It is proposed that the reactions proceed through the initial



Scheme 1. Oxidative addition at C4 and C5 in imidazolium cations to a Pt^0 center. nbe = norbornene.

[*] D. Bacciu, Prof. K. J. Cavell, Dr. I. A. Fallis, Dr. L.-l. Ooi
Department of Chemistry
Cardiff University
PO Box 912, Cardiff, Wales CF10 3TB (UK)
Fax: (+44) 29-2087-5899
E-mail: cavellkj@cf.ac.uk

[**] We thank Nicolas Clement for advice and helpful discussions, Rob Jenkins for technical assistance, and Dr. David Nielsen for help with the preparation of the manuscript. We are grateful to the Engineering and Physical Sciences Research Council (EPSRC) for financial support.

Supporting information for this article is available on the WWW under http://www.angewandte.org or from the author.

InterScience
© 2005 Wiley-VCH Verlag GmbH & Co. KGaA, Weinheim

formation of a [Pt(IMes)(norbornene)$_2$] complex, which then undergoes oxidative addition of the C4,5–H bond of the imidazolium salt. This one-pot reaction provides a potentially valuable route to "wrong-way" (hydrido)metal(carbene) complexes, which may have applications in catalysis.

Complexes **4** and **4′** were characterized by ^{1}H and ^{13}C NMR spectroscopic analysis, which revealed a mixture of two isomers in a ratio of 3:1. The platinum center in the minor component **4′** is connected to C4, which is the carbon atom closest to the *N*-propyl chain, whereas the platinum center in the major component **4** is connected to C5, which is the carbon atom adjacent to the *N*-methyl group. Steric influences may produce the observed regioselectivity.

The hydride ligands in **4** and **4′** appear in the ^{1}H NMR spectra (CD_2Cl_2) at $\delta = -18.29$ ppm (^1J(Pt-H) = 1714 Hz) and $\delta = -18.31$ ppm (^1J(Pt-H) = 1711 Hz), respectively. The ^{13}C NMR spectra of **4** and **4′** show characteristic signals from C2 of the IMes unit at $\delta = 180.9$ and 180.7 ppm, respectively, and from C4 and C5 of the abnormal carbene moiety at $\delta = 124.4$ and 151.6 ppm for **4**, respectively, and at $\delta = 152.4$ and 126.3 ppm for **4′**, respectively. The presence of a metal-bound carbene is also indicated by the ^{13}C{^{1}H} NMR spectra, in which the signals from C4 and C5 in **4** and **4′** are shifted downfield relative to **3**. The ^{13}C NMR resonances for C4 and C5 are comparable with previously reported abnormally bound carbenes.[5,13]

A mixture of crystalline needles (**4′**) and plates (**4**) was grown by slow diffusion of hexane into a saturated solution of the crude product in acetone. Only the needles were found to be suitable for single-crystal X-ray analysis, and they showed an abnormally bound Pt carbene complex (Figure 1). The crystal contains one acetone molecule and two Pt carbene complexes in the asymmetric unit. Both Pt carbene complexes in the crystal are identical within experimental error. The molecular structure of **4′**[14] shows a slightly distorted square-planar coordination around the Pt^{II} center, with *trans*-NHC moieties and hydride and bromide ligands occupying the remaining coordination sites. The Pt–C(carbene) bond lengths for the IMes ligand (Pt21–C21: 2.018(8) Å) and for the carbene ligand coordinated at C5 (Pt21–C223: 2.041(8) Å) are comparable and consistent with Pt–C single bonds.[5,6,13,15]

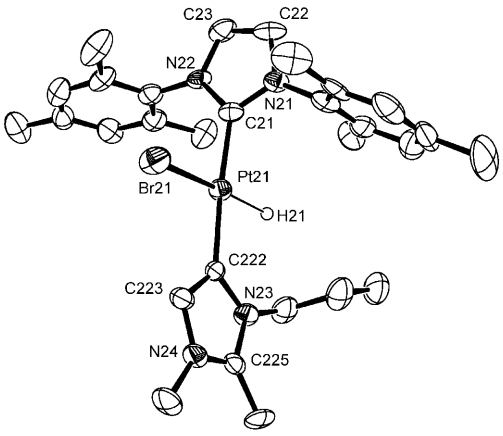
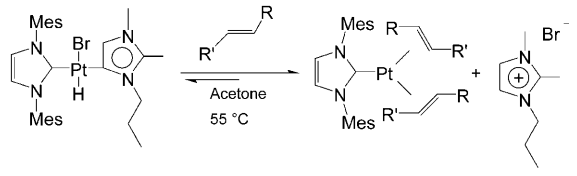


Figure 1. ORTEP diagram of **4′**. Some hydrogen atoms, the acetone molecule, and a molecule of **4′** are omitted for clarity. Selected bond lengths [Å] and angles [°]: Pt21-C21 2.018(8), Pt2-C222 2.041(8), Pt21-Br21 2.5622(9), Pt21-H21 1.8052, C21-Pt(21)-C222 175.6(3); C21-Pt21-Br21 91.4(2), C21-Pt21-H21 93.1, C222-Pt21-Br21 90.0(2), C222-Pt21-H21 85.2, Br21-Pt21-H21 173.2.

Although the mixture of **4** and **4′** is stable, both in the solid state and in solution with acetone at room temperature over two–three days, the mixture underwent reductive elimination[10,16,17] in the presence of alkenes (styrene or dimethyl fumarate) to regenerate **3** and form [Pt(η^2-alkene)$_2$(IMes)] complexes **5a** and **5b** (Scheme 2). Stirring a mixture of **4** and **4′** with five equivalents of dimethyl fumarate in acetone for three hours resulted in quantitative reductive elimination.[8] The equivalent reaction with styrene resulted in partial conversion with equilibrium concentrations of **4**, **4′**, **5**, and **3** being established.[16] The ^{1}H NMR spectrum of **5a** was identical to that observed for an authentic sample of [Pt(dimethyl fumarate)$_2$(IMes)] prepared by the reaction of [Pt(cod)$_2$] (cod = cyclooctadiene), IMes, and dimethyl fumarate.



5a: R = R' = COOMe t = 3 h 100%
5b: R = Ph, R' = H t = 8 h 50%

Scheme 2. Reductive elimination of imidazolium salts at C4/5–H from "abnormal" carbene complexes.

The observed reductive-elimination behavior is consistent with the π-acceptor ability of alkenes, the distribution of electron density within the complex, and the Pt–alkene bond strength. Interestingly, reductive elimination of the "normal" carbene and the products that result from insertion of alkenes into the Pt–H bond (e.g., Pt hydrocarbyl complexes or imidazolium salts substituted at C4/5) were not observed. The behavior reported herein provides clear indication that the substitution of ionic liquids at C2 may not be enough to prevent their involvement in reactions for which they are the solvent.[18]

Received: March 9, 2005
Published online: July 22, 2005

Keywords: azoles · ionic liquids · N-heterocyclic carbenes · oxidative addition · reductive elimination

[1] W. A. Herrmann, *Angew. Chem.* **2002**, *114*, 1342; *Angew. Chem. Int. Ed.* **2002**, *41*, 1290.
[2] D. Bourissou, O. Guerret, F. P. Gabbai, G. Bertrand, *Chem. Rev.* **2000**, *100*, 39; W. A. Herrmann, C. Köcher, *Angew. Chem.* **1997**, *109*, 2256; *Angew. Chem. Int. Ed.* **1997**, *36*, 2162; A. C. Hillier, W. J. Sommer, B. S. Yong, J. L. Petersen, L. Cavallo, S. P. Nolan, *Organometallics* **2004**, *23*, 4322.

 © 2005 Wiley-VCH Verlag GmbH & Co. KGaA, Weinheim

[3] D. S. McGuinness, K. J. Cavell, B. W. Skelton, A. H. White, *Organometallics* **1999**, *18*, 1596.
[4] S. Gründemann, A. Kovacevic, M. Albrecht, J. W. Faller, R. H. Crabtree, *J. Am. Chem. Soc.* **2002**, *124*, 10473.
[5] A. R. Chianese, A. Kovacevic, B. M. Zeglis, J. W. Faller, R. H. Crabtree, *Organometallics* **2004**, *23*, 2461.
[6] H. Lebel, M. K. Janes, A. B. Charette, S. P. Nolan, *J. Am. Chem. Soc.* **2004**, *126*, 5046.
[7] D. S. McGuinness, K. J. Cavell, B. F. Yates, B. W. Skelton, A. H. White, *J. Am. Chem. Soc.* **2001**, *123*, 8317.
[8] M. A. Duin, N. D. Clement, K. J. Cavell, C. J. Elsevier, *Chem. Commun.* **2003**, 400.
[9] N. D. Clement, K. J. Cavell, C. Jones, C. J. Elsevier, *Angew. Chem.* **2004**, *116*, 1297; *Angew. Chem. Int. Ed.* **2004**, *43*, 1277; D. S. McGuinness, K. J. Cavell, B. F. Yates, *Chem. Commun.* **2001**, 355.
[10] N. D. Clement, K. J. Cavell, *Angew. Chem.* **2004**, *116*, 3933; *Angew. Chem. Int. Ed.* **2004**, *43*, 3845.
[11] J. Dupont, J. Spencer, *Angew. Chem.* **2004**, *116*, 5408; *Angew. Chem. Int. Ed.* **2004**, *43*, 5296.
[12] L. E. Crascall, J. L. Spencer, *Inorg. Synth.* **1998**, *28*, 126.
[13] J. S. Owen, J. A. Labinger, J. E. Bercaw, *J. Am. Chem. Soc.* **2004**, *126*, 8247.
[14] Crystal data for **4′**: $C_{58}H_{78}Br_2N_8Pt_2{\cdot}C_3H_6O$, $M_r = 1495.36$ triclinic $P\bar{1}$, $a = 14.4027(3)$, $b = 14.4603(3)$, $c = 16.8198(4)$ Å, $\alpha = 75.582(1)$, $\beta = 68.713(1)$, $\gamma = 75.279(1)°$, $V = 3108.76(12)$ Å^3, $Z = 2$, $\rho_{calcd} = 1.597$ Mg m^{-3}, $\mu(Mo_{K\alpha}) = 0.71073$, $T = 150(2)$ K, 57703 reflections collected, 14183 (R(int) 0.1635), F^2 refinement $R_1 = 0.0616$, $wR_2 = 0.1111$ for ($I > 2\sigma$(I)), 24 restraints, and 687 parameters. CCDC-265475 contains the supplementary crystallographic data for this paper. These data can be obtained free of charge from the Cambridge Crystallographic Data Center via www.ccdc.cam.ac.uk/data_request/cif.
[15] A. A. Danopoulos, N. Tsoureas, J. A. Wright, M. E. Light, *Organometallics* **2004**, *23*, 166; X. Hu, I. C. Rodriguez, K. Meyer, *Organometallics* **2003**, *22*, 316.
[16] D. S. McGuinness, N. Saendig, B. F. Yates, K. J. Cavell, *J. Am. Chem. Soc.* **2001**, *123*, 4029.
[17] K. J. Cavell, D. S. McGuinness, *Coord. Chem. Rev.* **2004**, *248*, 671; M. Crudden, D. P. Allen, *Coord. Chem. Rev.* **2004**, *248*, 2247.
[18] Experimental details of the preparation, characterization of the complexes, and full details of the X-ray crystal structure of **4′** are available in the Supporting Information.

 © 2005 Wiley-VCH Verlag GmbH & Co. KGaA, Weinheim

Carbene Chemistry

DOI: 10.1002/anie.200501056

A Gold Catalyst for Carbene-Transfer Reactions from Ethyl Diazoacetate**

Manuel R. Fructos, Tomás R. Belderrain, Pierre de Frémont, Natalie M. Scott, Steven P. Nolan, M. Mar Díaz-Requejo,* and Pedro J. Pérez**

The use of transition-metal-based catalysts for the transfer of carbene units from diazo compounds constitutes a powerful tool in organic synthesis.[1] Several metals have been reported to mediate this transformation effectively, and the appropriate selection of ligands has permitted excellent selectivities. Highly chemo-, diastereo-, and/or enantioselective systems have been reported with rhodium-, copper-, or cobalt-containing catalysts. In fact, nearly all 12 elements of Groups 8–11 have been found to decompose diazo compounds and transfer a carbene unit to saturated or unsaturated organic substrates,[2] leading to the insertion or addition product, respectively (Scheme 1). Only one of these 12 elements remains unexplored in this chemistry: gold.[3] Although the other members of Group 11—copper and, to a lesser extent, silver—have been described to induce such transformations, conducting this type of catalytic reaction with gold remains a challenge. We therefore focused our attention on the development of a gold-based catalyst, as a result of our experience in the area of metal-catalyzed carbene transfer from ethyl diazoacetate (EDA).[4]

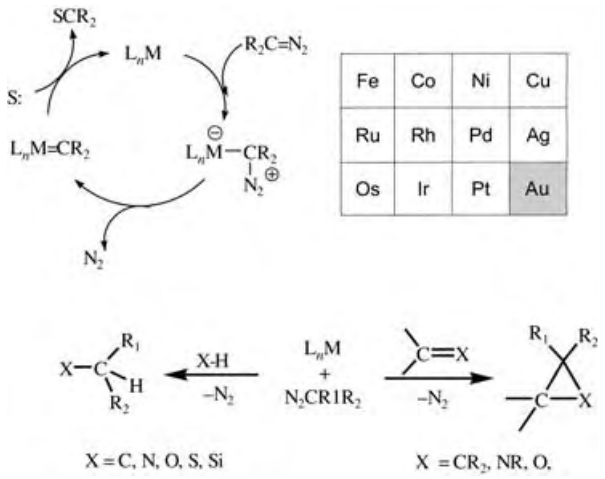
We recently reported the catalytic behavior of [(IPr)CuCl] (**1**, IPr = 1,3-bis(diisopropylphenyl)imidazol-2-ylidene) for the transfer of carbene from ethyl diazoacetate to olefins, amines, and alcohols to form cyclopropanes, amino acid derivatives, and ethers, respectively.[5] These promising results

[*] P. de Frémont, N. M. Scott, Prof. Dr. S. P. Nolan
Department of Chemistry
University of New Orleans
New Orleans, LA 70148 (USA)
Fax: (+1) 504-280-6860
E-mail: snolan@uno.edu
M. R. Fructos, Dr. T. R. Belderrain, Dr. M. M. Díaz-Requejo, Prof. Dr. P. J. Pérez
Departamento de Química y Ciencia de los Materiales
Campus de El Carmen s/n
Universidad de Huelva–Unidad Asociada al CSIC
21007 Huelva (Spain)
Fax: (+34) 959-219-942
E-mail: mmdiaz@dqcm.uhu.es
perez@dqcm.uhu.es

[**] We are grateful for financial support for this work (BQU2002–01114). We acknowledge the Universidad de Huelva (NMR Service), the MECD (M.R.F.), and the Ramon y Cajal Program (M.M.D.R.) as well as the National Science Foundation for work conducted at the University of New Orleans.

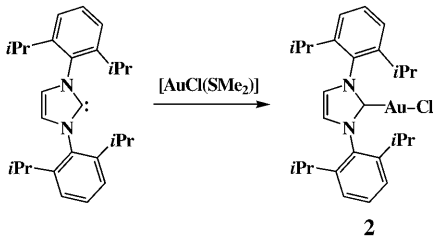
Supporting information for this article (general experimental procedures and product characterization data) is available on the WWW under http://www.angewandte.org or from the author.

 InterScience © 2005 Wiley-VCH Verlag GmbH & Co. KGaA, Weinheim



Scheme 1. Top left: Catalytic cycle proposed for the metal-catalyzed decomposition of diazo compounds and subsequent carbene transfer to a saturated or unsaturated substrate (S:). Top right: Metals of Groups 8–11 that have been described to induce such a transformation; gold still remained unreported. Bottom: The most common examples of organic transformations using the methodology of carbene transfer from diazo compounds.

prompted us to examine the potential role of the gold analogue [(IPr)AuCl] (**2**), which was prepared from equimolar amounts of the IPr ligand and [AuCl(SMe$_2$)] [Eq. (1)].[6]



(1)

This new compound was spectroscopically characterized, and its structure confirmed by X-ray diffraction studies (Figure 1). The gold(I) atom is two-coordinate in an essentially linear environment with C-Au-Cl bond angles close to 180°, an arrangement similar to that previously found for **1**.

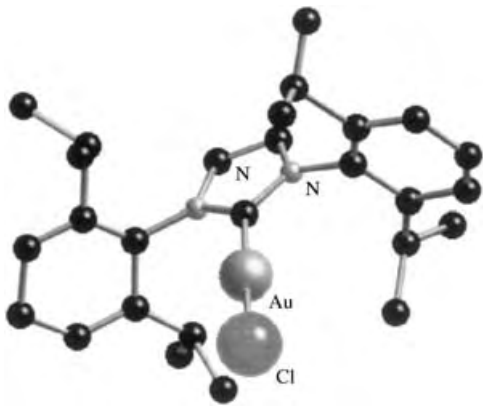
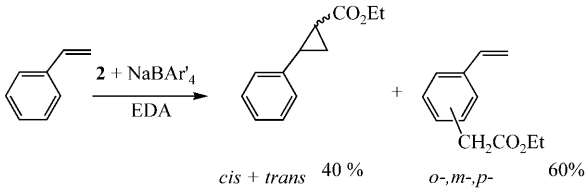
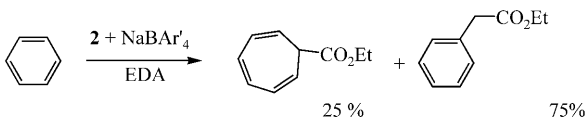


Figure 1. Ball-and-stick view of complex **2**; hydrogen atoms have been omitted for clarity.

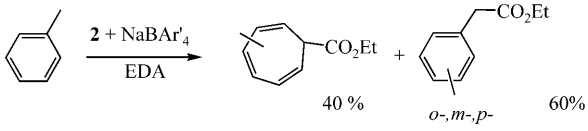
Once prepared and characterized, complex **2** was employed as a catalyst for the cyclopropanation of styrene with ethyl diazoacetate, a well-known model reaction. Our previous work with the copper complex **1** suggested that the chloride ion had to be removed from the metal center prior to reaction with EDA.[5] We therefore employed a modified method in which the active catalytic species was generated in situ by using an equimolar mixture of **2** and the sodium salt of the non-coordinating anion tetrakis(3,5-bis(trifluoromethyl)phenyl)borate (BAr′$_4$). The use of a 2.5% catalyst loading (with respect to EDA) in neat styrene (1 mL) led to the consumption of EDA within a few minutes (see the Experimental Section). Analysis of the reaction mixture by GC and GCMS showed, besides the expected *cis*- and *trans*-cyclopropanes, three other products with the same molar mass, namely, the *o*, *m*, and *p* isomers of the styryl acetate shown in Equation (2). These additional products are formed



(2)



(3)



(4)

by the formal insertion of the :CHCO$_2$Et unit into the sp^2 C–H bond of the aromatic ring of the styrene. To the best of our knowledge, this type of intermolecular reaction is unprecedented.[7] All published reports have shown that the double bond of styrene is preferentially converted into the cyclopropane product in this reaction. A second, but nonetheless important feature of this gold catalyst is that no diethyl fumarate or maleate formed as a result of EDA coupling, even though the diazo compound was added to the reaction mixture in one portion.

To see whether this unexpected insertion reaction can be generalized, we examined two common aromatic substrates, benzene and toluene [Eqs. (3), (4); yields determined by NMR spectroscopy]. Previous reports have shown that the metal-catalyzed addition of EDA to these compounds results in the formation of cycloheptatriene rings as the major product.[4h,8] In the case of toluene, a few catalysts have also promoted insertion into the methyl C–H bond to provide the dihydrocinnamate derivative[4h,8,9] but there are no examples of insertion into the aromatic sp^2 C–H bond. In contrast, the use of **2** and NaBAr′$_4$ as the catalyst precursor for the reaction

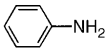
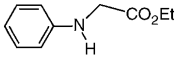
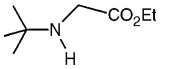
 © 2005 Wiley-VCH Verlag GmbH & Co. KGaA, Weinheim

of EDA and benzene led to a mixture of the expected cycloheptatriene as well as ethyl phenylacetate [Eq. (3)], the latter formed by formal insertion into the aromatic C–H bond. Similar behavior was observed with toluene as the substrate [Eq. (4)]: The expansion products were observed along with the three isomers of ethyl tolylacetate. The identities of the new products are unambiguous, as their spectroscopic and chromatographic data are identical to those of commercial samples (see the Experimental Section).

No EDA-coupling products—that is, diethyl fumarate and maleate—were observed in the above transformations, highlighting the chemoselectivity of this catalytic system. Even allowing EDA to react with complex **2** at room temperature for several hours did not lead to any transformation of the initial diazo compound. Heating of the reaction mixture at 60 °C and 80 °C did not induce any Au-catalyzed EDA decomposition, therefore indicating the stability of the diazo compound in the presence of **2**, as was observed for the copper analogue **1**.[5]

We next screened several substrates to explore the range of activity for the gold system (Table 1). The use of *cis*-cyclooctene as the olefin provided the expected mixture of *exo*- and *endo*-cyclopropanes. The insertion of EDA into N–H and O–H bonds was also studied with amines and alcohols; in all cases the corresponding amino acid derivatives and ethers were obtained quantitatively. Again, no EDA coupling products were detected in the mixture at the end of the reaction.

Table 1: The addition or insertion of EDA catalyzed by **2** + $NaBAr'_4$.

Substrate	Product	Yield [%][a]
		>99[b]
		>99[b]
		>99[b]
CH_3OH	$CH_3OCH_2CO_2Et$	>99[c]
CH_3CH_2OH	$CH_3CH_2OCH_2CO_2Et$	>99[c]

[a] No diethyl fumarate or maleate was detected in any experiment; see the Experimental Section for details. [b] Determined by NMR spectroscopy at the end of the reaction using an internal standard. [c] Determined by GC using an internal standard.

Kinetic experiments were performed using methanol as the substrate with complex **2** as the catalyst precursor both with and without the halide scavenger $NaBAr'_4$. First, the consumption of EDA was monitored in parallel experiments differing only in the presence or absence of $NaBAr'_4$. The two reactions lead to very similar decays that correspond to first-order behavior (Figure 2). Plots of ln[EDA] versus time provided k_{obs} values of 5.98×10^{-4} and $6.84\times10^{-4}\ s^{-1}$ for the experiments carried out in the absence and in the presence of the tetraarylborate anion, respectively; the latter reaction is slightly faster but of the same order of magnitude. Nearly identical values for k_{obs} were obtained from experiments in which the nitrogen evolution was measured (7.94×10^{-4} and $1.05\times10^{-3}\ s^{-1}$, respectively). These values compare well with those obtained from monitoring EDA consumption.

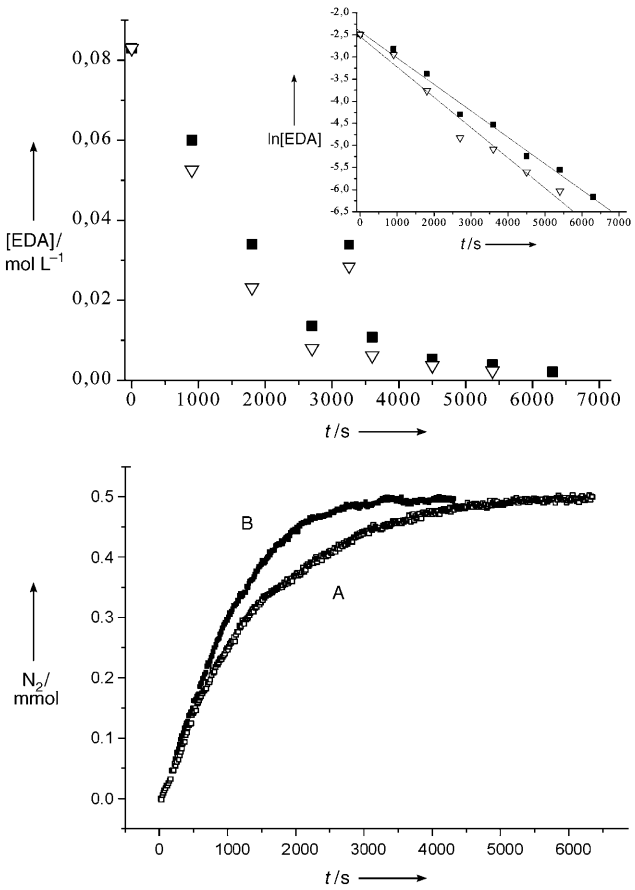
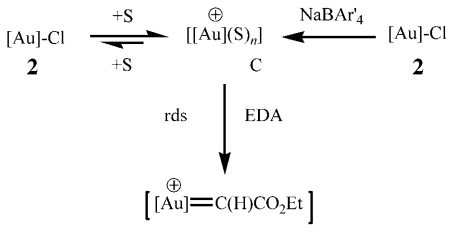


Figure 2. Top: Plot showing the consumption of EDA in the reaction of methanol and ethyl diazoacetate with **2** as catalyst in the absence (■) and presence of $NaBAr'_4$ (▽). Inset: Plot of ln[EDA] versus time t from which the following k_{obs} values were obtained: **2** as catalyst: $k_{obs}=5.98\times10^{-4}\ s^{-1}$; **2** + $NaBAr'_4$ as catalyst: $k_{obs}=6.84\times10^{-4}\ s^{-1}$. Bottom: Plot of nitrogen evolution under the same conditions. Exponential fitting provided the following values: $k_{obs}=7.94\times10^{-4}$ (**2** as catalyst, A), $k_{obs}=1.05\times10^{-3}\ s^{-1}$ (**2** + $NaBAr'_4$ as catalyst, B).

Scheme 2 illustrates a possible explanation for the experimental kinetic data. A cationic species **C**, probably containing coordinated methanol, is formed in both instances. The addition of $NaBAr'_4$ promotes the quantitative conversion of **2** into such a species; however, in the absence of $NaBAr'_4$, an equilibrium between the neutral **2** and the cationic **C** takes place. This also explains the slightly more sluggish reaction with **2** as catalyst since the amount of **C** is not equal to the



Scheme 2. Proposed mechanism for the generation of the catalytic species.

 © 2005 Wiley-VCH Verlag GmbH & Co. KGaA, Weinheim

initial amount of **2**. In contrast, the use of the arylborate salt ensures that $[\mathbf{C}] = [\mathbf{2}]_{init}$. The catalytic cycle starts from **C**, and the rate-determining step is the formation of a metallocarbene intermediate, as commonly proposed for this type of transformation.[1]. The observation of very similar rate constants from the monitoring of nitrogen generation and EDA consumption is in line with the absence of fumarate and maleate products.

In conclusion, we have described the first example of a gold-based catalyst for the decomposition of ethyl diazoacetate and the subsequent transfer of the :$CHCO_2Et$ unit to saturated and unsaturated substrates: Cyclopropanation of olefins as well as insertion into N–H and O–H bonds have been achieved. Even more interesting is the novel insertion of the carbene units into the C–H bonds of the aromatic ring of benzene, toluene, and styrene. Finally, this catalyst is very chemoselective, since no EDA coupling products are observed in any of the reactions studied.

Experimental Section

General: All reactions were carried out by using standard Schlenk techniques under an atmosphere of dry argon or in an MBraun glovebox containing dry argon or nitrogen. Anhydrous solvents were purchased from Aldrich and degassed prior to use. CD_2Cl_2 was either dried over CaH_2, or degassed with argon and dried over molecular sieves. The reagents (olefins, alcohols, amines) were also purchased from Aldrich and employed without further purification. IPr was synthesized by deprotonation of the imidazolium salt with base according to a literature procedure.[10] The immediate precursor, IPr·HCl, can be purchased from Strem Chemicals Inc. The ^1H and ^{13}C NMR spectra were collected on 400-MHz Varian Gemini and Varian Mercury spectrometers. The GC and GCMS were obtained in Varian 3800 and Saturn 2100 instruments, respectively. Elemental analyses were performed by Robertson Microlit Laboratories, Madison, NJ.

2: In a glove box a 100-mL Schenk flask was charged with IPr (686 mg, 1.8 mmol) and THF (35 mL), and then [AuCl(SMe_2)] (232 mg, 0.80 mmol) was added. The resulting solution was stirred at room temperature for 12 h. The solvent was removed under vacuum, and CH_2Cl_2 (5 mL) was added. The colorless solution was filtered, and hexane (10 mL) was added to the filtrate, resulting in precipitation of an off-white solid. The solid was washed with hexane (3×5 mL) and dried under vacuum. Yield: 770 mg (69 %). ^1H NMR (400 MHz, CD_2Cl_2): $\delta = 7.57$ (t, $J = 7.8$ Hz, 2H; ArH), 7.35 (d, $J = 7.8$ Hz, 4H; ArH), 7.24 (s, 2H; Imid-H), 2.57 (septet, $J = 6.8$ Hz, 4H; $CH(CH_3)_2$), 1.34 (d, $J = 6.8$ Hz, 12H; $CH(CH_3)_2$), 1.23 ppm (d, $J = 6.8$ Hz, 12H; $CH(CH_3)_2$); $^{13}C\{^1H\}$ NMR (125 MHz, CD_2Cl_2): $\delta =$ 175.09 ($C_{carbene}$), 145.78 (C_{Ar}), 134.05 (C_{Ar}), 130.68 (C_{Ar}), 124.28 (C_{Ar}), 123.32 (C_{imid}), 28.79 ($CH(CH_3)_2$), 24.17 ($CH(CH_3)_2$), 23.74 ppm ($CH(CH_3)_2$); elemental analysis: calcd for $C_{27}H_{36}N_2AuCl$ (621.69): C 52.11, H 5.79, N 4.50; found: C 51.70, H 5.61, N 4.38. Suitable crystals for crystallographic study were grown by slow evaporation of a saturated solution in acetone. CCDC-258274 (**2**) contains the supplementary crystallographic data for this paper. These data can be obtained free of charge from the Cambridge Crystallographic Data Centre via www.ccdc.cam.ac.uk/data_request/cif.

Catalytic experiments: The precatalyst **2** (0.025 mmol) was dissolved in neat substrate (1–3 mL), and $NaBAr'_4$[11] (1 equiv) was added to the solution. After 15 min of stirring, EDA (0.5 mmol) was added in one portion. After 1 h of additional stirring, the mixture was analyzed by GC and GCMS. The volatile components were then removed, and the residue analyzed by NMR spectroscopy to identify the products (see the Supporting Information). To establish the mass balance, an internal standard was employed.

Received: March 23, 2005
Revised: May 12, 2005
Published online: July 22, 2005

Keywords: C–H activation · carbenes · diazo compounds · gold · homogeneous catalysis

[1] M. P. Doyle, M. A. McKervey, T. Ye, *Modern Catalytic Methods for Organic Synthesis with Diazo Compounds*, Wiley, New York, **1998**.

[2] a) See reference [1] for examples based on Fe, Ru, Os, Co, Rh, Ni, Pd, Pt, and Cu; b) for iridium as catalyst, see: T. Kubo, S. Sakagushi, Y. Ishii, *Chem. Commun.* **2000**, 625; c) for Ag-based catalysts, see: J. Urbano, T. R. Belderraín, M. C. Nicasio, S. Trofimenko, M. M. Díaz-Requejo, P. J. Pérez, *Organometallics* **2005**, *24*, 1528, and references therein.

[3] For gold-based catalysts for other processes, see: a) A. S. K. Hashmi, *Gold Bull.* **2004**, *37*, 51; b) A. S. K. Hashmi, J. P. Weyrauch, M. Rudolph, E. Kurpejović, *Angew. Chem.* **2004**, *116*, 6707; *Angew. Chem. Int. Ed.* **2004**, *43*, 6545; c) Z. Shi, C. He, *J. Org. Chem.* **2004**, *69*, 3669; d) J. J. Kennedy-Smith, S. T. Staben, F. D. Toste, *J. Am. Chem. Soc.* **2004**, *126*, 4526; e) C. Nieto-Oberhuber, M. P. Muñoz, E. Buñuel, C. Nevado, D. J. Cárdenas, A. M. Echavarren, *Angew. Chem.* **2004**, *116*, 2456; *Angew. Chem. Int. Ed.* **2004**, *43*, 2402; f) V. Mamane, T. Gress, H.; Krause, A. Furstner, *J. Am. Chem. Soc.* **2004**, *126*, 8654; g) N. Morita, N. Krause, *Org. Lett.* **2004**, *6*, 4121; h) R. Casado, M. Contel, M. Laguna, P. Romero, S. Sanz, *J. Am. Chem. Soc.* **2003**, *125*, 11925; i) G. B. Shul'pin, A. E. Shilov, G. Süss-Fink, *Tetrahedron Lett.* **2001**, *42*, 7253; j) G. Dyker, *Angew. Chem.* **2000**, *112*, 4407; *Angew. Chem. Int. Ed.* **2000**, *39*, 4237; k) D. Thompson, *Gold Bull.* **1999**, *32*, 12; l) J. H. Teles, S. Brode, M. Chabanas, *Angew. Chem.* **1998**, *110*, 1475; *Angew. Chem. Int. Ed.* **1998**, *37*, 1415.

[4] For olefin cyclopropanation, see: a) M. M. Díaz-Requejo, T. R. Belderrain, S. Trofimenko, P. J. Pérez, *J. Am. Chem. Soc.* **2001**, *123*, 3167; b) M. M. Díaz-Requejo, A. Caballero, T. R. Belderrain, M. C. Nicasio, S. Trofimenko, P. J. Pérez, *J. Am. Chem. Soc.* **2002**, *124*, 978; For alkyne cyclopropenation, see: c) M. M. Díaz-Requejo, M. A. Mairena, T. R. Belderrain, M. C. Nicasio, S. Trofimenko, P. J. Pérez, *Chem. Commun.* **2001**, 1804; for C–H insertion, see: d) M. M. Díaz-Requejo, T. R. Belderrain, M. C. Nicasio, S. Trofimenko, P. J. Pérez, *J. Am. Chem. Soc.* **2002**, *124*, 896; e) A. Caballero, M. M. Díaz-Requejo, T. R. Belderrain, M. C. Nicasio, S. Trofimenko, P. J. Pérez, *J. Am. Chem. Soc.* **2003**, *125*, 1446; N-H insertion: f) M. E. Morilla, M. M. Díaz-Requejo, T. R. Belderrain, M. C. Nicasio, S. Trofimenko, P. J. Pérez, *Chem. Commun.* **2002**, 2998; g) for O–H insertion, see: M. E. Morilla, M. J. Molina, M. M. Díaz-Requejo, T. R. Belderrain, M. C. Nicasio, S. Trofimenko, P. J. Pérez, *Organometallics* **2004**, *23*, 2914; for addition to aromatic rings, see: h) M. E. Morilla, M. M. Díaz-Requejo, T. R. Belderrain, M. C. Nicasio, S. Trofimenko, P. J. Pérez, *Organometallics* **2004**, *23*, 293.

[5] M. R. Fructos, T. R. Belderrain, M. C. Nicasio, S. P. Nolan, H. Kaur, M. M. Díaz-Requejo, P. J. Pérez, *J. Am. Chem. Soc.* **2004**, *126*, 10846.

[6] See the Supporting Information for synthetic and structural details. For other members of the [(NHC)AuCl] family, see: P. de Frémont, N. M. Scott, E. D. Stevens, S. P. Nolan, *Organometallics* **2005**, *24*, in press.

[7] The intramolecular insertion of diazo ketones into aromatic C–H bonds has been extensively reported (see reference [1]). This process has been described as an electrophilic addition of the

 © 2005 Wiley-VCH Verlag GmbH & Co. KGaA, Weinheim

metallocarbene followed by 1,2-hydride migration: A. Padwa, D. J. Austin, A. T. Price, M. A. Semones, M. P. Doyle, M. N. Protopopova, W. R. Winchester, A. Tarn, *J. Am. Chem. Soc.* **1993**, *115*, 8669. The observed ratios for the products, particularly the *meta/para* ratios (lower than 2:1), shows a preference for the *para* position, a fact that would be in accord with such proposal.

[8] A. J. Anciaux, A. Demonceau, A. F. Noels, A. J. Hubert, R. Warin, P. H. Teyssie, *J. Org. Chem.* **1981**, *46*, 873.

[9] H. J. Callot, F. Metz, *Nouv. J. Chim.* **1985**, *9*, 167.

[10] M. S. Viciu, O. Navarro, R. F. Germaneau, R. A. Kelly III, W. Sommer, N. Marion, E. D. Stevens, L. Cavallo, S. P. Nolan, *Organometallics* **2004**, *23*, 1629, and references therein.

[11] M. Brookhart, B. Grant, A. F. Volpe, *Organometallics* **1992**, *11*, 3920.

 © 2005 Wiley-VCH Verlag GmbH & Co. KGaA, Weinheim

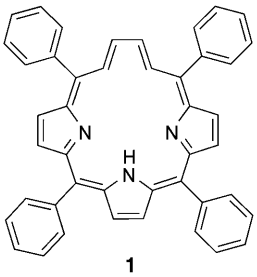
Porphyrinoids

DOI: 10.1002/anie.200501635

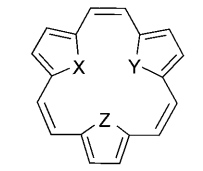
Dithiaethyneporphyrin: An Atypical [18]Triphyrin(4.1.1) Frame for Contracted Porphyrins**

Anna Berlicka, Lechosław Latos-Grażyński, and Tadeusz Lis*

The aza-deficent porphyrin 5,10,15,20-tetraaryl-21-vacataporphyrin (butadieneporphyrin, [18]triphyrin(6.1.1); **1**) is an



1

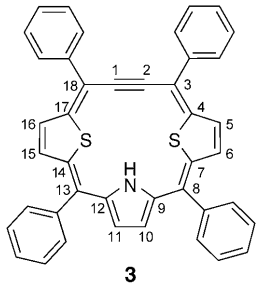


X, Y, Z = S, O, NH, NR

2

annulene–porphyrin hybrid.[1] In principle, vacataporphyrin **1** (paradoxically expanded porphyrin)[2–4] can be considered as a seminal molecule for the subclass of triphyrins, which are distinguished by the fact that they contain only three pyrrole or pyrrole-like rings, linked by two sp^2-hybridized *meso* carbon atoms to form the tripyrrolic brace. The macrocyclic structure of triphyrins is completed by a single chain of sp^2- and/or sp-hybridized carbon atoms. Besides vacataporphyrin, only [15]triphyrin(1.1.3), which was obtained serendipitously during the condensation of triisopropylsilyl propynal with 3,4-diethylpyrrole, meets the criterion outlined above.[5] Alternatively, the replacement of the six inner protons of [18]annulene by three oxygen, sulfur, or NH (NR) groups, or some combination of the three, as explored originally by Badger et al., leads to heteroatom-bridged annulenes **2**; that is, [18]triphyrin(2.2.2) or [18]heterotriphyrin(2.2.2).[6–8]

Herein, we report the synthesis and characterization of 3,8,13,18-tetraphenyl-19,21-dithiaethyneporphyrin (H(S_2-ETPP); **3**). This porphyrin derivative is a novel type of



3

contracted heteroporphyrin related to putative [18]triphyrin-(4.1.1) with an acetylene moiety embedded in the macrocyclic framework. It introduces a unique structural pattern for contracted porphyrins,[2,4] created by fusing the structural motifs of 21,23-dithiaporphyrin and acetylene.

The synthetic strategy for **3** (Scheme 1) resembles the [3+1] approach applied to prepare porphyrins, heteroporphyrins, and carbaporphyrinoids.[9] Retrosynthetic analysis led to the identification of 1,4-di(2-thienyl)-1,4-diphenyl-2-butyne (**7**) as the fundamental building block for the construction of **3**. Eventually, dithiaethyneporphyrin **3** was formed through a condensation reaction that is similar to the [3+1] procedure for porphyrins, although the *meso* carbon atoms here originated from **9** rather than the usual monopyrrolic fragment (12.7% yield).

The electronic spectrum of **3** (Figure 1) shows a distinct intense Soret-like band at $\lambda = 448$ nm accompanied by less-intense Q bands at 518, 553, 646, and 725 nm, resembling the spectroscopic features of aromatic 5,10,15,20-tetraphenyl-21,23-dithiaporphyrin, S_2TPP.[10] The ^{1}H NMR spectrum of **3** also resembled that of S_2TPP[10] and displayed resonances at positions consistent with an aromatic structure: porphyrinoid **3** retains macrocyclic aromaticity through an 18-π-electron delocalization motif. The scalar coupling detected between NH20 and the β-pyrrolic protons H10 and H11 confirms the molecular structure of **3** (Figure 2). The ^{13}C NMR chemical shifts of the four-carbon linker derived from 2-butyne reveals a symmetric structure, with $\delta = 116.8$ ppm for C1 and C2 and $\delta = 111.9$ ppm for C3 and C18.

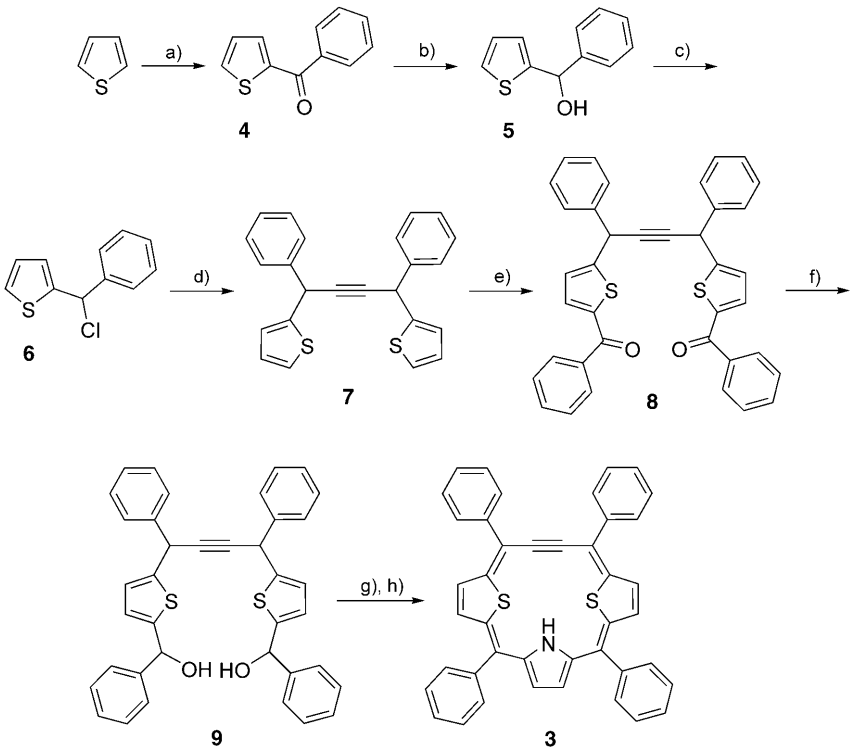
Two canonical structures of **3** define 18-π-electron macrocyclic delocalization pathways (Scheme 2). Accordingly, the

[*] A. Berlicka, Prof. Dr. L. Latos-Grażyński, Prof. Dr. T. Lis
Department of Chemistry
University of Wrocław
F. Joliot-Curie Street 14
50 383 Wrocław (Poland)
Fax: (+71) 32-823-48
E-mail: llg@wchuwr.chem.uni.wroc.pl

[**] Financial support from the Ministry of Scientific Research and Information Technology (Grant 3 T09A 162 28) is gratefully acknowledged.

Supporting information for this article is available on the WWW under http://www.angewandte.org or from the author.

InterScience
© 2005 Wiley-VCH Verlag GmbH & Co. KGaA, Weinheim



Scheme 1. Synthesis of dithiaethyneporphyrin **3**: a) PhCOCl, $AlCl_3$, CH_2Cl_2, RT→reflux, 6 h; b) $NaBH_4$, THF/MeOH (3:2 *V*/*V*); c) conc. HCl; d) BrMgC≡CMgBr, CuCl, THF, reflux, 2 h; e) PhCOCl, $AlCl_3$, CH_2Cl_2, room temperature, 14 h; f) $NaBH_4$, THF/MeOH (3:2 *V*/*V*); g) pyrrole, CH_3SO_3H, room temperature, 1 h; h) Et_3N, DDQ, room temperature, 1.5 h. DDQ = 2,3-dichloro-5,6-dicyano-1,4-benzoquinone.

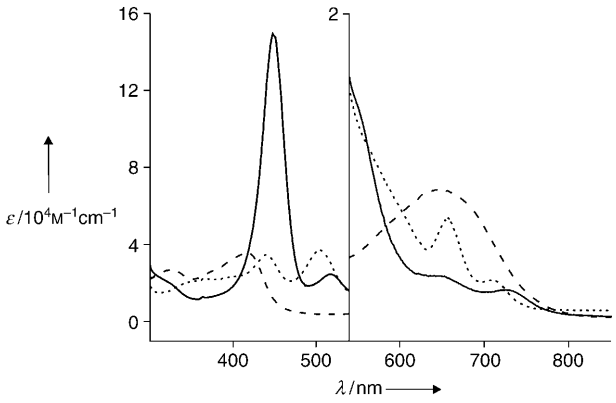
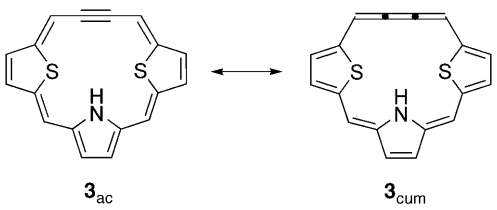


Figure 1. The electronic spectra of **3** (——, CH_2Cl_2), **10** (-----, $CHCl_3$), and **11** (– – –, CH_2Cl_2).



Scheme 2. Canonical structures of **3**.

electronic structure of **3** can be described as reflecting a combination of acetylene (=C–C≡C–C=) and cumulene (–C=C=C=C–) character of the C18-C1-C2-C3 fragment. The relevant chemical shift values of carbon atoms for acetylene or cumulene units attached adjacent to aryl or 2-thienyl moieties were considered for comparison. The sp-hybridized carbon atoms of intermediate **7** gave a ^{13}C NMR signal at $\delta = 84.4$ ppm, that is, in the $\delta = 70$–95 ppm range typical for acetylene. Similarly, the ^{13}C NMR chemical shifts of cumulene fragments vary over quite a wide range: $\delta = 140.5$ ppm for tetra(2-thienyl)butatriene,[11] $\delta = 152.0$ ppm for tetraphenylbutatriene,[12] and $\delta = 134.5$ ppm for 6,7,18,19-tetradehydrotetrathia[24]annulene(4.0.4.0) (some admixture of the acetylenic structure was suggested for the latter structure).[13] Thus the ^{13}C NMR chemical shifts of **3** point out that canonical structure $\mathbf{3}_{ac}$ and $\mathbf{3}_{cum}$ (ac = acetylene; cum = cumulene) contribute to the overall electronic structure, although the acetylene character of the C_{sp}–C_{sp} moiety prevails. The detected chemical shifts of **3** were fairly typical for acetylene–cumulene porphyrinoids[14,15] and acetylene–cumulene annulenes.[16]

The structure of **3** was determined by X-ray diffraction studies and is shown in Figure 3.[17] The S···S distance is short

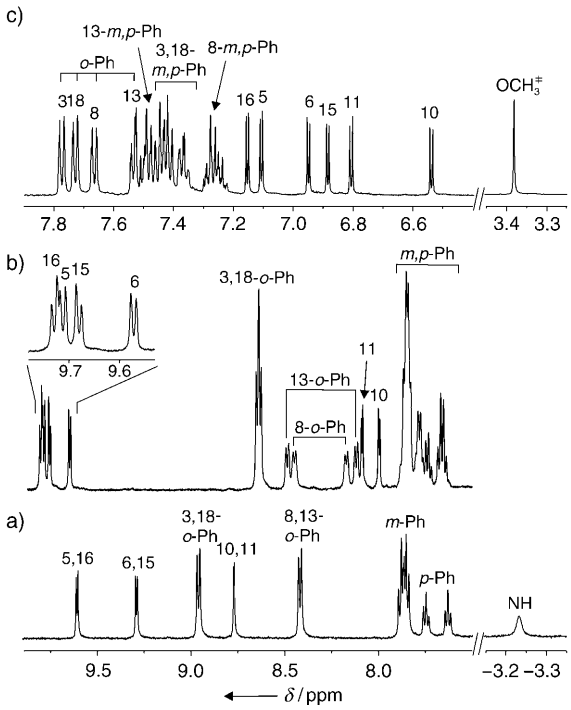


Figure 2. ^1H NMR spectra of a) **3** ($CDCl_3$, 298 K), b) **10** ($CDCl_3$, 240 K), and c) **11** (CD_2Cl_2, 298 K). Peak labels correspond to systematic position numbering or denote proton groups such as *o*,*m*,*p* positions of the *meso*-phenyl groups. Chemical shift values are relative to TMS (tetramethylsilane: $\delta = 0$ ppm). (≠): the intensity of the OCH_3 signal has been decreased by a factor of 5.

 © 2005 Wiley-VCH Verlag GmbH & Co. KGaA, Weinheim

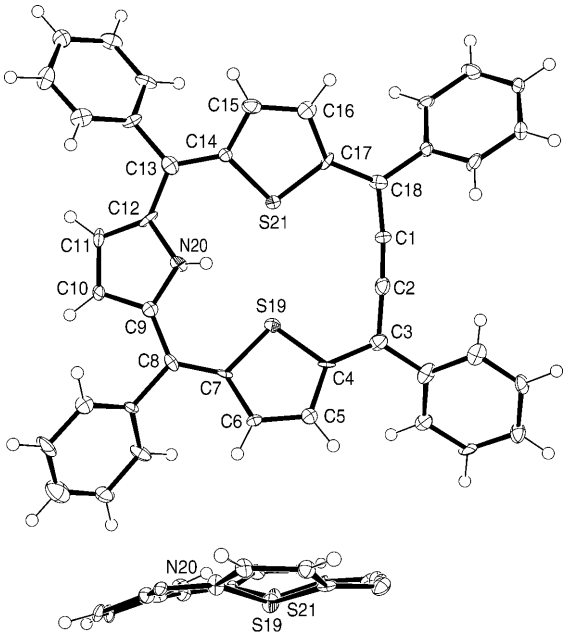
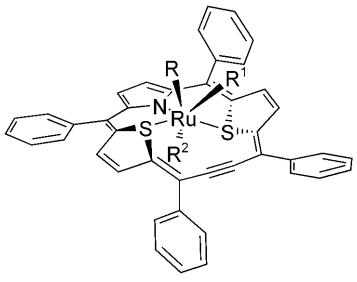


Figure 3. Crystal structure of dithiaethyneporphyrin **3**: a) top and b) side view (phenyl groups are omitted for clarity). The vibrational ellipsoids represent 50% probability. The bond lengths in the $C_{sp^2}C_{sp}C_{sp}C_{sp^2}$ (C18-C1-C2-C3) unit are 1.390(9) Å, 1.231(10) Å, and 1.418(10) Å, respectively. The dihedral angles between the plane defined by the four *meso* carbon atoms (C3, C8, C13, C18) and the planes of the five-membered rings are as follows: thiophene(S19) −19.0(2)°, pyrrole 17.6(3)°, thiophene(S21) −18.0(3)°.

(3.113(3) Å), and only a small number of compounds that contain such close sulfur–sulfur contacts have been reported.[13,18–20] The C_{sp^2}-C_{sp}-C_{sp}-C_{sp^2} butyne moiety reveals a slight distortion from linearity, showing a bowlike deformation directed outward of the macrocycle (C18-C1-C2: 174.0(9)°; C1-C2-C3: 176.6(9)°).

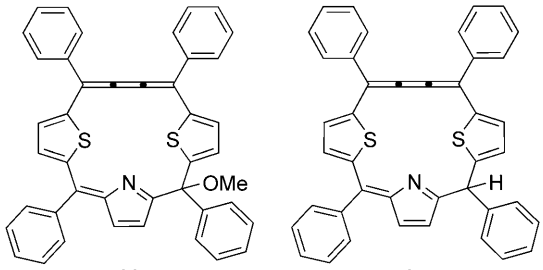
Treatment of **3** with $[Ru_3(CO)_{12}]$ in chlorobenzene resulted in formation of $[(S_2ETPP)Ru^{II}(CO)_2Cl]$ (**10**), as



10: R, R^1, R^2 equal Cl and two CO

confirmed by high-resolution mass spectrometry. The ^{1}H NMR spectrum of complex **10** revealed a lowering of symmetry relative to **3**. The geometry of **10** as inferred from the ^{1}H NMR spectroscopic pattern (Figure 2b) reflects the balance between constraints of the macrocyclic ligand and the coordination requirement of ruthenium(II) for octahedral geometry. Dithiaethyneporphyrin **3** has to distort to accommodate Ru^{II} binding. Consequently, the two thiophene rings are severely tilted in opposite directions with respect to the macrocyclic plane to allow the pyramidal side-on coordination of ruthenium(II), in a similar manner as detected for $[(S_2TPP)Ru^{II}Cl_2]$.[21] The puckering of dithiaethyneporphyrin and the difference in coordination above and below the porphyrin plane explains the observed lowering of symmetry of **10** relative to **3**. The 2-butyne fragment is not involved in coordination, as the ^{13}C chemical shifts of non-equivalent atoms C1 and C2 in **10** ($\delta = 111.1$ and 113.7 ppm) resemble those for **3**.

Dithiaethyneporphyrin **3** reacts regioselectively with methanol (or ethanol) in the presence of silver acetate to produce *iso*-8-methoxy-3,8,13,18-tetraphenyl-19,21-dithiaethyneporphyrin (**11**). Derivative **11** is related to a feasible



11 *iso*-**3**

non-aromatic isomer of **3**, that is, *iso*-dithiaethyneporphyrin, *iso*-**3**. The UV/Vis spectrum of **11** confirms a loss of aromaticity, as evident by the smaller extinction coefficients (Figure 1). The ^{1}H NMR resonances of **11** were detected in the region that is typical for the conjugated but non-aromatic system. The ^{13}C NMR shift of C8 ($\delta = 83.1$ ppm) is consistent with its tetrahedral geometry, whereas those of atoms C1 and C2 ($\delta = 143.8$ and 147.2 ppm) comply with a cumulenic structure. Treatment of **11** with gaseous HCl results in partial recovery of **3**.

In conclusion, dithiaethyneporphyrin—a new aromatic contracted porphyrinoid—has been synthesized and characterized and displays the unique features of an [18]dithiatriphyrin(4.1.1) frame.

Experimental Section

3: Pyrrole (0.11 mL, 1.58 mmol), **9** (0.9 g, 1.55 mmol), and freshly distilled CH_2Cl_2 (750 mL) were placed in a 1-L flask. Nitrogen was bubbled through the solution for 30 min, then CH_3SO_3H (0.2 mL, 3.1 mmol) was added, and the mixture was stirred in the dark for 1 h under N_2. Triethylamine (0.49 mL, 3.5 mmol) and DDQ (2.1 g, 9.3 mmol) were added and the solution was stirred for a further 1.5 h. The solvent was partly evaporated, and the reaction mixture was purified by chromatography on silica gel. The first orange-brown fraction (product **2**) was eluted with dichloromethane and repurified through a second chromatographic procedure on silica gel with hexane/benzene (1:1 *V*/*V*) as eluant. Product **2** was recrystallized from CH_2Cl_2/CH_3OH (120 mg, 12.7%); UV/Vis (CH_2Cl_2): λ_{max} (logε) = 448 (5.2), 518 (4.4), 553 (4.1), 646 (3.4), 725 nm (3.3); ^{1}H NMR (500 MHz, $CDCl_3$, 298 K, TMS): $\delta = 9.61$, 9.29 (AB, ^3J(H,H) = 4.4 Hz, 4H; H5,16, H6,15), 8.96 (d, ^3J(H,H) = 7.7 Hz, 4H; 3,18-*o*-Ph), 8.77 (d, ^4J(H,H) = 1.5 Hz, 2H; H10,11), 8.42 (d, ^3J(H,H) = 7.7 Hz, 4H; 8,13-*o*-

 © 2005 Wiley-VCH Verlag GmbH & Co. KGaA, Weinheim

Ph), 7.88 (t, ^3J(H,H) = 7.7 Hz, 4H; 3,18-*m*-Ph), 7.85 (t, ^3J(H,H) = 7.7 Hz, 4H; 8,13-*m*-Ph), 7.75 (t, ^3J(H,H) = 7.7 Hz, 2H; 8,13-*p*-Ph), 7.63 (t, ^3J(H,H) = 7.7 Hz, 2H; 3,18-*p*-Ph), −3.24 ppm (br s, 1H; NH); HR-MS (ESI): *m*/*z* calcd for $C_{42}H_{27}N^{32}S_2$ [M^+]: 609.1585; found: 609.1607; elemental analysis: calcd (%) for $C_{42}H_{27}NS_2$: C 82.27, H 4.65, N 2.50, S 10.45; found: C 82.72, H 4.46, N 2.30, S 10.52.

10: Compound **3** (20 mg, 0.033 mmol) and [$Ru_3(CO)_{12}$] (0.84 g, 1.32 mmol) in freshly distilled chlorobenzene (20 mL) were heated at reflux for 4 h under N_2. The solvent was evaporated to dryness and the residue was purified by chromatography on silica gel. After an initial orange-red fraction (recovered **3**) had been eluted with hexane/benzene (1:1 *V*/*V*), elution with benzene led to a second brown fraction, which was collected and identified as **10**. The second fraction was purified through a second column (silica gel with hexane/benzene (1:3 *V*/*V*) and recrystallized from $CHCl_3$/CH_3OH to yield the title product (9 mg, 34%). UV/Vis ($CHCl_3$): λ_{max} (logε) = 367 (4.3), 440 (4.5), 505 (4.6), 659 (3.8), 711 nm (3.4); ^{1}H NMR (500 MHz, $CDCl_3$, 240 K, TMS): δ = 9.83, 9.78 (AB, ^3J(H,H) = 5.2 Hz, 2H; H15, H16), 9.81, 9.67 (AB, ^3J(H,H) = 5.2 Hz, 2H; H5, H6), 8.65 (m, 4H; 3,18-*o*-Ph), 8.49 (d, ^3J(H,H) = 7.3 Hz, 1H; 13-*o*-Ph), 8.46 (d, ^3J(H,H) = 7.3 Hz, 1H; 8-*o*-Ph), 8.17 (d, ^3J(H,H) = 7.3 Hz, 1H; 8-*o*-Ph), 8.13 (d, ^3J(H,H) = 7.3 Hz, 1H; 13-*o*-Ph), 8.10, 8.00 (AB, ^3J(H,H) = 4.1 Hz, 2H; H10, H11), 7.85 (m, 7H; *m*-Ph), 7.78 (m, 2H; 8-*p*-Ph, 13-*m*-Ph), 7.74 (t, ^3J(H,H) = 7.3 Hz, 1H; 13-*p*-Ph), 7.66 ppm (m, 2H; 3,18-*p*-Ph); IR (KBr): $\tilde{\nu}$ = 2065, 2012 cm^{-1} (C≡O); HR-MS (ESI): *m*/*z* calcd for $^{12}C_{44}H_{26}NO_2{}^{32}S_2{}^{35}Cl^{102}Ru$ [M^+]: 801.0311; found: 801.0428; elemental analysis: calcd (%) for $C_{44}H_{26}NO_2S_2ClRu{\cdot}0.8\,CHCl_3{\cdot}1.4\,CH_3OH$: C 58.92, H 3.47, N 1.49; found: C 59.10, H 3.79, N 1.10.

11: UV/Vis (CH_2Cl_2): λ_{max} (logε) = 325 (4.4), 415 (4.6), 649 nm (3.9); ^{1}H NMR (500 MHz, CD_2Cl_2, 298 K, TMS): δ = 7.77 (d, ^3J(H,H) = 7.3 Hz, 2H; 3-*o*-Ph), 7.73 (d, ^3J(H,H) = 7.3 Hz, 2H; 18-*o*-Ph), 7.67 (d, ^3J(H,H) = 7.0 Hz, 2H; 8-*o*-Ph), 7.54 (d, ^3J(H,H) = 7.0 Hz, 2H; 13-*o*-Ph), 7.49 (m, 3H; 13-*m*,*p*-Ph), 7.45 (t, ^3J(H,H) = 7.3 Hz, 2H; 18-*m*-Ph), 7.42 (t, ^3J(H,H) = 7.3 Hz, 2H; 3-*m*-Ph), 7.37 (m, 2H; 3,18-*p*-Ph), 7.28 (m, 3H; 8-*m*,*p*-Ph), 7.16, 6.89 (AB, ^3J(H,H) = 4.0 Hz, 2H; H15, H16), 7.11, 6.95 (AB, ^3J(H,H) = 4.0 Hz, 2H; H5, H6), 6.81, 6.54 (AB, ^3J(H,H) = 4.4 Hz, 2H; H10, H11), 3.38 ppm (s, 3H; OCH_3); HR-MS (ESI): *m*/*z* calcd for $C_{43}H_{30}NO^{32}S_2$ [M−H]$^+$: 640.1769; found: 640.1793.

Received: May 12, 2005
Published online: July 25, 2005

Keywords: annulenes · aromaticity · heterocycles · NMR spectroscopy · porphyrinoids

[1] E. Pacholska, L. Latos-Grażyński, Z. Ciunik, *Chem. Eur. J.* **2002**, *8*, 5403.
[2] J. L. Sessler, S. J. Weghorn, *Expanded, Contracted, and Isomeric Porphyrins*, Elsevier Science, **1997**.
[3] J. L. Sessler, D. Seidel, *Angew. Chem.* **2003**, *115*, 5292; *Angew. Chem. Int. Ed.* **2003**, *42*, 5134.
[4] A system must be macrocyclic and contain pyrrole, furan, thiophene, or other heterocyclic subunits linked together by one or more spacer atoms in such a manner that the internal ring pathway contains minimum of 17 atoms. Once the number of atoms in the internal ring pathway is equal to or less than 15, the molecule can be classified as a contracted porphyrin.[3]
[5] A. Krivokapic, A. R. Cowley, H. L. Anderson, *J. Org. Chem.* **2003**, *68*, 1089.
[6] G. M. Badger, J. A. Elix, G. E. Lewis, *Proc. Chem. Soc.* **1964**, 82.
[7] G. M. Badger, J. A. Elix, G. E. Lewis, *Aust. J. Chem.* **1965**, *18*, 70.
[8] Z. Hu, J. L. Atwood, M. P. Cava, *J. Org. Chem.* **1994**, *59*, 8071.
[9] T. D. Lash, *Chem. Eur. J.* **1996**, *2*, 1197.
[10] A. Ulman, J. Manassen, *J. Am. Chem. Soc.* **1975**, *97*, 6540.
[11] T. Kawase, S. Muro, H. Kurata, M. Oda, *J. Chem. Soc. Chem. Commun.* **1992**, 778.
[12] J. P. C. M. van Dongen, M. J. A. de Bie, R. Steur, *Tetrahedron Lett.* **1973**, 1371.
[13] H. Kurata, H. Baba, M. Oda, *Chem. Lett.* **1997**, 571.
[14] N. Jux, P. Koch, H. Schmickler, J. Lex, E. Vogel, *Angew. Chem.* **1990**, *102*, 1429; *Angew. Chem. Int. Ed. Engl.* **1990**, *29*, 1385.
[15] D. O. Mártire, N. Jux, P. F. Aramendia, R. M. Negri, J. Lex, S. E. Braslavsky, K. Schaffner, E. Vogel, *J. Am. Chem. Soc.* **1992**, *114*, 9969.
[16] M. Nagawa, *Angew. Chem.* **1979**, *91*, 215; *Angew. Chem. Int. Ed. Engl.* **1979**, *18*, 202.
[17] X-ray crystal structure data for **3**·$CHCl_3$: crystals were prepared by slow diffusion of CH_3OH into a solution of **3** in $CHCl_3$ to yield dark brown crystals of $C_{42}H_{27}NS_2{\cdot}CHCl_3$, size 0.22 × 0.014 × 0.008 mm^3, monoclinic, space group $P2_1/n$, a = 14.726(6) Å, b = 8.536(3) Å, c = 27.761(9) Å, β = 105.02(3)°, V = 3370(2) Å^3, $\rho_{calcd.}$ = 1.437, Z = 4; Xcalibur PX κ-geometry diffractometer, $Cu_{K\alpha}$ radiation (λ = 1.5418 Å), T = 100 K, $2\theta_{max}$ = 153.88; total number of reflections collected: 23091; number of independent reflections: 6527, of which 6527 were included in the refinement of 419 parameters; an analytical numeric absorption correction was applied:[22] μ = 3.883 mm^{-1}, T_{min} = 0.661, T_{max} = 0.972. The structure was solved by using direct methods with SHELXS-97 and refined against $|F^2|$ using SHELXL-97 (G. M. Sheldrick, University of Göttingen, Germany, **1997**), final R_1/wR_2 indices (for $I > 2\sigma(I)$): 0.0691/0.1108; max/min residual electron density: +0.40/−0.42 e A^{-3}. The disordered molecule of chloroform is present. Hydrogen atoms except H20 (NH) were fixed in idealized positions using the riding model constraints. CCDC-265651 contains the supplementary crystallographic data for this paper. These data can be obtained free of charge from the Cambridge Crystallographic Data Centre via www.ccdc.cam.ac.uk/data_request/cif.
[18] L. Latos-Grażyński, J. Lisowski, L. Szterenberg, M. M. Olmstead, A. L. Balch, *J. Org. Chem.* **1991**, *56*, 4043.
[19] T. Kimura, K. Ishikawa, Y. Ueki, Y. Horie, N. Furukawa, *J. Org. Chem.* **1994**, *59*, 7117.
[20] T. Kawase, H. R. Darabi, R. Uchimiya, M. Oda, *Chem. Lett.* **1995**, 499.
[21] C.-H. Hung, C.-K. Ou, G.-H. Lee, S.-M. Peng, *Inorg. Chem.* **2001**, *40*, 6845.
[22] Xcalibur PX Software–CrysAlis CCD and CrysAlis RED version 1.171, Oxford Diffraction Ltd., Poland, Wrocław, Poland, **1995**–**2003**.

 © 2005 Wiley-VCH Verlag GmbH & Co. KGaA, Weinheim

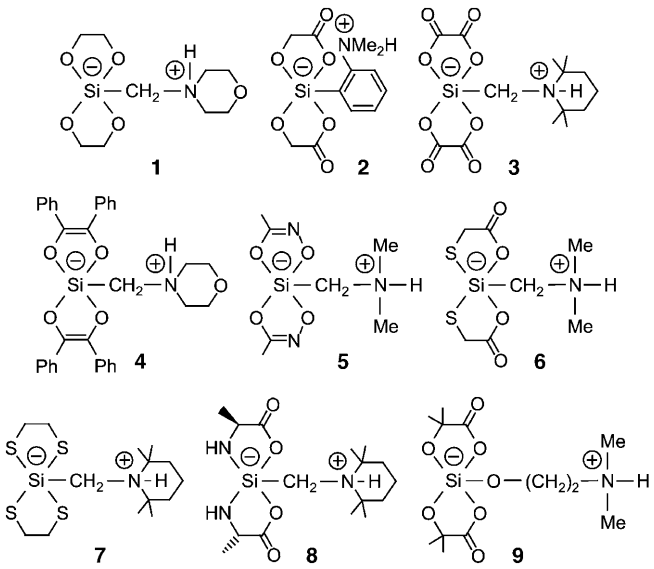
Higher-Coordinate Si Compounds

DOI: 10.1002/anie.200501164

A Zwitterionic Spirocyclic Pentacoordinate Silicon Compound Synthesized in Water by Si–O and Si–C Bond Cleavage**

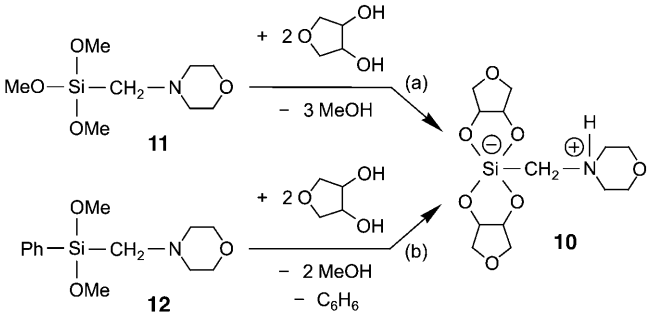
Reinhold Tacke, Rüdiger Bertermann, Christian Burschka, and Simona Dragota*

The chemistry of higher-coordinate silicon compounds is currently one of the main areas of research in silicon chemistry.[1] We have contributed to this field by systematic studies on zwitterionic λ^5*Si*-silicates that contain a pentacoordinate (formally negatively charged) silicon atom and a tetracoordinate (formally positively charged) nitrogen atom.[1d] The zwitterions **1**,[2] **2**,[3] **3**,[4] **4**,[5] **5**,[6] **6**,[7] **7**,[8] **8**,[9] and **9**[10] are examples of this type of compound. Generally,



these zwitterionic λ^5*Si*-silicates are quite sensitive to water and easily undergo hydrolytic Si–OC, Si–SC, and Si–NC bond cleavage. We have now succeeded in synthesizing a zwitterionic λ^5*Si*-silicate, namely, bis[*meso*-oxolane-3,4-diolato(2−)][(morpholinio)methyl]silicate (**10**), that shows remarkable stability in water.[11] Surprisingly, this pentacoordinate silicon compound could even be prepared in aqueous solution by Si–C bond cleavage. We report herein on the synthesis of **10** and its hydrate **10**·H_2O and their structural characterization in the solid state and in solution.

Compound **10** was synthesized according to Scheme 1, either through cleavage of three Si–O bonds (method a) or through cleavage of two Si–O bonds and one Si–C bond



Scheme 1. Syntheses of the zwitterionic λ^5*Si*-silicate **10**. For details see Experimental Section.

(method b), starting with trimethoxy[(morpholino)methyl]-silane (**11**)[12] (yield 87%) and dimethoxy[(morpholino)-methyl]phenylsilane (**12**)[12] (yield 53%), respectively. As the synthesis according to method b involves a relatively slow Si–C cleavage reaction as the rate-determining step,[13] product formation was significantly slower than with method a (see Experimental Section). The hydrate **10**·H_2O was synthesized analogously to **10** (Scheme 1, method a) by using water instead of acetonitrile as the solvent and was isolated, after crystallization from water, in 93% yield as a colorless crystalline solid.

The chiral λ^5*Si*-silicates crystallize in the space groups $P2_1/c$ (**10**) and *Cc* (**10**·H_2O), with one zwitterion (**10**) or with one zwitterion and one water molecule (**10**·H_2O) in the asymmetric unit.[14] As can be observed in Figure 1, the Si coordination polyhedra of **10** and **10**·H_2O in the crystal are strongly distorted trigonal bipyramids, in which each bidentate ligand spans one axial (O1, O3) and one equatorial site (O2, O4). The Si–O distances of the SiO_4C skeletons of **10** and **10**·H_2O range from 1.682(2) to 1.758(2) Å, and the axial Si–O bonds (1.7333(12)–1.758(2) Å) are significantly longer than the equatorial ones (1.682(2)–1.7114(11) Å). The Si–C distances are 1.913(3) (**10**) and 1.9168(14) Å (**10**·H_2O). Generally, the respective Si–O and Si–C bond lengths of **10** and **10**·H_2O are quite similar, whereas the distortions of the Si coordination polyhedra differ significantly (transition trigonal bipyramid→square pyramid: **10**, 26.8%; **10**·H_2O, 49.0%).[15]

Taking into account the different possible orientations of the two oxolane rings relative to the (morpholinio)methyl group, *syn*/*syn*, *anti*/*syn*, and *anti*/*anti* isomers must be considered for **10** (Figure 2). As can be seen in Figure 1, the *anti*/*syn* geometry is observed in the crystals of **10** and **10**·H_2O.

Hydrogen-bonding systems were observed in crystals of **10** and **10**·H_2O.[16] Compound **10** forms a trifurcate N–H···O1/O2/O3 hydrogen bond (intramolecular N–H···O1 and inter-

[*] Prof. Dr. R. Tacke, Dr. R. Bertermann, Dr. C. Burschka, Dipl.-Chem. S. Dragota
Institut für Anorganische Chemie
Universität Würzburg
Am Hubland
97074 Würzburg (Germany)
Fax: (+49) 931-888-4609
E-mail: r.tacke@mail.uni-wuerzburg.de

[**] This work was supported by the Fonds der Chemischen Industrie.

Supporting information for this article is available on the WWW under http://www.angewandte.org or from the author.

InterScience
© 2005 Wiley-VCH Verlag GmbH & Co. KGaA, Weinheim

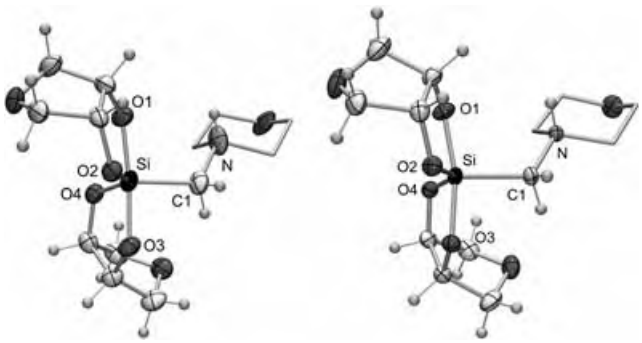


Figure 1. Molecular structure of **10** (Δ enantiomer, left) and the zwitterion of **10**·H_2O (Δ enantiomer, right) in the crystal (probability level of displacement ellipsoids 50%; morpholinio groups represented as stick model for clarity).[13] Selected bond lengths [Å] and angles [°] of **10** and **10**·H_2O (in parentheses): Si-O1 1.739(2) (1.7333(12)), Si-O2 1.702(2) (1.7114(11)), Si-O3 1.758(2) (1.7528(11)), Si-O4 1.682(2) (1.7007(11)), Si-C1 1.913(3) (1.9168(14)); O1-Si-O2 89.05(10) (89.01(5)), O1-Si-O3 172.98(10) (166.88(5)), O1-Si-O4 90.63(11) (87.96(5)), O1-Si-C1 95.17(13) (99.27(6)), O2-Si-O3 85.51(10) (84.85(5)), O2-Si-O4 130.78(10) (137.66(5)), O2-Si-C1 116.84(13) (111.59(6)), O3-Si-O4 89.57(10) (88.79(5)), O3-Si-C1 91.26(13) (93.78(6)), O4-Si-C1 112.20(12) (110.58(6)).

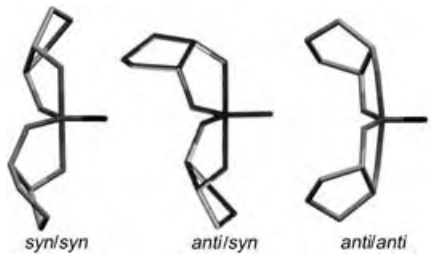


Figure 2. The three possible isomeric structures of the λ^5*Si*-silicate skeleton of **10** (*syn*/*syn*, *anti*/*syn*, *anti*/*anti*).

molecular N–H···O2/O3 interactions), and the zwitterion of **10**·H_2O forms a bifurcate intermolecular N–H···O2/O3 hydrogen bond, which lead to infinite one-dimensional chains along the [001] base vector in both crystal structures. In the case of **10**·H_2O, two additional intermolecular O–H···O hydrogen bonds between the water molecule (proton donor) and the zwitterion (proton acceptor) are observed.

Compounds **10** and **10**·H_2O were characterized by solution (^{1}H, ^{13}C, ^{29}Si) and solid-state (^{13}C, ^{15}N, ^{29}Si) NMR spectroscopy.[17] The solid-state NMR spectra were compatible with the crystal structures of the compounds. The isotropic ^{29}Si chemical shifts obtained in the solid-state NMR experiments (sharp resonance signals; full width at half height ca. 7.5–20 Hz) are very similar to those determined in aqueous solution (D_2O) and thus clearly demonstrate that the λ^5*Si*-silicate **10** exists in solution as well.

Upon dissolution of **10** and **10**·H_2O in D_2O, an equilibrium mixture of the *syn*/*syn*, *anti*/*syn*, and *anti*/*anti* isomers of the zwitterionic λ^5*Si*-silicate was observed. Whereas compounds **1–9** are hydrolytically sensitive, no tetracoordinate silicon species could be detected upon dissolution of **10** in water, that is, no hydrolytic decomposition occurred. This remarkable hydrolytic stability of **10** is emphasized by its direct synthesis in water in an NMR tube: upon addition of silane **11** to a solution of two molar equivalents of *meso*-oxolane-3,4-diol in D_2O, ^{1}H, ^{13}C, and ^{29}Si NMR measurements, performed 4 h after combining the reactants, afforded NMR spectra that were identical with those obtained upon dissolution of **10** and **10**·H_2O in water. A representative partial NMR spectrum resulting from a ^{29}Si,^{1}H HMQC experiment with a solution of **10** synthesized directly in an NMR tube is depicted in Figure 3.

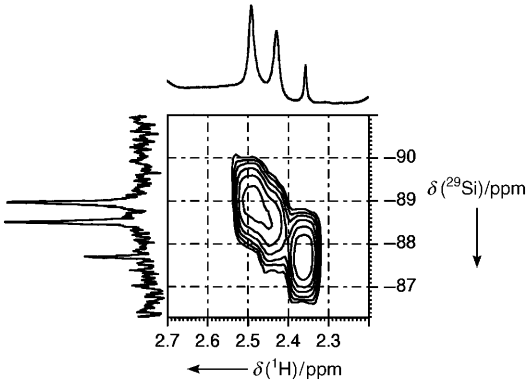


Figure 3. Partial spectrum obtained in a ^{29}Si,^{1}H HMQC experiment (23 °C, 300.1 MHz) with a 475 mM solution of **10** (pH 8.0 ± 0.1) synthesized directly in D_2O. The spectrum was measured 4 h after combining the reactants in an NMR tube. Top: ^{1}H NMR resonance signals of the $SiCH_2N$ protons of the three isomers of **10**. Left: ^{29}Si NMR signals of the three isomers of **10**.

To obtain more information on the stability of **10** in water, ^{1}H, ^{13}C, and ^{29}Si NMR experiments with a 475 mM solution in D_2O were carried out at various pH values. Upon dissolution of **10** in D_2O, a value of pH 8.0 was measured. This pH value was decreased stepwise by addition of small amounts of concentrated hydrochloric acid, and ^{1}H, ^{13}C, and ^{29}Si NMR experiments were performed at pH 7.4 and pH 7.0. As can be seen from Figure 4, the resulting partial ^{29}Si NMR spectra

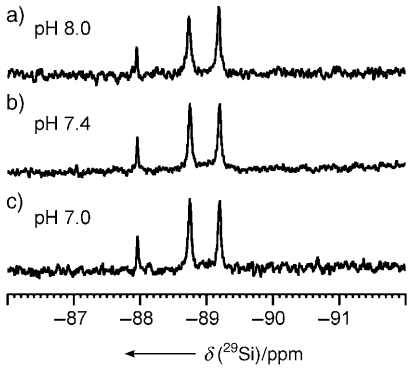
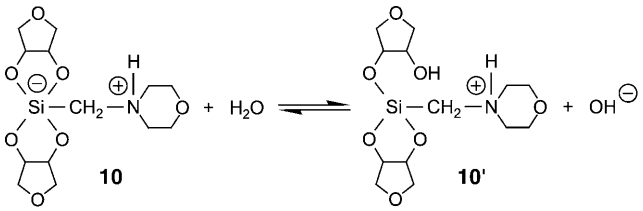


Figure 4. Partial spectra obtained in ^{29}Si NMR experiments (23 °C, 400.1 MHz) with 475 mM solutions of **10** (synthesized according to Scheme 1, method a) in D_2O at a) pH 8.0 ± 0.1, b) pH 7.4 ± 0.1, and c) pH 7.0 ± 0.1. The ^{29}Si NMR spectrum obtained for a 475 mM aqueous solution (D_2O) of **10** synthesized directly in the NMR tube was identical with spectrum a.

 © 2005 Wiley-VCH Verlag GmbH & Co. KGaA, Weinheim

indicate the existence of the three isomers of **10** in aqueous solution at all pH values studied (no tetracoordinate silicon species could be detected), and clearly demonstrate the stability of λ^5*Si*-silicate **10** in the range pH 7.0–8.0. The integrals extracted from the ^{1}H NMR spectra indicated that the ratio of the three isomers of **10** does not significantly depend on the pH value. Upon further acidification to pH 6, partial hydrolysis of **10** was observed (formation of tetracoordinate silicon species), and at pH 5, no ^{29}Si resonance signals for **10** could be detected at all (complete hydrolytic decomposition of **10**).

At first glance, the pH value of 8 measured for a 475 mM solution of **10** in water is quite surprising, because the ammonium moiety of the zwitterion should lead to an acidic milieu. The basic reaction of **10** in water might be explained by hydrolytic Si–OC cleavage to give the tetracoordinate silicon species **10′** and a hydroxide ion (Scheme 2); thus, one



Scheme 2. Equilibrium mixture of **10** and **10′** in aqueous solution.

could speculate on an equilibrium of the type **10**⇌**10′**. As can be observed from the measured pH value (8), this equilibrium should lie far to the left, and hence it should be very difficult (or even impossible) to detect the tetracoordinate silicon species **10′** by NMR spectroscopy.

Interestingly, aqueous solutions of **10** did not undergo gel formation at room temperature over a period of six months. Indeed, the hydrolytic stability of **10** in the pH range studied (pH 7.0–8.0) is quite remarkable, but cannot be satisfactorily explained so far. As the related λ^5*Si*-silicates **1**–**9** (including those with an SiO_4C skeleton) undergo spontaneous hydrolysis upon dissolution in water, special structural and/or electronic features of the *meso*-oxolane-3,4-diolato(2−) ligand must be considered to explain the hydrolytic stability of **10**. This particular ligand and related ligands derived from carbohydrates with *cis*-furanoidic diol moieties have already been reported to form anionic pentacoordinate silicon species in aqueous solution;[18,19] however, these anionic λ^5*Si*-silicates are only stable in strongly alkaline solution. Thus, it is likely that the zwitterionic nature of **10** (i.e., the presence of the (morpholinio)methyl group) also explains its hydrolytic stability. Future studies must elucidate whether this stability is a general feature of bis[*meso*-oxolane-3,4-diolato(2−)]-[(ammonio)organyl]silicates and if so, whether the chemistry of pentacoordinate silicon compounds in aqueous solution can be developed on the basis of this hydrolytic stability.

Experimental Section

10: Method a: **11**[12] (500 mg, 2.26 mmol) was added at 20 °C to a stirred solution of *meso*-oxolane-3,4-diol (471 mg, 4.52 mmol) in acetonitrile (10 mL), and the resulting mixture was transferred to a beaker (∅ 10 cm) and kept undisturbed at 20 °C for several hours (complete evaporation of the solvent). The solid residue was recrystallized from acetonitrile (40 mL) by cooling a boiling solution of **10** to 20 °C. After slow, complete evaporation of the solvent over a period of several hours, the solid product was washed with diethyl ether (3 × 20 mL) and recrystallized from dichloromethane/diethyl ether/*n*-pentane (1/1/1) at 20 °C (dissolution of **10** in dichloromethane (40 mL), subsequent addition of diethyl ether (40 mL) and *n*-pentane (40 mL), and slow evaporation of the solvent over 2 d). The resulting solid was washed with diethyl ether (3 × 20 mL) and dried in vacuo (0.01 Torr, 20 °C, 4 h) to give **10** in 87 % yield as a colorless crystalline solid (657 mg, 1.97 mmol); m.p. 180 °C; ^{13}C VACP/MAS NMR (ν_{rot} = 5 kHz; VACP: variable amplitude cross polarization): δ = 52.2 ($SiCH_2N$), 55.1 (NCH_2C), 59.8 (NCH_2C), 64.4 (2C, NCH_2CH_2O), 72.7 ($OCHC_2$), 73.2 ($OCHC_2$), 73.4 ($OCHC_2$), 74.0 ($OCHC_2$), 76.2 (2C, $CHCH_2O$), 76.5 ($CHCH_2O$), 77.3 ppm ($CHCH_2O$); ^{15}N VACP/MAS NMR (ν_{rot} = 5 kHz): δ = −327.7 ppm; ^{29}Si VACP/MAS NMR (ν_{rot} = 5.0 kHz): δ = −87.3 ppm; upon dissolution of **10** in D_2O (c = 475 mmol L^{-1}), the existence of three isomers was observed, with a molar equilibrium ratio **10a**:**10b**:**10c** of 0.65:0.24:0.11; NMR data for **10a**: ^{1}H NMR (D_2O, 400.1 MHz): δ = 1.81–2.06 (m, 2H, NCH_2C), 2.37 (s, 2H, $SiCH_2N$), 2.45–2.66 (m, 2H, NCH_2C), 3.40–3.48 (m, 4H, $CHCH_2O$), 3.45–3.64 (m, 4H, NCH_2CH_2O), 3.67–3.77 (m, 4H, $CHCH_2O$), 4.03–4.11 ppm (m, 4H, $OCHC_2$); ^{13}C NMR (D_2O, 100.6 MHz): δ = 45.8 (NCH_2C), 49.7 ($SiCH_2N$), 55.4 (NCH_2C), 65.8 (2C, NCH_2CH_2O), 70.8 (4C, $OCHC_2$), 71.3 ppm (4C, $CHCH_2O$); ^{29}Si NMR (D_2O, 79.5 MHz): δ = −89.2 ppm; NMR data for **10b**: ^{1}H NMR (D_2O, 400.1 MHz): δ = 2.30 ($SiCH_2N$), 2.80–2.95 (m, 2H, NCH_2C), 3.22–3.35 (m, 2H, NCH_2C), 3.22–3.35 (m, 4H, $CHCH_2O$), 3.45–3.66 (m, 4H, $CHCH_2O$), 3.45–3.66 and 3.78–3.90 (m, 4H, NCH_2CH_2O), 4.2 ppm (brs, 4H, $OCHC_2$); ^{13}C NMR (D_2O, 100.6 MHz): δ = 49.4 ($SiCH_2N$), 55.5 (2C, NCH_2C), 64.1 (NCH_2CH_2O), 64.3 (NCH_2CH_2O), 72.5 (4C, $OCHC_2$), 75.6 ppm (4C, $CHCH_2O$); ^{29}Si NMR (D_2O, 79.5 MHz): δ = −88.7 ppm; NMR data for **10c**: ^{1}H NMR (D_2O, 400.1 MHz): δ = 2.23 ($SiCH_2N$), 2.36–2.42 (m, 4H, NCH_2C), 3.22–3.35 (m, 4H, $CHCH_2O$), 3.45–3.66 (m, 4H, $CHCH_2O$), 3.45–3.66 and 3.78–3.90 (m, 4H, NCH_2CH_2O), 4.10–4.15 ppm (m, 4H, $OCHC_2$); ^{13}C NMR (D_2O, 100.6 MHz): δ = 48.9 ($SiCH_2N$), 53.8 (2C, NCH_2C), 63.8 (2C, NCH_2CH_2O), 72.4 (4C, $OCHC_2$), 75.1 ppm (4C, $CHCH_2O$); ^{29}Si NMR (D_2O, 79.5 MHz): δ = −87.9 ppm; elemental analysis (%) calcd for $C_{13}H_{23}NO_7Si$ (M_r = 333.41): C 46.83, H 6.95, N 4.20; found: C 46.6, H 6.8, N 4.2.

10: Method b: The synthesis was performed in a beaker (∅ 10 cm). Compound **12**[12] (500 mg, 1.87 mmol) was added at 20 °C to a stirred solution of *meso*-oxolane-3,4-diol (389 mg, 3.74 mmol) in water (6 mL), and an oily precipitate formed. The resulting mixture was kept undisturbed at 20 °C for 4 d (partial evaporation of water (ca. 3 mL)). The resulting oily residue was purified by crystallization from acetonitrile and then recrystallized from dichloromethane/diethyl ether/*n*-pentane as described for method a to give **10** in 53 % yield as a colorless crystalline solid (330 mg, 990 μmol); m.p. 180 °C; the NMR data of the product were identical with those obtained for the product prepared according to method a; elemental analysis (%) calcd for $C_{13}H_{23}NO_7Si$ (M_r = 333.41): C 46.83, H 6.95, N 4.20; found: C 46.4, H 6.8, N 4.1.

10·H_2O: The synthesis was performed in a beaker (∅ 10 cm). Compound **11**[12] (1.00 g, 4.52 mmol) was added at 20 °C to a stirred solution of *meso*-oxolane-3,4-diol (941 mg, 9.04 mmol) in water (2 mL), and the resulting mixture was stirred for 10 min (exothermic reaction) and then kept undisturbed at 20 °C for 2 d. The resulting precipitate was washed with water (3 × 0.3 mL) and dried in vacuo (0.01 Torr, 20 °C, 5 h) to give **10**·H_2O in 93 % yield as a colorless crystalline solid (1.48 g, 4.21 mmol); m.p. 179 °C; ^{13}C VACP/MAS NMR (ν_{rot} = 6 kHz): δ = 52.1 ($SiCH_2N$), 55.1 (NCH_2C), 59.8 (NCH_2C), 64.3 (2C, NCH_2CH_2O), 72.6 ($OCHC_2$), 73.2 ($OCHC_2$), 73.4 ($OCHC_2$), 74.0 ($OCHC_2$), 76.1 ($CHCH_2O$), 76.2 ($CHCH_2O$), 76.5

 © 2005 Wiley-VCH Verlag GmbH & Co. KGaA, Weinheim

($CHCH_2O$), 77.3 ppm ($CHCH_2O$); ^{15}N VACP/MAS NMR (ν_{rot} = 5 kHz): $\delta = -328.1$ ppm; ^{29}Si VACP/MAS NMR ($\nu_{rot} = 5.0$ kHz): $\delta = -87.5$ ppm; the solution NMR data of the product were identical with those obtained for compound **10**; elemental analysis (%) calcd for $C_{13}H_{25}NO_8Si$ ($M_r = 351.43$): C 44.43, H 7.17, N 3.99; found: C 44.3, H 6.8, N 3.9.

Received: April 1, 2005
Revised: May 27, 2005
Published online: July 26, 2005

Keywords: higher-coordinate compounds · silicates · silicon · zwitterions

[1] Selected reviews dealing with higher-coordinate silicon compounds: a) D. Kost, I. Kalikhman in *The Chemistry of Organic Silicon Compounds*, *Vol. 2*, *Part 2* (Eds.: Z. Rappoport, Y. Apeloig), Wiley, Chichester, UK, **1998**, pp. 1339–1445; b) V. Pestunovich, S. Kirpichenko, M. Voronkov in *The Chemistry of Organic Silicon Compounds*, *Vol. 2*, *Part 2* (Eds.: Z. Rappoport, Y. Apeloig), Wiley, Chichester, UK, **1998**, pp. 1447–1537; c) C. Chuit, R. J. P. Corriu, C. Reye in *Chemistry of Hypervalent Compounds* (Ed.: K. Akiba), Wiley, New York, **1999**, pp. 81–146; d) R. Tacke, M. Pülm, B. Wagner, *Adv. Organomet. Chem.* **1999**, *44*, 221–273; e) M. A. Brook, *Silicon in Organic*, *Organometallic*, *and Polymer Chemistry*, Wiley, New York, **2000**, pp. 97–114; f) R. Tacke, O. Seiler in *Silicon Chemistry: From the Atom to Extended Systems* (Eds.: P. Jutzi, U. Schubert), Wiley-VCH, Weinheim, **2003**, pp. 324–337; g) D. Kost, I. Kalikhman, *Adv. Organomet. Chem.* **2004**, *50*, 1–106.

[2] R. Bertermann, A. Biller, M. Kaupp, M. Penka, O. Seiler, R. Tacke, *Organometallics* **2003**, *22*, 4104–4110.

[3] R. Tacke, A. Lopez-Mras, P. G. Jones, *Organometallics* **1994**, *13*, 1617–1623.

[4] R. Tacke, M. Pülm, I. Richter, B. Wagner, R. Willeke, *Z. Anorg. Allg. Chem.* **1999**, *625*, 2169–2177.

[5] S. Dragota, R. Bertermann, C. Burschka, J. Heermann, M. Penka, I. Richter, B. Wagner, R. Tacke, *Silicon Chem.* **2002**, *1*, 291–297.

[6] R. Tacke, R. Bertermann, A. Biller, O. Dannappel, M. Penka, M. Pülm, R. Willeke, *Z. Anorg. Allg. Chem.* **2000**, *626*, 1159–1173.

[7] R. Willeke, R. Tacke, *Z. Anorg. Allg. Chem.* **2001**, *627*, 1537–1541.

[8] R. Tacke, M. Mallak, R. Willeke, *Angew. Chem.* **2001**, *113*, 2401–2403; *Angew. Chem. Int. Ed.* **2001**, *40*, 2339–2341.

[9] R. Tacke, R. Bertermann, C. Burschka, S. Dragota, M. Penka, I. Richter, *J. Am. Chem. Soc.* **2004**, *126*, 14493–14505.

[10] R. Tacke, B. Pfrommer, M. Pülm, R. Bertermann, *Eur. J. Inorg. Chem.* **1999**, 807–816.

[11] We use herein the terms "stability against hydrolysis" and "hydrolytic stability" to describe the overall stability in aqueous solution (no decomposition).

[12] J. Sperlich, J. Becht, M. Mühleisen, S. A. Wagner, G. Mattern, R. Tacke, *Z. Naturforsch. B* **1993**, *48*, 1693–1706.

[13] Si–C cleavage reactions leading to zwitterionic λ^5*Si*-silicates with SiO_4C skeletons: I. Richter, M. Penka, R. Tacke, *Organometallics* **2002**, *21*, 3050–3053, and references therein.

[14] Crystal structure analyses of **10** and **10**·H_2O: Suitable single crystals were mounted in inert oil (perfluoroalkyl ether, ABCR) on a glass fiber and then transferred to the cold nitrogen gas stream of the diffractometer (Stoe IPDS; graphite-monochromated $Mo_{K\alpha}$ radiation, $\lambda = 0.71073$ Å). The structures were solved by direct methods (SHELXS-97) and refined by full-matrix least-squares methods on F^2 for all unique reflections (SHELXS-97). For the CH hydrogen atoms, a riding model was employed, whereas the positions of the NH and OH hydrogen atoms were localized in difference Fourier syntheses and refined freely. CCDC-267545 (**10**) and CCDC-267546 (**10**·H_2O) contain the supplementary crystallographic data for this paper. These data can be obtained free of charge from the Cambridge Crystallographic Data Centre via www.ccdc.cam.ac.uk/data_request/cif. Selected data for **10**: single crystal of dimensions $0.4 \times 0.2 \times 0.1$ mm^3 obtained by crystallization from dichloromethane/diethyl ether/*n*-pentane (1/1/1; addition of diethyl ether and *n*-pentane to a solution of **10** in dichloromethane at 20 °C), $C_{13}H_{23}NO_7Si$, $M_r = 333.41$, analysis at 173(2) K, monoclinic, space group $P2_1/c$ (no. 14), $a = 9.941(2)$, $b = 17.028(3)$, $c = 10.100(2)$ Å, $\beta = 118.66(3)°$, $V = 1500.3(5)$ Å^3, $Z = 4$, $\rho_{calcd} = 1.476$ g cm^{-3}, $\mu = 0.192$ mm^{-1}, $F(000) = 712$, $2\theta_{max} = 49.48°$, 13821 collected reflections, 2538 unique reflections ($R_{int} = 0.0691$), 176 restraints, 248 parameters, $S = 1.198$, $R1$ ($I > 2\sigma(I)$) = 0.0521, $wR2$ (all data) = 0.1232, max./min. residual electron density +0.214/−0.250 e Å^{-3}. Selected data for **10**·H_2O: single crystal of dimensions $0.4 \times 0.4 \times 0.2$ mm^3 obtained by crystallization from water (slow evaporation of the solvent at 20 °C over a period of two months; before starting the evaporation, a pH value of 7 was adjusted by adding concentrated hydrochloric acid), $C_{13}H_{25}NO_8Si$, $M_r = 351.43$, analysis at 173(2) K, monoclinic, space group Cc (no. 9), $a = 9.9705(8)$, $b = 16.9981(12)$, $c = 10.4368(8)$ Å, $\beta = 117.356(8)°$, $V = 1571.0(2)$ Å^3, $Z = 4$, $\rho_{calcd} = 1.486$ g cm^{-3}, $\mu = 0.192$ mm^{-1}, $F(000) = 752$, $2\theta_{max} = 53.74°$, 9054 collected reflections, 3339 unique reflections ($R_{int} = 0.0313$), 3 restraints, 217 parameters, $S = 1.053$, $R1$ ($I > 2\sigma(I)$) = 0.0264, $wR2$ (all data) = 0.0692, absolute structure parameter 0.05(8), max./min. residual electron density +0.224/−0.207 e Å^{-3}.

[15] a) E. L. Muetterties, L. J. Guggenberger, *J. Am. Chem. Soc.* **1974**, *96*, 1748–1756; b) R. R. Holmes, J. A. Deiters, *J. Am. Chem. Soc.* **1977**, *99*, 3318–3326; c) the degree of distortion was calculated by using the dihedral angle method described in references [15a] and [15b]. All nine dihedral angles and the values for the reference geometry of the ideal square pyramid given in reference [15a] were considered for this calculation.

[16] The hydrogen-bonding systems were analyzed by using the program system PLATON: A. L. Spek, PLATON, University of Utrecht, Utrecht, The Netherlands, **1998**.

[17] NMR studies on **10** and **10**·H_2O: ^1H, ^{13}C, and ^{29}Si solution NMR spectra were recorded at 23 °C on a Bruker DRX-300 (^1H, 300.1 MHz; ^{13}C, 75.5 MHz; ^{29}Si, 59.6 MHz) or Bruker AVANCE-400 NMR spectrometer (^1H, 400.1 MHz; ^{13}C, 100.6 MHz; ^{29}Si, 79.5 MHz). D_2O was used as the solvent. Chemical shifts [ppm] were determined relative to internal HDO (^1H, $\delta = 4.70$ ppm) or external TMS (^{13}C, ^{29}Si; $\delta = 0$ ppm). Analysis and assignment of the ^1H NMR data was supported by ^1H,^1H COSY and ^{13}C,^1H, and ^{29}Si,^1H correlation experiments. Assignment of the ^{13}C NMR data was supported by DEPT 135 experiments. Solid-state ^{13}C, ^{15}N, and ^{29}Si VACP/MAS NMR spectra were recorded at 22 °C on a Bruker DSX-400 NMR spectrometer with bottom-layer rotors of ZrO_2 (∅ 7 mm) containing ca. 300 mg of sample (^{13}C, 100.6 MHz; ^{15}N, 40.6 MHz; ^{29}Si, 79.5 MHz); external standard TMS (^{13}C, ^{29}Si; $\delta = 0$ ppm) or glycine (^{15}N, $\delta = -342.0$ ppm); spinning rate 5–6 kHz; contact time 1 ms (^{13}C), 3 ms (^{15}N), or 5 ms (^{29}Si); 90° ^1H transmitter pulse length 3.6 μs; repetition time 4 s.

[18] Syntheses and X-ray diffraction studies: a) K. Benner, P. Klüfers, J. Schuhmacher, *Z. Anorg. Allg. Chem.* **1999**, *625*, 541–543; b) P. Klüfers, F. Kopp, M. Vogt, *Chem. Eur. J.* **2004**, *10*, 4538–4545.

[19] NMR studies: a) S. D. Kinrade, E. W. Deguns, A.-M. E. Gilson, C. T. G. Knight, *Dalton Trans.* **2003**, 3713–3716; b) S. D. Kinrade, R. J. Balec, A. S. Schach, J. Wang, C. T. G. Knight, *Dalton Trans.* **2004**, 3241–3243.

 © 2005 Wiley-VCH Verlag GmbH & Co. KGaA, Weinheim

Molecular Devices

DOI: 10.1002/anie.200501215

A Half Adder Based on a Photochemically Driven [2]Rotaxane**

*Da-Hui Qu, Qiao-Chun Wang, and He Tian**

Logic functions at the molecular scale are possible through a variety of approaches[1] that exploit the abilities of molecules to process information. The fundamental principles of logic operation have been demonstrated through detectable spectroscopic changes upon an ionic, electronic, or photonic input[1–6] and have led to the interpretation of complex molecular logic gates such as AND[2] and XOR functions.[3] Of course, mathematical calculations require the operation of several gates together. A half adder,[7] the combination of an AND gate and an XOR gate, could carry out elementary addition by using the XOR gate to generate the sum digit and the AND gate to generate the carry digit. Molecule-based logic gates with optical inputs and outputs would not require access for chemicals or wires and could operate on a fast timescale.[7d,f] Importantly, a single molecular platform that integrates multiple recognition sites for each input is expected to respond in parallel to a variety of reagents and thus provide logic functions at the molecular level.

Supramolecular systems[8–13] have attracted a great deal of attention in recent years because of their challenging construction as well as their potential application in molecular devices. Many supramolecular systems that function as simple logic gates have been reported.[1e,3,5] However, to the best of our knowledge, there has been no previous report of half adders based on a rotaxane system that uses light as an input. A rotaxane is a stable supramolecular system in which a linear subunit threads a macrocycle (wheel or bead) and is stoppered with two bulky end groups (dumbbell). Such a conformation is also similar to an abacus, the manual arithmetic calculator still used by some Chinese even today. Herein, we describe a new theoretical supramolecular half adder based on a [2]rotaxane, with optical inputs and outputs that can perform arithmetical functions directly by means of the position of the bead (wheel) on the axle. This abacus-type system can operate half-adder logic functions independently of any other reagents or chemical stimuli and may be the first step toward the construction of a supramolecular abacus for direct and complicated arithmetic.

[2]Rotaxane **1** comprises an α-cyclodextrin (α-CD) macrocycle locked onto a dumbbell that has two different photoswitchable binding sites, namely an azobenzene site and a stilbene site,[9,10a,13] and is end-trapped mechanically by two fluorescent naphthalimide moieties, 4-amino-1,8-naphthalimide-3,6-disulfonic disodium salt (stopper A) and 1,8-naphthalimide-5-sulfonic sodium salt (stopper B; Figure 1). The photoactive units can be switched independently by using light at different wavelengths (UV/Vis).[10c,14] The photochemical switching, which could mimic the function of a half adder that performs simple arithmetic addition, can be monitored by changes in the absorption of the supramolecular system and changes in the fluorescence of the end groups.

Molecular shuttle **1** is indeed a multistate [2]rotaxane that can be converted between a dynamic state and three static states in response to light and features dual fluorescence outputs. At room temperature in [D_6]DMSO, the state (*E*,*E*)-**1** as shown in Figure 1 is a dynamic state in which the α-CD bead moves back and forth between the azobenzene and stilbene units at a rate that cannot be followed on the NMR timescale. Rational nuclear Overhauser effects (NOEs)[14] can be observed between the resonances of the protons of the azobenzene and stilbene moities and protons H3 and H5 located inside the cyclodextrin annuli. This set of NOEs is not consistent with any single static geometry and shows that the cyclodextrin rapidly glides along the dumbbell. State (*E*,*E*)-**1** was converted into ($Z_{N=N}$,$E_{C=C}$)-**1** or ($E_{N=N}$,$Z_{C=C}$)-**1** by photoisomerization upon irradiation with at 380 nm or 313 nm, respectively. Finally, further irradiation of the $Z_{N=N}$,$E_{C=C}$ isomer at 313 nm or the $E_{N=N}$,$Z_{C=C}$ isomer at 380 nm can generate (*Z*,*Z*)-**1** (Figure 1).[15] Moreover, as shown in Figure 1, each photochemical reaction is fully reversible. The three *Z* isomers could be shifted back to the (*E*,*E*)-**1** isomer by irradiation with UV light of another wavelength, as shown in Figure 1, or by placing the sample in the dark for several hours. The initial *E*,*E* isomer could also be recovered upon heating solutions of each of the three *Z* isomers to 60 °C for 1 h and then cooling to room temperature. The various $E \rightarrow Z$ photoisomerization reactions of the [2]rotaxane **1** were also investigated by monitoring the changes in the ^{1}H NMR spectra and the two-dimensional ROESY spectra in [D_6]DMSO upon UV/Vis irradiation. Very different NOE patterns were observed for the three "Z" isomers,[14] consistent with the geometries of the three photostationary (PSS) states—$Z_{N=N}$,$E_{C=C}$ (PSS-ZE), $E_{N=N}$,$Z_{C=C}$ (PSS-EZ), and *Z*,*Z* (PSS-ZZ)—as shown in Figure 1. The NMR data[14] also support the idea that [2]rotaxane **1** can be photochemically converted between the dynamic-state *E*,*E* isomer (namely DS-EE)[16] and the three static states mentioned above.

The changes in absorption during the $E \rightarrow Z$ photoisomerism of [2]rotaxane **1** in solution were also investigated.[14] Compared with the absorption spectrum of the *E*,*E* isomer, those of the other three isomers were similar but showed an increased absorption at around 270 nm and a decrease in absorption at 350 nm with an isobestic point at 301 nm ($A_{301} = 0.165$). To indicate the magnitude of the change in absorption upon isomerization, the ratio of the difference in the

[*] D.-H. Qu, Dr. Q.-C. Wang, Prof. Dr. H. Tian
Laboratory for Advanced Materials and Institute of Fine Chemicals
East China University of Science & Technology
Shanghai 200237 (P.R. China)
Fax: (+86) 21-6425-2288
E-mail: tianhe@ecust.edu.cn

[**] H.T. acknowledges the support of the NSFC/China (20273020, 90401026) and the Education Committee of Shanghai. We thank Prof. A. Prasanna de Silva (Queen's University) for his valuable comments and suggestions. A half adder is a logic circuit that performs one-digit addition.

Supporting information for this article is available on the WWW under http://www.angewandte.org or from the author.

 InterScience © 2005 Wiley-VCH Verlag GmbH & Co. KGaA, Weinheim

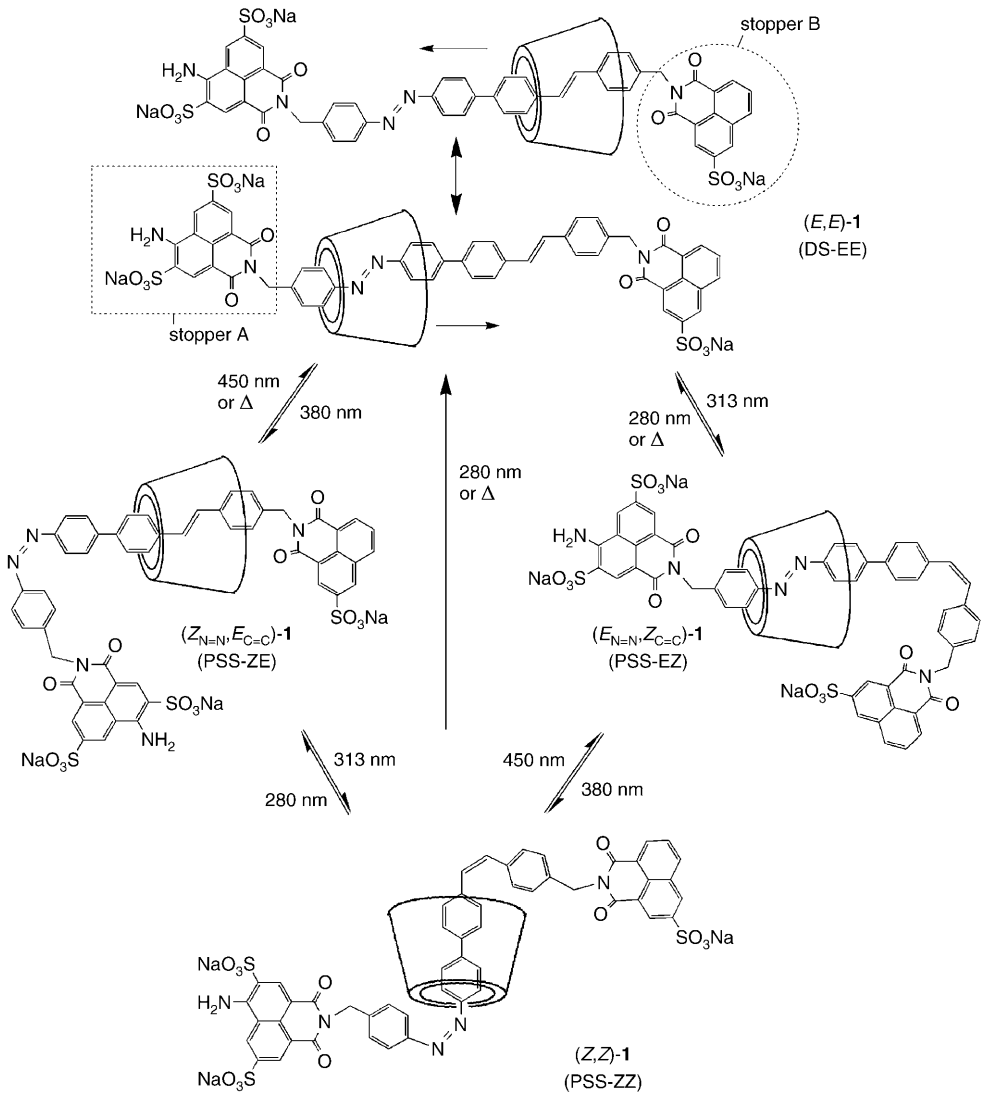


Figure 1. The intrinsic interconversion network of the α-cyclodextrin/azobenzene–stilbene [2]rotaxane **1** between the four states: one *E*,*E* isomer ((*E*,*E*)-**1**), two *E*,*Z* isomers (($Z_{N=N}$,$E_{C=C}$)-**1**), ($E_{N=N}$,$Z_{C=C}$)-**1**), and one *Z*,*Z* isomer ((*Z*,*Z*)-**1**). DS = dynamic state; PSS = photostationary state.

absorbances at 270 nm and 350 nm over the absorbance at 301 nm ($\Delta A = |A_{270} - A_{350}|/A_{301}$) was measured. For the *E* isomer, $\Delta A = 0.15$, whereas the values of ΔA calculated for the photostationary states (PSS-ZE, -EZ, and -ZZ) were 0.32 (PSS-ZE), 0.27 (PSS-EZ), and 0.73 (PSS-ZZ).[14]

A clear change was observed in the fluorescence spectra for [2]rotaxane **1** (see Supporting Information).[14] Relative to isomer (*E*,*E*)-**1**, the fluorescence intensity at $\lambda_{em} = 395$ nm (stopper B) increased by about 55% upon attaining the PSS-ZE state, while the fluorescence intensity at $\lambda_{em} = 520$ nm (stopper A) decreased by 14%. On the other hand, at the PSS-EZ state the fluorescence intensity at $\lambda_{em} = 520$ nm increased by about 52%, while a decrease of 15% in fluorescence intensity was observed at $\lambda_{em} = 395$ nm. For the PSS-ZZ state, the fluorescence intensities at both $\lambda_{em} = 395$ and 520 nm were similar to that of the *E* isomer but lower by 10%. The changes in the fluorescence spectra result from the rigidity of the α-CD ring. When the α-CD macrocycle is located near a fluorescent stopper, the vibrations and rotations of the methylene bonds between the stopper and the recognition site are hindered which leads to an increase in the fluorescence intensity of the stopper.[10] This was also confirmed by the weaker fluorescence observed for the lone dumbbell **2**, for which vibrations and rotations are relatively facile in the absence of the macrocycle.[14] Because of the total reversibility of the photoisomerization processes, the photoinduced shuttling motions of the α-CD ring on the dumbbell could be repeated and monitored by means of the reversible fluorescent output signals. By alternating irradiations at 380, 313, 450, and 280 nm, we verified that the photochemical processes are highly reproducible over more than 10 cycles.[14]

The above interconversions among the four states (*E*,*E*)-**1**, ($Z_{N=N}$,$E_{C=C}$)-**1**, ($E_{N=N}$, $Z_{C=C}$)-**1**, and (*Z*,*Z*)-**1** can be described with binary logic. The input (I) signals are UV light at wavelengths of 380 nm (I1) and 313 nm (I2). The difference in the absorption, ΔA, can be considered as one of the output signals, O1; O1 = 0 when ΔA is low (< 0.7), whereas O1 = 1 when ΔA is high (> 0.7). As mentioned above, only at the PSS-ZZ state does the photoisomerization about both azobenzene and stilbene occur. In this case, ΔA is high (> 0.7), but only upon simultaneous irradiation of both units at 380 nm and 313 nm (I1 = 1 and I2 = 1) is the output signal O1 = 1—otherwise, O1 = 0. Consequently, the difference in the change in absorption, ΔA, upon the external inputs of UV light at $\lambda = 380$ nm (I1) and 313 nm (I2) could be interpreted as an AND gate.

The change in the fluorescence intensity ΔF—defined as the difference in fluorescence intensity between two states at $\lambda_{em} = 520$ nm or at $\lambda_{em} = 395$ nm—of the rotaxane was selected as another output signal, O2. When the value of ΔF is low (< 50%), O2 = 0, whereas when the value of ΔF is high (> 50%), O2 = 1. Separate irradiation of the *E*,*E* isomer at either 380 nm (I1) or at 313 nm (I2) leads to the formation of either ($Z_{N=N}$,$E_{C=C}$)-**1** (PSS-ZE; $\Delta F = 55\%$ at $\lambda_{em} = 520$ nm)

 © 2005 Wiley-VCH Verlag GmbH & Co. KGaA, Weinheim

or ($E_{N=N}$,$Z_{C=C}$)-**1** (PSS-EZ, $\Delta F = 52\%$ at $\lambda_{em} = 395$ nm), respectively, and the ΔF output signal (O2) is high in both cases, that is, O2 = 1. Interestingly, under simultaneous irradiation at 380 nm (I1) and 313 nm (I2), (*Z*,*Z*)-**1** (PSS-ZZ) was formed and the resultant changes in the fluorescence intensity at $\lambda_{em} = 395$ and 520 nm were both small ($\approx 10\%$, therefore, O2 = 0). The changes in fluorescence (ΔF) in response to irradiation at 380 nm (I1) and 313 nm (I2) could be interpreted as an XOR gate.

The intrinsic network of the transformations of [2]rotaxane **1** between its four states leads to changes in absorption and fluorescence intensities of the two end groups, and these spectral changes can be interpreted as AND and XOR gates, respectively. The AND and XOR gates may function in parallel, as each photoswitchable unit (azobenzene or stilbene) in [2]rotaxane **1** can be switched with the inputs I1 and I2 independently.[14] Therefore, the spectral variations that result from the interconversion of the four states (DS-EE, PSS-ZE, PSS-EZ, PSS-ZZ) as shown in Figure 1 could be used to mimic the function of a half adder (Figure 2). Figure 2a shows a schematic diagram of the molecule-based half adder. In binary addition, the XOR gate output is the sum digit and the AND gate output is the carry digit. In the rotaxane-based half adder, the sum digit (n_S) is coded by the fluorescence change ΔF (O2) and the carry digit (n_C) is coded by the absorption change ΔA (O1). As shown in the truth table (Table 1) and Figure 2, each input and output of the half adder may be either ON (designated 1) or OFF (0). The AND gate gives an ON response only when both inputs I1 ($\lambda =$ 380 nm) and I2 ($\lambda = 313$ nm) are ON. The XOR gate generates an ON output when either input is ON but not when they are both ON or both OFF. After the readout, the half adder could be reset to its initial state by using light (280 nm) or heat energy. Because of the full reversibility of the photoisomerization processes, the current half adder can be used repeatedly.

Table 1: Truth table for a half adder with the sum digit n_S and the carry digit n_C.

I1 (380 nm)	I2 (313 nm)	O1 (ΔA) AND gate (n_C)	O2 (ΔF) XOR gate (n_S)	Binary sum
0	0	0	0	00
1	0	0	1	01
0	1	0	1	01
1	1	1	0	10

In summary, a photochemically driven (the inputs and the outputs are all photochemical) multistate [2]rotaxane that mimics a half adder with distinct AND and XOR logic gates has been demonstrated for the first time. After receiving inputs, the half adder remains in a static state for a while then gives rise to one of two optical outputs. The device can then be reset with light or heat, such that the half adder can be operated repeatedly. Most importantly, the realization that multistate [2]rotaxane operations which involve more than one logic expression are possible through a judicial choice of input and output signals has pointed a way to design complicated logic circuits based on one molecule. It is likely that by integrating these approaches, molecular logic gates with superior processing capabilities will emerge in the future.

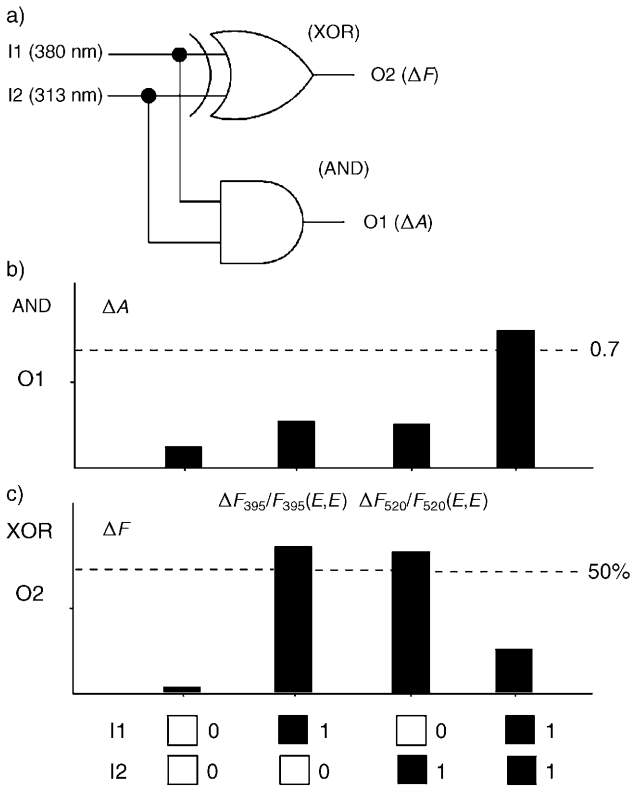


Figure 2. a) Schematic representation of the two-input half-adder logic circuit with [2]rotaxane **1** (I = input, O = output; *A* = absorbance, *F* = fluorescence). b) Experimental output O1 (ΔA) for the AND gate after irradiation of **1** at 380 nm (I1) and/or 313 nm (I2). c) Experimental output O2 (ΔF) for the XOR gate after irradiation at 380 nm (I1) and/or 313 nm (I2). The dashed line indicates the detection limit.

Received: April 7, 2005
Revised: June 9, 2005
Published online: July 22, 2005

Keywords: fluorescence · isomerization · molecular logic gates · photochemistry · rotaxanes

[1] a) P. Ball, *Nature* **2000**, *406*, 118–120; b) A. P. de Silva, H. Q. N. Gunaratne, C. P. McCoy, in *Molecular Switches* (Ed.: B. L. Feringa), Wiley-VCH, Weinheim, **2000**; c) B. L. Feringa, *Molecular Switches*, Wiley-VCH, Weinheim, **2001**; d) F. M. Raymo, *Adv. Mater.* **2002**, *14*, 401–414; e) V. Balzani, A. Credi, M. Venturi, *ChemPhysChem* **2003**, *4*, 49–59; f) V. Balzani, M. Venturi, A. Credi, *Molecular Devices and Machines*, Wiley-VCH, Weinheim, **2003**; g) A. P. de Silva, N. D. McClenaghan, *Chem. Eur. J.* **2004**, *10*, 574–586.

[2] For examples, see: a) A. P. de Silva, H. Q. N. Gunaratne, C. P. McCoy, *J. Am. Chem. Soc.* **1997**, *119*, 7891–7892; b) A. P. de Silva, N. D. McClenaghan, *Chem. Eur. J.* **2002**, *8*, 4935–4945.

[3] For examples, see: a) A. Credi, V. Balzani, S. J. Langford, J. F. Stoddart, *J. Am. Chem. Soc.* **1997**, *119*, 2679–2681; b) F. Pina, M. J. Melo, M. Maestri, P. Passaniti, V. Balzani, *J. Am. Chem. Soc.* **2000**, *122*, 4496–4498.

 © 2005 Wiley-VCH Verlag GmbH & Co. KGaA, Weinheim

[4] For examples, see: a) F. M. Raymo, S. Giordani, *J. Am. Chem. Soc.* **2001**, *123*, 4651 – 4652; b) F. M. Raymo, R. J. Alvarado, S. Giordani, M. A. Cejas, *J. Am. Chem. Soc.* **2003**, *125*, 2361 – 2364; c) H. Tian, B. Qin, R.-X. Yao, X.-L. Zhao, S.-J. Yang, *Adv. Mater.* **2003**, *15*, 2104 – 2107.

[5] For examples, see: a) C. P. Collier, E. W. Wong, M. Belohradsky, F. M. Raymo, J. F. Stoddart, P. J. Kuekes, R. S. Williams, J. R. Heath, *Science* **1999**, *285*, 391 – 394; b) C. P. Collier, M. Belohradsky, F. M. Raymo, J. F. Stoddart, J. R. Heath, *J. Am. Chem. Soc.* **2000**, *122*, 5831 – 5840.

[6] a) M. N. Stojanovic, D. Stefanovic, *Nat. Biotechnol.* **2003**, *21*, 1069 – 1074; b) A. Okamoto, K. Tanaka, I. Saito, *J. Am. Chem. Soc.* **2004**, *126*, 9458 – 9463.

[7] a) A. P. de Silva, N. D. McClenaghan, *J. Am. Chem. Soc.* **2000**, *122*, 3965 – 3966; b) F. Remacle, S. Speiser, R. D. Levine, *J. Phys. Chem. B* **2001**, *105*, 5589 – 5591; c) M. N. Stojanovic, D. Stefanovic, *J. Am. Chem. Soc.* **2003**, *125*, 6673 – 6676; d) J. Andréasson, G. Kodis, Y. Terazono, P. A. Liddell, S. Bandyopadhyay, R. H. Mitchell, T. A. Moore, A. L. Moore, D. Gust, *J. Am. Chem. Soc.* **2004**, *126*, 15926 – 15927; e) D. Margulies, G. Melman, C. E. Felder, R. Arad-Yellin, A. Shanzer, *J. Am. Chem. Soc.* **2004**, *126*, 15400 – 15401; f) X.-F. Guo, D.-Q. Zhang, G.-X. Zhang, D.-B. Zhu, *J. Phys. Chem. B* **2004**, *108*, 11942 – 11945.

[8] a) J.-M. Lehn, *Supramolecular Chemistry: Concepts and Perspectives*, Wiley-VCH, Weinheim, **1995**; b) V. Balzani, A. Credi, F. M. Raymo, J. F. Stoddart, *Angew. Chem.* **2000**, *112*, 3484 – 3530; *Angew. Chem. Int. Ed.* **2000**, *39*, 3348 – 3391; c) A. Harada, *Acc. Chem. Res.* **2001**, *34*, 456 – 464; d) C. A. Schalley, K. Beizai, F. Vögtle, *Acc. Chem. Res.* **2001**, *34*, 465 – 476; e) J.-P. Collin, C. Dietrich-Buchecker, P. Gavina, M. C. Jimenez-Molero, J.-P. Sauvage, *Acc. Chem. Res.* **2001**, *34*, 477 – 487.

[9] a) P. N. Taylor, M. J. O'Connell, L. A. McNeill, M. J. Hall, R. T. Aplin, H. L. Anderson, *Angew. Chem.* **2000**, *112*, 3598 – 3602; *Angew. Chem. Int. Ed.* **2000**, *39*, 3456 – 3460; b) C. A. Stanier, S. J. Alderman, T. D. W. Claridge, H. L. Anderson, *Angew. Chem.* **2002**, *114*, 1847 – 1850; *Angew. Chem. Int. Ed.* **2002**, *41*, 1769 – 1772.

[10] a) Q.-C. Wang, D.-H. Qu, J. Ren, K.-C. Chen, H. Tian, *Angew. Chem.* **2004**, *116*, 2715 – 2719; *Angew. Chem. Int. Ed.* **2004**, *43*, 2661 – 2665; b) D.-H. Qu, Q.-C. Wang, J. Ren, H. Tian, *Org. Lett.* **2004**, *6*, 2085 – 2088; c) D.-H. Qu, Q.-C. Wang, X. Ma, H. Tian, *Chem. Eur. J.* **2005**, DOI: 10.1002/chem.200401313.

[11] a) A. M. Brouwer, C. Frochot, F. G. Gatti, D. A. Leigh, L. Mottier, F. Paolucci, S. Roffa, G. W. H. Wurpel, *Science* **2001**, *291*, 2124 – 2128; b) M. Cavallini, F. Biscarni, S. León, F. Zerbetto, G. Bottari, D. A. Leigh, *Science* **2003**, *299*, 531; c) A. Altieri, G. Bottari, F. Dehez, D. A. Leigh, J. K. Y. Wong, F. Zerbetto, *Angew. Chem.* **2003**, *115*, 2398 – 2402; *Angew. Chem. Int. Ed.* **2003**, *42*, 2296 – 2300.

[12] a) C. P. Collier, M. Belohradsky, F. M. Raymo, J. F. Stoddart, J. R. Heath, *J. Am. Chem. Soc.* **2000**, *122*, 5831 – 5840; b) Y. Liu, A. H. Flood, J. F. Stoddart, *J. Am. Chem. Soc.* **2004**, *126*, 9150 – 9151; c) C. Seel, F. Vögtle, *Chem. Eur. J.* **2000**, *6*, 21 – 24; d) O. Lukin, A. Godt, F. Vögtle, *Chem. Eur. J.* **2004**, *10*, 1878 – 1883; e) M. C. Jimenez-Molero, C. Dietrich-Buchecker, J.-P. Sauvage, *Chem. Eur. J.* **2002**, *8*, 1456 – 1466; f) E. Katz, L. Sheeney-Haj-Ichia, I. Willner, *Angew. Chem.* **2004**, *116*, 3354 – 3362; *Angew. Chem. Int. Ed.* **2004**, *43*, 3292 – 3300; g) Y. Liu, Y.-L. Zhao, H.-Y. Zhang, H.-B. Song, *Angew. Chem.* **2003**, *115*, 3382 – 3385; *Angew. Chem. Int. Ed.* **2003**, *42*, 3260 – 3263; h) H. Shigekawa, K. Miyake, J. Sumaoka, A. Harada, M. Komiyama, *J. Am. Chem. Soc.* **2000**, *122*, 5411 – 5412; i) S. I. Jun, J. W. Lee, S. Sakamoto, K. Yamaguchi, K. Kim, *Tetrahedron Lett.* **2000**, *41*, 471 – 475.

[13] a) H. Murakami, A. Kawabuchi, K. Kotoo, M. Kunitake, N. Nakashima, *J. Am. Chem. Soc.* **1997**, *119*, 7605 – 7606; b) H. Meier, *Angew. Chem.* **2001**, *113*, 1903 – 1905; *Angew. Chem. Int. Ed.* **2001**, *40*, 1851 – 1853.

[14] The Supporting Information includes: ^{1}H NMR spectra, two-dimensional ^{1}H ROESY NMR spectra, and MALDI-TOF mass spectra of [2]rotaxane **1**; absorption and fluorescence spectra of dumbbell **2**, [2]rotaxane **1**, and the half-dumbbells; and detailed conditions for the photochemical reactions.

[15] The fractional conversion from (*E*,*E*)-**1** (DS-EE) to ($Z_{N=N}$,$E_{C=C}$)-**1** (PSS-ZE) is about 65%, and that to ($E_{N=N}$,$Z_{C=C}$)-**1** (PSS-EZ) is about 60%. The fractional conversion from ($Z_{N=N}$,$E_{C=C}$)-**1** (PSS-ZE) and ($E_{N=N}$,$Z_{C=C}$)-**1** (PSS-EZ) to (*Z*,*Z*)-**1** (PSS-ZZ) are slightly lower in comparison at about 53% and 57%, respectively.

[16] What station does the macrocycle prefer on the rotaxane: the azobenzene or the stilbene? The energy difference between the two translational isomers may determine the preferential location of the ring on one of the two sites. Fast shuttling of the ring between the two sites could make the determination of the population of the two translational isomers difficult, but if the entropy terms are sufficiently different then the relative binding affinity of the macrocycle for the two stations could be reversed by lowering the temperature.

 © 2005 Wiley-VCH Verlag GmbH & Co. KGaA, Weinheim

Green Chemistry

DOI: 10.1002/anie.200500346

Open-Framework Chalcogenides as Visible-Light Photocatalysts for Hydrogen Generation from Water**

*Nanfeng Zheng, Xianhui Bu, Hiep Vu, and Pingyun Feng**

The concern over the limited supply and the environmental effects of fossil fuels has led to increasing efforts directed towards the development of semiconductor photocatalysts for the production of hydrogen from water by using solar energy.[1–6] However, despite years of effort in this area of research, there are still many challenges that need to be met before such a photocatalytic process becomes economically feasible. The current limitations include the inadequate conduction-band energy levels for the photoreduction of

[*] N. Zheng, H. Vu, Prof. P. Feng
Department of Chemistry
University of California
Riverside, CA 92521 (USA)
Fax: (+1) 951-827-4713
E-mail: pingyun.feng@ucr.edu
Prof. X. Bu
Department of Chemistry and Biochemistry
California State University
1250 Bellflower Blvd.
Long Beach, CA 90840 (USA)

[**] We thank the NSF-DMR (P.F.) and the donors of the Petroleum Research Fund (administered by the ACS; X.B. and P.F.) for support of this work. P.Y. is an Alfred P. Sloan research fellow, Beckman Young Investigator, and Camille Dreyfus Teacher-Scholar.

 © 2005 Wiley-VCH Verlag GmbH & Co. KGaA, Weinheim InterScience

water and wide band gaps that correspond to UV light rather than visible light.[7]

Doping transition-metal cations or nitrogen anions into oxides is a commonly used strategy to create energy levels between valence and conduction bands so that the photocatalysts can be active in the visible-light region.[8–11] However, if the conduction-band level of a semiconductor is lower than the water-reduction potential, the doped semiconductor is usually photocatalytically inactive with respect to water reduction.

To overcome the above limitations and create a new generation of photocatalysts, it is necessary to develop a synthetic strategy that is capable of the systematic modification of both the electronic band gap and the energy level of each individual band. In addition, it is highly desirable to have a photocatalyst with a large number of active sites so as to increase quantum efficiency. Towards these goals, we have been developing methods for the synthesis of crystalline porous chalcogenide semiconductors with the expectation that such materials will have promising photocatalytic properties, particularly in the visible-light region.

We envision several unique advantages of photocatalysts based on crystalline porous semiconductors. By controlling framework architecture, it is possible to tune the band structure (both band positions and gap) of an open-framework solid within a given compositional domain. The open-framework construction also helps to increase the number of active reaction sites owing to a high surface area. The rate of charge recombination of the electron-hole pair is likely to be reduced because unlike a dense solid, the electron or hole does not need to travel all the way to the external surface of the catalyst particle for a reaction to occur. In addition to functioning as efficient photocatalysts on the basis of their framework composition and architecture, porous crystalline semiconductors can also serve as hosts for the incorporation of metal complexes, dyes, or other optically active species into their cavities. The synergetic effects in such hybrid materials are often highly desirable for enhancing photocatalytic efficiency.

Unfortunately, whereas open-framework materials have been extensively studied during the past several decades,[12–14] the vast majority of them are insulating oxides and therefore unsuitable for photocatalytic applications. There are also very few examples of hybrid materials between crystalline porous semiconductors and light-absorbing metal complexes (or dyes). Recently, a large family of crystalline chalcogenide open frameworks were developed.[15–19] These materials integrate tunable band gaps with an open-framework architecture and are potential candidates for efficient photocatalysts, particularly in the visible-light region. Herein we report photocatalytic properties of some select crystalline open-framework sulfides and demonstrate their unique features, particularly in comparison with some related dense semiconductors. This work represents our first step towards the development of efficient photocatalysts based on crystalline porous semiconductors.

The porous chalcogenides in this study were synthesized from solutions comprising In^{3+} and S^{2-} ions and one type of transition-metal cation (e.g., Cd^{2+}, Zn^{2+}, Mn^{2+}, Cu^{+}) under hydrothermal conditions. Two series of materials (denoted ICF-*m* and UCR-*m*) have been made. The ICF-*m* series contains hydrated inorganic cations (e.g., Li^{+}, Na^{+}) as extra-framework charge-balancing species and the UCR-*m* series contains protonated organic amines. The host framework of these materials is built from corner-sharing nanosized supertetrahedral clusters denoted as T*n*, in which *n* is the number of metal–sulfide layers in each cluster (Figure 1). UCR-7 has two interpenetrating cubic ZnS type lattices with T3 clusters

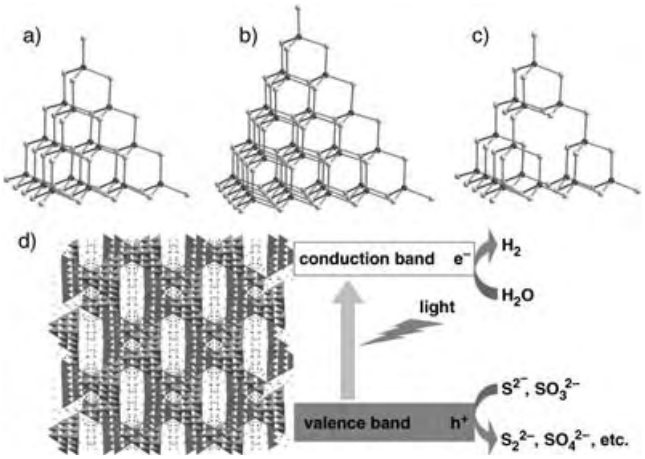


Figure 1. The structural and schematic diagrams of representative supertetrahedral clusters, chalcogenide frameworks, and their photocatalytic activity: a) T4 cluster; b) T5 cluster; c) coreless T4 cluster; d) the 3D diamond-type superlattice in ICF-5CuInS-Na: unconnected spheres are water molecules and Na^{+} sites.

($In_{10}S_{18}^{6-}$) at the tetrahedral nodes and UCR-20 has the sodalite-type structure with T2 clusters ($M_4S_8^{x-}$, M = In/Ge, In/Sn, Ga/Ge, and Ga/Sn) at the tetrahedral nodes. ICF-5, ICF-17, and ICF-22 all contain two interpenetrating cubic ZnS type lattices; however, tetrahedral nodes are occupied by T4 clusters (e.g., $Cu_3In_{17}S_{33}^{10-}$, $Cd_4In_{16}S_{33}^{10-}$) in ICF-5, T5 clusters (e.g., $Zn_{13}In_{22}S_{54}^{16-}$) in ICF-17, and the coreless T4 cluster ($In_{16}S_{32}^{16-}$) in ICF-22 (Figure 1). The size as measured between corner sulfur sites is 1.6 nm and 2.0 nm for T4 and T5 clusters, respectively. All these materials contain channels and cavities within 3D frameworks. A detailed discussion on the syntheses and structures of these materials was given elsewhere.[18–19]

A variety of compositions can be realized for these materials through the incorporation of different transition-metal cations, which provides a convenient route for the modification of the band gap. Figure 2 shows the UV/Vis–near-IR diffuse reflectance spectra of different ICF-*m* and UCR-*m* compounds and demonstrates how the band gap can be tuned from 2.0 to 3.6 eV. ICF-5InCuS-Na (formula: $Na_{14}In_{17}Cu_3S_{35}{\cdot}xH_2O$) is particularly interesting as it is compositionally related to $CuInS_2$, which is one of the most efficient photovoltaic materials. The introduction of Cu^{+} cations into the InS framework dramatically decreases the band gap to 2.0 eV, which makes this material particularly suitable for applications in the visible-light region.

 © 2005 Wiley-VCH Verlag GmbH & Co. KGaA, Weinheim

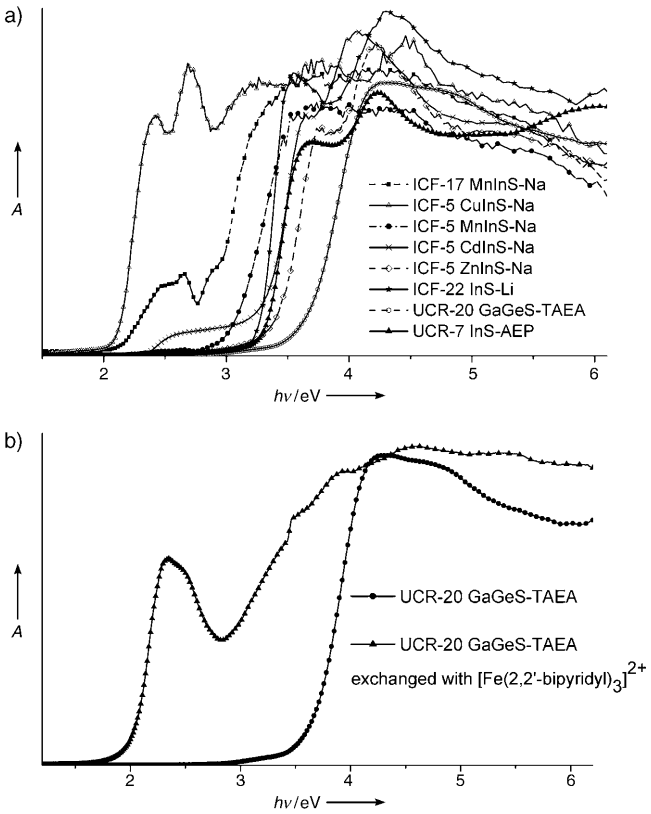


Figure 2. a) UV/Vis diffuse reflectance spectra of different open-framework chalcogenide materials. b) UV/Vis diffuse reflectance spectra of UCR-20GaGeS-TAEA before and after overnight ion exchange with 0.1 M $[Fe(2,2'\text{-bipyridine})_3]^{2+}$ solution. Data were measured on a Shimadzu UV-3101PC double-beam, double-monochromator spectrophotometer. $BaSO_4$ powder was used as reference (100% reflectance) and sometimes as base material for the coating of samples. Absorption (α/S) data were calculated from the reflectance data by using the Kubelka–Munk function: $\alpha/S=(1-R)^2/R$, in which R is the reflectance at a given wavelength, α is the absorption coefficient, and S is the scattering coefficient.

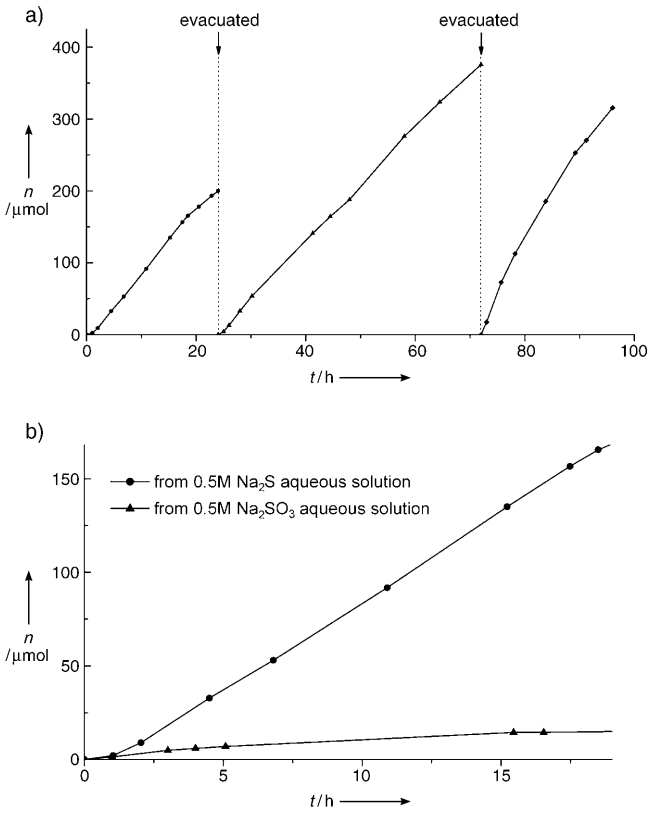


Figure 3. a) Photocatalytic H_2 evolution from an aqueous solution of Na_2S (0.5 M) over ICF-5 CuInS-Na (0.5 g); t: irradiation time, n: amount of H_2. b) Comparison of photocatalytic evolution of H_2 from an aqueous solution of Na_2S (0.5 M) and an aqueous solution of Na_2SO_3 (0.5 M) over ICF-5CuInS-Na (0.5 g). Light source: 300-W Xe lamp, $\lambda > 420$ nm.

A comparative study of porous sulfides and compositionally related dense phases showed that porous sulfides have a much higher photocatalytic activity. As shown in Figure 3 a, about 18 μmol h^{-1} g^{-1} of H_2 gas was produced over the ICF-5CuInS-Na catalyst under irradiation with the visible light. This activity was maintained for over 96 h and more than 890 μmol of H_2 gas evolved during this period. The turnover number—defined as the ratio between the moles of reacted electrons and the amount of the photocatalyst—exceeded 15 after 96 h, which indicates that the reaction proceeds photocatalytically. There was no difference in XRD patterns of the catalyst before and after the reaction. However, the light reddish reaction mixture might be related to the slow degradation of the catalyst. The quantum efficiency for ICF-5CuInS-Na was determined to be about 3.7% at 420 nm. Even though the number is lower than the quantum yield ($\approx$35%) of the well-known Pt/CdS photocatalyst, the efficiency is a considerable improvement on two anhydrous dense phases with similar compositions: $CuInS_2$ with the cubic ZnS structure; $CuIn_5S_8$ with the spinel structure. The quantum yield of $CuIn_5S_8$ with cocatalyst Ag_2S was reported smaller than 0.02% at 460 nm and 25 °C while the efficiency of $CuInS_2$ was even lower.[20]

When the photocatalytic reaction with ICF-5CuInS-Na was repeated under similar conditions but with 0.5 M Na_2SO_3 as the sacrificial agent instead of 0.5 M Na_2S, the amount of hydrogen produced was reduced substantially to about one tenth of that from the Na_2S solution (Figure 3 b). The production of hydrogen was negligible after 15 h of irradiation, which suggests that the SO_3^{2-} ion is a less effective sacrificial agent than the S^{2-} ion.

It is worth noting that ICF-5CuInS-Na is photocatalytically active without the use of a cocatalyst such as Pt. We have also observed hydrogen evolution over other porous chalcogenides such as ICF-17MnInS-Na (formula: $Na_{16}Mn_{13}In_{22}S_{54}{\cdot}x\,H_2O$) or ICF-5CdInS-Na (formula: $Na_{10}Cd_4In_{16}S_{33}{\cdot}x\,H_2O$) upon irradiation with visible light, again without any cocatalyst. Unlike typical dense semiconductors,[21–23] the presence of the Pt cocatalyst does not show an observable effect on the photocatalytic activity of these porous chalcogenides.

It is possible to engineer the band gap in the construction of an open framework. Similar to the effect that a decrease in conjugation leads to an increased energy gap in an organic

 © 2005 Wiley-VCH Verlag GmbH & Co. KGaA, Weinheim

conjugated system, the generation of porosity in crystalline semiconductors leads to an increase in the band gap and energy level of the conduction band. For example, $NaInS_2$ is a layered dense phase with a band gap of 2.3 eV;[24] in comparison, the band gap of ICF-22InS-Li (formula: $LiInS_2 \cdot x\,H_2O$) is 3.3 eV (Figure 2 a).

An increase in the energy of the conduction-band level, which may be made possible through the construction of a porous architecture, can help generate water-reduction photocatalysts from inactive semiconductors in a compositional domain with an inadequate conduction energy level. For example, even under UV irradiation, no photocatalytic activity for the evolution of hydrogen was observed from In_2S_3, a 3D dense structure.[24] However, UCR-7InS-AEP (framework formula: $In_{10}S_{18}^{6-}$; AEP = protonated 1-(2-aminoethyl)piperazine) showed high photocatalytic activity for the hydrogen evolution under UV irradiation (Figure 4). In

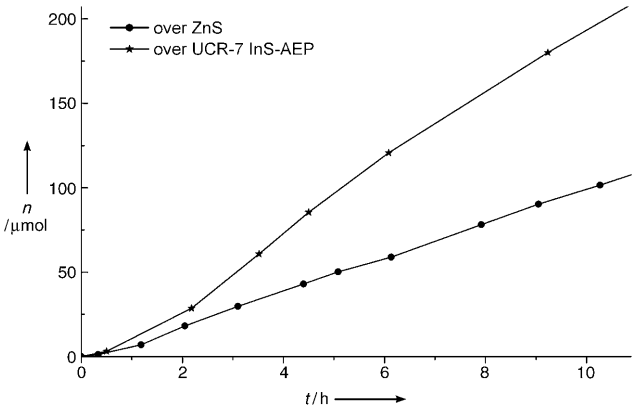


Figure 4. Comparison of photocatalytic H_2 evolution from 0.5 M Na_2SO_3 aqueous solution over 0.5 g UCR-7InS-AEP and ZnS. Light source, 300-W Xe lamp; *t*: irradiation time, *n*: amount of H_2.

the absence of any cocatalyst and under similar conditions, its activity is better than that of ZnS, a well-known UV-active photocatalyst.[25] A similar structural effect on photocatalytic activity has also been observed among oxide materials. For example, dense Nb_2O_5 shows little activity for the photoreduction of water due to its low conduction band. In comparison, a number of layered and tunneled structures based on niobium oxide are highly active in the UV region.[4]

In addition to the engineering of the band gap, the construction of an open framework makes it possible to create new composite visible-light photocatalysts by integrating porous semiconducting frameworks with optically active organic molecules or metal complexes. Upon incorporation into the pores of open-framework materials, dye molecules can function as sensitizers to enhance visible-light absorption and the subsequent transfer of energy to the semiconducting framework. The open-framework architecture can accommodate a high concentration of dye sensitizers, which is difficult to achieve by coating the surface of dense materials. The hybridization of crystalline porous semiconductors and metal complexes (or dyes) has the potential to make highly efficient use of solar energy and therefore significantly improve the photocatalytic efficiency.

In this work, the $[Fe(2,2'\text{-bipyridine})_3]^{2+}$ complex was incorporated into UCR-20GaGeS through ion exchange. XRD patterns before and after ion exchange were nearly identical; however, the absorption of the hybrid material was extended from the UV region to the visible-light region (Figure 2 b). The resulting red sample showed photocatalytic activity for the generation of hydrogen under irradiation with visible light ($\lambda > 420$ nm) for at least 24 h with SO_3^{2-} ions as the sacrificial agent. In comparison, the photocatalytic activity of both $[Fe(2,2'\text{-bipyridine})_3]^{2+}$ and UCR-20GaGeS-TAEA was also studied with SO_3^{2-} ions as the sacrificial agent (TAEA = protonated tris(2-aminomethyl)amine). They did not show observable activity in the visible-light region even though UCR-20 GaGeS-TAEA was found to exhibit activity under the UV light. Only after ion exchange of $[Fe(2,2'\text{-bipyridine})_3]^{2+}$ into UCR-20 did the resulting hybrid material show activity in visible light region.

In conclusion, a series of open-framework chalcogenides have been demonstrated to be efficient photocatalysts for the reduction of water. We have shown that novel hybrids of crystalline porous semiconductors and light-absorbing metal complexes can be prepared and these materials exhibit unique optical and photocatalytic properties. Compared with dense semiconductors, these porous semiconductors have received much less attention and their photocatalytic efficiency still requires further optimization. However, the unique advantages of porous semiconductors, such as having a high surface area and the easy incorporation of light sensitizers, provide new opportunities that can be explored to maximize photocatalytic efficiency, particularly in the visible-light region. We anticipate that the unique effects and advantages associated with the porous architecture are relevant to both porous sulfide and oxide semiconductor materials, which promise a new generation of photocatalysts for applications such as water reduction or splitting.

Experimental Section

The photocatalytic reactions were performed in a pyrex reaction cell connected to a closed gas-evacuation and circulation system.

In a typical procedure, the catalyst (0.5 g) was suspended in a solution of Na_2S or Na_2SO_3 (0.5 M, 270 mL). After the system had been evacuated, Ar gas was introduced into the reaction cell until a pressure of about 9.3 kPa was reached. The catalyst suspension was then irradiated with a 300 W Xe lamp equipped with an optical cut-off filter ($\lambda > 420$ nm) and a heat-absorbing filter. The amount of H_2 produced was analyzed by using an online gas chromatograph equipped with a thermal-conductivity detector (TCD). Quantum yield was measured at 420 nm by using a band-pass filter with a half width of 9.8 nm. The number of incident photons was determined by a chemical actinometry based on potassium ferrioxalate.

Received: January 29, 2005
Published online: July 22, 2005

Keywords: green chemistry · heterogeneous catalysis · microporous materials · photochemistry · reduction

 © 2005 Wiley-VCH Verlag GmbH & Co. KGaA, Weinheim

[1] A. Fujishima, K. Honda, *Nature* **1972**, *238*, 37 – 38.
[2] Z. G. Zou, J. H. Ye, K. Sayama, H. Arakawa, *Nature* **2001**, *414*, 625 – 627.
[3] T. Takata, A. Tanaka, M. Hara, J. N. Kondo, K. Domen, *Catal. Today* **1998**, *44*, 17 – 26.
[4] K. Domen, J. N. Kondo, M. Hara, T. Takata, *Bull. Chem. Soc. Jpn.* **2000**, *73*, 1307 – 1331.
[5] A. Kudo, *Catal. Surv. Asia* **2003**, *7*, 31 – 38.
[6] M. Ashokkumar, *Int. J. Hydrogen Energy* **1998**, *23*, 427 – 438.
[7] J. R. Bolton, *Science* **1978**, *202*, 705 – 711.
[8] A. K. Ghosh, H. P. Maruska, *J. Electrochem. Soc.* **1977**, *124*, 1516 – 1522.
[9] W. Choi, A. Termin, M. R. Hoffmann, *J. Phys. Chem.* **1994**, *98*, 13669 – 13679.
[10] R. Asahi, T. Morikawa, T. Ohwaki, K. Aoki, Y. Taga, *Science* **2001**, *293*, 269 – 271.
[11] S. U. M. Khan, M. Al-Shahry, W. B. Ingler, *Science* **2002**, *297*, 2243 – 2245.
[12] D. W. Breck, *Zeolite Molecular Sieves*, Wiley, New York, **1984**.
[13] M. E. Davis, *Nature* **2002**, *417*, 813 – 821.
[14] A. K. Cheetham, G. Ferey, T. Loiseau, *Angew. Chem.* **1999**, *111*, 3466 – 3492; *Angew. Chem. Int. Ed.* **1999**, *38*, 3268 – 3292.
[15] R. L. Bedard, S. T. Wilson, L. D. Vail, J. M. Bennett, E. M. Flanigen in *Zeolites: Facts, Figures, Future. Proceedings of the 8th International Zeolite Conference* (Eds.: P. A. Jacobs, R. A. van Santen) Elsevier, Amsterdam, **1989**, p. 375 – 387.
[16] a) H. Li, A. Laine, M. O'Keefe, O. M. Yaghi, *Science* **1999**, *283*, 1145 – 1147; b) H. Li, J. Kim, T. L. Groy, M. O'Keeffe, O. M. Yaghi, *J. Am. Chem. Soc.* **2001**, *123*, 4867 – 6868.
[17] a) C. L. Cahill, Y. Ko and J. B. Parise, *Chem. Mater.* **1998**, *10*, 19 – 21; b) C. L. Cahill, J. B. Parise, *J. Chem. Soc. Dalton Trans.* **2000**, 1475 – 1482.
[18] a) N. Zheng, X. Bu, B. Wang, P. Feng, *Science* **2002**, *298*, 2366 – 2399; b) C. Wang, Y. Li, X. Bu, N. Zheng, O. Zivkovic, C. Yang, P. Feng, *J. Am. Chem. Soc.* **2001**, *123*, 11506 – 11507.
[19] N. Zheng, X. Bu, P. Feng, *Nature* **2003**, *426*, 428 – 432.
[20] M. Matsumura, S. Furukawa, Y. Saho, T. Hiroshi, *J. Phys. Chem.* **1985**, *89*, 1327 – 1329.
[21] J.-F. Reber, M. Rusek *J. Phys. Chem.* **1986**, *90*, 824 – 834.
[22] K. Kobayakawa, A. Teranishi, T. Tsurumaki, Y. Sato, A. Fujishima, *Electrochim. Acta* **1992**, *37*, 465 – 467.
[23] A. Kudo, I. Tsuji, H. Kato, *Chem. Commun.* **2002**, 1958 – 1959.
[24] A. Kudo, A. Nagane, I. Tsuji, H. Kato, *Chem. Lett.* **2002**, 882 – 883.
[25] J.-F. Reber, K. Meier, *J. Phys. Chem.* **1984**, *88*, 5903 – 5913.

 © 2005 Wiley-VCH Verlag GmbH & Co. KGaA, Weinheim

DOI: 10.1002/anie.200463109

Trimethylyttrium and Trimethyllutetium**

*H. Martin Dietrich, Gabriele Raudaschl-Sieber, and Reiner Anwander**

Permethylated transition-metal complexes, as represented by neutral $M(CH_3)_x$ and anionic $[M(CH_3)_y]^{n-}$, have attracted considerable interest not only for displaying the simplest truly organometallic derivatives but also for their intrinsic bonding phenomena.[1,2] While structural and theoretical investigations have led to enormous progress for thermally labile homoleptic Group 4, 5, 6, and 7 derivatives, monometallic Group 3 and lanthanide congeners have remained elusive.[2,3] For example, the synthesis of rare-earth-metal–alkyl complexes such as $LnEt_3$ (Ln = Sc, Y) was claimed as early as 1938, however, striking evidence of their existence, be it spectroscopic data or clarifying follow-up chemistry, has never been reported.[4] Moreover, the ease of β-hydride elimination in such early transition-metal–alkyl complexes led to controversial discussions.[5,6] Nevertheless, a considerable number of silylalkyl complexes including homoleptic, donor-coordinated, donor-functionalized, and ate-type derivatives have been unambiguously identified.[7–11] In the early 1980s, Schumann et al. reported the synthesis of thermally stable ate complexes of the type $[Li_3(donor)_3][Ln(CH_3)_6]$ (donor = TMEDA (*N*,*N*,*N*′,*N*′-tetramethylethylenediamine), DME (1,2-dimethoxyethane)), which featured an octahedral coordination geometry, for the entire series of rare-earth metals.[12] Approximately ten years later, Evans et al. described permethylated derivatives $[Nd(GaMe_4)_3]$ and $[Ln(AlMe_4)_3]$ (Ln = Y, Nd, Sm) which can be viewed as trimethylgallium and trimethylaluminum adduct complexes, respectively, of the elusive $LnMe_3$.[13,14] Meanwhile, heterobimetallic derivatives $[Ln\{(\mu\text{-}Me)_2AlMe_2\}_3]$ are available for the entire Group 3 and 4f series except for scandium and promethium.[15,16] Herein, another ten years later, we describe the synthesis and derivatization of homoleptic trimethylyttrium and trimethyllutetium.

[*] H. M. Dietrich, Dr. R. Anwander
Department of Chemistry
University of Bergen
Allégaten 41, 5007 Bergen (Norway)
Fax: (+47) 5558-9490
E-mail: reiner.anwander@kj.uib.no
G. Raudaschl-Sieber
Anorganisch-chemisches Institut
Technische Universität München
Lichtenbergstraße 4, 85747 Garching (Germany)

[**] Financial support by the Deutsche Forschungsgemeinschaft (SPP 1166) and the Fonds der Chemischen Industrie is gratefully acknowledged. We thank M. Barth and co-workers for performing the elemental analyses.

Supporting information for this article is available on the WWW under http://www.angewandte.org or from the author.

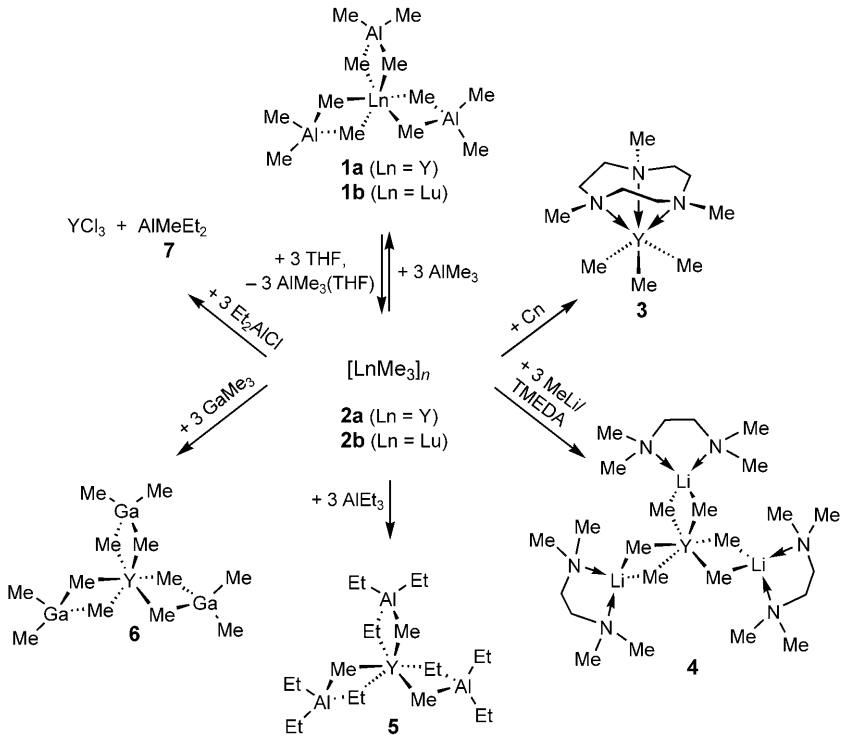
 © 2005 Wiley-VCH Verlag GmbH & Co. KGaA, Weinheim InterScience

Donor (Do)-induced cleavage of tetraalkylaluminates (Do = THF, diethyl ether, pyridine) has been previously applied to convert heteroleptic lanthanidocene and half-lanthanidocene complexes, $[Cp'_2Ln(AlR_4)]$ and $[Cp'Ln(AlR_4)_2]$ (Cp' = substituted cyclopentadienyl), into the corresponding σ-bonded alkyl derivatives [Eqs. (1) and (2)].[17–20]

$$2\,[Cp'_2Y\{Al(CH_3)_4\}] + 2\,Do \rightarrow [Cp'_2Y(\mu\text{-}CH_3)]_2 + 2\,Al(CH_3)_3(Do) \quad (1)$$

$$3\,[Cp'Y\{Al(CH_3)_4\}_2] + 6\,Do \rightarrow [Cp'Y(\mu\text{-}CH_3)_2]_3 + 6\,Al(CH_3)_3(Do) \quad (2)$$

We found that homoleptic $[Y(AlMe_4)_3]$ (**1a**) and $[Lu(AlMe_4)_3]$ (**1b**) are also amenable to this donor-induced tetraalkylaluminate cleavage. Accordingly, addition of a stoichiometric amount of THF (3 equiv) to a solution of **1a** in hexane at ambient temperature produced a white precipitate, which was insoluble in aliphatic and aromatic solvents (Scheme 1). After several washings with hexane and drying under high vacuum, the white powder was identified as polymeric $[YMe_3]_n$ (**2a**). Optimized conditions for this cleavage reaction comprised the use of freshly sublimed **1a** as well as the less Lewis basic donor diethyl ether as a cleavage reagent, and a low reaction temperature (−35 °C).[21] ^{1}H NMR experiments in C_6D_6 confirmed $Al(CH_3)_3(OEt_2)$ as the only soluble byproduct of the cleavage reaction (δ = −0.42 (s, 9H, $AlCH_3$), 0.73 (t, 6H, CH_3), 3.25 ppm (q, 4H, OCH_2)). Note that owing to its relatively low sublimation point (80 °C at 10^{-3} mbar; > 90 % yield), compound **1a** is among the most volatile of rare-earth metal compounds.[22]



Scheme 1. Synthesis and derivatization of $[LnMe_3]_n$ (**2**). Detailed reaction conditions are given in the Supporting Information (Cn = 1,4,7-trimethyl-1,4,7-triazacyclononane).

Such optimized reaction conditions were crucial for the synthesis of pure $[LuMe_3]_n$ (**2b**). The precursor $[Lu(AlMe_4)_3]$ (**1b**) was most efficiently separated from the coproduct of the synthesis, $[Me_2Al(\mu\text{-}NMe_2)]$, by fractional sublimation (ca. 90 °C at 10^{-3} mbar; > 20 % yield).[23] (*Caution*! Compound **2b** which is also obtained quantitatively as a white powder like the yttrium derivative **2a** detonates spontaneously when exposed to air; it also decomposes spontaneously at elevated temperature under high vacuum (ca. 80 °C at 10^{-4} mbar) to yield a black powder.) In addition to the C,H microanalytical data, unambiguous evidence for the formation of compounds **2a**,**b** stemmed from the complete reversibility of this donor-induced cleavage reaction (Scheme 1).[18] That is, treatment of the precipitated compounds **2** (non-isolated, as formed from the initial reaction mixture) and likewise the isolated compounds **2**, which were resuspended in hexane, with 3 equivalents of $AlMe_3$ both led to quantitative re-formation of the homoleptic complexes **1**. Visually, thus was indicated by the immediate formation of a clear solution.

A uniform coordination environment at the rare-earth-metal center in compounds **2** was confirmed by solid-state FTIR and MAS NMR spectroscopy. Nujol mulls of $[LnMe_3]_n$ gave IR spectra that displayed a characteristic vibration at $\tilde{\nu}$ = 1191 and 1202 cm^{-1} for the yttrium and lutetium derivatives, respectively, and a broad, intense low-energy band featuring three maxima at $\tilde{\nu}$ = 522, 431, and 361 cm^{-1} (**2a**). The ^{1}H MAS NMR spectrum of **2a** showed a broad resonance centered at δ = −0.3 ppm that exhibited two well-resolved shoulders at around δ = 0.1 and 1.0 ppm. The ^{13}C CPMAS NMR spectra of compounds **2** are shown in Figures 1 a and b. For each, one signal was detected for the methyl carbon atoms at δ = 28.3 (**2a**) and 31.4 ppm (**2b**). For comparison, the yttrium precursor complex **1a** revealed two signals at $\delta \approx -10$ and 18.0 ppm which can be assigned to Y-CH_3-Al bridging and Al-CH_3 terminal methyl ligands (Figure 1 c), whereas the half-yttrocene $[Cp^*Y(\mu\text{-}Me)_2]_3$ ($Cp^* = C_5Me_5$), which is discussed later, exhibits ^{13}C resonances at δ = 11.9, 30.3, and 118.7 ppm that are attributed to carbon atoms of $CH_3(Cp^*)$ substituents, Y-CH_3-Y bridging methyl ligands, and the Cp* ring, respectively (Figure 1 d).[19] Similar solid-state NMR chemical shifts have been previously reported for the complex $[Cp^*_2Th(CH_3)_2]$ (Cp*: δ = 123.1 and 12.0 ppm; Th-CH_3(terminal): δ = 68.4 ppm).[24] These findings clearly indicate the formation of homoleptic complexes **2** (ether donor ligands can be ruled out by the ^{13}C CPMAS NMR spectra) and to the absence of any methyl groups bonded to aluminum centers.[25,26] Carbon resonances of "Al-CH_3" moieties were previously shown to appear upfield,[27] and this is also corroborated by the spectrum of precursor compound **1a** (Figure 1 c).

Preliminary investigations into the reaction behavior of $[LnMe_3]_n$ were performed using the yttrium derivative **2a**

 © 2005 Wiley-VCH Verlag GmbH & Co. KGaA, Weinheim

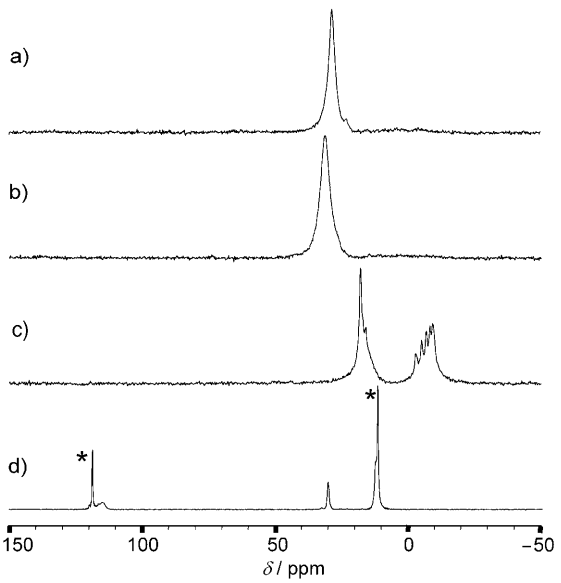


Figure 1. ^{13}C cross-polarization magic-angle-spinning (CPMAS) NMR spectra of a) neat $[YMe_3]_n$ (**2a**), b) neat $[LuMe_3]_n$ (**2b**), c) neat $[Y(AlMe_4)_3]$ (**1a**), and d) neat $[Cp^*YMe_2]_3$. Resonances due to C_5Me_5 (Cp*) are indicated by asterisks (*).

(Scheme 1). Although the isolation of simple ether adduct complexes, such as $[YMe_3(thf)_x]$, was not successful, addition of a stoichiometric amount of 1,4,7-trimethyl-1,4,7-triazacyclononane (Cn) to a suspension of $[YMe_3]_n$ in hexane gave $[CnYMe_3]$ (**3**) in almost quantitative yield.[28] The solid-state ^{13}C NMR spectrum of complex **3** (not shown) was similar to its spectrum in solution (C_6D_6) and gave signals at $\delta = 55.2$ (NCH_2), 48.7 (NCH_3), and 20.9 ppm (YCH_3). In the presence of TMEDA as an N-donor solvent, treatment of $[YMe_3]_n$ with 3 equivalents of MeLi gave Schumann's ate complex $[Li_3(tmeda)][Y(CH_3)_6]$ (**4**) in moderate yield.[12] Given the "reversibility" of the formation of $[LnMe_3]_n$, we anticipated that other strong Lewis acids might redissolve $[LnMe_3]_n$ as well. Accordingly, $AlEt_3$ and $GaMe_3$ form heterobimetallic/heteroleptic $[YAl_3Me_3Et_9]$ (**5**) and heterobimetallic/homoleptic $[YGa_3Me_{12}]$ (**6**) in almost quantitative yields (Scheme 1).[29] Whereas compound **5** was obtained as an oily residue, tetramethylgallate complex **6** yielded colorless crystals from solutions in hexane. Complex **6** shows a very broad ^1H NMR signal in C_6D_6 which is indicative of a decreased fluxional behavior of the bridging and terminal methyl ligands relative to tetramethylaluminate **2a**.

Instantaneous evolution of methane was observed when compound $[YMe_3]_n$ was treated with Brønsted acidic substrates such as $HN(SiMe_3)_2$, $HOCHtBu_2$, and HC_5Me_5 (HCp*) in hexane. The reactions of 3 equivalents of either the silylamine or the alcohol with **2a** gave the homoleptic complexes $[Y\{N(SiMe_3)_2\}_3]$ and $[Y(OCHtBu_2)_3]$, respectively, in high yields (see Supporting Information).[30,31] Owing to ligand scrambling, half-yttrocene complex $[Cp^*Y(\mu\text{-}Me)_2]_3$ did not form selectively upon addition of 1 equivalent of HCp* to compound **2a**, however, its presence could be identified by means of ^1H NMR spectroscopy.[19] A Me→Cl transformation with formation of YCl_3 occurred upon treatment of compound **2** with $AlMe_2Cl$ and documents the comparatively higher halophilicity of the rare-earth elements. Use of $AlEt_2Cl$ as a halogenating reagent afforded the mixed alkylaluminum $AlMeEt_2$ (**7**) as a coproduct.

In conclusion, we have shown that homoleptic rare-earth-metal–methyl complexes can be obtained through donor-induced tetraalkylaluminate cleavage of $[Ln\{(\mu\text{-}Me)_2AlMe_2\}_3]$ (Ln = Y, Lu). Compounds $[LnMe_3]_n$ are highly condensed materials. Notably, those derived from the smaller rare-earth-metal cations are stable at ambient temperature and accessible to a variety of ligand-exchange and addition reactions. Current investigations of $[LnMe_3]_n$ compounds are focused on 1) the accessibility of derivatives of the large rare-earth-metal cations, 2) the feasibility of controlled alkyl-elimination reactions, and 3) their potentials as catalysts.

Experimental Section

2a: In a glovebox, a solution of diethyl ether (3 equiv; 222 mg, 3.00 mmol) in hexane (5 mL) at −35 °C was added under vigorous stirring to a solution of $Y(AlMe_4)_3$ (**1a**; 350 mg, 1.00 mmol) in cold (−35 °C) hexane (10 mL). Instant formation of a white precipitate occurred. After stirring the reaction mixture for 10 min, the product was separated by centrifugation and washed three times with hexane to completely remove any soluble byproducts. After drying for 6 h under high vacuum, $[YMe_3]_n$ (**2a**) was obtained as a white powder in quantitative yield (133 mg). IR (Nujol): $\tilde{\nu} = 1191$ (vs), 522 (s), 431 (s), 361 (s), 320 cm^{-1} (w); far-IR (polyethylene): $\tilde{\nu} = 186$ cm^{-1} (w); ^1H MAS NMR (300.13 MHz, 25 °C): $\delta = 1.0$, 0.1, −0.3 ppm. ^{13}C MAS NMR (75.46 MHz, 25 °C): $\delta = 28.3$ ppm; elemental analysis (%): calcd for C_3H_9Y (134.010 g mol^{-1}): C 26.89, H 6.77; found: C 26.88, H 6.51.

Typical procedure for addition reactions, as shown for the synthesis of **6**: In a glovebox, a solution of $GaMe_3$ (3 equiv; 128 mg, 1.12 mmol) in hexane (5 mL) cooled to −35 °C was added under vigorous stirring to a suspension of $[YMe_3]_n$ (**2a**, 50 mg, 0.37 mmol) in hexane (5 mL) also cooled to −35 °C. The reaction mixture became clear after 15 min stirring. After a further 15 min, the reaction mixture was filtered, and the filtrate was retained. Evaporation of the solvent in vacuo yielded compound **6** as a white crystalline product (169 mg, 95%). IR (Nujol): $\tilde{\nu} = 1302$ (w), 1202 (s), 967 (w), 571 (s), 530 (s), 416 cm^{-1} (m); ^1H NMR (400 MHz, C_6D_6, 25 °C): $\delta = -0.10$ ppm; $^{13}C\{^1H\}$ NMR (100 MHz, C_6D_6, 25 °C): $\delta = 4.0$ ppm (v br); elemental analysis (%): calcd for $C_{12}H_{36}Ga_3Y$ (478.492 g mol^{-1}): C 30.12, H 7.58; found: C 31.30, H 7.34, N < 0.2.

Full experimental and physicochemical details for complexes **1–7** are available in the Supporting Information.

Received: December 31, 2004
Revised: March 1, 2005
Published online: July 22, 2005

Keywords: aluminum · lanthanides · NMR spectroscopy · yttrium

[1] P. J. Davidson, M. F. Lappert, R. Pearce, *Chem. Rev.* **1976**, *76*, 219.
[2] K. Seppelt, *Acc. Chem. Res.* **2003**, *36*, 147, and references therein.
[3] For a recent review on non-cyclopentadienyl organolanthanide complexes, see: F. T. Edelmann, D. M. M. Freckmann, H. Schumann, *Chem. Rev.* **2002**, *102*, 1851.

 © 2005 Wiley-VCH Verlag GmbH & Co. KGaA, Weinheim

[4] For a survey of the historical development of homoleptic σ-bonded organolanthanide compounds, see: a) H. Schumann, *J. Organomet. Chem.* **1985**, *281*, 95; b) H. Schumann, *J. Less-Common Met.* **1985**, *112*, 327.

[5] For donor-solvated neopentyl complexes, see: a) M. F. Lappert, R. Pearce, *J. Chem. Soc. Chem. Commun.* **1973**, 126; b) M. Niemeyer, *Z. Anorg. Allg. Chem.* **2000**, *626*, 1027.

[6] For homoleptic anionic *tert*-butyl ate complexes, see: a) A. L. Wayda, W. J. Evans, *J. Am. Chem. Soc.* **1978**, *100*, 7119; b) H. Schumann, W. Genthe, E. Hahn, J. Pickardt, H. Schwarz, K. Eckart, *J. Organomet. Chem.* **1986**, *306*, 215.

[7] For a homoleptic donor-functionalized dimethylaminopropyl ate complex, see: T. Herbrich, K.-H. Thiele, U. Thewalt, *Z. Anorg. Allg. Chem.* **1996**, *622*, 1609.

[8] a) P. B. Hitchcock, M. F. Lappert, R. G. Smith, R. A. Bartlett, P. P. Power, *J. Chem. Soc. Chem. Commun.* **1988**, 126; b) C. Eaborn, P. B. Hitchcock, K. Izod, J. D. Smith, *J. Am. Chem. Soc.* **1994**, *116*, 12071; c) J. R. van den Hende, P. B. Hitchcock, S. A. Holmes, M. F. Lappert, S. Tian, *J. Chem. Soc. Dalton Trans.* **1995**, 3933; d) C. Eaborn, P. B. Hitchcock, K. Izod, Z.-R. Lu, J. D. Smith, *Organometallics* **1996**, *15*, 4783; e) M. Westerhausen, M. Hartmann, W. Schwartz, *Inorg. Chim. Acta* **1998**, *269*, 91.

[9] a) J. L. Atwood, W. E. Hunter, R. D. Rogers, J. Holton, J. McMeeking, R. Pearce, M. F. Lappert, *J. Chem. Soc. Chem. Commun.* **1978**, 140; b) H. Schumann, J. Müller, *J. Organomet. Chem.* **1978**, *146*, C5 – C7; c) W. J. Evans, J. C. Brady, J. W. Ziller, *J. Am. Chem. Soc.* **2001**, *123*, 7711; d) H. Schumann, D. M. M. Freckmann, S. Dechert, *Z. Anorg. Allg. Chem.* **2002**, *628*, 2422.

[10] W. Clegg, C. Eaborn, K. Izod, P. O'Shaughnessy, J. D. Smith, *Angew. Chem.* **1997**, *109*, 2925; *Angew. Chem. Int. Ed. Engl.* **1997**, *36*, 2815.

[11] W. J. Evans, J. L. Shreeve, R. N. R. Broomhall-Dillard, J. W. Ziller, *J. Organomet. Chem.* **1995**, *501*, 7.

[12] a) H. Schumann, J. Müller, *Angew. Chem.* **1978**, *90*, 307; *Angew. Chem. Int. Ed. Engl.* **1978**, *17*, 276; b) H. Schumann, J. Pickardt, N. Bruncks, *Angew. Chem.* **1981**, *93*, 127; *Angew. Chem. Int. Ed. Engl.* **1981**, *20*, 120; c) H. Schumann, J. Müller, N. Bruncks, H. Lauke, J. Pickardt, H. Schwarz, K. Eckart, *Organometallics* **1984**, *3*, 69; d) H. Schumann, H. Lauke, E. Hahn, J. Pickardt, *J. Organomet. Chem.* **1984**, *263*, 29.

[13] W. J. Evans, R. Anwander, R. J. Doedens, J. W. Ziller, *Angew. Chem.* **1994**, *106*, 1725; *Angew. Chem. Int. Ed. Engl.* **1994**, *33*, 1641.

[14] a) W. J. Evans, R. Anwander, J. W. Ziller, *Organometallics* **1995**, *14*, 1107; b) W. T. Klooster, R. S. Lu, R. Anwander, W. J. Evans, T. F. Koetzle, R. Bau, *Angew. Chem.* **1998**, *110*, 1326; *Angew. Chem. Int. Ed.* **1998**, *37*, 1268.

[15] a) R. Anwander, O. Runte, J. Eppinger, G. Gerstberger, M. Spiegler, E. Herdtweck, *J. Chem. Soc. Dalton Trans.* **1998**, 847; b) A. Fischbach, PhD Thesis, Technische Universität München, **2003**; c) A. Fischbach, M. G. Klimpel, M. Widenmeyer, E. Herdtweck, W. Scherer, R. Anwander, *Angew. Chem.* **2004**, *116*, 2284; *Angew. Chem. Int. Ed.* **2004**, *43*, 2234; d) H. M. Dietrich, E. Herdtweck, R. Anwander, unpublished results.

[16] For the synthesis and structural characterization of tetraalkylaluminate complexes of the divalent rare-earth metals, $[Ln(AlR_4)_2]$ (R = Me, Et, *i*Bu), see: M. G. Klimpel, R. Anwander, M. Tafipolsky, W. Scherer, *Organometallics* **2001**, *20*, 3983.

[17] J. Holton, M. F. Lappert, D. G. H. Ballard, R. Pearce, J. L. Atwood, W. E. Hunter, *J. Chem. Soc. Dalton Trans.* **1979**, 54.

[18] M. G. Klimpel, J. Eppinger, P. Sirsch, W. Scherer, R. Anwander, *Organometallics* **2002**, *21*, 4021.

[19] $[Cp^*YMe_2]_3$ can be obtained in high yield through donor-induced cleavage of $[Cp^*Y(AlMe_4)_2]$ (see Supporting Information): H. M. Dietrich, E. Herdtweck, R. Anwander, unpublished results.

[20] C. J. Schaverien, *Organometallics* **1994**, *13*, 69.

[21] Nonstoichiometric reactions inevitably give Al-contaminated products as confirmed by atomic absorption spectroscopy. For example, an Al contamination of 0.6 wt%, which was observed for one of the donor-induced cleavage reactions of **1a** (23.11 wt% Al) would correspond to a Y/Al ratio of 33:1.

[22] R. Anwander, F. C. Munck, W. Scherer, T. Priermeier, O. Runte, W. A. Herrmann, *Inorg. Chem.* **1997**, *36*, 3545.

[23] $[Lu(AlMe_4)_3]$ (**1b**) is isostructrual to $[Nd(AlMe_4)_3]$[14a]: H. M. Dietrich, E. Herdtweck, R. Anwander, unpublished results.

[24] P. J. Toscano, T. J. Marks, *J. Am. Chem. Soc.* **1985**, *107*, 653.

[25] Preliminary X-ray diffraction studies revealed $[LnMe_3]_n$ to be amorphous powders.

[26] I. Nagl, M. Widenmeyer, E. Herdtweck, G. Raudaschl-Sieber, R. Anwander, *Microporous Mesoporous Mater.* **2001**, *44–45*, 311.

[27] R. Anwander, C. Palm, O. Groeger, G. Engelhardt, *Organometallics* **1998**, *17*, 2027.

[28] S. Hajela, W. P. Schaefer, J. E. Bercaw, *J. Organomet. Chem.* **1997**, *532*, 45.

[29] $Mg(n\text{Bu})_2$ also redissolves $[YMe_3]_n$ to form a heterobimetallic/heteroleptic YMg complex which was obtained as a colorless oil. For comparison, $ZnEt_2$ afforded no addition product.

[30] D. C. Bradley, J. S. Ghotra, F. A. Hart, *J. Chem. Soc. Dalton Trans.* **1973**, 1021.

[31] W. A. Herrmann, R. Anwander, W. Scherer, *Chem. Ber.* **1993**, *126*, 1533.

 © 2005 Wiley-VCH Verlag GmbH & Co. KGaA, Weinheim

Asymmetric Catalysis

DOI: 10.1002/anie.200501251

Highly Enantioselective Cu-Catalyzed Conjugate Additions of Dialkylzinc Reagents to Unsaturated Furanones and Pyranones: Preparation of Air-Stable and Catalytically Active Cu–Peptide Complexes**

*M. Kevin Brown, Sylvia J. Degrado, and Amir H. Hoveyda**

In recent years, a considerable amount of effort has been expended on the development of catalytic methods for asymmetric conjugate additions (ACA) of alkyl metal reagents to unsaturated carbonyls.[1] Research in these laboratories has led us to identify amino acid based phosphanes, such as **1**–**3** (Scheme 1), as chiral ligands for use in Cu-

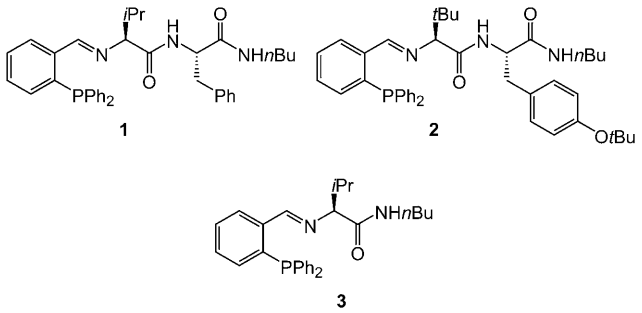
[*] M. K. Brown, S. J. Degrado, Prof. A. H. Hoveyda
Department of Chemistry
Merkert Chemistry Center, Boston College
Chestnut Hill, MA 02467 (USA)
Fax: (+1) 617-552-1442
E-mail: amir.hoveyda@bc.edu

[**] This research was supported by the United States National Institutes of Health (GM-47480). S.J.D. was a Bristol-Myers Squibb Graduate Fellow in Synthetic Organic Chemistry.

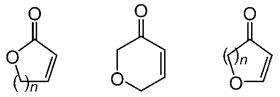
Supporting information for this article is available on the WWW under http://www.angewandte.org or from the author.

InterScience
© 2005 Wiley-VCH Verlag GmbH & Co. KGaA, Weinheim

Chiral phosphanes:



Substrates:



Scheme 1. Chiral amino acid based phosphanes used for Cu-catalyzed asymmetric conjugate additions (ACA) to various heterocyclic enones.

catalyzed ACA processes involving dialkylzinc reagents.[2] However, the majority of investigations have focused on transformations of unsaturated ketones;[2,3] more recently, a number of studies have involved Cu-catalyzed ACA of nitroalkenes.[4]

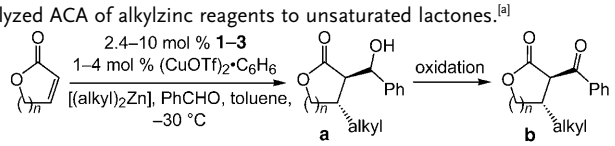
Catalytic ACA reactions of the less reactive cyclic or acyclic unsaturated carboxylic esters (e.g., **I**, Scheme 1) have received far less attention.[5] A number of studies have addressed the problem of catalytic additions of dialkylzinc reagents to unsaturated lactones.[6–8] In spite of high enantioselectivities (>90% *ee*) in select instances, the above disclosures address only reactions of one or two substrates (**I**, $n=1$ or 2) or nucleophiles (typically [Et_2Zn]; less frequently [Me_2Zn]). Due to complications that will be clarified later, in a number of cases, isolated yields are not indicated (only % conversion disclosed).[6a,b,d] In addition, two reports provide examples of Cu-catalyzed ACA of Grignard reagents to lactones (**I**, $n=2$);[9a–b] in one disclosure,[9a] high catalyst loading is required (32 mol%; 5–92% *ee*) and the other[9b] offers only a single example (82% *ee*). To the best of our knowledge, a report regarding catalytic ACA of an alkyl metal reagent to substrate types **II** or **III** (Scheme 1) has not appeared.

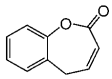
Herein, we disclose the first effective and general protocol for catalytic ACA of dialkylzinc reagents to unsaturated furanones and pyranones of varying steric and electronic properties (i.e., **I**–**III**, Scheme 1). Enantioselective additions proceed in the presence of optically pure phosphanes **1**–**3** to afford the desired products in high isolated yield and in up to >98% *ee*. We report the synthesis of catalytically active Cu^I–peptide complexes that are air stable, can be prepared from commercially available Cu salts and utilized after storage for at least a week.

Phosphanes **1**–**3** can be used to effect efficient and enantioselective ACA of alkylzinc reagents to small and medium ring unsaturated lactones (Table 1). A variety of dialkylzinc reagents, including the sterically demanding [$(i\text{Pr})_2Zn$] (entries 2 and 5) as well as the less reactive [Me_2Zn] can be employed (entries 3 and 7). To obtain high yield, reactions must be carried out in the presence of an aldehyde;[10] this is presumably due to adventitious ketene formation or intermolecular Michael addition if the enolate intermediate is not trapped in situ. The resulting aldol adduct can be oxidized to afford the corresponding diketone (>98% *anti*), or, as represented by the formation of **15** and **16** (Scheme 2), converted to the derived optically enriched β-alkyl carbonyl by an efficient retro-aldol process.

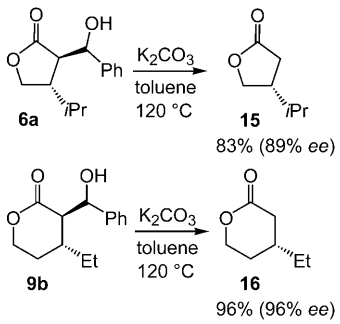
This phase of our studies pointed to a chiral ligand hierarchy: First, the simplest phosphane **3** was examined; in cases where ACA was sluggish, the more potent **1** was utilized (e.g., <10% conversion with 10 mol% **3** vs. >98% conversion with **1** in entry 7). Chiral phosphane **2** was employed when ACA products from reactions with **1** were judged not to

Table 1: Cu-catalyzed ACA of alkylzinc reagents to unsaturated lactones.[a]



Entry	Substrate		[(alkyl)$_2$Zn]	Ligand (mol%)	mol% Cu salt	Product	*t* [h]	Yield [%][b]	*ee* [%][c]
1		4	[Et_2Zn]	**2** (10)	4	**5b**	48	67	97
2			[$(i\text{Pr})_2Zn$]	**1** (10)	4	**6b**	48	85	89
3[d]		7	[Me_2Zn]	**1** (10)	4	**8b**	48	40	>98
4			[Et_2Zn]	**3** (2.4)	1	**9b**	6	90	96
5			[$(i\text{Pr})_2Zn$]	**2** (2.4)	1	**10b**	12	91	90
6			[{$Me_2CH(CH_2)_3$}$_2$Zn]	**3** (2.4)	1	**11b**	12	78	96
7		12	[Me_2Zn]	**1** (10)	4	**13b**	12	66	98
8			[Et_2Zn]	**3** (10)	4	**14b**	6	84	94

[a] Reactions were carried out under N_2. Oxidation step: PCC (pyridinium chlorochromate; 2.1 equiv), NaOAc, celite, 4-Å molecular sieves, CH_2Cl_2; products **a** are obtained in 0–60% *de*; see the Supporting Information for details. [b] >98% conversion in all cases, except entry 3 (65–70%); conversion determined by analysis of 400 MHz ^{1}H NMR spectra of unpurified products. Isolated yields for the ACA/aldol addition step; isolated yields for oxidations are >85%. [c] Determined by chiral HPLC analysis; see the Supporting Information for details. [d] Reaction was carried out at −15 °C.



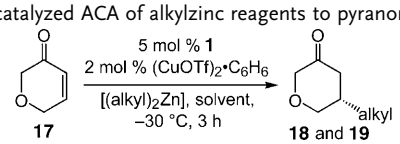
Scheme 2. Unmasking of ACA products.

 © 2005 Wiley-VCH Verlag GmbH & Co. KGaA, Weinheim

be of sufficient optical purity (e.g., **5b** formed in 84% *ee* in the presence of ligand **1** vs. 97% *ee* with phosphane **2**).

As illustrated in entries 1 and 4 of Table 2, under conditions identical to those used for reactions of lactones (see Table 1), Cu-catalyzed ACA of pyranone **17** proceed to

Table 2: Cu-catalyzed ACA of alkylzinc reagents to pyranone **17**.[a]



17 **18** and **19**

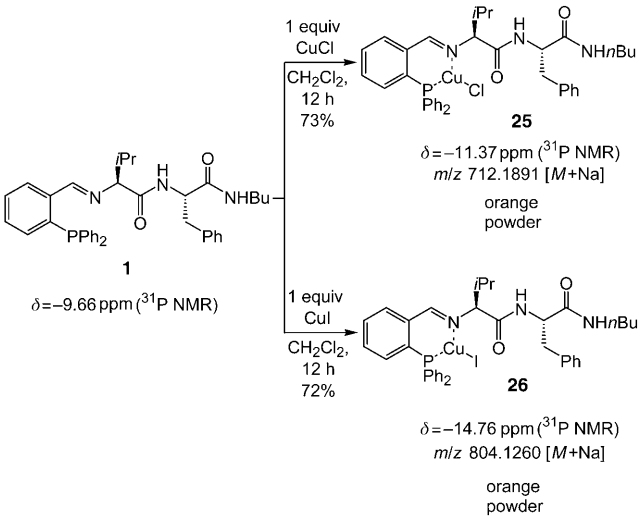
Entry	[(alkyl)$_2$Zn]	Solvent	Product	Yield [%][b]	*ee* [%][c]
1	[Et$_2$Zn]	toluene	**18**	n.d.	64
2	[Et$_2$Zn]	Et$_2$O	**18**	n.d.	72
3	[Et$_2$Zn]	THF	**18**	66	98
4	[Me$_2$Zn]	toluene	**19**	n.d.	56
5	[Me$_2$Zn]	THF	**19**	58	>98

[a] Reactions were carried out under N_2. [b] Isolated yields after silica gel chromatography. [c] All enantioselectivities determined by chiral GLC analysis; see the Supporting Information for details. n.d. = not determined.

>98% conversion but with inferior enantioselectivity (64% and 56% *ee*). We surmised that the diminished asymmetric induction might be due to the neighboring Lewis basic oxygen atom directing the enantioselective addition of an alkyl–copper complex to the electronically activated ketone.[11] Accordingly, we examined the effect of coordinating solvents to disrupt the purported O→Cu chelation. As illustrated in entries 3 and 5 of Table 2, when the catalytic ACA are performed in THF **18** and **19** are generated in ≥98% *ee*; as shown in entry 2, the less Lewis basic Et$_2$O does not have as pronounced an effect. Remarkably, in the case of the more electron rich unsaturated lactones (Table 1), there is <2% conversion when THF is used as the solvent.

Next, we turned our attention to the least electrophilic class of ACA substrates (**III**, Scheme 1). As the data summarized in Table 3 indicate, amino acid based chiral phosphanes are effective with this group of heterocyclic enones: ACA products are formed efficiently in ≥98% *ee*. As was the case with transformations involving unsaturated lactones, the presence of an aldehyde trap is required (to circumvent β elimination or intermolecular Michael addition). A similar ligand hierarchy, as mentioned for studies summarized in Table 1, holds here as well. Unlike reactions in Table 1, the products **a** of the three-component asymmetric process, are generated in high diastereoselectivity (80 to >98% *de*), and, as with transformations in Table 1, can be converted to ACA products **b** in high yield (Table 3).

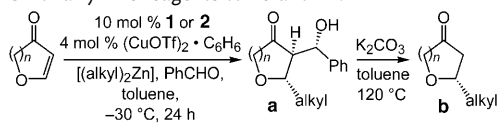
With an effective protocol for ACA of alkylzinc reagents to substrate classes **I**–**III** in hand, we focused our efforts on gaining insight regarding the nature of the chiral Cu complex. In this context, our efforts to synthesize and isolate a complex derived from a peptide phosphane and (CuOTf)$_2$·C$_6$H$_6$ was unsuccessful (presumably due to sensitivity of the Cu–triflate complexes). However, as depicted in Scheme 3, we have been



Scheme 3. Preparation of air-stable chiral Cu complexes **25** and **26**.

able to prepare the complexes derived from reaction of phosphane **1** with CuCl and CuI. Thus, treatment of unpurified commercial samples of CuCl and CuI with **1** at ambient temperature results in the formation of orange powders. These air-stable Cu complexes,[5c] for which we propose structures **25** and **26**, have been characterized spectroscopically (Scheme 3).[12] As the representative data summarized in Table 4 illustrate, not only are **25** and **26** effective ACA catalysts (entries 2 and 4), these chiral Cu complexes deliver improved enantioselectivity compared to when catalysts are prepared in situ (entries 1 and 3, Table 4). Higher catalyst loading (8 vs. 2 mol% in Table 1) is needed for reactions promoted by **25** and **26** (vs. **1**–**3**), likely due to lower activity of metal halide versus triflate complexes. Complex **25** is less stable than iodide **26**; whereas a week-old sample of **26** (stored in

Table 3: Cu-catalyzed ACA of alkylzinc reagents to **20** and **22**.[a]



Entry	Substrate		[(alkyl)$_2$Zn]	Ligand	Product	Conv. [%][b]	Yield [%][c]	*ee* [%][d]	*de* [%][e]	Product	Yield [%][c]
1		**20**	[Et$_2$Zn]	**1**	**21a**	>98	68	>98	>98	**21b**	74
2		**22**	[Et$_2$Zn]	**2**	**23a**	80	63	>98	80	**23b**	92
3			[(*i*Pr)$_2$Zn]	**2**	**24a**	71	54	98	80	**24b**	84

[a] Reactions were carried out under N_2. [b] Conversion determined by analysis of 400 MHz ^{1}H NMR spectra of unpurified products. [c] Isolated yields after silica gel chromatography. [d] Enantioselectivities determined by chiral GLC or HPLC analysis; see the Supporting Information for details. [e] See the Supporting Information for stereochemical assignments.

 © 2005 Wiley-VCH Verlag GmbH & Co. KGaA, Weinheim

Table 4: Representative ACA catalyzed by **25** and **26**.[a]

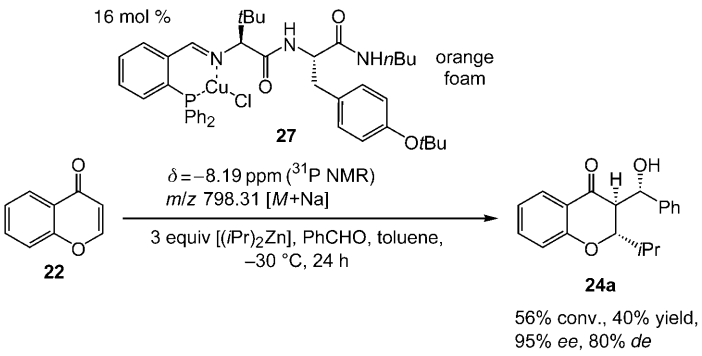
$$\mathbf{7} \xrightarrow[2)\ \text{PCC, NaOAc}]{1)\ 8\,\text{mol}\%\ \text{catalyst, [Et}_2\text{Zn], PhCHO}} \mathbf{9b}$$

Entry	Catalyst	Conv. [%][b]	Yield [%][c]	*ee* [%][d]
1	**1** + CuCl	92	51	90
2	**25**	92	87	94
3	**1** + CuI	57	24	63
4	**26**	92	74	89

[a] [Et_2Zn] (3 equiv), −30 °C, toluene, 12 h, N_2. [b] Conversion determined by analysis of 400 MHz ^{1}H NMR spectra of unpurified mixtures. [c] Isolated yields after silica gel chromatography; oxidations proceed in ≈90% isolated yield. [d] Enantioselectivities determined by chiral HPLC analysis.

air) promotes ACA with equal efficiency and enantioselectivity, a similar batch of **25** affords **9b** in 87% yield and 72% *ee* (vs. 94% with a freshly prepared sample).

An additional example, shown in Equation (1), illustrates that isolation of Cu-peptide chiral complexes is not limited to



(1)

the derivatives of phosphane **1**. Thus, in the presence of **27** (16 mol%), derived through reaction of **2** ($\delta = -10.7$ ppm, ^{31}P NMR) with CuCl (1 equiv, CH_2Cl_2, 22 °C; 84% yield), heterocyclic enone **22** can be converted to **24a** in 95% *ee* and 80% *de*. Similar to reactions with **25** and **26**, the copper chloride complex is less effective than when the chiral catalyst is prepared in situ from $(CuOTf)_2{\cdot}C_6H_6$ and phosphane **2** (see entry 3, Table 3).

In summary, we report the first generally effective method for catalytic ACA of dialkylzinc reagents to unsaturated furanones and pyranones with different steric and electronic properties. The present method significantly enhances the general utility of Cu-catalyzed ACA of alkylmetal reagents to unsaturated carbonyls. Synthesis, isolation, and characterization of catalytically active and air-stable chiral Cu–peptide complexes **25**–**27** enhance the practical utility of these protocols and set the stage for future mechanistic investigations.

Received: April 9, 2005
Published online: July 25, 2005

Keywords: asymmetric catalysis · conjugate addition · copper · enantioselectivity · zinc

[1] a) N. Krause, A. Hoffmann-Roder, *Synlett* **2001**, 171–196; b) A. Alexakis, C. Benhaim, *Eur. J. Org. Chem.* **2002**, 3221–3236; c) B. L. Feringa, R. Naasz, R. Imbos, L. A. Arnold in *Modern Organocopper Chemistry* (Ed.: N. Krause), Wiley-VCH, Weinheim, **2002**, pp. 224–258.

[2] a) S. J. Degrado, H. Mizutani, A. H. Hoveyda, *J. Am. Chem. Soc.* **2001**, *123*, 755–756; b) H. Mizutani, S. J. Degrado, A. H. Hoveyda, *J. Am. Chem. Soc.* **2002**, *124*, 779–781; c) S. J. Degrado, H. Mizutani, A. H. Hoveyda, *J. Am. Chem. Soc.* **2002**, *124*, 13362–13363; d) R. R. Cesati III, J. de Armas, A. H. Hoveyda, *J. Am. Chem. Soc.* **2004**, *126*, 96–101; for an overview, see: e) A. H. Hoveyda, A. W. Hird, M. A. Kacprzynski, *Chem. Commun.* **2004**, 1779–1785.

[3] For representative recent examples (subsequent to reviews in reference [1]), see: a) A. Alexakis, C. Benhaim, S. Rosset, M. Humam, *J. Am. Chem. Soc.* **2002**, *124*, 5262–5263; b) I. J. Krauss, J. L. Leighton, *Org. Lett.* **2003**, *5*, 3201–3203; c) A. P. Duncan, J. L. Leighton, *Org. Lett.* **2004**, *6*, 4117–4119; d) D. Pena, F. Lopez, S. R. Harutyunyan, A. J. Minnaard, B. L. Feringa, *Chem. Commun.* **2004**, 1836–1837.

[4] For representative recent examples (subsequent to reviews in reference [1]), see: a) C. A. Luchaco-Cullis, A. H. Hoveyda, *J. Am. Chem. Soc.* **2002**, *124*, 8192–8193; b) A. Duursma, A. J. Minnaard, B. L. Feringa, *J. Am. Chem. Soc.* **2003**, *125*, 3700–3701; c) U. Eilitz, F. Lessmann, O. Seidelmann, V. Wendisch, *Tetrahedron: Asymmetry* **2003**, *14*, 189–191; d) D. M. Mampreian, A. H. Hoveyda, *Org. Lett.* **2004**, *6*, 2829–2832; e) H. Choi, Z. Hua, I. Ojima, *Org. Lett.* **2004**, *6*, 2689–2691; f) J. Wu, D. M. Mampreian, A. H. Hoveyda, *J. Am. Chem. Soc.* **2005**, *127*, 4584–4585.

[5] For catalytic ACA of dialkylzinc reagents to acyclic unsaturated carboxylic acid derivatives, see: a) A. W. Hird, A. H. Hoveyda, *Angew. Chem.* **2003**, *115*, 1314–1317; *Angew. Chem. Int. Ed.* **2003**, *42*, 1276–1279; b) J. Schuppan, A. J. Minaard, B. L. Feringa, *Chem. Commun.* **2004**, 792–793; for a recent study involving alkyl Grignard reagents with an air-stable chiral Cu complex, see: c) F. Lopez, S. R. Harutyunyan, A. Meetsma, A. J. Minaard, B. L. Feringa, *Angew. Chem.* **2005**, *117*, 2812–2816; *Angew. Chem. Int. Ed.* **2005**, *44*, 2752–2756.

[6] a) M. Yan, Z-Y. Zhou, A. S. C. Chan, *Chem. Commun.* **2000**, 115–116; b) M. T. Reetz, A. Gosberg, D. Moulin, *Tetrahedron Lett.* **2002**, *43*, 1189–1191; c) L. Liang, L. Su, X. Li, A. S. C. Chan, *Tetrahedron Lett.* **2003**, *44*, 7217–7220; d) L. Liang, M. Yan, Y-M. Li, A. S. C. Chan, *Tetrahedron: Asymmetry* **2004**, *15*, 2575–2578; for Cu-catalyzed ACA of alkylzinc and alkylaluminium reagents to six-membered unsaturated lactams, see: e) M. Pineschi, F. Del Moro, F. Gini, A. J. Minnaard, B. L. Feringa, *Chem. Commun.* **2004**, 1244–1245; for Cu-catalyzed ACA of alkylzinc reagents to 4-piperidones, see: f) R. Sebesta, M. G. Pizzuti, A. J. Boersma, A. J. Minnaard, B. L. Feringa, *Chem. Commun.* **2005**, 1711–1713.

[7] For related approaches involving catalytic asymmetric hydride conjugate additions, see: a) G. Hughes, M. Kimura, S. L. Buchwald, *J. Am. Chem. Soc.* **2003**, *125*, 11253–11258; b) B. H. Lipshutz, J. M. Servesko, B. R. Taft, *J. Am. Chem. Soc.* **2004**, *126*, 8352–8353.

[8] For Rh-catalyzed enantioselective additions of arylzinc reagents to 4-piperidones, see: a) R. Shintani, N. Tokunaga, H. Doi, T. Hayashi, *J. Am. Chem. Soc.* **2004**, *126*, 6240–6241; for Rh-

 © 2005 Wiley-VCH Verlag GmbH & Co. KGaA, Weinheim

catalyzed enantioselective addition of arylboroxines to 4-piperidones, see: b) R. B. C. Jagt, J. G. de Vries, B. L. Feringa, A. J. Minnaard, *Org. Lett.* **2005**, *7*, 2433 – 2435; for Rh-catalyzed ACA of arylboronic acids to unsaturated lactones, see: c) M. Reetz, D. Moulin, A. Gosberg, *Org. Lett.* **2001**, *3*, 4083 – 4085; d) C. Defieber, J.-F. Paquin, S. Serna, E. M. Carreira, *Org. Lett.* **2004**, *6*, 3873 – 3876; e) Y. Otomaru, K. Okamaoto, R. Shintani, T. Hayashi, *J. Org. Chem.* **2005**, *70*, 2503 – 2508.

[9] For catalytic enantioselective ACA involving additions of Grignard reagents, see: a) M. Kanai, Y. Nakagawa, K. Tomioka, *Tetrahedron* **1999**, *55*, 3843 – 3854; b) B. L. Feringa, R. Badorrey, D. Pena, S. R. Harutyunyan, A. J. Minnaard, *Proc. Natl. Acad. Sci. USA* **2004**, *101*, 5834 – 5838; c) F. Lopez, S. R. Harutyunyan, A. J. Minaard, B. L. Feringa, *J. Am. Chem. Soc.* **2004**, *126*, 12784 – 12785.

[10] a) M. Kitamura, T. Miki, K. Nakano, R. Noyori, *Tetrahedron Lett.* **1996**, *37*, 5141 – 5144; b) L. A. Arnold, R. Naasz, A. J. Minaard, B. L. Feringa, *J. Am. Chem. Soc.* **2001**, *123*, 5841 – 5842.

[11] For proposed examples of O-directed Cu-catalyzed or Cu-mediated conjugate additions, see: a) R. Imbos, A. J. Minnaard, B. L. Feringa, *Tetrahedron* **2001**, *57*, 2485 – 2489; b) G. Hareau-Vittini, S. Hikichi, F. Sato, *Angew. Chem.* **1998**, *110*, 2221 – 2223; *Angew. Chem. Int. Ed.* **1998**, *37*, 2099 – 2101.

[12] See the Supporting Information for details.

 © 2005 Wiley-VCH Verlag GmbH & Co. KGaA, Weinheim

Zeolites

DOI: 10.1002/anie.200501250

Water Condensation in Hydrophobic Nanopores**

Nicolas Desbiens, Isabelle Demachy, Alain H. Fuchs, Helène Kirsch-Rodeschini, Michel Soulard, and Joël Patarin*

There are many intriguing situations in everyday life where water is confined to spaces of nanoscopic dimensions by hydrophilic as well as hydrophobic substrates such as in colloidal particles,[1–4] protein cavities,[5] and inorganic solid walls.[6,7] Fundamental interest stems from the fact that the properties of confined water are believed to be very different from those of the corresponding bulk fluid at the same temperature and chemical potential.[8–11] Recently, it was shown that storage or dissipation of mechanical energy could be achieved by forced intrusion/extrusion of water into/from hydrophobic porous materials.[12–14] Intrusion of water into silicalite-1 zeolite at a hydraulic pressure of about 100 MPa at room temperature results in its condensation. A spontaneous capillary evaporation (drying) took place upon release of the pressure. Similar behavior was observed very recently in the case of hydrophobized MCM-41 mesoporous materials.[15] Interestingly, the intrusion/extrusion cycle was accompanied by a hysteresis effect in the latter case, but not in the former one. Situations were also encountered in which no extrusion of water took place upon release of the pressure (zeolite β and wide-pore MCM-41).[12–15] To shed light on these phenomena we have undertaken a molecular simulation study of the intrusion/extrusion of water into/from hydrophobic silicalite-1 zeolite. Some new experimental data are also reported. We have been able to reproduce, for the first time to our knowledge,the spontaneous condensation of water that is observed experimentally, and thus to investigate the properties of confined water in these hydrophobic nanopores at the molecular level.

The intrusion/extrusion process was investigated with silicalite-1 by using two different experimental devices. The same silicalite-1 sample, prepared according to a literature method,[12] was used in both cases. In the first device the water/silicalite-1 system was placed in a cell of variable volume (1.20 cm^3 under atmospheric pressure) which was immersed in an oil-containing vessel able to withstand very high hydrostatic pressure. The volume changes were determined at constant temperature by increasing the pressure progressively, as described in reference [16]. The compressibility curve obtained corresponds to that obtained by Eroshenko et al.[12,14] (Figure 1; dashed line). The method used in this first set of experiments is believed to be accurate for determining the water intrusion pressure, but the absolute

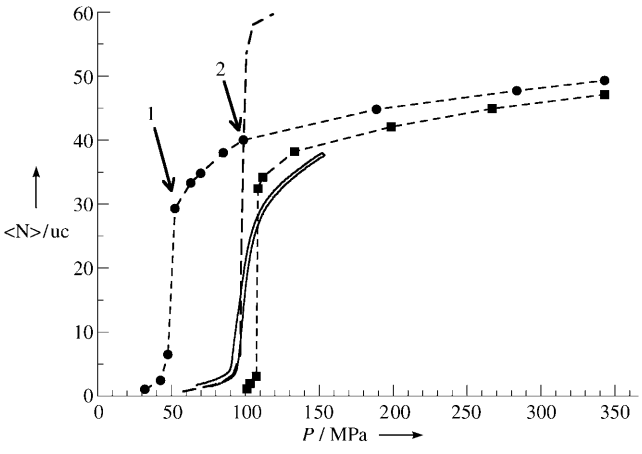


Figure 1. Condensation/drying isotherms of liquid water in silicalite-1 at 300 K. Solid line (displaying hysteresis): experimental data (this study); dashed line: experimental data;[12] circles: simulated isotherms with a silicon atomic charge of 1.4 a.u.; squares: simulated isotherm with a silicon atomic charge of 1.2 a.u. (see text). The dotted lines are a guide to the eye.

[*] N. Desbiens, Dr. I. Demachy, Prof. Dr. A. H. Fuchs
Laboratoire de Chimie Physique
CNRS and Université Paris-Sud
91405 Orsay (France)
Fax: (+33) 1-6915-6188
E-mail: fuchs@lcp.u-psud.fr
Ir. H. Kirsch-Rodeschini, Dr. M. Soulard, Dr. J. Patarin
Laboratoire de Matériaux à Porosité Contrôlée
CNRS, École Nationale Supérieure de Chimie de Mulhouse and Université de Haute-Alsace
68093 Mulhouse (France)

[**] Prof. Randy Snurr and Dr. Anne Boutin are gratefully acknowledged for fruitful discussions and correspondence.

InterScience
© 2005 Wiley-VCH Verlag GmbH & Co. KGaA, Weinheim

intruded volume seems to be overestimated. A second set of experiments was therefore performed which made use of a modified Carlo Erba mercury porosimeter, and a more realistic volume was obtained. In this case, the cell containing the water/zeolite system consisted of a 2-cm^3 polypropylene cylinder sealed by a mobile piston. This cell was introduced into the 15-cm^3 glass cell of the porosimeter which was filled with mercury. The variation in volume was determined from the conductivity measurement, which depends on the mercury height in the capillary tube of the glass cell. The maximum volume change was about 0.5 cm^3. We believe this methodology provides a more accurate measurement of the volume than the preceding case. The corresponding experimental intrusion/extrusion data are reported in Figure 1 (solid line). It is interesting to note that a porous volume of 0.18 cm^3 per gram of zeolite is obtained from the experimental intruded volume at 150 MPa and using the average computed water density of approximately 0.6 $kg\,m^{-3}$ (see below). This result is in complete agreement with the pore volume determined from nitrogen adsorption data.[12,13] This observation seems to demonstrate that the current volumetric data are much more accurate than the previously published ones. A very narrow hysteresis effect is observed during the intrusion/extrusion cycle; this effect was not observed in the first set of experiments. It is interesting to note that in a recent model proposed by Lefevre et al.,[15] it was predicted that the width of the intrusion/extrusion hysteresis in porous materials should progressively vanish as the pores get smaller. This prediction is in keeping with the current results.

We carried out Grand Canonical Monte Carlo (GCMC) simulations of the adsorption of water in silicalite-1. We used a rigid zeolite framework and used the atomic coordinates of the orthorhombic structure determined by Olson and et al.[17] We simulated a box of eight unit cells with periodic boundary conditions. We used the semiempirical TIP4P potential for water,[18] which was recently shown to provide a fairly good description of the adsorption of water in faujasite zeolites.[7,19] The host/guest potential is of the "Kiselev type":[20,21] It contains a single effective Lennard–Jones term that acts between the oxygen atoms of the framework and the oxygen atoms of the guest water molecules, together with a coulombic term that acts between the partial charges of the silicon and oxygen atoms and those of the guest molecules. We used the Lennard–Jones parameters for the zeolite oxygen atoms obtained from our previous work on the adsorption of hydrocarbons in silicalite-1[22] together with the Lorentz–Berthelot combining rules. The partial charge on the silicon atom was fixed at $+1.4$ a.u. (the zeolite oxygen atom bears a charge of -0.7 a.u. since the purely SiO_2 framework is neutral overall). There is an ongoing debate in the literature about the partial charge that a silicon atom should bear in silica-based materials; atomic charges have been reported in the range of 1.2 to 2.0 a.u., depending on the computational method used.[23–26] We found with the force-field model used here that the partial charge on the silicon atoms should be kept below approximately 1.7 a.u. for the silicalite-1 solid to exhibit hydrophobic character (namely, to prevent a capillary condensation phenomenon at a gas pressure below the saturation pressure of the bulk water). Details on this force-field adjustment will be reported elsewhere. We have chosen here the somewhat arbitrary value of 1.4 a.u. which corresponds to the Hartree–Fock calculation by Dovesi et al.[23] We have undertaken GCMC simulations of the adsorption of liquid water in silicalite-1. Thus, we have separately computed the relationship between the external pressure and the TIP4P chemical potential of liquid water at room temperature. GCMC simulations were then performed, at each pressure, by exchanging molecules between the zeolite sample and a fictitious external gas reservoir at the same chemical potential as the liquid water and at the pressure of interest. This method is similar to the one previously proposed by Snurr and coworkers for the adsorption of liquid alkanes.[27] Details of the GCMC algorithm and the statistical bias used can be found elsewhere.[22]

The adsorption data for the simulated liquid state at 300 K are reported in Figure 1. A stepwise condensation is observed at a pressure of about 50 MPa. The agreement with the experimental intrusion pressure is quite good, given that there is only a 3% difference in the chemical potential of liquid water between 50 and 100 MPa. An even better agreement with experimental data can be obtained by fixing an atomic charge of 1.2 a.u. on the silicon atom and -0.6 a.u. on each oxygen atom of the framework (Figure 1). The shape and the water loading of the computed intrusion isotherms are in good agreement with the currently reported experimental data. This observation is remarkable given the crudeness of the model used in the simulations. Simulations were also carried out using the MSPC/E semiempirical water potential model,[28] which is also known to reproduce quite well the saturation vapor pressure at room temperature. The computed adsorption curve (not shown here) was very similar to the TIP4P curve and also exhibited a stepwise, first-order-like condensation. This result is reminiscent of the two-state description of the water behavior in model carbon nanotubes[29] and nanoporous cylindrical channels[30] observed recently in molecular dynamics studies.

The computed isotherm shown in Figure 1 is reversible, within statistical uncertainties. This is generally what we expect for a Monte Carlo simulation, although it is known that GCMC adsorption isotherms may, in some special cases, exhibit hysteresis.[31] The computed isotherm displayed in Figure 1 can thus be considered as the equilibrium intrusion/extrusion curve of the model water/silicalite-1 system. It is the first time, to our knowledge, that this condensation/drying phenomenon has been reproduced theoretically.

We have examined in some detail the condensation mechanism in the molecular simulation model. The silicalite-1 framework (Figure 2) contains interconnected channels of pores of two types: straight channels which run in the direction of the *y*-axis and zigzag channels parallel to the *xz* plane. The Atlas of Zeolite structure types[32] denotes the silicalite-1 structure (MFI structure type) as being made of straight channels (SC) with a diameter of 5.4 Å, zigzag channels (ZC) with a diameter of 5.0 Å, and intersections (I). There are four SC, ZC, and I per unit cell, and they correspond to volume fractions of about 29, 33, and 38%, respectively. We have separately computed the local density of condensed water in these three subvolumes. This calcu-

 © 2005 Wiley-VCH Verlag GmbH & Co. KGaA, Weinheim

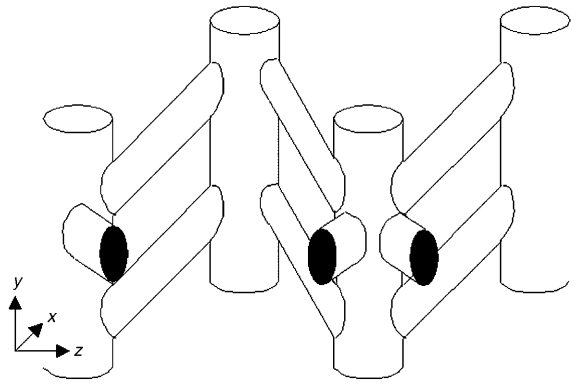


Figure 2. View of the interconnected pore channels in silicalite-1 (MFI-type structure).

lation is based on the determination of the void spaces in the zeolite model, which relies on a somewhat arbitrary definition of the "size" of the framework oxygen atoms. We have taken here a value of 1.5 Å for the van der Waals radius of the framework oxygen atoms. Consequently, the local density values shown in Figure 3, together with the average density

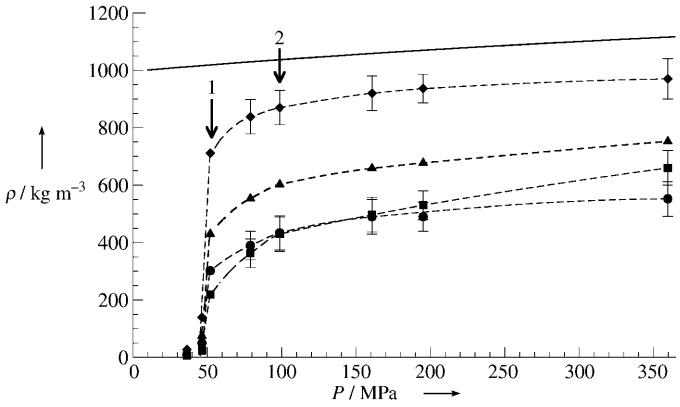


Figure 3. Density of condensed water in silicalite-1 as a function of pressure from GCMC simulations. Squares: local density in the zig-zag channels (ZC). Circles: local density in the straight channels (SC). Diamonds: local density in the intersections (I). Triangles: average water density in silicalite-1. Solid line: bulk water density. The dotted lines are a guide to the eye. No error bars are displayed for the average densities, for reasons of clarity.

and the bulk water density, depend on the criterion used for computing the void spaces, which leads to an uncertainty of about 10 % in the estimates of these local density values. The trends however (for example, the ratio of the intersection/straight channels densities and the way it changes with pressure) depend only weakly on this criterion.

The stepwise condensation phenomenon is observed in all three regions of the zeolite at a pressure of approximately 50 MPa. At this pressure (marked "1" in Figures 1 and 3) the average density of the condensed water is less than half that of the bulk water density under the same thermodynamic conditions. The condensed fluid is extremely inhomogeneous. The density in the intersections is three times as large as that of the fluid in the straight or zigzag channels. The average occupancy is 5 water molecules at an intersection, while there are only 1.5 molecules on average in the SC or ZC. At this stage, the filling of the channels (SC or ZC) is also highly inhomogeneous. Some of the sections of the channels are empty, while others contain 2–3 molecules. There is clearly a clustering effect in this first condensation step. The formation of water clusters in silicalite-1 was already suggested in some previous molecular dynamics studies.[33–35] The same behavior seems to hold true in the case of carbon nanopores.[36,37] The current results are in keeping with the observation of Vaitheeswaran et al.[37] that linear chains of water molecules inside a narrow cylindrical pore are less stable than the water clusters in a spherical nonpolar cavity of comparable volume.

A second condensation regime takes place as the pressure is increased from 50 to about 100 MPa. At the point marked "2" in Figures 1 and 3, each intersection is now occupied by six molecules and the SC and ZC by two water molecules. The channel filling now becomes homogeneous, with each channel section containing approximately the same number of molecules. At this stage, the water density in the intersection has reached 85 % of the bulk fluid value, while the density in the channels is lower by a factor of two.

A progressive filling of the silicalite-1 nanopores is observed upon pressure increases above 100 MPa. Given the uncertainties in the density calculations, it is hard to tell whether or not the density at the intersections reaches the bulk value at a sufficiently high pressure. However, it seems clear that the water density in the channels is always lower by a factor close to two. This fact can be interpreted by considering that the 3D-like geometry of the pore intersections enables water molecules to pile up in more or less the same way as in the bulk liquid. On the other hand, the pseudo-1D channel geometry prevents such a bulklike state from being reached. It is worth mentioning that the strong depletion of fluid observed in these simulations cannot simply be accounted for by a failure of the water force-field. The TIP4P intermolecular potential was checked to provide very accurate values for the density of bulk water at high pressure.

The observed water depletion is attributed to the hydrophobic (nonwetting) character of the purely siliceous nanopores studied here. Silicalite-1 zeolite consists of a three-dimensional network of SiO_4 tetrahedra connected to each other through shared oxygen atoms. This arrangement enables the build up of a purely siliceous open framework material without surface defects (bond breaking, presence of silanol groups).[12] Conversely, amorphous silica surfaces are highly defective, and thus display hydrophilic character. This is the case, for example, for the mesoporous MCM-41 materials. Hydrophobicity is generated in MCM-41 by covalent grafting of nonpolar siloxane chains.[15] In a recent study Engemann et al.[38] reported experimental evidence of interfacial melting of ice in contact with amorphous silica. The

 © 2005 Wiley-VCH Verlag GmbH & Co. KGaA, Weinheim

authors observed a quasiliquid layer with an enhanced density ($\rho \approx 1.2$) relative to bulk water. This fact can be tentatively attributed to the hydrophilic character of the amorphous silica surface.

One lesson that can be learned from this study is that simple models and simulation methods found useful for studying gas adsorption in nanoporous materials can be extended to describe the intrusion/extrusion cycle of a nonwetting fluid in a hydrophobic solid. We have reproduced for the first time the condensation transition of water in silicalite-1 zeolite at room temperature. The condensation process disclosed by computer simulations is much more complex than initially expected from the intrusion/extrusion experiments. The picture of water confined to hydrophobic spaces of nanoscopic dimensions that emerges from this study is one of a strongly depleted and highly inhomogeneous fluid.

Received: April 9, 2005
Published online: July 20, 2005

Keywords: adsorption · molecular modeling · phase transitions · water · zeolites

[1] P. Ball, *Nature* **2003**, *423*, 25 – 26.
[2] J. W. G. Tyrell, P. Attard, *Phys. Rev. Lett.* **2001**, *87*, 176104-1 – 176104-4.
[3] R. Steitz, T. Gutberlet, T. Hauss, B. Klösgen, R. Krastev, S. Schemmel, A. C. Simonsen, G. H. Findenegg, *Langmuir* **2003**, *19*, 2409 – 2418.
[4] D. Chandler, *Nature* **2002**, *417*, 491 – 491.
[5] B. Yu, M. Blaber, A. M. Gronenborn, G. M. Clore, D. L. D. Caspar, *Proc. Natl. Acad. Sci. USA* **1999**, *96*, 103 – 108.
[6] J. H. Walther, R. L. Jaffe, E. M. Kotsalis, T. Werder, T. Halicioglu, P. Koumoutsakos, *Carbon* **2004**, *42*, 1185 – 1194.
[7] C. Beauvais, A. Boutin, A. H. Fuchs, *ChemPhysChem* **2004**, *5*, 1791 – 1793.
[8] T. M. Truskett, P. G. Debenedetti, S. Torquato, *J. Chem. Phys.* **2001**, *114*, 2401 – 2418.
[9] P. Gallo, M. A. Ricci, M. Rovere, *J. Chem. Phys.* **2002**, *116*, 342 – 346.
[10] A. Giaya, R. W. Thompson, *J. Chem. Phys.* **2002**, *117*, 3464 – 3475.
[11] I. Brovchenko, A. Geiger, A. Oleinikova, *J. Chem. Phys.* **2004**, *120*, 1958 – 1972.
[12] V. Eroshenko, R.-C. Regis, M. Soulard, J. Patarin, *J. Am. Chem. Soc.* **2001**, *123*, 8129 – 8130.
[13] V. Eroshenko, R.-C. Regis, M. Soulard, J. Patarin, *C. R. Phys.* **2002**, *3*, 111 – 119.
[14] M. Soulard, J. Patarin, V. Eroshenko, R.-C. Regis, Proceedings of the 14th International Zeolite Conference, Cape Town (Eds.: E. Van Steen et al.), **2004**, pp. 1830–1837.
[15] B. Lefevre, A. Saugey, J. L. Barrat, L. Bocquet, E. Charlaix, P. F. Gobin, G. Vigier, *J. Chem. Phys.* **2004**, *120*, 4927 – 4938.
[16] V. Eroshenko, A. Fadeev, *Colloid J.* **1995**, *57*, 446 – 449.
[17] D. H. Olson, G. T. Kokotailo, S. L. Lawton, W. M. Meier, *J. Phys. Chem.* **1981**, *85*, 2238 – 2243.
[18] W. L. Jorgensen, J. Chandrasekhar, J. D. Madura, R. W. Impey, M. L. Klein, *J. Chem. Phys.* **1983**, *79*, 926 – 935.
[19] C. Beauvais, A. Boutin, A. H. Fuchs, *Adsorption* **2005**, in press.
[20] A. Bezus, A. V. Kiselev, A. A. Lopatkin, P. Q. Du, *J. Chem. Soc. Faraday Trans. 2* **1978**, *74*, 367 – 379.
[21] A. H. Fuchs, A. K. Cheetham, *J. Phys. Chem. B* **2001**, *105*, 7375 – 7383.
[22] P. Pascual, P. Ungerer, B. Tavitian, P. Pernot, A. Boutin, *Phys. Chem. Chem. Phys.* **2003**, *5*, 3684 – 3693.
[23] R. Dovesi, C. Pisani, C. Roetti, B. Silvi, *J. Chem. Phys.* **1987**, *86*, 6967 – 6971.
[24] L. Uytterhoeven, W. J. Mortier, P. Geerlings, *J. Phys. Chem. Solids* **1989**, *50*, 479 – 486.
[25] H. Heinz, U. W. Suter, *J. Phys. Chem. B* **2004**, *108*, 18341 – 18352.
[26] a) A. V. Larin, D. P. Vercauteren, *Int. J. Inorg. Mater.* **1999**, *1*, 201 – 207; b) A. V. Larin, L. Leherte, D. P. Vercauteren, *Chem. Phys. Lett.* **1998**, *287*, 169 – 177.
[27] S. Chempath, J. F. M. Denayer, K. M. A. De Meyer, G. V. Baron, R. Snurr, *Langmuir* **2004** *20*, 150 – 156.
[28] G. C. Boulougouris, I. G. Economou, D. N. Theodorou, *J. Phys. Chem. B* **1998**, *102*, 1029 – 1035.
[29] a) G. Hummer, J. C. Rasaiah, J. P. Noworyta, *Nature* **2001**, *414*, 188; S. Vaitheeswaran, J. C. Rasaiah, G. Hummer, *J. Chem. Phys.* **2004**, *121*, 7955 – 7965.
[30] R. Allen, J.-P. Hansen, S. Melchionna, *J. Chem. Phys.* **2003**, *119*, 3905 – 3919.
[31] F. Porcheron, P. Monson, *Langmuir* **2004**, *20*, 6482 – 6489.
[32] Atlas of zeolite Framework types http://www.iza-structure.org. Ch. Baerlocher, W. M. Meier, D. H. Olson, *Atlas of Zeolite Framework Types*, 5th rev. ed., Elsevier, Amsterdam, **2001**.
[33] P. Demontis, G. Stara, G. B. Suffritti, *J. Phys. Chem. B* **2003**, *107*, 4426 – 4436.
[34] C. Bussai, S. Fritzsche, R. Haberlandt, S. Hannonghua, *J. Phys. Chem. B* **2003**, *107*, 12444 – 12450.
[35] K. S. Smirnov, D. Bougeard, *Chem. Phys.* **2003**, *292*, 53 – 70.
[36] T. Ohba, H. Kanoh, K. Kaneko, *J. Phys. Chem. B* **2004**, *108*, 14964 – 14969; T. Ohba, H. Kanoh, K. Kaneko, *Nano Lett.* **2005**, *5*, 227 – 230.
[37] S. Vaitheeswaran, H. Yin, J. C. Rasaiah, G. Hummer, *Proc. Natl. Acad. Sci. USA* **2004**, *101*, 17002 – 17005.
[38] S. Engemann, H. Reichert, H. Dosch, J. Bilgram, V. Honkimäti, A. Snigirev, *Phys. Rev. Lett.* **2004**, *92*, 205701.

 © 2005 Wiley-VCH Verlag GmbH & Co. KGaA, Weinheim

Radical Cations

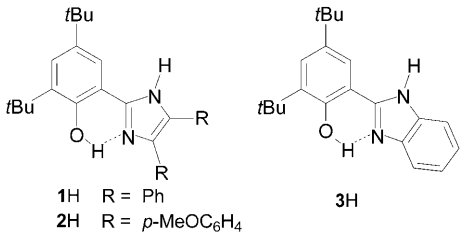
DOI: 10.1002/anie.200501132

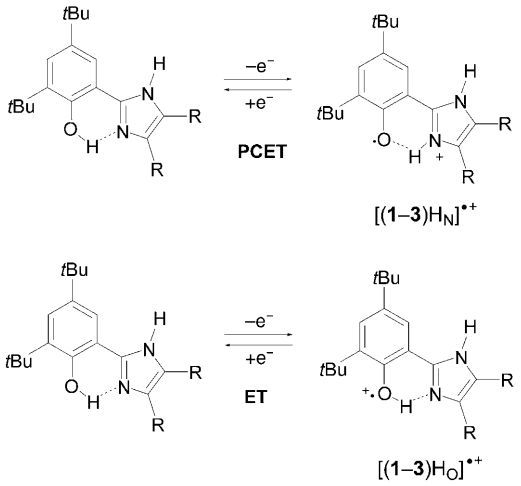
Phenoxyl Radicals Hydrogen-Bonded to Imidazolium: Analogues of Tyrosyl D· of Photosystem II: High-Field EPR and DFT Studies**

Laurent Benisvy, Robert Bittl, Eberhard Bothe, C. David Garner, Jonathan McMaster, Stephanie Ross, Christian Teutloff, and Frank Neese**

Tyrosyl radicals play a crucial role in many biological systems.[1] The remarkably stable tyrosyl radical, Tyr_D· in photosystem II (PSII)[2] is suggested to be hydrogen-bonded to an imidazol(ium) proton from a nearby histidine residue[3] (His 190 in higher plants; His 189 in cyanobacteria). Oxidation of Tyr_D to Tyr_D· probably proceeds via proton-coupled electron transfer (PCET) with migration of the phenoxyl proton to the imidazole group of the adjacent histidine.[4] Production of chemical analogues of Tyr_D· is of much current theoretical and experimental interest. Three recent studies have reported the oxidation of an α-alkylaminophenol derivative by a quasireversible PCET process, to form a phenoxyl radical hydrogen-bonded to an alkylammonium center.[5]

We have reported the synthesis and characterization of (**1**–**3**)H,[6] each of which has an intramolecular hydrogen bond involving the phenolic proton and an imidazole nitrogen atom. (**1**–**3**)H undergo a reversible, one-electron oxidation to form the corresponding radical cation, $[(\mathbf{1}–\mathbf{3})H]^{\bullet+}$. The oxidation of (**1**–**3**)H (see Scheme 1) could occur either by





Scheme 1. Possible mechanisms for the oxidation of (**1**–**3**)H to $[(\mathbf{1}–\mathbf{3})H]^{\bullet+}$.

PCET to produce an $R–O^{\bullet}\cdots H–N^{+}$ arrangement (designated $[(\mathbf{1}–\mathbf{3})H_N]^{\bullet+}$) or by electron transfer (ET) to produce an $R–O^{+\bullet}–H\cdots N$ arrangement (designated as $[(\mathbf{1}–\mathbf{3})H_O]^{\bullet+}$). Herein, we report the results of high-field EPR studies and DFT calculations that provide a definitive interpretation of the geometric and electronic structure of these $[(\mathbf{1}–\mathbf{3})H]^{\bullet+}$ radical cations.

The X-band EPR spectra of $[(\mathbf{1}–\mathbf{3})H]^{\bullet+}$ in CH_2Cl_2 at 77 K each consist of a single isotropic signal, centered at $g \approx 2.004$ with a linewidth of about 10 G and no discernible hyperfine splitting.[6] The absence of hyperfine splitting and the unresolved *g*-tensor anisotropy preclude any geometric and electronic structural information being obtained from the X-band EPR spectra alone. The lack of resolved proton hyperfine splittings may be taken as evidence for the presence of the $[(\mathbf{1}–\mathbf{3})H_N]^{\bullet+}$ forms of the radicals. However, a more positive experimental proof for this conjecture is required and is provided by high-field EPR. W-band (94.0 GHz) high-field EPR spectra, recorded for electrochemically generated $[(\mathbf{1}–\mathbf{3})H]^{\bullet+}$ in CH_2Cl_2 solution (1 mM) at 80 K (Figure 1 and Supporting Information) show three well-resolved *g* values; each spectrum was simulated successfully with $g_x = 2.0063–2.0067$, $g_y = 2.0043$, and $g_z = 2.0022/3$ (Table 1).

Density functional calculations were performed to interpret the W-band EPR spectra of $[(\mathbf{1}–\mathbf{3})H]^{\bullet+}$ and to investigate whether these data discriminate between the possible structures $[(\mathbf{1}–\mathbf{3})H_N]^{\bullet+}$ and $[(\mathbf{1}–\mathbf{3})H_O]^{\bullet+}$ (Scheme 1). As a calibration, the DFT calculations were performed initially for (**1**–**3**)H. In each case, the calculated structural parameters were in good agreement with the corresponding data obtained by X-ray crystallography;[6] the value of each bond length was reproduced to an accuracy of not worse than ±0.03 Å (see Supporting Information). For the corresponding $[(\mathbf{1}–\mathbf{3})H]^{\bullet+}(g)$ radical cations, DFT calculations were performed for the two forms $[(\mathbf{1}–\mathbf{3})H_N]^{\bullet+}$ and $[(\mathbf{1}–\mathbf{3})H_O]^{\bullet+}$, and in each

[*] Dr. L. Benisvy, Dr. E. Bothe, PD Dr. F. Neese
Max-Planck-Institut für Bioanorganische Chemie
Stiftstrasse 34–46, 45470 Mülheim an der Ruhr (Germany)
Fax: (+49) 208-306-3951
E-mail: benisvy@mpi-muelheim.mpg.de
neese@mpi-muelheim.mpg.de
Prof. C. D. Garner, Dr. J. McMaster, S. Ross
School of Chemistry
The University of Nottingham
University Park, Nottingham, NG72RD (UK)
Prof. Dr. R. Bittl, Dr. C. Teutloff
Institut für Experimentalphysik
Freie Universität Berlin
Arnimallee 14, 14195 Berlin (Germany)

[**] The authors thank Miss Petra Höfer for technical assistance and Dr. Sebastian Sinnecker for help with the electronic structure calculations. This work has been supported by Deutsche Forschungsgemeinschaft (Sfb 498 TP C5 and SPP 1137) and the Engineering and Physical Sciences Research Council (UK) (GR/R50325/01).

Supporting information for this article is available on the WWW under http://www.angewandte.org or from the author.

InterScience
© 2005 Wiley-VCH Verlag GmbH & Co. KGaA, Weinheim

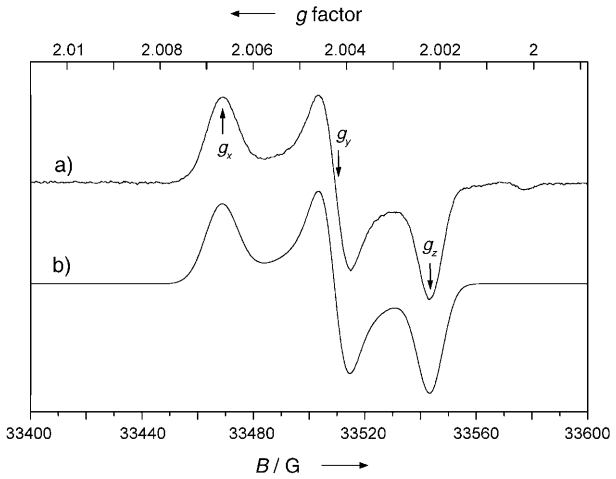


Figure 1. W-band EPR spectra of $[\mathbf{3}H]^{\bullet+}$. a) Spectrum recorded for electrochemically generated $[\mathbf{3}H]^{\bullet+}$ (1 mM) in CH_2Cl_2 at 80 K. b) Spectrum simulated by using the parameters listed in Table 1.

Table 1: Comparison of the experimental W-band g values obtained for $[(\mathbf{1}–\mathbf{3})H]^{\bullet+}$ and those calculated by DFT for $[(\mathbf{1}–\mathbf{3})H_O]^{\bullet+}$ and $[(\mathbf{1}–\mathbf{3})H_N]^{\bullet+}$.

Radical		g_x	g_y	g_z	g_{iso}
$[\mathbf{1}H]^{\bullet+}$	exptl	2.0065	2.0043	2.0022	2.0043
$[\mathbf{1}H_N]^{\bullet+}$	calcd	2.0066	2.0043	2.0023	2.0044
$[\mathbf{1}H_O]^{\bullet+}$	calcd	2.0034	2.0030	2.0023	2.0029
$[\mathbf{2}H]^{\bullet+}$	exptl	2.0063	2.0043	2.0023	2.0043
$[\mathbf{2}H_N]^{\bullet+}$	calcd	2.0064	2.0042	2.0023	2.0043
$[\mathbf{2}H_O]^{\bullet+}$	calcd	2.0036	2.0031	2.0024	2.0030
$[\mathbf{3}H]^{\bullet+}$	exptl	2.0067	2.0043	2.0022	2.0044
$[\mathbf{3}H_N]^{\bullet+}$	calcd	2.0068	2.0043	2.0023	2.0044
$[\mathbf{3}H_O]^{\bullet+}$	calcd	2.0044	2.0038	2.0022	2.0035

case convergence to a distinct energy minimum occurred. The difference in energy of the two forms of $[(\mathbf{1}–\mathbf{3})H]^{\bullet+}(g)$, $\Delta E = [E([(\mathbf{1}–\mathbf{3})H_N]^{\bullet+}) - E([(\mathbf{1}–\mathbf{3})H_O]^{\bullet+})]$, is calculated as -4.8, $+7.7$, and $-26.4\ kJ\,mol^{-1}$ for **1**H, **2**H, and **3**H, respectively. These results suggest that $[(\mathbf{1}–\mathbf{3})H_N]^{\bullet+}$ (the proton-transferred species) is favored for $[\mathbf{1}H]^{\bullet+}(g)$ and $[\mathbf{3}H]^{\bullet+}(g)$, but not for $[\mathbf{2}H]^{\bullet+}(g)$.

The bond lengths calculated for the geometry-optimized structures of $[(\mathbf{1}–\mathbf{3})H_N]^{\bullet+}$ and $[(\mathbf{1}–\mathbf{3})H_O]^{\bullet+}$ are listed in Table SI2. Each optimized structure involves an intramolecular hydrogen bond: for $[(\mathbf{1}–\mathbf{3})H_O]^{\bullet+}$, the H···N distances are calculated as 1.600 (**1**H), 1.623 (**2**H), and 1.435 Å (**3**H); for $[(\mathbf{1}–\mathbf{3})H_N]^{\bullet+}$, the O···H distances are calculated as 1.832 (**1**H), 1.781 (**2**H), and 1.867 Å (**3**H; see Supporting Information).

The g-tensor parameters calculated by DFT for $[(\mathbf{1}–\mathbf{3})H_N]^{\bullet+}$ and $[(\mathbf{1}–\mathbf{3})H_O]^{\bullet+}$ are compared with those observed experimentally in Table 1. In each case, the g values calculated for $[(\mathbf{1}–\mathbf{3})H_N]^{\bullet+}$ correspond very closely (within 100 ppm) to those observed experimentally; however, this is not true for the g values calculated for $[(\mathbf{1}–\mathbf{3})H_O]^{\bullet+}$: in particular, each g_x is calculated to be significantly lower (2000–3000 ppm) than the experimental value. Moreover, the W-band EPR spectrum of each $[(\mathbf{1}–\mathbf{3})H]^{\bullet+}$ is consistent with the presence of only a single species. Therefore, we conclude that all of the radical cations $[(\mathbf{1}–\mathbf{3})H]^{\bullet+}$ in CH_2Cl_2 solution at 80 K are present as $[(\mathbf{1}–\mathbf{3})H_N]^{\bullet+}$. Consequently, the slight energetic preference ($+7.7\ kJ\,mol^{-1}$) for $[\mathbf{2}H_O]^{\bullet+}(g)$ given by the DFT calculations is considered to be in error.

The nature of the singly occupied molecular orbital (SOMO) and the corresponding unpaired spin-density distribution were analyzed for both $[(\mathbf{1}–\mathbf{3})H_N]^{\bullet+}$ and $[(\mathbf{1}–\mathbf{3})H_O]^{\bullet+}$ (Figure 2 and Supporting Information). Each $[(\mathbf{1}–\mathbf{3})H_O]^{\bullet+}$

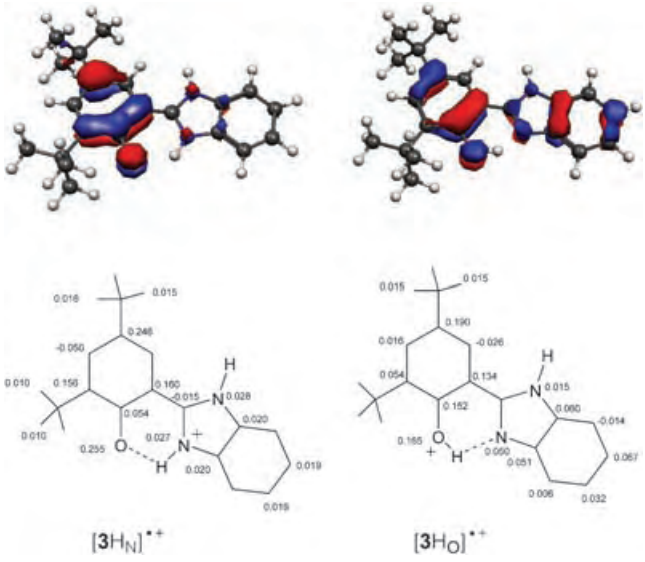


Figure 2. SOMO orbitals (top) and the spin populations (bottom) for $[\mathbf{3}H_N]^{\bullet+}$ and $[\mathbf{3}H_O]^{\bullet+}$.

involves a SOMO that extends over the phenol and imidazole rings with phenol/imidazole distributions of the unpaired spin population of approximately 70:30, 40:60, and 25:75 for $[\mathbf{3}H_O]^{\bullet+}$, $[\mathbf{1}H_O]^{\bullet+}$, and $[\mathbf{2}H_O]^{\bullet+}$, respectively. In contrast, the SOMO of each $[(\mathbf{1}–\mathbf{3})H_N]^{\bullet+}$ is localized primarily on the phenol ring, and the phenol/imidazole distribution of the unpaired spin population is approximately 90:10, 80:20, and 65:35 for $[\mathbf{3}H_N]^{\bullet+}$, $[\mathbf{1}H_N]^{\bullet+}$, and $[\mathbf{2}H_N]^{\bullet+}$, respectively. Thus, these calculations indicate that the electronic structure of $[\mathbf{3}H_N]^{\bullet+}$ is essentially that of a phenoxyl radical hydrogen-bonded to an imidazolium cation.

For the phenol ring of each $[(\mathbf{1}–\mathbf{3})H_N]^{\bullet+}$, the typical[5b,7] pattern of an alternating spin-density distribution is obtained with a significant amount of positive spin population located at the O, C_{ortho}, and C_{para} atoms (Figure 2 and Supporting Information). Also, there is a positive spin population at the phenolic carbon atom that is indicative of a redistribution of the spin density from that of an isolated phenoxyl radical and is attributed to hydrogen-bond formation.[7] The length of the C–O bond is calculated (Table SI2) to be significantly longer in $[(\mathbf{1}–\mathbf{3})H_O]^{\bullet+}$ (1.332 (**1**H), 1.343 (**2**H), and 1.307 Å (**3**H)) than in $[(\mathbf{1}–\mathbf{3})H_N]^{\bullet+}$ (1.265 (**1**H), 1.270 (**2**H), and 1.261 Å (**3**H)). The latter values are in excellent agreement with: 1) the length of the C–O bond of $\mathbf{1}^{\bullet}$ (1.264(5) Å) in the Cu^{II}–phenoxyl radical complex $[Cu(\mathbf{1}^{\bullet})(\mathbf{1})](BF_4)$[6a,b] and 2) those calculated (1.26–1.27 Å) for the C–O bond of a phenoxyl radical hydrogen-bonded to an imidazolium group.[7]

 © 2005 Wiley-VCH Verlag GmbH & Co. KGaA, Weinheim

The above analysis of the g tensors has illustrated that this approach represents a powerful tool for determining the nature of a phenoxyl radical. Theoretical[7,8] and experimental studies[4,5b,9] have indicated that hydrogen bonding to a phenoxyl (or tyrosyl) radical results in a considerable lowering of the g_x value but leaves g_y and g_z essentially unaffected. The g_x values observed for each $[(\mathbf{1}–\mathbf{3})H_N]^{\bullet+}$ (2.0065–2.0067, Table 1) are very similar to those observed for hydrogen-bonded tyrosyl radicals; for example, for γ-irradiated crystals of tyrosine·HCl, $g_x = 2.0067$;[10] $Tyr_D^{\bullet}$ of PSII, $g_x = 2.00643$ (radical generated at cryogenic temperature)[4] and $g_x = 2.00756$ (radical generated at physiological temperature);[11] $Tyr^{\bullet}$ of HSV1 RNR: $g_x = 2.0076$[12] and hydrogen-bonded phenoxyl radical compounds (g_x ranging from 2.0061 to 2.0066).[5b] These g_x values are significantly lower than those observed for non-hydrogen-bonded tyrosyl radicals; for example, $Tyr^{\bullet}$ of *E. coli* RNR, $g_x = 2.0087$,[9] or of *S. typhimurium* RNR,[13] $g_x = 2.0089$.

Theoretical studies of the g tensors of aromatic free radicals[14] indicate that variations in the g_x value of a phenoxyl radical may be understood as arising from a combination of two effects: 1) changes in the unpaired spin population at the oxygen atom, the constituent atom with the largest spin–orbit coupling constant; and 2) changes in the relative energies of two oxygen-based orbitals, the out-of-plane p_z orbital, which makes a significant contribution to the SOMO of a phenoxyl radical, and the in-plane p_y lone pair orbital, the contribution of which to the g shift arises as a result of spin–orbit coupling with the electron in the SOMO. This latter effect produces a magnetic moment along the C–O axis that increases the value of g_x. Formation of an in-plane hydrogen bond stabilizes the p_y lone pair, increases the energy difference between this orbital and the SOMO, and results in less effective spin–orbit coupling and a decrease in the g_x value (vide infra). In this respect, the species $[(\mathbf{1}–\mathbf{3})H_O]^{\bullet+}$ represent extreme cases in which the p_y lone pair is directly involved in the O–H bond and therefore, is not involved in efficient spin–orbit coupling with the SOMO, which explains the very low g_x values calculated for these species. For the $[(\mathbf{1}–\mathbf{3})H_N]^{\bullet+}$ radical cations, the DFT calculations indicate that the strength of the hydrogen bond increases across this series, that is, the O···HN distance decreases (1.867, 1.832, and 1.781 Å, respectively; see Supporting Information) and leads to a decreased g_x value. For these $[(\mathbf{1}–\mathbf{3})H_N]^{\bullet+}$ systems, in addition to the effect of hydrogen bonding on the g_x value, the extent of the delocalization of the unpaired electron onto the imidazole ring must be considered. Across this series, the unpaired spin population at the oxygen atom ($\rho(O) = 0.255$, 0.230, and 0.189, respectively; see Figure 2 and Supporting Information) decreases as a result of the increased delocalization of the unpaired spin density onto the imidazole ring (vide infra), and this also will lead to a decrease in the g_x value. Thus, these two effects operate in the same sense, consistent with the relative magnitudes of the g_x values of $[\mathbf{3}H_N]^{\bullet+}$ (2.0067), $[\mathbf{1}H_N]^{\bullet+}$ (2.0065), and $[\mathbf{2}H_N]^{\bullet+}$ (2.0063).

In conclusion, we have demonstrated that the one-electron oxidation of (**1**–**3**)H occurs by a PCET mechanism and produces the corresponding $[(\mathbf{1}–\mathbf{3})H_N]^{\bullet+}$; that is, a phenoxyl radical hydrogen-bonded to an imidazolium cation. The resolution of the principal g values by W-band EPR spectroscopy and the interpretation of these data by DFT calculations were essential in determining the nature of the $[(\mathbf{1}–\mathbf{3})H]^{\bullet+}$ radical cations. Furthermore, the DFT calculations provided valuable insight into the electronic structure of these species. The g_x value of the $[(\mathbf{1}–\mathbf{3})H_N]^{\bullet+}$ radical cations is lower than that of a simple phenoxyl radical owing to delocalization of the unpaired spin and orbital-stabilization effects, both of which are directly related to the formation of an O···HN hydrogen bond. These $[(\mathbf{1}–\mathbf{3})H_N]^{\bullet+}$ radical cations, notably $[\mathbf{3}H_N]^{\bullet+}$, represent valuable chemical analogues of $Tyr_D^{\bullet}$ in PSII, and further spectroscopic and theoretical studies of these species are currently being undertaken in our laboratories.

Experimental Section

Each radical cation was generated electrochemically by controlled potential coulometry with a platinum-grid working electrode, an $Ag/AgNO_3$ reference electrode, and a platinum brush in a counter electrode compartment. Each experiment was performed under dinitrogen at −25 °C with the compound (1 mM) in degassed CH_2Cl_2 containing $[n\mathrm{Bu_4N}](BF_4)$ (0.2 M) as background electrolyte. The solution was transferred under exclusion of dioxygen into a W-band quartz tube (inner diameter 0.7 mm, length 3 cm) with a microsyringe. Each tube was inserted into a cryovial which was immediately frozen and stored in liquid nitrogen.

All calculations were performed with the ORCA program.[15] Geometry optimizations were performed in redundant internal coordinates by using the pure density functional[16] BP[17] method with the TZVP[18] basis set on all atoms. For both the geometry optimization of the radical species and the g-tensor calculation, the CH_2Cl_2 solvent ($\varepsilon = 9.08$) was simulated by the COSMO dielectric continuum approach.[19] The B3LYP[20] hybrid DFT method, together with the EPR-II[21] basis set, was employed for the calculation of the magnetic properties at the optimized geometries of the radical species. Molecular g tensors were calculated by the coupled-perturbed Kohn–Sham method[22] and the multicenter, spin–orbit mean-field[23] (SOMF) spin-orbit coupling operator in the resolution-of-the-identity approximation.[24]

W-band (94 GHz) spectra were recorded on a Bruker Elexsys E680 spectrometer at 80 K with a microwave power of 0.32 μW, 5 G field modulation amplitude at 10 kHz modulation frequency, and a lock-in time constant of 82 ms. The magnetic field was calibrated against a LiLiF g standard[25] at microwave frequencies measured by the integrated frequency counter; all spectra were normalized to 94.0 GHz. The simulated spectra and the associated parameters were obtained with Bruker Simfonia software.

Received: March 30, 2005
Published online: July 22, 2005

Keywords: density functional calculations · electronic structure · EPR spectroscopy · hydrogen bonds · radical ions

[1] a) J. Stubbe, W. A. van der Donk, *Chem. Rev.* **1998**, *98*, 705–762; b) J. Stubbe, D. G. Nocera, C. S. Yee, M. C. Y. Chang, *Chem. Rev.* **2003**, *103*, 2167–2201.

[2] a) G. T. Babcock, M. Espe, C. Hoganson, N. Lydakis-Simantiris, J. McCracken, W. Shi, S. Styring, C. Tommos, K. Warncke, *Acta Chem. Scand.* **1997**, *51*, 533–540; b) G. M. Ananyey, I. Sakiyan, B. A. Diner, G. C. Dismukes, *Biochemistry* **2002**, *41*, 974–980; c) A. W. Rutherford, A. Boussac, P. Faller, *Biochim. Biophys. Acta* **2004**, *1655*, 222–230.

 © 2005 Wiley-VCH Verlag GmbH & Co. KGaA, Weinheim

[3] K. A. Campell, J. M. Peloquin, B. A. Diner, X.-S. Tang, D. A. Chisholm, R. D. Britt, *J. Am. Chem. Soc.* **1997**, *119*, 4787 – 4788.
[4] P. Faller, C. Goussias, A. W. Rutherford, S. Un, *Proc. Natl. Acad. Sci. USA* **2003**, *100*, 8732 – 8735.
[5] a) T. Maki, Y. Araki, Y. Ishida, O. Onomura, Y. Matsumura, *J. Am. Chem. Soc.* **2001**, *123*, 3371 – 3372; b) F. Thomas, O. Jarjayes, H. Jamet, S. Hamman, E. Saint-Aman, C. Duboc, J.-L. Pierre, *Angew. Chem.* **2004**, *116*, 604 – 607; *Angew. Chem. Int. Ed.* **2004**, *43*, 594 – 597; c) I. J. Rhile, J. M. Mayer, *J. Am. Chem. Soc.* **2004**, *126*, 12718 – 12719; d) I. J. Rhile, J. M. Mayer, *Angew. Chem.* **2005**, *117*, 1624 – 1625; *Angew. Chem. Int. Ed.* **2005**, *44*, 1598 – 1599.
[6] a) L. Benisvy, A. J. Blake, D. Collison, E. S. Davies, C. D. Garner, E. J. L. McInnes, J. McMaster, G. Whittaker, C. Wilson, *Chem. Commun.* **2001**, 1824 – 1825; b) L. Benisvy, A. J. Blake, D. Collison, E. S. Davies, C. D. Garner, E. J. L. McInnes, J. McMaster, G. Whittaker, C. Wilson, *Dalton Trans.* **2003**, 1975 – 1985; c) L. Benisvy, E. Bill, A. J. Blake, D. Collison, E. S. Davies, C. D. Garner, C. I. Guindy, E. J. L. McInnes, G. McArdle, J. McMaster, C. Wilson, J. Wolowska, *Dalton Trans.* **2004**, 3647 – 3653; d) L. Benisvy, E. Bill, A. J. Blake, D. Collison, E. S. Davies, C. D. Garner, E. J. L. McInnes, J. McMaster, S. Ross, C. Wilson, unpublished results; e) L. Benisvy, PhD Thesis, University of Nottingham, Nottingham, UK, **2001**.
[7] P. J. O'Malley, *J. Am. Chem. Soc.* **1998**, *120*, 11732 – 11737.
[8] a) J. R. Asher, N. L. Doltsinis, M. Kaupp, *J. Am. Chem. Soc.* **2004**, *126*, 9854 – 9861; b) M. Kaupp, T. Gress, R. Reviakine, O. L. Malkina, V. G. Malkin, *J. Phys. Chem. B* **2003**, *107*, 331 – 337; c) M. Engström, F. Himo, A. Gräslund, B. Minaev, O. Vahtras, H. Ågren, *J. Phys. Chem. A* **2000**, 104, 5149 – 5153.
[9] S. Un, M. Atta, M. Fontecave, A. W. Rutherford, *J. Am. Chem. Soc.* **1995**, *117*, 10713 – 10719.
[10] E. L. Fasanella, W. Gordy, *Proc. Natl. Acad. Sci. USA* **1969**, *62*, 299 – 304.
[11] P. Dorlet, A. W. Rutherford, S. Un, *Biochemistry* **2000**, *39*, 7826 – 7834.
[12] P. J. van Dam, J.-P. Willems, P. P. Schmidt, S. Pötsch, A.-L. Barra, W. R. Hagen, B. M. Hoffman, K. K. Andersson, A. Gräslund, *J. Am. Chem. Soc.* **1998**, *120*, 5080 – 5085.
[13] P. Allard, A.-L. Barra, K. K. Andersson, P. P. Schmidt, M. Atta, A. Gräslund, *J. Am. Chem. Soc.* **1996**, *118*, 895 – 896.
[14] a) A. J. Stone, *Mol. Phys.* **1963**, *6*, 509 – 515; b) A. J. Stone, *Mol. Phys.* **1964**, *7*, 311 – 316.
[15] F. Neese, ORCA, An ab initio, Density Functional and Semi-empirical Program Package, Version 2.4.13, Max-Planck-Institut für Bioanorganische Chemie, Mülheim an der Ruhr, Germany, **2004**.
[16] W. Koch, M. C. Holthausen, *A Chemist's Guide to Density Functional Theory*, Wiley-VCH, Weinheim, **2000**.
[17] a) A. D. Becke, *Phys. Rev. A* **1988**, 38, 3098 – 3100; b) J. P. Perdew, *Phys. Rev. B* **1986**, 33, 8822 – 8824.
[18] A. Schäfer, C. Huber, R. Ahlrichs, *J. Chem. Phys.* **1994**, *100*, 5829 – 5835.
[19] A. Klamt, G. Schüürmann, *J. Chem. Soc.*, *Perkin Trans.* 2 **1993**, 793 – 805.
[20] a) C. T. Lee, W. T. Yang, R. G. Parr, *Phys. Rev. B* **1988**, *37*, 785 – 789; b) A. D. Becke, *J. Chem. Phys.* **1993**, *98*, 5648 – 5652; c) P. J. Stephens, F. J. Devlin, C. F. Chabalowski, M. J. Frisch, *J. Phys. Chem.* **1994**, *98*, 11623 – 11627.
[21] V. Barone in *Recent Advances in Density Functional Methods* (Ed.: D. P. Chong), World Scientific Publishing, Singapore, **1996**.
[22] F. Neese, *J. Chem. Phys.* **2001**, *115*, 11080 – 11096.
[23] B. A. Hess, C. M. Marian, U. Wahlgren, O. Gropen, *Chem. Phys. Lett.* **1996**, *251*, 365 – 371.
[24] F. Neese, *J. Chem. Phys.* **2005**, *122*, 034107/1 – 13.
[25] A. Stesmans, G. van Gorp, *Rev. Sci. Instrum.* **1989**, *60* 2949 – 2952.

 © 2005 Wiley-VCH Verlag GmbH & Co. KGaA, Weinheim

Mesoporous Silicates

DOI: 10.1002/anie.200500113

Synthesis of Mesocage Structures by Kinetic Control of Self-Assembly in Anionic Surfactants**

Alfonso E. Garcia-Bennett, Natalia Kupferschmidt, Yasuhiro Sakamoto, Shunai Che, and Osamu Terasaki*

Molecular self-organization is the topic of numerous fundamental and applied studies for its potential in diverse applications in areas ranging from catalysis to photonic crystals, from biomimetic chemistry to sensor technology.[1–3] The study of such systems is central to physics, mathematics, biological systems, and materials chemistry alike. Innovative methods for the assembly of ordered structures with self-assembling building units at various length scales are constantly proposed. Among these, the self-assembly of lyotropic liquid crystals to form mesoporous structures, as pioneered by Kresge et al.,[4] is the center of a large academic and industrial effort due to the high potential to tailor porous properties of high-surface-area inorganic frameworks through variations in the self-assembling surfactant template and synthesis conditions. Functionalization of their internal surfaces renders them suitable for applications. New synthetic methods for the preparation of mesoporous structures are being developed. For example, the enlargement of pore sizes by the use of polymeric surfactants has led to mesoporous solids with enhanced diffusion and transport properties such as SBA-15 (*p6mm*), FDU-5 ($Ia\bar{3}d$), and SBA-16 ($Im\bar{3}m$).[5,6] Low-symmetry mesostructures have been reported previously, obtained using bolaform surfactants, as in the case of two-

[*] Dr. A. E. Garcia-Bennett, N. Kupferschmidt, Dr. Y. Sakamoto, Prof. O. Terasaki
Structural Chemistry, Arrhenius Laboratory
Stockholm University
10691 Stockholm (Sweden)
Fax: (+46) 8-163-118
E-mail: alf@struc.su.se
Prof. S. Che
Department of Chemistry
School of Chemistry and Chemical Technology
Shanghai Jiao Tong University
800 Dongchuan Road, Shanghai, 200240 (P. R. China)

[**] We are grateful to Dr. Bodo Zibrowius and Prof. Ferdi Schüth (Max-Planck-Institut für Kohlenforschung, Mülheim) for conducting NMR experiments and for helpful discussions, and to AminoScience Lab, Ajinomoto Co., Inc., for providing *N*-lauroyl glutamic acid. A.E.G.-B. is grateful to the European Research and Training Network "Nanocage Materials" for funding (grant no. HPRN-CT-2002-00193). This work was partly supported by the Swedish Science Council (VR) and by Core Research for Evolutional Science and Technology (CREST) of JST and BNRI, Japan (O.T.). The authors are grateful to Q. Chen (East China Normal University) for additional NMR experiments.

Supporting information for this article is available on the WWW under http://www.angewandte.org or from the author.

© 2005 Wiley-VCH Verlag GmbH & Co. KGaA, Weinheim

dimensional SBA-8 (*c2mm*),[7] and by evaporation-induced self-assembly (EISA).[8,9]

Recently, the preparation of highly ordered mesoporous structures using anionic surfactants and co-structure-directing agents (CSDAs) was reported.[10] This synthesis route has proven successful for the formation of several novel mesoporous phases. A face-centered cubic structure ($Fd\bar{3}m$), named anionic mesoporous solid (AMS-*n*) AMS-8, was identified and modeled by electron crystallography.[11] Furthermore, a hexagonal structure with chiral arrangement of the pores has been prepared.[12] The diversity of structure types that are possible using *N*-acyl amino acid anionic surfactants is already impressive, but little is known about the interaction of the CSDA with the anionic head group of the surfactant and its role in the synthesis mechanism.

A third structure, formed by the use of *N*-lauroyl glutamic acid as anionic surfactant and (3-aminopropyl)trimethoxysilane (APS) as CSDA, has been proposed. Named AMS-2, this mesocage silicate is composed of nonperiodic structural modulations observable as unit cell shifts of one-half.[13] Spherical micelles, which are used as templates for mesocage solids such as AMS-2, form in lipid/water and surfactant systems and undergo thermal, compositional, and time-dependent kinetically controlled structural transformations. Transitions can be described in terms of the surfactant packing parameter *g*, which is dependent on the kinetic surfactant chain length, the effective head-group area at the micelle surface, and the total surfactant volume. In practice, few phases are observed and it is difficult to control kinetics in structural transformations.[14]

Herein we demonstrate the possibility of inducing structural transformations in the synthesis of mesocage materials by delaying the time of addition of the silica source (tetraethyl orthosilicate, TEOS) with respect to the CSDA, the importance of which is clearly associated with precise control of the micellar (local) and structural (mesoscale) characteristics of the resulting porous solid.

A phase transformation expanding four different cubic structures was studied. Powder X-ray diffraction (XRD) data are unable to yield detailed structural information despite the increased order of AMS-*n* mesostructures. In contrast, electron microscopy investigations clearly show that it is possible to form mesoporous structures of lower symmetry with counterparts in atomic-scale materials such as intermetallic compounds.

These investigations open up avenues in synthesis, characterization, and application that are central to the development not only of mesoporous structured materials but also nanotechnology and materials engineering.

Figure 1 shows high-resolution transmission electron microscopy (HRTEM) images recorded along high-symmetry zone axes of calcined mesostructures synthesized with different APES-*t*-TEOS, for which *t* denotes the time in minutes between the addition of the CSDA and TEOS, *N*-lauroyl glutamic acid as self-assembling anionic surfactant, and aminopropyltriethoxysilane (APES) as CSDA. Tilt-series selected-area electron diffraction (SAED) patterns were recorded to determine the structural characteristics of each sample and confirmed the presence of four separate meso-

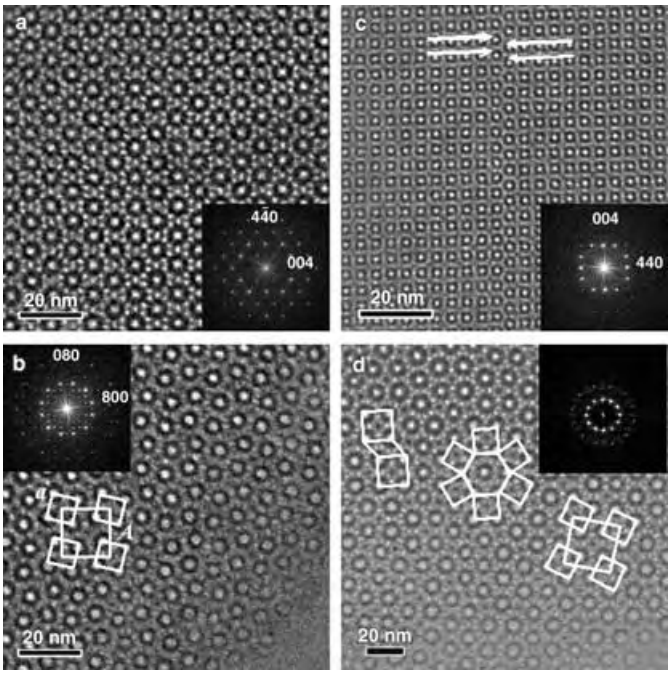


Figure 1. HRTEM images of mesocage structures synthesized by using *N*-lauroyl glutamic acid as surfactant and APES as CSDA. Images are viewed along a) [110] (AMS-8, $Fd\bar{3}m$), b) [001] (AMS-9, $P4_2/mnm$), c) [100] (SBA-1-type, $Pm\bar{3}n$), and d) (AMS-2; modulated structure). White insets show the periodic zigzag arrangement of cages in AMS-9 and the resulting superlattice, where $a = 84$ and $A = 168$ Å (b), and the nonperiodic arrangement of domains in AMS-2, composed of two distinct units, namely, slabs of $Pm\bar{3}n$ and $P4_2/mnm$ structures, as well as other motives and defects of the stacking-fault type (d). The insets show in all cases corresponding Fourier transform diffractograms.

structures in the *N*-lauroyl glutamic acid/APES system reported here. All samples display a high degree of periodicity over large areas and stability under the electron beam. Figure 1 a shows an HRTEM image recorded along the [110] orientation of APES-0-TEOS. Electron microscopy investigations are consistent with a cubic structure, and extinction conditions allow the space group symmetry to be confirmed as $Fd\bar{3}m$.

At first instance it is possible to deduce a lattice unit based on a cubic unit cell ($Pm\bar{3}n$) with $a = 84.0$ Å for a calcined sample of APES-2-TEOS (Figure 1 b). Periodic stacking faults characterized by unit cell shifts of one-half are clearly observed. The faults are arranged regularly to form a 2D antiphase boundary. From this image and the corresponding diffraction pattern a superlattice unit cell is easily determined, as outlined in Figure 1 b (inset). From a series of HRTEM tilt-series images and diffraction patterns it is possible to determine the crystal class and unit cell lattice parameters. The new superstructure is tetragonal, with lattice constants $(A)a = 167.9$ and $c = 84.0$ Å. This novel structure has been named AMS-9 (anionic surfactant-templated mesoporous silica 9). The formation of similar superstructures from cubic phases is well documented for intermetallic compounds and liquid crystals.[15,16] This strongly suggests that the formation of lower-symmetry 3D structures can be achieved at the mesoscale.

 © 2005 Wiley-VCH Verlag GmbH & Co. KGaA, Weinheim

Figure 2 shows SAED patterns recorded along the [001], [110], [101], and [111] directions of AMS-9. The unusually numerous reflection spots at higher scattering angles in comparison with other mesoporous materials indicate a highly ordered mesostructure and a sharp density boundary between cage cavity and wall. Observable reflections can be summarized with the following general conditions: hkl, $hk0$, hhl, $hh0$: no condition, $0kl$: $k+l=2n$, $00l$: $l=2n$, $0k0$: $k=2n$, reducing the possible space-group symmetry to $P4_2nm$, $P\bar{4}n2$, or $P4_2/mnm$. The latter was chosen for its highest symmetry.

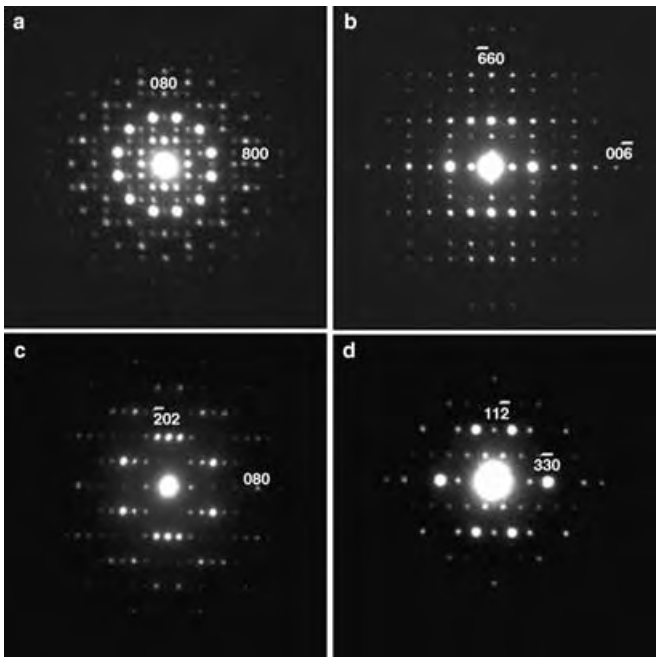


Figure 2. SAED patterns of calcined AMS-9 recorded along a) [001], b) [110], c) [101], and (d) [111] directions. Patterns are indexed on the basis of a tetragonal unit cell with lattice constants $a=167.9$ and $c=84.0$ Å. Reflection conditions are consistent with the space-group symmetry $P4_2/mnm$.

A 3D reconstruction of the structure,[17] based on analysis of Fourier transform (FT) diffractograms taken from thin parts of crystals (see Supporting Information), along high-symmetry zone axes of AMS-9 was conducted. Phase and amplitude of the structure factors were extracted from the 16 strongest reflections. Amplitudes were normalized by using common reflections obtained from images along [001], [101], [111], and [110] orientations. However, a unique set of phases could not be extracted from these four images due to the small number of common reflections encountered in tetragonal systems along these directions. The most probable data set (see Supporting Information) out of four possibilities can be deduced by considering neighboring cubic cage-type structures $Pm\bar{3}n$ and $Fd\bar{3}m$. From electrostatic potential density maps, it follows that cages in AMS-9 are arranged with space group $P4_2/mnm$. Figure 3a shows three 2D-sliced electrostatic potential density maps of the unit cell of AMS-9.

To obtain quantitative data about cage size and connectivity between cages from reconstructed data, an accurate estimation of the contrast transfer function (CTF) must be conducted. Almost all strong reflections of AMS-9 are at higher scattering angles than those of other mesoporous materials, so the relative intensity of each reflection is more sensitive to the CTF correction. A tentative model of the cage arrangement can be constructed based on $Pm\bar{3}n$ structural units (Figure 3b). The unit cell of AMS-9 is composed of 30 cages. Further analysis is being conducted to determine the size and connectivity of cages, and our findings will be reported shortly.

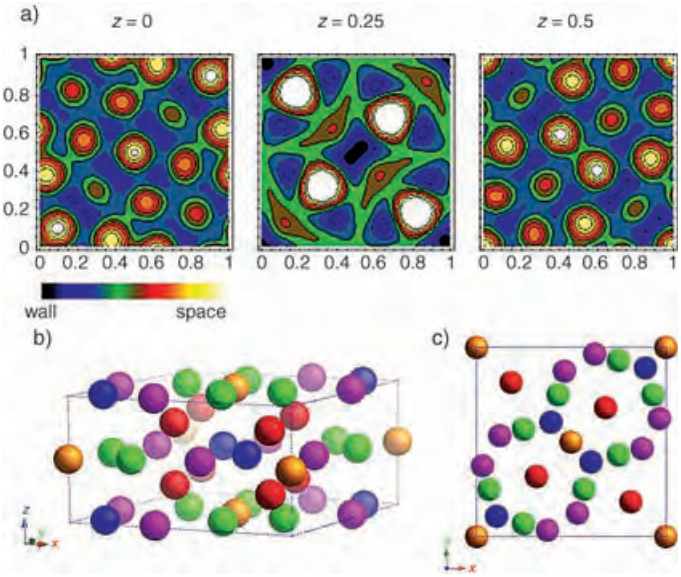


Figure 3. a) 2D electrostatic potential density maps derived from electron microscopy of the unit cell of AMS-9, shown parallel to the [001] plane. The unit cell slices are taken with $z=0$, 0.25, and 0.5. White contrast represents the pore space, and black contrast the silica wall. b), c) Model of the packing arrangement of cages in AMS-9, based on a $Pm\bar{3}n$ unit cell containing 30 cages (b), and viewed along the [001] direction (c). Each color represents a different crystallographic site of $P4_2/mnm$.

Samples synthesized in the range APES-6 $<t>$ 9-TEOS showed modulated structures that often contained a large number of defects of the stacking-fault type. Figure 1d shows a typical HRTEM image recorded on AMS-2 (APES-6-TEOS). Two structural units can be observed, based on $Pm\bar{3}n$ and $P4_2/mnm$ mesocage solids AMS-9 and SBA-1, in addition to stacking faults and motives showing the typical arrangement of cages.

A transition with time following the sequence $Fd\bar{3}m \rightarrow P4_2/mnm \rightarrow Pm\bar{3}n \rightarrow$ modulated structure $\rightarrow Fd\bar{3}m$ is observed when materials are prepared at 60 °C in the range APES-0 $<t>$ 10-TEOS. All structures obtained are mesocage materials. The apparent return to $Fd\bar{3}m$ is not fully understood. The proximity of all four structures in the phase diagram of *N*-lauroyl glutamic acid is a representation of the small differences in stabilization energy between each structure type. It is evident that small changes in the local environment of the spherical micelles caused by interaction and hydrolysis of the CSDA have a pronounced effect on the overall packing arrangement of the micelle. Similar structural transitions have been observed in systems using *N*-lauroyl glycine, lauric acid, and pluronics as surfactants, and APS, *N*-trimethoxysilyl-

 © 2005 Wiley-VCH Verlag GmbH & Co. KGaA, Weinheim

propyl-*N*,*N*,*N*-trimethylammonium chloride (TMAPS), and (3-mercaptopropyl)triethoxysilane (MPTS)[18] as CSDAs.

Mesostructures with $Fd\bar{3}m$ and $Pm\bar{3}n$ space-group symmetries have been reported previously,[11,16] and are the subject of continued structural and applied research as a result of their intricate 3D network of mesocages, connected to each other by small (< 20 Å) pore windows which can be used for the entrapment of functional guests such as dyes, metal oxides, or metal centers. The unit cell parameters for each of these structures as derived from TEM data are $a =$ 162.6 and $a = 82.8$ Å for the $Fd\bar{3}m$ and $Pm\bar{3}n$ phases, respectively. Both $Fd\bar{3}m$ (named AMS-8) and $Pm\bar{3}n$ (SBA-1-type) mesostructures (Figure 1a and c) are formed by self-assembly and cubic packing of spherical or pseudospherical micelles of different sizes. In the case of AMS-2 and AMS-9, the formation of new types of spherical cages is evident from electron microscopy. Evidence of a transition mechanism based on stacking faults can be clearly observed by electron microscopy (see Supporting Information). The connectivity and pore arrangement of intermediate phases are expected to be considerably different from samples that show no structural defects.

The structural and porous characteristics of samples reported here are summarized in Table 1. Raw-data nitrogen adsorption isotherms and pore size distribution curves are shown in the Supporting Information. From the capillary condensation steps it is possible to identify a structural change in samples synthesized with different APES-*t*-TEOS. An extra step is observed in the capillary condensation region of AMS-8, owing to a significant difference in cage size between its larger cage (44.5 Å) and smaller cage (40.3 Å). The adsorption curves of cubic structures SBA-1 and AMS-9 follow similar adsorption/desorption paths and show no hysteresis in the desorption branch; this indicates similarities in the packing arrangement of these two structures. However AMS-9 shows a higher total pore volume and a slight shift to higher pressures owing to the presence of larger cages. The modulated structure of AMS-2 shows decreased adsorption capacity and a smaller cage size. In this modulated structure it is possible that cages may be blocked to the external surface of the mesoporous particles, as a darkening of this sample is observed after calcination of the surfactant. Pore size distribution curves for all structures show additional peaks centered around 10 Å. These can be assigned to adsorption in the small connecting channels between cages.

The ^{29}Si MAS NMR spectra of calcined and extracted samples of AMS-9 are shown in Figure 4. The presence of T^3 and T^2 peaks between 50 and 65 ppm, attributed to $(R)Si(OSi)_3$ and $R(HO)Si(OSi)_2$, respectively, in the ^{29}Si MAS NMR spectra of a solvent-extracted sample of AMS-9 is evidence for the functionalization of the amorphous silicate framework with aminopropylsilane groups. The T^n/Q^n ratio of the as-synthesized (4.6:1) and extracted samples (3.2:1) of AMS-9 both indicate high incorporation of the CSDA. The data obtained by deconvolution agree well with the ratios derived from the integrals. This constitutes a direct method for incorporation of organic functional groups and offers considerable advantages for further functionalization of mesoporous structures over grafting and post-synthetic treatments.[19]

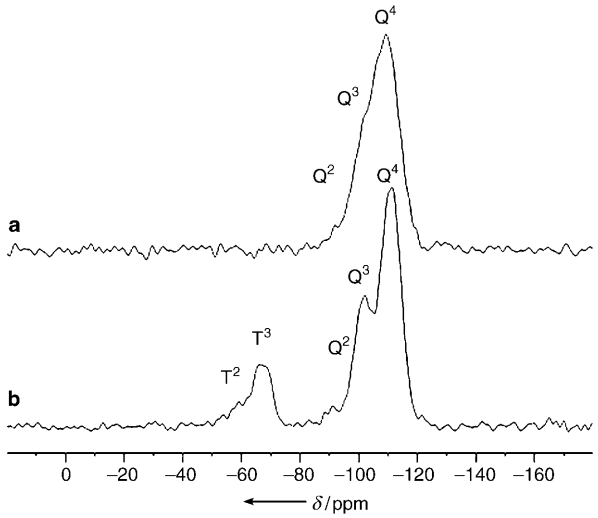


Figure 4. ^{29}Si CP-MAS NMR spectrum of calcined AMS-9 (a), and ^{29}Si MAS NMR spectrum of an extracted sample of AMS-9 (b). Peaks at $\delta = -92$, -100, and -109 ppm are attributed to Q^2, Q^3,and Q^4 silicon atoms ($Q^n = Si(OSi)_n(OH)_{4-n}$). T^3 and T^2 peaks can be attributed to $(R)Si(OSi)_3$ and $R(HO)Si(OSi)_2$, respectively.

Table 1: Structural and porous characteristics of mesocage solids synthesized with different APES-*t*-TEOS.

APES-*t*-TEOS (min)	Mesostructure (space group)	Unit cell parameter (TEM) [Å]	Unit cell parameter (XRD) [Å]	Pore size (DFT) [Å]	Total pore volume [cm^3g^{-1}]	Surface area [m^2g^{-1}]
0	3D cubic ($Fd\bar{3}m$)	162.6	154.9	42.4 40.2	0.58	755.3
2	3D tetragonal ($P4_2/mnm$)	167.9 (*c*) 84.0 (*a*)	172.0 (*c*) 90.2 (*a*)	38.3	0.60	872.2
4	3D cubic ($Pm\bar{3}n$)	88.8	94.8	36.0	0.58	890.4
6	modulated structure			34.2	0.43	710.0
10	3D cubic ($Fd\bar{3}m$)	145.6	152.5	44.5 40.3	0.59	724.5

Figure 5 shows XRD patterns of a structural transformation in the AMS-2 system induced by delaying addition of the silica source from 0 to 10 min (APES-*t*-TEOS). Clear structural transformations are observed. The XRD patterns obtained at APES-0-TEOS and APES-10-TEOS show similar diffraction peaks that can be indexed on the basis of a cubic unit cell with space group symmetry $Fd\bar{3}m$ with unit cell lattice constants of 154.9 and 152.5 Å for APES-0-TEOS and APES-10-TEOS, respectively. It is not possible to derive structural information directly from the XRD of samples prepared in the range APES-1-TEOS to APES-9-TEOS due

 © 2005 Wiley-VCH Verlag GmbH & Co. KGaA, Weinheim

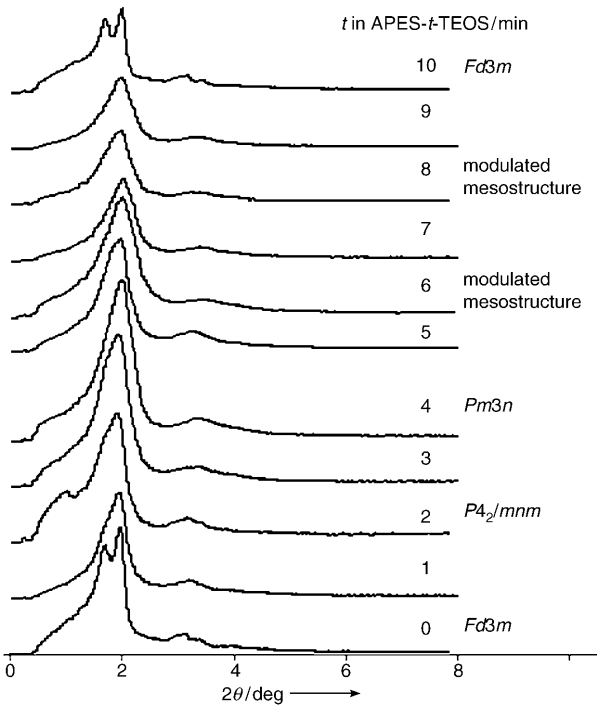


Figure 5. XRD patterns of calcined samples of mesostrucures synthesized by variation of the time of addition of the silica source with respect to the CSDA (APES-*t*-TEOS).

to the proximity of diffraction peaks at low scattering angles and the various defects associated with each structure. A typical example is the case of the $P4_2/mnm$ structure (APES-2-TEOS), where both SAED patterns show many very sharp reflections at low scattering angle.

In the system described herein the interaction between the CSDA and the hydrophilic head group of the anionic surfactant governs the phase transformation and allows control of the structural features of the desired phase. This might be due to an increase in the hydrophobicity at the interface between the surfactant head group and the CSDA. The use of organoalkoxysilanes has been noted to cause a stabilization of the structural properties of the resulting silicate products.[19] The rate of hydrolysis of the organoalkoxysilane (APES) is considerably slower than that of the tetraalkoxysilane (TEOS) due to the presence of the organic group bonded to Si. The addition of the latter allows the stabilizing anionic surfactant/CSDA micelle to "freeze" prior to condensation of the framework.

Bimodal spherical micelles are formed in this system in a ratio that varies considerably as the CSDA is hydrolyzed and interacts electrostatically with the surfactant head group, forcing the micellar interface to undergo conformational changes in shape and size. The possibility to study these changes through silicate intermediate phases offers the potential to control not only the structure but also the cage shape and connectivity with increased accuracy. This has been demonstrated by use of a CSDA to form a new structure, named AMS-9 ($P4_2/mnm$).

Analysis by HRTEM and fast Fourier transform (FFT) clearly shows the evolution with time of the CSDA effect. Ordered structures with long-range order are observed, in contrast to XRD evidence that reveals broad diffraction peaks suggesting disordered pore structures.

A fast and simple method with potential to form new structures, to design the extent of defects and size and shape of mesocages, and to functionalize the internal surface of mesoporous materials has been described. This approach has been applied in different anionic surfactant/CSDA systems and is largely extendable to different interactions by charge matching with the corresponding CSDA. Further synthetic and structural studies are being conducted and will be reported shortly.

Experimental Section

In a typical synthesis 0.2 g of *N*-lauroyl L-glutamic acid (C_{12}GlutA) was dissolved in 20 mL of deionized water with stirring at 80 °C overnight. The solution was cooled to 60 °C before 0.36 g of APES was added with rapid stirring (300 rpm). Tetraethyl orthosilicate (TEOS, 1.5 g) was added after a period of between 0 and 10 min (APES-*t*-TEOS) to give a final TEOS/APES/C_{12}GlutA/H_2O molar ratio in the gel of 1:0.21:0.085:154.

The pH value of the starting surfactant solution was 3.54 and rose rapidly to 9.30 (within seconds) on addition of the CSDA. The pH value of the reaction gel was 9.30 prior to the addition of TEOS. The pK_a values for the carboxylate groups in C_{12}GlutA were estimated on the basis of data for the free amino acid to be 2.19 and 4.25, while the isoelectronic point is 3.22. This implies that under the conditions of synthesis a strong electrostatic interaction between the surfactant head group and the CSDA is expected. The resultant silica gel solution was stirred for 10 min at 60 °C to promote hydrolysis of the CSDA and the silicate precursor. The reaction gel was then allowed to stand at 60 °C for 1 d with no stirring and for a further 2 days at 100 °C. After the reaction was complete the precipitate was collected by filtration, washed with 100 mL of H_2O, and dried overnight at room temperature. The surfactant was removed by calcination at 550 °C (1 h in flowing N_2, then 6 h in O_2) to give the porous AMS-*n* silicates. Alternatively, the surfactant was removed by solvent extraction in a Soxhlet apparatus with ethanol for 3 days.

XRD patterns were recorded on an STOE powder diffractometer equipped with $Cu_{K\alpha}$ radiation (40 kV, 20 mA) at a rate of 1.0 deg min^{-1} over the range of 1.0 to 10.0°.

The N_2 adsorption/desorption isotherms were measured at −196 °C on an ASAP 2020 Micromeritics Instrument. Calcined mesoporous AMS-*n* was outgassed for 6 h at 200 °C and 0.3 kPa. The BET specific surface area was evaluated from the adsorption data in the relative pressure range from 0.05 to 0.3. The total pore volume was estimated from the amount adsorbed at a relative pressure of 0.96. Pore size distribution curves were derived by NLDFT by assuming a spherical model of cages.

TEM was carried out with a JEOL JEM-3010 microscope operating at 300 kV ($C_s = 0.6$ mm, resolution 1.7 Å). Images were recorded with a CCD camera (model Keen View, SIS analysis, 1024 × 1024 pixels, pixel size 23.5 × 23.5 μm) at 30000–100000 × magnification under low-dose conditions.

^{29}Si MAS NMR spectra were measured on a Bruker Avance 500WB spectrometer with a 4-mm MAS probe under the following experimental conditions: 2.2 μs π/4 pulses, 30 s recycle delay, 2400 scans, and a spinning rate of 10 kHz.

Received: January 12, 2005
Revised: May 19, 2005
Published online: July 20, 2005

 © 2005 Wiley-VCH Verlag GmbH & Co. KGaA, Weinheim

Keywords: electron diffraction · electron microscopy · mesoporous materials · silicates · surfactants

[1] R. Vargas, P. Mariani, A. Gulik, V. Luzzati, *J. Mol. Biol.* **1992**, *225*, 137 – 145.
[2] N. Khazanovich, J. R. Granja, D. E. McRee, R. A. Milligan, M. R. Ghadiri, *J. Am. Chem. Soc.* **1994**, *116*, 6011 – 6012.
[3] E. A. Lord, A. L. Mackay, *Curr. Sci.* **2003**,*7*, 346 – 362.
[4] C. T. Kresge, M. E. Leonowicz, W. J. Roth, J. C. Vartuli, J. S. Beck, *Nature* **1992**, *359*, 710 – 712.
[5] D. Y. Zhao, J. Feng, Q. Huo, N. Melosh, G. H. Fredrickson, B. F. Chmelka, G. D. Stucky, *Science* **1998**, *279*, 548 – 552.
[6] F. Schüth, W. Schmidt, *Adv. Mater.* **2002**, *14*, 629 – 638.
[7] Q. Huo, D. Zhao, J. Feng, J. Kim, Y. Han, G. D. Stucky, *Chem. Mater.* **1999**, *11*, 2668.
[8] K. Yu, X. Wu, C. J. Brinker, J. Ripmeester, *Langmuir* **2003**, *19*, 7282.
[9] P. Falcaro, S. Costacurta, G. Mattei, H. Amenitsch, A. Marcelli, M. C. Guidi, M. Piccinini, A. Nucara, L. Malfatti, T. Kidchob, P. Innocenzi, *J. Am. Chem. Soc.* **2005**, *127*, 3838.
[10] S. Che, A. E. Garcia-Bennett, T. Yokoi, K. Sakamoto, H. Kunieda, O. Terasaki, T. Tatsumi, *Nat. Mater.* **2003**, *2*, 801 – 806.
[11] A. E. Garcia-Bennett, K. Miyasaka, S. Che, O. Terasaki, *Chem. Mater.* **2004**, *16*, 3597 – 3605.
[12] S. Che, Z. Liu, T. Ohsuna, K. Sakamoto, O. Terasaki, T. Tatsumi, *Nature* **2004**, *429*, 281 – 284.
[13] A. E. Garcia-Bennett, S. Che, T. Tatsumi, O. Terasaki, *Chem. Mater.* **2004**, *16*, 813 – 821.
[14] S. Kamiya, H. Tanaka, S. Che, T. Tatsumi, O. Terasaki, *Solid State Sci.* **2003**, *5*, 197 – 204.
[15] K. Hiraga, D. Shindo, M. Hirabayashi, O. Terasaki, D. Watanabe, *Acta Crystallogr.* **1980**, *36*, 2550 – 2554.
[16] X. Zeng, G. Ungar, Y. Liu, V. Percec, A. E. Dulcey, J. K. Hobbs, *Nature* **2004**, *428*, 157.
[17] Y. Sakamoto, M. Kaneda, O. Terasaki, D. Zhao, J.-M. Kim, G. D. Stucky, H. J. Shin, R. Ryoo, *Nature* **2000**, *408*, 449.
[18] R. P. Hodgkins, A. E. Garcia-Bennett, P. A. Wright, *Microporous Mesoporous Mater.* **2005**, *79*, 241 – 252.
[19] T. Yokoi, H. Yoshitake, T. Tatsumi, *J. Mater. Chem.* **2004**, *14*, 951 – 957.

 © 2005 Wiley-VCH Verlag GmbH & Co. KGaA, Weinheim

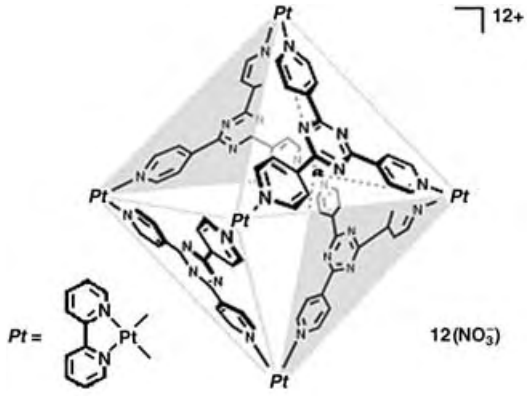
Host–Guest Systems

DOI: 10.1002/anie.200501568

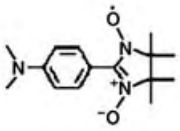
pH-Switchable Through-Space Interaction of Organic Radicals within a Self-Assembled Coordination Cage

Koji Nakabayashi, Masaki Kawano, and Makoto Fujita**

Whereas the control of the through-space interaction of organic radicals by external stimuli promises the development of a variety of molecular scale magnetic devices, it has been achieved only in the solid state and never in solution.[1] We recently reported the through-space interaction of non-associative stable organic radicals in aqueous solution by accommodating two organic radicals in a self-assembled coordination cage **1**.[2] Owing to restriction by the cage, two



1



2

organic radicals are fixed in the cavity such that the two radical centers are in close proximity. If such a through-space interaction could be switched by a slight change in the environment, molecular magnetic devices that are responsive

[*] K. Nakabayashi, Prof. Dr. M. Kawano, Prof. Dr. M. Fujita
Department of Applied Chemistry
School of Engineering
The University of Tokyo and CREST
Japan Science and Technology Agency (JST)
7-3-1 Hongo, Bunkyo-ku, Tokyo 113-8656 (Japan)
Fax: (+81) 3–5841–7257
E-mail: mkawano@appchem.t.u-tokyo.ac.jp
mfujita@appchem.t.u-tokyo.ac.jp

Supporting information for this article is available on the WWW under http://www.angewandte.org or from the author.

WILEY InterScience DISCOVER SOMETHING GREAT
© 2005 Wiley-VCH Verlag GmbH & Co. KGaA, Weinheim

to external stimuli in solution could be prepared. Accordingly, we demonstrate herein the pH-responsive switching of spin–spin interactions between stable organic radicals.[3] Radical **2**[4] has an amine group that may be protonated, and upon doing so the affinity of radical **2** for the host should be significantly lowered as a result of cationic repulsion.[5] We show that the pH response of the through-space magnetic interaction between accommodated **2** is quite sensitive and digitalized.[6]

An excess of powdered **2** (4.1 mg, 15×10^{-3} mmol) was suspended in a solution of **1** (20.5 mg, 5.0×10^{-3} mmol) in H_2O (1.0 mL) at 80 °C for 1 h. After filtration of surplus **2**, a solution of the clathrate compound **1**·(**2**)$_2$ (5 mM) remained.[7] The solution of the clathrate was diluted with H_2O (9 mL) and used for ESR and UV/Vis spectroscopy measurements. A single crystal of **1**·(**2**)$_2$ suitable for X-ray diffraction was obtained by slow evaporation of H_2O from the solution at room temperature for 2 days. The crystal structure of **1**·(**2**)$_2$ is shown in Figure 1.

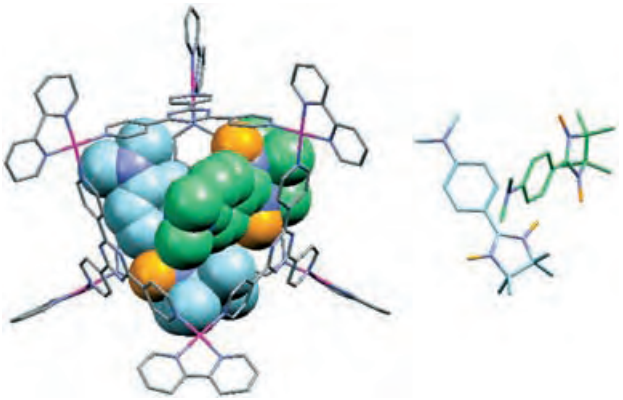
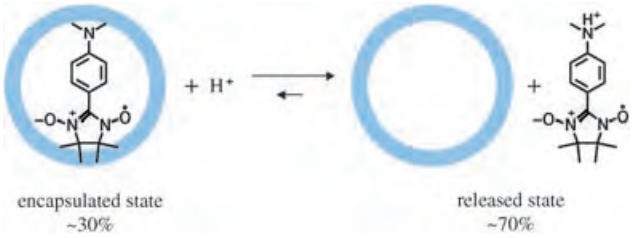


Figure 1. Molecular structure of the clathrate complex **1**·(**2**)$_2$ (left). Host **1**: stick representation (Pt magenta, N dark blue, C gray); guest **2**: space-filled representation (O yellow, N dark blue, C green/pale blue). The configuration of the radicals within the cage is shown more clearly by the stick representation on the right.

An advantage of using a discrete host is that the array of the guests is fixed regardless of whether they are in solution or in the solid state. Namely, the orientation of the guest depends upon the nature of the cavity in the host rather than the guest or the environment. In crystalline **1**·(**2**)$_2$, the guests are suitably oriented so that two spin centers[8] are in close proximity for efficient spin–spin interaction. The average distance between the spin centers is approximately 6.3 Å,[9] and we suggest that this orientation is fixed even in solution.

As expected from the X-ray diffraction study, the encapsulated guests in the cage showed intermolecular triplet-state spin–spin interactions. An intriguing feature of this clathrate complex is that the spin–spin interaction can be switched by pH.[10] As illustrated in Scheme 1, we observed the reversible process of release and reencapsulation of **2** in the pH range of 1.3 to 6.5 by ESR spectroscopy. Around pH 7, the ESR spectrum of the aqueous solution (frozen) of **1**·(**2**)$_2$ at 103 K[11] showed a split allowed transition ($\Delta m_s = 1$) at 321 mT and a forbidden transition ($\Delta m_s = 2$) at 160 mT; the



Scheme 1. Equilibrium in the acidified solution of host and guest, **1**·(**2**)$_2$.

observation of the latter is a proof of a triplet state that is derived from two interacting radicals in the cage (Figure 2a). When the solution was acidified to pH ≈ 1.3 with HNO_3, the

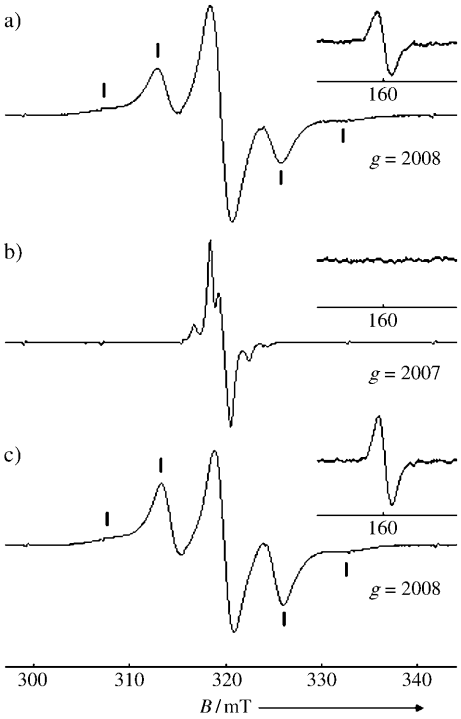


Figure 2. ESR spectra of clathrate compound **1**·(**2**)$_2$ (0.5 mM, 103 K): a) the initial solution (pH ≈ 6.5), b) the acidified solution (pH ≈ 1.3; with HNO_3), and c) the neutralized solution (pH ≈ 6.5; with K_2CO_3). The insets show forbidden transition; vertical bars indicate the signals derived from a triplet state. g = splitting factor.

triplet signal was completely suppressed and only a doublet signal with a hyperfine structure (due to coupling with the nitrogen nucleus) was observed. This observation strongly suggests that the protonated radical, **2**H$^+$, was released from the cage (Figure 2b). The profile of the doublet signal agreed with that of the signal of **2**H$^+$ in the absence of **1**.[12] The decapsulation of **2** from **1** is probably caused by a decreased hydrophobic interaction as well as coulombic repulsion between the host and the guest. When the solution was treated with K_2CO_3 to pH ≈ 6.5, the released guest returned to the cavity of **1** and the triplet signals reappeared (Figure 2c).

 © 2005 Wiley-VCH Verlag GmbH & Co. KGaA, Weinheim

The pH-dependent UV/Vis absorption spectra of $\mathbf{1}\cdot(\mathbf{2})_2$ also supported the pH-switchable encapsulation of **2**. Radicals **2** and $\mathbf{2}H^+$ showed absorption bands ascribed to an n–π* transition at 650 nm and 560 nm, respectively (Figure 3a).

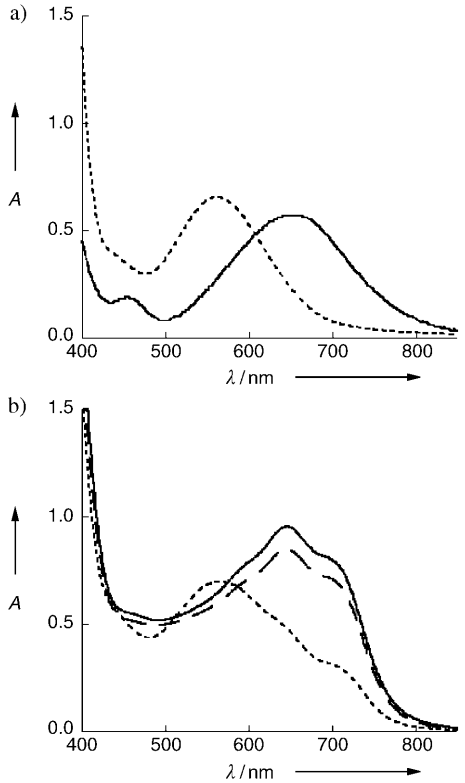


Figure 3. a) UV/Vis spectra of radical **2** (——, saturated solution, pH 6.5) and the protonated radical $\mathbf{2}H^+$ (-----, saturated solution, pH 1.3) at 293 K. b) UV/Vis spectra of clathrate compound $\mathbf{1}\cdot(\mathbf{2})_2$ (0.5 mM) at 293 K. ——: the initial solution at pH ≈ 6.5; -----: the acidified solution at pH ≈ 1.3 (HNO_3); – – –: the neutralized solution at pH ≈ 6.5 (K_2CO_3).

Under neutral conditions, $\mathbf{1}\cdot(\mathbf{2})_2$ showed an absorption band at 650 nm accompanied by a vibronic coupling derived from **2**. The presence of the vibronic coupling indicated that **2** remained in the hydrophobic environment (Figure 3b). The acidified solution of $\mathbf{1}\cdot(\mathbf{2})_2$ showed absorption bands at both 560 nm and 650 nm, which suggests that $\mathbf{2}H^+$ (out of the hydrophobic pocket of **1**) and **2** (encapsulated in **1**) were in equilibrium (Scheme 1). Deconvolution analysis of the spectrum of $\mathbf{1}\cdot(\mathbf{2})_2$ in acidified solution clarified that the ratio of the released and encapsulated guests was 7:3. When treated with K_2CO_3 (pH ≈ 6.5), the solution showed a similar spectrum to that observed initially, confirming that the released guest was reencapsulated in **1**.

In conclusion, we have demonstrated the pH-controlled doublet–triplet switching of organic radicals accommodated in a self-assembled coordination host. The facile solution-state control of the spin interaction is ascribed to the encapsulation effect of the cage: radicals are fixed in the host under neutral conditions, whereas they are expelled under acidic conditions. By applying such an encapsulation effect of a cage, new molecular magnetic materials that are responsive to other stimuli (particularly light) may be developed.

Experimental Section

$\mathbf{1}\cdot(\mathbf{2})_2$: An excess of powdered **2** (4.1 mg, 15×10^{-3} mmol, $M_w = 276.35$) was suspended in a solution of **1** (20.5 mg, 5.0×10^{-3} mmol, 5 mM) in H_2O (1.0 mL) at 80 °C for 1 h to give a solution of the clathrate compound (5 mM) after filtration of surplus **2**.[7] The solution of the clathrate was diluted tenfold with H_2O (9 mL) and was used for ESR and UV/Vis spectroscopy. A single crystal of $\mathbf{1}\cdot(\mathbf{2})_2$ suitable for X-ray diffraction studies was obtained by slow evaporation of H_2O from an aqueous solution of the clathrate at room temperature for 2 days. Elemental analysis (%): calcd for $C_{162}H_{182}N_{54}O_{61}Pt_6\cdot21\,H_2O$: C 38.67, H 3.65, N 15.03; found: C 38.95, H 3.81, N 14.66. Crystal data for $\mathbf{1}\cdot(\mathbf{2})_2$: $C_{162}H_{140}N_{50.50}O_{80.75}Pt_6$, $M_r = 5256.79$, tetragonal, $P4_12_12$, $a = b = 29.0831(9)$ Å, $c = 30.773(2)$ Å, $V = 26029(2)$ Å^3, $Z = 4$, $T = 90.0(1)$ K, $\rho_{calcd} = 1.341$ g cm^{-3}, $\lambda(Mo_{K\alpha}) = 0.71073$ Å; 404871 reflections were measured of which 40114 were unique ($R_{int} = 0.1341$) and were used in all calculations. The structure was solved by direct methods (SHELXL-97) and refined by full-matrix least-squares methods on F^2 with 1520 parameters. $R_1 = 0.0716$ ($I > 2\sigma(I)$) and $wR_2 = 0.1774$, GOF = 1.011, max./min. residual density 1.155/−0.831 e Å^{-3}.

Crystal data for **2**: $C_{15}H_{22}N_3O_2$, $M_r = 276.36$, monoclinic, $P2_1/n$, $a = 13.018(2)$ Å, $b = 9.434(1)$ Å, $c = 13.505(2)$ Å, $\alpha = \gamma = 90$, $\beta = 116.840(2)°$, $V = 1479.9(3)$ Å^3, $Z = 4$, $T = 90.0(1)$ K, $\rho_{calcd} = 1.258$ g cm^{-3}, $\lambda(Mo_{K\alpha}) = 0.71073$ Å; 5418 reflections were measured of which 3305 were unique ($R_{int} = 0.0919$) and were used in all calculations. The structure was solved by direct method (SHELXL-97) and refined by full-matrix least-squares methods on F^2 with 187 parameters. $R_1 = 0.0968$ ($I > 2\sigma(I)$) and $wR_2 = 0.2418$, GOF = 1.146; max./min. residual density 0.870/−0.494 e Å^{-3}. All the diffraction data were measured on a Siemens SMART/CCD diffractometer ($Mo_{K\alpha}$ radiation: $\lambda = 0.71073$ Å). Non-hydrogen atoms were refined anisotropically and hydrogen atoms were fixed at calculated positions and refined using a riding model. CCDC-271224 (**2**) and CCDC-271223 ($\mathbf{1}\cdot(\mathbf{2})_2$) contain the supplementary crystallographic data for this paper. These data can be obtained free of charge from the Cambridge Crystallographic Data Centre via www.ccdc.cam.ac.uk/data_request/cif.

Received: May 9, 2005
Published online: July 22, 2005

Keywords: clathrates · EPR spectroscopy · host–guest systems · radicals · self-assembly

[1] a) W. Fujita, K. Awaga, *Science* **1999**, *286*, 261–262; b) M. E. Itkis, X. Chi, A. W. Cordes, R. C. Haddon, *Science* **2002**, *296*, 1443–1445.
[2] K. Nakabayashi, M. Kawano, M. Yoshizawa, S. Ohkoshi, M. Fujita, *J. Am. Chem. Soc.* **2004**, *126*, 16694–16695.
[3] The Pt cage is proof against acidic conditions. Self-assembled coordination cage **1** was prepared by a procedure described in the following references: a) M. Yoshizawa, T. Kusukawa, M. Fujita, K. Yamaguchi, *J. Am. Chem. Soc.* **2000**, *122*, 6311–6312; b) T. Kusukawa, M. Fujita, *J. Am. Chem. Soc.* **2002**, *124*, 13576–13582.
[4] Radical **2** was prepared by a procedure described in the following references: a) H. Sakurai, A. Izuoka, T. Sugawara, *J. Am. Chem. Soc.* **2000**, *122*, 9723–9734; b) C. Hirel, K. E. Vostrikova, J. Pecaut, V. I. Ovcharenko, P. Rey, *Chem. Eur. J.* **2001**, *7*, 2007–2014.

 © 2005 Wiley-VCH Verlag GmbH & Co. KGaA, Weinheim

[5] For examples of a pH-responsive host–guest system, see: a) M. Haga, M. M. Ali, R. Arakawa, *Angew. Chem.* **1996**, *108*, 85–87; *Angew. Chem. Int. Ed. Engl.* **1996**, *35*, 76–78; b) D. E. Bergbreiter, J. G. J. Franchina, *Chem. Commun.* **1997**, 1531–1532; c) M.-V. Martínez-Díaz, N. Spencer, J. F. Stoddart, *Angew. Chem.* **1997**, *109*, 1991–1994; *Angew. Chem. Int. Ed. Engl.* **1997**, *36*, 1904–1907; d) D. Whang, J. Heo, J. H. Park, K. Kim, *Angew. Chem.* **1998**, *110*, 83–85; *Angew. Chem. Int. Ed.* **1998**, *37*, 78–80; e) F. Ibukuro, T. Kusukawa, M. Fujita, *J. Am. Chem. Soc.* **1998**, *120*, 8561–8562.

[6] The spin control of through-bond interactions by photoexcitation in the solution and solid states was achieved by the use of diarylethene with two nitronyl nitroxides; K. Matsuda, M. Irie, *J. Am. Chem. Soc.* **2000**, *122*, 8309–8310.

[7] Evaporation of a solution obtained by the same procedure gave a green powder whose elemental analysis agreed with complex **1**·(**2**)$_2$ (see Experimental Section), which suggests the quantitative formation of the 1:2 host–guest complex by this procedure.

[8] The spin center was defined as the oxygen atoms of the nitronyl nitroxides.

[9] From this distance (6.3 Å), the fine-structure constant of D was estimated to be 11.2 mT by a point-dipole approximation, in near-complete agreement with the observed value (12 mT). $D' = 3/2(\mu_0 g\beta)/(4\pi r^3)$, where $\mu_0 = 4\pi \times 10^{-7}\ \mathrm{H\,m^{-1}}$, $g = 2.008$, $\beta = 9.274 \times 10^{-24}\ \mathrm{J\,T^{-1}}$, and $r = 6.3$ Å, the average spin–spin distance between radicals within the cage.

[10] Both the acidified and neutral solutions of another stable radical that lacks an amino group gave identical ESR spectra (see Supporting Information).

[11] See Supporting Information for the ESR spectrum of an aqueous solution of **1**·(**2**)$_2$ at 293 K.

[12] See Supporting Information.

 © 2005 Wiley-VCH Verlag GmbH & Co. KGaA, Weinheim

Zeolites

DOI: 10.1002/anie.200500431

Förster-Type Energy Transfer along a Specified Axis**

*Claudia Minkowski and Gion Calzaferri**

Förster transfer of electronic excitation energy in 3D[1–3] and 2D[4,5] systems has been studied in many laboratories. Kuhn extended the Förster theory of long-range energy transfer in 3D systems to 2D and 1D systems.[6] The theory of the time dependence of this process in 1D and 2D cases was studied by Hauser et al.[7] and later extended to fractal dimensions by several groups.[8,9] Nevertheless, only little experimental evidence has been published to prove 1D energy transfer. In the strict sense, one-dimensionality can be understood as a transport along a line or at least along an isolated file. However, one-dimensionality in the 3D space of an object of, for example, cylindrical morphology can also mean that the nett transport of the individual transfer steps goes along the *c* axis of the cylinder, that is, along a well-defined axis. We call this quasi-1D to avoid any confusion.

One way to try to realize the conditions in which quasi-1D transport of excitation energy should be favored is by using dye molecules in a crystalline host that consists of 1D channels. Panchromatic chromophore mixtures in an $AlPO_4$–5 molecular sieve show interesting luminescence properties.[10] We have shown that zeolite L, with its 1D channels, is a very versatile material with which to build artificial host–guest antenna systems.[11] The channels are occupied by energy-transporting dyes (donors, D) and energy-trapping dyes (acceptors, A); strongly luminescent dyes are usually selected. The energy-transfer process that occurs when an excited donor transports its excitation energy to an unexcited acceptor proceeds with a Förster-type mechanism and its rate constant k_{DA} can be expressed according to Equation (1), in which ϕ_D and τ_D are the

$$k_{DA} \propto \frac{\phi_D}{\tau_D} J_{DA} \frac{\kappa^2_{DA}}{R^6_{DA}} \quad (1)$$

fluorescence quantum yield and lifetime, respectively, of the donor, J_{DA} is the spectral overlap integral between the donor emission and the acceptor absorption spectra, κ_{DA} describes the relative orientation of the electronic transition moments, and R_{DA} is the distance between D and A.

R_{DA} has a strong effect on the energy-transfer rate constant. It can be tuned, for example, by varying the loading of the dye molecules[12], which changes the overall dye–dye distance. Another elegant way to study the distance dependence of the transfer of excitation energy is to introduce a spacer molecule between the donors and the acceptors to separate them locally, as illustrated in Figure 1. To realize this introduction, a defined quantity of acceptor molecules was first incorporated into the channels of zeolite L. In the second step, different quantities of spacer molecules were incorporated into the channels that already contained acceptor dyes, thus forming spacer layers of different thicknesses. In the third step, the same quantity of donor dyes was always added. As the conditions are such that the dyes cannot glide past each other, the crystal is divided into compartments in which the density of one dye is dominant. By selectively exciting the donor, the behavior of the excitation energy can be observed as it depends on the amount of spacer molecules and therefore on the distance R_{DA}. Is the transport of electronic excitation energy preferentially quasi-1D along the cylinder axis?

With the dye molecules listed in Scheme 1, we investigated three systems. Two systems have been synthesized according to Figure 1 A, in which Py^+ acts as donor and Ox^+ as acceptor. Owing to its favorable spectral properties and its

[*] Dipl.-Chem. C. Minkowski, Prof. Dr. G. Calzaferri
Department of Chemistry and Biochemistry
University of Bern
Freiestrasse 3, 3012 Bern (Switzerland)
Fax: (+41) 31-631-39-94
E-mail: gion.calzaferri@iac.unibe.ch

[**] This work was supported by the Schweizerischer Nationalfonds zur Förderung der wissenschaftlichen Forschung NF 200020-105140/1 and NRP47 4047-57481. Zeolite L was synthesized by Dr. A. Khatyr and Dr. S. Megelski. Time-resolved measurements were carried out by K. Lutkouskaya.

 © 2005 Wiley-VCH Verlag GmbH & Co. KGaA, Weinheim

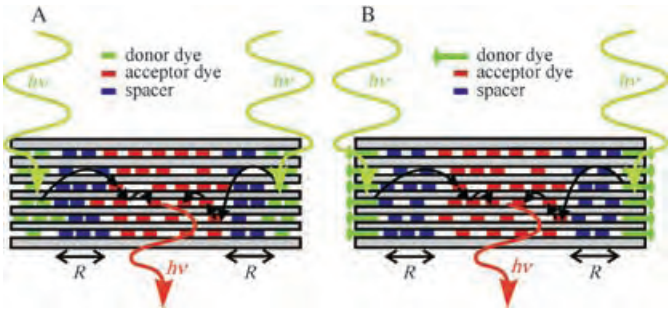
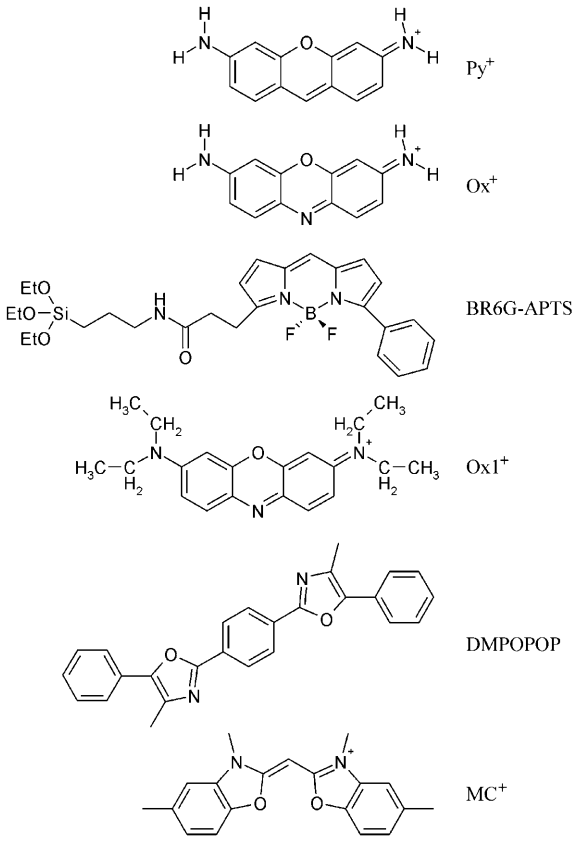


Figure 1. Schematic representation of zeolite L, which illustrates the parallel channels that run along the *c* axis of the crystal. The channels contain red-light-emitting dyes in the middle, followed by different amounts of spacer molecules (blue) that form spacer layers of different average thicknesses, and finally green-light-emitting donors at both ends. A) The donor–spacer and spacer–acceptor phase boundaries are diffuse. B) The donor dye is a stopper molecule with a tail that enters the channels but a head that is to large to enter. All donors are fixed at the same position and only the spacer–acceptor phase boundary is diffuse.



Scheme 1. Dyes used for the loading of zeolite L: Py^+ and BR6G-APTS (donors), Ox^+ and $Ox1^+$ (acceptors), and DMPOPOP and MC^+ (spacers).

high fluorescence quantum yields, this donor–acceptor pair exhibits a remarkable ability to transport excitation energy through Py^+ energy carriers to luminescent Ox^+ traps. The third system has been synthesized according to Figure 1B, in which BR6G-APTS acts as a "stopper" donor and $Ox1^+$ as the acceptor. Specific attachment of the triethoxysilyl group of this stopper donor at the entrance of the channels was carried out according to a previous report.[13] The spacer molecules—in our case dyes as well—must be chosen so that they do not participate in the energy-transfer process; that is, they should not absorb in the spectral region where the donor is excited and they should not trap the energy from the donor. In the first and third systems, DMPOPOP was used as the spacer to give the antenna systems Py^+/DMPOPOP/Ox^+–zeolite L (**1**) and BR6G-APTS/DMPOPOP/$Ox1^+$–zeolite L (**3**), whereas in the second system, MC^+ was used to give the antenna system Py^+/MC^+/Ox^+–zeolite L (**2**). For **1** and **2**, zeolite L crystals of 840 nm length were used, whereas for **3**, the crystals were 300 nm long. The left column of Figure 2 shows the excitation and emission spectra of the individual dye molecules inserted into zeolite L.

For each of the three systems, a series of four samples were synthesized. The amount of donor and acceptor was kept constant, whereas the amount of spacer, namely DMPOPOP and MC^+, was increased from samples 1 to 4 in each series. From the amount of spacer, the average number of spacer molecules per spacer layer (n) can be calculated. This value determines the mean distance between the donor and acceptor molecules. Emission spectra of the different samples were recorded. The donor was selectively excited and the spectra were scaled to the same height of the donor emission (Figure 2, right column). In all three systems, the first sample with the smallest spacer layer shows the highest acceptor fluorescence intensity. With an increasing number of spacer molecules per layer, less and less energy transfer occurs and thus the acceptor fluorescence intensity decreases.

The distance dependence of the probability P for Förster-type long-range energy transfer from an electronically excited donor to an acceptor can be simplified according to Equation (2). R_0 is the Förster radius; the exponent α is 6 for 3D

$$P = \frac{1}{1 + (R_{DA}/R_0)^{\alpha}} \qquad (2)$$

systems,[1] 4 for 2D systems,[3] and 2 for 1D systems.[6] We do not have direct access to the mean value of R_{DA} ($\bar{R}_{DA}$). However, the average number of spacer molecules per spacer layer is proportional to this mean distance. Therefore, we have plotted the acceptor fluorescence intensity versus $1/(1+n^{\alpha})$ for different values of α ranging from 6 to 1 and we found that all data obey an $\alpha = 2$ dependence (Figure 3). I_{rel} does not go to zero at $(1+n^2)^{-1} \rightarrow 0$ as the acceptor absorbs to a small degree at the wavelength of excitation. The numbers of spacer molecules in these experiments are reported in Table 1.

It is not possible to estimate $\bar{R}_{DA}$ by multiplying the number of spacer molecules by their lengths (2.02 nm for DMPOPOP and 1.48 nm for MC) as energy transfer is not restricted to individual channels (see Figure 1 and Figure 4). The spectral overlap integrals and the corresponding Förster radii in parenthesis, which are calculated for a numerically estimated κ^2_{DA} value of about 1 and an estimated refractive index of 1.4, are $J_{Py^+,Ox^+} = 2.3 \times 10^{-10}\ cm^6\,mol^{-1}$ (6.1 nm) and $J_{BR6G\text{-}APTS,Ox1^+} = 5.6 \times 10^{-10}\ cm^6\,mol^{-1}$ (7.1 nm).[14]

 © 2005 Wiley-VCH Verlag GmbH & Co. KGaA, Weinheim

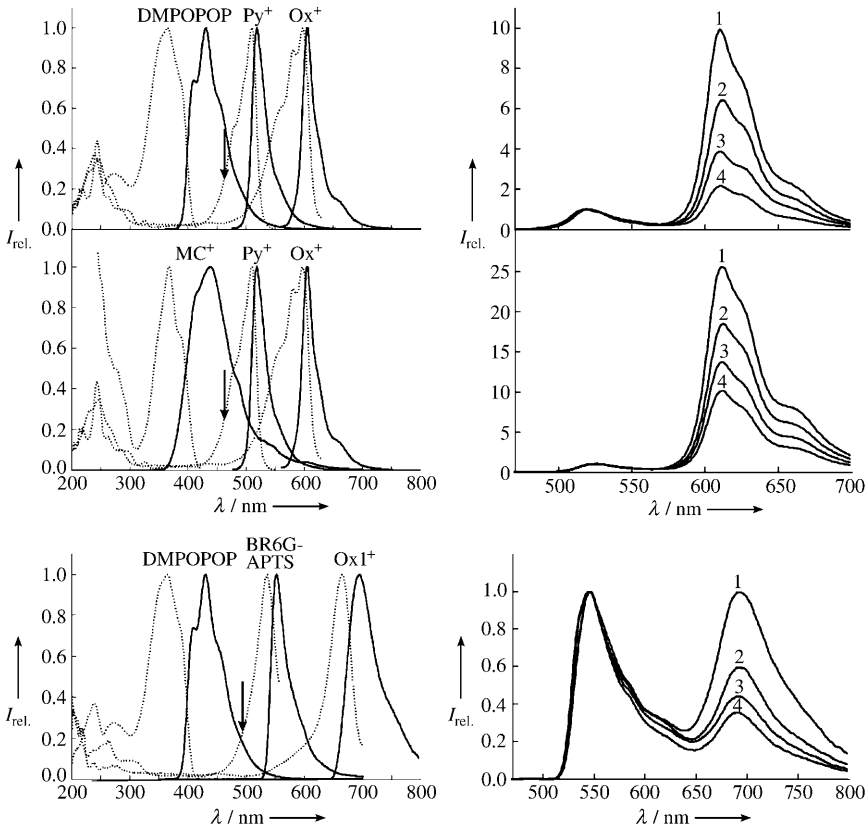


Figure 2. Left: Excitation (dotted lines) and emission (solid lines) spectra of the applied dye molecules. Right: Fluorescence spectra (scaled to the maximum of the donor emission) for **1** (top), **2** (middle), and **3** (bottom), with different amount of spacer, after selective excitation of the donor at the wavelengths indicated by the arrows in the left spectra. Average number of spacer molecules per spacer layer (n) for 1–4: top: 8.5, 11, 16, 22.5; middle: 15, 17.5, 24, 36.5; bottom: 2.7, 4, 6, 10.

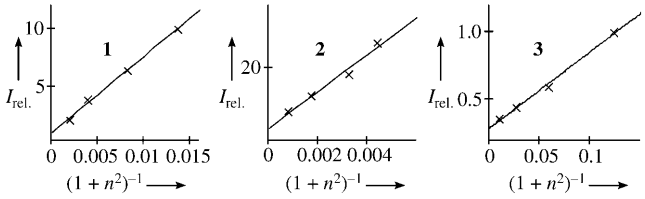


Figure 3. Intensities I_{rel} of the acceptor fluorescence versus the averaged number of spacer molecules per spacer layer (n) in **1**–**3** confirming the value of $\alpha = 2$.

Table 1: Values of n and the relative luminescence intensities of the acceptors for all the samples studied.

	1		**2**		**3**	
Sample	n	I_{rel}	n	I_{rel}	n	I_{rel}
1	8.5	9.92	15	25.55	2.7	0.99
2	11	6.4	17.5	18.44	4	0.59
3	16	3.86	24	13.70	6	0.44
4	22.5	2.15	36.5	11.10	10	0.35

One difficulty in analyzing the data in Figure 3 and Table 1 according to Equation (2) is that n is proportional but not equal to (R_{DA}/R_0). We can write this as follows $(R_{DA}/R_0) = cn$, in which c is a constant. What we know is that R_{DA} must be in the order of R_0 because the amount of energy transfer is substantial in all samples. R_0 is the radius at which the energy-transfer probability is 50%. From this we can estimate that c is less than 1 but we also know that R_{DA} cannot be smaller than the distance between the centers of two channels, which is 1.84 nm; thus $1 > c > 0.2$. With this range for c, it is easy to verify numerically that plotting the relative intensities versus $1/(1+n^{\alpha})$ allows us to discriminate between different α values and only $\alpha = 2$ is consistent with the measurements for all three materials.

In **1** and **2**, the donors are dyes that also enter the channels. The dyes cannot glide past each other within a channel, but their positions can overlap with neighboring channels to reveal a staggered profile of the phase boundaries (see Figure 1 and Figure 4). Replacing the donors with stopper molecules as in **3**, which have a tail that can enter the channel but a head too large to enter, results in a less-diffuse phase boundary. In this case, all stopper donors are fixed at the same position and only one staggered phase boundary from the spacer to the acceptor remains.

We report time-resolved data for the luminescence decay of the donor for each of the four samples of **1** and **2** (Table 2). The data were evaluated with a biexponential fit with lifetimes τ_1 and τ_2, with the factor f_1 indicating the number of photons that decay with lifetime τ_1. A Py^+–zeolite L sample with a loading of 0.02 decays with a mean lifetime $\langle\tau\rangle$ of 2.4 ns.[15] The decay of the donor in sample 4 of **1** is much faster than that of Py^+–zeolite L due to energy transfer, and the rate of decay increases from sample 4 to 1. This observation is in agreement with the steady-state emission spectra of these samples. The

Table 2: Decay [ns] of the luminescence of donor Py^+ in **1** and **2**.[a]

System	Sample	$\langle\tau\rangle$	τ_1	τ_2	f_1
Py^+–zeolite L		2.4			
1	1	0.13	0.007	1.26	0.90
1	2	0.27	0.105	2.00	0.91
1	3	0.45	0.11	1.43	0.75
1	4	0.89	0.24	2.16	0.66
2	1	0.21	0.05	2.96	0.95
2	2	0.22	0.04	3.07	0.94
2	3	0.25	0.04	2.47	0.91
2	4	0.29	0.04	2.75	0.91

[a] Excitation at 465 nm; detection at 520 nm.

 © 2005 Wiley-VCH Verlag GmbH & Co. KGaA, Weinheim

luminescence decay of the donor of **2** is already very fast for sample 4 and increases slightly from sample 4 to 1. As can be observed in the steady-state spectra (Figure 2), the acceptor fluorescence intensities of the samples of **2** are higher than those of **1**.

We have added some theoretical reasoning to explain better the system. First we focus on the distribution of the dye molecules at the phase boundaries. We can assume a uniform distribution of the dyes, as proposed by the results of a Monte Carlo calculation.[15] Figure 4A reveals the staggered profile of the borders. Figure 4B shows the same $\alpha = 2$ dependence for a calculated system in which the energy-migration and energy-transfer steps are described as a random walk by means of Markov chains.[16]

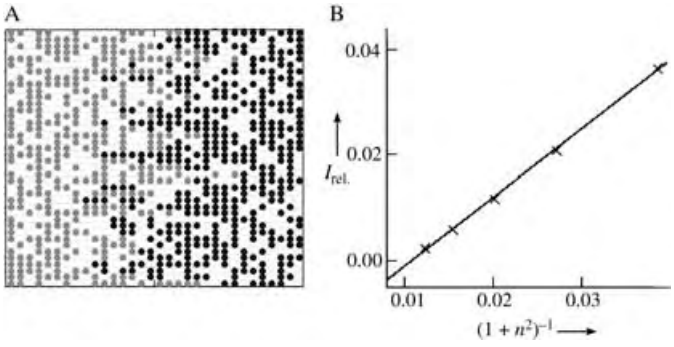


Figure 4. A) Simulated image of a zeolite L crystal containing 40 channels with each channel containing 32 sites, obtained by a Monte Carlo calculation; it illustrates the phase boundary. The sites are randomly filled with one type of dye molecule (dark dots), while after virtually sealing the right channel entrances another type of dye (light dots) was added from the left side. The overall occupation of both dye molecules per available site is 60%. The phase boundaries extend over about 10 sites. B) Calculated intensities of I_{rel} of the acceptor fluorescence versus averaged number of spacer molecules (n) between donor and acceptor for $\alpha = 2$.

The experimental data reported in Figures 2 and 3, and in Tables 1 and 2 can only be understood in terms of the long-range energy transfer of Förster. A trivial mechanism would not cause a shortening of the lifetime of the donor luminescence. There would also be no or a much weaker dependence on distance for the efficiency of the energy transfer because the change in distances is more than one order of magnitude smaller than the wavelength of the light. We found that varying n has a strong effect on the rate of energy transfer, as can be observed in the fluorescence intensities of the acceptors in samples in which the number of spacer molecules is different. This can also be observed in the time-resolved measurements in which the mean lifetimes $\langle\tau\rangle$ of the donor increase with an increase in n due to a decrease in energy transfer to the acceptor. System **2** has a much shorter $\langle\tau\rangle$ value than **1**, although the number of spacer molecules per layer is higher for **2** than for **1**. Thus we assume that MC^+ is more packed than DMPOPOP.

The correlation of the acceptor fluorescence intensity versus the number of spacer molecules per layer leads to a linearization at $1/(1+n^2)$. The same result is observed in the theoretical simulation. The individual transfer steps can also occur to a neighboring channel, but the statistical mean of the energy transfer in the dye-loaded zeolite L crystals is directed along the c axis of the cylinder. Hence, the transport of electronic excitation energy in all three systems is quasi-1D. This observation is of considerable interest for the development of highly anisotropic optoelectronic devices, some of which have already been proposed.[11]

Experimental Section

Zeolite L crystals were synthesized and characterized as described previously. [17]. The potassium-exchanged form was used, which had an average crystal length of 840 nm for **1** and **2**, and 300 nm for **3**. Py^+ and Ox^+ were synthesized and purified according to a reported procedure.[18]. DMPOPOP (Fluka), MC^+ (CIBA-GEIGY AG), and Cryptofix 222 (Fluka) were used as received. BR6G-APTS was made by substituting BODIPY-RG6 (succinimidyl ester of 4,4-difluoro-5-phenyl-4-bora-3a,4a-diaza-*s*-indacene-3-propionic acid, Molecular Probes), with (3-aminopropyl)triethoxysilane (Fluka). The two compounds were dissolved in CH_2Cl_2 and stirred for 1 h, the CH_2Cl_2 was removed by evaporation, and the resulting precipitate was washed twice with cyclohexane.[19]

1: Zeolite L was suspended in water and sonicated for 20 min to avoid aggregation of the crystals. An aqueous solution containing the required amount of Ox^+ was added and the resulting mixture was heated at reflux for 7 h. The Ox^+-loaded zeolite L crystals were washed with methanol to remove the Ox^+ from the surface. Insertion of DMPOPOP:[11] Ox^+-loaded zeolite L crystals were transferred into a glass ampoule and dehydrated under vacuum (3×10^{-2} mbar) at 80 °C for 24 h to empty the adsorption sites in the channels. The required amount of DMPOPOP was added and the ampoule was sealed. The sealed ampoule was heated in a rotating furnace at 150 °C for 6 days, after which the DMPOPOP/Ox^+-zeolite L crystals were washed with *n*-butanol and rehydrated in an exsiccator that contained a saturated solution of potassium acetate. Incorporation of Py^+: The DMPOPOP/Ox^+–zeolite L was suspended in water, and an aqueous solution of Py^+ was added and the mixture heated at reflux for 30 min. Compound **1** was washed again with methanol to remove dye molecules on the crystal surface.

2: First step as described for **1**. The incorporation of MC^+ was more involved and was carried out stepwise to obtain higher loadings: Ox^+-Zeolite L was suspended in a mixture of *n*-butanol and water (1:10) and sonicated for 20 min. A solution of MC^+ in the same *n*-butanol/water mixture was added to the suspension, which also contained an excess of Cryptofix 222.[18] The mixture was then heated at 65 °C for over 48 h to obtain a loading of about 40 to 50% of the preset amount of MC^+. The MC^+/Ox^+-zeolite L crystals were then washed with methanol and the insertion was repeated up to four times. MC^+/Ox^+-zeolite L was suspended in water and an aqueous solution containing the required amount of Py^+ was added; this mixture was heated at reflux for 30 min. Compound **2** was washed again with methanol.

3: Zeolite L was suspended in toluene and sonicated for 20 min. A solution of $Ox1^+$ in toluene and an excess of Cryptofix 222 was added and the resulting mixture was heated at 65 °C for 7 h. The $Ox1^+$-loaded zeolite L crystals were washed with methanol. Insertion of DMPOPOP as outlined for **1**. BR6G-APTS was added by dissolving the DMPOPOP/$Ox1^+$-zeolite L in Cl_2CH_2 and adding the required amount of the stopper molecule. The mixture was sonicated for 30 min and stirred at room temperature for 20 h.[13] Compound **3** was dried, dissolved in *n*-hexane, heated at reflux for 2 h, and again washed with methanol. The amount of dye molecules inside the channels was determined by destroying the zeolite framework with HF: A solution of HF (8%, 100 μL) was added to a solution of *n*-butanol (3.9 mL) containing the dye-loaded zeolite L (1 mg) in a

 © 2005 Wiley-VCH Verlag GmbH & Co. KGaA, Weinheim

polypropylene tube and this mixture was sonicated for 5 min. The amount of dye entering the solution was determined by UV/Vis spectroscopy.[12]

Thin-layer preparation: Dye-loaded zeolite L (100 μL) suspended in *n*-butanol (≈1 mg in 300 μL) was dropped onto a quartz plate (∅1.6 cm) and the solvent was evaporated in air. The quartz plate was then covered with a Petri dish. Emission and excitation spectra were recorded on a Perkin Elmer LS 50B luminescence photospectrometer. Compounds **1** and **2** were excited at 460 nm with a cut-off filter at 490 nm; compound **3** was excited at 490 nm with a cut-off filter at 510 nm. The samples were measured as thin layers on quartz. Time-resolved measurements were carried out according to a reported procedure.[15]. Samples were excited at 465 nm and detected at 520 nm; slit widths = 4 nm. Optical fluorescence microscopy images were carried out on an Olympus BX 60 device equipped with a Kappa CF 20 DCX Air K2 CCD camera.[11]

Received: February 4, 2005
Revised: June 7, 2005
Published online: July 25, 2005

Keywords: fluorescence · FRET (fluorescence resonant energy transfer) · host–guest systems · supramolecular chemistry · zeolites

[1] T. Förster, *Fluoreszenz organischer Verbindungen*, Vandenboeck & Ruprecht, Göttingen, **1951**.
[2] D. L. Andrews, A. A. Demidov, *Resonance Energy Transfer*, Wiley, New York, **1999**.
[3] a) B. Valeur, *Molecular Fluorescence*, Wiley-VCH, Weinheim, **2002**; b) J. R. Lakovicz, *Principles of Fluorescence Spectroscopy*, 2nd ed., Kluwer Academic-Plenum, New York, **1999**; c) X. F. Wang, B. Herman, *Fluorescence Imaging Spectroscopy and Microscopy*, Wiley, New York, **1996**.
[4] a) H. Bücher, K. H. Drexhage, M. Fleck, H. Kuhn, D. Möbius, F. P. Schäfer, J. Sondermann, W. Sperling, P. Tillmann, J. Wiegand, *Mol. Cryst.* **1967**, *2*, 199; b) H. Kuhn, D. Möbius, *Physical Methods of Chemistry*, *Vol. IXB* (Eds.: B. W. Rossiter, R. C. Baetzold), Wiley, New York, **1993**, pp. 375–542.
[5] a) G. Zumofen, A. Blumen, *J. Chem. Phys.* **1982**, *76*, 3713; b) P. Anfinrud, R. L. Crackel, W. S. Struve, *J. Phys. Chem.* **1984**, *88*, 5873; c) N. Tamai, T. Yamazaki, I. Yamazaki, *J. Phys. Chem.* **1987**, *91*, 841.
[6] H. Kuhn, *J. Chem. Phys.* **1970**, *53*, 101.
[7] M. Hauser, U. K. A. Klein, U. Gösele, *Z. Phys. Chem. Neue Folge* **1976**, *101*, 255.
[8] a) Z. Tang, B. Ozturk, Y. Wang, N. A. Kotov, *J. Phys. Chem. B* **2004**, *108*, 6927; b) D. Sendor, M. Hilder, T. Juestel, P. C. Junk, U. H. Kynast, *New J. Chem.* **2003**, *27*, 1070; c) B. Maliwal, J. Kusba, J. R. Lakowicz, *SPIE* **1992**, *1640*, 586; d) J. Grabowska, K. Sienicki, *Chem. Phys.* **1995**, *192*, 89.
[9] a) J. Klafter, J. M. Drake, *Molecular Dynamics in Restricted Geometries*, Wiley, New York, **1989**; b) S. E. Webber, *Chem. Rev.* **1990**, *90*, 1469; c) J. Klafter, A. Blumen, *J. Chem. Phys.* **1984**, *80*, 875; d) P. Levitz, J. M. Drake, *Phys. Rev. Lett.* **1987**, *58*, 686; e) J. P. S. Farinha, J. G. Spiro, M. A. Winnik, *J. Phys. Chem. B* **2001**, *105*, 4879.
[10] M. Ganschow, C. Hellriegel, E. Kneuper, M. Wark, C. Thiel, G. Schulz-Ekloff, C. Bräuchle, D. Wöhrle, *Adv. Funct. Mater.* **2004**, *14*, 269.
[11] G. Calzaferri, S. Huber, H. Maas, C. Minkowski, *Angew. Chem.* **2003**, *115*, 3860; *Angew. Chem. Int. Ed.* **2003**, *42*, 3732.
[12] S. Megelski, G. Calzaferri, *Adv. Funct. Mater.* **2001**, *11*, 277.
[13] T. Ban, D. Brühwiler, G. Calzaferri, *J. Phys. Chem. B* **2004**, *108*, 16348.
[14] S. Megelski, A. Lieb, M. Pauchard, A. Drechsler, S. Glaus, C. Debus, A. J. Meixner, G. Calzaferri, *J. Phys. Chem. B* **2001**, *105*, 25.
[15] M. M. Yatskou, M. Meyer, S. Huber, M. Pfenniger, G. Calzaferri, *ChemPhysChem* **2003**, *4*, 567.
[16] N. Gfeller, G. Calzaferri, *J. Phys. Chem. B* **1997**, *101*, 1396.
[17] A. Zabala Ruiz, D. Brühwiler, G. Calzaferri, *Monatsh. Chem.* **2005**, *136*, 77.
[18] H. Maas, A. Khatyr, G. Calzaferri, *Microporous Mesoporous Mater.* **2003**, *65*, 233.
[19] S. Huber, G. Calzaferri, *Angew. Chem.* **2004**, *116*, 6906; *Angew. Chem. Int. Ed.* **2004**, *43*, 6738.

 © 2005 Wiley-VCH Verlag GmbH & Co. KGaA, Weinheim

Structural Biochemistry

DOI: 10.1002/anie.200500903

Molecular Recognition of RNA by Neomycin and a Restricted Neomycin Derivative**

*Fang Zhao, Qiang Zhao, Kenneth F. Blount, Qing Han, Yitzhak Tor, and Thomas Hermann**

Aminoglycoside antibiotics such as neomycin (**1a**) and paromomycin (**1b**) bind to ribosomal RNA (rRNA) at the decoding site and thereby interfere with the accuracy of protein synthesis, ultimately leading to bacterial cell death (Figure 1). In addition to the decoding site in 16S rRNA, several other RNA motifs form well-defined complexes with individual aminoglycosides, which makes these antibiotics excellent model ligands for the study of RNA recognition.[1,2] The target "promiscuity" of the aminoglycosides has been attributed to two major factors: 1) their highly charged nature, which is responsible for their eletrostatically driven RNA-binding mode and 2) their conformational adaptability. Although rotation around the glycosidic bonds that link the saccharide building blocks is restricted, the remaining limited flexibility explains some adaptability toward diverse RNA targets.[2] This restricted conformational flexibility attenuates

[*] F. Zhao, Dr. K. F. Blount, Prof. Dr. Y. Tor, Dr. T. Hermann
Department of Chemistry and Biochemistry
University of California, San Diego
La Jolla, CA 92093 (USA)
Fax: (+1) 858-534-0202
E-mail: tch@chem.ucsd.edu
Dr. Q. Zhao, Dr. Q. Han
Department of Structural Chemistry
Anadys Pharmaceuticals, Inc.
3115 Merryfield Row, San Diego, CA 92121 (USA)

[**] F.Z. and Q.Z. contributed equally. This work was supported in part by the National Institutes of Health (Grant AI51104 to T.H. and AI47673 to Y.T.). We thank Dr. Daniel Wall and Ms. Jamie Froelich for antibacterial testing.

Supporting information for this article is available on the WWW under http://www.angewandte.org or from the author.

© 2005 Wiley-VCH Verlag GmbH & Co. KGaA, Weinheim

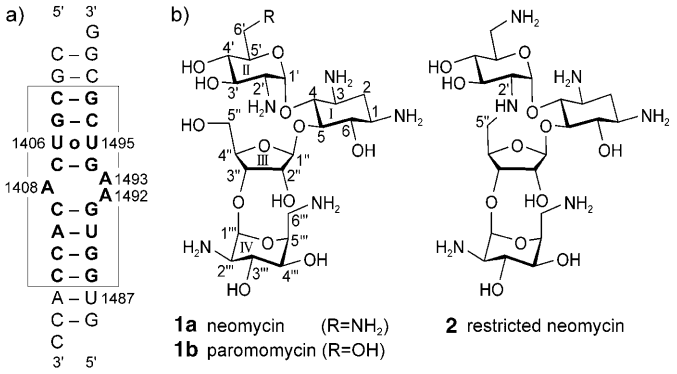


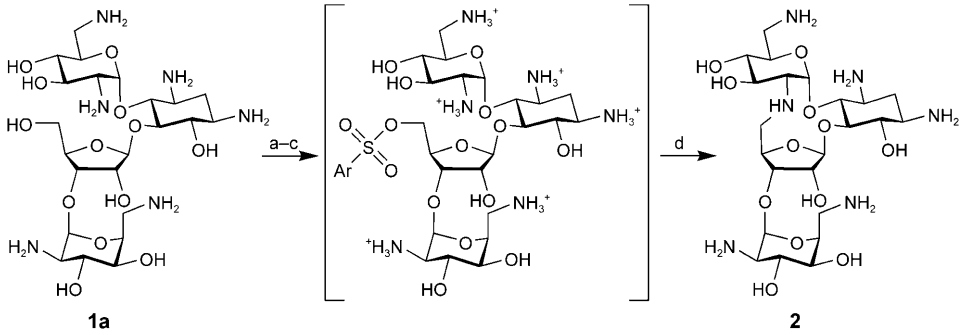
Figure 1. a) Secondary structure of the decoding-site oligonucleotide used for X-ray crystallography and structure determination. The box indicates the region that corresponds to the bacterial RNA sequence. Flanking nucleotides were added to enhance crystal packing. Residues are numbered according to the *Escherichia coli* 16S rRNA sequence. For multiwavelength anomalous diffraction experiments, U1487 was replaced by 5-Br-U. b) The natural aminoglycosides neomycin (**1a**) and paromomycin (**1b**) which differ at the 6′ position, and the semisynthetic restricted neomycin **2** in which rings II and III are linked through the 2′ and 5″ positions.

the contribution of charged interactions between RNA and the aminoglycosides, resulting in the formation of well-defined drug complexes that are distinct from nonspecific interactions of nucleic acids with flexible polyamines such as spermidine. The term structural electrostatic complementarity has been coined for this promiscuous yet target-specific binding of aminoglycosides to RNA.[2]

Aminoglycosides derived from 4,5-disubstituted 2-deoxystreptamine (2-DOS, ring I), including neomycin (**1a**) and paromomycin (**1b**), bind to a variety of RNA sequences. Examination of structurally characterized aminoglycoside complexes reveals that the relative orientation of rings I and II is very similar, whereas the conformation around the linkages to rings III and IV is significantly variable depending on the RNA target.[3] The apparent rigidity of the ring I/II system underlines the importance of this module for RNA recognition, attested by the fact that the 2-DOS and ring II moieties participate in key interactions that are responsible for target binding in decoding-site complexes with aminoglycosides.[1,4–6] Whereas higher thermal factors of rings III and IV in the crystal structure of paromomycin might suggest that these sugars generally contribute less to target-specific interactions,[4,5] the results presented herein suggest that the affinity of neomycin for the cognate decoding-site RNA and thus the antibacterial activity of this compound depend on an exquisitely balanced interplay of all four rings.

Previous investigations of aminoglycoside mimetics derived from neamine and paromamine, both of which lack rings III and IV, confirm the key role that the ring I/II core plays in decoding-site binding.[7,8] In the crystal structure of the related aminoglycoside paromomycin (**1b**) complexed with bacterial decoding-site RNA,[4,5] the distance between the 2′-amino group of ring II and the 5″-C atom of ring III is ≈3.7 Å, which suggests that cross-linking these positions may yield an aminoglycoside that retains the decoding-site-bound conformation of the parent drug. To support this hypothesis, we determined the X-ray crystal structures of neomycin (**1a**), among the most potent aminoglycoside antibiotics of therapeutic relevance, and its conformationally restricted analogue **2** bound to a decoding-site oligonucleotide (Figure 1a). Herein, we analyze the structural characteristics of both RNA–small-molecule complexes and discuss the structural basis of aminoglycoside ligand affinity along with general implications on the understanding of RNA recognition.

For the synthesis of restricted neomycin **2** we devised an intramolecular and regioselective cyclization strategy of an unprotected 5″-activated neomycin intermediate under high-dilution conditions that exploits the proximity of the 2′-amino and 5″-hydroxymethyl groups (Scheme 1).[3] The sulfonate-activated intermediate was obtained after Boc protection of the amino groups of neomycin, reaction of the primary alcohol at the 5″ position with 2,4,6-triisopropylbenzene sulfonyl chloride,[9] and cleavage of the Boc protecting groups with trifluoroacetic acid. High dilution of the activated intermediate to favor the intramolecular reaction and neutralization to deprotonate the ammonium groups for subsequent nucleophilic substitution eventually furnished the restricted aminoglycoside **2**.[3]



Scheme 1. Synthesis of restricted neomycin **2**: selective formation of **2** from neutralization of the unprotected sulfonate intermediate relied on the proximity of the 2′-amino and 5″-hydroxy groups. Neomycin (**1a**) was fully Boc-protected (a: Boc_2O, NEt_3, dioxane/H_2O; 75%) and activated as an aryl sulfonate at the 5″ position (b: 2,4,6-triispropylbenzenesulfonyl chloride, pyridine; 70%).[7] After acidic removal of the Boc protecting groups (c: TFA/$CHCl_3$ (1:1)), the sulfonate intermediate was highly diluted and neutralized to yield **2** (d: NEt_3, DMF, 10 days; 12% for steps c and d; a final Boc protection (not shown) was performed to facilitate purification).[3] Ar = 2,4,6-triisopropyl benzene; Boc = *tert*-butoxycarbonyl; TFA = trifluoroacetic acid; DMF = *N*,*N*-dimethylformamide.

 © 2005 Wiley-VCH Verlag GmbH & Co. KGaA, Weinheim

Both neomycin (**1a**) and restricted neomycin **2** were co-crystallized with an oligonucleotide that contains the decoding-site sequence and flanking bases, which facilitated crystal packing (Figure 1a). Similar small RNAs have been shown to provide authentic model systems that retain the structural and dynamic characteristics of the ribosomal decoding site.[5,6,10,11] Three-dimensional structures of the RNA complexes of **1a** and **2** were determined by X-ray diffraction by using anomalous dispersion of the halogen atom in the 5-Br-U1487 residue. For comparison, the structure of the unbound decoding site was solved as well (Supporting Information).

The electron density of the decoding-site complexes clearly revealed the identity of the bound aminoglycoside ligands (Figure 2a,b). Specifically, the 5″-hydroxymethyl group in neomycin gave rise to a characteristic extension of the electron density envelope which was lacking for the cyclized derivative **2**. Both **1a** and **2** bind to the decoding site at the same position as paromomycin (**1b**).[4,5] Complex formation induces a more compact structure of the RNA around the ligand-binding site as indicated by the base of A1408 and the sugar–phosphate backbone of A1492 and A1493 pulled closer to the aminoglycoside (Supporting Information). The hydrogen-bonding contacts between neomycin and the RNA are identical to those of paromomycin, including the interaction of the distinctive 6′ substituent (Figure 3a). The N1 atom of A1408 in the decoding site forms a hydrogen bond with either the 6′-hydroxy group of paromomycin or the 6′-amino substituent of neomycin which helps stabilize the base-pair-like interaction between ring II and the A1408 residue.[5]

The position of rings I and II within restricted neomycin **2** relative to the decoding-site RNA coincides with the binding site of these rings in the neomycin–RNA complex (Figure 2c). Consequently, the hydrogen-bonding network between the RNA and rings I and II is identical for the restricted derivative and neomycin as well as paromomycin (Figure 3). Distinct patterns are, however, observed for the interactions of rings III and IV. Intramolecular cyclization imparts to **2** with a slightly more compact overall structure than that of the parent neomycin, reflected by differences in the positioning of rings III and IV (see also Supporting Information). Ring IV of **2** interacts with the phosphate group of G1491, whereas hydrogen bonds are formed to the phosphate group of G1405 in the opposite RNA strand for the complexes formed with neomycin and paromomycin[5] (Figure 3). The covalent link between rings II and III in **2** pulls ring III away from the bottom of the RNA deep groove which leads to disruption of a hydrogen-bond interaction to C1407 that involves the 2″-hydroxy group; this interaction is present for complexes with neomycin and paromomycin. Another contact of the 5″-hydroxy substituent in the natural aminoglycosides with G1491 is absent for the restricted neomycin. Interestingly, the contacts to rings III and IV, which were considered to play a secondary role for decoding-site binding, are sacrificed upon binding of **2** to the decoding site. This is not the case for the interactions with rings I and II, the importance of which in RNA target recognition is underscored once again.

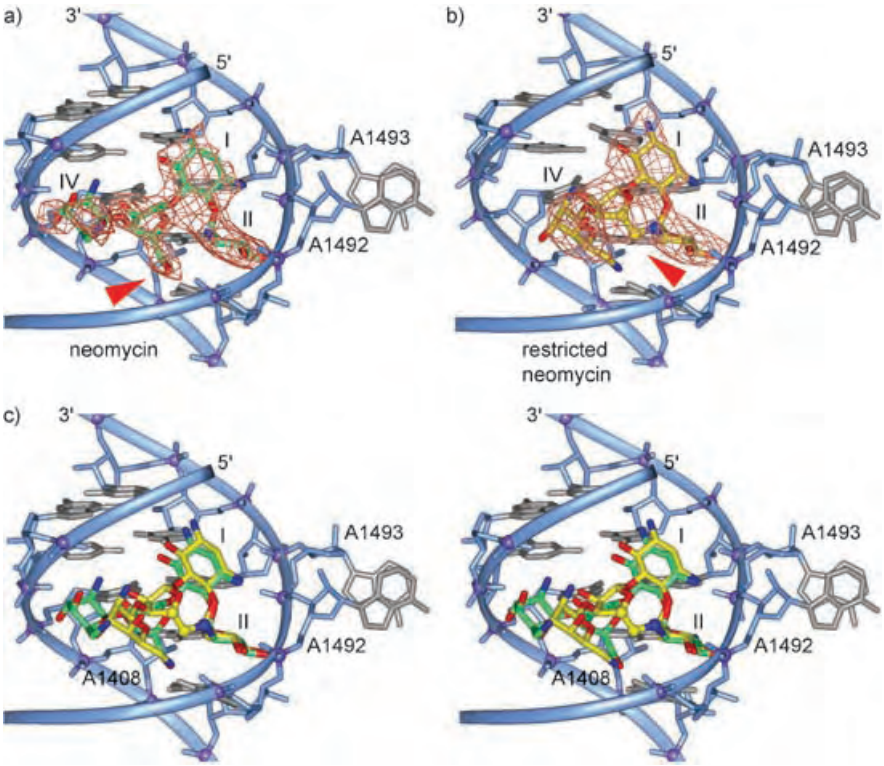


Figure 2. X-ray crystal structures of a) neomycin (**1a**) and b) restricted neomycin **2** complexed with decoding-site RNA. Aminoglycoside rings are numbered according to the structure shown in Figure 1b. Electron density ($2F_o-F_c$, contoured at 1.0σ around the ligands) reveals the identity of the aminoglycosides, specifically the extended 5″-hydroxymethylene group in neomycin, which is absent in the restricted ligand (red arrows). c) Stereo view of neomycin (**1a**, green) superimposed with its restricted derivative **2** (yellow) bound to the decoding site. (The superimposition is based on phosphate coordinates; only the RNA of the neomycin complex is shown.) The link between the 2′ and 5″ positions in **2** is highlighted in ball-and-stick representation.

Comparison of the binding affinities of neomycin (**1a**) with its cyclized derivative **2** for the decoding site revealed a 20-fold lower K_d value for the restricted derivative at pH 7.5,[3] in line with a similarly decreased antibacterial potency under physiological conditions.[12,13] The overall loss of direct hydrogen bonds between ring III and the RNA might explain the lower target affinity of **2**. However, at a lower pH value (5.8) similar to the crystallization conditions (pH 6.2), the K_d value of **2** decreased as a result of increasing protonation of the amino groups and thus domination of the ligand–RNA interaction by electrostatic forces.[3] It is well-documented

 © 2005 Wiley-VCH Verlag GmbH & Co. KGaA, Weinheim

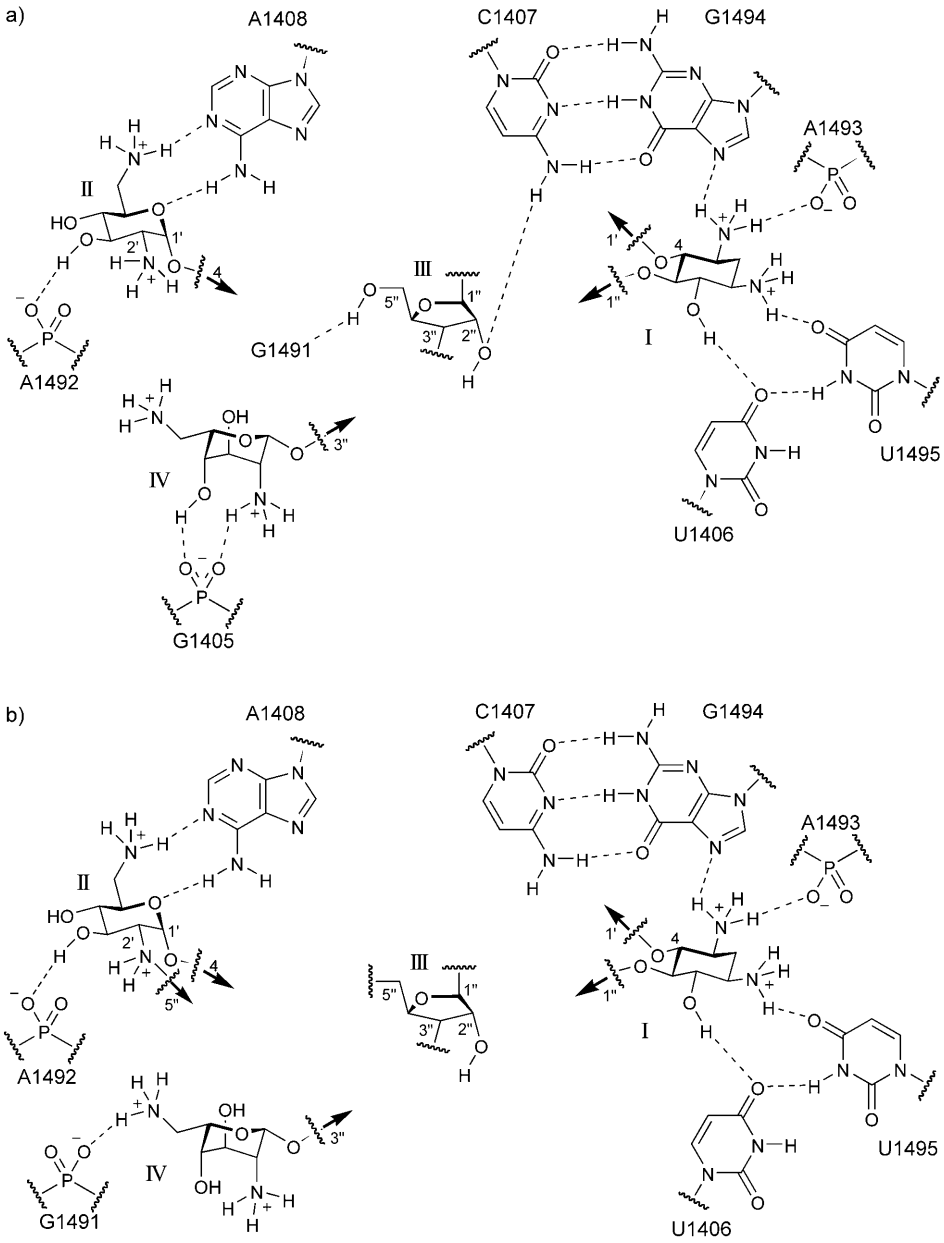


Figure 3. Schematic illustration of the dominant interactions of a) neomycin (**1a**) and b) restricted neomycin **2** with the decoding-site RNA. Unlike the case for the neomycin complex, the ribose moiety III of the restricted derivative does not participate in direct contacts with the target. The hydrogen-bonding network in the neomycin complex is identical to that previously observed in the decoding-site complex of paromomycin (**1b**).[4,5] Whereas there is a considerable range of pK_a values for the amino groups in **1a** and **2**,[3] protonated states dominate at the buffer conditions used (pH 6.2) which contribute an important electrostatic component to hydrogen-bonding interactions with the RNA.[3,21]

that the differences in RNA-binding affinities of various aminoglycosides carrying the same number of amino groups disappear at lower pH values, as electrostatic interactions of the protonated amino groups are the primary factors in complex formation.[3,19,20] Interestingly, the basicity of the secondary 2′-amino group, which covalently links rings II and III, is the lowest (pK_a 6.4 in **2**, versus pK_a 8.1 for the corresponding amine in **1a**).[3] Under physiological conditions, it is likely a combination of the decreased number of hydrogen-bond interactions between **2** and the decoding site, and diminished electrostatic contribution by the only partially protonated 2′-amino group that might cause the decreased binding affinity and antibacterial potency of the restricted neomycin derivative.[13]

A second aminoglycoside-binding site was observed in the crystal structure of both neomycin (**1a**) and restricted neomycin **2**. This site is located in the deep groove at the interface of two continuously stacking RNA constructs and displays features of ligand recognition that are radically different than those of the decoding site (Figure 4; and Supporting Information). Therefore, the complexes of **1a** and **2** described herein allow a direct comparison between distinct ligand-

 © 2005 Wiley-VCH Verlag GmbH & Co. KGaA, Weinheim

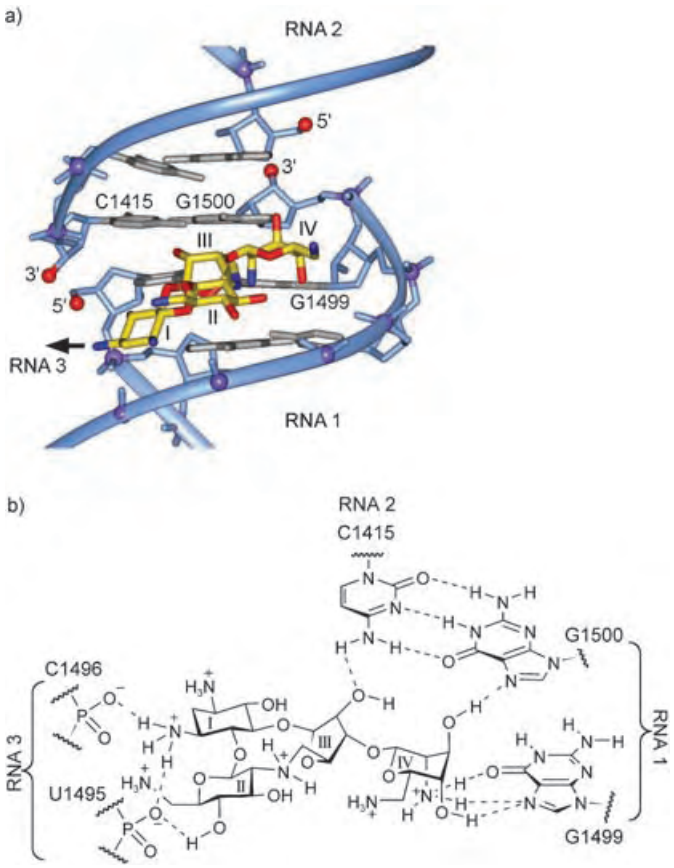


Figure 4. a) The second binding site of neomycin and restricted neomycin in the deep groove at the interface of coaxially stacked RNA helices (RNA 1 and 2). Only the structure of the complex with restricted neomycin is shown. The binding geometry at this site is identical to that of the complex with neomycin. Base-pair formation between the 3′-overhanging nucleotides of the decoding-site constructs promotes formation of pseudo-continuous helices in the crystal. A third, laterally docking RNA provides contacts with rings I and II of the aminoglycoside (RNA 3 not shown). b) Hydrogen-bonding interactions of **2** with RNA at the second binding site, which involves three RNA molecules.

recognition sites within the same RNA target. This provides the first "intramolecular" showcase for the promiscuity of aminoglycoside–RNA interactions.

At the interfacial site, the aminoglycoside forms hydrogen bonds with two mutually stacking RNA molecules and a third RNA helix that docks laterally. The interaction pattern differs remarkably from that observed at the decoding site in which rings I and II are involved in base-specific contacts, whereas rings III and IV play accessory roles. At the secondary binding site, ring IV docks in a coplanar manner between G1499 and G1500 and forms hydrogen bonds to the Hoogsteen edges of these bases. This is facilitated by a pyranose conformation that projects the 2‴, 3‴ and 4‴ substituents in an axial position (Figure 4). An additional hydrogen bond to the base of C1415 in a second RNA construct is provided by the 2″-hydroxy group of ring III. Rings I and II are projected outward from the RNA deep groove and are aligned along the sugar–phosphate backbone where they form hydrogen bonds exclusively with phosphate groups of a laterally docked third RNA helix (Figure 4). The geometry of the secondary aminoglycoside binding site is identical in the neomycin and restricted neomycin complexes. The small differences in the orientation of rings I and II that are induced by the intramolecular cyclization in **2** are accommodated by nonspecific interactions of these rings with phosphate groups. Interestingly, the docking site of ring IV at G1499 and G1500 in the aminoglycoside complexes corresponds to a magnesium ion binding site at the Hoogsteen face of consecutively stacked guanine residues. This metal ion binding site has been observed in RNA crystal structures, including the group I self-splicing intron[14] and 5S rRNA[15] (Supporting Information). The alternative occupancy of a magnesium binding site by neomycin, and the restricted derivative **2** is a further elegant example of structural electrostatic complementarity between cation binding sites in RNA and aminoglycosides.[2]

In summary, we have used X-ray crystallography to determine the three-dimensional structure of decoding-site RNA complexes of the aminoglycoside antibiotic neomycin (**1a**) and a synthetic restricted derivative **2** that was designed as a rigidified analogue of the natural product.[16] Conformational restriction by intramolecular cyclization is an established principle of drug design,[17] which we have applied to RNA-directed ligands.[3] The key requirement for conformational restriction is maintenance or induction of an active ligand conformation that allows target recognition. Our structural studies on RNA decoding-site complexes of neomycin (**1a**) and the restricted derivative **2** demonstrate that the intramolecular 2′–5″ cross-link introduced into the natural product is compatible with target binding. Comparison of the crystal structures of **1a** and **2** complexed to the decoding site reveals the exquisite sensitivity of aminoglycoside target recognition toward even slight modifications of the architecture of the natural product. Whereas key interactions of the aminoglycoside ligand are undisturbed by the modification, minimal differences in the overall conformation of **2** relative to **1a** disable hydrogen-bond contacts to the target.

Structural analysis revealed that neomycin, which is among the most potent aminoglycoside translation inhibitors, binds to the decoding site in the same conformation and at the same site as the structurally similar paromomycin, which is a considerably weaker inhibitor of bacterial translation.[7,18] The identical geometries for the decoding-site-bound neomycin and paromomycin suggest that the higher binding affinity of neomycin for the RNA target[7,18] may be due to the stronger N6′−H···$N1_{A1408}$ H bond relative to the O6′−H···$N1_{A1408}$ interaction in the paromomycin complex. A similar conclusion was drawn by Böttger and co-workers, who analyzed aminoglycoside binding to decoding-site mutants.[19] The identity of the 6′ substituent might also impact the basicity of other amino groups in the antibiotic, leading to a synergistic enhancement of neomycin binding over paromomycin. The interplay of amino group substitution pattern and basicity in aminoglycosides is well-established,[20] as is the importance of amino group protonation for ligand–RNA binding interactions.[21]

As an unexpected finding, a secondary aminoglycoside-binding site was discovered in the decoding-site complexes of both neomycin and the restricted derivative **2**. Interactions of the aminoglycosides at the secondary site involve the docking

 © 2005 Wiley-VCH Verlag GmbH & Co. KGaA, Weinheim

of an amino-sugar moiety of the ligand at a metal ion binding site of the RNA, following the principle of structural electrostatic complementarity.[2]

Received: March 11, 2005
Revised: April 22, 2005
Published online: July 22, 2005

Keywords: antibiotics · glycosides · RNA recognition · RNA · X-ray crystallography

[1] a) Q. Vicens, E. Westhof, *Biopolymers* **2003**, *70*, 42–57; b) Y. Tor, *ChemBioChem* **2003**, *4*, 998–1007; c) Q. Vicens, E. Westhof, *ChemBioChem* **2003**, *4*, 1018–1023.
[2] a) Y. Tor, T. Hermann, E. Westhof, *Chem. Biol.* **1998**, *5*, R277–R283; b) T. Hermann, E. Westhof, *J. Mol. Biol.* **1998**, *276*, 903–912; c) T. Hermann, E. Westhof, *Biopolymers* **1998**, *48*, 155–165.
[3] K. F. Blount, F. Zhao, T. Hermann, Y. Tor, *J. Am. Chem. Soc.* **2005**, *127*, 9818–9829.
[4] A. P. Carter, W. M. Clemons, D. E. Brodersen, R. J. Morgan-Warren, B. T. Wimberly, V. Ramakrishnan, *Nature* **2000**, *407*, 340–348.
[5] Q. Vicens, E. Westhof, *Structure* **2001**, *9*, 647–658.
[6] D. Fourmy, M. I. Recht, S. C. Blanchard, J. D. Puglisi, *Science* **1996**, *274*, 1367–1371.
[7] W. A. Greenberg, E. S. Priestley, P. S. Sears, P. B. Alper, C. Rosenbohm, M. Hendrix, S. C. Hung, C.-H. Wong, *J. Am. Chem. Soc.* **1999**, *121*, 6527–6541.
[8] K. B. Simonsen, B. K. Ayida, D. Vourloumis, M. Takahashi, G. C. Winters, S. Barluenga, S. Qamar, S. Shandrick, Q. Zhao, T. Hermann, *ChemBioChem* **2002**, *3*, 1223–1228.
[9] K. Michael, H. Wang, Y. Tor, *Bioorg. Med. Chem.* **1999**, *7*, 1361–1371.
[10] a) P. Purohit, S. Stern, *Nature* **1994**, *370*, 659–662; b) H. Miyaguchi, H. Narita, K. Sakamoto, S. Yokoyama, *Nucleic Acids Res.* **1996**, *24*, 3700–3706.
[11] S. Shandrick, Q. Zhao, Q. Han, B. K. Ayida, M. Takahashi, G. C. Winters, K. B. Simonsen, D. Vourloumis, T. Hermann, *Angew. Chem.* **2004**, *116*, 3239–3244; *Angew. Chem. Int. Ed.* **2004**, *43*, 3177–3182.
[12] Antibacterial potency of **1a** and **2** was tested by the serial dilution method described in: S. Barluenga, K. B. Simonsen, E. S. Littlefield, B. K. Ayida, D. Vourloumis, G. C. Winters, M. Takahashi, S. Shandrick, Q. Zhao, Q. Han, T. Hermann, *Bioorg. Med. Chem. Lett.* **2004**, *14*, 713–718. The minimum inhibitory concentration (MIC) was determined as the lowest compound concentration that prevented bacterial growth after 18 h of incubation at 37 °C. MIC values in $\mu g\,mL^{-1}$ for **1a**/**2**: 1/32 (*Escherichia coli* ATCC-25922 standard strain), 0.25/8 (*Staphylococcus aureus* ATCC-25923 standard strain), 0.5/16 (streptomycin-resistant *S. aureus* BAA-38), 64/>512 (gentamicin-resistant *S. aureus* BAA-40), 16/>512 (spectinomycin-resistant *S. aureus* BAA-44).
[13] Caution must be exercised in correlating antibacterial potency with in vitro target binding affinity and mode of interaction. Direct correlation with molecular parameters is difficult, as the apparent antibacterial potency might be affected by numerous parameters, including compound permeability and off-target effects.
[14] J. H. Cate, J. A. Doudna, *Structure* **1996**, *4*, 1221–1229.
[15] C. C. Correll, B. Freeborn, P. B. Moore, T. A. Steitz, *Cell* **1997**, *91*, 705–712.
[16] While this communication was under review, Asensio and coworkers published findings that intramolecular restriction of neomycin as in derivative **2** provides effective protection against aminoglycoside inactivation by a bacterial adenylate transferase resistance enzyme (ANT4): J. L. Asensio, A. Hidalgo, A. Bastida, M. Torrado, F. Corzana, J. L. Chiara, E. García-Junceda, J. Cañada, J. Jimenez-Barbero, *J. Am. Chem. Soc.* **2005**, *127*, 8278–8279.
[17] Conformational restriction by intramolecular cyclization has been applied almost exclusively to protein-directed ligands. For recent reviews that address the importance of conformational restriction in drugs, see: a) E. Perola, P. S. Charifson, *J. Med. Chem.* **2004**, *47*, 2499–2510; b) J. Clardy, C. Walsh, *Nature* **2004**, *432*, 829–837; Recently, semi-synthetic macrolide antibiotics that target the ribosomal peptidyl transferase center in 23S rRNA have been obtained by conformational restriction of natural products: c) Z. Ma, L. Li, M. Rupp, S. Zhang, X. Zhang, *Org. Lett.* **2002**, *4*, 987–990; d) G. Wang, D. Niu, Y. L. Qiu, L. T. Phan, Z. Chen, A. Polemeropoulos, Y. S. Or, *Org. Lett.* **2004**, *6*, 4455–4458.
[18] P. B. Alper, M. Hendrix, P. Sears, C.-H. Wong, *J. Am. Chem. Soc.* **1998**, *120*, 1965–1978.
[19] P. Pfister, S. Hobbie, C. Brüll, N. Corti, A. Vasella, E. Westhof, E. C. Böttger, *J. Mol. Biol.* **2005**, *346*, 467–475.
[20] a) H. Wang, Y. Tor, *J. Am. Chem. Soc.* **1997**, *119*, 8734–8735; b) H. Wang, Y. Tor, *Angew. Chem.* **1998**, *110*, 117–120; *Angew. Chem. Int. Ed.* **1998**, *37*, 109–111.
[21] a) M. Kaul, D. S. Pilch, *Biochemistry* **2002**, *41*, 7695–7706; b) M. Kaul, C. M. Barbieri, J. E. Kerrigan, D. S. Pilch, *J. Mol. Biol.* **2003**, *326*, 1373–1387.

 © 2005 Wiley-VCH Verlag GmbH & Co. KGaA, Weinheim

Supramolecular Chemistry

DOI: 10.1002/anie.200501467

Conservation of Chirality in a Hierarchical Supramolecular Self-Assembled Structure with Pentagonal Symmetry**

Marie-Christine Blüm, Elizabeta Ćavar, Marina Pivetta, François Patthey, and Wolf-Dieter Schneider*

Molecular and supramolecular chiral recognition governs fundamental processes in living systems.[1] Its importance for disciplines such as biology, pharmaceutics, chemistry, and physics stems from the different properties the two chiral forms exhibit in the presence of chiral phenomena, such as, for example, chiral enzymes and drugs,[2] β-rays,[3] circularly polarized light,[4] and spin-polarized electrons.[5] The differ-

[*] M.-C. Blüm, E. Ćavar, Dr. M. Pivetta, Dr. F. Patthey, Prof. Dr. W.-D. Schneider
Ecole Polytechnique Fédérale de Lausanne (EPFL)
Institut de Physique des Nanostructures
1015 Lausanne (Switzerland)
Fax: (+41) 21-693-0422
E-mail: marie-christine.bluem@epfl.ch

[**] We thank Alessandro de Vita and Massimiliano Stengel for stimulating discussions. This work was supported financially by the Swiss National Science Foundation.

InterScience
© 2005 Wiley-VCH Verlag GmbH & Co. KGaA, Weinheim

ences in physical and chemical characteristics should become important for the design of molecular electronic and optoelectronic devices.[6] The first steps have been made through the study of the self-organizing behavior of chiral organic molecules by scanning tunneling microscopy (STM) and the determination of the chirality of individual molecules and supramolecular assemblies.[7] Herein we present the first direct observation of all stages of a nested self-assembly of π-conjugated chiral molecules into cyclic supramolecular structures. We have followed by STM the hierarchical self-organization of single molecules into individual pentagonal supermolecules which then act as building blocks for the formation of supramolecular decagons. We show the spontaneous chiral resolution of the racemate into disjointed homochiral complex architectures and demonstrate the possibility to monitor directly the evolution of chiral recognition processes on the molecular and supramolecular level.

The aromatic hydrocarbon 5,6,11,12-tetraphenylnaphthacene (rubrene, $C_{42}H_{28}$) is chiral and nonplanar as a result of intramolecular steric hindrance[8] which causes a twisting of the central tetracene backbone around its axis and forces the four phenyl groups to rotate around their σ bonds (Figure 1a). Its highly efficient luminescence can be induced by a variety of methods, such as incident light,[9] chemical reactions,[10] and electronic excitation. The latter property established the success of rubrene as a dopant for organic light emitting diodes which led to the improvement of the efficiency and stability of the devices.[11] The high charge carrier mobility measured on the surface of the crystals[12] led to their integration into organic field-effect transistors[13] that can be switched by light[14] as a consequence of the reversible photooxidation behavior of the molecule.[15] Despite this growing interest in the application of rubrene, there have been no investigations of the self-assembly process and the molecular and supramolecular chirality of rubrene at the nanoscale.

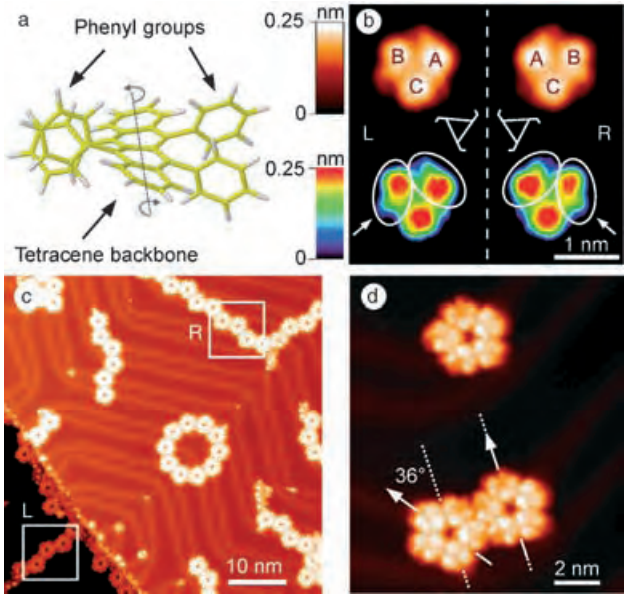


Figure 1. Monomers and self-assembled structures of rubrene on gold. a) Twisted 3D conformation of rubrene in the gas phase. b) STM image of two adsorbed monomers of opposite chirality represented in two different color codings. The arrows indicate the shoulders of feature B for the two enantiomers L and R. c) STM image showing the supramolecular structures on the herringbone-reconstructed Au(111) surface. Two terraces separated by a monatomic step are visible. The squares denoted L and R indicate areas shown in Figure 2c and d, respectively. d) STM image of an isolated supramolecular pentagon and two interlocked supermolecules resembling gear wheels.

Figure 1b shows an STM image of two individual molecules of rubrene adsorbed on an Au(111) surface. Three unequally shaped features (denoted by A, B, and C) with an apparent height of approximately 0.25 nm can be detected in each molecule. The monomer on the left has a counterclockwise arrangement of these lobes (BAC), while the one on the right follows a clockwise orientation (ABC), thus the molecules are mirror images of each other and reflect the chiral conformation of the molecule in the gas phase. The same STM image represented in a different color coding in the lower part of Figure 1b reveals the existence of shoulders (green/blue bulges) belonging to the features A and B which appear either on the left side of each maximum or on the right side, as viewed from the center of the molecule. This characteristic arrangement of asymmetric features determines the molecular chirality and allows the classification of the adsorbed molecules as L or R enantiomers, as shown schematically by the chiral triangles. The independence of these features on an applied voltage between -2 V and $+2$ V indicates that a modulation of the electronic substrate states by broadened molecular levels gives rise to the observed molecular contrast,[16] thus suggesting that the characteristic appearance of the molecules in the STM images reflects their nonplanar and twisted conformation.

The spontaneous self-assembly of single rubrene molecules results in the formation of complex supramolecular structures (Figure 1c). The STM image shows disjointed chains and rings which are constructed out of small building blocks. These structures are incommensurate with the hexagonal periodicity of the Au(111) substrate, but are stabilized by the domain walls of the herringbone-reconstructed surface and at step edges. A smaller scale image reveals that the observed building units of the supramolecular chains are molecular assemblies on their own (Figure 1d). More interestingly, they contain exactly five molecules which are linked into a pentagonal supermolecule with a radius of 1 nm. The appearance of regular pentagons in our experiment is very surprising, given that C_5 symmetries are mainly found in living organisms, but are a rarity in nonliving matter because of the impossibility of a periodic space-filling arrangement with pentagons. Supramolecular self-assembly of adsorbed molecules is the result of a competition between molecule–substrate interactions and noncovalent intermolecular attractions arising from van der Waals forces, hydrogen bonds, and electrostatic interactions. The absence of any permanent dipole in the molecule and the chemical structure of rubrene suggest that the observed self-assembly is the result of an interplay of van der Waals forces and CH···π hydrogen bonds. The incommensurability of the structures rules out site-specific bonding to the surface and indicates that the observed supramolecular assembly is determined by intermolecular forces.

© 2005 Wiley-VCH Verlag GmbH & Co. KGaA, Weinheim

A new level of supramolecular self-assembly is reached by a second organization step that follows the first assembly into stable fivefold structures (Figure 1d). The pentagonal supermolecules diffuse on the surface in a similar manner as the individual molecules and link to each other to form nanometer-sized gearlike wheels. This interlocking of the supermolecules is realized by one pentagonal gear wheel rotating by exactly 36° with respect to the other, which leads to a final distance of approximately 3 nm between their centers. This assembly of two individual supramolecular entities results in a stable individual structure to which other pentagons can join to build supramolecular architectures of higher complexity.

A fascinating aspect of this progression of supramolecular structures is that the molecular chirality is conserved and transferred to the next higher organizational level. A detailed analysis of the pentagonal supermolecules from the first assembly step reveals the existence of two different types of fivefold structures. Pentagons are found that consist of five L-type molecules (Figure 2a), while others are made out of five R-type molecules (Figure 2b). This observation shows that

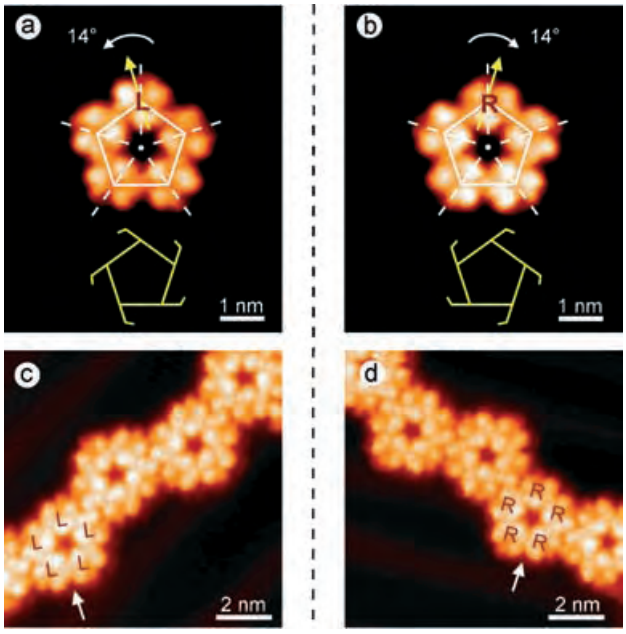


Figure 2. STM images of the enantioselective self-assembly into left- and right-handed supramolecular structures that are mirror images. a, b) Chiral pentagons formed by L-type (a) and R-type (b) molecules, rotated into opposite directions around their centers. c, d) Magnified image of the areas indicated in Figure 1c. Self-assembled chiral chains of interlocked L-type (c) and R-type (d) pentagons.

the spontaneous self-assembly of the individual chiral molecules is enantioselective, and results in two versions of homochiral pentagons. Furthermore, each molecule in the structures is rotated by approximately 14° around its center to optimize the interlocking between the molecules (Figure 2a, b). The direction of rotation is dependent on the molecular chirality: counterclockwise for the L-type molecules and clockwise of the R-type species. This rotation of the molecules, together with the homochirality of the whole assembly, results in the creation of L-type and R-type pentagons (Figure 2a, Figure 2b). The impact of this chiral property on the second step of self-assembly results in the formation of nested chiral structures. STM images of supramolecular chains (Figure 2c, 2d) clearly demonstrate that chirality is conserved in the spontaneous interlocking of pentagonal supermolecules. This observation proves that the two enantiomers of the molecule, as well as the pentagonal supermolecules, are not acting equally in the bonding process as this would result in chirally mixed supramolecular architectures. On the contrary, chiral recognition is of decisive importance for the supramolecular self-assembly and results in a spontaneous self-resolution of the original racemic mixture into nanometer-sized homochiral architectures.

An entirely new and especially beautiful result of the enantiomerically pure self-organization is the creation of a second generation of cyclic size-defined structures (Figure 3).

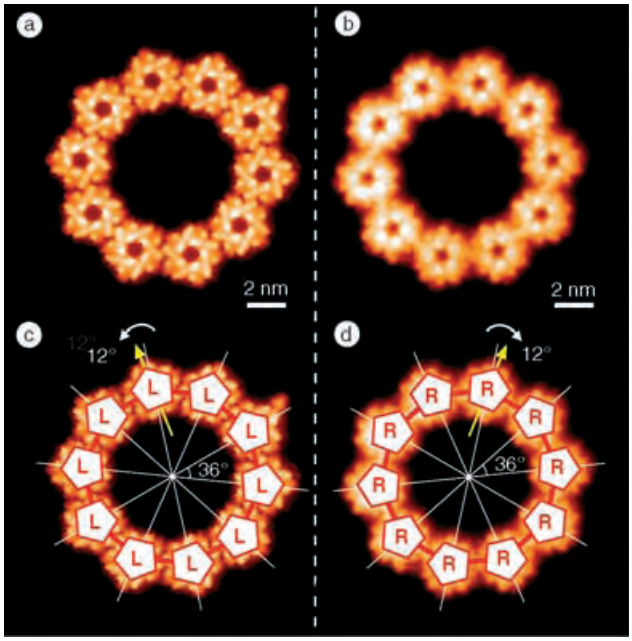


Figure 3. Formation of chiral supramolecular decagons of pentagonal supermolecules. a, b) STM images of a left-handed (a) and a right-handed (b) homochiral decagon. c, d) Construction of the decagons out of ten counterclockwise rotated L-type pentagons (c) and clockwise rotated R-type pentagons (d).

These planar decagons are composed of ten pentagonal supermolecules of the same chirality and rotated by approximately 12° around their centers. The orientation of the rotation depends on the chirality of the pentagonal building blocks and determines the chirality of the decagons (Figure 3a, Figure 3b). The overlaid picture in Figure 3c describes the finding that the decagon shown is a homochiral assembly of exclusively L-type pentagonal supermolecules. Since each pentagon is constructed out of five L-type molecules, we obtain a hierarchically organized architecture of $10 \times 5 = 50$ molecules of the same chirality. This fact, together with the counterclockwise orientation of each

 © 2005 Wiley-VCH Verlag GmbH & Co. KGaA, Weinheim

pentagon, yields an L-type chirality of the tenfold supramolecular structure. The creation of the mirror image of this chiral pattern, namely the R decagon made out of clockwise-rotated R pentagons, is the result of analogous but mirrored building rules as the L-type structure (Figure 3d). The rotation of neighboring pentagonal supermolecules by 36° illustrates that the chiral supramolecular decagons are a special result of the formation of supramolecular chains. The white arrows in Figure 2c and d indicate the docking sites the last pentagons of the chains would have to take to continue the arclike arrangement of the three previous ones. If ten such chirally selected pentagons join together in this way, their assembly leads to the construction of a supramolecular decagon with a diameter of 10 nm. In contrast to the combination of the first three pentagons, which always construct the basis for a cycle, the arriving supermolecules from the forth unit on have only a 50% chance of occupying the "correct" site. This reduces the probability for the development of a complete decagon to less than 1%, a value which explains the rarity of these nested patterns.

Our results demonstrate the surprising hierarchical complexity of the two-dimensional supramolecular assembly of rubrene on gold (Figure 4a). We have identified its three

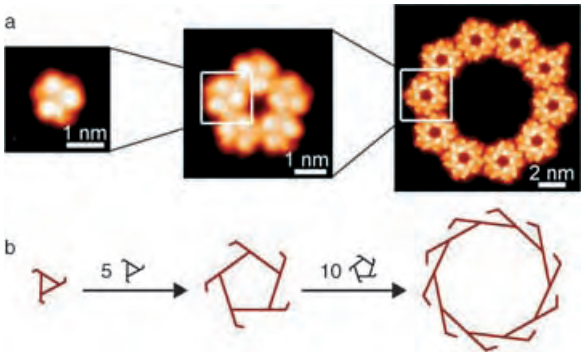


Figure 4. Hierarchy and conservation of chirality in the spontaneous two-dimensional supramolecular assembly. a) STM images representing the three generations of the nested two-staged self-organization. b) Enantioselective assembly from L-type monomers to L-type pentagons and further on to L-type decagons.

successive generations: single molecules, pentagonal supermolecules, and supramolecular decagons. The chirality of the individual molecules is conserved in both assembly steps, and both resulting generations of the progression are chiral as a result of the chirality-dependent rotation of the building blocks (Figure 4b). Since this self-organization of increasing complexity is enantioselective on the molecular and supramolecular level, we obtain a spontaneous resolution of the original racemic mixture of individual molecules into homochiral architectures. Our findings on the conservation and recognition of chirality at all stages of the supramolecular self-assembly of rubrene may have an impact on the development of chiral molecular electronic and optoelectronic devices, and exemplify the working principle of basic processes in nature.

Experimental Section

Experiments were performed using a home-built scanning tunneling microscope in an ultrahigh vacuum system at a base pressure of 2×10^{-11} mbar and a temperature of 5 K. Typical tunneling parameters were: $I_t = 20$ pA and $V_S = -0.8$ V. The rubrene molecules were deposited at low coverage (0.3 monolayers) in situ by sublimation from a home-built evaporator onto a clean Au(111) substrate at room temperature.

Received: April 28, 2005
Published online: July 22, 2005

Keywords: chirality · enantioselectivity · scanning probe microscopy · self-assembly · supramolecular chemistry

[1] J. Cohen, *Science* **1995**, *267*, 1265.
[2] J. M. Brown, S. G. Davies, *Nature* **1989**, *342*, 631.
[3] W. J. Meiring, *Nature* **1987**, *329*, 712.
[4] D. H. Metcalf, S. W. Snyder, S. Wu, G. L. Hilmes, J. P. Riehl, J. N. Demas, F. S. Richardson, *J. Am. Chem. Soc.* **1989**, *111*, 3082.
[5] K. Ray, S. P. Ananthavel, D. H. Waldeck, R. Naaman, *Science* **1999**, *283*, 814.
[6] a) E. W. Meijer, A. P. H. J. Schenning, *Nature* **2002**, *419*, 353; b) V. Percec, M. Glodde, T. K. Bera, Y. Miura, I. Shiyanovskaya, K. D. Singer, V. S. K. Balagurusamy, P. A. Heiney, I. Schnell, A. Rapp, H.-W. Spiess, S. D. Hudson, H. Duan, *Nature* **2002**, *419*, 384; c) Y. Wada, M. Tsukada, M. Fujihira, K. Matsushige, T. Ogawa, M. Haga, S. Tanaka, *Jpn. J. Appl. Phys.* **2000**, *39*, 3835.
[7] a) G. P. Lopinski, D. J. Moffatt, D. D. M. Wayner, R. A. Wolkow, *Nature* **1998**, *392*, 909; b) M. Böhringer, K. Morgenstern, W.-D. Schneider, R. Berndt, F. Mauri, A. De Vita, R. Car, *Phys. Rev. Lett.* **1999**, *83*, 324; c) M. Ortega Lorenzo, C. J. Baddeley, C. Muryn, R. Raval, *Nature* **2000**, *404*, 376; d) A. Kühnle, T. R. Linderoth, B. Hammer, F. Besenbacher, *Nature* **2002**, *415*, 891; e) R. Fasel, M. Parschau, K.-H. Ernst, *Angew. Chem.* **2003**, *115*, 5336; *Angew. Chem. Int. Ed.* **2003**, *42*, 5178; f) J. Weckesser, A. De Vita, J. V. Barth, C. Cai, K. Kern, *Phys. Rev. Lett.* **2001**, *87*, 096101; g) Q. Chen, D. J. Frankel, N. V. Richardson, *Langmuir* **2002**, *18*, 3219; h) S. M. Barlow, S. Louafi, D. Le Roux, J. Williams, C. Muryn, S. Haq, R. Raval, *Langmuir* **2004**, *20*, 7171.
[8] a) N. Sato, K. Seki, H. Inokuchi, *J. Chem. Soc. Faraday Trans. 2* **1981**, *77*, 1621–1633; b) P. U. Biedermann, A. Levy, J. J. Stezowski, I. Agranat, *Chirality* **1995**, *7*, 199.
[9] I. B. Berlman, *Handbook of fluorescence spectra of aromatic molecules*; Academic Press, New York, **1971**.
[10] D. M. Hercules, *Science* **1964**, *145*, 808.
[11] Z. Zhi-lin, J. Xue-yin, X. Shao-hong, T. Nagatomo, O. Omoto, *J. Phys. D* **1998**, *31*, 32.
[12] V. Podzorov, E. Menard, A. Borissov, V. Kiryukhin, J. A. Rogers, M. E. Gershenson, *Phys. Rev. Lett.* **2004**, *93*, 086602.
[13] V. C. Sundar, J. Zaumseil, V. Podzorov, E. Menard, R. L. Willett, T. Someya, M. E. Gershenson, J. A. Rogers, *Science* **2004**, *303*, 1644.
[14] V. Podzorov, V. M. Pudalov, M. E. Gershenson, *Appl. Phys. Lett.* **2004**, *85*, 6039.
[15] Y. Harada, T. Takahashi, S. Fujisawa, T. Kajiwara, *Chem. Phys. Lett.* **1979**, *62*, 283.
[16] A. J. Fisher, P. E. Blöchl, *Phys. Rev. Lett.* **1993**, *70*, 3263.

 © 2005 Wiley-VCH Verlag GmbH & Co. KGaA, Weinheim

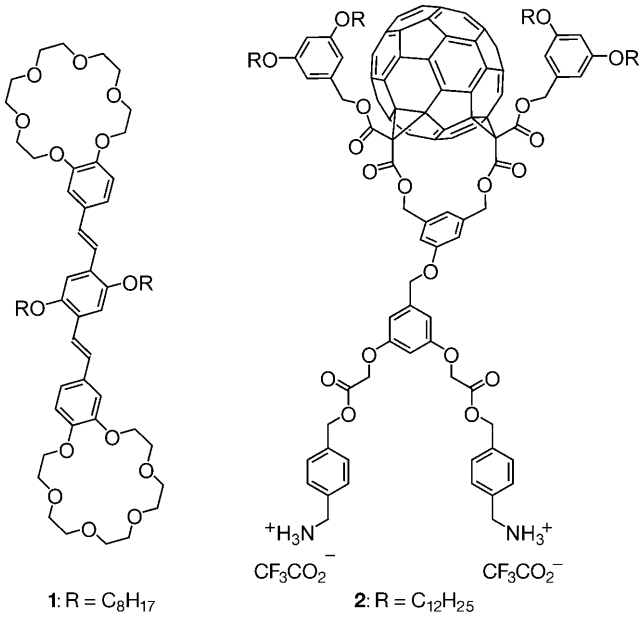
Host–Guest Chemistry

DOI: 10.1002/anie.200501249

Supramolecular Click Chemistry with a Bisammonium-C_{60} Substrate and a Ditopic Crown Ether Host**

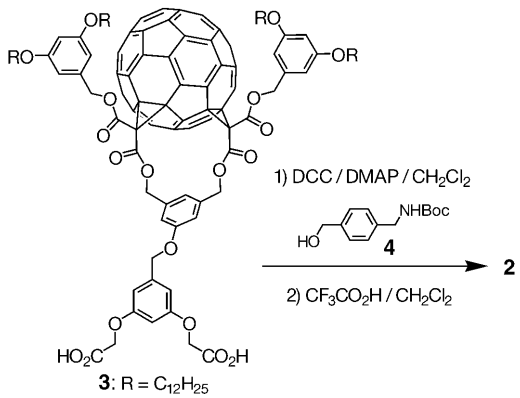
Uwe Hahn, Mourad Elhabiri, Ali Trabolsi, Haiko Herschbach, Emmanuelle Leize, Alain Van Dorsselaer, Anne-Marie Albrecht-Gary,* and Jean-François Nierengarten**

Fullerenes and their derivatives have shown a wide range of chemical and physical properties which make them attractive candidates for a variety of interesting applications in supramolecular chemistry.[1] Indeed, spectacular noncovalent architectures incorporating fullerene moieties have been described over the past few years. Examples include rotaxanes,[2] catenanes,[3] self-assembled coordination compounds,[4] liquid-crystalline inclusion complexes,[5] and photoactive supramolecular devices.[6–10] As part of this research, we have recently reported supramolecular donor-fullerene systems based on the self-assembly of C_{60} derivatives bearing an ammonium unit with crown ethers.[7–9] However, the ammonium–crown ether interaction is itself weak.[7] Consequently, the binding constants are rather low and only a small fraction of the two components are effectively associated in solution. This result prompted us to design systems with additional recognition elements to increase the binding constants.[8,9] For example, evidence of π-stacking interactions between the C_{60} sphere and the porphyrin moiety in a supramolecular array has been obtained from a porphyrin–crown ether conjugate and a fullerene derivative bearing an ammonium unit.[8] In this case, the association constant (K_a) for the complex is increased by two orders of magnitude relative to K_a values for the complexation of the same ammonium cation with other crown ether derivatives. We now report the preparation and the characterization of a very stable supramolecular complex obtained from bis(crown ether) receptor **1**[9] and bisammonium fullerene ligand **2**. As a result of the perfect complementarity of the two components, biscationic substrate **2** can be "clicked"[10] onto the ditopic crown ether derivative **1**, thus leading to a noncovalent macrocyclic 1:1 complex.



1: R = C_8H_{17} **2**: R = $C_{12}H_{25}$

The synthesis of **2** is depicted in Scheme 1. The C_s symmetrical fullerene bisadduct precursor **3** was prepared in nine steps according to a literature procedure.[11] Treatment of diacid **3** with alcohol **4**[7] and *N*,*N*′-dicyclohexylcarbodiimide (DCC) in the presence of 4-dimethylaminopyridine (DMAP) and 1-hydroxybenzotriazole (HOBt) gave bisamine **5** protected with *tert*-butyloxycarbonyl (Boc) groups in 37% yield.



3: R = $C_{12}H_{25}$

Scheme 1. Preparation of compound **2**.

[*] H. Herschbach, Dr. E. Leize, Dr. A. Van Dorsselaer
Laboratoire de Spectrométrie de Masse Bio-organique
Ecole de Chimie, Polymères et Matériaux (ECPM)
Université Louis Pasteur and CNRS
25 rue Becquerel, 67087 Strasbourg Cedex 2 (France)
Fax: (+33) 3-9024-2781
E-mail: vandors@chimie.u-strasbg.fr
Dr. M. Elhabiri, A. Trabolsi, Dr. A.-M. Albrecht-Gary
Laboratoire de Physico-Chimie Bioinorganique
Université Louis Pasteur et CNRS (UMR 7509)
Ecole Européenne de Chimie, Polymères et Matériaux (ECPM)
25 rue Becquerel, 67087 Strasbourg Cedex 2 (France)
Fax: (+33) 3-9024-2639
E-mail: amalbre@chimie.u-strasbg.fr
Dr. U. Hahn, Dr. J.-F. Nierengarten
Groupe de Chimie des Fullerènes et des Systèmes Conjugués
Laboratoire de Chimie de Coordination du CNRS
205 route de Narbonne, 31077 Toulouse Cedex 4 (France)
Fax: (+33) 5-6155-3003
E-mail: jfnierengarten@lcc-toulouse.fr

[**] This work was supported by the CNRS, a doctoral fellowship from the French Ministry of Research to A.T., a doctoral fellowship from the European Postgraduate School (GRK532) to H.H., and a postdoctoral fellowship from the Deutscher Akademischer Austausch Dienst (DAAD) to U.H.

Supporting information for this article is available on the WWW under http://www.angewandte.org or from the author.

InterScience
© 2005 Wiley-VCH Verlag GmbH & Co. KGaA, Weinheim

Subsequent treatment with CF_3CO_2H afforded **2** as its trifluoroacetate salt in 84% yield.

The binding behavior of bisammonium **2** with the bis(crown ether) receptor **1** in $CDCl_3$ was first investigated by ^{1}H NMR spectroscopy at 298 K. Comparison of the ^{1}H NMR spectra of **1**, **2**, and an equimolar mixture of both components revealed complexation-induced changes in chemical shifts (Figure 1). In particular, a dramatic downfield

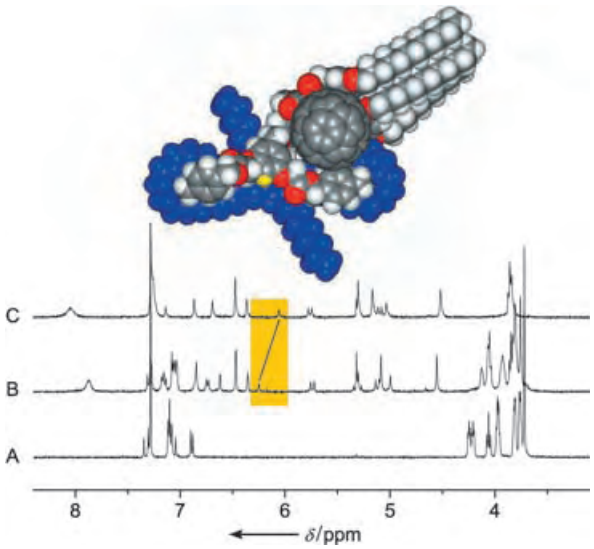


Figure 1. Top: calculated structure of the macrocyclic supramolecular complex [(**1**)·(**2**)] (molecular modeling studies were performed with Spartan). Bottom: ^{1}H NMR spectrum (400 MHz, 25 °C) of equimolar $CDCl_3$ solutions of **1** (A), **2** (C), and a 1:1 mixture of **1** and **2** (B); the downfield shift of the signal corresponding to proton H_K (shown in yellow) upon addition of **1** shows that this proton must be close to the π-conjugated system of **1** in the supramolecular complex, which is in good agreement with the proposed structure.

shift is seen for the signal of H_K of **2** upon addition of **1**. This downfield shift indicates the formation of a macrocyclic 1:1 supramolecular complex where proton H_K is located on top of the conjugated π system of **1**.

Further evidence for the formation of a 1:1 macrocyclic complex was obtained by electrospray mass spectrometry (ESMS).[12] The ES mass spectrum (positive mode; Figure 2) recorded under mild conditions (extracting cone voltage V_c = 200 V) of a 1:1 mixture of **1** and **2** is dominated by a doubly charged ion signal at *m*/*z* 1723.1 which can be assigned to the 1:1 complex after loss of the trifluoroacetate counteranions (calculated *m*/*z* 1723.11). A very minor signal corresponding to the 2:1 complex was also detected at *m*/*z* 2226.7 (calculated *m*/*z* 2226.76). Under harsher conditions (V_c = 400 V) the spectrum was still dominated by the doubly charged ion signal at *m*/*z* 1723.1 and no significant fragmentation of the supramolecular assembly [(**1**)·(**2**)] could be observed. Indeed, the spectra are almost identical regardless of the V_c value. This behavior is in sharp contrast to the ESMS analysis of supramolecular complexes of **2** with simple crown ether derivatives in which important fragmentation occurs at high V_c values (see Supporting Information). These observations

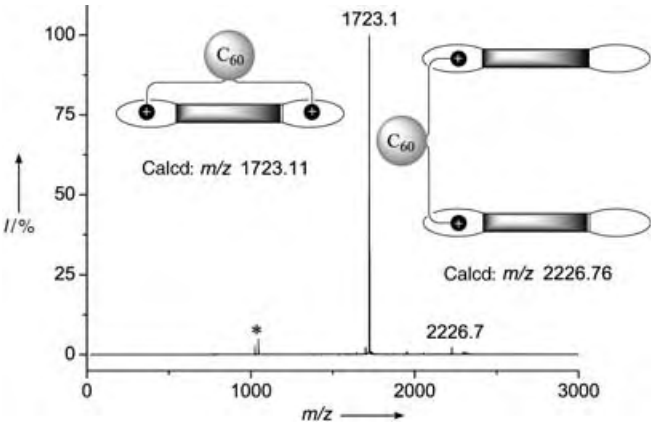


Figure 2. ES mass spectrum (V_c = 200 V) of a 1:1 mixture of **1** and **2** in CH_2Cl_2 ([(**1**)] = [(**2**)] = 5×10^{-6} M); the signal at *m*/*z* 1046.2 (*) is assigned to $[\mathbf{1}+K]^+$ (calculated *m*/*z* 1046.40).

show the high stability of the noncovalent array [(**1**)·(**2**)]. It is also worth noting that the major signal obtained in the ES mass spectra of a 10:1 mixture of **1** and **2** corresponds to the [(**1**)·(**2**)] complex. Under these conditions, the intensity of the signal corresponding to the 2:1 complex [(**1**)$_2$·(**2**)] is lower than 5% of the signal corresponding to the macrocyclic 1:1 complex, thus providing additional evidence for the high stability of [(**1**)·(**2**)].

To quantify the interactions between **1** and **2**, complexation was investigated in CH_2Cl_2 by UV/Vis binding studies, in which changes in the spectrum upon addition of increasing amounts of **2** to a solution of **1** in CH_2Cl_2 were monitored (see Supporting Information). The processing[13] of these data allowed the characterization of a single supramolecular complex [(**1**)·(**2**)] in solution ($\log K_1 = 6.3 \pm 0.4$), which is in excellent agreement with the ESMS and NMR spectroscopic data. Nevertheless, the rather weak complexation-induced changes in the adsorption spectrum prompted further investigation into the binding of **1** and **2** by luminescence experiments. As previously observed for related systems,[7–9] the strong emission of the π-conjugated system of **1** (λ_{em}^{max} = 450 nm, $\phi_{fluo} = 0.65 \pm 0.06$) is quenched upon binding of **2** through an efficient intramolecular process within the [(**1**)·(**2**)] complex, thus allowing the facile determination of the binding constant by luminescence titrations (Figure 3). Collisions and reabsorption events (see Supporting Information) could be neglected under our experimental conditions. Therefore, the decrease in the luminescence intensity observed in the presence of **2** (Figure 3) is attributed solely to intramolecular photochemical processes. By using a modified Stern–Volmer relationship[14] ($F_0/F = (1 + K_{SV}[(\mathbf{2})]) \times \exp(K_1[(\mathbf{2})])$) and assuming $K_{SV}[(\mathbf{2})] \ll 1$, the stability constant of [(**1**)·(**2**)] was obtained ($\log K_1 = 6.40 \pm 0.01$).[15] This value is in excellent agreement with the result obtained from the absorption binding studies.

Comparison of our results with thermodynamic data available in the literature show that coordination is more than three orders of magnitude stronger in the current system than in related systems (crown ethers and ammonium derivatives).[7] This result is mainly attributed to the two-center

 © 2005 Wiley-VCH Verlag GmbH & Co. KGaA, Weinheim

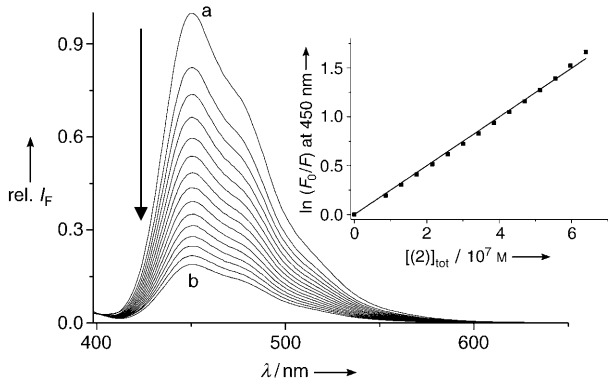


Figure 3. Luminescence titration of **1** with **2**. Solvent: CH_2Cl_2; $T = 25.0 \pm 0.2$ °C; $\lambda_{exc} = 398$ nm; emission and excitation slit widths 15 nm; 1% attenuator; a) $[(\mathbf{1})]_{tot} = 9.77 \times 10^{-7}$ M; b) $[(\mathbf{2})]_{tot}/[(\mathbf{1})]_{tot} = 0.7$. Inset: variation of $\ln(F_0/F)$ at 450 nm versus the concentration of **2**. The solid line is the result of the linear least-square fit of the experimental data according to $\ln(F_0/F) = K_1[(\mathbf{2})]$.

host–guest topography. In a similar manner to the "click chemistry" concept introduced by Sharpless and co-workers,[10] the "supramolecular click chemistry" principle described herein is a powerful and selective process for the preparation of stable macrocyclic noncovalent arrays. This approach is modular and it appears that it can be easily applied to a wide range of functional groups for the preparation of new supramolecular architectures with tunable structural and electronic properties.

Experimental Section

ESMS: High-resolution ESI mass spectra in the positive mode were acquired on a time of flight mass spectrometer (microTof, Bruker Daltonics, Bremen, Germany). The instrument was calibrated using a solution of cesium iodide (1 mg mL^{-1}) in water/isopropanol (50/50 (v/v)). CsI clusters of the types $[(CsI)_nCs]^+$ or $[(CsI)_nCs_2]^{2+}$ generate ions with m/z values up to about 16000. The ESI-source was heated to 100 °C. Sample solutions were introduced into the mass spectrometer source with a syringe pump (Cole Parmer, Vernon Hills, Illinois, USA) with a flow rate of 5 μL min^{-1}. Scanning was performed over an m/z range of 100–12000, and then the data were averaged for 1 min and smoothed using the Gaussian algorithm. To ensure that the species detected by ESI-MS reflect the species present in solution, the instrument parameters, for example, the sample cone voltage V_c, have been varied.

UV/Vis and luminescence binding studies: the experimental conditions have been described in detail in Ref. [9].

Received: April 9, 2005
Published online: July 25, 2005

Keywords: binding studies · crown compounds · fullerenes · host–guest systems · supramolecular chemistry

[1] For reviews on fullerene supramolecular chemistry, see: a) F. Diederich, M. Gómez-López, *Chem. Soc. Rev.* **1999**, *28*, 263–277; b) D. M. Guldi, N. Martin, *J. Mater. Chem.* **2002**, *12*, 1978–1992.

[2] a) F. Diederich, C. O. Dietrich-Buchecker, J.-F. Nierengarten, J.-P. Sauvage, *J. Chem. Soc. Chem. Commun.* **1995**, 781–782; b) N. Armaroli, F. Diederich, C. O. Dietrich-Buchecker, L. Flamigni, G. Marconi, J.-F. Nierengarten, J.-P. Sauvage, *Chem. Eur. J.* **1998**, *4*, 406–416; c) T. Da Ros, D. M. Guldi, A. F. Morales, D. A. Leigh, M. Prato, R. Turco, *Org. Lett.* **2003**, *5*, 689–691; d) N. Watanabe, N. Kihara, Y. Furusho, T. Takata, Y. Araki, O. Ito, *Angew. Chem.* **2003**, *115*, 705–707; *Angew. Chem. Int. Ed.* **2003**, *42*, 681–683; e) K. Li, D. I. Schuster, D. M. Guldi, M. A. Herranz, L. Echegoyen, *J. Am. Chem. Soc.* **2004**, *126*, 3388–3389; f) D. I. Schuster, K. Li, D. M. Guldi, J. Ramey, *Org. Lett.* **2004**, *6*, 1919–1922; g) H. Sasabe, N. Kihara, Y. Furusho, K. Mizuno, A. Ogawa, T. Takata, *Org. Lett.* **2004**, *6*, 3957–3960.

[3] a) P. R. Ashton, F. Diederich, M. Gómez-López, J.-F. Nierengarten, J. A. Preece, F. M. Raymo, J. F. Stoddart, *Angew. Chem.* **1997**, *109*, 1611–1614; *Angew. Chem. Int. Ed. Engl.* **1997**, *36*, 1448–1451; b) Y. Nakamura, S. Minami, K. Iizuka, J. Nishimura, *Angew. Chem.* **2003**, *115*, 3266–3270; *Angew. Chem. Int. Ed.* **2003**, *42*, 3158–3162.

[4] a) T. Habicher, J.-F. Nierengarten, V. Gramlich, F. Diederich, *Angew. Chem.* **1998**, *110*, 2019–2022; *Angew. Chem. Int. Ed.* **1998**, *37*, 1916–1919; b) F. Cardinali, H. Mamlouk, Y. Rio, N. Armaroli, J.-F. Nierengarten, *Chem. Commun.* **2004**, 1582–1583.

[5] D. Felder, B. Heinrich, D. Guillon, J.-F. Nicoud, J.-F. Nierengarten, *Chem. Eur. J.* **2000**, *6*, 3501–3507.

[6] a) N. Armaroli, F. Diederich, L. Echegoyen, T. Habicher, L. Flamigni, G. Marconi, J.-F. Nierengarten, *New J. Chem.* **1999**, *23*, 77–83; b) F. D'Souza, G. R. Deviprasad, M. S. Rahman, J.-P. Choi, *Inorg. Chem.* **1999**, *38*, 2157–2160; c) T. Da Ros, M. Prato, D. M. Guldi, E. Alessio, M. Ruzzi, L. Pasimeni, *Chem. Commun.* **1999**, 635–636; d) F. Diederich, L. Echegoyen, M. Gómez-López, R. Kessinger, J. F. Stoddart, *J. Chem. Soc. Perkin Trans. 2* **1999**, 1577–1586; e) E. H. A. Beckers, A. P. H. J. Schenning, P. A. van Hal, A. El-ghayoury, L. Sanchez, J. C. Hummelen, E. W. Meijer, R. A. J. Janssen, *Chem. Commun.* **2002**, 2888–2889; f) E. H. A. Beckers, P. A. van Hal, A. P. H. J. Schenning, A. El-ghayoury, E. Peeters, M. T. Rispens, J. C. Hummelen, E. W. Meijer, R. A. J. Janssen, *J. Mater. Chem.* **2002**, *12*, 2054–2060; g) F. Hauke, A. Swartz, D. M. Guldi, A. Hirsch, *J. Mater. Chem.* **2002**, *12*, 2088–2094; h) S. R. Wilson, S. MacMahon, F. T. Tat, P. D. Jarowski, D. I. Schuster, *Chem. Commun.* **2003**, 226–227; i) F. D'Souza, R. Chitta, S. Gadde, M. E. Zandler, A. S. D. Sandanayaka, Y. Araki, O. Ito, *Chem. Commun.* **2005**, 1279–1281.

[7] M. Gutiérrez-Nava, H. Nierengarten, P. Masson, A. Van Dorsselaer, J.-F. Nierengarten, *Tetrahedron Lett.* **2003**, *44*, 3043–3046.

[8] N. Solladié, M. E. Walther, M. Gross, T. M. Figueira Duarte, C. Bourgogne, J.-F. Nierengarten, *Chem. Commun.* **2003**, 2412–2413.

[9] M. Elhabiri, A. Trabolsi, F. Cardinali, U. Hahn, A.-M. Albrecht-Gary, J.-F. Nierengarten, *Chem. Eur. J.*, in press.

[10] For the concept of "click chemistry", see: H. C. Kolb, M. G. Finn, K. B. Sharpless, *Angew. Chem.* **2001**, *113*, 2056–2075; *Angew. Chem. Int. Ed.* **2001**, *40*, 2004–2021.

[11] D. Felder, M. Gutiérrez Nava, M. del Pilar Carreon, J.-F. Eckert, M. Luccisano, C. Schall, P. Masson, J.-L. Gallani, B. Heinrich, D. Guillon, J.-F. Nierengarten, *Helv. Chim. Acta* **2002**, *85*, 288–319.

[12] ESMS is a soft ionization technique ideally suited to characterize noncovalent complexes and is now commonly applied to the study of large supramolecular arrays; for examples, see: a) H. Nierengarten, J. Rojo, E. Leize, J.-M. Lehn, A. Van Dorsselaer, *Eur. J. Inorg. Chem.* **2002**, 573–579; b) M. Gutiérrez-Nava, M. Jaeggy, H. Nierengarten, P. Masson, D. Guillon, A. Van Dorsselaer, J.-F. Nierengarten, *Tetrahedron Lett.* **2003**, *44*, 3039–3042; c) C. A. Schalley, *Int. J. Mass Spectrom.* **2000**, *194*, 11–39.

 © 2005 Wiley-VCH Verlag GmbH & Co. KGaA, Weinheim

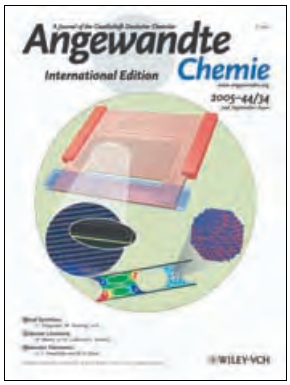
[13] a) R. A. Binsteadt, A. D. Zuberbühler, *Specfit, A Program for Global Least Squares Fitting of Equilibrium and Kinetics Systems Using Factor Analysis & Marquardt Minimisation*, Version 2-11 C, Spectrum Software Associates, Chapel Hill, **1998**; b) H. Gampp, M. Maeder, C. J. Meyer, A. D. Zuberbühler, *Talanta* **1985**, *32*, 95 – 101; c) H. Gampp, M. Maeder, C. J. Meyer, A. D. Zuberbühler, *Talanta* **1985**, *32*, 257 – 264; d) H. Gampp, M. Maeder, C. J. Meyer, A. D. Zuberbühler, *Talanta* **1986**, *33*, 943 – 951.

[14] a) *Biophysical and Biochemical Aspects of Fluorescence Spectroscopy* (Ed.: T. G. Dewey), Plenum, New York, **1991**; b) M. R. Eftink, C. A. Ghiron, *Biochemistry* **1976**, *15*, 672 – 680; c) M. R. Eftink, T. J. Selva, Z. Wasylewski, *Photochem. Photobiol.* **1987**, *46*, 23 – 30.

[15] Microcal Origin, Microcal Software, Inc., Northampton, USA.

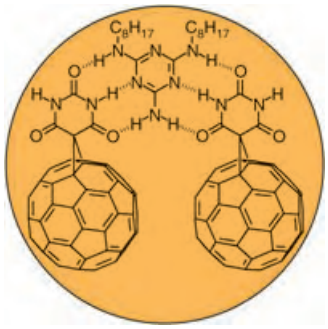
 © 2005 Wiley-VCH Verlag GmbH & Co. KGaA, Weinheim

Cover Picture



Brian K. H. Yen, Axel Günther, Martin A. Schmidt, Klavs F. Jensen,* and Moungi G. Bawendi*

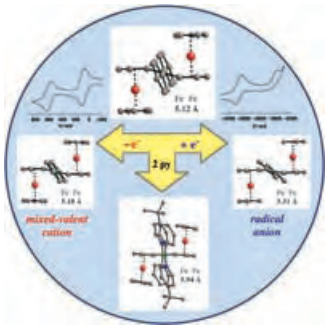
The two-phase flow of the gas–liquid segmented flow reactor with multiple temperature zones shown in the cover picture makes it possible to realize both rapid mixing of reagents and narrow residence-time distributions. The reactor design allows the preparation of colloidal CdSe quantum dots (bottom right) with excellent size distributions at high temperature. For more details, see the Communication by K. F. Jensen, M. G. Bawendi, and co-workers on page 5447 ff. (The authors thank Jane Rempel for assistance with the cover picture.)



Fullerene Chemistry
In their Minireview on page 5374 ff. N. Martín, D. M. Guldi, and L. Sánchez describe how supramolecular structures are formed and modulated by combinations of fullerenes and hydrogen bonds.



Biaryl Syntheses
Axially chiral biaryl compounds are increasingly common structural units. G. Bringmann, M. Breuning, and co-workers describe strategies for the atroposelective synthesis of these challenging compounds in their Review on page 5384 ff.



Ferrocenes
In their Communication on page 5428 ff., F. Jäkle and co-workers describe an electrochemical and structural study of a highly rigid 1,2-diborylated diferrocene that shows unusually strong electronic coupling between the ferrocene groups upon partial oxidation.

Contents

VIP *The following Communications have been judged by at least two referees to be "very important papers" and will be published online at www.angewandte.org soon:*

K. Haraguchi, H.-J. Li*
Control of the Coil-to-Globule Transition of Poly(*N*-isopropylacrylamide) and Ultrahigh Mechanical Properties in Nanocomposite Hydrogels

*T. Buskas, S. Ingale, G.-J. Boons**
Towards a Fully Synthetic Carbohydrate-Based Anticancer Vaccine: Synthesis and Immunological Evaluation of a Lipidated Glycopeptide Containing the Tumor-Associated Tn Antigen

A. C. Filippou, G. Schnakenburg, A. I. Philippopoulos, N. Weidemann*
Bonding Analysis of the M≡Ge–Ge≡M Chain in the Germylidyne Complexes *trans,trans*-[Cl(depe)$_2$M≡Ge–Ge≡M(depe)$_2$Cl]

*M. Veith**
Cubane-Type Li_4H_4 and $Li_3H_3Li(OH)$: Stabilized in Molecular Adducts with Alane

S. Protti, M. Fagnoni, A. Albini**
Photochemical Cross-Coupling Reactions of Electron-Rich Aryl Chlorides and Aryl Esters with Alkynes: A Metal-Free Alkynylation

*V. Lavallo, Y. Canac, C. Präsang, B. Donnadieu, G. Bertrand**
Stable Cyclic (Alkyl)(amino)carbenes as Rigid or Flexible, Bulky, Electron-Rich Ligands for Transition-Metal Catalysts

Meeting Reviews

Joint Meeting on Medicinal Chemistry in Vienna — R. E. Martin,* P. Mohr, W. Palmer, H. Stalder — **5364**

Books

Biocatalysts and Enzyme Technology — Klaus Buchholz, Volker Kasche, Uwe T. Bornscheuer — *reviewed by O. May* — **5367**

Handbook of RNA Biochemistry — Roland K. Hartmann, Albrecht Bindereif, Astrid Schön, Eric Westhof — *reviewed by W. Saenger* — **5367**

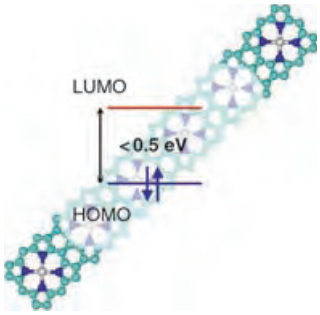
Highlights

Molecular Electronics

D. F. Perepichka,* M. R. Bryce* — **5370 – 5373**

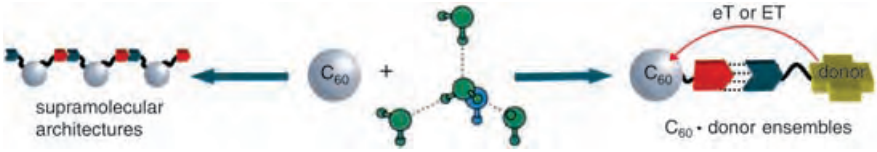
Molecules with Exceptionally Small HOMO–LUMO Gaps

Mind the gap: HOMO–LUMO gaps less than 0.5 eV have been recently engineered in small organic molecules through extended conjugation and donor–acceptor covalent coupling approaches (see picture). Such compounds reveal a number of unusual electronic properties such as thermo-excited intramolecular electron transfer (in solution) and metallic conductivity (in the solid state).



InterScience
© 2005 Wiley-VCH Verlag GmbH & Co. KGaA, Weinheim

Minireviews



Supramolecular chemistry of C_{60} is leading the way for the use of C_{60} as a unique photo- and electroactive building block. Arrays of hydrogen bonds ensure a high degree of order on the nanometer scale, a feature that will be critical in the application of the resulting noncovalently bound ensembles as molecular materials or supramolecular catalysts (see scheme; eT = electron transfer, ET = energy transfer).

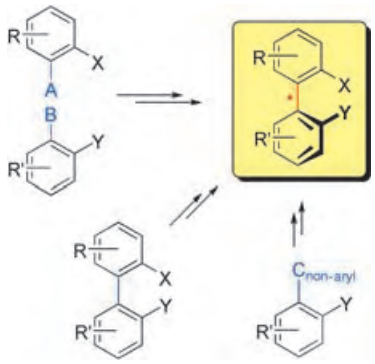
Fullerene Chemistry

L. Sánchez, N. Martín,*
D. M. Guldi* ——— **5374 – 5382**

Hydrogen-Bonding Motifs in Fullerene Chemistry

Reviews

Not only classic, atroposelective biaryl couplings lead to stereochemically pure, axially chiral biaryl compounds (see scheme); recently, novel, highly original strategies have also emerged. The authors present a discussion of the structural preconditions of axial chirality and the most successful and innovative of these strategies.

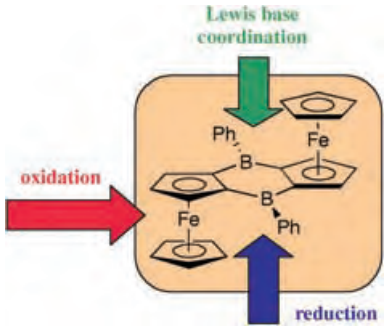


Biaryl Synthesis

G. Bringmann,* A. J. Price Mortimer,
P. A. Keller, M. J. Gresser, J. Garner,
M. Breuning* ——— **5384 – 5427**

Atroposelective Synthesis of Axially Chiral Biaryl Compounds

Communications



Two Bs in a pod: The first 1,2-diborylated ferrocene (see structure) was obtained upon reaction of $PhBCl_2$ with 1,1′-bis(trimethylstannyl)ferrocene. Conformational changes in this highly rigid species are triggered either through redox chemistry or the binding of nucleophiles, to render the complex an interesting candidate for the design of new types of molecular machines.

Ferrocenes

K. Venkatasubbaiah, L. N. Zakharov,
W. S. Kassel, A. L. Rheingold,
F. Jäkle* ——— **5428 – 5433**

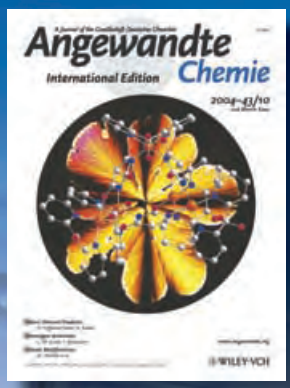
Reversible Expansion and Contraction of a 1,2-Diborylated Ferrocene Dimer Promoted by Redox Chemistry and Nucleophile Binding

For the USA and Canada:
ANGEWANDTE CHEMIE International Edition (ISSN 1433-7851) is published weekly by Wiley-VCH PO Box 191161, D 69451 Weinheim, Germany. Air freight and mailing in the USA by Publications Expediting Inc. 200 Meacham Ave., Elmont, NY 11003. Periodicals postage paid at Jamaica NY 11431. US POSTMASTER: send address changes to *Angewandte Chemie*, Wiley-VCH, 111 River Street, Hoboken, NJ 07030. Annual subscription price for institutions: US$ 4948.00/4498.00 (valid for print and electronic / print or electronic delivery); for individuals who are personal members of a national chemical society, or whose institution already subscribes, or who are retired or self-employed consultants, print only: US$ 394.00. Postage and handling charges included. All Wiley-VCH prices are exclusive VAT.

© 2005 Wiley-VCH Verlag GmbH & Co. KGaA, Weinheim

The best in chemistry –

for more than a hundred years



A Journal of the Gesellschaft Deutscher Chemiker

Angewandte
International Edition **Chemie**

www.angewandte.org

1888: ***The beginning of a success story***

Constant Innovations

1962: *First issue of the International Edition*
1976: *Graphical abstracts*
1979: *Cover pictures*
1988: *Centenary of Angewandte*
1989: *Routine use of color*
1991: *New section: Highlights*
1992: *Computerized editorial tracking system*
1995: *Internet service for readers*
1998: *Regular press service; full-text online*
2000: *New section: Essays; EarlyView: Communications available online ahead of the printed version*
2001: *New section: Minireviews*
2002: *Online submission of manuscripts*
2003: *Weekly publication; new section: News; new layout*
2004: *Backfiles (1962-1997); ManuscriptXpress: Online system for authors and referees*



Angewandte's advisors...

François Diederich
ETH Zürich

*»**Angewandte Chemie** has proven over the past two decades to be the most innovative of all chemical journals, taking leadership in both quality and presentation of the published material. Rapid, high visibility of important scientific work is readily ensured. It is a true privilege to serve on the Editorial Board.«*

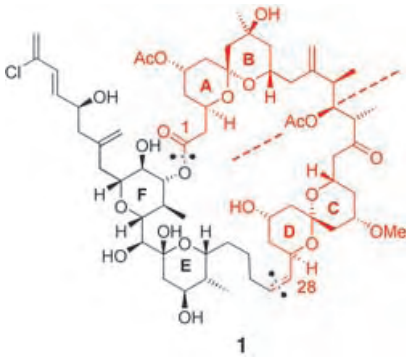
***Angewandte Chemie International Edition** is a journal of the German Chemical Society (GDCh)*

GDCh

WILEY InterScience® DISCOVER SOMETHING GREAT

WILEY-VCH

1811404_gu



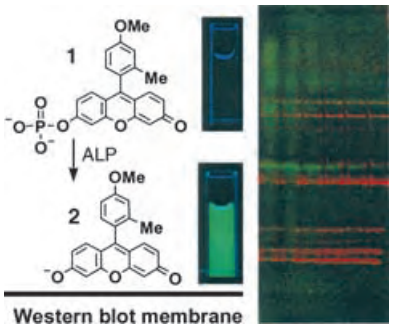
1

The challenging structure and potent growth inhibition properties against a variety of human cancer cell lines make Spongistatin 1 (**1**) an exciting target for total synthesis. Enantioselective total synthesis has been achieved by exploiting a latent element of pseudo-symmetry (-----= pseudo-C_2 axis) within the ABCD bis(spiroketal) fragment (red substructure).

Natural Product Synthesis

M. Ball, M. J. Gaunt, D. F. Hook, A. S. Jessiman, S. Kawahara, P. Orsini, A. Scolaro, A. C. Talbot, H. R. Tanner, S. Yamanoi, S. V. Ley* ____ **5433 – 5438**

Total Synthesis of Spongistatin 1: A Synthetic Strategy Exploiting Its Latent Pseudo-Symmetry

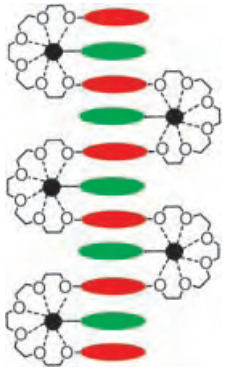


The new star of Westerns: A highly sensitive fluorescence probe for alkaline phosphatase (ALP) based on a fluorescein derivative has been prepared and found to be suitable for use in Western blot analysis. The probe **1** is nonfluorescent but undergoes hydrolysis in the presence of ALP to yield a green-fluorescent derivative **2** and may be used in multicolor labeling in combination with other probes.

Fluorescent Probes

M. Kamiya, Y. Urano, N. Ebata, M. Yamamoto, J. Kosuge, T. Nagano* ____ **5439 – 5441**

Extension of the Applicable Range of Fluorescein: A Fluorescein-Based Probe for Western Blot Analysis



Stack 'em high: A polyimide with pyromellitic diimide units linked by hexaoxyethylene segments can be made to fold by cooperative two-point interactions on addition of a folding agent (see scheme). The ammonium group of the folding agent forms complexes with the oxyethylene spacer which greatly facilitates the formation of charge-transfer complexes between the aromatic units of the two components.

Donor–Acceptor Systems

S. Ghosh, S. Ramakrishnan* ____ **5441 – 5447**

Small-Molecule-Induced Folding of a Synthetic Polymer



Monodisperse CdSe quantum dots (QDs) with excellent optical properties can be prepared with a gas–liquid segmented flow microreactor with multiple temperature zones (see picture; red = heated; blue = cooled quench zone). The enhanced mixing and narrow residence time distributions of segmented flow produce QDs superior to those prepared in single-phase operations.

Microreactor Fluidics

B. K. H. Yen, A. Günther, M. A. Schmidt, K. F. Jensen,* M. G. Bawendi* ____ **5447 – 5451**

A Microfabricated Gas–Liquid Segmented Flow Reactor for High-Temperature Synthesis: The Case of CdSe Quantum Dots

© 2005 Wiley-VCH Verlag GmbH & Co. KGaA, Weinheim

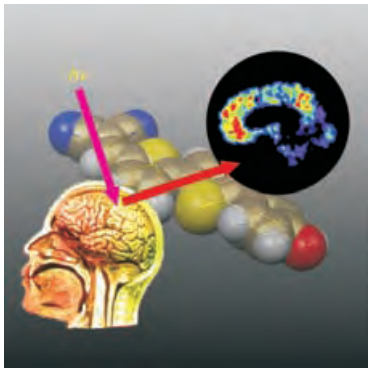
Contents

Fluorescent Probes

E. E. Nesterov, J. Skoch, B. T. Hyman, W. E. Klunk, B. J. Bacskai, T. M. Swager* _____ **5452 – 5456**

In Vivo Optical Imaging of Amyloid Aggregates in Brain: Design of Fluorescent Markers

Routine diagnostics and studies of Alzheimer's disease might benefit form the noninvasive optical imaging of amyloid-β plaques in the brain. A rational design strategy for in vivo amyloid-imaging agents that enter the brain and selectively stain amyloid plaques is presented (see picture), and properties of a promising lead biomarker candidate are reported.

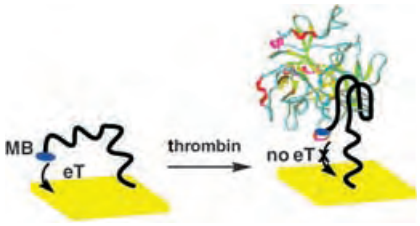


Electrochemical Biosensors

Y. Xiao, A. A. Lubin, A. J. Heeger, K. W. Plaxco* _____ **5456 – 5459**

Label-Free Electronic Detection of Thrombin in Blood Serum by Using an Aptamer-Based Sensor

Blue, gold, and DNA: A methylene blue (MB) tagged, thrombin-binding DNA aptamer immobilized on a gold surface undergoes a large conformational change upon target binding (see schematic representation; eT: electron transfer). This folding produces a large, readily measurable change in redox current and allows the electrochemical detection of thrombin in blood serum.

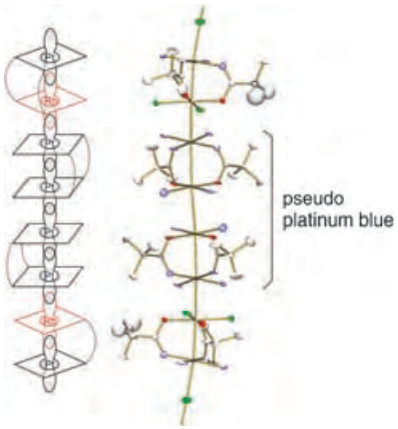


Metal Chains

K. Uemura, K. Fukui, H. Nishikawa, S. Arai, K. Matsumoto,* H. Oshio _ **5459 – 5464**

Paramagnetic Platinum–Rhodium Octamers Bridged by Halogen Ions To Afford a Quasi-1D System

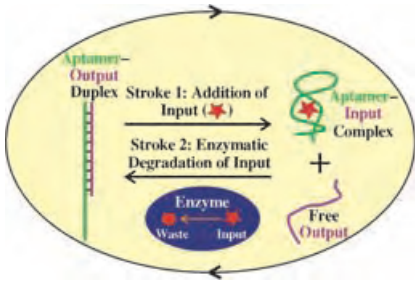
Down to the wire: A new class of 1D chain, $[\text{-Pt-Rh-Pt}_4\text{-Rh-Pt-Cl-}]_n$, composed of Pt–Pt and Pt–Rh dimeric complexes linked through metal–metal bonds has been prepared (see structure). This chain of mixed-valent metals (Pt^{II}/Pt^{III} and Rh^{II}/Rh^{III}) contains one unpaired electron in each octameric segment, leading to unique electrical and magnetic properties.



Molecular Motors

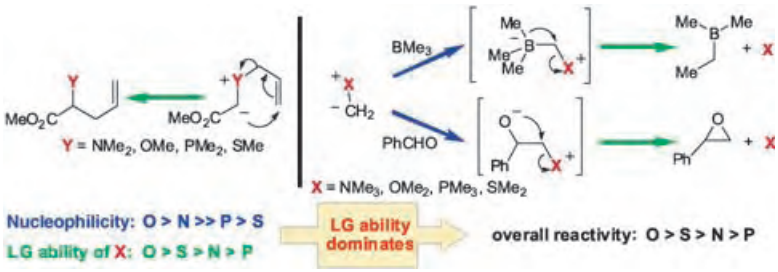
R. Nutiu, Y. Li* _____ **5464 – 5467**

A DNA–Protein Nanoengine for "On-Demand" Release and Precise Delivery of Molecules



A DNA aptamer (green in the scheme), an antisense DNA strand (purple), and an enzyme (blue) form a nanoengine that responds to a small-molecule input (red) and dispatches a DNA output. The addition of the input promotes the first stroke of the nanoengine, the action of the enzyme the second stroke. Joint exploration of all components could lead to bionanodevices that can detect a biological malfunction and initiate a repair.

© 2005 Wiley-VCH Verlag GmbH & Co. KGaA, Weinheim

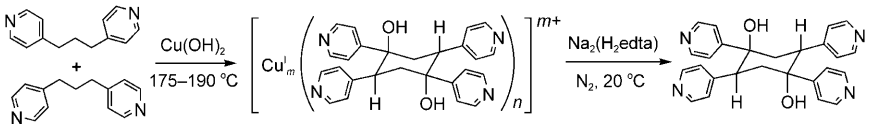


What controls reactivity of ylides? Computational data show that reactivity in the reactions shown in the scheme is mainly determined by the leaving group ability of the onium group, and this decreases for both intrinsic and thermochemical reasons in the order O > S > N > P. The results are consistent with experimental observations and account for the dearth of examples of phosphorus ylides in these reactions.

Reactivity Studies

V. K. Aggarwal,* J. N. Harvey,* R. Robiette ——— **5468 – 5471**

On the Importance of Leaving Group Ability in Reactions of Ammonium, Oxonium, Phosphonium, and Sulfonium Ylides



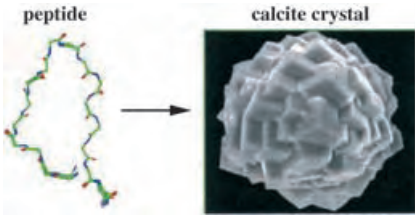
The hydrothermal reaction of 1,3-di(4-pyridyl)propane with $Cu(OH)_2$ in the presence of 1,4-cyclohexanedicarboxylic acid and dilute HCl generates an unprecedented tetratopic ligand (chtpy) and a family of interesting coordination networks in situ (see scheme). The topological diversification of the Cu^{I}–chtpy nets can be controlled simply by changing the molar ratio of the starting materials.

Coordination Polymers

S. Hu, J.-C. Chen, M.-L. Tong,* B. Wang, Y.-X. Yan, S. R. Batten ——— **5471 – 5475**

Cu^{2+}-Mediated Dehydrogenative Coupling and Hydroxylation of an N-Heterocyclic Ligand: From Generation of a New Tetratopic Ligand to the Designed Assembly of Three-Dimensional Copper(I) Coordination Polymers

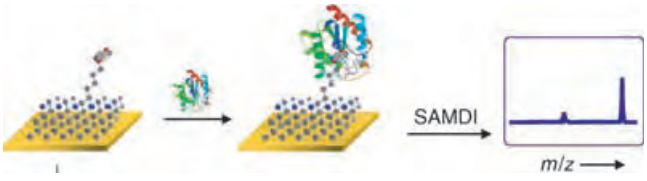
An eggshell finish: Designed peptides can be used as a tool to unravel the structure–activity relationships of eggshell matrix proteins. The ordered arrangement of doublets of charged residues on the peptide and its self-assembling characteristics play a key role in the biomimetic nucleation of polycrystalline calcite crystal aggregates (see picture), which models that initiated by the goose eggshell matrix protein, ansocalcin.



Biomineralization

P. K. Ajikumar, S. Vivekanandan, R. Lakshminarayanan, S. D. S. Jois, R. M. Kini, S. Valiyaveettil* **5476 – 5479**

Mimicking the Function of Eggshell Matrix Proteins: The Role of Multiplets of Charged Amino Acid Residues and Self-Assembly of Peptides in Biomineralization



Eliminating the middle-man: The combination of MALDI-TOF mass spectrometry and self-assembled monolayers on gold (SAMDI) offers a new detection method for protein–ligand (shown) and protein–protein interactions. Proteins and protein complexes are selectively bound to biochips and then directly analyzed by MALDI-TOF MS without the need for labels.

Protein Interactions

W.-S. Yeo, D.-H. Min, R. W. Hsieh, G. L. Greene, M. Mrksich* **5480 – 5483**

Label-Free Detection of Protein–Protein Interactions on Biochips

© 2005 Wiley-VCH Verlag GmbH & Co. KGaA, Weinheim

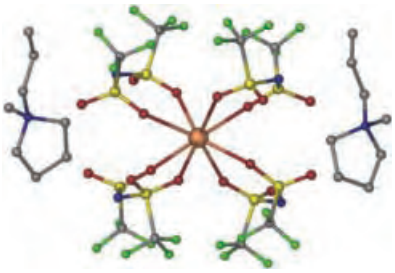
Contents

Structure Elucidation

A.-V. Mudring,* A. Babai, S. Arenz, R. Giernoth ——— **5485 – 5488**

The "Noncoordinating" Anion Tf_2N^- Coordinates to Yb^{2+}: A Structurally Characterized Tf_2N^- Complex from the Ionic Liquid [mppyr][Tf_2N]

Not as innocent as it looks: The first anionic Tf_2N^- complex, $[Yb(Tf_2N)_4]^{2-}$, has been prepared in the ionic liquid [mppyr][Tf_2N] (see crystal structure; blue: N, yellow: S, gray: C, green: F, orange: Yb, red: O; mppyr = 1-methyl-1-propyl-pyrrolidinium, Tf = trifloromethanesulfonyl). The coordination of the presumed noncoordinating ("innocent") Tf_2N^{2-} ion could have a decisive influence on reactions in ionic liquids.

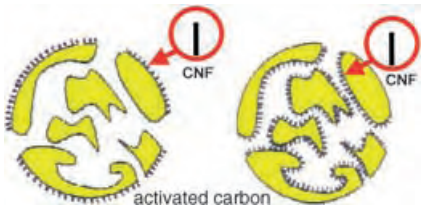


Carbon Nanoparticles

D. S. Su,* X. Chen, G. Weinberg, A. Klein-Hofmann, O. Timpe, S. B. A. Hamid, R. Schlögl **5488 – 5492**

Hierarchically Structured Carbon: Synthesis of Carbon Nanofibers Nested inside or Immobilized onto Modified Activated Carbon

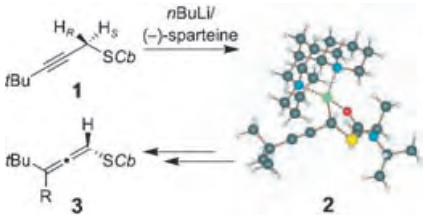
Filling in the gaps of activated carbon by chemical vapor decomposition of ethylene results in hierarchically structured carbon with carbon nanofibers (CNFs) nested inside and immobilized on the surface (see picture). The adsorption experiments show that this nanostructuring of carbon creates novel functions on the surface of activated carbon.



Asymmetric Synthesis

R. Otte, R. Fröhlich, B. Wibbeling, D. Hoppe* ——— **5492 – 5496**

Solid-State Structure and Enantioselective Reactions of a Complex of a 1-Thio-Substituted Propargyllithium and (−)-Sparteine

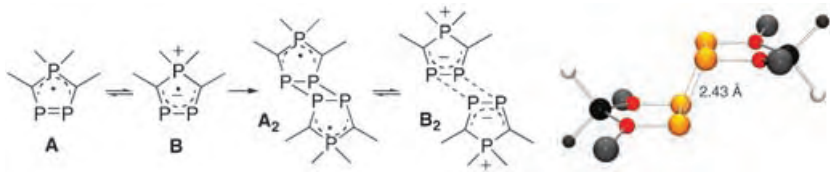


A useful transformation in enantioselective synthesis: (−)-Sparteine-assisted lithiation of the propargylic 1-thiocarbamate **1** (*Cb* = CON*i*Pr$_2$) forms the enantiomerically and diastereomerically pure lithium (−)-sparteine complex **2**. Its solid-state structure and application in the asymmetric synthesis of highly enantioenriched 1-thioallenes **3** were investigated.

Odd-Electron Bonds

T. Kato, H. Gornitzka, W. W. Schoeller, A. Baceiredo, G. Bertrand* **5497 – 5500**

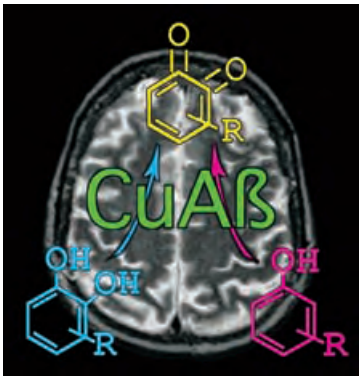
Dimerization of a Cyclo-1σ^4,3σ^2,4σ^2-Triphosphapentadienyl Radical: Evidence for Phosphorus–Phosphorus Odd-Electron Bonds



How odd! The title radical can be represented by resonance structures **A** and **B**. From **A**, dimerization refers to a [$\pi^2+\pi^2$] reaction and results in the formation of two inter-ring P–P single bonds, whereas from **B**, only one unpaired electron is supplied from each radical unit, which leads to two inter-ring P–P one-electron bonds. As a consequence, the isolated dimer features "short" P–P half-bonds.

© 2005 Wiley-VCH Verlag GmbH & Co. KGaA, Weinheim

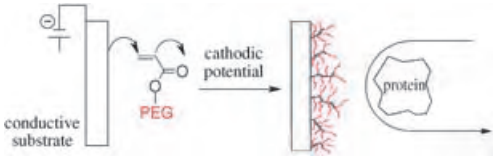
A gray area in gray matter: The Cu^{II} complex of a truncated β-amyloid, $CuA\beta_{1-20}$, catalyzes the oxidation of catechol and the hydroxylation and oxidation of phenol (see picture) with dramatic rate accelerations ($\approx 10^5$–10^6-fold increases). The Cu–oxygen chemistry of CuAβ may offer both a better understanding of the chemical effect in the brains of patients who suffer from Alzheimer's disease as well as possible treatment strategies of this disease.



Bioinorganic Chemistry

G. F. Z. da Silva, L.-J. Ming* **5501 – 5504**

Alzheimer's Disease Related Copper(II)-β-Amyloid Peptide Exhibits Phenol Monooxygenase and Catechol Oxidase Activities



Hydrophilic adherent coatings: Electrografting of acrylate end-capped poly(ethylene glycol) (PEG) is an important technique for the one-step coating of electroconductive substrates by an adherent hydrophilic coating (see figure). This technique is very efficient for the production of new protein-repellent surfaces.

Surface Chemistry

S. Gabriel, P. Dubruel, E. Schacht, A. M. Jonas, B. Gilbert, R. Jérôme, C. Jérôme* **5505 – 5509**

Electrografting of Poly(ethylene glycol) Acrylate: A One-Step Strategy for the Synthesis of Protein-Repellent Surfaces

Holding on to hydrido: The reactivity of the asymmetric dinuclear ruthenium species **1**, which is bridged by three different ligands, is studied. It undergoes ligand-exchange reactions, dehydration with protic acids, and decarboxylation by oxidative addition. Only the bridging hydrido ligand remains intact during all these reactions.



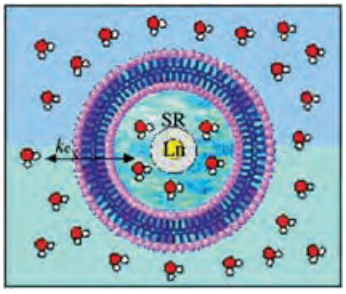
1

Organometallic Chemistry

Y. Arikawa, S. Nagae, J.-i. Morishita, K. Hiraki, M. Onishi* **5509 – 5513**

Formation of An Unsymmetrical Dinuclear Ruthenium Complex with μ-H, μ-OH, and μ-κ^2-CO_2 Bridges and Multiple Reactive Sites

Contrasting views: Entrapment of a paramagnetic shift reagent for water protons inside liposomes dramatically improves the sensitivity of chemical exchange saturation transfer agents. The chemical shift of the water entrapped within the liposomes, relative to bulk water, depends upon the nature and concentration of the shift reagent as well as on the permeability of the liposome membrane (see picture; SR = shift reagent, Ln = lanthanide ion).



Imaging Agents

S. Aime,* D. Delli Castelli, E. Terreno **5513 – 5515**

Highly Sensitive MRI Chemical Exchange Saturation Transfer Agents Using Liposomes

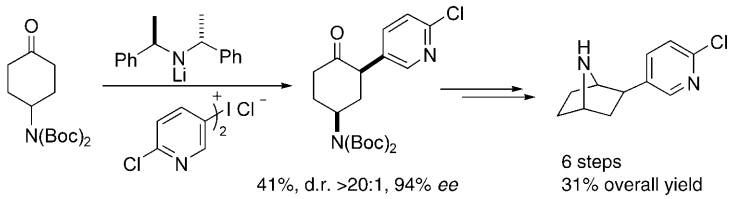
© 2005 Wiley-VCH Verlag GmbH & Co. KGaA, Weinheim

Contents

Synthetic Methods

V. K. Aggarwal,*
B. Olofsson ——— 5516 – 5519

Enantioselective α-Arylation of Cyclohexanones with Diaryl Iodonium Salts: Application to the Synthesis of (−)-Epibatidine

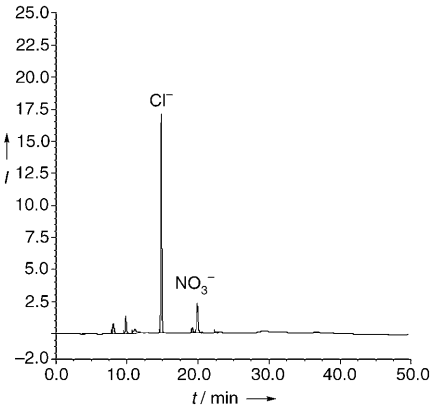


Short cut: Direct asymmetric α-arylation of prochiral ketones has been effected using chiral lithium amide bases and diaryl iodonium salts. The methodology has been employed in a short total synthesis of the alkaloid (−)-epibatidine (see scheme).

Homogeneous Catalysis

X. Liang,* D. Fu, R. Liu,* Q. Zhang, T. Y. Zhang, X. Hu* ——— 5520 – 5523

Highly Efficient $NaNO_2$-Catalyzed Destruction of Trichlorophenol Using Molecular Oxygen

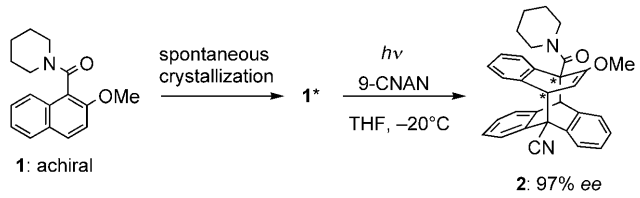


Cleaning up: $NaNO_2$, a simple, inexpensive and biodegradable inorganic compound, acts as a catalyst to activate molecular oxygen for the destruction of polychlorinated phenols. The $NaNO_2/O_2$ system efficiently oxidizes the recalcitrant trichlorophenol into CO_2 and/or CO and a small fraction of biodegradable organic products with a high rate of conversion (see ion chromatogram).

Asymmetric Synthesis

M. Sakamoto,* A. Unosawa, S. Kobaru, A. Saito, T. Mino, T. Fujita ——— 5523 – 5526

Asymmetric Photocycloaddition in Solution of a Chiral Crystallized Naphthamide

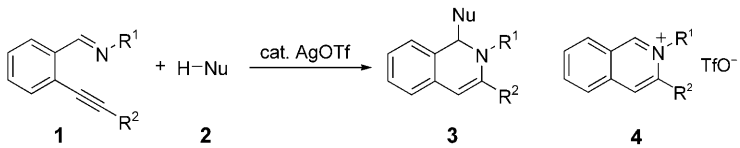


Frozen chirality: Achiral naphthamide **1** can be crystallized to give chiral **1***, whose chiral molecular conformation is retained ("frozen") after the crystals are dissolved in cold THF. Asymmetric photocycloaddition of **1*** with 9-cyanoanthracene (9-CNAN) in solution gives cycloadduct **2** with high enantioselectivity.

Nitrogen Heterocycles

N. Asao,* S. Yudha S., T. Nogami, Y. Yamamoto ——— 5526 – 5528

Direct Mannich and Nitro-Mannich Reactions with Non-Activated Imines: AgOTf-Catalyzed Addition of Pronucleophiles to *ortho*-Alkynylaryl Aldimines Leading to 1,2-Dihydroisoquinolines



A variety of 1,2-dihydroisoquinoline derivatives **3** have been prepared in good to high yields by the AgOTf-catalyzed reaction of *ortho*-alkynylaryl aldimines **1** with various pronucleophiles **2** (see scheme). Treatment of **1** with a stoichiometric amount of AgOTf followed by protonation with TfOH produced **4**, which suggests the formation of an isoquinolinium intermediate in the present direct addition reaction. Tf = trifluoromethanesulfonyl.

© 2005 Wiley-VCH Verlag GmbH & Co. KGaA, Weinheim

Sources

Product and Company Directory

You can start the entry for your company in "Sources" in any issue of *Angewandte Chemie*.

If you would like more information, please do not hesitate to contact us.

Wiley-VCH Verlag – Advertising Department
Tel.: 0 62 01 - 60 65 65
Fax: 0 62 01 - 60 65 50
E-Mail: MSchulz@wiley-vch.de

Service

Keywords ____ *5530*

Authors ____ *5531*

Angewandte's Sister Journals ____ *5532*

Preview ____ *5533*

Deadline for recruitment adverts

37/05 September 2 **Publication date: September 19**
38/05 September 9 **Publication date: September 26**

Angewandte Chemie International Edition
Advertising Sales Department:
Marion Schulz
Phone: 0 62 01 – 60 65 65
Fax: 0 62 01 – 60 65 50
E-Mail: MSchulz@wiley-vch.de

Place an advert in the printed version and have it made available online for 1 month, free of charge!

18 000 organic chemicals, 1 simple phone call !

TCI Europe, the European distribution centre in Antwerp, Belgium, guarantees a speedy delivery of all TCI products to European users, from university laboratories to corporate research facilities.



NEW

TCI 2005 Euro Catalogue

Ask your free copy today!

Visit us! "Annual Meeting GDCh 2005"
11 - 14 September 2005
Heinrich Heine University, Duesseldorf

TCI EUROPE N.V.
+800 46 73 86 67 • +32 (0)3 735 07 00
Fax +32 (0)3 735 07 01
sales@tcieurope.be • www.tcieurope.be
<Head Office> **TOKYO KASEI KOGYO CO., LTD.**
www.tokyokasei.co.jp

TCI has over 50 years of experience synthesizing fine organic chemicals

© 2005 Wiley-VCH Verlag GmbH & Co. KGaA, Weinheim



Joint Meeting on Medicinal Chemistry in Vienna**

Rainer E. Martin,* Peter Mohr, Wylie Palmer, and Henri Stalder

The fourth Austrian, German, Hungarian, Italian, Polish, and Spanish Joint Meeting on Medicinal Chemistry was held this year at the University of Vienna, the oldest university within the German-speaking part of Europe, founded in 1365 by Duke Rudolph IV. The conference was held in the magnificent banquet hall of the university, which holds recently restored paintings by Gustav Klimt (1862–1918), including the famous painting of Hygieia, who, according to the Greek mythology, was a daughter of Asclepius and the goddess associated with the prevention of sickness and the continuation of good health; could there have been a better location for a medicinal chemistry congress?

The meeting was attended by about 500 people from all over Europe, roughly two-thirds of whom come from academia with the remaining one-third from industry. In total, 25 lectures and 11 oral short communications covered a broad range of topics including chemogenomics, combinatorial chemistry, developing fields in medicinal chemistry, computer-aided molecular design, virtual screening, lead- and drug-likeness, oncology, Alzheimer's disease and central nervous system disorders, medicinal chemistry case studies, and natural product synthesis. The scientific discussion was further stimulated by two poster sessions with more than 200 contributions on display.

The synthesis of biologically relevant low molecular weight combinatorial compound libraries continues to be a challenge for the pharmaceutical industry, and numerous design strategies have been discussed over the past few years. The use of natural product scaffolds as biologically pre-validated and evolutionarily selected starting points for the design of molecules with potential in vivo activity seems to be a particularly appealing concept. The first plenary lecture was presented by Herbert Waldmann (Max Planck Institute for Molecular Physiology, Dortmund, Germany) on protein structure similarity clustering (PSSC) as a guiding principle for chemical genomics.[1] Recent results in structural biology and bioinformatics have shown that despite the wide diversity of proteins, their ligand binding pockets (folds) are fairly conserved. The idea that "similar folds bind to similar ligands" was exploited for the identification of an appropriate substructure for the generation of a compound library. A group of proteins (Cdc25A phosphatase, acetylcholinesterase (AChE), and 11β-hydroxysteroid dehydrogenase (11β-HSD1)) was clustered based on structural similarities of their domain cores and not by sequence homology, as is commonly done. The decalin substructure from dysidiolide, a known natural ligand of Cdc25A, was identified as an appropriate scaffold for library design. A focused library containing more than 500 compounds was synthesized providing hits for 11β-HSD1 with IC_{50} values in the nanomolar potency. The library also contained compounds with activity for Cdc25 and AChE, thereby validating the structural analysis method of identifying relevant templates.

The explosion of the number of solved protein structures and biological data in recent years has created the difficulty of efficiently organizing the flood of information for the extraction of knowledge in the form of trends, rules, or models that correlate chemical and biological properties. The ability to retrieve knowledge from databases is partly limited by the way data is stored. Jordi Mestres (University Pompeu Fabra, Barcelona, Spain) discussed options for data mining in the huge datasets available for receptors, enzymes, and their interactions with various ligands. An essential prerequisite for an efficient use of these data is a systematic application of hierarchical classification schemes for both chemical (e.g., the *m*olecular *eq*uivalence *num*ber (MEQNUM)) and biological entities. Knowledge generation based on well-organized and properly stored annotated biochemical data should also facilitate the shift from target-focused to pathway-directed drug discovery.

Exploration of the vast chemical space has just begun. If one considers only molecules with a molecular weight below 500 Da and less than seven rings, there are an unimaginable 65 quadrillion unique structure possibilities. Tudor I. Oprea (University of New Mexico School of Medicine, Albuquerque, USA) highlighted the large need for efficient tools to investigate and mine this huge chemical space to identify the most promising druglike seed structures. He provided a number of examples of how knowledge can be extracted from current databases to better guide the lead discovery process.[2]

Ulrich Stilz (Aventis Pharma, Frankfurt am Main, Germany) provided some illustrative examples of knowledge-based approaches for lead finding and lead optimization by using experimental and computational approaches such as 2D similarity searching, re-scaffolding and biased library design, and ligand- and structure-based modeling. These four approaches were successfully combined in the identification of a Kv1.5 channel inhibitor that targets atrial fibrillation. The result is a drug candidate which has recently entered phase II development.

Today G-protein-coupled receptors (GPCRs) constitute one of the largest families of physiologically relevant targets in the pharmaceutical industry. However, rhodopsin is the only three-dimensional structure of a GPCR available and unfortunately little is known

[*] Dr. R. E. Martin, Dr. P. Mohr, Dr. H. Stalder
F. Hoffmann-La Roche, Ltd.
Pharmaceuticals Division, Discovery Chemistry
PRBD-CM, 4070 Basel (Switzerland)
E-mail: rainer_e.martin@roche.com
Dr. W. Palmer
Roche Palo Alto
Medicinal Chemistry
Palo Alto, California 94304 (USA)

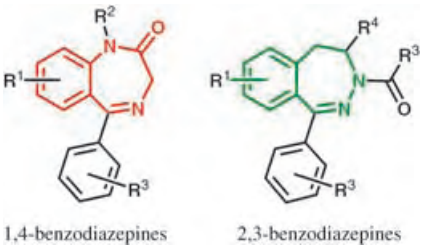
[**] Austrian – German – Hungarian – Italian – Polish – SpanishJoint Meeting on Medicinal Chemistry in Vienna, June 20–23, 2005.

InterScience © 2005 Wiley-VCH Verlag GmbH & Co. KGaA, Weinheim

about the higher-order structures of GPCRs and how they might relate to biologically important processes such as dimerization, internalization, and signal transduction within and between cells. By using in silico methods, Slawomir Filipek (International Institute of Molecular and Cell Biology, Warsaw, Poland) studied the cooperative interactions of rhodopsin. These studies revealed that rhodopsin can form dimeric, tetrameric, and even higher-order oligomeric structures. He also showed that proteins such as arrestin bind to rhodopsin dimers by a perfect geometrical and electrostatic match.[3] The lipid bilayer membrane can also play a critical role in the clustering and functioning of receptors. Wolfgang H. Binder (Vienna University of Technology, Austria) presented the latest advances on the use of artificial vesicle systems as models for biological membranes to study the mobility, distribution, and clustering of embedded lipid conjugates by using thermal, fluorescence, and AFM methods.[4]

Alzheimer's disease is a complex neurological disorder characterized by memory loss and progressive deficits in various cognitive abilities with a multifaceted etiology. Multiple explanations for the pathogenic process have been proposed, such as the cholinergic, amyloid-β, and tau-protein hypotheses; oxidative stress and disruption of cerebral metal ion homeostasis have also been suggested as causes. Carlo Melchiorre (University of Bologna, Italy) introduced the concept of a multifunctional drug in which distinct pharmacophores and properties of different drugs are combined into a single hybrid molecule. Memoquine is a symmetric tetraamine structure with a central quinone moiety that combines AChE inhibition, muscarinic M2 antagonism and antioxidative properties in a single molecule. It was demonstrated to effectively inhibit amyloid-β formation in vitro and thus might be an interesting lead structure for further optimization.

In contrast to this multitarget approach, researchers traditionally aim for highly selective chemical entities to avoid potential side effects caused by the action on non-disease-related targets. László G. Hársing (EGIS Pharmaceuticals Ltd., Budapest, Hungary) presented recent results in 2,3-benzodiazepine research. Despite their rich pharmacology mediated by binding to

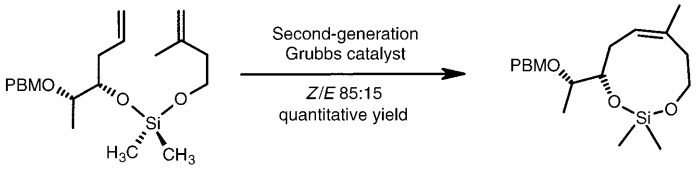


AMPA and $GABA_A$ receptors, 2,3-benzodiazepines have been explored much less than the well-known and intensely studied 1,4-benzodiazepine regioisomers. Fine tuning of the in vitro and in vivo properties led to the identification of EGIS-8858, a $GABA_A$-selective compound that elicited anxiety relief effects in two standard behavioral tests. Most interestingly, EGIS-8858 shows no signs of causing sedation, it does not induce dependency or amnesia, and anxiety symptoms do not return upon withdrawal.[5]

Barbara Malawska (Jagiellonian University, Kraków, Poland) discussed in detail the structure–activity relationship of arylpiperazines as potent antagonists of the α_1-, α_2- and α-adrenergic receptors. The distance between a phenyl ring and a basic nitrogen atom was found to be crucial for pharmacological activity. The most promising α_1-adrenergic receptor antagonists, with binding affinity in the low nanomolar range, are currently being profiled in animal models.

Angelo Carotti (University of Bari, Italy) showed that a comparative analysis of the two monoamine oxidase (MAO) A and B crystal structures, which only recently became available, allowed a ligand-based design of novel, orally bioavailable, nontoxic MAO-B inhibitors with potency in the low nanomolar range and more than 500-fold selectivity over MAO-A. These structures exhibit a favorable pharmacokinetic profile and might thus become interesting candidates for the treatment of Parkinson's disease.

Despite significant progress that has been made over the past few years, cancer is still a major cause of mortality in the industrialized world. Mario Varasi (Nerviano Medical Sciences, Milan, Italy) gave an interesting overview on the history of cancer treatment with all its hopes, hypes, and setbacks, starting in the middle of the last century, when only unselective cytotoxic treatments were available, to today's modern therapeutic agents, which selectively target cancerous cells. Sequencing the human genome has revealed more than 500 protein kinases, the selective modulation of which has become a cornerstone in the strategy to combat this human plague. New and promising CDK2 and Aurora inhibitors were designed based on the 3-aminopyrazole moiety, a well-known adenine mimetic that represents a widely used pharmacophore motif for kinase inhibitors. The most potent compounds displayed significant tumor-growth suppression in a human leukemia xenograft model. In his excellent presentation, Johann Mulzer (University of Vienna, Austria) referred to another promising class of anticancer agents: the microtubule-stabilizing epothilones. A key reaction in the synthesis of epothilone B was the intramolecular ring-closing metathesis reaction of a silicon-tethered precursor to produce a 9-membered advanced intermediate. With a second-generation Grubbs catalyst, the *Z*/*E* ratio was improved from 1:1 to 85:15 (Scheme 1). Another highlight was the synthesis of laulimalide, in which the application of an intramolecular Sharpless kinetic resolution obviated the need for a protecting-group strategy, thereby underscoring the power and reliability of this method.



Scheme 1. A key step in the synthesis of epothilone B in which an intramolecular ring-closing metathesis reaction increases stereoselectivity; PMB = *para*-methoxybenzyl.

© 2005 Wiley-VCH Verlag GmbH & Co. KGaA, Weinheim

The production of steroid hormones in the body is regulated by steroid sulfatase, an enzyme responsible for the hydrolysis of the sulfate esters of 3-hydroxy steroids. As Peter Nussbaumer (Novartis, Vienna, Austria) pointed out, it offers an attractive target for the treatment of estrogen- and androgen-dependent diseases. Nussbaumer not only provided a comprehensive overview of the current knowledge in this area, he also presented the endeavors of his own research group to transform a promising HTS hit into an interesting chromenone-based lead structure suited for further optimization toward a novel treatment for hormone-dependent hair loss and acne.[6]

An estimated 170 million people suffer from chronic hepatitis C virus (HCV) infection, a leading cause of the need for liver transplants in the US. In a showcase of modern drug discovery, Michael Bös (Boehringer Ingelheim, Laval, Canada) summarized the identification of specific antiviral benzimidazole 5-carboxamides that were demonstrated to specifically inhibit HCV RNA polymerase activity through a novel and specific mechanism. This may provide an opportunity for the development of novel HCV therapies.

A very entertaining lecture was delivered by Hugo Kubinyi (University of Heidelberg, Germany), who gave an excellent overview of lead optimization and general medicinal chemistry topics.[7] Among the many examples, he discussed the concept of privileged structures, (bio)isosteric replacement of atoms and groups, selective optimization of side activities (SOSA approach), fragment-based ligand design, and virtual screening methods. Especially informative were the case histories of Captopril, Sildenafil, Omeprazole, Imatinib and Tamiflu, which show in retrospect that successful development of a drug requires not only a lot of hard work and scientific excellence, but also a good slice of luck.

[1] R. Breinbauer, I. R. Vetter, H. Waldmann, *Angew. Chem.* **2002**, *114*, 3002 – 3015; *Angew. Chem. Int. Ed.* **2002**, *41*, 2878 – 2890.
[2] M. M. Hann, T. I. Oprea, *Curr. Opin. Chem. Biol.* **2004**, *8*, 255 – 263.
[3] P. S.-H. Park, S. Filipek, J. W. Wells, K. Palczewski, *Biochemistry* **2004**, *43*, 15643 – 15656.
[4] W. H. Binder, V. Barragan, F. M. Menger, *Angew. Chem.* **2003**, *115*, 5980 – 6007; *Angew. Chem. Int. Ed.* **2003**, *42*, 5802 – 5827.
[5] G. Szénási, L. G. Hársing, Jr., *Drug Discovery Today Therapeutic Strategies* **2004**, *1*, 69 – 76.
[6] P. Nussbaumer, A. Billich, *Med. Res. Rev.* **2004**, *24*, 529 – 576..
[7] See also http://www.kubinyi.de.

DOI: 10.1002/anie.200502439

 © 2005 Wiley-VCH Verlag GmbH & Co. KGaA, Weinheim

Molecular Electronics

DOI: 10.1002/anie.200500413

Molecules with Exceptionally Small HOMO–LUMO Gaps**

Dmitrii F. Perepichka and Martin R. Bryce**

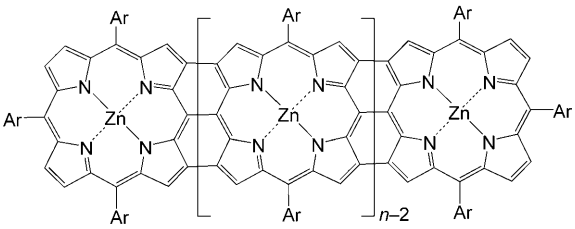
Keywords:
electrochemistry · electron transfer · fullerenes · HOMO–LUMO gap · tetrathiafulvalenes

The engineering of small band gaps in π-conjugated heteroaromatic polymers by chemical manipulation has been widely studied for the last 20 years in the search for materials with tailored optoelectronic properties,[1] such as intrinsic conductivity, infrared electrochromic displays, and charge-storage capability.[2] The two most successful approaches are 1) tuning bond-length alternation in the π-system by stabilizing quinonoid character (polyisothionaphthalene (PITN) is the classical example[3]) and 2) alternating heteroaromatic donor and acceptor units.[1,4] Most of these materials are modified thiophene derivatives, obtained by chemical or electrochemical polymerization. A band gap of 0.5 eV and smaller, usually determined by the on-set of absorption or the difference in oxidation/reduction on-set potentials, has been reported.[1] However, if the absorption or redox peak maxima are considered, rather than ill-defined on-set values, there are very few examples of polymers with electrochemical or optical gaps smaller than 1.0 eV.[4]

The attraction of molecular systems is their precise chemical structure and better defined frontier-orbital levels that are unperturbed by supramolecular band formation, which makes them ideal models for basic studies of electron-transfer phenomena as well as potential objects for molecular electronics.[5] There are two established approaches to decreasing the HOMO–LUMO gap (HLG) in a molecule: one is to extend the conjugation, the other is to covalently link electron-donor (high HOMO) and electron-acceptor (low LUMO) fragments. However, the design and synthesis of very-small-HLG systems (<0.5 eV) present considerable challenges.

Early predictions that large polyacenes (that is, conjugated polyaromatic hydrocarbons (PAHs) with linearly fused benzene rings) may behave as one-dimensional conductors with a zero band gap are contradicted by the most recent calculations.[6] The HOMO–LUMO gap of hexacene determined from both the UV/Vis spectra and density functional theory (DFT) calculations is approximately 1.8 eV; higher homologues are calculated to have an open-shell singlet ground state.[6] Also, the aromatic stabilization in graphene-type PAHs is predicted to keep the HLG above 1 eV even for large (over 200 carbon atoms) graphene molecules,[7] although the band formation in the solid state reduces the (band) gap for PAH $C_{222}H_{42}$ to about 0.6 eV (determined by absorption on-set).[8]

It was, however, demonstrated that conjugation over the planar π-electron platform in the triply linked, fused-porphyrin ribbons **1** results in exceptionally small HLGs which are manifested in remarkably red-shifted absorption spectra.[9] The longest fused array, a dodecamer $\mathbf{1}_{12}$ of approximately 10-nm length, has the longest wave-length absorption band at $\lambda_{max} \approx 2900$ nm (3500 cm^{-1}; Figure 1), which corresponds to an electron transition energy of as low as 0.45 eV to < -0.25 V versus $Ag/AgClO_4$. The one-electron-oxidation potential decreases progressively with an increase in the number of porphyrin units. Unfortunately, the electrochemical reduction of these molecules, which is expected to occur at easily accessible potentials, has not been investigated. Most unexpectedly, in spite of such low oxidation potentials the molecules are claimed to be air-stable, and prospective applications in near-IR and IR sensors, and conducting molecular wires, were suggested.



$\mathbf{1}_n$

Another way to attain a small HLG is to couple electron-donor (high HOMO) and electron-acceptor (low LU-

[*] Prof. D. F. Perepichka
INRS-ÉMT
Université du Québec
Varennes, J3X1S2 (Canada)
Fax: (+1) 450-929-8102
E-mail: perepichka@emt.inrs.ca
and
Institute of Physical Organic and Coal Chemistry
National Academy of Sciences of Ukraine
Donetsk 83114 (Ukraine)
Prof. M. R. Bryce
Department of Chemistry
University of Durham
Durham, DH1 3LE (UK)
Fax: (+44) 191-374-3848
E-mail: m.r.bryce@durham.ac.uk

[**] We thank the Royal Society of Chemistry for a Journals Grant for International Authors which funded a visit by D.F.P. to Durham.

InterScience
© 2005 Wiley-VCH Verlag GmbH & Co. KGaA, Weinheim

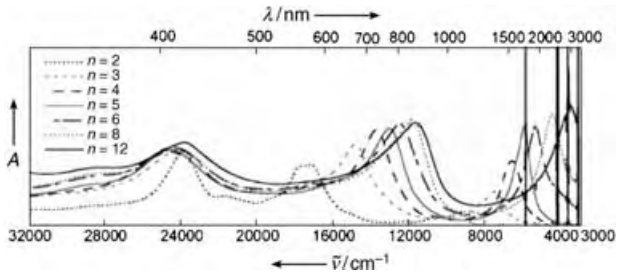
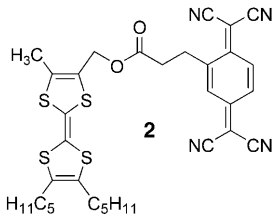


Figure 1. Electronic absorption spectra of porphyrin ribbons **1** with different numbers of units ($n = 2$–12).[9b]

MO) fragments in a single molecule. A significant difference between the previously described conjugated systems (which generally fit within a broader concept of small-band-gap materials) and the covalent donor–acceptor molecules is that different location of the HOMO and LUMO orbitals hinders the electron transition between them. Thus, a donor–acceptor molecule with zero HLG is not expected to show metallic (non-activated) conductivity, although this limited HOMO–LUMO interaction may be attractive for other applications. The first interest in such systems was presented in a famous proposal by Aviram and Ratner where a hypothetical TTF-σ-TCNQ molecule (TTF = tetrathiafulvalene; TCNQ = tetracyanoquinodimethane) with an HLG of 0.3 eV was predicted to act as a unimolecular rectifier.[10] Since then, this type of molecule has been a target for many research groups, although the challenge of preparing such a highly electrochemically amphoteric molecule was only overcome recently. Thus, the reaction of a TTF lithium alcoholate and a TCNQ acid chloride at −100 °C favored covalent coupling (i.e. ester formation) over electron-transfer processes, and the TTF–TCNQ diad **2** was prepared in



analytically pure form.[11,12] Two reversible oxidations and two reversible reductions in cyclic voltammetry (CV) experiments are characteristic of the TTF and TCNQ moieties, respectively, and the difference between the E^0_{1ox} and E^0_{1red} values suggests an HLG of only 0.17 eV (Figure 2a). Such a low barrier allowed the first observation of a thermo-excited electron-transfer in an organic molecule. Indeed, the solution ESR signal of **2** increases at higher temperatures (approximately 1% of the molecules are in a biradical form $TTF^{\bullet+}$-σ-$TCNQ^{\bullet-}$ at room temperature).

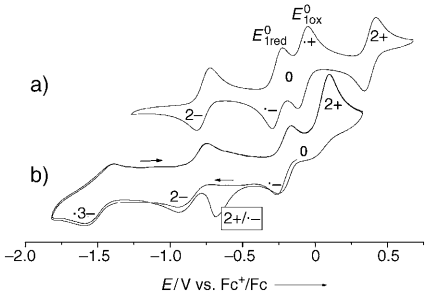
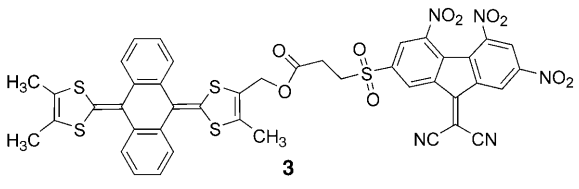


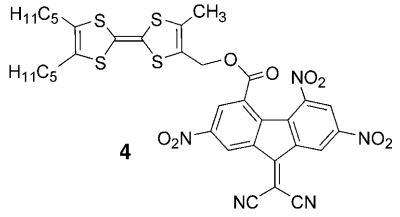
Figure 2. a) Amphoteric multiredox behavior of **2** in CV experiments; b) generation of a charge separated state $2+/^{\bullet-}$ of **3** in CV experiments at −15 °C; Fc = $[(\eta\text{-}C_5H_5)_2Fe]$.

Other novel electron-transfer phenomena are likely to arise in small-HLG molecules. Combining a π-extended TTF donor (TTFAQ) with a polynitrofluorene acceptor affords the diad **3**, in



which the small gap between the oxidation and reduction, combined with quasi-reversibility of the TTFAQ oxidation (that is, re-reduction of $TTFAQ^{2+}$ required a lower potential than the initial oxidation) result in a remarkable property:[13] When the potential was initially scanned in the positive region (forming the dication) and then reversed, the reduction peak (arising to formation of the fluorenone radical anion) preceded the re-reduction of the TTFAQ dication to the neutral species (Figure 2b). Consequently, a most unusual charge-separated state of **3**, D^{2+}-σ-$A^{\bullet-}$, was formed (D = donor, A = acceptor).[13]

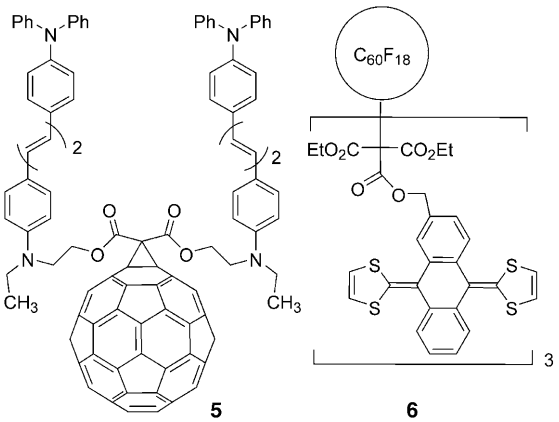
A molecular electronics application of TTF-based donor–acceptor diads with small HLG was recently demonstrated for the TTF–fluorene diad **4** (HLG 0.3 eV). When **4** was immobilized



in Langmuir–Blodgett monolayers between n-doped silicon and titanium or gold and thiol-protected mercury electrode pairs, asymmetric rectifying electrical characteristics were observed.[14] The molecular origin of the current–voltage (I–V) asymmetry was demonstrated by the alignment dependence of the rectification, which changed direction for monolayers transferred onto the electrode in opposite orientations (X and Z deposition).

Buckminsterfullerene is another prominent example of an electron-acceptor molecule, although its reduction potential (−1.06 V versus Fc/Fc^+) is too low to attain a gap of less than around 1 eV in diads with air-stable electron donors (donors with an oxidation potential less than approximately −0.1…−0.2 V vs. Fc/Fc^+ are usually doped when exposed to air). Numerous donor–C_{60} diads with gaps of 1–2 eV have been synthesized and used for fundamental studies of photoinduced electron-transfer processes, and as photovoltaic materials.[12,15] A fullerene–arylamine based D–A compound **5** with an electrochemical gap of about 1 eV was recently exploited as a

© 2005 Wiley-VCH Verlag GmbH & Co. KGaA, Weinheim



5 6

unimolecular rectifier.[16] The junctions prepared with Langmuir–Schaefer (horizontal transfer) monolayers sandwiched between two gold electrodes were found to be very robust up to ±5 V and reveal a rectification of approximately 16:1 at high biases (with a symmetric *I–V* behavior at lower voltage). Interestingly, the rectification direction is the same as found in other D-σ-A molecules (**4**), but opposite to that revealed by D-π-A molecules.

The HLG in fullerene systems can, however, be pushed below 1 eV by employing fluorinated C_{60} derivatives which are much stronger acceptors. Thus, the cyclic voltammetry of TTFAQ–$C_{60}F_{18}$ compound **6** (Figure 3) demonstrates high electrochemical amphotericity, with a reversible reduction of the fullerene moiety and a quasi-reversible two-electron oxidation of the TTFAQ moiety, with the gap between the oxidation and reduction peaks of the two-electron event being nearly 0.5 eV.[17] Time-resolved fluorescence studies suggested formation of a charge-separated state ((TTFAQ$^{\bullet+}$)-σ-($C_{60}F_{18}^{\bullet-}$)) whose low energy resulted in a very long life-time of around 1 μs.

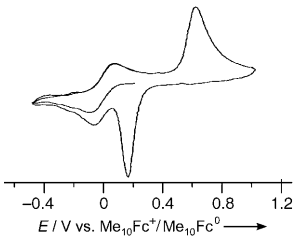
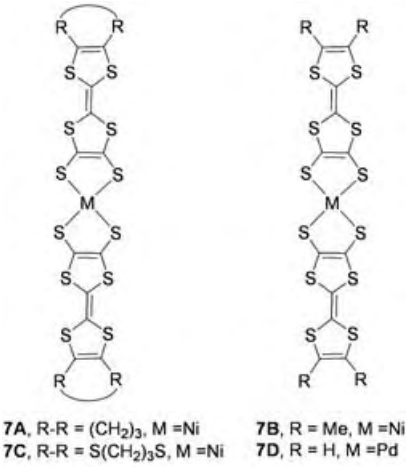


Figure 3. The cyclic voltammogram of compound **6**. Redrawn from ref. [17]; $Me_{10}Fc = [(\eta\text{-}C_5Me_5)_2Fe]$.

An approach which combines both the extended conjugation and the donor–acceptor concepts is exemplified by TTF–dithiolato metal complexes **7** (Figure 4). Based on electronic-absorption spectral bands that are shifted into the IR region, the neutral nickel complexes **7** are remarkably small-band-gap molecular solids.[18] The first electronic transition of dialkyl–TTF complexes **7A** and **7B** in the solid state occurs in the mid-IR region at $h\nu_{max} = 0.27$ eV and a nearly zero band gap can be assumed based on the absorption on-set (Figure 4). Performing band-structure calculations and fitting with the experimental spectral data, a molecular HLG of 0.14 ± 0.06 eV was predicted. Although the accuracy of the extended-Hückel calculations might be disputable, a D–A complexation in the solid state may result in increased optical gap versus the molecular HLG. Furthermore, electrochemical data for the anion of **7C** in which the difference between the first and the second oxidation potentials (0.3 V)[19] should correspond to the HLG of the neutral complexes, is also lower than the optical gap ($h\nu_{max}$) of the solid complex **7C** (0.58 eV).[18]



7A, R-R = $(CH_2)_3$, M =Ni **7B**, R = Me, M =Ni
7C, R-R = $S(CH_2)_3S$, M =Ni **7D**, R = H, M =Pd

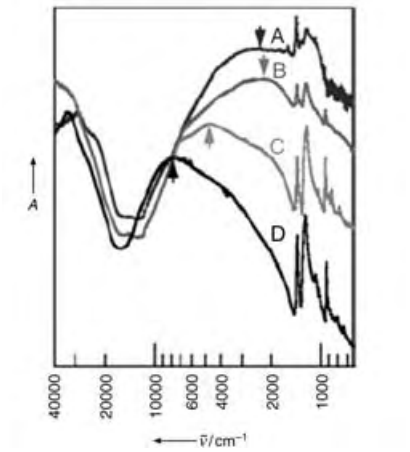


Figure 4. Electronic absorption spectra of TTF–M complexes **7A**–**D**.[18]

In contrast to small-band-gap polymers, where intrinsic conductivity was envisaged but has never been observed, the TTF–metal complexes with exceptionally small HLGs are single-component molecular metals with high conductivity down to 0.6 K ($\sigma_{rt} = 400\ S\,cm^{-1}$ for **7A**, $350\ S\,cm^{-1}$ for **7B**).[20] Notably, the higher HLG for the complexes **7C** and **7D** (optical gaps of 0.58 and 0.97 eV, respectively) results in semiconducting properties ($\sigma_{rt} = 7\ S\,cm^{-1}$ and $0.5\ S\,cm^{-1}$, respectively).[18]

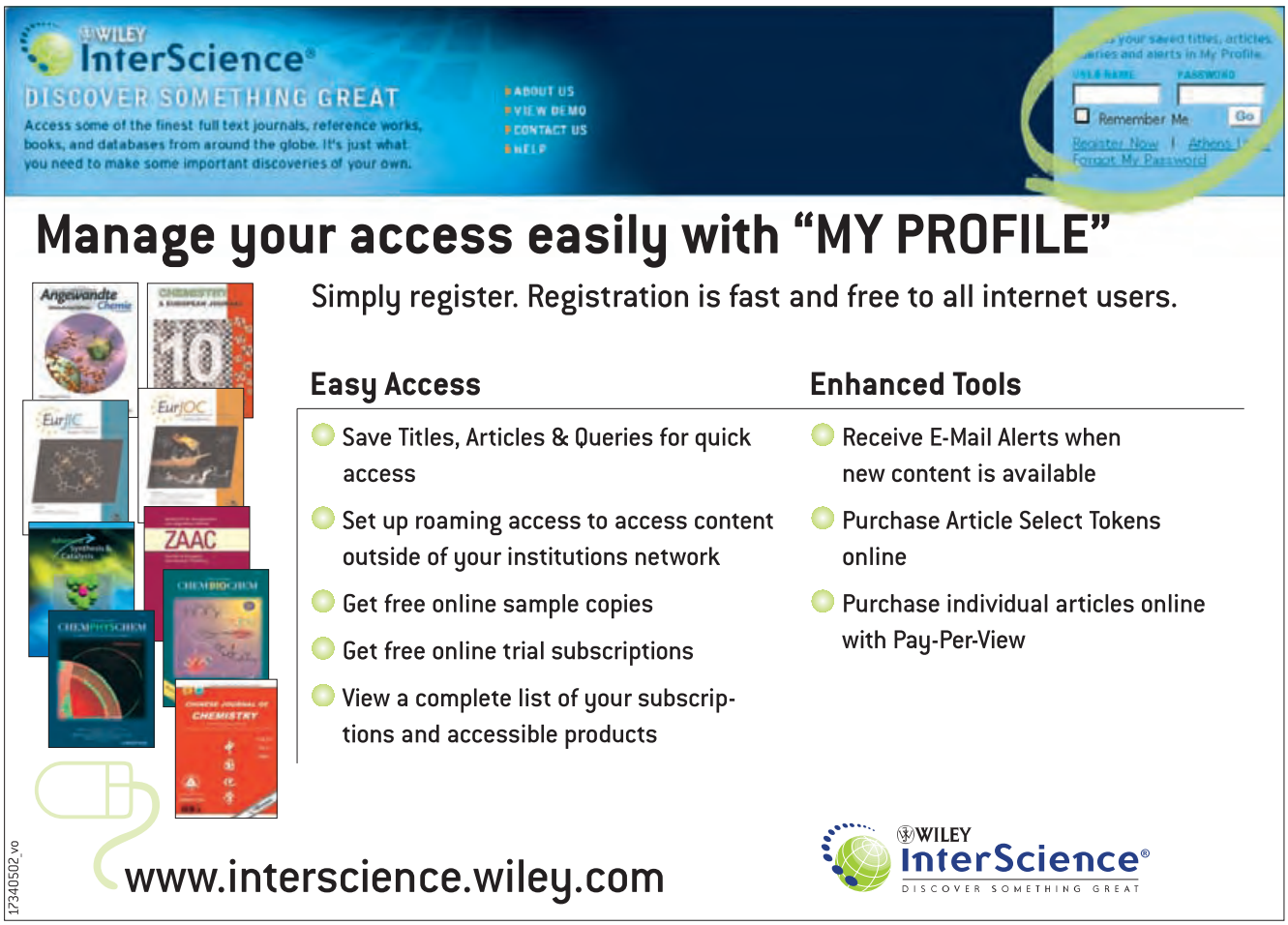
Thus, in the recent years molecules with exceptionally small (< 0.5 eV) HOMO–LUMO gaps have become synthetically achievable targets. A variety of unusual optoelectronic properties and electron-transfer phenomena have already been demonstrated for these compounds, making them as very desirable targets for further physical studies and electronics applications.

Published online: July 20, 2005

[1] J. Roncali, *Chem. Rev.* **1997**, *97*, 173.
[2] G. Sonmez, H. Meng, F. Wudl, *Chem. Mater.* **2003**, *15*, 4923.
[3] F. Wudl, M. Kobayashi, A. J. Heeger, *J. Org. Chem.* **1984**, *49*, 3382.
[4] A. Berlin, G. Zotti, S. Zecchin, G. Schiavon, B. Vercelli, A. Zanelli, *Chem. Mater.* **2004**, *16*, 3667.
[5] Review: R. Ll. Carroll, C. B. Gorman, *Angew. Chem.* **2002**, *114*, 4556; *Angew. Chem. Int. Ed.* **2002**, *41*, 4378.
[6] M. Bendikov, H. M. Duong, K. Starkey, K. N. Houk, E. A. Carter, F. Wudl, *J. Am. Chem. Soc.* **2004**, *126*, 7416; Correction/Addition: *J. Am. Chem. Soc.* **2004**, *126*, 10493.
[7] D. Moran, F. Stahl, H. F. Bettinger, H. F. Schaefer III, P. von R. Schleyer, *J. Am. Chem. Soc.* **2003**, *125*, 6746.

 © 2005 Wiley-VCH Verlag GmbH & Co. KGaA, Weinheim

[8] C. D. Simpson, J. D. Brand, A. J. Berresheim, L. Przybilla, H. J. Räder, K. Müllen, *Chem. Eur. J.* **2002**, *8*, 1424.
[9] a) A. Tsuda, A. Osuka, *Science* **2001**, *293*, 79; b) H. S. Cho, D. H. Jeong, S. Cho, D. Kim, Y. Matsuzaki, K. Tanaka, A. Tsuda, A. Osuka, *J. Am. Chem. Soc.* **2002**, *124*, 14642.
[10] A. Aviram, M. Ratner, *Chem. Phys. Lett.* **1974**, *29*, 277.
[11] D. F. Perepichka, M. R. Bryce, C. Pearson, M. C. Petty, E. J. L. McInnes, J. P. Zhao, *Angew. Chem.* **2003**, *115*, 4783; *Angew. Chem. Int. Ed.* **2003**, *42*, 4635.
[12] Review of HOMO–LUMO gap control in TTF derivatives: M. Bendikov, F. Wudl, D. F. Perepichka, *Chem. Rev.* **2004**, *104*, 4891.
[13] D. F. Perepichka, M. R. Bryce, I. F. Perepichka, S. B. Lyubchik, N. Godbert, C. A. Christensen, A. S. Batsanov, E. Levillain, E. J. L. McInnes, J. P. Zhao, *J. Am. Chem. Soc.* **2002**, *124*, 14227.
[14] G. Ho, J. R. Heath, M. Kondratenko, D. F. Perepichka, K. Arseneault, M. Pézolet, M. R. Bryce, *Chem. Eur. J.* **2005**, *11*, 2914.
[15] Review: N. Martín, L. Sánchez, B. Illescas, I. Pèrez, *Chem. Rev.* **1998**, *98*, 2527.
[16] A. Honciuc, A. Jaiswal, A. Gong, K. Ashworth, C. W. Spangler, I. R. Peterson, L. R. Dalton, R. M. Metzger, *J. Phys. Chem. B* **2005**, *109*, 857.
[17] G. A. Burley, A. G. Avent, O. V. Boltalina, I. V. Gol'dt, D. M. Guldi, M. Marcaccio, F. Paolucci, D. Paolucci, R. Taylor, *Chem. Commun.* **2003**, 148.
[18] A. Kobayashi, M. Sasa, W. Suzuki, E. Fujiwara, H. Tanaka, M. Tokumoto, Y. Okano, H. Fijiwara, H. Kobayashi, *J. Am. Chem. Soc.* **2004**, *126*, 426.
[19] M. Kumasaki, H. Tanaka, A. Kobayashi, *J. Mater. Chem.* **1998**, *8*, 301.
[20] H. Tanaka, Y. Okano, H. Kobayashi, W. Suzuki, A. Kobayashi, *Science* **2001**, *291*, 285.



 © 2005 Wiley-VCH Verlag GmbH & Co. KGaA, Weinheim

DOI: 10.1002/anie.200500321

Fullerene Chemistry

Hydrogen-Bonding Motifs in Fullerene Chemistry

Luis Sánchez, Nazario Martín, and Dirk M. Guldi**

Keywords:
fullerenes · hydrogen bonds · molecular devices · self-assembly · supramolecular chemistry

In memory of Juan C. del Amo

The combination of fullerenes and hydrogen-bonding motifs is a new interdisciplinary field in which weak intermolecular forces allow modulation of one-, two-, and three-dimensional fullerene-based architectures and control of their function. This Minireview aims to extend the scope of fullerene chemistry to a truly supramolecular level from which unprecedented architectures may evolve. It is shown that electronic communication in C_{60}-based hydrogen-bonded donor–acceptor ensembles is at least as strong as that found in covalently connected systems and that hydrogen-bonding fullerene chemistry is a versatile concept for the construction of functional ensembles.

1. Introduction

In Nature, both covalently and noncovalently bound motifs are widely spread organization principles that regulate the size, shape, and function of all living species on a molecular (nano-) scale. One of the most fascinating and cited examples is double-stranded DNA. In this biopolymeric dimer, cooperativity between noncovalent interactions—involving multiple hydrogen bonds—and hydrophobic interactions generates exceptionally stable architectures. Nature thus provides inspiration for the design of organized structures that perform specific functions.

To engineer multimolecular arrays of nanometer dimensions, a wealth of noncovalent interactions are at our disposal. These comprise ion–ion, ion–dipole, hydrogen-bond, dipole–dipole, and π–π-stacking interactions. Typically, their binding energies range from a few $kJ\,mol^{-1}$ up to several hundred $kJ\,mol^{-1}$.[1] Among these interactions, hydrogen bonding has emerged as the most useful, with binding energies between 4 and 120 $kJ\,mol^{-1}$. The specificity of hydrogen bonding and its high degree of directionality attracts a lot of attention, as it is responsible for governing many three-dimensional structures in chemical and biological systems.[2]

One approach to overcome the poor stability of single hydrogen bonds relies on arrays of multiple hydrogen bonds. Alternatively, high values of binding constants have been obtained by combining hydrogen bonds with additional supramolecular interactions such as hydrophobic or electrostatic forces. In this Minireview, we survey some of the most relevant hydrogen-bonding arrays that are known, as well as those few examples in which hydrogen bonds are combined with other noncovalent interactions, such as complementary guanidinium– or amidinium–carboxylate bridges (Figure 1a and b, respectively).[3] Association constants (K_a) of around $10\,M^{-1}$ are observed in $CHCl_3$ for the simplest donor–acceptor (DA) arrays that are built upon one donor (D) and one acceptor (A) site. Triple hydrogen-bonding motifs (e.g. DAD, see Figure 1c), as pioneered and tested by Whitesides et al.,[4] Zimmerman and Corbin,[5] and Meijer and co-workers,[6] reveal K_a values as large as 10^2–$10^3\,M^{-1}$($CHCl_3$). Even higher association constants of $K_a \approx 10^5\,M^{-1}$ ($CHCl_3$) are observed in self-complementary quadruple hydrogen-bonding motifs (e.g. DADA) as shown in Figure 1d.[7] If, however, association constants greater than $10^7\,M^{-1}$ ($CHCl_3$) are to be realized, self-complementary DDAA motifs become necessary. Meijer and co-workers[8a] demonstrated the unusual binding strength of a DDAA motif with 2-ureido-4-pyrimidinones (Figure 1e).

[*] Prof. Dr. L. Sánchez, Prof. Dr. N. Martín
Departamento de Química Orgánica I
Facultad de Química
Universidad Complutense
28040 Madrid (Spain)
Fax: (+34) 913-944-103
E-mail: nazmar@quim.ucm.es
Prof. Dr. D. M. Guldi
Institute for Physical and Theoretical Chemistry
Universität Erlangen-Nürnberg
Egerlandstr. 3, 91058 Erlangen (Germany)
Fax: (+49) 9131-852-8307
E-mail: dirk.guldi@chemie.uni-erlangen.de

InterScience
© 2005 Wiley-VCH Verlag GmbH & Co. KGaA, Weinheim

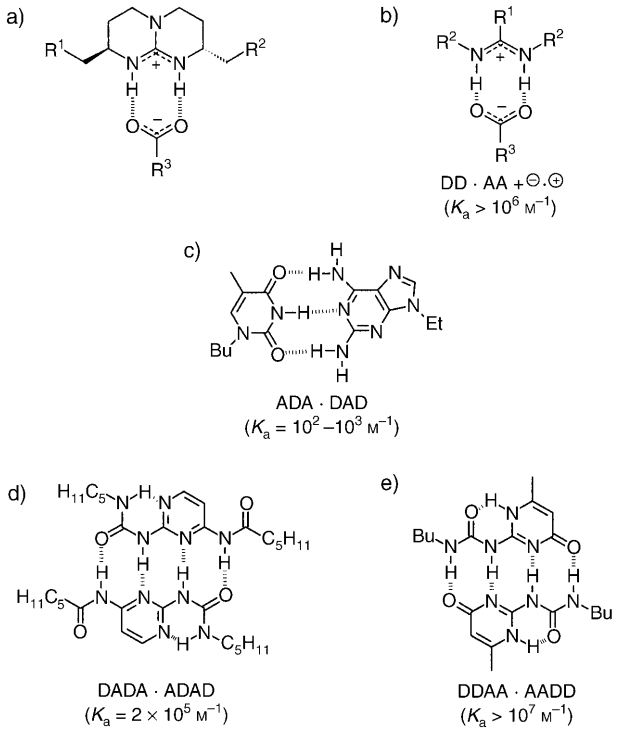


Figure 1. Hydrogen-bonding motifs that display high association constants. K_a values measured in 99:1 toluene/dimethyl sulfoxide (a, b) and in $CHCl_3$ (c–e). D = donor; A = acceptor.

Despite the importance of hydrogen-bonding motifs for the design of supramolecular architectures, their application to fullerenes has only recently been reported. This Minireview has three principle aims: 1) to extend the scope of fullerene chemistry to a truly supramolecular level from which unprecedented architectures evolve, 2) to show that electronic communication in C_{60}-based donor–acceptor ensembles that are connected through hydrogen bonds is at least as strong as that found in covalently connected systems, and 3) to highlight fullerene hydrogen-bonding chemistry as a versatile concept to construct functional ensembles such as molecular machines and optoelectronic devices.



Luis Sánchez received his PhD in organic chemistry in 1997 from the Universidad Complutense de Madrid (UCM; Spain). In 1998 he joined the faculty at the Department of Organic Chemistry at UCM and was promoted to Associate Professor in 2002. During 1999–2000 he was a postdoctoral researcher with Prof. Jan C. Hummelen (University of Groningen, The Netherlands) and worked on the synthesis of C_{60} derivatives and their application in the preparation of organic solar cells. His current research interests are focused on new supramolecular C_{60}-based ensembles in the study of electron-transfer processes and photovoltaic applications.



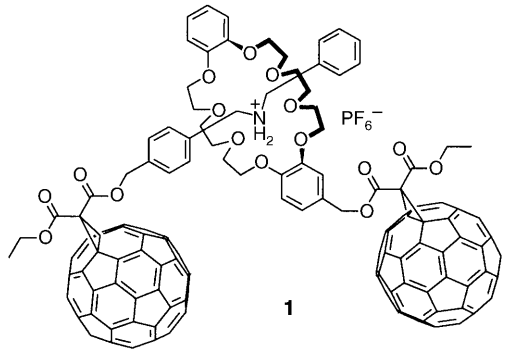
Nazario Martín received his PhD from the Department of Organic Chemistry at the Universidad Complutense de Madrid (Spain) in 1984. After a year in industry, he worked as a postdoctoral fellow (1987–1988) with Prof. M. Hanack at the Institut für Organische Chemie der Universität Tübingen (Germany) on electrically conducting organic materials. Since 1989 he has been Professor of Organic Chemistry at UCM. His research interests focus on electroactive molecules, with emphasis on the covalent and supramolecular chemistry of fullerenes, electron-donor tetrathiafulvalenes, and p-conjugated systems in the context of electron-transfer processes and photovoltaic applications.



Dirk M. Guldi studied chemistry at the University of Cologne (Germany) and received his PhD in 1990. He then carried out postdoctoral research at the National Institute of Standards and Technology (Gaithersburg, USA) and at the Hahn-Meitner-Institute, Berlin, and he joined the faculty at the Notre Dame Radiation Laboratory in 1995. He completed his Habilitation at the University of Leipzig in 1999, and since 2004 he is Professor of Physical Chemistry at the Friedrich-Alexander University in Erlangen. His primary research interests include new multifunctional carbon-based nanostructures within the context of light-induced charge separation and solar-energy conversion.

2. Hydrogen-Bonded Fullerene Ensembles

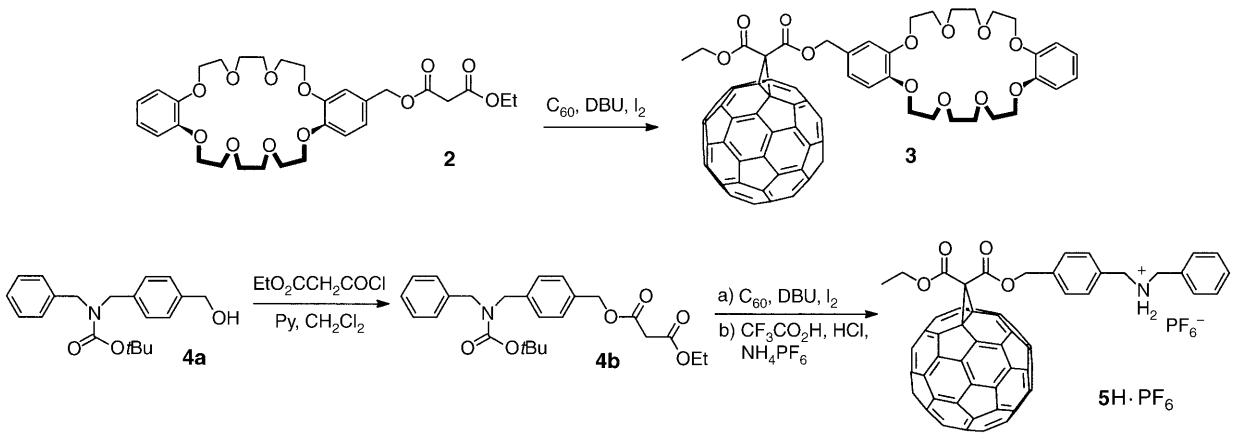
In 1999, Diederich et al. reported the dimer **1** (K_a = 970 M^{-1} in $CHCl_3$).[9] In this ensemble, N$^+$–H···O and C–H···O hydrogen bonds together with contributions from ion-pairing and dispersive interactions are the driving forces for noncovalent, pseudorotaxane-like geometries. On the way to supramolecular dimer **1**, Bingel reactions were carried out between C_{60} and malonate-appended crown **2** and dibenzylamido malonate **4b**, respectively, to afford the methanofullerene **3** and the precursor to **5**H·PF_6 (see Scheme 1). Consecutive deprotection (CF_3CO_2H/CH_2Cl_2), protonation (HCl), and ion exchange (NH_4PF_6/H_2O/acetone) led finally to **5**H·PF_6.



1

Highly stable hydrogen-bonded fullerene dimers **9** and **12** were prepared through self-complementary 2-ureido-4-pyrimidinone (UP) moieties (Scheme 2). The first step in the preparation of **9** was the 1,3-dipolar cycloaddition of the anion of *p*-tosylhydrazone **6** to C_{60}. Photoisomerization of the formed fulleroid quantitatively yielded methanofullerene **7a**, which was transformed into the acyl azide **7d** through routine chemistry. The final step involved heating of **7d** in the

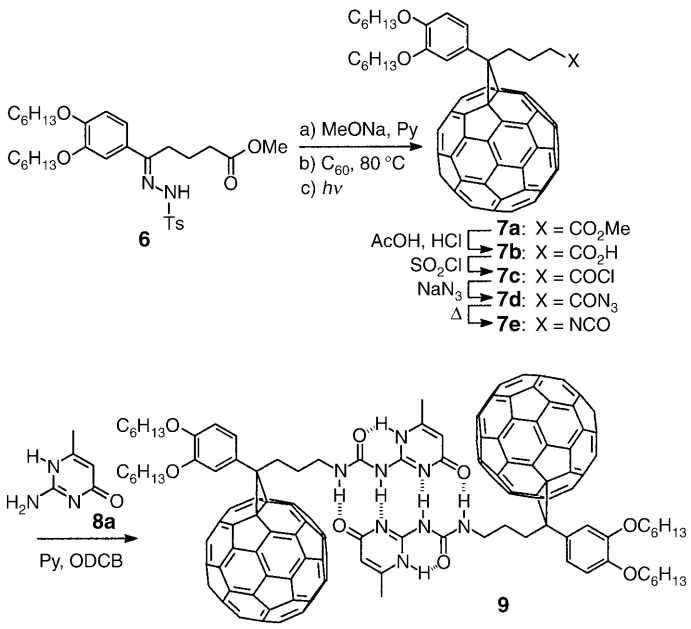
© 2005 Wiley-VCH Verlag GmbH & Co. KGaA, Weinheim



Scheme 1. Synthesis of precursors for noncovalently linked C_{60} dimer **1**. DBU = 1,8-diazabicyclo[5.4.0]undec-7-ene; Py = pyridine.

presence of 6-methylisocytosine (**8a**) to afford the monomeric unit of **9** in 71% yield (Scheme 2).[10]

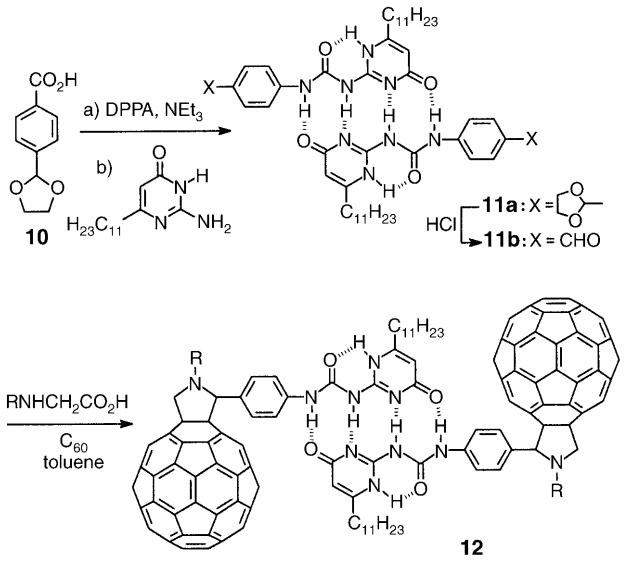
The key step in the synthesis of **12** was the reaction between C_{60} and a bisazomethine ylide generated in situ from dialdehyde **11b** (Scheme 3).[11] Electrochemical studies of **9** and **12** in the ground states confirmed the absence of



Scheme 2. Synthesis of supramolecular C_{60} dimer **9**. Ts = *p*-toluenesulfonyl; ODCB = *o*-dichlorobenzene.

interactions between the C_{60} units. However, differences were seen when the reactivity of the monomers and dimers in their excited states were studied.[11] Specifically, the photophysical findings pointed to strong electronic coupling between the C_{60} termini, mediated through the hydrogen-bonding edges.

Sánchez, Rispens, and Hummelen reported soon afterwards the synthesis of the supramolecular C_{60} polymer **15**[12] from the C_{60}-diester derivative **13** (Scheme 4). The dynamic behavior of **15** was investigated by ^{1}H NMR spectroscopy. At



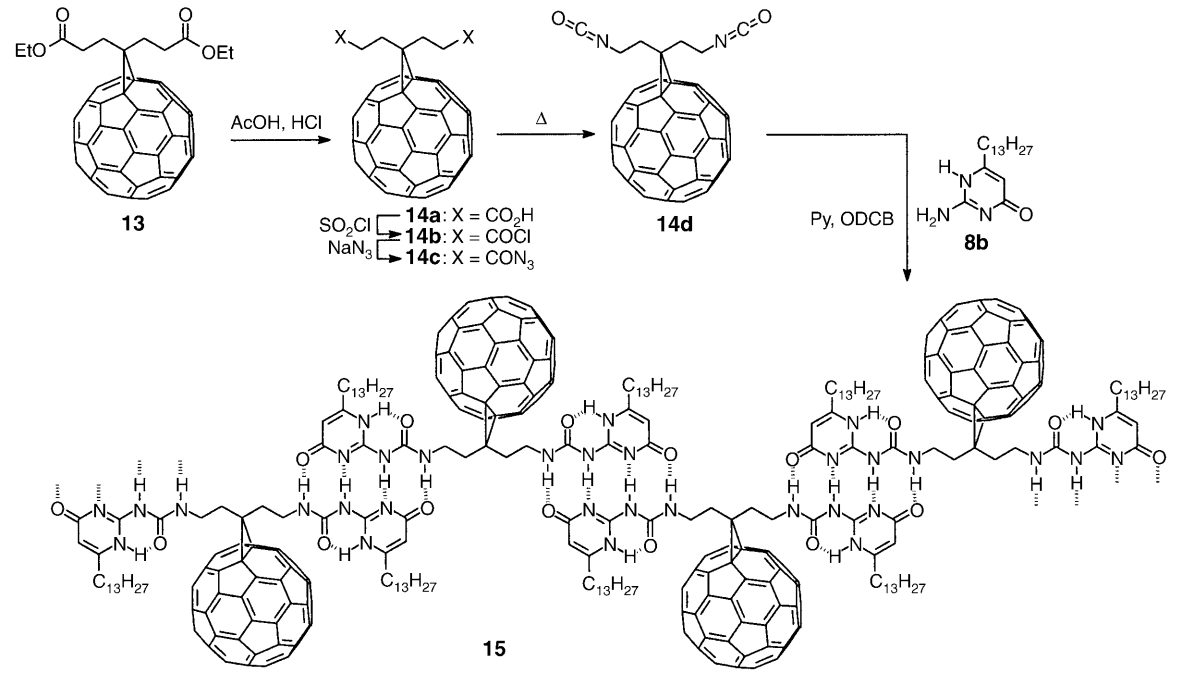
Scheme 3. Synthesis of supramolecular C_{60} dimer **12**. DPPA = diphenylphosphoryl azide; $R = CH_3(OCH_2CH_2)_3$.

low concentrations (10 mM) different sets of multiple signals were observed. A likely rationale infers the presence of polymeric and low-molecular-weight cyclic aggregates, as has been proposed for related systems.[13] A fairly high association constant, $K_a = 6 \times 10^7\,M^{-1}$, was determined for polymer **15** in chloroform.[14] The electrochemical behavior of polymer **15** was virtually identical to that of the analogous dimer **9**, and neither **9** nor **15** exhibit notable interactions between the fullerenes.

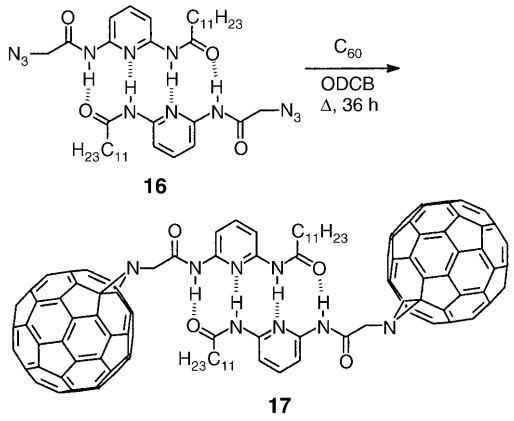
In line with the DADA concept, 2,6-bis(acylamino)pyridines were probed to integrate two aziridinofullerenes into the supramolecular C_{60} dimer **17**.[15] This dimer was prepared through 1,3-dipolar cycloaddition of the corresponding hydrogen-bonded azide **16** to C_{60} (Scheme 5). Interestingly, when dilute solutions of **17** were analyzed by scanning electron microscopy (SEM), spherical nanoparticles with diameters of typically around 15 nm were observed which resulted from aggregation.

Bassani and co-workers characterized a variety of supramolecular ensembles resulting from the reaction of fullerene-

© 2005 Wiley-VCH Verlag GmbH & Co. KGaA, Weinheim



Scheme 4. Synthesis of supramolecular C_{60}-based polymer **15**.



Scheme 5. Synthesis of DADA hydrogen-bonded C_{60}-based dimer **17**.

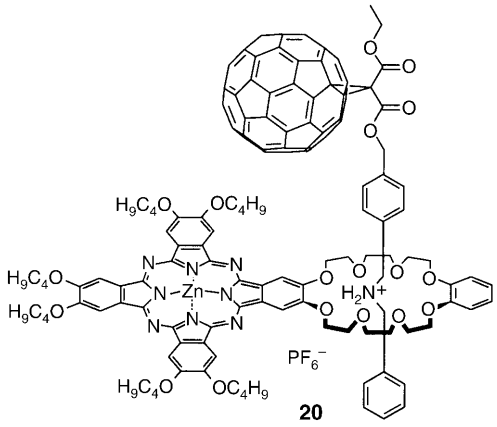
barbituric acid **18** and the melamine derivative triaminotriazine **19**.[16] Scheme 6, part a, shows several of the resulting architectures obtained. An interesting feature of [60]fullerenes is their susceptibility to undergo topologically controlled [2+2] photocycloaddition reactions. The resulting structures are similar to that obtained through the intermolecular photodimerization of the 1:2 complex formed from melamine template **19** and two molecules of **18** (Scheme 6, part b). Bassani's supramolecular approach represents the first instance of intermolecular photodimerization of a fullerene derivative in solution and an interesting example of supramolecular catalysis.

The above cases outline the structural sophistication obtained by combining noncovalent interactions with the covalent chemistry of fullerenes. The integration of hydrogen bonds has led to new supramolecular fullerene architectures that range from dimers to polymers.

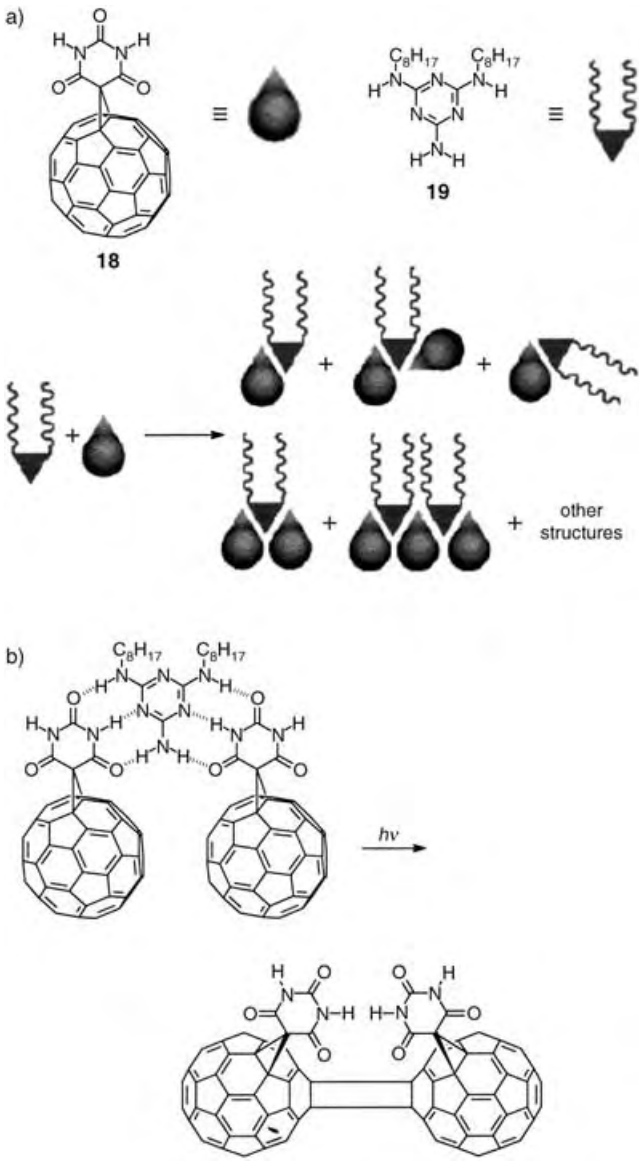
3. Hydrogen-Bonding C_{60}–Donor Ensembles

Given the importance of natural photosynthetic processes, the quest for simple models with focus on primary photosynthesis events is one of the most intriguing tasks in chemistry. In this regard, C_{60} is an excellent candidate for the preparation of photo- and redox-active model systems.

In electron-donor/electron-acceptor ensembles, light excitation typically forces a thermodynamically driven charge-separation (CS) process.[17] In the case of C_{60}, the lifetimes of such charge-separated radical-ion pairs lie between picoseconds and seconds. In the past, most of these donor–acceptor ensembles were covalently linked[18] and much less attention was given to hydrogen-bonded model systems.[19] Only recently did the first examples appear in which C_{60} is linked to an electron-donor unit through a hydrogen-bonding network. Pseudorotaxane-like molecular recognition motifs that lead to fullerene–(zinc phthalocyanine) (C_{60}-ZnPc) ensembles **20** were reported by Guldi, Torres, Prato, and co-



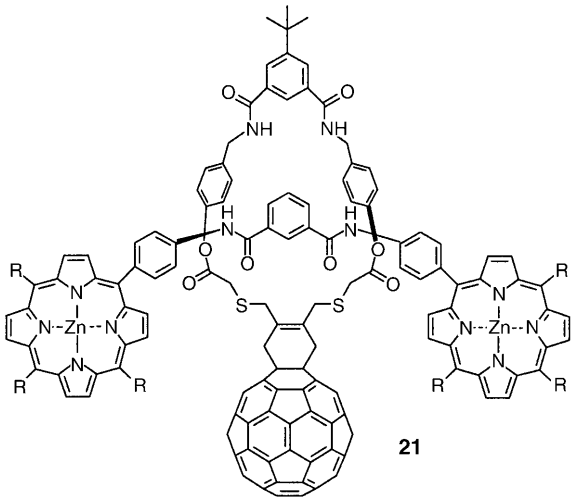
 © 2005 Wiley-VCH Verlag GmbH & Co. KGaA, Weinheim



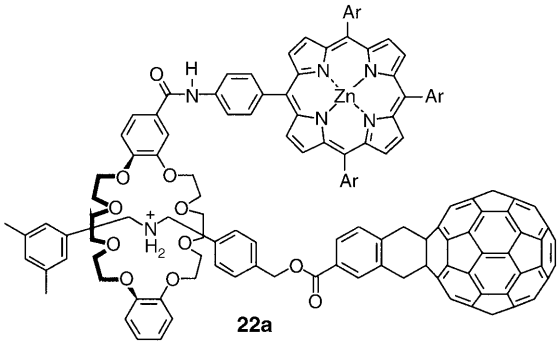
Scheme 6. a) Various supramolecular species formed by hydrogen bonding between C_{60}–barbituric acid **18** and melamine **19**. b) Intermolecular photodimerization process of $(\mathbf{18})_2 \cdot \mathbf{19}$, in which a noncovalently bonded species is transformed into one that is covalently bonded. Reprinted with permission from ref. [16]. Copyright (2003) American Chemical Society.

workers.[20] Charge-separated states (i.e. $C_{60}^{\bullet-} \cdot ZnPc^{\bullet+}$) with lifetimes of microseconds evolved from an efficient intracomplex electron-transfer process that started from the excited state of the ZnPc fragment. For the sake of comparison, a similar but covalently linked C_{60}-ZnPc dyad that exhibits lifetimes for the radical-ion pair of only 3 ns has been reported.[21]

Although numerous examples of porphyrin (P)-linked donor–acceptor systems are known,[22] including several that comprise C_{60} as an acceptor, no hydrogen-bonded fullerene–porphyrin (C_{60}-P) model systems were reported until recently. One such example was the rotaxane C_{60}-ZnP dyad **21** prepared by Takata, Ito, and co-workers.[23] Whereas **21** displays a lifetime of 180 ns for its radical-ion pair, covalently



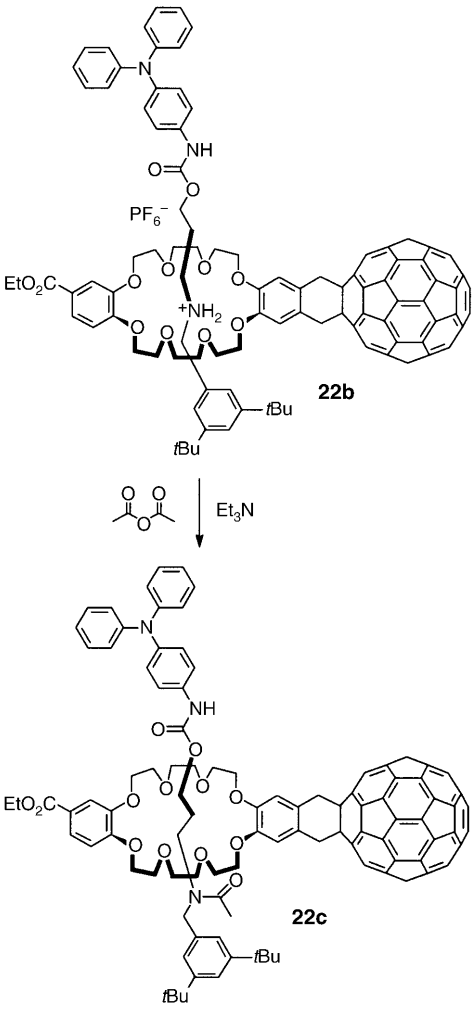
linked C_{60}-P dyads exhibit a longer lifetime of 770 ns.[24] Takata and co-workers have also synthesized new rotaxanes **22**, in which the [60]fullerene moiety makes up either the axle (**22a**)[25a] or the wheel (**22b**,**c**, Scheme 7)[25b] of the supra-



molecular structure. An attractive interaction between the two chromophores in **22a**, that is, C_{60} and ZnP, has been established. The consequence of this favorable interaction is noted through the acceleration of the end-capping process, which thus enhances its overall efficiency. Ensembles **22b**,**c**, which bear triphenylamine (TPA) electron-donor units, showed that noncovalent interactions can be modulated through the positive charge that is placed at the nitrogen atom in the middle of the axle (**22b**, Scheme 7). Acylation of the positively charged amine in **22b** to furnish the neutral amide group in **22c** evoked a shift of the axle with respect to the C_{60} wheel. In **22b**,**c** a through-space, intrarotaxane, photoinduced electron-transfer process gives rise to a long-lived CS state, $C_{60}^{\bullet-} \cdot TPA^{\bullet+}$, whose lifetimes range between 170 and 300 ns. Interestingly, the lifetimes of $C_{60}^{\bullet-} \cdot TPA^{\bullet+}$ in the rotaxanes appear to be longer than those measured for the corresponding covalently bound C_{60}-TPA dyad.[25b]

Highly stable supramolecular $C_{60} \cdots ZnP$ complexes **23**, held together through a two-point binding strategy, are well-defined with regards to distance and orientation.[26] Time-resolved emission and absorption studies have revealed efficient charge-separation processes, with rate constants of

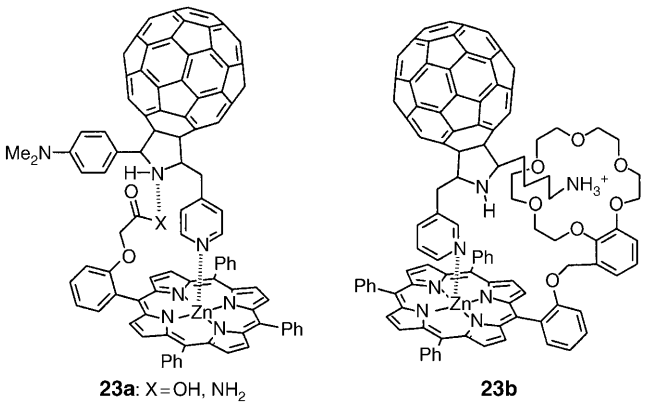
© 2005 Wiley-VCH Verlag GmbH & Co. KGaA, Weinheim

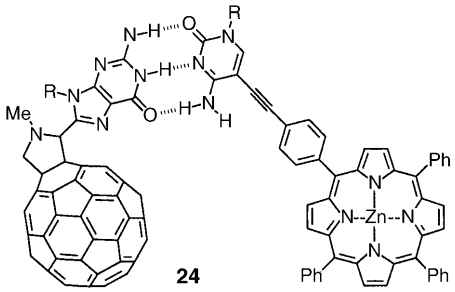


Scheme 7. C_{60}–TPA ensembles tethered by rotaxane structures.

6.3×10^7 and 3.1×10^9 s^{-1} observed for the formation of the CS states in **23a** and **23b**, respectively.

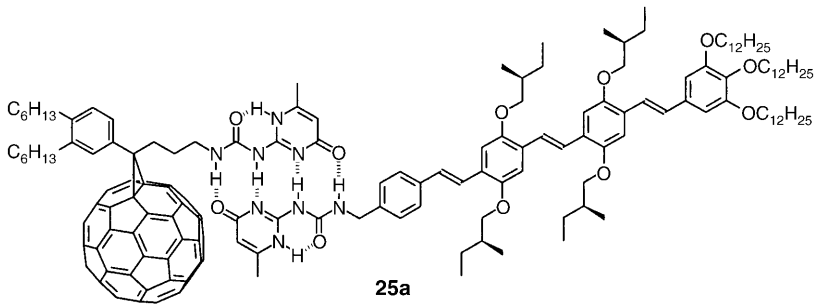
Another remarkable impact on the lifetime of the photogenerated radical-ion pair is seen when C_{60} is paired with a porphyrin moiety in the form of **24**. The lifetime of the radical-ion pair in **24**, in which C_{60} and ZnP are tethered by means of a guanosine–cytidine scaffold[27] is 2.02 μs. This value is higher than those reported for related covalently linked C_{60}-ZnP dyads[22–24] as a result of the beneficial effect of the hydrogen bonds.

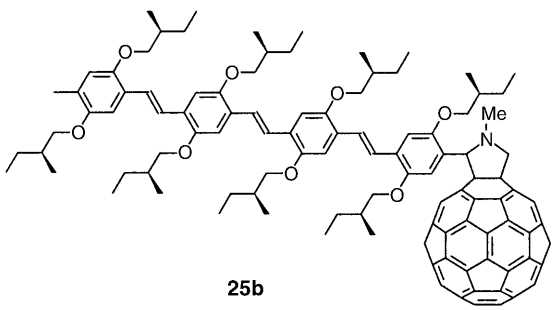




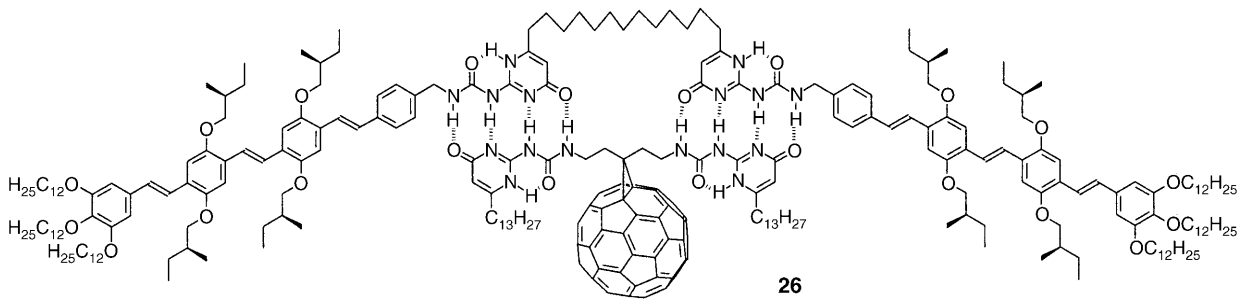
To control the organization in active layers of photovoltaic cells, **25a** is prepared by mixing **9** (Scheme 2) with an oligophenylene vinylene (OPV) system that bears complementary UP moieties.[28] In both **25a** and the "covalent" analogue **25b**,[29] a strong quenching of the OPV fluorescence is observed. Energy transfer from the singlet excited state of OPV to the fullerene is responsible for the quenching. In the covalently bound **25b**[29] an ultrafast electron-transfer process is followed by an intramolecular energy-transfer process, whereas this sequence does not occur in hydrogen-bonded **25a** as a consequence of the low electronic coupling between the electroactive units in **25a**.[30]

The combination of polymer **15** (Scheme 4) with OPVs functionalized with UP groups allowed the formation of heterodimers linked through quadruple hydrogen bonds. This strategy resulted in new supramolecular donor–acceptor dyads.[31] Remarkably, in contrast to previous examples in which the self-complementary nature of such hydrogen-bonding motifs led to a statistical mixture of homo- and heterodimers, dyad **26** represents the first example of





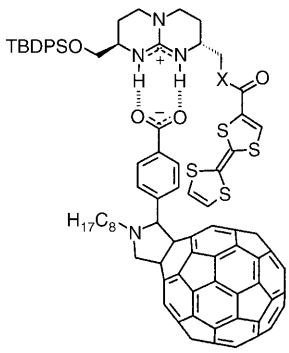
© 2005 Wiley-VCH Verlag GmbH & Co. KGaA, Weinheim



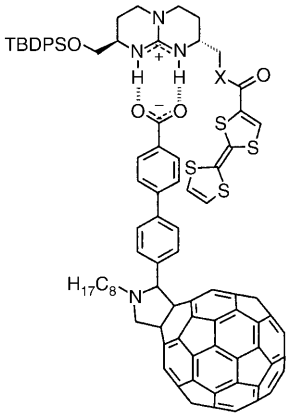
26

preferential formation of functional supramolecular heterodimers linked by UP moieties.

Recently, in collaboration with Mendoza's group we reported a series of hydrogen-bonded C_{60}·TTF ensembles, **27a–d** (TTF = tetrathiafulvalene, TBDPS = *tert*-butyldiphenylsilyl),[32] in which the tetrathiafulvalenes act as electron donors.[33] In these cases, the photoactive units are held together not only through complementary hydrogen bonds but also by strong electrostatic interactions through guanidinium and carboxylate ion pairs. To tune the molecular architecture, two chemical spacers of different lengths (phenyl versus biphenyl) as well as two functional groups (ester and amide) were used. The solvent-dependent nature of the fluorescence quenching in C_{60}·TTF dyads as well as the formation of the $C_{60}^{\bullet-}$·$TTF^{\bullet+}$ radical-ion pairs, together with the flexible nature of the spacer, reflect through-space electron-transfer processes. The lifetimes measured for the radical-ion pair states are in the range of hundred of nanoseconds, thus several orders of magnitude higher than those reported for covalently linked C_{60}-TTF dyads.[34]



27a: X = O
27b: X = NH

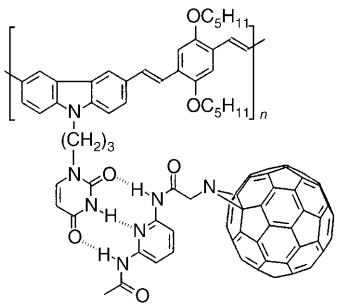


27c: X = O
27d: X = NH

4. Applications of Hydrogen-Bonded Supramolecular Fullerene Complexes

π-Conjugated oligomers/polymers as well as C_{60} are widely used as building blocks for optoelectronic devices such as light-emitting diodes (LEDs)[35] and organic solar cells.[36] In 2001, Meijer and co-workers reported hydrogen-bonded polymers that comprised oligo(*p*-phenylenevinylene) (PPV) moieties connected through multiple self-complementary fourfold hydrogen-bonding motifs.[37] A photovoltaic device was prepared by mixing this supramolecular polymer with a methanofullerene derivative, and the ensemble was successfully used in the preparation of bulk heterojunction organic solar cells.[36]

Li, Zhu, and co-workers presented a three-point hydrogen-bonding assembly between C_{60} and a π-conjugated PPV polymer (**28**·**29**).[38] In this particular case the noncovalent linkage was established between the uracil moiety, bound to polymer **28**, and 2,6-diacylamidopyridine **29**, linked to C_{60}. Fluorescence experiments revealed a strong interaction between PPV and C_{60}.



28 · 29

Perylene bisimides (PERYs) are another important class of materials for solar cells. The main features of PERYs include good electron-acceptor capabilities and good light absorption in the visible region. Both features are essential to guarantee good conversion efficiencies.[39] Diaminopyridine–C_{60} **29** has been used together with the tetraalkoxy-PERY system **30** (Figure 2a).[40] Irradiation of (**29**)$_2$·**30** films on indium tin oxide (ITO) electrodes with white light (63.2 mW cm^{-2}) generates a steady, rapid, and highly stable anodic photocurrent response. Importantly, the response to on/off cycling is prompt and reproducible (Figure 2b).

5. Summary and Outlook

In summary, the synthesis and applications of multiply hydrogen-bonded C_{60} derivatives have been reviewed here.

© 2005 Wiley-VCH Verlag GmbH & Co. KGaA, Weinheim

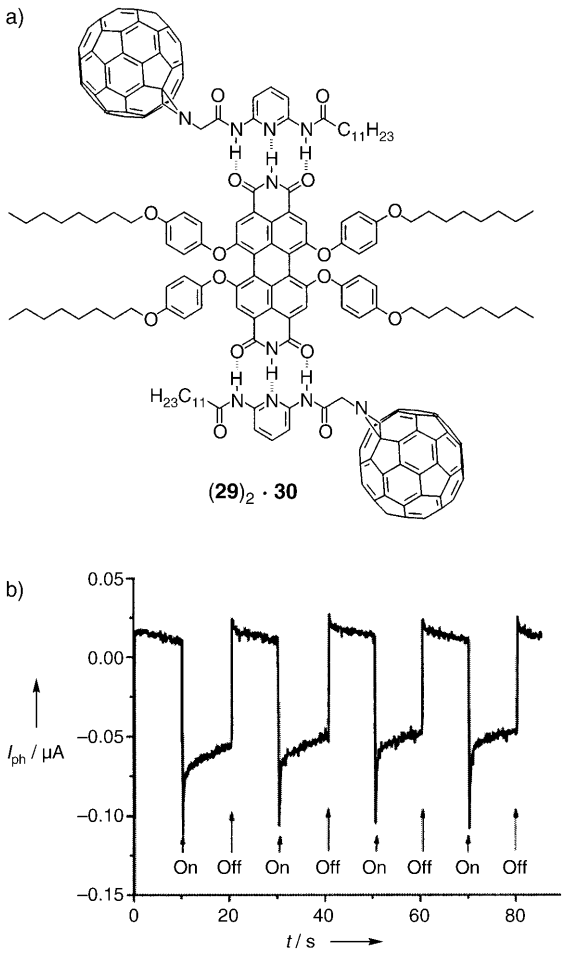


Figure 2. a) Structure of the three-point hydrogen-bonded C_{60}-PERY assembly $(\mathbf{29})_2$·**30**, and b) time-dependence of the photocurrent (I_{ph}) response of the self-assembled film. Reprinted with permission from ref. [40]. Copyright (2004) American Chemical Society.

Implementing the chemistry of fullerene into supramolecular chemistry has led to original examples of molecular organization that might find application in promising fields such as molecular materials or supramolecular catalysis. Supramolecular chemistry of fullerenes is a thriving field that should furnish future avenues for the integration of C_{60} as an outstanding photo- and electroactive building block in nanoscience and nanotechnology.

This work was supported by the MCYT of Spain, Comunidad de Madrid (Projects BQU2002-00855 and HSE/MAT0633-04). The US Department of Energy Basic Energy Sciences (NDRL 4613 from the Notre Dame Radiation Laboratory) is also acknowledged.

Received: January 27, 2005
Published online: July 5, 2005

[1] L. F. Lindoy, I. M. Atkinson, *Self-Assembly in Supramolecular Systems*, Royal Society of Chemistry, Cambridge, UK, **2000**.
[2] R. P. Sijbesma, E. W. Meijer, *Chem. Commun.* **2003**, 5 – 16.
[3] a) B. P. Orner, X. Salvatella, J. Sánchez-Quesada, J. de Mendoza, E. Giralt, A. D. Hamilton, *Angew. Chem.* **2002**, *114*, 125 – 127; *Angew. Chem. Int. Ed.* **2002**, *41*, 117 – 119; b) C. Schmuck, W. Wienand, *Angew. Chem.* **2001**, *113*, 4493 – 4499; *Angew. Chem. Int. Ed.* **2001**, *40*, 4363 – 4369.
[4] G. M. Whitesides, E. E. Simanek, J. P. Mathias, C. T. Seto, D. N. Chin, M. Mammen, D. M. Gordon, *Acc. Chem. Res.* **1995**, *28*, 37 – 44.
[5] S. C. Zimmermann, P. S. Corbin, *Struct. Bonding (Berlin)* **2000**, 63 – 94.
[6] F. H. Beijer, R. P. Sijbesma, J. A. J. M. Vekemans, E. W. Meijer, H. Kooijman, A. L. Spek, *J. Org. Chem.* **1996**, *61*, 6371 – 6380.
[7] F. H. Beijer, H. Kooijman, A. L. Spek, R. P. Sijbesma, E. W. Meijer, *Angew. Chem.* **1998**, *110*, 79 – 82; *Angew. Chem. Int. Ed.* **1998**, *37*, 75 – 78.
[8] a) F. H. Beijer, R. P. Sijbesma, H. Kooijman, A. L. Spek, E. W. Meijer, *J. Am. Chem. Soc.* **1998**, *120*, 6761 – 6769; b) D. C. Sherrington, K. A. Taskinen, *Chem. Soc. Rev.* **2001**, *30*, 83 – 93.
[9] a) F. Diederich, L. Echegoyen, M. Gómez-López, R. Kessinger, J. F. Stoddart, *J. Chem. Soc. Perkin Trans. 2* **1999**, 1577 – 1586; b) F. Diederich, M. Gómez-López, *Chem. Soc. Rev.* **1999**, *28*, 263 – 278.
[10] M. T. Rispens, L. Sánchez, J. Knol, J. C. Hummelen, *Chem. Commun.* **2001**, 161 – 162.
[11] J. J. González, S. González, E. Priego, C. Luo, D. M. Guldi, J. de Mendoza, N. Martín, *Chem. Commun.* **2001**, 163 – 164.
[12] L. Sánchez, M. T. Rispens, J. C. Hummelen, *Angew. Chem.* **2002**, *114*, 866 – 868; *Angew. Chem. Int. Ed.* **2002**, *41*, 838 – 840.
[13] For recent reviews on supramolecular polymers, see: a) A. Ciferri, *Supramolecular Polymers*, Marcel Dekker, New York, **2000**; b) J.-M. Lehn, *Polym. Int.* **2002**, *51*, 825 – 839; c) R. P. Sijbesma, E. W. Meijer, *Chem. Commun.* **2003**, 5 – 16.
[14] A. P. H. J. Schenning, P. Jonkheijm, E. Peeters, E. W. Meijer, *J. Am. Chem. Soc.* **2001**, *123*, 409 – 416.
[15] S. Xiao, Y. Li, H. Fang, H. Li, H. Liu, Z. Shi, L. Jiang, D. Zhu, *Org. Lett.* **2002**, *4*, 3063 – 3066.
[16] N. D. McClenaghan, C. Absalon, D. M. Bassani, *J. Am. Chem. Soc.* **2003**, *125*, 13004 – 13005.
[17] a) N. Martín, L. Sánchez, B. M. Illescas, I. Pérez, *Chem. Rev.* **1998**, *98*, 2527 – 2548; b) L. Sánchez, M. A. Herranz, N. Martín, *J. Mater. Chem.* **2005**, 1409 – 1421.
[18] a) M. R. Wasielewski, *Chem. Rev.* **1992**, *92*, 435 – 461; b) H. Kurreck, M. Huber, *Angew. Chem.* **1995**, *107*, 929 – 947; *Angew. Chem. Int. Ed. Engl.* **1995**, *34*, 849 – 866; c) D. Gust, T. A. Moore, A. L. Moore, *Acc. Chem. Res.* **2001**, *34*, 40 – 48.
[19] a) A. P. H. J. Schenning, J. v. Herrikhuyzen, P. Jonkheijm, Z. Chen, F. Würthner, E. W. Meijer, *J. Am. Chem. Soc.* **2002**, *124*, 10252 – 10253; b) D. M. Guldi, N. Martín, *J. Mater. Chem.* **2002**, *12*, 1978 – 1992; c) J. L. Sessler, M. Sathiosatham, C. T. Brown, T. A. Rhodes, G. Wiederrecht, *J. Am. Chem. Soc.* **2001**, *123*, 3655 – 3660; d) A. J. Myles, N. R. Branda, *J. Am. Chem. Soc.* **2001**, *123*, 177 – 178; e) T. H. Ghaddar, E. W. Castner, S. S. Isied, *J. Am. Chem. Soc.* **2000**, *122*, 1233 – 1234.
[20] D. M. Guldi, J. Ramey, M. V. Martínez-Díaz, A. de la Escosura, T. Torres, T. da Ros, M. Prato, *Chem. Commun.* **2002**, 2774 – 2775.
[21] D. M. Guldi, A. Gouloumis, P. Vázquez, T. Torres, *Chem. Commun.* **2002**, 2056 – 2057.
[22] a) H. Yamada, H. Imahori, Y. Nishimura, I. Yamazaki, T. K. Ahn, S. K. Kim, D. Kim, S. Fukuzumi, *J. Am. Chem. Soc.* **2003**, *125*, 9129 – 9139; b) D. Gust, T. A. Moore, A. L. Moore, *Acc. Chem. Res.* **2001**, *34*, 40 – 48; c) H. Imahori, Y. Sakata, *Adv. Mater.* **1997**, *9*, 537 – 546.
[23] N. Watanabe, N. Kihara, Y. Forusho, T. Takata, Y. Araki, O. Ito, *Angew. Chem.* **2003**, *115*, 705 – 707; *Angew. Chem. Int. Ed.* **2003**, *42*, 681 – 683.

 © 2005 Wiley-VCH Verlag GmbH & Co. KGaA, Weinheim

[24] H. Imahori, M. E. El-Khouly, M. Fujitsuka, O. Ito, Y. Sakata, S. Fukuzumi, *J. Phys. Chem. A* **2001**, *105*, 325 – 332.

[25] a) H. Sasabe, N. Kihara, Y. Forusho, K. Mizuno, A. Ogawa, T. Takata, *Org. Lett.* **2004**, *6*, 3957 – 3960; b) A. S. D. Sandanayaka, H. Sasabe, Y. Araki, Y. Forusho, O. Ito, T. Takata, *J. Phys. Chem. A* **2004**, *108*, 5145 – 5155.

[26] a) F. D'Souza, G. R. Deviprasad, M. E. Zadler, M. E. El-Khouly, F. Fujitsuka, O. Ito, *J. Phys. Chem. A* **2003**, *107*, 4801 – 4807; b) F. D'Souza, R. Chitta, S. Gadde, M. E. Zandler, A. S. D. Sandanayaka, Y. Araki, O. Ito, *Chem. Commun* **2005**, 1279 – 1281.

[27] J. L. Sessler, J. Jayawickramarajah, A. Gouloumis, T. Torres, D. M. Guldi, S. Maldonado, K. J. Stevenson, *Chem. Commun.* **2005**, 1892 – 1894.

[28] E. H. A. Beckers, P. A. van Hal, A. P. H. J. Schenning, A. El-ghayoury, E. Peeters, M. T. Rispens, J. C. Hummelen, E. W. Meijer, R. A. J. Janssen, *J. Mater. Chem.* **2002**, *12*, 2054 – 2060.

[29] a) P. A. van Hal, S. C. J. Meskers, R. A. J. Janssen, *Appl. Phys. Lett. A* **2004**, *79*, 41 – 46; b) E. Peeters, P. A. van Hal, J. Knol, C. J. Brabec, N. S. Sariciftci, J. C. Hummelen, R. A. J. Janssen, *J. Phys. Chem. B* **2000**, *104*, 10174 – 10191.

[30] For a recent review on PV materials by using the C_{60}/oligomer approach, see: J. L. Segura, N. Martín, D. M. Guldi, *Chem. Soc. Rev.* **2005**, *34*, 31 – 47.

[31] E. H. A. Beckers, A. P. H. J. Schenning, P. A. van Hal, A. El-ghayoury, L. Sánchez, J. C. Hummelen, E. W. Meijer, R. A. J. Janssen, *Chem. Commun.* **2002**, 2888 – 2889.

[32] M. Segura, L. Sánchez, J. de Mendoza, N. Martín, D. M. Guldi, *J. Am. Chem. Soc.* **2003**, *125*, 15093 – 15100.

[33] J. L. Segura, N. Martín, *Angew. Chem.* **2001**, *113*, 1416 – 1455; *Angew. Chem. Int. Ed.* **2001**, *40*, 1372 – 1409.

[34] a) D. M. Guldi, S. González, N. Martín, A. Antón, J. Garín, J. Orduna, *J. Org. Chem.* **2000**, *65*, 1978 – 1983; b) J. L. Segura, E. M. Priego, N. Martín, C. Luo, D. M. Guldi, *Org. Lett.* **2000**, *2*, 4021 – 4024; c) N. Martín, L. Sánchez, M. A. Herranz, D. M. Guldi, *J. Phys. Chem. A* **2000**, *104*, 4648 – 4657.

[35] a) J. H. Bourroughes, D. D. C. Bradley, A. R. Brown, R. N. Marks, K. MacKay, R. H. Friend, P. L. Burns, A. B. Holmes, *Nature* **1990**, *347*, 539 – 541; b) A. Kraft, A. C. Grimsdale, A. B. Holmes, *Angew. Chem.* **1998**, *110*, 416 – 443; *Angew. Chem. Int. Ed.* **1998**, *37*, 402 – **428**; c) S.-H. Jin, M.-Y. Kim, J. Y. Kim, K. Lee, Y.-S. Gal, *J. Am. Chem. Soc.* **2004**, *126*, 2474 – 2480.

[36] a) S. E. Shaheen, C. J. Brabec, N. S. Sariciftci, F. Padinger, T. Fromherz, J. C. Hummelen, *Appl. Phys. Lett.* **2001**, *78*, 841 – 843; b) N. S. Sariciftci, L. Smilowitz, A. J. Heeger, F. Wudl, *Science* **1992**, *258*, 1474 – 1476; c) G. Yu, J. Gao, J. C. Hummelen, F. Wudl, A. J. Heeger, *Science* **1995**, *270*, 1789 – 1790.

[37] A. El-ghayoury, A. P. H. J. Schenning, P. A. van Hal, J. K. J. van Duren, R. A. J. Janssen, E. W. Meijer, *Angew. Chem.* **2001**, *113*, 3772 – 3775; *Angew. Chem. Int. Ed.* **2001**, *40*, 3660 – 3663.

[38] a) Z. Shi, Y. Li, H. Gong, M. Liu, S. Xiao, H. Liu, H. Li, S. Xiao, D. Zhu, *Org. Lett.* **2002**, *4*, 1179 – 1182; b) H. Fang, S. Wang, S. Xiao, J. Yang, Y. Li, Z. Shi, H. Li, H. Liu, S. Xiao, D. Zhu, *Chem. Mater.* **2003**, *15*, 1593 – 1597.

[39] E. E. Neuteboom, S. C. J. Meskers, P. A. van Hal, J. K. J. van Duren, E. W. Meijer, R. A. J. Janssen, H. Dupin, G. Pourtois, J. Cornil, R. Lazzaroni, J.-L. Brédas, D. Beljonne, *J. Am. Chem. Soc.* **2003**, *125*, 8625 – 8638.

[40] Y. Liu, S. Xiao, H. Li, Y. Li, H. Liu, F. Lu, J. Zhuang, D. Zhu, *J. Phys. Chem. B* **2004**, *108*, 6256 – 6260.

 © 2005 Wiley-VCH Verlag GmbH & Co. KGaA, Weinheim

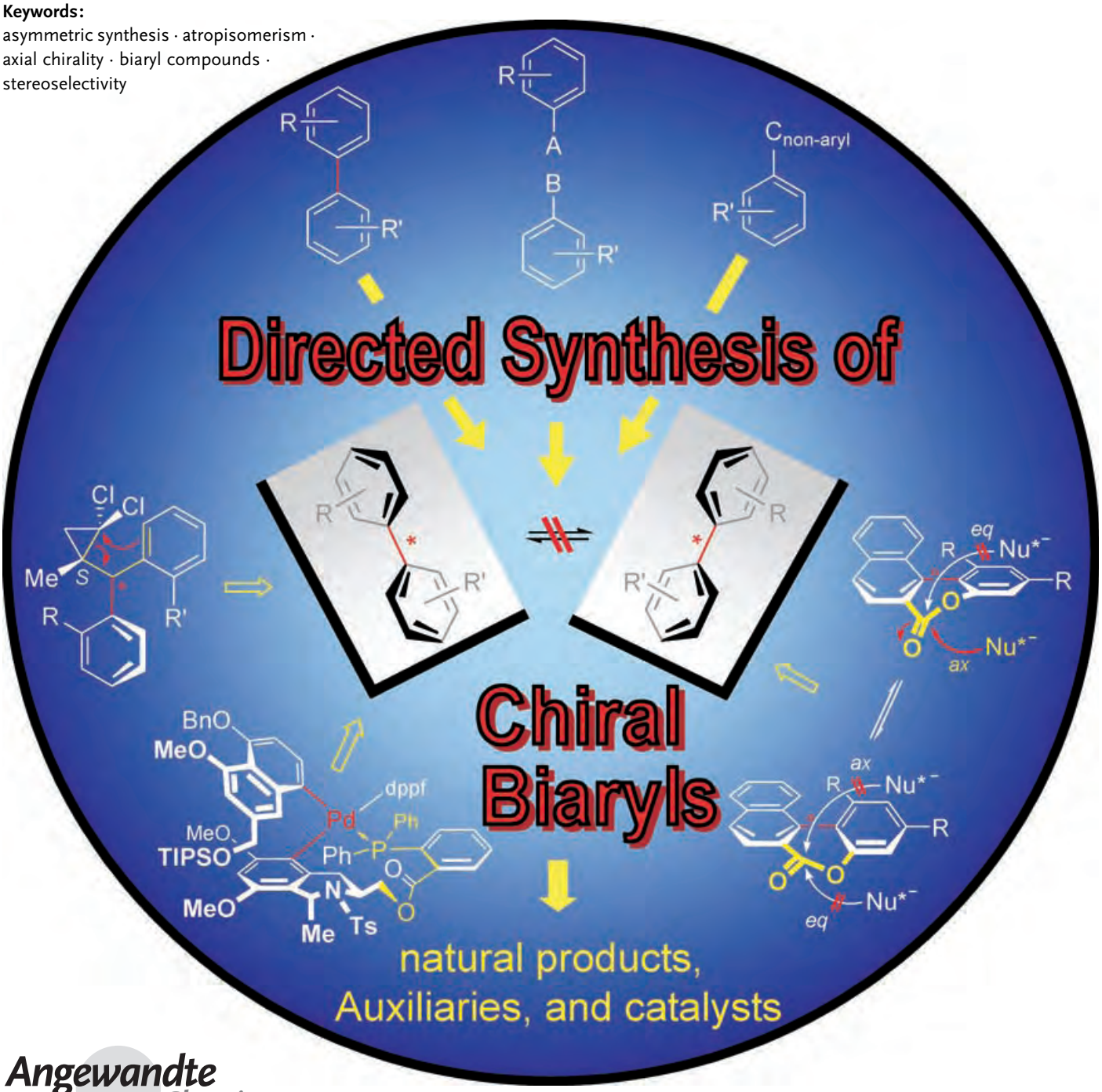
Biaryl Synthesis

DOI: 10.1002/anie.200462661

Atroposelective Synthesis of Axially Chiral Biaryl Compounds**

Gerhard Bringmann, Anne J. Price Mortimer, Paul A. Keller, Mary J. Gresser, James Garner, and Matthias Breuning**

Keywords:
asymmetric synthesis · atropisomerism · axial chirality · biaryl compounds · stereoselectivity



© 2005 Wiley-VCH Verlag GmbH & Co. KGaA, Weinheim

A rotationally hindered and thus stereogenic biaryl axis is the structurally and stereochemically decisive element of a steadily growing number of natural products, chiral auxiliaries, and catalysts. Thus, it is not surprising that significant advances have been made in the asymmetric synthesis of axially chiral biaryl compounds over the past decade. In addition to the classic approach (direct stereoselective aryl–aryl coupling), innovative concepts have been developed in which the asymmetric information is introduced into a preformed, but achiral—that is, symmetric or configurationally labile—biaryl compound, or in which an aryl–C single bond is stereoselectively transformed into an axis. This Review classifies these strategies according to their underlying concepts and critically evaluates their scope and limitations with reference to selected model reactions and applications. Furthermore, the preconditions required for the existence of axial chirality in biaryl compounds are discussed.

From the Contents

1. Introduction 5385
2. Preconditions for Axial Chirality and Mechanisms of Atropisomerization 5387
3. Biaryls by Asymmetric C–C Coupling 5391
4. Atroposelective Transformations of Prostereogenic Biaryl Compounds 5407
5. Asymmetric Biaryl Synthesis by Construction of an Aromatic Ring 5418
6. Summary and Outlook 5419

1. Introduction

Since the first resolution of tartaric acid by Louis Pasteur in 1848,[1] the stereoselective synthesis of compounds containing one or more stereogenic centers has emerged as one of the most important fields in chemistry. Numerous excellent diastereo- and enantioselective procedures have been developed which belong nowadays to the standard repertoire of synthetic chemistry.[2] Axial chirality, by contrast, as a stereogenic element in rotationally hindered biaryl compounds of natural and synthetic origin, has often been overlooked or treated as an "academic curiosity".[3] This, however, has changed with the recognition that the configuration at a biaryl axis can be a decisive factor in governing the pharmacological properties of a bioactive compound[4] and that axial chirality is the fundamental basis for useful reagents and catalysts in asymmetric synthesis.[5]

Natural products equipped with a rotationally hindered biaryl axis are far more widespread and structurally diverse than initially assumed.[4] Many representatives of this class of axially chiral metabolites exhibit remarkable bioactivities, like the famous antibiotic heptapeptide vancomycin (**1**, Figure 1).[6,7] This molecule contains three types of stereoelements—numerous stereogenic centers, two "chiral" planes, and a stereogenic biaryl axis, which together impose the rigid 3D structure necessary for an efficient binding to peptides of bacterial cell walls.[6] Knipholone[8] (**2**) possesses solely axial chirality and occurs with varying degrees of enantiomeric purity in nature;[9] compounds of this family of 1-phenylanthraquinones have recently been shown to exhibit good antimalarial[10] and antitumor[11] activities, the latter particularly when *M* configured. Mastigophorene A (**3**), a C_2-symmetric bisphenol bearing additional stereogenic centers, has been found to stimulate nerve growth.[12] The class of axially chiral natural products is, however, not restricted to C–C-coupled biaryl compounds. (*M*)-Murrastifoline-F ((*M*)-**4**), for example, is a biscarbazole with the two—otherwise identical—"halves" connected by a heterobiaryl C–N bond.[13]

Axially chiral biarylic auxiliaries and catalysts exhibit excellent chirality transfer properties.[5] A prime example is the diphosphine binap (**5**, Figure 2),[14] which is the ligand of choice in Ru-catalyzed asymmetric hydrogenations of C=C and C=O bonds.[15] The more complex epoxidation catalyst **6** possesses two axially chiral binaphthyl subunits embedded in a sterically demanding backbone.[16] More recently, attention has been focussed on non-C_2-symmetric biaryl compounds such as the tertiary aminophenol **7**, which catalyzes the enantioselective addition of diethylzinc to aldehydes.[17] The isoquinoline-containing phosphine quinap (**8**) is an example of an axially chiral heteroaromatic biaryl; it has been used as a ligand in Pd-catalyzed asymmetric allylic alkylation reactions.[18]

Owing to the importance of axially chiral biaryl compounds, a variety of excellent methods for their directed, atroposelective construction have been developed. Herein, we present an overview of the most efficient and practicable methods presently known for the atroposelective synthesis of axially chiral biaryl compounds.[19–24] Major consideration is

[*] G. Bringmann, A. J. Price Mortimer, M. Breuning
Institut für Organische Chemie
Universität Würzburg
Am Hubland, 97074 Würzburg (Germany)
Fax: (+49) 931-888-4755
E-mail: bringman@chemie.uni-wuerzburg.de
breuning@chemie.uni-wuerzburg.de
P. A. Keller, M. J. Gresser, J. Garner
Department of Chemistry
University of Wollongong
Wollongong 2522 (Australia)

[**] Novel Concepts in Directed Biaryl Synthesis, Part 110. Part 109: G. Bringmann, R.-M. Pfeifer, P. Schreiber, K. Hartner, N. Kocher, R. Brun, K. Peters, E.-M. Peters, M. Breuning, *Tetrahedron* **2004**, *60*, 6335–6355.

 © 2005 Wiley-VCH Verlag GmbH & Co. KGaA, Weinheim

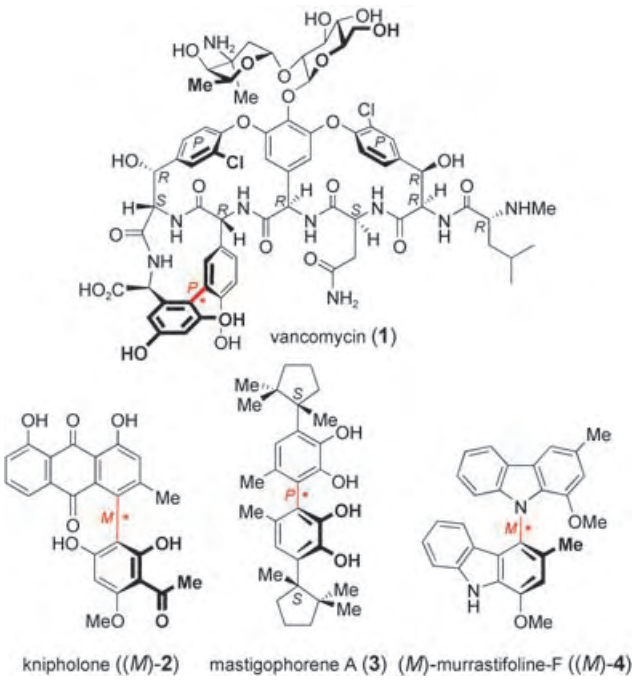


Figure 1. Selected examples of naturally occurring axially chiral biaryl compounds.

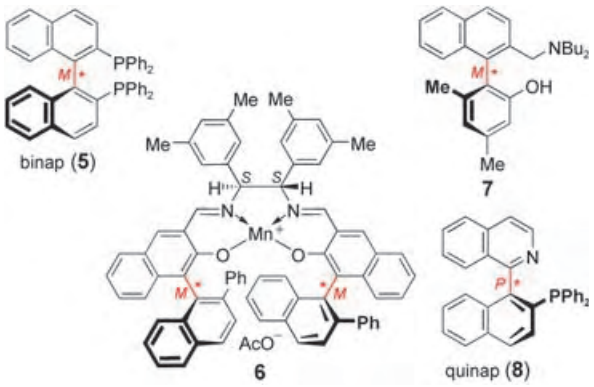


Figure 2. Selected examples of axially chiral ligands and catalysts.

given to the different fundamental strategies elaborated: their conceptual classification, the stereochemical principles that govern the asymmetric induction at the axis, their applicability, and their limitations.

As the phenomenon of axial chirality relies on the rotational stability of an aryl–aryl single bond, important preconditions for this stability, as well as the different mechanisms of atropisomerization, are discussed in Section 2. As outlined in Scheme 1, three fundamentally different strategies have, to date, been realized for the atroposelective synthesis of axially chiral biaryl compounds. The classic concept, which is discussed in Section 3, involves biaryl formation in a single step by C–C coupling, with the two aromatic portions being joined with simultaneous asymmetric induction (**9** + **10**→**11**).[19,22,23] The second approach, by contrast, relies on the atroposelective transformation of an existing, but stereochemically not yet defined, biaryl system (Section 4).[20,21] Within this two-step approach, a nonstereoselective coupling step thus precedes the introduction of the stereochemical information at the axis (**12**→**11**). Finally, Section 5 summarizes the few known methods in which a C–C bond between an arene and a precursor substituent is transformed into a chiral biaryl axis by construction of an



Gerhard Bringmann studied chemistry in Giessen and Münster (Germany) and received his PhD with Prof. B. Franck in 1978. After postdoctoral studies with Prof. Sir Derek H. R. Barton in Gif-sur-Yvette (France), and his habilitation in 1984 at the University of Münster. He became a full professor of Organic Chemistry at the University of Würzburg in 1987. In 1998 he declined an offer of the position of a director at the Leibniz Institute of Plant Biochemistry in Halle. His research interests lie in the field of analytical, synthetic, and computational natural products chemistry.



Paul Keller completed his BSc (Hons) (1985) and PhD (1991) at the University of New South Wales (Australia), before taking up an Alexander von Humboldt funded postdoctoral fellowship in Germany. Since 1994, he has worked at the University of Wollongong, Australia, and is currently Associate Professor in Organic and Medicinal Chemistry. His interests lie in drug design and development, the development of synthetic fullerenyl chemistry, and the design and synthesis of chiral catalysts.

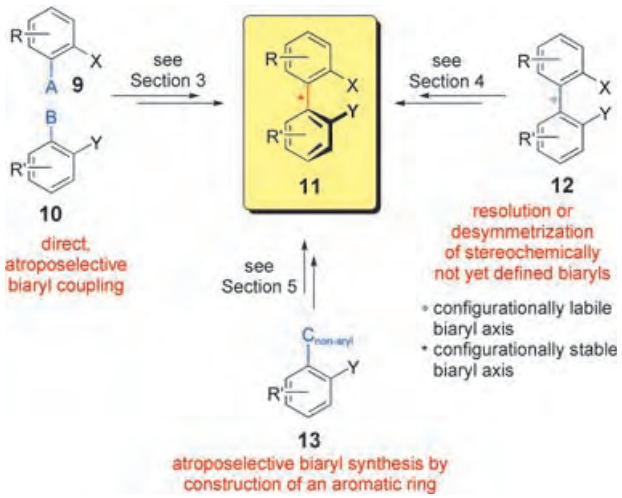


Anne J. Price Mortimer was born in Stoke-on-Trent (UK) in 1977. She studied chemistry at St. John's College, University of Oxford, before going on to complete a DPhil under the supervision of Prof. S. G. Davies in 2003, investigating the synthesis of β-amino acid natural products. From 2003 to 2005 she was a postdoctoral researcher in the group of Prof. G. Bringmann, developing novel methodologies for the synthesis of axially chiral biaryls, and held an Alexander von Humboldt research fellowship from 2004.



Mary J. Gresser, born in 1981, completed her BSc (Hons) at the University of Wollongong (Australia). She commenced her PhD in 2003 under the supervision of Associate Professor Paul A. Keller, investigating the synthesis of chiral ligands for palladium-based catalysis.

© 2005 Wiley-VCH Verlag GmbH & Co. KGaA, Weinheim



Scheme 1. Schematic overview of the existing strategies for atroposelective syntheses of axially chiral biaryl systems.

aromatic ring, usually with a central-to-axial chirality transfer (**13**→**11**).

2. Preconditions for Axial Chirality and Mechanisms of Atropisomerization

2.1. The Phenomenon of Axial Chirality

Optical activity due to axial chirality has been known since the early 20th century and was first correctly described by Christie and Kenner in 1922.[25] The term "atropisomerism" (from the Greek, *a* = not and *tropos* = turn) was introduced by Kuhn[26] in 1933 and originally referred solely to biaryl compounds. In general, there are two necessary preconditions for axial chirality in biaryl molecules (Figure 3):[27,28] a rotationally stable axis and the presence of

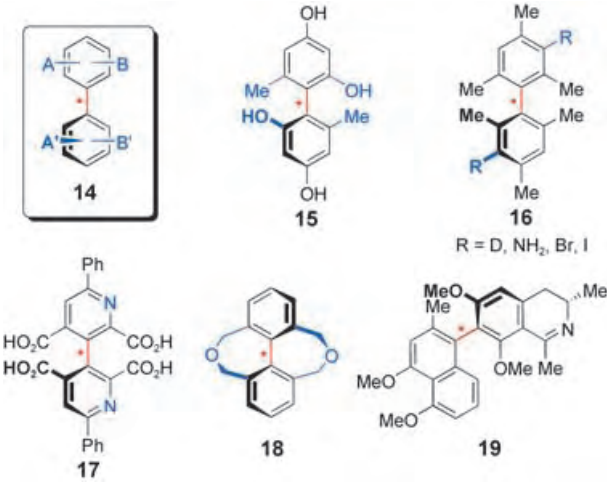


Figure 3. Selected substitution patterns that result in axial chirality.

different substituents on both sides of the axis as indicated in **14**, that is, A ≠ B and A′ ≠ B′. If A = A′ and B = B′, the molecule has C_2 symmetry (but is still chiral) as in **15**, **16**, and **17**. Surprisingly to the casual observer, even biaryl compounds with four constitutionally identical substituents may be chiral if these are connected pairwise through two bridges as in the D_2-symmetric diether **18**.[29] Axially chiral biaryl compounds that bear different *ortho* substituents, such as the dimeric orcinol (**15**),[30] are found ubiquitously (compare most of the biaryl species discussed in this article). Although less common, axial chirality may also result from an inequivalence of *meta* substituents, as found in the bimesityls **16**[31] and in the naphthylisoquinoline alkaloid ancistrocladisine (**19**).[32] Furthermore, heteroaromatic systems provide the possibility to introduce chirality merely from the position of the heteroatom, as found in the dipyridyl quateraryl **17**.[33]

The absolute axial configuration can be denoted by analysis of a Newman projection along the biaryl axis (Figure 4). After assignment of priority to the *ortho* (or *meta*) substituents according to the CIP rules,[34] the analysis is done by following the shortest 90° path from the substituent of highest priority at the proximal ring to the highest-ranking one at the distal ring (i.e. here from A to A′). If this 90° turn is counterclockwise as in **20**, the absolute configuration is *M* (for **m**inus); if it is clockwise as in *ent*-**20**, then the descriptor is *P* (for **p**lus).[35,36]

For the stereochemical assignment of pairwise enantiotopic substituents in prochiral biaryl compounds of type **21**, the arc between the substituent of interest and the substituent of highest priority on the other aryl ring is considered, giving rise to the descriptors pro-*M* and pro-*P* (see Figure 4, bottom), after the system of Hanson and Helmchen.[37,38]

The other crucial precondition for atropisomerism is the rotational stability of the biaryl axis. The temperature has a profound influence: On the one hand, even biaryl compounds



James Garner, born in 1976, studied chemistry at the University of Newcastle (Australia), before going on to complete a PhD in 2003 under the supervision of Dr Adam McCluskey, on the development of structurally unprecendented CRH_1 antagonists. He is currently a postdoctoral research fellow under the direction of Associate Professor Paul A. Keller, investigating the synthesis of 6,6′-bisindoles.



Matthias Breuning, studied chemistry at the University of Würzburg (Germany), where he completed his PhD in 1999 under Prof. G. Bringmann. After a postdoctoral stay with Prof. E. J. Corey at Harvard University (USA), he joined Bayer AG in 2001 as a senior research scientist. Since 2002 he has been working on his habilitation at the University of Würzburg, supported by an Emmy-Noether fellowship of the DFG. His main research interests lie in the field of asymmetric synthesis, in particular in the development of novel catalysts and their application in natural products synthesis.

© 2005 Wiley-VCH Verlag GmbH & Co. KGaA, Weinheim

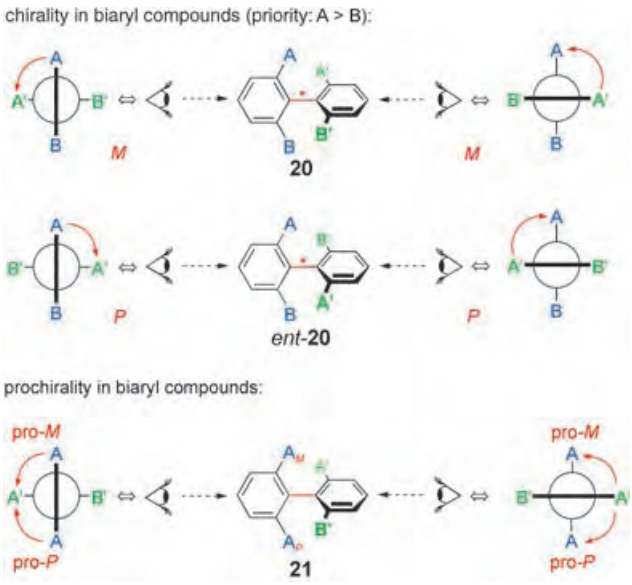


Figure 4. Assignment of absolute configuration in chiral biaryl species and descriptors for paired substituents in prochiral biaryl compounds (note that the same descriptor results, regardless of the position of the observer).[38]

with a low degree of steric hindrance will suffer impeded rotation if sufficiently cooled down,[39] and split up into atropoenantiomers or -diastereomers if unsymmetrically substituted; on the other hand, biaryl species that are axially chiral at room temperature may start to atropisomerize upon heating, resulting in thermodynamically controlled equilibrium mixtures (i.e. in a full loss of chiral information in the case of enantiomers).[40,41] As an arbitrary, but useful definition,[42] atropisomers are recognized as physically separable species when, at a given temperature, they have a half-life τ of at least 1000 s (16.7 min). Thus the minimum free energy barrier $\Delta G^{\ddagger}$ required varies with temperature (e.g. $\Delta G^{\ddagger}_{200\,K} = 61.6\ kJ\,mol^{-1}$, $\Delta G^{\ddagger}_{300\,K} = 93.5\ kJ\,mol^{-1}$, and $\Delta G^{\ddagger}_{350\,K} = 109\ kJ\,mol^{-1}$). The configurational stability of axially chiral biaryl compounds is determined by three major factors:

1) the (combined) steric demand of the substituents in proximity to the axis;
2) the existence, length, and rigidity of bridges; and
3) the involvement of atropisomerization mechanisms different from a merely physical rotation about the axis, for example, by photochemically or chemically induced processes.

2.2. Atropisomerization by Physical Rotation

Physical—that is, thermal—rotation about a biaryl axis has, in selected cases, been shown by quantum-chemical calculations to occur through twisted (i.e. nonplanar) transition states in which the bonds to the *ortho* substituents and the aryl rings are distorted, thus permitting the substituents to pass each other more easily than in a rigid planar transition state.[41,43–45] In many cases, the barrier to rotation can be rationalized in terms of substituent effects.

2.2.1. Effects of Nonbridging Substituents

ortho Substituents increase the atropisomerization barrier in nonbridged biaryl compounds by their steric repulsion (compare **22** and **25**, Figure 5), corresponding largely to the van der Waals radii of the substituents, that is, I > Br > Me > Cl > NO_2 > CO_2H > OMe > F > H.[46]

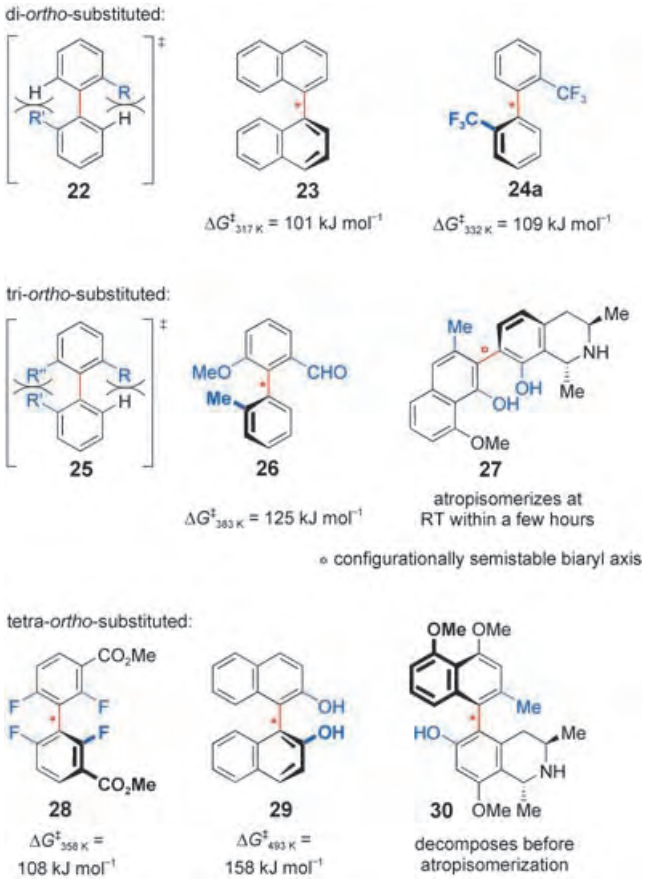


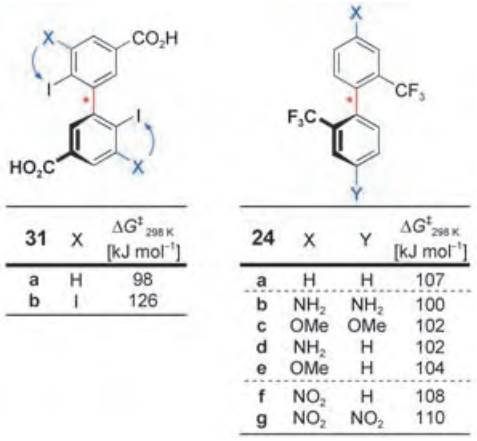
Figure 5. Configurational stability of di- to tetra-*ortho*-substituted biaryl compounds.

Open-chain (i.e. nonbridged), mono-*ortho*-substituted biaryl compounds do not form stable atropisomers at room temperature. With two substituents next to the axis, atropisomerism at room temperature is only observed if both groups are bulky, as in 1,1′-binaphthyl (**23**)[47] and in 2,2′-bis(trifluoromethyl)biphenyl (**24a**),[48] so that in the transition state **22** even the interactions of R and R′ with the small hydrogen atoms provide sufficient steric repulsion for restricted rotation.[49] As a rule, tri-*ortho*-substituted biaryl compounds form stable atropisomers; in the transition state **25**, two substituents now must pass one another for rotation to occur, rather than a substituent passing a hydrogen atom. The biphenyl **26**[50,51] is an example of such an axially chiral biaryl system. Nevertheless, sterically less demanding substituents may still permit slow axial rotation as observed with the

 © 2005 Wiley-VCH Verlag GmbH & Co. KGaA, Weinheim

naphthylisoquinoline alkaloid dioncophylline E (**27**), whose atropisomerization occurs within a few hours at room temperature.[52] Conformational stability is virtually guaranteed for tetra-*ortho*-substituted biaryl compounds, even if the substituents are all small, as in the tetrafluorobiphenyl **28** ($\Delta G^{\ddagger}_{358\,K} = 108\ kJ\,mol^{-1}$).[53] The rotational barriers can be extremely high, as in the auxiliary binol (**29**, $\Delta G^{\ddagger}_{493\,K} = 158\ kJ\,mol^{-1}$),[41] making these compounds configurationally stable even under forcing conditions; in many cases the atropisomerization temperature is so high that it cannot be reached without decomposition.[54] Ancistrocladine (**30**), as an example, can be dehydrogenated at 200 °C without loss of atropisomeric purity;[55] at higher temperatures, the molecule disintegrates.

Bulky substituents in the *meta* positions increase the configurational stability of biaryl compounds by "buttressing" the *ortho* substituents, thus preventing their bending out of the way in the transition state.[46,56,57] For example, rotation in the tetraiodobiphenyl **31b** (Figure 6) is considerably more difficult than in its diiodo analogue **31a** ($\Delta G^{\ddagger}_{298\,K} = 126\ kJ\,mol^{-1}$ vs. $\Delta G^{\ddagger}_{298\,K} = 98\ kJ\,mol^{-1}$).[56]



31	X	$\Delta G^{\ddagger}_{298\,K}$ [kJ mol^{-1}]
a	H	98
b	I	126

24	X	Y	$\Delta G^{\ddagger}_{298\,K}$ [kJ mol^{-1}]
a	H	H	107
b	NH_2	NH_2	100
c	OMe	OMe	102
d	NH_2	H	102
e	OMe	H	104
f	NO_2	H	108
g	NO_2	NO_2	110

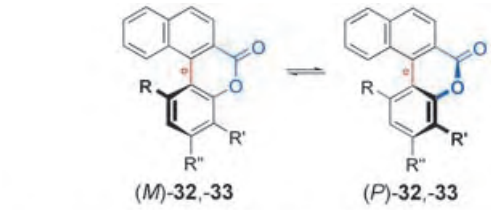
Figure 6. The effect of *meta* (left) and *para* (right) substituents on the configurational stability of biaryl compounds.

para Substituents influence the rotational barrier mainly by electronic effects,[43,57] as evidenced by the 4,4′-substituted biphenyls **24**.[57] Electron donation by resonance from the substituent at C4 increases the sp^3 character at C1, thus facilitating the out-of-plane bending at these positions. This decreases the strain in the transition state and, therefore, lowers the barrier to rotation (**24b–e**). By the same token, electron-withdrawing groups, which restrict the out-of-plane bending by decreasing the electron density at C1, raise the barrier (**24f,g**).[58]

2.2.2. *Bridged Biaryl Systems*

The effect of a bridging ring on the restricted rotation of a biaryl system varies greatly with the ring size. In systems in which two of the *ortho* substituents are replaced by a single bridging atom (i.e. a five-membered ring is formed), rotation is usually not hindered at room temperature.[59]

The presence of a six-membered bridge still considerably facilitates rotation, but to a lesser extent. A comparative study was done on the benzonaphthopyranones **32** and **33** (Figure 7), which exist as racemic mixtures of their helically



	32a	32b	32c	32d	32e	33a	33c	33f
R	H	OMe	Me	Et	*i*Pr	H	Me	*t*Bu
R'	*i*Pr	Et	*i*Pr	*i*Pr	Me	H	H	H
R"	H	H	H	H	H	H	Me	*t*Bu
$\Delta G^{\ddagger}_{298\,K}$ [kJ mol^{-1}]	–	54.4	73.9	83.7	92.3			104.4
$\tau_{298\,K}$	< ms	0.4 ms	1.0 s	52 s	28 min			2.2 d

X-ray crystal structures and torsion angles:

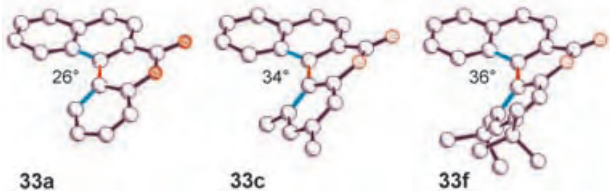


Figure 7. Atropisomerization barriers and structures of six-membered lactone-bridged biaryl compounds **32a–e** and **33a,c,f**. Note that the *M*/*P* descriptors given apply to **32a,c–e** and **33a,c,f**.[63]

distorted atropoenantiomers (*M*)- and (*P*)-**32** and -**33** (torsion angles from 26° for **33a** to 36° for **33f**).[45,60,61] $\Delta G^{\ddagger}_{298\,K}$ increases with the steric demand of the *ortho* substituent R.[62] Thus, **32a–d** (R = H, OMe, Me, Et) atropisomerize quickly at room temperature with half-lives $\tau_{298\,K} < 1$ min, whereas the lactone **32e** (R = *i*Pr) is at the brink of atropisomerism ($\tau_{298\,K} = 28$ min). The enantiomers of the largely distorted derivative **33f** (R = *t*Bu; see X-ray crystal-structure diagram, Figure 7, bottom) are configurationally stable and can be resolved by both physical and chemical methods.

Stereogenic centers in the bridge can strongly influence the—now atropodiastereomeric—equilibrium as, due to the exocyclic substituents (axial or equatorial), the bridge adopts the thermodynamically favorable conformation. In the acetal **34** (Figure 8), which has a single stereogenic center, the conformer with the methoxy group in an axial position is preferred (ax-**34**/eq-**34** = 91:9), apparently as a consequence of an *exo*-anomeric effect.[64] The atropodiastereomerization processes eq-**34**⇄ax-**34**, however, are still fast[62] and are comparable to those for the related lactone **32c** (see Figure 7). The biaryl compounds **35**[65] and **36**[66] are configurationally unstable at room temperature, and occur as 1:1 mixtures of atropodiastereomers, despite the presence of two stereogenic centers in the bridge, whereas **37**, with the dioxolane system enforcing a di-equatorial conformation, exists as a single diastereomer.[66]

© 2005 Wiley-VCH Verlag GmbH & Co. KGaA, Weinheim

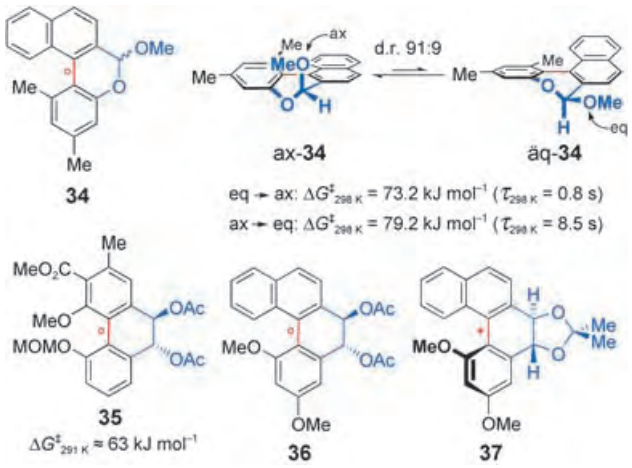


Figure 8. The configurational stability of six-membered bridged biaryl compounds that bear stereogenic centers in the bridge.

Biaryl compounds containing seven-membered rings exhibit rotational stabilities almost comparable to those of their unbridged analogues.[67] Larger bridges, including those formed by hydrogen bonding,[68] can induce atropisomerism by geometrical constraints of the ring, even in biaryl systems with relatively little axial hindrance. The synthetic biphenyls **38**[40,69] and **39**[70] are examples of such compounds that have just two substituents next to the axis, but are configurationally stable at room temperature (Figure 9). Even the tripeptide

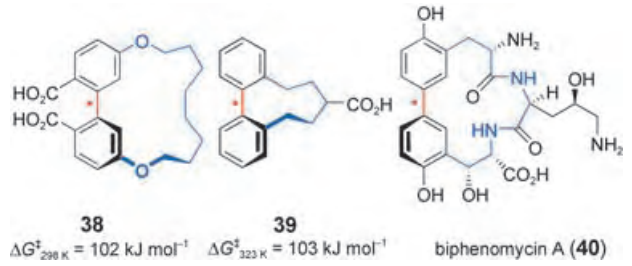


Figure 9. Macrocyclic bridged biaryl compounds that are axially chiral despite low steric hindrance in the proximity of the axis.

antibiotic biphenomycin A (**40**), which does not have any *ortho* substituents next to the axis, occurs as a single atropodiastereomer.[71] It is, however, not clear whether **40** is conformationally stable (high barrier) or, rather, labile with the atropodiastereomeric equilibrium completely shifted towards that isomer (thermodynamic effect).

2.3. Photochemically Induced Atropisomerization

In a number of cases, photoracemization of enantiomerically enriched biaryl compounds has been observed; the mechanisms suggested vary according to the particular molecular structure.[72–74] For example, 1,1′-binaphthyl (**23**), which is configurationally stable at room temperature (see Figure 5), racemizes readily via the triplet excited state **41** (Figure 10).[73] It has been proposed that, due to the diradical

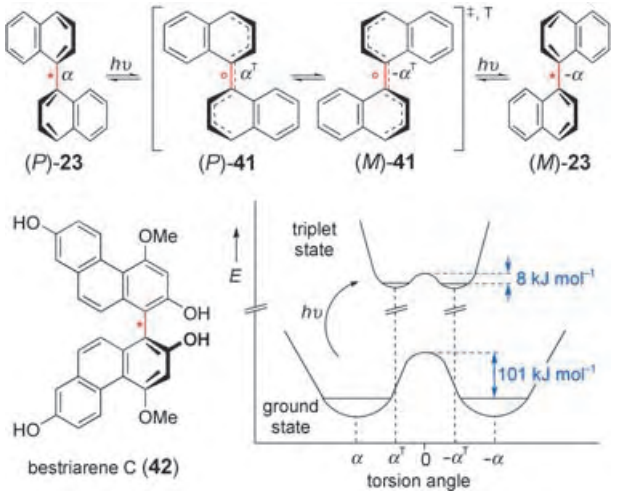


Figure 10. Photoracemization of 1,1′-binaphthyl (**23**) and bestriarene C (**42**).

character of the triplet state, the bond order of the aryl–aryl linkage increases, which causes a flattening of the structure (smaller torsion angle α^T); the electronic stabilization energy thus gained greatly lowers the rotational barrier ($E_{act,triplet} = 8\ kJ\,mol^{-1}$), despite the stronger steric interactions resulting from the shorter biaryl bond. The naturally occurring 1,1′-biphenanthrene, bestriarene C (**42**), undergoes remarkably swift photoracemization:[74] Illumination with a fluorescent lamp leads to a rapid loss of optical purity ($\tau_{295\,K} = 30$ min).

2.4. Chemically Induced Atropisomerization

The chemical conditions may substantially lower the rotational barrier of a biaryl compound if they lead to intermediates that are more prone to atropisomerization. The ubiquitously used chiral auxiliary binol (**29**) is configurationally stable even at elevated temperatures (see Figure 5); no loss of optical purity is observed upon heating at 100 °C for 24 h under neutral conditions.[75] In acidic media (e.g. 1.2 N HCl in dioxane/water), however, **29** racemizes within 24 h at 100 °C (Figure 11).[75] The de-aromatized cationic species **43**,

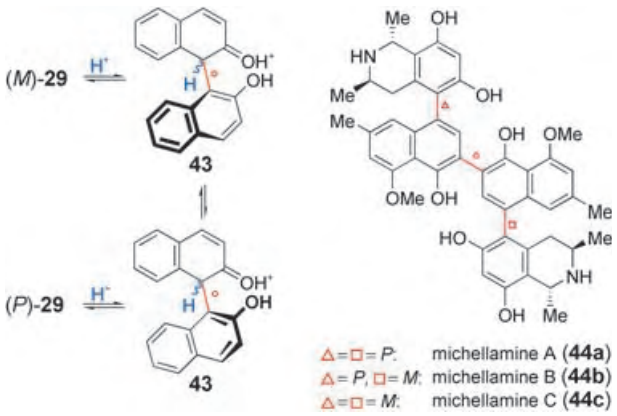


Figure 11. Acid-catalyzed racemization of binol (**29**) via the protonated intermediate **43**; structures of michellamines A–C (**44a–c**).

 © 2005 Wiley-VCH Verlag GmbH & Co. KGaA, Weinheim

which has a $C(sp^3)$–$C(sp^2)$ bond instead of the original biaryl axis, has been proposed as the intermediate that facilitates the racemization. The acid-catalyzed atropodiastereomerization of a binaphthyl-bridged bipyridyl in Scheme 55 is another example.[76,77] Binol (**29**) also racemizes upon heating in a basic environment (e.g. 0.67 N KOH in butanol); its dianionic bisphenolate has been suggested to promote the interconversion (for the electronic effects of donor groups on the rotational barrier, see Figure 6).[75,78] In a similar way, the michellamines A–C (**44a–c**), which possess a central axis that is configurationally unstable and two outer, configurationally stable ones, can be interconverted under basic conditions (0.5 M aq KOH, MeOH, RT, 6 days).[79] This led to the discovery that, in contrast to michellamines A and B (**44a,b**), michellamine C (**44c**), which had initially also been isolated, is not a natural product, but an artifact of the workup conditions.[79,80]

The seven-membered bridged biaryl lactam (*P*)-**45** (Figure 12), although configurationally stable at 140 °C for 7 days, undergoes acid-catalyzed atropisomerization to the

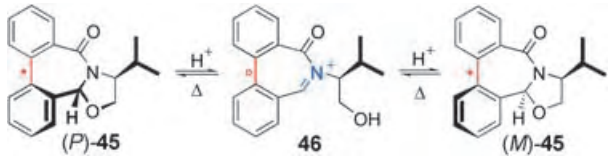


Figure 12. Proton-catalyzed atropodiastereomerization of the seven-membered bridged biaryl amide **45**.

thermodynamically more stable diastereomer (*M*)-**45** (46 % *de*) within 3 days upon addition of a catalytic amount of *p*-toluenesulfonic acid.[81] The acyliminium species **46**, formed reversibly by protonation, facilitates the interconversion due to its more planar structure (all bridging atoms sp^2 hybridized) and, in particular, due to the intermediate destruction of the five-membered oxazolidine ring annellated to the bridge, which rigidifies the biaryl system in **45** (compare also the dioxolane-annellated **37** and **36**, Figure 8).

In some cases, it is the reactivities of the *ortho* substituents themselves that are the origin of unexpectedly low rotational barriers. For example, the enantiomerically pure hydroxy aldehyde (*M*)-**47** (Figure 13), a fourfold *ortho*-substituted biaryl compound and thus anticipated to be configurationally fully stable, still racemizes slowly at room temperature even under neutral conditions ($\Delta G^{\ddagger}_{296\,K} = 99\ kJ\,mol^{-1}$, $\tau_{296\,K} = 6.5$ h).[62,82] Quantum-chemical calculations[83] and experimental work[64,82] show that the formation of the lactol intermediate **48** is the reason for this type of chemically induced atropisomerization. As a biaryl system bridged with a six-membered ring, **48** has a low atropisomerization barrier. A solely physical rotation about the axis can be excluded since the O-protected analogue (*M*)-**49** is configurationally stable.[82] Such a chemically induced atropisomerization process via a lactol-bridged species has been postulated[84] to be the reason for the lack of optical activity in the natural product cynandione A (**50**).[85]

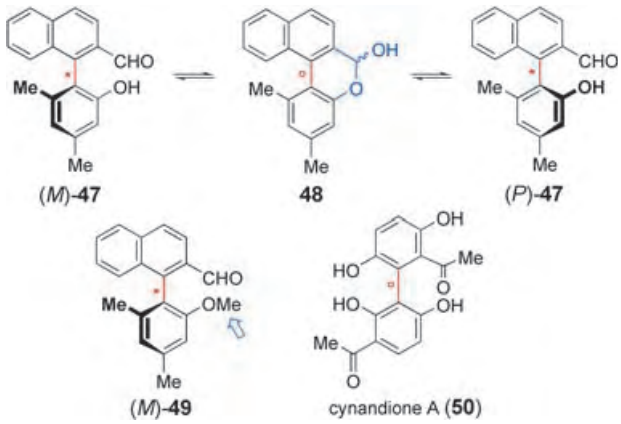


Figure 13. Atropisomerization of the biaryl hydroxyaldehyde **47** via its lactol **48**; structure of the natural product cynandione A (**50**).

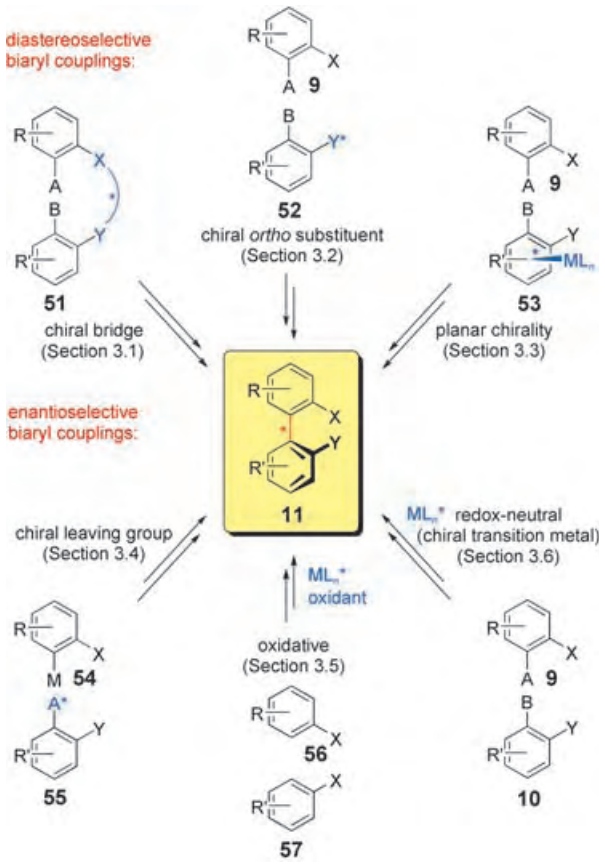
In summary, the occurrence of atropisomerism strongly depends on the temperature, the steric demand of the *ortho* substituents, and the length and rigidity of bridges, be they constitutive or transient. The effects of *meta* and *para* substituents and the chemical mechanism of atropisomerization also have to be taken into account.

3. Biaryls by Asymmetric C–C Coupling

The classic approach to the synthesis of axially chiral biaryl compounds entails a direct, atroposelective aryl–aryl coupling step, that is, the construction of the axis occurs simultaneously with the asymmetric induction. There are several options to introduce the stereochemical information, roughly divisible into diastereo- and enantioselective approaches (Scheme 2). Diastereoselective biaryl couplings have been realized by three different strategies: The simplest involves the incorporation of a chiral bridge (often sourced from the chiral pool) to prelink the two aryl substrates, subsequently permitting a favorable intramolecular reaction (**51**→**11**), as discussed in Section 3.1. Diastereoselective intermolecular coupling reactions can be effected by utilizing arenes that are modified by a chiral auxiliary, normally in one of the *ortho* positions next to the coupling site (as in **9** + **52**→**11**, see Section 3.2), or by using a (tracelessly) removable chiral element, for example, in the form of planar-chiral η^6-chromium complexes or *ansa* compounds (as for **9** + **53**→**11**, see Section 3.3).

An overall enantioselective approach has been achieved by employing a chiral leaving group, as in **55**, which is eliminated in the coupling step (**54** + **55**→**11**, see Section 3.4). An enantioselective biaryl coupling will also result if the stereochemical information is induced through a chiral additive. Both stoichiometric and catalytic oxidative dimerizations have been realized with metal-based reagents (e.g. with Cu) by using chiral ligands, usually amines, to induce the axial configuration (**56** + **57**→**11**, see Section 3.5). Furthermore, based on redox-neutral couplings (**9** + **10**→**11**, for example, Suzuki reactions), enantioselective procedures have

© 2005 Wiley-VCH Verlag GmbH & Co. KGaA, Weinheim



Scheme 2. Basic strategies for the direct, atroposelective construction of biaryl axes.

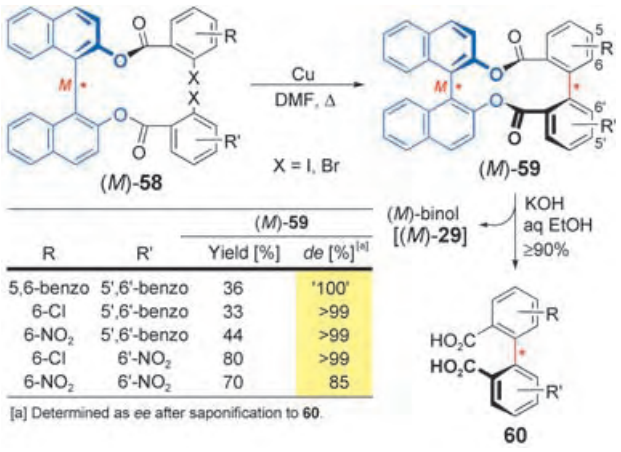
recently been developed, typically employing catalytic quantities of chiral bidentate N,P-ligands (see Section 3.6).

It is important to keep in mind that the construction of a configurationally stable biaryl compound is, by definition, a sterically hindered reaction, which often requires "forcing" conditions to provide the coupled products in reasonable yields. This, on the other hand, can cause a concomitant atropisomerization at the axis, hence leading to diminished atroposelectivities. Thus, care has to be taken that the reaction conditions employed are still mild enough not to interfere with the stereochemical integrity of the biaryl axis.

3.1. Intramolecular Coupling with Chiral Tethers

The coupling of two aryls units, pre-fixed through a chiral bridge, is a popular strategy in asymmetric biaryl synthesis since it provides two clear advantages: good yields for the intramolecular aryl–aryl bond formation, and the possibility to produce both homo- and cross-coupled biaryl compounds. The approaches of this type can be divided into two principal categories: those in which the bridge, or the chiral parts thereof, are part of the intended product, and those in which the tether is an artificial auxiliary (i.e. not part of the final target) that has to be eliminated in the end.

Miyano et al. pioneered this method in the early 1980s by employing diester-bridged systems of type (*M*)-**58** (Scheme 3); these are accessible from (*M*)-binol ((*M*)-**29**) and the corresponding aromatic diacids by twofold (symmetric, R = R′) or sequential (unsymmetric, R ≠ R′) esterification.[86] Ullmann coupling of (*M*)-**58** led to (*M*)-**59** with



R	R′	(*M*)-59 Yield [%]	*de* [%][a]
5,6-benzo	5′,6′-benzo	36	'100'
6-Cl	5′,6′-benzo	33	>99
6-NO_2	5′,6′-benzo	44	>99
6-Cl	6′-NO_2	80	>99
6-NO_2	6′-NO_2	70	85

[a] Determined as ee after saponification to **60**.

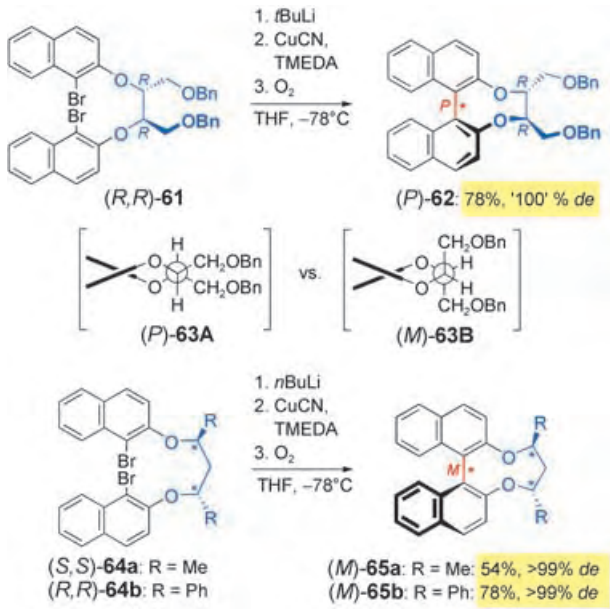
Scheme 3. Atroposelective preparation of the biaryl diacids **60** by Ullmann coupling of the (*M*)-binol-bridged diesters (*M*)-**58**.

excellent stereocontrol (up to "100%" *de*), albeit in low chemical yields if a sterically hindered axis was created. Hydrolysis of (*M*)-**59** afforded the biaryl diacids (*M*)-**60** with recovery of (*M*)-**29**. Further studies on other diester tethers revealed that the rigidity of the binol bridge is crucial to attain high asymmetric inductions.

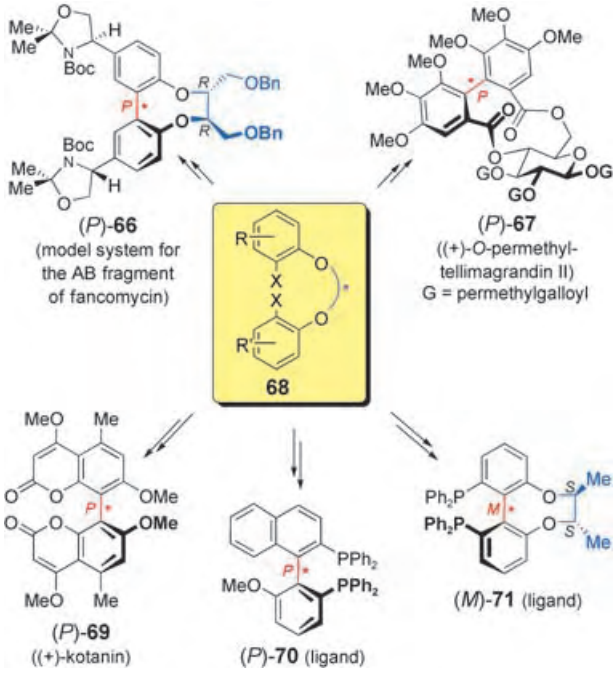
Significant progress was made in this area by Lipshutz et al.,[87] who introduced diether bridges combined with a more efficient coupling method via higher-order cuprates.[88] The best chirality transfers were obtained with C_2-symmetric bridges derived from tartaric acid which bear two stereogenic centers (Scheme 4),[89] as in the reaction of (*R*,*R*)-**61** to give (*P*)-**62** ("100%" *de*). The biaryl 2,2′-diol thus obtained are valuable both as ligands and as precursors to natural products. Sargent and co-workers proposed that the cyanocuprate intermediates preferentially adopt the *gauche* conformation **63A** rather than the diaxial conformation **63B**, thus leading to the observed stereochemical outcome.[90] Sugimura et al. successfully introduced 1,3-diol-derived tethers.[91] For example, the intramolecular coupling reactions of **64** gave (*M*)-**65** in 54% (R = Me) or 78% (R = Ph) yield with > 99% *de*.

This strategy has found application in the (partial) synthesis of natural products (and derivatives)[92–96] and ligands for catalytic asymmetric synthesis;[97–100] some examples are shown in Scheme 5. Lipshutz et al. synthesized (*P*)-**66**,[92] a model system for the AB system of vancomycin (**1**, Figure 1), and *O*-permethyltellimagrandin II ((*P*)-**67**),[96] a member of the ellagitannin family. The natural product kotanin ((*P*)-**69**) was constructed by Lin and co-workers.[93,94] The enantiomerically pure diphosphines (*P*)-**70** and (*M*)-**71**, used as the chiral ligands in catalytic asymmetric hydrogenations, were prepared by Genêt, Marinetti, and co-workers[97,98] and by Chan and co-workers,[99] respectively.

 © 2005 Wiley-VCH Verlag GmbH & Co. KGaA, Weinheim



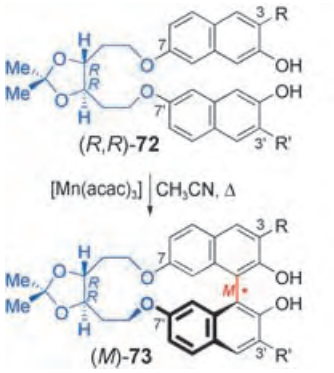
Scheme 4. The use of diether tethers bearing two stereogenic centers in the diastereoselective synthesis of biaryl compounds.



Scheme 5. Use of diethers of the type **68** in the atroposelective synthesis of biaryl ligands and natural products.

The use of 2,2′-linked chiral tethers allows an efficient and versatile preparation of axially chiral biaryl compounds. The asymmetric inductions observed are good to excellent, and, if atropodiastereomeric product mixtures are obtained, these are normally easy to resolve. Both C_2-symmetric and, by sequential etherification, heterocoupled products are obtainable, and although substitution patterns are constrained by the tethering site, a range of valuable products have been synthesized by this method. Drawbacks to this approach are the additional steps required to introduce and remove the tether, in combination with the harsh conditions (e.g. BBr_3) needed to cleave some of the ether bridges. In view of the fact that these are intramolecular coupling reactions, the yields are relatively modest in many cases (generally 50–80%).

Lipshutz and co-workers extended this methodology to 7,7′-bridged 2-naphthols of type (*R*,*R*)-**72** (Scheme 6),[101,102]



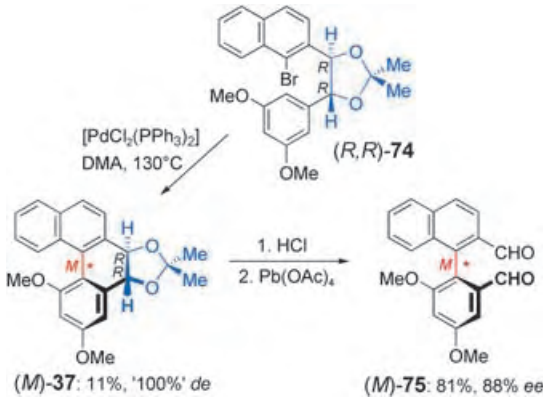
R	R′	Yield [%]	*de* [%]
H[a]	H	>90	85
Ph	H	73	95
Ph	*i*Pr	72	97
Ph	Ph	72	>95
$SiEt_3$	H	69	91

[a] Coupling conditions: CuCl(OH) • TMEDA, O_2.

Scheme 6. Atroposelective synthesis of the binaphthols (*M*)-**73** by using a remote 7,7′-tether.

with the option to prepare unsymmetrical biaryl compounds by sequential etherification. Oxidative biaryl coupling with Mn^{VI} gave the macrocyclic binaphthols (*M*)-**73** in good yields and excellent diastereoselectivities of up to 97%. Furthermore, the chiral bridge of (*M*)-**73** can be used as a linker for polymer attachment. The resulting solid-supported ligands were used successfully in a range of catalytic asymmetric reactions.[103] 2-Amino-2′-hydroxy binaphthyls (so-called "nobin"-ligands) have also been assembled through this route.[104]

Intramolecular coupling reactions of arenes employing an all-carbon chiral bridge have also been undertaken.[66,105] Our group made use of an acetonide-protected diol tether,[66] as in (*R*,*R*)-**74** (Scheme 7); the extra rigidity due to an additional ring annellated to the bridge creates a configurationally stable biaryl axis after coupling, thus compensating for the labilizing effect of the short bridge (compare Figure 8). Although biaryl

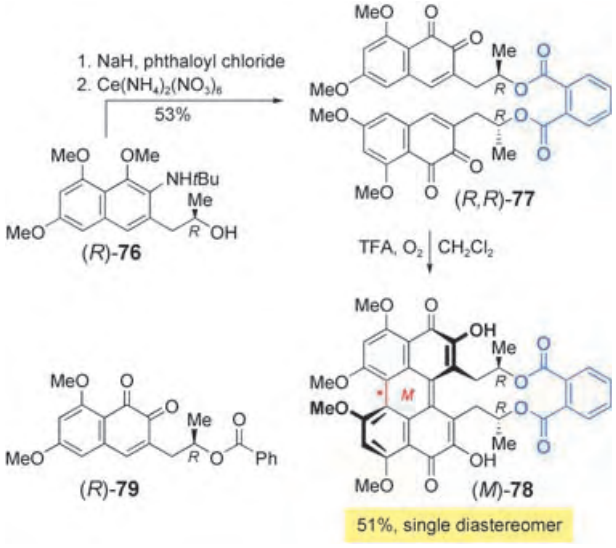


Scheme 7. Atroposelective intramolecular biaryl formation by using the all-carbon-tethered precursor (*R*,*R*)-**74**.

© 2005 Wiley-VCH Verlag GmbH & Co. KGaA, Weinheim

formation occurred with excellent stereocontrol to give (*M*)-**37** as a single diastereomer, the yield of the coupling reaction was low. Another problem was the lack of stereochemical integrity at the axis upon acetal cleavage in (*M*)-**37**, as the intermediate diol is configurationally semistable owing to the central six-membered ring, thus leading to a lower enantiopurity in the ring-opened product (*M*)-**75**.

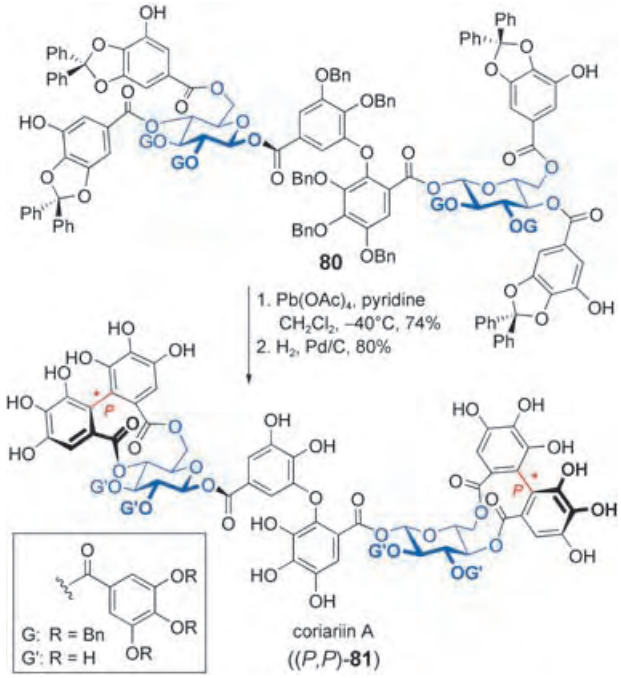
If the target biaryl system itself bears stereogenic centers, the artificial bridge between the two coupling partners does not need to carry stereochemical information. As part of their synthesis of derivatives of calphostine, Merlic et al. bridged the naphthalenes (*R*)-**76** with phthaloyl chloride to give, after oxidation, the bis(*ortho*-naphthoquinone) (*R*,*R*)-**77** (Scheme 8).[106] Oxidative coupling delivered the perylenequinone (*M*)-**78** as a single diastereomer in 51% yield. The additional rigidity induced by the phthaloyl linkage is responsible for the excellent stereocontrol, as evident from the analogous intermolecular coupling of the benzoyl derivative (*R*)-**79**, which proceeded with only 33% *de*.[107]



Scheme 8. Highly atropodiastereoselective intramolecular oxidative coupling in (*R*,*R*)-**77** to give the perylenequinone (*M*)-**78**.

The second large field of application of atropodiastereomeric intramolecular coupling reactions targets biaryl compounds that contain a chiral bridge as a structural element. Although very specialized, this (often biomimetic) approach has been used successfully in the synthesis of several complex natural products.

The ellagitannins are plant secondary metabolites characterized by one or more atropisomeric hexahydroxydiphenoyl moieties attached to a glucopyranose core,[108] which has been postulated to control the axial configuration in the biosynthetic oxidative coupling step.[109] Along these lines, Feldman and co-workers developed a biomimetic synthetic strategy, which, besides validating the theory, has led to the successful preparation of several simplified model biaryl compounds and a number of natural products under virtually complete stereocontrol.[110,111] For example, coriariin A ((*P*,*P*)-**81**),[112] a dimeric ellagitannin with antitumor activity,[113] was synthesized from **80** (74% yield). The stereochemically decisive step was a twofold oxidative biaryl formation, which afforded both axes in a *P*-configured form (Scheme 9).[114]

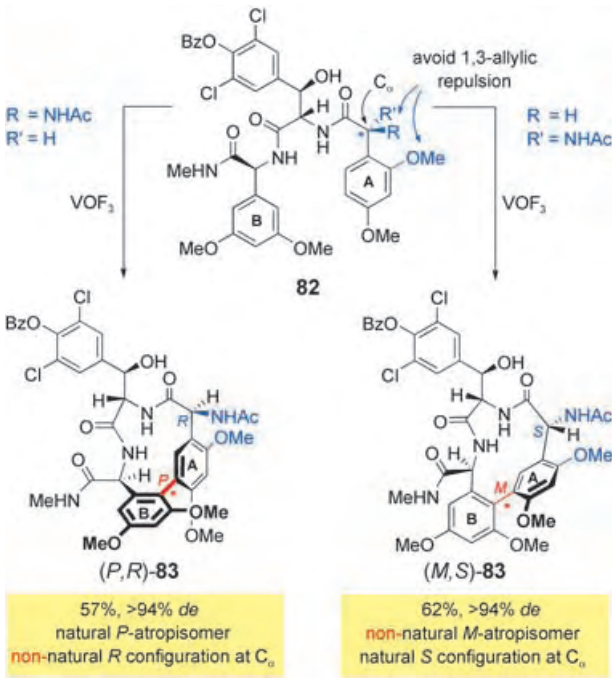


Scheme 9. Total synthesis of the ellagitannin coriariin A ((*P*,*P*)-**81**) through a twofold biomimetic oxidative biaryl coupling.

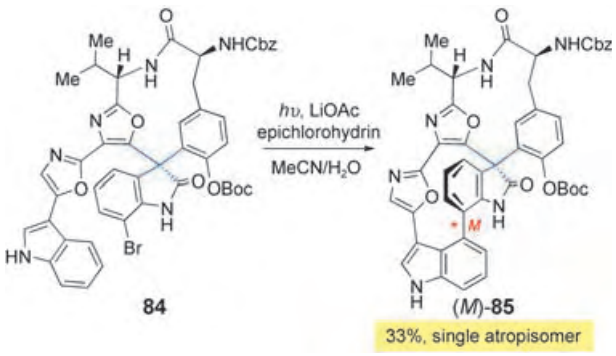
The atroposelective construction of the biarylic AB fragment was one of the major challenges in the total synthesis of vancomycin (**1**) and was successfully achieved by Evans et al.[115,116] In this biomimetic approach, the additional (non-natural) *ortho* methoxy group at the A ring of the tripeptide **82** (Scheme 10), as required to permit an oxidative biaryl coupling, had a strong impact on the asymmetric induction at the biaryl axis formed, as a result of its interaction with stereocenter C_α of the chiral backbone: The epimer (*S*)-**82**, with the natural *S* configuration at C_α (R = H, R′ = NHAc) delivered the non-natural atropodiastereomer (*M*,*S*)-**83** with 94% *de*, whereas the non-natural *R* epimer at C_α, (*R*)-**82** (R = NHAc, R′ = H), gave (*P*,*R*)-**83** with 94% *de* and the naturally occurring *P* configuration at the biaryl axis. It was argued that a *syn*-coplanar conformation of the artificial Ar–OMe bond and the hydrogen atom at C_α is maintained throughout the coupling step, thus avoiding the destabilizing 1,3-allylic repulsion between the larger NHAc group at C_α and Ar-OMe that would occur during formation of the minor atropisomers. For a subsequent "correction" of the wrong axial configuration, see Scheme 57.

More recently, Nicolaou et al. reported the completion of the first total synthesis of the complex, polycyclic secondary metabolite diazonamide A[117,118] (Scheme 11, for an alternative approach, see Scheme 53). Witkop-type[119] photocyclization of the chiral bridged aryl bromide **84** afforded the

 © 2005 Wiley-VCH Verlag GmbH & Co. KGaA, Weinheim



Scheme 10. Joint influence of the non-natural *ortho* methoxy group at the A-ring and the stereocenter at C_α on the configuration at the biaryl axis in the synthesis of the AB fragment of vancomycin (**1**, Figure 1).



Scheme 11. The photocyclization of **84** to give (*M*)-**85** in the synthesis of diazonamide A.

macrocyclic biaryl (*M*)-**85**. Although the yield was modest, (*M*)-**85** was the only atropodiastereomer observed.

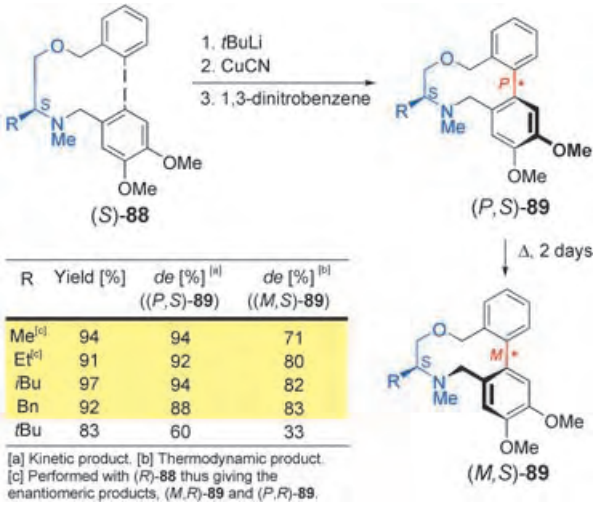
The stegane series of lignans is another family of axially chiral bridged biaryl compounds that can be synthesized atroposelectively through oxidative intramolecular coupling by taking advantage of stereogenic centers present in the bridge,[120] again following the biosynthetic pathway.[121] In a recent example shown in Scheme 12, Waldvogel and co-workers synthesized the lignan (*M*,*S*,*S*)-**87** in 50% yield from the precursor (*S*,*S*)-**86** in the presence of molybdenum pentachloride, with no evidence of formation of the diastereomeric product.[122]

Among the numerous biaryl coupling reactions mentioned in this Review, the only one directed at a diversity-



Scheme 12. Atropodiastereoselective synthesis of the lignan (*M*)-**87**.

oriented atroposelective preparation of a large number of axially chiral biaryl compounds (e.g. for the evaluation of structure–activity relationships in high-throughput assays) was published by Schreiber and co-workers.[123] A highly diverse family of N,O-bridged biaryl compounds **89** was prepared from (*S*)-**88** with good to excellent diastereoselectivities by coupling via higher-order cuprates (a small selection of substances of this library is shown in Scheme 13). The kinetic product (*P*,*S*)-**89** initially obtained gave rise to the other atropodiastereomer (*M*,*S*)-**89** upon heating, often with good *de* values.



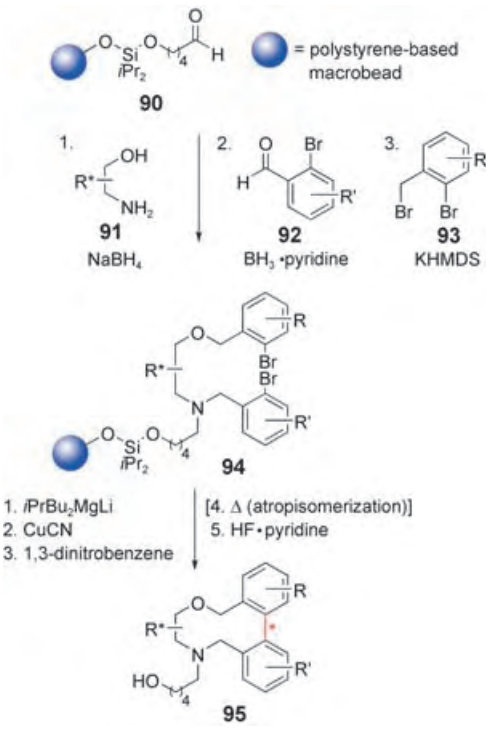
R	Yield [%]	*de* [%] [a] ((*P*,*S*)-**89**)	*de* [%] [b] ((*M*,*S*)-**89**)
Me[c]	94	94	71
Et[c]	91	92	80
*i*Bu	97	94	82
Bn	92	88	83
*t*Bu	83	60	33

[a] Kinetic product. [b] Thermodynamic product. [c] Performed with (*R*)-**88** thus giving the enantiomeric products, (*M*,*R*)-**89** and (*P*,*R*)-**89**.

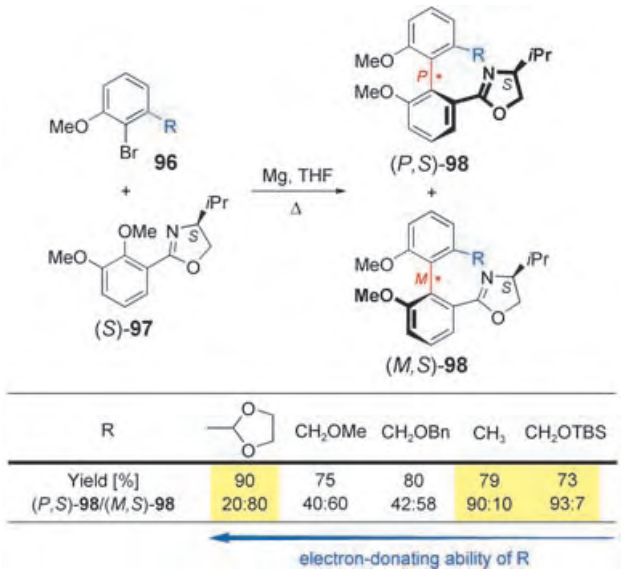
Scheme 13. Synthesis of a family of tethered biaryl compounds **89** with either desired axial configuration.

The method was applied to the polymer-supported synthesis of a library of >400 axially chiral biaryl compounds (Scheme 14). The chiral β-amino alcohols **91** and the two aryl subunits **92** and **93** were attached stepwise to the pregrafted linker **90** to give the polymer-fixed dibromide **94**. Biaryl coupling, optional atropisomerization, and eventual release afforded the compounds **95**. Points of diversity for this library were the substitutions at the biaryl compound (R, R′) and at the tether (R*) and the axial configuration. Biological testing of this archive in phenotype and protein-binding screens was moderately successful.

 © 2005 Wiley-VCH Verlag GmbH & Co. KGaA, Weinheim



Scheme 14. Synthesis of a library of axially chiral biaryl compounds of the type **95** on polystyrene-based macrobeads.



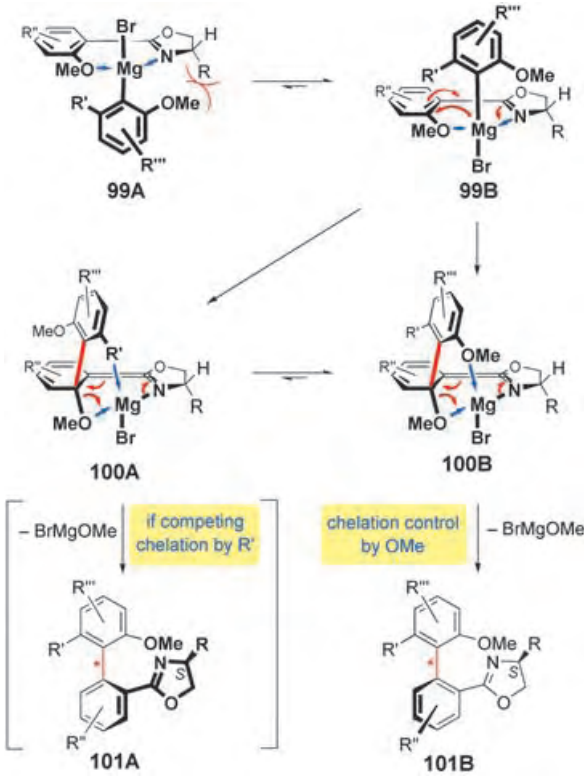
Scheme 15. Synthesis of axially chiral biphenyls **98** by S_N2 Ar reaction of oxazolinylbenzene (*S*)-**97** and influence of the electron-donating properties of the *ortho* substituent R of the aryl Grignard reagent on the asymmetric induction.

3.2. *Intermolecular Coupling with Chiral* ortho *Substituents*

In contrast to intramolecular diastereoselective biaryl coupling reactions, intermolecular variants require only one of the two aromatic moieties to be chemically modified (only by a chiral auxiliary, not by a bridge!), thus allowing a relatively free substitution pattern at the second arene ring. To ensure efficient chirality transfer, the asymmetric information is normally located in one of the *ortho* substituents, that is, close to the coupling site.

The coupling of aryl carboxylic esters that bear a chiral alcohol function should be a convenient access to axially chiral biaryl systems. All such attempts, however, have as yet failed to give atroposelectivities $>50\%$ *de*.[124,125] The major breakthrough in this field came from Meyers and co-workers, who developed an efficient method for the stereoselective construction of axially chiral biaryl compounds by nucleophilic aromatic substitution (S_N2 Ar) of chiral *ortho*-methoxy-(oxazolinyl)arenes with aryl Grignard reagents. The oxazoline moiety carries the chiral information and, additionally, facilitates the nucleophilic attack by stabilizing the developing negative charge.

L-Valinol-derived oxazolines such as (*S*)-**97** (Scheme 15), which are easily prepared from the corresponding benzoic acid, are the chiral coupling partners of choice in most cases.[126–129] Regioselective nucleophilic displacement of the *ortho*-methoxy function in (*S*)-**97** by aryl Grignard reagents (prepared from **96** and magnesium) delivered the tetra-*ortho*-substituted biphenyls **98**. The sense of the asymmetric induction and the levels of atropodiastereoselectivity strongly depend on the relative electron-donating abilities of the two *ortho* substituents of the aryl Grignard reagent.[127,130,131] In general, at least one *ortho* substituent with an accessible free electron pair (most commonly, OMe) is required to ensure a well-defined transition state (see mechanism, Scheme 16). Thus, the biphenyls (*P*,*S*)-**98** were obtained with $>80\%$ *de* if



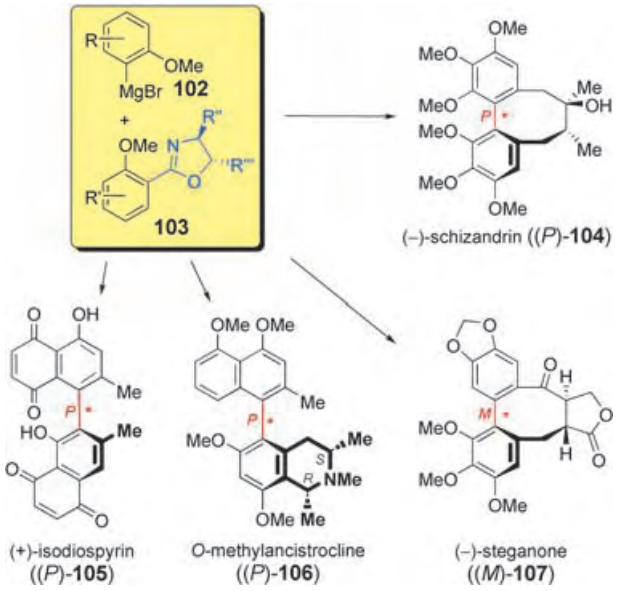
Scheme 16. The stereochemical course of the S_N2 Ar reaction of aryl Grignard reagents on chiral aryl oxazolines.

 © 2005 Wiley-VCH Verlag GmbH & Co. KGaA, Weinheim

the second *ortho* substituent R exhibited no (R = Me) or very low (R = CH_2OTBS) electron-donating abilities. The *M*-configured atropodiastereomer (*M*,*S*)-**98**, however, was preferentially formed (60% *de*) if the electron-donor character of R was superior to that of OMe (e.g. R = 1,3-dioxolan-2-yl). In the case of comparable donating abilities, as for R = CH_2OMe or CH_2OBn, the reactions proceeded with low stereocontrol ($\leq$20% *de*). Steric effects, such as the relative size of R and OMe, are of minor importance, as highlighted by the fact that with R = Me and R = CH_2OTBS the same *M*-configured diastereomers (*M*,*S*)-**98** were obtained, with similar asymmetric inductions.

As a consequence of these experimental observations, the reaction is believed to proceed through an addition–elimination mechanism, with the overall diastereoselectivity determined by both steps (Scheme 16).[127,130] Initially, a chelate complex is formed between the aryl Grignard reagent and the *ortho*-methoxy(oxazolinyl)arene. Of the two possible diastereomeric arrangements, **99B** is strongly favored over **99A**, as the former avoids the steric repulsion of the substituent R of the oxazoline moiety with the *ortho* substituents of the Grignard reagent. Nucleophilic addition in **99B** leads to the aza-enolates **100A** and **100B**. If the substituent R′ does not exhibit significant chelating abilities, complexation of the methoxy group to the magnesium center strongly favors the intermediate **100B**. After elimination of MeOMgBr, the stereochemical alignment of the two aryl moieties thus fixed is transferred into the axially chiral biaryl product **101B**. However, if R′ is also able to act as a chelator to Mg^{II}, the aza-enolates **100A** and **100B** are formed in ratios that reflect the relative donating abilities of R′ and OMe, thus leading preferentially to **101A** or **101B** or mixtures thereof.

This technique was used to produce several axially chiral biaryl natural products and derivatives,[128,132–135] some of which are shown in Scheme 17: (−)-schizandrin ((*P*)-**104**)[128] and (+)-isodiospyrin ((*P*)-**105**)[132] (both the non-natural enantiomers), *O*-methylancistrocline ((*P*)-**106**),[133] and (−)-steganone ((*M*)-**107**).[134]



Scheme 17. Biaryl natural products prepared by nucleophilic aromatic substitution of aryl Grignard reagents **102** on aryl oxazolines of type **103**.

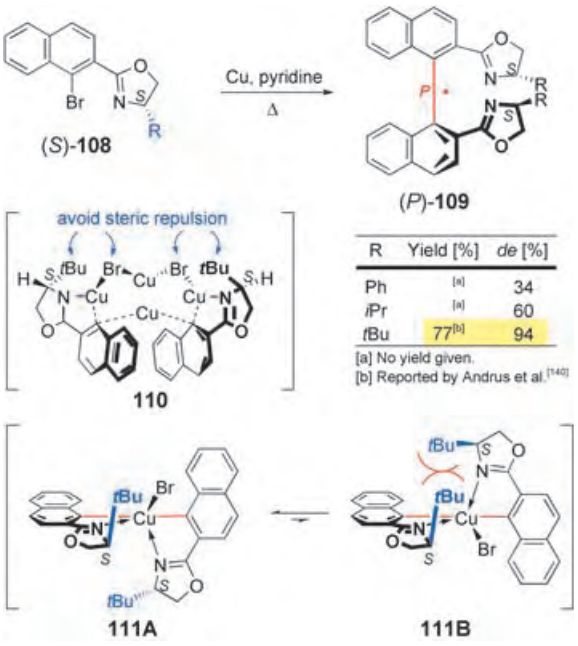
The main advantages of this method, which allows convenient access to cross-coupled (i.e. non-C_2-symmetric biaryl systems), are its simplicity, reliability, and robustness. The chiral oxazoline substituent is easily prepared from the corresponding aromatic acid and the amino alcohol, and can be transformed, after biaryl formation, into a variety of functional groups. Some limitations arise from the use of an aryl Grignard reagent and its structural requirements: To attain high atropodiastereoselectivities, one of the substituents *ortho* to the coupling position (usually OMe) must possess a free electron pair to chelate the magnesium, while the other one must not. However, the substitution pattern of the biaryl products formed, namely an *ortho*-methoxy group and a C_1 unit from the oxazoline in the *ortho′* position, is common to many natural products and so this route has a wide field of application.

Chiral *ortho*-bromo(oxazolinyl)arenes are also suitable starting materials for asymmetric Ullmann homocoupling reactions to give C_2-symmetric biaryl products with high diastereomeric purities. This section deals only with those cases that are known to proceed through a stereoselective aryl–aryl bond-formation step; many homocouplings of sterically less congested phenyls are first-order transformations,[136] that is, the (more or less) racemic biaryl compound initially produced is subsequently resolved by diastereoselective formation of a copper–chelate complex, and are, as such, treated in Section 4.2.4.

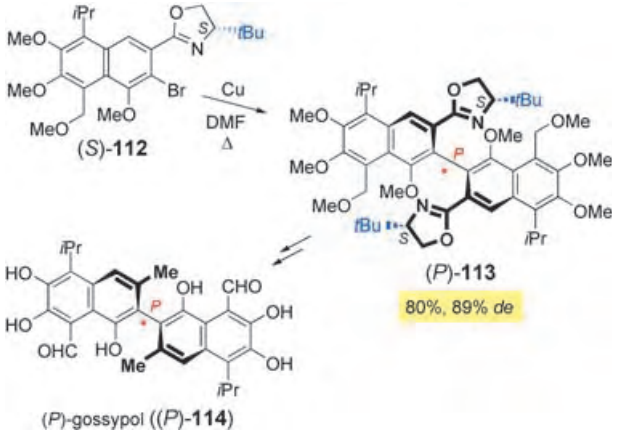
The Ullmann homocoupling of the 1-bromo-2-oxazolinylnaphthalenes (*S*)-**108** gave the binaphthyls (*P*)-**109** with diastereoselectivities that were strongly dependent on the steric demand of the substituent R of the oxazoline moiety;[126,137,138] only with the bulky *t*Bu group was an excellent 94% *de* achieved (Scheme 18).[139] Meyers and Nelson proposed the diaryl cuprates **111** as the stereochemically decisive species.[137,138] Intermediate **111A**, which leads to the observed product (*P*)-**109** by reductive elimination of Cu^I, avoids the steric repulsion between the two *t*Bu groups of the oxazoline portions and is, thus, energetically favored over **111B**. More recently, based on X-ray crystal structures of related aryl–copper species, Andrus et al. suggested an alternative intermediate.[140] It was argued that an eight-membered Cu_4 aggregate of type **110** might be formed, with the two naphthyl rings arranged in a more or less antiparallel fashion. According to this model, the stereoselectivity would be controlled by the steric interactions of the flanking *t*Bu groups with the bridged bromine atoms; intermediate **110**, in which these repulsions are avoided, is energetically favored over the diastereomer with *t*Bu and the bridging Br atom both on the same side (not shown).

The method has found application in the atroposelective synthesis of the cotton-seed-derived natural binaphthyl (*P*)-gossypol ((*P*)-**114**, Scheme 19).[141,142] Treatment of the naphthyl oxazoline (*S*)-**112** with copper in refluxing DMF delivered the biaryl (*P*)-**113** in 80% yield and with a high asymmetric induction of 89% *de*. Further transformation of (*P*)-**113** into the target (*P*)-**114** was straightforward.

 © 2005 Wiley-VCH Verlag GmbH & Co. KGaA, Weinheim



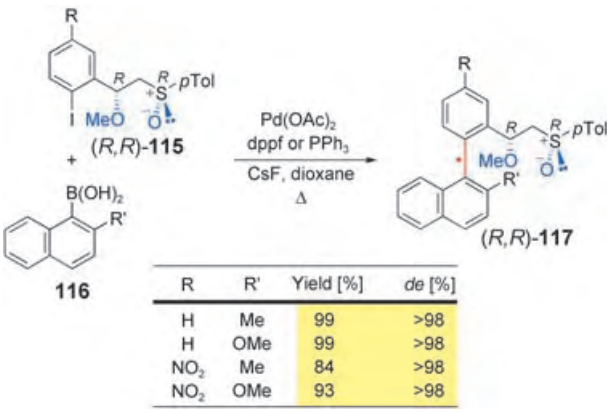
Scheme 18. Asymmetric Ullmann coupling of the 1-bromo-2-oxazolinylnaphthalenes (*S*)-**108** to give (*P*)-**109**.



Scheme 19. Atroposelective synthesis of the natural product (*P*)-gossypol ((*P*)-**114**).

The Ullmann coupling of aryl oxazolines provides efficient access to C_2-symmetric binaphthyls, but a drawback is the high price of the *tert*-leucinol-derived oxazoline required for high stereocontrol. It should be noted again that many examples of Cu-mediated reductive coupling reactions are not based on a stereoselective aryl–aryl bond-formation step, but on a subsequent deracemization of a biaryl species initially produced in a more or less racemic form (see Section 4.2.4).

Apart from these well-investigated cases with oxazolines as the chiral *ortho* substituents,[143] an α-methoxy-β-sulfinyl side chain next to the coupling position was found to be an effective asymmetric inductor in stereoselective Suzuki reactions, as demonstrated by Colobert and co-workers in 2003 (Scheme 20).[144] Coupling of the iodides (*R*,*R*)-**115**,



Scheme 20. The α-methoxy-β-sulfinyl side chain as an effective chiral controller in the atroposelective Suzuki coupling reactions of (*R*,*R*)-**115** with **116**; the absolute configuration of the products (*R*,*R*)-**117** at the biaryl axis is unknown.

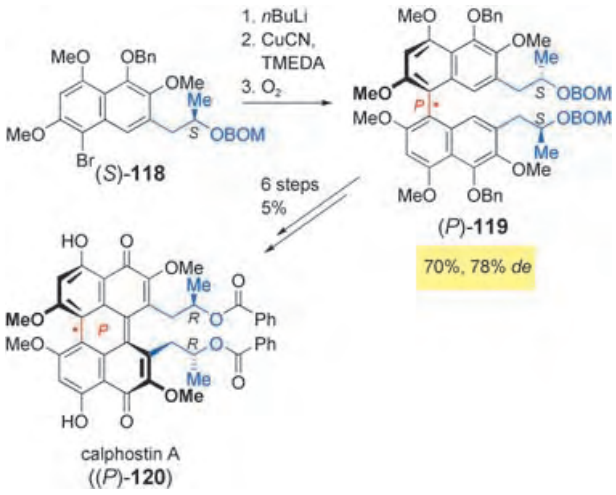
which are accessible in three steps from the corresponding esters, with the boronic acids **116** delivered the biaryl products (*R*,*R*)-**117** (absolute axial configuration unknown) in high to excellent yields (up to 99%) with almost complete asymmetric induction (>98% *de*). Both stereogenic elements in the side chain are required for the high chirality transfer: Removal of the stereocenter at the sulfoxide by oxidation to the sulfone led to diminished atropodiastereoselectivities (70% *de*), while inversion of the configuration of the methoxy-substituted C_α atom failed to give any significant asymmetric induction (10% *de*, "mismatched case"). The "opposite" couplings of phenyl boronic acids with 1-bromo-2-(α-methoxy-β-sulfinyl)naphthalenes were less stereoselective (only up to 70% *de*). Further investigations into the development of efficient procedures for desulfurization and removal of the chiral side chain are necessary to allow an extension of this promising method to the atroposelective synthesis of a wider range of biaryl systems.

Besides the element of axial chirality, many biaryl natural products bear additional stereocenters, which can be used as the chiral controlling units for the atroposelective construction of the biaryl axis. Two examples of such (rather special) approaches with internal asymmetric induction are described below.[145–147]

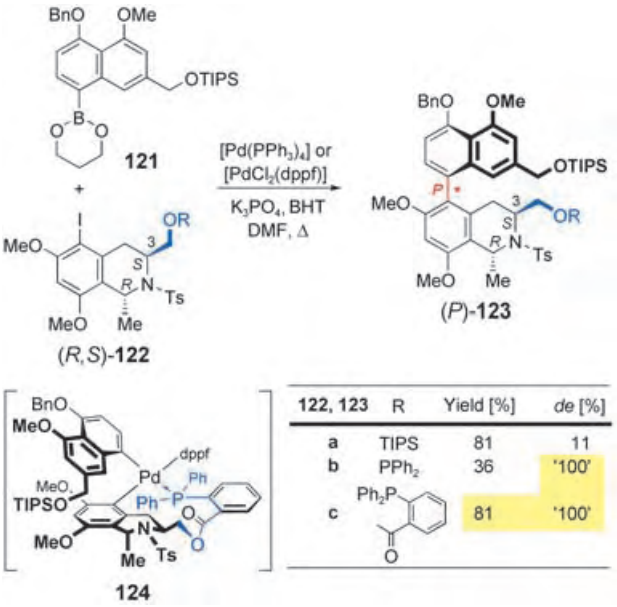
The perylenequinone calphostin A ((*P*)-**120**), a potent protein kinase C inhibitor, contains two chiral β-benzoyloxypropane side chains; this stereochemical information was used in the atroposelective total synthesis of (*P*)-**120** by Coleman et al. (Scheme 21).[145] Oxidative homocoupling of the chiral naphthalene (*S*)-**118** via a higher-order aryl cuprate delivered the binaphthalene (*P*)-**119** in 70% yield. In view of the remote position of the stereocenter, the 78% *de* obtained was remarkable. Transformation of (*P*)-**119** into the target (*P*)-**120** was achieved in six steps.

Most members of the rapidly growing class of naphthylisoquinoline alkaloids (for examples, see Schemes 26, 64, and 67) bear a methyl group at the C3 stereogenic center of the isoquinoline portion. Lipshutz et al. investigated whether an appropriate substituent at this position can induce a good central-to-axial chirality transfer (Scheme 22).[146] Suzuki

 © 2005 Wiley-VCH Verlag GmbH & Co. KGaA, Weinheim



Scheme 21. Atropodiastereoselective synthesis of the perylenequinone calphostin A ((*P*)-**120**).



122, 123	R	Yield [%]	*de* [%]
a	TIPS	81	11
b	PPh_2	36	'100'
c	Ph_2P	81	'100'

Scheme 22. Efficient atropodiastereoselective synthesis of the korupensamine A related naphthylisoquinolines (*P*)-**123b** and **c** by using the chelating properties of a linked PPh_2 unit.

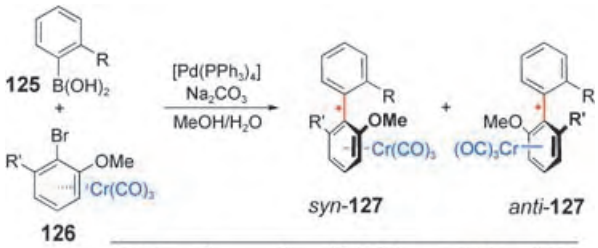
coupling of the naphthyl boronic ester **121** with the OTIPS derivative (*R*,*S*)-**122a** gave the biaryl product (*P*)-**123a** with low selectivity (11% *de*), thus indicating that steric bulk alone is not sufficient for good stereocontrol. The situation changed dramatically when a diphenylphosphanyl group, which can act as an additional binding site for the palladium catalyst, was attached, as in (*R*,*S*)-**122b** and **c**. In both cases, the *P*-configured biaryl compounds (*P*)-**123b** and **c** were obtained exclusively; the benzoic ester linked PPh_2 derivative (*R*,*S*)-**122c** showed an increased redox stability and gave a better yield than the diphenylphosphanyl alkoxide (*R*,*S*)-**122b**. The origin of the nearly complete chirality transfer in the reaction of (*R*,*S*)-**122b** with **121** was explained by formation of the intermediate **124**, in which the chelating PPh_2 group efficiently blocks the bottom face of the palladium atom. The naphthyl moiety is forced into a position above the face of the Pd center, with the bulky OTIPS substituent directed away from the dppf ligand. Reductive elimination of Pd^{II} in **124** should lead to the observed product (*P*)-**123**.

Even though the latter approaches have been developed for the atroposelective synthesis of relatively special target biaryl systems, they clearly demonstrate that remote stereogenic centers can also induce high levels of central-to-axial chirality transfer.

3.3. Intermolecular Coupling with the Element of Planar Chirality

The methods described in the preceding section require the presence of a chiral auxiliary attached to an appropriately modified *ortho* substituent. Thus, a worthwhile strategy would be based on a fixed (but not covalently bound), tracelessly removable stereogenic element. These conditions are fulfilled by planar-chiral transition-metal–arene complexes in which the metal fragment activates the arene by η^6-coordination and, at the same time, serves as a source of chiral information.

This concept was realized by Uemura and co-workers with [(arene)$Cr(CO)_3$] complexes such as **126** (Scheme 23).[22] For



Entry	R	R'	Yield [%]	*syn*-**127**/*anti*-**127**
1	Me	Me	96	'100:0'
2	Me	CH_2OH	77	'100:0'
3	OMe	Me	94	97:3
4	CHO	Me	95	'0:100'
5	CHO	CHO	43	'0:100'
6	OMe	CHO	85	4:96
7	Me	CHO	82	'100:0'

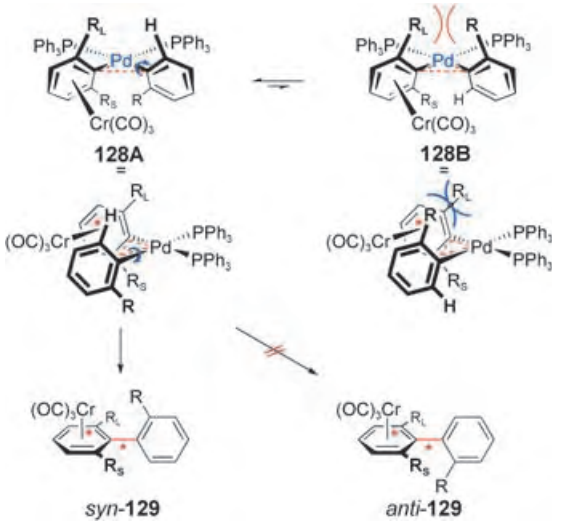
Scheme 23. Highly atropodiastereoselective Suzuki cross-couplings of the phenylboronic acids **125** with the planar-chiral [(arene)$Cr(CO)_3$] complexes **126** (all compounds racemic).

exploratory model reactions these planar-chiral substrates were used in a racemic form. Pd-catalyzed Suzuki coupling of the phenyl boronic acids **125** with **126** delivered the biaryl chromium complexes *syn*-**127** or *anti*-**127** with excellent atropodiastereoselectivities (up to "100% *de*"),[148–151] generally leading to the sterically more congested atropodiastereomer *syn*-**127**, in which the substituent R is directed towards the $Cr(CO)_3$ fragment (Scheme 23, entries 1–3). If an *ortho* carbonyl group is present, the thermodynamically more favored atropodiastereomer *anti*-**127** may also be obtained as the sole product (Scheme 23, entries 4 and 5), probably due to subsequent isomerization at the biaryl axis under the reaction conditions, as the consequence of the lower rotational barrier (see below). There is, however, no clear trend as the analogous reactions of [(*ortho*-formyl arene)$Cr(CO)_3$]

 © 2005 Wiley-VCH Verlag GmbH & Co. KGaA, Weinheim

complexes gave stereochemically inconsistent results (Scheme 23, entries 6 and 7). In general, the electron-withdrawing $Cr(CO)_3$ fragment must be located on the aryl halide portion as it accelerates the oxidative addition to Pd^0.[22,152] The alternative coupling of an aryl halide with a $\{Cr(CO)_3\}$-complexed aryl boronic acid resulted in poor coupling yields. Extension of the method to di-*ortho*-substituted aryl boronic acids and 2-substituted 1-naphthyl boronic acids led, in many cases, to diminished yields and stereoselectivities.[22,149,153]

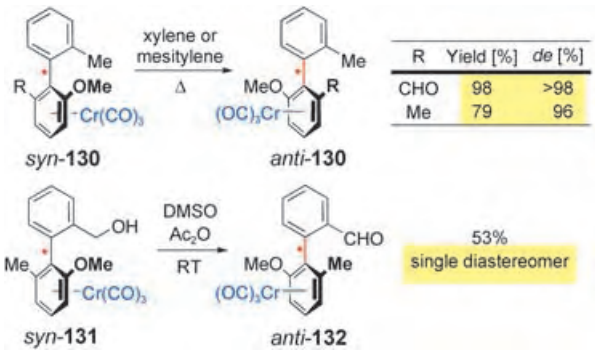
It has been proposed that the initial formation of the thermodynamically less stable *syn* product is caused by steric repulsions in the two relevant diastereomeric *cis*-diorganopalladium intermediates **128A** and **128B** (Scheme 24).[22,149]



Scheme 24. Stereochemical origin of the observed formation of the thermodynamically less stable [(biaryl)$Cr(CO)_3$] complexes *syn*-**129**. The blue arrow indicates the rotation that occurs upon biaryl-bond formation.

In both species, the $\{Cr(CO)_3\}$ fragment is directed towards the other arene moiety thus avoiding severe steric interactions with the bulky PPh_3 ligands, but **128A** is thermodynamically favored due to the weaker steric repulsions between H and R_L relative to those between R and R_L in **128B**. The rate-determining reductive elimination in **128A** leads, under kinetic control, to the chromium biaryl complex *syn*-**129** as the simultaneous rotation around the forming biaryl axis proceeds in a way that minimizes the steric interactions: The H atom is turned "outside" towards the bulky PPh_3 ligand and the substituent R moves "inside" towards the $\{Cr(CO)_3\}$ moiety.

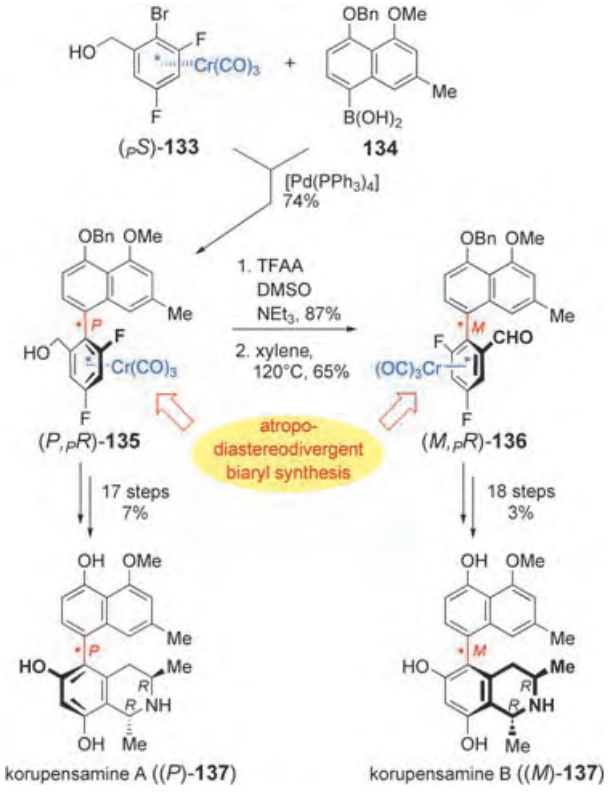
By heating in aromatic solvents, the trisubstituted biaryl compounds *syn*-**130** can be isomerized to give the thermodynamically more stable atropodiastereomers *anti*-**130** (Scheme 25, top).[149,154,155] Similar attempts with naphthalene biaryl chromium complexes resulted in lower conversion rates owing to increased steric bulk restricting rotation around the biaryl axis. Functionalization of one of the *ortho* substituents may also lead to a thermodynamically driven axial rotation, even at room temperature.[149,154,156] This occurs preferentially (but not necessarily)[154] if the steric demand of the substituent



Scheme 25. Atropodiastereomerization of *syn*-**130** to give *anti*-**130** under thermal conditions and axial rotation upon oxidation of *syn*-**131** to give *anti*-**132** (all compounds racemic).

decreases, for example, in the oxidation of the CH_2OH substituent of *syn*-**131** to the respective formyl group of *anti*-**132** (Scheme 25, bottom).

Planar-chiral [(arene)$Cr(CO)_3$] complexes have been used in the atropoenantioselective synthesis of the AB fragment of vancomycin (**1**, for the structure, see Figure 1),[157,158] of the naturally occurring biaryl compounds (−)-steganone ((*M*)-**107**; Scheme 17),[159] and of korupensamines A ((*P*)-**137**) and B ((*M*)-**137**).[160,161] The latter two were prepared in an atropodivergent approach (Scheme 26) from the enantiomerically pure planar-chiral [(arene)$Cr(CO)_3$] complex ($_PS$)-**133**.[160,162,163] Its Suzuki coupling with the naphthyl 1-boronic acid **134** delivered the planar and axially chiral biaryl ($P,_PR$)-



Scheme 26. Atropodivergent synthesis of korupensamines A ((*P*)-**137**) and B ((*M*)-**137**) starting from the enantiomerically pure [(arene)$Cr(CO)_3$] complex ($_PS$)-**133**.

 © 2005 Wiley-VCH Verlag GmbH & Co. KGaA, Weinheim

135 in 74% yield. After oxidation of the CH_2OH group to the aldehyde, the axial configuration can be inverted by thermal diastereomerization to give the *M*-configured biaryl (*M*,$_P$*R*)-**136** in 65% yield. Both biaryl compounds (*P*,$_P$*R*)-**135** and (*M*,$_P$*R*)-**136** were demetalated and used as intermediates in a total synthesis of (*P*)- and (*M*)-**137**.[164,165]

The major advantages of the "[(arene)Cr(CO)$_3$] method" are the high yields and the excellent, in many cases almost complete, stereoselectivities achieved in the aryl–aryl coupling step, and that both atropisomers are, in principle, accessible from a single planar-chiral precursor by thermal axial isomerization. The {Cr(CO)$_3$} fragment can be removed by photooxidative demetalation (*hv*, O_2) with yields between 50 and 90%, depending on the substrate. Besides the toxicity of the chromium compounds, the most problematic limitation is the restricted and laborious access to the enantiomerically pure [(aryl halide)Cr(CO)$_3$] complexes that are crucial for the preparation of stereochemically homogeneous biaryl systems.[166] Furthermore, the otherwise excellent coupling yields and diastereoselectivities decrease with increasing steric hindrance at the coupling sites, thus hampering the atroposelective synthesis of, for example, tetra-*ortho*-substituted biaryl compounds. The range of tolerated substituents is limited; there seems to be no general rule and extensive trials are required to find the respective optimum system. To date, Suzuki couplings of more-sophisticated (and, thus, harder-to-access) [(aryl halide)Cr(CO)$_3$] complexes have not been reported.

An elegant approach without any transition-metal complex was reported by Miyano and co-workers (Scheme 27).[167] Nucleophilic attack of enantiomerically pure dioxocyclophane ($_P$*R*)-**139** by the naphthyl Grignard reagents **140** and **141** with concomitant cleavage of the ansa chain delivered (*P*)-**138** and (*P*)-**142**, respectively, in high yields and *ee* values. The opposite stereoarrays at the biaryl axes of (*P*)-**138** and (*P*)-**142** appear to be a result of the coordination abilities of the *ortho*-methoxy group versus the steric demand of the naphthalene ring.[63]

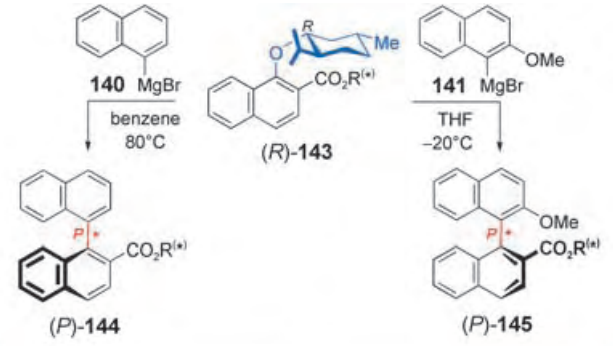


Scheme 27. Atroposelective synthesis of (*P*)-**138** and (*P*)-**142** by Grignard coupling of **140** and **141** with the planar-chiral dioxocyclophane ($_P$*R*)-**139**.[63]

3.4. Intermolecular Coupling with Chiral Leaving Groups

Biaryl synthesis by nucleophilic aromatic substitution (S_NAr) offers the chance to use a chiral leaving group as the source of the asymmetric information. This concept usually provides the advantage of an easy introduction of the chiral auxiliary into the molecule; it is then automatically replaced in the aryl–aryl bond formation, without the necessity of an additional removal step. Furthermore, with the asymmetric information located so close to the reaction center, high levels of chirality transfer should be achievable. This promising and—overall—enantioselective approach has been realized in the coupling of aryl Grignard compounds with chirally modified alkoxy arenes and aryl sulfoxides. As with the related Meyers methodology (see Schemes 15–17),[126,137] an ester (or oxazoline) function *ortho* to the leaving group is necessary to stabilize the intermediate negative charge and to ensure formation of a rigid and stereochemically well-defined transition state.

As early as 1982 Wilson and Cram screened several chiral alcohols for their suitability as chiral leaving groups, but only (*R*)-menthol was found to give satisfactory optical purity and chemical yields in the coupling step.[168] Later, Miyano and coworkers investigated coupling reactions of the alkyl 1-(*R*)-menthoxynaphthalene-2-carboxylates (*R*)-**143** with the naphthyl Grignard reagents **140** and **141**.[169] The binaphthyls (*P*)-**144** and (*P*)-**145** were obtained in high yields with up to 98% *ee* (Scheme 28). The influence of additional stereochemical information in the ester group on the enantioselectivity is inconsistent and negligible (see also beginning of Section 3.2).

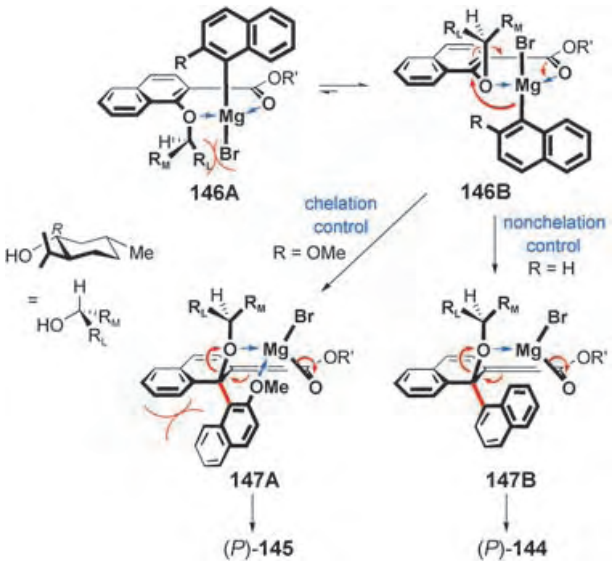


Yield [%]	*ee* [%]	R(*)	Yield [%]	*ee* [%]
95	80	*i*Pr	92	97
93	76	(*R*)-menthyl*	81	98
74	91	(*R*)-phenylethyl*	85	91

Scheme 28. Atropoenantio- or atropodiastereoselective biaryl synthesis by S_NAr on the chirally modified 1-(*R*)-menthoxy naphthalenes (*R*)-**143**.[63]

The two products, (*P*)-**144** and (*P*)-**145**, have opposite axial configurations (despite their identical stereodescriptors),[63] which was explained by chelate versus nonchelate control (Scheme 29):[169,170] Of the two possible chelate complexes **146** formed between the two reactants in the initial step, the diastereomer **146B** is thermodynamically favored over **146A** owing to the asymmetry of the menthol leaving group. Aryl migration in **146B** preferentially leads to the conformer **147A** if a coordinating group, in this case OMe, is present. Its strong intramolecular ligation to the magnesium center overrides the steric repulsion between the two naphthyl moieties. In the absence of a coordinating substitu-

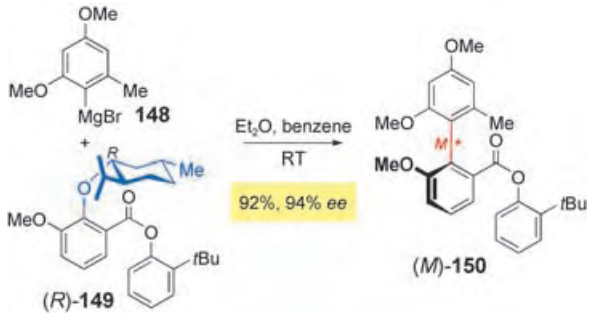
 © 2005 Wiley-VCH Verlag GmbH & Co. KGaA, Weinheim



Scheme 29. Chelation versus nonchelation control in atropoenantioselective biaryl formation through S_NAr reaction with chiral leaving groups.

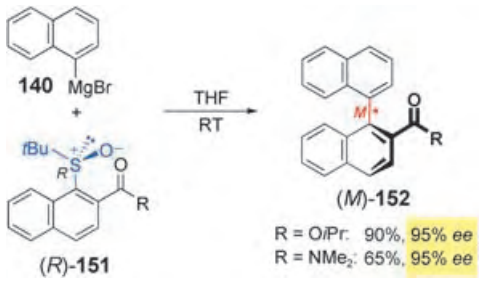
ent (R = H), conformer **147B** is favored, in which the destabilizing steric interactions are minimized. The respective axial twists are conserved into the products (*P*)-**145** and (*P*)-**144**.

In contrast to the formation of binaphthyls, the analogous preparation of biphenyls proved to be more difficult, with tri-*ortho*-substituted examples giving mainly modest atropoenantioselectivities.[171] The reaction of **148** with (*R*)-**149** to afford the tetra-*ortho*-substituted biphenyl (*M*)-**150** did, however, proceed in high chemical yield and optical purity (Scheme 30).



Scheme 30. Highly atropoenantioselective coupling of **148** with the aryl (*R*)-menthylether (*R*)-**149** to give (*M*)-**150**.

Chiral sulfoxides as non-ether-based leaving groups were evaluated by the groups of Baker and Sargent (Scheme 31).[172] Grignard coupling of **140** with the naphthyl 1-sulfoxides (*R*)-**151** delivered the binaphthyls (*M*)-**152** in good to high yields and with excellent stereocontrol (95% *ee*). Nevertheless, this approach is hampered by several disadvantages: No coupling reaction was observed with the sterically more demanding 2-methoxy derivative of **140**, and the preparation of (*R*)-**151** in enantiopure form is rather labor-



Scheme 31. Atropoenantioselective binaphthyl syntheses by using the chiral sulfoxides (*R*)-**151** as starting materials.

intensive. The more easily accessible tolyl analogue of (*R*)-**151**, in which *t*Bu is replaced by *p*Tol, is less suited for this type of biaryl coupling since it racemizes under the reaction conditions, thus leading to diminished atropoenantioselectivities (60–82% *ee*).

Even though the initial investigations were done more than 20 years ago, this approach is still in its infancy. Chiral leaving groups that are more widely applicable and easier to attach chiral leaving groups need to be developed to make this method, which relies on a stoichiometric use of the chiral auxiliary, more flexible and therefore competitive to other Grignard-based biaryl coupling reactions.

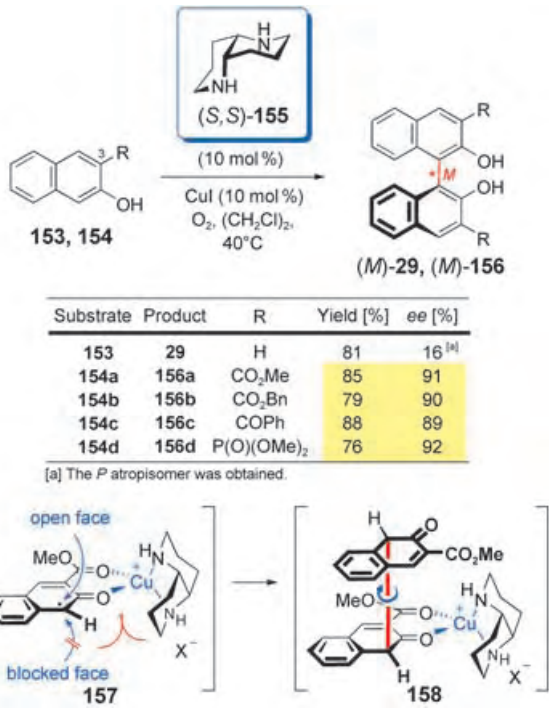
3.5. Oxidative Homocoupling in the Presence of Chiral Additives

The oxidative coupling of phenols is by far the most widespread pathway in the biosynthesis of biaryl natural products; it is also a common laboratory method for the formation of binol (1,1′-dinaphthalene-2,2′-diol) derivatives from the respective 2-naphthols.[173] Owing to the good availability of the "monomeric" substrates, the convenient reaction protocols, and the importance of the products as chiral auxiliaries in asymmetric synthesis, many attempts have been undertaken to translate this chemistry into atroposelective syntheses.

The most widely investigated catalysts to fulfill this goal have been chiral amine–copper salts, mainly due to the ease of ligand screening. It should be noted that the first preparation of highly enantiomerically pure binaphthyls reported by Brussee et al., by the homocoupling of 2-naphthol in the presence of $CuCl_2$ and amphetamine, was shown to be a dynamic kinetic resolution of binol and not the consequence of an atropoenantioselective biaryl coupling step, and will thus be covered in Section 4.2.4.[174]

Highly successful and truly enantioselective oxidative biaryl couplings[175] catalyzed by Cu^I in the presence of a chiral amine were published by Kozlowski and co-workers in 2001,[176–179] with the C_2-symmetric (*S*,*S*)-1,5-diazadecalin (*S*,*S*)-**155** as the ligand and O_2 as the stoichiometric oxidant (Scheme 32). In the presence of CuI and (*S*,*S*)-**155** (10 mol% each), the homocoupling of the 2-naphthol derivatives **154** to give (*M*)-**156** proceeded in good yields with up to 92% *ee*. A coordinating substituent at C3 (carboxylic or phosphonate ester, benzoyl) is crucial to attain high atroposelectivities, as is clear from the low stereocontrol achieved in the preparations

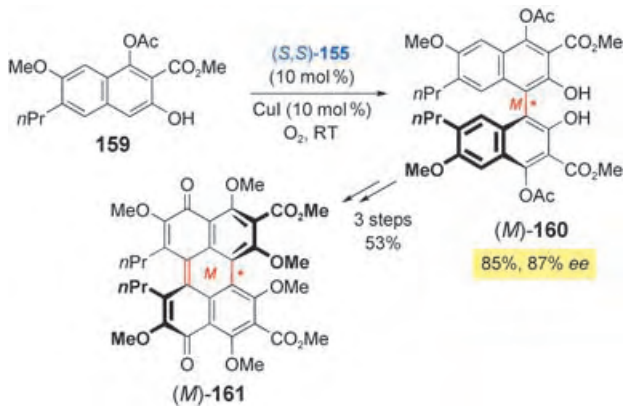
 © 2005 Wiley-VCH Verlag GmbH & Co. KGaA, Weinheim



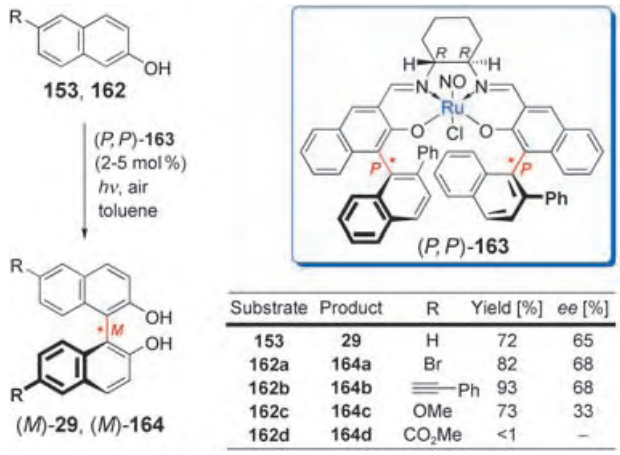
Substrate	Product	R	Yield [%]	*ee* [%]
153	29	H	81	16[a]
154a	156a	CO_2Me	85	91
154b	156b	CO_2Bn	79	90
154c	156c	COPh	88	89
154d	156d	$P(O)(OMe)_2$	76	92

[a] The *P* atropisomer was obtained.

Scheme 32. Cu^{I}-catalyzed oxidative homocoupling of 2-naphthols of type **154** in the presence of the chiral diamine (*S*,*S*)-**155** and O_2.



Scheme 33. Atropoenantioselective preparation of the perylenequinone (*M*)-**161** by using a CuI/(*S*,*S*)-**155**-catalyzed oxidative homocoupling as the stereochemical key step.



Substrate	Product	R	Yield [%]	*ee* [%]
153	29	H	72	65
162a	164a	Br	82	68
162b	164b	≡—Ph	93	68
162c	164c	OMe	73	33
162d	164d	CO_2Me	<1	–

Scheme 34. Oxidative homocoupling of 2-naphthols catalyzed by the $[Ru^{II}(salen)Cl(NO)]$ complex (*P*,*P*)-**163**.

of binol itself (**29**, 16% *ee*). Thus, the stereochemical outcome was rationalized by bidentate coordination of the substrate to the chiral amine–copper complex.[176,180] As exemplified for the homocoupling of **154a**, electron transfer should lead to the formation of the tetrahedral $[Cu^{I}]$ complex **157**, which carries a C-centered radical.[176] The second substrate should approach from the less-hindered top face to give **158** stereoselectively. Tautomerization along with clockwise rotation around the forming biaryl axis should then establish the observed axial configuration.

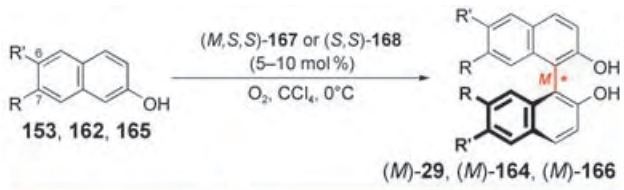
Although the requirement for a suitable substituent at C3 to aid bidentate coordination is an obvious limitation to its scope, this method does provide efficient catalytic enantioselective access to chiral binol derivatives. The synthetic potential of this approach was demonstrated by the enantioselective preparation of the perylenequinone (*M*)-**161** catalyzed by CuI/(*S*,*S*)-**155** (Scheme 33).[181,182]

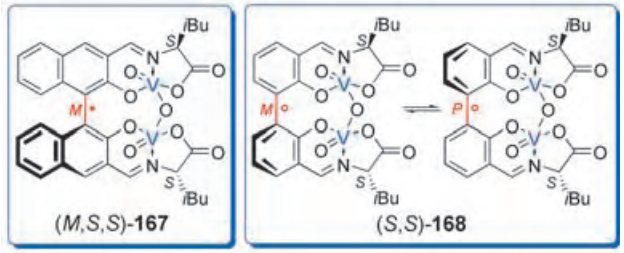
The oxidative homocoupling of 2-naphthols in the presence of ruthenium(II)–salen catalysts (Scheme 34) developed by Katsuki and co-workers involves a single-electron transfer upon irradiation with visible light.[183] (*M*)-Binol ((*M*)-**29**) and its derivatives (*M*)-**164a** and **b** were obtained in reasonable chemical yield and optical purity (65–68% *ee*), whereas a low *ee* value of 33% was found for the methoxy-substituted biaryl (*M*)-**164c**. The ester **162d** failed to give a coupling product. With regard to the structural requirements in the salen catalyst (*P*,*P*)-**163**, changes in the chiral bridge did not significantly affect the stereoselectivity. Substitution of the two axially chiral binaphthyl moieties by simple aryl groups, however, decreased the enantioselectivity considerably, indicating the crucial role of the two binaphthyl units around the metal center for the chirality transfer.

A variety of V^{IV}-based catalysts have also been studied for their application in asymmetric oxidative biaryl couplings.[184,185] Most successful so far have been "dimeric" oxovanadium(IV) complexes of chiral Schiff bases with a biaryl backbone (Scheme 35). With 5 or 10 mol% of (*M*,*S*,*S*)-**167** or (*S*,*S*)-**168** as the chiral catalyst and O_2 as the stoichiometric oxidant, the homocoupling of 2-naphthol (**153**) and its derivatives **162** and **165**, which bear substituents at C6 or C7, proceeded in high yields with excellent stereocontrol (up to 97% *ee*).[184] Intriguingly, the complex (*S*,*S*)-**168**, which contains a configurationally labile biphenyl axis and, thus, may exist as a mixture of (possibly interconverting) diastereomers, is as selective as (*M*,*S*,*S*)-**167** with its configurationally stable *M*-binaphthyl scaffold.

In general, all the oxidative couplings described so far[186] were performed on 2-naphthol-derived substrates to give homodimeric 2,2′-dihydroxy-1,1′-binaphthalenes. The recent development of more-effective catalytic systems resulted, in many cases, in high chemical yields and optical purities with model substrates, but the potential of these methods for application to more-sophisticated substrates remains to be proven, also in terms of a wider tolerance towards functional

 © 2005 Wiley-VCH Verlag GmbH & Co. KGaA, Weinheim



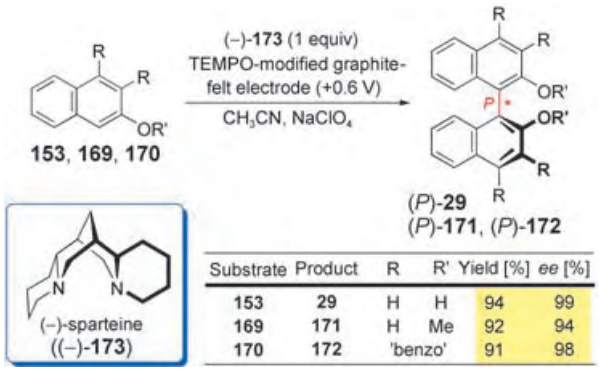


Substrate	Product	R	R'	(M,S,S)-167 Yield [%]	(M,S,S)-167 ee [%]	(S,S)-168 Yield [%]	(S,S)-168 ee [%]
153	29	H	H	95	83	89	89
162a	164a	H	Br	99	88	98	90
165a	166a	OMe	H	88	98	95	95
165b	166b	$OC_{12}H_{25}$	H	91	92	94	97

Scheme 35. Oxidative homocoupling of 2-naphthols catalyzed by the chiral oxovanadium(IV) complexes (*M*,*S*,*S*)-**167** and (*S*,*S*)-**168**.

groups. Despite the limited range, the synthetic importance of the products thus easily accessible may lead to prominent applications of the method to the large-scale production of enantiopure C_2-symmetric binaphthols in the future.

Besides such chemically induced oxidative biaryl couplings of 2-naphthols, there is a single report on an electrochemical variant, utilizing a TEMPO-modified graphite-felt electrode in the presence of a stoichiometric amount of (−)-sparteine ((−)-**173**, Scheme 36), by Osa et al.[187] (*P*)-Binol ((*P*)-**29**) and its derivatives (*P*)-**171** and (*P*)-**172** were obtained in high yields (>90%) and with excellent atropoenantioselectivities (99, 94, and 98% *ee*, respectively). This electro-oxidative method, however, has three disadvantages: 1) It is not catalytic with respect to the chiral auxiliary (−)-**173**; 2) the (+) enantiomer of (−)-**173**, which is necessary to produce the *M* atropoenantiomers, is not commercially available; and 3) the equipment needed is not found in standard synthetic laboratories.



Substrate	Product	R	R'	Yield [%]	ee [%]
153	29	H	H	94	99
169	171	H	Me	92	94
170	172	'benzo'		91	98

Scheme 36. Electrochemical oxidative homocoupling of 2-naphthols in the presence of (−)-sparteine ((−)-**173**).

3.6. Redox-Neutral Cross-Coupling Catalyzed by Chiral Metal Complexes

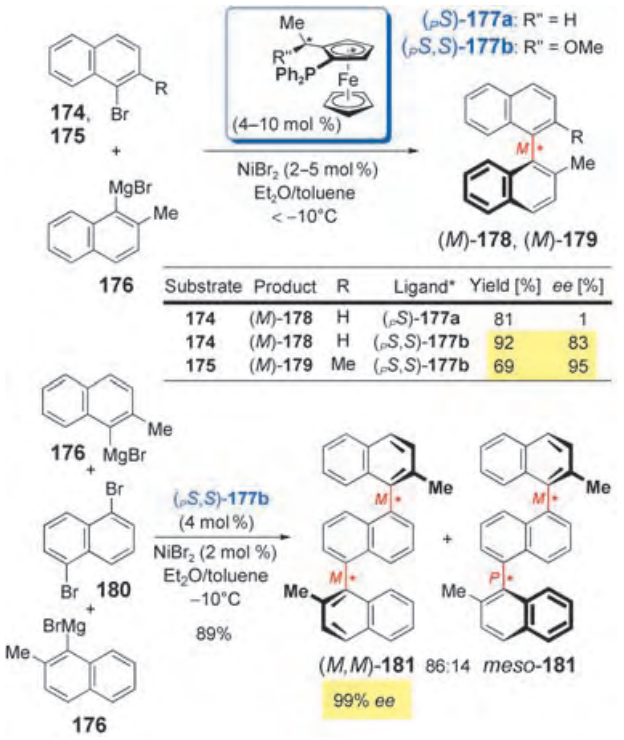
Redox-neutral biaryl couplings, widely used in nonstereoselective biaryl synthesis,[19] provide several benefits: They proceed under relatively mild conditions, they are not restricted to a specific substitution pattern, and they allow regioselective cross-coupling of two different aromatic moieties—in contrast to the homocouplings described in the preceding section. The catalytic enantioselective version offers two additional advantages, making such an approach a nearly ideal method: First, the target biaryls are often accessible with all the substituents required already in place, thus avoiding any subsequent modification, for example, as in the case of diastereoselective coupling procedures with an attached chiral auxiliary. Second, with a chirally modified transition metal as the carrier of asymmetric information, it is one of the few methods that allows the catalytic and, thus, highly economical use of the chiral information. Despite all these favorable premises, there has been, as yet, only limited research activity in the field.

Based on initial investigations by the Kumada group,[188] Hayashi, Ito, and co-workers achieved the first successful atropoenantioselective cross-coupling of aryl halides with aryl Grignard reagents (Kumada cross-coupling).[24,189] The axially chiral binaphthalenes (*M*)-**178** and (*M*)-**179** were obtained in excellent yields and enantiopurities (up to 95% *ee*) from **174** or **175** and **176** in the presence of ≤5 mol% of $NiBr_2$, chirally modified with the ferrocenylphosphine ($_P$*S*,*S*)-**177** (Scheme 37).[162,190,191] This principle was extended to the atroposelective preparation of ternaphthalenes.[192] Cross-coupling of 2 equivalents of **176** with 1,5-dibromonaphthalene (**180**) catalyzed by Ni–($_P$*S*,*S*)-**177b** delivered the desired ternaphthalene (*M*,*M*)-**181** and *meso*-**181** in a 84:16 ratio. The nearly complete stereocontrol (99% *ee*) in the formation of (*M*,*M*)-**181** was interpreted as a result of the twofold asymmetric induction over both cross-coupling steps.[193] The methoxy group in the ligand ($_P$*S*,*S*)-**177b** is crucial for a good chirality transfer (($_P$*S*)-**177a**: 1% *ee* vs. ($_P$*S*,*S*)-**177b**: 83% *ee*). It was postulated that this group functions as a coordination site for the magnesium cation of the incoming Grignard reagent in the transmetalation step, thus creating the required defined stereochemical array (see the Meyers mechanism, Scheme 16).[189]

Due to the very few examples to date of the atropoenantioselective Kumada cross-coupling,[191] an evaluation of the scope and limitation of this method is not yet possible. The use of aryl Grignard reagents, however, makes this approach incompatible with several usual functional groups.

The Suzuki cross-coupling[194] is a most convenient method for the preparation of biaryl compounds as it utilizes aryl boronic acids or esters as the nucleophilic arene species; these are easy to handle (air-stable and storable) and are tolerant of a wide range of other functional groups. On the other hand, the Suzuki coupling normally requires relatively high temperatures and is susceptible to steric hindrance, which hampered its application in asymmetric biaryl synthesis for a long time. Recent solutions to these problems,[195]

 © 2005 Wiley-VCH Verlag GmbH & Co. KGaA, Weinheim

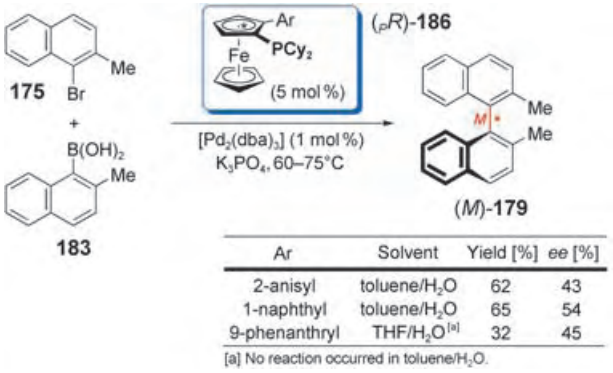


Scheme 37. Nickel-catalyzed atropoenantioselective Kumada cross-coupling of 1-bromonaphthalenes with the 2-methyl-1-naphthyl Grignard reagent **176** in the presence of the chiral ferrocenylphosphine ($_pS$,*S*)-**177b**.

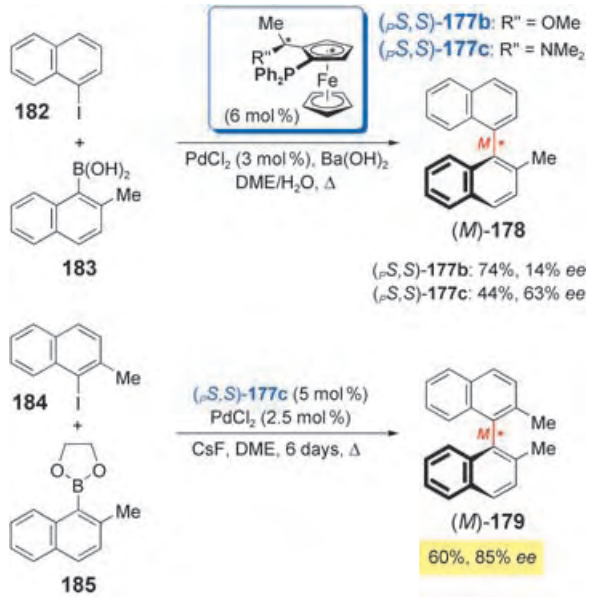
however, triggered exploratory research in asymmetric Suzuki cross-couplings.

First investigations by Cammidge et al. in 2000 used 1-iodonaphthalene (**182**) and 2-methylnaphthalene-1-boronic acid (**183**) as model substrates (Scheme 38) with $PdCl_2$ (3 mol %) modified by the ferrocene-derived bidentate ligands ($_pS$,*S*)-**177** (6 mol %) as the catalytic systems.[196,197] With ($_pS$,*S*)-**177b**, which bears a methoxy substituent, the binaphthyl (*M*)-**178** was obtained in a good yield but with a disappointingly low 14 % *ee*; the P,N-derivative ($_pS$,*S*)-**177c** allowed a reasonably good enantioselectivity (63 % *ee*), albeit compromised by a mediocre chemical yield (44 %). This result is in contrast to the Kumada coupling (see preceding Scheme), in which ($_pS$,*S*)-**177b** was used successfully and ($_pS$,*S*)-**177c** failed to promote the coupling.[197] It was proposed that the stronger donor character of the NMe_2 group is necessary to precoordinate the less basic boronic acid in the same way that the methoxy substituent does with the magnesium cation of the aryl Grignard reagent in the Kumada coupling.[197] Suzuki cross coupling of the sterically more demanding aryl iodide **184** with the cyclic boronic ester **185** delivered the bis-*ortho*-substituted binaphthyl derivative (*M*)-**179** in 60 % yield with a good 85 % *ee*.[196,197]

In the group of Johannsen, the air-stable ferrocenyl-derived monophosphines ($_pR$)-**186** have been utilized as the chiral ligands for the [Pd_2(dba)$_3$]-catalyzed preparation of (*M*)-**179**[198] from **175** and **183** (Scheme 39).[199] Depending on the aryl substituent of ($_pR$)-**186**, selectivities of 43–54 % *ee* were attained.



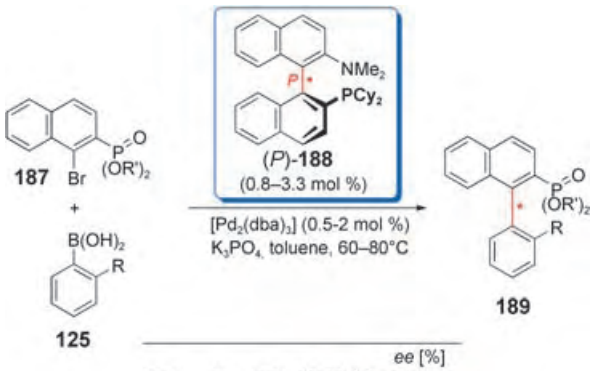
Scheme 39. Asymmetric synthesis of the dinaphthalene (*M*)-**179** in the presence of the planar chiral ferrocenyl monophosphine ($_pR$)-**186**.[198]



Scheme 38. Atropoenantioselective Suzuki couplings with the bidentate ferrocenylphosphines ($_pS$,*S*)-**177** as the chiral ligands.

The most successful[200] asymmetric Suzuki couplings have so far been published by Buchwald and co-workers.[201] Initial screening showed that [Pd_2(dba)$_3$] and the electron-rich biaryl aminophosphine (*P*)-**188** were the catalytic system of choice. As shown by the examples given in Scheme 40, cross-coupling of the naphthyl phosphonate **187** with several phenyl boronic acids **125** delivered the axially chiral biaryls (+)-**189** (absolute configuration not determined) in excellent yields (as high as 98 %) with up to 92 % *ee*. These are the only asymmetric Suzuki couplings reported so far in which a phenyl (instead of a naphthyl) boronic acid was used. The amount of Pd/(*P*)-**188** (ratio 1.2:1) can be lowered to as little as 0.2 mol % without any decrease in the optical purity (Scheme 40, entries 5 and 6). As shown in separate experiments, the phosphonate group is not necessary to achieve the high stereocontrol; it can, however, be converted into a PPh_2 substituent, thus permitting easy access to axially chiral monodentate phosphines.

 © 2005 Wiley-VCH Verlag GmbH & Co. KGaA, Weinheim



Entry	R	OR'	Yield [%]	*ee* [%] (rotation)
1	Me	OEt	98	87 (+)
2	Et	OEt	96	92 (+)
3	*i*Pr	OEt	89	85 (+)
4	Ph	OEt	74	74 (+)
5	Me	OMe	91	84 (+)
6[a]	Me	OMe	95	86 (+)

[a] 0.1 mol % $[Pd_2(dba)_3]$ were used.

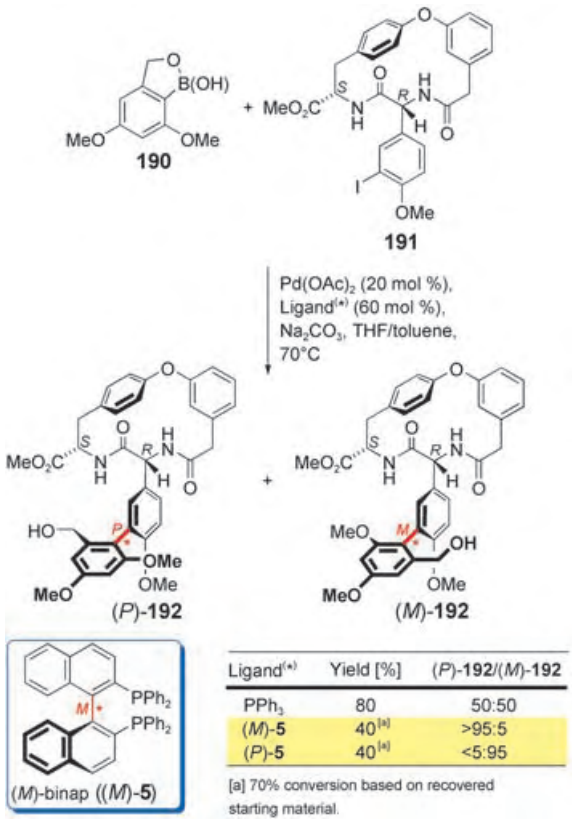
Scheme 40. Selected examples of the asymmetric Suzuki cross-coupling of **187** with different phenyl boronic acids **125** in the presence of the biaryl aminophosphine (*P*)-**188**.

There are very few applications of the asymmetric Suzuki cross-coupling in the directed synthesis of biaryl natural products; one notable example was reported by Nicolaou et al. (Scheme 41).[202,203] In model studies towards the atroposelective synthesis of the biaryl fragment of vancomycin (**1**), the Pd-catalyzed cross-coupling of the iodophenyl **191** and the cyclic boronic acid **190** to give **192** was investigated. Even though **191** is chiral, the two stereogenic centers do not influence the configuration at the biaryl axis in **192**, as is evident from the coupling in the presence of PPh_3 (0% *de*). However, (*M*)-**192** and (*P*)-**192** were obtained with high atroposelectivities (>90% *de*) in the presence of (*M*)-binap ((*M*)-**5**) and (*P*)-binap ((*P*)-**5**), respectively, as the chiral ligands.[204] Although the stereocontrol was excellent, the low chemical yields and the high amount of the chiral ligands used were not satisfactory.

The easy handling of the aryl precursors, the lack of dependence on particular substitution patterns, the relatively mild reaction conditions, and the catalytic nature of the reaction with regard to the chiral ligands all add up to make the asymmetric Suzuki coupling an attractive reaction strategy. However, only recent improvements have allowed its application in stereoselective biaryl synthesis, and there are, as yet, no standard procedures available; each new catalyst and substrate still requires time-consuming optimization of the particular reaction conditions (compare the different reaction conditions used in Schemes 38–41). Furthermore, the applicability of the method is often hampered by very long reaction times (up to 1 week) and the occurrence of hydrodeboronation, which requires excess aryl halide. New, more-effective ligands that deliver good and reliable chemical yields and optical purities under standardized conditions for a broad variety of substrates (including more-sophisticated systems) will have to be designed. The Suzuki cross-coupling could then become one of the most important methods for atroposelective biaryl coupling.

No asymmetric biaryl couplings with other aryl metal species such as aryl zinc (Negishi coupling) or aryl stannanes (Stille coupling) have so far been reported, but there is a single example of the use of a C_{arene}–$C(sp^3)$ cleavage with *ipso* substitution (Scheme 42).[205] Treatment of **193** with 2-(1-naphthyl)-2-propanol (**194**) in the presence of $Pd(OAc)_2$ and (*M*)-binap ((*M*)-**5**) delivered 2-methoxy-1,1′-binaphthalene (**195**) in 83% yield with a moderate 63% *ee* under extrusion of acetone. As this procedure avoids the use of any aryl metal species, it may offer new perspectives for atroposelective biaryl cross-couplings.

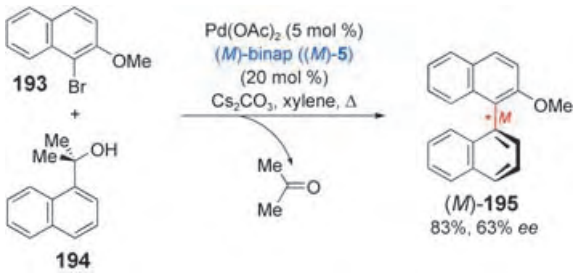
A different, Pd-free approach for the atropoenantioselective preparation of axially chiral biaryl compounds, with aryl lead compounds as the synthetic equivalents of aryl



Ligand[*]	Yield [%]	(*P*)-**192**/(*M*)-**192**
PPh_3	80	50:50
(*M*)-**5**	40[a]	>95:5
(*P*)-**5**	40[a]	<5:95

[a] 70% conversion based on recovered starting material.

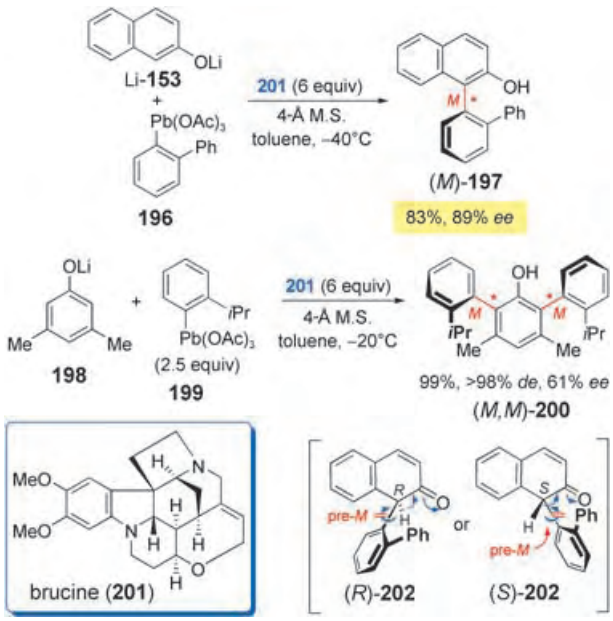
Scheme 41. Model studies towards the atroposelective synthesis of the biaryl fragment of vancomycin (**1**, Figure 1).



Scheme 42. Asymmetric biaryl coupling of **193** with the 2-(1-naphthyl)-2-propanol **194** in the presence of $Pd(OAc)_2$ and (*M*)-binap ((*M*)-**5**).

 © 2005 Wiley-VCH Verlag GmbH & Co. KGaA, Weinheim

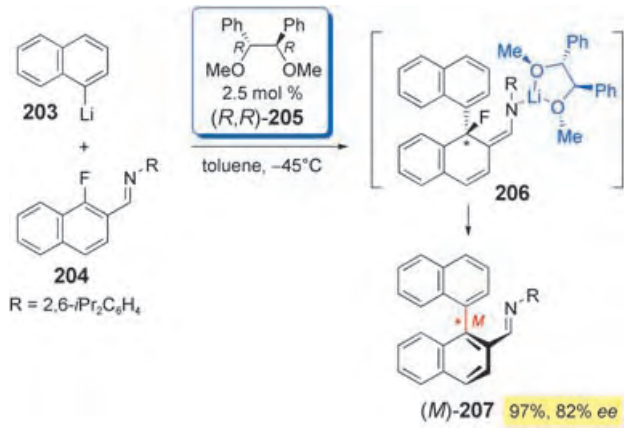
cations and lithiated phenols as the nucleophiles, was presented by Yamamoto and co-workers (Scheme 43).[206] In the presence of excess brucine (**201**) as the chiral auxiliary of choice, cross-coupling of lithiated 2-naphthol (Li-**153**) with



Scheme 43. Asymmetric coupling of aryl lead complexes with lithiated phenols in the presence of brucine (**201**).

the aryl lead **196** furnished the biaryl (*M*)-**197** in 83% yield with 89% *ee*, whereas the analogous reaction with aryl amines as the substrates occurred less stereoselectively, probably due to concomitant autocatalysis of the generated amine. The method was also applied successfully to the synthesis of teraryls. For example, treatment of **198** with **199** (2.5 equiv) in the presence of **201** delivered (*M*,*M*)-**200** in 99% yield with >98% *de* and 61% *ee*.[207] The use of brucine in catalytic amounts gave similar *ee* values but lower chemical yields. The observed selectivity was rationalized by coordination of brucine (**201**) and the phenolate to the lead atom to give, after reductive elimination of $Pb(OAc)_2$, either (*R*)-**202** or (*S*)-**202** as the intermediates, both of which have the correct stereochemical pre-*M* orientation at the future biaryl axis. Fast tautomerization conserves the axial configuration in the product (*M*)-**197**.

Tomioka and co-workers reported an efficient transition-metal-free asymmetric synthesis of biaryl compounds by nucleophilic aromatic substitution; the chiral information is provided by a catalytic amount of the chelating agent (*R*,*R*)-**205** (Scheme 44).[208] 1-Naphthyl lithium (**203**) forms a complex with (*R*,*R*)-**205** that adds stereoselectively to the 1-aryl fluoride **204** bearing an aldimine side chain, to give the postulated intermediate **206**. Elimination of LiF and central-to-axial chirality transfer affords (*M*)-**207**, with concomitant regeneration of the diether (*R*,*R*)-**205**. The reaction was, however, sensitive to small changes in the reaction conditions, and there has been little exploration of the substitution patterns tolerated.



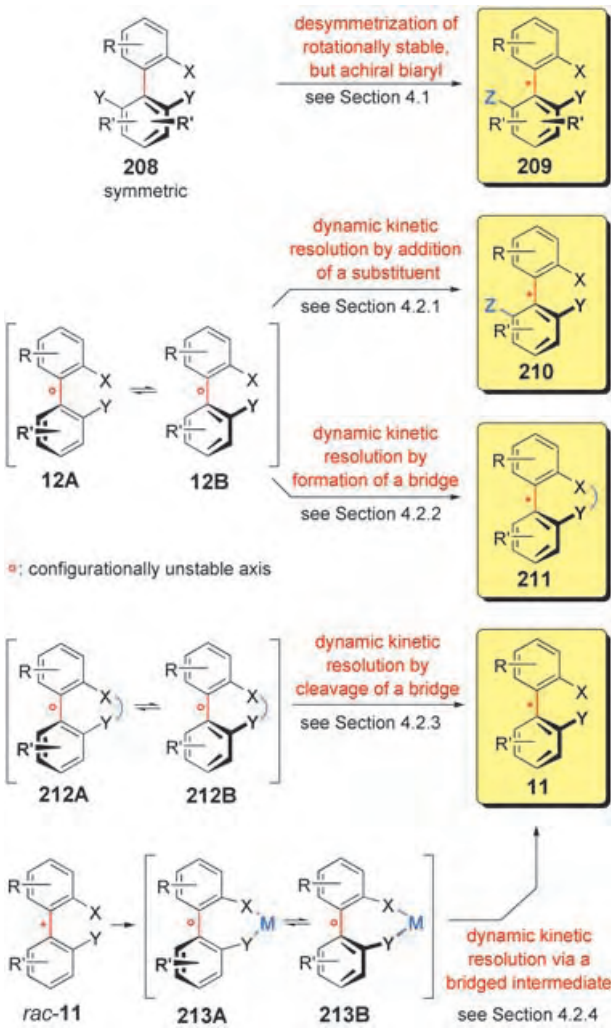
Scheme 44. Asymmetric biaryl synthesis by nucleophilic aromatic substitution with the chiral chelating agent (*R*,*R*)-**205**.

4. Atroposelective Transformations of Prostereogenic Biaryl Compounds

Besides the conventional approach of direct, atroposelective biaryl coupling described in the preceding section, highly efficient alternative strategies have been found in which the construction of the target biaryl species is carried out over two separate steps: a nonstereoselective C–C coupling reaction and a second step that finally establishes the absolute configuration at the biaryl axis. This concept permits an optimization of each of the two steps independently.

For such an introduction of the stereochemical information at a preformed axis, the biaryl substrate has to be either rotationally hindered but achiral or chiral but configurationally unstable. The first criterion is met if (at least) one of the two aromatic portions is constitutionally symmetric, as in **208** (Scheme 45). An enantiotopos-differentiating transformation of one substituent (here Y→Z) will reduce the symmetry and, thus, lead to axially chiral biaryl products of type **209**. Concrete realizations of this approach are discussed in Section 4.1. Nonsymmetric biaryl compounds such as **12** and **212** that are macroscopically achiral owing to rapid atropisomeric interconversion can be used as substrates for dynamic kinetic resolution. One option, though rarely used, is the atropoenantiomer-differentiating introduction of another *ortho* substituent, which establishes and simultaneously "locks" the axial conformation as in **210** (see Section 4.2.1). Alternatively, atropoenantiomer-differentiating bridging of the two aromatic "halves" of **12** delivers axially chiral biaryl species of the type **211** if this process is associated with an increase in the rotational barrier sufficient to reach configurational stability (see Section 4.2.2). Vice versa, the cleavage of a short bridge that causes configurational instability, as in **212 A**⇄**212 B**, allows an elegant access to axially chiral biaryl products (see Section 4.2.3). Moreover, biaryl compounds that are configurationally stable under normal conditions can undergo atropodiastereomerization if transiently bridged by a transition metal; this protocol can be used for the dynamic kinetic resolution of biaryl species that are stereochemically stable under ordinary conditions, for example, *rac*-**11**→(**213 A**⇄**213 B**)→**11** (see Section 4.2.4).

 © 2005 Wiley-VCH Verlag GmbH & Co. KGaA, Weinheim



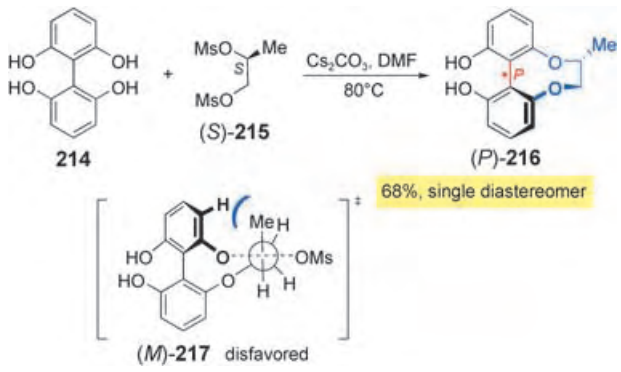
Scheme 45. Concepts for the atroposelective synthesis of biaryl compounds with preformed, but stereochemically not yet undefined biaryl precursors.

Before going into details, it should be noted that these methods, which rely on a separation of the coupling step and the introduction of the stereogenic information, are not necessarily more labor-intensive than the direct asymmetric coupling procedures described in the preceding section. The diastereoselective aryl–aryl bond-formation reactions, for example, necessitate the introduction and removal of a chiral auxiliary, and therefore require at least three steps for the atroposelective construction of a biaryl axis.

4.1. Desymmetrization of Configurationally Stable but Achiral Biaryl Compounds

The transformation of rotationally fixed, but symmetric (and hence achiral) biaryl species into axially chiral products requires a desymmetrization of the arene moiety which can be realized by an atropoenantiotopos or atropodiastereotopos modification of one of its substituents.

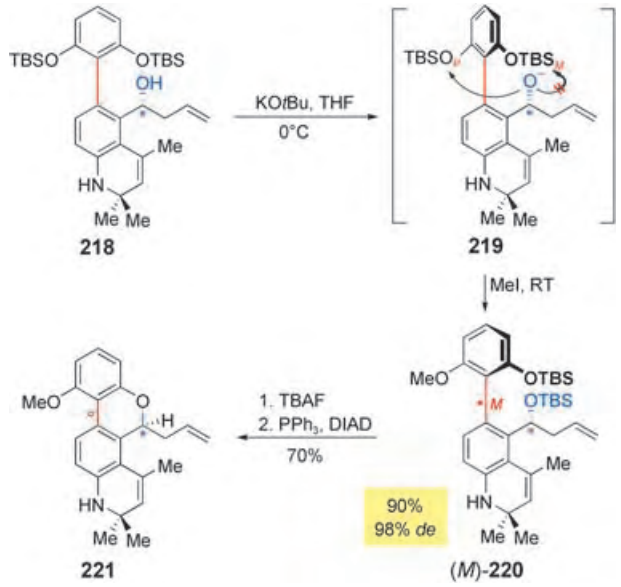
Harada and co-workers even succeeded in breaking the symmetry of the D_{2d}-symmetric tetra-*ortho*-hydroxybiphenyl (**214**) by atropodiastereoselective formation of an eight-membered diether bridge (Scheme 46).[209,210] Upon etherification of **214** with the chiral dimesylate (*S*)-**215**, the biaryl (*P*)-**216** was obtained in a diastereomerically pure form.[211]



Scheme 46. Desymmetrization of **214** by atropodiastereoselective formation of a diether bridge.

The excellent stereocontrol was rationalized to result during the formation of the second ether linkage: Of the two diastereomeric S_N2-type transition states, (*M*)-**217** is disfavored owing to the steric interactions of the methyl substituent with one of the aromatic rings. The method is limited to symmetrically substituted 2,2′,6,6′-tetrahydroxy biaryl compounds, but further modification of the two remaining hydroxy functions in the resulting biaryl diethers is possible[210,211] (e.g. by conversion into the corresponding ditriflates followed by Pd-catalyzed cross-coupling), thus broadening the scope of the method.

As part of the enantioselective synthesis of the antiinflammatory drug candidate A-240610.0 (**221**, Scheme 47), Ku and co-workers discovered an elegant central-to-axial chirality transfer. Upon O-deprotonation to **219**, the axially

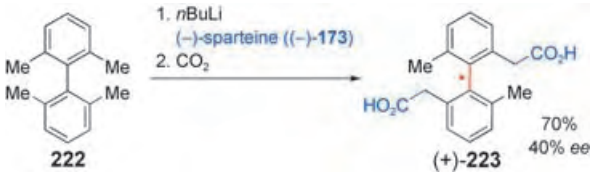


Scheme 47. Desymmetrization of **218** using an internal central-to-axial chirality transfer.

© 2005 Wiley-VCH Verlag GmbH & Co. KGaA, Weinheim

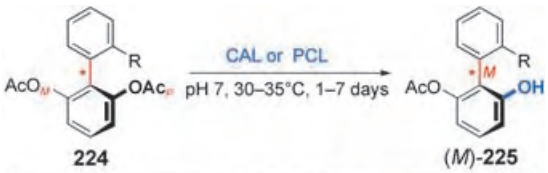
prostereogenic, but centrochiral biaryl **218** underwent an atropodiastereotopos-differentiating migration of the sterically more accessible $OTBS_B$, energetically driven by the formation of a phenolate from an alkoxide, with an excellent 98% *de*.[212] This remarkable reaction was, however, not taken advantage of stereochemically, as the targeted drug candidate **221** does not actually have a configurationally stable biaryl axis owing to the labilizing effect of the ether bridge. Nevertheless, the route via the axially chiral biaryl (*M*)-**220** was necessary to obtain good yields in the final etherification step.[213] Despite its limitation to compounds that bear an α-chiral alcohol substituent in the *ortho* position, the approach allows access to axially chiral biaryl compounds otherwise difficult to prepare.[212]

An enantioselective dilithiation of the "axially pro-prostereogenic" tetra-*ortho*-methylated biphenyl **222** in the presence of the chiral auxiliary (−)-sparteine ((−)-**173**), followed by an electrophilic quench with carbon dioxide, was reported by Raston and co-workers (Scheme 48).[214] The biaryl diacid (+)-**223** was obtained with moderate stereocontrol (40% *ee*).



Scheme 48. Desymmetrization of **222** via enantioselective di-lithiation; the absolute configuration of (+)-**223** is unknown.

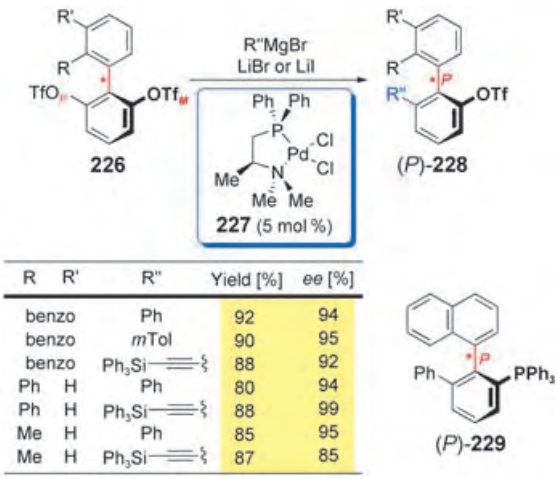
In an approach by Matsumoto et al. in which enzymes are used for the desymmetrization of prochiral biaryl compounds,[215] 2,6-diacetoxy-2′-alkyl biaryls **224** (Scheme 49) were enantioselectively monohydrolyzed at the OAc_P group with *Candida antarctica* lipase (CAL) and *Pseudomonas cepacia* lipase (PCL). The axially chiral 2-acetoxy-6-hydroxy-biaryls (*M*)-**225** were obtained in moderate to high yields (51–94%) and excellent enantioselectivities (≥96% *ee*), even for derivatives bearing small substituents R (e.g. R = Me). In all cases, the *M* atropisomer predominated, for which, however, no stereochemical rationalization was given.



R	Me	Et	CH_2OBn	2,3-benzo
CAL: *ee* [%] (yield [%])	97 (80)	99 (57)	99 (68)	97 (72)
PCL: *ee* [%] (yield [%])	99 (86)	96 (67)	98 (51)	98 (94)

Scheme 49. Desymmetrization of **224** by atropoenantiotopos-differentiating enzymatic O-deacetylation using CAL (*Candida antarctica* lipase) or PCL (*Pseudomonas capacia* lipase).

A remarkable enantiotopos-differentiating cross-coupling reaction was developed by Hayashi and co-workers.[216] Treatment of the achiral 2,6-ditriflates **226** (Scheme 50) with Grignard reagents in the presence of the chiral palladium



R	R′	R″	Yield [%]	*ee* [%]
benzo		Ph	92	94
benzo		*m*Tol	90	95
benzo		Ph_3Si—≡—	88	92
Ph	H	Ph	80	94
Ph	H	Ph_3Si—≡—	88	99
Me	H	Ph	85	95
Me	H	Ph_3Si—≡—	87	85

Scheme 50. Atropoenantiotopos-differentiating desymmetrization of **226** by cross-coupling in the presence of catalytic [$PdCl_2${(*S*)-alaphos}] (**227**).

complex **227** delivered the axially chiral biaryl compounds (*P*)-**228** in good yields and high to excellent enantioselectivities (up to 99% *ee*). The stereochemical origin of the asymmetric inductions observed was not discussed. Even though most cross-couplings were performed with the naphthyl derivative of **226** (R, R′ = benzo), biphenyls with smaller substituents such as R = Me also allowed good stereocontrol. Because bulky Grignard reagents R″MgBr were used exclusively, no statement is possible about the steric size of R″ necessary for attaining high enantioselectivities. The remaining OTf group in the products (*P*)-**228** can be subjected to a second cross-coupling reaction, thus providing access to a wider range of biaryl compounds. The method is of appreciable synthetic potential; it has, for example, been used in the synthesis of the biaryl monophosphine ligand **229**, a catalyst for asymmetric hydrosilylation reactions.

The pioneering work on the desymmetrization of configurationally stable, but achiral biaryl species has led to intriguing novel asymmetric approaches to axially chiral biaryl products. The enantioselectivities have been good to excellent. Still, all these methods lack a broader applicability due to the substitution patterns required in the starting materials and the not yet fully explored tolerance of functional groups and more-sophisticated substrates.

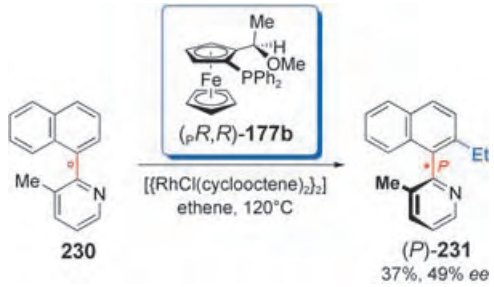
4.2. Atroposelective Conversion of Axially Chiral but Configurationally Unstable Biaryl Compounds

4.2.1. Atropoenantioselective Introduction of Another ortho *Substituent*

The conceptually simplest way to produce chiral biaryl compounds from configurationally labile biaryl species is to

© 2005 Wiley-VCH Verlag GmbH & Co. KGaA, Weinheim

introduce, in an enantiomer-differentiating manner, a further *ortho* substituent, thereby locking the axial configuration. Murai and co-workers reported the atropoenantioselective alkylation of 2-(1-naphthyl)-3-methylpyridine (**230**) through rhodium-catalyzed aryl C–H/olefin coupling (Scheme 51).[217] The yields and enantioselectivities were mediocre with all chiral catalysts screened; the best result (37 % yield, 49 % *ee*) was achieved with the planar- and centro-chiral catalyst (*pR*,*R*)-**177b**.



Scheme 51. Atroposelective *ortho* ethylation of **230**.

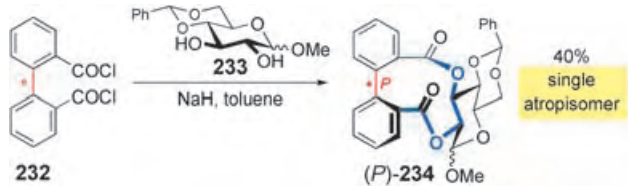
Owing to the aforementioned problems of enantioselectivity and the poor reactivity and regioselectivity, this direct approach has, as yet, been little used.

4.2.2. *Atropodiastereoselective Bridge Formation*

The bridging of *ortho* substituents to give medium to large rings can provide considerable rotational stability relative to the corresponding open-chain system (see **38** and **39**, Figure 9). Therefore, asymmetric syntheses have been envisaged in which the chiral information is introduced by a diastereoselective formation of a bridge, whereby an initially rotationally labile and hence macroscopically achiral biaryl system is "locked" into one of the two possible atropodiastereomeric forms.

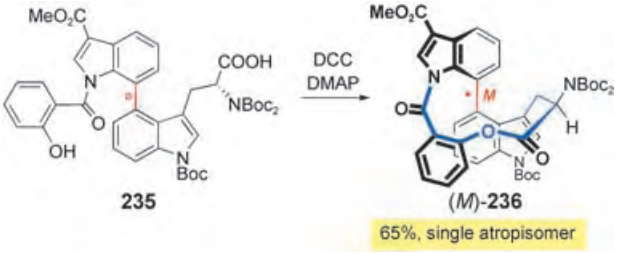
In their studies towards ellagitannin derivatives, Nativi and co-workers found that treatment of racemic, configurationally unstable 2,2′-dibenzoyl dichloride (**232**) with the glycopyranose derivative **233** resulted in the formation of the sugar-bridged biaryl product (*P*)-**234** as a single atropodiastereomer, albeit in low yield (40 %, Scheme 52).[218] The rigid scaffold of **233** was pivotal to ensure efficient resolution, as analogous esterifications of **232** with more flexible rhamnose derivatives led to low *de* values.

As part of their investigations towards the synthesis of the cytotoxic marine natural product diazonamide A, Feldman



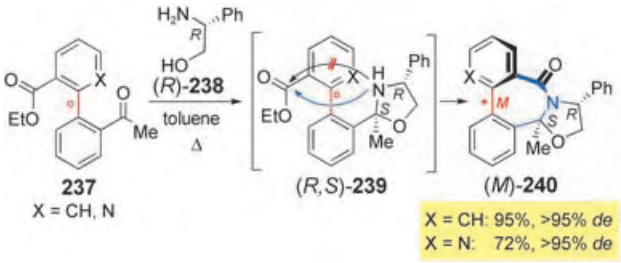
Scheme 52. Dynamic kinetic resolution of 2,2′-dibenzoyl dichloride (**232**) by a glucopyranose-based scaffold.

et al. discovered a noteworthy atropodiastereoselective macrolactonization reaction.[219] Ring closure of the configurationally flexible model bisindole **235** afforded (*M*)-**236** as a single isomer (Scheme 53). The bulk of the $NBoc_2$ group was found to be pivotal for the excellent atropodiastereomeric differentiation; with the sterically less demanding NHBoc substituent, no preferred axial configuration was obtained.



Scheme 53. Atropodiastereoselective synthesis of the diazonamide A model (*M*)-**236** by macrolactonization.

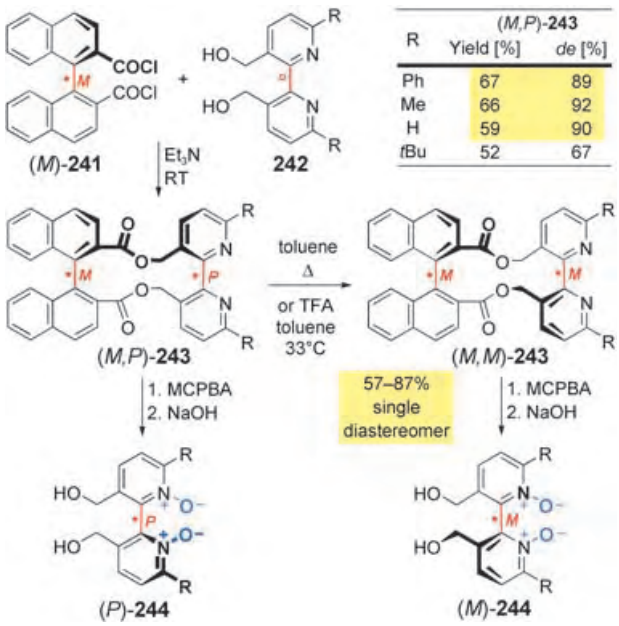
Levacher and co-workers discovered an intriguing dynamic kinetic resolution through the formation of a lactam bridge.[220,221] Thus, configurationally unstable iso- or heterocyclic biaryl compounds **237**, equipped with ester and keto functions in the *ortho* positions, react with (*R*)-phenylglycinol ((*R*)-**238**) to afford the bicyclic lactams (*M*)-**240** with excellent diastereoselectivities (> 95 % *de*; Scheme 54). The axial configuration is dictated by the newly generated N,O-acetal stereocenter in the oxazolidine moiety of the intermediate **239**.[222]



Scheme 54. Atropodiastereoselective synthesis of the biaryl lactams (*M*)-**240**.

An efficient reaction sequence in which the chiral bridge is used temporarily was developed by Hayashi and coworkers.[76] Upon esterification with the dichloride (*M*)-**241** of (*M*)-1,1′-binaphthyl-2,2′-dicarboxylic acid, the configurationally unstable bipyridine diols **242** gave the respective dilactones (*M*,*P*)-**243** with 67–92 % *de* (Scheme 55). These diastereomers constitute the kinetic products, since the axial configuration in the bipyridyl moieties can be completely inverted by thermal equilibration (accelerated considerably by addition of acid)[77] to give the pure atropodiastereomers (*M*,*M*)-**243**, without any decrease in stereochemical purity at the binaphthyl axis. Subsequent N-oxidation of (*M*,*P*)-**243** and (*M*,*M*)-**243** enhanced the rotational barrier at the bipyridine axis so that upon cleavage of the chiral auxiliary,

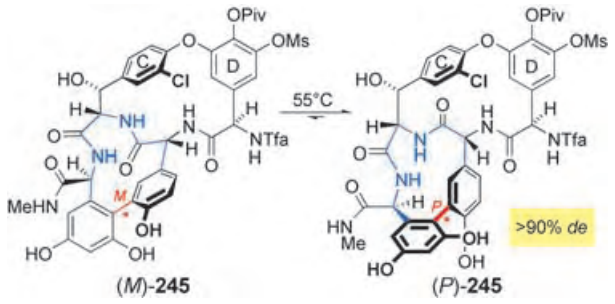
 © 2005 Wiley-VCH Verlag GmbH & Co. KGaA, Weinheim



Scheme 55. Synthesis of the 2,2′-bipyridine *N*,*N*′-dioxides (*P*)-**244** or, optionally, (*M*)-**244**.

the 2,2′-bipyridine *N*,*N*′-dioxides (*P*)-**244** and (*M*)-**244**, respectively, were obtained as configurationally stable products. Therefore, this is one of the very few overall enantiodivergent methods that permit access to either of the two biaryl atropoenantiomers in high purity by using the same chiral auxiliary. The obtained *N*,*N*′-dioxides (*M*)-**244** have been successfully applied as catalysts in enantioselective allylations of aldehydes.

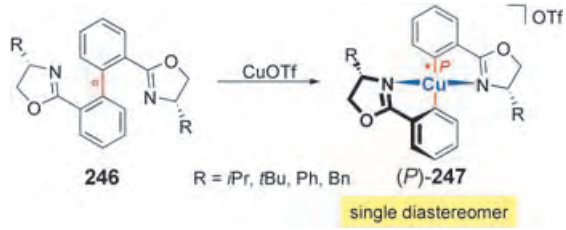
Such a secondary, thermodynamically driven inversion of an initially installed axial configuration was used in the synthesis of the aglycone of vancomycin (**1**, Figure 1) by Evans et al.,[116] as the biaryl axis formed at an earlier stage was of the undesired, non-natural *M* orientation (see Scheme 10). After construction of the planar-chiral CD ring system, the "wrong" axial configuration was elegantly "corrected" through complete axial inversion (Scheme 56): Thermal equilibration of (*M*)-**245** at 55 °C gave the desired natural axial isomer (*P*)-**245** with high diastereoselectivity.



Scheme 56. "Correcting" a "wrong" initial axial configuration by thermodynamic control: inversion of the axial configuration of (*M*)-**245** by thermal equilibration to give the naturally configured diastereomer (*P*)-**245**, a precursor to the vancomycin aglycone.

An alternative approach is the dynamic kinetic resolution of configurationally labile biaryl compounds by locking one of the two possible atropodiastereomeric conformations by chelation with a transition metal. This can be achieved if either the metal is chirally modified by another ligand[223] or if the biaryl substrate itself bears stereogenic centers.

A Cu^{I}-mediated deracemization of biaryl compounds was described by Ikeda and co-workers.[224,225] Upon addition of CuOTf, the 2,2′-bis(2-oxazolinyl)biphenyl derivatives **246**, which are configurationally labile at the axis (e.g., for R = *t*Bu: $\tau_{283\,K} = 0.07$ s), gave the complexes (*P*)-**247** as single diastereomers (Scheme 57). These complexes can be used as catalysts in asymmetric cyclopropanation reactions. The formation of the respective *M* atropisomers (*M*)-**247** is energetically disfavored owing to severe steric interactions between the substituents R (Scheme 69).



Scheme 57. Atropodiastereoselective bridging of the bisoxazoline-substituted biphenyls **246** by CuOTf.

More widely investigated is the dynamic kinetic resolution of configurationally labile biaryl–metal complexes by coordination of a second chiral ligand. This topic was recently reviewed[223] and thus will be dealt with only briefly here.

A classic example of such complexes, as given by Mikami, Noyori, and co-workers in 1999,[226,227] is the ruthenium complex **250** (Scheme 58), which was obtained by treatment



Scheme 58. Control of the axial configuration in the Ru-complex (*P*)-**250**.

of racemic, configurationally labile [$RuCl_2$(biphep)] (*rac*-**248**) with the enantiopure diamine (*S*,*S*)-**249**. Although initially there was no preference for one diastereomer, atropodiastereomerization occurred upon heating to give the thermodynamically more stable complex (*P*)-**250** in a diastereomerically pure form. Compounds of this type have been used as enantioselective hydrogenation catalysts.

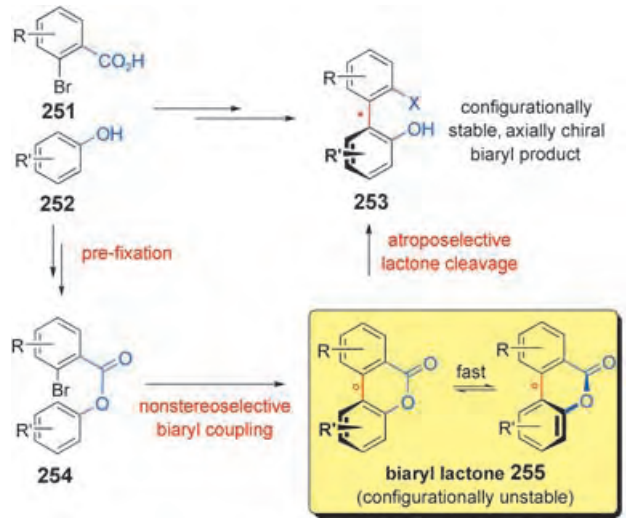
In summary, the bridging of conformationally flexible biaryl compounds can also provide stability in di-*ortho*-substituted biaryl systems at room temperature. An obvious

 © 2005 Wiley-VCH Verlag GmbH & Co. KGaA, Weinheim

synthetic limitation of this approach is that the auxiliary bridge must remain part of the ultimate product, as its cleavage will lead back to a configurationally unstable biaryl compound, unless further transformations are undertaken. Therefore, this strategy has found its main field of application in the synthesis of biaryl natural products (or analogues) that bear appropriate functionality (i.e. a bridge and a controlling stereoelement), but has so far found limited use in general asymmetric biaryl synthesis. The kinetic resolution of biaryl compounds by chelation to a chirally modified metal center allows the application of otherwise achiral ligands in asymmetric catalysis. The approach is normally restricted to the formation and thus use of only one of the two possible atropodiastereomeric complexes—thus excluding the possibility to differentiate between a matched and a mismatched situation for application in asymmetric synthesis. Still, the strategy takes advantage of the well-known benefits of a chiral biaryl backbone in such catalytic systems, whilst avoiding the costly asymmetric synthesis or resolution of rotationally stable biaryl ligands.

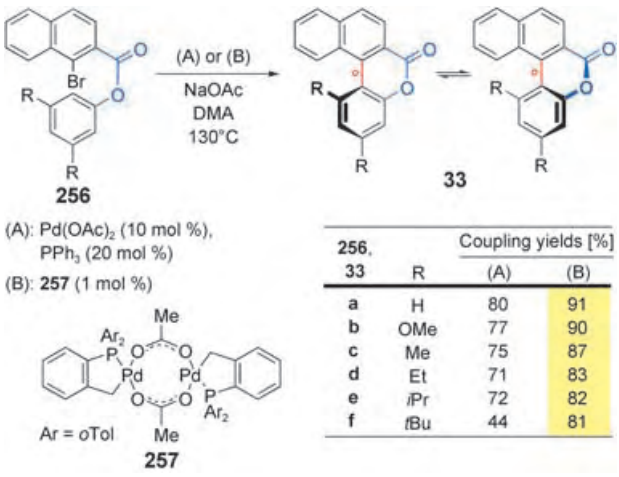
4.2.3. *Stereoselective Cleavage of a Bridge*

Stereochemically labile lactone-bridged biaryls are the key intermediates of a very efficient—and practicable—strategy developed by our group for the asymmetric synthesis of even highly hindered biaryl compounds.[20] As is the case with the other concepts described in this section, this approach separates the aryl–aryl bond formation from the introduction of the stereochemical information at the biaryl axis, thus avoiding a direct asymmetric biaryl-coupling step. The principle of this strategy is depicted in Scheme 59. Initial pre-fixation of *ortho*-bromobenzoic acids **251** and phenols **252** delivers bromoesters **254**, which give the configurationally unstable biaryl lactones **255** by Pd^{II}-catalyzed aryl–aryl coupling. Atropoenantio- or atropodiastereoselective cleavage of the bridge by using a variety of possible chiral nucleophiles establishes the axial configuration at the resulting, now configurationally stable (as it is open-chained) biaryl products **253**.



Scheme 59. The principle of the lactone strategy.

The first crucial step of this approach, the synthesis of the biaryl lactones, is straightforward, as demonstrated for a whole series of model compounds **33** with a variety of steric bulk at the axis (Scheme 60). The easily accessible esters **256**



256, 33	R	Coupling yields [%] (A)	(B)
a	H	80	91
b	OMe	77	90
c	Me	75	87
d	Et	71	83
e	*i*Pr	72	82
f	*t*Bu	44	81

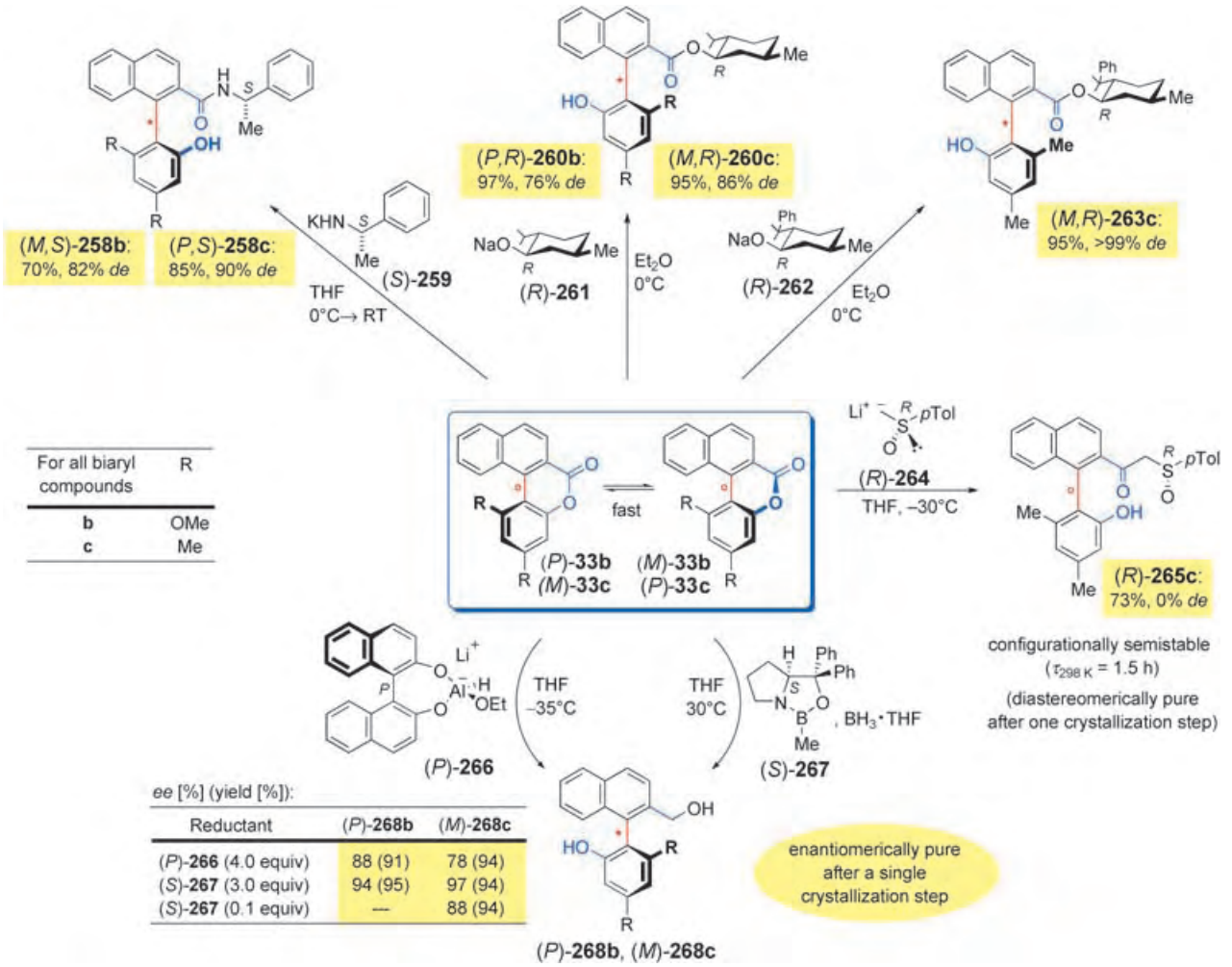
Scheme 60. Preparation of the biaryl lactones **33**.

undergo smooth aryl–aryl cross-coupling in the presence of catalytic amounts of $Pd(OAc)_2$ or the more reactive palladacycle **257**.[61,228] Owing to the favorable pre-fixation of the two aromatic units, the formation of the biaryl bond to form the six-membered ring occurs regioselectively and in high yields (up to 91%), even in cases of severe steric hindrance (for the structures and dynamics of such lactone-bridged biaryl species **33**, see Figure 7). As an example, the sterically severely distorted *t*Bu-substituted lactone **33f** is obtained in excellent yield (81%) with **257** as the catalyst.

The second crucial step requires the atroposelective transformation of the axially prostereogenic lactones **33** into configurationally stable biaryl compounds, which can be achieved simply by cleavage of the bridge with chiral O, N, or H nucleophiles (Scheme 61).[20,229,230] Potassium (*S*)-1-phenylethylamide ((*S*)-**259**) and sodium (*R*)-menthoxide ((*R*)-**261**) were the N and O nucleophiles of choice for the atropodiastereoselective ring opening of **33b** and **33c**, leading to the respective biaryl amides **258** and esters **260** in good yields (70–97%) and diastereoselectivity (74–90% *de*).[231–233] Almost complete control of the configuration at the biaryl axis was attained in the atropodiastereoselective cleavage of **33c** with the sterically more demanding sodium (*R*)-8-phenylmenthoxide ((*R*)-**262**), delivering exclusively the ester (*M*,*R*)-**263c** in 95% yield.[232]

The atropoenantioselective reduction of **33** was successfully accomplished either with (*P*)-binal-H ((*P*)-**266**) or, even better, with borane in the presence of the (*S*)-CBS reagent ((*S*)-**267**).[228,234] The biaryl diols (*P*)-**268b** and (*M*)-**268c** were obtained in high yields (>90%) and with up to 97% *ee*. Even if only catalytic amounts of (*S*)-**267** were used, the stereocontrol was preserved to a large degree (88% *ee* with 0.1 equiv vs. 97% *ee* with 3.0 equiv).[228,234] The size of the *ortho* substituent next to the axis (and the structure of the lactone **33** in general) usually has no influence on the

 © 2005 Wiley-VCH Verlag GmbH & Co. KGaA, Weinheim

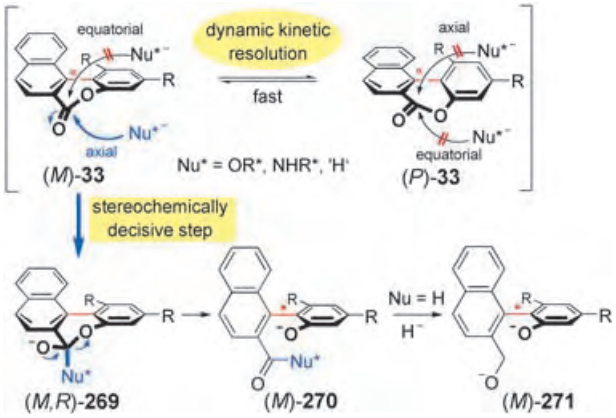


Scheme 61. Atroposelective ring opening of the lactones **33b,c** with chiral N, O, and H nucleophiles.[63]

direction of chirality transfer, making the ring-opening reactions not only efficient with respect to the chemical yields and optical purities, but also reliable with respect to the expected configuration.

No predominant axial configuration was found upon ring cleavage with chiral C nucleophiles.[235] The β-ketosulfoxide (*R*)-**265c**, for example, was obtained as a 1:1 mixture of its atropodiastereomers after treatment of **33c** with (*R*)-**264**. This is apparently not due to a nonstereoselective attack, but the consequence of the low configurational stability of (*R*)-**265c** at the axis. As is the case with most of the known biaryl compounds that bear an *ortho*-hydroxy and an *ortho'*-keto function,[62,64,82,84] (*R*)-**265c** is configurationally semistable at the axis ($\tau_{298\,K} = 1.5$ h; see also Figure 13), and thus rapidly loses any stereochemical information possibly attained in the ring-opening reaction. It can, however, be obtained diastereomerically pure by a single crystallization step.[236]

From a stereochemical point of view, the transformation of the lactones **33** into axially chiral biaryl compounds[20] can be considered as a dynamic kinetic resolution[237] (Scheme 62). The chiral nucleophile selectively attacks only one of the two atropoenantiomers of **33**, say (*M*)-**33**, which is steadily resupplied from the remaining enantiomer (*P*)-**33** through the rapid (*M*)-**33**⇄(*P*)-**33** equilibrium (see Figure 7),[238] thus allowing conversion of the entire racemic material of **33** into a stereochemically homogeneous product of either configuration. For the approach vector of the

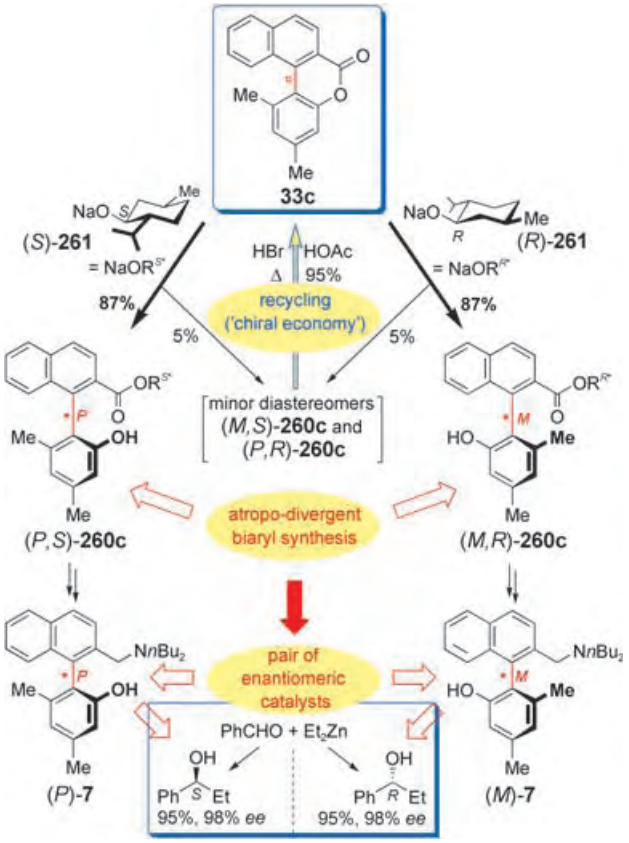


Scheme 62. The assumed mechanistic course of the lactone cleavage with chiral nucleophiles; the stereodescriptors have been arbitrarily given for R = H, alkyl.[63]

 © 2005 Wiley-VCH Verlag GmbH & Co. KGaA, Weinheim

nucleophile, an axial attack is strongly favored over an equatorial one, as predicted by quantum-chemical calculations.[239,240] Consequently, the initial attack of **33** with an ideal chiral N or O nucleophile Nu^{*-} leads to just a single tetrahedral (orthoester-like) intermediate, for example, only to (*M*,*R*)-**269**, which will—more or less irreversibly—burst open to give (*M*)-**270** and, after protonation, lead to the axially chiral biaryl ester or amide. The same pathway, followed by a rapid second hydride transfer to (*M*)-**270** to give (*M*)-**271**, probably also accounts for the atroposelective reduction of the lactones **33** with chiral H nucleophiles.[241]

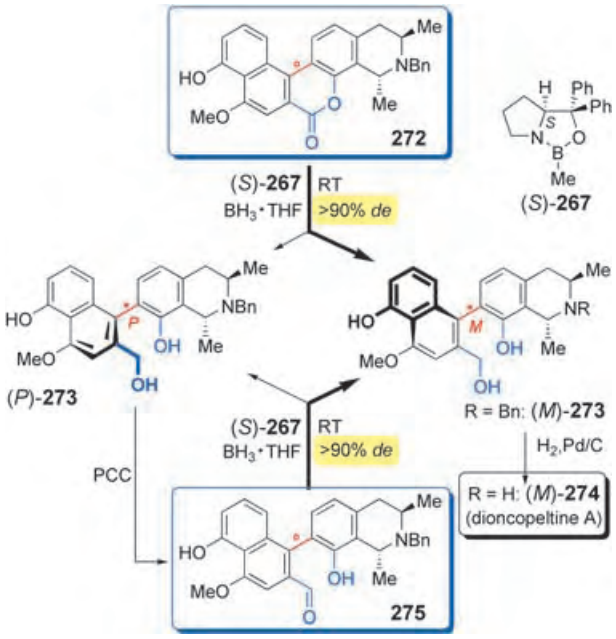
In addition to the versatility and the smooth conditions under which the atroposelective ring opening of **33** can be accomplished, the lactone approach offers another important advantage: the possibility to prepare either of the two atropisomers from the same precursor ("atropodivergence"). This feature is highly attractive in the synthesis of chiral auxiliaries and catalysts, which for a broad applicability of the method should be accessible in both enantiomeric forms. Such a demand is easily met with the lactone method as all the nucleophiles used to cleave the bridge (see Scheme 61) are commercially available in both enantiomeric forms. An example is the atroposelective synthesis of the biaryl amino alcohols (*P*)-**7** and (*M*)-**7** (Scheme 63), which have been demonstrated to be efficient catalysts for the enantioselective addition of diethylzinc to aldehydes (up to 98% *ee*).[17] In the key step, ring opening of **33c** with sodium (*S*)-menthoxide



Scheme 63. Two further advantages of the lactone method: atropodivergence and "chiral economy", illustrated in the directed synthesis of (*P*)-**7** or (*M*)-**7**.

((*S*)-**261**) delivered the ester (*P*,*S*)-**260c** in 87% yield, while the analogous reaction with the enantiomeric reagent (*R*)-**261** gave (*M*,*R*)-**260c**.[232] Furthermore, the minor product diastereomers, (*M*,*S*)-**260c** and (*P*,*R*)-**260c**, also obtained in the alcoholysis of **33c**, are not wasted, but can be easily recycled by acid-catalyzed recyclization back to the lactone.[242] Though not always required, this is a worthwhile option allowing economical use of precious material, for example, in multistep natural product syntheses.

The concept presented here is not restricted to six-membered biaryl lactones, but can be extended to other configurationally labile biaryl by the permanent or transient existence of short bridges, such as *ortho*-hydroxy-*ortho*′-aldehydes. An example is the naphthylisoquinoline **275** (Scheme 64). As discussed in Section 2 (Figure 13), these

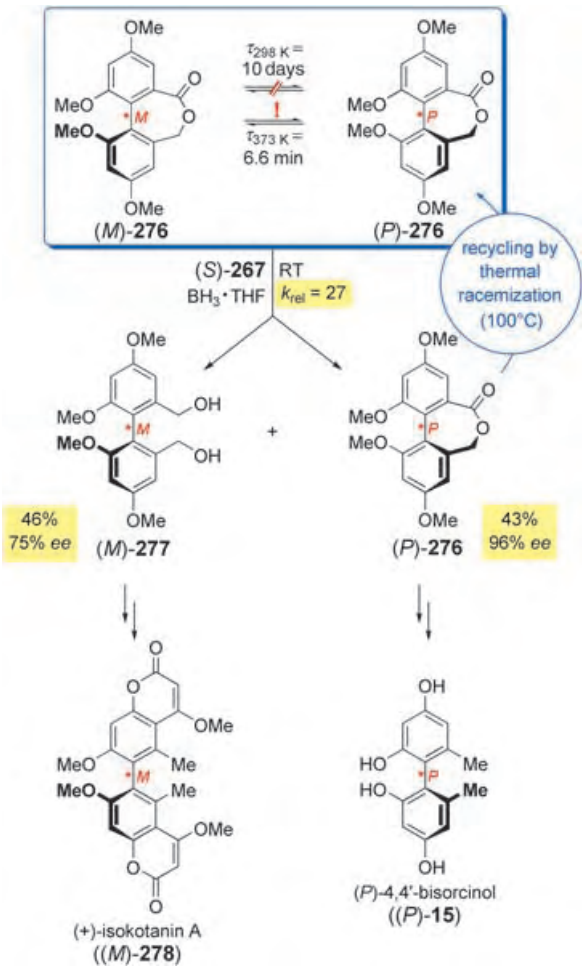


Scheme 64. The atroposelective reduction of biaryl hydroxyaldehydes as a complement to the lactone cleavage, in this case applied to the synthesis of the natural product dioncopeltine A ((*M*)-**274**).

compounds do not form stable atropisomers, despite their formally ring-opened structure, because they are in equilibrium with their cyclic—and thus configurationally labile—lactol isomers. If the substituents next to the axis are small,[243,64] the stereoselective reduction of such hydroxyaldehydes (**275**→(*M*)-**273**, >90% *de*) provides a useful alternative to the lactone reduction (**272**→(*M*)-**273**, >90% *de*), as illustrated in the atroposelective synthesis of the antimalarial naphthylisoquinoline alkaloid dioncopeltine A ((*M*)-**274**).[244]

The seven-membered lactones **276** (Scheme 65) have significantly higher atropisomerization barriers than their six-membered analogues **33** (Figure 7). The interconversion rate of **276** is too slow ($\tau_{298\,K} \approx 10$ days) to be used in a *dynamic* kinetic deracemization, but a normal (i.e. nondynamic) kinetic resolution with subsequent thermal recycling of the unconverted starting material is possible.[245,246] Thus, reduc-

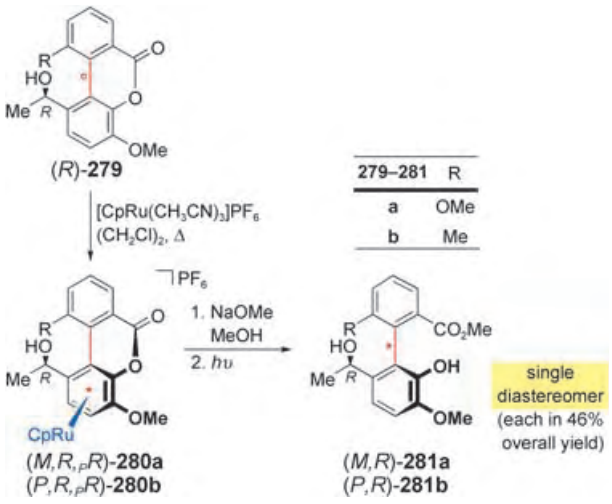
 © 2005 Wiley-VCH Verlag GmbH & Co. KGaA, Weinheim



Scheme 65. Atropoenantioselective synthesis of (*P*)-4,4′-bisorcinol ((*P*)-**15**) and (+)-isokotanin A ((*M*)-**278**) by kinetic resolution of the configurationally stable biaryl lactone **276**.

tion of racemic **276** with borane in the presence of the (*S*)-CBS reagent ((*S*)-**267**) delivered the diol (*M*)-**277** in 46% yield with 75% *ee* (95% *ee* after crystallization) and the lactone (*P*)-**276** in 43% yield with 96% *ee*, when the reaction was quenched at 56% conversion. The relative rate constant k_{rel} was calculated to be 27.[247] The lactone (*P*)-**276** can be recycled by thermal racemization at 100 °C ($\tau_{298\,K} = 6.6$ min) and resubmitted to a renewed ring cleavage with kinetic resolution; alternatively it can used as an enantiopure precursor for further synthesis. In the application presented here, (*P*)-**276** was converted into (*P*)-4,4′-bisorcinol ((*P*)-**15**), while the diol (*M*)-**277** was transformed into (+)-isokotanin A ((*M*)-**278**), both with high enantiomeric purities.

Within the lactone concept, a joint collaboration between Uemura and co-workers and our group showed that the element of planar chirality is excellently suited for transferring chiral information to the axis.[248] Treatment of the configurationally unstable lactones **279a** and **279b** (Scheme 66), which bear an *R*-configured 1-hydroxyethyl substituent *ortho* to the biaryl axis, with $[CpRu(CH_3CN)_3]PF_6$ delivered the centro-, axial-, and planar-chiral complexes (*M*,*R*,*pR*)-**280a** and (*P*,*R*,*pR*)-**280b**[163] regio- and diastereoselectively, owing to the directing effect of the OH function.



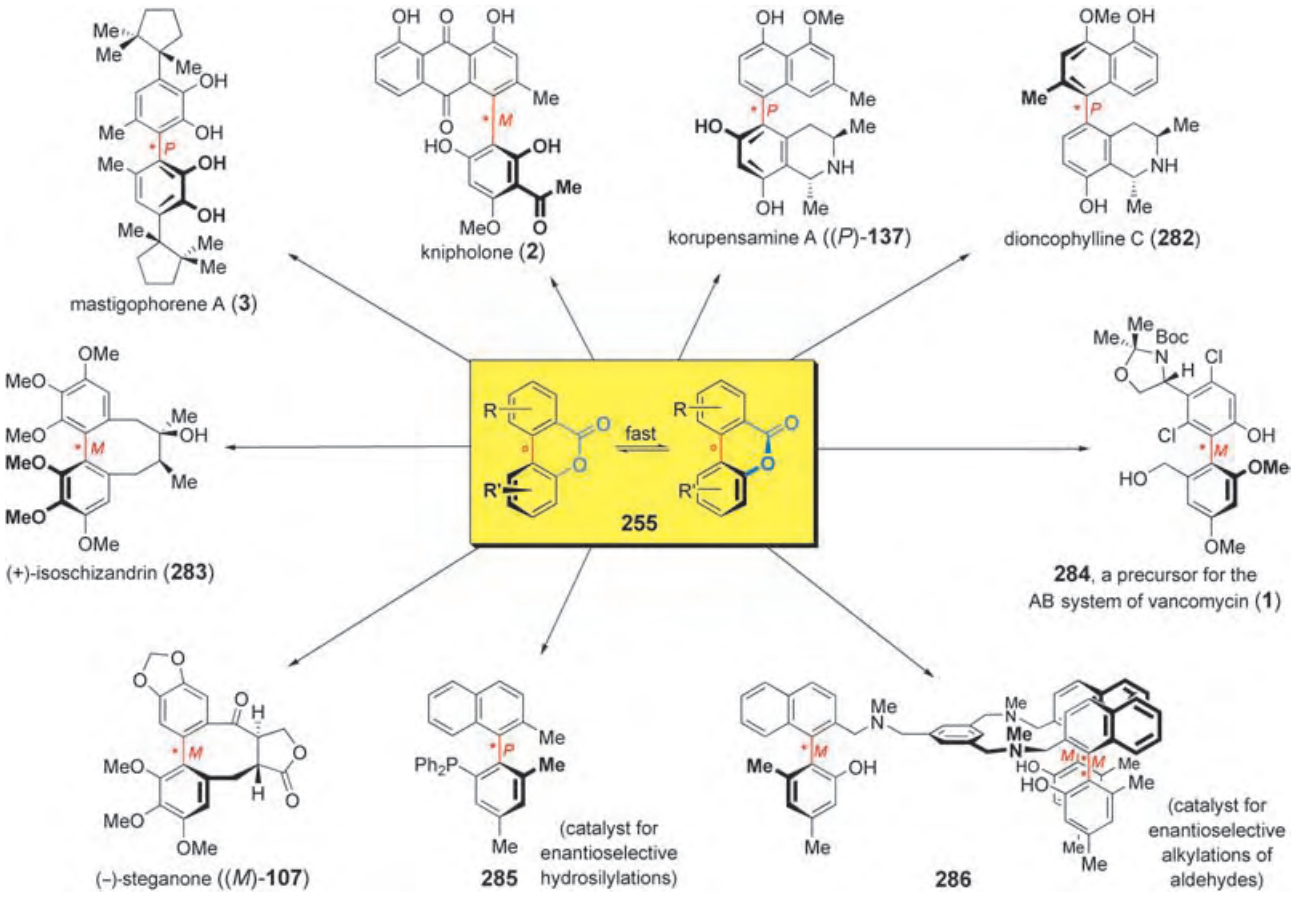
Scheme 66. Atropodiastereoselective biaryl lactone formation by using planar chirality as the chiral inductor, with subsequent ring cleavage and conversion into the metal-free biaryl products **281**.[63,162]

Cleavage of the lactone bridge with sodium methoxide and subsequent decomplexation gave the axially chiral biaryl compounds (*M*,*R*)-**281a** and (*P*,*R*)-**281b** as single diastereomers.

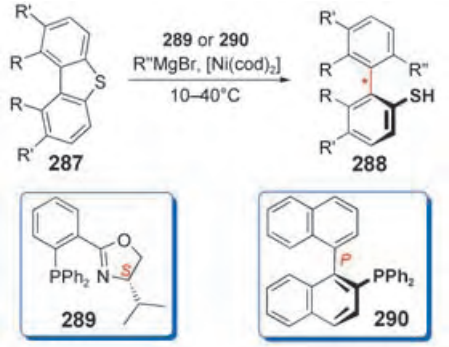
The potential and practicability of the lactone method has been demonstrated by its application in the atroposelective synthesis of more than 30 natural products and several useful catalysts,[20] some examples of which are presented in Scheme 67.[249–252] The lactone method is compatible with a variety of functional groups, works under mild conditions, and permits flexible and reliable access to a broad spectrum of structurally diverse biaryl species with any desired configuration at the axis. The carboxy- and phenol-derived *ortho* functions resulting from the ring-opening do not necessarily have to be part of the product, as they can easily be transformed or removed (see **282** and **285**). The lactone approach has also been used, among others, by Molander et al. in the total synthesis of (+)-isoschizandrin (**283**)[250] and by Abe, Harayama, and co-workers in a formal total synthesis of (−)-steganone ((*M*)-**107**).[251] Severe limitations of the method are not yet known.[253] The key six-membered biaryl lactone intermediates are C_1-symmetric and thus require the availability of two different building blocks (the phenolic moiety and the acid component). Hence the advantages of the method over other procedures are of particular significance for constitutionally *unsymmetrical* target molecules, whereas for simple C_2-symmetric products other procedures (e.g. homocoupling with subsequent racemate resolution if required) may be competing alternatives.

One other example in which an even shorter bridge—this time in a five-membered ring—is cleaved atropoenantioselectively, was reported by Hayashi and co-workers.[254] The asymmetric nickel-catalyzed cross coupling of the dibenzothiophenes **287** with Grignard reagents in the presence of chiral phosphines, including **289** and **290**, delivered the biaryl thiophenols **288** (Scheme 68). In some cases, both the chemical (up to 97%) and optical yields (up to 95% *ee*) were excellent, but this was not always true and the success of

 © 2005 Wiley-VCH Verlag GmbH & Co. KGaA, Weinheim



Scheme 67. A selection of C_1-, C_2-, and C_3-symmetric axially chiral biaryl natural products and catalysts that have been prepared by the lactone method;[249–252] further examples in this Review: N,O-ligands (*P*)-**7** and (*M*)-**7** (Scheme 63), dioncopeltine A ((*M*)-**274**, Scheme 64), (+)-isokotanin A ((*M*)-**278**), and (*P*)-4,4′-bisorcinol ((*P*)-**15**, Scheme 65).



R	R′	R"MgX	Catalyst	Yield [%]	*ee* [%]
benzo		*p*TolMgBr	**289**	97	95
benzo		*p*TolMgBr	**290**	93	14
benzo		PhMgBr	**289**	92	95
benzo		MeMgI	**289**	88	45
benzo		MeMgI	**290**	97	68
Me	H	*p*TolMgBr	**289**	– [a]	– [a]
Me	H	*p*TolMgBr	**290**	85	82

[a] No reaction observed.

Scheme 68. Atropoenantioselective ring-cleaving biaryl synthesis by Ni-catalyzed C-alkylation or -arylation in the presence of chiral phosphines.

this intriguing reaction varied both with the size of the Grignard reagent employed and the nature of the original *ortho* substituents. It is believed that the nickel catalyst first inserts into the C–S bond, with the stereochemically deciding step being the transmetalation of the Grignard reagent or the following reaction.

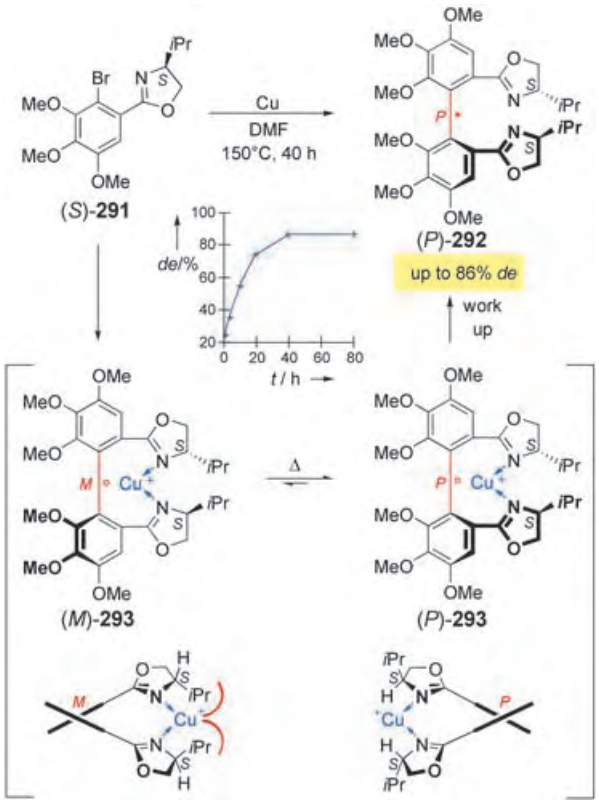
4.2.4. ***Transient Formation of a Short Metal Bridge***

As a rule, biaryl compounds with four *ortho* substituents are configurationally stable, even under forcing conditions (compare Figure 5). If equipped with two chelating groups next to the axis (e.g. binol (**29**)), however, an (albeit rather slow) atropisomerization can occur in the presence of an appropriate transition metal such as $Cu^{I/II}$, permitted by the resulting metallacycle with its (slightly) lower rotational barrier (see Section 2.2.2). If the metal or the substrate itself is chirally modified, this opens the possibility for the conversion of a racemic biaryl substrate into atropisomerically pure material by dynamic kinetic resolution, often already in situ, in the course of its formation.

Many Ullmann couplings of chiral *ortho*-halogenated oxazolinylbenzene derivatives, as developed by Meyers and co-workers,[126,137] are examples of the latter situation (for purely kinetically controlled atroposelective Ullmann cou-

 © 2005 Wiley-VCH Verlag GmbH & Co. KGaA, Weinheim

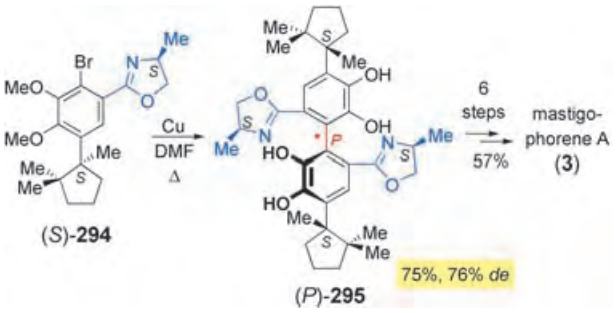
plings,[255] see Section 3.2). For example, the copper-mediated homocoupling of the L-valinol derived oxazoline (*S*)-**291** in DMF gave, after extended heating for 40 h, the atropodiastereomer (*P*)-**292** in 58% yield with 86% *de* (Scheme 69).[256,257] However, if the reaction was stopped



Scheme 69. Ullmann coupling of (*S*)-**291** with subsequent dynamic kinetic resolution by isomerization to the thermodynamically favored Cu^{I} complex (*P*)-**293**.

after 1 h, after which time all the starting material had already been consumed, (*P*)-**292** was isolated with much lower selectivity (24% *de*). As shown by the graph in Scheme 69, the *de* value of (*P*)-**292** increases with prolonged heating until a plateau is reached after 40 h. This proved that the high degree of stereoselectivity was not caused by an asymmetric coupling step, but was the consequence of a thermodynamically controlled deracemization (first-order asymmetric transformation).[136,258] It was postulated that the copper complexes formed initially, (*P*)-**293** and (*M*)-**293**, slowly interconvert at the elevated reaction temperature, thus leading to the preferred formation of the diastereomer (*P*)-**293** and alleviating the steric repulsion between the two isopropyl groups of the oxazoline moieties. The product (*P*)-**292** was further used in a short synthesis of an ellagitannin.[114,259]

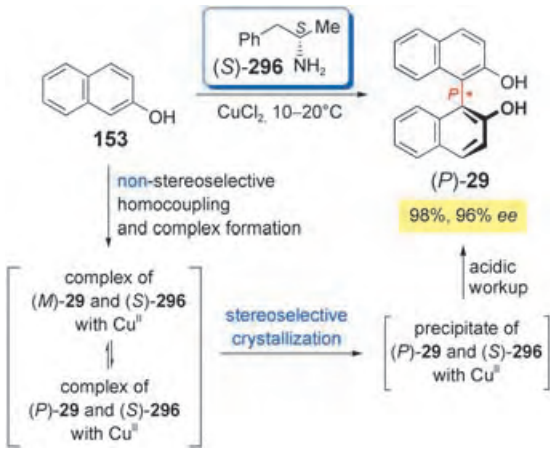
This strategy was further applied to the total synthesis of the axially chiral natural product mastigophorene A (**3**).[260] A key step of this approach was the asymmetric Ullmann homocoupling of the L-alaninol-derived aryl oxazoline (*S*)-**294**,[261] which gave the biaryl compound (*P*)-**295** in 75% yield with 76% *de* (Scheme 70).



Scheme 70. Total synthesis of mastigophorene A (**3**, Figure 1) by diastereoselective Ullmann coupling of the L-alaninol-derived aryl oxazoline (*S*)-**294**.

The Ullmann coupling of *ortho*-bromo(oxazolinyl)arenes with in situ dynamic kinetic resolution allows efficient access to axially chiral biaryl products with good to high stereocontrol. The prolonged heating required may, however, not be suitable for biaryl compounds with more-sensitive functional groups. Advantageously, the direct kinetically controlled Ullmann couplings of *ortho*-bromo(oxazolinyl)arenes (see Section 3.2) and the thermodynamic isomerizations described here always lead to the same stereochemical array at the biaryl axis, thus making the resulting axial configuration predictable and independent of the actual mechanism involved.

A spectacular early example of an atropoenantioselective biaryl synthesis by dynamic kinetic resolution was reported by Brussee et al.[174,262] (*P*)-Binol ((*P*)-**29**) was prepared in 98% yield with 96% *ee* by $CuCl_2$-induced oxidative homocoupling of 2-naphthol (**153**) in the presence of a large excess of amphetamine ((*S*)-**296**) (Scheme 71). The high enantiomeric purity, however, was not the result of an asymmetric coupling step, as initially assumed, but the consequence of stereoselective crystallization. Of the two intermediately formed diastereomeric complexes composed of Cu^{II}, (*S*)-**296**, and (*M*)- or (*P*)-**29** (no more details were given), only that containing the *P*-configured enantiomer of **29** crystallized,

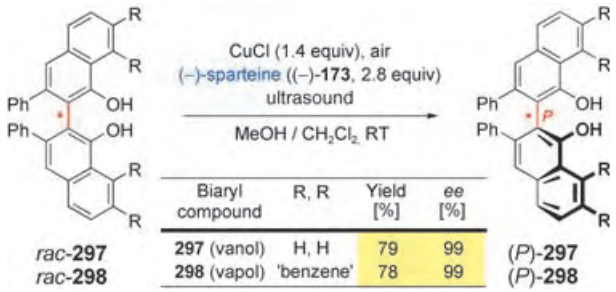


Scheme 71. Atropoenantioselective preparation of (*P*)-binol ((*P*)-**29**) by oxidative coupling of 2-naphthol (**153**) with concomitant stereoselective crystallization in the presence of amphetamine ((*S*)-**296**).

 © 2005 Wiley-VCH Verlag GmbH & Co. KGaA, Weinheim

steadily resupplied by concomitant atropisomerization of the remaining complex in solution (second-order asymmetric transformation).[136] The applicability of this reaction seems to be restricted to binol, and even in this important case, stereoselective crystallization only occurs within a narrow temperature range.

Recently, Wulff and co-workers published a highly enantioselective deracemization that is independent of any particular coupling step (Scheme 72).[263] Sonication of the

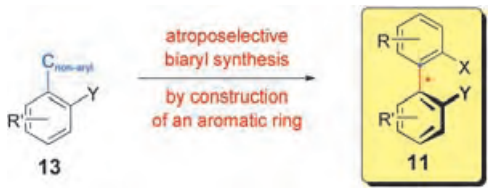


Scheme 72. Deracemization of *rac*-**297** and *rac*-**298** by using a complex of Cu^{2+} and (−)-sparteine ((−)-**173**).

racemic, *ortho*-dihydroxylated biaryl ligands vanol (**297**) and vapol (**298**)[264] in the presence of a chiral Cu^{II} complex, prepared in situ from CuCl and (−)-sparteine ((−)-**173**) by air oxidation, delivered the respective *P*-configured compounds nearly enantiopurely and in good yields. This deracemization, which occurred in homogeneous solution, is again a first-order asymmetric transformation that relies on the lowered rotational barrier and the relative thermodynamic stabilities of the intermediate Cu^{II} complexes formed. The mechanism is also supported by calculations that indicate that the complex [(*P*)-**297**/Cu^{II}/(−)-**173**] is more stable than its *M* diastereomer by as much as 16.4 kJ mol^{-1}. The deracemization also worked for binol (up to 94% *ee*). Such (−)-sparteine-mediated transformations are more generally applicable than that described above, which relies on a diastereoselective crystallization; nevertheless, despite the good *ee* values attained, definite drawbacks are the large excess of auxiliary required together with its availability in only one enantiomeric form.

5. Asymmetric Biaryl Synthesis by Construction of an Aromatic Ring

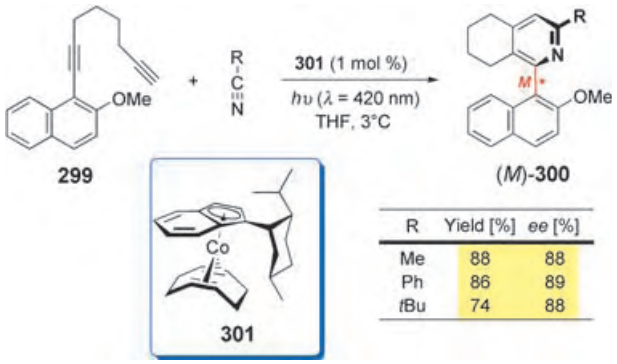
Besides the more classical direct asymmetric coupling reactions (as described in Section 3) and the atroposelective transformations on already prepared biaryl systems (see Section 4), a fundamentally new strategy for the construction of chiral biaryl compounds has emerged recently. In this concept, a preformed aryl–C single bond is transformed atroposelectively into the biaryl axis upon construction of the second arene ring from an aryl C substituent (Scheme 73). The chirality transfer to the axis results from a stereogenic center or by enantioselective catalysis. Only a few methods, which often involve asymmetric organometallic catalysis,



Scheme 73. The concept of atroposelective biaryl synthesis by construction of an aromatic ring.

have been used to realize this exciting—though less general—idea.

Thus, the groups of Gutnov and of Heller synthesized axially chiral 2-aryl pyridines by a catalytic asymmetric [2+2+2] cycloaddition.[265] The reaction of the 1-naphthyl diyne **299** with alkyl or aryl nitriles in the presence of the cobalt catalyst **301** (Scheme 74) gave the pyridines (*M*)-**300** in good



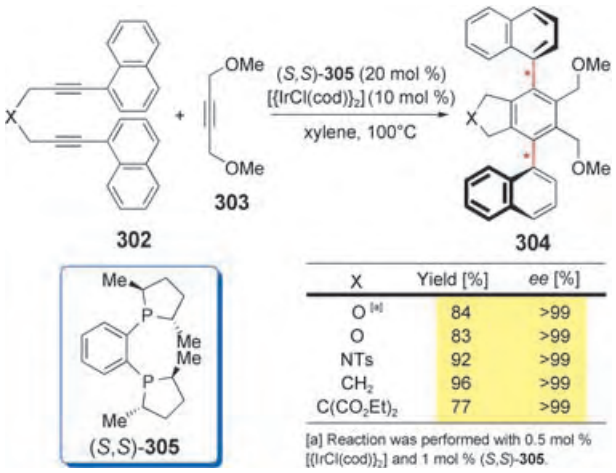
Scheme 74. Atropoenantioselective synthesis of the 1-aryl-5,6,7,8-tetrahydroisoquinolines (*M*)-**300** by asymmetric [2+2+2] cycloaddition.

chemical yields and optical purities (up to 89% *ee*). The analogous reaction of a naphthyl nitrile with an alkyl diyne, however, led only to poor yields and moderate *ee* values.

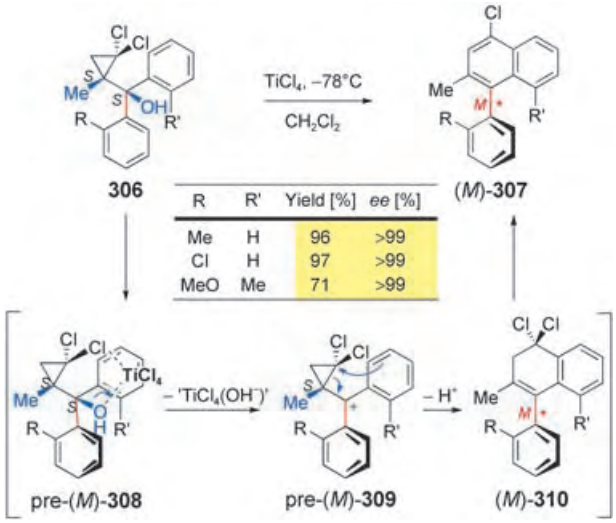
Independently, Shibata et al. reported related, but iridium-catalyzed [2+2+2] cycloadditions of diynes of type **302** with the alkyne **303** to construct the twofold axially chiral teraryls **304**. (*S*,*S*)-Me-duphos ((*S*,*S*)-**305**) was used as the chiral ligand (Scheme 75).[266] Excellent diastereoselectivities (the *meso* form was not observed) and enantioselectivities (> 99% *ee*) were achieved. Furthermore, the catalyst loading could be lowered to 0.5 mol% with no significant loss of selectivity. Besides such teraryls, a biaryl compound was also synthesized by this method, albeit with only up to 81% *ee*.

Nishii, Tanabe, and co-workers published a central-to-axial chirality transfer in the formation of (*M*)-1-arylnaphthalenes (*M*)-**307** from the enantiomerically pure dichlorocyclopropane precursors (*S*,*S*)-**306** (Scheme 76).[267] The Lewis acid promoted benzannellation produced chiral biaryl products with almost complete enantiomeric purity. The high degree of stereocontrol was rationalized by the conformational constraints upon formation of the intermediate carbocation (**306**→pre-(*M*)-**308**→pre-(*M*)-**309**), with the *ortho* substituent R being orientated away from the eliminating, Lewis acid bound hydroxy group. Conjugation between the cyclopropyl methyl cation and the benzene ring ensures that

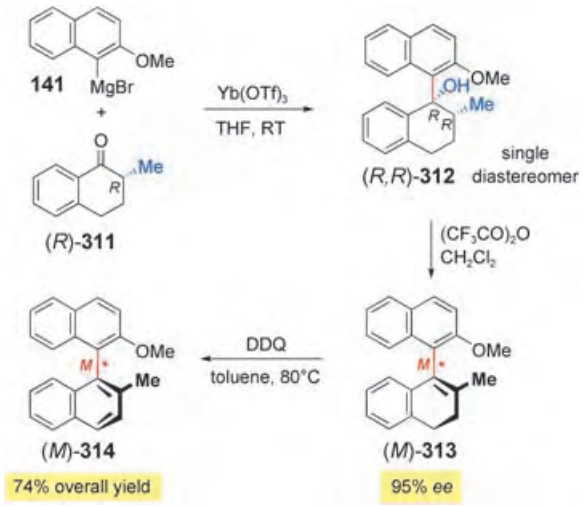
 © 2005 Wiley-VCH Verlag GmbH & Co. KGaA, Weinheim



Scheme 75. Atropoenantio- and atropodiastereoselective construction of teraryls by iridium-catalyzed [2+2+2] cycloaddition.

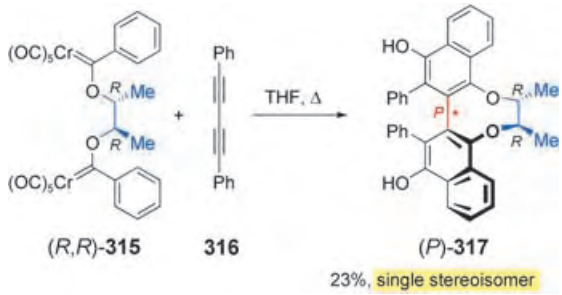


Scheme 76. Central-to-axial chirality transfer in benzannellation of the enantiomerically pure diaryl-2,2-dichlorocyclopropylmethanols **306**.



Scheme 77. Enantioselective synthesis of (*M*)-**314** from the α-substituted ketone (*R*)-**311** with an intermediate central-to-axial chiraliy transfer.

A reaction that has received much attention in this area is the Dötz benzannellation of Fischer carbenes with alkynes. The stereochemical array at the new biaryl axis was controlled by chiral bridges[270] and stereogenic centers in the *ortho* position.[271,272] In a pioneering study, Wulff and co-workers[270] treated two chromium carbenes connected by a chiral tether (i.e. (*R*,*R*)-**315**) with the 1,3-butadiyne **316** (Scheme 78). Both



Scheme 78. Double benzannellation of a bis(chromium carbene) species (*R*,*R*)-**315** to give (*P*)-**317**.

free rotation about the single bonds in pre-*M* carbocation **309** is sufficiently hampered such that this conformation is fully conserved in the axial configuration of the dihydronaphthalene (*M*)-**310** and, thus, in the biaryl product (*M*)-**307**.

Another efficient conversion of C centrochirality into axial chirality was utilized by the research groups of Hattori and Miyano to synthesize the 1,1′-binaphthalene (*M*)-**314** (Scheme 77).[268,269] In this case, the α-substituted chiral cyclohexanone (*R*)-**311** served as a precursor to the new aryl ring. Diastereoselective addition of the naphthyl Grignard **141** in the presence of $Yb(OTf)_3$ delivered (*R*,*R*)-**312**, which was dehydrated to give the axially chiral arene–olefin intermediate (*M*)-**313** with 95% *ee*. Oxidation with DDQ afforded the desired chiral biaryl species (*M*)-**314** in 74% overall yield. Although this method is somewhat indirect, it does have the advantage that chiral α-substituted ketones are accessible by standard procedures.

aromatic rings of (*P*)-**317** were assembled in a single step with essentially complete control of the configuration of the biaryl axis, albeit in low yield and with concomitant formation of other products.

The synthetic strategy for the construction of chiral biaryl compounds by the assembly of one (or both) of the aromatic rings is highly innovative. This work is still in its infancy and the generality of the concept is, as yet, largely limited in terms of functional-group compatibility and substitution patterns accessible.

6. Summary and Outlook

With the continuously increasing importance of axially chiral biaryl compounds as chiral auxiliaries and ligands for

 © 2005 Wiley-VCH Verlag GmbH & Co. KGaA, Weinheim

asymmetric synthesis and as the structurally decisive element in bioactive natural products, formidable efforts have been undertaken recently to develop efficient methods for their atroposelective synthesis. The approaches shown in this Review are characterized by their conceptual diversity and can be divided into three major classes:

1) the "classic" atroposelective aryl–aryl coupling reactions (Section 3), which allow the preparation of axially chiral biaryl compounds directly from their (suitably modified) aromatic halves;
2) approaches that rely on the atroposelective conversion of preformed, but stereochemically not yet differentiated (i.e. achiral or configurationally labile) biaryl species to give axially chiral products (Section 4); and
3) specialized methods in which a non-aryl substituent on an aromatic ring is atroposelectively converted into the second aromatic ring (Section 5).

Despite the originality and efficiency of some of these approaches and regardless of whether the aryl–aryl coupling and the asymmetric induction are achieved simultaneously or stepwise, the stereoselective preparation of (complex) biaryl compounds remains a challenging goal. Most currently available methods meet only some, but not all of the following demands:

1) excellent chemical yields and optical purities, even for biaryl compounds with high steric hindrance (e.g. tetra-*ortho*-substituted derivatives) and biaryl species in which the steric differentiation between the *ortho* substituents is small—or even in cases in which the *ortho* substituents are identical and axial chirality results only from groups in the *meta* position;
2) access to virtually any substitution pattern, and compatibility with common functional and protecting groups;
3) use of cheap and easily accessible starting materials, chiral catalysts, or auxiliaries (which should be available in both enantiomeric forms); the latter have to be easy to attach and remove;
4) mild and convenient reaction conditions that prevent undesired atropisomerization at the biaryl axis formed;
5) possibility to synthesize either atropisomer from the same precursor ("atropodivergence") and to recycle any unwanted minor atropisomer ("chiral economy"); and
6) the applicability to the atroposelective construction of concrete functionalized target molecules such as complex natural products.

Taking all this into account, it is understandable why, despite the intense efforts and enormous progress of the past decades, a reliable and generally applicable procedure that fulfills all these demands satisfactorily is still lacking. Many of the intriguing concepts described reflect the chemical creativity of the researchers and provide excellent approaches to a specific class of target biaryl compounds, but are restricted to a distinct substitution pattern (e.g. a particular functional group in the *ortho* position), or fail if the steric hindrance increases (e.g. tetra-*ortho*-substituted biaryl targets).

The methods that are currently most widely applied in the asymmetric synthesis of complex axially chiral biaryl compounds are the "lactone concept" (Section 4.2.3) among the stepwise (atropoenantio- or atropodiastereoselective) techniques, and the Meyers oxazoline method (Section 3.2) among the direct (atropodiastereoselective) coupling procedures. Catalytic enantioselective aryl–aryl couplings such as the Suzuki coupling (Section 3.6), although still hampered by several restrictions, are gradually improving and might, owing to the economical use of the chiral catalysts, become further methods of choice in the future.

Abbreviations

acac	acetylacetonate
BHT	2,6-di-*tert*-butyl-4-methylphenol
binap	2,2′-bis(diphenylphosphanyl)-1,1′-binaphthyl
binol	1,1′-binaphthyl-2,2′-diol
Bn	benzyl
Boc	*tert*-butyloxycarbonyl
BOM	benzyloxymethyl
Bz	benzoyl
Cbz	benzyloxycarbonyl
Cp	cyclopentadienyl
cod	1,5-cyclooctadiene
dba	dibenzylideneacetone
DCC	1,3-dicyclohexylcarbodiimide
DDQ	2,3-dichloro-5,6-dicyano-1,4-benzoquinone
DIAD	diisopropylazodicarboxylate
DMA	*N*,*N*-dimethylacetamide
DMAP	4-(dimethylamino)pyridine
DME	ethylene glycol dimethyl ether
DMF	*N*,*N*-dimethylformamide
DMSO	dimethyl sulfoxide
dppf	1,1′-bis(diphenylphosphanyl)ferrocene
KHDMS	potassium hexamethyldisilazide
MCPBA	*meta*-chloroperbenzoic acid
MOM	methoxymethyl
Ms	methanesulfonyl
M.S.	molecular sieves
NMP	1-methyl-2-pyrrolidinone
PCC	pyridinium chlorochromate
TBAF	tetra-*n*-butylammonium fluoride
TBS	*tert*-butyldimethylsilyl
Teoc	2-(trimethylsilyl)ethoxycarbonyl
TEMPO	2,2,6,6-tetramethyl-1-piperidinyloxy
tfa	trifluoroacetyl
TFA	trifluoroacetic acid
TFAA	trifluoroacetic acid anhydride
Tf	trifluoromethanesulfonyl
TIPS	triisopropylsilyl
TMS	trimethylsilyl
TMEDA	*N*,*N*,*N*′,*N*′-tetramethylethylenediamine
Tol	tolyl
Ts	4-toluenesulfonyl

For generous financial support of their own work in the field, the authors would like to thank the Deutsche Forschungsgemeinschaft (mainly SFB 347 "Selective Reactions of Metal-

 © 2005 Wiley-VCH Verlag GmbH & Co. KGaA, Weinheim

Activated Molecules" and an "Emmy-Noether" fellowship for M.B.), the Alexander von Humboldt Foundation (fellowship for A.J.P.M.), and the Fonds der Chemischen Industrie. G.B. thanks his scientific cooperation partners and, in particular, the numerous enthusiastic students and co-workers who have developed the "lactone concept" with great commitment and skill—their names can be seen in the literature citations.

Received: November 18, 2004
Revised: March 1, 2005

[1] G. B. Kauffman, R. D. Meyers, *J. Chem. Educ.* **1975**, *52*, 777 – 781, and references therein.

[2] a) *Asymmetric Synthesis* (Eds.: R. A. Aitkin, S. N. Kilényi), Blackie, Glasgow, **1992**; b) *Asymmetric Synthesis, Vols. 1–5* (Ed.: J. D. Morrison), Academic Press, Orlando, **1983–1985**; c) *Methods of Organic Chemistry (Houben-Weyl), Vol. 21a–f* (Eds.: G. Helmchen, R. W. Hoffmann, J. Mulzer, E. Schaumann), Thieme, New York, **1995**; d) *Comprehensive Asymmetric Catalysis I–III* (Eds.: E. N. Jacobsen, A. Pfaltz, H. Yamamoto), Springer, Berlin, **2000**.

[3] For some speculative early concepts about atropisomerism, see reference [27a].

[4] " *Biaryls in Nature*": G. Bringmann, C. Günther, M. Ochse, O. Schupp, S. Tasler, in *Progress in the Chemistry of Organic Natural Products, Vol. 82* (Eds.: W. Herz, H. Falk, G. W. Kirby, R. E. Moore), Springer, Vienna, **2001**, pp. 1 – 249.

[5] a) C. Rosini, L. Franzini, A. Raffaelli, P. Salvadori, *Synthesis* **1992**, 503 – 517; b) M. McCarthy, P. J. Guiry, *Tetrahedron* **2001**, *57*, 3809 – 3844.

[6] a) D. H. Williams, B. Bardsley, *Angew. Chem.* **1999**, *111*, 1264 – 1286; *Angew. Chem. Int. Ed.* **1999**, *38*, 1172 – 1193; b) K. C. Nicolaou, C. N. C. Boddy, S. Bräse, N. Winssinger, *Angew. Chem.* **1999**, *111*, 2230 – 2287; *Angew. Chem. Int. Ed.* **1999**, *38*, 2096 – 2152.

[7] B. K. Hubbard, C. T. Walsh, *Angew. Chem.* **2003**, *115*, 752 – 789; *Angew. Chem. Int. Ed.* **2003**, *42*, 730 – 765.

[8] E. Dagne, W. Steglich, *Phytochemistry* **1984**, *23*, 1729 – 1731.

[9] J. Mutanyatta, M. Bezabih, B. M. Abegaz, M. Dreyer, R. Brun, N. Kocher, G. Bringmann, *Tetrahedron*, **2005**, *61*, 8475 – 8484.

[10] a) G. Bringmann, D. Menche, M. Bezabih, B. M. Abegaz, R. Kaminsky, *Planta Med.* **1999**, *65*, 757 – 758; b) G. Bringmann, D. Menche, J. Kraus, J. Mühlbacher, K. Peters, E.-M. Peters, R. Brun, M. Bezabih, B. M. Abegaz, *J. Org. Chem.* **2002**, *67*, 5595 – 5610.

[11] M. Kuroda, Y. Mimaki, H. Sakagami, Y. Sashida, *J. Nat. Prod.* **2003**, *66*, 894 – 897.

[12] Y. Fukuyama, Y. Asakawa, *J. Chem. Soc. Perkin Trans. 1* **1991**, 2737 – 2741.

[13] a) C. Ito, Y. Thoyama, M. Omura, I. Kajiura, H. Furukawa, *Chem. Pharm. Bull.* **1993**, *41*, 2096 – 2100; b) G. Bringmann, S. Tasler, H. Endress, J. Kraus, K. Messer, M. Wohlfarth, W. Lobin, *J. Am. Chem. Soc.* **2001**, *123*, 2703 – 2711.

[14] A. Miyashita, A. Yasuda, H. Takaya, K. Toriumi, T. Ito, T. Souchi, R. Noyori, *J. Am. Chem. Soc.* **1980**, *102*, 7932 – 7934.

[15] a) R. Noyori, H. Takaya, *Acc. Chem. Res.* **1990**, *23*, 345 – 350; b) R. Noyori, *Acta Chem. Scand.* **1996**, *50*, 380 – 390.

[16] H. Sasaki, R. Irie, T. Hamada, K. Suzuki, T. Katsuki, *Tetrahedron* **1994**, *50*, 11 827 – 11 838.

[17] G. Bringmann, M. Breuning, *Tetrahedron: Asymmetry* **1998**, *9*, 667 – 679.

[18] a) J. M. Brown, D. I. Hulmes, P. J. Guiry, *Tetrahedron* **1994**, *50*, 4493 – 4506; b) N. W. Alcock, J. M. Brown, D. I. Hulmes, *Tetrahedron: Asymmetry* **1993**, *4*, 743 – 756.

[19] For comprehensive reviews on both stereoselective and non-stereoselective aryl–aryl coupling methods, see: a) J. Hassan, M. Sévignon, C. Gossi, E. Schulz, M. Lemaire, *Chem. Rev.* **2002**, *102*, 1359 – 1469; b) T. D. Nelson, R. D. Crouch, *Cu, Ni, and Pd Mediated Homocoupling Reactions in Biaryl Syntheses: the Ullmann Reaction* in *Organic Reactions, Vol. 63*, Wiley, New Jersey, **2004**, pp. 265 – 555.

[20] For reviews on the lactone method, see: a) G. Bringmann, M. Breuning, R.-M. Pfeifer, W. A. Schenk, K. Kamikawa, M. Uemura, *J. Organomet. Chem.* **2002**, *661*, 31 – 47; b) G. Bringmann, S. Tasler, R.-M. Pfeifer, M. Breuning, *J. Organomet. Chem.* **2002**, *661*, 49 – 65; c) G. Bringmann, D. Menche, *Acc. Chem. Res.* **2001**, *34*, 615 – 624; d) G. Bringmann, M. Breuning, S. Tasler, *Synthesis* **1999**, 525 – 558; e) G. Bringmann, S. Tasler in *Current Trends in Organic Synthesis* (Eds.: C. Scolastico, F. Nicotra), Plenum Publishing Corporation, New York, **1999**, pp. 105 – 116.

[21] For a review on the desymmetrization of achiral biaryl compounds and the dynamic kinetic resolution of configurationally unstable biaryl products, see: K. Khanbabaee, *Nachr. Chem.* **2003**, *51*, 163 – 166.

[22] For a review on planar-chirality-induced asymmetric biaryl syntheses, see: K. Kamikawa, M. Uemura, *Synlett* **2000**, 938 – 949.

[23] For a review on selected asymmetric biaryl couplings, see: P. Lloyd-Williams, E. Giralt, *Chem. Soc. Rev.* **2001**, *30*, 145 – 157.

[24] For a review on asymmetric Ni-catalyzed cross-couplings, see: T. Hayashi, *J. Organomet. Chem.* **2002**, *653*, 41 – 45.

[25] C. H. Christie, J. Kenner, *J. Chem. Soc.* **1922**, *121*, 614 – 620.

[26] "Moleculare Asymmetrie": R. Kuhn in *Stereochemie* (Ed.: K Freudenberg), Franz Deuticke, Leipzig, **1933**, pp. 803 – 824.

[27] For previous reviews on the configurational stability of biaryl compounds, see: a) R. Adams, H. C. Yuan, *Chem. Rev.* **1933**, *33*, 261 – 338; b) E. L. Eliel, S. H. Wilen, *Stereochemistry of Organic Compounds*, Wiley, New York, **1994**, 1142 – 1148; c) F. Leroux, *ChemBioChem* **2004**, *5*, 644 – 649.

[28] Normally, the lowest-energy conformation of a biaryl compound is neither completely planar nor with the rings orthogonal to each other, but has an intermediate angle. The stabilization gained from resonance between the two rings at coplanarity is balanced with the strain release in a perpendicular arrangement: F. Grein, *J. Phys. Chem. A* **2002**, *106*, 3823 – 3827, and references therein.

[29] K. Mislow, M. A. W. Glass, H. B. Hopps, E. Simon, G. H. Wahl, Jr., *J. Am. Chem. Soc.* **1964**, *86*, 1710 – 1733.

[30] H. Musso, W. Steckelberg, *Chem. Ber.* **1968**, *101*, 1510 – 1519.

[31] M. Bloch, N. Lau, H. Musso, U.-I. Záhorszky, *Chem. Ber.* **1972**, *105*, 1790 – 1797.

[32] a) T. R. Govindachari, P. C. Parthasarathy, H. K. Desai, *Indian J. Chem.* **1972**, *10*, 1117 – 1119; b) T. R. Govindachari, P. C. Parthasarathy, T. G. Rajagopalan, H. K. Desai, K. S. Ramachandran, E. Lee, *J. Chem. Soc. Perkin Trans. 1* **1975**, 2134 – 2136.

[33] E. H. Woodruff, R. Adams, *J. Am. Chem. Soc.* **1932**, *54*, 1977 – 1982.

[34] V. Prelog, G. Helmchen, *Angew. Chem.* **1982**, *94*, 614 – 631; *Angew. Chem. Int. Ed. Engl.* **1982**, *21*, 567 – 583.

[35] "Nomenclature and Vocabulary of Organic Stereochemistry": G. Helmchen in *Methods of Organic Chemistry (Houben-Weyl), Vol. 21a* (Eds.: G. Helmchen, R. W. Hoffmann, J. Mulzer, E. Schaumann), Thieme, New York, **1995**, pp. 10 – 13.

[36] This, now recommended, *M*/*P* nomenclature is more convenient than the older (and somewhat counterintuitive) *aR*/*aS* definition: If A-(via B′)→B→A′ is clockwise: *aR*; if anticlockwise: *aS*; in all cases, $aS = P$ and $aR = M$. The *M*/*P* convention does not need the more complicated 270° arc required for the *aR*/*aS* denotation and avoids any confusion with centrochiral

 © 2005 Wiley-VCH Verlag GmbH & Co. KGaA, Weinheim

elements—and it is in better agreement with the denotation for planar chirality.
[37] a) K. R. Hanson, *J. Am. Chem. Soc.* **1966**, *88*, 2731 – 2742; b) "Nomenclature and Vocabulary of Organic Stereochemistry": G. Helmchen in *Methods of Organic Chemistry (Houben-Weyl), Vol. 21a* (Eds.: G. Helmchen, R. W. Hoffmann, J. Mulzer, E. Schaumann), Thieme, New York, **1995**, pp. 17 – 21.
[38] It is important to remember that as for the pro-*R* and pro-*S* denotation, a modification of the pro-*M* or pro-*P* substituent does not necessarily give rise to a resulting *M* or *P* configuration at the axis.
[39] The rotational barrier in biphenyl itself has been estimated to be 8 kJ mol^{-1}: E. L. Eliel, S. H. Wilen, *Stereochemistry of Organic Compounds*, Wiley, New York, **1994**, p. 1147.
[40] For an older overview of racemization data on biaryl compounds, see: D. M. Hall, M. M. Harris, *J. Chem. Soc.* **1960**, 490 – 494.
[41] The chiral auxiliary binol (**29**), for example, racemizes readily at 220 °C ($\tau_{493\,K} = 60$ min): L. Meca, D. Řeha, Z. Havlas, *J. Org. Chem.* **2003**, *68*, 5677 – 5680; see also reference [75].
[42] "Recent Advances in Atropisomerism": K. Oki in *Topics in Stereochemistry, Vol. 14* (Eds.: N. L. Allinger, E. E. Eliel, S. H. Wilen), Wiley Interscience, New York, **1983**, pp. 1 – 76.
[43] C. C. K. Ling, M. M. Harris, *J. Chem. Soc.* **1964**, 1825 – 1835.
[44] A. C. T. van Duin, B. Hollanders, R. J. A. Smits, J. M. A. Baas, B. van de Graaf, M. P. Koopmans, J. P. Sinninghe Damsté, J. W. de Leeuw, *Org. Geochem.* **1996**, *24*, 587 – 591.
[45] G. Bringmann, H. Busse, U. Dauer, S. Güssregen, M. Stahl, *Tetrahedron* **1995**, *51*, 3149 – 3158.
[46] a) G. Bott, L. D. Field, S. Sternhell, *J. Am. Chem. Soc.* **1980**, *102*, 5618 – 5626; b) reference [27b].
[47] a) A. K. Coulter, L. M. Clemens, *J. Phys. Chem.* **1964**, *68*, 651 – 654; b) A. S. Cooke, M. M. Harris, *J. Chem. Soc.* **1963**, 2365 – 2373.
[48] C. Wolf, W. A. König, C. Roussel, *Liebigs Ann.* **1995**, 781 – 786.
[49] For an example in the field of naturally occurring biaryl compounds, see: K. Miura, T. Inagaki, N. Nakatani, *Chem. Pharm. Bull.* **1989**, *37*, 1816 – 1819.
[50] A. I. Meyers, R. J. Himmelsbach, *J. Am. Chem. Soc.* **1985**, *107*, 682 – 685.
[51] For the energy barriers of several 2,2′-binaphthalene derivatives, see: R. W. Baker, Z. Brkic, M. V. Sargent, B. W. Skelton, A. H. White, *Aust. J. Chem.* **2000**, *53*, 925 – 938.
[52] G. Bringmann, K. Messer, K. Wolf, J. Mühlbacher, M. Grüne, R. Brun, A. M. Louis, *Phytochemistry* **2002**, *60*, 389 – 397.
[53] N. Hasaka, M. Okigawa, I. Kouno, N. Kawano, *Bull. Chem. Soc. Jpn.* **1982**, *55*, 3828 – 3830; for a recent, similar example, see: F. Leroux, M. Maurin, N. Nicod, R. Scopelliti, *Tetrahedron Lett.* **2004**, *45*, 1899 – 1902.
[54] For the cotton-seed-derived, tetra-*ortho*-substituted biaryl natural product gossypol (**114**, Scheme 19), a rotational barrier of $\Delta G^{\ddagger} > 200$ kJ mol^{-1} was determined by MM2 calculations. Upon heating in organic solvents (e.g. 22 h at 149 °C in xylene), gossypol dehydrates to give anhydrogossypol: J. W. Jaroszewski, T. Strøm-Hansen, L. L. Hansen, *Chirality* **1992**, *4*, 216 – 221.
[55] J. Fleischhauer, A. Koslowski, B. Kramer, E. Zobel, G. Bringmann, K. P. Gulden, T. Ortmann, B. Peter, *Z. Naturforsch. B* **1993**, *48*, 140 – 148.
[56] M. Rieger, F. H. Westheimer, *J. Am. Chem. Soc.* **1950**, *72*, 19 – 28.
[57] C. Wolf, D. H. Hochmuth, W. A. König, C. Roussel, *Liebigs Ann.* **1996**, 357 – 363.
[58] The analogous di-*ortho*-isopropyl-substituted biaryls (i.e. CF_3 replaced by *i*Pr) showed the opposite effect.[57]
[59] a) S. Gladiali, A. Dore, D. Fabbri, O. De Lucchi, G. Valle, *J. Org. Chem.* **1994**, *59*, 6363 – 6371; b) D. Fabbri, A. Dore, S. Gladiali, O. De Lucchi, G. Valle, *Gazz. Chim. Ital.* **1996**, *126*, 11 – 18; c) A. A. Watson, A. C. Willis, S. B. Wild, *J. Organomet. Chem.* **1993**, *445*, 71 – 78; d) R. G. Harvey, J. Pataki, C. Cortez, P. Di Raddo, C. X. Yang, *J. Org. Chem.* **1991**, *56*, 1210 – 1217.
[60] K. Peters, E.-M. Peters, H. G. von Schnering, G. Bringmann, T. Hartung, O. Schupp, *Z. Kristallogr.* **1992**, *202*, 271 – 274.
[61] G. Bringmann, T. Hartung, L. Göbel, O. Schupp, C. L. J. Ewers, B. Schöner, R. Zagst, K. Peters, H. G. von Schnering, C. Burschka, *Liebigs Ann. Chem.* **1992**, 225 – 232.
[62] G. Bringmann, M. Heubes, M. Breuning, L. Göbel, M. Ochse, B. Schöner, O. Schupp, *J. Org. Chem.* **2000**, *65*, 722 – 728.
[63] Owing to the rules of the CIP denotion (see references [34] and [35]), stereochemically identical analogues (e.g. R = alkyl vs. R = alkoxy) can have opposite stereodescriptors and, vice versa, stereochemically opposite isomers can have identical stereodescriptors.
[64] G. Bringmann, M. Breuning, H. Endress, D. Vitt, K. Peters, E.-M. Peters, *Tetrahedron* **1998**, *54*, 10677 – 10690.
[65] K. Ohmori, M. Kitamura, K. Suzuki, *Angew. Chem.* **1999**, *111*, 1304 – 1307; *Angew. Chem. Int. Ed.* **1999**, *38*, 1226 – 1229.
[66] G. Bringmann, P. A. Keller, K. Rölfing, *Synlett* **1994**, 423 – 424.
[67] a) M. Hatsuda, H. Hiramatsu, S. Yamada, T. Shimizu, M. Seki, *J. Org. Chem.* **2001**, *66*, 4437 – 4439; b) S. Superchi, D. Casarini, A. Laurita, A. Bavoso, C. Rosini, *Angew. Chem.* **2001**, *113*, 465 – 468; *Angew. Chem. Int. Ed.* **2001**, *40*, 451 – 454; c) M. Tichý, L. Ridvan, P. Holý, J. Závada, I. Císařová, J. Podlaha, *Tetrahedron: Asymmetry* **1998**, *9*, 227 – 234.
[68] T. B. Freedman, X. Cao, L. A. Nafie, M. Kalbermatter, A. Linden, A. J. Rippert, *Helv. Chim. Acta* **2003**, *86*, 3141 – 3155.
[69] R. Adams, N. Kornblum, *J. Am. Chem. Soc.* **1941**, *63*, 188 – 200.
[70] K. Mislow, S. Hyden, H. Schaefer, *J. Am. Chem. Soc.* **1962**, *84*, 1449 – 1455.
[71] a) F. K. Brown, J. C. Hempel, J. S. Dixon, S. Amato, L. Mueller, P. W. Jeffs, *J. Am. Chem. Soc.* **1989**, *111*, 7328 – 7333; b) R. Kannan, D. H. Williams, *J. Org. Chem.* **1987**, *52*, 5435 – 5437.
[72] a) K. Mislow, A. J. Gordon, *J. Am. Chem. Soc.* **1963**, *85*, 3521 – 3521; b) H. E. Zimmerman, D. S. Crumrine, *J. Am. Chem. Soc.* **1972**, *94*, 498 – 506; c) M. Zhang, G. B. Schuster, *J. Phys. Chem.* **1992**, *96*, 3063 – 3067; d) M. Cavazza, M. Zandomeneghi, A. Ouchi, Y. Koga, *J. Am. Chem. Soc.* **1996**, *118*, 9990 – 9991; e) K. S. Burnham, G. B. Schuster, *J. Am. Chem. Soc.* **1998**, *120*, 12619 – 12625.
[73] M. Irie, K. Yoshida, K. Hayashi, *J. Phys. Chem.* **1977**, *81*, 969 – 972; see also: M. Irie, T. Yorozu, K. Yoshida, K. Hayashi, *J. Phys. Chem.* **1977**, *81*, 973 – 976.
[74] T. Hattori, Y. Shimazumi, H. Goto, O. Yamabe, N. Morohashi, W. Kawai, S. Miyano, *J. Org. Chem.* **2003**, *68*, 2099 – 2108.
[75] E. P. Kyba, G. W. Gokel, F. de Jong, K. Koga, L. R. Sousa, M. G. Siegel, L. Kaplan, G. D. Y. Sogah, D. J. Cram, *J. Org. Chem.* **1977**, *42*, 4173 – 4184.
[76] T. Shimada, A. Kina, T. Hayashi, *J. Org. Chem.* **2003**, *68*, 6329 – 6337.
[77] The atropodiastereomerization process is accelerated considerably by the addition of acid, as the reaction rate is enhanced 23000-fold in the presence of TFA ($\tau_{306\,K,\,TFA} = 3$ h vs. $\tau_{306\,K,\,no\,TFA} = 7.9$ years).[76]
[78] An octa-fluorinated analogue of binol, by contrast, showed no tendency to racemize under comparable conditions: A. K. Yudin, L. J. P. Marytn, S. Pandiaraju, J. Zheng, A. Lough, *Org. Lett.* **2000**, *2*, 41 – 44.
[79] M. R. Boyd, Y. F. Hallock, J. H. Cardellina II, K. P. Manfredi, J. W. Blunt, J. B. McMahon, R. W. Buckheit, Jr., G. Bringmann, M. Schäffer, G. M. Cragg, D. W. Thomas, J. G. Jato, *J. Med. Chem.* **1994**, *37*, 1740 – 1745.
[80] "The Naphthylisoquinoline Alkaloids": G. Bringmann, F. Pokorny in *The Alkaloids, Vol. 46* (Ed.: G. A. Cordell), Academic Press, San Diego, **1995**, pp. 127 – 271.

 © 2005 Wiley-VCH Verlag GmbH & Co. KGaA, Weinheim

[81] D. J. Edwards, R. G. Pritchard, T. W. Wallace, *Tetrahedron Lett.* **2003**, *44*, 4665 – 4668.
[82] G. Bringmann, T. Hartung, *Liebigs Ann. Chem.* **1994**, 313 – 316.
[83] G. Bringmann, D. Vitt, J. Kraus, M. Breuning, *Tetrahedron* **1998**, *54*, 10691 – 10698.
[84] See reference [4], p. 28.
[85] a) C.-N. Lin, P.-L. Huang, C.-M. Lu, M.-H. Yen, R.-R. Wu, *Phytochemistry* **1997**, *44*, 1359 – 1363; b) Y.-L. Lin, T.-C. Lin, Y.-H. Kuo, *J. Nat. Prod.* **1997**, *60*, 368 – 370.
[86] a) S. Miyano, M. Tobita, H. Hashimoto, *Bull. Chem. Soc. Jpn.* **1981**, *54*, 3522 – 3526; b) S. Miyano, S. Handa, K. Shimizu, K. Tagami, H. Hashimoto, *Bull. Chem. Soc. Jpn.* **1984**, *57*, 1943 – 1947; c) S. Miyano, H. Fukushima, S. Handa, H. Ito, H. Hashimoto, *Bull. Chem. Soc. Jpn.* **1988**, *61*, 3249 – 3254.
[87] B. H. Lipshutz, F. Kayser, Z.-P. Liu, *Angew. Chem.* **1994**, *106*, 1962 – 1964; *Angew. Chem. Int. Ed. Engl.* **1994**, *33*, 1842 – 1844.
[88] B. H. Lipshutz, K. Siegmann, E. Garcia, F. Kayser, *J. Am. Chem. Soc.* **1993**, *115*, 9276 – 9282.
[89] In early studies tethers with a single stereogenic center were used, resulting in 66–90% *de* in the coupling step.[87]
[90] R. V. Kyasnoor, M. V. Sargent, *Chem. Commun.* **1998**, 2713 – 2714.
[91] T. Sugimura, H. Yamada, S. Inoue, A. Tai, *Tetrahedron: Asymmetry* **1997**, *8*, 649 – 655.
[92] B. H. Lipshutz, P. Müller, D. Leinweber, *Tetrahedron Lett.* **1999**, *40*, 3677 – 3680.
[93] G.-Q. Lin, M. Zhong, *Tetrahedron: Asymmetry* **1997**, *8*, 1369 – 1372.
[94] For a similar strategy, see: G.-Q. Lin, M. Zhong, *Tetrahedron Lett.* **1997**, *38*, 1087 – 1090.
[95] For a partial synthesis of desertorin C, see: a) reference [90]; b) R. W. Baker, R. V. Kyasnoor, M. V. Sargent, B. W. Skelton, A. H. White, *Aust. J. Chem.* **2000**, *53*, 487 – 506.
[96] B. H. Lipshutz, Z.-P. Liu, F. Kayser, *Tetrahedron Lett.* **1994**, *35*, 5567 – 5570.
[97] G. Michaud, M. Bulliard, L. Ricard, J.-P. Genêt, A. Marinetti, *Chem. Eur. J.* **2002**, *8*, 3327 – 3330.
[98] J. Madec, G. Michaud, J.-P. Genêt, A. Marinetti, *Tetrahedron: Asymmetry* **2004**, *15*, 2253 – 2261.
[99] L. Qiu, J. Wu, S. Chan, T. T.-L. Au-Yeung, J.-X. Ji, R. Guo, C.-C. Pai, Z. Zhou, X. Li, Q.-H. Fan, A. S. C. Chan, *Proc. Natl. Acad. Sci. USA* **2004**, *101*, 5815 – 5820.
[100] For the synthesis of the teraryl ternol, see: T. Sugimura, S. Inoue, A. Tai, *Tetrahedron Lett.* **1998**, *39*, 6487 – 6490.
[101] a) B. H. Lipshutz, B. James, S. Vance, I. Carrico, *Tetrahedron Lett.* **1997**, *38*, 753 – 756; b) B. H. Lipshutz, Y.-J. Shin, *Tetrahedron Lett.* **1998**, *39*, 7017 – 7020.
[102] For a less atropodiastereoselective coupling of 7-deoxycholic acid 7,7′-bridged 2-naphthols, see: U. Maitra, A. K. Bandyopadhyay, *Tetrahedron Lett.* **1995**, *36*, 3749 – 3750.
[103] B. H. Lipshutz, Y.-J. Shin, *Tetrahedron Lett.* **2000**, *41*, 9515 – 9521.
[104] B. H. Lipshutz, D. J. Buzard, C. Olsson, K. Noson, *Tetrahedron* **2004**, *60*, 4443 – 4449.
[105] For a similar coupling strategy with a chiral all-carbon tether additionally bridged by a carbonate, see: V. H. Rawal, A. S. Florjancic, S. P. Singh, *Tetrahedron Lett.* **1994**, *35*, 8985 – 8988.
[106] C. A. Merlic, C. C. Aldrich, J. Albaneze-Walker, A. Saghatelian, J. Mammen, *J. Org. Chem.* **2001**, *66*, 1297 – 1309.
[107] For a similar, but more stereoselective intermolecular coupling, see Scheme 21.
[108] For a review on the ellagitannins, see: S. Quideau, K. S. Feldman, *Chem. Rev.* **1996**, *96*, 475 – 503.
[109] a) O. T. Schmidt, W. Mayer, *Angew. Chem.* **1956**, *68*, 103 – 115; b) E. Haslam in *Progress in the Chemistry of Organic Natural Products, Vol. 41* (Eds.: W. Herz, H. Grisebach, G. W. Kirby), Springer, New York, **1982**, pp. 1 – 46; c) R. K. Gupta, S. M. K. Al-Shafi, K. Layden, E. Haslem, *J. Chem. Soc. Perkin Trans. 1* **1982**, 2525 – 2534; d) E. A. Haddock, R. K. Gupta, E. Haslam, *J. Chem. Soc. Perkin Trans. 1* **1982**, 2535 – 2545.
[110] a) K. S. Feldman, S. M. Ensel, *J. Am. Chem. Soc.* **1993**, *115*, 1162 – 1163; b) K. S. Feldman, S. M. Ensel, *J. Am. Chem. Soc.* **1994**, *116*, 3357 – 3366; c) K. S. Feldman, S. M. Ensel, R. D. Minard, *J. Am. Chem. Soc.* **1994**, *116*, 1742 – 1745; d) K. S. Feldman, A. Sambandam, *J. Org. Chem.* **1995**, *60*, 8171 – 8178; e) K. S. Feldman, R. S. Smith, *J. Org. Chem.* **1996**, *61*, 2606 – 2612; f) K. S. Feldman, K. Sahasrabudhe, *J. Org. Chem.* **1999**, *64*, 209 – 216; g) K. S. Feldman, M. D. Lawlor, K. Sahasrabudhe, *J. Org. Chem.* **2000**, *65*, 8011 – 8019.
[111] For a similar approach in which a Ullmann coupling was used, see: D. Dai, O. R. Martin, *J. Org. Chem.* **1998**, *63*, 7628 – 7633.
[112] K. S. Feldman, M. D. Lawlor, *J. Am. Chem. Soc.* **2000**, *122*, 7396 – 7397.
[113] a) K. Miyamoto, N. Kishi, R. Koshiura, T. Yoshida, T. Hatano, T. Okuda, *Chem. Pharm. Bull.* **1987**, *35*, 814 – 822; b) K. S. Feldman, K. Sahasrrabudhe, R. S. Smith, W. J. Scheuchenzeuber, *Bioog. Med. Chem. Lett.* **1999**, *9*, 985 – 990.
[114] For a review describing the different approaches to the ellagitannins, see: K. Khanbabaee, T. van Ree, *Synthesis* **2001**, 1585 – 1610.
[115] D. A. Evans, C. J. Dinsmore, *Tetrahedron Lett.* **1993**, *34*, 6029 – 6032.
[116] a) D. A. Evans, M. R. Wood, B. W. Trotter, T. I. Richardson, J. C. Barrow, J. L. Katz, *Angew. Chem.* **1998**, *110*, 2864 – 2868; *Angew. Chem. Int. Ed.* **1998**, *37*, 2700 – 2704; b) D. A. Evans, C. J. Dinsmore, P. S. Watson, M. R. Wood, T. I. Richardson, B. W. Trotter, J. L. Katz, *Angew. Chem.* **1998**, *110*, 2868 – 2872; *Angew. Chem. Int. Ed.* **1998**, *37*, 2704 – 2708; c) a similar thermodynamically driven atropodiastereomerization was also observed in a total synthesis of the ristocetin aglycon: B. M. Crowley, Y. Mori, C. C. McComas, D. Tang, D. L. Boger, *J. Am. Chem. Soc.* **2004**, *126*, 4310 – 4317.
[117] K. C. Nicolaou, D. Y.-K. Chen, X. Huang, T. Ling, M. Bella, S. A. Snyder, *J. Am. Chem. Soc.* **2004**, *126*, 12888 – 12896.
[118] For a further total synthesis of diazonamide A, see: K. C. Nicolaou, J. Hao, M. V. Reddy, P. B. Rao, G. Rassias, S. A. Snyder, X. Huang, D. Y.-K. Chen, W. E. Brenzovich, N. Giuseppone, P. Giannakakou, A. O'Brate, *J. Am. Chem. Soc.* **2004**, *126*, 12897 – 12906.
[119] O. Yonemitsu, P. Cerutti, B. Witkop, *J. Am. Chem. Soc.* **1966**, *88*, 3941 – 3945.
[120] For some examples, see: a) K. Tomioka, T. Ishiguro, Y. Iitaka, K. Koga, *Tetrahedron* **1984**, *40*, 1303 – 1312; b) J. S. Buckleton, R. C. Cambie, G. R. Clark, P. A. Craw, C. E. F. Rickard, P. S. Rutledge, P. D. Woodgate, *Aust. J. Chem.* **1988**, *41*, 305 – 324; c) J. K. Burden, R. C. Cambie, P. A. Craw, P. S. Rutledge, P. D. Woodgate, *Aust. J. Chem.* **1988**, *41*, 919 – 933; d) M. Tanaka, H. Mitsuhashi, T. Wakamatsu, *Tetrahedron Lett.* **1992**, *33*, 4161 – 4164; e) D. Planchenault, R. Dhal, J.-P. Robin, *Tetrahedron* **1995**, *51*, 1395 – 1404; f) R. S. Ward, D. D. Hughes, *Tetrahedron* **2001**, *57*, 4015 – 4022.
[121] J.-P. Robin, Y. Landais, *J. Org. Chem.* **1988**, *53*, 224 – 226.
[122] B. Kramer, A. Averhoff, S. R. Waldvogel, *Angew. Chem.* **2002**, *114*, 3103 – 3104; *Angew. Chem. Int. Ed.* **2002**, *41*, 2981 – 92982.
[123] a) D. R. Spring, S. Krishnan, S. L. Schreiber, *J. Am. Chem. Soc.* **2000**, *122*, 5656 – 5657; b) D. R. Spring, S. Krishnan, H. E. Blackwell, S. L. Schreiber, *J. Am. Chem. Soc.* **2002**, *124*, 1355 – 1363; c) S. Krishnan, S. L. Schreiber, *Org. Lett.* **2004**, *6*, 4021 – 4024.
[124] a) S. Miyano, M. Tobita, S. Suzuki, Y. Nishikawa, H. Hashimoto, *Chem. Lett.* **1980**, 1027 – 1030; b) C. Qin, M. Liu, L.-K. Song, G.-B. Rong, *Chin. J. Org. Chem.* **2002**, *22*, 1013 – 1017.
[125] T. Hattori, H. Hotta, T. Suzuki, S. Miyano, *Bull. Chem. Soc. Jpn.* **1993**, *66*, 613 – 622.

© 2005 Wiley-VCH Verlag GmbH & Co. KGaA, Weinheim

[126] A. I. Meyers, T. D. Nelson, H. Moorlag, D. J. Rawson, A. Meier, *Tetrahedron* **2004**, *60*, 4459 – 4473.
[127] A. I. Meyers, A. Meier, D. J. Rawson, *Tetrahedron Lett.* **1992**, *33*, 853 – 856.
[128] A. M. Warshawsky, A. I. Meyers, *J. Am. Chem. Soc.* **1990**, *112*, 8090 – 8099.
[129] For earlier investigations, see: a) A. I. Meyers, K. A. Lutomski, *J. Am. Chem. Soc.* **1982**, *104*, 879 – 881; b) A. I. Meyers, R. J. Himmelsbach, *J. Am. Chem. Soc.* **1985**, *107*, 682 – 685.
[130] H. Moorlag, A. I. Meyers, *Tetrahedron Lett.* **1993**, *34*, 6989 – 6992.
[131] H. Moorlag, A. I. Meyers, *Tetrahedron Lett.* **1993**, *34*, 6993 – 6996.
[132] R. W. Baker, S. Liu, M. V. Sargent, B. W. Skelton, A. H. White, *Chem. Commun.* **1997**, 451 – 452.
[133] P. Chau, I. R. Czuba, M. A. Rizzacasa, G. Bringmann, K.-P. Gulden, M. Schäffer, *J. Org. Chem.* **1996**, *61*, 7101 – 7105.
[134] A. I. Meyers, J. R. Flisak, R. A. Aitken, *J. Am. Chem. Soc.* **1987**, *109*, 5446 – 5452.
[135] a) *O*-Methylancistrocladine: B. N. Leighton, M. A. Rizzacasa, *J. Org. Chem.* **1995**, *60*, 5702 – 5705; b) ancistrocladinine: M. A. Rizzacasa, M. V. Sargent, *J. Chem. Soc. Perkin Trans. 1* **1991**, 2773 – 2781; c) *O*-methylancistrocladine and *O*-methylhamatine: M. A. Rizzacasa, M. V. Sargent, *J. Chem. Soc. Perkin Trans. 1* **1991**, 845 – 854; d) M. A. Rizzacasa, M. V. Sargent, *J. Chem. Soc. Chem. Commun.* **1990**, 894 – 896; e) for studies towards desertorin C, see reference [95]; f) for studies towards dioncophylline C (**282**), see: R. W. Gable, R. L. Martin, M. A. Rizzacasa, *Aust. J. Chem.* **1995**, *48*, 2013 – 2021.
[136] J. Jacques, A. Collet, S. H. Wilen, *Enantiomers, Racemates, and Resolutions*, Wiley, New York, **1981**, pp. 369 – 371.
[137] A. I. Meyers, *J. Heterocycl. Chem.* **1998**, *35*, 991 – 1002.
[138] T. D. Nelson, A. I. Meyers, *J. Org. Chem.* **1994**, *59*, 2655 – 2658.
[139] A nonstereoselective coupling of (*S*)-**108** with subsequent resolution by diastereoselective formation of a copper/(*P*)-**109** complex can be excluded, as the diastereomeric ratio of (*P*)-**109** did not change upon heating in the absence of Cu^{I}/Cu^{II}.
[140] M. B. Andrus, D. Asgari, J. A. Sclafani, *J. Org. Chem.* **1997**, *62*, 9365 – 9368.
[141] a) A. I. Meyers, J. J. Willemsen, *Tetrahedron* **1998**, *54*, 10493 – 10511; b) A. I. Meyers, J. J. Willemsen, *Tetrahedron Lett.* **1996**, *37*, 791 – 792.
[142] For an application in the atroposelective preparation of a bis(bisthienyl benzene), see: K. Tanaka, H. Suzuki, H. Osuga, *J. Org. Chem.* **1997**, *62*, 4465 – 4470.
[143] For a highly atroposelective intermolecular biaryl coupling with a chiral sugar-based scaffold, see: M. Arisawa, S. Utsumi, M. Nakajima, N. G. Ramesh, H. Tohma, Y. Kita, *Chem. Commun.* **1999**, 469 – 470.
[144] P.-E. Broutin, F. Colobert, *Org. Lett.* **2003**, *5*, 3281 – 3284.
[145] a) R. S. Coleman, E. B. Grant, *J. Am. Chem. Soc.* **1995**, *117*, 10889 – 10904; b) R. S. Coleman, E. B. Grant, *J. Am. Chem. Soc.* **1994**, *116*, 8795 – 8796; the perylenequinone phleichrome was prepared by using the same strategy.
[146] B. H. Lipshutz, J. M. Keith, *Angew. Chem.* **1999**, *111*, 3743 – 3746; *Angew. Chem. Int. Ed.* **1999**, *38*, 3530 – 3533.
[147] For two further applications in natural products synthesis, see: a) K. C. Nicolaou, A. E. Koumbis, M. Takayanagi, S. Natarajan, N. F. Jain, T. Bando, H. Li, R. Hughes, *Chem. Eur. J.* **1999**, *5*, 2622 – 2647; b) O. Baudoin, A. Décor, M. Cesario, F. Guéritte, *Synlett* **2003**, 2009 – 2012.
[148] M. Uemura, K. Kamikawa, *J. Chem. Soc. Chem. Commun.* **1994**, 2697 – 2698.
[149] K. Kamikawa, T. Watanabe, M. Uemura, *J. Org. Chem.* **1996**, *61*, 1375 – 1384.
[150] For the atropodiastereoselective coupling of aryl Grignard reagents with [(arene)$Cr(CO)_3$] complexes, see: K. Kamikawa, M. Uemura, *Tetrahedron Lett.* **1996**, *37*, 6359 – 6362.
[151] For an application in the synthesis of 2,2′-disubstituted [(biaryl)$Cr(CO)_3$] complexes, see: S. G. Nelson, M. A. Hilfiker, *Org. Lett.* **1999**, *1*, 1379 – 1382.
[152] M. Uemura, H. Nishimura, K. Kamikawa, K. Nakayama, Y. Hayashi, *Tetrahedron Lett.* **1994**, *35*, 1909 – 1912.
[153] T. Watanabe, K. Kamikawa, M. Uemura, *Tetrahedron Lett.* **1995**, *36*, 6695 – 6698.
[154] K. Kamikawa, T. Watanabe, M. Uemura, *Synlett* **1995**, 1040 – 1042.
[155] Y. Tanaka, T. Sakamoto, K. Kamikawa, M. Uemura, *Synlett* **2003**, 519 – 521.
[156] In non-aromatic solvents, thermal migration of the {$Cr(CO)_3$} fragment to the opposite face of the arene ring can occur if a heteroatom (N or O) is present in the benzylic position of the *syn* biaryl chromium complex: a) K. Kamikawa, T. Sakamoto, Y. Tanaka, M. Uemura, *J. Org. Chem.* **2003**, *68*, 9356 – 9363; b) K. Kamikawa, T. Sakamoto, M. Uemura, *Synlett* **2003**, 516 – 518; in aromatic solvents, by contrast, decomplexation can take place.[156a]
[157] K. Kamikawa, A. Tachibana, S. Sugimoto, M. Uemura, *Org. Lett.* **2001**, *3*, 2033 – 2036.
[158] For a less sucessful approach towards the AB fragment of vancomycin (**1**) by using planar-chiral [(arene)$Cr(CO)_3$] complexes, see: Y.-L. Tan, A. J. P. White, D. A. Widdowson, R. Wilhelm, D. J. Williams, *J. Chem. Soc. Perkin Trans. 1* **2001**, 3269 – 3280.
[159] a) M. Uemura, A. Daimon, Y. Hayashi, *J. Chem. Soc. Chem. Commun.* **1995**, 1943 – 1944; b) K. Kamikawa, T. Watanabe, A. Daimon, M. Uemura, *Tetrahedron* **2000**, *56*, 2325 – 2337.
[160] T. Watanabe, Y. Tanaka, R. Shoda, R. Sakamoto, K. Kamikawa, M. Uemura, *J. Org. Chem.* **2004**, *69*, 4152 – 4158.
[161] For earlier atroposelective approaches to korupensamine derivatives by the same group, again by using η^6-chromium complexes, see: a) T. Watababe, M. Shakadou, M. Uemura, *Synlett* **2000**, 1141 – 1144; b) T. Watanabe, M. Uemura, *Chem. Commun.* **1998**, 871 – 872; c) reference [159b].
[162] Compound ($_{P}S$)-**133** was prepared in enantiomerically pure form in analogy to: L. A. Bromley, S. G. Davies, C. L. Goodfellow, *Tetrahedron: Asymmetry* **1991**, *2*, 139 – 156.
[163] The absolute configuration of the planar-chiral complexes was classified—for the highest ranking substituent—according to the CIP nomenclature: a) R. S. Cahn, C. K. Ingold, V. Prelog, *Angew. Chem.* **1966**, *78*, 413 – 447; *Angew. Chem. Int. Ed. Engl.* **1966**, *5*, 385 – 415; b) "Nomenclature and Vocabulary of Organic Stereochemistry": G. Helmchen in *Methods of Organic Chemistry (Houben-Weyl), Vol. E21a* (Eds.: G. Helmchen, R. W. Hoffmann, J. Mulzer, E. Schaumann), Thieme, New York, **1995**, pp. 33 – 34; c) for a consise explanation of these rules, see: S. E. Gibson, H. Ibrahim, *Chem. Commun.* **2002**, 2465 – 2473.
[164] The synthesis of korupensamine B ((*M*)-**137**) was a formal total synthesis that ended at the enantiomer of an intermediate of the total synthesis of *ent*-korupensamine B (*ent*-(*M*)-**137**) published in the same article.
[165] For an earlier atropodiastereodivergent total synthesis of korupensamines A ((*P*)-**137**) and B ((*M*)-**137**), see: G. Bringmann, M. Ochse, R. Götz, *J. Org. Chem.* **2000**, *65*, 2069 – 2077.
[166] For examples of the preparation of enantiomerically pure [(aryl halide)$Cr(CO)_3$] complexes, see: a) T. Watanabe, M. Shakadou, M. Uemura, *Inorg. Chim. Acta* **1999**, *296*, 80 – 85; b) references [159b], [161b], and [162].
[167] T. Hattori, N. Koike, Y. Okaishi, S. Miyano, *Tetrahedron Lett.* **1996**, *37*, 2057 – 2060.

 © 2005 Wiley-VCH Verlag GmbH & Co. KGaA, Weinheim

[168] a) J. M. Wilson, D. J. Cram, *J. Am. Chem. Soc.* **1982**, *104*, 881 – 884; b) J. M. Wilson, D. J. Cram, *J. Org. Chem.* **1984**, *49*, 4930 – 4943.

[169] a) T. Suzuki, H. Hotta, T. Hattori, S. Miyano, *Chem. Lett.* **1990**, 807 – 810; b) reference [125].

[170] This mechanism is a modified version of the mechanism published by Meyers et al. (see Scheme 16 and references [127], [130]).

[171] T. Hattori, N. Koike, S. Miyano, *J. Chem. Soc. Perkin Trans. 1* **1994**, 2273 – 2282.

[172] a) R. W. Baker, G. R. Pocock, M. V. Sargent, E. Twiss (née Stanojevic), *Tetrahedron: Asymmetry* **1993**, *4*, 2423 – 2426; b) R. W. Baker, M. V. Sargent, *Pure Appl. Chem.* **1994**, *66*, 2143 – 2150; c) R. W. Baker, D. C. R Hockless, G. R. Pocock, M. V. Sargent, B. W. Skelton, A. N. Sobolev, E. Twiss (née Stanojevic), A. H. White, *J. Chem. Soc. Perkin Trans. 1* **1995**, 2615 – 2629.

[173] For some examples of non-atroposelective couplings with various oxidants, see: a) G. Bringmann, S. Tasler, *Tetrahedron* **2001**, *57*, 331 – 343; b) T. Sakamoto, H. Yonehara, C. Pac, *J. Org. Chem.* **1994**, *59*, 6859 – 6861; c) M. Noji, M. Nakajima, K. Koga, *Tetrahedron Lett.* **1994**, *35*, 7983 – 7984; d) F. Toda, K. Tanaka, S. Iwata, *J. Org. Chem.* **1989**, *54*, 3007 – 3009; e) M. Smrčina, Š. Vyskočil, B. Máca, M. Polášek, T. A. Claxton, A. P. Abbott, P. Kočovský, *J. Org. Chem.* **1994**, *59*, 2156 – 2163; f) A. McKillop, A. G. Turrell, D. W. Young, E. C. Taylor, *J. Am. Chem. Soc.* **1980**, *102*, 6504 – 6512.

[174] a) J. Brussee, A. C. A. Jansen, *Tetrahedron Lett.* **1983**, *24*, 3261 – 3262; b) J. Brussee, J. L. G. Groenendijk, J. M. te Koppele, A. C. A. Jansen, *Tetrahedron* **1985**, *41*, 3313 – 3319.

[175] The first catalytic and genuinely asymmetric oxidative biaryl (cross-)coupling with $CuCl_2$ and (−)-sparteine [(−)-**173**] as the catalysts and AgCl as the stoichiometric cooxidant, was published in 1993; the chemical yield and optical purity, however, was low: M. Smrčina, J. Poláková, Š. Vyskočil, P. Kočovský, *J. Org. Chem.* **1993**, *58*, 4534 – 4538.

[176] a) X. Li, J. Yang, M. C. Kozlowski, *Org. Lett.* **2001**, *3*, 1137 – 1140; b) X. Li, J. B. Hewgley, C. A. Mulrooney, J. Yang, M. C. Kozlowski, *J. Org. Chem.* **2003**, *68*, 5500 – 5511.

[177] For an earlier, less successful approach, see: a) M. Nakajima, K. Kanayama, I. Miyoshi, S. Hashimoto, *Tetrahedron Lett.* **1995**, *36*, 9519 – 9520; b) M. Nakajima, I. Miyoshi, K. Kanayama, S. Hashimoto, N. Noji, K. Koga, *J. Org. Chem.* **1999**, *64*, 2264 – 2271.

[178] For the oxidative coupling of **154a** with up to 94% *ee* by using an octahydrobinaphthyl-2,2′-diamine as the ligand, see: K. H. Kim, D.-W. Lee, Y.-S. Lee, D.-H. Ko, D.-C. Ha, *Tetrahedron* **2004**, *60*, 9037 – 9042.

[179] Moderate enantioselectivities have also been achieved with catalytic amounts of chiral phosphoramides ligands and CuCl.[124b]

[180] M. C. Kozlowski, X. Li, P. J. Carroll, Z. Xu, *Organometallics* **2002**, *21*, 4513 – 4522.

[181] C. A. Mulrooney, X. Li, E. S. DiVirgilio, M. C. Kozlowski, *J. Am. Chem. Soc.* **2003**, *125*, 6856 – 6857.

[182] For applications in Glaser–Hay couplings, see: X. Xie, P.-W. Phuan, M. C. Kozlowski, *Angew. Chem.* **2003**, *115*, 2218 – 2220; *Angew. Chem. Int. Ed.* **2003**, *42*, 2168 – 2170.

[183] R. Irie, K. Masutani, T. Katsuki, *Synlett* **2000**, 1433 – 1436.

[184] a) Z. Luo, Q. Liu, L. Gong, X. Cui, A. Mi, Y. Jiang, *Angew. Chem.* **2002**, *114*, 4714 – 4717; *Angew. Chem. Int. Ed.* **2002**, *41*, 4532 – 4535; b) Z. Luo, Q. Liu, L. Gong, X. Cui, A. Mi, Y. Jiang, *Chem. Commun.* **2002**, 914 – 915.

[185] a) C.-Y. Chu, B.-J. Uang, *Tetrahedron: Asymmetry* **2003**, *14*, 53 – 55; b) N. B. Barhate, C.-T. Chen, *Org. Lett.* **2002**, *4*, 2529 – 2532; c) C.-Y. Chu, D.-R. Hwang, S.-K. Wang, B.-J. Uang, *Chem. Commun.* **2001**, 980 – 981; d) S.-W. Hon, C.-H. Li, J.-H. Kuo, N. B. Barhate, Y.-H. Liu, Y. Wang, C.-T. Chen, *Org. Lett.* **2001**, *3*, 869 – 872.

[186] There is one additional report on an asymmetric photocatalytic oxidative biaryl coupling with a centro- and helically chiral Ru catalyst to give (*M*)-binol ((*M*)-**29**) with low enantioselectivity (16% *ee*): T. Hamada, H. Ishida, S. Usui, Y. Watanabe, K. Tsumura, K. Ohkubo, *J. Chem. Soc. Chem. Commun.* **1993**, 909 – 911.

[187] T. Osa, Y. Kashiwaga, Y. Yanagisawa, J. M. Bobbit, *J. Chem. Soc. Chem. Commun.* **1994**, 2535 – 2537.

[188] Initial attempts by Kumada and co-workers gave only poor stereocontrol: a) K. Tamao, A. Minato, N. Miyake, T. Mastuda, Y. Kiso, M. Kumada, *Chem. Lett.* **1975**, 133 – 136; b) K. Tamao, H. Yamamoto, H. Matsumoto, N. Miyake, T. Hayashi, M. Kumada, *Tetrahedron Lett.* **1977**, *18*, 1389 – 1392.

[189] T. Hayashi, K. Hayashizaki, T. Kiyoi, Y. Ito, *J. Am. Chem. Soc.* **1988**, *110*, 8153 – 8156.

[190] The Kumada cross-coupling of **175** with **176** catalyzed by Ni/(*P*,*S*,*S*)-**177b** to give (*M*)-**179**, was successfully performed on a large scale (up to 20 g): a) S. L. Colletti, R. L. Halterman, *Tetrahedron Lett.* **1989**, *30*, 3513 – 3516; b) J. M. Harris, R. McDonald, J. C. Vederas, *J. Chem. Soc. Perkin Trans. 1* **1996**, 2669 – 2674.

[191] For less successful enantioselective Kumada cross-couplings of **175** with **176**, see: a) T. Frejd, T. Klingstedt, *Acta Chem. Scand.* **1989**, *43*, 670 – 675; b) A. Terfort, H. Brunner, *J. Chem. Soc. Perkin Trans. 1* **1996**, 1467 – 1479; c) L. Dahlenburg, V. Kurth, *Inorg. Chim. Acta* **2001**, *319*, 176 – 182.

[192] T. Hayashi, K. Hayashizaki, Y. Ito, *Tetrahedron Lett.* **1989**, *30*, 215 – 218.

[193] A large portion of the "wrong" *P* enantiomer of the intermediate binaphthyl initially formed will ultimately, by the strong renewed external asymmetric induction again with preferential formation of *M* in the second step, become the *meso*-configured *P,M* compound (and not the *P,P* product) and thus formally further enhance the *ee* value of the *M,M* product.

[194] For reviews on Suzuki cross-couplings, see: a) "Palladium-Catalyzed Aryl-Aryl Coupling" L. Anastasia, E. Negishi, in *Handbook of Organopalladium Chemistry for Organic Synthesis, Vol. I* (Eds. E. Negishi, A. de Meijere), Wiley, New York, **2002**, pp. 311 – 334; b) A. Suzuki, *J. Organomet. Chem.* **1999**, *576*, 147 – 168.

[195] a) S. D. Walker, T. E. Barder, J. R. Martinelli, S. L. Buchwald, *Angew. Chem.* **2004**, *116*, 1907 – 1912; *Angew. Chem. Int. Ed.* **2004**, *43*, 1871 – 1876; b) T. E. Barder, S. L. Buchwald, *Org. Lett.* **2004**, *6*, 2649 – 2652; c) J. Yin, M. P. Rainka, X.-X. Zhang, S. L. Buchwald, *J. Am. Chem. Soc.* **2002**, *124*, 1162 – 1163; d) J. P. Wolfe, S. L. Buchwald, *Angew. Chem.* **1999**, *111*, 2570 – 2573; *Angew. Chem. Int. Ed.* **1999**, *38*, 2413 – 2416; e) J. P. Wolfe, R. A. Singer, B. H. Yang, S. L. Buchwald, *J. Am. Chem. Soc.* **1999**, *121*, 9550 – 9561.

[196] A. N. Cammidge, K. V. L. Crépy, *Chem. Commun.* **2000**, 1723 – 1724.

[197] A. N. Cammidge, K. V. L. Crépy, *Tetrahedron* **2004**, *60*, 4377 – 4386.

[198] In the original literature (see reference [199]), although named correctly as (*aR*)-**179** = (*M*)-**179** (according to the measured α_D-value), it seems that the wrong enantiomer (*P*)-**179** was drawn.

[199] J. F. Jensen, M. Johannsen, *Org. Lett.* **2003**, *5*, 3025 – 3028.

[200] For less atropoenantioselective Suzuki couplings with binap and derivatives thereof, see: A.-S. Castanet, F. Colobert, P.-E. Broutin, M. Obringer, *Tetrahedron: Asymmetry* **2002**, *13*, 659 – 665.

[201] J. Yin, S. L. Buchwald, *J. Am. Chem. Soc.* **2000**, *122*, 12051 – 12052.

 © 2005 Wiley-VCH Verlag GmbH & Co. KGaA, Weinheim

[202] K. C. Nicolaou, H. Li, C. N. C. Boddy, J. M. Ramanjulu, T.-Y. Yue, S. Natarajan, X.-J. Chu, S. Bräse, F. Rübsam, *Chem. Eur. J.* **1999**, *5*, 2584 – 2601.
[203] For further applications in natural products synthesis, see: a) model system for (*M*)-rhazinilam: A. Herrbach, A. Marinetti, O. Baudoin, D. Guénard, F. Guéritte, *J. Org. Chem.* **2003**, *68*, 4897 – 4905; b) ancistrotanzanine B and ancistroealaine A: G. Bringmann, A. Hamm, M. Schraut, *Org. Lett.* **2003**, *5*, 2805 – 2808; c) G. Bringmann, R.-M. Pfeifer, P. Schreiber, K. Hartner, M. Schraut, M. Breuning, *Tetrahedron* **2004**, *60*, 4349 – 4360.
[204] The ring system in **191** is crucial to gain high atroposelectivities.[202]
[205] Y. Terao, H. Wakui, T. Satoh, M. Miura, M. Nomura, *J. Am. Chem. Soc.* **2001**, *123*, 10407 – 10408.
[206] a) S. Saito, T. Kano, H. Muto, M. Nakadai, H. Yamamoto, *J. Am. Chem. Soc.* **1999**, *121*, 8943 – 8944; b) T. Kano, Y. Ohyabu, S. Saito, H. Yamamoto, *J. Am. Chem. Soc.* **2002**, *124*, 5365 – 5373.
[207] The enantiomerically pure acetate of (*M*,*M*)-**200** was used as the chiral auxiliary in stereoselective aldol reactions: S. Saito, K. Hatanaka, T. Kano, H. Yamamoto, *Angew. Chem.* **1998**, *110*, 3579 – 3582; *Angew. Chem. Int. Ed.* **1998**, *37*, 3378 – 3381.
[208] M. Shindo, K. Koga, K. Tomioka, *J. Am. Chem. Soc.* **1992**, *114*, 8732 – 8733.
[209] For a less efficient desymmetrization of **220** via an (*R*)-menthone acetal, see: a) T. Harada, S. Ueda, T. Yoshida, A. Inoue, M. Takeuchi, N. Ogawa, A. Oku, M. Shiro, *J. Org. Chem.* **1994**, *59*, 7575 – 7576; b) T. Harada, S. Ueda, T. M. T. Tuyet, A. Inoue, K. Fujita, M. Takeuchi, N. Ogawa, A. Oku, M. Shiro, *Tetrahedron* **1997**, *53*, 16663 – 16678.
[210] For a related three-step protocol, see: a) T. Harada, T. M. T. Tuyet, K. Hashimoto, M. Hatsuda, A. Oku, *Synlett* **1997**, 1426 – 1428; b) T. M. T. Tuyet, T. Harada, K. Hashimoto, M. Hatsuda, A. Oku, *J. Org. Chem.* **2000**, *65*, 1335 – 1343.
[211] T. Harada, T. M. T. Tuyet, A. Oku, *Org. Lett.* **2000**, *2*, 1319 – 1322.
[212] a) Y.-Y. Ku, T. Grieme, P. Raje, P. Sharma, S. A. King, H. E. Morton, *J. Am. Chem. Soc.* **2002**, *124*, 4282 – 4286; b) Y.-Y. Ku, T. Grieme, *Curr. Opin. Drug Discovery Dev.* **2002**, *5*, 852 – 859.
[213] A similar central-to-axial chirality transfer was used successfully in the atropodiastereoselective preparation of an axially chiral phenylnaphthalene.[212a]
[214] L. M. Engelhardt, W.-P. Leung, C. L. Raston, G. Salem, P. Twiss, A. H. White, *J. Chem. Soc. Dalton Trans.* **1988**, 2403 – 2409.
[215] T. Matsumoto, T. Konegawa, T. Nakamura, K. Suzuki, *Synlett* **2002**, 122 – 124.
[216] a) T. Hayashi, S. Niizuma, T. Kamikawa, N. Suzuki, Y. Uozumi, *J. Am. Chem. Soc.* **1995**, *117*, 9101 – 9102; b) T. Kamikawa, Y. Uozumi, T. Hayashi, *Tetrahedron Lett.* **1996**, *37*, 3161 – 3164; c) T. Kamikawa, T. Hayashi, *Tetrahedron* **1999**, *55*, 3455 – 3466.
[217] F. Kakiuchi, P. Le Gendre, A. Yamada, H. Ohtaki, S. Murai, *Tetrahedron: Asymmetry* **2000**, *11*, 2647 – 2651.
[218] G. Capozzi, C. Ciampi, G. Delogu, S. Menichetti, C. Nativi, *J. Org. Chem.* **2001**, *66*, 8787 – 8792; for the opposite approach, the intramolecular atropodiastereoselective coupling of two gallic acid units prefixed to D-glucose as a chiral tether, see references [110–112], [114].
[219] K. S. Feldman, K. J. Eastman, G. Lessene, *Org. Lett.* **2002**, *4*, 3525 – 3528.
[220] M. Penhoat, V. Levacher, G. Dupas, *J. Org. Chem.* **2003**, *68*, 9517 – 9520.
[221] For a similar approach by Wallace and co-workers, see reference [81].
[222] For a related conformational locking, see compound **37** (Figure 8).
[223] a) K. Mikami, M. Yamanaka, *Chem. Rev.* **2003**, *103*, 3369 – 3400; b) K. Mikami, K. Aikawa, Y. Yusa, J. J. Jodry, M. Yamanaka, *Synlett* **2002**, 1561 – 1578.
[224] a) Y. Imai, W. Zhang, T. Kida, Y. Nakatsuji, I. Ikeda, *Tetrahedron Lett.* **1997**, *38*, 2681 – 2684; b) Y. Imai, W. Zhang, T. Kida, Y. Nakatsuji, I. Ikeda, *J. Org. Chem.* **2000**, *65*, 3326 – 3333.
[225] For an example involving silicon as the bridging atom, see: F. Fabris, O. De Lucchi, V. Lucchini, *J. Org. Chem.* **1997**, *62*, 7156 – 7164.
[226] For the dynamic kinetic resolution of a configurationally semistable [(biphenyldiphosphane)$PtCl_2$] complex by using (*P*)-binol, see: a) M. D. Tudor, J. J. Becker, P. S. White, M. R. Gagné, *Organometallics* **2000**, *19*, 4376 – 4384; b) J. J. Becker, P. S. White, M. R. Gagné, *J. Am. Chem. Soc.* **2001**, *123*, 9478 – 9479.
[227] a) K. Mikami, T. Korenaga, M. Terada, T. Ohkuma, T. Pham, R. Noyori, *Angew. Chem.* **1999**, *111*, 517 – 519; *Angew. Chem. Int. Ed.* **1999**, *38*, 495 – 497; b) T. Korenaga, K. Aikawa, M. Terada, S. Kawauchi, K. Mikami, *Adv. Synth. Catal.* **2001**, *343*, 284 – 288.
[228] a) G. Bringmann, M. Breuning, P. Henschel, J. Hinrichs, *Org. Synth.* **2002**, *79*, 72 – 83; b) reference [20a].
[229] Only some selected procedures will be reported here; for more detailed information, see the original literature.
[230] For an example of an atroposelective ring cleavage with an achiral hydride-transfer reagent in the presence of a chiral Lewis acid as the asymmetric inductor, see: W. A. Schenk, J. Kümmel, I. Reuther, N. Burzlaff, A. Wuzik, O. Schupp, G. Bringmann, *Eur. J. Inorg. Chem.* **1999**, 1745 – 1756; for the complementary approach, the coordination of an achiral Lewis acid with subsequent reduction with a chiral hydride-transfer reagent, see: G. Bringmann, A. Wuzik, J. Kümmel, W. A. Schenk, *Organometallics* **2001**, *20*, 1692 – 1694.
[231] G. Bringmann, M. Breuning, S. Tasler, H. Endress, C. L. J. Ewers, L. Göbel, K. Peters, E.-M. Peters, *Chem. Eur. J.* **1999**, *5*, 3029 – 3038.
[232] G. Bringmann, M. Breuning, R. Walter, A. Wuzik, K. Peters, E.-M. Peters, *Eur. J. Org. Chem.* **1999**, 3047 – 3055.
[233] For an atropoenantioselective ring-opening of **33c** with O-nucleophiles in the presence of a chiral catalyst, see: D. Seebach, G. Jaeschke, K. Gottwald, K. Matsuda, R. Formisano, D. A. Chaplin, M. Breuning, G. Bringmann, *Tetrahedron* **1997**, *53*, 7539 – 7556.
[234] a) G. Bringmann, T. Hartung, *Angew. Chem.* **1992**, *104*, 782 – 783; *Angew. Chem. Int. Ed. Engl.* **1992**, *31*, 761 – 762; b) G. Bringmann, M. Breuning, *Tetrahedron: Asymmetry* **1999**, *10*, 385 – 390; c) G. Bringmann, T. Hartung, *Synthesis* **1992**, 433 – 435; d) G. Bringmann, T. Hartung, *Tetrahedron* **1993**, *49*, 7891 – 7902.
[235] See references [20a,d].
[236] The axial configuration of atropisomerically pure (*P*,*R*)-**265c** obtained by crystallization can be preserved by quick transformation into a configurationally stable biaryl; see reference [62].
[237] H. Pellissier, *Tetrahedron* **2003**, *59*, 8291 – 8327.
[238] This does not apply to the *t*Bu-substituted lactone **33f**, which is configurationally stable ($\tau_{298\,K} = 2.2$ days, see Figure 7); however, **33f** can be reduced with high stereocontrol ($k_{rel} > 200$!) by a "normal" (nondynamic) kinetic resolution, with subsequent recycling of the nonreacting enantiomer by thermal racemization: G. Bringmann, J. Hinrichs, J. Kraus, A. Wuzik, T. Schulz, *J. Org. Chem.* **2000**, *65*, 2517 – 2527.
[239] G. Bringmann, S. Güssregen, D. Vitt, R. Stowasser, *J. Mol. Model.* **1998**, *4*, 165 – 175.
[240] G. Bringmann, D. Vitt, *J. Org. Chem.* **1995**, *60*, 7674 – 7681.
[241] For a more detailed discussion about the mechanism of the lactone reduction, including the existence of a "stereochemical

 © 2005 Wiley-VCH Verlag GmbH & Co. KGaA, Weinheim

leakage" at the level of the intermediates **269** and **270**, see references [20a,d,e], [240].

[242] Such a recycling is also possible for biaryl amides (e.g. **258**[231]) and biaryl diols (e.g. **268**[20a]).

[243] For more detailed investigations on the atropoenantioselective reduction of model biaryl hydroxyaldehydes, see: a) G. Bringmann, M. Breuning, *Synlett* **1998**, 634 – 636; b) reference [83].

[244] G. Bringmann, W. Saeb, M. Rübenacker, *Tetrahedron* **1999**, *55*, 423 – 432.

[245] G. Bringmann, J. Hinrichs, P. Henschel, J. Kraus, K. Peters, E.-M. Peters, *Eur. J. Org. Chem.* **2002**, 1096 – 1106.

[246] For further kinetic resolutions of configurationally stable biaryl lactones, see: a) G. Bringmann, J. Hinrichs, *Tetrahedron: Asymmetry* **1997**, *8*, 4121 – 4126; b) reference [238].

[247] On an analytical scale, even a k_{rel} value of 43 was attained.

[248] a) K. Kamikawa, K. Norimura, M. Furusyo, T. Uno, Y. Sato, A. Konoo, G. Bringmann, M. Uemura, *Organometallics* **2003**, *22*, 1038 – 1046; b) K. Kamikawa, M. Furusyo, T. Uno, Y. Sato, A. Konoo, G. Bringmann, M. Uemura, *Org. Lett.* **2001**, *3*, 3667 – 3670.

[249] a) Mastigophorene A (**3**): G. Bringmann, J. Hinrichs, T. Pabst, P. Henschel, K. Peters, E.-M. Peters, *Synthesis* **2001**, 155 – 167 and G. Bringmann, T. Pabst, P. Henschel, J. Kraus, K. Peters, E.-M. Peters, D. S. Rycroft, J. Connolly, *J. Am. Chem. Soc.* **2000**, *122*, 9127 – 9133; b) knipholone (**2**): reference [10b] and G. Bringmann, D. Menche, *Angew. Chem.* **2001**, *113*, 1733 – 1736; *Angew. Chem. Int. Ed.* **2001**, *40*, 1687 – 1690; c) korupensamine A ((*P*)-**137**): reference [165] and G. Bringmann, M. Ochse, *Synlett* **1998**, 1294 – 1296; d) dioncophylline C (**282**): G. Bringmann, J. Holenz, R. Weirich, M. Rübenacker, C. Funke, M. R. Boyd, R. J. Gulakowski, G. François, *Tetrahedron* **1998**, *54*, 497 – 512; e) AB system **284** of vancomycin (**1**): G. Bringmann, D. Menche, J. Mühlbacher, M. Reichert, N. Saito, S. S. Pfeiffer, B. H. Lipshutz, *Org. Lett.* **2002**, *4*, 2833 – 2836.

[250] (+)-Isoschizandrin (**283**): G. A. Molander, K. M. George, L. G. Monovich, *J. Org. Chem.* **2003**, *68*, 9533 – 9540.

[251] (−)-Steganone ((*M*)-**107**): H. Abe, S. Takeda, T. Fujita, K. Nishioka, Y. Takeuchi, T. Harayama, *Tetrahedron Lett.* **2004**, *45*, 2327 – 2329.

[252] a) MOP ligand **285**: G. Bringmann, A. Wuzik, M. Breuning, P. Henschel, K. Peters, E.-M. Peters, *Tetrahedron: Asymmetry* **1999**, *10*, 3025 – 3031; b) tripodal ligand **286**: G. Bringmann, R.-M. Pfeifer, C. Rummey, K. Hartner, M. Breuning, *J. Org. Chem.* **2003**, *68*, 6859 – 6863; see also: G. Bringmann, M. Breuning, R.-M. Pfeifer, P. Schreiber, *Tetrahedron: Asymmetry* **2003**, *14*, 2225 – 2228.

[253] There has been a single report in which the lactone method, whilst working in principle, failed to give good atroposelectivities.[212]

[254] a) T. Shimada, Y.-H. Cho, T. Hayashi, *J. Am. Chem. Soc.* **2002**, *124*, 13396 – 13397; b) Y.-H. Cho, A. Kina, T. Shimada, T. Hayashi, *J. Org. Chem.* **2004**, *69*, 3811 – 3823.

[255] For the asymmetric Ullmann coupling to either atropisomer of 8,8′-bis(oxazolinyl)-1,1′-binaphthalene from the same oxazolidine just by applying different conditions, see: a) A. I. Meyers, A. Price, *J. Org. Chem.* **1998**, *63*, 412 – 413; b) A. I. Meyers, M. J. McKennon, *Tetrahedron Lett.* **1995**, *36*, 5869 – 5872.

[256] T. D. Nelson, A. I. Meyers, *Tetrahedron Lett.* **1993**, *34*, 3061 – 3062.

[257] T. D. Nelson, A. I. Meyers, *Tetrahedron Lett.* **1994**, *35*, 3259 – 3262.

[258] The pivotal role of Cu^{I}/Cu^{II} in the atropodiastereomerization of di(oxazolinyl)-substituted biphenyls was also demonstrated.[126],[257]

[259] T. D. Nelson, A. I. Meyers, *J. Org. Chem.* **1994**, *59*, 2577 – 2580.

[260] A. P. Degnan, A. I. Meyers, *J. Am. Chem. Soc.* **1999**, *121*, 2762 – 2769; the atropodiastereomer mastigophorene B ((*M*)-**3**) was prepared accordingly.

[261] In this particular case, the normally used L-valinol-derived analogue of (*S*)-**294** gave a slightly lower selectivity (74% *de*).

[262] For a similar reaction, see: K. Yamamoto, H. Fukushima, H. Yumioka, M. Nakazaki, *Bull. Chem. Soc. Jpn.* **1985**, *58*, 3633 – 3634.

[263] a) Y. Zhang, S.-M. Yeung, H. Wu, D. P. Heller, C. Wu, W. D. Wulff, *Org. Lett.* **2003**, *5*, 1813 – 1816; b) S. Yu, C. Rabalakos, W. D. Mitchell, W. D. Wulff, *Org. Lett.* **2005**, *7*, 367 – 369; the 7,7′-dimethyl derivative of (*S*)-vapol was synthesized accordingly in 78% yield with 99% *ee*.

[264] Vanol (**297**) and vapol (**298**) were used as ligands in catalysts for asymmetric Baeyer–Villiger reactions: C. Bolm, J.-C. Frison, Y. Zhang, W. D. Wulff, *Synlett* **2004**, 1619 – 1621.

[265] A. Gutnov, B. Heller, C. Fischer, H.-J. Drexler, A. Spannenberg, B. Sundermann, C. Sundermann, *Angew. Chem.* **2004**, *116*, 3883 – 3886; *Angew. Chem. Int. Ed.* **2004**, *43*, 3795 – 3797.

[266] T. Shibata, T. Fujimoto, K. Yokota, K. Takagi, *J. Am. Chem. Soc.* **2004**, *126*, 8382 – 8383.

[267] Y. Nishii, K. Wakasugi, K. Koga, Y. Tanabe, *J. Am. Chem. Soc.* **2004**, *126*, 5358 – 5359.

[268] T. Hattori, M. Date, K. Sakurai, N. Morohashi, H. Kosugi, S. Miyano, *Tetrahedron Lett.* **2001**, *42*, 8035 – 8038.

[269] For a central-to-axial chirality transfer in the field of naturally occurring biaryl compounds, see: J. M. Wanjohi, A. Yenesew, J. O. Midiwo, M. Heydenreich, M. G. Peter, M. Dreyer, M. Reichert, G. Bringmann, *Tetrahedron* **2005**, *61*, 2667 – 2674.

[270] J. Bao, W. D. Wulff, M. J. Fumo, Eugene B. Grant, D. P. Heller, M. C. Whitcomb, S.-M. Yeung, *J. Am. Chem. Soc.* **1996**, *118*, 2166 – 2181.

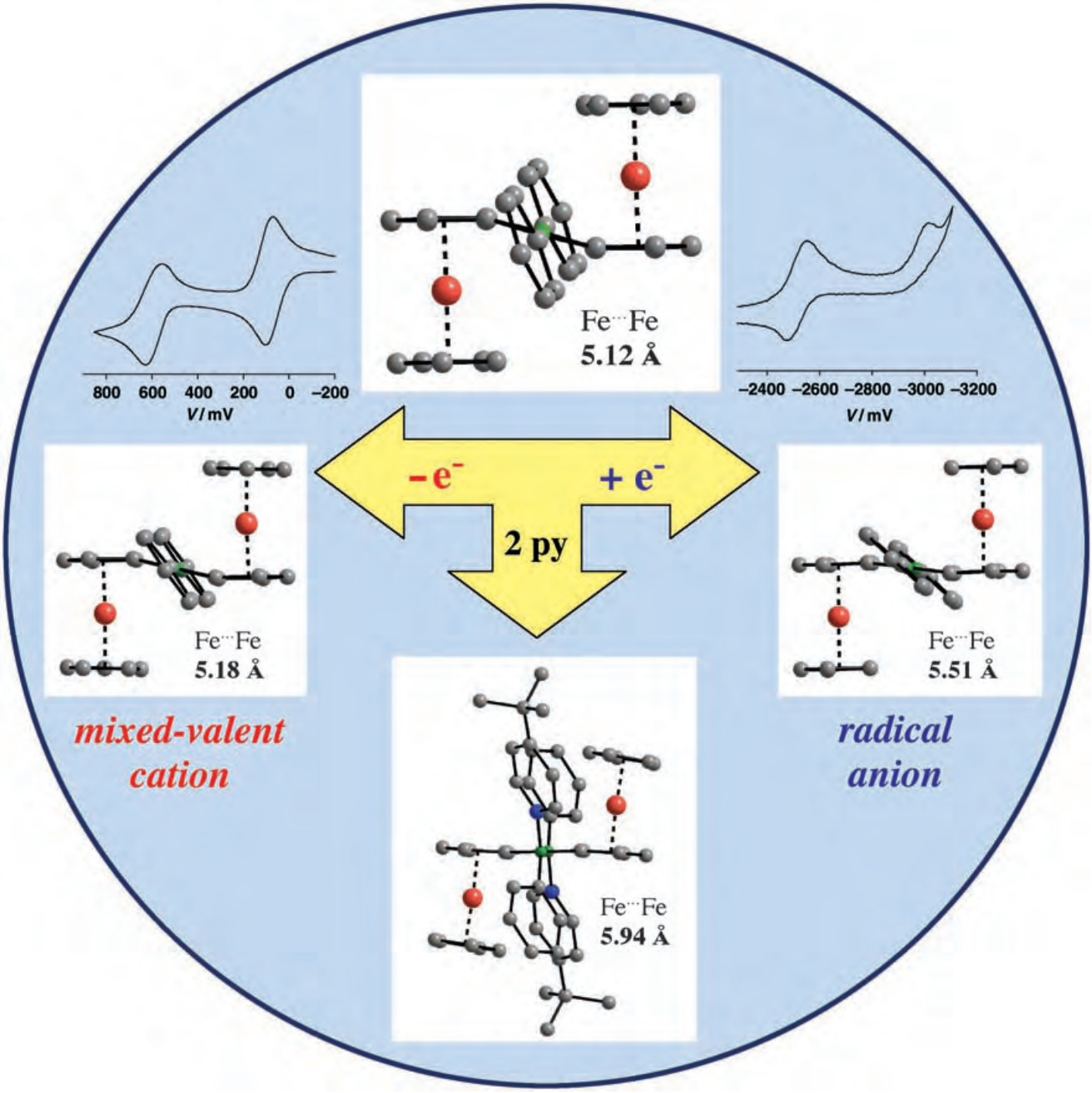
[271] A. V. Vorogushin, W. D. Wulff, H.-J. Hansen, *J. Am. Chem. Soc.* **2002**, *124*, 6512 – 6513.

[272] J. C. Anderson, J. W. Cran, N. P. King, *Tetrahedron Lett.* **2003**, *44*, 7771 – 7774.

© 2005 Wiley-VCH Verlag GmbH & Co. KGaA, Weinheim

Communications

DOI: 10.1002/anie.200502148



The doubly boron-bridged diferrocene [CpFe{$C_5H_3(BPh)_2C_5H_3$}FeCp] represents the first example of a 1,2-diborylated ferrocene. Controlled conformational changes in this rigid redox-active bifunctional Lewis acid species can be triggered either through redox chemistry or the binding of nucleophiles. For more details, see the Communication by F. Jäkle and co-workers on the following pages.

InterScience
© 2005 Wiley-VCH Verlag GmbH & Co. KGaA, Weinheim

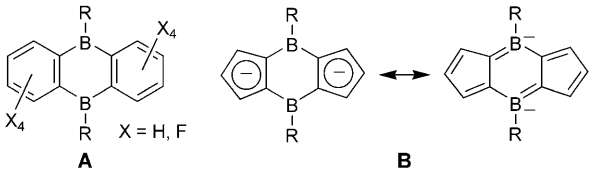
Ferrocenes

DOI: 10.1002/anie.200502148

Reversible Expansion and Contraction of a 1,2-Diborylated Ferrocene Dimer Promoted by Redox Chemistry and Nucleophile Binding**

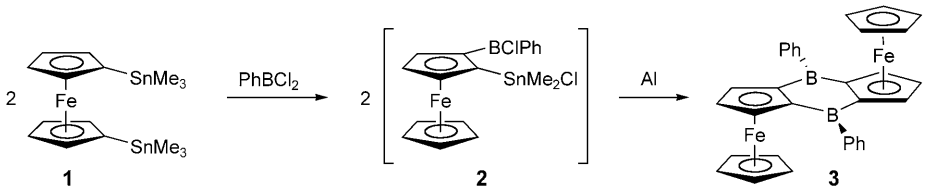
*Krishnan Venkatasubbaiah, Lev N. Zakharov, W. Scott Kassel, Arnold L. Rheingold, and Frieder Jäkle**

Diboraanthracenes **A** have been extensively used as precursors to various di- and multimetallic (and multidecker) sandwich complexes,[1–3] and more recently a perfluorinated derivative (X = H, R = C_6F_5) was employed as an activator in the polymerization of olefins.[4,5] Boracycles in general also serve as fluorescent materials, as probes for anions, and as building blocks for the assembly of new materials.[6] Finally, the "doping" of boron into larger organic π systems such as fullerenes and conjugated organic polymers continues to attract much interest owing to potentially interesting electronic effects.[7,8]



We previously showed that heteronuclear bidendate Lewis acids comprised of Lewis acidic boron and tin groups adjacent to one another are readily available through a rearrangement reaction from 1,1′-bis(trimethylstannyl)ferrocene (**1**) and boron halides.[9] For instance, the 1-stannyl-2-borylferrocene **2** is formed as the major product upon reaction of **1** with an excess of $PhBCl_2$ (Scheme 1). However, examples of ferrocenes that contain metals or semi-metals in neighboring positions at the same cyclopentadienyl (Cp) ring are generally still rare.[10] Among diborylated ferrocenes, for example, only 1,1′-diborylated species have been isolated and 1,3-diborylated isomers have been confirmed as minor byproducts by NMR spectroscopy.[11] Herein, we report the synthesis and properties of the first example of a 1,2-diborylated bisferrocene, in which two CpFe fragments are bridged by the novel dibora-*s*-indacenediyl ligand **B**.

When the reaction mixture of **1** and $PhBCl_2$ was kept for an extended period of time in an aluminum-capped vial, dark red crystals of the novel 1,2-diborylated ferrocene dimer **3** formed reproducibly in approximately 36% yield. The presence of aluminum was found to be critical, as confirmed by the lack of formation of product in the absence of a source of Al. While addition of Al powder to the reaction mixture accelerated the reaction, the selectivity for **3** was diminished. The ^{1}H NMR spectrum of **3** showed a doublet ($\delta = 4.89$ ppm, 4H) and a triplet ($\delta = 5.05$ ppm, 2H) with a coupling constant of $^3J = 2.5$ Hz, which is characteristic of a 1,2-disubstituted ferrocene.[10] A broad signal in the $^{11}B\{^1H\}$ NMR spectrum at $\delta = 57.7$ ppm is indicative of the formation of a triarylborane. The mass spectrum of **3** clearly shows a peak for the molecular ion at $m/z = 544$, which is consistent with the proposed dimeric structure.



Scheme 1. Formation of diboracycle **3**.

Single-crystal X-ray diffraction analysis of **3** confirmed that two ferrocene units are doubly bridged with two tricoordinate boron atoms (Figure 1).[12] The CpFe moieties adopt a *trans* configuration relative to the central B_2C_4 ring.[13] A pronounced tilting of the boron atoms towards the iron center (Cp_{cent}-C6-B1 = 167.9°; Cp_{cent}-C10-B1* = 164.4°) is evident, as is also observed in other ferrocenyl boranes; recent studies based on a combination of X-ray crystallography, cyclic voltammetry, Mössbauer spectroscopy, and theoretical calculations show that this feature results from a delocalized through-space interaction between iron and boron.[14] This interaction leads to a strong deviation from planarity for the diboraindacene ligand in **3** with an interplanar angle between the substituted Cp rings and the central B_2C_4 cycle of around 15.9° (see Figure 3a). In comparison, the related diboraanthracenes, **A**, are planar in the absence of steric strain.[2,4,15] The B–C bond lengths in **3** are similar to

[*] Dr. K. Venkatasubbaiah, Prof. F. Jäkle
Department of Chemistry
Rutgers University Newark
73 Warren Street, Newark, NJ 07102 (USA)
Fax: (+1) 973-353-1264
E-mail: fjaekle@rutgers.edu
Dr. L. N. Zakharov, Prof. A. L. Rheingold
Department of Chemistry and Biochemistry
University of California, San Diego
9500 Gilman Drive, La Jolla, CA 92093-0358 (USA)
Prof. W. S. Kassel
Department of Chemistry
Villanova University
Villanova, PA 19085 (USA)

[**] Acknowledgement is made to the National Science Foundation (CAREER award CHE-0346828 to F.J.), to the donors of the Petroleum Research Fund, administered by the American Chemical Society, and to the Rutgers University Research Council for support of this research. We are grateful to Prof. Nicholas J. Turro and Alberto Moscatelli for recording of the EPR spectrum and to Dr. Kakalis for acquisition of 2D NMR spectra. We would also like to thank Prof. Jack Norton for insightful discussions.

Supporting information for this article is available on the WWW under http://www.angewandte.org or from the author.

 © 2005 Wiley-VCH Verlag GmbH & Co. KGaA, Weinheim

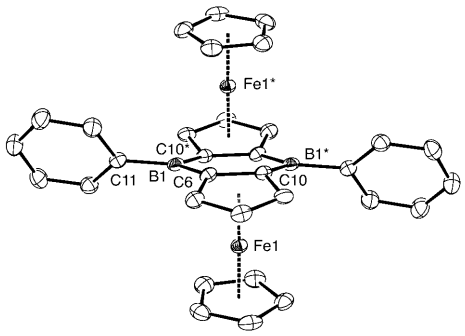


Figure 1. Molecular structure of **3** with thermal ellipsoids at the 50% probability level; hydrogen atoms are omitted for clarity. Selected interatomic distances [Å] and angles [°]: B1–C6 1.546(2), B1–C10* 1.546(2), B1–C11 1.564(2), B1···B1* 3.103, Fe1···B1 3.032, Fe1···B1* 2.957, Fe1···Fe1* 5.123, C6-B1-C10* 115.8(1), C6-B1-C11 123.7(1), C10*-B1-C11 120.4(1), C10-C6-B1 121.6(1), C6-C10-B1* 122.5(1).

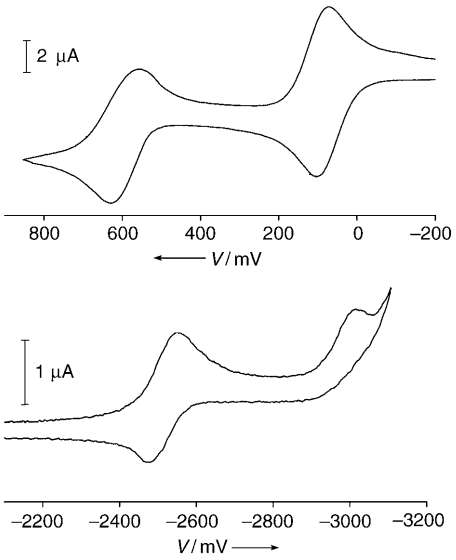


Figure 2. Cyclic voltammogram of **3** (vs. FcH/FcH^+). a) Oxidation waves of **3** (10^{-3} M) at 100 $mV s^{-1}$ with $Bu_4N^+B(C_6F_5)_4^-$ (0.1 M) in CH_2Cl_2 as the supporting electrolyte; b) reduction waves of **3** (10^{-3} M) at 100 $mV s^{-1}$ with $Bu_4N^+PF_6^-$ (0.1 M) in DME as the supporting electrolyte.

those in 9,10-diboraanthracenes **A** with organic substituents at the boron center (1.554–1.580 Å).[2,4,15] However, the B–C bonds to the Cp rings (1.546(2) Å) are significantly shorter than the exocyclic B–C bonds to the phenyl groups (1.564(2) Å), which suggests a significant contribution of the chinoid resonance structure of **B**.[9,16]

An intriguing feature of **3** is the presence of both redox-active ferrocene and triorganoborane moieties, which may allow one to electrochemically trigger conformational changes based on changes in the nature of the Fe···B interaction as suggested by DFT calculations by Wagner and co-workers[14] Such processes have attracted much interest recently with regard to the design of molecular machines that can be addressed through external stimuli.[17]

Cyclic voltammograms of **3** were recorded in $CH_2Cl_2/Bu_4N^+PF_6^-$ as well as $CH_2Cl_2/Bu_4N^+B(C_6F_5)_4^-$ (Figure 2a). In both cases two separate one-electron oxidation events were observed. However, improved chemical reversibility was achieved with $Bu_4N^+B(C_6F_5)_4^-$ as reported by Geiger and co-workers for related systems.[18] The first oxidation of **3** occurs at $E_{1/2} = +60$ mV (versus the ferrocene/ferrocenium (FcH/FcH^+) couple; $E_{1/2} = +88$ mV with PF_6^-), which is slightly higher than that reported for $FcBMe_2$ ($E = +9$ mV).[14] The second oxidation takes place at a much higher potential of $E_{1/2} = +570$ mV ($E_{1/2} = +432$ mV with PF_6^-). The pronounced difference between the results for the two electrolytes is due to differences in the degree of ion-pairing interactions.[18] In either case the separation between the two oxidation waves ($\Delta E = 510$ mV in $CH_2Cl_2/Bu_4N^+B(C_6F_5)_4^-$; $\Delta E = 344$ mV in $CH_2Cl_2/Bu_4N^+PF_6^-$) is considerably larger than those for the related doubly silyl-bridged ferrocenes [CpFe{Cp(SiR_2)$_2$Cp}FeCp] ($\Delta E = 195$–210 mV for R = Me, Et, and *n*Bu in propionitrile/$Bu_4N^+PF_6^-$),[19] which indicates unusually strong electronic coupling through the dibora-*s*-indacene bridge. However, the interaction is smaller than that for the all-carbon analogue, the *s*-indacene-bridged dimer [Cp*Fe{Cp(CH)$_2$Cp}FeCp*] (Cp* = pentamethylcyclopentadienyl), which shows a splitting of $\Delta E = 820$ mV and forms a fully valence-delocalized cation upon mono-oxidation.[20]

The mono-oxidized mixed-valence species $(\mathbf{3}^+)I_3 \cdot I_2$ was prepared in 85% yield upon treatment of **3** with an excess of I_2 in CH_2Cl_2/toluene and crystallization at −37 °C. The X-ray crystal structure shows two independent molecules, ($\mathbf{3}^+$)-1 and ($\mathbf{3}^+$)-2, along with I_3^- counterions and co-crystallized molecules of I_2.[12,21] There are two independent half cations on inversion centers, which render the Fe atoms in each of the dimers ($\mathbf{3}^+$)-1 and ($\mathbf{3}^+$)-2 equivalent. The latter has been shown to be indicative of valence delocalization owing to very rapid electron transfer.[22] In line with this interpretation, the Cp_{cent}–Cp_{cent} distances of 3.355 Å and 3.357 Å for ($\mathbf{3}^+$)-1 and ($\mathbf{3}^+$)-2, respectively, are intermediate between those of **3** (3.308 Å) and those of typical oxidized ferrocenes (ca. 3.4 Å). In contrast, the mixed-valent zwitterion ferricenyl(III)-trisferrocenyl(II)borate (Fc_4B), which contains a coordinatively saturated boron bridge, shows distinct ferrocene and ferrocenium moieties with Cp_{cent}–Cp_{cent} distances of 3.291–3.320 Å for the former and 3.428 Å for the latter.[23] The geometric parameters for ($\mathbf{3}^+$)-1 and ($\mathbf{3}^+$)-2 (Figure 3b) are similar apart from the tilting of the C_4B_2 ring relative to the Cp ring.[21] The interplanar angle of 16.5° for ($\mathbf{3}^+$)-1 is larger than that of 13.8° for ($\mathbf{3}^+$)-2 and even larger than in the free acid **3** itself. This unexpected feature is likely a result of packing effects involving the counterions, which form infinite helical chains $\{I_3^- \cdot I_2\}_n$ through short intermolecular I···I contacts.[21]

Hendrickson and co-workers have shown that IR spectroscopy may also serve as a convenient tool to evaluate the valence detrapping in diferrocene-type species. Particularly sensitive to oxidation of Fe is the perpendicular C–H bending vibration, which occurs at 815 cm^{-1} in ferrocene and is shifted to approximately 850 cm^{-1} in ferrocenium salts.[22a,b] A KBr pellet of the mixed-valence species $(\mathbf{3}^+)I_3 \cdot I_2$ shows a single broad band at 841 cm^{-1}, which is shifted relative to the neutral

 © 2005 Wiley-VCH Verlag GmbH & Co. KGaA, Weinheim

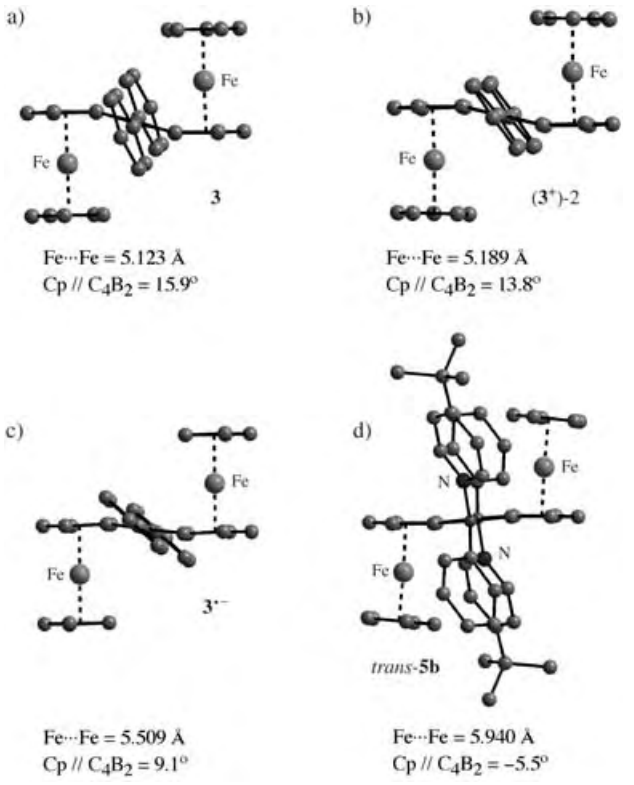


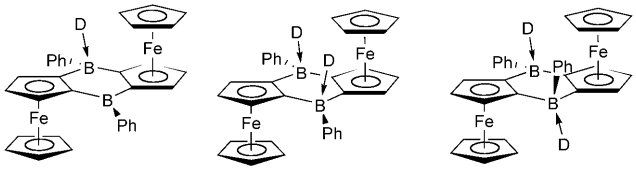
Figure 3. Comparison of structures of **3**, (**3**$^+$)-2, **3**$^{\bullet-}$, and *trans*-**5b**; hydrogen atoms are omitted for clarity; Cp//C_4B_2 denotes the interplanar angle between the Cp and C_4B_2 rings.

molecule **3** (820 cm^{-1}) and thus further indicates rapid electron transfer on the IR timescale (ca. 10^{12} s^{-1}).[21,22a,b]

The electrochemical reduction of **3** was studied by cyclic voltammetry in 1,2-dimethoxyethane (DME, Figure 2b) and revealed a quasi-reversible reduction wave at $E_{1/2} = -2.52$ V (vs. FcH/FcH$^+$) followed by an irreversible reduction at $E_{p2} = -3.02$ V. These data suggest the boracycle in **3** to be considerably more electron-rich than the respective diboraanthracene (**A**, R = Me), which was reported to show reversible reduction waves at −1.41 and −2.07 V in DME versus the saturated calomel electrode (SCE; or ca. −1.80/−2.46 V vs. FcH/FcH$^+$).[2] The latter is to be expected if extensive delocalization between the electron-rich ferrocene moieties and the boron atoms is present, which is evident from the relatively short endocyclic B–C bonds and the significant tilting of the boryl groups towards the iron atoms in the X-ray crystal structure of **3**.

The diboracycle **3** was chemically reduced by treatment with potassium in THF in the presence of 18-crown-6 (18-c-6). ESR spectroscopy of the solution in THF at −50 °C showed a signal, from which the ^{11}B hyperfine coupling could not be resolved. Dark brown thermally labile single crystals of the monoreduced species [K(18-c-6)(THF)$_2$][**3**$^{\bullet-}$] were obtained by crystallization from THF at −35 °C.[12,21] The bending of the boryl groups in **3**$^{\bullet-}$ towards Fe and the interplanar angle of 9.2° between the Cp rings and the C_4B_2 ring are significantly smaller than those in the parent compound **3** (interplanar angle: 15.9°), which in turn results in partial flattening of the dibora-*s*-indacene moiety and a significant increase in the Fe···Fe separation from 5.123 to 5.509 Å (Figure 3c). Both boryl groups are bent towards Fe at a similar angle (170.5° and 171.4°) which suggests that the electron is delocalized. A shortening of the B–C bond lengths within the six-membered diboracycle, as reported by Siebert and co-workers for the reduced diboraanthracene [K(18-c-6)(THF)$_2$][**A**$^{\bullet-}$] in comparison to the neutral diboraanthrancene **A** (R = Me),[2] is not observed. In this context, note that reduction of 1,8-bis(diphenylboryl)naphthalene, which shows a B···B separation of 3.002 Å similar to that of **3**, has been studied by Gabbaï and co-workers.[24] Upon chemical or electrochemical reduction, a monoanionic species was detected, for which a one-electron σ bond between the two boron centers has been proposed on the basis of EPR spectroscopy and DFT calculations. The calculations predict a shortening of the B···B distance upon reduction.[25] Although reduction apparently leads to a delocalized radical anion in our system, a decrease in the B···B distance (3.111 Å) in **3**$^{\bullet-}$ is not observed. The latter is due to incorporation of boron into the rigid ring system in **3**$^{\bullet-}$ which does not allow for direct overlap of the p orbitals of the two boron atoms.

Lewis acid/Lewis base binding offers yet another opportunity to trigger conformational changes in **3**.[14,26] Adducts **5a** and **5b** were obtained upon treatment of **3** with two equivalents of pyridine (py) and *tert*-butylpyridine (*t*Bu-py), respectively.[21] Weak binding of pyridine to **3** is evident from partial dissociation into the monoadducts **4** and the free acid **3** in solution. Single crystals of *trans*-**5b** were obtained by slow evaporation of solvent from a 1:2 mixture of **3** and *tert*-butylpyridine in chloroform.[12,21] A strong effect of the binding of pyridine on the geometric features is observed. In contrast to the free acid **3**, the central C_4B_2 ring of the dibora-*s*-indacene moiety is slightly bent away from the CpFe fragments, with interplanar angles between the Cp and C_4B_2 rings of 5.5° (Figure 3d). The latter is a result of electronic saturation and steric congestion around boron[26] which ultimately leads to expansion of the molecule and a much greater Fe···Fe distance of 5.940 Å relative to that of 5.123 Å in **3**.



In conclusion, the first 1,2-diboradiferrocene **3** was readily prepared from 1,1′-distannylferrocene and shows unusually strong electronic coupling between the ferrocene groups upon partial oxidation, which is indicative of fast electron transfer through the dibora-*s*-indacene ligand framework. Conformational changes in this highly rigid diferrocene can be triggered either through redox chemistry or through the binding of nucleophiles to render **3** an interesting candidate for the design of new types of molecular machines.

 © 2005 Wiley-VCH Verlag GmbH & Co. KGaA, Weinheim

Experimental Section

Experimental procedure for **3**: Neat $PhBCl_2$ (0.62 g, 3.90 mmol) was added to a solution of **1** (2.00 g, 3.90 mmol) in toluene (15 mL) at room temperature. The reaction mixture was kept for three months in an aluminum-capped vial. Large dark red crystals of **3** formed and were filtered off, washed with hexanes, and dried under high vacuum (0.38 g, 36 %). ^{1}H NMR (500 MHz, CD_2Cl_2, 25 °C): $\delta = 7.94$, 7.49–7.48 (m, 10H, Ph), 5.05 (t, $J = 2.5$ Hz, 2H, Cp-4), 4.89 (d, $J = 2.5$ Hz, 4H, Cp-3,5), 3.88 ppm (s, 10H, C_5H_5); ^{13}C NMR (125.69 MHz, CD_2Cl_2, 25 °C): $\delta = 144.5$ (br, *i*-Ph), 135.5 (*o*-Ph), 130.9 (*p*-Ph), 129.5 (*m*-Ph), 84.1 (br, Cp-1,2), 83.3 (Cp-3,5), 81.4 (Cp-4), 72.1 ppm (C_5H_5); ^{11}B NMR (160 MHz, CD_2Cl_2, 25 °C) $\delta = 57.7$ ($w_{1/2} = 1280$ Hz); GC-MS: *m*/*z*: 544 [M^+] (100 %); UV/Vis (CH_2Cl_2, 10^{-4} M): λ_{max} (ε) = 498 (6040), 411 (4360), 335 nm (5810 $cm^{-1}M^{-1}$); Elemental analysis (%) calcd for $C_{32}H_{26}Fe_2B_2$: C 70.67, H 4.82; found: C 70.72, H 4.78. See Supporting Information for further experimental details.

Received: June 20, 2005

Keywords: boron · cyclopentadienyl ligands · iron · Lewis acids · mixed-valent compounds

[1] W. Siebert, *Adv. Organomet. Chem.* **1993**, *35*, 187.
[2] P. Müller, S. Huck, H. Köppel, H. Pritzkow, W. Siebert, *Z. Naturforsch. B* **1995**, *50*, 1476.
[3] P. Müller, H. Pritzkow, W. Siebert, *J. Organomet. Chem.* **1996**, *524*, 41.
[4] M. V. Metz, D. J. Schwartz, C. L. Stern, P. N. Nickias, T. J. Marks, *Angew. Chem.* **2000**, *112*, 1368; *Angew. Chem. Int. Ed.* **2000**, *39*, 1312.
[5] V. C. Williams, C. Dai, Z. Li, S. Collins, W. E. Piers, W. Clegg, M. R. J. Elsegood, T. B. Marder, *Angew. Chem.* **1999**, *111*, 3922; *Angew. Chem. Int. Ed.* **1999**, *38*, 3695.
[6] a) S. Yamaguchi, T. Shirasaka, S. Akiyama, K. Tamao, *J. Am. Chem. Soc.* **2002**, *124*, 8816; b) D. J. H. Emslie, W. E. Piers, M. Parvez, *Angew. Chem.* **2003**, *115*, 1290; *Angew. Chem. Int. Ed.* **2003**, *42*, 1252; c) S. Kim, K.-H. Song, S. O. Kang, J. Ko, *Chem. Commun.* **2004**, 68; d) S. Bieller, F. Zhang, M. Bolte, J. W. Bats, H.-W. Lerner, M. Wagner, *Organometallics* **2004**, *23*, 2107.
[7] a) N. Matsumi, K. Naka, Y. Chujo, *J. Am. Chem. Soc.* **1998**, *120*, 5112; b) S. Yamanaka, T. Inoue, T. Aoyagi, T. Komatsu, *Synth. Met.* **1992**, *46*, 221; c) U. Salzner, J. B. Lagowski, P. G. Pickup, R. A. Poirier, *Synth. Met.* **1998**, *96*, 177.
[8] a) Z. Chen, H. Jiao, A. Hirsch, W. Thiel, *Chem. Phys. Lett.* **2000**, *329*, 47; b) L. Türker, A. Azizoglu, *Theochem* **2001**, *535*, 151; c) X. Xu, Y. Xing, Z. Shang, G. Wang, Z. Cai, Y. Pan, X. Zhao, *Chem. Phys.* **2003**, *287*, 317.
[9] J. A. Gamboa, A. Sundararaman, L. Kakalis, A. J. Lough, F. Jäkle, *Organometallics* **2002**, *21*, 4169.
[10] "Metallocene-Based Bidentate Lewis Acids": F. Jäkle, *ACS Symp. Ser.* **2002**, *822*, and references therein.
[11] a) B. Wrackmeyer, U. Dörfler, M. Herberhold, *Z. Naturforsch. B* **1993**, *48*, 121; b) B. Wrackmeyer, U. Dörfler, J. Rinck, M. Herberhold, *Z. Naturforsch. B* **1994**, *49*, 1403; c) B. Wrackmeyer, U. Dörfler, W. Milius, M. Herberhold, *Polyhedron* **1995**, *14*, 1425; d) A. Appel, H. Nöth, M. Schmidt, *Chem. Ber.* **1995**, *128*, 621; e) P. A. Deck, T. S. Fisher, J. S. Downey, *Organometallics* **1997**, *16*, 1193.
[12] X-ray crystal structure analyses: **3**: $C_{32}H_{26}B_2Fe_2$, $M_r = 543.85$, monoclinic, space group $P2_1/c$, $a = 9.1414(6)$, $b = 8.7739(6)$, $c = 15.1355(10)$ Å, $\beta = 101.4410(10)°$, $V = 1189.83(14)$ Å^3, $Z = 2$, $\rho_{calcd} = 1.518$ g cm^{-3}, $\lambda(Mo_{K\alpha}) = 0.71073$ Å, $T = 150(2)$ K, crystal dimensions $0.40 \times 0.30 \times 0.20$ mm^3, $\mu(Mo_{K\alpha}) = 1.240$ mm^{-1}, θ range from 2.27 to 28.28°, 7302 measured reflections, 2789 independent reflections ($R_{int} = 0.0206$), R_1 ($I > 2\sigma(I)$) = 0.0313, wR_2 ($I > 2\sigma(I)$) = 0.0777, GOF = 1.484, 163 parameters, final difference map within 0.517 and −0.353 e Å^{-3}. (**3**$^+$)I_3^-·I_2: $C_{32}H_{26}B_2Fe_2I_5$, $M_r = 1178.35$, monoclinic, space group $P2_1/n$, $a = 18.141(3)$, $b = 11.5344(19)$, $c = 18.752(3)$ Å, $\beta = 118.474(2)°$, $V = 3449.1(10)$ Å^3, $Z = 4$, $\rho_{calcd} = 2.269$ g cm^{-3}, $\lambda(Mo_{K\alpha}) = 0.71073$ Å, $T = 213(2)$ K, crystal dimensions $0.30 \times 0.10 \times 0.10$ mm^3, $\mu(Mo_{K\alpha}) = 5.338$ mm^{-1}, θ range from 2.15 to 28.19°, 25675 measured reflections, 8083 independent reflections ($R_{int} = 0.0300$), R_1 ($I > 2\sigma(I)$) = 0.0333, wR_2 ($I > 2\sigma(I)$) = 0.0946, GOF = 1.025, 370 parameters, final difference map within 1.532 and −0.735 e Å^{-3}. There are two independent half cations on inversion centers and one co-crystallized molecule of I_2. [K(18-c-6)(THF)$_2$][**3**$^-$]: $C_{52}H_{66}B_2Fe_2KO_8$, $M_r = 991.47$, triclinic, space group $P\bar{1}$, $a = 10.049(5)$, $b = 10.913(5)$, $c = 12.313(6)$ Å, $\alpha = 67.864(8)°$, $\beta = 79.656(8)°$, $\gamma = 86.403(8)°$, $V = 1230.4(10)$ Å^3, $Z = 1$, $\rho_{calcd} = 1.338$ g cm^{-3}, $\lambda(Mo_{K\alpha}) = 0.71073$ Å, $T = 100(2)$ K, crystal dimensions $0.14 \times 0.04 \times 0.04$ mm^3, $\mu(Mo_{K\alpha}) = 0.727$ mm^{-1}, θ range from 2.01 to 24.00°, 3900 measured reflections, 3480 independent reflections ($R_{int} = 0.0211$), R_1 ($I > 2\sigma(I)$) = 0.0967, wR_2 ($I > 2\sigma(I)$) = 0.2614, GOF = 1.092, 285 parameters, final difference map within 1.371 and −1.241 e Å^{-3}. *trans*-**5b**: $C_{50}H_{52}B_2Fe_2N_2$, $M_r = 814.26$, monoclinic, space group $C2/c$, $a = 28.2223(18)$, $b = 8.3188(5)$, $c = 21.8954(14)$ Å, $\beta = 127.6860(10)°$, $V = 4068.1(4)$ Å^3, $Z = 4$, $\rho_{calcd} = 1.329$ g cm^{-3}, $\lambda(Mo_{K\alpha}) = 0.71073$ Å, $T = 213(2)$ K, crystal dimensions $0.30 \times 0.20 \times 0.15$ mm^3, $\mu(Mo_{K\alpha}) = 0.751$ mm^{-1}, θ range from 1.82 to 28.22°, 14480 measured reflections, 4785 independent reflections ($R_{int} = 0.0362$), R_1 ($I > 2\sigma(I)$) = 0.0527, wR_2 ($I > 2\sigma(I)$) = 0.1257, GOF = 1.150, 253 parameters, final difference map within 0.517 and −0.423 e Å^{-3}. For all four structures, SADABS (Sheldrick, G. M. SADABS (2.01), Bruker/Siemens Area Detector Absorption Correction Program; Bruker AXS: Madison, WI, 1998) absorption correction was used. Non-hydrogen atoms were refined with anisotropic displacement coefficients, and hydrogen atoms were treated as idealized contributions. CCDC 275645, 275648, 275647, and 275646 (**3**, (**3**$^+$)I_3^-·I_2, [K(18-c-6)(THF)$_2$][**3**$^-$], and *trans*-**5b**, respectively) contain the supplementary crystallographic data for this paper. These data can be obtained free of charge from the Cambridge Crystallographic Data Centre via www.ccdc.cam.ac.uk/data_request/cif.
[13] *Cis* isomers are known for related doubly silyl-bridged species; see: M. Herker, F. H. Köhler, M. Schwaiger, B. Weber, *J. Organomet. Chem.* **2002**, *658*, 266. However, the Fe···B interactions for **3** would lead to severe steric congestion in the *cis* isomer.
[14] M. Scheibitz, M. Bolte, J. W. Bats, H.-W. Lerner, I. Nowik, R. H. Herber, A. Krapp, M. Lein, M. Holthausen, M. Wagner, *Chem. Eur. J.* **2005**, *11*, 584.
[15] H. Akutsu, K. Kozawa, T. Uchida, *Synth. Met.* **1995**, *70*, 1109.
[16] B. E. Carpenter, W. E. Piers, M. Parvez, G. P. A. Yap, S. J. Rettig, *Can. J. Chem.* **2001**, *79*, 857.
[17] a) V. Balzani, A. Credi, F. M. Raymo, J. F. Stoddart, *Angew. Chem.* **2000**, *112*, 3484; *Angew. Chem. Int. Ed.* **2000**, *39*, 3348; b) P. Jutzi, N. Lenze, B. Neumann, H.-G. Stammler, *Angew. Chem.* **2001**, *113*, 1469; *Angew. Chem. Int. Ed.* **2001**, *40*, 1423; c) Z. Dominguez, H. Dang, M. J. Strouse, M. A. Garcia-Garibay, *J. Am. Chem. Soc.* **2002**, *124*, 2398; d) M. F. Hawthorne, J. I. Zink, J. M. Skelton, M. J. Bayer, C. Liu, E. Livshits, R. Baer, D. Neuhauser, *Science* **2004**, *303*, 1849; e) D. Horinek, J. Michl, *J. Am. Chem. Soc.* **2003**, *125*, 11900.
[18] a) R. J. LeSuer, W. E. Geiger, *Angew. Chem.* **2000**, *112*, 254; *Angew. Chem. Int. Ed.* **2000**, *39*, 248; b) F. Barriere, N. Camire, W. E. Geiger, U. T. Mueller-Westerhoff, R. Sanders, *J. Am. Chem. Soc.* **2002**, *124*, 7262.
[19] F. H. Köhler, A. Schell, B. Weber, *J. Organomet. Chem.* **1999**, *575*, 33.

 © 2005 Wiley-VCH Verlag GmbH & Co. KGaA, Weinheim

[20] J. Kreisz, R. U. Kirss, W. M. Reiff, *Inorg. Chem.* **1994**, *33*, 1562.
[21] See Supporting Information for experimental details, ORTEP plots of $(\mathbf{3}^{+})I_3 \cdot I_2$, $[K(18\text{-c-}6)(THF)_2][\mathbf{3}^{\cdot-}]$, and *trans*-**5b**, a plot of the extended structure of $(\mathbf{3}^{+})I_3 \cdot I_2$, and a comparative plot of the IR spectra of **3** and $(\mathbf{3}^{+})I_3 \cdot I_2$.
[22] a) J. A. Kramer, D. N. Hendrickson, *Inorg. Chem.* **1980**, *19*, 3330; b) J. A. Kramer, F. H. Herbstein, D. N. Hendrickson, *J. Am. Chem. Soc.* **1980**, *102*, 2293; c) T.-Y. Dong, D. N. Hendrickson, C. G. Pierpont, M. F. Moore, *J. Am. Chem. Soc.* **1986**, *108*, 963; d) R. J. Webb, S. J. Geib, D. L. Staley, A. L. Rheingold, D. N. Hendrickson, *J. Am. Chem. Soc.* **1990**, *112*, 5031.
[23] D. O. Cowan, P. Shu, F. L. Hedberg, M. Rossi, T. J. Kistenmacher, *J. Am. Chem. Soc.* **1979**, *101*, 1304.
[24] a) J. D. Hoefelmeyer, F. P. Gabbaï, *J. Am. Chem. Soc.* **2000**, *122*, 9054; b) J. D. Hoefelmeyer, S. Solé, F. P. Gabbaï, *J. Chem. Soc. Dalton Trans.* **2004**, 1254.
[25] The X-ray crystal structure of the radical anion $(BMes_3)^{\cdot-}$ (Mes = mesityl) has been reported; see: M. M. Olmstead P. P. Power, *J. Am. Chem. Soc.* **1986**, *108*, 4235.
[26] M. Scheibitz, J. B. Heilmann, R. F. Winter, M. Bolte, J. W. Bats, M. Wagner, *Dalton Trans.* **2005**, 159.

 © 2005 Wiley-VCH Verlag GmbH & Co. KGaA, Weinheim

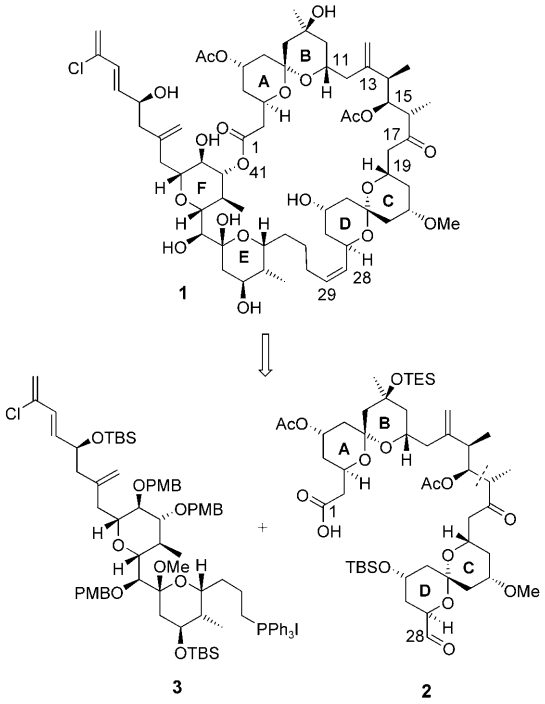
Natural Product Synthesis

DOI: 10.1002/anie.200502008

Total Synthesis of Spongistatin 1: A Synthetic Strategy Exploiting Its Latent Pseudo-Symmetry**

*Matthew Ball, Matthew J. Gaunt, David F. Hook, Alan S. Jessiman, Shigeru Kawahara, Paolo Orsini, Alessandra Scolaro, Adam C. Talbot, Huw R. Tanner, Shigeo Yamanoi, and Steven V. Ley**

The spongistatins comprise an important family of architecturally complex marine macrolides that display extraordinary antitumor activities against a variety of human cancer cell lines. These unique natural products were isolated independently by Pettit, Kitagawa and Fusetani in 1993,[1] although the absolute structure remained unknown until confirmation by synthesis in 1997.[2] The spongistatin family includes 9 macrolides, all of which possess remarkable growth inhibition properties against the US National Cancer Institute's panel of sixty human cancer cell lines. Spongistatin 1 (**1**) was extremely potent against a subset of highly chemoresistant tumor types, with typical GI_{50} values of $2.5–3.5 \times 10^{-1}$ M. Cell lines derived from human melanoma were also found to be especially sensitive to Spongistatin 1,[1f,h] the most active of this family of macrolides (Scheme 1).



Scheme 1. Structure and retrosynthetic analysis of Spongistatin 1 (**1**). TES = triethylsilyl, TBS = *tert*-butyldimethylsilyl, PMB = *p*-methoxybenzyl.

Spongistatin 1 (**1**) comprises a 42-membered macrolide ring, 24 asymmetric centers, a chlorodiene sidechain, two spiroketals (of which only one contains full anomeric stabilization) and two pyranyl units. The complex molecular architecture and exciting biological profile of these natural products have attracted significant interest resulting in total syntheses by six groups.[2–3] Our initial synthetic analysis for **1** was consistent with established endgame strategies and corresponded to a C1–C41(OH) macrolactonization and C28–C29 Wittig olefination, resulting in two advanced fragments (ABCD fragment **2** and EF fragment **3**) and hence enabling a convergent approach to the target (Scheme 1).[2–3] Furthermore, we recognized the utility of the *anti*-selective aldol coupling demonstrated by the groups of Evans,[2a] Paterson,[3d] Heathcock[3f] and more recently Smith[3a] and Crimmins,[3e] to join the AB and CD units together to form the basis of fragment **2** in their total syntheses. Accordingly, we envisaged that appropriately protected AB aldehyde **4** and

[*] Dr. M. Ball, Dr. M. J. Gaunt, Dr. D. F. Hook, A. S. Jessiman, S. Kawahara, P. Orsini, A. Scolaro, A. C. Talbot, H. R. Tanner, Dr. S. Yamanoi, Prof. Dr. S. V. Ley
Department of Chemistry, University of Cambridge
Lensfield Road, Cambridge, CB21EW (UK)
Fax: (+44) 122-333-6442
E-mail: svl1000@cam.ac.uk

[**] The authors thank Novartis for the Novartis Research Fellowship (S.V.L.) and a fully funded studentship (H.T.), the British Ramsey Trust and Magdalene College, Cambridge for a research fellowship (M.J.G.), Pfizer Global Research and Development, Sandwich (UK) (A.S.J.), Pharmacia, Italy (P.O. and A.S.), Ajinomoto Inc., Japan (S.K.), the Uehara Memorial Foundation for a postdoctoral fellowship (S.Y.), the EPSRC for studentships (A.C.T. and D.F.H.) and a postdoctoral fellowship (M.B.). We also acknowledge the contribution of Dr. Richard Turner (University of Cambridge) whose expertise in preparative HPLC proved invaluable.

 © 2005 Wiley-VCH Verlag GmbH & Co. KGaA, Weinheim

CD ketone **5** would be suitable coupling partners for this transformation (Scheme 2).

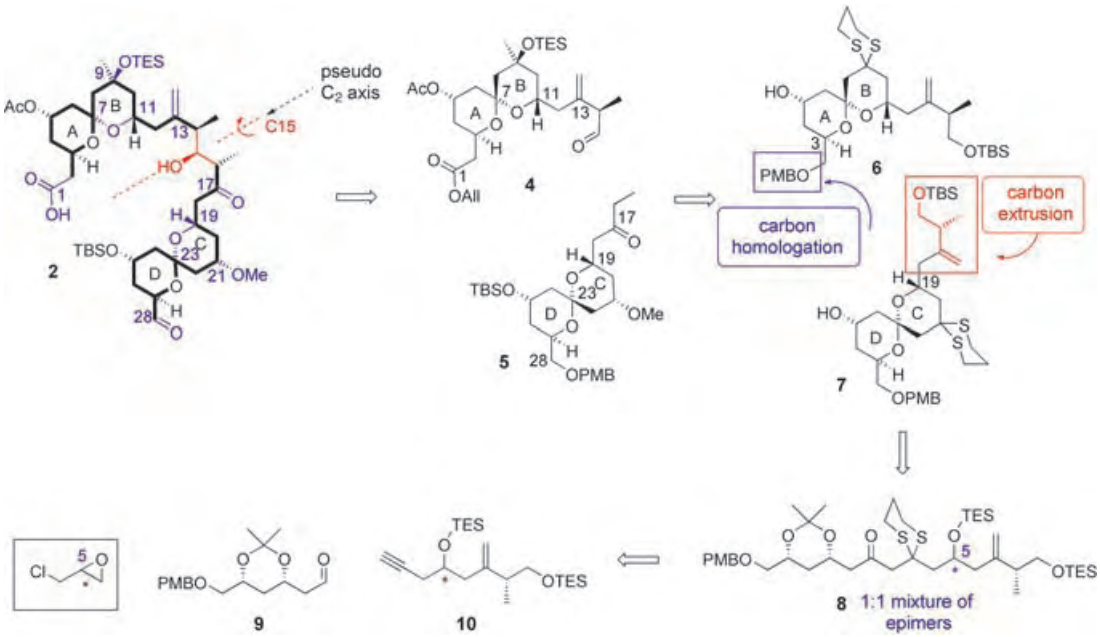
We have previously reported independent syntheses of both the AB (**4**) and CD (**5**) fragments,[4] employing acetylide–aldehyde C–C-bond formation–oxidation followed by addition of 1,3-propanedithiol to the resulting ynone as the key coupling approach for polyketide synthesis. Despite the high efficiency in these syntheses (average yield per step: 89% (**4**); 92% (**5**)), we felt that the overall sequence length, (64 discrete steps to assemble the ABCD precursors) precludes the synthesis of significant quantities of the spongistatins. As a result, we have developed an innovative second-generation route towards the ABCD bis(spiroketal) moiety **2**, which is reported here along with completion of the synthesis of the natural product.[5]

Close examination of the ABCD fragment **2** of Spongistatin 1 reveals a high level of latent C_2-symmetry about the C15 atom namely, the carbon framework from C1 to C14 is very similar to that of C16 to C28 (Scheme 2).[6] The A and D rings of the spiroketals are essentially identical and differ principally due to their anomeric arrangements and the C11 and C19 stereocenters, which are oppositely configured. We have already shown that the functionality at both C9 and C21 can be introduced through a carbonyl group interconversion.[4] Therefore, C1–C12 and C18–C28 differ by only one carbon atom and one stereocenter. Furthermore, the sp^2-carbon atoms at C13 and C17 are pseudo-symmetric about C15, as are the methyl groups at C14 and C16. These observations suggest that it may be possible to access the C1–C15 and C15–C28 fragments from an epimeric mixture of acyclic precursor **8**, dramatically decreasing the number of steps required to assemble the ABCD fragment (Scheme 2).

From an acyclic precursor **8**, one C5 epimer will furnish the AB spiroketal core **6**, whilst the opposite C5 epimer would yield the CD framework **7**. Post-spiroketalization modification should enable interception of our original routes to AB (**4**) and CD (**5**) subunits. Towards this goal, the AB spiroketal unit **6** requires one-carbon homologation in the C3 sidechain to generate the allyl ester **4**. In contrast, the CD unit **7** requires conversion of the exocyclic alkene into a ketone followed by effective formyl extrusion (via decarboxylation) from the C19 terminus to afford the ethyl ketone **5**. The utility of this pseudo-symmetric strategy hinges upon the ability to efficiently facilitate sidechain interconversion and is of central importance to the success of our second-generation synthetic strategy (Scheme 2).

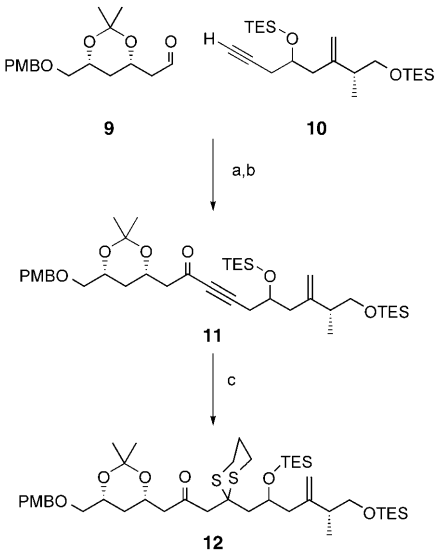
The synthesis begins with the preparation of the acyclic precursor **8**. We have previously prepared key aldehyde **9** from (*S*)-glycidol in the first-generation synthesis of the CD ketone.[4a] Formation of alkyne **10** as an epimeric mixture at C5 was achieved by adaptation of previously developed chemistry towards the AB spiroketal, in this case employing racemic epichlorohydrin as the central electrophilic component.[4b] Addition of the anion of alkyne **10** (formed through treatment with *i*PrMgCl) to aldehyde **9** generated a propargylic alcohol as a 1:1 mixture of diastereomers in 85% yield. Oxidation with Dess–Martin periodinane lead to ynone **11**, which afforded acyclic spiroketal precursor **12** in excellent yield by double conjugate addition of 1,3-propanedithiol (83% over 3 steps, Scheme 3).

Treatment of ketone **12** with dilute perchloric acid generated three different spiroketals corresponding to the AB double anomeric stabilized unit **13** (AB_{AA}) and the two CD anomeric isomers, bis-anomeric **14** (CD_{AA}) and mono-anomeric **15** (CD_{AE}), in a ratio of $AB_{AA}/CD_{AA}/CD_{AE}$ 1.00:0.74:0.26 (Scheme 4). The three spiroketals were separated by preparative HPLC[7] to afford the key cores of the AB and CD fragments in a total of only 26 discrete steps (17 longest linear sequence). The bis-anomeric **14** (CD_{AA}) spiroketal was equilibrated under calcium perchlorate epi-

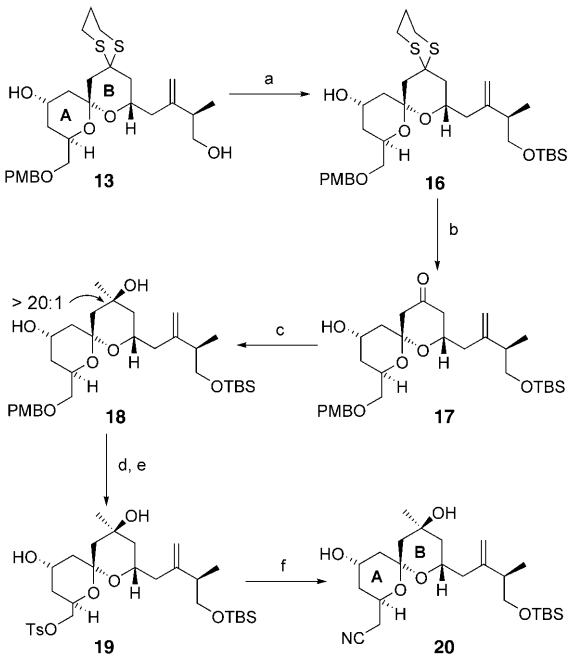


Scheme 2. Pseudo-symmetric retrosynthetic analysis of the ABCD bis(spiroketal) fragment **2**.

 © 2005 Wiley-VCH Verlag GmbH & Co. KGaA, Weinheim



Scheme 3. Reagents and conditions: a) *i*PrMgCl, **10**, THF, 2 h, RT; then **9**, THF, −20 °C, 1 h; b) Dess–Martin periodinane, CH_2Cl_2, RT, 1 h, 85 % over two steps; c) $HS(CH_2)_3SH$, NaOMe, MeOH–CH_2Cl_2, −10 °C→RT, 16 h, 97 %.

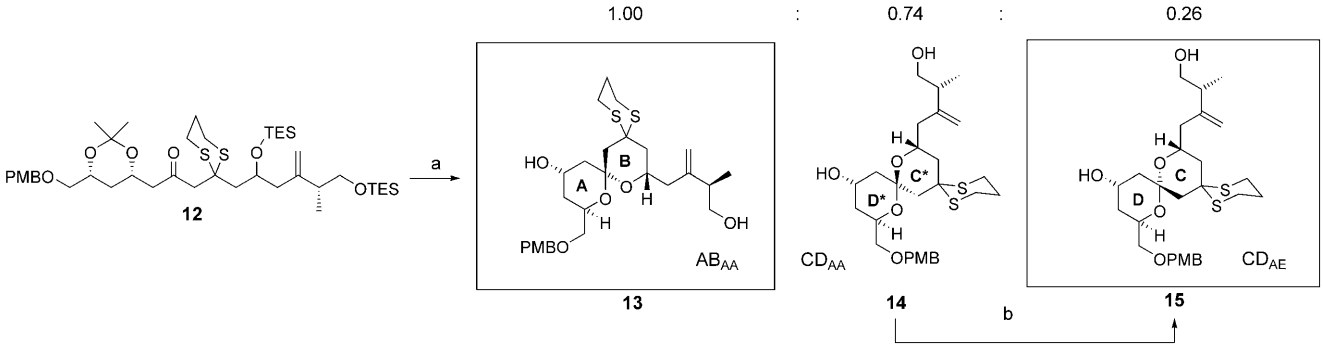


Scheme 5. Reagents and conditions: a) TBSCl, imidazole, CH_2Cl_2, RT, 17 h, 94 % ; b) I_2, aq. $NaHCO_3$, MeCN, 0 °C, 1 h, 99 %; c) MeLi, $CeCl_3$, THF, −78 °C, 1 h, 94 %; d) DDQ, pH 7 buffer, CH_2Cl_2, 2 h, RT, 98 %; e) *p*-TsCl, CH_2Cl_2, pyridine, RT, 19 h, 97 %; f) NaCN, DMF, 70 °C, 6 h, 80 %. DDQ = 2,3-dichloro-5,6-dicyano-*p*-benzoquinone; *p*-TsCl = *p*-toluenesulfonyl chloride; DMF = *N*,*N*-dimethylformamide.

merization conditions[3a,4] and cleanly converted into the desired mono-anomeric spiroketal **15** (CD_{AE}) (87 % yield after a 3-step recycle sequence). The equilibration process required 16 h to afford a 3:1 mixture in favor of the desired isomer. Interestingly, the presence of the primary hydroxy group in the C19 sidechain increased the proportion of **15** (CD_{AE}) after equilibration. This observation is in agreement with the results of Evans et al.[2a] and Smith et al.[3a] and in accord with our findings in our earlier CD fragment synthesis, which lacked oxygen substitution in the C19 sidechain[4a] (first generation $CD_{AA}/CD_{AE} = 1.0:2.2$, second generation $CD_{AA}/CD_{AE} = 1.0:3.0$). With an efficient method for the formation of both AB and CD spiroketal core structures now available, we investigated subsequent side-chain manipulation to afford the aldol-coupling fragments **4** and **5**.

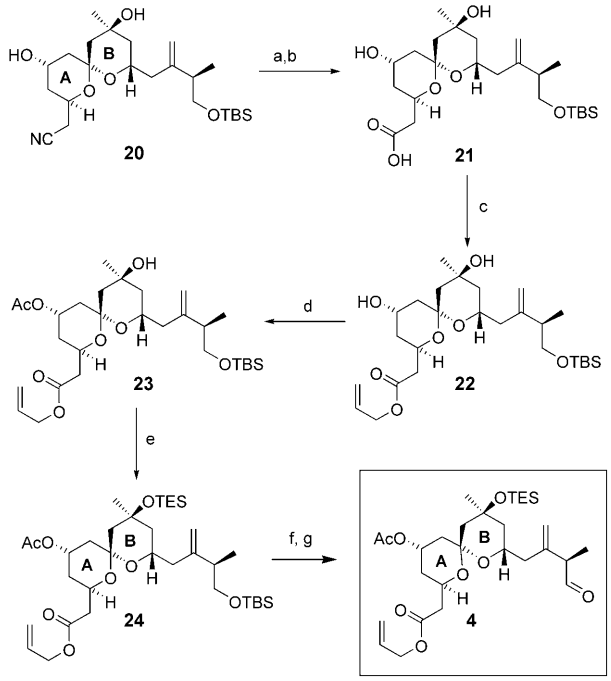
Elaboration of spiroketal **13** began by the selective protection of the primary hydroxy group as its silyl ether followed by iodine-facilitated cleavage of the dithiane unit[8] to afford the corresponding ketone **17** in excellent yield over two steps (Scheme 5). Methyl group addition mediated by the organocerium reagent derived from MeLi and $CeCl_3$ formed the tertiary alcohol **18** as a single diastereomer (d.r. > 20:1). Oxidative cleavage of the *p*-methoxybenzyl ether with DDQ and subsequent mono-tosylation of the resulting primary alcohol activated the C3 sidechain for carbon homologation. Tosylate displacement with NaCN[9] afforded **20** in good yield.

Cyanide **20** was converted into the corresponding acid **21** via reduction to the aldehyde followed by Pinnick oxidation (Scheme 6).[10] Alkylation of the carboxy group by allyl bromide–cesium carbonate furnished the full AB spiroketal skeleton **22**. Selective acetylation of the secondary alcohol followed by TES protection of the tertiary hydroxy group formed **24** in good yield over two steps. HF–pyridine complex removed the *tert*-butylsilyl group and subsequent oxidation of the primary hydroxy group using Dess–Martin periodinane[11]

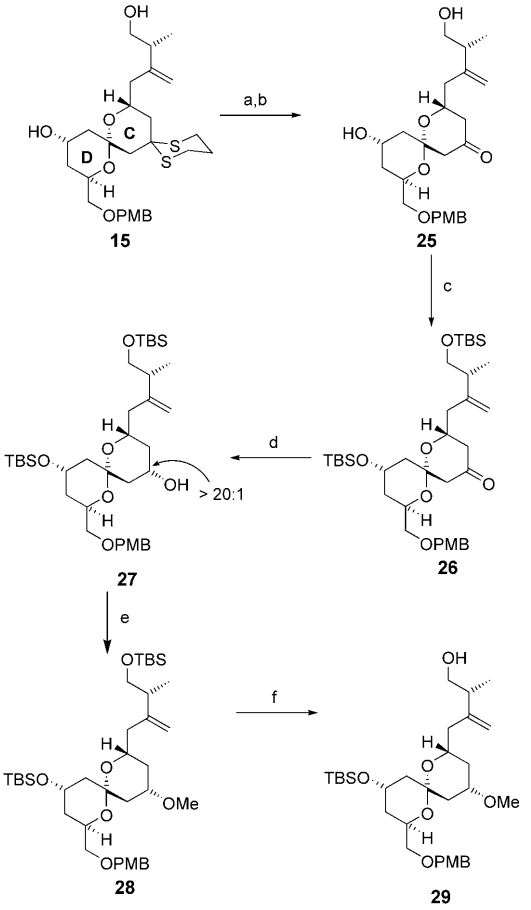


Scheme 4. Reagents and conditions: a) 10 % aq. $HClO_4$, MeCN–CH_2Cl_2, RT, 30 min, 86 %; b) 3.5 % aq. $HClO_4$, 5 equiv $Ca(ClO_4)_2 \cdot 4H_2O$, MeCN–CH_2Cl_2, RT, 18 h, 87 % after three recycles.

 © 2005 Wiley-VCH Verlag GmbH & Co. KGaA, Weinheim



Scheme 6. Reagents and conditions: a) DIBAL-H (1 M in CH_2Cl_2), CH_2Cl_2 −78 °C→RT, 6 h; b) $NaClO_2$, *t*BuOH, 2-methyl-2-butene, pH 7 buffer, RT, 2 h; c) allyl bromide, Cs_2CO_3, THF, RT, 17 h, 51% over three steps; d) Ac_2O, pyridine, DMAP, CH_2Cl_2, RT, 65 h, 86%; e) TESOTf, 2,6-lutidine, −78→0 °C, 1 h, 99%; f) HF·pyridine, pyridine–THF, RT 7 h; g) Dess–Martin periodinane, py, CH_2Cl_2, RT, 3 h, 66% over two steps. DIBAL-H = diisobutylaluminum hydride; DMAP = 4-(*N*,*N*-dimethylamino)pyridine; Tf = trifluoromethanesulfonyl.

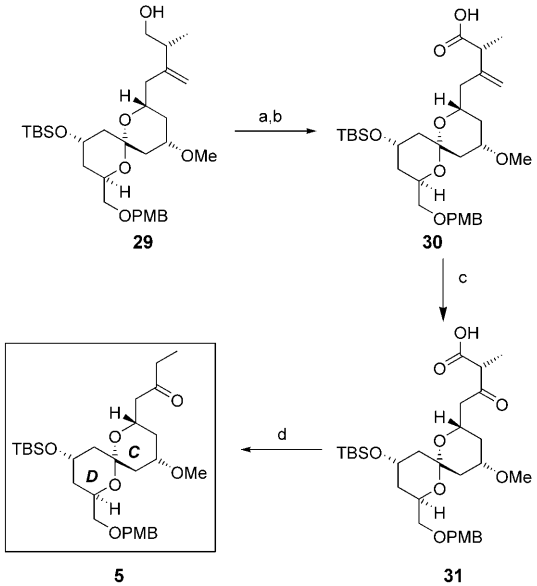


Scheme 7. Reagents and conditions: a) 2 equiv $PhI(Tfa)_2$, MeOH, 0 °C, 40 min; b) aq. $NaHCO_3$, AcOH–THF–H_2O, 30 °C, 6 h; c) TBSCl, imidazole, DMF, RT, 14 h, 82% over three steps; d) $NaBH_4$, $CeCl_3 \cdot 7H_2O$, THF, MeOH, −78 °C, 1 h, 87%; e) NaH, MeI, THF, 0 °C→RT, 22 h, 96%; f) HF·Pyridine, pyridine–THF, RT, 7 h, 75%. Tfa = trifluoroacetyl.

afforded key aldehyde **4** that was used immediately in the aldol coupling.

After efficient generation of the anomeric **15** (CD_{AE}) spiroketal unit we began its manipulation towards the CD ethyl ketone **5** (Scheme 7). Initially, two-step dithiane cleavage via the dimethylketal afforded ketone **25** in good yield; this procedure circumvents product decomposition that occurred under a variety of other cleavage conditions.[4a,12] Treatment of diol **25** with TBSCl and imidazole in DMF formed the bis(silyl ether) in excellent yield over the opening sequence (82% over 3 steps). Reduction under modified Luche conditions[13] afforded the desired equatorial C15 alcohol as essentially one diastereomer **27** (d.r. > 20:1), arising from the expected axial hydride delivery. Methylation proceeded with excellent yield, followed by selective primary silyl ether cleavage, forming the basis for investigation into the required carbon extrusion chemistry. Results from model studies on formyl group expulsion indicated that decarboxylation of a β-ketoacid would be the most reliable tactic.

To this end, oxidation of alcohol **29** with Dess–Martin periodinane[11] followed by Pinnick oxidation[10] afforded the acid **30**, and brief treatment with ozone in dichloromethane cleanly delivered the β-ketoacid **31** without affecting the primary *p*-methoxybenzyl ether (Scheme 8). The crude material could be smoothly decarboxylated with gentle heating in a toluene/pyridine (2:1) mixture, efficiently delivering the CD

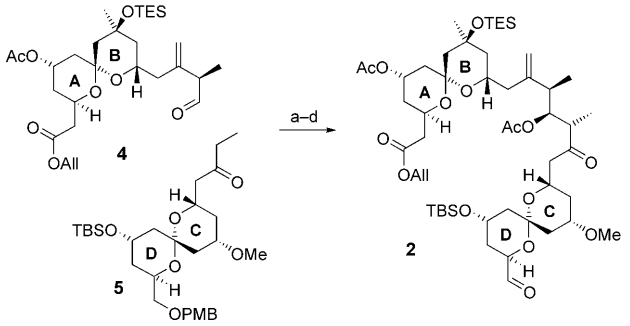


Scheme 8. Reagents and conditions: a) Dess–Martin periodinane, CH_2Cl_2, RT, 1 h; b) $NaClO_2$, *t*BuOH, 2-methyl-2-butene, pH 7 buffer, RT, 2 h; c) O_3, CH_2Cl_2, −78 °C, 3 min; then Me_2S, concentrate; d) toluene/pyridine (2:1), 40 °C, 3 h, 57% over four steps.

 © 2005 Wiley-VCH Verlag GmbH & Co. KGaA, Weinheim

ethyl ketone spiroketal unit **5** ready for use in the aldol coupling.

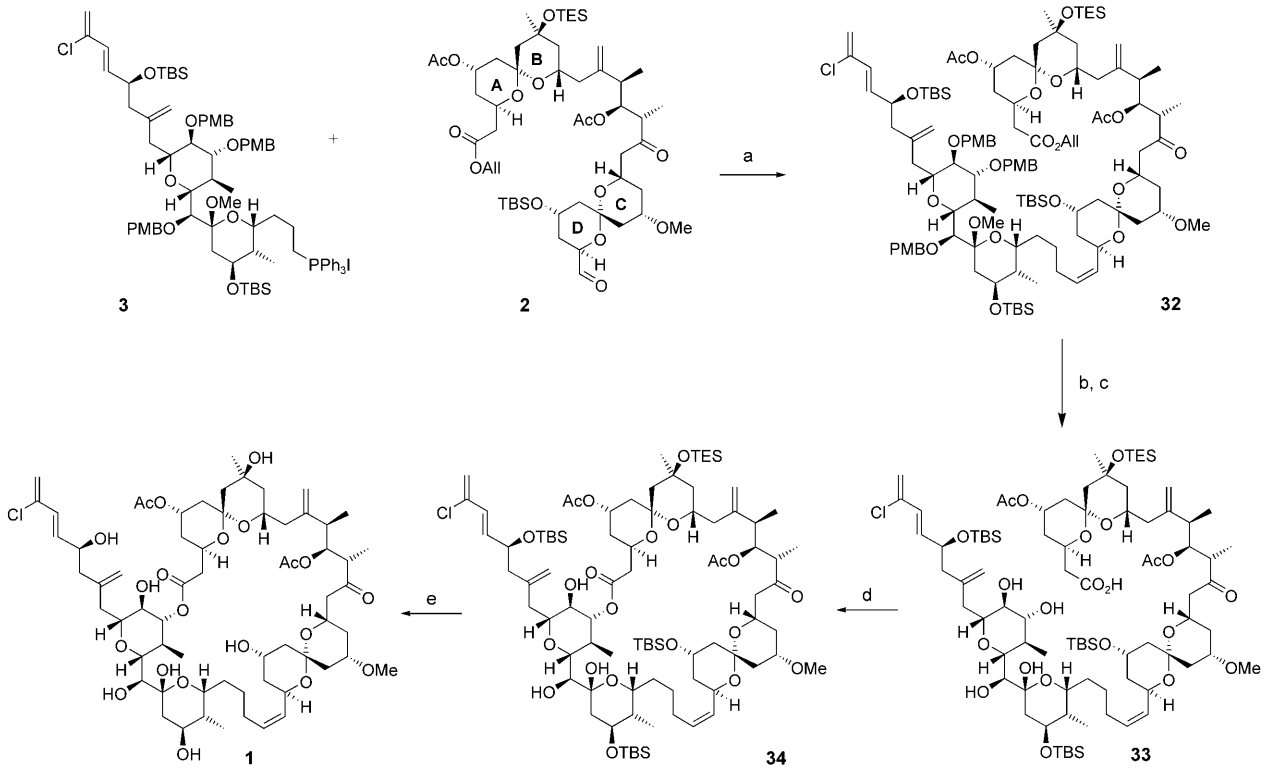
With gram-quantities of the key fragments available, we investigated the aldol union of the CD ketone **5** and AB aldehyde **4** (Scheme 9). Initially, we used the aldol conditions



Scheme 9. Reagents and conditions: a) BCy_2Cl, Et_3N, Et_2O, −78 °C→0 °C, 10 min; 0 °C→−78 °C; **4**, 1 h; −78 °C→−30 °C, 16 h, 78%, d.r. = 5:1; b) Ac_2O, pyridine, 0 °C→RT, 5 h; c) DDQ, CH_2Cl_2–pH 7 buffer, 0 °C, 5 h; d) Dess–Martin periodinane, CH_2Cl_2, RT, 3 h, 66% over three steps. Cy = cyclohexyl.

described by Evans' group employing pentane as the solvent. Treatment of ketone **5** with dicyclohexylboron chloride formed the *E*-boron enolate and following reaction with aldehyde **4** formed the *anti*-aldol product as an 8:1 mixture of diastereomers (45% yield of desired diastereoisomer). Given the subtle structural differences between our substrates and the Evans fragments[2a] we initiated a solvent screen which showed that upon switching to diethyl ether[3d] the reaction efficiency was greatly increased (78% yield) to afford a 5:1 mixture of diasterosiomers (65% of desired *anti*-adduct). Subsequent acetylation, PMB ether cleavage and oxidation proceeded in high yield to furnish ABCD aldehyde **2**, ready for Wittig coupling with the EF phosphonium salt **3**.

We have previously reported model studies[14] and recently the completion of the EF phosphonium Wittig salt **3**,[15] which we subsequently employed in hemisphere unification. The difficulties associated with late-stage Wittig coupling between ABCD aldehyde **2** and EF phosphonium salt **3** have been widely reported[2,3] and are in accord with our experience (Scheme 10). After experimentation with a variety of literature conditions, we used a modification of the procedure reported by Heathcock and co-workers[3f] (MeLi·LiBr), employing CaH_2 to remove residual water that may reduce yields due to hydrate formation. Furthermore, the addition of HMPA facilitated ylide formation and subsequent treatment with aldehyde **2** afforded the *cis* alkene **32** with comparable[3f] efficiency and selectivity (yield 50%). Oxidative removal of all *p*-methoxybenzyl protecting groups in a biphasic solvent system (CH_2Cl_2–THF–pH 7 buffer) was accompanied by complete hydrolysis of the C37 methoxyketal. Cleavage of the allyl ester protecting group with Pd^0 efficiently furnished the key secoacid intermediate **33**. Macrolactonization of **33** under modified Yamaguchi conditions[2a] yielded silyl-protected Spongistatin 1 **34**. Global



Scheme 10. Reagents and conditions: a) **3** treated with MeLi·LiBr, THF, −78 °C; then **2** (after drying over CaH_2), −78 °C→RT, 50%; b) DDQ, THF–CH_2Cl_2–pH 7 buffer, RT, 65%; c) $[Pd(PPh_3)_4]$, morpholine, RT; d) 2,4,6-trichlorobenzoylchloride, iPr_2NEt, DMAP, toluene, 90 °C, 56% over two steps; e) 48% HF, CH_3CN, −21 °C, 57%.

 © 2005 Wiley-VCH Verlag GmbH & Co. KGaA, Weinheim

silyl group removal by treatment with 48% HF yielded Spongistatin 1 (**1**), which was identical in all respects to an authentic sample.[16]

We have completed a synthesis of Spongistatin 1 (**1**) using established synthetic procedures and methods developed within our research group, including the introduction and subsequent manipulation of β-keto dithiane precursors. Furthermore, the pseudo-symmetric strategy used in forming the ABCD bis(spiroketal) unit **2** represents a new approach towards the family of Spongistatin natural products. The AB spiroketal unit **4** was prepared in 36 steps (overall yield 10% over a 27 step longest linear sequence, average yield 90% per step) and the CD fragment **5** in 37 steps (overall yield 6% over a 28 step longest linear sequence, average yield per step 89%). By applying the pseudo-symmetric approach we are able to access much larger quantities of the key ABCD fragment **2** than from our original route, hence providing the basis for a pragmatic and expedient assembly of the ABCD fragment. By application of the pseudo-symmetric strategy the route is decreased from 65 to only 46 discrete steps from commercially available starting materials. Ongoing work in our laboratories is focusing on further improving the efficiency and scale of the synthetic sequences towards the goal of producing significant quantities of Spongistatin 1.

Received: June 10, 2005
Published online: August 1, 2005

Keywords: dithianes · natural products · pseudo-symmetry · spongistatin 1 · total synthesis

[1] a) G. R. Pettit, *J. Nat. Prod.* **1996**, *59*, 812; b) G. R. Pettit, Z. A. Cichacz, F. Goa, C. L. Herald, M. R. Boyd, J. M. Schmidt, J. N. A. Hooper, *J. Org. Chem.* **1993**, *58*, 1302; c) G. R. Pettit, A. Z. Cichacz, F. Goa, C. L. Herald, M. R. Boyd, *J. Chem. Soc. Chem. Commun.* **1993**, 1166; d) G. R. Pettit, C. L. Herald, Z. A. Cichacz, F. Goa, M. R. Boyd, N. D. Christie, J. M. Schmidt, *Nat. Prod. Lett.* **1993**, *5*, 329; e) G. R. Pettit, Z. A. Cichacz, C. L. Herald, F. Goa, M. R. Boyd, E. Hamel, R. Bai, *J. Chem. Soc. Chem. Commun.* **1994**, 1605; f) R. Bai, Z. A. Cichacz, C. L. Herald, G. R. Pettit, E. Hamel, *Mol. Pharmacol.* **1993**, *44*, 757; g) R. K. Pettit, S. McAllister, G. R. Pettit, *Antimicrob. Agents* **1998**, *9*, 147; h) R. Bai, G. F. Taylor, Z. A. Chicacz, C. L. Herald, J. A. Keplar, G. R. Pettit, E. Hamel, *Biochemistry* **1995**, *34*, 9714; i) M. Kobayashi, S. Aoki, H. Sakai, K. Kawazoe, N. Kihara, T. Sasaki, I. Kitagawa, *Tetrahedron Lett.* **1993**, *34*, 2795; j) M. Kobayashi, S. Aoki, I. Kitagawa, *Tetrahedron Lett.* **1994**, *35*, 1243; k) M. Kobayashi, S. Aoki, H. Sakai, N. Kihara, T. Sasaki, I. Kitagawa, *Chem. Pharm. Bull.* **1993**, *41*, 989; l) M. Kobayashi, S. Aoki, I. K. Gato, I. Kitagawa, *Chem. Pharm. Bull.* **1996**, *44*, 2142; m) N. Fusetani, K. Shinoda, S. Matsunaga, *J. Am. Chem. Soc.* **1993**, *115*, 3977.

[2] a) D. A. Evans, P. J. Coleman, L. C. Dias, *Angew. Chem.* **1997**, *109*, 2951; *Angew. Chem. Int. Ed. Engl.* **1997**, *36*, 2737; D. A. Evans, B. W. Trotter, B. Côté, P. J. Coleman, *Angew. Chem.* **1997**, *109*, 2954; *Angew. Chem. Int. Ed. Engl.* **1997**, *36*, 2741; D. A. Evans, B. W. Trotter, B. Côté, P. J. Coleman, L. C. Dias, A. N. Tyler, *Angew. Chem.* **1997**, *109*, 2957; *Angew. Chem. Int. Ed. Engl.* **1997**, *36*, 2744; D. A. Evans, B. W. Trotter, P. J. Coleman, B. Côté, L. C. Dias, H. A. Rajapaske, A. N. Tyler, *Tetrahedron* **1999**, *55*, 8671; b) J. Guo, K. J. Duffy, K. L. Stevens, P. I. Dalko, R. M. Roth, M. M. Hayward, Y. Kishi, *Angew. Chem.* **1998**, *110*, 198; *Angew. Chem. Int. Ed.* **1998**, *37*, 187; M. M. Hayward, R. M. Roth, K. J. Duffy, P. I. Dalko, K. L. Stevens, J. Guo, Y. Kishi, *Angew. Chem.* **1998**, *110*, 202; *Angew. Chem. Int. Ed.* **1998**, *37*, 190.

[3] a) A. B. Smith III, V. A. Doughty, Q. Lin, L. Zhuang, M. D. McBriar, A. M. Boldi, W. H. Moser, N. Murase, K. Nakayama, M. Sobukawa, *Angew. Chem.* **2001**, *113*, 197; *Angew. Chem. Int. Ed.* **2001**, *40*, 191; b) A. B. Smith III, Q. Lin, V. A. Doughty, L. Zhuang, M. D. McBriar, J. K. Kerns, C. S. Brook, N. Murase, K. Nakayama, M. Sobukawa, *Angew. Chem.* **2001**, *113*, 202; *Angew. Chem. Int. Ed.* **2001**, *40*, 196; c) A. B. Smith III, V. A. Doughty, C. Sfouggatakis, C. S. Bennett, J. Koyanagi, M. Takeuchi, *Org. Lett.* **2002**, *4*, 783; d) I. Paterson, M. J. Coster, D. Y.-K. Chen, R. M. Oballa, D. J. Wallace, R. D. Norcross, *Org. Biomol. Chem.* **2005**, *3*, 2399; I. Paterson, M. J. Coster, D. Y.-K. Chen, K. R. Gibson, D. J. Wallace, *Org. Biomol. Chem.* **2005**, *3*, 2410; I. Paterson, M. J. Coster, D. Y.-K. Chen, J. L. Aceña, J. Bach, L. E. Keown, T. Trieselmann, *Org. Biomol. Chem.* **2005**, *3*, 2420; I. Paterson, D. Y.-K. Chen, M. J. Coster, J. L. Aceña, J. Bach, D. J. Wallace, *Org. Biomol. Chem.* **2005**, *3*, 2431; I. Paterson, D. Y.-K. Chen, M. J. Coster, J. L. Acena, J. Bach, K. R. Gibson, L. E. Keown, R. M. Oballa, T. Trieselmann, D. J. Wallace, A. P. Hodgson, R. D. Norcross, *Angew. Chem.* **2001**, *113*, 4179; *Angew. Chem. Int. Ed.* **2001**, *40*, 4055; e) M. T. Crimmins, J. D. Katz, D. G. Washburn, S. P. Allwein, L. F. McAtee, *J. Am. Chem. Soc.* **2002**, *124*, 5661; f) M. M. Claffey, C. J. Hayes, C. H. Heathcock, *J. Org. Chem.* **1999**, *64*, 8267, J. L. Hubbs, C. H. Heathcock, *J. Am. Chem. Soc.* **2003**, *125*, 12836; C. H. Heathcock, M. McLaughlin, J. Medina, J. L. Hubbs, G. A. Wallace, R. Scott, M. M. Claffey, C. J. Hayes, G. R. Ott, *J. Am. Chem. Soc.* **2003**, *125*, 12844.

[4] a) M. J. Gaunt, D. F. Hook, H. R. Tanner, S. V. Ley, *Org. Lett.* **2003**, *5*, 4815; b) M. J. Gaunt, A. S. Jessiman, P. Orsini, H. R. Tanner, D. F. Hook, S. V. Ley, *Org. Lett.* **2003**, *5*, 4819.

[5] First reported at the *Chemistry A European Journal* Symposium, Strasbourg, France, April 15, 2005.

[6] This structural feature has also been noted by Roush et al. who applied a double inversion tactic as the basis of forming the AB and CD spiroketal cores from a common intermediate. E. B. Holson, W. R. Roush, *Org. Lett.* **2002**, *4*, 3719–3722, E. B. Holson, W. R. Roush, *Org. Lett.* **2002**, *4*, 3723–3725.

[7] The spiroketals can also be separated by two successive column-chromatography operations. However in terms of overall efficiency, preparative HPLC proved to be the method of choice. Employing this separation method, multi-gram quantities of crude spiroketal reaction mixture could be purified and separated in one day.

[8] M.-K. Chen, G. E. Hardtmann, K. Prasad, O. Repic, M. J. Shapiro, *Tetrahedron Lett.* **1987**, *28*, 155.

[9] R. Baker, M. J. O'Mahony, C. J. Swain, *J. Chem. Soc. Perkin Trans. 1* **1987**, 1623.

[10] B. S. Bal, W. E. Childers, H. W. Pinnick, *Tetrahedron* **1981**, *37*, 2091.

[11] D. B. Dess, J. C. Martin, *J. Org. Chem.* **1983**, *48*, 4383.

[12] Conditions based on modification of procedure reported in G. Stork, K. Zhoa, *Tetrahedron Lett.* **1989**, *30*, 287.

[13] A. L. Gemal, J.-L. Luche, *J. Am. Chem. Soc.* **1981**, *103*, 5454.

[14] E. Fernandez-Megia, N. Gourlaouen, S. V. Ley, G. J. Rowlands, *Synlett* **1998**, 991.

[15] S. Kawahara, M. J. Gaunt, A. Scolaro, S. Yamanoi, S. V. Ley, *Synlett* **2005**, DOI: 10.1055/s-2005-871960.

[16] The authentic sample of Spongistatin 1 (**1**) was kindly provided by Professor Pettit.

 © 2005 Wiley-VCH Verlag GmbH & Co. KGaA, Weinheim

Fluorescent Probes

DOI: 10.1002/anie.200501542

Extension of the Applicable Range of Fluorescein: A Fluorescein-Based Probe for Western Blot Analysis**

*Mako Kamiya, Yasuteru Urano, Nobuyoshi Ebata, Masami Yamamoto, Jyunichi Kosuge, and Tetsuo Nagano**

Western blot immunoanalysis is a powerful method for detecting proteins of interest on a nitrocellulose or polyvinylidene fluoride (PVDF) membrane.[1–3] The presence of a target protein is usually detected by using a secondary antibody conjugated with an enzyme such as alkaline phosphatase (ALP), which allows marked signal amplification,[4] in combination with a chromogenic, fluorescent, or chemiluminescent probe.[5–7] Among these techniques, only fluorescence detection offers high sensitivity and the possibility of multicolor labeling.[8,9] Furthermore, fluorescence signals, unlike transient chemiluminescence signals, can be imaged several times and are stable on a dried blot. However, the range of fluorescence probes applicable to Western blot analysis is limited at the present time. In particular, probes based on the fluorescein molecule have rarely been used in this analysis despite their extensive exploitation in other biological techniques.[10–13] For example, fluorescein diphosphate (FDP),[14–17] a fluorescein-based ALP probe, is seldom used to detect the activity of the widely used secondary detection enzyme ALP in Western blot analysis. Nevertheless, the superior optical properties of fluorescein, such as high molar extinction coefficients and high quantum yields of fluorescence in aqueous media as well as efficient excitation by an argon ion laser (488 nm), make the development of fluorescein-based probes for ALP suitable for Western blot analysis highly desirable. Herein, we report a new probe for ALP based on a fluorescein derivative that we developed recently[18] which works effectively even on Western blots and makes it possible to perform multicolor labeling.

A critical requirement of probes for Western blot analysis is that the hydrolysis product has adequate affinity for the blot. We confirmed that fluorescein generated by ALP-catalyzed hydrolysis of FDP, lacks sufficient affinity for the blocked membrane in Western blotting (Figure 1), and we suggest that this low affinity may be attributed to the carboxylic group of the fluorescein molecule which makes the hydrophilicity rather high. We then examined the affinity of 2-Me TG, one of our recently reported fluorescein derivatives (TokyoGreens, TG),[18] in which the carboxylic group of the traditional fluorescein molecule is replaced with a methyl group. We found that a spot of a solution of 2-Me TG dropped onto the membrane remained well defined and was not readily washed out (see Supporting Information). This result suggested that TokyoGreens, which do not have a carboxylic group, are more suitable than traditional fluorescein as the fluorophore in probes for Western blot analysis. TokyoGreens also offer the advantage of precise control of the fluorescence emission output. We thus considered 2-Me-4-OMe TG (Figure 1), which shows strong fluorescence (as fluorescein does) and becomes essentially nonfluorescent upon alkylation of its phenolic group, as a suitable core fluorophore for our new probe. Incorporation of a phosphate group into the phenolic group of 2-Me-4-OMe TG gave TG-Phos, a new probe for ALP whose hydrolysis product has a high affinity for Western blots, unlike the hydrolysis product of FDP (Scheme 1).

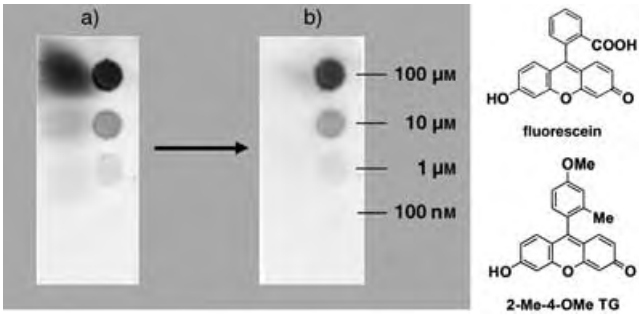


Figure 1. Difference in affinity for the blot between 2-Me-4-OMe TG and fluorescein. Solutions of various concentrations (100 μM, 10 μM, 1 μM, 100 nM) of 2-Me-4-OMe TG (right lane) and fluorescein (left lane) were dropped onto a blocked nitrocellulose membrane and imaged a) before and b) after washing.

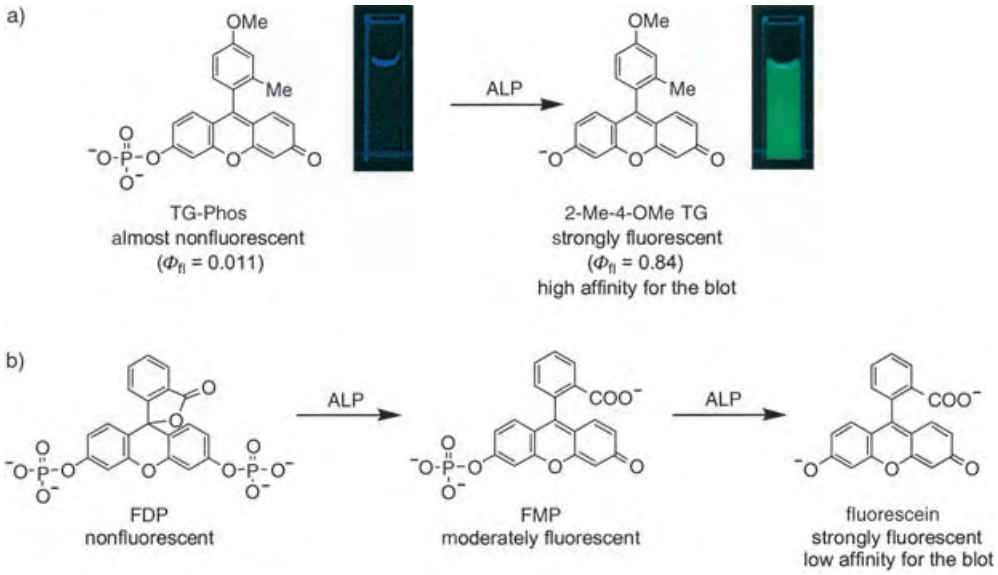
TG-Phos is stable and almost nonfluorescent, but is converted into strongly fluorescent 2-Me-4-OMe TG upon one-step hydrolysis by ALP (see Scheme 1a, Figure 2a, and Supporting Information). We observed a linear relationship between ALP activity and the initial rate of increase of fluorescence intensity (Figure 2b). In the case of FDP, which is hydrolyzed first to moderately fluorescent fluorescein monophosphate (FMP) and then to strongly fluorescent fluorescein, the rate of increase of fluorescence is slow (Scheme 1b, Figure 2a). Additionally, there is poor linearity

[*] M. Kamiya, Dr. Y. Urano,[+] Prof. Dr. T. Nagano
Graduate School of Pharmaceutical Sciences
The University of Tokyo
7-3-1 Hongo, Bunkyo-ku, Tokyo 113-0033 (Japan)
Fax: (+81) 3-5841-4855
E-mail: tlong@mol.f.u-tokyo.ac.jp
N. Ebata, M. Yamamoto, J. Kosuge
Development Department, Research Products Division
Daiichi Pure Chemicals Co., Ltd.
3-3-1 Koyodai, Ryugasaki-city, Ibaraki 301-0852 (Japan)
[+] PRESTO, Japan Science and Technology Agency
Kawaguchi, Saitama (Japan)

[**] This study was supported in part by a grant for Precursory Research for Embryonic Sciences and Technology from the JST Agency to Y.U., as well as research grants (grant nos. 13557209, 16651106, and 16689002) to Y.U. and a grant for the Advanced and Innovational Research Program in Life Sciences to T.N. from the Ministry of Education, Culture, Sports, Science, and Technology of the Japanese Government.

Supporting information for this article is available on the WWW under http://www.angewandte.org or from the author.

© 2005 Wiley-VCH Verlag GmbH & Co. KGaA, Weinheim



Scheme 1. Reaction scheme of a) TG-Phos and b) FDP with ALP to yield fluorescent hydrolyzed products.

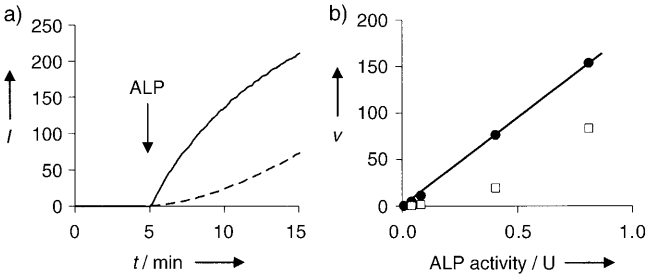


Figure 2. In vitro reaction of TG-Phos or FDP with ALP. a) Increase in fluorescence of 1 μM solutions of TG-Phos (——) and FDP (-----) upon reaction with ALP. b) Correlation between ALP activity and the initial rate of increase of fluorescence using TG-Phos (●) or FDP (□). I = increase in fluorescence (a.u.); v = initial rate of increase of fluorescence (a.u. min^{-1})

between ALP activity and the initial rate of increase of fluorescence owing to the involvement of the two-step hydrolysis (Figure 2b). The results of a dot-blot assay indicated that TG-Phos is greatly superior to ELF97 phosphate and shows about two-times higher sensitivity than DDAO phosphate, both of which have been used as fluorescence probes for Western blots (see Supporting Information). These results indicate that TG-Phos is a superior probe for ALP and allows the quantitative detection of ALP activity with high sensitivity.

We then examined if a protein of interest could be visualized on the blot by using TG-Phos after SDS-polyacrylamide gel electrophoresis (SDS-PAGE) and electroblotting. CYP3A2 was employed as the target protein, and detection with an ALP-labeled secondary antibody and TG-Phos yielded sharp, CYP3A2-specific green-fluorescent bands whose intensity was proportional to the amount of protein. The development of the fluorescence signal was very rapid, occurring in seconds to minutes, and CYP3A2 could be detected at the nanogram level. Furthermore, the fluorescence signal was not easily washed out and was stable on dried blots. In contrast, the green-fluorescent bands derived from FDP were poorly defined and could be easily washed out, making it difficult to detect CYP3A2 on the blot (see Supporting Information).

We next examined simultaneous green/red dual detection of CYP3A2 and total proteins on the same blot. The blot was stained with an amine-reactive BODIPY dye (BODIPY TR-X, succinimidyl ester) to detect total proteins, followed by TG-Phos in combination with an ALP-conjugated secondary antibody to visualize CYP3A2. We succeeded in visualizing all the proteins in the profile as red-fluorescent signals, together with CYP3A2 as a green-fluorescent signal at the same time on the same blot (Figure 3). Such simultaneous two-color detection is a powerful method because it becomes

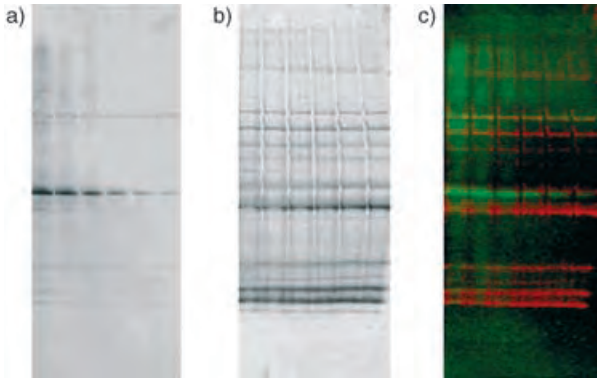


Figure 3. Green/red dual detection of CYP3A2 and total proteins on the same blot after SDS-PAGE and electroblotting onto a PVDF membrane. a) Specific staining of CYP3A2 using ALP-conjugated antibody and TG-Phos. b) Detection of total protein using BODIPY TR-X, succinimidyl ester. c) Simultaneous dual detection of CYP3A2 as green-fluorescent bands and total proteins as red-fluorescent bands. The six lanes contain protein molecular-weight standards (250 ng) and decreasing amounts of CYP3A2 (250 ng, 125 ng, 62.5 ng, 31.2 ng, 15.6 ng, 7.8 ng).

 © 2005 Wiley-VCH Verlag GmbH & Co. KGaA, Weinheim

possible to detect two kinds of proteins on a single blot and obviates the need to make a replica for visualizing total proteins, as is usually required for chemiluminescent or colorimetric detection.

In conclusion, we have developed a fluorescence probe for alkaline phosphatase based on the TokyoGreen scaffold which is suitable for Western blot analysis. The new probe, TG-Phos, yields the strongly fluorescent hydrolysis product, 2-Me-4-OMe TG, which has a high affinity for the blot, in a one-step reaction with ALP. Moreover, TG-Phos provides high sensitivity and a good linear response to ALP and is suitable for multicolor labeling. The design strategy presented here is not limited to ALP but could be extended to other detection enzymes and may provide a general method for simple and rapid detection of proteins on Western blots.

Received: May 5, 2005
Revised: June 7, 2005
Published online: July 26, 2005

Keywords: electrophoresis · enzymes · fluorescent probes · proteins · Western blot analysis

[1] S. Mimura, T. Seki, S. Tanaka, J. F. X. Diffley, *Nature* **2004**, *431*, 1118 – 1123.
[2] I. Dilova, S. Aronova, J. C. Y. Chen, T. J. Powers, *Biol. Chem.* **2004**, *279*, 46527 – 46535.
[3] R. Ricci, G. Sumara, I. Sumara, I. Rozenberg, M. Kurrer, A. Akhmedov, M. Hersberger, U. Eriksson, F. R. Eberli, B. Becher, J. Boren, M. Chen, M. I. Cybulsky, K. J. Moore, M. W. Freeman, E. F. Wagner, C. M. Matter, T. F. Lüscher, *Science* **2004**, *306*, 1558 – 1561.
[4] V. B. Paragas, J. A. Kramer, C. Fox, R. P. Haugland, V. L. Singer, *J. Microsc.* **2002**, *206*, 106 – 119.
[5] D. A. Knecht, R. L. Dimond, *Anal. Biochem.* **1984**, *136*, 180 – 184.
[6] B. J. Hanson, B. Schulenberg, W. F. Patton, R. A. Capaldi, *Electrophoresis* **2001**, *22*, 950 – 959.
[7] C. Delevoye, M. Nilges, A. Dautry-Varsat, A. Subtil, *J. Biol. Chem.* **2004**, *279*, 46896 – 46906.
[8] G. Larson, D. Thompson, *Biotechniques* **1992**, *12*, 656 – 658.
[9] K. Pretty On Top, G. Hatleberg, K. N. Berggren, D. Ryan, C. Kemper, R. P. Haugland, W. F. Patton, *Electrophoresis* **2001**, *22*, 896 – 905.
[10] A. Minta, J. P. Y. Kao, R. Y. Tsien, *J. Biol. Chem.* **1989**, *264*, 8171 – 8178.
[11] B. A. Griffin, S. R. Adams, R. Y. Tsien, *Science* **1998**, *281*, 269 – 272.
[12] H. Kojima, N. Nakatsubo, K. Kikuchi, S. Kawahara, Y. Kirino, H. Nagoshi, Y. Hirata, T. Nagano, *Anal. Chem.* **1998**, *70*, 2446 – 2453.
[13] K. Setsukinai, Y. Urano, K. Kakinuma, H. J. Majima, T. Nagano, *J. Biol. Chem.* **2003**, *278*, 3170 – 3175.
[14] B. Rotman, J. A. Zderic, M. Edelstein, *Proc. Natl. Acad. Sci. USA* **1963**, *50*, 1 – 6.
[15] Z. Huang, N. A. Olson, W. You, R. P. Haugland, *J. Immunol. Methods* **1992**, *149*, 261 – 266.
[16] C. T. Huang, K. D. Xu, G. A. Mcfeters, P. S. Stewart, *Appl. Environ. Microbiol.* **1998**, *64*, 1526 – 1531.
[17] Y. Murakami, T. Morita, T. Kanekiyo, E. Tamiya, *Biosens. Bioelectron.* **2001**, *16*, 1009 – 1014.
[18] Y. Urano, M. Kamiya, K. Kanda, T. Ueno, K. Hirose, T. Nagano, *J. Am. Chem. Soc.* **2005**, *127*, 4888 – 4894.

 © 2005 Wiley-VCH Verlag GmbH & Co. KGaA, Weinheim

Donor–Acceptor Systems

DOI: 10.1002/anie.200501448

Small-Molecule-Induced Folding of a Synthetic Polymer**

*Suhrit Ghosh and S. Ramakrishnan**

The remarkable range of chemical functions that evolution has elicited from biopolymers has inspired chemists to design synthetic systems that can mimic both the structural and functional features of these elegant long-chain molecules. Although the efforts to mimic functions such as molecular recognition, catalysis, and so forth has led to the development of systems such as molecular-imprint polymers,[1] the attempts to understand and emulate structural features has given rise to the area of foldamers.[2] In most such systems, the core design element utilizes multiple inter- or intramolecular noncovalent interactions that can be stabilized/destabilized by an external trigger. The cooperativity and reversibility of these weak noncovalent interactions are, thus, of paramount importance in the design of synthetic analogues that can emulate biological systems.

Supramolecular science, which deals with the design and utilization of noncovalent interactions to build superstructures with small molecular building blocks, has witnessed intense activity over the past decade.[3] The extension of these ideas has resulted in the generation of supramolecular polymers in solution, formed through multiple hydrogen-bonding interactions[4] or through metal–ion coordination between monomeric building blocks.[5] In the context of conventional polymer molecules, a similar approach in which noncovalent interactions occur between neighboring (or equispaced) segments within a single polymer chain, has been explored to stabilize specific conformations (secondary structures) in solution.[2] On the basis of these considerations, several research groups have examined new types of oligomers and polymers, which adopt well-defined conformations in solution guided by hydrogen-bonding interactions along the backbone,[6] steric and/or bond-angle constraints,[7] solvophobic effects, and so forth.[8] Although the large majority of foldamers are based on precisely defined oligomers with relatively rigid backbones, far fewer are based on flexible systems.[9]

Recently, we demonstrated that truly flexible synthetic macromolecules can be designed to fold under the influence

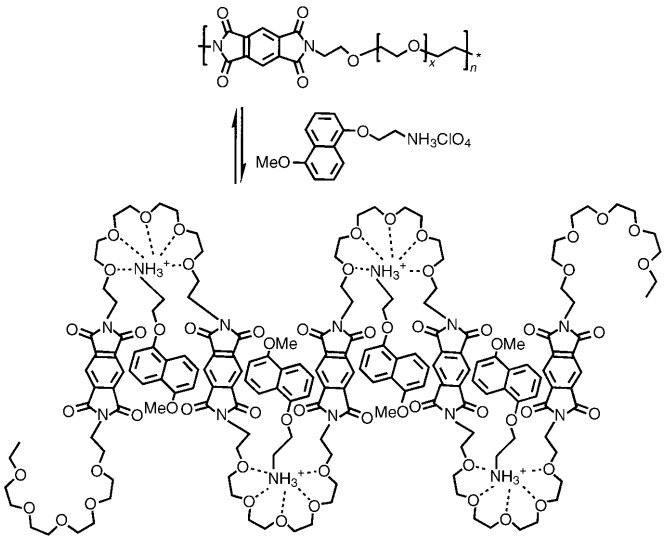
[*] S. Ghosh, Prof. S. Ramakrishnan
Department of Inorganic and Physical Chemistry
Indian Institute of Science
Bangalore 560012 (India)
Fax: (+91) 802-360-1552
E-mail: raman@ipc.iisc.ernet.in

[**] We would like to thank DST, New Delhi, and 3M India Ltd, for their financial support.

Supporting information for this article is available on the WWW under http://www.angewandte.org or from the author.

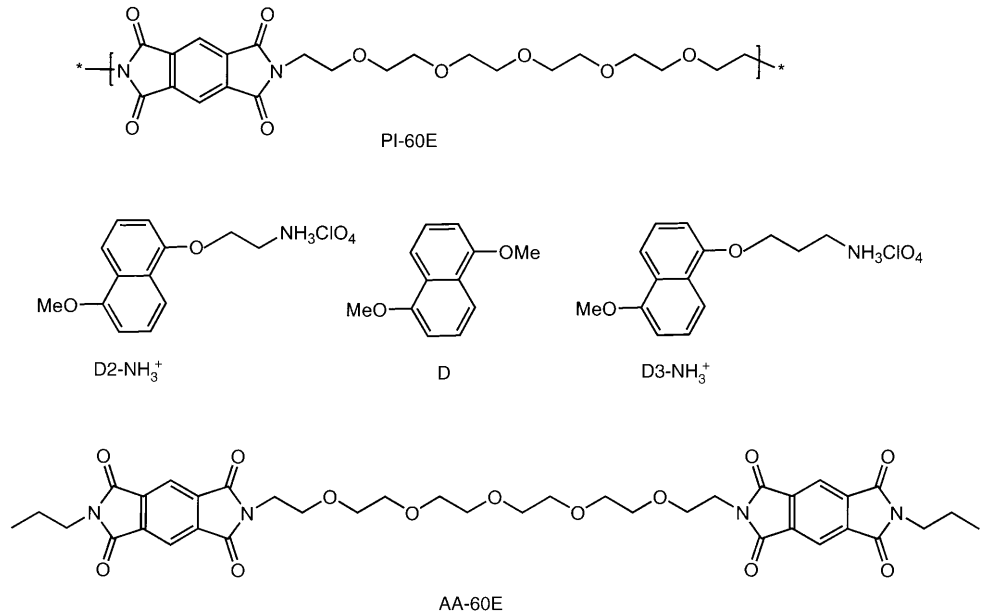
© 2005 Wiley-VCH Verlag GmbH & Co. KGaA, Weinheim

of several relatively weak intrachain intersegment interactions, such as formation of a charge-transfer (CT) complex, solvophobic effects, and metal–ion complexation, working in tandem.[10] Detailed spectroscopic studies of these (donor–spacer–acceptor–spacer)$_n$ type polymers, in conjunction with studies of model systems, have suggested the formation of extended donor–acceptor stacks by suitable folding of single polymer chains.[11] In a bid to develop simpler polymeric systems that can fold under similar conditions, we present herein a conceptually new approach for the folding of synthetic polymers based on a polyimide that contains only acceptor units linked by hexaoxyethylene (6OE) spacers of the type (acceptor–spacer)$_n$. In this design, we utilize an external small-molecule folding agent (donor type) that is designed to interact simultaneously with two adjacent segments along the polymer chain so that the polymer folds in a predetermined manner. As depicted in Scheme 1, the design specifically entails the formation of a CT complex between the donors of the folding agent and the acceptors along the polymer chain, in tandem with the complexation of the ammonium group of the folding agent with the 6OE spacer.[12] The latter interaction is expected to restrict the conformation of the flexible OE spacer so that the two adjacent acceptor units along the polymer chain can be brought close enough to form an effective CT interaction with the donor unit in the folding agent. Such a multiple-point interaction, which is key to the development of supramolecular science, has been extensively utilized to enhance associations between small molecules, as well as between polymers and small molecules.[13] An interesting example of the latter is the work of Meijer and co-workers,[14] in which they describe anchoring (clicking-in) small functional molecules onto the periphery of dendrimers through the simultaneous use of electrostatic and hydrogen-bonding interactions.



Scheme 1. Folding of a synthetic polymer aided by two-point interactions with a folding agent.

The polyimide PI-6OE was prepared from the appropriate diamine (derived from hexaethylene glycol)[15] and pyromellitic anhydride under standard conditions for polyimide synthesis.[16] Two folding agents, namely, D2-NH_3^+ and D3-NH_3^+, that contain a naphthalene donor linked to an ammonium group through a two- or a three-carbon-atom spacer, respectively, were prepared along with 1,5-dimethoxynaphthalene (D) that serves as a model donor which is devoid of the ammonium group (see Scheme 2). The structures of the various model compounds and polymer were confirmed by standard spectroscopic techniques, and the molecular weight M_n of PI-6OE was determined to be 20500 Da (polydispersity index (PDI) = 1.7) by gel-permeation chromatography (GPC).[17] PI-6OE forms a colorless solution, but an intense yellow color develops in the presence of D2-NH_3^+ because of the characteristic CT absorption band at 450 nm.



Scheme 2. Structures of the polymer, model compounds, and folding agents.

 © 2005 Wiley-VCH Verlag GmbH & Co. KGaA, Weinheim

The interaction of PI-6OE with the folding agents was investigated by monitoring the intensity of the CT band by UV/Vis spectroscopic analysis and by following the chemical shift of the aromatic protons of the pyromellitic diimide acceptor unit by ^{1}H NMR spectroscopic analysis. Figure 1 depicts the variation in the ^{1}H NMR spectra of PI-6OE with increasing amounts of D2-NH_3^+. The signal marked by an arrow, from the pyromellitic diimide unit in the polymer, is seen to move continuously upfield on addition of increasing amounts of the donor species. The remaining signals in the aromatic region are from the naphthalene ring of the folding agent, the intensities of which increase and are accompanied by a small downfield shift.[18]

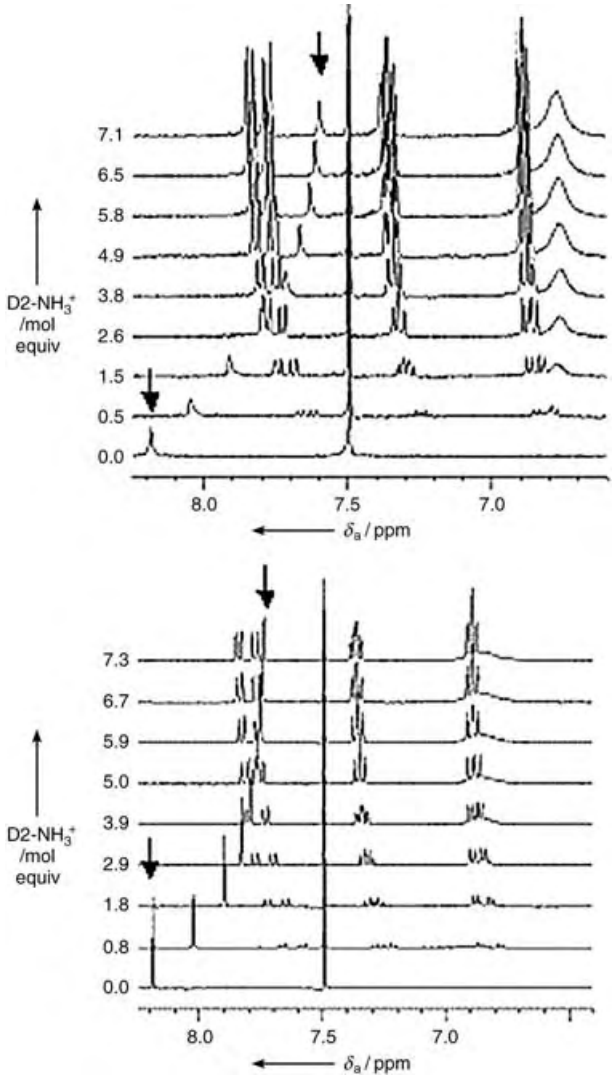


Figure 1. Variation in the aromatic region of the ^{1}H NMR spectra of PI-6OE (top) and AA-6OE (bottom) as a function of the addition of increasing amounts of D2-NH_3^+. The signal that arises from the pyromellitic diimide acceptor protons is indicated by an arrow. The solvent used is a $CDCl_3/CH_3CN$ mixture (1:1, v/v).

A plot of the variation in the chemical shift of the acceptor proton as a function of the concentration of the two different folding agents D2-NH_3^+ and D3-NH_3^+, along with the simple model donor D as a control experiment, is shown in Figure 2. It is evident that although both the folding agents that contain an ammonium group cause a dramatic change in the δ value, the simple donor molecule that does not contain this group causes only a marginal variation. This upfield shift of the acceptor proton suggests the formation of donor–acceptor CT stacks, as was elaborated in our earlier report.[11] Similarly, a significant increase in the intensity of the CT band in the UV/Vis spectra of the polymer solution occurs in the presence of the two donors that contain ammonium groups while only a marginal increase is seen in the presence of the simple donor (Figure 2), despite the fact that both the control experiments were done in the presence of an equimolar quantity of NH_4SCN with respect to D. The independent complexation of the ammonium ion with the OE loop would be expected to at least partially aid the CT interaction with D. These compa-

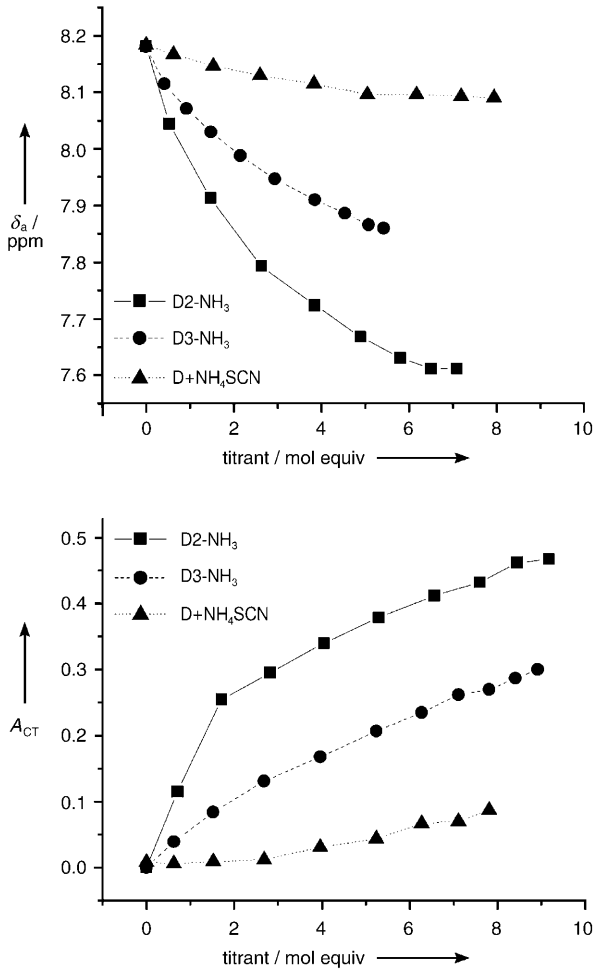


Figure 2. Variation in the chemical shift of the acceptor ring protons δ_a in PI-6OE in the presence of D + NH_4SCN, D2-NH_3^+, and D3-NH_3^+ (top) and variation in the CT band intensity A_{CT} in the presence of D + NH_4SCN, D2-NH_3^+, and D3-NH_3^+ (bottom). The solvent used is $CDCl_3/CH_3CN$ (1:1). The mole equivalents are calculated with respect to the polymer repeating unit.

 © 2005 Wiley-VCH Verlag GmbH & Co. KGaA, Weinheim

rative studies clearly demonstrate the importance of the cooperative two-point interaction, namely, the coordination of the ammonium group with the OE loop and the concomitant CT interaction between the donor and acceptor units, in the generation of the postulated folded structure. Furthermore, as anticipated, the length of the spacer that connects the ammonium group to the naphthalene donor also plays an important role in governing the efficacy of the CT interactions. It is apparent from the variations in the UV/Vis and NMR spectra that D2-NH_3^+ is a more effective folding agent than D3-NH_3^+ (see Figure 2).[19] This dependence on the spacer length reaffirms the importance of the crown ether type complexation of the ammonium group with the OE segment of the polymer in directing the formation of the postulated folded structure.

To probe the extent of the folding, model compound AA-6OE (see Scheme 2) which contains two acceptor units linked by a hexaoxyethylene spacer was synthesized[20] and its interaction with the folding agents studied by both UV/Vis and NMR spectroscopic analysis. The variation in the aromatic region of the ^{1}H NMR spectra of AA-6OE as a function of increasing concentration of the folding agent D2-NH_3^+ is compared with that of the polymer in Figure 1. It is apparent that a significant upfield shift of the acceptor protons is seen in this case as well, although the extent of the shift is clearly smaller in the model compound than in PI-6OE. The variation of the chemical shift of the acceptor proton upon interaction with the two folding agents in the case of the polymer is compared with that of the model compound AA-6OE in Figure 3. For both folding agents, it is clear that the extent of the shift is significantly higher for the polymer than for the model compound. This enhanced shift is clearly a reflection of the fact that the acceptor units in the model can never be sandwiched between two donors, unlike in the case of the polymer in which extended stacking would cause the acceptor units to be sandwiched between two donors. Interestingly, the final chemical shifts of the donor (naphthalene) protons are nearly identical for both the polymer and the model compound (see Figure 1), as expected, because in both cases the donor could become sandwiched between the acceptor units. In addition, as anticipated, the extent of folding exhibits strong temperature dependence, as is evident from the significant upfield shift upon cooling (see inset in Figure 3).[11] Again, it is seen that the polymer exhibits much stronger temperature dependence than the AA-6OE model, thus causing the difference in their chemical shifts to become as large as 0.3 ppm at the lowest temperature probed. We ascribe this difference to the formation of extended stacks in the case of the polymer.[21] To gain further insight into the extent of the stacking, a Job plot was constructed from the absorbance of the CT band, which suggested that the acceptor/donor ratio was 1:0.85 for the polymer PI-6OE (the maximum value in the Job plot was seen at approximately 0.46, see the Supporting Information). Although, in a general sense a ratio of 1:1 need not imply the formation of an extended stack, in our case, however, it can be reasoned that it does confirm the formation of a stack. It is apparent in the present system that the interaction of the ammonium group with the OE spacer is essential for the formation of a CT complex and, more importantly, leads to the sandwiching of the donor between two adjacent acceptors to form an acceptor-donor-acceptor type unit. Evidence for this sandwiching also comes from the Job plot of the model compound AA-6OE, which suggests the formation of an exact 1:1 complex (see the Supporting Information for details). Thus, an acceptor/donor ratio of 2:1 in case of the polymer would suggest the formation of only acceptor–donor–acceptor-type interactions with no extended stacking. On the other hand, if all the OE spacer sites form complexes with the ammonium group of the folding agent, as expected with an acceptor/donor ratio of 1:1, then the formation of an infinitely extended stack is implied. Although the exact scale of the stacking continues to be a challenging problem, a rough estimate on the basis of the Job plot of our polymer suggests the formation of stacks that consist of six donor–acceptor pairs on average.

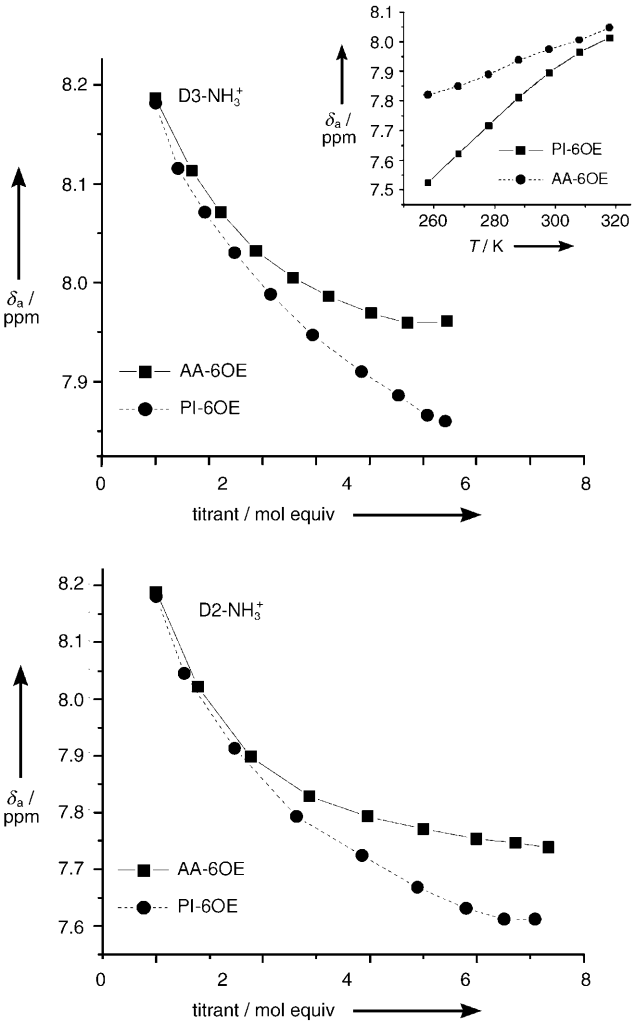


Figure 3. Variation in the chemical shift of the acceptor ring protons δ_a in PI-6OE and AA-6OE in the presence of D3-NH_3^+ (top) and D2-NH_3^+ (bottom). Inset: Effect of temperature on the chemical shift of PA-6OE and AA-6OE in presence of D3-NH_3^+ (the ratio of D3-NH_3^+ to polymer repeating unit/model compound was 4:1).

 © 2005 Wiley-VCH Verlag GmbH & Co. KGaA, Weinheim

To test the reversibility of such an interaction-induced folding, an experiment to extricate the folding agent with a crown ether was carried out. Thus, PI-6OE in the folded state (in the presence of 8 equiv of D2-NH_3^+) was titrated with [18]crown-6, which is known to bind very strongly with ammonium ions.[22] In Figure 4, the variation of the chemical shift is plotted, first for the addition of increasing amounts of the folding agent to the polymer and subsequently for the addition of increasing amounts of [18]crown-6. It is clear from the plot that there is a complete reversal of the chemical shift, as a signal with nearly the same value as that for the unfolded polymer is observed, although slightly more than one equivalent of [18]crown-6 was required to effect this complete reversal. The color of the solution changes from deep yellow to nearly colorless at the end of the titration with the crown ether, which is consistent with the complete disappearance of the CT band in the UV/Vis spectra (Figure 4). These experiments clearly confirm that the folding is completely reversible and also suggest that the folding/unfolding equilibrium can be controlled by an appropriate external agent.

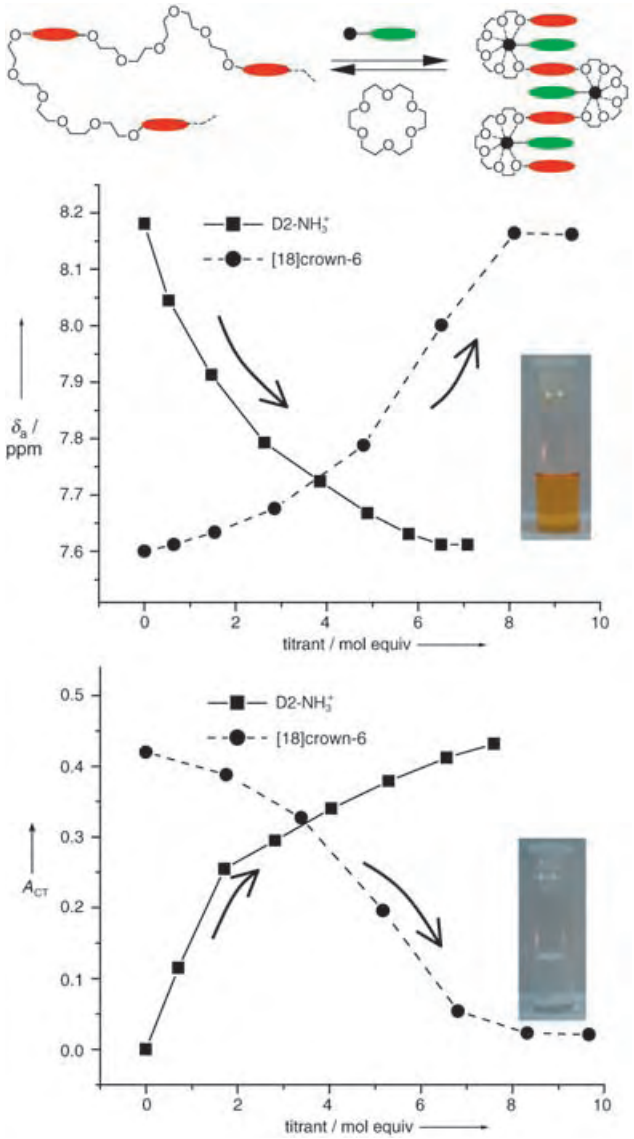


Figure 4. Reversal of the chemical shifts of the acceptor protons δ_a of PI-6OE (top) and the disappearance of CT absorption band (bottom) in the presence [18]crown-6. The mole equivalents were calculated with respect to the polymer repeating unit.

In conclusion, we have demonstrated a new approach to folding a flexible synthetic polymer in solution by utilizing a small molecule as a folding agent. The folding agent was designed to interact cooperatively with two adjacent segments of the polymer chain, such that one interaction facilitates the other, thus leading to the formation of a stacked structure. An ammonium cation in the folding agent forms a complex with a hexaoxyethylene spacer thereby aiding the CT interaction between a naphthalene donor and a pyromellitic diimide acceptor in the polymer. Control experiments with a model naphthalene donor, along with an equimolar amount of an ammonium salt, clearly helped delineate the importance of linking the two interacting subunits in the folding agent, and thereby confirmed the importance of cooperativity in such a folding process. Importantly, the folding was also shown to be completely reversible and the polymer unfolds when the folding agent is extricated by formation of a stronger complex with [18]crown-6. Further work to explore the generality and utility of such a small-molecule-induced folding of synthetic polymers would be of great interest and is currently being studied.

Experimental Section

Pyromellitic dianhydride and 1,5-dihydroxynaphthalene were purchased from the Aldrich Chemical Co. and were purified by sublimation and recrystallization (from nitromethane), respectively. Dry and purified solvents were used in all the syntheses and spectroscopic studies. All the solvents and common synthetic reagents were purified according to standard procedures.[23] The NMR experiments were performed using a Bruker 400 MHz spectrometer and UV/Vis spectra were measured using a Ocean Optics spectrometer. The molecular weights were determined by GPC with chloroform as the eluent at 35 °C, two PL-gel mixed-bed columns were used for separation, and a Viscotek TDA Model 300 was used as the detector. The universal calibration method based on a polystyrene standard was used to estimate the molecular weights. Isothermal titration calorimetry (ITC) experiments were performed with a VP-ITC Microcal LLC instrument in a $CHCl_3/CH_3CN$ solvent mixture (1:1). Mass-spectrometric data were obtained on a Q-TOP Micromass spectrometer. Elemental analysis was performed with a Carlo Erba 1106 CHN analyzer.

Folding studies: In a typical NMR titration experiment, a polymer solution (1.5 mL, 1.92 mM) was prepared in $CDCl_3/CH_3CN$ (1:1 v/v; solution A). An aliquot of this solution (0.6 mL) was placed in the NMR tube and a large excess ($\approx$10–15 equiv) of donor molecule was dissolved in the remaining solution (solution B). Solution A was then titrated with solution B (20–150-μL steps), which resulted in a series of solutions of fixed polymer concentration but with various amounts of donor. Similarly, the UV/Vis experiments were performed in $CHCl_3/CH_3CN$ (1:1).

In the experiment with the crown ether, a solution containing a polymer/donor mixture in a 1:7 ratio in $CHCl_3/CH_3CN$ (1:1) was titrated with a solution of [18]crown-6 in $CHCl_3/CH_3CN$ (1:1) that also contained a polymer/donor mixture in a 1:7 ratio. Therefore, the concentration and relative molar ratios of the polymer and donor molecules were kept constant, and the only variable was the

 © 2005 Wiley-VCH Verlag GmbH & Co. KGaA, Weinheim

concentration of [18]crown-6. The Job plot experiment based on UV/Vis spectroscopic analysis was performed in $CHCl_3/CH_3CN$ (1:1), and the total concentration (polymer + folding agent) was maintained at 12 mM for the polymer and 6 mM for the model compound.

Synthesis of the polymer: Hexaethylene glycol diamine[15] (0.494 g, 1.76 mmol) was placed in the reaction vessel and dissolved in freshly distilled *m*-cresol (3 mL). The purified pyromellitic dianhydride (0.384 g, 1.76 mmol) was added to this solution in one portion, and the reaction mixture was stirred at 85 °C for 2 h under a continuous flow of N_2 gas. The reaction mixture was cooled to room temperature, and *m*-cresol (2 mL), dry toluene (5 mL), and isoquinoline (8 drops) were added. The reaction mixture was stirred at 185 °C for another 6 h in an inert atmosphere with continuous azeotropic removal of water. The reaction mixture was cooled to room temperature, and the viscous liquid was poured into methanol (50 mL). The fine powdery precipitate was centrifuged, redissolved in a minimum volume of chloroform, and reprecipitated from methanol to obtain the desired polymer as a white fibrous material. The product was dried under vacuum at 100 °C for 3 h. Yield: 62 %.

For fractionation, methanol was added dropwise to a solution of the polymer (150 mg) in chloroform (10 mL) until the solution became cloudy. The mixture was stirred for another 15 min as a colorless oil separated and stuck to the walls of the vessel. The supernatant was decanted, and the oil was dissolved in chloroform (1 mL) and reprecipitated from methanol to form the fibrous colorless polymer. The product was dried under vacuum for 3 h at 100 °C, and the recovery was found to be approximately 30 %.

^{1}H NMR (400 MHz, $CDCl_3$): $\delta = 8.257$ (s, 2H, Ar-*H*), 3.950 (t, 4H, N-CH_2), 3.768 (t, 4H, N-CH_2-CH_2-), 3.658–3.581 ppm (m, 16H, rest of the oligoethylene protons); ^{13}C NMR: $\delta = 166.17$, 137.26, 118.27, 70.59, 70.53, 70.03, 67.68, 37.93 ppm. Elemental analysis (%) calcd for $C_{22}H_{26}N_2O_9$: C 57.14, H 5.66, N 6.06; found: C 56.82, H 5.51, N 5.93.

Received: April 27, 2005
Published online: July 29, 2005

Keywords: charge transfer · crown compounds · donor–acceptor systems · polymer folding

[1] a) G. Wulff, *Chem. Rev.* **2002**, *102*, 1; b) K. Haupt, K. Mosbach, *Chem. Rev.* **2000**, *100*, 2495; c) *Molecularly Imprinted Polymers, Man-Made mimics of Antibodies and their Application in Analytical Chemistry* (Ed.: B. Sellergren), Elsevier, New York, **2001**; d) S. C. Zimmerman, N. G. Lemcoff, *Chem. Commun.* **2004**, 5.

[2] a) S. H. Gellman, *Acc. Chem. Res.* **1998**, *31*, 173; b) D. J. Hill, M. J. Mio, R. B. Prince, T. S. Huges, J. S. Moore, *Chem. Rev.* **2001**, *101*, 3893; c) C. Schmuck, *Angew. Chem.* **2003**, *115*, 2552; *Angew. Chem. Int. Ed.* **2003**, *42*, 2448.

[3] a) J. M. Lehn, *Supramolecular Chemistry—Concepts and Perspectives*, Wiley-VCH, Weinheim, **1995**; b) C. A. Schalley, A. Lutzen, M. Albrecht, *Chem. Eur. J.* **2004**, *10*, 1072.

[4] a) J.-M. Lehn, *Supramolecular Polymers* (Ed.: A. Cifferi), Marcel Dekker, New York, **2000**, p. 615; b) S. C. Zimmerman, P. S. Corbin, *Struct. Bonding (Berlin)* **2000**, *96*, 63; c) L. Brunsveld, J. A. J. M. Vekemans, J. H. K. K. Hirschberg, R. P. Sijbesma, E. W. Meijer, *Proc. Natl. Acad. Sci. USA* **2002**, *99*, 4977; d) R. P. Sijbesma, E. W. Meijer, *Chem. Commun.* **2003**, 5; e) L. Brunsveld, B. J. B. Folmer, E. W. Meijer, R. P. Sijbesma, *Chem. Rev.* **2001**, *101*, 4071; f) V. Berl, M. Schmutz, M. J. Krische, R. G. Khoury, J.-M. Lehn, *Chem. Eur. J.* **2002**, *8*, 1227.

[5] a) D. Yu-Bin, W. Peng, H. Ru-Qi, D. S. Mark, *Inorg. Chem.* **2004**, *43*, 4727; b) U. S. Schubert, C. Eschbaumer, *Angew. Chem.* **2002**, *114*, 3016; *Angew. Chem. Int. Ed.* **2002**, *41*, 2892; c) H. Hofmeier, U. S. Schubert, *Chem. Soc. Rev.* **2004**, *33*, 373; d) P. R. Andres, U. S. Schubert, *Adv. Mater.* **2004**, *16*, 1043; e) B. J. Benjamin, J. J. R. Stuart, *J. Am. Chem. Soc.* **2003**, *125*, 13922.

[6] a) Y. Hamuro, S. J. Geib, A. D. J. Hamilton, *J. Am. Chem. Soc.* **1997**, *119*, 10587; b) Y. Hamuro, S. J. Geib, A. D. J. Hamilton, *J. Am. Chem. Soc.* **1996**, *118*, 7529; c) J. Zhu, R. D. Parra, H. Zeng, E. Skrzypczak-Jankun, X. C. Zeng, B. Gong, *J. Am. Chem. Soc.* **2000**, *122*, 4219; d) L. Yuan, H. Zeng, K. Yamato, A. R. Sanford, W. Feng, H. S. Atreya, D. K. Sukumaran, T. Szyperski, B. Gong, *J. Am. Chem. Soc.* **2004**, *126*, 16528.

[7] a) V. Berl, I. Huc, R. G. Khoury, J. M. Lehn, *Nature* **2000**, *407*, 720; b) A. Petitjean, L. A. Cuccia. J. M. Lehn, H. Nierengarten, M. Schmutz, *Angew. Chem.* **2002**, *114*, 1243; *Angew. Chem. Int. Ed.* **2002**, *41*, 1195.

[8] a) A. Tanatani, M. J. Mio. , J. S. Moore, *J. Am. Chem. Soc.* **2001**, *123*, 1792; b) R. B. Prince, L. Brunsveld, E. W. Meijer, J. S. Moore, *Angew. Chem.* **2000**, *112*, 234; *Angew. Chem. Int. Ed.* **2000**, *39*, 228; c) J. C. Nelson, J. G. Saven, J. S. Moore, P. G. Wolynes, *Science* **1997**, *277*, 1793; d) J. M. Heemstra, J. S. Moore, *J. Am. Chem. Soc.* **2004**, *126*, 1648; for related polymeric systems, see; e) R. S. Hecht, A. Khan, *Angew. Chem.* **2003**, *115*, 6203; *Angew. Chem. Int. Ed.* **2003**, *42*, 6021; f) L. Arnt, G. N. Tew, *Macromolecules* **2004**, *37*, 1283.

[9] a) W. Wang, L.-S. Li, G. Helms, H.-H. Zhou, A. D. Q. Li, *J. Am. Chem. Soc.* **2003**, *125*, 1120; b) A. D. Q. Li, W. Wang, L.-Q. Wang, *Chem. Eur. J.* **2003**, *9*, 4594; c) E. E. Neuteboom, S. C. J. Maskers, E. W. Meijer, R. A. J. Janssen, *Macromol. Chem. Phys.* **2004**, *205*, 217; d) R. S. Lokey, B. L. Iverson, *Nature* **1995**, *375*, 303; e) J. Q. Nguyen, B. L. Iverson, *J. Am. Chem. Soc.* **1999**, *121*, 2639; f) A. J. Zych, B. L. Iverson, *J. Am. Chem. Soc.* **2000**, *122*, 8898; g) G. J. Gabriel, B. L. Iverson, *J. Am. Chem. Soc.* **2002**, *124*, 15174; h) M. A. Balbo Block, S. Hecht, *Macromolecules* **2004**, *37*, 4761.

[10] S. Ghosh, S. Ramakrishnan, *Angew. Chem.* **2004**, *116*, 3326; *Angew. Chem. Int. Ed.* **2004**, *43*, 3264.

[11] S. Ghosh, S. Ramakrishnan, *Macromolecules* **2005**, *38*, 676.

[12] K^+ and NH_4^+ ions are known to have similar size-selective preferences on complexation with crown ethers. We have shown that a donor–acceptor polymer that contains a 6OE spacer forms complexes most strongly with K^+ ions.[10,11] Therefore, a polyimide that contains 6OE spacers was chosen in the present study. For reviews of the complexation of crown ethers and podands with cations, see: a) G. K. Gokel, W. M. Leevy, M. E. Weber, *Chem. Rev.* **2004**, *104*, 2723; b) H. G. Lohr, L. F. Vogtle, *Acc. Chem. Res.* **1985**, *18*, 65, and references therein; c) *Comprehensive Supramolecular Chemistry, Vol. 1* (Ed.: G. W. Gokel), Pergamon/Elsevier, Oxford, **1996**; d) R. M. Izatt, J. S. Bradshaw, S. A. Nielsen, J. D. Lamb, J. J. Christensen, *Chem. Rev.* **1985**, *85*, 271.

[13] a) G. Kaiser, T. Jarrosson, S. Otto, Y.-F. Ng, A. D. Bond, J. K. M. Sanders, *Angew. Chem.* **2004**, *116*, 1993; *Angew. Chem. Int. Ed.* **2004**, *43*, 1959; b) L. Kovbasyuk, R. Kramer, *Chem. Rev.* **2004**, *104*, 3161; c) F. Ithan, G. K. Blanchette, V. Rotello, *Macromolecules* **1999**, *32*, 6159; d) V. Berl, M. J. Krische, I. Huc, J. M. Lehn, R. Schmutz, *Chem. Eur. J.* **2000**, *6*, 1938.

[14] M. W. P. L. Baars, A. J. Karlsson, V. Sorokin, B. F. W. Waal, E. W. de Meijer, *Angew. Chem.* **2000**, *112*, 4432; *Angew. Chem. Int. Ed.* **2000**, *39*, 4262.

[15] For synthetic details, see the Supporting Information.

[16] J. G. Liu, M. H. He, Z. X. Li, Z. G. Qian, F. S. Wang, S. Y. J. J. Yang, *J. Polym. Sci. A* **2002**, *40*, 1572.

[17] All spectral data and gel-permeation chromatograms are available in the Supporting Information.

[18] The increase in intensity is simply a reflection of the increase in the concentration of the donor species, whereas the downfield shift arises from the mole-fraction weighted average of the free and complexed naphthalene units. It may be recalled that formation of a CT complex generally causes an upfield shift of

 © 2005 Wiley-VCH Verlag GmbH & Co. KGaA, Weinheim

both the donor and acceptor units,[11] however, the downfield shift of the donor protons in this case arises from the overwhelming presence of free donor species.

[19] The association constants of the two folding agents with AA-6OE were determined from the variation in the chemical shift of the acceptor ring protons as a function of the folding-agent concentration by using computer program EQNMR version 2.10. (Freeware, M. J. Hynes, Chemistry Department, University College Galway, Ireland). The *K* values were found to be 850 and 600 M^{-1} for D2-NH_3^+ and D3-NH_3^+, respectively, but only 30 M^{-1} for D + NH_4^+, thus confirming the cooperativity of the interaction, as well as the importance of the spacer length for effective binding and folding. The association constant for D2-NH_3^+ was also determined from ITC and was found to be 1050 M^{-1}, which is comparable to that obtained with NMR spectroscopic analysis. Similar attempts to determine the association constant for the polymer with ITC was difficult as a simple plot that assumed a single association constant failed to give a good fit. A probable reason for this failure is that several different values of association constants could, in principle, be required in the case of the polymer. Nevertheless, it is clear from the values of *K* obtained for the model AA-6OE that linking the two interacting segments in the folding agent is critical for the generation of a folded structure in the polymer.

[20] For synthetic details, see the Supporting Information.

[21] The variable temperature experiment was done using D3-NH_3^+ as the folding agent at a ratio of 4:1 molar equivalents with respect to the polymer repeating unit to ensure that the ammonium salt did not precipitate on cooling.

[22] [18]Crown-6 is known to form a very strong complex with ammonium ions with an association constant *K* in the order of 10^6 M^{-1}; see reference [12a].

[23] D. D. Perrin, W. L. F. Armarego, D. R. Perrin, *Purification of Laboratory Chemicals*, 2nd ed., Pergamon, Oxford, **1980**.

 © 2005 Wiley-VCH Verlag GmbH & Co. KGaA, Weinheim

Microreactor Fluidics

DOI: 10.1002/anie.200500792

A Microfabricated Gas–Liquid Segmented Flow Reactor for High-Temperature Synthesis: The Case of CdSe Quantum Dots**

Brian K. H. Yen, Axel Günther, Martin A. Schmidt, Klavs F. Jensen, and Moungi G. Bawendi**

Microfluidic reactors enable a number of advantages over conventional chemical processes including enhanced control of heat and mass transfer, lower reagent consumption during optimization, and sensor integration for in-situ reaction monitoring.[1,2] Reactors are usually fabricated from either silicon, glass, or polymers; those made of silicon or glass are advantageous because they can tolerate a broad range of chemistries and high temperatures. Microreactors for the large class of homogeneous liquid-phase reactions are often based on single-phase laminar flow designs in which reagent streams are brought into contact. However, such designs are limited in terms of slow diffusive reagent mixing and broad residence time distributions (RTDs). Recirculation within segments in a two-phase segmented flow approach (gas–liquid or liquid–liquid) overcomes such limitations by providing a mechanism of exchanging fluid elements located near the channel walls with those at the center.[3–5] This recirculatory motion has the dual effect of narrowing the RTD and improving reactant mixing. In contrast to single-phase designs, segmentation makes it possible to drive reactions to required yields over significantly shorter times owing to the enhanced mixing, while maintaining narrow RTDs.

[*] A. Günther, Prof. K. F. Jensen
Massachusetts Institute of Technology
Department of Chemical Engineering
Institute for Soldier Nanotechnologies
77 Massachusetts Avenue, 66–566, Cambridge, MA 02139 (USA)
Fax: (+1) 617-258-8224
E-mail: kfjensen@mit.edu

B. K. H. Yen, Prof. M. G. Bawendi
Massachusetts Institute of Technology
Department of Chemistry
Institute for Soldier Nanotechnologies
77 Massachusetts Avenue, 6–221, Cambridge, MA 02139 (USA)
Fax: (+1) 617-253-7030
E-mail: mgb@mit.edu

Prof. M. A. Schmidt
Massachusetts Institute of Technology
Microsystems Technology Laboratories
Department of Electrical Engineering and Computer Science
Cambridge, MA 02139 (USA)

[**] This research was funded in part by the NSF-CRC program (CHE-0209898), the Microchemical Systems Technology Center, and the U.S. Army through the Institute for Soldier Nanotechnologies (under contract DAAD-19-02-0002 with the U.S. Army Research Office). B.K.H.Y. acknowledges support from the NDSEG Fellowship Program. We thank the staff of the MIT Microsystems Technology Laboratories for assistance with microfabrication.

© 2005 Wiley-VCH Verlag GmbH & Co. KGaA, Weinheim
WILEY InterScience

Gas–liquid rather than liquid–liquid segmented flow offers the most versatility in terms of the range of chemistries that can be performed in a microfluidic system. Gas–liquid flow is preferable for performing reactions at elevated temperatures, as most solvents experience increased miscibility at higher temperatures. Moreover, it is possible to obtain uniform segmentation in gas–liquid flows over a very large range (over two orders of magnitude) of bubble velocities and therefore reaction timescales.[4,5] Liquid–liquid segmented flow systems are operated over a much narrower range with typical droplet velocities varying over one order of magnitude.[3,6] Finally, in gas–liquid segmented flow, the reaction solution is present as a continuous liquid phase within the channel (Figure 1) so that it is possible to

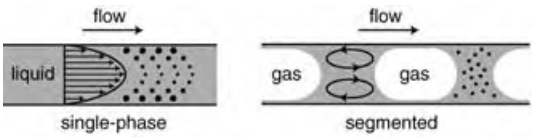


Figure 1. Mixing and residence time distribution (RTD) effects in a) single-phase and b) segmented gas–liquid flow. In the single-phase laminar flow, diffusion is the only means of mixing. As a result of the parabolic fluid-velocity profile, particles near the wall spend more time in the reactor than those in the center, resulting in broad RTDs. In the two-phase case, recirculation within each liquid slug brings material from the wall to the center of the channel. This facilitates mixing, which narrows the RTD, and results in narrower size distributions.

inject additional reactants or withdraw reaction aliquots in a continuous, controllable manner. In liquid–liquid segmented flow, the reaction solution is usually the dispersed (droplet) phase; subsequent addition of reactants is challenging, as it requires synchronized merging of discrete droplets.[6] The withdrawal of small aliquots without disturbing the flow is also difficult. Herein, we demonstrate a silicon-based microreactor that incorporates both gas–liquid segmented flow and multiple temperature zones. The reactor represents a general platform for high-temperature synthesis under very well-defined reaction conditions (mixing times and narrow RTDs).

As a model system for the reactor, the preparation of CdSe quantum dots (QDs) was chosen, as the chemistry a) requires high temperatures and b) highlights the advantages of the segmented-flow approach over single-phase and conventional batch processes. In the batch method, semiconductor QDs (diameters = 2–10 nm) are synthesized by the rapid injection of precursors into a heated flask containing a mixture of solvents and ligands.[7–10] Factors such as the injection process, local temperature and concentration gradients, mixing rate, and cooling rate strongly influence QD nucleation and growth, but are difficult to control. Single-phase continuous flow reactors in which precursor solutions are delivered into a heated reaction section have addressed some of these reproducibility problems.[11] However, these reactors suffer from slow mixing and broad RTDs, which are detrimental to the particle size distribution (Figure 1). It has been challenging to adapt QD chemistry to a chip-based segmented flow system owing mainly to the reaction temperatures required (> 250 °C). Liquid–liquid segmented flow has been used to prepare QDs at room temperature in a polydimethylsiloxane device,[6] but solvent miscibility and polymer degradation at high temperatures make it difficult to use this approach to prepare monodisperse, luminescent particles.

The introduction of segmenting gas into heated capillaries has also been implemented, but the uniformity of such gas–liquid flows and their effect on QD formation were not extensively characterized.[12,13] We demonstrate herein the success of our microreactor design in rapid mixing and extremely uniform segmentation behavior at the high temperatures required for QD synthesis. The QD sample size distributions and reaction yields are superior to those attainable in single-phase flow, with the improvement significantly more pronounced at short reaction times. As the improvement is a direct consequence of the rapid mixing and narrow RTD features of segmented flow, the reactor greatly decreases the time required to produce high-quality particles in comparison with existing single-phase approaches. Moreover, the reactor is applicable to a variety of nanoparticle chemistries because it offers access to a wide range of reaction timescales without a compromise in acceptable size distributions.

The reactor shown in Figure 2 allows rapid initial mixing of the precursors, controlled QD growth, and on-chip quenching of the reaction. The silicon reactor accommodates a reaction channel length of approximately 1 m (hydraulic diameter ≈ 380 μm) and two shallow side channels for collecting reaction aliquots. A halo etch region makes it possible to localize multiple temperature zones for reaction (> 260 °C) and quenching (< 70 °C) on the device. Precursor solutions are delivered separately into the heated section and an Ar gas stream introduced further downstream results in a segmented gas–liquid flow. Recirculation within the liquid slugs rapidly mixes the heated precursors, thereby initiating the reaction. The fluids initially pass through a meandering section to induce good mixing across the channel[3–5] before reaching a longer straight-channel section where the majority of the particle growth occurs. The reaction is stopped when the fluids enter the cooled outlet region of the device. The segment lengths are very uniform during conditions of a typical QD synthesis (Figures 2a and b). Figure 2c shows a long-time-exposure image of the cooled outlet region of the device under continuous UV excitation. At the high reaction temperatures, the QD photoluminescence (PL) is completely quenched (top portion of Figure 2c), but once the fluid reaches the cooled region (< 70 °C), yellow PL is observed. The image illustrates our ability to maintain the required ≈ 200 °C temperature gradient within a single reactor chip.

The quality of the segmentation shown in Figures 2a and b deserves further discussion, as the slug-length distribution can contribute to the RTD and therefore the ultimate QD size distribution. We systematically examined the slug statistics over a range of flow conditions by varying either the total fluid flow rate under conditions of constant gas-to-liquid flow rate (v_g/v_l) or by varying v_g under conditions of constant v_l.[14] The resulting liquid slug-length distributions over this range of residence times are shown in Figure 3a. The liquid lengths are on the order of the channel hydraulic diameter and typically have a relative standard deviation of ≤ 10 %.

 © 2005 Wiley-VCH Verlag GmbH & Co. KGaA, Weinheim

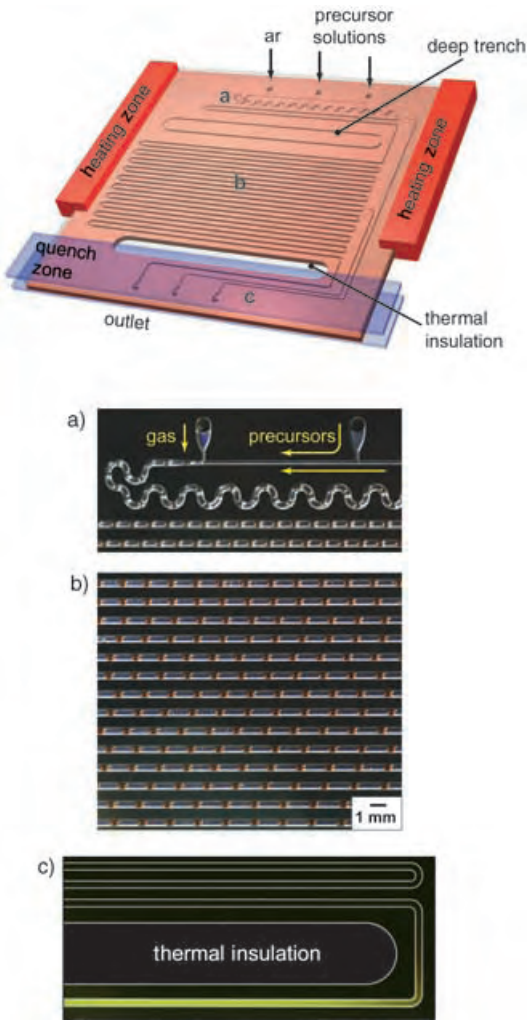


Figure 2. Reactor with heated reaction region and cooled outlet zone: a through-etch section ensures that the two regions are thermally isolated; a) heated inlets and b) main channel section: red segments = QD reaction solution; dark segments = Ar gas; c) time-exposure image of the cooled outlet region under UV irradiation. $T = 260\,°C$, $\nu_g = 60\ \mu L\,min^{-1}$, $\nu_l = 30\ \mu L\,min^{-1}$, Se/Cd = 5.0.

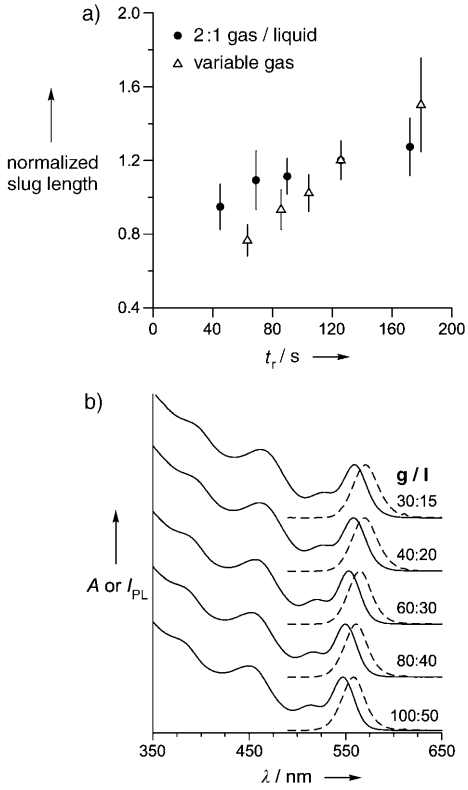


Figure 3. a) Ratio of average liquid slug length to hydraulic diameter (≈380 μm) over a range of flow rates (residence times, t_r) at 260 °C; error bars indicate the standard deviation of the liquid length for a given flow condition; ● = gas/liquid flow rates of: 100/50, 80/40, 60/30, 40/20, and 30/15 $\mu L\,min^{-1}$ (ratio kept equal to 2); △ = flow rates of: 100/20, 80/20, 60/20, 40/20, and 30/20 $\mu L\,min^{-1}$ (liquid flow rate kept at 20 $\mu L\,min^{-1}$). b) Absorbance (——) and photoluminescence (PL) (-----) spectra for QDs prepared under the flow conditions represented by (●) in part a).

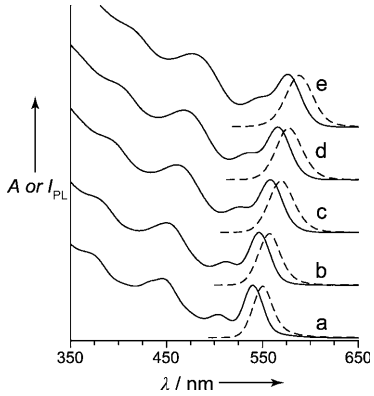


Figure 4. Absorbance (——) and photoluminescence (PL) (-----) spectra for QDs obtained by varying the precursor feed ratio ($T = 260\,°C$). The total gas and liquid flow rates were kept constant ($\nu_{l(Se)} + \nu_{l(Cd)} = 20\ \mu L\,min^{-1}$, $\nu_{g(Ar)} = 40\ \mu L\,min^{-1}$). Spectra correspond to the flow rates ($\nu_{l(Se)}/\nu_{l(Cd)}$) and resulting concentration ratios (Se/Cd) of a) 3.0 and 15, respectively; b) 1.67 and 8.3; c) 1.0 and 5.0; d) 0.60 and 3.0; e) 0.33 and 1.7.

This dispersion in the slug lengths is small enough so that it does not contribute to the overall RTD.[15] The resulting spectra of the QD samples indicate narrow size distributions (Figure 3b) and are similar to the best samples obtained by the batch process. The band-edge absorbance and several higher transitions are clearly resolved, and the PL line widths remain narrow over the entire range of flow rates. In the figure, the PL full-width-at-half-maximum (fwhm) varies between 28 and 31 nm (112 and 119 meV, depending on wavelength).

In Figure 3b, the QDs were prepared with a constant precursor composition and represent a fairly limited spectral range (< 10 nm variation in band-edge position). As discussed previously, it was found that size tuning is more readily accomplished through variation in the ratio Se/Cd rather than the reaction time.[12] Figure 4, illustrates such an effect from varying the Cd and Se precursor flow rates while the keeping the total liquid and gas flow rates constant (at 20 and 40 $\mu L\,min^{-1}$, respectively). In contrast to Figure 3b, a change in the ratio Se/Cd from 15 to 1.7 made it possible to tune the effective band gap of the QDs over a much larger spectral

 © 2005 Wiley-VCH Verlag GmbH & Co. KGaA, Weinheim

range of ≈40 nm yet maintain narrow size distributions. The average QD radius decreases with an increase in the Se/Cd ratio owing to the strong dependence of the nucleation rate on the precursor ratio. The samples represented in Figure 4 were produced by using the same temperature (260 °C) and mean residence time (≈140 s). By varying the temperature and reaction time in addition to the precursor feed ratios, it would be possible to tune the effective band gap over an even larger spectral window.

In general, it was found that spectra of QDs produced in single-phase operation ($\nu_g = 0$) were significantly broader than those obtained with gas–liquid flow. The poorer performance observed in the single-phase case results primarily from the combination of two effects: initial mixing and broad RTD. In single-phase flow, the two precursor streams combine slowly by diffusion, in contrast to the convective mixing induced by the introduction of a segmenting gas.[16] Slow initial mixing makes it difficult to realize a rapid nucleation burst, and the resulting QD samples are polydisperse. Once the reagents are completely mixed, the RTD effect is still present; QDs near the channel wall spend a longer time in the reactor than those in the channel center. In segmented flow, recirculation within the liquid brings fluid from the channel wall to the center which facilitates rapid mixing, lower dispersion in residence times, and therefore narrower QD size distributions (Figure 1).

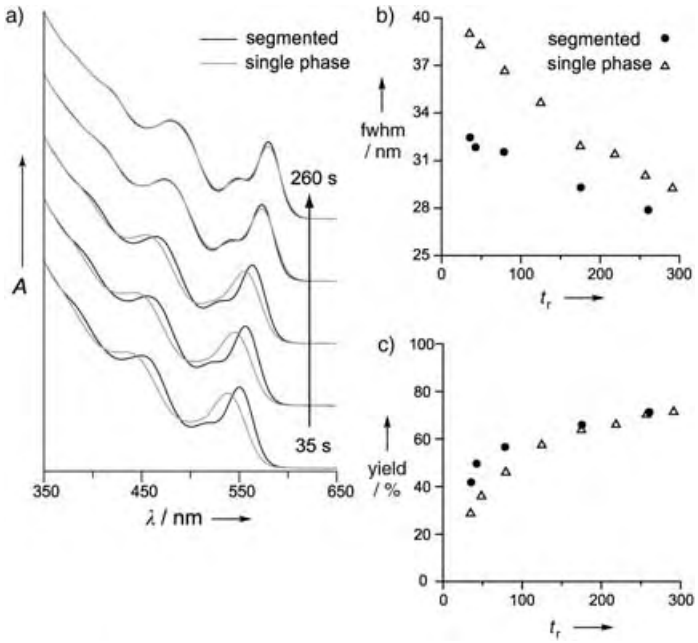


Figure 5. a) Absorbance spectra of QDs prepared with segmented and single-phase flow. Each pair of spectra corresponds to approximately the same mean residence time. b) PL full-width-at-half-maximum (fwhm) and c) reaction yield of QD samples prepared in segmented (●) and single-phase (△) flow. For segmented flow, ν_g/ν_l was varied between 15/10 and 100/40 μL min^{-1}. For single-phase flow, ν_l was varied between 34 and 250 μL min^{-1}. $T = 280$ °C, Se/Cd = 1.0.

To isolate the RTD contribution from the effects of initial mixing, we cooled the inlet region of the reactor and premixed the precursors inline with a miniature convective mixer. A deep trench feature (Figure 2) allowed us to keep the inlets thermally isolated from the main reaction channel. Cooling the inlets ensures that the pre-mixed precursors do not react until they reach the heated reaction section. In this way, we eliminated the effect of initial reagent mixing and were able to directly observe the RTD effect on the QD size distribution. The spectra in Figure 5a illustrate the improvement of the size distribution resulting from segmentation. Figure 5b is a plot of the fwhm of the PL peak for samples prepared at several flow conditions (mean residence times). For reaction times shown in Figure 5b, the PL fwhm varies between 28 and 32 nm (99–128 meV) for segmented flow, and 29 and 39 nm (104–158 meV) for single-phase flow. In both plots in Figure 5b, the PL peak width decreases with time, and this general trend (size distribution focusing) has been explained as evidence of the presence of a mass-transfer component in the particle growth rate.[17,18] However, the absorbance and PL spectra of QDs produced in gas–liquid flow are generally sharper in than those produced in single-phase scenarios. Furthermore, the difference shown in Figures 5a and b between single- and two-phase flow becomes more pronounced at shorter timescales. This behavior at short times results from the fact that the RTD broadens significantly with flow rate in single-phase flow,[12] whereas the RTD does not have such a strong flow-rate dependence in the segmented case. Notably, cooling the inlets is not the normal mode of operation for the device. Upon introduction of the gas at low temperature, the slug uniformity is substantially poorer than the uniform segments shown in Figures 2a and b. This flow destabilization results primarily from rapid expansion of gas and the large change in liquid viscosity when the fluids reach the heated section. In spite of such non-uniform segmentation, a significant improvement in QD size distribution is still observed.

Figure 5c reveals an additional reason for the larger improvement in size distribution at shorter reaction times. In segmented flow, the mixing timescale that is governed by recirculation within liquid slugs decreases almost linearly with flow rate.[5] Therefore, a shorter reaction time (faster flow rate) is compensated by more intense stirring, and vice versa. The inverse relationship between stirring intensity and reaction time is manifested in the reaction yield curves shown in Figure 5c. At shorter times (high flow rates), the QD reaction is driven to higher yields than those of the single-phase operation. The increased growth rate causes the QD population distribution to focus more quickly than in the single-phase case. Consequently, the difference in the two curves in Figure 5b is more pronounced at short times. At lower flow rates, the recirculatory stirring is slower, but the reaction time is longer, thus the yield curve converges with that for single-phase flow. Even at the longest reaction times (when the yields are similar for the two cases), the PL spectra for gas–liquid flow is still somewhat narrower, indicating that the improved RTD effect on size distribution is still present. In summary, the synthesis of acceptable QD samples by the single-phase approach requires long reaction times to allow the size distribution focusing and narrowing of the RTD time to fully develop. In segmented flow, the enhanced mixing

 © 2005 Wiley-VCH Verlag GmbH & Co. KGaA, Weinheim

accelerates the particle formation process, thereby decreasing the time required for focusing the size distribution, and a narrow RTD is sustained even at high flow rates. For example, from Figure 5b, the narrow size distribution obtained in 42 s with segmented flow requires over fourfold more time ($\approx$175 s) to achieve with single-phase flow.

In conclusion, we have designed a gas–liquid segmented flow reactor with multiple temperature zones. The reactor is applicable to a range of chemistries because it is possible to operate at high temperatures, yet maintain excellent mixing and RTD characteristics. To illustrate the unique features of the design, it was applied to the synthesis of CdSe QDs. Under the reaction conditions reported, segmentation is very uniform and the resulting monodisperse samples exhibit excellent optical properties. Relative to single-phase flow, the enhanced mixing and narrow RTD characteristics of the reactor result in a significant improvement in reaction yield and size distribution, especially at short reaction times. Such attributes are highly desirable from the standpoint of chemical production, as it is possible to increase throughput without sacrificing narrow size distributions. Furthermore, the reactor is applicable to particle systems in which the optimal reaction timescales are shorter than that of CdSe QDs, in contrast to single-phase devices, which are limited to long reaction times. In addition to its use as a synthesis tool, variation of the mean slug velocity and length in the reactor channel provides a way to reproducibly control the mass-transfer rate during particle formation, which is not possible in single-phase flow or the conventional batch method. This makes the reactor design ideally suited for the systematic study of the mechanism of QD formation.

Experimental Section

The reactor was fabricated with standard silicon micromachining techniques. Channels were fashioned by deep reactive ion etching (DRIE) of a silicon wafer ($\varnothing = 15$ cm; thickness = 0.65 mm). An oxide layer (0.5 μm) was grown on the silicon surface, and the entire device was capped and sealed with an anodically bonded pyrex wafer (thickness = 0.76 mm). High-temperature fluidic connections were made by using glass solder (Diemat) to seal Kovar tubing to the reactor inlets. Standard 1/16-inch (1.6 mm) chromatography fittings (Upchurch) were used to connect the Kovar tubing to gas and liquid lines. Syringe pumps (Harvard PHD 2000 and KD Scientific 210) were used to deliver both precursor solutions and segmenting gas. A heated aluminum block in contact with the reaction section of the device was used for thermal control. The inlet and quenching regions were cooled with water-chilled aluminum blocks. Images of the reactor channel were taken with a consumer digital camera equipped with a macro lens and flash. For each flow condition, several hundred individual slug lengths were measured. The liquid fraction (liquid volume/total channel volume) was determined from the average slug lengths, and the mean residence time was calculated from the fraction and syringe pump flow rates.

The Cd and Se precursors were prepared as described previously with a few minor modifications.[12] All manipulations were performed under air-free conditions. Briefly, the Cd precursor was prepared by heating a suspension of cadmium 2,4-pentanedionate (1 mmol, 98%, Alfa) in squalane (9 mL, 98%, Alfa) and oleic acid (2.2 mmol, >99%, Alfa) at 150°C for 10 min. The optically clear solution was then placed under vacuum at 100°C for $\approx$1.5 h before the addition of 4 mL oleylamine (97%, Pfaltz and Bauer). A stock solution of tri-*n*-octylphosphine selenide (TOPSe, 1.5 M) was prepared by dissolving an appropriate amount of selenium shot (99.999%, Alfa) in tri-*n*-octylphosphine (TOP, 97%, Strem). The Se precursor solution consisted of the suitable amount of TOPSe (1.5 M) diluted in squalane. The two precursor solutions were degassed thoroughly at 90°C before loading into separate syringes.

Samples for the measurement of absorbance and PL spectra were prepared by diluting the raw QD solutions in hexanes. Optical absorption spectra were acquired with a Hewlett-Packard 8452 diode array spectrometer. Photoluminescence spectra were acquired with an Ocean Optics SD2000 fiber-optic spectrometer and a handheld UV lamp as an excitation source. Reaction yields were determined from the optical density at $\lambda = 350$ nm and the measured absorbance cross-section for CdSe QDs.[19]

Received: March 3, 2005
Published online: June 20, 2005

Keywords: microreactors · nanostructures · nanotechnology · quantum dots · segmented flow

[1] K. F. Jensen, *Chem. Eng. Sci.* **2001**, *56*, 293.
[2] K. Jähnisch, V. Hessel, H. Löwe, M. Baerns, *Angew. Chem.* **2004**, *116*, 410; *Angew. Chem. Int. Ed.* **2004**, *43*, 406.
[3] H. Song, J. D. Tice, R. F. Ismagilov, *Angew. Chem.* **2003**, *115*, 792; *Angew. Chem. Int. Ed.* **2003**, *42*, 768.
[4] A. Günther, S. A. Khan, M. Thalmann, F. Trachsel, K. F. Jensen, *Lab Chip* **2004**, *4*, 278.
[5] A. Günther, M. Jhunjhunwala, M. Thalmann, M. A. Schmidt, K. F. Jensen, *Langmuir* **2005**, *21*, 1547.
[6] I. Shestopalov, J. D. Tice, R. F. Ismagilov, *Lab Chip* **2004**, *4*, 316.
[7] C. B. Murray, D. J. Norris, M. G. Bawendi, *J. Am. Chem. Soc.* **1993**, *115*, 8706.
[8] L. Qu, Z. A. Peng, X. Peng, *Nano Lett.* **2001**, *1*, 333.
[9] Z. A. Peng, X. Peng, *J. Am. Chem. Soc.* **2001**, *123*, 183.
[10] M. G. Bawendi, N. E. Stott, US Patent Number 6,821,337, **2004**.
[11] For a review of microreactors for nanoparticle synthesis, see: J. deMello, A. deMello, *Lab Chip.* **2004**, *4*, 11N.
[12] B. K. H. Yen, N. E. Stott, K. F. Jensen, M. G. Bawendi, *Adv. Mater.* **2003**, *15*, 1858.
[13] H. Nakamura, Y. Yamaguchi, M. Miyazaki, H. Maeda, M. Uehara, P. Mulvaney, *Chem. Commun.* **2002**, 2844.
[14] The reported gas flow rates do not include the significant, although steady, gas leakage from the syringe and tubing fittings leading up to the reactor. We found this to be the case even with nominally gas-tight syringes. However, the slug lengths were measured directly from images taken of the reactor channel, so the reported mean residence times are accurate.
[15] The standard deviation of the *mean* of the liquid slug length gives rise to an uncertainty in the residence time: $\sigma_{t_r}/t_r = \sigma_l/(l_{avg}\sqrt{N})$ in which t_r is the residence time, l is the length of an individual slug, and N is the number of liquid slugs in the reactor (typically $\approx$300). As $\sigma_l/l_{avg} \approx 10\%$, $\sigma_{t_r}/t_r < 0.6\%$. In other words, the liquid slug length distribution does not contribute significantly to the overall residence time dispersion.
[16] From Ref. [5], we estimate the mixing time for segmented flow in our system to be $\approx$1% of the average residence time. For the single-phase case, the diffusive mixing time can be >50% of the average residence time depending on the flow rate.
[17] X. Peng, J. Wickham, A. P. Alivisatos, *J. Am. Chem. Soc.* **1998**, *120*, 5343.
[18] D. V. Talapin, A. L. Rogach, M. Haase, H. Weller, *J. Phys Chem. B* **2001**, *105*, 12278.
[19] C. A. Leatherdale, W.-K. Woo, F. V. Mikulec, M. G. Bawendi, *J. Phys. Chem. B* **2002**, *106*, 7619.

 © 2005 Wiley-VCH Verlag GmbH & Co. KGaA, Weinheim

Fluorescent Probes

DOI: 10.1002/anie.200500845

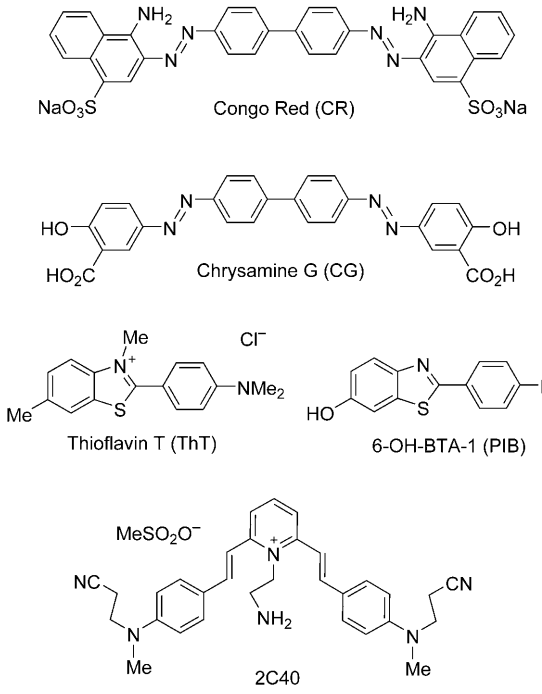
In Vivo Optical Imaging of Amyloid Aggregates in Brain: Design of Fluorescent Markers**

*Evgueni E. Nesterov, Jesse Skoch, Bradley T. Hyman, William E. Klunk, Brian J. Bacskai, and Timothy M. Swager**

Neuroimaging is emerging as a way to noninvasively identify and monitor neurodegenerative diseases during the preclinical and early clinical stages.[1] Alzheimer's disease (AD) stands out among the neurodegenerative diseases as the fourth leading cause of death in the United States and the most common cause of acquired dementia.[2] Early detection of AD is imperative in enabling the understanding and clinical treatment of this disorder, as well as in preventing its progression. The characteristic signature of AD is the deposition of amyloid-β plaques and neurofibrillary tangles in the patient's brain,[3] which parallel the disease but can only be diagnosed with certainty after death by an autopsy.

A significant advance in the field has been the development of radiolabeled small-molecule agents capable of entering the brain and specifically targeting plaques and tangles for imaging with positron emission tomography (PET) and single-photon emission computerized tomography (SPECT).[1] A major limitation of these methods is the requirement for the markers to be labeled with short-lived isotopes, such as ^{11}C with a half-life of about 20 min for PET. An attractive noninvasive alternative is in vivo optical imaging using specific far-red (near-IR) fluorescent contrast agents. These contrast agents make use of the inverse fourth-power relationship between the wavelength and light scattering, thus allowing the longer-wavelength light penetration through the living tissues necessary for direct brain imaging.[4a] Long-wavelength detection methods also benefit from the low auto-fluorescence of biological matter beyond 600 nm.[4] The requirements for a successful optical marker of AD are: 1) a suitable wavelength interval of absorption and emission (600–800 nm), 2) the ability to rapidly enter the brain after intravenous injection, and 3) specific labeling of the amyloid-β deposits with rapid clearing of the unbound dye. Another unique advantage of optical imaging is the possibility to attain substantial differences in the photophysical/optical properties between the bound and unbound forms of the marker (requirement 4). This would allow a significant increase in imaging contrast which cannot be exploited with techniques based on radioligands.

Among the known amyloid-staining compounds, Congo Red (CR) provides historically the most standardized way of staining amyloid plaques, and is still employed in post mortem histological analysis of AD brain, as the binding is specific.[5] Thioflavin T (ThT) is another dye to use in analysis of aggregated amyloid proteins. It binds slightly weaker than CR, but makes up for this deficiency by exhibiting a green fluorescence, that becomes more than 1000 times brighter upon binding to amyloid plaques.[6] The understanding of what makes these simple molecules so specific to senile plaques is the starting point for the rational design of improved markers. Studies[7] suggest that the origin of the specific binding of CR to amyloid-β aggregates is due to the combination of electrostatic interactions between the negatively charged CR's sulfonate groups with the positively charged amino acid residues in the antiparallel protein



[*] Dr. E. E. Nesterov,[+] Prof. Dr. T. M. Swager
Department of Chemistry and
Institute for Soldier Nanotechnologies
Massachusetts Institute of Technology
Cambridge, MA 02139 (USA)
Fax: (+1) 617-324-0505
E-mail: tswager@mit.edu
J. Skoch, Prof. Dr. B. T. Hyman, Dr. B. J. Bacskai
Department of Neurology/Alzheimer's Disease
Research Laboratory
Massachusetts General Hospital
114 16th Street, Charlestown, MA 02129 (USA)
Prof. Dr. W. E. Klunk
Department of Psychiatry
University of Pittsburgh School of Medicine
Pittsburgh, PA 15213 (USA)
[+] Current address:
Department of Chemistry
Louisiana State University
Baton Rouge, LA 70803 (USA)

[**] This research was supported by NASA and the U.S. Army through the Institute for Soldier Nanotechnologies, under contract DAAD-19-02-D-0002 with the U.S. Army Research Office (TMS), by NIH through grant EB00768 (BJB).

Supporting information for this article is available on the WWW under http://www.angewandte.org or from the author.

InterScience
© 2005 Wiley-VCH Verlag GmbH & Co. KGaA, Weinheim

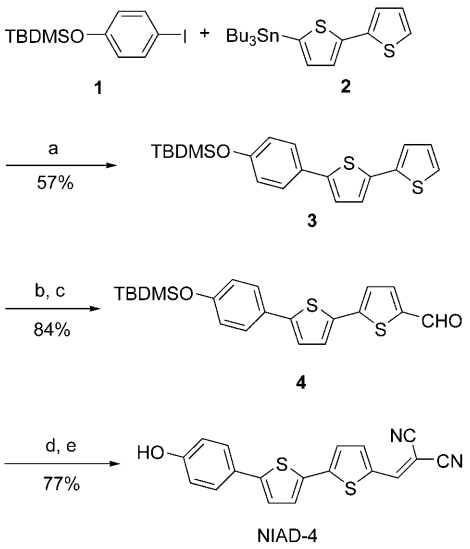
β sheets, and CR's shape is complementary to features in an amyloid fibril's surface. The latter recognition likely involves hydrophobic interactions with the planarized aromatic π system of the dye molecule.[7c] Although the binding of ThT to amyloids has received less attention, it is likely to involve similar shape-specific recognition.[6,8] Thus, it is our opinion that the presence of hydrophobic planarized (or easily planarizable) π system is an important design feature to obtain high binding specificity.

A potential biomarker must be able to rapidly enter the brain after an intravenous injection. To exhibit high blood–brain barrier (BBB) permeability, the molecule needs to be relatively lipophilic (but not highly lipophilic as this will lead to its aggregation and accumulation in blood proteins and red blood cell membranes), and should not bear ionic groups. High BBB permeability also requires the marker to be relatively small, with an upper molecular weight limit of about 600 Da. These simple empirical rules are extremely robust, and, for example, both CR and ThT, as charged molecules, are not capable of crossing the BBB. It is also highly probable that any charged molecules like compound 2C40, a recently proposed fluorescent marker for AD found by combinatorial screening of a library of 320 compounds,[9] will be similarly incapable of in vivo imaging. In contrast, substantial increase of the BBB permeability was achieved with uncharged analogues of CR and ThT. For example, in the CR analogue Chrysamine G (CG), the replacement of the sulfonate group by a less ionizable carboxy group significantly increased the BBB permeability without compromising the high binding specifity.[10] A ThT uncharged analogue, 6-OH-BTA-1, which is commonly referred to as Pittsburgh compound B (PIB), is highly efficient both in crossing the BBB and in selective binding to AD amyloid aggregates, and is currently under clinical tests as an amyloid marker with PET imaging.[11]

To develop an effective in vivo imaging dye, we have merged these empirical requirements with electronic structure design to produce a compound possessing a suitable spectral range of the absorption and emission bands along with a potential to produce additional imaging contrast. We have employed a classical push–pull architecture with terminal donor and acceptor moieties that are interconnected by a highly polarizable bridge. Various donor and acceptor groups can be used to manipulate the relative energies of HOMO and LUMO, with better donor and better acceptor leading to a smaller HOMO–LUMO gap and to the desired long wavelength absorption/emission bands. Finally, to obtain greater imaging contrast, we required a molecule to possess a substantial degree of conformational freedom when unbound in solution, but it would be conformationally restricted upon binding to the protein. Such a "rigidification" decreases the vibrational-rotational processes that couple the excited and ground states, thereby decreasing the radiationless decay rate and increasing the fluorescence quantum yield of the protein-bound molecule.[12]

The proof-of-approach near-IR Alzheimer's dye NIAD-4[13] was designed to satisfy all four of the requirements above. This dye with a molecular weight of 334 Da is likely to be among the simplest possible structures. It uses a dithienylethenyl π-conjugated bridge between donor and acceptor. The highly polarizable bridge was chosen to provide a substantial bathochromic shift in both absorption and emission spectra of the dye. The rigid rodlike aromatic core of NIAD-4 is hydrophobic and readily planarizable, and has a shape similar to that of ThT for achieving a high binding specificity to amyloid aggregates. In unbound NIAD-4 free rotation around the single bonds leads to facile vibrationally coupled radiationless excited-state deactivation. Reduction of these processes upon binding to the protein aggregate was expected to enhance its fluorescence quantum yield. The donor and acceptor groups were chosen to balance between the need for a high electron-donating/accepting ability to achieve a substantial spectral bathochromic shift and the requirement to avoid charged or easily ionizable groups to improve the BBB permeability. The dicyanomethylene group was chosen as the acceptor, and the hydrophilic *p*-hydroxyphenyl group was selected as a donor to compensate for the high hydrophobicity of the bridge. Both groups are relatively small and were instrumental in maintaining the low molecular weight of NIAD-4.

The synthesis of NIAD-4 is shown in Scheme 1. The silyl-protected aldehyde **4** was prepared by Stille coupling.



Scheme 1. Synthesis of dye NIAD-4: a) $[PdCl_2(PPh_3)_2]$ (3 mol%), toluene, 70°C, 36 h; b) *n*BuLi, TMEDA, hexanes, −70°C, 2 h; c) DMF, −70°C→RT, 12 h; d) $CH_2(CN)_2$, EtOH, piperidine (cat.), 60°C, 18 h; e) HCl, 60°C, 6 h. DMF: *N*,*N*-dimethylformamide; TMEDA: *N*,*N*,*N*′,*N*′-tetramethylethylenediamine.

Condensation with malononitrile followed by in situ deprotection afforded NIAD-4 as a dark-red material, which exhibits a bright red fluorescence in methanol solution (Figure 1). This contrast marker is slightly soluble in aqueous media, although it forms micelles/aggregates at the concentrations above 10 μM.[14] The aqueous solutions of NIAD-4 only have trace emission (quantum yield ≈0.00008), which may be in part due to the greater stabilization in aqueous media of the non-emissive intramolecular charge transfer state as opposed to the emissive planar excited state.[15] An in vitro spectral study with aggregated synthetic amyloid-β 1–

 © 2005 Wiley-VCH Verlag GmbH & Co. KGaA, Weinheim

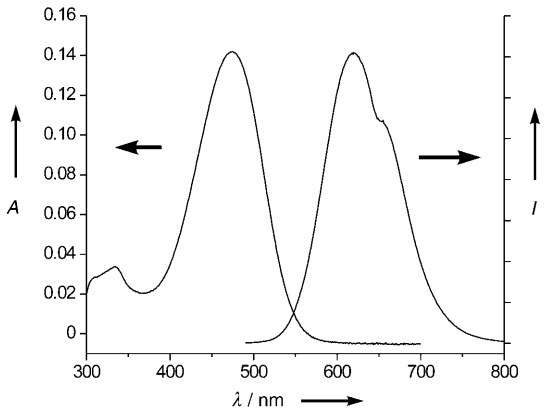


Figure 1. Absorption and fluorescence spectra of NIAD-4 in MeOH solution. (Extinction coefficient ε(475 nm) 35 700; fluorescence quantum yield 0.15.)

40 protein displayed a significant red shift ($\Delta\lambda \approx 70$ nm) of the absorption maximum along with about 1.3-fold increase in its extinction coefficient (Figure 2). This phenomenon is a

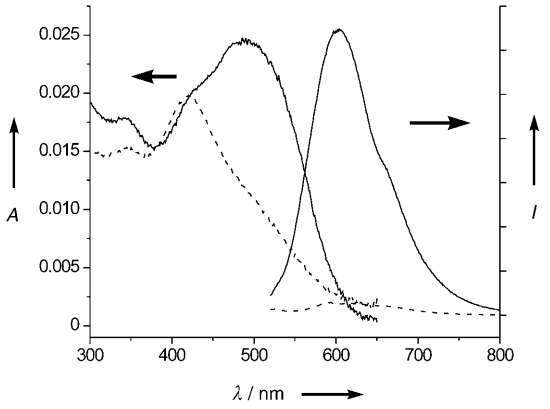


Figure 2. Absorption and fluorescence spectra of NIAD-4 in aqueous PBS solution in the presence of aggregated amyloid-β protein (solid line) and without the protein (dashed line). Concentrations: NIAD-4 4.1 μM, amyloid-β ≈10 μM. PBS: phosphate buffered saline.

consequence of the strong binding between the dye and the aggregated amyloid fibrils. The fluorescence maxima of the bound and unbound forms do not differ appreciably, and, as expected, the binding is accompanied by a dramatic enhancement of the fluorescent emission (about 400-fold, quantum yield 0.05), which is visible by simple visual inspection even at the micromolar concentrations used in the experiment. Apparently, the protein-bound dye is preorganized in a geometry that is similar to the planarized geometry of the emissive excited state after it has reached its equilibrium nuclear coordinates. Furthermore, binding to the amyloid fibrils places the dye in a lower dielectric constant environment that decreases detrimental relaxation into a non-emissive intramolecular charge transfer state.[15]

The binding studies with artificially aggregated amyloid protein assays revealed that NIAD-4 binds to the same site as BTA-1 with a binding affinity K_i of 10 nM. This affinity is much higher than that of ThT ($K_i = 580$ nM), and is close to that of high-affinity amyloid-binding compounds like PIB ($K_i = 4.3$ nM).[11b] The excellent performance of NIAD-4 for in vivo staining of amyloid plaques was demonstrated by using transgenic mice with AD-like pathology prepared with cranial windows to allow direct monitoring of the brain surface.[16] The dye readily crosses the BBB after an intravenous injection and labels specifically both the plaques and cerebrovascular amyloid angiopathy in the living brain thus making them easily detectable by the characteristic red fluorescence (see Figure 3 and Supporting Information). The high specificity of labeling the amyloid deposits is also clearly observed with in situ histochemical staining of fixed sections from transgenic mouse brain (Figure 3). In both in vivo and in situ experiments, the fluorescent images reveal exact position and size of the aggregated amyloid deposits, therefore providing the best demonstration of the high labeling specificity of NIAD-4.

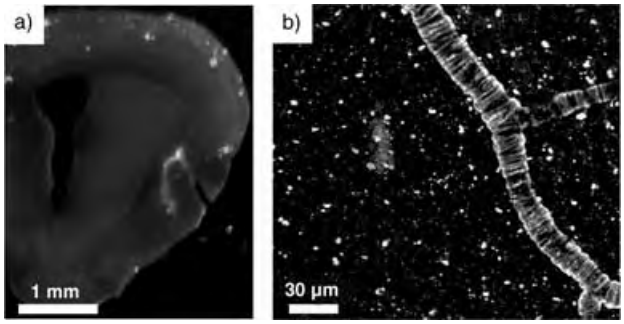


Figure 3. In vivo targeting and in situ specificity of NIAD-4 for amyloid deposits in the brain. a) A fluorescent image of a coronal section of brain from an aged APP transgenic mouse labeled with a 10 μM solution of NIAD-4 in DMSO/propylene glycol for 15 min at RT. b) In vivo fluorescent detection of both senile plaques and amyloid angiopathy using multiphoton microscopy immediately following intravenous injection of 2 mg kg^{-1} of NIAD-4. The images demonstrate the egress of dye through the BBB in a living mouse as well as the specific, sensitive targeting of amyloid-β deposits in the brain.

The remarkably strong bathochromic shift in absorption concomitant with the increase of absorption intensity upon binding combine for the high contrast optical imaging. To support our model that these changes are in part due to the planarization of NIAD-4 upon binding, we have calculated the geometry-optimized structure of the dye molecule (Figure 4a). Although both thienyl rings are nearly coplanar (dihedral angle 4.5°), the benzene ring is markedly twisted with respect to the plane of the neighboring thienyl group (dihedral angle 24.5°). This geometry still allows a π conjugation, and both HOMO and LUMO are substantially delocalized over the entire molecule (Figure 4c). Interestingly, just a small geometry change towards further planarization (which is likely to happen upon binding to amyloid fibrils) significantly increases the conjugation, resulting in even more delocalized frontier orbitals and a smaller HOMO–LUMO gap. The computed electrostatic potential distribution over the electron density surface (Figure 4b) is very similar to that of CR, with the highly hydrophobic neutral core and negative charge density localized at the

 © 2005 Wiley-VCH Verlag GmbH & Co. KGaA, Weinheim

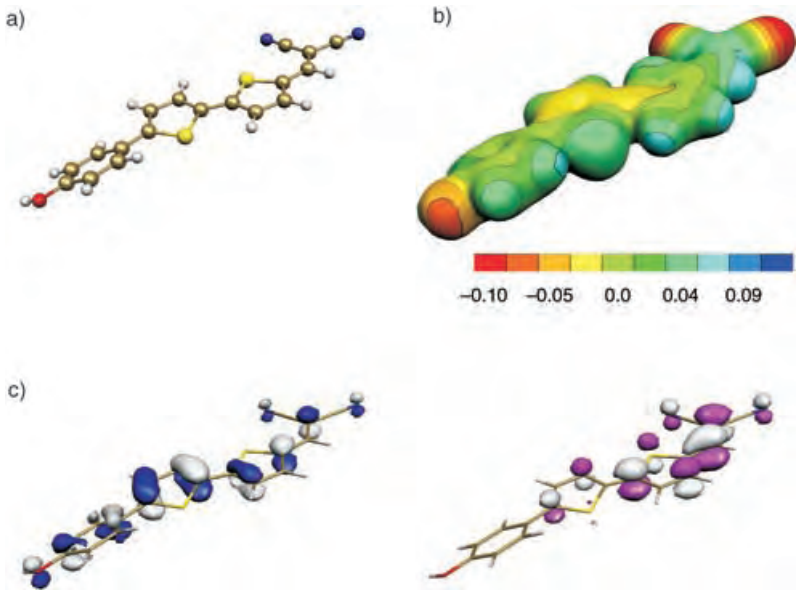


Figure 4. Optimized ground-state geometry of NIAD-4 (a), color-coded electrostatic potential mapped over electron density surface (b), and frontier molecular orbitals (c): HOMO (left) and LUMO (right). The computations were performed in gas phase at B3LYP/6-31G(df,p) level of theory. For this geometry, the computed absorption maximum (TD-B3LYP/6-31G(df,p)) was found to be 481 nm, which is in excellent agreement with the experimental value (475 nm).

molecule's termini. This feature may be in part responsible for the high binding selectivity of NIAD-4 to aggregated amyloid protein.[17]

In conclusion, we have demonstrated that the targeted rational design of in vivo fluorescent markers for amyloid protein aggregates can be successfully accomplished with a set of very simple qualitative rules. The designed contrast agent NIAD-4 shows remarkable promise for the optical imaging of amyloid plaques in brain. It may also be useful for the detection of peripheral amyloidoses. Clearly, its practical application in human Alzheimer's disease research and diagnostics requires further red-shifting of its spectral characteristics and increasing fluorescence quantum yield to allow truly noninvasive monitoring of the brain surface, without the need for the cranial window. It also requires detailed and thorough toxicity studies which we have not performed at this stage.[18] Still this is a remarkable milestone demonstrating great power of the simple design principles outlined herein for development of a practical AD biomarker. Regardless of the spectral properties of this new compound, a radiolabeled version of NIAD-4 may also be advantageous for PET or SPECT imaging. Directed modifications of the structure of NIAD-4 with the purpose to further red-shift the spectral characteristics, increase fluorescence quantum yields, and generally improve performance, as well as gain deeper understanding of these markers, are currently underway.

Received: March 7, 2005
Revised: July 16, 2005
Published online: August 1, 2005

Keywords: Alzheimer's disease · dyes/pigments · fluorescent probes · imaging agents · synthesis design

[1] S. T. DeKosky, K. Marek, *Science* **2003**, *302*, 830 – 834.
[2] "Alzheimer Disease": P. Nowotny, J. M. Kwon, A. M. Goate in *Encyclopedia of Life Sciences*, Macmillan Publishers, Nature Publishing Group, **2002**.
[3] P. M. Gorman, A. Chakrabartty, *Biopolymers* **2001**, *60*, 381 – 394.
[4] a) "Near-Infrared Dyes for High Technology Applications": E. Terpetschnig, O. S. Wolfbeis, *NATO ASI Ser. Ser. 3* **1998**, *52*, 161 – 182; b) A. Becker, C. Hessenius, K. Licha, B. Ebert, U. Sukowski, W. Semmler, B. Wiedenmann, C. Grötzinger, *Nat. Biotechnol.* **2001**, *19*, 327 – 331.
[5] G. T. Westermark, K. H. Johnson, P. Westermark, *Methods Enzymol.* **1999**, *309*, 3 – 25.
[6] E. S. Voropai, M. P. Samtsov, K. N. Kaplevskii, A. A. Maskevich, V. I. Stepuro, O. I. Povarova, I. M. Kuznetsova, K. K. Turoverov, A. L. Fink, V. N. Uverskii, *J. Appl. Spectrosc.* **2003**, *70*, 868 – 874.
[7] a) I. Roterman, M. Krol, M. Nowak, L. Konieczny, J. Rybarska, B. Stopa, B. Piekarska, G. Zemanek, *Med. Sci. Monit.* **2001**, *7*, 771 – 784; b) J. Sajid, A. Elhaddaoui, S. Turrell, *J. Mol. Struct.* **1997**, *408*/409, 181 – 184; c) R. Khurana, V. N. Uversky, L. Nielsen, A. L. Fink, *J. Biol. Chem.* **2001**, *276*, 22715 – 22721; d) D. B. Carter, K.-C. Chou, *Neurobiol. Aging* **1998**, *19*, 37 – 40; e) W. E. Klunk, J. W. Pettegrew, D. J. Abraham, *J. Histochem. Cytochem.* **1989**, *37*, 1273 – 1281.
[8] H. LeVine III, *Amyloid* **1995**, *2*, 1 – 6.
[9] Q. Li, J.-S. Lee, C. Ha, C. B. Park, G. Yang, W. B. Gan, Y.-T. Chang, *Angew. Chem.* **2004**, *116*, 6491 – 6495; *Angew. Chem. Int. Ed.* **2004**, *43*, 6331 – 6335.
[10] W. E. Klunk, M. L. Debnath, J. W. Pettegrew, *Neurobiol. Aging* **1995**, *16*, 541 – 548.
[11] a) W. E. Klunk, Y. Wang, G.-F. Huang, M. L. Debnath, D. P. Holt, C. A. Mattis, *Life Sci.* **2001**, *69*, 1471 – 1484; b) C. A. Mattis, Y. Wang, D. P. Holt, G.-F. Huang, M. L. Debnath, W. E. Klunk, *J. Med. Chem.* **2003**, *46*, 2740 – 2754; c) W. E. Klunk, H. Engler, A. Nordberg, Y. Wang, G. Blomqvist, D. P. Holt, M. Bergström, I. Savitcheva, G.-F. Huang, S. Estrada, B. Ausén, M. L. Debnath, J. Barletta, J. C. Price, J. Sandell, B. J. Lopresti, A. Wall, P. Koivisto, G. Antoni, C. A. Mathis, B. Långström, *Ann. Neurol.* **2004**, *55*, 306 – 319.
[12] The phenomenon of increasing the emission quantum yield in viscous solvents, where a conformationally labile molecule is vibrationally-restricted, is well documented for ThT (ref. [6]), as well as for some other fluorescent molecules (K. A. Willets, O. Ostroverkhova, M. He, R. J. Twieg, W. E. Moerner, *J. Am. Chem. Soc.* **2003**, *125*, 1174 – 1175).
[13] NIAD-4 is one of a series of contrast agents that we have been developing and testing. Additional NIAD compounds will be reported in the future.
[14] The 10 μM aggregation threshold, determined by a simple visual inspection, is a very approximate estimate, and strongly depends on the way the solution was prepared. The solutions used in the experiments reported herein had at least twice lower concentration, and their absorbance did not change after passing through a syringe filter with 0.2 μm pore size. Based on this, we can reasonably assume that NIAD-4 was not aggregated in the solutions.

 © 2005 Wiley-VCH Verlag GmbH & Co. KGaA, Weinheim

[15] We are currently conducting computational studies to gain further insight into this phenomenon.
[16] B. J. Bacskai, G. A. Hickey, J. Skoch, S. T. Kajdasz, Y. Wang, G.-F. Huang, C. A. Mathis, W. E. Klunk, B. T. Hyman, *Proc. Natl. Acad. Sci. USA* **2003**, *100*, 12462 – 12467.
[17] Alternatively, the spectral changes upon binding to amyloid may be explained by change in protonation of the phenolic hydroxy group upon binding of the dye to a protein aggregate. This behavior should be similar to the deprotonation at higher pH values, which can be employed to study the deprotonation effect. Although these experiments showed an anticipated change in optical properties at increasing pH (Figure S1 in the Supporting Information), the overall trend does not correspond to the spectral changes found upon binding to amyloid. This allowed us to safely rule out the explanation based on the protonation change.
[18] Injection of NIAD-4 into living mice did not result in any substantial alteration of their normally expected lifespan, or showed any visually detectable abnormalities. Although this does not exclude the need for thorough toxicology experiments, it may indicate that the dye is not significantly toxic.

 © 2005 Wiley-VCH Verlag GmbH & Co. KGaA, Weinheim

Electrochemical Biosensors

DOI: 10.1002/anie.200500989

Label-Free Electronic Detection of Thrombin in Blood Serum by Using an Aptamer-Based Sensor**

*Yi Xiao, Arica A. Lubin, Alan J. Heeger, and Kevin W. Plaxco**

Aptamers are DNA or RNA sequences selected in vitro for their ability to bind specific molecular targets.[1–3] Due to the ease with which novel aptamers can be fashioned and their generally impressive selectivity and affinity, they are widely regarded as ideal recognition elements for biosensor applications.[4,5] Consistent with this claim, aptamers have been employed in a variety of sensing technologies,[6–11] including a very promising optical approach termed "aptamer beacons". Aptamer beacons employ a large-scale, binding-induced conformational change in order to modulate the emission of a covalently bound fluorophore.[12] To date, aptamer beacons have been reported for such diverse targets as the small molecule cocaine[13] and the proteins Tat,[14] Taq DNA polymerase,[15] platelet-derived growth factor,[16] and thrombin.[6]

Aptamer beacons are rapid, label-free, and exceptionally selective.[12,17] As beacons are an optical approach, however, they suffer from several potential drawbacks relative to electronic-sensing strategies. These include a requirement for generally bulky, expensive, and power-intensive light sources, detectors, and monochromators, a susceptibility to photobleaching, and potential false signals arising from contaminating fluorophores or quenchers.[18] In contrast, the impressive miniaturization of modern microelectronics and the relative stability and environmental insensitivity of electroactive labels suggest that electronic sensors might avoid many of these pitfalls.[19] Previously described electronic aptamer-based sensors, however, require either the addition of exogenous reagents or are susceptible to interference from contaminants. For example, while impressive sensitivity and detection speed have been demonstrated by using aptamer sensors based on the quartz crystal microbalance[10] or on surface plasmon resonance,[20] both approaches are prone to false positives arising from nonspecific binding. Similarly, while the electrochemical detection of an aptamer–thrombin interaction has been reported, the approach requires complex, multistep preprocessing and the addition of an exogenous redox label.[11]

Here we describe a relatively general solution to the problem of electronic aptamer-based (E-AB) sensors. The sensor that we have developed, which is directed against the blood-clotting enzyme thrombin, is sensitive, selective, and reusable, and it does not require modification of the analyte. Instead, signal generation occurs upon a large, binding-induced conformational change in a redox-modified, electrode-attached aptamer upon target binding.

The E-AB sensor is analogous to the E-DNA sensor, a previously described, reagentless, electronic DNA sensing technology.[21] The E-AB sensor is constructed by covalently attaching a methylene blue (MB) labeled, thrombin-binding DNA aptamer (oligomer **1**) to a gold electrode by well-established self-assembling monolayer chemistry.[21] In the absence of target, the immobilized 32-base aptamer is thought to remain relatively unfolded,[6] thereby allowing the attached MB to collide with (or weakly bind to) the electrode and transfer an electron (Figure 1, left). Upon thrombin binding, electron transfer is inhibited, presumably due to a binding-induced conformational change in the aptamer (Figure 1, right)[6,22] that significantly alters the electron-tunneling distance and/or pathway (Figure 2, left). We assume that the immobilized aptamer (oligomer **1**) is in a conformational equilibrium between its unfolded state and the folded, binding-competent G-quartet conformation.[9] Since thrombin binds only the G-quartet conformation, the target protein

[*] A. A. Lubin, Prof. K. W. Plaxco
Department of Chemistry and Biochemistry
and Program in BioMolecular Science and Engineering
University of California
Santa Barbara, CA 93106 (USA)
Fax: (+1) 805-893-4120
E-mail: kwp@chem.ucsb.edu
Dr. Y. Xiao, Prof. A. J. Heeger
Department of Physics, Materials Department,
and Institute for Polymers and Organic Solids
University of California
Santa Barbara, CA 93106 (USA)

[**] This work was supported in part by the National Institutes of Health (Grant no.: EB002046) and by the Institute for Collaborative Biotechnologies (Grant no.: DAAD19-03-D-0004) from the U.S. Army Research Office. We gratefully acknowledge Brian Baker and Kevin Cash for providing critical commentary and Professor Pierre Petroff for his support.

 InterScience © 2005 Wiley-VCH Verlag GmbH & Co. KGaA, Weinheim

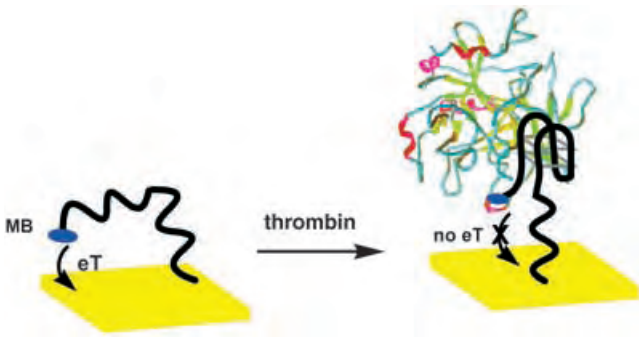


Figure 1. A schematic of the E-AB sensor. In the unbound state (left), the aptamer is thought to be highly dynamic,[6] allowing rapid collisions (or complex formation) between the MB redox tag and the electrode. This, in turn, presumably allows the efficient electron transfer (eT) that is observed in the absence of target. Upon target binding (right), electron transfer is inhibited, presumably because the aptamer forms a stable, rigid structure.

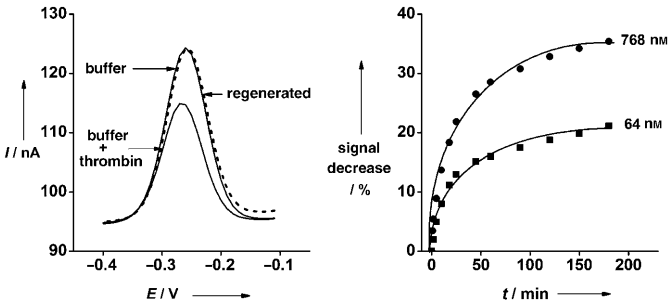


Figure 2. Left: The E-AB sensor responds robustly to 64 nM thrombin in buffered saline and can be regenerated by an eight-minute, room-temperature wash with 6 M guanidine hydrochloride. Even after two cycles of use and regeneration, we can recover 93% of the original sensor signal (dashed line). Right: Time dependence of the sensor response after a 3 h incubation ($t = 0$ min).

drives the equilibrium towards this state, thereby producing the observed signal.

As the modified aptamer is covalently attached to the sensing electrode, the E-AB sensor is readily regenerated (see dashed line in Figure 2, left). By contrast, several methods previously employed for the regeneration of antibody-based sensors (0.2 M NaOH; 0.25% sodium dodecyl sulfate at pH 10; 6 M urea; 0.2 M HCl; 0.2 M glycine, 30% methanol at pH 2; and 10% isopropyl alcohol in phosphate buffer at pH 7) produced little, if any, regeneration (data not shown). When compared to other, commonly employed sensing strategies, such as ELISAs,[23] the E-AB sensor is reasonably rapid; while a 3 h incubation is required to achieve signal saturation, the majority of the signal change occurs within minutes (Figure 2, right). The use of the Laviron equation[24] to calculate the interfacial electron-transfer rate between MB and the electrode gives rate constants of 88 s^{-1} and 58 s^{-1} before and after the reaction with thrombin, respectively (data not shown). The similarity in these rates suggests that unbound aptamers produce a similar electron-transfer rate irrespective of whether neighboring aptamers are bound to thrombin and that the electron-transfer rate becomes undetectably slow upon binding.

As signaling is based on a specific, binding-induced conformational change[25]—as opposed to a less specific physical change, such as adsorption—the E-AB sensor should be relatively insensitive to nonspecific binding. In order to test this, we have shown that 64 nM thrombin taken up in blood serum (diluted 50% with buffered saline)—a realistically complex and contaminant-ridden clinical material—produces a large (35%) reduction in peak current (Figure 3, right). By contrast, blood serum lacking exogenously added thrombin produces only a small ($\approx$7%) reduction in peak current (Figure 3, left).

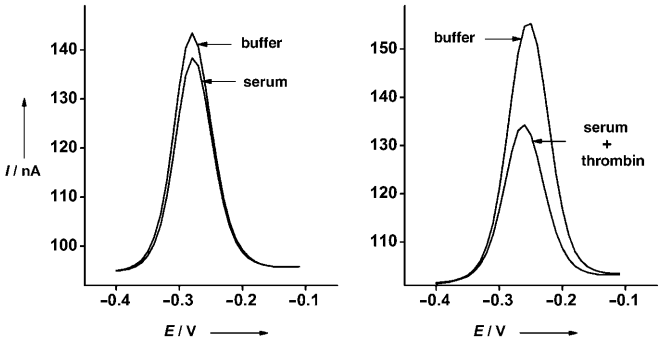


Figure 3. The E-AB sensor can detect thrombin even in a complex, contaminant-ridden sample such as blood serum. The sensor signals arising from thrombin-free buffered saline, from 50% fetal calf serum, and from 50% serum doped with 64 nM thrombin are shown.

The origin of the small signal drop observed in the absence of added thrombin is unclear. Possible sources include degradation of the aptamer or nonspecific interactions mimicking, to a limited extent, the binding-induced sequestration of the MB. However, neither an MB-tagged stem loop (oligomer **2**) nor a second, MB-tagged control oligonucleotide (oligomer **3**; of identical sequence composition and 81% sequence identity to oligomer **1**, but known not to bind thrombin[1]) exhibit any measurable signal drop when incubated in serum (data not shown), a result suggesting that these mechanisms are not significant. It is difficult to rule out the possibility that the signal change arises due to the presence of thrombin which, as a blood-clotting enzyme, may be present in the undoped serum; while resting (non-clotting) serum thrombin levels are very low, active concentrations soar to several hundred nanomolar during clotting.[26] Given that the blood serum employed is fetal calf serum (a safe proxy for human blood) that was harvested from calves in utero, some activation of the blood-clotting cascade may have occurred, thereby producing detectable levels of thrombin.

The sensitivity and dynamic range of the E-AB sensor span the physiological concentrations of thrombin in resting and activated blood, which range from low nanomolar to low micromolar, respectively.[8] Except at the very lowest thrombin concentration that we have investigated (6.4 nM), peak currents are linear with the logarithm of thrombin concentration (Figure 4). This linear relationship holds up to the highest thrombin concentrations that we have investigated (768 nM). Relative signal changes, however, are dependant on

 © 2005 Wiley-VCH Verlag GmbH & Co. KGaA, Weinheim

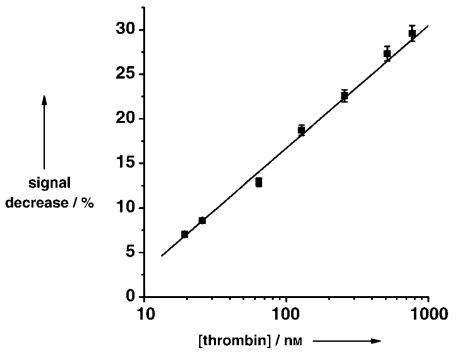


Figure 4. The dynamic range of the E-AB sensor covers physiologically relevant concentrations, which range from a few nanomolar (resting blood) to several hundred nanomolar (when the clotting cascade is activated). The error bars represent the standard deviation of four measurements conducted with a single electrode at each thrombin concentration. Multiple electrodes were used to collect this data set.

surface coverage; at lower surface coverage than that employed here, we observe smaller absolute signals but higher relative signal changes (data not shown). We presume this to be a consequence of reduced steric blocking of unbound aptamers by thrombin binding.

In conclusion, we have demonstrated a novel, label-free electronic method for the specific and quantitative detection of the blood-clotting factor thrombin. The E-AB sensor, which is based on a binding-induced conformational change in a highly selective, high-affinity thrombin-binding aptamer, detects the blood protein at nanomolar concentrations without any more cumbersome preprocessing than sample dilution with buffered saline. Moreover, because signal generation does not rely on simple physical adsorption, the sensor is quite insensitive to nonspecific binding and thus readily detects physiological thrombin levels, even in complex, contaminant-ridden samples such as blood serum. Lastly, the E-AB sensor is reasonably rapid and, given its label-free, fully covalent nature, readily regenerated.

The E-AB sensor platform is limited to targets for which DNA aptamers are available that undergo a large-scale, binding-induced conformational change. Such aptamers, however, may be relatively common. For example, as described above, a number of groups have reported optical aptamer-beacon sensors that utilize a ligand-induced folding event to segregate a fluorophore–quencher pair.[12] Additionally, Ellington and co-workers have reported an in vitro selection technique for the generation of aptamer-beacon-like molecules against arbitrary targets.[6b] The present study demonstrates a presumably general means by which the binding of such aptamers to their targets can be monitored electronically, thus opening a new direction for the development of rapid, reusable, and sensitive detection of multiple analytes in complex, contaminant-ridden clinical samples.

Experimental Section

Labeled DNA oligonucleotides were synthesized by BioSource Int. (Foster City, CA) and purified by C18 HPLC and PAGE; their structures were confirmed by mass spectrometry. The sequences of the three oligomers employed are:

1: 5′-HS-$(CH_2)_6$-TAAGTTCATCTCCCCGGTTGGTGTGGTTGGT-$(CH_2)_2$-MB-3′

2: 5′-HS-$(CH_2)_6$-GCGAGGTAAAACGACGGCCAGTCTCGC-$(CH_2)_7$-MB-3′

3: 5′-HS-$(CH_2)_6$-TAAGTTCATCTCCCCGGTGGTGGTTGTGGTT-$(CH_2)_2$-MB-3′

MB was conjugated to the 3′ end of these probes through succinimide ester coupling (MB–*N*-hydroxysuccinimide was obtained from EMP Biotech, Germany).[27] Inspection of a model of the solution structure of the thrombin–aptamer complex suggests that bases 4–12 of the aptamer bind to the anion-binding exosite of thrombin and that the remainder of the aptamer is relatively solvent-exposed.[22,28] This, in turn, suggests that the MB label, which is covalently attached to the 3′-terminal base, should not interfere with thrombin binding.

The human α-thrombin used in this study was purchased from Haematologic Technologies Inc. (Essex Junction, VT; specific activity: 3545 U mg^{-1}) and diluted with sterile water as appropriate. Fetal calf serum was purchased from Sigma-Aldrich, Inc. (USA) and used without further processing.

The E-AB sensor was fabricated by using polycrystalline gold disk electrodes (1.6 mm diameter; BAS, West Lafayette, IN). The electrodes were prepared by polishing with diamond and alumina (BAS), sonication in water, and electrochemical cleaning (a series of oxidation and reduction cycling in 0.5 M NaOH, 0.5 M H_2SO_4, 0.01 M KCl/0.1 M H_2SO_4, and 0.05 M H_2SO_4) before being modified with the probe DNA. The clean gold surface was interacted with a 0.1 μM solution of thrombin DNA aptamer (oligomer **1**) containing 1 μM tris-(2-carboxyethyl) phosphine hydrochloride (TCEP, which is included to reduce disulfide bound oligomers) in 100 mM tris(hydroxymethyl)aminomethane (Tris) buffer at pH 7.4 for 16 h. The surface was then rinsed with deionized water and subsequently passivated with 6-mercaptohexanol (1 mM in 10 mM Tris buffer, pH 7.4) for 3 h. The electrodes were rinsed again with 100 mM Tris buffer at pH 7.4 before being measured by alternating-current voltammetry with a CHI 603 potentiostat (CH Instruments, Austin, TX) in a standard cell with a platinum counter electrode and an Ag/AgCl reference electrode. Control electrodes modified with oligomers **2** and **3** were prepared on the gold surface as described for the immobilization of the thrombin aptamer (oligomer **1**). The surface coverage of the DNA was $(2.5 \pm 0.2) \times 10^{-12}$ mol cm^{-2}.

Sensor measurements were conducted by monitoring the electrode in buffered saline (0.1 M Tris (pH 7.4) with 140 mM NaCl, 20 mM MgCl, and 20 mM KCl). Neither increasing the final KCl concentration to 150 mM nor changing the pH value to 8.5 significantly affected the sensor response (data not shown). Thrombin detection was carried out either in buffered saline, or in fetal calf serum diluted with buffered saline. (The serum samples were diluted to 50% with 0.2 M Tris (pH 7.4). Saline (50 μL), 2.94 M in NaCl, 0.42 M in $MgCl_2$, and 0.42 M in KCl, was then added to this mixture (1 mL).) For all thrombin detection measurements, except the time-course study (Figure 2, right), electrodes were incubated in each sample for 3 h at room temperature. E-AB sensors were regenerated by soaking in 6 M guanidine hydrochloride (Pierce, Rockford, IL) for 8 min at room temperature, followed by rinsing with deionized water.

Received: March 17, 2005
Published online: July 26, 2005

Keywords: aptamers · biosensors · DNA structures · electron transfer · thrombin

[1] A. D. Ellington, J. W. Szostak, *Nature* **1990**, *346*, 818–822.
[2] a) C. Tuerk, L. Gold, *Science* **1990**, *249*, 505–510; b) M. P. Robertson, G. F. Joyce, *Nature* **1990**, *344*, 467–470.

 © 2005 Wiley-VCH Verlag GmbH & Co. KGaA, Weinheim

[3] B. Louis, G. Linda, L. John, V. Eric, T. John, *Nature* **1992**, *355*, 564 – 566.
[4] a) S. S. Iqbal, M. W. Mayo, J. G. Bruno, B. V. Bronk, C. A. Batt, J. P. Chambers, *Biosens. Bioelectron.* **2000**, *15*, 549 – 578; b) W. H. Tan, K. M. Wang, T. J. Drake, *Curr. Opin. Chem. Biol.* **2004**, *8*, 547 – 553.
[5] a) S. Tombelli, M. Minunni, E. Luzi, M. Mascini, *Anal. Lett.* **2004**, *37*, 1037 – 1052; b) M. Rajendran, A. D. Ellington, *Comb. Chem. High Throughput Screening* **2002**, *5*, 263 – 270.
[6] a) J. W. Li, X. H. Fang, W. H. Tan, *Biochem. Biophys. Res. Commun.* **2002**, *292*, 31 – 40; b) N. Hamaguchi, A. D. Ellington, M. Stanton, *Anal. Biochem.* **2001**, *294*, 126 – 131; c) W. U. Dittmer, A. Reuter, F. C. Simmel, *Angew. Chem.* **2004**, *116*, 3634 – 3637; *Angew. Chem. Int. Ed.* **2004**, *43*, 3550 – 3553.
[7] V. Pavlov, Y. Xiao, B. Shlyahovsky, I. Willner, *J. Am. Chem. Soc.* **2004**, *126*, 11 768 – 11 769.
[8] M. Lee, D. Walt, *Anal. Biochem.* **2000**, *282*, 142 – 146.
[9] H. A. Ho, M. Leclerc, *J. Am. Chem. Soc.* **2004**, *126*, 1384 – 1387.
[10] a) M. Minunni, S. Tombelli, A. Gullotto, E. Luzi, M. Mascini, *Biosens. Bioelectron.* **2004**, *20*, 1149 – 1156; b) S. Fukusho, H. Furusawa, Y. Okahata, *Chem. Commun.* **2002**, *1*, 88 – 89; c) M. Liss, B. Petersen, H. Wolf, E. Prohaska, *Anal. Chem.* **2002**, *74*, 4488 – 4495.
[11] T. Hianik, V. Ostatna, Z. Zajacova, E. Stoikova, G. Evtugyn, *Bioorg. Med. Chem. Lett.* **2005**, *15*, 291 – 295.
[12] a) M. Rajendran, A. D. Ellington, *Nucleic Acids Res.* **2003**, *31*, 5700 – 5713; b) J. Li, Z. W. Tang, K. M. Wang, W. H. Tan, *Curr. Proteomics* **2004**, *1*, 315 – 324; c) X. Fang, Y. Mi, J. J. Li, T. Beck, S. Schuster, W. Tan, *Cell Biochem. Biophys.* **2002**, *37*, 71 – 82.
[13] M. N. Stojanovic, P. de Prada, D. W. Landry, *J. Am. Chem. Soc.* **2001**, *123*, 4928 – 4931.
[14] R. Yamamoto, T. Baba, P. K. Kumar, *Genes Cells* **2000**, *5*, 389 – 396.
[15] C. A. Savran, S. M. Knudsen, A. D. Ellington, S. R. Manalis, *Anal. Chem.* **2004**, *76*, 3194 – 3198.
[16] X. H. Fang, A. Sen, M. Vicens, W. H. Tan, *ChemBioChem* **2003**, *4*, 829 – 834.
[17] a) J. Perlette, J. W. Li, X. H. Fang, S. Schuster, J. Lou, W. H. Tan, *Rev. Anal. Chem.* **2002**, *21*, 1 – 14; b) T. J. Drake, W. H. Tan, *Appl. Spectrosc.* **2004**, *58*, 269 A – 280 A.
[18] a) D. D. L. Bowtell, *Nat. Genet.* **1999**, *21*, 25 – 32; b) E. A. Winzeler, M. Schena, R. W. Davis, *Methods Enzymol.* **1999**, *306*, 3 – 18.
[19] a) I. Willner, *Science* **2002**, *298*, 2407 – 2408; b) A. J. Bard, L. R. Faulkner, *Electrochemical Method*, Wiley, New York, **2001**; c) S. A. Brazill, P. H. Kim, W. G. Kuhr, *Anal. Chem.* **2001**, *73*, 4882 – 4890; d) T. Hianik, V. Ostatna, Z. Zajacova, *J. Electroanal. Chem.* **2004**, *564*, 19 – 24.
[20] a) S. H. L. Verhelst, P. J. A. Michiels, G. A. van der Marel, C. A. A. van Boeckel, J. H. van Boom, *ChemBioChem* **2004**, *5*, 937 – 942; b) S. Tombelli, M. Minunni, M. Mascini, *Anal. Lett.* **2002**, *35*, 599 – 613.
[21] C. H. Fan, K. W. Plaxco, A. J. Heeger, *Proc. Natl. Acad. Sci. USA* **2003**, *100*, 9134 – 9137.
[22] a) R. F. Macaya, P. Schultze, F. W. Smith, J. A. Roe, J. Feigon, *Proc. Natl. Acad. Sci. USA* **1993**, *90*, 3745 – 3749; b) R. C. Buijsman, J. W. J. Schipperijn, E. K. Yeheskiely, G. A. van der-Marel, C. A. A. van Boeckel, J. H. van Boom, *Bioorg. Med. Chem. Lett.* **1997**, *7*, 2027 – 2032.
[23] J. Bichler, M. Siebeck, R. Maschler, H. Pelzer, H. Fritz, *Blood Coagulation Fibrinolysis* **1991**, *2*, 129 – 133.
[24] E. Laviron, *J. Electroanal. Chem.* **1979**, *101*, 19 – 28.
[25] a) K. Padmanabhan, K. P. Padmanabhan, J. D. Ferrara, J. E. Sadler, A. J. Tulinsky, *Biol. Chem.* **1993**, *268*, 17 651 – 17 654; b) I. Smirnov, R. H. Shafer, *Biochemistry* **2000**, *39*, 1462 – 1468; c) B. I. Kankia, L. A. Marky, *J. Am. Chem. Soc.* **2001**, *123*, 10 799 – 10 804.
[26] a) D. L. Aronson, L. Stevan, A. P. Ball, B. R. Franza, Jr., J. S. Finlayson, *J. Clin. Invest.* **1977**, *60*, 1410 – 1418; b) "Thrombin: Bioregulator Functions of Thrombin": J. W. Fenton II, *Ann. N. Y. Acad. Sci.* **1986**, 5.
[27] G. T. Hermanson, *Bioconjugate Techniques*, Academic Press, San Diego, **1996**.
[28] K. Y. Wang, S. McCurdy, R. G. Shea, S. Swaminathan, P. H. Bolton, *Biochemistry* **1993**, *32*, 1899 – 1904.

 © 2005 Wiley-VCH Verlag GmbH & Co. KGaA, Weinheim

Metal Chains

DOI: 10.1002/anie.200501049

Paramagnetic Platinum–Rhodium Octamers Bridged by Halogen Ions To Afford a Quasi-1D System**

Kazuhiro Uemura, Kôichi Fukui, Hiroyuki Nishikawa, Saiko Arai, Kazuko Matsumoto, and Hiroki Oshio*

One-dimensional (1D) materials have long fascinated physicists and chemists because of their unusual physical properties.[1,2] It has been recognized that stacks of mixed-valent organic and inorganic molecules exhibit unusual electrical properties owing to the alternate donor–acceptor interactions within the stack column, as found in [(TTF)(TCNQ)] (TTF = tetrathiafulvalene, TCNQ = tetracyanoquinodimethane), square-planar $[Pt(CN)_4]^{n-}$, and $K_2[Pt(CN)_4]X_{0.3}$ (X = Cl, Br).[3] The future goal in this area is to prepare "synthetic metals" and establish the superconducting state in low-dimensional materials.[2] To rationally synthesize 1D chains of conducting materials, a judicious choice of mixed-valent metal complexes (Pt, Rh, etc.) is necessary.[4] "Platinum blue" has a linear tetranuclear metal–metal bonded backbone with mixed valency $(Pt^{2.25+})_4$, and the one unpaired electron of the complex is delocalized over the four platinum centers,[5,6] whose redox properties based on $Pt^{III/II}$ have been well-studied and applied to catalysis.[5] Introduction of this fascinating structure into 1D conducting materials has, to our knowledge, not been attempted. Herein, we report the

[*] Dr. K. Uemura, Dr. K. Fukui, S. Arai, Prof. Dr. K. Matsumoto
Department of Chemistry, School of Science and Engineering
Advanced Research Institute for Science and Engineering
Waseda University
3-4-1, Ohkubo, Shinjuku, Tokyo 169-8555 (Japan)
Fax: (+81) 3-5273-3489
E-mail: kmatsu@waseda.jp
Dr. H. Nishikawa, Prof. Dr. H. Oshio
Department of Chemistry
University of Tsukuba
Tennoudai 1-1-1, Tsukuba, Ibaraki 305-8571 (Japan)

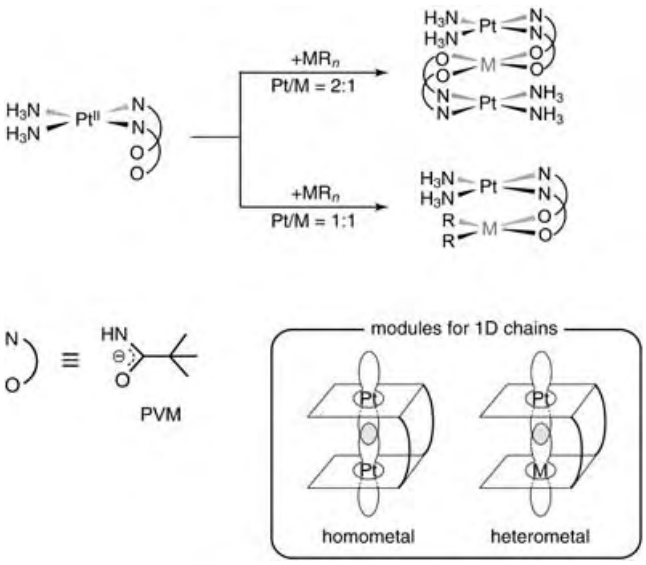
[**] This work was partially supported by the Nano COE and the 21COE program Practical Nano-Chemistry from MEXT, Japan.

Supporting information for this article is available on the WWW under http://www.angewandte.org or from the author.

© 2005 Wiley-VCH Verlag GmbH & Co. KGaA, Weinheim

synthesis, X-ray crystal structure analysis, and magnetic properties of the infinite chain of Pt_6Rh_2 moieties bridged by Cl^- ions.

Our strategy for the synthesis of a 1D chain is to rationally align dinuclear basic units doubly bridged with amidate ligands as found in platinum blue backbones. We previously reported the synthesis and structure of $[Pt(PVM)_2(NH_3)_2]\cdot 2H_2O$ (**1**, PVM = pivalamidate),[7] which can easily bind a second metal ion with the noncoordinated oxygen atoms of the amide moieties[8] to afford various dinuclear and trinuclear Pt complexes (Scheme 1).[7] For example, a simple mixture of **1** and $RhCl_3\cdot 3H_2O$ in MeOH provides the dinuclear complex, $[PtRh(PVM)_2(NH_3)_2Cl_3]$.[9,10] Such facile dimerization is attributed to the thermal instability of **1** in the solution state which is manifested by the release of PVM upon addition of excess $NaPF_6$ to **1** in MeOH[11] to give yellow-green crystals of $[Pt_2(PVM)_2(NH_3)_4](PF_6)_2\cdot H_2O$ (**2**). The oxidized **2**—platinum blue—was synthesized from the reaction of **1** and the hydrolysis product of *cis*-$[PtCl_2(NH_3)_2]$ and was isolated as dark green $[Pt_4(PVM)_4(NH_3)_8](PF_6)_4(ClO_4)\cdot 2H_2O$ (**3**). Figure 1 shows the crystal structures of **2** and **3**. Both single crystals of **2** and **3** consist of tetranuclear platinum chains (Figure 1 a and c). It is known that tetraplatinum chain structures are achieved only with head-to-head (HH) dimers and that dimer–dimer interactions are generally stabilized by a Pt–Pt bond and/or four hydrogen bonds formed between the oxygen atoms of the amidate and the hydrogen atoms of the ammine ligands. These tetranuclear structures are essentially identical to those reported previ-



Scheme 1. Reaction scheme for $[Pt(PVM)_2(NH_3)_2]\cdot 2H_2O$ (**1**), which can easily bind a second metal ion to afford various di- and trinuclear Pt complexes as shown.

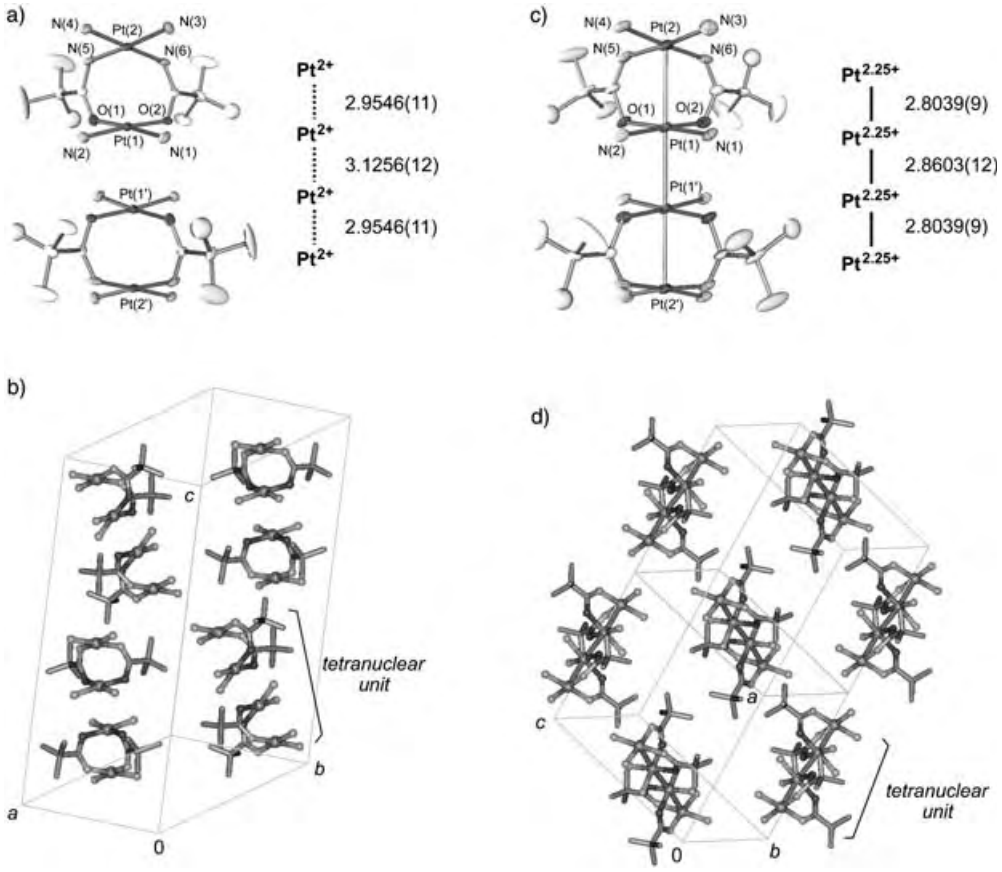


Figure 1. a) Crystal structure and b) packing diagram of $[Pt_2(PVM)_2(NH_3)_4](PF_6)_2\cdot H_2O$ (**2**), and c) crystal structure and d) packing diagram of $[Pt_4(PVM)_4(NH_3)_8](PF_6)_4(ClO_4)\cdot 2H_2O$ (**3**, platinum blue). Schematic drawings for the oxidation states of platinum atoms and metal–metal bonding lengths are also shown in (a) and (c). Hydrogen atoms, PF_6^- and ClO_4^- ions, and solvent molecules (H_2O) are omitted for clarity.

 © 2005 Wiley-VCH Verlag GmbH & Co. KGaA, Weinheim

ously with other amidate ligands.[6,12,13] Each platinum atom in the dimer is *cis*-coordinated to two ammine ligands and to either two oxygen atoms or two deprotonated nitrogen atoms of the PVM ligands. X-ray diffraction analysis revealed that four PF_6^- anions are present per tetranuclear unit in **2** and **3**, with an additional ClO_4^- ion present in the latter structure, and therefore the average oxidation state of platinum in **2** and **3** is +2 and +2.25, respectively. In both crystal structures, the tetrameric platinum units are packed without significant interaction with each other (Figure 1b and 1d).

The precursors to the two complexes, dinuclear $[PtRh(PVM)_2(NH_3)_2Cl_3]$ and tetranuclear **2**, were mixed together in a vessel, and brown single crystals of $\{[PtRh(PVM)_2(NH_3)_2Cl_{2.5}]_2[Pt_2(PVM)_2(NH_3)_4]_2(PF_6)_6{\cdot}2\,MeOH{\cdot}2\,H_2O\}_n$ (**4**) with metallic luster were successfully obtained upon evaporation of the solution in air. Figure 2 shows the crystal structure of **4**. The most remarkable structural feature is that the complex cation is an infinite repetition of the octameric segment of Pt_6Rh_2 bridged by the Cl^- ion, with a crystallographic inversion center at the center of the octamer. The Pt_6Rh_2 octameric segment consists of four dimeric units (inner dimers; Pt(1)–Pt(2), Pt(1′)–Pt(2′), outer dimers; Rh(1)–Pt(3), Rh(1′)–Pt(3′)), each doubly bridged by PVM ligands. The inner tetrameric platinum unit (Pt(2)-Pt(1)-Pt(1′)-Pt(2′)) has a structure that is quite similar to those of **2** and **3**. The central interdimer interaction is reinforced by four hydrogen bonds between the oxygen atoms of PVM and the hydrogen atoms of the ammine ligands. The distance between the PVM-bridged platinum atoms (Pt(1)–Pt(2): 2.8450(7) Å) is shorter by 0.218 Å than the inner Pt(1)–Pt(1′) distance of 3.0634(10) Å. The outer dimers, $[PtRh(PVM)_2(NH_3)_2Cl_2]^{n+}$ (Pt(3)–Rh(1) 2.5987(11) Å), are bonded to both ends of the tetranuclear platinum unit at a Pt(2)–Rh(1) distance of 2.7337(11) Å and a typical torsion angle of 45°. Additionally, the Pt_6Rh_2 octameric segments are bridged by Cl^- ligands (Pt(3)–Cl(3) 2.5959(6) Å) to give a very attractive pseudo-1D infinite chain expressed as $[\text{-Pt-Rh-Pt}_4\text{-Rh-Pt-Cl-}]_n$. Three types of crystal structures based similarly on the tetrameric platinum unit have been reported to date, namely 1) the octameric platinum oligomer,[14] 2) the Cl^--bridged platinum tan[6f] like M_4X-type chain, and 3) the infinite platinum wire.[4h] In contrast, the present system is a quasi-1D system, which is distinct from the previous systems on the grounds that two kinds of metals are conjugated in the system which leads to the unique metal–metal interactions and magnetic properties observed.

Table 1 summarizes the selected bond lengths and angles of the tetrameric platinum units in **2**–**4**. Both the inter- and intradimer Pt–Pt distances in **4** are slightly longer than the corresponding lengths of **3**, but still much shorter than those in **2**. Also, the lengths of the hydrogen bonds observed between the amide oxygen and ammine nitrogen atoms in the interdimers in **4** are intermediate between the lengths of the corresponding bonds in **2** and **3**. The tilt angle (τ) between the Pt(1) and Pt(2) coordination planes increases as the Pt–Pt distance increases, as observed also in the series α-pyrrolidonate-tan,[13a] -blue,[6f] and -yellow.[12e] The charge of +19 for the Pt_6Rh_2 octameric segment in **4** was determined from the number of independent PF_6^- ions, which is exactly

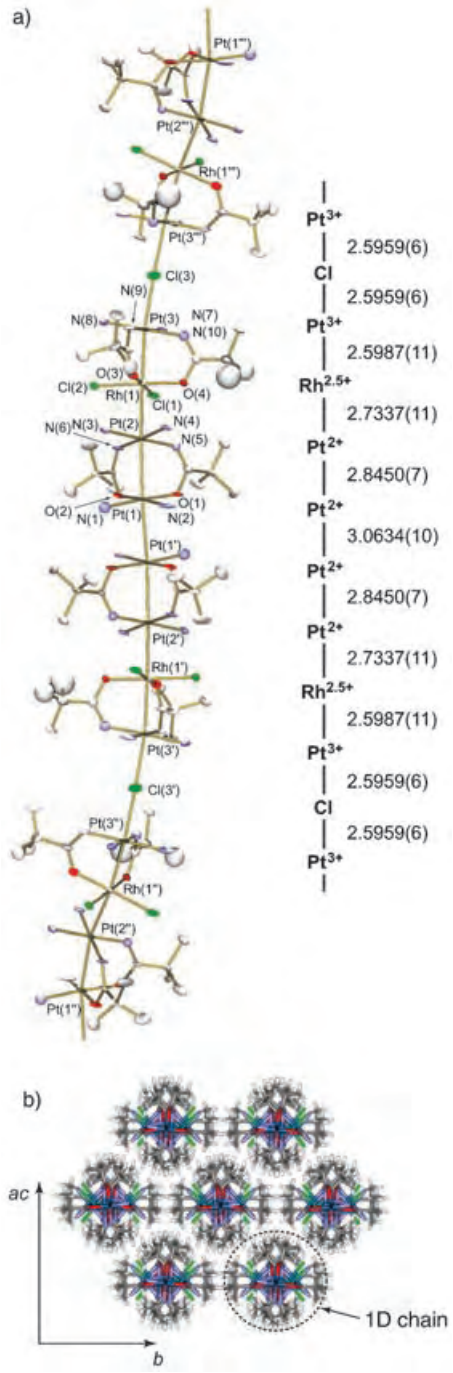


Figure 2. a) Crystal structure of $\{[PtRh(PVM)_2(NH_3)_2Cl_{2.5}]_2[Pt_2(PVM)_2(NH_3)_4]_2(PF_6)_6{\cdot}2\,MeOH{\cdot}2\,H_2O\}_n$ (**4**) with a schematic drawing of the metal–metal bond lengths (hydrogen atoms, PF_6^- ions, and solvent molecules (MeOH and H_2O) are omitted for clarity). b) Crystal packing diagram of the 1D chains in **4** (PF_6^- ions and solvent molecules (MeOH and H_2O) are omitted for clarity).

Table 1: Selected bond lengths [Å] and angles [°] for **2**, **3**, and **4**.

	2	**3**	**4**
Pt(1)–Pt(2)	2.9546(11)	2.8039(9)	2.8450(7)
Pt(1)–Pt(1′)	3.1256(12)	2.8603(12)	3.0634(10)
hydrogen bonds (NH···O)	2.96, 2.96, 2.98, 2.98	2.78, 2.78, 2.85, 2.85	2.91, 2.91, 2.91, 2.91
tilt angle (τ)	27.3	21.8	23.1

© 2005 Wiley-VCH Verlag GmbH & Co. KGaA, Weinheim

six, in the X-ray refinement of the ion occupancies. These results provide convincing evidence that the material is composed of Pt and Rh atoms with one unpaired electron per Pt_6Rh_2Cl unit. The increase in the Pt–Pt distance with a decrease in the average oxidation state of platinum is widely observed in this class of compound.[13a] Assuming this relationship holds in **4**, the average oxidation state of the inner tetrameric platinum unit in **4** appears to be between +2.0 and +2.25.

Figure 3 shows the EPR spectra of **3** in a water/ethylene glycol (1:1 v/v) glass and powder samples of **3** and **4** measured at 77 K. The EPR spectrum of **3** in the glass exhibits sharp perpendicular and parallel peaks, each split into at least nine lines due to ^{195}Pt nuclei ($I = 1/2$ with an abundance of 33.7 %). The EPR parameters have been determined by computer simulations as $g_\perp = 2.393$, $g_\parallel = 1.979$, $A_{1\perp} = 429$ MHz, $A_{1\parallel} = 499$ MHz, $A_{2\perp} = 861$ MHz, and $A_{2\parallel} = 679$ MHz. These values are similar to those reported for platinum blue.[6b,15] Powdered **3** shows a broad axial-type signal with no resolved hyperfine splittings ($g_\perp = 2.350$, $g_\parallel = 2.030$; peak-to-peak line width, $W_\perp = 12.5$ mT, $W_\parallel = 12.5$ mT), whereas the powder sample of **4** exhibits a much broader ($W = 45.0$ mT) signal centered at a smaller value of g_{av} ($g_{av} = 2.032$).

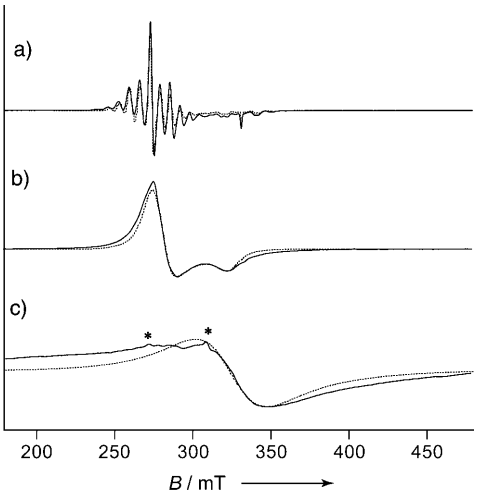
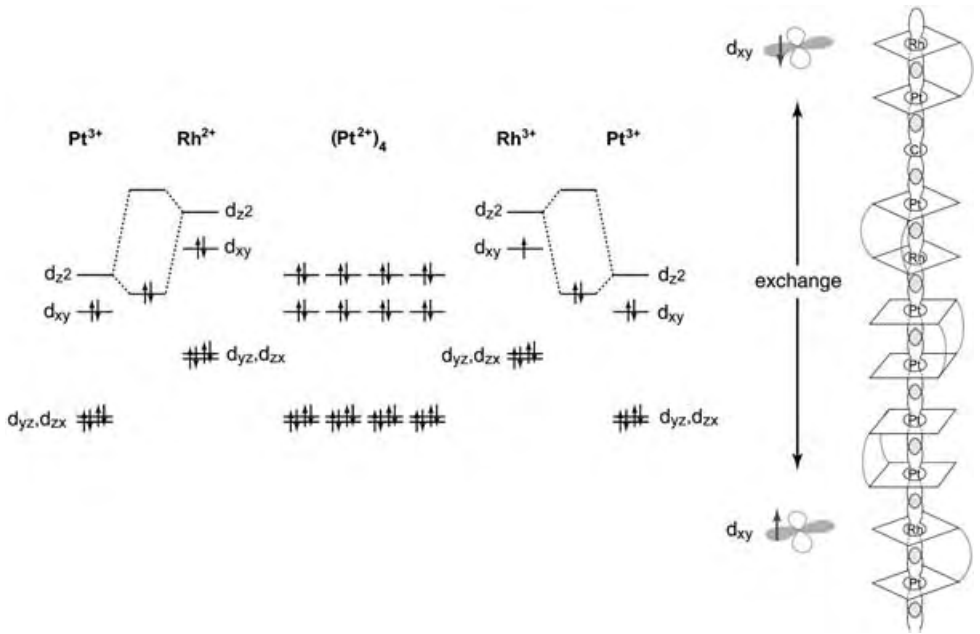


Figure 3. Continuous wave EPR spectra measured at 77 K for a) **3** in a water/ethylene glycol (1:1 v/v) glass, b) **3** (powder sample), and c) **4** (powder sample). Experimental settings: microwave frequency: 9.1826 (a), 9.2022 (b), and 9.1988 GHz (c); microwave power: 5 mW; field modulation (100 kHz): 0.1 mT. Asterisks indicate the platinum blue impurity (around 270 mT); solid lines are the measured spectra, and dotted lines are the simulations.

The g values obtained for **3** are well interpreted in terms of a d_{z^2}-hole state (the z axis lies along the mean Pt chain) with an admixture of the lower-lying d_{xz} and d_{yz} states due to spin–orbit coupling.[15] Typical examples for d_{z^2}-type Pt complexes are Pt^{IV}-doped $[Pt(NH_3)_4][PtCl_4]$ ($g_\perp = 2.504$, $g_\parallel = 1.939$, $g_{av} = 2.316$),[16] *cis*-diammineplatinum α-pyridone blue ($g_\perp = 2.381$, $g_\parallel = 1.975$, $g_{av} = 2.246$),[6b] and $[K_2Pt(CN)_4Br_{1/3}]\cdot 3H_2O$ (KCP, $g_\perp = 2.336$, $g_\parallel = 1.946$, $g_{av} = 2.206$).[17] All these values are attributed to the d_{z^2}-hole state of Pt^{III}. On the other hand, the EPR spectrum of **4** is quite different from that of **3** and features 1) a relatively small g_{av} value and 2) a broad spectrum profile. If it is taken into account that the g_{av} value of **4** ($g_{av} = 2.032$) is much smaller than those of the d_{z^2}-type Pt complexes, it is unlikely that the unpaired electron occupies the d_{z^2} state in **4**. It is important to note that the d_{z^2}-type Rh^{II} complexes exhibit a relatively large g_{av} value in similar fashion to Pt^{III} (e.g. $g_{av} = 2.176$ for [(TTiPP)Rh^{II}] (TTiPP = tetrakis(1,3,5-triisopropylphenyl)porphyrin)).[18] Considering the small g_{av} value of **4**, which is different from both Pt^{III} and Rh^{II}, the singly occupied orbital in **4** is attributed most likely to the Rh^{II} d_{xy} orbital, which is raised in energy above d_{z^2} through π interactions with the amidate ligands (Scheme 2). The broad nature of the EPR spectrum of



Scheme 2. Molecular orbital diagram of $\{[PtRh(PVM)_2(NH_3)_2Cl_{2.5}]_2[Pt_2(PVM)_2(NH_3)_4]_2(PF_6)_6\cdot 2\,MeOH\cdot 2H_2O\}_n$ (**4**) with schematic structural view.

 © 2005 Wiley-VCH Verlag GmbH & Co. KGaA, Weinheim

4 can be attributed to a long-distance exchange interaction. The magnetic susceptibility measurement of **4** shows that the μ_{eff} ($\propto (\chi T)^{1/2}$) value decreases with a decrease in temperature.[19] The plot of $1/\chi_m$ versus T follows the Curie–Weiss law with a Weiss constant $\theta = -31.9$ K, which indicates an antiferromagnetic interaction between the paramagnetic Pt_6Rh_2 segments.

Additionally, the single-crystal electrical conductivity of **4** (four probes, direct current) revealed semiconducting character of the material (3.52×10^{-6} S cm^{-1}) at room temperature.[20] Compound **4** shows a typical semiconducting behavior in the temperature range measured (267–295 K), and the activation energy was estimated as 1.0 eV (see Supporting Information).

In summary, the present results demonstrate that the linear chain structure of the amidate-bridged platinum tetramer can be extended to the octameric segment Pt_6Rh_2, which is further extended infinitely by Cl^- bridges. The Pt–Rh bond between the Pt–Rh dimer and the Pt tetramer is the first example of metal–metal bond formed between the tetranuclear platinum chain and any other metal, and suggests that by selecting suitable metal ions the tetranuclear platinum chain can be incorporated into a longer chain by metal–metal bonds. Note, in complex **4** the unpaired electron does not occupy the d_{z^2} orbital of the tetranuclear platinum chain[15] but, different from our expectation, occupies the d_{xy} orbital of the rhodium atom and hops from one rhodium atom to another. This type of long-distance exchange is rare and possibly leads to new electric and magnetic properties. Attempts to prepare a wider variety of heterometallic chain complexes by tailoring the ligands and selecting suitable metals are currently in progress.

Experimental Section

$[Pt_2(PVM)_2(NH_3)_4](PF_6)_2 \cdot H_2O$ (**2**): $NaPF_6$ (0.5 mmol, 0.084 g) was added to a solution of $[Pt(PVM)_2(NH_3)_2] \cdot 2H_2O$ (0.1 mmol, 0.047 g) in MeOH (2 mL). Yellow-green square crystals were obtained after one month (20% yield). Elemental analysis (%) calcd for $C_{20}H_{68}F_{24}N_{12}O_6P_4Pt_4$: C 12.43, H 3.55, N 8.70; found: C 12.58, H 3.34, N 8.08; IR (KBr pellet): $\tilde{\nu}$: C=O stretching, 1622 cm^{-1} (m), 1583 cm^{-1} (s); PF_6^- ion, 841 cm^{-1} (vs).

$[Pt_4(PVM)_4(NH_3)_8](PF_6)_4(ClO_4) \cdot 2H_2O$ (**3**): $AgClO_4$ (2 equiv, 1.0 mmol, 0.207 g) was added to an aqueous solution (2 mL) of *cis*-$[Pt(NH_3)_2Cl_2]$ (0.5 mmol, 0.150 g), and the mixture was stirred for 18 h in the dark. AgCl was then removed by filtration, and the colorless filtrate was warmed at 40 °C for 30 min before the addition of 1 equiv of $[Pt(PVM)_2(NH_3)_2] \cdot 2H_2O$ (0.5 mmol, 0.235 g) and $NaPF_6$ (1.0 mmol, 0.167 g). The mixture was stirred at 40 °C for a further 14 h, then the solution (dark blue) was left to stand for a week before dark blue crystals were separated (61% yield). Elemental analysis (%) calcd for $C_{20}H_{68}ClF_{24}N_{12}O_{10}P_4Pt_4$: C 11.82, H 3.37, N 8.27; found: C 11.89, H 3.27, N 7.73; UV/Vis (KBr pellet): $\lambda_{max} = 621$ nm; IR (KBr pellet): $\tilde{\nu}$: C=O stretching, 1637 cm^{-1} (m), 1583 cm^{-1} (s); ClO_4^- ion, 1097 cm^{-1} (s, br); PF_6^- ion, 843 cm^{-1} (vs).

$\{[PtRh(PVM)_2(NH_3)_2Cl_{2.5}]_2[Pt_2(PVM)_2(NH_3)_4]_2(PF_6)_6 \cdot 2MeOH \cdot 2H_2O\}_n$ (**4**): $RhCl_3 \cdot 3H_2O$ (0.05 mmol; 0.013 g) in MeOH (1 mL) was added to a solution of $[Pt(PVM)_2(NH_3)_2] \cdot 2H_2O$ (0.1 mmol, 0.047 g) and $NaPF_6$ (0.5 mmol, 0.084 g) in MeOH (1 mL). The mixture was placed in a tube for a month. Dark brown crystals formed during this time and were separated, washed with water, and dried (22% yield). Elemental analysis (%) calcd for $C_{42}H_{128}Cl_5F_{36}N_{20}O_{12}P_6Pt_6Rh_2$: C 14.29, H 3.66, N 7.94; found: C 14.07, H 3.57, N 8.16; UV/Vis (KBr pellet): $\lambda_{max} = 475$ nm, 599 nm, 720 nm (sh); IR (KBr pellet): $\tilde{\nu}$: C=O stretching, 1647 cm^{-1} (m), 1566 cm^{-1} (s); PF_6^- ion, 841 cm^{-1} (vs).

Crystal structure determination for **2**–**4**: Measurements were carried out on a Bruker SMART APEX CCD diffractometer equipped with a normal focus Mo-target X-ray tube ($\lambda = 0.71073$ Å) operated at 2000 W power (50 kV, 40 mA) and a CCD two-dimensional detector. A total of 1315 frames were collected with a scan width of 0.3° in ω with an exposure time of 20 (**2**), 40 (**3**), and 60 (**4**) s per frame. The frames were integrated with the SAINT software package with a narrow frame algorithm. Absorption correction was applied by using SADABS. All the structures were solved by direct methods with subsequent difference Fourier syntheses and refinement with the SHELXTL (version 5.1) software package. Non-hydrogen atoms were refined anisotropically, and all hydrogen atoms were placed in the ideal positions.

Crystal data for **2**: $C_{10}H_{20}F_{12}N_6O_3P_2Pt_2$, $M_w = 952.44$, monoclinic, space group $I2/a$, $a = 11.461(4)$, $b = 18.095(6)$, $c = 26.256(10)$ Å, $\beta = 98.543(6)°$, $V = 5385(3)$ Å^3, $Z = 8$, $\rho_{calcd} = 2.350$ g cm^{-3}, $\mu(Mo_{K\alpha}) = 10.605$ mm^{-1}, $F(000) = 3520$, crystal size: $0.60 \times 0.50 \times 0.05$ mm^3, $T = 120$ K; $\lambda(Mo_{K\alpha}) = 0.71073$ Å, $\theta_{min-max} = 1.4$–$27.5°$, total data = 14338, unique data = 5795, $R_{int} = 0.0583$, observed data ($I > 2\sigma(I)$) = 4898, $R = 0.0750$, $R_w = 0.1961$, GOF = 1.066.

Crystal data for **3**: $C_{20}H_{40}ClF_{24}N_{12}O_{10}P_4Pt_4$, $M_w = 2004.33$, triclinic, space group $P\bar{1}$, $a = 14.231(3)$, $b = 14.722(3)$, $c = 15.642(3)$ Å, $\alpha = 75.007(3)$, $\beta = 84.237(3)$, $\gamma = 73.648(4)°$, $V = 3036.3(10)$ Å^3, $Z = 2$, $\rho_{calcd} = 2.192$ g cm^{-3}, $\mu(Mo_{K\alpha}) = 9.457$ mm^{-1}, $F(000) = 1858$, crystal size: $0.50 \times 0.40 \times 0.10$ mm^3, $T = 120$ K; $\lambda(Mo_{K\alpha}) = 0.71073$ Å, $\theta_{min-max} = 2.4$–$26.9°$, total data = 18819, unique data = 12951, $R_{int} = 0.0433$, observed data ($I > 2\sigma(I)$) = 8401, $R = 0.0621$, $R_w = 0.1666$, GOF = 1.055.

Crystal data for **4**: $C_{42}H_{80}Cl_5F_{36}N_{20}O_{12}P_6Pt_6Rh_2$, $M_w = 3480.69$, monoclinic, space group $C2/c$, $a = 24.956(3)$, $b = 12.3284(14)$, $c = 34.205(4)$ Å, $\beta = 106.377(2)°$, $V = 10097(2)$ Å^3, $Z = 4$, $\rho_{calcd} = 2.290$ g cm^{-3}, $\mu(Mo_{K\alpha}) = 8.945$ mm^{-1}, $F(000) = 6500$, crystal size: $0.60 \times 0.05 \times 0.05$ mm^3, $T = 120$ K, $\lambda(Mo_{K\alpha}) = 0.71073$ Å, $\theta_{min-max} = 2.0$–$27.0°$, total data = 30284, unique Data = 11307, $R_{int} = 0.0844$, observed data ($I > 2\sigma(I)$) = 7669, $R = 0.0719$, $R_w = 0.1785$, GOF = 1.037.

For **2**, atoms C4, C8, and F10 were refined isotropically. For **3**, atoms C4, F24, O9, and O10 were found in the final stage, and thus their atom positions were isotropically refined under rigid condition. For **4**, atoms N1, N5, N10, C16, C19, and C20 were refined isotropically. CCDC-265911 (**2**), CCDC-265912 (**3**), and CCDC-265913 (**4**) contain the supplementary crystallographic data for this paper. These data can be obtained free of charge from The Cambridge Crystallographic Data Centre via www.ccdc.cam.ac.uk/data_request/cif.

UV/Vis reflection spectra were recorded on a Shimadzu UV-3101PC spectrophotometer over the range from 400 to 800 nm at room temperature. IR spectra were recorded on a JEOL WINSPEC-50 spectrometer with the samples prepared as KBr pellets. X-band EPR spectra were recorded on a JEOL JES-PX1060 spectrometer at 77 K. Magnetic susceptibility measurements were carried out in the temperature range 2–250 K with a magnetometer MPMS-7 (Quantum Design) equipped with a SQUID sensor.

Received: March 23, 2005
Published online: July 25, 2005

Keywords: chain structures · mixed-valent compounds · platinum · rhodium

[1] J. S. Miller, *Extended Linear Chain Compounds*, *Vols. 1–3*, **1982**, Plenum, New York.

 © 2005 Wiley-VCH Verlag GmbH & Co. KGaA, Weinheim

[2] a) J. K. Bera, K. R. Dunbar, *Angew. Chem.* **2002**, *114*, 4633; *Angew. Chem. Int. Ed.* **2002**, *41*, 4453; b) H. Kitagawa, T. Mitani, *Coord. Chem. Rev.* **1999**, *190–192*, 1169.

[3] J. S. Miller, A. J. Epstein, *Synthesis and Properties of Low-Dimensional Materials*, The New York Academy of Science, New York, **1978**.

[4] For recent reports on infinite 1D chains, see: a) G. M. Finniss, E. Canadell, C. Campana, K. R. Dunbar, *Angew. Chem.* **1996**, *108*, 2946; *Angew. Chem. Int. Ed. Engl.* **1996**, *35*, 2772; b) M. E. Prater, L. E. Pence, R. Clerac, G. M. Finniss, C. Campana, P. Auban-Senzier, D. Jerome, E. Canadell, K. R. Dunbar, *J. Am. Chem. Soc.* **1999**, *121*, 8005; c) K. Sakai, M. Takeshita, Y. Tanaka, T. Ue, M. Yanagisawa, M. Kosaka, T. Tsubomura, M. Ato, T. Nakano, *J. Am. Chem. Soc.* **1998**, *120*, 11353; d) H. Kitagawa, N. Onodera, T. Sonoyama, M. Yamamoto, T. Fukawa, T. Mitani, M. Seto, Y. Maeda, *J. Am. Chem. Soc.* **1999**, *121*, 10068; e) F. A. Cotton, E. V. Dikarev, M. A. Petrukhina, *J. Organomet. Chem.* **2000**, *596*, 130; f) F. A. Cotton, E. V. Dikarev, M. A. Petrukhina, *J. Chem. Soc. Dalton Trans.* **2000**, 4241; g) F. P. Pruchnik, P. Jakimowicz, Z. Ciunik, *Inorg. Chem. Commun.* **2001**, *4*, 726; h) K. Sakai, E. Ishigami, Y. Konno, T. Kajiwara, T. Ito, *J. Am. Chem. Soc.* **2002**, *124*, 12088; i) M. Mitsumi, S. Umebayashi, Y. Ozawa, M. Tadokoro, H. Kawamura, K. Toriumi, *Chem. Lett.* **2004**, *33*, 970; j) M. Yamashita, D. Kawakami, S. Matsunaga, Y. Nakayama, M. Sasaki, S. Takaishi, F. Iwahori, H. Miyasaka, K. Sugiura, Y. Wada, H. Miyamae, H. Matsuzaki, H. Okamoto, H. Tanaka, K. Marumoto, S. Kuroda, *Angew. Chem.* **2004**, *116*, 4867; *Angew. Chem. Int. Ed.* **2004**, *43*, 4763.

[5] a) C. Tejel, M. A. Ciriano, L. A. Oro, *Chem. Eur. J.* **1999**, *5*, 1131; b) K. Matsumoto, K. Sakai, *Adv. Inorg. Chem.* **2000**, *49*, 375.

[6] For tetranuclear $Pt^{2.25+}$ chains (platinum blue), see: a) J. K. Barton, H. N. Rabinowitz, D. J. Szalda, S. J. Lippard, *J. Am. Chem. Soc.* **1977**, *99*, 2827; b) J. K. Barton, D. J. Szalda, H. N. Rabinowitz, J. V. Waszczak, S. J. Lippard, *J. Am. Chem. Soc.* **1979**, *101*, 1434; c) T. V. O'Halloran, M. M. Roberts, S. J. Lippard, *J. Am. Chem. Soc.* **1984**, *106*, 6427; d) P. K. Mascharak, I. D. Williams, S. J. Lippard, *J. Am. Chem. Soc.* **1984**, *106*, 6428; e) K. Matsumoto, J. Matsunami, H. Urata, *Chem. Lett.* **1993**, 597; f) K. Sakai, Y. Tanaka, Y. Tsuchiya, K. Hirata, T. Tsubomura, S. Iijima, A. Bhattacharjee, *J. Am. Chem. Soc.* **1998**, *120*, 8366.

[7] a) W. Chen, K. Matsumoto, *Inorg. Chim. Acta* **2003**, *342*, 88; b) W. Chen, F. Liu, T. Nishioka, K. Matsumoto, *Eur. J. Inorg. Chem.* **2003**, 4234.

[8] a) A. Erxleben, I. Mutikainen, B. Lippert, *J. Chem. Soc. Dalton Trans.* **1994**, 3667; b) E. Zangrando, F. Pichierri, L. Randaccio, B. Lippert, *Coord. Chem. Rev.* **1996**, *156*, 275.

[9] K. Uemura, K. Matsumoto, unpublished results.

[10] For selected Pt–Rh dimers with other ligands, see: a) R. R. Guimerans, F. E. Wood, A. L. Balch, *Inorg. Chem.* **1984**, *23*, 1307; b) A. L. Balch, R. R. Guimerans, J. Linehan, F. E. Wood, *Inorg. Chem.* **1985**, *24*, 2021; c) A. L. Balch, V. J. Catalan, *Inorg. Chem.* **1992**, *31*, 3934.

[11] The dimerization process of **1** was monitored by ^{1}H NMR spectroscopy and ESI-MS (see Supporting Information).

[12] For tetranuclear Pt^{2+} chains, see: a) L. S. Hollis, S. J. Lippard, *J. Am. Chem. Soc.* **1981**, *103*, 1230; b) J.-P. Laurent, P. Lepage, F. Dahan, *J. Am. Chem. Soc.* **1982**, *104*, 7335; c) L. S. Hollis, S. J. Lippard, *Inorg. Chem.* **1983**, *22*, 2600; d) L. S. Hollis, S. J. Lippard, *J. Am. Chem. Soc.* **1983**, *105*, 3494; e) K. Matsumoto, H. Miyamae, H. Moriyama, *Inorg. Chem.* **1989**, *28*, 2959.

[13] For tetranuclear $Pt^{2.5+}$ chains (platinum tan), see: a) K. Matsumoto, K. Fuwa, *J. Am. Chem. Soc.* **1982**, *104*, 897; b) K. Matsumoto, H. Takahashi, K. Fuwa, *Inorg. Chem.* **1983**, *22*, 4086.

[14] a) K. Sakai, K. Matsumoto, *J. Am. Chem. Soc.* **1989**, *111*, 3074; b) K. Matsumoto, K. Sakai, K. Nishio, Y. Tokisue, R. Ito, T. Nishide, Y. Shichi, *J. Am. Chem. Soc.* **1992**, *114*, 8110.

[15] a) J. K. Barton, C. Caravana, S. J. Lippard, *J. Am. Chem. Soc.* **1979**, *101*, 7269; b) P. Arrizabalaga, P. Castan, M. Geoffroy, J.-P. Laurent, *Inorg. Chem.* **1985**, *24*, 3656.

[16] F. Mehran, B. A. Scott, *Phys. Rev. Lett.* **1973**, *31*, 99.

[17] F. Mehran, B. A. Scott, *Phys. Rev. Lett.* **1973**, *31*, 1347.

[18] A. G. Bunn, B. B. Wayland, *J. Am. Chem. Soc.* **1992**, *114*, 6917.

[19] See Supporting Information for the magnetic measurements of **4**.

[20] Only the electrical conductivity perpendicular to the chain direction was measured. It was impossible to measure the conductivity parallel to the chain, as the crystal is a thin plate (see Supporting Information).

 © 2005 Wiley-VCH Verlag GmbH & Co. KGaA, Weinheim

Molecular Motors

DOI: 10.1002/anie.200501214

A DNA–Protein Nanoengine for "On-Demand" Release and Precise Delivery of Molecules**

*Razvan Nutiu and Yingfu Li**

We demonstrate that artificial DNA probes can be merged with natural biological processes to create highly active nanomechanical devices by developing a DNA–enzyme hybrid nanoengine that is triggered by a small molecule as the input to cyclically dispatch and retrieve a DNA strand as the output. Moreover, the movement of the output can be accurately directed between two specific DNA destinations. Joint exploration of small molecules, nucleic acids, and enzymes may eventually lead to the engineering of bionanodevices that can both detect a biological malfunction and send out a messenger to initiate a repair mechanism.

Nucleic acids encode "smart" molecular recognition properties that commend their exploitation in bionanotechnology.[1,2] It has been proven that DNA or RNA can be used as structural material for building complex self-assembled objects,[3–7] computational devices,[8–13] or active machines and motors.[14–22] In the latter case, DNA also represents the "fuel" that triggers the function of the DNA machine. However, the

[*] R. Nutiu, Prof. Dr. Y. Li
Department of Biochemistry and Biomedical Sciences
and Department of Chemistry
McMaster University
Hamilton, ON L8N 3Z5 (Canada)
Fax: (+1) 905-522-9033
E-mail: liying@mcmaster.ca

[**] We thank the entire Li group as well as Dr. John Brennan, Dr. Eric Brown, and Dr. Gerard Wright for insightful discussions. This study was funded by the Canadian Institutes of Health Research (CIHR) and the Natural Sciences and Engineering Research Council of Canada (NSERC). Y.L. holds a Canada Research Chair. R.N. is the recipient of a CIHR Doctoral Research Award.

Supporting information for this article is available on the WWW under http://www.angewandte.org or from the author.

 InterScience © 2005 Wiley-VCH Verlag GmbH & Co. KGaA, Weinheim

need of artificial DNA molecules for the manipulation of DNA-based devices limits their potential for biological applications. Herein we show that an artificial DNA-aptamer nanoswitch can be coupled to an enzymatic reaction to create a hybrid DNA–enzyme nanoengine capable of transporting an antisense DNA molecule between two specific destinations under the control of a small-molecule input.

DNA aptamers are highly structured single strands of DNA that are capable of binding a ligand with great affinity and specificity. The nature of these aptamers makes them inherently capable of recognizing two different molecules: the cognate non-nucleic acid target for which the aptamer is created and an antisense DNA molecule through Watson–Crick base pairing. It has been shown that the addition of a target to a solution containing the properly engineered aptamer/antisense duplex can trigger rapid structure switching from the aptamer/antisense duplex to the aptamer/target complex.[23] The dual binding capability of DNA aptamers and the reversibility of the duplex–complex switching process are the two key elements exploited in the design of the DNA nanoswitch presented herein.

The molecular model of the DNA nanoswitch is illustrated in Figure 1 A. The nanoswitch has three components: a modified version of a previously described adenosine-binding DNA aptamer (black line),[24] a short complimentary DNA strand as the output (gray line), and adenosine as the input (red star). In the absence of adenosine, the system is in the "off" state, as the output molecule is docked onto the DNA aptamer through Watson–Crick base pairing. Upon addition of adenosine, the system is switched to the "on" state, as adenosine displaces the output from the aptamer. Therefore, the presence of one biological entity is transduced into the release of another.

The evidence for the output displacement by the input was obtained by using agarose gel electrophoresis (Figure 1 B). For this experiment, the output DNA strand was labeled with fluorescein at the 3′ end (green circle in Figure 1 A). DNA strands of 11 and 12 nucleotides in length (named "output 11" and "output 12") were studied as the output molecules at two concentrations. Figure 1 C plots the percentage release of the output versus the concentration of the input for each gel. In each case, a clear dependence of the output release on the input concentration was observed. The experiments with 20 nM output 12 and 100 nM output 11 gave higher release percentages at all tested concentrations than those with 100 nM output 12 and 500 nM output 11. It is important to note that, by using different concentrations of the nanoswitch, the absolute amount of the output to be released can be controlled independently of the concentration of the input. For example, 1 mM adenosine can cause the release of the output in four different amounts: 10.4 nM (52% of 20 nM output 12), 16 nM (16% of 100 nM output 12), 50 nM (50% of 100 nM output 11), or 80 nM (16% of 500 nM output 11). This suggests the possibility that a certain amount of input can be accurately transduced into a desired amount of output by utilizing different sizes of the DNA output along with different concentrations of the DNA nanoswitch.

As only physical interactions are involved in the function of the nanoswitch, the release of the output is a reversible

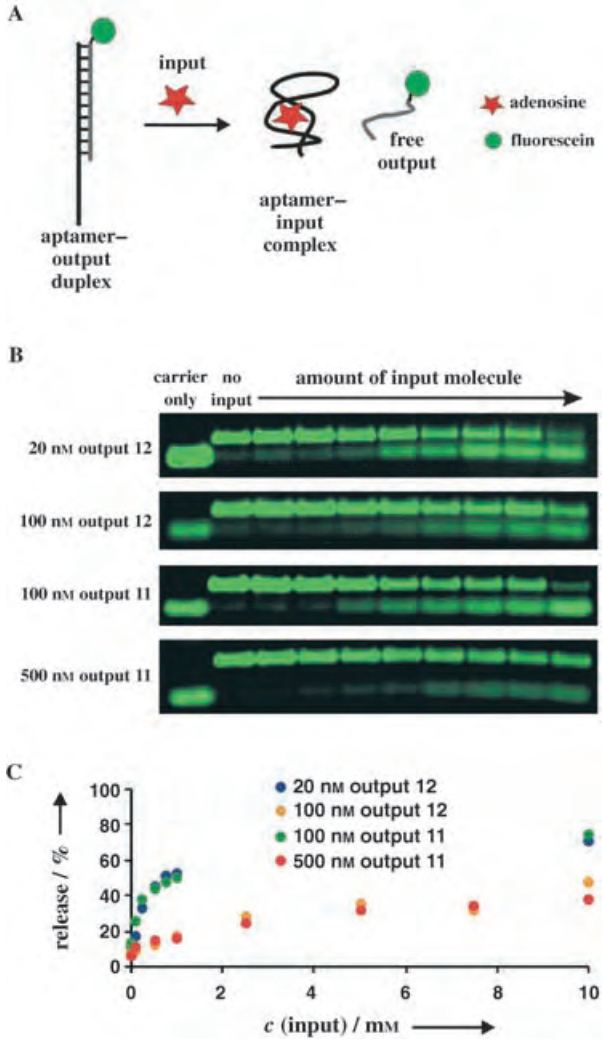


Figure 1. A DNA nanoswitch (see text). A) The working principle. B) Gel evidence for output release. Lanes 3–10 show the response of the nanoswitch to gradually increasing concentrations of the input (10^{-3}–10 mM). C) The dependence of output release on input concentration and overall concentration of the nanoswitch.

process. Therefore, the nanoswitch can be programmed to work cyclically when it is coupled to adenosine deaminase (ADA, blue oval in Figure 2 A)—an enzyme that converts adenosine (red star) into inosine (red pentagon), for which the aptamer has no affinity.[24] ADA is expected to convert free adenosine into inosine and this process should cause more and more aptamer–adenosine complexes to dissociate. Thus, freed aptamer molecules will then engage the output DNA molecules to reform the aptamer–output duplex. The inclusion of ADA in the system therefore converts the DNA nanoswitch into a two-stroke DNA nanoengine. The first stroke, triggered by the addition of adenosine, is represented by the release of the output; the second stroke, driven by the transformation of adenosine into inosine, is the return of the output to the aptamer.

A fluorescence quenching/dequenching experiment was performed to provide a physical readout of the cyclic function of the DNA nanoengine (Figure 2 B). First, the aptamer was

 © 2005 Wiley-VCH Verlag GmbH & Co. KGaA, Weinheim

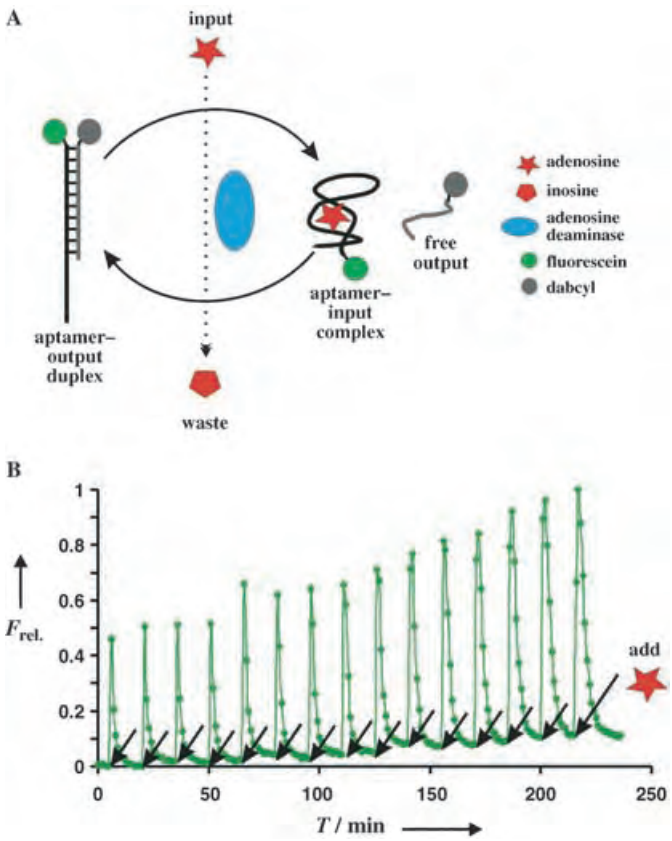


Figure 2. Transformation of the nanoswitch into a two-stroke DNA–enzyme nanoengine (see text). A) Cycling the nanoengine. B) A fluorescence quenching/dequenching experiment illustrates the working of the nanoengine. The figure presents the first 15 cycles of the nanoengine, where every cycle is initiated by the addition of fresh adenosine (black arrows).

labeled with fluorescein (green circle in Figure 2A) at its 5′ end and the output was labeled with 4-(4-(dimethylamino)-phenylazo)benzoic acid (dabcyl, a universal fluorescence quencher, gray circle) at its 3′ end. The fluorophore-labeled aptamer and the quencher-labeled output were then mixed with ADA and the fluorescence of the system was recorded over time. Prior to adenosine addition, the output was docked onto the aptamer, thereby bringing the quencher into close proximity with the fluorophore for efficient fluorescence quenching; therefore the system had a low fluorescence reading. The addition of adenosine after 5 min (the first black arrow in Figure 2B) elicited a rapid increase of the fluorescence intensity of the system, a result reflecting the fast release of the output (the first stroke of the engine). Slowly but gradually, ADA converted adenosine into inosine, thereby prompting the reannealing of the output onto the aptamer (the second stroke), which was indicated by the progressive decrease of the fluorescence intensity of the system.

A full cycle of the engine, under our experimental conditions, took about 15 min to complete. However, this interval could be easily altered by increasing or decreasing the amount of ADA in the system. Although only 15 cycles are shown in Figure 2B, each one triggered by the addition of fresh adenosine (black arrows), in theory the nanoengine should work for an indefinite period of time. However, in practice, the lack of an exhaust system will result in an accumulation of inosine and ammonia that will inhibit ADA[25] and will eventually arrest the engine. This may explain the gradual increase of the fluorescence intensity of the system as well as the steady peak widening observed in Figure 2B.

The above nanoengine could also be designed to include a defined destination for the output molecules upon their release. Two extra strands of DNA were introduced into the system to create two different destinations for the output: a mutagenized version of the aptamer as the desired destination and a control DNA strand as the unwanted destination. The mutant aptamer contained three mutations: A7→T7, G15→T15, and G27→T27. The first mutation, introduced into the output-binding site, caused the mutant aptamer to have a decreased affinity for the output, whereas the other two mutations, introduced into the adenosine-binding site, abolished the adenosine-binding ability. The control DNA had a sequence completely unrelated to that of the original aptamer. The active aptamer, the mutant aptamer, and the control DNA were labeled with Cy3, fluorescein, and Cy3.5, respectively, while the output was still labeled with the dabcyl quencher. Therefore, the arrival of the output at a given destination would be transduced into a decrease in the fluorescence intensity of the corresponding fluorophore.

When all the DNAs were mixed with ADA in the absence of adenosine, the high level of fluorescence of the mutant aptamer and the control DNA as well as the low level of fluorescence of the aptamer (Figure 3B) indicated that the output was docked onto the aptamer as planned. However, when adenosine was introduced, the rapid fluorescence increase of the active aptamer, coupled with the rapid fluorescence decrease of the mutant aptamer, confirmed the prearranged direction of movement of the output (Figure 3A). Importantly, the fluorescence of the control DNA remained unchanged, thereby demonstrating that the movement was indeed driven by specific molecular recognition. The action of ADA promoted the reverse movement of the output from the mutant aptamer to the active aptamer, reflected in the decrease of the fluorescence of the active aptamer and the increase of the fluorescence of the mutant aptamer. The dependence of the pattern of the fluorescence signal on the DNA sequence was verified by permutating the three fluorophores on the three DNA sequences (data not shown).

We have demonstrated above that a small molecule, an aptamer, an antisense DNA, and an enzyme can be configured into a two-stroke DNA nanoengine that can function in a cyclic fashion. The input-removing enzyme ADA is an essential component of our nanoengine. However, ADA functions independently of the output. A more desirable feature, particularly for real-world applications, that has yet to be demonstrated is the intricate linking of the enzyme activity with the freed output. Such a system can first detect a specific problem (input) and then dispatch a signal (output) for activating a rescuing protein or pathway (equivalent to ADA) for the correction of the problem. The completion of the final

 © 2005 Wiley-VCH Verlag GmbH & Co. KGaA, Weinheim

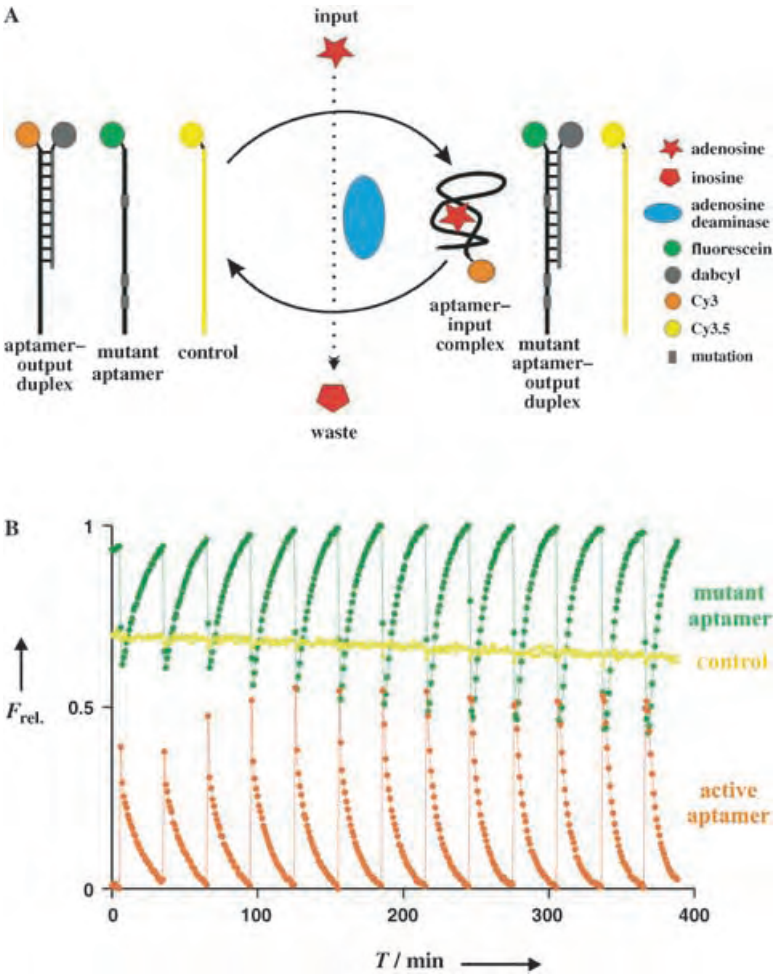


Figure 3. Precise delivery of the output (see text). A) Schematic representation. One cycle of the nanoengine is represented by the travel of the output from the aptamer to the mutant and back. B) A three-color fluorescence quenching/dequenching experiment.

step will deliver the output back to the aptamer, which resets the nanoengine for a new round of action, if necessary. Our nanoengine prototype does not offer a solution to this practical problem and can only dispatch a DNA strand as the output in response to a relatively high concentration of the small-molecule input. However, on the basis of the functional versatility of natural enzymes and the ease of in vitro selection with which diverse aptamers can be identified for virtually any target,[26,27] we speculate that highly practical nanoengines of a similar nature with a better input sensitivity and the ability to dispatch a desirable output will be created in the future for different input/output systems and that these nanoengines will offer new ways for the delivery of a drug or the regulation of a disease-causing biological process.

Received: April 6, 2005
Published online: July 25, 2005

Keywords: aptamers · DNA · enzymes · molecular devices · nanotechnology

[1] D. G. Anderson, J. A. Burdick, R. Langer, *Science* **2004**, *305*, 1923.
[2] C. M. Niemeyer, *Curr. Opin. Chem. Biol.* **2000**, *4*, 609; C. M. Niemeyer, *Angew. Chem.* **2001**, *113*, 4254; *Angew. Chem. Int. Ed.* **2001**, *40*, 4128; C. M. Niemeyer, M. Adler, *Angew. Chem.* **2002**, *114*, 3933; *Angew. Chem. Int. Ed.* **2002**, *41*, 3779.
[3] J. H. Chen, N. C. Seeman, *Nature* **1991**, *350*, 631.
[4] C. Mao, W. Sun, N. C. Seeman, *Nature* **1997**, *386*, 137.
[5] E. Winfree, F. Liu, L. A. Wenzler, N. C. Seeman, *Nature* **1998**, *394*, 539.
[6] W. M. Shih, J. D. Quispe, G. F. Joyce, *Nature* **2004**, *427*, 618.
[7] L. H. Eckardt, K. Naumann, W. M. Pankau, M. Rein, M. Schweitzer, N. Windhab, G. von Kiedrowski, *Nature* **2002**, *420*, 286; A. Chworos, I. Severcan, A. Y. Koyfman, P. Weinkam, E. Oroudjev, H. G. Hansma, L. Jaeger, *Science* **2004**, *306*, 2068.
[8] L. M. Adleman, *Science* **1994**, *266*, 1021.
[9] Q. Liu, L. Wang, A. G. Frutos, A. E. Condon, R. M. Corn, L. M. Smith, *Nature* **2000**, *403*, 175.
[10] C. Mao, T. H. LaBean, J. H. Reif, N. C. Seeman, *Nature* **2000**, *407*, 493.
[11] Y. Benenson, T. Paz-Elizur, R. Adar, E. Keinan, Z. Livneh, E. Shapiro, *Nature* **2001**, *414*, 430.
[12] R. S. Braich, N. Chelyapov, C. Johnson, P. W. K. Rothemund, L. Adleman, *Science* **2002**, *296*, 499.
[13] Y. Benenson, R. Adar, T. Paz-Elizur, Z. Livneh, E. Shapiro, *Proc. Natl. Acad. Sci. USA* **2003**, *100*, 2191.
[14] C. Mao, W. Sun, Z. Shen, N. C. Seeman, *Nature* **1999**, *397*, 144.
[15] B. Yurke, A. J. Turberfield, A. P. Mills, Jr., F. C. Simmel, J. L. Neumann, *Nature* **2000**, *406*, 605.
[16] H. Yan, X. Zhang, Z. Shen, N. C. Seeman, *Nature* **2002**, *415*, 62.
[17] P. Alberti, J. L. Mergny, *Proc. Natl. Acad. Sci. USA* **2003**, *100*, 1569.
[18] W. B. Sherman, N. C. Seeman, *Nano Lett.* **2004**, *4*, 1203.
[19] Y. Chen, M. Wang, C. Mao, *Angew. Chem.* **2004**, *116*, 3638; *Angew. Chem. Int. Ed.* **2004**, *43*, 3554.
[20] W. U. Dittmer, A. Reuter, F. C. Simmel, *Angew. Chem.* **2004**, *116*, 3634; *Angew. Chem. Int. Ed.* **2004**, *43*, 3550.
[21] J. S. Shin, N. A. Pierce, *J. Am. Chem. Soc.* **2004**, *126*, 10834.
[22] S. Liao, N. C. Seeman, *Science* **2004**, *306*, 2072.
[23] R. Nutiu, Y. Li, *J. Am. Chem. Soc.* **2003**, *125*, 4771; R. Nutiu, Y. Li, *Chem. Eur. J.* **2004**, *10*, 1868; R. Nutiu, J. M. Yu, Y. Li, *ChemBioChem* **2004**, *5*, 1139; R. Nutiu, Y. Li, *Angew. Chem.* **2005**, *117*, 1085; *Angew. Chem. Int. Ed.* **2005**, *44*, 1061.
[24] D. E. Huizenga, J. W. Szostak, *Biochemistry* **1995**, *34*, 656.
[25] A. A. Saboury, A. Divsalar, G. A. Jafari, A. A. Moosavi-Movahedi, M. R. Housaindokht, G. H. Hakimelahi, *J. Biochem. Mol. Biol.* **2002**, *35*, 302.
[26] D. S. Wilson, J. W. Szostak, *Annu. Rev. Biochem.* **1999**, *68*, 611.
[27] M. Famulok, G. Mayer, M. Blind, *Acc. Chem. Res.* **2000**, *33*, 591.

 © 2005 Wiley-VCH Verlag GmbH & Co. KGaA, Weinheim

Reactivity Studies

DOI: 10.1002/anie.200501526

On the Importance of Leaving Group Ability in Reactions of Ammonium, Oxonium, Phosphonium, and Sulfonium Ylides**

Varinder K. Aggarwal, Jeremy N. Harvey,* and Raphaël Robiette*

Dedicated to Professor Steven Ley on the occasion of his 60th birthday

Ammonium, phosphonium, and sulfonium ylides are powerful and versatile reagents in organic chemistry, which undergo three important types of reaction: olefination, cyclization to a three-membered ring, and rearrangement.[1] The reactivity and selectivity of the ylides in these reactions depend on the nature of the central heteroatom. The nucleophilicity of the carbon centre of the ylides is one important aspect of their reactivity, which is affected by the degree to which the onium group stabilizes the adjacent negative charge. It has been shown that stabilization increases in the order O < N ≪ P < S.[2] However, this feature alone does not explain all the observed reactivity. We present comparative computational data which suggest that the differences are mainly due to the differing leaving group ability of the respective onium groups. The calculations[3] are carried out using the accurate B3LYP density functional, which is known to describe trends of the kind studied here accurately.[4,5] We also include a continuum solvent model in all calculations as the gas-phase potential energy surfaces are qualitatively inaccurate for some of these very polar species.[5]

In the reaction with organoboranes, sulfonium ylides give homologation products at low temperature[6] while the more nucleophilic ammonium ylides react only at reflux of THF,[7] and phosphonium ylides require temperatures above 130 °C.[8] The energy profile[3] for the reaction of BMe_3 with ylides **1** involves barrierless addition to form ate complex **2**, followed by rate-determining 1,2-migration (Figure 1). The first step is most exothermic for the ammonium and oxonium ylides while the barrier for migration is smallest with the oxonium ylide and largest with the phosphonium derivative. Nucleophilicity of the onium ylides is clearly irrelevant for this process, with the key factor being instead the leaving group ability of the onium group, which decreases in the order O > S > N > P.

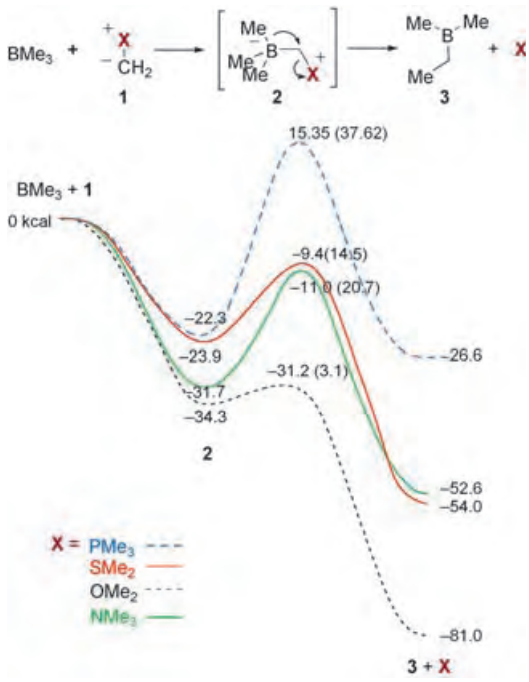


Figure 1. Calculated[3] energy surface (in kcal mol^{-1}) for reaction of BMe_3 with **1**. Values in parentheses are relative to **2**.

For epoxidation, observed reactivity does not correlate with carbon nucleophilicity either. Sulfonium ylides react with aldehydes at temperatures as low as −78 °C,[9] whilst room temperature is required using ammonium ylides.[10] This is consistent with the energy profile[3] for the reaction of the ylides **1** with benzaldehyde, and again, the higher reactivity of the sulfur-based species is due to a lower barrier in the intramolecular substitution step (Figure 2). In this reaction, the initial addition step is barrierless with the more nucleophilic ammonium ylide, and hence more favorable than with the sulfonium ylide, where a small barrier is observed. In the latter case, though, addition is the only demanding (and rate-limiting) step, whereas with nitrogen, betaine formation is followed by slower decomposition over a 15 kcal mol^{-1} barrier. This is consistent with the experimental observation that β-hydroxy ammonium salts are isolated upon work-up of the reaction of ammonium ylides at low temperature.[11] Wittig reaction leading to alkenes is the main pathway with phosphonium ylides. This difference in reaction behavior compared to sulfonium ylides has a number of reasons,[12] such as the fact that oxathietanes are not formed in the sulfur reaction.[5] One important effect is clearly leaving group ability: our calculations show that *trans* betaines can be formed from phosphorus ylides over a low barrier, but nucleophilic displacement of the phosphine involves a very significant barrier. Cyclization to the oxaphosphetane (see Figure S1, Supporting Information), or indeed facile direct formation of the latter, and subsequent phosphine oxide loss, therefore compete very effectively. As with the borane reaction, calculations suggest that the reaction with oxonium ylides would be very favorable, although no examples are

[*] Prof. V. K. Aggarwal, Dr. J. N. Harvey, Dr. R. Robiette
School of Chemistry
University of Bristol
Cantock's Close, Bristol BS8 1TS (UK)
Fax: (+44) 117-929-8611
E-mail: v.aggarwal@bristol.ac.uk
jeremy.harvey@bristol.ac.uk

[**] We thank EPSRC and Université catholique de Louvain (F.S.R. grant to R.R.) for financial support, and Merck and Pfizer for unrestricted grants.

Supporting information for this article is available on the WWW under http://www.angewandte.org or from the author.

InterScience
© 2005 Wiley-VCH Verlag GmbH & Co. KGaA, Weinheim

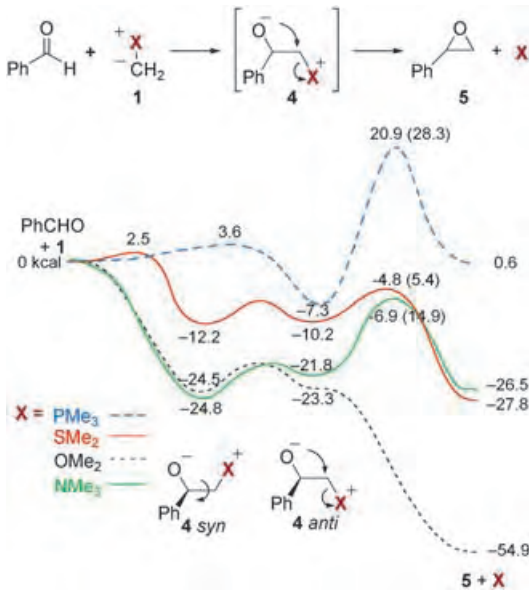
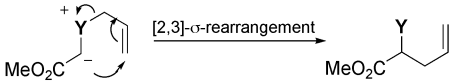


Figure 2. Computed[3] potential energy surface (in kcal mol^{-1}) for styrene oxide formation from **1**. Values in parentheses are relative to **4** *anti*.

reported in the literature. Overall, leaving group ability plays an extremely important role in determining reactivity and the nature of products formed in this set of reactions.

[2,3]-σ-Rearrangement is known for ammonium, oxonium, and sulfonium ylides[1] but only one low-yielding example has been reported for phosphonium ylides.[13] This process can in principle involve radical intermediates (Stevens rearrangement), but experimental evidence suggests a concerted pathway in most cases.[11,14] For the latter, the rate could be expected to depend both on nucleophilicity of the ylide carbon atom (which decreases in the order O > N > P > S) and on the leaving group ability of the corresponding onium (which should decrease as O > S > N > P, as in the other two reactions). Experimentally, the rearrangement is very facile even at low temperature for all but the phosphonium ylides. Our calculations[3] (Table 1) show that the barrier height follows the order O < S < N ≪ P, indicating that leaving group ability is the dominant effect in this case also. The magnitude of the barriers for the O, N, and S ylides confirms that their rearrangement should be rapid, while the high activation energy for phosphonium ylides accounts for the dearth of examples in this latter case. Considering the similarity in nucleophilicity of phosphonium and sulfonium ylides, the very different activation barriers for rearrangement emphasizes the dominant effect of leaving group ability.

Table 1: Computed[3] activation energies ($\Delta E^{\neq}$) and reaction energies (ΔE) of [2,3]-σ-rearrangements (in kcal mol^{-1}).



Y	$\Delta E^{\neq}$	ΔE
NMe_2	12.18	−27.29
OMe	2.94	−60.44
PMe_2	35.13	−4.71
SMe	7.83	−33.45

The consistent order of leaving group ability of the four onium groups in these three reactions is intriguing. Which factors cause ether and thioether groups to be excellent leaving groups, amines to be somewhat less good, and phosphines to be so poor? Nucleophilic substitution is one of the most important reactions in organic chemistry,[15] and extensive efforts have been made to develop a quantitative description of nucleophilicity,[16] and, to a lesser extent, the complementary kinetic property of leaving group ability.[17] It is generally recognized that both intrinsic factors and thermochemistry contribute to the barrier height. The combined impact of these two effects can be treated quantitatively using Marcus theory,[18] which has been applied successfully to group transfer reactions[19] and in particular to S_N2 reactions.[15,20] The intrinsic nucleophilicity of a given species is the same as its intrinsic leaving group ability, and can be measured by the rate or barrier height for the identity S_N2 reaction $X + CH_3X^+ \rightleftarrows X^+CH_3 + X$. The calculated[3] energy barriers for these reactions give a reactivity order similar to that found above, with O > S > N ≫ P (Table 2).[21,22]

Table 2: Intrinsic barrier heights (in kcal mol^{-1})[3] for the identity reaction $X + CH_3X^+ \rightleftarrows X^+CH_3 + X$; forward and reverse barrier heights and exothermicity for the reaction $H_2O + CH_3X^+ \rightleftarrows H_2O^+CH_3 + X$.

X =	OMe_2	SMe_2	NMe_3	PMe_3
		$X + CH_3X^+ \rightleftarrows X^+CH_3 + X$		
$\Delta E^{\neq}$	15.5	22.5	26.3	40.1
		$H_2O + CH_3X^+ \rightleftarrows H_2O^+CH_3 + X$		
$\Delta E^{\neq}$ forward	13.2	25.6	38.9	50.7
$\Delta E^{\neq}$ backward	10.6	9.4	2.1	4.8
ΔE	2.6	16.3	36.8	45.9

These intrinsic reaction barriers have been discussed for other nucleophiles previously, and depend on the strength of the C–X bond but also on the balance between bond-making and bond-breaking at the exchange transition state.[23] All other factors being equal, then, ether oxygens are (intrinsically) the best nucleophiles (and leaving groups), followed by sulfides and amines, with phosphines being poor for both types of reaction.

However, all factors are not equal: the thermodynamics of substitution vary considerably due to differences in the carbon–element bond strength, which decreases in the order P > N > S > O.[24] In trying to understand the trend in leaving group ability in reactions with a common nucleophile—the topic of the present study—these differences in bond energies need to be taken into account as well as the intrinsic reactivity, as the resulting changes in thermodynamics have an indirect impact on barrier heights. Assuming a constant intrinsic reaction barrier, leaving group ability would increase with decreasing bond energy, in the order P < N < S < O. In fact, the intrinsic barriers are not identical (Table 2), and indeed follow the same order of increased reactivity going from P to O, so that the two factors combine synergistically to yield an overall hierarchy of leaving group ability P < N < S < O.[25]

 © 2005 Wiley-VCH Verlag GmbH & Co. KGaA, Weinheim

This is shown for three different nucleophiles: an alkyl group in Figure 1, an alkoxide anion in Figure 2, and water in Table 2. To take another better known example, this trend explains the stability of alkyl phosphonium and ammonium salts in the presence of halide counterions, and the instability of the corresponding sulfonium salts.[26] A nucleophilic halide counterion can displace a good leaving group (sulfide), but not a poor one (amine, phosphine). It also accounts for why nature, with ready access to compounds containing N, O, S and P, has chosen a sulfonium salt (*S*-adenosyl methionine, SAM) for methyl group transfer.[27] Unlike oxonium salts, such species are stable enough to be formed without reacting instantaneously with water, yet have a higher alkylating reactivity than ammonium salts.

Although the focus of the present work is on leaving group ability, it is useful to note that the same two factors of intrinsic reactivity and thermochemistry account for the relative nucleophilicity of the different groups also. For example, phosphines are usually quite good nucleophiles despite their low intrinsic reactivity, because the strong C–P bond means that substitution is usually quite strongly exothermic. Calculated barriers for the reaction $X + CH_3OH_2^+ \rightarrow CH_3X^+ + H_2O$ are shown in Table 2. Because the exothermicity increases in the order ether < sulfide < amine < phosphine, the calculated nucleophilicity follows the well known[28] order $R_3N > R_3P > R_2S > R_2O$. The intrinsically weakest nucleophile, R_3P, has the second lowest barrier to reaction due to forming the most stable products. The ether group, on the other hand, is intrinsically reactive but the reaction is near thermoneutral and hence has a significant barrier.

In summary, the reactivity of sulfonium, ammonium, phosphonium, and oxonium ylides in a range of reactions is to a large part determined by the leaving group ability of the corresponding onium group, and this decreases for both intrinsic and thermochemical reasons in the order O > S > N > P. This means that when comparing reactions of, for example, ammonium and sulfonium ylides, the rate-limiting and selectivity-determining steps in a multistep mechanism may well be different. This insight should be of considerable use in designing new stereoselective synthetic transformations.

Received: May 4, 2005
Published online: August 4, 2005

Keywords: density functional calculations · leaving group ability · onium compounds · sigmatropic rearrangement · ylides

[1] a) J. S. Clark, *Nitrogen, Oxygen and Sulfur Ylide Chemistry: A Practical Approach in Chemistry*, Oxford University Press, Oxford, **2002**; b) O. I. Kolodiazhnyi, *Phosphorus Ylides: Chemistry and Application in Organic Synthesis*, Wiley-VCH, Wheinheim, **1999**; c) A.-H. Li, L.-X. Dai, V. K. Aggarwal, *Chem. Rev.* **1997**, *97*, 2341 – 2372.

[2] a) J.-P. Cheng, B. Liu, Y. Zhao, Y. Sun, X.-M. Zhang, Y. Lu, *J. Org. Chem.* **1999**, *64*, 604 – 610; b) T. Naito, S. Nagase, H. Yamataka, *J. Am. Chem. Soc.* **1994**, *116*, 10080 – 10088.

[3] Calculations were carried out at the B3LYP/6-311 + G**// B3LYP/6-31G* level of theory, including a continuum description of THF solvent for both the geometry optimization and the single point energy calculation using the Jaguar 4.0 pseudospectral program package (Jaguar 4.0, Schrödinger, Inc., Portland, OR, **1991**–**2000**). Relative energies correspond to electronic energies at the indicated levels of theory.

[4] a) A. Bottoni, M. Lombardo, A. Neri, C. Trombini, *J. Org. Chem.* **2003**, *68*, 3397 – 3405; b) A. A. Fokin, A. O. Kushko, A. V. Kirij, A. G. Yurchenko, P. von R. Schleyer, *J. Org. Chem.* **2000**, *65*, 2984 – 2995; c) G. D. Ruggiero, I. H. Williams, *J. Chem. Soc. Perkin Trans. 2* **2001**, *4*, 448 – 458.

[5] V. K. Aggarwal, J. N. Harvey, J. Richardson, *J. Am. Chem. Soc.* **2002**, *124*, 5747 – 5756.

[6] V. K. Aggarwal, G. Y. Fang, A. T. Schmidt, *J. Am. Chem. Soc.* **2005**, *127*, 1642 – 1643.

[7] W. K. Musker, R. R. Stevens, *Tetrahedron Lett.* **1967**, 995 – 997.

[8] M. E. Gurskii, D. G. Pershin, B. M. Mikhailov, *J. Organomet. Chem.* **1984**, *260*, 17 – 23.

[9] V. K. Aggarwal, C. L. Winn, *Acc. Chem. Res.* **2004**, *37*, 611 – 620.

[10] A. Kowalkowska, D. Sucholbiak, A. Joñczyk, *Eur. J. Org. Chem.* **2005**, 925 – 933.

[11] Y. Maeda, Y. Sato, *J. Chem. Soc. Perkin Trans. 1* **1997**,1491 – 1493.

[12] F. Volatron, O. Eisenstein, *J. Am. Chem. Soc.* **1987**, *109*, 1 – 14.

[13] J. E. Baldwin, M. C. H. Armstrong, *J. Chem. SOc. Chem. Commun.* **1970**, *11*, 631 – 632.

[14] For methodological studies, see: a) G. M. Blackburn, W. D. Ollis, J. D. Plackett, C. Smith, I. O. Sutherland, *J. Chem. Soc. Chem. Commun.* **1968**, *4*, 186 – 188; b) R. W. C. Cose, A. M. Dabies, W. D. Ollis, C. Smith, I. O. Sutherland, *J. Chem. Soc. Chem. Commun.* **1969**, *6*, 293 – 294; R. W. C. Cose, A. M. Dabies, W. D. Ollis, C. Smith, I. O. Sutherland, *J. Chem. Soc. Chem. Commun.* **1969**, *6*, 294 – 295.

[15] For reviews, see: a) J. K. Laerdahl, E. Uggerud, *Int. J. Mass Spectrom.* **2002**, *214*, 277 – 314; b) S. S. Shaik, H. B. Schlegel, S. Wolf, *Theoretical Aspects of Physical Organic Chemistry. The S_N2 Mechanism*, Wiley, New York, **1992**, p. 285.

[16] For reviews, see: a) H. Mayr, B. Kempf, A. R. Ofial, *Acc. Chem. Res.* **2003**, *36*, 66 – 77; b) H. Mayr, M. Patz, *Angew. Chem.* **1994**, *106*, 990 – 1010; *Angew. Chem. Int. Ed. Engl.* **1994**, *33*, 938 – 955.

[17] K. R. Fountain, K. D. Patel, T. W. Dunkin, J. A. Powers, D. A. Van Galen, *J. Org. Chem.* **1997**, *62*, 853 – 856, and references therein.

[18] R. A. Marcus, *Annu. Rev. Phys. Chem.* **1964**, *15*, 155 – 196.

[19] J. Donnella, J. R. Murdoch, *J. Am. Chem. Soc.* **1984**, *106*, 4724 – 4735.

[20] a) S. Wolfe, D. J. Mitchell, H. B. Schlegel, *J. Am. Chem. Soc.* **1981**, *103*, 7694 – 7696; b) M. L. Chabinyc, S. L. Craig, C. K. Regan, J. I. Brauman, *Science* **1998**, *279*, 1882 – 1886, and references therein.

[21] For previous results on the identity substitution reactions of N- and O-cationic leaving groups, see: a) J. K. Laerdahl, E. Uggerud, *Org. Biomol. Chem.* **2003**, *1*, 2935 – 2942; b) J. K. Laerdahl, L. Bache-Andreassen, E. Uggerud, *Org. Biomol. Chem.* **2003**, *1*, 2943 – 2950.

[22] A slightly different trend is observed in the barriers for the anionic reactions: S. Hoz, H. Basch, J. L. Wolk, T. Hoz, E. Rozental, *J. Am. Chem. Soc.* **1999**, *121*, 7724 – 7725.

[23] S. S. Shaik, A. Pross, *J. Am. Chem. Soc.* **1982**, *104*, 2708 – 2719.

[24] a) M. N. Glukhovtsev, J. E. Szulejko, T. B. McMahon, J. W. Gauld, A. P. Scott, B. J. Smith, A. Pross, L. Radom, *J. Phys. Chem.* **1994**, *98*, 13099 – 13101; b) P.-C. Nam, P. Gerbaux, M. T. Nguyen, *Eur. J. Mass Spectrom.* **2003**, *9*, 257 – 266.

[25] It has been noted previously that thermodynamic property of basicity correlates with leaving group ability (kinetic property): species with low basicity have high leaving group ability (see

 © 2005 Wiley-VCH Verlag GmbH & Co. KGaA, Weinheim

K. P. C. Vollhardt, N. E. Schore, *Organic Chemistry*, W. H. Freeman, New York, **1998**). However, this trend is not strictly followed by the present groups: phosphines and amines have similar basicity (pK_a of Et_3NH^+ and Et_3PH^+ are respectively 9.0 and 9.1 in DMSO; see D. H. Ripin and D. A. Evans pK_a's table at http://daecr1.harvard.edu/pdf/evans_pKa_table.pdf) yet phosphines are much poorer leaving groups.

[26] V. K. Aggarwal, A. Thompson, R. V. H. Jones, *Tetrahedron Lett.* **1994**, *35*, 8659 – 8660.

[27] D. Voet, J. G. Voet, *Biochemistry*, Wiley, New York, **1995**.

[28] F. A. Carey, R. J. Sundberg, *Advanced Organic Chemistry Part A: Structure and Mechanisms*, Plenum, New York, **1990**.

 © 2005 Wiley-VCH Verlag GmbH & Co. KGaA, Weinheim

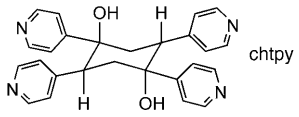
Coordination Polymers

DOI: 10.1002/anie.200501753

Cu^{2+}-Mediated Dehydrogenative Coupling and Hydroxylation of an N-Heterocyclic Ligand: From Generation of a New Tetratopic Ligand to the Designed Assembly of Three-Dimensional Copper(I) Coordination Polymers**

Sheng Hu, Jing-Cai Chen, Ming-Liang Tong, Bo Wang, Yun-Xin Yan, and Stuart R. Batten*

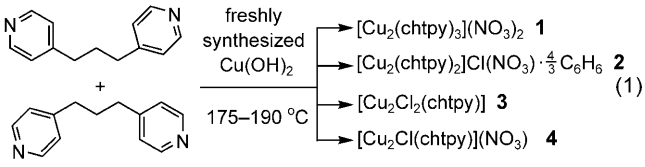
Great interest has been focused on the rapidly expanding field of crystal engineering of two- (2D) and three-dimensional (3D) coordination polymers due to their structural and topological diversity as well as their potential application as functional materials.[1] The main strategy popularly used in this area is a building-block approach,[2] and much effort has been made towards the connection of suitable, predetermined building blocks into networks in order to obtain the desired materials. In this regard, the development of new multitopic building blocks is one of the central tasks. Recently, we have been investigating a few in situ metal/organic reactions such as ligand oxidative coupling, hydrolysis, and substitution by hydrothermal methods,[3] which provide an intriguing pathway for generating new, functional building blocks and coordination polymers. In particular, we have isolated and structurally characterized covalent hydrates of N-heterocyclic ligands in delocalized mixed-valence Cu^{I}–Cu^{II} complexes, which are not only an important bridge between coordination chemistry and organic heterocyclic chemistry, but can also be successfully applied to the assembly of functional molecular solids.[3a,b] Following our recent report on the in situ metal/ligand redox reaction, in this communication we report a new Cu^{2+}-mediated dehydrogenative coupling and hydroxylation of an N-heterocyclic ligand (chtpy) in four Cu^{I} coordination



chtpy

polymers, namely $[Cu_2(chtpy)_3](NO_3)_2$ (**1**), $[Cu_2(chtpy)_2]Cl(NO_3)\cdot{}^4/_3\,C_6H_6$ (**2**), $[Cu_2Cl_2(chtpy)]$ (**3**), and $[Cu_2Cl(chtpy)](NO_3)$ (**4**; chtpy = *a*,*a*-1,4-dihydroxy-*e*,*e*,*e*,*e*-1,2,4,5-tetra(4-pyridyl)cyclohexane). This is the first time that simultaneous dehydrogenative coupling and hydroxylation of an N-heterocyclic ligand has been observed to generate a new, potentially tetratopic, coplanar ligand in situ.

Pale-yellow or reddish crystals of **1**–**4** (ca. 18–35 % yield) were obtained from the in situ hydrothermal treatment of $Cu(OH)_2$ (freshly synthesized from $Cu(NO_3)_2\cdot 3H_2O$ and NaOH) with 1,3-bis(4-pyridyl)propane (bpp), 1,4-cyclohexanedicarboxylic acid, and water in dilute HCl at 175–190 °C [Equation (1)]. The component diversification of the result-



(1)

ing Cu^{I}–chtpy nets can be controlled simply by tuning the molar ratio of the starting materials. Elemental analysis and PXRD (Figure S1 in the Supporting Information) confirmed the phase purity of the bulk materials. Compounds **1**–**4** are air-stable and insoluble in water and most organic solvents.

One of the most intriguing features regarding the synthesis is the direct observation of dehydrogenative coupling and hydroxylation of 1,3-bis(4-pyridyl)propane mediated by Cu^{2+}. It has been reported previously that dehydrogenative coupling of phenanthroline and 2,2′-bipyridine under hydrothermal conditions leads to two functional tetradentate ligands—biphenanthroline and quaterpyridine, respectively—that are difficult to obtain by common organic reactions.[4] Moreover, hydroxylation of N-heterocyclic ligands such as phenanthroline and 2,2′-bipyridine is now well understood and can be easily carried out under hydrothermal conditions.[3a,b] However, to the best of our knowl-

[*] S. Hu, J.-C. Chen, Prof. Dr. M.-L. Tong, Dr. B. Wang, Dr. Y.-X. Yan
School of Chemistry and Chemical Engineering
Institute of Optoelectronic and Functional Composite Materials and State Key Laboratory of Optoelectronic Materials and Technologies
Sun Yat-Sen University
Guangzhou 510275 (China)
Fax: (+86) 20-84112245
E-mail: cestml@zsu.edu.cn
Dr. S. R. Batten
School of Chemistry
Monash University
Victoria 3800 (Australia)

[**] We gratefully acknowledge the NSFC (grant nos. 20471069 and 20131020), the FANEDD and NCET of MOE, China, the NSF of Guangdong Province (04205405), and the Research Fund of Sun Yat-Sen University for financial support.

Supporting information for this article is available on the WWW under http://www.angewandte.org or from the author.

© 2005 Wiley-VCH Verlag GmbH & Co. KGaA, Weinheim

edge, the simultaneous dehydrogenative coupling and hydroxylation of an N-heterocyclic ligand is unprecedented.[5] The cyclohexane analogue having both hydroxyl and pyridyl substituent groups that is generated in situ may act as an important organic intermediate. Other interesting cases concerning tetradentate ligands generated in situ have been found in the reaction of silver(I) with 1,2-di(4-pyridyl)ethene,[6a] a template-directed solid-state [2+2] photodimerization of 4-chlororesorcinol with *trans*-1-(2-pyridyl)-2-(4-pyridyl)-ethylene,[6b] and the hydrothermal reaction of $Cd_{10}S_4(SPh)_{12}$ with 4,4′-trimethylenedipyridine and Na_2SO_4.[6c]

An X-ray crystallographic study[7] revealed unequivocally that a six-membered ring is formed by C–C coupling between four of the carbon atoms of each pair of bpp ligands in **1**–**4**. The six C–C bond distances of the ring fall in the range 1.503(8)–1.562(8) Å for **1**, 1.542(7)–1.552(5) Å for **2**, 1.491(9)–1.517(10) Å for **3**, and 1.536(3)–1.553(6) Å for **4**, characteristic of C–C single bonds.[8] Moreover, two hydroxy groups are also formed at the carbon atoms linking the pyridyl groups, with C–O bond lengths of 1.441(9)–1.458(8) Å for **1**, 1.437(11) Å for **2**, 1.466(10)–1.451(10) Å for **3**, and 1.423(4) Å for **4**, which are typical of a C–O single bond. Each cyclohexyl ring of the chtpy ligands in **1**–**4** adopts a chair conformation, with the four pyridyl groups located at the equatorial positions and the two hydroxy groups at the axial positions.

The structure of $[Cu_2(chtpy)_3](NO_3)_2$ (**1**) contains one crystallographically unique tetrahedral Cu^I atom, which lies on a general position, three unique L ligands, all of which lie across inversion centers, and one unique, uncoordinated nitrate counteranion. Two of the unique L ligands act as bidentate bridges between the copper atoms (Cu–N = 2.037(4) and 2.077(5) Å) by coordinating through their pyridyl groups *trans* to each other across the central six-membered ring; the other pyridyl groups are not coordinated. The third type of ligand acts as a tetradentate bridge (Cu–N = 2.050(5) and 2.054(4) Å) and coordinates through all four pyridyl groups (Figure 1a).

The ligands bridge the copper atoms to form three identical, interpenetrating 3D networks. The network topology can be simplified by considering just the tetrahedral copper atoms and the tetradentate ligands (represented by a square-planar node); the bidentate ligands can be represented simply as links between the copper nodes. The resulting net is shown in Figure 1b, and has the moganite topology,[9] which is a rare four-connected net with tetrahedral and square-planar nodes in the ratio 2:1. A topological analysis of this net was performed with OLEX.[10] The long topological (O'Keeffe) vertex symbol is $4.8_6.6.6.6.6$ for the Cu node, and $4.4.6_2.6_2.8_2.8_2$ for the chtpy node, which gives the short vertex symbol $(4^2.6^2.8^2)(4.6^4.8)_2$. The three interpenetrating networks are shown in Figure 1c. We are aware of only three examples of coordination polymers with this topology: the structures of $Cd(CN)_2(H_2O)_{2/3}\cdot t$BuOH and $[Cu_3(pytac)_6]\cdot 14H_2O$ (pytac = 2-(4-pyridyl)thiazole-4-carboxylate) contain a single moganite network,[11a,b] while the structure of $[Cu_2(TCNB)_3](PF_6)_2$ (TCNB = 1,2,4,5-tetracyanobenzene) contains two interpenetrating moganite nets.[11c] This structure is particularly relevant as, like the structure of **1**, it contains tetrahedral Cu^I atoms bridged by potential tetradentate ligands, only one-third of which are actually tetradentate and act as square-planar nodes, while the other two-thirds are simply bidentate.

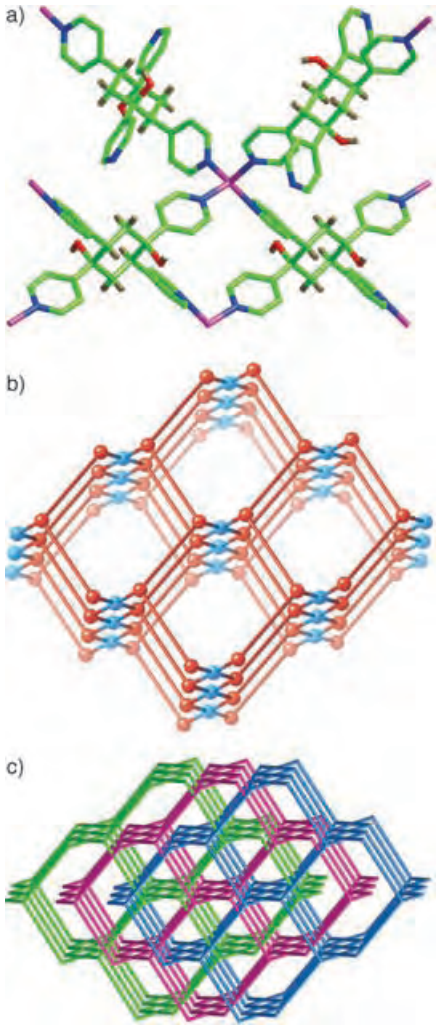


Figure 1. a) Local geometry in the structure of **1**. Each Cu^I center bonds to two crystallographically distinct bidentate ligands (top) and two symmetry-related tetradentate ligands (bottom). For clarity, pyridyl hydrogen atoms and nitrate counterions are not shown; pink Cu, blue N, red O, green C, gray H. b) The moganite topology of the 3D, four-connected nets in the structure of **1**. The red spheres represent copper atoms, while the blue spheres represent the tetradentate ligands. The bidentate ligands are represented by Cu···Cu links. c) The three interpenetrating moganite nets in the structure of **1**.

The nitrate anions, although uncoordinated, actually link the three interpenetrating networks together by hydrogen-bonding interactions between one of their oxygen atoms (O5) and the three different types of ligand hydroxide groups—one from each net for each nitrate anion ((O)H···O5 = 1.635(4), 1.871(5), and 1.865(6) Å, respectively). One of the hydroxide groups in fact participates in a bifurcated hydrogen bond and interacts with a second oxygen on the same nitrate anion ((O3)H3A···O6 = 2.140(5) Å).

The structure of **2** reveals an interesting porous 3D framework with the asymmetric unit consisting of one crystallographically unique tetrahedral Cu^I atom, which lies

 © 2005 Wiley-VCH Verlag GmbH & Co. KGaA, Weinheim

on a special position, one-quarter of a chtpy ligand with the hydroxy groups showing twofold disorder, one-sixth of a benzene guest molecule, and disordered uncoordinated nitrate and Cl^- counteranions, each with one-eighth occupancy. Each chtpy ligand acts as a tetradentate bridge (Cu–N = 2.025(3) Å) and coordinates through all four pyridyl groups (Figure 2a).

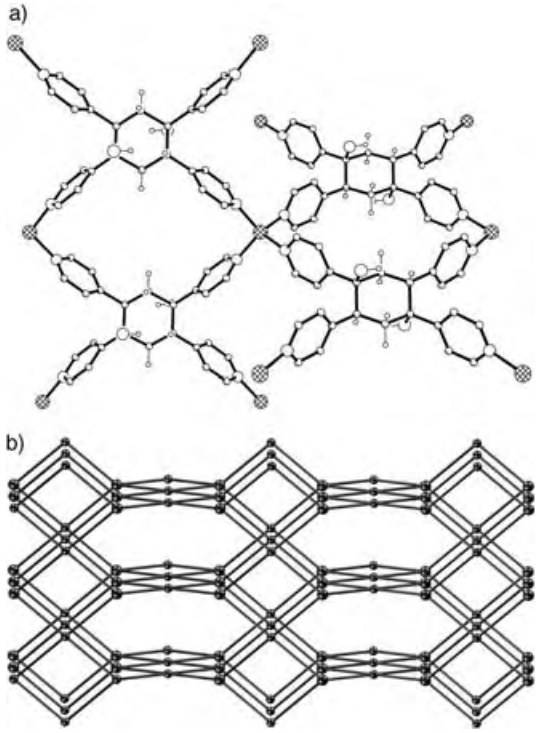


Figure 2. a) Local geometry in the structure of **2**. For clarity, pyridyl hydrogen atoms and counterions are not shown. b) The PtS topology of the 3D, four-connected, noninterpenetrating net in the structure of **2**.

The planar tetratopic chtpy ligands bridge the copper atoms into a noninterpenetrating 3D network. By considering just the copper atoms and the tetradentate ligands as tetrahedral and square-planar nodes, respectively, **2** can be defined as a rare four-connected net with tetrahedral and square-planar nodes in the ratio 1:1. The long topological (O'Keeffe) vertex symbol is $4.4.8_7.8_7.8_7.8_7$ for the Cu node and $4.4.8_2.8_2.8_8.8_8$ for the chtpy node, thus giving a short vertex symbol $4^2.8^4$, which is that of the PtS topology,[9] as shown in Figure 2b. It is worth noting that there are 3D channels running along the *a*-, *b*-, and *c*-axes in the cationic net structure of **2**, as shown in Figure 2b. An analysis using PLATON[12] suggested that the channels occupy 58.2% of the crystal volume. The guest benzene molecules and disordered NO_3^- and Cl^- counteranions are located within these channels. The calculated crystal density (in the presence of guest and the disordered counterions) of 0.914 g cm^{-3} is comparable to those found for some porous metal–polycarboxylate coordination materials.[1c]

Compound **3** consists of 2D coordination polymer sheets with the asymmetric unit containing one crystallographically unique Cu^I atom, which lies on a general position, one unique chtpy ligand, which lies across an inversion center, and one unique Cl^- counteranion. Each Cu atom is coordinated in a trigonal geometry by two pyridyl N atoms and one Cl atom (Cu–N = 1.978(5) and 1.993(5) Å; Cu–Cl = 2.167(2) Å; N–Cu–N/Cl = 113.9(2)–125.30(16)°). Each chtpy ligand acts as a tetradentate bridge to connect the CuCl motifs into a 2D (4,4) net (Figure 3). Adjacent (4,4) nets are each twofold interpenetrating in a diagonal/diagonal inclined fashion.[13]

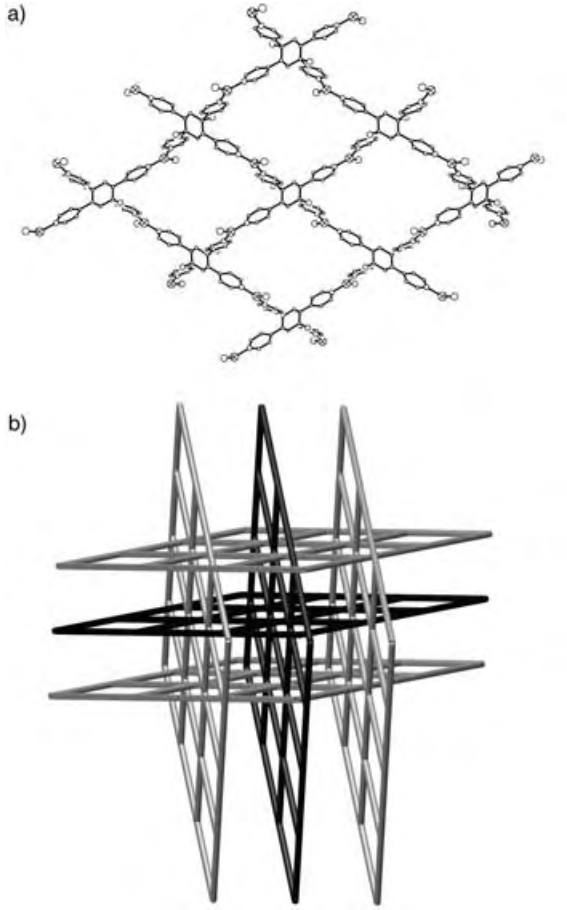


Figure 3. a) The 2D (4,4) coordination layer in the structure of **3**. b) The twofold interpenetrating 2D (4,4) nets in the structure of **3**.

Compound **4** is a 3D coordination network with the asymmetric unit consisting of one crystallographically unique tetrahedral Cu^I atom, which lies on a special position, one unique chtpy ligand, which lies across a fourfold axis, and one unique Cl^- atom and an uncoordinated nitrate, both of which lie on special positions. Similar to those in **3**, each Cu atom is coordinated in a Y-shaped geometry by two pyridyl N atoms and one Cl atom (Cu–N = 1.917(2) Å; Cu–Cl = 2.4802(7) Å; N–Cu–N/Cl = 101.99(8) and 156.01(17)°). Each chtpy ligand acts as a tetradentate bridge to connect the CuCl motifs into a 2D coordination layer of a (4,4) net (Figure 4a). The most interesting structural feature is that adjacent (4,4) nets are covalently connected by sharing the linear μ_2-Cl bridges, thereby generating two identical, interpenetrating 3D networks. The network topology can be simplified by considering

 © 2005 Wiley-VCH Verlag GmbH & Co. KGaA, Weinheim

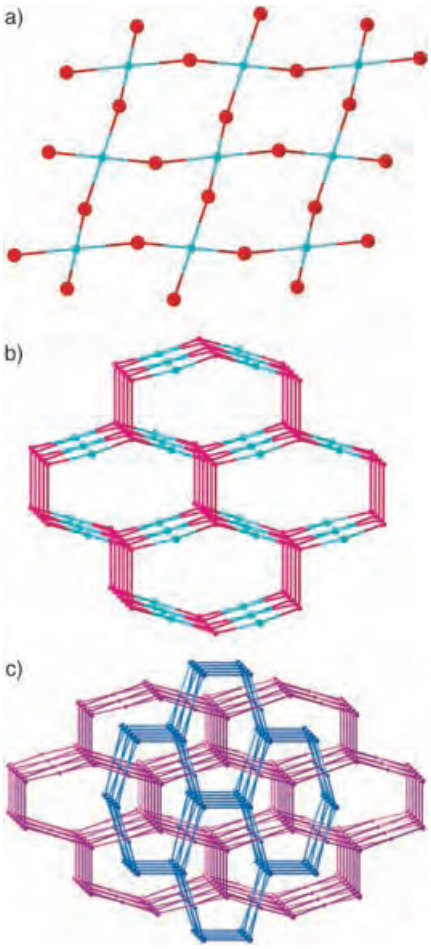


Figure 4. a) The 2D (4,4) coordination subnet motif in the structure of **4**; red Cu, cyan ligand. b) The 3D (3,4)-connected topological net constructed from the 2D (4,4) subnets. c) The two interpenetrating nets in the structure of **4**.

just the three-connected copper atoms and the tetradentate ligands as trigonal nodes and square-planar nodes; the bidentate μ_2-Cl bridges can be represented simply as links between the copper nodes. The resulting net is shown in Figure 4b, and is a rare (3,4)-connected net[14] with trigonal and square-planar nodes in the ratio 2:1. The long topological (O'Keeffe) vertex symbol is $6.6.8_2$ for the Cu node, and $6.6.8.8.10_2.10_2$ for the chtpy node, which gives the short vertex symbol $(6^2.8^2.10^2)(6^2.8)_2$. The twofold interpenetrating networks are shown in Figure 4c.

In order to obtain the newly generated multitopic building block, which will be of further use for the assembly of functional molecular solids, we separated the chtpy ligand from the metal center by treating **1** with $Na_2(H_2edta)$. An X-ray crystallographic study[7] clearly showed that the free chtpy molecule also adopts a chair conformation, with the four pyridyl groups located at the equatorial positions and the two hydroxy groups at the axial positions. Each unique chtpy molecule lies across a twofold axis (Figure 5). The six C–C bond distances of the cyclohexyl ring fall in the range 1.536(4)–1.543(4) Å, in agreement with those found in **1**–**4**

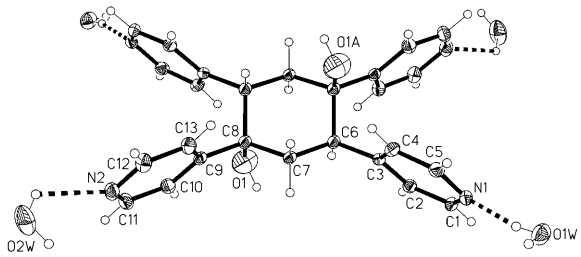


Figure 5. Crystal structure of chtpy·4 H_2O.

and characteristic of C–C single bonds.[8] The C–O bond length of 1.440(6) Å is indicative of a single-bond character.

In summary, we have prepared and characterized four new examples of copper(I) coordination networks with a new planar tetratopic ligand generated in situ and isolated this tetratopic ligand.[15] Extension of this functional, four-connected ligand to other metal salts and a further systematic investigation of their network connectivity and function is in progress.

Experimental Section

1: A mixture of $Cu(NO_3)_2{\cdot}3H_2O$ (0.061 g, 0.25 mmol), NaOH (0.02 g, 0.5 mmol), 1,4-cyclohexanedicarboxylic acid (0.086 g, 0.5 mmol), bpp (0.198 g, 1.0 mmol), and H_2O (9 mL) was placed in a Parr Teflon-lined, stainless-steel vessel and heated at 175 °C for 3 d to yield fine, pale-yellow crystals (yield ca. 25% based on Cu^{2+}). $C_{39}H_{36}CuN_7O_6$: calcd. C 61.45, H 4.76, N 12.86; found C 61.09, H 4.62 N 12.71.

2: A mixture of $Cu(NO_3)_2{\cdot}3H_2O$ (0.121 g, 0.5 mmol), NaOH (0.04 g, 1.0 mmol), 1,4-cyclohexanedicarboxylic acid (0.172 g, 1.0 mmol), bpp (0.198 g, 1.0 mmol), benzene (0.5 mmol), and H_2O (9 mL) was placed in a Parr Teflon-lined, stainless-steel vessel, acidified with HCl (0.25 mmol), then heated at 180 or 190 °C for 3 d to yield fine, pale-yellow crystals (yield 20–30%). $C_{60}H_{52}ClCu_2N_9O_7$: calcd. C 61.40, H 4.47, N 10.74; found C 61.14, H 4.36, N 10.65.

3: A mixture of $Cu(NO_3)_2{\cdot}3H_2O$ (0.484 g, 2.0 mmol), NaOH (0.08 g, 2.0 mmol), 1,4-cyclohexanedicarboxylic acid (0.172 g, 1.0 mmol), bpp (0.198 g, 1.0 mmol), and H_2O (9 mL) was placed in a Parr Teflon-lined stainless-steel vessel, acidified with HCl (0.25 mmol), then heated at 175 °C for 3 d to yield fine, primrose-yellow crystals (yield 18–22% based on bpp). $C_{26}H_{22}Cl_2Cu_2N_4O_2$: calcd. C 50.33, H 3.57, N 9.03; found C 50.10, H 3.42, N 8.95.

4: Compound **4** was prepared by a similar experimental procedure to that for **3** except for the molar ratio of HCl (0.5 mmol). Yield: 30–35% based on bpp. $C_{26}H_{22}ClCu_2N_5O_5$: calcd. C 48.26, H 3.43, N 10.82; found C 47.95, H 3.35, N 10.91.

chtpy: A solution of $Na_2(H_2edta)$ (0.149 g, 0.4 mmol) in water (10 mL) was added dropwise to a stirred suspension of **1** (0.145 g) in a mixture of dichloromethane (30 mL) and water (10 mL) at room temperature, followed by stirring for 48 h under nitrogen. The organic phase was then separated from the reaction mixture and the aqueous layers were extracted with dichloromethane (3 × 60 mL). The combined organic phase was concentrated in vacuo. The residue was dissolved in dichloromethane, purified by column chromatography, and dried with anhydrous Na_2SO_4 to give chtpy as a pale-yellow powder. Yield: 0.095 g (78%). (ESI-MS): $m/z = 425$, 213; ^{1}H NMR (300 MHz, $(CD_3)_2SO$): $\delta = 1.27$ (m, 4H, C7-H7a, C7-H7b), 2.18 (t, $J =$ 3.3 Hz, 2H, C6-H6), 7.14 (d, $J = 5.1$ Hz, 4H, C2-H2, C4-H4), 7.54 (d, $J = 5.4$ Hz, 4H, C10-H10, C13-H13), 8.56 ppm (d, $J = 3.6$ Hz, 8H, C1-H1, C5-H5, C11-H11, C12-H12); ^{13}C NMR (75 MHz, $(CD_3)_2SO$): $\delta =$ 30.9 (C-7), 34.6 (C-6), 79.9 (C-8), 121.9 (C-9), 124.5 (C-2), 150.1 (C-1), 151.1 ppm (C-3). $C_{26}H_{24}N_4O_2$: calcd. C 73.57, H 5.70, N 13.20; found C

 © 2005 Wiley-VCH Verlag GmbH & Co. KGaA, Weinheim

73.26, H 5.62, N 13.09. IR (KBr disk): $\tilde{\nu}=3228$ (m, OH), 1596, 1545 cm^{-1} (s, py). Colorless crystals of chtpy·4 H_2O were obtained by dissolution of the powder in acetonitrile at ambient temperature in air. $C_{26}H_{24}N_4O_2\cdot 4H_2O$: calcd. C 62.89, H 6.50, N 11.28; found C 62.71, H 6.62, N 11.03.

Received: May 20, 2005
Published online: July 29, 2005

Keywords: copper · hydrothermal synthesis · N ligands · organic–inorganic hybrid composites · topochemistry

[1] a) S. Kitagawa, R. Kitaura, S.-i. Noro, *Angew. Chem.* **2004**, *116*, 2388–2430; *Angew. Chem. Int. Ed.* **2004**, *43*, 2334–2375; b) C. N. R. Rao, S. Natarajan, R. Vaidhyanathan, *Angew. Chem.* **2004**, *116*, 1490–1521; *Angew. Chem. Int. Ed.* **2004**, *43*, 1466–1496; c) O. M. Yaghi, M. O'Keeffe, N. W. Ockwig, H. K. Chae, M. Eddaoudi, J. Kim, *Nature* **2003**, *423*, 705; d) C. Janiak, *Dalton Trans.* **2003**, 2781–2804; e) S.-L. Zheng, M.-L. Tong, X.-M. Chen, *Coord. Chem. Rev.* **2003**, *246*, 185–202; f) S. R. Batten, K. S. Murray, *Coord. Chem. Rev.* **2003**, *246*, 103–130; g) L. Carlucci, G. Ciani, D. M. Proserpio, *Coord. Chem. Rev.* **2003**, *246*, 247–289; h) J. Y. Lu, *Coord. Chem. Rev.* **2003**, *246*, 327–347; i) O. R. Evans, W. Lin, *Acc. Chem. Res.* **2002**, *35*, 511–522; j) B. Moulton, M. J. Zaworotko, *Chem. Rev.* **2001**, *101*, 1629–1658; k) S. Feng, R. Xu, *Acc. Chem. Res.* **2001**, *34*, 239–247; l) S. R. Batten, R. Robson, *Angew. Chem.* **1998**, *110*, 1558–1595; *Angew. Chem. Int. Ed.* **1998**, *37*, 1460–1494.

[2] a) B. F. Hoskins, R. Robson, *J. Am. Chem. Soc.* **1990**, *112*, 1546–1554; b) M. Eddaoudi, D. B. Moler, H. Li, B. Chen, T. M. Reineke, M. O'Keeffe, O. M. Yaghi, *Acc. Chem. Res.* **2001**, *34*, 319–330.

[3] a) X.-M. Zhang, M.-L. Tong, X.-M. Chen, *Angew. Chem.* **2002**, *114*, 1071–1073; *Angew. Chem. Int. Ed.* **2002**, *41*, 1029–1031; b) X.-M. Zhang, M.-L. Tong, M.-L. Gong, H.-K. Lee, L. Luo, K.-F. Li, Y.-X. Tong, X.-M. Chen, *Chem. Eur. J.* **2002**, *8*, 3187–3194; c) M.-L. Tong, L.-J. Li, K. Mochizuki, H.-C. Chang, X.-M. Chen, Y. Li, S. Kitagawa, *Chem. Commun.* **2003**, 428–429; d) J. Tao, Y. Zhang, M.-L. Tong, X.-M. Chen, T. Yuen, C.-L. Lin, X.-Y. Huang, J. Li, *Chem. Commun.* **2002**, 1342–1343; e) Y.-Z. Zheng, M.-L. Tong, X.-M. Chen, *New J. Chem.* **2004**, *28*, 1412–1415; f) S. M.-F. Lo, S. S.-Y. Chui, L.-Y. Shek, Z. Lin, X. X. Zhang, G.-H. Wen, I. D. Williams, *J. Am. Chem. Soc.* **2000**, *122*, 6293–6294; g) J. Y. Lu, B. R. Cabrera, R.-J. Wang, J. Li, *Inorg. Chem.* **1999**, *38*, 4608–4611.

[4] a) C.-M. Liu, S. Gao, H.-Z. Kou, *Chem. Commun.* **2001**, 1670–1671; b) D. Xiao, Y. Hou, E. Wang, J. Lu, Y. Li, L. Xu, C. Hu, *Inorg. Chem. Commun.* **2004**, *7*, 437–439.

[5] E. C. Constable, *Metals and Ligand Reactivity*, VCH, Weinheim, **1996**.

[6] a) A. J. Blake, N. R. Champness, S. S. M. Chung, W.-S. Li, M. Schröder, *Chem. Commun.* **1997**, 1675–1676; b) G. S. Papaefstathiou, L. R. MacGillivray, *Angew. Chem.* **2002**, *114*, 2174–2177; *Angew. Chem. Int. Ed.* **2002**, *41*, 2070–2073; c) N. Zheng, X. Bu, P. Feng, *J. Am. Chem. Soc.* **2002**, *124*, 9688–9689.

[7] Crystal data for **1**: $C_{39}H_{36}CuN_7O_6$, $M_r=762.29$, triclinic, space group $P\bar{1}$ (no. 2), $a=11.774(1)$, $b=13.475(1)$, $c=14.152(1)$ Å, $\alpha=97.358(2)$, $\beta=112.110(2)$, $\gamma=113.436(2)°$, $V=1803.8(2)$ Å^3, $Z=2$, $T=293(2)$ K, $F(000)=792$, $\rho_{calcd}=1.402$ g cm^{-3}, $\mu(Mo\,K_\alpha)=0.663$ mm^{-1} ($\lambda=0.71073$ Å); $R_1=0.0924$, $wR_2=0.2523$, and GOF = 1.040 for 478 parameters, 4724 reflections with $|F_o|\geq 4\sigma(F_o)$. Crystal data for **2**: $C_{30}H_{26}Cl_{0.5}CuN_{4.5}O_{3.5}$, $M=586.82$, orthorhombic, space group *Cccm* (no. 66), $a=11.399(2)$, $b=15.971(2)$, $c=23.417(3)$ Å, $V=4263.1(10)$ Å^3, $Z=4$, $T=123(2)$ K, $F(000)=1212$, $\rho_{calcd}=0.914$ g cm^{-3}, $\mu(Mo\,K_\alpha)=0.571$ mm^{-1} ($\lambda=0.71073$ Å); $R_1=0.1431$, $wR_2=0.3930$, and GOF = 1.736 for 120 parameters, 1470 reflections with $|F_o|\geq 4\sigma(F_o)$. Crystal data for **3**: $C_{26}H_{22}Cl_2Cu_2N_4O_2$, $M=620.46$, orthorhombic, space group *Pbcn* (no. 60), $a=11.489(1)$, $b=11.253(1)$, $c=19.881(2)$ Å, $V=2570.3(5)$ Å^3, $Z=4$, $T=293(2)$ K, $F(000)=1256$, $\rho_{calcd}=1.603$ g cm^{-3}, $\mu(Mo\,K_\alpha)=1.894$ mm^{-1} ($\lambda=0.71073$ Å); $R_1=0.0718$, $wR_2=0.2119$, and GOF = 1.088 for 172 parameters, 1315 reflections with $|F_o|\geq 4\sigma(F_o)$. Crystal data for **4**: $C_{26}H_{22}ClCu_2N_5O_5$, $M=647.02$, tetragonal, space group $P4_2/mbc$ (no. 135), $a=10.010(1)$, $c=26.540(2)$ Å, $V=2659.3(3)$ Å^3, $Z=4$, $T=293(2)$ K, $F(000)=1312$, $\rho_{calcd}=1.616$ g cm^{-3}, $\mu(Mo\,K_\alpha)=1.747$ mm^{-1} ($\lambda=0.71073$ Å); $R_1=0.0468$, $wR_2=0.1390$, and GOF = 1.104 for 103 parameters, 1383 reflections with $|F_o|\geq 4\sigma(F_o)$. Crystal data for chtpy·4 H_2O: $C_{26}H_{32}N_4O_6$, $M=496.56$, monoclinic, space group *C*2/*c* (no. 15), $a=15.5954(13)$, $b=11.3662(9)$, $c=14.0070(11)$ Å, $\beta=91.097(2)°$, $V=2482.4(3)$ Å^3, $Z=4$, $T=123(2)$ K, $F(000)=1056$, $\rho_{calcd}=1.329$ g cm^{-3}, $\mu(Mo\,K_\alpha)=0.095$ mm^{-1} ($\lambda=0.71073$ Å); $R_1=0.0965$, $wR_2=0.2794$, and GOF = 1.098 for 179 parameters, 2152 reflections with $|F_o|\geq 4\sigma(F_o)$. CCDC-261921 (**1**), -261922 (**2**), -261923 (**3**), -261925 (**4**), and -271176 (chtpy·4 H_2O) contain the supplementary crystallographic data for this paper. These data can be obtained free of charge from The Cambridge Crystallographic Data Center via www.ccdc.cam.ac.uk/data_request/cif.

[8] F. H. Allen, O. Kennard, D. G. Watson, L. Brammer, A. G. Orpen, R. Taylor, *J. Chem. Soc. Perkin Trans. 2* **1987**, S1–S19.

[9] a) M. O'Keeffe, M. Eddaoudi, H. Li, T. Reinke, O. M. Yaghi, *J. Solid State Chem.* **2000**, *152*, 3–20; b) O. Delgado-Friedrichs, M. O'Keeffe, O. M. Yaghi, *Solid State Sci.* **2003**, *5*, 73–78; c) O. Delgado-Friedrichs, M. O'Keeffe, *Acta Crystallogr. Sect. A* **2003**, *59*, 351–360; d) N. W. Ockwig, O. Delgado-Friedrichs, M. O'Keeffe, O. M. Yaghi, *Acc. Chem. Res.* **2005**, *38*, 176–182.

[10] O. V. Dolomanov, A. J. Blake, N. R. Champness, M. Schröder, *J. Appl. Crystallogr.* **2003**, *36*, 1283–1284.

[11] a) B. F. Abrahams, B. F. Hoskins, Y.-H. Lam, R. Robson, F. Separovic, P. Woodberry, *J. Solid State Chem.* **2001**, *156*, 51–56; b) C.-Y. Su, M. D. Smith, A. M. Goforth, H.-C. zur Loye, *Inorg. Chem.* **2004**, *43*, 6881–6883; c) M. Munakata, G. L. Ning, T. Kuroda-Sowa, M. Maekawa, Y. Suenaga, T. Horino, *Inorg. Chem.* **1998**, *37*, 5651–5656.

[12] A. L. Spek, *PLATON, A Multipurpose Crystallographic Tool*, Utrecht University, Utrecht, The Netherlands, **2003**.

[13] a) S. R. Batten, *CrystEngComm* **2001**, *3*, 1–7; b) M. J. Zaworotko, *Chem. Commun.* **2001**, 1–10.

[14] V. A. Blatov, L. Carlucci, G. Ciani, D. M. Proserpio, *CrystEngComm* **2004**, *6*, 377–395.

[15] By using $(NH_4)_2S$ as the precipitator, another new tetratopic ligand (1,2,4,5-tetra(4-pyridyl)benzene; phtpy) derived from chtpy was isolated by removal of the Cu^+ ions from complexes **1**–**4** at 60 °C in air. Crystal data for phtpy·2 H_2O: $C_{26}H_{22}N_4O_2$, monoclinic, space group *C*2/*c*, $M_r=422.48$, $a=16.344(6)$, $b=13.697(5)$, $c=9.748(3)$ Å, $\beta=97.171(6)°$, $V=2165.2(13)$ Å^3, $Z=4$. $R_1=0.0644$, $wR_2=0.1813$, and GOF = 1.071 for 151 parameters, 1669 reflections with $|F_o|\geq 4\sigma(F_o)$. This compound will be reported in a subsequent full paper.

 © 2005 Wiley-VCH Verlag GmbH & Co. KGaA, Weinheim

Biomineralization

DOI: 10.1002/anie.200500261

Mimicking the Function of Eggshell Matrix Proteins: The Role of Multiplets of Charged Amino Acid Residues and Self-Assembly of Peptides in Biomineralization**

*Parayil Kumaran Ajikumar, Subramanian Vivekanandan, Rajamani Lakshminarayanan, Seetharama D. S. Jois, R. Manjunatha Kini, and Suresh Valiyaveettil**

The molecular-level understanding and rationalization of nature's clues on how to produce complex, organized structures such as bone, teeth, and seashells at ambient temperature and in aqueous environments has resulted in the design and synthesis of novel materials.[1,2] The properties of the crystals such as size, shape, stability, polymorph selectivity, and crystallographic orientation are controlled by biomacromolecules, which are classified as "framework macromolecules" and "control macromolecules".[2,3] The complexities of the natural biomineralization process have resulted in research efforts being focused on "tailor-made" low-molecular-weight compounds and macromolecular additives for structure–function investigations by in vitro mineralization experiments.[4] So far, research efforts have been focused on auxiliary oligopeptides to probe the role of functional motifs in the kinetics, habit modifications, and polymorph selectivity during the crystal growth process.[5,6]

The structure–function sequence analysis of eggshell-specific proteins revealed that the presence of multiplets of charged amino acid residues and characteristic self-aggregation in solution influence the formation of biominerals.[7,8] We anticipate that the design and testing of peptides with multiplets of charged residues could mimic the functions of such proteins during in vitro experiments.[6c] Thus, to investigate the role of self-assembly and multiplets of charged amino acids in calcium carbonate mineralization, we designed a series of peptides (Table 1) and studied their structure–activity relationships. The first two groups (I, II) of peptides have an ordered arrangement of doublets of charged residues which resembles the primary structure of avian eggshell matrix proteins (a full sequence comparison is given in the Supporting Information).[7] The significant structural differences between the peptides involve replacing the arginine residue with lysine—a basic flexible residue with a primary amino group and hydrophobic side chain—and the incorporation of a proline residue in the middle of the peptides in group II. The proline residue is expected to limit the conformational flexibility,[6c] and organisms use such domains to form three-dimensional supramolecular structures of proteins.[2a,8,9] Among the three peptides in group III, $K_2E_2W_2D_2G$-17 and $K_2AE_2AW_2AD_2P$-23 have an ordered arrangement of doublets of charged residues. However, the incorporation of one glycine residue in the former and six alanine residues in the latter peptide is expected to disrupt the ordered, stable secondary structure of the peptides and impart flexibility to the peptide backbone. The peptide $(KE)_2(WD)_2$-16, with alternate acidic and basic residues, is designed as a control peptide for confirming the perceived critical role of multiplets of charged residues.

To understand the role of these designed peptides in calcite growth and habit modification, we carried out in vitro mineralization of calcium carbonate by slow diffusion of CO_2 and NH_3 gas to the peptide dissolved in $CaCl_2$ solution (7.5 mM).[10] The first two groups of peptides showed significant influence on the calcite crystal morphology and aggregation as compared with the group III peptides (compare images 2–5 with images 6–8 in Figure 1 and Supporting Information).

The $CaCO_3$ crystals formed in presence of group I and II peptides showed—similarly to those formed in the presence of ansocalcin[8]—concentration-dependent changes in crystal morphology (Figure 1 and Supporting Information). Polycrystalline aggregates of calcite crystals were formed as the concentration was increased to 2 mg mL^{-1}, and the size of the crystal aggregates obtained with $K_2E_2W_2D_2$-16 ($\approx$41 μm) and $K_2E_2W_2D_2P$-17 ($\approx$35 μm) was almost double that of crystals obtained with $R_2E_2W_2D_2$-16 ($\approx$20 μm) and $R_2E_2W_2D_2P$-17 ($\approx$21 μm). The observed superstructures are composed of smaller rudimentary calcite crystals assembled into spherical structures. The crystal lattice was further characterized by X-ray diffraction studies. In addition, the nucleation density (that is, the number of crystals per unit area) also increased with an increase in the peptide concentration. Group III peptides did not show significant influence on the calcite crystal nucleation, growth, or morphology. This finding indicates that not only the primary structural characteristics but also control of the spatial disposition of the functional sites on the peptide is important for the nucleation of crystal aggregates. Thus, the designed peptides $R_2E_2W_2D_2$-16, $R_2E_2W_2D_2P$-17, $K_2E_2W_2D_2$-16, and $K_2E_2W_2D_2P$-17 (2 mg mL^{-1}, $\approx$0.8 μM) induce the nucleation and formation

[*] Dr. P. K. Ajikumar, Dr. R. Lakshminarayanan, Prof. S. Valiyaveettil
Department of Chemistry and Singapore–MIT Alliance
National University of Singapore
3 Science Drive 3, Singapore 117543 (Singapore)
Fax: (+65) 6779-1669
E-mail: chmsv@nus.edu.sg
Dr. S. D. S. Jois
Department of Pharmacy
National University of Singapore
Singapore 117543 (Singapore)
Dr. S. Vivekanandan, Prof. R. M. Kini
Department of Biological Sciences
National University of Singapore
Singapore 117543 (Singapore)

[**] This work was supported by the Singapore–MIT Alliance. R.L. acknowledges Singapore Millennium Foundation for the award of a fellowship. The authors acknowledge technical support from the Departments of Chemistry, Biological Sciences, and Materials Sciences at National University of Singapore.

Supporting information for this article is available on the WWW under http://www.angewandte.org or from the author.

InterScience © 2005 Wiley-VCH Verlag GmbH & Co. KGaA, Weinheim

Table 1: Details of the amino acid sequences and structure–activity relationships of the model peptides.

Group	Model peptide	Primary structure	Results	
			Secondary structure	Activity in crystal growth
I	$R_2E_2W_2D_2$-16 (**I**)	RREEWWDDRREEWWDD	β sheet	polycrystalline calcite aggregate formation
	$K_2E_2W_2D_2$-16 (**III**)	KKEEWWDDKKEEWWDD	β sheet	
II	$R_2E_2W_2D_2$P-17 (**II**)	RREEWWDDPRREEWWDD	β sheet with turn	
	$K_2E_2W_2D_2$P-17 (**IV**)	KKEEWWDDPKKEEWWDD	β sheet with turn	
III	$K_2E_2W_2D_2$G-17 (**V**)	KKEEWWDDGKKEEWWDD	unordered	no influence on calcite growth or habit modification
	$K_2AE_2AW_2AD_2$P-23 (**VI**)	KKAEEAWWADDPKKAEEAWWADD		
	$(KE)_2(WD)_2$-16 (**VII**)	KEKEWDWDKEKEWDWD		

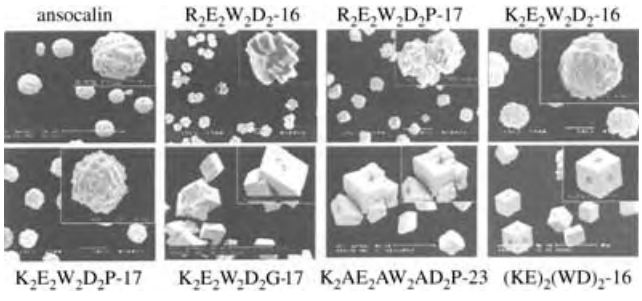


Figure 1. Crystal habit modification in the presence of the protein ansocalcin (500 μg mL^{-1}) and designed peptides (2 mg mL^{-1}). The scale bars represent 50 μm. Magnified images are given in the insets.

of polycrystalline calcite crystal aggregates similar to the parent protein ansocalcin.

For a detailed investigation of the structure–activity relationship, we investigated the self-assembly of the peptides in solution by dynamic light scattering (DLS), tryptophan fluorescence, circular dichroism (CD), NMR spectroscopy, and molecular modeling studies. The DLS and fluorescence analysis showed a concentration-dependent aggregation of group I and II peptides in $CaCl_2$ solution (Figure 2). The observed hydrodynamic radii of the group I peptides ($\langle R_H \rangle =$ 3.3 and 4.1 nm) are smaller than those of the corresponding proline-incorporated group II peptides ($\langle R_H \rangle = 6.4$ and 8.1 nm). However, a fourfold reduction in the size of the aggregate was observed when proline in $K_2E_2W_2D_2$P-17 (**IV**, 8.1 nm) was replaced with glycine in $K_2E_2W_2D_2$G-17 (**V**, 2.2 nm). These results highlight the expected role of proline toward decreasing the conformational flexibility and enhancing the oligomerization of peptides into large aggregates. The observed particle sizes for the group III peptides K_2AE_2-AW_2AD_2P-23 (**VI**, 2.2 nm) and $(KE)_2(WD)_2$-16 (**VII**, 1.8 nm) were low. Interestingly, alterations of the peptide sequences result in the enhancement of the mean diffusion coefficient ($\langle D \rangle$, Figure 2). In addition, the observed mean diffusion coefficient for the group I and II peptides is almost comparable to that of monomeric forms of ansocalcin and lithostathine.[8,11]

The study of the microenvironment around the tryptophan residues gives an insight into the self-aggregation tendency of the peptides. All the peptides showed distinct emission characteristics (see Supporting Information) and changes in intensity of the emission maximum with change in peptide concentration. The lysine-incorporated peptides $K_2E_2W_2D_2$-16 and $K_2E_2W_2D_2$P-17 showed weaker emission intensities than the peptides $R_2E_2W_2D_2$-16 and $R_2E_2W_2D_2$P-17. Notably, the intensity increased linearly with concentration up to 0.25 mg mL^{-1}, followed by an approximately 85% decrease in intensity for groups I and II peptides at a concentration of 2 mg mL^{-1}. This result might be a consequence of the quenching of the tryptophan fluorescence by the polar functional groups (CO_2H), which are brought into close proximity through aggregation of the peptide molecules.[12] However, in the case of the group III peptides, the emission intensity increased linearly with concentration up to 1 mg mL^{-1} followed by a small intensity drop at 2 mg mL^{-1}.

The CD spectra of the peptides were recorded in a concentration range of 0.05 to 2 mg mL^{-1} at 25 °C in $CaCl_2$ solution (Figure 3 and Supporting Information). It is clear that the secondary structure of the peptides $R_2E_2W_2D_2$-16 and $K_2E_2W_2D_2$-16 in solution is an extended β-sheet conformation

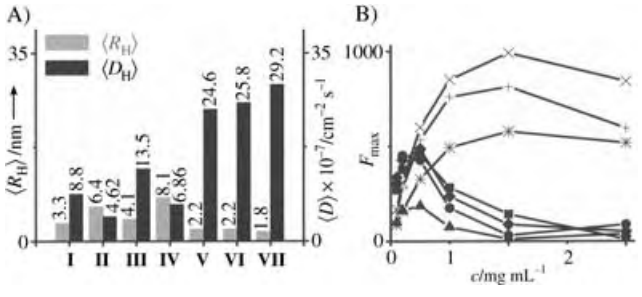


Figure 2. A) Mean hydrodynamic radius ($\langle R_H \rangle$) and diffusion coefficient ($\langle D \rangle$) of synthetic peptides **I**–**VII**. The *y* axis represents the $\langle R_H \rangle$ in nanometers or $\langle D \rangle \times 10^{-7}$ in cm^2 s^{-1}. B) Intensity (F_{max}) versus concentration profile of fluorescence emission of synthetic peptides **I** (◆), **II** (■), **III** (▲), **IV** (●), **V** (*), **VI** (+), and **VII** (×) in $CaCl_2$ solution (7.5 mM).

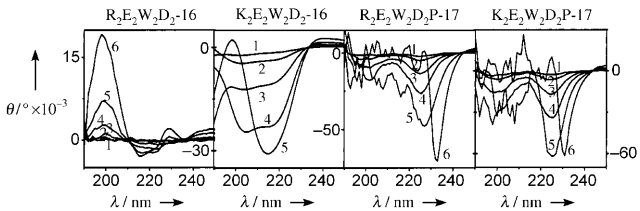


Figure 3. Circular dichroism spectra of group I and II peptides in $CaCl_2$ (7.5 mM) at various concentrations: 1) 50 μg mL^{-1}, 2) 100 μg mL^{-1}, 3) 250 μg mL^{-1}, 4) 500 μg mL^{-1}, 5) 1 mg mL^{-1}, and 6) 2 mg mL^{-1}. The instrument settings used were: scan range, 190 to 260 nm; scan rate, 50 nm min^{-1}; sensitivity, 10 millidegrees; response time, 1 s.

 © 2005 Wiley-VCH Verlag GmbH & Co. KGaA, Weinheim

at high peptide concentrations (2 mg mL^{-1}). However, the incorporation of the proline in the middle of the sequences ($R_2E_2W_2D_2$P-17 and $K_2E_2W_2D_2$P-17) disrupts the extended β-sheet structure. The CD spectra showed the appearance of an amide n–π* negative-transition band at 225 and 227 nm for the peptides, which corresponds to a β-turn conformation.[13] The replacement of proline with glycine in $K_2E_2W_2D_2$G-17 resulted in an unordered structure with turns (negative minimum at 201 and 223 nm).[14] Similarly, the CD spectra of the peptides $K_2AE_2AW_2AD_2$P-23 (negative minimum at 199 and 224 nm) and $(KE)_2(WD)_2$-16 (negative minimum at 199 nm and a weak positive maximum at 216 nm) also indicated unordered structures in solution.

The results obtained from CD spectrometry are supported by data from NMR experiments. The 1D NMR spectra of $R_2E_2W_2D_2$-16 and $K_2E_2W_2D_2$-16 showed a significant peak broadening (Figure 4A) as a result of the formation of an

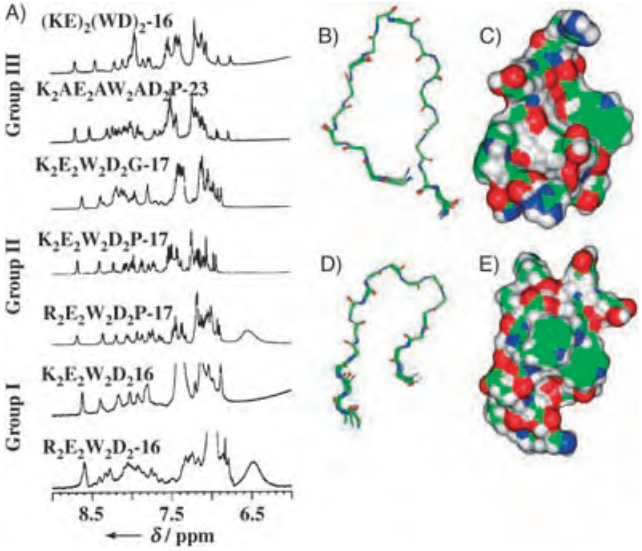


Figure 4. A) 1D pulsed-field gradient ^{1}H NMR spectra of the NH region of the model peptides; 300 K, in 90% H_2O/10% D_2O, pH 3.0. Proton chemical shifts are referenced from internal [2,2,3,3-D_4]TSP. B)–E) Conformational ensembles and surface structures obtained from molecular dynamics simulations of the peptides $R_2E_2W_2D_2$P-17 (B, C) and $K_2E_2W_2D_2$P-17 (D, E).

extended β-sheet conformation in solution. In contrast, the 1D NMR spectra of the peptides $R_2E_2W_2D_2$P-17 and $K_2E_2W_2D_2$P-17 showed sharp NH peaks within the range of $\Delta\delta = 1.3$ ppm, which indicates an ordered structure in solution. The NMR spectrum of $K_2E_2W_2D_2$G-17 showed a strong overlap of amide protons, thus indicating an unordered structure. Similarly, the peptides $(KE)_2(WD)_2$-16 and $K_2AE_2AW_2AD_2$P-23 also showed an extensive chemical shift overlap, which indicated an unordered structure in solution. The calculated proton chemical shift difference measured with TSP references (TSP = 3-(trimethylsilyl)propionate) showed deviation from the random coil values for the $R_2E_2W_2D_2$P-17 and $K_2E_2W_2D_2$P-17 peptides (see Supporting Information).[15]

The calculated δ values for residues E4-D7 and R/K10-D17 in the group II peptides are greater than random coil values by 0.1 ppm, which indicates that both peptides adopt a similar nonextended conformation with a turn structure for the backbone. The calculated ratio of $d_{\alpha N}(i,i+1)$:$d_{NN}(i,i+1)$ is greater than 1.4, which suggests an ordered peptide conformation. A long-range NOE cross-relaxation transfer ($d_{\alpha N}(i,i+2)$) was observed between the residues P9/R11 and E12/W14 for $R_2E_2W_2D_2$P-17 and D8/K10, P9/K11, and E12/W14 for $K_2E_2W_2D_2$P-17 (see Supporting Information). However, in the case of the glycine-containing peptide ($K_2E_2W_2D_2$G-17), no $d_{NN}(i,i+1)$ NOE connectivities were observed. Thus, from the above observations we conclude that the peptides $R_2E_2W_2D_2$P-17 and $K_2E_2W_2D_2$P-17 adopt a nonextended structure with a turn or kink on the backbone.

By using the available NMR restraints, the conformations of the peptides were calculated with the help of molecular-dynamics-simulated annealing/minimization experiments to determine a plausible lowest-energy conformational ensemble (ten structures) that fits the target NMR data set. The conformers with the fewest NOE violations were used to represent the structure. Figures 4B, D show the backbones of ten overlapped, energy-minimized structures of the peptides $R_2E_2W_2D_2$P-17 and $K_2E_2W_2D_2$P-17, whereas the surface structures (Figure 4C, E) represent the distribution of functional groups. Analysis of the ϕ,ψ distribution obtained for the ten conformational ensembles revealed that the dihedral pairs near proline consistently centered within the ϕ,ψ regions associated with a turn structure in polypeptides. Comparison of the dihedral angles shows a type II turn structure near P9-R10 residues of the peptide $R_2E_2W_2D_2$P-17 and a type I turn structure in the region of P9-R10 and E12 to E13 of $K_2E_2W_2D_2$P-17.

The observations from the CD and NMR spectra and molecular modeling studies are well-correlated and consistent. The peptides $R_2E_2W_2D_2$P-17 and $K_2E_2W_2D_2$P-17 exhibit a β-sheet-type structure with a turn near the proline residue. Such an unfolded conformation would minimize the electrostatic side-chain charge repulsion, orient the charged residues (D, E, R, and K), and make them accessible for complexation with calcium ions in solution.[16]

The observed extensive overlap of the NMR signals in the amide region of group III peptides indicates the presence of an unordered open structure with rapid conformational exchanges. In addition, the low hydrodynamic radius ($\langle R_H \rangle$) and high value of the mean diffusion coefficient ($\langle D \rangle$) obtained from the DLS experiments also corroborate the findings from the CD and NMR studies. Moreover, the fluorescence studies revealed the absence of concentration-dependent self-assembly of group III peptides in solution. The results from conformational studies of the peptides are consistent with the observed mineralization behavior in solution. Thus, in the nonaggregated form, the random movement of the peptides resulted in a nonspecific interaction with the $CaCO_3$ crystals, thereby inducing pits and truncation of the calcite crystal surfaces.

In conclusion, seven peptides were designed and fully characterized to mimic the function of the goose eggshell matrix protein, ansocalcin. The ordered arrangement of

 © 2005 Wiley-VCH Verlag GmbH & Co. KGaA, Weinheim

doublets of charged residues and the self-assembling characteristics of the group I and II peptides generated a functional-group-segregated surface which facilitates the nucleation, growth, and aggregation of calcium carbonate crystal nuclei to form polycrystalline calcite crystal aggregates. The group III peptides showed an unordered structure in solution and no activity toward mineralization. This finding is supported by evidence from DLS, NMR, CD, and fluorescence spectroscopy investigations.

Received: January 24, 2005
Revised: May 5, 2005
Published online: August 1, 2005

Keywords: biomineralization · eggshell · peptides · proteins · structure–activity relationships

[1] a) *Materials Synthesis Based on Biological Processes* (Eds.: M. Alper, P. D. Calvert, R. Frankel, P. C. Rieke, D. A. Tirrell), Materials Research Society, Pittsburgh, PA, **1991**; b) *Biomimetic Materials Chemistry* (Ed.: S. Mann), VCH, New York, **1996**; c) S. Zhang, *Nat. Biotechnol.* **2003**, *21*, 1171 – 1178.

[2] a) H. A. Lowenstam, S. Weiner, *On Biomineralization*, Oxford University Press, New York, **1989**; b) S. Mann, *Biomineralization: Principles and Concepts in Bioinorganic Materials Chemistry*, Oxford University Press, New York, **2001**.

[3] a) C. M. Zaremba, A. M. Belcher, M. Fritz, Y. L. Li, S. Mann, P. K. Hansma, D. E. Morse, J. S. Speck, G. D. Stucky, *Chem. Mater.* **1996**, *8*, 679 – 690; b) H. C. Lichtenegger, T. Schoberl, M. H. Bartl, H. Waite, G. D. Stucky, *Science* **2002**, *298*, 389 – 392; c) L. Addadi, S. Weiner, *Angew. Chem.* **1992**, *104*, 159 – 176; *Angew. Chem. Int. Ed. Engl.* **1992**, *31*, 153 – 169.

[4] a) A. P. Wheeler, C. S. Sikes in *Chemical Aspects of Regulation of Mineralization* (Eds.: C. S. Sikes, A. P. Wheeler), University of South Alabama, Mobile, AL, **1988**, pp. 9 – 13; b) A. P. Wheeler, C. S. Sikes in *Material Synthesis Utilizing Biological Process* (Eds.: P. C. Rieke, P. D. Calvert, M. Alper), Materials Research Society, Pittsburgh, PA, **1989**, pp. 45 – 50; c) S. Mann, D. D. Archibald, J. M. Didymus, T. Douglas, B. R. Heywood, F. C. Meldrum, N. J. Reeves, *Science* **1993**, *261*, 1286 – 1292; d) J. M. Didymus, P. Oliver, S. Mann, A. L. Devries, P. V. Hauschka, P. Westbroek, *J. Chem. Soc. Faraday Trans.* **1993**, *89*, 2891 – 2900; e) A. Wierzbicki, C. S. Sikes, J. D. Madura, B. Drake, *Calcif. Tissue Int.* **1994**, *54*, 133 – 141; f) C. Geffroy, A. Foissy, J. Persello, B. Cabane, *J. Colloid Interface Sci.* **1999**, *211*, 45 – 53; g) D. K. Keum, K.-M. Kim, K. Naka, Y. Chujo, *J. Mater. Chem.* **2002**, *12*, 2449 – 2452; h) K. Naka, *Top. Curr. Chem.* **2003**, *228*, 141 – 158.

[5] a) Y. Levi, S. Albeck, A. Brack, S. Weiner, L. Addadi, *Chem. Eur. J.* **1998**, *4*, 389 – 396; b) S. R. Whaley, D. S. English, E. L. Hu, P. F. Barbara, A. M. Belcher, *Nature* **2000**, *405*, 665 – 668; c) C. Li, G. D. Botsaris, D. L. Kaplan, *Cryst. Growth Des.* **2002**, *2*, 387 – 393; d) M. Gilbert, J. W. Shaw, J. R. Long, K. Nelson, G. P. Drobny, C. M. Giachelli, P. S. Stayton, *J. Biol. Chem.* **2000**, *275*, 16213 – 16218; e) B. Zhang, B. A. Wustman, D. E. Morse, J. S. Evans, *Biopolymers* **2002**, *63*, 358 – 372; f) B. Zhang, G. Z. Xu, J. S. Evans, *Biopolymers* **2000**, *54*, 464 – 475; g) B. A. Wustman, D. E. Morse, J. S. Evans, *Langmuir* **2002**, *18*, 9901 – 9906; h) B. A. Wustman, J. C. Weaver, D. E. Morse, J. S. Evans, *Connect. Tissue Res.* **2003**, *44*, 10 – 15; i) G. He, T. Dahl, A. Veis, A. George, *Nat. Mater.* **2003**, *2*, 552 – 558.

[6] a) D. B. DeOliveria, R. A. Laursen, *J. Am. Chem. Soc.* **1997**, *119*, 10627 – 10631; b) D. J. H. Gaskin, K. Starck, E. N. Vulfson, *Biotechnol. Lett.* **2000**, *22*, 1211 – 1216; c) P. K. Ajikumar, R. Lakshminarayanan, S. Valiyaveettil, R. M. Kini, *Biomacromolecules* **2003**, *4*, 1321 – 1326; d) D. Volkmer, M. Fricke, T. Huber, N. Sewald, *Chem. Commun.* **2004**, 1872 – 1873.

[7] a) R. Lakshminarayanan, S. Valiyaveettil, R. M. Kini, *Proc. Natl. Acad. Sci. USA* **2002**, *99*, 5155 – 5159; b) R. Lakshminarayanan, S. Valiyaveettil, V. S. Rao, R. M. Kini, *J. Biol. Chem.* **2003**, *278*, 2938 – 2946; c) R. Lakshminarayanan, J. S. Joseph, S. Valiyaveettil, R. M. Kini, *Biomacromolecules*, **2005**, *6*, 741 – 751.

[8] a) K. Mann, F. Siedler, *Biochim. Biophys. Acta Proteins Proteom.* **2004**, *1696*, 41 – 50; b) J. P. Reyes-Grajeda, A. Moreno, A. Romero, *J. Biol. Chem.* **2004**, *279*, 40876 – 40881; c) K. Mann, *Br. Poult. Sci.* **2004**, *45*, 483 – 490.

[9] a) M. Bergdoll, M. H. Remy, C. Cagnon, J. M. Masson, P. Dumas, *Structure* **1997**, *5*, 391 – 398; b) M. W. MacArthur, J. M. Thornton, *J. Mol. Biol.* **1991**, *218*, 397 – 412; c) S. C. Benson, F. H. Wilt in *Calcification in Biological Systems* (Ed.: E. Bonucci), CRC, Boca Raton, FL, **1992**, pp. 157 – 178; d) J. P. Gorski, *Calcif. Tissue Int.* **1992**, *50*, 391 – 396; e) J. Moradian-Oldak, J. Tan, A. G. Fincham, *Biopolymers* **1998**, *46*, 225 – 238; f) J. Moradian-Oldak, W. Leung, A. G. Fincham, *J. Struct. Biol.* **1998**, *122*, 320 – 327; g) C. E. Killian, F. C. Wilt, *J. Biol. Chem.* **1996**, *271*, 9150 – 9159.

[10] S. Albeck, J. Aizenberg, L. Addadi, S. Weiner, *J. Am. Chem. Soc.* **1993**, *115*, 11691 – 11697.

[11] C. Cerini, V. Peyrot, C. Garnier, L. Duplan, S. Veesler, J. P. Le Caer, J. P. Bernard, H. Bouteille, R. Michel, A. Vazi, P. Dupuy, B. Michel, Y. Berland, J. M. Verdier, *J. Biol. Chem.* **1999**, *274*, 22266 – 22274.

[12] a) A. P. Demchenko, *Topics in Fluorescence Spectroscopy*, *Vol. 3* (Ed.: J. R. Lackowicz), Plenum, New York, **1992**, pp. 77; b) L. W. Ruddock, T. R. Hirst, R. B. Freedman, *Biochem. J.* **1996**, *315*, 1001 – 1005.

[13] a) F. J. Blanco, G. Rivas, L. Serrano, *Nat. Struct. Biol.* **1994**, *1*, 584 – 590; b) M. C. Mannin, M. Illangasekare, R. W. Woody, *Biophys. Chem.* **1998**, *31*, 77 – 86.

[14] a) G. D. Fasman, *Circular Dichroism and the Conformational Analysis of Biomolecules*, Plenum, New York, **1996**; b) S. C. Shankaramma, S. K. Singh, A. Sathyamurthy, P. Balaram, *J. Am. Chem. Soc.* **1999**, *121*, 5360 – 5363.

[15] D. S. Wishart, B. D. Sykes, F. M. Richards, *J. Mol. Biol.* **1991**, *222*, 311 – 333.

[16] a) J. S. Evans, *Curr. Opin. Colloid Interface Sci.* **2003**, *8*, 48 – 54; b) B. A. Wustman, J. C. Weaver, D. E. Morse, J. S. Evans, *Langmuir* **2003**, *19*, 9373 – 9381.

 © 2005 Wiley-VCH Verlag GmbH & Co. KGaA, Weinheim

Protein Interactions

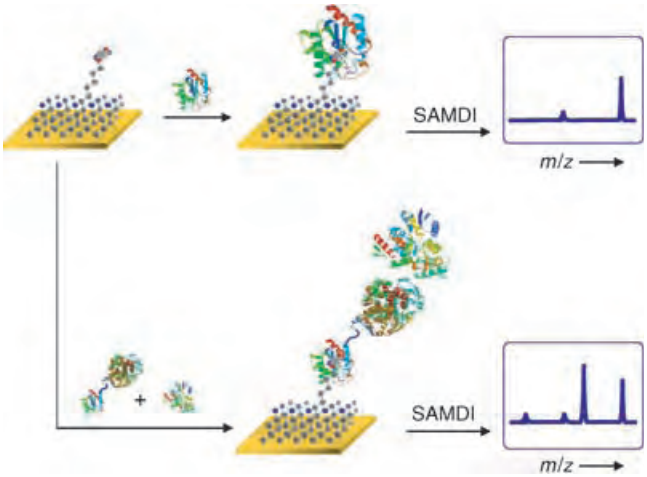
DOI: 10.1002/anie.200501363

Label-Free Detection of Protein–Protein Interactions on Biochips**

*Woon-Seok Yeo, Dal-Hee Min, Robert W. Hsieh, Geoffrey L. Greene, and Milan Mrksich**

The recent introduction of protein microarrays is now providing tools for the global profiling of biochemical activities.[1] Snyder and co-workers, for example, used yeast protein chips to identify kinase substrates and lipid-binding proteins.[2] Labaer and co-workers reported self-assembling protein microarrays to map pairwise interactions among 29 human DNA replication proteins.[3] Any application of a protein chip must involve a suitable labeling strategy that will permit the observation of activities. Common strategies include the use of radioisotopes to follow phosphorylation reactions[4] and fluorescent tags to identify protein–protein interactions.[5] The use of labels has limitations, including the need for additional steps in an assay, the difficulty in detecting certain biochemical activities, and the inability to identify unanticipated activities. These limitations have motivated the development of label-free formats for identifying the full range of biochemical activities on protein chips. Herein, we demonstrate that MALDI-TOF MS can be used to identify protein–ligand and protein–protein interactions on biochips that are prepared from self-assembled monolayers (SAMs) on gold. This work is significant because it extends the capacity of the SAMDI (self-assembled monolayers for MALDI) method from observation of low-molecular-weight species to proteins that are 50 kDa in size.

Our approach begins with a SAM of alkanethiolates on gold that presents maleimide groups amongst a background of tri(ethylene glycol) groups in a ratio of 1:20. The maleimide groups serve as a handle to immobilize thiol-derivatized small molecules,[6] and the tri(ethylene glycol) group ensures that the monolayers are inert to nonspecific protein adsorption.[7] Two model systems were used in the examples that follow: the binding of carbonic anhydrase (CA) to a benzenesulfonamide ligand and the binding of glutathione S-transferase (GST)-tagged protein complexes to a glutathione ligand (Scheme 1).



Scheme 1. Strategy for the label-free detection of protein–ligand (top) and protein–protein interactions (bottom) using MALDI-TOF MS on SAMs presenting capture ligands.

To immobilize the small molecules, monolayers were treated with either glutathione thiol (1 mM in tris(hydroxymethyl)-aminomethane (Tris) buffer, pH 7.5) or benzenesulfonamide thiol (2.5 mM in phosphate-buffered saline (PBS) containing 10% methanol, pH 7.4) (Figure 1a).[8] MS analysis of these monolayers showed peaks corresponding to the immobilized ligands and confirmed that the reactions proceeded in high yield (Figure 1b).[9]

Herein, we report several examples that establish the use of SAMDI for the direct observation of proteins bound to surface-immobilized ligands. A monolayer presenting glutathione groups was treated with GST (10 μM in Tris buffer containing 1 mM dithiothreitol (DTT), pH 7.5) for 1 hr, rinsed with distilled water, and dried under a stream of nitrogen. MS analysis of this monolayer showed two major peaks corresponding to the singly and doubly charged protein at m/z 28.0 kDa ($[M+H]^+$) and m/z 14.0 kDa ($[M+2H]^{2+}$), respectively (Figure 2a). A control experiment showed that the addition of soluble glutathione (1 mM in Tris buffer, pH 7.5) to the solution containing GST prevented binding of the protein to the monolayer. Indeed, MS data from the monolayer showed no major peaks, verifying the effectiveness of the monolayer in preventing nonspecific interactions (Figure 2b). Furthermore, no protein peaks were observed when a maleimide-presenting monolayer was treated with a cysteine-containing hexapeptide (CGRGDS) followed by incubation with GST (data not shown).

This experiment was repeated with several fusion proteins. A fusion between GST and a focal adhesion targeting domain (GST–FAT) bound to the monolayer, as evidenced by two major peaks corresponding to singly and doubly charged

[*] W.-S. Yeo, D.-H. Min, Prof. M. Mrksich
Department of Chemistry and
Institute for Biophysical Dynamics
The University of Chicago
5735 South Ellis Avenue, Chicago, IL 60637 (USA)
Fax: (+1) 773-702-0805
E-mail: mmrksich@uchicago.edu
R. W. Hsieh, Prof. G. L. Greene
The Ben May Institute for Cancer Research and
Department of Biochemistry and Molecular Biology
The University of Chicago
Chicago, IL 60637 (USA)

[**] This work was supported by the Nanoscale Science and Engineering Center (NSEC) and the Ludwig Fund for Cancer Research. R.W.H. was supported by The University of Chicago MSTP Unendowed Student Support. We thank Professor Benita S. Katzenellenbogen for providing the human ER_β LBD plasmid and Young-Sam Lee for providing the GST–FAT plasmid.

Supporting information for this article is available on the WWW under http://www.angewandte.org or from the author.

InterScience
© 2005 Wiley-VCH Verlag GmbH & Co. KGaA, Weinheim

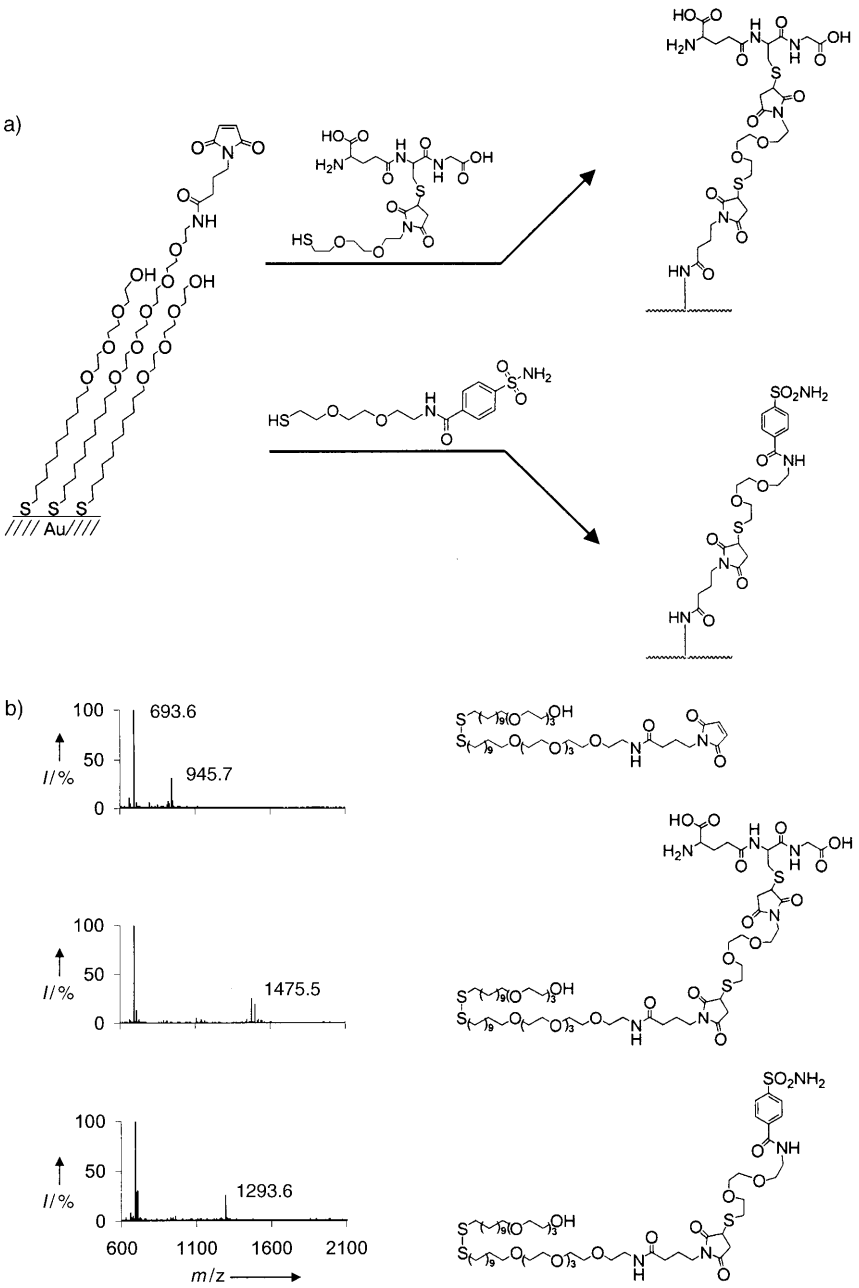


Figure 1. a) Protein-capture ligands were immobilized onto a maleimide-terminated SAM by reaction of the thiol-tagged ligands. b) MS data for the initial monolayer (top) displayed a peak at *m*/*z* 945.7, which corresponds to the mixed disulfide derived from a maleimide-terminated alkanethiolate and a tri(ethylene glycol)-terminated alkanethiolate. After treatment with ligands, the original peak disappeared and gave rise to a new peak at *m*/*z* 1475.5, which corresponds to the glutathione-conjugated product (middle) or at *m*/*z* 1293.6, which corresponds to the benzenesulfonamide-conjugated product (bottom).

bound GST–FAT at *m*/*z* 44.2 kDa ($[M+H]^+$) and *m*/*z* 22.1 kDa ($[M+2H]^{2+}$), respectively (Figure 2c).[10] We also found that a monolayer treated with a crude lysate of *E. coli* that had been transformed with the GST–FAT plasmid gave major peaks identical to those obtained from a purified GST–FAT protein (Figure 2d). This result gives further evidence that the immobilization of GST proteins is specific, and that the monolayer is inert to the nonspecific adsorption of proteins. In a separate experiment, a monolayer presenting the benzenesulfonamide ligand was treated with CA (5 μM in Tris buffer, pH 7.5). MS analysis of this monolayer revealed peaks corresponding to the bound protein, including a doubly charged monomer ($[M+2H]^{2+}$, *m*/*z* 14.5 kDa), a singly charged monomer ($[M+H]^+$, *m*/*z* 28.9 kDa), and a singly charged dimer ($[2M+H]^+$, *m*/*z* 57.9 kDa) (Figure 2e). Pre-incubation of CA with soluble benzenesulfonamide (500 μM) inhibited the binding of protein to the monolayer (data not shown). This latter example is significant because it suggests that SAMDI can be applied to the use of small-molecule arrays to identify inhibitors of target proteins.[11] Indeed, small arrays of carbohydrate ligands have been prepared on SAMs[12] and chemistries have been demonstrated for the immobilization of small molecules that have amine or thiol functional groups.[6,13]

This method is also well-suited for characterizing protein–protein interactions on biochips. We demonstrate this application with the interaction between estrogen receptor (ER) and steroid receptor coactivator (SRC).[14,15] ER serves as a molecular switch; its binding to SRC requires a small-molecule agonist.[16] The MALDI MS spectrum of a glutathione-presenting monolayer that was exposed to GST–SRC gave peaks corresponding to the singly and doubly charged fusion protein at *m*/*z* 44.7 kDa ($[M+H]^+$) and *m*/*z* 22.4 kDa ($[M+2H]^{2+}$), respectively (Figure 3a).[17] A solution containing GST–SRC (10 μM), ER (10 μM), and estradiol (E2, agonist, 50 μM) was applied to the monolayer and analyzed by MS. The analysis revealed peaks derived from both GST–SRC ($[M+H]^+$ at *m*/*z* 44.7 kDa, $[M+2H]^{2+}$ at *m*/*z* 22.4 kDa) and ER ($[M+H]^+$ at *m*/*z* 30.4 kDa, $[M+2H]^{2+}$ at *m*/*z* 15.2 kDa) (Figure 3b). However, a repeat of this experiment in which the E2 agonist was replaced with an antagonist (4-hydroxytamoxifen, OHT, 50 μM) that disrupts the protein–protein interaction, resulted in major MS peaks derived from GST–SRC and only minor peaks derived from ER (Figure 3c). As expected, the presence of the antagonist significantly diminished the recruitment of ER. These results indicate that the combination of SAMs presenting capture ligands and MALDI-TOF MS allows the detection of protein complexes without any

 © 2005 Wiley-VCH Verlag GmbH & Co. KGaA, Weinheim

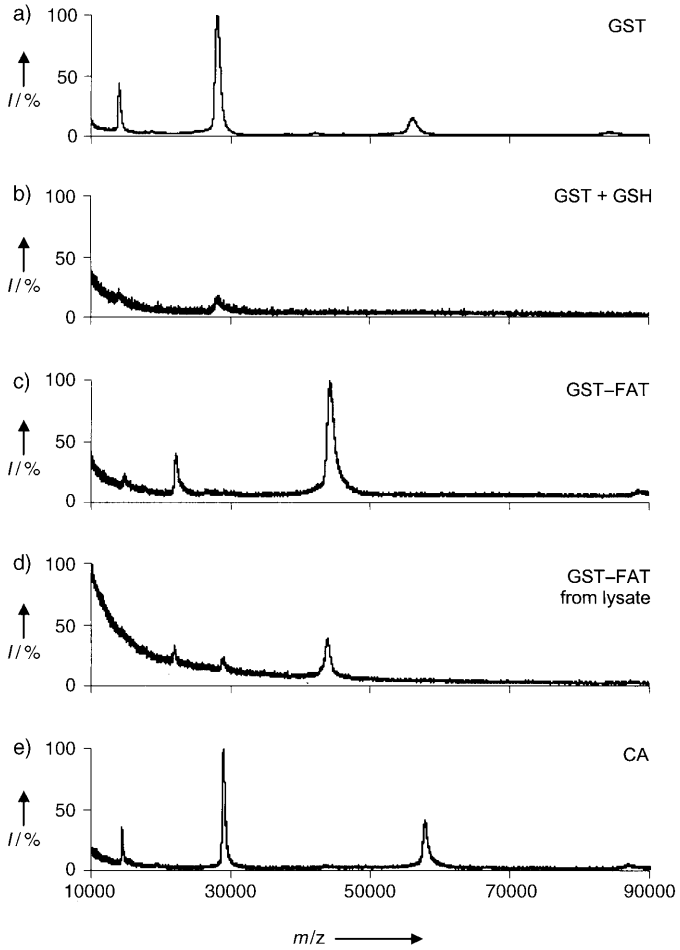


Figure 2. MS analysis of the binding of target proteins to monolayers presenting capture ligands. a) A monolayer presenting glutathione was treated with GST; the data show two major peaks corresponding to GST ions at m/z 28.0 kDa ($[M+H]^+$) and m/z 14.0 kDa ($[M+2H]^{2+}$), respectively. b) Pre-incubation of GST with soluble glutathione gave rise to no major peaks. c) An identical experiment was performed with GST–FAT, and the data show two major peaks corresponding to GST–FAT ions at m/z 44.2 kDa ($[M+H]^+$) and m/z 22.1 kDa ($[M+2H]^{2+}$), respectively. d) The monolayer was treated with a crude lysate from *E. coli* transformed with the GST–FAT plasmid and analyzed. The MS data show major peaks identical to those obtained from purified GST–FAT. e) A benzenesulfonamide-presenting monolayer was treated with CA; the resulting peaks correspond to the CA ions at m/z 14.5 kDa ($[M+2H]^{2+}$), m/z 28.9 kDa ($[M+H]^+$), and m/z 57.9 kDa ($[2M+H]^+$).

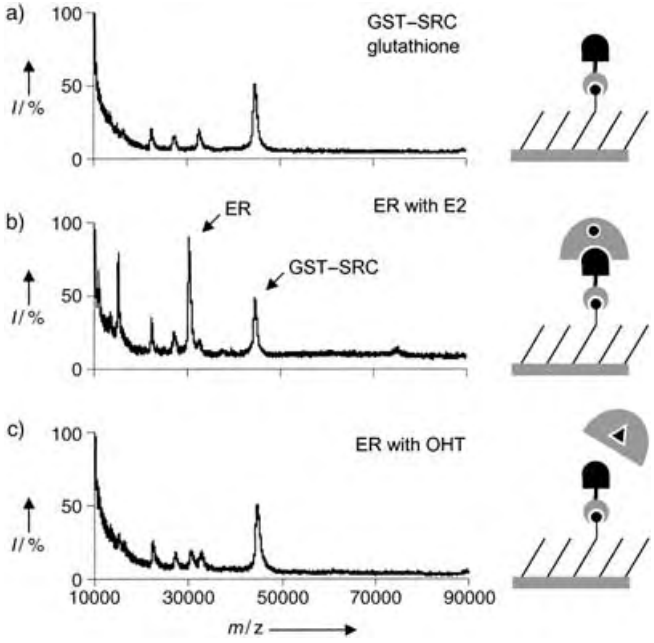


Figure 3. SAMDI analysis of protein- protein interactions on biochips. a) MS data from a glutathione-presenting monolayer treated with GST–SRC show peaks that correspond to bound-protein ions at m/z 44.7 kDa ($[M+H]^+$) and at m/z 22.4 kDa ($[M+2H]^{2+}$). b) A solution containing GST–SRC, ER, and E2 (agonist) was applied to a glutathione-presenting monolayer; the observed peaks derived from both GST–SRC ($[M+H]^+$ at m/z 44.7 kDa, $[M+2H]^{2+}$ at m/z 22.4 kDa) and ER ($[M+H]^+$ at m/z 30.4 kDa, $[M+2H]^{2+}$ at m/z 15.2 kDa). c) MS analysis of an identical experiment with OHT (antagonist) instead of E2 gave major peaks derived from GST–SRC and only minor peaks derived from ER.

labels. Furthermore, it differentiates agonist-induced and antagonist-blocked protein–protein interactions.

The combination of biochips and MALDI-TOF MS offers a powerful and flexible method for identifying protein–protein interactions on biochips and should be extendible to arrays. Importantly, the performance of this method is directly related to the use of self-assembled monolayers of alkanethiolates on gold as the substrate. The structural regularity and synthetic flexibility that are intrinsic to monolayer surface chemistries allow the properties of the interface to be optimized for biochip applications. In particular, the use of oligo(ethylene glycol)-terminated alkanethiols is very effective at controlling unwanted protein adsorption at the interface. This reduces false-positive signals and eliminates the need for usual blocking procedures.[7] Furthermore, a range of immobilization chemistries gives good control over the orientation, density, and activity of small molecules and proteins that are presented on the surface.[18] These factors make monolayers useful for quantitative assays of biochemical activities.[4b] The monolayers are also well-suited to analysis by MALDI-TOF MS. The gold substrate facilitates the release of alkanethiolates and bound proteins, and gives clean spectra that are readily interpreted. Whereas alternate methods based on porous silicon substrates share some of these properties,[19] only SAMDI allows MS detection of the interaction of both low-molecular-weight molecules (as in the case of immobilized peptides that report enzyme activities) and high-molecular-weight proteins, and is based on surface chemistries that are tailored for biochip applications.[20]

The work described herein offers a new opportunity for applying protein arrays to identify biomolecular interactions. The ability to identify protein–protein interactions without the need for labels will be particularly relevant for the observation of unanticipated activities. The SAMDI format also allows different classes of protein–protein (and enzyme–protein) interactions to be studied with a single array. Current methods, by contrast, often use labeling strategies that allow only a specific class of activity to be identified. These characteristics also suggest that SAMDI will be useful for

 © 2005 Wiley-VCH Verlag GmbH & Co. KGaA, Weinheim

chemical screenings that identify small-molecule inhibitors (or promoters) of protein–protein interactions.[20e]

Received: April 20, 2005
Published online: July 29, 2005

Keywords: bioinformatics · immobilization · mass spectrometry · monolayers · proteins

[1] a) T. Kodadek, *Chem. Biol.* **2001**, *8*, 105; b) Y.-S. Lee, M. Mrksich, *Trends Biotechnol.* **2002**, *20*, S14; c) M. F. Templin, D. Stoll, M. Schrenk, P. C. Traub, C. F. Vöhringer, T. O. Joos, *Trends Biotechnol.* **2002**, *20*, 160; d) D. S. Wilson, S. Nock, *Angew. Chem.* **2003**, *115*, 510; *Angew. Chem. Int. Ed.* **2003**, *42*, 494.

[2] H. Zhu, M. Bilgin, R. Bangham, D. Hall, A. Casamayor, P. Bertone, N. Lan, R. Jansen, S. Bidlingmaier, T. Houfek, T. Mitchell, P. Miller, R. A. Dean, M. Gerstein, M. Snyder, *Science* **2001**, *293*, 2101.

[3] N. Ramachandran, E. Hainsworth, B. Bhullar, S. Eisenstein, B. Rosen, A. Y. Lau, J. C. Walter, J. Labaer, *Science* **2004**, *305*, 86.

[4] a) H. Zhu, J. F. Klemic, S. Chang, P. Bertone, A. Casamayor, K. G. Klemic, D. Smith, M. Gerstein, M. A. Reed, M. Snyder, *Nat. Genet.* **2000**, *26*, 283; b) B. T. Houseman, J. H. Huh, S. J. Kron, M. Mrksich, *Nat. Biotechnol.* **2002**, *20*, 270.

[5] G. Macbeath, S. L. Schreiber, *Science* **2000**, *289*, 1760.

[6] B. T. Houseman, E. S. Gawalt, M. Mrksich, *Langmuir* **2003**, *19*, 1522.

[7] M. Mrksich, G. M. Whitesides, *American Chemical Society Symposium Series on Chemistry and Biological Applications of Polyethylene Glycol* **1997**, *680*, 361.

[8] Both glutathione thiol and benzenesulfonamide thiol were synthesized in eight steps from commercially available reagents. All intermediates gave satisfactory ^{1}H NMR spectra. Synthetic schemes and experimental details are provided in the Supporting Information.

[9] The peak at *m*/*z* 693.6 was derived from a symmetric disulfide of tri(ethylene glycol)-terminated alkanethiolates. Sodium adducts of disulfides are the major species, which are observed in MALDI spectra of SAMs of alkanethiolates; see: J. Su, M. Mrksich, *Angew. Chem.* **2002**, *114*, 4909; *Angew. Chem. Int. Ed.* **2002**, *41*, 4715 and J. L. Trevor, K. R. Lykke, M. J. Pellin, L. Hanley, *Langmuir* **1998**, *14*, 1664.

[10] GST fusions with src homology domain 3 (GST–SH3) and with green fluorescent protein (GST–GFP) were assayed with similar results.

[11] a) F. G. Kuruvilla, A. F. Shamji, S. M. Sternson, P. J. Hergenrother, S. L. Schreiber, *Nature* **2002**, *416*, 653; b) N. Winssinger, S. Ficarro, P. G. Schultz, J. L. Harris, *Proc. Natl. Acad. Sci. USA* **2002**, *99*, 11139.

[12] B. T. Houseman, M. Mrksich, *Chem. Biol.* **2002**, *9*, 443.

[13] W.-S. Yeo, M. Mrksich, *Adv. Mater.* **2004**, *16*, 1352.

[14] This work used the nuclear receptor interacting domain of SRC-1 and the ligand binding domain of ER_β.

[15] For a related example of chip-based assays of ER–SRC interactions using fluorescent labels, see: S. H. Kim, A. Tamrazi, K. E. Carlson, J. A. Katzenellenbogen, *Mol. Cell. Proteomics* **2005**, *4*, 267.

[16] a) S. A. Oñate, S. Y. Tsai, M.-J. Tsai, B. W. O'Malley, *Science* **1995**, *270*, 1354; b) Y. Kamei, L. Xu, T. Heinzel, J. Torchia, R. Kurokawa, B. Gloss, S.-C. Lin, R. A. Heyman, D. W. Rose, C. K. Glass, M. G. Rosenfeld, *Cell* **1996**, *85*, 403.

[17] In the MALDI MS data of GST–SRC, two other peaks at *m*/*z* 27.3 kDa and *m*/*z* 32.6 kDa were observed. We believe that these peaks represent GST and a degradation product of GST–SRC that still contains GST which were co-purified on a glutathione column.

[18] M. Mrksich, *Chem. Soc. Rev.* **2000**, *29*, 267.

[19] a) J. Wei J. M. Buriak, G. Siuzdak, *Nature* **1999**, *399*, 243; b) J. J. Thomas, Z. Shen, J. E. Crowell, M. G. Finn, G. Siuzdak, *Proc. Natl. Acad. Sci. USA* **2001**, *98*, 4932.

[20] a) C. D. Hodneland, Y.-S. Lee, D.-H. Min, M. Mrksich, *Proc. Natl. Acad. Sci. USA* **2002**, *99*, 5048; b) D.-H. Min, W.-S. Yeo, M. Mrksich, *Anal. Chem.* **2004**, *76*, 3923; c) Y. Kwon, Z. Han, E. Karatan, M. Mrksich, B. K. Kay, *Anal. Chem.* **2004**, *76*, 5713; d) D.-H. Min, J. Su, M. Mrksich, *Angew. Chem.* **2004**, *116*, 6099; *Angew. Chem. Int. Ed.* **2004**, *43*, 5973; e) D.-H. Min, W.-J. Tang, M. Mrksich, *Nat. Biotechnol.* **2004**, *22*, 717.

 © 2005 Wiley-VCH Verlag GmbH & Co. KGaA, Weinheim

Structure Elucidation

DOI: 10.1002/anie.200501297

The "Noncoordinating" Anion Tf_2N^- Coordinates to Yb^{2+}: A Structurally Characterized Tf_2N^- Complex from the Ionic Liquid [mppyr][Tf_2N]**

Anja-Verena Mudring, Arash Babai, Sven Arenz, and Ralf Giernoth*

Crystal structures of bis(trifluoromethanesulfonyl)amide (Tf_2N^-) complexes of transition or f elements are unknown to date. This is surprising, since a variety of bis(trifluoromethanesulfonyl)amide compounds have been identified to be excellent Lewis acid catalysts. The Tf_2N^- ion is the conjugate base of an extremely strong Brønsted acid and has the power to strengthen the Lewis acidity of a metal center when acting as a ligand.[1] Lanthanide bis(trifluoromethanesulfonyl)amide compounds are, for example, used as Lewis acid catalysts for Diels–Alder reactions, Friedel–Crafts acylations, Fries transpositions, and Baeyer–Villinger oxidations.[2] Much effort (although to no avail) has been put into the crystallization of lanthanide bis(trifluoromethanesulfonyl)amides, but so far the structural identity of these catalysts remains uncertain.[3] Attempts to crystallize an ytterbium–Tf_2N^- complex from *N*,*N*′-dimethylpropyleneurea (dmpu)/ethyl acetate yielded a crystal structure with Yb^{III} ions surrounded octahedrally by six dmpu ligands. The Tf_2N^- ion was, however, only incorporated into this structure as a noncoordinating anion.[4] It is, therefore, not surprising that the Tf_2N^- ion has often been considered as weakly or even noncoordinating. The Tf_2N^- ion shows the feature that is essential for an ion to have a low tendency to coordinate: delocalization of negative charge over an extended area of functional groups.[5] The extremely strong acidity of the corresponding acid Tf_2NH has been attributed to extensive electron delocalization. As a consequence, the term "gas-phase superacid" has been coined for Tf_2NH.[6]

The Tf_2N^- ion has recently gained much attention in the ongoing search for new room-temperature ionic liquids (RTILs), since it has become clear that anions with diffuse charges and negligible possibility to form hydrogen-bonding interactions have the highest potential to produce ionic compounds that are liquid at room temperature and below.[7] RTILs have attracted wide attention as "green" solvents for catalysis, chemical synthesis, and separations. They have many favorable properties that are tuneable through the choice of the cation/anion pair, such as negligible volatility, high chemical, thermal and (electro)chemical stability, viscosity, density, hydrophobicity. The Tf_2N^- ion has been found to frequently produce salts with low melting points that have high fluidity and high ionic conductivity.[8] Ionic liquids based on the Tf_2N^- ion have gained special attention as they improve the performance of lithium batteries and fuel cells.[9] Indeed, most crystal structures of ionic liquids with the Tf_2N^- ion reveal no substantial hydrogen bonding between the cation and anion.[10] Displacement factors and sometimes the tendency to disorder show that the anion is conformationally highly flexibile, which might be the reason for the low number of structure determinations containing the Tf_2N^- ion.[11]

In our ongoing studies to explore the reactivity of rare-earth compounds as reagents for organic synthesis and catalysis in ionic liquids we were able to structurally characterize the first ytterbium–Tf_2N^- complex. Here, we present the first homoleptic Tf_2N^- complex obtained by interaction of YbI_2 with the ionic liquid [mppyr][Tf_2N] (mppyr = 1-methyl-1-propylpyrrolidinium).[12]

The complex crystallizes in the monoclinic space group $P2_1/n$ with four formula units in the unit cell. The asymmetric unit of the crystal structure shows Yb^{II} being coordinated by four Tf_2N^- ions through their oxygen atoms (Figure 1), with two cations of the ionic liquid to balance the charge.[13] To our knowledge, this is the first structure showing the Tf_2N^- ion coordinating in a η^2-bidentate manner to a metal center to form discrete anionic molecules. The Yb atom is surrounded

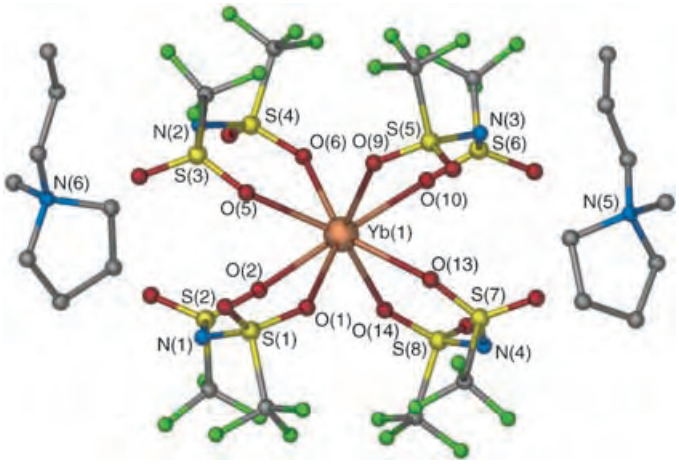


Figure 1. Asymmetric unit of the crystal structure of $[mppyr]_2[Yb(Tf_2N)_4]$; blue: N, yellow: S, gray: C, green: F, orange: Yb, red: O.

[*] Dr. A.-V. Mudring, Dipl.-Chem. A. Babai
Institut für Anorganische Chemie
Universität zu Köln
Greinstrasse 6, 50939 Köln (Germany)
Fax: (+49) 221-470-5083
E-mail: a.mudring@uni-koeln.de
Dipl.-Chem. S. Arenz, Dr. R. Giernoth
Institut für Organische Chemie
Universität zu Köln
Greinstrasse 4, 50939 Köln (Germany)

[**] This work has been supported by the Deutsche Forschungsgemeinschaft (SPP 1166 "Lanthanoidspezifische Funktionalitäten" and the Emmy Noether program (R.G.)) and by the Fonds der Chemischen Industrie (Liebig-Stipendium (A.V.M.) and Sachmittel (A.V.M. and R.G.)). We would especially like to thank Prof. Dr. G. Meyer and Prof. Dr. A. Berkessel for their continuous support.
Tf = trifluoromethanesulfonyl, mpyr = 1-methyl-1-propylpyrrolidinium.

Supporting information for this article is available on the WWW under http://www.angewandte.org or from the author.

© 2005 Wiley-VCH Verlag GmbH & Co. KGaA, Weinheim

by eight oxygen atoms that form a distorted square antiprism (Figure 1). The cations surround the anionic $[Yb(Tf_2N)_4]^{2-}$ units (d(N(5)-N(3)) = 473.3 pm, d(N(5)-N(4)) = 631.0 pm, d(N(6)-N(1)) = 625.3 pm, d(N(6)-N(2) = 453.4 pm) (Figure 1) and form a honeycomb-like structure.

The Yb–O bond lengths range from 241.0 to 251.7 pm, the latter being to our knowledge the longest Yb^{II}–O bond so far observed (Table 1). Bond lengths of 210–217 pm are found in

Table 1: Selected interatomic distances [pm] for $[mppyr]_2[Yb(Tf_2N)_4]$.

Yb(1)-O(1)	242.1(3)	S(1)-O(1)	144.5(3)
Yb(1)-O(2)	247.6(3)	S(1)-O(3)	142.1(4)
Yb(1)-O(5)	251.7(3)	S(2)-O(2)	144.3(3)
Yb(1)-O(6)	243.5(3)	S(2)-O(4)	141.9(3)
Yb(1)-O(9)	241.0(3)	S(3)-O(5)	143.9(3)
Yb(1)-O(10)	247.0(3)	S(3)-O(7)	142.0(3)
Yb(1)-O(13)	250.2(3)	S(4)-O(6)	144.7(3)
Yb(1)-O(14)	245.6(3)	S(4)-O(8)	140.5(4)
S(1)-N(1)	156.3(4)	S(5)-O(9)	145.0(3)
S(2)-N(1)	156.4(4)	S(5)-O(11)	141.6(3)
S(3)-N(2)	156.5(4)	S(6)-O(10)	144.1(3)
S(4)-N(2)	156.7(4)	S(6)-O(12)	141.5(4)
S(5)-N(3)	156.8(4)	S(7)-O(13)	143.6(3)
S(6)-N(3)	155.8(4)	S(7)-O(15)	141.7(3)
S(7)-N(4)	156.2(4)	S(8)-O(14)	144.1(3)
S(8)-N(4)	156.8(4)	S(8)-O(16)	141.8(4)

aryloxo–ytterbium complexes, while Yb–O bond lengths in bridging aryloxo ligands lie in the range 224–234 pm.[14] Yb–O bond lengths of 238–239 pm are reported for $[Yb(thf)_6]^{2+}$ with neutral tetrahydrofuran as a ligand.[15] Unfortunately there are no structural data for Yb^{II}–1,3-diketone complexes available for comparison. Considering that the ionic radius of an eightfold coordinate Yb^{2+} ion corresponds to the one for an eightfold coordinate La^{3+} ion, it might be possible to compare the average Yb–O bond length of 246.1 pm in $[mppyr]_2[Yb(Tf_2N)_4]$ to d(La-O) of 247 found for $[La(acac)_3(H_2O)_2]$ (acac = acetylacetonate).[16]

Surprisingly, all the ligands show a *cisoid* conformation with respect to the CF_3 groups, which fixes the $[Yb(Tf_2N)_4]^{2-}$ antiprisms along the crystallographic *b*-axis (Figure 2). The free acid Tf_2NH crystallizes with the CF_3 groups being oriented in a *transoid* banner to each other.[17] The Tf_2N ion also prefers the *transoid* conformation in the absence of suitable coordination centers.[10,11] This observation is backed by theoretical calculations (*transoid* Tf_2NH is about 8 kJ mol^{-1} more stable than *cisoid* Tf_2NH, and *transoid* Tf_2N^- about 4 kJ mol^{-1} more stable than *cisoid* Tf_2N^-).[18] It can thus be concluded that the *cisoid* conformation of the Tf_2N^- ion in [mppyr][Tf_2N] results from by Yb–Tf_2N^- interactions. The very weak interaction between the metal center and the oxygen atoms results in the average S–O bond lengths [144.3 pm (coordinating oxygen atoms) and 141.6 pm (non-coordinating oxygen atoms)] being only slightly affected by coordination to the Yb^{2+} ion, even when compared to the neutral amine (d(S-O) = 140.1 pm and 141.7 pm).[17]

The question that arises is: why does the Tf_2N^- ion coordinate through its oxygen atoms and not through the deprotonated nitrogen center? In this context, the often-cited

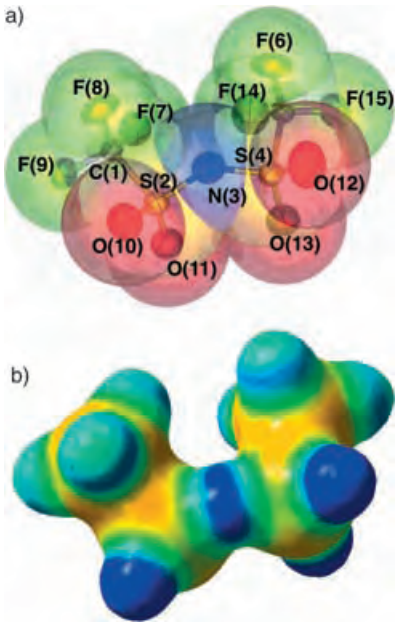


Figure 2. a) Space filling model of Tf_2N^- as found in $[mppyr]_2[Yb(Tf_2N)_4]$. b) Calculated electrostatic potential of *cisoid* Tf_2N^-.

Cruickshank model predicts that charge delocalization in these systems only occurs between the nitrogen and sulfur atoms.[19] In contrast, Mulliken charges as well as natural charges obtained from NBO analysis indicate that high partial charges occur not only at the nitrogen center but also at the oxygen atoms of the Tf_2N^- ion (Table 2). This charge

Table 2: Mulliken charges and natural charges for *cisoid* Tf_2N^- at the MP2 and B3LYP level of theory.

	Mulliken		Natural charges	
	B3LYP	MP2	B3LYP	MP2
C(1)	0.434	0.691	0.877	1.009
S(2)	1.016	1.373	2.137	2.353
N(3)	−0.715	−0.885	−1.209	−1.306
S(4)	1.014	1.378	2.128	2.343
C(5)	0.447	0.704	0.885	1.018
F(6)	−0.199	−0.284	−0.358	−0.399
F(7)	−0.186	−0.270	−0.352	−0.393
F(8)	−0.199	−0.283	−0.358	−0.399
F(9)	−0.206	−0.291	−0.363	−0.404
O(10)	−0.500	−0.637	−0.921	−1.008
O(11)	−0.504	−0.644	−0.918	−1.006
O(12)	−0.507	−0.647	−0.916	−1.003
O(13)	−0.495	−0.634	−0.917	−1.007
F(14)	−0.193	−0.276	−0.353	−0.394
F(15)	−0.207	−0.293	−0.363	−0.405

distribution is further backed by a plot of the electrostatic potential (Figure 2a).[20] Thus, electrostatic (high negative charge on the oxygen atoms, more favorable coordination to two sulfur atoms than to one nitrogen atom) and steric reasons (the nitrogen center is well shielded by its surroundings, Figure 2b) are the origin of the observed coordination mode of the Tf_2N^- ion.

 © 2005 Wiley-VCH Verlag GmbH & Co. KGaA, Weinheim

These observations show that ionic liquids containing the bis(trifluoromethanesulfonyl)amide anion (Tf_2N^-) are not as "innocent" or "noncoordinating" as they are often believed to be. In the absence of any stronger coordinating ligand, even the weak bis(trifluoromethanesulfonyl)amide anion coordinates to a metal cation present in solution. This observation is important, as many reactions in these solvents may be crucially influenced by complexation. Furthermore, our observation helps to understand the solvation process of inorganic salts in ionic liquids, since we are able to show that the metal cation, in our case Yb^{2+}, dissolves under complexation. The discovery of $[mppyr]_2[Yb(Tf_2N)_4]$ shows not only the high potential of ionic liquids for the synthesis of complex compounds with weakly coordinating anions but also the versatility of ionic liquids as solvents for highly reducing species as divalent rare-earth iodides.

Received: April 13, 2005
Published online: July 26, 2005

Keywords: coordination modes · fluorinated ligands · ionic liquids · lanthanides · rare earth metals

[1] K. Mikami, O. Kotera, Y. Motoyama, M. Tanaka, *Inorg. Chem. Commun.* **1998**, *1*, 10.

[2] a) H. Kobayashi, J. Nie, T. Sonoda, *Chem. Lett.* **1995**, 307; b) D. B. Baudry, A. Dormond, F. Duris, J. M. Bernard, J. R. Desmurs, *J. Fluorine Chem.* **2003**, *121*, 233; c) M. J. Earle, U. Hakala, B. J. McAuley, M. Nieuwenhuyzen, A. Ramani, K. R. Seddon, *Chem. Commun.* **2004**, 1368.

[3] D. B. Baudry, A. Dormond, F. Duris, J. M. Bernard, J. R. Desmurs, *J. Fluorine Chem.* **2003**, *121*, 233.

[4] Generally the crystallization of lanthanide sulfonylaminates seems to be difficult: see ref. [1] and Y. Hasegawa, T. Ohkubo, K. Sogabe, Y. Kawamura, Y. Wada, N. Nakashima, S. Yanagida, *Angew. Chem.* **2000**, *112*, 365; *Angew. Chem. Int. Ed.* **2000**, *39*, 357.

[5] a) I. Krossing, I. Raabe, *Angew. Chem.* **2004**, *116*, 2116; *Angew. Chem. Int. Ed.* **2004**, *43*, 2066; b) S. H. Strauss, *Chem. Rev.* **1993**, *93*, 927.

[6] a) I. A. Koppel, R. W. Taft, F. Ania, S.-Z. Zhu, L.-Q. Hu, K.-S. Sung, D. D. DesMarteau, L. M. Yagupolskii, Y. L. Yagupolskii, N. V. Ignatév, N. V. Kondratenko, A. Y. Volkonskii, V. M. Vlasov, R. Notario, P.-C. Maria, *J. Am. Chem. Soc.* **1994**, *116*, 3047; b) D. D. DesMarteau, *J. Fluorine Chem.* **1995**, *72*, 203.

[7] a) P. Bonhote, A. Dias, N. Papageorgiou, K. Kalyanasundaram, M. Grätzel, *Inorg. Chem.* **1996**, *35*, 1168; b) M. J. Earle, K. R. Seddon, *Pure Appl. Chem.* **2000**, *72*, 1391; c) P. Wasserscheid, W. Keim, *Angew. Chem.* **2000**, *112*, 3926; *Angew. Chem. Int. Ed. Engl.* **2000**, *39*, 3772; d) J. D. Holbrey, W. M. Reichert, R. D. Rogers, *Dalton Trans.* **2004**, 2267.

[8] V. R. Koch, C. Nanjundah, G. Battista Appetecchi, B. Scorsati, *J. Electrochem. Soc.* **1995**, *142*, L116.

[9] a) J. L. Nowinski, P. Lightfoot, P. G. Bruce, *J. Mater. Chem.* **1994**, *4*, 1579; b) J. R. Atloms, C. R. Sides, S. E. Creager, J. L. Harris, W. T. Pennington, B. H. Thomas, D. D. DesMarteau, *J. New Mater. Electrochem. Syst.* **2003**, *6*, 9.

[10] Crystal structures of purely organic compounds: a) J. J. Golding, D. R. MacFarlane, L. Spiccia, M. Forsyth, B. W. Skelton, A. H. White, *Chem. Commun.* **1998**, *15*, 1593; b) V. Montanari, D. D. DesMareteau, W. T. Pennington, *J. Mol. Struct.* **2000**, *550*/551, 337; c) C. M. Forsyth, D. R. MacFarlane, J. J. Golding, J. Huang, J. Sun, M. Forsyth, *Chem. Mater.* **2002**, *14*, 2103; d) J. A. Schlueter, U. Geiser, H. H. Wang, A. M. Kini, B. H. Ward, J. P. Parakka, R. G. Daugherty, M. E. Kelly, P. G. Nixon, R. W. Winter, G. L. Gard, L. K. Montgomery, H.-J. Koo, M.-H. Whangbo, *J. Solid State Chem.* **2002**, *168*, 524; e) M. G. Davidson, P. R. Raithby, A. L. Johnson, P. D. Bolton, *Eur. J. Inorg. Chem.* **2003**, 3445; f) D. D. DesMarteau, W. T. Pennington, V. Montanari, B. H. Thomas, *J. Fluorine Chem.* **2003**, *122*, 57; g) J. D. Holbrey, W. M. Reichert, R. D. Rogers, *Dalton Trans.* **2004**, 2267.

[11] Crystal structures of metal–organic compounds: a) J. L. Nowinski, P. Lightfoot, P. G. Bruce, *J. Mater. Chem.* **1994**, *4*, 1579; b) A. Haas, C. Klare, P. Betz, J. Bruckmann, C. Kruger, Y.-H. Tsay, F. Aubke, *Inorg. Chem.* **1996**, *35*, 1918; c) L. Xue, C. W. Padgett, D. D. DesMareau, W. T. Pennington, *Solid State Sci.* **2002**, *4*, 1535; d) D, Brouilette, D. E. Irish, N. J. Taylor, G. Perron, M. Odziemkowski, J. E. Desnoyers, *Phys. Chem. Chem. Phys.* **2002**, *4*, 6063; e) Z. Zak, A. Ruzicka, *Z. Kristallogr.* **1998**, *213*, 217; f) M. G. Davidson, P. R. Raithby, A. L. Johnson, P. D. Bolton, *Eur. J. Inorg. Chem.* **2003**, 3445; g) L. Xue, C. W. Padgett, D. D. DesMarteau, W. T. Pennington, *Acta Crystallogr. Sect. C* **2004**, *60*, m200; h) L. Xue, D. D. DesMarteau, W. T. Pennington, *Solid State Sci.* **2005**, *7*, 311; i) D. D. DesMarteau et al., CCDC-247563, private communication; j) A. Babai, A.-V. Mudring, *J. Alloys Compd.*, submitted; k) A. Babai, A.-V. Mudring, *Chem. Mater.*, in press.

[12] Synthesis: YbI_2 was prepared by reduction of YbI_3 with Yb metal in a sealed tantalum container jacketed with an evacuated silica tube. YbI_3 was prepared from ytterbium (chips, Chempur, 99.5%) and iodine (Riedel de Häen, 99.8%) according to the procedure described in: G. Meyer, *Chem. Rev.* **1988**, *88*, 93]. [mppyr][Tf_2N] was prepared according to the procedure in D. R. Mac Farlane, P. Meakin, J. Sun, N. Amini, M. Forsyth, *J. Phys. Chem. B* **1999**, *103*, 4164. Storage and manipulation of the starting materials and products were handled under dry-box conditions under dry argon (MBraun, Garching, Germany).
$YbI_2 + 4[mppyr][Tf_2N] \rightarrow [mppyr]_2[Yb(Tf_2N)_4] + 2[mppyr][I]$
The reaction of YbI_2 (0.2 mmol, 87 mg) with [mppyr][Tf_2N] (4.8 mmol, 1 g) was carried out in a evacuated and sealed silica tube at 393 K for 48 h. Colorless single crystals of $[mppyr]_2[Yb(Tf_2N)_4]$ formed as the single, insoluble product after subsequent cooling (2 K min^{-1}) of the mixture to room temperature. The product was separated by filtration. Estimated yield: 66%; m.p. 107 °C; IR (KBr): $\tilde{\nu}$ = 1473 (s), 1433 (s), 1352 (vs), 1331 (vs), 1231 (vs), 1197 (vs), 1144 (vs), 1058 (vs), 972 (w), 940 (w), 797 (m), 763 (w), 742 (m), 652 (s), 618 (s), 608 (s), 599 (s), 574 (s), 515 cm^{-1} (s).

[13] Crystal data: A suitable single crystal (0.3 × 0.2 × 0.2 mm) was mounted in a glass capillary. Intensity data were collected on an IPDS diffractometer (Stoe, Darmstadt, Germany) at 120(2) K. 120 K: monoclinic, space group $P2_1/n$; a = 1122.01(4), b = 2260.21(9), c = 2188.47(9) pm, β = 102.209(3)°, V = 5.4244(4) nm^3; Z = 4; ρ_{calcd} = 1.8978 g cm^{-3}; $1.80 < \theta < 27.19°$; IPDS II, $Mo_{K\alpha}$ radiation (λ = 71.073 pm); T = 120(2) K; $F(000)$ = 3056; μ = 2.177 mm^{-1}; 56375 reflections were measured, of which 11822 were unique. R_1 = 0.0436 and wR_2 = 0.1109 for [$I_0 > 2\sigma(I_0)$]. The data were processed with the program systems SHELX-97 [G. M. Sheldrick, SHELX-97, Universität Göttingen, **1997**] and X-Seed [L. J. Barbour, *J. Supramol. Chem.* **2001**, *1*, 189]. Numerical absorption correction after crystal shape optimization was performed by using the programs XRED and XSHAPE [Stoe, XRED 1.01 and XSHAPE 1.01, Darmstadt, **1996**]. CCDC-268479 contains the supplementary crystallographic data for this paper. These data can be obtained free of charge from the Cambridge Crystallographic Data Centre via www.ccdc.cam.ac.uk/data_request/cif.

[14] G. B. Deacon, C. M. Forsyth, P. C. Junk, B. W. Skelton, A. White, *Chem. Eur. J.* **1999**, *5*, 1452.

 © 2005 Wiley-VCH Verlag GmbH & Co. KGaA, Weinheim

[15] C. E. Pleènik, S. Liu, J. Liu, X. Chen, E. A. Meyers, S. G. Shore, *Inorg. Chem.* **2002**, *41*, 4936.
[16] T. Phillips, D. E. Sands, W. F. Wagner, *Inorg. Chem.* **1968**, *7*, 2295.
[17] A. Haas, C. Klare, P. Betz, J. Bruckmann, C. Kruger, Y.-H. Tsay, F. Aubke, *Inorg. Chem.* **1996**, *35*, 1918.
[18] All calculations were performed using the Gaussian03 program package [Gaussian 03 (Revision B.04), M. J. Frisch, G. W. Trucks, H. B. Schlegel, G. E. Scuseria, M. A. Robb, J. R. Cheeseman, J. A. Montgomery, Jr., T. Vreven, K. N. Kudin, J. C. Burant, J. M. Millam, S. S. Iyengar, J. Tomasi, V. Barone, B. Mennucci, M. Cossi, G. Scalmani, N. Rega, G. A. Petersson, H. Nakatsuji, M. Hada, M. Ehara, K. Toyota, R. Fukuda, J. Hasegawa, M. Ishida, T. Nakajima, Y. Honda, O. Kitao, H. Nakai, M. Klene, X. Li, J. E. Knox, H. P. Hratchian, J. B. Cross, C. Adamo, J. Jaramillo, R. Gomperts, R. E. Stratmann, O. Yazyev, A. J. Austin, R. Cammi, C. Pomelli, J. W. Ochterski, P. Y. Ayala, K. Morokuma, G. A. Voth, P. Salvador, J. J. Dannenberg, V. G. Zakrzewski, S. Dapprich, A. D. Daniels, M. C. Strain, O. Farkas, D. K. Malick, A. D. Rabuck, K. Raghavachari, J. B. Foresman, J. V. Ortiz, Q. Cui, A. G. Baboul, S. Clifford, J. Cioslowski, B. B. Stefanov, G. Liu, A. Liashenko, P. Piskorz, I. Komaromi, R. L. Martin, D. J. Fox, T. Keith, M. A. Al-Laham, C. Y. Peng, A. Nanayakkara, M. Challacombe, P. M. W. Gill, B. Johnson, W. Chen, M. W. Wong, C. Gonzalez, J. A. Pople, Gaussian, Inc., Pittsburgh, PA, **2003**]. The structure of *cisoid* Tf_2N has been fully optimized at the MP2/6-311+G* and B3LYP/6-311+G* levels of theory. MP2 = second-order Møller–Plesset perturbation theory (a) W. J. Hehre, L. Radom, P. v. R. Schleyer, J. A. Pople, *Ab Initio Molecular Orbital Theory*, Wiley, New York, **1986**; b) J. B. Foresman, E. Frisch, *Exploring chemistry with electronic structure methods*, 2nd ed., Gaussian, Pittsburgh, PA, **1996**), B3LYP is a density functional theory (DFT) method (R. G. Parr, Y. Yang, *Density-functional theory of atoms and molecules*, Oxford University Press, New York, **1989**) using Becke's three-parameter nonlocal exchange functional (A. D. Becke, *J. Chem. Phys.* **1993**, *98*, 5648) with the nonlocal correlation of Lee, Yang, and Parr (C. Lee, W. Yang, R. G. Parr, *Phys. Rev. B* **1988**, *37*, 785). All the stationary points were positively identified for minima (no imaginary frequency) or transition states (only one imaginary frequency).
[19] D. W. J. Cruickshank, *J. Chem. Soc.* **1961**, 5486.
[20] In order to evaluate second-order interactions natural bond orbital (NBO) analysis was performed at the respective level (a) A. E. Reed, R. B. Weinstock, F. Weinhold, *J. Chem. Phys.* **1985**, *83*, 735; b) J. E. Carpenter, F. Weinhold, *J. Mol. Struct. (THEOCHEM)* **1988**, *169*, 41). Atomic charges have been estimated using NPA method (A. E. Reed, L. A. Curtiss, F. Weinhold, *Chem. Rev.* **1988**, *88*, 899).

 © 2005 Wiley-VCH Verlag GmbH & Co. KGaA, Weinheim

Carbon Nanoparticles

DOI: 10.1002/anie.200500685

Hierarchically Structured Carbon: Synthesis of Carbon Nanofibers Nested inside or Immobilized onto Modified Activated Carbon

Dang Sheng Su, Xiaowei Chen, Gisela Weinberg, Achim Klein-Hofmann, Olaf Timpe, Sharifah Bee Abd. Hamid, and Robert Schlögl*

The rapidly expanding knowledge about the physical and chemical properties of carbon nanotubes and nanofibers (CNTs and CNFs) has led to a range of potential applications in nanotechnology[1–5] including field-effect transistors, one-dimensional quantum wires, field emitters, and hydrogen-storage devices. Most applications of CNTs/CNFs either use individual objects (in nanoelectronics) or embed the fibers into a host matrix. The outer surface of CNTs/CNFs can be tailored to display the desired chemical properties ranging from metallic (graphite layers parallel to the tube or fiber axis) and to acidic–basic (all prism faces are exposed along the fiber axis and saturated with hydroxy groups).[6,7] The selective chemisorption of undesired species from drinking water (Mn, As, Hg, Fe), the modification of the properties of polymers (heat conduction, electrical conduction, mechanical reenforcement), and the use of CNTs/CNFs as catalysts or catalyst supports are only some of the applications of chemical nanotechnology.[8–19] These applications require, however, large amounts of CNTs and CNFs with well-defined surface-chemical and mechanical properties. In addition, the nanocarbon particles must be formed into larger objects to optimize the hydrodynamic properties and allow effective contact with reacting matrices. Loose CNTs/CNFs are unsuitable as their suprastructural properties cannot be controlled, and operations of compaction can destroy or at least inhibit the access of the reactant medium to the nanostructures. On the molecular level it is potentially useful to grow dendritic structures of CNTs/CNFs onto each other to maximize the surface area exposed and to provide molecular roughness for entanglement of, for instance, polymer strands.

A hierarchical organization of the nanocarbon units on itself to form small objects and on a robust carrier structure on larger dimensions is therefore highly desirable. For chemical applications it is essential that only one chemical element is

[*] Dr. D. S. Su, Dr. X. Chen, G. Weinberg, A. Klein-Hofmann, Dr. O. Timpe, Prof. R. Schlögl
Department of Inorganic Chemistry
Fritz Haber Institute of the Max Planck Society
Faradayweg 4–6, 14195 Berlin (Germany)
Fax: (+49) 30-8413-4401
E-mail: dangsheng@fhi-berlin.mpg.de
Prof. S. B. A. Hamid
Combinatorial Technology and Catalysis Research Center
University of Malaya
50603 Kuala Lumpur (Malaysia)

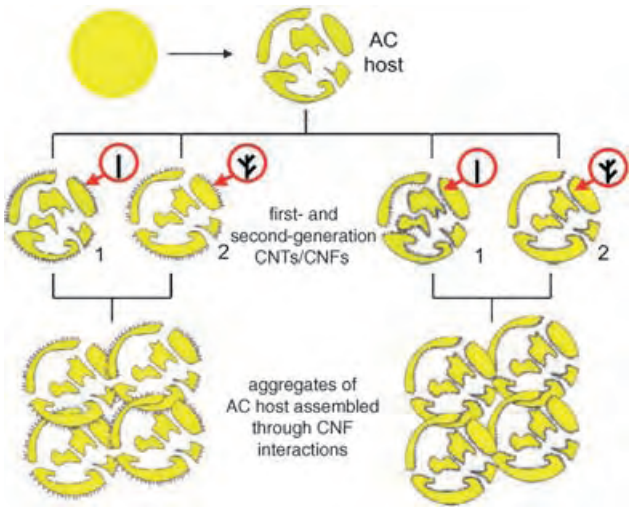
 WILEY InterScience DISCOVER SOMETHING GREAT © 2005 Wiley-VCH Verlag GmbH & Co. KGaA, Weinheim

used for the construction and that the combination of nanocarbon with the non-carbon support structures is avoided as the resulting discontinuities in transport and in chemical properties would lead to deterioration of the overall compound properties and chemical instability.

An ideal substrate is activated carbon from natural sources. Such bioinorganic polymers containing typically lignins and silicates are strong, well-structured in several dimensions, accessible for chemical modifications, and available in large amounts.[20] Natural precursors to activated carbons[21] utilize the biological cell structure to preset the disposition of the macropore network, and they benefit from inorganic additives as anchoring sites for the catalyst and therefore for the nanocarbon. It is essential that the chemical interaction between the nanocarbon and the activated carbon carrier is strong and inert to preserve the hierarchical structure during extended operation.

The present paper describes ways to modify the activated carbon obtained from the biowaste of palm oil production to serve as the support for the growth of nanocarbon. We obtained a family of immobilized CNFs in various modifications. Nanostructured carbon can be obtained on the outer surface of the activated carbon yielding a useful geometry for binder–filler applications. Alternatively, burning large pores into the bulk structure of the activated carbon and subsequently filling the pores with carbon nanostructures leads to hierarchically structured carbon materials with nested CNFs inside the activated carbon which are highly suitable for sorption and catalytic applications.

The concept behind the production of these hierarchically structured carbon materials is illustrated in Scheme 1. On the macroscopic level, bulk activated carbon aggregates are transformed into a macroporous scaffold by selectively removing the "soft" parts of the biopolymer. This is achieved by catalytic burning during or after carbonization. The catalyst particles are then deliberately embedded in the carbon matrix by transforming the oxidic form of the catalyst used for creating porosity into a metallic form. The metal particles gasify the support locally under a reducing atomosphere. This form is then used for growing nanocarbon by chemical vapor decomposition (CVD) of organic molecules in one or several generations; if needed additional catalyst is embedded. The resulting immobilized nanocarbon-activated carbon composite (NAC) can then be assembled into larger solid aggregates by growing nanocarbon on the outside of the activated carbon grains to bind NAC particles firmly to each other. The transport of matrix media can be well controlled by changing the density of the nanostructures and by varying the filling factor of the porous carbon support. A final stage of chemical surface modification that may be necessary is not shown in Scheme 1. The preferential location of catalyst deposition inside or outside of the activated carbon scaffold can be varied by changing the deposition conditions of the catalytic precursor from ion exchange to homogeneous precipitation.



Scheme 1. The synthesis of hierarchically structured carbon materials by modifying activated carbon with nanocarbon.

By varying the unit operations—1) impregnation with the catalyst, 2) calcinations of the support carbon, 3) reduction of the catalyst and growth of nanocarbon—a family of nested or immobilized CNTs/CNFs can be obtained. We use the CVD method for growing the CNTs/CNFs as it has several advantages over electric-arc discharge and laser ablation. For example, the CVD method leads not only to single-walled or multiwalled CNTs but also to aligned CNTs when different hydrocarbons are used. Carbon growth on inner surfaces is possible, large amounts of CNTs/CNFs can be synthesized at moderate temperatures and with low cost, and structure can be controlled by regulating the growth parameters. The CVD method is the most promising method for the large-scale synthesis of CNTs/CNFs.[1,22–26] A suitable choice for the catalyst system is iron, as it catalyzes both the oxidation of carbon and nanocarbon growth.

A typical carbonized precursor obtained from palm kernel shell exhibits a BET surface area of 1081 $m^2 g^{-1}$; the pore volume is 0.365 $cm^3 g^{-1}$. A scanning electron micrograph (SEM) of this activated carbon is displayed in Figure 1a. To prepare the host for the designed hierarchical structure, the as-obtained AC was oxidized under mild conditions at 400 °C in air for 4 h. The activated carbon suffered a weight loss of about 5.2 %. Figure 1b shows a SEM image of activated carbon after the mild oxidation. Oxidation at this temperature removes also carbon debris from the surface and cleans the pores of activated carbon. Furthermore the oxidation increases the pose size as is apparent by comparison of the electron micrographs in Figure 1a and 1b.

The SEM image in Figure 1c shows the iron catalyst particles observed on the surface of the AC catalyst after impregnation, oxidation, and reduction of the catalyst (see the Experimental Section). The specific BET surface area of the Fe/AC catalyst is 1490 $m^2 g^{-1}$, and the pore volume increases to 0.551 $cm^3 g^{-1}$. The plot of BJH pore-size distribution in Figure 2 shows that the volume of mesopores in the Fe/AC catalyst is substantially greater than that of the parent material. In parallel to the formation of mesopores, the micropores are also enlarged as evident in the BJH plot at a pore size of about 2 nm (Figure 2). After catalytic decomposition of a mixture of C_2H_4 and H_2 at 700 °C on the Fe/AC catalyst, carbon nanofibers form and cover the activated

 © 2005 Wiley-VCH Verlag GmbH & Co. KGaA, Weinheim

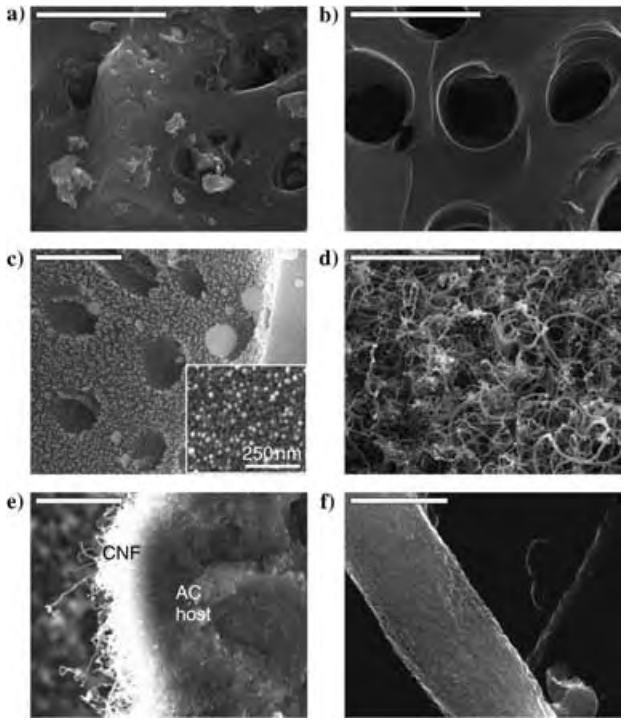


Figure 1. SEM images of a) activated carbon (AC); b) activated carbon calcined at 400 °C; c) 1 wt % Fe/activated carbon, the inset is a enlarged image of the catalyst particles; d) carbon nanofibers on activated carbon; e) a cross section of CNFs on the outer surface of activated carbon; f) a single CNF showing the rough surface morphology. Scale bars: 2 μm (a–c), 20 μm (d), 10 μm (e), and 500 nm (f).

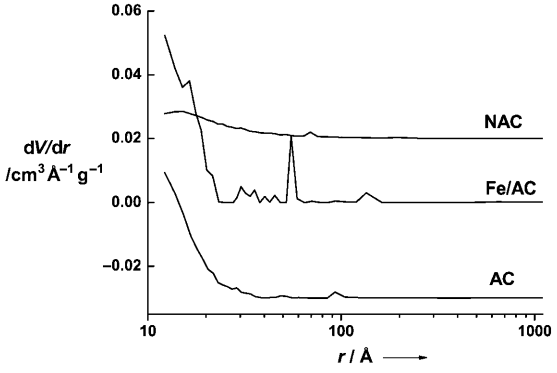


Figure 2. Pore-size distribution (determined by BJH adsorption) of the activated carbon, Fe/AC, and activated carbon with CNFs grown inside and outside. For distinction the plot of NAC is offset by 0.02 units; the plot of AD is offset −0.03 units.

carbon (as shown in Figure 1 d). They orient randomly and are entangled. The diameters of the fibers are widely distributed from 20 to 300 nm. The cross-section SEM image in Figure 1 e confirms that the CNFs are grown on the outer surface of the AC. The SEM image of a single CNF in Figure 1 f reveals the considerable roughness of the outer surface of the CNFs. Such a morphology is beneficial for the hydrodynamics of sorption processes from the liquid phase and provides mechanical and chemical anchoring sites when it is used as additive in polymer materials.

The yield of carbon nanofibers on an Fe/AC host reaches ca. 105 g of C per g of Fe. The growth mechanism is the same as that known for the CVD preparation of CNTs/CNFs, which consists of the dissolution, diffusion, and precipitation of carbon atoms on the catalyst particle.[27] Secondary electron and backscattered electron images of carbon nanofibers on the activated carbon are presented in Figures 3 a and 3 b,

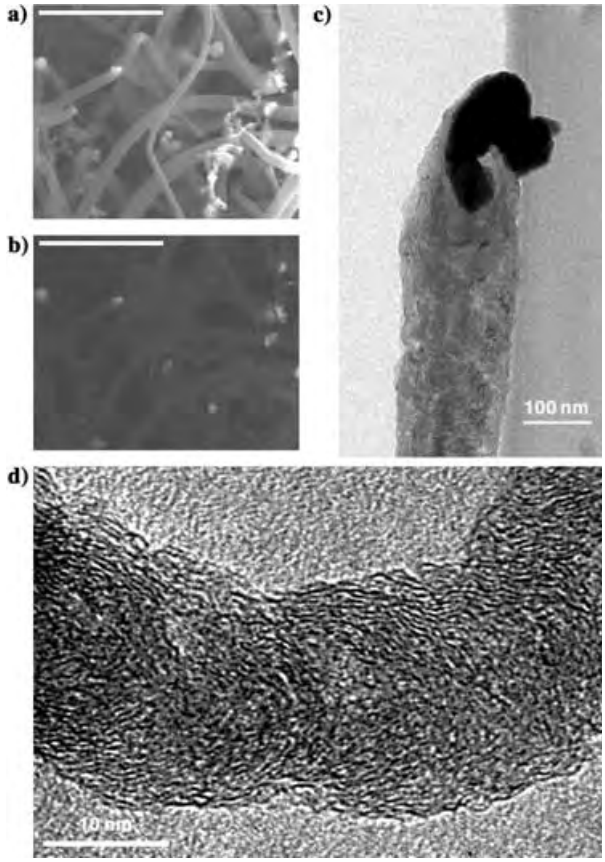


Figure 3. a, b) SEM images of immobilized CNFs with the Fe catalyst: a) SE mode, b) BSE mode; light spots correspond to Fe particles; c) TEM image of an immobilized CNF with a Fe particle on the tip; d) high-resolution TEM image showing the herringbone structure of a CNF. Scale bars: 5 μm (a, b).

respectively. From a comparison of the contrasts, the iron catalyst particles can be located as bright objects in the backscattered electron micrograph. The growth of CNFs follows the "tip-growing" model:[5,28] most of the iron catalyst particles are found on the tips of the CNFs (transmission electron micrograph (TEM) in Figure 3 c), although in few cases the iron particles are found not only at the tip but also in the middle of carbon nanofiber.

The high-resolution TEM image (Figure 3 d) of the carbon nanofibers reveals that the carbon nanofibers are of the herringbone type, which explains the origin of the surface roughness seen in SEM (Figure 1 f). Keeping in mind the intended applications, we wanted to expose as many prismatic faces as possible on the surface of the nanocarbon without losing mechanical stability. The shape and the size of the metal catalyst control the nanocarbon morphology.[29] Baker

 © 2005 Wiley-VCH Verlag GmbH & Co. KGaA, Weinheim

et al. reported that nanofibers are obtained from large Fe particles (>20 nm), while nanotubes were formed from smaller particles (<20 nm).[30,31] The high loading and the activation conditions caused the catalyst particles to aggregate (see Figure 3c) and form the desired rough surface of the CNFs.

Figure 4a presents a cross-section SEM image though an AC particle with a large pore in it after the CNF growth. Hair or microbrush structures are found inside the pore (cf. the SEM image Figure 1b). The enlarged SEM image in Figure 4b reveals that the dentritic structure results from entangled CNFs created during the CVD process. The cross-section TEM image of the pore in Figure 4c proves convincingly that CNFs were grown on the inner wall of the pore. Moreover, the distribution of diameters of CNFs in the pores is quite narrow, in the range of 20–50 nm. In addition, the CNFs grown inside the pores are shorter than those grown on the surface of the activated carbon. This could be a result of the limited transport of ethylene into the pores. The microstructure of the CNFs in the pores is revealed by high-resolution TEM (Figure 4d).

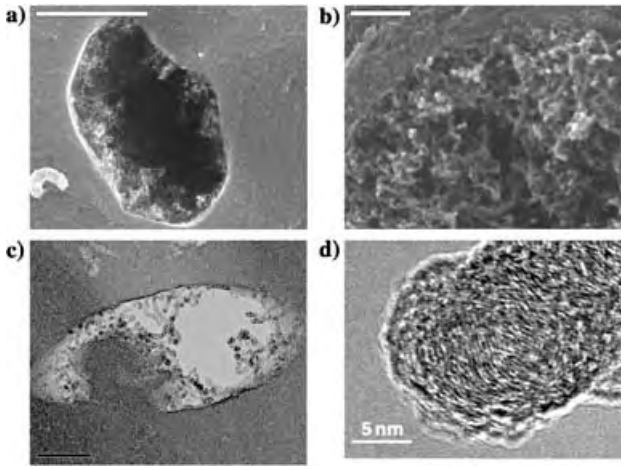


Figure 4. a) SEM image of cross section of CNFs on activated carbon, b) enlarged image of a; c) TEM image of cross section of CNFs on activated carbon; d) high-resolution image of a CNF in (c). Scale bars: 2 μm in a, 200 nm in b–c.

The microscopic data were confirmed by the specific BET surface area of activated carbon with CNFs inside which decreases to 305 $m^2 g^{-1}$ and is much smaller than that of activated carbon and of the Fe/AC catalyst. The pore volume decreases to 0.289 $cm^3 g^{-1}$. This is attributed to the partial filling of the pores in the matrix by CNFs. The pore-size distribution (Figure 2) changes drastically with a broad distribution of nanometer-sized pores being attributed to the desired voids between the entangled CNF fillers.

The surface of the freshly prepared CNFs should be poor in acidic oxygen functional groups due to the reductive reaction atmosphere of their growth. Chemisorption by ion exchange with OH groups should thus be negligible. On the other hand, the nanostructured voids between the entangled CNFs and their rough surfaces should support the agglomeration of condensable species and should thus allow the filtering of difficult-to-adsorb species, for example, the oxo anions of transition metals.

We tested this in a demonstration experiment comparing the adsorption of noncondensable chromate in basic solution and condensable heteropolymolybdate $H_3[PMo_{12}O_{40}]$ in solution. In Table 1 the adsorption capacities per unit mass and unit surface area are listed. The activated carbon adsorbs chromate by means of ion exchange with the acidic surface hydroxy groups. After treatment and growth of the CNFs these surface hydroxy groups are absent, depriving the material of its adsorption function. On the other hand, the polyoxomolybdate is poorly anchored to the hydroxy groups owing to its unfavorable charge-to-surface ratio. Sites for polycondensation of the anions into oxyhydroxide polymers are created by changing the surface texture of the activated carbon, and even better by introducing the CNF filling into the pore system. The absorption capacity of the activated carbon increases a factor of 5 when it is mildly oxidized at 400 °C, but by a factor of 27 when CNFs are grown on and inside the activated carbon (Table 1).

In summary, we have prepared hierarchically structured carbon with CNFs nested inside or immobilized onto modified activated carbon by means of chemical vapor decomposition of ethylene. The activated carbon is obtained from the biowaste of palm oil production, pretreated by mild oxidation, and impregnated with an iron catalyst. The method is cheap and can be scaled up. The preliminary results of adsorption experiments prove that the deliberate nanostructuring of a carbon surface can result in novel adsorbant properties. It is expected that the polymerization of metallic polyanions can be optimized by changing the pore-size distribution, adjusting roughness of the CNFs, and adding special surface functional groups.

Table 1: Adsorption of chromate and heteropolymolybdate in aqueous solution by activated carbon (AC), activated carbon calcined at 400 °C (AC-400), and nanocarbon-activated carbon composite (NAC).

	BET $[m^2 g^{-1}]$	Ads. $[CrO_4]^{2-}$ $[\mu mol\, g^{-1}]$[a]	Ads. $[CrO_4]^{2-}$ (rel.) $[\mu mol\, m^{-2}]$[b]	Ads. [PMo][c] $[\mu mol\, g^{-1}]$	Ads. [PMo] (rel.) $[\mu mol\, m^{-2}]$
AC-400	1490	67	0.016	15.5	0.120
AC	1081	73	0.034	2.5	0.024
NAC	305	55	–[d]	16.6	0.660
blank	–	55	–	0[e]	–

[a] Estimated from absorption at $\lambda = 420$ nm. [b] Values are based on difference to blank. [c] [PMo] = $[PMo_{12}O_{40}]^{3-}$. [d] The concentration after the experiment is identical to that of the blank. [e] In all solutions the absorption ($\lambda = 325$ nm) after the experiment was enhanced; adsorption of [PMo] for blank is used as the reference.

Experimental Section

The activated carbon used as the support was supplied by COMBI-CAT research center, University of Malaya (Malaysia). It was made from palm kernel shells, a waste product from palm oil production.

 © 2005 Wiley-VCH Verlag GmbH & Co. KGaA, Weinheim

Beside carbon, it contains substantial amounts of silicate and traces of iron as iron silicate after the activation. Palm kernel shells were carbonized in N_2 at 350 °C and activated in steam at 600 °C. The support activated carbon was calcined at 400 °C for 4 h in air. The Fe/AC precursor (1 wt % Fe) was prepared by impregnation with a 0.09 M aqueous solution of $Fe(NO_3)_3$ and activated carbon calcined at 400 °C with a loading of 1 % iron oxide onto dry carbon. A drying step at 60 °C overnight was followed by the autogeneous pore formation through calcination at 500 °C in N_2 for 4 h. The Fe-impregnated sample was reduced with H_2 at 700 °C for 4 h. The Fe/AC catalyst (100 mg, 1 wt % Fe) was put into the vertical quartz reactor and flushed with He overnight. The carbon nanofibers were grown by treating the Fe/AC catalyst at 700 °C in flowing 60 % C_2H_4/H_2 (125 mL min^{-1}) at atmospheric pressure for 2 h. The obtained sample was cooled to room temperature in a stream of He.

For the adsorption experiments, 10 mg of activated carbon or the NAC sample were suspended in 1.5 mL of aqueous $H_3PMo_{12}O_{40}$ or K_2CrO_4 (1 mM). The suspensions were stirred for 1 h at room temperature. The concentration of $[PMo_{12}O_{40}]^{3-}$ was measured by photometry ($\lambda = 325$ nm). The adsorption test was performed in an Eppendorf cap (Volume 2.0 mL, material is PE). The pH was not adjusted (with additional buffer); the pH calculated for heteropolymolybdate solution is around 3.0, for chromate solution around 8.5. SEM investigations were performed on a Hitachi S-4000 FEG in secondary-electron (SE) mode and backscattered-electron (BSE) mode at 15-kV accelerating voltage. TEM studies were performed on a Philips CM 200 LaB_6 operating at 200 kV.

Received: February 23, 2005
Published online: July 25, 2005

Keywords: activated carbon · adsorption · carbon nanofibers · hierarchical structure

[1] M. Terrones, *Annu. Rev. Mater. Res.* **2003**, *33*, 419.
[2] W. Qian, T. Liu, Z. Wang, H. Yu, Z. Li, F. Wei, G. Luo, *Carbon* **2003**, *41*, 2487.
[3] K. P. De Jong, J. W. Geus, *Catal. Rev. Sci. Eng.* **2000**, *42*, 481.
[4] A. Huczko, *Appl. Phys. A* **2002**, *74*, 617.
[5] C. Emmenegger, J.-M. Bonard, P. Mauron, P. Sudan, A. Lepora, B. Grobety, A. Züttel, L. Schlapbach, *Carbon* **2003**, *41*, 539.
[6] R. Schlögl in *Handbook of Porous Solids* (Eds.: F. Schüth, K. S. W. Sing, J. Weitkamp), Wiley-VCH, Weinhein, **2002**, pp. 1863 – 1900.
[7] H.-P. Boehm, *Angew. Chem.* **1966**, *78*, 617; *Angew. Chem. Int. Ed. Engl.* **1966**, *5*, 533.
[8] C. Pham-Huu, N. Keller, L. J. Charbonniere, R. Ziessel, M. J. Ledoux, *Chem. Commun.* **2000**, 1871.
[9] H. X. Luo, Z. J. Shi, N. Q. Li, Z. N. Gu, Q. K. Zhuang, *Anal. Chem.* **2001**, *73*, 915.
[10] R. Gao, C. D. Tan, R. T. K. Baker, *Catal. Today* **2001**, *65*, 19.
[11] R. Vieira, C. Pham-Huu, N. Keller, M. J. Ledoux, *Chem. Commun.* **2002**, 954.
[12] C. H. Liang, Z. L. Li, J. S. Qiu, C. Li, *J. Catal.* **2002**, *211*, 278.
[13] W. Z. Li, C. H. Liang, J. S. Qiu , W. J. Zhou, H. M. Han, Z. B Wei, G. Q. Sun, Q. Xin, *Carbon* **2002**, *40*, 787.
[14] T. G. Ros, A. J. van Dillen, J. W. Geus, D. C. Koningsberger, *Chem. Eur. J.* **2002**, *8*, 2868.
[15] M. L. Toebes, F. F. Prinsloo, J. H. Bitter, A. J. van Dillen, K. P. de Jong, *J. Catal.* **2003**, *214*, 78.
[16] V. Lordi, N. Yao, J. Wei, *Chem. Mater.* **2001**, *13*, 733.
[17] G. Mestl, N. I. Maksimova, N. Keller, V. V. Roddatis, R. Schlgöl, *Angew. Chem.* **2001**, *113*, 2122; *Angew. Chem. Int. Ed.* **2001**, *40*, 2066.
[18] R. Vieira, M.-J. Ledoux, C. Pham-Huu, *Appl. Catal. A* **2004**, *274*, 1.
[19] R. Vieira, D. Bastos-Netto, M.-J. Ledoux, C. Pham-Huu, *Appl. Catal. A* **2005**, *279*, 35.
[20] J.-B. Donnet, R. C. Bansal, M.-J. Wang in *Carbon Black, Science and Technology*, Marcel Dekker, New York, **1993**.
[21] F. J. Rodriguez-Reinoso in National Organic Standards Board Technical Advisory Panel Review, http://www.omri.org/AC_processing.pdf (**1995**).
[22] S. Zhu, C.-H. Su, S. L. Lehoczky, I. Muntele, D. Ila, *Diamond Relat. Mater.* **2003**, *12*, 1825.
[23] M. Pérez-Cabero, E. Romeo, C. Royo, A. Monzón, A. Guerrero-Ruíz, I. Rodríguez-Ramos, *J. Catal.* **2004**, *124*, 197.
[24] K. Otsuka, Y. Abe, N. Kanai, Y. Kobayashi, S. Takenaka, E. Tanabe, *Carbon* **2004**, *42*, 727.
[25] A. K. M. F. Kibria, Y. H. Mo, K. S. Nahm, *Catal. Lett.* **2001**, *71*, 229.
[26] L. C. Qin, *J. Mater. Sci. Lett.* **1997**, *16*, 457.
[27] J. C. Charlier, S. Iijima in *Topics in Applied Physics, Vol. 80* (Eds.: M. S. Dresslhaus, C. E. Ascheron, H. J. Koelsch), Springer, Berlin, **2001**, pp. 55 – 80.
[28] M. José-Yacamán, M. Miki-Yoshida, L. Rendón, J. G. Santiesteban, *Appl. Phys. Lett.* **1993**, *62*, 657.
[29] M. Audier, M. Coulon, A. Oberlin, *Carbon* **1980**, *18*, 73.
[30] R. T. K. Baker, M. A. Barber, P. S. Harris, F. S. Feates, R. J. Waite, *J. Catal.* **1972**, *26*, 51.
[31] R. T. K. Baker, N. M. Rodrigues in *Materials Research Society Symposium Proceeding*, *Vol. 2*, **1999**.

 © 2005 Wiley-VCH Verlag GmbH & Co. KGaA, Weinheim

Asymmetric Synthesis

DOI: 10.1002/anie.200501142

Solid-State Structure and Enantioselective Reactions of a Complex of a 1-Thio-Substituted Propargyllithium and (−)-Sparteine**

*Ralf Otte, Roland Fröhlich, Birgit Wibbeling, and Dieter Hoppe**

Organolithium (−)-sparteine complexes have become valuable tools in enantioselective synthesis.[1] Nevertheless, only few X-ray crystal structure analyses of lithium (−)-sparteine complexes with either chiral[2] or achiral carbanions[3] are known. Among these, there are no examples of an α-thio-

[*] Dipl.-Chem. R. Otte, Dr. R. Fröhlich,[+] B. Wibbeling,[+]
Prof. Dr. D. Hoppe
Organisch-Chemisches Institut
Westfälische Wilhelms-Universität Münster
Corrensstrasse 40, 48149 Münster (Germany)
Fax: (+49) 251-83-36531
E-mail: dhoppe@uni-muenster.de

[+] X-ray crystal structure analyses

[**] This work was supported by the Deutsche Forschungsgemeinschaft (Ho 577/13-3 and SFB 424), the Fonds der Chemischen Industrie (grant for R.O.), and the International NRW Graduate School of Chemistry.

Supporting information for this article is available on the WWW under http://www.angewandte.org or from the author.

WILEY InterScience DISCOVER SOMETHING GREAT
© 2005 Wiley-VCH Verlag GmbH & Co. KGaA, Weinheim

substituted carbanion complex.[4,5] Chiral α-thioalkyllithium and -benzyllithium complexes were found to racemize rapidly;[6–9] this is attributed to only a weak interaction between the cation and the anion in the ion pair.[10] In contrast, for α-carbamoylthio-substituted alkyllithium,[11] benzyllithium,[12] and cyclic allyllithium compounds,[13] a remarkably high configurational stability is recorded, presumably resulting from efficient chelation by the *S*-(*N*,*N*-dialkylcarbamoyl) group. The asymmetric deprotonation and substitution of thio-substituted compounds have been described recently in several publications.[14]

We investigated the (−)-sparteine-assisted lithiation of thiocarbamate **1** (Scheme 1).[15] In pentane at temperatures below −30 °C, a precipitate of complex (*S*)-**3**·**2** was formed, which provided suitable crystals for an X-ray analysis with anomalous dispersion (Figure 1).[16,17] Trapping the precipitate with trimethylsilyl triflate (TMSOTf) yielded the propargylsilane (*S*)-**4a** in 83 % yield with ≥95 % *ee*.[18] Similarly, the reaction with *tert*-butyldimethylsilyl triflate (TBSOTf) resulted in the crystalline silane (*S*)-**4b** (69 % yield, ≥95 % *ee*).[18] An X-ray crystal structure analysis with anomalous dispersion revealed the *S* configuration of **4b** (Figure 2).[17,19]

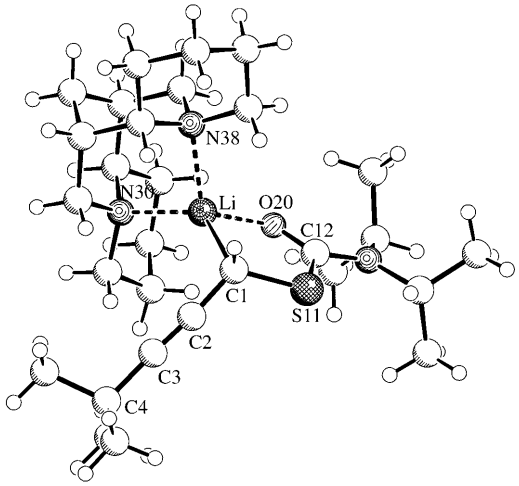


Figure 1. Molecular structure of (*S*)-**3**·**2** in the crystal. Selected bond lengths [pm] and angles [°]: Li–C1 217.3(10), Li–N30 203.8(9), Li–N38 205.0(9), Li–O20 189.7(9), C1–C2 141.7(7), C2–C3 119.8(7), C3–C4 149.5(8), C1–S11 176.1(5); N30-Li-N38 90.2(4), N30-Li-C1 127.8(4), N30-Li-O20 121.8(5), N38-Li-C1 115.1(4), N38-Li-O20 112.5(4), C1-Li-O20 91.0(4), Li-C1-S11 104.3(3), Li-C1-C2 103.3(4), S11-C1-C2 115.9(4), C1-C2-C3 175.2(5), C2-C3-C4 176.3(6), Li-C1-S11-C12 −1.9(4).

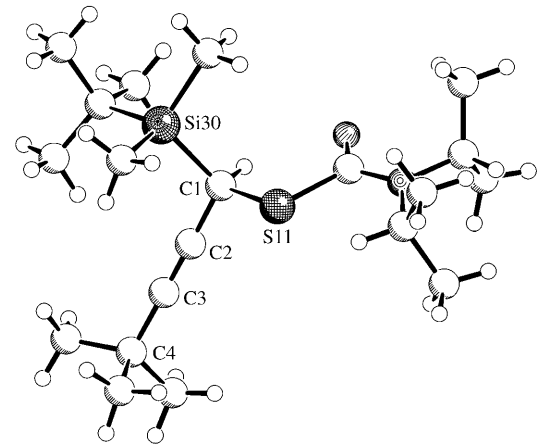
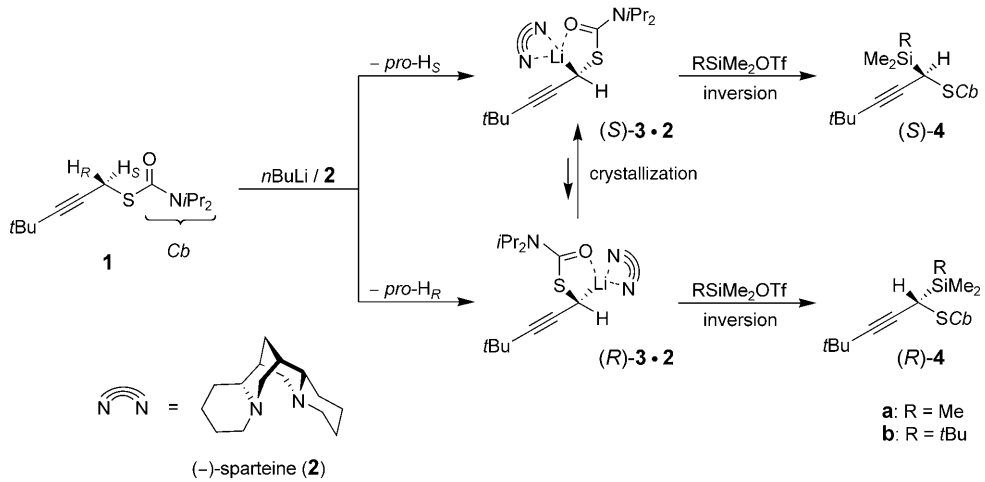


Figure 2. Molecular structure of (*S*)-**4b** in the crystal. Selected bond lengths [pm] and angles [°]: C1–C2 144.5(3), C1–S11 183.5(2), C1–Si30 190.6(2), C2–C3 120.3(3), C3–C4 147.1(3); C2-C1-S11 107.7(2), C2-C1-Si30 109.8(1), C3-C2-C1 176.2(3), C2-C3-C4 179.5(3).

As observed for all silylations of thio-substituted mesomerically stabilized carbanion/lithium–sparteine complexes the silylation proceeds with stereoinversion.[12,9]

Compound (*S*)-**3**·**2** crystallizes as a monomeric chelate complex with a tetragonally coordinated lithium cation, which is attached to the carbanionic center, the oxo group, and both nitrogen atoms of (−)-sparteine (Figure 1). The carbanionic center at C1 is *S*-configurated, and the stereogenic lithium cation has *S* configuration, as was also found for an allyllithium (−)-sparteine complex.[2b] Surprisingly, C1 is sp^3-hybridized: the sum of angles Li-C1-S11, Li-C1-C2, and S11-C1-C2 amounts to 323.5(11)° (the ideal values for sp^3



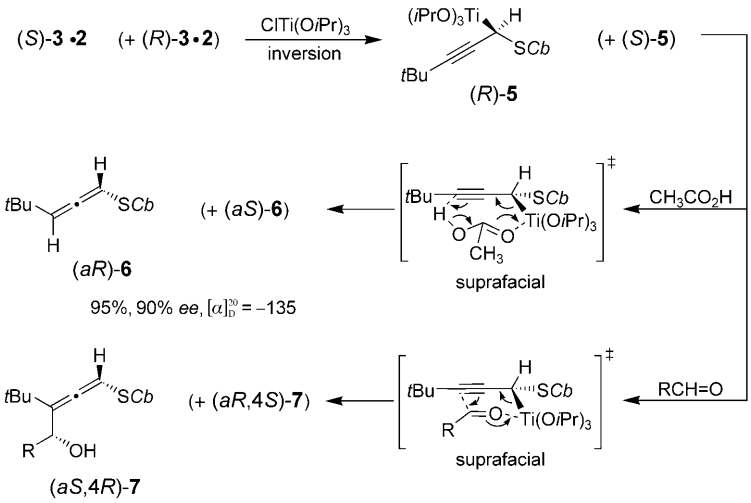
Scheme 1. Asymmetric deprotonation and silylation of **1**.

 © 2005 Wiley-VCH Verlag GmbH & Co. KGaA, Weinheim

hybridization are 328.4°, for sp^2 hybridization, 300.0°). This, in combination with the bond lengths for C1–C2 (141.7(7) pm) and C2–C3 (119.8(7) pm), leads us to the conclusion that mesomeric stabilization of the negative charge plays only a minor role. The lengths and angles in the vicinity of C1 to C3 are surprisingly similar for the lithium compound (*S*)-**3·2** and silane (*S*)-**4b** (Figure 2), which supports the lack of mesomeric stabilization in (*S*)-**3·2**.

The Li–C1 bond (217.3(10) pm) is relatively long and, consequently, the bonds to (−)-sparteine, $d_{\text{Li-N30}} = 203.8(9)$ pm and $d_{\text{Li-N38}} = 205.0(9)$ pm, are shorter than those in lithiated alkenyl carbamates.[20] Theoretical calculation on α-thio-substituted organolithium complexes[4c,14b,21] predict an antiperiplanar relationship between the bonds C1–Li and S–C12 for the conformation of lowest energy. In the cyclic complex (*S*)-**3·2** the dihedral angle Li-C1-S11-C12 is forced into synperiplanarity (−1.9(4)°).

Solid (*S*)-**3·2** undergoes transmetalation with $ClTi(OiPr)_3$ with stereoinversion to form the propargyltitanium intermediate (*R*)-**5**. This was the conclusion from some suprafacial reactions explored during the investigation of the *O*-carbamates analogous to **1**.[22] Quenching **5** with a solution of acetic acid in ether at −78 °C gave the allene (*aR*)-**6** in 95 % yield and 90 % *ee*[23] (Scheme 2). The absolute configuration of



7	R =	Yield [%]	d.r.	% *ee*	$[\alpha]_D^{20}$
a	2-naphthyl	79	≥ 98:2	96	−558
b	phenyl	82	≥ 98:2	98	−466
c	cyclohexyl	71	≥ 98:2	98	−77
d	2-propyl	66	≥ 98:2	97	−27

Scheme 2. Synthesis of enantioenriched 1-thio-substituted allenes **6** and **7**.

(*aR*)-**6** was elucidated by an X-ray crystal structure analysis,[17,24] again with anomalous dispersion (see Figure 3 in the Supporting Information).

At −78 °C the titanium intermediate **5** readily added to aldehydes and formed diastereomerically pure, highly enantioenriched 1-thio-substituted 4-hydroxy-1,2-alkadienes **7** with an (*aS*,4*R*) configuration, which arise from a Zimmerman–Traxler-type transition state (Scheme 2).[25] The reaction with naphthalene-2-carbaldehyde furnished the allene (*aS*,4*R*)-**7a** in 79 % yield and 96 % *ee*;[26] its absolute configuration was concluded from an X-ray crystal structure analysis (see Figure 4 in the Supporting Information).[27,17]

What is the mechanism resulting in enantiomeric enrichment?[28] When **1** was lithiated by *n*BuLi/**2** in toluene at −78 °C without crystallization and the soluble complexes **3·2** were trapped after 1 min with TMSOTf, (*S*)- and (*R*)-**4a** were formed in a ratio of 68:32 (36 % *ee*) and a yield of 84 %. The ratio shifted only slightly (71:29, 42 % *ee*) after 10 h of stirring at −78 °C. The precipitate of (*S*)-**3·2** formed by crystallization at −30 °C was dissolved in toluene and the solution kept for 6 h at −78 °C; the solution was treated with TMSOTf, and no decrease in the enantiomeric ratio of the silylated product (*S*)- and (*R*)-**4a** was observed (≤ 97.5:2.5, ≤ 95 % *ee*). These experiments demonstrate that there is only little preference for abstraction of *pro*-H_S under kinetically controlled conditions and essentially complete configurational stability. When the dissolved precipitate was stirred for 2 h at −30 °C, a ratio of 71:29 (42 % *ee*) was recorded, which is assumed to be close to the thermodynamically controlled ratio of (*S*)- and (*R*)-**3·2**. At −30 °C, epimerization is rapid enough so that the selection occurs by selective and complete crystallization of the major diastereomer (*S*)-**3·2** ("dynamic thermodynamic resolution").[29,30]

The reported results not only give deep insight into structural features of chiral substituted propargyllithium ion pairs and the stereochemistry of their reactions,[31,32] but also offer an efficient access to highly enantioenriched allenes.[33,34]

Experimental Section

The preparation of single crystals of (*S*)-**3·2** was performed under an argon atmosphere in a flame-dried Schlenk flask. A clear solution of **1** (0.128 g, 0.50 mmol, 1.00 equiv) and **2** (0.123 g, 0.53 mmol, 1.05 equiv) in dry pentane (8 mL) was prepared at room temperature. The reaction mixture was then cooled to −30 °C, and *n*BuLi (0.34 mL, 0.55 mmol, 1.1 equiv; 1.6 M in *n*-hexane) was added slowly over 5 min. Moderate stirring was stopped immediately when the addition was complete. The slightly yellow homogenous solution was kept undisturbed under argon at −30 °C for 1 h, and the first tiny crystals formed. These were allowed to grow by gradual evaporation of the solvent under vacuum (approx. 50 mbar). Under these conditions colorless crystals of suitable size formed over 4 h. The flask was back-filled with argon, and the remaining supernatant solution was removed carefully. The obtained crystals are stable below 0 °C under argon; at room temperature they decompose within hours. In solution, decomposition occurs much faster.

For experimental data for the substitution reactions see the Supporting Information.

Received: March 31, 2005
Published online: July 26, 2005

Keywords: allenes · asymmetric synthesis · carbanions · lithiation · sparteine

[1] For reviews, see: a) D. Hoppe, T. Hense, *Angew. Chem.* **1997**, *109*, 2376; *Angew. Chem. Int. Ed. Engl.* **1997**, *36*, 2282; b) D.

 © 2005 Wiley-VCH Verlag GmbH & Co. KGaA, Weinheim

Hoppe, F. Marr, M. Brüggemann, *Top. Organomet. Chem.* **2003**, *5*, 61 – 137; c) P. Beak, T. A. Johnson, D. D. Kim, S. H. Lim, *Top. Organomet. Chem.* **2003**, *5*, 139 – 176; d) D. Hoppe, G. Christoph in *The Chemistry of Organolithium Compounds* (Eds.: Z. Rappoport, I. Marek), Wiley, Chichester, **2004**, pp. 1055 – 1164.

[2] a) L. T. Bryne, L. M. Engelhardt, G. E. Jacobsen, W.-P. Leung, R. I. Papasergio, C. L. Raston, B. W. Skelton, P. Twiss, A. H. White, *J. Chem. Soc. Dalton Trans.* **1989**, 105; b) R. I. Papasergio, B. W. Skelton, P. Twiss, A. H. White, *J. Chem. Soc. Dalton Trans.* **1990**, 1161; c) M. Marsch, K. Harms, O. Zschage, D. Hoppe, G. Boche, *Angew. Chem.* **1991**, *103*, 338; *Angew. Chem. Int. Ed. Engl.* **1991**, *30*, 321; d) G. Boche, M. Marsch, J. Harbach, K. Harms, B. Ledig, F. Schubert, J. C. W. Lohrenz, H. Ahlbrecht, *Chem. Ber.* **1993**, *126*, 1887; e) I. Hoppe, M. Marsch, K. Harms, G. Boche, D. Hoppe, *Angew. Chem.* **1995**, *107*, 2328; *Angew. Chem. Int. Ed. Engl.* **1995**, *34*, 2158; f) I. Hoppe, D. Hoppe, M. Marsch, K. Harms, G. Boche, *Z. Kristallogr.* **1996**, *211*, 331; g) D. J. Pippel, G. A. Weisenburger, S. R. Wilson, P. Beak, *Angew. Chem.* **1998**, *110*, 2600; *Angew. Chem. Int. Ed.* **1998**, *37*, 2522.

[3] a) B. Ledig, M. Marsch, K. Harms, G. Boche, *Angew. Chem.* **1992**, *104*, 80; *Angew. Chem. Int. Ed. Engl.* **1992**, *31*, 79; b) C. Strohmann, T. Seibel, K. Strohfeldt, *Angew. Chem.* **2003**, *115*, 4669; *Angew. Chem. Int. Ed.* **2003**, *42*, 4531; c) C. Strohmann, K. Strohfeldt, D. Schildbach, *J. Am. Chem. Soc.* **2003**, *125*, 13672; d) C. Strohmann, K. Strohfeldt, D. Schildbach, M. McGrath, P. O'Brien, *Organometallics* **2004**, *23*, 5389; e) F. Marr, R. Fröhlich, D. Hoppe, *Tetrahedron: Asymmetry* **2002**, *13*, 2587.

[4] For selected crystal structures, see: a) D. Seebach, R. Amstutz, J. D. Dunitz, *Angew. Chem.* **1981**, *93*, 487; *Angew. Chem. Int. Ed. Engl.* **1981**, *20*, 465; b) D. Seebach, T. Maetzke, R. K. Haynes, M. N. Paddon-Row, S. S. Wong, *Helv. Chim. Acta* **1988**, *71*, 299; c) W. Zarges, M. Marsch, K. Harms, W. Koch, G. Frenking, G. Boche, *Chem. Ber.* **1991**, *124*, 543.

[5] For a review of structures of organolithiums, see: T. Stey, D. Stalke in *The Chemistry of Organolithium Compounds* (Eds.: Z. Rappoport, I. Marek), Wiley, Chichester, **2004**, pp. 47 – 120.

[6] a) R. W. Hoffmann, T. Rühl, J. Harbach, *Justus Liebigs Ann.* **1992**, 725; b) H. Ahlbrecht, J. Harbach, R. W. Hoffmann, T. Ruhland, *Liebigs Ann.* **1995**, 211; c) R. K. Dress, T. Rölle, R. W. Hoffmann, *Chem. Ber.* **1995**, *128*, 673; d) R. W. Hoffmann, R. K. Dress, T. Ruhland, A. Wenzel, *Chem. Ber.* **1995**, *128*, 861.

[7] a) H. J. Reich, R. R. Dykstra, *Angew. Chem.* **1993**, *105*, 1489; *Angew. Chem. Int. Ed. Engl.* **1993**, *32*, 1469; b) H. J. Reich, R. R. Dykstra, *J. Am. Chem. Soc.* **1993**, *115*, 7041; c) H. J. Reich, K. J. Kulicke, *J. Am. Chem. Soc.* **1995**, *117*, 6621; d) H. J. Reich, K. J. Kulicke, *J. Am. Chem. Soc.* **1996**, *118*, 273.

[8] R. W. Hoffmann, M. Julius, F. Chemla, T. Ruhland, G. Frenzen, *Tetrahedron* **1994**, *50*, 6049.

[9] For a review, see: T. Toru, S. Nakamura, *Top. Organomet. Chem.* **2003**, *5*, 177 – 216.

[10] T. Ruhland, R. W. Hoffmann, S. Schade, G. Boche, *Chem. Ber.* **1995**, *128*, 551.

[11] B. Kaiser, D. Hoppe, *Angew. Chem.* **1995**, *107*, 344; *Angew. Chem. Int. Ed. Engl.* **1995**, *34*, 323.

[12] a) D. Hoppe, B. Kaiser, O. Stratmann, R. Fröhlich, *Angew. Chem.* **1997**, *109*, 2872; *Angew. Chem. Int. Ed. Engl.* **1997**, *36*, 2784; b) O. Stratmann, B. Kaiser, R. Fröhlich, O. Meyer, D. Hoppe, *Chem. Eur. J.* **2001**, *7*, 423.

[13] a) F. Marr, R. Fröhlich, D. Hoppe, *Org. Lett.* **1999**, *1*, 2081; b) F. Marr, R. Fröhlich, B. Wibbeling, C. Diedrich, D. Hoppe, *Eur. J. Org. Chem.* **2002**, 2970.

[14] a) S. Nakamura, R. Nakagawa, Y. Watanabe, T. Toru, *Angew. Chem.* **2000**, *112*, 361; *Angew. Chem. Int. Ed.* **2000**, *39*, 353; b) S. Nakamura, R. Nakagawa, Y. Watanabe, T. Toru, *J. Am. Chem. Soc.* **2000**, *122*, 11340; c) S. Nakamura, A. Furutani, T. Toru, *Eur. J. Org. Chem.* **2002**, 1690; d) S. Nakamura, Y. Ito, L. Wang, T. Toru, *J. Org. Chem.* **2004**, *69*, 1581. See also ref. [9].

[15] Carbamate **1** was prepared in two steps starting from *S*-(4,4-dimethyl-pent-2-ynyl) thioacetate by reduction with $LiAlH_4$ to the corresponding thiol and subsequent carbamoylation with *N*,*N*-diisopropylcarbamoyl chloride. For the synthesis of *S*-(4,4-dimethyl-pent-2-ynyl) thioacetate, see: X. Cao, Y. Yang, X. Wang, J. *Chem. Soc. Perkin Trans. 1* **2002**, *22*, 2485.

[16] X-ray crystal structure analysis for (*S*)-**3·2**: $C_{29}H_{50}LiN_3OS$, $M_w = 495.72$, colorless crystal $0.15 \times 0.10 \times 0.05$ mm, $a = 12.923(1)$, $b = 13.038(1)$, $c = 18.067(1)$ Å, $V = 3044.1(4)$ Å^3, $\rho_{calcd} = 1.082$ g cm^{-3}, $\mu = 11.09$ cm^{-1}, empirical absorption correction ($0.851 \le T \le 0.947$), $Z = 4$, orthorhombic, space group $P2_12_12_1$ (No. 19), $\lambda = 1.54178$ Å, $T = 173$ K, ω and φ scans, 14321 reflections collected ($\pm h$, $\pm k$, $\pm l$), $[(\sin\theta)/\lambda] = 0.58$ Å^{-1}, 4740 independent ($R_{int} = 0.080$) and 3417 observed reflections [$I \ge 2\sigma(I)$], 323 refined parameters, $R = 0.063$, $wR^2 = 0.147$, Flack parameter 0.03(4), max. residual electron density 0.24(−0.26) e Å^{-3}, hydrogen atoms calculated and refined as riding atoms.

[17] Data sets were collected with Enraf-Nonius CAD4 and Nonius KappaCCD diffractometers. Programs used: data collection EXPRESS (Nonius B.V., 1994) and COLLECT (Nonius B.V., 1998), data reduction MolEN (K. Fair, Enraf-Nonius B.V., 1990) and Denzo-SMN (Z. Otwinowski, W. Minor, *Methods Enzymol.* **1997**, *276*, 307 – 326), absorption correction data for CCD data Denzo (Z. Otwinowski, D. Borek, W. Majewski, W. Minor, *Acta Crystallogr. Sect. A* **2003**, *59*, 228 – 234), structure solution SHELXS-97 (G. M. Sheldrick, *Acta Crystallogr. Sect. A* **1990**, *46*, 467 – 473), structure refinement SHELXL-97 (G. M. Sheldrick, Universität Göttingen, **1997**), graphics SCHAKAL (E. Keller, Universität Freiburg, **1997**). CCDC 267521 ((*S*)-**4b**), CCDC 267127 ((*aR*)-**6**), CCDC 267128 ((*aS*,4*R*)-**7a**), and CCDC 267129 ((*S*)-**3·2**) contain the supplementary crystallographic data for this paper. These data can be obtained free of charge from the Cambridge Crystallographic Data Centre via www.ccdc.cam.ac.uk/data_request/cif.

[18] The enantiomeric excess of **4a** and **4b** was determined by an ^{1}H NMR shift experiment with [Eu(hfc)$_3$] (hfc = 3-(heptafluoropropylhydroxymethylene)-D-camphorate).

[19] X-ray crystal structure analysis for (*S*)-**4b**: $C_{20}H_{39}NOSSi$, $M_w = 369.67$, colorless crystal $0.60 \times 0.30 \times 0.15$ mm, $a = 7.591(1)$, $b = 12.809(1)$, $c = 25.013(1)$ Å, $V = 2432.1(4)$ Å^3, $\rho_{calcd} = 1.010$ g cm^{-3}, $\mu = 16.84$ cm^{-1}, empirical absorption correction ($0.431 \le T \le 0.786$), $Z = 4$, orthorhombic, space group $P2_12_12_1$ (No. 19), $\lambda = 1.54178$ Å, $T = 223$ K, ω and φ scans, 26685 reflections collected ($\pm h$, $\pm k$, $\pm l$), $[(\sin\theta)/\lambda] = 0.58$ Å^{-1}, 3901 independent ($R_{int} = 0.037$) and 3870 observed reflections [$I \ge 2\sigma(I)$], 229 refined parameters, $R = 0.039$, $wR^2 = 0.108$, Flack parameter 0.00(2), max. residual electron density 0.41(−0.20) e Å^{-3}, hydrogen atoms calculated and refined as riding atoms.

[20] For calculations see: E.-U. Würthwein, D. Hoppe, *J. Org. Chem.* **2005**, *70*, 4443.

[21] a) J.-M. Lehn, G. Wipff, J. Demuynck, *Helv. Chim. Acta* **1977**, *60*, 1239; b) P. von R. Schleyer, T. Clark, A. J. Kos, G. W. Spitznagel, C. Rhode, D. Arad, K. N. Houk, N. G. Rondan, *J. Am. Chem. Soc.* **1984**, *106*, 6467; c) K. B. Wiberg, H. Castejon, *J. Am. Chem. Soc.* **1994**, *116*, 10489.

[22] C. Schultz-Fademrecht, B. Wibbeling, R. Fröhlich, D. Hoppe, *Org. Lett.* **2001**, *3*, 1221.

[23] The enantiomeric excess of **6** was determined by chiral GC, column: β-Dex 325.

[24] X-ray crystal structure analysis for (*aR*)-**6**: $C_{14}H_{25}NOS$, $M_w = 255.41$, colorless crystal $0.45 \times 0.25 \times 0.10$ mm, $a = 12.369(1)$, $b = 13.586(1)$, $c = 29.363(1)$ Å, $V = 4934.3(6)$ Å^3, $\rho_{calcd} = 1.635$ g cm^{-3}, $\mu = 16.35$ cm^{-1}, empirical absorption correction

 © 2005 Wiley-VCH Verlag GmbH & Co. KGaA, Weinheim

$(0.527 \le T \le 0.854)$, $Z = 12$, orthorhombic, space group $P2_12_12_1$ (No. 19), $\lambda = 1.54178$ Å, $T = 223$ K, ω and φ scans, 27969 reflections collected ($\pm h$, $\pm k$, $\pm l$), $[(\sin\theta)/\lambda] = 0.58$ Å^{-1}, 7697 independent ($R_{int} = 0.058$) and 6559 observed reflections [$I \ge 2\sigma(I)$], 481 refined parameters, $R = 0.049$, $wR^2 = 0.121$, Flack parameter −0.00(2), max. residual electron density 0.23(−0.14) e Å^{-3}, hydrogen atoms calculated and refined as riding atoms.

[25] a) D. Hoppe, C. Riemenschneider, *Angew. Chem.* **1983**, *95*, 64; *Angew. Chem. Int. Ed. Engl.* **1983**, *22*, 54; b) D. Hoppe, C. Gonschorrek, D. Schmidt, E. Egert, *Tetrahedron* **1987**, *43*, 2457.

[26] The enantiomeric excess of **7a**–**d** was determined by chiral HPLC, column: Chira Grom-2, solvent: hexane/2-propanol.

[27] X-ray crystal structure analysis for (*aS*,4*R*)-**7a**: $C_{25}H_{33}NO_2S$, $M_w = 411.58$, colorless crystal $0.25 \times 0.20 \times 0.20$ mm, $a = 6.066(1)$, $b = 22.381(3)$, $c = 8.598(1)$ Å, $\beta = 90.99(1)°$, $V = 1167.1(3)$ Å^3, $\rho_{calcd} = 1.171$ g cm^{-3}, $\mu = 13.74$ cm^{-1}, empirical absorption correction ($0.725 \le T \le 0.771$), $Z = 2$, monoclinic, space group $P2_1$ (No. 4), $\lambda = 1.54178$ Å, $T = 223$ K, $\omega/2\theta$ scans, 2666 reflections collected ($-h$, $+k$, $\pm l$), $[(\sin\theta)/\lambda] = 0.62$ Å^{-1}, 2440 independent ($R_{int} = 0.049$) and 2104 observed reflections [$I \ge 2\sigma(I)$], 270 refined parameters, $R = 0.039$, $wR^2 = 0.107$, Flack parameter 0.00(2), max. residual electron density 0.20(−0.23) e Å^{-3}, hydrogen atoms calculated and refined as riding atoms.

[28] A. Basu, S. Thayumanavan, *Angew. Chem.* **2002**, *114*, 740; *Angew. Chem. Int. Ed.* **2002**, *41*, 716.

[29] a) P. Beak, D. R. Anderson, M. D. Curtis, J. M. Laumer, D. J. Pippel, G. A. Weisenburger, *Acc. Chem. Res.* **2000**, *33*, 715; b) J. Clayden, L. W. Lai, M. Helliwell, *Tetrahedron* **2004**, *60*, 4399.

[30] For the first application in chiral anion chemistry, see: D. Hoppe, O. Zschage, *Angew. Chem.* **1989**, *101*, 67; *Angew. Chem. Int. Ed. Engl.* **1989**, *28*, 67.

[31] For NMR investigations see: H. J. Reich, J. E. Holladay, *J. Am. Chem. Soc.* **1995**, *117*, 8470.

[32] No solid-state structure of an η^1-2-alkynyllithium has been published yet, according to The Cambridge Structural Database: F. H. Allen, *Acta Crystallogr. Sect. B* **2002**, *58*, 380; Version 1.7 (December 2004).

[33] For quite recent reviews, see: a) A. Hoffmann-Röder, N. Krause, *Angew. Chem.* **2004**, *116*, 1216; *Angew. Chem. Int. Ed.* **2004**, *43*, 1196; b) N. Krause, A. S. K. Hashmi, *Modern Allene Chemistry*, Wiley-VCH, Weinheim, **2004**; c) N. Krause, A. Hoffmann-Röder, *Tetrahedron* **2004**, *60*, 11671.

[34] The method is also applicable to further *S*-2-alkynyl thiocarbamates: R. Otte, unpublished results.

 © 2005 Wiley-VCH Verlag GmbH & Co. KGaA, Weinheim

Odd-Electron Bonds

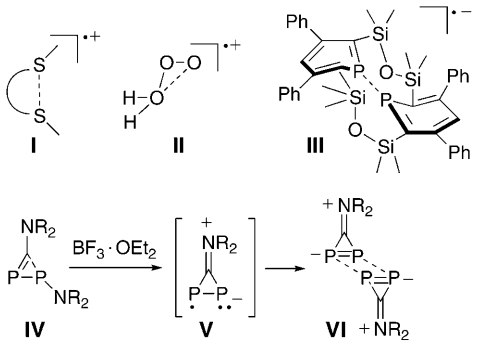
DOI: 10.1002/anie.200501369

Dimerization of a Cyclo-1σ⁴,3σ²,4σ²-Triphosphapentadienyl Radical: Evidence for Phosphorus–Phosphorus Odd-Electron Bonds**

*Tsuyoshi Kato, Heinz Gornitzka, Wolfgang W. Schoeller, Antoine Baceiredo, and Guy Bertrand**

Dedicated to Professor Herbert Roesky on the occasion of his 70th birthday

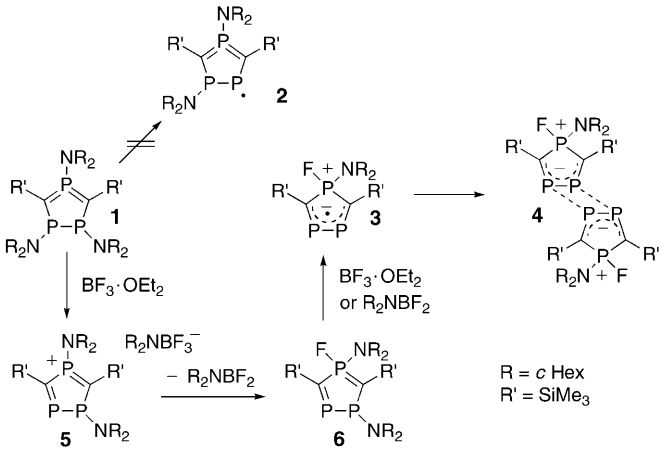
In hydrocarbon chemistry, carbon-centered radicals are rather short-lived intermediates and usually dimerize to give classical two-electron bonds.[1] If main group elements are involved, however, the situation is more diverse;[2] as predicted as early as 1931 by Pauling,[3] odd-electron bonds are sometimes formed. For Group 16 elements, the intensely studied radical cations of type **I**[4] are a good illustration of compounds that feature a two-center, three-electron bond, in which two electrons occupy a σ bonding orbital, and one electron occupies a σ* antibonding orbital (Scheme 1). Three-center, one-electron bonds have also been evoked to rationalize the formation of radical cation **II**;[5] in this case, the singly occupied π* orbital of O_2^+ interacts with an electron lone-pair orbital on water.



Scheme 1. Some examples of compounds that feature odd-electron bonds, and the synthetic route from **IV** to **VI**.

In phosphorus chemistry, only two examples of compounds that feature odd-electron bonds are known. Le Floch and co-workers[6] prepared the macrocyclic derivative **III**, which features a two-center, one-electron P–P bond in which the single electron is mainly located in a P–P σ bonding orbital. In 1998, we isolated derivative **VI**, which features a P_4 framework, which is best described as a four-center, six-π-electron system.[7] Four π electrons are present in the π orbitals of the two P=P bonds within each CP_2 ring, and the remaining two π electrons are used to join the two CP_2 units by two two-center, one-electron bonds. This description is consistent with the observation that the intra-ring P–P bonds are quite short (2.205 Å), whereas the inter-ring P–P bonds are very long (2.634 Å). Derivative **VI** resulted from the π*-π* dimerization[8] of diphosphirenyl radical **V**. Indeed, according to calculations, the unpaired electron of **V** is equally distributed over both phosphorus atoms and is localized in the π* orbital of the P=P bond.

In an attempt to prepare radical **2**, in which the unpaired electron would be distributed over a more extended π-conjugated framework, cyclic bis(methylene)phosphorane **1**[9] was treated with $BF_3{\cdot}OEt_2$ in a method used to homolytically cleave the P–N bond of diphosphirene **IV**. After removal of all the volatiles under vacuum and extraction with pentane, a new compound **4** was obtained in 40% yield as an air-sensitive purple solid (Scheme 2). Surprisingly, the ^{31}P NMR spectrum



Scheme 2. The synthesis of derivative **4**. *c*Hex = cyclohexyl.

showed a doublet of triplets at $\delta = 89$ ppm ($J_{P,F} = 938$ Hz and $J_{P,P} = 18$ Hz), characteristic of tetracoordinate phosphorus bearing a fluorine atom. It also had a very broad signal around 300 ppm in the region of phosphaalkene moieties. ^{19}F NMR spectroscopy gave a signal at $\delta = 23$ ppm as a doublet of triplets ($J_{F,P} = 938$ Hz and $J_{F,P} = 7$ Hz). The large P–F coupling constant confirms the direct P–F bond, and the triplet multiplicity of the signal is in good agreement with the presence of a P–P fragment. In solution at room temperature, no trace of paramagnetic species was detected by ESR spectroscopy.

[*] Prof. G. Bertrand
UCR-CNRS Joint Research Chemistry Laboratory (UMR 2282)
Department of Chemistry, University of California
Riverside, CA 92521-0403 (USA)
Fax: (+1) 951-827-2725
E-mail: gbertran@mail.ucr.edu
Dr. T. Kato, Dr. H. Gornitzka, Dr. A. Baceiredo, Prof. G. Bertrand
Laboratoire Hétérochimie Fondamentale et Appliquée du CNRS (UMR 5069)
Université Paul Sabatier
118, route de Narbonne, 31062 Toulouse Cedex 04 (France)
Prof. W. W. Schoeller
Fakultät für Chemie, Universität Bielefeld
Postfach 10 01 31
33615 Bielefeld (Germany)

[**] We are grateful to the NSF, USA (CHE 0213510), the CNRS, France, and the DFG, Germany, for financial support of this work.

 © 2005 Wiley-VCH Verlag GmbH & Co. KGaA, Weinheim

Dissolving **4** in hot toluene (≈60 °C) followed by slow cooling of the solution gave deep-red crystals suitable for a single-crystal X-ray diffraction study (Figure 1).[10] Compound **4** is organized around an inversion center located in the middle of the parallelogram described by four phosphorus atoms (P–P–P angles: 97.2° and 82.7°). The plane of the parallelogram is almost perpendicular (109 and 112°) to the two planar five-membered rings. All C–P bond lengths in the latter are equal (1.70 Å) and only slightly longer than C=P double bonds. The distance between the two five-membered rings of **4** is 2.427 Å, which is much longer than a classical P–P single bond,[11] but almost 0.2 Å shorter than that of the diphosphirenyl radical dimer **VI** (2.635 Å). In contrast, the P2–P3 bond length is short (2.157 Å), in fact even shorter than the analogous bond in **VI** (2.205 Å).

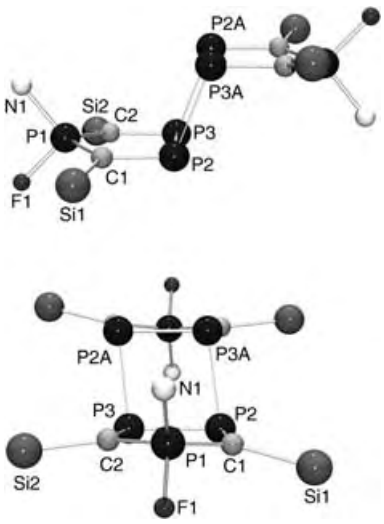


Figure 1. Simplified molecular views of **4** in the solid state. Selected bond lengths [Å] and angles [°]: P2–P3A 2.427(3), P1–C1 1.700(7), P1–C2 1.693(7), C1–P2 1.698(7), C2–P3 1.700(7), P2–P3 2.157(3), P1–N1 1.656(6), P1–F1 1.562(4), C1–Si1 1.851(7), C2–Si2 1.864(3); ∢C1-P1-C2 107.7(3), ∢P1-C1-P2 115.1(4), ∢P1-C2-P3 116.4(4), ∢C1-P2-P3 100.8(3), ∢C2-P3-P2 98.9(3), ∢P1-C1-Si1 128.6(4), ∢P2-C1-Si1 116.2(4), ∢P2-P3-P2A 82.7(11), ∢P3-P2-P3A 97.2(11), $\sphericalangle_{tors}$C1-P2-P3-P2A 109.1, $\sphericalangle_{tors}$C2-P3-P2-P3A 112.4.

Before performing a detailed investigation of the electronic structure of **4**, we studied the reaction leading to this unexpected compound. ^{31}P and ^{19}F NMR spectroscopy indicated that a small amount of cyclic ylide **6** was formed (Scheme 2). This compound was isolated by crystallization in THF, and its structure was unambiguously established by a single-crystal X-ray diffraction study (Figure 2).[10] Hence, it is reasonable to postulate that instead of the expected homolytic cleavage of a P–N bond, which would have led to **2**, heterolytic cleavage occurs to generate a cyclic methylenephosphonium salt **5**, as already observed by Grützmacher and Pritzkow in their work with analogous acyclic compounds.[12] The highly electrophilic cation **5** then abstracts a fluorine anion from the $R_2NBF_3^-$ counteranion to give the isolated cyclic ylide **6**. Finally, BF_3-catalyzed homolytic cleavage of the remaining σ^3-P–N bond leads to the transient cyclotriphosphapentadienyl radical **3**, which dimerizes to give **4**. Therefore, although we have not generated the desired radical **2**, we have, by serendipity, formed the radical **3** in which the unpaired electron is distributed over an extended π-conjugated framework, which was our primary aim.

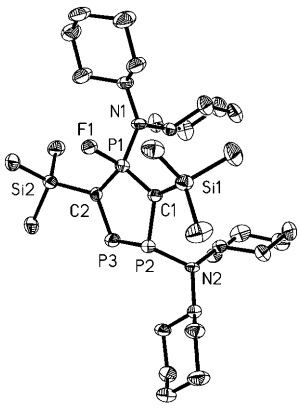


Figure 2. Molecular view of **6** in the solid state. Selected bond lengths [Å] and angles [°]: P1–C1 1.686(4), P1–C2 1.764(4), P2–C1 1.772(4), P3–C2 1.708(4), P2–P3 2.159(2), P1–N1 1.657(3), P1–F1 1.508(2), P2–N2 1.685(3), C1–Si1 1.854(4); ∢C1-P1-C2 109.0(2), ∢P1-C1-P2 111.5(2), ∢P2-P3-C2 97.2(1), ∢P1-C2-P3 116.0(2).

The single occupied molecular orbital (SOMO) of radicals of type **3** is, upon first estimate, the π_3 molecular orbital of a *cis*-oriented pentadiene unit with small contributions from the PR_2 fragment (Figure 3). Among the three symmetry-allowed dimerization processes that could occur from SOMO–SOMO (π_3–π_3) interactions, the [2+2] pathway clearly leads to the least sterically hindered and minimally strained product, namely **4**. In terms of canonical structures, radicals **3** can be represented as follows: the unpaired electron can reside at the carbon positions, as in **A**, or at the phosphorus atoms, as indicated in **B** (Scheme 3). As a consequence, a double bond is present between either the two phosphorus atoms (in **A**), or a phosphorus and a carbon atom (in **B**). From **A**, dimerization refers to a [π^2+π^2] reaction of two P=P double bonds and would result in a cyclotetraphosphane ring system with four

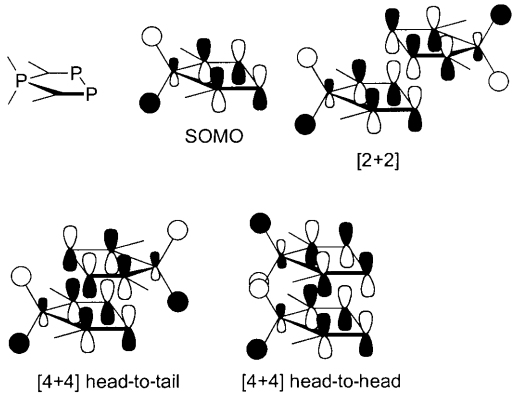
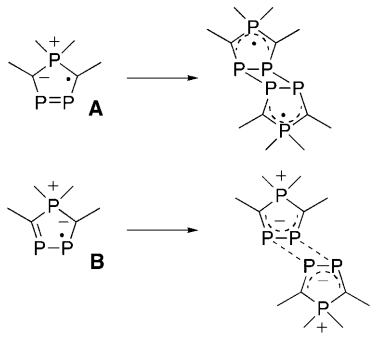


Figure 3. Representation of the SOMO for radical **3** and possible SOMO–SOMO interactions.

 © 2005 Wiley-VCH Verlag GmbH & Co. KGaA, Weinheim



Scheme 3. Canonical structures **A** and **B** for radical **3** and the respective canonical structures for the product dimer **4**.

P–P single bonds.[13] However, for the dimerization from **B**, only one unpaired electron is supplied from each radical unit. This results in an electron deficit for the resulting inter-ring P–P bonds, as only two electrons are available for forming two P–P bonds. The presence of the resonance form **A** in competition with **B** easily explains the differences observed in the P–P bond lengths between the four-membered-ring framework of dimers **VI** and **4**, and especially why the "long" P–P bond is shorter in **4**.

Another consequence of these two alternative resonance structures would be the ability to vary the P–P bond lengths in dimers of type **4** by changing the substituents attached to the carbon atoms. To substantiate these qualitative considerations, we performed quantum chemical calculations (Table 1). Various computational levels[14] were tested for the parent compound ($R^1 = R^2 = H$). Given the same DFT level (BP86) and increasing the quality of the basis set in the order SVP, TZVP causes only a slight shortening of the long P–P bonds. On the other hand, changing the electron correlation level from BP86 to MP2 exerts a stronger shrinking of the P–P bonds. The CBS-Q method (complete basis set method), considered to be a much better computational level,[14b] yields, for the parent dimer, a long inter-ring P–P distance of 2.592 Å and a concomitant dimerization energy of $-19.6\ kcal\,mol^{-1}$ (0 K). The effects of the different substituents were investigated with the less costly computational level (RI-BP86/SVP). Not surprisingly, the substituents at the carbon atoms which stabilize the canonical structure **A** and the electronegative substituents at phosphorus, shorten the inter-ring P–P distance. A drastic shortening is observed with an added exchange of substituents that can simultaneously stabilize a negative charge and an unpaired electron ($R^1 = NO_2$, SiH_3; $R^2 = F$). In contrast, strong electron-donating substituents at the carbon atoms, such as amino groups, elongate the inter-ring P–P distance. In all cases, a rhombic distortion of the central P_4 ring is observed. For the experimentally observed derivative ($R^1 = TMS$; $R^2 = F$ or $N(c\text{Hex})_2$), the calculated inter-ring P–P distance (2.599 Å) is still too large to agree well with the experimentally determined value of 2.427 Å; this probably means that DFT methods are not able to take weak bonds into account properly.[15]

A series of radical dimers of type **4** that feature different substituents at phosphorus and carbon positions are under current investigation. The possibility of finely tuning the interaction between such radicals might have implications in material sciences.[16]

Table 1: Substituent effects on P–P bond lengths and P-P-P bond angles for dimers of type **4** at the RI-BP86/SVP level.

R^1 (C)	R^2 (P)	$P–P_{interring}$ [Å]	$P–P_{intraring}$ [Å]	∢P-P-P [°]
H	H	2.702	2.220	87.8
		2.676[a]	2.221[a]	86.8[a]
		2.614[b]	2.215[b]	80.2[b]
		2.592[c]	2.209[c]	77.8[c]
		2.538[d]	2.222[d]	77.4[d]
NH_2	H	2.754	2.218	89.9
CH_3	H	2.718	2.214	89.8
SiH_3	H	2.635	2.226	82.3
phenyl	H	2.576	2.213	89.4
H	NH_2	2.655	2.241	88.7
H	F	2.588	2.255	89.9
NH_2	F	2.641	2.256	89.9
SiH_3	F	2.535	2.256	89.9
NO_2	F	2.484	2.258	83.2
SiH_3	F[f]/NH_2[g]	2.520	2.256	84.2
		2.473[b]	2.258[b]	79.1[b]
SiH_3	NH_2[f]/F[g]	2.550	2.252	84.9
		2.481[b]	2.254[b]	80.2[b]
TMS[e]	F[f]/$N(c\text{Hex})_2$[g]	2.599	2.229	87.1
TMS[e]	$N(c\text{Hex})_2$[f]/F[g]	2.601	2.247	88.0

[a] RI-BP86/TZVP; [b] RI-MP2(fc)/SVP; [c] CBS-Q (complete basis set method)[14]; [d] RI-MP2(fc)/TZVP; [e] TMS = trimethylsilyl; [f] *exo* with respect to the central four-membered-ring system; [g] *endo* with respect to the central four-membered-ring system.

Experimental Section

All manipulations were performed under an inert atmosphere of argon by using standard Schlenk techniques. Dry, oxygen-free solvents were employed. ^1H, ^{13}C, ^{19}F and ^{31}P NMR spectra were recorded on Bruker AC80, AC200, WM250 or AMX400 spectrometers.

4: $BF_3{\cdot}Et_2O$ (0.24 g, 1.30 mmol) was added at room temperature to a solution of **1** (0.45 g, 0.62 mmol) in toluene. The solution was heated at 30 °C for 2 days in the absence of light, and the reaction monitored by multinuclear NMR spectroscopy. When the starting materials were consumed, the volatiles were removed under vacuum and the product was extracted with toluene. After evaporation of toluene, the residue was recrystallized from hot toluene as deep-red crystals (0.12 g, 42 %); m.p. = 115 °C (decomp); $^{31}P\{^1H\}$ NMR (C_6D_6): $\delta = 88.9$ (dt, $^2J(P,P) = 15.3$ Hz, $^1J(P,F) = 939.8$ Hz, 1 P), 280 ppm (br, 2 P); ^1H NMR (C_6D_6): $\delta = 0.78$ (s, 36 H, $SiCH_3$), 1.2–2.2 (m, 20 H, CH_2), 3.04 (br, 4 H, CHN), 3.65 ppm (broad d, $^2J(P,H) = 13.8$ Hz, 4 H, CHN); $^{13}C\{^1H\}$ NMR (C_6D_6): $\delta = 3.9$ (s, $SiCH_3$), 25.5, 25.8, 26.7, 27.1 (s, CH_2), 34.3 (br, CH_2), 35.1 (d, $^2J(C,P) = 1.3$ Hz, CH_2), 57.4 (broad, NCH), 58.2 ppm (d, $^2J(C,P) = 5.1$ Hz, NCH), PCP (not observed); $^{19}F\{^1H\}$ NMR (C_6D_6): $\delta = 20.1$ ppm (dt, $^3J(F,P) = 60.0$ Hz, $^1J(F,P) = 939.8$ Hz). Computational procedures: quantum chemical calculations were performed with the Gaussian suite[14a] of programs as well as the Turbomole[14b] program systems. Various computational levels were studied. In general, RHF and B3LYP calculations yielded intermolecular bond lengths that were too large, whereas the BP86 density functional level yielded more satisfactory geometries, albeit with some P–P bond lengths too large for intermolecular bond formation between two radicals. At the MP2 level, shorter P–P bonds

 © 2005 Wiley-VCH Verlag GmbH & Co. KGaA, Weinheim

were observed, but this methodology is restricted to the study of the parent compound.

Received: April 20, 2005
Published online: July 29, 2005

Keywords: bond theory · computer chemistry · heterocycles · phosphorus · radicals

[1] M. Newcomb in *Reactive Intermediate Chemistry* (Eds.: M. Jones, R. A. Moss), Wiley-Interscience, Hoboken, **2004**, pp. 121–164.
[2] H. Grützmacher, F. Breher, *Angew. Chem.* **2002**, *114*, 4178; *Angew. Chem. Int. Ed.* **2002**, *41*, 4007.
[3] L. Pauling, *J. Am. Chem. Soc.* **1931**, *53*, 3225; L. Pauling, *The Nature of the Chemical Bond*, *3rd ed.*, Cornell University Press, Cornell, **1960**, pp. 340–343.
[4] R. S. Glass, *Top. Curr. Chem.* **1999**, *205*, 1; D. K. Maity, *J. Am. Chem. Soc.* **2002**, *124*, 8321; J. E. King, A. J. Illies, *J. Phys. Chem. A* **2004**, *108*, 3581.
[5] M. Zhou, A. Zeng, Y. Wang, Q. Kong, Z.-X. Wang, P. von R. Schleyer, *J. Am. Chem. Soc.* **2003**, *125*, 11512.
[6] L. Cataldo, S. Choua, T. Berclaz, M. Geoffroy, N. Mézailles, L. Ricard, F. Mathey, P. Le Floch, *J. Am. Chem. Soc.* **2001**, *123*, 6654.
[7] Y. Canac, D. Bourissou, A. Baceiredo, H. Gornitzka, W. W. Schoeller, G. Bertrand, *Science* **1998**, *279*, 2080.
[8] Although dimer **VI** is the only example of a phosphorus compound resulting from a π*-π* interaction, such interactions have been found in numerous inorganic molecules: a) T. Klapötke, J. Passmore, *Acc. Chem. Res.* **1989**, *22*, 234; b) J. M. Rawson, A. J. Banister, I. Lavender, *Ad. Heterocycl. Chem.* **1995**, *62*, 341; c) J. Beck, *Coord. Chem. Rev.* **1997**, *163*, 55; d) T. Drews, W. Koch, K. Seppelt, *J. Am. Chem. Soc.* **1999**, *121*, 4379; e) S. Brownridge, I. Krossing, J. Passmore, H. D. B. Jenkins, H. K. Roobottom, *Coord. Chem. Rev.* **2000**, *197*, 397.
[9] T. Kato, Dissertation Thesis Université Paul Sabatier, Toulouse, **2002**.
[10] Crystal data: **4**: $C_{20}H_{40}FNP_3Si_2$, $M = 462.62$, monoclinic, $P2_1/n$, $a = 11.192(4)$ Å, $b = 17.994(6)$ Å, $c = 12.621(5)$ Å, $\beta = 99.563(7)°$, $V = 2506.2(15)$ Å^3, $Z = 4$, $T = 193(2)$ K. 8658 reflections (3061 independent, $R_{int} = 0.1249$) were collected. Largest electron density residue: 0.379 e Å^{-3}, R_1 (for $I > 2\sigma(I)$) = 0.0709 and $wR_2 = 0.1411$ (all data) with $R_1 = \Sigma ||F_o| - |F_c|| / \Sigma |F_o|$ and $wR_2 = (\Sigma w (F_o^2 - F_c^2)^2 / \Sigma w (F_o^2)^2)^{0.5}$. **6**: $C_{32}H_{62}FN_2P_3Si_2$, $M = 642.93$, orthorhombic, *Pbca*, $a = 12.399(1)$ Å, $b = 21.421(1)$ Å, $c = 27.409(2)$ Å, $V = 7279.9(8)$ Å^3, $Z = 8$, $T = 193(2)$ K. 25920 reflections (4589 independent, $R_{int} = 0.1183$) were collected. Largest electron density residue: 0.257 e Å^{-3}, R_1 (for $I > 2\sigma(I)$) = 0.0454 and $wR_2 = 0.0910$ (all data). All data for the structures represented herein were collected at low temperatures with an oil-coated shock-cooled crystal on a Bruker-AXS CCD 1000 diffractometer with $Mo_{K\alpha}$ radiation ($\lambda = 0.71073$ Å). The structures were solved by direct methods[17] and all non-hydrogen atoms were refined anisotropically by using the least-squares method on F^2.[18] CCDC 269192 (for **4**) and CCDC 269193 (for **6**) contain the supplementary crystallographic data for this paper. These data can be obtained free of charge from The Cambridge Crystallographic Data Centre via www.ccdc.cam.ac.uk/data_request/cif.
[11] H. F. Allen, O. Kennard, D. G. Waston, L. Brammer, A. Orpen, *J. Chem. Soc. Perkin Trans. 2* **1987**, S1.
[12] H. Grützmacher, H. Pritzkow, *Angew. Chem.* **1989**, *101*, 768; *Angew. Chem. Int. Ed. Engl.* **1989**, *28*, 740.
[13] Such a [$\pi^2+\pi^2$] reaction of two P=P double bonds has already been observed for a 3H-diphosphirene. E. Niecke, R. Streubel, M. Nieger, *Angew. Chem.* **1991**, *103*, 103; *Angew. Chem. Int. Ed. Engl.* **1991**, *30*, 90.
[14] a) GAUSSIAN 03, Revision C.02, M. J. Frisch, G. W. Trucks, H. B. Schlegel, G. E. Scuseria, M. A. Robb, J. R. Cheeseman, J. A. Montgomery, Jr., T. Vreven, K. N. Kudin, J. C. Burant, J. M. Millam, S. S. Iyengar, J. Tomasi, V. Barone, B. Mennucci, M. Cossi, G. Scalmani, N. Rega, G. A. Petersson, H. Nakasuji, Y. Honda, O. Kitao, H. Nakai, M. Klene, X. Li, J. E. Knox, H. P. Hratchian, J. B. Cross, V. Bakken, C. Adamo, J. Jaramillo, R. Gomperts, R. E. Stratmann, O. Yazyev, A. J. Austin, R. Cammi, C. Pomelli, J. W. Ochterski, P. Y. Ayala, K. Morokuma, G. A. Voth, P. Salvador, J. J. Dannenberg, V. G. Zakrzewski, S. Dapprich, A. D. Daniels, M. C. Strain, O. Farkas, D. K. Malick, A. D. Rabuck, K. Raghavachari, J. B. Foresman, J. V. Ortiz, Q. Cui, A. G. Baboul, S. Clifford, J. Cioslowski, B. B. Stefanov, G. Liu, A. Liashenko, P. Piskorz, I. Komaromi, R. L. Martin, D. J. Fox, T. Keith, M. A. Al-Laham, C. Y. Peng, A. Nanayakkara, M. Challacombe, P. M. W. Gill, B. Johnson, W. Chen, M. W. Wong, C. Gonzalez, J. A. Pople, Gaussian, Inc., Wallingford CT, **2004**; b) TURBOMOLE, Program Package for ab initio Electronic Structure Calculations, Version 5.7, R. Ahlrichs, M. Bär, H.-P. Baron, R. Bauernschmitt, S. Böcker, M. Ehrig, K. Eichkorn, S. Elliott, F. Furche, F. Haase, M. Häser, C. Hättig, H. Horn, C. Huber, U. Huniar, M. Kattannek, A. Köhn, C. Kölmel, M. Kollwitz, K. May, C. Ochsenfeld, H. Öhm, A. Schäfer, U. Schneider, O. Treutler, K. Tsereteli, B. Unterreiner, M. von Arnim, F. Weigend, P. Weis, H. Weiss, Theoretical Chemistry Group, University of Karlsruhe, Karlsruhe, Germany, **2004**.
[15] The diamagnetic coupling of two radicals through π*–π* interactions usually leads to weak bonds. Consequently, the bond lengths in these dimers easily fluctuate. This is well-documented for the N_2O_2 dimer. For example, the N–N interatomic distance in the gas phase[15a] is 2.24 Å, whereas it is 2.18 Å in the solid state.[15b] a) S. G. Kukolich, *J. Am. Chem. Soc.* **1982**, *104*, 4715; b) W. N. Lipscomb, W. R. Wang, *Acta Cryst.* **1961**, *14*, 1100.
[16] M. E. Itkis, X. Chi, A. W. Cordes, R. C. Haddon, *Science* **2002**, *296*, 1443.
[17] G. M. Sheldrick, *Acta Cryst.* **1990**, *46*, 467.
[18] SHELXL 97, Program for Crystal Structure Refinement, G. M. Sheldrick, University of Göttingen **1997**.

 © 2005 Wiley-VCH Verlag GmbH & Co. KGaA, Weinheim

Bioinorganic Chemistry

DOI: 10.1002/anie.200501013

Alzheimer's Disease Related Copper(II)-β-Amyloid Peptide Exhibits Phenol Monooxygenase and Catechol Oxidase Activities**

*Giordano F. Z. da Silva and Li-June Ming**

Over the past few years an enormous effort has been directed toward the investigation of the metal-dependent mechanisms that lead to the neuropathology of Alzheimer's disease (AD).[1] The self-assembled metallo-β-amyloid (Aβ) peptide fibrils are the hallmark of this disease[2] and have been attributed to Fe^{III}- and Cu^{II}-centered generation of H_2O_2 under reducing conditions. The latter, H_2O_2, has been postulated to be of significant importance in connection with neuropathy in AD.[3,4] However, an area of oversight has been the detailed chemical processes associated with the neuropathology of AD, besides the generally acclaimed assault by ROS (reactive oxygen species; e.g. H_2O_2).[5] Hence, a better understanding of metal-centered redox chemistry and the mechanism for the generation of ROS and their fate can provide insight into potential strategies for the prevention and treatment of AD.

Several examples of redox chemistry in biological systems are known to be associated with di- or multinuclear "Type-3" Cu oxidases,[6] which may be related to the redox activity of $Cu^{II}A\beta$.[1–4] A number of chemical model systems that target Type-3 copper centers have successfully been demonstrated to contain highly active isoelectronic copper–dioxygen species (i.e. Cu_2^{II}-μ-η^1:η^1-peroxo, Cu_2^{II}-μ-η^2:η^2-peroxo, and Cu_2^{III}-bis-μ-oxo), which are responsible for copper-dependent oxidation and hydroxylation reactions.[6–9] Despite extensive modeling studies, peptide mimics of these enzymes have apparently been excluded from the studies. $Cu^{II}A\beta$ seems to fill the gap as it is a naturally occurring Cu–peptide complex demonstrated to exhibit oxygen-associated redox chemistry,[1–4] although details about its oxygen binding and activation mechanisms are lacking. Herein, we present results which bring together two distinct fields of research: Alzheimer's disease and Type-3 copper centers. The results elucidate that the Cu^{II} complex ($CuA\beta_{1-20}$) of the icosapeptidyl metal-binding domain of Aβ ($DAEFR^5HDSGY^{10}EVHHN^{15}$-$KLVFF^{20}$) exhibits metal-centered redox chemistry that is consistent with the mechanisms of the Type-3 copper enzymes, namely, phenol monooxygenase (e.g. tyrosinase) and catechol oxidase.

The metal-centered redox chemistry of $CuA\beta_{1-20}$ was probed using catechol and the more-inert phenol as substrates.[10,11] The oxidation of catechol under aerobic conditions reached a plateau at low mM concentrations, and the saturation profile fits well to pre-equilibrium kinetics [Eqs. (1) and (2)][12] to afford the rate constant $k_{cat} = 0.154\ s^{-1}$, the dissociation constant $K'_{app} = 0.35$ mM (Figure 1a), and a significant second-order rate constant $k_{cat}/K'_{app} = 440\ M^{-1}s^{-1}$ (cat = catalytic, app = apparent). As the formation of quinone from catechol is a two-electron oxidative process, the reaction is expected to follow the two-electron dinuclear reaction pathway for catechol oxidase,[13] wherein the binding of catechol to the active-site dicopper(II) center results in the reduction of the center to yield dicopper(I) with concomitant production of *o*-quinone. The reduced dicopper(I) center can bind dioxygen to afford the active peroxo-bridged dicopper(II) center, which can further oxidize a subsequently bound substrate. H_2O_2 can also be generated in this reaction pathway from the peroxo-bridged dicopper(II) center in the presence of a reducing agent such as the substrate itself. This pathway for the production of H_2O_2 under reducing conditions is consistent with previous observations in AD studies.[3] The catechol oxidase like mechanism has also been observed in kinetic studies of several chemical model systems[14] and in the oxidation of polyphenols by $CuA\beta_{1-20}$.[15] Note that a recent study based on density functional theory (DFT) pointed to mixed-valence Cu^{II}–Cu^{I} transition states,[16] which support the suggested reduction pathway for the Cu center.

We previously determined the $Cu^{II}/A\beta_{1-20}$ stoichiometry as 1:1 for oxidative activity with three N_ε-coordinated imidazole histidine rings as metal-binding ligands.[15] As activity is an excellent probe for determining stoichiometry, gradual replacement of Cu^{II} centers in $CuA\beta_{1-20}$ with redox-inactive Zn^{II} centers can serve as a practical method for addressing the nature of the active metal center by virtually "silencing" the active sites through dilution with Zn^{II}. A quadratic correlation between the activity and the extent of Zn^{II} dilution should be observed for simple 1:1 metal binding if there is no cooperativity and/or interactions between the Cu^{II} centers at the active site with different Aβ strands. Conversely, a sigmoidal activity profile was observed as a function of the mole fraction of Cu^{II} in $A\beta_{1-20}$ toward the oxidation of the catechol derivative 3,5-di-*tert*-butyl catechol (DTC, $k_{cat} = 0.411\ s^{-1}$ and $K'_{app} = 0.781$ mM) which can be fitted well to the Hill equation [Eq. (3)][17] with a Hill coefficient of $\theta = 2.40$ and $r^2 = 0.99$ (Figure 2a, solid line). The data clearly cannot be fitted well to a quadratic equation for 1:1 noncooperative binding mode ($r^2 = 0.91$; dashed line, Figure 2a). These results imply the possible presence of a cooperative dinuclear active Cu^{II} center during the catalytic

[*] G. F. Z. da Silva, Prof. L.-J. Ming
Department of Chemistry and
Institute for Biomolecular Science
University of South Florida
4202 E. Fowler Avenue, SCA400, Tampa, FL 33620-5250 (USA)
Fax: (+1) 813-974-3203
E-mail: ming@shell.cas.usf.edu

[**] G.F.Z.S. dedicates this work to his parents for their unyielding support. The authors dedicate this work to the Kelley and Sotolongo families for their unfortunate experience with Alzheimer's disease. Our research on the structure and activity of metallopeptides was partially supported by the Research and Creative Award of the University of South Florida and the Petroleum Research Fund administrated by the American Chemical Society (PRF AC #40851-AC3). We thank John Kelley for the modification of the picture for the Table of Contents.

 © 2005 Wiley-VCH Verlag GmbH & Co. KGaA, Weinheim

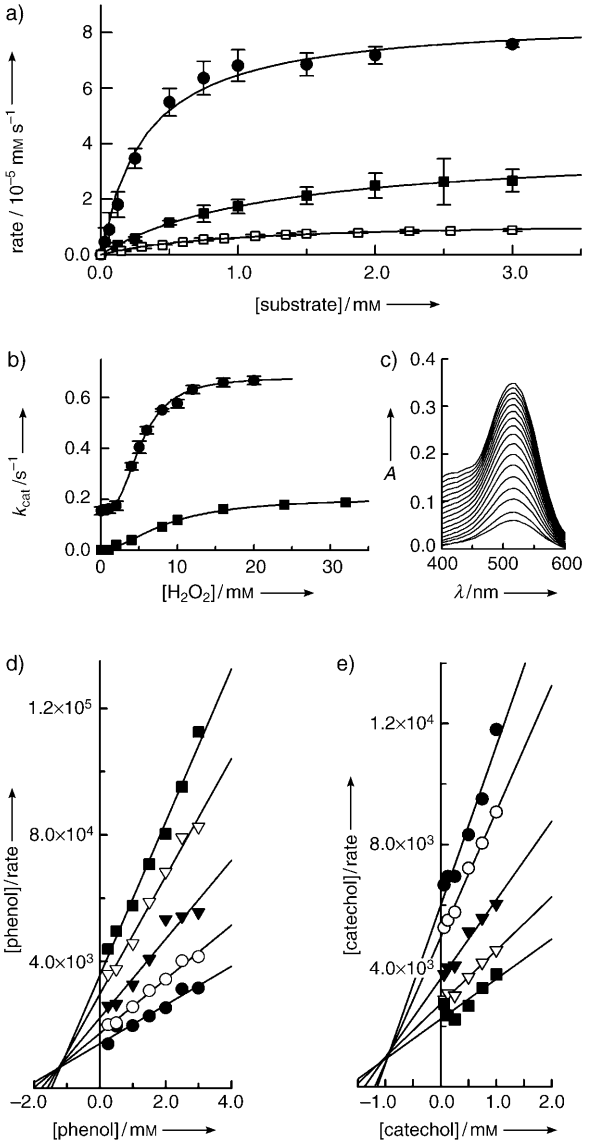


Figure 1. a) Saturation profile for the oxidation of phenol (■), deuterated phenol (□), and catechol (●) in the absence of H_2O_2. b) The effect of the concentration of H_2O_2 on the first-order rate constant k_{cat} toward the oxidation of phenol (■) and catechol (●). c) The production of *o*-quinone from phenol in the absence of H_2O_2 is monitored by the increase in the absorption as a result of the formation of its adduct with 3-methyl-2-benzothiazolinone hydrazone (MBTH). d, e) Hanes plot analysis of kinetic data from parts (a) and (b), with $[H_2O_2] = 0$, 5, 10, 20, and 30 mM from top to bottom.

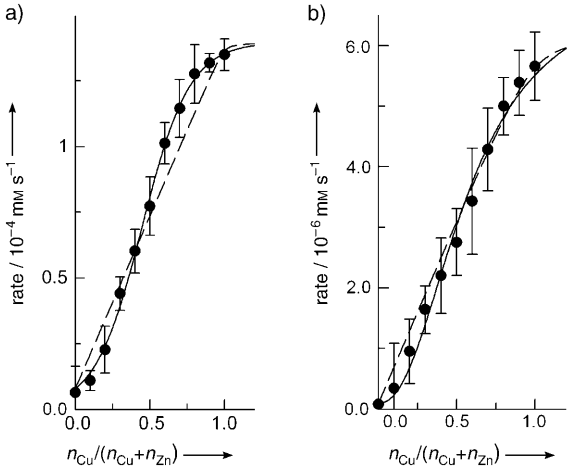


Figure 2. Oxidative activity of $CuA\beta_{1-20}$ toward the oxidation of a) DTC and b) phenol in the absence of H_2O_2 as a function of the mole fraction of Cu^{II} at a constant total concentration of Cu^{II} and Zn^{II} at pH 7.0 and 25 °C. The solid lines show the fit to the Hill equation, and the dotted lines are the fits to a quadratic binding pattern with a metal/ligand ratio of 1:1.

oxidation of catechol by $CuA\beta_{1-20}$, consistent with the catalytic cycle of catechol oxidase.[13]

The presence of the reactive oxygen species H_2O_2 (25 mM) significantly enhances the turnover and catalytic efficiency of $CuA\beta_{1-20}$ toward catechol oxidation, yielding $k_{cat} = 0.531\ s^{-1}$ and $K'_{app} = 0.342$ mM, and a significant second-order rate constant $k_{cat}/K' = 1.51 \times 10^3\ M^{-1} s^{-1}$ from the Hanes plot [Eq. (4) and Figure 1e][18,19] for a random two-substrate reaction, in which the binding of the two substrates H_2O_2 and catechol are independent of each other. Note, the second-order rate constant for catechol oxidation is only about 20 times lower than that for catechol oxidase extracted from gypsywort.[20] This pathway is consistent with the so-called peroxide shunt in the action of catechol oxidase in the presence of H_2O_2 for which a Cu^{II}_2-μ-η^2:η^2-peroxo intermediate is proposed to be the active species.[6] The oxidation of catechol to form *o*-quinone in the absence and presence of H_2O_2 exhibits remarkable rate accelerations (3.25×10^5 and 1.12×10^6 fold, respectively) in terms of the first-order rate constant k_{cat} relative to that for aerobic autooxidation of catechol in the absence of $CuA\beta_{1-20}$ ($k_o = 4.74 \times 10^{-7}\ s^{-1}$).

Owing to their inertness, metal-centered hydroxylation of phenol and its derivatives, particularly polychlorophenols, poses some challenging tasks in chemical synthesis and environmental detoxification and remediation[21] and may provide further insight into the action of those metalloenzymes for the monooxygenation of arenes.[8,22] Besides the oxidation of catechol described above, phenol was hydroxylated and oxidized by $CuA\beta_{1-20}$ in the presence of a saturating amount of H_2O_2 (> 50.0 mM). The formation of *o*-quinone exhibited rate and dissociation constants of $k_{cat} = 0.213\ s^{-1}$ and $K'_{app} = 1.31$ mM, respectively, and $k_{cat}/K' = 457\ M^{-1} s^{-1}$ from the Hanes plot (Figure 1a and d). This result represents a remarkable 4.6×10^6-fold rate acceleration for the hydroxylation/oxidation of phenol to form *o*-quinone in terms of k_{cat} relative to that for aerobic autooxidation of phenol ($k_0 = 4.6 \times 10^{-8}\ s^{-1}$). This reaction is expected to take place according to a dinuclear mechanism similar to the hydroxylation and oxidation of tyrosine by the dicopper enzyme tyrosinase, in which the active center is believed to contain dinuclear μ-η^2:η^2-peroxo-Cu^{II}_2 species on the basis of spectroscopic studies.[8,16]

Cooperativity of H_2O_2 in the oxidation of both catechol and phenol in terms of k_{cat} is observed upon titration of H_2O_2 and is reflected in the sigmoidal activity profile with respect to the concentration of H_2O_2 (Figure 1b). The data from the oxidation of catechol and phenol by H_2O_2 fit well to the Hill

 © 2005 Wiley-VCH Verlag GmbH & Co. KGaA, Weinheim

equation [Eq. (3)], yielding Hill coefficients of $\theta = 2.23$ and 1.78, respectively. Moreover, fitting of the rates to a random two-substrate reaction mechanism yields corrected K' values of 2.07 and 2.10 for phenol and catechol, respectively, and a cooperativity index based on the ratio K'_{app}/K' of 1.70 for H_2O_2 in both phenol and catechol oxidation reactions. These values suggest a small cooperativity of H_2O_2 and the independent binding of H_2O_2 and phenol or catechol to the active center.

Of particular interest is the observation of a scarcely reported process, namely, aerobic Cu^{II}-centered hydroxylation and oxidation of phenol in the absence of H_2O_2.[23] The production of *o*-quinone from phenol catalyzed by $CuA\beta_{1-20}$ follows pre-equilibrium kinetics, yielding $k_{cat} = 3.90 \times 10^{-3}\ s^{-1}$ and $K'_{app} = 1.23$ mM (Figure 1a) that represent an 8.67×10^4-fold first-order rate acceleration with respect to aerobic autooxidation of phenol. The k_{cat} value is lower than that for catechol oxidation and indicates that the hydroxylation step here must be the rate-limiting step. Otherwise, these two reactions would have similar k_{cat} values attributed to the oxidation of a bound catechol upon hydroxylation of a bound phenol. Moreover, the use of deuterated phenol as substrate reveals a significant kinetic isotope effect (KIE); k_{cat} values of 1.12×10^{-3} and $0.0442\ s^{-1}$ are obtained in the absence and presence, respectively, of H_2O_2 (100 mM) and represent KIE values of 3.46 and 4.77, respectively. The results indicate that hydroxylation and cleavage of the *o*-C–H bond of phenol is the rate-limiting step, which is followed by a faster step to form *o*-quinone. The different KIE values for the hydroxylation of phenol in the presence and absence of H_2O_2 suggest that the rate-determining step in these two cases may be different and/or possibly involve additional pathways. The K'_{app} values are not significantly different between phenol and deuterated phenol (1.31 and 1.23 mM for the latter in the presence and absence of H_2O_2, respectively) which suggests that k_{cat} does not significantly contribute to the magnitude of K'_{app} and that the two substrates may have a similar binding mode. The mechanistic reasoning for the conversion of phenol to *o*-quinone may be attributed to the fact that the Cu^{II}/Cu^{I} redox equilibrium can be achieved upon phenol binding, followed by electron transfer to afford a Cu^{I}–phenol radical, which is thought to be stabilized through resonance structures with delocalization of the free radical at the *ortho* and *para* positions[23a] (Figure 3, step a). This intermediate is then attacked by dioxygen and followed by electron transfer to possibly form a Cu^{II} superoxide center which may be further stabilized by a dinuclear center (step b). It was proposed previously that the free radical was attached directly by triplet dioxygen[23a] which, however, is not symmetrically favorable. Coupling of the superoxide radical to the bound phenol radical at an *ortho* position is then expected to be a favorable step (step c), which is followed by transfer of electrons and an oxygen atom to afford the final quinone product (step d). Involvement of a dinuclear center for the catalysis is possible as discussed below.

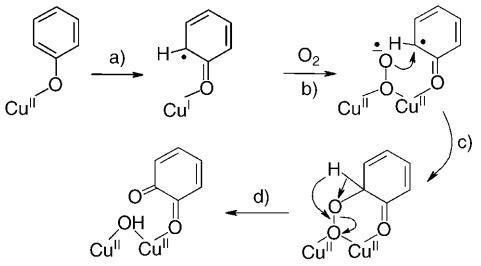


Figure 3. Proposed mechanism for aerobic hydroxylation and oxidation of phenol in the absence of H_2O_2, with the binding of phenol and reduction of the metal center as the key step (a). The binding of dioxygen and formation of superoxide (b) is proposed to be assisted by a dinuclear center. See text for details.

As the hydroxylation and oxidation of phenol is a multi-electron-transfer process, the involvement of two metal centers is suspected. The activity profile for phenol oxidation is similar to that for the Zn^{II} dilution experiment for catechol oxidation. The data can be fitted equally well to the Hill equation [Eq. (3)] to afford $\theta = 1.80$ ($r^2 = 0.98$) and a quadratic equation for single-metal binding ($r^2 = 0.98$), consistent with either a mononuclear oxidation[23] or a cooperative mechanism involving a dinuclear center,[16] or a combination of both pathways.

To monitor substrate binding, a "slow" substrate, 4,5-dichlorocatechol (DCC), which is approximately 200 times slower than catechol in terms of k_{cat}, was titrated into a solution of $CuA\beta_{1-20}$ (0.2 mM) in the presence or absence of H_2O_2 (100 mM) and monitored by UV/Vis spectroscopy at 25 °C at pH 7.0 (Figure 4). Similar spectra were obtained through the course of the titration, indicating that H_2O_2 was not involved in the binding of DCC to $Cu^{II}A\beta$ under the experimental conditions. The absorption at 437 nm increased upon addition of DCC to $(Cu^{II}A\beta)_2$ and reached saturation at more than 1.2 equivalents of DCC, and the data were fitted to a single-substrate binding model to yield a dissociation constant of 0.24 mM. The result provides direct evidence for catechol binding to a dicopper(II) center, consistent with the

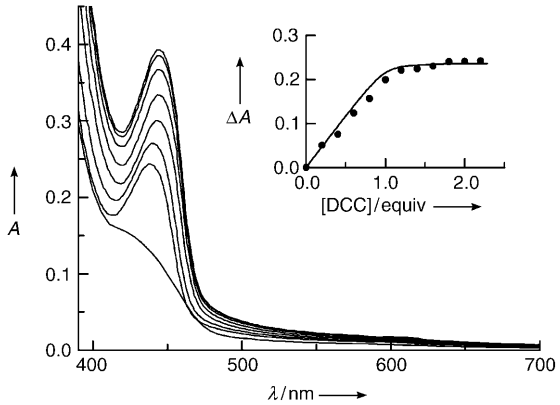


Figure 4. Titration of DCC to CuAβ (0.2 mM) in the presence of H_2O_2 (100 mM) in HEPES buffer (100 mM) at pH 7.0 monitored by UV/Vis spectroscopy. Analogous spectra were obtained in the absence of H_2O_2. The inset shows the change in absorbance at $\lambda = 437$ nm as a function of the number of equivalents of DCC added with respect to $(Cu^{II}A\beta)_2$, consistent with the formation of a 1:1 DCC–$(Cu^{II}A\beta)_2$ adduct.

 © 2005 Wiley-VCH Verlag GmbH & Co. KGaA, Weinheim

observations with a chemical model[24] and the mechanism proposed above.

In conclusion, we have established the catalytic activities of $CuA\beta_{1-20}$ toward the relatively inactive species (according to their k_0 values) catechol and phenol in the presence and absence of H_2O_2 in aqueous solutions at near-physiological conditions. The reaction patterns are consistent with the mechanisms carried out by Type-3 copper centers as observed with catechol oxidase and tyrosinase and their dinuclear model systems.[8,22] So far these results are unique in metal-centered redox chemistry related to Alzheimer's disease and are expected to offer further insight into the neuropathology of this disease, as it is suspected to be linked with, besides many other factors, the oxidation of mono- and diphenol-containing neurotransmitters such as dopamine, epinephrine, norepinephrine, and serotonin.[25,26] Furthermore, the association of this highly reactive Cu–oxygen chemistry with Alzheimer's disease can better define the role of metallo-β-amyloids in the neuropathology of this disease and possibly lead to different treatment strategies toward this disease.

Received: March 19, 2005
Published online: July 29, 2005

Keywords: β-amyloids · Alzheimer's disease · copper · oxidoreductases · peptides · redox chemistry

[1] A. I. Bush, *Trends Neurosci.* **2003**, *26*, 207 – 214.
[2] B. Tseng, M. Kitazawa, F. M. LaFerla, *Curr. Alzheimer Res.* **2004**, *1*, 231 – 239.
[3] X. Huang, C. S. Atwood, M. A. Hartshorn, G. Multhaup, L. E. Goldstein, R. C. Scarpa, M. P. Cuajungco, D. N. Gray, J. Lim, R. D. Moir, R. E. Tanzi, A. I. Bush, *Biochemistry* **1999**, *38*, 7609 – 7616.
[4] C. Opazo, X. Huang, R. A. Cherny, R. D. Moir, A. E. Roher, A. R. White, R. Cappai, C. L. Masters, R. E. Tanzi, N. C. Inestrosa, A. I. Bush, *J. Biol. Chem.* **2002**, *277*, 40302 – 40308.
[5] K. G. Manton, S. Volovik, A. Kulminski, *Curr. Alzheimer Res.* **2004**, *1*, 277 – 293.
[6] T. E. Machonkin, U. M. Sundaram, E. I. Solomon, *Chem. Rev.* **1996**, *96*, 2563 – 2605.
[7] W. B. Tolman, L. Que, Jr., *Angew. Chem.* **2002**, *114*, 1160 – 1185; *Angew. Chem. Int. Ed.* **2002**, *41*, 1114 – 1137.
[8] a) E. A. Lewis, W. B. Tolman, *Chem. Rev.* **2004**, *104*, 1047 – 1076; b) W. B. Tolman, *Acc. Chem. Res.* **1997**, *30*, 227 – 237.
[9] L. M. Mirica, X. Ottenwaelder, D. P. Stack, *Chem. Rev.* **2004**, *104*, 1013 – 1045.
[10] Phenol hydroxylation/oxidation and catechol oxidation were performed as previously reported[11] with minor changes to suit the current studies. The same molar concentrations of phenol or catechol and 3-methyl-2-benzothiazolinone hydrazone (MBTH, an indicator of *o*-quinone) were mixed in HEPES buffer (100 mM) at pH 7.00 in the presence of $CuA\beta_{1-20}$ at 5.0 μM (phenol hydroxylation/oxidation) or 0.50 μM (catechol oxidation). The red adduct of the *o*-quinone product was monitored at 500 nm ($\varepsilon = 32{,}500\ M^{-1}cm^{-1}$; see Figure 1c). The autooxidation of phenol and catechol were determined under the same conditions in the absence of $CuA\beta_{1-20}$. The 1–20 fragment of Aβ was synthesized at the Peptide Center of the University of South Florida. The identity of the peptide was confirmed with a Bruker MALDI-TOF mass spectrometer.
[11] S. G. Srivatsan, P. Nigamb, M. S. Raob, S. Verma, *Appl. Catal. A* **2001**, *209*, 327 – 334.
[12] Rates were determined on a Varian CARY50 spectrophotometer equipped with a temperature controller. The rate law for pre-equilibrium kinetics [Eq. (1)], as followed by $Cu^{II}A\beta$, is shown in Equation (2), in which k_{cat} and K'_{app} are the first-order rate constant and apparent dissociation constant, respectively, *S* is the substrate, P is the product, and v_{bg} is the autooxidation rate.

$$Cu^{II}A\beta + S \underset{k_{-1}}{\overset{k_1}{\rightleftharpoons}} A\beta Cu^{II}\text{–}S \xrightarrow{k_{cat}} Cu^{II}A\beta + P \quad (1)$$

$$v = v_{bg} + \frac{k_{cat}[CuA\beta][S]}{K'_{app} + [S]} \quad (2)$$

[13] A. Rompel, H. Fischer, D. Meiwes, K. Büldt-Karentzopoulos, R. Dillinger, F. Tuczek, H. Witzel, B. Krebs, *J. Biol. Inorg. Chem.* **1999**, *4*, 56 – 63.
[14] a) C. T. Yang, M. Vetrichelvan, X. Yang, B. Moubaraki, K. S. Murray, J. J. Vittal, *Dalton Trans.* **2004**, 113 – 121; b) A. Granata, E. Monzani, L. Casella, *J. Biol. Inorg. Chem.* **2004**, *9*, 903 – 913; c) R. Than, A. A. Feldmann, B. Krebs, *Coord. Chem. Rev.* **1999**, *182*, 211 – 241.
[15] G. F. Z. da Silva, W. T. Tay, L.-J. Ming, *J. Biol. Chem.* **2005**, *280*, 16601 – 16609.
[16] P. E. M. Siegbahn, *J. Biol. Inorg. Chem.* **2003**, *8*, 567 – 576.
[17] The Hill equation can serve as a general model for cooperativity as reflected by the Hill coefficient θ, which deviates from unity in the presence of cooperativity [Eq. (3); K_x is the intrinsic dissociation constant].

$$\frac{v_0}{v_{max}} = \frac{[CuA\beta]^{\theta}}{K_x + [CuA\beta]^{\theta}} \quad (3)$$

[18] In case of two-substrate catalysis, such as phenol hydroxylation/oxidation and catechol oxidation in the presence of H_2O_2, both substrates can interact with the metal center independently. The data are fitted to the Hanes plot [Eq. (4)] to yield true values of substrate dissociation constants K'.[19]

$$\frac{[S]}{v_0} = \frac{(1 + K\prime_{\alpha}/[H_2O_2])}{v_{max}}[S] + \frac{K'}{v_{max}}\left(1 + \frac{K_i}{[H_2O_2]}\right) \quad (4)$$

[19] V. Leskovac, *Comprehensive Enzyme Kinetics*, Kluwer, Boston, **2002**, p. 119.
[20] A. Rompel, H. Fischer, D. Meiwes, K. Buëldt-Karentzopoulos, A. Magrini, C. Eicken, C. Gerdemann, B. Krebs, *FEBS Lett.* **1999**, *445*, 103 – 110.
[21] M. Maumy, P. Capdevielle, *J. Mol. Catal. A* **1996**, *113*, 159 – 166.
[22] K. D. Karlin, S. Kaderli, A. D. Zuberbühler, *Acc. Chem. Res.* **1997**, *30*, 139 – 147.
[23] a) K.-Q. Ling, Y. Lee, D. Macikenas, J. D. Protasiewicz, L. M. Sayre, *J. Org. Chem.* **2003**, *68*, 1358 – 1366; b) S. R. Starck, J.-Z. Deng, S. M. Hecht, *Biochemistry* **2000**, *39*, 2413 – 2419.
[24] S. Torelli, C. Belle, S. Hamman, J. P. Pierre, *Inorg. Chem.* **2002**, *41*, 3983 – 3989.
[25] H. Umegaki, N. Tamaya, T. Shinkai, A. Iguchi, *Exp. Gerontology* **2000**, *35*, 1373 – 1382.
[26] W. Fu, H. Luo, S. Parthasarathy, M. P. Mattson, *Neurobiol. Dis.* **1998**, *5*, 229 – 243.

 © 2005 Wiley-VCH Verlag GmbH & Co. KGaA, Weinheim

Surface Chemistry

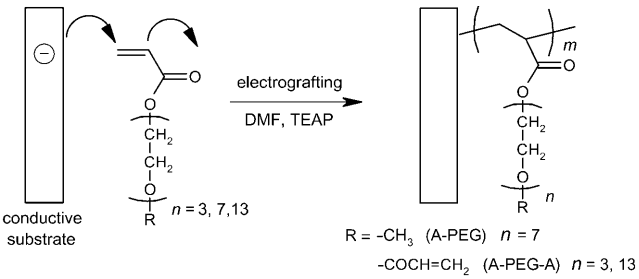
DOI: 10.1002/anie.200500639

Electrografting of Poly(ethylene glycol) Acrylate: A One-Step Strategy for the Synthesis of Protein-Repellent Surfaces**

*Sabine Gabriel, Peter Dubruel, Etienne Schacht, Alain M. Jonas, Bernard Gilbert, Robert Jérôme, and Christine Jérôme**

Nowadays, the availability of biocompatible surfaces is a key issue in the design and production of medical devices and implants to be used in contact with blood. Poly(ethylene glycol) (PEG) has the unique capacity to reduce protein adsorption and cell adhesion on a variety of hydrophobic substrates,[1] which explains the continuing efforts to develop new methods for the deposition of strongly adhering PEG coatings on gold[2] from thiols and disulfides, on silicon[3] and glass[4] from silanes or a poly(glycidyl methacrylate) primer,[5] and on metal oxides from poly(L-lysine)-g-poly(ethylene glycol)[6] or by plasma treatment.[7] In addition to these techniques, electrografting is often used for the chemisorption of poly(meth)acrylate chains onto electrically conductive substrates whatever their shape (plates, stents, fibers, powders,…).[8–11] Compared to the chemical methods, electrografting has the advantage of being applicable to a large variety of substrates, including metals and alloys, semiconductors, ITO-glass, and carbon. Although originally reported for acrylonitrile,[11] electrografting has been extended to a large variety of (meth)acrylates, thereby allowing the surface properties to be tuned by the appropriate choice of the ester substituent. For example, reactive, hydrophobic, and electroactive coatings have been deposited by the electrografting of various acrylates bearing *N*-succinimidyl,[12] norbornenyl,[13] and pyrrolyl[14] moieties, respectively. To the best of our knowledge, the one-step electrografting of highly hydrophilic coatings has not yet been reported.

Herein, we want to report the direct electrografting of acrylic end-capped PEG (macromonomers). In the following, A-PEG and A-PEG-A will be used as abbreviations for the number of polymerizable end-groups A (one or two, respectively; Scheme 1). The electropolymerization of PEG macromonomers was conducted by voltammetry in DMF containing a conducting salt (tetraethylammonium perchlorate, TEAP). As is usually observed for the cathodic polymerization of (meth)acrylates, two reduction phenomena can be distinguished[9] in solvents of a high donor number,[8] (Figure 1 A,



Scheme 1. Electrografting of PEG macromonomers by cathodic polarization of the conductive substrate.

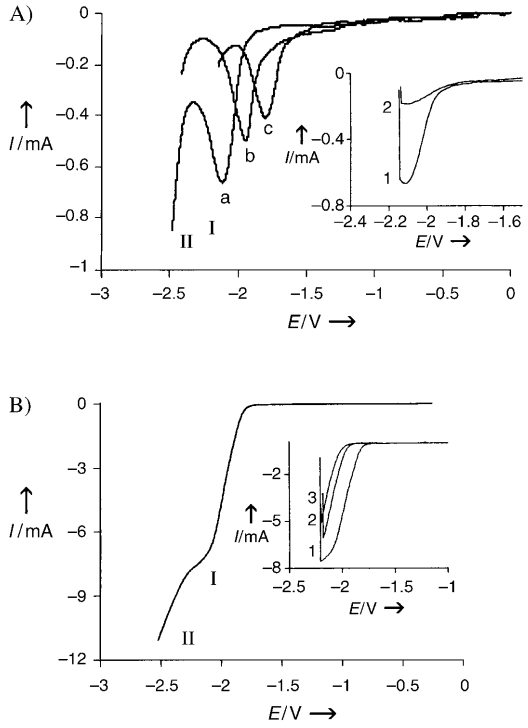


Figure 1. A) Voltammograms on glassy carbon for the reduction of A-PEG-A (M_n = 258): a) 0.1 M, b) 0.5 M, c) 1 M in DMF/5×10^{-2} M TEAP at 20 mVs^{-1}; I: grafting peak; II: polymerization in solution. Inset: Reduction of A-PEG-A (M_n = 258, 0.1 M): 1) first and 2) second scan. B) Voltammograms for the reduction of A-PEG (M_n = 454, 0.5 M) on glassy carbon in DMF/5×10^{-2} M TEAP at 20 mVs^{-1}; I: grafting peak; II: polymerization in solution. Inset: Reduction of A-PEG (M_n = 454, 0.5 M): 1) first, 2) second, and 3) third scan.

[*] S. Gabriel, Prof. R. Jérôme, Dr. C. Jérôme
Center for Education and Research on Macromolecules (C.E.R.M.)
University of Liege
B6 Sart-Tilman, 4000 Liège (Belgium)
Fax: (+32) 4-366-3497
E-mail: c.jerome@ulg.ac.be
Dr. P. Dubruel, Prof. E. Schacht
Department of Organic Chemistry
University of Gent
Krijgslaan 281, 9000 Gent (Belgium)
Prof. A. M. Jonas
Unité de Physique et de Chimie des Hauts Polymères
Université Catholique de Louvain
Place Croix de Sud 1, 1348 Louvain-la-Neuve (Belgium)
Prof. B. Gilbert
Laboratory of Analytical Chemistry and Electrochemistry
University of Liège
B6 Sart-Tilman, 4000 Liège (Belgium)

[**] The authors are grateful to the Belgian Science Policy for financial support in the framework of the Interuniversity Attraction Poles Programme (PAI V/03). C.J. is a research associate of the "Fonds National de la Recherche Scientifique" (FNRS).

 © 2005 Wiley-VCH Verlag GmbH & Co. KGaA, Weinheim

curve a). At the less-cathodic potential (peak I), a species is formed which is responsible for both the initiation of the macromonomer polymerization and the chemisorption of the growing chains,[11] whereas at a more-cathodic potential (Figure 1 A, signal II), the initiating species are also formed by electron transfer from the cathode to the monomer; however, the chains now propagate in solution and are no longer chemisorbed onto the cathode surface. Whenever the cathodic potential equals the maximum of peak I, the electrode is passivated within a few seconds as the result of the grafting of an insulating polyacrylate film. This polymer grafting was also confirmed by the extremely low current intensity observed during a second potential scan on the same electrode (curve 2 in the inset of Figure 1 A).

In a second part of the work, the macromonomer concentration was varied and the intensity of the passivation peak I (Ip1) was determined from the voltammograms, as exemplified in Figure 1 for A-PEG-A. As previously reported for ethyl acrylate electrografting,[8] the data summarized in Table 1 confirm that an increase in monomer concentration

Table 1: Current intensity at the potential of peak I in relation to the A-PEG-A concentration.[a]

[A-PEG-A]	0.1 M	0.5 M	1 M
Ip1 for A-PEG-A (M_n = 700) [mA]	−1.67	−1.28	−0.70
Ip1 for A-PEG-A (M_n = 258) [mA]	−0.66	−0.50	−0.40

[a] In a DMF solution of TEAP (0.05 M) at 20 mV s^{-1}.

results in a smaller Ip1 at a constant scan rate (20 mV s^{-1}). Indeed, only the polymerization initiation is an electrochemical process, in which only the adsorbed monomer participates. The kinetics of this step are thus weakly dependent on the monomer concentration. In contrast, chain propagation, and thus the increase of the degree of polymerization (DP) of the insulating brushes, is a chemical process which is fast when the monomer concentration is high. Therefore, passivation occurs rapidly when the chain propagation is fast and Ip1 decreases accordingly. In the case of the monoacrylate macromonomer, the voltammetric peaks I and II overlap and the passivation of the electrode is less efficient, as shown by the current intensity, which decreases more slowly when the potential scan is repeated (Figure 1 B, inset). These observations are consistent with a less-effective adsorption of the A-PEG macromonomer at the surface. The overlap of peaks I and II is indeed known to be extensive when the monomer concentration is low.[8] The lower efficiency of the electrografting of A-PEG also has a direct influence on the electrode passivation. As a rule, these electrochemical observations are observed irrespective of the substrate (glassy carbon, stainless steel, and gold).

Grafting of poly(ethylene glycol) was confirmed by ATR-FTIR analysis of the electrode surface after intensive washing with DMF, which is a good solvent for PEG; the three main absorptions at 2861, 1732, and 1106 cm^{-1} are characteristic of the CH_2, C=O, and C–O–C vibrations of poly(A-PEG), respectively (Figure 2). Moreover, a careful analysis of the spectra for all the electrografted films (PEG bands) shows

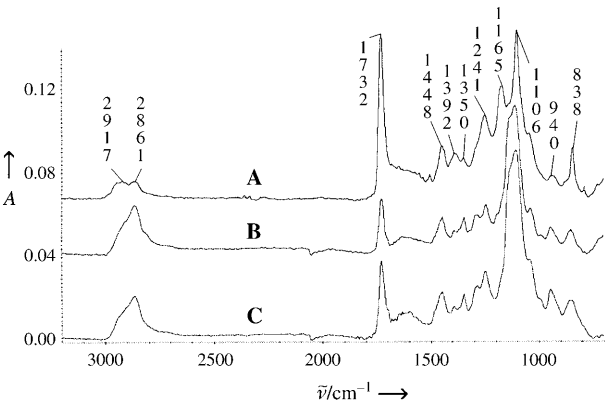


Figure 2. ATR-FTIR spectra for A-PEG-A (M_n = 258, 0.5 M) (A), A-PEG (M_n = 454, 1 M) (B), and A-PEG-A (M_n = 700, 0.1 M) (C) electrografted onto stainless steel.

that the CH_2 scissoring mode at 1448 cm^{-1} and the CH_2 twisting mode at 1241 cm^{-1} dominate the CH_2 wagging mode at 1350 cm^{-1}, which indicates that the PEG side chains are oriented parallel to the surface, as has been reported elsewhere.[6] Figure 3 illustrates this preferential

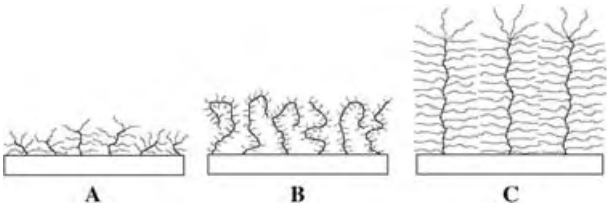


Figure 3. Expected architecture and conformation of poly(A-PEG) (A) and poly(A-PEG-A) (B and C) electrografted from A-PEG (M_n = 454, DP_{EG} = 7; A), A-PEG-A (M_n = 258, DP_{EG} = 3; B), and A-PEG-A (M_n = 700, DP_{EG} = 13; C). PEG side chains are in gray and the polyacrylic backbone in black.

orientation of the PEG teeth of the comb-like architectures. Interestingly, Raman analysis of the diacrylate PEG films showed that the electrografted coatings still contain unreacted acrylic functions. Indeed, although the intensity ratio of the C=C band at 1632 cm^{-1} to the C=O band at 1730 cm^{-1} has decreased, the C=C band does not disappear completely (Figure 4), which could offer a unique opportunity for further functionalization of the coating, for example by the Michael addition of nucleophiles.[15]

The film thickness was measured by ellipsometry at five distinct spots on the surface of films electrografted on stainless steel and glassy carbon (Table 2). The dispersion of the five data points for each film is lower than 10% error, which is a strong indication of the homogeneity of the films. Although the film thickness is systematically smaller when the substrate is stainless steel rather than glassy carbon (the difference being significant only for the A-PEG macromonomer), this characteristic feature depends more on the monomer concentration, as illustrated in Figure 5 for the glassy carbon substrate. The film thickness increases with the macromonomer concentration at a rate which is, however,

 © 2005 Wiley-VCH Verlag GmbH & Co. KGaA, Weinheim

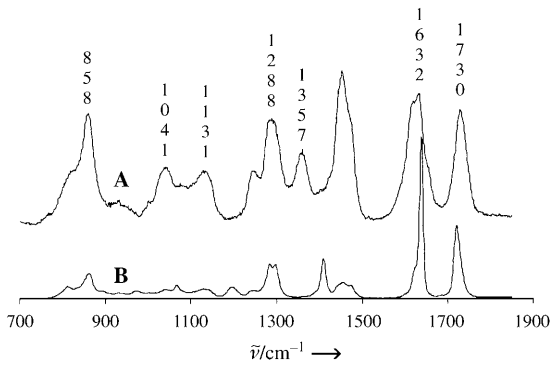


Figure 4. Raman spectra for A-PEG-A ($M_n = 258$, 1 M) electrografted (A) and solvent-cast (B) onto stainless steel.

Table 2: Thickness and contact angles of water (at 3 min) at the surface of PEG electrografted films.

		A-PEG-A ($M_n = 454$)			A-PEG-A ($M_n = 258$)		A-PEG-A ($M_n = 700$)	
		0.1 M	0.5 M	1 M	0.1 M	1 M	0.1 M	1 M
Carbon	Thickness [nm]	13 ± 1	24 ± 3	49 ± 5	14 ± 2	222 ± 20	112 ± 18	475 ± 37
	Contact angle [°]	43 ± 2	31 ± 3	25 ± 3	43 ± 3	48 ± 4	< 10	< 10
Stainless steel	Thickness [nm]	9 ± 1	18 ± 2	39 ± 4	11 ± 4	202 ± 31	98 ± 22	437 ± 39
	Contact angle [°]	45 ± 4	37 ± 4	29 ± 3	42 ± 4	50 ± 3	< 10	< 10

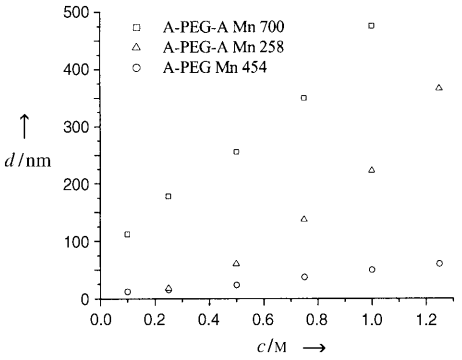


Figure 5. Dependence of the film thickness d on the macromonomer concentration c on polished glassy carbon.

much faster for the bifunctional than for the monofunctional macromonomer of comparable molecular weight. A greater thickness for the films formed by the bifunctional macromonomer was expected because the concentration of the polymerizable acrylic moieties is doubled in this case, thus making the propagation of the tethered chains much faster and, consequently, the DP and thickness greater, as illustrated in Figure 3 (A and B).

In the case of PEG monoacrylate films, a maximum thickness of 50 nm was observed for a coating prepared at high concentration (1M). This thickness is in agreement with the values previously measured for films synthesized starting from a monoacrylic monomer.[10,16] For example, for poly(ethyl acrylate)[10] or poly(acrylonitrile)[16] films, the thickness never exceeds 100 nm for a monomer concentration of 1M. In the case of PEG diacrylate, an increase in macromonomer concentration and molecular weight makes the coating thickness grow very rapidly such that a thickness of up to 500 nm can be reached when a macromonomer of $M_n = 700$ is used at a concentration of 1M.

This drastic evolution of the coating thickness can be explained by the peculiar architecture of the polymer chains that are formed by electrografting, namely a comblike polymer consisting of an acrylic backbone with PEG side chains grafted onto each acrylic unit. The conformation of such poly(acrylic) comblike polymers depends on the length of the macromonomer, i.e., on the size of the PEG side chain. As shown by Fredrickson,[17] the repulsive interaction between the side chains induces the rigidity of the comb polymer: the greater the length of the side chains, the higher the persistence length of the main chain. In other words, we can assume that when the M_n of the PEG side chains is increased, the stretching of the tethered chains is responsible for the rapid increase of the coating thickness (B and C in Figure 3). It should be emphasized that Figure 3 (B and C) does not consider the possible reaction of the second acrylic function of the macromonomer. However, this reaction most probably occurs and leads to additional branching of the brushes, cross-linking, loops, and/or network formation. All these additional reactions are also expected to increase the film thickness. These reactions have been neglected in Figure 3 for reasons of clarity as the extent of these reactions is limited, as already mentioned in the description of the Raman spectrum (Figure 4).

The water contact angles measured for the different PEG films are in good agreement with the thickness measurements. Table 2 shows that in the case of PEG diacrylate (thick films) the contact angles do not depend on the macromonomer concentration. These films fully cover the underlying substrate such that the contact angle only depends on the macromonomer composition and not on the macromonomer concentration, i.e., for A-PEG-A ($M_n = 258$), the DP of PEG is only 3, which makes the hydrophobic acrylic content quite high, and the contact angle levels at around 45°. When the M_n of the macromonomer is increased (from $M_n = 258$ to $M_n = 700$) very hydrophilic films are obtained (< 10°). As far as the monoacrylate PEG is concerned, the film thickness is low and concentration-dependent. As observed in Table 2, the contact angle decreases with increasing film thickness from 45 to 25°. When the films prepared with this hydrophilic macromonomer (A-PEG) are thin, the underlying hydrophobic substrate has an effect on the contact angle of water (Table 2), probably due to a weak tendency of these hydrophilic chains to spread out on the hydrophobic surface. For the thicker films, the contact angle reaches 25°, which is a value already lower than that usually reported for PEG monolayers 5–6 nm thick (30–35°).

The comblike architecture of the films obtained in this one-step process would be particularly interesting in cases where protein adsorption has to be avoided. Indeed, branched PEG chains, like PEG stars, have recently been shown to be more efficient at preventing unspecific protein adsorption

 © 2005 Wiley-VCH Verlag GmbH & Co. KGaA, Weinheim

than linear chains[3a,18] because they combine both high grafting density and high PEG segment mobility.

Based on contact angle and ellipsometry data, films of monoacrylate PEG prepared at a 1M concentration combine high hydrophilicity and low thickness, which are two key criteria for reliable measurements of protein adsorption by surface plasmon resonance (SPR). The poly(A-PEG-A) films were disregarded because of the possible Michael addition of the proteins to unreacted acrylate groups. Liedberg and coworkers, the pioneers in the SPR field, have demonstrated the utility of this practical and commonly used technique for the characterization of bio-interfaces.[19] SPR substrates (glass slides coated on one side by a thin gold film) were electrografted by ethyl acrylate (0.1M; reference sample) and PEG monoacrylate (1M) in a DMF solution containing TEAP (5×10^{-2}M). The sensorgrams showing the proteins' adsorption with time were compared for the hydrophobic poly(ethyl acrylate) (PEA) and hydrophilic poly(A-PEG) coatings. Figure 6 illustrates the adsorption of bovine serum albumin

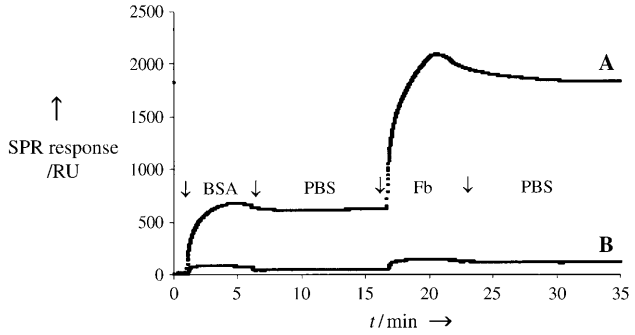


Figure 6. SPR adsorption profiles for bovine serum albumin (BSA; 0.5 mg mL^{-1}) and fibrinogen (Fb; 0.1 mg mL^{-1}) in a phosphate buffer (PBS; 10 mM, pH 7.4) on: A) electrografted PEA (0.1 M)[10] and B) electrografted A-PEG (M_n = 454, 1 M). Flow rate: 20 μL min^{-1}. Substrate: gold.

(BSA) (first injection) and fibrinogen (Fb) (second injection) on the two types of electrografted films. Curve B in Figure 6 is convincing evidence that electrografted PEG is very efficient in preventing protein adsorption. The electrografted PEG film decreases both the BSA and fibrinogen adsorption relative to the grafted PEA film: BSA adsorption is reduced by 93% (±3%), whereas fibrinogen adsorption is reduced by 92% (±2%). These results are highly reproducible, further indicating the homogeneous and reproducible coating process when using electrografting.

The one-step electrografting of PEG macromonomers is a technique that is very well suited for coating conductive substrates homogeneously with a strongly adhering hydrophilic coating. These electrografted chains, which have a comb-like architecture, have proven to be very efficient in preventing the adsorption of proteins. This very simple technique is thus highly promising in the field of coatings of biomedical devices and biosensors. In addition, the unreacted acrylic functions remaining in the PEG diacrylate films offer the opportunity of straightforward derivatization, for instance by Michael addition, with a variety of molecules of interest such as proteins. This opens the way to the easy elaboration of surfaces for the specific recognition of proteins or with sensor capabilities.

Experimental Section

PEG macromonomers (M_n = 258, 454, and 700; Aldrich) were dried by three azeotropic distillations with toluene. DMF and tetraethylammonium perchlorate (TEAP) were dried before use.[10] Electrochemical experiments were carried out in a three-compartment cell equipped with a Pt pseudo-reference electrode, a Pt counter-electrode, and a working electrode (1 cm^2) with a PAR EG&G potentiostat (Model 273A). All electrochemical experiments were carried out in a glovebox under a dry and inert atmosphere (N_2). All the electrografted films of PEG diacrylate and monoacrylate were prepared by, respectively, two or three scans of the potential between the initial potential of the open circuit and the potential at the top of the first peak, where it is kept for 5 s. The electrografted PEA films were prepared in the same way from ethyl acrylate (EA; 0.1M) solution in DMF/5×10^{-2}M TEAP, as reported previously.[10] This EA concentration was chosen such that the film thickness was similar to that prepared with the A-PEG macromonomer (1M). ATR-FTIR, Raman, and contact-angle measurements were carried out on the modified surface after rinsing with DMF to remove the monomer and the nongrafted polymer, and in acetonitrile to dry the coating. Ellipsometry was carried out with an Ellisel ellipsometer (Jobin-Yvon/Sofie instrument) operating at a wavelength of 632.8 nm. The film thickness was measured at 70.67° (incidence angle with respect to the normal of the substrate). At least five measurements were taken for each sample at different locations; the error in the thickness was about 10%. The refractive index for PEG was 1.506.[20] For thicker films (< 200 nm), the thickness was measured with a Sentech, SE 800 spectroscopic ellipsometer. SPR experiments were performed with a Biacore-X instrument equipped with an internal injection system (Hamilton syringe, 200 μL). The experiments were carried out with a phosphate buffer (10 mM, pH 7.4) at a flow rate of 20 μL min^{-1}. The concentration of the protein solutions was 0.5 mg mL^{-1} for bovine serum albumin (Sigma, Fraction V, 95%) and 0.1 mg mL^{-1} for fibrinogen (bovine, Sigma, Fraction I, 86%) rather than physiological protein concentrations. These low protein concentrations were chosen in order to avoid poisoning of the SPR signal by protein exchange phenomena. However, similar results were obtained for higher concentrations of fibrinogen (1 mg mL^{-1}). After each protein injection the SPR substrate was washed with a phosphate buffer (PBS). The percentage of absorbed protein was calculated based on the plateau levels after the PBS cleaning.

Received: February 21, 2005
Revised: June 13, 2005
Published online: July 29, 2005

Keywords: adsorption · electrochemistry · polymers · proteins · thin films

[1] a) J. H. Lee, H. B. Lee, J. D. Andrade, *Prog. Polym. Sci.* **1995**, *20*, 1043–1079; b) J. D. Andrade, V. Hlady, S. I. Jeon, *Adv. Chem. Ser.* **1996**, *248*, 51–59; c) P. Vermette, L. Meagher, *Colloids Surf. B* **2003**, *28*, 153–198.

[2] a) S. Herrwerth, T. Rosendahl, C. Feng, J. Fick, W. Eck, M. Himmelhaus, R. Dahint, M. Grunze, *Langmuir* **2003**, *19*, 1880–1887; b) N. Xia, Y. Hu, D. W. Grainger, D. G. Castner, *Langmuir* **2002**, *18*, 3255–3262; c) P. Harder, M. Grunze, R. Dadint, G. M. Whitesides, P. E. Laibinis, *J. Phys. Chem. B* **1998**, *102*, 426–436; d) K. Emoto, J. M. Van Alstine, J. M. Harris, *Anal. Chem.* **1996**,

 © 2005 Wiley-VCH Verlag GmbH & Co. KGaA, Weinheim

68, 3751 – 3757; e) K. L. Prime, G. M. Whitesides, *J. Am. Chem. Soc.* **1993**, *115*, 10714 – 10721.
[3] a) J. Groll, Z. Ademovic, T. Ameringer, D. Klee, M. Moeller, *Biomacromolecules* **2005**, *6*, 956 – 962; b) A. Papra, N. Gadegaard, N. B. Larsen, *Langmuir* **2001**, *17*, 1457 – 1460; c) Z. Yang, J. A. Galloway, H. Yu, *Langmuir* **1999**, *15*, 8405 – 8411; d) S. J. Sofia, V. Premnath, E. W. Merrill, *Macromolecules* **1998**, *31*, 5059 – 5070; e) M. Malmsten, K. Emoto, J. M. Van Alstine, *J. Colloid Interface Sci.* **1998**, *202*, 507 – 517; f) J. D. Andrade, V. Hlady, S. I. Jeon, *Adv. Chem. Ser.* **1996**, *248*, 51 – 59.
[4] a) E. V. Amirgoulova, J. Groll, C. D. Heyes, T. Ameringer, C. Roecker, M. Moeller, G. U. Nienhaus, *ChemPhysChem* **2004**, *5*, 552 – 555; b) S. Jo, K. Park, *Biomaterials* **2000**, *21*, 605 – 616; c) J. Piehler, A. Brecht, R. Valiokas, B. Liedberg, G. Gauglitz, *Biosens. Bioelectron.* **2000**, *15*, 473 – 481.
[5] B. Zdyrko, V. Klep, I. Luzinov, *Langmuir* **2003**, *19*, 10179 – 10187.
[6] N.-P. Huang, R. Michel, J. Voros, M. Textor, R. Hofer, A. Rossi, D. L. Elbert, J. A. Hubbell, N. D. Spencer, *Langmuir* **2001**, *17*, 489 – 498.
[7] a) X. Gong, L. Dai, H. J. Griesser, A. W. H. Mau, *J. Polym. Sci. B* **2000**, *38*, 2323 – 2332; b) Y. X. Qiu, D. Klee, W. Plüster, B. Severich, H. Höcker, *J. Appl. Polym. Sci.* **1996**, *61*, 2373 – 2382.
[8] N. Baute, P. Teyssié, L. Martinot, M. Mertens, P. Dubois, R. Jérôme, *Eur. J. Inorg. Chem.* **1998**, 1711.
[9] N. Baute, C. Jérôme, L. Martinot, M. Mertens, V. M. Geskin, R. Lazzaroni, J. L. Brédas, R. Jérôme, *Eur. J. Inorg. Chem.* **2001**, 1097.
[10] N. Baute, L. Martinot, R. Jérôme, *J. Electroanal. Chem.* **1999**, *472*, 83 – 90.
[11] M. Mertens, C. Calberg, L. Martinot, R. Jérôme, *Macromolecules* **1996**, *29*, 4910 – 4918.
[12] a) C. Jérôme, S. Gabriel, S. Voccia, C. Detrembleur, M. Ignatova, R. Gouttebaron, R. Jérôme, *Chem. Commun.* **2003**, 2500 – 2501; b) C. Jérôme, N. Willet, R. Jérôme, A.-S. Duwez, *ChemPhysChem* **2004**, *5*, 147 – 149.
[13] C. Detrembleur, C. Jérôme, M. Claes, P. Louette, R. Jérôme, *Angew. Chem.* **2001**, *113*, 1308 – 1311; *Angew. Chem. Int. Ed.* **2001**, *40*, 1268 – 1271.
[14] D. E. Labaye, C. Jérôme, V. M. Geskin, P. Louette, R. Lazzaroni, L. Martinot, R. Jérôme, *Langmuir* **2002**, *18*, 5222 – 5230.
[15] M. Heggli, N. Tirelli, A. Zisch, J. A. Hubbell, *Bioconjugate Chem.* **2003**, *14*, 967 – 973.
[16] C. Calberg, M. Mertens, R. Jérôme, X. Arys, A. M. Jonas, R. Legras, *Thin Solid Films* **1997**, *310*, 148 – 155.
[17] G. H. Fredrickson, *Macromolecules* **1993**, *26*, 2825.
[18] a) D. J. Irvine, A. M. Mayes, L. Griffith-Cima, *Macromolecules* **1996**, *29*, 6037 – 6043; b) D. J. Irvine, A. M. Mayes, S. K. Satija, J. G. Barker, S. J. Sofia-Allgor, L. G. Griffith, *J. Biomed. Mater. Res.* **1998**, *40*, 498 – 509.
[19] a) B. Liedberg, C. Nylander, I. Lundström, *Biosens. Bioelectron.* **1995**, *10*, i–ix; b) V. Silin, A. Plant, *Trends Biotechnol.* **1997**, *15*, 353; c) R. J. Green, J. Davies, M. C. Davies, C. J. Roberts, S. J. B. Tendler, *Biomaterials* **1997**, *18*, 405; d) R. J. Green, M. C. Davies, C. J. Roberts, S. J. B. Tendler, *Biomaterials* **1999**, *20*, 385.
[20] *Polymer Handbook*, *3rd ed.* (Eds.: J. Brandrup, E. H. Immergut), Wiley, New York, **1989**, p. VI–461.

 © 2005 Wiley-VCH Verlag GmbH & Co. KGaA, Weinheim

Organometallic Chemistry

DOI: 10.1002/anie.200501335

Formation of an Unsymmetrical Dinuclear Ruthenium Complex with μ-H, μ-OH, and μ-κ^2-CO_2 Bridges and Multiple Reactive Sites**

*Yasuhiro Arikawa, Shuichi Nagae, Jun-ichi Morishita, Katsuma Hiraki, and Masayoshi Onishi**

Hydrido ruthenium species and their organometallic derivatives play important roles as chemically active intermediates in the key steps of numerous catalytic reactions.[1] Judicious design and syntheses of model compounds for these processes have contributed to the rapid development of organoruthenium chemistry. We have exploited some versatile hydrido (phosphine) transition-metal compounds to obtain useful highly reactive catalysts[1,2] and to investigate the structural characteristics and chemical reactivities of organometallic intermediates derived from them through the incorporation of organic substrates, such as alkenes, alkynes, nitriles, and allylic compounds.[3] In the course of these studies, we treated ethanol solutions of some chloro(carbonyl)(phosphine) ruthenium(II) complexes $[RuCl_2(CO)_n(PR_3)_m]$ with a large excess of concentrated aqueous KOH solution, and from the reactions of the PMe_3 complexes, we succeeded in isolating and characterizing of an unprecedented dinuclear ruthenium complex with μ-H, μ-OH, and μ-κ^2-CO_2 bridges.[4] In contrast to this result, Lavigne and co-workers have described that reactions of the halo(carbonyl)ruthenium(II) complex $[RuCl_2(CO)_3(thf)]$ with methanolic solutions of KOH result in the formation of a hydroxycarbonyl species $[RuCl_2(CO)_2\{C(O)OH\}]^-$, and that subsequent thermal decarboxylation gives a transient hydride "$[RuCl_2(H)(CO)_2]^-$".[5] Our isolated dinuclear species is bridged not only by hydrido but also by hydroxo and κ^2-*O*,*C*- carbon dioxide ligands. Herein we report the synthesis of this complex and its chemical reactivity towards neutral monodentate donor molecules (i.e. Lewis bases), protic acids, and molecular iodine.

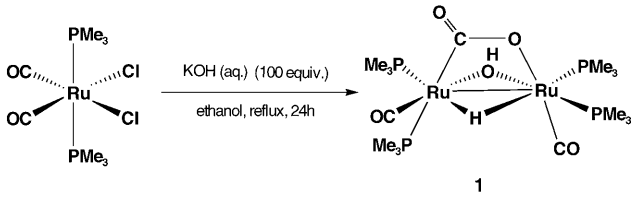
[*] Dr. Y. Arikawa, S. Nagae, J.-i. Morishita, Prof. Dr. K. Hiraki, Prof. Dr. M. Onishi
Department of Applied Chemistry
Faculty of Engineering
Nagasaki University
Bunkyo-machi 1-14, Nagasaki 852-8521 (Japan)
Fax: (+81) 95-819-2684
E-mail: onishi@net.nagasaki-u.ac.jp

[**] This work was supported by a Grant-in-Aid for Scientific Research on Priority Areas (No. 16033101, "Reaction Control of Dynamic Complexes") from the Ministry of Education, Culture, Sports, Science and Technology, Japan. We are grateful to Dr. Y. Esumi and Dr. M. Hoshino in the Institute of Physical and Chemical Research for assistance in mass spectrometry. We also thank Mr. K. Nishida and Mr. M. Okada in this Department for their technical assistance.

Supporting information for this article is available on the WWW under http://www.angewandte.org or from the author.

 © 2005 Wiley-VCH Verlag GmbH & Co. KGaA, Weinheim

Treatment of *cis*,*cis*,*trans*-$[RuCl_2(CO)_2(PMe_3)_2]$ with 100 equivalents of KOH (10 M aqueous solution) in refluxing ethanol was found to afford $[\{Ru(CO)(PMe_3)_2\}_2(\mu\text{-}H)(\mu\text{-}OH)\{\mu\text{-}\kappa^2\text{-}C(O)O\}]$ (**1**) as yellow brown powder in 59% yield (Scheme 1). The structural assignment of **1** was performed by an X-ray diffraction study of single crystals grown from benzene/hexane (Figure 1).[6]



Scheme 1. Synthesis of **1**.

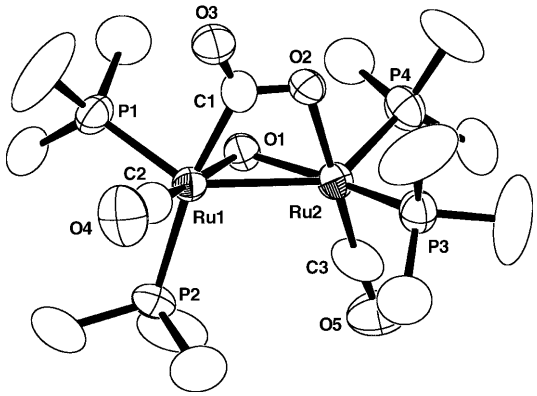


Figure 1. ORTEP diagram of complex **1** (thermal ellipsoids set at 50% probability). Selected bond lengths [Å] and angles [°]: Ru1-Ru2 2.788(1), Ru1-P1 2.282(2), Ru1-P2 2.402(2), Ru2-P3 2.273(3), Ru2-P4 2.312(3), Ru1-O1 2.089(5), Ru2-O1 2.089(5), Ru1-C1 2.089(9), Ru2-O2 2.105(5), O2-C1 1.320(10), O3-C1 1.248(10); O2-C1-O3 119.3(8).

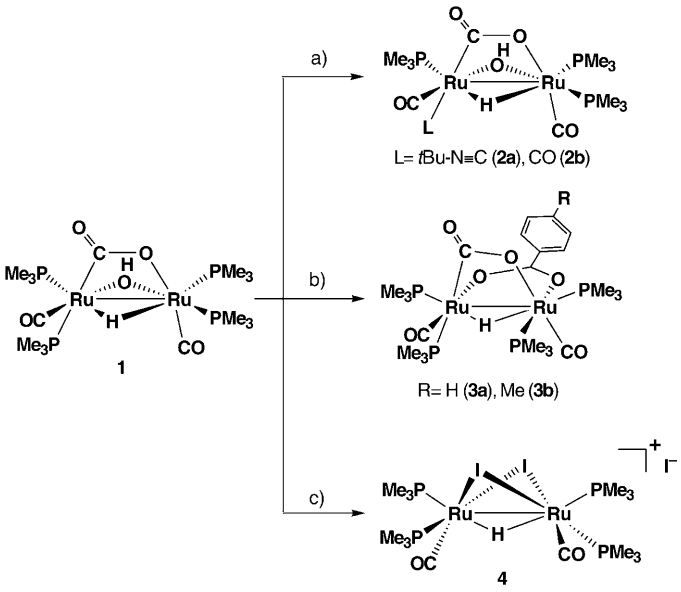
The molecule consists of two $[Ru(CO)(PMe_3)_2]$ units bridged by hydrido, hydroxo, and additionally κ^2-*O*,*C*-carbon dioxide ligands, resulting in an asymmetric dinuclear structure. Although some other dinuclear complexes containing CO_2 in a similar unsymmetrical bridging mode have been reported,[7] such a triply bridged dinuclear species is unprecedented. The geometry around each ruthenium atom is approximately octahedral. The coordinated carbon and oxygen atoms in the κ^2-*O*,*C*-CO_2 ligand are *trans* to a PMe_3 ligand (P2 of Ru1) and the CO ligand (of Ru2), respectively. The CO ligand of Ru1 and the PMe_3 (P3) ligand of Ru2 conform to the "A-frame" structure imposed by the bridging hydroxo group. Moreover, two positions *trans* to the bridging hydrido group are occupied by two PMe_3 ligands. Compound **1** has 34 cluster valence electrons with a typical Ru–Ru single bond of 2.788(1) Å.[8] The hydrido atom was located in a difference electron density map, but unfortunately its position was not refined. Bond lengths between the bridging hydroxo oxygen atom and two ruthenium atoms (Ru1-O1 2.089(5), Ru2-O1 2.089(5)) fall within the range of normal hydroxo bridge bonds in dinuclear complexes.[9] Whereas the Ru1-C1 bond length (2.089(9) Å) is comparable to that found in the only other structurally characterized metallacyclic CO_2-bridged diruthenium complex $[\{Ru(CO)_2\}_2\{\mu\text{-}\kappa^2\text{-}C(O)O\}\{\mu\text{-}(i\text{PrO})_2\text{PN(Et)P(O}i\text{Pr)}_2\}_2]$,[7a] but the Ru2-O2 bond (2.105(5) Å) of **1** is shorter. The C–O bond length of 1.248(10) Å for the noncoordinated carboxyl oxygen atom (O3), that is, the carbonyl oxygen, is shorter than the other C–O bond (C1–O2 1.320(10) Å) in the CO_2 ligand. The Ru1-P2 bond (2.402(2) Å) is the longest of the Ru–P bonds in **1**. The O···O separation of 2.758(8) Å between the hydroxo oxygen (O1)and neighboring non-coordinated carbonyl oxygen (O3) atoms indicates the presence of intermolecular hydrogen bonding.

The IR spectrum of **1** shows two ν(CO) bands at 1920 and 1906 cm^{-1}, together with a broad ν(OH) band near 3390 cm^{-1} which arises from the intermolecular hydrogen-bonding. The $^{31}P\{^1H\}$ NMR spectrum displays four non-equivalent signals at $\delta = 16.1$, 3.81, 0.21, and -18.4 ppm with multiple mutual couplings. In the ^1H NMR spectrum, a diagnostically split signal for the bridging hydrido atom which couples with these phosphorus atoms is observed at $\delta = -11.2$ ppm, in addition to a broad signal ($\delta = -0.61$ ppm) for the hydroxo proton. The latter signal diminished on addition of D_2O to the NMR sample. In the $^{13}C\{^1H\}$ NMR spectrum, the bridging CO_2 carbon atom resonated at $\delta = 205$ ppm and shows a large *trans*-phosphine coupling, in addition the spectrum also shows two lowfield resonances for the CO ligands. The FAB-MS spectrum supported the formulation of **1**.

While a similar reaction of the isomeric *trans*,*trans*,*trans*-$[RuCl_2(CO)_2(PMe_3)_2]$ failed to afford **1**, the use of another related ruthenium complex *trans*-$[RuCl_2(CO)(PMe_3)_3]$ gave rise to **1** in a low yield (4%). Thus, employment of *cis*,*cis*,*trans*-$[RuCl_2(CO)_2(PMe_3)_2]$ was essential for the successful isolation of the triply bridged diruthenium complex **1**, as the use of *cis*,*cis*,*trans*-stereoisomers with other phosphines PR_3 did not yield similar dinuclear complexes with the exception of $R_3 = Me_2Ph$, where formation of the corresponding dinuclear compound was detected in the solution, but it could not be isolated owing to its high instability. Use of a large excess of highly concentrated aqueous KOH solution was also a crucial factor in the successful formation of **1**. A reasonable mechanistic rationalization for the formation of **1** would involve initial generation of the five-coordinated hydroxycarbonyl species $[RuCl\{C(O)OH\}(CO)(PMe_3)_2]$, followed by its intermolecular unsymmetrical association as a dimer through two hydroxycarbonyl groups. Decarboxylation of one group and deprotonation of the other group would afford the μ-H and asymmetric μ-κ^2-*O*,*C*-CO_2 bridges, respectively.[10] A similar formation mechanism has been suggested by Lavigne and co-workers in the reaction of $[RuCl_2(CO)_3(thf)]$ with Et_4NOH to form polymeric carbonyl- and chloride-bridged diruthenium polyanions.[5b]

To examine the chemistry of the reactive sites in **1**, its reactivities toward neutral monodentate donor molecules were tested (Scheme 2). Treatment of **1** with excess *t*BuNC or CO in benzene gave rise to $[\{Ru_2(CO)_2(PMe_3)_3(L)\}(\mu\text{-}H)(\mu\text{-}OH)\{\mu\text{-}\kappa^2\text{-}C(O)O\}]$ (L = *t*BuNC (**2a**) and CO (**2b**)), respectively. Both $^{31}P\{^1H\}$ NMR spectra of **2a** and **2b** show a disappearance of the highest-field signal ($\delta = -18.4$ ppm) of

 © 2005 Wiley-VCH Verlag GmbH & Co. KGaA, Weinheim



Scheme 2. Reactions of **1** with various reagents. a) *t*BuNC or CO, b) benzoic acid or *p*-toluic acid, c) I_2.

the four observed for **1**, and in the ^{1}H NMR spectrum the resonances of the hydrido ligands were detected as doublet of doublet of doublet signals ($\delta = -11.0$ (**2a**), -10.9 ppm (**2b**)). Furthermore, the IR spectra of **2a** and **2b** show additional strong bands arising from ν(CN) at 2148 and ν(CO) at 2018 cm^{-1}.

Yellow crystals of **2a** were obtained and the molecular structure was determined by single-crystal X-ray structural analysis.[11] Complex **2a** has a similar framework to **1**, despite the use of excess *t*BuNC only the PMe_3 ligand situated *trans* to the bridging CO_2 carbon atom is selectively displaced by a *t*BuNC ligand. In contrast to this result, some hydrido-bridged dinuclear complexes have been reported to react with *t*BuNC to give μ-formimidoyl derivatives.[12] Moreover, it is noted that treatment of **1** with CO gas also resulted in displacement of the PMe_3 ligand at the same position (based on the ^{31}P{^{1}H} and ^{1}H NMR spectra) to give **2b**.

The reaction of **1** with benzoic acid as a protic acid was carried out to give [{Ru(CO)(PMe_3)$_2$}$_2$(μ-H)(μ-κ^2-O_2CPh){μ-κ^2-C(O)O}] (**3a**) in 49% yield (Scheme 2). The ^{31}P{^{1}H} NMR spectrum shows similar signal pattern arising from four non-equivalent phosphorus atoms, indicating the framework of **3a** is analogous to that of **1**. In the ^{1}H NMR spectrum, the aryl protons, the methyl protons of the PMe_3 groups, and the hydride are detected but there is no signal from the hydroxo proton. The *p*-toluic derivative [{Ru(CO)(PMe_3)$_2$}$_2$(μ-H)(μ-κ^2-O_2CC$_6$H$_4$Me){μ-κ^2-C(O)O}] (**3b**) was also isolated in 77% yield from reaction with *p*-toluic acid under the same conditions, and the molecular structure of the monohydrate of **3b** was revealed by X-ray crystallographic analysis.[13] Complex **3b** consists of two [Ru(CO)(PMe_3)$_2$] units connected by hydrido, κ^2-*O*,*C*-CO_2, and a new arylcarboxylato bridge. During this reaction, the configuration of the dinuclear structure remains intact. The bond lengths of **3b** are comparable to those of **1**, except for the elongation of the Ru–Ru bond to 3.0160(5) Å, which is still within the range of typical Ru–Ru single bonds.[8] FAB-MS and elemental analyses confirm the formulation.

When **1** was treated with HBAr$^F_4$ (Ar$^F_4$ = 3,5-C$_6$H$_3$(CF$_3$)$_2$) at -78 °C, four new signals were detected in the ^{31}P{^{1}H} NMR spectrum, these are at $\delta = 17.1$, 5.36–4.39 ppm (overlap of two signals), and $\delta = -14.0$ ppm, and the ^{1}H NMR spectrum showed the multiplet hydride signal at $\delta = -11.4$ ppm along with methyl protons of PMe_3 and aryl protons of BAr$^F_4$. The ESI-MS spectrum exhibited a parent peak at *m*/*z* 626 ascribed to [**1**+H]$^+$. Although complete purification of this product was unsuccessful due to its low stability in solution, these data probably indicate generation of an H_2O-bridged species [{Ru(CO)(PMe_3)$_2$}$_2$(μ-H)(μ-OH$_2$){μ-κ^2-C(O)O}]BAr$^F_4$ (**3′**), which would be the intermediate leading to **3a** and **3b**. Unfortunately, the μ-OH$_2$ protons were not detectable even at -60 °C in the ^{1}H NMR spectrum.

Treatment of **1** with I_2 at room temperature for 23 h afforded [{Ru(CO)(PMe_3)$_2$}$_2$(μ-H)(μ-I)$_2$]I (**4**) in 66% yield (Scheme 2). The ^{31}P{^{1}H} NMR spectrum exhibited only two multiplet signals, indicating a higher symmetry in **4** than **1**. A triplet of triplet signal of the hydrido ligand of **4** supports the presence of two pairs of PMe_3 ligands. Cooling the acetone solution of **4** afforded yellow crystals suitable for X-ray diffraction analysis.

The crystal structure of **4** (Figure 2)[14] which has a crystallographic two-fold axis verified the presence of two {Ru(CO)(PMe_3)$_2$} units symmetrically bridged by two iodide

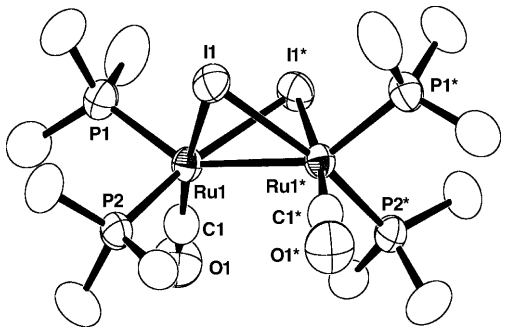


Figure 2. ORTEP diagram of complex **4** (thermal ellipsoids set at 50% probability). Selected bond lengths [Å]: Ru1-Ru1* 2.8955(8), Ru1-I1 2.7644(5), Ru1*-I1 2.7817(5), Ru1-P1 2.338(2), Ru1-P2 2.293(2).

and one hydrido ligands, accompanied by a counterion I$^-$. The hydrido atom was located in a difference electron density map, but unfortunately its position was not refined, however its presence was confirmed by the ^{1}H NMR spectrum (see Supporting Information). The Ru1–Ru1* distance of 2.8955(8) Å,which clearly indicates the presence of a metal–metal single bond,[8] is slightly longer than that of similar complex [{Ru(CO)(PPh_3)$_2$}$_2$(μ-H)(μ-Cl)$_2$]BF$_4$ (2.842(1) Å).[15] The cationic structure of [{Ru(CO)(PMe_3)$_2$}$_2$(μ-H)(μ-I)$_2$]$^+$ was also confirmed by the observation of the parent ion [*M*−1]$^+$ at *m*/*z* 817 in the positive ESI mass spectrum (acetone).

Interestingly, when **1** was treated with molecular iodine I_2 in dilute acetone solutions for only 30 min, the intermediate [{Ru(CO)(PMe_3)$_2$}$_2$(μ-H)(μ-OH)(μ-I)]I (**4′**) was detected

 © 2005 Wiley-VCH Verlag GmbH & Co. KGaA, Weinheim

with a small amount of **4** on the basis of NMR spectroscopy and ESI mass spectra. This result indicates that the mechanism of formation in the initial I_2 oxidation involves the release of CO_2 in **1** and coordination of I^- to the resulting vacant site generating the intermediate **4′**. Further reaction of the bridging OH group of **4′** with another mole of I_2 would proceed to produce **4**. However, isolation of **4′** failed owing to its facile conversion into **4** during the separation procedures.

In conclusion, we have isolated the novel dinuclear species **1** that is bridged by hydrido, hydroxo, and κ^2-*O*,*C*-CO_2, and which has multiple reactive sites. With *t*BuNC and CO **1** undergoes simple ligand replacement of one PMe_3 molecule to give **2a** and **2b**, respectively. The reactions with protic acids (benzoic and *p*-toluic acid) afford arylcarboxylato bridging complexes (**3a** and **3b**) in reactions that proceed through the selective protonation on the hydroxo ligand. A similar result was also observed in the reaction with $HBAr^F{}_4$. On the other hand, for the reaction of **1** with I_2, oxidative addition occurred to afford the decarboxylated complex **4** via the intermediate **4′**. Further investigations on other chemical reactivities of **1** are underway.

Experimental Section

Details on the syntheses as well as full spectroscopic characterization of **1**–**4** are given in the Supporting Information.

1: An aqueous 10 M KOH solution (76 mL, 760 mmol) was added to an ethanol solution (230 mL) of *cis*,*cis*,*trans*-$[RuCl_2(CO)_2(PMe_3)_2]$ (2.9 g, 7.6 mmol). The mixture was heated under reflux for 24 h and the resulting red brown solution was concentrated to one-third of its original volume to produce red brown oil. The supernatant colorless solution was then removed and the oily product was dried in vacuo. The residue was extracted with benzene and addition of hexane precipitated a yellow brown powder of **1** (1.4 g, 59%). ^{1}H NMR (C_6D_6, 400 MHz): $\delta = 1.51$ (d, $J = 9.4$ Hz, PMe_3), 1.30 (d, $J = 9.9$ Hz, PMe_3), 1.26 (d, $J = 9.8$ Hz, PMe_3), 1.15 (d, $J = 6.0$ Hz, PMe_3), −0.61 (s, μ-OH), −11.2 ppm (m, μ-H); ^{31}P{^{1}H} NMR (C_6D_6; 162 MHz): $\delta =$ 16.1 (d, $J = 26$ Hz, PMe_3), 3.81 (dd, $J = 11$, 41 Hz, PMe_3), 0.21 (dd, $J =$ 26, 41 Hz, PMe_3), −18.4 ppm (d, $J = 11$ Hz, PMe_3); ^{13}C{^{1}H} NMR (C_6D_6; 100 MHz): $\delta = 207$ (dd, $J = 7.9$, 16 Hz, CO), 205 (br, d, $J =$ 102 Hz, CO_2), 204 (t, $J = 14$ Hz, CO), 20.3 (d, $J = 31$ Hz, PMe_3), 19.4 (d, $J = 27$ Hz, PMe_3), 18.9 (d, $J = 16$ Hz, PMe_3), 15.8 ppm (d, $J =$ 27 Hz, PMe_3). IR (KBr, pellet): $\tilde{\nu} = \nu$(OH) 3390 (br); ν(C≡O) 1920 (s), 1906 (s); 951 (m) cm^{-1}. FAB-MS (*m*/*z*): 626 ($[M+1]^+$), 581 ($[M-CO_2-1]^+$), 505 ($[M-CO_2-PMe_3-1]^+$). Elemental analysis (%) calcd for $C_{15}H_{38}O_5P_4Ru_2$: C 28.97, H 6.60; found: C 28.85, H 6.13.

Received: April 18, 2005
Published online: July 26, 2005

Keywords: carbon dioxide · carbonyl complexes · hydrido species · hydroxides · ruthenium

[1] a) T. Naota, H. Takaya, S.-I. Murahashi, *Chem. Rev.* **1998**, *98*, 2599–2660; b) R. Noyori, T. Ohkuma, *Angew. Chem.* **2001**, *113*, 40–75; *Angew. Chem. Int. Ed.* **2001**, *40*, 40–73; c) B. M. Trost, F. D. Toste, A. B. Pinkerton, *Chem. Rev.* **2001**, *101*, 2067–2096; d) F. Kakiuchi, S. Murai, *Acc. Chem. Res.* **2002**, *35*, 826–834.

[2] a) H. Kawano, Y. Masaki, T. Matsunaga, K. Hiraki, M. Onishi, T. Tsubomura, *J. Organomet. Chem.* **2000**, *601*, 69–77; b) M. Onishi, M. Yonekura, K. Hiraki, M. Shugyo, H. Kawano, H. Kobayashi, *J. Mol. Catal. A* **1997**, *121*, 9–15; c) M. Onishi, M. Matsuda, I. Takaki, K. Hiraki, S. Oishi, *Bull. Chem. Soc. Jpn.* **1989**, *62*, 2963–2967.

[3] a) H. Kawano, Y. Nishimura, M. Onishi, *Dalton Trans.* **2003**, 1808–1812; b) H. Kawano, H. Narimatsu, D. Yamamoto, K. Tanaka, K. Hiraki, M. Onishi, *Organometallics* **2002**, *21*, 5526–5530; c) K. Hiraki, Y. Kinoshita, J. Kinoshita-Kawashima, H. Kawano, *J. Chem. Soc. Dalton Trans.* **1996**, 291–298; d) K. Hiraki, T. Matsunaga, H. Kawano, *Organometallics* **1994**, *13*, 1878–1885.

[4] Reactions of $[RuCl_2(CO)_2(PMe_3)_2]$ with $NaBH_4$ in alcohol have resulted in mononuclear hydrido complexes, $[RuCl(H)(CO)_2(PMe_3)_2]$ and $[Ru(H)_2(CO)_2(PMe_3)_2]$: a) M. P. Waugh, R. J. Mawby, *J. Chem. Soc. Dalton Trans.* **1997**, 21–33; b) D. Schott, C. J. Sleigh, J. P. Lowe, S. B. Duckett, R. J. Mawby, M. G. Partridge, *Inorg. Chem.* **2002**, *41*, 2960–2970.

[5] a) M. Faure, L. Maurette, B. Donnadieu, G. Lavigne, *Angew. Chem.* **1999**, *111*, 539–542; *Angew. Chem. Int. Ed.* **1999**, *38*, 518–522; b) L. Maurette, B. Donnadieu, G. Lavigne, *Angew. Chem.* **1999**, *111*, 3919–3922; *Angew. Chem. Int. Ed.* **1999**, *38*, 3707–3710.

[6] a) Crystal data for **1**: $C_{15}H_{37}O_5P_4Ru_2$ ($M_r = 623.49$); monoclinic, $P2_1/n$ (No. 14), $a = 11.663(5)$, $b = 12.589(3)$, $c = 18.762(2)$ Å, $\beta =$ 103.024(2)°, $V = 2683(1)$ Å^3, $Z = 4$, $\rho_{calcd} = 1.543$ g cm^{-3}, R (Rw) = 0.133 (0.137), GOF = 1.19 for 235 variables and 5947 unique reflections (all data).[6b] For crystallographic details, see Supporting Information; b) CCDC-268894 to 268897 contain the supplementary crystallographic data for this paper. These data can be obtained free of charge from the Cambridge Crystallographic Data Centre via www.ccdc.cam.ac.uk/data_request/cif.

[7] a) J. S. Field, R. J. Haines, J. Sundermeyer, S. F. Woollam, *J. Chem. Soc. Dalton Trans.* **1993**, 2735–2748; b) D. H. Gibson, *Chem. Rev.* **1996**, *96*, 2063–2095; c) D. H. Gibson, B. A. Sleadd, M. S. Mashuta, J. F. Richardson, *Organometallics* **1997**, *16*, 4421–4427; d) D. H. Gibson, Y. Ding, J. G. Andino, M. S. Mashuta, J. F. Richardson, *Organometallics* **1998**, *17*, 5178–5183; e) D. H. Gibson, X. Yin, *J. Am. Chem. Soc.* **1998**, *120*, 11200–11201.

[8] R. J. Haines in *Comprehensive Organometallic Chemistry II*, *Vol. 7* (Eds.: E. W. Abel, F. G. A. Stone, G. Wilkinson), Pergamon, Oxford, **1995**, pp. 625–681.

[9] a) R. A. Jones, G. Wilkinson, A. M. R. Galas, M. B. Hursthouse, K. M. A. Malik, *J. Chem. Soc. Dalton Trans.* **1980**, 1771–1778; b) E. G. Fidalgo, L. Plasseraud, H. Stoeckil-Evans, G. Süss-Fink, *Inorg. Chem. Commun.* **2001**, *4*, 308–310; c) K.-B. Shiu, J.-Y. Chen, G.-H. Lee, F.-L. Liao, B.-T. Ko, Y. Wang, S.-L. Wang, C.-C. Lin, *J. Organomet. Chem.* **2002**, *658*, 117–125.

[10] A probable mechanistic scheme is given in the Supporting Information.

[11] Crystal data for **2a**: $C_{17}H_{37}NO_5P_3Ru_2$ ($M_r = 630.54$); cubic, $Pa\bar{3}$ (No. 205), $a = 26.0919(3)$ Å, $V = 17763.0(4)$ Å^3, $Z = 24$, $\rho_{calcd} =$ 1.415 g cm^{-3}, R (Rw) = 0.073 (0.096), GOF = 1.90 for 253 variables and 6787 unique reflections (all data).[6b] For ORTEP diagram and crystallographic details, see Supporting Information.

[12] a) F. J. García Alonso, M. García Sanz, V. Riera, A. Anillo Abril, A. Tiripicchio, F. Ugozzoli, *Organometallics* **1992**, *11*, 801–808; b) N. Cabon, F. Y. Pétillon, P. Schollhammer, J. Talarmin, K. W. Muir, *Dalton Trans.* **2004**, 2708–2719; c) C. M. Alvarez, M. A. Alvarez, M. E. García, A. Ramos, M. A. Ruiz, M. Lanfranchi, A. Tiripicchio, *Organometallics* **2005**, *24*, 7–9.

[13] Crystal data for **3b**·H_2O: $C_{23}H_{35}O_7P_4Ru_2$ ($M_r = 749.56$); monoclinic, $P2_1/c$ (No. 14), $a = 17.586(2)$, $b = 11.408(2)$, $c =$ 17.5779(3) Å, $\beta = 103.0707(4)$°, $V = 3435.0(8)$ Å^3, $Z = 4$, $\rho_{calcd} =$ 1.449 g cm^{-3}, R (Rw) = 0.075 (0.101), GOF = 0.91 for 337 variables and 7523 unique reflections (all data).[6b] For ORTEP diagram and crystallographic details, see Supporting Information.

 © 2005 Wiley-VCH Verlag GmbH & Co. KGaA, Weinheim

[14] Crystal data for **4**: $C_{14}H_{37}O_2P_4Ru_2I_3$ ($M_r = 944.19$); monoclinic, $C2/c$ (No. 15), $a = 14.661(1)$, $b = 18.278(2)$, $c = 14.1796(4)$ Å, $\beta = 108.356(1)°$, $V = 3606.3(5)$ Å^3, $Z = 4$, $\rho_{calcd} = 1.739$ g cm^{-3}, R (Rw) = 0.061 (0.089), GOF = 1.32 for 114 variables and 4045 unique reflections (all data).[6b] For crystallographic details, see Supporting Information.

[15] R. A. Sánchez-Delgado, U. Thewalt, N. Valencia, A. Andriollo, R.-L. Márquez-Silva, J. Puga, H. Schöllhorn, H.-P. Klein, B. Fontal, *Inorg. Chem.* **1986**, *25*, 1097 – 1106.

 © 2005 Wiley-VCH Verlag GmbH & Co. KGaA, Weinheim

Imaging Agents

DOI: 10.1002/anie.200501473

Highly Sensitive MRI Chemical Exchange Saturation Transfer Agents Using Liposomes**

Silvio Aime, Daniela Delli Castelli, and Enzo Terreno*

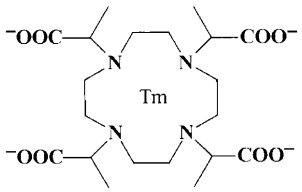
Chemical exchange saturation transfer (CEST) agents represent an emerging class of magnetic resonance imaging (MRI) contrast media that has huge potential. They act as negative agents by reducing the signal intensity of the water protons through a saturation transfer mediated by chemical exchange.[1] Saturation transfer occurs through selective irradiation at the absorption frequency of the exchanging protons of the agent. The great potential of CEST agents lies in the possibility of switching the contrast "on" and "off" at will, since each response is uniquely related to the specific absorption frequency of their mobile protons, thus making it possible to detect several agents in the same sample.[2] Basically, the saturation transfer efficiency is proportional to the exchange rate (k_{ex}) and to the number of mobile protons in the CEST agent. However, the value of k_{ex} must be smaller than the frequency separation ($\Delta\omega$) between the resonances of bulk water and the exchanging protons of the agent if the mobile protons are to be selectively irradiated. For this reason, it might be possible to find efficient CEST agents in the class of paramagnetic metal complexes (the so-called PARACEST agents),[3] in which the presence of unpaired electrons induce large $\Delta\omega$ values. However, the sensitivity of a PARACEST agent is still below that of the conventional relaxing agents based on the Gd^{III} ion, even when k_{ex} and $\Delta\omega$ are optimized.

[*] Prof. S. Aime, Dr. D. Delli Castelli, Dr. E. Terreno
Dipartimento di Chimica I.F.M.
Via P. Giuria 7, 10125, Torino (Italy)
Fax: (+39) 011-6707855
E-mail: silvio.aime@unito.it
and
Molecular Imaging Center
Via P. Giuria 15, 10125, Torino (Italy)

[**] Financial support from Bracco Imaging S.p.A., MIUR, NoE-EMIL, and DIMI are gratefully acknowledged. This work was carried out under the framework of the EU-COST D 18 action.

It has been suggested that an improved sensitivity may be obtained by increasing the number of exchangeable protons. Van Zijl and co-workers suggested the use of polymers, such as polyamino acids, polyamidoamine-based (PAMAM-based) dendrimers, and single-stranded RNA, containing a large number of labile amide protons.[4,5] We have further extended this approach by designing supramolecular adducts between a paramagnetic shift reagent and a substrate containing many, fast-exchanging protons.[6] The latter approach appears promising, but it bears the drawback of showing a severe broadening of the absorption corresponding to the exchangeable protons that, in turn, results in the need to apply a much more intense B_1 field to maximize their saturation.

To design a system with a well-defined paramagnetically shifted resonance that corresponds to a high number of exchangeable protons, we considered the use of liposomes containing a paramagnetic shift reagent for water protons in the aqueous inner cavities. In such systems, which we call LIPOCEST agents, the resonance of the water protons inside the liposomes is shifted from that of the external water to an extent that depends upon the structure and the concentration of the shift reagent entrapped within the liposomes. Thus, the ^1H NMR spectrum of such a suspension will display two signals for water that correspond to water confined in the liposome cavity and to the external solvent. The exchange of water molecules across the liposome membrane is usually slow and can be controlled, to some extent, by varying the composition of the lipidic bilayer. Suitable candidates for the shift reagent should be found among paramagnetic metal complexes containing at least one highly shifted and fast-exchanging water molecule. In principle, several macrocyclic lanthanide(III) chelates derived from 1,4,7,10-tetraaza-1,4,7,10-tetrakis(carboxymethyl)cyclododecane (DOTA), α,α′,α″,α‴-tetramethyl-1,4,7,10-tetraacetic acid (DOTMA), and related ligands display an axially coordinated water that nicely fulfills the latter requirement.[7] Herein we report the results obtained with the $[Tm(dotma)]^-$ complex, which has recently been proposed as a non-invasive MR probe for in vivo thermometry.[8]



[Tm(dotma)]⁻

$[Tm(dotma)]^-$ has been entrapped within a liposome formed from a blend of unsaturated/saturated phospholipids and cholesterol (palmitoyloleoylphosphatidylcholine (POPC)/dipalmitoylphosphatidylglycerol) sodium salt (DPPG)/cholesterol, 55:5:40 w/w/w). Previous studies on Gd(III) chelates entrapped within liposomes have shown that a mixture of cholesterol and unsaturated phospholipids results in a faster exchange of water across the liposome membrane relative to systems based only on saturated phospholipids.[9–11] When the preparation of the liposomes

 © 2005 Wiley-VCH Verlag GmbH & Co. KGaA, Weinheim InterScience

was carried out in the presence of 0.19 M [Tm(dotma)]$^-$, the water signal in the inner compartment resonated (at 312 K) at $\Delta\delta = 3.1$ ppm downfield of the signal of bulk water (Figure 1, top).

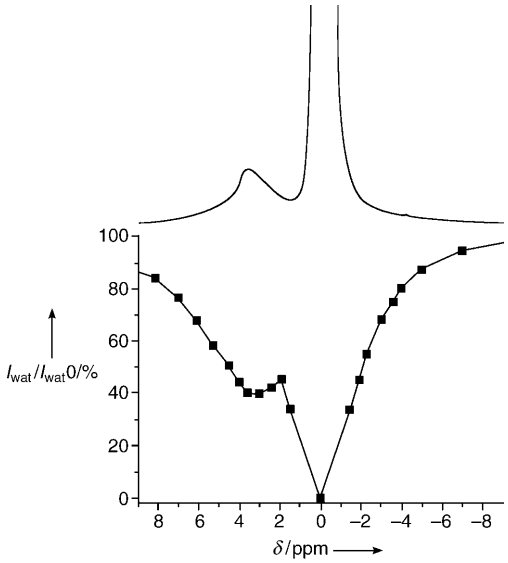


Figure 1. Top: ^{1}H NMR spectrum, recorded at 14.1 T and 312 K, of a suspension of the LIPOCEST agent entrapping [Tm(dotma)]$^-$. The signal at $\delta = 3.1$ ppm from the bulk water (off-scale signal at 0 ppm) corresponds to the water protons entrapped within the liposomes containing 0.1 M paramagnetic shift reagent, as demonstrated by the Z-spectrum (lower) obtained at 7 T and 312 K (liposome concentration 2.88 nM, B_1 field intensity 12 μT, irradiation time 3 s).

The difference in the chemical shift between the water resonances allows the actual concentration of the shift reagent in the liposome's inner cavity to be assessed, once the dependence of the paramagnetic shift of the bulk water resonance on the concentration of [Tm(dotma)]$^-$ has been determined by an independent experiment.[12] On this basis, it has been possible to determine that the experimental procedure used for the preparation of the liposomes led to an effective intraliposome [Tm(dotma)]$^-$ concentration of 0.1M. These liposomes showed a mean diameter of 270 ± 2.5 nm (polydispersity index 0.32) which gives a volume of the inner cavity of about 9.2×10^{-18} L. The ratio between the total concentration of the shift reagent in a given liposome suspension and its effective concentration inside the liposomes corresponds to the ratio between the volumes of the two compartments.

In this way the number of liposomes in the suspension, and thus their concentration, can be calculated by the ratio between the inner volume of a single liposome and the total volume of the compartment. The concentration of [Tm(dotma)]$^-$ in the the stock suspension of liposomes entrapping 0.1M shift reagent was 1.3 mM and the corresponding liposome concentration was 2.8 nM.

The Z-spectrum (7 T, 312 K, B_1 intensity 12 μT, irradiation time 3 s) of such a suspension is reported in Figure 1 (bottom). The profile confirms that the resonance $\Delta\delta =$ 3.1 ppm downfield from the bulk water protons corresponds to the pool of mobile water protons encapsulated within the liposomes.

Figure 2 shows the results of the saturation transfer (ST) experiments carried out at 7 T and 312 K upon irradiating the intraliposome water signal as a function of the liposome concentration. The data show the typical pseudohyperbolic

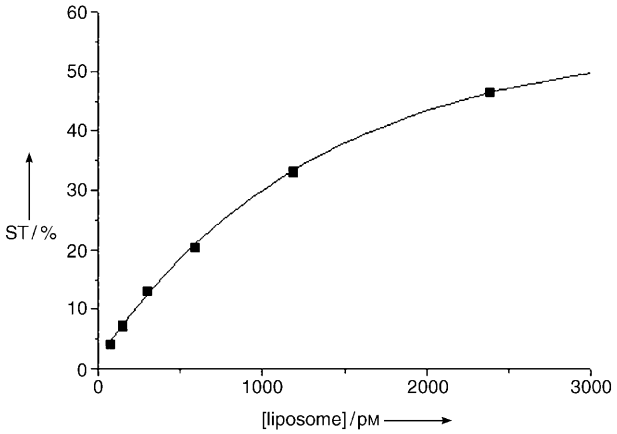


Figure 2. Saturation transfer assessment as a function of the liposome concentration for the LIPOCEST agent entrapping [Tm(dotma)]$^-$. Experimental conditions: 7 T, 312 K, irradiation pulse: train of 120 sinc3 pulses (25 ms each, B_1 field intensity 12 μT); the irradiation frequency was set at 930 Hz from the bulk water. The data points were fitted by using a simple hyperbolic function.

behavior[13] that leads to detectable ST effects down to picomolar concentrations of the LIPOCEST agent. If the threshold of the detectable saturation transfer is set at 5%, in analogy to previous works,[6,13] the agent reported herein can be detected down to about 90 pM!

As has been recently pointed out,[14,15] the intensity of the applied B_1 saturation field for attaining the maximum ST effect is directly related to the k_{ex} values of the mobile protons of the CEST agent. It is thus expected that the B_1 field necessary for transferring saturation in LIPOCEST agents is much lower than in other paramagnetic CEST probes containing fast-exchanging protons. In fact, the B_1 field used for liposomes entrapping [Tm(dotma)]$^-$ is about 20 times smaller than that used to saturate the metal-bound water protons in paramagnetic [Ln(dotamGly)]$^-$ complexes (dotam = 1,4,7,10-tetrakis(carbamoylmethyl)-1,4,7,10-tetraazacyclododecane).[13,16]

Figure 3 shows a difference (on/off) CEST image (see the Experimental Section) of a phantom made of eight capillaries containing different liposome concentrations to illustrate the dependence of the saturation transfer efficiency on the liposome concentration. The image clearly indicates that, for this agent, it is still possible to detect contrast at a liposome concentration of about 90 pM. The difference CEST images were acquired in about two minutes (with a total irradiation time of 3 s) by using a modified RARE pulse sequence.

In summary, the results reported here show that LIPOCEST agents represent an innovative class of MR imaging probes of outstanding sensitivity (per liposome). Moreover,

 © 2005 Wiley-VCH Verlag GmbH & Co. KGaA, Weinheim

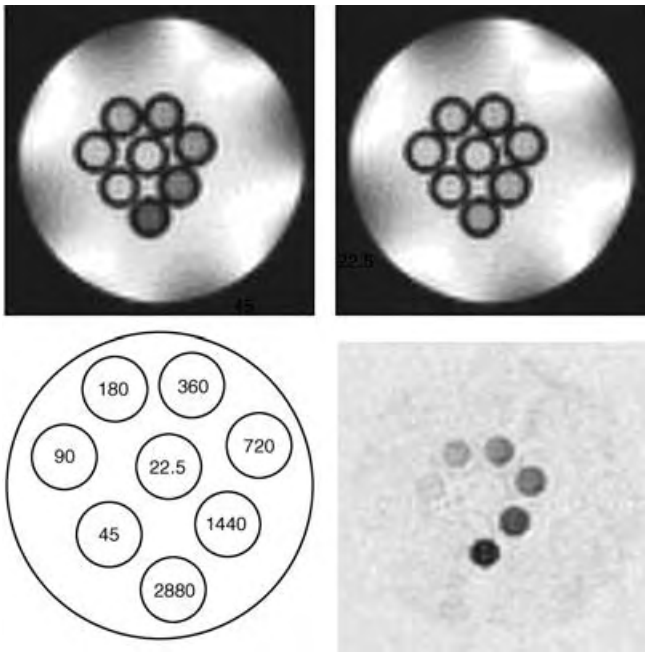


Figure 3. MRI-CEST images (matrix 64×64) of a phantom consisting of eight capillaries containing suspensions of the LIPOCEST agent entrapping $[Tm(dotma)]^-$ in the concentration range 22.5–2880 μM (see bottom left). Experimental conditions: 7 T, 312 K, RARE sequence: TR/TE/NE = 9 s/3.3 ms/1, rare factor = 8, irradiation pulse: train of 120 sinc3 pulses (25 ms each, B_1 field intensity 12 μT). Top left: On-image: irradiation frequency +930 Hz from bulk water. Top right: Off-image: irradiation frequency −930 Hz from bulk water. Bottom right: difference on/off image.

as the chemical shift of water entrapped within the liposomes depends upon the nature and concentration of the shift reagent as well as on the permeability of the liposome membrane, one may envisage facile access to a number of LIPOCEST agents with different absorption frequencies. This approach will allow a dramatic extension of the experiments that can be carried out by having the possibility of irradiating the various LIPOCEST agents present in the same sample specifically.

Experimental Section

The dotma ligand was provided by Bracco Imaging (Milano, Italy) and the corresponding Tm^{III} complex was prepared according to the published procedure, and characterized by ^1H NMR spectroscopy.[7] DPPG, POPC, and cholesterol were purchased from Sigma-Aldrich.

The liposomes were prepared according to the thin-film hydration method.[17]

The size of the liposomes were determined by photon correlation spectroscopy using a 90 Plus instrument (Brookheven, New York, USA) at a fixed scattering angle of 90° and 25 °C.

The total concentration of the Tm^{III} complex in the liposome suspension was determined by using the "bulk magnetic susceptibility" method (*tert*-butyl alcohol was used as the inert reference).[18]

Saturation transfer efficiency (ST%) was calculated by using Equation (1), where I_S and I_0 refer to the intensities of the bulk water signal when the irradiation pulse is set at the resonance frequency of the water protons entrapped within the liposomes (I_S) or on a frequency equally spaced with respect to the bulk water, but in the opposite direction (I_0).[6]

$$ST\% = (1-\frac{I_S}{I_0})100 \quad (1)$$

ST% values and the MR images were obtained on a Bruker Avance300 instrument operating at 7 T and equipped with a micro-imaging probe (inner diameter 10 mm). The image reported in Figure 3 (bottom right) is the difference between two images (top) obtained by irradiating the resonance frequency of the water protons inside the liposome (on-image, 930 Hz from bulk water) and acquired under off-resonance conditions (off-image, −930 Hz from water protons), respectively. Both images (matrix 64 × 64) were obtained by using a conventional RARE sequence (TR/TE/NE = 9 s/3.3 ms/1, RARE factor 8) preceded by a train of sinc3 pulses (120 pulses, 25 ms each, irradiation B_1 field 12 μT). The total acquisition time for each image was about 1 minutes.

Received: April 28, 2005
Published online: July 29, 2005

Keywords: imaging agents · lanthanides · liposomes · MRI · shift reagents

[1] K. M. Ward, A. H. Aletras, R. S. Balaban, *J. Magn. Reson.* **2000**, *143*, 79–87.
[2] S. Aime, C. Carrera, D. Delli Castelli, S. Geninatti Crich, E. Terreno, *Angew. Chem.* **2005**, *117*, 1847–1849; *Angew. Chem. Int. Ed.* **2005**, *44*, 1813–1815.
[3] S. Zhang, M. Merritt, D. E. Woessner, R. E. Lenkinski, A. D. Sherry, *Acc. Chem. Res.* **2003**, *36*, 783–790.
[4] N. Goffeney, J. W. M. Bulte, J. Duyn, L. H. Bryant, Jr, P. C. M. van Zjil, *J. Am. Chem. Soc.* **2001**, *123*, 8628–8629.
[5] K. Snoussi, J. W. M. Bulte, M. Gueron, P. C. M. van Zijl, *Magn. Reson. Med.* **2003**, *49*, 998–1005.
[6] S. Aime, D. Delli Castelli, E. Terreno, *Angew. Chem.* **2003**, *115*, 4665–4667; *Angew. Chem. Int. Ed.* **2003**, *42*, 4257–4259.
[7] D. Parker, R. S. Dickins, H. Puschmann, C. Crossland, J. A. K. Howard, *Chem. Rev.* **2002**, *102*, 1977–2010.
[8] S. K. Hekmatyar, P. Hopewell, S. K. Pakin, A. Babsky, N. Bansal, *Magn. Reson. Med.* **2005**, *53*, 294–303.
[9] C. Tilcock, P. MacDougall, E. Unger, D. Cardenas, L. Fajardo, *Biochim. Biophys. Acta* **1990**, *1022*, 181–186.
[10] S. L. Fossheim, A. K. Fahlvik, J. Klaveness, R. N. Muller, *Magn. Reson. Imaging* **1999**, *17*, 83–89.
[11] S. H. Koenig, Q. F. Ahkong, R. D. Brown, M. Lafleur, M. Spiller, E. Unger, C. Tilcock, *Magn. Reson. Med.* **1992**, *23*, 275–286.
[12] In principle, the chemical shift difference between the intra- and extraliposome water signals may be affected by chemical exchange. However, this effect may be reasonably neglected for the liposomes considered in this work, because of their relatively low water permeability.
[13] E. Terreno, D. Delli Castelli, G. Cravotto, L. Milone, S. Aime, *Invest. Radiol.* **2004**, *39*, 235–243.
[14] J. Zhou, D. A. Wilson, P. Z. Sun, J. A. Klaus, P. C. M. van Zijl, *Magn. Reson. Med.* **2004**, *51*, 945–952.
[15] D. E. Woessner, S. Zhang, M. E. Merritt, A. D. Sherry, *Magn. Reson. Med.* **2005**, *53*, 790–799.
[16] S. Aime, D. Delli Castelli, E. Terreno, *Angew. Chem.* **2002**, *114*, 4510–4512; *Angew. Chem. Int. Ed.* **2002**, *41*, 4334–4336.
[17] K.-E. Lokling, S. L. Fossheim, R. Skurtveit, A. Bjornerud, J. Klaveness, *Magn. Reson. Imaging* **2001**, *19*, 731–738.
[18] D. M. Corsi, C. Platas-Iglesias, H. van Bekkum, J. A. Peters, *Magn. Reson. Chem.* **2001**, *39*, 723–726.

 © 2005 Wiley-VCH Verlag GmbH & Co. KGaA, Weinheim

Synthetic Methods

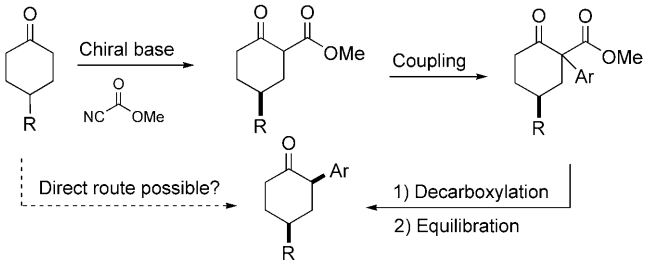
DOI: 10.1002/anie.200501745

Enantioselective α-Arylation of Cyclohexanones with Diaryl Iodonium Salts: Application to the Synthesis of (−)-Epibatidine**

Varinder K. Aggarwal and Berit Olofsson*

The enantioselective introduction of electrophiles α to carbonyl groups is a central topic in asymmetric synthesis. Although asymmetric α-alkylations have been well developed, high enantioselectivity in α-arylation of ketones has only been achieved in a very limited number of cases. These involve arylation of trisubstituted enolates using binap–Pd complexes which gives non-epimerizable, tetrasubstituted ketones.[1,2] However, this strategy cannot be used in the desymmetrization/arylation of cyclic ketones, since even if the enolate was generated enantioselectively, the ketone product would racemize the starting enolate (through proton transfer) at the high temperatures required for arylation.

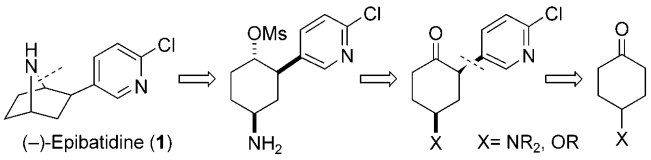
An alternative strategy involves α-arylation of β-ketoesters with aryl lead reagents (Scheme 1).[3] This strategy can be



Scheme 1. Possible asymmetric routes toward 2-aryl cyclohexanones.

rendered asymmetric through 1) desymmetrization/β-ketoester formation,[4] 2) arylation,[3] and 3) decarboxylation and subsequent equilibration.

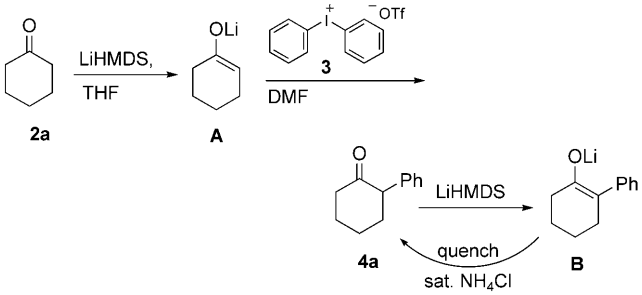
However, a direct asymmetric arylation of cyclohexanones would clearly be superior. If this could be achieved, we envisaged that this strategy could be applied to a short asymmetric synthesis of the alkaloid (−)-epibatidine (**1**) (Scheme 2). Herein, we describe our success in achieving these goals.



Scheme 2. Retrosynthesis of (−)-epibatidine.

As possible electrophilic sources of aryl reagents, we considered diaryl iodonium(III) salts since scattered reports existed of couplings with silyl enol ethers,[5] ketones,[6] and malonates,[7] albeit with varying yields. The scope and limitations of these couplings had not been investigated, and no successful asymmetric reactions have been reported.[8] Indeed, the dearth of examples of enolate arylations with diaryl iodonium(III) salts encouraged us to explore this area further.

The coupling conditions were optimized with cyclohexanone (**2a**) and the commercially available diphenyl iodonium salt **3** (Scheme 3).[9] Under optimized conditions arylation of cyclohexanone (**2a**) gave **4a** in 83% yield (entry 1, Table 1). It should be noted that 2 equivalents of base are required; the second equivalent is used to deprotonate the product ketone.[10] Despite the fact that part way through the reaction enolates **A** and **B** are both present, no bis-arylated product was observed under our optimized conditions (Scheme 3).[11]



Scheme 3. α-Arylation of cyclohexanone (**2a**); HDMS = hexamethyldisilazide.

When applied to 4-substituted cyclohexanones **2b–d**, the coupling reaction afforded 2,4-disubstituted products **4b–d** in high yields and with high diastereoselectivities (Table 1).[12] As expected, arylation of *tert*-butyl ketone **2b** resulted in **4b** with high *cis* selectivity (entry 2), whilst ketone **2c** yielded a 5:1 *cis*/*trans* mixture (entry 3). In contrast, reaction of the 4-silyloxy ketone **2d** led to **4d** with high *trans* selectivity, the 4-OTBDMS occupying the axial position (entry 4). It has been suggested that an attractive electrostatic interaction and/or an n,π* orbital overlap between the silyloxy group and the carbonyl carbon favors the axial orientation of 4-alkoxy substituents and so the *trans* isomer is likely to be the

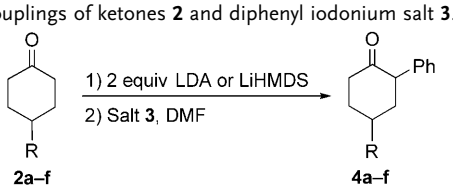
[*] Prof. V. K. Aggarwal, Dr. B. Olofsson
School of Chemistry
University of Bristol
Cantock's Close, Bristol, BS81TS (UK)
Fax: (+44) 117-929-8611
E-mail: v.aggarwal@bristol.ac.uk
Dr. B. Olofsson
Department of Organic Chemistry
Stockholm University (Sweden)

[**] We thank Merck and the Swedish Research Council for financial support.

Supporting information for this article is available on the WWW under http://www.angewandte.org or from the author.

InterScience
© 2005 Wiley-VCH Verlag GmbH & Co. KGaA, Weinheim

Table 1: Couplings of ketones **2** and diphenyl iodonium salt **3**.[a]

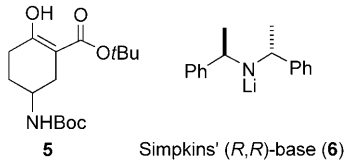


2a–f **4a–f**

Entry	Ketone (R)	Base	Yield of **4** [%][b]	*cis*/*trans*
1	**2a** (H)	LHMDS	83	–
2	**2b** (*t*Bu)	LDA	69	>20:1
3	**2c** (Ph)	LDA	76	5:1
4	**2d** (OTBDMS)	LDA	70	1:15
5	**2e** ($NBoc_2$)	LHMDS	18[c]	>20:1
6	**2f** (NHBoc)	LDA	31[d]	10:1

[a] Conditions: The ketone was treated with LHMDS or LDA at −78 °C in THF. Salt **3** was added in DMF and the reaction was stirred at −45 °C for 4–5 h. LDA = lithium diisopropylamide, TBDMS = *tert*-butyldimethylsilyl, Boc = *tert*-butoxycarbonyl. [b] Yields of isolated products. [c] The major product was Boc-transfer product **5**, see text. [d] 2,2-Diphenyl-4-NHBoc ketone (38%) and **2f** (30%) were also isolated.

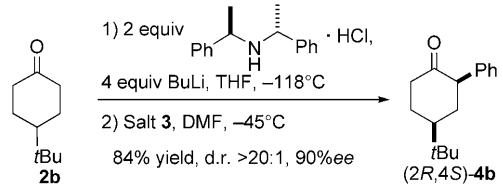
thermodynamically more stable product.[13,14] Application of this methodology to 4-aminoketone **2e**[15] was complicated by an unexpected intramolecular Boc-transfer reaction, yielding enol ester **5** as the major product (37%) (entry 5 and Scheme 4).[16] The Boc-transfer could be avoided by employing ketone **2f**, but the yield of **4f** was moderate due to competitive deprotonation of the carbamate nitrogen.[17] This entry shows that enolate **B** (Scheme 3) can indeed react to give disubstituted product when enolate **A** is absent, as the major product in this case was the corresponding diphenyl compound (38%).



5 Simpkins' (*R*,*R*)-base (**6**)

Scheme 4. Boc-transfer product **5** and chiral base **6** used in asymmetric reactions.

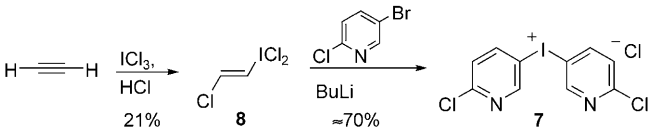
Employing Simpkins' (*R*,*R*)-base (**6**; Scheme 4) instead of LDA or LHMDS, we found that *tert*-butylcyclohexanone (**2b**) gave the arylated product (2*R*,4*S*)-**4b** in 84% yield and 90% enantiomeric excess (Scheme 5).[18] The enantioselectivity was in the range typical for this class of desymmetrization,[19,20] which clearly indicates that proton transfer between the product and the starting enolate was not occurring. Had this occurred, lower enantioselectivity would have been expected because the second equivalent of base would have deprotonated the ketone at −45 °C instead of −118 °C. Evidently, the second equivalent of base acted to directly deprotonate the arylated ketone.



Scheme 5. Asymmetric coupling with Simpkins' base.

Having established the asymmetric methodology for the α-arylation of cyclic ketones, we sought to apply it to a short enantioselective synthesis of epibatidine (**1**; Scheme 2). This alkaloid, which was isolated from the Ecuadorian poison frog *Epipedobates tricolor* in 1993, is 400 times more potent than morphine as an analgesic, and is also an extremely potent agonist of the nicotinic acetylcholine receptor.[21] Numerous syntheses of epibatidine have since been published, most of which are racemic.[22] One commonly employed strategy to introduce the pyridyl group involves an organometallic coupling with a 2-halosustituted cyclohexanone,[23,24] a reaction that cannot be rendered asymmetric (since the starting material is already chiral). As depicted in our retrosynthesis (Scheme 2), the direct coupling of a 4-substituted cyclohexanone with a pyridyl iodonium salt not only shortens the synthetic pathway but also renders the synthesis asymmetric.

Our strategy required a pyridyl iodonium salt that had not been previously prepared. After some experimentation, pyridyl salt **7** was synthesized in good yield from compound **8** and commercially available 2-chloro-5-bromopyridine (Scheme 6).[25]



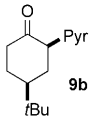
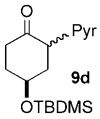
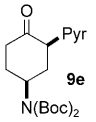
Scheme 6. Synthesis of pyridyl iodonium salt **7**.

Various cyclohexanones were treated with chiral base **6** and coupled with salt **7**, leading to the corresponding arylated ketones with high enantioselectivities and moderate to good yields (Table 2).[22,26] The pyridyl group on the iodonium salt had a negative impact on the yield of the coupling of ketones **2a** and **2b**. Whilst the diphenyl iodonium salt **3** gave **4a** in 83% yield, the pyridyl iodonium salt **7** only gave a 51% yield of coupling product **9a** (entry 1, Tables 1 and 2 respectively). Fortunately ketones **2d** and **2e**, both possible precursors to epibatidine, proved to be better substrates in the coupling reaction with the pyridyl iodonium salt **7**. Ketone **2d** has been previously employed in asymmetric desymmetrization reactions.[19,27] When this substrate was treated with base **6** and coupled with iodonium salt **7**, 2-pyridyl ketones **9d** were obtained in good yield and high enantioselectivity (entry 3). Interestingly, whilst the 2-phenyl ketone **4d** was formed with high *trans* diastereoselectivity (Table 1, entry 4), the 2-pyridyl ketone **9d** was produced with modest *cis* selectivity.[28]

Although asymmetric desymmetrization of ketone **2e** had not been previously reported, we expected that the steric bulk provided by the $N(Boc)_2$ moiety would lock the conformation of the cyclohexanone ring and thus lead to good asymmetric induction. Indeed, enantioselective deprotonation with base **6** and subsequent coupling afforded pyridyl ketone **9e** in 41%

 © 2005 Wiley-VCH Verlag GmbH & Co. KGaA, Weinheim

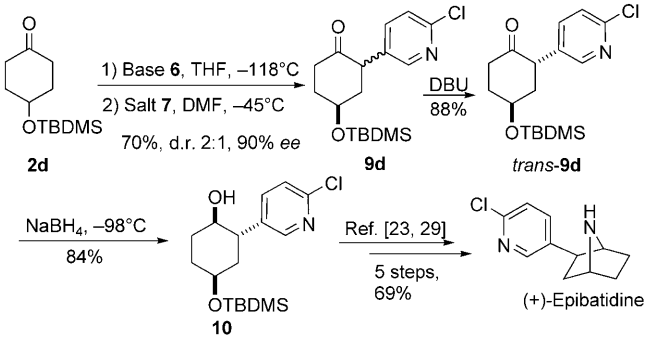
Table 2: Asymmetric couplings with pyridyl iodonium salt **7**.[a]

Entry	Ketone	Product[b]	Yield [%][c]	*ee* [%]
1	**2a**	 **9a**	51	–
2	**2b**	 **9b**	51	90
3	**2d**	 **9d**	70[d]	90
4	**2e**	 **9e**	41[e]	86 (94)[f]

[a] Conditions: The ketone was treated with base **6** at −118 °C in THF (entry 1: LHMDS at −78 °C). A solution of salt **7** in DMF was added and the reaction was stirred at −45 °C for 4 h. [b] Pyr = 5-(2-chloropyridyl). [c] Yields of isolated products. [d] *cis*/*trans* 2:1, 13% recovered **2d**. [e] Compound **5** isolated in 14% yield. [f] After recrystallization.

yield and 86% *ee* with complete *cis* selectivity (entry 4). Furthermore, a single recrystallization enhanced the enantiomeric excess of **9e** to 94%. This result indicates that salt **7** is more reactive than the diphenyl salt **3**, as much less of the Boc-transfer product was observed in this reaction.

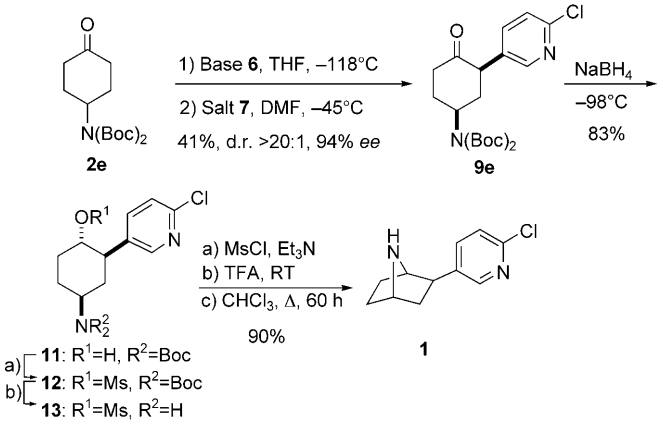
Having established the asymmetric α-arylation reaction we proceeded to complete the synthesis of epibatidine with ketones **2d** and **2e**. Commercially available ketone **2d** was employed in a formal synthesis of (+)-epibatidine (Scheme 7). As discussed above, the asymmetric iodonium



Scheme 7. Formal synthesis of (+)-epibatidine.

coupling afforded 2-pyridyl ketone **9d** as a kinetically formed 2:1 *cis*/*trans* mixture, which was equilibrated with DBU (1,8-diazabicyclo[5.4.0]undec-7-ene) to afford a separable 1:4 mixture with *trans*-**9d** as the major diastereomer. Ketone *trans*-**9d** was subsequently reduced with sodium borohydride to give the corresponding equatorial alcohol **10** in 84% isolated yield (d.r. 10:1 in crude). Alcohol **10** has previously been transformed into epibatidine in a further five steps,[23,29] thus providing a short and high-yielding formal synthesis of (+)-epibatidine. The optical rotation of **10** revealed that although the 4-OTBDMS group in **2d** prefers the axial conformation, it must be the *equatorial* conformation that becomes deprotonated by the chiral base.[30]

Alternatively, transformation of ketone **2e** to naturally occurring (−)-epibatidine could be performed in five straightforward steps (Scheme 8). 2-Pyridyl ketone **9e** was formed



Scheme 8. Synthesis of (−)-epibatidine. Ms = methanesulfonyl, TFA = trifluoroacetic acid.

with high enantiomeric excess, as discussed above, and reduced to alcohol **11** using sodium borohydride at low temperature with high diastereoselectivity (d.r. 7:1 in crude). Compound **11** was converted into (−)-epibatidine ($[\alpha]_D^{20} = -6.2$ ($c = 0.21$, CH_2Cl_2); literature value:[22b] $[\alpha]_D^{25} = -6.7$ ($c = 0.21$, CH_2Cl_2)) by sequential mesylation, deprotection and ring-closure in 90% yield over the three steps.[31] The total synthesis was thus accomplished in six steps and 31% overall yield from commercially available **2f** with essentially complete control of diastereoselectivity, thus providing the shortest and most efficient asymmetric route to this important compound to date.[32]

In summary, a direct asymmetric α-arylation of cyclohexanones has been developed. The method employs Simpkins' base to desymmetrize 4-substituted cyclohexanones by asymmetric enolization followed by coupling with diaryl iodonium salts, leading to 2-aryl ketones in moderate to good yields and high enantioselectivities. The method expands the scope of the desymmetrization strategy pioneered by Simpkins and Koga, and highlights the utility of iodonium salts for aryl transfer reactions in synthesis. This approach has been applied in a short and efficient total synthesis of (−)-epibatidine and a formal synthesis of (+)-epibatidine.

Received: May 20, 2005
Published online: July 29, 2005

Keywords: cyclohexanone · desymmetrization · enolates · epibatidine · iodonium salts

 © 2005 Wiley-VCH Verlag GmbH & Co. KGaA, Weinheim

[1] a) J. Åhman, J. P. Wolfe, M. V. Troutman, M. Palucki, S. L. Buchwald, *J. Am. Chem. Soc.* **1998**, *120*, 1918; b) T. Hamada, A. Chieffi, J. Åhman, S. L. Buchwald, *J. Am. Chem. Soc.* **2002**, *124*, 1261.

[2] For racemic or achiral examples of Pd-catalyzed arylation of ketones, see a) M. Kawatsura, J. F. Hartwig, *J. Am. Chem. Soc.* **1999**, *121*, 1473; b) B. C. Hamann, J. F. Hartwig, *J. Am. Chem. Soc.* **1997**, *119*, 12382; c) J. M. Fox, X. Huang, A. Chieffi, S. L. Buchwald, *J. Am. Chem. Soc.* **2000**, *122*, 1360; d) M. Palucki, S. L. Buchwald, *J. Am. Chem. Soc.* **1997**, *119*, 11108.

[3] G. I. Elliott, J. P. Konopelski, M. M. Olmstead, *Org. Lett.* **1999**, *1*, 1867.

[4] J. Busch-Petersen, E. J. Corey, *Tetrahedron Lett.* **2000**, *41*, 6941.

[5] a) T. Iwama, V. B. Birman, S. A. Kozmin, V. H. Rawal, *Org. Lett.* **1999**, *1*, 673; b) K. Chen, G. F. Koser, *J. Org. Chem.* **1991**, *56*, 5764.

[6] a) P. Gao, D. L. Larson, P. S. Portoghese, *J. Med. Chem.* **1998**, *41*, 3091; b) P. Gao, P. S. Portoghese, *J. Org. Chem.* **1995**, *60*, 2276; c) J. H. Ryan, P. J. Stang, *Tetrahedron Lett.* **1997**, *38*, 5061.

[7] C. H. Oh, J. S. Kim, H. H. Jung, *J. Org. Chem.* **1999**, *64*, 1338.

[8] One report of a coupling between a chiral diaryl iodonium salt and cyclic β-keto esters bearing chiral auxiliaries resulted in modest *ee*'s, see M. Ochiai, Y. Kitagawa, N. Takayama, Y. Takaoka, M. Shiro, *J. Am. Chem. Soc.* **1999**, *121*, 9233.

[9] The iodide salt was also tested and gave similar yields to the triflate salt.

[10] Both LiHMDS and LDA could be successfully employed, LiHMDS gave generally slightly higher yields.

[11] Significant double arylation was obtained at low temperature (up to 31%) but above −45°C only monoarylation was observed.

[12] The diastereoselectivity of the initial coupling is irrevelant, as the product is immediately deprotonated by the second equivalent of base, see Scheme 3. The diastereoselectivity is determined during the protonation (in the quench) under kinetic conditions.

[13] a) Y. Nagao, M. Goto, M. Ochiai, M. Shiro, *Chem. Lett.* **1990**, 1503; b) K. W. Baldry, M. H. Gordon, R. Hafter, M. J. T. Robinson, *Tetrahedron Lett.* **1976**, 2589.

[14] In the parent ketone, the C4 proton appears as a triplet of triplets in the ^{1}H NMR spectrum, $J = 5.2$ and 4.7 Hz, indicative of a predominant axial conformation of the silyloxy substituent.

[15] **2e** was obtained from commercially available NHBoc ketone **2f** by Boc-protection in quantative yield, see the Supporting information.

[16] When **2e** was treated with LDA without addition of iodonium salt, compound **5** was isolated in 75% yield. The intramolecular nature of the reaction was proved by a cross-over experiment with cyclohexanone. Only **5** and cyclohexanone were isolated; *tert*-butyl 2-oxocyclohexanecarboxylate was not observed.

[17] Ketone **2f** could be recovered in 30%. Use of 3 equiv base did not increase the yield of **4f**, instead more byproducts were formed.

[18] The enantiomeric excess was measured by chiral HPLC, see Supporting information. Absolute configurations were assigned by analogy with previous desymmetrizations of cyclohexanones with Simpkins' base.

[19] P. O'Brien, *J. Chem. Soc. Perkin Trans. 1* **1998**, 1439.

[20] a) N. S. Simpkins, *Pure Appl. Chem.* **1996**, *68*, 691; b) P. J. Cox, N. S. Simpkins, *Tetrahedron: Asymmetry* **1991**, *2*, 1.

[21] For a comprehensive review see: H. F. Olivo, M. S. Hemenway, *Org. Prep. Proced. Int.* **2002**, *34*, 1.

[22] For some recent asymmetric syntheses see: a) Y. Hoashi, T. Yabuta, Y. Takemoto, *Tetrahedron Lett.* **2004**, *45*, 9185; b) D. A. Evans, K. A. Scheidt, C. W. Downey, *Org. Lett.* **2001**, *3*, 3009; c) G. Pandey, S. K. Tiwari, R. S. Singh, R. S. Mali, *Tetrahedron Lett.* **2001**, *42*, 3947; d) S. Aoyagi, R. Tanaka, M. Naruse, C. Kibayashi, *J. Org. Chem.* **1998**, *63*, 8397; e) H. Kosugi, M. Abe, R. Hatsuda, H. Uda, M. Kato, *Chem. Commun.* **1997**, 1857.

[23] M. T. Barros, C. D. Maycock, M. R. Ventura, *J. Chem. Soc. Perkin Trans. 1* **2001**, 166.

[24] B. M. Trost, G. R. Cook, *Tetrahedron Lett.* **1996**, *37*, 7485.

[25] A modified procedure was developed from a) P. J. Stang, B. Olenyuk, K. Chen, *Synthesis* **1995**, 937; b) F. M. Beringer, R. A. Nathan, *J. Org. Chem.* **1969**, *34*, 685, see Supporting information. An unsymmetrical pyridyl-phenyl iodonium salt was also prepared, but this gave consistently lower yields in the couplings due to moderate selectivity of pyridyl-group transfer compared to phenyl transfer.

[26] The 2-chloro-5-iodopyridine formed from **7** can be recovered and used in the synthesis of **7**.

[27] M. Majewski, N. M. Irvine, J. MacKinnon, *Tetrahedron: Asymmetry* **1995**, *6*, 1837.

[28] The moderate diastereoselectivity could be explained by a diminished preference for the axial position in the enolate intermediate **A** (Scheme 1), which is quenched to give the product mixture.

[29] a) E. Albertini, A. Barco, S. Benetti, C. De Risi, P. Pollini, R. Romagnoli, V. Zanirato, *Tetrahedron Lett.* **1994**, *35*, 9297; b) A. Barco, S. Benetti, C. De Risi, P. Marchetti, G. P. Pollini, V. Zanirato, *Eur. J. Org. Chem.* **2001**, 975.

[30] Analytical data were in agreement with literature. Optical rotation differed in magnitude with the literature but had the same sign. Value observed by us: $[\alpha]_D = -7.2$ ($c = 0.32$, CH_2Cl_2); literature value:[23] $[\alpha]_D = -10.6$ ($c = 0.32$, CH_2Cl_2).

[31] The conversion of alcohol **11** to epibatidine follows the sequence described for the corresponding NHBoc compound.[24] Analytical data of **1** (see Supporting information) were in agreement with those reported in ref. [22].

[32] Compare ref. [22]; a) 9 steps, 21% yield; b) 13 steps, 13% yield; d) 10 steps, 5.9% yield.

 © 2005 Wiley-VCH Verlag GmbH & Co. KGaA, Weinheim

Homogeneous Catalysis

DOI: 10.1002/anie.200501470

Highly Efficient $NaNO_2$-Catalyzed Destruction of Trichlorophenol Using Molecular Oxygen**

Xinmiao Liang, Dongmei Fu, Renhua Liu,* Qing Zhang, Tony Y. Zhang, and Xinquan Hu**

Polychlorinated phenols (PCPs) are a class of compounds once widely used as wood preservatives, pesticides, insecticides, and defoliants. Moreover, an alarming amount of these compounds are produced by the pulp industry as a result of lignin chlorination by chlorine-based bleaching processes. The remarkable resistance of these compounds toward degradation led to their substantial release into the environment, even in treated pulp waste streams.[1,2] Their numerous and abundant points of entry, inherent toxicity, persistence, and their presence in significant quantities in the environment have resulted in chlorophenols becoming one of the worst offenders in the environment, and are listed by the US Environmental Protection Agency as priority pollutants.[3]

Eradication of these persisting pollutants from the environment has attracted much attention from academia, industry, and governmental agencies. However, for a number of reasons, decades of efforts aimed at the treatment of PCPs have met with a limited degree of success with regard to efficiency, complexity, and industrial viability. While biological methods for the treatment of PCPs have been intensively investigated,[4–6] progress in this field to date has been hampered by the inherent toxicity of PCPs against the organisms used. Adding to the frustration is the finding of the tendency of some microorganism to convert some PCPs into even more toxic and more persistent pollutants such as polychlorinated dibenzo-*p*-dioxins.[7] As a result of these limitations on bioremediation, environmental chemists have turned their attention to chemical methods for destroying these pollutants. Catalytic reductive dechlorination (CRD) has been extensively investigated as a direct method to decrease the level of PCPs, and high efficiency has been achieved.[8,9] A major drawback to this method is its inability to reduce the overall chemical oxygen demand (COD) in the waste, thus necessitating a secondary treatment of the waste stream after reductive dechlorination. In addition, catalysts for CRD are usually noble metals, which could be deactivated by complex pollutants. On the other hand, advanced oxidation processes (AOPs), which are designed to destroy the environmental pollutants and reduced COD level, are emerging as a versatile strategy to achieve this goal.[10–12] A representive example of an AOP highlighted by Meunier and co-workers is the H_2O_2-based oxidative degradation method.[2,13] In this process a degradation of 99% of trichlorophenol (TCP) was obtained with release of 70% chlorine and 14% carbon mineralization by using iron phthalocyanines as a catalyst, 30% H_2O_2 (5 equiv) as an oxidant, and acetonitrile as a cosolvent in a buffered solution. Lenoir, Collins, et al. have further demonstrated the effectiveness of this homogeneous oxidation pathway for PCPs.[14] They have demonstrated a degradation of 99% TCP by using an iron complex of a tetraamidomacrocyclic ligand (Fe-taml) with 100-fold excess of H_2O_2 at 25°C. In that process, 35% carbon mineralization was achieved, together with 46.5% conversion to low-molecular-weight acids and 83% of the chlorine atoms being released as free chloride. In light of these ground-breaking results, we sought to discover and develop innovative and economically feasible technologies that would be intrinsically easy to industrialize. Specifically, we focused our efforts on finding a catalytic system that uses inexpensive and easily available oxidants/catalysts, and are operationally economical in an industrial setting. As such, one key criterion is the use of minimum quantities or total elimination of transition metals, organic solvents, and hazardous oxidants. Herein we reported our preliminary results toward achieving these goals.

Recently we reported a highly efficient catalytic aerobic oxidation system for alcohols that did not necessitate a transition-metal catalyst.[15,16] Key to the newly developed oxidation process is the ability of a nitrite salt to activate molecular oxygen as well as the suitability of the system towards an aqueous environment. It was intriguing to see if this $NaNO_2$/molecular oxygen method could be adopted for the destruction of the environmental pollutants such as PCPs. Thus, we started our research with TCP as the prototypical PCP substrate in high dilution (thus mimicking the environmental contaminant level) with $NaNO_2$ under pressurized oxygen. After systematic investigation and optimization of the reaction conditions (temperature, oxygen pressure, and amount of $NaNO_2$), we developed an efficient and simple oxidative degradation method for TCP.

Several features of this simple yet robust system are worth noting. First, the catalytic system results in fairly efficient removal of TCP at a moderate reaction temperature (Table 1 entries 1–4). As the reaction temperature increases, the rate of TCP destruction increased correspondingly and the color of the reaction mixture underwent the anticipated changes: from colorless to pink, then to yellow, and finally to colorless,

[*] Prof. Dr. X. Liang, D. Fu, R. Liu, Dr. Q. Zhang, Dr. X. Hu
Dalian Institute of Chemical Physics
Chinese Academy of Sciences
Dalian 116023 (China)
Fax: (+86) 411-8437-9529
E-mail: liangxm@dicp.ac.cn
renhua@dicp.ac.cn
xinquan@dicp.ac.cn
Dr. T. Y. Zhang
Eli Lilly and Company
Indianapolis, Indiana 46285 (USA)

[**] We would like to thank the grant of Innovation Program of the Chinese Academy of Sciences (KGCX2-SW-213 and DICP 2004K05). We also thank Wei Pan at the Dalian Institute of Product Quality Supervision and Inspection for ion chromatographic analysis, Xiaoli Dong at the Dalian Institute of Light Industry for total organic carbon analysis, and Prof. Damuo Zhu for his helpful discussion of the GC-MS data.

Supporting information for this article is available on the WWW under http://www.angewandte.org or from the author.

InterScience
© 2005 Wiley-VCH Verlag GmbH & Co. KGaA, Weinheim

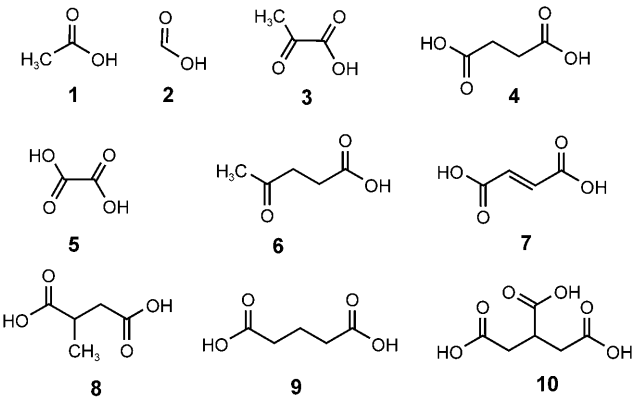
Table 1: Oxidation of TCP with $NaNO_2$ and oxygen under different reaction conditions.[a]

Entry	T [°C]	P [MPa]	t [h]	$NaNO_2$ [mol%]	Removal of TCP [%]	Removal of COD [%]	Mineralization of Cl [%]	Removal of TOC [%]
1	90	0.5	4	100	86	16	52	–
2	110	0.5	4	100	94	39	72	–
3	130	0.5	4	100	96	51	86	–
4	150	0.5	4	100	99	70	91	56
5	150	0.5	4	1	25	1	11	–
6	150	0.5	4	10	86	24	71	–
7	150	0.5	4	50	97	59	83	–
8	150	0.5	1	100	92	37	68	–
9	150	0.5	2	100	96	54	90	–
10	150	0.5	8	100	99	72	96	65
11	150	0.1	4	100	91	52	81	–
12	150	0.2	4	100	93	55	86	–
13	150	0.3	4	100	96	66	92	–
14	150	0.4	4	100	97	69	91	–
15[b]	150	1.5	4	100	97	60	90	–
16[c]	150	0.5	4	100	91	60	82	57
17[c]	170	0.5	4	100	92	64	82	63
18[c,d]	190	0.5	6	100	100	70	92	70
19[c]	210	0.5	6	100	100	73	90	76
20[c]	210	1.0	6	100	100	77	92	77

[a] Experimental conditions: TCP stock solution (20 mL) was treated with $NaNO_2$ and oxygen in the 50-mL teflon-lined autoclave. [b] Air was used as the oxidizing agent in the 50-mL teflon-lined autoclave. [c] The 100 times scale-up experiments were carried out in the 5-L Hastelloy autoclave. [d] The trace of dioxin in the TCP raw material was decreased by more than 80% under the above conditions. –: not determined. TCP: trichlorophenol; COD: chemical oxygen demand; TOC: total organic carbon.

as observed in previous research studies.[13,14] We were pleased to find that at a relatively mild reaction temperature (150 °C) with a stoichiometric amount of $NaNO_2$, 99% TCP was removed and 91% of the chlorine atoms of the TCP were released as innocuous inorganic chloride (entry 4). With a catalytic amount (1 mol%) of $NaNO_2$, 25% TCP degradation and 11% chlorine mineralization was observed (entry 5). This result clearly implicated the role of $NaNO_2$ as an active catalyst. Furthermore, a control experiment indicated that the oxidative destruction of TCP was totally ineffective in the absence of $NaNO_2$. This catalytic system also shows the degradation rate of TCP is rapid, for example, within only 1 hour, 92% TCP was removed and 68% chloride was released from the TCP (entry 8). Increasing the reaction time led to a slow increase in the removal of TCP, but a much greater extent of COD reduction. It is noteworthy that with 100 mol% $NaNO_2$, (which is within the feasible range given the relatively low environmental concentration of PCPs) under 0.5 MPa of O_2 and at 150 °C, more than 99% TCP was destroyed with 96% dechlorination and 72% COD reduction after 8 h (entry 10). The oxygen pressure had no significant influence on the reaction efficiency of the current catalytic system (entries 11–14). When air was used in place of pure oxygen, no apparent difference was observed (entry 15 versus entry 13). Finally, to demonstrate the viability of this new aerobic TCP degradation method for potential industrial applications, a scale-up experiment was carried out in a 5-L Hastelloy autoclave (entry 16). We observed a slightly lower degradation at this larger scale compared with the reaction in the small autoclave (entry 16 versus entry 4), which can be attributed to better agitation efficiency in the smaller vessel and can be easily compensated by a modest increase in temperature (entries 17–20). Overall, when all the facets of this new oxidation system is considered, the use of inexpensive $NaNO_2$ and air as reagents rendered it very attractive for potential application at an industrial scale for the treatment of these persistant environmental pollutants.

The extent of mineralization is also one of the critical factors for the evaluation of a new oxidative degradation system. Toward this end, we determined both the inorganic chloride released and the residual total organic carbon (TOC). The amount of chloride ions generated was measured by ion chromatography. As shown in Table 1, chlorine mineralization is up to 96% after 8 h at 150 °C (entry 10). TOC measurements indicated that 77% of the carbon in TCP was mineralized (entry 20). These analyses demonstrate that TCP was nearly completely destroyed and a considerable amount was mineralized; only a fraction of the TCP was converted into lower organic products (Scheme 1). The mass balance was determined by reduction of the TOC and some



Scheme 1. Products formed after TCP degradation by $NaNO_2$-catalyzed oxidation.

measurable reaction products such as acetic acid (**1**), formic acid (**2**), pyruvic acid (**3**), succinic acid (**4**), and oxalic acid (**5**) were identified and quantified with known standards by ion chromatography (Figure 1). The fate of 90% of the carbon atoms is accounted for (Table 2, entry 19). Gas chromatography/mass spectrometry (GC-MS) was used to identify residual organic compounds in the reaction mixture (Table 1, entry 18) and the results show that the major product is succinic acid (**4**), a fairly innocuous compound with a short environmental half-life. Other detectable minor

 © 2005 Wiley-VCH Verlag GmbH & Co. KGaA, Weinheim

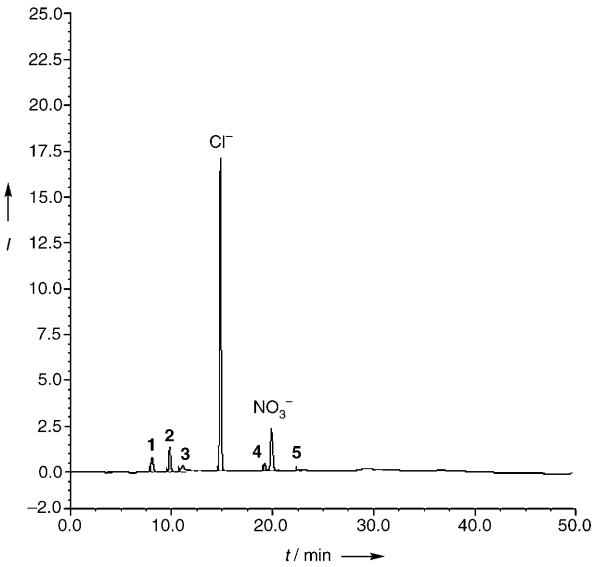


Figure 1. Products detected by ion chromatography after TCP degradation.

Table 2: Mass balance after the $NaNO_2$-catalyzed oxidation of TCP.

Compound	Entry 18[a]		Entry 19[a]		Entry 20[a]		Entry 10[a]	
	mM	% C	mM	% C	mM	% C	mM	% C
C + CO_2		70.0		75.6		77.4		65.0
acetic acid	0.15	4.9	0.16	5.3	0.16	5.4	0.19	6.3
formic acid	0.32	5.4	0.26	4.3	0.25	4.2	0.33	5.5
pyruvic acid	n.d.	n.d.	0.05	2.4	n.d.	n.d.	0.07	3.5
succinic acid	0.04	2.5	0.04	2.5	0.03	2.0	0.07	4.3
total		82.8		90.1		89.0		84.6

[a] From Table 1. n.d. = not detected.

components from the degraded mixture include levulinic acid (**6**), fumaric acid (**7**), 2-methylsuccinic acid (**8**), glutaric acid (**9**), and 3-carboxypentanedioic acid (**10**, Figure 2). Interestingly, the GC-MS results indicated that most detectable degradation products do not contain chlorine atoms, which is consistent with the extent of mineralization of the chlorine atoms. To the best of our knowledge, this is the first demonstration of $NaNO_2$, a simple, inexpensive and biodegradable inorganic compound, as a catalyst to activate molecular oxygen for the destruction of PCPs. Its remarkable effectiveness at attacking substances with low reduction potentials such as polychlorinated aromatic compounds has not been reported previously. However, several reports on biologically mediated systems[17–22] have provided useful insights for understanding the current oxidative degradation process. We postulate that peroxynitrite, which possesses activity similar to a hydroxyl radical, is most likely to be involved in the present catalytic system and acts as the veritable active oxidant for the degradation of TCP. Elucidation of the detailed mechanistic pathway will undoubtedly shed light on the pathway and allow further optimization of this aerobic oxidative degradation system.

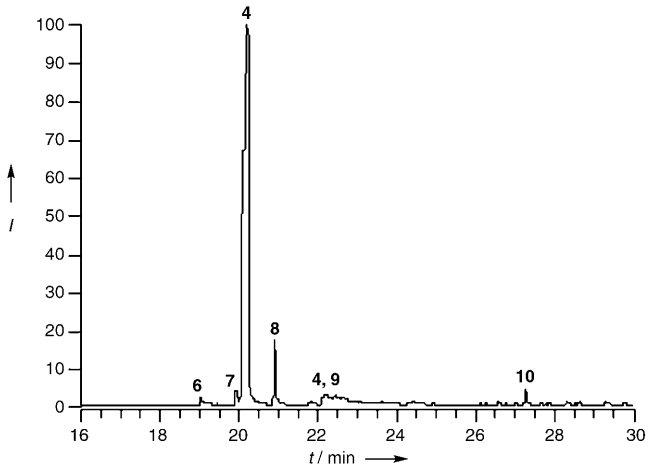


Figure 2. Products of TCP degradation detected by GC-MS after esterification.

The $NaNO_2/O_2$ system efficiently oxidizes the recalcitrant TCP into CO_2 and/or CO and a small fraction of biodegradable organic products with a high conversion rate. To the best of our knowledge, such a high extent of mineralization has not been reported previously without resorting to the extreme measure of high-temperature combustion. In addition, this system is intrinsically devoid of complications caused by other components found in industrial effluents, which tend to deactivate metal catalysts and render metal-based aerobic oxidation of pollutants ineffective. This non-transition-metal system is also free of the risk of secondary pollution during treatment as the catalyst, $NaNO_2$, was oxidized to $NaNO_3$. Therefore, this practical, inexpensive and efficient catalytic system represents a significant step forward in the fight against recalcitrant chlorinated organic pollutant and displays considerable promise for its practical application in an industrial setting.

Experimental Section

The catalytic oxidation of trichlorophenol (TCP) was carried out in a 50-mL teflon-lined stainless-steel autoclave. The reaction temperature was measured using a thermocouple and controlled by a PID regulator. TCP solution (20 mL, 1 mM) and $NaNO_2$ (20 μL, 1M) were added to the autoclave with a magnetic stirrer, thus, the mole ratio of TCP/$NaNO_2$ was 1:1. The autoclave was then closed and charged with pure oxygen to 0.5 MPa and then heated to the desired temperature. The stirring speed was set at 500 rpm. After reaction (heating time included), the autoclave was cooled to room temperature with a water bath, carefully depressurized, and sampled to perform further analysis. For scale-up experiments, TCP (395 mg, 1 equiv) and $NaNO_2$ (27.6 mg, 1 equiv) were added to the 5-L Hastelloy autoclave containing pure water (2 L, Millipore). The stirrer speed was set at 600 rpm. The rest of the procedure was similar to that described for the small-scale reaction.

Received: April 28, 2005
Published online: July 29, 2005

Keywords: chlorophenols · homogeneous catalysis · oxidation · oxygen · sodium nitrite

 © 2005 Wiley-VCH Verlag GmbH & Co. KGaA, Weinheim

[1] S. Ramamoorthy, S. Ramamoorthy, *Chlorinated Organic Compounds in the Environment*, Lewis, Boca Raton, FL, **1997**.
[2] A. Sorokin, S. De Suzzoni-Dezard, D. Poullain, J.-P. Noel, B. Meunier, *J. Am. Chem. Soc.* **1996**, *118*, 7410.
[3] http://oaspub.epa.gov/wqsdatabase/wqsi_epa_criteria.rep_parameter.
[4] T. Hatta, O. Nakano, N. Imai, N. Takizawa, H. Kiyohara, *J. Biosci. Bioeng.* **1999**, *87*, 267.
[5] N. Pal, G. Lewandowski, P. M. Armenante, *Biotechnol. Bioeng.* **1995**, *46*, 599.
[6] A. P. Annachhatre, S. H. Gheewala, *Biotechnol. Adv.* **1996**, *14*, 35.
[7] L. G. Oeberg, C. Rappe, *Chemosphere* **1992**, *25*, 49.
[8] C. Xia, J. Xu, W. Wu, X. Liang, *Catal. Commun.* **2004**, *5*, 383.
[9] F. Alonso, I. P. Beletskaya, M. Yus, *Chem. Rev.* **2002**, 102, 4009.
[10] W. Zhao, W. Ma, C. Chen, J. Zhao, Z. Shuai, *J. Am. Chem. Soc.* **2004**, *126*, 4782.
[11] M. Pera-Titus, V. Garcia-Molina, M. A. Banos, J. Gimenez, S. Esplugas, *Appl. Catal. B* **2004**, *47*, 219.
[12] G. Lente, J. H. Espenson, *Green Chem.* **2005**, *7*, 28.
[13] A. Sorokin, J. L. Seris, B. Meunier, *Science* **1995**, *268*, 1163.
[14] S. S. Gupta, M. Stadler, C. A. Noser, A. Ghosh, B. Steinhoff, D. Lenoir, C. P. Horwitz, K. W. Schramm, T. J. Collins, *Science* **2002**, *296*, 326.
[15] R. Liu, X. Liang, C. Dong, X. Hu, *J. Am. Chem. Soc.* **2004**, *126*, 4112.
[16] R. Liu, C. Dong, X. Liang, X. Wang, X. Hu, *J. Org. Chem.* **2005**, *70*, 729.
[17] P. C. Dedon, S. R. Tannenbaum, *Arch. Biochem. Biophys.* **2004**, *423*, 12.
[18] S. V. Lymar, R. F. Khairutdinov, J. K. Hurst, *Inorg. Chem.* **2003**, *42*, 5259.
[19] J. S. Beckman, T. W. Beckman, J. Chen, P. A. Marshall, B. A. Freeman, *Proc. Natl. Acad. Sci. USA* **1990**, *87*, 1620.
[20] P. Jenner, *Ann. Neurol.* **2003**, *53*, 26.
[21] S. Goldstein, G. L. Squadrito, L. Giuseppe, W. A. Pryor, G. Czapski, *Free Radical Biol. Med.* **1996**, *21*, 965.
[22] M. Kirsch, H. G. Korth, A. Wensing, R. Sustmann, H. Groot, *Arch. Biochem. Biophys.* **2003**, *418*, 133.

 © 2005 Wiley-VCH Verlag GmbH & Co. KGaA, Weinheim

Asymmetric Synthesis

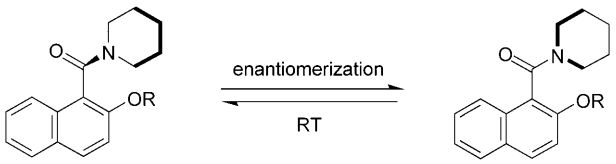
DOI: 10.1002/anie.200501156

Asymmetric Photocycloaddition in Solution of a Chiral Crystallized Naphthamide**

Masami Sakamoto, Atsushi Unosawa, Shuichiro Kobaru, Ayako Saito, Takashi Mino, and Tsutomu Fujita*

Asymmetric synthesis starting from an achiral material and in the absence of any external chiral agent has long been an intriguing challenge to chemists[1] and is also central to the origin of optical activity in Nature.[2] Stereospecific solid-state chemical reactions of chiral crystals formed by spontaneous crystallization of achiral materials are defined as "absolute" asymmetric synthesis, and most of the successful examples of such transformations involve photochemical reactions.[1,3] If the molecular chirality generated by chiral crystallization is retained even after the crystals are dissolved in a solvent, the "frozen" chirality is effectively transferred to the optically active products by various types of asymmetric reactions, besides the solid-state photochemical reaction.[4,5] Herein, we provide the first example of an asymmetric intermolecular photochemical reaction in solution through transfer of the chirality generated by chiral crystallization of an achiral naphthamide.

2-Alkoxy-1-naphthamides **1** were chosen to perform this asymmetric synthesis because the bond rotation between the naphthalene ring and the C=O(NR^1R^2) group corresponds to enantiomerization of **1**, and the rate is considerably affected by the substituents on both the naphthalene ring and the amide group (Scheme 1).[6] Naphthamides comprising a bulky



1a: R = CH_3
1b: R = C_2H_5

Scheme 1. Enantiomerization of naphthamides **1a**,**b** upon rotation about the naphthalene–C(=O) bond.

[*] Prof. M. Sakamoto, A. Unosawa, S. Kobaru, A. Saito, Dr. T. Mino, Prof. T. Fujita
Department of Applied Chemistry and Biotechnology
Faculty of Engineering
Chiba University
Yayoi-cho, Inage-ku, Chiba 263-8522 (Japan)
Fax: (+81) 43-290-3387
E-mail: sakamotom@faculty.chiba-u.jp

[**] This work was supported by a Grant-in-Aid for Scientific Research on Priority Area 417 from the Ministry of Education, Culture, Sports, Science, and Technology (MEXT) of the Japanese Government.

Supporting information for this article is available on the WWW under http://www.angewandte.org or from the author.

© 2005 Wiley-VCH Verlag GmbH & Co. KGaA, Weinheim

group such as *N*,*N*-diisopropylamide have stable axial chirality, which is used to advantage in many asymmetric synthesis methods.[7] Therefore, achiral naphthamides **1a** and **1b** that contain a relatively compact amide group derived from piperidine were prepared. X-ray crystallographic analysis of single crystals of **1a** and **1b** revealed that both amides adopt similar molecular conformations and, remarkably, that the carbonyl group in each is twisted such that it lies almost orthogonal to the naphthalene plane.

It was important that the achiral materials crystallized to yield chiral precursors for the proposed asymmetric synthesis. Fortunately, **1a** crystallized in a chiral space group, $P2_12_12_1$, and the constituent molecules adopted a chiral and helical conformation in the crystal lattice. On the other hand, ethoxy derivative **1b** formed a racemic crystalline system, $P2_1/c$.[8]

Recrystallization of **1a** from a mixed solvent system of hexane/chloroform gave colorless cubic crystals. X-ray analysis revealed that each single crystal was chiral and composed of one enantiomer. Circular dichroism (CD) spectra were measured to ascertain whether the chiral conformation was retained after the crystals were dissolved in an organic solvent. When a single crystal selected randomly was dissolved in THF at 5 °C using a cryostat apparatus, a strong Cotton effect was observed at below $\lambda = 350$ nm (Figure 1).

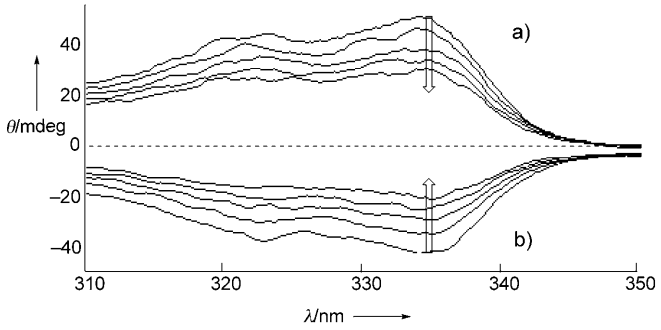


Figure 1. CD spectra of enantiomorphic crystals of **1a** in THF recorded at 5 °C using a cryostat apparatus: a) CD spectra of a solution of crystal (+)-**1a** measured every 10 minutes; b) CD spectra of a solution of a crystal (−)-**1a** measured every 12 minutes.

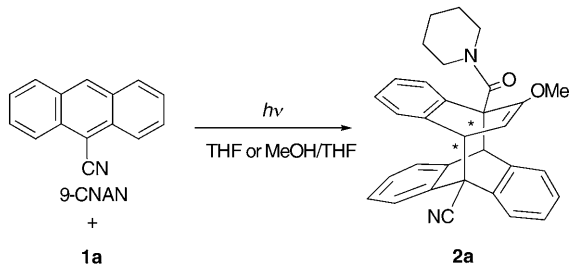
As expected, crystals of both enantiomers, which showed mirror-image CD curves, were easily obtained by crystallization from the solvent. One showed a positive Cotton effect (Figure 1 a), and the other showed a negative Cotton effect at the same wavelengths (Figure 1 b). Furthermore, the Cotton effect gradually decreased with racemization as a result of the rotation about the naphthalene–C(=O) bond.

To study how long naphthamide **1a** retained its molecular chirality after dissolving the crystals in a solvent, we measured the rate of racemization according to the changes in the CD spectra and calculated both the Gibbs free energy of activation ($\Delta G^{\neq}$) and the half-life of enantiomerization ($t_{1/2}$). The half-life was 11.8 minutes when the crystals were dissolved in THF at 15 °C, and the value increased upon lowering the temperature; $t_{1/2}$ values of 19.4 and 36.7 min were determined at 10 °C and 5 °C, respectively (Table 1). The free energy of activation was calculated as $\Delta G^{\neq} = 21.1$–21.2 kcal mol^{-1} from the temperature dependence of the kinetic constant, k (5 °C: $k = 4.90 \times 10^{-4}$; 10 °C: $k = 2.98 \times 10^{-4}$; 15 °C: $k = 1.58 \times 10^{-4}$). The rate of enantiomerization slowed considerably in a mixed solvent system of MeOH/THF. The half-life was 128.3 min at 15 °C and 21.2 min at 25 °C. In MeOH, naphthamide **1a** freezes its molecular conformation and maintains the molecular chirality derived from the crystal over a long period as result of the hydrogen-bonding interaction between the carbonyl group and methanol and also through the rather strong zwitterionic character of the amide group in a polar solvent. These facts indicate that achiral amide **1a** can retain the axial chirality induced in the crystal lattice after the crystallinity is lost and that the lifetime is long enough for application of **1a** in asymmetric synthesis.

Table 1: Kinetic parameters for enantiomerization of naphthamide **1a**.

Solvent	T [°C]	$t_{1/2}$ [min]	$\Delta G^{\neq}$ [kcal mol^{-1}]	$\Delta H^{\neq}$ [kcal mol^{-1}]	$\Delta S^{\neq}$ [cal mol^{-1} K^{-1}]
THF	5	36.7	21.08	17.53	−12.77
	10	19.4	21.11	17.52	−12.69
	15	11.8	21.21	17.51	−12.84
MeOH/	15	128.3	22.58	30.13	26.19
THF	20	62.6	22.46	30.12	26.11
(1:1)	25	21.2	22.32	30.11	26.13

To the best of our knowledge, there are no examples of photocycloaddition reactions of naphthamides with anthracene derivatives,[9,10] so the photocycloaddition of **1a** with 9-cyanoanthracene (9-CNAN) was first examined at room temperature. When a solution of naphthamide **1a** and 9-CNAN (0.05 M each) in THF was irradiated with a high-pressure mercury lamp under argon at room temperature, photocycloaddition occurred effectively and the [4+4] cycloadduct **2a** was obtained in quantitative yield (Scheme 2). The structure of the adduct **2a** was unequivocally established by X-ray crystallographic analysis.[11]



Scheme 2. Photochemical cycloaddition reaction of **1a** in the presence of 9-cyanoanthracene (9-CNAN).

Next, we attempted the asymmetric photocycloaddition using the frozen chirality. A number of chiral crystals of (+)-**1a** were dissolved in a cooled solution of 9-CNAN in THF (−20 °C), and the solution was irradiated with an ultrahigh-pressure mercury lamp for 30 minutes. Only one cycloadduct, (+)-**2a**, was obtained in 100 % yield with 95 % *ee* (Table 2,

 © 2005 Wiley-VCH Verlag GmbH & Co. KGaA, Weinheim

Table 2: Asymmetric photochemical cycloaddition reaction of (+)-**1a** with 9-cyanoanthracene (9-CNAN) using the frozen axial chirality.

Entry	Solvent	T [°C][a]	Conc. [M][b]	Conv. [%][c]	*ee* of (+)-**2a** [%][d]
1	THF	−20	0.05	52	95
2	THF	20	0.05	45	29
3	MeOH/THF[e]	−20	0.025	54	94
4	MeOH/THF[e]	20	0.025	40	88

[a] A solution of 9-CNAN was cooled to the cited temperature, and then powdered chiral crystals of (+)-**1a** were added. [b] Concentration of both **1a** and 9-cyanoanthracene. [c] Determined on the basis of the amount of **1a**. [d] *ee* value was determined by HPLC using a CHIRALCEL-ADH column. [e] A 1:1 mixture of MeOH/THF was used.

entry 1). When a mixed solvent system of MeOH and THF was used, a similar enantioselectivity was obtained (94% *ee*; entry 3). Even at 20°C, at which temperature the enantiomerization of **1a** occurs competitively with the photocycloaddition, the adduct from the reaction in THF was obtained with 29% *ee* (entry 2). The rate of enantiomerization is suppressed in MeOH/THF ($t_{1/2} = 62.6$ min at 20°C; Table 1) relative to pure THF, and, surprisingly, the cycloaddition product from the mixed solvent system was obtained with 88% *ee* at 20°C (Table 2, entry 4).

As the rate of racemization of naphthamide **1a** is slow, a high enantiomeric excess of the bulk crystals could not be obtained by recrystallization from a mixed solvent of hexane/chloroform. Therefore, crystals of **1a** used for the asymmetric photoreaction were prepared by stirred crystallization at high temperature,[12] by which the completely melted sample of **1a** at 120°C (m.p.: 110–112°C) was cooled and solidified by lowering the temperature to 100°C with stirring. Five independent crystallization experiments followed by photocycloaddition reactions with 9-CNAN were performed, and the photoadduct **2a** was obtained with enantioselectivities of 92, 97, 96, 94, and 97% *ee*. A high level of reproducibility of both chiral crystallization and asymmetric photoreaction was achieved by this method.

In many cases, the initially generated enantiomorphic crystal works in situ as a seed in the crystallization step such that all the subsequent crystals in the batch have the same absolute configuration.[12] The use of crystals generated in this fashion in the photocycloaddition reaction can lead to isolation of either of the enantiomers of the cycloadduct. For instance, from three independent experiments, (+)-**2a** was obtained on one occasion while (−)-**2a** was afforded in the other two reactions. Of course, the desired crystals of **1a** could be selectively prepared in large quantities by the addition of a corresponding seed crystal during the crystallization process.[13]

In conclusion, we have demonstrated asymmetric intermolecular photocycloadditions with high enantiomeric excess using the "frozen chirality" generated by spontaneous crystallization. The crystallization of achiral molecules in chiral space groups, while rare and unpredictable, is well documented.[1] Extension of spontaneous chiral crystallization to a variety of new systems is possible, and we believe that this methodology can be applied to the development of new absolute asymmetric syntheses.

Received: April 1, 2005
Revised: May 16, 2005
Published online: July 29, 2005

Keywords: asymmetric synthesis · chirality · cycloaddition · enantioselectivity · photochemistry

[1] For reviews, see: a) V. Ramamurthy, K. Venkatesan, *Chem. Rev.* **1987**, *87*, 433–481; b) J. R. Scheffer, M. Garcia-Garibay, O. Nalamasu in *Organic Photochemistry*, *Vol. 8* (Ed.: A. Padwa), Marcel Dekker, New York, **1987**, pp. 249–338; c) M. Vaida, R. Popovitz-Biro, L. Leiserowitz, M. Lahav in *Photochemistry in Organized and Constrained Media* (Ed.: V. Ramamurthy), Wiley, New York, **1991**, pp. 249–302; d) M. Sakamoto, *Chem. Eur. J.* **1997**, *3*, 384–389; e) B. L. Feringa, R. Van Delden, *Angew. Chem.* **1999**, *111*, 3624–3645; *Angew. Chem. Int. Ed.* **1999**, *38*, 3419–3438; f) M. Sakamoto in *Chiral Photochemistry* (Ed.: V. Ramamurthy), Marcel Dekker, New York, **2004**, pp. 415–461; g) A. G. Griesbeck, U. J. Meierhenrich, *Angew. Chem.* **2002**, *114*, 3279–3286; *Angew. Chem. Int. Ed.* **2002**, *41*, 3147–3154.

[2] a) L. Addadi, M. Lahav in *Origin of Optical Activity in Nature* (Ed.: D. C. Walker), Elsevier, New York, **1979**; b) S. F. Mason, *Nature* **1984**, *311*, 19–23; c) W. E. Wlias, *J. Chem. Educ.* **1972**, *49*, 448–454.

[3] A few examples involving solid–gas reactions were reported, however, the enantioselectivity is low. See: a) K. Penzein, G. M. J. Schmidt, *Angew. Chem.* **1969**, *81*, 628; *Angew. Chem.* **1969**, *8*, 608–609; b) B. S. Green, L. Heller, *Science* **1974**, *185*, 525–527; c) M. Garcia-Garibay, J. R. Scheffer, J. Trotter, F. Wireko, *Tetrahedron Lett.* **1988**, *29*, 1485–1488; d) R. Gerdil, L. Huiyou, B. Gerald, *Helv. Chim. Acta* **1999**, *82*, 418–434.

[4] Slow racemization of aromatic amides was reported, see: I. Azumaya, K. Yamaguchi, I. Okamoto, H. Kagechika, K. Shudo, *J. Am. Chem. Soc.* **1995**, *117*, 9083–9084.

[5] We previously reported asymmetric carbonyl addition using chirality of crystals; see: a) M. Sakamoto, T. Iwamoto, N. Nono, M. Ando, W. Arai, T. Mino, T. Fujita, *J. Org. Chem.* **2003**, *68*, 942–946; b) M. Sakamoto, S. Kobaru, T. Mino, T. Fujita, *Chem. Commun.* **2004**, 1002–1003.

[6] A. Ahmed, R. A. Bragg, J. Clayden, L. W. Lai, C. McCarthy, J. H. Pink, N. Westlund, S. A. Yasin, *Tetrahedron* **1998**, *54*, 13277–13294.

[7] a) J. Clayden, A. Lund, L. Vallverdu, M. Hellwell, *Nature* **2004**, *431*, 966–971; b) J. Clayden, *Angew. Chem.* **1997**, *109*, 986–988; *Angew. Chem. Int. Ed. Engl.* **1997**, *36*, 949–951.

[8] Crystal data for **1a**: Orthorhombic, space group $P2_12_12_1$, $a = 7.963(3)$ Å, $b = 11.713(3)$ Å, $c = 15.708(4)$ Å, $V = 1465.2(8)$ Å^3, $Z = 4$, $\rho = 1.221$ Mg m^{-3}; in the final least-squares refinement cycles on F^2, the model converged at $R_1 = 0.0499$, $wR_2 = 0.1316$, and GOF = 1.125 for 1611 reflections. Crystal data for **1b**: Monoclinic, space group $P2_1/n$, $a = 9.762(4)$ Å, $b = 12.702(4)$ Å, $c = 12.534(5)$ Å, $\beta = 99.84(3)$, $V = 1531.3(10)$ Å^3, $Z = 4$, $\rho = 1.229$ Mg m^{-3}; in the final least-squares refinement cycles on F^2, the model converged at $R_1 = 0.0683$, $wR_2 = 0.2369$, and GOF = 1.149 for 2903 reflections.

[9] For a report on the photochemical cycloaddition of anthracene and 1-cyanonaphthalene, see: A. Albini, E. Fasani, D. Faiardi, *J. Org. Chem.* **1987**, *52*, 155–157.

[10] For an example of intramolecular photocyloaddition reaction, see: S. Kohmoto, Y. Ono, H. Masu, K. Yamaguchi, K. Kishikawa, M. Yamamoto, *Org. Lett.* **2001**, *3*, 4153–4155.

 © 2005 Wiley-VCH Verlag GmbH & Co. KGaA, Weinheim

[11] Crystal data for **2a**: Monoclinic, space group $P2_1/c$, $a = 20.198(6)$ Å, $b = 9.073(3)$ Å, $c = 16.056(4)$ Å, $\beta = 96.08(2)$, $V = 2925.7(16)$ Å^3, $Z = 4$, $\rho = 1.237$ Mg m^{-3}; in the final least-squares refinement cycles on F^2, the model converged at $R_1 = 0.0894$, $wR_2 = 0.2242$, and GOF = 1.149 for 2903 reflections. CCDC 267437 (**1a**), 267438 (**1b**), and 267439 (**2a**) contain the supplementary crystallographic data for this paper. These data can be obtained free of charge from the Cambridge Crystallographic Data Centre via www.ccdc.cam.ac.uk/data_request/cif.

[12] a) M. Sakamoto, T. Utsumi, M. Ando, M. Saeki, T. Mino, T. Fujita, A. Katoh, T. Nishio, C. Kashima, *Angew. Chem.* **2003**, *115*, 4496 – 4499; *Angew. Chem. Int. Ed.* **2003**, *42*, 4360 – 4363; b) D. K. Kondepudi, J. Laudadio, K. Asakura, *J. Am. Chem. Soc.* **1999**, *121*, 1448 – 1451; c) J. M. McBride, R. L. Carter, *Angew. Chem.* **1991**, *103*, 298 – 300; *Angew. Chem. Int. Ed. Engl.* **1991**, *30*, 293 – 295.

[13] Seeding was carried out as follows: the melted sample of **1a** at 120 °C was gradually cooled, and a powdered single crystal (about 0.5 mm size) was added at below the melting point of 110–112 °C. The presence of the seed crystal induces the same conformation in the subsequent crystallization such that all the crystals in the batch have the same optical rotation.

 © 2005 Wiley-VCH Verlag GmbH & Co. KGaA, Weinheim

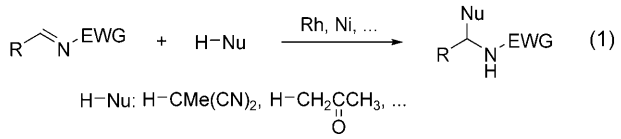
Nitrogen Heterocycles

DOI: 10.1002/anie.200500795

Direct Mannich and Nitro-Mannich Reactions with Non-Activated Imines: AgOTf-Catalyzed Addition of Pronucleophiles to *ortho*-Alkynylaryl Aldimines Leading to 1,2-Dihydroisoquinolines

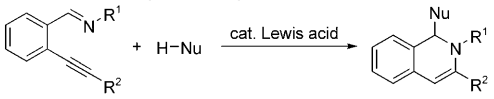
Naoki Asao, Salprima Yudha S., Tsutomu Nogami, and Yoshinori Yamamoto*

The Lewis acid and/or transition-metal-catalyzed addition of carbon nucleophiles to imines is one of the most important methods for the preparation of nitrogen-containing organic compounds.[1] In particular, the direct addition of carbon pronucleophiles to imines in the presence of catalysts is highly desirable as it represents an atom-economical approach. Previously, we reported the first example of the transition-metal-catalyzed direct addition of malononitrile derivatives and simple ketones, such as acetone, to activated imines [Eq. (1)].[2]



This transformation is useful for synthesizing amines and amino acid derivatives. However, activated imines that bear an electron-withdrawing group on the imine nitrogen atom have to be used as a substrate to induce the addition of pronucleophiles. Although direct Mannich-type reactions of activated ketones and malonates[3] and direct nitro-Mannich (aza-Henry) reactions catalyzed by metals and Brønsted acids were reported recently,[4] activated imines were also required in these cases. Herein, we report new direct Mannich and nitro-Mannich reactions of non-activated imines; AgOTf-catalyzed addition of carbon pronucleophiles to *ortho*-alkynylaryl aldimines **1** produces 1,2-dihydroisoquinoline derivatives **2** in good to high yields (Table 1).[5] Treatment of **1a** ($R^1 = R^2 = Ph$) with nitromethane (2 equiv) in the presence of AgOTf (3 mol%) in $(CH_2Cl)_2$ at 80°C for 1.5 h gave 1-nitromethyl-2,3-diphenyl-1,2-dihydro-isoquinoline (**2a**) in 85% yield (Table 1, entry 1). On the other hand, the reaction of benzylidene phenylamine, which bears no alkynyl group at the proximal position, under similar conditions did not give the corresponding addition product, and the starting material was recovered in 81% yield. This result clearly showed that the *ortho*-alkynyl group of **1a** is essential for the present direct addition of nitromethane to the imine moiety. Besides AgOTf, $Cu(OTf)_2$ was a suitable catalyst for the present reaction while the AuCl-catalyzed reaction gave **2a** in only 1% yield (Table 1, entries 2–3). Other starting materials **1b–e** were suitable for this reaction, and the corresponding

Table 1: Direct addition of pronucleophiles to **1**.[a]



Entry	1	R^1	R^2	Lewis acid	Nu-H	2	Yield [%][b]
1	**1a**	Ph	Ph	AgOTf	CH_3NO_2	**2a**	85
2	**1a**	Ph	Ph	$Cu(OTf)_2$	CH_3NO_2	**2a**	79
3	**1a**	Ph	Ph	AuCl	CH_3NO_2	**2a**	1
4[c]	**1b**	C_4H_9	Ph	AgOTf	CH_3NO_2	**2b**	56
5	**1c**	$PhCH_2$	Ph	AgOTf	CH_3NO_2	**2c**	58
6	**1d**	Ph	C_4H_9	AgOTf	CH_3NO_2	**2d**	72
7	**1e**	Ph	1-cC_6H_9	AgOTf	CH_3NO_2	**2e**	80
8	**1a**	Ph	Ph	AgOTf	$CH_3CH_2NO_2$	**2f**	72[d]
9	**1a**	Ph	Ph	AgOTf	acac	**2g**	77
10	**1a**	Ph	Ph	AgOTf	$CH_2(CO_2Me)_2$	**2h**	80
11	**1a**	Ph	Ph	AgOTf	$CH_2(CN)_2$	**2i**	84
12[e]	**1a**	Ph	Ph	AgOTf	acetone	**2j**	80
13[f]	**1a**	Ph	Ph	$[Rh(cod)(PPh_3)_2PF_6]$	CH_3CN	**2k**	61

[a] The reaction was carried out using **1** (1 equiv) and pronucleophiles (2 equiv) in the presence of Lewis acid (3 mol%) in $(CH_2Cl)_2$ at 80°C within 6 h unless otherwise noted. [b] Yields of isolated products. [c] The reaction was carried out at 60°C. [d] d.r. 84:16. [e] The reaction was carried out in acetone as a solvent at 70°C. [f] The reaction was conducted with $[Rh(cod)(PPh_3)_2PF_6]$ catalyst (2 mol%) using CH_3CN as a solvent. 1-cC_6H_9 = 1-cyclohexenyl; Tf = trifluoromethanesulfonyl; cod = 1,5-cyclooctadiene.

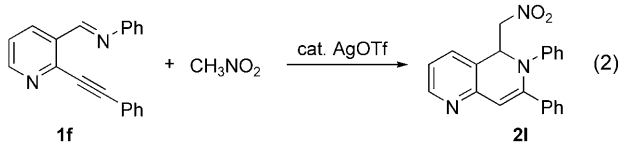
[*] Assoc. Prof. N. Asao, S. Yudha S., T. Nogami, Prof. Y. Yamamoto
Department of Chemistry
Graduate School of Science, Tohoku University
Sendai 980-8578 (Japan)
Fax: (+81) 22-795-6784
E-mail: asao@mail.tains.tohoku.ac.jp
yoshi@yamamoto1.chem.tohoku.ac.jp

Supporting information for this article is available on the WWW under http://www.angewandte.org or from the author.

InterScience
© 2005 Wiley-VCH Verlag GmbH & Co. KGaA, Weinheim

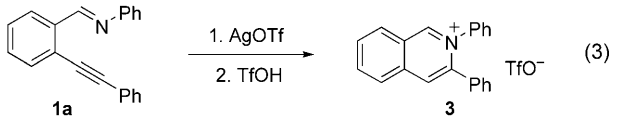
products **2b–e** were obtained in moderate to high yields (Table 1, entries 4–7). The reaction of **1a** with nitroethane gave **2f** as a mixture of diastereomers (d.r. 84:16, stereochemistry not determined; Table 1, entry 8). The reaction of **1a** with other pronucleophiles that bear activated methylene groups proceeded smoothly, and the corresponding dihydroisoquinoline derivatives **2g–i** were obtained in moderate to high yields (Table 1, entries 9–11). The reaction of **1a** with acetone (2 equiv) gave **2j** in a low yield. However, when acetone was used as the solvent, the direct addition proceeded smoothly, and **2j** was obtained in 80% yield (Table 1, entry 12). The reaction with CH_3CN proceeded in a low yield, even when the reaction was carried out in CH_3CN; however, when $[Rh(cod)(PPh_3)_2PF_6]$ was used as catalyst instead of AgOTf, the corresponding product **2k** was obtained in 61% yield (Table 1, entry 13).

Interestingly, the direct pronucleophile addition could also be applied to the pyridine derivative **1f**; treatment with nitromethane gave the naphthyridine derivative **2l** in 75% yield [Eq. (2)].



(2)

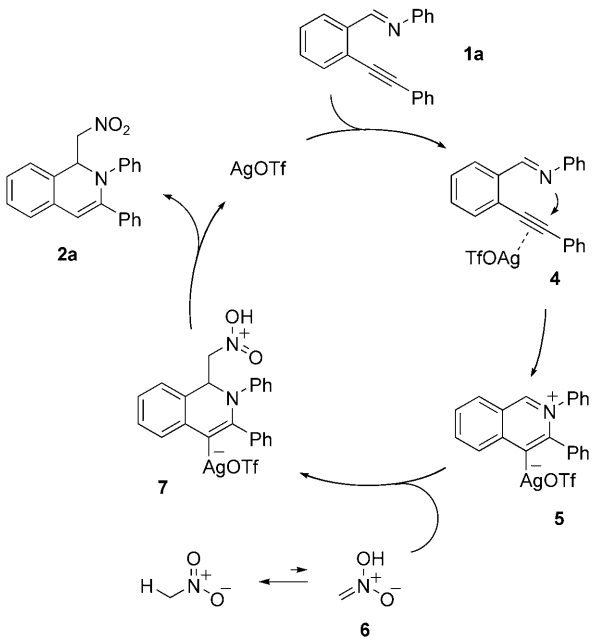
To clarify the mechanism of the process, we examined the reaction of **1a** with AgOTf in the absence of any pronucleophiles. Treatment of **1a** with AgOTf (1 equiv) in CH_2Cl_2, followed by addition of TfOH gave a crude material, which was recrystallized from a mixture of hexane and EtOH to give isoquinolinium salt **3** in 86% yield [Eq. (3)].[6]



(3)

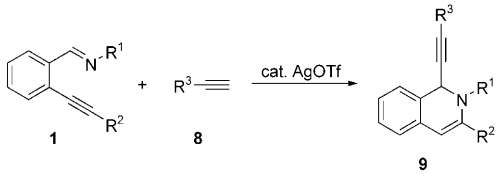
This result clearly indicates that at the beginning of the cyclization the triple bond coordinates to the Lewis acid, as shown in **4** (Scheme 1). Subsequent attack of the nitrogen atom at the electron-deficient triple bond leads to the isoquinolinium intermediate **5**. The addition of aci-nitromethane **6**, which is derived from nitromethane, gives the product **2** via **7**. As shown in Table 1, the AuCl-catalyzed reaction gave **2a** in a very low yield. Indeed, when **1a** was treated with AuCl (1 equiv) under similar reaction conditions as shown in Equation (3), the isoquinolinium salt **3** was obtained in 10% yield, which indicates that the formation of the isoquinolinium intermediate **5** is a key step in the present reaction.

Because the 1,2-dihydroisoquinoline derivatives **2** were produced unexpectedly easily from **1**, we were interested in whether the terminal alkynes **8** could be used as a pronucleophile. The results are summarized in Table 2. The reaction of **1a** with phenylacetylene **8a** under the similar reaction conditions as those given in Table 1 afforded 1-phenylethynyl-1,2-dihydroisoquinoline derivative **9a** in 93% yield. Analogously, the reaction proceeded smoothly with aliphatic



Scheme 1. Proposed mechanism for the AgOTf-catalyzed direct addition of nitromethane to **1a**.

Table 2: Direct addition of terminal alkynes **8** to **1**.[a]

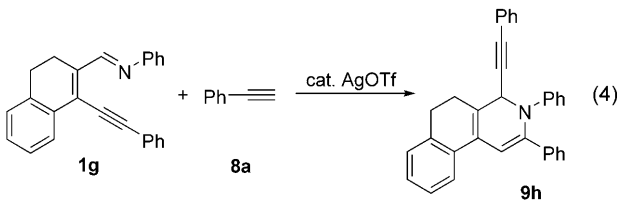


Entry	**1**	R^1	R^2	**8**	R^3	**9**	Yield [%][b]
1	**1a**	Ph	Ph	**8a**	Ph	**9a**	93
2	**1a**	Ph	Ph	**8b**	C_4H_9	**9b**	90
3	**1a**	Ph	Ph	**8c**	CO_2Et	**9c**	86
4	**1b**	C_4H_9	Ph	**8a**	Ph	**9d**	42
5	**1c**	$PhCH_2$	Ph	**8a**	Ph	**9e**	70
6	**1f**	Allyl	Ph	**8a**	Ph	**9f**	70
7	**1d**	Ph	C_4H_9	**8a**	Ph	**9g**	58

[a] The reaction was carried out with **1** (1 equiv) and terminal alkynes **8** (1.2 equiv) in the presence of AgOTf (3 mol%) in $(CH_2Cl)_2$ at 80°C within 6 h. [b] Yields of isolated products.

alkynes, such as hexyne (**8b**), and even with ethyl propanoate (**8c**), and the products **9b** and **9c**, respectively, were obtained in high yields (Table 2, entries 2 and 3). Not only **1a** but also the other substrates **1b**,**c**, and **f**, which have alkyl groups on the nitrogen atom of the imine moiety, were suitable for the present reaction (Table 2, entries 4–6). The reaction of **1d**, which has a butyl group at the end of the alkynyl group, with **8a** also gave **9g** in 58% yield (Table 2, entry 7). Interestingly, the reaction of **1g** with phenylacetylene (**8a**) gave the 3,4,5,6-tetrahydrobenzo[*f*]isoquinoline derivative **9h** in 62% yield [Eq. (4)]. Several methods for direct addition of terminal alkynes to imine compounds have been reported.[7–8] However, the direct addition of alkynes to benzylidene phenylamine, which bears no alkynyl group at the proximal position, did not proceed at all under the present reaction conditions.

 © 2005 Wiley-VCH Verlag GmbH & Co. KGaA, Weinheim



This result again indicates that the presence of an *ortho*-alkynyl group is essential for the imine addition, and the formation of the isoquinolinium intermediate **5** is a key step.

We are now in a position to synthesize functionalized 1,2-dihydroisoquinoline skeletons through the direct addition of various carbon pronucleophiles to *ortho*-alkynylaryl aldimines. Even without the use of the usual activated imines that bear an electron-withdrawing group, the addition to imines proceeded well, probably due to the formation of the reactive isoquinolinium intermediates **5** in situ. In general, the 1,2-dihydroisoquinoline framework can be constructed by nucleophilic addition to isoquinolinium salts, which are derived from the corresponding isoquinolines by acylation or alkylation.[9] Evidently, the present reaction proceeded without such activation, and the current transformation provides an alternative method for the construction of 1,2-dihydroisoquinolines.[10] Further studies to elucidate the precise mechanism of this reaction and to extend the scope of its synthetic utility are in progress in our laboratory.[11]

Received: March 4, 2005
Revised: May 31, 2005
Published online: July 26, 2005

Keywords: imines · Mannich reaction · nitrogen heterocycles · pronucleophiles · synthetic methods

[1] For reviews on catalytic asymmetric Mannich-type reactions, see: a) S. Kobayashi, H. Ishitani, *Chem. Rev.* **1999**, *99*, 1069–1094; b) A. E. Taggi, A. M. Hafez, T. Lectka, *Acc. Chem. Res.* **2003**, *36*, 10–19.

[2] a) Y. Yamamoto, Y. Kubota, Y. Honda, H. Fukui, N. Asao, H. Nemoto, *J. Am. Chem. Soc.* **1994**, *116*, 3161–3162; b) N. Shida, Y. Kubota, H. Fukui, N. Asao, I. Kadota, Y. Yamamoto, *Tetrahedron Lett.* **1995**, *36*, 5023–5026.

[3] For recent direct Mannich reactions, see: a) N. Kumagai, S. Matsunaga, M. Shibasaki *J. Am. Chem. Soc.* **2004**, *126*, 13632–13633; b) L.-W. Xu, C.-G. Xia, L. Li *J. Org. Chem.* **2004**, *69*, 8482–8484; c) T. Ooi, M. Kameda, J. Fujii, K. Maruoka, *Org. Lett.* **2004**, *6*, 2397–2399; d) D. Uraguchi, M. Terada, *J. Am. Chem. Soc.* **2004**, *126*, 5356–5357; e) S. Matsunaga, N. Kumagai, S. Harada, M. Shibasaki, *J. Am. Chem. Soc.* **2003**, *125*, 4712–4713; f) M. Marigo, A. Kjrsgaard, K. Juhl, N. Gathergood, K. A. Jørgensen, *Chem. Eur. J.* **2003**, *9*, 2359–2367; g) B. M. Trost, L. R. Terrell, *J. Am. Chem. Soc.* **2003**, *125*, 338–339; h) K. Juhl, N. Gathergood, K. A. Jørgensen, *Angew. Chem.* **2001**, *113*, 3083–3085; *Angew. Chem. Int. Ed.* **2001**, *40*, 2995–2997; i) H. Nemoto, R. Ma, H. Moriguchi, I. Suzuki, M. Shibuya, *J. Organomet. Chem.* **2000**, *611*, 445–448.

[4] For recent direct nitro-Mannich (aza-Henry) reactions, see: a) B. M. Nugent, R. A. Yoder, J. N. Johnston, *J. Am. Chem. Soc.* **2004**, *126*, 3418–3419; b) N. Tsuritani, K. Yamada, N. Yoshikawa, M. Shibasaki, *Chem. Lett.* **2002**, 276–277; c) N. Nishiwaki, K. R. Knudsen, K. V. Gothelf, K. A. Jørgensen, *Angew. Chem.* **2001**, *113*, 3080–3083; *Angew. Chem. Int. Ed.* **2001**, *40*, 2992–2995; d) C. Qian, F. Gao, R. Chen, *Tetrahedron Lett.* **2001**, *42*, 4673–4675; e) K. Yamada, S. J. Harwood, H. Gröger, M. Shibasaki, *Angew. Chem.* **1999**, *111*, 3713–3715; *Angew. Chem. Int. Ed.* **1999**, *38*, 3504–3506.

[5] Although the organocatalytic direct Mannich reaction proceeded well with non-activated imines to afford β-aminocarbonyl compounds, pronucleophiles were limited to aldehydes and ketones; see: a) A. Córdova, *Chem. Eur. J.* **2004**, *10*, 1987–1997; b) W. Notz, F. Tanaka, S. Watanabe, N. S. Chowdari, J. M. Turner, R. Thayumanavan, C. F. Barbas III, *J. Org. Chem.* **2003**, *68*, 9624–9634; c) Y. Hayashi, W. Tsuboi, I. Ashimine, T. Urushima, M. Shoji, K. Sakai, *Angew. Chem.* **2003**, *115*, 3805–3808; *Angew. Chem. Int. Ed.* **2003**, *42*, 3677–3680; d) A. Córdova, S.-i. Watanabe, F. Tanaka, W. Notz, C. F. Barbas III, *J. Am. Chem. Soc.* **2002**, *124*, 1866–1867; e) A. Córdova, W. Notz, G. Zhong, J. M. Betancort, C. F. Barbas III, *J. Am. Chem. Soc.* **2002**, *124*, 1842–1843; f) A. Córdova, C. F. Barbas III, *Tetrahedron Lett.* **2002**, *43*, 7749–7752; g) B. List, P. Pojarliev, W. T. Biller, H. J. Martin, *J. Am. Chem. Soc.* **2002**, *124*, 827–833; h) W. Notz, K. Sakthivel, T. Bui, G. Zhong, C. F. Barbas III, *Tetrahedron Lett.* **2001**, *42*, 199–201; i) B. List, *J. Am. Chem. Soc.* **2000**, *122*, 9336–9337.

[6] A Pd-catalyzed isoquinoline synthesis from *ortho*-alkynylaryl aldimines was reported; see: Q. Huang, R. C. Larock, *J. Org. Chem.* **2003**, *68*, 980–988, and references therein.

[7] For reviews, see: a) C. M. Wei, Z. G. Li, C. J. Li, *Synlett* **2004**, 1472–1483; b) P. G. Cozzi, R. Hilgraf, N. Zimmermann, *Eur. J. Org. Chem.* **2004**, 4095–4105.

[8] For recent examples, see: a) M. Benaglia, D. Negri, G. Dell'Anna, *Tetrahedron Lett.* **2004**, *45*, 8705–8708; b) B. M. Choudary, C. Sridhar, M. L. Kantam, B. Sreedhar, *Tetrahedron Lett.* **2004**, *45*, 7319–7321; c) C. Wei, J. T. Mague, C.-J. Li, *Proc. Natl. Acad. Sci. USA* **2004**, *101*, 5749–5754; d) C. Fischer, E. M. Carreira, *Synthesis* **2004**, 1497–1503; e) S. Sakaguchi, T. Mizuta, M. Furuwan, T. Kubo, Y. Ishii, *Chem. Commun.* **2004**, 1638–1639; f) L. Shi, Y.-Q. Tu, M. Wang, F.-M. Zhang, C.-A. Fan, *Org. Lett.* **2004**, *6*, 1001–1003; g) J. N. Rosa, A. G. Santos, C. A. M. Afonso, *J. Mol. Catal. A* **2004**, *214*, 161–165; h) C. Wei, C.-J. Li, *J. Am. Chem. Soc.* **2003**, *125*, 9584–9585; i) C. Wei, Z. Li, C.-J. Li, *Org. Lett.* **2003**, *5*, 4473–4475; j) B. Jiang, Y.-G. Si, *Tetrahedron Lett.* **2003**, *44*, 6767–6768; k) C. Koradin, N. Gommermann, K. Polborn, P. Knochel, *Chem. Eur. J.* **2003**, *9*, 2797–2811; l) C. Wei, C.-J. Li, *J. Am. Chem. Soc.* **2002**, *124*, 5638–5639; m) C.-J. Li, C. Wei, *Chem. Commun.* **2002**, 268–269; n) C. Koradin, K. Polborn, P. Knochel, *Angew. Chem.* **2002**, *114*, 2651–2654; *Angew. Chem. Int. Ed.* **2002**, *41*, 2535–2538; o) H. Z. S. Huma, R. Halder, S. S. Kalra, J. Das, J. Iqbal, *Tetrahedron Lett.* **2002**, *43*, 6485–6488; p) C. Fischer, E. M. Carreira, *Org. Lett.* **2001**, *3*, 4319–4321.

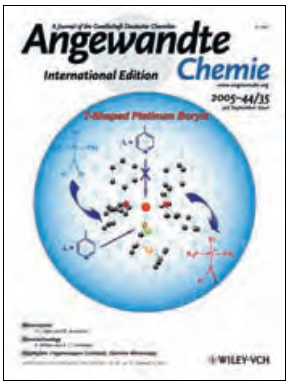
[9] For recent examples, see: a) F. Diaba, C. L. Houerou, M. Grignon-Dubois, B. Rezzonico, P. Gerval, *Eur. J. Org. Chem.* **2000**, 2915–2921; b) F. Diaba, I. Lewis, M. Grignon-Dubois, S. Navarre, *J. Org. Chem.* **1996**, *61*, 4830–4832.

[10] Recently, we developed a synthetic method for 1,2-dihydroisoquinoline derivatives in the presence of a bis-π-allylpalladium catalyst: M. Ohtaka, H. Nakamura, Y. Yamamoto, *Tetrahedron Lett.* **2004**, *45*, 7339–7341.

[11] The asymmetric version of the present reaction was investigated briefly. The reaction of **1** with nitromethane was carried out in the following catalytic systems; $Cu(OTf_2)$–(*R*)-(+)-2,2′-isopropylidenebis-(4-phenyl-2-oxazoline), $Cu(OTf_2)$–2,2′-isopropylidenebis[(4S)-4-*tert*-butyl-2-oxazoline], $Cu(OTf_2)$–2,6-bis[(4*S*)-(−)-isopropyl-2-oxazolin-2-yl]pyridine, and AgOTf–(*R*)-(+)-2,2′-bis(diphenylphosphanyl)-1,1′-binaphthalene. The reaction gave **2** in good yields, but the enantioselectivities were very low (≈1% *ee*).

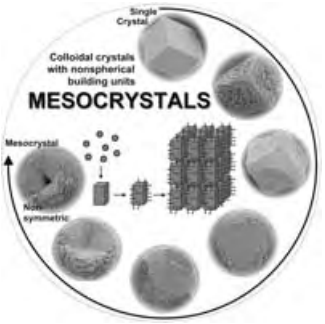
 © 2005 Wiley-VCH Verlag GmbH & Co. KGaA, Weinheim

Cover Picture



Holger Braunschweig,* Krzysztof Radacki, Daniela Rais, and David Scheschkewitz

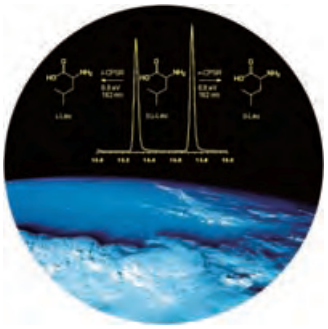
Cationic T-shaped platinum complexes are obtained because of the high *trans* influence of the ferrocenyl(bromo)boryl ligand. Addition of 4-methylpyridine to the platinum(II) boryl complex (as shown in the cover picture) causes displacement of the bromide ion at boron, leading to a cationic platinum complex with a 4-methylpyridine-stabilized borylene ligand (bottom right). For more information on this approach, see the Communication by H. Braunschweig et al. on page 5651 ff.



Mesocrystals
The formation and morphogenesis of mesocrystals apparently contradict the classical textbook knowledge on crystallization. This new type of colloidal crystals is discussed by H. Cölfen and M. Antonietti in their Review on page 5576 ff.



Organic Nanomaterials
One of the central roles of current materials research is a technology based on functional single molecules or small ensembles of molecules. The latest research is described by K. Müllen and A. C. Grimsdale in their Review on page 5592 ff.



Homochirality
U. Meierhenrich, L. Nahon et al. show in their Communication on page 5630 ff. that irradiation of solid D,L-leucine probes with right circularly polarized synchrotron radiation results in an enantiomeric excess of D-leucine.

Who Is Going To Read all This?

DOI: 10.1002/anie.200502730

Samuel Taylor Coleridge (the 18th century poet, critic, philosopher, and opium abuser) is said to have been the last man "to have read everything". Today it is no longer possible for scientists to even read everything (carefully) that is published in their own field, let alone in their discipline. As a result the questions of quality and selection of information become ever more pressing, and electronic search machines can only help a little. When we read a newspaper or watch a news program we want to be sure that the most important information is given quickly and reliably, it is no use finding out later which news was important and which was not. And it would be no help to put the news media to one side and to go directly to the vast amount of information that is made available by the news agencies, we would drown in information and in most cases we would lack the competence to differentiate important and right from unimportant and false.

The same situation exists in science. Today it is certainly possible to make all the research results (including all the raw data) of all scientists available without further selection or improvement as soon as the author has placed the last full stop. In chemistry alone this approach would give far in excess of the approximately 700000 articles currently covered per year by *Chemical Abstracts*[1] because, without barriers and filters, the manuscript output would increase unabated. Even using electronic search engines with stringently selected criteria would still deliver an immense amount of information, you would still have to sort and select yourself. And if, for the sake of curiosity, you wanted to inform yourself about developments in neighboring disciplines, you would be helplessly lost in an ocean of information.

The possibility of having a genuine and uncensored view of all information is one of the basic pillars of a democratic, enlightened society and in this point scientists see themselves as the avant-garde of such a society. However practicalities can not be ignored: Selection is necessary, more than ever! The main burden of responsibility lies with the authors, then with the publishers and editors, and finally, but also very importantly with the referees. The authors are the source of scientific information, and the others decide what information readers can find where; of course, scientists can be authors, editors, and referees all at the same time, but naturally all these roles can not be assumed for the same manuscript.

Selection is necessary, more than ever!

Authors: Their number has increased dramatically again in recent years because with China a new scientific giant has emerged onto the stage. In addition, the productivity of scientists has increased remarkably in the last two decades. Twenty years ago an X-ray structure analysis could take months, today it is usually a matter of hours. A similar trend is true across the whole breadth of instrumental analysis, and the productivity of computer chemists has without doubt risen at an even faster rate. Today, the rate-limiting step in chemistry seems no longer to be obtaining new scientific results, or their publication, but the writing of manuscripts. The high scientific productivity, which is not to be confused with an increase in knowledge, leads to an enormous pressure to publish. This pressure is increased further through the competition for positions, funding, and prizes. Today, authors must publish frequently and publish in respected journals. The quality of a journal is currently all to often reduced to "one with a high impact factor". The pressure of publishing lots has led to the search for the "Lowest Publishable Unit" (LPU) with a consequence that journals are flooded with "low-content/low-quality manuscripts". The hankering after the high impact factor has resulted in many authors giving up a healthy amount of self criticism and sending their manuscript first to a journal in which it has no chance of being accepted. This ideology is already producing fruit as can be seen

... Our manuscript was evaluated by three referees.

Referee 1 finds the work is important and recommends publication to Angewandte Chemie (**IF = 9.16**) after minor revision.

Referee 2 finds the scope of the work is directed to a journal such as Crystal growth and design (**IF = 2.74**)

Referee 3 finds the work of high quality and complements the authors, and feels that it would be a pity not to publish in its actual form. He or she recommends publication in Inorganic Chemistry. (**IF = 3.38**).

We were pleased to read that you spoke with Dr. Karen Hindson and recommended our paper for publication. However I would like to draw your attention that if you add up the values of the IF's of the three journals cited above and then divide by three you will obtain a value of **IF = 5.09**. The closet journal to this value would be *Chemistry A. European Journal*. (**IF = 4.517**). I therefore gently ask you to accept our paper in *Chemistry A. European Journal*, since you are the Editor in Chief...

InterScience
© 2005 Wiley-VCH Verlag GmbH & Co. KGaA, Weinheim

in the following: An author had a manuscript rejected from *Angewandte Chemie* after the assessment of three scientists. Deputy Editor Neville Compton recommended publication in the *European Journal of Inorganic Chemistry* (the editor of which is Karen J. Hindson) and shortly afterwards received a letter containing the passage reproduced on the previous page.

Clearly not only science administrators but also more and more scientists themselves are taking a completely uncritical view of impact factors. Naturally, journal impact factors can give a general impression about the importance of a journal and its articles, but very little about the quality of an individual article.

Angewandte Chemie
Impact Factor 2004: 9.161
Immediacy Index 2004: 1.966

How often an article is cited depends on many factors: Most important, is the number of researchers currently working on that topic; articles on unfashionable or highly specialized topics, which can certainly be or become very important, are naturally less cited than articles on current, main-stream research. *Angewandte Chemie* publishes articles from the full spectrum of chemistry and thus highly cited articles and less cited articles can stand side by side. The journal's very high impact factor, which increased still further in 2004 (Figure 1), should certainly not be interpreted as indicating that all the articles in *Angewandte Chemie* have the same "impact" or even the same quality—the most cited are perhaps not the most important. Authors should however use the high impact factor to decide, before they submit a manuscript, if their manuscript complies with the high expectations of the journal and its readers. In 2005, *Angewandte Chemie* once again has to cope with a huge increase in the number of manuscripts submitted. In the first six months alone we received 2069 Communications, which is nearly 30% more than in the first six months of 2004. This growth in submissions comes not only from China, but from almost all regions

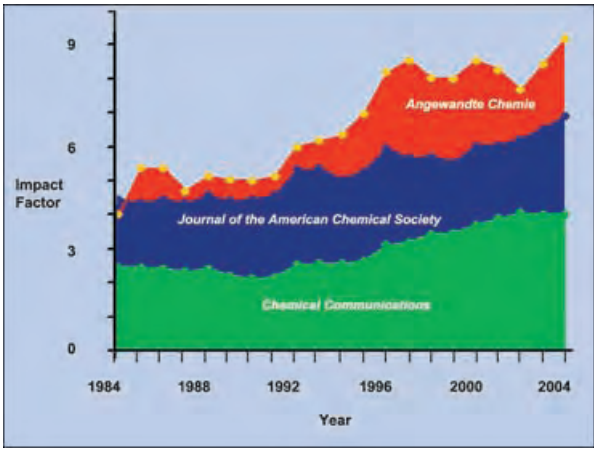


Figure 1. Impact factors of three important chemistry journals. The impact factors are determined by the Institute of Scientific Information (ISI); see http://www.isiknowledge.com

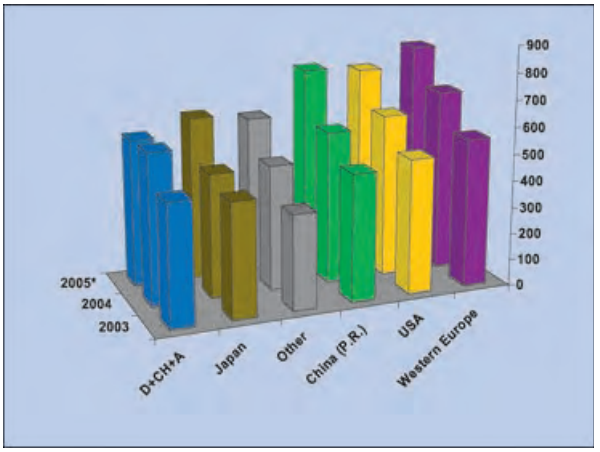


Figure 2. Country or region of origin for Communications submitted to *Angewandte Chemie* in 2003–2005. The values for 2005 are extrapolated on the basis of the first six months.

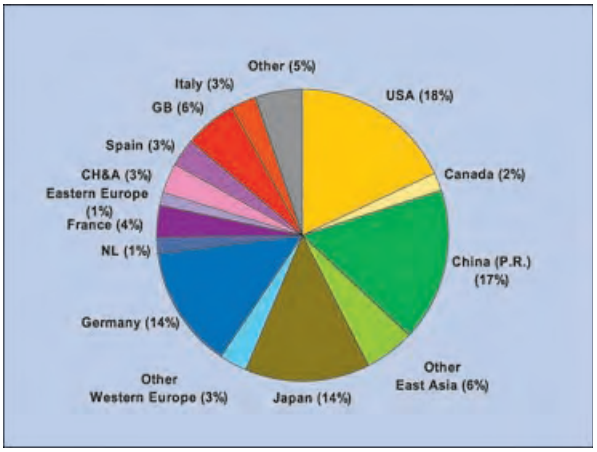


Figure 3. Country or region of origin for Communications submitted to *Angewandte Chemie* in 2004.

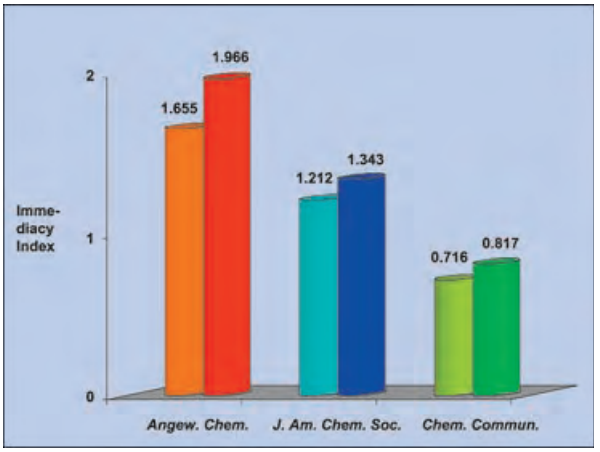


Figure 4. Immediacy indices 2003 and 2004; see http://isiknowledge.com

© 2005 Wiley-VCH Verlag GmbH & Co. KGaA, Weinheim



Dr. Neville Compton



Dr. Haymo Ross



Dr. Frank Maaß



Dr. José Oliveira



Dr. Guy Richardson



Dr. Diane Smith

of the world (see Figure 2). The land of origin for the submitted Communications in 2004 is shown in Figure 3. Currently, nearly 70% of submitted Communications are rejected, though the rejection rate for manuscripts from individual countries varies from 40% to 90%. We would be delighted if the high impact factor led to better journal selection by the authors.

Publishers and Editors (and their advisors from Editorial Boards etc.) are in the front line in dealing with the manuscript flood, and for most journals the selection occurs in several stages: At *Angewandte Chemie* around 10% of manuscripts are rejected immediately (and this figure is increasing), all the others are selected after refereeing. Controlling the manuscript flood requires ever more skilled and trained personnel. The fate of manuscripts and the selection of referees is determined by me, the two Deputy Editors, Neville Compton (Inorganic Chemistry) and Haymo Ross (Organic Chemistry), and four Senior Associate Editors, Frank Maass (Inorganic Chemistry), José Oliveira (Organic Chemistry), Guy Richardson (Inorganic Chemistry), and Diane Smith (Supramolecular Chemistry). All these editors have Doctorates in their specialist areas and in most cases postdoctoral research experience as well as many years experience as full-time editors. We select manuscripts in the interests of our readers—when our readers open an issue or look at Early View articles on the computer screen they should have the guarantee that they are reading something important and not wasting any time. "You've got to feel the heat when you read a journal" Peter Dervan, a member of the International Advisory Board of *Angewandte Chemie* once remarked.

Editors can make mistakes, and in the eyes of authors, almost every rejection is a mistake. However, a rebuttal should only follow if the decisive referee comments are inaccurate or wrong. When it is "only" a difference of opinion on the importance of an article then a rebuttal is usually rejected immediately. The decisions of editors are not based just on the simple mathematics of addition, that is, the receipt of one positive and one negative report does not mean that a third referee must be consulted. Not all referee reports are equally good. After reading the manuscript and the reports (or the only report in some cases) the editors in most cases are quite capable of deciding on the fate of a manuscript. In any case the decision has always to be justified if a member of the Editorial Board or the International Advisory Board asks for this.

Referees are naturally extremely important in the selection process. Working together, editors and referees are able to avoid making unjust and incorrect decisions. In the refereeing phase the system is placed under further pressure: Not only the pressure to publish lots in respected journals, but also the demand to publish quickly. Authors want to see their manuscripts published as fast as possible, even if the collection of the results took years and there is no competition on the horizon. Journals want to be the fastest, "instant publishing" seems to be desired. Referees complain that they have too many manuscripts to assess, and teaching, lectures, and administration can not wait. After the LPU comes the MRR (minimalistic referee report). Many reports for *Angewandte Chemie* demonstrate the expertise of the referees and the desire to help the authors even if the manuscript is recommended for publication in another journal. Regretfully, however, many of these manuscripts are then sent on to the next best journal without improvements—and the same referees might see it again and react accordingly. The refereeing load for *Angewandte Chemie* was carried by over 2000 scientists in the first half of 2005, although of these, round a half gave only one report in the six months. However, in this time 27 referees also had over 10 manuscripts to review (see Table 1). I would like to thank all our referees for their continued support and advice.

Table 1: Number of reports per referee for *Angewandte Chemie* in the first six months of 2005.

Referees	Reports
1	≥20
2	19–15
24	14–10
176	9–5
148	4
243	3
436	2

Several years ago, the then Editor in Chief of the *Journal of the American Chemical Society*, Allen J. Bard wrote that "quality should never be sacrificed for speed". There is no reason to change this view today. That in the first six months of 2005 we have been able to reduce publication times from first receipt to online publication for *Angewandte Chemie* from, on average 150 days to 110 days, has been made possible through the enormous efforts of the editorial staff and the decision that all manuscripts should be published online in the Early View mode as soon

© 2005 Wiley-VCH Verlag GmbH & Co. KGaA, Weinheim

as the corrections from the galley proofs have been incorporated. Many Communications are published (after critical refereeing and careful editing) within three months of submission, and when "danger is looming" in the form of competition, then manuscripts of high-enough quality can even be published in days. Instant publishing is not magic, with current technology any publisher can do it, it is the quality of the manuscript that makes the difference. Through fast publication (and high impact factors) most people forget that what is actually important is that the manuscript is promptly read by many and that its content is used rapidly and productively. A high immediacy index indicates these tendencies; its development from 2003 to 2004 is shown in Figure 4.

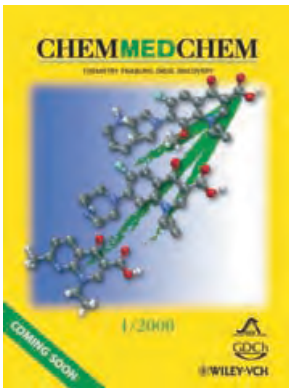
Chemistry creates new structures
Angewandte Chemie ***recognizes new structures***

"Chemistry creates new structures" is the motto of the Annual Conference of the Gesellschaft Deutscher Chemiker (German Chemical Society, GDCh) which takes place this year, September 11–14 in Düsseldorf. The excellent program helps, just like every issue of *Angewandte Chemie*, to recognize new structures. To help our readers see the trees *and* the wood, to ensure they do not miss important work in their own field, *and* to help them recognize the big discoveries in Chemistry, is what we aim to do.



Dr. Peter Gölitz

PS: As occasionally in the past, there is a new journal to introduce, which, with the help of *Angewandte Chemie*, should have a successful start. Following on from *ChemBioChem* (www.chembiochem.org) and *ChemPhysChem* (chemphyschem.org) comes *ChemMedChem* (www.chemmedchem.org). The Societá Chimica Italiana (SCI) will close its journal *Il Farmaco* at the end of the year and, from 2006, in conjunction with the GDCh and the publishers Wiley-VCH, will launch *ChemMedChem*.



The new journal, which will offer a European forum for articles from the whole world, will be dedicated to all aspects of drug discovery, with medicinal chemistry in the foreground. From bioinformatics and relevant chemical biology and molecular biology through to combinatorial chemistry, drug targeting, and toxicology a broad pallet of relevant articles (reviews and original research articles) will be presented. High quality is assured by the Editorial Board and the International Advisory Board which are headed by Professors R. Metternich (Schering, Berlin) and G. Tarzia (Università degli Studi di Urbino, Italy)

[1] L. R. Garson, *Acc. Chem. Res.* **2004**, *37*, 141 – 148.

© 2005 Wiley-VCH Verlag GmbH & Co. KGaA, Weinheim

VIP *The following Communications have been judged by at least two referees to be "very important papers" and will be published online at www.angewandte.org soon:*

*S. Majd, M. Mayer**
Hydrogel-Stamping of Arrays of Supported Lipid Bilayers with Various Lipid Compositions for Screening of Drug–Membrane and Protein–Membrane Interactions

*Y. Ishibashi, Y. Bessho, M. Yoshimura, M. Tsukamoto, M. Kitamura**
Origin of the Minor Enantiomeric Product in a Noyori Asymmetric Hydrogenation

H. Braunschweig, T. Herbst, D. Rais, F. Seeler*
Synthesis of Borirenes by Photochemical Borylene Transfer from $[(OC)_5M{=}BN(SiMe_3)_2]$ (M = Cr, Mo) to Alkynes

*Y. A. Yang, H. Wu, K. R. Williams, Y. C. Cao**
Synthesis of CdSe and CdTe Nanocrystals without Precursor Injection

*M. Nihei, M. Ui, M. Yokota, L. Han, A. Maeda, H. Kishida, H. Okamoto, H. Oshio**
Two-Step Spin Conversion in a Cyanide-Bridged Ferrous Square

S. F. Brady, J. Clardy*
Cloning and Heterologous Expression of Isonitrile Biosynthetic Genes from Environmental DNA

News

The Adolf von Baeyer Medal for A. de Meijere ____ 5554

The Karl Ziegler Prize for M. Reetz 5554

Bredereck Prize Goes to H.-A. Wagenknecht ____ 5554

August Wilhelm von Hofmann Medal Awarded to R. H. Grubbs and R. R. Schrock ____ 5555

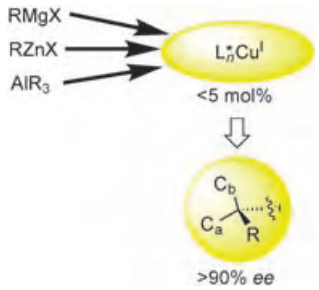
H. Vahrenkamp Receives Wilhelm Klemm Award ____ 5554

Arfvedson–Schlenk Prize Goes to D. Stalke ____ 5555

Meeting Reviews

Organometallics at Lake Geneva
H. Butenschön ____ 5556

Highlights

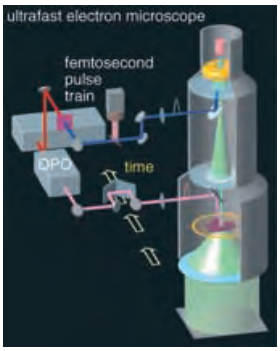


The organocopper craftsman's toolset is nearly complete with recent advances in ligand-based catalytic organocopper chemistry, which make viable enantioselective 1,4-conjugate additions and S_N2' substitutions of allylic halides using Grignard, RZnCl, and organoaluminum reagents (see scheme) at low loadings of copper(I) salts.

Organometallic Chemistry

S. Woodward* ____ 5560 – 5562

Organocopper for the Craftsman Cunning at His Trade



Ultrafast electron microscopy is a versatile technique that allows images and diffraction patterns of crystalline and amorphous materials as well as images of biological cells to be measured (see picture). Advances in the domain of time-resolved electron microscopy and the potential of the technique in various applications are discussed.

Electron Microscopy

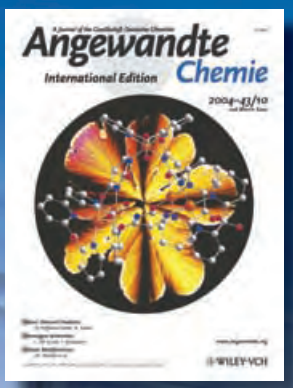
J. M. Thomas* ____ 5563 – 5566

A Revolution in Electron Microscopy

© 2005 Wiley-VCH Verlag GmbH & Co. KGaA, Weinheim

The best in chemistry –

for more than a hundred years



A Journal of the Gesellschaft Deutscher Chemiker

Angewandte
International Edition **Chemie**

www.angewandte.org

1888: ***The beginning of a success story***

Constant Innovations

1962: *First issue of the International Edition*
1976: *Graphical abstracts*
1979: *Cover pictures*
1988: *Centenary of Angewandte*
1989: *Routine use of color*
1991: *New section: Highlights*
1992: *Computerized editorial tracking system*
1995: *Internet service for readers*
1998: *Regular press service; full-text online*
2000: *New section: Essays; EarlyView: Communications available online ahead of the printed version*
2001: *New section: Minireviews*
2002: *Online submission of manuscripts*
2003: *Weekly publication; new section: News; new layout*
2004: *Backfiles (1962-1997); ManuscriptXpress: Online system for authors and referees*



Angewandte's advisors...

Manfred Reetz
Max-Planck-Institut für Kohlenforschung, Mülheim

*» **Angewandte Chemie** is extremely well-balanced in providing various types of information to the academic and industrial chemical community. If you inadvertently miss an issue, the mishap will catch up with you sooner or later. «*

Angewandte Chemie International Edition *is a journal of the German Chemical Society (GDCh)*

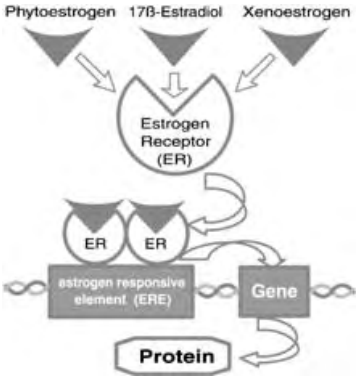
GDCh

WILEY InterScience® DISCOVER SOMETHING GREAT

WILEY-VCH

1188104_gu

Essays



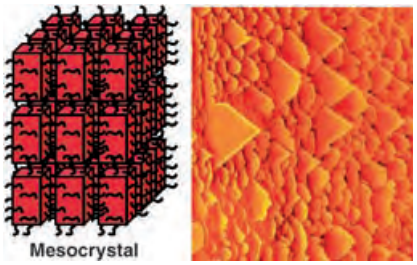
Horror scenarios have been conjured up, but how harmful, really, are the hormone-like compounds with which we come into contact daily in food, medications, and sunscreens? A xenobiotic can compete with a hormone at the hormone receptor and even block its action, as the picture shows for the estrogen receptor. To cause an observable effect, however, the potency and concentration of the xenobiotic must be sufficiently high, which fortunately is rarely the case.

Endocrine-Disrupting Substances

H. Greim* ——— **5568 – 5574**

Chemicals with Endocrine-Disrupting Potential: A Threat to Human Health?

Reviews

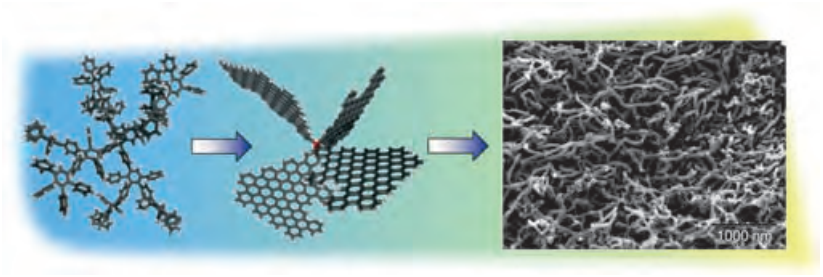


Nonclassical Crystallization: Mesocrystals are superstructures of well-aligned nanoparticles, which exhibit common outer faces on the mm or μm scale (see picture, right: SEM image of DL-alanine). They are usually built up from nonspherical nanoparticles which allows for further degrees of orientational freedom so that only very little is known about mesocrystal formation. Mesocrystals are examples of nonclassical crystallization, which were only recently discovered.

Mesocrystals

H. Cölfen,* M. Antonietti — **5576 – 5591**

Mesocrystals: Inorganic Superstructures Made by Highly Parallel Crystallization and Controlled Alignment



Smaller and better: Thanks to recent progress in organic nanomaterials, functional building blocks based on single molecules or small ensembles of molecules are no longer just the realm of science fiction, but are a realistically attainable goal. The picture shows the different organization steps of functional molecules, from a dendrimer, to a "nanopropeller", to nanotubes.

Nanotechnology

A. C. Grimsdale, K. Müllen* **5592 – 5629**

The Chemistry of Organic Nanomaterials

For the USA and Canada:
ANGEWANDTE CHEMIE International Edition (ISSN 1433-7851) is published weekly by Wiley-VCH PO Box 191161, D 69451 Weinheim, Germany. Air freight and mailing in the USA by Publications Expediting Inc. 200 Meacham Ave., Elmont, NY 11003. Periodicals postage paid at Jamaica NY 11431. US POSTMASTER: send address changes to *Angewandte Chemie*, Wiley-VCH, 111 River Street, Hoboken, NJ 07030. Annual subscription price for institutions: US$ 4948.00/4498.00 (valid for print and electronic / print or electronic delivery); for individuals who are personal members of a national chemical society, or whose institution already subscribes, or who are retired or self-employed consultants, print only: US$ 394.00. Postage and handling charges included. All Wiley-VCH prices are exclusive VAT.

© 2005 Wiley-VCH Verlag GmbH & Co. KGaA, Weinheim

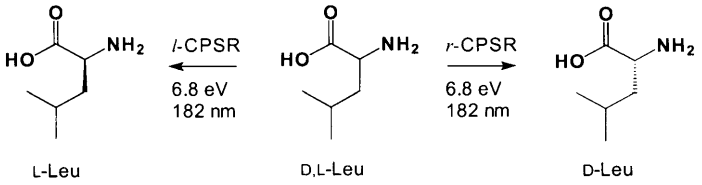
Contents

Communications

Homochirality

U. J. Meierhenrich,* L. Nahon,* C. Alcaraz, J. H. Bredehöft, S. V. Hoffmann, B. Barbier, A. Brack _____ 5630 – 5634

Asymmetric Vacuum UV Photolysis of the Amino Acid Leucine in the Solid State



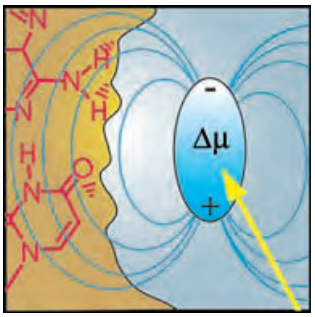
One hand clapping: Based on solid-state circular dichroism data, the leucine (π^*, π_1)-electronic transition is excited with right circularly polarized synchrotron radiation (*r*-CPSR) at 182 nm (see scheme). This treatment induced an enantiomeric excess of 2.6% of D-leucine. The results support the assumption that interstellar asymmetric photoreactions are capable of inducing significant enantiomeric enrichments in solid-state amino acids.

Femtosecond Spectroscopy

J. L. Pérez Lustres, S. A. Kovalenko, M. Mosquera, T. Senyushkina, W. Flasche, N. P. Ernsting* _____ 5635 – 5639

Ultrafast Solvation of *N*-Methyl-6-quinolone Probes Local IR Spectrum

A molecular dipole field (see picture) is created by femtosecond excitation of the title compound, and the response of the environment is observed by stimulated emission spectroscopy of the dye. Strong frequency modulation in the dynamic Stokes shift reflects coherent solvent motion. The IR spectrum of the solvent is related quantitatively to the experiment by dielectric continuum theory.

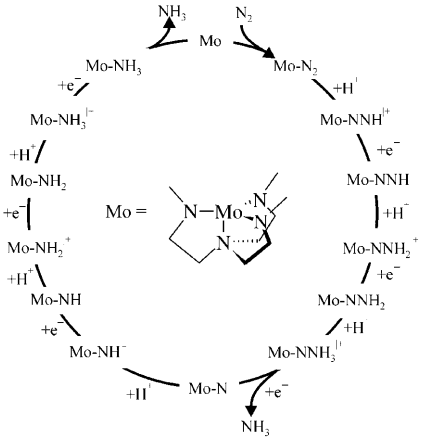


Nitrogenase Models

F. Studt, F. Tuczek* _____ 5639 – 5642

Energetics and Mechanism of a Room-Temperature Catalytic Process for Ammonia Synthesis (Schrock Cycle): Comparison with Biological Nitrogen Fixation

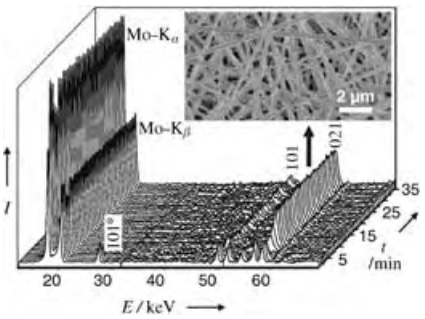
The transformation of N_2 to $2\,NH_3$ on a Mo^{III} complex containing a sterically shielding triamidoamine ligand is investigated with the help of DFT calculations, providing the energy profile and mechanism of the first truly catalytic process of ammonia synthesis working under ambient conditions and proceeding via well-defined intermediates (see catalytic cycle). It is shown that ammonia synthesis with this artificial system works with an energy expenditure comparable to that of biological nitrogen fixation.



Hydrothermal Synthesis

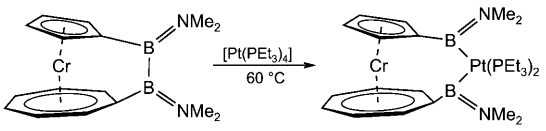
A. Michailovski, J.-D. Grunwaldt, A. Baiker, R. Kiebach, W. Bensch, G. R. Patzke* _____ 5643 – 5647

Studying the Solvothermal Formation of MoO_3 Fibers by Complementary In Situ EXAFS/EDXRD Techniques



Just a minute: The hydrothermal formation of fibrous MoO_3 is monitored with complementary in situ methods. The quantitative formation is complete within a few minutes, as shown by in situ EDXRD investigations (see picture: time-dependent powder diffractograms at 120 °C). A special in situ EXAFS cell permits the simultaneous observation of the solid and the liquid phase, thereby providing key information about the growth mechanism of the MoO_3 rods.

© 2005 Wiley-VCH Verlag GmbH & Co. KGaA, Weinheim

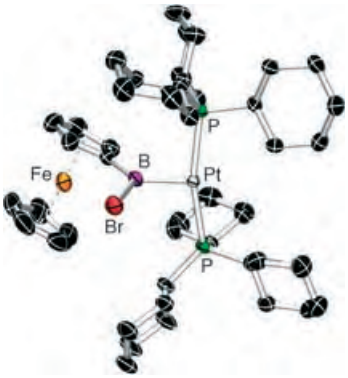


Chromium sandwich with "handles": A [2]boratrochrocenophane with diboron bridges was synthesized and oxidatively added to $[Pt(PEt_3)_4]$. The resulting [3]boraplatinatrochrocenophane, which is the first example of an *ansa*-[3]boraplatina sandwich complex, was characterized in solution and in the solid state.

Metallocenes

H. Braunschweig,* M. Lutz, K. Radacki ——— 5647 – 5651

Synthesis of *ansa*-[2]Boracyclopentadienylcycloheptatrienylchromium and Its Reaction to the *ansa*-Platinabis(boryl) Complex by Oxidative Addition of the Boron–Boron Bond



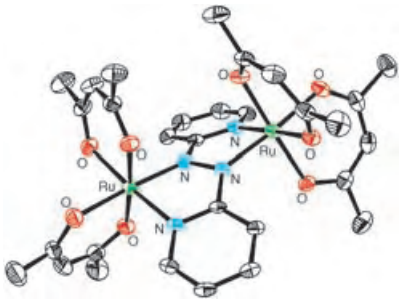
"T" time: A cationic, three-coordinate T-shaped platinum boryl complex (see structure) serves as the precursor to a cationic platinum complex featuring a base-stabilized borylene ligand.

Boron Ligands

H. Braunschweig,* K. Radacki, D. Rais, D. Scheschkewitz ——— 5651 – 5654

A T-Shaped Platinum(II) Boryl Complex as the Precursor to a Platinum Compound with a Base-Stabilized Borylene Ligand

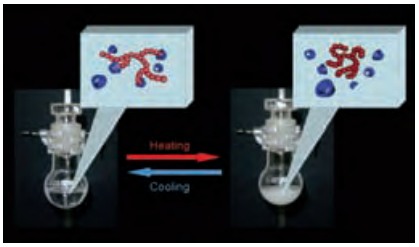
Valencies get remix: A unique kind of electronic structure $(M^{n+0.5})(\mu\text{-}L^{\bullet-})(M^{n+0.5})$ which was previously discussed only for metal–ligand charge-transfer (MLCT) excited states is established structurally and by quantum chemical analysis for both *rac* (see picture) and *meso* isomers of $[(\mu\text{-abpy})\{Ru(acac)_2\}_2]$ (abpy = 2,2′-azobispyridine, $acac^-$ = acetylacetonate).



Mixed-Valent Complexes

B. Sarkar, S. Patra, J. Fiedler, R. B. Sunoj, D. Janardanan, S. M. Mobin, M. Niemeyer, G. K. Lahiri,* W. Kaim* ——— 5655 – 5658

Theoretical and Experimental Evidence for a New Kind of Spin-Coupled Singlet Species: Isomeric Mixed-Valent Complexes Bridged by a Radical Anion Ligand



Clearing things up. Hydrophobic polymers that undergo complex formation with β-cyclodextrin in aqueous solution display reversible thermosensitive solubility. Supramolecular effects lead to a new kind of LCST behavior (LCST = lower critical solution temperature), which is evident from clouding and clearing points at defined temperatures (see picture). The polymer was synthesized by free-radical polymerization of the complexed monomer in water.

Supramolecular Chemistry

S. Schmitz, H. Ritter* ——— 5658 – 5661

Unusual Solubility Properties of Polymethacrylamides as a Result of Supramolecular Interactions with Cyclodextrin

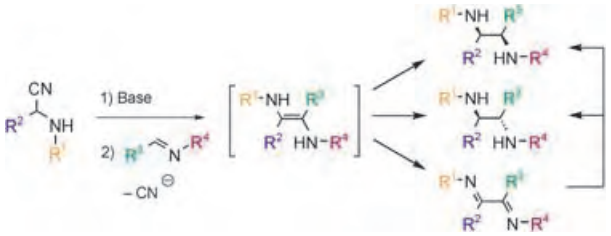
© 2005 Wiley-VCH Verlag GmbH & Co. KGaA, Weinheim

Contents

Cross-Couplings

C. Kison, N. Meyer,
T. Opatz* ——— **5662 – 5664**

An Aldimine Cross-Coupling for the Diastereoselective Synthesis of Unsymmetrical 1,2-Diamines

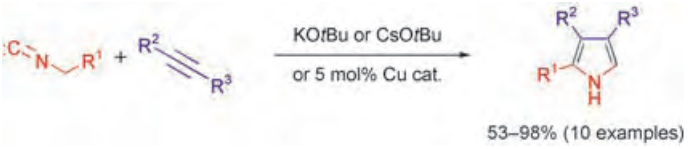


No protecting groups are required for the cross-coupling of *N*-monosubstituted α-aminonitriles with imines. Depending on the workup procedure, highly substituted unsymmetrical 1,2-diamines or 1,2-diimines can be prepared in a one-pot procedure. The diastereoselective reduction of the diimines furnishes either the *syn*- or the *anti*-configurated diamines (see scheme).

Heterocycles

O. V. Larionov,
A. de Meijere* ——— **5664 – 5667**

Versatile Direct Synthesis of Oligosubstituted Pyrroles by Cycloaddition of α-Metalated Isocyanides to Acetylenes

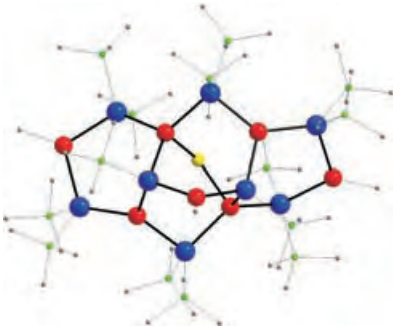


Acceptor-substituted pyrroles can be prepared from acetylenes and isocyanides in an efficient and direct manner by a formal cycloaddition under basic conditions or, even simpler, in the presence of catalytic amounts of nanosize copper powder or copper(I) benzenethiolate.

Organozinc Compounds

F. Thomas, S. Schulz,*
M. Nieger ——— **5668 – 5670**

Synthesis of Thermolabile Zinc–Pentel Compounds under Kinetically Controlled Reaction Conditions

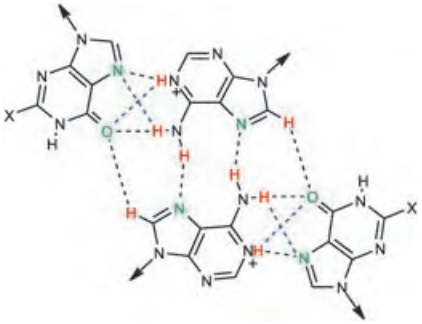


Base-stabilized aluminum–pentel compounds [(dmap)Al(Me$_2$)E(SiMe$_3$)$_2$] (dmap = 4-dimethylaminopyridine; E = P, As, Sb) are valuable reagents for the synthesis of zinc–pentel heterocycles of the type [{MeZnE(SiMe$_3$)$_2$}$_3$]. In addition, a novel Zn–Sb cluster was structurally characterized (see structure; blue Sb, red Zn, yellow Cl, green Si). The reactions proceed at low temperature, an essential factor for the synthesis of these thermolabile compounds.

Purine Quartets

P. Amo-Ochoa, P. J. Sanz Miguel, P. Lax, I. Alonso, M. Roitzsch, F. Zamora,*
B. Lippert* ——— **5670 – 5674**

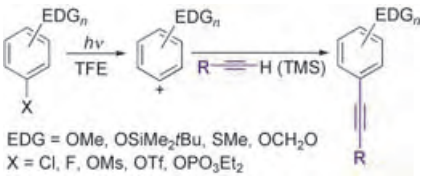
Models of Putative (AH)G(AH)G Nucleobase Quartets



Mispairs of protonated adenine and guanine (or hypoxanthine), AH$^+_{anti}$G/Hx$_{syn}$, can associate in various ways to give mixed purine quartets (see picture) as demonstrated by X-ray crystallography and ab initio calculations. The planar structure of such quartets implies that akin to established purine nucleobase quartets, these quartets could also play a role in natural DNA structures.

© 2005 Wiley-VCH Verlag GmbH & Co. KGaA, Weinheim

Photoheterolysis of aryl halides substituted with electron-donating groups (EDGs) or aryl esters in 2,2,2-trifluoroethanol (TFE) leads to phenyl cations, which can add to alkynes (see scheme, Tf = trifluoromethanesulfonyl). This reaction is an appealing metal-free alternative to the (sila)-Sonogashira reaction.

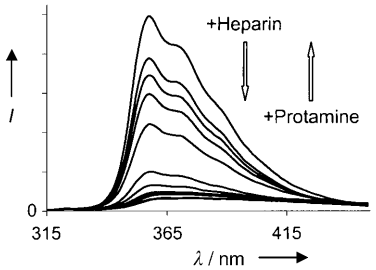


Addition Reactions

S. Protti, M. Fagnoni,*
A. Albini* ——— **5675 – 5678**

Photo-Cross-Coupling Reaction of Electron-Rich Aryl Chlorides and Aryl Esters with Alkynes: A Metal-Free Alkynylation

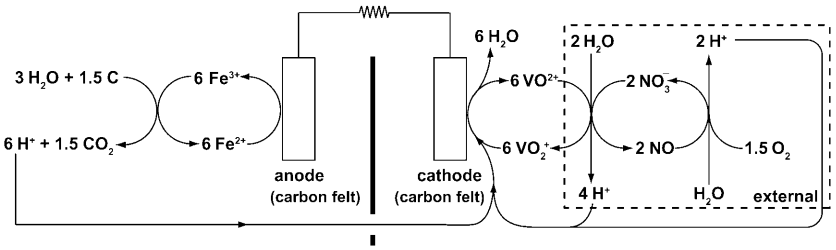
Excellent selectivity in highly competitive serum was displayed by a synthetic fluorescent receptor incorporating phenylboronic acid and ammonium groups for the therapeutic anticoagulant heparin. The concentration of heparin at clinically relevant dosing levels can be measured from the emission quenching. The binding is reversible as shown by the regeneration of the fluorescence on addition of protamine (see graph).



Molecular Recognition

A. T. Wright, Z. Zhong,
E. V. Anslyn* ——— **5679 – 5682**

A Functional Assay for Heparin in Serum Using a Designed Synthetic Receptor



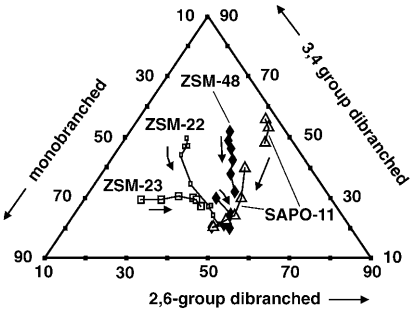
Redox Chemistry

D. B. Weibel, R. Boulatov, A. Lee, R. Ferrigno,
G. M. Whitesides* ——— **5682 – 5686**

Modeling the Anodic Half-Cell of a Low-Temperature Coal Fuel Cell

Mined over matter: The partial oxidation of sub-bituminous coal by Fe^{III} ions in 5 M H_2SO_4 at 100 °C was used in the anodic compartment in a prototype coal fuel cell, with a solution of VO_2^+/VO^{2+} in 5 M H_2SO_4 in the cathodic compartment (see scheme). The cell operated without loss of performance for 1000 h at 100 °C, with a maximum current density of 5 A L^{-1} and a power density of 0.6 W L^{-1}.

Slim through spatial constraints: A higher content of linear and monobranched propene trimers is obtained with ZSM-22 as catalyst than with many other zeolite catalysts (see picture). This is explained by the constraints imposed by the diameter of the tubular pores of ZSM-22. ZSM-22 also brings an important environmental benefit compared with the presently used industrial catalyst silica-supported phosphoric acid.



Industrial Catalysts

J. A. Martens,* W. H. Verrelst, G. M. Mathys, S. H. Brown, P. A. Jacobs ——— **5687 – 5690**

Tailored Catalytic Propene Trimerization over Acidic Zeolites with Tubular Pores

© 2005 Wiley-VCH Verlag GmbH & Co. KGaA, Weinheim

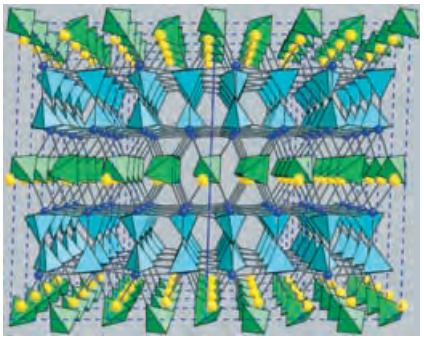
Contents

Phosphates

M. Nazaraly, G. Wallez, C. Chanéac, E. Tronc, F. Ribot,* M. Quarton, J.-P. Jolivet ——— **5691 – 5694**

The First Structure of a Cerium(IV) Phosphate: Ab Initio Rietveld Analysis of $Ce^{IV}(PO_4)(HPO_4)_{0.5}(H_2O)_{0.5}$

Layer apparent: Crystalline cerium(IV) phosphates have been studied for a long time as ion exchangers, but their structures have remained unknown. The structure of a cerium(IV) phosphate has been determined (see picture: tetrahedra PO_4, yellow Ce, blue O (water)) and clearly explains a notable feature of this compound, its inability to intercalate amines. The X-ray study is supported by solid-state NMR spectroscopy investigations.

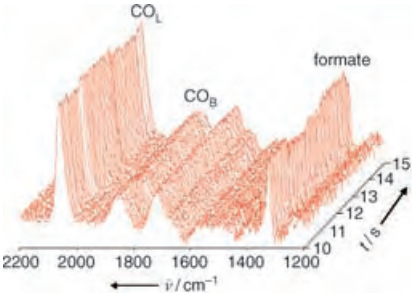


Electrochemical Oscillations

G. Samjeské, M. Osawa* ——— **5694 – 5698**

Current Oscillations during Formic Acid Oxidation on a Pt Electrode: Insight into the Mechanism by Time-Resolved IR Spectroscopy

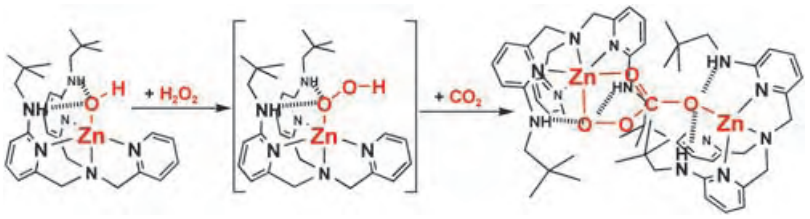
Revised model: Current oscillations in the electrooxidation of formic acid at a fixed potential can be observed by time-resolved surface-enhanced infrared absorption spectroscopy (see picture). Real-time probing of the reaction dynamics on the electrode surface provides new insight into the oscillations that are not accessible by conventional techniques. The reaction mechanism involves adsorbed formate as a reactive intermediate.



Bioinorganic Chemistry

A. Wada, S. Yamaguchi, K. Jitsukawa, H. Masuda* ——— **5698 – 5701**

Preparation of a Hydroperoxo Zinc(II) Intermediate

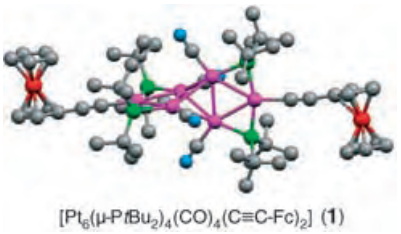


Three legs and four teeth: The tripodal tetradentate ligand bis[(6-neopentylamino-2-pyridyl)methyl][(2-pyridyl)methyl]amine (H_2bnpa) was used to prepare a novel {Zn—OOH} species. The intermediate of the reaction of $[Zn(H_2bnpa)(OH)]^+$ with H_2O_2 (see scheme) was characterized by a combination of ^{1}H NMR spectroscopy and ESI mass spectrometry; further treatment with CO_2 gave $[\{Zn^{2+}(H_2bnpa)\}_2(CO_4^{2-})](ClO_4)_2$.

Electron Transfer

A. Albinati, F. Fabrizi de Biani, P. Leoni,* L. Marchetti, M. Pasquali, S. Rizzato, P. Zanello* ——— **5701 – 5705**

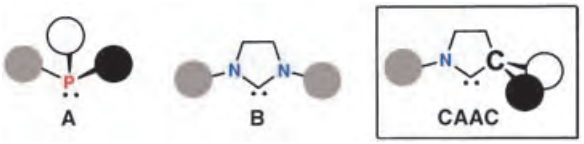
Redox Control of Light-Induced Platinum-Cluster-to-Iron Charge Transfer in a Bis(ferrocenylethynyl)-Substituted Hexanuclear Platinum Derivative



$[Pt_6(\mu\text{-}PtBu_2)_4(CO)_4(C{\equiv}C\text{-}Fc)_2]$ (**1**)

Give and take: Compound **1** (see structure: purple Pt, red Fe, green P, blue O; Fc = [(η-C_5H_5)Fe(η-C_5H_4)]) is prepared in good yields by the CuI-catalyzed coupling of two equivalents of ethynylferrocene with the hexanuclear cluster $[Pt_6(\mu\text{-}PtBu_2)_4(CO)_4Cl_2]$. Electrochemical and spectroelectrochemical data show the presence of photoelectrochemically triggered electron transfer from the $\{Pt_6\}$ core to the peripheral ferrocenyl subunits.

© 2005 Wiley-VCH Verlag GmbH & Co. KGaA, Weinheim



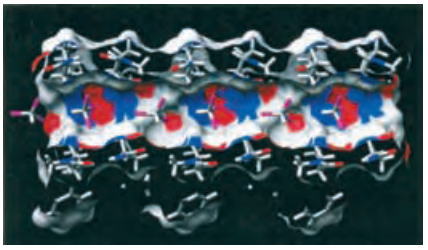
Like NHCs? Not quite: Cyclic (alkyl)(amino)carbenes (CAACs) are strong σ-donors and have steric environments that differ dramatically from those of bulky, electron-rich phosphines (**A**) and cyclic diaminocarbenes (**B**). These readily available carbenes are desirable ligands for catalysis, as illustrated by the first palladium-mediated α-arylation of ketones and aldehydes with non-activated aryl chlorides at ambient temperature.

Homogeneous Catalysis

V. Lavallo, Y. Canac, C. Präsang, B. Donnadieu, G. Bertrand* **5705 – 5709**

Stable Cyclic (Alkyl)(Amino)Carbenes as Rigid or Flexible, Bulky, Electron-Rich Ligands for Transition-Metal Catalysts: A Quaternary Carbon Atom Makes the Difference

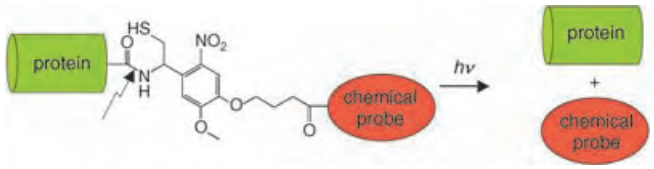
Cyclic peptides can dimerize through β-sheet-like hydrogen bonding. Heterodimerization is favored over homodimerization, which creates interesting combinatorial possibilities without detriment to the functionalization of amino acid side chains. These dimers represent a new class of self-assembling peptide nanotubes in which the hydrophobicity of the internal cavity (see picture) can be controlled.



Peptide Nanostructures

R. J. Brea, M. Amorín, L. Castedo, J. R. Granja* **5710 – 5713**

Methyl-Blocked Dimeric α,γ-Peptide Nanotube Segments: Formation of a Peptide Heterodimer through Backbone–Backbone Interactions

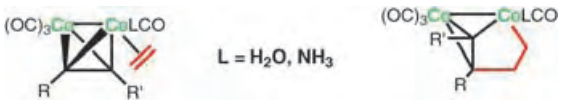


Design and light: A photocleavable synthetic moiety is ligated to the C terminus of a recombinant protein. In the ligated state, the chemical and protein components influence the properties of one another. Upon irradiation with light, both elements are released and their respective function is recovered. In this way a protein can be delivered into living cells and activated by UV irradiation at a desired time or location.

Photoactivatable Proteins

J.-P. Pellois, T. W. Muir* **5713 – 5717**

A Ligation and Photorelease Strategy for the Temporal and Spatial Control of Protein Function in Living Cells



Irreversiblity effect: The fundamental role of Lewis base promoters L in the Pauson–Khand reaction was studied by DFT calculations. Contrary to the currently held view, these promoters do not accelerate the departure of a second CO ligand from the acetylene dicobalt complex to create the requisite site for olefin coordination, but stabilize the olefin-insertion product (see scheme), so that product formation is essentially irreversible.

Reaction Mechanisms

C. Perez del Valle, A. Milet,* Y. Gimbert,* A. E. Greene **5717 – 5719**

Lewis Base Promoters in the Pauson–Khand Reaction: A Different Scenario

© 2005 Wiley-VCH Verlag GmbH & Co. KGaA, Weinheim

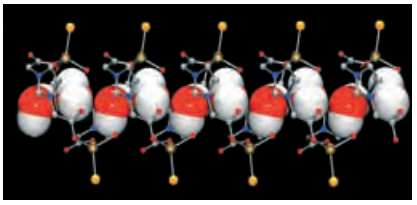
Contents

Coordination Polymers

Z. Fei, D. Zhao, T. J. Geldbach, R. Scopelliti, P. J. Dyson,* S. Antonijevic,* G. Bodenhausen ——— **5720 – 5725**

A Synthetic Zwitterionic Water Channel: Characterization in the Solid State by X-ray Crystallography and NMR Spectroscopy

Nanoscale plumbing: A zwitterionic, helical pipe of nanodimensions that contains a two-dimensional water chain (see picture; Br yellow, C gray, N blue, O red, H_{water} white, $H_{imidazolium}$ omitted) assembles from the reaction between zinc metal and *N*,*N*′-diacetic acid imidazolium bromide. A detailed study on the dynamics of the incorporated water molecules has been conducted by solid-state NMR spectroscopy.



VIP

Molecular Recognition

C. Li, S.-F. Ren, J.-L. Hou, H.-P. Yi, S.-Z. Zhu, X.-K. Jiang, Z.-T. Li* ——— **5725 – 5729**

F···H–N Hydrogen Bonding Driven Foldamers: Efficient Receptors for Dialkylammonium Ions

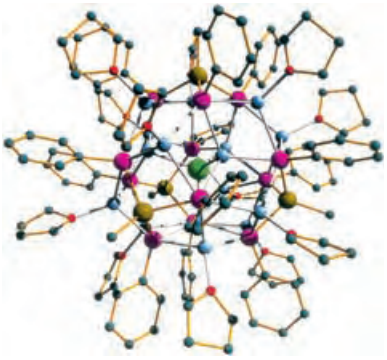


Intramolecular F···H–N hydrogen bonds have been utilized for the first time to construct a new series of foldamers from aromatic amides (see picture; $R^1 = H$, Me; $R^2 = CON(n\text{-}C_8H_{17})_2$). Moreover, the resulting crescent and helical architectures are good acceptors for binding dialkylammonium ions.

Cage Compounds

M. J. Duer, F. García, R. A. Kowenicki, V. Naseri, M. McPartlin, M. L. Stead, R. S. Stein, D. S. Wright* — **5729 – 5733**

Inverse Coordination of an Ionic Lattice by a Metal Host

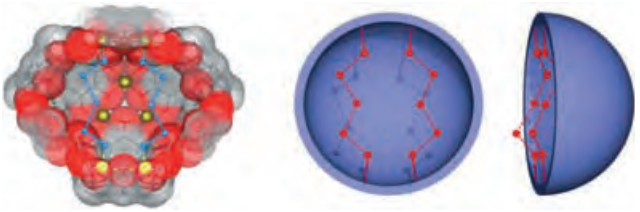


The solid-state structure of Li^+-$[\{MeAl(PPh)_3Li_4\}_4(\mu_4\text{-}Cl)(thf)_{12}]^-$ (see picture) dramatically illustrates the concept of lattice modification by "inverse" coordination of anions in an ionic lattice. A large change in the original NaCl-type lattice of LiCl results from the encapsulation of the Cl^- ions within heterometallic cages formed from four $[MeAl(PPh)_3Li_4]$ inverse ligands.

Molecular Capsules

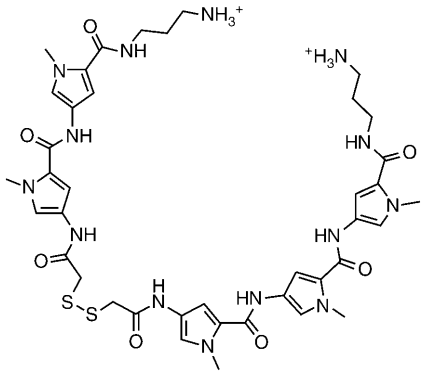
R. M. McKinlay, P. K. Thallapally, G. W. V. Cave, J. L. Atwood* **5733 – 5736**

Hydrogen-Bonded Supramolecular Assemblies as Robust Templates in the Synthesis of Large Metal-Coordinated Capsules



Uncommon water chain: A large neutral hexameric coordination cage $[Ga_{12}(H_2O)_{24}(C_{40}H_{42}O_{12})_6 \subset (acetone)_8(H_2O)_6]$ is assembled from six pyrogallol[4]arene ligands and twelve Ga^{III} ions. Found within the capsule structure are two pseudo-linear hydrogen-bonded water $(H_2O)_5$ chains (see picture, Ga gold, O red).

© 2005 Wiley-VCH Verlag GmbH & Co. KGaA, Weinheim



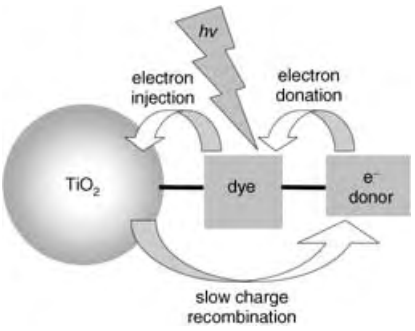
Reversible disulfide chemistry is used to identify ligands that stabilize either duplex or quadruplex DNA secondary structures from a dynamic combinatorial library of polyamide building blocks (example structure shown). Double-stranded DNA induces a larger amplification than quadruplex DNA, in accordance with the selectivity of the ligands for each DNA target.

Dynamic Combinatorial Chemistry

S. Ladame, A. M. Whitney, S. Balasubramanian* ——— **5736 – 5739**

Targeting Nucleic Acid Secondary Structures with Polyamides Using an Optimized Dynamic Combinatorial Approach

A trial separation: A dye-sensitized nanocrystalline TiO_2 film (see scheme) is prepared in which a remarkably long-lived (4 s) charge-separated state can be generated. The key parameter that controls charge transfer at the dye/TiO_2 interface is shown to be the spatial separation between the cation center of the dye and the electrode surface.



Supersensitizing Dyes

S. A. Haque,* S. Handa, K. Peter, E. Palomares, M. Thelakkat, J. R. Durrant ——— **5740 – 5744**

Supermolecular Control of Charge Transfer in Dye-Sensitized Nanocrystalline TiO_2 Films: Towards a Quantitative Structure–Function Relationship

Sources

Product and Company Directory

You can start the entry for your company in "Sources" in any issue of *Angewandte Chemie*.

If you would like more information, please do not hesitate to contact us.

Wiley-VCH Verlag – Advertising Department
Tel.: 0 62 01 - 60 65 65
Fax: 0 62 01 - 60 65 50
E-Mail: MSchulz@wiley-vch.de

Service

Keywords ——— *5746*

Authors ——— *5747*

Vacancies ——— *A53, A54*

Preview ——— *5749*

© 2005 Wiley-VCH Verlag GmbH & Co. KGaA, Weinheim



Awarded...

During its annual meeting between September 11 and 14, 2005 in Düsseldorf, the German Chemical Society (GDCh) will present numerous awards.

The Adolf von Baeyer Medal for A. de Meijere

Armin de Meijere (University of Göttingen, Germany) will be awarded the Adolf von Baeyer Medal. He will be recognized for his work with strained rings such as cyclopropane, for which he has become known as the "Lord of the Small Rings". His comprehensive chemistry with these strained compounds has led to the development of active agents and novel catalytic procedures. In *Chemistry—A European Journal*, for which he is a member of the editorial board, he recently reported the production of [D_{3d}]-octahedrane, the most stable $(CH)_{12}$ hydrocarbon.[1] De Meijere has literary versatility and is especially active in his capacity as an editor; his two-volume handbook of metal-catalyzed cross-coupling reactions, co-edited with F. Diederich, was published last year by Wiley-VCH.



A. de Meijere

De Meijere studied Chemistry at the Universities of Freiburg and Göttingen, and received his PhD in 1967 under the direction of W. Lüttke. He subsequently worked as a postdoc in the research group of K. B. Wiberg at Yale University in New Haven, Connecticut, USA. He returned to the University of Göttingen in 1969, where he obtained a habilitation in 1971. In 1974, he was named extraordinary professor and in 1977, he accepted a professorship at the University of Hamburg. He returned again to the University of Göttingen in 1989.

Bredereck Prize Goes to H.-A. Wagenknecht

The GDCh awards organic and bioorganic chemists working in the areas of hydrocarbons, heterocycles, nucleotides, and proteins with the Hellmuth Bredereck Endowment. This year, Hans-Achim Wagenknecht (Technical University of Munich, Germany) was honored for his research on charge-transfer mechanisms, the electronic properties of DNA, and the interactions of fluorescent probes in DNA. He recently reported in *Angewandte Chemie* the real-time spectroscopy and chemical probing of reductive electron transfer in DNA.[2]



H.-A. Wagenknecht

Wagenknecht studied Chemistry in Freiburg. He earned his PhD in 1998 in the group of W.-D. Woggon at the University of Basel from research with enzyme models and intermediates of the chloroperoxidase cycle. Over the following two years, he worked with J. K. Barton at the California Institute of Technology (Pasadena, USA). Since 2000 he has led a research group at the Institute for Organic Chemistry at the Technical University of Munich, where he obtained his habilitation in 2004 for his work on charge-transfer processes in DNA.

H. Vahrenkamp Receives Wilhelm Klemm Award

The GDCh gives out the Wilhelm Klemm Award for outstanding contributions to the field of inorganic chemistry. This year it went to Heinrich Vahrenkamp (University of Freiburg, Germany), in recognition of his work in organometallic chemistry. His past research interests dealt with electron transfer in multinuclear complexes, multinuclear carbonyl complexes, and in the potential application of coordination compounds as sensors and catalysts. His research group has focused more recently on the coordination chemistry and biological roles of zinc. Vahrenkamp recently reported on zinc thiolate complexes with tridentate ligands as models for thiolate alkylating enzymes.[3]

Vahrenkamp earned his PhD in 1967 on work with H. Nöth at the University of Munich, Germany, and worked as a postdoc with L. F. Dahl at the University of Wisconsin in Madison, USA. He received his 'habilitation' at the University of Munich in 1972. Since 1973 he has worked as a professor of inorganic chemistry at the University of Freiburg. From 1990 to 1997 he was co-editor of *Chemische Berichte*, one of the predecessors of the *European Journal of Inorganic Chemistry*.



H. Vahrenkamp

The Karl Ziegler Prize for M. Reetz

The Karl Ziegler Prize from the endowment of the same name is awarded by the GDCh in recognition of excellence in the field of inorganic and organic chemistry of catalysts and polymers. Manfred T. Reetz (Max Planck Institute for Coal Research in Mülheim/Ruhr) will receive the award for his work in test-tube evolution as a method for the generation of enantioselective biocatalysts and the development of new methods in asymmetric transition-metal catalysis. His recent report about a new method for expanding the substrate acceptance of



M. Reetz

InterScience
© 2005 Wiley-VCH Verlag GmbH & Co. KGaA, Weinheim

enzymes through a combinatorial active-site saturation test appears in *Angewandte Chemie*.[4]

Reetz studied at Washington University in St. Louis and the University of Michigan in Ann Arbor, USA. He received his PhD in 1969 at the University of Göttingen under the direction of U. Schöllkopf. He did his postdoctoral research with R. W. Hoffmann at the University of Marburg, where he earned his habilitation in 1974. In 1978, he accepted a position at the University of Bonn, and in 1980 he returned to the University of Marburg. He became a director at the Max Planck Institute for Coal Research in 1991. Reetz is a member of the academic advisory board for *Advanced Synthesis & Catalysis* and has served on the editorial board of *Angewandte Chemie* since 2002.

August Wilhelm von Hofmann Medal Awarded to R. H. Grubbs and R. R. Schrock

Every two years, the GDCh honors foreign chemists and German nonchemist-scientists with the August Wilhelm von-Hofmann Medal. This year, the honor went to Robert H. Grubbs (California Institute of Technology, Pasadena, USA) and Richard R. Schrock (Massachusetts Institute of Technology, Cambridge, USA). Both have made outstanding contributions to the field of organometallic chemistry through organic and polymer synthesis. Grubbs is famous for the development of a range of ruthenium-containing catalysts of olefin metathesis;[5] Schrock's name is associated with alkylidene complexes and ring-opening-metathesis polymerization.[6]



R. R. Schrock

Grubbs received his PhD in 1968 at Columbia University in New York under the direction of R. Breslow. In 1968 and 1969 he worked as a postdoc in the research group of J. P. Collman (Stanford University), and then as assistant and associate professor at Michigan State University in East Lansing. Since 1978 he has held a position as professor at the California Institute of Technology in Pasadena. He is the editor of the 2003 "Handbook of Metathesis" published by Wiley-VCH.



R. H. Grubbs

Schrock earned his PhD in 1971 at Harvard University with J. A. Osborn. He subsequently worked for a year at Cambridge University, and for three years at DuPont de Nemours. He has been active at the Massachusetts Institute of Technology since 1975, and as professor, since 1980. Both Grubbs and Schrock are members of the academic advisory board for *Advanced Synthesis & Catalysis*.

Arfvedson–Schlenk Prize Goes to D. Stalke

The GDCh awards excellence in lithium chemistry with the Arfvedson–Schlenk Prize. This year the honor goes to Dietmar Stalke (University of Göttingen). Stalke completed his PhD studies in chemistry at this university in 1987 with U. Klingebiel. He did his postdoctoral research with P. von R. Schleyer (University of Erlangen-Nürnberg) and at Cambridge University with R. Snaith and P. R. Raithby. In 1993 he obtained his habilitation in the research group of G. M. Sheldrick at the University of Göttingen and accepted a position at the University of Würzburg in 1995. In April of this year, he returned to the University of Göttingen.

Stalke's research is concentrated on the determination of electron densities through multipole refinement, sulfur–nitrogen chemistry, ligand design with N-heteroarenes, and low-temperature investigations of crystals. The award comes particularly for his development of cryotechniques that have enabled the elucidation of principles in structure and reactivity in the field of organolithium chemistry, among other things, of *n*- and *tert*-butyllithium. He recently reported on metal coordination to the formal P=N bond of an iminophosphorane.[7]



D. Stalke

[1] A. de Meijere, C.-H. Lee, M. A. Kuznetsov, D. V. Gusev, S. I. Kozhushkov, A. A. Fokin, P. R. Schreiner, *Chem. Eur. J.* August 1, **2005**, doi: 10.1002/chem.200500472.

[2] P. Kaden, E. Mayer-Enthart, A. Trifonov, T. Fiebig, H.-A. Wagenknecht, *Angew. Chem.* **2005**, *117*, 1662; *Angew. Chem. Int. Ed.* **2005**, *44*, 1636.

[3] M. Ji, H. Vahrenkamp, *Eur. J. Inorg. Chem.* **2005**, 1398.

[4] M. T. Reetz, M. Bocola, J. D. Carballeira, D. Zha, A. Vogel, *Angew. Chem.* **2005**, *117*, 4264; *Angew. Chem. Int. Ed.* **2005**, *44*, 4192.

[5] R. H. Grubbs, T. M. Trnka in *Ruthenium in Organic Synthesis* (Ed.: S.-I. Murahashi), Wiley-VCH, Weinheim, **2005**, pp. 153–177.

[6] R. R. Schrock, A. H. Hoveyda, *Angew. Chem.* **2003**, *115*, 4740; *Angew. Chem. Int. Ed.* **2003**, *42*, 4592.

[7] N. Kocher, D. Leusser, A. Murso, D. Stalke, *Chem. Eur. J.* **2004**, *10*, 3622.

DOI: 10.1002/anie.200502713

© 2005 Wiley-VCH Verlag GmbH & Co. KGaA, Weinheim



Organometallics at Lake Geneva**

Holger Butenschön*

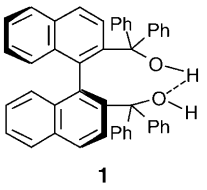
Between July 17 and 21, 2005 the 13th IUPAC International Symposium on Organometallic Chemistry Directed Towards Organic Synthesis (OMCOS-13) was held in Geneva. This biennial conference, organized this year by Peter Kündig and Alexandre Alexakis, was a success; OMCOS-13 was proven particularly attractive, as it gathered about 1200 participants from all over the world. Organometallic chemistry directed towards organic synthesis has been a rapidly developing area of high relevance, with asymmetric transition-metal catalysis still dominating the field.

L. Hegedus (Fort Collins, USA) won the audience over with his contribution in which he gave a nice review of OMCOS-1, which was held with his cooperation in Fort Collins in 1981. The list of speakers from OMCOS-1 shows how forward-looking the foundation of this series of conferences was: Posner, Noyori, Tsuji, Larock, Negishi, Semmelhack, Pearson, Heimbach, Chiusoli, Trost, Rosenblum, Nicholas, Murahashi, and others—the list reads like a Who's Who in Organometallic Chemistry! As has been the case for preceding OMCOS conferences, the organizers this year succeeded in acquiring a number of highly attractive speakers. In addition to 23 plenary lectures and one award lecture, 22 short communications were presented. The diversity of organometallic chemistry was represented by more than 620 poster presentations.

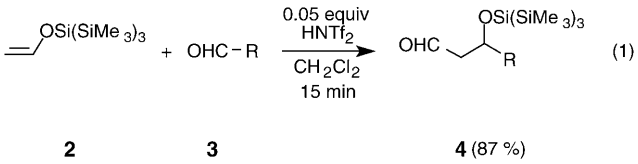
The conference was given a brilliant start by A. Fürstner (Mülheim an der Ruhr, Germany) with a plenary lecture on *Catalysis for Total Synthesis*. He presented the application of iron compounds as catalysts for coupling reactions as a current development. In the presence of iron(III) acetylacetonate, alkyl Grignard reagents can be coupled with aryl chlorides, bromides, or tosylates with high selectivity as was impressively demonstrated by Fürstner in the synthesis of amphidinolide X.[1] Interestingly, the process can be switched around to allow the coupling of secondary alkyl bromides with aryl Grignard reagents.

Catalytic enantioselective C–C bond-formation reactions based on chiral sulfoximines were presented by C. Bolm (Aachen, Germany). In particular, C_2-symmetric bissulfoximines and C_1-symmetric sulfoximines were used, a large variety of which are accessible through a building-block system. The potential of these catalysts was verified among others in Mukaiyama aldol and in carbonyl-ene reactions. Bidentate ligands with a chiral sulfoximine and a phosphane, phosphite, or amine co-ligand were successfully applied in iridium-catalyzed enantioselective reductions of imines to give enantiomeric excesses of up to 98%, thereby setting a new standard.

M. Murakami (Kyoto) impressed with a highly detailed study on the torquoselectivity of thermal conrotatory electrocyclic ring-opening reactions of silyl- and boryl-substituted cyclobutenes, which, in contrast to alkyl-substituted systems, prefer an inward opening. J. Maddaluno (Rouen) reported on chiral lithium amides and their application in asymmetric synthesis, whereby important aggregates were characterized by ^{6}Li NMR spectroscopy. H. Yamamoto (Chicago) introduced "designer acid catalysts", which are combinations of Lewis (L) and Brønsted (B) acids (A). The possible combinations BLA, LBA, LLA, and BBA lead to various kinds of activation. For example, diol **1** of the BBA type allows enantiomeric excesses up to 98% in hetero-Diels–Alder reactions.[2] Particularly interesting was the application in the enantioselective nitroso-aldol addition for the formation of 2-hydroxyketones. A remarkable increase in the nucleophilicity of silyl enol ethers was achieved with the tris(trimethylsilyl) (TTMSS) group, as shown by the Mukaiyama-aldol addition of **2** and **3** to **4** [Eq. (1); R = alkyl, Tf = trifluoromethanesulfonyl]. The silyl migration allows successive repetition similar to a cascade Mukaiyama aldol reaction, which proceeds with high *syn* selectivity.



1



2 **3** **4** (87%) (1)

Akin to preceding conferences, palladium-catalyzed reactions held a prominent position at OMCOS-13. G. Balme (Lyon) opened this field with a lecture on palladium-catalyzed multicomponent reactions for the construction of such heterocycles as furans, γ-lactones, and heterocyclic natural products. A true fireworks display of palladium-catalyzed reactions was then presented by this year's winner of the OMCOS award, S. Ma (Shanghai), who lectured on transition-metal-catalyzed reactions of allenes.[3] The carbometallation of allenes either leads to π-allyl complexes or to alkenyl metal compounds. A subsequent β-hydride elimination leads to new allenes. Ma also reported on multicomponent reactions. A special bonus at the end of his impressive lecture was a rhodium-catalyzed synthesis of steroid **6** from bisallene **5**, which was carried

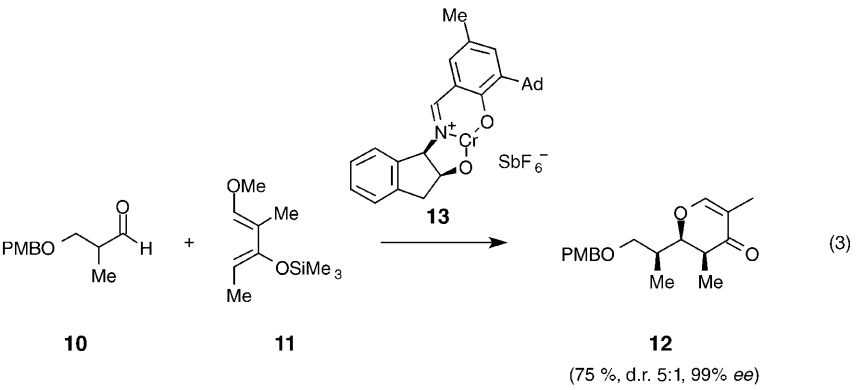
[*] H. Butenschön
Institut für Organische Chemie
Universität Hannover (Germany)

[**] 13th IUPAC International Symposium on Organometallic Chemistry Directed Towards Organic Synthesis (OMCOS-13) in Geneva, July 17–21, 2005.

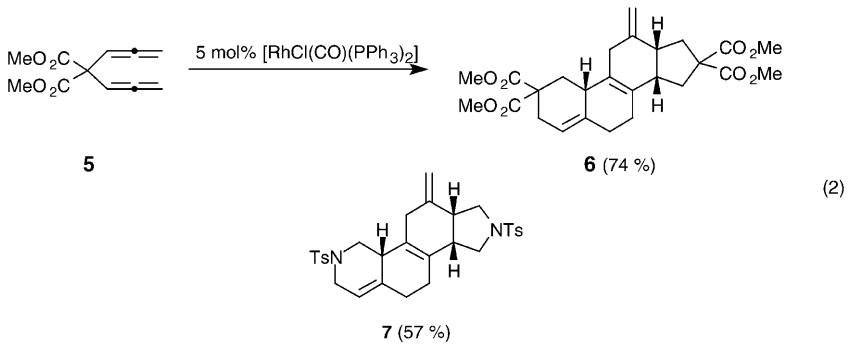
InterScience
© 2005 Wiley-VCH Verlag GmbH & Co. KGaA, Weinheim

out in 74% yield [Eq. (2)]. If the central $C(CO_2Me)_2$ unit in **5** is replaced by NTs (Ts = toluene-4-sulfonyl), diazasteroid **7** forms in 57% yield.

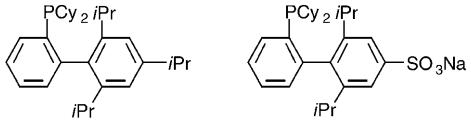
S. L. Buchwald (Cambridge, USA) presented a large number of special biphenyl-derived phosphanes such as **8**, which allow important palladium-catalyzed aminations and Suzuki–Miyaura coupling reactions, even with sterically hindered aryl chlorides. Interestingly, the similar phosphane **9** has recently proven valuable for Sonogashira coupling reactions in the aqueous phase.



10 **11** **13** **12** (75 %, d.r. 5:1, 99% *ee*) (3)



5 **6** (74 %) (2) **7** (57 %)



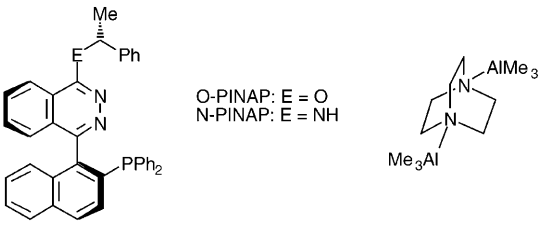
8 **9**

K. Oshima (Kyoto) reported on some interesting, cobalt-catalyzed reactions based on single-electron transfers, in which $[CoCl_2(dppe)]$ (dppe = ethane-l,2-diylbis(diphenylphosphane)) proved particularly successful. Cobalt Schiff-base complexes were the focus of the lecture by E. N. Jacobson (Cambridge, USA), who presented a large number of natural product syntheses. For example, the dynamic kinetic resolution for the hetero-Diels–Alder cycloaddition in the synthesis of the membrenone C building block **12** from **10** and **11** requires use of **13** as the hexafluoroantimonate [Eq. (3)].

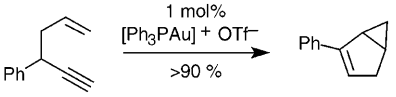
New ligands for the control of asymmetric catalysis were the central topic of the lecture by E. M. Carreira (Zürich). Chiral diene ligands have proven particularly useful in asymmetric rhodium-catalyzed Michael additions with 98% *ee*,[4] and Carreira gave proper credit to related work by Hayashi (Kyoto). For a number of other asymmetric catalyses such as hydroboration and dipolar addition reactions with azomethyne ylides, the group of PINAP ligands **14** were useful. S. Woodward convinced the audience with a very clear presentation on applications of aluminum reagents. For example, the 1,4-diazabicyclo[2.2.2]octane (DABCO) adduct DABAL (**15**) in the presence of chiral phosphane ligands of the Feringa type facilitates the stereoselective methylation of aldehydes.

Despite the dominant role of palladium among the catalytically important metals, there are frequent reports on remarkable catalyses by less-prominent metals. N. Chatani (Osaka) reported on gallium trichloride catalyzed cycloadditions of isocyanides, and F. D. Toste (Berkeley) presented a brilliant array of gold(I)-catalyzed reactions. The incentive for this research was the development of air-stable transition-metal catalysts. Next to $[(Ph_3PAu)_2O]$, which had been introduced by Schmidbaur, triphenylphosphane gold(I) triflate was used to facilitate the isomerization of enyne **16** to bicyclo[3.1.0]hexane **17** in greater than 90% yield [Eq. (4)]. Especially interesting is the isomerization of alkynylcyclopropanol **18** to 2-methylenecyclobutanone **19** (88–98%) with $[(4\text{-}F_3CC_6H_4)_3PAu]^+$ SbF_6^- (0.5–2.0 mol%) as catalyst [Eq. (5)]. The reaction was explained by a mechanism via a gold carbene intermediate.[5,6]

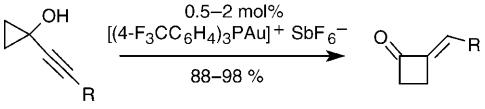
M. Sodeoka (Sendai, Japan) held the Chemical Communications 40th Anniversary Lecture on acid–base catalysis with chiral palladium catalysts. As in many other talks the 2,2′-bis(diphenylphosphanyl)-1,1′-binaphthyl (binap) ligand was featured prominently. The binap bis(aqua) complex of palladium shows Brønsted acidity at the aqua



14 **15**



16 **17** (4)

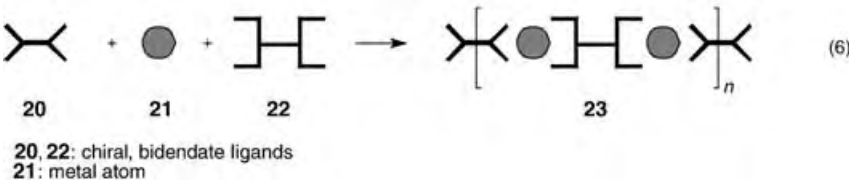


18 **19** (5)

© 2005 Wiley-VCH Verlag GmbH & Co. KGaA, Weinheim

ligands and Lewis acidity at the palladium atom. This allows an interaction that results in asymmetrically catalyzed aldol and Mannich reactions, and Michael additions with excellent yields and stereoselectivities. Remarkably, Michael additions are also possible with α,β-unsaturated aldehydes. Also notable is the catalytic enantioselective α-fluorination of α-monosubstituted β-dicarbonyl compounds and β-ketophosphonates with $(PhSO_2)_2NF$ with up to 97% yield and 96% *ee*, in which enolization and racemization are avoided. After a lecture by H. Lebel (Montréal) about nitrenes and their use in metal-catalyzed aziridinations, B. Lipshutz (Santa Barbara, USA) impressed the audience not only by the scientific content of his lecture but also by the enthusiastic style of his presentation. The focus of his talk was catalysis with the readily affordable nickel in charcoal and in graphite. Negishi coupling reactions, aminations of the Buchwald–Hartwig type, and Suzuki–Miyaura coupling reactions give high yields. These reactions can be accelerated remarkably upon microwave irradiation. The important aspect of planar chiral compounds was put forward by J. C. Carretero (Madrid), who investigated sulphenylphosphinylferrocenes as catalysts for asymmetric C–C bond formation and their use as catalysts for hetero-Diels–Alder cycloadditions.

A. S. C. Chan (Hong Kong) gave a lecture about "smart ligands" for C–C coupling reactions, in which chiral ligands are combined in such a way that the resulting synergism produces better results than is possible with single ligands only. Palladium catalysis was the focus of the talk given by M. Lautens (Toronto), who presented an interesting indole synthesis by a tandem coupling reaction of geminal dibromoalkanes and a vinylogous Mukaiyama–Mannich reaction. The direct α-alkylation or α-alkenylation of carbonyl compounds by treatment with ethene or ethyne was the target of N. Nakamura (Tokyo). This was finally successful by treatment of the respective imines with LDA, $ZnCl_2$, and butyl lithium followed by ethene via the zinc enolates. For the ethenylation of β-dicarbonyl compounds by treatment with ethyne, indium(III) triflate proved superior to the zinc salt. K. Ding (Shanghai) described his success in devising a way to decrease the amount of catalyst typically applied from 1–5 mol% to 0.1–0.05 mol%. He exploited the asymmetric activation of achiral ligands. His "self-supported ligands" are coordination polymers such as **23** that consist of two different chiral building blocks **20** and **22**, and the metal **21** [Eq. (6)][7] which combine the advantages of heterogeneous and homogeneous catalysis. The enantioselective epoxidation of enones, for example, gave 99% yield with 97.6% *ee*.



20, **22**: chiral, bidendate ligands
21: metal atom

After the lecture of C. Genari (Milan) about rhodium-catalyzed asymmetric hydrogenation reactions with monodentate phosphorous amidates, V. Aggarwal (Bristol, UK) completed the wide spectrum of organometallic chemistry by illustrating some possible uses for sulfur ylides which include asymmetric epoxidation and its application to the synthesis of natural products.

Next to the mostly excellent plenary lectures a number of short communications also had their place, among which were the impressive presentations by B. Breit (Freiburg, Germany) and J. Takacs (Lincoln, USA). Each described an approach to the field of self-organized bidentate ligands, yet from different starting ideas. The presentation of J. Williams (Bath, UK) about *Borrowing Hydrogen Using Transition Metal Catalysis* outlined a rather creative concept: a primary alcohol is oxidized to an aldehyde, which in turn is subjected to a Wittig olefination with formation of the respective alkene, which is finally reduced to the alkane—in summary, a primary alcohol has been alkylated. Interesting talks were also given by P. Chiu (Hong Kong) about copper-catalyzed (Stryker reagent: $[(Ph_3PCuH)_6]$) hydrostannylations of activated alkanes and the application of secondary phosphane oxides according to Li in titanium- and palladium-catalyzed amination reactions, which were the subjects of the communication of L. Ackermann (Munich).

Overall, it can be said that the application of organometallic chemistry to organic synthesis is still highly attractive. Various facets of asymmetric catalysis and cross-coupling reactions dominated many lectures. In addition to the frequently used palladium, other metals such as ruthenium or rhodium are playing an increasingly important role. The issue of practicability in catalysis was the topic of some contributions, in which the use of affordable metals (such as Ni and Fe) or heterogeneous catalysts without air exclusion were emphasized. The program was superbly arranged; the large number of poster contributions, which were presented at a great poster party and which were on display throughout the conference, inspired a highly communicative atmosphere. In summary, OMCOS-13 was a great success, and expectations are high for OMCOS-14 (August 2–6, 2007, in Nara, Japan).

[1] O. Lepage, E. Kattnig, A. Fürstner, *J. Am. Chem. Soc.* **2004**, *126*, 15970–15971.
[2] A. K. Unni, N. Takenaka, H. Yamamoto, V. H. Rawal, *J. Am. Chem. Soc.* **2005**, *127*, 1336–1337.
[3] S. Ma, *Acc. Chem. Res.* **2003**, *36*, 701–712.
[4] C. Fischer, C. Defieber, T. Suzuki, E. M. Carreira, *J. Am. Chem. Soc.* **2004**, *126*, 1628–1629.
[5] J. P. Markham, S. T. Staben, F. D. Toste, *J. Am. Chem. Soc.* **2005**, *127*, 9708–9709.
[6] X. Shi, D. J. Gorin, F. D. Toste, *J. Am. Chem. Soc.* **2005**, *127*, 5802–5803.
[7] Y. Liang, Q. Jing, X. Li, L. Shi, K. Ding, *J. Am. Chem. Soc.* **2005**, *127*, 7694–7695.

DOI: 10.1002/anie.200502598

 © 2005 Wiley-VCH Verlag GmbH & Co. KGaA, Weinheim

Organometallic Chemistry

DOI: 10.1002/anie.200501204

Organocopper for the Craftsman Cunning at His Trade**

*Simon Woodward**

Keywords:
aluminum · copper · Grignard reactions · nucleophilic substitution · zinc

Although modern organocopper chemistry emerged from the use of CuCl as a catalyst to promote 1,4-additions of Grignard reagents to enones by Kharasch and Tawney in 1941,[1] such reactivity has until recently remained the poorer cousin of stoichiometric cuprate reactivity, as exemplified by the use of Gilman's cuprate, $LiCuMe_2$, which recently celebrated its 50th birthday.[2] However, in the last twelve months an influx of papers that describe copper-catalyzed asymmetric reactions of organozinc, aluminum, and especially Grignard reagents has provided new, highly enabling methodologies. The exceptional utility of these reactions promises to displace stoichiometric cuprates from their preferred position as the reagents of choice for conjugate addition and S_N2' displacement reactions of allylic electrophiles.

The synthetic potential of general asymmetric 1,4-additions of RMgX species to enones has been recognized since the earliest days of organometallic chemistry. However, a near-enantiospecific catalyst for such reactions was considered viable "only in dreams", even as recently as 1997.[3e] Despite the screening of a wide range of ligands, including thiolates, phosphanes, and imines, the *R*/*S* selectivity in even the simple test reaction of 2-cyclohexenone and *n*BuMgX remained moderate for over a decade (Figure 1), and *ee* values remained persistently in the range 60–80%.[3] The benchmark result of

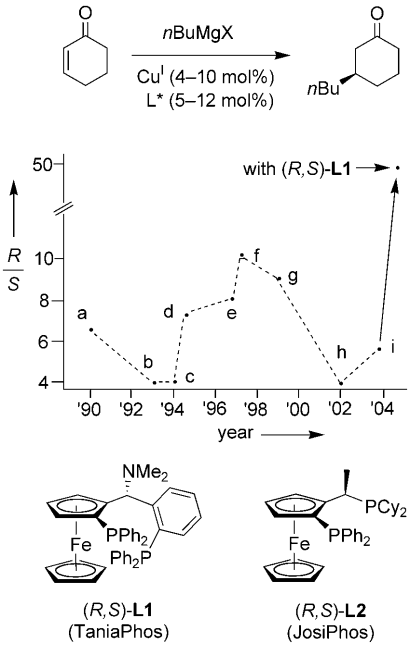


Figure 1. Selected maximum *ee* values for catalytic additions of BuMgX to 2-cyclohexenone, except (d), which involves addition of MeMgI to benzylideneacetone (< 10 mol% Cu^I; < 12 mol% chiral ligand, L*). Data points a–i correspond to References [3a–i], respectively. Cy = cyclohexyl.

van Koten and co-workers in this area on benzylideneacetone (76% *ee*) in 1994[3d] has also been included in Figure 1 for comparison. However, a huge improvement in *R*/*S* selectivity has very recently (2004–2005) been reported in a series of three publications by the group of Feringa.[4–6] Use of the key ferrocenyl ligands TaniaPhos (**L1**) and JosiPhos (**L2**) allows a wide range of Grignard 1,4-additions to cyclic and acyclic enones as well as α,β-unsaturated esters, with *R*/*S* selectivities that are 5–10 times higher than those seen with all previous catalysts. These ligands typically afford 85–95% *ee* for a wide range of substrates. The very high rate efficiency of the catalyst minimizes, or eliminates, the direct 1,2-addition of the Grignard reagent to the carbonyl group. Of additional note is the forgiving nature of these reactions with respect to their tolerance of traces of water and oxygen and that they can operate at very low catalyst loadings (down to 0.2 mol% in one case). Further synthetic simplicity in the form of an air-stable precatalyst prepared from **L2** and $CuBr{\cdot}SMe_2$ lead to near-optimal reaction conditions. The currently tolerated combinations of preferred ligands per substrate type are summarized in Table 1.

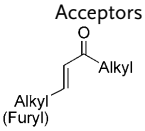
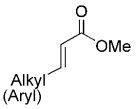
The current limitations of this system are few but are worth summarizing for those who are interested in using the reaction in target synthesis. 1) The presence of α branching in the Grignard component often leads to a catastrophic loss in enantioselectivity; 2) highly hindered enones, such as RCH=CHC(O)-*t*Bu (R = alkyl), lead to a poor selectivity (≈40% *ee*); 3) for the less-reactive α,β-unsaturated esters, the rate of addition of MeMgBr is slow (high *ee* values were still observed, but at low chemical yields); and 4) the presence of a double bond in the Grignard reagent leads to approximately 10% lower enantioselectivity than that observed for the parent hydrocarbon. These minor limitations represent goals for the future design of catalysts. However, the new methodology of Feringa and co-workers offers one last important advantage: as a result of the inherently high reactivity of the magnesium enolate formed in these reactions, great opportunities exist for

[*] Dr. S. Woodward
School of Chemistry
The University of Nottingham
Nottingham NG72RD (UK)
Fax: (+44) 115-951-3564
E-mail:
simon.woodward@nottingham.ac.uk

[**] Title taken from the opening line of the poem "Cold Iron" by Rudyard Kipling (1865–1936): "*Gold is for the mistress—silver for the maid—copper for the craftsman cunning at his trade*".

InterScience
© 2005 Wiley-VCH Verlag GmbH & Co. KGaA, Weinheim

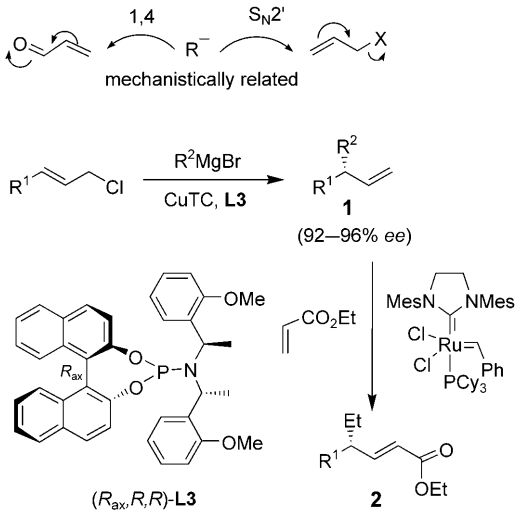
Table 1: Typical *ee* values (%) for Grignard reagents and substrates in 1,4-additions promoted by ligands **L1** and **L2**.

Grignard RMgX R =	Acceptors 		
Me	90 **L1**	97–98 **L2**	93 **L2** (slow)
n-Alkyl	94–96 **L1**	90–95 **L2**	84–99 **L2**
α-branched	54–92 **L1**	48–86 **L2**	[a]
β-branched	95 **L1**	92 **L2**	[a]
Ph	40 **L2**	76 **L2**	[a]

[a] Not reported.

one-pot consecutive trapping reactions and these will undoubtedly be realized in the near future.

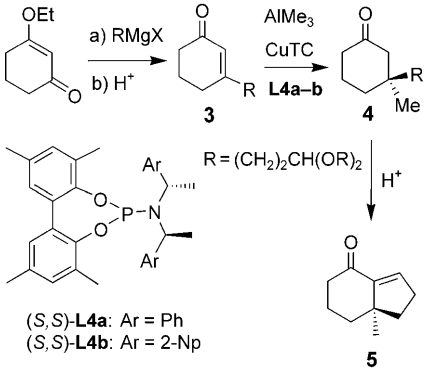
The use of Grignard nucleophiles has also allowed remarkable recent progress in S_N2' displacement reactions of allylic halides, as demonstrated by the group of Alexakis (Scheme 1).[7] Such reactions are mechanistically akin to 1,4-enone additions except that, in this case, the two-electron shift is accommodated by loss of "X^-" rather than its storage at the carbonyl oxygen atom.[8] The asymmetric transition state for ligand-promoted additions of organometallic reagents to (*E*)-RCH=$CHCH_2X$ species is presently not well understood and appears rather fragile. Despite intensive efforts in the last five years, catalytic systems have been able to afford stereoselectivities of over 90% only in special cases. However, the use of a combination of a Grignard reagent and a key chiral ligand has again led to a general strategy for this reaction. For a range of allylic chlorides and Grignard reagents, the α-chiral alkenes **1** are isolated in good yield and with outstanding enantioselectivity. The presence of the methoxy group in **L3** is crucial, but whether this unit can act as a bridging ligand to magnesium can only be speculated on at present. Direct exposure of the reaction mixture to ethyl acrylate and 5 mol% of the Grubbs II catalyst allows direct formation of the unsaturated esters **2** in moderate to good yield. Esters **2** would be excellent substrates for Josiphos (**L2**)-promoted addition of a further Grignard reagent using Feringa's system. The potential for creating one-pot multiple cascades that lead to two or three contiguous stereocenters is indeed very high.



Scheme 1. Preparation of chiral esters. R^1 = Ph, 4-Me-C_6H_4, Cy; R^2 = Et, 3-butenyl, 4-pentenyl; CuTC = copper(I) thiophene-2-carboxylate; Mes = 2,4,6-trimethylphenyl.

Unfortunately, the zinc analogues of Grignard reagents, RZnX, often lack sufficient reactivity to be useful in catalytic asymmetric 1,4- or S_N2' additions. Recently, we demonstrated a method to overcome this difficulty: By promoting the reverse Schlenk equilibrium, RZnCl can be transformed back into R_2Zn and $ZnCl_2$.[9] As the resultant diorganozinc reagent is of higher reactivity it could be utilized in copper-catalyzed S_N2' reactions of (*Z*)-ArCH=$C(CH_2Cl)CO_2Me$ to afford $ArCHRC(=CH_2)CO_2Me$ with good enantioselectivity (80–90% *ee*) in the presence of simple chiral amines. (Normally *Z*-allylic halides give far lower *ee* values in S_N2' chemistry, and to improve this remains a significant challenge in this area). The key trick in this chemistry of RZnCl is to add methylaluminoxane $[MeAlO]_n$ to the reaction mixture to scavenge $ZnCl_2$ and give ZnR_2 rather than the usual, highly thermodynamically favored RZnCl species. The formation of strong Al–Cl bonds probably accounts for the thermodynamic driving force. Thus, although this reaction does not use zinc Grignard reagents as such, the success of the approach is clearly related.

As a last example from this influx of organocopper-based methodology, Alexakis and co-workers have also exploited the strong Lewis acidity and oxophilicity of organoaluminum reagents to conquer another demanding class of substrates in classical organocuparate chemistry: β-disubstituted enones (Scheme 2).[10] Traditionally, the additional steric hindrance afforded by enones of type **3** leads to very poor reactivity. However, by using $AlMe_3$ and as little as 4 mol% of chiral ligands **L4a–b**, highly efficient catalytic syntheses of species **4** (91–95% *ee*), which contains a quaternary center, were reported. Interestingly, in this chemistry the presence of acetal groups is tolerated and allows rapid access to bicyclic structures such as **5**.



Scheme 2. Preparation of stereogenic quaternary centers with high enantiopurity by conjugate addition of $AlMe_3$. R = Et, *i*Bu, $(CH_2)_nCH{=}CH_2$ (n = 2,3), $(CH_2)_2CH(OR)_2$; Np = naphthyl.

All of the strategies described above have been attained with loadings of

 © 2005 Wiley-VCH Verlag GmbH & Co. KGaA, Weinheim

copper(I) salts of 5 mol% or less. It is clear that the nature of asymmetric copper-promoted reactivity is changing rapidly from a situation in which chiral stoichiometric reagents of low general utility (often targeting just a single substrate) were the norm to more-powerful, general catalytic asymmetric procedures. While some problematic combinations of organometallic reagents and substrates still exist in both conjugate addition and S_N2' chemistry, we can be confident that in the near future ligand structures will be identified to overcome these difficulties and an essentially complete set of synthetic methodologies in this area will be available.

Published online: July 29, 2005

[1] M. S. Kharasch, P. O. Tawney, *J. Am. Chem. Soc.* **1941**, *63*, 2308–2315.

[2] a) J. J. Eisch, *Organometallics* **2002**, *21*, 5439–5463; b) *Modern Organocopper Chemistry* (Ed.: N. Krause), Wiley-VCH, Weinheim, **2002**.

[3] a) K.-H. Ahn, R. B. Klassen, S. J. Lippard, *Organometallics* **1990**, *9*, 3178–3181 (74% *ee*, 3–5 mol% L*); b) M. Specha, G. Rihs, *Helv. Chim. Acta* **1993**, *76*, 1219–1230 (60% *ee*, 4–mol% L*); c) Q. Zhou, A. Pfaltz, *Tetrahedron* **1994**, *50*, 4467–4478 (60% *ee*, 5–10 mol% L*); d) M. van Klaveren, F. Lambert, D. J. F. M. Eijelkamp, D. M. Grove, G. van Koten, *Tetrahedron Lett.* **1994**, *35*, 6135–6138 (76% *ee*, 9 mol% L*); e) D. Seebach, G. Jaeschke, A. Pichota, L. Audergon, *Helv. Chim. Acta* **1997**, *80*, 2515–2519 (78% *ee*, 5 mol% L*); f) E. L. Strangeland, T. Sammakia, *Tetrahedron* **1997**, *53*, 16503–16510 (83% *ee*, 12 mol% L*); g) M. Kanai, Y. Nakagawa, K. Tomioka, *Tetrahedron* **1999**, *55*, 3831–3842 (81% *ee*, 10 mol% L*; improved to 92% *ee* but at 32 mol% L*); h) A. L. Braga, S. J. N. Silva, D. S. Lüdtke, R. L. Drekener, C. C. Silveira, J. B. T. Rocha, L. A. Wessjohann, *Tetrahedron Lett.* **2002**, *43*, 7329–7331 (62% *ee*, 10 mol% L*); i) S. A. Modin, P. Pinho, P. G. Andersson, *Adv. Synth. Catal.* **2004**, *346*, 549–553 (71% *ee*, 5 mol% L*).

[4] B. L. Feringa, R. Badorrey, D. Peña, S. R. Harutyunyan, A. J. Minnaard, *Proc. Natl. Acad. Sci. USA* **2004**, *101*, 5834–5838: Prior to this report, only hints existed that JosiPhos-type ligands may be powerful additives in asymmetric 1,4-addition chemistry. For example, see: H.-U Blaser, W. Brieden, B. Pugin, F. Spindler, M. Studer, A. Togni, *Top. Catal.* **2002**, *19*, 3–16.

[5] F. López, S. R. Harutyunyan, A. J. Minnaard, B. L. Feringa, *J. Am. Chem. Soc.* **2004**, *126*, 12784–12785.

[6] F. López, S. R. Harutyunyan, A. Meetsma, A. J. Minnaard, B. L. Feringa, *Angew. Chem.* **2005**, *117*, 2812–2816; *Angew. Chem. Int. Ed.* **2005**, *44*, 2752–2756.

[7] K. Tissot-Croset, D. Polet, A. Alexakis, *Angew. Chem.* **2004**, *116*, 2480–2482; *Angew. Chem. Int. Ed.* **2004**, *43*, 2426–2428.

[8] N. Krause, A. Gerold, *Angew. Chem.* **1997**, *109*, 194–213; *Angew. Chem. Int. Ed. Engl.* **1997**, *36*, 186–204.

[9] P. J. Goldsmith, S. J. Teat, S. Woodward, *Angew. Chem.* **2005**, *117*, 2275–2277; *Angew. Chem. Int. Ed.* **2005**, *44*, 2235–2237.

[10] M. d'Augustin, L. Palais, A. Alexakis, *Angew. Chem.* **2005**, *117*, 1400–1402; *Angew. Chem. Int. Ed.* **2005**, *44*, 1376–1378.

 © 2005 Wiley-VCH Verlag GmbH & Co. KGaA, Weinheim

Electron Microscopy

DOI: 10.1002/anie.200501466

A Revolution in Electron Microscopy**

*John Meurig Thomas**

Keywords:
electron diffraction · electron microscopy · femtochemistry · protein structures · structural dynamics

A paper on four-dimensional ultrafast electron microscopy published recently[1] reports breakthroughs and preliminary results that are of great potential significance to physical, materials, and biological scientists. A. H. Zewail and co-workers have described how to unite the time domain with the spatial domain in such a manner as to achieve unprecedented real-time and real-space capabilities. Adding the fourth dimension, time, to the three spatial ones that are retrievable by high-resolution electron microscopy opens up new vistas and applications by using timed, single-electron packets.

All this is achieved through coherent electron packets, which are liberated from a photocathode with femtosecond laser pulses, are accelerated at 120 keV, and contain as little as one electron per pulse. Such design ensures that no space–charge broadening of the electron beam occurs and that electron trajectories can be brought into sharp focus. The photocathode is illuminated with very weak ($E \approx 500$ pJ) femtosecond pulses—which constitute a high-frequency train (12.5 ns or longer separation)—such that the ultrafast electron microscope (UEM) provides, in principle, the ability to benefit from multiple pulsing with single-shot time resolution. For example, with a periodic sample, each electron pulse could, by dextrous manipulation, be applied to a different but equivalent region. Moreover, by lengthening the interval between pulses any reversible damage inflicted by an electron pulse on samples such as metals or other inorganic objects (e.g. Si, Ge, GaAs) may be allowed to self-heal prior to further repeated investigations. By obtaining diffraction patterns Zewail and co-workers[1] have reached atomic resolution, and by microscopy they have already obtained images that are resolved on the nanometer scale.

The conceptual design of the UEM, in which a femtosecond optical system is integrated with a high-resolution electron microscope, is depicted in Figure 1. The laser system consists of a diode-pumped mode-locked Ti:sapphire laser oscillator which generates sub-100-fs pulses at 800 nm with a repetition rate

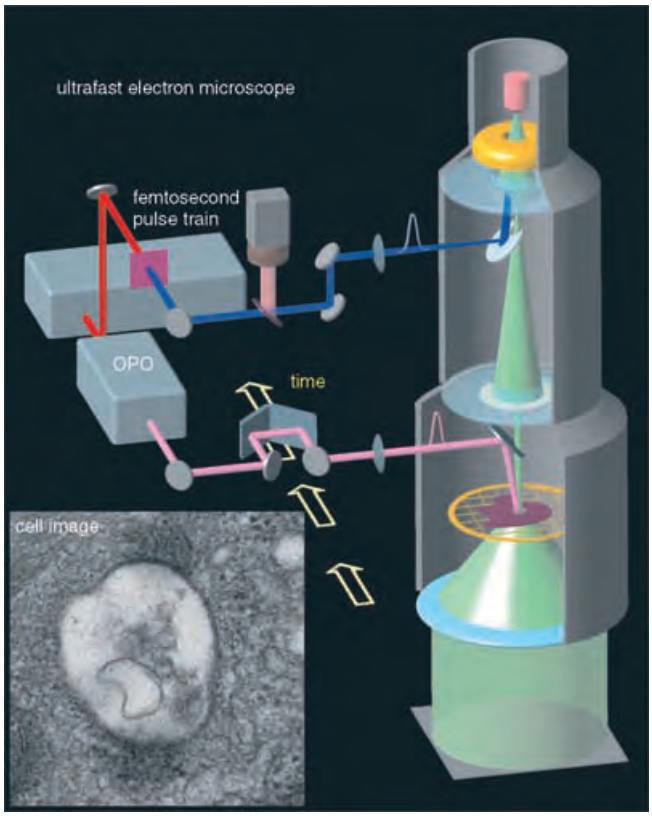


Figure 1. Design of the UEM (OPO = optical parametrical oscillator).[1] The inset shows the UEM image of a cell of rat intestine. Picture kindly provided by V. A. Lobastov.

[*] Prof. Sir J. M. Thomas
Department of Materials Science
University of Cambridge
Cambridge CB2 3QZ (UK)
Fax: (+44) 1223-334-567
E-mail: jmt2@cam.ac.uk
and
The Davy Faraday Laboratory
Royal Institution
21 Albemarle St., London W1S 4BS (UK)
and
The NanoCenter
University of South Carolina
Columbia, SC 29208 (USA)

[**] I am grateful to Professors K. D. M. Harris, R. M. Glaeser, and J. C. H. Spence for stimulating discussions.

© 2005 Wiley-VCH Verlag GmbH & Co. KGaA, Weinheim

of 80 MHz and an average power of 1 W. Part of the beam may be used to heat or excite the sample and to define the zero of time, while the remainder is frequency-doubled in a nonlinear crystal to yield 400-nm femtosecond pulses for generating the train of electron pulses. Single-electron detection is achieved by using a phosphor scintillator in conjunction with a charge-coupled device camera. Since 1990, the use of pulsed photoelectrons has been at the heart of the development of ultrafast gas-phase diffraction and ultrafast crystallography by Zewail and co-workers.

This approach is to be contrasted with the pioneering use of intense single pulses of nanosecond duration, also using photoelectrons, pursued by Bostanjoglo and co-workers[2–4] for the studies of texture of thin metallic films. In this case, the single pulse contains approximately 10^8 electrons, which is detrimental to time resolution because of Coulombic repulsion. It also limits spatial resolution to the micron level and to studies of, for example, melting and ablation. It differs also from the seminal work of Gai and Boyes,[5] who used continuous beams in a specially constructed microscope that could record high-resolution images of the migration of supported metal catalysts on oxide supports at elevated temperatures with millisecond resolution in an environmental cell. With their setup, Zewail and co-workers[1] demonstrated the versatility of their designated 4D UEM by recording images and diffraction patterns of amorphous carbon, polycrystalline aluminum, and single-crystal gold. They also obtained images of stained biological cells with an electron dose of around two electrons per $Å^2$.

In light of this major breakthrough and particularly the 4D capabilities, it is instructive to consider, along with some other recent advances, future possible implications for dynamic structural analyses of inorganic, organic, and biological materials. In the past, especially with regard to the determination of structures that are of interest to macromolecular biochemists and biophysicists, far greater use has been made of X-ray diffraction than electron diffraction and microscopy. Indeed, the structures determined were static ones, but, even so, they have sometimes conveyed deep insight into mechanism and function, and two outstanding examples are the structure of DNA and that of lysozyme. On the basis of the latter, Phillips and co-workers proposed a plausible (and still largely valid) mechanism for the mode of action of the proteolytic enzyme.[31] Equally, there have been many instances in which the detailed static structure deduced from X-ray studies gave no immediate clues as to the mechanism of its action—a noteworthy example is hemoglobin. As Max Perutz remarked when he solved the structure of this protein, the structure itself gave no suggestion as to how it functioned, and well-meaning friends to whom he proudly showed his model of hemoglobin hinted that the molecule that had yielded to his prolonged X-ray study might be that of an inconsequential impurity! With the ultrafast diffraction[6] and microscopy techniques introduced by Zewail and co-workers, dynamical evolution of structure and the concomitant charting of energy landscapes may be directly mapped so that there is reason to believe that greater appreciation of biological function may be gained by the application of 4D UEM.

With regards to sensitivity, X-rays are inferior to electrons as probing beams. Electron-scattering cross-sections are higher than those of X-ray scattering from molecules by some five to six orders of magnitude. Moreover, electrons are less damaging to specimens, per useful scattering event, than X-rays are.[7] In synchrotron studies that use intense X-ray beams, the question of beam damage of the specimen is often critical. Even so, synchrotron radiation readily permits time-resolved studies by means of the von Laue method of recording diffraction data. However, very few synchrotron sources are, as yet, capable of offering the timescale necessary to investigate the breaking and making of chemical bonds or the tracking of torsional and vibrational amplitudes, or of adaptation to enable direct, real-space imaging. Pulses of X-rays of 1 ps may be created with a laser-induced plasma, which generates a burst of X-rays from a tiny metal target, and these have recently been used[8] to such good effect in the study of multiple quantum wells that it has led to the possibility of making "X-ray movies of wiggling crystals".[9] Following simulations which indicated that the onset of radiation damage on the atomic scale in a typical protein occurs about 10 to 20 fs after significant diffraction has occurred, it has been suggested by Neutze et al.[10] that X-ray diffraction patterns could be collected from successive randomly oriented protein molecules in a stream that crosses an X-ray beam in synchrony with the X-ray pulses. This difficult experiment has not yet been carried out.

Ever since the landmark achievements of Klug,[11] who devised a way to deduce the structure of biological macromolecules by transmission electron microscopy, considerable use has been made of his general approach, notably by Henderson,[12] Unwin,[13] and others, to determine the structures of membranes and related materials. A recent triumph was the determination of the structure of the nicotinic acetylcholine receptor (at 4 Å resolution).[13] Spence et al.[14,15] have made the ingenious suggestion that electron-diffraction patterns from aligned molecular beams could be used to solve the structure of proteins, especially of those that are difficult to crystallize. Their arrangement consists of continuous, orthogonal, intersecting electron, molecular, and laser beams. This approach, which shows considerable promise, would greatly simplify the data-collection procedures over similar femtosecond-pulsed X-ray schemes proposed by Neutze et al.[10] To determine the structure of an enzyme such as lysozyme in this way, it has been estimated[15] that up to 1 kW of continuous-wave near-infrared laser power together with cooling to liquid N_2 temperatures may be needed to produce sufficiently accurate alignment for the direct observation of the secondary structure of the enzyme.

If—and this is the quintessential point—the suppression of electron-beam damage to be expected from the multiple and controlled pulsing, single-shot approach outlined above permits the collection of diffraction data at higher dose, one cannot but speculate that Zewail and co-worker's 4D UEM method will not only reveal new insight into the dynamics of biophysically relevant processes but also open up the possibility of arriving at structures of even higher resolutions than those re-

 © 2005 Wiley-VCH Verlag GmbH & Co. KGaA, Weinheim

cently obtained by utilizing cryogenic procedures.[16,17]

Prior to their development of 4D UEM, Zewail and co-workers had already reached atomic-scale resolutions in time and space by using ultrafast electron diffraction, which they applied to the study of different phases from gases and crystals to interfaces.[6,18–20] In a recent report, they completed a study of the atomic-scale dynamical structures of a fatty acid bilayer by using ultrafast electron crystallography. Apart from determining the structure of the two-dimensional assembly, they mapped structural dynamics by recording the diffraction frames every picosecond following a femtosecond temperature jump and found that coherent anisotropic expansion took place along the aliphatic chains of the bilayer, which itself is a 2D crystal (50 Å thick).

This level of resolution and sensitivity of electrons as probing beams coupled with the fact that, unlike X-rays, they may be readily focused makes 4D UEM unique as an investigative technique. Electron microscopy has often been able to reveal structural detail of great chemical interest when it is not possible to carry out single-crystal X-ray diffraction studies. The precise nanoporous nature of the key aluminosilicate, zeolitic (molecular sieve) catalyst, ZSM-5, for example, was determined[21] by electron microscopy long before a single-crystal structure was determined by X-ray studies. Moreover, because some 10^{15} unit cells need to be spatially averaged, in X-ray crystal structure determinations certain key microstructural details go undetected—they are obliterated by the process of spatial averaging. By using high-resolution microscopy, the number of unit cells explored is seldom more than 10^5 (and often much less) and a real-space picture of the local structure is recorded. In this way recurrent intergrowths of ZSM-5 and its symmetry-related analogue, ZSM-11, were first detected,[22] and many new structures, including such exotic samples as infinitely adaptive structures (where a fully ordered mixed oxide structure may be formed for every possible nonstoichiometric composition[23]), that remained unobserved by X-ray diffraction were subsequently discovered. Moreover, the structures of highly ordered mesoporous materials cannot be solved from X-ray patterns alone because of the paucity of reflections and their widths. Electron microscopy is the only reliable tool for the determination of such structures.[24]

In principle, the kind of experiment now rendered feasible by the inauguration of 4D UEM should enable unprecedented detail to be retrieved in the study of inorganic, organic, and biological materials. For example, the femtosecond-scale heating (or photoexciting) pulse opens up the possibility of the direct study of a wide range of phase transitions including such phenomena as martensitic transformations, the dynamics of which have hitherto proved inordinately difficult to record directly by other experimental means. For solid-state and materials chemists, the phenomenon of diffusionless reactions[25,26] (such as photostimulated dimerizations and polymerizations) in organic molecular crystals, with its related strategy of crystal engineering, should be a rich pasture to explore. Likewise, the investigation of redox metalloenzymes by dynamic electron microscopy should shed new light on the mechanisms of action of cytochrome P450, manganese oxidase, the hydrogenases, and many other enzymes because it will be possible to record electron-energy-loss spectra[27] (and to reveal oxidation states of the metal ions at active centers, even though the measurements may be complicated by the reducing environment created by the secondary electrons within the sample). Also, with open-structure, single-site heterogeneous catalysts[28,29] the "breathing" of nanopores and nanocages and the amplitudes of atomic motion of the active center grafted onto them, which are crucial determinants in catalytic performance, should be directly recordable. Because of the high sensitivity of 4D UEM it should also be possible to uncover new facts about the enigmatic catalytic activity of nanoparticle gold (supported on certain oxides). Bulk gold is catalytically inactive, but nanoparticles of the metal (diameter ≈ 5 nm) supported on TiO_2 catalytically oxidize[30] carbon monoxide in air at below room temperature. What are the structural dynamics of the terrace, step, and kink sites of this remarkable material? And what are the ultrastructural characteristics of macromolecular assemblies, nanocomposites, grain boundaries, and quantum dots?

The development at Caltech of 4D diffraction, crystallography, and microscopy is indeed revolutionary. The door is now open for myriad explorations in the physical and biological sciences.

Published online: July 26, 2005

[1] V. A. Lobastov, R. Srinivasan, A. H. Zewail, *Proc. Natl. Acad. Sci. USA* **2005**, *102*, 7069.
[2] O. Bostanjoglo, R. E. Elschner, Z. Mao, T. Nink, M. Weingärtner, *Ultramicroscopy* **2000**, *81*, 141.
[3] H. Dömer, O. Bostanjoglo, *Rev. Sci. Instrum.* **2003**, *74*, 4369.
[4] O. Bostanjoglo, *Adv. Imaging Electron Phys.* **2002**, *121*, 1.
[5] P. L. Gai, E. D. Boyes, *Ultramicroscopy* **1997**, *67*, 219.
[6] A. H. Zewail, *Philos. Trans. R. Soc. London Ser. A* **2005**, *364*, 315.
[7] R. Henderson, *Q. Rev. Biophys.* **1995**, *28*, 171.
[8] M. Bargheer, N. Zhavoronkov, Y. Gritsai, J. C. Woo, D. S. Kim, M. Woerner, T. Elsaesser, *Science* **2004**, *306*, 1771.
[9] P. H. Bucksbaum, *Science* **2004**, *306*, 1691.
[10] R. Neutze, R. Wouts, D. van der Spoel, E. Weckert, J. Hajdu, *Nature* **2000**, *406*, 752.
[11] A. Klug in *Nobel Lectures, Chemistry 1981–1990* (Ed.: B. G. Malmström), World Scientific, Singapore, **1991**, pp. 77.
[12] R. Henderson, *Q. Rev. Biophys.* **2004**, *37*, 3.
[13] N. Unwin, *J. Mol. Biol.* **2005**, *346*, 967.
[14] J. C. H. Spence, R. B. Doak, *Phys. Rev. Lett.* **2004**, *92*, 198102.
[15] J. C. H. Spence, K. Schmidt, J. S. Wu, G. Hembree, U. Weierstall, B. Doak, P. Fromme, *Acta Crystallogr. Sect. A* **2005**, *61*, 237.
[16] W. Chiu, A. McGough, M. B. Sherman, M. F. Schmid, *Trends Cell Biol.* **1999**, *9*, 154.
[17] A. Sali, R. Glaeser, T. Earnest, W. Baumeister, *Nature* **2003**, *422*, 216.
[18] F. Vigliotti, S. Chen, C.-Y. Ruan, V. A. Lobastov, A. H. Zewail, *Angew. Chem.* **2004**, *116*, 2759; *Angew. Chem. Int. Ed.* **2004**, *43*, 2705.
[19] J. M. Thomas, *Angew. Chem.* **2004**, *116*, 2658; *Angew. Chem. Int. Ed.* **2004**, *43*, 2606.
[20] C.-Y. Ruan, V. A. Lobastov, F. Vigliotti, S. Chen, A. H. Zewail, *Science* **2004**, *304*, 80.

 © 2005 Wiley-VCH Verlag GmbH & Co. KGaA, Weinheim

[21] J. M. Thomas, G. R. Millward, L. A. Bursill, *Philos. Trans. R. Soc. London Ser. A* **1981**, *300*, 43.
[22] J. M. Thomas, G. R. Millward, *J. Chem. Soc. Chem. Commun.* **1982**, 1380.
[23] J. S. Anderson, *J. Chem. Soc. Dalton Trans.* **1973**, 1107.
[24] Y. Sakamoto, T. W. Kim, R. Ryoo, O. Terasaki, *Angew. Chem.* **2004**, *116*, 5353; *Angew. Chem. Int. Ed.* **2004**, *43*, 5231.
[25] J. M. Thomas, *Nature* **1981**, *289*, 633.
[26] J. M. McBride, B. E. Segmuller, M. D. Hollingsworth, D. E. Mills, B. A. Weber, *Science* **1986**, *234*, 830.
[27] J. M. Thomas, P. A. Midgley, *Chem. Commun.* **2004**, 1253.
[28] T. Maschmeyer, F. Rey, G. Sankar, J. M. Thomas, *Nature* **1995**, *378*, 159.
[29] J. M. Thomas, R. Raja, D. W. Lewis, *Angew. Chem.* **2005**, *117*, in press; *Angew. Chem. Int. Ed.* **2005**, *44*, in press.
[30] M. S. Chen, D. W. Goodman, *Science* **2004**, *306*, 252.
[31] C. C. F. Blake, D. F. Koenig, G. A. Mair, A. C. T. North, D. C. Phillips, V. R. Sarma, *Nature* **1965**, *206*, 757.

 © 2005 Wiley-VCH Verlag GmbH & Co. KGaA, Weinheim

Endocrine-Disrupting Substances

DOI: 10.1002/anie.200502138

Chemicals with Endocrine-Disrupting Potential: A Threat to Human Health?**

*Helmut Greim**

Keywords:
endocrine system · environmental chemistry · hormones · toxicology

1. Introduction

In 1996 the book "Our Stolen Future: Are We Threatening Our Fertility, Intelligence, and Survival?" by Colborn, Dumanoski, and Myers was published.[1] Thereafter, reports of decreased human sperm counts and increased incidences of testicular cancer in males and breast tumors in females aroused intense discussions in the public and the scientific community. Previously, Carlsen et al.[2] had evaluated a total of 61 studies on sperm count and had established that there was a decrease from 113 million to 66 million sperm per milliliter of semen between 1938 and 1990. This led Sharpe and Skakkebaek[3] to present the hypothesis that the dysfunctions and diseases of the male sex organs (such as testicular cancer, malformations of the urethra, and cryptorchidism), which have been observed with increasing frequency in the course of the last three to five decades, could be associated with chemicals that mimic the action of estrogen. In particular, medications that mimic the action of estrogen, phytoestrogens, estrogens in cows' milk, and certain industrial chemicals have been considered. This assumption is supported by observations in wild animals. DDT, for example, accumulates in the bodies of birds of prey, which are at the end of the food chain, and leads to reproductive disorders. Colborn et al.[4] described smaller penises in alligators and unfertilized eggs that had been laid as the result of an industrial accident in Florida. In this case, large quantities of the insecticide Dicofol had been discharged into a lake. In other regions, more female than male offspring had been counted for several species of fish and the gulls that ate these fish. These observations and hypotheses resulted in a multitude of studies to identify hormonally active chemicals and to explain their mechanism of action and their significance for humans and the environment.

The different effects have been described and discussed by various authors and committees[5–14] as well as the consequences for appropriate testing.[15,16] In a continuous flow of reports, the chemical exposure of children is linked to hormone-related disorders. These include

- birth defects,
- developmental disorders,
- declining proportion of male newborns,
- mental deficiencies in families of pesticide workers,[17,18]
- testicular dysgenesis syndrome as a result of the disruption of embryonal programming and gonadal development during fetal life by adverse environmental influences,[19]
- insufficient androgen action in the male fetus with subsequent undervirilization and hypospadias in the newborn as a result of intrauterine exposure to environmental hormonal disruptors.[20]

However, except for obvious associations such as the Yusho disease after high exposure to polychlorinated biphenyls, dibenzodioxins, and dibenzofurans,[21,22] none of these suggested associations demonstrated a sufficiently robust correlation between exposure and effects so that increasingly other causes for the observed effects have been discussed like sociodemographic characteristics[23] and combinations of more than one problem.[19]

It is impossible to review all of the available information and add to the detailed reports of the different review panels. Therefore, in this Essay the possible mechanisms and criteria to evaluate the plausibility of a correlation between adverse effects in children and exposure to endocrine-disrupting chemicals will be described. Possible effects of endocrine disruptors in the environment have been discussed recently by Lintelmann et al.[24]

2. Substances Mimicking the Action of Hormones

An "endocrine disrupter" is defined as an exogenous substance or mixture that alters function(s) of the endocrine system and consequently causes adverse health effects in an intact organism, or its progeny, or (sub-) populations.[7,25] Interaction with endogenous hormones may occur by different mechanisms. Xenobiotics can influence hormone synthesis and the release, transport, effect, metabolism, and excretion of hormones. A further group of natural and synthetic substances interferes with the hormones at receptors. Phytoestrogens such as coumestrol, daidzein, and genistein,

[*] Prof. Dr. H. Greim
Institut für Toxikologie und Umwelthygiene
Technische Universität München
Hohenbachernstrasse 15–17
85350 Freising Weihenstephan (Germany)
Fax: (+49) 8161-715618
E-mail: helmut.greim@lrz.tum.de

[**] An explanation of some of the biological and medical terms used in this article is given in the Glossary at the end of the Essay.

InterScience
© 2005 Wiley-VCH Verlag GmbH & Co. KGaA, Weinheim

medications such as diethylstilbestrol, ethinyl estradiol, and tamoxifen, and industrial chemicals such as DDT, 4-nonylphenol, and bisphenol A belong to this group. They bind to the estrogen receptor and interact with the binding of the hormone. A third group of substances, for example, the DDT metabolite *p,p′*-DDE and vinclozoline metabolites, interact with the androgen receptors, that is, the receptors for the male hormone testosterone. Speculations that xenoestrogens may act through unique cellular receptors that do not bind endogenous endocrine modulators lack support.

Compounds that interact with a receptor trigger a cascade of events, which are regulated by the receptor. Substances that compete with the physiological ligand such as a hormone at the receptor and imitate its effect are called agonists, those which block the receptor are antagonists. The kinetics of interactions of xenobiotics with an endogenous compound at a receptor are well understood and are the basis for the evaluation of drug effects via a receptor (see textbooks of pharmacology). The interaction of a ligand with a receptor is described by Equation (1) (see also Figure 1)

$$\text{Ligand} + \text{Receptor} \rightleftharpoons \text{Ligand} - \text{Receptor Complex} \quad (1)$$

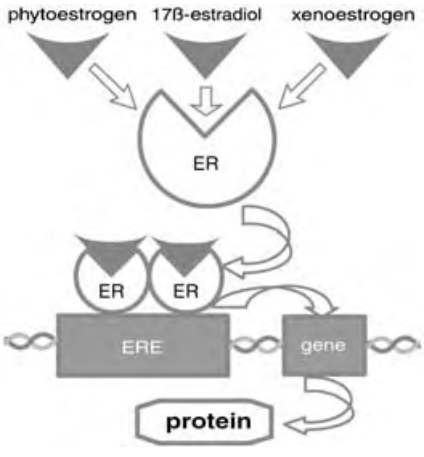


Figure 1. Competition of xenoestrogens and phytoestrogens with 17β-estradiol at an estrogen receptor (ER). The ligand–receptor complex interacts with the estrogen responsive element (ERE), which activates the response gene that in turn triggers the estrogen-dependent production of proteins.

Replacement of a physiological ligand such as an estrogen from the receptor by a competitor such as a xenoestrogen depends on its relative affinity to the receptor and its concentration. For example, replacement of the physiological ligand from the receptor by a compound of 1000-fold lower affinity requires a 1000-fold higher concentration. Although this oversimplifies the competitive interaction of compounds at a receptor, it demonstrates that information on the relative binding affinities of the compounds in question and their concentration in the organism are major criteria to evaluate possible effects of endocrine-disrupting compounds.

The Scientific Committee on Toxicology, Ecotoxicology and the Environment (CSTEE)[7] of the European Commission has compared the potency of xenoestrogen concentrations detected in human blood as a surrogate for concentrations at the receptor with the potency of estradiol concentrations in blood. It appears that the relative potency of *o,p′*-DDT, 4-nonylphenol, and bisphenol A are about millionfold lower than that of estradiol. Only the phytoestrogen genistein showed a potency exceeding that of estradiol. From this it was concluded that an interaction of the compounds at the receptor with physiological consequences is unlikely.

In addition to the reproductive organs, the liver, kidneys, adrenal glands, central nervous system, immune system, cardiovascular system, and bones are target tissues of the effect of steroid hormones; the corresponding receptors have been identified in these tissues. Moreover, there are indications of a concentration-dependent stimulation (low concentrations) and inhibition (high concentrations) of tumor growth by steroid hormones.[10,26,27] For example, xenoestrogens stimulate mitotic activity by interacting with specific receptors of cells in the female genital tract. Many chemicals that humans ingest with their diet have estrogen-like effects, which have been identified in a multitude of test systems.[28] Among these are industrial chemicals such as certain herbicides, fungicides, organochlorine insecticides, nematocides, organophosphates, pyrethroids, heavy metals, polychlorinated biphenyls, and phthalates. Colborn et al.[4] compiled a list of 45 chemicals, including the polychlorinated biphenyls, dibenzodioxins, dibenzofurans, and DDT, to which they attribute an influence on the reproductive system in humans. Also included are the phytoestrogens, that is, naturally occurring plant substances.

3. Test Systems for Identifying Endocrine-Disrupting Chemicals

A great variety of test systems are being used with different experimental modifications, and it is difficult to directly compare the results.[28,15] In most cases standardization is required. The in vitro tests are suitable for identifying the intrinsic hormone-like potential (hazard identification) of a chemical and its relative potency. However, they do not include toxicokinetics of the chemical and its metabolites so that results have to be verified by in vivo testing. Some of the tests are briefly described in this section.

3.1. In Vitro Test Systems

The recombinant yeast estrogen assay uses yeast cells that are transfected with the human estrogen receptor α gene, together with expression plasmids (estrogen-responsive elements and the *lac*-Z reporter gene encoding β-galactosidase). The cells are incubated with the test compound and a chromogenic compound. Active ligands that bind to the receptor induce the expression of β-galactosidase, changing the chromogen to yellow, which is quantified by a spectrophotometer.[29]

In the E-SCREEN test the human MCF-7 breast cancer cell line is incubated with the test compound for several days to allow proliferation. Thereafter the number of cells is quantified, for example, by measuring optical density.[30]

In the estrogen-R(α) competitor screening test the human estrogen receptor is fixed to the 96 wells of a microtiter plate. The test compound and fluorescein-labeled 17β-estradiol are added. After incubation and washing, the fluorescence of 17β-estradiol attached to the receptor is measured.[31]

© 2005 Wiley-VCH Verlag GmbH & Co. KGaA, Weinheim

The placental aromatase assay utilizes aromatase cytochrome P450 mediated conversion of C19 androgens to aromatic C18 estrogens. Androgens have been shown to inhibit this reaction.[32]

The androgen binding or reporter gene assay and the thyroid receptor binding assay determine the affinity of androgen-like and thyroid hormone-like compounds, respectively, to the specific receptors relative to that of the endogenous hormones.

It has to be stressed that these and other in vitro tests are screening tests for the determination of relative potencies of the test chemicals, which must be verified by appropriate studies in animals.[33]

3.2. In Vivo Test Systems

The traditional Hershberger test was originally designed to differentiate between anabolic and androgenic effects of drugs by determining the weights of the *musculus levator ani* and seminal vesicles in mice after treatment for several weeks. Other workers have used a wide range of treatment regimens to determine the androgenic potential of chemicals in intact and castrated laboratory animals. The endpoints used are, for example, prostatic weight, seminal vesical weight, and DNA/RNA contents of male reproductive organs.[34]

In the uterotrophic assay juvenile female rats are treated with the test compound, and uterine growth is monitored after several days of treatment. Since several experimental designs are used, the test requires standardization.[35]

The OECD 407 Test is a repeated-exposure test in rats over 28 days in which histopathological alterations in the gonads can be observed. To better detect endocrine effects of the test chemicals, the OECD 421/422 Screening Tests can be performed to determine the weight and histopathology of hormone-regulated organs and analyze epididymal sperms, the estrous cycle, and a battery of hormones.

The OECD 416 reproductive test in rodents permits an in-depth study of the growth, development, and sexual functionality of the F_1 generation and includes the monitoring of the subsequent F_2 generation through to weaning. The recently revised protocol is considered to include parameters like weights and pathological examinations of the reproductive organs, and detailed spermatogenesis and sperm investigations of the parental generation and their offspring. Evaluation of physical, sexual, and behavioral development and the learning and memory abilities of the offspring is also included.

4. The Relative Potency of Xenoestrogenic Effects

The intensity of the effect of substances, particularly in comparison to the endogenous hormones or natural hormone-like chemicals, is critical for an evaluation. Sonnenschein et al.[36] studied the proliferative effect in estrogen-sensitive cells and found that the estrogenic potency of chemicals such as 4-octylphenol and bisphenol A was considerably less than that of endogenous estradiol by a factors of 3000 and 30000, respectively (Table 1). In view of the low amounts of these chemicals found in the organism, the resulting intensity of effect is very low. Safe[37] calculated the estrogenic and antiestrogenic potencies of xenoestrogens that may be ingested daily relative to 17β-estradiol. A woman taking a birth control pill ingests about 17000 equivalents per day, during postmenopausal estrogen therapy 3300 equivalents. In contrast, ingestion of estrogenic flavonoids in food amounts to 102 equivalents and of environmental organochlorine estrogens 2.5×10^{-6} equivalents. Similar data have been obtained with antiestrogens.

Table 1: Estrogenic potency in the E-SCREEN assay. Proliferation of breast cancer cells MCF-7.[36,51]

Substance	Concn[a] [nmol L^{-1}]	Potency [%][b]
estradiol	0.03	100
4-octylphenol	100	0.03
4-nonylphenol	1000	0.003
bisphenol A	1000	0.003
bisphenol A dimethacrylate	1000	0.003
benzyl butyl phthalate	10000	0.0003
tert-butylhydroxyanisole	50000	0.00006

[a] Lowest concentration that elicits maximal proliferation. [b] Relative proliferative potency ($concn_{estradiol}$/$concn_{test\ substance}$) × 100.

Bolt et al.[33] compared the potencies of the estimated daily intake of 4-nonylphenol and bisphenol A (each 1 μg kg^{-1} body weight) with that of the phytoestrogen daidzein (1 mg kg^{-1} body weight) and ethinyl estradiol (0.5 μg kg^{-1} body weight), which was ingested daily as a low-dosage contraceptive pill. The estrogenic potencies of nonylphenol and bisphenol A were 125–250 and 1000 times lower, respectively, than the daidzein intake, whereas that of ethinyl estradiol was 20 times higher. Daidzein penetrates the placenta.[38] Since soy is the major source of phytoestrogens in human food, which can amount up to 8 mg kg^{-1} body weight in babies fed with soy-based infant formula,[39] the consequences of these exposures carry far more weight than the exposure to xenoestrogens.

The CSTEE[7] in its opinion on endocrine-disrupting chemicals calculated the relative estrogenic potencies of several compounds in humans. Based on their concentration in human serum and their estrogenic potencies as determined in the recombinant yeast estrogen assay, the potencies were shown to be several orders of magnitude lower than that of estradiol (Table 2).

Specific low-dosage effects indicated by experiments reported by the group of vom Saal[40,41] on bisphenol A and nonylphenol could not be verified.[16,42] Attempts to demonstrate the potentiation of low-dosage effects by the presence of several compounds also failed. McLachlan's research group[43] reported that in an in vitro system with yeast cells the effect of two separate, weakly active estrogens was 1000 times higher in combination. Other research groups were not able to repeat these results.[44] Finally McLachlan et al. officially retracted the results and any inferences drawn from them.[45]

Considering this, a toxicologically relevant effect on the prenatal or post-

 © 2005 Wiley-VCH Verlag GmbH & Co. KGaA, Weinheim

Table 2: Estrogenic potency of endocrine modulators detected in the recombinant yeast estrogen assay.[7]

Substance	$Concn_{effect.}$ [mol L^{-1}][a]	$Concn_{hs}$ [ng L^{-1}][b]	Rel. potency
estradiol	2.25×10^{-10}	187	1.0
testosterone	5.09×10^{-5}	6	1.3×10^{-4}
o,p'-DDT	1.80×10^{-3}	0.006	3.0×10^{-9}
4-nonylphenol	1.00×10^{-6}	< 1	1.5×10^{-6}
bisphenol A	3.40×10^{-6}	< 1	4.0×10^{-7}

[a] Effective concentration. [b] Concentration in human serum.

natal phase from synthetic chemicals is not plausible or likely. However, the potential beneficial or adverse effects of phytoestrogens and other natural compounds with hormone-like effects must be considered in the toxicological evaluation.

5. Phytoestrogens in the Human Diet

Phytoestrogens occur naturally in plants. Common classes comprise isoflavones, lignans, coumestans, and resorcylic acid lactones; they are structurally similar to the mammalian estrogen and have a weak estrogenic potency ranging from 500 to 1000 times less than that of 17β-estradiol. A major phytoestrogen source in the human diet is soybean-derived products, which contain the isoflavones daidzein and genistein. As a result of great differences in the consumption of such products, adults in the UK and the USA ingest about 1 mg of isoflavons per day, whereas Asians ingest 50–100 mg daily.[46] Infants who are fed soy-based formula as a sole source of nutrition ingest 22 to 45 mg per day.[47]

The beneficial effects of phytoestrogens in women have been investigated in several studies.[46,48] These indicate that phytoestrogens in the diet have a beneficial effect with respect to breast cancer most likely by prolonging the menstrual cycle. Mean cycle length in Western countries with high breast cancer risk is 28 to 29 days. In Japan it is 32 days, and breast cancer risk is four times lower. Since the division rate of breast cells is four times slower during the follicular phase of the cycle, the authors hypothesize that longer menstrual cycles result in longer follicular phases with reduced cell division during the premenopausal years. Other beneficial effects reported may be reduced serum cholesterol levels, low rates of cardiovascular disease, cancer, and, especially in postmenopausal women, conservation of bone mass.[49]

In newborns fed a soy-based formula during the first three to six months no clinical effects such as feminization have been reported so far. Essex[50] assumes that in babies the hypothalamic–pituitary–gonadal axis (Figure 2) is more active than in older children and adults, which compensates the estrogenic effects of the high intake of isoflavons. However, the author concludes that breast-feeding obviously is best for babies.

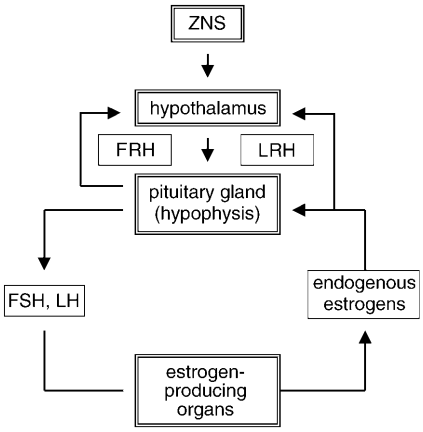


Figure 2. Representation of the hypothalamic–pituitary–gonadal axis. CNS: central nervous system; FSHRH: follicle stimulating hormone releasing hormone; LHRH: lutinizing hormone releasing hormone; FSH: follicle stimulating hormone; LH: lutinizing hormone.

6. Questionable Correlation between Diseases and Endocrine-Disrupting Chemicals

Several well-respected institutions have evaluated the evidence for adverse health effects resulting from human exposure to endocrine disruptors.[7,51,52] They conclude that analysis of the human data so far has failed to provide firm evidence of direct causal association between low-level exposure of endocrine disruptors measured in the general population and adverse health effects. The specific conclusions of the CSTEE[7] and the IPCS[52] are:

- Temporal increases in the frequency of developmental abnormalities of the male reproductive tract, particularly cryptorchidism and hypospadias have been reported, but no causative role for endocrine-disrupting chemicals has been determined. The data on temporal trends in the incidence of hypospadias and cryptorchism should be interpreted with considerable caution, given the lack of longitudinal studies and the consequent difficulties in comparing data from separate studies, in which definition, ascertainment, and registration of these defects may have differed substantially.
- The reports on the declining proportion of male newborns during the last decades remain unexplained.
- Concerns have been raised about the influence of endocrine-disrupting chemicals on the timing of puberty, but the possible mechanisms of action and role of other factors such as nutrition need to be clarified.
- High accidental exposure of pregnant women to certain organochlorine compounds, for example, polychlorinated biphenyls, has led to delays in the physical and mental development of the offspring. Some of these effects appear to result from altered thyroid or neurotransmitter function, but in most instances endocrine mechanisms have not been demonstrated.
- A number of studies report a decline (since 1939) in human sperm quality in several countries. Several re-analyses of these data has indicated possible bias and confounding, and have reached different conclusions with respect to sperm quality, depending on the methodology used. Recent, well-designed studies have shown large regional differences in overall sperm quality and time trends, both within and between countries. Even if semen quality

 © 2005 Wiley-VCH Verlag GmbH & Co. KGaA, Weinheim

has deteriorated, this would not necessarily be due to endocrine disruption.

- Temporal increases in the incidence of testicular cancer have been reported in certain countries, but rates vary considerably among countries. The underlying reason(s) for the increased incidences has not been determined. However, exposure data on endocrine-disrupting chemicals for critical periods are lacking.
- Exposure to certain pesticides and organochlorine compounds has been linked to increases in the incidence of prostate cancer in a few limited studies, but most studies have found no association and the mechanism is unknown.
- There has been a steady increase in breast cancer incidence rates over the last decades (in Europe). The available data associating breast cancer development with exposure to organochlorine compounds do not support a causal relationship. Adult women currently at risk may have been exposed to endocrine-disrupting chemicals in utero or during infancy, childhood, and adolescence in the mid-twentieth century, when contaminant levels of these compounds were higher.

7. Ongoing Evaluation by the European Commission

In June 2000 the Commission established a first priority list of 553 substances. Evidence of endocrine disruption or potential endocrine disruption was found for 118 of these substances. However, when the CSTEE evaluated the list, it concluded that the source of the material, the methodology, and the selection criteria used to establish the list were not scientifically adequate.[53,54] In particular, the omission of dose–response/potency and exposure considerations have been criticized as well as the fact that synthetic hormones released into the environment were not considered. Several suggestions for improving the current approach have been made, including a stepwise approach for the selection of substances for further evaluation and prioritization.

Thereafter, the Commission initiated an in-depth evaluation of a group of 12 candidate substances consisting of 9 industrial compounds and 3 natural/synthetic hormones. At the same time information was gathered on the persistence, production volume, and legal status of another 435 substances for which there was insufficient data to decide on their potential for endocrine disruption. The two studies were presented to the CSTEE for a determination of scientific soundness.

For the first group of 12 substances the CSTEE reached the following conclusions:

- BADGE, carbon disufide, 4-chloro-3-methylphenol, 2,4-dichlorophenol, 4-nitrotoluene, and 2-phenylphenol do not appear to cause critical endocrine-disrupting effects in humans and wildlife.
- 4-(5,5-Dimethylhexyl)phenol and resorcinol do not appear to cause critical endocrine-disrupting effects in humans, but there is a potential risk to aquatic organisms near discharge points.
- The data for 4-chloro-3-methylphenol, 2,4-dichlorophenol, 2-phenylphenol, 4-nitrotoluene, and 4-(5,5-dimethylhexyl)phenol were quite limited, especially regarding environment impact.
- Further testing for potential endocrine-disrupting effects is needed for resorcinol, both on human health and the environment.
- Since the control of 2,2′,4,4′-tetrabromodiphenyl ether (tetra-BDE) can be extracted from the control of penta-BDE (particularly given that tetra-BDE is not produced commercially), it was not considered necessary to review this substance in further detail.
- As expected, the hormones estrone, 17β-estradiol, and ethinyl estradiol cause critical endocrine-disrupting effects in the environment.

The report on the 435 substances now adequately applies selection criteria such as exposure and persistency data, and missing data such as environmental impact have been identified. A preliminary evaluation indicates that of the 435 compounds, 30 are listed in Category 1 (at least one positive in vivo study); of these, 2,3,7,8-TBDD shows a higher endocrine-disrupting potency, whereas the others show 50- to 1000000-fold lower potencies. Of the 57 listed in Category 3, 19 did not show scientific basis for inclusion (3a), the others were classified as having "no data" (3b). Since the report now evaluates reproduction toxicity as part of other systemic toxic effects, further evaluation of the data will allow a comparison of the relative sensitivity of the endocrine system to a compound as compared to other toxic effects. Again, information on wildlife generally is insufficient, and no final conclusion on the impact of endocrine-disrupting chemicals to wildlife populations can be drawn at present.

From both of these reports it can be concluded that although many chemicals have the intrinsic potential for endocrine-disrupting effects, a more detailed evaluation reveals that the NOELs (no observed effect levels) of these effects are usually higher than those of the effects on other organs. Thus, environmental control levels and occupational exposure levels that are based on other endpoints protect humans from endocrine disruption. Because of insufficient information on environmental effects, this conclusion cannot be drawn about possible endocrine-disrupting effects on the environment.

8. Estrogenicity of Sunscreens

Recently Schlumpf et al.[55] investigated a number of compounds that are used as UV absorbers in sunscreen formulations in vitro in the E-SCREEN assay in MCF-7 breast cancer cells and the uterotrophic assay using immature Long Evans rats in vivo. As shown in Table 3 five out of six chemicals indicated estrogenic effects[55] in vitro, whereas three of the six compounds were positive in the uterotrophic assay. However, in the uterotrophic assay the estrogenic potency of benzophenone-3 (Bp-3) was 1500000 times lower than that of ethinyl estradiol, that of 4-methylbenzylidene camphor (4-MBC) 300000 times lower, and of octylmethoxycinnamate (OMC) 1000000 times lower.

 © 2005 Wiley-VCH Verlag GmbH & Co. KGaA, Weinheim

Table 3: Estrogenic activity of compounds in sunscreens (UV-screens).[55]

	BP-3	HMS	4-MBC	OMC	OD-PABA	B-MDM	EE_2
E-SCREEN assay *MCF-7* cells	+	+	+	+	+	negative	+
uterotr. assay [ED_{50}]	1.525 mg kg^{-1}	negative	309 mg kg^{-1}	935 mg kg^{-1}	negative	negative	0.8 μg kg^{-1}
Rel. Potency [ED_{50} EE_2/ED_{50} UV-screen]	1:1.5×10^{-6}	negative	1:0.3×10^{-6}	1:1×10^{-6}	negative	negative	1

[a] BP-3: benzophenone-3 (2-hydroxy-4-methoxybenzophenone); HMS: homosalate (3,3,5-trimethylcyclohexyl 2-hydroxybenzoate); 4-MBC: 4-methylbenzylidene camphor; OMC:octyl methoxycinnamate; PABA: 4-aminobenzoic acid; OD-PABA: octyl-dimethyl-PABA; B-MDM: butylmethoxydibenzoylmethane; EE_2: ethinyl estradiol

However, in the in vitro test the potency of the compounds was similar to that of other industrial chemicals and thus low relative to endogenous estrogens. Bolt et al.[33] criticized these findings since a nonstandardized and non-GLP (good laboratory practice) protocol and uncommon rat strains (Long Evans and Nu rats) had been used. When these authors repeated the work using standardized and GLP protocols, they did not see estrogenic effects for 4-MBC, Bp-3, and OMC in the uterotrophic assay.

Moreover, Nakagawa and Suzuki[31] generally questioned the in vitro test systems used to determine the estrogenic potency of chemicals. In an investigation of 2-hydroxy-4-methoxybenzophenone (HMB) in metabolically competent rat hepatocytes, HMB was hydroxylated to 2,4-dihydroxy-4-methoxybenzophenone (DHMB) and the hydroxylated intermediate, which was tentatively identified as an isomer of 2,2′-dihydroxy-4-methoxybenzophenone (DHP). Both metabolites and the parent compound were rapidly conjugated to glucuronic acid. The metabolites had higher estrogenic activities than the starting HMB in MCF-7 cells (HMB (no activity) < DHMB (weak) < DHP). These findings further indicate that in vitro tests do not mirror the complexity of the intact organism, and that any results must be verified by in vivo testing before any conclusion can be drawn.

9. Conclusion

A great number of endocrine-disrupting chemicals have been identified by in vitro test systems. Since toxicokinetics and metabolism, which are not or insufficiently represented in these tests, affect the toxic potency of a substance, the results from in vitro test systems must be verified by in vivo studies. With such test systems like the improved 28-day toxicity test in rodents (OECD 407), the screening tests on reproduction (OECD 421/422), and the two-generation reproduction toxicity test (OECD 416), endocrine disrupters either showed no effects or the effects appeared only at very high doses exceeding those of other toxic endpoints.

Considering the relative low exposure of humans to endocrine-disrupting chemicals, it is not plausible that low-affinity compounds can displace high-affinity compounds from a receptor unless they reach sufficiently high concentrations. Such high exposure in humans has occurred only after industrial accidents. Thus, the assumption that the binding of a compound to a receptor per se has biological consequences is not acceptable.

There is overwhelming experience from the therapeutic use of very potent synthetic estrogens during pregnancy in order to prevent spontaneous abortion, for contraception, and to treat menopausal or postmenopausal disorders. All of these treatments require sufficiently high therapeutic doses to modulate the endocrine system. No one would expect that a dose more than 1000 times less than the therapeutic dose would be effective.

Overall, the science-based knowledge on the robustness of the endocrine system, the well-understood principles of substrate—receptor interactions, and the generally low exposure of humans to potentially endocrine-disrupting chemicals make it unlikely that the latter play a causative role in diseases and abnormalities observed in children and in the human population in general.

The array of in vitro test systems that covers relevant endpoints of endocrine disrupters is useful for mechanistic studies and helps in setting priorities for further testing. Since these tests do not evaluate the toxicokinetics of the chemical and its metabolites, they may generate false-negative as well as false-positive effects, so that the results must be verified by in vivo studies. Therefore, instead of supporting the further development of in vitro screening tests, it is recommended to improve available long-term in vivo tests like the enhanced OECD 407 28-day test and the OECD 416 two-generation study. These tests are considered relevant for the detection of hormone-like effects of chemicals. They usually demonstrate that endocrine-disrupting effects of chemicals are weaker than other effects like hepatotoxicity and neurotoxicity. Due to insufficient information on environmental effects, such conclusions cannot be drawn about possible endocrine-disrupting effects on wildlife populations.

10. Glossary

Explanation of some biological and medical terms:

- Cryptorchidism: failure of the testes to descend into the scrotum.
- Hypospadias: developmental anomaly in which the urethra opens on the underside of the penis or the peritoneum.
- Testicular dysgenesis syndrome: syndrome that encompasses low sperm quality, hypospadias, cryptorchidism, and testicular cancer.
- Hypothalamic–pituitary–gonadal axis: different feedback mechanisms between CNS (hypothalamus) and the hormone system (pituitary gland, gonads) for the regulation of endogenous sexual hormones; for example, a decrease in blood levels of estrogens stimulates their production in the ovary while an increase

 © 2005 Wiley-VCH Verlag GmbH & Co. KGaA, Weinheim

results in diminished estrogen release.

[1] T. Colborn, D. Dumanoski, J. P. Myers, *Our Stolen Future: Are We Threatening Our Fertility, Intelligencen, and Survival?*, Dutton, New York, **1996**.

[2] E. Carlsen, A. Giwercman, N. Keiding, N. E. Skakkebaek, *Br. Med. J.* **1992**, *305*, 609 – 613.

[3] R. M. Sharpe, N. E. Skakkebaek, *Lancet* **1993**, *341*, 1392 – 1395.

[4] T. Colborn, F. S. vom Saal, A. M. Soto, *Environ. Health Perspect.* **1993**, *101*, 378 – 384.

[5] S. Barlow, R. J. Kavlock, J. A. Moore, S. L. Schanz, D. M. Sheehan, D. L. Shuey, J. M. Lary, *Teratology* **1999**, *60*, 365 – 375.

[6] R. D. Combes, *ATLA Altern. Lab. Anim.* **2000**, *28*, 81 – 118.

[7] CSTEE Opinion on human and wildlife health effects of endocrine-disrupting chemicals, with emphasis on wildlife and on ecotoxicology test methods, European Commission, March **1999**, http://europa.eu.int/comm/health/ph_risk/committees/sct/sct_en.htm.

[8] G. H. Degen, H. M. Bolt, *Int. Arch. Occup. Environ. Health* **2000**, *73*, 433 – 441.

[9] J. M. Goldman, S. C. Laws, S. K. Balchak, R. L. Cooper, R. J. Kavlock, *Crit. Rev. Toxicol.* **2000**, *30*, 135 – 196.

[10] J. J. A. Mendes, *Fd. Chem. Toxicol.* **2002**, *40*, 781 – 788.

[11] National Research Council. Hormonally active agents in the environment. Washington, D.C. (USA), National Academy Press, **1999**.

[12] R. Nilsson, *Toxicol. Pathol.* **2000**, *28*, 420 – 431.

[13] S. H. Safe, *Environ. Health Perspect.* **2000**, *108*, 487 – 493.

[14] J. G. Vos, E. Dybing, H. Greim, O. Ladefoged, C. Lambre, J. V. Tarazona, I. Brandt, A. D. Vethaak, *Crit. Rev. Toxicol.* **2000**, *30*, 71 – 133.

[15] C. A. Kimmel, S. L. Makris, *Toxicol. Lett.* **2001**, *82*, 73 – 82.

[16] C. W. Schmidt, *Environ. Health Perspect.* **2001**, *109*, 420 – 421.

[17] V. F. Garry, M. E. Harkins, L. L. Erickson, L. K. Long-Simpson, S. E. Holland, B. L. Burroughs, *Environ. Health Perspect.* **2002**, *110*, 441 – 449.

[18] E. A. Guilette, *Cent. Eur. J. Public Health* **2000**, *8*, 58 – 59.

[19] N. E. Skakkebaek, E. Rajpert-De Meyts, K. M. Main, *Hum. Reprod.* **2001**, *16*, 972 – 978.

[20] C. Sultan, F. Paris, B. Terouanne, P. Balaguer, V. Georget, N. Poujol, C. Jeandel, S. Lumbruso, J. C. Nicolas, *Hum. Reprod. Update* **2001**, *7*, 314 – 322.

[21] Y. Aoki, *Environ. Res. A* **2001**, *86*, 2 – 11.

[22] M. P. Longnecker, M. A. Kiebanoff, H. Zhou, J. W. Brock, *Lancet* **2001**, *358*, 110 – 114.

[23] M. Martuzzi, N. D. DiTanno, R. Bertollini, *Arch. Environ. Health* **2001**, *56*, 358 – 364.

[24] J. Lintelmann, A. Katayama, N. Kuhihara, L. Shore, A. Wenzel, *Pure Appl. Chem.* **2003**, *75*, 631 – 681.

[25] IPCS (International Programme on Chemical Safety): Report of IPCS/OECD scoping meeting on endocrine disruptors (EDCs). Washington, D.C. (USA), March **1998**.

[26] *Hormonally active agents in food. Symposium organized by the DFG Senate Commission on the Evaluation of Food Safety* (Ed.: G. Eisenbrand), Wiley-VCH, Weinheim, **1998**.

[27] W. G. Foster, *Can. J. Public Health* **1998**, *89*, Suppl. 1, 37 – 41.

[28] ECETOC (European Centre for Ecotoxicology and Toxicology of Chemicals). Environmental Oestrogens: A compendium of test methods. ECETOC Document No. 33, Brussels, **1996**.

[29] E. J. Routledge, J. P. Sumpter, *Environ. Toxicol. Chem.* **1996**, *15*, 241 – 248.

[30] A. M. Soto, C. Sonnenschein, K. L. Chung, M. F. Fernandez, N. Olea, M. F. Serrano, *Environ. Health Perspect.* **1995**, *103*, 113 – 122.

[31] Y. Nakagawa, T. Suzuki, *Chem. Biol. Interact.* **2002**, *139*, 115 – 128.

[32] M. J. O'Reilly, N. Li, L. W. Duax, W. R. Brueggemeier, *J. Med. Chem.* **1995**, *38*, 2842 – 2850.

[33] H. M. Bolt, P. Janning, H. Michna, G. H. Degen, *Arch. Toxicol.* **2001**, *74*, 649 – 662.

[34] W. Kuhnz, S. Beier, *Contraception* **1994**, *49*, 275 – 289.

[35] J. Odum, P. A. Lefevre, S. Tittensor, D. Patton, E. J. Routledge, N. A. Beresford, J. P. Sumpter, J. Ashby, *Regul. Toxicol. Appl. Pharmacol.* **1997**, *25*, 176 – 188.

[36] C. Sonnenschein, A. M. Soto, M. F. Fernandez, N. Olea, M. F. Olea-Serrano, M. D. Ruiz-Lopez, *Clin. Chem.* **1995**, *41*, 1888 – 1895.

[37] S. H. Safe, *Environ. Health Perspect.* **1995**, *103*, 346 – 351.

[38] G. H. Degen, P. Janning, P. Diel, H. Michna, H. M. Bolt, *Arch. Toxicol.* **2002**, *76*, 23 – 29.

[39] K. D. R. Setchell, L. Zimmer-Nechemias, J. Cai, J. E. Heubi, *Am. J. Clin. Nutr.* **1998**, *68*, 1453S – 1461S.

[40] S. C. Nagel, F. S. vom Saal, K. A. Thayer, M. G. Dhar, M. Boechler, W. V. Welshons, *Environ. Health Perspect.* **1997**, *105*, 70 – 76.

[41] F. S. vom Saal, P. S. Cooke, D. L. Buchanan, P. Palanza, K. A. Thayer, S. C. Nagel, S. Parmigiani, W. V. Welshons, *Toxicol. Ind. Health* **1998**, *14*, 239 – 260.

[42] R. W. Tyl, C. B. Myers, M. C. Marr, B. F. Thomas, A. R. Keimowitz, D. R. Brine, M. M. Veselica, P. A. Fail, T. Y. Chang, J. C. Seely, R. L. Joiner, J. H. Butala, S. S. Dimond, S. Z. Cagen, R. N. Shiotsuka, G. D. Stropp, J. M. Waechter, *Toxicol. Sci.* **2002**, *45*, 121 – 146.

[43] S. F. Arnold, D. M. Klotz, B. M. Collins, P. M. Vonier, J. R. Guilette, J. A. McLachlan, *Science* **1996**, *272*, 1489 – 1492.

[44] K. W. Gaido, D. P. McDonnell, K. S. Korach, S. H. Safe, *CIIT Activities* **1997**, *17*,1–7.

[45] J. A. McLachlan, *Science* **1997**, *277*, 462 – 463.

[46] A. Cassidy, *Proc. Nutr. Soc.* **1996**, *55*, 399 – 417.

[47] K. D. R. Setchell, L. Zimmer-Nechemias, J. Cai, J. E. Heubi, *Lancet* **1997**, *350*, 23 – 27.

[48] A. Cassidy, S. Bingham, K. Setchell, *Br. J. Nutr.* **1995**, *74*, 587 – 601.

[49] D. M. Tham, C. D. Gardner, W. L. Haskell, *J. Clin. Endocrinol. Metab.* **1998**, *83*, 2232 – 2235.

[50] C. Essex, *Br. Med. J.* **1996**, *313*, 507 – 508.

[51] BUA Reports 212 and 228: GDCh Advisory committee on Existing Chemicals (Beratergremium für Altstoffe: BUA): Biological impact of synthetic and natural endocrine active substances—Effects on human health, Hirzel, Stuttgart, **1999** and **2001**.

[52] *IPCS (International Programme on Chemical Safety): Global assessment of the state-of-the-science of endocrine disruptors* (Ed.: T. Damstra, S. Barlow, A. Bergman, R. Kavlock, G. Van Der Kraak), World Health Organization, **2002**.

[53] CSTEE Opinion on BKH Consulting Engineers Report "Towards the establishment of a priority list of substances for further evaluation of their role in endocrine disruption" European Commission, September, **2000**, http://europa.eu.int/comm/health/ph_risk/committees/sct/sct_en.htm.

[54] CSTEE Opinion on "Two study reports on endocrine disruptors by WRc-NSF and BKH Consulting Engineers" (WRc-NSF ref: UC 6052; BKH Ref: MO355037). European Commission, September **2003**, http://europa.eu.int/comm/health/ph_risk/committees/sct/sct_en.htm.

[55] M. Schlumpf, B. Cotton, M. Conscience, V. Haller, B. Steinmann, W. Lichtensteiger, *Environ. Health Perspect.* **2001**, *109*, 239 – 244.

 © 2005 Wiley-VCH Verlag GmbH & Co. KGaA, Weinheim

H. Cölfen and M. Antonietti

DOI: 10.1002/anie.200500496

Mesocrystals

Mesocrystals: Inorganic Superstructures Made by Highly Parallel Crystallization and Controlled Alignment

Helmut Cölfen and Markus Antonietti*

Keywords:
aggregation · colloidal crystal · crystal growth · mesocrystal · self-assembly

Dedicated to Professor Rüdiger Kniep on the occasion of his 60th birthday



© 2005 Wiley-VCH Verlag GmbH & Co. KGaA, Weinheim

Controlled self-organization of nanoparticles can lead to new materials. The colloidal crystallization of non-spherical nanocrystals is a reaction channel in many crystallization reactions. With additives, self-organization can be stopped at an intermediary step—a mesocrystal—in which the primary units can still be identified. Mesocrystals were observed for various systems as kinetically metastable species or as intermediates in a crystallization reaction leading to single crystals with typical defects and inclusions. The control forces and mechanism of mesocrystal formation are largely unknown, but several mesocrystal properties are known. Mesocrystals are exiting examples of nonclassical crystallization, which does not proceed through ion-by-ion attachment, but by a modular nanobuilding-block route. This path makes crystallization more independent of ion products or molecular solubility, it occurs without pH or osmotic pressure changes, and opens new strategies for crystal morphogenesis.

From the Contents

1. Introduction	5577
2. Early Reports on Mesocrystals	5578
3. One- and Two-Dimensional Mesocrystals	5580
4. Three-Dimensional Mesocrystals	5580
5. Conclusions	5589

1. Introduction

Alignment of nanoparticle building blocks into ordered superstructures by bottom-up approaches is one of the key topics of modern colloid and materials chemistry.[1] In this area, much can be learned from the processes of biomineralization, which lead to well defined organic–inorganic hybrid materials with superior materials properties, complex morphologies. and hierarchical order.[2–4] Biominerals are often single crystals with amazingly complex morphologies such as the hammer-shaped building units of coccoliths[5] or the skeletal plates of sea urchins.[6] Although it is known that organic scaffolds, as in the case of coccoliths, play an important role,[5] the actual crystallization mechanism of the inorganic phase remains largely unexplored. Recently, increasing evidence was found that biomineralization takes place through amorphous precursor particles, for example, as reported for sea urchin spines.[7] In this way large amounts of material can be stored in metastable precursor particles, which are readily available to a crystallization event in a confined reaction environment. Further advantages of this crystallization pathway are highly efficient mass fluxes that are independent of solubility-products, the coupled high crystallization speeds, and crystallization without change of the pH value and the osmotic pressure. These are key features for mineralization especially in biological systems. This pathway is in stark contrast to the classical crystallization, which postulates an ion-by-ion or single-molecule attachment to a critical crystal nucleus and is therefore bound to solubility products and diffusion limitations. Mesoscale transformation processes towards crystalline phases were recently reviewed.[8]

By mesoscale transformation, not only single crystals with complex morphologies but also superstructures made up of nanoparticles interspaced by organic additives can be formed. The fusion of the building blocks leads to single-crystalline structures with included organic additives as defects. Support for this view comes from biomineral examples, which, although single crystalline, often contain minor amounts of included biopolymers. This inclusion is not understandable from the viewpoint of an ion-mediated crystallization process, as additives are generally considered to adsorb at edges and kinks of the developing crystal surface stopping it from further growth.[9]

Mesocrystal formation and the process of mesoscale transformation seem, however, not to be limited only to biominerals. It looks like nature only employs this advantageous physico-chemical construction principle, gaining speed and flexibility of construction. For example, similar to biomineralization, inclusions of additives up to 30 wt % are observed in synthetically grown crystals, too.[10,11] Revisiting the existing literature shows indeed that comparable observations have been made in synthetic inorganic chemistry much earlier, even in the absence of additives,[12,13] and the question can be raised if precursor particles and their superstructures also play a role—at least as intermediates—in crystallization in a much broader context.

In this Review we revisit the existing literature and examine it from the viewpoint of nonclassical, nanoparticle-mediated crystallization. A mesocrystal in this context is defined as a superstructure of crystalline nanoparticles with external crystal faces on the scale of some hundred nanometers to micrometers (Figure 1).

Mesocrystal intermediates can also lead by fusion to the formation of single crystals with included organic additives, sometimes allowing the observation of highly oriented nanoparticle-based intermediates. This scenario is shown in Figure 1.

It has to be noted that the term "mesocrystal" has already been used in the literature, but in the less restricted sense of a mutual three-dimensional translational order of various nanocrystals. As templates, pore systems of the MCM-41

[*] Dr. H. Cölfen, Prof. Dr. M. Antonietti
Max-Planck-Institute of Colloids and Interfaces
Colloid Chemistry, Research Campus Golm
14424 Potsdam (Germany)
Fax: (+49) 331-5679502
E-mail: Coelfen@mpikg.mpg.de

 © 2005 Wiley-VCH Verlag GmbH & Co. KGaA, Weinheim

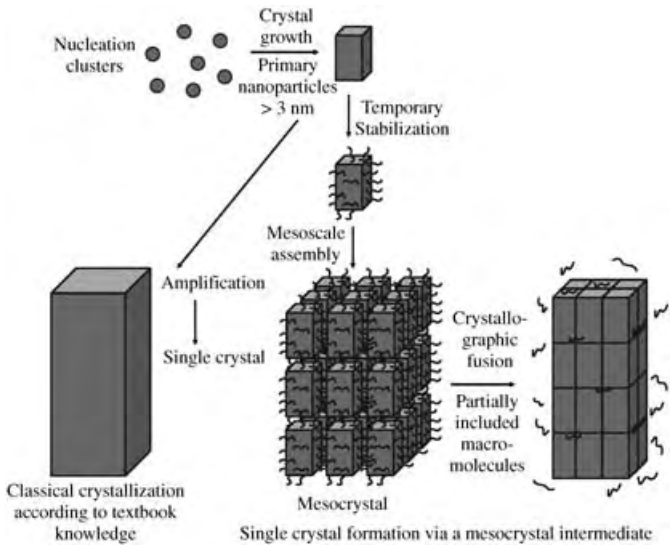


Figure 1. Classical crystallization (left) by ion-by-ion addition versus single-crystal formation by a mesocrystal intermediate formed by nanoparticle self-assembly. Image based upon ref. [8]

type were used for the deposition of size-quantized $BaTiO_3$[14–16] or $SrBi_2Ta_2O_9$.[15,17] Our definition is more restricted as it also involves orientational order (vectorial alignment) and the self assembly to facetted microstructures.

Mesocrystals are a special case of colloidal crystals. The latter have received considerable attention in recent years, as they result from the formal substitution of atoms or molecules in a classical crystallization event by defined and monodisperse nanoparticles this leads to superlattices with new and desirable properties such as photonic band gaps[18] or altered electronic and optical properties as in the case of semiconductors.[19] In addition to colloidal crystals made from SiO_2 which are a convenient model case, semiconductor and metal nanoparticles have been intensively investigated, owing to their electronic and optical applications.[20–24] Usually, the nanoparticle building blocks can be regarded as spherical core–shell nanoparticles with an inorganic core and an organic surfactant/ligand shell, both of which play a role for the crystallographic symmetry of the superlattice. Even colloidal crystals from two different nanocrystal systems could be prepared.[24] If inorganic and slightly prolate building units such as CdSe were used, an almost perfect crystallographic alignment of the nanocrystals was detected[19]—a feature which is also observed in mesocrystals as will be discussed later. Nevertheless, colloidal crystals were so far only self-assembled from spherical nanoparticles or by covalent linkage of clusters,[25] although it is clear that nonspherical nanoparticle building units should provide additional opportunities for self-assembly. Concepts to design such colloidal crystals, for example by orientation of nonspherical nanoparticles through magnetic fields are just being developed, and have to date not been experimentally verified.[26] It is important to remember that the mesocrystals described below already manifest the applicability of such concepts as they consist of highly oriented nonspherical building units and are formed through a pure self-assembly approach.

2. Early Reports on Mesocrystals

Although particle aggregates have been observed since the advent of crystallization experiments, particle aggregates with defined morphology and size were much less reported. For a Review by one of the pioneers in this field, see ref. [27]. One of the very first indications of mesocrystal intermediates was deduced from the porous internal structure of $BaSO_4$[28] which—according to the classical crystallization theory—should crystallize to a defect-free single crystal.

First indications of mesocrystals, although without perfectly flat external faces, were reported by Matijevic et al. in a synthetic study on various Ce^{IV} compounds in absence of any organic additives.[13] Figure 2 shows some of these rod-like particles of Ce^{IV} minerals.

These structures are clearly nanoparticle aggregates but without a well facetted external morphology. Nevertheless, the single rodlike or platelike nanoparticles mutually align with high positional and vectorial precision to give a reproducible superstructure.

Another example is reported for the same components[13] as well as for CuO, depicted in Figure 3 (right).[29] For CuO, the aggregation from primary nanoparticles could be revealed in a kinetic study which already indicated the general self-assembly mechanism for mesocrystals, although a faceting of the nanocrystal aggregates is generally lacking (Figure 3,



Helmut Cölfen studied Chemistry at the university Duisburg and completed his PhD in 1993 supervised by Werner Borchard. After a Postdoc at the NCMH Nottingham with Stephen Harding, he joined the Max Planck Institute of Colloids and Interfaces in 1995 and finished his Habilitation on "Biomimetic Mineralization" in 2001 with Markus Antonietti. He is now a lecturer at the University of Potsdam and head of the analytical service in the colloid chemistry department of the MPI. His current research is focused on the synthesis and analysis of double hydrophilic block copolymers, biomimetic mineralization, and nonclassical crystallization. In his spare time he plays music in a band.



Markus Antonietti studied Chemistry in Mainz and did his doctorate with Hans Sillescu. His habilitation about nanostructured polymergels in 1990 filled him with enthusiasm for complex materials. After his professorship for Chemistry at the University of Marburg he was appointed director for the department of Colloid Chemistry at the Max Planck Institute of Colloids and Interfaces in 1993. His main academic interest is in the creativity in research. He loves to share and impart this passion. He likes cooking with his family and loud music.

 © 2005 Wiley-VCH Verlag GmbH & Co. KGaA, Weinheim

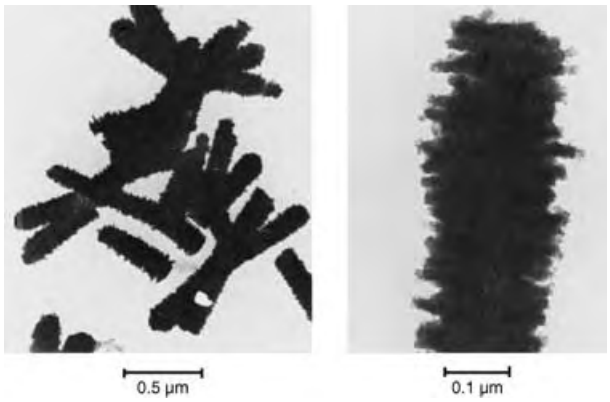


Figure 2. Transmission electron microscope (TEM) images of rodlike Ce^{IV} sulfate particles obtained by aging 2.5×10^{-9} mol dm^{-3} $Ce(SO_4)_2$, 4.5 mol dm^{-3} H_2SO_4, and 0.45 mol dm^{-3} Na_2SO_4 at 90 °C for 12 h. Figure reproduced from ref. [13] with kind permission of the American Chemical Society.

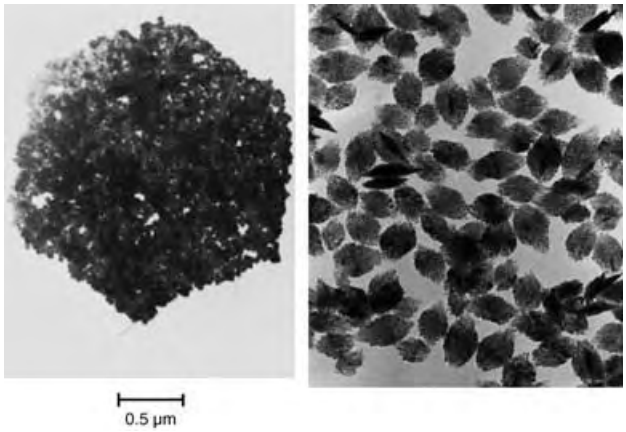


Figure 3. Left: TEM of a minor part of CeO_2 precipitates obtained by aging 1.5×10^{-3} mol dm^{-3} $(NH_4)_2[Ce(NO_3)_6]$, 6.4×10^{-2} mol dm^{-3} H_2SO_4, and 1.6×10^{-2} mol dm^{-3} Na_2SO_4 pH 1.4 at 90 °C for 12 h. Figure reproduced from ref. [13] with kind permission of the American Chemical Society. Right: CuO particle aggregates obtained via double jet precipitation,[29] reproduced with permission from Academic Press.

right). For CeO_2, a two-dimensional hexagonal platelet is formed from not very homogeneous and not very well-defined spherical nanoparticles (Figure 3, left). Clearly, the mutual interaction forces drive the single nanoparticles to form a hexagonal superstructure. It is remarkable that CeO_2 possesses a primitive triclinic unit cell, that is, it has especially no hexagonal symmetry axis. It will be shown below that mesocrystals very often have a higher symmetry than their constituting tectons. This occurrence is speculatively assigned to multiple twinning of primitive units and the resulting symmetry average on the mesoscale.[30] In these early experiments, the hexagon superstructure however just represented a minor part of the precipitates and its formation mechanism remained as unclear as for the rods shown in Figure 1. Nevertheless, it was an early observation of crystalline superstructures with an external structure and symmetry differing from that of the nanoparticle building units, but with a not too well ordered nanoparticle interior. For the sake of completeness, it should be mentioned that very similar observations on the oriented aggregation of CuO were just recently published,[31] however with a more precise view of the relevant phenomena.

As early as 1986, mesocrystals with even higher definition were reported for $CaCO_3$ made in silica gels.[32] In this case, fibers built from a set of cleaved calcite rhombohedra arranged along their *c*-axis were reported. Although each fiber was an aggregate of crystalline subunits, the observed behavior by polarization microscopy was that of a single crystal indicating the high orientational alignment of the subunits in this one-dimensional mesocrystal.[32] Interestingly, these mesocrystal fibers were only an outer part of a hierarchical structure, the so called "sheaf of wheat" morphology.[32] From different sheaves, mesocrystal fibers with a very different morphology radially splayed out from the sheaf center. Again, the mesocrystals behaved like single crystals in polarization microscopy and exhibited a complicated morphology (Figure 4). The reason for this unusual aggregate morphology remained unexplained, although the morphogenesis process was assumed to be of importance.

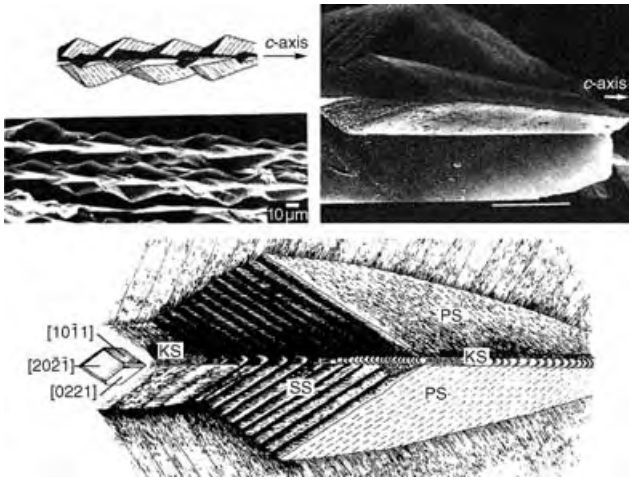


Figure 4. $CaCO_3$ formed in a silica gel. Top left: SEM view of a set of serrated fibers and a diagram of one fiber. Top right: Enlarged view of the left SEM image showing a morphological unit form by two domes (scale bar = 10 μm. Bottom: Diagrammatic representation of a morphological unit of the structures shown in the top part revealing the orientation of the aggregating rhombohedra. PS = planar surfaces, KS = kinked surfaces, SS = stepped surfaces. Reprinted from ref. [32] with permission of Elsevier Science publishers B.V.

Such work has stimulated experiments where otherwise stable nanoparticles of anatase were destabilized in a controlled fashion, either by hydrothermal treatment[33] or by the addition of face-specific organic molecules called "assemblers".[34,35] Indeed, a few years ago, the first nanoparticle-based structuration mechanism was identified.[33] In this so called "oriented attachment", nanoparticles fuse together with their high-energy surfaces under crystallographic fusion and elimination of the high-energy faces under energy gain, thus creating extended structures.[33] Addition of assembler throughout this process even improves the control

 © 2005 Wiley-VCH Verlag GmbH & Co. KGaA, Weinheim

over the aggregation process;[34,35] similar levels of control were also found with polymeric additives.[36–39] Such an oriented attachment mechanism was then suggested also to hold true for iron hydroxide biomineralization products.[40]

3. One- and Two-Dimensional Mesocrystals

One- and two dimensional particle arrays such as those shown above were also reported by Mann and co-workers but in a difference to the previous studies, they used a surfactant microemulsion-mediated approach. In this case, presumably a combined action of nanoparticle crystallization and surfactant interactions led to the self assembly of these remarkable low-dimensional structures, and a surfactant-mediated aggregation mechanism was suggested for the growth of these structures, as shown in Figure 5.[41]

The structures shown in Figure 5 quite nicely illustrate some of the building principles of mesocrystals (shown as a sketch in Figure 1) in one or two dimensions: the primary crystalline building blocks are mutually aligned, following common crystallographic coordinates. The structure in itself is not exactly crystalline, as minor differences in length or size are tolerated and taken up in the structure. It is a mutual self-organization principle, which can tolerate lattice defects.

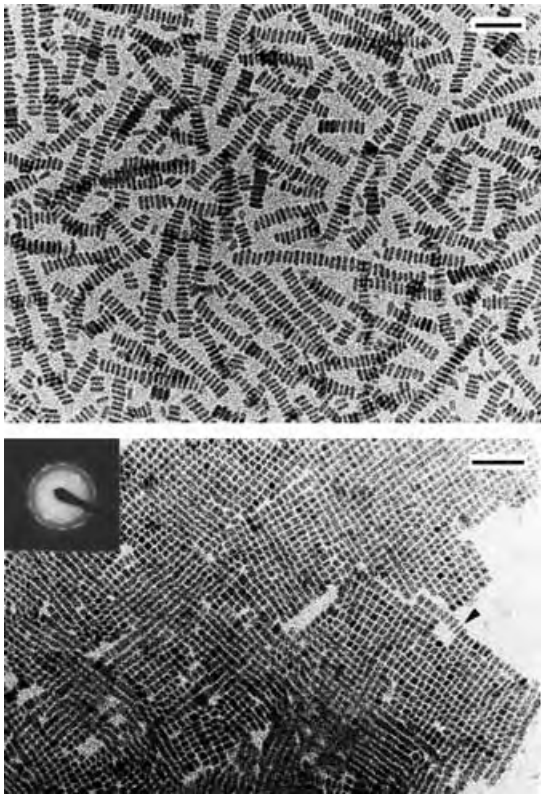


Figure 5. TEM images showing top: ordered chains of prismatic $BaCrO_4$ nanoparticles and bottom: rectangular superlattice of $BaCrO_4$ nanoparticles[41] prepared in a reverse microemulsion. Scale bars = 50 nm . The arrow indicates dislodged particles revealing the prismatic morphology of individual crystallites. Inset: The electron diffraction pattern gives the superimposition of reflections from zone axes approximately parallel to the [100] direction. Reproduced from ref. [41] with kind permission of Nature Publishing Group.

4. Three-Dimensional Mesocrystals

Examinations on defined particle aggregation by hydrophilic molecules[42] or double hydrophilic block copolymers (DHBCs) as especially powerful surface-active agents to control crystallization and superstructure formation of inorganic compounds,[43] have subsequently multiplied the reported observations of diverse mesocrystal systems. Herein, it will be shown that the restrictions on additive design for mesocrystal formation are not too strict, as even just a preferential attachment to specific surfaces of the primary crystals can lead to strongly anisotropic mutual interactions. Among these interactions, dipole fields were first suggested by Busch, Kniep, et al. to be of importance for the structuration process of inorganic matter.[44,45]

The formation mechanisms of three dimensional mesocrystals are largely unexplored. One of the difficulties maybe the high lattice energy of inorganic crystals, which in many cases leads to the crystallographic fusion of the oriented nanocrystal building units to a single crystal (Figure 1) through the three-dimensional oriented attachment mechanism.[33] Another difficulty maybe the homogeneous aqueous environment, where it is difficult to predict how hydrophilic nanoparticles can be arranged to defined three-dimensional mesocrystals. Herein we will try to reveal a general mesocrystal formation mechanism, that is clearly distinguishable from the default case of uncontrolled primary particle aggregation.

One of the first three-dimensional mesocrystals and probably the most perfect to date was reported by Busch and Kniep in form of an elongated, hexagonal-prismatic fluoroapatite seed crystal formed in a double diffusion experiment at ambient temperature in a gelatine gel (Figure 6).[44–46] The hexagonal seed crystal was not directly recognizable as a mesocrystal, as it showed a well-facetted, single-crystal-like morphology (Figure 6). Even X-ray diffraction showed features of a fluorapatite single crystal oriented along the *c*-axis,[47,48] because of the very high vectorial order of its nanoparticulate building units. Although the hexagonal crystals contain approximately 2 wt-% intracrystalline gelatine, the polymer does not modulate the crystal structure, so it was concluded that the gelatine adapts to the fluoroapatite structure.[47]

Kniep et al. were able to reveal the radial inner structure of this seed crystal by a hexagonal cross section perpendicular to the seed axis, thus disproving the existence of a classical single crystal.[45] It was concluded that the hexagonal seed crystal with single-crystalline appearance and scattering behavior is a hierarchically ordered inorganic–organic composite superstructure with periodic orientation of hexagonal primary apatite nanocrystals,[49] or, in our words, a mesocrystal (see also Figure 1).

In a more recent study, the internal nature of the hexagonal seed crystals (Figure 7, left) was investigated in more detail.[50] Figure 7 (right) shows the growth model for the observed radial outgrowth. It agrees with the mesocrystal scheme presented in Figure 1 but modified for the case of hexagonal building units.[50]

 © 2005 Wiley-VCH Verlag GmbH & Co. KGaA, Weinheim

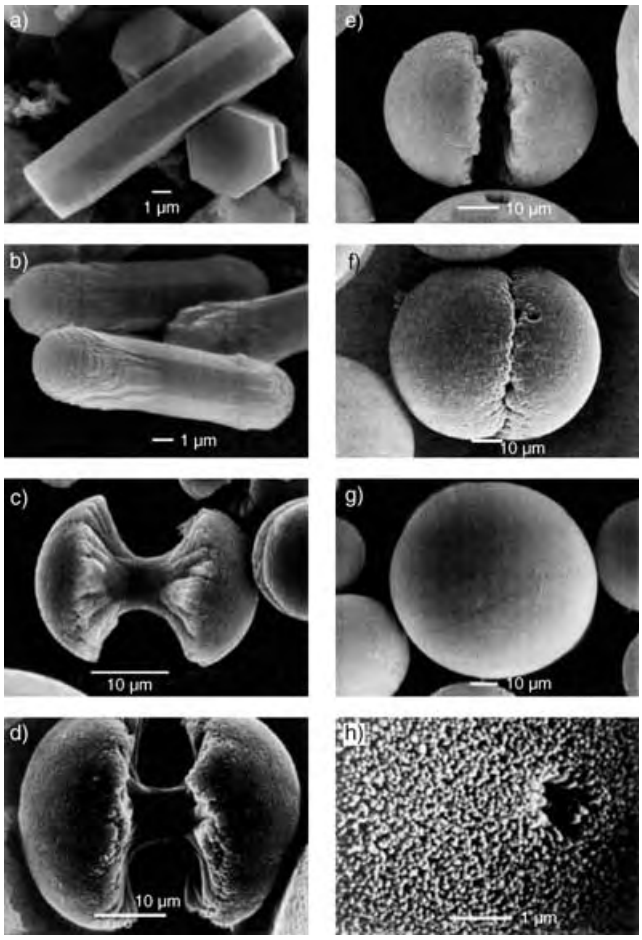


Figure 6. Selected sequence of SEM images of progressive stages of self-assembled (hierarchical) growth of fluorapatite aggregates in a gelatin gel (morphogenesis): from an elongated hexagonal-prismatic seed (a) through dumbbell shapes (c–f) to spheres (g); the surface of a just closed sphere also consists of needlelike units (h) following the general principles of self-similarity. Intrinsic electric fields were suggested control factor for the rod–dumbbell–sphere fractal growth. Picture reproduced from ref. [45].

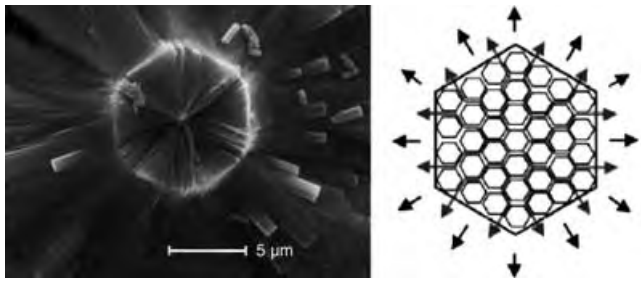


Figure 7. Left: SEM image of the fracture area of a central seed of a fractal composite aggregate. The fracture surface is dominated by a radial pattern. SEM (vacuum) was used instead of "environmental SEM" (freezing of sample) because areas of structural weakness are made visible more clearly by shrinking effects during evacuation (drying). Right: Idealized two-dimensional arrangement of hexagonal nanoparticles forming a hexagonal nanoensemble (nanosuperstructure). The organic component inside and between the crystalline building units is omitted for clarity. The inner lines in the right Figure indicate possible directions of preferred cleavage, the outer arrows show the radial structure of the cleavage. Reprinted from ref. [50] with permission of the Royal Society of Chemistry.

The hexagonal pattern, already known from X-ray diffraction studies,[47,48] was also found in high-resolution micrographs with subsequent fast Fourier transform (FFT) analysis (Figure 8, top). Electronic filtering and enhancement of this image revealed structural defects, which were attributed to a collagen triple-helix strand (white circle Figure 8, bottom),[50] the memory of the former grain boundaries that are stabilized by organic material.

In addition, a superstructure periodicity of 10 nm was revealed, in good agreement with a tecton or primary nanoparticle size of about 10 nm.[50] Furthermore, TEM of a focused ion beam milled sample showed pores and channels at the grain boundaries containing an amorphous phase,[51] giving final evidence for the mesocrystalline nature of the well facetted hexagonal superstructure (see also Figure 1).

Reactions in gels appear to be well suited for the generation of mesocrystals as crystal growth in gels takes place under very high supersaturation[52] leading to increased nucleation of small clusters—the building units for the mesocrystals. Simultaneously, convection or turbulence throughout crystallization can be suppressed, thus allowing the interaction potentials between the particles to dominate the mutual alignment of the particles. This process explains why many of the most defined mesocrystals are observed in gels.

Whereas gelatine gels can be considered to interact with inorganic crystals, at least through their charged groups, polyacrylamide gels can be considered to be essentially inert. The growth of $CaCO_3$ in polyacrylamide gels led to remarkable pseudo-octahedral calcite mesocrystal morphologies built up of rhombohedral primary nanocrystallites (Figure 9).[53,54] The external faces of the superstructure could even be indexed and a growth model based on hierarchical aggregation of rhombohedral subunits was proposed.[53] As already found for the fluorapatite hexagonal seeds, the crystallographic orientation of the subcrystallites is almost perfect, and the organic matrix appears to be interspaced between individual crystallites (Figure 9).[53] However, whereas the fluoroapatite diffraction pattern was that of a single crystal,[47] the calcite mesocrystals indicated a slight orientational distortion of the diffraction spots (Figure 9) corresponding to an average mosaic spread of 3.9 ± 1.1 degrees. This result nevertheless still confirms a high orientational order of the subunits in the mesocrystal.[53] We attribute this difference to the fact that the calcite system contains many vacancies and is potentially twinned (to allow construction of an octahedra from rhombohedra), whereas the particles from Kniep et al. have a higher symmetry and are clearly rather tightly packed.

Varying the polyacrylamide hydrogels by copolymerization with charged acrylamidopropanesulfonate (AMPS) to give polyacrylamide-co-acrylamidopropanesulfonate (PAAm-co-PAMPS), the morphology of the calcite mesocrystals could be tuned from the pseudo-octahedral[53] towards a cubooctahedral morphology with increasing

 © 2005 Wiley-VCH Verlag GmbH & Co. KGaA, Weinheim

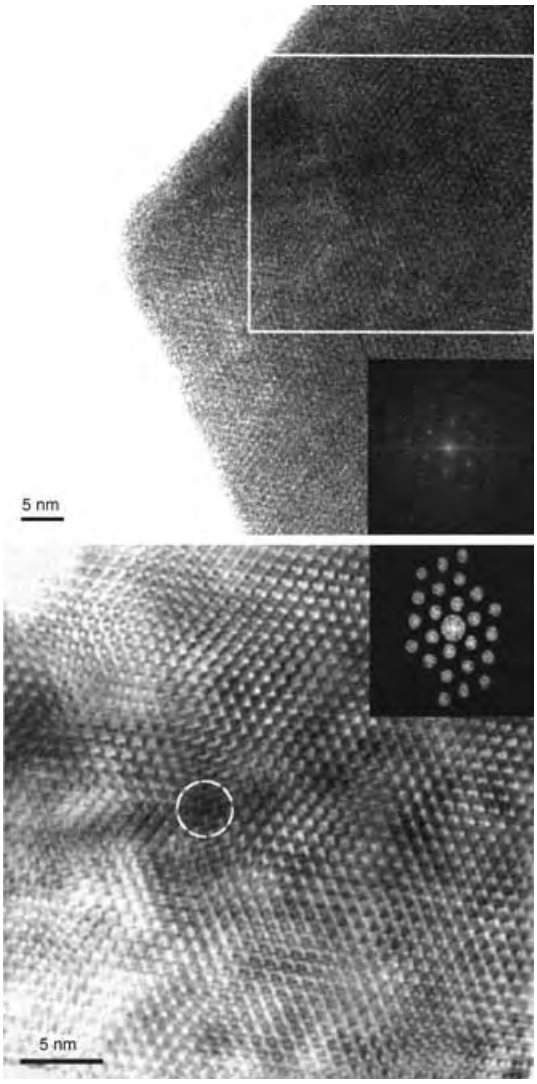


Figure 8. Top: High-resolution electron micrograph of a composite seed (fast ion bombardment (FIB) preparation) viewed along [001]. The FFT (inset, bottom right) is characterized by hexagonal symmetry. Structural disorder of the composite (defects, mosaic structure) is indicated by diffuse reflections and by vanishing of higher order peaks. Bottom: Filtered and enhanced view of the white-framed area of the top image. The overall hexagonal pattern is significantly broken inside the area of the white circle. The inset represents the mask used for the filter process (reflections observed). Reproduced from ref. [50] with permission of the Royal Society of Chemistry.

amounts of the charged AMPS in the copolymer gel (Figure 10).[55] The substructure of the mesocrystals from aligned smaller crystals could be nicely visualized (Figure 10c,d).

One important conclusion of this study was that the alteration of the functional groups in the hydrogel changed not the mesocrystal formation as such, but the morphogenesis process, shedding some light onto the question why mesocrystals exhibit defined outer faces and how they can be influenced.[55]

Mesocrystals can not only be formed in gel matrices with their special slow transport conditions, they can also form

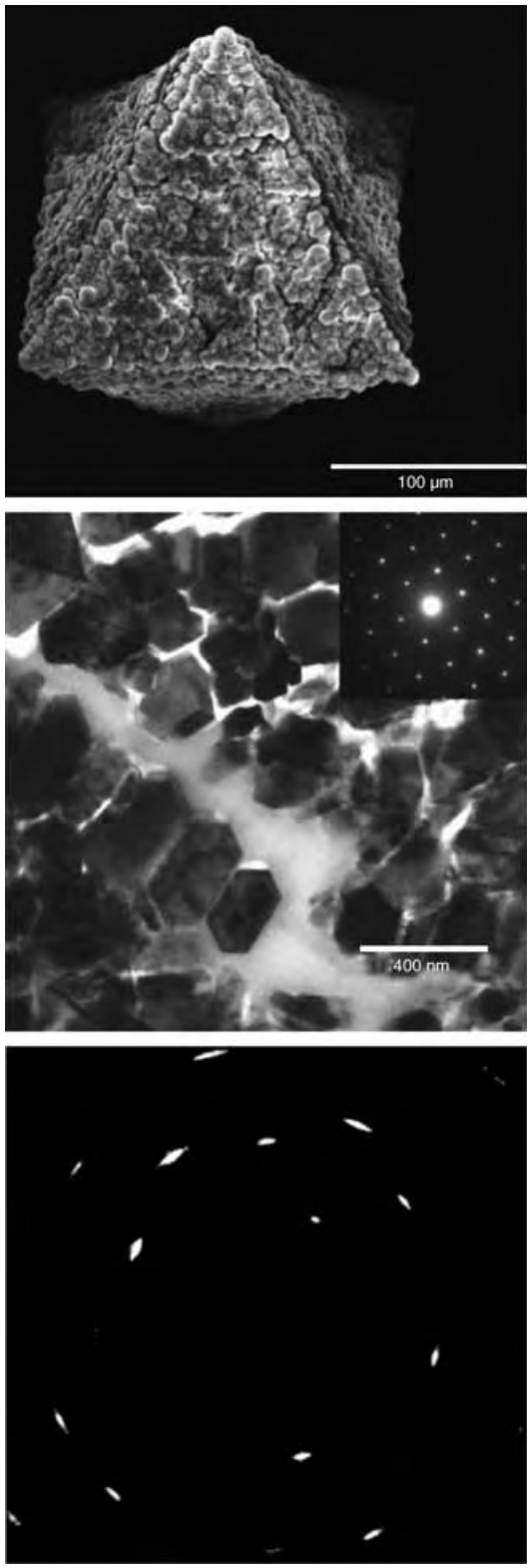
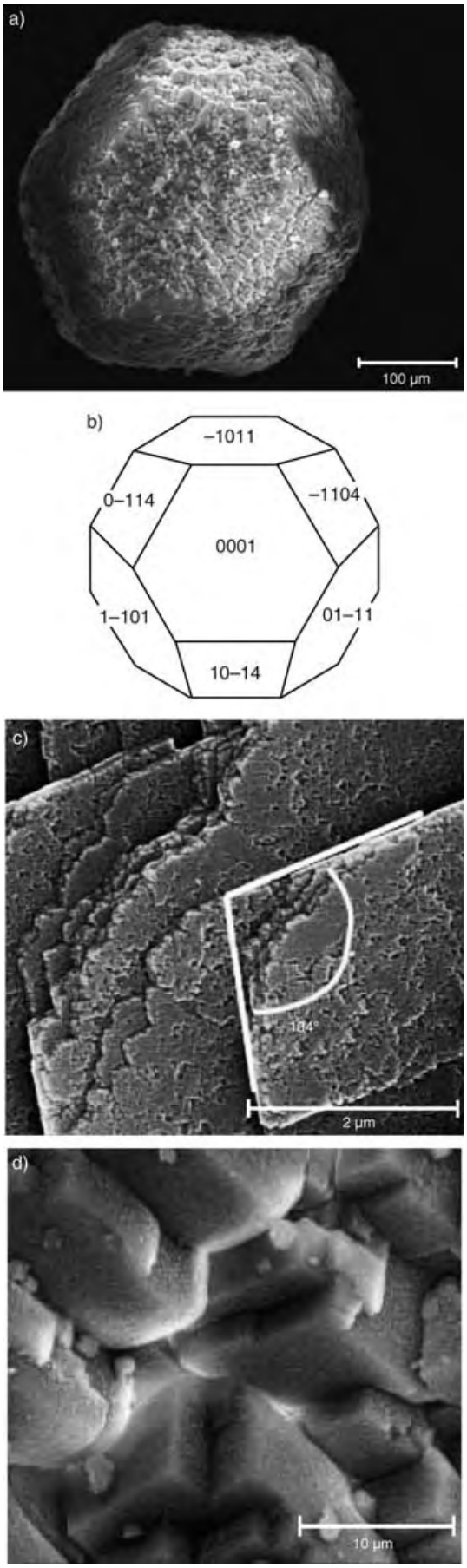


Figure 9. Top: SEM-image of a calcite aggregate grown in a polyacrylamide gel with characteristic pseudooctahedral morphology. Middle: TEM image of the microstructure of one such aggregate grown in polyacrylamide and showing the alignment of individual crystallites. (inset: an electron diffraction pattern of an individual calcite crystal). bottom: Single-crystal-like diffraction pattern of the calcite aggregate. Reprinted from ref. [53] with permission of the American Mineralogical Society.

 © 2005 Wiley-VCH Verlag GmbH & Co. KGaA, Weinheim



directly in solution. Among the first reported three-dimensional mesocrystals was a pseudocubic hematite (α-Fe_2O_3) particle.[56–59] For this crystal, the typical but remarkable high orientational alignment of the nanoparticle subunits as well as the iso-aligned nanoparticle building units was clear even from electron-diffraction images (Figure 11).[59] However the result were interpreted as being from single-crystal particles with internal discontinuities.[59] According to this interpretation, it was noted that the reported monodisperse polycrystalline hematite particles grow through a dissolution–recrystallization mechanism and not through an aggregation-based mechanism, although a "characteristic internal structure" of the pseudocubic particles was suggested. Furthermore, it was noted that the adsorption of anions plays an important role for the morphology and internal structure control where Cl^- ions were suggested to remain in the mesocrystal interior.[59] In our opinion, these nice results could also be explained by the controlled aggregation of primary nanoparticles and mesocrystal formation, analogous to the other cases. The experimental results however clearly reveal the nanocrystalline substructure as well as the radial alignment of elongated subcrystals (Figure 12) resulting in different crystal orientations according to their position.

Another example for mesocrystals formed directly from solution without any additive is $(NH_4)_3PW_{12}O_{40}$.[60–64] In these crystals, nanocrystals were unidirectionally aligned and epitaxially connected to form dodecahedral aggregates, and the analogy of the mesocrystal aggregate to a single crystal in terms of diffraction analysis was underlined. In addition, the mesocrystals were found to be porous.[62] Comparison of the cesium and ammonium salts which precipitated at different temperatures allowed a variation of the degree of order in the mesocrystals. [65] The solubility of the salts was considered to be responsible for the control of the microstructure morphology with the higher solubility favoring the regular polyhedral shape.[65] This result is qualitatively in agreement with the finding that the mesocrystal morphogenesis in gels is influenced by the functional groups of the gel, which in turn determines the gel–crystal surface interaction and therefore the surface conditions of the mesocrystal.

Mesocrystal formation was also observed for Zeolites.[66,67] In these experiments, the zeolite first forms "nanoslabs" containing 2, 6, 12, or 48 zeolithic unit cells, which then vectorially align to larger structures. TEM however clearly revealed that those bigger units are composed of the smaller building blocks, with all the textures and defects typical for mesocrystals.

A very detailed study on mesocrystal formation directly in solution and subsequent fusion to iso-oriented crystals was reported for copper oxalate.[68,69] In this case, nanoparticles

Figure 10. Pseudocubooactaedral calcite mesocrytals grown in a PAAm-co-PAMPS hydrogel containing 10 mol% of monomers bearing sulfonate groups. a) SEM micrograph, b) schematic illustration of the pseudocubooctaedral morphology, c) flattened vertices of pseudo cubooctahedral particles showing calcite rhombohedra faces, d) orientation of rhombohedral subcrystals on aggregate faces. Images (c) and (d) clearly show the substructure of the mesocrystal. Figure reproduced from ref. [55].

 © 2005 Wiley-VCH Verlag GmbH & Co. KGaA, Weinheim

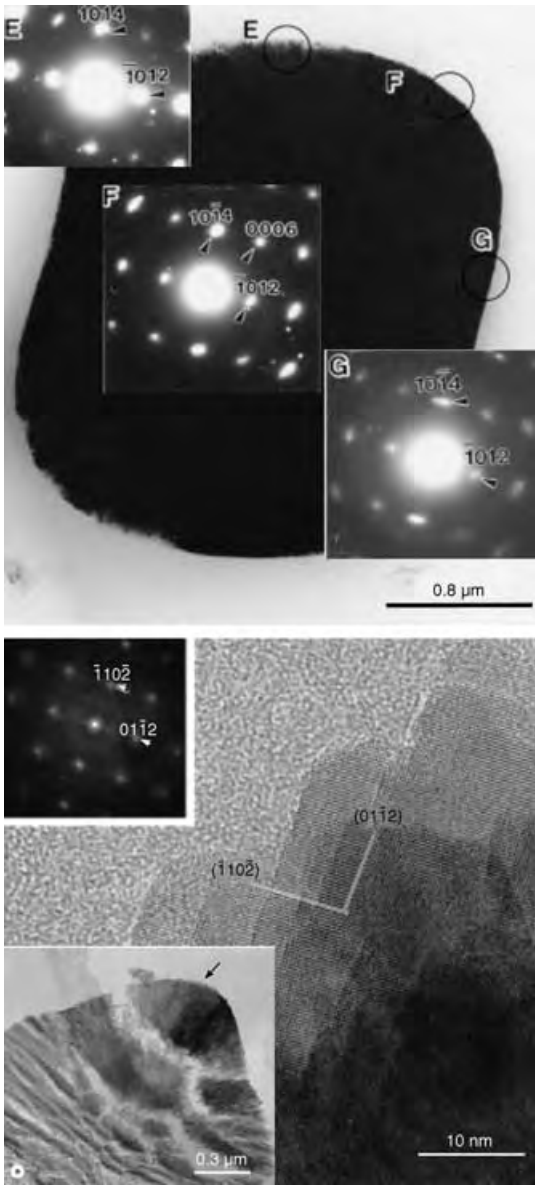


Figure 11. Hematite (α-Fe_2O_3) mesocrystals: top: Transmission electron micrograph of a thin section and electron diffraction patterns obtained from the parts E, F, and G. Bottom: inset lower left is the transmission electron micrograph of a section around a corner of a pseudocubic particle; main photo: High-resolution electron micrograph of the area indicated by an arrow in the lower left inset. Upper left inset is the Fourier diffractogram of the lower inset. Figure reproduced from ref. [59] with permission of Academic Press.

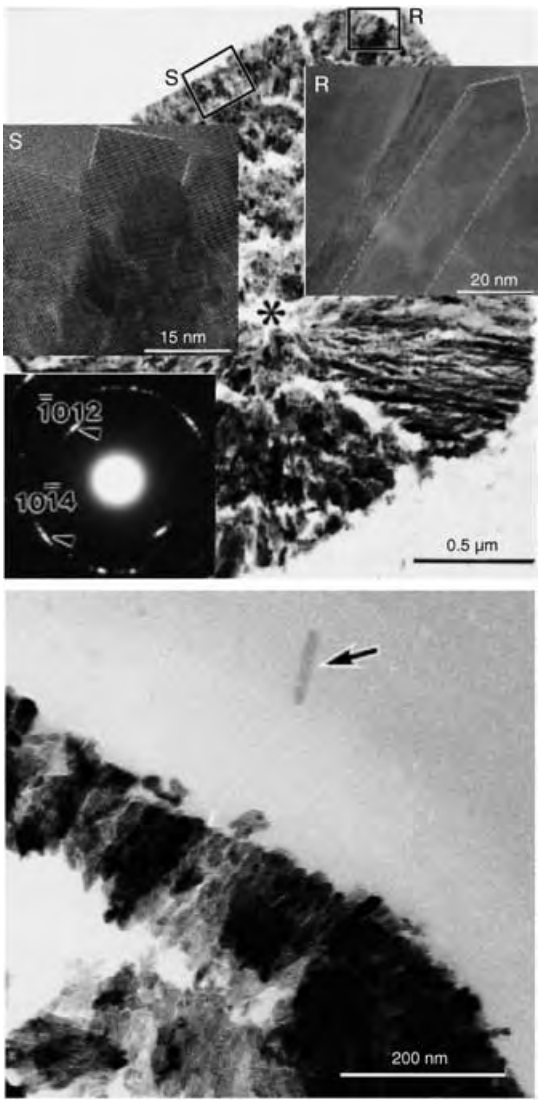


Figure 12. Hematite (α-Fe_2O_3) mesocrystals: top: Transmission electron micrograph of a thin section together with HRTEM pictures of areas S and R as insets. The $\star$ notes the position where the electron diffraction data (shown in the lower inset) was taken. Bottom: TEM micrograph of a thin section of a pseudocubic particle. An arrow indicates a subcrystal separated from the solution. Figure reproduced from ref. [59] with permission of Academic Press.

were found to arrange almost perfectly to a mesocrystal, which could be influenced in terms of morphology by hydroxymethylpropylcellulose (HPMC, Figure 13). It was found that the polymer influences nucleation, nanocrystal growth, and aggregation by selective interaction of the polymer with the more hydrophobic lateral (110)/(1$\bar{1}$1) ε-faces of an [001] elongated nanocrystal as compared to the hydrophilic (001) α-face.[69]

Increasing polymer concentration led to the formation of more but smaller crystal nuclei as a result of the decrease of the interfacial tension between nuclei and solution. The specific HPMC adsorption to the lateral ε-surfaces of the growing nanocrystals, once a sufficient HPMC concentration was reached, led to the formation of anisotropic shapes. Upon aggregation of these nanocrystals, a mesocrystal is formed as intermediate but is apparently not stable because of the low repulsive electrostatic and steric forces. Depletion flocculation of the weakly adsorbed polymer layers was suggested to be the reason for the depletion of the polymer from the inner mesocrystal surfaces to the outer mesocrystal faces resulting in attraction of the nanoparticles with subsequent nanoparticle fusion to give an iso-oriented crystal.[69] Nevertheless, this iso-oriented crystal was shown to be not single crystalline, as line width analysis in wide-angle X-ray scattering (WAXS)

 © 2005 Wiley-VCH Verlag GmbH & Co. KGaA, Weinheim

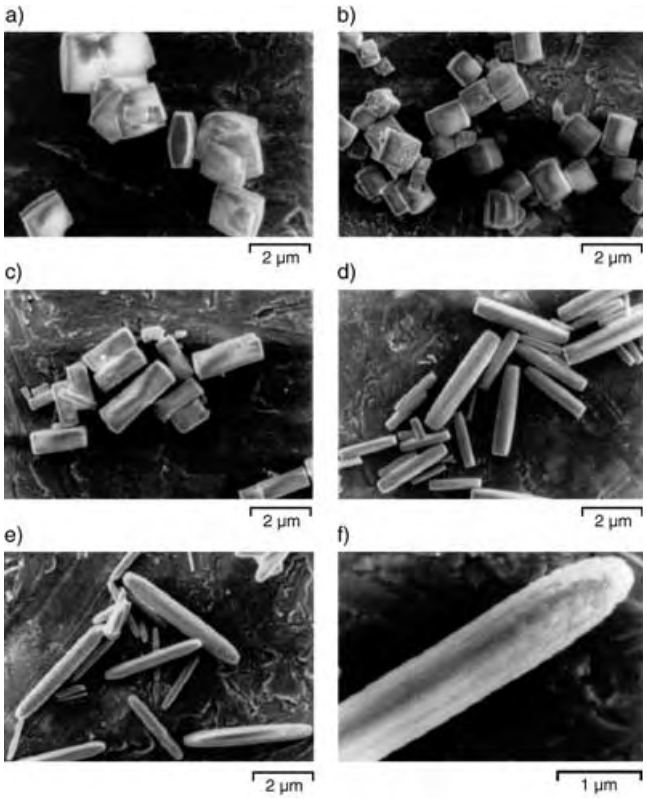


Figure 13. SEM micrographs of copper oxalate powders prepared a) without HPMC, b) with 0.005 g L^{-1} HPMC, c) 0.0195 g L^{-1} HPMC, d) 0.156 g L^{-1} HPMC, e) 0.625 g L^{-1} HPMC, and f) a higher magnification of (e) showing the mesocrystal structure. Figure reproduced from ref. [69] with permission of Academic Press.

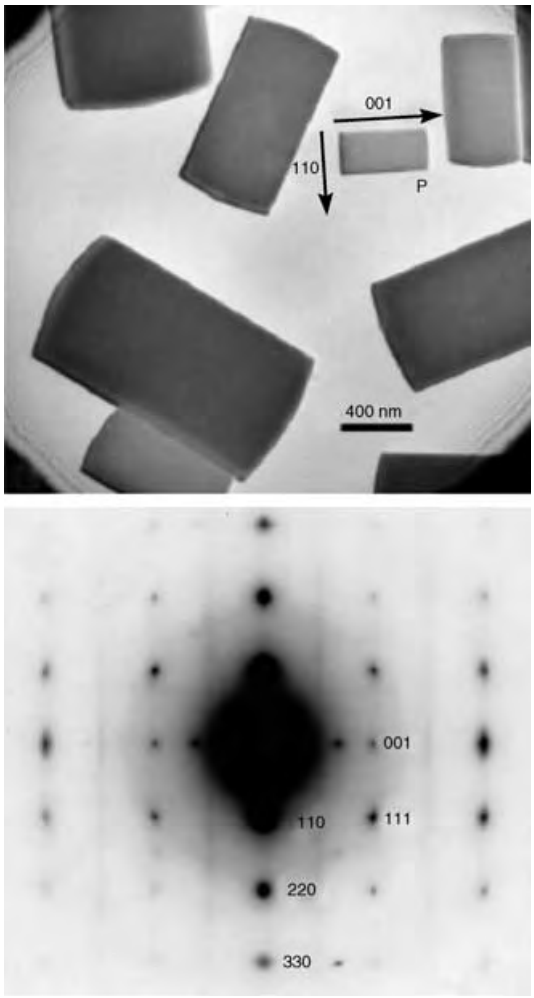


Figure 14. Top: TEM micrograph of copper oxalate with a square rod shape, precipitated in presence of 0.0195 g L^{-1} HPMC (Figure 13c) and bottom: electron diffraction pattern of the smallest particle on the micrograph, zone axis [1$\bar{1}$0]. Figure reproduced from ref. [69] with permission of Academic Press.

reveals the nanometer size of the primary building units, which get smaller with increasing HPMC concentration. As typical for mesocrystals, electron diffraction indicated a minor, but detectable orientational disorder, in this case along the [001] direction, which also supports the nanoparticle-aggregation-based mechanism of mesocrystal formation (Figure 14).

The whole mesocrystal formation process originally proposed is illustrated in Figure 15. In this case, the role of the polymeric additive on nucleation, growth, and organized aggregation to a mesocrystal is shown, and a coding of the mesocrystal morphology by tuning the surface energies of the nanocrystal building units and thus the nanocrystal morphology is suggested (that is, the morphology of the nanocrystal is a major influence on the shape of the resulting mesocrystal). In this particular case, the mesocrystal appears to adopt the same morphology as the nanoparticles. It is remarkable to note that the copper oxalate mesocrystals retain their morphology and nanometric substructure throughout decomposition into copper oxide.[70]

In a later and more detailed study on the copper oxalate system,[71,72] the "brick-by-brick" aggregation mechanism could be revealed in a time-dependent study.[71] However, the mesocrystal core parallel to the [110] direction showed poor organization with increasing order towards the particle surface and with increasing nanoparticle size. The particle density was higher at the hydrophobic ε-surfaces than the hydrophilic α-surface. Kinetic studies revealed a fast nucleation, growth, and agglomeration onset of primary mesocrystals leading to the relatively unordered particle core. This step is followed by a much slower growth stage with controlled aggregation as the predominant growth mechanism, which amplifies the mesocrystal morphology. Secondary particle nucleation was found as a competing event. Upon extended ripening, likely by dissolution–recrystallization, high-energy surfaces were eliminated.[71] This study implies that a mesocrystal is more a kinetic, metastable intermediate than a thermodynamically stable product.

The studies were extended onto the related cobalt oxalate dihydrate.[73] As was found for copper oxalate, WAXS showed the crystals were composed from nanometer building units. Atomic force microscopy (AFM) revealed strings of nanodomains oriented along the principal axis of the particle (Figure 16) and that the lateral and basal faces of the precipitate are composed of stacked nanoparticle layers with a thickness between 5–7 nm.

 © 2005 Wiley-VCH Verlag GmbH & Co. KGaA, Weinheim

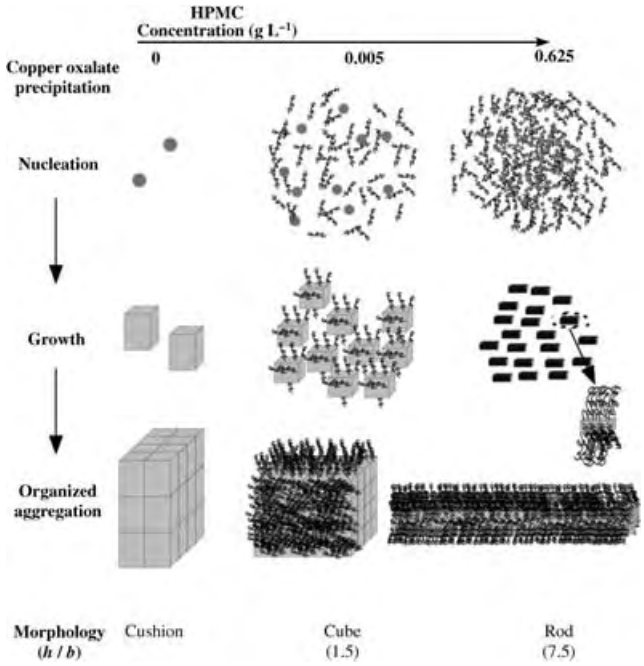


Figure 15. Schematic representation copper oxalate precipitation showing the influence of HPMC on the three major steps of particle formation (h = height, b = breadth). Figure reproduced from ref. [69] with permission of Academic Press.

A time resolved HRSEM study revealed the formation mechanism of the mesocrystal (Figure 16).[73] Poorly crystalline primary particles (10 nm) first aggregate to form secondary particles (23 nm). The latter subsequently aggregate to form polydisperse elongated particles (Figure 16, middle). These elongated particles also aggregate at the end and center of a growing particle (Figure 16, bottom) building the mesocrystal. Afterwards, there is a layer-by-layer growth by aggregation of primary particles onto the lateral external faces. Thus the mesocrystal is a core–shell particle or core–shell mesocrystal, where the core is quite disordered owing to the polydispersity of the nanoparticle building units.[73] The presence of steps and kinks on the external faces is reminiscent of classical crystallization models—except that the atoms or molecules are replaced by nanoparticles. The changes in supersaturation and thus ionic strength, which is closely associated to colloidal stability of nanoparticles, were suggested to play a major role in the process of ordering the nanocrystals into a mesocrystal because the ordered mesocrystal shells were formed at a lower supersaturation than the disordered cores. However, the ordering of nanoparticles to a mesocrystal can certainly not be reduced to the nanoparticle colloidal stability issue alone. An example are $CaCO_3$ mesocrystals, which are formed by the selective adsorption of poly(styrene sulfonate) PSS onto the highly polar calcite (001) nanoparticle faces.[74] If the nanocrystal is considered as a dielectric, adsorption of PSS onto one (001) face results in repulsion of negative ions from the opposite (001) face so that a dipole field is built up. It was argued that this situation can lead to a controlled arrangement of the nanoparticle subunits to give mesocrystals (Figure 17). These mesocrystals are

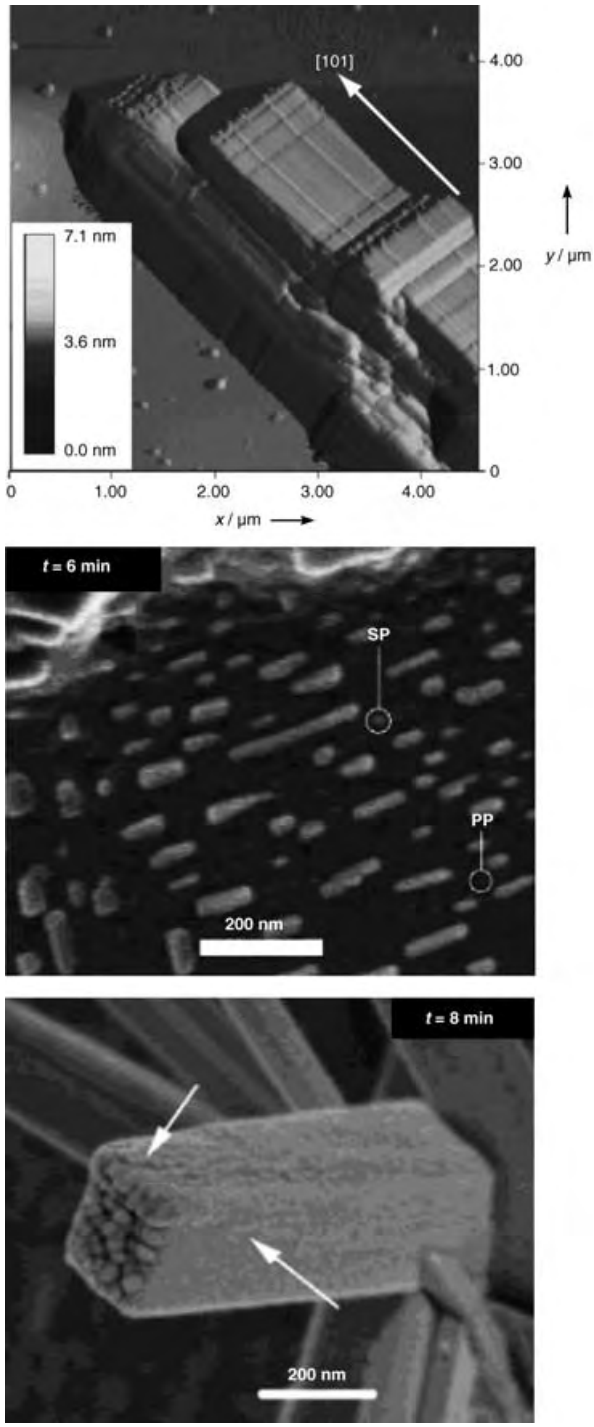
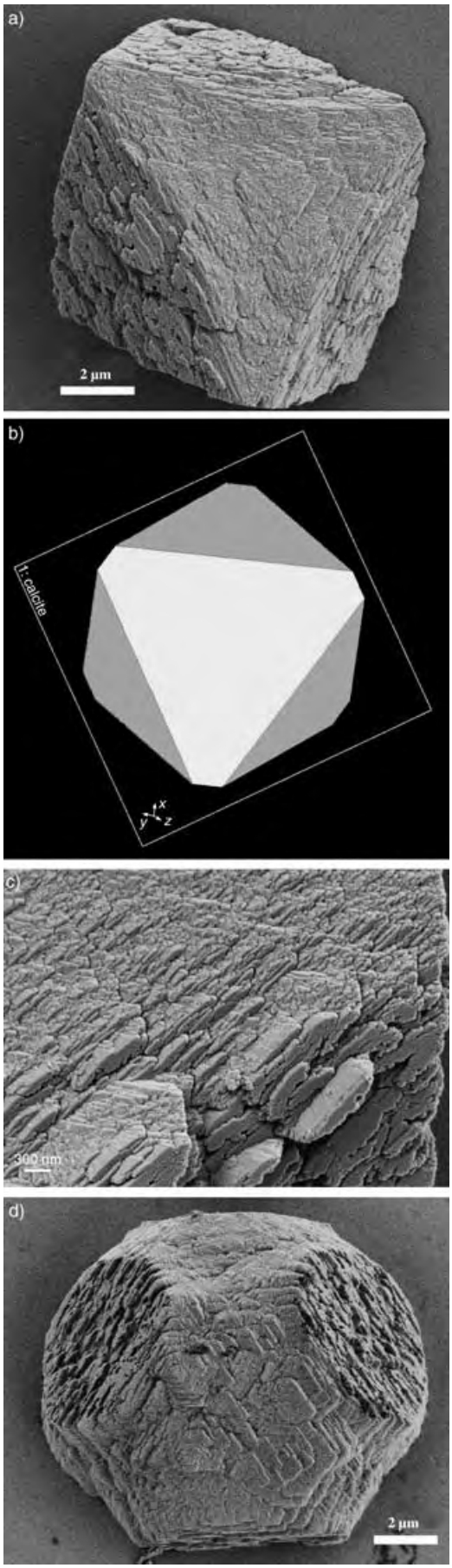


Figure 16. Top: AFM image of a $CoC_2O_4 \cdot 2H_2O$ particle aged 1 h in suspension. Middle: Low-voltage high-resolution (LVHR) scanning electron micrograph of uncoated cobalt oxide dihydrate primary (PP) and secondary (SP) particles after 4 min reaction time. Bottom: LVHRSEM micrograph of cobalt oxide dihydrate mesocrystal formed from secondary particle aggregates. The arrow pointing towards the end of the growing particle shows the agglomeration of polydisperse nanoparticles of 23 nm size, whereas the other arrow pointing at the lateral external faces indicated the layer-by-layer growth on these faces. Figure reproduced from ref. [73] with permission of the American Chemical Society.

 © 2005 Wiley-VCH Verlag GmbH & Co. KGaA, Weinheim



highly porous but show their common mutual high orientation by a rather perfect tensorial birefringence under crossed polarizers. Note that calcite is highly birefringent except when observed from the [001] direction (white plane in the Cerius model, Figure 17).

Variation of the $CaCO_3$/PSS ratio resulted in very systematic variations of the mesocrystal morphology, including a whole family of highly defined rounded structures (for one case with six elliptic faces, see Figure 17). Higher PSS concentrations lead to increasing exposition of the highly polar (001) face, finally resulting in a multicurved convex–concave structure with broken symmetry along the [001] direction at high Ca^{2+} and PSS concentrations. This result shows the importance of dipole fields as ordering forces for mesocrystal formation.[74]

Interestingly, there is evidence that some biominerals are also mesocrystals. For example, sea urchin calcite skeletal elements scatter like single crystals but have a nearly isotropic fracture behavior, which is untypical for single-crystalline calcite. Indeed, in a very recent study, an AFM investigation of a fracture pattern of sea urchin skeletal elements revealed a rough, clusterlike pattern without any preferred plane orientation.[75] The detected subunit size was in the range of 30–50 nm. In the same study, a synthetic calcite mesocrystal was reported, which was grown from an amorphous precursor in presence of polyaspartic acid. This calcite crystal consisted of uniformly shaped, oriented, and interlocked planar triangular growth domains with a length of 80–150 nm, width 40–100 nm, and a thickness of 3–6 nm.

Mesocrystals can not only be obtained for inorganic but also for organic crystals. An advantage of using organic nanocrystals is that these are molecular crystals, where a dipole moment as well as an anisotropic polarizability can be encoded in the molecule. Such mesocrystals are particularly well suited to learn about the mechanism of mesocrystal formation. For example, alanin is dipolar, and thus mesocrystals can be formed using a block-copolymer additive that has an anionic polyelectrolyte block which selectively adsorbs onto the positive (001) face of DL-alanine. This process creates platelets with a dipole moment along the *c*-axis (Figure 18).[30] The dipole moment along the [001] axis leads to the observed stacking of the nanocrystal platelets forming the mesocrystal where the individual building units are interspaced by the adsorbed polymer on (001).

A model example for a mesocrystal formed by anisotropic van der Waals attraction was reported by Taden et al. for dyes with an anisotropic polarizability.[76] Amorphous particle precursors were made in a size-controlled fashion by cooling the liquid nanodroplets of a miniemulsion. Spontaneous

Figure 17. $CaCO_3$ mesocrystals formed in presence of PSS ($Ca^{2+} = 2.5$ mM, PSS = 1 g L^{-1}) a) SEM micrograph of a single mesocrystal. b) Cerius^2 calculated morphology of a $CaCO_3$ single crystal with the mesocrystal morphology (gray = (104), white = (001)). c) higher magnification clearly indicating the alignment of primary particles and the porous nature of the mesocrystal. d) lowering the PSS concentration ($Ca^{2+} = 2.5$ mM, PSS = 0.5 g L^{-1}) results in a curving of the (001) planes. The former (104) planes are now six ellipses, illustrating that mesocrystals can easily exhibit highly defined curved morphologies.

 © 2005 Wiley-VCH Verlag GmbH & Co. KGaA, Weinheim

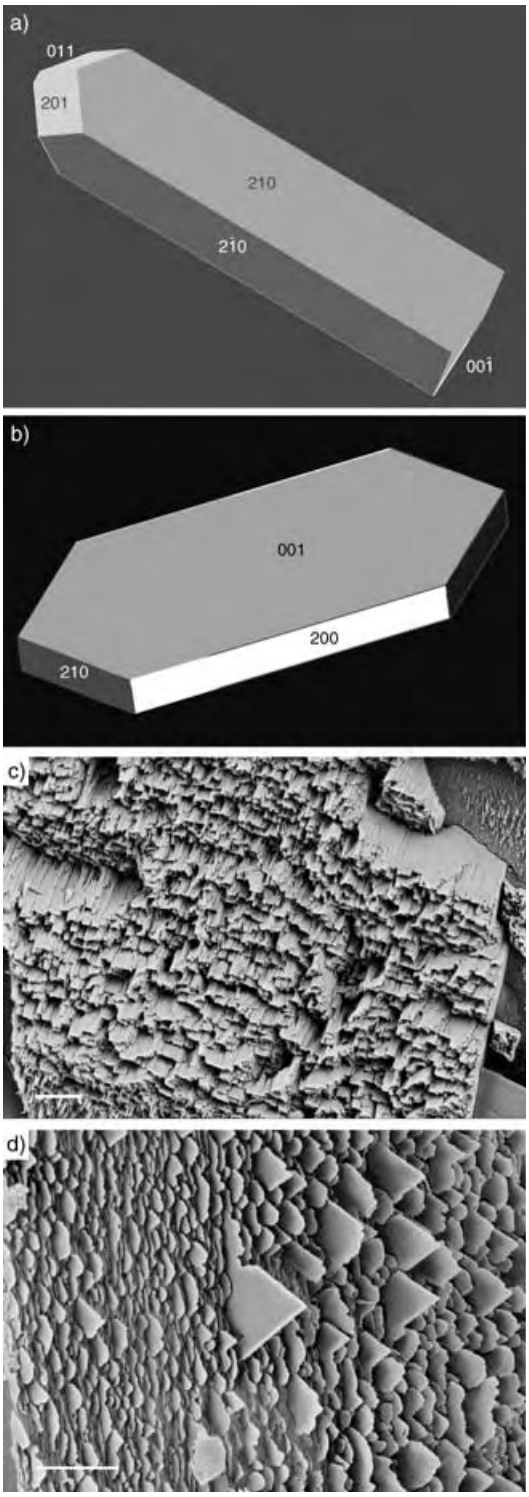


Figure 18. DL-alanine crystals through crystallization of 10 mL of a supersaturated solution (from 65 °C to 20 °C) a) default experiment without additive. b) Suggested mesocrystal subunit by addition of 1.0 wt% anionic blockcopolymer and selective adsorption onto (001). c) High-resolution SEM of DL-alanine crystals through crystallization by addition of 1.0 wt% block copolymer (scale bar = 2 μm). d) Different cut of the same structure revealing the high orientational order of the nanocrystalline platelets (scale bar = 3 μm). Figure reproduced from ref. [30].

rearrangement of many nanodroplets towards well-defined linear mesocrystal aggregates was observed, which was accompanied by significant color changes of the dye superstructures. These rodike particles could be ripened to larger three-dimensional mesocrystals that retained the almost perfect molecular orientation found in the nanoparticle aggregate. This orientation could be demonstrated on turning the ripened mesocrystals under crossed polarizers (Figure 19, bottom).

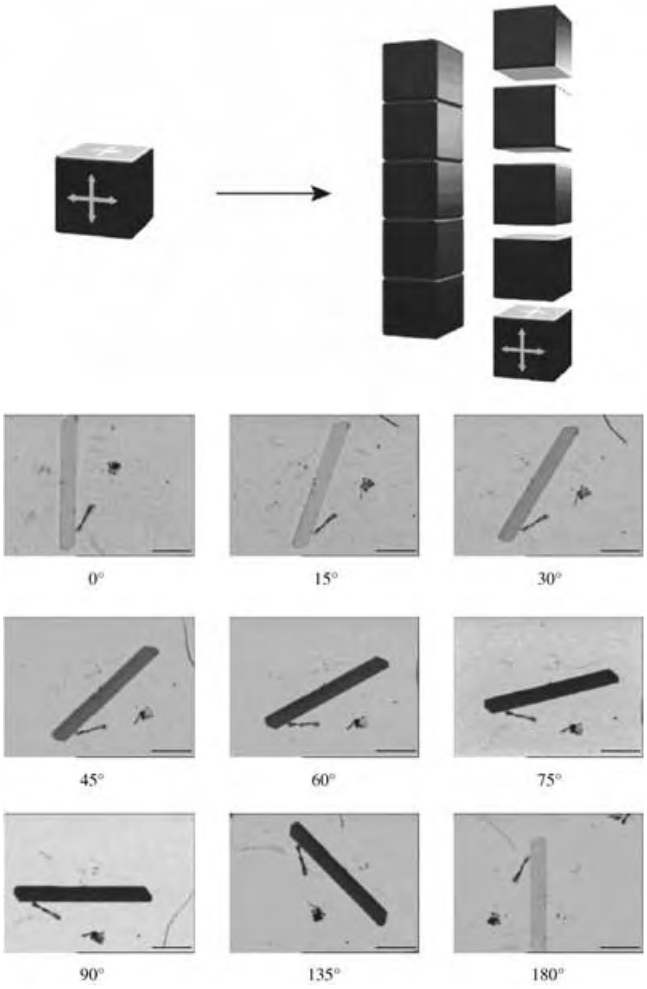


Figure 19. Top: Scheme to illustrate the directed mesoscale aggregation of dye nanoparticles. Because of the symmetry of the unit cell the primary nanocrystals formed show different polarizabilities along different planes. As is typical for van der Waals forces, similar polarizabilities attract each other optimally ("attraction of the same"). In this representation the light faces with the highest polarizability give the strongest van der Waals force. As a result, aggregation and mesocrystal formation occurs only in this direction. Bottom: series of polarization tilts of a selected large crystal of oil blue (scale bar = 20 mm). Figure reproduced from ref. [76] with permission of the American Chemical Society.

The fact that the dipole moment of such dyes is along the molecular axis and coupled to the maximum color allows the difference between polarizability and dipole moment as the driving force for organization to be studied. A high polarizability will lead to a high van der Waals attraction (light

 © 2005 Wiley-VCH Verlag GmbH & Co. KGaA, Weinheim

faces in Figure 19, top), a dipole moment will lead to an attraction of different dipoles. As the dye molecules are perfectly aligned perpendicular to the main axis of the mesocrystal, these experiments revealed tensorial differences in the polarizability of various nanocrystal faces to be the driving force for the formation of mesocrystals with the observed high orientational order. Whether or not the nanocrystalline building units in the mesocrystals fused together by oriented attachment[33] to form a single crystal was not revealed.

In addition to the above examples, where mesocrystals are sufficiently long-lived to be isolated at least as kinetically stable intermediates, there are also examples where mesocrystals can only be postulated as short-lived intermediates by indirect evidence in a "classical crystallization" event,[77] which is usually expected to occur by molecule or ion-by-ion attachment.

In most cases, however, the speed of crystallization events makes the classical molecule- or ion-mediated crystallization picture unrealistic. For example, Rieger et al. have demonstrated that the particle formation from highly supersaturated boehmite solutions is determined by the mixing process, which is orders of magnitude too fast to be covered by classical nucleation and growth theories.[78] Even in the crystallization process of a mineral such as $BaSO_4$, which has been intensively studied in the past and which was assumed as a model case for ion-mediated crystallization, strong experimental evidence was found that crystallization also progresses by organized mesoscale aggregation and alignment. Judat and Kind analyzed the additive-free crystallization of $BaSO_4$ for various supersaturation conditions[77] and found clear evidence for a nanoparticle-mediated crystallization mechanism contradicting the classical ion-mediated mechanism. Electron microscopy and diffraction revealed a polycrystalline, but almost perfectly oriented mesocrystalline superstructure of primary $BaSO_4$ nanocrystal subunits with the typical slight orientational distortions of the superstructure (data not shown; similar to Figure 8, right). It was proposed that a mesocrystal formed as an intermediate on the way to a porous $BaSO_4$ crystal and various evidence for the absence of the classical crystallization pathway for this example was collected.[77] However, in other regions of supersaturation, crystallization according to the classical mechanism was also observed.

These examples indicate that the evidence for mesoscale aggregation and organization towards mesocrystals should increase dramatically in the next few years as mesocrystals also appear to be regular intermediates in ordinary crystallization reactions, which to date were assumed to be ion mediated. Typical areas in the parameter space to expect mesocrystals are high supersaturation ratios or corresponding low solubilities or ion products.

5. Conclusions

In summary, mesocrystals are oriented superstructures of nanocrystals with common outer faces, and are a new type of colloidal crystals formed from nonspherical, crystalline building units. Both the formation as well as the morphogenesis of mesocrystals apparently contradict the classical textbook knowledge on crystallization, where growth of shapes is based on the integration of atomic or molecular building blocks into energetically favorable sites on a growing crystal face.[79,80] The adsorption of ions or molecules onto the crystal face is followed by subsequent diffusion across the surface to steps and kink sites[81] which leads to a plane-by-plane growth of a single crystal. The relevant parameters for classical crystallization are molecular solubility (defining the speed of crystallization) and crystal-face-specific interface tensions (defining growth rates, relative exposure, and therefore the morphology of the crystal).

This type of crystallization is clearly not observed for mesocrystals, which are built from nanoparticle building units, where speed of crystallization and morphology of the superstructure are only encoded in colloidal stabilization and vectorial long-ranged interaction potentials. This principle delivers new tools and possibilities into the hands of chemists, as it is now possible to generate crystalline nano- and mesostructures in a much broader and potentially useful way. The universal applicability of the classical crystallization picture was already questioned for a few years,[82] partly as a result of the careful observation of biominerals.

In addition, mesocrystal formation processes may even be a common crystallization pathway in the formation of single crystals, especially in systems with very low molecular solubilities or high supersaturations. As a result of the progress in instrumentation, direct evidence for such mesocrystals was recently discovered, which appear to be valid over a wide parameter space. The reason for the remarkable, almost perfect order of the nanocrystalline subunits which results in diffraction patterns similar to single crystals is still unknown, but tensorial polarization forces and dipole fields are discussed.[45,74] Indeed, theoretical studies suggest that a nonspherical charged object in an electrolyte creates a screened electrostatic potential that is anisotropic at any distance[83] so that mutual ordering can be induced.

There are however some criteria by which the presence of a mesocrystal either as an intermediate or as the final product can be identified. Even if the nanoparticle orientational order is almost perfect, the porosity in mesocrystals can be quite high as a result of nanoparticle polydispersity and stacking defects during mesocrystal formation. These defects are transformed into pores with organic or foreign-ion inclusions upon ripening to a single connected crystal.[77] Organized grain defects or amorphous interlayers can occur in the same way.

The reasons for the formation of the external mesocrystal faces are still unknown. In the most simple case, they maybe simply the reflection of the nanocrystal morphology[69] but in the majority of cases, mesocrystals exhibit external morphologies not related to the primary crystal symmetry, sometimes they have the typical rough faces, but a higher symmetry than the primary units, sometimes they even have curved, parabolic, or elliptic faces, as shown in Section 4.

In an extreme case, a mesocrystal can, although vectorially quite perfectly aligned, completely loose any macroscopic crystalline appearance and can exhibit morphologies

© 2005 Wiley-VCH Verlag GmbH & Co. KGaA, Weinheim



Figure 20. SEM image of helical $BaCO_3$ fibers formed in presence of a stiff phosphonated block copolymer. Reproduced from ref. [84] with permission of Nature Publishing Group.

like the $BaCO_3$ helices shown in Figure 20, which were formed after selective encoding of special faces of the orthorhombic primary nanoparticle building units by additive adsorption.[84] Not only the high alignment of elongated nanoparticles in these helices is remarkable, also the apparent "communication" between the two helices is. Identical morphologies and irregular helix pitch strongly indicate the presence of ordering electric fields in addition to the constraints exerted by the face-selective polymer adsorption. Helices from twisted twin subunits were also reported for triclinic $K_2Cr_2O_7$ and H_3BO_3, formed in a diffusion field created around a growing crystal in poly(acrylic acid) or poly(vinyl alcohol) gels[85] or orthorhombic K_2SO_4 in a viscous poly(acrylic acid) solution (PAA).[86] In the latter case, the crystal habit was modified by selective PAA adsorption leading to tilted platelike crystals. This effect is in addition to the diffusion-limited growth condition, which controls the assembly of the tilted subunits. Even the direction of the helical turn could be influenced for $K_2Cr_2O_7$ in a gel medium by molecular recognition of the enantiomeric triclinic subunit surfaces by glutamic acid enantiomers.[87]

Nanoparticle surface interactions appear to be of importance for the formation of a mesocrystal and possibly are also responsible for the formation of external faces, which can be indexed like those of a single crystal. Mesocrystals are a new type of nanostructured matter with potentially exciting applications, either in construction materials (as exploited by nature for biominerals) or as functional ceramics (e.g. with color or magnetic properties). However, there is still much to be learned about the forces guiding mesocrystal assembly and the exact formation mechanisms.

We thank the Max Planck Society for financial support. Dr. Tong Xin Wang is acknowledged for the material in Figure 17 and the frontispiece.

Received: February 9, 2005
Published online: July 20, 2005

[1] M. Antonietti, G. Ozin, *Chem. Eur. J.* **2004**, *10*, 28.
[2] H. A. Lowenstam, S. Weiner, *On Biomineralization*, Oxford University Press, New York, **1989**.
[3] S. Mann, *Biomineralization*, Oxford University Press, Oxford, **2001**.
[4] *Biomineralization, Progress in Biology, Molecular Biology and Application*, *2nd completely revised and extended ed.* (Ed.: E. Bäuerlein), Wiley-VCH, Weinheim, **2004**.
[5] M. E. Marsh in *Biomineralization, Progress in Biology, Molecular Biology and Application*, *2nd completely revised and extended ed.*, Wiley-VCH, Weinheim, **2004**, p. 197.
[6] G. Donnay, D. L. Pawson, *Science* **1969**, *166*, 1147.
[7] Y. Politi, T. Arad, E. Klein, S. Weiner, L. Addadi, *Science* **2004**, *306*, 1161.
[8] H. Cölfen, S. Mann, *Angew. Chem.* **2003**, *115*, 2452; *Angew. Chem. Int. Ed.* **2003**, *42*, 2350.
[9] G. Wegner, P. Baum, M. Müller, J. Norwig, K. Landfester, *Macromol. Symp.* **2001**, 175.
[10] L. Qi, H. Cölfen, M. Antonietti, *Angew. Chem.* **2000**, *112*, 617; *Angew. Chem. Int. Ed.* **2000**, *39*, 604.
[11] A. Taubert, D. Palms, Q. Weiss, M. T. Piccini, D. N. Batchelder, *Chem. Mater.* **2002**, *14*, 2594.
[12] E. Matijevic, P. Schreiner, *J. Colloid Interface Sci.* **1978**, *63*, 509.
[13] W. P. Hsu, L. Rönnquist, E. Matijevic, *Langmuir* **1988**, *4*, 31.
[14] K. Yamada, S. Kohiki, *Phys. E* **1999**, 228.
[15] S. Kohiki, S. Takada, A. Shimizu, K. Yamada, H. Higashijima, *J. Appl. Phys.* **2000**, *87*, 474.
[16] S. Kohiki, S. Takada, K. Yamada, Y. Adachi, A. Shimizu, M. Oku, M. Mitome, *Phys. E* **2000**, 161.
[17] H. Higashijima, S. Kohiki, S. Takada, A. Shimizu, K. Yamada, *Appl. Phys. Lett.* **1999**, *75*, 3189.
[18] C. M. Soukoulis, *Photonic Band Gap Materials*, Kluwer, Boston, MA, **1996**.
[19] C. B. Murray, C. R. Kagan, M. G. Bawendi, *Science* **1995**, *270*, 1335.
[20] C. P. Collier, T. Vossmeyer, J. R. Heath, *Annu. Rev. Phys. Chem.* **1998**, *49*, 271.
[21] C. B. Murray, C. R. Kagan, M. G. Bawendi, *Annu. Rev. Mater. Sci.* **2000**, *30*, 545.
[22] C. B. Murray, S. H. Sun, W. Gaschler, H. Doyle, T. A. Betley, C. R. Kagan, *IBM J. Res. Dev.* **2001**, *45*, 47.
[23] H. Weller, *Philos. Trans. R. Soc. Lond. A* **2003**, *361*, 229.
[24] F. X. Redl, K. S. Cho, C. B. Murray, S. O. Brien, *Nature* **2003**, *423*, 968.
[25] T. Vossmeyer, G. Reck, L. Katsikas, E. T. K. Haupt, B. Schulz, H. Weller, *Science* **1995**, *267*, 1476.
[26] Y. Lu, Y. D. Yin, Y. N. Xia, *Adv. Mater.* **2001**, *13*, 415.
[27] E. Matijevic, *J. Eur. Ceram. Soc.* **1998**, *18*, 1357.
[28] J. J. Petres, G. Dezelic, B. Tezak, *Croat. Chem. Acta* **1969**, *41*, 183.
[29] S. H. Lee, Y. S. Her, E. Matijevic, *J. Colloid Interface Sci.* **1997**, *186*, 193.
[30] S. Wohlrab, N. Pinna, M. Antonietti, H. Cölfen, *Chem. Eur. J.* **2005**, *11*, 2903.
[31] Z. Zhang, H. Sun, X. Shao, D. Li, H. Yu, M. Han, *Adv. Mater.* **2005**, *17*, 42.
[32] S. Dominguez Bella, J. M. Garcia-Ruiz, *J. Cryst. Growth* **1986**, *79*, 236.
[33] R. L. Penn, J. F. Banfield, *Geochim. Cosmochim. Acta* **1999**, *63*, 1549.
[34] J. Polleux, N. Pinna, M. Antonietti, M. Niederberger, *Adv. Mater.* **2004**, *16*, 436.
[35] J. Polleux, N. Pinna, M. Antonietti, C. Hess, U. Wild, R. Schlögl, M. Niederberger, *Chem. Eur. J.*, **2005**, *11*, 3541.
[36] L. Qi, H. Cölfen, M. Antonietti, M. Li, J. D. Hopwood, A. J. Ashley, S. Mann, *Chem. Eur. J.* **2001**, *7*, 3526.
[37] S.-H. Yu, H. Cölfen, M. Antonietti, *Chem. Eur. J.* **2002**, *8*, 2937.

 © 2005 Wiley-VCH Verlag GmbH & Co. KGaA, Weinheim

[38] S.-H. Yu, H. Cölfen, M. Antonietti, *Adv. Mater.* **2003**, *15*, 133.
[39] S.-H. Yu, M. Antonietti, H. Cölfen, J. Hartmann, *Nano Lett.* **2003**, *3*, 379.
[40] J. F. Banfield, S. Welch, H. Zhang, T. Thomsen Ebert, R. L. Penn, *Science* **2000**, *289*, 751.
[41] M. Li, H. Schnablegger, S. Mann, *Nature* **1999**, *402*, 393.
[42] S.-H. Yu, H. Cölfen, *J. Mater. Chem.* **2004**, *14*, 2124.
[43] H. Cölfen, *Macromol. Rapid Commun.* **2001**, *22*, 219.
[44] S. Busch, Dissertation, Technische Universität (Darmstadt), **1998**.
[45] S. Busch, H. Dolhaine, A. DuChesne, S. Heinz, O. Hochrein, F. Laeri, O. Podebrad, U. Vietze, T. Weiland, R. Kniep, *Eur. J. Inorg. Chem.* **1999**, *10*, 1643.
[46] R. Kniep, S. Busch, *Angew. Chem.* **1996**, *108*, 2788; *Angew. Chem. Int. Ed. Engl.* **1996**, *35*, 2624.
[47] S. Busch, U. Schwarz, R. Kniep, *Adv. Funct. Mater.* **2003**, *13*, 189.
[48] R. Kniep in *Facetten einer Wissenschaft* (Eds.: A. Müller, H. J. Quadbeck-Seeger, E. Diemann), Wiley-VCH, Weinheim, **2004**, p. 221.
[49] S. Busch, U. Schwarz, R. Kniep, *Chem. Mater.* **2001**, *13*, 3260.
[50] P. Simon, W. Carillo-Cabrera, P. Formanek, C. Göbel, D. Geiger, R. Ramlau, H. Tlatlik, J. Buder, R. Kniep, *J. Mater. Chem.* **2004**, *14*, 2218.
[51] C. A. Volkert, S. Busch, B. Heiland, G. Dehm, *J. Microsc.* **2004**, *214*, 208.
[52] A. Putnis, M. Prieto, L. Fernandez-Diaz, *Geol. Mag.* **1995**, *132*, 1.
[53] O. Grassmann, R. B. Neder, A. Putnis, P. Löbmann, *Am. Mineral.* **2003**, *88*, 647.
[54] O. Grassmann, G. Müller, P. Löbmann, *Chem. Mater.* **2002**, *14*, 4530.
[55] O. Grassmann, P. Löbmann, *Chem. Eur. J.* **2003**, *9*, 1310.
[56] D. Shindo, G. S. Park, Y. Waseda, T. Sugimoto, *J. Colloid Interface Sci.* **1994**, *168*, 478.
[57] G. S. Park, D. Shindo, Y. Waseda, *J. Electron Microsc.* **1994**, *43*, 208.
[58] D. Shindo, S. Aita, G. S. Park, T. Sugimoto, *Mater. Trans. JIM* **1993**, *24*, 1226.
[59] G. S. Park, D. Shindo, Y. Waseda, T. Sugimoto, *J. Colloid Interface Sci.* **1996**, *177*, 198.
[60] K. Inumaru, H. Nakajima, T. Ito, M. Misono, *Chem. Lett.* **1996**, *7*, 559.
[61] T. Ito, I. K. Song, K. Inumaru, M. Misono, *Chem. Lett.* **1997**, *8*, 727.
[62] T. Ito, K. Inumaru, M. Misono, *J. Phys. Chem. B* **1997**, *101*, 9958.
[63] T. Ito, K. Inumaru, M. Misono, *Chem. Lett.* **2000**, *11*, 830.
[64] T. Ito, K. Inumaru, M. Misono, *Chem. Mater.* **2001**, *13*, 824.
[65] K. Inumaru, T. Ito, M. Misono, *Microporous Mesoporous Mater.* **1998**, *21*, 629.
[66] C. E. A. Kirschhock, R. Ravishankar, P. A. Jacobs, J. A. Martens, *J. Phys. Chem. B* **1999**, *103*, 11021.
[67] C. E. A. Kirschhock, V. Buschmann, S. Kremer, R. Ravishankar, C. J. Y. Houssin, B. L. Mojet, R. A. van Santen, P. J. Grobet, P. A. Jacobs, J. A. Martens, *Angew. Chem.* **2001**, *113*, 2707; *Angew. Chem. Int. Ed.* **2001**, *40*, 2637.
[68] N. Jongen, J. Lemaitre, P. Bowen, H. Hofmann, Proceedings of 5th World Congress of Chemical Engineering, San Diego, **1996**, pp. 31.
[69] N. Jongen, P. Bowen, J. Lemaitre, J. C. Valmalette, H. Hofmann, *J. Colloid Interface Sci.* **2000**, *226*, 189.
[70] N. Jongen, H. Hofmann, P. Bowen, J. Lemaitre, *J. Mater. Sci. Lett.* **2000**, *19*, 1073.
[71] L. C. Soare, P. Bowen, J. Lemaitre, H. Hofmann, M. Pijolat, F. Valdivieso, Materials Research Society Symposium Proceedings. Proceedings of 2003 MRS Fall Meeting, Boston, MA, **2003**, p. L1.4.
[72] L. C. Soare, PhD thesis 3083, Ecole Polytechnique Federale de Lausanne, **2004**.
[73] O. Pujol, P. Bowen, P. A. Stadelmann, H. Hofmann, *J. Phys. Chem. B* **2004**, *108*, 13128.
[74] T. X. Wang, H. Cölfen, M. Antonietti, *J. Am. Chem. Soc.* **2005**, *127*, 3246.
[75] I. Sethmann, A. Putnis, O. Grassmann, P. Löbmann, *American Mineralogist* **2005**, *90*, 1213.
[76] A. Taden, K. Landfester, M. Antonietti, *Langmuir* **2004**, *20*, 957.
[77] B. Judat, M. Kind, *J. Colloid Interface Sci.* **2004**, *269*, 341.
[78] J. Rieger, D. Franke, T. Frechen, H. Haberkorn, W. Goesele, Proceedings BIWIC. Proceedings of 9th Workshop on Industrial Crystallization, Halle-Wittenberg, **2002**, p. 13.
[79] "Zur Theorie des Kristallwachstums": W. Kossel, *Nachr. Ges. Wiss. Goettingen Math.-Phys. Kl.* **1927**, 135.
[80] I. N. Stranski, *Z. Phys. Chem. A* **1928**, *136*, 259.
[81] W. K. Burton, N. Cabrera, F. C. Frank, *Philos. Trans. R. Soc. Lond. A* **1951**, *243*, 299.
[82] A. P. Alivisatos, *Science* **2000**, *289*, 736.
[83] R. Agra, F. van Wijland, E. Trizac, *Phys. Rev. Lett.* **2004**, *93*, 018301.
[84] S.-H. Yu, H. Cölfen, K. Tauer, M. Antonietti, *Nat. Mater.* **2005**, *4*, 51.
[85] Y. Oaki, H. Imai, *Angew. Chem.* **2004**, *116*, 1387; *Angew. Chem. Int. Ed.* **2004**, *43*, 1363.
[86] Y. Oaki, H. Imai, *Langmuir* **2005**, *21*, 863.
[87] Y. Oaki, H. Imai, *J. Am. Chem. Soc.* **2004**, *126*, 9271.

© 2005 Wiley-VCH Verlag GmbH & Co. KGaA, Weinheim

K. Müllen and A. C. Grimsdale

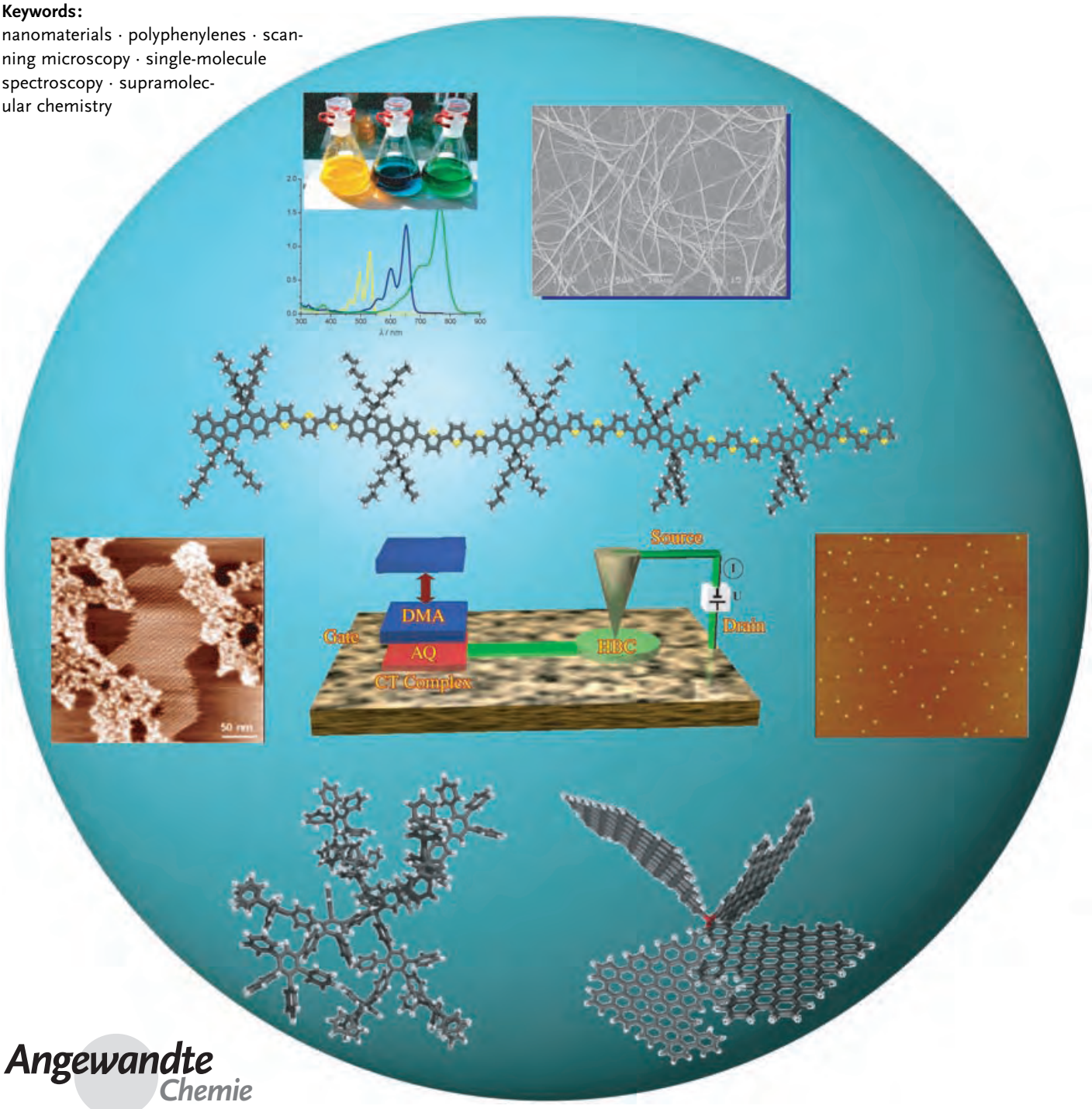
DOI: 10.1002/anie.200500805

Nanotechnology

The Chemistry of Organic Nanomaterials

*Andrew C. Grimsdale and Klaus Müllen**

Keywords:
nanomaterials · polyphenylenes · scanning microscopy · single-molecule spectroscopy · supramolecular chemistry



© 2005 Wiley-VCH Verlag GmbH & Co. KGaA, Weinheim

The development of nanotechnology using organic materials is one of the most intellectually and commercially exciting stories of our times. Advances in synthetic chemistry and in methods for the investigation and manipulation of individual molecules and small ensembles of molecules have produced major advances in the field of organic nanomaterials. The new insights into the optical and electronic properties of molecules obtained by means of single-molecule spectroscopy and scanning probe microscopy have spurred chemists to conceive and make novel molecular and supramolecular designs. Methods have also been sought to exploit the properties of these materials in optoelectronic devices, and prototypes and models for new nanoscale devices have been demonstrated. This Review aims to show how the interaction between synthetic chemistry and spectroscopy has driven the field of organic nanomaterials forward towards the ultimate goal of new technology.

From the Contents

1. Introduction 5593
2. Probing, Visualizing, and Manipulating Single Molecules by Single-Molecule Spectroscopy and Scanning Probe Microscopy 5595
3. Rigid-Rod Polymer Chains as Nanoobjects 5596
4. Two-Dimensional Polyphenylenes: Graphene Molecules as Nanosized Semiconductors 5600
5. Rylene Dyes for Single-Molecule Spectroscopy 5604
6. Dendrimers as Vessels for Chemistry, Physics, and Biology 5608
7. Dye-Loaded Dendrimers: Emissive Nanoparticles 5614
8. Combining One-, Two-, and Three-Dimensional Polyphenylene Nanostructures 5620
9. From Discotic Mesophases to Carbon Nano- and Microstructures 5620

1. Introduction

1.1. Nanomaterials, Nanotechnology, and Nanoscience

Nanomaterials are functional materials comprised of objects with at least one dimension below 100 nm. These objects may be either nanoparticles (small ensembles of molecules) or even individual molecules. Functional nanoparticles have an ancient pedigree. Soot, which contains nanosized (< 1 μm) carbon particles, was used as a colorant by the earliest humans, while colloidal gold particles have served as a pigment, for example, for ruby-colored stained glass, since the middle ages.[1] Nanoobjects, such as polymer latices or pigment particles and technology dependent upon the unique properties of nanomaterials, have today acquired great economic importance. However, it is something of a paradox that nanotechnology, which we define as technology that is dependent upon the unique properties of nanomaterials, is seen as an ultramodern technology even though, from a chemistry point of view, these materials are anything but new.

One of the most exciting aspects of nanoobjects is that their properties may differ very significantly from those of the corresponding bulk materials, for example, silver nanoparticles show biological (antimicrobial) activity whereas silver metal does not.[2] Similarly the conductivity of metal particles undergoes a marked change as their size decreases,[1] and the optical and electronic properties of inorganic semiconductor nanoparticles are known to depend upon the particle size.[3] It is therefore justified to assert that the study of the properties and manipulation of individual nanoobjects constitutes a scientific discipline (nanoscience) in its own right. It should be noted that while there is an accepted standard definition for a nanomaterial as given above, there is as yet no consensus as to the exact meaning of the terms nanoscience and nanotechnology, as clearly shown by the varying definitions given in two recent overviews by leading figures in their development;[4,5] the above descriptions are our personal attempts at defining them. Nanotechnology and nanoscience, however they may be defined, must also include more complex functions of nanoobjects, such as the development of devices with dimensions of less than 100 nm. It is this aspect that has captured the public imagination, and spurred funding agencies all over the world to launch programs for both fundamental and industrial research. As a result "nano" is one of the current buzzwords driving investment in research and development. (As an aside it should be noted that "nano-" is the form used by physical scientists, whereas the biological sciences use the prefix "nanno-", for example, in nannoplankton.[6]) Public excitement, and also concern about the environmental and other aspects of the development of nanotechnology, has led to the publication of major reports by the Royal Society in London,[7] and the Academies of Science and Technology in Paris,[8] into the social and other impacts of these emerging technologies. There have also been a number of general reviews and books on nanoscience and nanotechnology, as well as on various aspects and applications of

[*] Dr. A. C. Grimsdale, Prof. Dr. K. Müllen
Max-Planck-Institute for Polymer Research
Ackermannweg 10, 55128 Mainz (Germany)
Fax: (+49) 6131-379-350
E-mail: muellen@mpip-mainz.mpg.de

 © 2005 Wiley-VCH Verlag GmbH & Co. KGaA, Weinheim

them ranging from catalysis to food science.[9–23] The excitement about the construction of nanosized devices, and especially those using single molecules,[24] stems in part from the fact that they represent the logical endpoint for the ongoing miniaturization of devices, for example, of the integrated circuits in computers, which underlies the whole electronics revolution that has changed the face of our world. As Richard Feynman famously pointed out,[25] if 100 atoms were sufficient to store one bit (binary digit) of information then all the books ever written could be stored in a cube with edges 6 mm long, so the potential impact of nanotechnology on information storage and processing is hard to overstate. Another exciting point is that if nanoelectronic devices can be made by chemical synthesis and processing, then more devices could be made in a single day than have ever been made by lithographic methods!

Given that the definition of nanoobjects by size is somewhat diffuse—and also embraces materials with only one dimension in the nanometer range, such as functional self-assembled monolayers[26,27]—much nanoscience therefore focuses on the properties of *single* molecules or particles rather than the properties of the ensembles, but it must always be borne in mind that nanoobjects also include supramolecular aggregates held together by intermolecular forces. The study of single molecules is a special challenge which has become possible through the development of new physical methods for probing their electronic and optical properties, in particular single-molecule spectroscopy (SMS) and scanning tunnelling microscopy (STM). These technical developments have prompted chemists to investigate ways to efficiently and reproducibly synthesize materials which perform optimally at the single-molecule level, or which can self-assemble to form well-defined functional nanostructures; indeed to a chemist the design and synthesis of the latter is one of the key aspects of nanoscience. The further advancement of nanoscience and nanotechnology will thus require an integrated combination of synthesis and physical methods.

1.2. Scope of the Review

In this Review we present an overview of our recent work towards the development of organic nanomaterials. In particular we want to show how an integrated approach combining many fields of structural chemistry (conjugated polymers, polycyclic aromatic hydrocarbons, dyestuffs, dendrimers, and biomaterials) can lead to significant advances. Of equal importance is the close collaboration between our synthetic efforts and the development of means for visualizing, manipulating, and addressing molecules and small aggregates of molecules. When one considers how many publications have appeared in the last decade reporting SMS and STM studies of the commercially available perylene tetracarboxydiimides and dianhydrides, and reflects that these molecules have been chosen in large part simply because they are available, one can immediately see the tremendous scope for synthetic chemists to advance nanoscience.

There are three issues that must be considered in designing and synthesizing a new compound that will act as a nanomaterial. First there are the properties of individual molecules (or even of individual functional groups within multifunctional molecules); these correspond to those of isolated molecules either in a dilute solution, in a matrix, or upon a surface. Second the interactions between these molecules (or functional groups) and how they affect the properties of discrete ensembles of the molecules must be considered. Finally the interface with the outside world must be designed, that is, how the input of the energy or charge is going to be achieved, and how an output is going to be received or detected. In principle the properties of a single molecule (or functional group) are much simpler to predict and control than those of a group of molecules, as in the latter case it has to be considered how the individual molecules interact, which in turn may depend in subtle ways upon the size and shape of the molecule. Thus, the design of a nanomaterial involves both the optimization of the functional units and the control of their supramolecular order. The ultimate aim is to produce hierarchies of structures with different types of order on different length scales,[28,29] as are seen in living organisms.

Light and/or charge can be used as potential interface mechanisms as these are highly controllable and are detectable even at the very low levels associated with the output from individual molecules or nanoparticles. Our approach therefore involves the combination of new functional and



Klaus Müllen received his Diploma in 1969 from the University of Cologne for work with Prof. E. Vogel, and in 1972 he completed his PhD with Prof. F. Gerson at the University of Basel, Switzerland for research on EPR spectroscopy. He pursued postdoctoral research on dynamic NMR spectroscopy and electrochemistry with Prof. J. F. M. Oth at the ETH, Zurich, and in 1977 completed his habilitation there. In 1979 he became a Professor of Organic Chemistry in Cologne, and in 1983 he accepted a chair in Organic Chemistry at the University of Mainz. In 1989 he became one of the directors of the Max-Planck Institute for Polymer Research. His research interests focus on synthetic macromolecular chemistry and materials science.

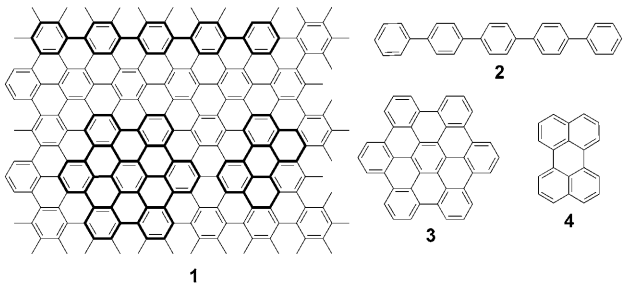


Andrew Grimsdale was born in Waiouru, New Zealand, and graduated from the University of Auckland. He completed his PhD there in 1990 with Prof. R. C. Cambie for work on the synthesis of analogues of biologically active drimane sesquiterpenes. After postdoctoral work on photochromic and electroactive materials with Prof. A. Pelter at the University of Wales in Swansea, and on electroluminescent polymers with Prof. A. B. Holmes at the University of Cambridge, in 1999 he joined Prof. Müllen at the Max-Planck Institute for Polymer Research at Mainz. In 2005 he rejoined Prof. Holmes, now at the University of Melbourne. His research involves the synthesis of polyphenylene-based materials for optoelectronic applications.

 © 2005 Wiley-VCH Verlag GmbH & Co. KGaA, Weinheim

structural units into new compounds and materials in which the supramolecular order of the functional elements is engineered to maximize beneficial and minimize undesirable interactions.

We begin by briefly introducing the methods by which the optical, mechanical, and electronic properties of materials can be probed at the nanolevel: SMS, STM, and atomic force microscopy (AFM). Then we survey each of the main classes of building units which we have used for making nanomaterials: rigid-rod phenylene-based conjugated polymers and oligomers (1-D polyphenylenes), planar polycyclic aromatic hydrocarbons (PAHs), and rylene-based dyes. An emphasis has been placed on their materials properties at the nanoscale. An interesting feature of these classes of materials is that many of the compounds involved can be thought of as molecular subunits of graphite (Scheme 1). Thus, examination of a single sheet of graphite (a graphene sheet; **1**) enables one to readily pick out subunits such as the 1-D oligophenylene quinquephenyl (**2**) or a an all-benzenoid (classification according to E. Clar)[382] PAH ("2-D polyphenylene"; see Section 4.1) such as hexabenzocoronene (HBC, **3**), or a subunit not belonging to this type such as perylene (**4**). As graphite is a conductor and strongly absorbs light, it is not surprising that its molecular subunits often have notable optoelectronic properties.



Scheme 1. One- and two-dimensional polyphenylenes and rylenes as subunits of graphite

By contrast in the next class of materials, polyphenylene dendrimers (3-D polyphenylenes), the benzene rings are nearly nonconjugated (see Figures 7 and 9). Thus, whereas the previous materials are all functional units, dendrimers are used more as structural elements in nanomaterials.

We then move on to various combinations of these building blocks: dye-substituted dendrimers, polymers and discs as nanoemissive materials, and then molecules containing combinations of one-, two-, and three-dimensional polyphenylene nanostructures with controllable sizes and shapes. As a logical extension of the research into carbon-rich fibers and columnar superstructures we finally discuss our new methods for making carbon nanoparticles. The key aim here was to obtain better control over the morphology of the products by pyrolysis of polyphenylenes in ordered mesophases or confined geometries.

In this Review we show not only how we can optimize each of the potential components of nanomaterials (graphenes, dyestuffs, dendrimers etc.), but also how we can combine them to optimize the properties of the final materials. In particular we will illustrate the value of collaborative research with physicists that utilize the most up-to-date SMS, STM, and other techniques to probe the optical and electronic properties of these materials.

2. Probing, Visualizing, and Manipulating Single Molecules by Single-Molecule Spectroscopy and Scanning Probe Microscopy

An SMS experiment[30,31] requires the emissive molecules to be isolated. This is usually achieved by dispersing them highly diluted ($< 10^{-10}$ M) in a solid transparent matrix, for example, polystyrene. SMS measurements can also be performed in very dilute liquid solutions, but this presents problems arising from the Brownian motion of the molecules, especially at room temperature. The absorption and emission of the chromophores are then probed, often at low temperature, by excitation with short pulses of laser light. Whereas an averaged result for the absorption and emission of the chromophores is typically recorded in bulk measurements, spectra for each individual species are observed in SMS experiments; the species may even display distinct blinking[383] as individual chromophores "switch" on and off. SMS experiments are generally performed on a number of individual molecules and histograms of the results are compiled, which can provide information about the distribution of states not obtainable from the bulk data. Furthermore the broadening of the signals in the bulk spectra produced by disorder is absent so that individual spectral features may be more clearly resolved. Time-resolved measurements may provide insights into the nature of excitation energy transfer that may not be available from studies of the bulk materials; for example, it has been possible to observe quantum jumps between singlet and triplet states of terrylene directly by SMS.[32] SMS is thus of great importance for investigating multichromophoric species, in particular the kinetics of interchromophore interactions can be determined. Attachment of fluorescent tags to biologically active molecules also enables biological processes to be studied by SMS. For example, the infection pathway of fluorescently labeled virus particles into a cell has been monitored in this way.[33,34]

Scanning probe microscopy[35] can be used to visualize single molecules in real space and to investigate their chemical and electronic properties. It is possible to scan across molecules deposited on a surface with resolutions down to the sub-nanometer range, and to manipulate individual nanoobjects. The breakthrough in investigating the electronic properties of individual molecules or particles came with the invention of scanning tunneling microscopy (STM).[36,37] An STM experiment involves scanning a sharp tip across a sample on a conducting substrate, for example, highly ordered pyrolytic graphite (HOPG), while determining at each point the probability that electrons can tunnel between the tip and the substrate, and so gain insight into the local electronic density of states.

The visualization of individual molecules by STM is performed after their immobilization on a surface, often as

 © 2005 Wiley-VCH Verlag GmbH & Co. KGaA, Weinheim

part of an ordered monomolecular layer. The combination of scanning tunneling microscopy with scanning tunneling spectroscopy offers the possiblity of recording current–potential curves for individual molecules or even parts of molecules.[35,38] The STM tip has also been used to manipulate nanoobjects, for example, metal atoms or organic molecules, and even to perform nanochemistry by making and breaking individual chemical bonds,[35] or initiating a polymerization.[39] STM is also an important tool for investigating supramolecular self-assembly of molecules within monolayers and epitaxial growth of double and multilayers[40] and has even been used to study photoinduced chemical reactions within monolayers.[39,41,42]

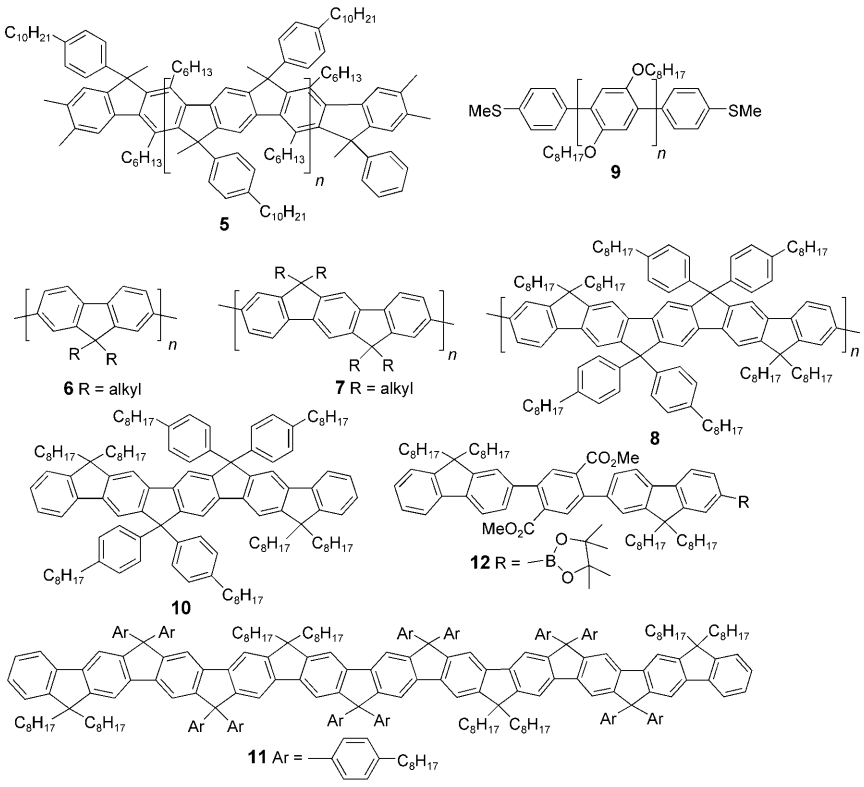
Another scanning technique that is used to investigate nanostructures is atomic force microscopy (AFM)[43]—sometimes also called scanning force microscopy (SFM). In an AFM experiment the contact force between a tip and the surface is measured at each point as the surface is scanned. The advantage of AFM over STM is that it can be used to study the surfaces of insulating substrate materials, whereas STM requires the surface being examined to be electrically conductive. The AFM tip can also be used for manipulating nanoobjects, for example, polymer chains,[35] or be chemically modified to measure the strengths of bonds, for example, the rupture forces of ruthenium complexes linked to both an AFM tip and a substrate have been measured.[44] AFM has also been used to estimate directly the molecular weight of polymer chains within a Langmuir–Blodgett film.[45] It should be kept in mind, however, that scanning probe methods do not replace, but complement classical techniques, such as electron microscopy or various spectroscopy techniques, in an integrated approach toward the investigation of nanomaterials.

3. Rigid-Rod Polymer Chains as Nanoobjects

Conjugated polymers have attracted attention in recent years as organic semiconductors for use in devices such as light-emitting diodes (LEDs),[46] solar cells,[47] and field-effect transistors (FETs).[48] There has also been interest in monodisperse conjugated oligomers, both as active materials and as models for polymers.[49,50] Since these materials are well-defined molecular species, reliable structure–property relationships can more easily be obtained from them than from the corresponding polydisperse polymers. A desirable feature for the conjugated materials to be useful is that they can self-assemble into well-defined nanostructures. A number of approaches have been adopted to direct the assembly of conjugated polymers and oligomers. For example, hydrogen bonding can be used to induce self-assembly of oligo(phenylenevinylene)s to form polymers, including chiral helical polymers,[51] and such materials have served as active components in a photovoltaic device.[52] Rod-coil or coil-rod-coil block copolymers offer another way to control assembly processes through variation of the number, nature, and size of the coil units.[53–65] A wide range of topologies, including sheets of mushroomlike aggregates;[56,64] spherical, vesicular, cyclindrical, and lamellar aggregates;[58–61,66] and porous membranes,[53,62,63] have been obtained in this way.

3.1. One-Dimensional Polyphenylenes and Poly(phenyleneethynylene)s

One-dimensional polyphenylenes are generally rodlike materials, whose degree of rigidity depends upon their structure. The rigidity has been controlled by linking of some or all adjacent benzene rings through methine bridges introduced by intramolecular Friedel–Crafts alkylations. Thus ladder-type poly(*para*-phenylene)s such as Me-LPPP (**5**, Scheme 2) in which the bridges are formed in a polymer-analogous Friedel–Crafts reaction,[67] are rigid linear ribbon-like molecules, whereas the partially bridged polyfluorenes (PFs, **6**)[68] can form coils because of their nonlinear monomer units. Other partially bridged structures such as polyindenofluorenes (PIFs, **7**)[69,70] or poly(ladder-type pentaphenylenes) (**8**)[71] have linear monomers and so are rigidly linear. The rigidity of these materials has been confirmed by dynamic light scattering experiments which have shown them to



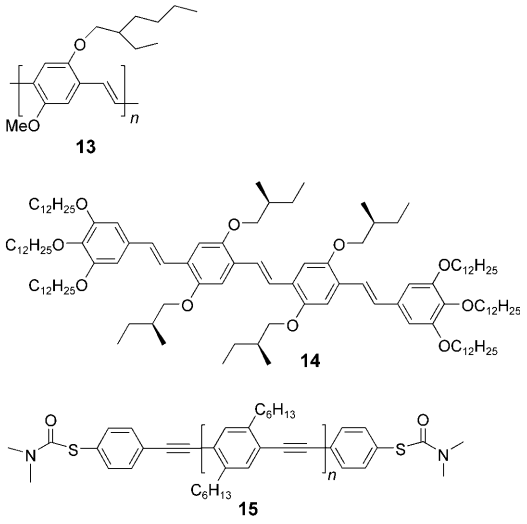
Scheme 2. One-dimensional polyphenylenes and oligomers.

 © 2005 Wiley-VCH Verlag GmbH & Co. KGaA, Weinheim

possess persistence lengths ranging from 8 nm for PFs (**6**) up to 25 nm for the pentaphenylene-based polymer **8**.[72] These polymers can be prepared by nickel(0)-mediated coupling of dihaloarenes,[73] or by Suzuki polycondensation of dihaloarenes with diboronates,[74] with very high ($>100000\,g\,mol^{-1}$) molar masses and have lengths of ten to several hundreds of nanometers. Methods have been established by which functional groups can be attached to the ends of the polymer chains by adding suitable endcapping reagents to the polymerization reactions.[75–78] Such groups can be used to help bind the chain end to a surface, for example, the thiol endgroups in compound **9** assist in its attachment to gold electrodes. These endcapping procedures also offer a way in which to control the molecular mass and thus chain length of the polymer and to synthesize rod-coil block copolymers.[75,76,78]

Oligomers of fluorene up to hexadecamers are known,[79,80] but the nonlinearity of the fluorene monomer means that these are not rigidly linear species. The ladder-type pentaphenylene (**10**)[71] is also readily available, This oligomer is already a 2-nm long linear rigid rod, and can be difunctionalized to permit attachment of other building units such as dyes. The largest ladder-type oligophenylene made to date is the undecamer **11**,[81] which is 4.5 nm long and with 11 benzene rings is of comparable size to the estimated effective conjugation length of polymer **5**.[82] The key intermediate was a pentaphenylene monoboronate **12** which was treated with a dibromoterephthalate to produce an undecaphenylene, which was converted into **11** by addition of several equivalents of an aryllithium and a subsequent Friedel–Crafts ring closure. The synthesis and purification of asymmetrically substituted intermediates such as **12** are the main challenges in the synthesis of larger bridged oligomers.

Phenylenevinylene polymers, such as MEH-PPV (**13**), and oligomers, such as the chiral OPV **14** (Scheme 3), are not rotationally restricted about the C–C bonds, and so the polymers can form coils, whereas the alkyne linkages in poly(phenyleneethynylene)s (PPEs)[83] are linear so that these polymers are rigid rods. Endcapping with functional groups has also been accomplished, for example, in polymer **15**,[84,85] and suitable endgroups have been used to make rod-coil block copolymers.[86]



Scheme 3. Polymers and oligomers from phenylenevinylene and phenyleneethynylene.

3.2. Studying the Self-Asembly of Polymers and Oligomers by AFM and STM

The microscopic surface morphology of polymer films can best be investigated by tapping-mode AFM. This method is unable to distinguish individual molecules or polymer chains, and so molecular modeling studies also need to be done to understand the supramolecular organization producing the observed morphology. The self-assembly of conjugated phenylene-based homopolymers and rod-coil copolymers has been probed in such a combined AFM/molecular modeling approach.[87] The most commonly observed organized structures in drop-cast films of these polymers are nanoribbons or nanofibres produced by π stacking of the chains. For example, poly(dioctylfluorene) (**6**, R = *n*-octyl) displays a fibrillar morphology (Figure 1, left) with straight fibrils.[87] These

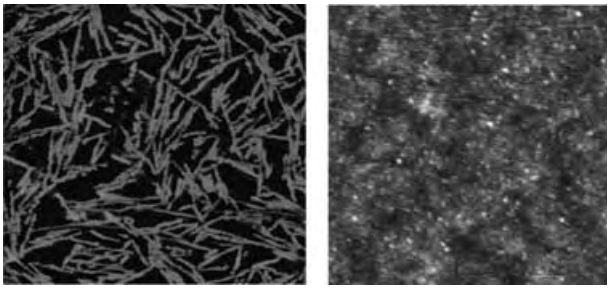


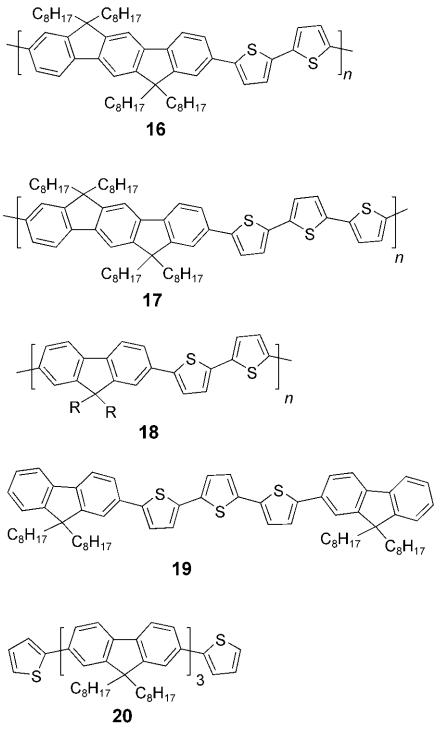
Figure 1. Morphologies of thin films of poly(dioctylfluorene) (**6**, left), poly(tetra(2-ethylhexyl)indenofluorene) (**7**, right) as revealed by AFM.

fibrils typically have heights of only a few nm and widths of tens of nm, which is equivalent to the lengths of individual chains, thus indicating that the chains are oriented perpendicular to the main axis of the fibers. A similar morphology is observed for the corresponding polyindenofluorene (**7**, R = *n*-octyl), whereas the polyindenofluorene with a branched alkyl substituent (**7**, R = 2-ethylhexyl) displays a smooth featureless morphology (Figure 1, right).[88,89] These differences can readily be explained by modeling studies, which show that the bulkier branched alkyl or aryl substituents hinder π stacking of the chains.[87,89,90] Another effect of the substituents is in controlling the thermotropic phase forming properties of these polymers. Thus PFs and PIFs with *n*-alkyl substituents typically form two nematic liquid-crystalline (LC) phases, while ethylhexyl-substituted polymers exhibit only a single nematic phase.[69,91–93] Annealing films of PFs on rubbing-aligned polyimide alignment layers has been used to obtain aligned films which exhibit polarized luminescence.[94]

Such differences have significance for the bulk optoelectronic properties of conjugated polymers: close packing enhances exciton diffusion to defect sites, which can suppress

© 2005 Wiley-VCH Verlag GmbH & Co. KGaA, Weinheim

fluorescence or cause the dominant emission to arise from emissive defects. As a result the amount of green emissions arising from defects in films of PIFs (**7**) correlates with the degree of π stacking as evidenced by a fibrillar morphology in AFM studies.[88] Thus, hindering interchain interactions is clearly desirable to achieve stable blue emission from materials such as PIFs. By contrast, strong π stacking is beneficial if efficient charge transport is desired. It has been demonstrated that a fibrillar morphology correlates to a relatively high charge-carrier mobility in copolymers of fluorene and indenofluorene with oligothiophenes such as **16**, **17**, and **18** (Scheme 4).[95–97] Modeling studies on the



Scheme 4. Copolymers of oligothiophenes with indenofluorene and fluorene.

polymer chain packing show that whereas the chains in polymers **17** and **18** have extended linear conformations and can undergo face-to-face packing between the oligothiophene and oligophenylene units to form closely packing ensembles (Figure 2), polymer **16** has a bent lowest energy chain conformation and cannot close-pack in this way.[98] The terthienyl oligomer **19** forms ordered striplike nanostructures when dropcast on glass, mica, or graphite. The height of these stripes (ca. 3 nm) matches the length of the molecules, thus indicating that they were aligned perpendicular to the surfaces. In contrast, the terfluorenyl oligomer **20** produced only disordered structures.[99]

Layers formed upon physisorption of PPE **15** from solution showed an interesting feature: polymer chains of similar sizes formed clusters.[84,100,101] This observed fractionation is attributed to formation of such clusters in solution,

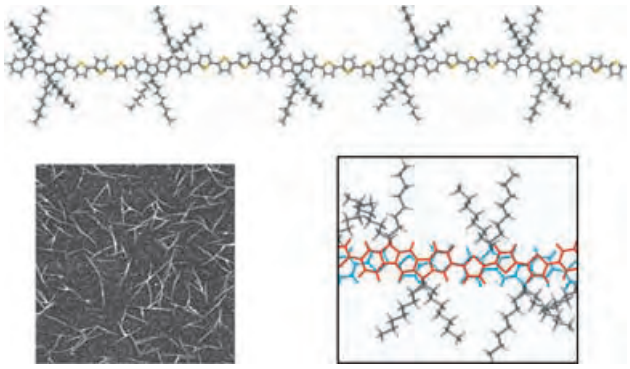


Figure 2. AFM image of a deposit of **17** from THF on mica, as well as simulations of the chain conformation and packing of **17**.

followed by their adsorption, and later exchange between adsorbed and non-adsorbed molecules at the solid–liquid interface which favors larger molecules being adsorbed where permitted sterically. The size and shape of the ribbons was independent of the substrate, thus indicating that the growth of the architectures from solution was largely governed by intermolecular interactions. The rod-coil block copolymers with polyphenylene or PPE blocks show fibrillar morphologies when deposited from solvents that are good for the conjugated blocks, but deposition of a polyphenylene–poly(ethylene oxide) (PPP-PEO) block copolymer from methanol, which solubilizes the coil but not the rod, produces apparently hollow, round-shaped deposits.[87] This result again confirms that the fibrillar morphology is a clear sign of π stacking of conjugated units. Self-assembly of chiral oligo(phenylenevinylene)s and oligothiophene-oligo(ethylene oxide) block copolymers on silicon produces chiral helical fibrils.[90,102,103]

STM has also been used to investigate conjugated phenylene-based oligomers and polymers at the single-molecule level. Chiral oligo(phenylenevinylene)s, such as **14**, were found to form ordered monolayers in which the packing in **14** was directed by the alkyl chains so as to induce an end-to-end arrangement, whereas in longer oligomers the conjugated backbones were the dominant influence and produced a closely packed columnar phase.[104] A similar close packing was seen for polymer **15**.[84] Trimeric phenyleneethynylenes, which were used as model systems, were synthesized by stepwise Hagihara–Sonogashira coupling and both their 2D and 3D solid-state structures determined.[84] The formation of tightly packed 2D crystals grown epitaxially on the basal plane of graphite was visualized by STM. The stiffness of the backbone and the conformational mobility of hexyl side chains were key structure-forming parameters. Two kinds of defects were recorded on the nanometer and subnanometer scale: missing molecules within a crystallite and domain boundaries surrounding such crystallites. Both defects turned out to be dynamic and Ostwald ripening occurred. This packing information is important since it helps to tune interchain distances and thus interchain hopping processes. STM studies on less rigid materials such as polythiophenes show a lamellar close-packing of the long linear segments that are linked together by hairpinlike folds

 © 2005 Wiley-VCH Verlag GmbH & Co. KGaA, Weinheim

of the polymer chain, thus suggesting that π-π interactions are the dominant force in their packing also.[105]

3.3. Nanostructured Devices

The next step required is to utilize the nanomaterials described above to make nanostructured devices. For example, field-effect transistors (FETs) could be fabricated either by aligning the structures between predeposited electrodes or by attaching electrodes to prealigned structures. Three methods for such alignment are available: 1) Cooling a liquid-crystalline material from the ordered mesophase has been used to align bulk materials, for example, PF-T2 (**18**), in FETs. This approach requires that the material be liquid-crystalline at a temperature significantly above room temperature, but not so high as to damage the other components of the device. 2) Oxidative nanolithography of silicon has been used to create a silicon dioxide array of parallel lines of width 30–50 nm and lengths of several micrometers. This array then acted as a template for the growth of a monolayer of an oligothiophene.[106] 3) The final approach uses lithographically controlled wetting, in which a stamp is placed in contact with a liquid thin film. Capillary forces cause the liquid to distribute itself only under the protrusions of the stamp, so that the solute forms patterns with the same length scale as the stamp upon evaporation of the solvent. In this approach a stamp with sub-micrometer features produces nanostructures with dimensions of several 10s of nanometers.[107,108] This method has been utilized to construct an FET using stripes of the oligomer **19**.[109] It must be noted that while self-assembled nanostructures can be made with dimensions considerably smaller than the smallest currently accessable devices, the devices discussed above are no smaller than those obtained using conventional materials, because of the need to fabricate stamps and/or deposit electrodes by conventional methods. Further advances in minaturization will thus require new methods for deposition of electrodes, for example, by advances in microcontact printing.

3.4. Optical and Electrical Measurements on Isolated Polymer Chains

Single-molecule spectroscopy gives fundamental insights into the photophysics of multichromophoric species. For example, the emission from individual chromophore subunits of Me-LPPP (**5**) can be resolved at low temperature and the interactions between them investigated.[110] The spectral diffusion dynamics of individual chromophores in Me-LPPP and the totally different conjugated polymer MEH-PPV (**13**) appears to be identical, but emission from multiple chromophores is possible only from the latter, which indicates that the major differences in the bulk behaviour of the polymers can be ascribed to morphological differences in the chain, and thus that structure–property relationships in conjugated polymers are extrinsic to the nature of the chromophores.[111] Comparison of the oligomer **10** with the polymer **5** by SMS shows that while there are individual chromophores of the same size on the polymer as on the oligomer (as shown by their emission maxima), their fluorescence intensity is much higher, and their line widths are narrower. The fluorescence dynamics of the oligomer and polymer are different in ensemble measurements, with the polymer showing appreciably shorter lifetimes of the excited state. These important differences between the oligomer and polymer chromophores are attributed to the excited states on the polymer having excitonic character, while the oligomer exhibits a molecular excitation.[81]

A new direction for single-molecule studies is the application of SMS on single chains of a conjugated polymer in a LED structure under a controllably varied electrical bias to probe the oxidation/reduction processes that occur in these devices.[112,113] Such techniques may lead to the optimization of LEDs by providing greater understanding of the mechanisms for their operation and breakdown.

Since the first proposal that rectifiers could be constructed using individual molecules linking two electrodes,[114] there has been interest in utilizing conjugated molecules, and even biomolecules, as so-called "molecular wires".[115–119] In such a case, charge-carrier transport would occur along a conjugated chain and not along their π-stacked aggregates as discussed above. The methods that have been used to measure the electrical characteristics of individual or small ensembles of molecules have recently been reviewed.[120] In most studies the molecules are tested as a self-assembled monolayer (SAM), for example, by scanning a self-assembled monolayer (SAM) on a gold electrode or other conductive surfaces with an STM or conducting AFM tip. Groups such as isonitriles or thiols are used as so-called "alligator clips" to attach the molecules to the conductive surface, and the position of these anchoring groups on the molecule has been shown to affect the detected electric current.[121] The reproducibility of results from single-molecule measurements is limited, so that statistical analysis of a number of individual measurements provides the best means for comparing the electronic properties of single molecules of different substances.[122] The thiol endgroups on polymers **9** and **11** enable them to bind to gold electrodes. It is possible to measure the electrical properties of individual polymer chains by using them to bridge two electrodes. The thiol-endcapped poly(*para*-phenylene) (PPP, **9**) with an average length of about 8 nm has been deposited between two electrodes in a transistor structure. Weak transistor behavior was observed upon altering the gate voltage, thus showing that in principle isolated conjugated polymer chains can be used in single-molecule FETs, although the transistor properties will need considerable improvement.[123]

3.5. Conjugated Polymers for Chemical Sensors

An important emerging area of nanotechnology is the use of sensors based on self-assembled monolayers.[26] As shown above, conjugated polymers can form ordered monolayers, and chemical sensors utilizing conjugated polymers may show greater sensitivity than small molecules.[124–126] The principle behind most of this work is that interactions between the

 © 2005 Wiley-VCH Verlag GmbH & Co. KGaA, Weinheim

analyte and the polymer induce a change in the conformation of the polymer chain which in turn affects its electrical and optical properties. These interactions are detected as changes in the conductivity, redox behavior (measured by cyclic voltammetry), absorption, or fluorescence of the polymer. The materials that can be detected by such methods include halide ions,[127,128] chemical warfare agents,[129] proteins,[130,131] nucleic acids,[132–135] and even bacteria.[136] The sensitivity of these methods is such that as few as 220 DNA molecules in 180 μL (2.4×10^{-18} M) can be detected.[134] Another DNA-sensing approach uses a polycationic fluorene–phenylene copolymer and a peptide nucleic acid (PNA) strand bearing a chromophore dye.[137] The PNA can hybridize with a strand of complementary DNA to form a polyanion which is then electrostatically attracted to the copolymer. In this case energy transfer can occur form the polymer to the dye and lead to intense fluorescence from the dye, whereas in the presence of noncomplementary DNA such complexation and energy transfer cannot occur. A third approach to DNA sensing is to attach two identical sequences of single-stranded DNA to a conjugated rigid rod.[138] Hybridization with the complementary sequences induces a marked augmentation in the fluorescence from the conjugated moiety. Even single nucleotide polymorphisms can be detected efficiently.

It can be seen from these results that rigid-rod one-dimensional conjugated materials will play a considerable future role as the active components in nanoelectronic devices such as FETs. Transistors with channel lengths of 100 nm or below are conceivable (compared with the multi-micrometer channel lengths seen in conventional devices). A key feature of these compounds as nanomaterials is their self-assembly behavior which arises from the π-π interactions of the "hard" aromatic backbone, but is heavily influenced by attachment of "soft" alkyl substituents or ethylene oxide coils. This combination of a hard aromatic core whose self-assembly through π stacking is controlled by a soft alkyl shell is seen in more extreme form in the case of "two-dimensional polyphenylenes", which will be considered in the next section.

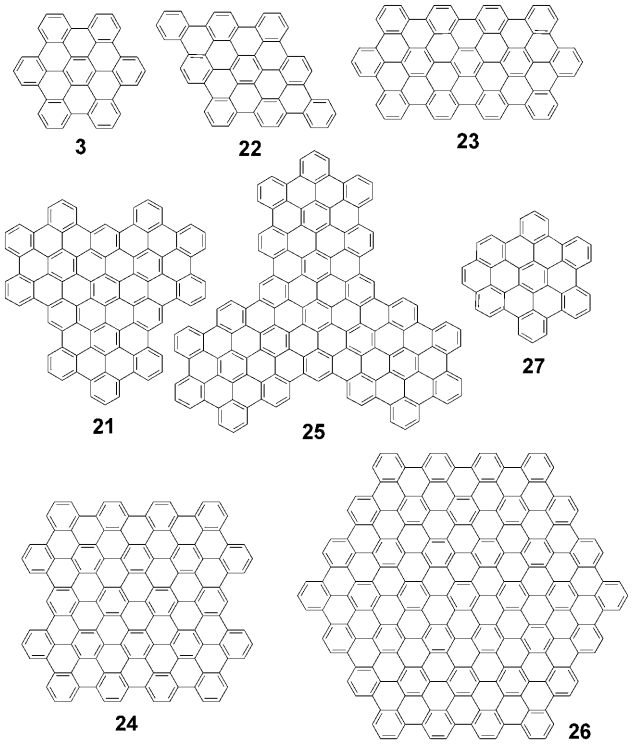
4. "Two-Dimensional Polyphenylenes": Graphene Molecules as Nanosized Semiconductors

4.1. PAHs as Molecular Subunits of Graphite

Planar polycyclic aromatic hydrocarbons (PAHs)[139] can be regarded as molecular subunits of graphite that consist of fused benzene rings. Such molecules have long played an important role as models in molecular orbital theory and, more recently, have become important objects in the visualization of single molecules by STM.[35] PAHs can be divided into two types according to the model of Clar, in which the π electrons are distributed among the benzene rings so as to form the greatest possible number of "full" rings, that is, π-electron sextets.[140] In all-benzenoid PAHs all the π electrons in the PAH can be distributed so that each benzene ring contains either 6 or 0 π electrons (which means such molecules must have a number of ring carbon atoms divisible by 6). All-benzenoid PAH molecules are more stable, less reactive, and have larger HOMO–LUMO gaps than isomeric compounds that do not satisfy this criterion.[139]

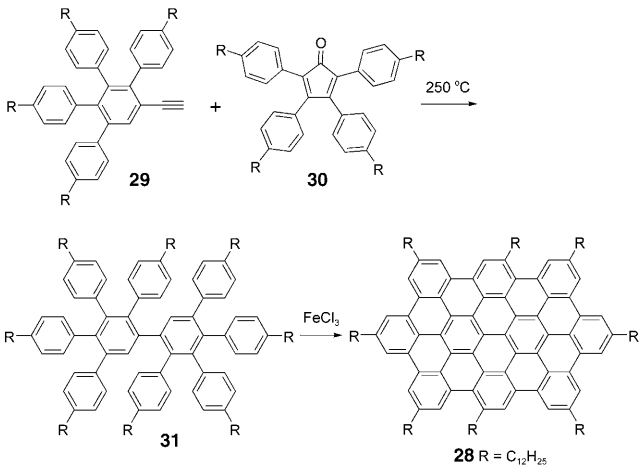
Efficient routes have been developed to a large variety of graphene molecules with different molecular topologies (Scheme 5; substituents are not shown). The diameters of these molecules range from 1.4 nm (**3**) to 3.5 nm (**26**). Of the skeletons shown, C_{42} (HBC, **3**),[141] C_{96} "superphenalene" (**21**),[142] C_{54} (**22**),[143] C_{78} (**23**),[143] C_{132} (**24**),[143] C_{150} (**25**),[144] and C_{222} (**26**)[145] are all-benzenoid, whereas C_{44} (**25**)[146] is not. The PAHs are all made in good yield by oxidative cyclodehydrogenation of a soluble three-dimensional polyphenylene dendrimer precursor, as illustrated in Scheme 6 for the substituted C_{60} molecule **28**.[147] The branched oligophenylene precursor **31** was synthesized by Diels–Alder addition between tetraphenylcyclopentadienone (**30**) and the monoethynyl-substituted pentaphene **29**. Oxidative cyclodehydrogenation of this precursor by treatment with iron(III) chloride then afforded the planar C_{60} molecule **28** in nearly quantitative yield.[147] This simple and efficient route is suitable for the large-scale synthesis of all-benzenoid PAHs, which are now obtained as structurally perfect nanosized 2D π systems. PAHs bearing solubilizing groups such as alkyl groups can be processed in solution. Large unsubstituted PAHs such as **22** are insoluble but thin films can be obtained by ultrahigh vacuum deposition at high temperature (550–650 °C) because of their excellent thermal stability.

As would be expected, the size and shape of the PAHs have major effects upon their optoelectronic properties.



Scheme 5. Graphene molecules.

 © 2005 Wiley-VCH Verlag GmbH & Co. KGaA, Weinheim



Scheme 6. Synthesis of a disc-type C_{60}-molecule **28**.

Increasing size leads to greater delocalization of the π electrons and a decrease in the bandgap as reflected in the UV/Vis spectra. A linear relationship is seen between the absorption maximum of the α band and the number of "full" aromatic rings.[139,148] As illustrated in Figure 3, this change is also

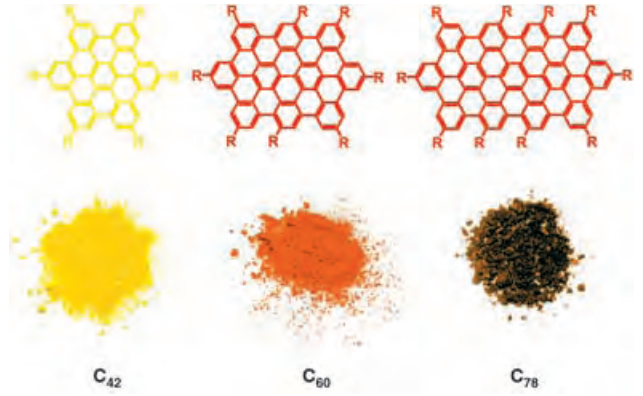


Figure 3. Examples of PAHs showing the bathochromic shift in the spectra with increasing size of the molecule.

readily visible in the color of the materials. Thus C_{42} (HBC) is a yellow powder, while C_{132} **24** possesses a red color in solution,and the parent compound C_{222} **26** is a black powder with a broad absorption band extending up to 1200 nm. The introduction of extra π center—such as in **25**—produces a strong perturbation of the π-electron cloud, so that additional bands are seen in the UV/Vis spectrum and the intensity of the lowest band of the α transition is greatly enhanced as a result of the loss of symmetry.[146] The Raman spectra of PAHs reflect both the size and shape of the molecules,[149,150] and have been used as models for simulating and interpreting the spectra of complex carbon materials, for example, amorphous carbon and graphite.[149,151,152] An important question concerns the relation between the size of the PAHs and the charge-carrier mobility within their columnar superstructures (see Section 4.2.2).[148]

4.2. Liquid-Crystalline Graphite Molecules as Building Blocks for Nanostructured Arrays

Soluble discotic graphite molecules such as alkyl-substituted HBCs **32** (Figure 4) can form thermotropic liquid-crystalline phases, in which the molecules align into ordered

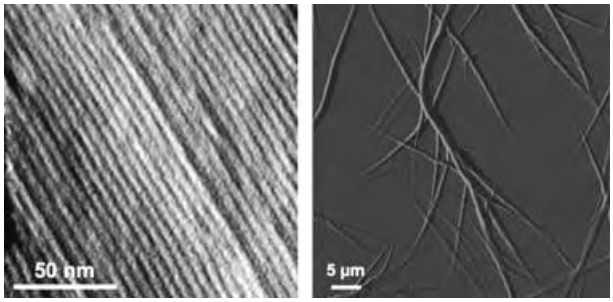


Figure 4. Zone-cast films (left) and microfibres (right) of HBCs cast from THF solution onto glass substrates.

nanosized columns.[153] While the π interaction of the aromatic cores leads to self-assembly into columnar structures, the side chains are partially organized at the core periphery and produce nanophase-separated arrays. The supramolecular order is strongly dependent on the thermal behavior of the compound. Thus, the aromatic cores of the discs have reduced molecular dynamics in the crystalline state and arrange in a herringbone structure which is characterized by a molecular tilting with respect to the columnar axis. Heating to the liquid-crystalline phase results in the molecular arrangement changing to an orthogonal intracolumnar packing. Longitudinal and lateral displacements of the molecules are possible within the stacks as a result of a high side-chain mobility and the increase in their steric requirements. The self-organized molecules are typically about 0.35 nm apart, which allows for efficient overlap of the π orbitals on adjacent discs and the generation of high charge-carrier mobility along the axis of the column.[148,153–155] This arrangement means that a column of HBCs acts like a nanowire with a conductive core and an insulating shell of alkyl substituents. As a result, the highest efficiencies will be attained in electronic devices when the columns are aligned perpendicular to the electrodes; in FETs this means the discs are edge-on to the substrate (heterotropic alignment) and for a solar cell they are face-on (homeotropic alignment). Whereas the former is the favored orientation for discs deposited from solution, it has been shown that the latter can be achieved by cooling an HBC layer from the isotropic phase between two substrates.[153,156] Here again the size of the molecules plays an important role. Although discotic mesophases have been obtained for a large number of disc-type molecules[153] it is the size of the PAHs which leads to anistropic LC phases that are stable over a broad temperature range as well as to increased charge-carrier mobilities.

Two methods have been used for producing aligned films of HBCs. In the first the material is spin-cast upon a pre-aligned polytetrafluoroethylene (PTFE) layer,[157] while the

 © 2005 Wiley-VCH Verlag GmbH & Co. KGaA, Weinheim

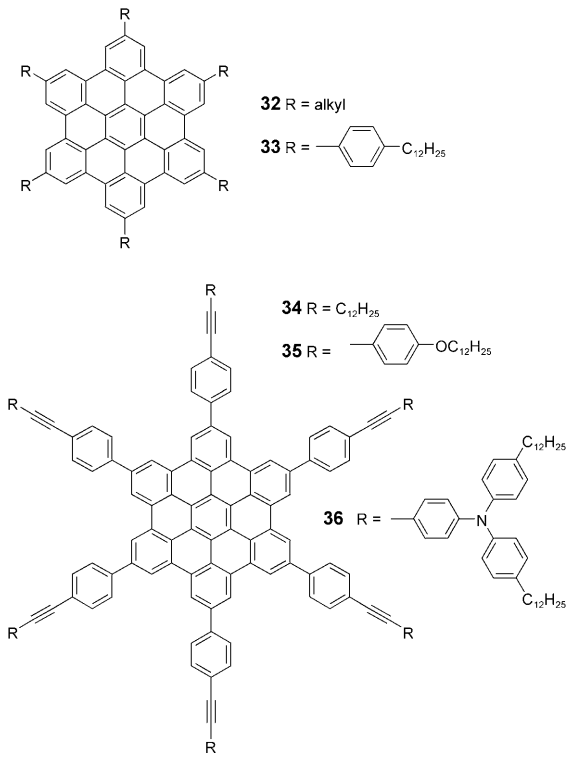
second utilizes zone-casting from solution.[158] In this simple procedure, a solution is deposited through a nozzle onto a moving substrate, with both nozzle and substrate being thermally stabilized. The concentration and temperature gradients suffice to uniaxially align the columnar nanostructures along the deposition direction. The casting conditions can be varied to obtain either continuous films with a "quasi-single-crystalline", long-range ordered surface layer (Figure 4, left) or highly oriented microfibres (right). Zone crystallization from the melt has also been used to obtain highly aligned films.[159]

Both methods have been used to construct efficient FETs using films of HBCs **32** which have been aligned between the electrodes (method for the pre-alignment PTFE layer: $\mu = 10^{-3}$ cm^2 Vs^{-1};[157] zone-casting: $\mu = 10^{-2}$ cm^2 Vs^{-1}).[160] A blend of the aryl-substituted HBC **33** with an electron-accepting perylenediimide dye showed high efficiency in a photovoltaic device with an external quantum efficiency (EQE) of 34% being seen at 460 nm.[161] The partial phase separation of the two components to provide separate percolation pathways for holes and electrons seems to be the main reason for the good efficiency. Thus, optimizing the performance of FETs and photovoltaic cells with PAHs as the active components requires increasingly complex supramolecular hierarchies.

The parent HBC could be sublimed under ultrahigh vacuum and the thin films deposited on MoS_2, HOPG, Au(111), and copper surfaces. The films produced displayed epitaxial order with the HBC normal perpendicular to the surface.[162] Highly ordered, several nanometers thick films of alkylated discs could also be grown on a MoS_2 surface by solution processing.[163] These films exhibited a two-dimensional lateral arrangement of columns standing on the surface. The planar arrangement of the first layer might be the reason for the observed epitixal growth. Angle-resolved photoelectron spectra revealed a highly anisotropic quasi-one-directional electronic structure with an extended π-electronic wave function. An intermolecular dispersion of the highest occupied band of at least 0.15 eV along the stacking direction has been measured.

The charge transport in columns of HBCs can be optimized by attaining the maximum degree of intracolumnar order and thus the best overlap of orbitals. One way of increasing the order of the columns is to replace the alkyl substituents in **32** with (di)arylethyne units, as in **34**–**35** (Scheme 7).[164] Compound **35** displays helical stacking with each successive disc rotated by 15° about the columnar axis. Very high charge-carrier mobility is also achieved by attaching hole-accepting triarylamine units, as in **36**.[165] Here the HBC cores and triarylamine units provide two coaxial pathways for the charges to move along.

AFM studies on spin-cast films of **34** revealed individual columns of discs as stripes with widths of about 3.4 nm (corresponding to the intercolumnar distance seen from X-ray diffraction measurements on the bulk material) and lengths of up to several hundred nanometers within larger ordered domains.[164] The height of these objects also conformed to the calculated diameter of the HBC units, thus suggesting that they were comprised of individual columns with the column axis approximately parallel to the substrate

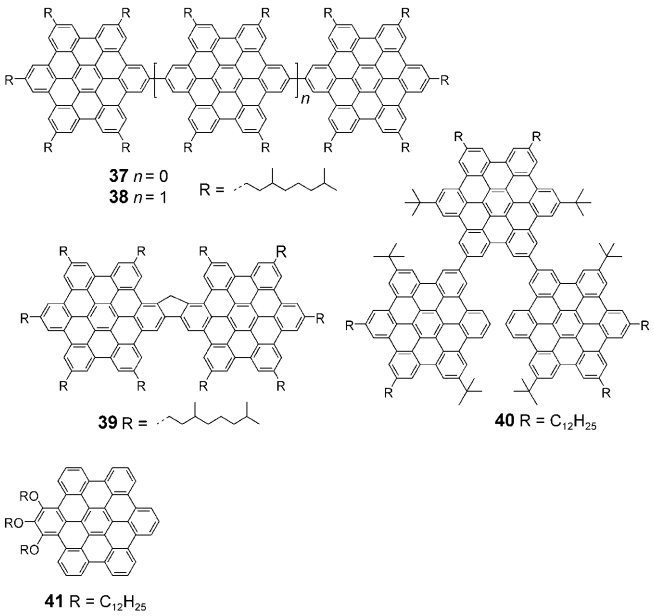


Scheme 7. Discotic liquid-crystalline HBCs.

surface. Drop-casting films of **35** produced nanoribbons several micrometers in length, with widths of about 21 nm and heights of about 4 nm, which we interpret as being arrays of 5–6 columns. Similar self-assembled fibres have been seen for dendrimers and dendronized polymers (see Section 6.5). The next problem to be solved is to align individual HBC fibres or columns between two electrodes and so fabricate a nano-FET. The lithographically controlled wetting technique described in Section 3.3 offers one way to achieve this.

The above materials illustrate how we can optimize intracolumnar order in HBCs, but the control of intercolumnar order is equally important if more than a single column is to be used in a device. One method to achieve this is to combine one- and two-dimensional structural motifs by preparing HBCs with rigid conjugated linkers which might be blended with other HBCs and thus link together the columns in which they are incorporated. These conjugated links might also allow charge to be transferred between columns, thus by-passing any defects in the columns. To this end the HBC dimer **37** and linear "*para*-trimer" **38**, the "superfluorene" **39**, and the nonlinear "*ortho*-trimer" **40** (Scheme 8) have been prepared and their phase-forming behavior investigated.[166] Compounds **37**–**39** self-assemble into ordered columnar mesophases as shown by X-ray diffraction experiments. By contrast the nonlinear trimer **40** does not form an ordered columnar array, presumably because the HBCs in this material are twisted even more out-of-plane by steric interactions than the rings in the other materials. An "unwrapped" HBC molecule **41** was also synthesized which displays a stable columnar liquid-crystalline phase with a low isotropization temperature (190 °C).[167]

 © 2005 Wiley-VCH Verlag GmbH & Co. KGaA, Weinheim

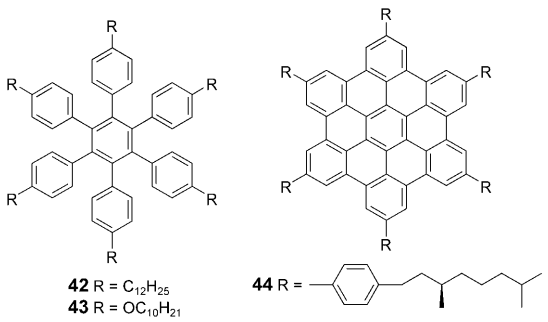


Scheme 8. Oligomers of HBC and "unwrapped" HBC **41**.

In addition, it possesses a good solubility in common solvents and can be used as active components in field-effect transistors. Thus, the interactions between unsubsituted aromatic cores should allow for better intercolumnar charge transport.

4.3. Scanning Tuneling Microscopy on Monolayers of Polycyclic Aromatic Hydrocarbons

The STM visualization of individual molecules in real space is performed after their immobilization, often as part of an ordered monomolecular layer.[35] The formation of the monolayer (a so-called 2D crystal) is a sensitive function of the size and shape of the molecule, and is controlled by the symmetries of both the adsorbate and substrate. Such layers are obtainable either by ultrahigh vacuum (UHV) deposition[168] or by physisorption from solution. Since the formation of monolayers competes with the occurrence of double and multilayers, complex problems of epitaxial growth arise both for single and for multicomponent deposition.[168] The interactions between molecules can be probed by STM of the resulting films to determine how the molecules stack within the layers. Thus STM has established that the chiral PAH heptahelicene forms SAMs consisting of chiral molecular clusters when deposited under UHV conditions.[169] In the deposition of alkyl-substituted PAHs upon HOPG it was determined that π interactions between the adsorbate and substrate, as well as the adhesion of the alkyl chains to the surface play a role. It is interesting that the alkyl chains can easily change their conformation upon adsorption so as to obtain the best packing arrangement. An ordered monolayer of **32** ($R = C_{12}H_{25}$) has even been created by depositing the hexaphenylbenzene (HPB) precursor **42** (Scheme 9) on



Scheme 9. PAH precursors and PAHs visualized by STM.

HOPG, and then converting it into the HBC with iron(III) chloride.[170] In this case STM could not be used to monitor the reaction because of the presence of the metal ions, but the similarity in the unit cells of **42** and **32** suggested that it proceeded at the surface. Thus, this technique might be useful for depositing ordered films of larger, less soluble, PAHs through conversion of their soluble precursors.

STM was also used to confirm the thermally induced cyclodehydrogenation of the hexadecyloxy HPB **43** on a copper surface at 550–710 K.[171] The cyclodehydrogenation was accompanied by loss of the alkyl groups, and the molecules became anchored to the surface through the oxygen atoms of the ether groups during the course of the reaction. Very large PAHs are formed upon copper surfaces by heating diphenylacetylene or HPB to 550–700 K.[172] STM visualization has been used to prove the rhomoboidal shape of the C_{54} molecule **22**,[143,173] which was difficult by conventional spectroscopic means, and the biaryl nature of a "superbiphenylene" (**36**, $R = C_{12}H_{25}$).[174] The contrast within the STM images of the C_{60} molecule **28** appears to reflect the nodal properties of the frontier orbitals and so enables the π bonding within the molecule to be described as a combination of three weakly coupled terphenyl and quaterphenyl chains.[147] The "thickness" of the PAH monolayers can be controlled by the branching within the alkyl chains and the presence of additional (twisted) phenyl rings. Thus, deposition of the HBC **44** creates a staircase pattern in which each molecule can adopt one of three different heights (that is, different positions between the substrate and the tip).[175] Each molecule thus has a different position within the pattern and gives a different tunneling current. Such a site-specific contrast becomes even more important since some of the positions within the pattern remain vacant which allow the displacement of molecules between positions with different currents, thus creating a kind of register.

While the visualization and manipulation of nanometer-sized molecules in real space described above are fascinating experiments, it is important to go one step further and utilize the electronic function of single molecules. Graphene molecules have played an important role in this key step towards molecular electronics. By combining STM with STS it has become possible to record current–potential curves for single PAH molecules.[35,38] These curves displayed a typical diode-like asymmetry when the tip was passed over the aromatic

 © 2005 Wiley-VCH Verlag GmbH & Co. KGaA, Weinheim

cores, whereas the aliphatic chains produced a symmetrical curve.[38] The shapes of the curves vary in going from C_{42} to C_{60} and C_{78} to C_{114}, and indicates how the increased core size changes the frontier orbitals.[176]

Current–potential curves were recorded separately for the donor and acceptor components of molecule **45**—with an HBC core as the electron donor surrounded by six alkyl chains bearing electron-accepting anthraquinone (AQ) groups (Figure 5). The curves showed characteristic differences in their slope, thus indicating that the tunneling currents were strongly influenced by the resonant enhancement of the HBC HOMO and the quinone LUMO. Remarkably, transistor activity has been demonstrated for a single molecule of **45** on a surface, in which the HBC and anthraquinone both lie flat on the surface. The addition of 9,10-dimethoxyanthracene (DMA, **46**) resulted in the formation of a charge-transfer complex with the anthraquinone, whose dipole changed the substrate work function by about 120 meV, and so induced a detectable change in the I/V characteristics of the HBC core as measured by a STM tip. In this way a chemical gate effect[177] was produced with a nanometer-sized gate. In this system the dipole was parallel to the channel direction of the transistor, and thus perpendicular to the surface. Attachment of a dipole to the HBC with its direction parallel to the surface had no effect on the HBC I/V behavior.[178] Although it is certainly a fascinating experiment to demonstrate a FET function on a nanometer scale, the currents involved are much too small to be of practical value in a real FET.

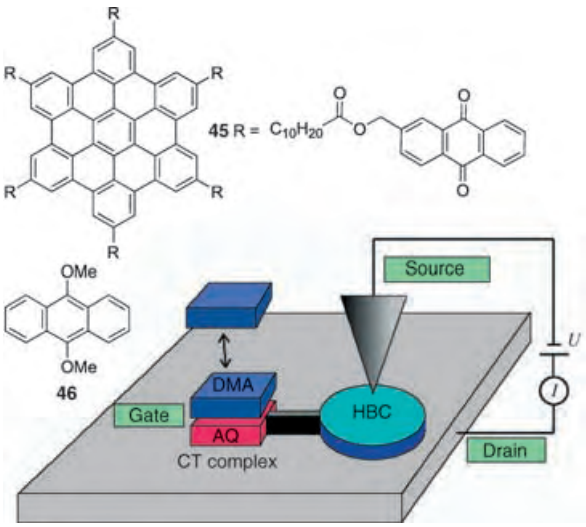


Figure 5. A single-molecule chemical FET.

In this section we have considered the behavior of PAHs with various molecular topologies. The effects of different topologies upon properties are even more clearly seen with rylenes, a class of not all-benzenoid graphite subunits which display excellent performance as colorants, particularly when substituted with auxochromic anhydride and imide groups.

5. Rylene Dyes for Single-Molecule Spectroscopy

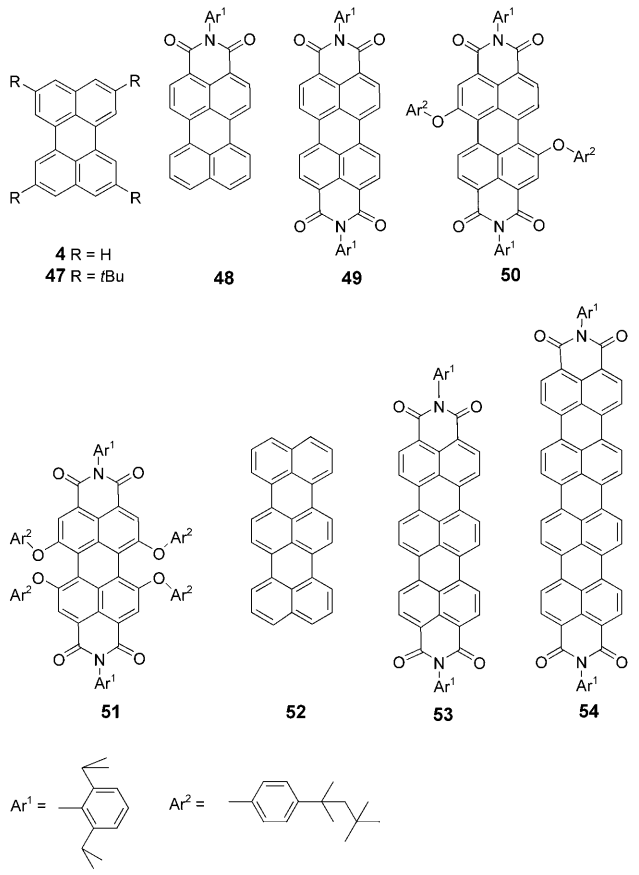
Soluble (dyes) or insoluble (pigments) colorants may be used to add color to materials. The insolubility of pigments means they are generally employed as dispersions of particles (most commonly micrometer sized) within the material they are coloring. Smaller particles give a more even distribution of color and so, as mentioned in the Introduction, colored nanoparticles have long been used as pigments. In recent years there has been much industrial interest in developing pigment nanoparticles and particularly nanocrystals as colorants.[179] A second point of interest beyond the colorant aspect is the use of "functional dyes" as active components for xerography,[180] optical switches,[181] laser-dyes,[182] photovoltaic cells,[161] optical recording,[183] light-emitting diodes,[184] or as tracers in fluorescence analytical assays.[185]

A third, more recent, research field arises from the idea of using light as a way to address single molecules. Our ability to control light is now so developed that even single photons can be detected and manipulated reliably, either as an input or output; thus optical addressing of nanomaterials in devices is an attractive option. In parallel with this came the development of single-molecule spectroscopy (SMS) as a powerful tool for the investigation of the photophysics of materials, particularly in conjunction with confocal microscopy. The necessary requirements for this technique are chromophores, whether molecular or polymeric, which show strong absorption and/or emission in appropriate regions of the electromagnetic spectrum. Other requirements are good photo- and chemical stability, and for some applications, for example, bioassays, water solubility and anchoring to a biologically active moiety may also be needed. The issue of stability is particularly vital for chromophores for use in nanomaterials. In bulk materials there are many "surplus" molecules present to compensate for any which fail, and so the failure of a certain amount of the material may not have an immediate effect on the overall properties of the materials. In nanomaterials, where there are only a limited number of molecules present, every molecule matters. Molecules or assemblies with multiple chromophores, in which there is thus a certain amount of "back-up" functionality, might therefore be more desirable for nanoapplications than single-chromophore compounds. Such molecules will also show more absorption and emission per molecule, thus increasing the detection sensitivity and making them better for studies by SMS. Before we investigate the SMS of dyes, we must first take a detour into classical dyestuff chemistry whose origins go back to the early 20th century.[186] The class of dyes examined are rylenes, which perfectly satisfy the above-mentioned criteria and additionally can be readily functionalized by simple, high-yielding procedures to enhance their solubility and to permit them to be attached to various other chemical or biological systems.

5.1. Tuning the Properties of Rylenes

Rylene dyes have a backbone consisting of *peri*-linked naphthalene units (Scheme 10). The emission color of these

 © 2005 Wiley-VCH Verlag GmbH & Co. KGaA, Weinheim



Scheme 10. Representative rylene dyes.

dyes can be tuned from blue through to the NIR by varying the number of naphthalene units and/or the number, type, and pattern of the substituents. Thus, of the compounds with two naphthalene units, the parent compound perylene (**4**)[187] and the tetra-*tert*-butyl derivative **47** are blue-green and blue emitters, respectively.[187] Substitution with imide units produces a red-shift so that perylenemonoimide (PMI, **48**) is a yellow emitter with an emission maximum at 506 nm, while the diimide (PDI, **49**) is an orange emitter ($\lambda_{max} = 526$ nm). Attachment of substituents in the bay positions also induces a bathochromic shift in the absorption and emission maxima, as well as markedly improving the solubility of the dyes. The diphenoxylated PDI **50** and tetraphenoxylated PDI **51** are thus orange ($\lambda_{max} = 575$ nm) and red emitters ($\lambda_{max} = 610$ nm) respectively.[188]

Higher rylenes are made by aryl–aryl coupling of naphthalene or perylene units followed by a ring closure of the bisaryl precursors to the ladder-type rylene structure. Homocoupling of bromoperylenes with nickel(0) provides an efficient route to bisperylenes,[189] while Stille or Suzuki coupling are the optimal methods for the heterocoupling of naphthalene or perylene units.[190,191] The synthesis of the boronate or stannyl intermediates is a crucial step in these routes. Since functional groups such as the imide structure are sensitive towards organolithium compounds the synthesis of boronic acids or esters with organolithium reagents are not applicable here. Therefore, mild palladium-catalyzed methods have to be used to form a boronate[192] or organostannane.[193] Base-promoted cyclizations in the presence of strong electron-withdrawing groups, such as imides, provide the rylenes in nearly quantitative yields,[189,191,194] while for materials without such groups oxidative cyclodehydrogenation of the coupled biaryls to the rylenes can be efficiently performed with aluminum trichloride or iron(III) chloride.[195,196] Increasing the number of rylene units produces a red-shift in the emission so that terrylene (**52**) is a green emitter ($\lambda_{max} = 573$ nm)[195] and the emission maxima for the terrylenediimide (TDI, **53**)[190] and quaterrylene (QDI, **54**)[189,197] are at 650 and 760 nm, respectively (Figure 6). However, while the emission quantum yields for PDI and TDI are close to unity, that for QDIis only 5%.[197] This low quantum yield is attributed to the increased possibility of nonradiative loss of energy by means of vibrationally induced torsion between adjacent rylene units.

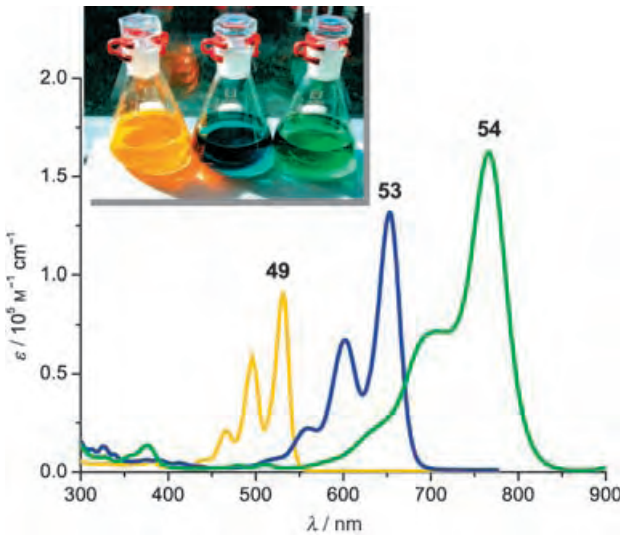
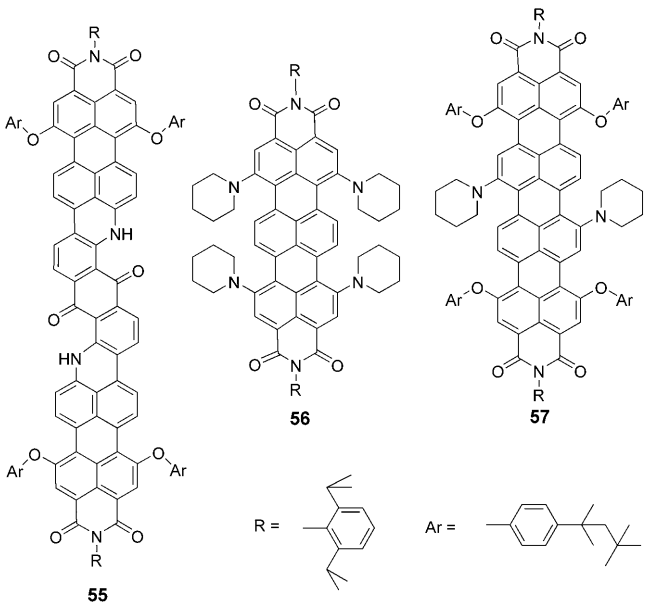


Figure 6. UV/Vis absorption spectra of PDI, TDI, and QDI.

The even greater bathochromic shifts needed to obtain absorption in the NIR have been achieved by other means. Aryl amination of two equivalents of a bromo-substituted PMI with a diaminoanthraquinone followed by oxidative ring closure produced compound **55**, which possesses an absorption maximum at 1000 nm with a shoulder at 1106 nm (Scheme 11).[194] Introduction of piperidine substituents in the bay positions of TDI and QDI has been used to make the dyes **56** and **57** which possess absorption maxima at 765 and 910 nm, respectively.[198]

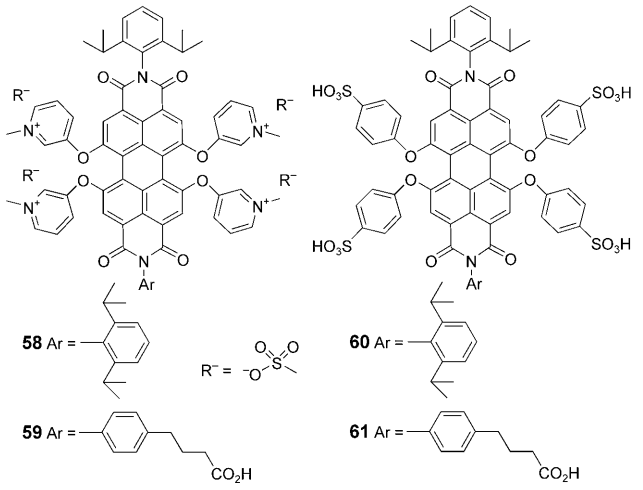
The next question to be addressed is that of water solubility (with retention of high fluorescence efficiency), which is necessary if the dyes are to be used in bioapplications. The excellent efficiency and stability (and also the nontoxicity) of PDI were utilized in the development of water-soluble PDI-based chromophores by introduction of highly hydrophilic units into the bay position of PDI (by phenoxylation of tetrachloro-PDIs). Aromatic nucleophilic substitution with 3-pyridinol followed by quaternization with

 © 2005 Wiley-VCH Verlag GmbH & Co. KGaA, Weinheim



Scheme 11. Rylene dyes with adsorption maxima in the NIR region.

iodomethane gave the positively charged dyes **58** and **59** (Scheme 12), while phenoxylation followed by sulfonation gave the tetrasulfonates **60** and **61**.[199] All of these possessed



Scheme 12. Water-soluble perylenediimide dyes.

good solubilty in water and the photoluminescence quantum yields in aqueous solution varied from 0.66 for **58** to 0.49 for **61**. The biological applicability of these materials was demonstrated with cardiac cell cultures. After staining, the cells were intensely fluorescent and no sign of a structural degradation could be observed. Furthermore, the cells continued to proliferate, thus underlining the nontoxicity of the label. Fluorescence intensity remained for a long period of time after contact with cell cultures, and demonstrates the suitability of perylene dyes as labels in biological studies.[200]

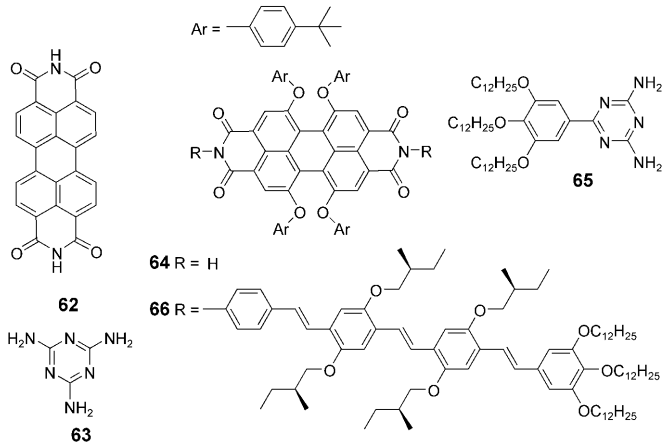
Another way to introduce charges around the perylenediimide chromophore and achieve water solubility is the attachment of oligonucleotides as polyanions. In general, DNA allows the formation of well-defined supramolecular aggregates of small organic molecules by base pairing.[201–204] Structurally defined chromophore dimers, trimers, tetramers, and pentamers with equidistant spacing of the dyes were realized by introducing two identical oligonucleotide sequences into the imide structures. Two of these biological–organic hybrid structures with complementary sequences form linear assemblies by hybridization.[205] These arrays containing only one type of chromophore are the first step towards the rational bottom-up approach of DNA-based supramolecular structures for controlled excitation energy transfer.

Water-soluble PDIs can also be obtained by coupling with polypeptide chains which can be achieved by functionalization of the phenoxy groups in the bay and subsequent "grafting-from" reactions of the peptide fragments.[206,207]

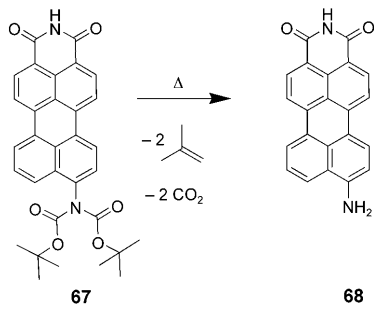
5.2. Self-Assembly Using Perylenediimides

Self-assembly of chromophores is of great interest because such assemblies are models for natural light-harvesting systems,[208–210] and because they have potential application in solar cells.[211] Perylene is a planar molecule and so in the absence of bulky substituents PDIs will readily aggregate through π stacking. The introduction of phenoxy substituents, such as in **50**—**51**, thus markedly improves their solubility by suppressing this aggregation. Attaching suitable functionality at the imide positions enables the PDI derivatives to be used as building units for supramolecular architectures held together by noncovalent forces such as hydrogen bonding, ionic interactions, or metal–ligand coordination.[212] The folding of copolymers of perylenediimides with flexible chains, including nucleotides, can be controlled by means of the temperature-dependent stacking of the dye units.[213] The thermally induced folding can be reversed by DNA hybridization, thus offering a new approach towards biosensors based on color change. PDIs with a thiol substituent have been shown by AFM to self-assemble on gold surfaces.[214] The fluorescence from these aggregates was much stronger on patterned than on unpatterned surfaces which enabled the structure of gold surfaces to be probed by simple fluorescence methods. The self-assembly of monolayers (both vacuum deposited and from solution) of PDIs has been studied by STM. While PDI **62** (Scheme 13) forms an array with quasihexagonal symmetry,[215] co-deposition with melamine (**63**) produces an extended hydrogen-bonded hexagonal network.[216] A mixture of the substituted PDI **64** with the triazine **65** gives a partially ordered monolayer containing local domains of linear complexes of the two components that coexist with uncomplexed dimers of **65**.[217] The two conjugated systems in the OPV-perylene compound **66** could be distinguished by their bias-dependent tunneling currents, which are higher for the OPV group at negative bias and for the PDI unit at positive bias as a result of resonant enhancement by the HOMO of the OPV and the LUMO of the PDI.[218]

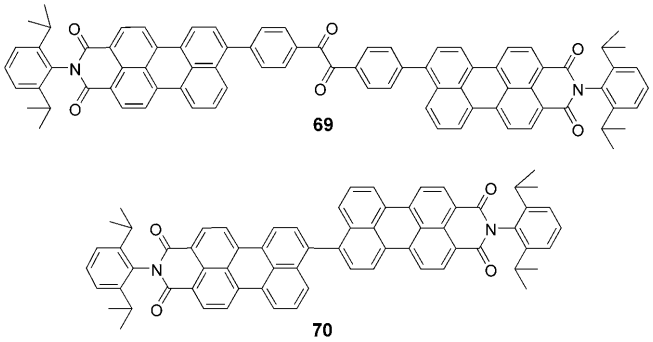
 © 2005 Wiley-VCH Verlag GmbH & Co. KGaA, Weinheim



Scheme 13. Perylenediimides that can form self-assembled monolayers.



Scheme 14. Interconversion of dyes studied by single-molecule spectroscopy.



Scheme 15. Bisperylene molecules studied by single-molecule spectroscopy.

5.3. SMS on Rylene-Based Chromophores

Rylenes possess most of the properties desired for SMS—including strong absorption, high fluorescence efficiency, low photobleaching efficiency—and so have been the object of much attention. There were several early SMS studies on terrrylene (**52**),[219–223] including, as mentioned in the Introduction, the direct observation of quantum jumps between singlet and triplet states.[32] Isolated molecules of TDI **53** have been studied by frequency-selective high-resolution laser spectroscopy at liquid helium temperatures and by confocal fluorescence microscopy between 100 K and room temperature, and their spectral dynamics determined.[224–226] Most of the molecules showed several (up to 10^7) on-off-on (blinking) transitions before permanent bleaching occurred. From the point of view of photostability, the main advantage of TDI **53** is its low-lying triplet state. SMS studies on the tetraphenoxy-PDI **51** have been used to investigate its conformational changes[227] and by comparing these in different environments to probe the local free space inside various polymer glasses.[228,229] The water-soluble PDI **60** could be imaged inside living cells by one-photon confocal microscopy and fluorescence lifetime microscopy with two-photon excitation. A good example of how SMS can be used to obtain information not derivable from ensemble measurements is presented by the dyes **48**, **67**, and **68**.[230–232] The spectra of solutions of **48** and **67** are almost indistinguishable but they can be clearly distinguished by SMS. Even different conformations of **68** can be detected by single-molecule fluorescence measurements. Since **67** undergoes a thermally induced fragmentation to give **68** (Scheme 14), the course of this reaction can be monitored at a single-molecule level, and information derived about the nature of intermediates.

A logical extension of SMS studies of individual rylene chromophores is to include bischromophores made up from identical dyes. This theme will be extended in Section 6 to the study of vectorial Förster-type energy transfer in bis- and multichromophores and in Section 7 to the SMS study of linear oligophenylenes by using dyes as labels. The first such system to be studied was compound **69** (Scheme 15) in which two perylenemonoimides are attached to the *para* positions of a benzil spacer. Collective off-times of both chromophores could be seen in SMS studies as a result of single–triplet annihilation, and the probability of coincident emission of two photons vanished because of singlet–singlet annihilation.[233]

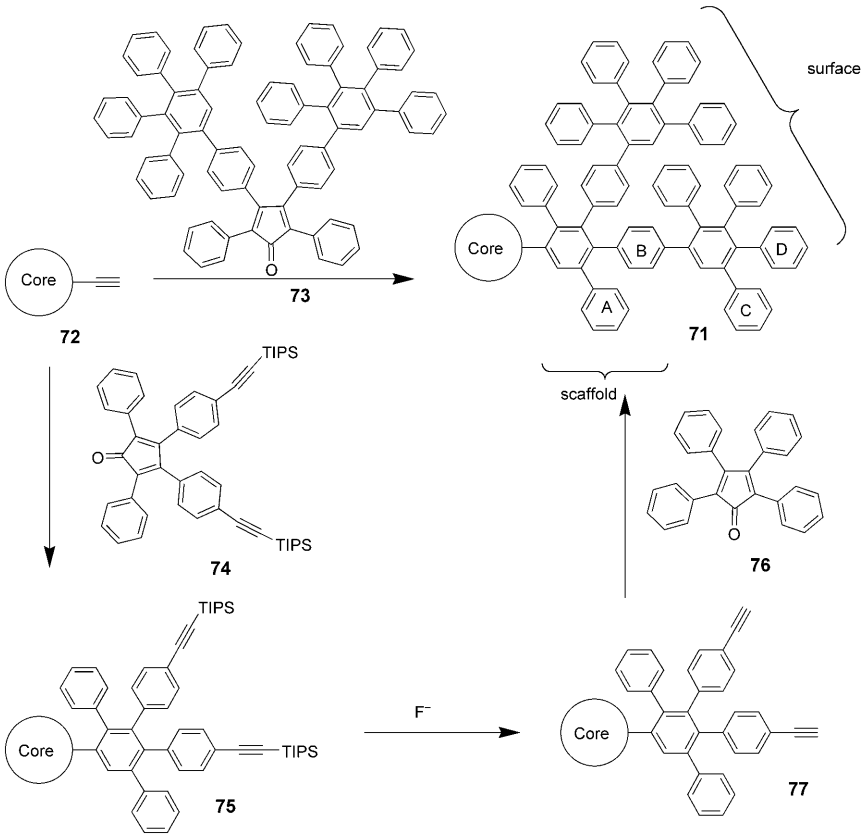
Single bischromophores (as a first approximation to collective effects) allow the distribution of cooperative radiative decay rates in bis- and multichromophoric aggregates to be studied. Coherent energy transport has been a matter of dispute in J-aggregates,[234] light-harvesting complexes,[235] and polymers.[236] SMS succeeded in identifying molecules of bisperylenylmonoimide **70** with the excitation either delocalized (superradiant emission) or localized. Transitions between both states could be seen for a single molecule of **70** under the influence of structural fluctuations of the guest matrix system, another phenomenon which would not be detectable in the ensemble.[237]

The above results confirm that rylene-based chromophores are particularly suitable for use as emissive groups in nanomaterials and for SMS studies. A question remaining to be resolved is the suppression of interchromophore interactions in the aggregated state. This problem has stimulated the concept of shielding the dyes by encapsulating them within a dendrimeric polyphenylene structure. Before we can discuss the perfect site definition of single fluorophores we must first consider the synthesis and properties of functional polyphenylene dendrimers.

 © 2005 Wiley-VCH Verlag GmbH & Co. KGaA, Weinheim

6. Dendrimers as Vessels for Chemistry, Physics, and Biology

Dendrimers,[238–240] unlike hyperbranched polymers are regular macromolecules with well-defined structures, and have served as functional objects in nanotechnology and nanoscience,[241–243] including as vehicles for drug delivery[244,245] and as light-harvesting materials.[246] Most types of dendrimers possess flexible branches which are easily deformed by external stimuli, and can even bend back towards the center of the molecule. As a result of this backbending they are usually denser at the center than on the periphery.[247,248] By contrast polyphenylene dendrimers[249] are rigid, shape-persistent compounds which can be visualized as discrete nanoobjects by AFM (see Section 6.5).[250,251] Neutron diffraction experiments have shown that they are denser at the periphery than at the core.[252] As a result of this rigidity any two groups within the dendrimer or upon its surface are in well-defined spatial relationships to each other, which is of great importance for controlling their electronic interactions, particularly the transfer of excitation energy between them. It also means that the shape of the empty space between groups in the interior of the dendrimer is well-defined and, as a consequence of the limited mobility of the benzene rings within the structure, relatively invariant, which offers the possibility of manipulating this space by synthetic design so as to produce great selectivity for guest molecules. This specificity in host–guest interactions could then be used for sensing, for example, by selective incorporation of molecules, or to create a nanoreactor in which reactions could occur selectively, similar to the use of pores in inorganic materials such as zeolites to induce chemo- or regioselectivity in reactions.



Scheme 16. Convergent (top) and divergent approaches to second-generation polyphenylene dendrimers.

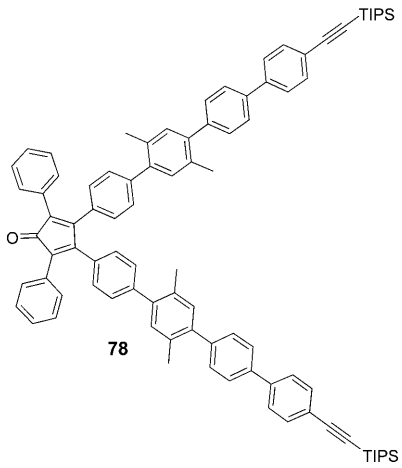
6.1. Synthesis of Polyphenylene Dendrimers

The two basic approaches to the synthesis of polyphenylene dendrimers[249] are shown in Scheme 16 for a second-generation dendrimer **71**. Both routes utilize Diels–Alder cycloadditions of cyclopentadienones to alkynes. In the convergent approach the ethynyl-substituted core **72** is treated with a cyclopentadienone **73** substituted with dendrons to make **71** directly. In the divergent approach the dendrons are grown outwards from the core in an iterative manner by addition of a cyclopentadienone **74** with silyl-protected ethynyl functionality to **72** to make **75**, followed by deprotection and addition of a second cyclopentadienone **76** to the resulting ethynyl-substituted first-generation dendrimer **77**. It must again be emphasized that the inherent stiffness of the structure means that these macromolecules are well-defined shape-persistent nanoobjects. Molecular modeling studies[253] predict sizes of 7 nm for the fourth-generation dendrimers, which have been confirmed by light-scattering, TEM, and AFM measurements.[250,251] A spectacular increase in the size of these nanoobjects is obtained by employment of the branching unit **78** (Scheme 17), in which a rigid spacer is inserted between the cyclopentadienone and the ethynyl groups on **74** to increase the distance between successive layers of the dendrimer. Dendrimers with a complete fifth generation can now be made as spherical monodisperse objects with diameters up to 22 nm by using **78**.[254]

As can be seen from Scheme 16, functionality can be introduced into the dendrimer at three places: at the core, in the scaffold (rings A and B in **62**), and at the surface (rings C and D in **62**). Functionalization of the core requires synthesis of a ethynyl-substituted core molecule on which the dendrons can be constructed. Functionalization of the scaffold and surface requires suitably functionalized cyclopentadienones.

Functionalization of the scaffold enables multiple functional groups to be built into the dendrimer in well-defined relationships to each other and to whatever groups are at the core and the surface. This approach requires modification of the ethynylcyclopentadienone **74** used to build the higher

 © 2005 Wiley-VCH Verlag GmbH & Co. KGaA, Weinheim

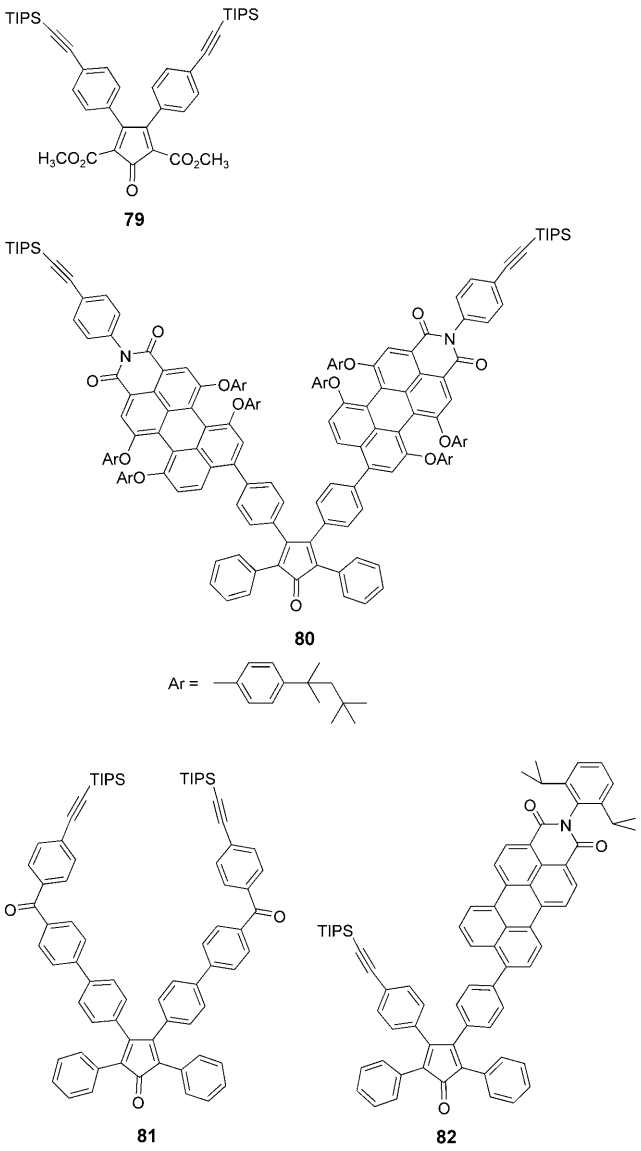


Scheme 17. Expanded dendrimers can be synthesized by incorporating a cyclopentadienone.

generation dendrimers. There are two ways in which this can be achieved (Scheme 18): 1) Functional groups can be added into **74** either at the α-positions by replacement or substitution of the phenyl rings (for example, in **79**),[255] or by inserting them between the β phenyl rings and the ethyne bonds (for example, in **80** or **81**);[256] 2) **74** can be desymmetrized by replacing one of the ethynyl groups with a functional group, for example **82** with one perylene monomimide dye.[257] This is achieved by using a Knoevenagel condensation of diphenylacetone with an assymmetrically functionalized benzil.

The effect of the substituents in **79** and **80** is to introduce functionality within the scaffold which may affect the internal density of the dendrimer and the chemical properties of the cavities without affecting the possible number of branches or the number of potential functional groups at the surface. Thus, ester groups can be incorporated within a dendrimer by using the reagent **79** which can then be hydrolyzed to carboxylates, thus producing charged cavities of defined sizes which could be used to form complexes with cationic species within the dendrimers.[258] The perylenediimide groups in **80** not only introduce functionality, but also act to extend the space between the adjacent layers, which has the effect of reducing the peripheral density of the molecules. In this way the total number of chromophores in the dendrimers can be significantly increased and thus the intensity of their overall absorption or emission increased. The effect of using desymmetrized reagents such as **82** is to introduce bulky functional groups into a layer of the scaffold without increasing the space between the layers.

The introduction of many functional groups also provides a way of ensuring efficient energy or charge transfer occurs between the core and the surface in larger dendrimers. Furthermore, the ketone groups on **81** are sites for subsequent chemistry, for example, conversion to trityl radicals which would enable radical interactions within a nanosized dendrimer cage to be studied.

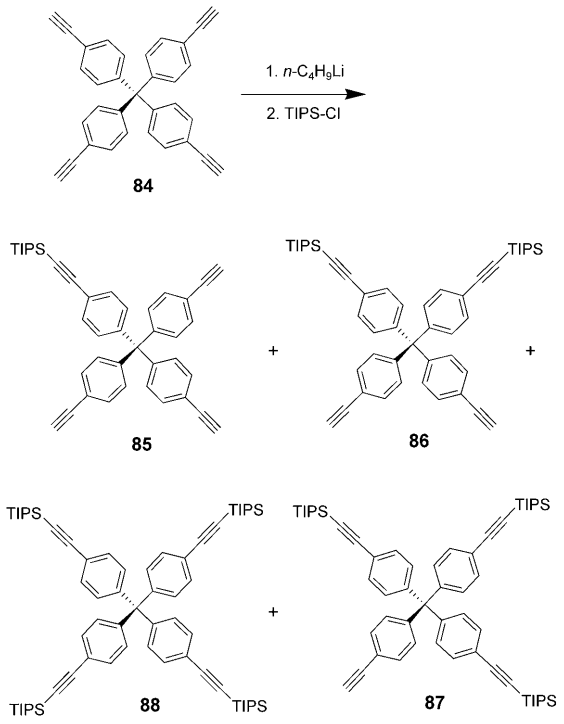


Scheme 18. Modified cyclopentadienones for introduction of functionality into scaffold.

6.2. Desymmetrized Dendrimers

An exciting possibility for tailoring the properties of functional dendrimers is desymmetrization, that is, to have different functional groups on different regions of the nanoparticle surface.[259] For example, a dendrimer with part of its surface substituted with groups capable of binding to a biologically active material, while other parts bear chromophores has applications in bioassays. To prepare such dendrimers one requires a desymmetrized core. Treatment, for example, of tetra(4-ethynylphenyl)methane (**84**) with less than four equivalents of *n*-butyllithium followed by an excess of triisopropyl chloride (TIPS-Cl) gives a statistical mixture of the readily separable mono- (**85**), di- (**86**), tri- (**87**), and tetrasilylated (**88**; this is unreactive and so is converted back into **84**) cores (Scheme 19).[260] The free ethyne groups can

 © 2005 Wiley-VCH Verlag GmbH & Co. KGaA, Weinheim

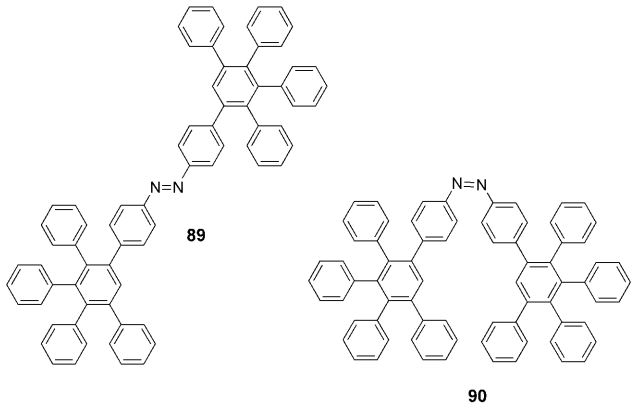


Scheme 19. Synthesis of desymmetrized dendrimer cores.

now be used to create dendrons, and then the protected ethynes can be deprotected and used to build other dendrons, thus leading to a range of new molecular topologies.[260]

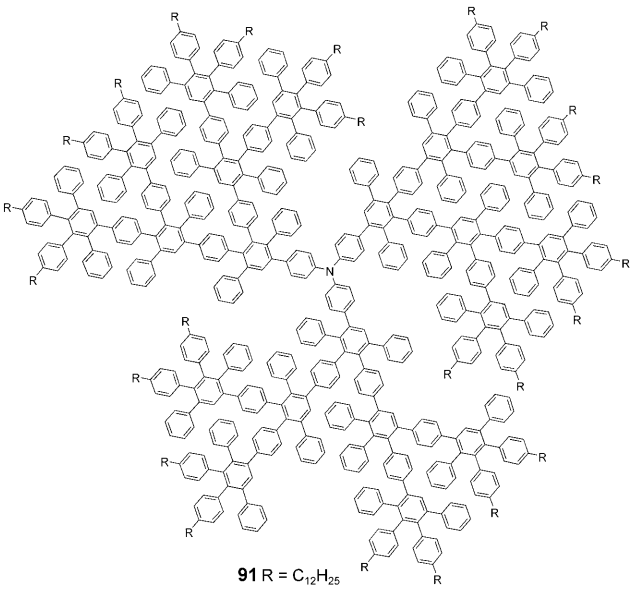
6.3. Polyphenylene Dendrimers with Functional Cores

An example of a dendrimer with a functional core is a first-generation dendrimer **89**/**90** (Scheme 20) with a photochromic azobenzene core, which isomerises from the *trans* to the *cis* form upon irradiation with ultraviolet light.[261] It can be clearly seen that the *trans* form **89** and *cis* form **90** have markedly different volumes. Gel permeation chromotography (GPC) measurements show an increased retention time of the *cis* isomer **90** on the column because of its markedly decreased (24–38%) hydrodynamic volume. These dendrimers thus represent an example of a nanosized so-called "smart material", in that they show a clear reproducible response to an external stimulus (in this case light). The rate of light-induced *trans–cis* isomerization and the proportion of the *cis* isomer in the photostationary state decrease with increasing generation or increasing branching of the dendrimer, while the rate of the thermally induced reverse isomerization increases. Dendrimers with azobenzene cores have also been prepared by other research groups,[261] but the flexibility of their dendrons results in their photoisomerization not causing a marked, well-defined change in the dendrimer shape.



Scheme 20. First-generation azobenzene-cored dendrimers showing the marked change in volume of the nanoobject upon *trans–cis* isomerization.

The dendrons are not expected to be good charge transporters because of the twists between adjacent benzene rings. This has been confirmed by cyclic voltammetry (CV) studies; for example, dendrimer **91** with a triphenylamine core (Scheme 21)[262,263] showed an increase in the potential of the anodic peak in the oxidation cycle in going from the first- to the third-generation dendrimer together with a two-thirds reduction in the peak current.[262] This observation shows that the effect of the dendrons is to hinder electron transfer from the hole-accepting triphenylamine core. Thus, the shell should not be made too large when encapsulating an electrically active unit within a dendrimer.

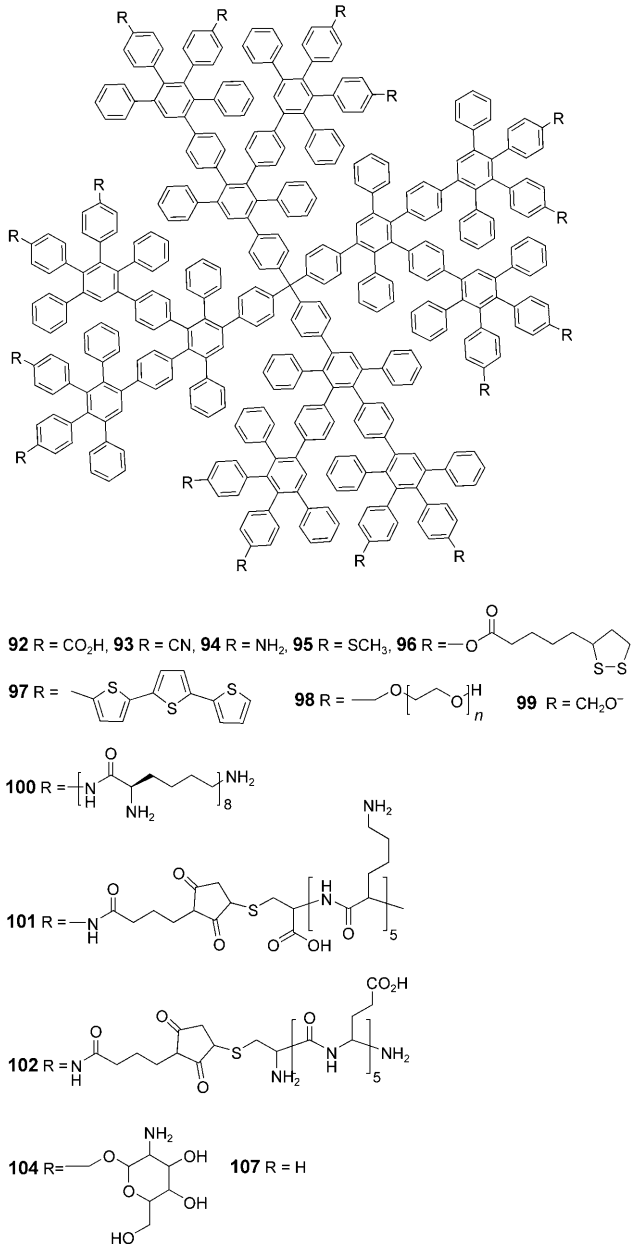


Scheme 21. Third-generation dendrimer with a triphenylamine core.

6.4. Dendrimers with Functionalized Surfaces and Scaffolds

Dendrimers have been prepared bearing a variety of polar groups, for example, carboxylic acids (**92**), nitriles (**93**), amines (**94**), and thiols (**95**, **96**; Scheme 22).[249] Such substituents can be used to confer water solubility (**92**) or to assist in binding to substrates, for example, the thiol-substituted dendrimers **95** and **96** bind to gold. Dendrimers **92–94**

 © 2005 Wiley-VCH Verlag GmbH & Co. KGaA, Weinheim



Scheme 22. Second-generation dendrimers with peripheral substituents.

selectively include volatile organic molecules within their internal free space, so that layers of these dendrimers on a quartz microbalance act as chemical vapor sensors, with sensitivities as high as 5 ppm for some analytes.[264] Dendrimer **95** with thiomethyl substituents serves as a template for the formation of gold nanoparticles.[265] Electron microscopy studies reveal that all the particles are spherical with average diameters of about4 nm. The particles self-assemble to form porous nanocomposites in which the randomly arranged gold nanoparticles are separated by dendrimer "nanolinkers". Similar nanocomposites have been made by layer-by-layer deposition of gold nanopartcles (ca. 4 nm in diameter) and the dithiane-substituted dendrimer **96**.[266] The electrical resistance of films of these porous nanocomposites was found to increase dramatically and reproducibly upon exposure to organic vapors. Much greater sensitivity was observed for nonpolar solvents because of their much greater sorption onto the hydrophobic dendrimers.[266,267]

Conjugated rods can also be attached to the surface of dendrimers. Such functionalized dendrimers could assemble to form three-dimensional networks of conjugated rods. As an example, dendrimers such as **97** with terthiophene subtituents have been prepared (Figure 7).[268] Two processes occur during electrochemical oxidation of **97**: coupling of the terthiophene chains to sexithiophene bridges with formation of an oligothiophene–dendrimer 3D network and, at higher potential, partial cyclodehydrogenation of the dendrimers to furnish a unique polythiophene–graphite hybrid. In situ conductivity measurements of the resulting nanocomposites revealed two well-separated electrical conductivity processes which correspond to the different electroactive components of the network. Both processes can be addressed by applying the correct electrical charge to the material.

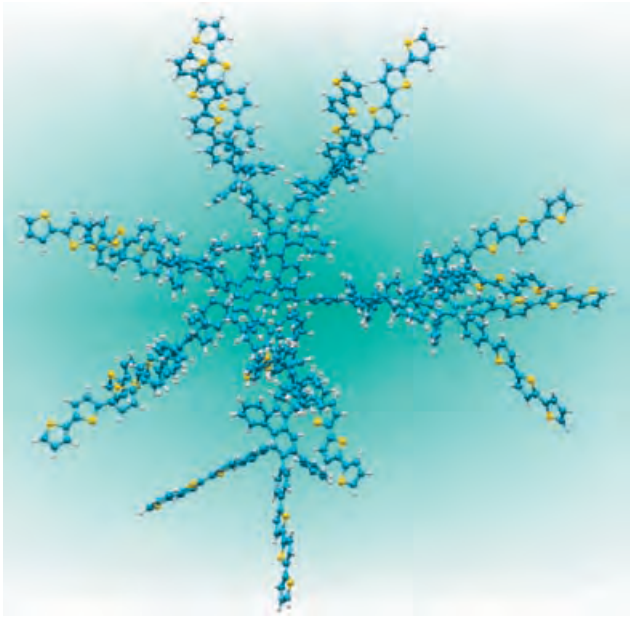


Figure 7. Molecular model of the terthienyl-substituted dendrimer **97**.

Solid-supported metallocenes have great industrial importance as catalysts for the polymerization of olefins.[269] The product morphology is controlled by immobilizing the metal catalyst on the surface of a support by use of latex particles (typically 80–100 nm in diameter) with poly(ethylene oxide) (PEO) chains on their surface.[270] These form secondary particles as a result of interactions with methylalumoxane which bind the catalyst. A key concern in making high quality polyolefins is that the solid support must fragment during the course of the polymerization to make catalyst sites accessible for the monomer.

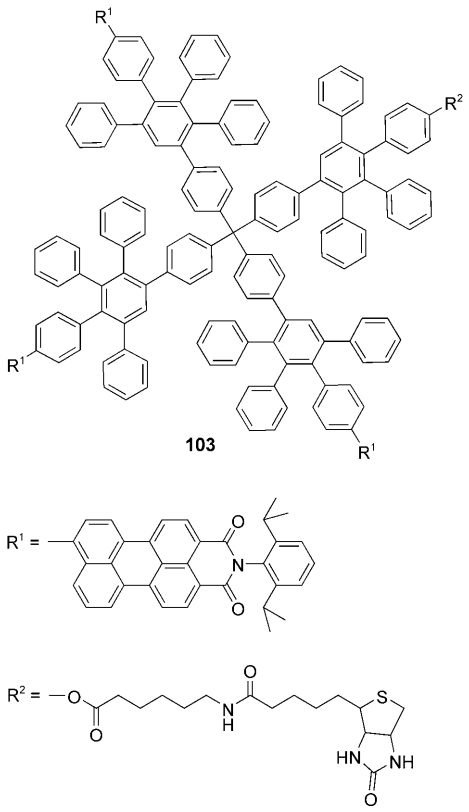
As polyphenylene dendrimers are small discrete particles (less than 10 nm in diameter) they are attractive models for carriers of metallocene systems, and we have shown that zirconocene catalysts for olefin polymerization can be

 © 2005 Wiley-VCH Verlag GmbH & Co. KGaA, Weinheim

attached to the surface of a polyphenylene dendrimer.[249] Dendrimer-based core-shell systems, for example, **98**, with a rigid polyphenylene core surrounded by a PEO shell have been prepared by both a "grafting-from" approach using **99** as a macroinitiator for anionic polymerization of ethylene oxide and a "grafting-onto" approach in which the ethylene oxide chains are attached to a substituted dendrimer.[271] These dendrimer models can then be compared with the latex versions.

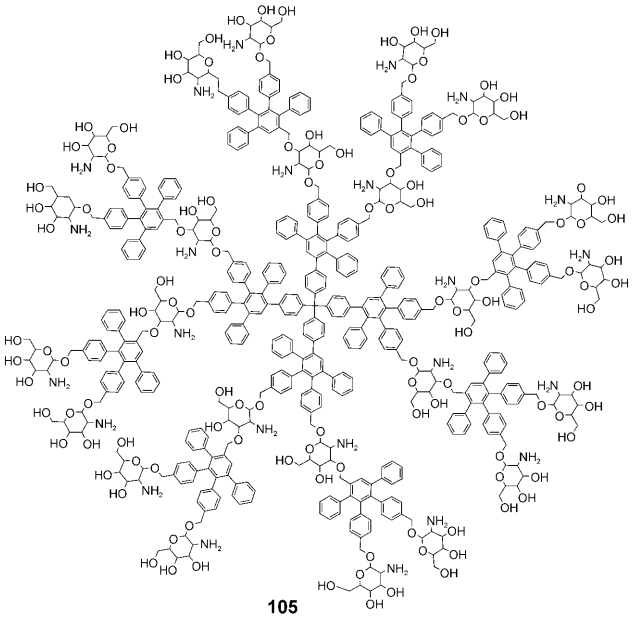
Dendrimers have been the subject of much interest as possible delivery agents for drugs or DNA.[244,245] Polyphenylene dendrimers are particularly suitable substrates for biological applications as they are biologically inert and thus nontoxic, but can be readily and controllably functionalized. Dendrimers bearing oligopeptide chains have been prepared either by using peptide-substituted cyclopentadienones (for example, dendrimer **100**) or by functionalizing an amino-substituted dendrimer such as **94** with an *N*-alkyl maleimide followed by a Michael reaction with a thiol-endcapped peptide (for example, dendrimers **101** and **102**).[272] Such dendrimers are being used as model compounds for studying DNA complexation, and as agents for the introduction of RNA into cells (transfection).[273]

By utilizing the desymmetrization method discussed in Section 6.2 dendrimers can be made bearing both a biologically active functionality and an optically or electrically active functional group in a nanosized array. In the resulting bioassay the former group binds to a target biological moiety and the latter group is used for visualization. The rigidity and shape-persistence of the dendrimers are important as they maintain the biologically active moieties in fixed, well-defined relationships to each other and to the other active substituents. For example, the asymmetrically functionalized dendrimer **103** (Scheme 23) bears one biotin unit which binds strongly with the protein streptavidin, and three dye units which act as fluorescent markers.[274] The dendrimer has to be mixed with a non-ionic detergent to obtain water solubility. The solubilized dendrimer binds strongly to streptavidin in aqueous media to create a highly fluorescent complex, which remains intact in the presence of proteins, thus demonstrating the potential of this approach for bioassay applications.



Scheme 23. Biotin-substituted dendrimer for applications in bioassays.

It is possible to incorporate sugar groups not only on the periphery of a polyphenylene dendrimer (as in **104**, Scheme 22), but also within the dendrimer scaffold (as in **105** (Scheme 24).[275] The role of the peripheral sugar groups is to impart water solubility to the dendrimer. Fluorescence probe experiments show that the interior sugar groups in **105** are encased within a hydrophobic environment of the nanosized molecule, reminiscent of an active center situated within a hydrophobic pocket, as seen in enzymes. It is anticipated that these interior sugar groups can form stable hydrogen bonds to a guest and so lead to molecular recognition.



Scheme 24. Glycodendrimers with sugar groups at the periphery and in the scaffold.

6.5. AFM Studies and Self-Assembly of Dendrimers

As mentioned, above, polyphenylene dendrimers can be visualized as discrete nanoobjects by AFM (Figure 8).[250,251] Unlike other flexible dendrimers, the height of these objects matches that calculated by molecular modeling studies,[253] which confirms their rigidity (the height of "soft" objects is usually underestimated by AFM because of deformation). Their stiffness was further confirmed by pulsed-force mode AFM experiments. Just as flexible dendritic structures have

 © 2005 Wiley-VCH Verlag GmbH & Co. KGaA, Weinheim

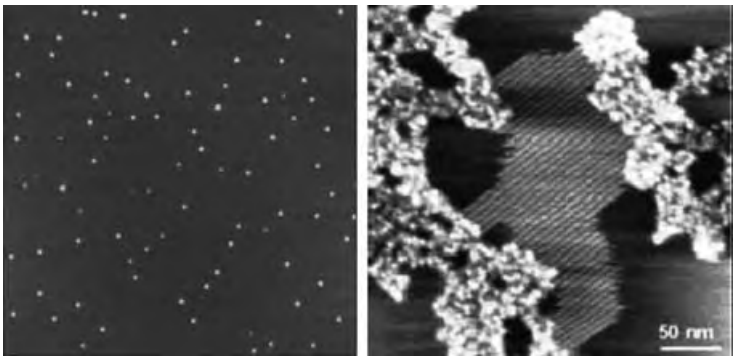
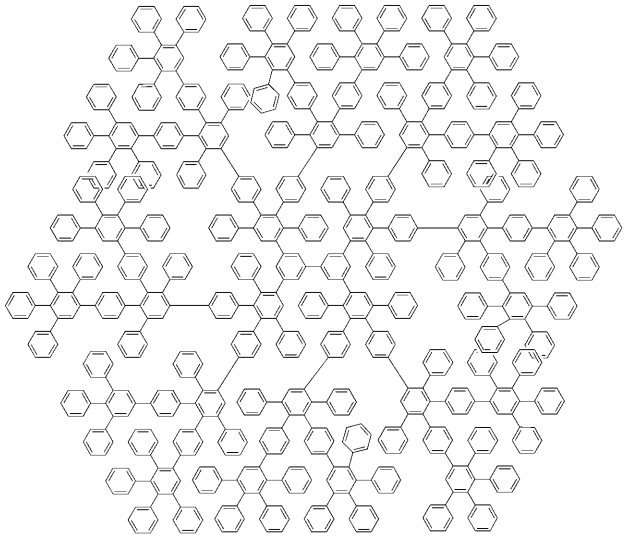


Figure 8. AFM images of: single third-generation unsubstituted dendrimers with a tetrahedral core (left) and nanorods of second-generation dendrimers with tetrahedral cores and alkyl substituents (right).

been demonstrated to form self-assembled monolayers and a variety of complex structures,[276] polyphenylene dendrimers can also self-assemble to form more complex architectures. The dumbbell-shaped third-generation dendrimer **106** with a biphenyl core (Scheme 25) forms globular clusters on mica with heights of about 6 nm when spin-cast and about 47 nm



106

Scheme 25. Dendrimer with a biphenyl core that forms globular aggregates on mica and fibers on HOPG.

when drop-cast.[277] In contrast spin-casting produced monolayers on HOPG or silanized mica surfaces, while drop-casting resulted in the formation of nanofibres with widths of up to several hundred nanometers, heights of up to 100 nm, and lengths of up to 400 μm. Similar micrometer-sized fibers have also been reported from the self-assembly of nonrigid dendrimers.[278] Stable, pinhole-free monolayers are also formed from alkyl-substited dendrimers on graphite surfaces.[263,279,280] Dendrimers up to the fourth generation with biphenyl (for example, **106**) or *trans*-azobenzene (for example, **89**) cores have also been shown to give rise to such globular cluster or nanofibers.[281,282] The formation of nanofibers was found to be favored by lower dendrimer generations and more-separated dendrimer branches. The major driving forces for aggregation are π interactions between the dendrimers as a result of interdigitation of the branches.

The dendrimer **92** substituted with carboxylic acid groups also forms aggregates, as shown by light-scattering experiments. AFM analysis of thin deposits from very dilute solutions reveal objects with heights corresponding to three to eight dendrimer layers.[250] Ionized molecules of **92** have been visualized by AFM after adsorption onto a SAM terminated with carboxylic acid groups through linkage with copper(II) ions.[283] Deformation of the SAM and a decrease in the measured height of the dendrimer ions compared to the calculated dimensions of the dendrimer were observed as a result of the strong interactions between the ions and the SAM. This dendrimer also undergo Decher-style layer-by-layer self-assembly[284] with poly(allylamine) which can be followed by surface plasmon spectroscopy.[285] A similar self-assembly process has been seen with the lysine-substituted dendrimer **101**,[258] while the glutamate-substituted dendrimer **102** forms complexes with cationic polyionenes.[286] The size and shape of larger polyphenylene dendrimers can also be determined by transmission electron microscopy. Single-molecule detection is possible, but size determination depends upon how the macromolecules are lying upon the substrate surface.[251]

6.6. SMS Studies on Dendrimer–Dye Host–Guest Systems

The torsions between adjacent phenylene units in polyphenylene dendrimers means that they have only limited conjugation and so such dendrimers fluoresce in the near ultraviolet with maxima around 365 nm.[287] Increases in the quantum efficiency of the emission are observed with increasing generation number as well as increased crowding and rigidity of the structure which reduce nonradiative decay pathways. SMS studies on host–guest systems in which cyanine dyes are incorporated within dendrimer **92** substituted with carboxylic acid groups[288,289] show that the absorption band of the dyes are red-shifted upon incorporation into the dendrimer as a result of the change in the polarizability of the environment. The incorporation of two different dyes enabled the energy transfer between to be studied. The energy-transfer efficiency was observed to fluctuate with time, which could be interpreted as arising from changes in the free volume within the host, or to variation in the transfer modes possible at the single-molecule level.

Now that we have introduced the properties of both perylene dyes and poylphenylene dendrimers we will examine the benefits of combining these classes of materials.

 © 2005 Wiley-VCH Verlag GmbH & Co. KGaA, Weinheim

7. Dye-Loaded Dendrimers: Emissive Nanoparticles

Attaching dyes to polyphenylene dendrimers results in the formation of emissive nanoparticles. Such nanoparticles are of interest for a number of present and putative applications. An example of the former is that the attachment of dyes to the nanoparticles described in Section 6.4 generates supports for metallocene catalysts in polyolefin synthesis. Here the fragmentation of the catalyst particles within the product can be monitored by confocal fluorescence spectroscopy[290] to gain insight into the polymerization process.

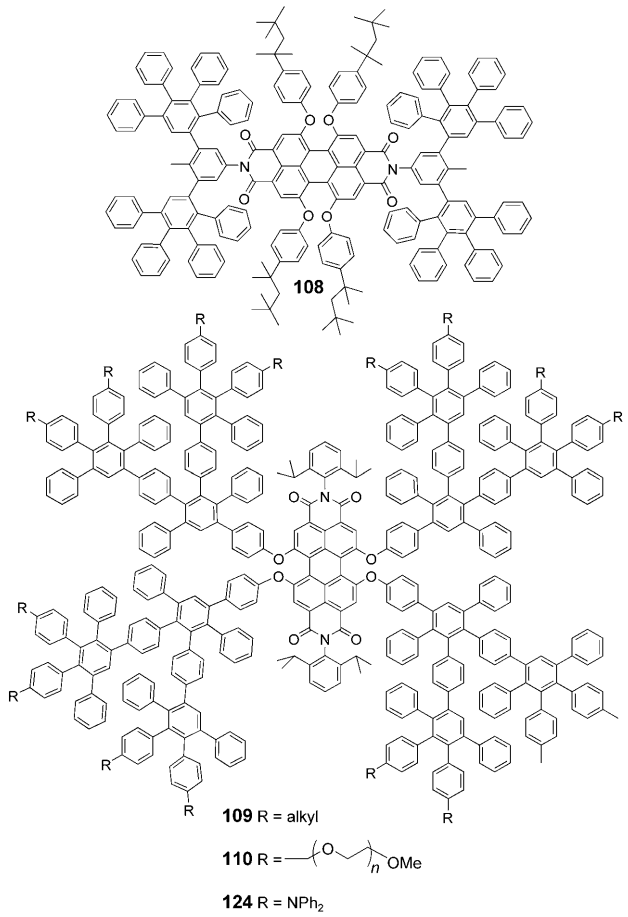
A possible future application is the use of light emission from single molecules in molecular electronics. The aim here is to manipulate excited states to encode or transmit information. For example, if a degenerate and vectorial energy-transfer process is considered, then allowing or not-allowing energy transfer between two dyes of a multichromophore would allow a read-out to be controlled at the molecular level. Two key problems of the approach are 1) the limited time before irreversible photobleaching occurs and 2) the limited excursion to the triplet state which renders the molecule dark for extended periods of time. The former aspect suggests that the lifetime of the multichromophores needs to be increased upon laser irradiation, for example, by rigorously excluding oxygen. The latter problem explains why control of the spin statistics have recently attracted the most interest in the optimization of molecular light systems.[291]

The combination of dyes with rigid dendrimers in host–guest systems has several potential advantages: 1) the dendrimer can be used as a shield around an emissive core to prevent chromophore interactions, which are well-known to lead to quenching of photoluminescence or to red-shifting in absorption or emission spectra as a result of the formation of aggregates or excimers.[292] 2) Multiple dyes can be attached in the scaffold and/or at the surface to produce materials with very high absorption and luminance. 3) Different dyes can be attached at different parts of the dendrimer, and/or the dyes can be combined with other functionality. 4) All the chromophores are in well-defined positions with respect to each other and to other substituents. Since energy (or charge) transfer between two chromophores is heavily dependent upon their distance and relative orientation, interactions between them can be finely controlled.

As single photon sources, multichromophoric dendrimers would, despite limited lifetimes, have distinct advantages over the existing materials: 1) the absorption cross-section can be increased by increasing the number of identical dye units. This means that 2) every laser pulse should result in at least one excited state being generated on the dendrimer, and that 3) the geometric conditions for energy transfer can be tuned. This last point is important since singlet–singlet annihilation processes need to be efficient to ensure only one photon is emitted.

7.1. Dendronised Dyes: Isolated Chromophores

Dendrimers with rylene dyes as cores have been made (Scheme 26) to demonstrate the efficient suppression of chromophore interactions by dendronization. Emissive PDI cores have been used with dendrons of increasing size attached to either the imide moieties[293] or in the bay positions.[294] Molecular models of the nanosized emitters such as **108** (Figure 9) and **109** clearly show that the dendrons in these materials shield the perylene core to hinder aggregation of the chromophores. The shielding is more effective for the materials with the dendrons in the bay positions. The dendrimer **110** bearing poly(ethylene oxide) chains has been used as a support for metallocene catalysts in polyolefin synthesis. The emissive core enables the fragmentation of the catalyst particles inside the polyolefin to be studied by confocal fluorescence microscopy.[295]



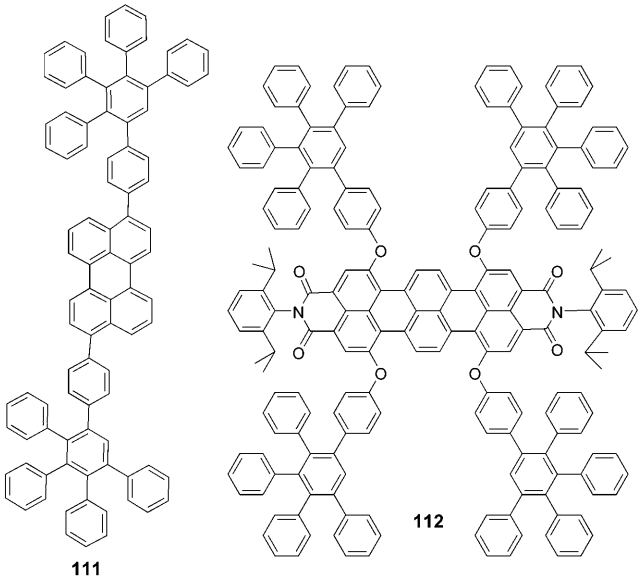
Scheme 26. Representative first- and second-generation dendrimers with PDI cores.



Figure 9. Molecular models of **108** (left) and its second- (middle) and third-generation (right) analogues.

 © 2005 Wiley-VCH Verlag GmbH & Co. KGaA, Weinheim

In both cases the effect of the dendronization is to produce a blue-shift in the solid-state absorption and emission spectra relative to an undendronized perylenediimide, thus showing that the chromophores have been prevented from aggregating.[293,296] The photoluminescence quantum yield of the dyes dendronized at the imide decrease with increasing dendrimer generation. This observation is attributed to the opening up of new nonradiative deactivation pathways by the dendrons.[293] It has also been shown that excitation of the dendrons stimulates emission from the PDI core as a result of efficient energy transfer between them; the calculated Förster radius is about 2.4 nm.[287] Light-emitting diodes (LEDs) have been prepared using these dendronized dyes[296,297] but show low efficiencies, especially for the higher-generation dendrimers, which is attributed to poor charge transport through the dendrimer shell. Blending the imide-dendronized dyes such as **108** with polyfluorenes improves the electroluminescence yield because of better charge injection and transport.[297] Blends of dyes dendronized at the bay position, for example, **109** in a poly(*N*-vinylcarbinol) (PVK) matrix show a more intense electroluminescence because of the charge-transporting properties of PVK.[296] A similar suppression of interchromphore effects occurs for other dendrimers with perylene (for example, **111**)[298] or TDI cores (for example, **112**,[299] Scheme 27; only first generation dendrimers shown).

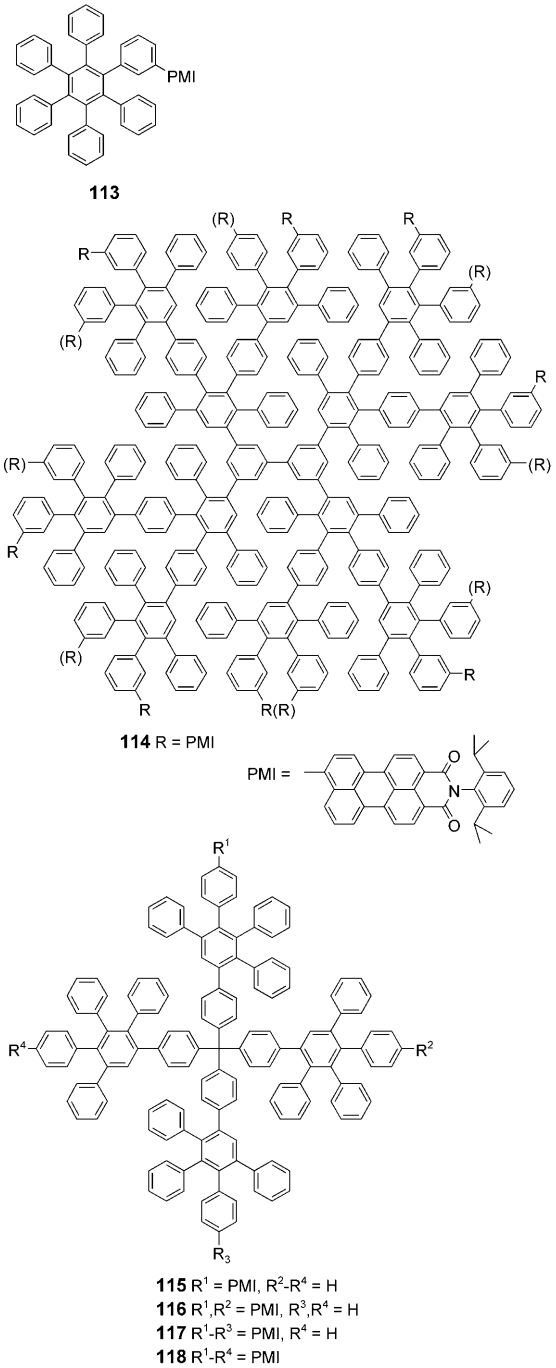


Scheme 27. Examples of first-generation dendrimers with rylene dyes as cores.

7.2. Dendrimers with Dyes on the Surface and/or in the Scaffold

Polyphenylene dendrimers can have multiple chromophores attached at their peripheries, thus producing strongly emissive nanoparticles. The well-defined spatial positions and orientations of the attached chromophores makes these materials particularly suitable subjects for single-molecule spectroscopy (SMS) studies on the intramolecular interactions between chromophores. Studying such chromophore interactions is essential for the understanding of the photophysical processes that occur in solid-state optical systems and in multichromophore systems such as the light-harvesting systems involved in photosynthesis.

A broad range of dendrimers with perylenemonoimide (PMI) chromophores have been used in SMS studies—from the isomeric hexaphenylbenzene model compound **113** with one PMI group to the second-generation dendrimer **114** with a biphenyl core bearing eight PMI chromophores (Scheme 28).[300] The dessymmetrization procedures discussed in Section 6.2 can be used to prepare dendrimers with dyes on only part of the surface, such as in dendrimers **115**–**118**.[260]

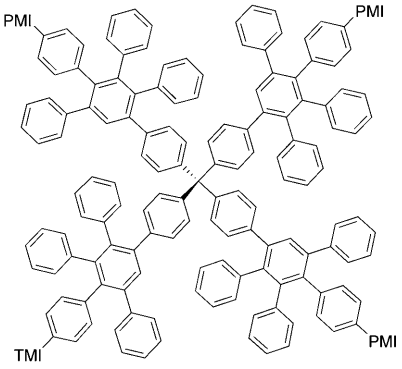


Scheme 28. Dendrimers with PMI chromophores on the periphery.

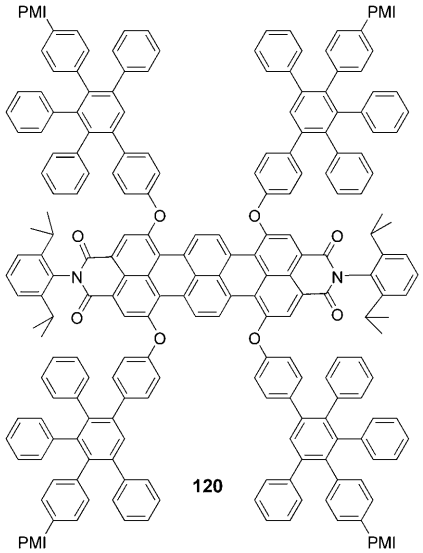
© 2005 Wiley-VCH Verlag GmbH & Co. KGaA, Weinheim

Better models for light-harvesting systems are dendrimers containing both donor and acceptor chromophores for energy transfer. Both dyes can be attached to a dessymmetrized surface or each can be incorporated separately in different layers, that is, as the core, in the scaffold, or at the surface. Both approaches have been used successfully, as exemplified by the dessymmetrized dendrimer **119**,[260] and the dyad **120** (Scheme 29).[301]

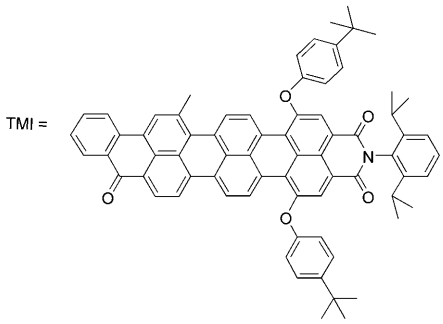
The most sophisticated example of this approach is the triad **121**, which incorporates three different dyes at the core, in the scaffold, and at the periphery (Scheme 30).[257] The



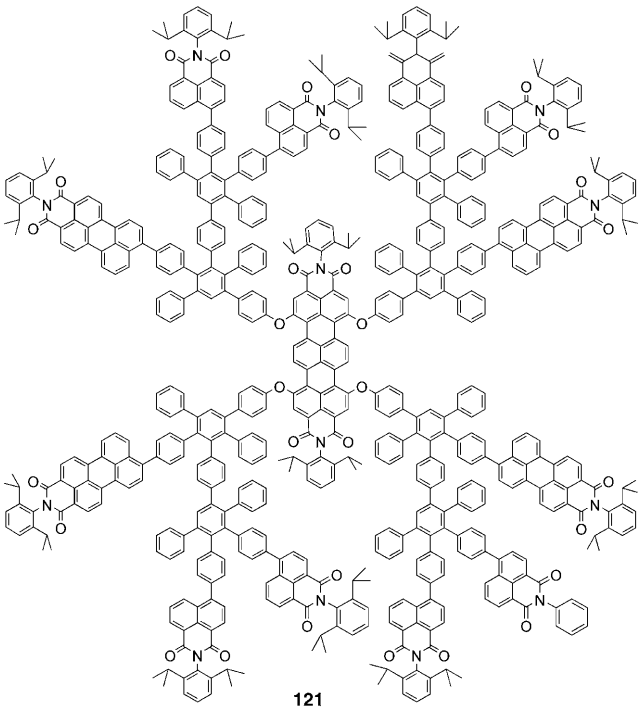
119



120



Scheme 29. Dendrimers with both perylene and terrylene chromophores.



121

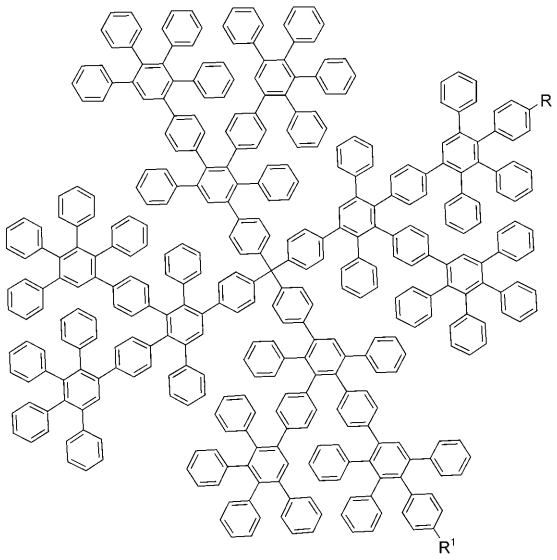
Scheme 30. Triad system with an energy-harvesting unit.

overlap between the emission spectrum of the chromophore in each layer with the absorption spectrum of the chromophore in the next layer towards the core is designed to promote efficient energy transfer from the periphery to the core in **121**. This triad is made by first adding the desymmetrized cyclopentadienone **82** bearing a perylenecarboxydiimide dye unit (Scheme 18) to a terrylenetetracarboxdiimide core, then deprotecting with fluoride ions, and finally treating the deprotected alkynes with a cyclopentadienone bearing naphthalimide dye units. Highly efficient intramolecular energy transfer is demonstrated in all three molecules **119**, **120**, and **121**, with the photoluminescence emission coming almost exclusively from the terrylenediimide units. A blend of the triad (5 wt %) in charge-transporting violet-emitting PVK matrix produces red electroluminescence, which shows that efficient energy transfer can also occur under electrical stimulation, and thus leads to the possibility of building a single-molecule LED.[302]

7.3. Self-Assembly of Fluorescent Dendrimers

As mentioned in Section 6.5, polyphenylene dendrimers can self-assemble to form fibers (Figure 8). Long fluorescent nanofibers have been obtained from such an assembly of the third-generation dendrimer analogue of **116** and the second-generation dendrimer **122** bearing one PMI unit.[282] The emission from **122** is red-shifted relative to that of the solution and indicates that aggregation of the chromophores is occurring. In contrast, the dendrimer **123** with two dye units (Scheme 31) does not form such nanofibers, only nanorods.

 © 2005 Wiley-VCH Verlag GmbH & Co. KGaA, Weinheim



122 R = PMI, R^1 = H
123 R, R^1 = PMI

Scheme 31. Dye-loaded dendrimers that form fluorescent nanofibres.

Mixtures of **123** with the nonfluorescent dendrimer **107**, however, do form nanofibers. The emission from nanofibers containing mixtures of **107** and **122** or **123** is blue-shifted as the dye content decreases. No polarization of the emission is seen from any of the nanofibers, thus indicating that the chromophores are randomly oriented.

7.4. SMS Studies on Emissive Dendrimers

SMS measurements of the chromophores in the nanoemitters described in the previous section allow detailed investigations of processes such as energy or electron transfer.[303,304] SMS can provide important insights even for the model compound **113**. Single molecules of **113** show a reversible on-off "blinking" effect with two different time scales.[305] The shorter off-times of 10–100 μs are ascribed to formation of non-emissive triplet states, while the longer times of 100 ms to tens of seconds may arise from formation of radical anions or cations by electron tunneling. Energy hopping and transfer to the chromophore with the lowest singlet state is observed in studies of the multichromophoric systems such as **114**[300,306–311] and **115**–**118**[312–323]. Multichromophoric dendrimers such as **115** can be shown by their Mandel parameter to act as a single-photon emitters with sub-Poissonian characteristics when embedded in a polymer matrix and subjected to coincidence measurements.[324] These dendrimers (like the bischromophores mentioned in Section 5.3) behave as single photon sources, as efficient singlet–singlet annihilation means only one photon is emitted at a time even when more than one chromophore is excited simultaneously.[317,321,323,324] Both singlet–singlet and singlet–triplet annihilation have been detected in these systems by SMS, but only the former can be visualized in studies on the ensemble.[301,303,304,310]

Single-photon emission, in which light pulses each consisting of a single photon are produced at a user-determined time is a particularly exciting concept in modern electronics. Quantum dots[325,326] and color centers in diamond single crystals[327] have been used as single-photon sources. Quantum logic gates based upon single photons[328] and a sort of quantum cryptography based on the polarization of a single photon[329] are examples of the potential utility of such sources. Multichromophoric dendrimers meet some of the requirements for a single-photon cryptography source, but future research needs to address, besides the issue of stability, additional challenges, such as controlling the polarization of single photons and sending an encryption key with the photons emitted from the single dendrimer.

One unexpected result was that dendrimer **114**, in which the chromophores are only weakly coupled, showed collective on/off fluorescence, which is usually seen only in strongly coupled systems. This result has been attributed to energy transfer between the chromophores on **114**, with the collective off periods arising from a triplet state on one of the chromophores acting as a nonradiative trap.[310] This concept has been used as a model for understanding the energy-transfer processes seen in natural light-harvesting systems.[310] Regioisomerism in dendrimers such as **114** means that there are a range of interchromophore distances and orientations which leads to a loss of structure in the fluorescence spectra from **114**, and the appearance of extra components in time-resolved spectra. The spectra of two isomers of a first-generation dendrimer **117** bearing only three chromophores have been distinguished in SMS experiments.[312]

There are a wider variety of interchromophore relationships available for study in systems containing different chromophores, as not only can degenerate energy transfer between identical chromophores, but also Förster or Dexter transfer between the different chromophores can occur. Both ensemble and SMS measurements have been used to probe the photophysics of systems such as **119**[260,330] and **120**[301,331–335] that contain both perylene and terrylene units. Efficient (95%) energy transfer from the perylenes (donor) to the terrylene (acceptor) chromophore has been demonstrated in both cases.[330,332–335] For the dendrimers with a terrylene core, such as **120**, two independent energy-transfer processes were identified, whose rates correlated with the size of the dendrimers: 4 and 25 ps for the first-generation (**120**) to 22 and 68 ps for the corresponding second-generation dendrimer.[331] Singlet–singlet annihilation was found to compete with energy transfer at low excitation powers so that emission was only seen from the terrylene core. At high excitation powers, an exciton blockade was observed in which several perylene units were simultaneously excited and not all underwent singlet–singlet annihilation so that emission from both donor and acceptor chromophores was seen.[333] Frequency-selective excitation in SMS measurements of **120** at low temperature enables the addressing of individual perylene donors and the terrylene acceptor and thus allows the energy-transfer times for each donor to be defined. The interrogation of both the energy donors and energy acceptors

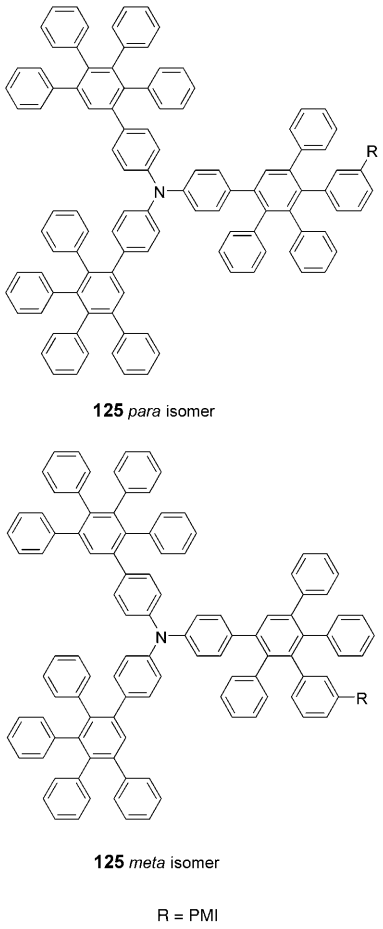
 © 2005 Wiley-VCH Verlag GmbH & Co. KGaA, Weinheim

should allow fluctuations in the transfer rate caused by spectral shifts in the emissions from either type of chromopore to be detected.[331] SMS studies of the triad **121** show that energy transfer between the naphthalene and terrylene chromophores may proceed by either a direct or a cascade route.[336]

7.5. Electron Transfer in Emissive Dendrimers containing Triarylamine Units

Perylenecarboxydiimide chromophores are good electron acceptors, and both energy and electron transfer from the amines to the dye have been seen in ensemble and SMS studies in dendrimers, such as **124** (Scheme 26), with peripheral electron-donating triphenylamine units.[294,337,338] As would be expected from the distance-dependence, the electron transfer is more favorable in first- than in second-generation dendrimers, as well as in more polar solvents. Similarly, ensemble and SMS measurements on dendrimer **125** (Scheme 32) with an electron-donating triarylamine core and a dye on the periphery show that reversible electron transfer occurs between the core and the dyes.[339–341] The single-molecule emission spectra of the two isomers resulting from the Diels–Alder addition are again resolvable: the electron-transfer processes have different kinetics because of the different distances between donor and acceptor in the isomers (1.5 and 1.7 nm for the *meta* and *para* isomers, respectively).

Understanding the kinetics of such electron-transfer processes is important in the study of photosynthesis and other natural processes involving charge transfer between active units. One futuristic concept that has yet to be realized is to use donor–acceptor molecules as single-molecule photovoltaic devices. The major hurdle to be overcome is collecting the charges in dendrimers with one of the active units at the core, as any charges at a totally enclosed active core would be inaccessible. Dessymmetrized dendrimers with donors on one dendron and acceptors on another, or with only a partially enclosed core are promising solutions to the problem.



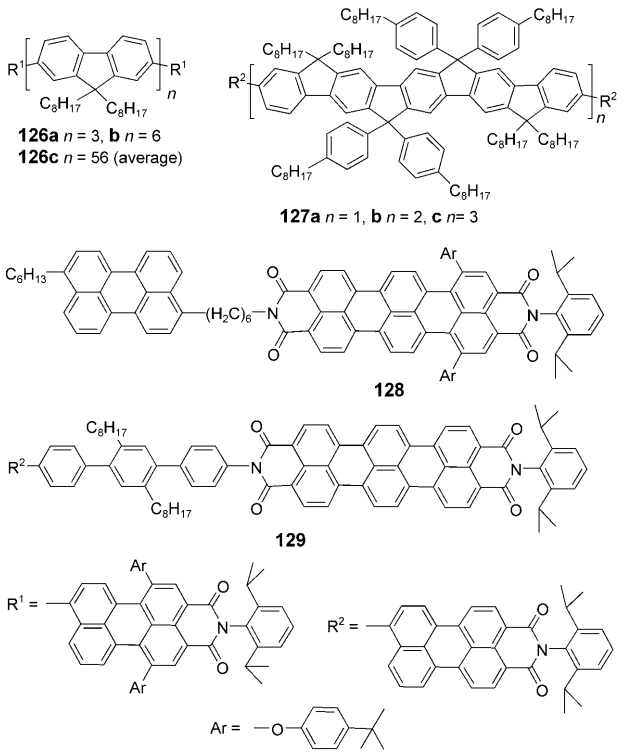
Scheme 32. Dendrimer with a triarylamine core and a perylene chromophore at the periphery.

7.6. Combining Dyes with One- and Two-Dimensional Polyphenylenes

We showed in the previous section that perylene dyes can be combined with three-dimensional polyphenylene dendrimers to make strongly emissive compounds. They can also be combined with polyphenylenes of lower dimensionality to make emissive materials with different topologies. One-dimensional oligo- and polyphenylenes are rigid rods and thus they are clearly suitable scaffolds to which chromophores can be attached to produce nanoemitters.

One-dimensional polyphenylenes are wide-bandgap materials which emit in the violet, blue, or blue-green regions of the spectrum, and so can transfer excitation energy to a smaller bandgap chromophore such as a rylene dye. Thus, perylene dyes can be incorporated into polyfluorenes as random co-monomers within the chain, on side-chains, or at the termini of the chains.[188] In all three cases efficient Förster energy transfer between the blue-emitting polyfluorene and the dyes results in emission coming from the latter. This principle has enabled the fabrication of efficient polyfluorene-based LEDs whose emission color can be tuned across the visible spectrum. The energy transfer is much more efficient in the solid state, and occurs in thin films even when the mole fraction of dye is only 1%. Unlike the emissive dendrimers described above, these emissive polymers do not possess multiple chromophores in well-defined positions with respect to each other. The polymers with dyes at the chain ends are polydispserse and so the distances between the two dye units are also random. Therefore, oligofluorenes **126a**,**b** have been prepared with dyes at the ends so as to have materials with well-defined interchromophore distances (Scheme 33). Both compounds were studied at the ensemble and single-molecule levels and compared with the dye-endcapped polymer **126c**.[342,343] Energy hopping, and singlet–singlet and singlet–triplet annihilation processes could all be detected in the oligomers. In contrast, only some chains showed singlet–singlet annihilation in the dye-endcapped polymer, presumably because the chain length was too short or the chain conformations were such that the two dye units

 © 2005 Wiley-VCH Verlag GmbH & Co. KGaA, Weinheim



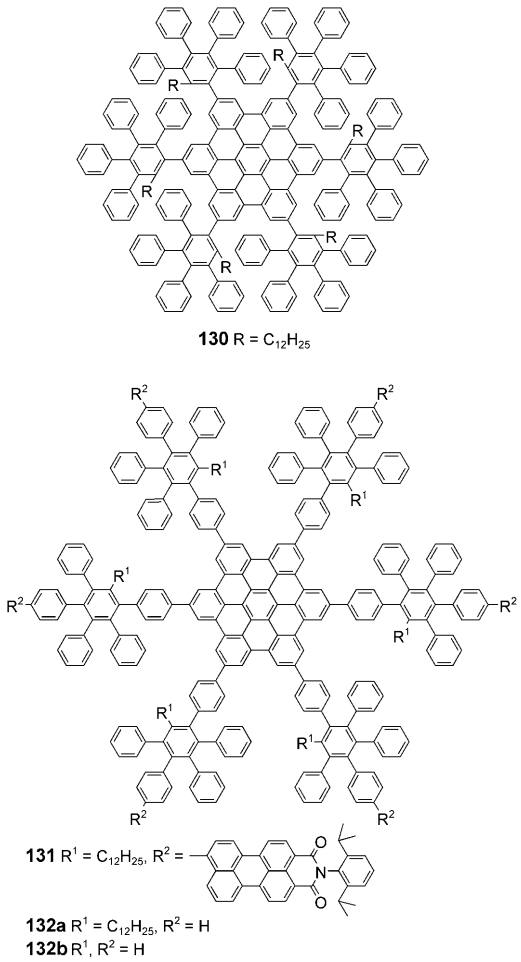
Scheme 33. Oligophenylenes with a rylene chromophore at each end.

were brought close to each other; polyfluorenes are not rigidly linear and can adopt coiled conformations.

SMS studies on the trimer **126a** in a zeonex matrix showed that the angle between the dipoles of the chromophore was 70°, thus indicating it had a bent conformation. This arrangement is attributed to the lipophobicity of the matrix inducing aggregation of the alkyl side chains.[344] This determination of the conformation of an isolated molecule illustrates the power of SMS techniques. Whereas oligofluorenes can adopt nonlinear conformations, which makes the interchromophore distances difficult to predict, the oligomers **127** based on ladder-type pentaphenylenes are rigidly linear. Here the distance between the dyes can be tuned from 2.2 nm (**127a**)[71] to 6.7 nm (**127c**)[345] by varying the number of pentaphenylene units. An SMS study on **127a** in a poly(methylmethacrylate) (PMMA) matrix revealed that 44% of molecules switched between the locally excited state and an emissive charge-transfer state by a reversible electron transfer from the pentaphenylene to the dye. The same switching ratio was detectable in ensemble experiments performed in polar solvents.[346]

SMS studies have been performed on systems such as **128**[347] and **129**[348] that contain a perylene and a terrylene chromophore separated by short spacers. Förster energy transfer was observed in both cases, with a calculated Förster radius of 3.3 nm for **128**. Somewhat unexpectedly the dipoles of the two chromophores were found not to be colinear (maximum in the distribution of deviation angles observed at 22°). This observation was tentatively attributed to the transition dipole not being aligned with the long molecular axes of the chromophores. The key advantage of bichromophores such as **129** is that the distance and relative orientation of the donor and acceptor dyes can be controlled. These dyads then serve as important models for complex multichromophores such as the dye–dendrimer hybrids described above. The aim of further studies is to increase the length of the oligophenyl spacer and to introduce a kink by incorporating in *meta*-phenylene units.[349]

Two-dimensional polyphenylenes offer a wider range of topologies than the rodlike one-dimensional conjugated polymers and can also have more positions to which dye units can be attached. Such a multichromophore combining a disc-type PAH with perylene-based dyes is the hexa-*peri*-hexabenzocoronene (HBC) derivative **131** (Scheme 34) in



Scheme 34. HBCs with dye-loaded dendron substituents.

which the chromophores are attached to six dendron substituents. HBCs are good hole-accepting units and perylene imides are good electron acceptors and so efficient electron transfer from the HBC core to the dyes is seen.[350] An important motivation for the development of HBC–perylenemide hybrids is the combination of light-induced charge separation with charge-carrier transport in supramolecular architectures.

 © 2005 Wiley-VCH Verlag GmbH & Co. KGaA, Weinheim

Compound **131** combines phenylene nanostructures of two different dimensionalities, in this case a two-dimensional disc and a three-dimensional dendrimer. As shown in the next section, this combination approach furnishes increasingly complex nanoarchitectures.

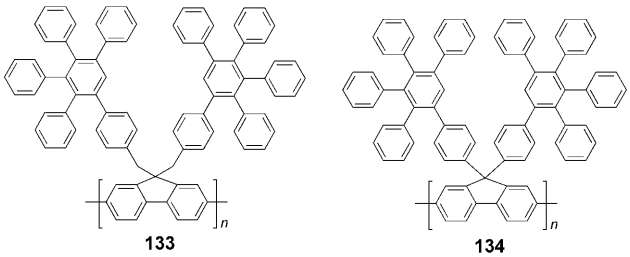
8. Combining One-, Two-, and Three-Dimensional Polyphenylene Nanostructures

A combination of one-dimensional and two-dimensional structural motifs has already been shown in the HBC oligomers **32**–**35** in Section 4.2 above. We have also demonstrated that dendronization of rylene dyes offers a way to prevent interchromophore interactions in the solid state. An extension of this concept is to use dendronization of conjugated polymers and of PAHs to control their packing. Also, since lithium ions can intercalate between,[351] and hydrogen molecules can adsorb to, graphene sheets[352,353] materials containing well-defined three-dimensional arrays of such sheets might have applications in lithium batteries or hydrogen storage.

8.1. Controlling the Stacking of HBCs and Conjugated Polymers by Dendronization

As was discussed in Section 4, optimizing the mobilities of electrons and electron defects by the intra- and intercolumnar order of HBCs is a major research goal. However, if bulky groups are attached to an HBC then the stacking of the discs can be restricted (Scheme 34). Such compounds cannot be used in existing electronic devices but exemplify how the self-assembly of molecules is controllable by means of varying the substituents.The dendronized HBC **130** cannot stack and so exists as isolated discs. Attaching the dendrons through an intermediate phenylene ring reduces the steric hindrance to stacking so that **131** forms stable dimers, while **132a** displays an equilibrium between the monomer and dimer which can be studied by NMR spectroscopy.[354]

Whereas the most important properties of discotic molecules such as HBCs are associated with assemblies of molecules, those of emissive conjugated polymers arise from individual molecules so that restricting their stacking has fewer negative ramifications and is likely to be beneficial as it can suppress undesirable interchain interactions such as those leading to excimer emission or to enhancement of non-radiative decay pathways. The aim of wrapping conjugated polymers in polyphenylene dendrimers is to have the polymers encased within a protective shell so that the polymer chains are electronically isolated but without preventing the charge hopping from chain to chain necessary for obtaining electroluminescence. Polyfluorenes in which first-generation dendrons are attached to the bridgehead carbon atoms either by a benzyl linker (**133**) or directly (**134**; Scheme 35)[355,356] exhibit much stabler blue emission from LEDs than corresponding nondendronized PFs.[355,357] This effect is attributed to the reduction in exciton migration as a result of defects and the greater resistance of the arylated bridgeheads in **134** towards oxidation to form emissive defects. The dendrons have been shown to alter the exciton dynamics in the polymers,[358] and in particular to increase the triplet lifetimes[359] and reduce triplet migration.[360]



133 134

Scheme 35. Polyfluorenes with phenylene dendrimer side chains.

The dendronized polymers described here are highly rigid and, similar to polyphenylene dendrimers, can assemble to form nanofibers.[361] This assembly does not result from π stacking as seen for alkylfluorene polymers, and so should not affect the electronic properties of the individual chains.

8.2. Nanopropeller Molecules with Three-Dimensional Arrays of Graphene Sheets

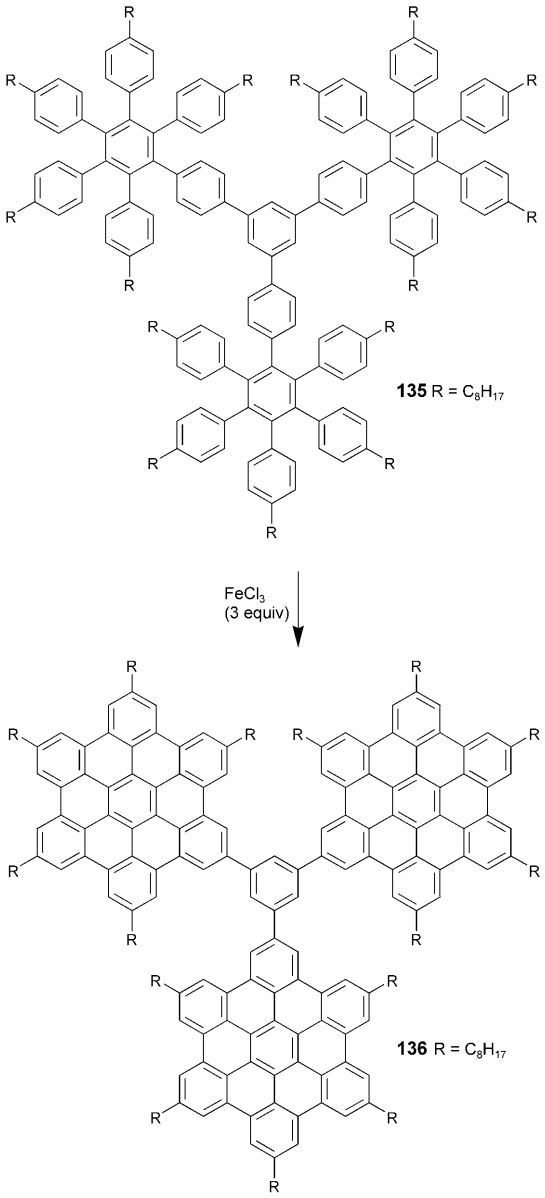
Another class of molecules in which polyphenylene nanostructures of different dimensionalities are combined are "propeller" molecules in which a number of 2D polyphenylene units (graphene sheets) are linked through a nonplanar core.[362] These molecules are made by the partial dehydrogenation of polyphenylene dendrimers, as illustrated in Scheme 36 for the preparation of a soluble model compound **136** from the dendrimer **135**. The three HBC units In **136** are not coplanar as shown by the fact that Raman and UV/Vis spectra closely match those for individual HBCs (Figure 10). Propellers **139** and **140** with larger blades have been made from their dendrimer precursors **137** and **138** (Figure 11). However, these materials are insoluble and have been characterized only by solid-state UV/Vis and Raman spectroscopy, as well as by mass spectrometry. Thus, the cyclodehydrogenation must be conducted in such a way as to restrict the planarization to the separate dendron arms. Separation of the enantiomers of propeller **137** (4.5 nm diameter) was not possible because of its insolubility.

As can be seen from these results, the combination of polyphenylene nanostructures of various dimensionalities opens up a whole new range of molecular architectures, but there remains one class of carbon-rich materials we have not yet addressed, that is, carbon nanotubes.

9. From Discotic Mesophases to Carbon Nano- and Microstructures

Carbon nanotubes (CNTs)[363] are discrete particles that belong to a broad family of carbonaceous materials which have a long history and have proven of great industrial importance. CNTs may comprise either a single graphite

 © 2005 Wiley-VCH Verlag GmbH & Co. KGaA, Weinheim



Scheme 36. Partial cyclodehydrogenation of a C_{132} dendrimer **136** to a model "propeller" molecule **135**.

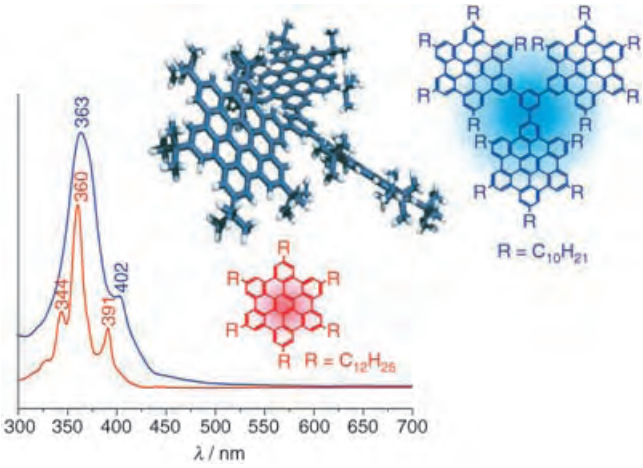


Figure 10. UV/Vis spectra of model propeller compound **135** (blue) compared with an alkylated HBC (red).

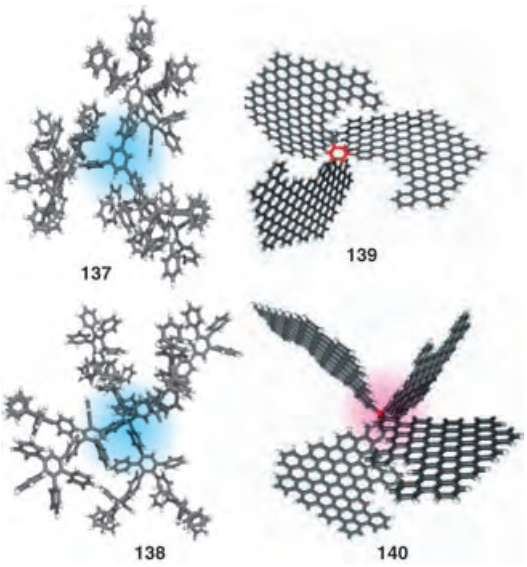


Figure 11. Formation of larger nanopropellers from dendrimer precursors.

sheet (single walled nanotubes, SWNTs) or an array of such nanotubes concentrically nested in a similar way as the rings in a tree trunk (multiwalled nanotubes, MWNT).[364] CNTs (and the related fullerenes) have become of intense academic and industrial interest recently because of their outstanding electronic (they can be either metallic or semiconducting) and physical (high tensile strength) characteristics, and potential use in electronic devices, or as chemical sensors, but there remain difficulties in obtaining these materials, particularly the SWNTs in both high yield and purity.[353,365–372] The standard methods for preparing carbon nanotubes and fullerenes typically involve high temperatures or pressures, for example, electric arc discharge of graphite electrodes[363] or laser ablation of graphite.[373] The chemical vapor deposition method is particularly attractive for the synthesis of aligned CNTs from the gas phase.

A new milder method has now been developed for preparing carbon nanoparticles by a two-stage pyrolysis of an alkyl-HBC (**32** $R = C_{12}H_{25}$).[374] The first stage of the pyrolysis occurs at 400 °C—a temperature at which the HBCs are still in an ordered liquid-crystalline mesophase (a carbomesophase). This results in the formation of large PAH intermediates (detected by MALDI-TOF) which preserve some mesomorphic order as shown by polarizing optical microscopy studies. In the second step, pyrolysis at 800 °C results in mild graphitization to produce carbon nano- and microparticles with graphitic nanostructures, including fibers and rods (Figure 12).[375]

Pyrolysis on mica afforded a mixture of films coated on the surface and discrete nanoparticles, whose preferred shape appeared to be a hexagonally symmetric zigzag, for example, large microobjects with cross-sections of 1–10 mm, and lengths in the micrometer range (Figure 11, bottom left), and rootlike microobjects with cross-sections of 400 nm–1 μm and lengths of > 30 μm (Figure 12, bottom right).

Metal particles are known to catalyze the formation of the aryl–aryl bonds in CNTs, and thus an organometallic complex

 © 2005 Wiley-VCH Verlag GmbH & Co. KGaA, Weinheim

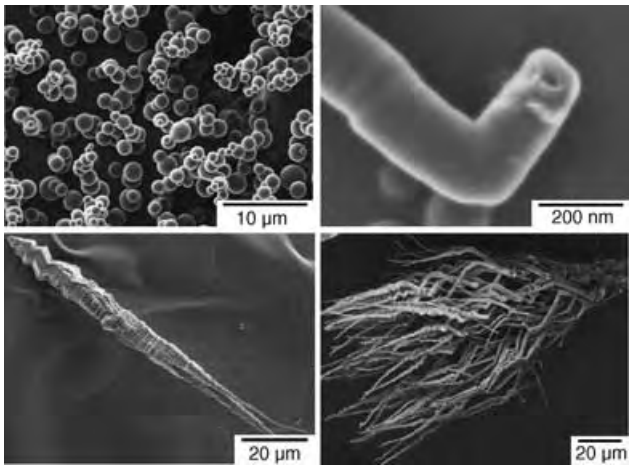


Figure 12. Top: Spherical (left) and rodlike (right) particles obtained by pyrolysis of HBC on quartz. Bottom: microobjects formed by pyrolysis of HBC on mica.

can serve as both a carbon source and a catalyst precursor in a pyrolysis. The solid-state pyrolysis of organometallic compounds such as metallo-dehydro[*n*]annulenes has emerged as a new method for making CNTs (primarily MWNTs).[376–379] The pyrolysis of an HBC–cobalt complex **141** in the solid-state produces carbon nanotubes (Figure 13).[380] Nearly quantitative yields of either "bamboo-shaped" or straight nanotubes are obtained. The shape and yield of the carbon nanostructures can be finely controlled by regulation of the heating process. The precursor **141** contains both a graphite carbon source (HBC) and a catalyst precursor, and at high temperatures the graphite islands form tubelike graphene structures on the cobalt catalyst units.

The next progression is to use the ordering of graphene molecules such as HBC to induce order in the nanotube pyrolysis products. Thus, a well-controlled pyrolysis of HBC molecules has been performed in a porous alumina membrane which acts as a template.[381] The HBC molecules were introduced to the nanochannnels within the alumina template by a simple wetting process, whereby it is important that the HBC discs adopt an edge-on arrangement of the template surface. Pyrolysis then furnishes carbon nanotubes. After dissolution of the template, high-resolution TEM studies (Figure 14) showed that the carbon nanotubes were formed with graphite layers perpendicular to the nanotube axis, that is, matching the alignment of the original HBCs. It was found

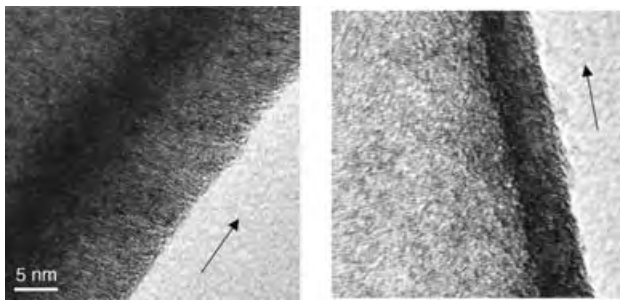


Figure 14. TEM pictures of the nanotubes showing the aligned graphene layers.

that the ordered preorganization of the liquid-crystalline HBC molecules on the surface of the membrane played a key role in obtaining carbon nanotubes with controlled orientation of the graphene layer. This special alignment of the graphene sheets is expected to induce significantly different properties in these nanotubes compared with those made by the previously known methods.

Further development of these concepts aims to produce nanotubes with controllable size, morphology, and electronic properties. For example, pyrolysis of materials containing heteroatoms could be used to selectively produce n- or p-type semiconductors.

10. Summary and Outlook

Though the emergence of a technology based on nanometer-sized devices still lies some time in the future, useful progress has been made. Hand-in-hand with the development of new methods for visualizing and manipulating matter at the nanoscale has come progress in the chemistry of nanomaterials—that is, in the design, synthesis, processing, and characterization of materials capable of performing as func-

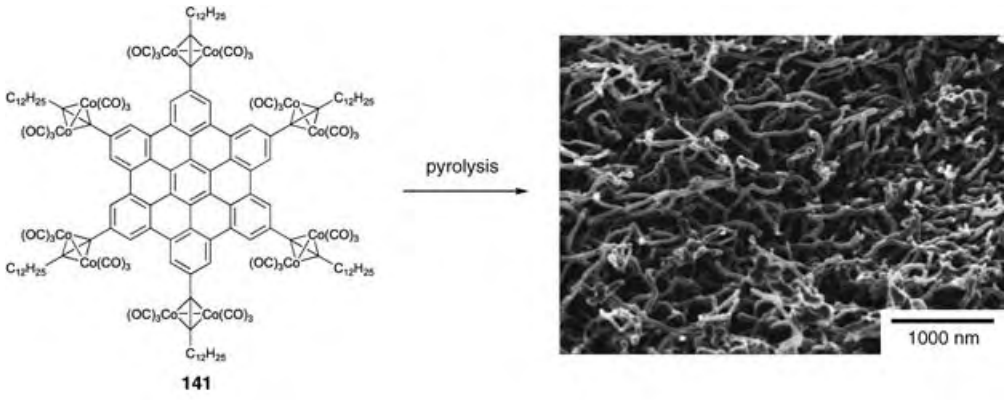


Figure 13. High-yielding synthesis of carbon nanotubes by pyrolysis of an HBC–cobalt complex in the solid state.

 © 2005 Wiley-VCH Verlag GmbH & Co. KGaA, Weinheim

tional elements in putative nanodevices. In this Review we have presented our work on the development of such materials within the context of the wider ongoing research into the nanosciences.

Thus, we have shown how the optical, electronic, and phase-forming properties of rigid-rod one-dimensional polyphenylenes, discotic polycyclic aromatic hydrocarbons, rylene dyes, and polyphenylene dendrimers as well as of molecules containing various combinations of these structural elements can be manipulated by synthetic means. Crucial feedback for the synthetic design has been obtained by our research colleagues who have visualized individual molecules or small ensembles of these materials and probed their optical and electronic properties by means of single-molecule spectroscopy and scanning probe microscopy techniques. In this way, valuable insights have been gained into the fundamental processes of charge transport as well as of energy and charge transfer within and between molecules. This knowledge not only permits the design of improved nanomaterials but also provides valuable information about the behavior of the wonderfully sophisticated light-harvesting and other systems found within living organisms. It should not be forgotten that, in addition to the development of nanosized devices, there is still considerable scope for improvement in bulk organic electronic devices through investigation and optimization of the behavior of their component materials at the nanoscale. For example, the design of organic solar cells requires a control not only of the electronic properties of components absorbing light and acting as electron donors and acceptors, but also of phase-separated morphologies, preferably at the nanoscale, for charge transport.

Some initial steps have also been taken towards proving the viability of advanced nanotechnology. For example, a chemically gated transistor has been demonstrated for individual molecules of a substituted hexa-*peri*-hexabenzocoronene. On a more immediately practical level, fibers consisting of small bundles of columns of HBCs have been obtained which might plausibly be used in a nanosized FET. Polyphenylene dendrimers have been developed as highly stable shape-persistent nanoobjects which can be functionalized at the core, in the scaffold, and/or at the surface with a range of groups. This diversity offers the possibility of making functional nanoparticles with a wide range of possible applications including as nanoemitters, chemical sensors, drug-delivery systems, bioassays, and supports for catalysts.

New stable dyes with very efficient absorption and/or emission across the whole visible range and into the near infrared region have been developed which are both of great practical importance and are suitable for study by single-molecule spectroscopy techniques. These dyes can be combined with polyphenylenes of various dimensionalities to make highly emissive materials. In particular, they can be combined with polyphenylene dendrimers to make materials which act as single-photon sources and meet some of the requirements for single-photon cryptography.

An area that holds great promise for the development of complex nanostructures containing novel molecular topologies is the combination of one-, two-, and three-dimensional polyphenylene nanostructures. We have demonstrated that attaching dedrimers to one- and two-dimensional polyphenylenes can be used to control their assembly and thus their electronic properties. Finally we have shown that pyrolysis of ordered mesophases of HBCs is a practical way to make novel carbon nanoparticles with well-defined, synthetically controlled properties.

All of these results suggest that functional devices using individual molecules or small ensembles of molecules should no longer be regarded as the stuff of science fiction but as a realistically attainable goal. Further advances in techniques for the manipulation of matter at the nanoscale are needed, and the issue of electronically addressing nanoparticles or single molecules must be solved. However, if progress continues at the current rate and driven by the fruitful interaction between chemists and physicists, we may soon be rewarded with an advanced nanotechnology.

We thank all the many people who performed the work we have presented. First we thank all our co-workers, past and present, at Mainz. Second we cannot acknowledge too deeply the invaluable contributions from our distinguished collaborators, in particular Thomas Basché, Steven De Feyter, Frans De Schryver, Richard Friend, Johan Hofkens, Roberto Lazzaroni, Emil List, John Lupton, Jürgen Rabe, and Paolo Samori. The assistance and advice of Roland Bauer, Andreas Herrmann, Lileta Gherghel, Marcel Kasker, Markus Klapper, Christopher Kohl, Wojciech Pisula, and Jishan Wu in the preparation of this manuscript is also gratefully acknowldeged. Financial support for this research from the Max Planck Society for the Advancement of Science, the European Commission, the Bundesministerium für Bildung und Forschung, the Deutsche Forschungsgemeinschaft, the Volkswagen Stiftung, BASF, Merck, SONY, Roche and DuPont Displays is also gratefully acknowledged.

Received: March 4, 2005

[1] C. N. R. Rao, G. U. Kulkarni, P. J. Thomas, P. P. Edwards, *Chem. Soc. Rev.* **2000**, *29*, 27.
[2] C. Aymonier, U. Schlotterbeck, L. Antonietti, P. Zacharias, R. Thomann, J. C. Tiller, S. Mecking, *Chem. Commun.* **2002**, 3018.
[3] A. L. Rogach, D. V. Talapin, H. Weller in *Colloids and Colloid Assemblies* (Ed.: F. Caruso), Wiley-VCH, Weinheim, **2004**, p. 52.
[4] G. M. Whitesides, *Small* **2005**, *1*, 172.
[5] V. Balzani, *Small* **2005**, *1*, 278.
[6] C. Joachim, *Nat. Mater.* **2005**, *4*, 107.
[7] *Nanoscience and Nanotechnology: Opportunities and Uncertainties*, Royal Society, London, **2004**.
[8] R. Corriu, P. Nozières, C. Weisbuch, *Nanoscience, Nanotechnologies*, Académie des Sciences & Académie des Technologies, Paris, **2004**.
[9] Z. L. Wang in *Characterization of Nanophase Materials* (Ed.: Z. L. Wang), Wiley-VCH, Weinheim, **2000**, p. 1.
[10] R. Ellialtioglu, *NATO Sci. Ser. Ser. C* **2000**, *559*, 449.
[11] M. F. Hochella, *Geochim. Cosmochim. Acta* **2002**, *66*, 735.
[12] R. E. Palmer, *Surf. Interface Anal.* **2002**, *25*, 3.
[13] A. T. Bell, *Science* **2003**, *299*, 1688.
[14] J. Grunes, J. Zhu, G. A. Somorjal, *Chem. Commun.* **2003**, 2257.
[15] S.-W. Hla, K.-H. Rieder, *Annu. Rev. Phys. Chem.* **2003**, *54*, 307.
[16] P. V. Kamat, D. Meisel, *Comptes Rendu Chimie* **2003**, *6*, 999.

 © 2005 Wiley-VCH Verlag GmbH & Co. KGaA, Weinheim

[17] E. Dickinson, *Curr. Opin. Colloid Interface Sci.* **2003**, *8*, 346.
[18] C. P. Poole, Jr., F. J. Owens, *Introduction to Nanotechnology*, Wiley-Interscience, Hoboken, **2003**.
[19] J. Grunes, J. Zhu, G. A. Somorjal in *Nanotechnology in Catalysis* (Eds.: B. Zhou, S. Hermans, G. A. Somorjal), Kluwer, New York, **2004**, p. 1.
[20] R. Corriu, A. Mehdi, C. Reye, *J. Organomet. Chem.* **2004**, *689*, 4437.
[21] J. Chen, Y. Miao, N. He, X. Wu, S. Li, *Biotechnol. Adv.* **2004**, *22*, 505.
[22] H. Rauter, V. Matyushin, Y. Alguel, F. Pittner, T. Schmalkhammer, *Macromol. Symp.* **2004**, *217*, 104.
[23] P. Wagner in *Nanoscale Technology in Biological Systems* (Eds.: R. S. Greco, F. B. Prinz, R. L. Smith), CRC, Boca Raton, **2005**, p. 39.
[24] C. Joachim, J. K. Gimzewski, A. Aviram, *Nature* **2000**, *408*, 541.
[25] R. P. Feynman, *Eng. Sci.* **1960**, *23*, 22.
[26] S. Flink, F. C. J. M. van Veggel, D. N. Reinhoudt, *Adv. Mater.* **2000**, *12*, 1315.
[27] X.-M. Li, J. Huskens, D. N. Reinhoudt, *J. Mater. Chem.* **2004**, *14*, 2954.
[28] J. A. A. W. Elemans, A. E. Rowan, R. J. M. Nolte, *J. Mater. Chem.* **2003**, *13*, 2661.
[29] M. A. Mateos-Timoneda, M. Crego-Calama, D. N. Reinhoudt, *Chem. Soc. Rev.* **2004**, *33*, 363.
[30] T. Baschè, W. E. Moerner, M. Orrit, U. P. Wild, *Single Molecule Optical Detection, Imaging, and Spectroscopy*, Wiley-VCH, Weinheim, **1997**.
[31] W. E. Moerner, M. Orrit, *Science* **1999**, *283*, 1670.
[32] T. Basché, S. Kummer, C. Bräuchle, *Nature* **1995**, *373*, 132.
[33] G. Seisenberger, M. U. Ried, T. Endress, H. Büning, M. Hallek, C. Bräuchle, *Science* **2001**, *294*, 1929.
[34] C. Bräuchle, G. Seisenberger, T. Endress, M. U. Ried, H. Büning, M. Hallek, *ChemPhysChem* **2002**, *3*, 299.
[35] P. Samori, *J. Mater. Chem.* **2004**, *14*, 1353.
[36] G. Binning, H. Rohrer, C. Gerber, E. Weibel, *Helv. Phys. Acta* **1982**, *55*, 726.
[37] G. Binning, H. Rohrer, C. Gerber, E. Weibel, *Appl. Phys. Lett.* **1982**, *40*, 178.
[38] A. Stabel, P. Herwig, K. Müllen, J. P. Rabe, *Angew. Chem.* **1995**, *107*, 1768; *Angew. Chem. Int. Ed. Engl.* **1995**, *34*, 1609.
[39] A. Miura, S. De Feyter, M. M. S. Abdel-Mottaleb, A. Gesquière, P. C. M. Grim, G. Moessner, M. Sieffert, M. Klapper, K. Müllen, F. C. De Schryver, *Langmuir* **2003**, *19*, 6474.
[40] S. De Feyter, F. C. De Schryver, *Chem. Soc. Rev.* **2003**, *32*, 139.
[41] S. De Feyter, A. Gesquière, M. M. Abdel-Mottaleb, P. C. M. Grim, F. C. De Schryver, C. Meiners, M. Sieffert, S. Valiyaveettil, K. Müllen, *Acc. Chem. Res.* **2000**, *33*, 520.
[42] S. De Feyter, J. Hofkens, M. Van der Auweraer, R. J. M. Nolte, K. Müllen, F. C. De Schryver, *Chem. Commun.* **2001**, 585.
[43] G. Binning, C. F. Quate, C. Gerber, *Phys. Rev. Lett.* **1986**, *56*, 930.
[44] M. Kudera, C. Eschbaumer, H. E. Gaub, U. S. Schubert, *Adv. Funct. Mater.* **2003**, *13*, 615.
[45] S. S. Sheiko, M. da Silva, D. Shirvaniants, I. LaRue, S. Prokhorovka, M. Möller, K. Beers, K. Matyjaszewski, *J. Am. Chem. Soc.* **2003**, *125*, 6725.
[46] A. Kraft, A. C. Grimsdale, A. B. Holmes, *Angew. Chem.* **1998**, *110*, 416; *Angew. Chem. Int. Ed.* **1998**, *37*, 402.
[47] C. J. Brabec, N. S. Sariciftci, J. C. Hummelen, *Adv. Funct. Mater.* **2001**, *11*, 15.
[48] C. D. Dimitrakopoulos, P. R. L. Malenfant, *Adv. Mater.* **2002**, *14*, 99.
[49] K. Müllen, G. Wegner, *Electronic Materials: The Oligomer Approach*, Wiley-VCH, Weinheim, **1998**.
[50] R. F. Martin, F. Diederich, *Angew. Chem.* **1999**, *111*, 1440; *Angew. Chem. Int. Ed.* **1999**, *38*, 1350.
[51] J. H. K. K. Hirschberg, L. Brunsveld, A. Ramzi, J. A. J. M. Vekemans, R. P. Sijbesma, E. W. Meijer, *Nature* **2000**, *407*, 167.
[52] A. El-ghayoury, A. P. H. J. Schenning, P. A. van Hal, J. K. J. van Duren, R. A. J. Janssen, E. W. Meijer, *Angew. Chem.* **2001**, *113*, 3772; *Angew. Chem. Int. Ed.* **2001**, *40*, 3660.
[53] G. Widawski, M. Rawiso, B. François, *Nature* **1994**, *369*, 387.
[54] L. H. Radzilowski, S. I. Stupp, *Macromolecules* **1994**, *27*, 7747.
[55] G. Mao, C. K. Ober, *Acta Polym.* **1997**, *48*, 405.
[56] L. H. Radzilowski, B. O. Carragher, S. I. Stupp, *Macromolecules* **1997**, *30*, 2110.
[57] M. A. Hempenius, B. M. W. Langeveld-Voss, J. A. E. H. van-Haare, R. A. J. Janssen, S. S. Sheiko, J. P. Spatz, M. Möller, E. W. Meijer, *J. Am. Chem. Soc.* **1998**, *120*, 2798.
[58] S. A. Jenekhe, X. L. Chen, *Science* **1998**, *279*, 1903.
[59] S. A. Jenekhe, X. L. Chen, *Science* **1999**, *283*, 372.
[60] S. A. Jenekhe, X. L. Chen, *J. Phys. Chem. A* **2000**, *104*, 6332.
[61] H. Wang, H. H. Wang, V. S. Urban, K. C. Littrell, P. Thiyagarajan, L. Yu, *J. Am. Chem. Soc.* **2000**, *122*, 6855.
[62] U. Stalmach, B. de Boer, C. Videlot, F. F. Vercuateen, J. J. L. van der Want, G. Hadziioannou, *J. Am. Chem. Soc.* **2000**, *122*, 5464.
[63] B. De Boer, U. Stalmach, H. Nijland, G. Hadziioannou, *Adv. Mater.* **2000**, *12*, 1581.
[64] E. R. Zubarev, M. U. Pralle, E. D. Sone, S. I. Stupp, *J. Am. Chem. Soc.* **2001**, *123*, 4105.
[65] J. L. M. Cornelissen, M. Fischer, R. van Waes, R. van Heerbeck, P. C. J. Kamer, J. N. H. Reek, N. A. J. M. Sommerdijk, R. J. M. Nolte, *Polymer* **2004**, *45*, 7417.
[66] D. M. Vriezma, A. Kros, R. de Gelder, J. J. L. M. Cornelissen, A. E. Rowan, R. J. M. Nolte, *Macromolecules* **2004**, *37*, 4736.
[67] U. Scherf, *J. Mater. Chem.* **1999**, *9*, 1853.
[68] D. Neher, *Macromol. Rapid Commun.* **2001**, *22*, 1365.
[69] S. Setayesh, D. Marsitzky, K. Müllen, *Macromolecules* **2000**, *33*, 2016.
[70] J. Jacob, J. Zhang, A. C. Grimsdale, K. Müllen, M. Gaal, E. J. W. List, *Macromolecules* **2003**, *36*, 8240.
[71] J. Jacob, S. Sax, T. Piok, E. J. W. List, A. C. Grimsdale, K. Müllen, *J. Am. Chem. Soc.* **2004**, *126*, 6987.
[72] E. Somma, B. Loppinet, F. G. S. Setayesh, J. Jacob, A. C. Grimsdale, K. Müllen, *Colloid Polym. Sci.* **2004**, *282*, 867.
[73] T. Yamamoto, Y. Hayashi, A. Yamamoto, *Bull. Chem. Soc. Jpn.* **1978**, *51*, 2091.
[74] S. Schlüter, J. Frahn, B. Karakaya, A.-D. Schlüter, *Macromol. Chem. Phys.* **2000**, *201*, 139.
[75] D. Marsitzky, M. Klapper, K. Müllen, *Macromolecules* **1999**, *32*, 8685.
[76] D. Marsitzky, T. Brand, Y. Geerts, M. Klapper, K. Müllen, *Macromol. Rapid Commun.* **1998**, *19*, 385.
[77] T. Miteva, A. Meisel, W. Knoll, H. G. Nothofer, U. Scherf, D. C. Müller, K. Meerholz, A. Yasuda, D. Neher, *Adv. Mater.* **2001**, *13*, 565.
[78] M. Surin, D. Marsitzky, A. C. Grimsdale, K. Müllen, R. Lazzaroni, P. Leclère, *Adv. Funct. Mater.* **2004**, *14*, 708.
[79] Y. Geng, K. Trayovska, D. J. D. Ou, S. W. Culligan, S. H. Chen, *J. Am. Chem. Soc.* **2002**, *124*, 8337.
[80] J. Jo, C. Chi, S. Höger, G. Wegner, D. Y. Yoon, *Chem. Eur. J.* **2004**, *10*, 2681.
[81] F. Schindler, J. Jacob, A. C. Grimsdale, J. M. Lupton, U. Scherf, K. Müllen, J. Feldmann, *Angew. Chem.* **2005**, *117*, 1544; *Angew. Chem. Int. Ed.* **2005**, *44*, 1520.
[82] J. Grimme, M. Kreyenschmidt, F. Uckert, K. Müllen, U. Scherf, *Adv. Mater.* **1995**, *7*, 292.
[83] U. H. F. Bunz, *Chem. Rev.* **2000**, *100*, 1605.
[84] P. Samori, V. Francke, K. Müllen, J. P. Rabe, *Chem. Eur. J.* **1999**, *5*, 2312.
[85] P. Samori, V. Francke, V. Enkelmann, K. Müllen, J. P. Rabe, *Chem. Mater.* **2003**, *15*, 1032.

 © 2005 Wiley-VCH Verlag GmbH & Co. KGaA, Weinheim

[86] V. Francke, H.-J. Räder, Y. Geerts, K. Müllen, *Macromol. Rapid Commun.* **1998**, *19*, 275.
[87] P. Leclère, E. Hennbicq, A. Calderone, P. Brocorens, A. C. Grimsdale, K. Müllen, J. L. Brédas, R. Lazzaroni, *Prog. Polym. Sci.* **2003**, *28*, 55.
[88] A. C. Grimsdale, P. Leclère, R. Lazzaroni, J. D. MacKenzie, C. Murphy, S. Setayesh, C. Silva, R. H. Friend, K. Müllen, *Adv. Funct. Mater.* **2002**, *12*, 729.
[89] M. Surin, E. Henebicq, C. Ego, D. Marsitzky, A. C. Grimsdale, K. Müllen, J.-L. Brédas, R. Lazzaroni, P. Leclère, *Chem. Mater.* **2004**, *16*, 994.
[90] P. Leclère, M. Surin, P. Jonheijm, O. Henze, A. P. H. J. Schenning, F. Biscarini, A. C. Grimsdale, W. J. Feast, E. W. Meijer, K. Müllen, J. L. Brédas, R. Lazzaroni, *Eur. Polym. J.* **2004**, *40*, 885.
[91] M. Grell, D. D. C. Bradley, M. Inbasekaran, E. P. Woo, *Adv. Mater.* **1997**, *9*, 798.
[92] J. Teetsov, M. A. Fox, *J. Mater. Chem.* **1999**, *9*, 2117.
[93] M. Grell, W. Knoll, D. Lupo, A. Meisel, T. Miteva, D. Neher, H.-G. Nothofer, U. Scherf, A. Yasuda, *Adv. Mater.* **1999**, *11*, 671.
[94] M. Grell, D. D. C. Bradley, *Adv. Mater.* **1999**, *11*, 895.
[95] P. Sonar, A. C. Grimsdale, K. Müllen, M. Surin, R. Lazzaroni, P. Leclère, J. Pinto, L.-L. Chua, H. Sirringhaus, R. H. Friend, unpublished results.
[96] H. Sirringhaus, T. Kawase, R. H. Friend, T. Shimoda, M. Inbasekaran, W. Wu, E. P. Woo, *Science* **2000**, *290*, 2123.
[97] H. Sirringhaus, R. J. Wilson, R. H. Friend, M. Inbasekaran, W. Wu, E. P. Woo, M. Grell, D. D. C. Bradley, *Appl. Phys. Lett.* **2000**, *77*, 406.
[98] M. Surin, P. Sonar, A. C. Grimsdale, K. Müllen, P. Leclère, R. Lazzaroni, *Adv. Funct. Mater.* submitted.
[99] M. Surin, P. Sonar, A. C. Grimsdale, K. Müllen, S. De Feyter, S. Habuchi, S. Sarzi, M. Van der Auweraer, F. C. De Schryver, M. Cavallini, F. Biscarini, E. da Como, R. Lazzaroni, P. Leclère, *Adv. Funct. Mater.*, submitted.
[100] P. Samori, I. Sikharulidze, V. Francke, K. Müllen, J. P. Rabe, *Nanotechnology* **1999**, *10*, 77.
[101] P. Samori, N. Severin, K. Müllen, J. P. Rabe, *Adv. Mater.* **2000**, *12*, 579.
[102] P. Leclère, M. Surin, R. Lazzaroni, A. F. M. Kilbinger, O. Henze, P. Jonkheijm, F. Biscarini, M. Cavallini, W. J. Feast, E. W. Meijer, A. P. H. J. Schenning, *J. Mater. Chem.* **2004**, *14*, 1959.
[103] P. Leclère, M. Surin, P. Viville, R. Lazzaroni, A. F. M. Kilbinger, O. Henze, W. J. Feast, M. Cavallini, F. Biscarini, A. P. H. J. Schenning, E. W. Meijer, *Chem. Mater.* **2004**, *16*, 4452.
[104] A. Gesquière, P. Jonkheijm, A. P. H. J. Schenning, E. Mena-Osteritz, P. Bäuerle, S. De Feyter, F. C. De Schryver, E. W. Meijer, *J. Mater. Chem.* **2003**, *13*, 2164.
[105] E. Mena-Osteritz, A. Meyer, B. M. W. Langeveld-Voss, R. A. J. Janssen, E. W. Meijer, P. Bäuerle, *Angew. Chem.* **2000**, *112*, 2791; *Angew. Chem. Int. Ed.* **2000**, *39*, 2680.
[106] R. Garcia, M. Tello, J. F. Moulin, F. Biscarini, *Nano Lett.* **2004**, *4*, 1115.
[107] M. Cavallini, F. Biscarini, *Nano Lett.* **2003**, *3*, 1269.
[108] M. Cavallini, M. Facchini, M. Massi, F. Biscarini, *Synth. Met.* **2004**, *146*, 283.
[109] M. Cavallini, P. Stoliar, M. Facchini, F. Biscarini, M. Surin, R. Lazzaroni, P. Leclère, P. Sonar, A. C. Grimsdale, K. Müllen, unpublished results.
[110] J. G. Müller, U. Lemmer, G. Raschke, M. Anni, U. Scherf, J. M. Lupton, J. Feldmann, *Phys. Rev. Lett.* **2003**, *91*, 267403.
[111] F. Schindler, J. M. Lupton, J. Feldmann, U. Scherf, *Proc. Natl. Acad. Sci. USA* **2004**, *101*, 14695.
[112] S.-J. Park, A. J. Gesquiere, J. Yu, P. F. Barbara, *J. Am. Chem. Soc.* **2004**, *126*, 4116.
[113] A. J. Gesquiere, S.-J. Park, P. F. Barbara, *J. Phys. Chem. B* **2004**, *108*, 10301.
[114] A. Aviram, M. A. Ratner, *Chem. Phys. Lett.* **1974**, *29*, 277.
[115] J. Roncali, *Acc. Chem. Res.* **2000**, *33*, 147.
[116] J. M. Tour, *Acc. Chem. Res.* **2000**, *33*, 791.
[117] J. M. Tour, A. M. Rawlett, M. Kozaki, Y. Yao, R. C. Jagessar, S. M. Dirk, D. W. Price, M. A. Reed, C. Zhou, J. Chen, W. Wang, I. Campbell, *Chem. Eur. J.* **2001**, *7*, 5118.
[118] N. Robertson, C. A. McGowan, *Chem. Soc. Rev.* **2003**, *32*, 96.
[119] J. M. Tour, *Molecular Electronics: Commercial Insights, Chemistry, Devices, Architecture and Programming*, World Scientific, River Edge, NJ, **2003**.
[120] D. K. James, J. M. Tour, *Chem. Mater.* **2004**, *16*, 4423.
[121] M. Mayor, H. B. Weber, J. Reichert, M. Elbing, C. von Hänisch, D. Beckmann, M. Fischer, *Angew. Chem.* **2003**, *115*, 1614; *Angew. Chem. Int. Ed.* **2003**, *42*, 5834.
[122] M. Mayor, H. B. Weber, *Angew. Chem.* **2004**, *116*, 2942; *Angew. Chem. Int. Ed.* **2004**, *43*, 2882.
[123] J.-O. Lee, G. Lietschnig, F. G. H. Wiertz, M. Struijk, R. A. J. Janssen, R. Egberink, D. N. Reinhoudt, A. C. Grimsdale, K. Müllen, P. Hadley, C. Dekker, *Ann. N.Y. Acad. Sci.* **2003**, *1006*, 122.
[124] D. T. McQuade, A. E. Pullen, T. M. Swager, *Chem. Rev.* **2000**, *100*, 2537.
[125] K. Kuroda, T. M. Swager, *Macromol. Symp.* **2003**, *201*, 127.
[126] M. Leclerc, H. A. Ho, *Synlett* **2004**, 380.
[127] T.-H. Kim, T. M. Swager, *Angew. Chem.* **2003**, *115*, 4951; *Angew. Chem. Int. Ed.* **2003**, *42*, 4803.
[128] H. A. Ho, M. Leclerc, *J. Am. Chem. Soc.* **2003**, *125*, 4412.
[129] S.-W. Zhang, T. M. Swager, *J. Am. Chem. Soc.* **2003**, *125*, 3420.
[130] L. Kumpumbu-Kalemba, M. Leclerc, *Chem. Commun.* **2000**, 1847.
[131] D. T. McQuade, A. H. Hegedus, T. M. Swager, *J. Am. Chem. Soc.* **2000**, *122*, 12389.
[132] H.-A. Ho, M. Boissinot, M. G. Bergeron, G. Corbeil, K. Dore, D. Boudreau, M. Leclerc, *Angew. Chem.* **2002**, *114*, 1618; *Angew. Chem. Int. Ed.* **2002**, *41*, 1548.
[133] H.-A. Ho, M. Leclerc, *J. Am. Chem. Soc.* **2004**, *126*, 1384.
[134] K. Dore, S. Dubus, H.-A. Ho, I. Levesque, M. Brunette, G. Corbeil, M. Boissinot, G. Boivin, M. G. Bergeron, D. Boudreau, M. Leclerc, *J. Am. Chem. Soc.* **2004**, *126*, 4240.
[135] H.-A. Ho, M. Boissinot, M. G. Bergeron, G. Corbeil, K. Dore, D. Boudreau, M. Leclerc, *ACS Symp. Ser.* **2005**, *888*, 359.
[136] M. D. Disney, J. Zheng, T. M. Swager, P. H. Seeberger, *J. Am. Chem. Soc.* **2004**, *126*, 13343.
[137] B. S. Gaylord, A. J. Heeger, G. C. Bazan, *J. Am. Chem. Soc.* **2003**, *125*, 896.
[138] E. Ergen, J. Jacob, A. Herrmann, K. Müllen, unpublished results.
[139] M. D. Watson, A. Fechtenkötter, K. Müllen, *Chem. Rev.* **2001**, *101*, 1267.
[140] E. Clar, *The Aromatic Sextet*, Wiley, London, **1972**.
[141] P. T. Herwig, C. W. Kayser, K. Müllen, H. W. Spiess, *Adv. Mater.* **1996**, *8*, 510.
[142] Z. Tomovic, M. D. Watson, K. Müllen, *Angew. Chem.* **2004**, *116*, 773; *Angew. Chem. Int. Ed.* **2004**, *43*, 755.
[143] M. Müller, C. Kübel, K. Müllen, *Chem. Eur. J.* **1998**, *4*, 2099.
[144] J. Wu, Z. Tomovic, V. Enkelmann, K. Müllen, *J. Org. Chem.* **2004**, *69*, 5179.
[145] C. D. Simpson, J. D. Brand, A. J. Berresheim, L. Przybilla, H.-J. Räder, K. Müllen, *Chem. Eur. J.* **2002**, *8*, 1424.
[146] Z. Wang, Z. Tomovic, M. Kastler, R. Pretsch, F. Negri, V. Enkelmann, K. Müllen, *J. Am. Chem. Soc.* **2004**, *126*, 7794.
[147] V. S. Iyer, K. Yoshimura, V. Enkelmann, R. Epsch, J. P. Rabe, K. Müllen, *Angew. Chem.* **1998**, *110*, 2843; *Angew. Chem. Int. Ed.* **1998**, *37*, 2696.
[148] M. G. Debije, J. Piris, M. P. de Haas, J. M. Warman, Z. Tomovic, C. D. Simpson, M. D. Watson, K. Müllen, *J. Am. Chem. Soc.* **2004**, *126*, 4641.

 © 2005 Wiley-VCH Verlag GmbH & Co. KGaA, Weinheim

[149] C. Castiglioni, C. Mapelli, F. Negri, G. Zerbi, *J. Chem. Phys.* **2001**, *114*, 963.
[150] E. Di Donato, M. Tommasini, G. Fustella, L. Brambilla, C. Castiglioni, G. Zerbi, C. D. Simpson, K. Müllen, F. Negri, *Chem. Phys.* **2004**, *301*, 81.
[151] C. Castiglioni, F. Negri, M. Tommasini, E. Di Donato, G. Zerbi, *AIP Conf. Proc.* **2002**, *633*, 394.
[152] C. Castiglioni, E. Di Donato, M. Tommasini, F. Negri, G. Zerbi, *Synth. Met.* **2003**, *139*, 885.
[153] C. D. Simpson, J. Wu, M. D. Watson, K. Müllen, *J. Mater. Chem.* **2004**, *14*, 494.
[154] A. M. van de Craats, J. M. Warman, K. Müllen, Y. Geerts, J. D. Brand, *Adv. Mater.* **1998**, *10*, 36.
[155] A. M. van de Craats, J. M. Warman, A. Fechtenkötter, J. D. Brand, M. A. Harbison, K. Müllen, *Adv. Mater.* **1999**, *11*, 1469.
[156] C.-y. Liu, A. Fechtenkötter, M. D. Watson, K. Müllen, A. J. Bard, *Chem. Mater.* **2003**, *15*, 124.
[157] A. M. van de Craats, N. Stutzmann, O. Bunk, M. M. Nielsen, M. Watson, K. Müllen, H. D. Chanzy, H. Sirringhaus, R. H. Friend, *Adv. Mater.* **2003**, *15*, 495.
[158] A. Tracz, J. K. Jeszka, M. D. Watson, W. Pisula, K. Müllen, T. Pakula, *J. Am. Chem. Soc.* **2003**, *125*, 1682.
[159] W. Pisula, M. Kastler, D. Wasserfallen, T. Pakula, K. Müllen, *J. Am. Chem. Soc.* **2004**, *126*, 8074.
[160] W. Pisula, A. Menon, M. Stepputat, I. Lieberwirth, U. Kolb, A. Tracz, H. Sirringhaus, T. Pakula, K. Müllen, *Adv. Mater.* **2005**, *17*, 684.
[161] L. Schmidt-Mende, A. Fechtenkötter, K. Müllen, E. Moons, R. H. Friend, J. D. MacKenzie, *Science* **2001**, *293*, 1119.
[162] M. Keil, P. Samori, D. A. Dos Santos, T. Kugler, S. Stafström, J. D. Brand, K. Müllen, J. L. Brédas, J. P. Rabe, W. R. Salaneck, *J. Phys. Chem. B* **2004**, *108*, 3967.
[163] R. Friedlein, X. Crispin, C. D. Simpson, M. D. Watson, F. Jäckel, W. Osikowicz, S. Marciniak, M. P. De Jong, P. Samori, S. K. M. Jönsson, M. Fahlman, K. Müllen, J. P. Rabe, W. R. Salaneck, *Phys. Rev* **2003**, *68*, 195414.
[164] J. Wu, M. D. Watson, L. Zhang, Z. Wang, K. Müllen, *J. Am. Chem. Soc.* **2004**, *126*, 177.
[165] J. Wu, M. Baumgarten, M. G. Debije, J. M. Warman, K. Müllen, *Angew. Chem.* **2004**, *116*, 5445; *Angew. Chem. Int. Ed.* **2004**, *43*, 5331.
[166] J. Wu, M. D. Watson, N. Tchebotareva, Z. Wang, K. Müllen, *J. Org. Chem.* **2004**, *69*, 8194.
[167] Z. Wang, M. D. Watson, J. Wu, K. Müllen, *Chem. Commun.* **2004**, 336.
[168] S. R. Forrest, *Chem. Rev.* **1997**, *97*, 1793.
[169] R. Fasel, M. Parschau, K.-H. Ernst, *Angew. Chem.* **2003**, *115*, 5336; *Angew. Chem. Int. Ed.* **2003**, *42*, 5178.
[170] P. Samori, C. D. Simpson, K. Müllen, J. P. Rabe, *Langmuir* **2002**, *18*, 4183.
[171] K. Weiss, G. Beernink, F. Dötz, A. Birkner, K. Müllen, C. H. Wöll, *Angew. Chem.* **1999**, *111*, 3974; *Angew. Chem. Int. Ed.* **1999**, *38*, 3748.
[172] G. Beernink, M. Gunla, F. Dötz, H. Öström, K. Weiss, K. Müllen, C. Wöll, *ChemPhysChem* **2001**, *2*, 317.
[173] C. Günther, N. Karl, J. Pflaum, R. Strohmaier, B. Gompf, W. Eisenmenger, M. Müller, K. Müllen, *Langmuir* **2005**, *21*, 656.
[174] S. Ito, P. T. Herwig, T. Böhme, J. P. Rabe, W. Rettig, K. Müllen, *J. Am. Chem. Soc.* **2000**, *122*, 7698.
[175] P. Samori, A. Fechtenkötter, F. Jäckel, T. Böhme, K. Müllen, J. P. Rabe, *J. Am. Chem. Soc.* **2001**, *123*, 11462.
[176] T. Böhme, C. Simpson, J. P. Rabe, K. Müllen, unpublished results.
[177] F. Jäckel, M. D. Watson, K. Müllen, J. P. Rabe, *Phys. Rev. Lett.* **2004**, *92*, 1883031.
[178] F. Jäckel, Z. Wang, M. D. Watson, K. Müllen, J. P. Rabe, *Synth. Met.* **2004**, *146*, 269.
[179] D. Horn, J. Rieger, *Angew. Chem.* **2001**, *113*, 4460; *Angew. Chem. Int. Ed.* **2001**, *40*, 4330.
[180] J. Fabian, R. Zahradnik, *Angew. Chem.* **1989**, *101*, 693; *Angew. Chem. Int. Ed. Engl.* **1989**, *28*, 677.
[181] M. P. O'Niell, M. P. Niemczyk, W. A. Svec, D. Goszrola, G. L. Gaines III, M. R. Wasielewski, *Science* **1992**, *257*, 63.
[182] R. Gvishi, R. Reisfeld, Z. Bursheim, *Chem. Phys. Lett.* **1993**, *213*, 338.
[183] P. Gregory, *High-Technology Applications of Organic Colorants*, Plenum, New York, **1991**.
[184] J. Kalinowski, P. D. Marco, V. Fattori, L. Guiletti, M. Cochi, *J. Appl. Phys.* **1998**, *83*, 4242.
[185] H. Langhals, *Heterocycles* **1995**, *40*, 477.
[186] H. Zöllinger, *Color Chemistry*, Wiley-VCH, Weinheim, **2003**.
[187] A. Bohnen, K. H. Koch, W. Lüttke, K. Müllen, *Angew. Chem.* **1990**, *102*, 548; *Angew. Chem. Int. Ed. Engl.* **1990**, *29*, 525.
[188] C. Ego, D. Marsitzky, S. Becker, J. Zhang, A. C. Grimsdale, K. Müllen, J. D. MacKenzie, C. Silva, R. H. Friend, *J. Am. Chem. Soc.* **2003**, *125*, 437.
[189] H. Quante, K. Müllen, *Angew. Chem.* **1995**, *107*, 1487; *Angew. Chem. Int. Ed. Engl.* **1995**, *34*, 1323.
[190] F. O. Holtrup, G. R. J. Müller, H. Quante, S. De Feyter, F. C. De Schryver, K. Müllen, *Chem. Eur. J.* **1997**, *3*, 219.
[191] F. Nolde, J. Qu, C. Kohl, N. G. Pschirer, E. Reuther, K. Müllen, *Chem. Eur. J.* **2005**, *11*, 3959.
[192] T. Tshigama, M. Murata, N. Migaura, *J. Org. Chem.* **1995**, *60*, 7508.
[193] H. Azizian, C. Eaborn, A. Pidcock, *J. Organomet. Chem.* **1981**, *215*, 49.
[194] C. Kohl, S. Becker, K. Müllen, *Chem. Commun.* **2002**, 2778.
[195] K. H. Koch, K. Müllen, *Chem. Ber.* **1991**, *124*, 2091.
[196] C. Former, S. Becker, A. C. Grimsdale, K. Müllen, *Macromolecules* **2002**, *35*, 1576.
[197] Y. Geerts, H. Quante, H. Platz, R. Mahrt, M. Hopmeier, A. Böhm, K. Müllen, *J. Mater. Chem.* **1998**, *8*, 2357.
[198] J. Qu, PhD Thesis, Johannes-Gutenberg-University, Mainz, **2004**.
[199] C. Kohl, T. Weil, J. Qu, K. Müllen, *Chem. Eur. J.* **2004**, *10*, 5297.
[200] J. Qu, C. Kohl, M. Pottek, K. Müllen, *Angew. Chem.* **2004**, *116*, 1554; *Angew. Chem. Int. Ed.* **2004**, *43*, 1528.
[201] S. M. Waybright, C. P. Singleton, J. M. Tour, C. J. Murphy, U. H. F. Bunz, *Organometallics* **2000**, *19*, 368.
[202] S. M. Waybright, C. P. Singleton, K. Wachter, C. J. Murphy, U. H. F. Bunz, *J. Am. Chem. Soc.* **2001**, *123*, 1828.
[203] M. Scheffler, A. Dorenbeck, S. Jordan, M. Wustefeld, G. von Kiedrowski, *Angew. Chem.* **1999**, *111*, 3513; *Angew. Chem. Int. Ed.* **1999**, *38*, 3312.
[204] L. H. Eckhardt, K. Naumann, W. M. Pankau, M. Rein, M. Schweitzer, N. Windhab, G. von Kiedrowski, *Nature* **2002**, *420*, 286.
[205] M. A. Abdalla, J. Bayer, J. O. Rädler, K. Müllen, *Angew. Chem.* **2004**, *116*, 4057; *Angew. Chem. Int. Ed.* **2004**, *43*, 3967.
[206] H.-A. Klok, S. Becker, F. Scuch, T. Pakula, K. Müllen, *Macromol. Biosci.* **2003**, *3*, 729.
[207] J. Rodriguez-Hernandez, J. Qu, E. Reuther, H.-A. Klok, K. Müllen, *Polym. Bull.* **2004**, *52*, 57.
[208] A. Jesorka, T. S. Balaban, A. R. Holzwarth, K. Schaffner, *Angew. Chem.* **1996**, *108*, 3019; *Angew. Chem. Int. Ed. Engl.* **1996**, *35*, 2861.
[209] T. S. Balaban, A. Eichhofer, J.-M. Lehn, *Eur. J. Org. Chem.* **2000**, 4047.
[210] T. S. Balaban, M. Linke-Schaetzel, A. D. Bhise, N. Vanthuyne, C. Roussel, *Eur. J. Org. Chem.* **2004**, 3919.
[211] M. Linke-Schaetzel, A. D. Bhise, H. Gliemann, T. Koch, T. Schimmel, T. S. Balaban, *Thin Solid Films* **2004**, *451–452*, 16.
[212] F. Würthner, *Chem. Commun.* **2004**, 1564.

 © 2005 Wiley-VCH Verlag GmbH & Co. KGaA, Weinheim

[213] W. Wang, W. Wan, H.-H. Zhou, S. Niu, A. D. Q. Li, *J. Am. Chem. Soc.* **2003**, *125*, 5248.
[214] U. Haas, C. Thalacker, J. Adams, J. Fuhrmann, S. Riethmüller, U. Beginn, U. Ziener, M. Möller, R. Dobrawa, F. Würthner, *J. Mater. Chem.* **2003**, *13*, 767.
[215] C. Ludwig, B. Gompf, J. Petersen, R. Strohmaier, W. Eisenmenger, *Z. Phys. B* **1994**, *93*, 365.
[216] J. A. Theobald, N. S. Oxtoby, M. A. Phillips, N. R. Champness, P. H. Beton, *Nature* **2003**, *424*, 1029.
[217] S. De Feyter, A. Miura, S. Yao, Y. Chen, F. Würthner, P. Jonkheijm, A. P. H. J. Schenning, E. W. Meijer, F. C. De Schryver, *Nano Lett.* **2005**, *5*, 77.
[218] A. Miura, Z. Chen, H. Uji-i, S. De Feyter, M. Zdanowska, P. Jonkheijm, A. P. H. J. Schenning, E. W. Meijer, F. Würthner, F. C. De Schryver, *J. Am. Chem. Soc.* **2003**, *125*, 14968.
[219] S. Kummer, T. Basché, C. Bräuchle, *Chem. Phys. Lett.* **1994**, *229*, 309.
[220] R. Kettner, J. Tittel, T. Basché, C. Bräuchle, *J. Phys. Chem.* **1994**, *98*, 6671.
[221] C. Bräuchle, T. Basché, *Proc. SPIE* **1994**, *2144*, 66.
[222] C. Bräuchle, T. Basché, *J. Inform. Rec. Mater.* **1994**, *21*, 491.
[223] J. Tittel, R. Kettner, T. Basché, C. Bräuchle, H. Quante, K. Müllen, *J. Lumin.* **1995**, *26*, 1.
[224] S. Mais, J. Tittel, T. Basché, C. Bräuchle, W. Göhde, H. Fuchs, G. Müller, K. Müllen, *J. Phys. Chem. A* **1997**, *101*, 8435.
[225] W. Göhde, U. C. Fischer, H. Fuchs, J. Tittel, T. Basché, C. Bräuchle, A. Herrmann, K. Müllen, *J. Phys. Chem. A* **1998**, *102*, 9109.
[226] S. Mais, T. Basché, G. Müller, K. Müllen, C. Bräuchle, *Chem. Phys.* **1999**, *247*, 41.
[227] J. Hofkens, T. Vosch, M. Maus, F. Köhn, M. Cotlet, T. Weil, A. Herrmann, K. Müllen, F. C. De Schryver, *Chem. Phys. Lett.* **2001**, *333*, 255.
[228] R. A. L. Vallée, M. Cotlet, M. Van der Auweraer, J. Hofkens, K. Müllen, F. C. De Schryver, *J. Am. Chem. Soc.* **2004**, *126*, 2296.
[229] R. A. L. Vallée, M. Cotlet, J. Hofkens, F. C. De Schryver, K. Müllen, *Macromolecules* **2003**, *36*, 7752.
[230] F. Stracke, C. Blum, S. Becker, K. Müllen, A. J. Meixner, *Chem. Phys. Lett.* **2000**, *325*, 196.
[231] C. Blum, F. Stracke, S. Becker, K. Müllen, A. J. Meixner, *J. Phys. Chem. A* **2001**, *105*, 6983.
[232] F. Stracke, C. Blum, S. Becker, K. Müllen, A. J. Meixner, *Chem. Phys.* **2004**, *300*, 153.
[233] T. Christ, F. Petzke, P. Bordat, A. Herrmann, E. Reuther, K. Müllen, T. Basché, *J. Lumin.* **2002**, *98*, 23.
[234] H. Fidder, J. Knoester, D. Wiersma, *J. Chem. Phys.* **1991**, *95*, 7880.
[235] A. M. van Oijen, M. Ketelaars, J. Köhler, T. J. Aartsma, J. Schmidt, *Science* **1999**, *285*, 400.
[236] J. Yu, D. H. Hu, P. F. Barbara, *Science* **2000**, *289*, 1327.
[237] M. Lippitz, C. G. Hübner, T. Christ, H. Eichner, P. Bordat, A. Herrmann, K. Müllen, T. Basché, *Phys. Rev. Lett.* **2004**, *92*, 103001.
[238] E. Buhleier, W. Wehner, F. Vögtle, *Synthesis* **1978**, 155.
[239] D. A. Tomalia, H. Baker, J. Dewald, M. Hall, G. Kallos, S. Martin, J. Roeck, J. Ryder, P. Smith, *Macromolecules* **1986**, *19*, 2466.
[240] S. M. Grayson, J. M. J. Fréchet, *Chem. Rev.* **2001**, *101*, 3819.
[241] J. M. J. Fréchet, *Macromol. Symp.* **2003**, *201*, 11.
[242] J. M. J. Fréchet, *J. Polym. Sci. A* **2003**, *41*, 3713.
[243] A.-M. Caminade, J.-P. Majoral, *Acc. Chem. Res.* **2004**, *37*, 341.
[244] M. Liu, J. M. J. Fréchet, *Pharm. Sci. Technol. Today* **1999**, *2*, 393.
[245] J. D. Eichman, A. U. Bieleinska, J. F. Kurowska-Latallo, B. W. Donovan, J. R. Baker, Jr. in *Dendrimers and other Dendritic Polymers* (Eds.: J. M. J. Fréchet, D. A. Tomalia), Wiley, **2001**, p. 441.
[246] A. Adronov, J. M. J. Fréchet, *Chem. Commun.* **2000**, 170.
[247] D. Boris, M. Rubinstein, *Macromolecules* **1996**, *29*, 7251.
[248] L. Cavallo, F. Fraternali, *Chem. Eur. J.* **1998**, *4*, 927.
[249] U. M. Wiesler, T. Weil, K. Müllen, *Top. Curr. Chem.* **2001**, *212*, 1.
[250] H. Zhang, P. C. M. Grim, T. Vosch, U. M. Wiesler, A. J. Berresheim, K. Müllen, F. C. De Schryver, *Langmuir* **2000**, *16*, 9294.
[251] H. Zhang, P. C. M. Grim, P. Foubert, T. Vosch, P. Vanoppen, U. M. Wiesler, A. J. Berresheim, K. Müllen, F. C. De Schryver, *Langmuir* **2000**, *16*, 9009.
[252] S. Rosenfeldt, N. Dingenouts, D. Pötschke, M. Ballauff, A. J. Berresheim, K. Müllen, P. Lindner, *Angew. Chem.* **2004**, *116*, 111; *Angew. Chem. Int. Ed.* **2004**, *43*, 109.
[253] P. Brocorens, E. Zojer, J. Cornil, Z. Shuai, G. Leising, K. Müllen, J. L. Brédas, *Synth. Met.* **1999**, *100*, 141.
[254] E. Andreitchenko, C. J. Clark, R. E. Bauer, K. Müllen, unpublished results.
[255] R. Bauer, K. Müllen, unpublished results.
[256] S. Bernhardt, I. Oesterling, K. Müllen, unpublished results.
[257] T. Weil, E. Reuther, K. Müllen, *Angew. Chem.* **2002**, *114*, 1980; *Angew. Chem. Int. Ed.* **2002**, *41*, 1900.
[258] G. Mihov, R. E. Bauer, N. Tchebotareva, W. Knoll, M. Schmidt, A. F. Thüneman, K. Müllen, *Polym. Mater. Sci. Eng.* **2004**, *90*, 66.
[259] A. C. Grimsdale, R. Bauer, T. Weil, N. Tchebotareva, J. S. Wu, M. Watson, K. Müllen, *Synthesis* **2002**, 1229.
[260] T. Weil, U. M. Wiesler, A. Herrmann, R. Bauer, J. Hofkens, F. C. De Schryver, K. Müllen, *J. Am. Chem. Soc.* **2001**, *123*, 8101.
[261] D. Grebel-Koehler, D. J. Liu, S. De Feyter, V. Enkelmann, T. Weil, C. Engels, C. Samyn, K. Müllen, F. C. De Schryver, *Macromolecules* **2003**, *36*, 578.
[262] C. Hampel, PhD Thesis, Johannes-Gutenberg-University, Mainz, **2001**.
[263] S. Loi, H. J. Butt, C. Hampel, R. Bauer, U. M. Wiesler, K. Müllen, *Langmuir* **2002**, *18*, 2398.
[264] M. Schlupp, T. Weil, A. J. Berresheim, U. M. Wiesler, J. Bargon, K. Müllen, *Angew. Chem.* **2001**, *113*, 4124; *Angew. Chem. Int. Ed.* **2001**, *40*, 4011.
[265] A. Taubert, U. M. Wiesler, K. Müllen, *J. Mater. Chem.* **2003**, *13*, 1090.
[266] T. Vossmeyer, B. Guse, I. Besnard, R. E. Bauer, K. Müllen, A. Yasuda, *Adv. Mater.* **2002**, *14*, 238.
[267] N. Krasteva, I. Besnard, B. Guse, R. E. Bauer, K. Müllen, A. Yasuda, T. Vossmeyer, *Nano Lett.* **2002**, *2*, 551.
[268] R. E. Bauer, P. Espindola, H. John, P. Sonar, J. Heinze, K. Müllen, *Angew. Chem.* **2005**, *117*; *Angew. Chem. Int. Ed.* **2005**, *44*, in press.
[269] F. Langhauser, J. Kerth, M. Kersting, P. Kölle, D. Lilge, P. Müller, *Angew. Makromol. Chem.* **1994**, *223*, 155.
[270] M. Koch, A. Falcou, N. Nenov, M. Klapper, K. Müllen, *Macromol. Rapid Commun.* **2001**, *22*, 1455.
[271] V. Atanasov, V. Sinigersky, M. Klapper, K. Müllen, unpublished results.
[272] A. Herrmann, G. Mihov, G. W. M. Vandermeulen, H.-A. Klok, K. Müllen, *Tetrahedron* **2003**, *59*, 3925.
[273] G. Mihov, A. Herrmann, D. Prawitt, L. Brixel, J. G. Hengsler, K. Müllen, unpublished results.
[274] C. Minard-Basquin, T. Weil, A. Hohner, J. O. Rädler, K. Müllen, *J. Am. Chem. Soc.* **2003**, *125*, 5832.
[275] J. Sakamoto, K. Müllen, *Org. Lett.* **2004**, *6*, 4277.
[276] T. Emrick, J. M. J. Fréchet, *Curr. Opin. Colloid Interface Sci.* **1999**, *4*, 15.

 © 2005 Wiley-VCH Verlag GmbH & Co. KGaA, Weinheim

[277] D. J. Liu, H. Zhang, P. C. M. Grim, S. De Feyter, U. M. Wiesler, A. J. Berresheim, K. Müllen, F. C. De Schryver, *Langmuir* **2002**, *18*, 2385.
[278] A. El Ghzaoui, F. Gauffre, A.-M. Caminade, J.-P. Majoral, H. Lannibois-Drean, *Langmuir* **2004**, *20*, 9348.
[279] S. Loi, U. M. Wiesler, H. J. Butt, K. Müllen, *Macromolecules* **2001**, *34*, 3661.
[280] S. Loi, U. M. Wiesler, H. J. Butt, K. Müllen, *Chem. Commun.* **2000**, 1169.
[281] D. J. Liu, S. De Feyter, P. C. M. Grim, T. Vosch, D. Grebel-Koehler, U. M. Wiesler, A. J. Berresheim, K. Müllen, F. C. De Schryver, *Langmuir* **2002**, *18*, 8223.
[282] D. Liu, S. De Feyter, M. Cotlet, U.-M. Wiesler, T. Weil, A. Herrrmann, K. Müllen, F. C. De Schryver, *Macromolecules* **2003**, *36*, 8489.
[283] H. Zhang, P. C. M. Grim, D. Liu, T. Vosch, S. De Feyter, U.-M. Wiesler, A. J. Berresheim, K. Müllen, C. Van Haesendonck, N. Vandamme, F. C. De Schryver, *Langmuir* **2002**, *18*, 1801.
[284] G. Decher, J. D. Hong, *Macromol. Chem.* **1991**, *46*, 321.
[285] J. L. Hernandez-Lopez, R. E. Bauer, W.-S. Chang, G. Glasser, D. Grebel-Koehler, M. Klapper, M. Kreiter, J. Leclaire, J.-P. Majoral, S. Mittler, K. Müllen, K. Vasilev, T. Weil, J. Wu, T. Zhu, W. Knoll, *Mater. Sci. Eng. C* **2003**, *11*, 267.
[286] G. Mihov, M. Chelmecka, F. Gröhn, K. Müllen, unpublished results.
[287] D. Liu, S. De Feyter, M. Cotlet, A. Stefan, U.-M. Wiesler, A. Herrmann, D. Grebel-Koehler, J. Qu, K. Müllen, F. C. De Schryver, *Macromolecules* **2003**, *36*, 5918.
[288] F. Köhn, J. Hofkens, U.-M. Wiesler, M. Cotlet, M. van der-Auweraer, K. Müllen, F. C. De Schryver, *Chem. Eur. J.* **2001**, *7*, 4126.
[289] F. Köhn, J. Hofkens, R. Gronheid, M. Cotlet, K. Müllen, M. Van der Auweraer, F. C. De Schryver, *ChemPhysChem* **2002**, *3*, 1005.
[290] M. Klapper, Y.-J. Jang, K. Bieber, T. Namnich, N. Nenov, K. Müllen, *Macromol. Symp.* **2004**, *213*, 131.
[291] I. Bergenti, V. Dediu, E. Arisi, T. Mertelj, M. Murgia, A. Riminucci, G. Ruani, M. Solzi, C. Taliani, *Org. Electron.* **2004**, *5*, 309.
[292] M. Pope, C. A. Swenberg, *Electronic Processes in Organic Crystals*, Oxford University Press, Oxford, **1998**.
[293] A. Herrmann, T. Weil, V. Sinigersky, U. M. Wiesler, T. Vosch, J. Hofkens, F. C. De Schryver, K. Müllen, *Chem. Eur. J.* **2001**, *7*, 4844.
[294] J. Qu, N. G. Pschirer, D. Liu, A. Stefan, F. C. De Schryver, K. Müllen, *Chem. Eur. J.* **2004**, *10*, 528.
[295] Y.-J. Jang, V. Atanasov, M. Klapper, K. Müllen, unpublished results.
[296] J. Qu, J. Zhang, A. C. Grimsdale, K. Müllen, F. Jaiser, X. Yang, D. Neher, *Macromolecules* **2004**, *37*, 8287.
[297] A. Meisel, A. Herrmann, T. Miteva, H.-G. Nothofer, U. Scherf, K. Müllen, D. Neher, unpublished results.
[298] J. Qu, D. Liu, S. De Feyter, J. Zhang, F. C. De Schryver, K. Müllen, *J. Org. Chem.* **2003**, *68*, 9802.
[299] T. Weil, PhD Thesis, Johannes-Gutenberg-University, Mainz, **2001**.
[300] T. Gensch, J. Hofkens, A. Heirmann, K. Tsuda, W. Verheijen, T. Vosch, T. Christ, T. Basche, K. Müllen, F. C. De Schryver, *Angew. Chem.* **1999**, *111*, 3970; *Angew. Chem. Int. Ed.* **1999**, *38*, 3752.
[301] R. Gronheid, J. Hofkens, F. Kohn, T. Weil, E. Reuther, K. Müllen, F. C. De Schryver, *J. Am. Chem. Soc.* **2002**, *124*, 2418.
[302] J. Zhang, A. C. Grimsdale, K. Müllen, unpublished results.
[303] A. C. Grimsdale, T. Vosch, M. Lor, M. Cotlet, S. Habuchi, J. Hofkens, F. C. De Schryver, K. Müllen, *J. Lumin.* **2005**, *111*, 239.
[304] F. C. De Schryver, T. Vosch, M. Cotlet, M. Van der Auweraer, K. Müllen, J. Hofkens, *Acc. Chem. Res.* **2005**, *38*, 514.
[305] M. Haase, C. G. Hübner, E. Reuther, A. Herrmann, K. Müllen, T. Basché, *J. Phys. Chem. B* **2004**, *108*, 10445.
[306] Y. Karni, S. Jordens, G. De Belder, J. Hofkens, G. Schweitzer, F. C. De Schryver, A. Herrmann, K. Müllen, *J. Phys. Chem. B* **1999**, *103*, 9378.
[307] Y. Karni, S. Jordens, G. De Belder, G. Schweitzer, J. Hofkens, T. Gensch, M. Maus, F. C. De Schryver, A. Hermann, K. Müllen, *Chem. Phys. Lett.* **1999**, *310*, 73.
[308] J. Hofkens, L. Latterini, G. De Belder, T. Gensch, M. Maus, T. Vosch, Y. Karni, G. Schweitzer, F. C. De Schryver, A. Hermann, K. Müllen, *Chem. Phys. Lett.* **1999**, *304*, 1.
[309] J. Hofkens, M. Maus, T. Gensch, T. Vosch, M. Cotlet, F. Kohn, A. Herrmann, K. Müllen, F. De Schryver, *J. Am. Chem. Soc.* **2000**, *122*, 9278.
[310] J. Hofkens, W. Schroeyers, D. Loos, M. Cotlet, F. Kohn, T. Vosch, M. Maus, A. Herrmann, K. Müllen, T. Gensch, F. C. De Schryver, *Spectrochim. Acta A* **2001**, *57*, 2093.
[311] T. Gensch, J. Hofkens, F. Köhn, T. Vosch, A. Herrmann, K. Müllen, F. C. De Schryver, *Single Mol.* **2001**, *2*, 35.
[312] T. Vosch, J. Hofkens, M. Cotlet, F. Köhn, H. Fujiwara, R. Gronheid, K. Van Der Biest, T. Weil, A. Herrmann, K. Müllen, S. Mukamel, M. Van der Auweraer, F. C. De Schryver, *Angew. Chem.* **2001**, *113*, 4779; *Angew. Chem. Int. Ed.* **2001**, *40*, 4643.
[313] G. De Belder, G. Schweitzer, S. Jordens, M. Lor, S. Mitra, J. Hofkens, S. De Feyter, M. Van der Auweraer, A. Herrmann, T. Weil, K. Müllen, F. C. De Schryver, *ChemPhysChem* **2001**, *2*, 49.
[314] G. De Belder, S. Jordens, M. Lor, G. Schweitzer, R. De, T. Weil, A. Herrmann, U. M. Wiesler, K. Müllen, F. C. De Schryver, *J. Photochem. Photobiol. A* **2001**, *145*, 61.
[315] M. Maus, S. Mitra, M. Lor, J. Hofkens, T. Weil, A. Herrmann, K. Müllen, F. C. De Schryver, *J. Phys. Chem. A* **2001**, *105*, 3961.
[316] M. Lor, R. De, S. Jordens, G. De Belder, G. Schweitzer, M. Cotlet, J. Hofkens, T. Weil, A. Herrmann, K. Müllen, M. Van Der Auweraer, F. C. De Schryver, *J. Phys. Chem. A* **2002**, *106*, 2083.
[317] P. Tinnefeld, K. D. Weston, T. Vosch, M. Cotlet, T. Weil, J. Hofkens, K. Müllen, F. C. De Schryver, M. Sauer, *J. Am. Chem. Soc.* **2002**, *124*, 14310.
[318] T. Christ, F. Kulzer, T. Weil, K. Müllen, T. Basche, *Chem. Phys. Lett.* **2003**, *372*, 878.
[319] T. Vosch, M. Cotlet, J. Hofkens, K. Van Der Biest, M. Lor, K. Weston, P. Tinnefeld, M. Sauer, L. Latterini, K. Müllen, F. C. De Schryver, *J. Phys. Chem. A* **2003**, *107*, 6920.
[320] S. Jordens, G. De Belder, M. Lor, G. Schweitzer, M. Van der-Auweraer, T. Weil, A. Herrmann, U.-M. Wiesler, K. Müllen, F. C. De Schryver, *Photochem. Photobiol. Sci.* **2003**, *2*, 177.
[321] P. Tinnefeld, J. Hofkens, D.-P. Herten, S. Masuo, T. Vosch, M. Cotlet, S. Habuchi, K. Müllen, F. C. De Schryver, M. Sauer, *ChemPhysChem* **2004**, *5*, 1786.
[322] W. Schroeyers, R. Valleé, D. Patra, J. Hofkens, S. Habuchi, T. Vosch, C. M. , K. Müllen, J. Enderlein, F. C. De Schryver, *J. Am. Chem. Soc.* **2004**, *126*, 14310.
[323] S. Masuo, T. Vosch, M. Cotlet, P. Tinnefeld, S. Habuchi, T. D. M. Bell, I. Oesterling, D. Beljonne, B. Champagne, K. Müllen, M. Sauer, J. Hofkens, F. C. De Schryver, *J. Phys. Chem. B* **2004**, *108*, 16686.
[324] T. D. M. Bell, S. Habuchi, S. Masuo, I. Oesterling, K. Müllen, P. Tinnefeld, M. Sauer, M. Van der Auweraer, J. Hofkens, F. C. De Schryver, *Aust. J. Chem.* **2004**, *57*, 1169.
[325] G. S. Solomon, M. Pelton, Y. Yamamoto, *Phys. Rev. Lett.* **2001**, *86*, 3903.
[326] D. Fattal, C. Santori, J. Vuckovic, G. S. Solomon, *Phys. Status Solidi B* **2003**, *238*, 305.

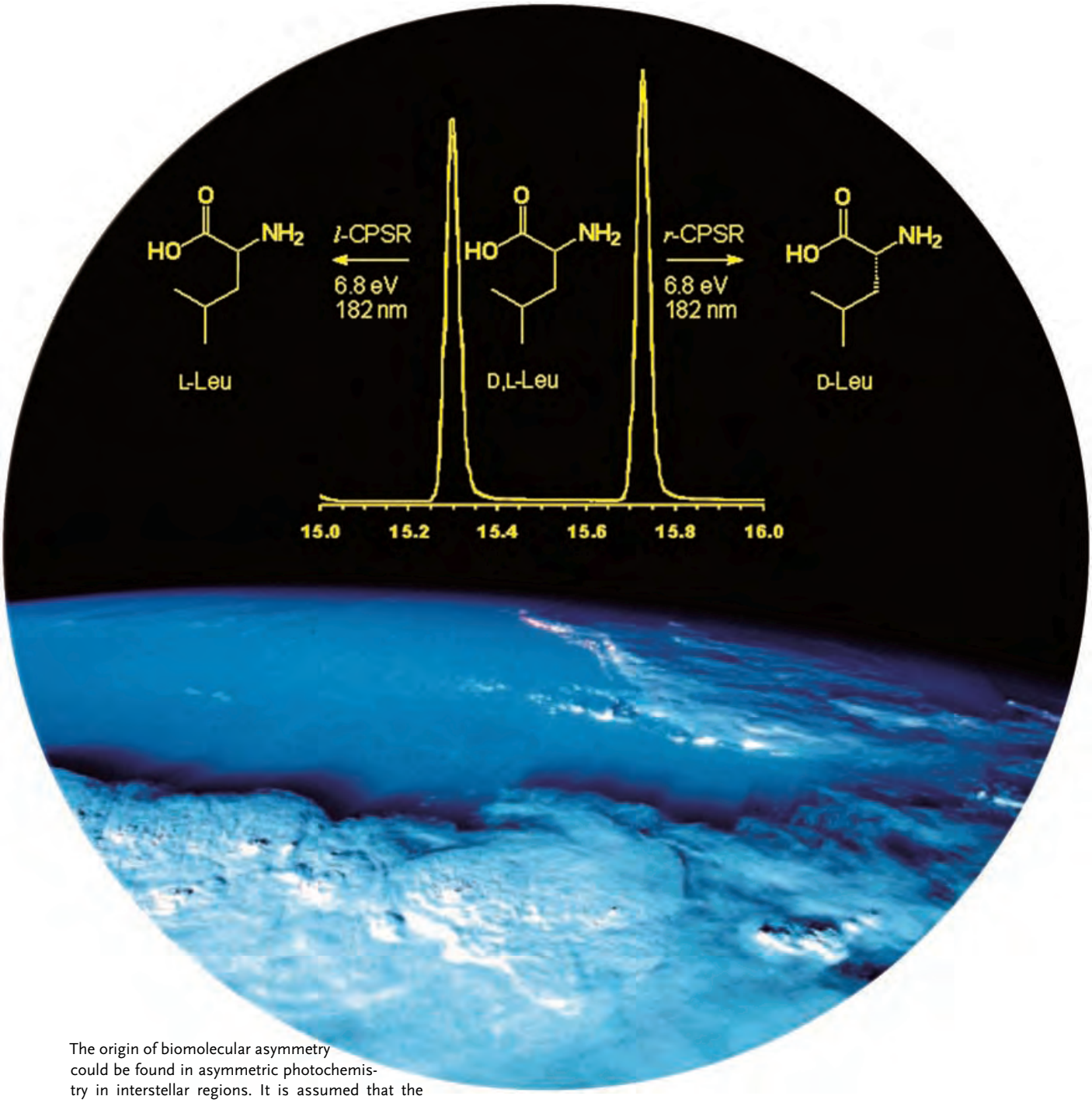
 © 2005 Wiley-VCH Verlag GmbH & Co. KGaA, Weinheim

[327] A. Beveratos, R. Brouri, T. Gacoin, J.-P. Poizat, P. Grangier, *Phys. Rev. A* **2001**, *64*, 061802.
[328] Q. A. Turchette, C. J. Hood, W. Lange, H. Mabuchi, H. J. Kimble, *Phys. Rev. Lett.* **1995**, *75*, 4710.
[329] A. Beveratos, R. Brouri, T. Gacoin, A. Villing, J.-P. Poizat, P. Grangier, *Phys. Rev. Lett.* **2002**, *89*, 187901.
[330] M. Maus, R. De, M. Lor, T. Weil, S. Mitra, U. M. Wiesler, A. Herrmann, J. Hofkens, T. Vosch, K. Müllen, F. C. De Schryver, *J. Am. Chem. Soc.* **2001**, *123*, 7668.
[331] G. Schweitzer, R. Gronheid, S. Jordens, M. Lor, G. De Belder, T. Weil, E. Reuther, K. Müllen, F. C. De Schryver, *J. Phys. Chem. A* **2003**, *107*, 3199.
[332] S. Jordens, G. De Belder, M. Lor, G. Schweitzer, M. Van der-Auweraer, T. Weil, E. Reuther, K. Müllen, F. C. De Schryver, *Photochem. Photobiol. Sci.* **2003**, *2*, 177.
[333] M. Cotlet, R. Gronheid, S. Habuchi, A. Stefan, A. Barabfina, K. Müllen, J. Hofkens, F. C. De Schryver, *J. Am. Chem. Soc.* **2003**, *125*, 13609.
[334] R. Métivier, F. Kulzer, T. Weil, K. Müllen, T. Basché, *J. Am. Chem. Soc.* **2004**, *126*, 14364.
[335] R. Métivier, T. Christ, F. Kulzer, T. Weil, K. Müllen, T. Basché, *J. Lumin.* **2004**, *110*, 217.
[336] M. Cotlet, T. Vosch, S. Habuchi, T. Weil, K. Müllen, J. Hofkens, F. C. De Schryver, *J. Am. Chem. Soc.* **2005**, *127*, in press.
[337] R. Gronheid, A. Stefan, M. Cotlet, J. Hofkens, J. Qu, K. Müllen, M. Van der Auweraer, J. W. Verhoeven, F. C. De Schryver, *Angew. Chem.* **2003**, *115*, 4341; *Angew. Chem. Int. Ed.* **2003**, *42*, 4209.
[338] M. Cotlet, S. Masuo, G. Luo, J. Hofkens, M. Van der Auweraer, J. Verhoeven, K. Müllen, X. S. Xie, F. De Schryver, *Proc. Natl. Acad. Sci. USA* **2004**, *101*, 14343.
[339] M. Lor, J. Thielemans, L. Viaene, M. Cotlet, J. Hofkens, T. Weil, C. Hampel, K. Müllen, J. W. Verhoeven, M. Van der Auweraer, F. C. De Schryver, *J. Am. Chem. Soc.* **2002**, *124*, 9918.
[340] M. Lor, S. Jordens, G. De Belder, G. Schweitzer, E. Fron, L. Viaene, M. Cotlet, T. Weil, K. Müllen, J. W. Verhoeven, M. Van der Auweraer, F. C. De Schryver, *Photochem. Photobiol. Sci.* **2003**, *2*, 501.
[341] M. Lor, L. Viaene, R. Pilot, E. Fron, S. Jordens, G. Schweitzer, T. Weil, K. Müllen, J. W. Verhoeven, M. Van der Auweraer, F. C. De Schryver, *J. Phys. Chem. B* **2004**, *108*, 10721.
[342] J. Hofkens, M. Cotlet, T. Vosch, P. Tinnefeld, K. D. Weston, C. Ego, A. Grimsdale, K. Müllen, D. Beljonne, J. L. Brédas, S. Jordens, G. Schweitzer, M. Sauer, F. De Schryver, *Proc. Natl. Acad. Sci. USA* **2003**, *100*, 13146.
[343] M. Cotlet, T. Vosch, S. Masuo, M. Sauer, K. Müllen, J. Hofken, F. De Schryver, *Proc. SPIE-Int. Soc. Opt. Eng.* **2004**, *5322*, 20.
[344] F. Jäckel, S. De Feyter, J. Hofkens, F. Köhn, F. C. De Schryver, C. Ego, A. C. Grimsdale, K. Müllen, *Chem. Phys. Lett.* **2002**, *362*, 534.
[345] J. Jacob, A. C. Grimsdale, K. Müllen, unpublished results.
[346] M. A. Izquierdo, T. D. M. Bell, S. Habuchi, E. Fron, R. Pilot, T. Vosch, S. De Feyter, J. Verhoeven, J. Hofkens, F. C. De Schryver, J. Jacob, K. Müllen, *Chem. Phys. Lett.* **2005**, *401*, 503.
[347] P. Schlichting, B. Duchscherer, G. Seisenberger, T. Basché, C. Bräuchle, K. Müllen, *Chem. Eur. J.* **1999**, *5*, 2388.
[348] C. G. Hübner, V. Ksenofontov, F. Nolde, K. Müllen, T. Basché, *J. Chem. Phys.* **2004**, *120*, 10867.
[349] G. Hinze, M. Haase, F. Nolde, K. Müllen, T. Basché, *J. Phys. Chem. A*, submitted.
[350] J. Wu, J. Qu, N. Tchebotareva, K. Müllen, *Tetrahedron* **2005**, *49*, 1565.
[351] K. Sato, M. Noguchi, A. Demachi, N. Ok, M. Endo, *Science* **1994**, *264*, 556.
[352] L. Schlapbach, A. Züttel, *Nature* **2001**, *414*, 353.
[353] R. H. Baughman, A. A. Zakhidov, W. A. de Heer, *Science* **2002**, *297*, 787.
[354] J. Wu, A. Fechtenkötter, J. Gauss, M. D. Watson, M. Kastler, C. Fechtenkötter, M. Wagner, K. Müllen, *J. Am. Chem. Soc.* **2004**, *126*, 11311.
[355] S. Setayesh, A. C. Grimsdale, T. Weil, V. Enkelmann, K. Müllen, F. Meghdadi, E. J. W. List, G. Leising, *J. Am. Chem. Soc.* **2001**, *123*, 946.
[356] J. Jacob, L. Oldridge, J. Zhang, M. Gaal, E. J. W. List, A. C. Grimsdale, K. Müllen, *Curr. Appl. Phys.* **2004**, *4*, 339.
[357] A. F. Pogantsch, F. P. Wenzl, E. W. J. List, G. Leising, A. C. Grimsdale, K. Müllen, *Adv. Mater.* **2002**, *14*, 1061.
[358] J. M. Lupton, P. Schouwink, P. E. Keivanidis, A. C. Grimsdale, K. Müllen, *Adv. Funct. Mater.* **2003**, *13*, 154.
[359] A. Pogantsch, F. P. Wenzl, U. Scherf, A. C. Grimsdale, K. Müllen, E. J. W. List, *J. Chem. Phys.* **2003**, *119*, 6904.
[360] A. Pogantsch, C. Gadermaier, G. Cerullo, G. Lanzani, U. Scherf, A. C. Grimsdale, K. Müllen, E. J. W. List, *Synth. Met.* **2003**, *139*, 847.
[361] D. Liu, A. C. Grimsdale, K. Müllen, S. De Feyter, F. C. De Schryver, unpublished results.
[362] C. D. Simpson, G. Mattersteig, K. Martin, L. Gherghel, R. E. Bauer, H. J. Räder, K. Müllen, *J. Am. Chem. Soc.* **2004**, *126*, 3139.
[363] S. Ijima, *Nature* **1991**, *354*, 56.
[364] C. N. R. Rao, B. C. Satishkumar, A. Givindaraj, M. Nath, *ChemPhysChem* **2001**, *2*, 78.
[365] H. Dai, E. W. Wong, C. M. Lieber, *Science* **1996**, *272*, 523.
[366] S. Subramoney, *Adv. Mater.* **1998**, *10*, 1157.
[367] C. Journet, P. Bernier, *Appl. Phys. A* **1998**, *67*, 1.
[368] M. Fan, M. G. Chapline, N. R. Franklin, T. W. Tombler, A. M. Cassell, H. Dai, *Science* **1999**, *283*, 512.
[369] P. Chen, X. Wu, J. Lin, K. L. Tan, *Science* **1999**, *285*, 91.
[370] C. Liu, Y. Y. Fan, M. Liu, T. Cong, H. M. Cheng, M. S. Dresselhaus, *Science* **1999**, *286*, 1127.
[371] J. Kong, N. R. Franklin, C. Zhou, M. R. Chapline, S. Peng, K. Cho, H. Dai, *Science* **2000**, *287*, 622.
[372] H. Dai, *Surf. Sci.* **2002**, *500*, 218.
[373] A. Thess, R. Lee, P. Nikolaev, H. J. Dai, P. Petit, J. Robert, C. H. Xu, Y. H. Lee, S. G. Kim, A. G. Rinzler, D. T. Colbert, G. E. Scuseria, D. Tomanek, J. E. Fischer, R. E. Smalley, *Science* **1996**, *273*, 483.
[374] L. Gherghel, C. Kübel, G. Lieser, H.-J. Räder, K. Müllen, *J. Am. Chem. Soc.* **2002**, *124*, 13130.
[375] A. Oberlin, *Carbon* **1984**, *22*, 521.
[376] P. I. Dosa, C. Erben, V. S. Iyer, K. P. C. Vollhardt, I. M. Wasser, *J. Am. Chem. Soc.* **1999**, *121*, 10430.
[377] M. Laskoski, W. Steffen, J. G. M. Morton, M. D. Smith, U. H. F. Bunz, *J. Am. Chem. Soc.* **2002**, *124*, 13814.
[378] C. N. R. Rao, A. Govindaraj, *Acc. Chem. Res.* **2002**, *35*, 998.
[379] V. S. Iyer, K. P. C. Vollhardt, R. Wilhelm, *Angew. Chem.* **2003**, *115*, 4515; *Angew. Chem. Int. Ed.* **2003**, *42*, 4379.
[380] J. Wu, B. El Hamaoui, J. Li, L. Zhi, U. Kolb, K. Müllen, *Small* **2005**, *1*, 210.
[381] L. Zhi, J. Wu, J. Li, U. Kolb, K. Müllen, *Angew. Chem.* **2005**, *117*; *Angew. Chem. Int. Ed.* **2005**, *44*, in press.
[382] E. Clar, *The Aromatic Sextett*, Wiley, New York, **1972**.
[383] W. Göhde, Jr., U. C. Fischer, H. Fuchs, J. Tittel, T. Basché, C. Bräuchle, A. Herrmann, K. Müllen, *J. Phys. Chem. A* **1998**, *102*, 9106.

 © 2005 Wiley-VCH Verlag GmbH & Co. KGaA, Weinheim

Communications

DOI: 10.1002/anie.200501311



The origin of biomolecular asymmetry could be found in asymmetric photochemistry in interstellar regions. It is assumed that the amino acids were formed in these regions. The irradiation of solid D,L-leucine probes with right circularly polarized synchrotron radiation at 182 nm produced an enantiomeric excess of the D enantiomer of 2.6%. For more details see the Communication by Meierhenrich, Nahon et al. on the following pages. The image was taken in June 1998 on the space shuttle Discovery.

InterScience
© 2005 Wiley-VCH Verlag GmbH & Co. KGaA, Weinheim

Homochirality

DOI: 10.1002/anie.200501311

Asymmetric Vacuum UV photolysis of the Amino Acid Leucine in the Solid State**

Uwe J. Meierhenrich, Laurent Nahon,* Christian Alcaraz, Jan Hendrik Bredehöft, Søren V. Hoffmann, Bernard Barbier, and André Brack*

The origin of biomolecular asymmetry, the fact that biological molecules such as amino acids show the same chirality, still requires an explanation and might be traced back to interstellar low-temperature processes.[1–6] Under interstellar conditions, chiral solid-state amino acids might have been subjected to circularly polarized vacuum ultraviolet (VUV) electromagnetic radiation before and during their space journey to Earth. However, to date, experimental data on chiroptical properties of amino acids were limited to aqueous solutions, which is not relevant in terms of astrophysical conditions.

Amino acids, the chiral building blocks of proteins, probably played a key role in both the appearance of life on Earth and the emergence of biomolecular asymmetry. Some of these amino acids were discovered in carbonaceous meteorites,[1,2] with enantiomeric excesses (*ee* values) and isotopic composition[3] indicating an extraterrestrial origin of biomolecular asymmetry. Amino acids have also been synthesized in the laboratory by simulating interstellar/circumstellar ice photochemistry.[4,5] Proteins are exclusively based on L-amino acid monomer units. The use of homochiral monomers is generally considered as advantageous for the prebiotic construction of their structure.[7–9] Interestingly, even small *ee* values can be amplified by autocatalytic reactions leading to near homochirality.[10,11]

Numerous asymmetric mechanisms have been suggested and tested experimentally, including the influence of circularly polarized light (CPL) as an external chiral force.[12–14] Astronomical sources of CPL,[15,16] which might produce enantiomeric selection in interstellar organic molecules, were observed in the IR range.[17] Electromagnetic radiation from magnetic white dwarfs and white-dwarf binaries (Polars) can be circularly polarized up to 12% and 50%, respectively.[18] CPL might also be produced by dust grains aligned by a magnetic field in the reflection nebulae in star-formation regions.

Since the pioneering work of Kuhn et al. who studied the enantioselective photodecomposition of ethyl-α-bromopropionate and *N*,*N*-dimethyl-α-azidopropionamide via electronically excited states,[19,20] asymmetric photolysis experiments on several chiral compounds have been reported.[21,22] In 1977, the amino acids alanine[23] and leucine[24] were decomposed enantioselectively in aqueous solution by excitation of the (π^*,n)-transition at 213 nm, and gave *ee* values of 2.5%.[24] The corresponding photolysis mechanism was recently examined.[25,26] To date, no higher *ee* value has been generated in amino acids.

So far, experiments using CPL have been performed in solution, which is less relevant with respect to astrophysical conditions. Because of the solvent absorption below 200 nm, such studies have been restricted to excitations of the (π^*,n)-electronic transition (213 nm on leucine), so that only part of the UV/VUV absorption spectrum was accessible. This situation is unfortunate since in general amino acids exhibit stronger absorption cross-sections for the (π^*,π_1)-electronic transitions, which are therefore interesting to investigate. It is noteworthy that Inoue et al.[27] irradiated pentane solutions of racemic (*E*)-cyclooctene with left circular polarized synchrotron radiation (*l*-CPSR) or right-CPSR (*r*-CPSR) at 190 nm and observed an enantioselective photoisomerization effect. Herein we report on chiroptical properties and asymmetric photolysis of D,L-leucine that was exposed, for the first time in the solid state, to VUV *l*-CPSR and *r*-CPSR at 170 nm and 182 nm, inducing asymmetric photochemistry via (π^*,π_1)-electronic transitions.

[*] Priv.-Doz. Dr. U. J. Meierhenrich
Laboratoire A.S.I. et Laboratoire de Chimie Bioorganique
UMR 6001 CNRS–UNSA
Université de Nice–Sophia Antipolis
Faculté des Sciences
Parc Valrose, 06108 Nice (France)
Fax: (+33) 4-9207-6125
E-mail: uwe.meierhenrich@unice.fr

Dr. L. Nahon,[+] Dr. C. Alcaraz
Laboratoire pour l'Utilisation du Rayonnement Electromagnétique
LURE
Université Paris-Sud
Bâtiment 209D, B.P. 34, 91898 Orsay (France)
Fax: (+33) 1-6446-4148
E-mail: laurent.nahon@synchrotron-soleil.fr

Dr. L. Nahon[+]
CEA/DRECAM/SPAM and
LFP/CNRS URA 2453
CE de Saclay, 91191 Gif sur Yvette (France)

Priv.-Doz. Dr. U. J. Meierhenrich, J. H. Bredehöft
Department of Physical Chemistry
University of Bremen
Leobener Strasse, 28359 Bremen (Germany)

Dr. S. V. Hoffmann
Institute for Storage Ring Facilities
University of Aarhus
Ny Munkegade, 8000 Aarhus C (Denmark)

Dr. B. Barbier, Dr. A. Brack
Centre de Biophysique Moléculaire CNRS
Rue Charles-Sadron, 45071 Orléans (France)

[+] Present address:
SOLEIL, l'Orme des Merisiers
St Aubin, BP48, 91192 Gif sur Yvette Cedex (France)

[**] This work was funded by the EU, CNES, FNAD, Région Centre, and the Département du Cher (France). We acknowledge the support of Mai Julie Nguyen, Romain Jacquet, Bertrand Pilette, and the synchrotron-teams of ASTRID and LURE. We thank Wolfram H.-P. Thiemann, Henri B. Kagan, and Odile Dutuit. U.J.M. is grateful to Le Studium for a C.B.M. postdoctoral position, to the DFG, Bonn (Germany) for funding his research group at the University of Bremen, and for a CNRS position at the University of Nice.

Supporting information for this article is available on the WWW under http://www.angewandte.org or from the author.

 © 2005 Wiley-VCH Verlag GmbH & Co. KGaA, Weinheim

The amino acid leucine was chosen for the study of solid-state asymmetric photodecomposition experiments for the following reasons: 1) The photochemistry of the (π^*,n)-electronic transition is well-known. 2) Leucine shows the largest anisotropy factor g ($g = \Delta\varepsilon/\varepsilon$) among proteinaceous amino acids.[24] It has been established that the gain in *ee* value achievable during photolysis of a racemate is a function of the magnitude of g and of the extent of reaction.[22] 3) Enantiomeric separation techniques provide a high separation factor α and a high resolution R_S. 4) Leucine has a slow racemization rate compared to other amino acids.[28]

To establish the most suitable conditions for the enantioselective photodecomposition of solid-state leucine, electronic transitions and circular dichroism (CD) features were studied in the VUV photon energy range. VUV absorption spectra of solid films of leucine (1 μm film thickness deposited on an MgF_2 window) were recorded between 110 and 220 nm by synchrotron radiation (SR) absorption spectroscopy on beamline SA-61 of the Super-ACO storage ring of LURE in Orsay (France). A weak (π^*,n)-transition of leucine was detected at 211 nm, and a strong (π^*,π_1)-transition at 183 nm, about five-times more intense. Additional electronic transitions were determined below 150 nm.

A VUV CD spectrum of L-leucine in solution in 1,1,1,3,3,3-hexafluoroisopropanol has been reported.[29] It shows a positive (π^*,n)-electronic transition at 194 nm and a negative (π^*,π_1)-electronic transition at 168 nm. As part of our study VUV-CD spectra of solid-state D-leucine films, with estimated thickness ranging from 0.2 to 1 μm deposited on MgF_2 windows, were run below 200 nm at the Institute for Storage Ring Facilities, University of Aarhus (Denmark) using the synchrotron beamline UV1-ASTRID. The obtained CD spectrum is given in Figure 1 (top). It shows a negative band at 207 nm and a positive band at 191 nm, noticeably different from the spectrum recorded in solution. Comparing the CD data with the absorption spectrum, we conclude that the (π^*,π_1)-electronic transition splits into three CD bands, a negative band above 200 nm which overlaps with the negative (π^*,n)-band, and two positive bands, at 191 nm and at 175 nm.

The CD band splitting is assumed to arise from an excitation coupling based on coupling processes between leucine molecules in the solid state. We deduce from the CD data that the (π^*,n)-electronic transition of D-leucine is induced preferentially by right-handed circularly polarized light (*r*-CPL) and the two positive (π^*,π_1)-electronic transitions of D-leucine are preferentially excited by *l*-CPL. Since VUV electronic excitations lead to leucine photolysis, mainly by decarboxylation, irradiation of D,L-leucine with *r*-CPL at the (π^*,n)-electronic transition should theoretically produce an enantiomeric excess of L-leucine. Conversely, irradiation at the positive (π^*,π_1)-electronic transitions with *r*-CPL should lead to an enantiomeric excess of D-leucine by photodecomposition of the L-leucine. Opposite enantioenrichments are expected when using the opposite photon helicity *l*-CPL.

To achieve VUV asymmetric photodecomposition of solid state D,L-leucine, intense and quasi-perfect CPSR (Figure 2) as emitted by the OPHELIE Undulator[30] of the VUV SU5 beamline[31] was used to irradiate the samples. The photon energy was first set at 6.8 eV (182 nm; see Figure 1 bottom) and then at 7.3 eV (170 nm), so that information about the energy-dependence of the process could be gained. The first energy closely matches the middle of the two CD positive bands of the (π^*,π_1)-electronic transitions, while the second

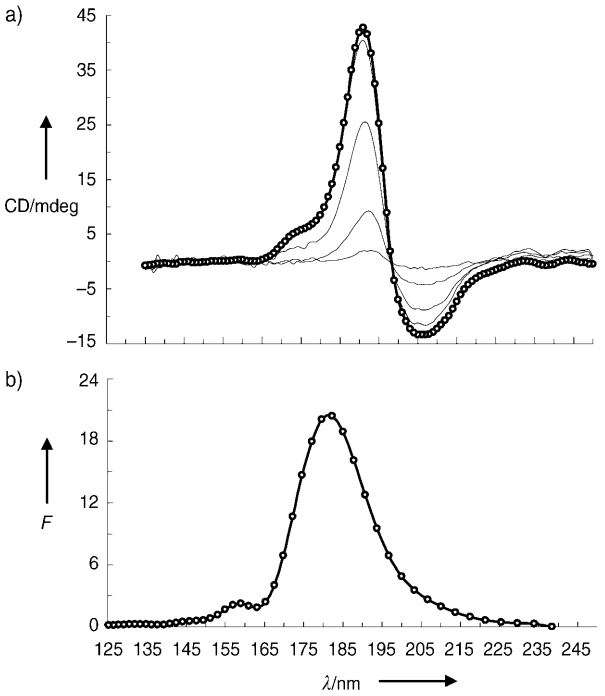


Figure 1. Spectral dependence of leucine CD and SR-irradiation. a) VUV CD spectrum of solid-state D-leucine recorded at the Synchrotron Facility ISA, University of Aarhus (Denmark). High-resolution measurement of D-leucine, film thickness 1 μm (bold line); low-resolution measurements of D-leucine, film thickness 0.2, 0.4, 0.6, and 0.8 μm (thin line); leucine films were immobilized on MgF_2. b) Spectral flux (F) of the OPHELIE undulator of the SU5 beamline at LURE (Orsay, France) in arbitrary units used for irradiation with CPSR centered at 6.8 eV (182 nm).

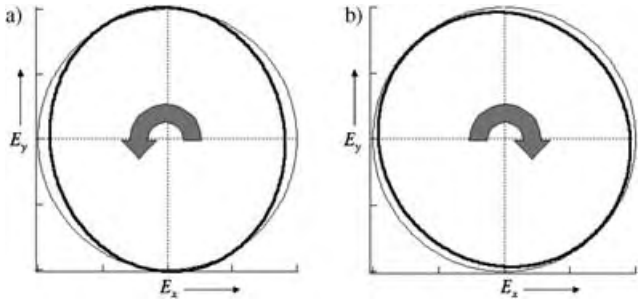
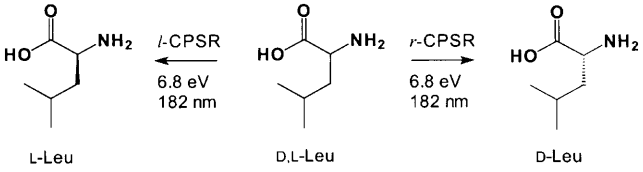


Figure 2. Measured polarization ellipses (thick lines) at the sample location. They were measured for a SR centered at 6.8 eV (182 nm), for a) *l*-CPSR and b) *r*-CPSR, as produced by the OPHELIE undulator of the SU5 beamline. Absolute circular polarization rates are of 91% for *r*-CPSR and 94% for *l*-CPSR. Thin lines are guide to the eye illustrating the perfect CP light case and the dashed lines indicate the normal ellipse axes corresponding to the two components (E_x, E_y) of the electric field associated with the light. The curved arrows indicate the helicity of the photons as seen by an observer facing the beam coming out of the plane of the Figure.

 © 2005 Wiley-VCH Verlag GmbH & Co. KGaA, Weinheim

corresponds to the almost absent CD contribution on the short-wavelength side. Solid films of D,L-leucine were irradiated with *r*-CPSR and with *l*-CPSR in separate experiments. After photodecomposition, the remaining leucine was extracted and analyzed by enantioselective CG-MS. As summarized in Table 1, five samples were used: sample 1 was not irradiated and was used as a normalization sample, while the other samples were irradiated with different photon energies and CPL helicities. Sample numbers 1, 3, and 4 were analyzed six times in parallel, sample number 2 was analyzed three times, and sample number 5 was analyzed four times (see Table S1 in the Supporting Information). Overlaid chromatograms of the irradiated and separated leucine enantiomers are presented in Figure 3. No decomposition products of leucine could be identified with the GC-MS technique used, the expected volatile decomposition products, CO_2 and primary amines, would be evacuated in the high-vacuum synchrotron beamline and avoid detection.

Table 1: Enantiomeric excesses (averaged over three to six samples for the same irradiation conditions) obtained after irradiation of D,L-leucine with *l*-CPSR and *r*-CPSR.[a]



Sample	E_{photon} [eV]/λ [nm]	Irradiation	*ee* (D-leucine) [%]	CI_{95}[b]
1[c]	–	–	0.00	0.38
2	6.8/182	*l*-CPSR	−0.88	0.28
3	6.8/182	*r*-CPSR	2.60	0.16
4	7.3/170	*r*-CPSR	0.75	0.36
5	7.3/170	*l*-CPSR	0.53	0.48

[a] Complete set of data in the Supporting Information. [b] CI_{95} = confidence interval at 95% determined by multiple analyses of each sample. [c] Not irradiated, control sample.

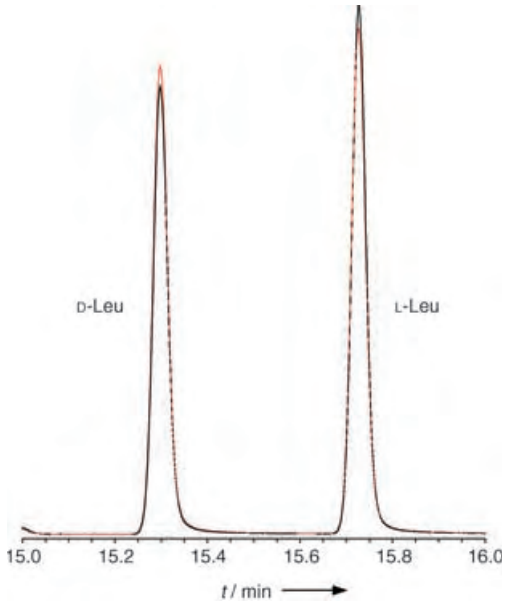


Figure 3. Overlaid gas chromatograms of irradiated D,L-leucine depicting the separated enantiomers after irradiation at 6.8 eV (182 nm) with *l*-CPSR (black line) and *r*-CPSR (red line) on the SU5 beamline at the Synchrotron Facility LURE, Orsay (France). The first eluting enantiomer is D-leucine. D,L-Leucine irradiated with *r*-CPSR, shows a marked enantioselective photodecomposition of L-leucine, the *ee* value for D-leucine being 2.60%. Chromatograms were measured in the single-ion monitoring mode at *m/z* 158 amu. For chromatographic overlay, the area of the sample irradiated with *r*-CPSR was multiplied by a factor of 1.61. *t* = retention time.

The highest gain in *ee* value was found to be +2.6% in D-leucine when irradiating with *r*-CPSR at 6.8 eV (182 nm), that is, near the two positive (π^*,π_1)-electronic transitions. Irradiation with *l*-CPSR at 6.8 eV resulted in an *ee* value of +0.88% in L-leucine. Samples were irradiated for 3 h each with a decreasing photon flux, owing to the decrease of the electron current in the Super-ACO storage ring. The photon flux was measured during the irradiation by monitoring the photoemission current from a highly transparent gold mesh inserted in the SR beam just upstream of the samples. From this measurement, we can determine that the total dose of irradiation (flux × duration) received by sample 2 is about 25% lower than for sample 3. This result explains parts of the observed difference between the absolute *ee* value for the two light helicities. The remaining part could be explained by a likely difference in the spatial transverse flux density and pointing between *r*-CPSR and *l*-CPSR owing to non-perfect symmetry of the OPHELIE undulator.[32] The result of these effects being that irradiation would not have the same efficiency for the different helicities. Beside this, tiny inhomogeneities of the solid-state leucine samples 2 and 3 resulting in a nonsymmetrical alignment within the synchrotron beamline may account for some of the differences.

The results demonstrate that a significant enantiomeric enrichment can be induced in solid-state D,L-amino acids by irradiation with energies closely matching the positive (π^*,π_1)-electronic transitions. Irradiation of solid-state D,L-leucine with CPSR at a higher energy, 7.3 eV (170 nm), did induce a minor *ee* value, which in addition does not change sign by switching photon helicity. This observation is coherent with the fact that the CD signal of leucine (see Figure 1) at 170 nm is vanishing.

In conclusion, enantiomeric excesses were induced in samples of leucine by VUV asymmetric photochemical reactions, such as enantioselective photolysis, under realistic interstellar/circumstellar conditions. These experimental data support the assumption that tiny interstellar/circumstellar ice grains can experience asymmetric reactions when irradiated by circularly polarized ultraviolet light. Various families of amino acids have been identified in carbonaceous meteorites,[1,2,33] with *ee* values and isotopic composition[3] indicating an extra-terrestrial origin of biomolecular asymmetry. A systematic study of asymmetric VUV photolysis in the solid state for different amino acids would help us to better understand the processes leading to their asymmetric formation and their role in prebiotic chemistry. Based on the present data, it is possible to conclude that asymmetric interstellar/circumstellar solid-state photochemical processes

 © 2005 Wiley-VCH Verlag GmbH & Co. KGaA, Weinheim

in the VUV might have triggered the appearance of biomolecular asymmetry and thus could have assisted the start of life.

Experimental Section

Information on VUV circularly polarized synchrotron radiation and enantioselective GC-MS analyses are given in the Supporting Information. For the preparation of the solid-state leucine sample D,L-leucine (space group $P\bar{1}$, triclinic; 600 μg) were lyophilized and suspended in *m*-xylene (1,3-dimethylbenzene; 200 μL). A 2.5-μL sample of the suspension was introduced into a 1×5 mm cavity carved out at the surface of a VUV-transparent MgF_2 window. The samples were dried in a desiccator filled with P_2O_5 at ambient pressure. By this technique, a homogeneous film of leucine was deposited on the surface of the MgF_2 window.

VUV CPSR was produced by the recently developed electromagnetic polarizing undulator OPHELIE[30] installed on the Super-ACO storage ring of LURE in Orsay (France), feeding the VUV high resolution variable polarization SU5 beamline,[31] whose monochromator was set to deliver only the zeroth order diffraction of its gratings. Under these conditions, the spectrum of the synchrotron radiation (SR) impinging on the sample, as depicted in Figure 1 (bottom), corresponds to a peak centered on the tunable central photon energy ε_c with a 11% relative bandwidth ($\Delta\lambda/\lambda_c$) proving an integrated flux in the range of 10^{14} photon per second as derived from a VUV photodiode signal. Absolute circular polarization rates, measured at the sample location with a dedicated VUV polarimeter, vary from 90 to 100% over the 6 to 28 eV range.[32] For both photon energies, 6.8 eV and 7.3 eV, corresponding to two different undulator settings, they reach 91% for *r*-CPSR and 94% for *l*-CPSR. The corresponding polarization ellipses are shown in Figure 2.

After CPSR irradiation the remaining leucine was extracted from the MgF_2 window cavity with 0.1M hydrochloric acid (3×20 μL). The extract was transferred into a reaction vial (1 mL volume) and an ethanol–pyridine mixture (3:1, v/v; 30 μL) was added. To this solution, ethyl chloroformate (6 μL) was added, the vial was capped tightly, and shaken vigorously for 10 s to form *N*-ethoxycarbonyl leucine ethyl esters (leucine-ECEE).[34,35] Chloroform (18 μL) was added and the vial was shaken again for extraction of the leucine-ECEE into the (lower) organic layer. Finally, 1 μL of the organic phase was withdrawn by a microliter syringe and injected directly into the gas chromatographic Agilent 6890/5973 GC-MSD system equipped with a 25 m chiral stationary Chirasil-L-Val phase.

Received: April 14, 2005
Revised: May 27, 2005
Published online: July 20, 2005

Keywords: amino acids · astrochemistry · homochirality · photochemistry · synchrotron radiation

[1] J. R. Cronin, S. Pizzarello, *Science* **1997**, *275*, 951 – 955.
[2] M. H. Engel, S. A. Macko, *Nature* **1997**, *389*, 265 – 268.
[3] S. Pizzarello, M. Zolensky, K. A. Turk, *Geochim. Cosmochim. Acta* **2003**, *67*, 1589 – 1595.
[4] G. M. Muñoz Caro, U. J. Meierhenrich, W. A. Schutte, B. Barbier, A. Arcones Segovia, H. Rosenbauer, W. H.-P. Thiemann, A. Brack, J. M. Greenberg, *Nature* **2002**, *416*, 403 – 406.
[5] M. P. Bernstein, J. P. Dworkin, S. A. Sandford, G. W. Cooper, L. J. Allamandola, *Nature* **2002**, *416*, 401 – 403.
[6] M. Crisma, A. Moretto, F. Formaggio, B. Kaptein, Q. B. Broxterman, C. Toniolo, *Angew. Chem.* **2004**, *116*, 6863 – 6867; *Angew. Chem. Int. Ed.* **2004**, *43*, 6695 – 6699.
[7] M. Idelson, E. R. Blout, *J. Am. Chem. Soc.* **1958**, *80*, 2387 – 2393.
[8] V. I. Goldanskii, V. V. Kuz'min, *Z. Phys. Chem.* **1988**, *269*, 216 – 274.
[9] G. Spach, A. Brack, *Structure, dynamics, interactions and evolution of biological macromolecules* (Ed.: C. Hélène), D. Reidel Publishing, Dordrecht, **1983**, pp. 383 – 394.
[10] T. Shibata, J. Yamamoto, N. Matsumoto, S. Yonekubo, S. Osanai, K. Soai, *J. Am. Chem. Soc.* **1998**, *120*, 12157 – 12158.
[11] C. Girard, H. B. Kagan, *Angew. Chem.* **1998**, *110*, 3088 – 3127; *Angew. Chem. Int. Ed.* **1998**, *37*, 2922 – 2959.
[12] O. Burchardt, *Angew. Chem.* **1974**, *86*, 222 – 228; *Angew. Chem. Int. Ed. Engl.* **1974**, *13*, 179 – 185.
[13] A. G. Griesbeck, U. J. Meierhenrich, *Angew. Chem.* **2002**, *114*, 3279 – 3286; *Angew. Chem. Int. Ed.* **2002**, *41*, 3147 – 3154.
[14] U. J. Meierhenrich, W. H.-P. Thiemann, *Origins Life Evol. Biosphere* **2004**, *34*, 111 – 121.
[15] S. F. Mason, *Nature* **1997**, *389*, 804.
[16] C. Cerf, A. Jorissen, *Space Sci. Rev.* **2000**, *92*, 603 – 612.
[17] J. Bailey, A. Chrysostomou, J. H. Hough, T. M. Gledhill, A. McCall, S. Clark, F. Ménard, M. Tamura, *Science* **1998**, *281*, 672 – 674.
[18] J. Bailey, *Origins Life Evol. Biosphere* **2001**, *31*, 167 – 183.
[19] W. Kuhn, E. Braun, *Naturwissenschaften* **1929**, *17*, 227 – 228.
[20] W. Kuhn, E. Knopf, *Naturwissenschaften* **1930**, *18*, 183.
[21] A. Moradpour, J. F. Nicoud, G. Balavoine, H. B. Kagan, G. Tsoucaris, *J. Am. Chem. Soc.* **1971**, *93*, 2353 – 2354.
[22] G. Balavoine, A. Moradpour, H. B. Kagan, *J. Am. Chem. Soc.* **1974**, *96*, 5152 – 5158.
[23] B. Norden, *Nature* **1977**, *266*, 567 – 568.
[24] J. J. Flores, W. A. Bonner, G. A. Massey, *J. Am. Chem. Soc.* **1977**, *99*, 3622 – 3625.
[25] H. Nishino, A. Kosaka, G. A. Hembury, H. Shitomi, H. Onuki, Y. Inoue, *Org. Lett.* **2001**, *3*, 921 – 924.
[26] H. Nishino, A. Kosaka, G. A. Hembury, F. Aoki, K. Miyauchi, H. Shitomi, H. Onuki, Y. Inoue, *J. Am. Chem. Soc.* **2002**, *124*, 11618 – 11627.
[27] Y. Inoue, H. Tsuneishi, T. Hakushi, K. Yagi, K. Awazu, H. Onuki, *Chem. Commun.* **1996**, *23*, 2627 – 2628.
[28] H. N. Poinar, M. Hoss, J. L. Bada, S. Paabo, *Science* **1996**, *272*, 864 – 866.
[29] P. A. Snyder, P. M. Vipond, W. C. Johnson, *Biopolymers* **1973**, *12*, 975 – 992.
[30] L. Nahon, M. Corlier, P. Peaupardin, F. Marteau, O. Marcouillé, P. Brunelle, C. Alcaraz, P. Thiry, *Nucl. Instrum. Methods Phys. Res. Sect. A* **1997**, *396*, 237 – 250.
[31] L. Nahon, C. Alcaraz, J.-L. Marlats, B. Lagarde, F. Polack, R. Thissen, D. Lepère, K. Ito, *Rev. Sci. Instrum.* **2001**, *72*, 1320 – 1329.
[32] L. Nahon, C. Alcaraz, *Appl. Opt.* **2004**, *43*, 1024 – 1037.
[33] U. J. Meierhenrich, G. M. Muñoz Caro, J. H. Bredehöft, E. K. Jessberger, W. H.-P. Thiemann, *Proc. Natl. Acad. Sci. USA* **2004**, *101*, 9182 – 9186.
[34] I. Abe, N. Fujimoto, T. Nishiyama, K. Terada, T. Nakahara, *J. Chromatogr. A* **1996**, *722*, 221 – 227.
[35] Z.-H. Huang, J. Wang, D. A. Gage, J. T. Watson, C. C. Sweeley, *J. Chromatogr. A* **1993**, *635*, 271 – 281.

 © 2005 Wiley-VCH Verlag GmbH & Co. KGaA, Weinheim

Femtosecond Spectroscopy

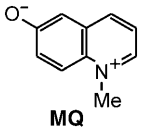
DOI: 10.1002/anie.200501397

Ultrafast Solvation of *N*-Methyl-6-quinolone Probes Local IR Spectrum**

*J. Luis Pérez Lustres, Sergey A. Kovalenko, Manuel Mosquera, Tamara Senyushkina, Wolfgang Flasche, and Nikolaus P. Ernsting**

Solvation is a matter of central interest in chemistry. It influences the energetics of chemical reactivity because the reactants, transition state, and products may be stabilized differently by the solvent, and it creates frictional forces for the dynamics. Here we consider charge-transfer reactions in polar media. Usually the polarity of the environment is in equilibrium with the charge distribution along the reaction path. But ultrafast reactions may even "leave the solvent behind", the polarity can no longer stay adjusted, and the energy barrier is crossed in a nonequilibrated environment.[1] The time behavior of adjustment, or "polar solvation dynamics",[2–10] is a key to understanding many reactions in the condensed phase. In liquids at room temperature, individual solvent molecules respond to charge redistribution on a timescale of 10–100 femtoseconds (fs). The collective answer comes slower, and restructuring of solvent shells may take picoseconds or longer.

Measurements of polar solvation dynamics aim to observe the process directly, independent of reactive motion, and for this purpose one needs a suitable molecular probe. Usually these are solvatochromic dye molecules whose color depends strongly on the surrounding because the ground and excited electronic states interact differently with it. Using the novel probe *N*-methyl-6-quinolone (**MQ**), we show that its solvation in water and methanol is reproduced quantitatively, both in magnitude and time behavior, by the bulk dielectric dispersion $\varepsilon(\nu)$ of the liquid, the connection being continuum theory.[11–16] The surprising ability of a simple model to describe the dynamics was already noted.[8,11,13] It is now substantiated with the detection of solvent oscillations which modulate the emission frequency.



MQ

The match of observed, time-resolved solvation with prediction from continuum theory is at once puzzling and a chance. For one, the solvation process is microscopic by its very nature, as shown by numerous molecular dynamics simulations. The solute disturbs the liquid structure, and liquid dynamics around the probe is therefore expected to deviate from the bulk. It is far from trivial to relate the solvation response of a chromophore to solvent properties such as $\varepsilon(\nu)$, and this problem has been addressed by statistical theories.[17,18] Deviations from continuum theory are termed "molecularity of solvation".[14] The new dye does not exhibit molecularity towards collective solvent motion at the accuracy of present experiments, and this could lead to specific applications in characterizing water dynamics in restricted or biological environments on molecular dimensions. For this purpose **MQ** has several advantages over other probes. It is not charged, hence does not polarize the surrounding more than is needed for measurement. The solvent polarity couples mainly through dipole moment change, allowing straightforward evaluation of experiments. Most importantly, there is no interfering solute motion at frequencies relevant for aqueous solvation. Finally, the molecule is small enough to replace natural bases in nucleic acids or tryptophan in proteins. If continuum theory holds in such environments, femtosecond solvation measurements will provide the local IR spectrum.

Water and methanol are used here as benchmark solvents. Water deserves attention owing to its unique features. It can stabilize polar reactants within 100 fs and thus is the "fastest" solvent known. The interest in water extends from the properties of the pure solvent to its behaviour in complex environments[19–21] and especially to biopolymers where "biological water"[21] is expected to be involved in important primary reaction steps. Methanol is interesting because of its amphiphilic character. For both solvents, $\varepsilon(\nu)$ is known to high accuracy, and conclusions about the ability of continuum theory to describe **MQ** solvation can be drawn.

Femtosecond solvation experiments are explained in Figure 1. The molecule is suddenly promoted into the S_1 state by a short laser pulse. The ensuing relaxation of the excited state in terms of the free energy gap $\Delta E(t) = E_1(t) - E_0(t)$ is central to optical spectroscopy in the condensed phase. How $\Delta E(t)$ is accessed by time-resolved interaction of femtosecond optical pulses depends on the nonlinear optical signal that is detected. The fluorescence band provides probably the most direct view of relaxation in the excited state. Its time-resolved dynamic Stokes shift is a linear image of the solvation process, provided that intramolecular reorganization is either absent because the molecular structures in S_1 and S_0 are the same, or else avoided by excitation into S_1 without excess energy. Here we monitor stimulated emission which is strictly related to spontaneous fluorescence.

The continuum theory of polar solvation is also sketched in Figure 1. Consider first the pure liquid in an external electric field (not shown) which partially orients the solvent molecules, generally represented by their dipole moments (arrows). Continuum theory replaces the microscopic liquid

[*] Dr. J. L. Pérez Lustres, Dr. S. A. Kovalenko, Dr. T. Senyushkina, W. Flasche, Prof. N. P. Ernsting
Department of Chemistry, Humboldt University
Brook-Taylor-Strasse 2, 12489 Berlin (Germany)
Fax: (+49) 30-2093-5553
E-mail: nernst@chemie.hu-berlin.de
Prof. M. Mosquera
Department of Physical Chemistry
University of Santiago de Compostela
15782 Santiago de Compostela (Spain)

[**] This work was supported by the Deutsche Forschungsgemeinschaft, the Volkswagen Foundation, the Fonds der Chemischen Industrie, and the Xunta de Galicia. We also thank John E. Bertie (University of Alberta, Edmonton, Canada) for providing the optical constants of the investigated solvents.

Supporting information for this article is available on the WWW under http://www.angewandte.org or from the author.

 © 2005 Wiley-VCH Verlag GmbH & Co. KGaA, Weinheim

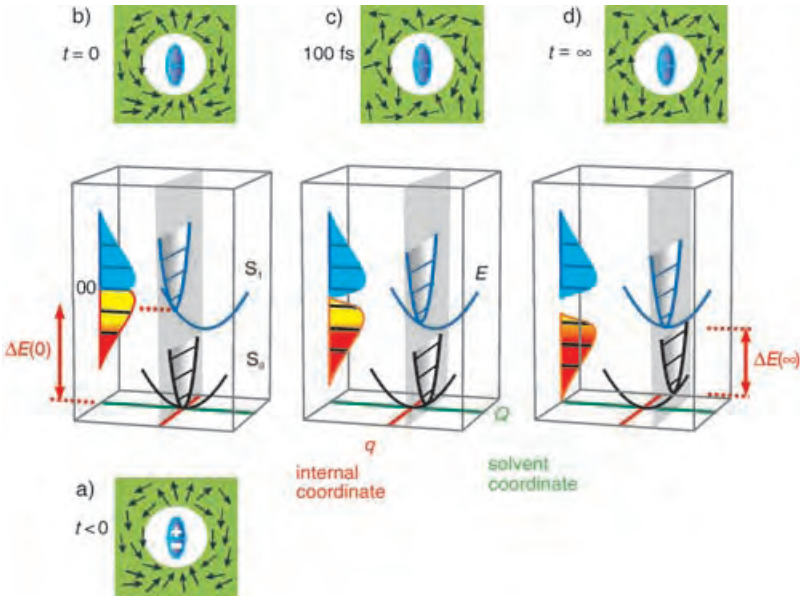


Figure 1. The dynamic Stokes shift of fluorescence (yellow–red band) images the relaxation of the surrounding solvent in the S_1 state of the solute. Solvent coordinate Q represents the configurational state of the environment and is treated classically. High-frequency motion along internal coordinate q for bond lengths and angles is quantized in vibrational states. Before femtosecond excitation (a) the solute is in the equilibrated ground state S_0 and the (blue) absorption band extends over a Franck–Condon progression for upward optical transitions. Immediately after excitation (b) the emission overlaps the absorption band at the electronic absorption origin 00. Partially relaxed $E_1(Q)$ (c) corresponds to solvent configurations that have raised $E_0(Q)$. The fluorescence therefore changes from yellow to red as solvation proceeds. After several picoseconds (d) a new equilibrium is reached for the S_1 state. A point dipole in a spherical polarizable cavity represents the solute, while a continuum with dielectric dispersion $\varepsilon(\nu)$ represents the surrounding liquid.

structure with an average, smooth, dipole density—the polarization P. The latter responds to changes in the field, and from such measurements at frequencies ν in the microwave, far-infrared, and infrared spectral regions one obtains the polarization susceptibility $\chi(\nu)=\varepsilon(\nu)-1$, where $\varepsilon(\nu)$ is the dielectric dispersion. For solvation, the field is instead derived from the charge distribution of the chromophore (Figure 1 a). It polarizes the surrounding medium, which in turn creates a reaction field R which stabilizes the solute. Analogous to the previous consideration, R responds to changes in the solute charge distribution at frequency ν. Equivalently the charge distribution may be switched from one form into another by femtosecond excitation $S_1 \leftarrow S_0$, and the solvent configuration and R are thus driven towards a new equilibrium.

Altogether the free energy of solvation can be calculated. In continuum theory a cavity is carved out of the solution, with the solute charge distribution inside and a homogeneous medium characterized by $\varepsilon(\nu)$ outside. A simple version is obtained when the cavity is taken to be spherical with radius r and the solute charge distribution is approximated by its dipole moment μ at the center. In this case the susceptibility of the reaction field to changes in the dipole moment[11,12] is given by Equation (1).

$$\chi_{\mathrm{dip}}(\nu)=\frac{2(n_{\mathrm{cav}}^2+2)}{3r^3}\left(\frac{\varepsilon(\nu)-1}{2\varepsilon(\nu)+n_{\mathrm{cav}}^2}-\frac{n^2-1}{2n^2+n_{\mathrm{cav}}^2}\right) \quad (1)$$

Here n and n_{cav} are the refractive indices of the solvent and the cavity, respectively, due to electronic response at optical frequencies. The latter is related to the polarizability α_1 of the solute in the S_1 state through the Clausius–Mosotti equation [Eq. (2)]

$$\frac{\alpha_1}{r^3}=\frac{n_{\mathrm{cav}}^2-1}{n_{\mathrm{cav}}^2+2} \quad (2)$$

Equation (1) is needed below to calculate the time-dependent Stokes shift.

The absorption and stationary stimulated emission spectra of **MQ** in water are shown in Figure 2 a. Femtosecond transient absorption was measured with the pump—supercontinuum–probe technique. Typical transient spectra are shown in Figure 2 b. They have three contributions: excited-state absorption ($S_n \leftarrow S_1$, ESA), stimulated emission ($S_1 \rightarrow S_0$, SE), and negative absorption due to the ground-state hole ($S_1 \leftarrow S_0$, bleach). The time-dependent red shift of the SE band is easily recognized together with a blue shift of the ESA band at 350 nm.

The stimulated emission band at delay time t is extracted from the corresponding transient absorption spectrum, and the peak frequency $\nu(t)$ is adopted as a measure of the free-energy gap. $\nu(t)$ is the desired time-resolved Stokes shift. The experiment thus provides a normalized relaxation function [Eq. (3)]

$$S_\nu(t)\equiv\frac{\nu(t)-\nu(\infty)}{\nu(0)-\nu(\infty)} \quad (3)$$

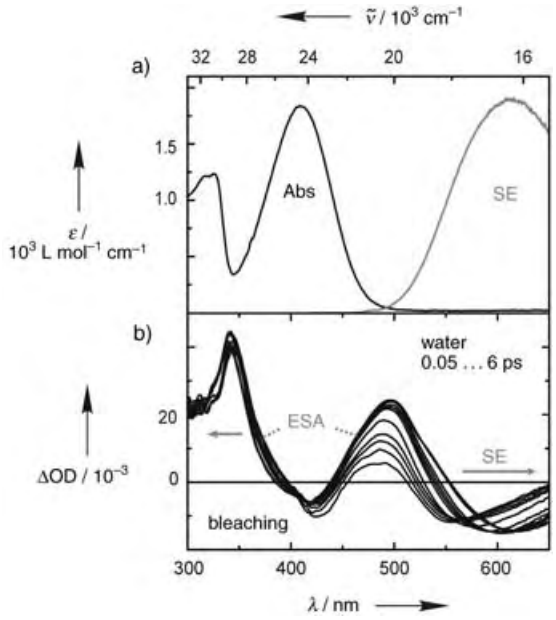


Figure 2. Optical spectra of **MQ** in water (pH 9). a) Stationary absorption (Abs) and stimulated emission (SE). b) Femtosecond transient absorption recorded with a time resolution of 30 fs after excitation at 430 nm. Induced change of optical density $\Delta OD < 0$ indicates stimulated emission in the fluorescence region and bleach in the absorption region where excited-state absorption (ESA) dominates. Transient spectra between 0.05 and 1 ps are shown in 0.1-ps steps and between 1 and 6 ps in 1-ps steps.

 © 2005 Wiley-VCH Verlag GmbH & Co. KGaA, Weinheim

Here $\nu(0)$ is the peak emission frequency immediately after excitation and $\nu(\infty)$ the frequency at a later time; the full Stokes shift is $\Delta\nu = \nu(0) - \nu(\infty)$.

To calculate the time-dependent Stokes shift from dielectric dispersion we consider the energy gap $\Delta E_{dip}(t)$ of an ideal dipolar chromophore in a cavity (Figure 1a). Equilibrium solvent motion causes fluctuations $\delta\Delta E_{dip}$ of the energy gap, and the classical correlation function is given by Equation (4)

$$S_{dip}(t) \equiv \frac{\langle \delta\Delta E_{dip}(0)\, \delta\Delta E_{dip}(t)\rangle}{\langle \delta\Delta E_{dip}(0)\, \delta\Delta E_{dip}(0)\rangle} \tag{4}$$

where $\langle\rangle$ is the ensemble average. The same time behavior is expected, essentially, for the nonequilibrium relaxation of $\Delta E_{dip}(t)$. The full spectral density of the correlation function for the energy gap is accessible through the fluctuation–dissipation theorem [Eq. (5)] (see the Supporting Information):

$$C_{dip}(\nu) = \left\{1 + \coth\left(\frac{h\nu}{2\,k_B\,T}\right)\right\}\chi''_{dip}(\nu) \tag{5}$$

Finally, the quantity defined in Equation (4) is given a theoretical curve [Eq. (6)]

$$S_{dip}(t) \propto \int_{-\infty}^{+\infty} d\nu\, C_{dip}(\nu)\cos(2\pi\nu t) \tag{6}$$

which can be compared to experimental $S_\nu(t)$.

The procedure is illustrated for water in Figure 3.[11,22,23] Our main observation is that the measured relaxation of **MQ** in water is identical, within measurement error, with the calculated dipole solvation relaxation. For the moment let us treat this as an hypothesis and replace $S_\nu(t)$ in Equation (3) by $S_{dip}(t)$ to obtain Equation (7)

$$\nu(t) = \Delta\nu\, S_{dip}(t) + \nu(\infty) \tag{7}$$

where the full Stokes shift is given by Equation (8)

$$\Delta\nu = \chi_{dip}(0)\mu_1(\mu_1 - \mu_0)/h\,c \tag{8}$$

(in wavenumbers, with c speed of light, h Planck's constant, and molecular dipole moments μ_i of **MQ**). In order to prove the hypothesis the theoretical curve [red line, Eq. (7)] is mapped onto the measured curves (gray dots, blue, green, and black lines) in Figure 4, where we summarize our results. For example, Figure 4a shows several measurements in water. The peak emission frequency sweeps precipitously from ca. 19400 cm^{-1} at $t = 0$ to 18200 cm^{-1} at $t = 100$ fs and further to equilibrium with $\nu(\infty) = 16340$ cm^{-1}. Optimal values for the cavity index and Stokes shift are found by simultaneous fit of all measurements, and they are consistent with the molecular properties of the probe (see the Supporting Information). The red curve shows the calculation with $n_{cav} = 2.3$ and $\Delta\nu =$

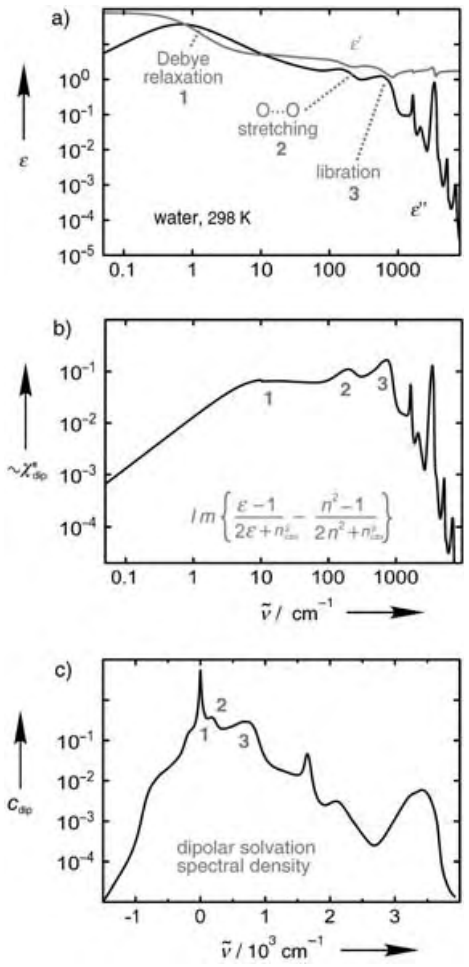


Figure 3. Calculations for the solvation of a molecular dipole by dielectric continuum theory. a) Real (ε') and imaginary (ε'') parts of water dielectric dispersion. Sharp structure results from intramolecular IR activity and broad bands 1–3 are caused by collective motion. b) Susceptibility χ''_{dip} of solute stabilization to solvent motion. The transformation from ε enhances high-frequency contributions and reduces low-frequency contributions. c) The spectral density for dipole solvation $C_{dip}(\nu)$ is constructed from the susceptibility. From here the theoretical relaxation function $S_{dip}(t)$ is reached by Fourier transformation.

3050 cm^{-1}. Increasing solute polarizability slows down the relaxation as already noted from molecular dynamics simulations.[24–26]

The initial relaxation dynamics in water is particularly interesting. The dynamic Stokes shift across this range is best seen in the insert of Figure 4a. Oscillations during the first picoseconds come from vibrational modes in the excited chromophore. But around 170 fs a shoulder can be discerned underneath. Dipolar solvation predicts a weakly underdamped relaxation feature at precisely the same time and with the same relative amplitude. Indeed, if the intramolecular vibrations are removed by spectral filtering, an underlying relaxation curve emerges that exactly matches the predicted one. (Deviations before $t = 100$ fs are caused by a coherent contribution to transient absorption during pump-and-probe overlap in time[27]). It follows that the oscillation feature around 170 fs is due to coherent nuclear motion in the solvent shell. The motion can be traced to a broad band in the

 © 2005 Wiley-VCH Verlag GmbH & Co. KGaA, Weinheim

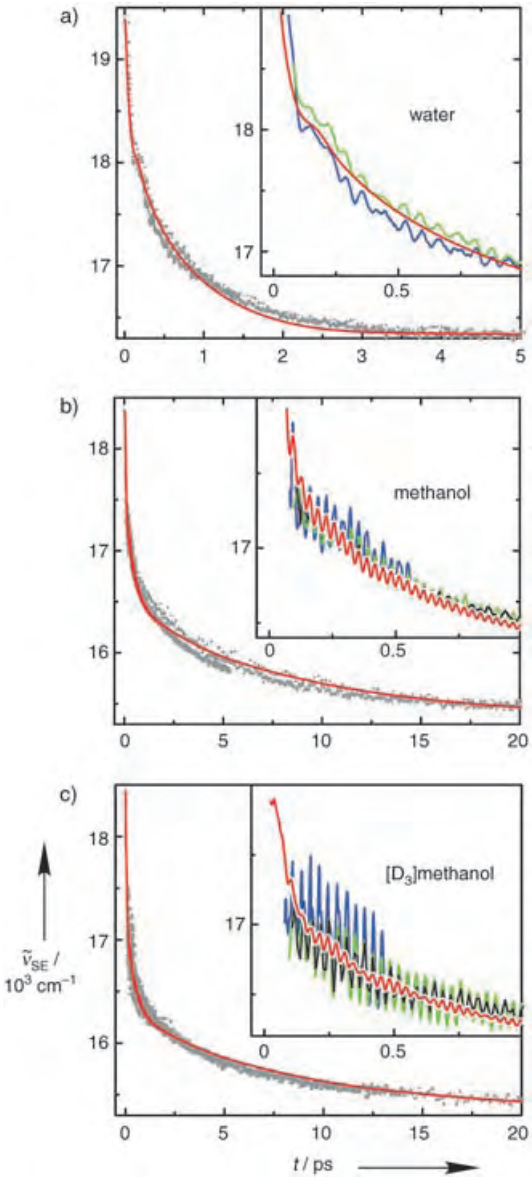


Figure 4. The time-dependent, measured peak position of the stimulated emission band (gray points, blue, green, and black lines) is well described by continuum theory (red). a) **MQ** in water. Here high-frequency oscillations correspond to intramolecular modes at 460 and 580 cm^{-1}. If they are removed by spectral filtering, an underlying relaxation curve emerges that matches the (red) predicted curve exactly. An oscillation hump at ≈170 fs marks the coherent O···O stretching period in the water shell. b, c) **MQ** in methanol and [D_3]methanol after excitation at 540 nm. Fast frequency modulation is caused by coherent C–O stretching motion of solvent molecules (1100 and 930 cm^{-1}, respectively). A hump at ≈0.25 ps indicates the period for collective libration.

dielectric dispersion of water, around 200 cm^{-1}, from intermolecular O···O stretching of the hydrogen-bonded network.[28,29]

Measurements for **MQ** in methanol and [D_3]methanol are analyzed in Figure 4b and c. In this case the excitation was tuned to the very red absorption edge to avoid creating *intra*molecular wavepackets. The emission peak relaxes from 18450 (fitted) to 17320 cm^{-1} (measured) during the first 100 fs. A slower stage with strong oscillations—that is, frequency modulation of the emission band—follows up to 2 ps. As with water, simple continuum theory describes quantitatively the shape of the relaxation curve.[30] Strong oscillations correspond to the IR band from C–O stretching in methanol at 1030 cm^{-1}, or at 980 cm^{-1} in [D_3]methanol (Figure 4c).

We conclude: 1) ultrafast excitation of **MQ** launches and reports coherent solvent motion in the surrounding liquid, and 2) solvation dynamics is well described by dipolar change $\Delta\mu$ in a sphere of radius r and refractive index n_{cav} surrounded by a dielectric continuum. Eventually the dynamic Stokes shift may be inverted into the dielectric dispersion $\varepsilon(\nu)$ in the vicinity of the probe, and the imaginary part will give the local IR spectrum $\nu\varepsilon''(\nu)$.

Received: April 22, 2005
Published online: August 1, 2005

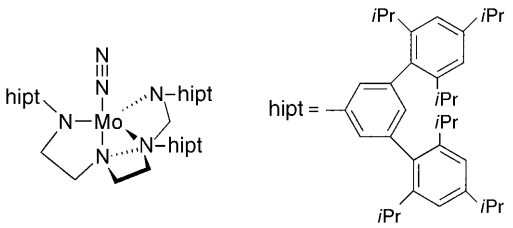
Keywords: femtochemistry · fluorescence · IR spectroscopy · solvatochromism

[1] K. Yoshihara, K. Tominaga, Y. Nagasawa, *Bull. Chem. Soc. Jpn.* **1995**, *68*, 696–712.
[2] R. Jimenez, G. R. Fleming, P. V. Kumar, M. Maroncelli, *Nature* **1994**, *369*, 471–474.
[3] M. L. Horng, J. A. Gardecki, A. Papazyan, M. Maroncelli, *J. Phys. Chem.* **1995**, *99*, 17311–17337.
[4] L. Zhao, J. L. Pérez Lustres, V. Farztdinov, N. P. Ernsting, *Phys. Chem. Chem. Phys.* **2005**, *7*, 1716–1725.
[5] G. R. Fleming, M. Cho, *Annu. Rev. Phys. Chem.* **1996**, *47*, 109–134.
[6] M. J. Lang, X. J. Jordanides, X. Song, G. R. Fleming, *J. Chem. Phys.* **1999**, *110*, 5884–5892.
[7] H. Bürsing, S. Kundu, P. Vöhringer, *J. Phys. Chem. B* **2003**, *107*, 2404–2414.
[8] J. Ruthmann, S. A. Kovalenko, N. P. Ernsting, D. Ouw, *J. Chem. Phys.* **1998**, *109*, 5466–5468.
[9] C. Silva, P. K. Walhout, K. Yokoyama, P. F. Barbara, *Phys. Rev. Lett.* **1998**, *80*, 1086 1089.
[10] P. Changenet-Barret, C. T. Choma, E. F. Gooding, W. F. DeGrado, R. M. Hochstrasser, *J. Phys. Chem. B* **2000**, *104*, 9322–9329.
[11] C. P. Hsu, X. Song, R. A. Marcus, *J. Phys. Chem. B* **1997**, *101*, 2546–2551.
[12] C. J. F. Böttcher, P. Bordewijk, *Theory of Electric Polarization*, Elsevier, Amsterdam, **1996**, Vol. 1, Eq. (4.31).
[13] C. P. Hsu, Y. Georgievskii, R. A. Marcus, *J. Phys. Chem. A* **1998**, *102*, 2658–2666.
[14] M. Maroncelli, G. R. Fleming, *J. Chem. Phys.* **1987**, *86*, 6221–6239.
[15] D. L. Beveridge, G. W. Schnuelle, *J. Phys. Chem.* **1975**, *79*, 2562–2566.
[16] X. Song, D. Chandler, *J. Chem. Phys.* **1998**, *108*, 2594–2600.
[17] F. O. Raineri, H. Resat, B.-C. Perng, F. Hirata, H. L. Friedman, *J. Chem. Phys.* **1994**, *100*, 1477–1491.
[18] S. Roy, B. Bagchi, *J. Chem. Phys.* **1994**, *101*, 4150–4155.
[19] N. Nandi, K. Bhattacharyya, B. Bagchi, *Chem. Rev.* **2000**, *100*, 2013–2046.
[20] E. O. Potma, W. P. De Boeij, D. A. Wiersma, *Biophys. J.* **2001**, *80*, 3019–3024.
[21] S. K. Pal, A. H. Zewail, *Chem. Rev.* **2004**, *104*, 2099–2124.

 © 2005 Wiley-VCH Verlag GmbH & Co. KGaA, Weinheim

[22] M. L. T. Asaki, A. Redondo, T. A. Zawodzinski, A. J. Taylor, *J. Chem. Phys.* **2002**, *116*, 8469 – 8482.
[23] J. E. Bertie, Z. Lan, *Appl. Spectrosc.* **1996**, *50*, 1047 – 1057.
[24] M. Maroncelli, *J. Mol. Liq.* **1993**, *57*, 1 – 37.
[25] P. V. Kumar, M. Maroncelli, *J. Chem. Phys.* **1995**, *103*, 3038 – 3060.
[26] B. D. Bursulaya, D. A. Zichi, H. J. Kim, *J. Phys. Chem.* **1996**, *100*, 1393 – 1405.
[27] A. D. Dobryakov, S. A. Kovalenko, N. P. Ernsting, *J. Chem. Phys.*, in press.
[28] I. Ohmine, H. Tanaka, *Chem. Rev.* **1993**, *93*, 2545 – 2566.
[29] V. I. Gaiduk, D. S. F. Crothers, Ch. M. Briskina, B. M. Tseitlin, *J. Mol. Struct.* **2004**, *689*, 11 – 23.
[30] In methanol the relaxation in the ps range is faster than predicted for a filled cavity; we find $n_{cav} \approx 1$. This and other deviations (see the Supporting Information) may indicate molecularity of solvation.

 © 2005 Wiley-VCH Verlag GmbH & Co. KGaA, Weinheim



Scheme 1. The $[(hiptN_3N)Mo(N_2)]$ complex.

Nitrogenase Models

DOI: 10.1002/anie.200501485

Energetics and Mechanism of a Room-Temperature Catalytic Process for Ammonia Synthesis (Schrock Cycle): Comparison with Biological Nitrogen Fixation**

*Felix Studt and Felix Tuczek**

A room temperature catalytic process for ammonia synthesis analogous to biological nitrogen fixation has for a long time presented a challenge of fundamental chemical importance.[1–4] The recent discovery by Schrock et al. of the first truly catalytic system for ammonia synthesis working under ambient conditions and involving well-defined intermediates marks a historic breakthrough in this respect.[5–10] It is based on the molybdenum complex $[Mo(hiptN_3N)]$ (**I**) with the specially designed triamidoamine ligand $hiptN_3N$ (tris(hexaisopropylterphenyl)triamidoamine) which provides the metal center with a sterically shielded site for dinitrogen bonding and reactivity (Scheme 1). This system has allowed the catalytic generation of ammonia from N_2 at room temperature and atmospheric pressure using $(LutH)BAr'_4$ (Lut = 2,6-dimethylpyridine, Ar'_4 = 3,5-bis(trifluoromethyl)-phenyl) as a proton source and decamethylchromocene ($[Cp^*_2Cr]$, $Cp^* = C_5Me_5$) as reductant. To date six catalytic turnovers have been achieved. Apart from establishing the physicochemical conditions under which the room-temperature catalytic synthesis of ammonia is feasible, the molybdenum triamidoamine system also allows insight into the mechanism of this process at the molecular level. This aspect is of particular interest for a comparison with the mechanistic pathway of the enzyme nitrogenase (which converts N_2 into NH_3) on which important information has been obtained by theoretical calculations recently.[11,12]

A number of intermediates relevant to the molybdenum triamidoamine catalytic cycle have been isolated and characterized: $[Mo(hiptN_3N)N_2]$, $[Mo(hiptN_3N)NNH]$, $[Mo(hiptN_3N)NNH_2]^+$, $[Mo(hiptN_3N)N]$, $[Mo(hiptN_3N)NH]^+$, $[Mo(hiptN_3N)NH_3]^+$, and $[Mo(hiptN_3N)NH_3]$.[7,9] Based on the available experimental information, a mechanism has been proposed (Schrock cycle).[6,9] Herein we present density functional theory (DFT) calculations on all the possible intermediates that can appear in the catalytic transformation of N_2 to ammonia mediated by the molybdenum triamidoamine complex **I**, including those invoked by Schrock et al. On the basis of these calculations the detailed mechanistic pathway and the free energy profile of the entire cycle are determined. The calculations are performed on complexes **1**–**14** where the hipt groups have been replaced by hydrogen atoms (Figure 1). Applying this simplification and the model chemistry described in reference [13], the observed structural and spectroscopic data have been reproduced.[14] A comparison of calculated and measured vibrational frequencies is given in the Supporting Information, structural parameters of the optimized model complexes (some of which are shown in Figure 1, lower left) are collected and compared to available X-ray data in the Supporting Information). Energies for reduction and protonation steps are explicitly calculated relative to the processes $[Cp^*_2Cr] \rightarrow [Cp^*_2Cr]^+$ and $LutH^+ \rightarrow$ Lut, respectively, which have been theoretically treated without any simplification of the molecules involved. All the energies are evaluated at the B3LYP/TZVP level and are zero-point energy (ZPE), thermal, as well as solvent corrected (see Supporting Information);[13] corresponding standard free enthalpies have been determined and are plotted in Figure 1 against the reaction coordinate ρ.

The starting complex $[(N_3N)Mo]$ (**1**; $(N_3N)^{3-} = [(HNCH_2CH_2)_3N]^{3-}$) gives rise to $S = 1/2$ and $S = 3/2$ states

[*] Dipl.-Chem. F. Studt, Prof. Dr. F. Tuczek
Institut für Anorganische Chemie
Christian Albrechts Universität Kiel
Ohlshausenstrasse 40, 24098 Kiel (Germany)
Fax: (+49) 431-880-1520
E-mail: ftuczek@ac.uni-kiel.de

[**] Financial support of this research by Deutsche Forschungsgemeinschaft (DFG Tu58-12/1 and Fonds der Chemischen Industrie (FCI) is gratefully acknowledged.

Supporting information for this article is available on the WWW under http://www.angewandte.org or from the author.

 © 2005 Wiley-VCH Verlag GmbH & Co. KGaA, Weinheim

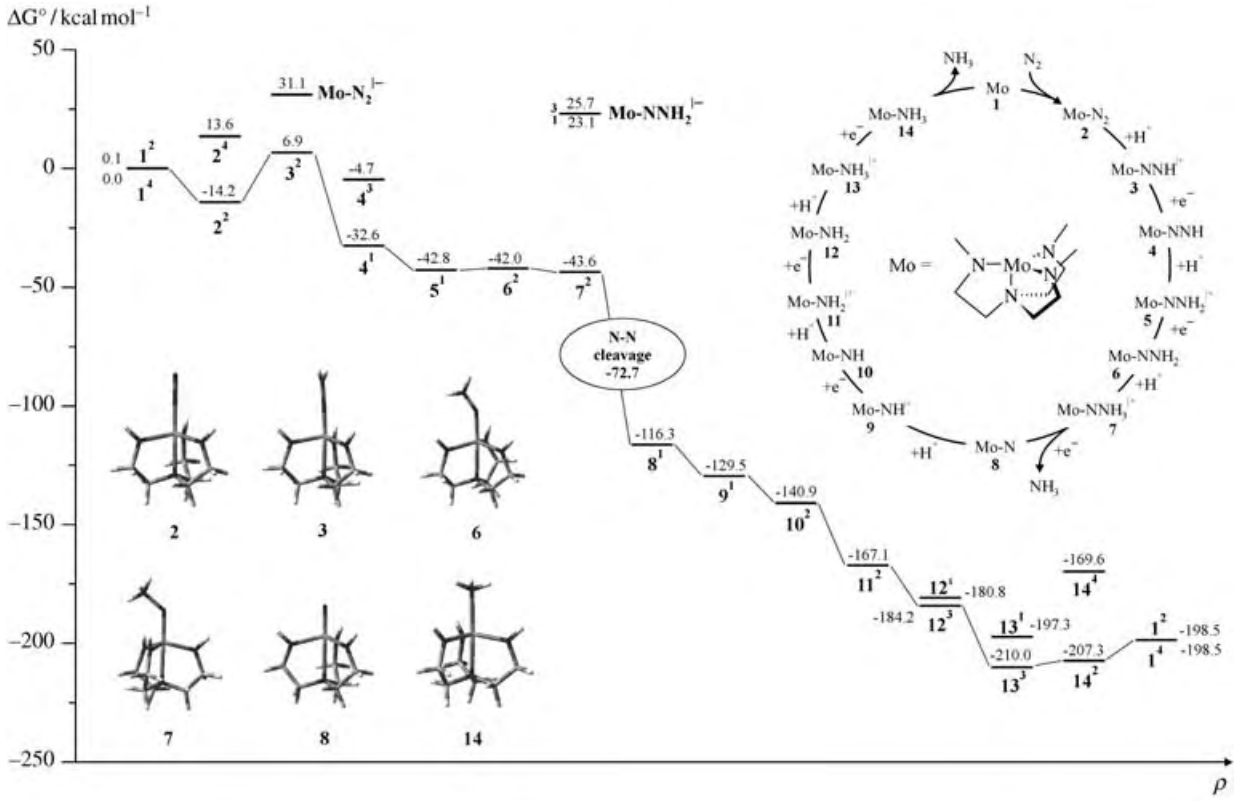


Figure 1. Catalytic cycle (upper right) and energy profile (center) of the reduction of N_2 to ammonia in the molybdenum triamidoamine system. All energies correspond to standard free enthalpies and are in kcal mol^{-1}. Lower left: optimized structures of selected intermediates.

which are about isoenergetic (calculated energy splitting between $\mathbf{1}^{\mathbf{2}}$ and $\mathbf{1}^{\mathbf{4}}$ 0.1 kcal mol^{-1}). Addition of dinitrogen to **1** leads to $[(N_3N)Mo^{III}–N_2]$ (**2**) which is found to have an $S = 1/2$ ground state; the $S = 3/2$ state is 27.8 kcal mol^{-1} higher in energy. The coordination of dinitrogen is calculated to be exergonic by 14.2 kcal mol^{-1}, which is in agreement with the observation that **2** is thermally stable towards loss of N_2.[5] The next step in the catalytic cycle is the protonation of **2** to $[(N_3N)Mo^{V}–NNH]^+$ (**3**) which is endergonic by 21.1 kcal mol^{-1}, reflecting a "moderate" activation of **2** towards protonation.[15] Subsequent reduction of **3** in an exergonic reaction gives the neutral molybdenum(IV) species $[(N_3N)Mo–NNH]$ (**4**) which exhibits an $S = 0$ ground state; the $S = 1$ state is found to be 27.9 kcal mol^{-1} higher in energy. The next two steps (protonation and reduction of **4**) are about thermoneutral, leading to complexes $[(N_3N)Mo–NNH_2]^+$ (**5**) and $[(N_3N)Mo–NNH_2]$ (**6**).

Complex **6** is susceptible to further protonation, as evident from the weakly exergonic character of the reaction **6**→$[(N_3N)Mo^{V}–NNH_3]^+$ (**7**). Direct reduction of **6** to the anionic molybdenum(IV) complex $[(N_3N)Mo–NNH_2]^-$ can be discounted based on the highly endergonic character of this reaction. Judging from its very large N–N distance of 1.57 Å, complex **7** has a highly activated N–N bond (see Supporting Information), this activated bond initiates N–N cleavage which is the next step in the reaction sequence. In fact, geometry optimization of **7** after addition of one electron spontaneously leads to splitting of the N–N bond under generation of the nitrido complex $[(N_3N)Mo^{VI}–N]$ (**8**) and the first equivalent of ammonia. This process is calculated to be highly exergonic (72.7 kcal mol^{-1}) and is predicted to occur without an activation barrier, in analogy to molybdenum–NNH_3 systems with phosphine ligands.[14]

The next protonation and reduction steps are exergonic as well. Thus, protonation of the nitrido complex **8** leads to the molybdenum(VI) complex $[(N_3N)Mo–NH]^+$ (**9**). Reduction of **9** and protonation of the resulting neutral molybdenum(V) imido complex $[(N_3N)Mo–NH]$ (**10**) generates $[(N_3N)Mo–NH_2]^+$ (**11**) which is reduced to the neutral molybdenum(IV) amido complex $[(N_3N)Mo–NH_2]$ (**12**). The two d-electrons of **12** give rise to an $S = 0$ and an $S = 1$ state, the latter being found at 3.4 kcal mol^{-1} lower energy. Protonation of **12** generates the Mo^{IV} complex $[(N_3N)Mo–NH_3]^+$ (**13**) which also exhibits an $S = 1$ ground state; in this case the $S = 0$ state is calculated to be 12.7 kcal mol^{-1} higher in energy. Complete reduction of **13** was experimentally determined to require the presence of $[Cp^*_2Cr]$ whereas all other reductions could be performed by the weaker reductant $[Cp_2Co]$ ($Cp = C_5H_5$) as well.[5,8] Even for $[Cp^*_2Cr]$ this step is calculated to be slightly endergonic (+2.7 kcal mol^{-1}). If less-strongly reducing agents are employed the endergonic character of this reaction concomitantly increases (e.g. $\Delta G° = +27.9$ kcal mol^{-1} if $[Cp_2Co]$ is used), eventually causing the total suppression of the reaction. The resulting molybdenum(III) ammine complex

 © 2005 Wiley-VCH Verlag GmbH & Co. KGaA, Weinheim

$[(N_3N)Mo–NH_3]$ (**14**) exhibits an $S = 1/2$ ground state with the $S = 3/2$ state being 37.7 kcal mol^{-1} higher in energy. At this stage, the dinitrogen complex **2** has been reduced by six $[Cp^*_2Cr]$ molecules and protonated by six molecules of $LutH^+$. To close the catalytic cycle the NH_3 ligand of **14** has to be replaced by N_2. Dissociation of **14** under formation of **1** and ammonia is endergonic by 8.8 kcal mol^{-1}. Subsequent bonding of N_2 under formation of the dinitrogen complex **2**, however, is exergonic ($\Delta G° = -14.2$ kcal mol^{-1}, see above), rendering the overall substitution of NH_3 by N_2 exergonic by 5.4 kcal mol^{-1}.

Thus, the catalytic cycle consists of a sequence of strictly alternating protonation and reduction steps. This agrees with the mechanism proposed by Schrock et al.,[6,9] except for the conversion of the dinitrogen complex **2** into the neutral NNH complex **4** (see below). All the relevant intermediates therefore are either neutral or positively charged and the formation of negative species appears to be excluded. Moreover, most reactions are exergonic. By far the most exergonic step is the cleavage of the N–N bond which in addition is predicted to proceed spontaneously. Only three steps (**2**→**3**, **13**→**14**, and **14**→**1**) of the cycle are endergonic. The transformation of **13** to **14** is found to be the most difficult of all the reduction steps, in agreement with the experiment (see above). The endergonic dissociation of **14** to **1** + ammonia is part of the exchange of NH_3 for N_2 on complex **1** that is calculated to be weakly exergonic overall. Experimentally this exchange reaction is found to be about thermoneutral.[9] Energetically the most demanding of all reactions of the cycle is the protonation of the dinitrogen complex **2** to the cationic intermediate **3** ($\Delta G° = +21.1$ kcal mol^{-1}). The subsequent reduction of **3**, however, is strongly exergonic, providing the driving force for the net conversion of **2** into **4**. Schrock et al., in contrast, have postulated a primary reduction of **2** to the complex $[(N_3N)Mo–N_2]^-$ followed by protonation to **4**.[9] Based on the much higher energy of the negatively charged intermediate in comparison to **3**, this scenario appears less likely.[16]

The exergonic character of most of the elementary reactions involved in the Schrock cycle is also evident from the fact that the total free reaction enthalpy $\Delta G°_R$ of one turnover corresponding to the reaction in Equation (1) is strongly negative (−198.5 kcal mol^{-1}; see Figure 1 from left to right and Figure 2a). Formally the six reduced $[Cp^*_2Cr]$ and six protonated $LutH^+$ molecules needed in Equation (1) can be considered to result from the reaction in Equation (2) for which the calculation gives a $\Delta G°$ value of +186.2 kcal mol^{-1} (in heptane).

$$N_2 + 6\,[Cp^*_2Cr] + 6\,LutH^+ \rightarrow 2\,NH_3 + 6\,[Cp^*_2Cr]^+ + 6\,Lut \quad (1)$$

$$3\,H_2 + 6\,[Cp^*_2Cr]^+ + 6\,Lut \rightarrow 6\,[Cp^*_2Cr] + 6\,LutH^+ \quad (2)$$

Equations (1) and (2) combine to give the net reaction in Equation (3) for which the calculation gives a standard free enthalpy change $\Delta G°_f$ of −12.3 kcal mol^{-1} (in heptane).[17]

$$N_2 + 3\,H_2 \rightarrow 2\,NH_3 \quad (3)$$

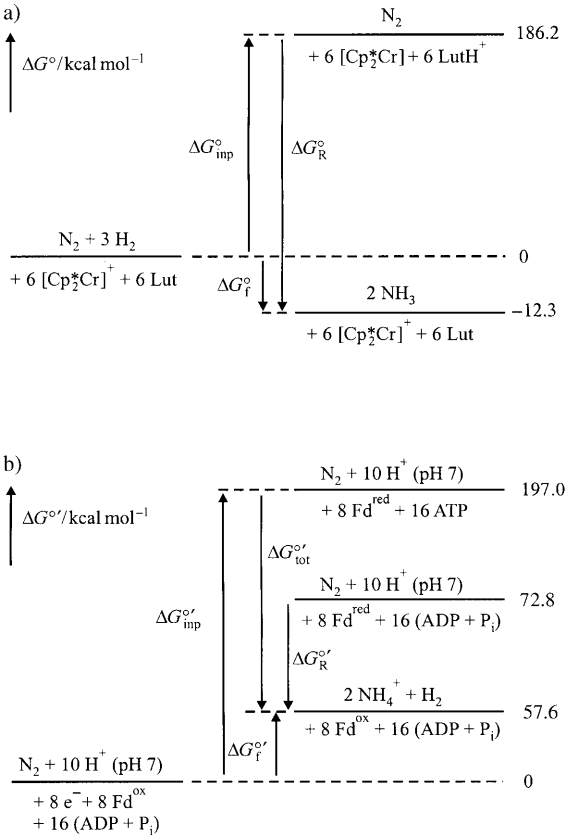


Figure 2. Free enthalpies for the formation of ammonia from N_2 at room temperature and normal pressure in the molybdenum triamidoamine system (a) and nitrogenase (b). Energies not to scale.

The synthetic system thus is calculated to require a standard free enthalpy input $\Delta G°_{inp}$ of +186.2 kcal per mol N_2 to generate ammonia at room temperature and normal pressure (Figure 2a). This energy expenditure is very large, but is also required in nitrogen fixation mediated by the enzyme nitrogenase. In the biological system, ammonia is produced along with H_2 according to Equation (4) where Fd = Ferredoxin.[18–21]

$$N_2 + 10\,H^+ + 8\,Fd^{red} \rightarrow 2\,NH_4^+ + H_2 + 8\,Fd^{ox} \quad (4)$$

Under standard conditions this reaction is associated with a free enthalpy change $\Delta G°_R$ of −110.8 kcal mol^{-1};[22] changing to pH 7 yields a transformed standard free reaction enthalpy $\Delta G°'_R$ of −15.2 kcal mol^{-1} (Figure 2b).[23] Moreover, the biological process requires the hydrolysis of two molecules of ATP per transferred electron such that the total reaction [Eq. (5)] is associated with a reaction enthalpy $\Delta G°'_{tot}$ of −139.4 kcal mol^{-1} at pH 7.[24]

$$N_2 + 10\,H^+(pH\,7) + 8\,Fd^{red} + 16\,ATP \rightarrow 2\,NH_4^+ + H_2 + 8\,Fd^{ox} + 16\,(ADP + P_i) \quad (5)$$

Under this condition the free enthalpy change for the formation of NH_4^+ and H_2 according to Equation (6) is

 © 2005 Wiley-VCH Verlag GmbH & Co. KGaA, Weinheim

positive ($\Delta G_f^{\circ\prime} = 57.6\ \text{kcal mol}^{-1}$).[23]

$$N_2 + 10\,H^+(pH\,7) + 8\,e^- \rightarrow 2\,NH_4^+ + H_2 \quad (6)$$

In order to make the overall reaction in Equation (5) exergonic by 139.4 kcal mol^{-1}, a free energy input $\Delta G_{inp}^{\circ\prime}$ of +197.0 kcal is needed which is associated with the reaction in Equation (7).

$$8\,e^- + 8\,Fd^{ox} + 16\,(ADP + P_i) \rightarrow 8\,Fd^{red} + 16\,ATP \quad (7)$$

This value is close to that of the artificial system.[25] In both cases the (free) energy input of approximately 190 kcal per mol N_2 is used for the generation of the respective reduction equivalents; the hydrolysis of 16 ATP molecules in nitrogenase thereby acts to lower the reduction potential of the iron protein.[19] The energy profile presented in Figure 1 shows that the strongly negative reduction potential is primarily necessary to activate N_2 towards protonation; once the first protonation of N_2 has been achieved, most of the following steps are exergonic. This situation is similar to that calculated for the conversion of N_2 into NH_3 at the iron–molybdenum cofactor (FeMoco) of nitrogenase in which, however, combined protonation–reduction steps corresponding to hydrogenation reactions were considered.[11,12] Moreover, the N–N cleavage reaction in this process is exothermic and activationless, in agreement with the same reaction in the molybdenum triamidoamine system.

In summary, the energy profile of the first room-temperature catalytic process for ammonia synthesis from N_2 proceeding via well-defined intermediates has been determined, and a theoretically founded mechanism for this reaction established. Salient features of the calculated reaction course correctly reproduce experimental observations. The reaction pathway exhibits strong similarities to that obtained theoretically for nitrogenase. Importantly, the energy input of approximately 190 kcal calculated to be involved in the conversion of 1 mol N_2 into 2 mol NH_3 is found to be very near to that obtained empirically for biological nitrogen fixation, underlining the significance of the molybdenum triamidoamine system as a functional model of nitrogenase.

Received: April 29, 2005
Published online: August 5, 2005

Keywords: ammonia · density functional calculations · molybdenum · nitrogen fixation · N ligands

[1] B. A. MacKay, M. D. Fryzuk, *Chem. Rev.* **2004**, *104*, 385.
[2] M. Hidai, *Coord. Chem. Rev.* **1999**, *185–186*, 99.
[3] T. A. Bazhenova, A. E. Shilov, *Coord. Chem. Rev.* **1995**, *144*, 69.
[4] C. J. Pickett, J. Talarmin, *Nature* **1985**, *317*, 652.
[5] D. V. Yandulov, R. R. Schrock, *J. Am. Chem. Soc.* **2002**, *124*, 6252.
[6] D. V. Yandulov, R. R. Schrock, *Science* **2003**, *301*, 76.
[7] D. V. Yandulov, R. R. Schrock, A. L. Rheingold, C. Ceccarelli, W. M. Davis, *Inorg. Chem.* **2003**, *42*, 796.
[8] V. Ritleng, D. V. Yandulov, W. W. Weare, R. R. Schrock, A. S. Hock, W. M. Davis, *J. Am. Chem. Soc.* **2004**, *126*, 6150.
[9] D. V. Yandulov, R. R. Schrock, *Inorg. Chem.* **2005**, *44*, 1103.
[10] G. J. Leigh, *Science* **2003**, *301*, 55.
[11] B. Hinnemann, J. K. Nørskov, *J. Am. Chem. Soc.* **2004**, *126*, 3920.
[12] T. H. Rod, J. K. Nørskov, *J. Am. Chem. Soc.* **2000**, *122*, 12751.
[13] For details see the Supporting Information.
[14] K. Mersmann, K. H. Horn, N. Böres, N. Lehnert, F. Studt, F. Paulat, G. Peters, I. Ivanovic-Burmazovic, R. van Eldik, F. Tuczek, *Inorg. Chem.* **2005**, *44*, 3031.
[15] F. Tuczek, N. Lehnert, *Angew. Chem.* **1998**, *110*, 2780; *Angew. Chem. Int. Ed.* **1998**, *37*, 2636.
[16] There are precedents for the protonation of neutral N_2 complexes to positively charged NNH_x intermediates: C. M. Habeck, N. Lehnert, C. Näther, F. Tuczek, *Inorg. Chim. Acta C* **2002**, *337*, 11, and references therein
[17] Calculated gas-phase value: 9.22 kcal mol^{-1}; reported gas-phase value: 7.7 kcal mol^{-1}: M. W. Chase, Jr., C. A. Davies, J. R. Downe, Jr., D. J. Frurip, R. A. McDonald, A. N. Syverue, *J. Phys. Chem. Ref. Data* **1985**, *14*, Suppl. No. 1.
[18] O. Einsle, F. A. Tezcan, S. L. A. Anrade, B. Schmidt, M. Yoshida, J. B. Howard, D. C. Rees, *Science* **2002**, *297*, 1696.
[19] B. K. Burgess, D. J. Lowe, *Chem. Rev.* **1996**, *96*, 2983.
[20] J. B. Howard, D. C. Rees, *Chem. Rev.* **1996**, *96*, 2965.
[21] There are nitrogenases where other electron donors are involved, for example, flavodoxin.
[22] Based on an $E^{\circ\prime}$ for Fd of −0.395 V for *Clostridium pasteurianum*.
[23] R. A. Alberty, *J. Biol. Chem.* **1994**, *269*, 7099.
[24] R. A. Alberty, R. N. Goldberg, *Biochemistry* **1992**, *31*, 10610.
[25] Note in this comparison that the efficiency of the Schrock cycle has been determined to be 65% (see ref. [6] and [9]). On the other hand, the consumption of 16 ATP per transferred electron in nitrogenase is a lower limit (see ref. [19,20]). Moreover, the transformation of N_2 to NH_3 in nitrogenase probably does not proceed at the molybdenum atom but on one or more iron centers of the FeMoco (ref. [11,12] and [18–20]).

 © 2005 Wiley-VCH Verlag GmbH & Co. KGaA, Weinheim

Hydrothermal Synthesis

DOI: 10.1002/anie.200500514

Studying the Solvothermal Formation of MoO_3 Fibers by Complementary In Situ EXAFS/EDXRD Techniques**

*Alexej Michailovski, Jan-Dierk Grunwaldt, Alfons Baiker, Ragnar Kiebach, Wolfgang Bensch, and Greta R. Patzke**

The reliable and straightforward fabrication of nanoparticles is essential for developing future nanotechnology.[1–5] Nanoscale transition-metal oxides provide a wide spectrum of important properties,[6,7] and their functionalization and alignment is greatly facilitated by anisotropic morphologies.[8] Among the transition-metal oxides, MoO_3 is the focus of much attention owing to its numerous applications, for example, in catalysis[9–11] or sensor technology.[12,13] We have recently developed a solvothermal procedure that provides a convenient access to highly anisotropic nanoscale MoO_3 fibers.[14,15]

The solvothermal process[16] is famous for its unique control facilities regarding the particle size of the material produced.[17,18] Its major drawback, however, is that the predictive and rational preparation of a desired solid remains a major preparative challenge—especially if the morphology of the product is to be tuned as well. This problem is because of the tremendous impact of the synthetic parameters on the course of the reaction. Thus, the development of solvothermal nanomaterials syntheses may require considerable "trial and error" work. The elucidation of solvothermal reaction mechanisms is therefore vital for devising more predictive strategies so that the resulting materials can be optimized for commercial purposes. As solvothermal reactions are usually performed in thick-walled reaction containers, sophisticated in situ techniques employing high-intensity synchrotron radiation are required for their direct monitoring.[19–22] Generally, the development of high-pressure, in situ spectroscopic approaches is a challenging topic of chemistry and materials science.[23] Orientating kinetic studies may also be performed by quenching hydrothermal reactions, but this information is only valid if the recovered material is not affected by any irreversible changes upon cooling and isolation. Among the multitude of solvothermally generated materials, special emphasis has been placed upon the in situ study of zeolites,[24–26] open-framework compounds,[27,28] silicate minerals,[29,30] and sulfide-based systems.[22,31] For the transition-metal oxides, the main focus has been on ternary compounds of industrial interest (e.g. bismuth molybdates[32] or $BaTiO_3$[33]), whereas considerably fewer binary oxides (such as ZrO_2[34]) have been investigated by solvothermal in situ methods. Very little mechanistic information is available on their solvothermal transformation into nanomaterials.

Herein, we report the first comprehensive in situ study on the growth of MoO_3 fibers by complementary EDXRD (energy dispersive X-ray diffraction) and XANES/EXAFS (X-ray absorption near edge structure/extended X-ray absorption fine structure) techniques. While XRD allows the long-range order to be monitored, XANES/EXAFS provides information on the short-range order.[35–37] This information is indispensable for describing the solvothermal crystallization of nanostructured matter, because amorphous solids and small particles (typically below 50 Å) cannot be detected by Bragg diffraction. Moreover, the simultaneous observation of both the solid and the liquid phase during the reaction is vital for proposing a reaction pathway. For this purpose, a special in situ-EXAFS cell was used (see Supporting Information).[38] The EXAFS technique is ideally suited to monitor both crystalline and amorphous solid intermediates as well as species in solution, whereas all crystalline components can be fully characterized in terms of the complementary EDXRD method.

The solvothermal access to MoO_3 nanorods is quite straightforward: yellow molybdic acid, $MoO_3 \cdot 2H_2O$, is quantitatively transformed into the fibrous product after a few hours of autoclave treatment at 180–220 °C in water or acetic acid.[14] The fibers often display high aspect ratios with lengths above 10 μm and diameters between 100 and 150 nm. Although the parameters (e.g. time, acid concentration, or temperature) can be varied quite widely, the presence of $MoO_3 \cdot 2H_2O$ is a prerequisite for the formation of MoO_3 fibers.[14] MoO_3 and $MoO_3 \cdot 2H_2O$ both have layered crystal structures that are topotactically related by a stepwise dehydration proceeding via β-$MoO_3 \cdot H_2O$.[39] Preliminary experiments covering the formation of MoO_3 fibers in various media point to a different formation pathway under solvothermal conditions.[14]

The temperature interval for the onset of MoO_3 rod formation from $MoO_3 \cdot 2H_2O$ in acetic acid was evaluated with

[*] Dipl-Chem. A. Michailovski, Dr. G. R. Patzke
Laboratory of Inorganic Chemistry
ETH Hönggerberg
8093 Zürich (Switzerland)
Fax: (+41) 1633-4692
E-mail: patzke@inorg.chem.ethz.ch
Dr. J.-D. Grunwaldt, Prof. Dr. A. Baiker
Institute for Chemical and Bioengineering
ETH Hönggerberg, 8093 Zürich (Switzerland)
Dipl.-Chem. R. Kiebach, Prof. Dr. W. Bensch
Institut für Anorganische Chemie
Universität Kiel, 24098 Kiel (Germany)

[**] We thank Prof. Dr. R. Nesper (Laboratory of Inorganic Chemistry, ETH Zürich) for his steady interest and continuous support of this work. We gratefully acknowledge HASYLAB (DESY, Hamburg) for providing beamtime at beamline X1 and F3 for in situ EXAFS and XRD experiments, respectively. The beamline staff, Julia Wienold and M. Herrmann, as well as Matteo Caravati and Michael Ramin (ICAB, ETH Zürich) are gratefully acknowledged for their help during the EXAFS measurements. This work was supported by the ETH Zurich, by the Swiss National Science Foundation (MaNEP: Materials with Novel Electronic Properties), and by the National Research Program "Supramolecular Functional Materials".
EXAFS = extended X-ray absorption fine structure, EDXRD = energy dispersive X-ray diffraction.

Supporting information for this article is available on the WWW under http://www.angewandte.org or from the author.

 © 2005 Wiley-VCH Verlag GmbH & Co. KGaA, Weinheim

ex situ quenching experiments between 80 °C and 180 °C (Experimental Section). The reaction can be monitored visually because the bright yellow starting material is converted into a gray-blue product by a partial reduction of MoO_3 (the amount of product falls below the detection limit of standard analytical techniques). At 80 °C, the yellow color was maintained, whereas a sharp color change was observed after 12 min of treatment at 100 °C. When the reaction temperature was raised, this time interval further decreased to 6 min (120 °C) and 2 min (180 °C). These observations are supported by the corresponding scanning electron micrograph (SEM) images and powder diffraction patterns (Figure 1 I): at 80 °C, $MoO_3{\cdot}2H_2O$ (JCPDS 39–363; $P2_1/n$, $a = 10.618(5)$, $b = 13.825(7)$, $c = 10.482(5)$ Å, $\beta = 91.61(4)°$) undergoes no significant structural (Figure 1 Ia, bottom) or morphological (Figure 1 Ia, top) changes. However, at 100 °C, the dehydration to MoO_3 is finished (Figure 1 Ib, bottom) and the formation of a fibrous material sets in (Figure 1 Ib, top). Between 100 °C and 180 °C both the fibrous morphology (Figure 1 Ic, d, top) and the crystallinity (compare the (061), (002) and (112) reflections in Figure 1 Ic,d, bottom) improve further. The analogous quenching series in water proceeded on a similar timescale and led to the quantitative formation of MoO_3 nanorods at 150 °C within 3–4 min. (Figure 1 IId, top/bottom). The powder diffraction patterns of the flat, fibrous products display intensities different from the literature data (JCPDS 35–609; *Pbnm*, $a = 3.963$, $b = 13.856$, $c = 3.697$ Å). This deviation may be due to the presence of stacking faults in the [001] growth direction[40] together with a preferred orientation of the MoO_3 rods on the flat sample holder.

The presence of stacking faults in the as-synthesized rods grown after 20 min of ex situ treatment was confirmed by TEM investigations and may account for the broadened reflections occurring in the powder diffraction patterns (Figure 1). Figure 2 demonstrates that separated rods with

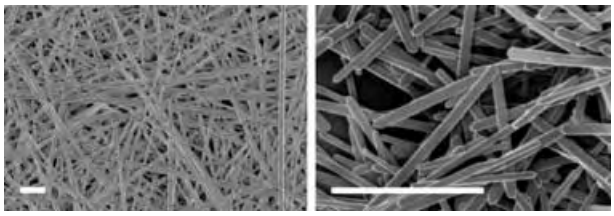


Figure 2. Representative SEM images of MoO_3 nanorods (scale bar = 2 μm) after prolonged solvothermal treatment.

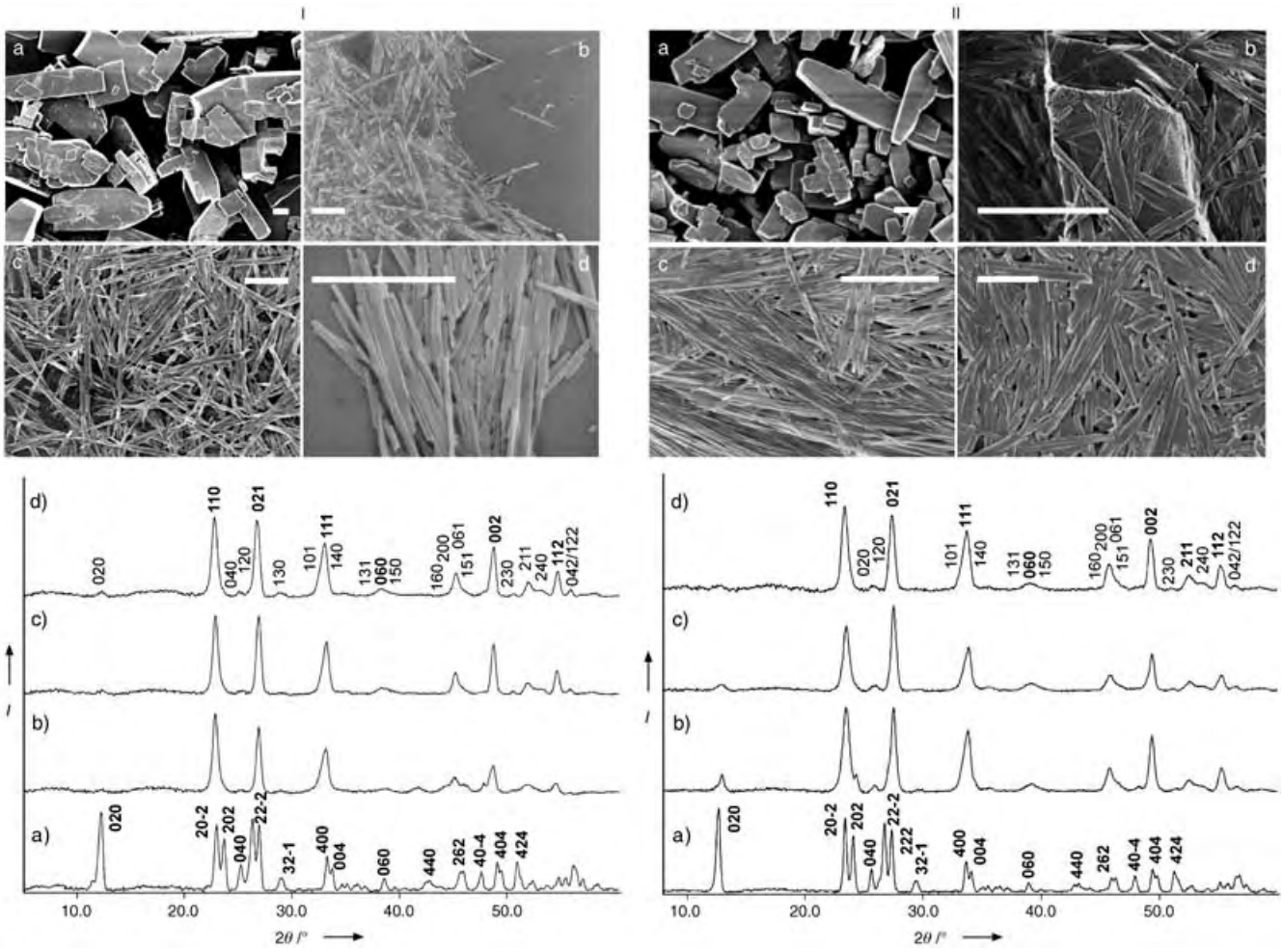


Figure 1. SEM images (top: I and II, scale bar = 1 μm) and XRD patterns (bottom: I and II) of the products resulting from mixtures of $MoO_3{\cdot}2H_2O$ and acetic acid (I) or water (II) at 80 °C (a), 100 °C (b), 120 °C (c) and 180 °C (acetic acid) or 150 °C (H_2O) (d).

 © 2005 Wiley-VCH Verlag GmbH & Co. KGaA, Weinheim

well-defined edges and tips are accessible after prolonged solvothermal treatments (16–24 h at 180 °C). Even at 100 °C, only few residual microcrystals of $MoO_3 \cdot 2H_2O$ are still present (see powder XRD pattern (Figure 1 II b, bottom) and SEM images (Figure 1-II b, top)).

The temperature-dependent formation of MoO_3 rods was studied with in situ X-ray absorption spectroscopy. Our novel autoclave cell allows the study of the liquid phase and the solid/liquid interface. The cell can be positioned so that the X-ray beam probes either the liquid phase or the solid/liquid interface (see Supporting Information). In the present case, the monitoring of the liquid phase is essential to distinguish a strictly topotactic dehydration from alternative dissolution–precipitation mechanisms. XANES spectra at the molybdenum K edge of the reaction of $MoO_3 \cdot 2H_2O$ in water were taken both at the bottom of the cell (mainly solid part, Figure 3 a,b) and the middle of the cell (liquid part, Figure 3 c) between 25 °C and 150 °C. Up to 50 °C no molybdenum-containing species were observed in solution (Figure 3 c) and the solid phase displayed the XANES spectrum of pure $MoO_3 \cdot 2H_2O$. The first slight changes were observed at 90 °C, and the reaction sets in around 99 °C (Figure 3 a,b). The XANES and Fourier transformed EXAFS spectra (Figure 3 a,b) demonstrate the continuous transformation of $MoO_3 \cdot 2H_2O$ into MoO_3 nanorods at 99 °C and do not indicate the presence of any intermediates (for reference spectra see the Supporting Information). Furthermore, the concentration of water-soluble species increases significantly at around 95 °C and rises continuously up to 150 °C. Note that the separation into individual MoO_3 nanorods proceeds at these elevated temperatures (cf. Figure 1-I/II d, top). The reaction starts as soon as the first soluble Mo species are detected and it accelerates at higher temperature so that the concentration of Mo species in solution increases. Furthermore, the rod formation is diffusion limited, as shown by the reaction being slower when performed in glass wool (see Experimental Section). All these observations strongly support a solution-based mechanism rather than a topotactic transformation of $MoO_3 \cdot 2H_2O$ into MoO_3.

In situ-EDXRD techniques were employed to study the time-resolved formation of MoO_3 rods from $MoO_3 \cdot 2H_2O$. A typical result of the time-dependent evolution of the diffraction patterns at 120 °C in acetic acid is shown in Figure 4 a. The Mo signals and the characteristic reflections of $MoO_3 \cdot 2H_2O$ (Figure 4 a, inset) are visible from the start. After a temperature-dependent induction time (in this case: 8 min) during which the signals of the starting material vanish, the first reflections of the product are observed and the product starts to form without the occurrence of a crystalline intermediate. All the reflections of the material grow simultaneously. The reaction is complete after another 7–8 min. The crystallization curve ($\alpha(t)$ vs. time) has a sigmoidal shape (Figure 4 b) which is typical for the kinetics of many solid-state reactions. Compared to other solid-state reactions, the velocity of the MoO_3 rod formation is very high. Therefore, a further evaluation of the observed kinetic data was not possible.

In summary, the formation of MoO_3 rods is a rapid process that is finished within minutes at temperatures well below 180 °C. All the experimental results point to a quick dissolution–precipitation mechanism without a crystalline intermediate phase. Thus, the high anisotropy of the MoO_3

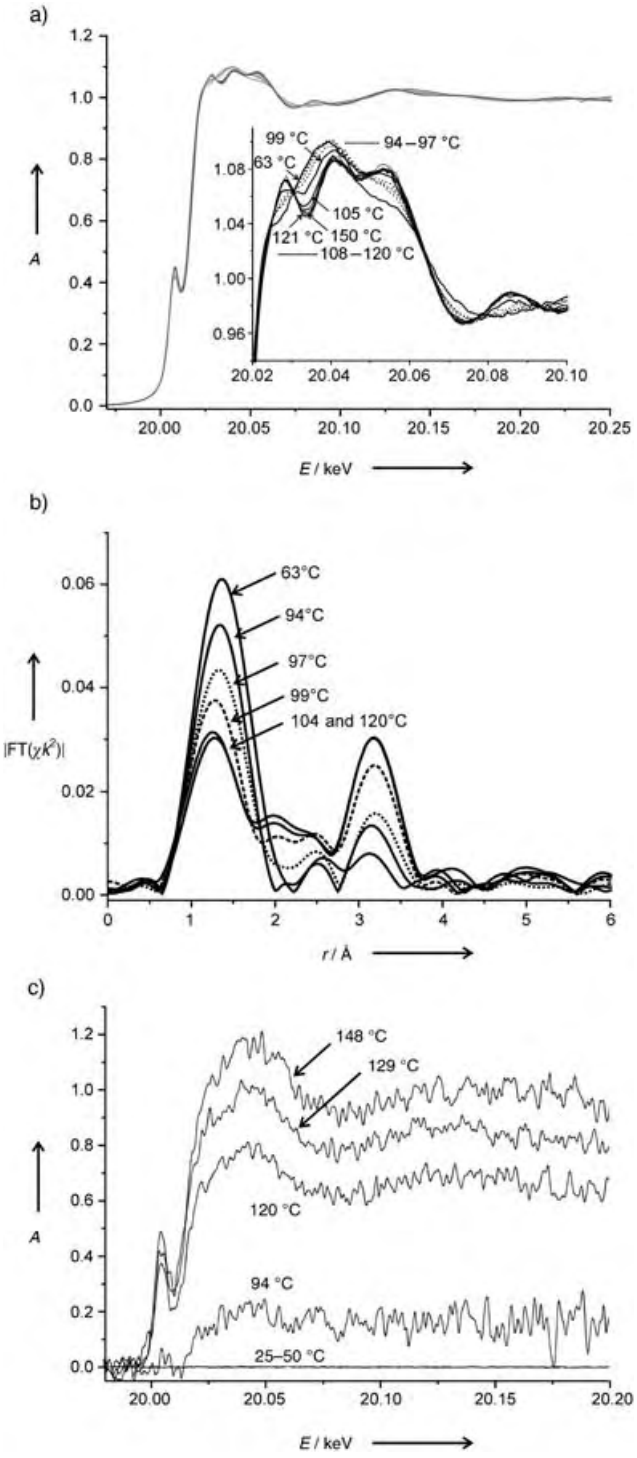


Figure 3. a) Molybdenum K-edge X-ray absorption near edge spectra during the hydrothermal reaction of $MoO_3 \cdot 2H_2O$ to MoO_3 fibers (solid phase), inset: expansion of the 20.02–20.1 region, b) Fourier transforms of the EXAFS spectra, c) molybdenum K-edge XANES spectra of the liquid phase during the reaction. The intensity of the absorption step is referenced against the spectrum recorded at 150 °C. *A* and $|FT(\chi k^2)|$ in arbitrary units.

 © 2005 Wiley-VCH Verlag GmbH & Co. KGaA, Weinheim

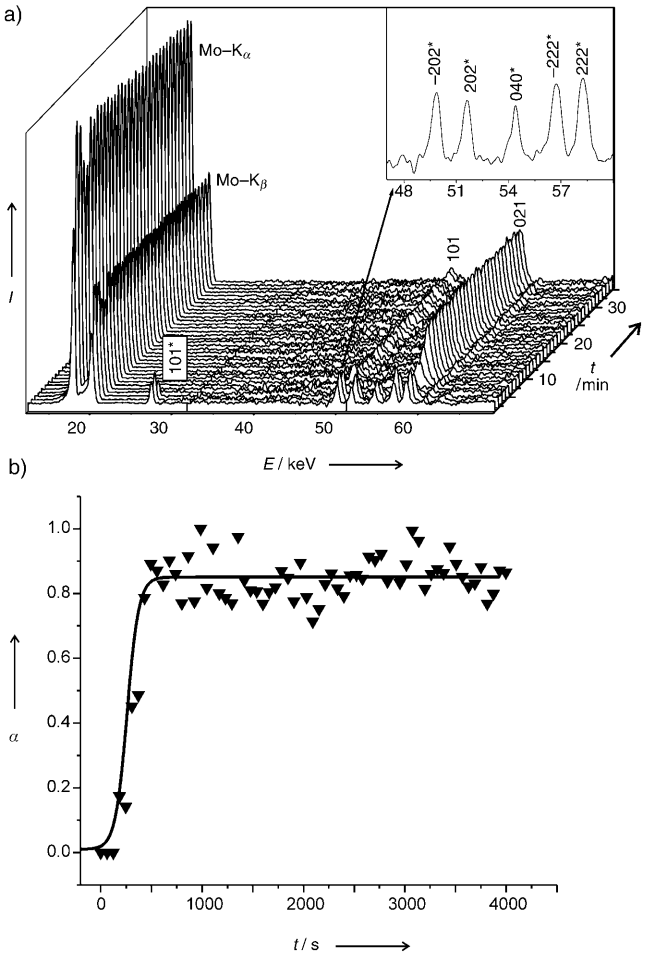


Figure 4. a) Time-resolved, background-corrected powder patterns recorded at 120 °C. The indices of the starting material (*), the product, and the Mo fluorescences are marked (the inset shows a magnification of the first spectrum), b) time dependence of the extent of reaction α for reflection (021) at 120 °C. The crystallization curve has a sigmoidal fit.

fibers presumably arises from the higher growth velocity of the [001] crystal direction in the orthorhombic α-MoO_3 lattice cell (*Pbnm*, $a = 3.9630$, $b = 13.856$, $c = 3.6966$ Å).[41,42] Our approach provides a versatile strategy towards understanding solvothermal reactions. After a series of orientating ex situ quenching experiments, the temperature-dependent solid–liquid equilibria of a given reaction can be monitored with a newly developed autoclave suitable for in situ-EXAFS spectroscopy. A kinetic study based on in situ-EDXRD provides the essential complementary information. In this way, the solvothermal mechanisms and the role of the precursor material are analyzed from different perspectives. Such insights are essential for optimizing syntheses for industrial scale-up processes. In conclusion, the presented approach is a step towards the rational solvothermal design of nanomaterials and of syntheses proceeding by amorphous and/or liquid phases in general.

Experimental Section

For the quenching experiments, $MoO_3 \cdot 2H_2O$ (180 mg, 1 mmol), glacial acetic acid (0.5 mL), and water (1.5 mL) were added to a glass ampoule (volume 23 mL) that was sealed under atmospheric pressure. The ampoules were heated for 20 min at 80, 100, 120, or 180 °C and subsequently quenched at −8 °C in a NaCl/ice mixture. The products were centrifuged several times in water, ethanol, and acetone and then subjected to scanning electron microscopy (SEM, LEO 1530 (FEG) microscope with 1 kV electrons) and to X-ray powder analysis (STOE STADI-P2 diffractometer, flat sample holders, $Cu_{K\alpha}$ radiation).

The in situ EXAFS and XANES experiments were performed at the beamline X1 at HASYLAB (DESY, Hamburg, Germany). $MoO_3 \cdot 2H_2O$ (50 mg) was embedded between glass wool plugs to fix the solid phase and were loaded together with water (3 mL) into a newly designed spectroscopic cell (see Supporting Information). The EXAFS scans around the molybdenum K edge were recorded between 19850 and 21200 eV under stationary conditions (liquid solution and solid phase) and were calibrated with a Mo reference foil. Faster spectra during the change of the reaction conditions were recorded in the QEXAFS mode between 19950 and 20450 eV (110 s/spectrum). The following procedure was applied: Heating to 150 °C in 1.5 °C min^{-1} steps from RT to 50, 94, 120, and 150 °C. The raw data were energy-calibrated with the according reference foil, background corrected and normalized (WINXAS 3.0 software[43]). Fourier transformation for EXAFS data during dynamic changes was applied to the k^3-weighted functions in the interval $k = 3.5$–9.3 $Å^{-1}$.

MoO_3 nanorods were obtained during the in situ EDXRD experiments (HASYLAB beamline F3, Hamburg, Germany) from (230.0 mg, 1.27 mmol) $MoO_3 \cdot 2H_2O$ in a solution of glacial acetic acid (0.4 mL) and H_2O (1.1 mL). The reaction was carried out under autogeneous pressure and isothermal conditions in sealable glass tubes as inserts for autoclaves (see Supporting Information).[22,31] The reaction vessel was transferred into the autoclave, and the reaction time was started after a delay time of approximately 1 min. The reaction temperatures were then reached after about 30 s, and X-ray powder patterns were recorded with acquisition times of 120 s. The spectra were evaluated with EDXPow.[44] The reflection profiles were modeled with a Gaussian peak shape, and the intensities of the product reflections were normalized against the peak intensities of the $Mo_{K\alpha}$ resonance.

Received: February 10, 2005
Revised: May 17, 2005
Published online: August 1, 2005

Keywords: EXAFS spectroscopy · hydrothermal synthesis · in situ spectroscopy · molybdenum oxide · nanostructures

[1] *Encyclopaedia of Nanoscience and Nanotechnology* (Ed.: H. S. Nalwa), American Scientific Publishers, Stevenson Ranch, CA, **2004**.
[2] *Nanoparticles* (Ed.: G. Schmid), Wiley-VCH, Weinheim, **2004**.
[3] *The Chemistry of Nanostructured Materials* (Ed.: P. Yang), World Scientific Publishers, Singapore, **2003**.
[4] R. Tenne, *Angew. Chem.* **2003**, *115*, 5280; *Angew. Chem. Int. Ed.* **2003**, *42*, 5124.
[5] C. N. R. Rao, A. K. Cheetham, *J. Mater. Chem.* **2001**, *11*, 2887.
[6] C. N. R. Rao, B. Raveau, *Transition Metal Oxides*, VCH, New York, **1995**.
[7] C. N. R. Rao, F. L. Deepak, G. Gundiah, A. Govindaraj, *Prog. Solid State Chem.* **2003**, *31*, 5.
[8] G. R. Patzke, F. Krumeich, R. Nesper, *Angew. Chem.* **2002**, *114*, 2554; *Angew. Chem. Int. Ed.* **2002**, *41*, 2446.
[9] J. Haber, E. Lalik, *Catal. Today* **1997**, *33*, 119.

 © 2005 Wiley-VCH Verlag GmbH & Co. KGaA, Weinheim

[10] J. B. Wagner, S. B. Abd Hamid, D. Othman, O. Timpe, S. Knobl, D. Niemeyer, D. S. Su, R. Schlögl, *J. Catal.* **2004**, *225*, 87.
[11] A. Baiker, P. Dollenmeier, A. Reller, *J. Catal.* **1987**, *103*, 394.
[12] A. K. Prasad, P. I. Gouma, *J. Mater. Sci.* **2003**, *38*, 4347.
[13] S. S. Sunu, E. Prabhu, V. Jayaraman, K. J. Guanasekar, T. K. Seshariji, T. Guanasekaran, *Sens. Actuators B* **2004**, *101*, 161.
[14] G. R. Patzke, A. Michailovski, F. Krumeich, R. Nesper, J.-D. Grunwaldt, A. Baiker, *Chem. Mater.* **2004**, *16*, 1126.
[15] A. Michailovski, F. Krumeich, G. R. Patzke, *Helv. Chim. Acta* **2004**, *87*, 1029.
[16] K. Byrappa, M. Yoshimura, *Handbook of Hydrothermal Technology*, Noyes, Park Ridge, NJ, **2001**.
[17] R. I. Walton, *Chem. Soc. Rev.* **2002**, *31*, 230.
[18] G. Demazeau, *J. Mater. Chem.* **1999**, *9*, 15.
[19] R. I. Walton, D. O'Hare, *Chem. Commun.* **2000**, 2283.
[20] A. K. Cheetham, C. F. Mellot, *Chem. Mater.* **1997**, *9*, 229.
[21] R. I. Walton, A. Norquist, R. I. Smith, D. O'Hare, *Faraday Discuss.* **2002**, *122*, 331.
[22] L. Engelke, M. Schaefer, M. Schur, W. Bensch, *Chem. Mater.* **2001**, *13*, 1383.
[23] J.-D. Grunwaldt, R. Wandeler, A. Baiker, *Catal. Rev. Sci. Eng.* **2003**, *45*, 1.
[24] R. I. Walton, T. Loiseau, D. O'Hare, G. Férey, *Chem. Mater.* **1999**, *11*, 3201.
[25] R. E. Morris, S. J. Weigel, P. Norby, J. C. Hanson, A. K. Cheetham, *J. Synchrotron Radiat.* **1996**, *3*, 301.
[26] D. Hooper, P. Barnes, J. K. Cockcroft, A. C. Jupe, S. D. M. Jacques, S. P. Bailey, F. Lupo, M. Vickers, M. Hanfland, *Phys. Chem. Chem. Phys.* **2003**, *5*, 4946.
[27] R. J. Francis, S. O'Brien, A. M. Fogg, P. Shiv Halasyamani, D. O'Hare, T. Loiseau, G. Férey, *J. Am. Chem. Soc.* **1999**, *121*, 1002.
[28] P. Norby, J. C. Hanson, *Catal. Today* **1998**, *39*, 301.
[29] S. Shaw, S. M. Clark, C. M. B. Henderson, *Chem. Geol.* **2000**, *167*, 129.
[30] S. Shaw, M. B. Henderson, S. M. Clark, *Am. Mineral.* **2002**, *87*, 533.
[31] L. Engelke, M. Schaefer, F. Porsch, W. Bensch, *Eur. J. Inorg. Chem.* **2003**, 506.
[32] A. M. Beale, G. Sankar, *Chem. Mater.* **2003**, *15*, 146.
[33] R. I. Walton, F. Millange, R. I. Smith, T. C. Hansen, D. O'Hare, *J. Am. Chem. Soc.* **2001**, *123*, 12547.
[34] F. Lupo, J. K. Cockcroft, P. Barnes, P. Stukas, M. Vickers, C. Norman, H. Bradshaw, *Phys. Chem. Chem. Phys.* **2004**, *6*, 1837.
[35] B. S. Clausen, H. Topsøe, R. Frahm, *Adv. Catal.* **1998**, *42*, 315.
[36] J.-D. Grunwaldt, B. S. Clausen, *Top. Catal.* **2002**, *18*, 37.
[37] G. Sankar, J. M. Thomas, *Top. Catal.* **1999**, *8*, 1.
[38] J.-D. Grunwaldt, M. Ramin, M. Rohr, A. Michailovski, G. R. Patzke, A. Baiker, *Rev. Sci. Instrum.* **2005**, *76*, 054104.
[39] J. R. Günter, *J. Solid State Chem.* **1972**, *5*, 354.
[40] D. B. Williams, C. B. Carter, *Transmission Electron Microscopy*, Plenum, New York, **1996**.
[41] J. Li, P. Wei, W. Ruigang, J. Chen, *Key Eng. Mater.* **2002**, *224–226*, 367.
[42] G. Andersson, A. Magneli, *Acta Chem. Scand.* **1950**, *4*, 793.
[43] T. Ressler, *J. Synchrotron Radiat.* **1998**, *5*, 118.
[44] F. Porsch, *EDXPow*, V. 3.15, RTI GmbH, Paderborn **2002**.

 © 2005 Wiley-VCH Verlag GmbH & Co. KGaA, Weinheim

Metallocenes

DOI: 10.1002/anie.200500686

Synthesis of *ansa*-[2]Boracyclopentadienylcycloheptatrienylchromium and Its Reaction to the *ansa*-Platinabis(boryl) Complex by Oxidative Addition of the Boron–Boron Bond**

Holger Braunschweig, Matthias Lutz, and Krzysztof Radacki*

Metalation reactions are of great importance in metallocene chemistry since they provide access to a wide variety of functionalized sandwich complexes. Among those, the dilithiation of ferrocene[1] and related compounds such as bis(benzene)chromium,[2] for which an alkyllithium base is employed in the presence of a chelating amine (typically *N*,*N*,*N*′,*N*′-tetramethylethylenediamine = tmeda), are the most prominent examples to accomplish this goal. Recently, Mulvey and co-workers reported the selective tetrametalation of ferrocene[3] and monometalation of bis(benzene)chromium[4] by the use of mixed alkali-metal–magnesium amide bases.

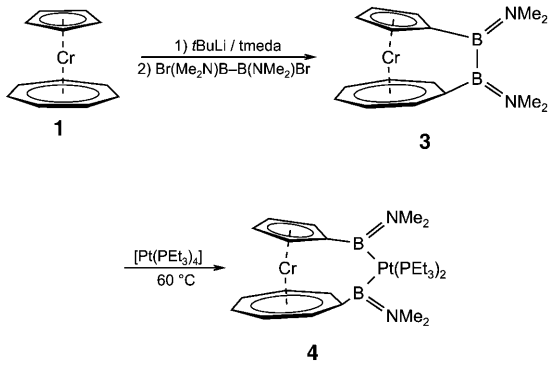
Our interest focused on cyclopentadienylcycloheptatrienylchromium $[(\eta^5\text{-}C_5H_5)Cr(\eta^7\text{-}C_7H_7)]$ (trochrocene **1**),[5] which is isoelectronic to bis(benzene)chromium and was intensively studied by Fischer and co-workers.[6,7] Although the metalation of trochrocene was the subject of a series of studies, in which either *n*-amylsodium[7] or mixtures comprising *n*BuLi/tmeda[8] were employed, there is no precedence for the metalation of both the Cp and the Cht ring. We achieved the double lithiation of trochrocene by using a *t*BuLi/tmeda mixture, which resulted in the formation of the base-stabilized compound $[(\eta^5\text{-}C_5H_4Li)Cr(\eta^7\text{-}C_7H_6Li)]\cdot$tmeda (**2**) in yields of up to 80%. The ^{1}H NMR spectrum of **2** is in agreement with an overall C_S-symmetric compound in solution and features two signals for the Cp ligand ($\delta = 3.51$ and 3.86 ppm) and two signals for the Cht ring ($\delta = 5.23$–5.30 and 5.70 ppm) with a relative intensity of 2:2:4:2. However, the ^{13}C NMR spectrum exhibits only five resonances for the aromatic carbon atoms; the *ipso*-carbon atoms are undetectable at room temperature, a fact which is probably due to the quadrupolar moment of the Li atom.[9]

Dilithiotrocrocene (**2**) was subsequently treated with stoichiometric amounts of $Br(NMe_2)B{-}B(NMe_2)Br$ to afford the [2]boratrochrocenophane **3**, which was isolated from pentane solutions at −30 °C as green crystals in 35–45% yields (Scheme 1). The most noteworthy feature in the ^{1}H NMR spectrum of **3** is the splitting of the Cp resonances

[*] Prof. Dr. H. Braunschweig, Dr. M. Lutz, Dr. K. Radacki
Institut für Anorganische Chemie
Bayerische Julius-Maximilians-Universität Würzburg
Am Hubland, 97074 Würzburg (Germany)
Fax: (+49) 931-888-4623
E-mail: h.braunschweig@mail.uni-wuerzburg.de

[**] This work was supported by the DFG and EPSRC.

 © 2005 Wiley-VCH Verlag GmbH & Co. KGaA, Weinheim



Scheme 1. Synthesis of the [2]boratrochrocenophane **3** and Pt^0-mediated oxidative cleavage of the boron–boron bond.

into two apparent triplets ($\delta = 3.90$ and 4.05 ppm) and of the Cht resonances into three multiplets ($\delta = 5.51$–5.52, 5.57–5.60 and 5.78–5.79 ppm), which are significantly lowfield shifted compared to the corresponding resonances in trochrocene ($\delta = 3.66$ ppm, C_5H_5, 5.45 ppm, C_7H_7). Owing to chemical inequivalence and hindered rotation, four resonances are detected for the aminomethyl groups of **3** in the ^{1}H and ^{13}C NMR spectra. As for the dilithio compound **2**, there are only five resonances detectable for the aromatic carbon atoms between $\delta = 77.58$ and 93.06 ppm. Moreover, the two expected ^{11}B NMR resonances were detected at $\delta = 45.05$ and 48.90 ppm.[10]

To gain more detailed insight into the structural properties of **3**, the compound was subjected to a single-crystal X-ray diffraction analysis (Figure 1).[11] In accord with the molecular geometry of $[(\eta^5\text{-}C_5H_5)Cr(\eta^7\text{-}C_7H_7)]$,[12] the metal–carbon distances to the seven-membered ring (2.1370(18)–2.1683(20) Å) are not markedly different from those to the five-membered ring (2.1616(20)–2.2056(18) Å). In contrast, the corresponding nonbridged titanium and vanadium congeners display a metal–(η^7-C_7H_7) separation that is markedly smaller than the metal–(η^5-C_5H_5) distance.[12] Since a decrease of the interatomic metal–carbon distance greatly increases the overlap of the e_2 orbital of the ligand with the $d_{x^2-y^2}$ orbitals of the metal, these findings emphasize the importance of the δ bonding in the Ti–(η^7-C_7H_7) moiety, which is more pronounced than in the case of Cr.[8,13] The incorporation of the [2]bora bridge into the framework of trochrocene imposes moderate molecular strain, which is manifested in the tilt angle $\alpha = 8.9°$. This value is comparable to that for previously reported [2]boraarenophanes[14] but significantly smaller than that for highly strained [1]boraferrocenophanes.[15]

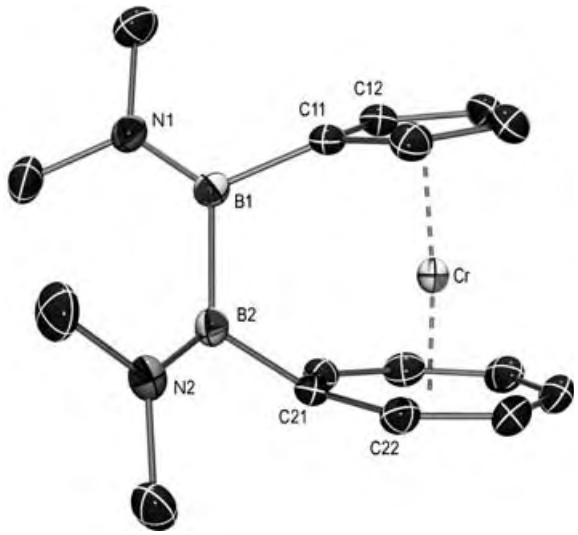


Figure 1. Molecular structure of **3**.[11] Selected bond lengths [Å] and angles [°]: Cr-C11 2.1806(18), Cr-C12 2.1932(18), Cr-C13 2.2056(18), Cr-C14 2.1939(20), Cr-C15 2.1616(20), Cr-C21 2.1370(18), Cr-C22 2.1683(20), Cr-C23 2.1597(19), Cr-C24 2.1676(19), Cr-C25 2.1649(19), Cr-C26 2.1559(18), Cr-C27 2.1386(17), B1-B2 1.7260(29), B1-C11 1.5957(27), B2-C21 1.6062(27), B1-N1 1.3902(26), B2-N2 1.3837(27), Cr-X_{Cp} 1.823, Cr-X_{Cht} 1.416; X_{Cp}-Cr-X_{Cht} 173.1, C21-B2-B1-C11 −40.5 (X = centroid).

Especially in the case of Si-bridged *ansa* complexes, the oxidative addition of the bridging Si–C bond to late transition metals has led to very interesting heterodinuclear complexes, which are key intermediates of the metal-catalyzed ring-opening polymerization (ROP) of such metallocenophanes.[16] Extending this reactivity pattern to B-bridged metallocenophanes would be highly desirable, for example, to provide an alternative to the commonly applied thermally induced ROP, which unfortunately fails in the case of thermally labile complexes.[14,15] The corresponding oxidative addition of a [1]borametallocenophane, however, is precluded by the strength of the B–C bond, which significantly exceeds that of a Si–C linkage.[17] Moreover, the reversed reaction, that is, the reductive elimination of B–C bonds from late transition-metal centers, is thermodynamically favorable and is known to be a key step in metal-catalyzed hydroboration.[18]

B–B bonds, however, are prone to undergo facile oxidative addition reactions with a variety of low-valent transition-metal complexes[18d,19] with concomitant formation of bisboryl–metal species $M(BR_2)_2$.[20] Hence, diboranes(4) have been very successfully applied to the transition-metal-catalyzed diboration of alkenes,[21] alkynes,[22] and 1,3-dienes.[23]

These findings have prompted us to further investigate [2]boratrochrocenophane **3** as a suitable candidate for a boron–boron bond cleavage. To this end, treatment of **3** with stoichiometric amounts of $[Pt(PEt_3)_4]$ in benzene at elevated temperature for two days afforded the oxidative addition product **4** as a green, crystalline solid in 85 % yield. The NMR spectroscopic data of **4** are in full agreement with the formulation of a C_1-symmetric compound. Interestingly, the ^{31}P NMR spectrum exhibits two singlets at $\delta = 10.69$ and 11.76 ppm with a peak widths at half height of about 70 Hz, which are flanked by characteristic ^{31}P–^{195}Pt satellites with coupling constants of $J_{P,Pt} = 1139.45$ Hz and $J_{P,Pt} = 1186.22$ Hz, respectively. However, no coupling between the nonequivalent phosphorus atoms could be observed. Previously, $^2J_{P,P}$ couplings of 19 Hz have been reported for a [2]platinasilaferrocenophane bearing an unsymmetrically substituted *cis*-$\{Pt(PEt_2)_2\}$ moiety.[24] The absence of ^{31}P–^{31}P couplings in the ^{31}P NMR spectrum between the two chemically nonequivalent ^{31}P atoms in **4** is presumably attributable to the

 © 2005 Wiley-VCH Verlag GmbH & Co. KGaA, Weinheim

quadrupolar moment imposed by the ^{11}B nuclei.[20b] Two ^{11}B resonances ($\delta = 60.63$ and 66.95 ppm) are recorded on a high-field NMR spectrometer.[10]

To confirm the structural details of **4** in the solid state, a single-crystal structure analysis was carried out (Figure 2).[11] As to be expected the incorporation of the $Pt(PEt_3)_2$ subunit

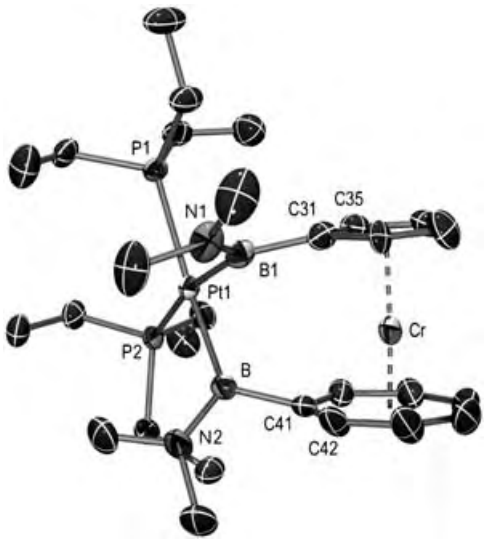


Figure 2. Molecular structure of **4**.[11] Selected bond lengths [Å] and angles [°]: Cr-C31 2.181, Cr-C32 2.181, Cr-C33 2.173, Cr-C34 2.174, Cr-C35 2.152, Cr-C41 2.178, Cr-C42 2.158, Cr-C43 2.156, Cr-C44 2.157, Cr-C45 2.158, Cr-C46 2.144, Cr-C47 2.130, B1-C31 1.5956(41), B2-C41 1.6029(39), B1-Pt1 2.1081(28), B2-Pt1 2.0963(28), B1-N1 1.4187(40), B2-N2 1.4246(36), Pt1-P1 2.3463(7), Pt1-P2 2.3399(6); B1-Pt1-P1 90.27(8), B2-Pt1-P2 94.53(8), B1-Pt1-B2 76.42(12), P1-Pt1-P2 99.18(2), B2-Pt1-P1 165.98(9), B1-Pt1-P2 168.92(9), Cr-X_{Cp} 1.800, Cr-X_{Cht} 1.422, X_{Cp}-Cr-X_{Cht} 176.91 (X = centroid).

leads to a drastic release of molecular strain, as illustrated by the tilt angle $\alpha = 3.48(0.15)°$, thus allowing the arene ligands in **4** to be in an almost parallel arrangement. Notable pertinent metric parameters around the platinum center, which displays a distorted square-planar environment, include the Pt–B bond lengths (Pt1–B1 2.108(3), Pt1–B2 2.096(3) Å), the Pt–P distances (Pt1–P1 2.3463(7), Pt1–P2 2.3399(6) Å), the B-Pt-B angle (76.42(12)°), and the P-Pt-P bond angle (99.18(2)°) all of which lie within previously reported ranges.[19c,20a,20b,22c,22e]

Herein, we have reported the synthesis and structural characterization of the first [2]boratrochrocenophane **3** and its reaction with the low-valent species $[Pt(PEt_3)_4]$, which yields the [3]boraplatinatrochrocenophane **4** by oxidative addition of the boron–boron bond. This reaction is of particular interest, since **4** has the potential for subsequent diboration reactions of alkynes, thus leading to polymers bearing the trochrocene moiety in its backbone. Corresponding studies are currently ongoing in our laboratories and will be reported elsewhere.

Experimental Section

2: A solution of *t*BuLi in pentane (12.42 mL, 1.7 M) was added slowly at 0 °C to a suspension of **1** (2.00 g, 9.60 mmol) in pentane (50 mL) and tetramethylethylenediamine (tmeda) (2.45 g, 3.15 mL, 21.1 mmol). The yellow suspension was allowed to warm up to ambient temperature and stirred overnight. The green-yellow precipitate was filtered off, washed with pentane (2 × 20 mL), and dried in vacuo (2.54 g, yield 79 %). ^1H NMR (500 MHz, [D$_8$]THF, 297 K): $\delta = 2.08$ (s, 12 H; $((CH_3)_2NCH_2)_2$), 2.23 (s, 4 H; $((CH_3)_2NCH_2)_2$), 3.51 (s, 2 H; C_5H_4), 3.86 (s, 2 H; C_5H_4), 5.23–5.30 (m, 4 H; C_7H_6), 5.70 ppm (m, 2 H; C_7H_6); $^7Li\{^1H\}$ NMR (117 MHz, [D$_8$]THF, 297 K): $\delta =$ 2.39 ppm (br. s); $^{13}C\{^1H\}$ NMR (126 MHz, [D$_8$]THF, 297 K)): $\delta =$ 46.30 ($(CH_3)_2NCH_2)_2$), 58.69 ($(CH_3)_2NCH_2)_2$), 78.82 (C_5H_4), 85.75 (C_7H_6), 86.33 (C_5H_4), 91.48 (C_7H_6), 97.77 ppm (C_7H_6).

3: A solution of $B_2Br_2(NMe_2)_2$ (1.70 g, 5.95 mmol) in pentane (20 mL) at −78 °C was added dropwise over a period of 30 min to a suspension of **2** (2.00 g, 5.95 mmol) in pentane (50 mL). After complete addition, the reaction mixture was stirred for 2 h at −78 °C and subsequently allowed to warm up to ambient temperature over a period of 6 h, during which time the color of the suspension changed from pale yellow to dark green. The suspension was filtered through Celite, and **3** was isolated by crystallization at −30 °C as a dark green solid (846 mg, 45 %). ^1H NMR (500.13 MHz, C_6D_6, 297 K): $\delta = 2.67$ (s, 3 H; $N(CH_3)_2$), 2.88 (s, 3 H; $N(CH_3)_2$), 2.91 (s, 3 H; $N(CH_3)_2$), 3.12 (s, 3 H; $N(CH_3)_2$), 3.90 (m, 2 H; C_5H_4), 4.05 (m, 2 H; C_5H_4), 5.51–5.52 (m, 2 H; C_7H_6), 5.57–5.60 (m, 2 H; C_7H_6), 5.78–5.79 ppm (m, 2 H; C_7H_6); $^{11}B\{^1H\}$ NMR (161 MHz, C_6D_6, 297 K): $\delta =$ 45.05, 48.90 ppm; $^{13}C\{^1H\}$ NMR (126 MHz, C_6D_6, 297 K): $\delta = 40.31$ ($N(CH_3)_2$), 40.98 ($N(CH_3)_2$), 43.66 ($N(CH_3)_2$), 43.94 ($N(CH_3)_2$), 77.58 (C_5H_4), 81.70 (C_5H_4), 86.70 (C_7H_6), 92.04 (C_7H_6), 93.06 ppm (C_7H_6); elemental analysis (%) calcd for $C_{16}H_{22}B_2CrN_2$ (315.98): C 60.82, H 7.02, N 8.87; found: C 61.07, H 6.84, N 9.03.

4: A resealable bulb was charged with $[Pt(PEt_3)_4]$ (235 mg, 0.352 mmol) and heated for 20 min at 60 °C under vacuum. Compound **3** (100 mg, 0.352 mmol) and benzene (2 mL) were added to the resulting red oil. The mixture was heated at 60 °C for two days and subsequently dried in vacuo. The residue was taken up in heptane (20 mL) and filtered through a short pad of Celite. The solution was concentrated to about 3 mL and then cooled to −78 °C. The greenish crystals that separated were decanted from the mother liquid, washed with pentane (2 × 3 mL), and dried in vacuum. Yield 200 mg (0.268 mmol, 85 %). ^1H NMR (500.13 MHz, C_6D_6, 297 K): $\delta = 0.90$ (dt, $J = 13.85$, 7.60 Hz, 9 H; $P(CH_2CH_3)_3$), 1.13 (dt, $J = 14.15$, 7.60 Hz, 9 H; $P(CH_2CH_3)_3$), 1.52 (m, 6 H; $P(CH_2CH_3)_3$), 1.79 (m, 6 H; $P(CH_2CH_3)_3$), 2.94 (d, $^5J_{P,H} = 1.60$ Hz, 3 H; $N(CH_3)_2$), 3.12 (d, $^5J_{P,H} =$ 1.55 Hz, 3 H; $N(CH_3)_2$), 3.32 (s, $^4J_{Pt,H} = 4.45$ Hz, 3 H; $N(CH_3)_2$), 3.41 (s, $^4J_{Pt,H} = 5.05$ Hz, 3 H; $N(CH_3)_2$), 4.04 (m, 1 H; C_5H_4), 4.06 (m, 1 H; C_5H_4), 4.26 (m, 1 H; C_5H_4), 4.58 (m, 1 H; C_5H_4), 5.65 (t, $J = 7.55$ Hz, 1 H; C_7H_6), 5.67 (t, $J = 7.25$ Hz, 1 H; C_7H_6), 5.74 (t, $J = 7.25$ Hz, 2 H; C_7H_6), 5.85 (t, $J = 7.55$ Hz, 1 H; C_7H_6), 6.25 ppm (d, $J_{H,H} = 7.55$, $^4J_{H,H} =$ 17.65 Hz, 1 H; C_7H_6); $\{^1H\}^{11}B$ NMR (160.47 MHz, C_6D_6, 297 K): $\delta =$ 60.63, 66.95 ppm; $^{13}C\{^1H\}$ NMR (125.77 MHz, C_6D_6, 297 K): $\delta = 8.59$ (s, $J_{C,Pt} = 14.66$ Hz; $P(CH_2CH_3)_3$), 9.03 (s, $J_{C,Pt} = 16.49$ Hz; $P(CH_2CH_3)_3$), 20.01 (dd, $J_{C,P} = 18.32$, 5.50 Hz, $J_{C,Pt} = 20.63$ Hz; $P(CH_2CH_3)_3$), 21.12 (dd, $J_{C,P} = 17.41$, 5.50 Hz, $J_{C,Pt} = 21.01$ Hz; $P(CH_2CH_3)_3$), 41.35 (d, $J_{C,P} = 3.66$ Hz, $J_{C,Pt} = 32.99$ Hz; $N(CH_3)_2$), 43.17 (d, $J_{C,P} = 3.67$ Hz, $J_{C,Pt} = 32.99$ Hz; $N(CH_3)_2$), 48.72 (d, $J_{C,P} =$ 3.67, $J_{C,Pt} = 98.99$ Hz, $N(CH_3)_2$), 49.75 (d, $J_{C,P} = 3.67$, $J_{C,Pt} =$ 105.39 Hz; $N(CH_3)_2$), 76.99 (s, $J_{C,Pt} = 9.16$ Hz; C_5H_4), 78.15 (s, C_5H_4), 81.37 (d, $J_{C,P} = 2.75$, $J_{C,Pt} = 19.26$ Hz; C_5H_4), 85.43 (s, C_7H_6), 87.25 (s, C_7H_6), 87.43 (s, C_7H_6), 88.07 (s, $J_{C,Pt} = 32.09$ Hz, C_5H_4), 90.59 (s, C_7H_6), 91.18 (s, C_7H_6), 94.89 ppm (s, $J_{C,Pt} = 22.92$ Hz, C_7H_6); $^{31}P\{^1H\}$ NMR (202 MHz, C_6D_6, 297 K): $\delta = 10.69$ (s, $J_{P,Pt} = 1139.45$ Hz, $\Delta\nu_{1/2} =$ 70 Hz), 11.76 ppm (s, $J_{P,Pt} = 1186.22$ Hz, $\Delta\nu_{1/2} = 66$ Hz); elemental

 © 2005 Wiley-VCH Verlag GmbH & Co. KGaA, Weinheim

analysis (%) calcd for $C_{28}H_{52}B_2CrN_2P_2Pt$ (747.37): C 45.00 H 7.01 N 3.75; found: C 45.12, H 7.23, N 3.86.

Received: February 23, 2005
Published online: July 13, 2005

Keywords: boron · chromium · metalation · oxidative addition · platinum

[1] M. Rausch, D. Ciappenelli, *J. Organomet. Chem.* **1967**, *13*, 127 – 136.
[2] C. Elschenbroich, *J. Organomet. Chem.* **1968**, *14*, 157 – 163.
[3] a) W. Clegg, K. W. Henderson, A. R. Kennedy, R. E. Mulvey, C. T. O'Hara, R. B. Rowlings, D. M. Tooke, *Angew. Chem.* **2001**, *113*, 4020 – 4023; *Angew. Chem. Int. Ed.* **2001**, *40*, 3902 – 3906; b) P. C. Andrikopoulos, D. R. Armstrong, W. Clegg, C. J. Gilfillan, E. Hevia, A. R. Kennedy, R. E. Mulvey, C. T. O'Hara, J. A. Parkinson, C. M. Tooke, *J. Am. Chem. Soc.* **2004**, *126*, 11 612 – 11 620.
[4] E. Heiva, G. W. Honeyman, A. R. Kennedy, R. E. Mulvey, D. C. Sherrington, *Angew. Chem.* **2005**, *117*, 70 – 74; *Angew. Chem. Int. Ed.* **2005**, *44*, 68 – 72.
[5] For the sandwich complex $[(\eta^5\text{-}C_5H_5)Cr(\eta^7\text{-}C_7H_7)]$, we wish to introduce the trivial name "trochrocene", which stands for [(η⁷-*tro*pylium)*chro*mium(η⁵-cyclop*en*tadi*en*yl)] and is in accord with the naming of $[(\eta^5\text{-}C_5H_5)V(\eta^7\text{-}C_7H_7)]$ as "trovacene" and $[(\eta^5\text{-}C_5H_5)Ti(\eta^7\text{-}C_7H_7)]$ as "troticene", see for example: C. Elschenbroich, O. Schiemann, O. Burghaus, K. Harms, *J. Am. Chem. Soc.* **1997**, *119*, 7452 – 7457; M. Tamm, A. Kunst, T. Bannenberg, E. Herdtweck, P. Sirsch, C. J. Elsevier, J. M. Ernsting, *Angew. Chem.* **2004**, *116*, 5646 – 5650; *Angew. Chem. Int. Ed.* **2004**, *43*, 5530 – 5534.
[6] E. O. Fischer, S. Breitschaft, *Angew. Chem.* **1963**, *75*, 94 – 95; *Angew. Chem. Int. Ed. Engl.* **1963**, *2*, 44 – 45.
[7] E. O. Fischer, S. Breitschaft, *Chem. Ber.* **1966**, *99*, 2905 – 2917.
[8] C. J. Groenenboom, H. J. De Liefde, Meijer, F. Jellinek, *J. Organomet. Chem.* **1974**, *69*, 235 – 240.
[9] M. Herberhold, U. Dörfler, B. Wrackmeyer, *J. Organomet. Chem.* **1997**, *530*, 117 – 120.
[10] Two separated signals could only be detected at 161 MHz. At lower fields the compounds displayed one broad resonance in the ^{11}B NMR spectra (**3**: $\delta = 47.7$ ppm, **4**: $\delta = 62.5$ ppm).
[11] The crystal data for **3** and **4** were collected on a Bruker APEX diffractometer with a CCD area detector and graphite-monochromated $Mo_{K\alpha}$ radiation. The structure was solved by using direct methods, refined with the Shelx software package (G. Sheldrick, University of Göttingen, **1997**) and expanded by using Fourier techniques. All non-hydrogen atoms were refined anisotropically. Hydrogen atoms were assigned at idealized positions and were included in structure factor calculations. Crystal data for **3**: $C_{16}H_{22}B_2CrN_2$ $M_r = 315.98$, green rods, $0.25 \times 0.18 \times 0.12$ mm, orthorhombic, space group $P2(1)2(1)2(1)$, $a = 10.6876(7)$ Å, $b = 11.7017(7)$ Å, $c = 12.3316(8)$ Å, $V = 1542.23(17)$ Å^3, $Z = 4$, $\rho_{calcd} = 1.361$ g cm^{-3}, $\mu = 0.734$ cm^{-2}, $F(000) = 664$, $T = 173(2)$ K, $R_1 = 0.0305$, $wR^2 = 0.0780$, 3559 independent reflections [$2\theta \leq 55.06°$] and 190 parameters. Crystal data for **4**: $C_{28}H_{52}B_2CrN_2P_2Pt$ $M_r = 747.37$, green plates, $0.31 \times 0.28 \times 0.17$ mm, monoclinic, space group $P2(1)/n$, $a = 8.5981(6)$ Å, $b = 17.6203(13)$ Å, $c = 21.1762(16)$ Å, $\beta = 91.3130(10)°$, $V = 3207.4(4)$ Å^3, $Z = 4$, $\rho_{calcd} = 1.548$ g cm^{-3}, $\mu = 4.815$ cm^{-2}, $F(000) = 1504$, $T = 193(2)$ K, $R_1 = 0.0206$, $wR^2 = 0.0505$, 6339 independent reflections [$2\theta \leq 52.12°$] and 325 parameters. Details of the X-ray crystal structure determination can be found in the Supporting Information. CCDC-263858 (**3**) and CCDC-263859 (**4**) contain the supplementary crystallographic data for this paper. These data can be obtained free of charge from the Cambridge Crystallographic Data Centre via www.ccdc.cam.ac.uk/data_request/cif.
[12] K. A. Lyssenko, M. Yu. Antipin, S. Yu. Ketkov, *Russ. Chem. Bull. Int. Ed.* **2001**, *50*, 130 – 141.
[13] a) C. J. Groenenboom, H. J. De Liefde, Meijer, F. Jellinek, *J. Organomet. Chem.* **1974**, *80*, 229 – 234; b) D. W. Clack, K. D. Warren, *J. Organomet. Chem.* **1978**, *152*, C60 – C62; c) D. W. Clack, K. D. Warren, *J. Organomet. Chem.* **1978**, *162*, 83 – 88; d) D. W. Clack, K. D. Warren, *Inorg. Chim. Acta* **1978**, *30*, 251 – 258.
[14] H. Braunschweig, M. Homberger, C. Hu, X. Zheng, E. Gullo, G. Glentsmith, M. Lutz, *Organometallics* **2004**, *23*, 1968 – 1970.
[15] a) H. Braunschweig, R. Dirk, M. Müller, P. Nguyen, R. Resendes, D. P. Gates, I. Manners, *Angew. Chem.* **1997**, *109*, 2433 – 2435; *Angew. Chem. Int. Ed. Engl.* **1997**, *36*, 2338 – 2340; b) H. Braunschweig, R. Dirk, U. Englert, A. Berenbaum, J. C. Green, A. J. Lough, I. Manners, *J. Am. Chem. Soc.* **2000**, *122*, 5765 – 5774.
[16] a) I. Manners, *Angew. Chem.* **1996**, *108*, 1712 – 1731; *Angew. Chem. Int. Ed. Engl.* **1996**, *35*, 1602 – 1621; b) P. Nguyen, P. Gomez-Felipe, I. Manners, *Chem. Rev.* **1999**, *99*, 1515 – 1548; c) I. Manners, *Chem. Commun.* **1999**, 857 – 865; d) I. Manners, *Adv. Organomet. Chem.* **1995**, *37*, 131 – 168.
[17] *Comprehensive Organometallic Chemistry, Vol. 1* (Eds.: E. W. Abel, F. G. A. Stone, G. Wilkinson, C. E. Housecroft), Pergamon, Oxford, **1982**, p. 5.
[18] a) K. Burgess, M. J. Ohlmeyer, *Chem. Rev.* **1991**, *91*, 1179 – 1191; b) I. Beletskaya, A. Pelter, *Tetrahedron* **1997**, *53*, 4957 – 5026; c) T. B. Marder, N. C. Norman, *Top. Catal.* **1998**, *5*, 63 – 73; d) T. Ishiyama, N. Miyaura, *J. Organomet. Chem.* **2000**, *611*, 392 – 402.
[19] For reviews on the formation of metal–boron bonds including oxidative addition of diboranes(4): a) H. Braunschweig, M. Colling, *Coord. Chem. Rev.* **2001**, *223*, 1 – 51; b) H. Braunschweig, *Angew. Chem.* **1998**, *110*, 1883 – 1898; *Angew. Chem. Int. Ed. Engl.* **1998**, *37*, 1737 – 1801; c) G. I. Irvine, M. J. G. Lesley, T. B. Marder, N. C. Norman, C. R. Rice, E. G. Robins, W. R. Roper, G. R. Whittell, L. J. Wright, *Chem. Rev.* **1998**, *98*, 2685 – 2722; d) M. R. Smith III, *Prog. Inorg. Chem.* **1999**, *48*, 505 – 567.
[20] a) N. Lu, N. C. Norman, A. G. Orpen, M. J. Quayle, P. L. Timms, G. R. Whittell, *J. Chem. Soc. Dalton Trans.* **2000**, 4032 – 4037; b) D. Curtis, M. J. G. Lesley, N. C. Norman, A. G. Orpen, J. Starbuck, *J. Chem. Soc. Dalton Trans.* **1999**, 1687 – 1694; c) W. Clegg, F. J. Lawlor, T. B. Marder, P. Nguyen, N. C. Norman, A. G. Orpen, M. J. Quayle, C. R. Rice, E. G. Robins, A. J. Scott, F. E. S. Souza, G. Stringer, G. R. Whittel, *J. Chem. Soc. Dalton Trans.* **1998**, 301 – 309; d) B. P. Cleary, R. Eisenberg, *Organometallics* **1995**, *14*, 4525 – 4534; e) J. C. Calbrese, S. A. Westcott, P. Nguyen, T. B. Marder, *J. Am. Chem. Soc.* **1993**, *115*, 4367 – 4368; f) J. F. Hartwig, X. M. He, *Angew. Chem.* **1996**, *108*, 352 – 353; *Angew. Chem. Int. Ed. Engl.* **1996**, *35*, 315 – 317; g) W. Clegg, F. J. Lawlor, G. Lesley, T. B. Marder, N. C. Norman, A. G. Orpen, M. J. Quayle, C. R. Rice, A. J. Scott, F. E. S. Souza, *J. Organomet. Chem.* **1998**, *550*, 183 – 192.
[21] a) R. T. Baker, P. Nguyen, T. B. Marder, S. A. Westcott, *Angew. Chem.* **1995**, *107*, 1451 – 1452; *Angew. Chem. Int. Ed. Engl.* **1995**, *34*, 1336 – 1338; b) T. Ishiyama, M. Yamamoto, N. Miyaura, *Chem. Commun.* **1997**, 689 – 690; c) C. N. Iverson, M. R. Smith, *Organometallics* **1997**, *16*, 2757 – 2760; d) T. B. Marder, N. C. Norman, C. R. Rice, *Tetrahedron Lett.* **1998**, *39*, 155 – 158; e) C. Dai, E. G. Robins, A. J. Scott, W. Clegg, D. S. Yufit, J. A. K. Howard, T. B. Marder, *Chem. Commun.* **1998**, 1983 – 1984; f) P. Nguyen, R. B. Coapes, A. D. Woodward, N. J. Taylor, J. M. Burke, J. A. K. Howard, T. B. Marder, *J. Organomet. Chem.* **2002**, *652*, 77 – 85; g) J. B. Morgan, S. P. Miller, J. P. Morken, *J. Am. Chem. Soc.* **2003**, *125*, 8702 – 8703; h) S. P. Miller, J. B. Morgan, F. J. Nepveux, J. P. Morken, *Org. Lett.* **2004**, *6*, 131 – 133.

 © 2005 Wiley-VCH Verlag GmbH & Co. KGaA, Weinheim

[22] a) T. Ishiyama, N. Matsuda, N. Miyaura, A. Suzuki, *J. Am. Chem. Soc.* **1993**, *115*, 11018 – 11019; b) T. Ishiyama, N. Matsuda, M. Murata, F. Ozawa, A. Suzuki, N. Miyaura, *Organometallics* **1996**, *15*, 713 – 720; c) C. N. Iverson, M. R. Smith, *J. Am. Chem. Soc.* **1995**, *117*, 4403 – 4404; d) C. N. Iverson, M. R. Smith, *Organometallics* **1996**, *15*, 5155 – 5165; e) G. Lesley, P. Nguyen, N. J. Taylor, T. B. Marder, A. J. Scott, W. Clegg, N. C. Norman, *Organometallics* **1996**, *15*, 5137 – 5154; f) R. L1. Thomas, F. E. S. Souza, T. B. Marder, *J. Chem. Soc. Dalton Trans.* **2001**, 1650 – 1656.

[23] T. Ishiyama, M. Yamamoto, N. Miyaura, *Chem. Commun.* **1996**, 2073 – 2074.

[24] a) N. P. Reddy, N. Choi, S. Shirnada, M. Tanaka, *Chem. Lett.* **1996**, *25*, 649 – 650; b) J. B. Sheridan, A. J. Lough, I. Manners, *Organometallics* **1996**, *15*, 2195 – 2197.

 © 2005 Wiley-VCH Verlag GmbH & Co. KGaA, Weinheim

Boron Ligands

DOI: 10.1002/anie.200501588

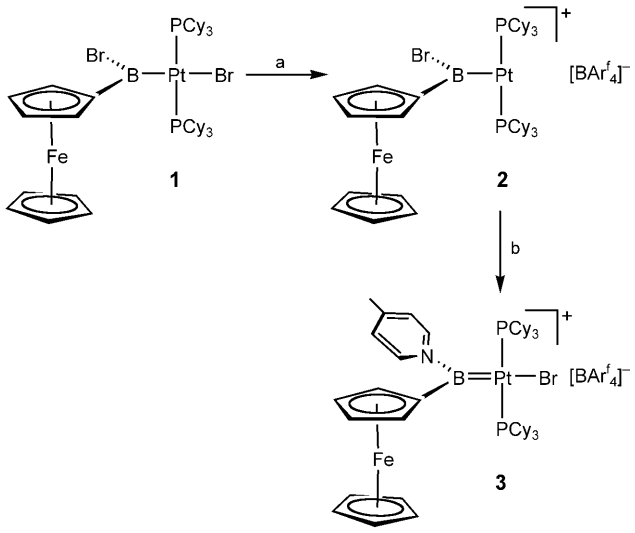
A T-Shaped Platinum(II) Boryl Complex as the Precursor to a Platinum Compound with a Base-Stabilized Borylene Ligand**

Holger Braunschweig, Krzysztof Radacki, Daniela Rais, and David Scheschkewitz*

Transition-metal boryl complexes constitute an abundant and important class of boron-containing transition-metal compounds,[1] in view of their intermediacy in the catalyzed hydro-[2] and diboration[3] of unsaturated organic substrates, as well as the selective C–H bond activation of alkanes and arenes.[4] A number of synthetic routes have been applied to the generation of boryl complexes.[1] Among these, that involving B–X (X = Cl, Br) bond oxidative addition has seldom been employed, and examples of rhodium and iridium,[5] palladium,[6] and platinum[7] boryl complexes synthesized in this fashion have only relatively recently appeared in the literature.

We previously reported the synthesis of *trans*-$[(Cy_3P)_2Pt(Br)\{B(Fc)Br\}]$ (Fc = ferrocenyl, Cy = cyclohexyl) (**1**) by reaction of $[Pt(PCy_3)_2]$ with $FcBBr_2$.[7b] A remarkable structural feature of crystalline **1** is the rather long Pt–Br bond length (2.6183(8) Å), which provides an indication of the high *trans* influence of the B(Fc)Br group. Indeed, on account of its strong σ-donor character, the boryl ligand exerts a higher *trans*-labilizing influence[8] than that of other σ donors, such as hydrido[7a,9] and stannyl groups,[6a] or π acceptors, such as CO.[10] Herein, we demonstrate how strongly this property influences the reactivity of **1**. Thus, the reaction of **1** with $Na[BAr^f_4]$ (Ar^f = 3,5-$C_6H_3(CF_3)_2$) leads to the T-shaped, three-coordinate platinum complex *trans*-$[(Cy_3P)_2Pt\{B(Fc)Br\}][BAr^f_4]$ (**2**). Such a species constitutes the precursor to the cationic, base-stabilized borylene complex *trans*-$[(Cy_3P)_2Pt(Br)\{B(Fc)(NC_5H_4\text{-}4\text{-}Me)\}][BAr^f_4]$ (**3**), which is obtained upon addition of 4-methylpyridine, via an overall 1,2-bromide migration from the boron center to the platinum center.

Treatment of a solution of **1** in CD_2Cl_2 with $Na[BAr^f_4]$ led to an immediate color change from bright orange to cherry red, with concomitant precipitation of NaBr (Scheme 1, a).



Scheme 1. a) $Na[BAr^f_4]$ in CD_2Cl_2; b) 4-methylpyridine in CD_2Cl_2.

The $^{31}P\{^1H\}$ NMR spectrum of the reaction mixture conclusively revealed the quantitative formation of a new compound within a few minutes, with the presence of a single signal at δ = 41.7 ppm (^1J(P,Pt) = 2914 Hz), strongly downfield shifted with respect to that of **1** (δ = 21.5 ppm, ^1J(P,Pt) = 2892 Hz).

In the ^1H NMR spectrum, two broad signals for the protons of the $[BAr^f_4]^-$ ion appeared at δ = 7.74 and 7.58 ppm, alongside a new set of signals for the ferrocenylboryl ligand, namely two multiplets at δ = 4.71 ppm (2H) and δ = 4.52 ppm (2H), and a singlet at δ = 4.26 ppm (5H). Surprisingly, no resonance signal was observed in the $^{11}B\{^1H\}$ NMR spectrum, probably due to broadening of the signal as a consequence of unresolved coupling to the platinum and phosphorus nuclei.[11]

Orange bricklike crystals of **2** were obtained by layering a solution of the complex in CD_2Cl_2 with hexane and cooling the solution to −36 °C. The X-ray diffraction study performed

[*] Prof. Dr. H. Braunschweig, Dr. K. Radacki, Dr. D. Rais, Dr. D. Scheschkewitz
Institut für Anorganische Chemie
Bayerische Julius-Maximilians-Universität Würzburg
Am Hubland 97074 Würzburg (Germany)
Fax: (+49) 931-888-4623
E-mail: h.braunschweig@mail.uni-wuerzburg.de

[**] This work was supported by the Deutsche Forschungsgemeinschaft and the Engineering and Physical Sciences Research Council. D.R. thanks the Alexander-von-Humboldt Foundation for a postdoctoral fellowship. The authors thank Dr. G. R. Whittell, Bristol, for helpful discussions.

Supporting information for this article is available on the WWW under http://www.angewandte.org or from the author.

 © 2005 Wiley-VCH Verlag GmbH & Co. KGaA, Weinheim

on a suitable single crystal confirmed that complex **2** was a three-coordinate platinum(II) boryl compound that displayed a distorted T-shaped geometry (P1-Pt1-P2 162.96(3)°; Figure 1).[12]

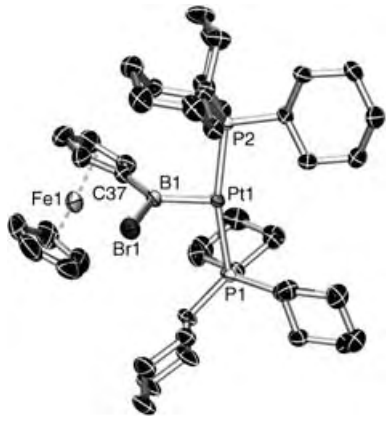


Figure 1. Molecular structure of **2**. Hydrogen atoms and the $[BAr^f_4]^-$ ion were omitted for clarity. Selected bond lengths [Å] and angle [°]: Pt1–B1 1.966(4), Pt1–P2 2.3071(8), Pt1–P1 2.3323(8), B1–Br1 1.955(4); P1-Pt1-P2 162.96(3).

Despite the absence of a ligand *trans* to the boryl group, the B1–Pt1 distance (1.966(4) Å) in **2** is, unexpectedly, only slightly shorter than that in crystalline **1** (1.9963(34) Å).[7b] This is presumably a consequence of the steric bulk of the tricyclohexylphosphane ligands, which prevents a closer approach of the boryl group to the metal center. The threefold coordination at the platinum center in the cationic portion of **2** is remarkable. It is well-established that the highly unsaturated, Lewis acidic nature of the metal center in 14-electron d^8ML_3 compounds greatly enhances the reactivity of these species, leading to interactions even with weak nucleophiles, such as solvent molecules, weakly coordinating anions,[13] or agostic C–H bonds.[14] In **2**, however, no such interaction is observed. Particularly noteworthy is the absence of any efficient agostic interaction between the metal center and the C–H bonds of the cyclohexyl groups. The shortest Pt···H–C distance is 2.542 Å (Pt···C–H 3.117 Å), which is considerably longer than corresponding distances in the complexes $[PtMe(P\textit{i}Pr_3)_2][1\text{-H-}\textit{closo}\text{-}CB_{11}Me_{11}]$ (Pt–H 2.24, Pt–C 2.859 Å)[14g] and $[Pt\{P(2,6\text{-}Me_2C_6H_3)Cy_2\}\{\kappa^2\text{-}P,C\text{-}P(2\text{-Me-6-}CH_2\text{-}C_6H_3)Cy_2\}][BAr^f_4]$ (Pt–C 2.432 Å)[14f] and in the range of those observed in truly three-coordinate *neutral* palladium complexes, in which the presence of agostic interactions was excluded.[15] Indeed, theoretical calculations on 14-electron d^8ML_3 boryl complexes of the type $[(R_3P)_2Rh(BX_2)]$ support the reluctance of such compounds to bind C–H bonds in the site opposite to the boryl group, owing to the extremely strong *trans* influence of the boryl ligand.[16] Thus, compound **2** represents a structurally characterized example of this class of complexes, and provides experimental confirmation of what was predicted from theoretical studies.

The absence of agostic interactions in **2** was supported by density functional calculations[17] and variable-temperature NMR studies. No appreciable change in the NMR spectra of **2** was observed upon cooling the sample to −60 °C. At lower temperatures, the signal in ^{1}H NMR spectrum at $\delta = 4.52$ ppm for two of the ferrocenyl protons broadened. At −90 °C, coalescence occurred, consistent with restricted rotation of the ferrocenyl group around the B–C(Fc) bond. Concomitant broadening of the initial singlet at $\delta = 41.7$ ppm was observed in the $^{31}P\{^1H\}$ NMR spectrum, and two separate broad signals at $\delta = 42.5$ and 38.3 ppm could be detected at −90 °C. However, none of these processes was accompanied by the appearance of a high-field resonance signal that could be assigned to an agostic hydrogen atom, suggesting the decreased fluxionality of the molecule at low temperatures as the likely origin of the spectral phenomena.

The bulky tricyclohexylphosphane ligands and the high *trans*-labilizing boryl ligand cooperate to inhibit coordination of more efficient nucleophiles, such as THF or CH_3CN, at the platinum center. Negligible decomposition of a solution of **2** in CD_2Cl_2 containing an excess (>10 equiv) of THF or CH_3CN was observed by NMR spectroscopy over the course of 24 h. Upon addition of the stronger Lewis base 4-methylpyridine, however, gradual darkening of the solution from cherry red to dark purple occurred within 2 h, and the predominant formation of a new species, **3**, which incorporated the added ligand was observed by NMR spectroscopy. Although binding of the pyridine unit to the platinum center might have been expected, on account of the electronic unsaturation at the metal center and its affinity for nitrogen donors,[13b–d] an X-ray diffraction study[12] performed on purple crystals of **3** revealed a different outcome of the reaction. As displayed in Figure 2, the constitution of complex **3** is that of a four-coordinate, cationic *trans*-bis(tricyclohexylphosphino)platinum complex, with the two remaining sites occupied by a bromide ligand and a 4-methylpyridine-stabilized ferrocenylborylene moiety. As such, **3** represents a unique example of a cationic[18] platinum(II) borylene complex and a rare instance of a base-stabilized borylene

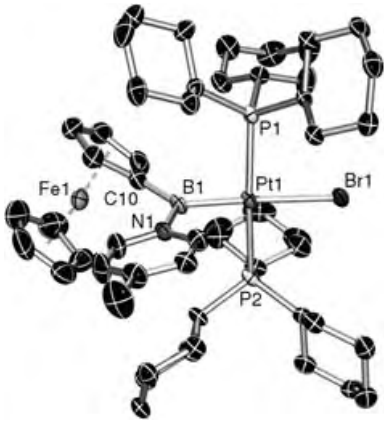


Figure 2. Molecular structure of **3**. The hydrogen atoms and the $[BAr^f_4]^-$ ion have been omitted for clarity. Selected bond lengths [Å] and angles [°]: Pt1–B1 2.014(5), Pt1–P2 2.3452(11), Pt1–P1 2.3564(11), Pt1–Br1 2.6057(5), N1–B1 1.582(6); P2-Pt1-P1 171.83(4), C10-B1-N1 114.4(4), C10-B1-Pt1 131.0(3), N1-B1-Pt1 113.6(3).

 © 2005 Wiley-VCH Verlag GmbH & Co. KGaA, Weinheim

compound.[10b,19] Previously, Roper et al. described formation of the only other reported organic base-stabilized borylene compounds, upon reaction of the osmium dichloroboryl precursor $[Os(BCl_2)Cl(CO)(PPh_3)_2]$ with 8-aminoquinoline[10b] or 2-aminopyridine.[19a] In analogy with the formation of the osmium system, it can be inferred that formation of **3** occurs by a Lewis base induced, formal 1,2-halide shift from boron to platinum, by which a strong B–N bond (B1–N1 1.582(6) Å) is formed within the borylene moiety and concomitantly the coordinative unsaturation at the metal center is relieved upon coordination of the bromide ligand. The latter appears to be an important factor. For example, intramolecular, particularly α-hydrogen, migrations within organometallic compounds are thought to be kinetically favorable, if through the shift a coordinatively unsaturated species can be converted into coordinatively more strongly saturated compound.[20] This principle, which plays a significant role in organometallic chemistry,[21] provided a viable route to silylene complexes of platinum.[22] The isolation of complex **3** and of the osmium compounds demonstrates that analogous 1,2-halide migrations might be similarly powerful synthetic tools in borylene chemistry.[23]

In contrast to the very short Fe–B distance (1.792(8) Å) in $[(\eta^5\text{-}C_5Me_5)(OC)_2Fe{=}BMes][BAr^f_4]$ (Mes = 2,4,6-$Me_3C_6H_2$),[18] the only other reported cationic terminal borylene complex, the Pt1–B1 distance (2.014(5) Å) in **3** is only slightly longer than that in the three-coordinate platinum precursor **2** (1.966(4) Å) and comparable to that in the four-coordinate boryl compound **1** (1.9963(34) Å).[7b] This is in line with the increased coordination number at the metal center and the enhanced steric congestion at the boron center.

Nonetheless, it must be stated that the comparable Pt–B bond lengths and angles at boron in the T-shaped complex **2** and the tetracoordinate complex **3** make the description of **2** as a boryl and of **3** as a borylene complex somewhat ambiguous. A similar ambiguity was pointed out by Roper et al. with regard to the "boryl" character of their base-stabilized borylene compounds of osmium,[10b,19a] and found to apply to base-stabilized silylene compounds, whose silylene character was judged to be limited.[24a,c] Hence, while the utilized description of complex **3** is based on the formalism that defines the B–R group a borylene, and hence a B(L)R group, where L is a Lewis base, a base-stabilized borylene ligand, this is only one of the possible descriptions. Elucidation of the bonding interactions that characterize complex **3** awaits theoretical calculations and reactivity studies, both of which are currently in progress.

The increased steric congestion at the boron center brought about by the coordination of pyridine is likely to be responsible for the nearly orthogonal disposition (78.42(13)°) of the plane of the borylene ligand with respect to the coordination plane of the platinum center. An analogous orientation of the boron-containing group was observed in the molecular structures of the boryl complexes **1** and **2**, as well as in those of square-planar platinum carbene[25] and silylene[24b] compounds, and attributed to steric interactions with the phosphane ligands. The Pt1–Br1 distance (2.6057(5) Å) in **3** is rather long and comparable to that in the neutral boryl complex **1** (2.6183(8) Å), in line with the high *trans* influence of the boron-containing ligand.

The spectroscopic data of complex **3** were in agreement with its solid-state structure. The $^{31}P\{^1H\}$ NMR spectrum exhibited a singlet at $\delta = 25.0$ ppm ($^1J(P,Pt) = 2554$ Hz), strongly high-field-shifted with respect to the corresponding signal of **2**. In the room-temperature ^1H NMR spectrum, broad signals were observed at $\delta = 7.90$ and 7.82 ppm for two of the 4-methylpyridine protons, as well as at $\delta = 4.54$ ppm for two of the ferrocenyl protons and for some of the cyclohexyl protons; this indicates slow hindered rotation of the methylpyridine ligands and of the ferrocenyl groups around the B–N and B–C bonds, respectively, with respect to the NMR time scale. At −20 °C, the four pyridine protons gave rise to two overlapping doublets at $\delta = 10.45$–10.42 ppm and two more doublets at $\delta = 7.92$ and 7.79 ppm ($^3J(H,H) = 6$ Hz). Only after the sample had been cooled to −60 °C were four separate signals for the four protons of the boron-bound cyclopentadienyl ring observed at $\delta = 4.92$, 4.88, 4.73, and 4.04 ppm. Finally, as for complex **2**, extreme broadening of the resonance in the $^{11}B\{^1H\}$ NMR spectrum of **3** prevented observation of a detectable signal.

In conclusion, we have described the synthesis of the T-shaped, three-coordinate boryl complex *trans*-$[(Cy_3P)_2Pt\{B(Fc)Br\}][BAr^f_4]$ (**2**) and its conversion into the cationic base-stabilized borylene complex *trans*-$[(Cy_3P)_2Pt(Br)\{B(Fc)(NC_5H_4\text{-}4\text{-}Me)\}][BAr^f_4]$ (**3**) by an overall 1,2-migration of bromide from the boron to the platinum center. Experiments aimed at verifying the generality of this approach to the synthesis of borylene complexes, as well as at exploiting the high *trans* influence of the boryl ligand to access highly unsaturated compounds are currently underway.

Received: May 10, 2005

Keywords: boron · boryl ligands · borylene ligands · platinum · structure elucidation

[1] a) H. Braunschweig, *Angew. Chem.* **1998**, *110*, 1882–1898; *Angew. Chem. Int. Ed.* **1998**, *37*, 1786–1801; b) G. J. Irvine, M. G. J. Lesley, T. B. Marder, N. C. Norman, C. R. Rice, E. G. Robins, W. R. Roper, G. R. Whittell, L. J. Wright, *Chem. Rev.* **1998**, *98*, 2685–2722; c) H. Braunschweig, M. Colling, *Coord. Chem. Rev.* **2001**, *223*, 1–51; d) S. Aldridge, D. L. Coombs, *Coord. Chem. Rev.* **2004**, *248*, 535–559.

[2] a) K. Burgess, M. J. Ohlmeyer, *Chem. Rev.* **1991**, *91*, 1179–1191; b) I. Beletskaya, A. Pelter, *Tetrahedron* **1997**, *53*, 4957–5026.

[3] T. B. Marder, N. C. Norman, *Top. Catal.* **1998**, *5*, 63–73.

[4] a) J.-Y. Cho, M. K. Tse, D. Holmes, R. E. Maleczka, Jr., M. R. Smith III, *Science* **2002**, *295*, 305–308; b) T. Ishiyama, N. Miyaura, *J. Organomet. Chem.* **2003**, *680*, 3–11; c) T. Ishiyama, Y. Nobuta, J. F. Hartwig, N. Miyaura, *Chem. Commun.* **2003**, 2924–2925; d) D. N. Coventry, A. S. Batsanov, A. E. Goeta, J. A. K. Howard, T. B. Marder, R. N. Perutz, *Chem. Commun.* **2005**, 2172–2174; e) J. F. Hartwig, K. S. Cook, M. Hapke, C. D. Incarvito, Y. Fan, C. E. Webster, M. B. Hall, *J. Am. Chem. Soc.* **2005**, *127*, 2538–2552, and references therein.

[5] F. E. S. Souza, P. Nguyen, T. B. Marder, A. J. Scott, W. Clegg, *Inorg. Chim. Acta* **2005**, *358*, 1501–1509.

 © 2005 Wiley-VCH Verlag GmbH & Co. KGaA, Weinheim

[6] a) S.-Y. Onozawa, Y. Hatanaka, T. Sakakura, S. Shimada, M. Tanaka, *Organometallics* **1996**, *15*, 5450 – 5452; b) S.-Y. Onozawa, M. Tanaka, *Organometallics* **2001**, *20*, 2956 – 2958.

[7] a) W. Clegg, F. J. Lawlor, G. Lesley, T. B. Marder, N. C. Norman, A. G. Orpen, M. J. Quayle, G. C. Rice, A. J. Scott, F. E. S. Souza, *J. Organomet. Chem.* **1998**, *550*, 183 – 192; b) H. Braunschweig, K. Radacki, D. Rais, F. Seeler, *Organometallics* **2004**, *23*, 5545 – 5549.

[8] a) G. Sivignon, P. Fleurat-Lessard, J.-M. Onno, F. Volatron, *Inorg. Chem.* **2002**, *41*, 6656 – 6661; b) K. C. Lam, W. H. Lam, Z. Lin, T. B. Marder, N. C. Norman, *Inorg. Chem.* **2004**, *43*, 2541 – 2547.

[9] C. Dai, G. Stringer, T. B. Marder, R. T. Baker, A. J. Scott, W. Clegg, N. C. Norman, *Can. J. Chem.* **1996**, *74*, 2026 – 2031.

[10] a) C. E. F. Rickard, W. R. Roper, A. Williamson, L. J. Wright, *Organometallics* **1998**, *17*, 4869 – 4874; b) G. J. Irvine, C. E. F. Rickard, W. R. Roper, A. Williamson, L. G. Wright, *Angew. Chem.* **2000**, *112*, 978 – 980; *Angew. Chem. Int. Ed.* **2000**, *39*, 948 – 950.

[11] C. N. Iverson, M. R. Smith III, *J. Am. Chem. Soc.* **1995**, *117*, 4403 – 4404.

[12] Crystal data for **2**: $C_{78}H_{87}B_2BrF_{24}FeP_2Pt\cdot 1.5\,CH_2Cl_2\cdot 0.25\,C_6H_{14}$, orange brick, $0.093\times0.210\times0.250$ mm^3, triclinic, space group $P\bar{1}$, $a=12.8443(9)$, $b=17.7059(12)$, $c=19.5664(13)$ Å, $\alpha=102.7860(10)$, $\beta=91.0560(10)$, $\gamma=91.9000(10)°$, $V=4335.5(5)$ Å^3, $Z=2$, $\rho_{calcd}=1.566$ g cm^{-3}, $T=173(2)$ K; Bruker-Apex platform with CCD detector, graphite-monochromated $Mo_{K\alpha}$ radiation, $2\theta_{max}=52.79$; 39023 reflections, 17675 independent ($R_{int}=0.0266$), direct methods, absorption correction SADABS ($\mu=2.462$ cm^{-1}). Residual electron density was attributed to 1.5 dichloromethane and 0.25 hexane molecules per asymmetric unit. Refinement on split positions, and DFIX, DANG, and DELU restraints were applied to all solvents molecules. All non-hydrogen atoms were refined anisotropically. Hydrogen atoms were refined on idealized positions. $R_1=0.0347$ ($I>2\sigma$), $wR_2=0.0885$ (all data), GoF = 1.044, restrained GoF = 1.046, max/min residual electron density: $2.059/-0.485\times10^{30}$ e m^{-3}. Crystal data for **3**: $C_{84}H_{94}NB_2BrF_{24}FeP_2Pt$, red plate, $0.06\times0.15\times0.30$ mm^3, triclinic, space group $P\bar{1}$, $a=14.2217(17)$, $b=15.7319(19)$, $c=21.014(3)$ Å, $\alpha=110.284(2)$, $\beta=103.702(2)$, $\gamma=93.827(2)°$, $V=4226.9(9)$ Å^3, $Z=2$, $\rho_{calcd}=1.562$ g cm^{-3}, $T=173(2)$ K; Bruker-Apex platform with CCD detector, graphite-monochromated $Mo_{K\alpha}$ radiation, $2\theta_{max}=52.08$; 35533 reflections, 16491 independent ($R_{int}=0.0287$), absorption correction SADABS ($\mu=2.432$ cm^{-1}). The structure was solved by direct methods. All non-hydrogen atoms were refined anisotropically. Hydrogen atoms were refined on idealized positions. $R_1=0.0412$ ($I>2\sigma$), $wR_2=0.0995$ (all data), GoF = 1.068, max/min residual electron density: $1.833/-1.362\times10^{30}$ e m^{-3}. CCDC-271343 (**2**) and CCDC-271344 (**3**) contain the supplementary crystallographic data for this paper. These data can be obtained free of charge from the Cambridge Crystallographic Data Centre via www.ccdc.cam.ac.uk/data_request/cif.

[13] a) M. D. Butts, B. L. Scott, G. J. Kubas, *J. Am. Chem. Soc.* **1996**, *118*, 11831 – 11843; b) S. D. Ittel, L. K. Johnson, M. Brookhart, *Chem. Rev.* **2000**, *100*, 1169 – 1204; c) H. A. Zhong, J. A. Labinger, J. E. Bercaw, *J. Am. Chem. Soc.* **2002**, *124*, 1378 – 1399; d) U. Fekl, K. I. Goldberg, *Adv. Inorg. Chem.* **2003**, *54*, 259 – 320.

[14] a) F. M. Conroy-Lewis, L. Mole, A. D. Redhouse, S. A. Litster, J. L. Spencer, *J. Chem. Soc. Chem. Commun.* **1991**, 1601 – 1603; b) L. Mole, J. L. Spencer, N. Carr, A. G. Orpen, *Organometallics* **1991**, *10*, 49 – 52; c) N. Carr, L. Mole, A. G. Orpen, J. L. Spencer, *J. Chem. Soc. Dalton Trans.* **1992**, 2653 – 2662; d) J. L. Spencer, G. S. Mhinzi, *J. Chem. Soc. Dalton Trans.* **1995**, 3819 – 3824; e) L. Huff Shultz, M. Brookhart, *Organometallics* **2001**, *20*, 3975 – 3982; f) W. Baratta, S. Stoccoro, A. Doppiu, E. Herdtweck, A. Zucca, P. Rigo, *Angew. Chem.* **2003**, *115*, 109 – 113; *Angew. Chem. Int. Ed.* **2003**, *42*, 105 – 108; g) M. J. Ingleson, M. F. Mahon, A. S. Weller, *Chem. Commun.* **2004**, 2398 – 2399.

[15] J. P. Stambuli, M. Bühl, J. F. Hartwig, *J. Am. Chem. Soc.* **2002**, *124*, 9346 – 9347.

[16] W. H. Lam, K. C. Lam, Z. Lin, S. Shimada, R. N. Perutz, T. B. Marder, *Dalton Trans.* **2004**, 1556 – 1562.

[17] See Supporting Information.

[18] For the only other example of cationic terminal borylene complex, see: D. L. Coombs, S. Aldridge, C. Jones, D. J. Willock, *J. Am. Chem. Soc.* **2003**, *125*, 6356 – 6357.

[19] a) C. E. F. Rickard, W. R. Roper, A. Williamson, J. L. Wright, *Organometallics* **2002**, *21*, 4862 – 4872; b) For an example of terminal borylene complex stabilized by a transition metal-base, see: H. Braunschweig, D. Rais, K. Uttinger, *Angew. Chem.* **2005**, *117*, 3829 – 3832; *Angew. Chem. Int. Ed.* **2005**, *44*, 3763 – 3766.

[20] a) R. J. Goddard, R. Hoffman, E. D. Temmis, *J. Am. Chem. Soc.* **1980**, *102*, 7667 – 7676; b) T. Ziegler, L. Versluis, V. Tschinke, *J. Am. Chem. Soc.* **1986**, *108*, 612 – 617.

[21] R. H. Crabtree, *The Organometallic Chemistry of the Transition Metals*, Wiley, New York, 2nd ed., **1994**.

[22] a) G. P. Mitchell, T. D. Tilley, *J. Am. Chem. Soc.* **1998**, *120*, 7635 – 7636; b) G. P. Mitchell, T. D. Tilley, *Angew. Chem.* **1998**, *110*, 2602 – 2605; *Angew. Chem. Int. Ed.* **1998**, *37*, 2524 – 2526.

[23] We wish to point out that the definition "1,2-halide migration" refers here to the overall outcome of the reaction that from compound **2** leads to compound **3**, and is not intended to hold any mechanistic implication which, in the absence of appropriate studies, would only be purely speculative.

[24] a) T. D. Tilley in *The Silicon-Heteroatom Bond* (Eds.: S. Patai, Z. Rappaport), Wiley, New York, **1991**, chaps. 9 and 10; b) S. D. Grumbine, T. D. Tilley, *J. Am. Chem. Soc.* **1993**, *115*, 7884 – 7885; c) S. K. Grumbine, D. A. Straus, T. D. Tilley, A. L. Rheingold, *Polyhedron* **1995**, *14*, 127 – 148, and references therein.

[25] U. Schubert, *Coord. Chem. Rev.* **1984**, *55*, 261 – 286.

 © 2005 Wiley-VCH Verlag GmbH & Co. KGaA, Weinheim

Mixed-Valent Complexes

DOI: 10.1002/anie.200501075

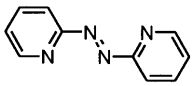
Theoretical and Experimental Evidence for a New Kind of Spin-Coupled Singlet Species: Isomeric Mixed-Valent Complexes Bridged by a Radical Anion Ligand**

Biprajit Sarkar, Srikanta Patra, Jan Fiedler, Raghavan B. Sunoj, Deepa Janardanan, Shaikh M. Mobin, Mark Niemeyer, Goutam Kumar Lahiri, and Wolfgang Kaim**

Singlet species composed from clearly identified odd-electron components have long been known in the form of antiferromagnetically spin–spin coupled transition-metal centers (M) of d^{2n+1} configuration bridged by ligands μ-L, giving rise to the phenomenon of "superexchange" in (M•)(μ-L)(M•) species.[1] More recently,[2] the reverse situation (L•)(M)(L•) with a bridging diamagnetic metal center was described and referred to in terms of "singlet diradical" species. Herein we present another alternative [Eq. (1)], involving the strong intramolecular interaction between a bridging anion radical ligand $L^{\bullet-}$ and two mixed-valent metal centers.

$$(M^{\cdot})(L^{\cdot-})(M) \leftrightarrow (M)(L^{\cdot-})(M^{\cdot}) \quad (1)$$

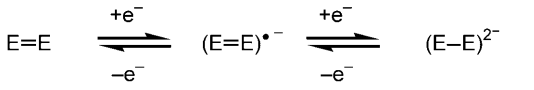
Evidence for the formulation in Equation (1) comes from structure determination in conjunction with density functional theory (DFT) calculations. Structural criteria have been increasingly used to establish the oxidation states of "non-innocent" ligands[3] and, by implication, of metal centers in the coordination compounds. Prominent examples include the bidentate 1,2-dioxolene chelate ligands $Q/Q^{\bullet-}/Q^{2-}$ for which structure–valency correlations were reported[4,5] and applied, and simple diatomic ligands such as the potentially metal–metal bridging redox system $O_2/O_2^{\bullet-}/O_2^{2-}$, a textbook case.[6] Related to the latter by the relation O ≙ NR are organic azo compounds $(NR)_2$ which in the *E* configuration can act as reducible bis-bidentate bridges if R is a coordinating group, such as 2-pyridyl to form 2,2′-azobispyridine (abpy).[7]



abpy

Abpy was first described by Lever and co-workers as a strongly π accepting but otherwise normal bridging ligand,[7b] a special feature of its complexes being the relatively short metal–metal distance of about 5 Å.[7a,c,e]

As with the O_2^{n-} system,[6] the addition of electrons to abpy causes a lengthening of the central N–N bond from double-bond values of about 1.25 Å via approximately 1.35 Å in the anion radicals[8] to approximately 1.42 Å for single bonds in the two-electron-reduced forms (Scheme 1).[9]



E=O:	1.21 Å	1.23–1.35 Å	1.40–1.50 Å
E=NR:	1.23–1.30 Å	ca. 1.35 Å	1.40–1.45 Å

Scheme 1. Bond lengths in E_2^{n-} systems.

Whereas coordination of π back-donating metal centers can result in a slight increase of the double-bond length relative to that in the free ligand,[7a] the lengthening caused by successive electron addition is so large and well documented through supporting spectroscopic data[8] that these criteria can be unequivocally applied to establish the bonding situation.

In the search for unusual mixed-valent configurations involving ruthenium and other platinum metals[10] we have now obtained the compound $[(\mu\text{-abpy})\{Ru(acac)_2\}_2]$ from abpy[7] and the neutral precursor $[Ru(acac)_2(CH_3CN)_2]$ ($acac^- = 2,4$-pentanedionate),[11] separated the *meso* and *rac* isomers[12] by chromatography, characterized them by ^1H NMR spectroscopy,[13] and identified them by crystal-structure analysis (Figure 1, Table 1).[14]

The molecules show the expected "S-frame" configurations[7a] with the bis-chelating abpy variably twisted; the C-N-N-C torsional angles are 26.1° in the *rac* form but only 15.5° and 0.0° for the two crystallographically independent molecules of the *meso* form. As expected,[7a] the bonds from the metal centers to the stronger π-accepting azo nitrogen atoms (ca. 1.965 Å) are shorter than those to the pyridine N centers (average 2.010 Å). Most remarkably, the central N–N bonds of the abpy ligand are considerably lengthened to 1.372(4) Å in the *rac* form and to 1.374(11) Å and 1.352(17) Å in the *meso* form whereas the adjacent C–N bonds are slightly shortened to about 1.395 Å. The average N–N distance of 1.366 Å lies in the same range as the 1.345(7) Å determined for a structurally and electronically well identified dicopper(I) complex containing the radical anion of the closely related 2,2′-bis(5-chloropyrimidine) (abcp) ligand.[8] A reduced N–N bond order of 1.5 would be compatible with the ease of twisting around the central CNNC backbone of abpy.

The abpy and related ligands are known to effect rather short metal–metal distances of about 5 Å.[7a,c] The unusually[7a,c] short metal–metal distances observed for *rac* (4.664 Å)

[*] S. Patra, Prof. Dr. R. B. Sunoj, D. Janardanan, S. M. Mobin, Prof. Dr. G. K. Lahiri
Department of Chemistry
Indian Institute of Technology-Bombay
Powai, Mumbai-400076 (India)
Fax: (+91) 22-2572-3480
E-mail: lahiri@chem.iitb.ac.in
Dr. B. Sarkar, Priv.-Doz. Dr. M. Niemeyer, Prof. Dr. W. Kaim
Institut für Anorganische Chemie
Universität Stuttgart
Pfaffenwaldring 55, 70550 Stuttgart (Germany)
Fax: (+49) 711-685-4165
E-mail: kaim@iac.uni-stuttgart.de
Dr. J. Fiedler
J. Heyrovský Institute of Physical Chemistry
Academy of Sciences of the Czech Republic
Dolejškova 3, 18223 Prague (Czech Republic)

[**] This work was supported by the DFG, the DAAD (Germany), the DST (New Delhi, India), and by the GACR (Czech Republic; grant no. 203/03/0821).

 © 2005 Wiley-VCH Verlag GmbH & Co. KGaA, Weinheim

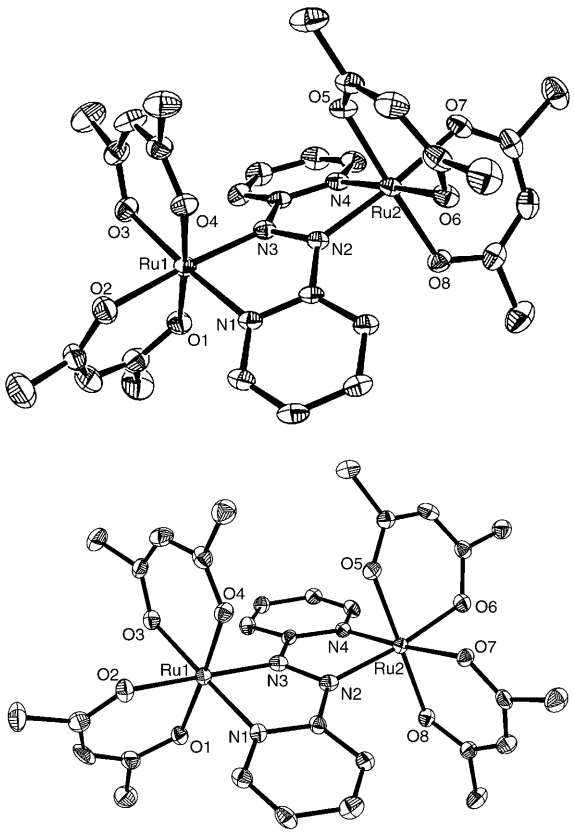


Figure 1. Crystal structures of *rac* (top) and one of the *meso* forms (bottom) of $[(\mu\text{-abpy})\{Ru(acac)_2\}_2]$.

Table 1: Comparison of experimental and computed (DFT[a]) structural parameters[b] for different isomers of $[(\mu\text{-abpy})\{Ru(acac)_2\}_2]$.

Parameter	Experimental[c]			DFT			
	rac	*meso*1	*meso*2	^{1}*rac*	^{3}*rac*	^{1}*meso*	^{3}*meso*
C-N=N-C[d]	26.1	15.5	0.0	18.3	24.8	0.0	0.0
N=N	1.372(4)	1.374(11)	1.352(17)	1.344	1.410	1.339	1.408
$C\text{-}N_{azo}$	1.390(5)	1.382(12)	1.420(12)	1.390	1.365	1.391	1.365
	1.390(5)	1.391(12)					
$Ru\text{-}N_{azo}$	1.963(3)	1.961(8)	1.962(9)	2.014	2.000	2.029	2.015
	1.954(3)	1.997(8)					
$Ru\text{-}N_{py}$	2.008(3)	1.995(8)	2.027(9)	2.027	2.055	2.021	2.046
	2.007(3)	2.001(8)					

[a] Optimized parameters for singlet and triplet states obtained at the B3LYP/SDD/6-31G* level. [b] Bond lengths [Å] and angles [°]. [c] Two independent molecules in the unit cell of the crystallized *meso* isomer. [d] Torsional angle.

and *meso* forms (4.698 and 4.780 Å) are partly caused by the CNNC twisting. The structural data thus clearly indicate the presence of a one-electron reduced (i.e. radical anion) ligand bridge, leaving a $Ru^{II}Ru^{III}$ mixed-valent formulation for the metal centers. Since structural and spectroscopic results for this diamagnetic compound point to a symmetrical situation, this mixed valency would then have to be described as a Class III system (fully valence delocalized, that is, $Ru^{2.5}Ru^{2.5}$)[15] with strong antiferromagnetic coupling between metal- and ligand-based spins in accord with the observed diamagnetism. As noted previously,[7d] mixed-valent complexes with radical anion bridging ligands ($L^{\bullet-}$) can be invoked as metal-to-ligand charge transfer (MLCT) excited states of symmetrical dinuclear complexes [Eq. (2)].[16]

$$[M^n(\mu\text{-}L)M^n] \xrightarrow[MLCT]{h\nu} *[M^{n+1}(\mu\text{-}L^{\bullet-})M^n] \text{ or } *[M^{n+0.5}(\mu\text{-}L^{\bullet-})M^{n+0.5}] \qquad (2)$$

Reversible oxidation and reduction processes of both the *meso* and *rac* forms of $[(\mu\text{-abpy})\{Ru(acac)_2\}_2]$ occur at 0.05 (oxidation) and −1.03 V (reduction; versus saturated calomel electrode (SCE) in CH_3CN/0.1 M Bu_4NClO_4), yielding a very large comproportionation constant K_c of $10^{18.3}$. Reduction produces EPR signals at $g = 1.990$ that are indicative of a radical,[17a] and thus suggesting a $\{Ru^{II}(abpy^{\bullet-})Ru^{II}\}$ configuration. Oxidation produces EPR signals at $g = 2.25$, 2.14 and 1.98 (*rac* isomer) or $g = 2.35$, 2.15 and 1.81 (*meso* isomer) that are indicative of the presence of an Ru^{III} center,[17b] which would be compatible with a $\{Ru^{III}(abpy^{\bullet-})Ru^{III}\}$ or $\{Ru^{II}(abpy)Ru^{III}\}$ formulation. Absence of the near infrared band expected for a conventional mixed-valent compound[10,12,15] suggests the $\{Ru^{III}(abpy^{\bullet-})Ru^{III}\}$ alternative, implying metal-based electron transfer within the redox system $[(\mu\text{-abpy})\{Ru(acac)_2\}_2]^{+/0/-}$ as befits a mixed-valency situation for the neutral form $\{Ru^{2.5}(abpy^{\bullet-})Ru^{2.5}\}$.

The UV/Vis spectra of the neutral compounds are characterized by very intense bands ($\varepsilon = 29000\ M^{-1}\,cm^{-1}$) at 835 (*rac*) and 848 nm (*meso*) which are assigned to MLCT/MMCT (metal-to-ligand/metal-to-metal charge transfer) transitions between a metal-based occupied molecular orbital and a mixed abpy/metal LUMO.

DFT calculations at the B3LYP level were performed for both isomers.[18a] The calculated bond characteristics for the singlet ground states (Table 1) are in reasonable agreement with the experimental values, in addition, triplet states with longer N–N and shorter C–N distances (Table 1) were found comparatively close (*rac*: 840 cm^{-1}; *meso*: 1535 cm^{-1}) to the singlet ground states. The higher singlet–triplet gap for the *meso* isomer reflects the invariant coplanar CNNC backbone structure. Conversely, the energy difference between the singlet isomers is only 330 cm^{-1} whereas it increases to 1026 cm^{-1} between the triplet isomers, in both cases in favor of the *rac* form.

The wave functions were further analyzed using the natural bond orbital (NBO) method to probe the electron occupancies of the key orbitals as well as the extent of delocalization.[18f,g] The $\pi_{(N=N)}$ occupancies for both *rac* and *meso* isomers are about 1.87 e while $\pi^*_{(N=N)}$ was found to have a substantial population of 0.73 e. The corresponding values for the neutral ligand are 1.90 and 0.16 e, respectively. Although the change in occupancy is negligible for the π orbital on complex formation, it is significantly higher for the

 © 2005 Wiley-VCH Verlag GmbH & Co. KGaA, Weinheim

π* molecular orbital, reflecting a substantial metal-to-ligand charge shift in the ground state. The donor–acceptor interaction energies obtained from the NBO analysis suggest that the cumulative effects of ligand-to-metal donation and π back-donation make the azo nitrogen atoms slightly better donors than pyridyl nitrogen atoms. This result is in agreement with the experimental differences in the Ru–N bond lengths. The high values for the metal-to-ligand donation together with the substantial population of $\pi^*_{(N=N)}$ clearly justify a description of the bridging ligand as a radical anion.

In summary, X-ray structure, spectroscopy, and DFT calculations have clearly established that the new stereoisomeric compounds *rac*- and *meso*-[(μ-abpy){Ru(acac)$_2$}$_2$] must be formulated as [Ru$^{2.5}$(abpy$^{\bullet-}$)Ru$^{2.5}$] complexes, thus constituting both a new kind of unconventional mixed-valent compound and a new class of singlet species composed from metal/ligand/metal intramolecular spin-spin coupling. The occurrence of radical anions as ligands,[19] either as small molecules such as $O_2^{\bullet-}$ [6] or $CO_2^{\bullet-}$ [20] or as larger entities,[2,4,5] has thus been extended to yield unprecedented electronic structures, using the rather simple inorganic complex fragment {Ru(acac)$_2$}. The additional feature of two separable stereoisomers will stimulate further investigations into configurational aspects of intramolecular interactions in these unconventional mixed-valent species.

Received: March 24, 2005
Published online: August 3, 2005

Keywords: azobispyridine · bridging ligands · mixed-valent complexes · N ligands · ruthenium

[1] J. B. Goodenough, *Magnetism and the Chemical Bond*, Wiley Interscience, New York, **1963**.
[2] a) D. Herebian, K. E. Wieghardt, F. Neese, *J. Am. Chem. Soc.* **2003**, *125*, 10997; b) V. Bachler, G. Olbrich, F. Neese, K. Wieghardt, *Inorg. Chem.* **2002**, *41*, 4179.
[3] M. D. Ward, J. A. McCleverty, *J. Chem. Soc. Dalton Trans.* **2002**, 275.
[4] S. Bhattacharya, P. Gupta, F. Basuli, C. G. Pierpont, *Inorg. Chem.* **2002**, *41*, 5810.
[5] D. Herebian, E. Bothe, F. Neese, T. Weyhermüller, K. Wieghardt, *J. Am. Chem. Soc.* **2003**, *125*, 9116.
[6] F. A. Cotton, G. Wilkinson, C. A. Murillo, M. Bochmann, *Advanced Inorganic Chemistry*, 6th ed., Wiley, New York, **1999**, pp. 468–471.
[7] a) W. Kaim, *Coord. Chem. Rev.* **2001**, *219–221*, 463; b) D. A. Baldwin, A. B. P. Lever, R. V. Parish, *Inorg. Chem.* **1969**, *8*, 107; c) H. Hartmann, T. Scheiring, J. Fiedler, W. Kaim, *J. Organomet. Chem.* **2000**, *604*, 267; d) S. D. Ernst, W. Kaim, *Inorg. Chem.* **1989**, *28*, 1520; e) C. S. Campos-Fernández, J. R. Galán-Mascarós, B. W. Smucker, K. R. Dunbar, *Eur. J. Inorg. Chem.* **2003**, 988.
[8] a) N. Doslik, T. Sixt, W. Kaim, *Angew. Chem.* **1998**, *110*, 2521; *Angew. Chem. Int. Ed.* **1998**, *37*, 2403; b) W. Kaim, N. Doslik, S. Frantz, T. Sixt, M. Wanner, F. Baumann, G. Denninger, H.-J. Kümmerer, C. Duboc-Toia, J. Fiedler, S. Zalis, *J. Mol. Struct.* **2003**, *656*, 183.
[9] D. Chan, L. Cronin, S. B. Duckett, P. Hupfield, R. N. Perutz, *New J. Chem.* **1998**, *22*, 511.
[10] W. Kaim, A. Klein, M. Glöckle, *Acc. Chem. Res.* **2000**, *33*, 755.
[11] T. Kobayashi, Y. Nishina, K. G. Shimizu, G. P. Satô, *Chem. Lett.* **1988**, 1137.
[12] Compare isomerism in [(μ-abpy){Ru(bpy)$_2$}$_2$]$^{4+}$: a) S. Ernst, V. Kasack, W. Kaim, *Inorg. Chem.* **1988**, *27*, 1146; b) L. S. Kelso, D. A. Reitsma, F. R. Keene, *Inorg. Chem.* **1996**, *35*, 5144; c) M. Heilmann, S. Frantz, W. Kaim, J. Fiedler, C. Duboc, *Inorg. Chim. Acta*, in press.
[13] [Ru(acac)$_2$(CH$_3$CN)$_2$][11] (0.10 g, 0.26 mmol) and abpy[7a] (0.022 g, 0.12 mmol) were combined in ethanol (10 mL) and heated to reflux for 4 h under a dinitrogen atmosphere. The color of the solution gradually changed from orange to dark brown. The solvent was removed and the residue was subjected to chromatography on a silica gel column. Initially, a red compound corresponding to [Ru(acac)$_3$] was eluted with CH$_2$Cl$_2$/CH$_3$CN (10:1). With CH$_2$Cl$_2$/CH$_3$CN (5:1), a green band corresponding to a mixture of *rac* and *meso* isomers was eluted. The *rac* and *meso* isomers were separated on a silica gel preparatory thin layer chromatography (TLC) plate using CH$_2$Cl$_2$/CH$_3$CN (7:1). *rac* Isomer: Yield 20 mg (20%); elemental analysis (%) calcd for C$_{30}$H$_{36}$N$_4$O$_8$Ru$_2$ (782.77): C 45.91, H 4.63, N 7.14; found: C 46.54, H 4.36, N 7.51; ESI MS (CH$_2$Cl$_2$): *m*/*z*: 783.08 [*M*$^+$] (calcd *m*/*z* 782.78). *meso* Isomer: Yield 25 mg (25%); Calcd: C 45.91, H 4.63, N 7.14; found: C 45.62, H 4.99, N 7.28; ESI-MS (CH$_2$Cl$_2$): *m*/*z*: 784.19 [*M*$^+$] (calculated *m*/*z* 782.78). ^{1}H NMR ((CD$_3$)$_2$SO; 300 MHz) for *rac* Isomer: δ = 8.55 (d, J = 8.5 Hz, H3), 7.97 (d, J = 6.3 Hz, H6), 7.70 (t, J = 7.2 and 8.1 Hz, H4), 7.56 (t, J = 6.4 and 7.2 Hz, H5), 5.31 (s, CH(acac)), 4.74 (s, CH(acac)), 2.11 (s, CH$_3$(acac)), 1.97 (s, CH$_3$(acac)), 1.64 (s, CH$_3$(acac)), 1.52 ppm (s, CH$_3$(acac)). *meso*-Isomer: δ = 8.32 (d, J = 5.1 Hz, H6), 8.26 (d, J = 8.4 Hz, H3), 7.75 (t, J = 6.9 and 7.2 Hz, H4), 7.44 (t, J = 6.3 and 6.6 Hz, H5), 5.47 (s, CH(acac)), 5.39 (s, CH(acac)), 2.28 (s, CH$_3$(acac)), 2.09 (s, CH$_3$(acac)), 1.78 (s, CH$_3$(acac)), 1.69 ppm (s, CH$_3$(acac)).
[14] a) Single crystals of the isomers C$_{30}$H$_{36}$N$_4$O$_8$Ru$_2$ (M_r = 782.77) were measured using Mo$_{K\alpha}$ radiation (0.71073 Å). The structures were solved and refined by full-matrix least-squares on F^2 using SHELX-97 (SHELXTL).[21] Hydrogen atoms were included in the refinement process as per the riding model. CCDC-265479 and CCDC-266238 contain the supplementary crystallographic data for this paper. These data can be obtained free of charge from The Cambridge Crystallographic Data Centre via www.ccdc.cam.ac.uk/data_request/cif. b) *rac* Isomer: Single crystals grown by slow evaporation of a dichloromethane solution, crystal size 0.35 × 0.30 × 0.30 mm^3, monoclinic, space group $P2_1/c$, a = 20.5490(10), b = 11.8440(8), c = 25.695(3) Å, β = 149.040(8)°, V = 3217.1(4) Å^3, T = 293 (2) K, Z = 4, ρ_{calcd} = 1.616 g cm^{-3}, μ = 0.993 mm^{-1}, $2\theta_{max}$ = 49.86°, 4898 independent reflections (R(int) = 0.0000), $R1$ = 0.0328, $wR2$ = 0.0758 [$I > 2\sigma(I)$], $R1$ = 0.0431, $wR2$ = 0.0814 (all data), GOF (F^2) = 1.044, data/restraints/parameters = 4898/0/397, largest differential peak and hole 0.394 and −0.647 e Å^{-3}. c) *meso* Isomer: Single crystals grown by slow evaporation of an acetonitrile solution, crystal size 0.85 × 0.85 × 0.40 mm^3, monoclinic, space group $P2_1/c$, a = 26.296(9), b = 12.593(6), c = 15.018(7) Å, β = 104.20(4)°, V = 4821(4) Å^3, T = 173(2) K, Z = 6 (1.5 independent molecules), ρ_{calcd} = 1.618 g cm^{-3}, μ = 0.994 mm^{-1}, $2\theta_{max}$ = 52.02°, 9434 independent reflections (R(int) = 0.0885), $R1$ = 0.0852, $wR2$ = 0.1947 [for 6659 reflections with $I > 2\sigma(I)$], $R1$ = 0.1272, $wR2$ = 0.2146 (all data), GOF (F^2) = 1.653, data/restraints/parameters = 9434/0/609, largest differential peak and hole 9.556 and −2.613 e Å^{-3}.
[15] a) C. Creutz, *Prog. Inorg. Chem.* **1983**, *30*, 1; b) D. E. Richardson, H. Taube, *Coord. Chem. Rev.* **1984**, *60*, 107; c) R. J. Crutchley, *Adv. Inorg. Chem.* **1994**, *41*, 273; d) W. Kaim, A. Klein, M. Glöckle, *Acc. Chem. Res.* **2000**, *33*, 755; e) K. D. Demadis, C. M. Hartshorn, T. J. Meyer, *Chem. Rev.* **2001**, *101*, 2655.

 © 2005 Wiley-VCH Verlag GmbH & Co. KGaA, Weinheim

[16] For a discussion of organic systems see J. V. Lockard, J. I. Zink, A. E. Konradsson, M. N. Weaver, S. F. Nelsen, *J. Am. Chem. Soc.* **2003**, *125*, 13471.
[17] a) W. Kaim, S. Ernst, V. Kasack, *J. Am. Chem. Soc.* **1990**, *112*, 173; b) S. Patra, B. Sarkar, S. M. Mobin, W. Kaim, G. K. Lahiri, *Inorg. Chem.* **2003**, *42*, 6469.
[18] a) Density functional theory calculations were performed using the Gaussian 98 suite of quantum chemical programs[18b] employing the SDD basis set[18c] for Ru and 6-31G* for the other elements using the hybrid Hartree-Fock density functional theory (B3LYP).[18d,e] Optimized geometries were then used for the Natural Bond Orbital (NBO) analysis with the NBO 3.1 program[18f,g] as implemented in Gaussian 98; b) Gaussian 98 (Revision A.11), M. J. Frisch, G. W. Trucks, H. B. Schlegel, G. E. Scuseria, M. A. Robb, J. R. Cheeseman, V. G. Zakrzewski, J. A. Montgomery, R. E. Stratmann, J. C. Burant, S. Dapprich, J. M. Millam, A. D. Daniels, K. N. Kudin, M. C. Strain, O. Farkas, J. Tomasi, V. Barone, M. Cossi, R. Cammi, B. Mennucci, C. Pomelli, C. Adamo, S. Clifford, J. Ochterski, G. A. Petersson, P. Y. Ayala, Q. Cui, K. Morokuma, D. K. Malick, A. D. Rabuck, K. Raghavachari, J. B. Foresman, J. Cioslowski, J. V. Ortiz, B. B. Stefanov, G. Liu, A. Liashenko, P. Piskorz, I. Komaromi, R. Gomperts, R. L. Martin, D. J. Fox, T. Keith, M. A. Al-Laham, C. Y. Peng, A. Nanayakkara, C. Gonzalez, M. Challacombe, P. M. W. Gill, B. Johnson, W. Chen, M. W. Wong, J. L. Andres, M. Head-Gordon, E. S. Replogle, J. A. Pople, Gaussian, Inc., Pittsburgh, PA, **2002**; c) D. Andrae, U. Häußermann, M. Dolg, H. Stoll, H. Preuss, *Theor. Chim. Acta* **1990**, *77*, 123; d) A. D. Becke, *J. Chem. Phys.* **1993**, *98*, 5648; e) C. Lee, Y. Wang, R. G. Parr, *Phys. Rev. B* **1988**, *37*, 785; f) NBO Version 3.1, E. D. Glendening, A. E. Reed, J. E. Carpenter, F. Weinhold; g) A. E. Reed, L. A. Curtiss, F. Weinhold, *Chem. Rev.* **1988**, *88*, 899.
[19] W. Kaim, *Coord. Chem. Rev.* **1987**, *76*, 187.
[20] I. Castro-Rodriguez, H. Nakai, L. N. Zakharov, A. L. Rheingold, K. Meyer, *Science* **2004**, *305*, 1757.
[21] G. M. Sheldrick, SHELX-97 Program for Crystal Structure Solution and Refinement, University of Göttingen, Göttingen, Germany, **1997**.

 © 2005 Wiley-VCH Verlag GmbH & Co. KGaA, Weinheim

Supramolecular Chemistry

DOI: 10.1002/anie.200501374

Unusual Solubility Properties of Polymethacrylamides as a Result of Supramolecular Interactions with Cyclodextrin

*Sarah Schmitz and Helmut Ritter**

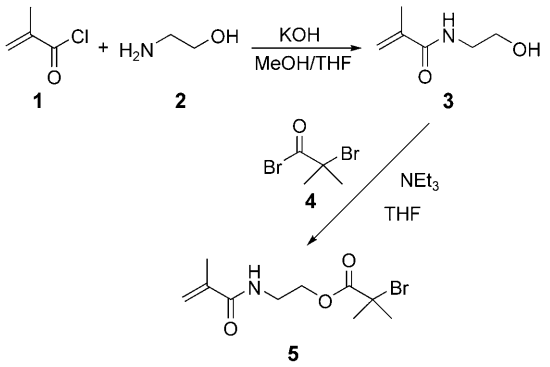
Hydrophilic polymers with so-called LCST behavior are soluble within a certain temperature range but undergo phase separation or a change in volume above a critical temperature value, the lower critical solution temperature (LCST).[1] These phenomena can also be observed when other parameters are changed such as pH value,[2] electric field, and ionic strength.[3] For example, poly(*N*-isopropylacrylamide) shows a LCST at 34 °C in pure aqueous solution. This means that the polymer is soluble in water below 34 °C and precipitates simply when the solution is heated above that critical temperature.[4] The LCST value can be influenced, for example, by copolymerization of *N*-isopropylacrylamide or by chemical modification of the acrylamide polymer itself. The slightly cross-linked LCST polymers, so-called hydrogels, find potential application in the medical and biochemical fields, for controlled drug delivery[5] and as materials for bioreactors.[6] Although this LCST behavior of polymers cannot yet be explained, many studies have focused on this topic. One general explanation of the LCST effect is that strong hydrogen bonds exist between water molecules and the hydrophilic groups of the polymer at low temperature.[7] With increasing temperature, intramolecular interactions between hydrophobic chain components of the polymer increase. Reaching the LCST, polymer aggregation takes place, and the solubility in water decreases suddenly. We report here on a similar LCST-type solubility effect based on the reversible complexation of suitable polymers with β-cyclodextrin. Although the formation of complexes of hydrophobic polymers with cyclodextrins (CDs) has already been reported,[8] a characteristic LCST-type behavior has not yet been observed.

A functionalized polymer suitable for complexation with β-CD was prepared by the synthesis and radical polymerization of monomer **5** according to Scheme 1. Intermediate **3** was obtained from the reaction of **1** and **2** (Scheme 1).[9] The esterification of **3** with **4** led to formation of methacrylamide monomer **5**, which contains a bulky group suitable for complexation with CD and a bromine atom, which opens up the possibility of further modification by atom-transfer radical polymerization (ATRP).[10]

[*] Dipl.-Chem. S. Schmitz, Prof. Dr. H. Ritter
Institut für Organische Chemie und Makromolekulare Chemie II
Heinrich-Heine-Universität Düsseldorf
Universitätsstrasse 1, 40225 Düsseldorf (Germany)
Fax: (+49) 211-8115-840
E-mail: h.ritter@uni-duesseldorf.de

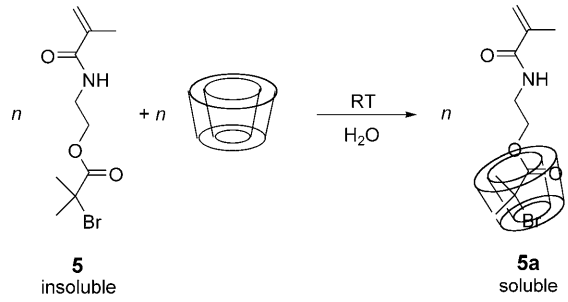
Supporting information for this article is available on the WWW under http://www.angewandte.org or from the author.

WILEY InterScience DISCOVER SOMETHING GREAT
© 2005 Wiley-VCH Verlag GmbH & Co. KGaA, Weinheim



Scheme 1. Synthesis of monomer **5**.

The water-insoluble monomer **5** was treated with β-CD, and the resulting complex **5a** was soluble in water (Scheme 2). With a [CD]/[**5**] ratio of less than 1.5:1, it was



Scheme 2. Complex formation of monomer **5** with β-CD at room temperature in water.

possible to complex the monomer, but the polymer precipitated afterward polymerization. At larger [CD]/[**5**] ratios the polymer remained in the aqueous phase as a result of sufficient complexation.

The preferred stoichiometry of the monomer/β-CD complex can be evaluated by using Job's method[11,12] which was transferred to NMR spectroscopy by Blanda et al.[13] In this case monomer **5** represents the guest molecule, while β-CD corresponds to the host molecule. (For further information on the method see the Supporting Information.) A curve with a maximum around 0.4 was obtained (Figure 1a), which suggests that the stoichiometry of the **5**/β-CD complex is 1.5:1. That means that a temporary complexation of two monomer molecules by one β-CD ring takes place. The increase in the chemical shift of the NMR signal of the methyl protons with an increasing amount of β-CD is shown in Figure 1b. A 2D ROESY NMR spectrum indicates the interactions between the β-CD ring and the monomer **5** (Figure 2). The protons of the two methyl groups ($CBr(CH_3)_2$) at $\delta = 1.9$ ppm are directly correlated to the protons of β-CD at $\delta = 3.3$–3.9 ppm. We can assume that β-CD preferably includes the $CBr(CH_3)_2$ group of **5** (see the Supporting Information).

The free-radical polymerization of the complexed monomer **5a** was carried out in presence of a redox initiator at room temperature (Scheme 3). The average molar masses $\bar{M}$

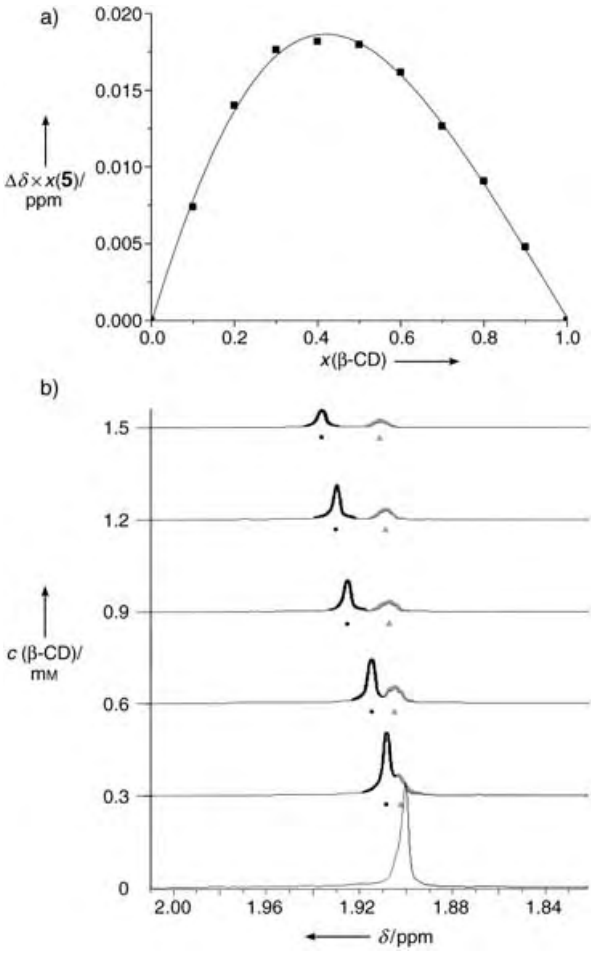


Figure 1. a) Job plot of monomer **5**: the chemical shift of the six protons of the methyl groups ($CBr(CH_3)_2$) was observed. b) Stacked plot of the NMR spectra. The chemical shift of the six protons [$CBr(CH_3)_2$ group (●)] and of the three protons [$C(CH_3)=CH_2$ group (▲)] of monomer **5** was observed with increasing amount of β-CD (500 MHz, D_2O).

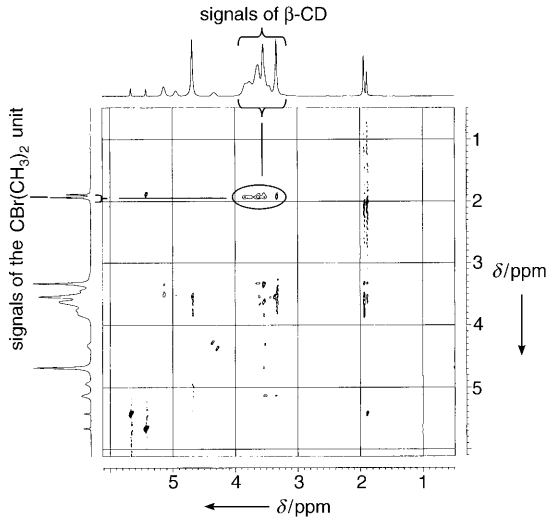
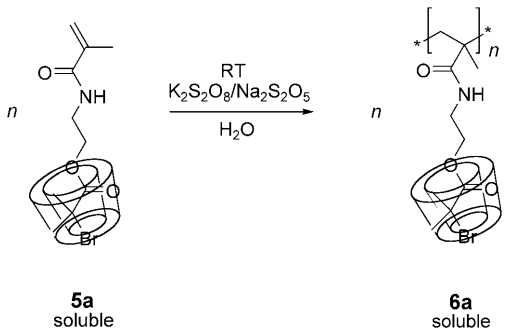


Figure 2. 2D ROESY NMR experiment with a monomer/β-CD solution (**5a**).

 © 2005 Wiley-VCH Verlag GmbH & Co. KGaA, Weinheim



Scheme 3. Free-radical polymerization of the monomer/β-CD complex **5a** to give the complexed water-soluble polymer **6a**.

of the obtained polymers, as determined by MALDI-TOF measurements, are in the range between 4300 (**7**) and 5400 g mol^{-1} (**6**) depending on the amount of initiator (Table 1). In the mass spectrum (Figure 3) the differences between the signals of the main series correspond to the molar mass of the monomer unit, 278 g mol^{-1}, as expected.

Table 1: Pseudo-LCST behavior of the polymers.

Polymer	Initiator [mol %]	$\bar{M}$ [g mol^{-1}][a]	Clouding point [°C][b]	Clearing point [°C][c]
6	2.5	5400	54	50
7	5	4300	68	61

[a] Determined by MALDI-TOF mass spectrometry. [b] Determined by turbidity measurement during heating. [c] Determined by turbidity measurement during cooling.

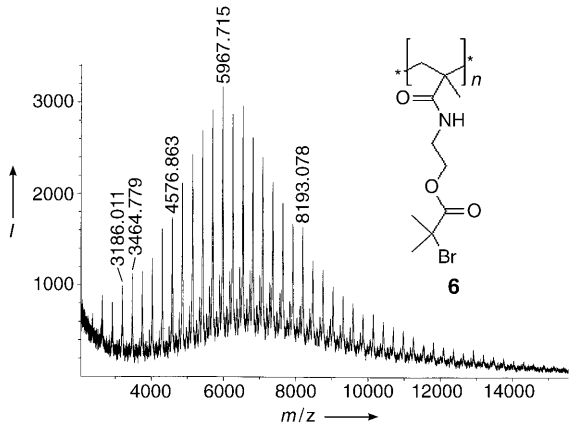


Figure 3. MALDI-TOF mass spectrum of polymer **6**.

When the optically clear aqueous solutions of the complexed polymers **6a** (see the Experimental Section for the synthesis of polymer **6**) were heated above 70 °C, a sudden turbidity was observed. Surprisingly, when the solution was cooled, transparency was completely restored. Exact turbidity measurements were performed to evaluate the solubility as a function of the temperature. We found that the complexed monomer **5a** is completely soluble in the temperature range from 10 up to 85 °C. This means that the monomer complex is stable enough to keep the monomer in solution independent of temperature. In contrast, the polymer complex **6a** showed a definite clouding point at a temperature of 54 °C for the heating run (Figure 4a) and a clearing point of about 50 °C for

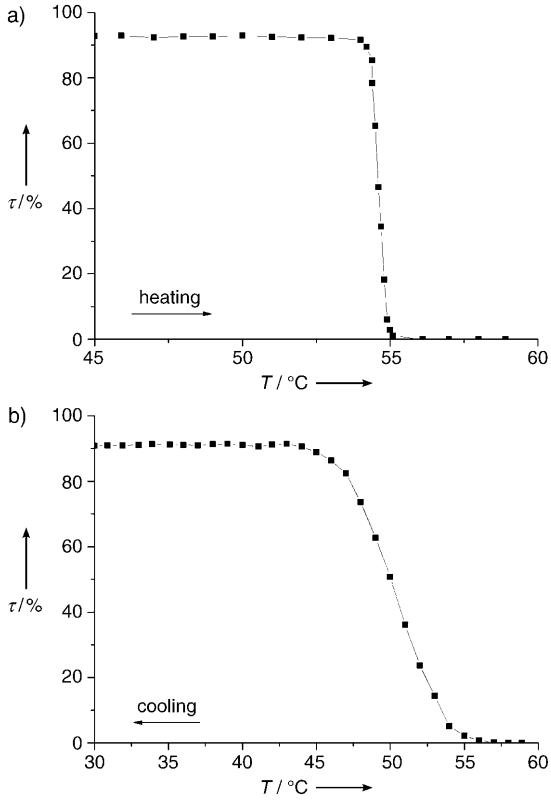
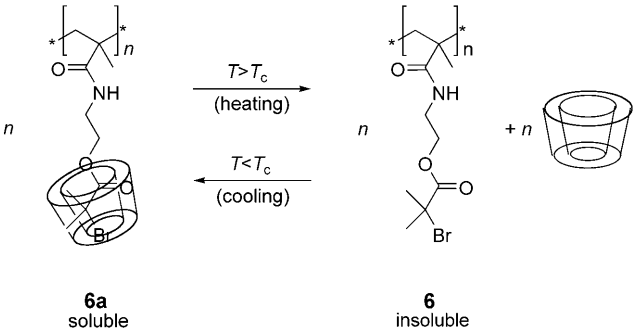


Figure 4. Transmittance of a solution of complexed polymer **6a** versus temperature during a) heating and b) cooling.

the cooling run (Figure 4b). These temperatures were found to be a function of the molecular mass $\bar{M}$ of the β-CD-free polymers. The corresponding values are listed in Table 1. Scheme 4 shows the reversible decomplexation–complexation process of polymer **6** in water.

The transmittance change of a solution of **6a** is plotted as a function of temperature in Figure 4. The decrease in the transmittance of the complexed polymer to 0 % occurs within a temperature interval of roughly 5 °C. In the subsequent



Scheme 4. Temperature-dependent reversible unthreading of CD from the bulky side group of **6a** during the heating procedure.

 © 2005 Wiley-VCH Verlag GmbH & Co. KGaA, Weinheim

cooling step the polymer returns to solution by new formation of polymer/β-CD complex. In contrast, the β-CD-free polymer is not soluble in water at any temperature in this range. The interesting polymer-solubility behavior led us to compare this phenomenon with classical LCST effects. In our case, because of the reversible complex formation between the polymer **6** and cyclodextrin, the optical effect is based on supramolecular interactions. This means that the discovered pseudo-LCST behavior is a result of noncovalent interactions between the CD host and polymer guest. Furthermore, in this system competitive inhibition or control of the LCST is possible by addition of other suitable guest molecules of low molecular weight, for example, potassium 1-adamantylcarboxylate. CD complexes these molecules preferably, and the polymer precipitates. This special effect cannot be observed in "normal" LCST systems.

To prove the postulated dissociation of the polymer/CD complex at temperatures higher than the clouding point, the total amount of β-CD in solution was determined by ^{1}H NMR measurements before polymerization and after filtration of the precipitated polymer. DMSO was added to the monomer/β-CD solution as an internal standard. After polymerization, the solution was heated and the precipitated polymer was filtered off. Integration of the NMR signals showed the same amount of β-CD relative to DMSO at each time. The filtered polymer was nearly free of CD. This is in accordance with the "pseudo-LCST" effect described above which is caused by reversible complex formation.

These experiments and results clearly show that the investigated system of β-CD and polymethacrylamide (**5**) reveals new opportunities in the field of thermosensitive systems based on noncovalent interactions between host and guest compounds. The noncovalently attached β-CD ring keeps the insoluble polymer in aqueous solution at lower temperature. At higher temperatures the CD ring slips off and the polymer precipitates; this process is reversible. Currently detailed studies about the temperature-dependent formation of aggregates and changes in viscosity are underway for a better understanding of the observed phenomenon and to investigate the suitability of polymer/β-CD solutions as novel thermosensitive gels.

Experimental Section

For materials and methods, see the Supporting Information. Monomer **3** was synthesized according to the work of Bertozzi and coworkers.[9]

Monomer **5**: 2-Bromoisobutyryl bromide (**4**; 10.12 mL, 81.9 mmol) was added dropwise to a cold mixture of **3** (8.8 g, 68.2 mmol) and triethylamine (14.1 mL, 100.8 mmol) in 180 mL of THF over 20 min. The mixture was stirred for 4 h at 0 °C and 42 h at room temperature. The precipitated salt was removed by filtration. The solvent was removed under vacuum, and the resulting yellow oil was then purified by column chromatography (silica gel, ethyl acetate/petroleum ether 1:1) ($R_f = 0.4$). Yield: 85 %. For elemental analysis and NMR and IR data, see the Supporting Information.

Complex **5a**: Monomer **5** (1 g, 3.6 mmol) was added to a stirred aqueous solution of β-CD (40 wt %; 7.2 g of β-CD in 10.8 mL of doubly distilled water). The molar ratio of monomer **5** to β-CD was 1:1.5.

Polymer **6**: Monomer **5** (1 g, 3.6 mmol) was added to a stirred aqueous solution of β-CD (40 wt %). After the solution had been flushed with argon for 20 min, a mixture of potassium peroxodisulfate (24.3 mg) and sodium disulfite (17.1 mg, 2.5 mol %) was added. The polymerization was carried out at room temperature for 12 h. The synthesized polymer was purified by several precipitation cycles in a low concentrated sodium chloride solution first from the crude solution and then from methanol. NMR and IR data are given in the Supporting Information.

Received: April 21, 2005
Published online: July 29, 2005

Keywords: cyclodextrins · host–guest systems · LCST · polymers

[1] P. R. Washington, O. Steinbock, *J. Am. Chem. Soc.* **2001**, *123*, 7933 – 7934.
[2] J. Zhang, N. A. Peppas, *Macromolecules* **2000**, *33*, 102 – 107.
[3] H.-C. Chin, Y.-F. Lin, S.-H. Hung, *Macromolecules* **2002**, *35*, 5235 – 5242.
[4] E. Tepper, O. Sadowski, H. Ritter, *Angew. Chem.* **2003**, *115*, 3279 – 3281; *Angew. Chem. Int. Ed.* **2003**, *42*, 3171 – 3173.
[5] J. H. Han, J. M. Krochta, M. J. Kurth, Y. -L. Hsieh, *J. Agric. Food Chem.* **2000**, *48*, 5278 – 5282.
[6] J. Heo, K. J. Thomas, G. Seong, R. M. Crooks, *Anal. Chem.* **2003**, *75*, 22 – 26.
[7] H. Feil, Y. H. Bae, J. Feijen, S. W. Kim, *Macromolecules* **1993**, *26*, 2496 – 2500.
[8] H. Ritter, M. Tabatabai, "Cyclodextrin in Polymer Synthesis" in *Encyclopaedia of Polymer Science and Technology*, Wiley-Interscience, New York, **2004**, published online.
[9] J. Song, E. Saiz, C. R. Bertozzi, *J. Am. Chem. Soc.* **2003**, *125*, 1236 – 1243.
[10] K. Matyjaszewski, T. P. Davis in *Handbook of Radical Polymerization*, Wiley-Interscience, New York, **2002**.
[11] P. Job, *C. R. Hebd. Seances Acad. Sci.* **1925**, *180*, 928 – 930.
[12] K. A. Connors, *Binding Constants, The Measurement of Molecular Complex Stability*, Wiley, New York, **1987**.
[13] M. T. Blanda, J. H. Horner, M. Newcomb, *J. Org. Chem.* **1989**, *54*, 4626 – 4636.

 © 2005 Wiley-VCH Verlag GmbH & Co. KGaA, Weinheim

Cross-Couplings

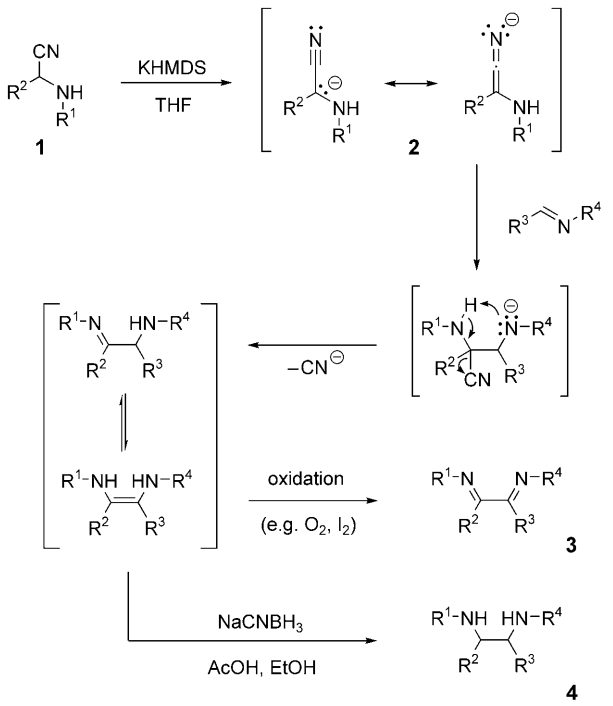
DOI: 10.1002/anie.200501705

An Aldimine Cross-Coupling for the Diastereoselective Synthesis of Unsymmetrical 1,2-Diamines**

*Coralie Kison, Nino Meyer, and Till Opatz**

Procedures for the reversible umpolung of the natural reactivity of functional groups are valuable additions to organic chemists' repertoire of methods.[1–3] One of the most prominent examples of such a reversal of polarity is the benzoin condensation, in which an electrophilic aromatic aldehyde is converted into a CH-acidic cyanohydrin, and hence a pronucleophile, by addition of cyanide. Because of the fast reversibility of cyanohydrin formation under the basic reaction conditions, the addition of the α-deprotonated cyanohydrin to an aldehyde cannot be used for the selective preparation of unsymmetrical benzoins. To assign unambiguous roles to the reactants during the course of the reaction, the temporary introduction of a hydroxy protecting group is necessary.[4] While the OH acidity of cyanohydrins is higher or at least equal to their CH acidity, the CH acidity of α-aminonitriles should surpass their NH acidity. This holds true in particular for Strecker products derived from aromatic aldehydes. Therefore, it should be possible to convert *N*-mono- and *N*-unsubstituted α-aminonitriles into their conjugate anions avoiding the base-induced elimination of HCN (retro-Strecker reaction).

Indeed, α-aryl-substituted aminonitriles yield the ketene iminates **2** upon deprotonation with potassium hexamethyldisilazide (KHMDS; Scheme 1), while lithium bases such as LDA lead to deprotonation at nitrogen and thus to the irreversible retro-Strecker reaction. Only *N*,*N*-disubstituted α-aminonitriles can be converted into stable lithium salts, which may be used as acylanion equivalents.[5–8] In contrast to these and other α-amino-substituted carbanion equivalents,[9] the ketene iminates **2** have the advantage that after their addition to an electrophile, no additional deprotection steps are necessary to liberate the amino function. The cyano group can be removed from the addition products under mild conditions,[10] thus rendering these ketene iminates easily accessible α-amino carbanion equivalents bearing a variable N substituent.[11] Upon addition of the carbanions **2** to imines, amide ions are formed which undergo an intramolecular



Scheme 1. Mechanism of the diamine synthesis.

elimination of cyanide, finally yielding α-aminoimines or the tautomeric enediamines (Scheme 1).

The course of the reaction is similar to that of the aldimine coupling, the aza analogue of the benzoin condensation, which requires only catalytic amounts of cyanide but does not allow the selective cross-coupling of two different imines.[12–16] Oxidative workup of the reaction mixture by addition of iodine or oxygen yields diimines **3**, which can serve as starting materials for the preparation of highly substituted imidazolium salts or nucleophilic carbenes.[17,18] On the other hand, the one-pot reduction of the addition products with sodium cyanoborohydride in the presence of acetic acid leads to the formation of the diamines **4** (Table 1). In accordance with a chelated transition state, the *anti*-configurated products are predominantly formed, albeit with low diastereoselectivity: At best, an *anti*/*syn* ratio of 4.3:1 was observed. The relative configuration of the main products could be determined based on the reported characteristic ^{1}H and ^{13}C chemical shifts of vicinal diamines as well as the NOE data of the diastereomeric formaldehyde aminals of the diamines **4a** and **4m**.[19–22]

In attempts to improve the diastereoselectivity of the reduction, we found that the reaction of the pure diimines **3** with BH_3·THF containing $NaBH_4$ furnishes preferentially the *syn*-configurated diamines **4** in quantitative yield (Table 2, Method A). Compounds of this type may be applied as combinatorially diverse pseudo-C_2-symmetric N,N ligands for asymmetric aldol reactions,[23] dihydroxylations,[24] and reductions.[25] If, on the other hand, phthalic acid is added to the reaction mixture instead of $NaBH_4$ (Table 2, Method B),[26] the reduction of the diimines yields the *anti*-configurated products.[27]

[*] C. Kison, N. Meyer, Dr. T. Opatz
Institut für Organische Chemie
Johannes Gutenberg-Universität Mainz
Duesbergweg 10–14
55128 Mainz (Germany)
Fax: (+49) 6131-392-4786
E-mail: opatz@uni-mainz.de

[**] This work was supported by the Fonds der Chemischen Industrie and the University of Mainz. We thank H. Kolshorn for performing the 2D-NMR experiments and the NOE measurements.

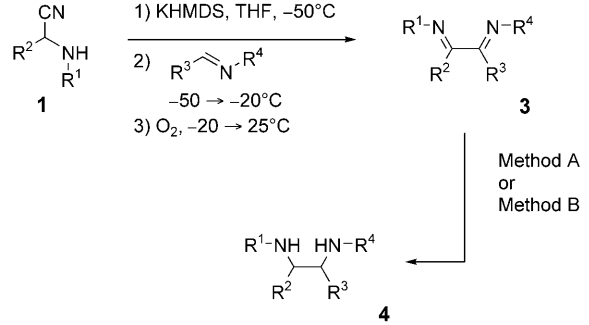
InterScience
© 2005 Wiley-VCH Verlag GmbH & Co. KGaA, Weinheim

Table 1: 1,2-Diamines obtained by aldimine cross-coupling.[a]

No.	R^1	R^2	R^3	R^4	Prod.	Yield [%][b]	d.r. (*anti*:*syn*)
1	Ph_2CH	Ph	4-ClC_6H_4	Ph	**4a**	63	1.2:1
2	Ph_2CH	Ph	4-ClC_6H_4	4-Tol	**4b**	64	1.3:1
3	Ph_2CH	Ph	Ph	4-Tol	**4c**	34	1.2:1
4	Ph_2CH	Ph	4-Py	Ph	**4d**	41	1.2:1
5	Ph_2CH	Ph	Ph	4-ClC_6H_4	**4e**	68	1.7:1
6	$Ph(CH_2)_2$	Ph	4-ClC_6H_4	Ph	**4f**	60	1.7:1
7	$Ph(CH_2)_2$	Ph	4-ClC_6H_4	4-Tol	**4g**	55	1.6:1
8	$Ph(CH_2)_2$	Ph	Ph	4-ClC_6H_4	**4h**	59	1.7:1
9	$Ph(CH_2)_2$	Ph	1-Naph	4-ClC_6H_4	**4i**	42	2.3:1
10	Me	2-Naph	4-ClC_6H_4	Ph	**4j**	60	2.4:1
11	Me	2-Naph	4-ClC_6H_4	4-Tol	**4k**	55	1.6:1
12	Me	2-Naph	Ph	4-ClC_6H_4	**4l**	58	1.5:1
13	Me	2-Naph	1-Naph	4-ClC_6H_4	**4m**	55	3.2:1
14	*i*Pr	Ph	4-ClC_6H_4	Ph	**4n**	35	2:1
15	*i*Pr	Ph	4-ClC_6H_4	4-Tol	**4o**	37	1.4:1
16	*i*Pr	Ph	Ph	4-ClC_6H_4	**4p**	33	1.6:1
17	*i*Pr	Ph	1-Naph	4-ClC_6H_4	**4q**	32	4.3:1

[a] Naph = naphthyl, Py = pyridyl, Tol = tolyl. [b] Yield after purification by preparative thin-layer chromatography.

Table 2: 1,2-Diamines obtained by diastereoselective reduction of diimines.



No.	Prod.	Method	Yield [%][a]	d.r. (*anti*:*syn*)
1	**4a**	A	65	1:5.5
2	**4b**	A	69	1:20
3	**4e**	A	67	1:6
4	**4l**	A	55	1:11
5	**4m**	A	73	3:10
6	**4a**	B	65	27:1
7	**4b**	B	69	9:1
8	**4e**	B	67	3.5:1

[a] Method A: BH_3·THF, $NaBH_4$; Method B: BH_3·THF, phthalic acid. [b] Overall yield after chromatographic purification of the diimine. The reduction is quantitative.

Compared to other methods[28] that employ the attachment of amino groups to preexisting carbon frameworks such as alkenes,[29,30] aziridines,[31] epoxides,[32] and diols,[33] the selective aldimine cross-coupling has the advantage that a single regioisomer is formed independent of the substitution pattern of the reactants. The reaction sequence does not require protecting-group operations and can be performed in one pot. In addition, either the *syn*- or *anti*-configurated vicinal diamine can be obtained, depending on the choice of the workup and reduction conditions. Therefore, the aldimine cross-coupling represents a simple and flexible method for the synthesis of a class of highly substituted unsymmetrical 1,2-diamines, of which only a few members are known.

Experimental Section

Diamines **4** (general procedure): To a stirred solution of the aminonitrile **1** (1.7 mmol) in anhydrous THF (1.5 mL) was added a solution of KHMDS (373 mg, 1.87 mmol) in anhydrous THF (2 mL) at −50 °C under an argon atmosphere. After 3 min, a solution of the imine (1.7 mmol) in anhydrous THF (1 mL) was added, and the reaction mixture was allowed to warm up to −20 °C within 100 min. Solid $NaCNBH_3$ (427 mg, 6.8 mmol) was added to the solution followed by a mixture of acetic acid (0.6 mL, 10.5 mmol) and ethanol (6.4 mL, 109 mmol). The reaction mixture was stirred overnight at room temperature. After addition of ethyl acetate (40 mL) and phase separation, the organic layer was washed several times with 1N NaOH and finally with brine and dried over Na_2SO_4, and the solvent was removed in vacuo. The product was purified by preparative thin-layer chromatography.

For the preparation of the diimines **3**, the argon atmosphere was replaced by air when the reaction mixture reached −20 °C. The solution was allowed to warm up to room temperature, and after extraction with ethyl acetate and washing with brine, the product was isolated in analogy to the procedure described for the diamines **4**.

Analytical data of **4b** (mixture of diastereomers, *anti*/*syn* 1.3:1): weakly reddish solid, R_f (silica gel 60; cyclohexane/EtOAc 10:1 + 1% $EtNMe_2$): 0.70. ^{1}H NMR (300 MHz, $CDCl_3$), COSY, HMQC, HMBC: $\delta = 7.34$–6.56 (m, 44H, *anti* + *syn*), 6.40 (pseudo-d, 2H, aniline-2,6-H *syn*, $J_{app} = 8.5$ Hz), 6.31 (pseudo-d, 2H, aniline-2,6-H *anti*, $J_{app} = 8.5$ Hz), 4.58 (s, 1H, Ph_2CH *anti*), 4.56 (s, 1H, Ph_2CH *syn*), 4.45 (d, 1H, 1-H *anti*, $J = 5.3$ Hz), 4.30 (d, 1H, 1-H *syn*, $J = 7.5$ Hz), 3.88 (d, 1H, 2-H *anti*, $J = 5.3$ Hz), 3.63 (d, 1H, 2-H *syn*, $J = 7.5$ Hz), 2.17 (s, 3H, Ph-CH_3 *syn*), 2.15 ppm (s, 3H, Ph-CH_3 *anti*). ^{13}C NMR, DEPT (75.5 MHz, $CDCl_3$), HMQC, HMBC: $\delta = 145.2$ (aniline-C1 *syn*), 144.5 (aniline-C1 *anti*), 144.1 (2C), 142.9, 142.4, 140.0, 139.9, 139.2, 138.6, 132.8, 132.6, 129.5–126.6 (partly overlapping signals), 114.0 (2C, aniline-C2,6 *syn*), 113.6 (2C, aniline-C2,6 *anti*), 65.6 (C2 *syn*), 64.4 (C2 *anti*), 63.9 (C1 *syn*), 63.5 (Ph_2CH *anti*), 63.4 (Ph_2CH *syn*), 62.5 (C1 *anti*), 20.3 ppm (2C, Ph-CH_3). IR (NaCl, film): $\tilde{\nu} = 3405$ (m, NH), 3347 (m, NH), 3060 (m), 3026 (m), 2917 (m), 2863 (m), 1616 (m), 1519 (s), 1490 (s), 1453 (m), 1090 (m), 700 (s) cm^{-1}. FD-MS: *m*/*z* (%) = 230.4 (16) [Cl-PhCH=NHPh-CH_3]$^+$, 231.4 (2), 232.4 (7), 272.5 (42) [Ph_2CH-NH=CHPh]$^+$, 273.5 (9), 503.0 (100) [*M*+H]$^+$, 504.0 (44), 505.0 (37), 506.0 (10). ESI-HRMS: calcd for [$C_{34}H_{31}ClN_2$+H]$^+$: 503.2254, found: 503.2246.

Reduction of the diimines **3** (Method A): To a stirred solution of the diimine **3** (0.5 mmol) in anhydrous THF (4 mL) was added solid $NaBH_4$ (9.5 mg, 0.25 mmol) under argon atmosphere, and the mixture was cooled to 0 °C. A fresh solution of BH_3·THF (0.75 mL, 1M in THF) was added, and stirring was continued for 30 min at 0 °C and for a further 15 h at room temperature. After addition of ethanolamine (0.5 mL), the mixture was stirred for 3–18 h and partitioned between ethyl acetate and water. The organic layer was washed with water and dried over Na_2SO_4, and the solvent was removed in vacuo.

Reduction of the diimines **3** (Method B): A stirred solution of the diimine **3** (0.5 mmol) and phthalic acid (166 mg, 1 mmol) in anhydrous THF (4 mL) was cooled to −20 °C under argon atmosphere.

 © 2005 Wiley-VCH Verlag GmbH & Co. KGaA, Weinheim

After addition of a BH_3·THF solution (1 mL, 1M in THF), the mixture was gradually warmed to room temperature, and stirring was maintained for a further 15 h. The workup procedure and the isolation of the product were performed as described for Method A.

Received: February 15, 2005
Revised: May 17, 2005
Published online: July 29, 2005

Keywords: C–C coupling · carbanions · diamines · reduction · umpolung

[1] D. Seebach, *Angew. Chem.* **1979**, *91*, 259 – 278; *Angew. Chem. Int. Ed. Engl.* **1979**, *18*, 239 – 258.
[2] D. Seebach, *Angew. Chem.* **1969**, *81*, 690 – 700; *Angew. Chem. Int. Ed. Engl.* **1969**, *8*, 639 – 649.
[3] H. Stetter, *Angew. Chem.* **1976**, *88*, 695 – 704; *Angew. Chem. Int. Ed. Engl.* **1976**, *15*, 639 – 647.
[4] K. Deuchert, U. Hertenstein, S. Hünig, *Synthesis* **1973**, 777 – 779.
[5] C. R. Hauser, H. M. Taylor, T. G. Ledford, *J. Am. Chem. Soc.* **1960**, *82*, 1786 – 1789.
[6] J. D. Albright, *Tetrahedron* **1983**, *39*, 3207 – 3233.
[7] D. Enders, J. P. Shilvock, *Chem. Soc. Rev.* **2000**, *29*, 359 – 373.
[8] J. Kant, *J. Heterocycl. Chem.* **1990**, *27*, 2129 – 2132.
[9] P. Beak, W. J. Zajdel, D. B. Reitz, *Chem. Rev.* **1984**, *84*, 471 – 523.
[10] C. H. Mitch, *Tetrahedron Lett.* **1988**, *29*, 6831 – 6834.
[11] N. Meyer, F. Werner, T. Opatz, *Synthesis* **2005**, 945 – 956.
[12] H. H. Strain, *J. Am. Chem. Soc.* **1928**, *50*, 2218 – 2223.
[13] M. Cariou, R. Carlier, J. Simonet, *Bull. Soc. Chim. Fr.* **1986**, 781 – 792.
[14] J. Correia, *J. Org. Chem.* **1983**, *48*, 3343 – 3344.
[15] H.-D. Becker, *J. Org. Chem.* **1970**, *35*, 2099 – 2102.
[16] J. S. Walia, L. Guillot, J. Singh, M. S. Chatta, M. Satyanarayana, *J. Org. Chem.* **1972**, *37*, 135 – 137.
[17] A. J. Arduengo III, R. Krafczyk, R. Schmutzler, H. A. Craig, J. R. Goerlich, W. J. Marshall, M. Unverzagt, *Tetrahedron* **1999**, *55*, 14523 – 14534.
[18] F. Glorius, WO 2004007465, **2004**.
[19] P. Mangeney, T. Tejero, A. Alexakis, F. Grosjean, J. Normant, *Synthesis* **1988**, 255 – 257.
[20] M. Largeron, M.-B. Fleury, *J. Org. Chem.* **2000**, *65*, 8874 – 8881.
[21] M. Periasamy, G. Srinivas, G. V. Karunakar, P. Bharathi, *Tetrahedron Lett.* **1999**, *40*, 7577 – 7580.
[22] B. Hatano, A. Ogawa, T. Hirao, *J. Org. Chem.* **1998**, *63*, 9421 – 9424.
[23] S. Kobayashi, H. Uchiro, Y. Fujishita, I. Shiina, T. Mukaiyama, *J. Am. Chem. Soc.* **1991**, *113*, 4247 – 4252.
[24] E. J. Corey, P. DaSilva Jardine, S. Virgil, P.-W. Yuen, R. D. Connell, *J. Am. Chem. Soc.* **1989**, *111*, 9243 – 9244.
[25] N. Uematsu, A. Fujii, S. Hashiguchi, T. Ikariya, R. Noyori, *J. Am. Chem. Soc.* **1996**, *118*, 4916 – 4917.
[26] Z.-H. Lu, N. Bhongle, X. Su, S. Ribe, C. H. Senanayake, *Tetrahedron Lett.* **2002**, *43*, 8617 – 8620.
[27] Notably, the diastereoselectivity of the reduction with commercially available $NaBH_4$-stabilized BH_3·THF depends on the age of the reagent: While a fresh solution predominantly yields the *syn* product, aged batches of the reagent lead to the formation of the *anti* product. See: J. Kollonitsch, *J. Am. Chem. Soc.* **1961**, *83*, 1515.
[28] D. Lucet, T. Le Gall, C. Mioskowski, *Angew. Chem.* **1998**, *110*, 2724 – 2772; *Angew. Chem. Int. Ed. Engl.* **1998**, *37*, 2580 – 2627.
[29] A. Chong, K. Oshima, K. B. Sharpless, *J. Am. Chem. Soc.* **1977**, *99*, 3420 – 3426.
[30] J. Barluenga, F. Aznar, M. C. S. De Mattos, W. B. Kover, S. Garcia-Granda, E. Perez-Carreno, *J. Org. Chem.* **1991**, *56*, 2930 – 2932.
[31] M. Egli, L. Hoesch, A. S. Dreiding, *Helv. Chim. Acta* **1985**, *68*, 220 – 230.
[32] P. O'Brien, P. Poumellec, *Tetrahedron Lett.* **1996**, *37*, 5619 – 5622.
[33] D. Pini, A. Iuliano, C. Rosini, P. Salvadori, *Synthesis* **1990**, 1023 – 1024.

 © 2005 Wiley-VCH Verlag GmbH & Co. KGaA, Weinheim

Heterocycles

DOI: 10.1002/anie.200502140

Versatile Direct Synthesis of Oligosubstituted Pyrroles by Cycloaddition of α-Metalated Isocyanides to Acetylenes**

*Oleg V. Larionov and Armin de Meijere**

Dedicated to Professor Rolf Huisgen on the occasion of his 85th birthday

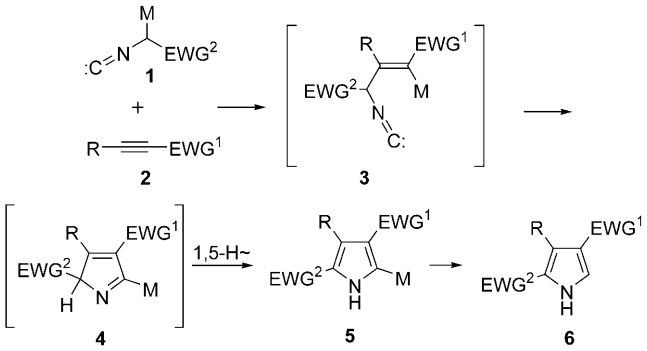
Oligofunctional pyrroles play a pivotal role among five-membered heterocycles, being basic constituents of numerous natural products,[1] potent pharmaceuticals,[2] molecular sensors, and devices.[3] We envisaged that formal cycloaddition of an α-metalated isocyanide **1** across a C–C triple bond in an electron-acceptor-substituted acetylene **2** (Scheme 1) might furnish a transient 2*H*-pyrrole **4**, which would undergo a 1,5-hydrogen shift and protonation to give a 2,3,4-trisubstituted pyrrole **6**. Although a number of pyrrole syntheses[4] from alkenes and isocyanides via pyrrolines, which contain a leaving group appropriate for elimination, have been described,[5] a direct access to pyrroles from acetylenes has been elusive so far.[6]

Methyl isocyanoacetate (**7a**) and methyl cyclopropylpropiolate (**8**-Me) were chosen for a test reaction, because the expected cyclopropyl-substituted pyrroles would supplement other cyclopropyl-substituted heterocycles, which are relevant for the pharmaceutical industry[7] (Scheme 2). Screening of various reaction conditions (Table 1) showed that most of

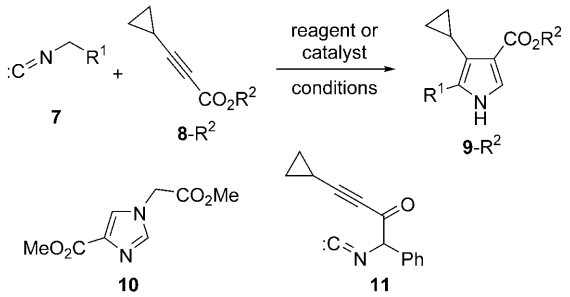
[*] Dipl.-Chem. O. V. Larionov, Prof. Dr. A. de Meijere
Institut für Organische und Biomolekulare Chemie
Georg-August-Universität Göttingen
Tammannstrasse 2, 37077 Göttingen (Germany)
Fax: (+49) 551-399-475
E-mail: Armin.deMeijere@chemie.uni-goettingen.de

[**] This work was supported by the Deutsche Forschungsgemeinschaft (SFB 416, Project A3) and the Fonds der Chemischen Industrie. O.V.L. is indebted to the Degussa-Hermann-Schlosser-Stiftung for a graduate fellowship. The authors are grateful to the companies BASF AG, Bayer AG, Chemetall GmbH, and Degussa AG for generous gifts of chemicals, and to Dr. B. Knieriem, Göttingen, for his careful proofreading of the final manuscript.

WILEY InterScience DISCOVER SOMETHING GREAT
© 2005 Wiley-VCH Verlag GmbH & Co. KGaA, Weinheim



Scheme 1. Key steps of the presented pyrrole synthesis.



Scheme 2. Formal cycloaddition of acceptor-substituted methyl isocyanides **7** to cyclopropylpropiolates **8**-R^2. For further details see Table 1.

the protocols, which had successfully been employed for isocyanide cycloadditions across double bonds,[8] proved inefficient in the case of alkynes. Thus, silver(I) acetate, and gold(I) and copper(I) chlorides gave the isocyanide dimer **10** as the sole product in $>80\%$ yield,[9] whereas no reaction was observed in the presence of zinc halides and scandium(III) triflate. On the other hand, the desired pyrrole **9a**-Me was obtained with an equimolar amount of 1,8-diazabicyclo-[5.4.0]undec-7-ene (DBU) present, albeit in a poor yield of 17%. Finally, added copper powder (10 mol%) in DMF at 70°C led to the desired product **9a**-Me in 51% yield. These promising results were used as starting points for further optimization.

Under the assumption that the low yield of pyrrole **9a**-Me could be due to the insufficient basicity of DBU, potassium *tert*-butoxide was employed. Indeed, the reaction proceeded cleanly and was complete within 2 h at ambient temperature to give **9a**-Me in 96% yield (Table 1, entry 3). With *p*-toluenesulfonylmethyl isocyanide (TOSMIC, **7b**) under these conditions, the reaction was also efficient and gave the 2-tosylpyrrole **9b**-Me in a 93% yield.

Benzyl isocyanide (**7c**), however, only produced a trace of the 2-phenylpyrrole **9c**-Me along with the unexpected isocyanobenzyl ketone **11** as the major product, which apparently arose by addition of the isocyanobenzyl anion to the carbonyl group of the propiolate **8**-Me and subsequent elimination of methoxide. This type of reaction was not observed with the carbanions derived from methyl isocyanoacetate (**7a**) and TOSMIC (**7b**), and this must have to do with their being softer nucleophiles. This undesired reaction mode could not be completely suppressed by switching to the more sterically encumbered *tert*-butyl ester **8**-*t*Bu. At best, **8**-*t*Bu in the presence of potassium hexamethyldisilazide (KHMDS) at −78°C gave a mixture of **9c**-*t*Bu and **11** in a ratio of 56:44 (Table 1). Switching from potassium to sodium and lithium hexamethyldisilazide led to vastly predominant formation of the formal substitution product **11** again (92 and 96%, respectively), even from the *tert*-butyl ester **8**-*t*Bu and at −78°C. This dependence of the **9c**-*t*Bu/**11** ratio on the nature of the alkali-metal ion is in line with the hard and soft acids and bases (HSAB) principle.[12] As a consequence, cesium *tert*-butoxide was employed, and indeed the ratio **9c**-*t*Bu/**11** increased to 96:4, so that the 2-phenylpyrrole **9c**-*t*Bu could be isolated in 91% yield (Table 1, entry 11).

With this base-mediated cycloaddition of acceptor-substituted methyl isocyanides to acetylenes in hand, our attention was turned to the copper-catalyzed variant (Table 1, entry 2), because it might bring along certain advantages in cost efficiency and compatibility with base-sensitive substrates. In a screening of various copper catalysts,

Table 1: Formal cycloadditions of acceptor-substituted methyl isocyanides **7** to cyclopropylpropiolates **8**-R^2; see Scheme 2.[10][a]

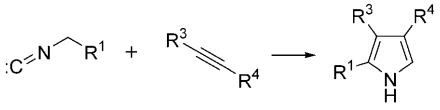
Entry	Isocyanide	R^1	Acetylene **8**-R^2	Reagent or catalyst (equiv)	Solvent	*t* [h]	*T* [°C]	Product(s)	Yield [%] (ratio)
1	**7a**	CO_2Me	**8**-Me	DBU (1.0)	THF	24	60	**9a**-Me	17
2	**7a**	CO_2Me	**8**-Me	Cu^0 (0.1)	DMF	6	70	**9a**-Me	51
3	**7a**	CO_2Me	**8**-Me	KO*t*Bu (1.1)	THF	2	20	**9a**-Me	96[b,c]
4	**7b**	SO_2Tol	**8**-Me	KO*t*Bu (1.1)	THF	2	20	**9b**-Me	93[b]
5	**7c**	Ph	**8**-Me	KO*t*Bu (1.1)	THF	2	20	**9c**-Me/**11**	96 (5:95)
6	**7c**	Ph	**8**-*t*Bu	KO*t*Bu (1.1)	THF	2	20	**9c**-*t*Bu/**11**	96 (51:49)
7	**7c**	Ph	**8**-*t*Bu	KHMDS (1.1)	THF	2	20	**9c**-*t*Bu/**11**	93 (47:53)
8	**7c**	Ph	**8**-*t*Bu	KHMDS (1.1)	THF	2	−78	**9c**-*t*Bu/**11**	86 (44:56)
9	**7c**	Ph	**8**-*t*Bu	NaHMDS (1.1)	THF	2	−78	**9c**-*t*Bu/**11**	98 (6:94)
10	**7c**	Ph	**8**-*t*Bu	LiHMDS (1.1)	THF	2	−78	**9c**-*t*Bu/**11**	98 (2:98)
11	**7c**	Ph	**8**-*t*Bu	CsO*t*Bu (1.1)	THF	2	20	**9c**-*t*Bu/**11**	91 (96:4)
12	**7a**	CO_2Me	**8**-Me	CuSPh (0.05)	DMF	12	85	**9a**-Me	93
13	**7a**	CO_2Me	**8**-Me	Cu^0-NP[d] (0.05)	DMF	16	70	**9a**-Me	92
14	**7a**	CO_2Me	**8**-Me	Cu_2O (0.05)	DMF	12	85	**9a**-Me	78

[a] Reactions were performed on a 0.5 mmol scale. Yields determined by integration of the corresponding peaks in the ^1H NMR spectra with hexamethylbenzene as an internal standard unless stated otherwise. [b] Yield of isolated product. [c] The yield was 91% on a 5 mmol scale. [d] Preactivated nanosize copper powder was used.[11]

 © 2005 Wiley-VCH Verlag GmbH & Co. KGaA, Weinheim

copper(I) benzenethiolate and preactivated nanosize metallic copper powder in dimethylformamide at 85 °C turned out to be equally efficient, providing the pyrrole **9a**-Me in 93 and 92 % yield, respectively (Table 1, entries 12 and 13, respectively). With copper(I) oxide[13] as a catalyst, **9a**-Me was obtained in a slightly lower yield of 78 %, whereas other copper compounds (e.g. copper(I) *n*-hexanethiolate (52 %), benzeneselenide (45 %), and diphenylphosphide (39 %)) gave inferior results. Benzenethiolates of gold(I) and silver(I), as well as copper(I) cyanide and halides gave rise to complex mixtures of products.

The scope and limitations of both the base-mediated and the copper-catalyzed new pyrrole synthesis were tested with a series of different acetylenes and various acceptor-substituted methyl isocyanides (Table 2, Scheme 3). Apparently, quite a number of differently 2,3,4-trisubstituted pyrroles, bearing sulfonyl, dialkoxyphosphoryl, trifluoromethyl, cyano, and secondary amino groups are easily accessible in one step from readily available acetylenes and commercial acceptor-substituted methyl isocyanides. Some of the prepared pyrroles are intermediates in the synthesis of biologically active compounds. Several can also easily be transformed into pyrroles of higher or lower order of substitution according to established protocols.[14,15]



7 12 13

Scheme 3. Preparation of 2,3,4-trisubstituted pyrroles **13** by formal cycloaddition of acceptor-substituted methyl isocyanides to acetylenes. For details see Table 2.

Experimental Section

Synthesis of **9a**-Me under base mediation (method A): To a solution of **8**-Me (620 mg, 5.0 mmol) and **7a** (545 mg, 5.5 mmol) in THF (60 mL) was added dropwise at 20 °C within 1 h a solution of KO*t*Bu (616 mg, 5.5 mmol) in THF (35 mL). The mixture was stirred at 20 °C for 1 h, the reaction was then quenched with AcOH (1 mL), and the mixture concentrated under reduced pressure. The residue was triturated with CH_2Cl_2 (3 × 30 mL) at 20 °C to extract the crude product, which was purified by column chromatography (cyclohexane/ethyl acetate (4:1)) to give **9a**-Me (1.01 g; 91 %) as a colorless solid, m.p. 123 °C. ^{1}H NMR (300 MHz, $CDCl_3$): $\delta = 0.83$–0.96 (m, 4H), 2.17–2.27 (m, 1H), 3.76 (s, 3H), 3.82 (s, 3H), 7.43 (d, $J = 3.6$ Hz, 1H), 9.78 ppm (br s, 1H); ^{13}C NMR (75.5 MHz, $CDCl_3$): $\delta = 7.3$ (CH), 8.2 (CH_2), 51.0 (CH_3), 51.45 (CH_3), 116.9 (C), 121.3 (C), 127.5 (CH), 135.4 (C), 161.4 (C), 164.5 ppm (C); IR (KBr): $\tilde{\nu} = 3325$, 3146, 3010, 2951, 1719, 1696, 1541, 1437, 1276, 1199, 1059, 785 cm^{-1}; LRMS (EI): *m*/*z*: 223.1 [M^+]; HRMS (ESI): calcd for $C_{11}H_{14}NO_4$ [M+H$^+$] 224.0923, found 224.0917.

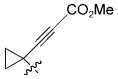
The formal cycloaddition of benzyl isocyanide (**7c**) to *tert*-butyl cyclopropylpropiolate (**8**-*t*Bu) to give **9c**-*t*Bu can be performed by the same protocol except that potassium *tert*-butoxide has to be replaced with cesium *tert*-butoxide.

Synthesis of **13g** by copper-catalyzed formal cycloaddition (method B; Table 2, entry 9): The copper catalyst (preferably preactivated nanosize copper powder (3 mg, 0.05 mmol, 5 mol %), or copper(I) benzenethiolate (9 mg, 0.05 mmol, 5 mol %)) was added to a solution of **7a** (109 mg, 1.1 mmol) and **12f** in DMF (2 mL), and the mixture was vigorously stirred at 70 °C (with preactivated nanosize copper powder) or 85 °C (with CuSPh) for 16 h. The solvent was removed in vacuo (0.05 mbar), and the residue was purified by column chromatography (cyclohexane/ethyl acetate (4:1)) to give pyrrole **13g** (277 mg; 91 %) as a pale yellow solid, m.p. 141 °C. ^{1}H NMR (300 MHz, $CDCl_3$): $\delta = 1.22$ (dd, $J = 4.8$, 7.6 Hz, 2H), 1.64 (dd, $J = 5.1$, 7.9 Hz, 2H), 3.67 (s, 3H), 3.81 (s, 3H), 3.87 (s, 3H), 7.40 (d, $J = 3.5$ Hz, 1H), 9.73 ppm (br s, 1H); ^{13}C NMR (75.5 MHz, $CDCl_3$): $\delta = 7.6$ (C), 21.2 (CH_2), 51.2 (CH_3), 51.8 (CH_3), 52,3 (CH_3), 67.2 (C), 94.9 (C), 117.2 (C), 122.5 (C), 127.0 (CH), 129.4 (C), 154.6 (C), 160.4 (C), 163.6 ppm (C); IR (KBr): $\tilde{\nu} = 3298$, 3014, 2954, 2229, 1707, 1559, 1437, 1271, 1196, 1023, 749 cm^{-1}; LRMS (EI): *m*/*z*: 305.1 [M^+]; HRMS (ESI): calcd for $C_{15}H_{16}NO_6$ [M+H$^+$] 306.0978, found 306.0981.

Received: June 20, 2005

Keywords: cesium · copper · heterocycles · homogeneous catalysis · isocyanides

Table 2: Synthesis of 2,3,4-trisubstituted pyrroles **9** and **13** by formal cycloaddition of substituted methyl isocyanides **7** to acetylenes **8** and **12**, respectively (see Schemes 2 and 3).

Entry	Isocyanide		Acetylene		Product	Yield [%]	
		R^1		R^3	R^4		Method A[a] (base)	Method B[b] (cat., [mol %])
1	**7a**	CO_2Me	**8**-*t*Bu	*c*Pr	CO_2tBu	**9a**-*t*Bu	97 (KO*t*Bu)	94 (CuSPh, 5)
2	**7b**	SO_2Tol	**8**-*t*Bu	*c*Pr	CO_2tBu	**9b**-*t*Bu	93 (KO*t*Bu)	91 (CuSPh, 5)
3	**7d**	CO_2tBu	**12a**	Me	CO_2Me	**13a**	76[c] (KO*t*Bu)	83 (Cu^0-NP, 5)
4	**7e**	CN	**8**-*t*Bu	*c*Pr	CO_2tBu	**13b**	83 (KHMDS)	[d]
5	**7a**	CO_2Me	**12b**	$MeOCH_2$	$P(O)(OEt)_2$	**13c**	53 (KO*t*Bu)	47 (Cu^0-NP, 5)
6	**7b**	SO_2Tol	**12c**	CF_3	CO_2Et	**13d**	76 (KHMDS)	–
7	**7d**	CO_2tBu	**12d**		CO_2Me	**13c**	45 (KO*t*Bu)	[d]
8	**7d**	CO_2tBu	**12e**	Ph	CO_2Et	**13f**	–	78 (Cu^0-NP, 5)[e,f]
9	**7a**	CO_2Me	**12f**		CO_2Me	**13g**	87[g] (KO*t*Bu)	91[g] (CuSPh, 5)

[a] Method A: Addition of base (1.2 equiv), 1 h, then 1 h at 20 °C, THF. [b] Method B: Cu catalyst (Cu^0-NP stands for preactivated nanosize copper powder), DMF, 85 °C, 12 h. [c] An intermediate in the synthesis of an inhibitor of DNA gyrase,[2a] and antagonist of CHO cells expressing metabotropic glutamate receptor 1a.[2b] [d] Not performed due to instability of the acetylene and/or the substituted isocyanide. [e] A possible intermediate for the synthesis of a potent inhibitor of HMG-CoA reductase.[2b] [f] The reaction was performed at 120 °C. [g] Only the monoaddition product was obtained.

 © 2005 Wiley-VCH Verlag GmbH & Co. KGaA, Weinheim

[1] D. E. N. Jacquot, M. Zöllinger, T. Lindel, *Angew. Chem.* **2005**, *117*, 2336 – 2338; *Angew. Chem. Int. Ed.* **2005**, *44*, 2295 – 2298; H. Garrido-Hernandez, M. Nakadai, M. Vimolratana, Q. Li, T. Doundoulakis, P. G. Harran, *Angew. Chem.* **2005**, *117*, 775 – 779; *Angew. Chem. Int. Ed.* **2005**, *44*, 765 – 769; H. Hoffmann, T. Lindel, *Synthesis* **2003**, 1753 – 1783; D. Seidel, V. Lynch, J. L. Sessler, *Angew. Chem.* **2002**, *114*, 1480 – 1483; *Angew. Chem. Int. Ed.* **2002**, *41*, 1422 – 1425; J. A. Johnson, N. Li, D. Sames, *J. Am. Chem. Soc.* **2002**, *124*, 6900 – 6903; G. Dannhardt, W. Kiefer, *Arch. Pharm. Pharm. Med. Chem.* **2001**, *334*, 183 – 188; T. Lindel, M. Hochgürtel, M. Assmann, M. Köck, *J. Nat. Prod.* **2000**, *63*, 1566 – 1569; M. Adamczyk, D. D. Johnson, R. E. Reddy, *Angew. Chem.* **1999**, *111*, 3751 – 3753; *Angew. Chem. Int. Ed.* **1999**, *38*, 3537 – 3539; S. Depraetere, M. Smet, W. Dehaen, *Angew. Chem.* **1999**, *111*, 3556 – 3558; *Angew. Chem. Int. Ed.* **1999**, *38*, 3359 – 3361; J. M. Gottesfeld, L. Neely, J. W. Trauger, E. E. Baird, P. B. Dervan, *Nature* **1997**, *387*, 202 – 205.

[2] K. Yamaji, M. Masubuchi, F. Kawahara, Y. Nakamura, A. Nishio, S. Matsukuma, M. Fujimori, N. Nakada, J. Watanabe, T. Kamiyama, *J. Antibiot.* **1997**, *50*, 402 – 411; B. Fournier, D. C. Hooper, *Antimicrob. Agents Chemother.* **1998**, *42*, 121 – 128; D. Perrin, B. van Hille, J.-M. Barret, A. Kruczynski, C. Etievant, T. Imbert, B. T. Hill, *Biochem. Pharmacol.* **2000**, *59*, 807 – 819; F. Micheli, R. Di Fabio, R. Benedetti, A. M. Capelli, P. Cavallini, P. Cavanni, S. Davalli, D. Donati, A. Feriani, S. Gehanne, M. Hamdan, M. Maffeis, F. M. Sabbatini, M. E. Tranquillini, M. V. A. Viziano, *Farmaco* **2004**, 175 – 183; B. D. Roth, C. J. Blankley, A. W. Chucholowski, E. Ferguson, M. L. Hoefle, D. F. Ortwine, R. S. Newton, C. S. Sekerke, D. R. Slikovic, C. D. Stratton, M. W. Wilson, *J. Med. Chem.* **1991**, *34*, 357 – 366.

[3] D. W. Yoon, H. Hwang, C.-H. Lee, *Angew. Chem.* **2002**, *114*, 1835 – 1837; *Angew. Chem. Int. Ed.* **2002**, *41*, 1757 – 1759; J. O. Jeppesen, J. Becher, *Eur. J. Org. Chem.* **2003**, 3245 – 3266; H. Miyaji, W. Sato, J. L. Sessler, *Angew. Chem.* **2000**, *112*, 1847 – 1850; *Angew. Chem. Int. Ed.* **2000**, *39*, 1777 – 1780; F.-P. Montforts, O. Kutzki, *Angew. Chem.* **2000**, *112*, 612 – 614; *Angew. Chem. Int. Ed.* **2000**, *39*, 599 – 601.

[4] For recent pyrrole syntheses see: D. Tejedor, D. González-Cruz, F. García-Tellado, J. J. Marrero-Tellado, M. L. Rodríguez, *J. Am. Chem. Soc.* **2004**, *126*, 8390 – 8391; B. Ramanathan, A. J. Keith, D. Armstrong, A. L. Odom, *Org. Lett.* **2004**, *6*, 2957 – 2960; Y. Nishibayashi, M. Yoshikawa, Y. Inada, M. D. Milton, M. Hidai, S. Uemura, *Angew. Chem.* **2003**, *115*, 2785 – 2788; *Angew. Chem. Int. Ed.* **2003**, *42*, 2681 – 2684; J. T. Kim, A. V. Kel'in, V. Gevorgyan, *Angew. Chem.* **2003**, *115*, 102 – 105; *Angew. Chem. Int. Ed.* **2003**, *42*, 98 – 101; M. Yu, B. L. Pagenkopf, *Org. Lett.* **2003**, *5*, 5099 – 5101; N. D. Smith, D. Huang, N. D. P. Cosford, *Org. Lett.* **2002**, *4*, 3537 – 3539; A. V. Kel'in, A. W. Sromek, V. Gevorgyan, *J. Am. Chem. Soc.* **2001**, *123*, 2074 – 2075; H. Kagoshima, T. Akiyama, *J. Am. Chem. Soc.* **2000**, *122*, 11741 – 11742; C.-F. Lee, L.-M. Yang, T.-Y. Hwu, A.-S. Feng, J.-C. Tseng, T.-Y. Luh, *J. Am. Chem. Soc.* **2000**, *122*, 4992 – 4993.

[5] A. M. van Leusen, H. Siderius, B. E. Hoogenboom, D. van Leusen, *Tetrahedron Lett.* **1972**, 5337 – 5340; D. H. R. Barton, J. Kervagoret, S. Z. Zard, *Tetrahedron* **1990**, *46*, 7587 – 7598; D. van Leusen, E. van Echten, A. M. van Leusen, *J. Org. Chem.* **1992**, *57*, 2245 – 2249; H. Uno, K. Sakamoto, T. Tominaga, N. Ono, *Bull. Chem. Soc. Jpn.* **1994**, *67*, 1441 – 1448; A. R. Katritzky, L. Zhu, H. Y. Lang, O. Denisko, Z. Q. Wang, *Tetrahedron* **1995**, *51*, 13271 – 13276; M. Adamczyk, R. E. Reddy, *Tetrahedron* **1996**, *52*, 14689 – 14700; J. Boëlle, R. Schneider, P. Gérardin, B. Loubinoux, *Synthesis* **1997**, 1451 – 1456; R. Di Santo, R. Costi, S. Massa, M. Artico, *Synth. Commun.* **1998**, *28*, 1801 – 1816; H. P. Dijkstra, R. ten Have, A. M. van Leusen, *J. Org. Chem.* **1998**, *63*, 5332 – 5338, and references therein; J. O. Brower, D. A. Lightner, A. F. McDonagh, *Tetrahedron* **2001**, *57*, 7813 – 7827.

[6] A single report described reactions of dimethyl acetylenedicarboxylate and methyl propiolate, respectively, with *p*-tosylmethyl isocyanide in the presence of DBU furnishing correspondingly substituted pyrroles in 7 and 12% yields: H. Saikachi, T. Kitagawa, H. Sasaki, *Chem. Pharm. Bull.* **1979**, *27*, 2857 – 2861.

[7] V. Costantino, E. Fatorusso, M. Menna, O. Taglialatella-Scafari, *Curr. Med. Chem.* **2004**, *11*, 1671 – 1692; P. A. Seymour, A. W. Schmidt, D. W. Schulz, *CNS Drug Rev.* **2003**, *9*, 57 – 96; J. J. Starling, R. L. Shepard, J. Cao, K. L. Law, B. H. Norman, J. S. Kroin, W. J. Ehlhardt, T. M. Baughman, M. A. Winter, M. G. Bell, C. Shih, J. Gruber, W. F. Elmquist, A. H. Dantzig, *Adv. Enzyme Regul.* **1997**, *37*, 335 – 347.

[8] Isocyanide cycloadditions across double bonds. Lewis acid catalysis: a) T. Saegusa, Y. Ito, H. Kinoshita, S. Tomita, *J. Org. Chem.* **1971**, *36*, 3316 – 3323; b) Y. Ito, T. Matsuura, T. Saegusa, *Tetrahedron Lett.* **1985**, *26*, 5781 – 5784; c) R. Grigg, M. I. Lansdell, M. Thornton-Pett, *Tetrahedron* **1999**, *55*, 2025 – 2044; base-mediated formal cycloadditions: d) D. Hoppe, *Angew. Chem.* **1974**, *86*, 778 – 793; *Angew. Chem. Int. Ed. Engl.* **1974**, *13*, 789 – 804; see also ref. [4].

[9] The isocyanide dimer **11** was reported to be formed in the presence of an equimolar amount of AgOAc (see ref. [8c]). The rapid dimerization observed here may be due to the strong influence of the acetylene component on the catalytic activity of Ag^{I}.

[10] Further metal compounds were tested but proved inefficient: CuOTf, $Cu(OTf)_2$, AgOTf, $Yb(OTf)_3$, PdO, Ag_2O, $GaCl_3$, $BF_3{\cdot}OEt_2$, $MgBr_2$, $CoCl_2$.

[11] Commercial nanosize copper powder (Aldrich) was preactivated by heating in vacuo (0.05 mbar) at 150 °C overnight, and was stored under argon. The activity of thus prepared catalyst does not deteriorate within at least two weeks.

[12] R. G. Pearson, *Coord. Chem. Rev.* **1990**, *100*, 403 – 425; T. L. Ho, *Chem. Rev.* **1975**, *75*, 1 – 20; J. Seyden-Penne, *Bull. Soc. Chim. France* **1968**, 3871 – 3878.

[13] T. Saegusa, I. Murase, Y. Ito, *Bull. Chem. Soc. Jpn.* **1972**, *45*, 830 – 833.

[14] For some recently published transformations of pyrroles see: direct C-arylation of pyrroles with free NH groups: a) X. Wang, B. S. Lane, D. Sames, *J. Am. Chem. Soc.* **2005**, *127*, 4996 – 4997; b) R. D. Rieth, N. P. Mankad, E. Calimano, J. P. Sadighi, *Org. Lett.* **2004**, *6*, 3981 – 3983; addition of pyrroles to unfunctionalized enediynes: c) A. Odedra, C.-J. Wu, T. B. Pratap, C.-W. Huang, Y.-F. Ran, R.-S. Liu, *J. Am. Chem. Soc.* **2005**, *127*, 3406 – 3412; oxidative cyanation of pyrroles: d) T. Dohi, K. Morimoto, Y. Kiyono, H. Tohma, Y. Kita, *Org. Lett.* **2005**, *7*, 537 – 540.

[15] Shortly after submission of this manuscript we have become aware of a very recent publication by Yamamoto et al., who have independently discovered a formal cycloaddition of isocyanides to alkynes: S. Kamijo, C. Kanazawa, Y. Yamamoto, *J. Am. Chem. Soc.* **2005**, *127*, 9260 – 9266.

 © 2005 Wiley-VCH Verlag GmbH & Co. KGaA, Weinheim

Organozinc Compounds

DOI: 10.1002/anie.200500688

Synthesis of Thermolabile Zinc–Pentel Compounds under Kinetically Controlled Reaction Conditions**

Florian Thomas, Stephan Schulz, and Martin Nieger*

Dedicated to Professor Herbert W. Roesky on the occasion of his 70th birthday

Several general reaction pathways have been established for the synthesis of transition metal/Group 15 and main-group metal/Group 15 compounds with the metathesis reaction showing the most potential. Amide, phosphide, and arsenide groups ER_2 (E = N, P, As) can be introduced readily to main-group and transition-metal centers by reaction of metal halides MX_n and the corresponding organolithium compound $LiER_2$. In sharp contrast, the synthesis of metal–antimony and metal–bismuth compounds is rather problematic because of the tendency of lithium stibides and bismuthides $LiER_2$ (E = Sb, Bi) to undergo redox reactions with formation of elemental Sb and Bi. Comparable trends have been observed for dehalosilylation reactions between $E(SiMe_3)_3$ (E = Sb, Bi) and transition-metal halides, which typically yield low-valent compounds such as distibanes and dibismuthanes.[1] Only recently, we reported on reactions of $[\{Me_2AlE(SiMe_3)_2\}_x]$ (E = P, As, Sb, Bi)[2] and Me_3M-dmap (dmap = 4-dimethylaminopyridine; M = Ga, In, Tl), which proceed with Al/M exchange and subsequent formation of the corresponding Group 13/15 heterocycles $[\{Me_2ME(SiMe_3)_2\}_x]$.[3] This novel reaction type generally allows the synthesis of Group 13/15 compounds under kinetic control, as is typical for salt-elimination reactions using organolithium compounds, but does not require redox-sensitive reagents. Consequently, extremely thermolabile compounds such as $[\{Me_2InBi(SiMe_3)_2\}_3]$ and $[\{Me_2TlE(SiMe_3)_2\}_2]$ (E = P, As) could be synthesized and structurally characterized for the first time.[4]

[*] Prof. Dr. S. Schulz
Chemistry Department, University of Paderborn
Warburger Strasse 100, J6.214, 33098 Paderborn (Germany)
Fax: (+49) 5251-60-3423
E-mail: stephan.schulz@upb.de
Dr. F. Thomas
BASF AG
Ludwigshafen (Germany)
Dr. M. Nieger
Institute of Inorganic Chemistry
University of Bonn (Germany)

[**] S. Schulz gratefully acknowledges generous financial support from the Deutsche Forschungsgemeinschaft (DFG), the Fonds der Chemischen Industrie (FCI), the Bundesministerium für Bildung, Wissenschaft, Forschung und Technologie (BMBF), and Prof. E. Niecke, Universität Bonn. F. Thomas is grateful to the Fonds der Chemischen Industrie for a fellowship award.

To investigate whether this specific transmetalation reaction is applicable only for the synthesis of Group 13/15 heterocycles or if it can be used generally for the synthesis of metal–pentel compounds, we became interested in reactions with organozinc compounds. Consequently, we investigated the reaction of $[\{Me_2AlE(SiMe_3)_2\}_x]$ (E = P, As, Sb) with $[(dmap)_2ZnMe_2]$ (**1**, Figure 1), which was obtained from the reaction of Me_2Zn and two equivalents of dmap in hexane.[5]

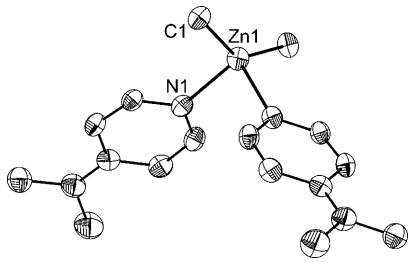


Figure 1. Solid-state structure of **1** (one of two independent molecules, data for the second molecule in square brackets); H atoms are omitted for clarity). Selected bond lengths [Å] and angles [°]: Zn1–C1 2.022(2) [2.023(2)], Zn1–N1 2.177(2) [2.169(2)]; C1-Zn1-C1A 137.2(1) [137.7(1)], C1-Zn1-N1 105.6(1) [104.4(1)], C1-Zn1-N1A 102.3(1) [105.0(1)], N1-Zn1-N1A 97.4(1) [90.9(1)].

The central Zn atom in **1** (crystallographic C_2 symmetry, two independent half molecules in the elemental cell, space group *Pccn*) shows a distorted tetrahedral environment. The Zn–N bond lengths (2.177(2) [2.169(2)] Å) are in between those observed for Me_2Zn adducts with bidentate N-donor ligands (2.20–2.41 Å;[6] coordination number 4) and $[(thf)_2Li\{(NtBu)_3SMe\}\text{-}ZnMe_2]$ (2.137(2) Å), the only structurally characterized Me_2Zn adduct with a threefold-coordinated Zn center.[7]

The reactions of **1** with $[\{Me_2AlE(SiMe_3)_2\}_x]$ (E = P, As, Sb) [Eq. (1a)] and $[(dmap)Al(Me_2)E(SiMe_3)_2]$ with Me_2Zn [Eq. (1b)] occur with Al/Zn exchange and subsequent formation of the desired heterocycle $[\{MeZnE(SiMe_3)_2\}_x]$ (E = P, As, Sb **2**).

$$3/x\,[\{Me_2AlE(SiMe_3)_2\}_x] + 3\,[(dmap)_2ZnMe_2] \xrightarrow[-3\,[(dmap)AlMe_3],\,-3\,dmap]{} [\{MeZnE(SiMe_3)_2\}_3] \quad (1a)$$

$$3\,[(dmap)Al(Me_2)E(SiMe_3)_2] + 3\,Me_2Zn \xrightarrow[-3\,[(dmap)AlMe_3]]{} [\{MeZnE(SiMe_3)_2\}_3] \quad (1b)$$

$[\{MeZnP(SiMe_3)_2\}_3]$ and $[\{MeZnAs(SiMe_3)_2\}_3]$, which have been synthesized previously,[8] were identified by ^1H, ^{31}P, and ^{13}C NMR spectroscopy. Because of the thermolability of **2**, NMR spectra of the reaction solution were recorded directly at −30 °C.[9] Characteristic resonances of $[(dmap)AlMe_3]$ are observed, which is proof of the transmetalation. In addition, resonances arising from the ZnMe and $SiMe_3$ groups with an intensity ratio of 3:18 (^1H NMR) confirm the formation of **2**. Unfortunately, crystals suitable for a single-crystal X-ray analysis have not been obtained to date. However, we obtained single crystals of a rather unexpected compound **3** (Figures 2 and 3) in very low yield (about 4%)

 InterScience © 2005 Wiley-VCH Verlag GmbH & Co. KGaA, Weinheim

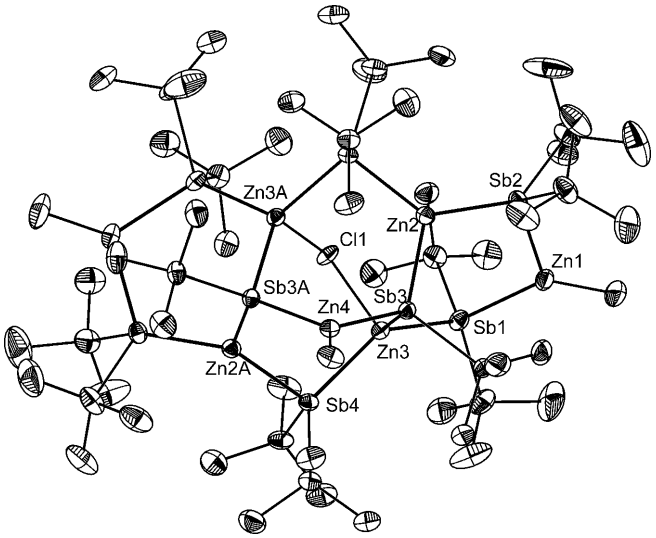


Figure 2. Solid-state structure of **3** (H atoms are omitted for clarity). Selected bond lengths [Å] and angles [°]: Sb1–Zn1 2.644(1), Sb1–Zn3 2.644(1), Sb2–Zn2 2.646(1), Sb2–Zn1 2.656(1), Sb3–Zn2 2.604(1), Sb3–Zn3 2.616(1), Sb3–Zn4 2.629(1), Sb4–Zn3 2.686(1), Sb4–Zn2A 2.604(1), Sb1–Si1 2.542(1), Sb1–Si2 2.553(1), Sb3–Si5 2.544(1), Zn1–C22 1.974(4), Zn4–C23 1.974(5), Zn3–Cl1 2.474(1); Zn1-Sb1-Zn3 118.3(1), Zn1-Sb2-Zn2 110.0(1), Zn2-Sb3-Zn3 90.6(1), Zn2-Sb3-Zn4 117.5(1), Zn3-Sb3-Zn4 109.7(1), Zn2A-Sb4-Zn3 96.8(1), Sb1-Zn1-Sb2 107.2(1), Sb2-Zn2-Sb3 113.6(1), Sb1-Zn3-Sb3 111.0(1), Sb3-Zn3-Sb4 117.9(1), Sb1-Zn3-Sb4 121.5(1), Sb4A-Zn2-Sb2 133.0(1), Sb4A-Zn2-Sb3 113.3(1), Sb3-Zn4-Sb3A 102.5(1), Zn3-Cl1-Zn3A 117.2(1).

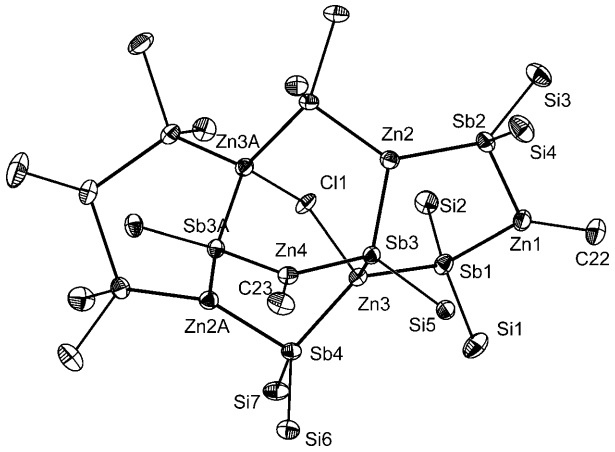


Figure 3. Representation of the central cluster framework of **3**.

from a reaction solution of $[(dmap)Al(Me_2)Sb(SiMe_3)_2]$ and $ZnMe_2$ after storage for six weeks at −30 °C.[5]

The novel cluster **3** contains a central Zn_5Sb_4Cl unit, which is bridged by two additional $ZnSb_2$ moieties. Alternatively, the central framework of **3** can be described as an assembly of three annelated Zn_3Sb_3 rings, in which the outer rings are bridged by a $Sb(SiMe_3)_2$ group (Zn3-Sb4-Zn2A) and a chlorine atom (Zn3-Cl1-Zn3a). Consequently, the central core of **3** is composed completely of six-membered rings. The molecule contains a diadic rotational axis along the atoms Cl1-Zn4-C23. The Sb atoms show distorted tetrahedral coordination spheres, whereas the Zn atoms display different coordination environments. Zn atoms that are bound only to Sb atoms are threefold coordinated, whereas those that are bound to the Cl bridges (Zn3, Zn3A), are fourfold coordinated. The Zn–Sb bond lengths within the heterocyclic Zn_3Sb_3 moieties range from 2.604(1) to 2.656(1) Å. In contrast, the Zn–Sb bond lengths to the bridging $Sb(SiMe_3)_2$ group differ more significantly by about 0.08 Å (Zn2A–Sb4 2.604(1); Zn3–Sb4 2.686(1) Å). These findings as well as the pronounced pyramidalization of Sb4 (sum of bond angles: 312.6° (Zn2A-Sb4-Si6/7 + Si6-Sb4-Si7), 346.6° (Zn3-Sb4-Si6/7 + Si6-Sb4-Si7)) point to rather dative bonding character between Sb4 and Zn3. The endocyclic Zn-Sb-Zn bond angles vary significantly between 90.6(1) and 118.3(1)°, whereas the Sb-Zn-Sb bond angles differ only by 6.4° (107.2(1)–113.6(1)°). The Zn–Cl distance of 2.474(1) Å is rather long, the Zn–C (1.974(5) Å) and Sb–Si bond lengths (2.542(2)–2.577(2) Å) are within typical ranges.

The formation of **3** is attributed to contaminating Cl ions in the Me_2Zn solution used in the reaction with $[(dmap)Al(Me_2)Sb(SiMe_3)_2]$. Apparently these react with $Sb(SiMe_3)_2$ groups in analogy to the reactions of $ZnCl_2$ and ZnI_2 with $E(SiMe_3)_3$ (E = P, As; formation of Me_3SiX, dehalosilylation reaction).[10] Currently, we are investigating the general applicability of this particular reaction type for the synthesis of novel cluster compounds by reaction of defined mixtures of Me_2Zn and $ZnCl_2$ with $[(dmap)Al(Me_2)Sb(SiMe_3)_2]$.[11]

The novel metal-exchange reaction has been extended to the synthesis of Zn–pentel heterocycles. This is a very promising result with respect to the development of a general synthetic pathway for metal–pentel compounds. The reactions can be performed under kinetically controlled reaction conditions at low temperatures. Consequently, previously unknown compounds containing the heaviest Group 15 elements Sb and Bi, as well as novel metal–pentel clusters, might become accessible in the near future.

Experimental Section

1: 4-Dimethylaminopyridine (dmap; 2.44 g, 20 mmol) dissolved in hexane (30 mL) was combined with a 2 M solution of $ZnMe_2$ in toluene (5 mL, 10 mmol) and stirred for 2 h at ambient temperature. The resulting colorless solution was concentrated under vacuum and stored at −30 °C. After 24 h, **1** was obtained as a colorless crystalline solid. Yield: 2.92 g, 8.6 mmol, 86 %. ^{1}H NMR (300 MHz, C_6D_6, 30 °C): $\delta = -0.01$ (s, 6H; $ZnMe_2$), 2.10 (s, 6H; NMe_2), 5.87 (dd, $^3J_{H,H} = 5.3$, $^4J_{H,H} = 1.4$ Hz, 4H; C3-H), 8.21 ppm (dd, $^3J_{H,H} = 5.2$, $^4J_{H,H} = 1.4$ Hz, 4H; C2-H); ^{13}C NMR (75 MHz, 30 °C, C_6D_6): $\delta = -11.9$ ($ZnMe_2$), 36.8 (NMe_2), 105.2 (C3), 147.5 (C2), 153.3 ppm (C4); MS (EI, 15 eV, 100 °C): *m/z* (%): 217 (6) [M^+−dmap], 122 (100) [$dmap^+$], 95 (35) [$ZnMe_2^+$], 80 (56) [$ZnMe^+$].

2: A suspension of $[\{Me_2AlSb(SiMe_3)_2\}_3]$ (0.49 g, 0.5 mmol) in toluene (15 mL) was cooled to −30 °C and then combined with a solution of **1** (0.56 g, 1.5 mmol) in pentane (15 mL). The brownish solution was stirred for 30 min at −10 °C and then stored for 12 h at −30 °C, which resulted in the precipitation of $[(dmap)AlMe_3]$. The solid was removed by decantation, and the remaining solution was concentrated to dryness under vacuum. The resulting waxy solid was dissolved in precooled pentane (10 mL), filtered, and stored for 24 h at −60 °C. Compound **2** was obtained as a colorless, thermolabile, light-sensitive solid. Yield: 0.21 g, 0.21 mmol, 41 %. M.p. 45 °C (decomp). ^{1}H NMR (300 MHz, [D_8]toluene, −30 °C): $\delta = 0.19$ (s, 3H; ZnMe), 0.52 ppm (s, 18H; $SiMe_3$); ^{13}C{^{1}H} NMR (75 MHz,

 © 2005 Wiley-VCH Verlag GmbH & Co. KGaA, Weinheim

[D_8]toluene, −30 °C): $\delta = -17.4$ (s; ZnMe), 12.4 ppm (s; $SiMe_3$); MS (EI, 12 eV, 75 °C): *m/z* (%): 267 (5) $[Sb(SiMe_3)_2]^+$, 94 (100) $[ZnMe_2]^+$, 79 (80) $[ZnMe]^+$.

Received: February 23, 2005
Revised: April 27, 2005
Published online: August 1, 2005

Keywords: heterocycles · metathesis · pentels · transmetalation · zinc

[1] a) P. Sharma, N. Rosas, S. Hernández, A. Cabrera, *J. Chem. Soc. Chem. Commun.* **1995**, 1325; b) D. Fenske, A. Rothenberger, S. Wieber, *Z. Anorg. Allg. Chem.* **2003**, *629*, 929.

[2] These can be prepared easily by dehydrosilylation. See, for instance, "Group 13 Chemistry. I: Fundamental New Developments": S. Schulz, *Struct. Bonding (Berlin)* **2002**, *103*, 117.

[3] F. Thomas, S. Schulz, M. Nieger, *Organometallics* **2003**, *22*, 3471.

[4] F. Thomas, S. Schulz, M. Nieger, *Angew. Chem.* **2003**, *115*, 5800; *Angew. Chem. Int. Ed.* **2003**, *42*, 5641.

[5] Single-crystal X-ray diffraction: Nonius KappaCCD diffractometer ($Mo_{K\alpha}$ radiation, $\lambda = 0.71073$ Å; $T = 123(2)$ K). The structures were solved by direct methods (SHELXS-97, G. M. Sheldrick, *Acta Crystallogr. Sect. A* **1990**, *46*, 467) and refined by full-matrix least-squares on F^2 (SHELXL-97, Program for Crystal Structure Refinement, G. M. Sheldrick, Universität Göttingen, **1997**). All non-hydrogen atoms were refined anisotropically and hydrogen atoms were refined by a riding model. Empirical absorption corrections were applied. **1**: $[(dmap)_2ZnMe_2]$ ($C_{16}H_{26}N_4Zn$, $M_r = 339.78$), colorless crystal ($0.50 \times 0.30 \times 0.20$ mm^3); orthorhombic, space group *Pccn* (no. 56); $a = 13.9127(2)$, $b = 14.5494(2)$, $c = 17.5015(3)$ Å, $V = 3542.68(9)$ Å^3; $Z = 8$; $\mu = 1.386$ mm^{-1}; $\rho_{calcd} = 1.274$ g cm^{-3}; 27766 reflections ($2\theta_{max} = 50°$), 3119 unique ($R_{int} = 0.054$), 195 parameters; largest max./min. in the final difference Fourier synthesis 0.340 e Å^{-3}/−0.514 e Å^{-3}; max./min. transmission 0.68936/0.63695; $R_1 = 0.032$ ($I > 2\sigma(I)$), $wR_2 = 0.098$. **3**: $[\{(MeZn)\{Sb(SiMe_3)_2\}_3Zn_2(SbSiMe_3)\}_2(ZnMe)Cl]$ ($C_{45}H_{135}ClSb_8Si_{14}Zn_7$·toluene, $M_r = 2628.96$), colorless crystal ($0.35 \times 0.20 \times 0.15$ mm^3); monoclinic, space group *C*2/*c* (no. 15); $a = 16.4669(1)$, $b = 20.6864(2)$, $c = 30.8325(3)$ Å, $\beta = 94.050(1)°$, $V = 10476.58(16)$ Å^3; $Z = 4$; $\mu = 3.806$ mm^{-1}; $\rho_{calcd} = 1.667$ g cm^{-3}; 64863 reflections ($2\theta_{max} = 50°$), 9252 unique ($R_{int} = 0.061$), 371 parameter, 52 restraints; largest max./min. in the final difference Fourier synthesis 0.791 e Å^{-3}/−0.888 e Å^{-3}; max./min. transmission 0.44589/0.36300; $R_1 = 0.025$ ($I > 2\sigma(I)$), $wR_2 = 0.059$. CCDC-262593 (**1**) and CCDC-262594 (**3**) contain the supplementary crystallographic data for this paper. These data can be obtained free of charge from the Cambridge Crystallographic Data Centre via www.ccdc.cam.ac.uk/data_request/cif.

[6] a) M. Kaupp, H. Stoll, H. Preuss, W. Kaim, T. Stahl, G. van Koten, E. Wissing, W. J. J. Smeets, A. L. Spek, *J. Am. Chem. Soc.* **1991**, *113*, 5606; b) P. O'Brien, M. B. Hursthouse, M. Motevalli, J. R. Walsh, A. C. Jones, *J. Organomet. Chem.* **1993**, *449*, 1; c) E. Wissing, M. Kaupp, J. Boersma, A. L. Spek, G. van Koten, *Organometallics* **1994**, *13*, 2349.

[7] a) B. Walfort, A. P. Leedham, C. A. Russell, D. Stalke, *Inorg. Chem.* **2001**, *40*, 5668; b) M. B. Hursthouse, M. Motevalli, P. O'Brien, J. R. Walsh, A. C. Jones, *Chem. Mater.* **1991**, *3*, 139; c) H. Mimoun, J. Y. de Saint Laumer, L. Giannini, R. Scopelliti, C. Floriani, *J. Am. Chem. Soc.* **1999**, *121*, 6158.

[8] a) B. Rademacher, W. Schwarz, M. Westerhausen, *Z. Anorg. Allg. Chem.* **1995**, *621*, 287; b) B. Rademacher, W. Schwarz, M. Westerhausen, *Z. Anorg. Allg. Chem.* **1995**, *621*, 1439.

[9] Compound **2** decomposes at 0 °C giving $Sb(SiMe_3)_3$, $Sb_2(SiMe_3)_4$, and a brownish insoluble solid, which could not yet be identified.

[10] O. Fuhr, D. Fenske, *Z. Anorg. Allg. Chem.* **1999**, *625*, 1229.

[11] $[\{Me_2AlSb(SiMe_3)_2\}_3]$ reacts with three equivalents of dmap and $ZnCl_2$ at 0 °C to form a dark brown insoluble solid, which contains Si, Cl (both about 5–8 %), Sb, and Zn according to EDX analysis. The formation of Me_3SiCl was verified by NMR spectroscopy.

 © 2005 Wiley-VCH Verlag GmbH & Co. KGaA, Weinheim

Purine Quartets

DOI: 10.1002/anie.200500896

Models of Putative (AH)G(AH)G Nucleobase Quartets**

Pilar Amo-Ochoa, Pablo J. Sanz Miguel, Patrick Lax, Inés Alonso, Michael Roitzsch, Félix Zamora, and Bernhard Lippert**

The existence of homo(nucleobase) quartets such as those of guanine (G), adenine (A), thymine (T), and uracil (U) in multistranded nucleic acid structures is well-established, and the awareness of the potential relevance of such quartets (also known as tetrads) in biology and medicine is steadily increasing.[1–3] Guanine quartets (G_4) can be formed through the folding of an individual single-stranded oligonucleotide or through the association of either four single-stranded oligo-

[*] Dr. F. Zamora
Departamento de Química Inorgánica
Universidad Autónoma de Madrid
28049 Madrid (Spain)
Fax: (+34) 91-497-4833
E-mail: felix.zamora@uam.es

Dipl.-Chem. P. J. Sanz Miguel, Dipl.-Chem. P. Lax, Dipl.-Chem. M. Roitzsch, Prof. B. Lippert
Fachbereich Chemie
Universität Dortmund
44221 Dortmund (Germany)
Fax: (+49) 231-755-3797
E-mail: bernhard.lippert@uni-dortmund.de

Dr. P. Amo-Ochoa
Departamento de Tecnología Industrial
Universidad Alfonso X "El Sabio"
28691 Villanueva de la Cañada, Madrid (Spain)

Dr. I. Alonso
Departamento de Química Orgánica
Universidad Autónoma de Madrid
28049 Madrid (Spain)

[**] We thank the Deutsche Forschungsgemeinschaft, the Fonds der Chemischen Industrie, UAM (CS13-541A-9-640), and MAT (2004-05589-C02-02) for financial support, and César Pastor for his contribution to the solution of the structure of **1**.
AH = adeninium ion, G = guanine.

Supporting information for this article is available on the WWW under http://www.angewandte.org or from the author.

InterScience
© 2005 Wiley-VCH Verlag GmbH & Co. KGaA, Weinheim

nucleotides, two hairpins, or two cyclic oligonucleotides. The exceptional stability of G_4 quartets facilitates the formation of further quartets through stacking. This also applies to mixed nucleobase quartets such as CGCG,[1] TATA,[2a] and even GCAT.[4] Surprisingly, the existence of AGAG quartets is still controversial[5] despite the observation and characterization of four different AG mispair types in nucleic acid structures.[6]

Herein, we report the X-ray crystal structure analyses of two closely related quartets, each with two protonated adenine model nucleobases (9-methyladeninium, 9-MeAH$^+$, "AH") and two 6-oxopurine bases (9-ethylguanine, 9-EtGH, "G" or 9-methylhypoxanthine, 9-MeHxH, "Hx"). Additionally, ab initio calculations for the model quartet consisting of two 9-ethyladeninium and two 9-methylguanine bases are reported which confirm the existence of the quartet observed in the solid-state structure and at the same time, point to the existence of a second variant.

$[\{(9\text{-MeAH})(9\text{-EtGH})\}_2](BF_4)_2$ (**1**) and $[\{(9\text{-MeAH})(9\text{-MeHxH})\}_2](ClO_4)_2$ (**2**) were isolated from an ethanol/water mixture.[7] Figure 1 shows **1** in two perspectives. The

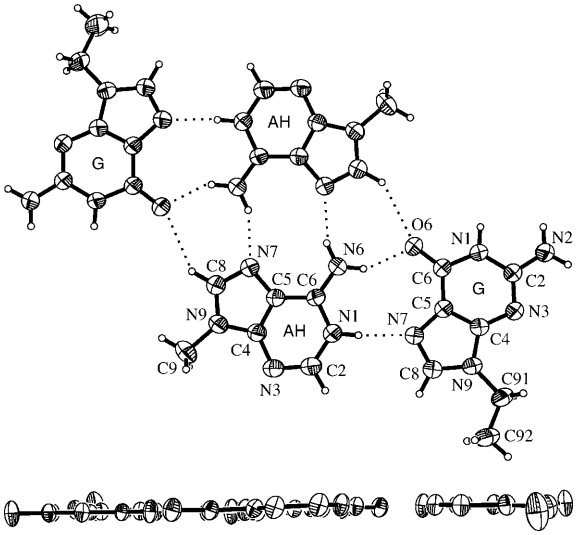


Figure 1. The cationic nucleobase quartet $[\{(9\text{-MeAH})(9\text{-EtGH})\}_2]^{2+}$ (**1**) viewed a) from the top and b) from the side, with atom numbering scheme and eight intramolecular hydrogen bonds between the bases shown. The structure of $[\{(9\text{-MeAH})(9\text{-MeHxH})\}_2]^{2+}$ (**2**) is virtually identical (not shown).

structure of **2** is closely related and is provided in the Supporting Information. Both quartets[8] consist of a central centrosymmetric 9-methyladeninium dimer with hydrogen bonds between the ^{AH}N7 and ^{AH}N6H$_2$ sites. Each of the two 6-oxopurine bases are hydrogen bonded through ^{G}N7 and ^{G}O6 to the ^{AH}N1H and ^{AH}N6H$_2$ sites of adeninium. The distances between the nitrogen and oxygen atoms in the hydrogen bonds NH···N and NH···O of **1** and **2** are listed in Table 1. They are well within the range of distances typically observed in nucleobase pairing motifs, including Watson–Crick base pairs, for example.[9] In **1**, the hydrogen bonds between the G$\cdot$AH$^+$ pairs are shorter than those within the central AH$^+\cdot$AH$^+$ pair. A similar trend is observed in **2**. Moreover, the heteroaromatic ^{AH}CH8 proton of the adeninium ions of

Table 1: Hydrogen-bond lengths [Å] between bases in nucleobase quartets **1** and **2** and in the calculated structure **I**.

Intramolecular hydrogen bonds				
	1	**I**		**2**
^{AH}N7···^{AH}N6	2.860(4)	3.082	^{AH}N7···^{AH}N6	2.842(7)
^{AH}N6···^{G}O6	2.749(4)	2.875	^{AH}N6···^{Hx}O6	2.739(7)
^{AH}N1···^{G}N7	2.833(4)	2.966	^{AH}N1···^{Hx}N7	2.838(7)
^{AH}C8···^{G}O6	3.350(4)	4.085[a]	^{AH}C8···^{Hx}O6	3.318(8)
Intermolecular hydrogen bonds				
	1			**2**
^{G}N2···^{G}N3	3.008(4)	–	^{Hx}C2···^{Hx}N3	3.284(9)

[a] Average values (max. difference $\pm$0.002 Å).

both **1** and **2** are involved in weak hydrogen bonds to the $^{G/Hx}$O6 atoms of guanine and hypoxanthine, respectively. These contacts, although markedly longer than common NH···N and NH···O hydrogen bonds (Table 1), still clearly qualify for CH···O hydrogen bonds as observed in other nucleobase associations.[10]

Both quartets are almost completely flat; the maximal deviation of individual atoms from the best plane amounts to $\leq$0.03 Å. The base quartets are linked through pairs of hydrogen bonds involving the so-called "sugar edges" of the 6-oxopurines (^{G}N3 and ^{G}N2H$_2$ in **1**, and ^{Hx}N3 and ^{Hx}C2H in **2**) and thus form infinitely long tapes (see Figure 2 and

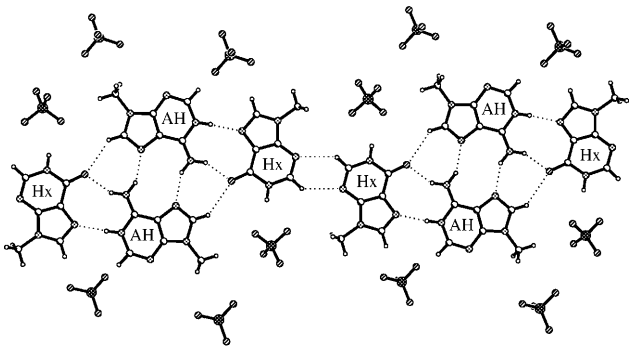


Figure 2. Association pattern of base quartet **2** leading to an infinite tape structure. Structure **1** displays a rather similar arrangement. Perchlorate anions connect adjacent tapes of base quartets.

Supporting Information). The presence of a CH···N contact (in **2**) is noteworthy. Similar hydrogen-bonding patterns and lengths are also realized in Pt^{II} complexes of these nucleobases.[11] Excluding the long hydrogen-bonding contacts between ^{AH}C8H of 9-MeAH$^+$ and ^{G}O6 of the 6-oxopurines in **1** and **2**, the intermolecular separations through ^{AH}N3 and ^{G}N2H$_2$ (**1**), and ^{AH}N3 and ^{Hx}C2H (**2**) are clearly longer than analogous distances observed in other quartet structures, which supports the consideration of **1** and **2** as true base quartets.

The packing of individual tapes in **1** and **2** is different. In both cases the tapes are stacked on top of each other at a distance of $\approx$3.4 Å, to produce stacks. The stacks are slightly inclined (75° in **1**, 77° in **2**) and separated by the tetrahedral counterions (BF_4^- in **1**, ClO_4^- in **2**). Whereas adjacent stacks

 © 2005 Wiley-VCH Verlag GmbH & Co. KGaA, Weinheim

are oriented in a parallel fashion in **1**, only every second stack is parallel in **2**. Directly adjacent stacks form angles of 65° with each other in **1** (see Supporting Information). An analysis of the hydrogen-bonding interactions in **2** reveals that with the exception of ^{Hx}C8H, all remaining protons of the two nucleobases not already engaged in hydrogen-bond formation between bases are involved in hydrogen bonds between the quartet and the ClO_4^- anions (the ClO_4^- anions do not display rotational disorder). Specifically, ^{Hx}N1H and ^{Hx}C9CH$_3$ as well as ^{A}C2H and ^{A}C9CH$_3$ of 9-MeAH$^+$ form such contacts, the lengths of which range between ≈3.0–3.4 Å (see Supporting Information).

Formation of the base quartets **1** and **2** can be envisaged as an association of two AH$^+_{anti}$G/Hx$_{syn}$ mispairs[12] (Figure 3). There are two principal arrangements (**I**, **II**) of dimerization, which are interrelated by a simple sliding motion of the two mispairs. In both cases, hydrogen-bonding interactions between donor (Do) and acceptor (A) sites can form, which give rise to favorable secondary electrostatic interactions,[13] even though their distribution is different in the two cases. Arrangement **I** is realized in **1** and **2**. Arrangement **II** combines two of the four possible mispairs between A and G, namely AH$^+_{anti}$G$_{syn}$[12] and A$_{syn}$G$_{anti}$,[14] ignoring the fact that in this second pair, the adenine is likewise protonated. Both mismatches have been shown to be easily accommodated within double-stranded B-form DNA.

By using the Gaussian suite of programs,[15] energy-minimized structures of **I** and **II** (+2 charged each) were calculated and fully optimized (RHF/6-31G* level, see Supporting Information). In all cases, frequency calculations were carried out to confirm that the geometries represented energy minima. Results for **I** and **II** are respectively shown in Figure 4 and Figure 5. Arrangement **I** is slightly less stable than **II** by 23.29 kJ mol^{-1}.[16] Hydrogen-bond lengths in the calculated structure **I** show trends similar to those found in **1** (Table 1), but absolute values are longer in the calculated structure. This applies in particular to the central pair of intermolecular hydrogen bonds between ^{AH}N7 and ^{AH}N6 sites

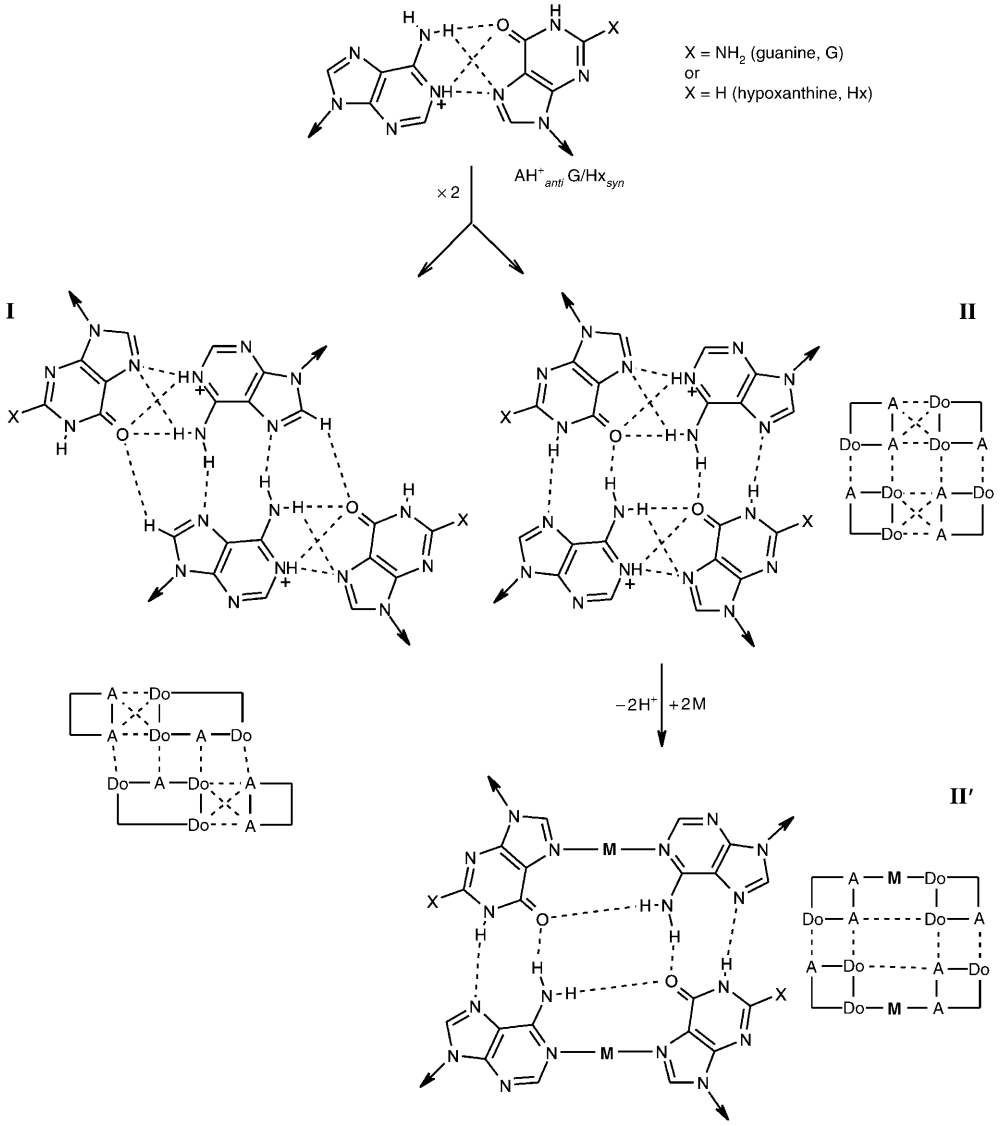


Figure 3. Formal relationship between the AH$^+_{anti}$G/Hx$_{syn}$ mispair (top), base quartets **I** and **II** (middle), and a metal-containing base quartet **II′** (bottom). Favorable secondary electrostatic interactions in hydrogen bonds are indicated by crossed dashed lines.

 © 2005 Wiley-VCH Verlag GmbH & Co. KGaA, Weinheim

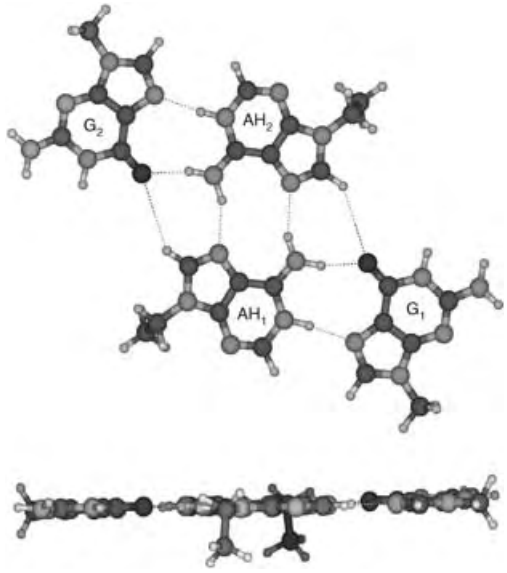


Figure 4. Energy-minimized gas-phase structure (Gaussian) of $[\{(9\text{-EtAH})(9\text{-MeGH})\}_2]^{2+}$ (**I**) with views from top (above) and side (bottom). Calculated hydrogen-bond lengths are listed in Table 1.

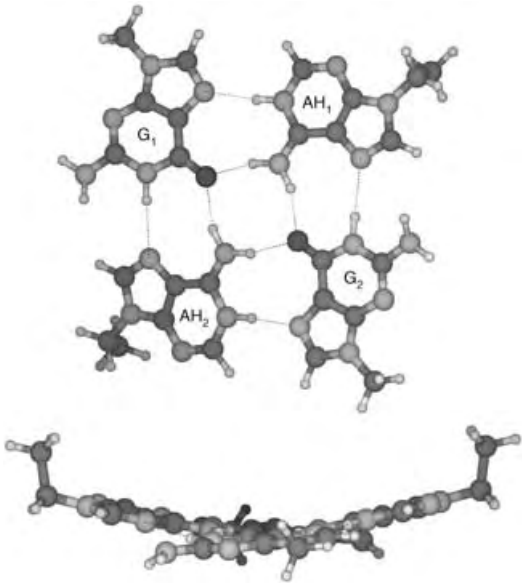


Figure 5. Energy-minimized gas-phase structure (Gaussian) of $[\{(9\text{-EtAH})(9\text{-MeGH})\}_2]^{2+}$ (**II**) with views from top (above) and side (bottom). Calculated hydrogen-bond lengths [Å]: ^{AH_1}N6···^{G_1}O6, 2.877 Å; ^{AH_1}N1···^{G_1}N7, 3.013 Å; ^{AH_1}N6···^{G_2}O6, 2.910 Å; ^{AH_1}N7···^{G_2}N1, 3.212 Å. The other hydrogen bonds are either identical or agree within 0.001 Å. The quartet is slightly saddle shaped, with two guanine bases pointing downward (dihedral angle 12.6°), and the two adeninium ions pointing upward (dihedral angle 20.6°).

of the adeninium bases. In the calculations of **I** and **II**, the combinations of the bases used (9-EtAH$^+$ and 9-MeGH) were applied for a more direct structural comparison with a metal-containing mixed adenine/hypoxanthine quartet which we recently characterized by X-ray crystallography (**II′** in Figure 3).[17] For **II′**, in which the acidic ^{AH}N1 protons of the two adeninium ions are replaced by linear [*trans*-$(NH_3)_2Pt^{II}$] units, the four nucleobases are perfectly planar. The situation in **II′** stands in sharp contrast to the AGAG quartet, which contains neutral bases only. As reported by Gu and Leszczynski[5d] and confirmed by our calculations, the AGAG quartet is V-shaped and far from planar (see Supporting Information). Consequently this quartet has been considered unlikely to play a role in biologically relevant base quartets. Our calculations clearly indicate that protonation of the two adenine bases in AGAG to give (AH)G(AH)G as realized in **II** causes the V-shaped quartet to flatten appreciably (Figure 5). Furthermore, if the four bases in **II** are constrained to coplanarity, the energy penalty is only 4.50 kJ mol^{-1}. This strongly suggests that **II** can be incorporated into a four-stranded structure.

It is less clear how structure **I** fits into a four-stranded DNA. However, the fact that base sextets can be accommodated into a DNA quadruplex[18] implies that a shift from a square **II** to a parallelogram **I** should not present an insurmountable obstacle. Moreover, the central symmetric AH$^+$AH$^+$ pair corresponds to that realized in the double helix of poly(AH$^+$)poly(AH$^+$).[19] Stacking of two of these quartets **I** is feasible, as shown by molecular modeling with HyperChem 6.02 (Figure 6).[20] In this model, the four central adeninium dinucleotides are parallel in alignment and the two layers are rotated by 25°.

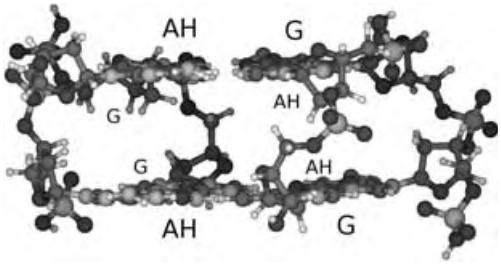


Figure 6. Calculated structure (HyperChem 6.02) of the stacked arrangement of two base quartets (AH)G(AH)G (**I**) joined by phosphodiester bonds between identical bases. Bases closer to viewer are indicated by larger letters.

In conclusion, we have shown that unlike the case for the purine quartet resulting from the dimerization of the neutral $A_{syn}G_{anti}$ pair, the bases that form the purine quartet derived from two $AH^+_{anti}G_{syn}$ pairs are completely (structure **I**) or almost (structure **II**) coplanar. The exocyclic $^{G}N2H_2$ groups are not involved in quartet formation and the hypoxanthine base behaves analogously. How realistic is the protonation of a nucleobase, in this case A, at physiological pH? There is no doubt that protonation equilibria of nucleobases can be significantly disturbed; consequently nucleobase pK_a values can be shifted if favorable hydrogen bonding stabilizes the protonated base.[21] The presence of hemiprotonated cytosine mismatches at physiological pH[1] is yet another example of this principle.

Received: March 10, 2005
Published online: August 5, 2005

 © 2005 Wiley-VCH Verlag GmbH & Co. KGaA, Weinheim

Keywords: DNA structures · hydrogen bonds · nucleobases · purine quartets

[1] D. J. Patel, S. Bouaziz, A. Kettani, Y. Wang in *Oxford Handbook of Nucleic Acid Structure* (Ed.: S. Neidle), Oxford University Press, Oxford, **1999**, p. 389.

[2] a) G. N. Parkinson, M. P. H. Lee, S. Neidle, *Nature* **2002**, *417*, 876; b) P. K. Patel, A. S. R. Koti, R. V. Hosur, *Nucleic Acids Res.* **1999**, *27*, 3836; c) B. Pan, Y. Xiong, K. Shi, M. Sundaralingam, *Structure* **2003**, *11*, 825; d) B. Pan, Y. Xiong, K. Shi, J. Deng, M. Sundaralingam, *Structure* **2003**, *11*, 815.

[3] J. T. Davis, *Angew. Chem.* **2004**, *116*, 684; *Angew. Chem. Int. Ed.* **2004**, *43*, 668.

[4] N. Escaja, J. L. Gelpi, M. Orozco, M. Rico, E. Pedroso,, C. Gonzalez, *J. Am. Chem. Soc.* **2003**, *125*, 5654.

[5] a) A. I. H. Murchie, D. M. J. Lilley, *EMBO J.* **1994**, *13*, 993; b) D. Mohanty, M. Bansal, *Biophys. J.* **1995**, *69*, 1046; c) M. C. Shiber, E. H. Braswell, H. Klump, J. R. Fresco, *Nucleic Acids Res.* **1996**, *24*, 5004; d) J. Gu, J. Leszczynski, *J. Phys. Chem. A* **2000**, *104*, 1898. In ref. [5b] the possibility of adenine protonation is briefly mentioned, yet is not further elaborated.

[6] W. N. Hunter, T. Brown in *Oxford Handbook of Nucleic Acid Structure* (Ed.: S. Neidle), Oxford University Press, Oxford, **1999**, p. 389.

[7] **1** was obtained from a water/ethanol mixture (1:1, 15 mL) solution containing 9-EtGH, 9-MeA (0.21 mmol each) and $Zn(BF_4)_2$ (0.8 mmol) after heating at 80 °C for 24 h, filtration, and keeping the solution for 2 days at 5 °C. Colorless crystals of **1** were obtained in 63 % yield. Elemental analysis for C, H, and N was satisfactory. Colorless crystals of **2** were isolated from a mixture of $HClO_4$ (0.1 mol L^{-1}) in water/ethanol (1:1, 20 mL) containing 9-MeHxH and 9-MeA (0.15 mmol each) after few days at room temperature. The composition of **2** was established by X-ray crystallographic analysis.

[8] Crystal structure data for **1**: $C_{26}H_{34}N_{20}O_2B_2F_8$, $M_r = 832.35$, colorless crystals, triclinic $P\bar{1}$, $a = 8.4649(2)$, $b = 9.1145(2)$, $c = 12.2988(2)$ Å, $\alpha = 95.261(1)$, $\beta = 105.124(1)$, $\gamma = 97.024(1)°$, $V = 901.56(3)$ Å^3, $Z = 2$, $\rho_{calcd} = 2.161$ Mg m^{-3}, $Cu_{K\alpha}$ radiation, $\lambda = 1.54178$ Å, $\mu = 4.085$ mm^{-1}, $T = 296$ K. 2988 data (2514 unique, $R_{int} = 0.07$, $3.75 < \theta < 70.31°$) were collected on a Bruker SMART 6K CCD area-detector three-circle diffractometer with a Rigaku Rotating Anode by using narrow frames (0.3° in ω) and were corrected empirically (SADABS: G. M Sheldrick, Bruker AXS Inc., Madison, WI, **2000**) for absorption. The raw intensity data frames were integrated with the SAINT program (SAINT + NT Version 6.04, SAX Area Detector Integration Program, Bruker AXS Inc., Madison, WI, **1997–2001**), which also applied corrections for Lorentz and polarization effects. Crystal structure data for **2**: $C_{48}H_{56}N_{36}O_{20}Cl_4$, $M_r = 1595.06$, colorless crystals, monoclinic, space group $P21/c$, $a = 8.804(2)$, $b = 8.193(2)$, $c = 24.008(6)$ Å, $\beta = 102.85(3)°$, $V = 1688.4(6)$ Å^3, $Z = 1$, $\rho_{calcd} = 1.573$ Mg m^{-3}, $Mo_{K\alpha}$ radiation, $\lambda = 0.71073$ Å, $\mu = 0.276$ mm^{-1}, $T = 296$ K. 2946 data (891 unique, $R_{int} = 0.05$, $2.37 < \theta < 26.41°$) were collected on an Enraf-Nonius Kappa CCD diffractometer. Data reduction and cell refinement were carried out by using the programs DENZO and SCALE-PACK (Z. Otwinowski, W. Minor, *Methods Enzymol.* **1997**, *276*, 307). Both structures were solved by standard Patterson methods and refined by full-matrix least-squares methods based on F^2 with the SHELXTL-PLUS (G. M. Sheldrick, Siemens Analytical X-ray Instruments, Inc., Madison, WI, **1990**) and SHELXL (G. M. Sheldrick, SHELXL 97, University of Göttingen, Germany, **1997**) programs. All non-hydrogen atoms in the structures were refined anisotropically. The fluoride ligands in BF_4^- of **1** displayed rotational disorder over five positions. The hydrogen atoms were either included in geometrically calculated positions and refined with isotropic displacement parameters according to the riding model, or found with difference Fourier synthesis, and refined isotropically. CCDC-265600 and CCDC-265403 (**1** and **2**) contain the supplementary crystallographic data for this paper. These data can be obtained free of charge from the Cambridge Crystallographic Data Centre via www.ccdc.cam.ac.uk/data_request/cif.

[9] W. Saenger, *Principle of Nucleic Acid Structure*, Springer, New York, **1984**, p. 123.

[10] a) M. C. Wahl, S. T. Rao, M. Sundaralingam, *Nat. Struct. Biol.* **1996**, *3*, 24; b) B. Auffinger, S. Louise-May, E. Westhof, *J. Am. Chem. Soc.* **1996**, *118*, 1181; c) G. R. Desiraju, T. Steiner, *The Weak Hydrogen Bond*, Oxford University Press, Oxford, **1999**.

[11] a) R. K. O. Sigel, E. Freisinger, S. Metzger, B. Lippert, *J. Am. Chem. Soc.* **1998**, *120*, 12000; b) E. Freisinger, I. B. Rother, M. S. Lüth, B. Lippert, *Proc. Natl. Acad. Sci. USA* **2003**, *100*, 3748.

[12] X. Gao, D. J. Patel, *J. Am. Chem. Soc.* **1988**, *110*, 5178.

[13] a) J. Pranata, S. G. Wierschke, W. L. Jorgensen, *J. Am. Chem. Soc.* **1991**, *113*, 2810; b) J. Sartorius, H.-J. Schneider, *Chem. Eur. J.* **1996**, *2*, 1446.

[14] T. Brown, W. N. Hunter, G. Kreale, O. Kennard, *Proc. Natl. Acad. Sci. USA* **1986**, *83*, 2402.

[15] a) Gaussian 98 (Revision A.7), M. J. Frisch et al., see Supporting Information; b) Gaussian 03, (Revision C.02), M. J. Frisch et al., see Supporting Information.

[16] This value refers to electronic energy only. If zero-point energies are considered as well, **I** is less stable than **II** by only 17.23 kJ mol^{-1}.

[17] M. Roitzsch, B. Lippert, *Inorg. Chem.* **2004**, *43*, 5483.

[18] A. Kettani, A. Gorin, A. Majumdar, T. Hermann, E. Skripkin, H. Zhao, R. Jones, D. J. Patel, *J. Mol. Biol.* **2000**, *297*, 627.

[19] A. Rich, D. R. Davies, F. H. C. Crick, J. D. Watson, *J. Mol. Biol.* **1961**, *3*, 71.

[20] Hyper Chem Program (Release 6.02), Hypercube, 1115 NW 4th Street, Gainesville, FL 32601, USA. Following an optimization of the base quartet by applying the PM3(tm) method, alkyl groups were removed from the N9 positions and substituted by deoxyribose units. The layer was then duplicated and bonded to the first one through phosphate groups (through 5′ and 3′ ends, pairs of $(AH)_2G_2$ helices, right-handed and antiparallel). External sugar-phosphate chains were selected and optimized by AMBER. In this situation, the nucleobases were frozen (AMBER: W. D. Cornell, P. Cieplak, C. I. Bayly, I. R. Gould, K. Merz, D. M. Ferguson, D. C. Spellmeyer, T. Fox, J. W. Caldwell, P. A. Kollman, *J. Am. Chem. Soc.* **1995**, *117*, 5179).

[21] P. C. Bevilacqua, T. S. Brown, S.-i. Nakano, R. Yajima, *Biopolymers* **2004**, *73*, 90, and references therein.

 © 2005 Wiley-VCH Verlag GmbH & Co. KGaA, Weinheim

Addition Reactions

DOI: 10.1002/anie.200501541

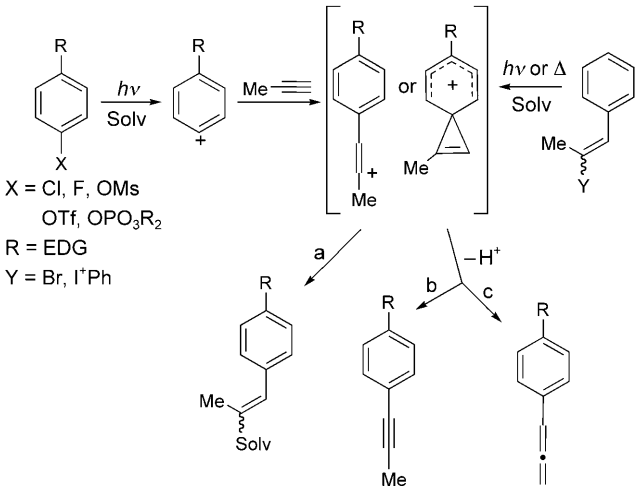
Photo-Cross-Coupling Reaction of Electron-Rich Aryl Chlorides and Aryl Esters with Alkynes: A Metal-Free Alkynylation**

Stefano Protti, Maurizio Fagnoni, and Angelo Albini**

Aryl acetylenes are versatile intermediates in organic synthesis in view of the easy derivatization of their triple bonds[1] and find application in molecular electronics.[2] The elective method for the synthesis of these compounds is the Sonogashira reaction, which involves the Pd/Cu-mediated formation of a $C(sp^2)$–C(sp) bond. Despite many efforts to improve this method, the most popular protocol in use today still consists of a mixture of an aryl iodide or bromide, a terminal alkyne, $[PdCl_2(PPh_3)_2]$, an amine, and CuI: the same protocol as introduced many years ago by Sonogashira et al.[3,4]

There has been growing interest into extending the reaction to different aryl precursors; for example, aryl triflates (or nonaflates) were introduced about 20 years ago,[5] and more recently aryl tosylates[6] and aryl boronic acids were also used (in the latter case the presence of air is tolerated).[7] However, the inexpensive aryl chlorides have been employed with success in only a few cases, but necessitated the use of high temperatures.[6,8] The use of a single metal compound is possible, and palladium-free[9] and copper-free[10] protocols have also been investigated for some aryl bromides and iodides. In some cases, copper salts cause an adverse effect on the reaction and do not result in the intended catalysis. Thus, copper can either inhibit the reaction[6] or promote oxidative homocoupling.[11] An effective metal-free reaction is clearly desirable and a step in this direction was recently achieved by using microwave-assisted reactions,[12] although satisfying results have been obtained only in one case, namely the reaction between aryl iodides and phenylacetylenes. The Sonogashira reaction generally involves non-activated terminal alkynes, although tetraalkynyl aluminates[13a] and alkynyl trifluoroborates[13b] make the coupling reaction with aryl halides (or triflates) cleaner. A "sila"-Sonogashira reaction starting from alkynylsilanes has also found limited application.[14]

A radically different approach for the synthesis of aryl acetylenes is presented here, and is based on the use of phenyl cations. In the last few years we have demonstrated that these intermediates (in the triplet state) are obtained smoothly by photolysis of aryl halides substitued with electron-donating groups (for example, chlorophenol[15] or fluoroanilines[16]), aryl sulfonates, and aryl phosphates (for example, methoxyphenyl mesylate or *N*,*N*-dimethylaminophenyl phosphate),[17] and add to alkenes to form an aryl–C bond via a phenonium ion.[15a,18] We surmised that phenyl cations would react with triple bonds to yield β-phenylvinyl cations, or more probably cyclic vinylenebenzenium ions (Scheme 1). The last species have been invoked as intermediates in the thermal solvolysis of styryliodonium tetrafluoroborate[19] and in the photoheterolysis of (*E*)-bromostyrene[20] (Scheme 1).



Scheme 1. Hypothesized photogeneration and reaction of the vinylenebenzenium ion. Ms = methanesulfonyl, Tf = trifluoromethanesulfonyl, EDG = electron-donating group.

The usual literature methods for the generation of vinylenebenzenium ions employ a nucleophilic solvent, usually an alcohol. Under these conditions, addition to form an alkoxystyryl derivative occurred (path a, see Scheme 1 for the case of propyne),[19,21] although proton elimination competed to a variable extent and led either to an aryl alkyne (path b) or an aryl allene (path c). Thus, the choice of the conditions is critical so that the desired elimination occurs to form an aryl alkyne.

In view of the above findings, we studied the photolysis of various precursors of the 4-methoxyphenyl cation, namely, the corresponding chloride (**1a**), mesylate (**1b**), triflate (**1c**), diethylphosphate (**1d**), and fluoride (**1e**; 0.05 M) in the presence of 1-hexyne (**2**, a terminal alkyne), ethynyltrimethylsilane (**3**, a partially silylated alkyne), and trimethylsilylpropyne (**4**, a precursor lacking acetylenic hydrogen atoms; 0.5 M). The results of the irradiation experiments are shown in Table 1.

We were happy to find that cross-coupling with 1-hexyne took place upon irradiation ($\lambda_{exc} = 310$ nm, 36 h) of **1** in 2,2,2-trifluoroethanol (TFE) in the presence of an equimolar amount of base (triethylamine, TEA[22]) to yield 4-(1-hexynyl)anisole (**5**) in more than 60% yield (90% when using

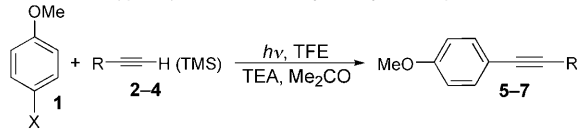
[*] S. Protti, Dr. M. Fagnoni, Prof. A. Albini
Department of Organic Chemistry
University of Pavia
Via Taramelli 10, 27100 Pavia (Italy)
Fax: (+39) 0382-987323
E-mail: fagnoni@unipv.it
angelo.albini@unipv.it

[**] Partial support of this work by Murst, Rome, is gratefully acknowledged.

Supporting information for this article is available on the WWW under http://www.angewandte.org or from the author.

 © 2005 Wiley-VCH Verlag GmbH & Co. KGaA, Weinheim

Table 1: Photolysis of 4-methoxyphenyl derivatives **1** (0.05 M) in the presence of 0.5 M alkyne.



1 (X=)	Alkyne	t_{IRR} [h]	ArX consumption [%]	Product	Yield [%][a]
1a (Cl)	C_4H_9 **2**	36	100	MeO—C_4H_9 **5**	62
1b[b] (OMs)		60	75[c]	**5**	73
1c[b] (OTf)		60	80[c]	**5**	83
1d (OPO_3Et_2)		60	80[c]	**5**	90
1e (F)		60	65[c]	**5**	60
1a	$SiMe_3$ **3**	36	100	MeO—$SiMe_3$ **6**	71
1b[b]		60	75[c]	**6**	54
1c[b]		60	80[c]	**6**	62
1d		60	80[c]	**6**	70
1a	Me—$SiMe_3$ **4**	36	100	MeO—Me **7**	51 (20)
1b[b]		60	75[c]	**7**	75 (14)
1c[b]		60	80[c]	**7**	67
1d		60	80	**7**	50 (10)

[a] Yields of isolated compounds based on consumed aryl halide or ester. The yield of anisole is shown in parentheses, and is not quoted when less than 5%. [b] Reaction sensitized by 0.9 M acetone and buffered by 0.1 M TEA. [c] The consumption of ArX was not increased after prolonged irradiation.

phosphate **1d**). The use of other solvents, such as MeCN or MeCN/H_2O, gave poor yields.

Esters **1b** and **1c** absorbed poorly at 310 nm and underwent a sluggish reaction under these conditions. Acetone (0.9 M) sensitization was adopted and enabled a high conversion to be obtained (>75% in 60 h), provided that the amount of base was doubled (0.1 M). To our knowledge, these are the first examples reported of an alkynylation reaction using an aryl phosphate,[23] a mesylate, or, noteworthy, an aryl fluoride, which is usually an unreactive derivative.

The photoinduced arylation of alkyne **3** by compounds **1** led to the silicon-containing alkyne (*p*-methoxyphenylethynyl)trimethylsilane, **6**).[24] However, arylation of alkyne **4** occurred with elimination of the trimethylsilyl (TMS) group and gave 4-(1-propynyl)anisole (**7**) in a medium to good yield. When this alkyne was used, the aryl derivatives **1** were in part reduced to anisole, except for the case of triflate **1d**.

Aromatic alkynes could not be used conveniently in this procedure because they absorbed a significant fraction of the incident light and underwent photoreactions to give strongly absorbing products. Thus, irradiation of phenylacetylene in TFE led to darkening and clouding of the reaction mixture; under these conditions the consumption of **1a** after 36 h was limited to 37% and the only significant product was anisole (12%).

The generation of phenyl cations from aromatic compounds substituted with other electron-donating groups[25] was then explored by using the readily accessible chlorides **8**–**10** (Table 2). The reaction was successful also in these cases (44–71% yield). However, the use of 4-chlorothioanisole **8** resulted in clouding of the solution during the irradiation, which hindered the complete consumption of the halide and prolonged the required irradiation time. This problem was in part overcome by irradiating at 254 nm. Although 4-chlorophenol gave poor results in the reaction, the *tert*-butyldimethylsilyl-protected derivative **9** gave aryl alkynes in 51–71% yield. The chlorinated benzodioxole **10** reacted in a similar way with 1-hexyne and gave arylated compound **17** in 52% yield after 30 h of irradiation.

Finally, we explored the reaction of **1a** with the propargylic alcohol 2-methyl-3-butyn-2-ol (**18**). In this case, an unexpected route was followed and the *Z*-enone **19** was obtained as the only product (35% yield, Scheme 2).

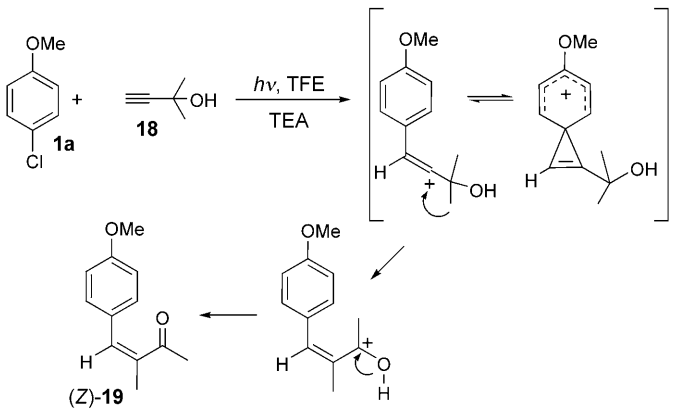
Table 2: Photoinduced synthesis of electron-rich aromatic alkynes.

Electron-rich precursor	Alkyne	t_{IRR} [h]	ArX consumption [%]	Product	Yield [%][a]
MeS—Cl **8**	**2**	72[b]	90	MeS—C_4H_9 **11**	55
8	**3**	72[b]	80	MeS—$SiMe_3$ **12**	58
8	**4**	72[b]SUP>	100	MeS—Me **13**	44
R_3SiO—Cl **9**	**2**	45	100	R_3SiO—C_4H_9 **14**	51
9	**3**	45	100	R_3SiO—$SiMe_3$ **15**	64
9	**4**	45	100	R_3SiO—Me **16**	71
O,O—Cl **10**	**2**	30	100	O,O—C_4H_9 **17**	52

[a] Yields of isolated compounds based on consumed aryl chloride; the corresponding dehalogenated aromatic compounds (<10%) were identified in the irradiated solutions by GC analysis. [b] Irradiation carried out at 254 nm. Cloudy solutions were obtained after irradiation.

The above results show that aryl alkynes are obtained by reaction of aryl cations with terminal acetylenes or their silylated derivatives. The cations are readily obtained by photolysis of electron-rich aryl esters or aryl halides, with the readily available chlorides being a particularly convenient choice. Furthermore, aromatic compounds bearing an SMe,

 © 2005 Wiley-VCH Verlag GmbH & Co. KGaA, Weinheim

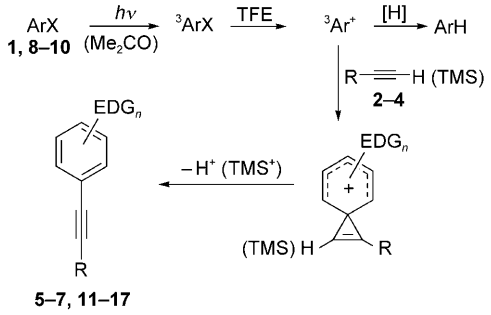


Scheme 2. Addition of the 4-methoxyphenyl cation onto propargylic alcohol **18**.

an *O*-trialkylsilyl (as a protected OH group), or a dioxolanyl group were used for the first time in the generation of aryl cations,[25] thus broadening the scope of the arylation reaction.

Alkynes are known to be less reactive with electrophiles than the corresponding alkenes. However, Mayr et al. reported that 1-hexyne is less reactive by one order of magnitude than 1-hexene in the reaction with $(p\text{-}MeC_6H_4)_2CH^+$ at −70 °C,[26a] but that the difference is reduced at higher temperatures. In some cases the reactivity towards the carbenium ion is similar or even higher than that of alkenes.[26b] In the present case, the reactions involving alkynes **1**–**3** required a longer irradiation time (> 30 h) than alkenes (14 h),[15a] but this can probably be attributed to a stronger filter effect of the product formed (conjugated phenylalkynes versus alkyl benzenes) rather than to a less-efficient reaction. The photolysis requires a polar (preferably a protic) medium for reaction to occur.[27] TFE was found to be the best solvent for the arylation of alkynes, but the same products were formed in lower yields in MeCN, MeOH, MeCN/TFE, and MeCN/H_2O. Among these, MeCN/H_2O (5:1) gave the best results, although reduction of the aryl cations was competitive with the reaction with the alkynes[28] (for example, the reaction between **1a** and **4** gave 34% of **7** and 30% of anisole).

The mechanism of the reaction is outlined in Scheme 3. The vinylenebenzenium ion resulting from the trapping of $^3Ar^+$[29,30] by the alkyne does not undergo solvent addition in TFE (a poor nucleophile),[31] nor indeed in a more nucleophilic medium such as MeCN/H_2O. Rearrangement to yield allenes also does not compete, and the straightforward formation of the alkynes is by far the preferred pathway and involves elimination of the acetylenic hydrogen atom. Of particular note is that deprotonation is the only process observed in the arylation of ethynyltrimethylsilane—to the exclusion of the elimination of the other potential electrofugal group TMS^+.[32] Nevertheless, when the TMS^+ ion is the only leaving group present (as in the case of **4**), this is eliminated and an aryl alkyne is again formed in a good yield,[33] although in this case reduction of the phenyl cation to anisole plays a greater role.[28]



Scheme 3. Mechanism of the photoinduced metal-free formation of aryl alkynes.

A new cationic path was found in the reaction with propargylic alcohol **18**, where a methyl group migrated onto the vinyl cation intermediate (Scheme 2). In this case the driving force is the stability of the α-hydroxy cation formed, and no deprotonation occurred to give an alkyne. Precedents for the migration of a methyl (or a methylene) group adjacent to a vinyl cation have been reported,[34] but examples that lead to an α-hydroxy cation are rare.[35] Moreover, formation of the enone **19** as the *Z* isomer demonstrates a new route to the synthesis of related compounds which are currently accessible by the Rupe or Meyer–Schuster rearrangement.[36]

To summarize, a metal-free protocol for the mild alkynylation of aromatic compounds substituted with electron-donating groups has been developed. The reaction proceeds via a phenyl cation formed by photoheterolysis and allows for the use of a variety of precursors, such as readily available aryl chlorides as well as aryl esters (mesylates or phosphates). Interestingly, aryl fluorides, which are virtually unreactive under metal catalysis in the Sonogashira reaction, could also be used, although the consumption of the reagent was incomplete. Phenylalkynes are obtained in good, although not excellent, yields in TFE. Despite some limitation, this method has distinct advantages over the thermal alternatives, since the reaction is carried out at room temperature, with no need of a sensitive and/or expensive metallic catalyst or of water-free or oxygen-free conditions, and the experimental procedure is quite simple.[37]

The complete H^+ versus TMS^+ selectivity coupled with the successful application to silylated alkynes when no acetylene proton is present is an appealing characteristic of the reaction. The thermal-catalyzed sila-Sonogashira reaction has been exploited to a limited degree up to now, but the use of a silyl derivative may be advantageous for application to complex derivatives where protection is required, as well as making it easier to handle low-boiling alkynes (for example, **4**).[38] Finally, the synthesis of a β-aryl-substituted enone by addition onto a propargylic alcohol opens up yet a new synthetic pathway.

Experimental Section

Typical procedure for the photochemical synthesis of arylalkynes: A solution of an aryl ester or halide (**1**, **8**–**10**, 1.5 mmol, 0.05 M), triethylamine (TEA, 0.05 M), and an alkyne (**2**–**4**, 0.5 M) in TFE (30 mL) was poured into two quartz tubes and purged for 10 min with argon, serum capped, and irradiated with six 15-W phosphor-coated lamps (emission centered at 310 or 254 nm). The photolyzed solution

 © 2005 Wiley-VCH Verlag GmbH & Co. KGaA, Weinheim

was concentrated under reduced pressure and purified by column chromatography (cyclohexane/ethyl acetate as eluant). Acetone (3 mL, 0.9 M) was added to the reaction mixtures involving esters **1b**,**c** and the amount of TEA was increased to 0.1 M.

Received: May 5, 2005
Published online: August 5, 2005

Keywords: alkynes · aryl cations · arylation · cross-coupling · photochemistry

[1] L. Brandsma, S. F. Vasilevsky, H. D. Vekruijsse, *Application of Transition Metal Catalysts in Organic Synthesis*, Springer, Berlin, **1998**, pp. 179 – 225; K. C. Nicolaou, E. J. Sorensen, *Classics in Total Synthesis*, Wiley-VCH, Weinheim, **1996**, pp. 582 – 586.
[2] J. M. Tour, *Acc. Chem. Res.* **2000**, *33*, 791 – 804.
[3] R. R. Tykwinski, *Angew. Chem.* **2003**, *115*, 1604 – 1606; *Angew. Chem. Int. Ed.* **2003**, *42*, 1566 – 1568.
[4] K. Sonogashira, Y. Tohda, N. Hagihara, *Tetrahedron Lett.* **1975**, 4467 – 4470.
[5] Q.-Y. Chen, Z.-Y. Yang, *Tetrahedron Lett.* **1986**, *27*, 1171 – 1174.
[6] D. Gelman, S. L. Buchwald, *Angew. Chem.* **2003**, *115*, 6175 – 6178; *Angew. Chem. Int. Ed.* **2003**, *42*, 5993 – 5996.
[7] G. Zou, J. Zhu, J. Tang, *Tetrahedron Lett.* **2003**, *44*, 8709 – 8711.
[8] A. Köllhofer, T. Pullmann, H. Plenio, *Angew. Chem.* **2003**, *115*, 1086 – 1088; *Angew. Chem. Int. Ed.* **2003**, *42*, 1056 – 1058; M. R. Eberhard, Z. Wang, C. M. Jensen, *Chem. Commun.* **2002**, 818 – 819; D. Mery, K. Heuzé, D. Astruc, *Chem. Commun.* **2003**, 1934 – 1935.
[9] M. B. Thathagar, J. Beckers, G. Rothenberg, *Green Chem.* **2004**, *6*, 215 – 218.
[10] J. Cheng, Y. Sun, F. Wang, M. Guo, J.-H. Xu, Y. Pan, Z. Zhang, *J. Org. Chem.* **2004**, *69*, 5428 – 5432; A. Soheili, J. Albaneze-Walker, J. A. Murry, P. G. Dormer, D. L. Hughes, *Org. Lett.* **2003**, *5*, 4191 – 4194.
[11] P. Siemsen, R. C. Livingston, F. Diederich, *Angew. Chem.* **2000**, *112*, 2740 – 2767; *Angew. Chem. Int. Ed.* **2000**, *39*, 2632 – 2657.
[12] N. E. Leadbetter, M. Marco, B. J. Tominack, *Org. Lett.* **2003**, *5*, 3919 – 3922; P. Appukkuttan, W. Dahaen, E. Van der Eycken, *Eur. J. Org. Chem.* **2003**, 4713 – 4716.
[13] a) D. Gelman, D. Tsvelikhovsky, G. A. Molander, J. Blum, *J. Org. Chem.* **2002**, *67*, 6287 – 6290; b) G. A. Molander, B. W. Katona, F. Machrouhi, *J. Org. Chem.* **2002**, *67*, 8416 – 8423.
[14] Y. Nishihara, K. Ikegashira, A. Mori, T. Hiyama, *Chem. Lett.* **1997**, 1233 – 1234.
[15] a) S. Protti, M. Fagnoni, M. Mella, A. Albini, *J. Org. Chem.* **2004**, *69*, 3465 – 3473; b) I. Manet, S. Monti, M. Fagnoni, S. Protti, A. Albini, *Chem. Eur. J.* **2005**, *11*, 140 – 151.
[16] B. Guizzardi, M. Mella, M. Fagnoni, A. Albini, *J. Org. Chem.* **2003**, *68*, 1067 – 1074.
[17] M. De Carolis, S. Protti, M. Fagnoni, A. Albini, *Angew. Chem.* **2005**, *117*, 1258 – 1262; *Angew. Chem. Int. Ed.* **2005**, *44*, 1232 – 1236.
[18] S. Milanesi, M. Fagnoni, A. Albini, *J. Org. Chem.* **2005**, *70*, 603 – 610.
[19] T. Okuyama, *Acc. Chem. Res.* **2002**, *35*, 12 – 18.
[20] R. Gronheid, H. Zuilhof, M. G. Hellings, J. Cornelisse, G. Lodder, *J. Org. Chem.* **2003**, *68*, 3205 – 3215.
[21] In some cases a hydride shift within the β-phenylvinyl cation led to the more stable α-phenylvinyl cation, as revealed by the formation of 1-alkoxystyrenes.
[22] The presence of a base is required to buffer the acidity generated in the reaction; omitting TEA led to a rapid darkening of the solution.
[23] Vinyl but not aryl phosphates have been used to some extent in thermal-catalyzed reactions, see: F. Lo Galbo, E. G. Occhiato, A. Guarna, C. Faggi, *J. Org. Chem.* **2003**, *68*, 6360 – 6368; F. Lepifre, C. Buon, P. Bouyssou, G. Coudert, *Heterocycl. Commun.* **2000**, *6*, 397 – 402.
[24] This observation parallels the result from the classical Sonogashira reaction with a Pd catalyst, where **6** was obtained from the reaction of 4-bromoanisole and **3**; see: T. Hundertmark, A. F. Littke, S. L. Buchwald, G. C. Fu, *Org. Lett.* **2000**, *2*, 1729 – 1732.
[25] The 2,6-dimethyl analogue of **9** has been used succesfully in the arylation of allyltrimethysilane; see ref. [15b].
[26] a) H. Mayr, J. L. Gozalez, K. Lüdtke, *Chem. Ber.* **1994**, *127*, 525 – 531; b) G. Melloni, G. Modena, U. Tonellato, *Acc. Chem. Res.* **1981**, *14*, 227 – 233.
[27] M. Freccero, M. Fagnoni, A. Albini, *J. Am. Chem. Soc.* **2003**, *125*, 13182 – 13190.
[28] Reduction of phenyl cations is often a main pathway in the absence of an effective nucleophilic trap; see: B. Guizzardi, M. Mella, M. Fagnoni, M. Freccero, A. Albini, *J. Org. Chem.* **2001**, *66*, 6353 – 6363.
[29] The attack is favored by the 2-propenyl cation formed being about 21–25 kcal mol^{-1} (in the gas phase) more stable than the initial phenyl cation; see: Y. Apeloig, D. Arad, *J. Am. Chem. Soc.* **1985**, *107*, 5285 – 5286.
[30] The formation of aryl alkynes by attack of an aryl radical onto a non-activated triple bond can be excluded on two grounds: first, homolytic clevage of the Ar–X bond is an endothermic process for all of the precursors considered (e.g. **1e**)[27] and second, the generation of the 4-methoxyphenyl radical (by irradiation of 4-bromoanisole in TFE) in the presence of hexyne did not lead to the formation of **5**; for further comments see also note 28 in ref. [17].
[31] S. Minegishi, S. Kobayashi, H. Mayr, *J. Am. Chem. Soc.* **2004**, *126*, 5174 – 5181.
[32] Vinyl cations are known to be stabilized by both an α- and by a β-trimethylsilyl substituent; see: G. A. McGibbon, M. A. Brook, J. K. Terlouw, *J. Chem. Soc. Chem. Commun.* **1992**, 360 – 362.
[33] Alkynes such as **4** are reported to yield disubstituted alkynes in the reaction with *tert*-butyl or adamantyl cations; see: G. Capozzi, G. Romeo, F. Marcuzzi, *J. Chem. Soc. Chem. Commun.* **1982**, 959 – 960.
[34] A. G. Martinez, M. Hanack, R. H. Summerville, P. von R. Schleyer, P. J. Stang, *Angew. Chem.* **1970**, *82*, 323 – 324; *Angew. Chem. Int. Ed. Engl.* **1970**, *9*, 302 – 303; P. J. Stang, T. E. Deuber, *Tetrahedron Lett.* **1977**, 563 – 566.
[35] A shift of a dialkylaminophenyl group after addition of the arene–ruthenium(II) derivatives onto propargylic alcohols has been reported; see: D. Pilette, S. Moreau, H. Le Bozec, P. H. Dixneuf, J. F. Corrigan, A. J. Carty, *J. Chem. Soc. Chem. Commun.* **1994**, 409 – 410.
[36] G. Sartori, A. Sartorio, R. Maggi, F. Bigi, *Tetrahedron* **1996**, *52*, 8287 – 8296.
[37] For example, the reaction between **1a** and **3** was slower (by about 20%) in an air-equilibrated rather than in an argon-equilibrated solution, but the product distribution did not change significantly.
[38] Only a few reports (all of them using aryl iodides) are available concerning the sila-Sonogashira reaction using trimethylsilylpropine; see: M. Krause, X. Ligneau, H. Stark, M. Garbarg, J.-C. Schwartz, W. Schunack, *J. Med. Chem.* **1998**, *41*, 4171 – 4176; A. K. Dutta, M. C. Davis, X.-S. Fei, P. M. Beardsley, C. D. Cook, M. E. A. Reith, *J. Med. Chem.* **2002**, *45*, 654 – 662.

 © 2005 Wiley-VCH Verlag GmbH & Co. KGaA, Weinheim

Molecular Recognition

DOI: 10.1002/anie.200501437

A Functional Assay for Heparin in Serum Using a Designed Synthetic Receptor**

*Aaron T. Wright, Zhenlin Zhong, and Eric V. Anslyn**

A common objective when developing synthetic receptors is high binding affinity and specificity for an analyte. This aim is challenging when targeting a complex analyte in a competitive crude medium such as serum, urine, or saliva.[1] We report herein the development of a synthetic receptor with high affinity and selectivity in human and equine serum for the clinical anticoagulant heparin.[2]

Two forms of heparin are in clinical use: unfractionated heparin (UFH) with a molecular weight range from 3000–30000 Da, and low-molecular-weight heparin (LMWH) with a mean molecular weight of 5000 Da. Heparin concentration and activity is monitored during surgery, and in postoperative therapy, to prevent complications such as hemorrhaging.[3] Current methods for heparin quantification employ the activated clotting time (ACT), activated partial thromboplastin time (aPTT), chromogenic antifactor Xa assay, electrochemical and piezoelectric assays, and complexation with protamine.[4] Although these are proven methods, they are often arduous, inaccurate, costly, and not always amenable to clinical settings.[5] Recently, an engineered GST fusion protein containing three hyaluronan binding domains from a heparin binding protein was used to accurately measure heparin in plasma at clinically relevant values, but it has not been employed clinically.[6]

Heparin cannot be expressed exactly using a conventional chemical formula. It is a heterogeneous mixture of diverse chain lengths consisting of repeating copolymers of 1→4-linked iduronic acid and glucosamine residues in a semi-random order (Figure 1b). Heparin has the highest anionic charge to mass ratio of any biopolymer, as a result of numerous sulfate and carboxylate functionalities in the biopolymer chain. Its activity occurs by binding to antithrombin III, a naturally occurring protease inhibitor, which accelerates the rate of inhibition of coagulation proteases factor Xa and thrombin by antithrombin III.[7] Clinically administered heparin binds to its natural substrate antithrombin III primarily through cationic ion-pairing interactions with the sulfate and carboxylate groups.[8] Similarly, the cationic protein protamine is an excellent ligand for heparin and is often used for the calibration of aPTT reagents. The highly anionic nature of heparin makes it an ideal target for synthetic receptors that incorporate functional groups for molecular recognition which participate in ion-pairing or other anion-binding interactions.

The design of heparin receptor **1** (Figure 1a) builds upon the successes of synthetic receptors reported previously. For example, we recently created receptor **2** (Figure 2), which incorporates phenylboronic acids and ammonium groups, for the complexation of anionic polysaccharides such as heparin, hyaluronic acid, and chondroitin-4-sulfate.[9] Phenylboronic acids with an *ortho*-aminomethyl group are known to form boronate esters with alcohols in aqueous media, and have been used extensively for the molecular recognition of saccharides.[10] It has been found that these boronate esters have particularly high affinity for anions with closely appended hydroxy groups.[11] Furthermore, ion pairing is anticipated between the ammonium functionalities and the carboxylate and sulfate groups. Receptor **2** had good selectivity for heparin relative to the other anionic polysaccharides. However, because heparin does not consist of a single entity, its concentration must be defined by considering

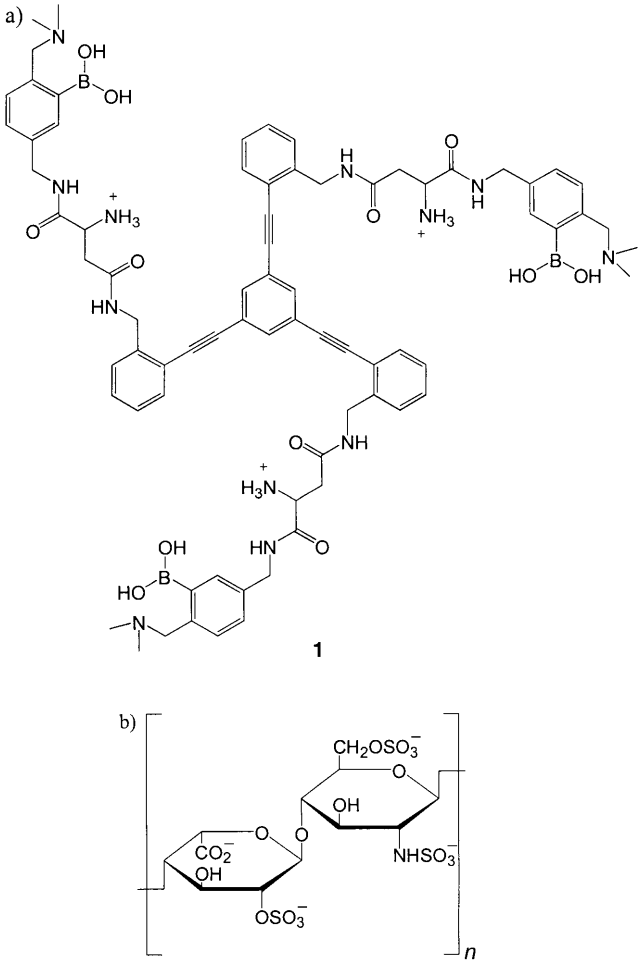


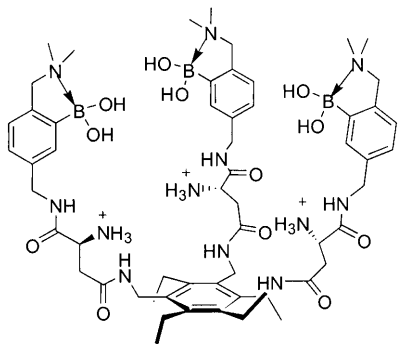
Figure 1. a) Heparin receptor **1**. b) Major unit of heparin.

[*] A. T. Wright, Dr. Z. Zhong, Dr. E. V. Anslyn
Department of Chemistry and Biochemistry
The University of Texas at Austin
Austin, TX 78712 (USA)
Fax: (+1) 512-471-8696
E-mail: Anslyn@ccwf.cc.utexas.edu

[**] We gratefully acknowledge support for this work from the US NIH (EB00549).

Supporting information for this article is available on the WWW under http://www.angewandte.org or from the author.

 © 2005 Wiley-VCH Verlag GmbH & Co. KGaA, Weinheim



2

Figure 2. Previously reported receptor that had insufficient sensitivity to be active and accurate in a biological medium.

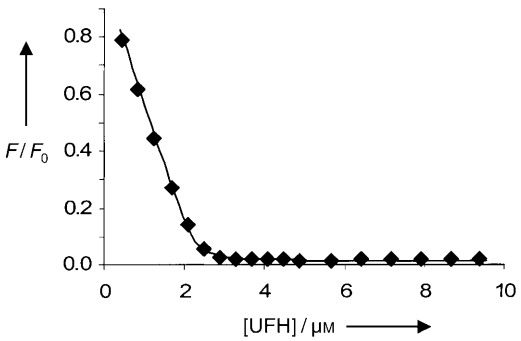


Figure 3. 1:1 binding isotherm for **1** and UFH. The K_a value obtained from the curve was $1.4\times10^{8}\,\text{M}^{-1}$.

various subunits so that a binding constant can be measured. A binding affinity of $3.8\times10^{4}\,\text{M}^{-1}$ was calculated when using a heparin concentration that is defined by the concentration of each disaccharide unit. This affinity was insufficient to allow quantification of heparin in serum at physiologically relevant concentrations. Moreover, although an indicator-displacement assay with **2** gave a dramatic yellow to purple color change in response to heparin,[12] we found that the indicator bound nonspecifically with proteins in crude serum, and thereby skewed the quantitative results.

From the lessons gleaned from the studies using **2**, we designed a second-generation heparin receptor with two goals in mind, both of which are embodied in the structure of **1**. First, the cavity was enlarged to allow the arms containing the boronic acid and ammonium groups to encompass a larger surface of the oligosaccharide, which we predicted would raise the affinity by cooperatively increasing the number of interactions. Second, a fluorescent scaffold was incorporated into the design of the receptor, thereby avoiding the use of an indicator-displacement assay. This new signaling technique should also increase the overall sensitivity of the system. We used 1,3,5-triphenylethynylbenzene as the core unit to satisfy both requirements. However, because of the excellent selectivity previously found for **2** with heparin, we retained the side arms containing the boronic acid and ammonium groups.

An assay for UFH or LMWH in serum requires a binding interaction between **1** and heparin in the nM range. Titrations of **1** with UFH and LMWH in water buffered with 10 mM 2-[4-(2-hydroxyethyl]-1-piperazinyl]ethanesulfonic acid (HEPES) at pH 7.4 were monitored by fluorescence spectroscopy to determine the affinity of **1** for UFH and LMWH. The binding of UFH and LMWH with **1** caused a decrease in the emission intensity, which resulted in a near complete quenching of the receptor's emission. Presumably, the interaction of heparin with **1** leads to conformational restriction of the receptor "arms", thereby modulating the fluorescence—a technique used routinely by Finney and co-workers for creating chemosensors.[13] Titration data at 357 nm was used to generate a binding isotherm, which was analyzed by using a standard 1:1 binding algorithm (Figure 3). As discussed above, the heterogeneous structure of heparin means that one must define a repeating unit with which the receptor interacts. The binding isotherm shown in Figure 3 was achieved by defining the concentration of heparin to be that of four saccharide units (an integral number of saccharides is not required to fit the binding isotherm). The number four supports a stoichiometry where each receptor on average spans four saccharide units along the heparin biopolymer. The calculated association constant between **1** and UFH is $1.4\times10^{8}\,\text{M}^{-1}$. This value corresponds to an increase in affinity of nearly 10^{4} for **1** over **2**, which was gained by increasing the size of the scaffold. It should be noted that the glycosaminoglycuronans hyaluronic acid and chondroitin-4-sulfate did not bind to **1** at low μM concentrations. This result is further evidence for the high selectivity of **1** for UFH and LMWH.

As noted above, several clinical methods (such as aPTT) are calibrated by titration with protamine. Protamine sequesters heparin, thereby lowering its bioavailability to bind antithrombin III. Therefore, if there is a specific binding interaction between heparin and **1** as postulated above, protamine should strip heparin from receptor **1**, thereby restoring the fluorescence. Indeed, fluorescence could be fully reestablished by titration of the complex formed between receptor **1** and either UFH or LMWH with protamine (Figure 4). This observation illustrates that the binding between **1** and heparin is reversible, and acts in an analogous way to that between heparin and antithrombin III.

Our last study targeted the creation of calibration curves for monitoring UFH and LMWH in serum. Heparin is administered intravenously or subcutaneously at therapeutic dosing levels of 2–8 U mL^{-1} (0.8–3.2 μM) during cardiopulmonary surgery and emergency deep venous thrombosis (DVT) conditions to prevent excessive clotting. However, patients are treated at therapeutic dosing levels of 0.2–2 U mL^{-1} (0.08 μM–0.8 μM) in post-operative and long-term anticoagulant care of DVT. Human and equine serums were doped with UFH and LMWH at these dosing levels to simulate monitoring conditions in a clinical setting. A serum sample (32 μL) doped with UFH or LMWH was added to a fluorimeter cell containing a total volume of 1.5 mL HEPES (10 mM) in deionized water. To this was added 2 μL of **1** ($2.24\times10^{-3}\,\text{M}^{-1}$). The fluorescence stabilized over a period of 18 minutes, which contrasts the instantaneous response found

 © 2005 Wiley-VCH Verlag GmbH & Co. KGaA, Weinheim

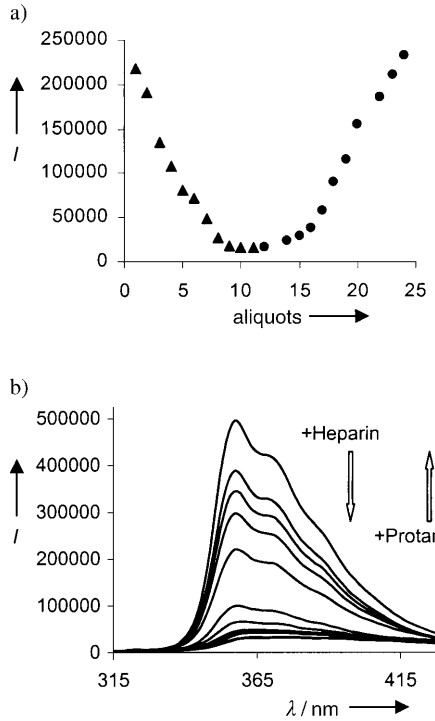


Figure 4. Reversibility of LMWH:**1** binding upon titration with protamine. a) Emission intensity at 357 nm. Dilution was carried out with aliquots of buffered water (HEPES, pH 7.4). First 11 aliquots of heparin were added (▲), and then 12 aliquots of protamine were added (●). The fluorescent emission was reestablished upon titration. b) Emission spectrum of **1** upon addition of LMWH. The addition of protamine reverses the spectrum.

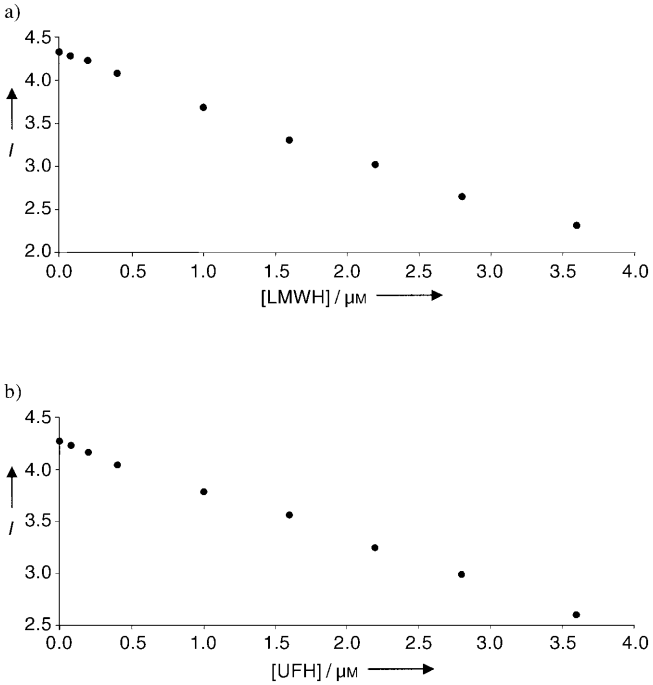


Figure 5. Calibration curves for a) LMWH in human serum and b) UFH in human serum. Conformational changes to **1** upon binding to heparin result in a diminished fluorescence emission. Greater concentrations of UFH and LMWH result in increased fluorescent quenching. The range of detection for both UFH and LMWH was 0–9 U mL^{-1} (0–3.6 μM).

in buffered water, and indicates that the formation of the complex with heparin in serum was slow on the laboratory timescale. This result is potentially a consequence of the kinetics of release of heparin from natural receptors in the sera. Emission spectra were recorded after 18 minutes for each of nine samples with various heparin concentrations to generate calibration curves (355 nM, Figure 5). Increased levels of heparin in serum correlated linearly with lower emission responses for both UFH and LMWH within the range of clinically relevant concentrations, as was observed for the fluorimetric titrations using pure heparin in buffered water. Furthermore, the method worked in both equine and human samples, thus illustrating that the affinity of the synthetic receptor for heparin is independent of the mammalian source, and could potentially be used for either human or veterinary applications.

In summary, we have demonstrated a functional synthetic fluorescent assay for the clinically administered anticoagulant heparin. The synthetic receptor highlighted herein showed remarkable selectivity and affinity for heparin, even in crude serum. The fluorescence emission was used to generate calibration curves for UFH and LMWH in serum at clinically relevant dosing levels (0.2–8.0 U mL^{-1}). These calibration curves allow the heparin concentration in an unknown sample to be determined by comparative analysis of the fluorescence emission. This study demonstrates that synthetic receptors can be created to target very complex bioanalytes, and function successfully in physiological settings.

Received: April 26, 2005
Published online: August 5, 2005

Keywords: fluorescence · heparin · host–guest systems · receptors · supramolecular chemistry

[1] a) S. L. Tobey, E. V. Anslyn, *Org. Lett.* **2003**, *5*, 2029–2031; b) Z. Zhong, E. V. Anslyn, *Angew. Chem.* **2003**, *115*, 3113–3116; *Angew. Chem. Int. Ed.* **2003**, *42*, 3005–3008.

[2] G. J. Despotis, G. Gravlee, K. Filos, J. Levy, *Anesthesiology* **1999**, *91*, 1122–1151.

[3] J. Hirsh, J. E. Dalen, D. Deykin, L. Poller, *Chest* **1992**, *102*, 337S–352S.

[4] a) T.-J. Cheng, T.-M. Lin, T.-H. Wu, H.-C. Chang, *Anal. Chim. Acta.* **2001**, *432*, 101–111; b) J. M. Thomson, L. Poller in *Blood Coagulation and Haemostasis* (Ed.: J. M. Thomson), Churchill Livingstone, Edinburgh, Scotland, **1989**, pp. 301–339; c) S.-C. Ma, V. C. Yang, M. E. Meyerhoff, *Anal. Chem.* **1992**, *64*, 694–697; d) V. C. Yang, W.-C. Ma, B. Fu, M. E. Meyerhoff, *Anal. Chem.* **1993**, *65*, 2078–2084; e) N. Ramamurthy, N. Baliga, J. A. Wahr, U. Schaller, V. C. Yang, M. E. Meyerhoff, *Clin. Chem.* **1998**, *44*, 606–613; f) N. Ramamurthy, N. Baliga, T. W. Wakefield, P. C. Andrews, V. C. Yang, M. E. Meyerhoff, *Anal. Biochem.* **1999**, *266*, 116–124; g) S. Mathison, E. Bakker, *Anal. Chem.* **1999**, *71*, 4614–4621; h) G. A. Mitchell, R. J. Gargiulo, R. M. Huseby, D. E. Lawson, S. P. Pochron, J. A. Sehuanes, *Thromb. Res.* **1978**, *13*, 47–52; i) E. Homer, *Thromb. Haemost.* **1985**, *54*, 29–31.

 © 2005 Wiley-VCH Verlag GmbH & Co. KGaA, Weinheim

[5] a) R. J. Linhardt, T. Toida in *Carbohydrates in Drug Design* (Eds.: Z. J. Witczak, K. A. Nieforth), Marcel Dekker, New York, New York, **1997**, pp. 277 – 341; b) L. Poller, J. M. Thomson, K. F. Yee, *Br. J. Haematol.* **1980**, *44*, 161 – 165; c) S. Kitchen, *Br. J. Haematol.* **2000**, *111*, 397 – 406.
[6] S. Cai, J. L. Dufner-Beattie, G. D. Prestwich, *Anal. Biochem.* **2004**, *326*, 33 – 41.
[7] a) J. I. Weitz, *N. Engl. J. Med.* **1997**, *337*, 688 – 698; b) I. Bjork, U. Lindahl, *Mol. Cell. Biochem.* **1982**, *48*, 161; c) R. Jordan, D. Beeler, R. Rosenberg, *J. Biol. Chem.* **1979**, *254*, 2902 – 2913.
[8] R. H. Lorentsen, J. H. Graversen, N. R. Caterer, H. C. Thøgersen, M. Etzerodt, *Biochem. J.* **2000**, *347*, 83 – 87.
[9] Z. Zhong, E. V. Anslyn, *J. Am. Chem. Soc.* **2002**, *124*, 9014 – 9015.
[10] S. L. Wiskur, J. J. Lavigne, H. Ait-Haddou, V. Lynch, Y. H. Chiu, J. W. Canary, E. V. Anslyn, *Org. Lett.* **2001**, *3*, 1311 – 1314.
[11] a) S. L. Wiskur, J. J. Lavigne, A. Metzger, S. L. Tobey, V. Lynch, E. V. Anslyn, *Chem. Eur. J.* **2004**, *10*, 3792 – 3804; b) K. Burgess, A. M. Porte, *Angew. Chem.* **1994**, *106*, 1218 – 1220; *Angew. Chem. Int. Ed. Engl.* **1994**, *33*, 1182 – 1184; c) J. J. Lavigne, E. V. Anslyn, *Angew. Chem.* **1999**, *111*, 3903 – 3906; *Angew. Chem. Int. Ed.* **1999**, *38*, 3666 – 3669.
[12] S. L. Wiskur, H. Ait-Haddou, E. V. Anslyn, J. J. Lavigne, *Acc. Chem. Res.* **2001**, *34*, 963 – 972.
[13] a) S. A. McFarland, N. S. Finney, *J. Am. Chem. Soc.* **2001**, *123*, 1260 – 1261; b) J. V. Mello, N. S. Finney, *Angew. Chem.* **2001**, *113*, 1584 – 1586; *Angew. Chem. Int. Ed.* **2001**, *40*, 1536 – 1538.

 © 2005 Wiley-VCH Verlag GmbH & Co. KGaA, Weinheim

Redox Chemistry

DOI: 10.1002/anie.200501192

Modeling the Anodic Half-Cell of a Low-Temperature Coal Fuel Cell**

*Douglas B. Weibel, Roman Boulatov, Andrew Lee, Rosaria Ferrigno, and George M. Whitesides**

Herein we examine the reduction of Fe^{III} ions by subbituminous coal (SBC) having a composition $CH_{0.81}O_{0.22}$ in 5 M H_2SO_4 at 100 °C. The reaction proceeds with a maximum rate constant of 8×10^{-4} cm s^{-1},[1] which is 15–160 times greater than those reported previously.[2,3] We used this reaction in the anode compartment of a prototype of a coal fuel cell that operated at 100 °C and at atmospheric pressure with VO_2^+ as the model oxidant. The cell produced a maximum current (power) density of 5 A (0.6 W) per liter of a slurry of electrolyte and coal, and 100 mA (11 mW) at the scale at which we carried out experiments (19 mL).

Attempts to develop a process for generating electricity directly from the oxidation of coal date back to the late 19th century.[4] Recent work on coal-powered fuel cells has been motivated by two facts: 1) the worldwide reserves of coal significantly exceed those of other fossil fuels,[5] and 2) the environmental benefits of converting coal into electricity directly in a fuel cell rather than by generating steam in turbines have been perceived as significant.[6] The oxidation of carbon electrochemically has a large activation energy (26 kcal mol^{-1}),[7] and proceeds at room temperature at detectable rates only at an overpotential of greater than 1 V.

Two strategies have been used to overcome the intrinsically slow kinetics of the oxidation of carbon in a coal fuel cell. One strategy is to oxidize a carbonaceous fuel (e.g., graphite) electrochemically at high temperatures (> 600 °C)—the majority of recent research on coal fuel cells has been based on this approach.[2,7–9] Molten carbonates are typically used as electrolytes in high-temperature cells; molten hydroxides, borates and silicates, and solid oxides have also been used. One of the most advanced examples of a direct carbon–air fuel cell operated at 630 °C for 500 h with molten KOH/NaOH as the electrolyte, a graphite anode that also served as the fuel, and a Fe–Ti alloy as the cathode at which O_2 was reduced. The cell produced current and power densities of 30 A L^{-1} (270 mA cm^{-2} of anode) and 2.5 W L^{-1} (0.12 W cm^{-2} of anode), respectively.[10] The high operating temperature of this class of cells tends to result in their corrosion, particularly in the presence of oxygen.[10] Other technical problems with these cells include: 1) the high resistivity of molten salts (up to 100 Ω cm);[11] 2) the consumption of carbon by reaction with CO_2 to produce CO;[7] and 3) the clogging of cells by ash and other components of the fuel that are not oxidized.[9] The high resistivity and poor mechanical stability of carbon fuels such as bituminous coal make them impractical as consumable anodes in coal fuel cells—the use of coal slurries in molten electrolytes requires vigorous stirring.[6] Zecevic et al. have argued that high-temperature coal fuel cells cannot be made practical because of these problems.[10]

An alternative strategy for overcoming the slow kinetics of the direct electrochemical oxidation of coal is based on the observation that several transition-metal ions, including Fe^{III}, Sn^{IV}, Cu^{II}, and Ce^{IV}, oxidize coal slurries with an activation energy of 7–16 kcal mol^{-1}, which is significantly lower than that for the direct electrooxidation of coal.[12,13] Although the electrolysis of coal slurries in the presence of transition-metal ions has been studied extensively,[2,3,12,13] we are not aware of any coal-powered fuel cells that use a secondary redox couple (e.g., Fe^{III}/Fe^{II}). This type of cell—in which metal ions would be reduced by the coal and reoxidized at the anode electrochemically—has been considered impractical because of the

[*] Dr. D. B. Weibel,[+] Dr. R. Boulatov,[+] A. Lee, Dr. R. Ferrigno, Prof. G. M. Whitesides
Department of Chemistry and Chemical Biology
Harvard University
Cambridge, MA 02138 (USA)
Fax: (+1) 617-495-9857
E-mail: gwhitesides@gmwgroup.harvard.edu

[+] These authors contributed equally to the work.

[**] This research was supported by the DoE (DE-FG02-OOER45852) and DARPA. D.B.W. was a recipient of a postdoctoral fellowship from the National Institutes of Health (GM067445). R.F. was a recipient of a postdoctoral fellowship from the Swiss National Science Foundation. We thank Wyodak Resources, Williams Coal & Oil, Dakota Westmoreland Corporation, and the American Coal Foundation for samples of coal.

Supporting information for this article is available on the WWW under http://www.angewandte.org or from the author.

InterScience
© 2005 Wiley-VCH Verlag GmbH & Co. KGaA, Weinheim

slow turnover ($< 7\times10^{-7}$–$2\times10^{-5}\,s^{-1}$) observed under a variety of conditions with all but the strongest oxidants (Ce^{IV} and Br_2).[13]

We found that Fe^{II} ions can be generated by reducing a saturated solution of Fe^{III} ions in 5 M H_2SO_4 (5 mL) with a suspension of SBC (5 g, 70 mesh) at a maximum rate of 4 mM s^{-1};[14] at this rate and temperature, the reaction becomes kinetically suitable for use in a coal fuel cell operating at atmospheric pressure (although problems with the overall conversion of coal to energy remain; see below).

Among the carbonaceous fuels tested, sub-bituminous coal and Kraft lignin were oxidized most rapidly by Fe^{III} ions.[15] The rates of oxidation by Fe^{III} ions decreased in the order: peat, lignite, activated charcoal, anthracite, and bituminous coal. Graphite felt was inert to oxidation by Fe^{III} ions under these conditions. The oxidation of SBC at 100 °C by Cu^{II} ions (0.16 V versus the normal hydrogen electrode (NHE)) and Sn^{IV} ions (0.15 V versus NHE)—both weaker oxidants than Fe^{III} ions (0.72 V versus NHE at 100 °C)—was too slow to be useful.[16]

Up to approximately 0.1 mol of Fe^{III} was reduced to Fe^{II} ions with 1 g of SBC (ca. 100 mesh) at 100 °C in 5 M H_2SO_4.[15] This amount corresponds to approximately 40 % of the electrons available (0.24 mol or 24 kC) from the complete oxidation of 1 g of SBC to CO_2 and H_2O [Eq. (1)].

$$CH_{0.81}O_{0.22} + 1.78\,H_2O \rightleftharpoons CO_2 + 4.37\,H^+ + 4.37\,e^- \quad (1)$$

The reaction between SBC and Fe^{III} ions produced CO_2, traces of CO, and a solid with the chemical composition $CH_{0.58}O_{0.33}$; the mass of this more highly oxidized residue was 75 % of the initial mass of coal. Equation (2) describes the empirical stoichiometry of the oxidation of SBC by Fe^{III} ions under these conditions.

$$CH_{0.81}O_{0.22} + 0.61\,H_2O + 1.62\,Fe^{III} \rightleftharpoons 0.70\,CH_{0.58}O_{0.33} + 0.30\,CO_2 + 1.62\,H^+ + 1.62\,Fe^{II} \quad (2)$$

The rate of reduction of Fe^{III} ions by SBC is given by Equation (3), where $[Fe^{III}]$ is the concentration of Fe^{III} ions (M); m is the mass of coal (g); l is the average "size" of coal particles based on the mesh size of coal (cm);[17] ρ is the density of coal (g cm^{-3});[18] and v is the volume of the reaction mixture (the volume of the solution and the coal, cm^3). In Equation (3) the term $m/l\rho$ is proportional to the total surface area of the coal; for spherical particles the coefficient of proportionality is 0.75.

$$\frac{d[Fe^{II}]}{dt} = k\frac{[Fe^{III}]\left(\frac{m}{l\rho}\right)}{v} \quad (3)$$

The maximum rate of reduction of Fe^{III} to Fe^{II} ions was 4×10^{-3} M s^{-1} at 100 °C in a reaction mixture containing 5 g of SBC (ca. 70 mesh) and 5 mL of a solution of Fe^{III} ions (0.385 M) in 5 M H_2SO_4 (this slurry contained approximately 1:1 electrolyte/SBC (v/v)). The corresponding heterogeneous rate constant k [Eq. (3)] was 8×10^{-4} cm s^{-1}, which is 15–160 times greater than those reported previously for the oxidation of various types of coal by Fe^{III} ions in H_2SO_4 at 100 °C.[2,3]

The kinetic data suggest that the reduction of Fe^{III} ions by SBC under these conditions might provide a method of regenerating Fe^{II} ions in the anodic compartment of a redox fuel cell that uses the Fe^{III}/Fe^{II} couple. To explore this possibility, and to identify some of the limitations of such a cell, we built a prototype of a coal fuel cell. In the anodic chamber, Fe^{III} ions were reduced to Fe^{II} ions by SBC, and Fe^{II} ions were oxidized to Fe^{III} ions electrochemically at a carbon felt anode. The anodic oxidation of the Fe^{II} ions was coupled to the reduction of VO_2^+ to VO^{2+} at the cathode (carbon felt) through an external circuit. We separated the cathodic and anodic compartments with a nafion-112 membrane (Figure 1). VO_2^+ is a more suitable oxidant for academic studies than O_2—the species used in commercial fuel cells—because VO_2^+ is a strong oxidant (the standard potential of the VO_2^+/VO^{2+} couple is only 0.2 V less oxidizing than that of the O_2/H_2O couple) that is reduced much more rapidly than O_2 at carbon electrodes.

VO^{2+} ions accumulated in the cathodic compartment during the operation of the cell. To regenerate VO_2^+ ions, the solution in the cathodic compartment was pumped into a separate vessel where the VO^{2+} ions were oxidized aerobically in the presence of nitrate at 80 °C.[19]

We ran the cell until the desired fraction of electrons (up to 40 %) available from the complete oxidation of SBC to H_2O and CO_2 had been extracted as electric current. We then separated the remaining solid from the electrolyte by centrifugation, and added a fresh batch of SBC. The content of the cathodic compartment was replaced with a regenerated solution of VO_2^+ ions as frequently as necessary to maintain the cathodic potential within 0.1 V. We observed maximum volumetric current and power densities of 5 A per liter of slurry and 0.6 W per liter of slurry, respectively, using 15 mL of 5 M H_2SO_4 saturated with $Fe_2(SO_4)_3$ and 4 g of SBC (ca. 100 mesh; electrolyte/SBC ≈ 4:1 (v/v)). The current/potential curves (Figure 2 a) indicate that the performance of the cell was not limited by the cathodic reaction or by mass transport.

To understand the relative contributions of 1) the reaction between Fe^{III} ions and SBC, 2) anodic oxidation of Fe^{II} ions,

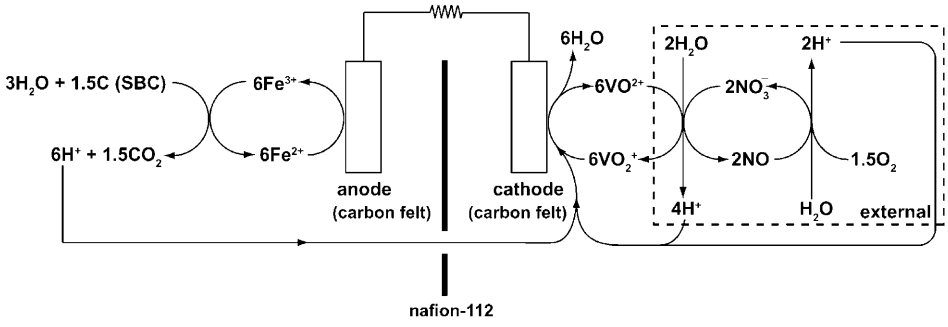


Figure 1. Schematic representation of the coal fuel cell which simplifies the stoichiometry of the reaction between SBC and Fe^{III} ions given in Equation (2).

 © 2005 Wiley-VCH Verlag GmbH & Co. KGaA, Weinheim

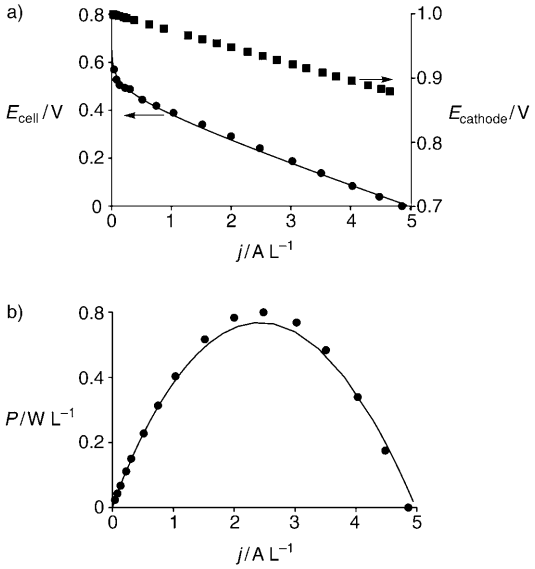


Figure 2. Current and power output of the cell. a) A plot of the potential of the cell E_{cell} (◆, left axis) and the cathodic potential $E_{cathode}$ versus NHE (■, right axis) as a function of the current density j. b) A plot of the power density P as a function of the current density j. The solid lines are fits to Equation (4) using $(km/\rho l) = 0.1\ cm^3\,s^{-1}$, k_{ET}-$S_{an} = 0.01\ cm^3\,s^{-1}$, $v = 0.019$ L, $r = 3.90\ \Omega$. The anodic compartment contained 15 mL of a saturated solution of ferric sulfate in 5 M H_2SO_4 and 4 g of SBC; the cathodic compartment contained 60 mL of a solution of VO_2^+ and VO^{2+} (ca. 1:1) in 5 M H_2SO_4. The temperature of the cell was 100 °C. The arrows indicate the axes corresponding to each plot.

and 3) cell resistance to the performance of the cell at various currents we analyzed the current/potential and current/power data (Figure 2) with a kinetic model in which Fe^{III} ions were reduced to Fe^{II} ions by SBC with a composite rate constant $km/l\rho$, and Fe^{II} ions were oxidized anodically with a rate constant $k_{ET}S_{an}$; the variables k, m, l, and ρ are defined in Equation (3), k_{ET} is the standard heterogenous rate constant[16] for electron transfer between the $Fe^{III/II}$ couple and carbon felt ($> 1\times10^{-5}$ cm s^{-1}, see Supporting Information), and S_{an} is the surface area of the anode (2000 cm^2 for graphite felt with dimensions 13 cm^2 × 0.3 cm).[20] In this model the volumetric current density j [A L^{-1}] is given by Equation (4), where [Fe] is the total concentration of iron (M); v_{an} is the volume of the anolyte (L); E_{cell} is the potential of the cell (V); $E_{cathode}$ is the potential of the cathode (versus NHE, V); $E^{o\prime}$ is the formal potential of the Fe^{III}/Fe^{II} couple under the experimental conditions (0.72 V versus NHE, V); r is the internal resistance of the cell (Ω); F and R are Faraday and gas constants, respectively, and T is absolute temperature (K).

$$j = \frac{1}{v_{an}} \frac{10^{-3} F\,[\mathrm{Fe}]}{\left(\frac{e^{-\frac{0.5F}{RT}(E_{cathode} - E_{cell} - j v_{an} r - E^{o\prime})}}{(k_{ET} S_{an})}\right) + \left(\frac{1+e^{-\frac{F}{RT}(E_{cathode} - E_{cell} - j v_{an} r - E^{o\prime})}}{\left(\frac{km}{T\rho}\right)}\right)} \qquad (4)$$

The fit of experimental current/potential curves to Equation (4) (Figure 2) suggests that at potentials below 0.5 V the performance of this prototype fuel cell is limited primarily by the internal resistance (3.9 Ω, a value corresponding to an areal resistance of 50 Ω cm^{-2}). The carbon felt electrodes were responsible for 95% of this resistance; we estimate the resistance of the nafion membrane and the electrolyte to be less than 0.1 Ω.

At a cell potential between 0.5 and 0.65 V, the rate of the reaction between Fe^{III} ions and SBC limited the current. Our calculations suggest that at the ratio of the area of the anode to the total surface area of SBC used in our experiments $S_{an}/(m/l\rho)$ the electrochemical oxidation of Fe^{II} ions at the anode was not rate-limiting, even at the largest cell potentials.

The open-circuit voltage of our fuel cell was about 350 mV lower than the estimated formal potential of the SBC/O_2 couple.[21] The anodic half-cell was responsible for 150 mV of this overpotential, with the steady-state oxidation of Fe^{II} ions by O_2, hot H_2SO_4, or both being probable side reactions.[22] The cathodic half-cell contributed approximately 200 mV to the overpotential, because we regenerated the catholyte only until its potential reached 1 V (versus NHE). The aerobic oxidation of VO^{2+} is relatively slow, and impractically long times were required to achieve $[VO_2^+]/[VO^{2+}] \gg 1$ that would correspond to more oxidizing potentials. The crossover currents were small (0.5–2 μA cm^{-2} M^{-1}) and contributed little to the overpotential; for example, the loss in a cell comprising two 70-mL compartments separated by a membrane having an area of 13 cm^2 was less than 1 mV per minute when the cell was at open circuit.

As a batch of SBC oxidized, the maximum current density and power produced by the cell decreased as an exponential function of the charge per gram of SBC passed through the cell, because the rate constant for the reaction between Fe^{III} ions and SBC decreased (see Supporting Information).

We ran our prototype fuel cell continuously for 10^3 h (corresponding to the total turnover number of Fe^{III} ions of 10^3) and produced a current that was approximately constant by periodically adding SBC (5 g/100 mL added every 96 h) to the anode compartment and replacing the solution in the cathodic compartment at a frequency that maintained its potential within 0.1 V. The fraction of SBC not oxidized by Fe^{III} ions remained in the anodic compartment during the experiment. We observed no significant degradation in the performance of the cell during this prolonged run.

In summary, we have characterized the kinetics of the oxidation of SBC with Fe^{III} ions at 100 °C and have tested this reaction in a model of the anodic compartment of coal-powered fuel cell. The cell, which contained approximately 4 g of SBC (ca. 100 mesh) and 15 mL of saturated iron sulfate in 5 M H_2SO_4, delivered a maximum current of 100 mA and a power of 11 mW, which correspond to volumetric densities of 5 A L^{-1} and 0.6 W L^{-1}, respectively. It should be possible to lower the internal resistance of our prototype cell to less than 1 Ω and thereby increase the maximum volumetric current and power densities to over 90 A L^{-1} and 7 W L^{-1}, respectively, simply by optimizing the design of the electrodes, provided that limitations of mass-transport can be avoided. These values compare favorably with the maximum current and power densities reported in the literature for high-temperature coal fuel cells: 30 A L^{-1} and 2.5 W L^{-1}.[23]

The conditions described in the manuscript for the oxidation of SBC do not yet form the basis of a practical

 © 2005 Wiley-VCH Verlag GmbH & Co. KGaA, Weinheim

coal fuel cell, because of the small fraction of the enthalpy of SBC that can be converted into electrical power. The reversible electrochemical oxidation of 1 g of SBC with O_2 as the terminal oxidant would produce 24 kC of current at 1 V, which corresponds to 24 kJ of electrical energy. The oxidation of the same amount of SBC by Fe^{III} ions at 100 °C in 5 M H_2SO_4 produces 10 kC of current (40 %); the remaining 60 % of the reducing equivalents are contained in the solid that is oxidized by Fe^{III} ions at a rate below the detection limit of our experiments. At maximal power output, 1.3 kJ of electrical work is extracted from 1 g of SBC (ca. 100 mesh) in our cell; this amount constitutes 5 % of the enthalpy of the aerobic oxidation of SBC. Forty-five percent of the remaining enthalpy resides in the unoxidized solid residue. Ohmic resistance dissipates another 5 % of the enthalpy (1.3 kJ). The remaining losses (ca. 45 %, 11 kJ) arise during the operation of the cell because an equilibrium cannot be maintained between the terminal oxidant (O_2) and the redox couple in the cathodic half-cell (VO_2^+/VO^{2+}) and between the terminal reductant (SBC) and the redox couple in the anodic half-cell (Fe^{III}/Fe^{II}). As a result, the electrolyte in the cathodic compartment is reduced to a greater extent than it would be if it was in equilibrium with O_2, and the anodic compartment is oxidized to a greater extent than it would be if the Fe^{III}/Fe^{II} couple was in equilibrium with SBC. The efficiency of the conversion increases to 7 % (2 kJ) if the cell operates at 10 % of the maximum power output (high potential); in this regime, the currents are low and the irreversible non-electrochemical oxidation of Fe^{II} ions in side reactions dominates the energy losses. The efficiency of converting the enthalpy into electrical power correlates with the power output only as long as the rate of electrochemical oxidation of Fe^{II} ions exceeds the total rate of non-electrochemical processes in which Fe^{II} ions are oxidized, such as oxidation of Fe^{II} ions by air or H_2SO_4.

The primary reason for the inefficient conversion of enthalpy into power is the exponential decrease in the rate constant with the amount of charge extracted from SBC; this relationship indicates that the rapid initial rate of the reaction between SBC and Fe^{III} ions arises from the oxidation of a small fraction of highly reactive functional groups in coal (probably at or near the surface). As these groups are consumed, less-reactive groups at the surface or in the solid core of the particle are oxidized, with an observed corresponding decrease in the apparent rate constant.

Our analysis of Equation (3) suggests that it should be possible (but untested experimentally) to increase the initial rate of oxidation of coal with Fe^{III} ions by: 1) using smaller particles of coal (decreasing l); 2) using a larger ratio of coal to electrolyte (increasing m/v); and 3) using a different carbonaceous fuel or different electrolyte (increasing k). Improvements (1) and (3) may also increase the number of reducing equivalents of SBC extractable by Fe^{III} ions (namely, > 40 %). For example, if, following Equation (3), we assume that using particles of SBC with diameters of 1 μm would increase the initial rate of the reaction 200-fold over that with 200-μm particles (100 mesh)—without affecting how rapidly the rate constant k decays with the amount of charge extracted per gram of SBC—the enthalpy of conversion would be 9 % at maximum power output (17 % at 10 % of the maximum power output). If we assume that the rate constant for oxidation of particles of SBC with diameters of 1 μm with Fe^{III} ions decays 200-fold more slowly than for particles with diameters of 200 μm, the efficiency of converting enthalpy into useable electrical energy would become 18 % at maximum power output (40 % at 10 % of the maximum output).[24] By comparison, the corresponding conversion for an internal combustion engine is about 30 % and for a proton-exchange membrane (PEM) cell is approximately 45 %.[25]

The low efficiency observed in our studies is certainly not inevitable, and can be improved by using a better catalyst for the oxidation of coal than the transition-metal ions screened so far (Fe^{III}, Cu^{II}, Sn^{IV}).

It is possible that the kinetics and extent of oxidation of carbonaceous materials with Fe^{III} ions can be improved by using different fuels. The reactivity of carbon towards the direct electrochemical oxidation in high-temperature coal fuel cells correlates inversely with its degree of crystallinity;[9] a carbon fuel that is more amorphous than SBC may be more reactive to Fe^{III} ions in 5 M H_2SO_4 at 100 °C. If the oxidation of coal by Fe^{III} ions requires the coordination of ferric ions to active sites on the surface of coal, H_2SO_4 may not be the optimal electrolyte—Fe^{III} ions are present in H_2SO_4 primarily as $[Fe(HSO_4)_x]^{(3-x)+}$ complexes and the concentration of coordinatively unsaturated ions available for the oxidation of coal is low.[26]

Ultimately, to be practical, the anodic half-cell based on the transition-metal-catalyzed oxidation of a carbonaceous fuel should be integrated with a (half) membrane-electrode assembly (MEA) for the direct reduction of O_2 at the cathode. This integration would be possible only if MEAs are 1) stable to corrosive electrolytes (e.g., 5 M H_2SO_4 at 100 °C), and 2) have a low permeability to solutes (e.g., H_2SO_4 and the transition-metal ions).

This study does not provide the basis for a practical low-temperature, coal-powered fuel cell—it demonstrates a significant yield of electrons using what is, in essence, a liquid reformer (the $Fe^{III/II}$ component of this system), and provides a benchmark and starting point against which further studies in this area can be compared.

Received: April 5, 2005
Published online: August 5, 2005

Keywords: carbon · electrochemistry · fuel cells · redox chemistry

[1] The units of the rate constant are $cm\,s^{-1}$, and arise from the fact that the rate at which Fe^{II} ions are produced is given by $d[Fe]/dt = k[Fe]$(surface area of coal)/(reaction volume) or $[M\,s^{-1}] = k[M][cm^2][cm^{-3}]$. These are the same units used for a rate constant for heterogenenous electron transfer between a redox couple in solution and a solid electrode.

[2] P. M. Dhooge, D. E. Stilwell, S.-M. Park, *J. Electrochem. Soc.* **1982**, *129*, 1719–1724.

[3] a) K. E. Anthony, H. G. Linge, *J. Electrochem. Soc.* **1983**, *130*, 2217–2219; b) we estimated a rate constant for the oxidation of lignite coal (mesh > 250) at 100 °C of $2–3 \times 10^{-5}\,cm\,s^{-1}$ by recalculating data from Figure 1 of reference [16] and by using an activation energy of $12\,kcal\,mol^{-1}$. We estimated a rate

 © 2005 Wiley-VCH Verlag GmbH & Co. KGaA, Weinheim

constant for the oxidation of bituminous charcoal (ca. 75 mesh) at 100 °C of 5×10^{-6} cm s^{-1} by recalculating data from Figure 7 in reference [6] using the reported activation energy of 13.3 kcal mol. The elemental composition of this coal was $CHO_{0.29}$ and the ash content 33 %.

[4] See for example: E. Chen in *Fuel Cell Technology Handbook* (Ed.: G. Hoogers), CRC, Boca Raton, FL, **2003**, pp. 2.

[5] a) World Energy Council, "Survey of Energy Resources", can be found under http://www.worldenergy.org/wec-geis/publications/reports/ser/overview.asp, **1998**; b) Energy Information Administration, "International Energy Outlook", can be found under http://www.eia.doe.gov/oiaf/ieo/coal.html, **2004**.

[6] The perceived environmental benefit of converting coal directly into electricity in a fuel cell versus by means of a temperature gradient is the amount of CO_2 released per unit of electrical output. At present, no more than 60 % of the enthalpy of the aerobic combustion of carbon can be converted into electricity as a result of the finite top temperature that can be utilized by turbines. A coal fuel cell can convert all of the enthalpy for the aerobic oxidation of coal thermodynamically into CO_2 because of the positive entropy change upon combustion of C to CO_2.

[7] D. G. Vutetakis, D. R. Skidmore, H. J. Byker, *J. Electrochem. Soc.* **1987**, *134*, 3027 – 3035.

[8] S. Benson, *Fuel Cells: Use with Coal and Other Solid Fuels*, IEA, London, **2001**.

[9] N. J. Cherepy, R. Krueger, K. J. Fiet, A. F. Jankowski, J. F. Cooper, *J. Electrochem. Soc.* **2005**, *152*, A80 – A87.

[10] S. Zecevic, E. M. Patton, P. Parhami, *Carbon* **2004**, *42*, 1983 – 1993.

[11] W. H. A. Peelen, M. Olivry, S. F. Au, J. D. Fehribach, K. J. Hemmes, *J. Appl. Electrochem.* **2000**, *30*, 1389 – 1395.

[12] A. M. Posner, *Fuel* **1955**, *34*, 330 – 338.

[13] S.-M. Park, *J. Electrochem. Soc.* **1984**, *131*, 363C – 373C.

[14] The composition of SBC after drying was $CH_{0.81}O_{0.22}$; the loss upon drying and ash content were both approximately 10 %.

[15] a) This method of burning coal at low temperature reminds us of prior work on oxidatively removing (namely low-temperature burning) lignin from cellulose using polyoxometalates; see, for example: V. Grigoviev, C. L. Hill, I. A. Weinstock in *Fundamentals and Catalysis* (Ed.: D. S. Argyropoulos), American Chemical Society Symposium Series, Washington, DC, **2001**, pp. 297 – 312; b) lignin, cellulose, and other biomass feedstocks may be particularly attractive fuels in fuel cells because they minimize the emission of CO_2 per unit output of electrical energy.

[16] The standard potential of the $[Fe(H_2O)_6]^{2+}/[Fe(H_2O)_6]^{3+}$ couple is 0.77 V versus NHE: A. J. Bard, L. R. Faulkner, *Electrochemical Methods: Fundamentals and Applications*, Wiley, New York, **2001**, 2nd ed. We measured the formal potential in 25 % H_2SO_4 at 100 °C as 0.57 V versus standard Ag/AgCl, or 0.72 V versus NHE using the potential of the Ag/AgCl reference electrode of 0.15 versus NHE at 100 °C: D. J. G. Ives, *Reference Electrodes, Theory and Practice*, Academic Press, New York, **1961**, p. 189.

[17] Mesh refers to the number of openings per linear inch of a screen. The mesh size of a particle is the mesh screen having the largest openings on which the particle is retained. The mesh size of the American Sieve Series is related to the size of the opening, in cm as: (size in cm) = 2/(mesh size) for mesh sizes above 50, and (size in cm) = (1.5)/(mesh size) for mesh sizes below 40. In kinetic equations, we used the size of the opening in cm as the characteristic size of a particle of coal l because the linear size is not defined for a particle of an arbitrary shape.

[18] The choice of the parameters $m/l\rho$ to represent the accessible surface is discussed in the Supporting Information.

[19] J. T. Kummer, *Inorg. Chim. Acta* **1983**, *76*, L291 – L292.

[20] The measured value for k_{ET} is on the low end of rate constants for electron transfer between the $Fe^{III/II}$ couple and different forms of carbon reported in the literature. See for example, P. Chen, M. A. Frying, R. L. McCreery, *Anal. Chem.* **1995**, *67*, 3115 – 3122.

[21] We were unable to find data in the literature on the standard redox potential of the reaction in Equation (1) or its temperature dependence. We estimated the potential of this reaction at 100 °C from the combustion analysis of SBC, according to the formula: $E_{SBC}(T) = \frac{\Delta G_{combustion}(T)}{nF} - 1.2\ V \approx \frac{LHV}{nF} \approx -0.25\ V$, where the low-heat value (LHV) is the enthalpy of the combustion of coal generating steam and $n = 4.37$.

[22] At open circuit voltage, which corresponds to a potential of the anodic half-cell of about 350 mV versus NHE, the oxidation of Fe^{II} ions by H_2SO_4 becomes thermodynamically favorable at a partial pressure of $SO_2 \leq 600$ Pa (≤ 0.6 % of atmospheric pressure). The aerobic oxidation of Fe^{II} ions is thermodynamically unfavorable at any potential of the cell, but it may be driven by the highly exergonic decomposition of HO_2, which results from reaction between the Fe^{II} ions and O_2. Assuming that the rate of the reduction of the Fe^{III} ions by SBC equals the total rate of oxidation of Fe^{II} ions in side-reactions at open circuit, the apparent first-order rate constant for the non-electrochemical oxidation of Fe^{II} is about 10^{-9} s^{-1} for a reaction mixture containing 1 g of SBC per 4 mL of 5 M H_2SO_4 saturated with iron sulfate at 100 °C.

[23] We cannot compare the sustained current and power output of our cell with similar values reported for high-temperature CFCs. The literature on high-temperature CFCs does not specify the fraction of electrons available from the complete oxidation of fuel in the cell that was consumed while the "sustained" performance of the cell was characterized.

[24] The fraction of oxidizable functional groups that are on the surface of a particle of coal is inversely proportional to the radius of the particle when the groups are distributed homogeneously throughout the particle.

[25] a) J. Larminie, A. Dicks, *Fuel Cell Systems Explained*, Wiley, Hoboken, **2003**, pp. 61 – 108; b) R. Stone, *Introduction to Internal Combustion Engines*, MacMillan, New York, **1985**, pp. 22 – 46.

[26] A. F. Gil, L. Galicia, I. Gonzalez, *J. Electroanal. Chem.* **1996**, *417*, 129 – 134.

 © 2005 Wiley-VCH Verlag GmbH & Co. KGaA, Weinheim

Industrial Catalysts

DOI: 10.1002/anie.200463045

Tailored Catalytic Propene Trimerization over Acidic Zeolites with Tubular Pores**

Johan A. Martens, Wim H. Verrelst, Georges M. Mathys, Stephen H. Brown, and Pierre A. Jacobs*

Oligomerization of short alkenes is applied in large-scale petrochemical processes for a variety of products including liquid hydrocarbon fuels, lubricants, detergent precursors, solvents, and plasticizers.[1–4] Whereas longer-chain linear alkenes result from homogeneous catalytic processes that use transition metal complexes,[5] chain-branched alkenes in the C_6–C_{12} range stem from the oligomerization of C_3 or C_4 alkenes using a fixed bed of silica-supported phosphoric acid (SSPA),[1–4,6] at temperatures and pressures amounting to about 520 K and 12 MPa, respectively.[7,8] Despite drawbacks related to the maintenance of a critical feed hydration level, catalyst clogging, and corrosion problems caused by phosphoric acid leaching, SSPA processes are still widely operated.[1–4] We have now discovered that acidic ZSM-22 zeolite allows the synthesis of propene trimers of intermediate degree of chain branching, suitable as feedstock for oxyfunctionalization processes. The narrow tubular pores of this zeolite impose preferential formation of the slimmer linear and monobranched oligomers. Though the in-time stability of ZSM-22 is similar to that of SSPA, the former catalyst does not present the numerous disadvantages encountered with the latter.

Difficulties in finding a viable substitute for SSPA are not only related to the fact that cheap, impure alkene feedstocks are used, but also to the critical product specification with respect to molecular weight and chain branching of the oligomers. Acidic zeolites through their molecular shape selectivity properties can meet these stringent catalyst requirements. For fuel and lubricant applications, a technology based on ZSM-5 has been developed.[9] More recently, ZSM-57 with its unique lobate pore structure was reported to be a stable and selective dimerization catalyst for C_4–C_6 alkenes.[10] With a ZSM-57-type catalyst, the number of chain branchings (NCB) of the alkene dimers is high and similar to that of processes using SSPA. In oxyfunctionalization processes, olefins with two and especially with three or more chain branchings show decreased reactivity.[11] We now report the advantageous use of ZSM-22 for the synthesis of propene trimers with appropriate low NCB.

Zeolite pore architecture is characterized by the dimensionality and size of the channel system, the latter being determined by the number of oxygen atoms in the ring circumscribing the opening. Candidate zeolite topologies categorized according to micropore architecture were screened in the propene trimerization reaction using a mixture of 12 wt % of propene in propane fed in supercritical state at 6.8 MPa and 473–513 K. Contact time was adapted to reach at least initially a high conversion level. With respect to trimerization yield (Y_{C9}) and limitation of NCB, zeolites with a tubular 10-membered ring (10-MR) channel system devoid of large lobes or intersections outperformed all others (Figure 1, bottom). On the majority of zeolite structure types known today, with intersecting 10-MR channels, side pockets, or pronounced lobes or with 12-MRs,[12] Y_{C9} at high conversion was reduced, while the NCB was close to 2.0 (Figure 1, top), a value typical for SSPA processes.

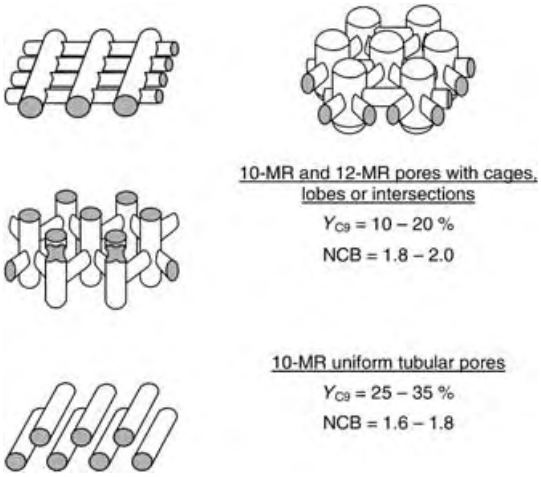


Figure 1. Influence of the micropore system of the acidic zeolite at propene conversions exceeding 80% on propene trimer yield (Y_{C9}) and number of chain branchings (NCB).

Uniform 10-MR tubular pores are encountered in ZSM-22, ZSM-23, SAPO-11 with TON, MTT, and AEL topology, respectively,[12] as well as in the ZSM-48 family of zeolites.[13,14] With ZSM-22, initially all propene was converted. Though the activity showed some decay with time-on-stream, an amount of propene corresponding to 400 times the catalyst weight could be converted easily (see Experimental Section). The three other zeolites showed decreased initial activity, with similar (ZSM-23) or higher rates of decay (ZSM-48 and SAPO-11).

Under the presently used reaction conditions, typical for industrial processes, the tubular 10-MR zeolite catalysts yielded mainly dimers, trimers, and tetramers as reaction products. This is evident from Figure 2, which also clearly

[*] Prof. J. A. Martens, Dr. W. H. Verrelst, Prof. P. A. Jacobs
Centre for Surface Chemistry and Catalysis
Catholic University of Leuven
Kasteelpark Arenberg 23, 3001 Leuven (Belgium)
Fax: (+32) 16-32-19-98
E-mail: johan.martens@agr.kuleuven.ac.be
Dr. G. M. Mathys, Dr. S. H. Brown
ExxonMobil Chemical Europe, Inc.
European Technology Center
Hermeslaan 2, 1831 Machelen (Belgium)

[**] J.A.M. and P.A.J. acknowledge the Flemish Government for support in the frame of a Concerted Research Action on Catalysis (GOA), as well as the Federal Services of Science Policy for support in the frame of a IAP-PAI Network on Supramolecular Catalysis.

 © 2005 Wiley-VCH Verlag GmbH & Co. KGaA, Weinheim

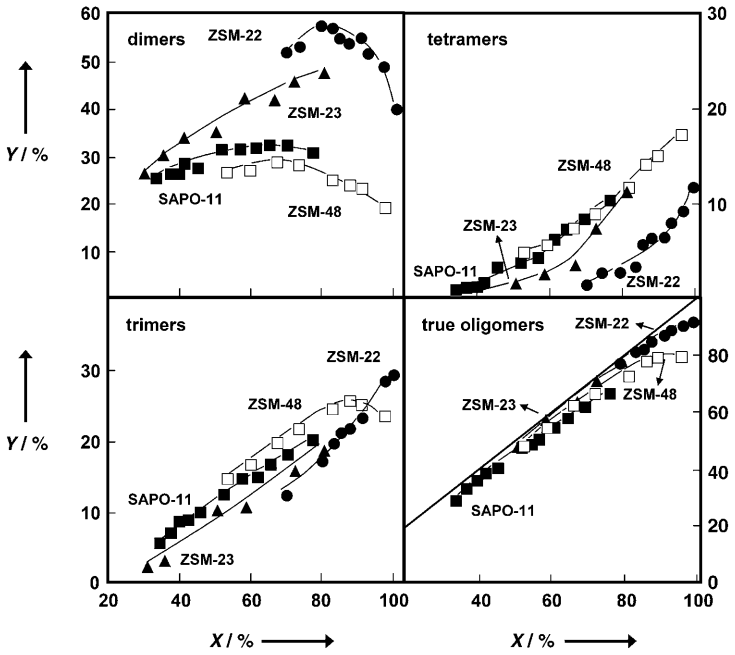
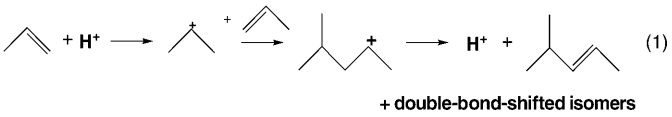


Figure 2. Yield (*Y*) of propene dimers, trimers, tetramers, and of total true oligomers (di- to hexamers, without products with intermediate carbon numbers obtained by cracking and recombination of fragments) against propene conversion (*X*) with ZSM-22, ZSM-23, ZSM-48, and SAPO-11.

indicates that on all four catalysts the true oligomers remain the largest product fraction up to high conversion—for ZSM-23 and ZSM-22 even more pronounced than for SAPO-11 and ZSM-48. Despite the high conversion, also oligomer chain growth was limited. On ZSM-22, the dimer yield peaked at around 80% propene conversion; the trimer yield close to 100% (Figure 2). The highest trimer yields were obtained with ZSM-22. Chain growth was more pronounced on ZSM-23, SAPO-11, and ZSM-48, as noted from the more abundant formation of tetramers and the occurrence of dimer and trimer yield maxima at lower propene conversion.

Given the multitude of possible double-bond and skeletal isomers, the molecular reaction network for propene oligomerization is complex. As double bond positions in the individual dimers were always at equilibrium, selectivity discussions can be limited to the rationalization of the branching of the alkane skeleton obtained after saturation of the double bond. Chain branching was analyzed using gas chromatography with sample hydrogenation (see Experimental Section). In the dimer fraction obtained on ZSM-22 (Figure 3), primary products dominating at low conversion have a carbon skeleton with a methyl branch at C2, as expected for an acid-catalyzed alkylation [Eq. (1)].



(1)

Skeletal isomers with methyl branching at C3 are secondary products obtained by methyl shifts on 2-methyl-

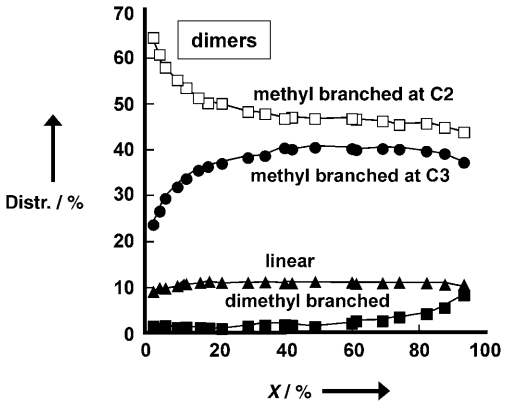


Figure 3. Skeletal distribution of the dimer fraction obtained at increasing propene conversion with ZSM-22.

branched isomers (Figure 3). With ZSM-22, methyl shifts on alkylcarbenium ions were found to be substantially slower than de-branching reactions in which one branch vanishes.[15] Linear dimers observed over the entire conversion range (Figure 3) stem from fast de-branching reactions of 2-methylpentenes. Above 40% propene conversion, linear and methyl-branched dimers are found at equilibrium with ZSM-22 as catalyst (Figure 3). Dimers with dimethyl-branched carbon skeleton were obtained only at high feed conversion. Similar dimers fractions were obtained on the other 10-MR tubular zeolites, except for the more pronounced formation of dibranched dimers on SAPO-11 and ZSM-48.

The NCB in the trimer fractions obtained with 10-MR tubular zeolites is displayed in Figure 4 and compared with that of a typical trimer fraction obtained on SSPA, representative for an oligomerization without any confinement in micropores. The large majority of trimers show a dibranched carbon skeleton (Figure 4), which can be explained by acid-catalyzed oligomerization causing an additional branching upon addition of a novel propene unit to a methyl-branched dimer. Especially with ZSM-23 and ZSM-22, the fraction of

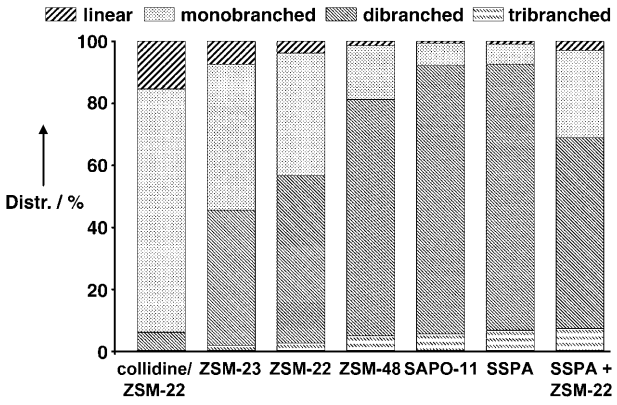


Figure 4. Skeletal distribution of trimer fractions at 30% propene conversion, obtained on collidine-treated ZSM-22, ZSM-23, ZSM-22, ZSM-48, SAPO-11, SSPA, and on successive layers of SSPA and ZSM-22.

© 2005 Wiley-VCH Verlag GmbH & Co. KGaA, Weinheim

trimers with monobranched or linear carbon skeleton is larger than with SSPA. Propene trimers are methyl-branched at carbon positions 3 and 4 (3,4-group isomers) unless the branchings are shifted (2,6-group isomers) or eliminated to give monobranched and linear isomers (monobranched-group isomers).[16] Among the 10-MR tubular pore zeolites the formation of monobranched-group nonene isomers decreases in the series ZSM-23 > ZSM-22 > ZSM-48 > SAPO-11 (Figure 5). The skeletal distribution of the trimer fraction obtained with SAPO-11 is already very similar to that encountered with SSPA (Figure 4).

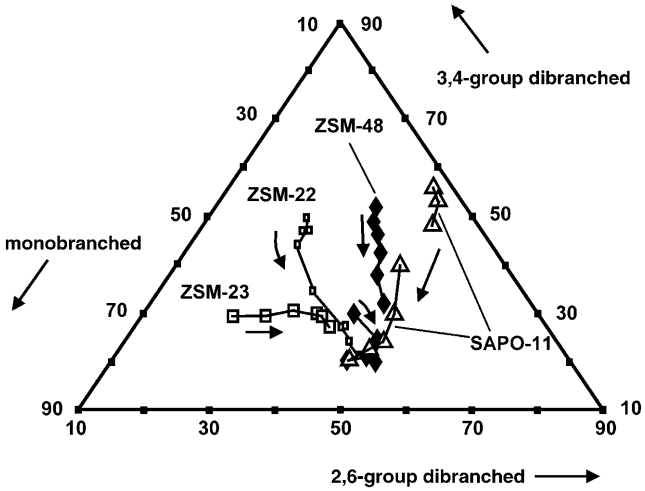


Figure 5. Compositional diagram showing the evolution of the skeletal structures of propene trimers obtained with 10-MR tubular pore zeolites at increasing conversions indicated by the arrows.

Among the known zeolite structure types, those with tubular 10-MRs having a free diameter of around 0.5 nm exhibit the highest heats of adsorption for linear hydrocarbons.[17–22] The free diameters of ZSM-23 pores of $0.45 \times 0.52\ nm^2$ [12] preclude methyl-branched alkanes from entering.[17] The penetration of the same methyl-branched alkanes into the slightly wider ZSM-22 pores with cross sections of $0.44 \times 0.55\ nm^2$ is possible, depending on conditions.[17–20] SAPO-11 belongs to the AEL zeolite family, has a little wider 10-MR of $0.40 \times 0.65\ nm^2$, and readily adsorbs isoalkanes.[21,22] Sorption data on ZSM-48 with its relatively wide 10-MR of $0.53 \times 0.56\ nm^2$ are not available. Catalytic test reactions such as the determination of the constraint index[23] and of the refined constraint index[24] reveal that there is less steric limitation inside SAPO-11 and ZSM-48 pores than inside ZSM-22 and ZSM-23 pores. Thus the observed tendency of debranching of propene trimers in the zeolite sequence of SAPO-11 < ZSM-48 < ZSM-22 < ZSM-23 (Figures 4 and 5) reflects the order of decreasing effective pore width.

The stronger limitation of oligomer chain growth in ZSM-22 compared with ZSM-23 (Figure 2) can be explained as follows: Inside the pores of these two zeolites, the formation of tetramers most likely occurs through propene addition to linear trimers. As ZSM-23 exhibits a stronger tendency to trimer linearization, it shows a more pronounced chain growth. In ZSM-48 and SAPO-11, chain growth can probably also proceed on monobranched trimer chains, explaining why in these zeolites tetramer formation is also more pronounced than in ZSM-22.

As the ZSM-22 crystals are micrometer-sized and the specific external surface area amounts to about $40\ m^2 g^{-1}$, pore mouth sites of ZSM-22 may contribute significantly to catalysis, for example, in catalytic isodewaxing.[25] Acidic sites on the external surfaces and pore mouths of ZSM-22 can be selectively poisoned with collidine (2,4,6-trimethylpyridine), a bulky amine that cannot penetrate the pores of 10-MR zeolites. Whereas the collidine-poisoned ZSM-22 catalyst was about five times less active than the parent sample, the trimer fraction was very rich in monobranched nonenes (80%) and contained a significant amount of linear nonenes (15%) (Figure 4), confirming that catalytic sites located inside the tubular pores are responsible for the formation of monobranched and linear trimers, and that sites accessible to collidine are responsible for the formation of di- and tribranched nonenes. ZSM-22 also shows "coke selectivation" as partially deactivated catalysts were found to be more selective for linear and monobranched nonenes than fresh catalysts, owing to a gradual loss of the contribution of the external sites.

ZSM-22 can be used as hydroisomerization catalyst for converting long-chain *n*-alkanes into mono- and dibranched skeletal isomers,[25] as it establishes the internal equilibrium between the linear alkane, its monobranched isomers, and specific dibranched isomers.[25] This property of ZSM-22 can be exploited to reduce the NCB of the C_9 products obtained from propene oligomerization with SSPA as was shown for the trimer fraction produced in a process with SSPA for which the NCB was reduced from 2.0 to 1.7 during a typical catalytic run (473 K, 6.8 MPa, $W/F_0 = 280\ kg\,s\,mol^{-1}$). The reduction resulted primarily from conversion of dibranched into monobranched and linear nonenes (Figure 4, columns 6 and 7). Tribranched isomers have too little adsorption affinity in pore mouths and are not converted. Dibranched isomers undergo a first de-branching in pore mouths and eventually entire linearization deeper inside the pores.

The ZSM-22 catalysis was also run using feedstock of 50 wt% propene in propane, similar to a process with SSPA. Though with this propene-rich feed, pronounced exothermicity in the catalyst bed was observed, deactivation was minor. Propene conversion remained complete until an amount of propene of at least 400 times the catalyst weight was fed. An incremental increase of catalyst temperature was sufficient to reestablish complete propene conversion. Finally, the experiment was interrupted after the formation of more than 600 kg of oligomer product per kg of catalyst, which is in the range of oligomer yields with SSPA processes. ZSM-22 also brings an important environmental benefit, as it is reusable many times after regeneration and has a much longer lifetime than SSPA which can only be used once. Thus, the use of ZSM-22 in propene oligomerization adds to the sustainability of the petrochemical industry.

 © 2005 Wiley-VCH Verlag GmbH & Co. KGaA, Weinheim

Experimental Section

Zeolite samples were synthesized according to published methods: ZSM-22,[26] ZSM-23 was run 4 of reference [27], ZSM-48,[28] SAPO-11[29] was sample S-11/2 of reference [30]. The Si/Al ratio of ZSM-22, -23, and -48 was 42, 44, and 50, respectively. The phase purity was confirmed by XRD and SEM. Gram quantities of as-synthesized zeolite powder were pelletized (0.25–0.50 mm) by compression, loaded in a quartz tube, and calcined, first under flowing nitrogen at 400 °C for 5 h and subsequently under oxygen at 550 °C for 15 h. The samples were exchanged with 0.5 M aqueous NH_4Cl solution and calcined at 400 °C. This procedure resulted in acidic zeolites with more than 99.5 % of the aluminum tetrahedrally coordinated according to ^{27}Al MAS-NMR (signal at 54 ppm against aluminum nitrate reference with a Bruker Avance 400 MHz instrument; spinning frequency of 20 kHz). The FT-IR spectra of the zeolites displayed absorptions at about 3595 and 3745 cm^{-1}, assigned to bridging Al–OH–Si groups with Brønsted acid character and framework-terminating silanol groups, respectively. IR absorption bands at about 3655 cm^{-1}, which are characteristic of hydroxy groups on aluminum atoms that are partially dislodged from the framework and responsible for Lewis acidity, were absent.

The chemical composition of the SAPO-11 material corresponds to $(Si_{0.21}Al_{0.43}P_{0.36})0_2$. The SAPO-11 crystals are composed of 28 % aluminosilicate (AS) and 72 % silicoaluminophosphate (SAP) domains.[30] The catalytic activity of SAPO-11 is mainly due to Brønsted acid sites at the interphase between the AS and SAP domains.

Catalytic experiments in a fixed-catalyst-bed continuous-flow reactor: catalyst pellets of compressed zeolite powder with diameters of 0.25–0.50 mm were loaded in a stainless steel reactor tube with an internal diameter of 9 mm and a length of 300 mm. Empty volume was filled with alumina beads of the same diameter. Reaction conditions: $T = 473$ K; $P = 6.8$ MPa; feedstock: 12 wt % propene in propane; $W/F_0 = 34$ kg s mol^{-1} (W: catalyst weight; F_0: molar propene flow at reactor inlet); liquid feedstock delivered with a liquid mass flow controller (Brooks Instruments). The reactor outlet was sampled online at high pressure using a 4-port HPLC sampling valve (Valco) with an internal volume of 0.1 μL, and analyzed with capillary gas chromatography. Product NCB was determined offline on a gas chromatograph with sample hydrogenation module.

Received: December 23, 2004
Revised: February 23, 2005
Published online: August 1, 2005

Keywords: oligomerization · propene · shape selectivity · silica-supported phosphoric acid · zeolites

[1] K. Tanabe, W. F. Höldrich, *Appl. Catal. A* **1999**, *181*, 399 – 434.
[2] K. Weissermel, H. J. Arpe, *Industrial Organic Chemistry*, 4th ed., Wiley-VCH, Weinheim, **2003**, pp. 83 – 85.
[3] S. Matar, L. F. Hatch, *Chemistry of Petrochemical Processes*, 2nd ed., Butterworth-Heinemann, Woburn, MA, **2001**, chap. 8.
[4] D. York, J. C. Scheckler, D. G. Tajbl in *Handbook of Petroleum Refining Processes*, 3rd ed. (Ed.: R. A. Meyers), McGraw-Hill, New York, **2003**, pp. 1.21 – 1.30.
[5] J. Skupinska, *Chem. Rev.* **1991**, *91*, 613 – 648.
[6] V. N. Ipatieff, B. B. Corson, G. Egloff, *Ind. Eng. Chem.* **1935**, *27*, 1077 – 1081.
[7] K. G. Wilshier, P. Smart, R. Western, T. Mole, T. Behrsing, *Appl. Catal.* **1987**, *31*, 339 – 359.
[8] C. T. O'Connor, M. Kojima, *Catal. Today* **1990**, *6*, 329 – 349.
[9] S. A. Tabak, F. J. Krambeck, W. E. Garwood, *AICHE J.* **1986**, *32*, 1526 – 1531.
[10] J. A. Martens, R. Ravishankar, I. E. Mishin, P. A. Jacobs, *Angew. Chem.* **2000**, *112*, 4547 – 4550; *Angew. Chem. Int. Ed.* **2000**, *39*, 4376 – 4379.
[11] B. Cornils in *New Synthesis with Carbon Monoxide* (Ed.: J. Falbe), Springer, Berlin, **1980**, p. 96.
[12] C. Baerlocher, W. M. Meier, D. H. Olson, *Atlas of Zeolite Framework Types*, 5th ed., Elsevier, Amsterdam, **2001**.
[13] J. L. Schlenker, W. J. Rohrbaugh, P. Chu, E. W. Valyocsik, G. T. Kokotailo, *Zeolites* **1985**, *5*, 355 – 358.
[14] R. F. Lobo, H. van Koningsveld, *J. Am. Chem. Soc.* **2002**, *124*, 13222 – 13230.
[15] C. S. L. Narasimhan, J. W. Thybaut, G. B. Marin, P. A. Jacobs, J. A. Martens, J. F. Denayer, G. V. Baron, *J. Catal.* **2003**, *220*, 399 – 413.
[16] After hydrogenation, the 3,4-group comprises the following isomers: 3,4-, 2,3- and 4,4-dimethylheptane; 3-ethyl-2-methyl- and 3-ethyl-3-methylhexane; 2,3,4-trimethylhexane. The 2,6-group comprises 2,6-, 2,5-, 3,5-, 2,4-, and 2,2-dimethylheptane.
[17] J. F. Denayer, A. R. Ocakoglu, W. Huybrechts, J. A. Martens, J. W. Thybaut, G. B. Marin, G. V. Baron, *Chem. Commun.* **2003**, *15*, 1880 – 1881.
[18] M. Schenk, B. Smit, T. J. H. Vlugt, T. L. M. Maesen, *Angew. Chem.* **2001**, *113*, 758 – 761; *Angew. Chem. Int. Ed.* **2001**, *40*, 736 – 739.
[19] F. Eder, J. A. Lercher, *J. Phys. Chem. B* **1997**, *101*, 1273 – 1278.
[20] J. A. Z. Pieterse, S. Veefkind-Reyes, K. Seshan, J. A. Lercher, *J. Phys. Chem. B* **2000**, *104*, 5715 – 5723.
[21] F. Eder, J. A. Lercher, *J. Phys. Chem.* **1996**, *100*, 16460 – 16462.
[22] H. Stach, K. Fiedler, J. Janchen, *Pure Appl. Chem.* **1993**, *65*, 2193 – 2200.
[23] V. J. Frilette, W. O. Haag, R. M. Lago, *J. Catal.* **1981**, *67*, 218 – 223.
[24] P. A. Jacobs, J. A. Martens, *Pure Appl. Chem.* **1986**, *58*, 1329 – 1338.
[25] J. A. Martens, W. Souverijns, W. Verrelst, R. Parton, G. F. Froment, P. A. Jacobs, *Angew. Chem.* **1995**, *107*, 2726 – 2728; *Angew. Chem. Int. Ed. Engl.* **1995**, *34*, 2528 – 2530.
[26] S. Ernst, J. Weitkamp, J. A. Martens, P. A. Jacobs, *Appl. Catal.* **1989**, *48*, 137 – 148.
[27] S. Ernst, R. Kumar, J. Weitkamp, *Catal. Today* **1988**, *3*, 1 – 10.
[28] P. A. Jacobs, J. A. Martens, *Stud. Surf. Sci. Catal.* **1987**, *33*, 22.
[29] M. Mertens, J. A. Martens, P. J. Grobet, P. A. Jacobs in *Guidelines for Mastering the Properties of Molecular Sieves* (Ed.: D. Barthomeuf), Plenum, New York, **1990**, p. 1.
[30] J. A. Martens, P. J. Grobet, P. A. Jacobs, *J. Catal.* **1990**, *126*, 299 – 305.

 © 2005 Wiley-VCH Verlag GmbH & Co. KGaA, Weinheim

Phosphates

DOI: 10.1002/anie.200501871

The First Structure of a Cerium(IV) Phosphate: Ab Initio Rietveld Analysis of $Ce^{IV}(PO_4)(HPO_4)_{0.5}(H_2O)_{0.5}$**

Micaela Nazaraly, Gilles Wallez, Corinne Chanéac, Elisabeth Tronc, François Ribot, Michel Quarton, and Jean-Pierre Jolivet*

Since the investigations by König and Alberti in the late 1960s and those by Clearfield in the 1970s, several studies have continued to show that cerium(IV) phosphates (CePs) are interesting inorganic materials for cation exchange, amine intercalation, trapping of radioactive elements, and proton conduction.[1–12] Very recently, cerium(IV) phosphate nanotubes have also been reported.[13] Compared with zirconium, titanium, and tin phosphates, which are well-documented materials used in various fields (ion exchange, intercalation, proton conduction, heterogeneous catalysis, molecular sorption),[14] CePs appear to be much more complex. While the former exhibit two well-characterized lamellar structures, that is, $Zr(HPO_4)_2{\cdot}H_2O$ (α-ZrP)[15] and $Zr(H_2PO_4)(PO_4){\cdot}2H_2O$ (γ-ZrP),[16] based on six-coordinate metal centers, cerium(IV) phosphates appear to adopt several crystalline structures, with P/Ce ratios ranging from 1.1:1 to 3.0:1.[1–12] Despite some efforts and evidences that the structures do not correspond to the α- or γ-ZrP types,[7,9] all these cerium(IV) phosphates structures have remained unknown until now. This lack of information has often made the interpretation of results much more difficult or even impossible. Moreover, in some cases, the chemical composition remains a matter of debate. Indeed, according to its powder X-ray diffraction pattern a unique crystalline compound has, depending on authors, been considered to be $Ce_2O(HPO_4)_3{\cdot}H_2O$, $(CeOH)_2(HPO_4)_3$, $Ce(HPO_4)(PO_4)_{0.5}(OH)_{0.5}$, or $Ce(PO_4)(HPO_4)_{0.5}(H_2O)_{0.5}$.[1a,4a,6,7,9]

This peculiar CeP, which exhibits a P/Ce ratio of 1.5:1 has been described several times in the literature.[1a,3a,4a,6,7,9] A unit cell and possible space groups have even been proposed.[7,9] Moreover, its structure was supposed to be a layered one, even though no amine could be intercalated.[7] However no other structural details were available. As it has been obtained from various cerium(IV) salts (sulfate, ammonium nitrate) or derivatives (hydroxide, oxide) either under reflux or hydrothermal ageing in H_3PO_4 solutions, this crystalline compound seems to exhibit a high degree of thermodynamic stability and, therefore, should offer a relevant first entry in the field of CePs structures. Herein, the structure of $Ce(PO_4)(HPO_4)_{0.5}(H_2O)_{0.5}$ is solved by ab initio Rietveld analysis. It consists of $[Ce(PO_4)^+]_n$ slabs bridged by hydrogenphosphate tetrahedra. The chemical nature of the (hydrogen)phosphates is also unambiguously established from the P–O distances and ^{31}P NMR spectroscopy. Importantly, this is the first time a CeP structure is presented.

$Ce(PO_4)(HPO_4)_{0.5}(H_2O)_{0.5}$ was synthesized from CeO_2, H_3PO_4, and H_2O. It consists of crystalline platelets a few microns long in the longest dimension. The compound was found to be monoclinic, with a strong cell elongation along the *a* axis, consistent with the (100) platelet habit of the crystallites. The unit cell parameters were refined from the X-ray powder diffraction data ($a = 21.0142(3)$, $b = 6.55082(7)$, $c = 6.94382(6)$ Å, $\beta = 91.983(1)°$, $V = 955.32(2)$ Å^3) and the results agreed with those reported.[7,9] The structure was solved with the space group *C*2/*c* (No. 15). It can be described as dense $[Ce(PO_4)^+]_n$ slabs, extending parallel to the (*b*,*c*) plane, with cerium atoms on both surfaces (Figure 1). Each cerium atom is connected to four phosphate tetrahedra belonging to the same side and to one phosphate tetrahedron on the opposite surface of the slab. These slabs are bridged by HPO_4^{2-} units and water molecules are also present in the interslab region, which results in eight-coordinate cerium atoms. This structure bears absolutely no resemblance with the α- or γ-ZrP structures.[15,16] The $\{(P1)O_4\}^{3-}$ (slab) tetrahedron is regular (Figure 1), except for the outstandingly small O13-P1-O14 angle (97.1(8)°), which results from the sharing of the O13–O14 edge with a cerium atom. The long P2–O24 distance and the absence of Ce–O24 contact indicate that O24 is the protonated vertex of the $\{H(P2)O_4\}^{2-}$ hydrogenphosphate tetrahedron. The water molecule fills a structural cavity surrounded by eight oxygen atoms of (hydrogen)phosphates and one cerium atom.

Actually, the absence of superstructure peaks indicates some form of disorder in the array of the HPO_4^{2-} and H_2O units. The distances between an HPO_4^{2-} tetrahedron (e.g., the white one (P2) near the center of the cell in Figure 2) and its three closest equivalents (shaded in Figure 2) are too short to allow the occupation of these closest positions. Likewise, the occupation of an HPO_4^{2-} site precludes the presence of a water molecule in the closest H_2O site (d(P2)-O_W) 1.21(1) Å). These two conditions, along with the 50% occupancy of the interslab sites, lead to consideration of two equiprobable sets of alternate HPO_4^{2-} and H_2O units, forming fully ordered zigzags along the *c* axis, shown in different tones in Figure 2. In terms of symmetry, each zigzag still obeys the *c*-mirror axis, but ignores the inversion center and the twofold symmetry. Although neighbor zigzags in the same (*b*,*c*) plane are far enough apart to prevent any overlapping of their sites, the *b* parameter is small and the interactions should be strong

[*] M. Nazaraly, Dr. C. Chanéac, Dr. E. Tronc, Dr. F. Ribot, Prof. Dr. J.-P. Jolivet
Chimie de la Matière Condensée–UMR CNRS 7574
Université Pierre et Marie Curie
4, place Jussieu, cc 174, F-75252 Paris Cedex 05 (France)
Fax: (+33) 1-44-27-47-69
E-mail: fri@ccr.jussieu.fr
Dr. G. Wallez, Prof. Dr. M. Quarton
Laboratoire de Cristallochimie du Solide - UMR CNRS 7574
Université Pierre et Marie Curie
4, place Jussieu, cc 176, F-75252 Paris Cedex 05 (France)

[**] M.N. is indebted to Rhodia for her PhD fellowship. The authors are grateful to Dr W. van Beck (ESRF) for his help in collecting the diffraction data and to J. Maquet for her assistance with solid-state NMR spectroscopy.

 © 2005 Wiley-VCH Verlag GmbH & Co. KGaA, Weinheim

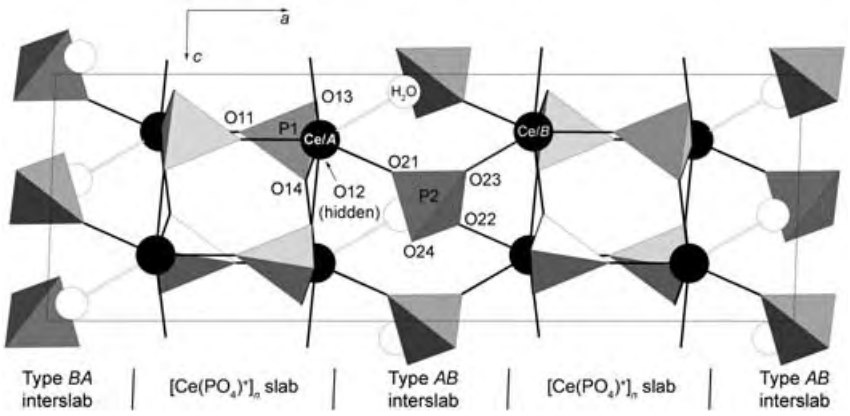


Figure 1. (010) projection of the $Ce(PO_4)(HPO_4)_{0.5}(H_2O)_{0.5}$ structure. The random succession of the interslab regions along the stacking *a* axis illustrates the disorder. P–O interatomic distances [Å]: P1-O11 1.543(6), P1-O12 1.518(9), P1-O13 1.52(1), P1-O14 1.53(1), P2-O21 1.50(1), P2-O22 1.51(2), P2-O23 1.52(2), P2-O24 1.61(2). Gray tetrahedra PO_4. The positions Ce/*A* and Ce/*B* are discussed in the text as are the *BA* and *AB* interslab units.

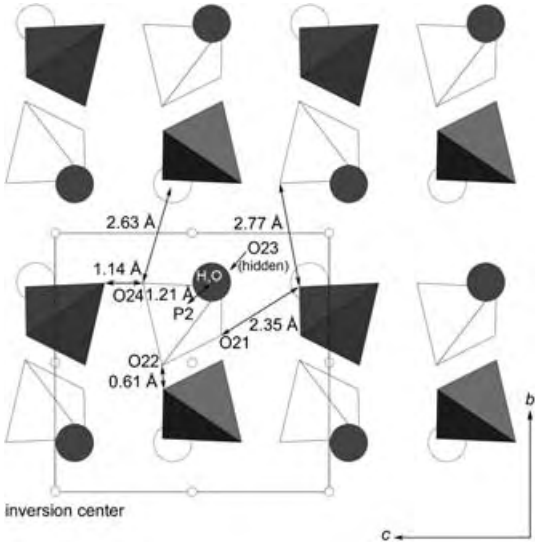


Figure 2. (100) projection of the interslab regions near $x = 1/2$ for the $Ce(PO_4)(HPO_4)_{0.5}(H_2O)_{0.5}$ structure. White and shaded units ($H(P2)O_4^{2-}$ tetrahedra and O_w (water oxygen) atoms) represent the two possible and equipropable zigzag models.

enough to keep the structure ordered along the *b* axis (see distances in Figure 2). So, the whole interslab region obeys a *c* symmetry instead of 2/*c*. In contrast, the thickness of the $[Ce(PO_4)^+]_n$ slabs prevents the cerium atom from "seeing" both neighbor layers, thus reducing strongly the ordering interactions along the *a* axis. Indeed, the disorder is likely to affect the stacking axis. The drop of symmetry of the zigzags has repercussions for the cerium atoms. If a pair of cerium atoms that should be equivalent by a twofold symmetry operation is considered for example, Ce/*A* and Ce/*B* in Figure 1, Ce/*A* is linked to atom O21 and the water molecule, while Ce/*B* is connected to atoms O22 and O23 of two different HPO_4^{2-} tetrahedra. Therefore, two different environments must be taken into account for the cerium atoms. They are noted *A* and *B*, hereafter (Figure 3). Note that all cerium atoms on one side of a slab are of the same type, while those facing them on the nearest slab are of the other type. Therefore, each interslab layer has an "*A*" and a "*B*" side, but is randomly either of "*AB*" or "*BA*" type, as shown in Figure 1.

In the course of the Rietveld refinements, attempts were made to measure the effect on the slabs of the disorder in the interslab regions by splitting the cerium atom and the $\{(P1)O_4\}^{3-}$ tetrahedron onto two sites. The cerium atom appeared slightly delocalized along the *a* axis onto two positions, 0.169(5) Å apart, as could be guessed from the two environment types, while the split positions of the P1 and connected oxygen atoms remained very close, but with larger estimated standard deviations (esds). Because this model did not allow correlations between the environment and the position of a slab atom to be established, this model was abandoned. The cerium atom was simply modeled as lying on a single position, with anisotropic harmonic displacement factors, resulting in an *a*-axis elongated thermal ellipsoid (B_{11} 1.27(7), B_{22} 0.10(6), B_{33} 0.12(5), B_{12} 0.1(1), B_{13} 0.04(5), B_{23} 0.10(8) Å^2). Note that the cerium atoms are octacoordinate in both environments (Figure 3), and exhibit

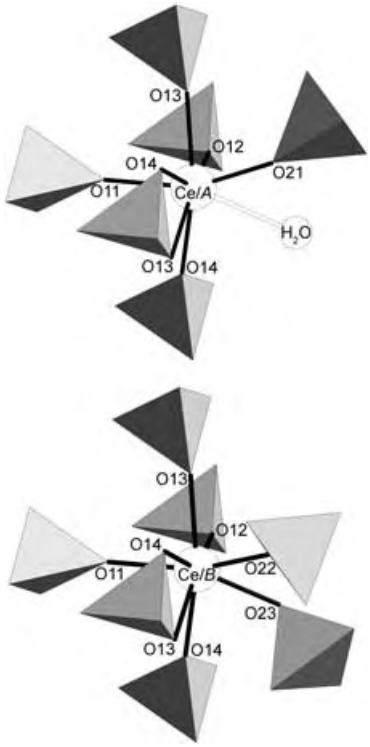


Figure 3. The two possible and equiprobable environments of the cerium atom (top: type *A*, bottom: type *B*) in the $Ce(PO_4)(HPO_4)_{0.5}(H_2O)_{0.5}$ structure. Ce–O interatomic distances [Å]: Ce*A*/*B*-O11^{I} 2.235(5), Ce*A*/*B*-O12^{II} 2.206(7), Ce*A*/*B*-O13 2.44(1), Ce*A*/*B*-O13^{III} 2.384(9), Ce*A*/*B*-O14 2.44(1), Ce*A*/*B*–O14^{IV} 2.334(8), Ce*A*-O21 2.22(1), Ce*B*-O22^{V} 2.32(2), Ce*B*-O23^{VI} 2.38(2), Ce*A*-O_w 2.92(2) (with the following symmetry operations: I = 1/2−*x*, 1/2+*y*, 1/2−*z*; II = *x*, 1+*y*, *z*; III = *x*, 1−*y*, 1/2+*z*; IV = *x*, 1−*y*, *z*−1/2; V = 1−*x*, 1−*y*, 1−*z*; VI = 1−*x*, *y*, 1/2−*z*).

 © 2005 Wiley-VCH Verlag GmbH & Co. KGaA, Weinheim

nearly equal valences (3.35 and 3.51 for *A* and *B* type cerium, respectively).[17] The slight but non-negligible contribution of the O_W atom in environment *A* accounts for a structural role of the water molecule.

This very same compound, according to its X-ray powder diffraction, has been described in previous works as a cerium(IV) hydroxy(hydrogen)phosphate with the formula $Ce(HPO_4)(PO_4)_{0.5}(OH)_{0.5}$.[4a,6,7] The present structure, and especially the P–O distances, indicate quite clearly that the compound is in fact a cerium(IV) (hydrogen)phosphate hydrate, with the formula $Ce(PO_4)(HPO_4)_{0.5}(H_2O)_{0.5}$. The nature of phosphate units was however confirmed by ^{31}P MAS and CP-MAS NMR spectroscopy (CP-MAS = cross polarization magic-angle spinning), a result of the high sensitivity of such techniques to phosphorus environment.[18,19] The ^{31}P MAS NMR spectrum of $Ce(PO_4)(HPO_4)_{0.5}(H_2O)_{0.5}$ (Figure 4) shows three resolved resonance signals at $\delta = -15.7$, -27.3, and -29.2 ppm, with an intensity ratio of 1:1:1. A similar spectrum was previously reported but incorrectly interpreted.[6] Variation of the contact time in ^1H–^{31}P CP-MAS NMR (Figure 4) spectra shows that the signal at $\delta = -15.7$ ppm has a steep magnetization build up, while the two others ($\delta = -27.3$ and -29.2 ppm) have slower ones. From these results it can be inferred that the signal at $\delta = -15.7$ ppm corresponds to a hydrogenphosphate while the others correspond to fully deprotonated phosphates. Accordingly the amount of phosphate is twice the amount of hydrogenphosphate and the formula $Ce(PO_4)(HPO_4)_{0.5}(H_2O)_{0.5}$ must be considered. These ^{31}P chemical shifts fall within the regions found for the α- and γ-$M^{IV}P$ structures (M = Zr, Ti) and agree with the generally observed highfield shift of about 10 ppm for the removal of one proton.[19] While there is only one fully deprotonated phosphate environment in the structure, $\{(P1)O_4\}^{3-}$, ^{31}P NMR spectroscopy indicates two similar but different environments. This feature can be related to the occupancy in the interslab region. Indeed, depending on the surface of the slab, that is, corresponding to type *A* or type *B* cerium atoms, P1 has two possible and equiprobable environments which also exhibit different magnetization sources for CP experiments. A P1 atom belonging to a type *A* plane has one $H(P2)O_4$ tetrahedron (P1-O24 3.50 Å) and one water molecule (P1-O_W 3.68 Å) in its near environment, while a P1 atom in a type *B* plane has only one more remote H(P2)O4 tetrahedron (P1-O24 4.07 Å). Accordingly, the signal with the slower magnetization build up ($\delta = -29.2$ ppm) can be assigned to the phosphates in the type *B* planes which have the less-protonated environment.

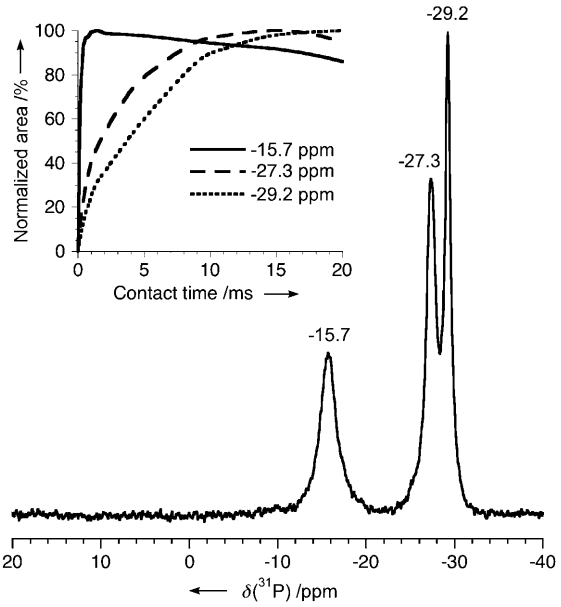


Figure 4. ^{31}P MAS NMR spectrum of $Ce(PO_4)(HPO_4)_{0.5}(H_2O)_{0.5}$ ($\nu_{MAS} = 14$ kHz). The inset shows the area of each signal versus the contact time in ^1H–^{31}P CP-MAS NMR experiments.

In conclusion, $Ce(PO_4)(HPO_4)_{0.5}(H_2O)_{0.5}$ can be considered to have a layered structure, as previously proposed from sedimentation experiments.[7] However, the bridging hydrogenphosphates hold the slabs tightly together and this simply explains why amine could not be intercalated in such a compound. Of note is that $U_2(PO_4)_2(HPO_4)\cdot H_2O$ and $Th_2(PO_4)_2(HPO_4)\cdot H_2O$, which both exhibit a powder diffraction pattern similar to the one of the homologous compound $Ce(PO_4)(HPO_4)_{0.5}(H_2O)_{0.5}$ studied here,[9] must have an identical structure to this first reported CeP structure.

Experimental Section

$Ce(PO_4)(HPO_4)_{0.5}(H_2O)_{0.5}$: Cerium oxide nanoparticles (2.6 g)[20] were dispersed in 1.96 M H_3PO_4 (15 mL; $PO_4/Ce \approx 2.4$). The preparation was then treated hydrothermally at 200 °C for 5 h. The yellow product obtained was collected by filtration, washed several times with distilled water, and dried under a flow of nitrogen.

X-ray powder diffraction (XRD) patterns were recorded on the BM01B line of the European Synchrotron Radiation Facility (Grenoble, France). The instrument parameters were previously refined from a LaB_6 pattern. The powder sample was placed in a 0.3 mm capillary and the data were collected at 293 K, using a wavelength of 0.69947 Å and a Ge(111) rear monochromator. The data were scanned between 4.062 and 55.488° (2θ), with a step of 0.006°, and 1247 reflections were observed. Assuming, as a rule of thumb, a rough 20 $Å^3$ volume per oxygen atom, the number of formula units in the cell was found to be $Z = 4$. Systematic extinctions led space groups *Cc* and *C*2/*c* to be considered, and the structure resolution was initiated with the *Cc*. FullProf.2k[21] was run in profile-matching mode to extract the diffracted intensities and to correct them from absorption. The broadening of the *h*-dependent peaks, resulting from the crystallite shape (platelet), was taken into account when modeling the peaks shapes. The background fitting was made by interpolation between selected points. Eight positions and profile parameters were used. The profile model was a Thompson–Cox–Hasting with anisotropic size and strain effect. A Patterson synthesis performed with Shelx-97[22] allowed the cerium atoms to be located, the other atoms were found by observation of the Fourier maps.[23] The cerium atoms and some of the phosphates appeared to form dense $[Ce(PO_4)^+]_n$ blocks extending parallel to the (*b*,*c*) plane. At this point, the presence of a twofold symmetry between the cerium atoms, as well as between the electron densities became so obvious that the space group was changed for *C*2/*c*. HPO_4^{2-} units and the oxygen atom O_W of the H_2O molecules were found in the interblock spaces, on half-occupied sites in agreement with the stoichiometry and the symmetry (indeed, a joint refinement gave a 0.47(1) occupancy for the interblock sites). To reduce the number of parameters, anisotropic

 © 2005 Wiley-VCH Verlag GmbH & Co. KGaA, Weinheim

thermal factors were only used for the cerium atom. A single isotropic displacement factor was used for both phosphorus atoms and an other isotropic displacement factor for all the oxygen atoms. Finally, 44 parameters were refined and gave satisfactory reliability factors ($R_P = 0.060$, $R_{WP} = 0.084$, $R_{Bragg} = 0.055$, $R_{exp} = 0.053$, $R_F = 0.029$, and $\chi^2 = 9.5$).[24] Note that because of the low electron weight of the HPO_4^{2-} unit, the O-P-O angles and P–O distances had to be put under soft constraints, taking those of K_2HPO_4 as reference.[25]

^{31}P MAS NMR spectroscopy was performed at 121.5 MHz on a Bruker Avance 300 spectrometer, using a 4-mm locked Bruker probe. Chemical shifts are quoted relative to 85 % H_3PO_4.

Received: May 30, 2005
Published online: August 3, 2005

Keywords: cerium · layered compounds · NMR spectroscopy · phosphates · structure elucidation

[1] a) K. H. König, E. Meyn, *J. Inorg. Nucl. Chem.* **1967**, *29*, 1153 – 1160; b) K. H. König, E. Meyn, *J. Inorg. Nucl. Chem.* **1967**, *29*, 1519 – 1526; c) K. H. König, G. Eckstein, *J. Inorg. Nucl. Chem.* **1969**, *31*, 1179 – 1188; d) K. H. König, G. Eckstein, *J. Inorg. Nucl. Chem.* **1972**, *34*, 3771 – 3779.

[2] E. M. Larsen, W. A. Cilley, *J. Inorg. Nucl. Chem.* **1968**, *30*, 287 – 293.

[3] a) G. Alberti, U. Costantino, F. Di Gregorio, P. Galli, E. Torracca, *J. Inorg. Nucl. Chem.* **1968**, *30*, 295 – 304; b) G. Alberti, U. Costantino, L. Zsinka, *J. Inorg. Nucl. Chem.* **1972**, *34*, 3549 – 3560.

[4] a) R. G. Herman, A. Clearfield, *J. Inorg. Nucl. Chem.* **1975**, *37*, 1697 – 1704; b) R. G. Herman, A. Clearfield, *J. Inorg. Nucl. Chem.* **1976**, *38*, 853 – 858; c) R. G. Herman, A. Clearfield, *J. Inorg. Nucl. Chem.* **1977**, *39*, 143 – 146.

[5] M. Tsuhako, M. Danjo, Y. Baba, M. Murakami, H. Nariai, I. Motooka, *Bull. Chem. Soc. Jpn.* **1997**, *70*, 143 – 148.

[6] H. Hayashi, K. Torii, S. Nakata, *J. Mater. Chem.* **1997**, *7*, 557 – 562.

[7] M. Kaneyoshi, W. Jones in *Advances in Ion Exchange for Industry and Research* (Eds.: P. A. Williams, A. Dyer), The Royal Society of Chemistry, Cambridge, **1999**, pp. 176 – 186.

[8] H. Nakayama, A. Hayashi, M. Tsuhako, T. Eguchi, N. Nakamura, *Phosphorus Res. Bull.* **1998**, *8*, 89 – 94.

[9] V. Brandel, N. Clavier, N. Dacheux, *J. Solid State Chem.* **2005**, *178*, 1054 – 1063.

[10] P. Barboux, R. Morineau, J. Livage, *Solid State Ionics* **1988**, *27*, 221 – 225.

[11] Y. Xu, S. Feng, W. Pang, G. Pang, *Chem. Commun.* **1996**, 1305 – 1306.

[12] S. Pajkoff, *Monatsh. Chem.* **1968**, *99*, 1400 – 1408.

[13] C. Tang, Y. Bando, D. Goldberg, R. Ma, *Angew. Chem.* **2005**, *117*, 582 – 585; *Angew. Chem. Int. Ed.* **2005**, *44*, 576 – 579.

[14] a) G. Alberti in *Inorganic Ion Exchange Materials* (Ed.: A. Clearfield), CRC, Boca Raton, FL, **1982**, chap. 2; b) A. Clearfield in *Inorganic Ion Exchange Materials* (Ed.: A. Clearfield), CRC, Boca Raton, FL, **1982**, chap. 1; c) G. Alberti, U. Costantino in *Intercalation Chemistry* (Eds.: M. S. Wittingham, A. J. Jacobsen), Academic Press, New York, **1987**, pp. 147 – 180.

[15] J. M. Troup, A. Clearfield, *Inorg. Chem.* **1977**, *16*, 3311 – 3314.

[16] D. M. Poojary, B. Shpeizer, A. Clearfield, *J. Chem. Soc. Dalton Trans.* **1995**, 111.

[17] N. E. Brese, M. O'Keeffe, *Acta Crystallogr. Sect. B* **1991**, *47*, 192.

[18] a) A. R. Grimmer, U. Haubenreisser, *Chem. Phys. Lett.* **1983**, *99*, 487; b) T. M. Duncan, D. C. Douglas, *Chem. Phys.* **1984**, *87*, 339; c) A. K. Cheetham, N. J. Clayden, C. M. Dobson, R. J. B. Jakeman, *J. Am. Chem. Soc.* **1985**, *107*, 6249 – 6252; d) R. J. B. Jakeman, A. K. Cheetham, N. J. Clayden, C. M. Dobson, *J. Chem. Soc. Chem. Commun.* **1986**, 195 – 197.

[19] H. Nakayama, T. Eguchi, N. Nakamura, S. Yamaguchi, M. Danjyo, M. Tsuhako, *J. Mater. Chem.* **1997**, *7*, 1063 – 1066.

[20] Cerium oxide was provided by Rhodia in the form of crystalline nanometric particles (diameter ≈ 6 nm) that can be easily redispersed in water. Its formula corresponds to $CeO_{1.8}(NO_3)_{0.4}$-$(H_2O)_{1.1}$ ($M_w = 213.5$ g mol^{-1}).

[21] J. Rodriguez-Carvajal, *FullProf.2k: Rietveld, profile matching and integrated intensity refinement of X-ray and neutron data, V 1.9c*, Laboratoire Léon Brillouin, CEA, Saclay, France, **2001**.

[22] G. M. Sheldrick, *Shelx-97: a program for crystal structure determination*, Göttingen, Germany, **1997**.

[23] J. Gonzalez-Platas, J. Rodriguez-Carvajal, *Gfourier: Fourier maps calculation program, V 3.20*, Universidad de La Laguna, Tenerife, Spain, and Laboratoire Léon Brillouin, CEA, Saclay, France, **2003**.

[24] $R_P = \Sigma \mid y_o^i - y_c^i \mid / \Sigma y_o^i$, $R_{WP} = \Sigma w^i \mid y_o^i - y_c^i \mid / \Sigma w^i y_o^i$, $R_{\mathrm{Bragg}} = \Sigma \mid I_o^i - I_c^i \mid / \Sigma I_o^i$, $R_{\mathrm{exp}} = ((n-p)/\Sigma w_i y_o^i)^{1/2}$, $R_F = \Sigma \mid (I_o^i)^{1/2} - (I_c^i)^{1/2} \mid / \Sigma (I_o^i)^{1/2}$, $\chi^2 = (R_{WP}/R_{\mathrm{exp}})^2$. Further details on the crystal structure investigation may be obtained from the Fachinformationszentrum Karlsruhe, 76344 Eggenstein-Leopoldshafen, Germany (fax: (+49) 7247-808-666; e-mail: crysdata@fiz-karlsruhe.de), on quoting the depository number CSD-415465.

[25] T. Lis, *Acta Crystallogr. Sect. C* **1994**, *50*, 484.

 © 2005 Wiley-VCH Verlag GmbH & Co. KGaA, Weinheim

Electrochemical Oscillations

DOI: 10.1002/anie.200501009

Current Oscillations during Formic Acid Oxidation on a Pt Electrode: Insight into the Mechanism by Time-Resolved IR Spectroscopy**

*Gabor Samjeské and Masatoshi Osawa**

Various types of instabilities occur in chemical systems maintained under nonequilibrium conditions,[1] and this is also the case for several electrochemical systems.[1,2] In the

[*] Dr. G. Samjeské, Prof. Dr. M. Osawa
Catalysis Research Center, Hokkaido University
Kita 21 Nishi 10, Kita-Ku, Sapporo 001-0021 (Japan)
Fax: (+81) 11-706-9124
E-mail: osawam@cat.hokudai.ac.jp
and
CREST-JST
Kawaguchi Center Building
4-1-8 Honcho, Kawaguchi, Saitama 332-0012 (Japan)

[**] This work was supported by the Core Research for Evolutional Science and Technology (CREST) of the Japan Science and Technology Agency (JST) as well as by the Ministry of Education, Culture, Sports, Science, and Technology of Japan (Grant-in-Aid for Basic Research No. 14205121 and for Scientific Research on Priority Areas 417), the Research Institute of the Innovative Technology for the Earth, and the Asahi Glass Foundation. Valuable discussions with Prof. Hiroshi Okamoto are acknowledged.

Supporting information for this article is available on the WWW under http://www.angewandte.org or from the author.

 WILEY InterScience DISCOVER SOMETHING GREAT

© 2005 Wiley-VCH Verlag GmbH & Co. KGaA, Weinheim

electrochemical oxidation of formic acid on Pt and Pt-group metals, instabilities can cause spontaneous potential and current oscillations under galvanostatic (constant current) and potentiostatic (constant potential) conditions, respectively. The electrooxidation of formic acid is one of the most fundamental electrocatalytic systems and has a great relevance to low-temperature fuel cells; therefore, the mechanism of the oscillations has long been the focus of experimental[3] and theoretical[3b,c,4] investigations.

It is generally accepted that the oxidation of formic acid follows the so-called "dual-pathway" mechanism[5]: one path involves a fast reaction via a reactive intermediate (direct path) and the other path includes a step in which an inhibiting intermediate is formed (indirect path). The reactive intermediate is generally assumed to be a carboxylic acid species (COOH) adsorbed on the surface through the C atom, whereas adsorbed CO produced by dehydration of formic acid has definitely been identified as the poisonous species by in situ IR reflection–absorption spectroscopy (IRAS).[6] The electrochemical oscillations in the oxidation of formic acid have been explained basically in terms of the dual-pathway mechanism: the periodic adsorption and oxidative removal of CO inhibits and accelerates, respectively, the direct path. The ohmic drop (iR, where i is the current and R is the resistance of the electrochemical system) also plays an important role, and current oscillations result from the interplay of chemical and electrical variables.[2,3g,4a,4c] Nevertheless, the details of the oscillations are still controversial[2–4] and further investigations are required.

The identification of the reactive intermediate and probing of the reaction dynamics are essential for a full understanding of the oscillations. Infrared spectroscopy is suitable for this purpose. Honda et al.[7] studied current oscillations by time-resolved IRAS and reported that CO coverage does not change during the oscillations. This result is inconsistent with the general consensus, and these authors proposed a model in which the periodic adsorption and desorption of the OH species ($H_2O \rightleftarrows OH_{ads} + H^+ + e^-$) results in current oscillations. However, the observed current is much larger than that expected from the adsorption and desorption of the OH species. We reexamined the current oscillations by an alternative IR spectroscopy method having a sensitivity higher than that of IRAS, namely, surface-enhanced infrared absorption spectroscopy (SEIRAS) in a Kretschmann-type attenuated-total-reflection (ATR) mode,[8] and found that the reactive intermediate is not COOH but formate (HCOO) adsorbed on the electrode surface through two oxygen atoms. Note that formate is different from the COOH species in molecular structure. On the basis of the results reported herein, we propose a new mechanism of current oscillations that is largely different from those suggested earlier.[3,4]

Figure 1a shows a typical current oscillation pattern observed in 0.5 M H_2SO_4 + 1 M formic acid solution after stepping the electrode potential (E) from 0.05 to 1.1 V versus a reversible hydrogen electrode (RHE, to which all potentials hereafter are referred). The electrode used was a thin ($\approx$50 nm) polycrystalline Pt film deposited on the reflecting plane of a Si ATR prism by an electroless deposition technique.[9] A 30-Ω resistor was connected to the electrochemical system in series for observing the oscillations.[2,3g,4a,4c]

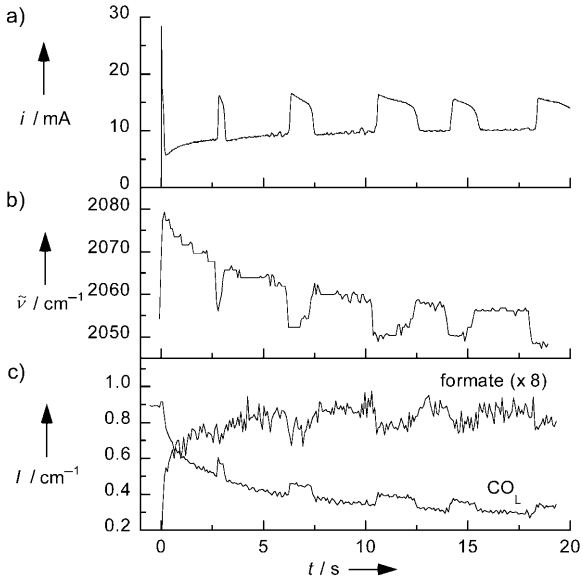


Figure 1. a) Current oscillations observed in the oxidation of formic acid at a constant potential of 1.1 V (RHE) in 0.5 M H_2SO_4 + 1 M HCOOH with a 30-Ω external resistor. b) Peak position of CO adsorbed at an atop site (CO_L). c) Integrated band intensities of CO_L and formate taken from a series of SEIRA spectra acquired simultaneously with the current–time curve.

The high sensitivity of ATR-SEIRAS enabled the time-resolved monitoring of the reaction processes occurring on the Pt electrode during the current oscillations with a time resolution of 80 ms (Figure 2). The spectral data correspond to the 10–15 s region in Figure 1a. A spectrum collected at 0.05 V in the pure electrolyte without formic acid was used as the reference. Other details of the spectral measurements have been described elsewhere.[8–10] Three bands at $\approx$2060, $\approx$1850, and 1320 cm^{-1} change their intensities and/or peak positions periodically. These bands have been assigned, from

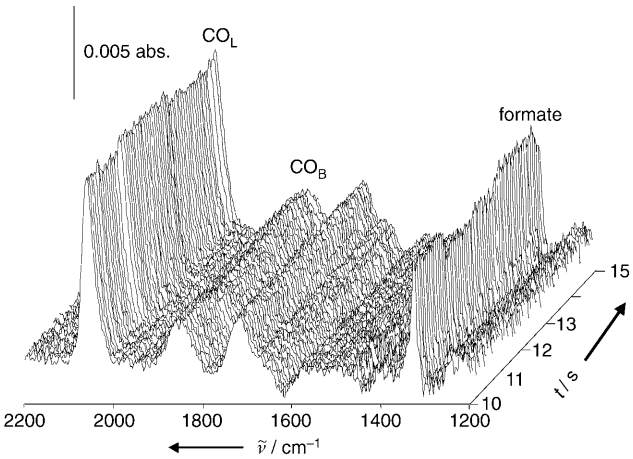


Figure 2. Time-resolved SEIRA spectra of the Pt electrode surface acquired during the current oscillations with a time resolution of 80 ms, which corresponds to the 10–15 s region in Figure 1a. A spectrum of the bare Pt surface collected at 0.05 V in the pure supporting electrolyte without formic acid was used as the reference.

 © 2005 Wiley-VCH Verlag GmbH & Co. KGaA, Weinheim

higher to lower, to the stretching modes of CO molecules adsorbed at atop and bridge sites (denoted as CO_L and CO_B, respectively) and to the symmetric OCO stretching mode of formate adsorbed in a bridging configuration (bonded through both oxygen atoms to two Pt surface atoms).[9a] The band at 1720 cm^{-1} corresponds to the C=O stretching mode of formic acid in the bulk solution and thus does not change its intensity. The peak position ($\tilde{\nu}$) of the CO_L band and the integrated intensities (I) of the CO_L and formate bands are plotted in Figure 1 b and c, respectively, as a function of time. The intensity data for CO_B are omitted owing to their negligibly small change. The temporal changes of the spectral features are synchronized with the current oscillations. The CO_L band increases in intensity and decreases in peak position when the current increases (and vice versa), while the change of the formate band intensity is the opposite.

It is well-known that the CO_L band shifts to higher frequencies as the electrode potential increases as a result of the Stark effect and/or electron back-donation from the metal to the $2\pi^*$ orbital of CO.[11] Note that the potential that determines the peak position of the CO vibration is not the externally applied potential E but the potential drop across the double layer, ϕ ($= E - iR$). The peak shift observed during the oscillations can be explained by the change in ϕ; by taking into account the total resistance of the system of 35 Ω (the external resistance of 30 Ω + the measured solution resistance of 5 Ω), ϕ is roughly estimated to be 0.6 and 0.8 V in the high- and low-current states ($i \approx 15$ and ≈ 10 mA), respectively. Consequently, the peak position of the CO_L band is shifted in association with the current oscillations. The global red-shift of the peak position can be ascribed to the gradual decrease of CO_L coverage (nearly proportional to the band intensity, Figure 1 c) through the changes in the dipole–dipole interaction among CO molecules and in the electron back-donation.[11,12]

The temporal changes of the band intensities of CO_L and formate can also be explained by the change of ϕ. The linear-sweep voltammogram shown in Figure 3 a (solid curve) was recorded in the same solution at a sweep rate of 50 mV s^{-1} without the external resistor and by correcting for the ohmic drop arising from the solution resistance (that is, $E = \phi$). The oxidation current is found to be higher at 0.6 than at 0.8 V, which is consistent with the current–time curve (Figure 1 a). Associated with the increase of the potential, the band intensity of CO_L decreases by oxidation and that of formate increases, which is also consistent with the spectral changes observed for the transient from the high-current state to the low-current state. A SEIRAS measurement for a potential step from 0.8 to 0.6 V, which corresponds to the reverse transient from the low-current to the high-current state, showed that the formate band intensity decreases quickly and the CO_L band intensity increases slowly.[13] The slow kinetics of CO formation explains the gradual decrease of the global CO band intensity during the oscillations (Figure 1 c).[14]

It is well-established that formic acid is decomposed to CO_2 through adsorbed formate on Pt in ultrahigh vacuum (UHV) and in the gas phase (CO is also produced by a side reaction).[15] Different from the reaction scheme under these conditions, COOH has long been assumed to be the reactive

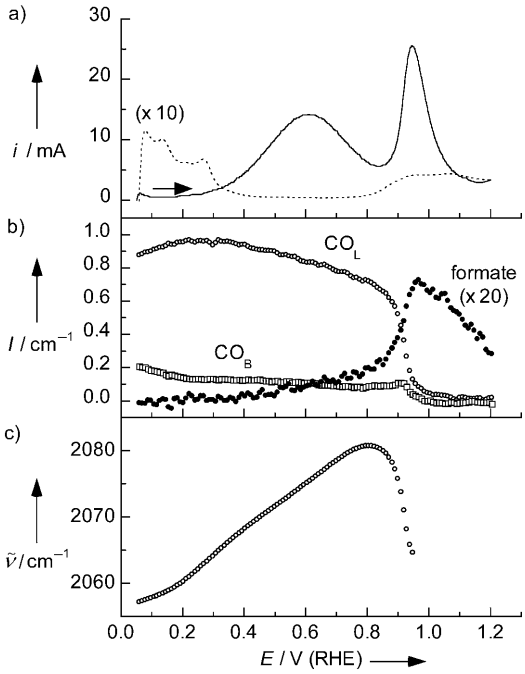


Figure 3. a) Linear-sweep voltammograms for the Pt electrode in 0.5 M H_2SO_4 with (——) and without (-----) 1 M HCOOH recorded at a sweep rate of 50 mV s^{-1} by correcting for ohmic drops. b) Integrated band intensities of CO_L, CO_B, and formate and c) peak position of CO_L plotted as a function of potential. The spectral data were taken from a series of SEIRA spectra acquired simultaneously with the solid-line voltammogram.

intermediate in the electrooxidation of formic acid without any clear experimental evidence. Despite the very high sensitivity of ATR-SEIRAS and very careful examinations, we could not detect any bands corresponding to this species. Instead we observed that formic acid is chemisorbed on the electrode as formate during the oxidation. Adsorbed formate has not been detected by IRAS, as a consequence of the limited mass transfer arising from the thin-layer geometry required for IRAS as discussed in our previous paper.[9b] As shown in Figure 3, the rapid oxidative removal of CO at $E >$ 0.8 V results in sharp increases of the formate band intensity and the oxidation current, which suggests that adsorbed formate is a reactive intermediate. With reference to the well-established reaction mechanism of formic acid oxidation in UHV and the gas phase, the electrooxidation scheme via adsorbed formate is very likely, and quite reasonable. Support for the oxidation via formate was obtained by a quick solution-exchange experiment (from $H^{13}COOH$ to $H^{12}COOH$, or the reverse) at a fixed potential of 0.6 V,[13] which showed that adsorbed formate species are completely replaced by those supplied from the solution within 1 s. The rate is fast enough to explain the observed current. An additional potential-step experiment from 1.5 V, where no carbonaceous species exist on the electrode surface, to 0.6 V showed that adsorption of formate is very fast and saturates within 80 ms (the time resolution used). Therefore, the decomposition of formate to CO_2 is believed to be the rate-determining step. However, isotopic substitution for adsorbed

 © 2005 Wiley-VCH Verlag GmbH & Co. KGaA, Weinheim

CO was negligibly slow and thus the indirect path scarcely contributes to formic acid oxidation.

Adsorbed CO can suppress the oxidation of formic acid by blocking vacant sites for formate adsorption. Consequently, the rapid oxidative removal of CO at $E > 0.8$ V leads to an increase of formate coverage and results in a sharp increase of the oxidation current (Figure 3). However, the situation is different in the potential range of 0.6–0.8 V where the current oscillations occur: the oxidation current decreases despite the decrease of CO and the increase of formate. This result indicates that the reaction rate (that is, current) is not a simple function of formate coverage. The suppression of the reaction at $0.6 < E < 0.8$ V, often termed as the negative differential resistance (NDR), plays a decisive role in the oscillation and has been discussed extensively in earlier studies.[2–4] Adsorbed OH species have generally been assumed to cause the NDR. For example, Strasser et al.[3g,4c] proposed that all CO species are oxidized in the NDR region and the adsorption of OH species at vacant sites generated by CO removal block the direct path via COOH formation. This proposal is, however, inconsistent with our data (Figure 3). In addition, the current arising from OH adsorption is not observed at $E < 0.8$ V in the pure supporting electrolyte (Figure 3, dashed curve). Even if the adsorption of OH species could be possible, it would be suppressed by the adsorption of formate.

A hint to help understand the NDR has been given by UHV studies of the decomposition of formate and acetate to CO_2 on transition-metal surfaces.[16] The rate of the decomposition is remarkably slowed down at high formate (or acetate) coverage (θ_f), and once the reaction is initiated the rate is increased *explosively*, which is called surface explosion.[16] The suppression of the reaction before the explosion has been explained by the adsorbed species themselves blocking each other's decomposition by steric hindrance.[16b,c] The necessity for the suppression is high *local* coverage (practically independent of the global coverage).[16b,c] This condition is likely to be fulfilled in the electrooxidation of formic acid, judging by the potential dependence of the CO_L vibrational frequency (Figure 3c). Recalling that the vibrational frequency is a function of both potential and coverage,[11,12] the linear potential dependence up to 0.8 V indicates that CO_L is oxidized without changing the dipole–dipole interactions. This result can be understood by assuming that CO is oxidized to form islands of vacant sites (that is, through a nucleation-and-growth mechanism) and formate is adsorbed at the generated vacant sites (by forming islands of formate).

The rate of decomposition of formate (or acetate) is given by the second-order rate equation (1) by modifying the original rate equation[16] to include CO coverage ($\theta_{CO} = \theta_{CO_L} + 2\,\theta_{CO_B}$).

$$-\frac{d\theta_f}{dt} = k\,\theta_f(1-2\,\theta_f-\theta_{CO}) \qquad (1)$$

The factor 2 of θ_f and θ_{CO_B} arises from the requirement of two vacant sites for the adsorption of these species. The θ_f dependence of the reaction rate is schematically shown in Figure 4 for low and high CO coverages. These plots show that the rate decreases with an increase of CO coverage and also with an increase of θ_f crossing $(1-\theta_{CO})/4$ (the coverage at which the reaction rate is maximal). Formate coverage

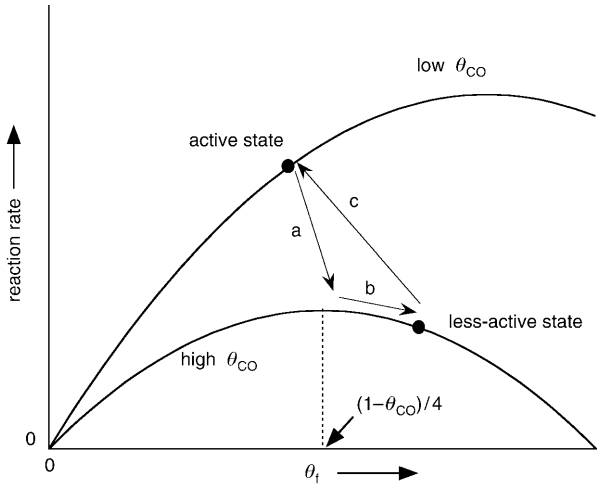


Figure 4. Schematic drawing of the formate coverage (θ_f) dependence of the reaction rate for high and low CO coverages (θ_{CO}) calculated by Equation (1).

increases almost linearly with the potential and CO coverage does not change significantly at $E < 0.8$ V (Figure 3). Therefore, the curves can be regarded as voltammograms by replacing θ_f coverage with potential, although the actual system is more complicated on account of the potential dependence of rate constants and the effect of the diffusion of formic acid.[4] The second-order rate equation (1) can reasonably explain the voltammmetric behavior in the low-potential region (that is, the current peak centered at 0.6 V and the NDR). By using this figure, the current oscillation can be explained as follows. Starting from the active (high-current) state, CO adsorption decreases the reaction rate (a), which results in an increase of ϕ and leads to an increase of formate coverage (b). The increase of formate coverage suppresses formate decomposition and increases ϕ further (that is, autocatalytically) to reach the less-active (low-current) state. Once ϕ reaches a certain high value, both CO oxidation and formate decomposition are accelerated, and the system is shifted to the initial active state (c).

Notably, Wojtowicz et al.[3b] proposed a nonlinear rate equation similar to Equation (1) to explain oscillations in the electrooxidation of formic acid, and they showed mathematically that such nonlinear rate equations are indispensable for oscillations, although the reaction mechanism assumed was totally different from that found herein. A mathematical analysis by the same procedure showed that sustained oscillations are possible in the framework of our new mechanism.[13]

In conclusion, we observed that formic acid is oxidized to CO_2 on Pt electrodes via adsorbed formate and that the decomposition of formate is rate-determining. The result forced us to revise earlier models of current oscillations to include adsorbed formate. The central part of the model proposed herein is that formate species suppress each other's

 © 2005 Wiley-VCH Verlag GmbH & Co. KGaA, Weinheim

decomposition. Adsorbed CO acts not only as a site-blocking species but also suppresses the decomposition of formate. Coupled with the change in ϕ, the oxidation and formation of CO modify the rate of formate decomposition and lead to current oscillations.

Received: March 19, 2005
Revised: June 6, 2005
Published online: August 1, 2005

Keywords: electrochemistry · formic acid · IR spectroscopy · oxidation · surface chemistry

[1] For example, see: U. F. Franck, *Angew. Chem.* **1978**, *90*, 1; *Angew. Chem. Int. Ed. Engl.* **1978**, *17*, 1.
[2] a) J. L. Hudson, T. T. Tsotsis, *Chem. Eng. Sci.* **1994**, *49*, 1493; b) M. T. M. Koper in *Advances in Chemical Physics*, *Vol. 92* (Eds.: I. Prigogine, S. A. Rice), Wiley, New York, **1996**, p. 161; K. Krischer in *Modern Aspects of Electrochemistry*, *Vol. 32* (Eds.: B. E. Conway, J. O. M. Bockris, R. E. White), Kluwer Academic/Plenum, New York, **1999**, p. 1.
[3] a) E. Müller, S. Tanaka, *Z. Elektrochem.* **1928**, *34*, 256; b) J. Wojtowicz, N. Marincic, B. E. Conway, *J. Chem. Phys.* **1968**, *48*, 4333; c) F. N. Albahadily, M. Schell, *J. Electroanal. Chem.* **1991**, *308*, 151; d) N. Markovic, P. N. Ross, *J. Phys. Chem.* **1993**, *97*, 9771; e) H. Okamoto, *Electrochim. Acta* **1992**, *37*, 37; f) F. Raspel, M. Eiswirth, *J. Phys. Chem.* **1994**, *98*, 7613; g) P. Strasser, M. Lübke, F. Raspel, M. Eiswirth, G. Ertl, *J. Chem. Phys.* **1997**, *107*, 979; h) T. J. Schmidt, B. N. Grgur, N. M. Markovic, P. N. Ross, *J. Electroanal. Chem.* **2001**, *500*, 36.
[4] a) M. T. M. Koper, J. H. Sluyters, *J. Electroanal. Chem.* **1994**, *371*, 149; b) H. Okamoto, *Chem. Phys. Lett.* **1996**, *248*, 289; c) P. Strasser, M. Eiswirth, G. Ertl, *J. Chem. Phys.* **1997**, *107*, 991.
[5] A. Capon, R. Parsons, *J. Electroanal. Chem.* **1973**, *45*, 205.
[6] a) K. Kunimatsu, H. Kita, *J. Electroanal. Chem.* **1987**, *218*, 155; b) D. S. Corrigan, M. J. Weaver, *J. Electroanal. Chem.* **1988**, *241*, 143.
[7] Y. Honda, M.-B. Song, M. Ito, *Chem. Phys. Lett.* **1997**, *273*, 141.
[8] a) M. Osawa, *Bull. Chem. Soc. Jpn.* **1997**, *70*, 2861; b) M. Osawa in *Vibrational Spectroscopy*, *Vol. 1* (Eds.: J. Charmers, P. R. Griffiths), Wiley, Chichester, **2002**, p. 785.
[9] a) A. Miki, S. Ye, M. Osawa, *Chem. Commun.* **2002**, 1500; b) A. Miki, S. Ye, T. Senzaki, M. Osawa, *J. Electroanal. Chem.* **2004**, *563*, 23.
[10] a) M. Osawa, K. Ataka, K. Yoshii, T. Yotsuyanagi, *J. Electron Spectrosc. Relat. Phenom.* **1993**, *64*/65, 371; b) K. Ataka, T. Yotsuyanagi, M. Osawa, *J. Phys. Chem.* **1996**, *100*, 10664.
[11] For example, see: R. J. Nichols in *Adsorption of Molecules at Metal Electrodes* (Eds.: J. Lipkowski, P. N. Ross), VCH, New York, **1992**, p. 347.
[12] F. M. Hoffmann, *Surf. Sci. Rep.* **1983**, *3*, 107.
[13] See the Supporting Information.
[14] The rate of CO formation decreases as the potential is increased or the oxidation overwhelms the adsorption at high potentials. Consequently, the slow growth of the CO_L band is not observed clearly in the high-current state where ϕ increases gradually with time. Nevertheless, it can lead to the long-term gradual decrease of the global CO_L band intensity.
[15] a) M. R. Columbia, A. M. Crabtree, P. A. Thiel, *J. Am. Chem. Soc.* **1992**, *114*, 1231; b) M. R. Columbia, P. A. Thiel, *J. Electroanal. Chem.* **1994**, *369*, 1.
[16] a) J. L. Falconer, R. J. Madix, *Surf. Sci.* **1974**, *46*, 473; b) T. J. Cassidy, M. D. Allen, Y. Li, M. Bowker, *Catal. Lett.* **1993**, *21*, 321; c) R. G. Sharpe, M. Bowker, *J. Phys. Condens. Matter* **1995**, *7*, 6379.

 © 2005 Wiley-VCH Verlag GmbH & Co. KGaA, Weinheim

Bioinorganic Chemistry

DOI: 10.1002/anie.200501157

Preparation of a Hydroperoxo Zinc(II) Intermediate**

*Akira Wada, Syuhei Yamaguchi, Koichiro Jitsukawa, and Hideki Masuda**

Among biological transition-metal ions, in many cases, a Zn^{II} ion serves as a Lewis acid without participating in an electron-transfer reaction. In the late 1960s, it was discovered that copper/zinc-containing proteins (copper zinc superoxide dismutase, CuZn SOD) were capable of catalyzing the disproportionation of a superoxide ion to give molecular oxygen and hydrogen peroxide. The mechanism is considered to progress by alternating reduction/oxidation of the copper atom at the active site (first step, $O_2^{\cdot-} + Cu^{II} \rightarrow O_2 + Cu^{I}$; second step, $Cu^{I} + O_2^{\cdot-} + 2H^{+} \rightarrow Cu^{II} + H_2O_2$).[1,2] As the crystal structure of CuZn SOD indicates an imidazolate-bridged heteronuclear Cu–Zn center at the active site,[3,4] many model complexes that include copper and/or zinc ions have been synthesized and studied to understand the mechanism of disproportionation of superoxide.[5,6] However, these studies have yielded a limited amount of useful information on the formation and physicochemical properties of a metal hydroperoxide intermediate that is suggested in the second step of the SOD reaction.[7]

We have previously synthesized a mononuclear copper(II) hydroperoxide complex by using a new ligand, bis[(6-pivalamido-2-pyridyl)methyl][(2-pyridyl)methyl]amine (H_2bppa).[8] Previous investigations have suggested that copper hydroperoxide complexes tend to decompose in air to generate highly toxic hydroxyl or hydroperoxyl radicals.[9,10] Such a copper hydroperoxide species appears to be unable to release H_2O_2 efficiently with the acceptance of a proton. Thus, it would be very significant to characterize a Zn–OOH species. There is no report for the preparation of a zinc(II) hydroperoxide complex hitherto, although the preparation of a zinc(II) alkylperoxide complex was reported recently.[11] Herein, we describe the preparation and characterization of a Zn^{II}–OOH species by using a tripodal pyridylamine ligand, bis[(6-neopentylamino-2-pyridyl)methyl][(2-pyridyl)methyl]-

[*] Dr. A. Wada, Dr. S. Yamaguchi, Prof. K. Jitsukawa, Prof. H. Masuda
Department of Applied Chemistry
Graduate School of Engineering
Nagoya Institute of Technology
Gokiso-cho, Showa-ku, Nagoya 466-8555 (Japan)
Fax: (+81) 52-735-5209
E-mail: masuda.hideki@nitech.ac.jp

[**] This work was supported partly by a Grant-in-Aid for Scientific Research from the Ministry of Education, Science, Sports, and Culture of Japan and supported in part by a grant from the NITECH 21st Century COE Program, to which our thanks are due.

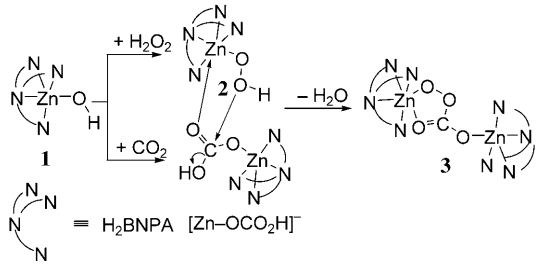
Supporting information for this article is available on the WWW under http://www.angewandte.org or from the author.

© 2005 Wiley-VCH Verlag GmbH & Co. KGaA, Weinheim

amine (H_2bnpa), and we compare the Zn complex with the corresponding Cu–OOH complex.

The initial mononuclear Zn^{II} hydroxide complex, [Zn(H_2bnpa)(OH)]$^+$ (**1**),[12] was prepared from the reaction of the ligand H_2bnpa with [Zn^{II}–OH]$^+$ in methanol/water. The crystal structure obtained from a single crystal of recrystallized **1**-ClO_4 revealed a trigonal-bipyramidally coordinated Zn^{II} with the hydroxide ion in an axial position (see Supporting Information).[12] The coordination of an hydroxide ion was also confirmed by the ^{1}H NMR spectrum of the product, which had a signal from the hydroxide hydrogen atom at 2.04 ppm (singlet) in [D_3]MeCN (see Supporting Information), and by the IR spectrum, which had ν(O-H) stretching vibration at $\bar{\nu} = 3626\ cm^{-1}$.

The reaction of **1** with H_2O_2 (approximately 20 equiv) in [D_3]MeCN solution at 20 °C gave new ^{1}H NMR signals characteristic of a trigonal-bipyramidal Zn^{II} complex, **2** (Scheme 1), which were accompanied by the disappearance



Scheme 1. Synthesis of **2** and **3** from **1**.

of the Zn–OH proton signal and appearance of a new singlet at 7.77 ppm. This signal falls within the range found for protons of HOO^- ions bound to metal centers that were reported previously.[13,14] The intensity of the singlet signal decreased with gradual addition of D_2O ($\approx 6\ \mu L$). Furthermore, upon treatment with D_2O_2, the signal at 7.77 ppm was not detected, although signals associated with the H_2bnpa ligand of **2** were obtained. Thus, these observations allow us to assign the proton signal as a resonance derived from a hydroperoxide ion coordinated to the zinc complex.

The formation of the Zn–OOH species was also monitored by ESI mass spectrometry (see Supporting Information). A solution of **1** in MeCN treated with $H_2{}^{16}O_2$ or $H_2{}^{18}O_2$ afforded prominent positive-ion peak clusters at *m*/*z* 557 or 561, respectively. These observed masses and isotope patterns correspond to the [Zn(H_2bnpa)($^{16}O_2$H)]$^+$ and [Zn(H_2bnpa)($^{18}O_2$H)]$^+$ ions. With D_2O_2 instead of H_2O_2, the peak at *m*/*z* 557 shifts to 560, which suggests that [Zn(D_2bnpa)(O_2D)]$^+$ is generated. These spectroscopic data provide strong evidence for the formation of a mononuclear Zn^{II} hydroperoxide complex, [Zn(H_2bnpa)(OOH)]$^+$ (**2**), in solution. The robust ligation of the hydroperoxide ion to Zn^{II} appears to be stabilized by hydrogen-bonding interactions between the amino hydrogen atoms of **2** and a hydroperoxo oxygen atom. This hydrogen-bonding interaction is confirmed by a larger down-field shift ($\delta = 4.43$ ppm) of the amine proton signals relative to that of free ligand H_2bnpa.

At this stage, it is very important to examine which of the metal hydroperoxide species has higher basicity, Zn^{II}–OOH or Cu^{II}–OOH, because in the second step of the CuZn SOD mechanism, efficient protonation of the hydroperoxide ion is required for rapid liberation of H_2O_2.[3,4,7] To investigate the nucleophilicity/basicity of mononuclear hydroperoxo complexes of Zn^{II} and Cu^{II}, the reaction with CO_2 was carried out according to previously reported procedures.[15] Bubbling CO_2 into an acetonitrile solution of **1** treated with H_2O_2 produced an ESI mass spectrum with a new peak cluster at *m*/*z* 564, whose isotope pattern corresponds to [{Zn(H_2bnpa)}$_2$-(CO_4^{2-})]$^{2+}$ (**3**). Compound **1** reacts with CO_2 to form a species containing {Zn–OCO_2H}$^-$;[16] the resulting change in the ESI spectra (see Supporting Information) implies that the {Zn^{II}–OCO_2H}$^-$ species once formed immediately reacts with the generated peroxide complex **2**, followed by release of water to afford the stable dinuclear zinc complex **3** (see Scheme 1). The formation of **3** observed under very low concentrations of CO_2 is ascribed to an extraordinary high nucleophilicity/basicity of a hydroperoxide ion bound to a Zn^{II} center.

A colorless single crystal of **3**-2ClO_4 suitable for X-ray diffraction analysis was obtained from a THF/Et_2O solution of **2** kept at 0 °C under atmospheric CO_2. As shown in Figure 1, the crystal structure of **3** indicates that the peroxy-

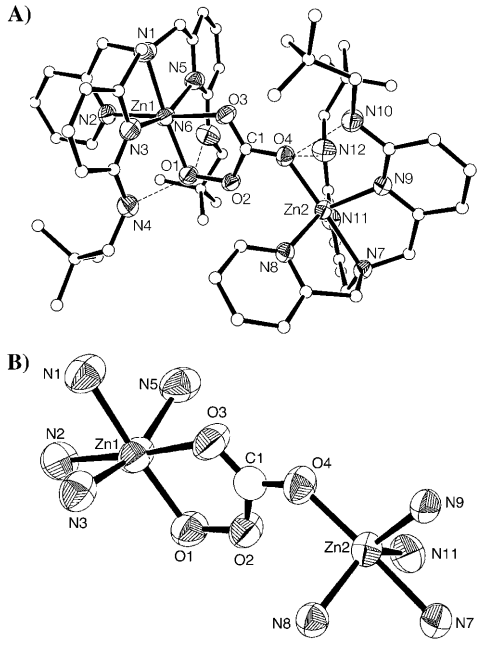


Figure 1. A) ORTEP view of the structure of **3**; thermal ellipsoids are set at the 30% level of probability. B) ORTEP view of the [ZnOO-C(O)OZn]$^{2+}$ core in **3**; hydrogen atoms, counteranions, and solvent molecules are omitted for clarity; thermal ellipsoids are set at the 30% level of probability. Selected bond lengths [Å] and angles [°]: Zn1-N1 2.139(6), Zn1-N2 2.144(5), Zn1-N3 2.213(7), Zn1-N5 2.210(7), Zn1-O1 2.002(4), Zn1-O3 2.111(4), Zn2-N7 2.148(4), Zn2-N8 2.081(5), Zn2-N9 2.084(5), Zn2-N11 2.092(5), Zn2-O4 1.987(4), C1-O2 1.320(7), C1-O3 1.212(7), C1-O4 1.290(6), O1-O2 1.474(5); O1-O2-C1 114.6(4), O2-C1-O3 123.1(5), O2-C1-O4 112.7(5), O3-C1-O4 124.1(6). Hydrogen bonding interactions are observed for O1···N4 (2.928 Å), O1···N6 (2.954 Å), O4···N10 (2.884 Å), and O4···N12 (3.004 Å).

 © 2005 Wiley-VCH Verlag GmbH & Co. KGaA, Weinheim

carbonate ion bridges the Zn1 and Zn2 sites, whose coordination environments are distorted octahedral and trigonal-bipyramidal, respectively, in a μ-η^1:η^2 fashion. The two exchangeable coordination sites of the Zn1 center are occupied by the peroxide and carbonyl oxygen atoms of the peroxycarbonate ion in a bidentate fashion with Zn1–O1 and Zn1–O3 bond lengths of 2.002(4) and 2.111(4) Å, respectively, and a O2-C1-O3 angle of 123.1(5)°. The remaining carboxylate oxygen atom of the peroxycarbonate ion is coordinated to the Zn2 site with a Zn2–O4 bond length of 1.987(4) Å.

The O1–O2 bond length is 1.474(5) Å, which is within the range for known metal alkylperoxide complexes (1.36–1.52 Å) and close to that of H_2O_2 (1.49 Å).[17] This bond is slightly longer than those of the previously reported peroxycarbonate metal complexes, $KH(O_2C(O)O)\cdot H_2O_2$ (1.457(2) Å)[18] and $Ph_4P[Fe(quinaldate)_2(O_2C(O)O)]\cdot 1.5\,CH_3OH\cdot 0.5\,(CH_3)_2NCHO$ (1.455(5) Å),[19] which suggests that the peroxy oxygen atoms of the peroxycarbonate ion are derived from hydroperoxide bonded to **2**. For the shortest bond of the peroxycarbonate ligand, C1–O2 (1.320(7) Å) compared with C1–O3 (1.212(7) Å) and C1–O4 (1.290(6) Å), some double-bond character can be assumed. Moreover, as demonstrated by ^{1}H NMR spectroscopic analysis for **2**, the two amine hydrogen atoms stabilize the binding of the peroxycarbonate ion, which is also evidenced by the hydrogen-bond lengths (2.928(8), 2.954(8), 2.884(7), and 3.004(8) Å; see Figure 1). This structure determination is the first of a dinuclear zinc(II) complex with a peroxycarbonate ion in μ-η^1:η^2-coordination mode.

The behavior described above suggests that the hydroperoxo group of complex **2** is nucleophilic towards CO_2. Next, we examined the reactivity of the corresponding Cu^{II} complex with H_2bnpa to compare the nucleophilicity/basicity of the Cu–OOH and Zn–OOH species. However, both $[Cu(H_2bnpa)(OOH)]^+$ and the previously reported complex $[Cu(H_2bppa)(OOH)]^+$ did not show such a nucleophilic reactivity,[8] although the carbonate complex is also generated by the reaction of Cu–OH(H_2bnpa/H_2BPPA) with CO_2. This result suggests lower nucleophilicity/basicity of a hydroperoxide ion bound to Cu^{II}, which is reasonably interpreted in terms of the decrease in electron density on the hydroperoxide oxygen atom due to its stronger binding to Cu^{II} than to Zn^{II}. Thus, only hydroperoxide bound to Zn^{II} may be sufficiently nucleophilic/basic to attract electrophilic molecules such as CO_2.

In summary, we have described the generation, spectroscopic characterization, and reactivity of a novel mononuclear Zn^{II} hydroperoxide intermediate. We have also performed the first X-ray crystallographic characterization of a dinuclear zinc peroxycarbonate complex. A comparison of the electronic and structural properties of the hydroperoxo complexes of Zn^{II} and Cu^{II} may indicate the role of Zn^{II} in the second step of the catalytic cycle of CuZn SOD.

Experimental Section

General: All reagents and solvents were obtained from commercial sources and were used as received unless otherwise noted.

Caution! The perchlorate salts used in this study are all potentially explosive and should be handled with care.

Preparation of **1**-ClO_4: A solution (pH 6.5–7, 300 mL) containing {Zn(OH)} species was prepared by mixing $Zn(ClO_4)_2\cdot 6H_2O$ (178.8 mg, 0.48 mmol) and KOH in methanol/water (1:1). A solution of H_2bnpa (184.3 mg, 0.4 mmol) in a mixture of methanol and water (1:1, 80 mL) was added dropwise to the reaction mixture at room temperature. After 30 min, the solvent was removed in vacuo to leave a white powder. Recrystallization from methanol at 25 °C afforded colorless crystals of $[Zn(H_2bnpa)(OH)]ClO_4$ (0.19 g, 74% yield) suitable for X-ray diffraction measurements (the structure of **1**-ClO_4 is the same as that reported previously, see Supporting Information).[12b]). ^{1}H NMR: see Supporting Information. Elemental analysis (%) calcd for $C_{28}H_{41}N_6O_5ZnCl$: C 52.34, H 6.43, N 13.08; found: C 52.40, H 6.43, N 13.10. MS (ESI) m/z: 541 $[Zn(H_2bnpa)(OH)]^+$.

Preparation of **3**-$(ClO_4)_2$: The treatment of **1** (12.8 mg, 20 μmol) with H_2O_2 in MeCN (0.4 mL) afforded a solution containing **2**. CO_2 dissolved in THF (0.1 mL) was added dropwise to this solution at 0 °C. Crystallization from MeCN/THF/Et_2O in air gave colorless crystals of $[\{Zn(H_2bnpa)\}_2(CO_4)](ClO_4)_2\cdot(CH_3CH_2)_2O\cdot CH_3CN$ (2.63 mg, 38% yield). Elemental analysis (%) calcd for $C_{63}H_{93}N_{13}O_{13}Zn_2Cl_2$: C 52.46, H 6.49, N 12.62; found: C 52.54, H 6.21, N 12.44. MS (ESI): m/z: 564 $[\{Zn(H_2bnpa)\}_2(CO_4)]^{2+}$, 1227 $[\{Zn(H_2bnpa)\}_2(CO_4)(ClO_4)]^+$. ^{13}C NMR (100 MHz, [D$_3$]MeCN, 25 °C, TMS): δ = 207.8 ppm (s, OC(O)OO).

Preparation of $[Cu(H_2bnpa)(OOH)]^+$: The treatment of $Cu(ClO_4)_2\cdot 6H_2O$ (148.2 mg, 0.4 mmol) with H_2bnpa (184.3 mg, 0.4 mmol) and KOH (22.4 mg, 0.4 mmol) in MeCN (0.4 mL) afforded a solution containing $[Cu(H_2bnpa)(OH)]^+$. H_2O_2 (4.0 mmol) was added dropwise to the solution of $[Cu(H_2bnpa)(OH)]^+$ at −40 °C. The mononuclear hydroperoxo copper(II) complex $[Cu(H_2bnpa)(OOH)]^+$ was characterized spectroscopically. UV/Vis (MeCN): λ_{max} = 380 nm (hydroperoxide-to-copper(II) charge transfer transition); ESR: $g_\perp$ = 2.22, $g_\parallel$ = 2.00, $|A_\perp|$ = 94 G, $|A_\parallel|$ = 100 G at 77 K; ESI MS: m/z: 556 $[Cu(H_2bnpa)(^{16}O_2H)]^+$, 560 $[Cu(H_2bnpa)(^{18}O_2H)]^+$; resonance Raman spectra: $\tilde{\nu}$ = 847, 800 cm^{-1} ($\nu(^{18}O\text{-}^{18}O)$); see Supporting Information.

X-ray crystal-structure analysis of **3**-$(ClO_4)_2$: A colorless single crystal suitable for X-ray structure analysis was obtained from a THF/Et_2O solution. Crystal data: $C_{61}H_{90}N_{12}O_{13}Cl_2Zn_2$, M_r = 1401.12, triclinic, space group $P\bar{1}$ (no. 2), a = 13.355(2), b = 26.039(5), c = 10.785(3) Å, α = 101.72(2), β = 98.93(2), γ = 75.39(1)°, V = 3510.5(7) Å^3, Z = 2, ρ_{calcd} = 1.325 g cm^{-3}, μ = 8.26 cm^{-1}, $Mo_{K\alpha}$ radiation (λ = 0.71070 Å), T = 173 K, R_1 = 0.059, R_w = 0.084. CCDC-267192 contains the supplementary crystallographic data for this paper. These data can be obtained free of charge from the Cambridge Crystallographic Data Centre via www.ccdc.cam.ac.uk/data_request/cif.

Received: April 1, 2005
Revised: June 13, 2005
Published online: August 1, 2005

Keywords: mass spectrometry · peroxides · peroxo ligands · tripodal ligands · zinc

[1] J. M. McCord, I. Fridovich, *J. Biol. Chem.* **1969**, *244*, 6049.
[2] D. Klug-Roth, I. Fridovich, J. Rabani, *J. Am. Chem. Soc.* **1973**, *95*, 2786.
[3] J. A. Tainer, E. D. Getzoff, J. S. Richardson, D. C. Richardson, *Nature* **1983**, *306*, 284.
[4] P. J. Hart, M. M. Balbirnie, N. L. Ogihara, A. M. Nersissian, M. S. Weiss, J. S. Valentine, D. Eisenberg, *Biochemistry* **1999**, *38*, 2167, and references therein.

 © 2005 Wiley-VCH Verlag GmbH & Co. KGaA, Weinheim

[5] H. Ohtsu, Y. Shimazaki, A. Odani, O. Yamauchi, W. Mori, S. Itoh, S. Fukuzumi, *J. Am. Chem. Soc.* **2000**, *122*, 5733, and references therein.
[6] J.-L. Pierre, P. Chautemps, S. Refaif, C. Beguin, A. E. Marzouki, G. Serratrice, E. Saint-Aman, P. Rey, *J. Am. Chem. Soc.* **1995**, *117*, 1965.
[7] J. A. Fee, R. L. Ward, *Biochem. Biophys. Res. Commun.* **1976**, *71*, 427.
[8] A. Wada, M. Harata, K. Hasegawa, K. Jitsukawa, H. Masuda, M. Mukai, T. Kitagawa, H. Einaga, *Angew. Chem.* **1998**, *100*, 874; *Angew. Chem. Int. Ed.* **1998**, *37*, 798.
[9] E. K. Hodgson, I. Fridovich, *Biochemistry* **1975**, *14*, 5294.
[10] D. T. Sawyer, J. S. Valentine, *Acc. Chem. Res.* **1981**, *14*, 393, and references therein.
[11] a) J. Lewiński, Z. Ochal, E. Bojarski, E. Tratkiewicz, I. Justyniak, J. Lipkowski, *Angew. Chem.* **2003**, *115*, 4791; *Angew. Chem. Int. Ed.* **2003**, *42*, 4643; b) L. Lewiński, W. Marciniak, J. Lipkowski, I. Justyniak, *J. Am. Chem. Soc.* **2003**, *125*, 12698.
[12] a) H. Masuda, I. Tokairin, K. Jitsukawa, H. Einaga, *J. Inorg. Biochem.* **1999**, *74*, 225; b) J. C. Mareque-Rivas, R. Prabaharan, S. Parsons, *Dalton Trans.* **2004**, 1648.
[13] D. D. Wick, K. I. Goldberg, *J. Am. Chem. Soc.* **1999**, *121*, 11900.
[14] M. Akita, T. Miyaji, S. Hikichi, Y. Moro-oka, *Chem. Lett.* **1999**, 813.
[15] D. A. Palmer, R. van Eldik, *Chem. Rev.* **1983**, *83*, 651.
[16] S. Yamaguchi, I. Tokairin, Y. Wakita, Y. Funahashi, K. Jitsukawa, H. Masuda, *Chem. Lett.* **2003**, *32*, 406.
[17] O. Bain, P. A. Giguére, *Can. J. Chem.* **1955**, *33*, 527.
[18] A. Adam, M. Mehta, *Angew. Chem.* **1988**, *100*, 1457; *Angew. Chem. Int. Ed.* **1988**, *37*, 1387.
[19] K. Hashimoto, S. Nagatomo, S. Fujinami, H. Furutachi, S. Ogo, M. Suzuki, A. Uehara, Y. Maeda, Y. Watanabe, T. Kitagawa, *Angew. Chem.* **2002**, *114*, 1250; *Angew. Chem. Int. Ed.* **2002**, *41*, 1202.

 © 2005 Wiley-VCH Verlag GmbH & Co. KGaA, Weinheim

Electron Transfer

DOI: 10.1002/anie.200501714

Redox Control of Light-Induced Platinum-Cluster-to-Iron Charge Transfer in a Bis(ferrocenylethynyl)-Substituted Hexanuclear Platinum Derivative**

Alberto Albinati, Fabrizia Fabrizi de Biani, Piero Leoni, Lorella Marchetti, Marco Pasquali, Silvia Rizzato, and Piero Zanello**

Placing equivalent redox-active groups as end-caps in molecular arrays is often used to evaluate whether intramolecular electronic communication occurs through organic[1] or metal-containing fragments.[2–9] To this end, ferrocenyl (Fc = [(η-C_5H_5)Fe(η-C_5H_4)]) pendant groups (often as ferrocenylethynyl termini),[3–5] are commonly used because of their chemical robustness, synthetic versatility, and reversible redox properties. They have been attached to mono-[2,3,6,10] or dinuclear[4,7] organometallic and coordination compounds. However examples of metal clusters capped by equivalent ferrocenyl groups are rare. To our knowledge, structurally characterized examples are limited[8a] to the following compounds: $[Mo_6Cl_8(O_2C{-}Fc)_6]^{2-}$, which contains an octahedral core of Mo^{II} centers $\{Mo_6Cl_8\}^{4+}$,[9a] $[Ru_3(CO)_7(\mu_2\text{-S-Fc})_4]$,[9b] $[Cu_3(dppm)_3(\mu_3\text{-}\eta^1\text{-}C{\equiv}C{-}Fc)_2]^+$, (dppm = methylenebis-[(diphenyl)phosphine]) with two terminal (Fc-C≡C)$^-$ groups bridging the opposite sides of a triangular Cu^I_3 core in an μ_3-η^1 fashion,[5a] $[M_6(\mu\text{-dppm})_2(\mu_3\text{-}\eta^1\text{-}C{\equiv}C{-}Fc)_4(L)_2]X_2$ (M = Ag, L = CH_3OH, X = BF_4; M = Cu, L = none, X = ClO_4)[5b] and $[Pt_2Au(dppm)_2X(\eta^1\text{-}C{\equiv}C{-}Fc)_2]$.[4a] Electron transfer from, to, or across the cluster-containing spacer, triggered by external stimuli, would make these units promising candidates for the preparation of connector elements in nanoscale switchable molecular devices.[11] Indeed, the utilization of carbonyl

[*] Prof. P. Leoni, Dr. L. Marchetti, Prof. M. Pasquali
Dipartimento di Chimica e Chimica Industriale
Università di Pisa
Via Risorgimento 35, 56126 Pisa (Italy)
Fax: (+39) 050-2219246
E-mail: leoni@dcci.unipi.it
Dr. F. Fabrizi de Biani, Prof. P. Zanello
Dipartimento di Chimica dell'Università di Siena
Via A. Moro, 53100 Siena (Italy)
Fax: (+39) 0577-234254
E-mail: zanello@unisi.it
Prof. A. Albinati, Dr. S. Rizzato
Dipartimento di Chimica Strutturale e Stereochimica Inorganica (DCSSI)
Università di Milano
Via Venezian 21, 20133 Milano (Italy)

[**] A.A., P.L., and P.Z. gratefully acknowledge the financial support from Ministero dell'Istruzione, dell'Università e della Ricerca (PRIN 2003).

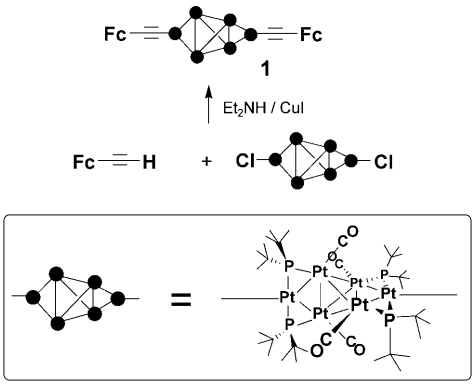
Supporting information for this article is available on the WWW under http://www.angewandte.org or from the author.

 © 2005 Wiley-VCH Verlag GmbH & Co. KGaA, Weinheim

clusters as single-electron tunneling transistors has been reported,[12a] and their employment as molecular capacitors[12b] is also under scrutiny. However, well-documented examples of electron transfer in molecular frameworks containing cluster subunits are exceedingly rare; in all the above-mentioned compounds the metal-cluster spacers do not allow significant electronic communication between the ferrocene units. However, in those derivatives containing one or two ferrocenyl units linked to a hexamolybdate spacer, through π-conjugated arms, a photoinduced charge transfer from the Fc to the polyoxometalate unit was observed,[13] while in a derivative containing a Os_3 core bonded to a viologen-containing acceptor, a photoinduced charge transfer from the triosmium cluster to the acceptor ligand was observed.[11]

Herein, we report the synthesis and structural characterization of $[Pt_6(\mu\text{-}P\textit{t}Bu_2)_4(CO)_4(C{\equiv}C{-}Fc)_2]$ (**1**), in which the hexaplatinum core $[Pt_6(\mu\text{-}P\textit{t}Bu_2)_4(CO)_4]^{2+}$ (hereafter $\{Pt_6\}$) is capped by two ferrocenylethynyl groups, and the results of an electrochemical and spectroelectrochemical study, which shows the presence of photo-electrochemically triggered electron transfer from the $\{Pt_6\}$ core to the peripheral Fc subunits. To our knowledge, this is the first example in which a metallic cluster behaves as electron donor towards a ferrocenium acceptor.

The disubstituted complex **1** was easily prepared from its dichloride precursor $\{Pt_6\}Cl_2$[14] (Scheme 1) and was isolated



Scheme 1. Synthesis of complex **1**.

as a red microcrystalline solid which yielded X-ray quality crystals upon recrystallization from $CHCl_3$ (Figure 1).[15] The structure shows that **1** retains the main structural features which are quite rare for other hexanuclear clusters and that we have found in closely related derivatives.[14,16] The structure consists of a slightly distorted tetrahedral platinum cluster capped, on each of two opposite edges, by a platinum atom linked to a terminally bonded (σ, η^1) ferrocenylethynyl moiety (other possible (π) bonding modes of the alkynyl units are hindered by the bulky phosphido ligands).[16] The ferrocenyl units lie on opposite sides of the plane defined by atoms Pt1, Pt2, Pt3, and Pt6 (Figure 1). Moreover the C_5 ring Cp1–Cp5 is approximately coplanar with the Pt1-Pt2-Pt3 plane (dihedral angle 172(1)°), while the other ethynyl-bound

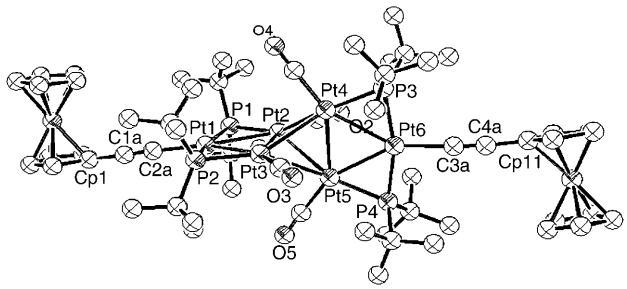


Figure 1. ORTEP view of compound **1**. Thermal ellipsoids set at 50% probability. Selected bond lengths [Å] and angles [°]: Pt1-Pt2 2.7196(5), Pt1-Pt3 2.7196(5), Pt4-Pt6 2.7389(6), Pt5-Pt6 2.7287(5), Pt2-Pt3 2.6875(6), Pt2-Pt5 2.8380(6), Pt2-Pt4 2.8389(5), Pt3-Pt4 2.8421(5), Pt3-Pt5 2.8440(6), Pt4-Pt5 2.6734(5); Pt1-C2a-C1a 178(1), Pt6-C3a-C4a 178(1), C2a-C1a-Cp1 176(1), C3a-C4a-Cp11 173(1).

C_5 ring (Cp11–Cp15) is almost perpendicular to the P4-Pt5-Pt6 plane (dihedral angle 102(2)°).

The structure of **1** is retained in solution, as confirmed by IR and NMR spectra, which show diagnostic signals at the expected positions (IR: $\tilde{\nu} = 2126, 2106$ (ν_{CC}), 2009 (ν_{CO}) cm^{-1}; ^{31}P NMR: $\delta = 333.6$ ppm; ^{195}Pt NMR: $\delta = -4663$ (2 Pt), -2997 ppm (4 Pt)).[14,16]

In CH_2Cl_2 solution the platinum cluster undergoes three reversible, and coulometrically measured, redox processes (Table 1): two slightly separated one-electron reductions

Table 1: Formal electrode potentials (V, vs. SCE) for the redox changes exhibited by $[Pt_6(\mu\text{-}P\textit{t}Bu_2)_4(CO)_4(\eta^1\text{-}C{\equiv}C{-}Fc)_2]$ and related species in CH_2Cl_2.

Compound	$\{Pt_6\}$-centered ox.	Fc-centered ox.	$\{Pt_6\}$-centered red.	
1	+1.26[a,b]	+0.30[a]	−1.50	−1.64
$[Pt_6(P\textit{t}Bu_2)_4(CO)_4(C_2Ph)_2]$[c]	+1.05[a,b]		−1.45	−1.54
Fc-C≡CH[d]		+0.52		

[a] Two-electron process. [b] Peak-potential for irreversible processes. [c] Ref. [18]. [d] Ref. [20].

($E^{\circ\prime} = -1.50$ V and -1.64 V versus saturated calomel electrode (SCE)) and one two-electron oxidation ($E^{\circ\prime} = +0.30$ V).[17] A further, apparently irreversible, two-electron oxidation is also present ($E_p = +1.26$ V) (see Supporting Information).

On the basis of the redox behavior of the parent dication $[\{Pt_6\}(CO)_2]^{2+}$ and its substituted product $[\{Pt_6\}(C_2Ph)_2]$[16b,18] both the two one-electron reductions and the irreversible oxidation are assigned as $\{Pt_6\}$ centered. The reversible two-electron removal event can be reliably assigned to the simultaneous one-electron oxidation of each of the two ferrocenyl units. This simultaneous process does not split into two separated one-electron events, even when a very low-coordinating electrolyte (e.g. $[NBu_4][B(C_6F_5)_4]$) is used.[19] This observation confirms that no electronic (through-space or through-bond) communication between the two ferrocenyl units is allowed by the $\{Pt_6\}$ spacer. The more anodic (irreversible) two-electron oxidation takes place at a potential

 © 2005 Wiley-VCH Verlag GmbH & Co. KGaA, Weinheim

approximately 200 mV more positive than in the parent complex $[Pt_6(\mu\text{-}PtBu_2)_4(CO)_4(C_2Ph)_2]$. At the same time, the ferrocenyl-centered oxidations occur at a potential approximately 200 mV less positive than in free acetylferrocene.[20] These redox shifts suggest that the acetilyde bridging ligands exert cooperative electronic effects inside the molecular frame.[21]

As shown in Figure 2, the most significant spectroelectrochemical change upon stepwise two-electron oxidation of

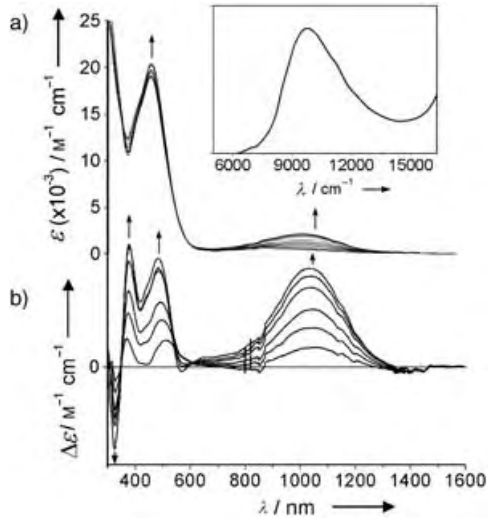


Figure 2. a) UV/Vis/NIR spectra and b) difference spectra recorded upon stepwise oxidation of **1** in an OTTLE cell, CH_2Cl_2/$[NBu_4][PF_6]$ (0.2 mol dm^{-3}) solution. Arrows indicate the change on oxidation. Inset: NIR band in (a) replotted in cm^{-1} to show the asymmetry of this band.

complex **1** is the progressive appearance of a broad band in the NIR region ($\lambda = 1025$ nm; $\varepsilon = 2.1 \times 10^3$ M^{-1} cm^{-1}). Upon exhaustive two-electron oxidation, the UV/Vis region of the spectrum does not change and does not exhibit the typical blue-to-green ferrocenium absorption ($\lambda = 698$ nm for $[FcCCH]^+$)[20]; the solution remains cherry-red. In the stepwise oxidation, the NIR band keeps growing and does not change position or shape even upon removal of the second electron. Such behavior suggests consecutive metal-to-metal charge transfers (MMCT) from the Pt_6 cluster to the peripheral ferrocenium subunits [Eq. (1) and Eq. (2)]

$$\overset{+}{Fc}\text{-}C{\equiv}C\text{-}\{Pt_6\}\text{-}C{\equiv}C{-}Fc \xrightarrow{h\nu} Fc\text{-}C{\equiv}C\text{-}\{\overset{+}{Pt_6}\}\text{-}C{\equiv}C\text{-}Fe \quad (1)$$

$$\overset{+}{Fc}\text{-}C{\equiv}C\text{-}\{Pt_6\}\text{-}C{\equiv}C\text{-}\overset{+}{Fc} \xrightarrow{h\nu} Fc\text{-}C{\equiv}C\text{-}\{\overset{2+}{Pt_6}\}\text{-}C{\equiv}C{-}Fc \quad (2)$$

Our preliminary observations show that a band at the same position in the NIR develops upon one-electron oxidation of the corresponding monoferrocenyl complex $[\{Pt_6\}(C{\equiv}C{-}Fc)I]$,[22] giving further support to the assumption that this absorption cannot arise from the interaction between the two ferrocene subunits.

We attempted to check the solvent dependence of the NIR band, but our efforts were frustrated by the impossibility of finding different useful solvents and the pertinent supporting electrolytes. Nevertheless, the change of the supporting electrolyte from $[NBu_4][PF_6]$ to the low-coordinating $[NBu_4][B(C_6F_5)_4]$ maintained unchanged the high-energy bands, but causes a red shift ($\lambda = 1108$ nm) of the low-energy band, thus confirming the sensitivity of the actual absorption to the medium, as expected for a MMCT intervalence transfer (IT) absorption.

As can be seen in the inset of Figure 2, when the spectrum is plotted in cm^{-1}, the asymmetry of the MMCT band becomes evident. Indeed, such a cut-off on the low-energy side of IT absorptions is predicted in the case of sizeable electronic coupling between the states involved in the electron transfer (although different factors, such as vibronic progressions or band overlaps, can cause asymmetry of IT bands).[23]

According to the Hush treatment of dinuclear asymmetric derivatives,[24] the limiting value[25] of the bandwidth at half height ($\Delta\bar{\nu}_{1/2}$) for the IT band of a partially delocalized mixed-valent species is theoretically expected to be given by Equation (3) where the free-energy difference between the initial and the final state after the electron transition, $\Delta G°$, is usually approximated as the separation $\Delta E°$ of the redox potentials of the processes centered on the isolated units involved in the electron transfer. Significantly narrower IT absorptions are expected for a completely delocalized mixed-valent species.

$$\Delta\bar{\nu}_{1/2} = 48\,(\bar{\nu}_{max} - \Delta G^o)^{1/2} \quad (3)$$

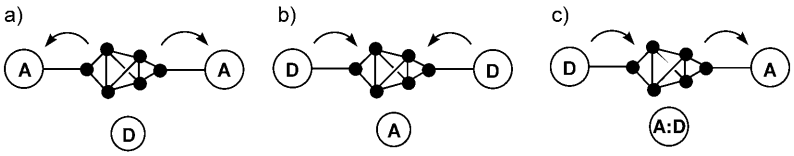
On placing the values in Equation (3) it follows that $\Delta\bar{\nu}_{1/2}$ in the present case is given by Equation (4) where $\Delta G° \approx \Delta E° = 4195$ cm^{-1} has been calculated on the basis of the formal electrode potentials of $[\{Pt_6\}(C{\equiv}C\text{-}Ph)_2]^{2+/0}$ and $[HC{\equiv}C{-}Fc]^{+/0}$.[18,20]

$$\Delta\bar{\nu}_{1/2\,theoretical} = 48(9760-4195)^{1/2} = 3580\,cm^{-1} \quad (4)$$

The experimental bandwidth, taken as twice the difference between the band maximum and the half-height point on the high-energy side, is $\Delta\bar{\nu}_{1/2\,experimental} = 4470$ cm^{-1}, which is much larger than the theoretical limiting value of 3580 cm^{-1}. This result suggests that both the singly and doubly oxidized species (the monocation and the dication) can be regarded as valence-trapped systems.

As a final consideration, we underline that compounds that can absorb light in the NIR region may, in principle, be used in optical data-storage devices that are able to read and write through proper diode lasers (that is, operating in the NIR region of the spectrum),[26] in particular when the NIR absorption can be triggered by external perturbations. Even though the intensity of the present NIR transition is too weak[26] for practical applications in data-storage devices, these compounds offer the appealing possibility of easily tuning both the redox capacity of the attached ferrocenyl units and the resulting MMCT NIR absorption. Moreover, the ability of the $\{Pt_6\}$ unit to be both oxidized and reduced[14a] suggests the possibility of building systems in which, based on the proper calibration of redox potentials of the end-cap

 © 2005 Wiley-VCH Verlag GmbH & Co. KGaA, Weinheim



Scheme 2. Electron transfer from (a), to (b), or across (c) the $\{Pt_6\}$ cluster unit. See text for details.

donor (D) and/or acceptor (A) units, the electron transfer might be driven through the different paths illustrated in Scheme 2.

Received: May 18, 2005
Published online: August 4, 2005

Keywords: alkynyl ligands · cluster compounds · electron transfer · ferrocenes · platinum

[1] a) A. Tarraga, P. Molina, D. Curiel, M. D. Velasco, *Organometallics* **2001**, *20*, 2145–2152; b) C. Patou, C. Coudret, J.-P. Launay, C. Joachim, A. Gourdon, *Inorg. Chem.* **1997**, *36*, 5037–5049.

[2] a) J. Jiao, G. J. Long, F. Grandjean, A. M. Beatty, T. P. Fehlner, *J. Am. Chem. Soc.* **2003**, *125*, 7522–7523; b) M. Tanabe, M. Horie, K. Osakada, *Organometallics* **2003**, *22*, 373–376; c) J. A. Mata, E. Peris, R. Llusar, S. Uriel, M. P. Cifuentes, M. G. Humphrey, M. Samoc, B. Luther-Davies, *Eur. J. Inorg. Chem.* **2001**, 2113–2122; d) O. Clot, M. O. Wolf, G. P. A. Yap, *J. Organomet. Chem.* **2001**, *637–639*, 145–150.

[3] a) W.-Y. Wong, K.-Y. Ho, K.-H. Choi, *J. Organomet. Chem.* **2003**, *670*, 17–26; b) U. Siemeling, J. Vor der Brüggen, U. Vorfeld, B. Neumann, A. Stammler, H.-G. Stammler, A. Brockhinke, R. Plessow, P. Zanello, F. Laschi, F. Fabrizi de Biani, M. Fontani, S. Steenken, M. Stapper, G. Gurzadyan, *Chem. Eur. J.* **2003**, *9*, 2819–2833; c) C. Lebreton, D. Touchard, L. Le Pichon, A. Daridor, L. Toupet, P. H. Dixneuf, *Inorg. Chim. Acta* **1998**, *272*, 188–196.

[4] a) J. H. K. Yip, J. Wu, K.-Y. Wong, K. P. Ho, C. S.-N. Pun, J. J. Vittal, *Organometallics* **2002**, *21*, 5292; b) E. Champeil, S. M. Draper, *J. Chem. Soc. Dalton Trans.* **2001**, 1440–1447; c) M. I. Bruce, B. W. Skelton, M. E. Smith, A. H. White, *Aust. J. Chem.* **1999**, *52*, 431–436.

[5] a) J. H. K. Yip, J. Wu, K.-Y. Wong, K.-W. Yeung, J. J. Vittal, *Organometallics* **2002**, *21*, 1612–1621; b) Q.-H. Wei, L.-Y. Zhang, L.-X. Shi, Z.-N. Chen, *Inorg. Chem. Commun.* **2004**, *7*, 286–288.

[6] a) C. Bucher, J.-C. Moutet, J. Pecaut, G. Royal, E. Saint-Aman, F. Thomas, S. Torelli, M. Ungureanu, *Inorg. Chem.* **2003**, *42*, 2242–2252; b) S. L. Guo, F. Peters, F. Fabrizi de Biani, J. W. Bats, E. Herdtweck, P. Zanello, M. Wagner, *Inorg. Chem.* **2001**, *40*, 4928–4936; c) M. Sato, H. Anano, *J. Organomet. Chem.* **1998**, *555*, 167–175.

[7] a) M. W. Cooke, T. S. Cameron, K. N. Robertson, J. C. Swarts, M. A. S. Aquino, *Organometallics* **2002**, *21*, 5962–5971; b) W.-M. Xue, F. E. Kuhn, E. Herdtweck, Q. Li, *Eur. J. Inorg. Chem.* **2001**, 213–221; c) H. Matsuzaka, J.-P. Qö, T. Ogino, M. Nishio, Y. Nishibayashi, Y. Ishii, S. Uemura, M. Hidai, *J. Chem. Soc. Dalton Trans.* **1996**, 4307–4312; d) A. A. Koridze, A. I. Yanovsky, Yu. T. Struchkov, *J. Organomet. Chem.* **1992**, *441*, 277–284.

[8] a) Loosely related systems contain Fc-$(C{\equiv}C)_n$-Fc units π-bonded to Os_3[8b,c] or Ru_3[8d] carbonyl clusters. In these compounds the main charge-carrier chain is the polyalkynyl skeleton, which is only "modified" by the cluster unit.[8c] In only one of these derivatives[8c] has a significant electronic communication between the terminal Fc groups been observed; b) R. D. Adams, B. Qu, M. D. Smith, *Organometallics* **2002**, *21*, 3867–3872; c) R. D. Adams, B. Qu, M. D. Smith, T. A. Albright, *Organometallics* **2002**, *21*, 2970–2978; d) M. I. Bruce, B. W. Skelton, A. H. White, N. N. Zaitseva, *J. Organomet. Chem.* **2002**, *650*, 188–197.

[9] a) N. Prokopuk, D. F. Shriver, *Inorg. Chem.* **1997**, *36*, 5609–5613; b) W. R. Cullen, S. J. Rettig, T. C. Zheng, *Polyhedron* **1995**, *14*, 2653–2661.

[10] P. Zanello in *Ferrocenes: From Homogeneous Catalysis to Material Science* (Eds.: T. Hayashi, A. Togni), VCH, Weinheim, **1995**, chapt. 7.

[11] F. W. Vergeer, C. J. Cleverlaan, P. Matousek, M. Towrie, D. J. Stufkens, F. Hartl, *Inorg. Chem.* **2005**, *44*, 1319–1331.

[12] a) S. P. Gubin, Y. V. Gulayev, G. B. Khomutov, V. V. Kislov, V. V. Kolesov, E. S. Soldatov, K. S. Sulaimankulov, A. S. Trifonov, *Nanotechnology* **2002**, *13*, 185–194; b) C. Femoni, M. C. Iapalucci, G. Longoni, P. H. Svensson, P. Zanello, F. Fabrizi De Biani, *Chem. Eur. J.* **2004**, *10*, 2318–2326.

[13] J. Kang, J. A. Nelson, M. Lu, B. Xie, Z. Peng, D. R. Powell, *Inorg. Chem.* **2004**, *43*, 6408–6413.

[14] a) F. Fabrizi de Biani, A. Ienco, F. Laschi, P. Leoni, F. Marchetti, L. Marchetti, C. Mealli, P. Zanello, *J. Am. Chem. Soc.* **2005**, *127*, 3076–3089; b) P. Leoni, F. Marchetti, L. Marchetti, M. Pasquali, S. Quaglierini, *Angew. Chem.* **2001**, *113*, 3729–3730; *Angew. Chem. Int. Ed.* **2001**, *40*, 3617–3618.

[15] Crystal data for **1**·(0.5 $CHCl_3$): $C_{56.5}H_{90.5}Cl_{1.5}Fe_2O_4P_4Pt_6$, M_r = 2293.08. Monoclinic, space group $C2/c$, a = 24.424(2), b = 17.604(1), c = 33.489(2) Å, β = 105.250(2)°, V = 13892(2) Å^3, Z = 8, ρ_{calcd} = 2.193 g cm^{-3}, $\mu(Mo_{K\alpha})$ = 126.10 cm^{-1}, dimensions 0.4 × 0.4 × 0.3 mm^3. 63429 reflections were collected, at 120 K (on a Bruker SMART CCD diffractometer), of which 13675 were unique (R_{int} = 0.0875). An empirical absorption correction was applied using the program SADABS (transmission factors in the range 1.000–0.522). Structure solution was by direct and Fourier methods and refinement by full-matrix least squares on F^2 (programs WinGx vs. 1.70 and SHELX-PC). Isotropic displacement parameters were used for the carbon atoms of the C_5 rings of the Fc units and of the ethynyl moieties; the Pt, Fe, and P atoms, and the remaining carbon atoms were refined using anisotropic displacement parameters. From the difference Fourier maps a solvent molecule (CH_2Cl_2) was found, disordered across a crystallographic inversion center, and its contribution was taken into account. Final agreement factors were R_1 = 0.0403, R_{w2} = 0.0890 for 9178 observed reflections [$I \geq 2\sigma(I)$] and 582 refined parameters; GOF = 1.011. CCDC-272174 (**1**) contains the supplementary crystallographic data for this paper. These data can be obtained free of charge from the Cambridge Crystallographic Data Centre via www.ccdc.cam.ac.uk/data_request/cif.

[16] a) A. Albinati, P. Leoni, L. Marchetti, S. Rizzato, *Angew. Chem.* **2003**, *115*, 6172–6175; *Angew. Chem. Int. Ed.* **2003**, *42*, 5990–5993; b) P. Leoni, F. Marchetti, L. Marchetti, M. Pasquali, *Chem. Commun.* **2003**, 2372–2373.

[17] P. Zanello, *Inorganic Electrochemistry: Theory, Practice and Application*, RSC, Cambridge, UK, **2003**.

[18] C. Bonaccorsi, F. Fabrizi de Biani, P. Leoni, F. Marchetti, L. Marchetti, P. Zanello, unpublished results.

[19] R. J. LeSuer, W. E. Geiger, *Angew. Chem.* **2000**, *112*, 254–256; *Angew. Chem. Int. Ed.* **2000**, *39*, 248–250.

[20] H. Fink, N. J. Long, A. J. Martin, G. Opromolla, A. J. P. White, D. J. Williams, P. Zanello, *Organometallics* **1997**, *16*, 2646–2650.

[21] V. Balzani, A. Juris, M. Venturi, S. Campagna, S. Serroni, *Chem. Rev.* **1996**, *96*, 759.

[22] [$\{Pt_6\}$(C≡C–Fc)I] was prepared by coupling the unsymmetrical dihalide [$\{Pt_6\}$(Cl)I] with one equivalent of Fc-C≡CH (see

 © 2005 Wiley-VCH Verlag GmbH & Co. KGaA, Weinheim

Supporting Information) and it exhibits spectroelectrochemical intervalence transfer (IT) absorptions nearly identical to those given by complex **1**. Full details of the synthesis, and the cyclic voltammetric and spectroelectrochemical characterization will be given elsewhere.

[23] B. S. Brunschwig, C. Creutz, N. Sutin, *Chem. Soc. Rev.* **2002**, *31*, 168 – 184.

[24] a) N. S. Hush in *Progress in Inorganic Chemistry*, *Vol. 8* (Ed.: F. A. Cotton), Wiley, New York, **1967**, p. 391; b) N. Dowling, P. M. Henry, N. A. Lewis, H. Taube, *Inorg. Chem.* **1981**, *20*, 2345 – 2348.

[25] This has to be considered as the lower limit for the bandwidth, since anharmonicity and/or spin–orbit coupling can also broaden the band.

[26] a) M. Emmelius, G. Pawlowski, H. W. Vollmann, *Angew. Chem.* **1989**, *101*, 1475 – 1502; *Angew. Chem. Int. Ed. Engl.* **1989**, *28*, 1445 – 1475; b) J. Fabian, R. Zahradnik, *Angew. Chem.* **1989**, *101*, 693 – 710; *Angew. Chem. Int. Ed. Engl.* **1989**, *28*, 677 – 694.

 © 2005 Wiley-VCH Verlag GmbH & Co. KGaA, Weinheim

Homogeneous Catalysis

DOI: 10.1002/anie.200501841

Stable Cyclic (Alkyl)(Amino)Carbenes as Rigid or Flexible, Bulky, Electron-Rich Ligands for Transition-Metal Catalysts: A Quaternary Carbon Atom Makes the Difference**

*Vincent Lavallo, Yves Canac, Carsten Präsang, Bruno Donnadieu, and Guy Bertrand**

The availability of catalysts to perform specific transformations is critical for both industry and academia. Over the years, the success of homogeneous catalysis can be attributed largely to the development of a diverse range of ligand frameworks that have been used to tune the behavior of a variety of metal-containing systems. Advances in ligand design have allowed not only for improvements of known processes in terms of scope, mildness, and catalyst loadings, but also for the discovery of new selective reactions. A good illustration is given by palladium-catalyzed coupling reactions, which are applied to a wide area of endeavors ranging from synthetic organic chemistry to materials science.[1] For these catalytic processes, which represent some of the most powerful and versatile tools available for synthetic chemists, major advances have recently been reported thanks to the use of bulky, electron-rich, phosphines **A** and cyclic diaminocarbenes (N-heterocyclic carbenes (NHCs)) **B** (Figure 1).[2] These ligands stabilize the active catalytic species, and accelerate the important catalytic steps, namely oxidative addition, transmetallation, and reductive elimination. On the other hand, excessive steric hindrance can present some drawbacks for the coupling of bulky reactants.[3] To overcome this problem Glorius and co-workers have successfully developed ligands with "flexible steric bulk" using the conformational flexibility of cyclohexane.[4]

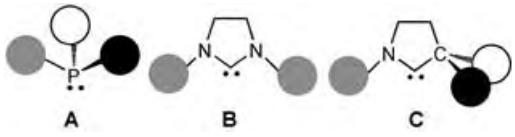
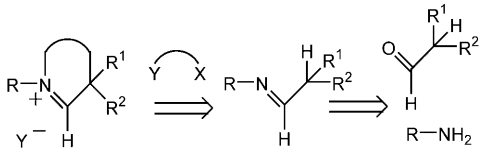


Figure 1. Schematic view of ligands **A**–**C** showing their different steric demands.

Herein we report the synthesis of stable cyclic (alkyl)(amino)carbenes (CAACs) **C** (Figure 1). The replacement of one of the electronegative amino substituents of NHCs **B** by a strong σ-donor alkyl group makes the CAAC ligands **C** even more electron-rich than **A** and **B**. Moreover, owing to the presence of a quaternary carbon atom in a position α to the carbene center, carbenes **C** feature steric environments that differentiate them dramatically from both ligands **A** and **B** (Figure 1), and amplifies flexible steric bulk effect. We show that the peculiar electronic and steric properties of carbenes **C** allow for the synthesis of CAAC-palladium complexes that are highly efficient for the catalytic α-arylation of carbonyl compounds.

Direct detection of singlet alkyl carbene compounds usually requires matrix-isolation conditions or nanosecond time-resolved laser flash photolysis techniques.[5] However, last year we reported that, provided a tertiary alkyl group is bonded to the carbene center, acyclic (alkyl)(amino)carbenes are isolable and, importantly, behave as strong σ-donors toward transition-metal centers.[6] NHCs **B** are more robust and give rise to more active catalysts, when used as ligands for transition metals, than their acyclic counterparts.[7] Therefore it was reasonable to believe that CAACs **C** would also be more stable than their acyclic variants, and would have interesting ligand properties.

The method used to prepare the precursor of acyclic (alkyl)(amino)carbenes, namely the alkylation of the corresponding enamines, is very limited in its scope. Therefore, we have designed a new synthetic approach, which is very versatile (Scheme 1). The choice of R, R^1, and R^2 substituents



Scheme 1. Retrosynthetic analysis for the preparation of CAACs.

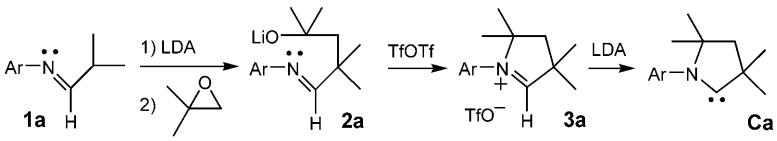
[*] V. Lavallo, Dr. Y. Canac, Dr. C. Präsang, B. Donnadieu, Dr. G. Bertrand
UCR-CNRS Joint Research Chemistry Laboratory (UMR 2282)
Department of Chemistry
University of California
Riverside, CA 92521-0403 (USA)
Fax: (+1) 951-827-2725
E-mail: gbertran@mail.ucr.edu

[**] We are grateful to the NIH (R01 GM 68825) and RHODIA for financial support of this work, and to the Alexander von Humboldt Foundation (C.P.).

© 2005 Wiley-VCH Verlag GmbH & Co. KGaA, Weinheim

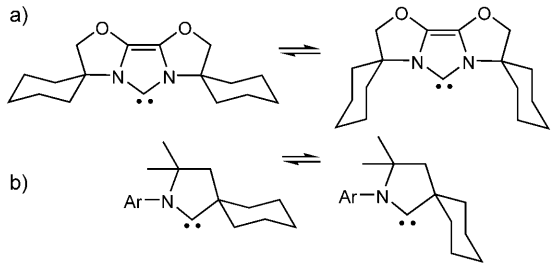
is virtually unlimited (except that R^1 and R^2 cannot be H) and the ring skeleton can be modified at will.

This synthetic strategy was first tested with imine **1a** (Scheme 2) prepared from 2,6-diisopropylaniline and the simplest aldehyde featuring a secondary alkyl substituent, 2-methylpropanal. Deprotonation of **1a** with lithium diisopropylamide (LDA) afforded the aza-allyl anion, which readily induces the ring opening of 1,2-epoxy-2-methylpropane leading to the corresponding alkoxide **2a**. Subsequent treatment with triflic anhydride (TfOTf) at −78 °C gives rise to the triflate derivative, which upon warming to room temperature affords the aldiminium salt **3a** in 58% yield (based on the imine). Lastly, deprotonation with LDA quantitatively affords carbene **Ca** as a white solid (Scheme 2). CAAC **Ca** is perfectly stable at room temperature in the solid state and in solution, for at least two weeks.



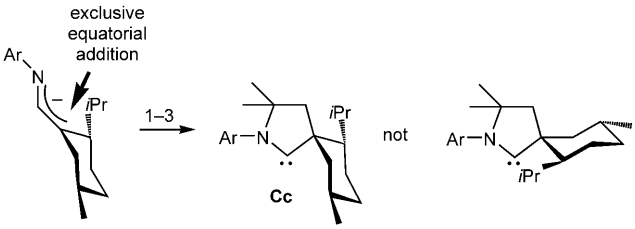
Scheme 2. Synthesis of CAAC **Ca**. Ar = 2,6-diisopropylphenyl.

The presence of the tertiary carbon center next to the carbene center offers the possibility of constructing ligands featuring different types of steric environment. Spiro-CAAC **Cb**, readily prepared in a manner similar to that used for **Ca**, but using cyclohexyl carbaldehyde, illustrates how the concept of flexible steric bulk can be incorporated into this ligand family. In fact, compared to the NHCs **B** developed by Glorius and co-workers,[4] the cyclohexane ring of **Cb** is closer to the carbene and to an ensuing metal center, and therefore the effects of the "flexible wing" should be amplified (Scheme 3).



Scheme 3. Flexible steric bulk for a) NHCs (**B**) and b) CAACs (**Cb**). Ar = 2,6-diisopropylphenyl.

In contrast to **Cb**, carbene **Cc** (Scheme 4) exemplifies the rigidity and extreme steric bulk that CAACs can provide to metal centers to which they are bound. As a starting material, we chose the imine **1c** derived from (−)-menthone. The key step of the synthesis is based on the propensity of relatively bulky reactants to approach the cyclohexane moiety from the equatorial direction. This effect is reinforced by the presence of the *iso*-propyl group, and therefore the reaction with the



Scheme 4. Stereoselective synthesis of CAAC **Cc**. 1) Dimethyloxirane; 2) TfOTf; 3) LDA; Ar = 2,6-diisopropylphenyl.

oxirane is completely diastereoselective (Scheme 4). It leads to the diastereomer affording the best protection for the carbene and the ensuing metal center to which it is bound. Moreover, in contrast with **Cb**, the chair conformation is locked. Indeed, the other chair conformation would put both the *iso*-propyl and methyl groups in unfavorable axial positions (even a boat conformation would be highly adverse). It is apparent from the molecular structure, obtained by a single-crystal X-ray diffraction study (Figure 2)[8] that the steric environment of this

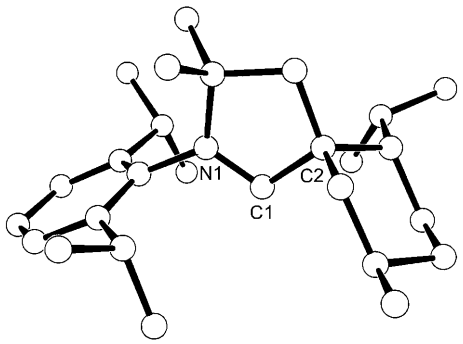


Figure 2. Molecular view of the crystal structure of **Cc**. Selected bond lengths [Å] and angles [°]: N1-C1 1.315(3), C1-C2 1.516(3); N1-C1-C2 106.54(18).

CAAC is very different from that of phosphines (described as a cone) and NHCs (defined as fan-like):[9] the locked cyclohexane moiety constitutes a "wall of protection" not only for the carbene center, but also for a metal if **Cc** is being used as a ligand (Figure 2). It is noteworthy that **Cc** is enantiomerically pure and has been prepared without time-consuming enantio- or diastereoselective separation.

The carbonyl stretching frequencies of *cis*-[IrCl(CO)$_2$(L)] complexes are recognized as an excellent measure of the σ-donor and π-acceptor properties of the ligand L.[10] Addition of half an equivalent of [{IrCl(cod)}$_2$] (cod = 1,5-cyclooctadiene) to a THF solution of carbene **Cc** led to the formation of [IrCl(cod)(**Cc**)], which upon treatment with CO at room temperature afforded *cis*-[IrCl(CO)$_2$(**Cc**)] (**4c**) in high yield. The average value of the carbonyl stretching frequencies for complex **4c** (ν_{av}(CO) = 2013 cm^{-1}) indicates that the donor power of **Cc** is higher than that of electron-rich phosphines (PCy$_3$: ν_{av}(CO) = 2028 cm^{-1}) and even NHC ligands (2017–

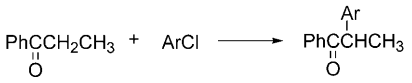
 © 2005 Wiley-VCH Verlag GmbH & Co. KGaA, Weinheim

2020 cm^{-1}); only the abnormal C5-bound NHCs are stronger donors (2003 cm^{-1}).[10]

The steric and electronic properties of CAACs should benefit the numerous catalytic processes which require bulky electron-rich ligands at the metal center. As an example of such a process, we chose to study the palladium-catalyzed α-arylation of ketones, discovered concurrently in 1997 by the groups of Buchwald,[11] Hartwig,[12] and Miura.[13] This reaction has not yet been achieved at room temperature with non-activated aryl chlorides; moreover there are no examples with sterically hindered di-*ortho*-substituted aryl chlorides. The use of CAAC ligands **C**, indeed, overcomes these limitations. The [PdCl(allyl)(CAAC)] complexes **5a–c** (Figure 3) were readily prepared in high yields by addition of [{Pd(allyl)(Cl)}$_2$] to the corresponding carbenes **Ca–c**, and isolated as air stable colorless crystals; they can even be purified by column chromatography on silica gel.

Table 1 summarizes the results obtained using complexes **5a–c** for the α-arylation of propiophenone, the classical substrate for the palladium-catalyzed α-arylation of ketones.[11–14] With nonhindered aryl chlorides the superior catalytic activity of CAAC complex **5c** over **5a**,**b** is demonstrated (entries 1–8). A turn over number (TON) of up to 7200 has been obtained at room temperature. This compares extremely favorably with the best TON reported to date: 4200 at 120 °C.[14c] When a di-*ortho*-substituted aryl chloride is used (entries 9–14), no catalytic activity has been observed with **5a** and **5c**, but in marked contrast **5b** is active, even at room temperature. Entries 11 and 13 indicate the thermal stability of the catalyst.

Table 1: Palladium-mediated α-arylation of propiophenone with aryl chlorides.[a]



Entry	Aryl chloride	Catalyst ([mol%])	*T* [°C]	*t* [h]	Yield [%][b]
1	PhCl	**5a** (0.5)	23	70	22
2	PhCl	**5b** (0.5)	23	70	29
3	PhCl	**5c** (0.5)	23	1	100
4	PhCl	**5c** (0.1)	23	1	83
5	PhCl	**5c** (0.01)	23	38	72
6	2-MePhCl	**5a** (0.5)	23	70	0
7	2-MePhCl	**5b** (0.5)	23	36	10
8	2-MePhCl	**5c** (0.5)	23	36	82
9	2,6-Me$_2$PhCl	**5a** (0.5)	23	70	0
10	2,6-Me$_2$PhCl	**5b** (0.5)	23	36	32
11	2,6-Me$_2$PhCl	**5b** (0.5)	70	4	56
12	2,6-Me$_2$PhCl	**5b** (1)	23	16	61
13	2,6-Me$_2$PhCl	**5b** (1)	50	20	81
14	2,6-Me$_2$PhCl	**5c** (0.5)	50	20	0

[a] Conditions: THF (1 mL), NaO*t*Bu (1.1 mmol), propiophenone (1.0 mmol), aryl chloride (1.0 mmol); all reactants (Aldrich) were used as received. [b] Yields as determined by NMR spectroscopy.

The dramatic differences observed in the catalytic activity of complexes **5a–c** can be rationalized by the different steric environments created by ligands **Ca**, **Cb**, and **Cc**. Carbene **Ca** is not sterically hindered enough to favor reductive elimination at room temperature. This step is easily promoted, for relatively small substrates, by the very rigid and bulky **Cc** ligand. However, entry 14 shows that **Cc** gives rise to a catalyst very sensitive to excessive steric hindrance. The molecular structures shown in Figure 3 clearly show that the steric environment around the metal is very similar for **5a** and **5b**, and therefore cannot explain the superior catalytic activity of **5b**. However, in solution, the cyclohexane moiety of **5b** can easily undergo a ring flip, which leads to a steric environment similar to that of **5c**.[15] This flexibility also explains the superiority of **5b** over **5c** in accommodating sterically demanding substrates in the coupling process.

Although the α-arylation of carbonyl compounds has a broad scope of application,[16] very little success has been reported with aldehydes,[17] mostly because of the competing aldol condensation. It was reasonable to believe that this side reaction could be reduced by taking advantage of the mild conditions allowed by CAAC palladium complexes. Indeed, 2-chlorotoluene is coupled with isobutanal with high efficiency at ambient temperature. Using 1 mol% of **5c**, the desired product was obtained after 16 h in 98% yield, and no evidence of aldol condensation products was observed. This is the first example of α-arylation of an aldehyde with an aryl chloride.

In recent years, several different types of stable carbene compounds have been prepared,[18] but only the "pure" σ-donor NHCs, when used as ligands, have led to highly active and robust catalysts,[19] which compete or even surpass their

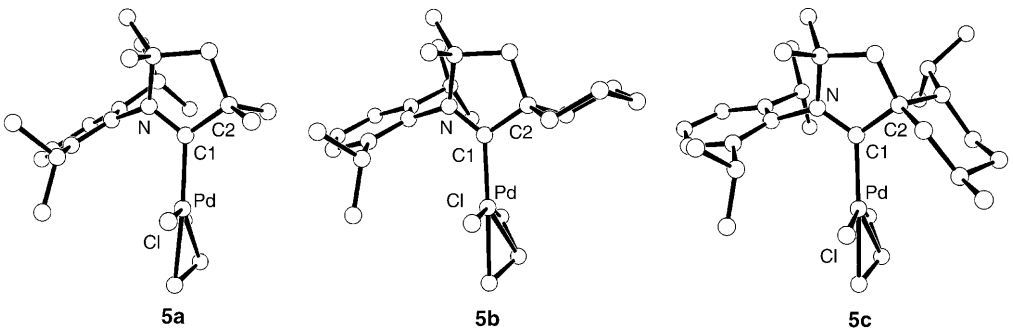


Figure 3. Molecular view of the crystal structures of **5a–c**. Selected lengths [Å] and angles [°]: **5a**: N-C1 1.3133(11), C1-C2 1.5298(12), C1-Pd 2.0246(9); N-C1-C2 108.51(8). **5b**: N-C1 1.310(4), C1-C2 1.526(4), C1-Pd 2.020(3); N-C1-C2 108.7(2). **5c**: N-C1 1.315(5), C1-C2 1.543(5), C1-Pd 2.045(4); N-C1-C2 108.8(3).

 © 2005 Wiley-VCH Verlag GmbH & Co. KGaA, Weinheim

bulky, electron-rich phosphine counterparts. It is generally believed that in contrast to NHCs, Fischer-type carbenes would not survive the standard conditions of organometallic catalysis, because of the cleavage of the metal–carbon bond;[20,21] moreover they are regarded as weak σ-donors and good π-acceptors. Our work demonstrates that the readily available CAACs are strong σ-donors, weak π-acceptors, and form highly catalytically active "cyclic Fischer carbene complexes". Their unique steric and electronic properties, in addition to the broad range of structural features possible, which arise as a result of the presence of a tertiary carbon in a position α to the carbene center, makes these carbenes highly desirable as ligands for various catalytic processes, including asymmetric variants.

Experimental Section

All manipulations were performed under an inert atmosphere of argon using standard Schlenk techniques. Dry, oxygen-free solvents were employed. ^{1}H and ^{13}C NMR spectra were recorded on Varian Inova 300, 500, and Brucker Avance 300 spectrometers.

3a,**b**: A solution of LDA (4.66 g, 43.5 mmol) in Et_2O (40 mL) was added at 0 °C to a stirred solution of imine **1a** or **1b** (43.5 mmol) in Et_2O (40 mL). The solution was warmed to room temperature and stirred for 2 h. After evaporation of the solvent under vacuum, the residue was dissolved in Et_2O (80 mL), and 1,2-epoxy-2-methylpropane (4.06 mL, 45.7 mmol) was added dropwise. After stirring for 12 h at room temperature, trifluoromethane sulfonic anhydride (7.68 mL, 45.7 mmol) was added at −78 °C. The solution was warmed to room temperature and stirred for 1 h. After filtration, the residue was washed with Et_2O (80 mL). Extraction of the solid with CH_2Cl_2 (40 mL) afforded **3a**,**b** as white solids. **3a**: 58 %, m.p. 198–200 °C; ^{1}H NMR ($CDCl_3$, 25 °C, 300 MHz): $\delta = 9.48$ (s, 1H, CH), 7.53 (m, 1H, H_{ar}), 7.34 (m, 2H, H_{ar}), 2.63 (sept, 2H, C*H*CH_3, $J =$ 6.9 Hz), 2.43 (s, 2H, CH_2), 1.68 (s, 6H, CH_3), 1.54 (s, 6H, *C*H_3), 1.35 (d, 6H, CHC*H*$_3$, $J = 6.9$ Hz), 1.17 ppm (d, 6H, CHC*H*$_3$, $J = 6.9$ Hz); ^{13}C NMR (CD_3CN, 25 °C, 75 MHz): $\delta = 192.2$ (CH), 145.6, 133.1, 130.1, 126.6, 122.2 (q, $J = 321.6$ Hz), 85.8, 66.3, 48.8, 30.4, 28.5, 26.3, 26.2, 22.2 ppm. **3b**: 48 %, m.p. 268–270 °C; ^{1}H NMR (CD_3CN, 25 °C, 300 MHz): $\delta = 8.91$ (s, 1H, CH), 7.67 (m, 1H, H_{ar}), 7.52 (m, 2H, H_{ar}), 2.78 (sept, 2H, C*H*CH_3, $J = 6.9$ Hz), 2.53 (s, 2H, CH_2), 1.19–2.11 (m, 10H, CH_2), 1.59 (s, 6H, CH_3), 1.40 (d, 6H, CHC*H*$_3$, $J = 6.9$ Hz), 1.15 ppm (d, 6H, CHC*H*$_3$, $J = 6.9$ Hz); ^{13}C NMR (CD_3CN, 25 °C): $\delta =$ 191.3 (CH), 145.4, 132.9, 130.0, 126.4, 122.2 (q, $J = 321.2$ Hz), 85.0, 53.6, 45.9, 34.6, 30.2, 28.7, 26.1, 25.3, 22.1 ppm.

3c: A solution of the lithium salt of dimethylamine (1.56 g, 30.5 mmol) in THF (40 mL) was added at 0 °C to a stirred solution of imine **1c** (10.00 g, 30.5 mmol) in THF (40 mL). The solution was warmed to room temperature and stirred for 18 h. After evaporation of the solvent and then heating under vacuum at about 200 °C for 10 min, to remove the THF complexed to the lithium, the residue was dissolved in toluene (100 mL). After adding dropwise 1,2-epoxy-2-methylpropane (2.85 mL, 32.0 mmol), the solution was stirred for 12 h at room temperature. Then Tf_2O (5.39 mL, 32.0 mmol) was added at −78 °C and the suspension was allowed to warm to room temperature and stirred for 2 h. After filtration, the oily residue was washed with boiling toluene (90 mL). Extraction of the residue with CH_2Cl_2 (60 mL) afforded **3c** as a white solid, which was recrystallized in CH_2Cl_2/Et_2O at −20 °C. 6.65 g, 41 %, m.p. 258–260 °C; $[\alpha]_D^{23} = -38°$ ($CHCl_3$); ^{1}H NMR ($CDCl_3$, 25 °C, 500 MHz): $\delta = 9.73$ (s, 1H, CH), 7.53 (m, 1H, H_{ar}), 7.34 (m, 2H, H_{ar}), 2.64 (m, 3H, CH), 2.20 (m, 2H), 2.04 (m, 2H), 1.90 (m, 2H), 1.78 (m, 2H), 1.59 (s, 3H, CH_3), 1.55 (s, 3H, CH_3), 1.35 (d, 3H, CHC*H*$_3$, $J = 7.0$ Hz), 1.34 (d, 3H, CHC*H*$_3$, $J =$ 6.0 Hz), 1.21 (d, 3H, CHC*H*$_3$, $J = 6.5$ Hz), 1.17 (d, 3H, CHC*H*$_3$, $J =$ 6.0 Hz), 1.06 (d, 3H, CHC*H*$_3$, $J = 7.0$ Hz), 1.00–1.10 (m, 2H), 0.94 (d, 3H, CHC*H*$_3$, $J = 6.5$ Hz), 0.83 ppm (d, 3H, CHC*H*$_3$, $J = 6.5$ Hz); ^{13}C NMR ($CDCl_3$, 25 °C, 125 MHz): $\delta = 192.64$ (CH), 144.7, 144.5, 131.7, 129.0, 125.6, 125.1, 120.6 (q, $J = 321.6$ Hz), 81.6, 58.5, 52.2, 51.0, 45.4, 34.7, 29.9, 29.5, 29.2, 28.1, 27.1, 26.7, 25.5, 22.8, 22.7, 22.3, 22.2, 22.1, 18.7 ppm.

Ca–Cc: A 1/1 mixture of LDA and iminium salt **3** (5.0 mmol) was cooled to −78 °C and THF was added (30 mL). The suspension was warmed to room temperature and stirred for 30 min. After evaporation of the solvent under vacuum, a solid residue containing the corresponding carbene **C** and LiOTf was obtained and used for the complexation reaction without further purification, except for **Cc**. In this case, the solid residue was extracted with hexane (30 mL), and after evaporation of the solvent under vacuum, **Cc** was obtained as a white microcrystalline solid. **Ca**: ^{13}C NMR ([D$_8$]THF, 25 °C, 125 MHz): $\delta = 304.2$ (C), 145.8, 137.5, 128.0, 123.8, 82.5, 57.7, 50.3, 29.1, 28.9, 27.5, 21.7 ppm. **Cb**: ^{13}C NMR ([D$_8$]THF, 25 °C, 125 MHz): $\delta = 309.4$ (C), 145.8, 137.8, 127.9, 123.6, 81.2, 63.3, 47.7, 35.8, 29.3, 29.1, 26.4, 23.0, 21.5 ppm. **Cc**: 92 %, m.p. 115 °C; $[\alpha]_D^{23} = +113°$ (hexane); ^{1}H NMR (C_6D_6, 25 °C, 500 MHz): $\delta = 7.13$–7.25 (m, 3H, H_{ar}), 3.18 (sept, 2H, C*H*CH_3, $J = 6.9$ Hz), 2.54–2.78 (m, 2H), 2.11 (m, 1H), 1.72–1.97 (m, 4H), 1.41 (dd, 1H, $J = 12.3$ and $J = 3.3$ Hz), 1.11–1.27 (m, 21H), 1.06 (d, 3H, CHC*H*$_3$, $J = 6.9$ Hz), 1.02 (d, 3H, CHC*H*$_3$, $J =$ 6.9 Hz), 0.96 ppm (3H, CHC*H*$_3$, $J = 6.6$ Hz); ^{13}C NMR ([D$_8$]THF, 25 °C, 125 MHz): $\delta = 319.0$ (C), 146.6, 145.7, 138.1, 127.6, 123.8, 123.3, 79.7, 69.4, 53.1, 52.0, 48.0, 36.9, 30.2, 29.8, 29.1, 29.0, 28.6, 27.7, 27.0, 25.4, 24.1, 23.6, 22.8, 21.9, 21.2, 18.7 ppm.

4c: A solution of carbene **Cc** (0.34 g, 0.90 mmol) in THF (5 mL) was added at −78 °C to a stirred THF solution (5 mL) of [{IrCl(cod)}$_2$] (0.27 g, 0.41 mmol). The solution was warmed to room temperature and stirred for 3 h. After evaporation of the solvent under vacuum, the residue was washed with hexane (15 mL), dissolved in THF (5 mL), and carbon monoxide was bubbled through the solution (45 min) at room temperature. After evaporation of the solvent under vacuum, carbene complex **4c** was obtained as a brown powder. 0.42 g, 71 %; ^{1}H NMR ($CDCl_3$, 25 °C, 300 MHz): $\delta = 7.55$ (m, 1H, H_{ar}), 7.36 (m, 2H, H_{ar}), 2.61–2.76 (m, 3H), 2.38 (d, 1H, $J = 14.4$ Hz), 2.06–2.24 (m, 3H), 1.67–1.95 (m, 6H), 1.64 (s, 3H), 1.60 (s, 3H), 1.36 (d, 6H, CHC*H*$_3$, $J = 6.6$ Hz), 1.19–1.27 (m, 6H), 1.08 (d, 3H, CHC*H*$_3$, $J =$ 6.9 Hz), 0.97 (d, 3H, CHC*H*$_3$, $J = 5.4$ Hz), 0.85 ppm (d, 3H, CHC*H*$_3$, $J = 6.9$ Hz); ^{13}C NMR ($CDCl_3$, 25 °C, 75 MHz): $\delta = 191.3$ (CO), 190.9 (C), 167.8 (CO), 144.8, 144.6, 132.3, 129.0, 126.1, 125.6, 82.4, 58.7, 58.6, 52.3, 51.1, 45.8, 34.6, 30.4, 30.1, 29.7, 28.6, 27.6, 27.4, 26.6, 23.3, 23.0, 22.9, 22.5, 22.2, 19.4 ppm. IR (CH_2Cl_2): $\tilde{\nu} =$ 2055, 1971 (ν(CO)) cm^{-1}.

5a–c: A solution of carbene **C** (5.2 mmol) in THF (15 mL) was added at −78 °C to a stirred solution of [{Pd(allyl)(Cl)}$_2$] (0.95 g, 2.6 mmol) in THF (15 mL). The solution was warmed to room temperature and stirred for 3 h. After evaporation of the solvent under vacuum, the solid residue was washed with hexane (40 mL). Extraction with CH_2Cl_2 (20 mL) afforded a gray solid, which was recrystallized in THF (**5a**) or hexane (**5b**,**c**) at −20 °C. Carbene complexes **5** were obtained as colorless crystals. **5a**: 71 %, m.p. 162–163 °C; ^{1}H NMR ($CDCl_3$, 25 °C, 300 MHz): $\delta = 7.27$–7.42 (m, 3H, H_{ar}), 5.05 (m, 1H, H_{allyl}), 4.18 (d, 1H, H_{allyl}, $J = 7.5$ Hz), 3.19 (m, 3H, C*H*CH_3 and 2H_{allyl}), 3.01 (m, 1H, C*H*CH_3), 2.02 (s, 3H, H_{allyl}, CH_2), 1.64 (s, 6H, *C*H_3), 1.23–1.40 ppm (m, 18H, CH_3); ^{13}C NMR ($CDCl_3$, 25 °C, 75 MHz): $\delta = 267.4$ (C), 146.5, 135.8, 129.1, 125.1, 115.5, 81.5, 76.8, 57.5, 50.5, 48.6, 31.7, 30.6, 29.3, 28.6, 28.1, 27.5, 25.1 ppm. **5b**: 74 %, m.p. 176–178 °C; ^{1}H NMR ($CDCl_3$, 25 °C, 300 MHz): $\delta = 7.21$–7.63 (m, 3H, H_{ar}), 5.04 (m, 1H, H_{allyl}), 4.18 (d, 1H, H_{allyl}, $J = 7.5$ Hz), 3.29 (m, 1H, C*H*CH_3), 3.15 (m, 2H, H_{allyl}), 2.98 (m, 1H, C*H*CH_3), 2.45 (m, 2H, CH_2), 1.22–2.05 (m, 17H, H_{allyl}, CH_2, CH_3), 1.30 ppm (d, 12H, CHC*H*$_3$, $J = 6.9$ Hz); ^{13}C NMR ($CDCl_3$, 25 °C, 75 MHz): $\delta = 267.8$ (C), 146.5, 136.3, 129.0, 125.1, 115.6, 80.5, 77.0, 62.9, 48.3, 45.7, 38.8, 37.2, 31.3, 29.5, 28.6, 28.0, 27.0, 25.4, 25.3, 22.9, 22.4 ppm. **5c**: 70 %, m.p. 157–159 °C; $[\alpha]_D^{23} = -1°$ ($CHCl_3$); ^{1}H NMR ($CDCl_3$, 25 °C, 300 MHz): $\delta = 7.20$–7.38 (m, 3H, H_{ar}), 5.04 (m, 1H, H_{allyl}), 4.21 (d, 1H, H_{allyl}, $J = 7.5$ Hz), 3.70 (sept, 1H, C*H*CH_3, $J = 6.3$ Hz), 3.15 (d,

 © 2005 Wiley-VCH Verlag GmbH & Co. KGaA, Weinheim

1H, H_{allyl}, $J = 14.1$ Hz), 2.82–2.98 (m, 4H), 2.32 (m, 1H), 1.70–2.09 (m, 7H), 1.35–1.45 (m, 8H), 1.30 (d, 6H, $CHCH_3$, $J = 6.6$ Hz), 1.29 (s, 3H), 1.20 (d, 3H, $CHCH_3$, $J = 6.9$ Hz), 0.99 (t, 6H, $CHCH_3$, $J = 6.9$ Hz), 0.93 ppm (d, 3H, $CHCH_3$, $J = 6.6$ Hz); ^{13}C NMR ($CDCl_3$, 25 °C, 75 MHz): $\delta = 272.0$ (C), 148.3, 145.6, 137.5, 129.0, 126.4, 124.7, 114.9, 78.7, 78.0, 67.4, 54.2, 52.0, 51.2, 48.1, 33.7, 33.6, 30.7, 30.1, 29.2, 29.0, 28.6, 28.0, 27.2, 26.0, 25.7, 23.8, 22.4, 20.9 ppm.

α-Arylation procedure: Glass vials were charged under inert atmosphere in the glovebox with NaO*t*Bu (1.1 mmol) in THF (0.5 mL). Then a mixture of the palladium catalyst (see Table 1 for amounts), aryl halide (1.0 mmol) and propiophenone or isobutanal (1.0 mmol) in THF (0.5 mL) was added at room temperature. Then the reaction were stirred at the temperature for the period of time indicated in Table 1. The reactions were quenched with aqueous solution of NH_4Cl and extracted with Et_2O. The organic layer was dried over $MgSO_4$. All compounds were identified by ^{1}H NMR spectroscopy. The reported yields are determined by NMR spectroscopy.

Received: May 27, 2005
Published online: August 1, 2005

Keywords: arylation · carbenes · homogeneous catalysis · palladium

[1] a) *Metal-Catalyzed Cross-Coupling Reactions* (Eds.: A. de Meijere, F. Diederich), Wiley-VCH, Weinheim, **2004**; b) *Handbook of Organopalladium Chemistry for Organic Synthesis* (Ed.: E. Negishi), Wiley, Hoboken, NJ, **2002**.
[2] a) A. F. Littke, G. C. Fu, *Angew. Chem.* **2002**, *114*, 4350; *Angew. Chem. Int. Ed.* **2002**, *41*, 4176; b) A. Zapf, M. Beller, *Chem. Commun.* **2005**, 431; c) M. Muira, *Angew. Chem.* **2004**, *116*, 2251; *Angew. Chem. Int. Ed.* **2004**, *43*, 2201.
[3] C. W. K. Gstöttmayr, V. P. W. Böhm, E. Herdtweck, M. Grosche, W. A. Herrmann, *Angew. Chem.* **2002**, *114*, 1421; *Angew. Chem. Int. Ed.* **2002**, *41*, 1363.
[4] a) G. Altenhoff, R. Goddard, C. W. Lehmann, F. Glorius, *J. Am. Chem. Soc.* **2004**, *126*, 15195; b) G. Altenhoff, R. Goddard, C. W. Lehmann, F. Glorius, *Angew. Chem.* **2003**, *115*, 3818; *Angew. Chem. Int. Ed.* **2003**, *42*, 3690.
[5] a) *Reactive Intermediate Chemistry* (Eds.: R. A. Moss, M. S. Platz, M. Jones, Jr.), Wiley-Interscience, Hoboken, NJ, **2004**; b) R. S. Sheridan, R. A. Moss, B. K. Wilk, S. Shen, M. Wlostowski, M. A. Kesselmayer, R. Subramanian, G. Kmiecik-Lawrynowicz, K. Krogh-Jespersen, *J. Am. Chem. Soc.* **1988**, *110*, 7563.
[6] V. Lavallo, J. Mafhouz, Y. Canac, B. Donnadieu, W. W. Schoeller, G. Bertrand, *J. Am. Chem. Soc.* **2004**, *126*, 8670.
[7] W. A. Herrmann, K. Ofele, D. von Preysing, E. Herdtweck, *J. Organomet. Chem.* **2003**, *684*, 235.
[8] CCDC-265858 (**Cc**), -265854 (**5a**), -265855 (**5b**), and -265856 (**5c**) contain the supplementary crystallographic data for this paper. These data can be obtained free of charge from the Cambridge Crystallographic Data Centre via www.ccdc.cam.ac.uk/data_request/cif.
[9] J. Huang, H. J. Schanz, E. D. Stevens, S. P. Nolan, *Organometallics* **1999**, *18*, 2370.
[10] A. R. Chianese, A. Kovacevic, B. M. Zeglis, J. W. Faller, R. H. Crabtree, *Organometallics* **2004**, *23*, 2461.
[11] M. Palucki, S. L. Buchwald, *J. Am. Chem. Soc.* **1997**, *119*, 11108.
[12] B. C. Hamann, J. F. Hartwig, *J. Am. Chem. Soc.* **1997**, *119*, 12382.
[13] T. Satoh, Y. Kawamura, M. Miura, M. Nomura, *Angew. Chem.* **1997**, *109*, 1820; *Angew. Chem. Int. Ed. Engl.* **1997**, *36*, 1740.
[14] a) M. S. Viciu, R. F. Germaneau, S. P. Nolan, *Org. Lett.* **2002**, *4*, 4053; b) J. M. Fox, X. H. Huang, A. Chieffi, S. L. Buchwald, *J. Am. Chem. Soc.* **2000**, *122*, 1360; c) A. Ehrentraut, A. Zapf, M. Beller, *Adv. Synth. Catal.* **2002**, *344*, 209.
[15] Indeed, the methyl and *iso*-propyl group of the menthyl ring are far from the metal.
[16] D. A. Culkin, J. F. Hartwig, *Acc. Chem. Res.* **2003**, *36*, 234.
[17] A 50% conversion of isobutanal was reported after 3 h at 110 °C using an aryl bromide with 5 mol% $Pd(OAc)_2$ and 10 mol% $P(tBu)_3$, the reaction also produced a significant amount of aldol side products: Y. Terao, Y. Fukuoka, T. Satoh, M. Miura, M. Nomura, *Tetrahedron Lett.* **2002**, *43*, 101.
[18] For reviews on stable carbene compounds: a) W. Kirmse, *Angew. Chem.* **2004**, *116*, 1799; *Angew. Chem. Int. Ed.* **2004**, *43*, 1767; b) R. W. Alder, M. E. Blake, M. E Chaker, J. N. Harvey, F. Paolini, J. Schütz, *Angew. Chem.* **2004**, *116*, 6020; *Angew. Chem. Int. Ed.* **2004**, *43*, 5896; c) Y. Canac, M. Soleilhavoup, S. Conejero, G. Bertrand, *J. Organomet. Chem.* **2004**, *689*, 3857; d) D. Bourissou, O. Guerret, F. P. Gabbaï, G. Bertrand, *Chem. Rev.* **2000**, *100*, 39.
[19] For reviews on stable carbene compounds in catalysis: a) N. M. Scott, S. P. Nolan, *Eur. J. Inorg. Chem.* **2005**, 1815; b) E. Peris, R. H. Crabtree, *Coord. Chem. Rev.* **2004**, *248*, 2239; c) C. M. Crudden, D. P. Allen, *Coord. Chem. Rev.* **2004**, *248*, 2247; d) V. César, S. Bellemin-Laponnaz, L. H. Gade, *Chem. Soc. Rev.* **2004**, *33*, 619; e) D. Enders, T. Balensiefer, *Acc. Chem. Res.* **2004**, *37*, 534; f) M. C. Perry, K. Burgess, *Tetrahedron: Asymmetry* **2003**, *14*, 951; g) W. A. Herrmann, *Angew. Chem.* **2002**, *114*, 1342; *Angew. Chem. Int. Ed.* **2002**, *41*, 1290; h) L. Jafarpour, S. P. Nolan, *Adv. Organomet. Chem.* **2001**, *46*, 181; i) D. Enders, H. Gielen, *J. Organomet. Chem.* **2001**, *617–618*, 70.
[20] a) W. A. Herrmann, C. Köcher, *Angew. Chem.* **1997**, *109*, 2256; *Angew. Chem. Int. Ed. Engl.* **1997**, *36*, 2162; b) A. C. Albeniz, P. Espinet, R. Manrique, A. Perez-Mateo, *Chem. Eur. J.* **2005**, *11*, 1565.
[21] Recently, the catalytic activity of acyclic Fischer carbene complexes of palladium and nickel has been reported: D. Kremzow, G. Seidel, C. W. Lehmann, A. Fürstner, *Chem. Eur. J.* **2005**, *11*, 1833.

 © 2005 Wiley-VCH Verlag GmbH & Co. KGaA, Weinheim

Peptide Nanostructures

DOI: 10.1002/anie.200501555

Methyl-Blocked Dimeric α,γ-Peptide Nanotube Segments: Formation of a Peptide Heterodimer through Backbone–Backbone Interactions**

*Roberto J. Brea, Manuel Amorín, Luis Castedo, and Juan R. Granja**

In recent years, considerable effort has been devoted to the synthesis of organic and inorganic nanotubes.[1] Among a number of other nanotube design concepts, self-assembling peptide nanotubes (SPNs)[1–6] have attracted attention for some time because of the probable ease with which they may be endowed with structural and functional properties of interest for applications in biology and materials science.[7] SPNs are formed by stacking cyclic peptides whose amino acid residues have configurations that impart the peptide ring backbone with an essentially flat shape and that orient the C=O and NH groups roughly perpendicular to the ring plane. This allows β-sheet-like hydrogen bonding between antiparallel rings (Figure 1). In particular, SPNs based on cyclic α,γ peptides (α,γ CPs) such as **1a** and **2a**, in which the requisite all-*trans* conformation is achieved by the alternation of (1*R*,3*S*)-3-aminocyclohexanecarboxylic acids (γ-Ach) with D-α-amino acids,[8] hold considerable promise for the design of nanotubes with novel structural and internal cavity properties.

The results reported herein support the possibility of constructing SPNs by using α,γ CPs of type **3**, in which the γ-amino acid is not γ-Ach but (1*R*,3*S*)-3-aminocyclopentanecarboxylic acid (γ-Acp).[9] We show that heterodimerization between γ-Ach-based and γ-Acp-based α,γ CPs is not only possible, but is favored over homodimerization for the compounds used herein. In nature, heterodimerization of peptides is common[10–12] and appears to constitute an economical means toward structural diversity and functional versatility; the same benefits may be expected to accrue from the development of a battery of α,γ CPs that are capable of forming hetero-oligomers with each other. However, whereas in all known natural cases the selectivity for hetero- rather than homodimerization is mainly due to interactions between the side chains of the component monomers, interactions of this kind are not necessary for preferential heterodimerization of the α,γ CPs studied herein. This is fortunate, because it means that the combinatorial advantages of heterodimerization are available without detriment to the possibility of exploiting side chains for other purposes.

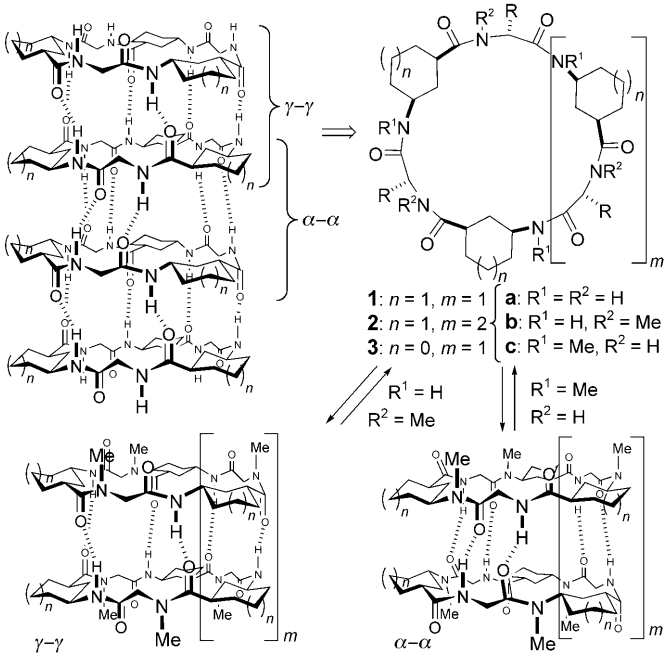


Figure 1. Design for self-assembling peptide nanotubes composed of *cyclo*[(D-Aa-(1*R*,3*S*)-γ-Aa)$_3$-] or *cyclo*[(D-Aa-(1*R*,3*S*)-γ-Aa)$_4$-] units, involving two different (α–α and γ–γ) Hydrogen-bonding patterns (Aa = amino acid). Dimer models of the two hydrogen-bonding patterns are shown at the bottom of the figure. Amino acid side chains have been omitted in the nanotube and dimer structures for clarity.

The construction of an SPN from α,γ CPs involves two different sets of β-sheet-like hydrogen bonds: one exclusively involves the NH and C=O groups of the γ-amino acid (γ–γ bonding, Figure 1) and the other, those of the α-amino acid (α–α bonding). In previous work with hexameric and octameric γ-Ach-based α,γ CPs, we found that α–α bonding was stronger than γ–γ bonding.[8] Herein, we accordingly focused on α–α bonding with the preparation of α,γ dimers in which γ–γ bonding was prevented by *N*-methylation of all the γ-amino acids as in **1c**–**3c** to avoid complications that would be irrelevant to this preliminary work.[13]

(1*R*,3*S*)-*N*-Boc-γ-Acp (**5**) was prepared from Vince's lactam (**4**)[14] by hydrogenation, acidic hydrolysis, and *N*-protection (Scheme 1) followed by successive recrystallizations from chloroform containing 0.7 equivalents of (+)-α-phenylethylamine, and was obtained with an enantiomeric purity greater than 97 %[15]. The *N*-methylated amino acid **6a** (^{Me}*N*-γ-Acp) was then obtained by treatment of **5** with sodium hydride and iodomethane in THF, and its fluorenyl-protected ester **6b** by reaction of **6a** with fluorenylmethanol.

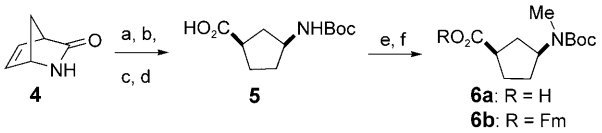
The α,γ CP *cyclo*[(D-Leu-(1*R*,3*S*)-^{Me}*N*-γ-Acp)$_3$-] (**7a**, Figure 2) was synthesized by standard procedures and characterized by NMR spectroscopy and mass spectrometry (see Supporting Information). Its ^{1}H NMR spectra in polar and nonpolar solvents (CCl_4, $CDCl_3$, MeOH, DMSO) are well-defined, reflect a high degree of symmetry, and show a $J_{NH,H\alpha}$

[*] R. J. Brea, M. Amorín, Prof. Dr. L. Castedo, Dr. J. R. Granja
Departamento de Química Orgánica e Unidade Asociada ó C.S.I.C.
Facultade de Química, Universidade de Santiago
15782 Santiago de Compostela (Spain)
Fax: (+34) 981-595012
E-mail: qojuangg@usc.es

[**] This work was supported by the Ministerio de Ciencia y Tecnología (SAF2001-3120, SAF2004-01044) and the Xunta de Galicia (PGIDT02BTF20901PR, PGIDT04BTF209006PR). M.A. and R.J.B. thank the Ministerio de Ciencia y Tecnología for their FPU grants.

Supporting information for this article is available on the WWW under http://www.angewandte.org or from the author.

InterScience
© 2005 Wiley-VCH Verlag GmbH & Co. KGaA, Weinheim



Scheme 1. Synthesis of (1*R*,3*S*)-Boc-^{Me}*N*-γ-Acp-OH (**6a**) and (1*R*,3*S*)-Boc-^{Me}*N*-γ-Acp-OFm (**6b**) from Vince's lactam (**4**); a) H_2, Pd/C, MeOH, 99%; b) HCl (10%), 90%; c) $(Boc)_2O$, *N*,*N*-diisopropylethylamine, H_2O/dioxane, 89%; d) resolution: (+)-α-phenylethylamine, $CHCl_3$/hexanes: $[\alpha]_D = -16.8$ ($c = 1.0$ in MeOH), >97% *ee*; e) NaH, MeI, THF, 98%; f) FmOH, 1-(3-dimethylaminopropyl)-3-ethylcarbodiimide, 1-hydroxybenzotriazole, 4-(dimethylamino)pyridine, CH_2Cl_2, 92%. Boc = *tert*-butoxycarbonyl, Fm = fluorenylmethyl.

coupling constant of 9.4 Hz, which is typical of the all-*trans* backbone conformation required for the flatness of the peptide ring (which, in turn, favors the formation of hydrogen-bonded assemblies such as the SPN shown in Figure 1). In nonpolar solvents, the formation of a dimer ($\mathbf{8}_{7a}$) is reflected by the downfield shift of the NH signal of Leu. The fact that the location of this signal ($\delta = 8.23$ ppm) remains constant at concentrations as low as 1×10^{-4} M, regardless of methanol composing up to 30% of the solvent or heating at 323 K, shows that the association constant for dimer formation must be at least $10^5\,M^{-1}$. FTIR spectra recorded in chloroform display bands at 1626, 1534, and 3304 cm^{-1} which, like analogous bands observed for other all-*trans* cyclic peptides linked by hydrogen bonds in dimers or SPNs,[2,8,13] resemble the amide I, amide II_{II}, and amide A bands typical of protein β sheets.

X-ray crystallography of a colorless prismatic crystal obtained from a solution of peptide **7a** in chloroform by vapor-phase equilibration with hexane confirmed the α–α dimerization of essentially flat, antiparallel rings by means of a β-sheet-like array of six hydrogen bonds with interatomic N···O distances of 2.88–2.98 Å (Figure 3a,b). The drum-shaped dimer has an approximate van der Waals internal diameter of 5.4 Å, and its cavity is occupied by a partially disordered chloroform molecule. The body-centered struc-

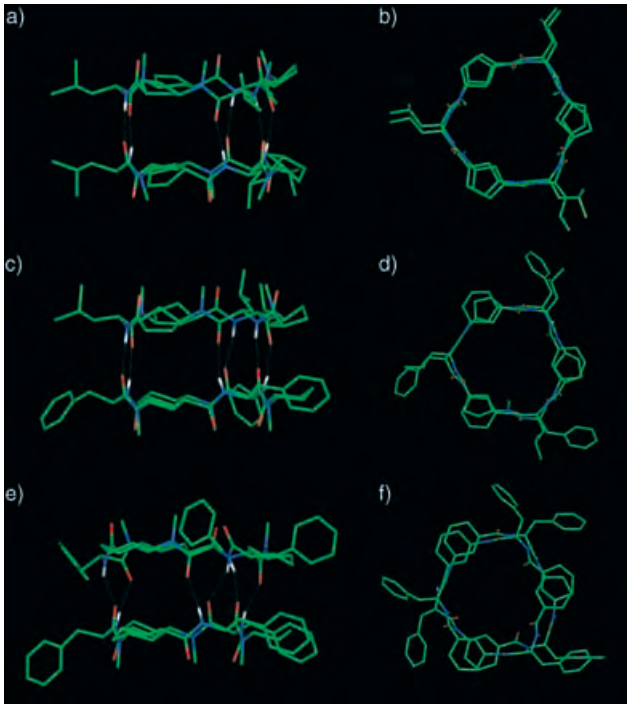


Figure 3. a) Views from the sides (a, c, e) and down the axes (b, d, f) of a,b) homodimers $\mathbf{8}_{7a}$ and e,f) **10**[8a], and of c,d) heterodimer $\mathbf{11}_{7a-9}$ in the solid state; chloroform molecules in the central cavities have been removed for clarity.

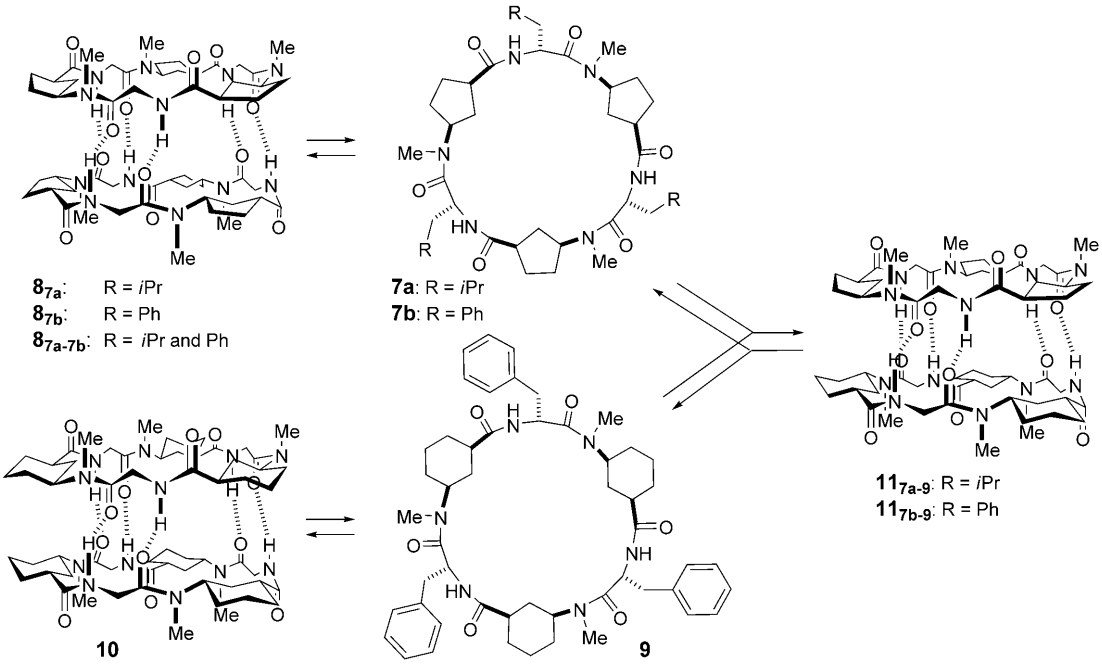


Figure 2. Homo- and heterodimerization of *cyclo*[(D-Leu-(1*R*,3*S*)-^{Me}*N*-γ-Acp)$_3$-] (**7a**), *cyclo*[(D-Phe-(1*R*,3*S*)-^{Me}*N*-γ-Acp)$_3$-] (**7b**) and *cyclo*[(D-Phe-(1*R*,3*S*)-^{Me}*N*-γ-Ach)$_3$-] (**9**).

 © 2005 Wiley-VCH Verlag GmbH & Co. KGaA, Weinheim

ture of the crystal forms channels by stacking the dimers along the crystallographic *a* axis, each dimer making van der Waals contacts with the next through its γ face carbonyl and *N*-methyl groups.

The γ-Ach-based **7a** analogue *cyclo*[(D-Phe-(1*R*,3*S*)-^{Me}*N*-γ-Ach)$_3$-] (**9**) also forms stable homodimers **10** in nonpolar solvents, with an association constant estimated to be at least $10^5\,M^{-1}$, as in the case of **7a** (Figure 2).[8] The possibility of heterodimer formation was confirmed upon the addition of 0.8 equivalents of **7a** to a solution of **9** (2.1 mM) in chloroform, which resulted in the appearance of a new species with a ^{1}H NMR spectrum that did not correspond to either of the possible homodimers. The dimeric nature of the new species, $\mathbf{11}_{\mathbf{7a\text{-}9}}$, was shown by NOE cross-peaks between the signals of $H\gamma_{Acp}$ (at $\delta = 4.92$ ppm) and $H\alpha_{Ach}$ (at $\delta = 2.62$ ppm). Definitive evidence of heterodimerization in the solid state was obtained by X-ray crystallography of the colorless prismatic single crystals recovered from a 1:1 solution of **7a** and **9** in chloroform. As expected, the monomeric cyclic peptides form heterodimers in which the two essentially flat rings are antiparallel, with their α faces linked in β-sheet fashion through six hydrogen bonds with N···O interatomic distances of 2.82–2.90 Å (Figure 3). The dimers stack closely along the *a* axis, each making van der Waals contacts with its neighbor with γ-face carbonyl and *N*-methyl groups. The resulting channel contains two chloroform molecules per unit, one in the cavity of the heterodimer and a second at variable sites between successive dimers.

Notably, the heterodimer $\mathbf{11}_{\mathbf{7a–9}}$ was in fact about 30-fold more abundant than the homodimer if prepared as described above from a mixture of **7a** and $\mathbf{9}$,$\mathbf{8}_{\mathbf{7a}}$ (0.8:1) which at 298 K corresponds to an energy difference of 2.0 kcal mol^{-1}. To determine whether this selectivity was derived from interactions between the side chains of the monomers, we investigated the dimerization of **7a** with *cyclo*[(D-Phe-(1*R*,3*S*)-^{Me}*N*-γ-Acp)$_3$-] (**7b**).[16] If the stability of $\mathbf{11}_{\mathbf{7a–9}}$ were the result of side-chain–side-chain interactions, the potential heterodimer $\mathbf{8}_{\mathbf{7a–7b}}$, in which the side chains are the same as those of $\mathbf{11}_{\mathbf{7a–9}}$ yet not the two backbones, is expected to be at least as stable as is $\mathbf{11}_{\mathbf{7a–9}}$ relative to $\mathbf{8}_{\mathbf{7a}}$. Nevertheless, the ^{1}H NMR spectrum of a 1:1 mixture of **7a** and **7b** in chloroform showed the presence of dimers $\mathbf{8}_{\mathbf{7a}}$, $\mathbf{8}_{\mathbf{7b}}$, and $\mathbf{8}_{\mathbf{7a–7b}}$ in almost equal concentrations, which implies that all three species have similar stabilities. This rules out the possibility of significant interactions between the side chains of opposing rings. Consistent with this conclusion, the addition of 0.9 equivalents of **9** to a solution of **7b** (4.6 mM) in chloroform resulted in the formation of heterodimer $\mathbf{11}_{\mathbf{7b–9}}$ without any observable trace of the homodimer **10**; this shows an even greater difference in stability between hetero- and homodimers than in the case of $\mathbf{11}_{\mathbf{7a–9}}$ and **10**.

The cause of the higher stability of the heterodimers is unclear. However, inspection of the crystal structures of $\mathbf{8}_{\mathbf{7a}}$, **10**[8a] and $\mathbf{11}_{\mathbf{7a–9}}$ (Figure 3) suggests that the heterodimer is more stable through an improved alignment of hydrogen-bond donors and acceptors. This could be due in part to more favorable packing between cyclopentyl and cyclohexyl than cyclopentyl–cyclopentyl or cyclohexyl–cyclohexyl ring packing. This hypothesis is supported by the intradimer distances between CPs in the crystals (see Supporting Information) and by those calculated from the N–H stretch frequencies ($\tilde{\nu} =$ 3304, 3309, and 3300 cm^{-1} in $\mathbf{8}_{\mathbf{7a}}$, **10** and $\mathbf{11}_{\mathbf{7a–9}}$, respectively; see Supporting Information). However, further studies might clarify this issue.

In conclusion, NMR and FTIR spectroscopy and X-ray diffraction data show conclusively that cyclic α,γ hexapeptides containing three γ-Acp units can form stable cylindrical dimers in which antiparallel peptide rings are linked by a β-sheet-like set of six hydrogen bonds. Even greater stability is shown by the heterodimers of these γ-Acp α,γ CPs with γ-Ach α,γ CPs. Potential applications for nanotubes developed from appropriately functionalized α,γ CPs include their use as logic gates, biosensors, catalysts, molecular receptors, and molecule containers.

Received: May 6, 2005
Revised: June 7, 2005
Published online: August 4, 2005

Keywords: amino acids · dimerization · nanotubes · peptides · self-assembly

[1] a) "Self-Assembly of Cyclic Peptides in Hydrogen-Bonded Nanotubes": R. J. Brea, J. R. Granja in *Dekker Encyclopedia of Nanoscience and Nanotechnology*, Marcel Dekker, **2004**, pp. 3439–3457; b) G. R. Patzke, F. Krumeich, R. Nesper, *Angew. Chem.* **2002**, *114*, 2554–2571; *Angew. Chem. Int. Ed.* **2002**, *41*, 2446–2461; c) D. T. Bong, T. D. Clark, J. R. Granja, M. R. Ghadiri, *Angew. Chem.* **2001**, *113*, 1016–1041; *Angew. Chem. Int. Ed.* **2001**, *40*, 988–1011; d) P. M. Ajayan, O. Z. Zhou, *Top. Appl. Phys.* **2001**, 80, 391–425.

[2] a) M. R. Ghadiri, J. R. Granja, R. A. Milligan, D. E. McRee, N. Khazanovich, *Nature* **1993**, *366*, 324–327; b) N. Khazanovich, J. R. Granja, D. E. McRee, R. A. Milligan, M. R. Ghadiri, *J. Am. Chem. Soc.* **1994**, *116*, 6011–6012; c) M. R. Ghadiri, J. R. Granja, L. K. Buehler, *Nature* **1994**, *369*, 301–304; d) J. D. Hartgerink, J. R. Granja, R. A. Milligan, M. R. Ghadiri, *J. Am. Chem. Soc.* **1996**, *118*, 43–50.

[3] a) D. Seebach, J. L. Matthews, A. Meden, T. Wessels, C. Baerlocher, L. B. McCusker, *Helv. Chim. Acta* **1997**, *80*, 173–182; b) T. D. Clark, L. K. Buehler, M. R. Ghadiri, *J. Am. Chem. Soc.* **1998**, *120*, 651–656.

[4] For recent examples of nanotubes made of δ-amino acids, see: a) D. Gauthier, P. Baillargeon, M. Drouin, Y. L. Dory, *Angew. Chem.* **2001**, *113*, 4771–4774; *Angew. Chem. Int. Ed.* **2001**, *40*, 4635–4638; b) S. Leclair, P. Baillargeon, R. Skouta, D. Gauthier, Y. Zhao, Y. L. Dory, *Angew. Chem.* **2004**, *116*, 353–357; *Angew. Chem. Int. Ed.* **2004**, *43*, 349–353.

[5] For a novel peptide nanotube made of 1,2,3-triazole-ε-amino acids, see: W. S. Horne, C. D. Stout, M. R. Ghadiri, *J. Am. Chem. Soc.* **2003**, *125*, 9372–9376.

[6] For peptide nanotubes made of linear peptides, see: M. Reches, E. Gazit, *Science* **2003**, *300*, 625–627.

[7] a) For a review of biotechnological nanotube applications, see: C. R. Martin, P. Kohli, *Nat. Rev.* **2003**, *2*, 29–37; b) C. Steinem, A. Janshoff, M. S. Vollmer, M. R. Ghadiri, *Langmuir* **1999**, *15*, 3956–3964; c) S. Fernández-López, H.-S. Kim, E. C. Choi, M. Delgado, J. R. Granja, A. Khasanov, K. Kraehenbuehl, G. Long, D. A. Weinberger, K. Wilcoxen, M. R. Ghadiri, *Nature* **2001**, *412*, 452–455; d) K. Motesharei, M. R. Ghadiri, *J. Am. Chem. Soc.* **1998**, *120*, 1347–1351.

 © 2005 Wiley-VCH Verlag GmbH & Co. KGaA, Weinheim

[8] a) M. Amorín, L. Castedo, J. R. Granja, *J. Am. Chem. Soc.* **2003**, *125*, 2844 – 2845; b) M. Amorín, V. Villaverde, L. Castedo, J. R. Granja, *J. Drug Delivery Sci. Technol.* **2005**, *15*, 87 – 92; c) M. Amorín, L. Castedo, J. R. Granja, *Chem. Eur. J.* **2005**, *11*, in press.
[9] For foldamers based on *cis*-γ-aminoproline, see: J. Farrera-Sinfreu, L. Zaccaro, D. Vidal, X. Salvatella, E. Giralt, M. Pons, F. Albericio, M. Royo, *J. Am. Chem. Soc.* **2004**, *126*, 6048 – 6057.
[10] a) P. M. Bowers, S. J. Cokus, D. Eisenberg, T. O. Yeates, *Science* **2004**, *306*, 2246 – 2249; b) A. Tsuchisaka, A. Theologis, *Proc. Natl. Acad. Sci. USA* **2004**, *101*, 2275 – 2280; c) For a recent heteromeric peptide nanotube, see: K. Rosenthal-Aiman, G. Svensson, A. Undén, *J. Am. Chem. Soc.* **2004**, *126*, 3372 – 3373; d) For the use of heteromeric nanotubes as ion channel rectifiers, see: J. Sanchez-Quesada, M. P. Isler, M. R. Ghadiri, *J. Am. Chem. Soc.* **2002**, *124*, 10004 – 10005.
[11] a) M. R. Young, H-S. Yang, N. H. Colburn, *Trends Mol. Med.* **2003**, *9*, 36 – 41; b) R. Eferl, R. Ricci, L. Kenner, R. Zenz, J.-P. David, M. Rath, E. F. Wagner, *Cell* **2003**, *112*, 181 – 192.
[12] a) S. K. Nair, S. K. Burley, *Cell* **2003**, *112*, 193 – 205; b) D. W. Felsher, *Nat. Rev. Cancer* **2003**, *3*, 375 – 380.
[13] a) M. R. Ghadiri, K. Kobayashi, J. R. Granja, R. K. Chadha, D. E. McRee, *Angew. Chem.* **1995**, *107*, 76 – 78; *Angew. Chem. Int. Ed. Engl.* **1995**, *34*, 93 – 95; b) K. Kobayashi, J. R. Granja, M. R. Ghadiri, *Angew. Chem.* **1995**, *107*, 79 – 81; *Angew. Chem. Int. Ed. Engl.* **1995**, *34*, 95 – 98; c) D. T. Bong, M. R. Ghadiri, *Angew. Chem.* **2001**, *113*, 2221 – 2224; *Angew. Chem. Int. Ed.* **2001**, *40*, 2163 – 2166; d) M. Saviano, A. Lombardi, C. Pedone, B. Di Blasio, X. C. Sun, G. P. Lorenzi, *J. Inclusion Phenom. Mol. Recognit. Chem.* **1994**, *18*, 27 – 36; e) X. C. Sun, G. P. Lorenzi, *Helv. Chim. Acta* **1994**, *77*, 1520 – 1526; f) W. S. Horne, N. Ashkenasy, M. R. Ghadiri, *Chem. Eur. J.* **2005**, *11*, 1137 – 1144; g) V. Pavone, E. Benedetti, B. Di Blasio, A. Lombardi, C. Pedone, L. Tomasich, G. P. Lorenzi, *Biopolymers* **1989**, *28*, 215 – 223.
[14] J. C. Jagt, A. M. Van Leusen, *J. Org. Chem.* **1974**, *39*, 565 – 566.
[15] P. Marfey, *Carlsberg Res. Commun.* **1984**, *49*, 591 – 596.
[16] In the absence of other peptides, **7b** formed highly stable homodimers ($\mathbf{8}_{\mathbf{7b}}$) in chloroform and other nonpolar solvents.

 © 2005 Wiley-VCH Verlag GmbH & Co. KGaA, Weinheim

Photoactivatable Proteins

DOI: 10.1002/anie.200501244

A Ligation and Photorelease Strategy for the Temporal and Spatial Control of Protein Function in Living Cells**

*Jean-Philippe Pellois and Tom W. Muir**

The temporal and spatial regulation of protein function is central to biological processes. Hence, the ability to artificially trigger molecular events in a biologically relevant context is useful for the study of living organisms. By chemically modifying a protein with groups that can respond to an external input such as light, control of protein function inside live cells can in principle be achieved. For instance, peptides or proteins that contain photolabile protecting groups appended to functionalities required for biological activity can be delivered into live cells and activated by UV irradiation at a desired time or location, and a cellular response can subsequently be measured.[1] This can be accomplished within single cells or in the context of whole organisms.[2] Although protein photocaging is a powerful tool to investigate biological systems, this approach has been limited by the difficulties associated with the preparation of the caged protein reagents.

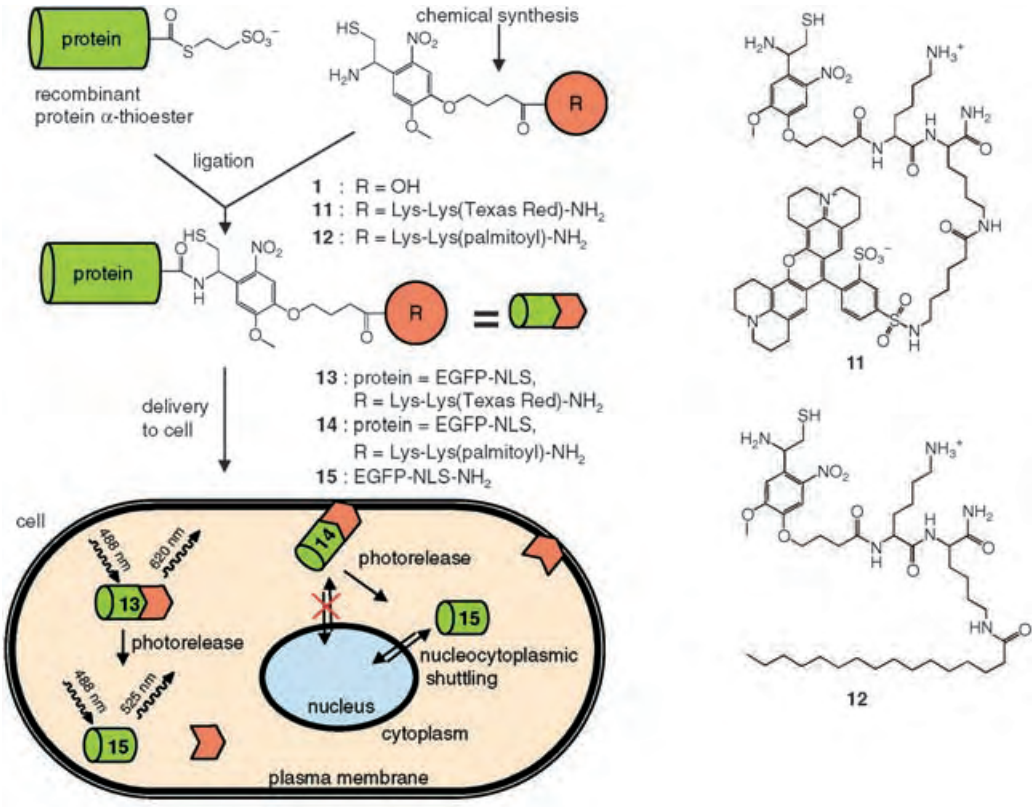
To facilitate the semisynthesis of caged proteins and expand the repertoire of suitable chemical reagents, we report the design, synthesis, and use of a ligation and photorelease (LPR) molecule suitable for the introduction of a light-activatable cleavage site within a semisynthetic protein (Scheme 1). In contrast to previously reported strategies relying on site-specific photochemical cleavage,[3] our LPR approach is based on the ligation of a photocleavable synthetic moiety to the C terminus of a recombinant protein. In principle, the chemical and protein components may influence the properties of one another in the ligated state. Irradiation with light and subsequent photorelease of each element may then lead to the recovery of their respective function. We demonstrate that such chimeric semisynthetic proteins can be efficiently prepared and photocleaved in vitro. We also demonstrate that photocleavage of protein constructs microinjected in live cells can be triggered in a

[*] Dr. J.-P. Pellois, Prof. T. W. Muir
The Laboratory of Synthetic Protein Chemistry
The Rockefeller University
Box 223, 1230 York Avenue, New York, NY 10021 (USA)
Fax: (+1) 212-327-7358
E-mail: muirt@mail.rockefeller.edu

[**] We gratefully acknowledge Dr. Alison North for her assistance at the bio-imaging center of The Rockefeller University. We thank Dr. Jianxin Shi, Edmund Schwartz, and Amy Tyszkiewicz for help with cloning procedures. This work was supported by NIH grant GM55843-07.

Supporting information for this article is available on the WWW under http://www.angewandte.org or from the author.

© 2005 Wiley-VCH Verlag GmbH & Co. KGaA, Weinheim



Scheme 1. Schematic representation of the semisynthesis and applications of protein constructs in which a photoactivatable cleavage site is introduced. A synthetic moiety (e.g. peptide, small molecule) is ligated to a recombinant protein through molecule **1**. The semisynthetic protein is then delivered into living cells where the protein and chemical components can be photoreleased from one another with temporal and spatial control.

dosable manner and that the subcellular localization of a protein can be controlled with light.

The LPR molecule **1** was designed to combine a 2-aminoethanethiol group required for native chemical ligation, an *o*-nitrobenzyl chromophore required for bond cleavage,[4] and a carboxylic acid tether for facile conjugation to amine-containing compounds (Scheme 1).[5] For synthetic purposes, the thiol and amine groups were protected as *S*-*tert*-butyl disulfide and *tert*-butyl carbamate, respectively. The protected molecule was synthesized in seven steps from vanillin (24% overall yield), essentially according to the route developed by Dawson and co-workers for the synthesis of a native chemical ligation auxiliary.[6,7] The product is suitable for solid-phase peptide synthesis (SPPS) using Boc (*tert*-butyloxycarbonyl) or Fmoc (9-fluorenylmethoxycarbonyl) protecting groups. Once deprotected, the 2-aminoethanethiol moiety should be compatible with native chemical ligation and expressed protein ligation (EPL).[8]

The native chemical ligation and photocleavage reactions were characterized using a model α-thioester peptide, Gly-Lys(TAMRA)-Gly-$SCH_2CH_2SO_3Na$ (**7**; TAMRA = 5-carboxytetramethylrhodamine), and a peptide synthesized with **1** at its N terminus, **1**-Lys-Lys(Fl)-NH_2 (**8**; Fl = 6-carboxyfluorescein).[7] The two peptides were incubated in phosphate-buffered saline (PBS), 100 mM 2-mercaptoethanesulfonic acid sodium salt (MESNa; pH 7.5), and the expected product, Gly-Lys(TAMRA)-Gly-**1**-Lys-Lys(Fl)-NH_2 (**9**), was obtained in near-quantitative yield in less than 1 h. Subsequent irradiation of **9** (in 1 mM in PBS, pH 7.5) at 325 nm with a He–Cd laser for 2 s was sufficient for quantitative photolysis and led to the formation of a single N-terminal product, Gly-Lys(TAMRA)-Gly-NH_2 (**10**). The LPR molecule was thus shown to react rapidly with thioesters and to efficiently generate the corresponding amide upon photolysis.[7]

The applicability of our caging strategy was next tested in the context of EPL. The enhanced green fluorescent protein (EGFP) containing the SV40 T-antigen Lys-Lys-Lys-Arg-Lys-Val nuclear localization signal (NLS) at its C terminus was used as a model protein and obtained as the recombinant protein α-thioester (from transthioesterification of an EGFP-NLS-GyrA intein fusion expressed in *E. coli*, see ref. [11]).[9,10] The peptides **1**-Lys-Lys(TR) (**11**) and **1**-Lys-Lys(Palm) (**12**; TR = Texas Red-X, Palm = palmitoyl) were synthesized by SPPS and used as model small molecules. The ligation reactions between the EGFP-NLS α-thioester and peptides **11** and **12** were monitored by reverse-phase HPLC, electrospray mass spectrometry (ES-MS), and sodium dodecyl sulfate/polyacrylamide gel electrophoresis (SDS-PAGE) and were complete in less than 12 h (Figure 1a). The products, EGFP-NLS-**1**-Lys-Lys(TR) (**13**) and EGFP-NLS-**1**-Lys-Lys-(Palm) (**14**), were purified and their identity confirmed by ES-MS. Protein **13** is labeled with a fluorophore that can undergo intramolecular fluorescence resonant energy transfer (FRET) with EGFP.[12] Protein **14** is modified with a non-hydrolyzable

 © 2005 Wiley-VCH Verlag GmbH & Co. KGaA, Weinheim

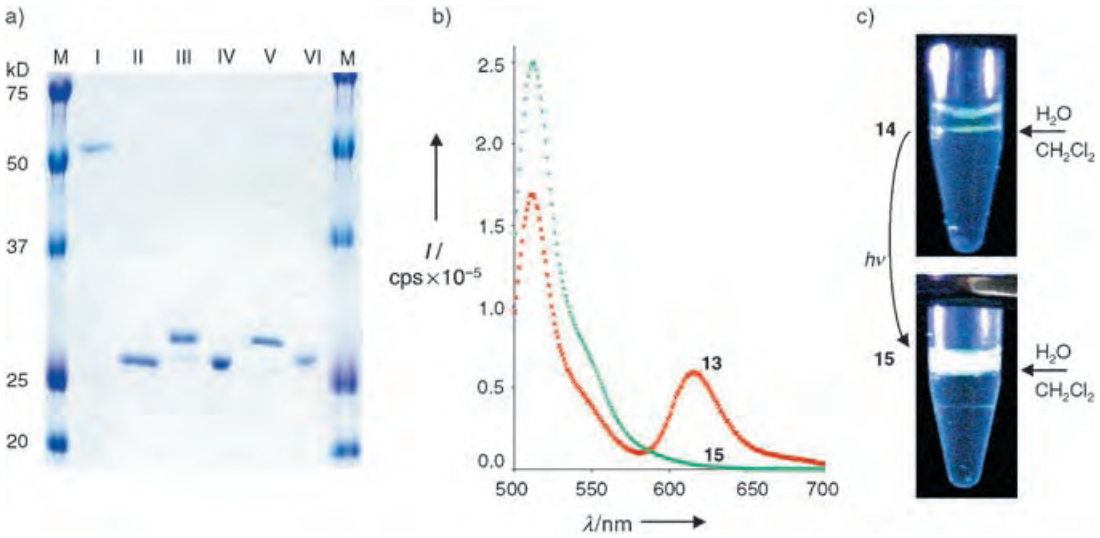


Figure 1. In vitro characterization of the semisynthetic proteins and their photocleaved products. a) SDS-PAGE analysis, Lanes M = marker; I = EGFP-NLS-GyrA-CBD; II = EGFP-NLS α-thioester; III = EGFP-NLS-**1**-Lys-Lys(TR) (**13**); IV = **13** + UV irradiation (**15**); V = EGFP-NLS-**1**-Lys-Lys-(Palm) (**14**); VI = **14** + UV irradiation (**15**). For all samples, UV irradiation was performed with a He–Cd laser at 325 nm for 2 s. Proteins were detected by coomassie staining. b) Fluorescence spectra of protein **13** before and after (→**15**) UV irradiation. Fluorescence excitation was performed at 488 nm. c) Images of test tubes containing protein **14**, before and after UV irradiation, in a two-phase system of water and dichloromethane. An arrow indicates the interface of the two solvents.

lipid, thereby mimicking a widespread post-translational phenomenon found in eukaryotic organisms.[13]

The photocleavage of **13** and **14** was first tested in vitro. Both constructs were irradiated with UV light, and the photolysis products were analyzed by HPLC, ES-MS, and SDS-PAGE. Under the conditions tested, the photolytic conversion was found to be quantitative, with the EGFP-NLS amide **15** (from **13** + UV or **14** + UV) identified as the only proteinogenic product (Figure 1a). The fluorescence spectrum of **13** showed FRET ($\lambda_{ex} = 488$ nm, $\lambda_{em} = 620$ nm) between EGFP and TR with an efficiency of 33%. Protein **13** was used to determine the kinetics and quantum yield of photolysis by using the decrease in FRET intensity as a direct measure of photocleavage between the FRET pair (Figure 1b).[14] Using irradiation at 365 nm and 1 mW cm^{-2}, the kinetics of photolysis was first-order with a half-life of $t_{1/2} = 178$ s and an observed quantum yield of 0.11. Photolysis was quantitative in less than 2 s when a high-intensity laser was used. The behavior of **14** before and after photorelease of the lipid moiety was tested by monitoring the affinity of the protein for a hydrophobic environment. When dichloromethane was added to **14** dissolved in PBS containing 10 mM 3-[(3-cholamidopropyl)dimethylammonio]-1-propane-sulfonate (CHAPS, pH 7.5), the protein localized exclusively at the interface of the two solvents (Figure 1c). Upon irradiation with UV light, the EGFP-NLS moiety was released from the interface and diffused in the aqueous phase.

Protein **13** was microinjected into Hela cells cultured on glass slides and live-cell imaging was performed on a confocal microscope. A FRET signal ($\lambda_{ex} = 488$ nm, $\lambda_{em} = 620$ nm) with an efficiency of 30% was observed accompanied with perfect colocalization of the signals from the green ($\lambda_{ex} = 488$ nm, $\lambda_{em} = 525$ nm) and red ($\lambda_{ex} = 565$ nm, $\lambda_{em} = 620$ nm) channels (Figure 2a). Upon

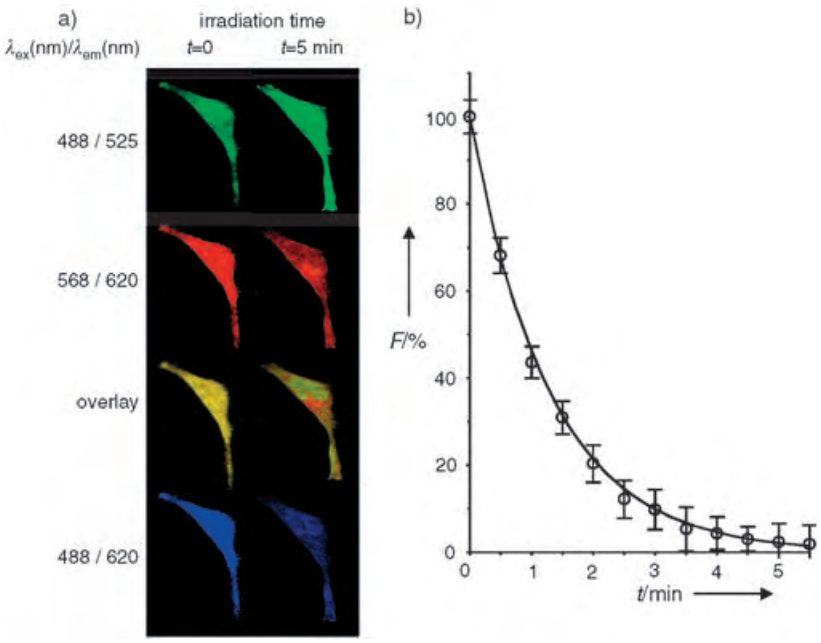


Figure 2. FRET assay. Hela cells were microinjected with **13** and exposed to low-intensity UV light (360 nm) at varying irradiation times. a) Pseudo-color images from confocal microscopy. The fluorescence signal from EGFP ($\lambda_{ex} = 488$ nm, $\lambda_{em} = 525$ nm), Texas Red ($\lambda_{ex} = 568$, $\lambda_{em} = 620$ nm), and FRET between EGFP and Texas Red ($\lambda_{ex} = 488$ nm, $\lambda_{em} = 620$ nm) were recorded before and immediately following UV irradiation. b) Time course of photocleavage. The FRET intensity F (averaged over the cytoplasmic area and normalized at t(irradiation) = 0) is plotted versus time of irradiation, along with an exponential curve of best fit, which yielded a first-order rate constant for photolysis of 1.3×10^{-2} s^{-1}. Error bars represent the standard deviation obtained from the averaging of two experiments.

© 2005 Wiley-VCH Verlag GmbH & Co. KGaA, Weinheim

irradiation of the whole cell at 360 nm (5 μW), the FRET intensity diminished and EGFP fluorescence inversely increased. The observed kinetics of photolysis was first-order with a half-life of $t_{1/2} = 53$ s (Figure 2b). This demonstrates that photolysis of a protein in a cell can be achieved in a dosable manner with low-intensity UV light.[15] This is especially relevant if different concentrations of a photocleaved species would be expected to trigger different responses. Interestingly, the red and green signals accumulated in different subcellular locations after UV irradiation (Figure 2). These results demonstrate that a protein and a small molecule can be photoreleased from one another, thereby triggering changes in their respective function or localization.

The possibility of photocontrolled cellular localization was further explored with protein **14**. It was expected that the modification of EGFP with a lipid would target the protein to cellular membranes.[16] Indeed, when microinjected in Hela cells, **14** localized with great specificity at the plasma membrane, with less than 6 and 2.5% of the total signal present in the cytoplasm and nucleus, respectively (Figure 3).

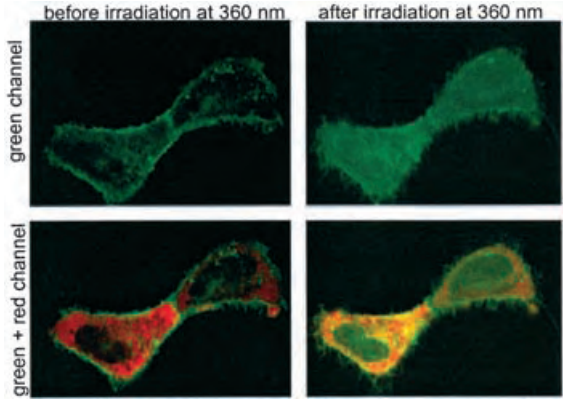


Figure 3. Representative images illustrating the photocontrol of the subcellular localization of a protein. Hela cells were microinjected with **14** and Dextran-TMR (70 kDa). Dextran-TMR was used as a red fluorescent marker that is excluded from the nucleus when injected in the cytoplasm. The images were acquired on a confocal microscope with green ($\lambda_{ex} = 488$ nm, $\lambda_{em} = 525$ nm) and red ($\lambda_{ex} = 568$, $\lambda_{em} = 620$ nm) channels and pseudo-colored. The fluorescence signals were recorded before and immediately following UV irradiation (360 nm).

When the cells were irradiated with UV light, the cleaved product **15** diffused in the cytoplasm and nucleus with respective 11- and 15-fold increases in signal. Even though an NLS was present in the construct, the protein did not accumulate in the nucleus presumably because its low molecular weight (28 kDa) allowed it to diffuse through the nuclear pore complex (NPC).[17] It is therefore interesting to note that the photocaging of a functional lysine present in the NLS sequence might not be sufficient to achieve photocontrol of the nuclear import of a small protein such as EGFP.[18] Indeed, a protein with a molecular weight below the NPC diffusion limit (≈ 40 kDa) might diffuse in and out of the nucleus in both its caged-NLS and uncaged-NLS states. In contrast, using a non-hydrolyzable but photocleavable lipid, EGFP was excluded from the nucleus in the absence of light but underwent free nucleocytoplasmic shuttling after irradiation. Hence, these results raise the possibility of the photocontrol of a protein's activity not by the caging of a critical group required for function but rather by control of its location.[19]

In summary, we have reported the synthesis of a LPR molecule and demonstrated its utility in the synthesis of caged proteins. We demonstrated that a photoactivatable cleavage site can be introduced in a semisynthetic protein containing complex chemical modifications. Furthermore, we showed that photocleavage can be achieved in a dosable manner to generate a controlled amount of cleaved product inside a living cell. Finally, we demonstrated that the localization of an EGFP-NLS construct can be controlled by photochemically releasing a lipid moiety from its C terminus. The chemical diversity that can be introduced by this approach should permit the manipulation of a protein in a variety of ways and the generation of a variety of responses upon photocleavage. Such caging strategies hold potential for the characterization of complex biological processes in their native context, single cells or whole organisms. Direct applications might involve the photoregulation of proteins containing photocleavable localization signals and post-translational modifications.

Received: April 8, 2005
Published online: August 1, 2005

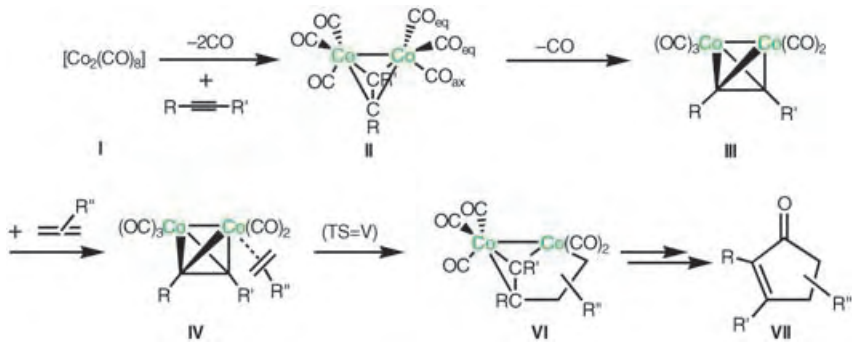
Keywords: bioorganic chemistry · drug delivery · photoactivation · proteins

[1] a) K. Curley, D. S. Lawrence, *Curr. Opin. Chem. Biol.* **1999**, *3*, 84; b) S. N. Cook, W. E. Jack, X. Xiong, L. E. Danley, J. A. Ellman, P. G. Schultz, C. J. Noren, *Angew. Chem.* **1995**, *107*, 1736; *Angew. Chem. Int. Ed. Engl.* **1995**, *34*, 1629; c) K. D. Philipson, J. P. Gallivan, G. S. Brandt, D. A. Dougherty, H. A. Lester, *Am. J. Physiol. Cell Physiol.* **2001**, *281*, C195; d) K. Zou, W. T. Miller, R. S. Givens, H. Bayley, *Angew. Chem.* **2001**, *113*, 3139; *Angew. Chem. Int. Ed.* **2001**, *40*, 3049; e) M. Ghosh, X. Song, G. Mouneimne, M. Sidani, D. S. Lawrence, J. S. Condeelis, *Science* **2004**, *304*, 743; f) A. Nguyen, D. M. Rothman, J. Stehn, B. Imperiali, M. B. Yaffe, *Nat. Biotechnol.* **2004**, *22*, 993; g) J. P. Pellois, M. E. Hahn, T. W. Muir, *J. Am. Chem. Soc.* **2004**, *126*, 7170; h) M. E. Hahn, T. W. Muir, *Angew. Chem.* **2004**, *116*, 5924; *Angew. Chem. Int. Ed.* **2004**, *43*, 5800.
[2] S. B. Cambridge, R. L. Davis, J. S. Minden, *Science* **1997**, *277*, 825.
[3] a) P. M. England, H. A. Lester, N. Davidson, D. A. Dougherty, *Proc. Natl. Acad. Sci. USA* **1997**, *94*, 11025; b) M. Endo, K. Nakayama, Y. Kaida, T. Majima, *Angew. Chem.* **2004**, *116*, 5761; *Angew. Chem. Int. Ed.* **2004**, *43*, 5643.
[4] a) A. Patchornik, B. Amit, R. B. Woodward, *J. Am. Chem. Soc.* **1970**, *92*, 6333; b) S. R. Adams, R. Y. Tsien, *Annu. Rev. Physiol.* **1993**, *55*, 755.
[5] C. P. Holmes, *J. Org. Chem.* **1997**, *62*, 2370.
[6] C. Marinzi, J. Offer, R. Longhi, P. E. Dawson, *Bioorg. Med. Chem.* **2004**, *12*, 2749.
[7] See the Supporting Information for experimental details.
[8] T. W. Muir, *Annu. Rev. Biochem.* **2003**, *72*, 249.
[9] R. Y. Tsien, *Annu. Rev. Biochem.* **1998**, *67*, 509.
[10] M. R. Fontes, T. Teh, B. Kobe, *J. Mol. Biol.* **2000**, *297*, 1183.

 © 2005 Wiley-VCH Verlag GmbH & Co. KGaA, Weinheim

[11] The fusion protein was cloned into the pTXB1 bacterial expression vector (New England Biolab, Beverly, MA) upstream of the *Mycobacterium xenopi* GyrA intein and a chitin binding domain. Following overexpression in *E. coli*, the soluble fraction of the cell lysate was purified on chitin resin. The EGFP-NLS moiety was cleaved from the resin by incubation of the beads with MESNa to yield an EGFP-NLS with a C-terminal α-thioester.
[12] P. R. Selvin, *Methods Enzymol.* **1995**, *246*, 301.
[13] M. D. Resh, *Cell. Signalling* **1996**, *8*, 403.
[14] Irradiation was performed with either a He–Cd laser (325 nm and 4.74 $W cm^{-2}$) or a Hg lamp equipped with a narrow-bandwidth filter (365 nm and 1 $mW cm^{-2}$).
[15] Rapid (< 2 s) and quantitative photocleavage was observed when irradiation with high-intensity light (365 nm, 50 mW) was performed.
[16] a) D. Kadereit; J. Kuhlmann, H. Waldmann, *ChemBioChem* **2000**, *1*, 144; b) R. Reents, M. Wagner, S. Schlummer, J. Kuhlmann, H. Waldmann, *ChemBioChem* **2005**, *6*, 86.
[17] a) O. Rosorius, P. Heger, G. Stelz, N. Hirschmann, J. Hauber, R. H. Stauber, *BioTechniques* **1999**, *27*, 350; b) D. Görlich, U. Kutay, *Annu. Rev. Cell Dev. Biol.* **1999**, *15*, 607.
[18] Y. Watai, I. Sase, H. Shiono, Y. Nakano, *FEBS Lett.* **2001**, *488*, 39.
[19] P. J. Belshaw, S. N. Ho, G. R. Crabtree, S. L. Schreiber, *Proc. Natl. Acad. Sci. USA* **1996**, *93*, 4604.

 © 2005 Wiley-VCH Verlag GmbH & Co. KGaA, Weinheim



Scheme 1. Pauson–Khand mechanism.

Reaction Mechanisms

DOI: 10.1002/anie.200500955

Lewis Base Promoters in the Pauson–Khand Reaction: A Different Scenario**

Carlos Perez del Valle, Anne Milet, Yves Gimbert,* and Andrew E. Greene*

The Pauson–Khand reaction,[1] a dicobalt octacarbonyl mediated process for joining an olefin and an acetylene to produce a cyclopentenone (Scheme 1), is enjoying increased application in synthesis because of recent improvements that permit a broad range of substrates to be used successfully.[2–5] Spectacular rate and yield increases in both the intra- and intermolecular versions of the reaction have been found to result, in particular, from the addition of Lewis bases,[6] such as amines[3] and thioethers[4] as well as alcohols, ethers, and water.[5]

Although the fundamental role of these Lewis base additives has received little study, it has been widely assumed that they function by accelerating the departure of a second CO ligand from the acetylene cobalt complex to create the requisite vacant site for olefin coordination, and in this way overcome the putative limiting factor.[6] Current reports abound with statements such as "[certain] Lewis bases in low-valent organotransition-metal complexes make the existing ligands labile and produce the reactive complexes"[6b] and "when amines coordinate to low-valent organotransition metals, the existing ligands on the metal become labile".[6a] However, do these spectacular increases really derive from a facilitated departure of a CO ligand to liberate a site for olefin coordination? We questioned this interpretation as it seemed clear that the obligatory loss of the first CO ligand would be energetically the same in the absence or presence of the promoter;[7] the fact that similar temperatures[8] are required for the reaction with and without a promoter being present provides evidence for this reasoning. Moreover, simple Lewis bases, essentially σ donors, should increase backdonation toward the remaining CO ligands by electronic enrichment of the metal, thus making the loss of the second CO ligand at best comparable, if not more difficult.[9] Herein, the prevailing view is shown to be incorrect and a new interpretation based on theoretical studies at the DFT level is outlined.

Yamanaka and Nakamura[10a] and our group[10b] have described the Pauson–Khand reaction pathway at the DFT level. Three particularly important findings resulted: First, the step that requires the most energy (ca. 26.4 kcal mol^{-1}) is decarbonylation,[10c] which occurs at the outset of the reaction (**II**→**III**, Scheme 1); second, equatorial (eq; $\mathbf{IV}_{eq}$) and axial (ax; $\mathbf{IV}_{ax}$) olefin coordination modes are possible (Figures 1 and 2), with the energies of activation for the formation of the cobaltacycle (**VI**) in the range 10.0–14.4 kcal mol^{-1} (the lowest-energy transition state is $\mathbf{V}_{ax}$);[10b] third, the formation of the cobaltacycle is reversible.[11]

In the present study, a CO ligand in complex **II** was replaced with a molecule of water, which occupies a lower-energy equatorial position ($\Delta E = 5$ kcal mol^{-1}, complex $\mathbf{III}_{H_2O}$; Figure 3, blue data).[13] Based on examination of the Co–CO bond lengths in $\mathbf{III}_{H_2O}$, extraction of a second

[*] Dr. C. Perez del Valle, Dr. A. Milet, Dr. Y. Gimbert, Dr. A. E. Greene
Université Joseph Fourier de Grenoble
Chimie Recherche (LEDSS)
38041 Grenoble Cedex (France)
Fax: (+33) 4-76-51-44-94
E-mail: Anne.Milet@ujf-grenoble.fr
Yves.Gimbert@ujf-grenoble.fr

[**] We acknowledge the Université Joseph Fourier (UJF) and the CECIC for providing computer facilities. We also express our gratitude to Dr. P. Vatton for the installation of the applied software programs. Financial support from the UJF and the CNRS (UMR 5616, FR 2607) are gratefully acknowledged.

Supporting information for this article is available on the WWW under http://www.angewandte.org or from the author.

© 2005 Wiley-VCH Verlag GmbH & Co. KGaA, Weinheim

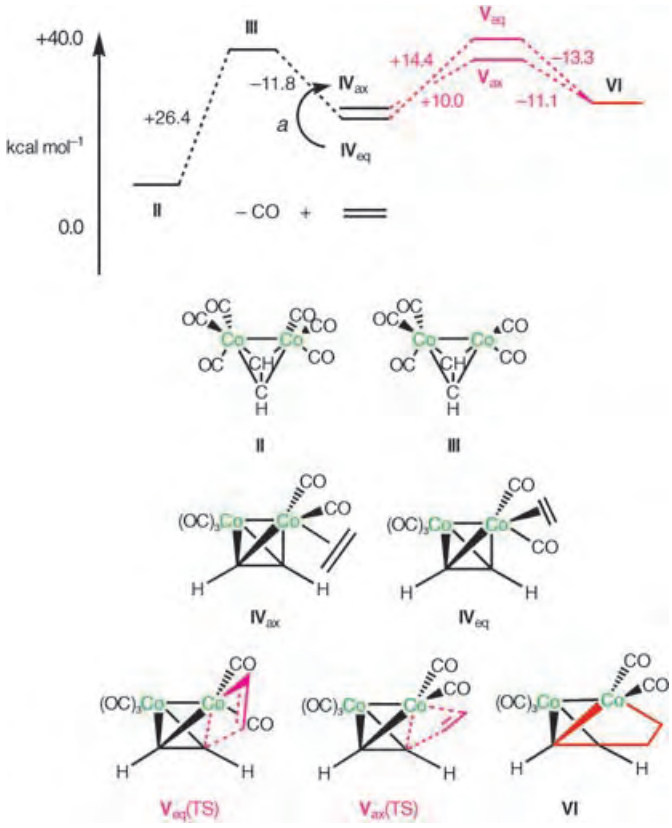


Figure 1. Energy barrier for formation of **VI** without a promoter. *a*) See Figure 2 for the transformation of $\mathbf{IV}_{eq}$ into $\mathbf{IV}_{ax}$. TS = transition state.

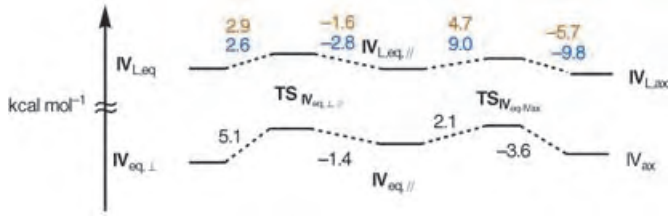


Figure 2. Transformation of $\mathbf{IV}_{eq}$ into $\mathbf{IV}_{ax}$. L = Ligand; ⊥, // are perpendicular and parallel coordination modes, respectively (with respect to the Co–Co axis).

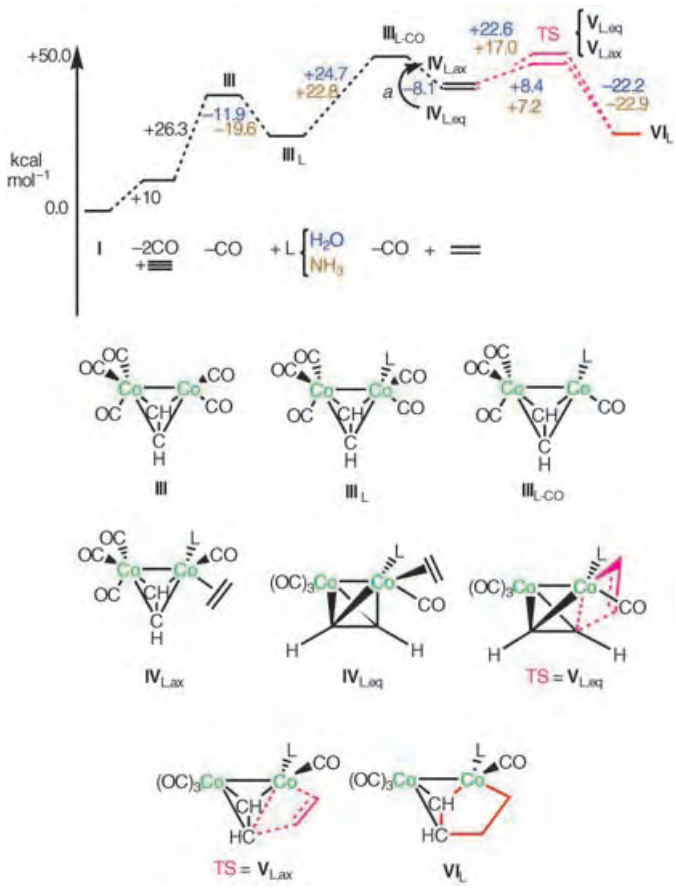


Figure 3. Energy barrier for formation of **VI** with promoter. *a*) See Figure 2 for the transformation of $\mathbf{IV}_{L,eq}$ into $\mathbf{IV}_{L,ax}$.

molecule of CO from $\mathbf{III}_{H_2O}$ was found to engender complex $\mathbf{III}_{H_2O\text{–}CO}$, in which the CO ligand has been lost from the remaining equatorial position on the water-associated cobalt atom (24.7 versus 31.5 kcal mol^{-1} for removal of a CO ligand from the next lowest-energy position, which is in the *trans*-equatorial position on the water-free cobalt atom). It is perfectly clear that water does not facilitate the loss of a second CO ligand, as only 1.6 kcal mol^{-1} separates the loss of the first and second CO ligands.[14] Next, association of complex $\mathbf{III}_{H_2O\text{–}CO}$ with ethylene at the vacant site on the water-associated cobalt atom produced complexes $\mathbf{IV}_{H_2O,ax}$ and $\mathbf{IV}_{H_2O,eq}$ (Figure 3).[15] The former confronts an activation-energy barrier of 8.4 kcal mol^{-1} for the formation of cobaltacycle $\mathbf{VI}_{H_2O}$ via transition-state $\mathbf{V}_{H_2O,ax}$, whereas the latter must overcome an activation-energy barrier of 22.6 kcal mol^{-1} via $\mathbf{V}_{H_2O,eq}$. Thus, it can be assumed that olefin insertion in the presence of water occurs from the axial position with an activation-energy barrier of 8.4 kcal mol^{-1}. This activation-energy barrier is lower than when the water is absent (then the olefin insertion is 10.0 kcal mol^{-1} from an axial position and 14.4 kcal mol^{-1} from an equatorial),[10b,16] but is nevertheless too high to explain the substantial acceleration of the reaction in its presence. A comparison of Figures 1 and 3, however, clearly reveals the remarkable ability of the promoter to stabilize the cobaltacycle: $\mathbf{VI}_{H_2O}$ is more than 22 kcal mol^{-1} lower than the transition state $\mathbf{V}_{H_2O,ax}$. As only 8.4 kcal mol^{-1} is required to reach this transition state in the forward direction, the formation of the cobaltacycle is in essence irreversible[17] in the presence of water. This irreversibility is the major effect of this promoter in the Pauson–Khand reaction.

Ammonia has also been studied at the DFT level to probe the remarkable accelerating effect of amines in the Pauson–Khand reaction, and the results have been found to parallel those obtained above with water as the promoter. Once again, removal of a second CO ligand from the complex ($\mathbf{III}_{NH_3}$) is energetically comparable to removal of the first ligand (Figure 3, brown data). The lower activation energy leading to the cobaltacycle transition state $\mathbf{V}_{NH_3}$ in the forward direction is 7.2 kcal mol^{-1} (Figure 3) and starting from the cobaltacycle $\mathbf{VI}_{NH_3}$, the activation energy is 22.9 kcal mol^{-1}, which effectively makes the insertion, as before, irreversible.

 © 2005 Wiley-VCH Verlag GmbH & Co. KGaA, Weinheim

In conclusion, it has been shown for the first time that most simple Lewis base promoters are likely to achieve their dramatic rate effects in the Pauson–Khand reaction by imposing irreversibility on olefin insertion, rather than by facilitating the departure of a CO ligand to create a vacant site for olefin coordination, as previously believed. This discovery may help in the design of new ligands for improved efficacy and/or asymmetric induction in this important transformation.

Received: March 15, 2005
Revised: April 20, 2005
Published online: August 3, 2005

Keywords: coordination modes · cycloaddition · density functional calculations · insertion · ligand effects

[1] For recent reviews, see: a) O. Geis, H. G. Schmalz, *Angew. Chem.* **1998**, *110*, 955 – 958; *Angew. Chem. Int. Ed.* **1998**, *37*, 911 – 914; b) N. Jeong, *Trans. Met. Org. Synth.* **1998**, *1*, 560 – 577; c) Y. K. Chung, *Coord. Chem. Rev.* **1999**, *188*, 297 – 341; d) K. M. Brummond, J. L. Kent, *Tetrahedron* **2000**, *56*, 3263 – 3283; e) A. J. Fletcher, S. D. R. Christie, *J. Chem. Soc. Perkin Trans. 1* **2000**, 1657 – 1668; f) J. Blanco-Urgoiti, L. Anorbe, L. Perez-Serrano, G. Dominguez, J. Perez-Castells, *Chem. Soc. Rev.* **2004**, *33*, 32 – 42; g) S. E. Gibson, N. Mainolfi, *Angew. Chem.* **2005**, *117*, 3082 – 3097; *Angew. Chem. Int. Ed.* **2005**, *44*, 3022 – 3037.

[2] Dry-support adsorption: W. A. Smit, S. O. Simonyan, G. S. Tarasov, G. S. Mikaelian, A. S. Gybin, I. I. Ibragimov, R. Caple, O. Froen, A. Kraeger, *Synthesis* **1989**, 472 – 476; photochemistry: B. L. Pagenkopf, T. Livinghouse, *J. Am. Chem. Soc.* **1996**, *118*, 2285 – 2286; amine oxides: S. Schambayati, W. E. Crowe, S. L. Schreiber, *Tetrahedron Lett.* **1990**, *31*, 5289 – 5292; N. Jeong, Y. K. Chung, B. Y. Lee, S. H. Lee, S. E. Yoo, *Synlett* **1991**, 204 – 206; phosphine oxides: D. C. Billington, I. M. Helps, P. L. Pauson, W. Thomson, D. Willson, *J. Organomet. Chem.* **1988**, *354*, 233 – 242; sulfoxides: Y. K. Chung, B. Y. Lee, N. Jeong, M. Hudecek, P. L. Pauson, *Organometallics* **1993**, *12*, 220 – 223.

[3] Amines: a) T. Rajesh, M. Periasamy, *Tetrahedron Lett.* **1998**, *39*, 117 – 118; b) T. Sugihara, M. Yamada, H. Ban, M. Yamaguchi, C. Kaneko, *Angew. Chem.* **1997**, *109*, 2884 – 2886; *Angew. Chem. Int. Ed. Engl.* **1997**, *36*, 2801 – 2804.

[4] Thioethers: M. E. Kraft, I. L. Scott, R. H. Romero, S. Feibelmann, C. E. Van Pelt, *J. Am. Chem. Soc.* **1993**, *115*, 7199 – 7203; T. Sugihara, M. Yamada, M. Yamaguchi, M. Nishizawa, *Synlett* **1999**, 771 – 773; W. J. Kerr, D. M. Lindsay, M. McLaughlin, P. L. Pauson, *Chem. Commun.* **2000**, 1467 – 1468.

[5] Alcohols, ethers, and water: B. E. La Belle, M. J. Knudsen, M. M. Olmstead, H. Hope, M. D. Yanuck, N. E. Shore, *J. Org. Chem.* **1985**, *50*, 2515 – 2517; T. Sugihara, M. Yamaguchi, *Synlett* **1998**, 1384 – 1386.

[6] For reviews, see: a) T. Sugihara, M. Yamaguchi, M. Nishizawa, *Rev. Heteroat. Chem.* **1999**, *21*, 179 – 194; b) T. Sugihara, M. Yamaguchi, M. Nishizawa, *Chem. Eur. J.* **2001**, *7*, 1589 – 1595.

[7] It is important to point out that there is apparently no pathway (eventually of lower energy) that involves a concerted exchange[12] or direct attack of the promoter on a CO ligand.

[8] For example, the Pauson–Khand reaction of 1-(hept-6-en-1-ynyl)benzene in the presence of cyclohexylamine required 3 days at 25 °C to obtain the expected adduct in 46% yield, whereas at 83 °C, typical thermal conditions, the reaction was complete after 5 min and afforded the adduct in 99% yield.[3b]

[9] Although phosphines and phosphites can be considered Lewis bases, as they coordinate to the metal center through σ donation, the relatively low-energy phosphorus d orbitals, which permit overlap with the metal d orbitals, also make them π acceptors. For this reason, they cannot be treated in the present context as simple Lewis bases. Thioethers, which are also π acceptors although weaker than phosphines, appear from preliminary results to behave as H_2O and NH_3, namely, as pure σ donors (A. Milet, C. Perez del Valle, unpublished results).

[10] a) M. Yamanaka, E. Nakamura, *J. Am. Chem. Soc.* **2001**, *123*, 1703 – 1708; b) T. J. M. de Bruin, A. Milet, F. Robert, Y. Gimbert, A. E. Greene, *J. Am. Chem. Soc.* **2001**, *123*, 7184 – 7185; c) for the influence of the acetylene substituents in determining the CO ligand that is lost, see: F. Robert, A. Milet, Y. Gimbert, D. Konya, A. E. Greene, *J. Am. Chem. Soc.* **2001**, *123*, 5396 – 5400.

[11] Reversibility seems probable on closer examination, although the contrary was assumed[10b] based on earlier work.[1c,10a] This possibility is supported by a subsequent mass-spectrometric study[12] that detected in two separate experiments the insertion product prior to incorporation of any of the CO present and follows from the low CO concentration generally present in the Pauson–Khand reaction medium. (Reversibility does not affect the conclusion given in reference [10b].)

[12] Y. Gimbert, D. Lesage, A. Milet, F. Fournier, A. E. Greene, J.-C. Tabet, *Org. Lett.* **2003**, *5*, 4073 – 4075.

[13] Computational details: All calculations were performed with the Gaussian 98 suite of programs with a restricted B3LYP functional and the LANL2DZ for the Co centers and a D95 split valence basis set for C, O, and H atoms, with an augmentation of d-polarization functions on the C and O atoms. The basis set is denoted as LANL2DZ*; a) Gaussian 98 (Revision A.6): M. J. Frisch, et al. (see the Supporting Information); b) restricted B3LYP functional: A. D. Becke, *J. Chem. Phys.* **1993**, *98*, 5648 – 5652; C. Lee, W. Yang, R. G. Parr, *Phys. Rev. B* **1988**, *37*, 785 – 789; c) LANL2DZ: P. J. Hay, W. R. Wadt, *J. Chem. Phys.* **1985**, *82*, 270–283; d) D95 split valence: T. H. Dunning, Jr., P. J. Hay in *Modern Theoretical Chemistry* (Ed.: H. F. Schaefer, III), Plenum, New York, **1976**, pp. 1 – 28.

[14] This finding is fully consistent with recent calculations (supported by X-ray structure determinations) carried out by Frenking et al. on the octahedral complexes $[M(CO)_6]$ and $[M(CO)_5L]$ (M = Cr, Mo, W; L = H_2O, NH_3). In this investigation, it was shown that replacing a CO ligand with a Lewis base (L) significantly shortens the M–CO bond *trans* to L and slightly shortens those *cis*. On the reasonable assumption that the length of a M–CO bond reflects its strength, the results of Frenking et al. imply that removal of a second CO ligand from $[M(CO)_5L]$ is at best no easier than removal of the first; see: G. Frenking, S. Dapprich, T. Meisterknet, J. Uddin, *Metal–Ligand Interactions in Chemistry, Physics and Biology* (Eds.: N. Russo, D. R. Salahub), Kluwer, Dordrecht, **2000**, pp. 73 – 89.

[15] Pseudorotation[10b] in the equatorially coordinated olefin complex $\mathbf{IV}_{H_2O,eq}$ to give the axially coordinated complex $\mathbf{IV}_{H_2O,ax}$ was determined to be energetically feasible (see Figure 2).

[16] This lowering of the energy of activation is because of a reduction in the gap energy between the highest occupied molecular orbital (HOMO) of the alkyne–$Co_2(CO)_4H_2O$ fragment and the lowest unoccupied molecular orbital (LUMO) of ethylene in $\mathbf{IV}_{H_2O}$ (0.211 versus 0.224 eV in the complex without the promoter, **IV**). As this interaction is involved in the formation of the new C–C bond of the cobaltacycle, it follows that the better overlap in $\mathbf{IV}_{H_2O}$ should translate into a lower activation energy.

[17] For a discussion on the effect of imposing irreversibility on a step in a reversible, multistep transformation, see: T. Baer, W. L. Hase in *Unimolecular Reaction Dynamics* (Eds.: M. L. H. Green, J. Halpem, S. V. Ley, T. Mukaiyama, J. P. Simons), Oxford University Press, Oxford, **1996**.

 © 2005 Wiley-VCH Verlag GmbH & Co. KGaA, Weinheim

Coordination Polymers

DOI: 10.1002/anie.200500207

A Synthetic Zwitterionic Water Channel: Characterization in the Solid State by X-ray Crystallography and NMR Spectroscopy**

Zhaofu Fei, Dongbin Zhao, Tilmann J. Geldbach, Rosario Scopelliti, Paul J. Dyson, Sasa Antonijevic,* and Geoffrey Bodenhausen*

Bio-inspired supramolecular frameworks are of both fundamental value as models and of practical importance in areas such as materials science, catalysis, and molecular electronics.[1–3] Many of these synthetic materials are constructed from metal ions as connectors and ligands as linkers, and are referred to as coordination polymers.[4] Porous materials are of particular interest, as the nanosized cavities lead to novel phenomena, with applications in separation, storage, and catalysis. In this respect, attempts to generate synthetic water channels that mimic aquaporin water channels[5] have met with some success.[6–10] Here we describe a zwitterionic, helical tube of nanodimensions that to some extent mimics aquaporin, and provide a detailed study of the water incorporated inside the channel over a wide temperature range by solid-state ^{2}H NMR spectroscopy.

Reaction of the carboxy-functionalized imidazolium salt *N*,*N*′-diacetic acid imidazolium bromide[11] with zinc in aqueous solution affords zwitterionic coordination polymer **1** in crystalline form. The structure of **1** was characterized by single-crystal X-ray diffraction at 140 K and is shown in Figure 1. To ensure that the encapsulated water does not undergo any structural changes at ambient temperature, the structure was also determined at 293 K (see Supporting Information). The macrostructure is formed from $ZnBr(H_2O)$ units linked by bridging dicarboxylate anions, which assemble into helical channels and appear to be supported by weak π-stacking interactions between the imidazolium moieties and by intrahelical hydrogen bonds. The strongest hydrogen bonds stem from contacts of the carboxy oxygen atom O2 to H3 and H6 in the next layer. Two molecules constitute a full cycle within the helix with distances between the layers of 6.234 Å. The cavity of the channel is occupied by water molecules, which form a one-dimensional chain with distances between the oxygen atoms of 3.157 Å.

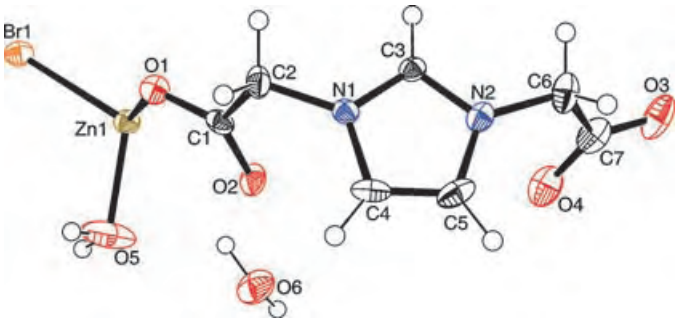


Figure 1. Structure of the asymmetric unit of **1** (ORTEP plot; ellipsoids are drawn at the 50% probability level). Selected bond lengths [Å] and angles [°]: Zn1–Br1 2.3677(6), Zn–O1 1.977(2), Zn–O4 1.983(3), Zn–O5 2.014(3), C1–O1 1.270(4), C1–O2 1.243(4), C7–O3 1.199(5), C7–O4 1.287(5); O1-C1-O2 124.9(3), O3-C7-O4 126.2(4), Br1-Zn1-O1 109.73(7), Br1-Zn1-O5 111.0(1), Br1-Zn1-O4 114.88(8), O1-Zn1-O5 110.4(1), O1-Zn1-O4 117.1(1), O4-Zn1-O5 92.5(2).

The coordination sphere around the zinc anion in **1** is best described as a distorted tetrahedron with angles between 92.5(2) and 117.1(1)°. Zinc–oxygen bond lengths lie between 1.997(2) and 2.014(3) Å, and both angles and bond lengths are in good agreement with those of comparable zinc dicarboxylate polymers.[12]

The helices are packed in a hexagonal-based array with pronounced interhelical hydrogen bonding (Figure 2b). Each asymmetric unit has five contacts shorter than 3 Å to neighboring helices, which arise from medium-strength interactions from O1 and O3 and weaker contacts from the bromide ligands. The hydrogen atoms H61 and H62 of the encapsulated water molecule are engaged in strong hydrogen

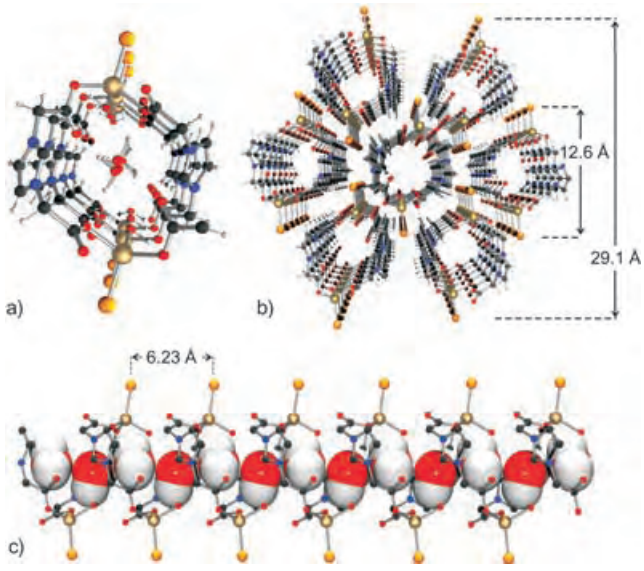


Figure 2. a) View into the helical tube of **1** with the one-dimensional water chain in the center. b) View into the helical tube of **1** with the free water molecules removed for clarity. c) View along the *y* axis showing the encapsulated water drawn with van der Waals radii. Hydrogen atoms on the imidazolium moiety have been omitted for clarity.

[*] Dr. Z. Fei, D. Zhao, Dr. T. J. Geldbach, Dr. R. Scopelliti, Prof. Dr. P. J. Dyson, Dr. S. Antonijevic, Prof. Dr. G. Bodenhausen
Institut des Sciences et Ingénierie Chimiques
Ecole Polytechnique Fédérale de Lausanne, EPFL-BCH
1015 Lausanne (Switzerland)
Fax: (+41) 21-693-9885
E-mail: paul.dyson@epfl.ch
Sasa.Antonijevic@epfl.ch

[**] We thank the EPFL and Swiss National Science Foundation for financial support and Dr. P. G. Anil Kumar at the ETH (Zürich) for solution diffusion measurements.

Supporting information for this article is available on the WWW under http://www.wiley-vch.de/home/angewandte/ or from the author.

InterScience
© 2005 Wiley-VCH Verlag GmbH & Co. KGaA, Weinheim

bonding to oxygen atoms O2 and O4 on the inner wall of the tube, both of which bear a delocalized negative charge. As a result of these quite strong interactions the oxygen atoms of the water molecules are in relatively close contact and are not bridged by a hydrogen atom. A summary of the more important hydrogen-bonding interactions (< 3 Å) is given in Table 1.

Table 1: Hydrogen-bonding distances [Å] in **1**.

Interhelical contacts		Intrahelical contacts		Contacts from free water	
Br–H2	2.952	O2–H3	2.461	O2–H62	1.728
Br–H4	2.823	O2–H6	2.908	O4–H61	2.194
Br–H6	2.960			O5–H61	2.261
O1–H2	2.405				
O3–H5	2.353				

The inner dimensions of the imidazolium–zinc channel are 5.656 and 6.515 Å between adjacent oxygen atoms O2 and O4, respectively, resulting in a cavity of about 2.656×3.513 Å^2 if van der Waals radii are taken into account.[13]

In the mass spectrum, no evidence of aggregates is observed, and pulsed-field-gradient spin-echo (PGSE) diffusion measurements on **1** in D_2O solution confirmed that **1** exists as a monomer in solution. The estimated diffusion coefficient is 5.65×10^{-10} m^2 s^{-1}, which corresponds to a hydrodynamic radius of about 3.8 Å. This value is in good agreement with that of 3.6 Å for the analogous zwitterionic imidazolium carboxylate (see Supporting Information).

To gain a more comprehensive understanding of the properties of the one-dimensional water chain and to characterize the local mobility of the two different types of water molecules in the helix, **1** was studied by solid-state ^{13}C and ^{2}H NMR spectroscopy. Figure 3 shows the ^{13}C cross-polarized (CP) magic-angle spinning (MAS) NMR spectrum of **1**. Seven nicely resolved resonance signals are associated with seven crystallographically different carbon atoms in the asymmetric unit cell as follows: C1 and C7 at $\delta = 174.07$ and 175.46 ppm; C2 and C6 at $\delta = 53.56$ and 54.78 ppm; C3 at $\delta = 139.67$; and C4 and C5 at $\delta = 125.07$ and 125.77 ppm. The linewidths (full width at half-height, FWHH) of C1 and C7 are only 30 Hz and could be obtained by very accurate

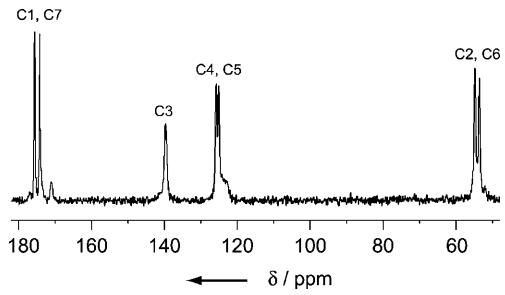


Figure 3. ^{13}C CPMAS NMR spectrum of **1** displays seven resolved resonance signals that are assigned to seven crystallographically different carbon atoms in the asymmetric unit cell. The spectrum is the result of averaging 8000 transients.

adjustment of the magic angle (better than $\pm 0.004°$).[14,15] Such narrow ^{13}C resonances suggest that the helical framework structure of this coordination polymer experiences very little structural disorder, if any.[16] The linewidths of the other carbon atoms are in the range of 50–80 Hz, and are due in part to residual dipolar splittings (or second-order quadrupole–dipole cross-terms) to neighboring ^{14}N atoms.[17–19] The assignment of the chemical shifts of pairs of chemically identical carbon atoms is not feasible from the ^{13}C CPMAS spectrum alone.

Understanding the motional behavior of water molecules that constitute a one-dimensional chain may prove important for the rationalization of various biological processes. To distinguish the two different types of water molecules in **1** and individually examine their motional behavior, they were replaced by D_2O by recrystallization of **1** from heavy water to give the deuterated material **1-D**. The water content of **1-D** amounts to 98% of the theoretical value, as determined by thermogravimetric analysis.

Motional disorder can be readily probed by static and MAS ^{2}H NMR experiments over a wide range of correlation rates, namely, 10^2 s$^{-1} < k < 10^9$ s^{-1}.[20–22] The high-resolution ^{2}H MAS spectra of **1-D** in Figure 4 show three resonances at isotropic chemical shifts $\delta_{iso} = 2.19$, 3.24, and 7.09 ppm. The very narrow resonance at $\delta = 2.19$ ppm (marked with $*$) is assigned to residual [D_6]acetone, which was used in the preparation of **1-D**. This resonance, which in comparison to the other two resonances displays only a center band, makes a negligible contribution to the overall signal. The other two resonances are assigned to water molecules and exhibit different linewidths due to structural disorder of water molecules and/or motional broadening. The considerable difference in the local magnetic fields, reflected in a relatively large difference in isotropic chemical shift, is due to the very different electronic environments of the two types of water molecules. One is coordinated to zinc ($\delta = 7.09$ ppm), whereas the other is located in the middle of the channel ($\delta =$ 3.24 ppm).

Variable-temperature ^{2}H MAS NMR spectra of **1-D** reveal changes in the linewidths of the ^{2}H resonances of both types of water molecules and thus indicate their mobility. Increasing temperature results in line narrowing, and this suggests that both types of water molecules move in the fast motional regime, typically $k \geq 10^7$ s^{-1}.[21–23] Decreasing the temperature leads to line broadening, and the linewidths observed at 246 K for both water resonances are so large that spinning sidebands are barely observable. The rate of the motions in this intermediate regime is typically in the range 10^7 s$^{-1} \geq k \geq 10^4$ s^{-1}. Figure 4b shows a ^{2}H MAS spectrum of **1-D** that was exposed to high vacuum (0.01 mbar) for 4 min. The loss of about 10% of the total amount of water indicates that water molecules can be relatively easily removed from the channel. Both deuterium resonances arising from deuterons of water molecules in Figure 4b are narrower than in Figure 4a. The narrowing of the resonance at $\delta = 3.24$ ppm is more pronounced, most probably due to increased mobility of the free water molecules.

It is expected that water molecules bound to zinc have restricted motional freedom and undergo a reorientational

 © 2005 Wiley-VCH Verlag GmbH & Co. KGaA, Weinheim

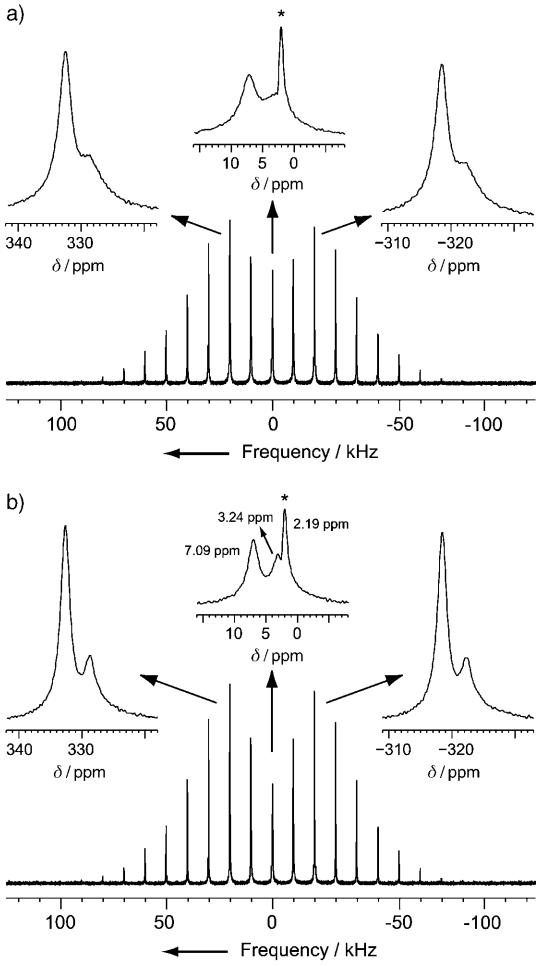


Figure 4. ^{2}H MAS NMR spectra of **1-D**: a) as synthesized and b) treated under high vacuum (0.01 mbar) for 4 min. The center band of (b) displays three resolved signals: two water molecules at $\delta = 7.09$ and 3.24 ppm and a narrow signal at $\delta = 2.19$ ppm (marked with *) originating from traces of [D_6]acetone. The spectra are the result of averaging 640 transients. A line broadening of 10 Hz was applied to both spectra.

motion which is often a 180° flip around the DOD bisector.[24] The free water in the channel, on the other hand, is expected to have more motional freedom, even to the extent of fast isotropic tumbling.[20] Both types of motion lead to averaging of the quadrupolar interaction. The former yields an averaged quadrupolar interaction that is comparable in magnitude to the quadrupolar interaction in the absence of the motion. The latter results in a more pronounced averaging of the quadrupolar interaction, and in extreme cases only a tiny residual quadrupolar interaction is observed. Note that not only reorientation and/or tumbling of the actual deuteron results in averaging of the quadrupolar interaction, but molecular motions of the nearest neighbors can also introduce a time-dependent electric field gradient and hence a time-dependent quadrupolar interaction.

Figure 5 shows the experimental ^{2}H NMR spectra of **1-D** (solid line) recorded at different temperatures under static conditions. They display a complex lineshape resulting from an overlap of several resonances. The narrow resonance at

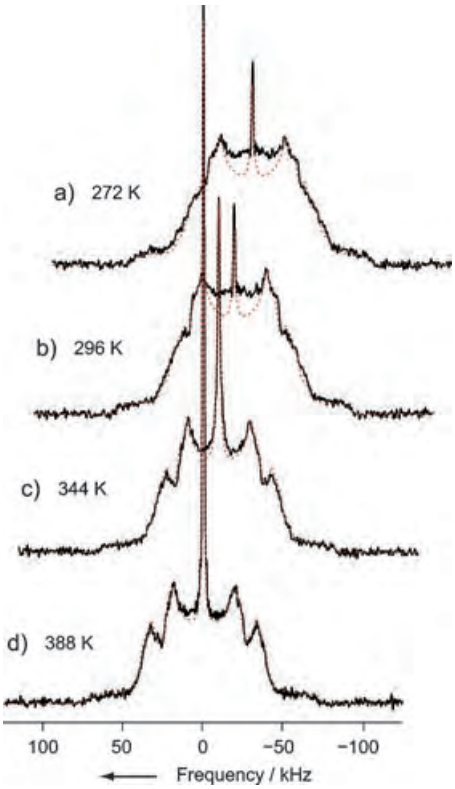


Figure 5. Experimental (solid) and simulated (dashed) static ^{2}H NMR spectra of **1-D** recorded as a function of temperature. The narrow signal at $\delta = 2.19$ ppm in a) and b) purely arises from residual [D_6]acetone. The spectra are the result of averaging 640 transients.

$\delta = 2.19$ ppm in the two spectra at lower temperatures is assigned to traces of [D_6]acetone. This resonance is also present in the spectra recorded at higher temperatures, but here it overlaps with newly formed narrow resonances, as shown in Figure 5c and d. The broad features of the spectra resemble superposition of two deuterium powder patterns. The narrower powder pattern has $\delta_{iso} = 3.24$ ppm, while the broader powder pattern has $\delta_{iso} = 7.09$ ppm, as found from the spectra in Figure 4. They are assigned to free and bound water molecules, respectively. Each powder pattern can be represented by an averaged quadrupolar coupling constant C_Q and an asymmetry parameter η_Q. Simulated spectra obtained by using the averaged quadrupolar parameters listed in Table 2 are in a very good agreement with the experimental spectra (Figure 5). In the absence of motions, C_Q for deuterons of D_2O in solids is typically in the range $240 \geq C_Q \geq 180$ kHz.[25] Evidently, the quadrupolar interaction for the free water molecules is averaged to a greater extent. Bound-water

Table 2: Quadrupolar parameters C_Q and η_Q of **1-D** as determined from static ^{2}H NMR spectra recorded at different temperatures.

T [K]	Bound water ($\delta_{iso} = 7.09$ ppm)		Free water ($\delta_{iso} = 3.24$ ppm)	
	C_Q [kHz]	η_Q	C_Q [kHz]	η_Q
272	98.4	0.14	64.5	0.16
296	96.7	0.12	62.9	0.15
344	96.7	0.09	60.5	0.14
388	96.7	0.09	57.6	0.11

 © 2005 Wiley-VCH Verlag GmbH & Co. KGaA, Weinheim

deuterons experience a slight decrease of averaged quadrupolar parameters with increasing temperature, which indicates that there is little change in motional freedom. However, the significant change in C_Q and η_Q for free-water deuterons is indicative of a significant change in motional freedom of these water molecules. Curiously, neither of the two averaged powder patterns corresponds to that which would arise for 180° flips around the DOD bisector, which normally results in averaged values of $\eta_Q \approx 1$.[24]

The intensity ratio of the two powder patterns at lower temperatures is estimated to be 1:1, while at higher temperatures (Figure 5c, d) the intensity of the narrower pattern (free water molecules) decreases by conversion to a newly formed narrow resonance. This "sudden" formation of a new narrow resonance is observed between 336 and 345 K. It has a linewidth typical for water undergoing isotropic motion and cannot result only from an increased rate of motion or deuterium transfer, that is, in the fashion of a proton (deuteron) wire. The observed increase in motional freedom might occur either due to some structural change or to water "rattling" (i.e., diffusing into unoccupied positions) through the channel. A structural change could be expected to result in an increase of motional freedom for *all* free water molecules, but this was not observed. On the other hand, unoccupied water sites represent an opportunity for some water molecules to undergo a translational "hopping" motion. We find that any changes observed in ^{2}H spectra of **1-D** exposed to temperatures in the range from 240 to 390 K are reversible. In samples of **1-D** with 100% water content, where there are no vacant sites in the helix, another very sharp resonance (FWHH of 5 Hz) at $\delta = 5.0$ ppm is observed at 353 K (see Supporting Information). This very narrow resonance is characteristic of water that tumbles very rapidly and was therefore assigned to adsorbed or surface water. It is not clear if these water molecules are released from the channel as a direct consequence of water transport through the channel, as found in other one-dimensional water-channel systems,[26–28] or due to a rather unlikely diffusion process through the "walls" of the nanotubes. In samples with less than 100% water content, water molecules do not appear to leave the tubes when the temperature increases, but move along the vacant sites. The existence of vacant sites was shown to be critical for diffusion processes observed in zeolites containing one-dimensional water channels.[27]

Studies on helical zinc complexes of carboxylic acids have been previously reported,[29,30] including conducting helical polymers,[31] of which zwitterionic polymers are of special interest.[32] In this work, however, the water molecules in the helical channel have been studied by ^{2}H NMR spectroscopy, and it was possible to differentiate the two different types of water molecules. One is assigned to deuterons of free water molecules found in the middle of the channels, while the other corresponds to water coordinated to zinc. Both undergo fast motions ($k \geq 10^7\ s^{-1}$) at room temperature. The quadrupolar interaction of free-water deuterons in **1-D** is scaled to a greater extent, and this indicates different motional behavior than for the bound water molecules. Furthermore, the motional freedom of free water molecules increases with increasing temperature, since the quadrupolar parameters decrease, while they remain the same for the bound-water deuterons. Neither of the two deuterium powder patterns corresponds to simple 180° flips around the DOD bisector. Partial displacement of water molecules from the channel seems to be a process with a low activation energy barrier, since a significant fraction of the water molecules can be removed by short exposure to high vacuum. The change in the motional behavior of a fraction of the free water molecules in **1-D** that occurs between 336 and 345 K results in a dramatic averaging of C_Q. This is most probably due the water "rattling" along the channel, permitted by the existence of vacant water positions, in addition to already existing motional degrees of freedom. Proton (deuteron) transfer can be ruled out as a source of such an observation. The very narrow peak at $\delta = 5.0$ ppm observed at 353 K for **1** without water vacancies is related to water molecules that are delivered to the outside of the channels and have a liquidlike motional behavior. It is likely that these water molecules either diffuse out of the channels or escape as a result of water transfer through the channel. Finally, a possible exchange of deuterons between two different types of water molecules may occur, but on a timescale with a rate constant that is much smaller than the quadrupolar splitting.

It is interesting to compare **1** to other systems that contain water in a confined channel. For example, aquaporin water channels (AQP1) are composed of an hourglass structure with a narrowest constriction of 2.8 Å (Figure 6); the narrowest gap in the channel of **1** is 2.656 Å.

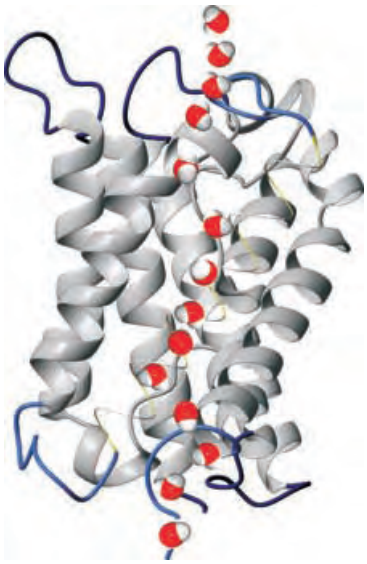


Figure 6. Schematic representation of water flow through an aquaporin channel.

Although **1** resembles an aquaporin channel in that the water molecules form a single file and the diameter of the tube is of approximately the same size as the narrowest part of the pore in the protein, there are also fundamental differences. Owing to the presence of strong hydrogen bonds between the hydrogen atoms of the encapsulated water molecules and oxygen atoms of the inner wall, both water

 © 2005 Wiley-VCH Verlag GmbH & Co. KGaA, Weinheim

hydrogen atoms point towards the wall of the tube, rather than to neighboring water molecules. In contrast, each water molecule in aquaporin water channels forms one hydrogen bond with the wall of the protein and one with an adjacent water molecule. Furthermore, the water molecules in the aquaporin channel undergo a fliplike motion while passing through the pore. This change in orientation is crucial for proton exclusion and it thereby preserves the electrochemical potential across the cell membrane.[33] Owing to the uniformity of the zwittertube, no comparable conformational change is observed along the chain of water molecules. As the wall of the nanotube consists of zwitterionic residues, interactions between the water molecules are much stronger than in the biological system, where dipole–dipole interactions dominate. This has implications with respect to the efficiency with which the channel can transport water. It was previously demonstrated in carbon nanotubes that the high affinity of water molecules to charged moieties significantly decreases their mobility.[34] While the rate of water transport at room temperature in aquaporin is on the order of one molecule per nanosecond,[35] it is believed to be slower in the zwittertube.

Experimental Section

Synthesis of **1**: A mixture of elemental zinc (1.50 g, 23 mmol) and **2** (2.65 g, 10 mmol) in water (20 mL) was stirred for 10 days at room temperature, after which time no further evolution of hydrogen gas could be observed. The mixture was filtered, and the filtrate concentrated to half of its volume and left at room temperature for seven days to afford big colorless crystals. Yield: 96%. ESI-MS: m/z: 328 $[M-2H_2O]^+$, 344 $[M-H_2O]^+$; ^{1}H NMR (400.1 MHz, D_2O): $\delta =$ 8.68 (s, 1H), 7.36 (s, 2H), 4.80 ppm (s, 4H); ^{13}C NMR (100.6 MHz, D_2O): $\delta = 172.33, 137.18, 123.17, 51.94$ ppm; IR: $\tilde{\nu} = 3150, 3108, 3017, 2950, 1622, 1589, 1565, 1437, 1397, 1298, 1177, 1162, 1101, 971, 765, 681$ cm^{-1}; elemental analysis (%) calcd for $C_7H_{11}BrN_2O_6Zn$ (364.46): C 23.07, H 3.04, N 7.69; found: C 23.11, H 3.07, N 7.75.

Synthesis of **1-D**: A sample of **1** was dissolved in D_2O followed by immediate removal of the solvent at low temperature (2–5 °C) to afford **1-D**. The solid was washed with [D_6]acetone to remove residual water absorbed on the surface. The water content was determined to be 98% of the theoretical value by thermogravimetric analysis and was confirmed by elemental analysis. Unwanted exchange of protons at C3 was observed when the sample of **1-D** was prepared at room temperature with slow evaporation of the solvent. The D3 deuteron of this material results in an additional ^{2}H NMR resonance at $\delta =$ 9.1 ppm (see Supporting Information), which makes interpretation of the NMR spectra more complicated. Similarly, if the reaction of the acid with elemental zinc was carried out in D_2O, unwanted exchange of H2, H3, and H6 is observed.

Crystallography: Single crystals of **1** were measured on a KUMA CCD diffractometer. Data reduction was performed with CrysAlis RED.[36] Structure solution and refinement were performed with the SHELX97 software package;[37] graphical representations of the structures were made with ORTEP32.[38] Structures were solved by direct methods and successive interpretation of the difference Fourier maps, followed by full-matrix least-squares refinement (against F^2). An empirical absorption correction (DELABS)[39] was applied. All non-hydrogen atoms were refined anisotropically. Hydrogen atoms on the imidazolium moiety were placed in their geometrically generated positions and refined with a riding model. Water hydrogen atoms were located on the Fourier map and refined by using the HTAB command with a fixed O–H distance of 0.98 Å and with an additional H···H restraint (1.60 Å) by using the DFIX command in SHELX97.

Crystal data of $C_7H_7BrN_2O_4Zn\cdot 2H_2O$ (**1**): Crystal dimensions $0.19\times0.10\times0.06$ mm^3, monoclinic, space group $P2(1)/n$, $a =$ 9.9025(8), $b = 6.2345(4)$, $c = 19.3319(15)$ Å, $\beta = 99.314(7)°$, $V =$ 1177.76(15) Å^3, $\rho_{calcd} = 2.055$ Mg m^{-3}, $Z = 4$, $\mu = 5.496$ mm^{-1}, $\theta_{max} =$ 3.44 to 25.03, $Mo_{K\alpha}$ radiation ($\lambda = 0.71070$ Å), $T = 140$ K, $F(000) =$ 720, total reflections 6384, independent reflections 1971 ($R_{int} =$ 0.0400), observed data 1677 ($I > 2\sigma(I)$). The final anisotropic full-matrix least-squares refinement on F^2 for 166 variables converged at $R_1 = 0.0271$ and $wR_2 = 0.0636$ with a GOF of 1.061. CCDC-251434 contains the supplementary crystallographic data for this paper. These data can be obtained free of charge from The Cambridge Crystallographic Data Centre via www.ccdc.cam.ac.uk/data_request/cif.

Solid-state NMR measurements: Spectra were recorded on a Bruker Avance 400 spectrometer equipped with a wide-bore 9.4 T magnet, operating at a Larmor frequency of $\nu_0 = 61.4$ MHz for ^{2}H ($S = 1$) and 100.6 MHz for ^{13}C ($S = 1/2$). Cross-polarized (CP) ^{13}C{^{1}H} MAS NMR spectra were recorded with a standard Bruker 2.5 mm CPMAS probe with a spinning rate of 30 kHz, a ^{1}H radio-frequency (RF) field strength of 85 kHz, a contact time of 1 ms, and a recycle interval of 3 s. The best performance of TPPM proton decoupling during acquisition was obtained with pulse widths of 3.9 μs at 100 kHz ^{1}H RF field and a phase difference between two successive pulses of 35°. The magic angle was adjusted first by minimizing the residual quadrupolar splitting in the rotor-synchronized ^{2}H MAS spectrum of α-oxalic acid [D_6]dehydrate.[12] The subsequent fine adjustment was carried out by maximizing the height of the ST_1-CT shifted-echo signal in a one-dimensional STMAS experiment.[12,15] Static and MAS deuterium spectra were recorded with a Bruker 4 mm MAS probe. A 500 W RF amplifier was used to give a ^{2}H 90° pulse duration of 2.9 μs. The static wide-line deuterium powder patterns were recorded by using "Exorcycled" quadrupolar echo pulse sequence to avoid distortions due to chemical shift anisotropy (CSA).[40] The variable-temperature ^{2}H MAS experiments were performed at a spinning rate of 10 kHz. A recycle interval of 1 s was appropriate for all deuterium resonances. The temperature was calibrated by using $Pb(NO_3)_2$ as a chemical shift thermometer.[41] Chemical shifts are reported in ppm relative to adamantane (high-frequency resonance at $\delta = 38.56$ ppm) for ^{13}C and TMS for ^{2}H. The frequency-domain simulated spectra were produced by a home-written program which does not take finite pulse duration effects into account, and does not include any time dependence of the quadrupolar interaction.[42]

Received: January 19, 2005
Revised: April 25, 2005
Published online: August 1, 2005

Keywords: coordination polymers · helical structures · NMR spectroscopy · supramolecular chemistry · water channels

[1] C. T. Kresge, M. E. Leonowicz, W. J. Roth, J. C. Vartuli, J. S. Beck, *Nature* **1992**, *359*, 710–712.
[2] R. S. Meissner, J. Rebek, Jr., J. de Mendoza, *Science* **1995**, *270*, 1485–1488.
[3] S. Mann, *Biomimetic Materials Chemistry*, VCH, New York, 1996.
[4] S. Kitagawa, R. Kitaura, S.-i. Noro, *Angew. Chem.* **2004**, *116*, 2388–2430; *Angew. Chem. Int. Ed.* **2004**, *43*, 2334–2375.
[5] P. Agre, *Angew. Chem.* **2004**, *116*, 4377–4390; *Angew. Chem. Int. Ed.* **2004**, *43*, 4278–4290.
[6] V. Videnova-Adrabinska, *J. Mater. Chem.* **2002**, *12*, 2931–2935.
[7] L. E. Cheruzel, M. S. Pometun, M. R. Cecil, M. S. Mashuta, R. J. Wittebort, R. M. Buchanan, *Angew. Chem.* **2003**, *115*, 5610–5613; *Angew. Chem. Int. Ed.* **2003**, *42*, 5452–5455.

 © 2005 Wiley-VCH Verlag GmbH & Co. KGaA, Weinheim

[8] P. S. Sidhu, K. A. Udachin, J. A. Ripmeester, *Chem. Commun.* **2004**, 1358 – 1359.
[9] B. Sreenivasulu, J. J. Vittal, *Angew. Chem.* **2004**, *116*, 5893 – 5896; *Angew. Chem. Int. Ed.* **2004**, *43*, 5769 – 5772.
[10] A. Mukherjee, M. K. Saha, M. Nethaji, A. R. Chakravarty, *Chem. Commun.* **2004**, 716 – 717.
[11] Prepared in an analogous method to the chloride salt, by using $BrCH_2CO_2Me$ and HBr in place of $ClCH_2CO_2Me$ and HCl, as described in Z. Fei, D. Zhao, T. J. Geldbach, R. Scopelliti, P. J. Dyson, *Chem. Eur. J.* **2004**, *10*, 4886 – 4893.
[12] a) N. J. Burke, A. D. Burrows, A. S. Donovan, R. W. Harrington, M. F. Mahon, C. E. Price, *Dalton Trans.* **2003**, 3840 – 3849; b) A. D. Burrows, R. W. Harrington, M. F. Mahon, C. E. Price, *J. Chem. Soc. Dalton Trans.* **2000**, 3845 – 3854.
[13] R. D. Shannon, *Acta Crystallogr. Sect. A* **1976**, *32*, 751 – 767.
[14] S. Antonijevic, G. Bodenhausen, *Angew. Chem.* **2005**, *117*, 2995 – 2998; *Angew. Chem. Int. Ed.* **2005**, *44*, 2935 – 2038.
[15] S. E. Ashbrook, S. Wimperis, *J. Magn. Reson.* **2002**, *156*, 269 – 281.
[16] D. Sakellariou, S. P. Brown, A. Lesage, S. Hediger, M. Bardet, C. A. Meriles, A. Pines, L. Emsley, *J. Am. Chem. Soc.* **2003**, *125*, 4376 – 4380.
[17] J. G. Hexem, M. H. Frey, S. J. Opella, *J. Am. Chem. Soc.* **1981**, *103*, 224 – 226.
[18] A. Naito, S. Ganapathy, C. A. McDowell, *J. Chem. Phys.* **1981**, *74*, 5393 – 5397.
[19] C. A. McDowell in *Encyclopedia of Nuclear Magnetic Resonance*, *Vol. 5* (Eds.: D. M. Grant, R. K. Harris), Wiley, Chichester, **1996**, p. 2901.
[20] M. J. Duer, H. He, W. Kolodziejski, J. Klinowski, *J. Phys. Chem.* **1994**, *98*, 1198 – 1204.
[21] J. H. Kristensen, G. L. Hoatson, R. L. Vold, *Solid State Nucl. Magn. Reson.* **1998**, *13*, 1 – 37.
[22] J. H. Kristensen, G. L. Hoatson, R. L. Vold, *J. Chem. Phys.* **1999**, *110*, 4533 – 4553.
[23] S. E. Ashbrook, S. Antonijevic, A. J. Berry, S. Wimperis, *Chem. Phys. Lett.* **2002**, *364*, 634 – 642.
[24] T. Chiba, *J. Chem. Phys.* **1963**, *39*, 947 – 953.
[25] L. G. Butler, T. L. Brown, *J. Am. Chem. Soc.* **1981**, *103*, 6541 – 6549.
[26] G. Hummer, J. C. Rasaiah, J. P. Noworyta, *Nature* **2001**, *414*, 188 – 190.
[27] P. Demontis, G. Stara, G. B. Suffritti, *J. Chem. Phys.* **2004**, *120*, 9233 – 9244.
[28] S. Nair, Z. Chowdhuri, I. Perla, D. A. Neumann, L. C. Dickinson, G. Tompsett, H-K. Jeong, M. Tsapatsis, *Phys. Rev. B* **2005**, *71*, 104301 – 104308.
[29] P. Jiang, Z. Guo, *Coord. Chem. Rev.* **2004**, *248*, 205 – 229.
[30] A. Erxleben, *Coord. Chem. Rev.* **2003**, *246*, 203 – 228.
[31] T. Hatano, A.-H. Bae, M. Takeuchi, N. Fujita, K. Kaneko, H. Ihara, M. Takafuji, S. Shinkai, *Angew. Chem.* **2004**, *116*, 471 – 475; *Angew. Chem. Int. Ed.* **2004**, *43*, 465 – 469.
[32] H. Terao, T. Sugawara, Y. Kita, N. Sato, E. Kaho, S. Takeda, *J. Am. Chem. Soc.* **2001**, *123*, 10468 – 10474.
[33] E. Tajkhorshid, P. Nollert, M. Ø. Jensen, L. J. W. Miercke, J. O'Connell, R. M. Stroud, K. Schulten, *Science* **2002**, *296*, 525 – 530.
[34] F. Zhu, K. Schulten, *Biophys. J.* **2003**, *85*, 236 – 244.
[35] a) M. Borgnia, S. Nielsen, A. Engel, P. Agre, *Annu. Rev. Biochem.* **1999**, *68*, 425 – 458; b) M. Ø. Jensen, E. Tajkhorshid, K. Schulten, *Biophys. J.* **2003**, *85*, 2884 – 2899.
[36] Oxford Diffraction Ltd, 68 Milton Park, Abingdon, OX144RX, UK, **2003**.
[37] G. M. Sheldrick, SHELX-97, Structure Solution and Refinement Package, Universität Göttingen, **1997**.
[38] L. J. Farrugia, *J. Appl. Crystallogr.* **1997**, *30*, 565.
[39] N. Walker, D. Stuart, *Acta Crystallogr. Sect. A* **1983**, *39*, 158 – 166.
[40] S. Antonijevic, S. Wimperis, *J. Magn. Reson.* **2003**, *164*, 343 – 350.
[41] A. Bielecki, D. P. Burum, *J. Magn. Reson. A* **1995**, *116*, 215 – 220.
[42] S. Antonijevic, S. Wimperis, *J. Chem. Phys.* **2005**, *122*, 044312 – 044314.

 © 2005 Wiley-VCH Verlag GmbH & Co. KGaA, Weinheim

Molecular Recognition

DOI: 10.1002/anie.200500982

F···H–N Hydrogen Bonding Driven Foldamers: Efficient Receptors for Dialkylammonium Ions**

*Chuang Li, Shi-Fang Ren, Jun-Li Hou, Hui-Ping Yi, Shi-Zheng Zhu, Xi-Kui Jiang, and Zhan-Ting Li**

An essential attribute of biomacromolecules such as proteins and nucleic acids is their accurate control over the noncovalent forces that govern folding and self-assembly processes.[1] In recent years, chemists have been engaged in the development of foldamers,[2] artificial molecules that utilize noncovalent forces to modulate folding or helical structures. Among other noncovalent forces, the O···H–N hydrogen bonding motif has been widely utilized for this purpose,[3,4] a number of pyridine-N···H–N hydrogen-bonded folding architectures have also been developed.[5] Although it has been well established that the fluoride ion acts as a very strong proton acceptor,[6,7] it has been reported that covalently bound fluorine is a very weak intermolecular hydrogen-bonding acceptor.[8,9] We recently found that intramolecular F···H–N hydrogen bonding could be used to promote the stability of hydrazide-based quadruply hydrogen-bonded heterodimers.[10] We envisioned that rationally designed, intramolecular F···H–N hydrogen bonding might provide a novel approach for the formation of new rigid, well-established conformations. Herein, we demonstrate how intramolecular F···H–N hydrogen bonding controls the crescent and helical conformations of aromatic amides to such an

[*] C. Li, S.-F. Ren, J.-L. Hou, H.-P. Yi, Prof. Dr. S.-Z. Zhu, Prof. Dr. X.-K. Jiang, Prof. Dr. Z.-T. Li
State Key Laboratory of Bio-Organic and Natural Products Chemistry
Shanghai Institute of Organic Chemistry
Chinese Academy of Sciences
354 Fenglin Lu, Shanghai 200032 (China)
Fax: (+86) 21-6416-6128
E-mail: ztli@mail.sioc.ac.cn

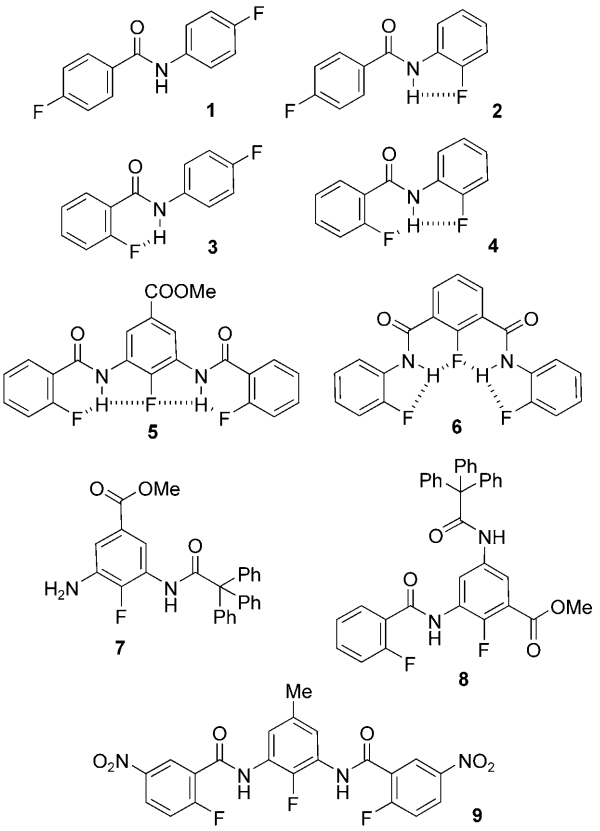
[**] We thank the Ministry of Science and Technology (G2000078101), the National Natural Science Foundation of China, and the Chinese Academy of Sciences for financial support.

Supporting information for this article is available on the WWW under http://www.angewandte.org or from the author.

© 2005 Wiley-VCH Verlag GmbH & Co. KGaA, Weinheim

extent that the new foldamers can strongly bind dialkylammonium ions.

The molecular design was based on the recently established three-centered O···H–N hydrogen-bond motif.[11,12] Compounds **1**–**6** were prepared and a comparison of the



chemical shift of the amide proton in **2**–**6** with that in **1**, which cannot form intramolecular hydrogen bonds (Table 1), reveals a significant downfield shift of their NH signals, suggesting the formation of an intramolecular hydrogen bond in **2**–**6**. Larger changes with respect to **1** are exhibited for **4**–**6** than for **2** and **3**, indicating that the NH protons in **4**–**6** are involved in two hydrogen bonds simultaneously, as observed in the RO-related systems.[11–13]

Numerous attempts to crystallize **2**–**6** were unsuccessful. Given the well-known crystallinity of triphenylmethyl and nitro compounds,[14,15] compounds **7**–**9** were prepared. Crystals of **7**–**9** suitable for X-ray analysis were grown by slow evaporation of a dichloromethane/ethyl acetate solution of **7**–**9**. All three compounds adopt a well-defined planar conformation, which is rigidified by intramolecular F···H–N hydrogen bonds (Figure 1). For **7**, the F···H (amide) distance

Table 1: Chemical shifts (ppm) of the NH signals of **1**–**8**, **10**, and **11a** in $CDCl_3$ (1.0 mM) at 25 °C.[a]

Compound	Chemical shift	Compound	Chemical shift
1	7.78	**6**	8.57 (0.79)
2	8.00 (0.22)	**7**	8.43 (0.65)
3	8.47 (0.69)	**8**	8.88 (1.10)
4	8.83 (1.05)	**10**	8.91 (1.13)
5	8.92 (1.14)	**11a**	9.04 (1.26)

[a] The value in parentheses is the downfield change of the chemical shift relative to that of **1**.

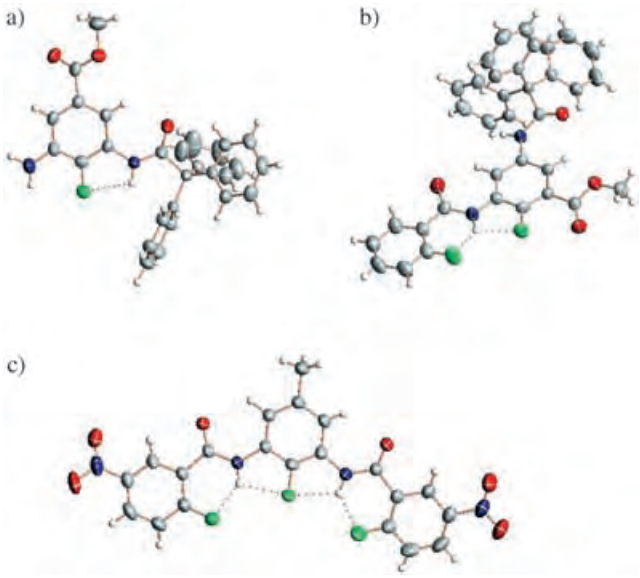


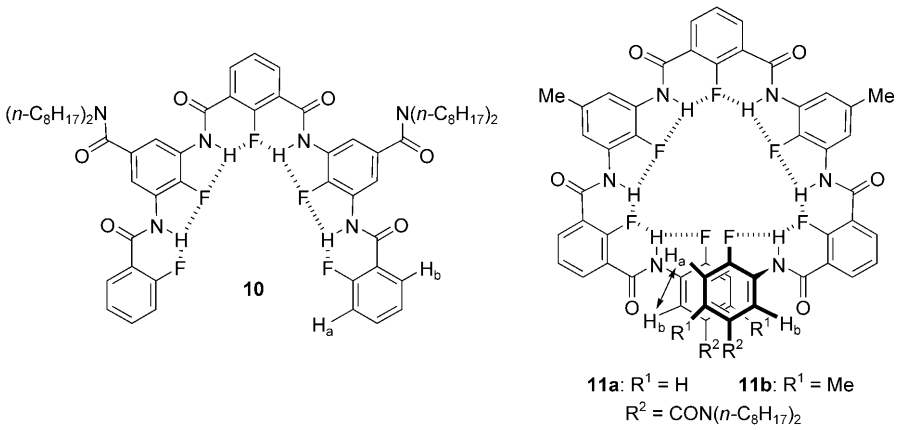
Figure 1. The crystal structures of a) **7**, b) **8**, and c) **9**.

is 2.227 Å, and the F···H–N angle is 106.37°. The fluorine atoms of both **8** and **9** are located in the proximity of the amide hydrogen atom due to the formation of the three-centered hydrogen bonds. The F···H (amide) distance in the six- and five-membered hydrogen bonds is 1.935 and 2.184 Å for **8**, and 1.968 and 2.183 Å for **9**, respectively, and the corresponding F···H–N angles are 135.72 and 107.59° for **8** and 135.98 and 111.21° for **9**. All these values fall in the range considered acceptable for F···H–N hydrogen bonds, namely, the F···HN distance is less than 2.3 Å and the F···H–N angle is greater than 90°.[9a] In contrast, the F···HN distance for the amine group in **7** is 2.385 Å, which is outside the acceptable range given above. In addition, the skeleton of 3-mer **9** adopts a folding conformation.

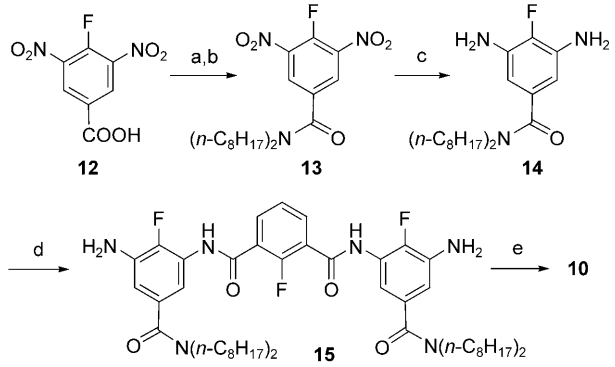
The three-centered F···H–N hydrogen-bonding motif, which is present both in solution and in the solid state, is an ideal candidate for the construction of foldamers. To explore this possibility, 5-mer **10** and 7-mers **11a** and **11b** (Scheme 1) were synthesized, as shown in Scheme 2 and Scheme 3. Thus, acid **12** was first transformed to amide **13**, which was then reduced to diamine **14**. Treatment of **14** with 2-fluoroisophthaloyl chloride afforded **15**. Finally, reaction of **15** with 2-fluorobenzoyl chloride yielded **10**. For the preparation of **11a**, **16** was first reduced to amine **17**, which was acylated to yield **18**. The latter was then hydrolyzed to acid **19**, followed by a coupling reaction to give **20**. Treatment of **20** with 2-fluoroisophthaloyl chloride afforded **11a** (Scheme 3). Compound **11b** was prepared according to the similar route.

The peaks in the ^{1}H NMR spectrum of **10**, **11a**, and **11b** in $CDCl_3$ are sharp. Their signals have been assigned based on 2D-NOESY and COSY experiments. As expected, their NH signals are also shifted downfield substantially (Table 1) and

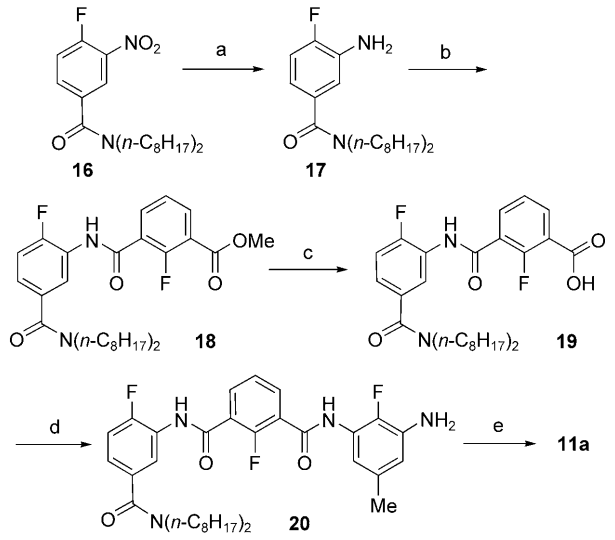
 © 2005 Wiley-VCH Verlag GmbH & Co. KGaA, Weinheim



Scheme 1. The structure of crescent **10** and helical **11a** and **11b**. Compound **11b** displayed intramolecular end-to-end NOE values (500 MHz, 2.5 mM in $CDCl_3$ at 25 °C), which support a helical conformation for **11**.



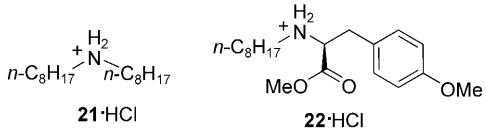
Scheme 2. The synthesis of **10**: a) oxalyl chloride, DMF (cat.), THF, RT, 0.5 h; b) $NH(n\text{-}C_8H_{17})_2$, NEt_3, THF, −10 °C, 1 h, 59%; c) H_2, Pd/C, MeOH/THF, RT, 48 h, 92%; d) 2-fluoroisophthaloyl chloride, NEt_3, CH_2Cl_2, RT, 0.5 h, 33%; e) 2-fluorobenzoyl chloride, NEt_3, CH_2Cl_2, RT, 1 h, 47%.



Scheme 3. The synthesis of **11a**: a) H_2, Pd/C, MeOH/THF, RT, 24 h, 98%; b) 2-fluoro-3-(methoxycarbonyl)benzoyl chloride, NEt_3, CH_2Cl_2, 0.5 h, 91%; c) LiOH, THF/H_2O, RT, 5 h, 98%; d) 2-fluoro-5-methylbenzene-1,3-diamine, EDCI, DMAP (cat.), CH_2Cl_2, RT, 12 h, 45%; e) 2-fluoroisophthaloyl chloride, NEt_3, CH_2Cl_2, RT, 1 h, 55%.

the values are comparable to those of the shorter oligomers **4**, **5**, and **8**. The results indicate that three-centered F···H–N hydrogen bonding also occurs in these oligomers. Moderate NOE values between H_a and H_b of the terminal benzene rings was observed for **11b** (Scheme 1). Because similar NOE values were not revealed for **10** even at the higher concentration of 10 mM, the observed NOE between H_a and H_b in **11b** can only be ascribed to that produced by an end-to-end arrangement, as shown in Scheme 1. This cross-ring NOE strongly supports a rigidified helical conformation of **11b** in chloroform.[4a,b] In contrast, 5-mer **10** is not long enough for its two end benzene units to stack or even to be in close proximity. In principle, a similar NOE might also be displayed in **11a**, but this could not be assigned due to signal overlap for the terminal benzene groups.

Molecular modeling revealed a crescent planar conformation for **10** and a helical conformation for **11a** and **11b**, in which the fluorine atoms converge towards the center of their skeletons creating a polar internal cavity of 6.5 and 6.6 Å diameter, respectively. Such a cavity appears well suited to complex secondary $R_2NH_2^+$ ions in a manner similar to that of dibenzo[24]crown-8.[16] The interactions of **10** and **11a** with symmetrical **21**·HCl were first investigated by means of ESI-MS analysis of their 1:1 solutions (1.0 mM) in chloroform.



Strong peaks for the complexes **10**·**21**·HCl and **11a**·**21**·HCl were observed (Figure 2). The ^{1}H NMR NOESY spectrum also revealed intermolecular a NOE of modest strength for the 1:1 solution of **10** and **21**·HCl as well as **11a** and **21**·HCl in $CDCl_3$ (Scheme 4). These results clearly indicate that strong intermolecular F···H electrostatic interactions or hydrogen bonding also exist between the new F···H–N hydrogen-bonded foldamers and **21**·HCl.[17]

Addition of **21**·HCl to the solution of **10** and **11a** in chloroform remarkably decreased the intensity of the emission for the folding oligomers in the fluorescent spectrum. Similar quenching was not observed when **21**·HCl was replaced with $n\text{Bu}_4\text{N}^+\text{Cl}^-$ under identical conditions. This result rules out the possibility of a salt effect at a higher concentration of ammonium and indicates that the reduction of the emission intensity was caused by the complexation of the folding molecules around the ammonium ion. As an example, the titration spectra of **11a** with **21**·HCl are provided in Figure 3. By fitting the data to a 1:1 binding mode, the association constant K_{assoc} of complexes **10**·**21**·HCl and

 © 2005 Wiley-VCH Verlag GmbH & Co. KGaA, Weinheim

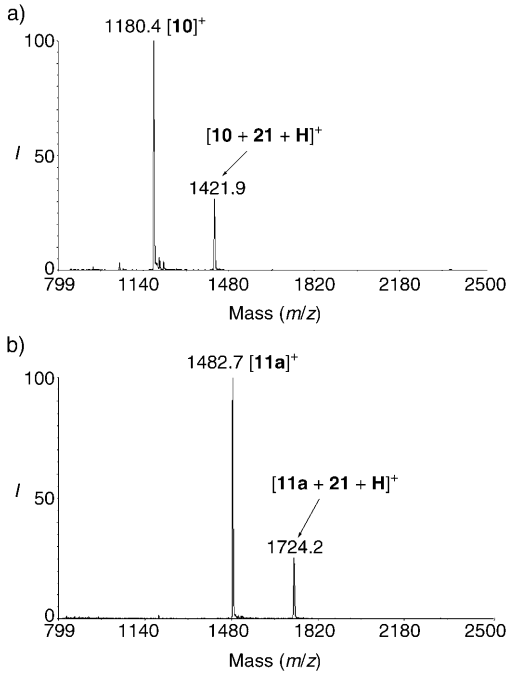
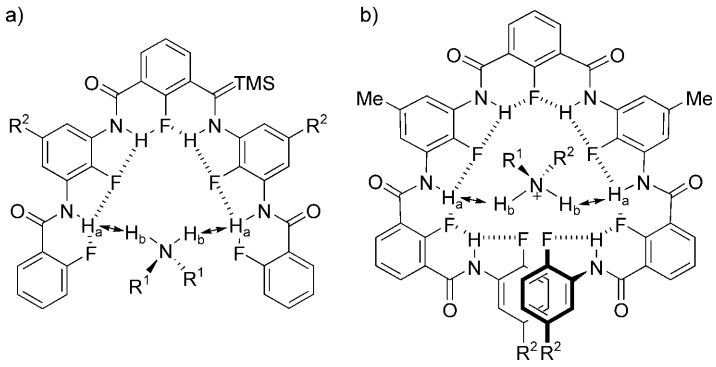


Figure 2. ESI mass spectrum obtained from the 1:1 solution (1.0 mM) of a) **10** and **21**·HCl and b) **11a** and **21**·HCl in chloroform.



Scheme 4. Intermolecular NOE connections revealed by the NOESY spectrum (500 MHz) of the 1:1 solution of a) **10** and **21**·HCl and b) **11a** and **21**·HCl in $CDCl_3$ (4.0 mM) at 23 °C (mixing time: 0.5 s).

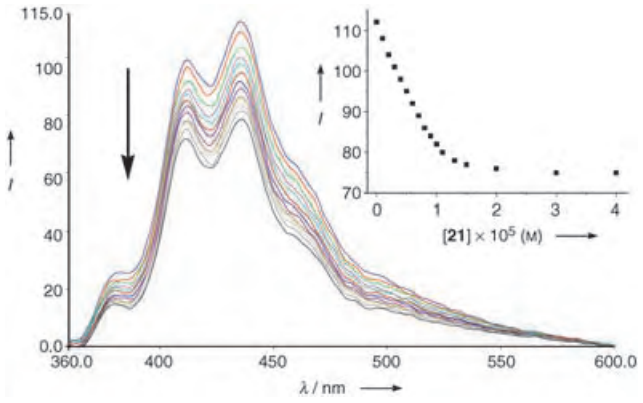


Figure 3. Fluorescent spectra of **11a** (1.5×10^{-5} M, excitation wavelength = 330 nm) in $CHCl_3$ at 25 °C, decreased gradually on addition of **21**·HCl (0 to 4.0×10^{-5} M).

11a·**21**·HCl was determined to be $4.9(\pm0.6)\times10^6$ and $8.1(\pm0.9)\times10^6\,M^{-1}$, respectively.[4b] The 1:1 stoichiometry of the complexes was estimated based on Job plots. The binding constants are considerably larger than that of the complex between dibenzo[24]crown-8 and dialkylammonium ions (ca. $2.7\times10^4\,M^{-1}$ in chloroform),[18] suggesting that highly efficient electrostatic interactions or hydrogen bonding could occur intermolecularly between fluorine and ammonium protons due to the rigidified conformation of the oligomers. By using the same method, the K_{assoc} values for the complexes of **10** with chiral **22**·HCl as well as **11a** with chiral **22**·HCl were determined to be $2.4(\pm0.2)\times10^5$ and $7.3(\pm0.8)\times10^5\,M^{-1}$, respectively. The values are notably lower than those of the respective complexes with **21**·HCl, but still larger than that of the complex between dibenzo[24]crown-8 and dialkylammonium ions.

Given the above strong binding features, chirality induction through complexation of **10** and **11a** with chiral L-tyrosine-derived ammonium **22**·HCl was investigated.[4b,19] The guest molecule itself (**22**·HCl) exhibits a CD signal at about 277 nm. Therefore, induced CD spectra generated from the interaction of **22**·HCl with **10** and **11a** were obtained by subtracting the spectrum of **22**·HCl from that of the complex. Figure 4 shows the typical CD curves of the complexes. Both

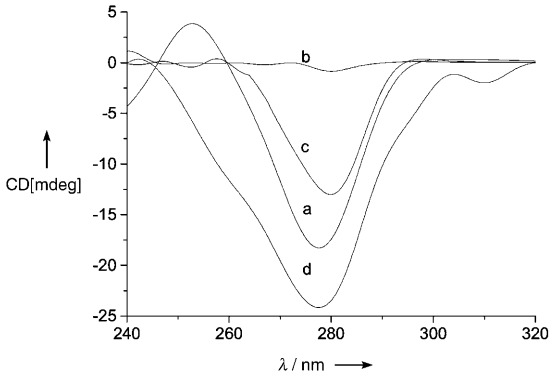


Figure 4. Induced CD spectra of complexes of **22**·HCl (1.0 mM) with a) **10** (1.0 mM), b) **11a** (0.01 mM), c) **11a** (0.05 mM), and **11a** (0.2 mM) in chloroform at 25 °C.

complexes gave rise to negative CD signals, which increased with the increase of the concentration of the foldamers. The intensity of the CD signals decreased on addition of polar methanol in the solvent and vanished in a mixture of methanol and chloroform (1:3 (v/v)), indicating that the signals were generated through intermolecular electrostatic interactions or hydrogen bonding. The different shape of the signals of the two complexes presumably reflects the different binding environments for both complexes.

In conclusion, we have demonstrated that intramolecular F···H–N hydrogen bonds can be utilized to construct a new generation of folding architectures. The new foldamers strongly bind dialkylammonium ions by means of intermolecular electrostatic interactions or F···H–N hydrogen bonding, which can give rise to chiral induction or amplification through complexation with chiral L-tyrosine-derived ammonium ions. It has been proposed that organic fluorine hardly ever accepts hydrogen bonds, the present work reveals that

 © 2005 Wiley-VCH Verlag GmbH & Co. KGaA, Weinheim

relatively stable F···H–N hydrogen bonds can be formed, at least, in elaborately designed aromatic amides. This opens new possibilities in supramolecular chemistry. Future work will be aimed at the construction of helical and tubular systems with deeper and larger cavities. It also remains to be shown whether intra- or intermolecular F···H–O hydrogen bonds can be formed in organofluorine molecules.

Received: March 17, 2005
Published online: August 3, 2005

Keywords: fluorine · foldamers · hydrogen bonds · molecular recognition

[1] D. S. Lawrence, T. Jiang, M. Levett, *Chem. Rev.* **1995**, *95*, 2229.
[2] a) D. Seebach, J. L. Matthews, *Chem. Commun.* **1997**, 2015; b) S. H. Gellman, *Acc. Chem. Res.* **1998**, *31*, 173; c) K. D. Stigers, M. J. Soth, J. S. Nowick, *Curr. Opin. Chem. Biol.* **1999**, *3*, 714; d) D. J. Hill, M. J. Mio, R. B. Prince, T. S. Hughes, J. S. Moore, *Chem. Rev.* **2001**, *101*, 3893; e) M. S. Cubberley, B. L. Iverson, *Curr. Opin. Chem. Biol.* **2001**, *5*, 650; f) A. R. Sanford, B. Gong, *Curr. Org. Chem.* **2003**, *7*, 1649; g) C. Schmuck, *Angew. Chem.* **2003**, *115*, 2552; *Angew. Chem. Int. Ed.* **2003**, *42*, 2448; h) I. Huc, Ivan, *Eur. J. Org. Chem.* **2004**, 17.
[3] a) P. S. Corbin, S. C. Zimmerman, P. A. Thiessen, N. A. Hawryluk, T. J. Murray, *J. Am. Chem. Soc.* **2001**, *123*, 10475; b) K. Gademann, A. Hane, M. Rueping, B. Jaun, D. Seebach, *Angew. Chem.* **2003**, *115*, 1573; *Angew. Chem. Int. Ed.* **2003**, *42*, 1534; c) J. S. Nowick, J. O. Brower, *J. Am. Chem. Soc.* **2003**, *125*, 876; d) J. S. Park, H. S. Lee, J. R. Lai, B. M. Kim, S. H. Gellman, *J. Am. Chem. Soc.* **2003**, *125*, 8539.
[4] a) B. Gong, H. Zeng, J. Zhu, L. Yuan, Y. Han, S. Cheng, M. Furukawa, R. D. Parra, A. Y. Kovalevsky, J. L. Mills, E. Skrzypczak-Jankun, S. Martinovic, R. D. Smith, C. Zheng, T. Szyperski, X. C. Zeng, *Proc. Natl. Acad. Sci. USA* **2002**, *99*, 11583; b) J.-L. Hou, X.-B. Shao, G.-J. Chen, Y.-X. Zhou, X.-K. Jiang, Z.-T. Li, *J. Am. Chem. Soc.* **2004**, *126*, 12386; c) D. Kanamori, T. Okamura, H. Yamamoto, N. Ueyama, *Angew. Chem.* **2005**, *117*, 995; *Angew. Chem. Int. Ed.* **2005**, *44*, 969.
[5] a) Y. Hamuro, S. J. Geib, A. D. Hamilton, *J. Am. Chem. Soc.* **1996**, *118*, 7529; b) E. Kolomiets, V. Berl, I. Odriozola, A.-M. Stadler, N. Kyritsakas, J.-M. Lehn, *Chem. Commun.* **2003**, 2868; c) B. Huang, M. A. Prantil, T. L. Gustafson, J. R. Parquette, *J. Am. Chem. Soc.* **2003**, *125*, 14518; d) H. Jiang, J.-M. Léger, I. Huc, *J. Am. Chem. Soc.* **2003**, *125*, 3448; e) J. Garric, J.-M. Léger, I. Huc, *Angew. Chem.* **2005**, *117*, 1990; *Angew. Chem. Int. Ed.* **2005**, *44*, 1954.
[6] a) S. A. Harrell, D. H. McDaniel, *J. Am. Chem. Soc.* **1964**, *86*, 4497; b) S. J. Coles, J. G. Frey, P. A. Gale, M. B. Hursthouse, M. E. Light, K. Navakhun, G. L. Thomas, *Chem. Commun.* **2003**, 568.
[7] a) L. Pauling, *The Nature of the Chemical Bond*, 3rd ed., Cornell University Press, Ithaca, NY, **1960**, p. 464; b) B. Dietrich, J.-M. Lehn, J. Guilhem, C, Pascard, *Tetrahedron Lett.* **1989**, *30*, 4125.
[8] H. A. K. Howard, V. J. Hoy, D. O'Hagan, G. T. Smith, *Tetrahedron* **1996**, *52*, 12613.
[9] a) J. D. Dunitz, R. Taylor, *Chem. Eur. J.* **1997**, *3*, 89; b) J. D. Dunitz, *ChemBioChem* **2004**, *5*, 614.
[10] X. Zhao, X.-Z. Wang, X.-K. Jiang, Y.-Q. Chen, Z.-T. Li, G.-J. Chen, *J. Am. Chem. Soc.* **2003**, *125*, 15128.
[11] B. Gong, *Chem. Eur. J.* **2001**, *7*, 4337.
[12] a) Z.-Q. Wu, X.-K. Jiang, S.-Z. Zhu, Z.-T. Li, *Org. Lett.* **2004**, *6*, 229; b) J. Zhu, X.-Z. Wang, Y.-Q. Chen, X.-K. Jiang, X.-Z. Chen, Z.-T. Li, *J. Org. Chem.* **2004**, *69*, 6221.
[13] The proximity of the F and HN groups in **2** and other compounds may be partially caused by the repulsion of the F and C=O groups. Nevertheless, the coplanarity of the benzene units in **7–9** in the solid state supports the formation of intramolecular hydrogen bonds. We thank the referees for the stimulating comments on this issue.
[14] P. S. Corbin, L. J. Lawless, Z.-T. Li, Y. Ma, M. J. Witmer, S. C. Zimmerman, *Proc. Natl. Acad. Sci. USA* **2002**, *99*, 5099.
[15] Z. Yin, L. Jiang, J. He, J.-P. Cheng, *Chem. Commun.* **2003**, 2326.
[16] P. R. Ashton, P. T. Glink, J. F. Stoddart, P. A. Tasker, A. J. P. White, D. J. Williams, *Chem. Eur. J.* **1996**, *2*, 729.
[17] Complexes between fluorine-containing cyclophanes and ammonium, based on intermolecular F···HN^+ hydrogen bonding has been reported, see: H. Takemura, N. Kon, M. Yasutake, S. Makashima, T. Shinmyozu, T. Inazu, *Chem. Eur. J.* **2000**, *6*, 2334.
[18] This is the largest value for the dialkylammonium ions investigated, see: P. R. Ashton, P. J. Campbell, E. J. T. Chrystal, P. T. Glink, P. S. Menzer, D. Philip, N. Spencer, J. F. Stoddart, P. A. Tasker, D. J. Williams, *Angew. Chem.* **1995**, *107*, 1902; *Angew. Chem. Int. Ed. Engl.* **1995**, *34*, 1865.
[19] a) A. Tanatani, T. S. Hughes, J. S. Moore, *Angew. Chem.* **2002**, *114*, 335; *Angew. Chem. Int. Ed.* **2002**, *41*, 325; b) A. Petitjean, H. Nierengarten, A. van Dorsselaer, J.-M. Lehn, *Angew. Chem.* **2004**, *116*, 3781; *Angew. Chem. Int. Ed.* **2004**, *43*, 3695.

 © 2005 Wiley-VCH Verlag GmbH & Co. KGaA, Weinheim

Cage Compounds

DOI: 10.1002/anie.200501198

Inverse Coordination of an Ionic Lattice by a Metal Host**

*Melinda J. Duer, Felipe García, Richard A. Kowenicki, Vesal Naseri, Mary McPartlin, Matthew L. Stead, Robin S. Stein, and Dominic S. Wright**

There is considerable interest in the effects of modifying the structures of ionic compounds into molecular arrangements, to give materials with unusual properties such as low melting points and solubility in organic solvents.[1] Fragmentation of

[*] Dr. M. J. Duer, F. García, R. A. Kowenicki, V. Naseri, M. L. Stead, R. S. Stein, Dr. D. S. Wright
Chemistry Department
Cambridge University
Lensfield Road, Cambridge CB21EW (UK)
Fax. (+44) 122-333-6362
E-mail: dsw1000@cus.cam.ac.uk
Prof. M. McPartlin
Department of Health and Human Sciences
London Metropolitan University
Holloway Road, London N78DB (UK)

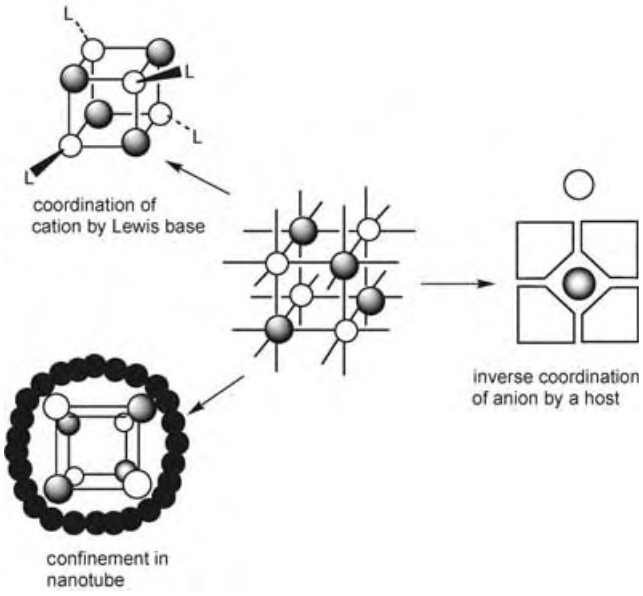
[**] We thank the EPSRC (F.G., M.M., D.S.W.), the EU (Erasmus grant, V.N.), the Cambridge European Trust and Newton Trust (F.G.), the Gates Foundation (R.S.S.), and the States of Guernsey and the Domestic and Millennium Fund (R.A.K.) for financial support. Acknowledgement is made to the donors of the American Chemical Society Petroleum Research Fund for partial support of this research (M.L.S.). We also thank Dr. J. E. Davies (Cambridge) for collecting X-ray data for **1**.

© 2005 Wiley-VCH Verlag GmbH & Co. KGaA, Weinheim

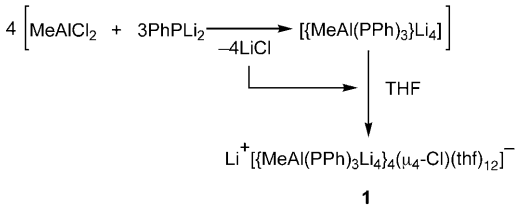
an ionic lattice can be achieved by replacing some or all of the cation–anion bonding with Lewis base coordination (Scheme 1).[1] In notable cases, the molecular species produced have a close resemblance to the parent lattice.[2] A further strategy is the confinement of a salt lattice within another framework. Recent research has focused on the growth of salt lattices within carbon nanotubes (Scheme 1).[3] Remarkably, novel lattice arrangements can be formed which are different to the bulk materials. A third way by which alkali metal salt lattices can, in theory, be modified is by coordination of the anion (Scheme 1).

This approach is the opposite to the conventional coordination of the cation using a Lewis base and thus can be termed as "inverse coordination".[4] Although there are many examples of anion receptors based on organic frameworks, in these anion receptors interactions are relatively weak compared to the lattice energies of simple metal salts.[5] The obvious candidates for strong anion receptors are inorganic metal hosts. Recent studies by Mulvey[4] and Hawthorne and Zheng[6] have illustrated the power of inverse coordination of this type using macrocyclic hosts.

As part of our studies into the structural and materials properties of p-block-metal phosphides,[7–9] we recently investigated the synthesis of Group 13 anions $[RE(PR)_3]^{4-}$ (E = Al, Ga, In).[10] From the reaction of "$PhPLi_2$"[11] with $MeAlCl_2$ in tetrahydrofuran (THF) the ion-separated compound Li^+-$[\{MeAl(PPh)_3Li_4\}_4(\mu_4\text{-}Cl)(thf)_{12}]^-$ (**1**) was obtained as a crystalline product in 43% yield (first batch; see Scheme 2 and Experimental Section).



Scheme 1. Modification of ionic lattices, as illustrated for the fragmentation of the NaCl-type lattice.



Scheme 2. Synthesis of **1**.

Although **1** was characterized by spectroscopic and analytical investigations, its elaborate structure was not fully apparent until a later low-temperature X-ray study.[12] This study showed that the heterometallic cage anion of **1** has a $[Al_4P_{12}Li_{16}(\mu_4\text{-}Cl)]$ core (Figure 1 a), in which an interstitial Cl^- anion is effectively coordinated by four of the anticipated $[MeAl(PPh)_3Li_4]$ units. Although templating of inorganic cages by halide ions has been seen before,[13] to our knowledge **1** is the first example in which a lattice of a simple binary salt is modified by inverse coordination exclusively of one ion.

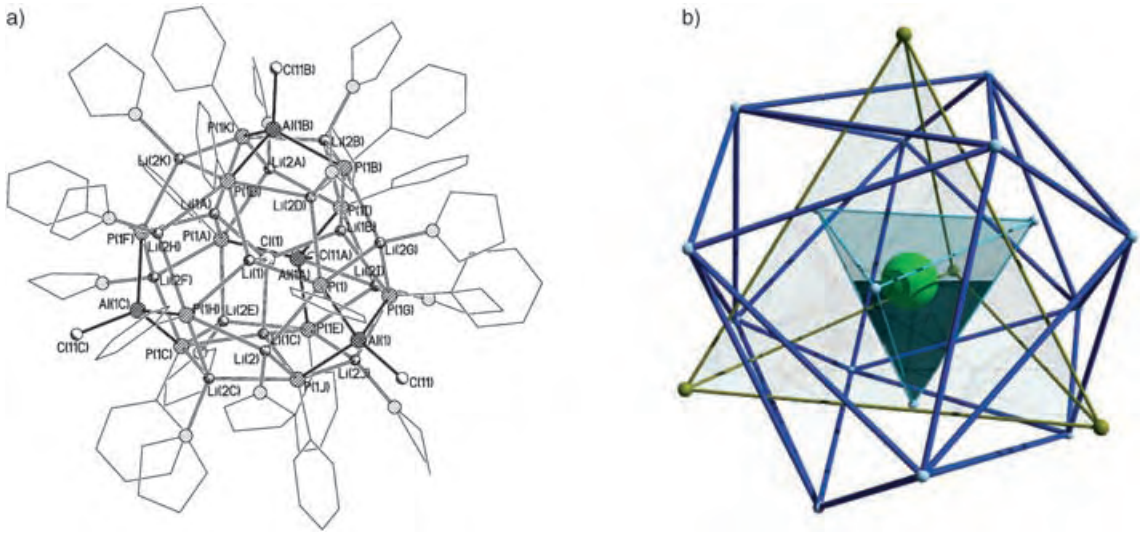


Figure 1. a) Structure of the heterometallic anion of **1**. Selected bond lengths [Å] and angles [°]: Al(1)–C(10) 2.01(2), Al(1)–P(1) 2.461(3), P(1)–Li(1) 2.530(5), P(1)–Li(2) 2.63(1), P(1)–Li(2D) 2.47(2), P(1)–Li(2G) 2.71(2), Li(1)–Cl(1) 2.45(2); P(1)-Al(1)-P(1G) 103.0(1), C(10)-Al(1)-P(1) 115.33(9), Li-Cl(1)-Li(mean) 109.5. Symmetry transformations used to generate equivalent atoms: **A** $x, -y+1, -z+1$; **B** $-x+1, -y+1, z$; **C** $-x+1, y, -z+1$; **D** $-z+1, x, -y+1$; **E** $y, -z+1, -x+1$; **F** z, x, y; **G** y, z, x; **H** $-x+{}^3/_2, -z+1, y+0$; **I** $-x+{}^3/_2, z+0, -y+1$; b) Polyhedral Li (outer shell: blue), Al (gold), Li (inner shell: light blue).

 © 2005 Wiley-VCH Verlag GmbH & Co. KGaA, Weinheim

Interestingly, lithium complexes containing the related nitrogen anions $[R'Al(NAr)_3]^{4-}$ (R′ = Et, *n*Bu; Ar = 2-MeO-C_6H_4) adopt the ion-separated arrangements $[Li(thf)_4]^+{}_2$-$[\{R'Al(NR)_3\}_2Li_6]^{2-}$, in which no encapsulation of Cl^- ion occurs even though LiCl was also present as a byproduct in their formation.[10] This difference may reflect the lower ligand bite angle of the $[RAl(NAr)_3]^{4-}$ anions (average N···N distance 2.91 Å) compared to the $[MeAl(PPh)_3]^{4-}$ analogue (P···P 3.85 Å).[14] The tetrahedral $[MeAl(PPh)_3]^{4-}$ anions of **1** are arranged in a supramolecular tetrahedron (gold, Figure 1b), which defines the polyhedral arrangement of Li^+ cations. The twelve phosphorus atoms of the cage are all six-coordinate, each being bonded to four Li^+ cations within the core (Li–P 2.47(2)–2.71(2) Å). The twelve symmetry-related ions Li(1) to Li(1K) (dark blue, Figure 1b) form an outer shell of ions that are each bonded to three phosphorus centers and to the oxygen atom of a thf ligand. The inner sphere of Li ions Li(1) to Li(1C) (light blue, Figure 1b) have a similar tetrahedral environment, but their fourth coordination site is occupied by the central Cl^- anion (Li(1–1C)–Cl(1) 2.45(2) Å) rather than an O atom from thf.

A single, unsolvated Li^+ countercation is present in the lattice of **1** for each of the cage anions (the charge of each anion being −1). Owing to the cubic space group there is inherent uncertainty as to the location of these Li^+ cations, however, their most likely location is midway between cluster anions (along the edges of the cubic unit cell and the central face-to-face diagonals), that is, $^1/_3$ Li^+ occupancy in each of these 24 symmetry-related sites balancing the −8 charge of the 8 anions. Eight anions are depicted in Figure 2.[12] The Li^+ cations loosely bind two cluster anions together through agostic C–H···Li interactions with two pairs of symmetry-related thf molecules (C···Li 2.82–2.84 Å).[15] The resulting zeolite-like structure contains large voids (ca. 17 Å in diameter) and has nearest neighbor Li^+ and encapsulated Cl^- ions separated by 8.76 Å. The absence of further disordered thf molecules or $[Li(thf)_4]^+$ cations in these voids was shown by elemental analysis and ^{1}H NMR spectroscopic studies of bulk samples of **1** (analyzed both before and after exposure to a vacuum). We assume that **1** adopts this open arrangement in order to minimize anion–anion repulsion, while allowing efficient anion–cation interactions between the polyhedra. Clearly, anion–anion repulsion would be significantly greater in the close-packed structure of the original LiCl lattice.

Solid-state ^{6}Li and ^{7}Li magic-angle-spinning (MAS) NMR studies of **1** are consistent with the X-ray study,[16] showing the expected presence of a highly mobile Li^+ cation as a result of its weak coordination. Two resonances are found in the ^{6}Li NMR spectrum at $\delta = 3.8$ ($w_{1/2} = 50$ Hz, 10 Hz line broadening) and 2.2 ppm (very broad). At least two overlapping resonances are apparent in the ^{7}Li NMR spectrum at $\delta = 3.6$ and 0.4 ppm.[17] The ^{7}Li relaxation-assisted separation (2D-RAS) spectrum[18] shows that the peak at $\delta = 0.4$ ppm has a longitudinal relaxation time constant $t_1 = 107$ s, which is consistent with a mobile lithium ion without strong interactions to other nuclei (Li(3)), while the peak at $\delta = 3.6$ ppm has $t_1 = 6$ s. The peak at $\delta = 0.4$ ppm does not appear in a ^{7}Li{^{1}H} CPMAS NMR spectrum, confirming that lithium is not bound strongly to any protons in the crystal. Furthermore, the peak at $\delta = 3.6$ ppm is very broad and likely contains the peaks appearing at $\delta = 3.8$ and 2.2 ppm observed in the ^{6}Li NMR spectrum which are assigned to the cage lithium atoms Li(1) and Li(2). It can be noted that all three Li environments are observed for **1** in solution in THF.

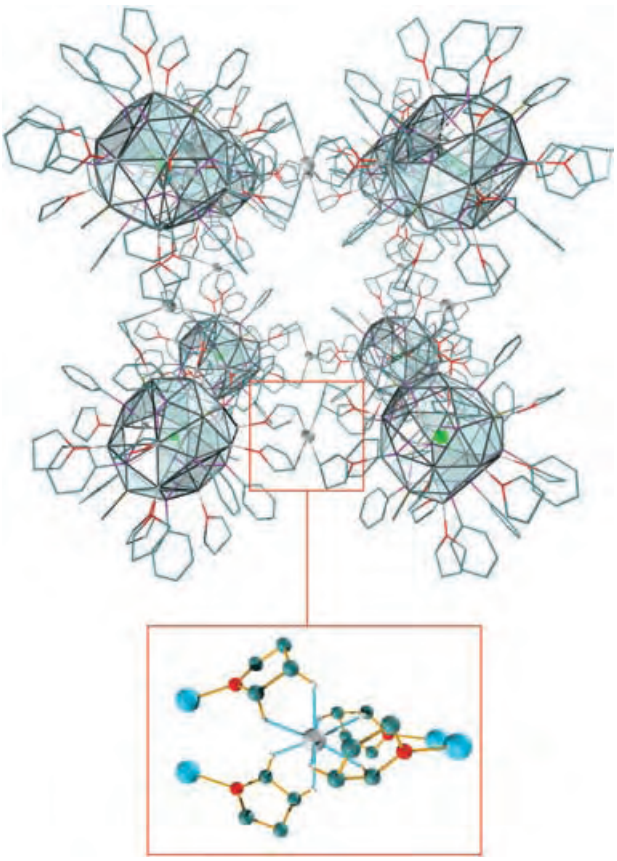


Figure 2. Formation of cube-shaped cavities within the structure of **1**, showing the partial occupancy Li(3) sites between adjacent cluster anions. The insert shows the thf C–H···Li^+ interactions that anchor the Li^+ counterions in the lattice: C···Li 2.81–2.84 Å (H···Li 2.09–2.16 Å).

The structure of **1** dramatically illustrates the concept of lattice modification using inverse coordination of a simple ionic salt. A large expansion of the NaCl-type lattice of LiCl results from the encapsulation of the Cl^- ions within the cages, with a loss of the original close packing of the chloride ion array. This type of structural modification provides a potentially general new strategy for crystal engineering. Such a strategy should lead to a novel approach to fast-ion conductors.[19,20] The generalization of this synthetic approach using inorganic frameworks with building blocks related to the $[MeAl(PPh)_3]^{4-}$ anions in **1** is therefore an exciting prospect both from a theoretical and technological standpoint.[21]

Experimental Section

1: All manipulations were performed under dry, O_2-free argon. *n*BuLi (8.25 mL, 1.60 M in hexane, 13.2 mmol) was added to a stirred solution of $PhPH_2$ (0.66 mL, 6.00 mmol) in diethyl ether (50.0 mL) at −78 °C.

 © 2005 Wiley-VCH Verlag GmbH & Co. KGaA, Weinheim

The reaction mixture was allowed to warm to room temperature and stirred for a further 1 h, producing a yellow precipitate, then the reaction mixture was heated at reflux (14 h). The resulting suspension was cooled to −78 °C, and $MeAlCl_2$ (2.00 mL, 1.00 M in hexane, 2.00 mmol) was added. The mixture was allowed to warm to room temperature and then heated at reflux (14 h) to give a yellow solution and white precipitate. After replacing the solvent by toluene (50.0 mL) and filtration (Celite, P4) to remove LiCl, the solvent was removed under vacuum and a yellow precipitate was obtained. Crystallization from THF at room temperature (14 h) led to light yellow cube-shaped crystals of **1** (0.54 g yield, 43 % first batch of crystals); decomp. ca. 210 °C (red) to ca. 270 °C (black solid); IR (Nujol, NaCl), $\tilde{\nu}$ = 3030(w) (C–H aryl stretch), 1570(w) (C=C stretch), 1022(s) cm^{-1}; no P–H stretching band was observed; ^1H NMR (500.2 MHz, 298 K, C_6D_6): δ = 8.3 (m, *m*-CH Ph), 7.22 (q, *p*-CHPh), 0.40 ppm (br s, Me-Al); ^{31}P NMR (202.5 MHz, 298 K, THF/[D_6]acetone capillary, 85 % H_3PO_4/D_2O): δ = −161.8 ppm; ^7Li NMR (194.4 MHz, 298 K, THF/[D_6]acetone capillary, sat. LiCl/D_2O): δ = 2.25 (br s, $w_{1/2}$ = 29 Hz, Li(3)), 1.82 (br s, $w_{1/2}$ = 29 Hz, Li(1)), 0.36 ppm (s, $w_{1/2}$ = 10 Hz, Li(2)); assignments were made solely on the basis of the approximate integration of the spectrum, 1:4:8 ratio of the resonances (theoretical 1:4:12). The ^{31}P and ^7Li NMR solution spectra do not change with concentration or temperature (180–298 K), proving that no fragmentation of the anion of **1** occurs in solution. Solid state MAS-NMR, ^7Li (155.406 MHz, 32 scans, 15-s recycle delay): δ = 3.6 (Li(1) and Li(2)), 0.4 ppm (Li(3)); $^7Li\{^1H\}$ CPMAS (399.87 MHz for ^1H, 4-ms contact time, 8 scans): δ = 3.6 ppm; $^6Li\{^1H\}$ CPMAS (58.89 MHz/399.87 MHz for ^1H, 3-ms contact time, 4096 scans): δ = 3.8 (Li(1)), 2.2 ppm (Li(2)); assignments made on the basis of approximate 2:1 integration. Sixty logarithmically spaced τ values were collected between 0.01 s and 160 s for the RAS spectrum; twenty-four transients were collected for each τ value;[22] elemental analysis (%) calcd for **1**: C 60.0, H 6.8, P 15.0; found (typical): C 59.0, H 7.6, P 12.7.

Received: April 5, 2005
Revised: June 24, 2005
Published online: August 3, 2005

Keywords: aluminum · cage compounds · inverse coordination · lithium · X-ray diffraction

[1] R. Snaith, D. S. Wright in *Lithium Chemistry: A Theoretical and Experimental Overview* (Eds.: A.-M. Sapse, P. von R. Schleyer), Wiley, New York, **1994**, chap. 8, p. 227.
[2] D. Barr, W. Clegg, R. E. Mulvey, R. Snaith, *J. Chem. Soc. Chem. Commun.* **1984**, 79.
[3] J. Sloan, A. I. Kirkland, J. L. Hutchison, M. L. H. Green, *Chem. Commun.* **2002**, 1319.
[4] Mulvey and co-workers have coined the term "inverse crowns" to describe a series of macrocycles composed of Group 1 and/or 2 metal acceptors linked by amide groups, see: R. E. Mulvey, *Chem. Commun.* **2001**, 1049.
[5] For examples of organic receptors of this type, see: J. L. Sessler, J. M. Davis, *Acc. Chem. Res.* **2001**, *34*, 984.
[6] For "metallacarborane" macrocycles composed of acceptor Hg^{II} ions linked by C_2B_{10} icosahedra, see: M. F. Hawthorne, Z. Zheng, *Acc. Chem. Res.* **1997**, *30*, 267.
[7] A. D. Hopkins, J. A. Wood, D. S. Wright, *Coord. Chem. Rev.* **2001**, *216*, 155.
[8] M. A. Beswick, C. A. Harmer, A. D. Hopkins, M. McPartlin, J. A. Wood, D. S. Wright, *Science* **1998**, *281*, 150.
[9] F. García, A. D. Hopkins, C. M. Pask, D. S. Wright, *J. Mater. Sci.* **2004**, *39*, 3093.
[10] Isoelectronic nitrogen analogues $[R'Al(NAr)_3]^{4-}$ have recently been reported, see: M. C. Copsey, J. C. Jeffery, C. A. Russell, J. M. Slattery, J. A. Slaughan, *Chem. Commun.* **2003**, 2306.
[11] The dilithiation procedure is the same as that reported previously for a range of other primary phosphines, see: K. Niediek, B. Neumüller, *Z. Anorg. Allg. Chem.* **1993**, *619*, 885. Whether the reaction of $PhPH_2$ with *n*BuLi produces a genuine dilithiate could not be ascertained by NMR spectroscopy owing to the low solubility of the product. Attempts to prepare **1** by stepwise reaction of $MeAlCl_2$ with $PhPH_2$ followed by reaction with *n*BuLi failed. The presence of 2 equivalents of *n*BuLi in the reaction mixture prior to reaction with $MeAlCl_2$ is necessary to prevent an alternative pathway involving P–P bond formation; see: F. García, S. M. Humphrey, R. A. Kowenicki, M. McPartlin, D. S. Wright, *Dalton Trans.* **2004**, 977.
[12] Crystal data for **1**: $C_{124}H_{168}Al_4ClLi_{17}O_{12}P_{12}$, M = 2483.57, cubic, space group $F\bar{4}3c$, Z = 8, a = 35.037(4) Å, V = 43011(9) Å^3, $\mu(Mo_{K\alpha})$ = 0.158 mm^{-1}, ρ_{calcd} = 0.767 $Mg\,m^{-3}$, T = 180(2) K. Data were collected on a Nonius Kappa CCD diffractometer. Of a total of 10442 reflections collected, 1674 were unique (R_{int} = 0.170). The structure was solved by direct methods, and all non-hydrogen atoms of the cluster anion, centered by a chlorine atom at $^1/_2$, $^1/_2$, $^1/_2$ (site symmetry 23), were readily located. The location of the lithium countercation proved more problematic. Initially it seemed possible that a solvated $[Li(thf)_4]^+$ cation might be located in the giant cavity (centered at $^1/_4$, $^1/_4$, $^1/_4$) defined by the cubelike arrangement of the clusters, giving a pseudo-CsCl-type structure. Although there was no significant electron density apparent within the cavity, this might have been explained by a complete randomization of the position of the $[Li(thf)_4]^+$ cation (radius, $r \approx 5$ Å) which is considerably smaller than the cavity ($r \approx 8$ Å, to the closest hydrogen atom). This possibility is ruled out by the elemental analysis, which is consistent with an unsolvated Li^+ cation (with no further THF being present). The only site suitable for a naked cation is at $^1/_4$, 0, 0 (site symmetry −4) which gives reasonable $Li^+\cdots$thf interactions. A lithium atom of occupancy $^1/_3$ was included at this site in the refinement by full-matrix least squares on F^2 with anisotropic displacement parameters assigned to all full occupancy non-hydrogen atoms (G. M. Sheldrick, *SHELX-97*, Göttingen, Germany, **1997**). Relatively high displacement parameters for two carbon atoms indicated some unresolved conformational disorder of the thf ligand. Final R_1 = 0.076 ($I > 2\sigma(I)$) and wR_2 = 0.201 (all data). CCDC 267276 contains the supplementary crystallographic data for this paper. These data can be obtained free of charge from The Cambridge Crystallographic Data Centre via www.ccdc.cam.ac.uk/data_request/cif.
[13] For examples of templating of metal cages with halide ions, see: P. J. M. W. Birker, J. Reedijk, G. C. Verschoor, *Inorg. Chem.* **1981**, *20*, 2877; R. Wang, T. Jin, Z. Zheng, R. J. Staples, *Angew. Chem.* **1999**, *111*, 1929; *Angew. Chem. Int. Ed.* **1999**, *38*, 1813; A. Müller, R. Rohlfing, R. Krichemeyer, E. Penk, H. Bögge, *Angew. Chem.* **1993**, *105*, 916; *Angew. Chem. Int. Ed. Engl.* **1993**, *32*, 909.
[14] As a result, the phosphorus anions in **1** are more capable of supporting a larger cage arrangement than their nitrogen counterparts. A similar structural trend has been observed previously in the antimony complexes $[Sb(ER)_3]^{3-}$ (E = N or P); see: M. A. Beswick, N. Choi, C. N. Harmer, A. D. Hopkins, M. A. Paver, M. McPartlin, D. S. Wright, *Inorg. Chem.* **1998**, *37*, 2177; M. A. Beswick, C. N. Harmer, P. R. Raithby, D. S. Wright, *Chem. Commun.* **1997**, 1897.
[15] The C···Li distances involved are typical of agostic interactions as observed for a range of organolithium compounds, see: W. Setzer, P. von R. Schleyer, *Adv. Organomet. Chem.* **1985**, *24*, 353.

 © 2005 Wiley-VCH Verlag GmbH & Co. KGaA, Weinheim

[16] Two-pulse phase-modulation decoupling used throughout, see: A. E. Bennett, C. Rienstra, M. Auger, K. V. Lakshmi, R. Griffin, *J. Chem. Phys.* **1995**, *103*, 6951.
[17] Relaxation times of ^{6}Li nuclei are typically larger than those of ^{7}Li, and ^{6}Li is much less sensitive to NMR spectroscopy than ^{7}Li, so it is not surprising that the peak at $\delta = 0.4$ ppm in the ^{7}Li NMR spectrum does not appear in the ^{6}Li NMR spectrum.
[18] A. Lupulescu, M. Kotecha, L. Frydman, *J. Am. Chem. Soc.* **2003**, *125*, 3376.
[19] S. M. Ivanova, B. G. Nolan, Y. Kobayashi, S. M. Miller, O. P. Anderson, S. H. Strauss, *Chem. Eur. J.* **2001**, *7*, 503.
[20] F. Kita, H. Sakata, S. Sinomoto, A. Kawakami, H. Kamizori, T. Sonoda, H. Nagashima, J. Nie, N. V. Pavlenko, Y. Yagupolskii, *J. Power Sources* **2000**, *90*, 27.
[21] M. A. Beswick, D. S. Wright, *Coord. Chem. Rev.* **1998**, *176*, 373.
[22] The data were processed by applying an inverse Laplace transformation using Genereg. See: J. Weese, *Comput. Phys. Commun.* **1992**, *99*, 69.

 © 2005 Wiley-VCH Verlag GmbH & Co. KGaA, Weinheim

Molecular Capsules

DOI: 10.1002/anie.200501491

Hydrogen-Bonded Supramolecular Assemblies as Robust Templates in the Synthesis of Large Metal-Coordinated Capsules**

*Robert M. McKinlay, Praveen K. Thallapally, Gareth W. V. Cave, and Jerry L. Atwood**

The synthesis of large multicomponent spheroid cage structures that offer the possibility of encapsulating numerous molecules is an important theme in supramolecular chemistry.[1] Strategies developed in their construction have mainly relied on self-assembly by means of multiple hydrogen bonds[2] or metal–ligand coordination.[3] Although there are numerous reports[4] of metal coordination to calixarene-based macrocycles, the formation of larger molecular cage structures involving more than two units remains limited.[5]

The bowl-shaped resorcin[4]arene and pyrogallol[4]arene macrocycles lend themselves amenable to the formation of large hexameric cage structures by hydrogen bonding.[6] From a pictorial point of view, substitution of hydrogen atoms for metal ions within these hexameric capsules[6] would result in structural preservation of the hexameric assembly while introducing new variables such as inorganic functionality. Indeed, limited consideration has been given to using pyrogallol[4]arene units as multibranched chelate ligands. Caulder and Raymond have shown the concept of using multibranched chelate ligands in the synthesis of cage structures, however, these structures contain relatively small cavities.[7] Herein we report the formation of a large neutral hexameric coordination cage structure assembled from six pyrogallol[4]arene ligands and twelve Ga^{III} ions.

Treatment of *C*-propyl-pyrogallol[4]arene (Figure 1) with four equivalents of $Ga(NO_3)_3 \cdot H_2O$ in a mixture of acetone and water resulted in the metal-directed self-assembly of $[Ga_{12}(H_2O)_{24}(C_{40}H_{42}O_{12})_6 \subset (acetone)_8(H_2O)_6]$ (**1**; Figure 2). Single-crystal X-ray analysis shows that **1** is assembled from 18 components: 6 pyrogallol[4]arene ligands and 12 Ga^{III} ions.[8] This large "rugby ball" shaped coordination cage is arranged such that the centroids of the six pyrogallol[4]arene ligand components reside on the vertices of a skewed octahedron and encloses approximately 1150 $Å^3$ of space.[9] The cage structure within **1** is held together by four slightly curved six-membered $[Ga_3O_3]$ arrays ($Ga\cdots O_{equatorial}$: 1.886–

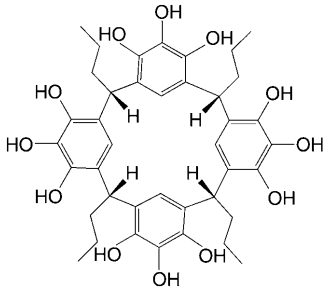


Figure 1. *C*-propyl-pyrogallol[4]arene macrocycle.

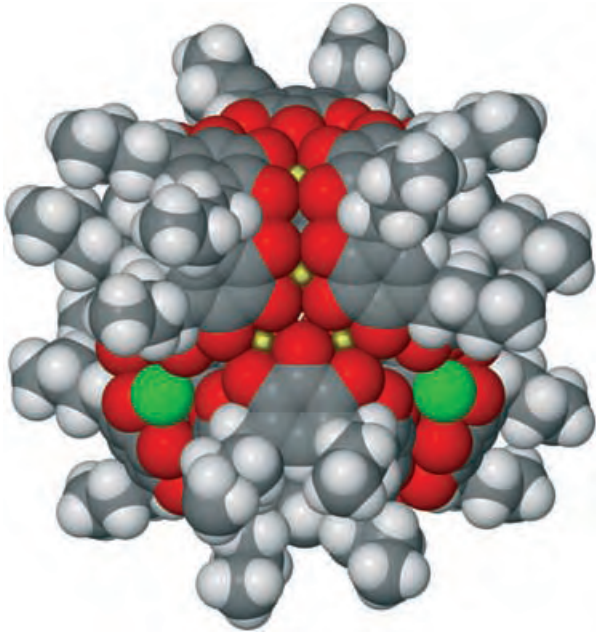


Figure 2. Space-filling representation of **1**. Surface-coordinated water molecules represented in green, gallium in gold; axial-coordinated water molecules and phenol hydrogen atoms removed for clarity.

[*] R. M. McKinlay, Dr. P. K. Thallapally, Dr. G. W. V. Cave, Prof. J. L. Atwood
Department of Chemistry
University of Missouri-Columbia
Columbia, Missouri 65211 (USA)
Fax: (+1) 573-884-9606
E-mail: AtwoodJ@missouri.edu

[**] This work was supported by the National Science Foundation.

© 2005 Wiley-VCH Verlag GmbH & Co. KGaA, Weinheim

2.009 Å, O–Ga–O: 85.18–98.77°, Ga–O–Ga: 137.97–148.07°; Figure 3). All four equatorial positions on each octahedral gallium center are occupied by oxygen atoms from the macrocycle framework, with the axial positions (Ga···O_{axial}

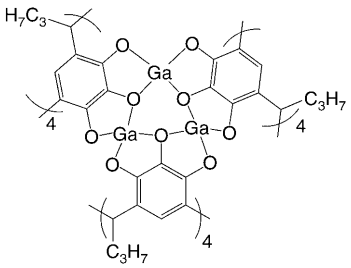


Figure 3. One of the four [Ga_3O_3] six-membered arrays that hold **1** together.

1.924–2.104 Å) occupied by water molecules, twelve of them pointing inwards towards the cavity center. These axial bond distances correspond clearly to Ga···OH_2 coordination rather than Ga···OH bonds.[10] Embedded on the surface of **1** are four water molecules that participate in intermolecular hydrogen bonding with the upper-rim framework of the macrocycle which seals up potential surface voids. Indeed, these surface-coordinated water molecules may be viewed as occupying gates to the interior of the capsule.

The previously reported metal-directed self-assembly of pyrogallol[4]arene macrocycles with four equivalents of Cu^{II} ions resulted in the formation of a large spherical coordination cage $[Cu_{24}(C_{40}H_{40}O_{16})_6]$ (**2**).[11] Each face within the octahedral structure was capped by eight six-membered $[Cu_3O_3]$ planar arrays. In contrast to the Cu^{II} structure **2**, only half of the octahedral faces within **1** are capped with $[Ga_3O_3]$ arrays (Figure 4).

Within the hydrogen-bonded hexameric structure previously determined, there are 24 intramolecular hydrogen bonds, that is, 4 intramolecular hydrogen bonds per macrocycle that seam the capsule together.[6] These intramolecular hydrogen bonds are important for holding and stabilizing each macrocycle into its rigid cone or bowl-shaped conformation. Indeed, within the spherical Cu^{II} coordination capsule **2**, there are 24 intramolecular hydrogen bonds of the type OH···O^- that hold the framework together. However, from a pictorial view, the addition of 12 Ga^{III} metal ions into the hydrogen-bonded hexameric framework results in the substitution of 36 hydrogen atoms. It should be noted that 36 phenol groups, 6 from each macrocycle, remain to participate in hydrogen bonding as determined by ^1H NMR spectral analysis. Therefore, within **1** there are 48 Ga–O coordination bonds, 16 intramolecular hydrogen bonds of the type OH···O^-, 4 intramolecular hydrogen bonds of the type OH···OH, and 16 phenol groups remaining that can participate in intermolecular hydrogen bonding. Thus, the gallium coordination capsule **1** has only a total of 20 intramolecular hydrogen bonds that seam the framework together. A reasonable explanation for the structural difference between **1** and **2** is the loss of four intramolecular hydrogen bonds as a result of Ga^{III} versus Cu^{II}, which has the possibility of

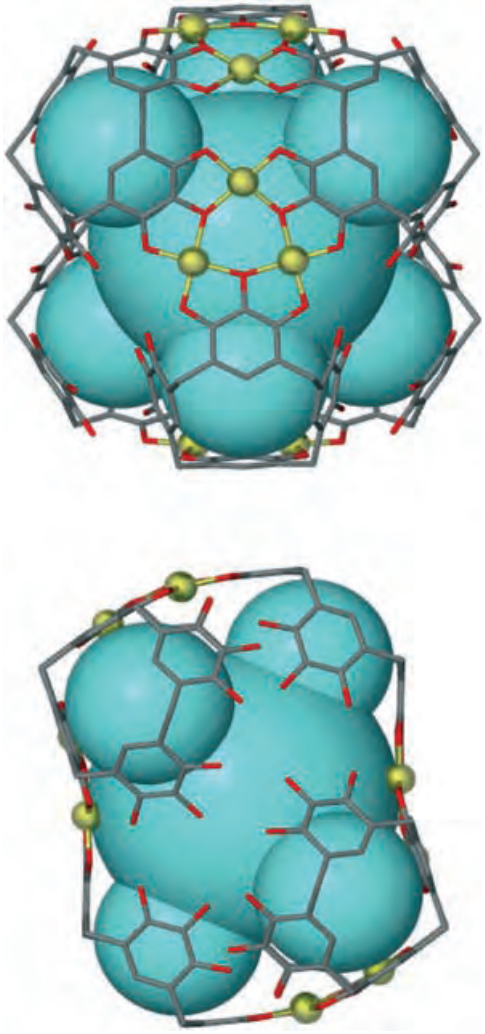


Figure 4. Structure **1** showing half of the octahedral faces capped with [Ga_3O_3] arrays. Axial coordinated water molecules, hydrogen atoms, and alkyl tails removed for clarity.

introducing greater flexibility and decreasing structural rigidity within the cone conformation. This flexibility alters the spherical topology framework found within **2** to a "rugby ball" topology **1**. Since the "rugby ball" topology distorts the remaining phenol framework, further insertion of metal ions is less favored.

The combination of hydrogen bonds and metal–ligand coordination that hold supramolecular cage frameworks together is limited.[12] The advantage of using combinations of noncovalent interactions is a greater degree of freedom and control to build interesting supramolecular assemblies. For example, by alternating the number of intramolecular hydrogen bonds within the metal-coordinated hexameric structure by changing the oxidation state of the metal ion, slightly different structures are formed.

Steric interactions tend to be the main force in organizing guest molecules within large spheroid supramolecular cage assemblies, although there are some exceptions.[13] This implies that many guest molecules within large cavities are highly disordered as determined from X-ray analysis. How-

 © 2005 Wiley-VCH Verlag GmbH & Co. KGaA, Weinheim

ever, within structure **1**, the axial metal-coordinated sites from the corresponding Ga^{III} ions are advantageously located orthogonal to the surface framework. These coordination sites have a profound influence on guest arrangements within **1**. Embedded within the large cavity are eight acetone molecules, twelve metal-coordinated water molecules, and six noncoordinated water molecules yielding an effective encapsulation of approximately 66%.[9] The packing coefficient within various molecular recognition systems is calculated to be approximately 55%.[14] The metal-coordinated water molecules within the cavity form hydrogen bonds with each acetone guest molecule. Interestingly, within the asymmetric unit, two axial metal-coordinated water molecules demonstrate evidence of a strong hydrogen bond (O···O 2.501 Å) that connects two neighboring $[Ga_3O_3]$ units together. Furthermore, the metal-coordinated water molecules show hydrogen bonding to each other within each $[Ga_3O_3]$ array (O···O 2.797–2.913 Å). Thus the Ga^{III} geometry is distorted sufficiently away from octahedral symmetry (O_{axial}-Ga-$O_{equatorial}$: 82.85–97.44°).

Found within **1** are two pseudo-linear hydrogen-bonded water $(H_2O)_5$ chains; hydrogen bonds are inferred from short O···O distances. The adjacent O···O distances are 2.711–2.823 Å and the O···O···O angles are 91.01–133.18°. X-ray analysis could not determine the position of hydrogen atoms within the water chain. The free water molecules adjacent to the Ga^{III}-coordinated water molecules also form hydrogen bonds to the phenol groups from the macrocycle framework. The free water molecules within the cavity do not form hydrogen bonds with acetone guest molecules. Within each linear water $(H_2O)_5$ chain, the three non-metal-coordinated water molecules, as a supramolecular entity, in effect act as a bridging ligand by connecting two opposite $[Ga_3O_3]$ arrays within **1** by hydrogen bonding to a metal-coordinated water molecule from each $[Ga_3O_3]$ array (Figure 5). The prevailing

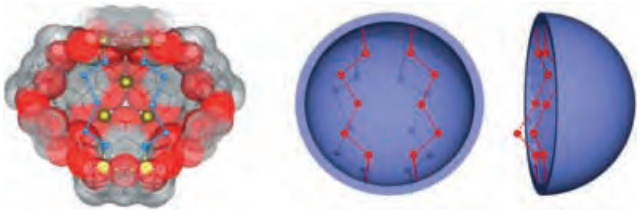


Figure 5. The pseudo-linear hydrogen-bonded water $(H_2O)_5$ chains within **1**. Acetone guest molecules within **1** removed for clarity.

knowledge is that the global minima of hydrogen-bonded water $(H_2O)_n$ clusters with $3 \le n \le 6$ have a general tendency to associate into two-dimensional planar ringlike architectures which is supported by both theoretical and experimental observations.[15] However, it is possible that confined space can offer an alternative environment to enforce different water topologies.

In conclusion, we have demonstrated the synthesis of a large hexameric cage structure stitched together from a combination of metal coordination and hydrogen bonds. Thus, the advantageous structural features from the hydrogen-bonded capsules are preserved while introducing new variables such as inorganic functionality. Indeed, this resulting combination of binding forces has led to architectures that organize the enclosed guest molecules in unique ways.

Experimental Section

Butyraldehyde (11.4 g, 0.16 mol) was added dropwise over a period of 2 h to a solution of pyrogallol (20 g, 0.16 mol) in ethanol (100 mL) and conc. HCl (10 mL) under N_2 gas. The resulting mixture was heated at reflux for 24 h, filtered, washed with water (3 × 500 mL), and recrystallized from methanol. *C*-propyl-pyrogallol[4]arene (14.2 g, 49%) was collected as a colorless powder. ^{1}H NMR (300 MHz, [D_6]acetone): $\delta = 0.95$ (12H, t, $^3J = 7.4$ Hz), 1.32 (8H, sextet, $^3J = 7.4$ Hz), 2.26 (8H, q, $^3J = 7.5$ Hz), 4.37 (4H, t, $^3J = 7.9$ Hz), 7.14 (4H, s), 7.18 (4OH, s), 8.09 ppm (8OH, brs); ^{13}C NMR ([D_6]acetone): $\delta = 13.3$, 20.8, 33.6, 34.9, 113.5, 124.7, 132.6, 139.1 ppm.

Single colorless crystals of **1** suitable for X-ray crystallographic analysis were grown from a sealed container, with a solution of *C*-propyl-pyrogallol[4]arene (0.20 g) in acetone (5 mL) added to a solution of $Ga(NO_3)_3 \cdot H_2O$ (0.28 g) in water (2 mL).[8] Yield: 48%, based on pyrogallol[4]arene ligand. ^{1}H NMR of **1** (300 MHz, CD_3CN): $\delta = 0.98$ (72H, t, $^3J = 7.5$ Hz), 1.29 (48H, m), 2.22 (48H, m), 4.26 (24H, t), 6.89 (12OH + 24Ar, brs), 7.38 ppm (24OH, brs); ^{1}H NMR of **1** (CD_3CN + D_2O): the peak at $\delta = 6.89$ ppm reduces to 24Ar.

Received: April 29, 2005
Published online: August 4, 2005

Keywords: gallium · hydrogen bonds · molecular capsules · self-assembly · supramolecular chemistry

[1] J. Rebek, Jr., *Angew. Chem.* **2005**, *117*, 2104; *Angew. Chem. Int. Ed.* **2005**, *44*, 2068.
[2] L. J. Prins, D. N. Reinhoudt, P. Timmerman, *Angew. Chem.* **2001**, *113*, 2446; *Angew. Chem. Int. Ed.* **2001**, *40*, 2382.
[3] M. Fujita, M. Tominaga, A. Hori, B. Therrien, *Acc. Chem. Res.* **2005**, *38*, 369.
[4] a) R. Pinalli, V. Cristini, V. Sottili, S. Geremia, M. Campagnolo, A. Caneschi, E. Dalcanale, *J. Am. Chem. Soc.* **2004**, *126*, 6516; b) K. Kobayashi, Y. Yamada, M. Yamanaka, Y. Sei, K. Yamaguchi, *J. Am. Chem. Soc.* **2004**, *126*, 13896; c) F. A. Cotton, P. Lei, C. Lin, C. A. Murillo, X. Wang, S.-Y. Yu, Z.-Z. Zhang, *J. Am. Chem. Soc.* **2004**, *126*, 1518; d) Z. Zhong, A. Ikeda, M. Ayabe, S. Shinkai, S. Sakamoto, K. Yamaguchi, *J. Org. Chem.* **2001**, *66*, 1002; e) S. J. Park, J.-I. Hong, *Chem. Commun.* **2001**, 1554; f) O. D. Fox, J. F.-Y. Leung, J. M. Hunter, N. K. Dally, R. G. Harrison, *Inorg. Chem.* **2000**, *39*, 783; g) O. D. Fox, N. K. Dalley, R. G. Harrison, *J. Am. Chem. Soc.* **1998**, *120*, 7111; h) P. Jacopozzi, E. Dalcanale, *Angew. Chem.* **1997**, *109*, 665; *Angew. Chem. Int. Ed. Engl.* **1997**, *36*, 613.
[5] a) O. D. Fox, M. G. B. Drew, P. D. Beer, *Angew. Chem.* **2000**, *112*, 139; *Angew. Chem. Int. Ed.* **2000**, *39*, 135; b) O. D. Fox, M. G. B. Drew, E. J. S. Wilkinson, P. D. Beer, *Chem. Commun.* **2000**, 391.
[6] a) G. W. V. Cave, J. Antesberger, L. J. Barbour, R. M. McKinlay, J. L. Atwood, *Angew. Chem.* **2004**, *116*, 5375; *Angew. Chem. Int. Ed.* **2004**, *43*, 5263; b) J. L. Atwood, L. J. Barbour, A. Jerga, *J. Supramol. Chem.* **2001**, *1*, 131; c) T. Gerkensmeier, W. Iwanek, C. Agena, R. Fröhlich, S. Kotila, C. Näther, J. Mattay, *Eur. J. Org. Chem.* **1999**, 2257; d) L. R. MacGillivray, J. L. Atwood, *Nature* **1997**, *389*, 469.
[7] D. L. Caulder, K. N. Raymond, *Acc. Chem. Res.* **1999**, *32*, 975.
[8] Crystal data for $[Ga_{12}(H_2O)_{24}(C_{40}H_{42}O_{12})_6] \cdot 19(CH_3COCH_3) \cdot 16(H_2O)$, $M_r = 6949.4$, monoclinic, $a = 23.579(3)$, $b = 27.299(3)$, $c = 27.025(3)$ Å, $\beta = 93.886(2)°$, $V = 7356(4)$ Å^3, space group $P21/n$,

 © 2005 Wiley-VCH Verlag GmbH & Co. KGaA, Weinheim

$Z = 4$, $\rho_{calcd} = 1.308\ g\,cm^{-3}$, $\lambda(Mo_{K\alpha}) = 0.70930$ Å, $F(000) = 7073$, $T = 173(2)$ K, 38365 unique reflections ($2\theta \leq 56°$), of which 18300 were observed [$I_o > 2\sigma(I)$]. Final R factors: $R_1 = 0.0872$, $wR_2 = 0.2380$ for 2230 parameters. Data were collected on a Bruker SMART 1000 CCD diffractometer with $Mo_{K\alpha}$ radiation using the ω-scan mode. Data were corrected for absorption using the SADABS program, and solution and refinement of the structure were performed using the SHELX-97 software package. All non-hydrogen atoms and non-guest molecules were refined anisotropically, whereas the hydrogen atoms were included at geometrically calculated positions and allowed to ride on their parent atoms. The hydrogen atoms from water molecules were not assigned. CCDC 243837 contains the supplementary crystallographic data for this paper. These data can be obtained free of charge from the Cambridge Crystallographic Data Centre via www.ccdc.cam.ac.uk/data_request/cif.

[9] L. J. Barbour, **2003** MCAVITY, program for calculating the molecular volume of closed capsules, University of Missouri-Columbia, Missouri, USA. http://www.x-seed.net/cavity.html. Maximum free volume within the cavities was calculated with guest molecules removed. It was assumed that the molecular volume of acetone and water is 61.3 and 14.7 Å^3, respectively. The volume of cavity **1** was subject to an error of $\pm 10\,\%$ as the capsule was distorted from perfect spheroid geometry.

[10] O. Jarjayes, A. Du Moulinet D'Hardemare, A. Durif, M.-T. Averbuch-Pouchot, *Acta Crystallogr. Sect. C* **1998**, *54*, 931.

[11] R. M. McKinlay, G. W. V. Cave, J. L. Atwood, *Proc. Natl. Acad. Sci. USA* **2005**, *102*, 5944.

[12] a) R. Garía-Zarracino, H. Höpfl, *Angew. Chem.* **2004**, *116*, 1533; *Angew. Chem. Int. Ed.* **2004**, *43*, 1507; b) M. A. Alam, M. Nethaji, M. Ray, *Angew. Chem.* **2003**, *115*, 1984; *Angew. Chem. Int. Ed.* **2003**, *42*, 1940.

[13] J. L. Atwood, L. J. Barbour, A. Jerga, *Proc. Natl. Acad. Sci. USA* **2002**, *99*, 4837.

[14] A. S. Mecozzi, J. Rebek, Jr., *Chem. Eur. J.* **1998**, *4*, 1016.

[15] K. Liu, J. D. Cruzan, R. J. Saykally, *Science* **1996**, *271*, 929.

 © 2005 Wiley-VCH Verlag GmbH & Co. KGaA, Weinheim

Dynamic Combinatorial Chemistry

DOI: 10.1002/anie.200501450

Targeting Nucleic Acid Secondary Structures with Polyamides Using an Optimized Dynamic Combinatorial Approach**

*Sylvain Ladame, Andrew M. Whitney, and Shankar Balasubramanian**

Nucleic acids can adopt a variety of well-defined conformations. DNA exists predominantly as a double-stranded right-handed helix but can also adopt alternative structures such as bulges, hairpins, and four-stranded quadruplexes. Such DNA secondary structures have been identified in genomic DNA and many of these are associated with regulatory mechanisms. DNA secondary structures in regulatory regions are potentially attractive targets for chemical intervention by agents that bind and either block or enhance the binding of transcription factors. Thus far, the most successful approaches for the development of artificial transcriptional repressors have included both small molecules and proteins that recognize RNA or DNA structures. These transcriptional antagonists include oligonucleotides (or oligonucleotide mimics) that recognize the major groove of double-stranded DNA through triple-helix[1] or synthetic pyrrole/imidazole-based polyamides that recognize the minor groove of the DNA double helix.[2] Recently, a small molecule was reported to suppress expression of the oncogene *c-myc* by targeting a proximal four-stranded G-quadruplex DNA secondary structure element.[3]

It is desirable to develop new approaches and new molecules that recognize particular nucleic acid structure(s) with both high affinity and specificity. Dynamic covalent chemistry (DCC) is a reversible exchange process that allows noncovalent interactions to template covalent bond formation.[4] Since its conception, there have been very few examples that have used biologically relevant nucleic acids as a template.[5] We recently reported the use of dynamic covalent chemistry for the generation of G-quadruplex ligands from a small library of nine different species.[6] Herein, we demonstrate the general application of DCC as both a qualitative and quantitative method for the selection and discrimination of ligands that bind distinct nucleic acid structures (quadruplex and duplex DNA).

Distamycin-like polyamides containing *N*-methylpyrrole and *N*-methylimidazole amino acids can bind to the minor groove of double-stranded DNA with an affinity similar to naturally occurring DNA-binding proteins in a sequence-specific manner.[7] During the past decade, extensive work, particularly by Dervan and co-workers, has demonstrated that covalently linking polyamides that contain three pyrrole or imidazole units along a γ-aminobutyric acid turn can lead to a six-heterocycle hairpin that recognizes five base pairs with increased affinity and specificity.[8] More recently, it was shown that distamycin can recognize the G-quadruplex motif.[9,10] Initial studies by NMR spectroscopy and mass spectrometry suggested that distamycin interacts as a dimer with two opposing grooves of a quadruplex with an overall stoichiometry of 4:1.[9] However, recent NMR spectroscopic studies proposed a structurally distinct model in which two distamycin molecules are stacked on the terminal planar G quartet of a quadruplex.[10] Herein, we describe the selection of dimers of pyrrole-based polyamides that bind duplex and/or quadruplex DNA by using an optimized dynamic combinatorial approach. Based on previous studies by ourselves and others, thiol-disulfide chemistry was chosen to mediate the reversible exchange process because it is water-compatible, relatively fast, and pH-controlled.[6,11]

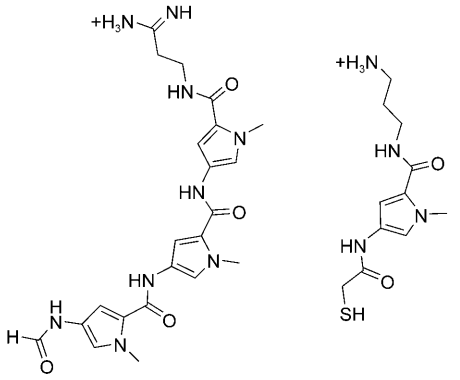
Polyamides **P1**, **P2**, and **P3**, which respectively contain one, two, and three *N*-methylpyrrole heterocycles, were designed to closely mimic the chemical structure of distamy-

[*] Dr. S. Ladame, Dr. A. M. Whitney, Dr. S. Balasubramanian
University Chemical Laboratory, University of Cambridge
Lensfield Road, Cambridge CB2 1EW (UK)
Fax: (+44) 1223-336-913
E-mail: sb10031@cam.ac.uk

[**] This work was funded by the BBSRC and Cancer Research U.K. We thank Dr. A. Bugaut for proofreading the manuscript.

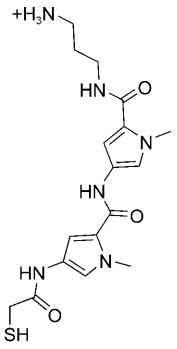
InterScience
© 2005 Wiley-VCH Verlag GmbH & Co. KGaA, Weinheim

cin. The formyl group present at the terminus of distamycin was replaced with a β-thiocarbonyl group that provides the

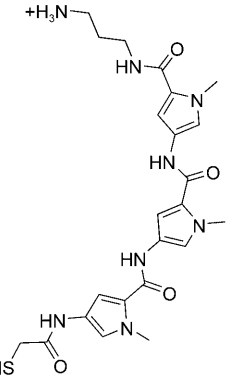


distamycin

P1



P2



P3

aliphatic thiol, and the amidine function at the other terminus of distamycin was replaced by an amino group. Previous studies on distamycin and distamycin analogues suggest that such molecules have the potential to bind quadruplex and duplex DNA as dimers.[7] We set out to optimize the number of heteroaromatic units for binding to each of the two DNA templates. The molecular targets for this study were: 1) a four-stranded intramolecular G quadruplex formed by human telomeric DNA, which is a target under study for anticancer agents,[12] and 2) an A/T-rich duplex DNA sequence identified in the promoter region of the oncogene *c-kit*,[13] which could serve as a site for intervention of transcriptional regulation.

The Fmoc-protected *N*-methylpyrrole monomers were synthesized as previously reported[14] and assembled on a 1,3-diaminopropane-derivatized trityl resin (Merck Biosciences, loading 1.19 mmol g^{-1}) by using standard solid-phase Fmoc chemistry (Fmoc = 9-fluoromethoxycarbonyl). Three distamycin analogues containing either one, two, or three *N*-methylpyrrole units were end-derivatized with *S*-trityl-β-thioacetic acid. Treatment with a solution of TFA/TIS/H_2O (95:2.5:2.5) afforded the desired molecules, which were subsequently purified by HPLC (TFA = trifluoroacetic acid, TIS = triisopropylsilane). The nucleic acid targets used were the intramolecular human telomeric quadruplex formed from the folded deoxyoligonucleotide 5′-biotin-$(GTTAGG)_5$,[15] and an 11-mer duplex DNA formed from 5′-biotin-(CTTTTATTTTG) hybridized with its complementary sequence (also 5′-biotinylated). The experimental design principles were essentially the same as those we reported previously.[6] Briefly, an equimolar mixture of monomers **P1**, **P2**, and **P3** were allowed to react at pH 7.4 in an exchange buffer containing an excess of both oxidized (**G–G**) and reduced (**G**) glutathione. Once equilibrium was reached, the exchange process was stopped by lowering the pH to 2, and the biotinylated target, with associated ligands, was isolated by immobilization onto magnetic streptavidin beads. The DNA was then heat-denatured to release any bound ligands; HPLC was used to identify and quantify each species represented in the dynamic combinatorial library (DCL). Comparison of the DCL composition with that obtained in a parallel control experiment that lacked nucleic acid target enabled the identification of the species that were amplified by the presence of template.

A major limitation of the DCC concept is the possibility for library components to strongly self-associate or to associate with another building block in the absence of template.[11] This effect could mask the template-induced amplification of species that are already present in large quantities in the absence of template.[16] To overcome this intrinsic limitation, we reasoned that a large excess of a competing thiol such as glutathione could be used to drive the thermodynamic equilibrium toward the formation of glutathione conjugates in the absence of target, thus decreasing the presence of stable disulfide adducts of library components. This was expected to sensitize the system toward the detection of amplified species that are otherwise significantly pre-formed in the absence of template.

We initially used reduced glutathione (**G**, 1.5 mM) and oxidized disulfide-bridged glutathione (**G–G**, 0.375 mM) in Tris-HCl buffer (300 mM, pH 7.4), KCl (150 mM), and 100 μM of each monomer to mediate thiol–disulfide exchange. Under such conditions, monomer **P3**, in particular, existed predominantly as the homodisulfide **P3–P3** (representing 73% of the total amount of thiol **P3**) at equilibrium (Figure 1a, blue trace). In such conditions, further amplification of **P3–P3** induced by the addition of DNA target would have been very difficult to observe. Exchange experiments were then carried out with a 10-fold increase in the glutathione concentration (**G**, 15 mM; **G–G**, 3.75 mM) as well as a corresponding 20-fold increase in concentration (**G**, 30 mM; **G–G**, 7.5 mM). The HPLC traces representing the composition of the DCL mixtures at equilibrium are shown in Figure 1a (red and green traces). Elevated glutathione concentrations caused the amounts of **P3** and **P2** glutathione conjugates and free thiols to increase significantly at the expense of both homodisulfides and of heterodisulfide **P3–P2**. For example, whereas the **P3–P3** homodisulfide represented 75% of thiol **P3** at the lowest concentration of glutathione (**G**, 1.5 mM; **G–G**, 0.375 mM) it represented only 15% when the amount of glutathione was increased 20-fold.

Among the conditions tested, the highest glutathione concentrations were optimal for the detection of DNA-template-induced amplification of species containing either

 © 2005 Wiley-VCH Verlag GmbH & Co. KGaA, Weinheim

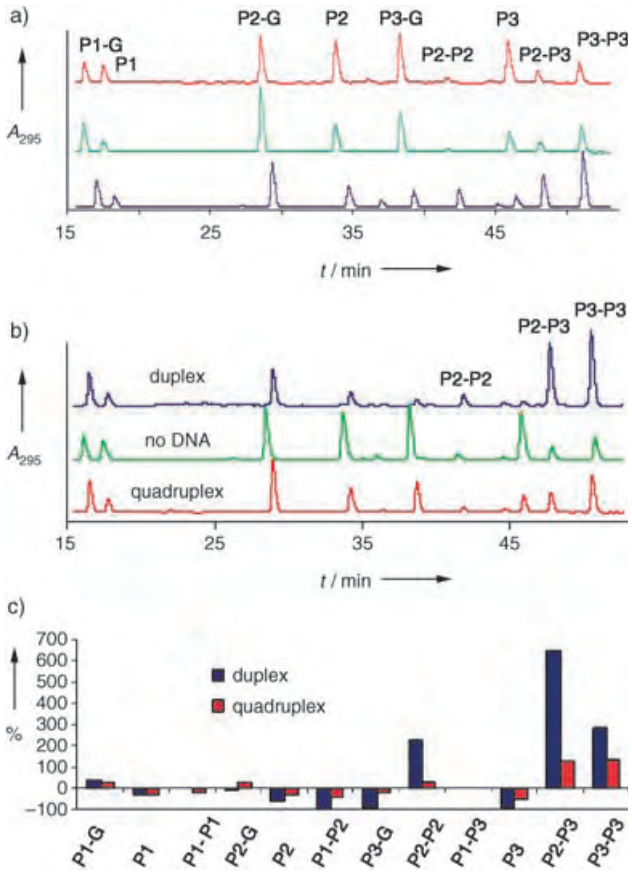


Figure 1. a) HPLC traces showing the component composition at equilibrium after 18 h for exchange experiments starting from **P1**, **P2**, and **P3** as thiols (100 μM each) in Tris buffer (300 mM Tris-HCl pH 7.4, 150 mM KCl) containing different concentrations of glutathione (**G**). From top to bottom: **G** 30 mM + **G**–**G** 7.5 mM, **G** 15 mM + **G**–**G** 3.75 mM, and **G** 1.5 mM + **G**–**G** 0.375 mM; b) HPLC traces showing the component composition at equilibrium after 18 h for exchange experiments starting from **P1**, **P2**, and **P3** as thiols (100 μM each) in Tris buffer (300 mM Tris-HCl pH 7.4, 150 mM KCl) containing **G** (30 mM) + **G**–**G** (7.5 mM) and either in the absence of template or in the presence of quadruplex DNA (100 μM, bottom) or duplex DNA (100 μM, top). c) Histogram showing the percent change in each species of the equilibrium mixture upon introduction of either quadruplex (red) or duplex DNA (blue).

P2 or **P3**. The concept of dynamic combinatorial chemistry strictly requires the system under study to establish equilibrium under the conditions of the selection experiments. To confirm true thermodynamic equilibrium for the disulfide exchange, the experiment was repeated starting from **P1**, **P2**, and **P3**–**P3**, instead of **P1**, **P2**, and **P3** thiol. The same distribution of thiols and disulfides was obtained after 18 h despite the change from initial conditions, which confirms that the system was reversible and under thermodynamic control. Parallel experiments were then carried out with conditions identical to those described above, but in the presence of 100 μM biotinylated quadruplex or duplex DNA. Equilibrium was reached within 24 h and the same distribution of species was observed starting with either all three monomers as thiols or **P1** and **P2** as thiols and **P3** in disulfide form. This confirmed a true equilibration of the system in the presence of template. HPLC traces showing the distribution of every species at equilibrium in the presence of either quadruplex or double-stranded DNA are shown in Figure 1b.

Compared with the experiment carried out in the absence of template, a moderate amplification of disulfides **P2**–**P3** and **P3**–**P3** (130% and 140%, respectively) was observed upon the addition of quadruplex DNA. The quantities of all other DCL species were either unchanged or significantly decreased. Interestingly, substantially greater amplification effects were observed with double-stranded DNA as a template. In the presence of duplex DNA (Figure 1c) the amounts of disulfides **P2**–**P3**, **P3**–**P3** and **P2**–**P2** at equilibrium increased significantly, corresponding to amplifications of 660, 295, and 220%, respectively. These results suggest that homo- and heterodisulfides of **P2** and **P3** are amplified, albeit to varying extents, in the presence of quadruplex and duplex DNA templates. Duplex DNA elicits a much stronger amplification of these selected species than does quadruplex DNA (for example, the increase in **P2**–**P3** is 660% with duplex DNA and 130% for quadruplex DNA), which also suggests that the disulfides of **P2** and **P3** show a much greater affinity for duplexes than for quadruplexes.

Pyrrole polyamides have already been shown to bind A/T-rich duplexes as antiparallel dimers with a very high affinity (K_d values in the nM range). Our results suggest such polyamides bind quadruplex DNA with much lower affinity, in accordance with a comparative NMR spectroscopic study, which showed that both distamycin and netropsin possess a higher affinity for duplex DNA than for quadruplex DNA.[17] To confirm the relative binding of selected species (amplified or not) to both DNA targets, thermal melting studies were carried out under conditions similar to those of the DCC experiments (100 μM DNA, 300 mM Tris-HCl, 150 mM KCl) in the absence or presence of 100 μM selected disulfide ligand (Figure 2). The melting temperature of the duplex alone was found to be 43.5 °C. No stabilization effect was observed upon incubation of DNA with disulfide **P1**–**P1**, which was not amplified. However, addition of either **P2**–**P2** or **P2**–**P3** to the double-stranded DNA produced an increase in the T_m value

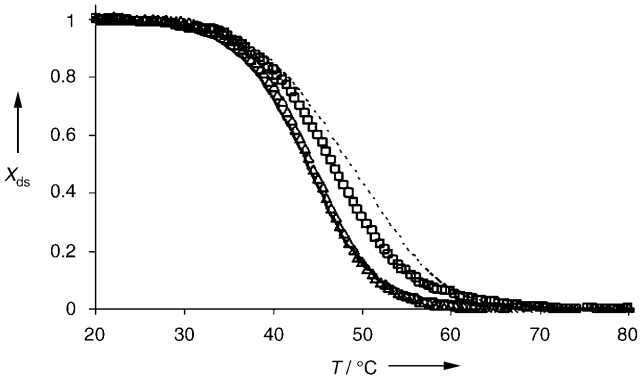


Figure 2. UV/Vis thermal denaturation curves obtained from 100 μM duplex DNA alone (——) and in the presence of either **P1**–**P1** (△), **P2**–**P2** (□), or **P2**–**P3** (••••) at a concentration of 100 μM. Experiments were carried out in duplicate in buffer (300 mM Tris-HCl, pH 7.4 containing 150 mM KCl) in a cuvette with a 1-mm path length. X_{ds} = fraction double-stranded DNA.

 © 2005 Wiley-VCH Verlag GmbH & Co. KGaA, Weinheim

to 46.5 °C ($\Delta T_m = +3$ °C) and 48.5 °C ($\Delta T_m = +5$ °C), respectively. No significant shift in melting temperature was observed with quadruplex DNA and either **P1**–**P1** or **P2**–**P3** (data not shown), which may be a consequence of weaker (or less-stabilized) binding. This shows a correlation between the melting temperature values and the level of amplification observed in the DCC experiment, consistent with observations reported previously by Bugaut et al. for the dynamic combinatorial selection of nucleic acid modifications that stabilize DNA duplexes.[5c]

Recently, Poulin-Kerstien and Dervan showed that double-stranded DNA is capable of accelerating the irreversible formation of tandem hairpin dimers.[18] There is also a significant body of work on the use of DNA or RNA as a template for directing chemical reactions, primarily under irreversible conditions.[19] The study reported herein shows that DNA secondary structures (duplex or quadruplex) can also be used as templates that are capable of inducing, under reversible conditions, the formation of ligands that are thermodynamically stabilized through interactions with the DNA. A key feature of our studies is the demonstration that an increase in the concentration of buffering thiol (glutathione) is an effective means to sensitize the dynamic selection process to amplifications of pre-stabilized disulfide species. This may be particularly useful for more complex and larger libraries, in which there is an increased likelihood for mutual recognition between library members. Theoretical studies have demonstrated that the correlation between host–guest binding and amplification could vary from poor (with template in large excess) to good (with substoichiometric template).[20] The optimized dynamic combinatorial approach reported herein could facilitate the detection of only the strongest-binding ligands by preventing the formation of weaker-binding ligands with a large excess of competitor glutathione. This study also suggests that it is possible to compare the level of amplification of the same species obtained in experiments carried out in parallel but with *different* templates. This will be of particular interest for the discovery of DNA-binding ligands that bind selectively and with high-affinity.

Received: April 27, 2005
Published online: August 3, 2005

Keywords: combinatorial chemistry · DNA recognition · DNA structures · nucleic acids · template synthesis

[1] K. M. Vasquez, P. M. Glazer, *Quart. Rev. Biophys.* **2002**, *35*, 89.
[2] J. M. Gottesfeld, L. Neely, J. W. Trauger, E. E. Baird, P. B. Dervan, *Nature* **1998**, *396*, 202.
[3] A. Siddiqui-Jain, C. L. Grand, D. J. Bearss, L. H. Hurley, *Proc. Natl. Acad. Sci. USA* **2002**, *99*, 11593.
[4] For selected reviews, see: a) J.-M. Lehn, *Chem. Eur. J.* **1999**, *5*, 2455; b) O. Ramstrom, T. Bunyapaiboonsri, S. Lohmann, J.-M. Lehn, *Biochim. Biophys. Acta* **2002**, *1572*, 178; c) S. J. Rowan, S. J. Cantrill, G. R. L. Cousins, J. K. M. Sanders, J. F. Stoddart, *Angew. Chem.* **2002**, *114*, 938; *Angew Chem. Int. Ed.* **2002**, *41*, 898.
[5] a) B. Klekota, B. L. Miller, *Tetrahedron* **1999**, *55*, 11687; b) C. Karan, B. L. Miller, *J. Am. Chem. Soc.* **2001**, *123*, 7455; c) A. Bugaut, J. J. Toulmé, B. Rayner, *Angew. Chem.* **2004**, *116*, 3206; *Angew. Chem. Int. Ed.* **2004**, *43*, 3144; d) A. Bugaut, K. Bathany, J.-M. Schmitter, B. Rayner, *Tetrahedron Lett.* **2005**, *46*, 687.
[6] A. M. Whitney, S. Ladame, S. Balasubramanian, *Angew. Chem.* **2004**, *116*, 1163; *Angew. Chem. Int. Ed.* **2004**, *43*, 1143.
[7] For a recent review, see: P. B. Dervan, B. S. Edelson, *Curr. Opin. Struct. Biol.* **2003**, *13*, 284.
[8] E. D. Baird, P. B. Dervan, *J. Am. Chem. Soc.* **1996**, *118*, 6141.
[9] a) A. Randazzo, A. Galeone, L. Mayol, *Chem. Commun.* **2001**, 1030; b) W. M. David, J. Brodbelt, S. M. Kerwin, P. W. Thomas, *Anal. Chem.* **2002**, *74*, 2029.
[10] M. J. Cocco, L. A. Hanakahi, M. D. Huber, N. Maizels, *Nucleic Acids Res.* **2003**, *31*, 2944.
[11] Y. Krishnan-Ghosh, S. Balasubramanian, *Angew. Chem.* **2003**, *115*, 2221; *Angew. Chem. Int. Ed.* **2003**, *42*, 2171.
[12] J. Cuesta, M. A. Read, S. Neidle, *Mini-Rev. Med. Chem.* **2003**, *3*, 11.
[13] K. Yamamoto, A. Tojo, N. Aoki, M. Shibuya, *Jpn. J. Cancer Res.* **1993**, *84*, 1136.
[14] N. R. Wurtz, J. M. Turner, E. E. Baird, P. B. Dervan, *Org. Lett.* **2001**, *3*, 1201.
[15] The G quadruplex was folded under standard conditions. The single-stranded oligonucleotide, 5′-biotinylated $(GTTAGG)_5$, was heated in buffer at 90 °C and slowly cooled to room temperature overnight. Its fully folded structure was confirmed by circular dichroism spectroscopy and UV/Vis melting experiments.
[16] I. Huc, R. Nguyen, *Comb. Chem. High Throughput Screening* **2001**, *4*, 53.
[17] A. Randazzo, A. Galeone, V. Esposito, M. Varra, L. Mayol, *Nucleosides Nucleotides Nucleic Acids* **2002**, *21*, 535.
[18] A. T. Poulin-Kerstien, P. B. Dervan, *J. Am. Chem. Soc.* **2003**, *125*, 15811.
[19] a) X. Li, D. R. Liu, *Angew. Chem.* **2004**, *116*, 4956; *Angew. Chem. Int. Ed.* **2004**, *43*, 4848; b) Z. J. Gartner, B. N. Tse, R. Grubina, J. B. Doyon, T. M. Snyder, D. R. Liu, *Science* **2004**, *305*, 1601.
[20] a) P. T. Corbett, S. Otto, J. K. M. Sanders, *Chem. Eur. J.* **2004**, *10*, 3139; b) P. T. Corbett, S. Otto, J. K. M. Sanders, *Org. Lett.* **2004**, *6*, 1825.

 © 2005 Wiley-VCH Verlag GmbH & Co. KGaA, Weinheim

Supersensitizing Dyes

DOI: 10.1002/anie.200500363

Supermolecular Control of Charge Transfer in Dye-Sensitized Nanocrystalline TiO_2 Films: Towards a Quantitative Structure–Function Relationship**

Saif A. Haque, Samantha Handa, Katja Peter, Emilio Palomares, Mukundan Thelakkat, and James R. Durrant*

The attachment of redox or photoactive molecules to solid surfaces is important for the development of many applications. One area of research that is receiving extensive interest at present is the immobilization of molecular dyes on mesoporous nanocrystalline metal oxide electrodes. Such functionalized films are currently under investigation for device applications ranging from solar cells to chemical and biological sensors.[1–6] Recently there has been interest in the use of more complex supramolecular or multifunctional sensitizers to build a range of new applications including heterosupramolecular devices.[7–14] The use of such materials is particularly attractive as it enables the development of electroactive structures that exhibit a remarkable degree of structural organization, improved stability, redox reversibility, and a greater functional diversity.[14–16] A key requirement for the exploitation of such materials in electronic devices is the ability to electrically interface the supramolecular or multifunctional materials to the metal oxide electrode whilst achieving control over key device parameters such as interfacial charge transfer. Such issues have been considered in great detail for molecular-based adsorbates,[17] but are yet to be addressed systematically for functionalized films that comprise more complex, supramolecular or multifunctional sensitizer dyes. This understanding is both of fundamental interest and essential to the design and application of such materials in electronic devices. Herein we address this issue by exploring a class of multifunctional sensitizer dyes that exhibit multistep charge-transfer cascades. We show that by careful design of the "supersensitizer" dye it is possible to modulate the charge-recombination dynamics by five orders of magnitude and achieve remarkably long-lived photoinduced charge separation at a dye/TiO_2 interface. These studies enable us to address the relationship between supermolecular dye structure and interfacial charge transfer and provide an insight into the fundamental processes that govern charge-transfer dynamics at the supermolecular sensitizer dye/TiO_2 interface.

We have used sensitizer dyes in which the dye chromophore is modified by the covalent attachment of secondary electron donors. By introducing such secondary electron-transfer cascades within the dye structure, as illustrated in Figure 1, it is possible to retard the charge-recombination dynamics by increasing the physical separation between the dye–cation moiety and the surface of the TiO_2 surface. Such an approach has been recently adopted, however in all cases reported to date, only simple monomeric electron-donor groups have been employed.[9,14,18] Herein we consider the influence of structure of the electron-donating moiety upon the charge-recombination dynamics. In particular we address the influence of extended π-conjugation within the electron-transfer cascade and the use of polymeric electron-donating units which allows us to address the relationship between supermolecular dye structure and interfacial charge-transfer dynamics. Density functional theory (DFT) ab initio calculations are performed to determine the spatial distribution of the HOMO orbitals of the dyes. These slow charge-recombination dynamics observed herein are shown to be consistent with the increased physical separation of the HOMO orbitals of dye molecules from the TiO_2 surface as indicated by the DFT calculations.

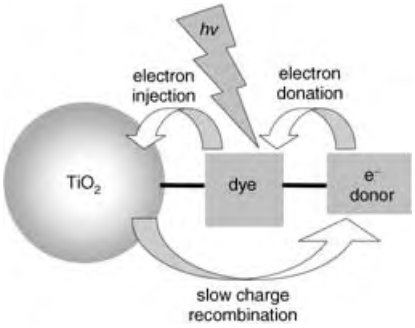


Figure 1. The heterosupermolecular structure and the charge-transfer processes occurring at the dye/TiO_2 interface.

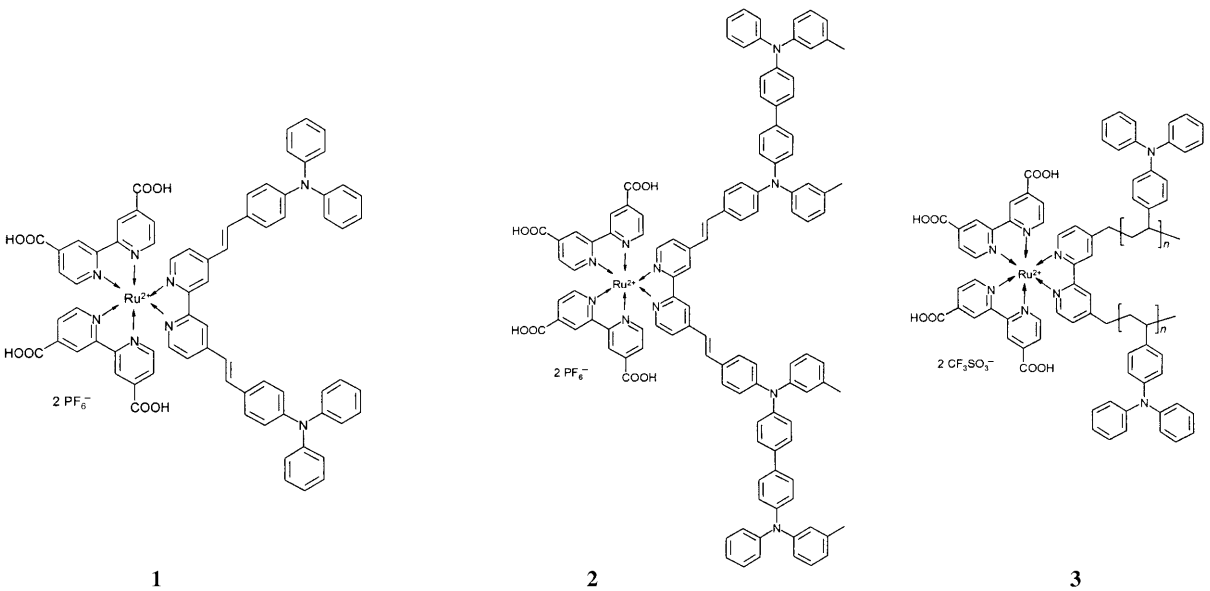
We have employed three bifunctional dyes that differ in the structure of electron-donor component (Scheme 1). Our dyes are built with carboxylated ruthenium (II) polypyridyl chromophores and carry aromatic-amine-based electron-donor groups attached on the 4 and 4′ positions of the bipyridyl (bpy) ligand. Such electron-donor groups are ideal

[*] Dr. S. A. Haque, S. Handa, Dr. J. R. Durrant
Centre for Electronic Materials and Devices
Department of Chemistry
Imperial College of Science Technology and Medicine
London SW72AZ (UK)
Fax: (+44) 207-594-5801
E-mail: s.a.haque@imperial.ac.uk
Dr. E. Palomares
Institut de Ciencia Molecular (IcMol)
Universitat de Valencia
461000 Burjassot, Valencia (Spain)
K. Peter, Dr. M. Thelakkat
Makromoleculare Chemie 1
Universitat Bayreuth
95440 Bayreuth (Germany)

[**] We thank the Engineering and Physical Sciences Research Council (EPSRC), BP Solar Ltd, and the European Commission (project 'Molycell, SE56-CT-2003-502783) for financial support. M.T. would like to thank Deutsche Forschungsgemeinschaft (SFB 481 project B4) for the financial support. We would also like to thank Dr. Ian Gould for help with the Gaussian HOMO orbital calculations.

Supporting information for this article is available on the WWW under http://www.angewandte.org or from the author.

 InterScience © 2005 Wiley-VCH Verlag GmbH & Co. KGaA, Weinheim



1 2 3

Scheme 1. The structure of the three dyes employed in this study [Ru^{II}(dcbpy)$_2$(TPAbpy)] (**1**), [Ru^{II}(dcbpy)$_2$(TPDbpy)] (**2**), and [Ru^{II}(dcbpy)$_2$(poly-TPAbpy)] (**3**); dc = dicarboxylate.

for this purpose as they possess low ionization potentials which facilitate the formation of cation radicals, thereby allowing multistep charge transfers. Dyes **1** and **2** comprise low-molecular-weight electron-donating units, namely, triphenylamine (TPA) and *N*,*N*′-diphenyl-*N*,*N*′-bis(3-methylphenyl)-[1,1′-biphenyl]-4,4′-diamine (TPD), respectively. Dye **3** comprises of poly(vinyl triphenylamine) chains (poly-TPA) with approximately 100 repeat units attached to one of the bipyridine units of the Ru^{II} core.[19] Details of the synthesis of these dyes and characterization are provided in the Supporting Information. The attachment of the dyes to the nanocrystalline TiO_2 films was achieved by immersion of the preformed metal oxide electrodes in solutions of the dyes at 25 °C, for 2 h for dyes **1** and **2** and overnight for dye **3**. All three dyes incorporate carboxylate groups (-COOH) to achieve direct binding to the TiO_2 surface. All three dyes were found to result in strong adsorption to the surface of the electrode.

Transient absorption spectroscopy was employed to monitor the charge-recombination dynamics following photo-excitation of the dye. Details of the transient absorption apparatus have been described previously.[20–22] The dye-sensitized films were incorporated into a sealed glass cell and degassed with argon gas prior to transient absorption studies to ensure an anaerobic environment. Experiments employed low excitation energy densities ($\approx 25\ \mu J\ cm^{-2}$ at 430 nm for all three dyes), these excitation densities being selected to ensure matched densities of absorbed photons for the three dyes, this corresponding to approximately 0.5 injected electron per TiO_2 particle.

The recombination dynamics were monitored by observing the decay of the photoinduced cation absorption of the three dyes. Typical data for the dyes are shown in Figure 2 employing a probe wavelength of 850 nm for all three dye/TiO_2 film combinations. The transient absorption traces

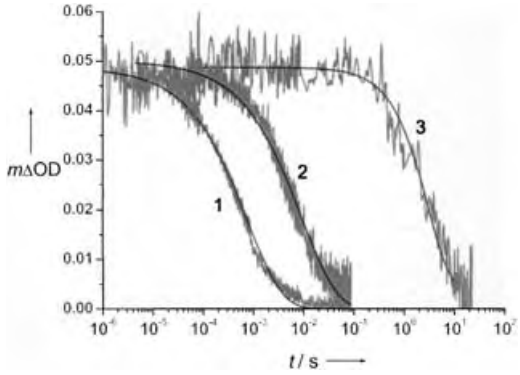


Figure 2. Transient absorption data obtained for nanocrystalline TiO_2 films sensitized with dyes **1**–**3**. The decay kinetics are assigned to the charge recombination of the photo-generated dye cations with the electrons in the TiO_2 [Eq. (2)]. The black lines indicate the fit, see text for details.

shown in Figure 2 follow the formation of the supermolecular-dye cations [Eq. (1)] and their recombination with photo-injected electrons [Eq. (2)].

$$Dye \xrightarrow{h\nu} Dye^* \rightarrow Dye^+ + e^-_{TiO_2} \quad (1)$$

$$Dye^+ + e^-_{TiO_2} \rightarrow Dye \quad (2)$$

The absence of any grow-in of the transient signal is indicative that both the electron injection and arylamine oxidation by the $\{Ru(bpy)_3\}^{3+}$ component of the dye occurs within the time resolution of our apparatus; this result is consistent with previous studies.[23–26] However it is apparent that the recombination dynamics observed for all three dyes differ significantly, with dyes **1**, **2**, and **3** exhibiting recombination half-times ($t_{50\%}$) of 350 μs, 5 ms, and 4 s, respectively. It

 © 2005 Wiley-VCH Verlag GmbH & Co. KGaA, Weinheim

is noteworthy that dye **3**/TiO_2 combination exhibits the longest lifetime reported to date for a dye-sensitized metal oxide film.

We attribute the retardation of the charge recombination observed for dyes **2** and **3** to an increase in the physical separation of dye cation from the metal oxide surface as a result of the multistep translation of the oxidized moiety away from the TiO_2 surface. To support this argument we have performed DFT ab initio calculations to determine the spatial distribution of the HOMO orbitals of **1**–**3**. These calculations were carried out using the Gaussian visualizer with a Gaussian View 3.08 program running on an AMD Athlon 64-bit processor computer. The DFT calculations employed Becke's (B3) three parameter hybrid functional with (LYP) correlation functional (B3LYP). The electronic structures of the complexes were determined using a general basis set with 6-31G(d) for nitrogen, oxygen, and carbon atoms, 6-31G for hydrogen atoms, and an effective core potential basis set LANL2DZ for the ruthenium atoms, full details of which are given in the Supporting Information. The HOMO orbital profiles for the three dyes are shown in Figure 3. The HOMO distribution in $[Ru^{II}(dcbpy)_3]$ dyes without any electron donating groups are centered entirely at the ruthenium core and not on the ligands. However, the HOMO orbitals of **1** are delocalized partially over the bipyridyl group and TPA units.

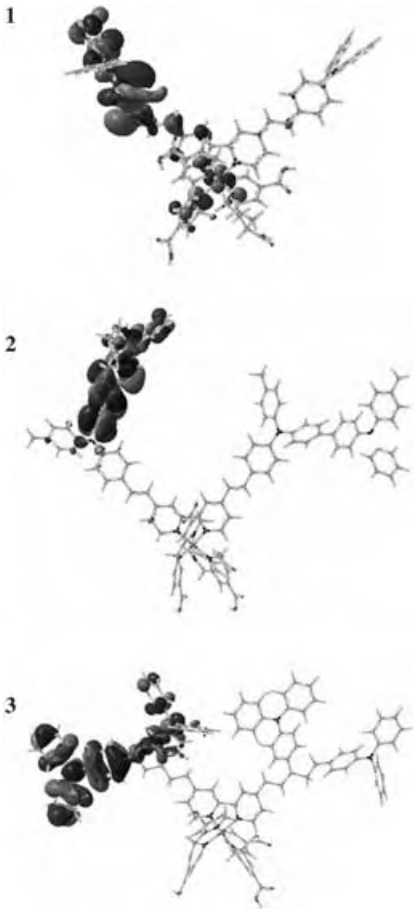


Figure 3. Graphical representation of the HOMOs of dyes **1**–**3** as determined from DFT ab initio calculations.

In contrast, for **2** and **3** the HOMO orbitals are located only on the phenylamine moieties, resulting in an increased separation of the HOMO orbitals from the TiO_2 surface compared to dye **1**. The approximate distances of the excited-state HOMO from the TiO_2 surface, as obtained from these calculations, were 10.8 Å for **1**, 15.6 Å for **2**, and 16.7 Å for **3**.[26] These calculations were complimented by cyclic voltammetry (CV) measurements which indicate a translation of the oxidizing moiety onto the aryl-amine components of the dye and thus further away from the surface of the TiO_2, resulting in an increased physical separation; this result is in agreement with previous CV studies of analogous dyes.[18]

We have recently shown that one of the key factors controlling the charge-recombination dynamics in molecular dye-sensitized nanocrystalline TiO_2 films is the spatial separation of the dye cation from the electrode surface.[17] More specifically we have demonstrated a linear correlation between the logarithm of the experimentally observed charge recombination half-time ($t_{50\%}$) and the spatial separation r of the molecular dye cation from the TiO_2 surface;[17] this is consistent with the expected exponential dependence of electron-transfer rate upon spatial separation ($k_{et} \propto e^{-\beta r}$, where β is the barrier height to electron tunneling and r is the spatial separation) from electron-tunneling theory.[27] Such data for the molecular sensitizers is shown in Figure 4 (points **A**–**E**) with the inclusion of the three supermolecular sensitizers **1**–**3** studied herein. Also included in the same plot is a supramolecular dye rotaxane **5**, based upon cyclodextrin encapsulated azobenzene chromophore and supermolecular dye **4** we have studied previously.[7,9] It is apparent that all

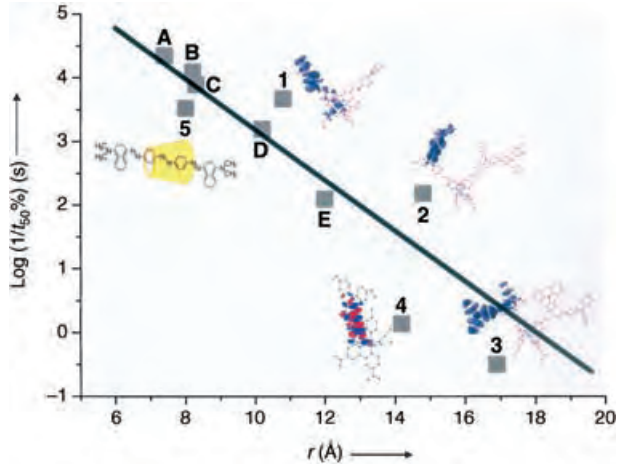


Figure 4. Plot of the logarithm of $1/t_{50\%}$ versus the spatial separation r of the dye cation from the TiO_2 surface for a series of dyes. Letters **A**–**E** represent series of molecular dyes studied previously:[17,29] **A** = [Ru(dcbpy)$_2$Cl$_2$], **B** = [Ru(dcbpy)$_2$(DTC)$_2$], **C** = [Ru(dcbpy)$_2$CN$_2$], **D** = [Ru(dcbpy)$_2$NCS$_2$], **E** = titanium phthalocyanine; DTC = $S_2CHN(C_2H_5)_2$. **1**–**3** are the supermolecular dyes studied herein, **4** is a supersensitizer dye[9] and **5** is a supramolecular dye,[7] both previously studied. The straight line is a linear fit to the experimental data following the theoretical treatment for electron-tunneling theory.[26] The slope of the line is indicative of the barrier height to tunneling $\beta = 0.95 \pm 0.2$ Å^{-1} as determined previously.[17] The influence of the free energy driving force ΔG has been factored into $t_{50\%}$ data shown here to give "free energy optimized" values as previously discussed.[17]

 © 2005 Wiley-VCH Verlag GmbH & Co. KGaA, Weinheim

these five supermolecular dyes **1**–**5** lie reasonably well along the straight line, further indicating that the key parameter controlling the charge-recombination dynamics for the supersensitizers **1**–**4**, and also the supramolecular dye **5**, is the spatial separation of the dye cation from the surface of the electrode. Thus our quantitative relationship for the molecular dyes can be extended to the more complex supermolecular sensitizers. This is the first time such a quantitative relationship has been shown for nanocrystalline metal oxides sensitized with more complex supermolecular or supramolecular sensitizers.[27] Moreover we expect the present findings to have implications for the design of sensitizers for electronic applications such as dye-sensitized solar cells. A key requirement for the efficient operation of such devices is minimization of charge recombination. It is clear from Figure 4 that the more complex "supersensitizers" and in particular dyes **2**–**4**, exhibit considerably slower charge-recombination rates than the more simple molecular dyes. Our results suggest that to achieve a long-lived charge-separated life-time the sensitizer dye can be engineered such that the oxidizing equivalent "hole" resides further away from the TiO_2 surface after charge separation. As such, the use of sensitizer dyes with multistep charge-transfer cascades provides an attractive option for this purpose. Furthermore it is apparent from the data shown in Figure 2 that the temporal shape of the charge-recombination kinetics differs significantly between the three sensitizer dyes. The transient decays in Figure 4 were fitted to a stretched exponential function ($\Delta OD \propto \exp^{-(\omega\tau)}$) with $\alpha \approx 0.4$, $\alpha \approx 0.9$, and $\alpha = 1$ for dyes **1**, **2**, and **3**, respectively, as illustrated by the black lines in Figure 2. This shift is indicative of a transition from more inhomogeneous, transport-limited recombination dynamics to more homogeneous, interfacial electron-transfer-limited recombination dynamics as the spatial separation of the dye cation from the TiO_2 surface is increased, consistent with our previous observations.[7,17,18,28] We note that this shift has potentially important advantages for device optimization as the less dispersive (more mono-exponential) recombination dynamics observed for dyes **2** and **3** offer more potential for precise optimization of the kinetics and energetics of device function.

In summary we have reported a supermolecular dye-sensitized nanocrystalline TiO_2 film in which we are able to achieve a remarkably long-lived (4 s) charge-separated state. Our approach is based upon bifunctional sensitizer dyes. We find that the key parameter that controls charge transfer at the supermolecular-dye/TiO_2 interface is the spatial separation between the cation center of the dye and the electrode surface. More specifically the retardation in charge-recombination kinetics observed for dye **3** compared to dyes **2** and **1** results from a greater physical separation between the dye cation and TiO_2 film surface, which is consistent with the multistep translation of the oxidizing equivalent "hole" away from the surface, and in agreement with our DFT ab initio calculations. We note that the aryl-amine-based electron-donor groups used herein can be expected to electrically interface well with organic hole-transporting materials making our approach attractive for applications in solid-state dye-sensitized solar cells. Moreover, the wetting property of hole conductors may be improved as a result of the matching of the polarity at this interface. We further note that the hybrid integration of multifunctional materials with metal oxide surfaces and the ability of these structures to generate remarkably long-lived charge separation, may also provide a platform for the development of nanostructured optically driven data storage devices. The present findings show that the use of multifunctional dyes provides a versatile approach to the control of interfacial charge transfer.

Received: January 31, 2005
Revised: May 6, 2005
Published online: August 1, 2005

Keywords: dye sensitization · dyes/pigments · electron transfer · ruthenium · titanium oxide

[1] B. O'Regan, M. Grätzel, *Nature* **1991**, *353*, 737.
[2] U. Bach, D. Lupo, P. Compte, J. E. Moser, F. Weissortel, J. Salbeck, H. Spreitzer, M. Grätzel, *Nature* **1998**, *395*, 583.
[3] J. Krüger, R. Plass, L. Cevey, M. Piccirelli, M. Grätzel, U. Bach, *Appl. Phys. Lett.* **2001**, *79*, 2085.
[4] S. A. Haque, E. Palomares, H. Upadhyaya, L. Ottley, R. J. Potter, A. B. Holmes, J. R. Durrant, *Chem. Commun.* **2003**, 3008.
[5] E. Topoglidis, C. J. Campbell, E. Palomares, J. R. Durrant, *Chem. Commun.* **2002**, 1518.
[6] E. Palomares, R. Villar, J. R. Durrant, *Chem. Commun.* **2004**, 362.
[7] S. A. Haque, J. S. Park, M. Srinivasarao, J. R. Durrant, *Adv. Mater.* **2004**, *16*, 1177.
[8] K. Peter, H. Wietasch, B. Peng, M. Thelakkat, *Appl. Phys. A* **2004**, *79*, 65.
[9] N. Hirata, J. J. Lagref, E. J. Palomares, J. R. Durrant, M. K. Nazeeruddin, M. Grätzel, D. D. Censo, *Chem. Eur. J.* **2004**, *10*, 595.
[10] G. Will, J. Sotomayor, S. N. Rao, D. Fitzmaurice, *J. Mater. Chem.* **1999**, *9*, 2297.
[11] J. Sotomayer, G. Will, D. Fitzmaurice, *J. Mater. Chem.* **2000**, *10*, 685.
[12] A. Merrins, C. Kleverlaan, G. Will, S. N. Rao, F. Scandola, D. Fitzmaurice, *J. Phys. Chem. B* **2001**, *105*, 2998.
[13] A. Merrins, X. Marguerettaz, S. N. Rao, D. Fitzmaurice, *Chem. Eur. J.* **2001**, *7*, 1309.
[14] R. Argazzi, N. Y. M. Iha, H. Zabri, F. Odobel, C. A. Bignozzi, *Coord. Chem. Rev.* **2004**, *248*, 1299.
[15] H. Hofmeier, U. S. Schubert, *Chem. Soc. Rev.* **2004**, *33*, 373.
[16] V. Balzani, M. G. Lopez, J. F. Stoddart, *Acc. Chem. Res.* **1999**, *32*, 405.
[17] J. N. Clifford, E. Palomares, M. K. Nazeeruddin, M. Grätzel, J. Nelson, X. Li, N. Long, J. R. Durrant, *J. Am. Chem. Soc.* **2004**, *126*, 5225.
[18] J. N. Clifford, G. Yahioglu, L. R. Milgrom, J. R. Durrant, *Chem. Commun.* **2002**, 1260.
[19] K. Peter, M. Thelakkat, *Macromolecules* **2003**, *36*, 1779.
[20] S. A. Haque, Y. Tachibana, R. L. Willis, J. E. Moser, M. Grätzel, D. R. Klug, J. R. Durrant, *J. Phys. Chem. B* **2000**, *104*, 538.
[21] E. Palomares, J. N. Clifford, S. A. Haque, T. Lutz, J. R. Durrant, *J. Am. Chem. Soc.* **2003**, *125*, 475.
[22] S. A. Haque, T. Park, C. Xu, S. Koops, N. Schultes, R. J. Potter, A. B. Holmes, J. R. Durrant, *Adv. Funct. Mater.* **2004**, *14*, 435.
[23] G. Benko, J. Kallioinen, J. E. I. Korppi-Tommola, A. P. Yartsev, V. Sundstrom, *J. Am. Chem. Soc.* **2002**, *124*, 489.
[24] J. Ashbury, E. Hao, Y. Wang, H. N. Ghosh, T. Lian, *J. Phys. Chem. B* **2001**, *105*, 4545.

 © 2005 Wiley-VCH Verlag GmbH & Co. KGaA, Weinheim

[25] Y. Tachibana, S. A. Haque, I. P. Mercer, J. E. Moser, D. R. Klug, J. R. Durrant, *J. Phys. Chem. B* **2001**, *105*, 7424.

[26] The spatial separation of the HOMO orbitals from the TiO_2 surface was determined by calculating the geometric distance between the carboxylate groups and each atom of the dye and by weighting this value with the square of the percentage contribution of each atom to the HOMO orbital. The spatial separation from the dye-cation moiety to the electrode surface was also calculated in three alternative ways: 1) by calculating the geometric distance between the carboxylate groups and the "edge" of the HOMO distribution, 2) by calculating the geometric distance between the Ti atom at surface of TiO_2 nanoparticle and each atom of the dye and by weighting this value with the square of the percentage HOMO orbital contribution, and 3) by calculating the geometric distance between the Ti atom at surface of TiO_2 nanoparticle and the "edge" of the HOMO distribution. All four methods yielded almost identical linear dependence of the charge-recombination rate upon spatial separation. We further note that the deviations of the data from the straight line fit in Figure 4 may be due to uncertainties in exact orientation of the anchored dyes on the TiO_2 electrode surface. We also note that for dye **3**, the DFT calculation was performed in a condition where the number of TPA units was 2. This therefore represents a lower limit for the extent of delocalization of the dye cation away from the ruthenium metal center and subsequently from the TiO_2 surface.

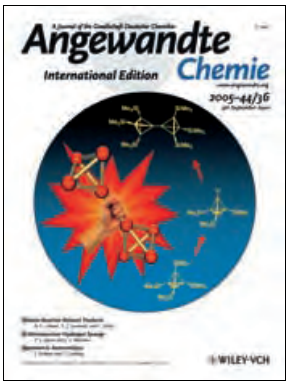
[27] D. S. Bendal in *Protein Electron Transfer, Outline of Theory of Protein Electron Transfer* (Eds.: C. C. Moser, P. L. Dutton), BIOS Scientific Publishers, Oxford, **1996**, chap. 1.

[28] J. Nelson, S. A. Haque, D. R. Klug, J. R. Durrant, *Phys. Rev. B* **2001**, *63*, 205321.

[29] E. Palomares, M. V. Martinez-Diaz, S. A. Haque, T. Torres, J. R. Durrant, *Chem. Commun.* **2004**, 2112.

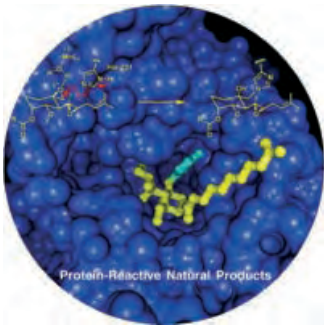
 © 2005 Wiley-VCH Verlag GmbH & Co. KGaA, Weinheim

Cover Picture

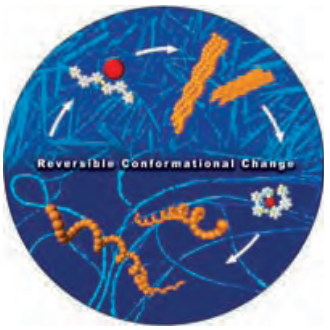


Masanobu Tanaka and Akira Sekiguchi*

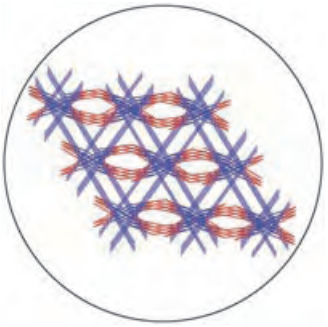
Extreme shortening of a C–C bond results from an increase in the s character of the bond orbitals, as is found in hexakis(trimethylsilyl)tetrahedranyltetrahedrane, which is depicted in the cover picture. Although a decade ago nobody assumed that such a derivative could be isolated, in their Communication on page 5821 ff. A. Sekiguchi and M. Tanaka describe the synthesis and characterization of this highly sought after target, which agrees perfectly with theoretical predictions.



Bioorganic Chemistry
In their Review on page 5788 ff., B. F. Cravatt, E. J. Sorensen, and C. Drahl describe the mechanisms and consequences of covalent modification of amino acid residues in the active sites of proteins by small-molecule natural products.



Coordination Polymers
In their Communication on page 5810 ff., M. Lee and co-workers introduce cationic coordination polymers that respond to the type of counteranions bound by undergoing a conformational change. As a result, the solution's bulk properties can be reversibly switched between gel and liquid states.



Coordination Networks
Three different coordination networks from nickel salts, 4,4′-bipyridine, and a V-shaped 4,4′-oxybis(benzoate) ligand are described by E.-B. Wang, Z.-M. Su, L. Carlucci et al. in their Communication on page 5824 ff.

Contents

The following Communications have been judged by at least two referees to be "very important papers" and will be published online at www.angewandte.org soon:

*Sheereen Majd, Michael Mayer**
Hydrogel-Stamping of Arrays of Supported Lipid Bilayers with Various Lipid Compositions for the Screening of Drug–Membrane and Protein–Membrane Interactions

*Yoshitaka Ishibashi, Yuhki Bessho, Masahiro Yoshimura, Masaki Tsukamoto, Masato Kitamura**
Origin of the Minor Enantiomeric Product in a Noyori Asymmetric Hydrogenation

Holger Braunschweig, Thomas Herbst, Daniela Rais, Fabian Seeler*
Synthesis of Borirenes by Photochemical Borylene Transfer from $[(OC)_5M{=}BN(SiMe_3)_2]$ (M = Cr, Mo) to Alkynes

*Y. Andrew Yang, Huimeng Wu, K. R. Williams, Y. Charles Cao**
Synthesis of CdSe and CdTe Nanocrystals without Precursor Injection

*Masayuki Nihei, Mayumi Ui, Mizuho Yokota, Lingqin Han, Atsushi Maeda, Hideo Kishida, Hiroshi Okamoto, Hiroki Oshio**
Two-Step Spin Conversion in a Cyanide-Bridged Ferrous Square

Sean F. Brady, Jon Clardy*
Cloning and Heterologous Expression of Isonitrile Biosynthetic Genes from Environmental DNA

Meeting Reviews

Fluorous Chemistry and Technology—A Symposium Showcases Ever-Broadening Frontiers — *J. A. Gladysz** — **5766**

Books

Multicomponent Reactions — Jieping Zhu, Hugues Bienyamé — *reviewed by V. Nair* — **5769**

Protein Microarray Technology — Dev Kambhampati — *reviewed by J. Eppinger* — **5770**

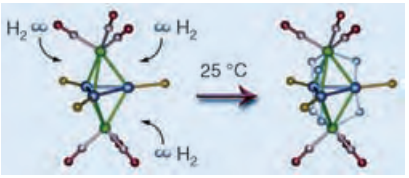
Highlights

Cluster Compounds

P. J. Dyson,* J. S. McIndoe* **5772 – 5774**

Hydrogen Sponge? A Heteronuclear Cluster That Absorbs Large Quantities of Hydrogen

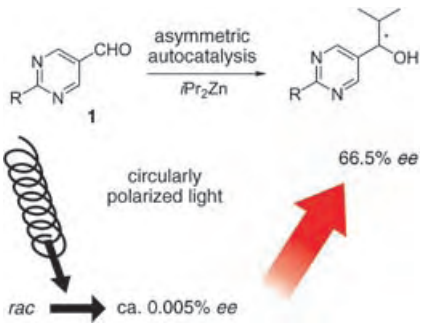
After a very long wait two arrive together: Following the recent highlight of a late-transition-metal octahedral cluster with 12 hydride ligands and 10 too few electrons, an equally remarkable highly electron-deficient pentanuclear cluster based on a triplatinum–dirhenium trigonal-bipyramidal core has been discovered which undergoes oxidative addition with three equivalents of H_2 (see scheme)



Asymmetric Amplification

J. Podlech,* T. Gehring **5776 – 5777**

New Aspects of Soai's Asymmetric Autocatalysis



Photolysis with circularly polarized light combined with Soai's asymmetric autocatalysis in the reaction of 2-(*tert*-butylethynyl)pyrimidine-5-carbaldehyde (**1**, R = C≡CtBu) with iPr_2Zn results in the amplification of ≈0.005% *ee* to about 65% *ee* in one step (see scheme). This reaction may serve as a model for how chiral amplification occurred in the prebiotic era.

InterScience
© 2005 Wiley-VCH Verlag GmbH & Co. KGaA, Weinheim

Essays



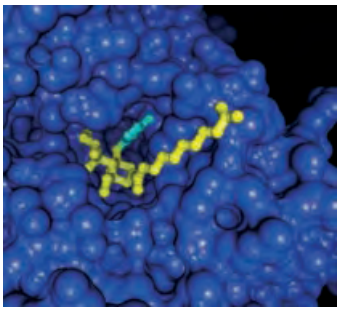
An explosive history: Diphenylketene was isolated and identified by Staudinger (see photo) in 1905, as the first example of this class of highly reactive compounds. Others had previously generated these species, but missed the opportunity to claim their discovery. This Essay provides an enlightening view of the history behind these useful reagents.

Reactive Intermediates

T. T. Tidwell* _____ **5778 – 5785**

The First Century of Ketenes (1905–2005): The Birth of a Versatile Family of Reactive Intermediates

Reviews



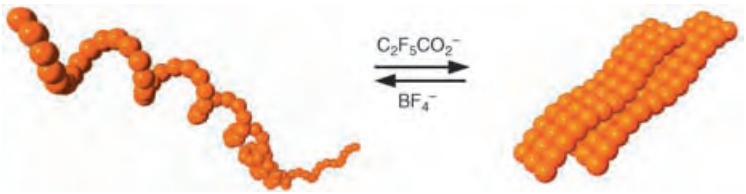
Permanently arrested—that is, when small-molecule natural products inhibit enzymes by covalent modification of an amino acid residue in the active site. An example of this is the complex of human MetAP-2 (blue) with fumagillin (yellow) in which the natural product is linked to a histidine residue (cyan) of the protein by a C–N bond.

Natural Products Chemistry

C. Drahl, B. F. Cravatt,*
E. J. Sorensen* _____ **5788 – 5809**

Protein-Reactive Natural Products

Communications



Sol–gel switching is triggered by counter-anion guest exchange. The secondary structures of reversible coordination polymers can interconvert from a folded helical conformation (gel) into an unfolded zigzag conformation (sol) and back again in aqueous media (see picture).

Supramolecular Chemistry

H.-J. Kim, J.-H. Lee, M. Lee* **5810 – 5814**

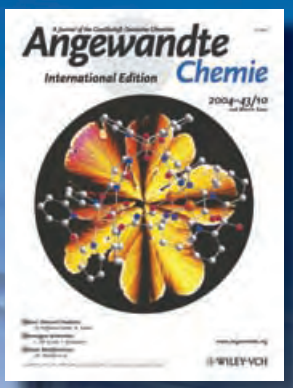
Stimuli-Responsive Gels from Reversible Coordination Polymers

For the USA and Canada:
ANGEWANDTE CHEMIE International Edition (ISSN 1433-7851) is published weekly by Wiley-VCH PO Box 191161, D 69451 Weinheim, Germany. Air freight and mailing in the USA by Publications Expediting Inc. 200 Meacham Ave., Elmont, NY 11003. Periodicals postage paid at Jamaica NY 11431. US POSTMASTER: send address changes to *Angewandte Chemie*, Wiley-VCH, 111 River Street, Hoboken, NJ 07030. Annual subscription price for institutions: US$ 4948.00/4498.00 (valid for print and electronic / print or electronic delivery); for individuals who are personal members of a national chemical society, or whose institution already subscribes, or who are retired or self-employed consultants, print only: US$ 394.00. Postage and handling charges included. All Wiley-VCH prices are exclusive VAT.

© 2005 Wiley-VCH Verlag GmbH & Co. KGaA, Weinheim

The best in chemistry –

for more than a hundred years



A Journal of the Gesellschaft Deutscher Chemiker

Angewandte
International Edition **Chemie**

www.angewandte.org

1888: ***The beginning of a success story***

Constant Innovations

1962: First issue of the International Edition
1976: Graphical abstracts
1979: Cover pictures
1988: Centenary of Angewandte
1989: Routine use of color
1991: New section: Highlights
1992: Computerized editorial tracking system
1995: Internet service for readers
1998: Regular press service; full-text online
2000: New section: Essays; EarlyView: Communications available online ahead of the printed version
2001: New section: Minireviews
2002: Online submission of manuscripts
2003: Weekly publication; new section: News; new layout
2004: Backfiles (1962-1997); ManuscriptXpress: Online system for authors and referees



Angewandte's advisors...

Robert Langer
Massachusetts Institute of Technology

*»**Angewandte Chemie** is one of the top chemistry journals in the world. As such, I try to publish there frequently and am honored to be a member of its International Advisory Board.«*

Angewandte Chemie International Edition *is a journal of the German Chemical Society (GDCh)*

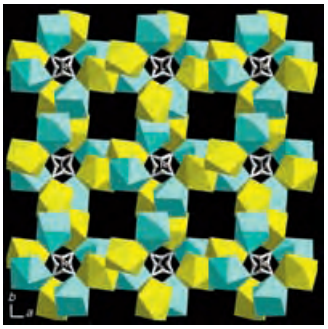
GDCh

WILEY InterScience® DISCOVER SOMETHING GREAT

WILEY-VCH

1841404_gu

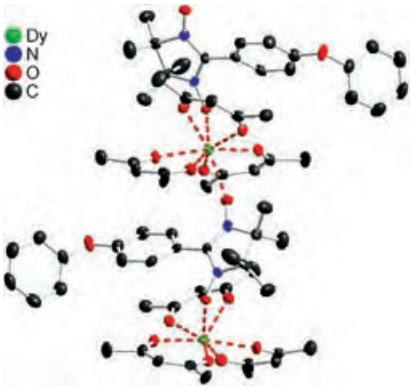
Achiral channels as well as left- and right-handed helical tubes are present in novel lanthanide-organic frameworks prepared under hydrothermal conditions from lanthanide oxides. In the three-dimensional coordination polymers, the Ln atoms (Ln = Eu, Dy, Y, Pr, Nd, Sm, Gd, Tb, Er) are linked by 4,5-imidazoledicarboxylic acid ligands with skew coordination orientation (see picture).



Coordination Polymers

Y.-Q. Sun, J. Zhang, Y.-M. Chen, G.-Y. Yang* ——— **5814 – 5817**

Porous Lanthanide–Organic Open Frameworks with Helical Tubes Constructed from Interweaving Triple-Helical and Double-Helical Chains



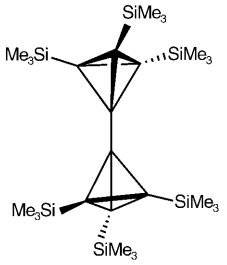
Single-chain magnets: A rational approach to decrease magnetic dipolar interactions led to the chain compound $[Dy(hfac)_3\{NIT(C_6H_4OPh)\}]$ (see structure; NIT(R): 2-(4′-R)-4,4,5,5-tetramethylimidazoline-1-oxyl-3-oxide), the first rare-earth-radical-based single-chain magnet. The compound shows slow relaxation behavior, a dynamical crossover resulting from finite-size effects, and a very rich static magnetic behavior.

One-Dimensional Magnets

L. Bogani, C. Sangregorio, R. Sessoli, D. Gatteschi* ——— **5817 – 5821**

Molecular Engineering for Single-Chain-Magnet Behavior in a One-Dimensional Dysprosium–Nitronyl Nitroxide Compound

On the short side: Hexakis(trimethylsilyl)tetrahedranyltetrahedrane (see formula) was synthesized by the oxidative coupling of tris(trimethylsilyl)tetrahedranyllithium via a cuprate complex. The exocyclic C–C bond between the two tetrahedrane units is the shortest known C–C single bond (1.436(3) Å) owing to the increased s character of the bond orbitals.



Short C–C Bonds

M. Tanaka, A. Sekiguchi* ——— **5821 – 5823**

Hexakis(trimethylsilyl)tetrahedranyltetrahedrane

Caught in a net: Self-assembly of nickel salts with 4,4′-bipyridine and the long V-shaped 4,4′-oxybis(benzoate) ligand has led to three different coordination networks: a parallel polycatenation of nanotube motifs to give a layered framework (see picture), a 2D→3D polythreaded array involving five polymeric units at a time, and a 3D self-penetrating binodal network with an unprecedented $(4.8^2)(4.6^4.8^4.10)$ topology.



Supramolecular Chemistry

X.-L. Wang, C. Qin, E.-B. Wang,* Y.-G. Li, Z.-M. Su,* L. Xu, L. Carlucci* ——— **5824 – 5827**

Entangled Coordination Networks with Inherent Features of Polycatenation, Polythreading, and Polyknotting

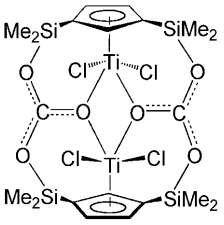
© 2005 Wiley-VCH Verlag GmbH & Co. KGaA, Weinheim

Contents

Polynuclear Complexes

D. Santamaría, J. Cano, P. Royo,*
M. E. G. Mosquera, T. Cuenca,*
L. M. Frutos, O. Castaño ___ **5828 – 5830**

Carbon Dioxide Activation Assisted by a Bis(chlorodimethylsilyl)cyclopentadienyl Titanium Compound



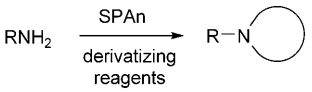
A helping hand: The assisted fixation of CO_2 and its transformation into a carbonato ligand has been achieved using a di(silyl)cyclopentadienyl titanium(IV) complex. In the presence of water and under air, a dinuclear carbonato titanium(III) complex (see picture) is formed. Theoretical investigations into the electronic properties of this titanium(III) complex explain its high stability and diamagnetism.

Combinatorial Chemistry

R. E. Dolle,* C. MacLeod,
B. Martinez-Teipel, W. Barker, P. R. Seida,
T. Herbertz _____ **5830 – 5833**

Solid/Solution-Phase Annulation Reagents: Single-Step Synthesis of Cyclic Amine Derivatives

Spanning the diversity gap: The conversion of primary amines into cyclic derivatives is achieved by using a family of amine-derivatizing reagents, termed SPAn reagents (see scheme). The reagents, which require no further chemical manipulation or activation, are used to prepare discrete compounds or a library collection

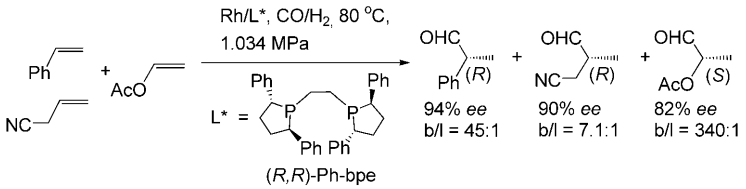


of diverse heterocycles. SPAn reagents have application in finding new lead compounds and the development of structure–activity relationships.

Asymmetric Catalysis

A. T. Axtell, C. J. Cobley, J. Klosin,*
G. T. Whiteker, A. Zanotti-Gerosa,
K. A. Abboud _____ **5834 – 5838**

Highly Regio- and Enantioselective Asymmetric Hydroformylation of Olefins Mediated by 2,5-Disubstituted Phospholane Ligands

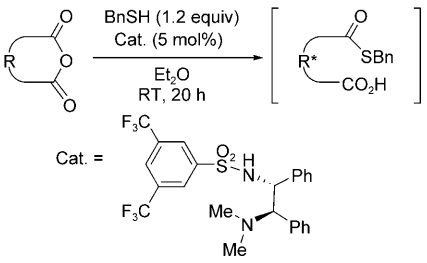


Off the shelf: The commercially available ligand (*R*,*R*)-1,2-bis(2,5-diphenylphospholano)ethane ((*R*,*R*)-Ph-bpe) has been identified as an excellent ligand for asymmetric hydroformylation. State-of-the-art regio- and enantioselectivities are obtained for reactions with styrene, allyl cyanide, and vinyl acetate as substrates while high reaction rates (> 4000 turnovers h^{-1}) are maintained (see scheme; Ac = acetate, b/l = branched/linear).

Asymmetric Synthesis

T. Honjo, S. Sano, M. Shiro,
Y. Nagao* _____ **5838 – 5841**

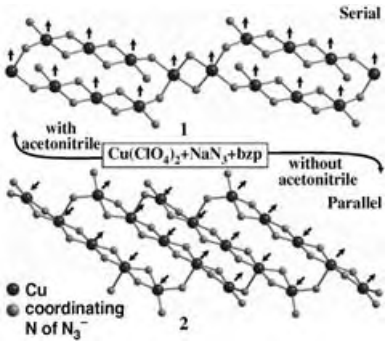
Highly Enantioselective Catalytic Thiolysis of Prochiral Cyclic Dicarboxylic Anhydrides Utilizing a Bifunctional Chiral Sulfonamide



A catalytic desymmetrization is achieved for various prochiral dicarboxylic anhydrides with yields of 87–100% and *ee* values of 83–98% through the title reaction (see scheme; Bn = benzyl). The bifunctional effect of the chiral sulfonamide catalyst was clarified on the basis of unsuccessful asymmetric induction by using the related chiral sulfonamides.

© 2005 Wiley-VCH Verlag GmbH & Co. KGaA, Weinheim

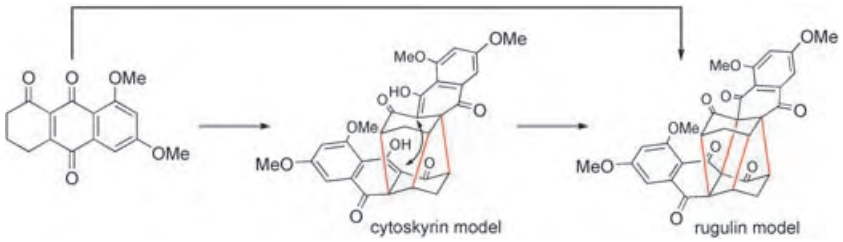
Magnetic attraction: The exotic 1D molecular tapes $[Cu_4(N_3)_8(CH_3CN)_3(bzp)_2]_n$ (**1**) and $[Cu_5(N_3)_{10}(bzp)_2]_n$ (**2**) were obtained from a solution of methanol or methanol/acetonitrile (see scheme; bzp = 2-benzoylpyridyl). The end-on azide bridges in **1** transmit ferromagnetic interaction, whereas in **2**, the central copper center of a linear Cu_5 unit is antiferromagnetically coupled with its neighboring Cu ions.



Polynuclear Complexes

Y.-Z. Zhang, H.-Y. Wei, F. Pan, Z.-M. Wang, Z.-D. Chen,* S. Gao* ——— **5841 – 5846**

Two Molecular Tapes Consisting of Serial or Parallel Azido-Bridged Eight-Membered Copper Rings



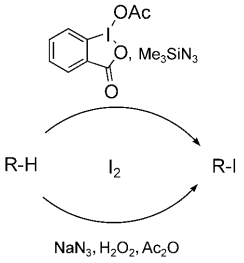
Models revealed: A series of model systems, for example, for cytoskyrin and rugulin, were prepared from an anthraquinone (see scheme). The cascade sequence features Michael additions and oxidation reactions.

Natural Products Synthesis

K. C. Nicolaou,* C. D. Papageorgiou, J. L. Piper, R. K. Chadha ——— **5846 – 5851**

The Cytoskyrin Cascade: A Facile Entry into Cytoskyrin A, Deoxyrubroskyrin, Rugulin, Skyrin, and Flavoskyrin Model Systems

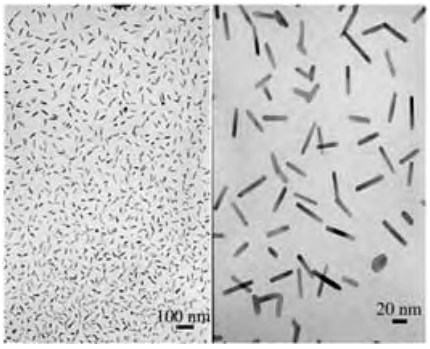
Unactivated C–H bonds react with iodine when exposed to trimethylsilyl azide in the presence of a hypervalent iodine reagent or, alternatively, to aqueous H_2O_2, acetic anhydride, and sodium azide (see scheme).



C–H Activation

J. Barluenga,* E. Campos-Gómez, D. Rodríguez, F. González-Bobes, J. M. González ——— **5851 – 5854**

New Iodination Reactions of Saturated Hydrocarbons



Highly uniform, single-crystalline PbTe nanorods with a diameter of 7 nm and an aspect ratio of 7 can be obtained by using a sonoelectrochemical method. The metal ion/ligand ratio controls the purity of the PbTe nanostructures through the redox chemistry of the ions involved in the growth process. Transmission electron microscopy of the nanorods reveals the highly uniform morphology obtained (see picture).

Nanostructures

X. Qiu, Y. Lou, A. C. S. Samia, A. Devadoss, J. D. Burgess, S. Dayal, C. Burda* ——— **5855 – 5857**

PbTe Nanorods by Sonoelectrochemistry

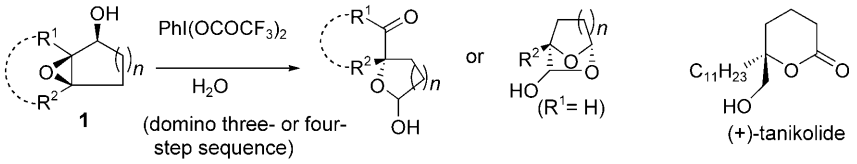
© 2005 Wiley-VCH Verlag GmbH & Co. KGaA, Weinheim

Contents

Hypervalent Iodine Reagents

Y. Kita,* S. Matsuda, E. Fujii, M. Horai, K. Hata, H. Fujioka ——— **5857 – 5860**

Domino Reaction of 2,3-Epoxy-1-alcohols and PIFA in the Presence of H_2O and the Concise Synthesis of (+)-Tanikolide

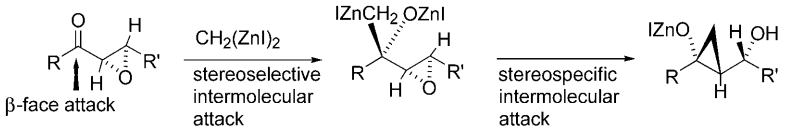


Lactols are prepared by a single operation, in which 2,3-epoxy-1-alcohols are treated with phenyliodine(III) bis(trifluoroacetate) (PIFA) in the presence of H_2O. Thus, an efficient domino three- or four-step sequence has been developed and applied to the concise synthesis of (+)-tanikolide (see scheme).

Diastereoselectivity

K. Nomura, K. Oshima, S. Matsubara* ——— **5860 – 5863**

Stereospecific and Stereoselective Preparation of 2-(1-Hydroxyalkyl)-1-alkylcyclopropanols from α,β-Epoxy Ketones and Bis(iodozincio)methane



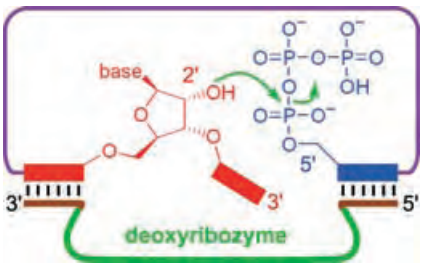
A coordinated attack: The reaction of α,β-epoxy ketones with bis(iodozincio)methane produces 2-(1-hydroxyalkyl)-1-alkylcyclopropanols diastereoselectively (see scheme). The reaction proceeds by the coordination and diastereoselective addition of the zinc reagent to the carbonyl group followed by a stereospecific intramolecular attack on the epoxide ring.

DNA Catalysis

Y. Wang, S. K. Silverman* ——— **5863 – 5866**

Efficient One-Step Synthesis of Biologically Related Lariat RNAs by a Deoxyribozyme

Closing the loop: The artificial 6BX22 deoxyribozyme (in green) synthesizes naturally occurring lariat RNAs in one step from readily available linear RNA substrates. The exquisite site selectivity of this macrocyclization reaction—which can form a 1597-membered ring in 72% yield with <0.1% side products—highlights the utility of catalytic DNA for transformations that are not possible with traditional synthetic methods.



Annulation

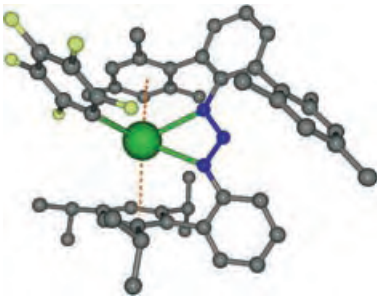
C. P. Davie, R. L. Danheiser* ——— **5867 – 5870**

Stereoselective Synthesis of Highly Substituted Cyclopentenones through [4+1] Annulations of Trialkylsilyl Vinyl Ketenes with α-Benzotriazolyl Organolithium Compounds

Closing the ring: Highly functionalized cyclopentenones are prepared by the reaction of readily available metalated benzotriazole derivatives with trialkylsilyl vinyl ketenes (see scheme; Z = heteroatom substituent). Dienolate intermediates are generated which form the five-membered ring. Most transformations proceed with high stereoselectivity by a mechanism believed to involve stereospecific 4π-electrocyclic ring closure.



© 2005 Wiley-VCH Verlag GmbH & Co. KGaA, Weinheim

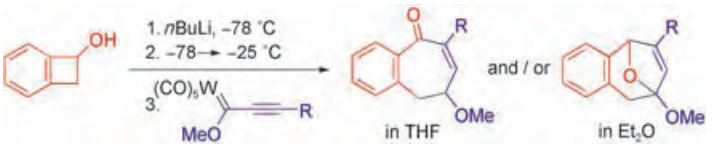


Pentafluorophenyl complexes of the heavier alkaline-earth metals (Ca, Sr, Ba) are stabilized by a novel sterically crowded triazenido ligand. The pendent arene rings of the aryl-substituted triazenide are π bonded to the alkaline-earth metal atoms, thereby suppressing decomposition pathways or ligand redistribution reactions and allowing the isolation of solvent-free derivatives (see picture; Ba: green; N: blue; F: light green; C: gray).

Alkaline-Earth Metal Complexes

S.-O. Hauber, F. Lissner, G. B. Deacon, M. Niemeyer* _____ 5871 – 5875

Stabilization of Aryl–Calcium, –Strontium, and –Barium Compounds by Designed Steric and π-Bonding Encapsulation



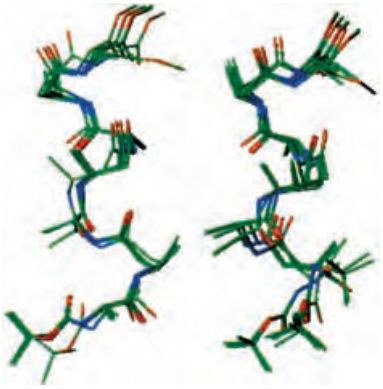
The reaction of alkynyl Fischer carbene complexes with the *ortho*-quinodimethane obtained from lithium benzocyclobuteneoxide leads to the preparation of highly functionalized seven-membered benzocarbocycles (see scheme). The position and the nature of the functional groups in the product are solvent controlled: benzocycloheptenones are selectively formed in THF, whereas benzocycloheptene ketals are exclusively synthesized in diethyl ether.

Synthetic Methods

J. Barluenga,* P. García-García, M. A. Fernández-Rodríguez, E. Aguilar, I. Merino _____ 5875 – 5878

Lithium Benzocyclobuteneoxide as a Precursor of a Vinylogous Enolate: Solvent-Controlled Synthesis of Highly Functionalized Seven-Membered Benzocarbocycles

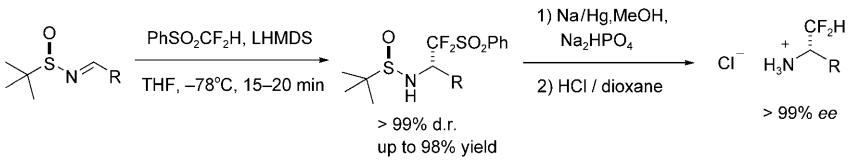
A new twist: The α/β hybrid dipeptide repeats prepared from alternating C-linked carbo-β³-amino acid and L-Ala residues show a high propensity for mixed helices and produce hitherto unknown right-handed 11/9 and 9/11 helical structures (see picture).



Peptide Helices

G. V. M. Sharma,* P. Nagendar, P. Jayaprakash, P. Radha Krishna, K. V. S. Ramakrishna, A. C. Kunwar* _____ 5878 – 5882

9/11 Mixed Helices in α/β Peptides Derived from C-Linked Carbo-β-Amino Acid and L-Ala Repeats



Nucleophilic (phenylsulfonyl)difluoromethylation of (*R*)-(*N*-*tert*-butylsulfinyl)-aldimines with difluoromethyl phenyl sulfone affords the corresponding products in excellent yields and with high diastereoselectivity (see scheme). The facile and convenient deprotection of both *tert*-butylsulfinyl and phenylsulfonyl groups affords the target α-difluoromethyl amines with high enantiomeric purity.

Synthetic Methods

Y. Li, J. Hu* _____ 5882 – 5886

Facile Synthesis of Chiral α-Difluoromethyl Amines from *N*-(*tert*-Butylsulfinyl)aldimines

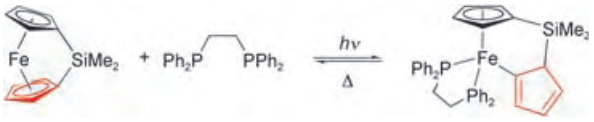
© 2005 Wiley-VCH Verlag GmbH & Co. KGaA, Weinheim

Contents

Coordination Modes

M. Tanabe, S. C. Bourke, D. E. Herbert, A. J. Lough, I. Manners* — **5886 – 5890**

Reversible, Strain-Controlled Haptotropic Shifts of Cyclopentadienyl Ligands in [1]- and [2]Metallocenophanes

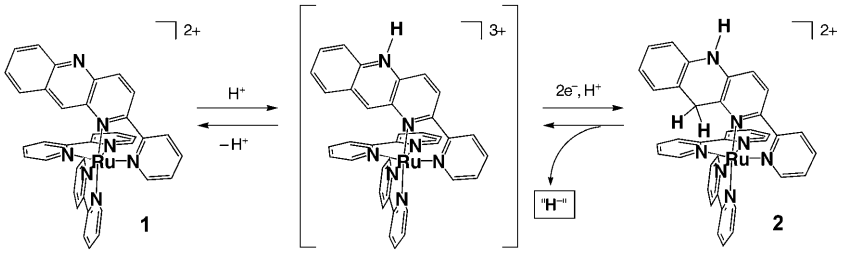


Slipping rings: A reversible shift from η^5-Cp to η^1-Cp and back has been established for ring-strained metallocenophanes (see scheme) and the dependence of the reversibility on the degree of ring strain has been probed. The presence of phosphane ligands has allowed the isolation of novel η^1-Cp ring-slipped Fe and Ru complexes.

Redox Chemistry

T.-a. Koizumi, K. Tanaka* — **5891 – 5894**

Reversible Hydride Generation and Release from the Ligand of $[Ru(pbn)(bpy)_2](PF_6)_2$ Driven by a pbn-Localized Redox Reaction



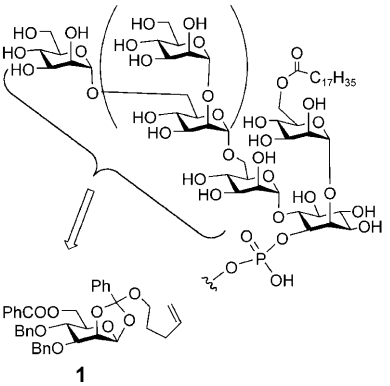
Electrochemical reduction of $[Ru(pbn)(bpy)_2]^{2+}$ (**1**, pbn = 2-(2-pyridyl)benzo[*b*]-1,5-naphthyridine, bpy = 2,2′-bipyridine) in an acidic solvent gives $[Ru(pbnH_2)(bpy)_2]^{2+}$ (**2**), which releases the hydrogen as "hydride" (see scheme). This catalytic system reduces substrates (for example, acetone) with two electrons and protons from water, and thus operates in a similar way to the NAD^+/NADH redox couple.

Carbohydrate Synthesis

K. N. Jayaprakash, J. Lu, B. Fraser-Reid* — **5894 – 5898**

Synthesis of a Lipomannan Component of the Cell-Wall Complex of *Mycobacterium tuberculosis* Is Based on Paulsen's Concept of Donor/Acceptor "Match"

The perfect match: A mannosidyl *n*-pentenylorthoester **1** is the sole donor and acceptor source for a branched oligomannan array (see picture). An iterative process of regioselective glycosidation of polyol acceptors virtually eliminates the need for protecting-group manipulations, thereby permitting a rapid, high-yielding route to the mycobacterial lipomannan phosphoinositide.



VIP Communications labeled with this symbol have been judged by two referees as being "very important papers".

© 2005 Wiley-VCH Verlag GmbH & Co. KGaA, Weinheim

Sources

Product and Company Directory

You can start the entry for your company in "Sources" in any issue of *Angewandte Chemie*.

If you would like more information, please do not hesitate to contact us.

Wiley-VCH Verlag – Advertising Department
Tel.: 0 62 01 - 60 65 65
Fax: 0 62 01 - 60 65 50
E-Mail: MSchulz@wiley-vch.de

Service

Keywords ____ 5900
Authors ____ 5901
Vacancies ____ A53
Preview ____ 5903

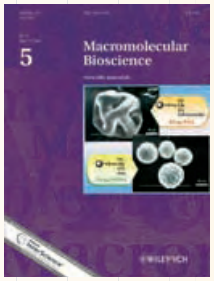


Think Macro

Excellence in Specialized Macromolecular Science

Research in the interdisciplinary field of macromolecular science and biology

ISI Impact Factor 2003 2.439



www.mbs-journal.de
ISSN Print 1616-5187
ISSN Online 1616-5195
Volume 5, 12 issues

- Covers all aspects of biomaterials from basic research to applications, from chemistry to physics and from biotechnology to medicine.
- Listed in *Index Medicus*, MEDLINE, *ISI Web of Science®*, *Science Citation Index ExpandedTM*, *ISI Alerting ServicesTM*, *Chemistry Citation IndexTM*, *Materials Science Citation Index®*, *Biochemistry & Biophysics Citation IndexTM*.
- Presents Feature Articles/Reviews, Full Papers, Communications.

Macromolecular Bioscience is available **separately** and as part of the *Macromolecular* Full Package, *Macromolecular Basic* Package + *Macromolecular* Materials and Engineering, *Macromolecular Basic* Package + *Macromolecular* Symposia , *Macromolecular Basic* Package.



For more details and pricing information please visit
www.mbs-journal.de

WILEY InterScience® WILEY WILEY-VCH

John Wiley & Sons, Inc. • Tel.: +1-800-825-7550 (US only) or +1-201-748-6645 • Fax: +1-201-748-5915 • E-Mail: subinfo@wiley.com
John Wiley & Sons, Ltd. • Tel.: +44 (0) 1243-843335 • Fax: +44 (0) 1243-843232 • E-Mail: cs-journals@wiley.co.uk
Wiley-VCH • Tel.: +49 (0) 6201 606-400 • Fax: +49 (0) 6201 606-184 • E-Mail: service@wiley-vch.de

20591506_ps

© 2005 Wiley-VCH Verlag GmbH & Co. KGaA, Weinheim



Fluorous Chemistry and Technology—A Symposium Showcases Ever-Broadening Frontiers**

John A. Gladysz*

Only an infinitesimal fraction of publications in chemistry directly spawn new research fields. However, one good case in point is the report by I. Horváth and J. Rábai from 1994 that coined the term "fluorous" and provided the first example of fluorous biphasic catalysis.[1] Fluorous substances are simultaneously hydrophobic and lipophobic, and researchers quickly recognized a variety of useful applications for this phase-orthogonality, which in many cases has the additional benefit of being temperature-dependent. Indeed, biological and physical chemists had been crafting and studying fluorous materials for some time (cloaked in other nomenclature), and they found eager new partners among synthetic chemists who took up the quest for novel recyclable catalysts and reagents, tagging strategies for mixture synthesis and separations, and other objectives.

Today, there are over 800 papers in the literature that contain the word fluorous in the title or abstract. Along the way, a company, "Fluorous Technologies Incorporated" was founded (2000), and a "Handbook of Fluorous Chemistry" has appeared (2004).[2] Clearly, eleven years after the seminal paper, the time for a meeting dedicated to this field had arrived. Accordingly, over 75 scientists from Europe, Asia, and North America made the trek to the scenic venue of Bordeaux in early July. The co-chairmen J.-M. Vincent (University of Bordeaux) and R. H. Fish (Lawrence Berkeley National Laboratory) expertly handled the organizational details. Despite the lure of the vineyards and châteaux, science held the center stage for three exciting days.

The opening talk by I. Horváth (Eötvös Lórand University, Budapest) was both a retrospective and a prospective, and challenged the audience to find ways of addressing the environmental persistence associated with most $(CF_2)_n$-based fluorous compounds. A quest for fluorocarbon-degrading microorganisms was recommended. Subsequent presentations by G. Fontana (Solvay Solexis, Milan) and J. Rábai (Eötvös Lórand University) highlighted new types of oxygen-containing solvents, ponytails, and tags that are more promising in terms of biodegradability, and which have other attractive properties. Nonetheless, a recurrent theme during the entire conference involved fluorous-solvent-free protocols for the recovery of fluorous catalysts and reagents.

One novel approach was reported by P. Pollet (Georgia Institute of Technology; collaborators: C. Eckert, C. Liotta, and P. Jessop). She described the use of CO_2 pressure (sub-supercritical) as a "solubility switch" for fluorous solutes in organic solvents (Figure 1). Furthermore, these "gas expanded" media could desorb fluorous rhodium catalysts from fluorous silica gel, which redeposited upon pressure release. M. Contel (University of Zaragoza; collaborators: J.-M. Vincent and R. H. Fish) and J. A. Gladysz; detailed new thermomorphic catalysts that could be used under homogeneous conditions in alkane, arene, or ether solvents at elevated temperatures, and can be recovered by a simple liquid–solid phase separation at lower temperatures.



Figure 1. Use of CO_2 pressure to homogenize organic (toluene, above) and fluorous (FC-72, below) liquid phases. A colored solute was added to the latter. Note the progressive volume increase. Fluorous solids can be similarly solubilized in organic solvents.

New types of fluorous supports were described, also with the idea of facilitating fluorous-solvent-free procedures. These included fluorous zirconium phosphates (E. Hope, University of Leicester), and garden-variety Teflon tape. Both J. Nishikido (Noguchi Institute, Tokyo) and A. Biffis (University of Padua) reported on fluorous catalysts that had been immobilized on fluorous silica gel (main group or early transition metal Lewis acids and dirhodium complexes); the latter presentation also detailed protocols with fluorous solid ion exchangers.

The use of fluorous tags in discovery synthesis and strategic separations continues to undergo remarkable growth. The state-of-the-art in parallel synthesis was represented in talks by W. Zhang (Fluorous Technologies) and D. Curran (University of Pittsburgh). Attention-getting developments included the emergence of fluorous aryl sulfonates ($ArOSO_2(CF_2)_7CF_3$) as versatile building blocks, and the simultaneous use of fluorous and polyethylene-glycol-like tags[3] that allow two-dimensional separations and enable much more complex libraries to be processed (Figure 2). Fluorous protecting groups can often serve as phase tags, as demonstrated in elegant syntheses of cyclic peptides by S. Takeuchi (Niigata University). Heavy fluorous tags that facilitate oligosaccharide and oligodeoxyribonucleotide syntheses were reported by T. Inazu (Tokai University) and T. Wada (University of Tokyo).

A lecture by W. Bannwarth (University of Freiburg) showed how fluorous tags can be used to immobilize DNA fragments on fluorous silica gel, allowing the facile purification of synthetic oligonucleotides. His data indicated a high potential for the fixation of biomolecules on surfaces by fluorous–fluorous interactions, and applications in molecular biology and proteomics are believed to be just around the corner. Taking the

[*] Prof. Dr. J. A. Gladysz
Institut für Organische Chemie
Friedrich-Alexander-Universität
Erlangen-Nürnberg
Henkestraße 42, 91054 Erlangen
(Germany)
Fax: (+49) 9131-8526865
E-mail: gladysz@organik.uni-erlangen.de

[**] 1st International Symposium on Fluorous Technologies in Bordeaux-Talence (France), July 3–6, 2005

InterScience
© 2005 Wiley-VCH Verlag GmbH & Co. KGaA, Weinheim

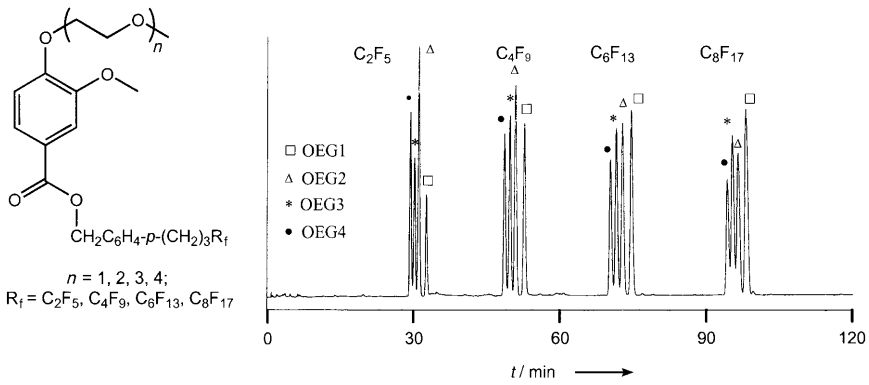


Figure 2. Double demixing of a sample with both fluorous and oligomeric ethylene glycol (OEG) tags on a FluoroFlash PF-C8 HPLC column.

biological interface one step further, K. Hatanaka (University of Tokyo) described fluorous-tagged glycoside primers in which the saccharide chains can be elongated by cellular enzymes. This demonstrates for the first time that fluorous-tagged compounds can be taken up in the cell to participate in the biosynthetic machinery without the need for protection and deprotection steps usually required for chemical oligosaccharide synthesis.

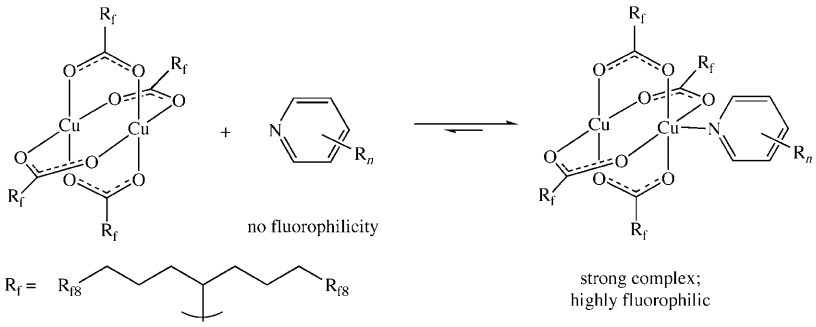
J. Riess (UC San Diego and Alliance Pharmaceutical) then shifted the theme into the clinic—by no means a new venue for fluorous chemistry—and described the search for fluorous ultrasound contrast agents that optimize microbubble lifetime. The physical–biochemical interface was also represented in presentations by M. P. Krafft (Institut Charles Sadron, Strasbourg) and V. Percec (University of Pennsylvania). The former detailed the unique properties associated with phospholipids that contain fluorocarbon–hydrocarbon diblocks, and applications in lung surfactant therapy for neonatal respiratory distress syndrome. The latter featured wedge-shaped building blocks for supramolecular chemistry that contain fluorous domains, and self-assembly processes leading to channels that conduct water and ions.

Additional self-assembly phenomena that involve "halogen bonding" and lead to fluorous solid-state networks were described by P. Metrangolo (Milan Polytechnic; collaborator: G. Resnati). Many other types of phase phenomena received attention, such as design strategies for fluorous gelators, in the lecture of J.-L. Pozzo (University of Bordeaux; collaborator: J.-M. Vincent). B.-J. Deelman (ARKEMA, The Netherlands) reported new theoretical approaches to optimizing fluorophilicities. M. F. Costa Gomes (University of Clermont-Ferrand) explained how thermodynamicists rigorously measure and model phase equilibria, particularly with respect to gas solubilities in fluorous liquids. Differences between nonpolar, polar, and quadrupolar solutes were emphasized. Unusually selective brominations were effected by J. Iskra (Jozef Stefan Institute, Ljubljana) by layering reacting species (substrate and Br_2) on the opposite sides of a fluorocarbon interface, the so-called "phase vanishing" technique. Applications of reversible "phase switching" (Scheme 1) were featured in posters from the J.-M. Vincent research group.

Oxidations with molecular oxygen were also well-represented. K. Pamin (Polish Academy of Sciences, Krakow; collaborator: J. Haber) disclosed new families of fluorous porphyrin catalysts for the oxidation of alkenes, and E. Magnier (University of Versailles), R. H. Fish and M. Contel detailed manganese, cobalt, and copper complexes of cyclic polyamine ligands for the oxidation of alkanes, alkenes, alcohols, and other functional groups. Another approach, relayed by O. Holczknecht (CNR Institute, Milan; collaborator: G. Pozzi), used fluorous derivatives of TEMPO in conjunction with NaOCl or $ArI(OAc)_2$.

Many additional advances in catalysis were reported. One new direction involved the use of fluorous crown ethers and phosphonium salts as phase-transfer catalysts, as recounted by A. Stuart (Leicester). G. Pozzi described highly enantioselective transition metal catalysts based on heavy fluorous chiral nitrogen donor ligands. The lecture of J. Otera (Okayama University) featured fluorous organotin catalysts that are unparalleled for transesterifications and that have a variety of unusual phase properties. G. Vlád (Eötvös Lórand University; collaborator: I. Horváth) detailed improved routes to a variety of fluorous phosphines that see extensive use in catalysis.

At the banquet, I. Horváth and J. Rábai were presented with the first International Award for Fluorous Technologies, in recognition of their groundbreaking contributions noted above. The program concluded with a free-spirited panel discussion. There was unanimous sentiment that fluorous chemistry is a wide-open field that will continue to rapidly grow and expand into new applications. An important message for readers is that there are abundant



Scheme 1. Reversible phase switching: a fluorous dicopper complex that binds pyridines and extracts them into fluorous phases; applications in histamine detection were described.

© 2005 Wiley-VCH Verlag GmbH & Co. KGaA, Weinheim

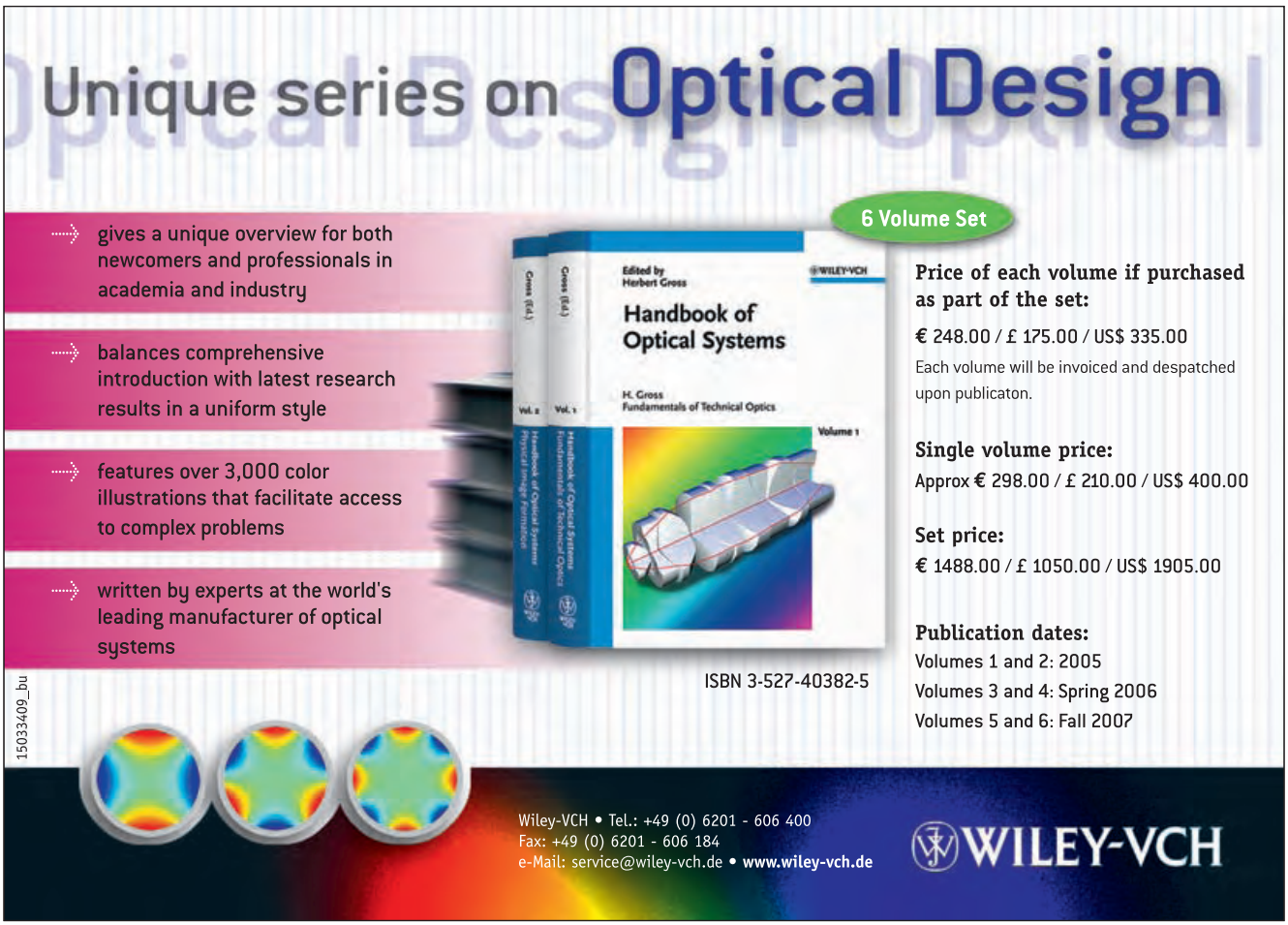
opportunities for newcomers. The natives are friendly (not to mention hospitable), cooperation abounds, and there is a conspicuous lack of turf battles. For those interested in climbing on board, one opportunity will be the second Symposium, which is scheduled to be held in Kamakura, Japan in July of 2007.

[1] I. T. Horváth, J. Rábai, *Science* **1994**, *266*, 72.

[2] *Handbook of Fluorous Chemistry* (Eds.: J. A. Gladysz, D. P. Curran, I. T. Horváth), Wiley-VCH, New York, **2004**.

[3] C. S. Wilcox, S. Turkyilmaz, *Tetrahedron Lett.* **2005**, *46*, 1827.

DOI: 10.1002/anie.200502639



 © 2005 Wiley-VCH Verlag GmbH & Co. KGaA, Weinheim

Cluster Compounds

DOI: 10.1002/anie.200501549

Hydrogen Sponge? A Heteronuclear Cluster That Absorbs Large Quantities of Hydrogen**

Paul J. Dyson and J. Scott McIndoe**

Keywords:
cluster compounds · hydride ligands · hydrogen storage · platinum · rhenium

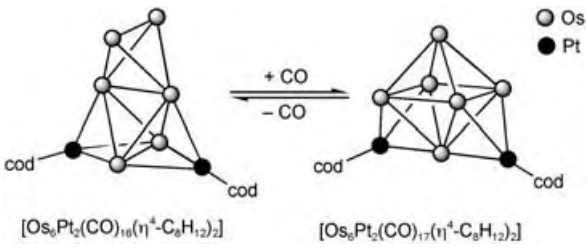
Clusters offer unique possibilities in reactivity that are not possible with mononuclear complexes, and different to that of nanoparticles and the bulk metallic state.[1] For example, while both mononuclear and cluster species can undergo ligand-substitution reactions by associative, dissociative, or intermediate mechanisms, ligand substitution in clusters can also be driven by metal–metal bond scission/reformation mechanisms (which in fact may be viewed as a special case of an associative reaction).[2] While activation by metal–metal bond scission could conceivably take place at the surface of a nanocluster, such a process would be very difficult to demonstrate experimentally. In contrast, clusters are soluble in common organic solvents and accordingly can be studied in solution by high-resolution spectroscopic techniques in situ.[3] Electronically unsaturated transition-metal carbonyl clusters open up further mechanistic possibilities, providing alternative mechanisms for ligand addition, substitution, and C–X (and other) bond activation, which differ from those of clusters that obey the usual electron-counting rules, that is, the effective atomic number (EAN) rule and the polyhedral skeletal electron pair theory (PSEPT).[4]

A classic example of a low nuclearity (EAN) cluster that contains two electrons less than expected is $[Os_3H_2(CO)_{10}]$. This cluster undergoes addition reactions with, for example, phosphines, to form clusters of formula $[Os_3H_2(CO)_{10}(PR_3)]$. It can also undergo a more complicated addition/Si–H bond activation process with the functionalized phosphine $HMe_2SiC_6H_4CH_2PPh_2$ to afford $[Os_3H(CO)_8(Me_2SiC_6H_4CH_2PPh_2)]$.[5] In both reactions the resulting cluster core comprises a triangle in which all the Os–Os bond lengths are typical of single bonds.

An interesting example of a high nuclearity cluster with two electrons less than the expected number is $[Os_6Pt_2(CO)_{16}(\eta^4\text{-}C_8H_{12})_2]$ (see Scheme 1).[6] The geometry can be described in various ways, but perhaps the simplest way to view the core is as four fused tetrahedra. The addition of two electrons in the form of a CO ligand does not result in a simple transformation, instead a major structural rearrangement takes place, resulting in a cluster with a bicapped-octahedral core. Clusters with excessive electron counts are also known, for example, $[Ni_6(\eta^5\text{-}Cp)_6]$ ($Cp = C_5H_5$) has an octahedral structure but has 90 electrons, four more than expected.[7]

The cationic tetrahedral platinum hydride clusters $[Pt_4H_2(PtBu_3)_4]^{2+}$ and $[Pt_4H(PtBu_3)_4]^{+}$ react rapidly with H_2 to give the heptahydride cluster $[Pt_4H_7(PtBu_3)_4]^{2+}$, in which a Pt–Pt bond has been broken to afford a cluster with a butterfly geometry.[8] This process can be reversed by reaction with ethene.

Very recently Weller and co-workers reported a late-transition-metal cluster that is not just short of two electrons, but deficient by an electron count of 10 (though exactly comparable to the early-transition-metal cluster $[Nb_6Cl_{18}]$).[9,10] The compound in question, $[Rh_6(\mu\text{-}H)_{12}(PiPr_3)_6]^{2+}$, has a regular octahedral geometry in which each vertex has a phosphine ligand and each edge is bridged by a hydride ligand. Now, Adams and Captain have discovered an equally remarkable cluster, $[Pt_3Re_2(CO)_6(PtBu_3)_3]$ (**1**) that is also deficient by 10 electrons, but contains only five metal atoms—three platinum and two rhenium atoms.[11] The cluster was isolated from the reaction of $[Pt(PtBu_3)_2]$ with $[Re_2(CO)_{10}]$ in refluxing octane in 18% yield. The trigonal bi-



Scheme 1. Polyhedral rearrangement observed on the formation of $[Os_6Pt_2(CO)_{17}(\eta^4\text{-}C_8H_{12})_2]$ from $[Os_6Pt_2(CO)_{16}(\eta^4\text{-}C_8H_{12})_2]$ following association of one CO ligand (cod = C_8H_{12}; CO ligands omitted for clarity).

[*] Prof. Dr. P. J. Dyson
Institut des Sciences et Ingénierie Chimiques
Ecole Polytechnique Fédérale de Lausanne (EPFL)
1015 Lausanne (Switzerland)
Fax: (+41) 21-6939885
E-mail: paul.dyson@epfl.ch
Prof. Dr. J. S. McIndoe
Department of Chemistry
University of Victoria
P.O. Box 3065, Victoria, BC V8W 3V6 (Canada)
Fax: (+1) 250-721-7147
E-mail: mcindoe@uvic.ca.

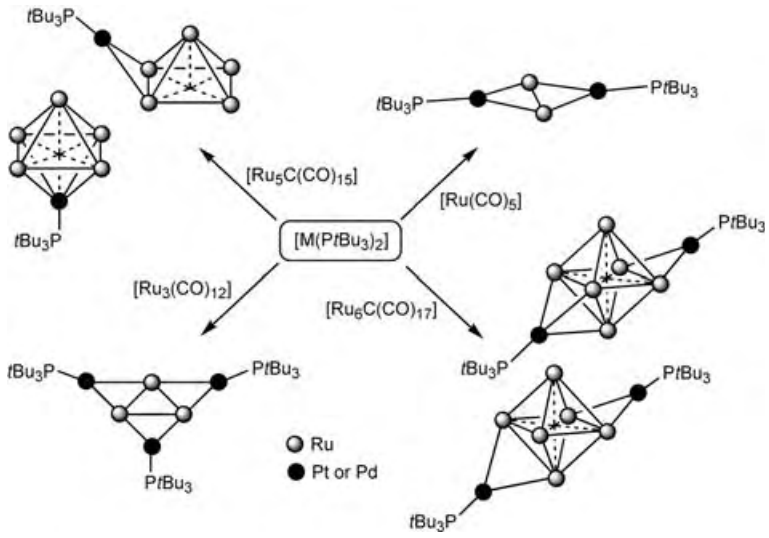
[**] We would like to thank Prof. Richard Adams for supplying the graphic used in the Table of Contents.

InterScience
© 2005 Wiley-VCH Verlag GmbH & Co. KGaA, Weinheim

pyramidal geometry presented by this cluster is shown in Figure 1a. The surface of the cluster is decorated with carbonyl and phosphine ligands and the space-filling diagram (Figure 1b) reveals essentially complete encapsulation of the metal core by the ligand sphere.

In the presence of H_2 at room temperature the cluster reacts to form $[Pt_3Re_2(\mu\text{-}H)_6(CO)_6(PtBu_3)_3]$ (**2**). The cluster retains essentially the same geometry, including the original trigonal-bipyramidal core, and the crystal structure of **2** shows that all six of the Re–Pt bonds are bridged by hydride ligands. The hydride ligands were located in the high-quality X-ray structure, and significantly, the Pt–Re bond lengths had considerably lengthened (from an average of 2.648 in **1** to 2.909 Å in **2**).

The 14 valence-electron (VE) complex $[Pt(PtBu_3)_2]$, and the palladium analogue, have been used by Adams and co-workers to produce an array of fascinating new heteronuclear clusters, many with unusual electron counts. In their earlier work they described the reaction of $[Pd(PtBu_3)_2]$ with $[Ru_3(CO)_{12}]$ to afford the remarkable near-planar cluster $[Ru_3(CO)_{12}\{Pd(PtBu_3)\}_3]$ (Scheme 2).[12] The utility of the reactive fragment was further demonstrated in the reaction with $[Ru_6C(CO)_{17}]$ affording $[Ru_6C(CO)_{17}\{Pd(PtBu_3)\}_2]$, which exists as two isomers in the solid state, and with $[Ru(CO)_5]$ yielding the complex $[Ru_2(CO)_9\{Pd(PtBu_3)\}_2]$, a dipalladium adduct of unstable $[Ru_2(CO)_9]$. Subsequently other compounds have been reported including $[Ru_5C(CO)_{15}\{Pt(PtBu_3)\}]$, which consists of two interconverting isomers in solution,[13] and some rhodium–platinum,[14] and iridium–platinum[15] clusters containing up to 12 metal atoms.



Scheme 2. Examples of condensation reactions between the highly reactive 14 VE complexes $[M(PtBu_3)_2]$ (M = Pd or Pt) and various ruthenium carbonyl compounds recently reported by Adams and co-workers (CO ligands omitted for clarity).

Efficient hydrogen production and storage is of considerable importance in a world where cheap and renewable energy source are urgently needed, and although clusters are unlikely to be used for hydrogen storage, they should certainly serve as excellent models for this process. The replacement of nanoclusters in fuel cells by molecular clusters can also be envisaged and it is likely to be clusters such as $[Pd_{28}(CO)_{27}(H_{12})\{Pt(PMe_3)\}\{Pt(PPh_3)\}_{12}]$,[16] $[Pt_4H_8(PPhiPr_2)_4]$,[17] $[Rh_6(\mu\text{-}H)_{12}(PiPr_3)_6]^{2+}$, and $[Pt_3Re_2(\mu\text{-}H)_6(CO)_6(PtBu_3)_3]$ that drive such possibilities forward. The heavy transition metals are of course unlikely candidates for H_2 storage by themselves, setting aside the fact that they are among the most rare and expensive of elements, to meet the US Department of Energy's recommendation for mobile applications of 6% hydrogen by weight,[18] each metal atom alone would have to reversibly absorb many hydrogen molecules. However, the rate and extent of adsorption of H_2 on more promising substrates (light and cheap materials with high surface area, such as carbon) may be increased by using metal particles, which enhance hydrogen storage through hydrogen spillover.[19] Metal nanoparticles with a strong propensity for hydrogen absorption may prove to be useful models and/or precursors for this process. Furthermore, there will certainly be a demand for hydrogen storage beyond mobile applications.

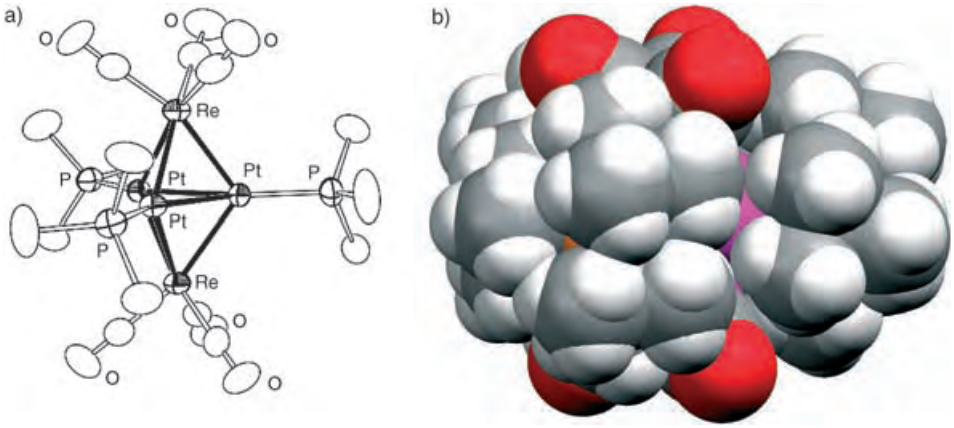


Figure 1. The structure of **1**; a) ORTEP plot, b) space-filling model.

Science follows trends, and not so long ago molecular clusters were in vogue, not just because of their fascinating structures, but also because of their potential to revolutionize catalysis and exhibit novel material properties. While the sheer quantity of publications in this area has certainly decreased from the heights of the late 1980s, fascinating new discoveries continue to be made. Notable synthetic develop-

 © 2005 Wiley-VCH Verlag GmbH & Co. KGaA, Weinheim

ments in cluster chemistry include the isolation of a nanosized, three-shelled spherical Pd_{145} cluster;[20] giant polyoxomolybdate wheels,[21] a spectacular, protein-sized Mo_{368} "nanohedgehog",[22] and the exotic inorganic fullerenes $[P_{60}(FeCp^*)_{12}Cu_{25}Cl_{25}(MeCN)_{10}]$[23] ($Cp^* = C_5Me_5$) and $[As@Ni_{12}@As_{20}]^{3-}$.[24] In addition, the employment of clusters as precursors to well defined supported nanoparticles has been elegantly demonstrated.[25] Indeed, part of the renaissance in molecular-cluster chemistry has been driven by the development of nanotechnology; the emphasis in this area of research is on objects whose size is between 0.1 to 100 nm, and the larger molecular clusters fit firmly into the lower end of this range. While nanotechnology is now in fashion, on a scale that molecular clusters never witnessed (metaphorically and in terms of absolute size), in many ways the aspirations remain the same, that is, catalysis, material science, but also in diagnostics and medicine. However, potential biomedical applications of clusters have also been recognized,[26] and it is not unreasonable to assume that as miniaturization continues, a natural regression in size may well mean that clusters fulfill their initial promise in an unexpected context.

It will certainly be interesting to see what Adams and Captain can do with their nascent discovery. The palladium analogue is an obvious target, given that the chemistry of $[Pd(PtBu_3)_2]$ appears to parallel the platinum analogue. The ability of palladium metal to behave as a hydrogen sponge provides further impetus. The cluster **1** uptakes about 75 times its volume of H_2 (about 10% of the efficiency of palladium metal at a stoichiometry of $PdH_{0.6}$, though much of this difference is due to the higher density of Pd—the % hydrogen by weight is 0.33% for **1** compared to 0.56% for $PdH_{0.6}$), and finding a way of making this process reversible will be a key advance. The trigonal bipyramidal cluster **1** should be able to accommodate a further two equivalents of H_2 and still give a satisfactory electron count (and indeed, Adams and Captain found **1** has five low-lying unoccupied molecular orbitals of which three are filled on formation of **2**). Whether the space is available for these four hydride ligands is less obvious—certainly three could occupy the remaining unbridged M–M edges, but the likely position of a fourth is not immediately clear. However, studies by Weller et al. have shown that octahedral rhodium clusters (12 M–M bonds) can possess up to 16 hydride ligands[27] so the possibility of having more hydrogen atoms than edges is certainly feasible. Clusters rich in hydrogen with both terminal and bridging hydride ligands are also known.[17] In such cases, neutron diffraction studies to discern the exact locations of the hydride ligands are desirable. Many questions can be asked about the chemistry of a cluster as unsaturated as **1**. For example, is the oxidative addition of substrates other than hydrogen possible? It is possible to imagine, for example, the oxidative addition or association of different substrates onto the cluster framework followed by recombination in new and different ways to those possible with existing systems.

Published online: August 18, 2005

[1] *Metal Clusters in Chemistry* (Eds.: P. Braunstein, L. A. Oro, P. R. Raithby), Wiley, New York, **1999**.

[2] D. H. Farrar, A. J. Poe, Y. Zheng, *J. Am. Chem. Soc.* **1994**, *116*, 6252.

[3] a) For a recent example demonstrating such a process see, D. Blazina, S. B. Duckett, P. J. Dyson, J. A. B. Lohman, *Chem. Eur. J.* **2003**, *9*, 1045; b) B. F. G. Johnson, J. S. McIndoe, *Coord. Chem. Rev.* **2000**, *200–202*, 901.

[4] D. M. P. Mingos, *Inorg. Chem.* **1985**, *24*, 114.

[5] H. G. Ang, B. Chang, W. L. Kwik, *J. Chem. Soc. Dalton Trans.* **1992**, 2161.

[6] C. Couture, D. H. Farrar, *J. Chem. Soc. Dalton Trans.* **1986**, 1395.

[7] M. S. Paquette, L. F. Dahl, *J. Am. Chem. Soc.* **1980**, *102*, 6621.

[8] R. J. Goodfellow, E. M. Hamon, J. A. K. Howard, J. L. Spencer, D. G. Turner, *J. Chem. Soc. Chem. Commun.* **1984**, 1604.

[9] M. J. Ingleson, M. F. Mahon, P. R. Raithby, A. S. Weller, *J. Am. Chem. Soc.* **2004**, *126*, 4784.

[10] P. J. Dyson, J. S. McIndoe, *Angew. Chem.* **2004**, *116*, 6152; *Angew. Chem. Int. Ed.* **2004**, *43*, 6028.

[11] R. D. Adams, B. Captain, *Angew. Chem.* **2005**, *117*, 2587; *Angew. Chem. Int. Ed.* **2005**, *44*, 2531.

[12] a) R. D. Adams, B. Captain, W. Fu, M. D. Smith, *J. Am. Chem. Soc.* **2002**, *124*, 5628; b) R. D. Adams, B. Captain, W. Fu, M. B. Hall, J. Manson, M. D. Smith, C. E. Webster, *J. Am. Chem. Soc.* **2004**, *126*, 5253.

[13] R. D. Adams, B. Captain, W. Fu, P. J. Pellechia, M. D. Smith, *Inorg. Chem.* **2003**, *42*, 2094.

[14] R. D. Adams, B. Captain, P. J. Pellechia, M. D. Smith, *Inorg. Chem.* **2004**, *43*, 3921.

[15] R. D. Adams, B. Captain, M. B. Hall, J. L. Smith, Jr., C. E. Webster, *J. Am. Chem. Soc.* **2005**, *127*, 1007.

[16] J. M. Bemis, L. F. Dahl, *J. Am. Chem. Soc.* **1997**, *119*, 4545.

[17] P. W. Frost, J. A. K. Howard, J. L. Spencer, D. G. Turner, *J. Chem. Soc. Chem. Commun.* **1981**, 1104.

[18] United States Department of Energy, Hydrogen Posture Plan, February **2004**. Online: http://www.eere.energy.gov/hydrogenandfuelcells/pdfs/hydrogen_posture_plan.pdf (accessed April 2005). Interim targets of 6% by 2010 and 9% by 2015.

[19] A. D. Lueking, R. T. Yang, *Appl. Catal. A* **2004**, *265*, 259.

[20] N. T. Tran, D. R. Powell, L. F. Dahl, *Angew. Chem.* **2000**, *112*, 4287; *Angew. Chem. Int. Ed.* **2000**, *39*, 4121.

[21] A. Müller, C. Serain, *Acc. Chem. Res.* **2000**, *33*, 2.

[22] A. Müller, E. Beckmann, H. Bögge, M. Schmidtmann, A. Dress, *Angew. Chem.* **2002**, *114*, 1210; *Angew. Chem. Int. Ed.* **2002**, *41*, 1162.

[23] J. Bai, A. V. Virovets, M. Scheer, *Science* **2003**, *300*, 781.

[24] M. J. Moses, J. C. Fettinger, B. W. Eichhorn, *Science* **2003**, *300*, 778.

[25] For example see, a) F. Schweyer-Tihay, P. Braunstein, C. Estournes, J. L. Guille, B. Lebeau, J. L. Paillaud, M. Richard-Plouet, J. Rose, *Chem. Mater.* **2003**, *15*, 57; b) J. M. Thomas, B. F. G. Johnson, R. Raja, G. Sankar, M. A. Midgley, *Acc. Chem. Res.* **2003**, *36*, 20.

[26] Several examples are described in, C. S. Allardyce, A. Dorcier, C. Scolaro, P. J. Dyson, *Appl. Organomet. Chem.* **2005**, *19*, 1.

[27] S. K. Brayshaw, M. Ingleson, J. C. Green, P. R. Raithby, G. Kociok-Köhn, J. S. McIndoe, A. S. Weller, *Angew. Chem.* **2005**, *117*; *Angew. Chem. Int. Ed.* **2005**, *44*, in press.

 © 2005 Wiley-VCH Verlag GmbH & Co. KGaA, Weinheim

Asymmetric Amplification

DOI: 10.1002/anie.200501742

New Aspects of Soai's Asymmetric Autocatalysis

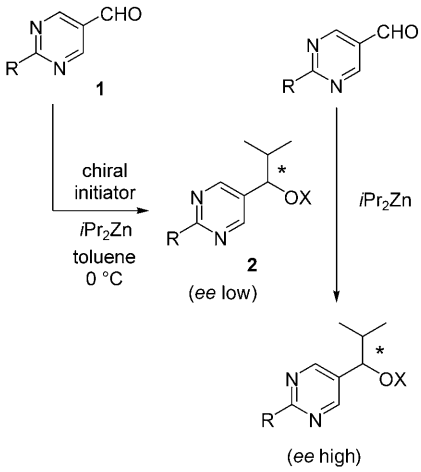
Joachim Podlech and Timo Gehring*

Keywords:
asymmetric amplification · asymmetric photolysis · autocatalysis · nonlinear effects · zinc

The origin of the homochirality of biomolecules (e.g., amino acids and carbohydrates) is still puzzling. While mechanisms have been found for the formation of enantiomerically enriched biomolecules without the help of enzymes or other chiral biocatalysts, it is still not clear how these generally small enantiomeric excesses could have been amplified under prebiotic conditions.[1] In this context, an example of asymmetric autocatalysis reported by Soai and co-workers in 1990[2] has found ongoing interest. Though was featured in a Highlight back in 1996,[3] significant and stunning improvements since then justify an updated treatise.

In Soai's example heteroaromatic carbaldehydes react with organozinc compounds, and the product serves as an asymmetric catalyst for its own formation (Scheme 1). Soai and co-workers tested a plethora of substrates, and the best results were obtained with 2-(*tert*-butylethynyl)pyrimidine-5-carbaldehyde (**1**).[4] Addition of diisopropylzinc in toluene or cumene at 0 °C led to the nonracemic secondary alcohol **2** even when no source of chirality had been added (15–91 % *ee*). In a series of runs the sense of rotation in the product was randomly distributed.[5]

Similar results were obtained by Singleton et al., but in some experiments they observed a nonrandom distribution of enantiomers even without any chiral inductor added.[6] This has been explained by trace amounts of optically active impurities present but not detectable in the solvents.



Scheme 1. Asymmetric autocatalysis in the formation of secondary alcohols. R = C≡C*t*Bu; X = H, Zn*i*Pr.

Even higher enantioselectivities were obtained when a small amount of product with a small enantiomeric excess was added. Addition of the *S* alcohol **2** (0.8 % with ≈0.00005 % *ee*) led to product **2** with 57 % *ee* (*S* configuration).[7]

Soai et al. observed that not only the product itself but also other chiral sources can be used to induce high selectivities (Figure 1). These chiral sources initiated the formation of product with a small enantiomeric excess, which promoted the faster and more selective formation of further product. Almost every imaginable chiral source has been tested over the last decade:[5] compounds with chiral centers, including chiral alcohols, amines, epoxides, carboxylic esters, and amino acids can be used as chiral initiators. Even an almost negligible asymmetry, as in (*S*)-α-deuterobenzyl alcohol (0.02–0.05 mol %, >95 % *ee*), is sufficient to produce the *R* product with 95 % *ee*.[8]

Furthermore, compounds with planes of chirality (e.g., substituted [2.2]paracyclophanes), with axes of chirality (e.g., [5]- and [6]helicenes and allenes), chiral complexes (K-[Co(edta)·2H$_2$O], edta = ethylenediaminetetraacetate), and crystals with enantiomorphous faces (e.g., sodium chlorate and quartz) were also applicable. The latter used as *d* quartz led to an *S* product with 80–90 % *ee*; *l* quartz

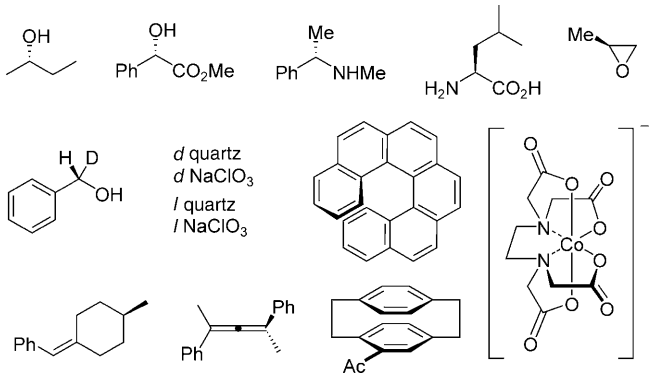


Figure 1. A selection of chiral initiators used in the Soai reaction.[5]

[*] Prof. Dr. J. Podlech, T. Gehring
Institut für Organische Chemie
Universität Karlsruhe (TH)
Fritz-Haber-Weg 6
76131 Karlsruhe (Germany)
Fax: (+49) 721-608-7652
E-mail: joachim.podlech@ioc.uka.de

InterScience
© 2005 Wiley-VCH Verlag GmbH & Co. KGaA, Weinheim

resulted in 84–89% *ee* *R* product.[9] The enantiopurity of product **2** was even higher when the product of a first run was used as catalyst in a second run. Usually after three consecutive runs, the product was obtained with >99.5% *ee*.

A recent publication by Soai et al. describes an especially interesting two-step protocol.[10] A minimal enantiomeric excess (estimated to be about 0.005% *ee*) of the standard product was obtained by asymmetric photolysis of racemic alcohol **2** with *r* circularly polarized UV light. The resulting actually nonracemic alcohol **2** (the authors use the term "cryptochiral" for a non-detectable deviation from the racemate) was used as a catalyst (1%) in the standard reaction to yield the *R* product **2** with 65% *ee*. This result is especially interesting since the enantiomeric excesses of amino acids in meteorites were attributed to a similar photolysis. These amino acids might have been a source for nonracemic organic material in the prebiotic era.[11]

Although the principle of asymmetric autocatalysis is very simple, functional examples are scarce, if not restricted to Soai's system.[5] Autocatalysis occurs when a chiral product acts as a catalyst for its own formation (Figure 2). Nevertheless, the mechanism of the Soai reaction is still not completely understood. The kinetic models presented in literature[12–14,17] considering the formation of catalytically active dimers or higher oligomers[14] are in line with the experimental data, but experimental proof of these proposed intermediates is lacking.

It is obvious that the reaction has to be significantly faster in the presence of the catalyst. But the mechanism for asymmetric autocatalysis should include both the catalysis of the formation of one enantiomer and an inhibition of the generation of the other enantiomer. This inhibition might be possible through removal of the catalyst's minor enantiomer by formation of inactive heterodimers $(R)\cdot(S)$ (or higher oligomers). Similar nonlinear effects have been discussed for dialkylzinc additions in the presence of nonracemic amino alcohols first described by the groups of Noyori[15] and Kagan.[16]

The Soai reaction was obviously not a prebiotic process since the reaction conditions (utilization of highly hygroscopic organometallic compounds) are not very likely in the primordial broth. Nevertheless, one might think of other reactions with greater biological relevance proceeding by means of similar mechanisms. The chemical community is looking forward to further examples of this fascinating type of reaction.

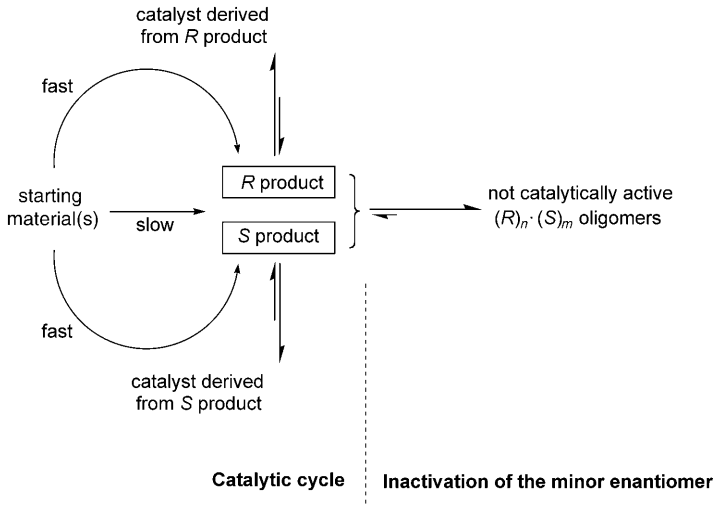


Figure 2. General scheme for asymmetric autocatalysis.

Published online: August 3, 2005

[1] J. Podlech, *Cell. Mol. Life Sci.* **2001**, *58*, 44–60; B. L. Feringa, R. A. van Delden, *Angew. Chem.* **1999**, *111*, 3624–3645; *Angew. Chem. Int. Ed.* **1999**, *38*, 3418–3438.

[2] K. Soai, S. Niwa, H. Hori, *J. Chem. Soc. Chem. Commun.* **1990**, 982–983.

[3] C. Bolm, F. Bienewald, A. Seger, *Angew. Chem.* **1996**, *108*, 1767–1769; *Angew. Chem. Int. Ed. Engl.* **1996**, *35*, 1657–1659.

[4] T. Shibata, S. Yonekubo, K. Soai, *Angew. Chem.* **1999**, *111*, 746–748; *Angew. Chem. Int. Ed.* **1999**, *38*, 659–661.

[5] K. Soai, T. Shibata, I. Sato, *Bull. Chem. Soc. Jpn.* **2004**, *77*, 1063–1073.

[6] D. A. Singleton, L. K. Vo, *J. Am. Chem. Soc.* **2002**, *124*, 10010–10011; D. A. Singleton, L. K. Vo, *Org. Lett.* **2003**, *5*, 4337–4339.

[7] I. Sato, H. Urabe, S. Ishiguro, T. Shibata, K. Soai, *Angew. Chem.* **2003**, *115*, 329–331; *Angew. Chem. Int. Ed.* **2003**, *42*, 315–317.

[8] I. Sato, D. Omiya, T. Saito, K. Soai, *J. Am. Chem. Soc.* **2000**, *122*, 11739–11740.

[9] K. Soai, S. Osanai, K. Kadowaki, S. Yonekubo, T. Shibata, I. Sato, *J. Am. Chem. Soc.* **1999**, *121*, 11235–11236.

[10] T. Kawasaki, M. Sato, S. Ishiguro, T. Saito, Y. Morishita, I. Sato, H. Nishino, Y. Inoue, K. Soai, *J. Am. Chem. Soc.* **2005**, *127*, 3274–3275.

[11] J. Podlech, *Angew. Chem.* **1999**, *111*, 501–502; *Angew. Chem. Int. Ed.* **1999**, *38*, 477–478.

[12] I. Sato, D. Omiya, H. Igarashi, K. Kato, Y. Ogi, K. Tsukiyama, K. Soai, *Tetrahedron: Asymmetry* **2003**, *14*, 975–979.

[13] T. Buhse, *Tetrahedron: Asymmetry* **2003**, *14*, 1055–1061.

[14] D. G. Blackmond, *Proc. Natl. Acad. Sci. USA* **2004**, *101*, 5732–5736.

[15] M. Kitamura, S. Okada, S. Suga, R. Noyori, *J. Am. Chem. Soc.* **1989**, *111*, 4028–4036.

[16] C. Girard, H. B. Kagan, *Angew. Chem.* **1998**, *110*, 3088–3127; *Angew. Chem. Int. Ed.* **1998**, *37*, 2922–2959.

[17] I. D. Gridnev, J. M. Serafimov, J. M. Brown, *Angew. Chem.* **2004**, *116*, 4992–4995; *Angew. Chem. Int. Ed.* **2004**, *43*, 4884–4887.

© 2005 Wiley-VCH Verlag GmbH & Co. KGaA, Weinheim

Reactive Intermediates

DOI: 10.1002/anie.200500098

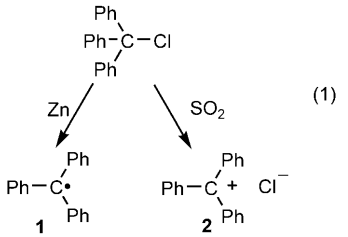
The First Century of Ketenes (1905–2005): The Birth of a Versatile Family of Reactive Intermediates**

*Thomas T. Tidwell**

Keywords:
cycloaddition · history of chemistry · ketenes · reactive intermediates · Wolff rearrangement

Discovery

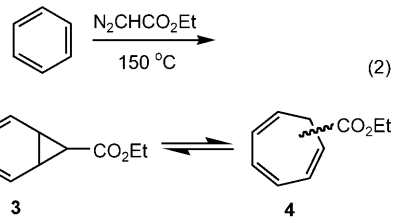
Organic reactive intermediates[1] are the species involved in multistep organic reactions, and the beginning of the 20th century saw convincing experimental evidence for these entities become available. The discovery by Gomberg in 1900 that triphenylmethyl chloride and zinc formed the stable triphenylmethyl radical (**1**) [Eq. (1)],[2] was widely noted, and Gomberg narrowly missed the award of the Nobel prize for his discovery.[2c] This was quickly followed in 1901 by the demonstration that triphenylmethyl chloride in an ionizing solvent also formed the triphenylmethyl cation **2** [Eq. (1)].[3]



(1)

A carbanion intermediate was suggested by Clarke and Lapworth in 1907 to occur in the benzoin condensation,[4a] and the conversion of **1** or triphenylmethyl chloride with sodium into triphenylmethylsodium was demonstrated in 1914 by Schlenk and Marcus, who studied the ion pairing of the intermediate by measuring the conductivity.[4b] The name carbanion was coined by Wallis and Adams in 1933.[4c]

The intervention of carbenes was inferred to explain the Buchner reaction [Eq. (2)][5a–d] and analogous reactions of diazomethane.[5e] Many examples of stable carbocations, carbanions, and carbon-centered free radicals have been isolated, as have carbenes,[5f,g] which formerly seemed the most unruly of the reactive intermediates.



(2)

These findings combined with an emerging understanding of the theory of organic chemistry incorporating reaction kinetics and stereochemical and structural studies created what came to be known as physical organic chemistry. After decades of work, argument, and controversy the pivotal role of reactive intermediates was well recognized by 1940, marked by the text "Physical Organic Chemistry" by Hammett.[6] As pointed out by Leffler in 1956[1a] reactive intermediates in reactions were assumed "which have not been isolable for direct experimental study" but whose existence could be inferred by comparison to observable species "of the same type as the hypothetical intermediate" and which "have a great variety of degrees of stability, depending upon their structures. The extrapolation to the properties of the hypothetical intermediate is therefore a continuous one." Now with vastly improved methodology many formerly hypothetical intermediates have been observed directly, and even isolated. There are still hold-outs which are too short-lived for observation, or whose preparation has eluded the synthetic skills of the investigators, and these provide a continuing challenge.

Diphenylketene

In 1903 a young instructor (Unterrichts-Assistent) Hermann Staudinger joined the laboratory of Thiele at the Kaiser-Wilhelms-Universität of Strassburg (Strasbourg in French) in the Alsace.[7a] Strasbourg occupies a strategic position on the Rhine River on the border between Germany and France and over the centuries has been part of one or the other, depending on the political and military situation. After the Franco-Prussian war of 1870–1871 it had become part of the new Germany, and the University was endowed with an imposing chemical laboratory (Figure 1), which still stands.[7b] The University is now a prominent center of chemistry in France, the Université Louis Pasteur.

In 1905 Staudinger reported the discovery of the first example of an

[*] T. T. Tidwell
Department of Chemistry
University of Toronto
Toronto, Ontario M5S 3H6 (Canada)
Fax: (+1) 416-978-3585
E-mail: ttidwell@chem.utoronto.ca

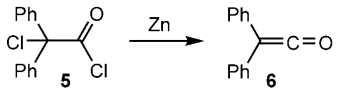
[**] Professor P. Federlin is thanked for helpful comments and a copy of Ref. [7b]. The assistance of Annette Allen, Professor Jean-Marie Lehn, and Dr. Valerij Nikolaev is gratefully acknowledged, as is financial support by the Natural Sciences and Engineering Research Council of Canada, the Petroleum Research Fund administered by the American Chemical Society, and a Killam Fellowship from the Canada Council for the Arts.

InterScience
© 2005 Wiley-VCH Verlag GmbH & Co. KGaA, Weinheim



Figure 1. Chemical laboratory at the University of Strasbourg, around 1960.
Courtesy of Professor Jean-Marie Lehn.

unexpected new family of reactive intermediates, diphenylketene (**6**).[8a] As described later by Staudinger in his scientific autobiography[8b] he was inspired by the work of Gomberg to attempt the preparation of new free radicals. He examined the reaction of α-chlorodiphenylacetyl chloride (**5**) with zinc and was rewarded with the isolation of **6**, the first demonstrated example of these highly reactive organic compounds [Eq. (3)]. Diphenylketene (**6**)



(3)

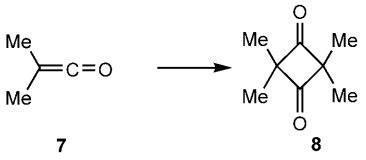
was obtained as a low-melting-point solid, and so the identity of this species was secure, although ketenes are in general highly reactive, and the existence of some examples is still in doubt.

Staudinger seized the opportunity and pursued the study of ketenes for the next 20 years (Figure 2), after which he



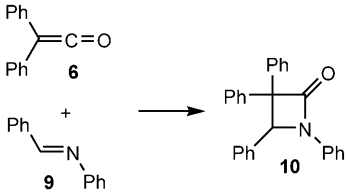
Figure 2. Hermann Staudinger (1881–1965).
Courtesy of the GDCh (Gesellschaft Deutscher Chemiker (German Chemical Society)).

devoted himself fulltime to the exploration of polymer chemistry, for which he won the Nobel Prize in 1953. Within two years of the initial discovery dimethylketene (**7**) had also been prepared and found to undergo [2+2] dimerization to give the symmetrical cyclobutanedione **8** [Eq. (4)],[9a] and **6** was found to



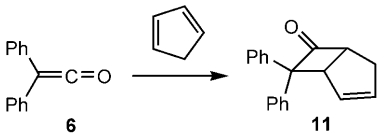
(4)

participate in cycloadditions with the imine **9** to form β-lactam **10** (Staudinger reaction) [Eq. (5)] and with carbonyl



(5)

compounds to form reactive β-lactones.[9b] The reaction of **6** with cyclopentadiene gave a product[9b] that was later proven to be the [2+2] cycloaddition adduct **11** [Eq. (6)]. These discov-

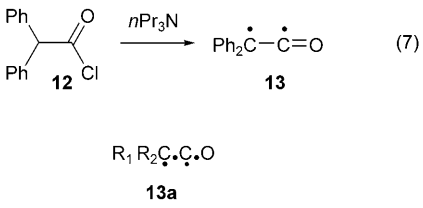


(6)

eries were made two decades before the development of the Diels–Alder reaction, and are still mainstays of synthetic organic chemistry. Cycloadditions have remained the most distinctive, useful, and intellectually stimulating aspect of ketene chemistry.

Staudinger, Wedekind, or Wolff

The discovery by Staudinger had, however, been foreshadowed by the investigations of Wedekind, who in 1901 at the University of Tübingen reacted diphenylacetyl chloride (**12**) with nPr$_3$N, and noted the formation of nPr$_3$NHCl. He proposed the formation of the intermediate **13** (this was represented as **13a**) [Eq. (7)], which appears equivalent to ketene **6** but was not isolated or characterized.[10a] Wedekind wrote "Herewith is made the hypothesis,



(7)

that the atomic grouping $(R_1.R_2).C_2O.$ is temporarily capable of existence in solution."[10a] This was 15 years before the proposal of the electron pair bond by Lewis, but the idea of the tetravalence of carbon was well established. However, in the next year Wedekind was more equivocal about the existence of the ketene.[10b] This work was known to Staudinger and frequently acknowledged by him,[8a] but Wedekind missed his chance to be recognized as the discoverer of ketenes. He worked in this area for a decade, but there is no mention of this research in his obituary.[10c,d]

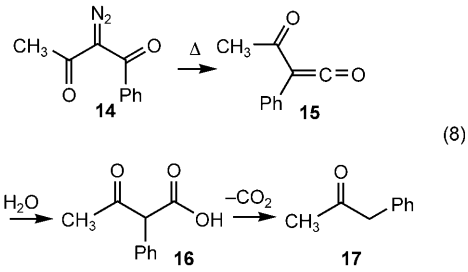
Ketenes had also been generated by a completely different route by Ludwig Wolff (Figure 3) at the University of



Figure 3. Ludwig Wolff (1857–1919).
Courtesy of the GDCh.

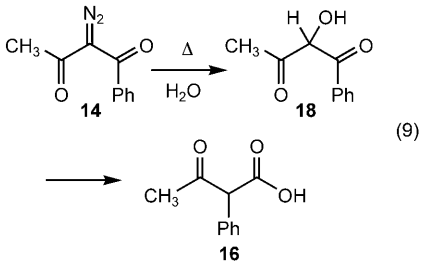
Jena in 1902, by a reaction that became known as the Wolff rearrangement.[11] This involved heating the diazo ketone **14** (formulated at that time as having a cyclic structure) at refux in water to form the ketene **15**. The latter led to the unobserved acid **16**, which underwent decarboxylation to give **17** [Eq. (8)].[11a] Wolff recognized that rearrangement had occurred and that the acid **16** was a key intermediate. But rather than assuming ketene formation, he pro-

© 2005 Wiley-VCH Verlag GmbH & Co. KGaA, Weinheim



(8)

posed that the addition of water occurred to give **18**, which underwent a double migration to form **16**, and cited the analogy of the pinacol and benzilic acid rearrangements [Eq (9)].[11a] The



(9)

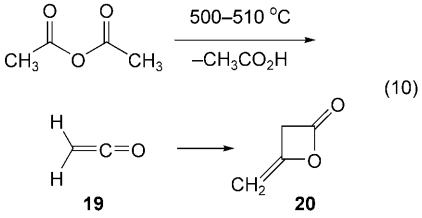
proposal of a ketene intermediate in the reaction was made by Schröter in 1909, after ketenes had become well-recognized intermediates.[11c] This reaction was adapted as the Arndt–Eistert reaction for chain elongation, with a proposal for a carbene intermediate,[11d] and was developed for photochemical ketene generation by Horner.[11e,f] The photochemical version of the reaction is particularly valuable for the study of reactive intermediates, as highly reactive ketenes can be generated in various media from the reasonably stable diazo ketones. Addition of water to the ketenes gives observable acid enols as further observable reactive intermediates, which then form the carboxylic acids.

Why is Staudinger and not Wedekind or Wolff credited with the discovery of ketenes? Recognition of priority for discoveries is of intense interest to scientists, but there is no apparent record of dispute between Staudinger, Wedekind, and Wolff. Staudinger was a highly prolific investigator, and with more than 50 papers and a book on ketenes[12a] following his 1905 work in rapid order, his position as the founder of ketene studies has not been challenged. The nature of chemical discovery has been discussed by Berson,[12b] and Staudinger's clear recognition of what he had discovered and extensive further study established him as the founder of the field. Wedekind had correctly identified the structure of the ketene as an unisolated reactive intermediate,[10a] but was not firm in his conviction and missed his opportunity.

Staudinger's further career in the tumultuous development of polymer chemistry, as well as his complex personal life and sometimes outspoken political views, have generated much comment.[12c–e] Wolff has the honor of two well-known named reactions, the Wolff-rearrangement and the Wolff–Kishner reaction, and can be satisfied that every student of organic chemistry still sees his name. Ironically Berson's comments on the need to recognize a discovery were directed at Fittig, Thiele's predecessor and Wolff's supervisor at Strassburg, who had discovered the rearrangement of pinacol with acid, but did not recognize what had occurred, and so the reaction is known as the pinacol rearrangement, an example of the broader class of Wagner–Meerwein rearrangement. As noted above Schröter was the first to formulate the ketene intermediate in the Wolff rearrangement,[11c] and by Berson's criterion Wolff does not deserve credit for the ketene discovery.[12b]

Ketene and Its Dimer: Wilsmore's Contribution

Staudinger was not alone for long in the study of ketenes, for in 1907 from a completely different perspective Wilsmore (Figure 4) prepared $CH_2=C=O$ (**19**) from the thermolysis of acetic anhydride or acetone with a hot platinum wire [Eq. (10)].[13a] The parent



(10)

ketene is a noxious and poisonous gas, and its preparation at University College (London) inspired "The Ketene



Figure 4. N. T. M. Wilsmore (1868–1940). Courtesy of Dr. Andrea Stella.

The Ketene Song

There is a new substance discovered
In a room that's just over the way.
—The inventor's assistant recovered,
Though it was a near squeak, doctors say—.
But though it is ages & ages
E'er the world saw as much as a grain,
Later on you will hear, say the sages,
Of keten again.

It has quite a good constitution
—C twice and H twice and an O—:
And even in weakest dilution
Of its presence you will very soon know.
For the smell of that simple creation
Will grasp at your nose & remain
And hours after you'll sneeze in iration
At ketene again.

It's a simple enough preparation.
You stick in acetic a wire
Which gives the required dehydration
When raised to a red heat or high'r.
Then out comes a torrent of gases
Bearing liquid along in their train:
When this you have trapped ere it passes,
You've keten again

When the O.L. in slumber reposes
And room No 7 is asleep
Dr. Wilsmore, as usual, proposes
To let loose the winds on the deep.
And the sleepers, awakened, grab vainly
After beakers that scatter like rain,
While A and B rage quite insanely
At ketene again.
S.

(A & B were two small research labs, and O. L. refers to the Organic Lab.)

© 2005 Wiley-VCH Verlag GmbH & Co. KGaA, Weinheim

Song", perhaps sung at the occasion of a departmental party.[13b]

Staudinger and Klever shortly thereafter reported the preparation of ketene by the zinc debromination of bromoacetyl bromide.[13c] There was a brisk dispute between Staudinger and Wilsmore as to the priority for this discovery as well as to the purity of Wilsmore's sample of ketene and whether it had the formula $CH_2{=}C{=}O$ or $HC{\equiv}COH$, another possibility noted by Wilsmore. This was resolved in favor Wilsmore and the ketene structure.[13d,e]

The development of ketene chemistry has been bedeviled with controversy, most prominently with the structure of ketene dimer **20** [Eq. (10)], originally suggested by Wilsmore in 1908[14a] to have the acetylketene structure $CH_3COCH{=}C{=}O$. This debate lasted for more than 40 years, and elicited the comment from one worker in the field "The extraordinary chemical behavior of the ketene dimers has lent exceptional interest to that class of substances, and the controversy which has raged for decades over the structures of the compounds is without parallel in the study of small molecules."[14b] This was finally settled definitively by chemical investigations,[14c] electron diffraction,[14d] and X-ray diffraction.[14e] The continual dispute regarding the chemistry of ketenes may be attributed to their extraordinary reactivity and unique structures.

Hurd (Figure 5) was active in the discussion of the structure of diketene, and carried out many studies in ketene chemistry.[15] He modified Wilsmore's procedure for ketene preparation by



Figure 5. Charles D. Hurd (1899–1997). Courtesy of Northwestern University.

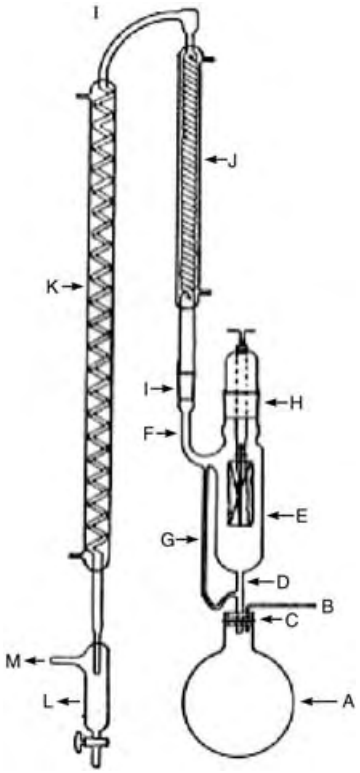


Figure 6. Hurd lamp for ketene preparation (reproduced from Ref. [15e] with the permission of the American Chemical Society).

pyrolysis of acetone with the widely used apparatus known as the "Hurd lamp" (Figure 6).[15e] This method was also used for the industrial preparation of ketene for conversion into acetic anhydride.

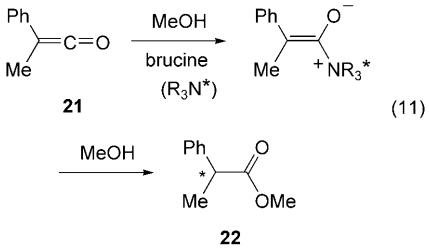
Asymmetric Reactions

Additions of nucleophiles to unsymmetrical ketenes generate new stereogenic centers, and this led to a long-lasting interest in steroselective reactions of ketenes. In an early study of asymmetric synthesis Richard Weiss at the University of Vienna treated phenyl(4-tolyl)ketene with the optically active alcohol menthol, and after saponification claimed to have obtained an acid with optical activity.[16a] The chirality of the acid arises from the different aryl groups in $Ph(4\text{-}Tol)CHCO_2H$, and the claim that this compound exhibited significant optical activity was improbable and was eventually disproven.[16b,c] Even though this initial effort was not successful, the idea was to prove fruitful, and was later developed by Pracejus (Figure 7) at the University of Rostock



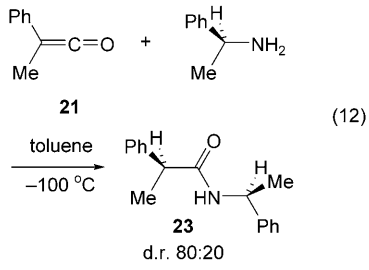
Figure 7. Horst Pracejus (1927–1987). Courtesy of Professor Matthias Beller, Universität Rostock.

into a practical reaction for aryl(alkyl)ketenes. Pracejus observed significant stereoselectivity in the addition of methanol to phenyl(methyl)ketene (**21**) catalyzed by the chiral base brucine to



form **22** [Eq. (11)]. Ester **22** is a precursor of α-arylalkanoic acids, which are of major pharmaceutical importance.[16d,e] The Gesellschaft Deutscher Chemiker (German Chemical Society) established the Horst Pracejus Prize for advancement of research in chirality in his honor, first awarded in 1999.

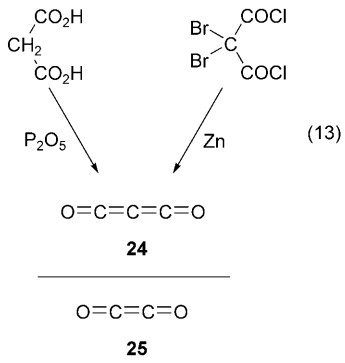
Stereoselective addition of chiral amines to aryl(alkyl)ketenes was also studied by Pracejus,[16f] and reaction of phenyl(methyl)ketene (**21**) with (*S*)-1-phenylethylamine in toluene at −100 °C gave the chiral amide (*S*,*S*)-**23** [Eq. (12)].[16f]



© 2005 Wiley-VCH Verlag GmbH & Co. KGaA, Weinheim

Bisketenes

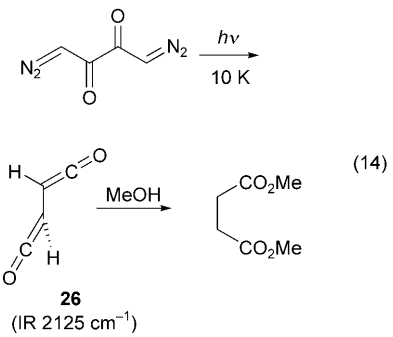
Many types of ketenes have been made, including bisketenes,[17a] that bear two ketene groupings in the same molecule. The first example, carbon suboxide (**24**) was prepared in 1906 by Diels and Wolf by the dehydration of malonic acid [Eq. (13)],[17b] and then in 1908 by



(13)

Staudinger and Bereza by dehalogenation [Eq. (13)].[17c] However, the isolation of further bisketenes proved difficult, and the simplest example, the carbon monoxide dimer **25**, has been the object of continuing theoretical[17d,e] and experimental[17f] examination. Although an energy minimum structure for this molecule has been calculated,[17f] it is still unknown experimentally. It was concluded that this species is an intrinsically short-lived molecule that would rapidly dissociate to CO within a few nanoseconds.[17f]

Staudinger made a sustained effort to prepare other bisketenes, but was unsuccessful in efforts to obtain the linear α,ω-bisketenes, including the 1,2-bisketene **26**.[9b,12a,18a] This was eventually observed in 1982 when it was formed by a double Wolff rearrangement of bis(diazo ketone) in an argon matrix at 10 K. The species was identified by the IR absorption at 2125 cm^{-1}

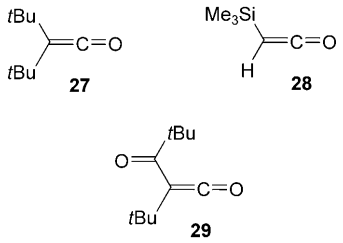


(14)

and its conversion into the diester with methanol [Eq. (14)].[18b] Surprisingly, such 1,2-bisketenes were shown by computational studies and confirmed by X-ray crystal-structure determination to have twisted, almost perpendicular conformations instead of the typical coplanar structures of 1,3-butadienes.[18c,d]

Substituent Effects

Among the distinctive characteristics of ketenes are their propensity for dimerization and their sensitivity towards hydration, but a notable exception is di-*tert*-butylketene (**27**). This ketene, which was prepared in the



laboratory of Newman (Figure 8) at Ohio State University in 1960,[19a] is



Figure 8. Melvin Newman (1908–1993). Courtesy of Professor J. D. Roberts.

protected by its bulky substituents. Another exception is trimethylsilylketene (**28**), discovered by Shchukovskaya, Pal'chik, and Lazarev in 1965 in Leningrad (now St. Petersburg; Russia) (Figures 9 and 10).[19b,c] Neither of these ketenes is known to dimerize,[19a,b] and both are much less reactive towards



Figure 9. Lidiya L. Shchukovskaya (1926–2002). Courtesy of Dr. Valerij Nikolaev, St. Petersburg State University.



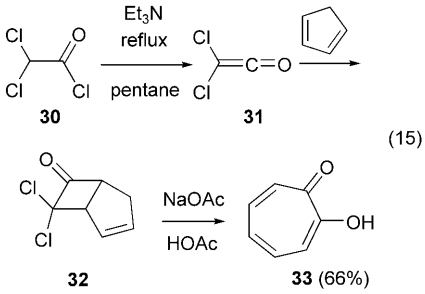
Figure 10. Adrian N. Lazarev (1928–1993). Courtesy of Dr. Valerij Nikolaev, St. Petersburg State University.

water than CH_2=C=O. The stabilization by the trimethylsilyl group in **28** is due to the β-silicon effect and the general tendency of ketenes to be stabilized by electropositive groups through electron donation from ketenyl C–M σ bonds to the in-plane carbonyl π orbital.[19d] The first acylketene was EtO_2CCEt=C=O, also discovered by Staudinger in 1909,[19e] which was only stable at −80 °C, while the crowded example **29**, first prepared in 1978 in Leningrad, appeared to be stable indefinitely as a neat liquid.[19f]

Just as ketenes are stabilized by electropositive groups they are destabilized by electronegative groups. Thus halo ketenes are highly reactive, and despite early efforts directed toward their preparation,[20a–c] were unknown until 1965–1966, when their formation as unobserved intermediates was reported from three different laboratories.[20d–f] Dichloroketene (**31**) was prepared by

 © 2005 Wiley-VCH Verlag GmbH & Co. KGaA, Weinheim

the dehydrochlorination of dichloroacetyl chloride (**30**), and trapped with cyclopentadiene by [2+2] cycloaddition to form bicyclo[3.2.0]pent-2-ene-6-one **32** [Eq. (15)].[20d] Hydrolysis of **32** is a



(15)

simple and efficient method for the preparation of tropolone (**33**) [Eq. (15)].[20d,g] Brady of the University of North Texas (Figure 11)[20e] was a leading pioneer in the development of haloketene chemistry, including fluoro, chloro, and bromo derivatives.



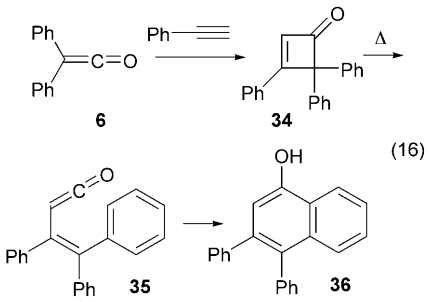
Figure 11. William T. Brady (*1933). Courtesy of Professor Brady.

Cycloadditions

Novel routes to ketenes were found by the reversal of cycloadditions, and these reactions have been extensively exploited in mechanistic studies and in the synthesis of complex molecules. Thus it was discovered by Smith (Figure 12) at the University of Minnesota that cyclobutenone **34**, obtained from [2+2] cycloaddition of diphenylketene with phenylacetylene, undergoes thermal ring opening to the alkenylketene **35**, which gives intramolecular [4+2] cycloaddition with the pendant phenyl group to form **36** (Smith–Hoehn reaction) [Eq. (16)].[21a] Barton (Figure 13) and Quinkert discovered the facile photochemical ring opening of cyclohexadienones to give dienylketenes (Barton–Quinkert reaction).[21b] This process has even been observed with the parent **37**, a tautomer of phenol generated at 77 K, to form **38** [Eq. (17)].[21c]



Figure 12. Lee Irvin Smith (1891–1973). Courtesy of the University of Minnesota.

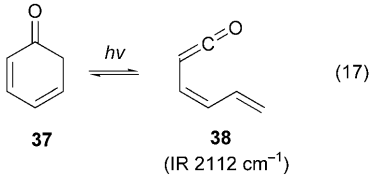


(16)



Figure 13. Derek H. R. Barton (1918–1998). Courtesy of Professor Harold Hart, Michigan State University.

The exquisite stereochemistry observed in the [2+2] cycloaddition of



(17)

ketenes was one of the cornerstones of the development of the rules of orbital symmetry by Woodward and Hoffmann,[22a] and the investigation of these reactions was pursued in many mechanistic studies, particularly by Huisgen (Figure 14) in München (Germany).[22b,c] One of the first examples of the [2+2] cycloaddition of a ketene with a carbon–



Figure 14. Rolf Huisgen (*1920). Courtesy of the Universität München.

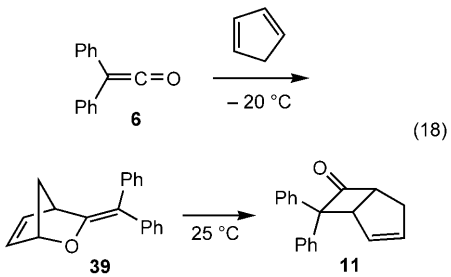
carbon double bond was the reaction of diphenylketene (**6**) with cyclopentadiene [Eq. (6)].[9b] Surprisingly it was found by Machiguchi (Figure 15) at Saitama University that the net [2+2]



Figure 15. Takahisa Machiguchi (*1940). Courtesy of Professor Machiguchi.

© 2005 Wiley-VCH Verlag GmbH & Co. KGaA, Weinheim

cycloaddition observed in this canonical process was not the initial reaction in the sequence, but that instead (as observed at low temperature) a [4+2] cycloaddition to carbonyl oxygen formed **39**, which upon warming underwent Claisen rearrangement to **11** [Eq. (18)].[22d]



(18)

Overview

Ketene chemistry in its first 100 years has been a microcosm of organic chemistry as a whole, with useful contributions in synthesis, theory, mechanisms, and practical applications. The major types of ketenes and their typical reactions as described above are now being increasingly applied in new and ingenious ways. Ketenes have always attracted many of the most talented individuals in chemistry, including many Nobel prize winners.[23] Ketenes have found many industrial applications, ranging from the seemingly mundane manufacture of acetic acid and acetic anhydride, to the widespread use of ketene dimers from fatty acids as coatings for paper,[24a] the sophisticated application of the Süs photochemical Wolff rearrangement[24b] for the manufacture of the integrated circuits used in computer chips,[24c,d] and the use of ketenes in the preparation of drug candidates. The unique structural features of ketenes and their high reactivity ensure the vitality of these species in their second century.

[1] Many books entitled as dealing with reactive intermediates have appeared between 1956[1a] and 2004:[1b] a) J. E. Leffler, *The Reactive Intermediates of Organic Chemistry*, Wiley-Interscience, New York, **1956**; b) *Reactive Intermediate Chemistry* (Eds.: R. A. Moss, M. S. Platz, M. Jones, Jr.), Wiley, Hoboken, NJ, **2004**.

[2] a) M. Gomberg, *Ber. Dtsch. Chem. Ges.* **1900**, *33*, 3150 – 3163; b) M. Gomberg, *J. Am. Chem. Soc.* **1900**, *22*, 757 – 771; c) L. Eberson, *Chem. Intell.* **2000**, *44–49*, 57; d) for the history of this discovery, see: J. M. McBride, *Tetrahedron* **1974**, *30*, 2009 – 2022; e) for a history of free radical chemistry in the 20th century, see: T. T. Tidwell, *Adv. Phys. Org. Chem.* **2001**, *36*, 1 – 58.

[3] a) F. Kehrmann, F. Wentzel, *Ber. Dtsch. Chem. Ges.* **1901**, *34*, 3815 – 3819; b) J. F. Norris, *Am. Chem. J.* **1901**, *25*, 54 – 62; c) for a history of carbocation chemistry, see: C. D. Nenitzescu in *Carbonium Ions, Vol. 1*, (Eds.: G. A. Olah, P. von R. Schleyer), Wiley-Interscience, New York, **1968**, pp. 1 – 75.

[4] a) R. W. L. Clarke, A. Lapworth, *J. Chem. Soc.* **1907**, *91*, 694 – 705; b) W. Schlenk, E. Marcus, *Ber. Dtsch. Chem. Ges.* **1914**, *47*, 1664 – 1687; c) E. S. Wallis, F. H. Adams, *J. Am. Chem. Soc.* **1933**, *55*, 3838 – 3851.

[5] a) E. Buchner, T. Curtius, *Ber. Dtsch. Chem. Ges.* **1885**, *18*, 2377 – 2379; b) E. Buchner, *Ber. Dtsch. Chem. Ges.* **1896**, *29*, 106 – 109; c) E. Buchner, S. Hediger, *Ber. Dtsch. Chem. Ges.* **1903**, *36*, 3502 – 3509; d) for an obituary of Eduard Buchner (1860–1917), see: *Ber. Dtsch. Chem. Ges.* **1917**, *50*, 1844 – 1876. Buchner was awarded the Nobel Prize in 1907 for studies of noncellular fermentation, and died in 1917 from wounds sustained in the war while serving in a field hospital. He also devised the ubiquitous Buchner funnel. e) H. Staudinger, O. Kupfer, *Ber. Dtsch. Chem. Ges.* **1912**, *45*, 501 – 509; f) W. Kirmse, *Angew. Chem.* **2004**, *116*, 1799 – 1801; *Angew. Chem. Int. Ed.* **2004**, *43*, 1767 – 1769; g) R. W. Alder, M. E. Blake, L. Chaker, J. N. Harvey, F. Paolini, J. Schuetz, *Angew. Chem.* **2004**, *116*, 6020 – 6036; *Angew. Chem. Int. Ed.* **2004**, *43*, 5896 – 5911.

[6] L. P. Hammett, *Physical Organic Chemistry*, Wiley, New York, **1940**.

[7] a) Staudinger recounted[8b] that he went to Strassburg in the fall of 1903, but initially worked in the inorganic chemistry department of Kohlschütter; b) for a history of chemistry in the Alsace, see: P. Federlin, "La Chimie, une passion des scientifiques Strasbourgeios et Alsaciens" in *Les Sciences en Alsace 1538–1988*, Oberlin, Strasbourg, **1989**.

[8] a) H. Staudinger, *Ber. Dtsch. Chem. Ges.* **1905**, *38*, 1735 – 1739; b) H. Staudinger, *From Organic Chemistry to Macromolecules*, Wiley, New York, **1970**.

[9] a) H. Staudinger, H. Klever, *Ber. Dtsch. Chem. Ges.* **1906**, *39*, 968 – 971; b) H. Staudinger, *Justus Liebigs Ann. Chem.* **1907**, *356*, 51 – 123.

[10] a) "Hierbei ist die Voraussetzung gemacht, dass die Atomgruppirung $(R^1.R^2).C_2O$. vorübergehend in Lösung als solche existenzfähig ist.": E. Wedekind, *Ber. Dtsch. Chem. Ges.* **1901**, *34*, 2070 – 2077; b) E. Wedekind, *Justus Liebigs Ann. Chem.* **1902**, *323*, 246 – 257; c) In 1909, Wedekind succeeded Kohlschütter as professor in the inorganic chemistry department in Strassburg, where Staudinger had originally been associated: *Chem. Zeit.* **1930**, *54*, 90; d) for an obituary notice of Wedekind (1870–1938), see: *Ber. Dtsch. Chem. Ges. A* **1938**, *71*, 196 – 198.

[11] a) L. Wolff, *Justus Liebigs Ann. Chem.* **1902**, *325*, 129 – 195; b) for a review of the Wolff rearrangement, see: W. Kirmse, *Eur. J. Org. Chem.* **2002**, 2193 – 2256; c) G. Schröter, *Ber. Dtsch. Chem. Ges.* **1909**, *41*, 2336 – 2349; d) F. Arndt, B. Eistert, *Ber. Dtsch. Chem. Ges. A* **1935**, *68*, 200 – 208; e) L. Horner, E. Spiestchka, A. Gross, *Justus Liebigs Ann. Chem.* **1951**, *573*, 17 – 30; f) W. Kirmse, L. Horner, *Chem. Ber.* **1956**, *89*, 2759 – 2765; g) for an obituary notice of Wolff (1857–1919), see: *Ber. Dtsch. Chem. Ges. A* **1929**, *62*, 145 – 159; Wolff received his PhD at Strassburg in 1882 for work with Rudolf Fittig, and was Unterrichts-Assistent (teaching assistant) and Privat-Dozent (junior lecturer) there until 1891.

[12] a) H. Staudinger, *Die Ketene*, Enke, Stuttgart, **1912**; b) J. A. Berson, *Angew. Chem.* **2002**, *114*, 4848 – 4854; *Angew. Chem. Int. Ed.* **2002**, *41*, 4655 – 4659; c) H. Ringsdorf, *Angew. Chem.* **2004**, *116*, 1082 – 1095; *Angew. Chem. Int. Ed.* **2004**, *43*, 1064 – 1076; d) R. Mülhaupt, *Angew. Chem.* **2004**, *116*, 1072 – 1080; *Angew. Chem. Int. Ed.* **2004**, *43*, 1054 – 1063; e) Y. Furukawa, *Chem. Heritage*, **1993–1994**, *11*, 4 – 6.

[13] a) N. T. M. Wilsmore, *J. Chem. Soc.* **1907**, *91*, 1938 – 1941; b) due to A. W. Stewart, later professor in Belfast, and supplied by Professor Alwyn Davies, University College, London; c) H. Staudinger, H. Klever, *Ber. Dtsch. Chem. Ges.* **1908**, *41*, 594 – 600; d) N. T. M. Wilsmore, A. W. Stewart, *Ber. Dtsch. Chem. Ges.* **1908**, *41*, 1025 – 1027; e) H. Staudinger, H. Klever, *Ber. Dtsch. Chem. Ges.* **1908**, *41*, 1516 – 1517; f) for an obituary notice of N. T. M. Wilsmore (1868–1940), see: *J. Chem. Soc.* **1941**, 59 – 60

[14] a) F. Chick, N. T. M. Wilsmore, *J. Chem. Soc.* **1908**, *93*, 946 – 950; b) R. B. Woodward, G. Small, Jr., *J. Am. Chem. Soc.* **1950**, *72*, 1297 – 1304; c) J. R. Johnson, V. J. Shiner, Jr., *J. Am. Chem. Soc.* **1953**, *75*, 1350 – 1355; d) J. Bregman, S. H. Bauer, *J. Am. Chem. Soc.* **1955**, *77*,

 © 2005 Wiley-VCH Verlag GmbH & Co. KGaA, Weinheim

1955 – 1965; e) L. Katz, W. N. Lipscomb, *J. Org. Chem.* **1952**, *17*, 515 – 517.

[15] a) C. D. Hurd, P. D. Cochran, *J. Am. Chem. Soc.* **1923**, *45*, 515 – 521; b) C. D. Hurd, C. Kocour, *J. Am. Chem. Soc.* **1923**, *45*, 2167 – 2171; c) C. D. Hurd, *J. Am. Chem. Soc.* **1923**, *45*, 3095 – 3101; d) C. D. Hurd, *Org. Synth. Coll.* **1932**, *1*, 330 – 334; e) J. W. Williams, C. D. Hurd, *J. Org. Chem.* **1940**, *5*, 122 – 125.

[16] a) R. Weiss, *Monatsh. Chem.* **1919**, *40*, 391 – 402; b) A. McKenzie, E. W. Christie, *J. Chem. Soc.* **1934**, 1070 – 1075; c) J. D. Morrison, H. S. Mosher, *Asymmetric Organic Reactions*, Academic Press, New York, **1971**, pp. 276 – 281, 295, 322, 326; d) H. Pracejus, *Justus Liebigs Ann. Chem.* **1960**, *634*, 9 – 22; e) H. Pracejus, G. Kohl, *Justus Liebigs Ann. Chem.* **1969**, *722*, 1 – 11; f) H. Pracejus, *Fortschr. Chem. Forsch.* **1967**, *8*, 493 – 553; g) H. Pracejus, A. Tille, *Chem. Ber.* **1963**, *96*, 854 – 865.

[17] a) The name bisketenes is used because the alternative diketene is applied to the ketene dimer **20**; b) O. Diels, B. Wolf, *Ber. Dtsch. Chem. Ges.* **1906**, *39*, 689 – 697; c) H. Staudinger, S. Bereza, *Ber. Dtsch. Chem. Ges.* **1908**, *41*, 4461 – 4465; d) D. A. Dixon, A. J. Arduengo III, K. D. Dobbs, D. V. Khasnis, *Tetrahedron Lett.* **1995**, *36*, 645 – 648; e) R. Glaser, R. K. Murmann, C. L. Barnes, *J. Org. Chem.* **1996**, *61*, 1047 – 1058; f) D. Schröder, C. Heinemann, H. Schwarz, J. N. Harvey, S. Dua, S. J. Blanksby, J. H. Bowie, *Chem. Eur. J.* **1998**, *4*, 2550 – 2556.

[18] a) H. Staudinger, W. Kreis, *Helv. Chim. Acta* **1923**, *39*, 689 – 697; b) G. Maier, H. P. Reisenauer, T. Sayrac, *Chem. Ber.* **1982**, *115*, 2192 – 2201; c) A. D. Allen, M. A. McAllister, T. T. Tidwell, D. Zhao, *Acc. Chem. Res.* **1995**, *28*, 265 – 271; d) A. D. Allen, A. J. Lough, T. T. Tidwell, *Chem. Commun.* **1996**, 2171 – 2172.

[19] a) M. S. Newman, A. Arkell, T. Funkanaga, *J. Am. Chem. Soc.* **1960**, *82*, 2498 – 2501; b) L. L. Shchukovskaya, R. I. Pal'chik, A. N. Lazarev, *Dokl. Akad. Nauk SSSR* **1965**, *164*, 357 – 360; *Engl. Transl.* **1965**, *164*, 884 – 890; c) This work was contained in the dissertation of Rachel Pal'cik at the Leningrad State University (1969). L. L. Shchukovskaya was a synthetic chemist at the Grebenschikov Institute of Silicate Chemistry in Leningrad (now St. Petersburg, Russia) of the Academy of Sciences of the USSR, and her husband A. N. Lazarev carried out the spectroscopic investigations; d) M. A. Brook, *Silicon in Organic, Organometallic, and Polymer Chemistry*, Wiley, New York, **2000**, pp. 485 – 496; e) H. Staudinger, S. Bereza, *Ber. Dtsch. Chem. Ges.*, **1909**, *42*, 4098 – 4818; f) V. A. Nikolaev, Y. Frenkh, I. K. Korobitsyna, *Zh. Org. Khim.* **1978**, *14*, 1433 – 1441; *Russ. J. Org. Chem.* **1978**, *14*, 1338 – 1346.

[20] a) H. Staudinger, E. Anthes, H. Schneider, *Ber. Dtsch. Chem. Ges.* **1913**, *46*, 3539 – 3541; b) E. Ott, *Justus Liebigs Ann. Chem.* **1913**, *401*, 159 – 177; c) H. Staudinger, H. Schneider, *Helv. Chim. Acta* **1923**, *6*, 304 – 315; d) H. C. Stevens, D. A. Reich, D. R. Brandt, K. R. Fountain, E. J. Gaughan, *J. Am. Chem. Soc.* **1965**, *87*, 5257 – 5259; e) W. T. Brady, H. G. Liddell, W. L. Vaughn, *J. Org. Chem.* **1966**, *31*, 626 – 628; f) L. Ghosez, R. Montaigne, P. Mollet, *Tetrahedron Lett.* **1966**, 135 – 139; g) R. A. Minns, *Org. Synth. Coll.* **1988**, 6, 1037 – 1040 (Ed.: W. E. Noland).

[21] a) L. I. Smith, H. H. Hoehn, *J. Am. Chem. Soc.* **1939**, *61*, 2619 – 2624; b) D. H. R. Barton, G. Quinkert, *J. Chem. Soc.* **1960**, 1 – 9; c) D. M. Jerina, B. Witkop, C. L. McIntosh, O. L. Chapman, *J. Am. Chem. Soc.* **1974**, *96*, 5579 – 5580.

[22] a) R. B. Woodward, R. Hoffmann, *Angew. Chem.* **1969**, *81*, 797 – 869; *Angew. Chem. Int. Ed. Engl.* **1969**, *8*, 781 – 853; b) R. Huisgen, *Acc. Chem. Res.* **1977**, *10*, 117 – 124; c) R. Huisgen, *Pure Appl. Chem.* **1980**, *52*, 2283 – 2302; d) T. Machiguchi, T. Hasegawa, A. Ishiwata, S. Terashima, S. Yamabe, T. Minato, *J. Am. Chem. Soc.* **1999**, *121*, 4771 – 4786.

[23] Nobel prize winners who have published work on ketene chemistry include R. B. Woodward, E. J. Corey, R. G. W. Norrish, G. Porter, K. Fukui, G. Olah, R. W. Holley, V. Prelog, O. Diels, H. Staudinger, D. Barton, R. Hoffmann, J. Pople, A. Zewail, G. Natta, R. F. Curl, Jr, L. Ruzicka, J. C. Polanyi, and W. N. Lipscomb.

[24] a) C. Abaecherli, R. J. Miller, *Kirk-Othmer Encyclopedia of Chemical Technology*, Wiley, New York, **1995**; b) O. Süs, *Justus Liebigs Ann. Chem.* **1944**, *556*, 65 – 84; c) A. Reiser, H.-Y. Shih, T.-F. Yeh, J.-P. Huang, *Angew. Chem.* **1996**, *108*, 2610 – 2622; *Angew. Chem. Int. Ed. Engl.* **1996**, *35*, 2429 – 2440; d) A. Reiser, J. P. Huang, X. He, T. F. Yeh, S. Jha, H. Y. Shih, M. S. Kim, Y. K. Han, K. Yan, *Eur. Polym. J.* **2002**, *38*, 619 – 629.

 © 2005 Wiley-VCH Verlag GmbH & Co. KGaA, Weinheim

B. F. Cravatt, E. J. Sorensen, and C. Drahl

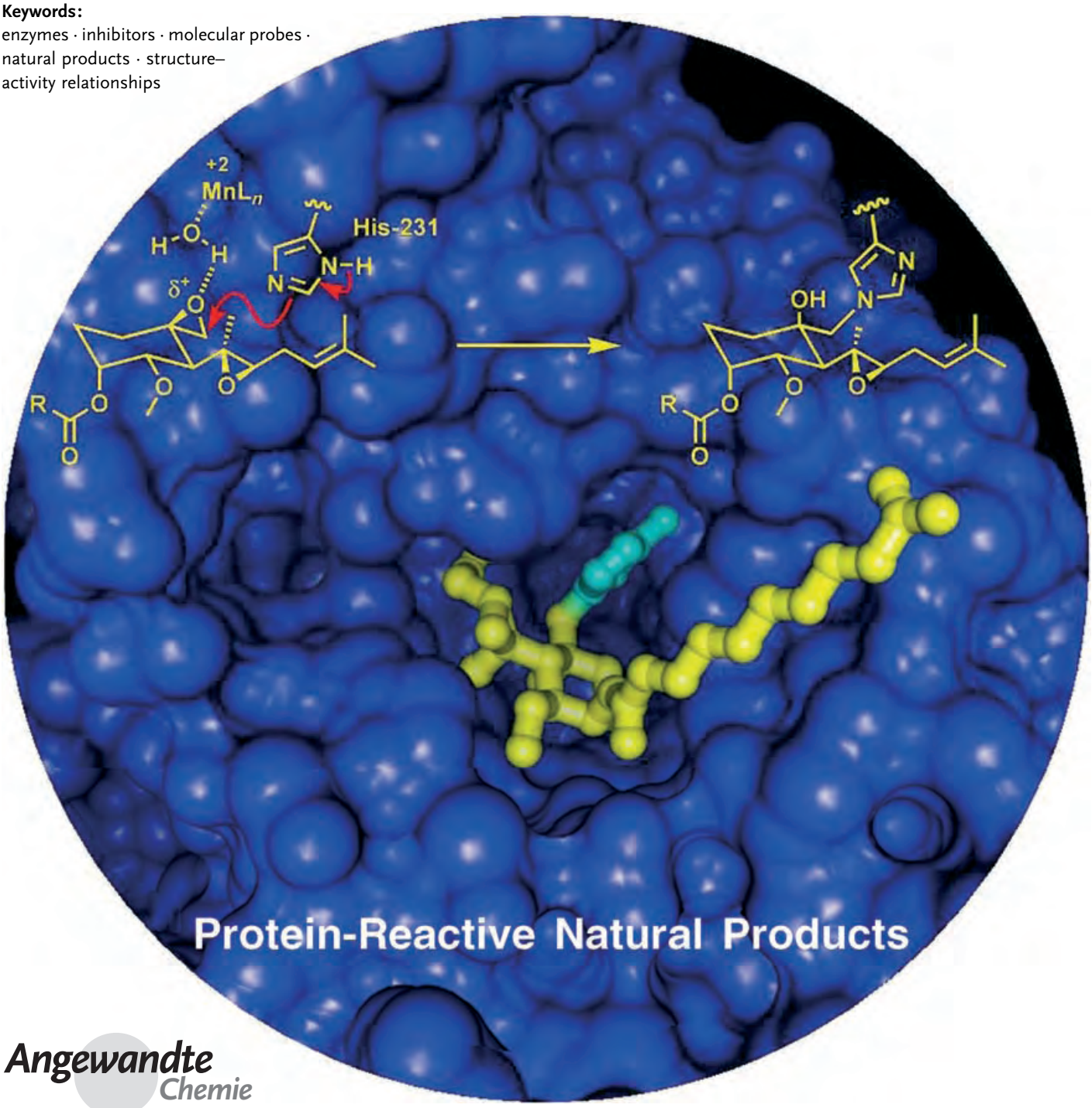
DOI: 10.1002/anie.200500900

Natural Products Chemistry

Protein-Reactive Natural Products

Carmen Drahl, Benjamin F. Cravatt, and Erik J. Sorensen**

Keywords:
enzymes · inhibitors · molecular probes · natural products · structure–activity relationships



© 2005 Wiley-VCH Verlag GmbH & Co. KGaA, Weinheim

Researchers in the post-genome era are confronted with the daunting task of assigning structure and function to tens of thousands of encoded proteins. To realize this goal, new technologies are emerging for the analysis of protein function on a global scale, such as activity-based protein profiling (ABPP), which aims to develop active site-directed chemical probes for enzyme analysis in whole proteomes. For the pursuit of such chemical proteomic technologies, it is helpful to derive inspiration from protein-reactive natural products. Natural products use a remarkably diverse set of mechanisms to covalently modify enzymes from distinct mechanistic classes, thus providing a wellspring of chemical concepts that can be exploited for the design of active-site-directed proteomic probes. Herein, we highlight several examples of protein-reactive natural products and illustrate how their mechanisms of action have influenced and continue to shape the progression of chemical proteomic technologies like ABPP.

From the Contents

1. Introduction 5789

2. Natural Products that Target Catalytic Nucleophiles in Enzyme Active Sites 5790

3. Natural Products that Target Non-Nucleophilic Residues in Enzyme Active Sites 5794

4. Targeting Nonenzymatic Proteins 5802

5. Summary and Outlook 5803

1. Introduction

The sequencing of the human genome has transformed the way in which scientists think about biology. However, there is a vast gulf between the wealth of gene sequence information and our knowledge of gene function. Researchers are now confronting the task of understanding the cellular and molecular functions of thousands of predicted gene products. The genome gives rise to the proteome, and it is the combinatorial interactions among proteins that make living organisms so complex at the molecular level. Elucidating the three-dimensional structures and cellular functions of all proteins encoded by prokaryotic and eukaryotic genomes and deciphering the architectures of protein–protein interaction networks of cells and tissues are among the great challenges and opportunities facing new generations of life scientists. To reach this understanding, the development of new technologies and concepts to expedite global analyses of protein function is required.[1] A growing number of research laboratories are exploring biology with chemistry-based strategies that are capable of yielding insight into the role of individual proteins in complex biological systems. The field of chemical synthesis has often played a major role in this process, perhaps most visibly through facilitating the identification of protein targets of bioactive natural products.[2]

For centuries, natural products have been used for medicinal purposes.[3] Life forms that lack immune systems, in particular, biosynthesize natural products of unparalleled structural diversity, some of which modulate biological function with exquisite specificity. It is tantalizing to consider the wealth of secondary metabolites that remains undiscovered. Microorganisms, for example, are a fertile and diverse source for new chemical entities, and researchers are actively developing ways to exploit their metabolic diversity.[4] A provocative subset of biologically active natural products is endowed with electrophilic functional groups that covalently modify nucleophilic residues in specific protein targets. Lipstatin,[5] fumagillin,[6] and microcystin[7] embody the chemistry of the carbonyl group, the epoxide, and the electron-deficient alkene, respectively, and are prominent examples of protein-reactive natural products. These and related secondary metabolites are important because they have yielded insight into the cellular functions of key enzymes. Most natural products that covalently modify proteins possess structural features that render them chemically reactive, whereas others bear latent reactivity; by posing as innocuous substrates, they are activated only by catalytic turnover in their enzyme targets.[8]

Protein-reactive natural products are highly attractive as molecular probes for protein activity profiling experiments, because they provide information about enzyme active sites in complex proteomes. Moreover, the diversity of mechanisms employed by reactive natural products to target enzyme active sites can serve as a valuable guide for the de novo design of affinity agents for the proteomic profiling of specific classes of enzymes. Such activity-based protein profiling (ABPP) endeavors[9] provide a more direct readout of enzyme activity in proteomes, as opposed to inferring this critical parameter from mRNA or protein levels, neither of which reflect the myriad post-translational mechanisms that regulate enzyme function in vivo.[10]

[*] Prof. B. F. Cravatt
The Skaggs Institute for Chemical Biology and
The Departments of Chemistry and Cell Biology
The Scripps Research Institute
10550 North Torrey Pines Road, La Jolla, CA 92037 (USA)
Fax: (+1) 858-784-8023
E-mail: cravatt@scripps.edu

C. Drahl, Prof. E. J. Sorensen
Department of Chemistry
Princeton University
Princeton, NJ 08544 (USA)
Fax: (+1) 609-258-1980
E-mail: ejs@princeton.edu

© 2005 Wiley-VCH Verlag GmbH & Co. KGaA, Weinheim

Nature engages protein targets with reactive small molecules in many ways, and the number of natural products that covalently modify proteins is likely very large. In coming to grips with this subject, we have chosen to address selected reactive natural products for which the protein targets are well-characterized, and we have placed particular emphasis on natural products that exert their activities in eukaryotic systems. For a more detailed discussion of classical examples of protein-reactive natural products that target prokaryotic enzymes, such as the β-lactam family of antibiotics, which inhibit peptidases involved in cell wall biosynthesis, the reader is referred to some authoritative review articles.[11] Furthermore, natural products such as DNA-alkylating agents that covalently modify non-protein biomolecules have been extensively reviewed elsewhere, and are not discussed herein.[12] Finally, throughout this review, we attempt to emphasize themes that may be useful in conceiving novel chemical proteomics probes; as will become apparent, the target of natural product action need not be a catalytic nucleophile, or for that matter even an enzyme. Strategies other than the general electrophile–nucleophile interaction offer valuable lessons that may be harnessed by chemical biologists to further expand the proteome space amenable to analysis by ABPP.[13] From the examples below, we hope it is evident that bioactive natural products provide key tools and concepts that can be exploited for the characterization of protein function on a global scale.

2. Natural Products that Target Catalytic Nucleophiles in Enzyme Active Sites

Many natural products have cleverly exploited the catalytic mechanisms of enzymes to elicit selective, covalent inhibition. In this section, we highlight representative natural products that modify key catalytic residues in enzyme active sites.

2.1. Lipstatin

Lipstatin was isolated from *Streptomyces toxytricini* on the basis of its potent, selective, and irreversible inhibition of pancreatic lipase (Scheme 1).[14] The structure of lipstatin was determined by a combination of spectroscopic and chemical methods,[15] and was confirmed by chemical synthesis.[16] Lipstatin features a β-lactone ring with two linear carbon chains of six and thirteen atoms, respectively. The longer of the two is doubly unsaturated and contains an *N*-formylleucine ester side chain. Structural analysis revealed a striking similarity between lipstatin and esterastin, a reported inhibitor of esterase which features a different amino acid side chain, *N*-acetylasparagine.[17] Other members of this β-lactone enzyme inhibitor family include the panclicins,[18] the ebelactones,[19] and valilactone (Scheme 1).[20] The research group of Bacher later found that lipstatin is derived biosynthetically from 3-hydroxytetradeca-5,8-dienoic acid,[21] which forms from a condensation of two mycolic acid[22] components of 14 and 8 carbon atoms, both of which originate from fatty acid catabolism. Protons at the C2 and C3 positions, and one proton at C4 are derived from water.[21c] This is in contrast with the initial assumption that lipstatin had a polyketide origin; early [^{13}C]acetate feeding experiments were inconclusive.[21d] A total synthesis of lipstatin from (*S*)-*N*-formylleucine and dimethyl-(*S*)-(−)-malate was recently described,[23] and there is also a comprehensive body of synthetic work on tetrahydrolipstatin,[16,24] which is obtained by the catalytic hydrogenation of lipstatin.[15]

Pancreatic lipase is the target of lipstatin and its derivatives. This lipase possesses an active-site charge-relay system similar to serine proteases; it features the catalytic triad of His263, Asp176, and Ser152.[25] Pancreatic lipase is responsible for the hydrolysis of dietary triacylglycerols to fatty acids and monoacylglycerols.[26] This catabolic process is critical for proper fat absorption; inhibition of pancreatic lipase activity results in the passage of fats through the stool. Tetrahydrolipstatin limits the absorption of dietary fat by blocking the activity of pancreatic lipase, as well as carboxylester lipase, human milk lipase, and gastric lipase.[22a] Now available under the trade names orlistat or xenical, tetrahydrolipstatin was approved by the Food and Drug Administration in March 1999 and has been successful in helping obese patients lose weight.[26b,27] Obesity affects approximately one third of the U.S. population,[26b] and many problems are thought to stem from this chronic condition, including diabetes mellitus type II. This disease may be prevented or brought under control with an Orlistat regimen.[28]

Tetrahydrolipstatin is also an inhibitor of the thioesterase domain of fatty acid synthase (FAS), an enzyme associated with tumor cell proliferation.[29] Administration of orlistat to prostate tumor cells causes apoptosis; the drug also halts growth of xenograft tumors in mice. Interestingly, it was an

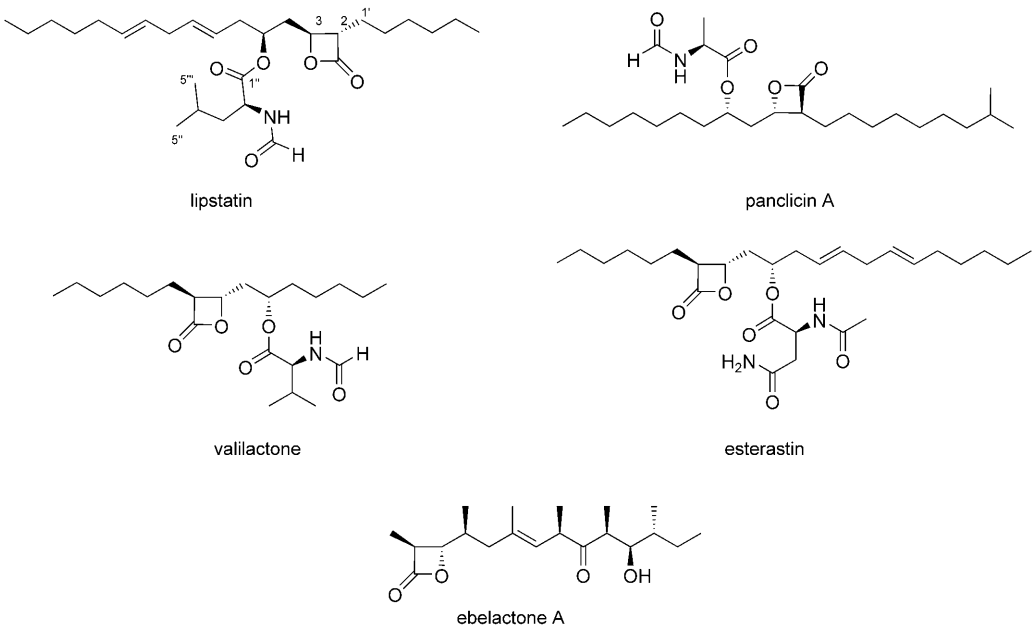


Carmen Drahl obtained her BA in chemistry at Drew University in 2002. She received her MA at Princeton University in the laboratory of G. McLendon. Currently, she is conducting graduate studies at Princeton under the direction of E. J. Sorensen. Her research interests include the synthesis and biological evaluation of reactive natural products. She is the recipient of a Barry M. Goldwater Fellowship, as well as predoctoral fellowships from Eli Lilly and the National Science Foundation.



Benjamin Cravatt studied biological sciences (BS) and history (BA) at Stanford University. He then conducted research with D. Boger and R. Lerner and received his PhD from The Scripps Research Institute (TSRI) in 1996. He joined the faculty at TSRI in 1997 as a member of the Skaggs Institute for Chemical Biology and the departments of Cell Biology and Chemistry. His research group is developing and applying new technologies to elucidate the roles of enzymes in the physiological and pathological processes of the nervous system and in cancer.

 © 2005 Wiley-VCH Verlag GmbH & Co. KGaA, Weinheim



Scheme 1. The lipstatin family of natural products; all members feature a four-membered β-lactone ring.

ABPP screen of prostate cancer cell proteomes with a fluorophosphonate–rhodamine probe that allowed researchers to characterize Orlistat as a FAS thioesterase inhibitor and a potential antitumor therapeutic.[29]

The chemical reactivity of the β-lactone group of tetrahydrolipstatin and its analogues is the basis for their biological effects. The catalytic active-site serine nucleophile of pancreatic lipase attacks the electrophilic β-lactone at the carbonyl carbon C1 to form a β-hydroxy serine ester (Scheme 2, route a).[5,30] Theoretically, attack could also occur at C3 to form a stable serine ether (Scheme 2, route b). Modified tetrahydrolipstatins (as obtained after enzyme attack and following adduct hydrolysis) were synthesized and then compared with the enzyme reaction results. Products with inverted stereochemistry at C3, which would result from nucleophilic attack at this atom, were observed in trace amounts at most. These data support the carbonyl carbon atom as the site of attack.[30] The carbonyl carbon atom may be activated by a hydrogen-bond donor in the active site of the lipase, or the relief of ring strain alone may be sufficient to drive the ring-opening process. In the absence of a water-insoluble substrate and at pH 7.0, the acyl-enzyme intermediate hydrolyzes very slowly to a hydroxy acid that still bears the formylleucine side chain, thus almost completely restoring enzyme activity within 24 hours.[22a,30a]

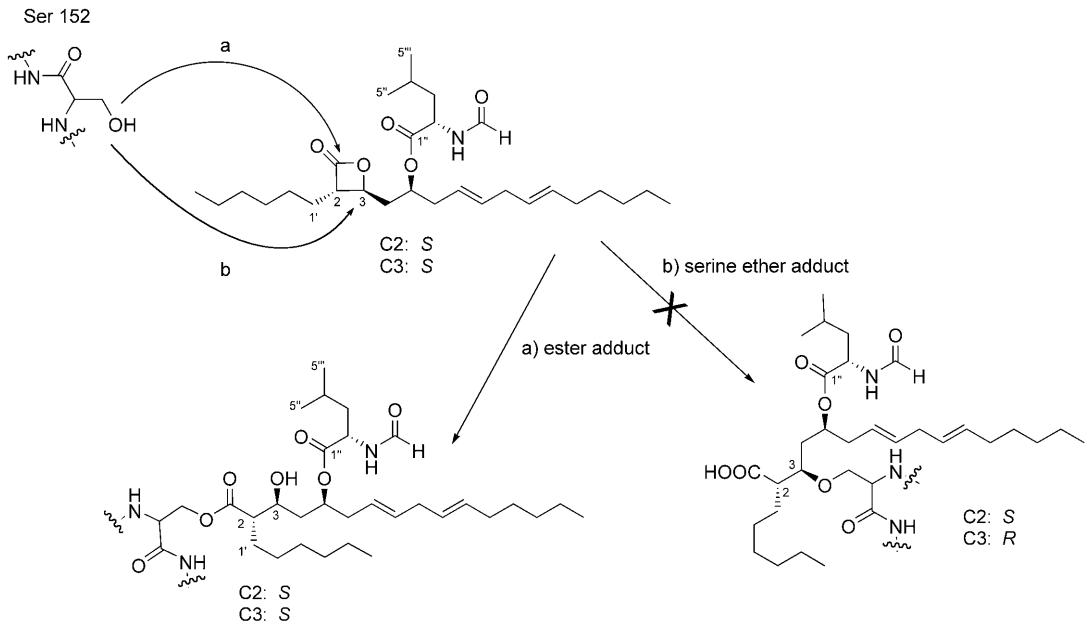


Erik J. Sorensen received his BA degree from Syracuse University. Under the guidance of K. C. Nicolaou at the University of California, San Diego, he obtained his PhD in 1995 and co-authored the book Classics in Total Synthesis. He subsequently worked as a postdoctoral fellow with S. Danishefsky. In 1997, he began his independent career at The Scripps Research Institute and became associate professor in 2001. In 2003, he moved to Princeton University, where he is the Arthur Allan Patchett Professor in organic chemistry.

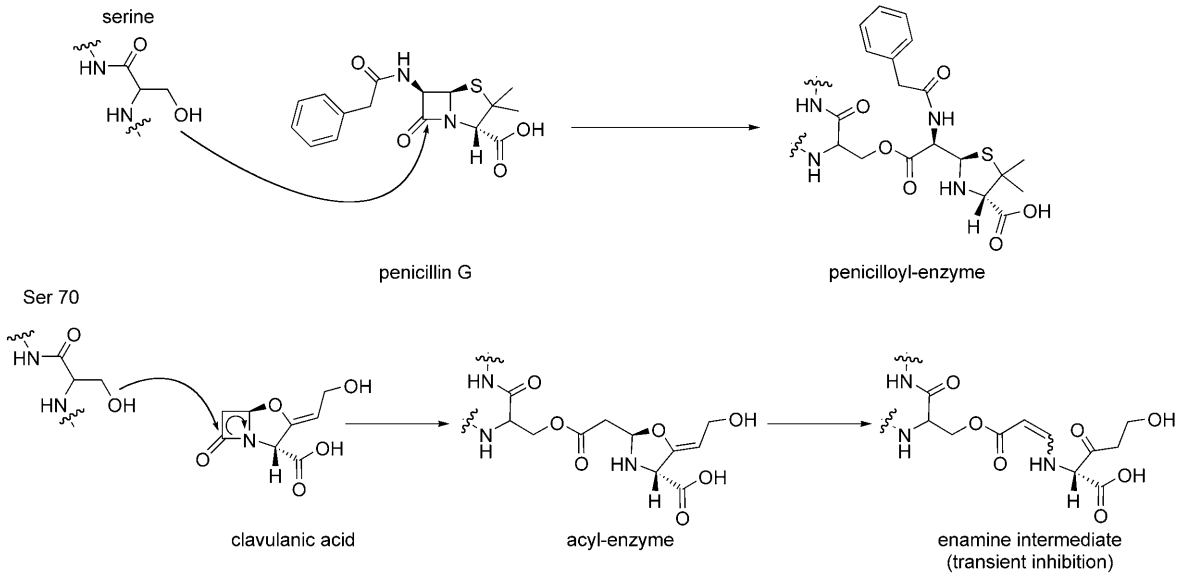
This type of reactivity is similar to that of the β-lactam antibiotics, which target peptidases involved in bacterial cell-wall biosynthesis (Scheme 3). The active-site serine nucleophile in the proteins targeted by penicillin is believed to attack the carbonyl carbon of the lactam ring to furnish a ring-opened penicilloyl-enzyme.[31] Clavulanic acid has a more complicated proposed mechanism, but it shares with lipstatin the principal features of inhibition through ring opening and recovery of enzyme activity through the slow subsequent hydrolysis of an enamine.[32]

The simplicity of the reactive motif in the lipstatin family is as instructive as the scaffold that frames it. Many physiological nucleophiles could conceivably react with and open the lactone ring. The long alkyl chains of these natural products presumably direct them toward enzymes with lipid substrates. The reactivation period for pancreatic lipase by hydrolysis of the acyl-enzyme intermediate is interesting, particularly in light of a study that demonstrated a threefold increase in the reactivation rate constant (k_r) in the presence of lipid–water interfaces (k_r increased from 2000 to 6000 min^{-1}).[33] Enzymes found in different environments might therefore have different turnover rates. Part of the noted selectivity of lipstatin may come not only from selective targeting of the small molecule to pancreatic lipase, but also from the selected lack of turnover of the lipase–lipstatin complex. Variation of the scaffold around the reactive β-lactone motif should allow lipstatin-like chemical probes to be redirected to target other lipase enzymes or even other enzyme families altogether.

 © 2005 Wiley-VCH Verlag GmbH & Co. KGaA, Weinheim



Scheme 2. Two possible mechanisms for the covalent modification of pancreatic lipase by lipstatin. The reaction occurs exclusively at the β-lactone carbonyl group.



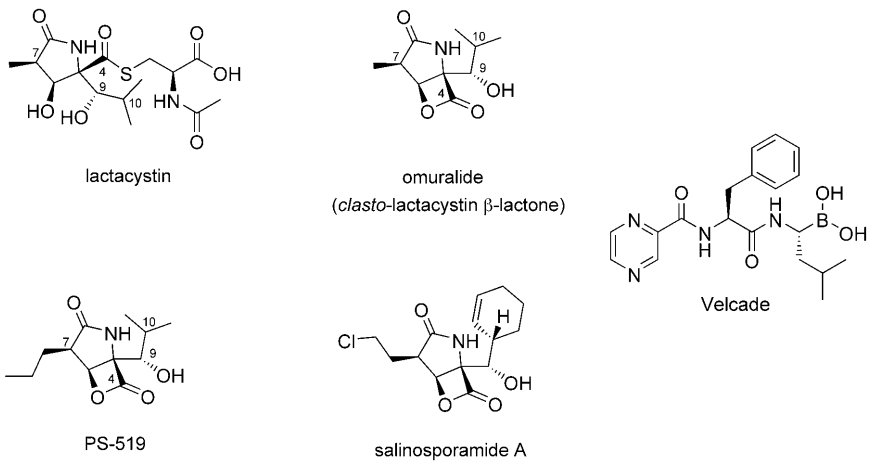
Scheme 3. Principal features of β-lactam antibiotic reactivity.

2.2. Lactacystin

Lactacystin (Scheme 4) was isolated by Omura and co-workers from a *Streptomyces* strain in a screen for natural products that induce neurite outgrowth.[34] Its interesting structure was elucidated by X-ray crystallography and NMR spectroscopy,[35] and confirmed by the total syntheses carried out by several research groups.[36] Lactacystin is biosynthesized from three units: leucine, isobutyrate (and/or valine), and cysteine.[37]

Further investigations showed that lactacystin does not mimic nerve growth factor;[38] instead, it reacts specifically with the proteasome, binding covalently to the hydroxy group of the highly conserved N-terminal threonine residue to inhibit the chymotrypsin-like and trypsin-like proteasome activities in irreversible fashion.[38b] The proteasome is an abundant ATP-dependent cellular protease that degrades damaged proteins.[39] With few exceptions, proteasomes act on proteins that are tagged for destruction through the covalent attachment of the small protein ubiquitin.[39] The proteasome consists of a barrel-like core, in which controlled proteolysis takes place. The core is capped at each end by a regulatory protein.[39] The N-terminal threonine residue modified by lactacystin serves as the active-site nucleophile of the proteasome.[38b,40] The proteasome lacks a catalytic triad, but requires a basic group to accept a proton from threonine in

 © 2005 Wiley-VCH Verlag GmbH & Co. KGaA, Weinheim

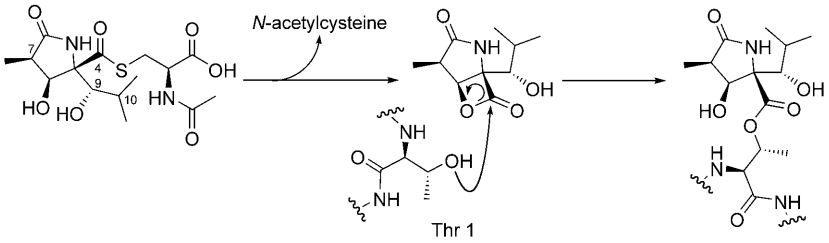


Scheme 4. Lactacystin and related proteasome inhibitors. Velcade is a synthetic inhibitor clinically approved for the treatment of multiple myeloma.

the transition state. This is most likely the job of the α-amino group of Thr 1, which is ideally situated to accept a proton in the crystal structure of the proteasome in complex with lactacystin.[41] Alternatively, the conserved Lys 33 residue may fulfill this role, since mutation of this residue abolishes proteasome activity.[42] Lactacystin inhibits neither the serine proteases trypsin and chymotrypsin, nor the cysteine proteases papain, the calpains, or cathepsin B;[38b] it does, however, covalently inhibit the serine protease cathepsin A.[43] As a fairly selective proteasome inhibitor, lactacystin has proven to be a valuable probe to study the cellular role of the ubiquitin–proteasome pathway.[44]

Different families of proteasome inhibitors have been developed over the years to better understand the ubiquitin–proteasome system. The earliest synthetic inhibitors, the C-terminal peptide aldehydes, showed too little selectivity for the proteasome over serine and cysteine proteases.[40] Certain tripeptides modified at the C terminus by a vinyl sulfone or glyoxal act as mechanism-based inhibitors of the proteasome.[39b,45] Boronic acid peptides (in which the aldehyde pharmacophore has been replaced by a boronate group) are more potent and selective for the proteasome. The flagship boronate compound, PS-341,[40,46] was recently clinically approved for the treatment of multiple myeloma (velcade (bortezomib), Scheme 4). This validates the proteasome as a therapeutic target for at least this type of cancer and potentially other forms as well.[47] Unlike lactacystin, however, Velcade reversibly inhibits the chymotrypsin-like activity of the proteasome.[40] The most clinically advanced lactacystin analogue is PS-519 (Scheme 4), a cell-permeable variant that features an *n*-propyl substitution at C7. This compound is more potent than the natural product and has entered phase II clinical trials for acute stroke.[40,48]

The reactivity of lactacystin is brought about by its latent β-lactone group, termed *clasto*-lactacystin β-lactone or omuralide (Scheme 4).[49] Derivatives that cannot form the β-lactone are inactive. Omuralide is formed in the extracellular fluid from cyclization (lactonization) of lactacystin with loss of the *N*-acetylcysteine leaving group. The resulting omuralide is more cell-permeable than the parent compound,[40,49] and it inhibits proteasome activities 15 to 20-fold faster than lactacystin.[38] Carbon atom C4 of this intermediate lactone is electrophilic and is presumed to undergo attack by the hydroxy group of the catalytic threonine residue[44b] to yield an ester-linked omuralide–proteasome adduct (Scheme 5). The "masking" of the reactive β-lactone in its open thioester form is important, as it may help lactacystin avoid spurious targets. Several research groups have shown that lactacystin labels all active proteasome β subunits.[39b,50] Interestingly, it was



Scheme 5. Lactacystin is lactonized to its cell-permeable, protein-reactive derivative, omuralide, which then covalently inactivates the proteasome.

demonstrated that replacement of the catalytic N-terminal threonine group with serine produced a fivefold increase in the rate of proteasome inactivation by omuralide. This replacement also increased the rate of hydrolysis of the acyl-enzyme intermediate.[51] This result may explain why omuralide and lactacystin inhibit very few serine proteases, as serine–omuralide adducts may undergo rapid hydrolysis to relieve inhibition.[44a] It is instructive to note how the activity and selectivity of lactacystin are exquisitely controlled by intrinsic chemical reactivity.

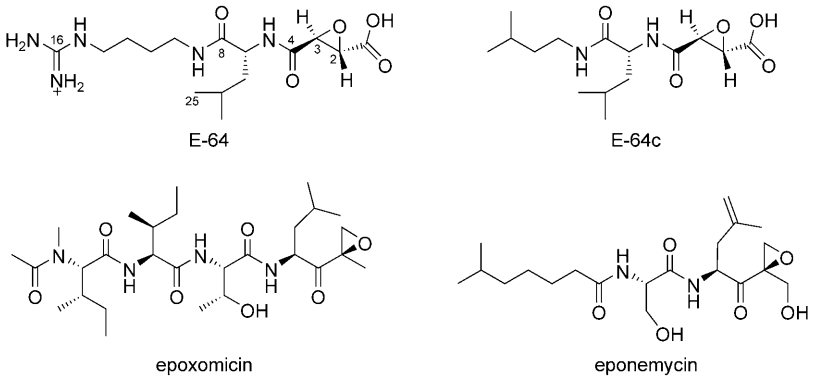
The structure of the proteasome from *Saccharomyces cerevisiae* co-crystallized with omuralide[41] was determined by X-ray analysis, and confirmed the covalent linkage between the threonine side chain hydroxy group and omuralide. The N-terminal amino group is not modified by the natural product. Omuralide makes four hydrogen-bond contacts with the main chain of the proteasome catalytic subunit. The C9 isopropyl moiety of omuralide projects into a hydrophobic pocket of the proteasome to lend additional binding affinity. Corey and co-workers have shown that replacement of the omuralide C9 isopropyl group with a phenyl group abolishes all activity.[52] Interestingly, salinosporamide A (Scheme 4), a natural product 35-fold more potent than omuralide, possesses a cyclohexene moiety in place of the isopropyl group, yet it shares the bicyclic ring structure of omuralide.[53] Feling and co-workers suggested that this may be indicative of the different ways by which omuralide and salinosporamide A interact with the protea-

 © 2005 Wiley-VCH Verlag GmbH & Co. KGaA, Weinheim

some.[53] Corey and co-workers recently reported the first enantiospecific total synthesis of salinosporamide A[54] with a procedure that yields sufficient material to carry out biological analyses of the efficacy of salinosporamide A as a potential anticancer agent. Moreover, congeners of salinosporamide A were recently prepared for the possible treatment of proteasome-mediated disease.[55] It will be interesting to learn whether salinosporamide A has improved upon the delicately balanced chemistry of lactacystin.

2.3. E-64

In 1978, the Hanada group pursued a specific inhibitor of cysteine proteases to expedite investigation of protease biological functions. They succeeded in isolating a highly potent and irreversible inhibitor, E-64, from the mold *Aspergillus japonicus*.[56] The structure of E-64 was determined principally through classical chemical reactivity testing, IR spectroscopy, and ^{1}H NMR spectroscopy, and was subsequently confirmed by a chemical synthesis of its enantiomer.[57] The structure contains agmatine, the arginine decarboxylation product 1-amino-4-guanidinobutane (Scheme 6). To identify an E-64 pharmacophore, a comprehensive library of derivatives and fragments was synthesized. Both the epoxide and the carboxyl group derived from L-*trans*-(*S*,*S*)-epoxysuccinic acid were found to be indispensable for inhibition of papain.[58] Notably, other peptidyl epoxide natural products that act as covalent inhibitors of the proteasome have also been identified, including epoxomicin[59] and eponemicin[60] (Scheme 6).



Scheme 6. E-64 and other L-*trans*-(*S*,*S*)-epoxysuccinic acid derivatives.

In addition to papain, E-64 is a covalent inhibitor of several other cysteine proteases, including cathepsins B, H, and L, stem bromelain, and ficin.[61] The revelation that the high affinity, active-site-directed reversible inhibitor leupeptin decreased the rate of E-64 binding cemented the idea that E-64 is an active-site-directed inhibitor of cysteine proteases.[61] These proteases exert their catalytic activity with the assistance of an active-site ion pair between cysteine and histidine residues.[62] In papain, these residues are Cys 25 and His 159.[62]

Aberrant cysteine protease activity leads to many disease states. Inflammatory and traumatic processes, muscular dystrophy, Alzheimer's disease, cancer, and cataract formation all have a putative link to cysteine protease dysfunction.[63] In addition, because cysteine proteases are a critical component of the *Plasmodium* life cycle, they are regarded as viable targets for potential antimalarial drugs.[64] In an effort to improve the cell permeability of leads, the agmatine group was replaced with neutral moieties, such as isoamylamine in the case of E-64c (Scheme 6).[65] In 1986, the ethyl ester of E-64c was removed from phase III clinical trials in Japan for muscular dystrophy indications because its efficacy did not meet expectations, and the drug covalently modified proteins of other mechanistic classes.[63d,66] However, by virtue of its inhibition of calpain, this same E-64 derivative has found use in eye drops for the prevention and treatment of cataracts.[67] E-64 is still frequently used to facilitate discovery and classification of newly isolated papain-class enzymes.[68]

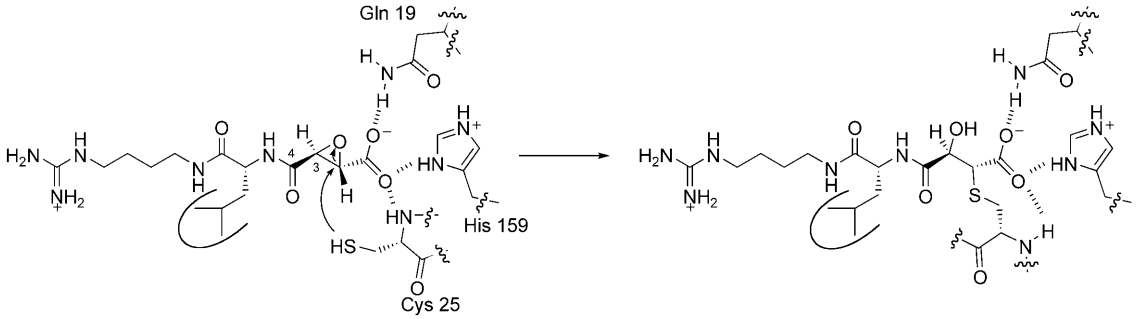
Molecular probes for ABPP inspired by the E-64 motif have proven to be of great value for tracking the activities of both animal and plant cysteine proteases in whole proteomes, and in the design and screening of inhibitors for these enzymes.[68a,b] For example, a screen of plant extracts revealed cysteine protease activity for three proteins that had not been previously characterized.[68a] In a comparative screen of mature and senescent leaf extracts, ABPP demonstrated that a change in mRNA transcript levels does not always correlate with protease activity.[68a] In addition, a cell-permeable E-64 probe revealed that increased cathepsin activity is associated with the angiogenic vasculature and invasive fronts of carcinomas.[69] Based on these results, administration of a broad-spectrum cathepsin inhibitor was performed, which impaired tumor growth and invasiveness.

The reaction of the E-64 epoxide with papain was elucidated by ^{13}C NMR spectroscopy.[70] Attack by the catalytic cysteine nucleophile occurs at the epoxide C2 atom.[70,71] Backside attack in S_N2 fashion inverts the configuration at C2 of the product thioether (Scheme 7). The key contacts between cysteine proteases and E-64 that are responsible for situating the inhibitor's epoxide group for regioselective nucleophilic attack have been extensively characterized in a series of crystal structures.[57,71,72] In the structure of the E-64–papain complex, the N-terminal carboxyl group of E-64 is positioned in the oxyanion hole, while the carbonyl group adjacent to the epoxide group interacts with the histidine catalytic base.[71] The mechanistic characterization of the interaction between E-64 and cysteine proteases of the papain class is an excellent example of the power of convergent research efforts in chemical synthesis, classical biochemistry, and structural biology.

3. Natural Products that Target "Non-Nucleophilic" Residues in Enzyme Active Sites

Several natural products inhibit enzymes through the covalent modification of active-site residues that are not essential for catalysis. Although some of these residues appear to perform supportive catalytic roles, they do not

 © 2005 Wiley-VCH Verlag GmbH & Co. KGaA, Weinheim



Scheme 7. The active-site cysteine residue of papain attacks the electrophilic epoxide of E-64 in an S_N2 fashion.

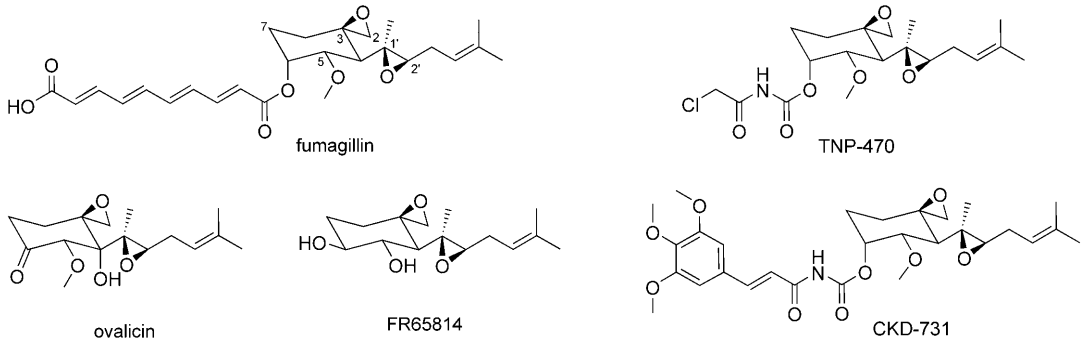
participate as nucleophiles directly; other residues seem altogether superfluous for catalysis. In either case, however, covalent modification of these residues results in enzyme inactivation. Herein, we highlight selected examples of natural products that target "non-nucleophilic" residues in enzyme active sites.

3.1. Fumagillin

A 1949 report demonstrated that concentrates of *Aspergillus fumigatus* cultures possessed antibiotic activity against *Staphylococcus aureus*.[73] Tarbell and co-workers characterized the chemical behavior of the active component, fumagillin, including the acid sensitivity of its characteristic spiroepoxide unit.[74] The constitution and stereochemistry of fumagillin were confirmed by X-ray crystallography (Scheme 8).[75] In 1972, Corey and Snider described their elegant studies that culminated in the first chemical synthesis of this natural product.[76] Subsequent work has produced a 26-step synthesis of (−)-fumagillol,[77] the saponification product of fumagillin, and a 13-step racemic synthesis of fumagillol.[78] Fumagillin and its close relatives ovalicin[79] and FR65814 (Scheme 8)[80] possess a rare sesquiterpene carbon skeleton that has been shown by labeling experiments to originate biosynthetically from β-*trans*-bergamotene, which arises from farnesyl pyrophosphate.[81] Other natural products not necessarily in the fumagillin family, but which contain a spiroepoxide moiety include curvularol[82] and FR901464.[83]

Fumagillin and other members of its family target methionine aminopeptidase 2 (MetAP-2), but not the closely related enzyme methionine aminopeptidase 1 (MetAP-1).[6b,84] Methionine aminopeptidases are metalloproteases responsible for co-translational removal of the N-terminal methionine residue in specific protein targets.[6b,85] These enzymes were originally thought to use cobalt as the active-site metal center, but more recent studies indicate that manganese is likely the physiologically relevant cofactor.[86] In the enzyme active site, the metal ions are coordinated by Asp251, Asp262, His331, Glu364, Glu459, and a water molecule.[87] The nucleophilicity of the water molecule is enhanced by coordination to the manganese ion; it attacks the scissile amide bond of the substrate.[88] MetAP-mediated removal of methionine is necessary for post-translational modifications such as myristoylation.[89] A single amino acid residue in MetAP-2, Ala362, confers sensitivity to ovalicin, and a Thr362Ala mutation of the human MetAP-1 gene inserted into yeast results in ovalicin-sensitive yeast colonies.[90]

The connection between inhibition of MetAP-2 and the medicinal utility of fumagillin appears complex and remains unclear.[91] It has been speculated that a connection exists at the level of protein myristoylation.[92] Without removal of N-terminal methionine residues, proteins cannot be myristoylated in vivo, which in turn, could disrupt their localization and function. Therefore, the hypothesis is that fumagillin indirectly causes cell-cycle arrest by interfering with myristoylation, which leads to aberrant subcellular localization of proteins that are not yet identified.[92] Despite a mechanism of action that remains enigmatic, fumagillin is firmly established as a potent antiparasitic agent.[93] During the 1950s, fumagillin was used for treatment of amoebiasis in humans, caused by *Endamoeba histolytica*, and is still used today for Nosema disease in honeybees, caused by the protozoan *Nosema*



Scheme 8. Fumagillin and other protein-reactive spiroepoxides. TNP-470 and CKD-731 are synthetic compounds.

 © 2005 Wiley-VCH Verlag GmbH & Co. KGaA, Weinheim

apis.[93a,b] More recently, fumagillin has shown efficacy against microsporidial keratoconjunctivitis of the eye, caused by a single-celled fungus.[94] Fumagillin and its semisynthetic derivative TNP-470 (Scheme 8) are the only treatments for microsporidiosis in HIV-positive patients[95] and block the in vitro growth of *Plasmodium falciparum* and *Leishmania donavani*, the organisms that cause malaria and leishmaniasis, respectively.[96] The broad anti-infective activity of fumagillin does not come without a price; it is toxic to mammals which indicates its low selectivity for parasitic over mammalian MetAP-2.[97]

The research group of Folkman stimulated a renaissance of interest in fumagillin with their discovery that this natural product inhibits tumor-induced angiogenesis.[98] TNP-470 is also a promising small-molecule inhibitor of angiogenesis and has progressed into clinical trials as a potential anticancer drug.[99] By using a homology modeling approach from the crystal structure of MetAP-2, Han and co-workers designed CKD-731 (Scheme 8), an analogue that is 1000-fold more potent against endothelial cell proliferation than TNP-470.[100]

New data suggest that MetAP-2 may not be the biologically relevant target of fumagillin, and that MetAP-2 function is not necessary for the growth of endothelial cells.[101] However, this study could not completely rule out a functional role for MetAP-2, because knockdown of the peptidase by siRNA was incomplete. The authors raised the intriguing possibility that another MetAP family member may exist in humans that could also act as a target for fumagillin.[101]

The key reactive motif of fumagillin is its spiroepoxide structure.[6] Removal of the spiroepoxide unit results in a 1000-fold decrease in MetAP-2 inhibition.[84] Fumagillin also possesses a side chain epoxide group; this epoxide was demonstrated to be dispensable for MetAP-2 inhibitory activity.[84] In the X-ray crystal structure of human MetAP-2 complexed with fumagillin, a covalent bond between the imidazole nitrogen ($N^{\varepsilon}2$) of a histidine residue (His231) and the methylene of the spiroepoxide is evident (Figure 1).[87] It has been speculated that His231 acts as a general base during catalysis, as it serves as a nucleophile to open the spiroepoxide ring.[84] It was thought that His231, along with the binuclear metal center, could activate a water molecule for attack at the scissile amide bond, after which another histidine in the active site, His339, could protonate the leaving group.[84] However, the active site geometry in *E. coli* MetAP-2 does not corroborate this proposal.[102] Scheme 9 depicts one model for fumagillin-mediated labeling of MetAP-2.[103] Transition-

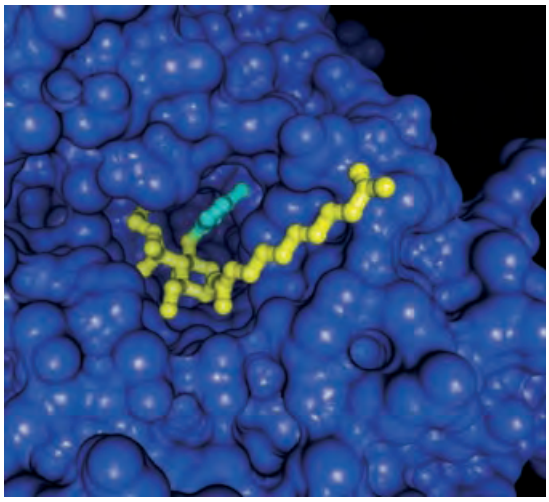
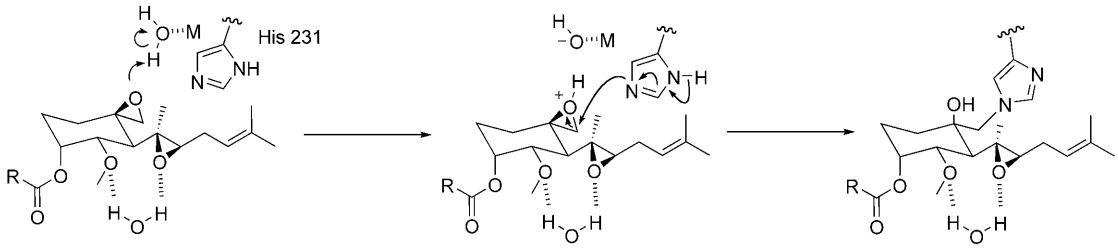


Figure 1. X-ray crystal structure of human MetAP-2 complexed with fumagillin. The covalent bond between C11 of the natural product (yellow) and $N^{\varepsilon}2$ of the active site His231 (cyan) is shown; the rest of the molecular surface of MetAP-2 is colored blue.

state analogues and crystallographic analysis yielded further insight into the catalytic mechanism of *E. coli* MetAP,[102–104] suggesting that His79 of *E. coli* MetAP (equivalent to His231 of human MetAP-2) actually stabilizes the tetrahedral intermediate that results when the peptide is attacked by an activated hydroxide through direct interaction with the nitrogen atom of the scissile peptide bond. Thus, the histidine residue modified by fumagillin appears to play an important supportive role in catalysis, consistent with the dramatic reduction in enzyme activity observed for a His231Asn MetAP-2 mutant.[84] More generally, fumagillin targeting of MetAP-2, which uses a metal-activated water molecule as the nucleophile for peptide-bond hydrolysis, underscores the remarkable ability of natural products to selectively label the active sites of enzymes that do not themselves engage in covalent catalysis.

3.2. Wortmannin

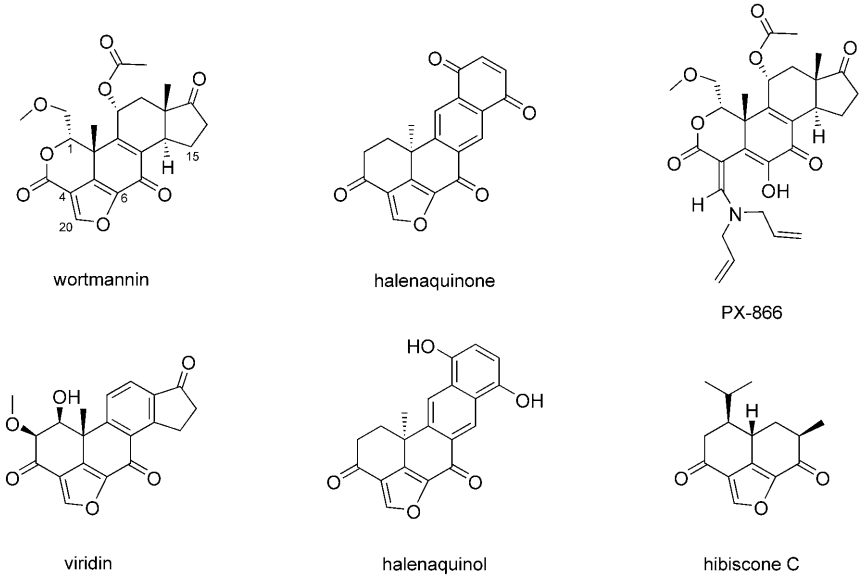
The antifungal antibiotic wortmannin (Scheme 10) was isolated from *Penicillium wortmanii* and its complex structure was elucidated by chemical degradation and NMR spectroscopic methods.[105] The hallmark of wortmannin is its reactive furan ring, which is fused between C4 and C6 of a steroid



Scheme 9. In one model for MetAP-2 modification by fumagillin, a histidine group in the MetAP-2 substrate binding site is able to open a protonated epoxide. Fumagillin binding is enhanced at low pH.[103]

 © 2005 Wiley-VCH Verlag GmbH & Co. KGaA, Weinheim

framework.[106] This feature is also found in viridin, demethoxyviridin, the marine-derived pp60$^{v\text{-}src}$ protein tyrosine kinase inhibitors halenaquinone and halenaquinol, and hibiscone C (gmelofuran), which is found in the heartwood of *Gmelina arborea* and the Jamaican Blue Mahoe (Scheme 10).[107]



Scheme 10. The wortmannin family of steroidal natural products. PX-866 was synthesized from wortmannin.

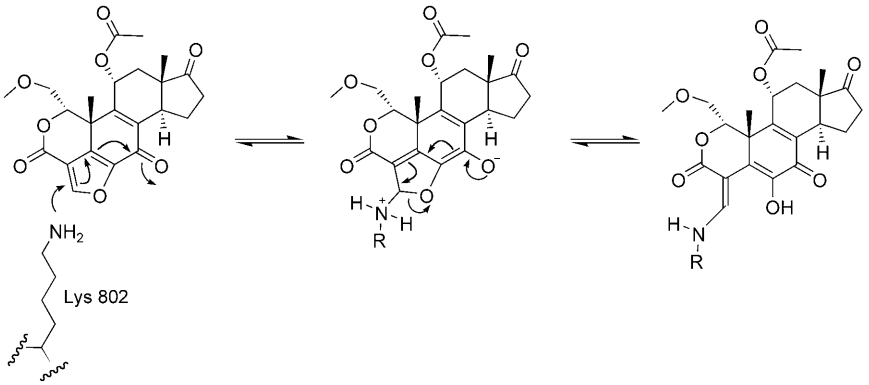
Wortmannin[108] and its structural relative viridin[109] are biosynthesized from the triterpenoid alcohol lanosterol[110] and are potent cell-permeable inhibitors of the lipid kinase phosphatidylinositol 3-kinase (PI 3-kinase). This enzyme is a central component of two major receptor-mediated signal transduction pathways:[111] the G-protein-coupled receptor pathway and the receptor tyrosine kinase pathway. PI 3-kinase phosphorylates at position 3 of the inositol ring of phosphatidylinositol (PtdIns), leading to the production of the second messengers PtdIns-3-phosphate, PtdIns-3,4-bisphosphate, and PtdIns-3,4,5-triphosphate. The precise nature of the PI 3-kinase catalytic mechanism is unknown.[112] In porcine PI 3-kinase, contact with the α- and β-phosphate groups of ATP is mediated by the conserved Lys 833 and Ser 806 side chains, respectively. An early mechanistic model involved deprotonation of the lipid substrate hydroxy group by Asp 946 to generate a nucleophile that attacks the γ-phosphate of ATP. Although mutations of this amino acid abolish activity, the crystal structure of PI 3-kinase indicates that this particular aspartate is not positioned properly for a role as catalytic base. Another residue, His 948, has been offered as an alternative base, but there is no experimental evidence to support this claim.[112b] Alternatively, PI 3-kinase may not possess a base catalyst. Instead, it may operate through a dissociative transition state.[113]

In addition to its well-studied lipid kinase target, wortmannin has been demonstrated to inhibit other serine/threonine kinases, including the mammalian target of rapamycin (mTOR), DNA-dependent protein kinase (DNA-PK),[114] myosin light chain kinase (MLCK), the gentamicin resistance enzyme AAC(6′)-APH(2″), and a membrane-bound PI 4-kinase.[115]

PI 3-kinases are involved in a large number of fundamental cellular processes, including apoptosis, proliferation, cell motility, and adhesion, and have been implicated in the malignant transformation of cells. Increased levels of PI 3-kinase products have been observed in colorectal tumors and in breast cancers.[116] It was also reported that dephosphorylation of PI 3-kinase products suppresses tumor formation.[117] As inhibitors of PI 3-kinase in vertebrates, wortmannin and its structural relatives are considered to have potential as therapeutic agents for the treatment of human neoplasms and other disease states such as diabetes, inflammation, platelet aggregation, atherosclerosis, and osteoporosis. A semisynthetic wortmannin library yielded ten compounds that were advanced to pharmacokinetic and toxicity studies.[118] PX-866 (Scheme 10), a diallylamino wortmannin derivative lacking the furan ring, demonstrated good pharmacokinetics and toxicity and exhibited prolonged inhibition of PI 3-kinase in vivo. This compound also augmented the antitumor effects of the established chemotherapeutic agent cisplatin.[119] It was speculated that loss of the furan ring was redeemed by improved chemical stability or a better fit in the ATP-binding pocket.[118]

Amine nucleophiles react efficiently with the doubly activated and highly electrophilic strained furan ring of wortmannin by attacking C20 to give vinylogous carbamates through an addition–elimination mechanism.[120] Wipf and co-workers recently synthesized a library of 94 C20-substituted semisynthetic wortmannin derivatives by reaction of the natural product with a wide variety of amine and thiol nucleophiles.[118] Wymann and co-workers discovered that this chemistry also occurs in the active site of PI 3-kinase.[121] The ε-amino group of Lys 802 of PI 3-kinase (Lys 833 in porcine PI 3-kinase)[122] attacks C20 of wortmannin which results in furan ring-opening to form a vinylogous carbamate (Scheme 11). This covalent bond-forming event irreversibly inhibits the enzyme. The acid lability of the vinylogous carbamate group complicated efforts to isolate wortmannin-labeled peptides. Fortunately, this group could be reduced with sodium cyanoborohydride to give a considerably more stable amine–wortmannin adduct. ATP, adenine, and FSBA (5′-*para*-fluorosulfonylbenzoyladenosine) each at 1 mM interfered with the alkylation of PI 3-kinase by wortmannin when added before the inhibitor, although substances containing nucleophilic amino acid side chain groups had no effect at the same concentration. FSBA is a derivative of adenine that reacts covalently with nucleophilic amino acids and has been

 © 2005 Wiley-VCH Verlag GmbH & Co. KGaA, Weinheim



Scheme 11. Lysine 802 in PI 3-kinase opens the doubly activated furan ring of wortmannin by an addition–elimination mechanism to yield a vinylogous carbamate.

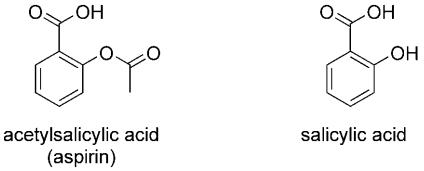
used to map nucleotide binding sites.[121] The PI 3-kinase substrate PtdIns-4,5-bisphosphate also effectively competes with wortmannin binding. These findings led Wymann and coworkers to conclude that the wortmannin target site in PI 3-kinase is in a nucleotide binding site in proximity to the substrate binding site. These postulates were confirmed by the X-ray crystal structure of a complex between wortmannin and porcine PI 3-kinase.[122]

The role of Lys 802, as mentioned above, may be the stabilization of the α-phosphate of ATP in the binding pocket, as has been speculated for Lys 72 in protein kinase A (PKA).[121] Lysine 72 anchors the nonlabile phosphate groups of ATP and neutralizes their charges by a salt bridge. Replacement of Lys 72 with Ala in yeast PKA leads to an 800-fold decrease in the V_{max} value.[123] Whereas Lys 72 of PKA and perhaps Lys 802 of PI 3-kinase appear important for enzyme activity, they probably participate in a primarily structural role rather than through direct involvement in catalysis. The protein microenvironment may be responsible for an enhanced nucleophilicity of the targeted lysine; alternatively, the positioning of wortmannin in kinase active sites may preclude productive interactions with catalytic residues. Regardless, the potency of wortmannin should encourage consideration of cofactor binding sites as targets for small-molecule probes. This may expand the menu of proteins amenable to functional proteomic methods like ABPP. Indeed, quite recently, a rhodamine-tagged wortmannin analogue was synthesized and used in proteomic studies to identify mammalian polo-like kinase as an additional target of this natural product.[124] This kinase is an important protein for mitosis that is known to be overexpressed in various human cancers. The wortmannin-based probe successfully detected kinase activity changes due to treatment with drugs and in different stages of the cell cycle. Importantly, these results suggest that wortmannin is a good lead for the development of polo-like kinase inhibitors for cancer therapy.

3.3. Aspirin

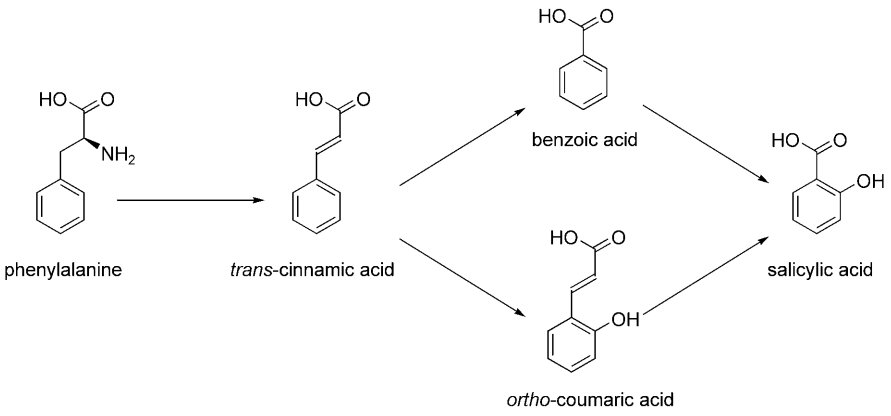
In a letter to the Right Honorable George, Earl of Macclesfield and President of the Royal Society, the Reverend Edward Stone wrote on April 25, 1763: "There is a bark of an English tree, which I have found by experience to be a powerful astringent, and very efficacious in curing aguish and intermitting disorders."[125]

Stone was not the first to observe the fever and pain-reducing properties of the extracts of the willow tree. In the year 200 B.C., the Greek physician Hippocrates prescribed willow bark and leaves for pain relief. Willow leaves were described by the Roman Pliny the Elder in his *Natural History*. Today, a modified version of salicylic acid, the active constituent in willow bark, named acetylsalicylic acid or aspirin (Scheme 12),[126] is one of the most widely used remedies in the world.



Scheme 12. Aspirin and salicylic acid, the natural product from which the drug was first synthetically derived.

Salicylic acid and structurally related secondary metabolites, the salicylates, are major defensive compounds that are present in nearly all higher plants,[127] and deter the feeding of a variety of herbivores.[127] The biosynthesis of salicylic acid (Scheme 13) may be traced to the phenylpropanoid pathway,[127] which begins with the formation of *trans*-cinnamic acid through the phenylalanine ammonia lyase-catalyzed elimination of ammonia from phenylalanine.[127a] From this point, two pathways are possible, and different plant species may use either or both.[127b] The first involves the removal of a two-carbon unit from cinnamic acid, leading to benzoic acid, followed by *ortho*-hydroxylation to salicylic acid. The second



Scheme 13. Two biosynthetic pathways for salicylic acid in plants.

 © 2005 Wiley-VCH Verlag GmbH & Co. KGaA, Weinheim

reverses the order of the two steps, resulting first in *ortho*-coumaric acid. The decarboxylation step is thought to proceed in a fashion similar to the β-oxidation events of fatty acid breakdown.[127] This was supported by studies in which the decarboxylation step in cell-free plant extracts was found to be ATP and CoA-dependent.[128]

In 1860, Hermann Kolbe of Marburg University in Germany carried out a laboratory synthesis of salicylic acid and its sodium salt from phenol, carbon dioxide, and sodium. Kolbe's student, Friedrich von Heyden, established a factory for the bulk production of salicylates in Radebeul, near Dresden. The unpleasant side effect of salicylate, gastric irritation, revealed itself quite rapidly as the drug became widely available. Felix Hoffmann, a chemist at Bayer, ameliorated the problem in 1897 by synthesizing a more easily tolerated derivative, acetylsalicylic acid.[129] Heinrich Dreser, the director of research at Bayer, coined the term "aspirin" from a combination of Spirsäure (salicylic acid) with an initial "a" for acetyl, and a patent was granted in 1899.

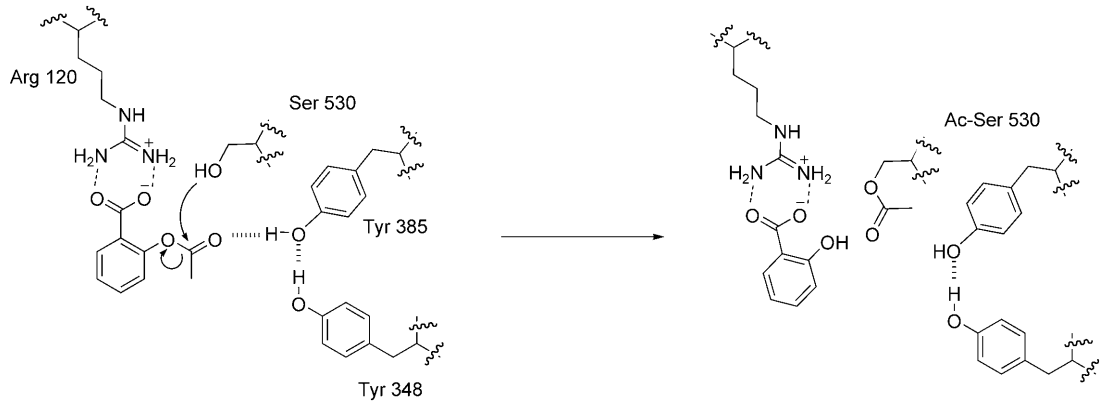
For nearly a century, the molecular mechanism of aspirin remained a mystery. However, in 1971, research by Vane indicated that aspirin inhibits prostaglandin biosynthesis.[130] This seminal finding explained both the beneficial properties and side effects of aspirin, and culminated in the awarding of a share of the 1982 Nobel Prize in Physiology or Medicine to Vane.[131] The prostaglandins are paracrine hormones that act on cells proximal to their place of synthesis. A trauma to cells results in an increase in local biosynthesis of prostaglandins, which cause elevated body temperature, inflammation, and pain.[132] Aspirin was found to acetylate and irreversibly inactivate prostaglandin endoperoxide (PGG/H) synthase, also termed cyclooxygenase (COX).[133] In addition, aspirin acetylates human hemoglobin and human serum albumin.[134]

The COX enzyme has two known isoforms, the constitutive COX-1 and the inducible COX-2.[135] COX enzymes catalyze the first two steps in the metabolism of arachidonic acid to prostaglandins. The cyclooxygenase activity incorporates two oxygen atoms into arachidonic acid to produce prostaglandin G_2 (PGG_2). PGG_2 is then subjected to the peroxidase section of these enzymes, which catalyzes a reduction of the hydroperoxy group of PGG_2 to the hydroxy endoperoxide, PGH_2.[133b,136]

It is recognized that aspirin inhibits the cyclooxygenase activity of the COX enzymes, but not their peroxidase activity.[137] Aspirin appears to exert its inhibitory effects by disrupting substrate (arachidonic acid) binding to the cyclooxygenase active site, as the serine residue acetylated by aspirin (Ser530 in COX-1, Ser516 in COX-2) is not critical for catalysis.[133b]

Studies of active-site COX residues have provided insight into the mechanism of COX enzymes, as well as that of aspirin acetylation. The mechanism of acetyl transfer involves several amino acids in the COX active site, including conserved tyrosine and arginine residues (Scheme 14).[138] In 1990, spectral and biochemical studies revealed that Tyr385 is essential for COX-1 cyclooxygenase activity.[139] Structurally, this tyrosine is properly positioned to perform the rate-limiting step of cyclooxygenation: abstraction of the 13-pro-*S* hydrogen atom from arachidonate.[139,140] A Tyr385Phe mutant of COX-2 displays virtually no serine acetylation by aspirin, and a Tyr348Phe mutant displays reduced activity and aspirin acetylation.[141] The latter result confirms the importance of Tyr348, which forms a hydrogen bond to Tyr385 and helps to position the substrate. Arginine 120 of COX-1 is an important residue for both substrate recognition and imparting sensitivity to inhibitors that contain a free carboxylic acid.[142] Analysis of a crystal structure of COX-1 suggests that the guanidino moiety interacts with the arachidonate carboxylate group.[143] Furthermore, reversible inhibitors with a free carboxylic acid, such as flurbiprofen, were ineffective against COX-1 enzymes with a mutation at Arg120.[142,143] The corresponding COX-2 Arg-to-Gln mutant was later found to have a 73% reduction of acetylation of Ser516 in COX-2.[141]

Based on the above experimental data, researchers have described a best possible mechanism for serine acetylation by aspirin (Scheme 14). The amino acid numbering scheme presented in the following paragraph corresponds to COX-1. Initial interaction of the carboxylate group of aspirin with Arg120 stabilizes its location in the substrate-binding pocket. The hydroxy groups of Tyr385 and Tyr348 then act as an extended hydrogen-bonding network. This directs the acetyl group of aspirin toward Ser530, and increases the reactivity of aspirin by stabilizing the developing negative charge of the



Scheme 14. An intricate network of hydrogen bonds and other interactions position aspirin to acetylate Ser530 of cyclooxygenase-1.

© 2005 Wiley-VCH Verlag GmbH & Co. KGaA, Weinheim

tetrahedral addition intermediate. The possibility of transient tyrosine acetylation was excluded by testing the acetylation of a Ser530Ala mutant, for which no *O*-acetyltyrosine was detected.[141] These data are all corroborated by the X-ray crystal structure of COX-1 inactivated by bromoaspirin (bromoacetylsalicylic acid). Bromoaspirin was used so that its location could be identified definitively in a relatively low-resolution (3.4 Å) crystal structure from the presence of the heavy bromine atom. The phenolic oxygen atom of Tyr385 is within hydrogen-bonding distance to the acetyl group.[144]

In summary, an elaborate scheme of hydrogen bonding and ionic interactions serves to position aspirin in the COX active site, increasing its effective concentration and enhancing its reactivity, which leads to the selective acetylation of Ser530. The X-ray structure also lends insight into the inhibitory effect of aspirin acetylation. Ser530 lies in a highly conserved region[133b] along a hydrophobic channel that leads from the surface of the enzyme to the catalytic tyrosine. The aspirin acetyl group extends outward into the channel, perhaps in a manner sufficient to prevent arachidonic acid from reaching the active site.[133b,144]

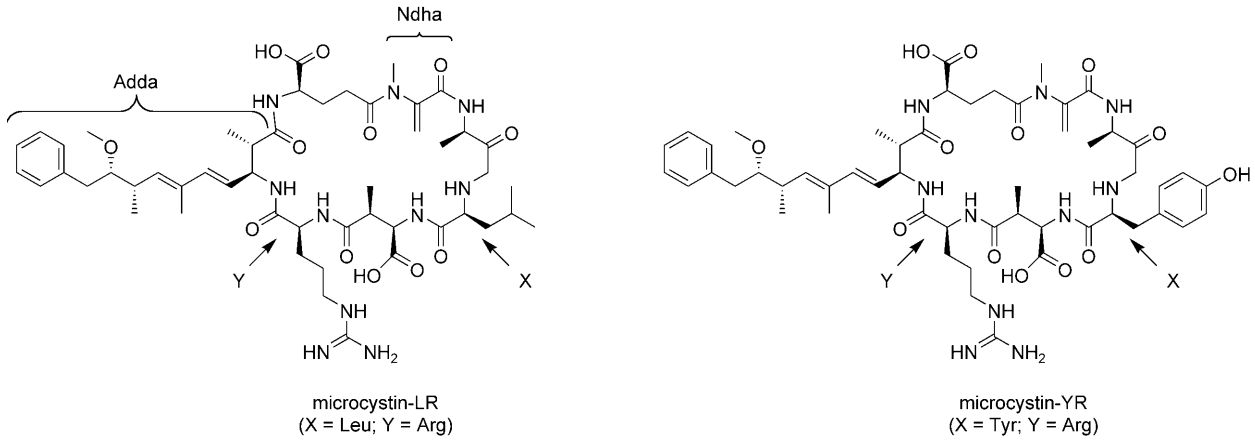
Finally, it is important to note that salicylic acid also possesses anti-inflammatory effects, but does not itself covalently modify COX enzymes. Discussion concerning the precise mechanism of action of salicylate is ongoing.[145] Thus, the conversion of this natural product to its semisynthetic derivative aspirin had the fortuitous effects of conferring mechanistic irreversibility and anointing principal protein targets for therapeutic intervention.

3.4. Microcystin

Cyanobacteria in the blue-green algae blooms of contaminated drinking water have been the cause of many animal deaths. Beginning in 1878,[146] it became evident that blooms of the genera *Oscillatoria*, *Anabaena*, *Nostoc*, and *Microcystis* in freshwater and marine environments were to blame for related incidents of acute toxicity.[147] The active components, a family of potent hepatotoxins, were isolated and a vigorous research effort initiated toward determining their structure.[148] Although the peptidic nature of the toxins was confirmed in 1959,[149] their amino acid compositions were not determined until many years later.[150] The first complete structure was determined by NMR spectroscopy and MS in 1984,[151] and was soon followed by characterization of other family members.[152] The toxins are cyclic heptapeptides with variable L-amino acid residues at two positions labeled X and Y. They contain an Adda residue, an unusual aromatic β-amino acid featuring an unsaturated alkyl chain (Scheme 15). An unambiguous determination of the configuration of Adda was published in 1988, confirming the structure as (2*S*,3*S*,8*S*,9*S*)-3-amino-9-methoxy-2,6,8-trimethyl-10-phenyl-(4*E*,6*E*)-decadienoic acid.[153] Various names were present in the literature for Adda-containing cyclic peptide natural products, but ultimately the name microcystin was chosen (Scheme 15).[154]

The microcystin family comprises more than sixty members;[155] the vast majority differ in the nature of two variable amino acids, or in the methylation states of the dehydroalanine and/or aspartic acid groups. In naming new microcystins, two letters are appended to abbreviate amino acids at the variable positions. Biosynthetic studies on microcystins were particularly focused on the identification of the origin of the carbon atoms in the Adda unit and the methylaspartic acid residue. Methylaspartic acid originates from acetyl-CoA and pyruvic acid via a methylsuccinic acid intermediate, and the Adda unit derives from acetate; certain methyl groups are methionine-derived.[156] Typically, microcystins are biosynthesized non-ribosomally.[157] Analyses of microcystin synthetase genes have yielded genes for polyketide synthases.[158]

Researchers also sought to understand the molecular nature of the toxicity of microcystins, and not long after the structures of these natural products were revealed, it was determined that they are potent inhibitors of serine/threonine phosphatases 1 and 2A,[7,147b,159] and other less-thoroughly characterized phosphatase family members.[160] Reversible protein phosphorylation is a critical mechanism for the regulation of cellular processes.[161] More than 98% of protein phosphorylation in eukaryotic cells occurs on serine and threonine residues.[160] Serine/threonine phosphatases 1 and 2A (PP1 and PP2A) have been implicated in the regulation of



microcystin-LR
(X = Leu; Y = Arg)

microcystin-YR
(X = Tyr; Y = Arg)

Scheme 15. Two prototypical microcystin family members; positions X and Y may represent any of several different amino acids. Ndha = *N*-methyl dehydroalanine.

 © 2005 Wiley-VCH Verlag GmbH & Co. KGaA, Weinheim

such diverse events as glycogen metabolism, synaptic plasticity, cell-cycle progression, embryogenesis, apoptosis and smooth-muscle contraction.[162] The structures, activities, and inhibition properties of PP1 and PP2A have been reviewed extensively.[163] Significantly, these enzymes do not possess a catalytic nucleophile; instead, they activate a water molecule for catalysis with protein-bound metal ion cofactors.[163]

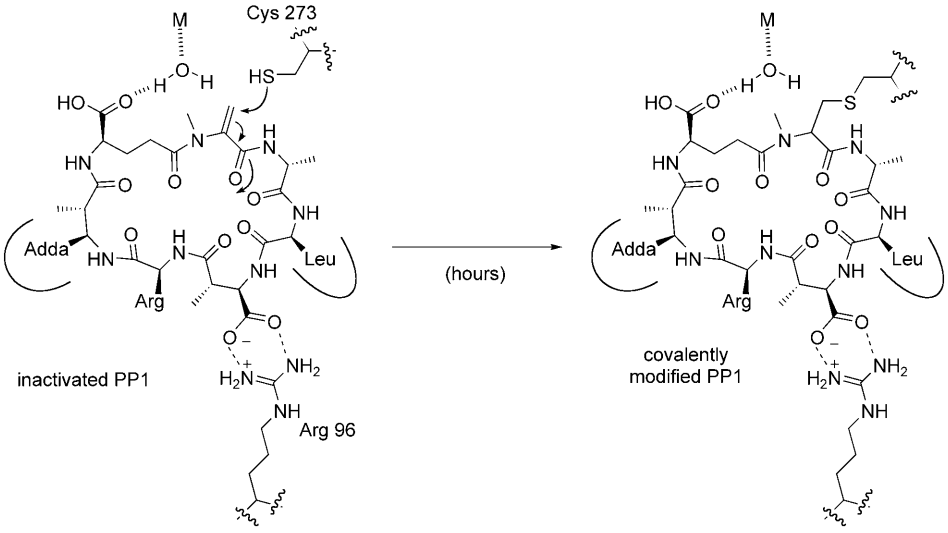
Indiscriminate inhibition of the many essential functions performed by PP1 and PP2A may contribute to the severe toxicity of the microcystins; between one and two micrograms constitutes a lethal intraperitoneal dose in mice.[147b] Although the broad toxicity of microcystins undermines their potential as therapeutic agents, research groups have synthesized variants and truncated versions of the toxin family to better understand the properties that confer toxicity and specificity.[164] So far, only one total synthesis of a microcystin family member has been completed.[165] These natural products have facilitated the functional characterization of phosphatases and phosphatase–protein complexes in proteomes.[159b,166] A microcystin-LR–rhodamine conjugate reacted with and detected numerous serine/threonine phosphatases in a crude cell lysate sample, and could record changes in phosphatase activity levels.[166] These probes expanded the list of enzyme families amenable to functional proteomic analysis.

Several bioactive natural products, such as leptomycin B,[167] isoavenaciolide,[168] and pironetin[169] have been shown to act as carbon-based electrophiles, similar to the α,β-unsaturated carbonyl element of the methyl-dehydroalanine residue of microcystin. In 1995, two research groups simultaneously published work confirming the conjugate addition chemistry of the dehydroalanine moiety of microcystin with PP1 at Cys 273 near the enzyme C terminus.[7,159a] In PP2A, the analogous Cys 266 is the targeted residue.[159a] The amino acid sequence Ser-Ala-Pro-Asn-Tyr-Cys, which includes the cysteine residue modified by microcystin, is highly conserved in Ser/Thr phosphatases.[7] The covalent linkage between the various microcystins and PP1 is stable to heat and acid. However, covalent binding of microcystin-YR to phosphatases was not observed when the proteins were denatured with sodium dodecyl sulfate prior to the addition of the natural product, indicating that the interaction depends on an intact active site.[7]

Microcystins bind to PP1 with subnanomolar affinity;[170] in the crystal structure of microcystin-LR bound to PP1, the Adda side chain makes contacts with a conserved hydrophobic groove, and the carboxyl group of glutamate and the adjacent carbonyl oxygen atom coordinate the metal-binding site indirectly through water molecules.[171] The leucine side chain of the toxin is situated in a loop of the C-terminal domain; in addition, the carboxyl group of methylaspartate hydrogen bonds to Arg 96, a residue crucial for interactions with phosphate groups on substrates. Hence, access to the active site is completely blocked.

The extensive interactions between microcystins and phosphatase active sites suggest that covalent reactivity contributes only partly to the mode of action of these natural products. Microcystins immobilized to a Sepharose bead through an aminoethanethiol adduct retained inhibitory activity over PP1 and PP2A.[159b] Microcystins-LR, YR, and RR were converted synthetically to their glutathione and cysteine conjugates; both of these thiols reacted with the dehydroalanine group, yet the 1,4-addition products retained a measure of in vivo toxicity ($LD_{50} = 38\ \mu g\,kg^{-1}$ for microcystin-LR; $LD_{50} = 630\ \mu g\,kg^{-1}$ for its glutathione conjugate).[171] Notably, such adducts may not be resistant toward retro-Michael reaction in vivo, and reversible adduct formation may explain the observed biological activity.[172] These results imply that the dehydroalanine residue probably does not play a role in early enzyme–inhibitor interactions.

Mechanistic studies by Craig and co-workers confirmed a two-step mechanism for irreversible inhibition by microcystins (Scheme 16).[173] In the first step, the rapid noncovalent binding and inhibition occurs with all the contacts detailed above. The slower covalent modification of Cys 273 occurs over the course of hours.[173] The tendency for the conjugate addition reaction is likely enhanced by the high



Scheme 16. Microcystin inactivates PP1 prior to the slow covalent attachment to Cys 273. However, the network of noncovalent interactions is essential for a successful conjugate addition.

© 2005 Wiley-VCH Verlag GmbH & Co. KGaA, Weinheim

effective concentration of microcystin in the well-folded binding pocket, as evidenced by the control reaction with denatured protein discussed above. It is also not out of the question that the nucleophilicity of the target cysteine may be enhanced in its local protein environment. Regardless, it is important to note that mutagenesis studies have found that Cys 273 is not required for catalysis; in fact, the activity of a Cys 273 Ser mutant is indistinguishable from that of the wild-type enzyme.[174] Thus, microcystins provide a salient example of how an intricate architecture of noncovalent interactions with enzymes can facilitate covalent modification on non-catalytic active-site residues. Notably, similar strategies have been employed to convert tight-binding reversible inhibitors into covalent inactivators of the EGF receptor[175a–c] and p90 ribosomal protein S6 kinase[175d] by the introduction of electrophilic groups in proximity to cysteine residues in the active sites of these proteins.

4. Targeting Nonenzymatic Proteins

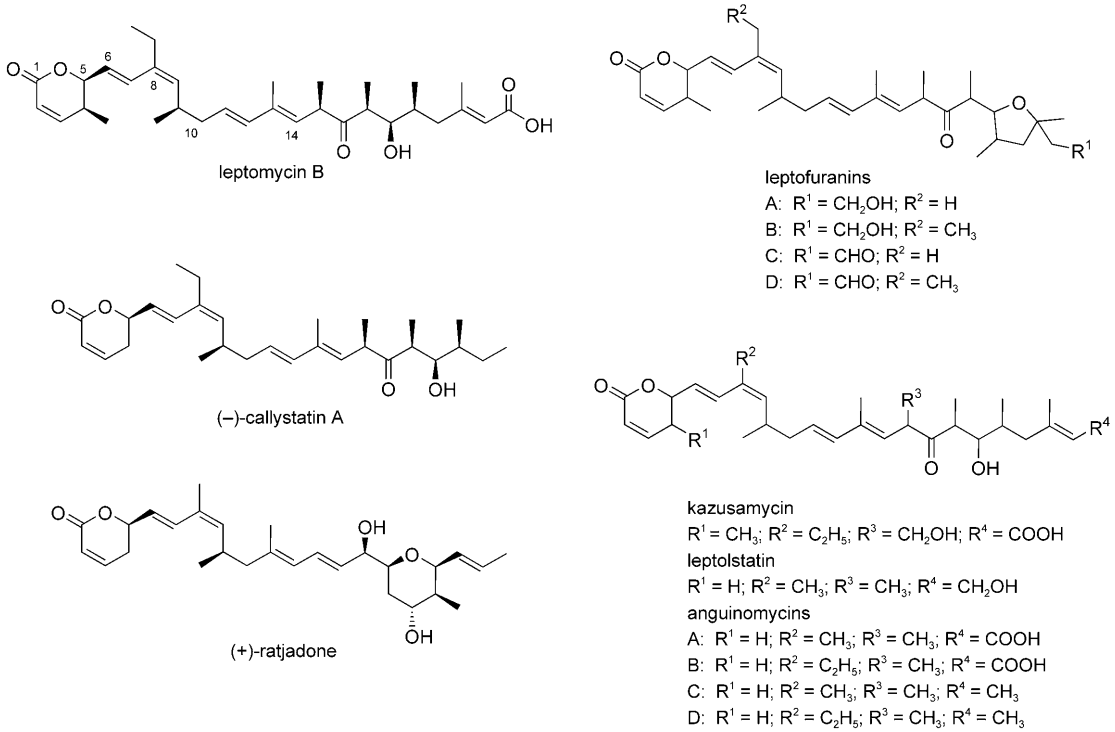
Although most protein-reactive natural products target the active sites of enzymes, there are exceptions. Here, we highlight one such natural product, leptomycin B, which covalently modifies a receptor protein involved in nuclear transport.

4.1. Leptomycin B

A *Streptomyces* strain isolated from soil samples yielded two novel antifungal antibiotics. The active components were purified, isolated, and termed leptomycins A and B.[176] These compounds constitute part of a family of structurally similar natural products, including callystatin A, ratjadone, kazusamycin, anguinomycin, leptofuranin and leptolstatin (Scheme 17).[177] Structures of the leptomycins were determined by NMR spectroscopy, MS, and IR spectroscopy.[178] They feature an unsaturated fatty acid with a terminal δ-lactone ring. Leptomycin B has a polyketide origin; it may be traced back to four acetate units, seven propionate units, and one butyrate unit.[179] Leptomycin B interferes with DNA synthesis stages of the cell cycle,[180] presumably a result of its inhibitory effect on nuclear transport.[181] A nanomolar binding partner for leptomycin B was discovered and named chromosome maintenance region 1 (CRM1).[182] CRM1, also known as exportin 1, is an evolutionarily conserved receptor for the leucine-rich nuclear export signal (NES)[183] of proteins and is an essential mediator of NES-dependent nuclear export of proteins and ribonucleoprotein complexes in eukaryotic cells.[182,184]

In conjunction with CRM1, the protein Rev allows partially processed HIV mRNAs to be transported outside the nucleus for translation, enabling the HIV virus to hijack the cellular protein synthesis machinery.[182,185] Agents like leptomycin B that block the interaction of Rev with nuclear transport proteins have the potential to inhibit HIV-1 replication.[186] Leptomycin B has also been used to accumulate the tumor suppressor p53 in the nucleus.[187] This subcellular localization leads to p53 activation, cell-cycle arrest, and apoptosis. Hence, leptomycin could represent a novel therapeutic approach for HIV and cancer treatment.[187,188]

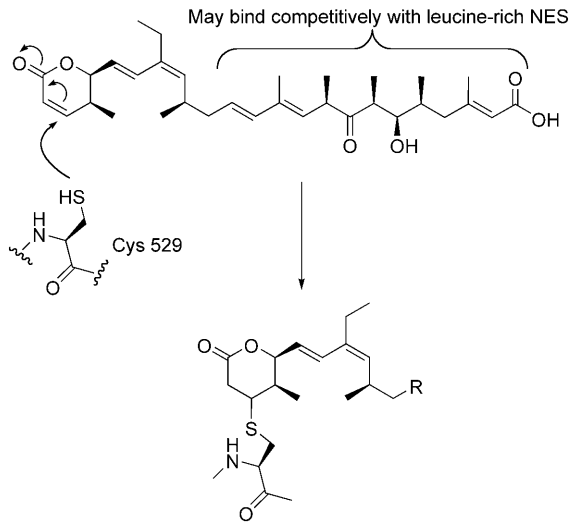
Leptomycin B binds to CRM1 and covalently modifies Cys 529 in a central conserved region of the protein, which inhibits recognition of the NES; ratjadone was recently found



Scheme 17. The leptomycin family of natural products.

 © 2005 Wiley-VCH Verlag GmbH & Co. KGaA, Weinheim

to share this mechanism (Scheme 18).[167,181,186a,189] Researchers found that a single mutation, Cys529Ser, in *Schizosaccharomyces pombe* was sufficient to greatly reduce sensitivity to leptomycin B.[167,190] To determine which portion of the



Scheme 18. The α,β-unsaturated lactone of leptomycin reacts by conjugate addition with Cys529 of exportin.

natural product serves as the pharmacophore, Kobayashi and colleagues performed extensive studies on a series of analogues of callystatin. The α,β-unsaturated lactone was found to be the crucial reactive element.[191] Other research groups reduced the lactone moiety to a saturated analogue[192] or formed a Michael adduct with nitromethane;[185a] both of these events greatly decreased inhibition.[192] Furthermore, *N*-acetylcysteine methyl ester and leptomycin B reacted to give a stable 1,4-addition product, as determined by NMR spectroscopy.[167] All these results lend credence to the idea that leptomycin binds covalently through an attack on its electrophilic α,β-unsaturated lactone function by the thiol group of CRM1 Cys529 (Scheme 18).

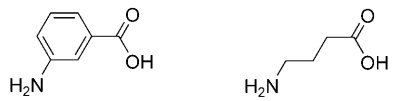
The role of Cys529 in CRM1 is not yet clear. This residue does not seem to be necessary for CRM1 to function. The Cys529Ser mutant mediates nuclear export just as effectively as wild-type CRM1, and it is not temperature-sensitive.[167] Moreover, wild-type *Saccharomyces cerevisiae* CRM1 has a threonine in place of cysteine at the analogous position.[167]

It is difficult to speculate further about the nature of the CRM1–leptomycin B interaction, as a structure of the complex has yet to be determined.[188,193] This information is crucial to the development of new drug candidates for the inhibition of nuclear translocation. Leptomycin B itself has a high toxicity profile, as demonstrated in a phase I clinical trial, and was not recommended for further development.[194] Several syntheses of leptomycin B and its relatives have been carried out in an effort to understand the function of this family of compounds.[191a,195] The premise that some of these reagents might selectively shut down transport of specific mRNA molecules is enticing and warrants further research.

In summary, CRM1 is a particularly notable target for a protein-reactive natural product, because this protein is not an enzyme. Despite this, leptomycin B labels Cys529 with exquisite specificity, suggesting that this residue resides in a structured small-molecule binding site. One intriguing possibility is that the central conserved region of CRM1 contains a hydrophobic pocket that is capable of interacting with both leucine-rich NESs and the distinct architecture of leptomycin B in a manner similar to enzyme active sites that bind substrates and inhibitors that often share little structural homology.[167]

5. Summary and Outlook

In this review, we have attempted to highlight the diversity of mechanisms by which natural products engage and covalently modify proteins and protein active sites. The specific compounds discussed are meant to serve as representatives of the different classes of protein-reactive natural products discovered so far, rather than as a comprehensive list. Notably, the reactivity of these natural products is not restricted to a specific type of amino acid, but rather can occur on a range of active-site residues, including serine (lipstatin, aspirin), threonine (lactacystin), lysine (wortmannin), cysteine (E-64, microcystin), and histidine (fumagillin). Moreover, these residues do not need to serve a catalytic function in the target enzyme class (for example, Cys273 in PP1) or, for that matter, to be part of an enzyme active site (as is the case for Cys529 in CRM1). This underscores the creative ability of nature to exploit "spurious" nucleophiles in small-molecule binding sites for the selective modification of proteins. Although all the natural products discussed herein inactivate their cognate protein targets by modifying amino acid residues, other mechanisms of enzyme inhibition are possible. For example, gabaculine (Scheme 19), a rare amino acid



Scheme 19. The natural product gabaculine is a conformationally constrained GABA analogue. GABA = γ-aminobutyric acid.

isolated from the mold *Streptomyces toyocaensis*,[196] inactivates several related aminotransferases by covalently reacting with the enzyme's pyridoxal phosphate cofactor (Table 1).[8c,197]

What lessons might be learned from protein-reactive natural products that could assist in the design of chemical probes for the burgeoning field of activity-based protein profiling (ABPP)?[9] ABPP is a functional proteomic method that aims to develop active-site-directed probes that label many enzymes in parallel, thereby facilitating their collective functional characterization in samples of high biological complexity. The application of ABPP methods has so far enabled the discovery of enzyme activities that are upregulated in diseases like cancer,[69,198] obesity,[199] and malaria;[200] it has also enabled the design of selective inhibitors for these enzymes.[201]

 © 2005 Wiley-VCH Verlag GmbH & Co. KGaA, Weinheim

Table 1: Representative protein-reactive natural products and their targets.

Natural product	Target	Labeled residue	Catalytic nucleophile?
lipstatin	pancreatic lipase	Ser 152	yes
lactacystin	proteasome β subunits	Thr 1	yes
E-64	papain (Cys proteases)	Cys 25	yes
fumagillin	MetAP-2	His -231	no
wortmannin	PI 3-kinase	Lys 802	no
aspirin	COX-1	Ser 530	no
	COX-2	Ser 516	no
microcystin	PP1	Cys 273	no
	PP2A	Cys 266	no
leptomycin B	CRM1	Cys 529	no
gabaculine	aminotransferases	PLP cofactor[a]	no

[a] PLP = pyridoxal phosphate.

The profound influence of protein-reactive natural products on the maturation of ABPP can be discerned at several levels. First, and perhaps most clear, many ABPP probes are themselves derivatives of natural products, including biotin/fluorophore-tagged reagents that target cysteine proteases (based on E-64),[68a,b,201b] phosphatases (based on microcystin),[166] and kinases (based on wortmannin).[124] A second class of ABPP probes also borrows a strategy of natural products by modifying conserved catalytic nucleophiles in enzyme active sites. These probes, which include fluorophosphonate and electrophilic ketone reagents for serine[202] and cysteine[203] hydrolases, respectively, typically exhibit a broad target spectrum within a given family of enzymes. Even ABPP probes that incorporate photoreactive (rather than electrophilic) groups could be considered as followers of the precedents set by natural products, as they too exploit class-selective functional groups to bind conserved elements of enzyme active sites.[204] Finally, the principles derived from protein-reactive natural products have also inspired the emergence of a third approach for ABPP that explores the proteome reactivity of structurally diverse libraries of electrophilic agents.[199,205] In this combinatorial, or "nondirected" approach for ABPP, probe libraries have been designed to contain carbon electrophiles, based in large part on the rich diversity of natural products that have exploited this versatile reactive group, to label enzyme active sites (for example, fumagillin, wortmannin, and microcystin). To date, nondirected ABPP efforts have identified active-site proteomics probes for more than 10 mechanistically distinct enzyme classes.[9,199] Remarkably, most of these enzymes lack cognate affinity agents, underscoring the value of nondirected ABPP for the discovery of novel molecular probes of enzyme function.

Looking forward, we anticipate that our understanding of the full spectrum of mechanisms employed by natural products to target protein active sites is still far from complete. Given the central role that natural products have played in the elucidation of the biochemical and cell-biological activities of proteins, we strongly advocate the sustained pursuit of these special pharmacological agents. Their discovery and characterization should continue to offer fascinating insight into the seemingly endless array of small-molecule–protein interactions that occur in nature. The lessons learned from these studies should in turn guide chemical biologists in their efforts to achieve a paramount objective of post-genomic science—the design of selective small-molecule probes for the functional analysis of every protein.

We thank K. Barglow and Dr. E. C. Taylor for critical reading of this manuscript, and Dr. M. H. Bracey for assistance with the generation of figures. This research was supported by the NIH (CA087660), NIGMS (GM065483), a Bristol Myers-Squibb Unrestricted Grant in Synthetic Organic Chemistry, the Skaggs Institute for Chemical Biology, and Princeton University. C.D. gratefully acknowledges predoctoral fellowships from Eli Lilly and the National Science Foundation.

Received: March 10, 2005

[1] a) A. Pandey, M. Mann, *Nature* **2000**, *405*, 837–846; b) N. L. Anderson, N. G. Anderson, *Electrophoresis* **1998**, *19*, 1853–1861.
[2] a) D. T. Hung, T. F. Jamison, S. L. Schreiber, *Chem. Biol.* **1996**, *3*, 623–639; b) R. F. Standaert, A. Galat, G. L. Verdine, S. L. Schreiber, *Nature* **1990**, *346*, 671–674.
[3] K. Nakanishi in *Comprehensive Natural Products Chemistry, Vol. 1* (Eds.: D. Barton, K. Nakanishi, O. Meth-Cohn, U. Sankawa), Elsevier, New York, **1999**, pp. xxiii-xl.
[4] N. Kasanah, M. T. Hamann, *Expert Opin. Invest. Drugs* **2004**, *5*, 827–837.
[5] P. Hadvary, W. Sidler, W. Meister, W. Vetter, H. Wolfer, *J. Biol. Chem.* **1991**, *266*, 2021–2027.
[6] a) W. T. Lowther, D. A. McMillen, A. M. Orville, B. W. Matthews, *Proc. Natl. Acad. Sci. USA* **1998**, *95*, 12153–12157; b) N. Sin, L. H. Meng, M. Q. W. Wang, J. J. Wen, W. G. Bornmann, C. M. Crews, *Proc. Natl. Acad. Sci. USA* **1997**, *94*, 6099–6103.
[7] R. W. Mackintosh, K. N. Dalby, D. G. Campbell, P. T. W. Cohen, P. Cohen, C. Mackintosh, *FEBS Lett.* **1995**, *371*, 236–240.
[8] a) R. B. Silverman, *Methods Enzymol.* **1995**, *249*, 240–283; b) R. R. Rando, *Pharmacol. Rev.* **1984**, *36*, 111–142; c) C. Walsh, *Tetrahedron* **1982**, *38*, 871–909.
[9] a) A. E. Speers, B. F. Cravatt, *ChemBioChem* **2004**, *5*, 41–47; b) G. C. Adam, E. J. Sorensen, B. F. Cravatt, *Mol. Cell. Proteomics* **2002**, *1*, 781–790; c) B. F. Cravatt, E. J. Sorensen, *Curr. Opin. Chem. Biol.* **2000**, *4*, 663–668.
[10] P. R. Graves, T. A. J. Haystead, *Microbiol. Mol. Biol. Rev.* **2002**, *66*, 39–63.
[11] a) J. F. Fisher, S. Q. Meroueh, S. Mobashery, *Chem. Rev.* **2005**, *105*, 395–424; b) S. J. Coulthurst, A. M. L. Barnard, G. P. C. Salmond, *Nat. Rev. Microbiol.* **2005**, *3*, 295–306; c) B. F. Gherman, S. D. Goldberg, V. W. Cornish, R. A. Friesner, *J. Am. Chem. Soc.* **2004**, *126*, 7652–9664; d) J. R. Knowles, *Acc. Chem. Res.* **1985**, *18*, 97–104.
[12] a) D. L. Boger, R. M. Garbaccio, *Acc. Chem. Res.* **1999**, *32*, 1043–1052; b) K. S. Gates in *Comprehensive Natural Products Chemistry, Vol. 7* (Eds.: D. Barton, K. Nakanishi, O. Meth-Cohn, E. T. Kool), Elsevier, New York, **1999**, pp. 491–552; c) D. L. Boger, D. S. Johnson, *Angew. Chem.* **1996**, *108*, 1542–1580; *Angew. Chem. Int. Ed. Engl.* **1996**, *35*, 1438–1474.
[13] J. A. Gerlt, *Nat. Biotechnol.* **2002**, *20*, 786–787.

 © 2005 Wiley-VCH Verlag GmbH & Co. KGaA, Weinheim

[14] a) P. Hadvary, H. Lengsfeld, H. Wolfer, *Biochem. J.* **1988**, *256*, 357 – 361; b) E. K. Weibel, P. Hadvary, E. Hochuli, E. Kupfer, H. Lengsfeld, *J. Antibiot.* **1987**, *40*, 1081 – 1086.

[15] E. Hochuli, E. Kupfer, R. Maurer, W. Meister, Y. Mercadal, K. Schmidt, *J. Antibiot.* **1987**, *40*, 1086 – 1091.

[16] a) P. Barbier, F. Schneider, *Helv. Chim. Acta* **1987**, *70*, 196 – 202; b) P. Barbier, F. Schneider, U. Widmer, *Helv. Chim. Acta* **1987**, *70*, 1412 – 1418.

[17] H. Umezawa, T. Aoyagi, T. Hazato, K. Uotani, F. Kojima, M. Hamada, T. Takeuchi, *J. Antibiot.* **1978**, *31*, 639 – 641.

[18] K. Yoshinari, M. Aoki, T. Ohtsuka, N. Nakayama, Y. Itezono, M. Mutoh, J. Watanabe, K. Yokose, *J. Antibiot.* **1994**, *47*, 1376 – 1384.

[19] a) K. Uotani, H. Naganawa, S. Kondo, T. Aoyagi, H. Umezawa, *J. Antibiot.* **1982**, *35*, 1495 – 1499; b) K. Uotani, H. Naganawa, T. Aoyagi, H. Umezawa, *J. Antibiot.* **1982**, *35*, 1670 – 1674; c) H. Umezawa, T. Aoyagi, K. Uotani, M. Hamada, T. Takeuchi, S. Takahashi, *J. Antibiot.* **1980**, *33*, 1594 – 1596.

[20] M. Kitahara, M. Asano, H. Naganawa, K. Maeda, M. Hamada, T. Aoyagi, H. Umezawa, Y. Iitaka, H. Nakamura, *J. Antibiot.* **1987**, *40*, 1647 – 1650.

[21] a) C. A. Schuhr, W. Eisenreich, M. Goese, P. Stohler, W. Weber, E. Kupfer, A. Bacher, *J. Org. Chem.* **2002**, *67*, 2257 – 2262; b) M. Goese, W. Eisenreich, E. Kupfer, P. Stohler, W. Weber, H. G. Leuenberger, A. Bacher, *J. Org. Chem.* **2001**, *66*, 4673 – 4678; c) M. Goese, W. Eisenreich, E. Kupfer, W. Weber, A. Bacher, *J. Biol. Chem.* **2000**, *275*, 21192 – 21196; d) W. Eisenreich, E. Kupfer, W. Weber, A. Bacher, *J. Biol. Chem.* **1997**, *272*, 867 – 874.

[22] a) B. Borgstrom, *Biochim. Biophys. Acta* **1988**, *962*, 308 – 316; b) F. H. Stodola, A. Lesuk, R. J. Anderson, *J. Biol. Chem.* **1938**, *126*, 505 – 513.

[23] A. Pommier, J. M. Pons, P. J. Kocienski, *J. Org. Chem.* **1995**, *60*, 7334 – 7339.

[24] a) J. A. Bodkin, E. J. Humphries, M. D. McLeod, *Tetrahedron Lett.* **2003**, *44*, 2869 – 2872; b) A. K. Ghosh, S. Fidanze, *Org. Lett.* **2000**, *2*, 2405 – 2407; c) P. J. Parsons, J. K. Cowell, *Synlett* **2000**, 107 – 109; d) A. K. Ghosh, C. F. Liu, *Chem. Commun.* **1999**, 1743 – 1744; e) C. Lowe, J. C. Vederas, *Org. Prep. Proced. Int.* **1995**, *27*, 305 – 346; f) A. Pommier, J. M. Pons, P. I. Kocienski, L. Wong, *Synthesis* **1994**, 1294 – 1300.

[25] F. K. Winkler, A. D'Arcy, W. Hunziker, *Nature* **1990**, *343*, 771 – 774.

[26] a) M. E. Lowe, *J. Lipid Res.* **2002**, *43*, 2007 – 2016; b) A. M. Heck, J. A. Yanovski, K. A. Calis, *Pharmacotherapy* **2000**, *20*, 270 – 279; c) M. E. Lowe, *Annu. Rev. Nutr.* **1997**, *17*, 141 – 158; d) S. Ransac, Y. Gargouri, F. Marguet, G. Buono, C. Beglinger, P. Hildebrand, H. Lengsfeld, P. Hadvary, R. Verger, *Methods Enzymol.* **1997**, *286*, 190 – 231.

[27] a) P. Hollander, *Prim Care.* **2003**, *30*, 427 – 440; b) K. H. Lucas, B. Kaplan-Machlis, *Ann. Pharmacother.* **2001**, *35*, 314 – 328; c) A. Ballinger, *Expert Opin. Pharmacother.* **2000**, *1*, 841 – 847.

[28] a) L. M. Prisant, *J. Clin. Pharmacol.* **2004**, *44*, 406 – 413; b) D. E. Kelley, M. Jneidi, *Expert Opin. Pharmacother.* **2002**, *3*, 599 – 605; c) L. J. Aronne, *Prog. Cardiovasc. Nurs.* **2001**, *16*, 98 – 106, 115; d) G. M. Keating, B. Jarvis, *Drugs* **2001**, *61*, 2107 – 2119.

[29] S. J. Kridel, F. Axelrod, N. Rozenkrantz, J. W. Smith, *Cancer Res.* **2004**, *64*, 2070 – 2075.

[30] a) H. Stalder, G. Oesterhelt, *Helv. Chim. Acta* **1992**, *75*, 1593 – 1603; b) Q. Q. Luthipeng, H. P. Marki, P. Hadvary, *FEBS Lett.* **1992**, *299*, 111 – 115; c) H. Stalder, P. R. Schneider, G. Oesterhelt, *Helv. Chim. Acta* **1990**, *73*, 1022 – 1036.

[31] D. J. Waxman, J. L. Strominger, *Annu. Rev. Biochem.* **1983**, *52*, 825 – 869.

[32] C. Therrien, R. C. Levesque, *FEMS Microbiol. Rev.* **2000**, *24*, 251 – 262.

[33] A. Lookene, N. Skotlova, G. Olivecrona, *Eur. J. Biochem.* **1994**, *222*, 395 – 403.

[34] S. Omura, T. Fujimoto, K. Otoguro, K. Matsuzaki, R. Moriguchi, H. Tanaka, Y. Sasaki, *J. Antibiot.* **1991**, *44*, 113 – 116.

[35] S. Omura, K. Matsuzaki, T. Fujimoto, K. Kosuge, T. Furuya, S. Fujita, A. Nakagawa, *J. Antibiot.* **1991**, *44*, 117 – 118.

[36] a) C. E. Masse, A. J. Morgan, J. Adams, J. S. Panek, *Eur. J. Org. Chem.* **2000**, 2513 – 2528; b) E. J. Corey, W.-D. Z. Li, G. A. Reichard, *J. Am. Chem. Soc.* **1998**, *120*, 2330 – 2336; c) E. J. Corey, W. D. Li, T. Nagamitsu, *Angew. Chem.* **1998**, *110*, 1784 – 1787; *Angew. Chem. Int. Ed.* **1998**, *37*, 1676 – 1679; d) N. Chida, J. Takeoka, K. Ando, N. Tsutsumi, S. Ogawa, *Tetrahedron* **1997**, *53*, 16287 – 16298; e) H. Uno, J. E. Baldwin, I. Churcher, A. T. Russell, *Synlett* **1997**, 390 – 392; f) T. Nagamitsu, T. Sunazuka, H. Tanaka, S. Omura, P. A. Sprengeler, A. B. Smith, *J. Am. Chem. Soc.* **1996**, *118*, 3584 – 3590; g) N. Chida, J. Takeoka, N. Tsutsumi, S. Ogawa, *J. Chem. Soc. Chem. Commun.* **1995**, 793 – 794; h) H. Uno, J. E. Baldwin, A. T. Russell, *J. Am. Chem. Soc.* **1994**, *116*, 2139 – 2140; i) T. Sunazuka, T. Nagamitsu, K. Matsuzaki, H. Tanaka, S. Omura, A. B. Smith, *J. Am. Chem. Soc.* **1993**, *115*, 5302 – 5302; j) E. J. Corey, G. A. Reichard, *J. Am. Chem. Soc.* **1992**, *114*, 10677 – 10678.

[37] a) A. Nakagawa, M. Kainosho, S. Omura, *Pure Appl. Chem.* **1994**, *66*, 2411 – 2413; b) A. Nakagawa, S. Takahashi, K. Uchida, K. Matsuzaki, S. Omura, A. Nakamura, N. Kurihara, T. Nakamatsu, Y. Miyake, K. Take, M. Kainosho, *Tetrahedron Lett.* **1994**, *35*, 5009 – 5012.

[38] a) L. R. Dick, A. A. Cruikshank, L. Grenier, F. D. Melandri, S. L. Nunes, R. L. Stine, *J. Biol. Chem.* **1996**, *271*, 7273 – 7276; b) G. Fenteany, R. F. Standaert, W. S. Lane, S. Choi, E. J. Corey, S. L. Schreiber, *Science* **1995**, *268*, 726 – 731; c) G. Fenteany, R. F. Standaert, G. A. Reichard, E. J. Corey, S. L. Schreiber, *Proc. Natl. Acad. Sci. USA* **1994**, *91*, 3358 – 3362.

[39] a) B. Alberts, A. Johnson, J. Lewis, M. Raff, K. Roberts, P. Walter, *Molecular Biology of the Cell, 4th ed.*, Garland Science, New York, **2002**, pp. 358 – 359; b) M. Bogyo, M. Gaczynska, H. L. Ploegh, *Biopolymers* **1997**, *43*, 269 – 280.

[40] P. J. Elliott, T. M. Zollner, W. H. Boehncke, *J. Mol. Med.* **2003**, *81*, 235 – 245.

[41] M. Groll, L. Ditzel, J. Loewe, D. Stock, M. Bochter, H. D. Bartunik, R. Huber, *Nature* **1997**, *386*, 463 – 471.

[42] a) E. Seemüller, A. Lupas, D. Stock, J. Löwe, R. Huber, H. Baumeister, *Science* **1995**, *268*, 579 – 582; b) O. Coux, K. Tanaka, A. L. Goldberg, *Annu. Rev. Biochem.* **1996**, *65*, 801 – 847.

[43] a) L. Kozlowski, T. Stoklosa, S. Omura, C. Wojcik, M. Z. Wojtukiewicz, K. Worowski, H. Ostrowska, *Tumor Biol.* **2001**, *22*, 211 – 215; b) H. Ostrowska, C. Wojcik, S. Wilk, S. Omura, L. Kozlowski, T. Stoklosa, K. Worowski, P. Radziwon, *Int. J. Biochem. Cell Biol.* **2000**, *32*, 747 – 757; c) H. Ostrowska, C. Wojcik, S. Omura, K. Worowski, *Biochem. Biophys. Res. Commun.* **1997**, *234*, 729 – 732.

[44] a) A. F. Kisselev, A. L. Goldberg, *Chem. Biol.* **2001**, *8*, 739 – 758; b) G. Fenteany, S. L. Schreiber, *J. Biol. Chem.* **1998**, *273*, 8545 – 8548.

[45] a) D. H. Lee, A. L. Goldberg, *Trends Cell Biol.* **1998**, *8*, 397 – 403; b) M. Bogyo, J. S. McMaster, M. Gaczynska, D. Tortorella, A. L. Goldberg, H. L. Ploegh, *Proc. Natl. Acad. Sci. USA* **1997**, *94*, 6629 – 6634; c) M. C. Sousa, B. M. Kessler, H. J. Overkleeft, R. B. McKay, *J. Mol. Biol.* **2002**, *318*, 779 – 785.

[46] G. Martinelli, P. Tosi, E. Ottaviani, S. Soverini, S. Tura, *Haematologica* **2001**, *86*, 908 – 917.

[47] R. Twombly, *J. Natl. Cancer Inst.* **2003**, *95*, 845.

[48] F. Soucy, L. Grenier, M. L. Behnke, A. T. Destree, T. A. McCormack, J. Adams, L. Plamondon, *J. Am. Chem. Soc.* **1999**, *121*, 9967 – 9976.

© 2005 Wiley-VCH Verlag GmbH & Co. KGaA, Weinheim

[49] a) E. J. Corey, W.-D. Z. Li, *Chem. Pharm. Bull.* **1999**, *47*, 1–10; b) L. R. Dick, A. A. Cruikshank, A. T. Destree, L. Grenier, T. A. McCormack, F. D. Melandri, S. L. Nunes, V. J. Palombella, L. A. Parent, L. Plamondon, R. L. Stein, *J. Biol. Chem.* **1997**, *272*, 182–188.

[50] A. Craiu, M. Gaczynska, T. Akopian, C. F. Gramm, G. Fenteany, A. L. Goldberg, K. L. Rock, *J. Biol. Chem.* **1997**, *272*, 13437–13445.

[51] A. F. Kisselev, Z. Songyang, A. L. Goldberg, *J. Biol. Chem.* **2000**, *275*, 14831–14837.

[52] E. J. Corey, W. D. Z. Li, T. Nagamitsu, G. Fenteany, *Tetrahedron* **1999**, *55*, 3305–3316.

[53] R. H. Feling, G. O. Buchanan, T. J. Mincer, C. A. Kaufmann, P. R. Jensen, W. Fenical, *Angew. Chem.* **2003**, *115*, 369–371; *Angew. Chem. Int. Ed.* **2003**, *42*, 355–357.

[54] L. R. Reddy, P. Saravanan, E. J. Corey, *J. Am. Chem. Soc.* **2004**, *126*, 6230–6231.

[55] M. Stadler, S. Seip, H. Mueller, A. Mayer-Bartschmid, M.-A. Bruenig, J. Benet-Buchholz, H. Togame, R. Dodo, P. Reinemer, K. Bacon, K. Fuchikami, S. Matsukawa, K. Urbahns, *PCT Int. Appl.* **2004**, 79 pp. CODEN: PIXXD2 WO 2004071382 A2 20040826 CAN 141:224070 AN 2004:701941.

[56] K. Hanada, M. Tamai, M. Yamagishi, S. Ohmura, J. Sawada, I. Tanaka, *Agric. Biol. Chem.* **1978**, *42*, 523–528.

[57] K. Hanada, M. Tamai, S. Ohmura, J. Sawada, T. Seki, I. Tanaka, *Agric. Biol. Chem.* **1978**, *42*, 529–536.

[58] K. Hanada, M. Tamai, S. Morimoto, T. Adachi, S. Ohmura, J. Sawada, I. Tanaka, *Agric. Biol. Chem.* **1978**, *42*, 537–541.

[59] a) L. H. Meng, R. Mohan, B. H. B. Kwok, M. Elofsson, N. Sin, C. M. Crews, *Proc. Natl. Acad. Sci. USA* **1999**, *96*, 10403–10408; b) N. Sin, K. B. Kim, M. Elofsson, L. H. Meng, H. Auth, B. H. B. Kwok, C. M. Crews, *Bioorg. Med. Chem. Lett.* **1999**, *9*, 2283–2288.

[60] L. H. Meng, B. H. B. Kwok, N. Sin, C. M. Crews, *Cancer Res.* **1999**, *59*, 2798–2801.

[61] A. J. Barrett, A. A. Kembhavi, M. A. Brown, H. Kirschke, C. G. Knight, M. Tamai, K. Hanada, *Biochem. J.* **1982**, *201*, 189–198.

[62] M. J. Harrison, N. A. Burton, I. H. Hillier, *J. Am. Chem. Soc.* **1997**, *119*, 12285–12291.

[63] a) M. Lee, R. Fridman, S. Mobashery, *Chem. Soc. Rev.* **2004**, *33*, 401–409; b) A. Baruch, D. Greenbaum, E. T. Levy, P. A. Nielsen, N. B. Gilula, N. M. Kumar, M. Bogyo, *J. Biol. Chem.* **2001**, *276*, 28999–29006; c) J. G. Tidball, M. J. Spencer, *Int. J. Biochem. Cell Biol.* **2000**, *32*, 1–5; d) H. H. Otto, T. Schirmeister, *Chem. Rev.* **1997**, *97*, 133–171.

[64] B. K. Na, T. S. Kim, P. J. Rosenthal, J. K. Lee, Y. Kong, *Parasitol. Res.* **2004**, *94*, 312–317.

[65] T. Noda, K. Isogai, N. Katunuma, Y. Tarumoto, M. Ohzeki, *J. Biochem.* **1981**, *90*, 893–896.

[66] a) Y. Shoji-Kasai, M. Senshu, S. Iwashita, K. Imahori, *Proc. Natl. Acad. Sci. USA* **1988**, *85*, 146–150; b) M. Tamai, K. Matsumoto, S. Omura, I. Koyama, Y. Ozawa, K. Hanada, *J. Pharmacobio-Dyn.* **1986**, *9*, 672–677.

[67] a) *Drugs Future* **1994**, *19*, 1040; b) P. Mathur, S. K. Gupta, A. R. Wegener, W. Breipohl, M. H. Ahrend, Y. D. Sharma, Y. K. Gupta, R. B. Vajpayee, *Curr. Eye Res.* **2000**, *21*, 926–933; c) M. Inomata, H. Hayashi, S. Shumiya, S. Kawashima, Y. Ito, *J. Biochem.* **2000**, *128*, 771–776.

[68] a) R. A. L. van der Hoorn, M. A. Leeuwenburgh, M. Bogyo, M. H. A. J. Joosten, S. C. Peck, *Plant Physiol.* **2004**, *135*, 1170–1178; b) D. Greenbaum, K. F. Medzihradszky, A. Burlingame, M. Bogyo, *Chem. Biol.* **2000**, *7*, 569–581; c) H. Cheng, C. A. Parish, B. A. Gilbert, R. R. Rando, *Biochemistry* **1995**, *34*, 16662–16671; d) G. Velasco, A. A. Ferrando, X. S. Puente, L. M. Sanchez, C. Lopezotin, *J. Biol. Chem.* **1994**, *269*, 27136–27142.

[69] J. A. Joyce, A. Baruch, K. Chehade, N. Meyer-Morse, E. Giraudo, F. Y. Tsai, D. C. Greenbaum, J. H. Hager, M. Bogyo, D. Hanahan, *Cancer Cell* **2004**, *5*, 443–453.

[70] Y. Yabe, D. Guillaume, D. H. Rich, *J. Am. Chem. Soc.* **1988**, *110*, 4043–4044.

[71] K. Matsumoto, K. Mizoue, K. Kitamura, W. C. Tse, C. P. Huber, T. Ishida, *Biopolymers* **1999**, *51*, 99–107.

[72] a) K. Matsumoto, M. Murata, S. Sumiya, K. Mizoue, K. Kitamura, T. Ishida, *Biochim. Biophys. Acta* **1998**, *1383*, 93–100; b) A. Fujishima, Y. Imai, T. Nomura, Y. Fujisawa, Y. Yamamoto, T. Sugawara, *FEBS Lett.* **1997**, *407*, 47–50; c) B. G. Zhao, C. A. Janson, B. Y. Amegadzie, K. D'Alessio, C. Griffin, C. R. Hanning, C. Jones, J. Kurdyla, M. McQueney, X. Y. Qiu, W. W. Smith, S. S. Abdel-Meguid, *Nat. Struct. Biol.* **1997**, *4*, 109–111; d) N. A. Katerelos, M. A. J. Taylor, M. Scott, P. W. Goodenough, R. W. Pickersgill, *FEBS Lett.* **1996**, *392*, 35–39; e) K. I. Varughese, Y. Su, D. Cromwell, S. Hasnain, N. H. Xuong, *Biochemistry* **1992**, *31*, 5172–5176; f) D. Yamamoto, K. Matsumoto, H. Ohishi, T. Ishida, M. Inoue, K. Kitamura, K. Hanada, *FEBS Lett.* **1990**, *263*, 134–136; g) D. Yamamoto, K. Matsumoto, T. Ishida, M. Inoue, S. Sumiya, K. Kitamura, *Chem. Pharm. Bull.* **1989**, *37*, 2577–2581.

[73] F. R. Hanson, E. Eble, *J. Bacteriol.* **1949**, *58*, 527–529.

[74] a) J. R. Turner, D. S. Tarbell, *Proc. Natl. Acad. Sci. USA* **1962**, *59*, 733–735; b) D. S. Tarbell, R. M. Carman, D. D. Chapman, S. E. Cremer, A. D. Cross, K. R. Huffman, M. Kunstmann, N. J. McCorkindale, J. J. G. McNally, A. Rosowsky, F. H. L. Varino, R. L. West, *J. Am. Chem. Soc.* **1961**, *83*, 3096–3113; c) D. S. Tarbell, R. M. Carman, D. D. Chapman, K. R. Huffman, N. J. McCorkindale, *J. Am. Chem. Soc.* **1960**, *82*, 1005–1007.

[75] N. McCorkindale, J. G. Sime, *Proc. Chem. Soc. London* **1961**, 331.

[76] a) B. B. Snider, PhD thesis, Harvard University **1973**; b) E. J. Corey, B. B. Snider, *J. Am. Chem. Soc.* **1972**, *94*, 2549–2550.

[77] a) D. Kim, S. K. Ahn, H. Bae, W. J. Choi, H. S. Kim, *Tetrahedron Lett.* **1997**, *38*, 4437–4440; for other syntheses of fumagillin/fumagillol, see: b) O. Bedel, A. Haudrechy, Y. Langlois, *Eur. J. Org. Chem.* **2004**, 3813–3819; c) D. F. Taber, T. E. Christos, A. L. Rheingold, I. A. Guzei, *J. Am. Chem. Soc.* **1999**, *121*, 5589–5590.

[78] D. A. Vosburg, S. Weiler, E. J. Sorensen, *Angew. Chem.* **1999**, *111*, 1024–1027; *Angew. Chem. Int. Ed.* **1999**, *38*, 971–974.

[79] a) P. Bollinger, H. P. Sigg, H. P. Weber, *Helv. Chim. Acta* **1973**, *56*, 819–830; b) H. P. Sigg, H. P. Weber, *Helv. Chim. Acta* **1968**, *51*, 1395–1408.

[80] a) H. Hatanaka, T. Kino, M. Hashimoto, Y. Tsurumi, A. Kuroda, H. Tanaka, T. Goto, M. Okuhara, *J. Antibiot.* **1988**, *41*, 999–1008; b) S. Amano, N. Ogawa, M. Ohtsuka, N. Chida, *Tetrahedron* **1999**, *55*, 2205–2224.

[81] a) D. E. Cane, D. B. McIlwaine, *Tetrahedron Lett.* **1987**, *28*, 6545–6548; b) D. E. Cane, S. L. Buchwald, *J. Am. Chem. Soc.* **1977**, *99*, 6132–6134; c) D. E. Cane, G. G. S. King, *Tetrahedron Lett.* **1976**, *17*, 4737–4740; d) D. E. Cane, R. H. Levin, *J. Am. Chem. Soc.* **1976**, *98*, 1183–1188; e) D. E. Cane, R. H. Levin, *J. Am. Chem. Soc.* **1975**, *97*, 1282–1284; f) M. Tanabe, K. T. Suzuki, *Tetrahedron Lett.* **1974**, *15*, 4417–4420; g) A. J. Birch, S. F. Hussain, *J. Chem. Soc. C* **1969**, 1473–1474.

[82] Y. Honda, M. Ueki, G. Okada, R. Onose, R. Usami, K. Horikoshi, H. Osada, *J. Antibiot.* **2001**, *54*, 10–16.

[83] H. Nakajima, S. Takase, H. Terano, H. Tanaka, *J. Antibiot.* **1997**, *50*, 96–99.

[84] E. C. Griffith, Z. Su, S. Niwayama, C. A. Ramsay, Y. H. Chang, J. O. Liu, *Proc. Natl. Acad. Sci. USA* **1998**, *95*, 15183–15188.

[85] E. C. Griffith, Z. Su, B. E. Turk, S. P. Chen, Y. H. Chang, Z. C. Wu, K. Biemann, J. O. Liu, *Chem. Biol.* **1997**, *4*, 461–471.

 © 2005 Wiley-VCH Verlag GmbH & Co. KGaA, Weinheim

[86] J. Y. Wang, G. S. Sheppard, P. P. Lou, M. Kawai, C. Park, D. A. Egan, A. Schneider, J. Bouska, R. Lesniewski, J. Henkin, *Biochemistry* **2003**, *42*, 5035 – 5042.
[87] S. P. Liu, J. Widom, C. W. Kemp, C. M. Crews, J. Clardy, *Science* **1998**, *282*, 1324 – 1327.
[88] M. D. Vaughan, P. B. Sampson, J. F. Honek, *Curr. Med. Chem.* **2002**, *9*, 385 – 409.
[89] a) R. A. Bradshaw, W. W. Brickey, K. W. Walker, *Trends Biochem. Sci.* **1998**, *23*, 263 – 267; b) R. L. Kendall, R. Yamada, R. A. Bradshaw, *Methods Enzymol.* **1990**, *185*, 398 – 407.
[90] C. M. Brdlik, C. M. Crews, *J. Biol. Chem.* **2004**, *279*, 9475 – 9480.
[91] a) A. Catalano, M. Romano, I. Robuffo, L. Strizzi, A. Procopio, *Am. J. Pathol.* **2001**, *159*, 721 – 731; b) N. Wernert, A. Stanjek, S. Kiriakidis, A. Hügel, H. C. Jha, R. Mazitschek, A. Giannis, *Angew. Chem.* **1999**, *111*, 3432 – 3435; *Angew. Chem. Int. Ed.* **1999**, *38*, 3228 – 3231; c) B. E. Turk, Z. Su, J. O. Liu, *Bioorg. Med. Chem.* **1998**, *6*, 1163 – 1169.
[92] J. Taunton, *Chem. Biol.* **1997**, *4*, 493 – 496.
[93] a) H. Katznelson, C. A. Jamieson, *Science* **1952**, *115*, 70 – 71; b) J. H. Killough, G. B. Magill, R. C. Smith, *Science* **1952**, *115*, 71 – 72; c) M. C. McCowen, M. E. Callender, J. F. Lawlis, *Science* **1951**, *113*, 202 – 203.
[94] J. H. Wilkins, N. Joshi, T. P. Margolis, V. Cevallos, C. R. Dawson, *Eye* **1994**, *8*, 703 – 704.
[95] a) J. M. Molina, M. Tourneur, C. Sarfati, S. Chevret, A. de Gouvello, J. G. Gobert, S. Balkan, F. Derouin, *N. Engl. J. Med.* **2002**, *346*, 1963 – 1969; b) J. M. Molina, J. Goguel, C. Sarfati, J. F. Michiels, I. Desportes-Livage, S. Balkan, C. Chastang, L. Cotte, C. Maslo, A. Struxiano, F. Derouin, J. M. Decazes, *AIDS* **2000**, *14*, 1341 – 1348.
[96] P. Zhang, D. E. Nicholson, J. M. Bujnicki, X. Z. Su, J. J. Brendle, M. Ferdig, D. E. Kyle, W. K. Milhous, P. K. Chiang, *J. Biomed. Sci.* **2002**, *9*, 34 – 40.
[97] a) E. S. Didier, M. E. Stovall, L. C. Green, P. J. Brindley, K. Sestak, P. Didier, *Vet. Parasitol.* **2004**, *126*, 145 – 166; b) E. S. Didier, *Antimicrob. Agents Chemother.* **1997**, *41*, 1541 – 1546.
[98] D. Ingber, T. Fujita, S. Kishimoto, K. Sudo, T. Kanamaru, H. Brem, J. Folkman, *Nature* **1990**, *348*, 555 – 557.
[99] a) G. Bergers, K. Javaherian, K. M. Lo, J. Folkman, D. Hanahan, *Science* **1999**, *284*, 808 – 812; b) R. Offodile, T. Walton, M. Lee, A. Stiles, M. Nguyen, *Tumori* **1999**, *85*, 51 – 53; c) M. Kusaka, K. Sudo, E. Matsutani, Y. Kozai, S. Marui, T. Fujita, D. Ingber, J. Folkman, *Br. J. Cancer* **1994**, *69*, 212 – 216; d) T. Yanase, M. Tamura, K. Fujita, S. Kodama, K. Tanaka, *Cancer Res.* **1993**, *53*, 2566 – 2570.
[100] C. K. Han, S. K. Ahn, N. S. Choi, R. K. Hong, S. K. Moon, H. S. Chun, S. J. Lee, J. W. Kim, C. I. Hong, D. Kim, J. H. Yoon, K. T. No, *Bioorg. Med. Chem. Lett.* **2000**, *10*, 39 – 43.
[101] S. Kim, K. LaMontagne, M. Sabio, S. Sharma, R. W. Versace, N. Yusuff, P. E. Phillips, *Cancer Res.* **2004**, *64*, 2984 – 2987.
[102] W. T. Lowther, A. M. Orville, D. T. Madden, S. J. Lim, D. H. Rich, B. W. Matthews, *Biochemistry* **1999**, *38*, 7678 – 7688.
[103] C. D. P. Klein, R. Schiffmann, G. Folkers, S. Piana, U. Rothlisberger, *J. Biol. Chem.* **2003**, *278*, 47862 – 47867.
[104] W. T. Lowther, Y. Zhang, P. B. Sampson, J. F. Honek, B. W. Matthews, *Biochemistry* **1999**, *38*, 14810 – 14819.
[105] a) J. MacMillan, A. E. Vanstone, S. K. Yeboah, *J. Chem. Soc. Perkin Trans. 1* **1972**, 2892 – 2898; b) J. MacMillan, T. J. Simpson, A. E. Vanstone, S. K. Yeboah, *J. Chem. Soc. Perkin Trans. 1* **1972**, 2898 – 2903; c) J. MacMillan, T. J. Simpson, S. K. Yeboah, *J. Chem. Soc. Chem. Commun.* **1972**, 1063; d) J. MacMillan, A. E. Vanstone, S. K. Yeboah, *J. Chem. Soc. Chem. Commun.* **1968**, 613 – 614; e) P. W. Brian, P. J. Curtis, H. G. Hemming, G. L. F. Norris, *Trans. Br. Mycol. Soc.* **1957**, *40*, 365 – 368.
[106] a) P. Wipf, R. J. Halter, *Org. Biomol. Chem.* **2005**, 2053 – 2061; b) J. R. Hanson, *Nat. Prod. Rep.* **1995**, *12*, 381 – 384.
[107] a) R. H. Lee, D. L. Slate, R. Moretti, K. A. Alvi, P. Crews, *Biochem. Biophys. Res. Commun.* **1992**, *184*, 765 – 772; b) M. A. Ferreira, T. J. King, S. Ali, R. H. Thomson, *J. Chem. Soc. Perkin Trans. 1* **1980**, 249 – 256; c) K. C. Joshi, P. Singh, R. T. Pardasani, A. Pelter, R. S. Ward, R. Reinhardt, *Tetrahedron Lett.* **1978**, *19*, 4719 – 4722.
[108] a) T. Mizutani, S. Honzawa, S. Tosaki, M. Shibasaki, *Angew. Chem.* **2002**, *114*, 4874 – 4876; *Angew. Chem. Int. Ed.* **2002**, *41*, 4680 – 4682; b) S. Sato, M. Nakada, M. Shibasaki, *Tetrahedron Lett.* **1996**, *37*, 6141 – 6144.
[109] a) P. W. Brian, J. C. McGowan, *Nature* **1945**, *156*, 144 – 145; b) For a racemic total synthesis of viridin, see: E. A. Anderson, E. J. Alexanian, E. J. Sorensen, *Angew. Chem.* **2004**, *116*, 2032 – 2035; *Angew. Chem. Int. Ed.* **2004**, *43*, 1998 – 2001.
[110] W. S. Golder, T. R. Watson, *J. Chem. Soc. Perkin Trans. 1* **1980**, 422 – 425.
[111] C. P. Downes, A. N. Carter, *Cell. Signalling* **1991**, *3*, 501 – 513.
[112] a) E. H. Walker, O. Perisic, C. Reid, L. Stephens, R. L. Williams, *Nature* **1999**, *402*, 313 – 320; b) J. Djordjevic, P. C. Driscoll, *Trends Biochem. Sci.* **2002**, *27*, 426 – 432.
[113] K. Kim, P. A. Cole, *J. Am. Chem. Soc.* **1997**, *119*, 11096 – 11097.
[114] a) G. J. Brunn, J. Williams, C. Sabers, G. Wiederrecht, J. C. Lawrence, R. T. Abraham, *EMBO J.* **1996**, *15*, 5256 – 5267; b) S. Boulton, S. Kyle, L. Yalcintepe, B. W. Durkacz, *Carcinogenesis* **1996**, *17*, 2285 – 2290.
[115] a) D. D. Boehr, W. S. Lane, G. D. Wright, *Chem. Biol.* **2001**, *8*, 791 – 800; b) S. Corvera, M. P. Czech, *Trends Cell Biol.* **1998**, *8*, 442 – 446; c) S. Nakanishi, S. Kakita, I. Takahashi, K. Kawahara, E. Tsukuda, T. Sano, K. Yamada, M. Yoshida, H. Kase, Y. Matsuda, Y. Hashimoto, Y. Nonomura, *J. Biol. Chem.* **1992**, *267*, 2157 – 2163.
[116] a) E. S. Gershtein, V. A. Shatskaya, V. D. Ermilova, N. E. Kushlinsky, M. A. Krasil'nikov, *Clin. Chim. Acta* **1999**, *287*, 59 – 67; b) W. A. Phillips, F. St. Clair, A. D. Munday, R. J. S. Thomas, C. A. Mitchell, *Cancer* **1998**, *83*, 41 – 47.
[117] C. P. Downes, D. Bennett, G. McConnachie, N. R. Leslie, I. Pass, C. MacPhee, L. Patel, A. Gray, *Biochem. Soc. Trans.* **2001**, *29*, 846 – 851.
[118] P. Wipf, D. J. Minion, R. J. Halter, M. I. Berggren, C. B. Ho, G. G. Chiang, L. Kirkpatrick, R. Abraham, G. Powis, *Org. Biomol. Chem.* **2004**, *2*, 1911 – 1920.
[119] N. T. Ihle, R. Williams, S. Chow, W. Chew, M. I. Berggren, G. Paine-Murrieta, D. J. Minion, R. J. Halter, P. Wipf, R. Abraham, L. Kirkpatrick, G. Powis, *Mol. Cancer Ther.* **2004**, *3*, 763 – 772.
[120] a) B. H. Norman, C. Shih, J. E. Toth, J. E. Ray, J. A. Dodge, D. W. Johnson, P. G. Rutherford, R. M. Schultz, J. F. Worzalla, C. J. Vlahos, *J. Med. Chem.* **1996**, *39*, 1106 – 1111; b) B. H. Norman, J. Paschal, C. J. Vlahos, *Bioorg. Med. Chem. Lett.* **1995**, *5*, 1183 – 1186; c) W. Haefliger, Z. Kis, D. Hauser, *Helv. Chim. Acta* **1975**, *58*, 1620 – 1633.
[121] M. P. Wymann, G. Bulgarelli-Leva, M. J. Zvelebil, L. Pirola, B. Vanhaesebroeck, M. D. Waterfield, G. Panayotou, *Mol. Cell. Biol.* **1996**, *16*, 1722 – 1733.
[122] E. H. Walker, M. E. Pacold, O. Perisic, L. Stephens, P. T. Hawkins, M. P. Wymann, R. L. Williams, *Mol. Cell* **2000**, *6*, 909 – 919.
[123] Madhusudan, E. A. Trafny, N. H. Xuong, J. A. Adams, L. F. Teneyck, S. S. Taylor, J. M. Sowadski, *Protein Sci.* **1994**, *3*, 176 – 187.
[124] Y. Liu, K. R. Shreder, W. Gai, S. Corral, D. K. Ferris, J. S. Rosenblum, *Chem. Biol.* **2005**, *12*, 99 – 107.
[125] E. Stone, *Philos. Trans. R. Soc. London* **1763**, *53*, 195 – 200.
[126] a) G. Weissman, *Sci. Am.* **1991**, *264*, 84 – 90; b) K. D. Rainsford, *Aspirin and the Salicylates*, Thetford, England, **1984**.

 © 2005 Wiley-VCH Verlag GmbH & Co. KGaA, Weinheim

[127] a) T. M. Ruuhola, M. R. K. Julkunen-Tiitto, *Plant Physiol.* **2000**, *122*, 895 – 905; b) H. I. Lee, J. Leon, I. Raskin, *Proc. Natl. Acad. Sci. USA* **1995**, *92*, 4076 – 4079; c) S. Z. El-Basyouni, D. Chen, R. K. Ibrahim, A. C. Neish, G. H. N. Towers, *Phytochemistry* **1964**, *3*, 485 – 492.

[128] G. Alibert, R. Ranjeva, *FEBS Lett.* **1971**, *19*, 11 – 14.

[129] H. Dreser, *Pfluegers Arch. Gesamte Physiol. Menschen Tiere* **1899**, *76*, 306.

[130] J. R. Vane, *Nature New Biol.* **1971**, *231*, 232 – 235.

[131] J. A. Oates, *Science* **1982**, *218*, 765 – 768.

[132] D. L. Nelson, M. M. Cox, *Lehninger Principles of Biochemistry, 3rd ed.*, Worth, New York, **2000**, p. 378.

[133] a) W. L. Smith, D. L. Dewitt, T. Shimokawa, *Adv. Prostaglandin Thromboxane Leukotriene Res.* **1991**, *21*, 77 – 80; b) D. L. Dewitt, E. A. El-Harith, S. A. Kraemer, M. J. Andrews, E. F. Yao, R. L. Armstrong, W. L. Smith, *J. Biol. Chem.* **1990**, *265*, 5192 – 5198.

[134] a) A. S. L. Xu, Y. O. L. Vida, R. J. Labotka, R. E. London, *Biochem. Pharmacol.* **2000**, *60*, 917 – 922; b) J. E. Walker, *FEBS Lett.* **1976**, *66*, 173 – 175; c) D. Hawkins, R. N. Pinckard, R. S. Farr, *Science* **1968**, *160*, 780 – 781.

[135] L. P. Wennogle, H. Liang, J. C. Quintavalla, B. R. Bowen, J. Wasvary, D. B. Miller, A. Allentoff, W. Boyer, M. Kelly, P. Marshall, *FEBS Lett.* **1995**, *371*, 315 – 320.

[136] a) S. W. Rowlinson, J. R. Kiefer, J. J. Prusakiewicz, J. L. Pawlitz, K. R. Kozak, A. S. Kalgutkar, W. C. Stallings, R. G. Kurumbail, L. J. Marnett, *J. Biol. Chem.* **2003**, *278*, 45763 – 45769; b) W. L. Smith, D. L. DeWitt, R. M. Garavito, *Annu. Rev. Biochem.* **2000**, *69*, 149 – 182.

[137] F. J. van der Ouderaa, M. Buytenhek, D. H. Nugteren, D. A. Vandorp, *Eur. J. Biochem.* **1980**, *109*, 1 – 8.

[138] E. D. Thuresson, K. M. Lakkides, C. J. Rieke, Y. Sun, B. A. Wingerd, R. Micielli, A. M. Mulichak, M. G. Malkowski, R. M. Garavito, W. L. Smith, *J. Biol. Chem.* **2001**, *276*, 10347 – 10357.

[139] T. Shimokawa, R. J. Kulmacz, D. L. DeWitt, W. L. Smith, *J. Biol. Chem.* **1990**, *265*, 20073 – 20076.

[140] a) R. G. Kurumbail, J. R. Kiefer, L. J. Marnett, *Curr. Opin. Struct. Biol.* **2001**, *11*, 752 – 760; b) M. G. Malkowski, S. L. Ginell, W. L. Smith, R. M. Garavito, *Science* **2000**, *289*, 1933 – 1937.

[141] G. P. Hochgesang, S. W. Rowlinson, L. J. Marnett, *J. Am. Chem. Soc.* **2000**, *122*, 6514 – 6515.

[142] J. A. Mancini, D. Riendeau, J. P. Falgueyret, P. J. Vickers, G. P. O'Neill, *J. Biol. Chem.* **1995**, *270*, 29372 – 29377.

[143] D. K. Bhattacharyya, M. Lecomte, C. J. Rieke, M. Garavito, W. L. Smith, *J. Biol. Chem.* **1996**, *271*, 2179 – 2184.

[144] P. J. Loll, D. Picot, R. M. Garavito, *Nat. Struct. Biol.* **1995**, *2*, 637 – 643.

[145] R. Amann, B. A. Peskar, *Eur. J. Pharmacol.* **2002**, *447*, 1 – 9.

[146] G. Francis, *Nature* **1878**, *18*, 11 – 12.

[147] a) L. Zhou, H. Yu, K. Chen, *Biomed. Environ. Sci.* **2002**, *15*, 166 – 171; b) C. Mackintosh, K. A. Beattie, S. Klumpp, P. Cohen, G. A. Codd, *FEBS Lett.* **1990**, *264*, 187 – 192.

[148] D. G. Steyn, *S. Afr. J. Sci.* **1945**, *41*, 243 – 244.

[149] C. T. Bishop, E. F. L. J. Anet, P. R. Gorham, *Can. J. Biochem. Physiol.* **1959**, *37*, 453 – 471.

[150] a) S. Santikarn, D. H. Williams, R. J. Smith, S. J. Hammond, D. P. Botes, A. Tuinman, P. L. Wessels, C. C. Viljoen, H. Kruger, *J. Chem. Soc. Chem. Commun.* **1983**, 652 – 654; b) D. P. Botes, C. C. Viljoen, H. Kruger, P. L. Wessels, D. H. Williams, *S. Afr. J. Sci.* **1982**, *78*, 378 – 379; c) T. C. Elleman, I. R. Falconer, A. R. B. Jackson, M. T. Runnegar, *Aust. J. Biol. Sci.* **1978**, *31*, 209 – 218.

[151] D. P. Botes, A. A. Tuinman, P. L. Wessels, C. C. Viljoen, H. Kruger, D. H. Williams, S. Santikarn, R. J. Smith, S. J. Hammond, *J. Chem. Soc. Perkin Trans. 1* **1984**, 2311 – 2318.

[152] a) W. W. Carmichael, J. W. He, J. Eschedor, Z. R. He, Y. M. Juan, *Toxicon* **1988**, *26*, 1213 – 1217; b) D. P. Botes, P. L. Wessels, H. Kruger, M. T. C. Runnegar, S. Santikarn, R. J. Smith, J. C. J. Barna, D. H. Williams, *J. Chem. Soc. Perkin Trans. 1* **1985**, 2747 – 2748.

[153] K. L. Rinehart, K. Harada, M. Namikoshi, C. Chen, C. A. Harvis, M. H. G. Munro, J. W. Blunt, P. E. Mulligan, V. R. Beasley, A. M. Dahlem, W. W. Carmichael, *J. Am. Chem. Soc.* **1988**, *110*, 8557 – 8558.

[154] W. W. Carmichael, V. Beasley, D. L. Bunner, J. N. Eloff, I. Falconer, P. Gorham, K. I. Harada, T. Krishnamurthy, M. J. Yu, R. E. Moore, K. Rinehart, M. Runnegar, O. M. Skulberg, M. Watanabe, *Toxicon* **1988**, *26*, 971 – 973.

[155] a) L. A. Lawton, C. Edwards, *J. Chromatogr. A* **2001**, *912*, 191 – 209; b) M. Namikoshi, B. W. Choi, R. Sakai, F. Sun, K. L. Rinehart, W. W. Carmichael, W. R. Evans, P. Cruz, M. H. G. Munro, J. W. Blunt, *J. Org. Chem.* **1994**, *59*, 2349 – 2357; c) M. Craig, T. L. McCready, H. A. Luu, M. A. Smillie, P. Dubord, C. F. B. Holmes, *Toxicon* **1993**, *31*, 1541 – 1549.

[156] R. E. Moore, J. L. Chen, B. S. Moore, G. M. L. Patterson, W. W. Carmichael, *J. Am. Chem. Soc.* **1991**, *113*, 5083 – 5084.

[157] a) M. Kaebernick, E. Dittmann, T. Börner, B. A. Neilan, *Appl. Environ. Microbiol.* **2002**, *68*, 449 – 455; b) E. Dittmann, B. A. Neilan, T. Börner, *Appl. Microbiol. Biotechnol.* **2001**, *57*, 467 – 473; c) L. H. Du, C. Sanchez, B. Shen, *Metab. Eng.* **2001**, *3*, 78 – 95; d) D. Tillett, E. Dittmann, M. Erhard, H. von Dohren, T. Börner, B. A. Neilan, *Chem. Biol.* **2000**, *7*, 753 – 764.

[158] a) G. Christiansen, J. Fastner, M. Erhard, T. Borner, E. Dittmann, *J. Bacteriol.* **2003**, *185*, 564 – 572; b) T. Nishizawa, A. Ueda, M. Asayama, K. Fujii, K. Harada, K. Ochi, M. Shirai, *J. Biochem.* **2000**, *127*, 779 – 789.

[159] a) M. Runnegar, N. Berndt, S. M. Kong, E. Y. C. Lee, L. F. Zhang, *Biochem. Biophys. Res. Commun.* **1995**, *216*, 162 – 169; b) G. Moorhead, R. W. Mackintosh, N. Morrice, T. Gallagher, C. Mackintosh, *FEBS Lett.* **1994**, *356*, 46 – 50; c) R. Matsushima, S. Yoshizawa, M. F. Watanabe, K. Harada, M. Furusawa, W. W. Carmichael, H. Fujiki, *Biochem. Biophys. Res. Commun.* **1990**, *171*, 867 – 874; d) R. E. Honkanen, J. Zwiller, R. E. Moore, S. L. Daily, B. S. Khatra, M. Dukelow, A. L. Boynton, *J. Biol. Chem.* **1990**, *265*, 19401 – 19404.

[160] R. E. Honkanen, T. Golden, *Curr. Med. Chem.* **2002**, *9*, 2055 – 2075.

[161] W. P. Taylor, T. S. Widlanski, *Chem. Biol.* **1995**, *2*, 713 – 718.

[162] a) P. T. W. Cohen, *J. Cell Sci.* **2002**, *115*, 241 – 256; b) D. M. Virshup, *Curr. Opin. Cell Biol.* **2000**, *12*, 180 – 185.

[163] a) H. Ceulemans, M. Bollen, *Physiol. Rev.* **2004**, *84*, 1 – 39; b) V. Janssens, J. Goris, *Biochem. J.* **2001**, *353*, 417 – 439; c) J. Goldberg, H. B. Huang, Y. G. Kwon, P. Greengard, A. C. Nairn, J. Kuriyan, *Nature* **1995**, *376*, 745 – 753; d) S. Shenolikar, *Annu. Rev. Cell Biol.* **1994**, *10*, 55 – 86.

[164] B. M. Gulledge, J. B. Aggen, H. B. Huang, A. C. Nairn, A. R. Chamberlin, *Curr. Med. Chem.* **2002**, *9*, 1991 – 2003.

[165] J. M. Humphrey, J. B. Aggen, A. R. Chamberlin, *J. Am. Chem. Soc.* **1996**, *118*, 11759 – 11770.

[166] K. R. Shreder, Y. Liu, T. Nomanhboy, S. R. Fuller, M. S. Wong, W. Z. Gai, J. Wu, P. S. Leventhal, J. R. Lill, S. Corral, *Bioconjugate Chem.* **2004**, *15*, 790 – 798.

[167] N. Kudo, N. Matsumori, H. Taoka, D. Fujiwara, E. P. Schreiner, B. Wolff, M. Yoshida, S. Horinouchi, *Proc. Natl. Acad. Sci. USA* **1999**, *96*, 9112 – 9117.

[168] K. Ueda, T. Usui, H. Nakayama, M. Ueki, K. Takio, M. Ubukata, H. Osada, *FEBS Lett.* **2002**, *525*, 48 – 52.

[169] T. Usui, H. Watanabe, H. Nakayama, Y. Tada, N. Kanoh, M. Kondoh, T. Asao, K. Takio, H. Watanabe, K. Nishikawa, T. Kitahara, H. Osada, *Chem. Biol.* **2004**, *11*, 799 – 806.

[170] C. F. B. Holmes, J. T. Maynes, K. R. Perreault, J. F. Dawson, M. N. G. James, *Curr. Med. Chem.* **2002**, *9*, 1981 – 1989.

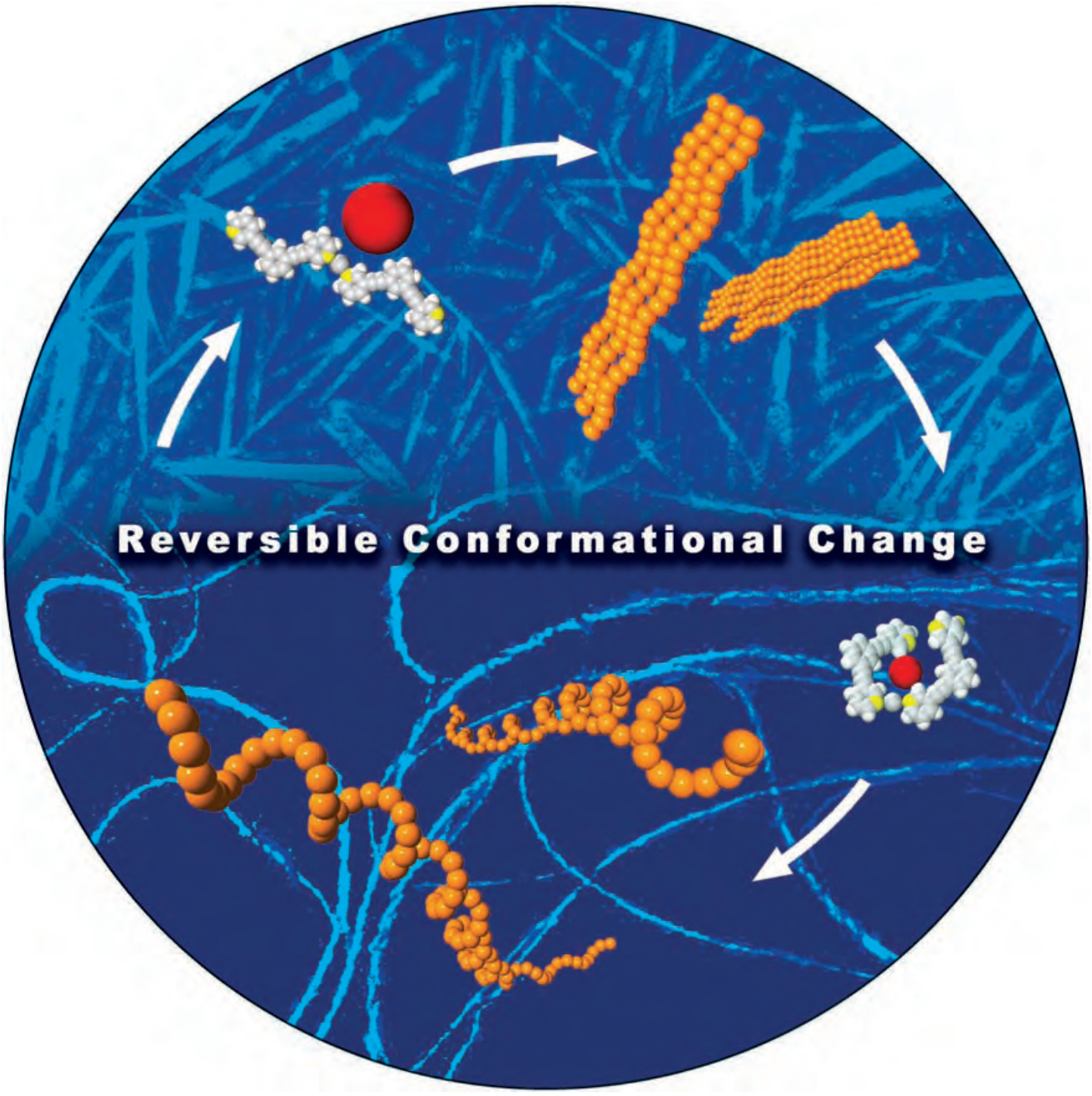
 © 2005 Wiley-VCH Verlag GmbH & Co. KGaA, Weinheim

[171] F. Kondo, Y. Ikai, H. Oka, M. Okumura, N. Ishikawa, K. Harada, K. Matsuura, H. Murata, M. Suzuki, *Chem. Res. Toxicol.* **1992**, *5*, 591 – 596.
[172] M. van Iersel, PhD Thesis, Wageningen Universiteit **1998**.
[173] M. Craig, H. A. Luu, T. L. McCready, D. Williams, R. J. Andersen, C. F. B. Holmes, *Biochem. Cell Biol.* **1996**, *74*, 569 – 578.
[174] Z. Zhang, S. Zhao, S. Deans-Zirattu, G. Bai, E. Y. Lee, *Mol. Cell. Biochem.* **1993**, *127–128*, 113 – 119.
[175] a) J. B. Smaill, H. D. Showalter, H. Zhou, A. J. Bridges, D. J. McNamara, D. W. Fry, J. M. Nelson, V. Sherwood, P. W. Vincent, B. J. Roberts, W. L. Elliott, W. A. Denny, *J. Med. Chem.* **2001**, *44*, 429 – 440; b) J. B. Smaill, B. D. Palmer, G. W. Rewcastle, W. A. Denny, D. J. McNamara, E. M. Dobrusin, A. J. Bridges, H. Zhou, H. D. Showalter, R. T. Winters, W. R. Leopold, D. W. Fry, J. M. Nelson, V. Slintak, W. L. Elliot, B. J. Roberts, P. W. Vincent, S. J. Patmore, *J. Med. Chem.* **1999**, *42*, 1803 – 1815; c) D. W. Fry, A. J. Bridges, W. A. Denny, A. Doherty, K. D. Greis, J. L. Hicks, K. E. Hook, P. R. Keller, W. R. Leopold, J. A. Loo, D. J. McNamara, J. M. Nelson, V. Sherwood, J. B. Smaill, S. Trumpp-Kallmeyer, E. M. Dobrusin, *Proc. Natl. Acad. Sci. USA* **1998**, *95*, 12022 – 12027; d) M. S. Cohen, C. Zhang, K. M. Shokat, J. Taunton, *Science* **2005**, *308*, 1318 – 1321.
[176] T. Hamamoto, S. Gunji, H. Tsuji, T. Beppu, *J. Antibiot.* **1983**, *36*, 639 – 645.
[177] a) Y. Hayakawa, K. Sohda, H. Seto, *J. Antibiot.* **1996**, *49*, 980 – 984; b) Y. Hayakawa, K. Sohda, K. Shin-ya, T. Hidaka, H. Seto, *J. Antibiot.* **1995**, *48*, 974 – 979; c) K. Gerth, D. Schummer, G. Höfle, H. Irschik, H. Reichenbach, *J. Antibiot.* **1995**, *48*, 973 – 976; d) D. Schummer, K. Gerth, H. Reichenbach, G. Höfle, *Liebigs Ann.* **1995**, 685 – 688; e) K. Abe, M. Yoshida, S. Horinouchi, T. Beppu, *J. Antibiot.* **1993**, *46*, 728 – 734; f) K. Abe, M. Yoshida, H. Naoki, S. Horinouchi, T. Beppu, *J. Antibiot.* **1993**, *46*, 735 – 740; g) Y. Hayakawa, K. Adachi, N. Komeshima, *J. Antibiot.* **1987**, *40*, 1349 – 1352; h) K. Komiyama, K. Okada, Y. Hirokawa, K. Masuda, S. Tomisaka, I. Umezawa, *J. Antibiot.* **1985**, *38*, 224 – 229; i) K. Komiyama, K. Okada, H. Oka, S. Tomisaka, T. Miyano, S. Funayama, I. Umezawa, *J. Antibiot.* **1985**, *38*, 220 – 223.
[178] T. Hamamoto, H. Seto, T. Beppu, *J. Antibiot.* **1983**, *36*, 646 – 650.
[179] T. Hamamoto, T. Uozumi, T. Beppu, *J. Antibiot.* **1985**, *38*, 533 – 535.
[180] T. Hamamoto, T. Uozumi, T. Beppu, *J. Antibiot.* **1985**, *38*, 1573 – 1580.
[181] a) T. Meissner, E. Krause, U. Vinkemeier, *FEBS Lett.* **2004**, *576*, 27 – 30; b) B. Wolff, J. J. Sanglier, Y. Wang, *Chem. Biol.* **1997**, *4*, 139 – 147.
[182] M. Fukuda, S. Asano, T. Nakamura, M. Adachi, M. Yoshida, M. Yanagida, E. Nishida, *Nature* **1997**, *390*, 308 – 311.
[183] E. A. Nigg, *Nature* **1997**, *386*, 779 – 787.
[184] a) D. Goerlich, U. Kutay, *Annu. Rev. Cell Dev. Biol.* **1999**, *15*, 607 – 660; b) B. Ossareh-Nazari, F. Bachelerie, C. Dargemont, *Science* **1997**, *278*, 141 – 144; c) K. Stade, C. S. Ford, C. Guthrie, K. Weis, *Cell* **1997**, *90*, 1041 – 1050.
[185] a) N. Kudo, B. Wolff, T. Sekimoto, E. P. Schreiner, Y. Yoneda, M. Yanagida, S. Horinouchi, M. Yoshida, *Exp. Cell Res.* **1998**, *242*, 540 – 547; b) M. Fornerod, M. Ohno, M. Yoshida, I. W. Mattaj, *Cell* **1997**, *90*, 1051 – 1060.
[186] a) T. J. Hope, *Arch. Biochem. Biophys.* **1999**, *365*, 186 – 191; b) A. Heguy, *Front. Biosci.* **1997**, *2*, 283 – 293.
[187] S. Lain, C. Midgley, A. Sparks, E. B. Lane, D. P. Lane, *Exp. Cell Res.* **1999**, *248*, 457 – 472.
[188] T. R. Kau, P. A. Silver, *Drug Discovery Today* **2003**, *8*, 78 – 85.
[189] a) M. Köster, S. Lykke-Andersen, Y. A. Elnakady, K. Gerth, P. Washausen, G. Höfle, F. Sasse, J. Kjems, H. Hauser, *Exp. Cell Res.* **2003**, *286*, 321 – 331; ratjadone exhibits additional features not observed for leptomycin. It leads to G1 phase arrest as opposed to G1 and G2 arrest shown by leptomycin and callystatin: b) M. Kalesse, K. P. Chary, M. Quitschalle, A. Burzlaff, C. Kasper, T. Scheper, *Chem. Eur. J.* **2003**, *9*, 1129 – 1136; the configuration at C10 of ratjadone is crucial for its activity: c) M. Kalesse, M. Christmann, U. Bhatt, M. Quitschalle, E. Claus, A. Saeed, A. Burzlaff, C. Kasper, L. O. Haustedt, E. Hofer, T. Scheper, W. Beil, *ChemBioChem* **2001**, *2*, 709 – 714; d) A. Burzlaff, M. Kalesse, C. Kasper, T. Scheper, *Appl. Microbiol. Biotechnol.* **2003**, *62*, 174 – 179.
[190] M. Neville, M. Rosbash, *EMBO J.* **1999**, *18*, 3746 – 3756.
[191] a) M. Kalesse, M. Christmann, *Synthesis* **2002**, 981 – 1003; b) N. Murakami, M. Sugimoto, M. Kobayashi, *Bioorg. Med. Chem.* **2001**, *9*, 57 – 67; c) N. Murakami, M. Sugimoto, T. Nakajima, M. Kawanishi, Y. Tsutsui, M. Kobayashi, *Bioorg. Med. Chem.* **2000**, *8*, 2651 – 2661.
[192] M. Kuhnt, F. Bitsch, M. Ponelle, J. J. Sanglier, Y. Wang, B. Wolff, *Appl. Environ. Microbiol.* **1998**, *64*, 714 – 720.
[193] K. Weis, *Cell* **2003**, *112*, 441 – 451.
[194] E. S. Newlands, *Br. J. Cancer* **1996**, *74*, 648 – 649.
[195] M. Kobayashi, W. Q. Wang, Y. Tsutsui, M. Sugimoto, N. Murakami, *Tetrahedron Lett.* **1998**, *39*, 8291 – 8294.
[196] K. Kobayashi, S. Miyazawa, A. Terahara, H. Mishima, H. Kurihara, *Tetrahedron Lett.* **1976**, *17*, 537 – 540.
[197] a) S. A. Shah, B. W. Shen, A. T. Brunger, *Structure* **1997**, *5*, 1067 – 1075; b) G. Burnett, K. Yonaha, S. Toyama, K. Soda, C. Walsh, *J. Biol. Chem.* **1980**, *255*, 428 – 432; c) R. R. Rando, F. W. Bangerter, *J. Am. Chem. Soc.* **1977**, *99*, 5141 – 5145; d) R. R. Rando, F. W. Bangerter, *Biochem. Biophys. Res. Commun.* **1977**, *76*, 1276 – 1281; e) R. R. Rando, *Biochemistry* **1977**, *16*, 4604 – 4610; f) R. R. Rando, F. W. Bangerter, *J. Am. Chem. Soc.* **1976**, *98*, 6762 – 6764.
[198] a) N. Jessani, M. Humphrey, W. H. McDonald, S. Niessen, K. Masuda, B. Gangadharan, J. R. Yates, B. M. Mueller, B. F. Cravatt, *Proc. Natl. Acad. Sci. USA* **2004**, *101*, 13756 – 13761; b) N. Jessani, Y. S. Liu, M. Humphrey, B. F. Cravatt, *Proc. Natl. Acad. Sci. USA* **2002**, *99*, 10335 – 10340.
[199] K. T. Barglow, B. F. Cravatt, *Chem. Biol.* **2004**, *11*, 1523 – 1531.
[200] D. C. Greenbaum, A. Baruch, M. Grainger, Z. Bozdech, K. F. Medzihradszky, J. Engel, J. DeRisi, A. A. Holder, M. Bogyo, *Science* **2002**, *298*, 2002 – 2006.
[201] a) D. Leung, C. Hardouin, D. L. Boger, B. F. Cravatt, *Nat. Biotechnol.* **2003**, *21*, 687 – 691; b) D. Greenbaum, A. Baruch, L. Hayrapetian, Z. Darula, A. Burlingame, K. F. Medzihradszky, M. Bogyo, *Mol. Cell. Proteomics* **2002**, *1*, 60 – 68.
[202] a) M. P. Patricelli, D. K. Giang, L. M. Stamp, J. J. Burbaum, *Proteomics* **2001**, *1*, 1067 – 1071; b) D. Kidd, Y. S. Liu, B. F. Cravatt, *Biochemistry* **2001**, *40*, 4005 – 4015; c) Y. S. Liu, M. P. Patricelli, B. F. Cravatt, *Proc. Natl. Acad. Sci. USA* **1999**, *96*, 14694 – 14699.
[203] a) L. Faleiro, R. Kobayashi, H. Fearnhead, Y. Lazebnik, *EMBO J.* **1997**, *16*, 2271 – 2281; b) N. A. Thornberry, E. P. Peterson, J. J. Zhao, A. D. Howard, P. R. Griffin, K. T. Chapman, *Biochemistry* **1994**, *33*, 3934 – 3940.
[204] a) E. W. Chan, S. Chattopadhaya, R. C. Panicker, X. Huang, S. Q. Yao, *J. Am. Chem. Soc.* **2004**, *126*, 14435 – 14446; b) A. Saghatelian, N. Jessani, A. Joseph, M. Humphrey, B. F. Cravatt, *Proc. Natl. Acad. Sci. USA* **2004**, *101*, 10000 – 10005.
[205] a) G. C. Adam, J. Burbaum, J. W. Kozarich, M. P. Patricelli, B. F. Cravatt, *J. Am. Chem. Soc.* **2004**, *126*, 1363 – 1368; b) G. C. Adam, E. J. Sorensen, B. F. Cravatt, *Nat. Biotechnol.* **2002**, *20*, 805 – 809; c) G. C. Adam, B. F. Cravatt, E. J. Sorensen, *Chem. Biol.* **2001**, *8*, 81 – 95.

© 2005 Wiley-VCH Verlag GmbH & Co. KGaA, Weinheim

Communications

DOI: 10.1002/anie.200501270



Cationic coordination polymers adopt two distinct conformations in response to the nature of the anions bound. Therefore, a simple exchange of anion type results in a reversible change in the bulk properties of the solution, from liquid to gel and back. M. Lee and co-workers describe the characterization of these polymers in their Communication on the following pages.

InterScience
© 2005 Wiley-VCH Verlag GmbH & Co. KGaA, Weinheim

Supramolecular Chemistry

DOI: 10.1002/anie.200501270

Stimuli-Responsive Gels from Reversible Coordination Polymers**

*Ho-Joong Kim, Jung-Hoon Lee, and Myongsoo Lee**

The design of supramolecular helices that mimic the macromolecular organization observed in biological systems is a topic of great interest.[1] Therefore, considerable effort has been made to introduce helicity into artificial systems.[2] The most widely used strategy for generating supramolecular helices requires a noncovalent motif, which can provide the desired connectivity of the building blocks in a predictable manner.[3] For example, relatively strong directional interactions, such as complexation between bent ligands and transition-metal atoms that adopt a linear coordination geometry can give rise to extended polymeric chains with a helical secondary structure.[4,5] Especially for conformationally flexible ligands, one can envisage the formation of linear coordination chains that can adopt folded or unfolded secondary structures as a function of counteranion binding to cationic polymeric backbones through electrostatic interactions.[6,7] Indeed, a folded helical conformation has been reported to transform directly into an unfolded state in response to external stimuli.[8] These observations led us to investigate whether the secondary structure of cationic coordination chains can interconvert in aqueous solution from a folded helical conformation into an unfolded zigzag conformation in response to a counteranion guest to exhibit a reversible sol–gel transition.[9]

Herein, we report reversible sol–gel interconversion of coordination polymers in aqueous media, from folded helical chains into an unfolded zigzag conformation with counteranion exchange; the process is driven by depolymerization or conformational change (Figure 1). The synthesis of the bent ligands (**1**–**3**) containing hydrophilic dendritic side groups was performed stepwise according to previously reported methods.[10,11] The resulting pyridine ligands were complexed with silver tetrafluoroborate to afford the coordination chains, [Ag-***n***]BF_4, in which ***n*** is one of the ligands, **1**–**3**. All of the analytical data are in full agreement with the chemical structures presented. In the solid state, all of the coordination polymers self-assembled into a hexagonal columnar structure (see Supporting Information), which suggests that the size of the BF_4^- ion is compatible with the internal cavity of the helical columns.

In contrast to [Ag-**1**]BF_4, which precipitates in water, [Ag-**2**]BF_4 and [Ag-**3**]BF_4 form dilute aqueous solutions that undergo spontaneous gelation at concentrations above

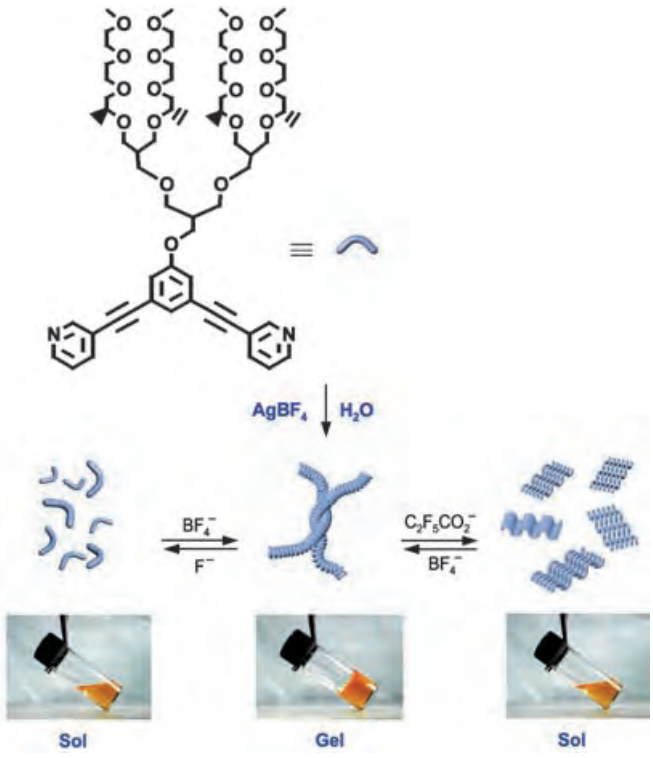
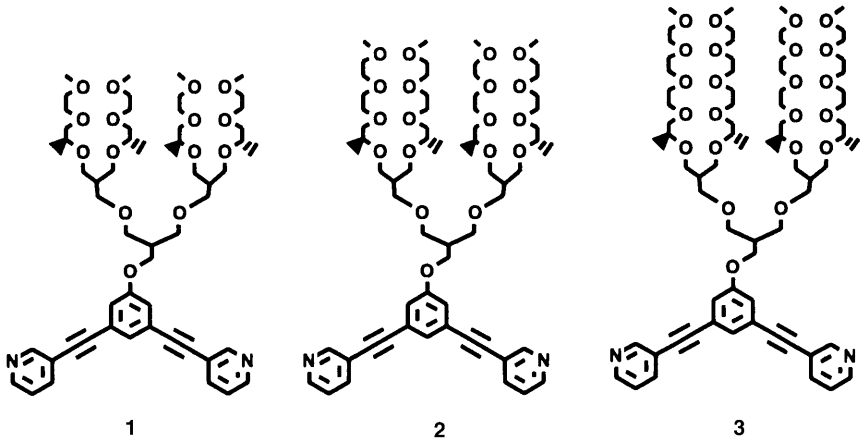


Figure 1. Schematic representation of reversible polymerization and reversible conversion between folded and unfolded conformations of a coordination chain upon counteranion exchange.



[*] H.-J. Kim, J.-H. Lee, Prof. M. Lee
Center for Supramolecular Nano-Assembly and
Department of Chemistry, Yonsei University
Shinchon 134, Seoul 120-749 (Korea)
Fax: (+82) 2-393-6096
E-mail: mslee@yonsei.ac.kr

[**] This work was supported by the Creative Research Initiative Program of the Ministry of Science and Technology, Korea and Pohang Accelerator Laboratory, Korea (synchrotron radiation). H.-J.K. thanks the Seoul Science Fellowship Program.

Supporting information for this article is available on the WWW under http://www.angewandte.org or from the author.

© 2005 Wiley-VCH Verlag GmbH & Co. KGaA, Weinheim

2.5 wt%. Upon addition of 1.2 equivalents of tetra-*n*-butylammonium fluoride $Bu_4N^+F^-$ to the gels, which drives the coordination polymers to depolymerize through a strong electrostatic interaction between the Ag^+ and F^- ions, the gels rapidly become a fluid solution. After the addition of 1.2 equivalents of F^- ions, the signals corresponding to aromatic protons in the ^{1}H NMR spectrum of [Ag-**2**]BF_4 show an upfield shift relative to those of the coordination polymer solution (1 wt% in CD_3OD), which indicates that the addition of F^- ions leads to decomplexation of the coordination polymer to give free ligands (Figure 2a). Upon addition of 1.2 equivalents of $Bu_4N^+BF_4^-$, the solution returns to the gel state; thus the polymerization is reversible.

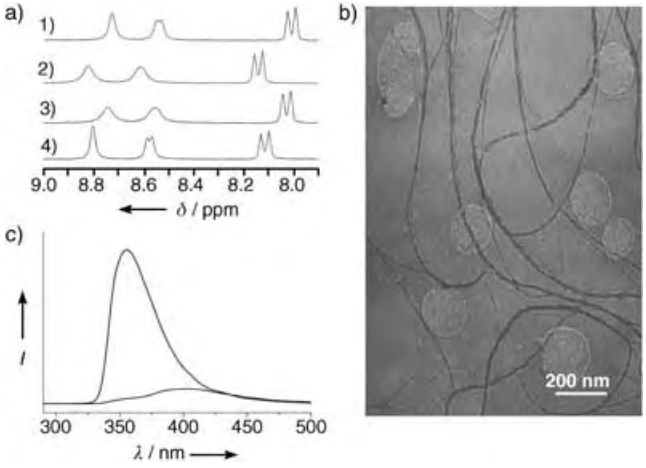


Figure 2. a) ^{1}H NMR spectra (250 MHz, 298 K) in CD_3OD (1 wt%) of 1) **2**; 2) [Ag-**2**]BF_4; 3) [Ag-**2**]BF_4 and 1.2 equiv $Bu_4N^+F^-$; 4) same as (3) after the addition of 1.2 equiv $Bu_4N^+BF_4^-$. b) TEM image of dried gel from [Ag-**2**]BF_4 in H_2O (0.3 wt%) stained with RuO_4. c) Fluorescence spectra of **2** and gel of [Ag-**2**]BF_4 (5 wt% in H_2O; λ_{ex} = 275 nm).

TEM analysis of the gels revealed right-handed helical bundles of elongated fibers with diameters of 6–30 nm, which in turn form an entangled fibrillar network (Figure 2b). The gels reveal a significant Cotton effect in the chromophore of the aromatic unit, which supports the presence of elongated helical aggregates in aqueous solution.[12,13] These results demonstrate that the complexes self-assemble into a helical secondary structure that forms a coiled-coil superstructure, and the fibrous aggregates entangle to form gels. This aggregation of the coordination chains is further supported by fluorescence measurements, which showed a strong red-shift of the emission maximum[14] and a significant decrease in the emission intensity of the gel state relative to that of the ligand (Figure 2c).[15] The formation of the helical secondary structure in aqueous solution can be rationalized by considering supramolecular polymerization through coordination bonding and subsequent binding of counteranions through the *cis*-like conformation of the monomeric units. Molecular models indicate that the size of the BF_4^- ion is compatible with the internal cavity formed by the *cis*-like conformation of the ligands. To maximize electrostatic interactions of the cationic chains with the counteranions, the coordination chains adopt a folded helical conformation, which is responsible for the formation of the entangled fibrillar network.

More importantly, the gels reversibly transform into a fluid solution with counteranion exchange of BF_4^- with a larger ion, $C_2F_5CO_2^-$. Upon addition of 1 equivalent of $Bu_4N^+C_2F_5CO_2^-$ to the [Ag-**2**]BF_4 gel, it transforms rapidly into a fluid solution (Figure 1).[16] CD spectra of the [Ag-**2**]BF_4/$C_2F_5CO_2$ solution shows no Cotton effect (Figure 3a), thus demonstrating the absence of helical aggregation in this condition. The fluorescence spectrum of the gel of [Ag-**2**]BF_4 exhibits an emission maximum at 400 nm, which is indicative of a helical aggregation as described above. However, upon addition of up to 0.8 equivalent of $C_2F_5CO_2^-$ ions, the emission maximum gradually red-shifts (20 nm) with respect

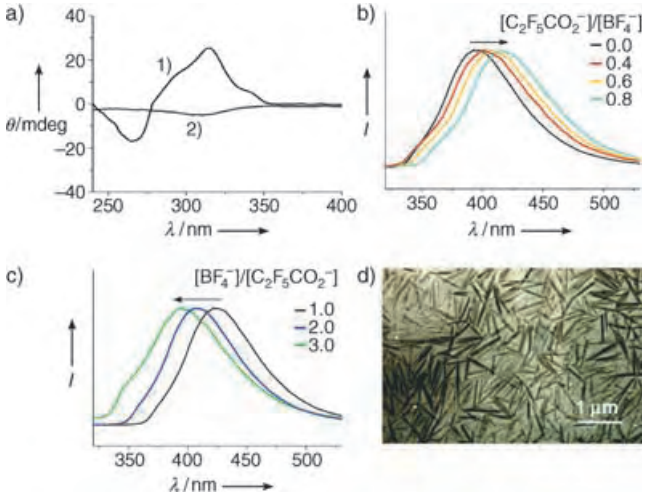


Figure 3. a) Circular dichroism (CD) spectra of: 1) [Ag-**2**]BF_4 (5 wt%); 2) [Ag-**2**]BF_4 (5 wt%) after the addition of 1 equiv $Bu_4N^+C_2F_5CO_2^-$. b) Fluorescence spectra of [Ag-**2**]BF_4 (5 wt%) with increasing amounts of $Bu_4N^+C_2F_5CO_2^-$. c) Fluorescence spectra of a mixture of [Ag-**2**]BF_4 (5 wt%) and $Bu_4N^+C_2F_5CO_2^-$ (1:1) with increasing amounts of $Bu_4N^+BF_4^-$. d) TEM image of [Ag-**2**]$C_2F_5CO_2$ in H_2O (0.3 wt%) stained with RuO_4.

to that observed in the gel state (Figure 3b), thus demonstrating that the chain conformation transforms into a *trans*-like state.[10] It should be noted that the addition of more $C_2F_5CO_2^-$ ions (up to 2 equivalents) did not further change the spectrum. This process was reversed by the addition of BF_4^- ions to give a gel (Figure 3c). Remarkably, TEM images indicate that there is a dramatic change in morphology on replacing BF_4^- with $C_2F_5CO_2^-$ ions. In contrast to that of the gel of [Ag-**2**]BF_4, the TEM image of the homologous complex, [Ag-**2**]$C_2F_5CO_2$, shows discrete ribbonlike aggregates with lengths of 0.7–1.3 μm and widths of 20–40 nm (Figure 3d), which indicates that the size of counteranion has a profound effect on the nanoscale structure and macroscopic properties of the complex. In light of the *trans*-like conformation of the coordination chains as confirmed by fluorescence spectroscopy, we consider these ribbonlike aggregates to be based on a discrete layered structure in which the coordination chains adopt an unfolded zigzag conformation. An inspection of the molecular models indi-

 © 2005 Wiley-VCH Verlag GmbH & Co. KGaA, Weinheim

cates that the $C_2F_5CO_2^-$ ion is too large for the cavity formed by the *cis*-like conformation of the polymer chains and thus the chain conformation is likely to adopt an unfolded *trans*-like state for efficient binding of the larger counteranion while maintaining close packing of the rigid segments.

We performed ^{19}F NMR spectroscopic experiments to further investigate the role of added $C_2F_5CO_2^-$ ions in the structural change. The ^{19}F NMR spectrum of a D_2O gel of complex [Ag-**2**]BF_4 shows a resonance at $\delta = -151.85$ ppm along with a resonance from a minor isotope at $\delta = -151.80$ ppm, which is downfield with respect to those of free BF_4^- ion (Figure 4). This result suggests that BF_4^- ions

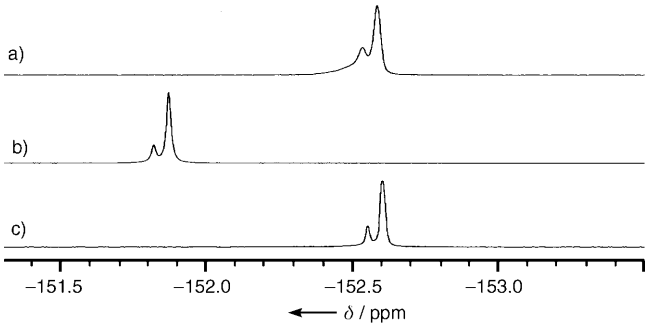


Figure 4. Comparison of ^{19}F NMR spectra in D_2O (470 MHz, 298 K): a) free $AgBF_4$; b) [Ag-**2**]BF_4 (5 wt%); c) [Ag-**2**]BF_4 (5 wt%) after the addition of 1 equiv of $Bu_4N^+C_2F_5CO_2^-$. The chemical shifts were measured as upfield shifts relative to that of $CFCl_3$ as an external standard.

are entrapped within the helical chains.[17] The downfield shift observed for the entrapped anions is due to their coordination to Ag^+ ions. Upon addition of 1 equivalent of $Bu_4N^+C_2F_5CO_2^-$ to the gel of [Ag-**2**]BF_4, however, the signal at $\delta = -151.85$ ppm shifts to -152.60 and the signal from the minor isotope, $\delta = -151.80$ ppm, shifts to -152.55 ppm. These shifts indicate the release of entrapped BF_4^- ions through the modification of the helical conformation. Together with fluorescence spectra, these results demonstrate that this anion exchange triggers release of the entrapped BF_4^- ions with concomitant transformation of the folded helical structure into an unfolded zigzag conformation. Consequently, this conformational change of the coordination chains gives rise to a significant structural change from elongated fibers into discrete ribbonlike aggregates thereby sol–gel interconversion. Therefore, the helical conformation of the coordination chain is most probably the principal driving force for the gelation of the complexes in water.

The results described herein demonstrate that the reversible coordination polymers self-assemble into a helical structure which, in turn, forms an entangled fibrillar network thereby immobilizing the solvent. Remarkably, the aqueous gels were observed to transform rapidly into fluid solutions with counteranion exchange of BF_4^- with F^- or $C_2F_5CO_2^-$, which can be used to trigger reversible sol–gel phase transition. This sol–gel interconversion in response to external stimuli is attributed to depolymerization or transformation of the folded helical conformation into an unfolded zigzag conformation of the coordination chains; there is subsequent structural change from elongated fibers to discrete ribbons with counteranion exchange. These results are a significant example of changing the size of an entrapped guest in a self-assembling system providing a useful strategy to create stimuli-responsive smart nanoscale materials with functions that can be produced at any time on demand.

Received: April 12, 2005
Revised: June 1, 2005

Keywords: coordination modes · host–guest systems · ion exchange · sol–gel processes · supramolecular chemistry

[1] S. H. Gellman, *Acc. Chem. Res.* **1998**, *31*, 173–180.
[2] a) D. J. Hill, M. J. Mio, R. B. Prince, T. S. Hughes, J. S. Moore, *Chem. Rev.* **2001**, *101*, 3893–4011; b) L. Brunsveld, B. J. B. Folmer, E. W. Meijer, R. P. Sijbesma, *Chem. Rev.* **2001**, *101*, 4071–4097.
[3] a) M. Barboiu, G. Vaughan, R. Graff, J.-M. Lehn, *J. Am. Chem. Soc.* **2003**, *125*, 10257–10265; b) F. Würthner, S. Yao, U. Beginn, *Angew. Chem.* **2003**, *115*, 3368–3371; *Angew. Chem. Int. Ed.* **2003**, *42*, 3247–3250; c) M. Enomoto, A. Kishimura, T. Aida, *J. Am. Chem. Soc.* **2001**, *123*, 5608–5609; d) T. Hatano, A.-H. Bae, M. Takeuchi, N. Fujita, K. Kaneko, H. Ihara, M. Takafuji, S. Shinkai, *Angew. Chem.* **2004**, *116*, 471–475; *Angew. Chem. Int. Ed.* **2004**, *43*, 465–469.
[4] L. Carlucci, G. Ciani, D. W. V. Gudenberg, D. M. Proserpio, *Inorg. Chem.* **1997**, *36*, 3812–3813.
[5] Y. Cui, S. J. Lee, W. Lin, *J. Am. Chem. Soc.* **2003**, *125*, 6014–6015.
[6] C. Piguet, G. Bernardinelli, G. Hopfgartner, *Chem. Rev.* **1997**, *97*, 2005–2062.
[7] B. Hasenknopf, J.-M. Lehn, B. O. Kneisel, G. Baum, D. Fenske, *Angew. Chem.* **1996**, *108*, 1987–1990; *Angew. Chem. Int. Ed. Engl.* **1996**, *35*, 1838–1840.
[8] a) N. Giuseppone, J.-L. Schmitt, J.-M. Lehn, *Angew. Chem.* **2004**, *116*, 5010–5014; *Angew. Chem. Int. Ed.* **2004**, *43*, 4902–4906; b) R. B. Prince, T. Okada, J. S. Moore, *Angew. Chem.* **1999**, *111*, 245–249; *Angew. Chem. Int. Ed.* **1999**, *38*, 233–236; c) C. Dolain, V. Maurizot, I. Huc, *Angew. Chem. Int. Ed.* **2003**, *115*, 2844–2846; *Angew. Chem. Int. Ed.* **2003**, *42*, 2738–2740; d) M. Inouye, M. Waki, H. Abe, *J. Am. Chem. Soc.* **2004**, *126*, 2022–2027.
[9] a) S.-I. Kawano, N. Fujita, S. Shinkai, *J. Am. Chem. Soc.* **2004**, *126*, 8592–8593; b) K. Kuroiwa, T. Shibata, A. Takada, N. Nemoto, N. Kimizuka, *J. Am. Chem. Soc.* **2004**, *126*, 2016–2021; c) J. B. Beck, S. J. Rowan, *J. Am. Chem. Soc.* **2003**, *125*, 4224–4225.
[10] H.-J. Kim, W.-C. Zin, M. Lee, *J. Am. Chem. Soc.* **2004**, *126*, 7009–7014.
[11] C.-J. Jang, J.-H. Ryu, J.-D. Lee, D. Sohn, M. Lee, *Chem. Mater.* **2004**, *16*, 4226–4231.
[12] R. B. Prince, J. G. Savan, P. G. Wolynes, J. S. Moore, *J. Am. Chem. Soc.* **1999**, *121*, 3114–3121.
[13] A. F. M. Kilbinger, A. P. H. J. Schenning, F. Goldoni, W. J. Feast, E. W. Meijer, *J. Am. Chem. Soc.* **2000**, *122*, 1820–1821.
[14] W. Y. Yang, R. B. Prince, J. Sabelko, J. S. Moore, M. Gruebele, *J. Am. Chem. Soc.* **2000**, *122*, 3248–3249.
[15] A. P. H. J. Schenning, P. Jonkheijm, E. Peeters, E. W. Meijer, *J. Am. Chem. Soc.* **2001**, *123*, 409–416.
[16] Dynamic light scattering (DLS) experiments performed with this solution (1 wt%) indicated the presence of aggregates of a narrow size distribution with an average hydrodynamic radius of about 1.1 μm (Supporting Information).

 © 2005 Wiley-VCH Verlag GmbH & Co. KGaA, Weinheim

[17] a) S. Hiraoka, T. Yi, M. Shiro, M. Shionoya, *J. Am. Chem. Soc.* **2002**, *124*, 14510 – 14511; b) S. O. Kang, D. Van der Velde, D. Powell, K. Bowman-James, *J. Am. Chem. Soc.* **2004**, *126*, 12272 – 12273.

 © 2005 Wiley-VCH Verlag GmbH & Co. KGaA, Weinheim

Coordination Polymers

DOI: 10.1002/anie.200500453

Porous Lanthanide–Organic Open Frameworks with Helical Tubes Constructed from Interweaving Triple-Helical and Double-Helical Chains**

*Yan-Qiong Sun, Jie Zhang, Yong-Mei Chen, and Guo-Yu Yang**

In recent years, the construction of metal-organic coordination polymers has attracted considerable attention in supramolecular and materials chemistry due to the formation of fascinating structures and potential applications as optoelectronic, magnetic, and porous materials.[1] However, most of the work has so far focused on the assembly of the d-block metal-organic open frameworks,[2] while the analogous chemistry of the lanthanides remains less developed.[3] This is attributed to the tendency of the lanthanide ions for high coordination, which favors the formation of condensed structures with[4] or without guest species.[3b,5] To date, no systematic investigation on lanthanide-based porous materials with luminescent properties has been documented.[6] In addition, lanthanide-organic frameworks with channels from which the guest species can be removed and reintroduced reversibly without collapse of the framework are rare.[7]

Among the reported network lanthanide carboxylates, 4,5-imidazoledicarboxylic acid (H_3ImDC), which remains largely unexplored,[8] was chosen as the multidentate ligand for the following reasons: 1) The flexible, multifunctional coordination sites provide a high likelihood for generation of structures with high dimensions. 2) It can be deprotonated to generate H_2ImDC^-, $HImDC^{2-}$, and $ImDC^{3-}$, which allow various, acidity-dependent coordination modes. 3) The skew coordination orientation of the carboxy groups is favorable for constructing a helical structure.

Accordingly, our aim was to synthesize novel lanthanide-organic open frameworks by using the H_3ImDC ligand. Here we report the syntheses, structures, and luminescent and magnetic properties of two novel lanthanide-organic coordination polymers of $[Ln_2(ImDC)_2(H_2O)_3]\cdot 1.625\,H_2O$ (Ln = Eu (**1**) and Dy (**2**)). The structures of **1** and **2** not only display one-dimensional achiral channels, but also contain alternately arranged left- and right-handed helical tubular channels.

White prism crystals of **1** and **2** were obtained by the hydrothermal reaction of Ln_2O_3 and H_3ImDC in water in the presence of HNO_3 at pH 2 and 170 °C. The X-ray crystal structure analyses reveal that **1** and **2** are isostructural and crystallize in the high symmetry tetragonal space group $I4_1/a$.[9] Therefore, only the structure of **1** is described in detail. In the asymmetrical unit of **1**, there are two crystallographically independent Eu^{3+} ions and two unique ImDC ligands with two different coordination modes (Figure 1 and see the Supporting Information). The Eu1 ion (mode **I**, Scheme 1) is eight-coordinate and is described as a dodecahedron (see the Supporting Information): Two imidazole nitrogen (N_{Im}) and four carboxylate oxygen (O_{COO^-}) atoms from three ImDC moieties as well as two terminal water molecules. The coordination geometry for the nine-coordinate Eu2 ion (mode **II** in Scheme 1) is close to that of a tricapped trigonal prism (see the Supporting Information): six O_{COO^-} and two

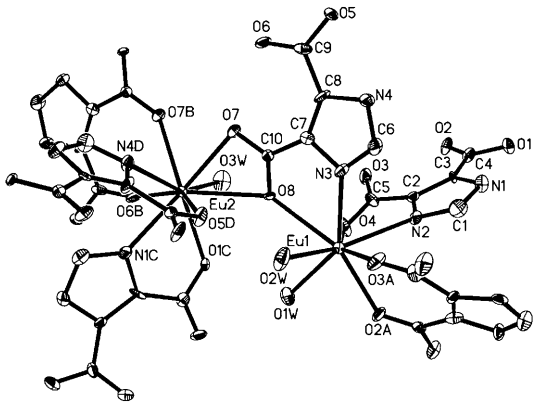
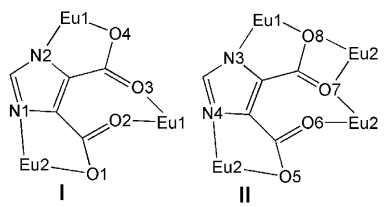


Figure 1. The coordination environments of Eu1 and Eu2 atoms in **1**. Atoms with "A" or "B" in their labels are symmetry-generated.



Scheme 1. Coordination modes of the ImDC ligands in **1**.

[*] Y.-Q. Sun, Prof. Dr. J. Zhang, Prof. Dr. G.-Y. Yang
State Key Laboratory of Structural Chemistry
Fujian Institute of Research on the Structure of Matter
Chinese Academy of Sciences
Fuzhou, Fujian 350002 (P.R. China)
Fax: (+86) 591-8371-0051
E-mail: ygy@fjirsm.ac.cn
Dr. Y.-M. Chen
Department of Applied Chemistry
Faculty of Science
Beijing University of Chemical Technology
Beijing 100029 (P.R. China)

[**] This work was supported by the NNSF of China (nos. 20271050 and 20473093), the Talents Program of Chinese Academy of Sciences, and the NSF of Fujian Province (nos. E0510030 and E0210029).

Supporting information for this article is available on the WWW under http://www.angewandte.org or from the author.

InterScience
© 2005 Wiley-VCH Verlag GmbH & Co. KGaA, Weinheim

N_{Im} atoms from four ImDC units as well as one terminal water molecule. The O7 and O8 atoms in mode **II** are simultaneously coordinated to two Eu^{3+} ions, while the O3 and O4 atoms in mode **I** are not further coordinated (Scheme 1). Thus, the O7/O8 atoms play a key role in the formation of **1** with an open framework. The Eu–O bond lengths range from 2.328(9) to 2.702(8) Å, whereas the Eu–N distances vary from 2.432(11) to 2.572 (10) Å.

The most striking features of **1** are the linkages between the Eu^{3+} ions and the two unusual coordinate modes of the ImDC moieties to form a unprecedented three-dimensional framework with achiral channels and two types of helical tubes with opposite chirality (Figure 2a and see the Supporting Information). The helical tubes of **1** can be understood in terms of two distinct parts: The helical tubular walls and the fillers. Thus, the Eu^{3+} ions linked through four carboxyl groups of two types of ImDC units form the achiral channels and the helical tubular walls that are made of triple-helical chains and double-helical chains (Figure 2b,c and see the Supporting Information). In the structure, the left- and right-handed helical channels, which are made of triple-helical chains, are further weaved by double-helical chains having the reverse orientation to the triple-helical chains to make the tubular walls with opposite chirality (Figure 2b,c and see the Supporting Information). These tubular walls are further linked together by O7 and O8 atoms from mode **II** to form the achiral channels (Figure 2a, and Figures S5 and 6b in the Supporting Information). In addition, the helical channels constructed from the triple-helical chains have a 32-membered ring opening along the [001] direction (Figure 3). In fact, there is no closed 32-membered ring present in the structure. The open 32-membered ring consisting of four repeating O2-C4-O1-Eu2-O7-C10-O8-Eu1 linkages—which are built up from the Eu1 and Eu2 atoms as well as two bridging carboxy groups containing C4 and C10 atoms—gives rise to two types of helical ribbons of three equivalent helical chains with opposite chirality (Figure 2b,c and see the Supporting Information). The separation between the adjacent chains in the helical ribbon is the same as the length of the *c* axis (16.176 Å). The pitch of the helical ribbon running along the *c* axis is three times the length of the *c* axis. In contrast, the double-helical chain consists of two distinct helical chains with a 16-membered ring made of four repeating Eu1-O3-C5-O4 (Eu2-O5-C9-O6) linkages, which are only built up from Eu1 (Eu2) atoms and one carboxy bridge containing C5 (C9) atoms (see the Supporting Information). The shortest Eu···Eu distance, bridged by carboxy groups, is 4.24 Å.

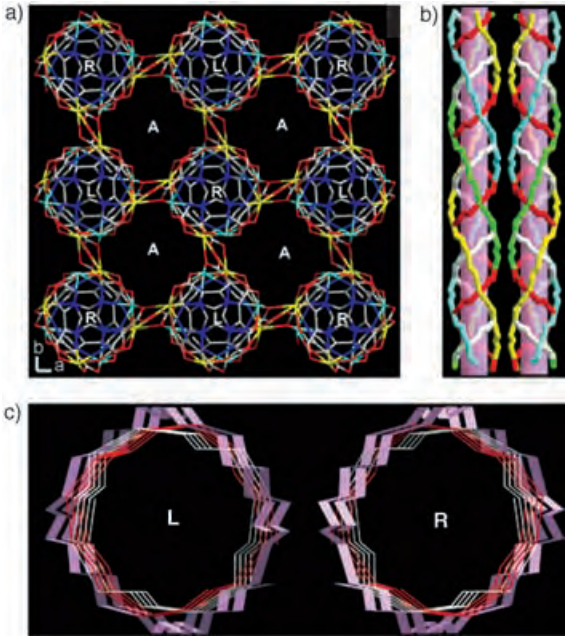


Figure 2. a) The framework of **1** viewed along the *c* axis, showing two types of helical tubular and achiral channels arranged alternately along the *a* and *b* axes. A: achiral channel, L and R indicate the left- and right-handed helical tubular channels. Hydrogen atoms are omitted for clarity. b) View of the helical tubular combination with opposite chirality, constructed from channels of triple-helical chains weaved by double-helical chains with the reverse helical orientation (*b* axis). The triple-helical chains are marked yellow, green, and cyan. The double-helical chains are displayed with red and white helical chains. The imidazole rings are omitted for clarity. c) The helical ribbon representation for the aggregate of triple-helical chains in the helical tube with opposite chirality along the [001] (left) and [00−1] directions (right). The white and red helical chains present two distinct helical chains of double-helical chains weaved across the ribbon.

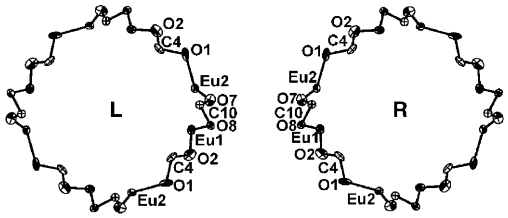


Figure 3. Views of the two types of helical channels containing triple-helical chains in **1** along the [001] (left) and [00−1] directions (right). L and R indicate the left- and right-handed helical channels.

Remarkably, the two types of imidazole rings of the ImDC ligands that act as the fillers are alternately trapped inside the helical tubes and coordinated to adjacent Eu1 and Eu2 atoms from the walls through N_{Im} atoms to form a pair of helical chains with the same helical orientation as the triple-helical chain (see the Supporting Information). The shortest Eu···Eu distance, bridged by an imidazole ring, is about 6.96 Å.

The guest water molecules are suspended in the achiral channels (dimensions 4.58 × 4.58 Å; see the Supporting Information), and the coordinated water molecules point away from the Eu–ImDC hybrid framework and into the achiral channels. There are strong hydrogen bonds between the guests, as well as between the guests and the oxygen atoms from the ImDC moieties and the coordinated water molecules (O···O 2.168(22)–3.344(15) and 2.735(19)–2.976(13) Å, respectively).

Complex **1** displays intense red luminescence (Figure 4a, and see the Supporting Information) and exhibits the characteristic transition of $^5D_0 \rightarrow {}^7F_J$ ($J = 0$–4) of the Eu^{3+}

 © 2005 Wiley-VCH Verlag GmbH & Co. KGaA, Weinheim

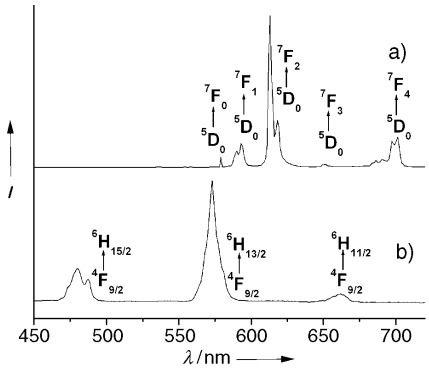


Figure 4. Emission spectra of **1** (a) and **2** (b) in the solid state at room temperature (excitation at 394 and 325 nm for **1** and **2**, respectively). *I* = intensity.

ion with a decay lifetime of 251.2 μs. The appearance of the symmetry-forbidden emission $^5D_0 \rightarrow {}^7F_0$ at 580 nm indicates that the Eu^{3+} ions in **1** occupy sites with low symmetry and have no inversion center,[10] which is further confirmed by the intensity ratio of about 5.5 for $I(^5D_0 \rightarrow {}^7F_2)/I(^5D_0 \rightarrow {}^7F_1)$.[11] This is in agreement with the result of the single-crystal X-ray analysis. Complex **2** is yellow-luminescent in the solid state with typical Dy^{3+} emissions at 480, 573, and 622 nm (decay lifetime 1.21 μs), corresponding to the characteristic emission $^4F_{9/2} \rightarrow {}^6H_J$ transitions of the Dy^{3+} ion ($J = 15/2$, 13/2, and 11/2; Figure 4b and Figure S11b in the Supporting Information). The yellow emission of the $^4F_{9/2} \rightarrow {}^6H_{13/2}$ transition has a stronger intensity than the blue emission of $^4F_{9/2} \rightarrow {}^6H_{15/2}$ for **2**, while the red emission of the $^5D_0 \rightarrow {}^7F_2$ transition is the most intense for **1**, suggesting that the ImDC ligand is suitable for the sensitization of yellow and red luminescence for Dy^{3+} and Eu^{3+}, respectively. With respect to H_3ImDC, the strongest emission peak is located at 490 nm ($\lambda_{ex} = 296$ nm; see Figure S11c in the Supporting Information). The absence of the ligand-based emission in the fluorescence spectra of **1** and **2** suggests that the energy transfer from the ligand to the lanthanide center is very effective and can sensitize the lanthanide emission to a large extent.

The magnetic susceptibilities of **1** and **2** were measured in the temperature range 5–300 K. For **1**, the room temperature value of $\chi_M T$ is 2.77 $cm^3\,K\,mol^{-1}$, slightly less than the value of 3.0 $cm^3\,K\,mol^{-1}$ for two Eu^{3+} ions calculated from the van Vleck equation allowing for population of the excited state with higher values of *J* at 293 K.[3d] As the sample is cooled, $\chi_M T$ continuously decreases due to the depopulation of the Stark levels for a single Eu^{3+} ion, and tends to a value very close to zero as the temperature approaches absolute zero, which indicates a $J = 0$ ground state for the Eu^{3+} ion ($^7F_0$) at the lowest temperature (see Figure S12a in the Supporting Information). The $\chi_M T$ value per molecule of **2** is 30.37 $cm^3\,K\,mol^{-1}$ at room temperature, comparable to the expected value of 28.34 $cm^3\,K\,mol^{-1}$ for two free Dy^{3+} ions with a $^6H_{15/2}$ ground state. As the temperature is lowered, the $\chi_M T$ product increases slightly to a maximum of 31.91 $cm^3\,K\,mol^{-1}$ at about 120 K, and then decreases gradually to 24 $cm^3\,K\,mol^{-1}$ at 5 K, suggesting a dominant ferromagnetic interaction between adjacent Dy^{3+} ions. The fitting above 100 K to Curie–Weiss equation yields a positive Weiss constant $\theta = 7.12$ K, which confirms a ferromagnetic coupling between Dy^{3+} centers (see Figure S12b in the Supporting Information). The further decrease of $\chi_M T$ at low temperature is mainly attributed to the splitting of the ligand field of the Dy^{3+} ion because of strong spin-orbital coupling.[12]

In summary, we have successfully constructed two novel lanthanide metal coordination polymers with an open framework under hydrothermal conditions from lanthanide oxide as the source of lanthanide and multidentate ImDC as a bridging ligand; the synthetic procedure has been well established.[13] The linkages between Ln centers through the ImDC ligands in two unique coordination modes result in a series of unusual lanthanide-organic open frameworks containing not only two types of helical tubular channels with opposite chirality but also achiral channels. To the best of our knowledge, this is the first time lanthanide metal coordination polymers with ImDC ligands have been prepared.

Experimental Section

1 and **2**: A mixture of Ln_2O_3 (0.5 mmol; Eu_2O_3, 0.176 g; Dy_2O_3, 0.187 g), H_3ImDC (1 mmol, 0.156 g), and H_2O (8 mL) in the presence of HNO_3 (0.33 mL 8.4 wt%) in a molar ratio of about 1:2:889:0.92 (pH 2) was sealed in a 30-mL stainless steel reactor with a Teflon liner and heated at 170 °C for 10 days, and then cooled to room temperature. White prismatic crystals of **1** and **2** were recovered by filtration, washed with distilled water, and dried in air.

1: Yield: 60% (based on Eu_2O_3); elemental analysis (%) calcd for $C_{10}H_{11.25}Eu_2N_4O_{12.63}$: C 17.32, H 1.64, N 8.08; found: C 17.31, H 1.63, N 8.14; IR (KBr pellet): $\tilde{\nu} = 1573$, 1389, 1108 cm^{-1}.

2: Yield: 37% (based on Dy_2O_3); elemental analysis (%) calcd for $C_{10}H_{11.25}Dy_2N_4O_{12.63}$: C 16.79, H 1.59, N 7.84; found: C 16.30, H 1.61, N 7.59; IR (KBr pellet): $\tilde{\nu} = 1579$, 1392, 1111 cm^{-1}.

Received: February 6, 2005
Published online: August 1, 2005

Keywords: coordination polymers · helical structures · lanthanides · N ligands · O ligands

[1] a) O. M. Yaghi, H. Li, C. Davis, D. Richardson, T. L. Groy, *Acc. Chem. Res.* **1998**, *31*, 474–484; b) B. Moulton, M. J. Zaworotko, *Chem. Rev.* **2001**, *101*, 1629–1658; c) M. Eddaoudi, D. B. Moler, H. Li, B. Chen, T. M. Reineke, M. O'Keeffe, O. M. Yaghi, *Acc. Chem. Res.* **2001**, *34*, 319–330; d) W. Lin, Z. Wang, L. Ma, *J. Am. Chem. Soc.* **1999**, *121*, 11249–11250; e) O. Kahn, *Acc. Chem. Res.* **2000**, *33*, 647–657; f) M. Eddaoudi, J. Kim, N. Rosi, D. Vodak, J. Wachter, M. O'Keeffe, O. M. Yaghi, *Science* **2002**, *295*, 469–472; g) S. M. Kuznicki, V. A. Bell, S. Nair, H. W. Hillhouse, R. M. Jacubinas, C. M. Braunbarth, B. H. Toby, M. Tsapatsis, *Nature* **2001**, *412*, 720–724; h) S. Noro, S. Kitagawa, M. Kondo, K. Seki, *Angew. Chem.* **2000**, *112*, 2161–2164; *Angew. Chem. Int. Ed.* **2000**, *39*, 2081–2084.

[2] a) O. R. Evans, R. Xiong, Z. Wang, G. K. Wong, W. Lin, *Angew. Chem.* **1999**, *111*, 557–559; *Angew. Chem. Int. Ed.* **1999**, *38*, 536–538; b) S. R. Batten, R. Robson, *Angew. Chem.* **1998**, *110*, 1558–1595; *Angew. Chem. Int. Ed.* **1998**, *37*, 1460–1494; c) W. Lin, O. R. Evans, R. G. Xiong, Z. Wang, *J. Am. Chem. Soc.* **1998**, *120*, 13272–13273; d) C. Janiak, *Angew. Chem.* **1997**, *109*, 1499–1502; *Angew. Chem. Int. Ed. Engl.* **1997**, *36*, 1431–1434; e) M. J. Zaworotko, *Chem. Soc. Rev.* **1994**, *23*, 283–288;

 © 2005 Wiley-VCH Verlag GmbH & Co. KGaA, Weinheim

f) G. B. Gardner, D. Venkataraman, J. S. Moore, S. Lee, *Nature* **1995**, *374*, 792 – 795; g) M. Fujita, Y. J. Kwon, S. Washizu, K. Ogura, *J. Am. Chem. Soc.* **1994**, *116*, 1151 – 1152.

[3] a) M. R. Bürgstein, M. T. Gamer, P. W. Roesky, *J. Am. Chem. Soc.* **2004**, *126*, 5213 – 5218, and references therein; b) T. M. Reineke, M. Eddaoudi, M. O'Keeffe, O. M. Yaghi, *Angew. Chem.* **1999**, *111*, 2712 – 2716; *Angew. Chem. Int. Ed.* **1999**, *38*, 2590 – 2594; c) D.-L. Long, A. J. Blake, N. R. Champness, C. Wilson, M. Schröder, *Angew. Chem.* **2001**, *113*, 2509 – 2513; *Angew. Chem. Int. Ed.* **2001**, *40*, 2443 – 2447; d) Y. Wan, L. Zhang, L. Jin, S. Gao, S. Lu, *Inorg. Chem.* **2003**, *42*, 4985 – 4994; e) X.-J. Zheng, L.-P. Jin, S.-Z. Lu, *Eur. J. Inorg. Chem.* **2002**, 3356 – 3363.

[4] a) O. M. Yaghi, H. Li, T. L. Groy, *Z. Kristallogr.* **1997**, *212*, 457 – 458; b) L. P. Wu, M. Munakata, T. Kuroda-Sowa, M. Maekawa, Y. Suenaga, *Inorg. Chim. Acta* **1996**, *249*, 183 – 189; c) J. A. Seddon, A. R. W. Jackson, R. A. Kresinski, A. W. G. Platt, *Polyhedron* **1996**, *15*, 1899 – 1902; d) E. Huskowska, T. Glowiak, J. Legendziewicz, G. Oremek, *J. Alloys Compd.* **1992**, *179*, 13 – 25; e) S. J. L. Ribeiro, R. R. Goncalves, L. F. C. de Oliveira, P. S. Santos, *J. Alloys Compd.* **1994**, *216*, 61 – 66.

[5] a) L. Pan, N. Zheng, Y. Wu, S. Han, R. Yang, X. Huang, J. Li, *Inorg. Chem.* **2001**, *40*, 828 – 830; b) L. Pan, E. B. Woodlock, X. Wang, C. Zheng, *Inorg. Chem.* **2000**, *39*, 4174 – 4178.

[6] a) T. M. Reineke, M. Eddaoudi, M. Fehr, D. Kelley, O. M. Yaghi, *J. Am. Chem. Soc.* **1999**, *121*, 1651 – 1657; b) F. Millange, C. Serre, J. Marrot, N. Gardant, F. Pellé, G. Férey, *J. Mater. Chem.* **2004**, *14*, 642 – 645.

[7] a) L. Pan, K. M. Adams, H. E. Hernandez, X. Wang, C. Zheng, Y. Hattori, K. Kaneko, *J. Am. Chem. Soc.* **2003**, *125*, 3062 – 3067; b) L. Pan, X. Huang, J. Li, Y. Wu, N. Zheng, *Angew. Chem.* **2000**, *112*, 537 – 540; *Angew. Chem. Int. Ed.* **2000**, *39*, 527 – 530.

[8] a) M. T. Caudle, J. W. Kampf, M. L. Kirk, P. G. Rasmussen, V. L. Pecoraro, *J. Am. Chem. Soc.* **1997**, *119*, 9297 – 9298; b) P. Sengupta, R. Dinda, S. Ghosh, W. S. Sheldrick, *Polyhedron* **2001**, *20*, 3349 – 3354; c) T. M. Rajendiran, M. L. Kirk, I. A. Setyawati, M. T. Caudle, J. W. Kampf, V. L. Pecoraro, *Chem. Commun.* **2003**, 824 – 825; d) J. C. Bayón, G. Net, P. G. Rasmussen, J. B. Kolowich, *J. Chem. Soc. Dalton Trans.* **1987**, 3003 – 3007; e) C.-F. Wang, E.-Q. Gao, Z, He, C.-H. Yan, *Chem. Commun.* **2004**, 720 – 721, and references therein.

[9] Crystal data for **1** ($C_{10}H_{11.25}Eu_2N_4O_{12.63}$): $M_r = 693.40$, tetragonal, space group $I4_1/a$, $a = 20.2950$ (11), $b = 20.2950(11)$, $c = 16.1760(12)$ Å, $V = 6662.7(7)$ Å^3, $Z = 16$, $\rho = 2.765$ g cm^{-3}, $\mu = 7.543$ cm^{-1}, $F(000) = 5220$, GOF = 1.187. Of 7971 total reflections collected, 2947 were unique ($R_{int} = 0.0700$). $R1$ ($wR2$) = 0.0473 (0.0966) for 259 parameters and 2115 reflections [$I > 2\sigma(I)$]. Crystal data for **2** ($C_{10}H_{11.25}Dy_2N_4O_{12.63}$): $M_r = 714.48$, tetragonal, space group $I4_1/a$, $a = 20.187(3)$, $b = 20.187$ (3), $c = 15.992(3)$ Å, $V = 6517.0(19)$ Å^3, $Z = 16$, $\rho = 2.913$ g cm^{-3}, $\mu = 9.185$ cm^{-1}, $F(000) = 5316$, GOF = 1.191. Of 19395 total reflections collected, 2873 were unique ($R_{int} = 0.0353$). $R1$($wR2$) = 0.0265 (0.0568) for 264 parameters and 2783 reflections [$I > 2\sigma(I)$]. The intensity data were collected on a Smart CCD diffractometer with graphite-monochromated $Mo_{K\alpha}$ radiation ($\lambda = 0.71073$ Å) at room temperature. All absorption corrections were performed by using the SADABS program. The structures were solved by direct methods and refined by full-matrix least squares on F^2 using the SHELXTL-97 program package. CCDC-238992 (**1**) and CCDC-238946 (**2**) contain the supplementary crystallographic data for this paper. These data can be obtained free of charge from the Cambridge Crystallographic Data Centre via www.ccdc.cam.ac.uk/data_request/cif.

[10] B. Zhao, X.-Y. Chen, P. Cheng, D.-Z. Liao, S.-P. Yan, Z.-H. Jiang, *J. Am. Chem. Soc.* **2004**, *126*, 15394 – 15395, and references therein.

[11] J.-C. G. Bünzli in *Lanthanide Probes in left, Chemical and Earth Sciences. Theory and Practice* (Eds.: J.-C. G. Bünzli, G. R. Choppin), Elsevier Scientific Publishers, Amsterdam, **1989**, charp. 7.

[12] B. Ma, D. Zhang, S. Gao, T. Jin, C. Yan, G. Xu, *Angew. Chem.* **2000**, *112*, 3790 – 3792; *Angew. Chem. Int. Ed.* **2000**, *39*, 3644 – 3646.

[13] Other phase-pure lanthanides polymers, $[Ln_2(ImDC)_2(H_2O)_3]\cdot n\,H_2O$ (Ln = Y, Pr, Nd, Sm, Gd, Tb, and Er; CCDC-271490–271496) were also obtained as single crystals. X-ray diffraction proves that these compounds are analogous to the title compound. Further investigation on the fluorescent, magnetic, and adsorption properties of these compounds is in progress.

 © 2005 Wiley-VCH Verlag GmbH & Co. KGaA, Weinheim

One-Dimensional Magnets

DOI: 10.1002/anie.200500464

Molecular Engineering for Single-Chain-Magnet Behavior in a One-Dimensional Dysprosium–Nitronyl Nitroxide Compound**

*Lapo Bogani, Claudio Sangregorio, Roberta Sessoli, and Dante Gatteschi**

The discovery of single molecule magnets (SMMs), about a decade ago,[1] opened up a very lively scientific area where still both physicists and chemists join their efforts to better understand and selectively change the magnetic properties of matter.[2] On one side, the interest aroused by these materials is due to the fact that they allow us to directly address questions of fundamental interest,[3] and, on the other side, their proposed applications make them appealing candidates for future devices.[4] The field was further expanded by the discovery, some years ago, of a polymeric compound, [Co(hfac)$_2${NIT(C_6H_4OMe)}][5] (hfac = hexafluoroacetylacetonate; NIT(R): 2-(4′-R)-4,4,5,5-tetramethylimidazoline-1-oxyl-3-oxide), which displays a hysteresis behavior above the temperature of liquid He without undergoing three-

[*] L. Bogani, Dr. C. Sangregorio, Prof. R. Sessoli, Prof. D. Gatteschi
Department of Chemistry and INSTM Research Unit
Università di Firenze
Via della Lastruccia 3, 50019 Sesto Fiorentino (Italy)
Fax: (+39) 055-457-3372
E-mail: dante.gatteschi@unifi.it

[**] This work was financially supported by the Human Potential Program RTN-QUEMOLNA (FP6-504880), the Italian MIUR (FIRB and PRIN projects), and the German DFG (SPP1137). We acknowledge Prof. A. Rettori, Dr. M. G. Pini, and Prof. C. Benelli for many stimulating discussions and Dr. P. Rosa for his assistance in ac magnetic measurements.

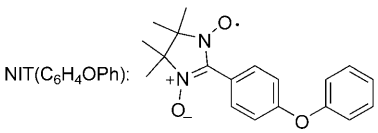
Supporting information for this article is available on the WWW under http://www.angewandte.org or from the author.

© 2005 Wiley-VCH Verlag GmbH & Co. KGaA, Weinheim

dimensional (3D) magnetic ordering. This slow dynamics of the magnetization was explained with Glauber's model[5] for Ising spin chains and, while the physics underlying these systems is revealing interesting aspects,[6] much effort is devoted to the synthesis of new chain compounds of this kind, known as single-chain magnets (SCMs).[7] The two requirements needed to observe Glauber dynamics, that is, a strong Ising anisotropy and a very low ratio of interchain/intrachain interactions, are difficult to balance, and only a few compounds have been proposed as SCMs up to now.[8]

Rare-earth-radical-based chains are very appealing candidates for SCMs owing to the Ising anisotropy of their metallic centers, and $[Dy(hfac)_3\{NIT(Et)\}]$ (**1**) displays a transition to 3D magnetic order at 4.3 K.[9] However, the interchain interactions are relatively weak, as the shortest metal–metal distances are 10.76 Å, and only through-space (dipolar) interchain interactions are active. It should be possible to further increase these distances by varying the radical, thus determining a passage from 3D order to SCM behavior. This can shed light on the delicate balance between the exchange, structural features, and magnetic anisotropy required for SCM behavior. This idea proved to work well, and we wish to report herein the first complete structural and magnetic characterization of a rare-earth-based SCM synthesized by a rational approach. Frequency-dependent data on a Tb-based compound have been reported in a previous work, but structural evidence was lacking.[10]

The radical $NIT(C_6H_4OPh)$ was an appealing candidate to increase the separation of neighboring chains because it possesses two rather mobile aromatic rings, as spacers, and an



ether group in between that enriches the electron density of these rings. The presence of such electron-rich groups alternating with the electron-poor rings formed when hfac ligands coordinate to a metal center favors stacking interactions along the chain, thus stabilizing the polymeric compound.[11]

The reaction of $[Dy(hfac)_3(H_2O)_2]$ with the $NIT(C_6H_4OPh)$ radical in hot *n*-heptane afforded single crystals of the chain compound $[Dy(hfac)_3\{NIT(C_6H_4OPh)\}]$ (**2**) suitable for X-ray analysis. This compound, whose structure is depicted in Figure 1,[12] consists of chains, parallel to *b*, of octacoordinated $Dy(hfac)_3$ centers connected by radical units, which act as bis-monodentate ligands.

The coordination geometry around the Dy atom is a distorted dodecahedron with triangular faces, where the two radical oxygen atoms occupy the apical positions of two distorted pentagons. The distances between the metal center and these oxygen atoms were found to be very similar to each other (2.329(4) Å and 2.385(4) Å). The stacking interactions between the inner aromatic ring of the spacer and an hfac ligand can be clearly identified,[13] as the distance between the two aromatic planes is 3.75(5) Å and the angle between them

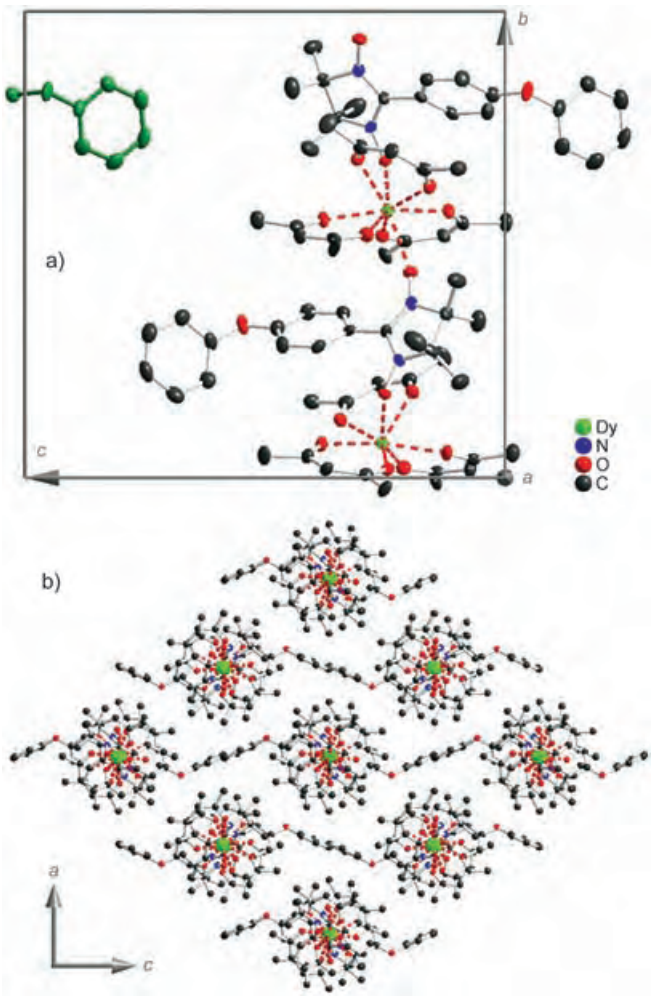


Figure 1. Views of the structure of **2**: a) along the *a* axis, showing the chain structure together with the unit cell. The aromatic tail of the radical of an adjacent chain is also shown (in green); b) along the crystallographic *b* axis, showing the packing of the chains. Ellipsoids are drawn at 50% probability and fluorine and hydrogen atoms have been omitted for clarity.

is 14.6(2)°, in agreement with the situation observed in other metal NIT(R) derivatives.[11] The outer aromatic ring of the spacer, on the other hand, is placed between the chains, with the normal tilted with respect to the inner ring (65.84°) and oriented almost perpendicularly to the chain axis (86.71°). This ring lies isolated in a niche between two other chains, surrounded by the fluorine atoms of four hfac ligands, with a distance of 5.90(5) Å from the centroid of the nearest ligand. In this way, as can be observed from Figure 1, the free volume between the chains is alternatively occupied by the spacers of two different chains, thereby minimizing any weak magnetic interactions between the radicals. Our strategy leads to an increased volume per metal center, which grows from 881 $Å^3$ in **1** to 1001 $Å^3$ in **2** and, more importantly, to a lengthening of all distances between different chains. Analysis of the distances between a chain and the six neighboring ones showed the presence, in both cases, of three couples of equally distant chains. All three distances increase, with the shortest distance between two Dy centers growing from 10.76 to

 © 2005 Wiley-VCH Verlag GmbH & Co. KGaA, Weinheim

11.35 Å, and the next two shortest separations increasing from 11.23 to 11.38 Å and from 11.43 to 14.31 Å. In other words, there is a change from a pseudo-hexagonal arrangement of the chains in **1** to a pseudo-tetragonal one in **2**. Considering the r^{-3} dependence of magnetic dipolar interactions, such changes in the crystal structure, although they may not seem dramatic, reduce the interactions along the shortest distance by 15% and those along the longest distance by up to 49%. This analysis reveals that the engineering of the compound has led to an efficient suppression of interchain interactions independent of the orientation of the magnetic easy axis.

The effect of this crystal engineering strategy on the magnetic properties is evident from Figure 2, in which we show the dc magnetic susceptibility measured for a powder

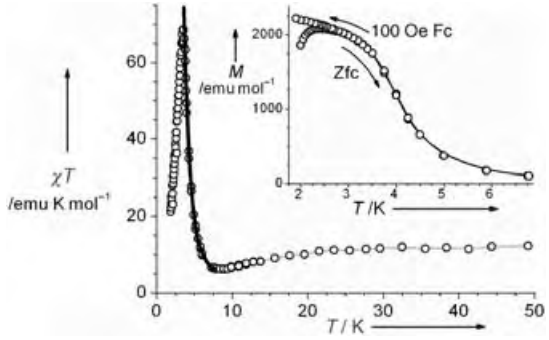


Figure 2. Low-temperature dependence of the χT product from dc magnetic measurements performed in a 100 Oe applied field. The black line represents the calculated curve, as described in the text. In the inset we show the gap that opens up below 2.6 K between the zero-field-cooled and the 100-Oe-cooled curves.

sample. The radicals are $S = 1/2$ isotropic magnetic centers, while Dy^{III}, a $^6H_{15/2}$ ion, is usually treated, at low temperature, as an effective $S = 1/2$ anisotropic center. The high-temperature χT value, 12.2 emu K mol^{-1} at 300 K, is slightly lower than the expected theoretical value for two such noninteracting magnetic centers, but consistent with the data available for **1**.[9] The temperature dependence of χT shows a minimum at 8.6 K and a rounded peak of 68.5 emu K mol^{-1} at 3.6 K, typical of 1D behavior, while the cusp found in the 3D-ordered compound[9] is not observed.

The magnetism of this type of lanthanide–radical chain is characterized by the presence of nearest-neighbor (NN) ferromagnetic metal–radical and next-nearest-neighbor (NNN) antiferromagnetic metal–metal or radical–radical magnetic couplings (J_{Mr}, J_{MM}, and J_{rr}, respectively).[9] The overall behavior at low temperature depends on the ratio between ferro- and antiferromagnetic interactions.[14] The low-temperature powder data of **2** suggest that ferromagnetic interactions dominate. A scaling procedure of the χT data[15] clearly indicates a linear regime characteristic of Ising 1D systems (see Supporting Information). The data between 8.5 and 3.6 K were therefore reproduced with a spin-1/2 Ising model with alternating Landé g-factors (g_r and g_{Dy} for the radical and the Dy centers, respectively) and three exchange interactions. A good agreement ($R = 0.999$) between the calculated and experimental curves in this region was found with the values $g_r = 2.0$, $g_{Dy} = 8.0$ (vide infra), ferromagnetic $J_{Mr} = 19$ K, and antiferromagnetic $J_{rr} = -6.5$ and $J_{MM} = -4$ K. A similar agreement was also observed with other sets of parameters, thereby suggesting a strong correlation between them, with the difference between the ferromagnetic and antiferromagnetic interactions being the key point. Moreover, due to the presence of a strong anisotropy of the magnetization, single-crystal measurements as a function of the orientation will be needed to give a completely reliable set of values.

1D Ising systems are expected to follow Glauber slow dynamics with a thermally activated reversal of the magnetization, $\tau = \tau_0 \exp(\Delta/k_B T)$, where the energy barrier, Δ, depends on the exchange interaction, that is, $\Delta = |J|$ for $S = 1/2$. The ac magnetic susceptibility curves, measured in zero static field, display a frequency-dependent peak for both in-phase χ' and out-of-phase χ'' signals below 4.5 K, as shown in Figure 3, thus indicating the presence of a thermally activated mechanism. A frequency-independent peak at the transition

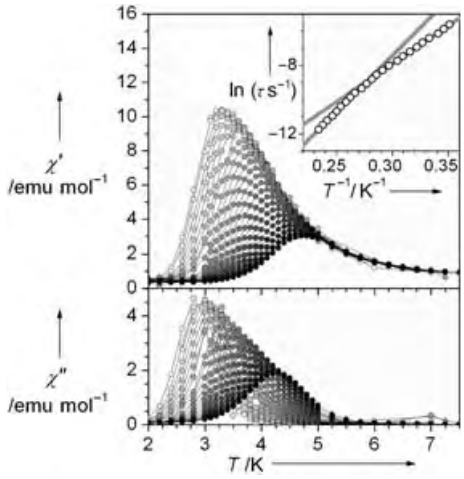


Figure 3. Temperature dependence of the real (top) and imaginary (bottom) components of the ac magnetic susceptibility measured in zero applied field in the frequency range 25 Hz–20 kHz. The inset shows the obtained Arrhenius plot and the crossover.

temperature would be found for a 3D-ordered compound. The dynamic behavior of **2** can be reproduced with the generalized Debye model (Supporting Information) by taking into account a narrow distribution of relaxation times, $\alpha = 0.16$, a value compatible with those observed for other SCMs.[8]

The Arrhenius plot extracted from these data, reproduced in the inset of Figure 3, shows the presence of a crossover between two different activated regimes, both of which give best-fits with physical τ_0 values (5.6×10^{-10} and 1.9×10^{-12} s for the low- and high-temperature regimes, respectively) and two different barriers (42 and 69 K, respectively). The presence of a crossover in the Arrhenius plot of SCMs that halves the Glauber activation barrier due to finite-size effects has been predicted[16] and experimentally observed for systems with a slow relaxation of single monomeric units.[15]

 © 2005 Wiley-VCH Verlag GmbH & Co. KGaA, Weinheim

Below 2.6 K, irreversibility effects also appear in static magnetic measurements as a discrepancy between the magnetization curve cooled in zero field and the curve cooled in an applied external field, as shown in the inset of Figure 2. The magnetization curve taken at 1.60 K, depicted in Figure 4, reveals the opening of a hysteresis loop and a very rich magnetic behavior with two different steps, an unprecedented feature in rare-earth polymeric systems. The fact that such steps do not change on varying the field sweep rate indicates that they are associated with static properties. While we cannot totally exclude that the first step around $H = 50$ Oe is due to residual antiferromagnetic interchain interactions, it is interesting to note that the slow relaxation of the magnetization observed above 2 K in zero field also persists above the step. This is consistent with a very "robust" Glauber dynamic regime that is unaffected by possible weak interchain interactions.[17]

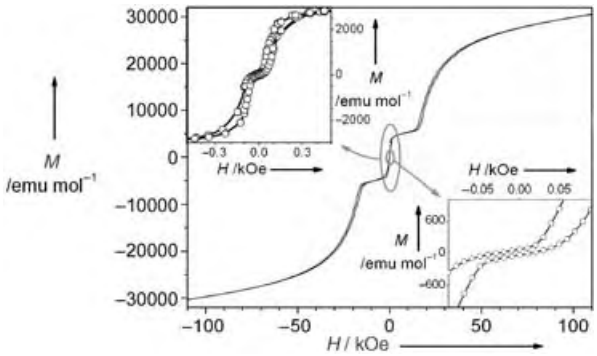


Figure 4. Magnetization curve versus applied field measured at 1.60 K. The nested hysteresis cycles are shown in the two insets.

The step at around $H = 15$ kOe is more difficult to rationalize. The presence of competing NN and NNN interactions could stabilize states that do not correspond to the ferromagnetic alignment of all the spins. A state that has been previously discussed can be described by the spin arrangement …↓↓↑↑↓↑…, in which the red arrows represent Dy magnetic moments and the black arrows represent radical sites.[9] This state has a magnetization corresponding to $(M_{Dy}-M_r)/3$, and is not too far from that observed in Figure 4, assuming that the high-field value tends to $(M_{Dy}+M_r)$, thus providing an average g_{Dy} value of around 8. However, we could not successfully reconcile this picture with the ferromagnetic behavior observed between 4 and 10 K using a simple Ising model; further investigations with single crystals are necessary to clarify this point.

In conclusion, we have prepared and structurally characterized the first rare-earth-radical-based coordination polymer to exhibit SCM behavior, namely [Dy(hfac)$_3${NIT(C$_6$H$_4$OPh)}] (**2**). A critical reconsideration of previously known compounds was a key point to rationally plan the synthesis to enhance the stacking along the chains and to weaken the interchain magnetic interactions. To the best of our knowledge, this is the first successful preparation of an SCM from a material known to undergo 3D magnetic ordering. The chains exhibit all the features of a slowly relaxing system, including a crossover between two Arrhenius regimes, and a hysteresis loop opens below 3 K. The observation of such a crossover in **2**, if due to finite-size effects, would suggest a significant contribution to the barrier coming from the anisotropic building blocks, as the barrier is not exactly halved.[15] This would open the possibility to study the effect of the recently observed dynamics of rare-earth single-ion units[18] when arranged in chains. These dynamic features are accompanied by a very rich static behavior that could be due to the interplay of NN and NNN interactions, with the presence of several low-energy states. Finally, thanks to the synthetic possibilities opened up here, the chemical reactivity of rare-earth metals can now be exploited to study the role of the anisotropy and magnetic multiplicity of the rare-earth ion on the slow dynamics of both monomers and chains.

Experimental Section

Synthesis of **2**: [Dy(hfac)$_3$(H$_2$O)$_2$] (1 mmol) was dissolved in boiling dry *n*-heptane (30 mL). The solution was left to boil for 20 min and then cooled down to 75 °C, whereupon 1 mmol of the crystalline solid radical NIT(C$_6$H$_4$OPh) was slowly added whilst stirring followed by 3 mL of CH$_2$Cl$_2$. The final solution was cooled down to room temperature and was left to stand for about 24 h to give green, needle-like crystals. C$_{34}$H$_{24}$DyF$_{18}$N$_2$O$_9$: calcd C 36.89, H 2.18, N 2.52; found: C 37.10, H 2.50, N 2.79.

Physical measurements: The dc magnetic susceptibility measurements were performed on solid polycrystalline samples with a Cryogenic S600 SQUID magnetometer and were all corrected for the diamagnetic contribution as calculated with Pascal's constants. Magnetization curves with fields over 60 kOe were measured with an Oxford VSM system after inclusion of the sample in grease to prevent orientation of the crystallites. Data were corrected for the magnetism of the grease, which was independently determined at the same temperature and fields. The ac magnetic susceptibility was measured by using a homemade probe operating in the range 20–20 000 Hz.[19] Crystal structure data were collected with an Oxford Diffraction Xcalibur3 diffractometer.

Received: February 7, 2005
Revised: June 6, 2005
Published online: August 5, 2005

Keywords: lanthanides · magnetic properties · one-dimensional magnets · radicals · rational synthesis design

[1] R. Sessoli, D. Gatteschi, A. Caneschi, M. A. Novak, *Nature* **1993**, *365*, 141.
[2] D. Gatteschi, R. Sessoli, *Angew. Chem.* **2003**, *115*, 278; *Angew. Chem. Int. Ed.* **2003**, *42*, 268.
[3] a) P. C. E. Stamp, *Nature* **1996**, *383*, 125; b) E. M. Chudnovsky, *Science* **1998**, *280*, 229; c) W. Wernsdorfer, R. Sessoli, *Science* **1999**, *284*, 133.
[4] M. N. Leuenberger, D. Loss, *Nature* **2001**, *410*, 789.
[5] A. Caneschi, D. Gatteschi, N. Lalioti, C. Sangregorio, R. Sessoli, G. Venturi, A. Vindigni, A. Rettori, M. G. Pini, M. A. Novak, *Angew. Chem.* **2001**, *113*, 1810; *Angew. Chem. Int. Ed.* **2001**, *40*, 1760.
[6] L. Bogani, A. Caneschi, M. Fedi, D. Gatteschi, M. Massi, M. A. Novak, M. G. Pini, A. Rettori, R. Sessoli, A. Vindigni, *Phys. Rev. Lett.* **2004**, *92*, 207204.

 © 2005 Wiley-VCH Verlag GmbH & Co. KGaA, Weinheim

[7] R. Clerac, H. Miyasaka, M. Yamashita, C. Coulon, *J. Am. Chem. Soc.* **2002**, *124*, 12837.
[8] a) R. Lescouezec, J. Vaissermann, C. Ruiz-Perez, F. Lloret, R. Carrasco, M. Julve, M. Verdaguer, Y. Dromzee, D. Gatteschi, W. Wernsdorfer, *Angew. Chem.* **2003**, *115*, 1521; *Angew. Chem. Int. Ed.* **2003**, *42*, 1483; b) T. Liu, D. Fu, S. Gao, Y. Zhang, H. Sun, G. Su, Y. Liu, *J. Am. Chem. Soc.* **2003**, *125*, 13976; c) L. M. Toma, R. Lescouezec, F. Lloret, M. Julve, J. Vaissermann, M. Verdaguer, *Chem. Commun.* **2003**, 1850; d) E. Pardo, R. Ruiz-Garcia, F. Lloret, J. Faus, M. Julve, Y. Journaux, F. Delgado, C. Ruiz-Perez, *Adv. Mater.* **2004**, *16*, 1597.
[9] a) C. Benelli, A. Caneschi, D. Gatteschi, R. Sessoli, *Adv. Mater.* **1992**, *4*, 504; b) C. Benelli, A. Caneschi, D. Gatteschi, R. Sessoli, *Inorg. Chem.* **1993**, *32*, 4797; c) C. Benelli, A. Caneschi, D. Gatteschi, R. Sessoli, *J. Appl. Phys.* **1993**, *73*, 5333; d) C. Benelli, A. Caneschi, D. Gatteschi, L. Pardi, P. Rey, *Inorg. Chem.* **1990**, *29*, 4223.
[10] J. P. Costes, J. M. Clemente-Juan, F. Dahan, J. Milon, *Inorg. Chem.* **2004**, *43*, 8200.
[11] A. Caneschi, D. Gatteschi, N. Lalioti, C. Sangregorio, R. Sessoli, *J. Chem. Soc. Dalton Trans.* **2000**, 3907.
[12] Crystal structure data for **2**: $C_{34}H_{24}DyF_{18}N_2O_9$ ($0.28\times0.09\times0.02\ mm^3$), $M_r=1109.05$, orthorhombic, space group $P2_12_12_1$ (no. 19), $a=14.313(1)$, $b=16.472(1)$, $c=16.974(1)$ Å, $V=4001.9(6)$ Å^3, $Z=4$, $\rho_{calcd}=1.841\ g\,cm^{-3}$, $\mu=2.006\ mm^{-1}$, min./max. transmission = 0.675, $Mo_{K\alpha}$ radiation ($\lambda=0.71069$ Å), $T=150$ K, 25285 collected reflections of which 7273 were unique ($R_{int}=0.0397$), and 574 parameters, $R1=0.0338$ and $wR2=0.0694$ using 5565 reflections with $I>2\sigma(I)$, $R1$ (all data) = 0.0449, GooF = 0.947. Lorentzian polarization and absorption corrections were applied to the data set. The structure was solved by direct methods (SIR97), and was refined by Fourier difference syntheses using SHELXL97 with a full-matrix least-squares method against $|F^2|$ data. During the final iterations, hydrogen atoms were added in calculated positions assuming idealized bond geometries. CCDC-262704 contains the supplementary crystallographic data for this paper. These data can be obtained free of charge from the Cambridge Crystallographic Data Centre via www.ccdc.cam.ac.uk/data_request/cif.
[13] C. Janiak, *J. Chem. Soc. Dalton Trans.* **2000**, 3885.
[14] a) M. G. Pini, A. Rettori, *Phys. Rev. B* **1993**, *48*, 3240; b) I. Harada, *J. Phys. Soc. Jpn.* **1983**, *52*, 4099.
[15] a) C. Coulon, R. Clerac, L. Lecren, W. Wernsdorfer, H. Miyasaka, *Phys. Rev. B* **2004**, *69*, 132408; b) M. Ferbinteanu, H. Miyasaka, W. Wernsdorfer, K. Nakata, K. Sugiura, M. Yamashita, C. Coulon, R. Clerac, *J. Am. Chem. Soc.* **2005**, *127*, 3090.
[16] a) J. Kamphorst Leal da Silva, A. G. Moreira, M. Silvério - Soares, F. C. Sá Barreto, *Phys. Rev. E* **1995**, *52*, 4527; b) J. H. Luscombe, M. Luban, J. P. Reynolds, *Phys. Rev. E* **1996**, *53*, 5852.
[17] S. Žumer, *Phys. Rev. B* **1980**, *21*, 1298.
[18] a) R. Giraud, W. Wernsdorfer, A. M. Tkachuk, D. Mailly, B. Barbara, *Phys. Rev. Lett.* **2001**, *87*, 057203; b) N. Ishikawa, M. Sugita, T. Ishikawa, S. Koshihara, Y. Kaizu, *J. Am. Chem. Soc.* **2003**, *125*, 8694; c) T. Ishikawa, M. Sugita, W. Wernsdorfer, *J. Am. Chem. Soc.* **2005**, *127*, 3650; d) T. Ishikawa, M. Sugita, W. Wernsdorfer, *Angew. Chem.* **2003**, *115*, 2991; *Angew. Chem. Int. Ed.* **2005**, *44*, 2931.
[19] S. Midollini, A. Orlandini, P. Rosa, L. Sorace, *Inorg. Chem.* **2005**, *44*, 2060.

 © 2005 Wiley-VCH Verlag GmbH & Co. KGaA, Weinheim

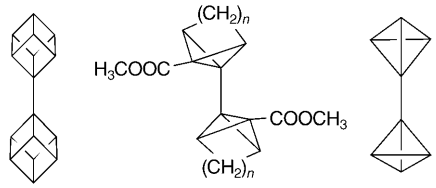
Short C–C Bonds

DOI: 10.1002/anie.200501605

Hexakis(trimethylsilyl)tetrahedranyltetrahedrane**

*Masanobu Tanaka and Akira Sekiguchi**

The most important factor for bond shortening is the increase in s character of the bond orbital.[1] In 1988, Eaton and coworkers succeeded in the synthesis and structural characterization of cubylcubane (**1**).[2] The bond length between the



1 **2**: $n=2$, **3**: $n=3$ **4**

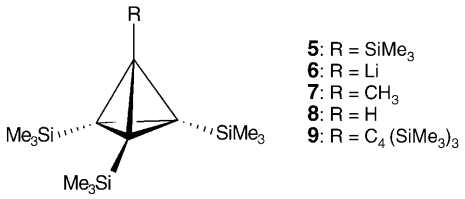
two cubane units (1.458 Å) was significantly shorter than the usual carbon–carbon single-bond length (1.54 Å). This bond shortening was attributed to the high s character of the bond orbitals. Later, Ermer et al. synthesized coupled bicyclo[1.1.0]butane derivatives **2** and **3**,[3] in which the corresponding C–C bonds have higher s character than that in cubylcubane. As expected, the linking C–C bond lengths in these coupled bicyclo[1.1.0]butane derivatives are further shortened (1.445 and 1.440 Å). Tetrahedrane is the most strained cage compound with the highest degree of s character in the exocyclic bond. Therefore, the linking C–C bond length in tetrahedranyltetrahedrane (**4**) is expected to be even shorter. Indeed, theoretical studies suggest compound **4** as a candidate for the molecule with the shortest carbon–carbon single bond in a saturated hydrocarbon system.[4] However, treatment of substituted tetrahedranes is extremely difficult because of its high strain and, consequently, high reactivity.[5,6] Until now, no tetrahedranyltetrahedrane derivative has been synthesized.

Recently, we succeeded in the synthesis and characterization of trimethylsilyl-substituted tetrahedrane derivatives.[7,8] Electropositive silyl groups significantly release the inherent ring strain of the tetrahedrane skeleton. For

[*] Dr. M. Tanaka, Prof. Dr. A. Sekiguchi
Department of Chemistry
Graduate School of Pure and Applied Sciences
University of Tsukuba
Tsukuba, Ibaraki 305-8571 (Japan)
Fax: (+81) 298-53-4314
E-mail: sekiguch@staff.chem.tsukuba.ac.jp

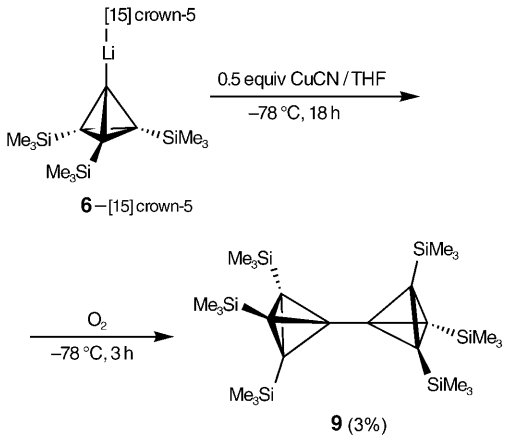
[**] This work was supported by a Grant-in-Aid for Scientific Research (Nos. 14707820 4, 16205008) from the Ministry of Education, Science, and Culture of Japan, a JSPS Research Fellowship for Young Scientists (M.T.), and a COE (Center of Excellence) program. We thank Professor Günther Maier for helpful discussions and advice.

 © 2005 Wiley-VCH Verlag GmbH & Co. KGaA, Weinheim



example, tetrakis(trimethylsilyl)tetrahedrane (**5**) is stable in the presence of air and moisture at temperatures up to 300 °C. We also synthesized and isolated tetrahedranyllithium **6** as a thermally stable compound which is a good precursor for other tetrahedrane derivatives.[8] Indeed, we succeeded in the synthesis of methyl- and hydrogen-substituted tetrahedranes (**7** and **8**, respectively) from tetrahedranyllithium. Surprisingly, tetrahedranes with smaller substituents and hence a lower steric protection were stable in air and at temperatures up to 100 °C. In the ^{1}H NMR spectrum of hydrogen-substituted tetrahedrane **8**, a very large ring C–H coupling constant was observed which is comparable to that of acetylene. From the empirical correlation, we estimated the s character of the ring C–H bond to be 48 %.[8] These results indicate that the C–C link should also have high s character and a very short C–C bond in silyl-substituted tetrahedranyltetrahedrane. Herein, we report the synthesis of hexakis(trimethylsilyl)-tetrahedranyltetrahedrane (**9**) as well as the structural characterization by X-ray crystallography.

Tetrahedrane **9** was synthesized by the oxidative coupling of **6** via a cuprate complex (Scheme 1). First, tetrahedranyllithium **6** was prepared by the reaction of **5** with excess methyllithium in THF, and the ligand of **6** was changed from



Scheme 1. Synthesis of hexakis(trimethylsilyl)tetrahedranyltetrahedrane (**9**).

THF to [15]crown-5 to remove the remaining methyllithium completely. Reaction of **6** with CuCN (0.5 equiv) at −78 °C in THF gave the cuprate complex, which was subsequently oxidized with oxygen at −78 °C. The reaction mixture was purified consecutively by gel-permeation chromatography (toluene) and HPLC (MeOH/*t*BuOMe 1:1) equipped with a recycling system, and finally **9** was isolated as a colorless solid in 3 % yield in a pure form. Several other methods to synthesize **9** by the oxidation of **6** with various reagents such as dichlorodicyano-*p*-benzoquinone, tetracyano-*p*-benzoquinone, $NO^+PF_6^-$, and $(C_6F_5)_3B$ were performed; however, no trace amount of **9** was formed.

Compound **9** was stable in air and up to 200 °C. The most important stabilizing factor can be attributed to the electronic effect of the trimethylsilyl groups, as found in **5**.[7] The ^{1}H, ^{29}Si, and ^{13}C NMR spectra of **9** in [D$_6$]benzene demonstrated its high symmetry. Only one signal was observed for the trimethylsilyl groups in the ^{1}H NMR ($\delta = 0.22$ ppm) and ^{29}Si NMR ($\delta = -2.5$ ppm) spectra, and three signals appeared at $\delta = -18.0$ (ring C–Si), −4.7 (linking ring C), and 0.07 ppm ($SiMe_3$) in the ^{13}C NMR spectrum. The large upfield shift of the ring C atom is typical for tetrahedrane.[7–10] The linking carbon atom shows a remarkably downfield shift relative to that of the silicon-substituted skeletal carbon atom because of the different electronegativities of the Si and C substituents and the high s character of the linking carbon atoms.

The molecular structure of tetrahedranyltetrahedrane **9** was determined by X-ray crystallographic analysis without disorder phenomena. X-ray-quality single crystals were obtained by crystallization from ethanol at 5 °C. As shown in Figure 1,[11] the bulky trimethylsilyl groups sterically

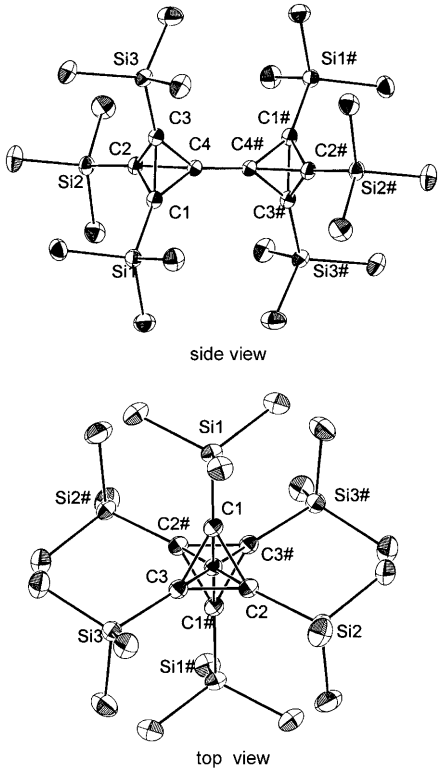


Figure 1. Structure of **9** (ORTEP plot; thermal ellipsoids set at 30 % probability; hydrogen atoms omitted for clarity). Selected bond lengths [Å] and angles [°]: C1–C2 1.523(2), C1–C3 1.528(2), C1–C4 1.483(2), C2–C3 1.511(2), C2–C4 1.484(2), C3–C4 1.484(2), C4–C4# 1.436(3), Si1–C1 1.8260(18), Si2–C2 1.8271(18), Si3–C3 1.8250(19); C4-C1-C2 59.13(11), C4-C1-C3 59.05(11), C2-C1-C3 59.39(11), C4-C1-Si1 153.45(14), C2-C1-Si1 140.76(13), C3-C1-Si1 140.42(14), C1-C4-C2 61.76(11), C1-C4-C3 61.97(11), C2-C4-C3 61.21(11), C4#-C4-C1 144.5(2), C4#-C4-C2 142.8(2), C4#-C4-C3 143.87(19).

 © 2005 Wiley-VCH Verlag GmbH & Co. KGaA, Weinheim

protect the tetrahedranyltetrahedrane skeleton, and the two tetrahedrane units have a staggered conformation owing to steric repulsion.

As expected, the linking C–C bond length (1.436(3) Å) is shortened considerably, and this experimental value of the bond length is practically identical to the theoretical one.[4] To our knowledge, this is the shortest noncyclic (unbent) C–C single bond between saturated C atoms observed to date. The calculated s character of the linking C–C bond in **9** at the NBO/B3LYP/6-31G level is $sp^{1.53}$, which supports the suggestion that this shortening arises from the high s character of the bond. When the electronegativity increases (from Si to C), the s character of the exocyclic bond decreases. This electronic effect changes the structure of the tetrahedrane skeleton.[12] Whereas tetrahedrane **5** has a regular tetrahedral structure, the tetrahedrane units in **9** have a distorted tetrahedral structure. The endocyclic C(C)–C($SiMe_3$) bond lengths (C4–C1, C4–C2, C4–C3) in **9** range from 1.483(2) to 1.484(2) Å (average 1.484(2) Å), whereas the endocyclic C($SiMe_3$)–C($SiMe_3$) bond lengths (C1–C2, C1–C3, C2–C3) range from 1.511(2) to 1.528(2) Å (average 1.521(2) Å), which are longer than those of C–C bond lengths of tetrahedrane **5** (average 1.501(4) Å). The endocyclic C($SiMe_3$)–C($SiMe_3$) bond lengths of **9** (average 1.521(2) Å) are somewhat longer than those of **5** (average 1.501(4) Å) and **6**·$(tmeda)_{1.5}$ (average 1.4986(15) Å).

It is interesting to compare the lengths of the endocyclic C($SiMe_3$)–C(R) bond: R = Li for **6** (average 1.5425(15) Å), R = $SiMe_3$ for **5** (average 1.501(4) Å), R = $C_4(SiMe_3)_3$ for **9** (average 1.484(2) Å); certainly, the electronegativity of R affects the structural features of the tetrahedrane skeleton. In the case of the most electropositive Li atom the C($SiMe_3$)–C(Li) bond has a high p character, thus leading to the elongation of the C–C bond, whereas in the case of more-electronegative substituents (from $SiMe_3$ to $C_4(SiMe_3)_3$) the tendency is the opposite: increase in s character and shortening of the C–C bond.

Experimental Section

9: Tetrakis(trimethylsilyl)tetrahedrane (**5**)[7] (53 mg, 0.16 mmol) and a tenfold excess of methyllithium were placed in a reaction tube. Dry oxygen-free THF (3.0 mL) was introduced by vacuum transfer and stirred for 24 h. After the solvent was removed, dry oxygen-free hexane (5 mL) was introduced and the insoluble methyllithium in hexane was filtered through celite in a glove box. [15]Crown-5 (0.03 mL) was introduced as a solution in hexane, and the deposited methyllithium was filtered through celite in a glove box. The solvent was placed in a reaction tube and removed in vacuo. The colorless solid **6** was obtained. CuCN (4.5 mg, 0.05 mmol) was added to the reaction tube and dry oxygen-free THF (4 mL) was introduced by vacuum transfer and stirred at −78 °C for 18 h, and oxygen gas was bubbled in the solution at −78 °C. After the solvent was removed, the reaction mixture was purified by gel-permeation chromatography (toluene) and HPLC (MeOH/*t*BuOMe 1:1) equipped with a recycling system. The solvent was removed in vacuo and **9** was obtained as a colorless solid (2.5 mg, 3 %); m.p. 209–211 °C; ^{1}H NMR (400 MHz, [D_6]benzene, TMS): δ = 0.22 ppm (s, 54 H, $SiMe_3$); ^{13}C{^{1}H} NMR (100 MHz, [D_6]benzene, TMS): δ = −18.0 (C), −4.7 (C), 0.07 ppm ($SiMe_3$); ^{29}Si{^{1}H} NMR (80 MHz, [D_6]benzene, TMS): δ = −2.5 ppm; MS (70 eV, EI): *m*/*z*: 534 [M^+], 461 [M^+−$SiMe_3$), 73 ($SiMe_3$); HRMS: calcd for $C_{26}H_{54}Si_6$: 534.2841; found: 534.2806. The very low yield of **9** is due to the formation of tetrahedrane **5** and hydrogen-substituted tetrahedrane **8**, which were also produced under the reaction conditions together with **9**.

Received: May 11, 2005
Published online: July 25, 2005

Keywords: silicon · small ring systems · solid-state structures · strained molecules · tetrahedranes

[1] S. Osawa, M. Sakai, E. Osawa, *J. Phys. Chem. A* **1997**, *101*, 1378.
[2] a) R. Glilardi, M. Maggini, P. E. Eaton, *J. Am. Chem. Soc.* **1988**, *110*, 7230; b) R. Glilardi, M. Maggini, P. E. Eaton, *J. Am. Chem. Soc.* **1988**, *110*, 7232.
[3] O. Ermer, P. Bell, J. Schäfer, G. Szeimies, *Angew. Chem.* **1989**, *101*, 503; *Angew. Chem. Int. Ed. Engl.* **1989**, *28*, 473.
[4] a) Y. Xie, H. F. Schaefer III, *Chem. Phys. Lett.* **1989**, *161*, 516; b) Y. Xie, H. F. Schaefer III, *Chem. Phys. Lett.* **1990**, *168*, 249.
[5] G. Maier, *Angew. Chem.* **1988**, *100*, 317; *Angew. Chem. Int. Ed. Engl.* **1988**, *27*, 309.
[6] a) R. F. Peterson, Jr., R. T. K. Baker, R. L. Wolfgang, *Tetrahedron Lett.* **1969**, 4749; b) P. B. Shevlin, A. P. Wolf, *J. Am. Chem. Soc.* **1970**, *92*, 406; c) L. B. Rodewald, H. Lee, *J. Am. Chem. Soc.* **1973**, *95*, 623; d) G. Maier, M. Hoppe, K. Lanz, H. P. Reisenauer, *Tetrahedron Lett.* **1984**, *25*, 5645.
[7] G. Maier, J. Nuedert, O. Wolf, D. Pappusch, A. Sekiguchi, M. Tanaka, T. Matsuo, H. Watanabe, *J. Am. Chem. Soc.* **2002**, *124*, 13819.
[8] A. Sekiguchi, M. Tanaka, *J. Am. Chem. Soc.* **2003**, *125*, 12684.
[9] a) G. Maier, S. Pfriem, U. Schäfer, R. Matusch, *Angew. Chem.* **1978**, *90*, 552; *Angew. Chem. Int. Ed. Engl.* **1978**, *17*, 520; b) G. Maier, S. Pfriem, U. Schäfer, K. D. Malsch, R. Matusch, *Chem. Ber.* **1981**, *114*, 3965.
[10] G. Maier, D. Born, *Angew. Chem.* **1989**, *101*, 1085; *Angew. Chem. Int. Ed. Engl.* **1989**, *28*, 1050.
[11] Crystal structure analysis of **9**: single crystals were grown from a solution in ethanol. A colorless crystal ($\approx 0.4 \times 0.3 \times 0.2$ mm^3) was used for X-ray diffraction data collection on a MacScience DIP2030 K Image Plate Diffractometer with graphite-monochromated $Mo_{K\alpha}$ radiation (λ = 0.71070 Å). Crystal data for **9** at 120 K: $C_{26}H_{54}Si_6$, M_r = 535.23, triclinic, space group = $P\bar{1}$, a = 9.5100(7), b = 10.0500(9), c = 11.6350 (12) Å, α = 102.488(5), β = 104.540(5), γ = 114.754(5)°, V = 909.8(1) Å^3, Z = 1, ρ_{calcd} = 0.997 g cm^3, total reflections collected = 9434, unique reflections = 4051 (R_{int} = 0.029), $2\theta_{max}$ = 56.06, completeness to θ = 91.9 %, GOF = 1.042. The final R factor was 0.0471 (R_W = 0.1367 for all data) for 3325 reflections $I_o > 2\sigma(I_o)$. The structure was solved by direct methods and refined by the full-matrix least-squares method by using the SHELXL-97 program. CCDC-265873 contains the supplementary crystallographic data for **9**. These data can be obtained free of charge from the Cambridge Crystallographic Data Centre via www.ccdc.cam.ac.uk/data_request/cif.
[12] a) J. D. Dill, A. Greenberg, J. F. Liebman, *J. Am. Chem. Soc.* **1979**, *101*, 6814; b) T. Clark, G. W. Spitznagel, R. Klose, P. von. R. Schleyer, *J. Am. Chem. Soc.* **1984**, *106*, 4412; c) D. Cremer, E. Kraka, *J. Am. Chem. Soc.* **1985**, *107*, 3811.

 © 2005 Wiley-VCH Verlag GmbH & Co. KGaA, Weinheim

Supramolecular Chemistry

DOI: 10.1002/anie.200501373

Entangled Coordination Networks with Inherent Features of Polycatenation, Polythreading, and Polyknotting**

Xin-Long Wang, Chao Qin, En-Bo Wang, Yang-Guang Li, Zhong-Min Su,* Lin Xu, and Lucia Carlucci**

The current interest in coordination polymer frameworks not only stems from their potential applications in microelectronics, nonlinear optics, porous materials, and catalysis, but also from their intriguing variety of topologies and entanglement motifs.[1] Interpenetration has been the most investigated type of entanglement, as shown by the two comprehensive reviews by Batten and Robson.[2] More recently, a complete analysis of all the 3D interpenetrated structures contained in the CSD database was also carried out with a rationalization and classification of the topology of the interpenetration.[3] The increasing number of coordination polymers reported in the literature has led to new and more complex types of entanglement being recognized[2b,4,5] in polycatenated, polythreaded, and polyknotted species that are reminiscent of molecular catenanes, rotaxanes, and knots, respectively.

According to Ciani and co-workers,[5] polycatenation differs from interpenetration in that the whole catenated array has a higher dimensionality than that of the component motifs, and that each individual motif is catenated only with the surrounding ones and not with all the others. Polythreaded structures are characterized by the presence of closed loops, as well as of elements that can thread through the loops, and can be considered as extended periodic analogues of molecular rotaxanes and pseudorotaxanes, depending on the "ideal" possibility of being extricated. Polyknotting is typical of self-penetrating nets, that is, single nets having the peculiarity that the smallest topological rings are catenated by other smallest rings belonging to the same net.

Apart from their intrinsic aesthetic appeal, interest in these new families of entangled structures has been heightened by the fact that their resulting overall architectures are more flexible than the usual networks based entirely on coordination bonds[6]—a functional property that has potential applications ranging from drug-delivery vehicles to sensor devices.[7] Therefore, the exploitation of such species not only increases the structural diversity of coordination polymers, but also provides new insights into the relationships between the structure and function of these materials.

We report here three new entangled frames that were obtained from the use of the rigid 4,4′-bipyridine (bpy) and the long V-shaped 4,4′-oxybis(benzoate) (oba) ligands: $[Ni_2(oba)_2(bpy)_2(H_2O)_2]\cdot bpy$ (**1**) is the first example of a polycatenated array of 1D nanotubes, $[Ni_3(oba)_2(bpy)_2(Hoba)_2(H_2O)_2]\cdot bpy\cdot 2H_2O$ (**2**) is a new type of 2D polythreaded architecture involving five polymeric units at a time, and $[Ni(oba)(bpy)]\cdot 2H_2O$ (**3**) is an intriguing self-penetrating 3D net with an unprecedented topology. The magnetic susceptibilities of compounds **1**–**3** were also investigated (see the Supporting Information).

The crystal structure of compound **1**[8] consists of cationic $[\{Ni(bpy)\}_4]^{8+}$ squares (crystallographically equivalent in pairs), with Ni···Ni separations of 11.180(7) and 11.269(5) Å; these square units are joined by anionic oba^{2-} bridges to give one-dimensional nanotubes containing large cubelike boxes of approximate dimensions $11.2\times11.3\times14.9$ Å (Figure 1, top). The two differnt types of nickel(II) centers are coordi-

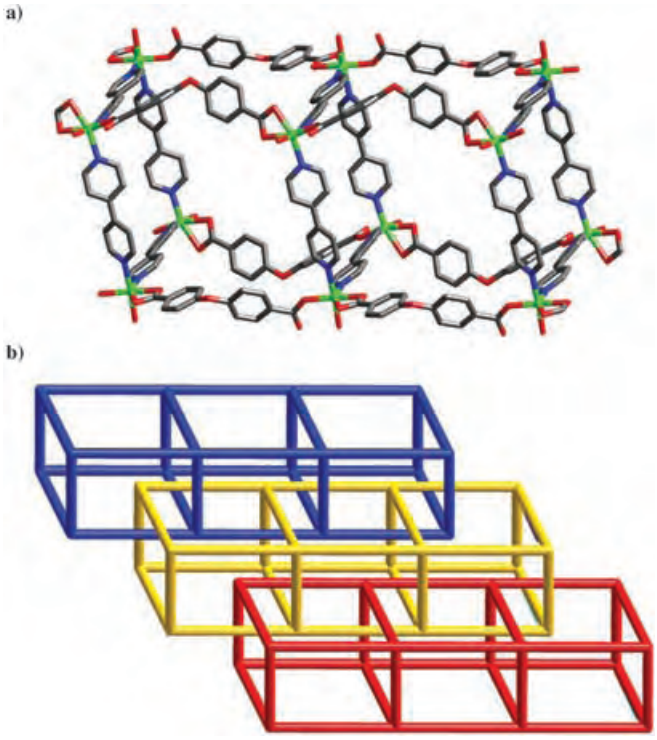


Figure 1. Compound **1**: a) a portion of two cubelike boxes of a single nanotube; b) a schematic view of the parallel polycatenation of three different nanotube motifs.

[*] Dr. X.-L. Wang, Dr. C. Qin, Prof. E.-B. Wang, Dr. Y.-G. Li, Prof. Z.-M. Su, Prof. L. Xu
Institute of Polyoxometalate Chemistry
Department of Chemistry
Northeast Normal University
Changchun 130024 (China)
Fax: (+86) 431-5098787
E-mail: wangenbo@public.cc.jl.cn
zmsu@nenu.edu.cn
Dr. L. Carlucci
Dipartimento di Chimica Strutturale e Stereochimica Inorganica
Università di Milano
Via G. Venezian 21, Milano 20133 (Italy)
Fax: (+39) 0250314454
E-mail: lucia.carlucci@istm.cnr.it

[**] This work was supported financially by the National Natural Science Foundation of China (No. 20371011).

Supporting information for this article is available on the WWW under http://www.angewandte.org or from the author.

InterScience
© 2005 Wiley-VCH Verlag GmbH & Co. KGaA, Weinheim

nated in a distorted octahedral geometry to two oba ligands (one monodentate: Ni-O 1.998(3) and 2.033(3) Å, and one chelate: Ni-O in the range 2.064(3)–2.200(4) Å), two bpy ligands (Ni-N 2.066(4)–2.159(4) Å), and one water molecule (Ni-O 2.045(4) and 2.103(4) Å). A large number of molecular squares have been thoroughly investigated to date,[9] all of which were held together by van der Waals interactions except in one case, in which cationic squares were interconnected by axial chloride bridges into a 3D network.[10] Therefore, to our knowledge, this is the first nanosized tubular structure constructed by the covalent linkage of molecular squares.

The most fascinating and peculiar structural feature of **1** is that each nanotube, which is aligned parallel to the *b* axis, is interlocked in a parallel fashion (along the *a* axis) with the two nearest neighboring ones to give rise to a 2D polycatenated layer (Figure 1, bottom). This kind of entanglement is still quite uncommon and the known examples are based exclusively on infinite 1D molecular ladders.[4,11] Therefore, compound **1**, besides providing a remarkable new structural motif, represents the first example of a 2D array of such motifs polycatenated in a parallel manner. It is also a rare example having both polyrotaxane and polycatenane characteristics[12] and could equally well be considered as formed by interconnected 1D polyrotaxane columns. Free void space is also present within the structure (25.5 % of the crystal volume as calculated by PLATON) which is occupied by guest molecules, with each "box" encapsulating two uncoordinated bpy molecules.

Compound **2** is an extended threaded framework involving 2D coordination layers of square (4^4) topology with dangling ligands. The nodes within the layers are alternately represented by single metal centers (Ni2) of distorted octahedral geometry (Ni-O in the range 2.051(3)–2.119(3) and Ni-N $2\times2.100(4)$ Å), and dinuclear units of Ni1 atoms that are bridged by two pairs of oba carboxylate ligands into a paddle wheel moiety (Ni-O in the range 1.971(3)–1.993(4), Ni-N 2.075(4), and Ni···Ni 2.6174(13) Å). All the nodes are connected through oba and bpy ligands to give a 2D motif with very large rhombic windows (dimensions 12.50×15.00 Å); dangling oba ligands are coordinated in the axial sites of dinuclear nodes only, and disposed in a mutual *anti* orientation with respect to the layer plane (Figure 2a). The layers are stacked in a parallel manner along the [−1 −1 2] direction in an ABCABC sequence at a distance of approximately 5.4 Å. Each dangling arm has an effective length of about 13.5 Å. As result, the dangling oba ligands of each layer are threaded into the rhombic voids of the two adjacent layers above and below, thus every rhombic window of each layer is threaded by only two dangling ligands that come from opposite directions (this is expected considering that the dangling arms reside on the dinuclear nodes only, Figure 2a). Finally, this unique simultaneous threading fashion of five adjacent polymeric motifs gives the novel (2D→3D) polythreaded array observed for compound **2** (Figure 2b).

Polythreaded structures containing finite components are, at present, rare.[5] The few species known include polythreaded 0D rings with side arms that give 1D[13a] or 2D arrays,[13b] as well as molecular ladders with dangling arms

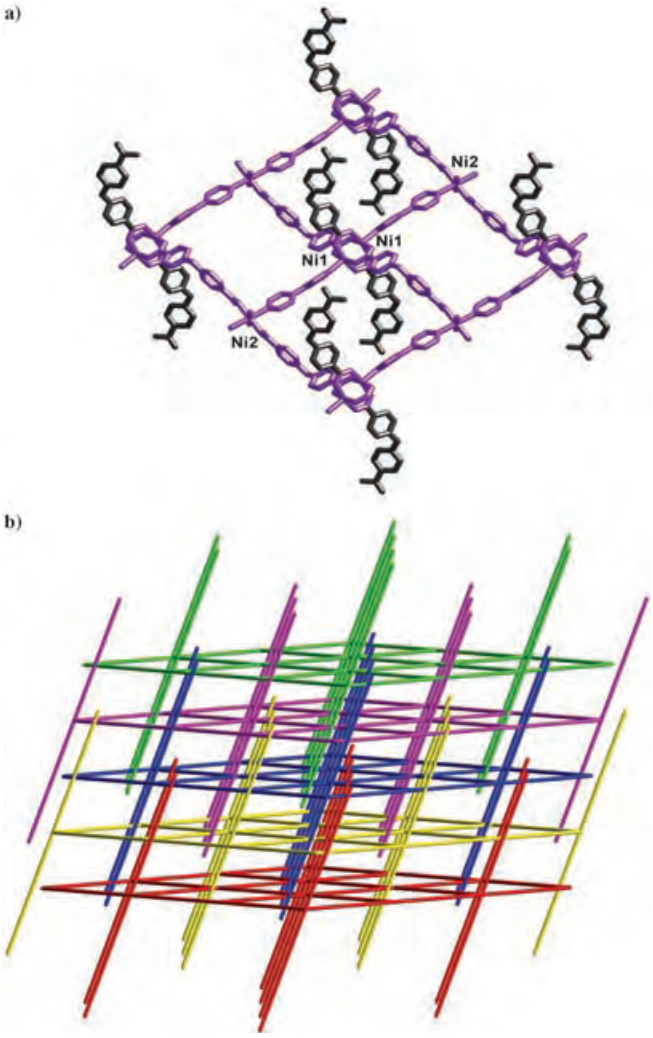


Figure 2. Compound **2**: a) a single 2D square (4^4) layer showing the alternating nodes: single Ni2 atoms and $(Ni1)_2$ paddle wheel units which carry the dangling arms; b) a schematic illustration of the mutual polythreading of five layers.

that result in (1D→2D)[13c] or (1D→3D)[13d] polythreaded arrays. Until now, the only known example of a (2D→3D) polythreaded network assembled from 2D motifs is the complex $[Zn(Hbtc)(4,4'\text{-bpy})]_n$ (btc = 1,2,4-benzenetricarboxylate) reported by us very recently,[14] in which the threading involves the two nearest layers only because of the shorter length of the dangling arms.

The threading observed in **2** is stabilized by two weak interactions: a π–π stacking arising from the aromatic rings of the oba ligands penetrating into the same void (interplanar distance: 3.65 Å, offset: 1.39 Å), and strong hydrogen bonding involving the uncoordinated carbonyl oxygen atoms from a dangling ligand and a coordinated water molecule of a mononuclear metal center on the third nearest neighboring layer (O···O 2.82 Å). When these hydrogen bonds are taken into account, the resulting structure displays a threefold interpenetrated 3D 6-connected net with α-Po (primitive cubic, pcu) ($4^{12}.6^3$) topology. A distorted cubelike unit of the resulting α-Po nets (Figure 3a) shows dimensions of $12.5\times$

 © 2005 Wiley-VCH Verlag GmbH & Co. KGaA, Weinheim

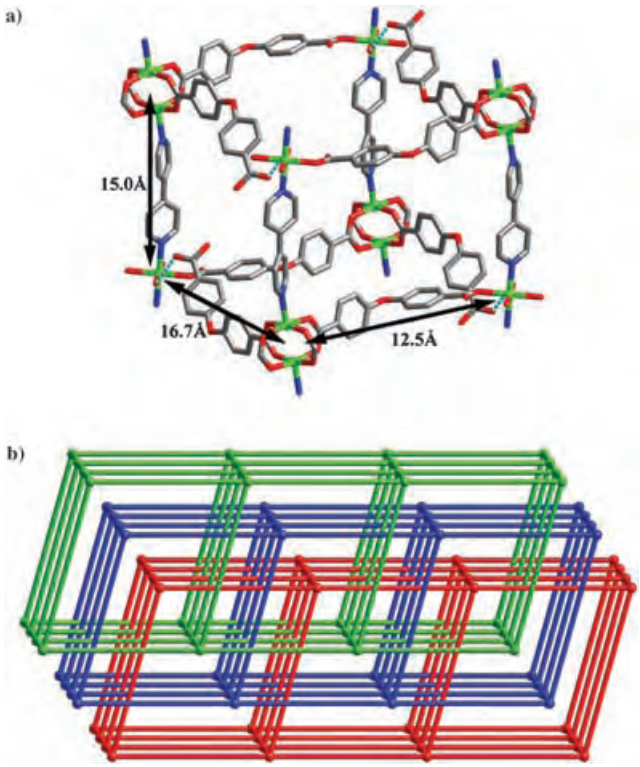


Figure 3. Compound **2**: a) a single distorted cubelike unit of the α-Po net with the relative dimensions 12.5 × 15.0 × 16.7 Å; b) a schematic view of the threefold interpenetrating α-Po network that is formed when H bonds are taken into account.

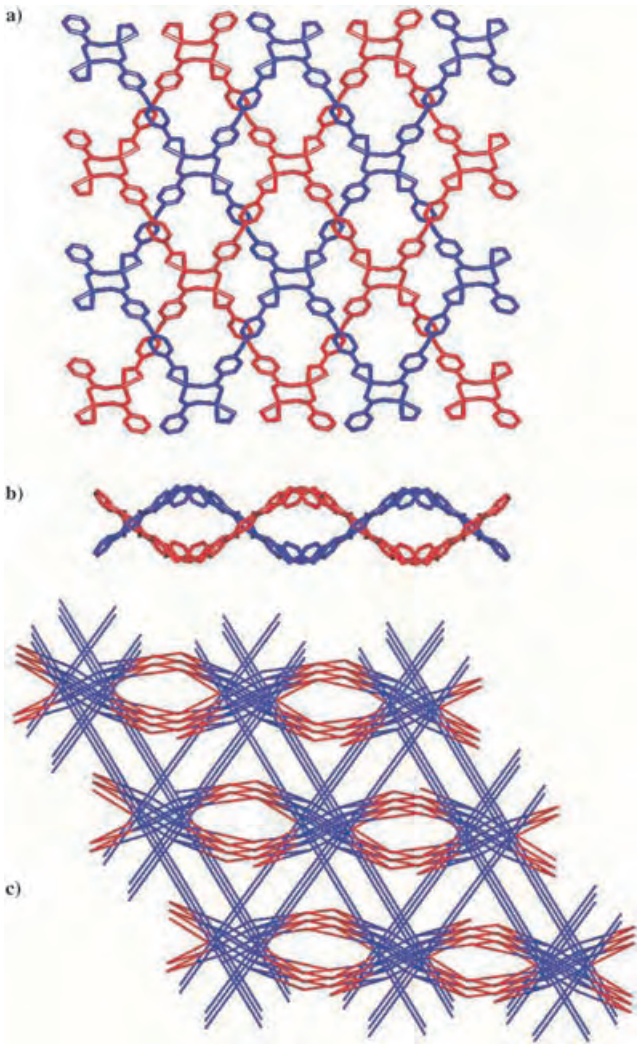


Figure 4. Compound **3**: a) twofold parallel interpenetrating layers of (4.8^2) topology; b) a view down the *c* axis of the twofold interpenetrating layers showing the elliptic-shaped channels; c) a schematic representation of the (3,5)-connected self-penetrating 3D net of (4.8^2)($4.6^4.8^4.10$) topology.

15.0 × 16.7 Å. The three interpenetrating nets of the 3D array originate from layers of A, B, and C type (Figure 3b). An analysis of the topology of interpenetration according to a recent classification[3] reveals that compound **2** belongs to Class Ia (all the interpenetrated nets are generated only by translation and the translating vector is [100] (9.90 Å). The overall entanglement still leaves voids that are occupied by two water molecules and one bpy guest molecule that form an intricate net of H bonds across different layers.

Compound **3** is a new (3,5)-connected 3D self-penetrating network with an unprecedented topology whose structure can be described as follows. First of all, it comprises neutral layers of composition [Ni(oba)]. Within these layers the nickel atoms are coordinated by four oxygen atoms from one chelating and two μ_2-bridging carboxylate ions of oba ligands (Ni-O in the range 2.004(3)–2.162(4) Å) to give dinuclear units that are further extended by bridging oba ligands into 2D layers (Figure 4a). From consideration of the Ni and C atoms of the μ_2-carboxylate groups as nodes, we can see that the layers are comprised of octagonal and rhombic meshes with a 3-connected (4.8^2) topology. The diagonals of the distorted rhombic windows are about 4.3 and 4.4 Å, while the dimensions of the distorted octagonal windows, estimated from the maximum distances between opposite vertices, are about 16.9 × 22.9 Å. The resulting layers are highly undulated as a consequence of the bent geometry of the dicarboxylate ligands and the twisting of its phenyl rings (dihedral angle of ca. 83°). The corrugation of the sheets makes the parallel interpenetration of two such layers possible (the average planes of the layers are coincident) to give a twofold interpenetrated array. Entanglement of layers with (4.8^2) topology are rare compared to layers that show the more common square (4^4) or hexagonal (6^3) topologies, and only few examples are known that include sheets that are interpenetrated in a parallel twofold[15] and threefold[16] manner. These sets of twofold interpenetrated layers generate elliptic-shaped channels running along the *c* axis (Figure 4b) that are populated by the guest water molecules. The twofold layers stack in an ABAB sequence parallel to the plane defined by the (**a**,**b**) and **c** vectors, and are interconnected to the two closest layers (above and below the average plane) through bpy bridges disposed along the crystallographic *a* and *b* axes. Two bpy ligands are *trans*-coordinated to each metal center in an axial position (Ni···N 2.096(3) Å) to give a unique (3,5)-connected 3D framework with an unprecedented (4.8^2)($4.6^4.8^4.10$) topology. In this simplification the 5-con-

 © 2005 Wiley-VCH Verlag GmbH & Co. KGaA, Weinheim

nected nodes are the metal atoms and the 3-connected ones are the carbon atoms of the oba ligands bridging the dimetallic unit (Figure 4c).

The network of compound **3** clearly results in self-penetrating since it is generated from linking twofold-interpenetrated sheets. The self-penetration feature is not very common within coordination polymers and only a limited number of self-penetrated nets have been reported to date.[4] A drastic simplification of compound **3** is that it is a 6-connected uninodal net with an unprecedented topology.[17]

In conclusion, although the three compounds described herein were obtained from the same starting building blocks they display quite different structures (ranging from 1D to 3D) and show unusual features of polycatenation, polythreading, and polyknotting. Thus, this study highlights an intriguing feature of coordinative network chemistry in producing rich architectures and topologies.

Experimental Section

1–**3**: A mixture of $Ni(NO_3)_2 \cdot 6H_2O$ (145 mg, 0.5 mmol for **1**–**3**), 4,4′-oxybisbenzoate (129 mg, 0.5 mmol for **1**–**3**), 4,4′-bipyridyl (156 mg, 1 mmol for **1** and **2**; 78 mg, 0.5 mmol for **3**), and water (10 mL) was placed in a 23-mL teflon reactor. After the pH values had been adjusted to 6.5, 5.5, and 7.8 for **1**, **2**, and **3**, respectively, by addition of triethylamine, the mixture was heated at 140 °C for 3 days. Green crystals of **1**–**3** were obtained on cooling the mixture to room temperature at 10 °C h^{-1}.

Received: May 20, 2005

Keywords: coordination modes · networks · nickel · self-assembly · supramolecular chemistry

[1] For recent reviews, see: a) B. Moulton, M. J. Zaworotko, *Chem. Rev.* **2001**, *101*, 1629; b) O. R. Evans, W. Lin, *Acc. Chem. Res.* **2002**, *35*, 511; c) C. Janiak, *Dalton Trans.* **2003**, 2781; d) S. Kitagawa, R. Kitaura, S. I. Noro, *Angew. Chem.* **2004**, *116*, 2388; *Angew. Chem. Int. Ed.* **2004**, *43*, 2334; e) C. N. R. Rao, S. Natarajan, R. Vaidhyanathan, *Angew. Chem.* **2004**, *116*, 1490; *Angew. Chem. Int. Ed.* **2004**, *43*, 1466; f) N. W. Ockwig, O. Delgado-Friederichs, M. O'Keeffee, O. M. Yaghi, *Acc. Chem. Res.* **2005**, *38*, 176.

[2] a) S. R. Batten, R. Robson, *Angew. Chem.* **1998**, *110*, 1558; *Angew. Chem. Int. Ed.* **1998**, *37*, 1460; b) S. R. Batten, *CrystEngComm.* **2001**, *3*, 67.

[3] V. A. Blatov, L. Carlucci, G. Ciani, D. M. Proserpio, *CrystEngComm* **2004**, *6*, 377.

[4] L. Carlucci, G. Ciani, D. M. Proserpio, *Coord. Chem. Rev.* **2003**, *246*, 247.

[5] L. Carlucci, G. Ciani, D. M. Proserpio, *CrystEngComm* **2003**, *5*, 269.

[6] a) M. Fujita, O. Sasaki, K. Watanabe, K. Ogura, K. Yamaguchi, *New J. Chem.* **1998**, *22*, 189; b) L. Carlucci, G. Ciani, M. Moret, D. M. Proserpio, S. Rizzato, *Angew. Chem.* **2000**, *112*, 1566; *Angew. Chem. Int. Ed.* **2000**, *39*, 1506.

[7] a) J.-P. Sauvage, *Acc. Chem. Res.* **1998**, *31*, 611; b) K. Kim, *Chem. Soc. Rev.* **2002**, *31*, 96.

[8] Crystal data for **1** ($C_{58}H_{44}Ni_2N_6O_{12}$): $M_r = 1134.41$, triclinic, space group $P\bar{1}$, $a = 12.430(3)$, $b = 14.913(16)$ Å, $c = 15.905(5)$ Å, $\alpha = 88.04(3)$, $\beta = 73.07(3)$, $\gamma = 70.08(3)°$, $V = 2644.6(9)$ Å^3, $Z = 2$, $\rho_{calcd} = 1.425$ mg m^{-3}, final $R1 = 0.0785$ for 11611 independent reflections $[I > 2\sigma(I)]$. Crystal data for **2** ($C_{86}H_{66}Ni_3N_6O_{24}$): $M_r = 1743.58$, triclinic, space group $P\bar{1}$, $a = 9.903(2)$ Å, $b = 12.966(3)$ Å, $c = 16.223(3)$ Å, $\alpha = 92.44(3)$, $\beta = 92.66(3)$, $\gamma = 106.50(3)°$, $V = 1991.7(7)$ Å^3, $Z = 1$, $\rho_{calcd} = 1.454$ mg m^{-3}, final $R1 = 0.0733$ for 8648 independent reflections $[I > 2\sigma(I)]$. Crystal data for **3** ($C_{24}H_{20}NiN_2O_7$): $M_r = 507.13$, monoclinic, space group $C2/c$, $a = 18.911(4)$ Å, $b = 12.318(5)$ Å, $c = 19.885(4)$ Å, $\beta = 95.58(3)°$, $V = 4610(2)$ Å^3, $Z = 8$, $\rho_{calcd} = 1.461$ mg m^{-3}, final $R1 = 0.0663$ for 5272 independent reflections $[I > 2\sigma(I)]$. The data were collected at 173(2) K on a Rigaku R-AXIS RAPID IP diffractometer with $Mo_{K\alpha}$ monochromated radiation ($\lambda = 0.71073$ Å). The structures were solved by direct method using SHELXS-97 and extended using Fourier techniques. CCDC-266679–266681 contain the supplementary crystallographic data for this paper. These data can be obtained free of charge from The Cambridge Crystallographic Data Centre via www.ccdc.cam.ac.uk/data_request/cif.

[9] a) P. J. Stang, B. Olenyuk, *Acc. Chem. Res.* **1997**, *30*, 502; b) F. A. Cotton, C. Lin, C. A. Murillo, *Acc. Chem. Res.* **2001**, *34*, 759.

[10] L. Carlucci, G. Ciani, D. M. Proserpio, S. Rizzato, *Chem. Commun.* **2002**, 1198.

[11] a) A. J. Blake, N. K. Champness, A. Khlobystov, D. A. Lemenovskii, W.-S. Li, M. Schröder, *Chem. Commun.* **1997**, 2027; b) M. Meakawa, H. Konaka, Y. Suenaga, T. Kuroda-Sowa, M. Munakada, *J. Chem. Soc. Dalton Trans.* **2000**, 4160; c) L. Carlucci, G. Ciani, D. M. Proserpio, *J. Chem. Soc. Dalton Trans.* **1999**, 1799; d) B. Dong, R. C. Layl, N. G. Pschirer, M. D. Smith, U. H. F. Bunz, H.-C. zur Loye, *Chem. Mater.* **1999**, *11*, 1413.

[12] a) B. F. Hoskins, R. Robson, D. A. Slizys, *Angew. Chem.* **1997**, *109*, 2430; *Angew. Chem. Int. Ed. Engl.* **1997**, *36*, 2336; b) D. M. L. Goodgame, S. Menzer, A. M. Smith, D. J. Williams, *Angew. Chem.* **1995**, *107*, 605; *Angew. Chem. Int. Ed. Engl.* **1995**, *34*, 574; c) L. Carlucci, G. Ciani, D. M. Proserpio, *Cryst. Growth Des.* **2005**, *5*, 37.

[13] a) S. Banfi, L. Carlucci, E. Caruso, G. Ciani, D. M. Proserpio, *J. Chem. Soc. Dalton Trans.* **2002**, 2714; b) G. F. Liu, B. H. Ye, Y. H. Ling, X. M. Chen, *Chem. Commun.* **2002**, 1442; c) L. Carlucci, G. Ciani, D. M. Proserpio, *Chem. Commun.* **1999**, 449; d) M. L. Tong, H. J. Chen, X. M. Chen, *Inorg. Chem.* **2000**, *39*, 2235.

[14] C. Qin, X. L. Wang, L. Carlucci, M. L. Tong, E. B. Wang, C. W. Hu, L. Xu, *Chem. Commun.* **2004**, 1876.

[15] a) S. Y. Wan, J. Fan, T. Okamura, H. F. Zhu, X. M. Ouyang, W. Y. Sun, N. Ueyama, *Chem. Commun.* **2002**, 2520; b) S. A. Barnett, A. J. Blake, N. R. Champness, J. E. B. Nicolson, C. Wilson, *J. Chem. Soc. Dalton Trans.* **2001**, 567.

[16] J. Fan, W. Y. Sun, T. Okamura, W. X. Tang, N. Ueyama, *Inorg. Chem.* **2003**, *42*, 3168.

[17] If the dinuclear units are simplified to their baricentres (new nodes) joined by pairs of bpy ligands (new links) the net becomes 6-connected self-penetrating with a ($4^4.6^{11}$) topology, unprecedented within coordination polymers.[1f]

 © 2005 Wiley-VCH Verlag GmbH & Co. KGaA, Weinheim

Polynuclear Complexes

DOI: 10.1002/anie.200500716

Carbon Dioxide Activation Assisted by a Bis(chlorodimethylsilyl)cyclopentadienyl Titanium Compound**

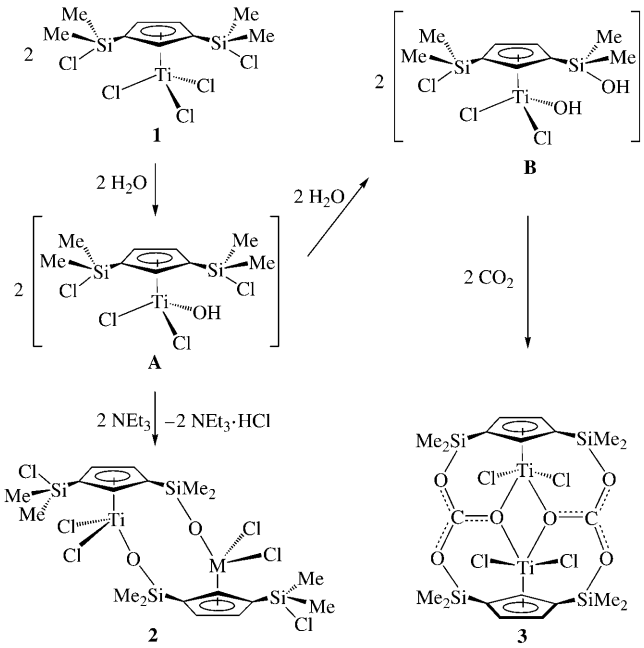
David Santamaría, Jesús Cano, Pascual Royo, Marta E. G. Mosquera, Tomás Cuenca,* Luis M. Frutos, and Obis Castaño*

A great deal of interest has focused on the role of metal ions as the active centers in the fixation of CO_2 and its transformation.[1] Activation of CO_2 by hydroxo and oxo metal complexes to afford metal hydrogencarbonato and carbonato species, respectively, is related to the function of the carbonic anhydrase metalloenzyme,[2] which catalyzes the physiologically important hydration of CO_2 to hydrogencarbonate [Eq. (1)].

$$\text{[M]-OH or [M]-O-[M]} \xrightarrow{CO_2} \text{[M]-CO}_3\text{H or [M]-CO}_3\text{-[M]} \quad (1)$$

This type of reaction is common for the late-transition metals[3] and is known for main-group organometallic species.[4] Nevertheless, the carbonato derivatives reported for complexes of Group 4–6 metals are synthesized by alternative methods[5] based on reactions of metal precursor compounds with carbonate salts X_2CO_3 (X = K, Bu_4N) and NH_4HCO_3 or by methods that involve the disproportionation of CO_2.

Herein, we describe the use of the bis(chlorodimethylsilyl)cyclopentadienyl titanium(IV) compound **1**,[6] which was reported previously for the in situ activation of CO_2. The carbonato titanium(III) derivative **3** was serendipitously obtained when a dilute solution of **1** in wet toluene was exposed to air for several days (Scheme 1). This reaction proceeded in better yield (43% after purification) when a solution of **1** in toluene was treated with a saturated aqueous solution of CO_2 to give **3**, which was isolated as an analytically pure and highly air-stable diamagnetic orange crystalline solid. However, hydrolysis of **1** carried out in the presence of NEt_3 resulted in no reaction with CO_2 and the μ-oxo titanium(IV) derivative **2** and NEt_3·HCl being obtained (Scheme 1). The reaction of **1** with K_2CO_3 in THF or toluene afforded a mixture of unidentified compounds that did not contain **3**.



Scheme 1. Possible reaction pathways for the synthesis of **2** and **3**.

Hydrolysis of the Group 4 metal/chloro complexes usually proceeds with initial transformation of the metal–chlorine bonds so that intermediate complexes are formed which contain rather uncommon, discrete terminal Group 4 metal–hydroxo bonds.[7] These species subsequently condense to give polynuclear compounds stabilized by μ-oxo bridges.[8] We propose that the carbonato complex **3** results from the in situ formation of intermediate Si–OH/Ti–OH terminal bonds (see **A** and **B** in Scheme 1) and a further insertion reaction of CO_2 with simultaneous reduction to the highly stable titanium(III) compound **3**. This mechanism of formation is consistent with the high stability of **3**, which remains unaltered when left for weeks in air; with the formation of the μ-oxo complex **2** in the presence of a deprotonating agent; and also with the observed stability of **2**, as it did not react with CO_2 to give **3** after several days at temperatures higher than 120 °C.

The ^{1}H NMR spectrum ($CDCl_3$, 25 °C) of complex **3** shows behavior expected for a C_{2h}-symmetric molecule with an A_2B spin system for the cyclopentadiene (Cp) protons and with two resonances of the two nonequivalent methyl groups of the four equivalent {$SiMe_2$} fragments (see Experimental Section). The resonances of the carbon atoms of the two equivalent bridging carbonato ligands are observed in the ^{13}C NMR spectrum as one signal at $\delta = 183.7$ ppm. The IR spectrum shows the characteristic ν(C–O) absorption of the carbonato ligand at 1375 cm^{-1}. The ^{1}H and ^{13}C NMR spectra ($CDCl_3$, 25 °C) of complex **2** show behavior expected for a disymmetric molecule with two resonances for the diastereotopic methyl groups of two equivalent {$SiMe_2O$} fragments rather than the singlet observed for the related symmetrical complex [{$TiCl_2$[μ-($OSiMe_2$-η^5-C_5H_4)]}$_2$][9] reported previ-

[*] D. Santamaría, Dr. J. Cano, Prof. P. Royo, Dr. M. E. G. Mosquera, Prof. T. Cuenca
Departamento de Química Inorgánica
Universidad de Alcalá
Campus Universitario, 28871 Alcalá de Henares (Spain)
Fax: (+34) 918-854-683
E-mail: pascual.royo@uah.es
tomas.cuenca@uah.es
Dr. L. M. Frutos, Prof. O. Castaño
Departamento de Química-Física
Universidad de Alcalá
Campus Universitario, 28871 Alcalá de Henares (Spain)

[**] Financial Support by the Spanish MEC (project MAT2004-02614) and MCyT (project BQU2003-07281) is acknowledged.

Supporting information for this article is available on the WWW under http://www.angewandte.org or from the author.

InterScience
© 2005 Wiley-VCH Verlag GmbH & Co. KGaA, Weinheim

ously. The resonances for the $SiMe_2Cl$ protons of **2** appear as two singlets with chemical shifts analogous to those observed for **1** and for $[TiCl_3(\eta^5\text{-}C_5H_4SiMe_2Cl)]$.[9]

The molecular structure of **3**[10] was determined by X-ray diffraction (Figure 1), which indicates a square-base pyramid coordination for the titanium center. The $\{Ti_2O_2\}$ core is planar, with the two carbonato ligands and the four Si atoms also located in a second plane (maximum deviation = 0.0447 Å) with the dihedral angle between the planes at 128°. The Ti–Ti distance (3.2901(9) Å) is longer than that expected for a conventional Ti–Ti bond (ca. 2.68–2.85 Å).[11]

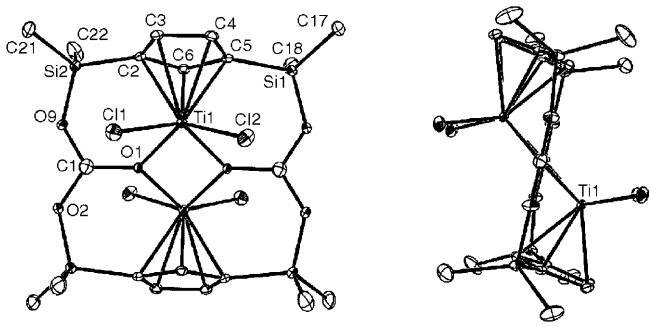


Figure 1. ORTEP view of **3**, with 30% probability ellipsoids. Selected bond lengths [Å] and angles [°]. Ti-Ti 3.2901(9), C1-O2 1.353(3), C1-O9 1.357(3), C1-O1 1.407(3), Ti1-O1 2.0495(14); O2-C1-O9 116.9(2), O2-C1-O1 121.6(2), O9-C1-O1 121.4(2), Cl2-Ti1-Cl1 89.21(3).

To clarify the nature of the $Ti(d^1)$–$Ti(d^1)$ electron coupling and, consequently, the diamagnetism of the molecule, we carried out a theoretical investigation of the electronic properties of **3**. Single-determinant wave functions (Hartree–Fock), as well as DFT methods,[12] failed to explain the stability of the singlet state of this molecule.[13] This fact reflects the importance of the correlation energy in the study of the d^1–d^1 electron coupling. Only by including the correlation energy[14] through the second-order-perturbation method (MP2)[15] is it possible to explain the high stability of the singlet species, which is 57.6 kcal mol^{-1} more stable than the triplet state (49.2 kcal mol^{-1}, as obtained from the X-ray crystal structure), and hence its diamagnetic character. The d^1–d^1 electron coupling basically arose from the in-phase interacting d_{z^2}-like orbitals located in each Ti atom (Figure 2). This in-phase orbital interaction collects almost all of the electronic density between the two Ti atoms,[16] as it is the principal interaction responsible for the spin pairing. Also, minor contributions from the two bridging oxygen atoms increase the strength of the interaction (Figure 2).

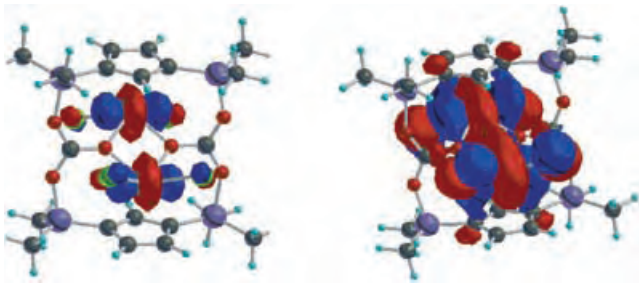


Figure 2. Depiction of the highest-occupied molecular orbitals showing the Ti–Ti in-phase orbital interaction at two different wave-function amplitudes (0.04 and 0.02 (left and right, respectively)). Minor contributions from the two annular oxygen atoms are present.

The Ti–Ti in-phase orbital interaction is strong enough to provide a high stability to the singlet species, as this state is only populated at room temperature. An S_0/T_1 intersystem crossing should not be an efficient path to populate the triplet state, as a result of low spin-orbit coupling[17] as well as the high S_0–T_1 energy gap.

In summary, we have demonstrated that a bis(chlorodimethylsilyl)cyclopentadienyl titanium(IV) derivative can fix CO_2 and transform it into a carbonato ligand with simultaneous reduction to give an air-stable diamagnetic titanium(III) compound. A theoretical investigation of the electronic properties of the molecule demonstrates the high stability of the singlet versus the triplet state and justifies the diamagnetism exhibited by the carbonato complex **3**.

Experimental Section

2: Distilled and degassed water (27 μL, 1.49 mmol) and NEt_3 (0.42 mL, 2.96 mmol) were added to a solution of **1** (0.6 g, 1.48 mmol) in toluene (50 mL). The cloudy reaction mixture was stirred over 24 h at room temperature and then filtered to give a pale-orange solution. The solvent was removed under vacuum and the residue was extracted with hexane. The resulting solution was concentrated to 20 mL and cooled to −35 °C to give a light-orange solid which was isolated by filtration and identified as **2** (0.58 g, 0.827 mmol) 56% yield. Elemental analysis (%) calcd for $C_{18}H_{30}O_2Si_4Ti_2Cl_6$: C 30.92, H 4.32; found: C 30.75, H 4.48; ^{1}H NMR (300 MHz, $CDCl_3$): $\delta = 0.55$, 0.60, 0.78, 0.83 (4 s, 4 × 6H, $SiMe_2$), 7.06, 7.19, 7.35 ppm (3 m, 3 × 2H, C_5H_3); ^{13}C NMR (300 MHz, $CDCl_3$): $\delta = 0.2$, 0.6, 2.5, 2.9 (4 × $SiMe_2$), 127.4, 130.7, 134.0 (C_5H_3), 133.7, 135.4 ppm (C_{ipso}, C_5H_3).

3: An excess of distilled and degassed water (67 μL, 3.70 mmol) was added to a pale-yellow solution of **1** (0.3 g, 0.74 mmol) in toluene (200 mL) saturated with CO_2. Formation of the same white solid suspension described above was observed. The reaction mixture was stirred over 42 h at room temperature. After that time, the reaction mixture changed to pale orange. The solvent was removed to give an orange solid that was extracted with a mixture of toluene/pentane and isolated as an orange crystalline solid identified as **3** (0.27 g, 0.086 mmol) 43% yield. Single crystals of **3** suitable for X-ray diffraction studies were grown from a solution of $CHCl_3$. Elemental analysis (%) calcd for $C_{22}H_{32}O_6Si_4Ti_2Cl_{10}$: C 27.67, H 3.38; found: C 27.87, H 3.44; ^{1}H NMR (300 MHz, $CDCl_3$): $\delta = 0.51$, 0.60 (2s, 2 × 12H, $SiMe_2$), 6.88 (m, 2H, C_5H_3), 7.88 ppm (m, 4H, C_5H_3); ^{13}C NMR (300 MHz, $CDCl_3$): $\delta = -1.39$, −0.50 ($SiMe_2$), 135.6, 136.5 (C_5H_3), 141.4 (C_{ipso}, C_5H_3), 183.7 ppm (CO_3); IR: $\tilde{\nu} = 3218$, 2961 (C–H (C_5H_3)), 1375 (C=O (CO_3^{2-})), 1262, 1221 (Si–CH_3 ($SiMe_2$)), 834, 800 (Ti-O-Ti), 676 cm^{-1} (Si–Cp ligand).

Received: February 25, 2005
Published online: August 4, 2005

Keywords: ab initio calculations · carbon dioxide fixation · silicon · titanium

[1] a) D. H. Gibson, *Chem. Rev.* **1996**, *96*, 2063; b) W. Leitner, *Coord. Chem. Rev.* **1996**, *153*, 257; c) X. Ling, J. R. Moss *Coord. Chem. Rev.* **1999**, *181*, 27.

[2] a) G. Parkin, *Chem. Rev.* **2004**, *104*, 699; b) S. Schenk, J. Kesselmeier, E. Anders, *Chem. Eur. J.* **2004**, *10*, 3091; c) H. Strasdeit, *Angew. Chem.* **2001**, *113*, 730; *Angew. Chem. Int. Ed.*

 © 2005 Wiley-VCH Verlag GmbH & Co. KGaA, Weinheim

2001, *40*, 707; d) J. T. Cullen, T. W. Lane, F. M. M. Morel, R. M. Sherrell, *Nature* **1999**, *402*, 165.
[3] a) N. Kitajima, S. Hikichi, M. Tanaka, Y. Morooka, *J. Am. Chem. Soc.* **1993**, *115*, 5496; b) A. Escuer, R. Vicente, S. B. Kumar, X. Solans, M. Font-Bardía, *J. Chem. Soc. Dalton Trans.* **1997**, 403; c) R. A. Allred, L. H. McAlexander, A. M. Arif, L. M. Berreau, *Inorg. Chem.* **2002**, *41*, 6790; d) C. Bergquist, T. Fillebeen, M. M. Morlok, G. Parkin, *J. Am. Chem. Soc.* **2003**, *125*, 6189; e) E. García-España, P. Gavina, J. Latorre, C. Soriano, B. A. Verdejo, *J. Am. Chem. Soc.* **2004**, *126*, 5082.
[4] J. Beckmann, D. Dakternieks, A. Duthie, N. A. Lewcenko, C. Mitchell, *Angew. Chem.* **2004**, *116*, 6851; *Angew. Chem. Int. Ed.* **2004**, *43*, 6683.
[5] a) T. C. W. Mak, P. J. Li, C. M. Zheng, K. Y. Huang, *J. Chem. Soc. Chem. Commun.* **1986**, 1597; b) M. C. Suen, G. W. Tseng, J. D. Chen, T. C. Keng, J. C. Wang, *Chem. Commun.* **1999**, 1185; c) F. A. Cotton, C. Lin, C. A. Murillo, *J. Am. Chem. Soc.* **2001**, *123*, 2670; d) G. Fachinetti, C. Floriani, A. Chiesivilla, C. Guastini, *J. Am. Chem. Soc.* **1979**, *101*, 1767; e) V. V. Burlakov, F. M. Dolgushin, A. I. Yanovsky, Y. T. Struchkov, V. B. Shur, U. Rosenthal, U. Thewalt, *J. Organomet. Chem.* **1996**, *522*, 241.
[6] M. Sudupe, J. Cano, P. Royo, E. Herdtweck, *Eur. J. Inorg. Chem.* **2004**, 3074.
[7] a) V. Ugrinova, G. A. Ellis, S. N. Brown, *Chem. Commun.* **2004**, 468; b) R. Bortolin, V. Patel, I. Munday, N. J. Taylor, A. J. Carty, *J. Chem. Soc. Chem. Commun.* **1985**, 456.
[8] G. Hidalgo, M. A. Pellinghelli, P. Royo, R. Serrano, A. Tiripicchio, *J. Chem. Soc. Chem. Commun.* **1990**, 1118.
[9] S. Ciruelos, T. Cuenca, P. Gómez-Sal, A. Manzanero, P. Royo, *Organometallics* **1995**, *14*, 177.
[10] Crystal data for **3**: ($C_{11}H_{16}Cl_5O_3Si_2Ti$), $M_r = 477.57$, monoclinic, space group $P2_1/c$, $a = 10.5230(3)$, $b = 9.5400(10)$, $c = 19.787(3)$ Å, $\beta = 96.016(6)°$, $V = 1975.5(4)$ Å^3, $Z = 4$, $\rho_{calcd} = 1.606$ g cm^{-3}, F(000) = 964, $Mo_{K\alpha}$ radiation ($\lambda = 0.71073$ Å), $\mu = 1.236$ mm^{-1}; crystal dimensions $0.51 \times 0.36 \times 0.16$ mm. R_1 ($F^2 > 2\sigma(F^2)$) = 0.0311, $wR_2(F^2 > 2\sigma(F^2)) = 0.0703$, $R_1(F^2) = 0.0452$, $wR_2(F^2) = 0.0741$). Final-difference Fourier maps showed no peaks higher than 0.537 nor deeper than −0.701 e Å^{-3}. CCDC-262845 contains the supplementary crystallographic data for this paper. These data can obtained free of charge from the Cambridge Crystallographic Data Center via www.ccdc.cam.ac.uk/data request/cif.
[11] a) A. Decker, D. Fenske, K. Maczek, *Angew. Chem.* **1996**, *108*, 3025; *Angew. Chem. Int. Ed. Engl.* **1996**, *35*, 2863; b) A. Roth, C. Floriani, A. Chiesivilla, C. Guastini, *J. Am. Chem. Soc.* **1986**, *108*, 6823.
[12] Single point from the X-ray structure as well as geometrical optimization with the Hartree–Fock (HF) and B3Lyp methods with the 3-21G(d) basis set were performed by using the Gaussian 98 suite of programs (see ref. [23]).
[13] All the theoretical calculations were made with: Gaussian 98, (Revision A.7): M. J. Frisch, et al. (see Supporting Information).
[14] Multiconfigurational CASSCF(2,2)/LANL2DZ calculations describe only qualitatively (not quantitatively) the energy of the singlet and triplet states, whereas geometrical optimization at this level gives a very accurate structure compared with the X-ray data (see Supporting Information).
[15] Moller–Plesset up to second-order calculation (MP2) with a LANL2DZ basis set were used to determine the energetics by using the optimized CASSCF(2,2)/LANL2DZ geometry.
[16] The calculated difference of the density matrix elements between the S_0 and T_1 states reflects a high depopulation of the Ti–Ti shared density in the excitation to T_1 (approximately 0.8 e; see Supporting Information).
[17] Spin-orbit coupling calculated at CASSCF(2,2)/3-21G(d) for the S_0 equilibrium geometry is equal to 16.80 cm^{-1}.

 © 2005 Wiley-VCH Verlag GmbH & Co. KGaA, Weinheim

Combinatorial Chemistry

DOI: 10.1002/anie.200501665

Solid/Solution-Phase Annulation Reagents: Single-Step Synthesis of Cyclic Amine Derivatives

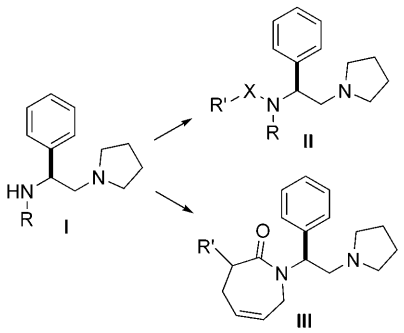
Roland E. Dolle, Calum MacLeod, Blanca Martinez-Teipel, William Barker, Pamela R. Seida, and Torsten Herbertz*

Single-step amine-derivatization chemistry is one of the most powerful and practical streamlined synthetic techniques available to the medicinal and combinatorial chemist. Acylation, sulfonylation, ureidoation, heteroarylation, reductive amination, and alkylation are used extensively to create libraries of amine derivatives.[1] Researchers involved in drug discovery particularly appreciate the importance of such high-throughput chemistries used to create nascent structure–activity relationships (SARs) and to expand the intellectual property field around a novel biologically active lead. Amine derivatization is conveniently carried out in the solution phase with a scavenger resin(s) to assist in the removal of the excess derivatizing reagent and/or product purification.[2] Activated resins have also been developed in which an amine is treated with a resin-bound functional-group-transfer reagent suspended in a suitable solvent.[3a] Following filtration, which removes both the spent and excess reagent, and solvent evaporation, derivatives are generally produced in over 75% purity, which is suitable for biological screening. Examples of this type of reagent are the commercially available carboxyl- and sulfonyl-activated tetrafluorophenol (TFP) resins developed by Salvino et al. for amide and sulfonamide synthesis.[3b]

During the course of a drug-discovery program directed toward the identification of peripherally restricted κ-opioid receptor agonists, we conducted a high-throughput *N*-derivatization campaign for diamine **I**, including the use of TFP resins, to define the SAR in this region of the pharmacophore (**I**→**II**; X = CO, SO_2, HNCO; Scheme 1). In related SAR studies, conformationally restricted analogues **III** were prepared by ring-closing metathesis as the method for the generation of the azepinone ring.[4] In contrast to the hours of labor required to generate acyclic analogues **II** by semi-automated parallel synthesis, the synthesis of cyclic analogues **III** required a multistep sequence and several months of labor. Access to robust reagents to carry out single-step amine annulations would have accelerated the synthesis and biological evaluation of **III** and related heterocyclic analogues. However, there are no generally recognized "off-the-shelf"

[*] Dr. R. E. Dolle, Dr. C. MacLeod, Dr. B. Martinez-Teipel, W. Barker, Dr. P. R. Seida, Dr. T. Herbertz
Department of Chemistry
Adolor Corporation
700 Pennsylvania Drive, Exton, PA 19341 (USA)
Fax: (+1) 484-595-1551
E-mail: rdolle@adolor.com

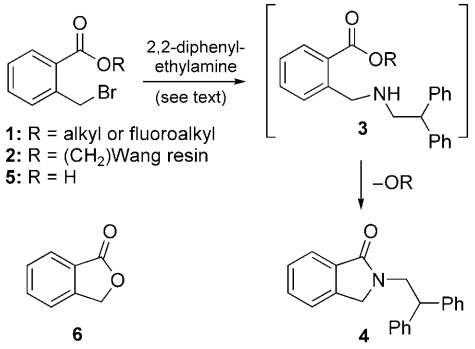
 InterScience © 2005 Wiley-VCH Verlag GmbH & Co. KGaA, Weinheim



Scheme 1. Amine derivatization leading to κ-opioid receptor agonists.[4]

reagents for high-throughput amine annulation. An exploratory chemical-technology program was initiated to address this gap in methodology, and so develop reagents for rapid amine annulation. Approaches were sought to produce monocyclic, bicyclic, spirocyclic, and polycyclic ring systems from primary amines in one step that would be amenable to semiautomated library production in a manner analogous to the acyclic derivatization protocols. The acronym SPAn, derived from solid/solution-phase annulation, collectively refers to the technology, reagents, and products thereof. The first examples of this conceptually new family of SPAn reagents, which yield five-, six-, and seven-membered heterocycles from primary amines, are introduced.

A tandem *N*-alkylation/intramolecular acylation reaction that yields an isoindolinone was selected as the prototypical annulation reaction to be investigated (**1/2**→**3**→**4**; Scheme 2).[5] The results of the initial solution-phase experi-



Scheme 2. Annulation strategy for isoindolinone **4**.

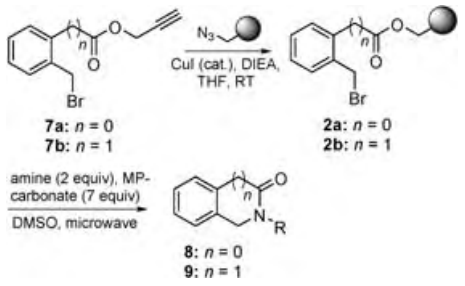
ments with assorted esters **1** and 2,2-diphenylethylamine in a range of solvents under both thermal and microwave reaction conditions were unsatisfactory. As a result, our attention turned to the employment of a cyclorelease strategy[6] and the preparation of resin-bound reagent **2**. The dilemma that immediately surfaced with this approach was the efficient loading of acid **5**. Direct coupling of **5** to Wang resin by employing a range of coupling reagents and reaction conditions resulted in capricious loading, even when **5** was used in large excess. Substantial amounts of lactone **6** formed, which is a testament to the reactivity and instability of this material. In light of this experience and the potential for the troublesome loading of other reactive esters of interest, an alternative method for the generation of the resin-bound reagent was required. The copper(I)-catalyzed 1,3-dipolar cycloaddition of azides and terminal alkynes is a robust ligation method that occurs under very mild reaction conditions.[7] Gmeiner and co-workers recently employed this approach to create new amide-backbone[8a,b] and acrylate-based (REM) linkers[8c] for solid-phase organic synthesis. With this methodology in mind, bromide **7a** (5 equiv; prepared from 2-bromomethylbenzoic acid (1 equiv), propargyl alcohol (3 equiv), *N*,*N*′-diisopropylcarbodiimide (1.2 equiv), and dimethylaminopyridine (cat.) in 48% yield) was added to a suspension of Merrifield azide resin[8a] in dichloromethane followed by the addition of excess diisopropylethylamine (DIEA) and 0.02 equivalents of CuI. The reaction was monitored by single-bead FTIR (disappearance of absorption at 2096 cm^{-1}), and resin **2a** was obtained in good yield (65% as determined by elemental analysis) after 20 hours on an orbital shaker. Importantly, the loading was reproducible (5 runs, 65–70% yield). Subsequent reaction of **2a** with 2,2-diphenylethylamine (2 equiv) in dimethyl sulfoxide (DMSO) with excess MP-carbonate (7 equiv; Polymere Labs) under microwave conditions (150°C for 15 min following a 30-min temperature ramp-up from 25 to 150°C) afforded the desired annulated product **4** in 90% crude purity (UV: $\lambda 1 = 220$ nm; $\lambda 2 = 254$ nm) and 33% yield of the isolated product. It was subsequently found that both the chloro and iodo ester analogues of **2** also load efficiently, but only the iodo resin gave equivalent or higher yields and purity of **4**. For this reason, bromide and iodide were the preferred halogen leaving groups in the SPAn reagents. Unlike **1**, which spontaneously decomposed to **6** and other unidentified materials, the resin-bound reagent **2a** was stable for months when stored at ambient temperature and humidity.

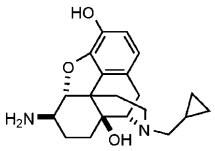
Given the success of this first annulation reaction, the chemistry was expanded to include homologue **2b** and the preparation of a 20-member library of isoindolinones **8** and isoquinolones **9** (Table 1). A range of primary amine substrates was successfully annulated in a single step, including substituted alkyl- **A1**, **A4**; alkylaryl- **A2**, **A9**; heteroarylalkyl- **A3**, **A6–8**; and heterocycloalkylamines **A5** and the sterically demanding 6β-naltrexamine (**A10**). An average yield of 30% and a purity of greater than 90% was obtained following chromatographic purification.

To explore the scope of the SPAn chemistry in terms of ring sizes that may be obtained, iodo esters **10a–d** were synthesized (Scheme 3). Reaction of the resins with a representative amine, phenoxyethylamine (**A1**), under the reaction conditions defined above afforded pyrrolidinone (**11c**; 29%) and piperidinone (**11d**; 24%; Scheme 4). Azetidinone (**11a**) and azepinone (**11b**) were not detected in the crude reaction mixtures. Seven-membered-ring annulation products were obtained, however, provided that a conformational constraint biased the system toward cyclization. For example, reagents **10m–o**, in which the acyl and haloalkyl groups are *ortho*-disposed on an aromatic ring, furnished **11m**, **11n**, and **11o** (21, 23, and 12%, respectively) upon annulation of **A1**.

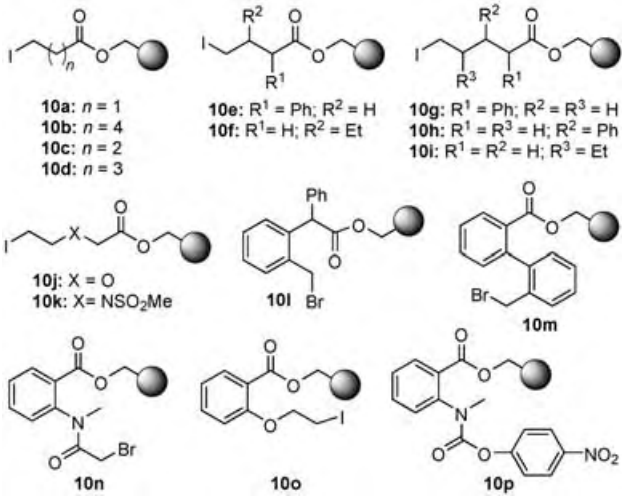
 © 2005 Wiley-VCH Verlag GmbH & Co. KGaA, Weinheim

Table 1: Isoindolinone **8** and isoquinolone **9** library from SPAn reagents **2a,b**.



Amine		SPAn reagent	Annulation product	Yield [%][a]
2-phenoxyethylamine	**A1**	**2a**	**8a**	32
		2b	**9a**	32
2-(4-chlorophenyl)ethylamine	**A2**	**2a**	**8b**	29
		2b	**9b**	30
(pyridin-3-yl)methylamine	**A3**	**2a**	**8c**	24
		2b	**9c**	32
2-(*N*-morpholino)ethylamine	**A4**	**2a**	**8d**	24
		2b	**9d**	36
4-amino-(*N*-Boc-piperidine)	**A5**	**2a**	**8e**	42
		2b	**9e**	30
(thiophen-2-yl)methylamine	**A6**	**2a**	**8f**	61
		2b	**9f**	26
(5-methylfuran-2-yl)methylamine	**A7**	**2a**	**8g**	40
		2b	**9g**	25
(5-methylisoxazol-3-yl)-methylamine	**A8**	**2a**	**8h**	21
		2b	**9h**	22
(*S*)-methylbenzylamine	**A9**	**2a**	**8i**	45
		2b	**9i**	31
	**A10**	**2a**	**8j**	33
		2b	**9j**	17

[a] Yield of isolated product, as purified by HPLC.



Scheme 3. Additional selected examples of SPAn reagents.

The introduction of substituents into these reagents adds elements of stereochemical and shape diversity in the annulation products. SPAn reagents **10e–i** with pendent aryl (phenyl) or alkyl (ethyl) groups furnishes substituted pyrrolidinones **11e,f** and piperidinones **11g–i** (**A1**; 23–62% yield). This result is significant for two reasons: First, the chemical reactivity of the SPAn reagents was expanded to include displacement of less-reactive nonbenzylic halogen centers in the tandem alkylation/intracyclization process. Second, the unique three-dimensional disposition of the ring functionalities present in **11e–i** permits a thorough interrogation of biological space. The differential display of the chemical functionalities by the annulation products is ideal for the development of a SAR against a given molecular target. These results are analogous, albeit accentuated by the conformational rigidity of the cyclic derivatives, to SAR information that may be obtained when traditional acyclic derivatization is performed. The swath of chemical space occupied by the SPAn products is assessed visually by examination of the overall topography of all of the annulation products listed in Scheme 4 (Figure 1a). The importance of shape sampling in relation to biological activity is illustrated in the derivatization of 6β-naltrexamine (**A10**) with reagents **2a,b**. The α-phenylpyrrolidinone derivative **8j** exhibits a K_i value of 1.6 nM against the μ-opioid receptor, whereas $K_i =$

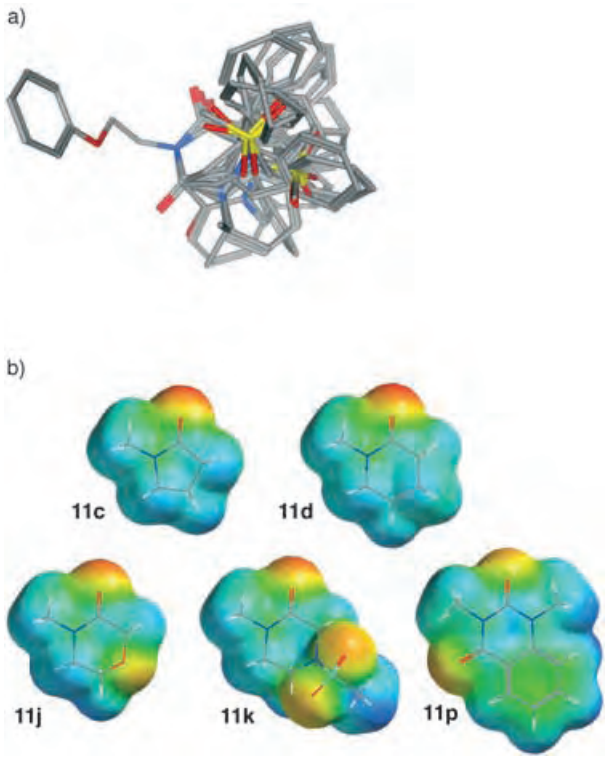
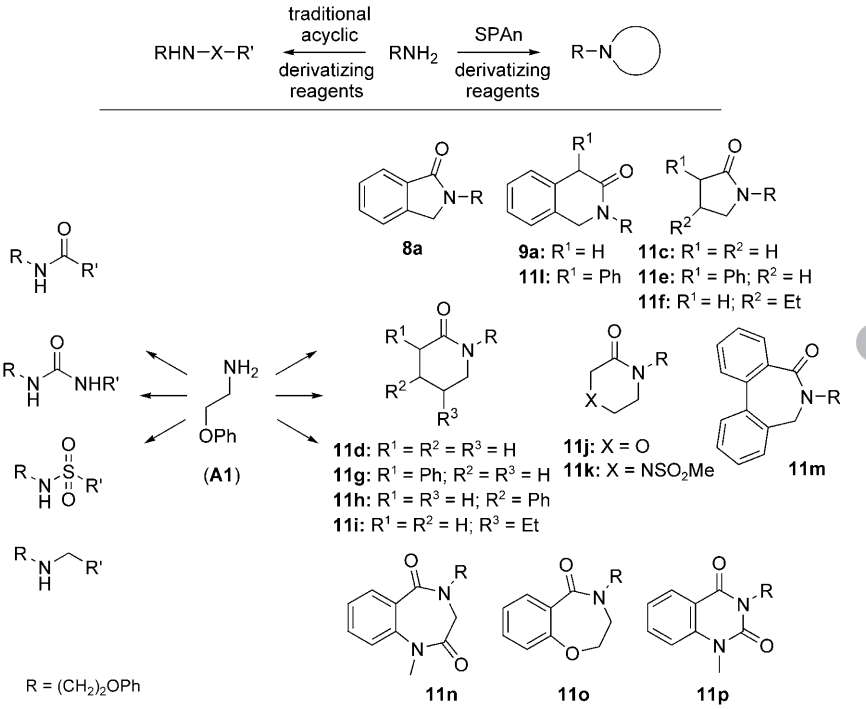


Figure 1. a) The collective topology of SPAn products given in Scheme 4 indicates dense interrogation of chemical space. The phenoxyamide linkage was kept fixed and low-energy conformations of the side chains of **11c–p** were calculated by using the MMFF94x forcefield in the molecular operating environment (MOE; Chemical Computing Group). The structures were aligned with respect to the atoms making up the phenoxyamide linker. b) Graphical comparison of electrostatic potential surfaces of **11c,d** versus **11j,k,p**, as derived from HF/3-21g* calculations by using Spartan '04. The electrostatic potential values range from −67 (red) to 37 kcal mol^{-1} (blue). The phenoxyethyl group is replaced with a methyl group for clarity.

 © 2005 Wiley-VCH Verlag GmbH & Co. KGaA, Weinheim



Scheme 4. Use of SPAn reagents for cyclic amine derivatization.

56 nM for the α-phenylpiperidinone derivative **9j** at this receptor. The increase in ring size by a single methylene unit causes a remarkable 35-fold decrease in binding affinity.

Replacement of the methylene carbon atoms in **10b**,**c** by a heteroatom generates reagents **10j**,**k** which afford morpholinone **11j** (**A1**; 29%) and piperazinone **11k** (**A1**; 21%). These cyclic and related heteroatom-containing derivatives **11n–p**, give rise to electrostatic potential (EP) surfaces, distinct from their carbon congeners.[9] This result is again evident upon visual inspection of the EP surfaces generated for **11j**,**k**,**p** and carbon congeners **11c**,**d** (Figure 1b). The complementarity of the EP surface and molecular shape are two mutually inclusive determinants for high-affinity binding. Both of these molecular attributes are readily probed by employing the annulation chemistry.

A new family of reagents for amine derivatization, termed SPAn reagents, enables the single-step conversion of primary amines to cyclic derivatives. The annulation protocol, together with existing protocols for the preparation of amides, sulfonamides, ureas, and other acyclic derivatives in one step (Scheme 4), represents a powerful ensemble for streamlined synthesis. Resin loading, a major obstacle in reagent preparation, was overcome through the 1,3-dipolar cycloaddition reaction of solution-prepared propargyl esters and Merrifield azide resin. The reagents require no further chemical manipulation or activation for their use and display excellent shelf stability. Microwave heating was essential to obtain the annulation products as discrete compounds **11c–p** or in a library format (**2a**,**b**→**8/9a–j**, respectively). Tandem *N*-alkylation/intramolecular acylation is utilized in this report as the annulation manifold to yield heterocyclic lactams. Reagents that afford cycloalkylamines, diazaspirocycles, and other non-lactams have also been developed by us, thus increasing the molecular diversity of the cyclic derivatives obtained. Application of SPAn chemistry in the context of finding new lead compounds and SAR development will be reported subsequently.[10]

Received: May 13, 2005
Published online: August 3, 2005

Keywords: amines · annulation · combinatorial chemistry · cycloaddition · heterocycles

[1] R. E. Dolle, *J. Comb. Chem.* **2003**, *6*, 623–679, and references therein.
[2] S. Bhattacharyya, *Curr. Opin. Drug Discovery Dev.* **2004**, *7*, 752–764.
[3] a) J. M. Salvino, R. E. Dolle in *Methods in Enzymology*, *Vol. 369*, *Part B* (Eds.: G. A. Morales, B. A. Bunin), Elsevier Academic Press, Amsterdam, **2003**, pp. 151–163; b) J. M. Salvino, N. V. Kumar, E. Orton, J. Airey, T. Kiesow, K. Crawford, R. Mathew, P. Krolikowski, M. Drew, D. Engers, D. Krolinkowski, T. Herpin, M. Gardyan, G. McGeehan, R. Labaudiniere, *J. Comb. Chem.* **2000**, *2*, 691–697.
[4] P. A. Tuthill, P. R. Seida, W. Barker, J. A. Cassel, S. Belanger, R. N. DeHaven, M. Koblish, S. L. Gottshall, P. J. Little, D. L. DeHaven-Hudkins, R. E. Dolle, *Bioorg. Med. Chem. Lett.* **2004**, *14*, 5693–5697.
[5] V. A. Kovtunenko, A. K. Tyltin, T. T. Dobrenko, F. S. Babichev, *Ukr. Khim. Zh.* **1983**, *49*, 1099–1103.
[6] J. H. van Maarseveen, *Comb. Chem. High Throughput Screening* **1998**, *1*, 185–214.
[7] H. C. Kolb, M. G. Finn, K. B. Sharpless, *Angew. Chem. Int. Ed.* **2001**, *40*, 2004–2021.
[8] a) S. Lober, P. Rodriguez-Loaiza, P. Gmeiner, *Org. Lett.* **2003**, *5*, 1753–1755; b) L. Bettinetti, S. Lober, H. Huebner, P. Gmeiner, *J. Comb. Chem.* **2005**, *7*, 309–316; c) S. Lober, P. Gmeiner, *Tetrahedron* **2004**, *60*, 8699–8702.
[9] J. S. Murray, P. Politzer, *Methods Princ. Med. Chem.* **2003**, *17*, 233–254.
[10] The authors wish to acknowledge P. C. Kambhampati, D. Subrahmanyam, V. S. Ponnapalli, L. M. Kolukuluri, Y. Deraje, and M. R. Motatipally, of GVK Biosciences PVT, Ltd., Hyderabad, India, for their assistance in the preparation of propargyl esters, the details of which will be reported separately.

 © 2005 Wiley-VCH Verlag GmbH & Co. KGaA, Weinheim

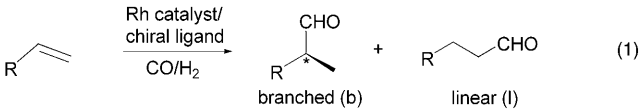
Asymmetric Catalysis

DOI: 10.1002/anie.200501478

Highly Regio- and Enantioselective Asymmetric Hydroformylation of Olefins Mediated by 2,5-Disubstituted Phospholane Ligands**

Alex T. Axtell, Christopher J. Cobley, Jerzy Klosin, Gregory T. Whiteker, Antonio Zanotti-Gerosa, and Khalil A. Abboud*

Asymmetric hydroformylation (AHF) is a powerful synthetic methodology that allows conversion of olefins into optically active aldehydes in a single step [Eq. (1)].[1] The aldehyde



(1)

group is one of the most versatile functional groups and can be readily transformed into a variety of high-value-added chiral chemicals, such as amines, imines, alcohols, and acids.[2] Even though AHF offers great promise to the fine-chemical industry, this reaction has not been utilized on a commercial scale because of several remaining technical challenges; among the most important to overcome are a) low reaction rates at low temperatures for reactions in which good selectivities are usually observed, b) difficulties in controlling the regio- and enantioselectivities simultaneously, and c) limited substrate scope for any single ligand.

The reaction rates of Rh-catalyzed hydroformylations are commonly slower than those of asymmetric hydrogenations that are conducted near ambient temperature. Commercially viable rates in AHF can be achieved at 80–120 °C (turnover rates of several thousand per hour); however, lower regio- and enantioselectivities are usually observed at these high temperatures. Thus, the most desired characteristic of the new generation of AHF ligands should be the ability to produce optically active aldehydes at high temperatures without compromising product selectivity.

Only a few chiral ligands have been successfully applied in AHF reactions (Scheme 1). Among the most effective are (2*R*,4*R*)-chiraphite (**1**)[3] and its analogues,[4] which exhibit enantioselectivities of up to 90 % *ee* for the hydroformylation of styrene at low temperatures; (*R*,*S*)-binaphos (**2**),[5] which shows high enantioselectivities for the hydroformylation of many structurally diverse olefins; (*S*,*S*)-kelliphite (**3**), which is effective for the hydroformylation of allyl cyanide[6] and vinyl acetate;[7] and (*S*,*S*)-esphos (**5**), which displays a high enantioselectivity for the hydroformylation of vinyl acetate.[8] Together with Landis and co-workers, we recently reported[9] the application of diazaphospholane ligands **4** in AHF reactions which showed outstanding hydroformylation rates and very high enantioselectivities for reactions with styrene and allyl cyanide substrates. Diazaphospholane **4** is especially selective for vinyl acetate at 80 °C (96 % *ee*, b/l = 35). This ligand family is structurally related to 1,2-bis(2,5-dialkylphospholano)benzene (duphos; **6**–**8**), 1,2-bis(2,5-dialkylphospholano)ethane[10] (bpe; **9**–**11**), and especially the recently reported (*R*,*R*)-1,2-bis(2,5-diphenylphospholano)ethane ((*R*,*R*)-Ph-bpe; **12**) Scheme 2).[11] The duphos and bpe ligands[12] have been proven to be exceptional ligands for the asymmetric hydrogenation[13] of dehydroamino acids and mono- and disubstituted itaconates, among numerous other applications, but their use has not been reported for AHF reactions.

Herein, we report that **12** is an excellent ligand for the rhodium-catalyzed AHF of styrene, allyl cyanide, and vinyl acetate at high temperatures (80–100 °C). (*R*,*R*)-Ph-bpe (**12**) displays the best regio- and enantioselectivities reported to date for the hydroformylation of styrene and allyl cyanide and the second best for the hydroformylation of vinyl acetate. The reaction rates obtained at these elevated temperatures render this catalytic system amenable to industrial applications.

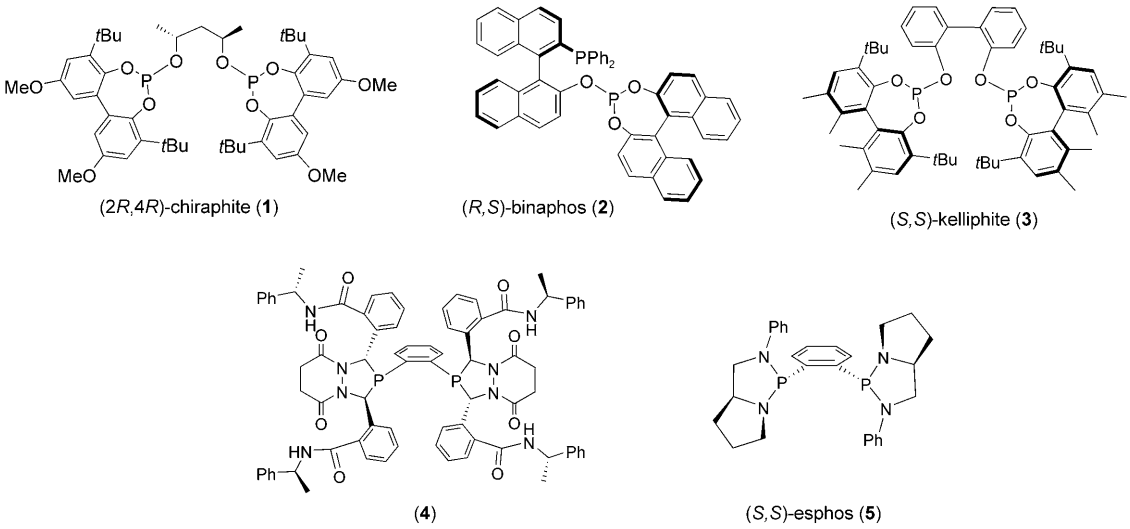
The hydroformylation reactions were carried out at 80 °C and 1.034 MPa CO/H_2 pressure with substrate/catalyst molar ratios of 5000:1 and a catalyst concentration of 0.37 mM. Phospholane and phosphetane ligands **6**–**16** (Scheme 2) and previously reported ligands **1**–**4** were evaluated under identical conditions for comparison. Active catalysts were prepared by combining $[Rh(acac)(CO)_2]$ (acac = acetylacetonate) with 1.2 equivalents of each bidentate ligand (2.1 equiv for **16**) in toluene followed by pressurizing the resulting solution with syngas (CO/H_2, molar ratio of 1:1). Styrene, allyl cyanide, and vinyl acetate underwent simultaneous hydroformylation under constant pressure, with the gas uptake being monitored continuously. Olefin conversion, together

[*] A. T. Axtell, Dr. J. Klosin
Chemical Sciences
The Dow Chemical Company
1776 Building, Midland, MI 48674 (USA)
Fax: (+1) 989-638-6225
E-mail: jklosin@dow.com
Dr. C. J. Cobley, Dr. A. Zanotti-Gerosa[+]
Dowpharma
Chirotech Technology Limited
321 Cambridge Science Park, Cambridge CB4 0WG (UK)
Dr. G. T. Whiteker
Chemical Sciences
The Dow Chemical Company
740 Building, South Charleston, WV 25303 (USA)
Dr. K. A. Abboud
Department of Chemistry
University of Florida
Gainesville, FL 32611 (USA)
[+] Current address:
Johnson Matthey Catalysts
28 Cambridge Science Park
Cambridge CB4 0FP (UK)

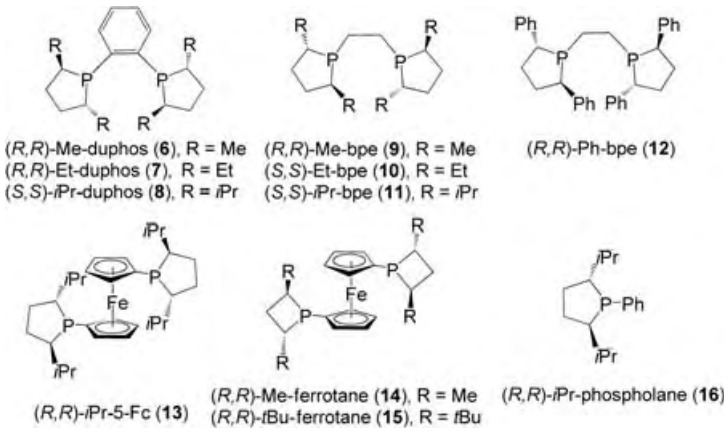
[**] We thank Dr. Mark Jackson for providing a sample of the Ph-bpe ligand, Prof. Clark Landis from the University of Wisconsin—Madison, and Dr. Cynthia Rand, Dr. Ian Lennon, and Dr. Guy Casy from Dowpharma for helpful discussions.

Supporting information for this article is available on the WWW under http://www.angewandte.org or from the author.

InterScience
© 2005 Wiley-VCH Verlag GmbH & Co. KGaA, Weinheim



Scheme 1. Chiral ligands that have been successfully applied in AHF reactions.



Scheme 2. Phospholane and phosphetane ligands.

with the regio- and enantioselectivities of the products, was determined by using gas chromatography on a chiral stationary phase, as previously described.[7] The syngas uptake curves demonstrate that all the phospholane ligands screened exhibited low hydroformylation rates except for **12** (Figure 1). The lowest hydroformylation rates were observed for the ferrocenyl phospholane and phosphetane[14] ligands **13**–**15** (Table 1, entries 12–14). (*R*,*R*)-Ph-bpe (**12**) exhibits an average turnover frequency of 1139 h^{-1}, which is about five times more active than the second fastest phospholane **11** and only about two times slower than **1** and **2**. The most likely reason for the increased activity of **12** compared with the other phospholane ligands is the presence of the electron-withdrawing phenyl rings that reduce the overall basicity of the phosphine moiety. The IR spectroscopic data ν_{CO} obtained for [Mo(CO)$_4${(*S*,*S*)-Me-bpe}], [Mo(CO)$_4${(*S*,*S*)-*i*Pr-bpe}], and [Mo(CO)$_4${(*R*,*R*)-Ph-bpe}] (2012, 2011, and 2015 cm^{-1}, respectively)[15] support the assertion that (*R*,*R*)-Ph-bpe is the least basic phosphine amongst the bpe ligands. It is well established that electron-poor phosphines lead to more active catalysts in Rh-catalyzed hydroformylation.[1a]

The olefin conversion and regio- and enantioselectivity data for the ligands investigated in this study are summarized in Table 1. The olefin conversion data are in close agreement with the syngas uptake curves and clearly demonstrate that **12** exhibits the fastest hydroformylation rates of all the phospholane and phosphetane ligands in this study (Table 1, entry 11 versus entries 6–10 and 12–15). The enantioselectivity data show that bpe and duphos ligands with larger substituents in the 2,5-positions of the phospholane rings (*i*Pr and Ph versus Me and Et) lead to noticeably higher enantioselectivities. Importantly, the selectivities observed for styrene, allyl cyanide, and vinyl acetate are comparable for a given phospholane ligand, thus suggesting the potential for broad applicability of phospholane ligands to a wide range of substrates. Monodentate ligand **16** has a very poor activity and selectivity, which indicates that the bidentate nature of the ligand is necessary for achieving high regio- and enantioselectivities. Phospholane **12** is the most enantioselective ligand in this study giving 94, 90, and 82% *ee* for the

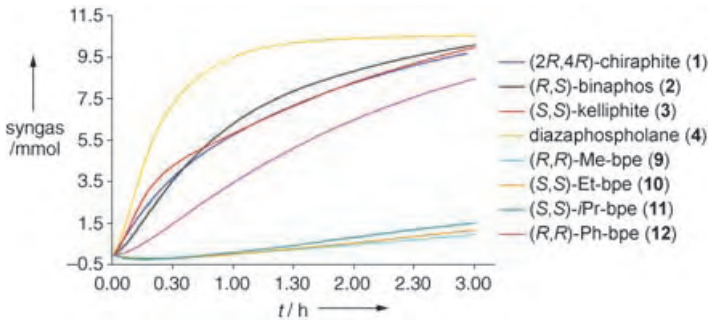


Figure 1. Syngas-uptake curves for reactions performed with a olefin/catalyst ratio of 5000:1 (at 80 °C in toluene with 1.034 MPa of CO/H_2 (1:1) and a L/Rh ratio of 1.2:1).

 © 2005 Wiley-VCH Verlag GmbH & Co. KGaA, Weinheim

Table 1: Percentage conversion (conv.), branched/linear ratio (b/l), and enantioselectivities of the hydroformylation reactions of styrene, allyl cyanide, and vinyl acetate.

Entry	Ligand	Styrene			Allyl cyanide			Vinyl acetate		
		conv. [%]	b/l	*ee* [%]	conv. [%]	b/l	*ee* [%]	conv. [%]	b/l	*ee* [%]
1	(2*R*,4*R*)-chiraphite (**1**)	89	9.1:1	50 (*R*)	98	5.8:1	14 (*R*)	76	246:1	49 (*R*)
2	(*R*,*S*)-binaphos (**2**)	96	4.5:1	82 (*R*)	98	2.1:1	72 (*R*)	72	8.2:1	48 (*S*)
3	(*S*,*S*)-kelliphite (**3**)	82	8.4:1	3 (*S*)	98	9.9:1	68 (*S*)	83	65:1	72 (*R*)
4	diazaphospholane **4**	100	6.6:1	82 (*R*)	100	4.1:1	87 (*R*)	100	37:1	96 (*S*)
5	(*R*,*R*)-Me-duphos (**6**)	10	15.7:1	44 (*S*)	42	6.6:1	32 (*S*)	26	176:1	51 (*R*)
6	(*R*,*R*)-Et-duphos (**7**)	14	13.7:1	52 (*S*)	49	7.8:1	35 (*S*)	27	371:1	66 (*R*)
7	(*S*,*S*)-*i*Pr-duphos (**8**)	15	11.3:1	83 (*S*)	55	7.2:1	82 (*S*)	29	322:1	74 (*R*)
8	(*R*,*R*)-Me-bpe (**9**)	8	14.0:1	43 (*S*)	36	5.8:1	37 (*S*)	23	97:1	59 (*R*)
9	(*S*,*S*)-Et-bpe (**10**)	10	11.3:1	55 (*R*)	40	6.2:1	49 (*R*)	23	152:1	66 (*S*)
10	(*S*,*S*)-*i*Pr-bpe (**11**)	11	9.5:1	82 (*S*)	48	6.7:1	83 (*S*)	28	142:1	70 (*R*)
11	(*R*,*R*)-Ph-bpe (**12**)	57	45.0:1	94 (*R*)	96	7.1:1	90 (*R*)	52	340:1	82 (*S*)
12	(*R*,*R*)-*i*Pr-5-Fc (**13**)	9	3.2:1	15 (*R*)	28	3.9:1	49 (*R*)	22	94:1	29 (*R*)
13	(*R*,*R*)-*t*Bu-ferrotane (**14**)	10	1.7:1	55 (*R*)	31	5.3:1	73 (*R*)	23	29:1	27 (*R*)
14	(*R*,*R*)-Me-ferrotane (**15**)	9	3.6:1	18 (*S*)	28	2.3:1	53 (*S*)	22	8.5:1	39 (*R*)
15	(*R*,*R*)-*i*Pr-phospholane (**16**)	11	4.4:1	11 (*R*)	30	3.5:1	7 (*R*)	17	21:1	8 (*S*)

[a] All the reactions were performed at 80 °C in toluene with 1.034 MPa of CO/H_2 (1:1), L/Rh = 1.2:1 (2.1:1 for **16**), substrate/Rh = 5000:1, catalyst concentration of 0.037 mol %, and a reaction time of 3 h.

reactions of styrene, allyl cyanide, and vinyl acetate, respectively.[16] Phospholane **12** is not only the most enantioselective ligand for the hydroformylation of styrene (including previously reported ligands **1**–**4**), but it also gives an unprecedented high regioselectivity (b/l = 45:1). Under identical conditions, **2**, for example, exhibits a significantly lower regioselectivity (b/l = 4.5:1). The ability of a ligand to give high regioselectivities in AHF (high ratio of branched to linear isomers) is a very important attribute as any amount of achiral linear isomer can be regarded as an additional impurity that must be separated from the desired chiral product. To put the regioselectivities of the styrene products into perspective, the amount of the undesired linear isomer formed with (*R*,*R*)-Ph-bpe (**12**) is 2.2 % (b/l = 45:1), whereas with (*R*,*S*)-binaphos (**2**) it is 18.2 % (b/l = 4.5:1; Table 1, entries 11 and 2). Phospholane **12** also gives the highest enantioselectivity (90 % *ee*, b/l = 7.1:1) in the case of the hydroformylation of allyl cyanide. Under the same conditions, diazaphospholane **4** gives a similar enantioselectivity (87 % *ee*) but a noticeably lower regioselectivity (b/l = 4.1:1). For ligands **1**–**4**, only **3** gives a higher regioselectivity for the hydroformylation of allyl cyanide (b/l = 9.9:1), although with a much lower enantioselectivity (68 % *ee*). Phospholane **12** gives the second best enantioselectivity (82 % *ee*) for the hydroformylation of vinyl acetate but with a high regioselectivity (b/l = 340:1) that is unprecedented. The only ligand that shows higher enantioselectivity for the hydroformylation of vinyl acetate is the recently reported diazaphospholane **4** (96 % *ee*, b/l = 37:1).[9]

A second set of hydroformylation reactions was conducted to compare ligand **12** with ligands **1**–**4** using mixtures of neat olefins at 80 °C and 1.034 MPa pressure of syngas with substrate/catalyst molar ratios of 30000:1 and a catalyst concentration of 0.062 mM. At these very low catalyst loadings, the rate of hydroformylation with **12** (an average turnover frequency of 4467 h^{-1}) was virtually identical to those of **1** and **2** and only slower than **3** and **4** (see Figure 2). The regio- and enantioselectivities achieved under these conditions were comparable to those obtained at the substrate/catalyst ratio of 5000:1 (see Table 2).

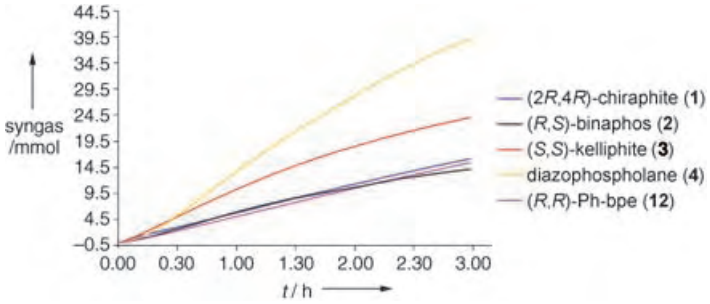


Figure 2. Syngas-uptake curves for reactions were performed with a ratio of olefin/catalyst = 30000:1 (at 80 °C in toluene with 1.034 MPa of CO/H_2 (1:1) and a L/Rh ratio of 1.2:1).

Hydroformylation experiments conducted with the isolated rhodium complex [Rh(acac){(*R*,*R*)-Ph-bpe}], prepared by the reaction of **12** and [Rh(cod)(acac)] (cod = cyclooctadiene), gave identical results to experiments in which the rhodium complex was prepared in situ prior to the hydroformylation reaction. The solid-state structures of **12** and [Rh(acac){(*R*,*R*)-Ph-bpe}] were determined by single-crystal X-ray analysis (Figures 3 and 4).[17]

A preliminary investigation into the reaction conditions (olefin concentration, CO and H_2 pressures, and temperature) reveals that the hydroformylation rate with **12** is first order in olefin concentration, zero order in ligand concentration (ligand/Rh = 1:1–5:1), zero order in H_2 pressure, and negative first order in CO pressure. These observations are consistent with the dissociation of CO from a five-coordinate rhodium dicarbonyl complex as a pre-equilibrium step prior to the rate-limiting insertion of the olefin into the Rh–H bond.[18] Interestingly, the enantioselectivities of all the products were

 © 2005 Wiley-VCH Verlag GmbH & Co. KGaA, Weinheim

Table 2: Percent conversion (conv.), branched/linear ratio (b/l), and enantioselectivities of the hydroformylation reactions of styrene, allyl cyanide, and vinyl acetate.

Entry	Ligand	Styrene			Allyl cyanide			Vinyl acetate		
		conv. [%]	b/l	*ee* [%]	conv. [%]	b/l	*ee* [%]	conv. [%]	b/l	*ee* [%]
1	(2*R*,4*R*)-chiraphite (**1**)	32	10.8:1	51 (*R*)	74	5.8:1	13 (*R*)	34	204:1	50 (*R*)
2	(*R*,*S*)-binaphos (**2**)	35	4.6:1	81 (*R*)	58	2.1:1	68 (*R*)	23	7.1:1	58 (*S*)
3	(*S*,*S*)-kelliphite (**3**)	32	9.2:1	3 (*S*)	99	10.1:1	66 (*S*)	32	100:1	75 (*R*)
4	diazaphospholane (**4**)	73	5.7:1	80 (*R*)	100	3.9:1	80 (*R*)	92	47:1	95 (*S*)
5	(*R*,*R*)-Ph-bpe (**12**)	33	45.0:1	92 (*R*)	67	7.6:1	90 (*R*)	34	263:1	82 (*S*)

[a] All the reactions were performed at 80 °C in toluene at 1.034 MPa of CO/H_2 (1:1) with L/Rh = 1.2:1, substrate/Rh = 30000:1, a reaction time of 3 h, and 4.43 mL of a mixture of styrene/allyl cyanide/vinyl acetate/dodecane (1:1:1:0.3 molar ratio).

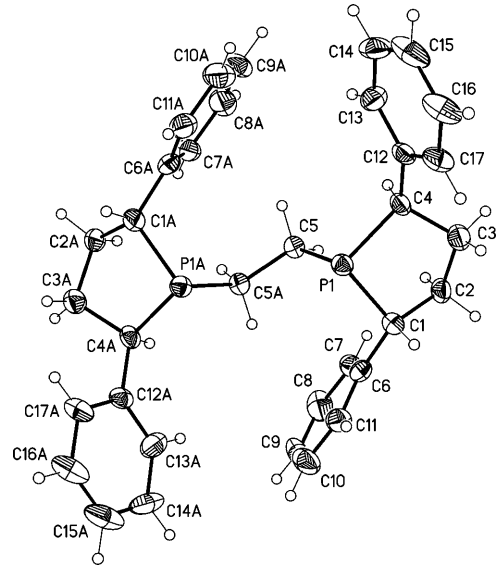


Figure 3. Molecular structure of (*R*,*R*)-Ph-bpe (**12**), with the thermal ellipsoids set at 40% probability.

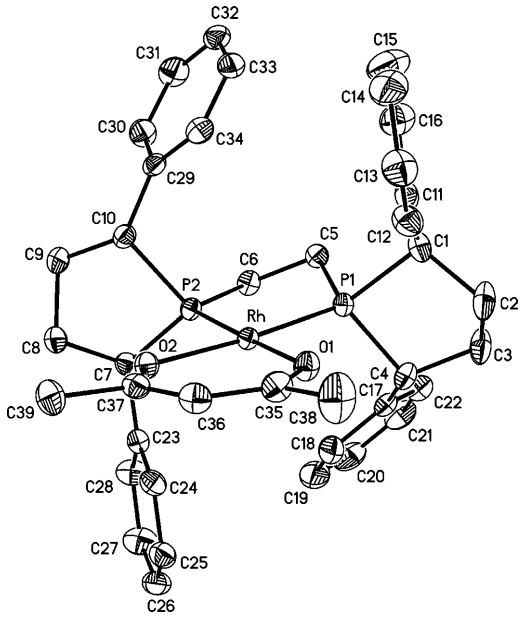


Figure 4. Molecular structure of [Rh(acac){(*R*,*R*)-Ph-bpe}], with the thermal ellipsoids set at 40% probability.

unaffected by variations in the syngas pressure (0.345–3.102 MPa), whereas the regioselectivities were dependent upon pressure, with b/l ratios of 40:1– 45:1 for the styrene products and b/l ratios of 1060:1–155:1 for the vinyl acetate products being observed over these pressures.

In conclusion, (*R*,*R*)-Ph-bpe (**12**) was identified as an excellent ligand for asymmetric hydroformylation which gives state-of-the-art regio- and enantioselectivities for styrene, allyl cyanide, and vinyl acetate, while maintaining commercially viable turnover rates over 4000 h^{-1} at 80 °C. The remarkable ability of phospholane-based ligands **12** and **4** to yield very high enantioselectivities at high temperatures renders these ligands suitable for large-scale industrial applications.

Received: April 28, 2005
Published online: August 12, 2005

Keywords: asymmetric catalysis · hydroformylation · P ligands · rhodium

[1] a) *Rhodium Catalyzed Hydroformylation* (Eds.: C. Claver, P. W. N. M. van Leeuwen), Kluwer Academic Publishers, Dordrecht, **2000**; b) M. Diéguez, O. Pàmies, C. Claver, *Tetrahedron: Asymmetry* **2004**, *15*, 2113–2122.
[2] J. K. Stille in *Comprehensive Organic Synthesis, Vol. 4* (Eds.: B. M. Trost, I. Flemming, L. A. Paquette), Pergamon, Oxford, **1991**, p. 913.
[3] a) J. E. Babin, G. T. Whiteker (Union Carbide Corporation), WO 9303839, **1993**; b) G. T. Whiteker, J. R. Briggs, J. E. Babin, B. A. Barner, *Chemical Industries, Vol. 89*, Marcel Dekker, New York, **2003**, pp. 359–367.
[4] M. Diéguez, O. Pàmies, A. Ruiz, S. Castillón, C. Claver, *Chem. Eur. J.* **2001**, *7*, 3086–3094.
[5] K. Nozaki, N. Sakai, T. Nanno, T. Higashijima, S. Mano, T. Horiuchi, H. Takaya, *J. Am. Chem. Soc.* **1997**, *119*, 4413–4423.
[6] C. J. Cobley, K. Gardner, J. Klosin, C. Praquin, C. Hill, G. T. Whiteker, A. Zanotti-Gerosa, J. L. Petersen, K. A. Abboud, *J. Org. Chem.* **2004**, *69*, 4031–4040.
[7] C. J. Cobley, J. Klosin, C. Qin, G. T. Whiteker, *Org. Lett.* **2004**, *6*, 3277–3280.
[8] S. Breeden, D. J. Cole-Hamilton, D. F. Foster, G. J. Schwarz, M. Wills, *Angew. Chem.* **2000**, *112*, 4272–4274; *Angew. Chem. Int. Ed.* **2000**, *39*, 4106–4108.
[9] T. P. Clark, C. R. Landis, S. L. Freed, J. Klosin, K. A. Abboud, *J. Am. Chem. Soc.* **2005**, *127*, 5040–5042.
[10] a) M. J. Burk, J. E. Feaster, W. A. Nugent, R. L. Harlow, *J. Am. Chem. Soc.* **1993**, *115*, 10125–10138; b) M. J. Burk, *Acc. Chem. Res.* **2000**, *33*, 363–372.

 © 2005 Wiley-VCH Verlag GmbH & Co. KGaA, Weinheim

[11] C. J. Pilkington, A. Zanotti-Gerosa, *Org. Lett.* **2003**, *5*, 1273 – 1275.
[12] Chiraphite (**1**), duphos, and bpe ligands, including (*R*,*R*)-Ph-bpe (**12**), are available from Strem Chemicals.
[13] W. Tang, X. Zhang, *Chem. Rev.* **2003**, *103*, 3029 – 3069.
[14] For synthesis and application of ferrocene-based phospholane ligands, see : a) A. Marinetti, F. Labrue, J.-P. Genet, *Synlett* **1999**, *12*, 1975 – 1977; b) U. Berens, M. J. Burk, A. Gerlach, W. Hems, *Angew. Chem.* **2000**, *112*, 2057 – 2060; *Angew. Chem. Int. Ed.* **2000**, *39*, 1981 – 1984; c) C. J. Cobley, I. C. Lennon, C. Praquin, A. Zanotti-Gerosa, R. B. Appell, C. T. Goralski, A. C. Sutterer, *Org. Process Res. Dev.* **2003**, *7*, 407 – 411.
[15] For IR spectroscopic data of other [$Mo(CO)_4$(diphosphine)] complexes, see: a) M. F. Ernst, D. M. Roddick, *Inorg. Chem.* **1989**, *28*, 1624 – 1627; b) K. G. Moloy, J. L. Petersen, *J. Am. Chem. Soc.* **1995**, *117*, 7696 – 7710; c) S. L. Mukerjee, S. P. Nolan, C. D. Hoff, R. Lopez de la Vega, *Inorg. Chem.* **1988**, *27*, 81 – 85.
[16] Hydroformylation experiments conducted with individual olefins gave the same selectivities for all three substrates as those obtained from simultaneous hydroformylations of these olefins, except for the regioselectivity for the reaction of vinyl acetate, which was lowered to b/l = 260:1.
[17] X-ray diffraction data for **12**: $M_r = C_{34}H_{36}P_2$, $T = 173$ K, $\lambda = 0.71073$ Å, monoclinic, $C2$, $a = 19.394(1)$, $b = 18.956(1)$, $c = 24.752(2)$ Å, $\beta = 104.717(1)°$, $Z = 12$, no. reflections = 14755 ($7283 > 2\sigma(I)$), refinement on $F2$, $R1(>2\sigma(I)) = 0.0363$, $R1$(all data) = 0.086, GOF = 0.756; [Rh(acac){(*R*,*R*)-Ph-bpe}]: $M_r = C_{80}H_{89}NO_4P_4Rh_2$, $T = 173$ K, $\lambda = 0.71073$ Å, monoclinic, $P2_1$, $a = 10.3863(6)$, $b = 19.9915(12)$, $c = 17.8855(10)$ Å, $\beta = 105.370(1)°$, $Z = 2$, no. reflections = 14572 ($13725 > 2\sigma(I)$), refinement on $F2$, $R1(>2\sigma(I)) = 0.0209$, $R1$(all data) = 0.0229, GOF = 1.000. CCDC-270008 and -270009 contain the supplementary crystallographic data for this paper. These data can be obtained free of charge from the Cambridge Crystallographic Data Centre via www.ccdc.cam.ac.uk/data_request/cif.
[18] a) P. W. N. W. van Leeuwen, C. P. Casey, G. T. Whiteker, *Rhodium Catalyzed Hydroformylation* (Eds.: C. Claver, P. W. N. M. van Leeuwen), Kluwer Academic Publishers, Dordrecht, **2000**, pp. 63 – 105; b) A. van Rooy, E. N. Orij, P. C. J. Kamer, P. W. N. M. van Leeuwen, *Organometallics* **1995**, *14*, 34 – 43.

 © 2005 Wiley-VCH Verlag GmbH & Co. KGaA, Weinheim

Asymmetric Synthesis

DOI: 10.1002/anie.200501408

Highly Enantioselective Catalytic Thiolysis of Prochiral Cyclic Dicarboxylic Anhydrides Utilizing a Bifunctional Chiral Sulfonamide**

*Takashi Honjo, Shigeki Sano, Motoo Shiro, and Yoshimitsu Nagao**

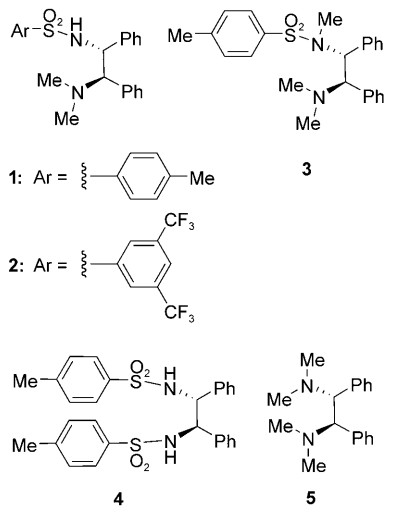
Asymmetric differentiation between two identical carbonyl groups of prochiral σ-symmetric dicarboxylic acid derivatives by using an enzymatic or a nonenzymatic procedure is a rational and useful strategy for the asymmetric synthesis of biologically active compounds and medicines. The resultant chiral products can be subjected to further so-called "enantioconvergent" and "enantiodivergent" transformations on the basis of latent σ symmetry.[1] Previously, we disclosed remarkable nonenzymatic asymmetric induction methods for various prochiral σ-symmetric dicarboxylic acid derivatives based on highly diastereoselective aminolysis and Dieckmann-type cyclizations using functional heterocycles, such as the C4-chiral 1,3-thiazolidine-2-thiones.[2] Recent efforts in this field have been directed towards the development of methods for the catalytic desymmetrization of prochiral cyclic dicarboxylic anhydrides, such as enantioselective ring opening with methanol and carbon nucleophiles in the presence of a catalytic amount of chiral reagents.[3] We have focused on the development of simple and versatile chiral sulfonamides that are available for various catalytic asymmetric reactions. Very recently, Wang et al. reported highly enantioselective Michael addition reactions catalyzed by a chiral pyrrolidine sulfonamide[4] and Ishihara et al. disclosed an attractive method for the kinetic resolution of racemic alcohols that utilized an L-histidine sulfonamide derivative.[5] Ikariya and co-workers also carried out catalytic enantioselective Michael addition reactions that employed chiral Ru amido complexes.[6] However, to the best of our knowledge, there has been no report of a catalytic asymmetric desymmetrization of prochiral dicar-

[*] Prof. Dr. Y. Nagao
Graduate School of Pharmaceutical Sciences
The University of Tokushima
Sho-machi, Tokushima 770-8505 (Japan)
Fax: (+81) 88-633-9503
E-mail: ynagao@ph.tokushima-u.ac.jp
T. Honjo, Dr. S. Sano
Graduate School of Pharmaceutical Sciences
The University of Tokushima
Sho-machi, Tokushima 770-8505 (Japan)
Dr. M. Shiro
Rigaku Corporation
3-9-12 Matsubaracho
Akishima, Tokyo 196-8666 (Japan)

[**] This work was supported by a Grant-in-Aid for Scientific Research(B)(2) from the Japan Society for the Promotion of Science.

Supporting information for this article is available on the WWW under http://www.angewandte.org or from the author.

InterScience
© 2005 Wiley-VCH Verlag GmbH & Co. KGaA, Weinheim



boxylic anhydrides by sulfur nucleophiles. Herein, we describe the highly enantioselective thiolysis of prochiral cyclic dicarboxylic anhydrides with benzyl mercaptan (BnSH) in the presence of a catalytic amount of chiral bifunctional sulfonamide.

First, we inspected the molecular structure of two chiral sulfonamide catalysts **1** and **2** expecting to observe bifunctional catalytic effects, namely, both acid- and base-like properties. The nucleophilicity of the SH group can be enhanced by an amine base, and the electrophilicity of the carbonyl group may be activated by an acidic proton from the sulfonamide moiety.[4,5] On the basis of an X-ray crystallographic analysis of **2** (see below), we envisaged that chiral sulfonamides **1** and **2** would not only show acid- and base-like catalytic functions but may also provide suitable conditions for the enantioselective molecular recognition between a prochiral dicarboxylic anhydride and BnSH based on hydrogen-bonding interactions. Chiral sulfonamides **1** and **2** were readily synthesized as follows: The treatment of (1*R*,2*R*)-*N*,*N*-dimethyl-1,2-diphenyl-1,2-ethanediamine[7] with *p*-toluenesulfonyl chloride or 3,5-bis(trifluoromethyl)benzenesulfonyl chloride in the presence of Et_3N in CH_2Cl_2 afforded the desired products **1** and **2** (89 and 76% yields, respectively).[8] Figure 1 shows the X-ray crystal structure[9] of **2**, in which the three phenyl groups are positioned alongside each other, two of which are organized in a stacked manner,[13] whereas the third occupies a more open position. Thus, the acidic (-SO_2NH-) and basic (Me_2N-) bifunctional groups are located beside each other opposite the phenyl groups and may be suitable for trapping both reactants, namely, the anhydride and thiol moieties, through hydrogen-bonding interactions at the thiolysis site. To verify the bifunctionality of **1** and **2** based on the hypothesis described above, the related chiral compounds **3**–**5** were also synthesized from (1*R*,2*R*)-1,2-diphenyl-1,2-ethanediamine.[8,14]

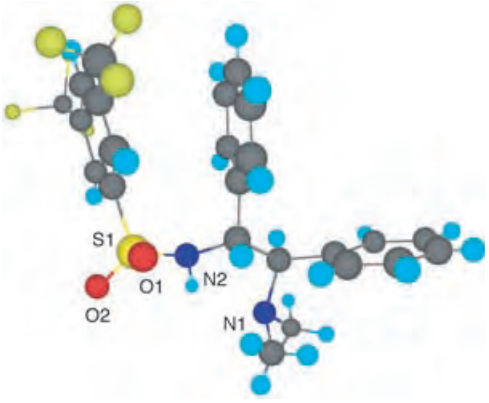
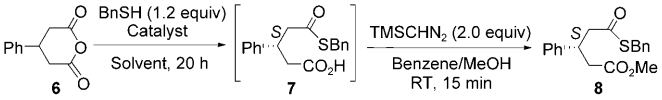


Figure 1. Computer-generated drawing derived from the X-ray coordinates of sulfonamide **2**.

Thus, the asymmetric thiolysis of 3-phenylglutaric anhydride **6** with BnSH (1.2 equiv) was examined in the presence of 10 mol% of chiral catalysts **1**–**5** in toluene at room temperature for 20 h. Then, the resultant crude *S*-benzyl thioester monocarboxylic acid **7** was converted into its methyl ester **8** without isolation of **7** for easy handling to determine the *ee* (Table 1). The desired catalytic asymmetric thiolysis of **6** with 1.2 equivalents of BnSH in the presence of 10 mol% of the bifunctional sulfonamides **1** and **2** smoothly proceeded to afford the chiral product **8** in 78 and 88% yields with 83 and 90% *ee*, respectively (Table 1, entries 1 and 2). However, the thiolysis of **6** with BnSH in the presence of *N*-methyl sulfonamide **3**, containing an *N*,*N*-dimethylamino basic functionality, or bisamino sulfonamide **4**, without an *N*,*N*-dimethylamino group, did not proceed at all (Table 1, entries 3 and 4). In the case of (1*R*,2*R*)-*N*,*N*,*N*′,*N*′-tetramethyl-1,2-diphenyl-1,2-ethanediamine (**5**), the thiolysis proceeded slightly to give **8** in 20% yield with 6% *ee* (Table 1, entry 5). On the basis of the experimental results (Table 1, entries 1–5), we conclude that both the acid catalysis resulting from the sulfonamide proton and the base catalysis resulting from the *N*,*N*-dimethylamino group in the exploitation of catalysts **1** and **2** were equally effected through this facile catalytic and enantioselective thiolysis of **6** with BnSH.

The reaction conditions were optimized with an investigation of the influence of the solvent, reaction temperature, and amount of catalyst **2** on the yield and enantioselectivity of the thiolysis of **6** with 1.2 equivalents of BnSH (Table 1,

Table 1: Investigation of the reaction conditions for the enantioselective thiolysis of 3-phenylglutaric anhydride **6** with benzyl mercaptan in the presence of chiral catalysts.



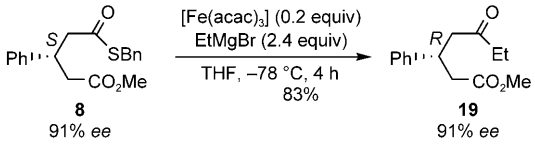
Entry	Catalyst (mol%)	Solvent	*T* [°C]	Yield [%][a]	*ee* [%][b]
1	**1** (10)	toluene	RT	78	83
2	**2** (10)	toluene	RT	88	90
3	**3** (10)	toluene	RT	NR[c]	–
4	**4** (10)	toluene	RT	NR[c]	–
5	**5** (10)	toluene	RT	20	6
6	**2** (10)	CH_2Cl_2	RT	61	83
7	**2** (10)	MeCN	RT	88	38
8	**2** (10)	THF	RT	87	84
9	**2** (10)	Et_2O	RT	94	92
10	**2** (10)	Et_2O	0	94	92
11	**2** (10)	Et_2O	−30	93	92
12	**2** (5)	Et_2O	RT	95	91
13	**2** (1)	Et_2O	RT	87	87

[a] Yield of isolated product. [b] Determined by HPLC analysis. [c] NR = no reaction. Bn = benzyl, TMS = trimethylsilyl.

© 2005 Wiley-VCH Verlag GmbH & Co. KGaA, Weinheim

entries 6–13). Among the solvents used (namely, toluene, CH_2Cl_2, MeCN, THF, and Et_2O), Et_2O at room temperature provided the best result, thus giving the chiral product **8** in 94% yield with 92% *ee* (Table 1, entries 2 and 6–9). At reaction temperatures lower than room temperature (0 and −30 °C), the enantioselective thiolysis was almost the same as at room temperature (Table 1, entries 9–11). Interestingly, this catalytic enantioselective thiolysis even proceeded in the presence of 5 and 1 mol% of **2** at room temperature to afford **8** in 95 and 87% yields with 91 and 87% *ee*, respectively (entries 12 and 13). Similar enantioselective thiolysis of **6** with 1.2 equivalents of ethanethiol or thiophenol in the presence of 5 mol% of **2** in Et_2O at room temperature followed by methylation with $TMSCHN_2$ gave the corresponding *S*-ethyl and *S*-phenyl thioesters in 61 and 90% yields with 78 and 16% *ee*, respectively.

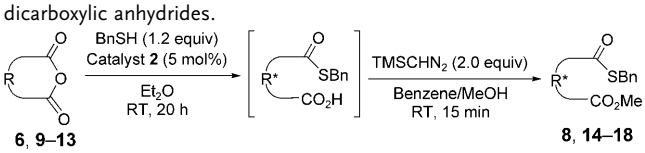
Thus, highly enantioselective thiolysis of prochiral dicarboxylic anhydrides **6** and **9–13** with 1.2 equivalents of BnSH was performed in the presence of 5 mol% of **2** in Et_2O at room temperature for 20 h followed by methylation of the resultant corresponding monocarboxylic acids with $TMSCHN_2$. The corresponding chiral monomethyl esters **8** and **14–18** were efficiently obtained in yields of 87–100% with *ee* values of 83–98% (Table 2). The absolute configuration of the newly formed chiral carbon atom(s) in **8** and **14–18** was determined by conversion[8] into known chiral compounds.[15] Although the detailed reaction mechanism of this catalytic and highly enantioselective thiolysis in the presence of chiral sulfonamides remains unclear, this quite simple catalytic desymmetrization procedure should be a fascinating method for the practical syntheses of chiral synthons (synthetic building blocks). Using the active monothioester character, **8** (91% *ee*) was tentatively treated with 0.2 equivalents of $[Fe(acac)_3]$ (acac = acetylacetonate) and 2.4 equivalents of EtMgBr in THF at −78 °C to give chemoselectively the

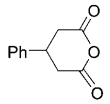
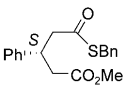
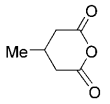
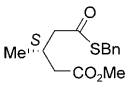
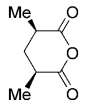
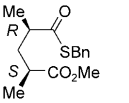
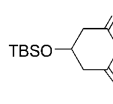
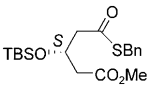
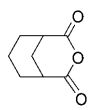
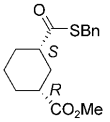
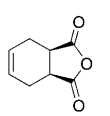
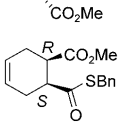


desired chiral ketoester **19** in 83% yield with 91% *ee*.[16]

The chiral monothioesters **8** and **14–18** will be exploited for the asymmetric synthesis of macrocyclic antibiotic drugs and biologically active natural products.[17] Newly designed bifunctional chiral sulfonamides, including **2**, seem to be promising for the development of various catalytic asymmetric induction methods.

Table 2: Catalytic, enantioselective thiolysis of various prochiral cyclic dicarboxylic anhydrides.



Entry	Anhydride		Product		Yield [%][a]	*ee* [%][b]
1		**6**		**8**	95	91
2		**9**		**14**	87	91
3		**10**		**15**	100	90
4		**11**		**16**	88	93
5		**12**		**17**	90	98
6		**13**		**18**	90	83

[a] Yield of isolated product. [b] Determined by HPLC analysis. TBS = *tert*-butyldimethylsilyl.

Experimental Section

A typical procedure of the catalytic enantioselective thiolysis: Benzyl mercaptan (141 μL, 1.2 mmol) was added to a solution of 3-phenylglutaric anhydride **6** (190 mg, 1.0 mmol) and chiral sulfonamide **2** (25.8 mg, 0.05 mmol) in Et_2O (10 mL) at room temperature. The mixture was stirred at room temperature under Ar for 20 h and treated with 10% HCl followed by extraction with $CHCl_3$. The $CHCl_3$ extracts were dried over $MgSO_4$ and filtered. After evaporation of the filtrate in vacuo, the residue was dissolved in benzene/MeOH (7:2; 9 mL) and a solution of $TMSCHN_2$ in Et_2O (2.0 M, 1 mL, 2.0 mmol) was added. The mixture was stirred at room temperature for 15 min and then evaporated in vacuo to give an oily residue. Purification of the residue by column chromatography on silica gel with EtOAc/*n*-hexane (1:4) afforded compound **8** (312 mg, 95% yield, 91% *ee*) as a white solid (m.p. 34.5–35 °C).

Received: April 25, 2005
Published online: August 4, 2005

Keywords: anhydrides · asymmetric synthesis · homogeneous catalysis · sulfonamides · thiolysis

[1] a) Y. Nagao, E. Fujita, *Yuki Gosei Kagaku Kyokai Shi* **1984**, *42*, 622–634; b) E. Fujita, Y. Nagao, *Advances in Heterocyclic Chemistry*, *Vol. 45* (Ed.: A. R. Katritzky), Academic Press, New York, **1989**, pp. 1–36; c) R. S. Ward, *Chem. Soc. Rev.* **1990**, *19*, 1–19; d) S. Sano, H. Ushirogochi, K. Morimoto, S. Tamai, Y. Nagao, *Chem. Commun.* **1996**, 1775–1776; e) S. Sano, K. Hayashi, T. Miwa, T. Ishii, M. Fujii, H. Mima, Y. Nagao, *Tetrahedron Lett.* **1998**, *39*, 5571–5574; f) M. C. Willis, *J. Chem. Soc. Perkin Trans. 1* **1999**, 1765–1784; g) Y. Nagao, *Yakugaku Zasshi* **2002**, *122*, 1–27.

[2] a) Y. Nagao, T. Ikeda, M. Yagi, M. Shiro, E. Fujita, *J. Am. Chem. Soc.* **1982**, *104*, 2079- 2081; b) Y. Nagao, T. Inoue, E. Fujita, S. Terada, M. Shiro, *J. Org. Chem.* **1983**, *48*, 132–133; c) Y. Nagao, T. Inoue, E. Fujita, S. Terada, M. Shiro, *Tetrahedron* **1984**, *40*, 1215–1223; d) Y. Nagao, T. Ikeda, T. Inoue, M. Yagi, M. Shiro,

 © 2005 Wiley-VCH Verlag GmbH & Co. KGaA, Weinheim

E. Fujita, *J. Org. Chem.* **1985**, *50*, 4072 – 4080; e) Y. Nagao, Y. Hagiwara, T. Tohjo, Y. Hasegawa, M. Ochiai, M. Shiro, *J. Org. Chem.* **1988**, *53*, 5983 – 5986; f) Y. Nagao, Y. Hagiwara, H. Hasegawa, M. Ochiai, T. Inoue, M. Shiro, E. Fujita, *Chem. Lett.* **1988**, 381 – 384.

[3] a) Y. Chen, S.-K. Tian, L. Deng, *J. Am. Chem. Soc.* **2000**, *122*, 9542 – 9543; b) A. C. Spivey, B. I. Andrews, *Angew. Chem.* **2001**, *113*, 3227 – 3230; *Angew. Chem. Int. Ed.* **2001**, *40*, 3131 – 3134; c) Y. Chen, P. McDaid, L. Deng, *Chem. Rev.* **2003**, *103*, 2965 – 2983; d) S. -K. Tian, Y. Chen, J. Hang, L. Tang, P. McDaid, L. Deng, *Acc. Chem. Res.* **2004**, *37*, 621 – 631; e) E. A. Bercot, T. Rovis, *J. Am. Chem. Soc.* **2004**, *126*, 10248 – 10249.

[4] W. Wang, J. Wang, H. Li, *Angew. Chem.* **2005**, *44*, 1393 – 1395; *Angew. Chem. Int. Ed.* **2005**, *44*, 1369 – 1371.

[5] K. Ishihara, Y. Kosugi, M. Akakura, *J. Am. Chem. Soc.* **2004**, *126*, 12212 – 12213.

[6] a) M. Watanabe, A. Ikagawa, H. Wang, K. Murata, T. Ikariya, *J. Am. Chem. Soc.* **2004**, *126*, 11148 – 11149; b) H. Wang, M. Watanabe, T. Ikariya, *Tetrahedron Lett.* **2005**, *46*, 963 – 966.

[7] J. M. Mitchel, N. S. Finney, *Tetrahedron Lett.* **2000**, *41*, 8431 – 8434.

[8] See Supporting Information.

[9] Crystallographic study for compound **2**: Intensity data were collected on a Rigaku RAXIS-RAPID imaging plate diffractometer with $Cu_{K\alpha}$ radiation at a temperature of 93.2 K. The program of PROCESS-AUTO[10] was used during data collection. The structure was solved by direct methods with SIR97[11] and refined by least-squares methods with CRYSTALS.[12] **2**: crystallized from MeOH/$CHCl_3$, $C_{24}H_{22}F_6N_2O_2S$, $M_r = 516.50$, colorless block $0.30 \times 0.20 \times 0.10$ mm, monoclinic, $P2_1(4)$, $a = 11.6363(11)$, $b = 8.2929(9)$, $c = 12.4374(13)$ Å, $\beta = 96.404(6)°$, $V = 1192.7(2)$ Å^3, $Z = 2$, $\rho_{calcd} = 1.438$ g cm^{-3}, 2θmax 136.5°, measured reflections = 12702, independent reflections = 4013 ($R_{int} = 0.029$), $R1 = 0.0307$ for 3797 reflections with $I > 2\sigma(I)$, $wR2 = 0.0812$ for all reflections with $I > 2\sigma(I)$, GOF = 1.054. The absolute configuration was determined based on the Flack parameter (0.004(14)) refined using 1684 Friedel pairs. CCDC-269460 (**2**) contains the supplementary crystallographic data for this paper. These data can be obtained free of charge from the Cambridge Crystallographic Data Centre via www.ccdc.cam.ac.uk/data_request/cif.

[10] Rigaku (1998) PROCESS-AUTO: Automatic data acquisition and processing package for imaging plate diffractometer, Rigaku Corporation, Tokyo, Japan.

[11] SIR97 (1999): Crystal structure determination and refinement: A. Altomare, M. C. Burla, M. Camalli, G. L. Cascarano, C. Giacovazzo, A. Guagliardi, A. G. G. Moliterni, G. Polidori, R. Spagna, *J. Appl. Crystallogr.* **1999**, *32*, 115 – 119.

[12] D. C. Watkin, C. K. Prout, J. R. Carruthers, P. W. Betteridge, CRYSTALS, *Issure 10*, Chemical Crystallography Laboratory, Oxford, UK, **1996**.

[13] a) G. Basu, M. Kubasik, D. Anglos, B. Secor, A. Kuki, *J. Am. Chem. Soc.* **1990**, *112*, 9410 – 9411; b) Y. Nagao, S. Sano, S. Nakagawa, M. Tanaka, M. Shiro, T. Taga, *Chem. Lett.* **1992**, 915 – 918.

[14] a) E. J. Corey, R. Imwinkelried, S. Pikul, Y. B. Xiang, *J. Am. Chem. Soc.* **1989**, *111*, 5493 – 5495; b) K. Tomioka, M. Shindo, K. Koga, *J. Am. Chem. Soc.* **1989**, *111*, 8266 – 8268.

[15] The absolute stereochemistry of the chiral thiolysis products was determined by conversion into known chiral compounds; see: for compound **8**: D. Enders, K. Paradopoulos, *Tetrahedron Lett.* **1983**, *24*, 4967 – 4970; for **14**: Y. Shi, W. D. Wulff, G. P. A. Yap, A. L. Rheingold, *Chem. Commun.* **1996**, 2601 – 2602; for **15**: C.-S. Chen, Y. Fujimoto, C. J. Sih, *J. Am. Chem. Soc.* **1981**, *103*, 3580 – 3582; for **16** and **17**: R. Shintani, G. C. Fu, *Angew. Chem.* **2002**, *114*, 1099 – 1101; *Angew. Chem. Int. Ed.* **2002**, *41*, 1057 – 1059; for **18**: I. J. Jokovac, H. B. Goodbrand, K. P. Lok, J. B. Jones, *J. Am. Chem. Soc.* **1982**, *104*, 4659 – 4665.

[16] W. Oppolzer, C. Darcel, P. Rochet, S. Rosset, J. D. Brabander, *Helv. Chim. Acta* **1997**, *80*, 1319 – 1337.

[17] *Recent Progress in the Chemical Synthesis of Antibiotics* (Eds.: G. Lukacs, M. Ohno), Springer, Berlin, **1990**.

 © 2005 Wiley-VCH Verlag GmbH & Co. KGaA, Weinheim

Polynuclear Complexes

DOI: 10.1002/anie.200501327

Two Molecular Tapes Consisting of Serial or Parallel Azido-Bridged Eight-Membered Copper Rings**

Yuan-Zhu Zhang, Hai-Yan Wei, Feng Pan, Zhe-Ming Wang, Zhi-Da Chen, and Song Gao**

The construction of low-dimensional coordination polymers has received intense attention for a long time because of their structural diversity and unusual properties as well as their magneto–structural correlations.[1] Among them, some one-dimensional (1D) expanded chains with exotic topologies have been reported, such as ladders,[2] ropes,[3] and cluster-based chains.[4] They provide an intermediate step from 1D chains towards 2D networks, thus potentially helping the magnetic behavior at the border of 1D to 2D systems to be understood. As a versatile bridging ligand, the azido ion could link two or more metal ions in various modes, for example, μ-1,1 (end-on (EO)), μ-1,3 (end-to-end (EE)), μ-1,1,1, μ-1,1,3, and so forth, thus giving rise to a variety of zero- to three-dimensional polynuclear complexes.[5–9] As far as 1D chains are concerned, many unusual alternating chains with different combinations of these modes have been obtained.[7,8]

However, the synthesis of 1D chains of increasing width is still a big challenge. In our opinion, utilizing the diverse coordination geometry of the copper ion and the versatile bridging modes of the azide moiety might be key to facing the challenge. From the viewpoint of magneto–structural correlation, the azido–copper system might be one of the most complicated systems because of the various bridging modes of the azido ion and the Jahn–Teller effect of the copper ion in an

[*] Y.-Z. Zhang, H.-Y. Wei, F. Pan, Prof. Z.-M. Wang, Prof. Z.-D. Chen, Prof. S. Gao
College of Chemistry and Molecular Engineering
State Key Laboratory of Rare Earth Materials Chemistry and Applications
Peking University, Beijing 100871 (P.R. China)
Fax: (+86) 10-6275-1708
E-mail: zdchen@pku.edu.cn
gaosong@pku.edu.cn

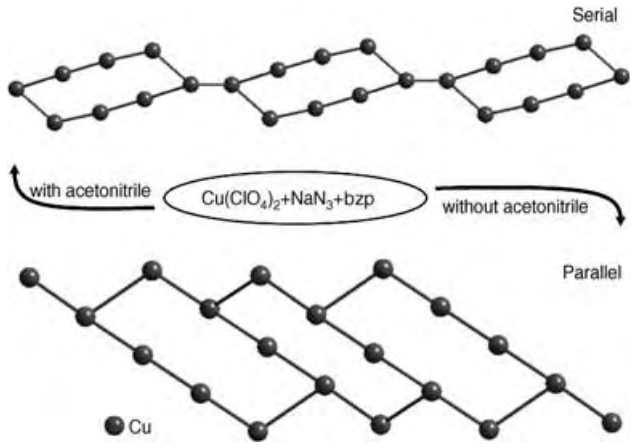
[**] This work was supported by the National Science Fund for Distinguished Young Scholars (20125104), NSFC (nos. 20221101 and 20490210), and the National Basic Research Program of China (2006CB601102).

Supporting information for this article is available on the WWW under http://www.angewandte.org or from the author.

© 2005 Wiley-VCH Verlag GmbH & Co. KGaA, Weinheim

elongated octahedral or square-pyramidal geometry. Although it has been well stated both theoretically and experimentally that the exchange is ferromagnetic (F) or antiferromagnetic (AF) depending on the angle of Cu-N-Cu for the EO mode,[10] the correlation seems to be open ended for continuous exceptions.[11–12] In addition, to obtain an isolated 1D magnetic chain, a blocking coligand with stereochemical character, as well as an effective bridging ligand, is often needed to reduce the structural dimension and decrease the intermolecular interactions.

2-Benzoylpyridyl (bzp) has been used as a terminal/convergent coligand to form a 1D azido–manganese chain with interchain Mn···Mn distances of 10 Å.[13] We employed this coligand in an azido–copper system on the basis of these considerations and obtained an exotic 1D molecular tape, $[Cu_4(N_3)_8(CH_3CN)_3(bzp)_2]_n$ (**1**), with serial-connected cyclic azido-bridged eight-membered copper rings from the reaction solution of methanol/acetonitrile. Noticing that coordinated acetonitrile molecules might prevent further expansion of the tape, we changed the experimental conditions to 100% methanol as the solvent. Fortunately, we obtained another more interesting molecular tape, $[Cu_5(N_3)_{10}(bzp)_2]_n$ (**2**), with parallel eight-membered copper rings (Scheme 1). Herein, we report the synthesis, structure,[14] and magneto–structural correlations of these copper rings.



Scheme 1. Formation of molecular tapes **1** and **2**.

The single-crystal X-ray determination revealed that **1** consists of neutral 1D azido–copper chains with serial octanuclear repeating units (Figure 1a). There are four crystallographically independent Cu^{II} ions, with each assuming an elongated octahedral geometry; eight nonequivalent azido ligands, five (N5, N8, N11, N20, and N23) which adopt the EO bridging mode and the other three (N14, N17, and N26) which adopt the μ-1,1,1 mode; and three terminal acetonitrile molecules (N2, N3, and N4). For the Cu2 center, three azido atoms (N11, N17, and N20) and one pyridine nitrogen atom (N1) from the bzp ligand are in the basal sites, whereas the oxygen atom (O1) of the bzp ligand and one μ-1,1,1-azido ion are in the apical positions (Cu2–O1: 2.442 Å, Cu2–N14: 2.400 Å). The environment around the other three Cu^{II} ions are similar, with the nonequivalent apical positions occupied by one acetonitrile molecule ($Cu–N_{CH_3CN}$: 2.38–2.43 Å) and one μ-1,1,1-azido ion ($Cu–N_{azido}$: 2.71–2.82 Å)

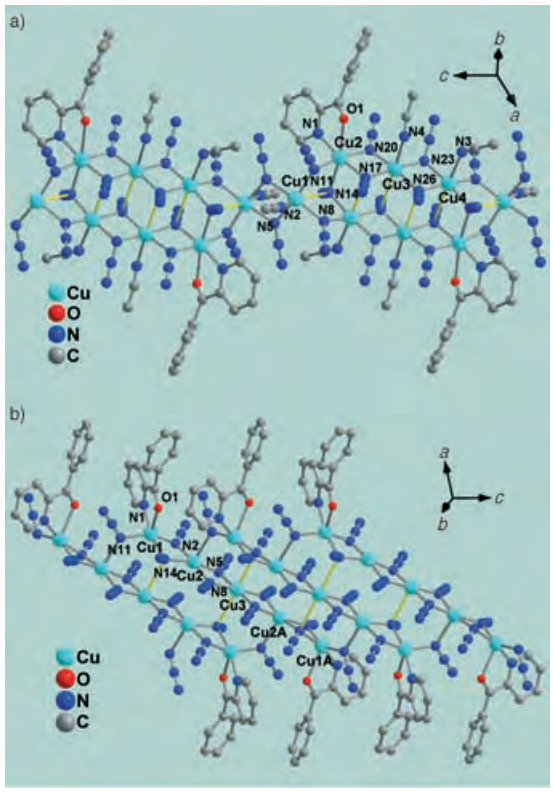


Figure 1. a) The ball and stick structure of the tape **1** with serial cyclic azido-bridged octanuclear copper clusters along the *c* axis (the yellow bonds are approximately 2.8 Å). b) The ball and stick structure of the tape **2** with the parallel linear azido-bridged pentanuclear copper units along the *c* axis (the yellow bonds are longer than 2.65 Å).

and the basal sites furnished by four azido ions ($Cu–N_{azido}$: 1.98–2.03 Å), thus the basal bonds are significantly shorter than the axial ones. Here, the distortion of the basal planes of the octahedral or square-pyramidal Cu^{II} ions could be described by a geometrical parameter τ in accord with the method of Addison et al. with $\tau = |\beta - \alpha|/60$, in which β and α are the bond angles that involve *trans* donor atoms in the basal plane.[15] All the τ values are around 0.05 for the Cu^{II} ions. The Cu-N-Cu angles vary from 82.85 to 102.74°, except for Cu1-N11-Cu2 and Cu1-N8-Cu4A which are 116.78 and 116.38°, respectively, and the dihedral angles ϕ between the basal planes of Cu1 and Cu2, Cu2 and Cu3, Cu3 and Cu4, and Cu4 and Cu1A are 68.9, 1.9, 6.9, and 72.8°, respectively. Thus, a unique centrosymmetric cyclic azido-bridged eight-membered copper ring $[Cu_8(N_3)_{14}(CH_3CN)_6(bzp)_2]^{2+}$ is formed, within which the metal ions are bridged by eight EO azido groups outside, whereas each of the three closest copper ions are bridged by one asymmetric μ-1,1,1-azido ligand inside. The adjacent rings are further linked in a serial mode to an exotic 1D chain by double EO bridges along the *c* axis. The chains of **1** are well isolated as the shortest Cu···Cu interchain distance is 8.3 Å, which is between the Cu2 and Cu2 centers ($-x+1$, $-y+1$, $-z+2$; see the Supporting Information).

The structure of **2** reveals a more interesting neutral azido–copper tape. There are three crystallographically independent Cu^{II} ions (Cu1, Cu2, and Cu3) and five non-

 © 2005 Wiley-VCH Verlag GmbH & Co. KGaA, Weinheim

equivalent azido ligands, which include three basal–basal EO azido (N2, N5, and N8) ligands, one basal–apical EO azido (N11) ligand, and one asymmetric μ-1,1,1-azido (N14) ligand (Figure 1b). Both the Cu1 and Cu2 ions are five-coordinate with distorted square-pyramidal geometry (4+1): For the Cu1 center, three azido nitrogen atoms (N11, N2, and N14) and one pyridine nitrogen atom (N1) of the bzp ligand occupy the basal sites, thus leading to significantly shorter Cu–N bond lengths (1.89–1.92 Å), and the oxygen atom of the bzp ligand occupies the apical position (Cu1–O1: 2.27 Å). For the Cu2 center, only the azido ions are involved in the coordination, with the N11A atom at the apical position (Cu2–N11A: 2.275 Å). The values of τ are 0.28 and 0.18 for the Cu1 and Cu2 centers, respectively. The Cu3 ion ($\tau = 0$) lies in the symmetric center with an elongated octahedral geometry furnished by six azido ions, and the apical sites are occupied by two μ-1,1,1-azido (N14) atoms (Cu–N: 2.683 Å, which is much longer than the basal bonds as well as the apical bonds of the square-pyramidal Cu ions). Thus, the five copper ions (Cu1, Cu2, Cu3, Cu2A, and Cu1A) are bridged by double basal–basal EO azides to form a linear unit, in which the dihedral angles ϕ are 25.4° for the Cu1 and Cu2 centers and 5.8° for the Cu2 and Cu3 centers, and the bridge angles are 107.0° (∢ Cu1-N2-Cu2), 104.5° (∢ Cu1-N14-Cu2), and 107.7° (∢ Cu2-N5/N8-Cu3). The intraunit metal distances are Cu1···Cu2: 3.05 Å and Cu2···Cu3: 3.07 Å. The parallel neighboring units are further connected to a tape along the *c* axis through two basal–apical EO azido bridges (∢ Cu1-N11-Cu2B: 118°) and two asymmetric μ-1,1,1-azido bridges with an inter-unit metal distance of Cu1···Cu2B: 3.59 Å. The tapes are well isolated, with the shortest Cu···Cu intertape distance of 8.13 Å occurring between the Cu1 and Cu2 centers ($2-x$, $y-0.5$, $0.5-z$; see the Supporting Information). It is of note that if the weak Cu3–N_{azido} bonds (the yellow bonds in Figure 1b) are omitted, the tape can also be viewed as a 1D chain that consists of parallel eight-membered copper rings (Scheme 1).

The magnetic susceptibilities of **1** and **2** (2–300 K) were measured at 1 kOe on a Quantum Design MPMS XL-5 SQUID system (Figure 2). For **1**, the $\chi_M T$ value per {Cu_4} unit increases gradually on cooling, thus suggesting an overall ferromagnetic coupling between the adjacent Cu^{II} ions, and there is an decrease in $\chi_M T$ below 4 K that may be because of an interchain AF and/or a zero-field splitting (ZFS) effect. The data above 70 K fit well with the Curie–Weiss law ($\chi_M = C/(T-\theta)$), thus giving $C = 1.79\ cm^3 mol^{-1} K$ (which corresponds to four uncoupled Cu^{II} ions with $g = 2.18$) and $\theta = 22.5$ K. No long-range ordering was observed above 1.9 K from the magnetization–temperature (*M*–*T*) curve at 20 Oe and *ac* susceptibilities versus the *T* curves (see the Supporting Information). The observed magnetization curve at 1.9 K is above the calculated Brillouin function for the sum of four isolated Cu^{II} ions ($S = 1/2$) below 50 kOe, thus confirming further the ferromagnetic coupling between the copper ions (see the Supporting Information).

For **2**, the $\chi_M T$ value of 2.2 $cm^3 mol^{-1} K$ at 300 K per {Cu_5} unit decreases gradually on lowering the temperature and reaches a plateau at 1.5 $cm^3 mol^{-1} K$ at 10–20 K (Figure 2b), which is close to the $S = 3/2$ state (it was expected that $\chi_M T =$ 1.875 $cm^3 mol^{-1} K$ at this point; however, the observed value is lower than the expected one, probably as a result of interpentanuclear AF interactions). The $\chi_M T$ value then decreases sharply, possibly because of the interpentanuclear interactions, and/or interchain AF interactions, and/or the ZFS effect as the field-saturation effect has been excluded by the similar decrease found in the $\chi_M T$–*T* curve at the fairly low field of 20 Oe (see the Supporting Information). Fitting the data above 100 K with the Curie–Weiss law gives $C = 2.26\ cm^3 mol^{-1} K$ (which corresponds to five independent spin-only Cu^{II} ions with $g = 2.19$) and a negative θ value of −12 K, thus indicating a net AF coupling among the metal ions. The magnetization value of $2.6 N\beta$ per {Cu_5} unit at 50 kOe and 1.9 K, which is close to and slightly lower than the expected value of $2.9 N\beta$ from the Brillouin function for a $S = 3/2$ system with $g = 2$, also implies a ferrimagnetic-like state in which $S = 3/2$, thus further suggesting the coexistence of antiferromagnetic and ferromagnetic couplings within the pentanuclear subunit. The AF interaction between the subunits was estimated to be −2.4 K by fitting magnetization–magnetic field (*M*–*H*) data by using a modified Brillouin function (see the Supporting Information).

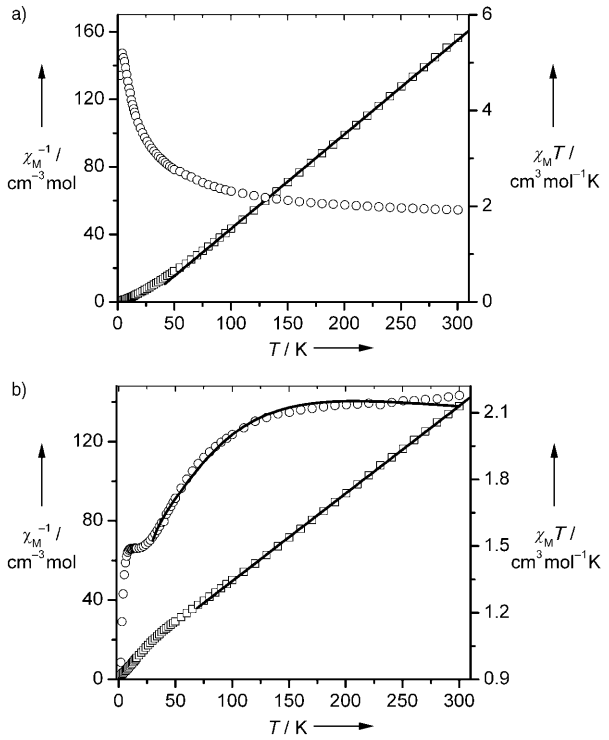


Figure 2. $\chi_M T$ and $1/\chi_M$ versus *T* in an applied field of 1 kOe for a) **1** and b) **2**. The lines are the best fits to the Curie–Weiss law and are an approximate uniform-chain model.

The magnetic behaviors of **1** and **2** can be rationalized on the basis of their structures. The EO bridges in the azido–copper system could be further divided into two types: 1) basal–basal bridges, in which the azido bridges are involved in two basal planes of Cu^{II} ions; 2) asymmetric basal–apical bridges, in which the azido group is located at the apical position of one of the Cu^{II} ions and the basal position of the other. It has been well documented that the exchange is F or

 © 2005 Wiley-VCH Verlag GmbH & Co. KGaA, Weinheim

AF depending on the Cu-N-Cu angle for the basal–basal bridges (the calculated critical angle is 104° and experimentally derived angle is 108°)[10] and that the interaction through the basal–apical bridges is either negligible or weakly F/AF depending on the distortion of the basal planes of the Cu^{II} ions.[12] Taking into account the structure of **1**, interaction through the basal–apical bridges (between the $\{Cu_4\}$ units) is negligible because of very small distortions ($\tau \approx 0.05$). Figure 3 shows the resulting magnetic chain of **1,** in which

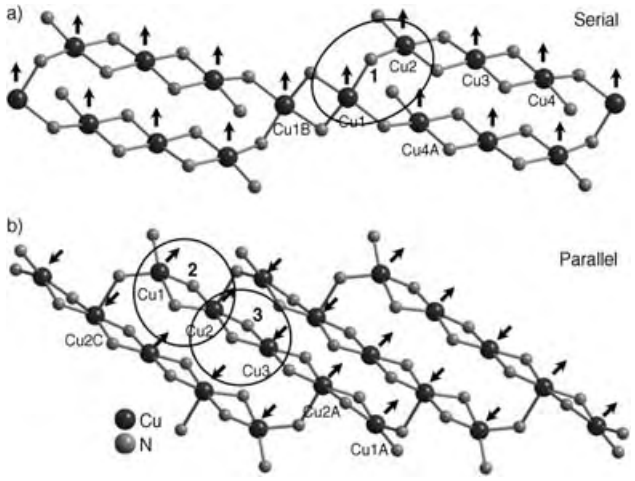


Figure 3. The magnetic chains of a) **1** and b) **2**.

the bridge angles are in the range 98.8–102.7°, except for the ∢ Cu1-N11-Cu2 and ∢ Cu1-N8-Cu4A angles of 116.5° which are anticipated to transmit strong AF coupling. Surprisingly, our magnetic measurements suggest that all the copper ions are F. To understand the unusual F interaction through the Cu1-N11-Cu2 bridges, preliminary theoretical studies were performed for the Cu1–Cu2 "dimer" model **1** formed from **1** (see the Supporting Information) by using the broken-symmetry approach under a DFT framework (DFT-BS).[16,17] The calculated results show that the "local magnetic orbitals" are mainly located at paramagnetic centers (Cu1 and Cu2); describe the distribution of the active spin electrons at each local magnetic center, that is to say, are beside the Cu1 and Cu2 centers, which also contain possible components of bridging and/or terminal ligands; and show that the $d_{x^2-y^2}$ orbitals occupied by nonpaired electrons in the Cu1 and Cu2 ions are located at the basal planes of the Cu1 and Cu2 centers. From the point of view of the molecular orbital theory, the two local magnetic orbitals on the Cu1 and Cu2 ions further constitute the singly occupied molecular orbitals in the triplet state (Figure 4). It is worth noting that the Cu1-N11-Cu2 bridge is different from other usual basal–basal EO bridges because of a large dihedral angle of 68.9° between the basal planes of the Cu1 and Cu2 centers, thus leading no doubt to a small overlap integral (calculated value of 0.0263) between the two local magnetic orbitals on the Cu1 and Cu2 centers. On the basis of the relationship[18] between the exchange constant J and the overlap integral S_{ab} between the local magnetic orbitals of a and b, $J = J_F + J_{AF} = 2K - US_{ab}^2$, in which K is the ferromagnetic contribution and U is the

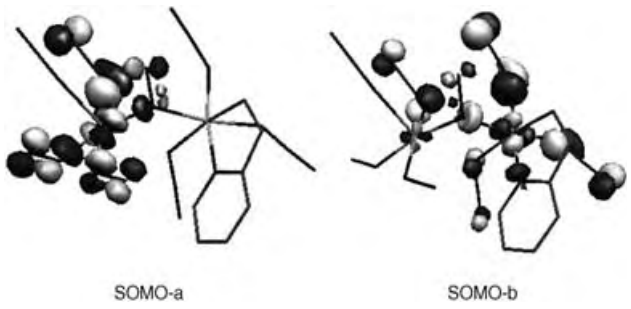


Figure 4. Singly occupied molecular orbitals of model **1** in the triplet state.

charge-transfer energy difference between the covalent and the ionic configurations, the small overlap integral should be responsible for the ferromagnetic interaction between the Cu1 and Cu2 centers. Additionally, we obtained the calculated exchange constant $J = 28.6\ cm^{-1}$ ($H = -2JS_1S_2$), which accounts just for the experimentally ferromagnetic interaction, by using the DFT-BS method.

Figure 3b shows the structure of the magnetic chain of **2**, which is based on the following rational considerations: 1) interactions through the basal–apical bridges that occupy the apical positions of the Cu3 ions (the yellow bonds in Figure 1b) can be safely omitted; 2) the coupling through the Cu1-N11-Cu2C bridges between the adjacent pentanuclear units should be considered as J_1 because the distortion of the basal plane of the Cu1 and Cu2 ions cannot be considered as being small ($\tau \approx 0.18$–0.28); 3) J_2 and J_3 are used to calculate the magnetic exchange interactions for Cu1···Cu2 and Cu2···Cu3, respectively. On the basis of an approximate model,[19] **2** can be treated as a uniform chain with linear pentanuclear $\{Cu_5\}$ as a subunit, for which $H = -2J_2(S_{Cu1}S_{Cu2} + S_{Cu1A}S_{Cu2A}) - 2J_3(S_{Cu2}S_{Cu3} + S_{Cu3}S_{Cu2A})$ (for $\{Cu_5\}$); $H = -2J_1\Sigma S_{p,i}S_{p,i+1}$ (S_p for $\{Cu_5\}$ as a classical system). Fixing $g = 2.19$, the best fitting of the data at 25–300 K gives $J_1 = -1.5$, $J_2 = 112$, and $J_3 = -29\ cm^{-1}$, with $R = 8 \times 10^{-5}$ ($R = \Sigma[(\chi_M T)_{obsd} - (\chi_M T)_{calcd}]^2/\Sigma(\chi_M T)_{obs}^2$). The negative J_1 value of $-1.5\ cm^{-1}$, which indicates AF coupling between the pentanuclear units, is consistent with the estimated value of -2.4 K from the M–H fitting (see the Supporting Information). The theoretical calculations of the "dimer" models of Cu1–Cu2 and Cu2–Cu3 in **2** are also performed by using the DFT-BS approach (see the Supporting Information). The calculated results of $J_2 = 113$ and $J_3 = -22\ cm^{-1}$ reproduced the experimentally derived F and AF characteristics well for Cu1–Cu2 and Cu2–Cu3, respectively. Further inspection of the calculated overlap integrals between the local magnetic orbitals $d_{x^2-y^2}$ on the Cu^{II} ions shows that the small overlap integral (0.0139) between the Cu1 and Cu2 centers and the larger overlap integral (0.136) between the Cu2 and Cu3 centers are responsible for these magnetic coupling characteristics. The large difference might come from three possibilities: 1) using **1**, which has a large ϕ value, as a ferromagnetic reference, the ϕ value of 25.4° between the Cu1 and Cu2 centers in **2**, which cannot be considered as small, might also contribute to the ferromagnetic coupling; 2) the large distortion ($\tau = 0.28$ and 0.18 for Cu1 and Cu2, respectively) also could cause a small overlap between the

 © 2005 Wiley-VCH Verlag GmbH & Co. KGaA, Weinheim

local magnetic orbitals on the Cu1 and Cu2 centers; 3) as the magnetic coupling J often has a strong dependence on the Cu-N-Cu angle θ and as $2J = 4440–41.94\ \theta(cm^{-1})$,[10d] it is evident that the small angles of Cu1-N-Cu2 (104.5 and 107°) would transfer a ferromagnetic interaction more readily than Cu2-N-Cu3 (107.7 and 107.7°). However, it is unclear which is the dominant reason at the present stage.

In summary, we have obtained two exotic 1D molecular tapes with serial and parallel cyclic azido-bridged eight-membered copper rings $[Cu_4(N_3)_8(CH_3CN)_3(bzp)_2]_n$ (**1**) and $[Cu_5(N_3)_{10}(bzp)_2]_n$ (**2**) in solution with methanol, either with or without the addition of acetonitrile. It is of note that the EO bridge in **1**, in which the Cu-N-Cu angle is 116° and $\phi =$ 68.9°, is observed to transmit ferromagnetic interactions and that the central copper center of the linear pentanulear $\{Cu_5\}$ unit in **2** is antiferromagnetically coupled with its neighboring Cu ions and has a ground state S of 3/2. The magneto–structural correlation for a basal–basal EO azido bridge in the azido–copper system is not only dependent on the Cu-N-Cu angle; therefore, more factors should be taken into account, such as the dihedral angle ϕ between the basal planes of the two bridged copper ions as well as the distortion from square-pyramidal to trigonal-bipyramidal geometry for the Cu^{II} ion.

Experimental Section

1: A solution of $Cu(ClO_4)_2{\cdot}6H_2O$ (185 mg, 0.5 mmol) in acetonitrile (15 mL) was mixed with a solution of bzp (92 mg, 0.25 mmol) and NaN_3 (65 mg, 1 mmol) in methanol (15 mL). The resulting solution was kept undisturbed at room temperature. Brown platelike single crystals of **1** were obtained after several days. Yield: 58 mg, 52%. Elemental analysis (%) calcd for $C_{18}H_{18}Cu_4N_{28}O$: C 24.11, H 2.02, N 43.74; found: C 23.73, H 2.14, N 43.14; IR: $\tilde{\nu} = 2046$, 2080, and 2089 (vs) for the azide group and 2262 and 2295 cm^{-1}(w) for CH_3CN.

2: A solution of $Cu(ClO_4)_2{\cdot}6H_2O$ (185 mg, 0.5 mmol) in methanol (15 mL) was mixed with a solution of bzp (92 mg, 0.5 mmol) and NaN_3 (45 mg, 0.7 mmol) in methanol (15 mL). The resulting solution was left at room temperature. Green blocklike single crystals were isolated and brown striplike single crystals of **2** were obtained after 2 weeks. Yield: 18 mg, 24%. Elemental analysis (%) calcd for $C_{24}H_{18}Cu_5N_{32}O_2$: C 26.10, H 1.64, N 40.59; found: C 26.54, H 1.91, N 40.15. IR $\tilde{\nu} = 2052$, 2076, 2095, and 2119 cm^{-1} (v s) for the azide group.

All theoretical calculations were performed by the Amsterdam Density Functional (ADF) program, version 2004.01.[16] The VWN local density approximation,[20] and Operdew nonlocal density corrections[21] are used. The calculations on the magnetic-exchange constant J are based on the broken-symmetry approach developed by Noodleman.[17] The details of the method used for the calculation are described elsewhere.[22] The geometry of the dimer models **1**–**3** was adapted according to the experimentally crystal structure data, in which the bzp ligand was simplified (see the Supporting Information).

Received: April 16, 2005
Published online: August 12, 2005

Keywords: azides · coordination modes · copper · inorganic polymers · magnetism · polynuclear complexes

[1] a) O. Kahn, *Molecular Magnetism*, VCH, New York, **1993**; b) J. S. Miller, M. Drillon, *Magnetism: Molecules to Materials I*, Wiley-VCH, Weinheim, **2002**; c) L. K. Thompson, *Coord. Chem. Rev.* **2002**, *233–234*, 193–206; d) L. M. C. Beltran, J. R. Long, *Acc. Chem. Res.* **2005**, *38*, 325–334.

[2] a) Y. Akhriff, J. Server-Carrió, A. Sancho, J. García-Lozano, E. Escrivá, J. V. Folgado, L. Soto, *Inorg. Chem.* **2000**, *39*, 1174–1185; b) B. W. Sun, S. Gao, Z. M. Wang, *Chem. Lett.* **2001**, 2–3; c) R. Lescouëzec, J. Vaissermann, L. M. Toma, R. Carrasco, F. Lloret, M. Julve, *Inorg. Chem.* **2004**, *43*, 2234–2236; d) Y. Z. Zhang, S. Gao, Z. M. Wang, G. Su, H. L. Sun, F. Pan, *Inorg. Chem.* **2005**, *44*, 4534–4545.

[3] a) M. Ohba, N. Maruono, H. Ōkawa, T. Enoki, J. M. Latour, *J. Am. Chem. Soc.* **1994**, *116*, 11566–11567; b) M. Ohba, N. Fukita, H. Ōkawa, *J. Chem. Soc. Dalton Trans.* **1997**, 1733–1737; c) Y. S. You, D. Kim, Y. Do, S. J. Oh, C. S. Hong, *Inorg. Chem.* **2004**, *43*, 6899–6901.

[4] a) J. R. Galán-Mascarós, C. Giménez-Saiz, S. Triki, C. J. Gómez-García, E. Coronado, L. Ouahab, *Angew. Chem.* **1995**, *107*, 1601–1603; *Angew. Chem. Int. Ed. Engl.* **1995**, *34*, 1460–1462; b) D. F. Sun, R. Cao, Y. Q. Sun, W. H. Bi, D. Q. Yuan, Q. Shi, X. Li, *Chem. Commun.* **2003**, 1528–1529; c) T. S. Lobana, R. Sharma, R. Sharma, S. Mehra, A. Castineiras, P. Turner, *Inorg. Chem.* **2005**, *44*, 1914–1921.

[5] a) J. Ribas, A. Escuer, M. Monfort, R. Vicente, R. Corte's, L. Lezama, T. Rojo, *Coord. Chem. Rev.* **1999**, *193–195*, 1027–1068, and references therein.

[6] a) Z. E. Serna, L. Lezama, M. K. Urtiaga, M. I. Arriortua, M. G. B. Barandika, R. Cortés, T. Rojo, *Angew. Chem.* **2000**, *112*, 352–354; *Angew. Chem. Int. Ed.* **2000**, *39*, 344–346; b) G. S. Papaefstathiou, S. P. Perlepes, A. Escuer, R. Vicente, M. Font-Bardia, X. Solans, *Angew. Chem.* **2001**, *113*, 908–910; *Angew. Chem. Int. Ed.* **2001**, *40*, 884–886; c) Y. F. Song, C. Massera, O. Roubeau, P. Gamez, A. M. M. Lanfredi, J. Reedijk, *Inorg. Chem.* **2004**, *43*, 6842–6847.

[7] a) G. Viau, M. G. Lombardi, G. D. Munno, M. Julve, F. Lloret, J. Faus, A. Caneschi, J. M. Clemente-Juan, *Chem. Commun.* **1997**, 1195–1196; b) A. Escuer, R. Vicente, F. A. Mautner, M. A. S. Goher, *Inorg. Chem.* **1997**, *36*, 1233–1236; c) L. K. Thompson, S. S. Tandon, F. Lloret, J. Cano, M. Julve, *Inorg. Chem.* **1997**, *36*, 3301–3306; d) F. A. Mautner, S. Hanna, R. Cortés, L. Lezama, M. G. Barandika, T. Rojo, *Inorg. Chem.* **1998**, *37*, 4647–4652.

[8] a) A. Escuer, R. Vicente, M. S. El Fallah, M. A. S. Goher, F. A. Mautner, *Inorg. Chem.* **1998**, *37*, 4466–4469; b) M. A. S. Goher, J. Cano, Y. Journaux, M. A. M. Abu-Youssef, F. A. Mautner, A. Escuer, R. Vicente, *Chem. Eur. J.* **2000**, *6*, 778–784; c) A. Escuer, M. A. S. Goher, F. A. Mautner, R. Vicente, *Inorg. Chem.* **2000**, *39*, 2107–2112; d) M. A. M. Abu-Youssef, A. Escuer, M. A. S. Goher, F. A. Mautner, G. J. Reiß, R. Vicente, *Angew. Chem.* **2000**, *112*, 1681–1683; *Angew. Chem. Int. Ed.* **2000**, *39*, 1624–1626; e) L. Zhang, L. F. Tang, Z. H. Wang, M. Du, M. Julve, F. Lloret, J. T. Wang, *Inorg. Chem.* **2000**, *39*, 3619–3622; f) E. Q. Gao, S. Q. Bai, C. F. Wang, Y. F. Yue, C. H. Yan, *Inorg. Chem.* **2003**, *42*, 8456–8464.

[9] a) F. A. Mautner, R. Cortes, L. Lezama, T. Rojo, *Angew. Chem.* **1996**, *108*, 96; *Angew. Chem. Int. Ed. Engl.* **1996**, *35*, 78; b) M. Monfort, I. Resino, J. Ribas, H. Stoeckli-Evans, *Angew. Chem.* **2000**, *112*, 197–199; *Angew. Chem. Int. Ed.* **2000**, *39*, 191–193; c) Z. Shen, J. L. Zuo, S. Gao, Y. Song, C. M. Che, H. K. Fu, X. Z. You, *Angew. Chem.* **2000**, *112*, 3779–3781; *Angew. Chem. Int. Ed.* **2000**, *39*, 3633–3635; d) M. A. S. Goher, F. A. Mautner, M. A. M. Abu-Youssef, A. K. Hafez, A. M. A. Badra, *J. Chem. Soc. Dalton Trans.* **2002**, 3309–3312; e) A. Escuer, F. A. Mautner, M. A. S. Goher, M. A. M. Abu-Youssef, R. Vicente, *Chem. Commun.* **2005**, 605–606; f) Y. Z. Zhang, S. Gao, H. L. Sun, G. Su, Z. M. Wang, S. W. Zhang, *Chem. Commun.* **2004**, 1906–1907.

[10] a) J. Comarmond, P. Plumeré, J. M. Lehn, Y. Agnus, R. Weiss, O. Kahn, I. Morgenstern-Badarau, *J. Am. Chem. Soc.* **1982**, *104*,

 © 2005 Wiley-VCH Verlag GmbH & Co. KGaA, Weinheim

6330 – 6340; b) S. Sikorav, I. Bkouche-Waksman, O. Kahn, *Inorg. Chem.* **1984**, *23*, 490 – 495; c) S. S. Tandon, L. K. Thompson, M. E. Manuel, J. N. Bridson, *Inorg. Chem.* **1994**, *33*, 5555 – 5570; d) L. K. Thompson, S. S. Tandon, M. E. Manuel, *Inorg. Chem.* **1995**, *34*, 2356 – 2366; e) M. A. Aebersold, B. Gillon, O. Plantevin, L. Pardi, O. Kahn, P. Bergerat, I. Seggern, F. Tuczek, L. Öhrström, A. Grand, E. Lelièvre-Berna, *J. Am. Chem. Soc.* **1998**, *120*, 5238 – 5245; f) E. Ruiz, J. Cano, S. Alvarez, P. Alemany, *J. Am. Chem. Soc.* **1998**, *120*, 11122 – 11129.

[11] a) P. S. Mukherjee, T. K. Maji, G. Mostafa, T. Mallah, N. R. Chaudhuri, *Inorg. Chem.* **2000**, *39*, 5147 – 5150; b) S. Koner, S. Saha, K. I. Okamoto, J. P. Tuchagues, *Inorg. Chem.* **2003**, *42*, 4668 – 4672; c) S. Koner, S. Saha, T. Mallah, K. I. Okamoto, *Inorg. Chem.* **2004**, *43*, 840 – 842.

[12] a) T. R. Felthouse, D. N. Hendrickson, *Inorg. Chem.* **1978**, *17*, 444 – 456; b) P. Manikandan, R. Muthukumaran, K. R. Justin - Thomas, B. Varghese, G. V. R. Chandramouli, P. T. Manoharan, *Inorg. Chem.* **2001**, *40*, 2378 – 2389; c) E. Q. Gao, Y. F. Yue, S. Q. Bai, Z. He, C. H. Yan, *Cryst. Growth Des.* **2004**, *4*, 513 – 516; d) M. S. Ray, A. Ghosh, S. Chaudhuri, M. G. B. Drew, J. Ribas, *Eur. J. Inorg. Chem.* **2004**, 3110 – 3117.

[13] M. A. M. Abu-Youssef, A. Escuer, D. Gatteschi, M. A. S. Goher, F. A. Mautner, R. Vicente, *Inorg. Chem.* **1999**, *38*, 5716 – 5723.

[14] Crystal data for **1**: $C_{18}H_{18}Cu_4N_{28}O$, $M_r = 896.76$, monoclinic, space group $P2_1/c$, $a = 11.8532(2)$, $b = 21.4355(4)$, $c = 14.2472(2)$ Å, $\beta = 113.7515(11)°$, $V = 3313.31(10)$ Å^3, $Z = 4$, ρcalcd $= 1.798$ g cm^{-3}, $\lambda = 0.71073$ Å, $\mu(Mo_{K\alpha}) = 2.598$ mm^{-1}, $F(000) = 1784$, GOF $= 1.015$. A total of 49774 reflections were collected and 7610 are unique ($R_{int} = 0.0759$). $R1$ and $wR2$ are 0.0381 and 0.0831, respectively, for 462 parameters and 7610 reflections ($I > 2\sigma(I)$). **2**: $C_{24}H_{18}Cu_5N_{32}O_2$, $M_r = 1104.40$, monoclinic, space group $C2/c$, $a = 22.9413(6)$, $b = 14.4026(4)$, $c = 10.7951(3)$ Å, $\beta = 97.2433(12)°$, $V = 3538.39(16)$ Å^3, $Z = 4$, $\rho_{calcd} = 2.073$ g cm^{-3}, $\lambda = 0.71073$ Å, $\mu(Mo_{K\alpha}) = 3.039$ mm^{-1}, $F(000) = 2188$, GOF $= 0.861$. A total of 36150 reflections were collected and 4062 are unique ($R_{int} = 0.1019$). *R1* and $wR2$ are 0.0336 and 0.0724, respectively, for 286 parameters and 4062 reflections ($I > 2\sigma(I)$). The data were collected on an Enraf-Nonius Kappa CCD with $Mo_{K\alpha}$ radiation ($\lambda = 0.71073$ Å) at 293 K. The structures were solved by direct methods and refined with full-matrix least-squares on F^2 by using the SHELX-97 program. All non-hydrogen atoms were refined anisotropically. CCDC-268022 (**1**) and -268023 (**2**) contain the supplementary crystallographic data for this paper. These data can be obtained free of charge from the Cambridge Crystallographic Data Centre via www.ccdc.cam.ac.uk/data_request/cif.

[15] W. Addison, T. N. Rao, J. Reedijk, J. van Rijn, G. C. Verschoor, *J. Chem. Soc. Dalton Trans.* **1984**, 1349 – 1356.

[16] Amsterdam density functional (ADF), version 2004.01; Scientific Computing and Modelling, Theoretical Chemistry, Vrije Universiteit, Amsterdam, **2004**.

[17] a) L. Noodleman, *J. Chem. Phys.* **1981**, *74*, 5737 – 5743; b) J. Li, L. Noodleman, D. A. Case in *Inorganic Electronic Structure and Spectroscopy, Vol. 1* (Eds.: E. I. Solomon, A. B. P. Lever), Wiley, New York, **1999**, pp. 661 – 724; c) C. Adamo, V. Barone, A. Bencini, F. Totti, I. Ciofini, *Inorg. Chem.* **1999**, *38*, 1996 – 2004; d) E. Ruiz, P. Alemany, S. Alvarez, J. Cano, *J. Am. Chem. Soc.* **1997**, *119*, 1297 – 1303; e) E. Ruiz, P. Alemany, S. Alvarez, S. J. Cano, *Inorg. Chem.* **1997**, *36*, 3683 – 3688.

[18] a) O. Kahn, B. Briat, *J. Chem. Soc. Faraday Trans II* **1976**, *72*, 268 – 275; b) L. Noodleman, *J. Chem. Phys.* **1981**, *74*, 5737 – 5743; c) J. M. Mouesca, *J. Chem. Phys.* **2000**, *113*, 10505 – 10511.

[19] a) A. Caneschi, D. Gatteschi, M. C. Melandri, P. Rey, R. Sessoli, *Inorg. Chem.* **1990**, *29*, 4228 – 4234; b) B. Chiari, A. Cinti, O. Piovesana, P. F. Zanazzi, *Inorg. Chem.* **1995**, *34*, 2652 – 2657; c) G. Wrzeszcz, L. Dobrzańska, A. Wojtczak, A. Grodzicki, *J. Chem. Soc. Dalton Trans.* **2002**, 2862 – 2867; d) H. Z. Kou, B. C. Zhou, S. Gao, D. Z. Liao, R. J. Wang, *Inorg. Chem.* **2003**, *42*, 5604 – 5611.

[20] S. H. Vosko, L. Wilk, M. Nusair, *Can. J. Phys.* **1980**, *58*, 1200 – 1211.

[21] a) J. P. Perdew, Y. Wang, *Phys. Rev. B* **1986**, *33*, 8822 – 8824; b) N. C. Handy, A. J. Cohen, *Mol. Phys.* **2001**, *99*, 403 – 412.

[22] a) Q. H. Ren, Z. D. Chen, J. Ren, H. Y. Wei, W. T. Fen, L. Zhang, *J. Phys. Chem. A* **2002**, *106*, 6161 – 6166; b) H. Y. Wei, Z. C. Hu, Z. D. Chen, *J. Mol. Struct.* **2005**, *733*, 145 – 151.

 © 2005 Wiley-VCH Verlag GmbH & Co. KGaA, Weinheim

Natural Products Synthesis

DOI: 10.1002/anie.200502011

The Cytoskyrin Cascade: A Facile Entry into Cytoskyrin A, Deoxyrubroskyrin, Rugulin, Skyrin, and Flavoskyrin Model Systems**

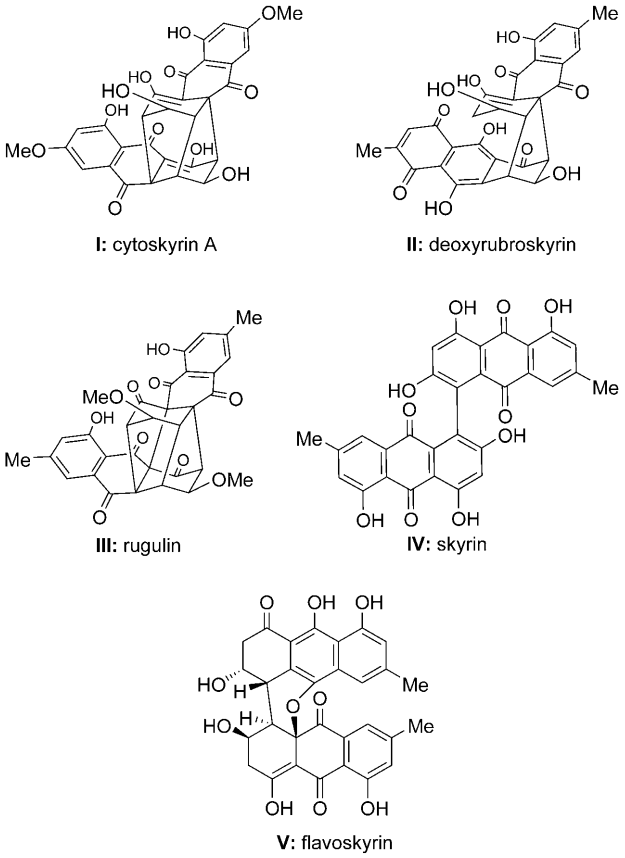
K. C. Nicolaou, Charles D. Papageorgiou, Jared L. Piper, and Raj K. Chadha*

The collection of naturally occurring compounds shown in Scheme 1 (**I**: cytoskyrin A,[1] **II**: deoxyrubroskyrin,[2a] **III**: rugulin,[3] **IV**: skyrin,[2b,4] and **V**: flavoskyrin[2a]) represents a growing class of natural products often referred to as bisanthraquinones. Notable among them are cytoskyrin A,[1] the newest member of the class whose striking biological activity includes potency down to 12.5 ng mL^{-1} in the biochemical induction assay (BIA), and rugulin, whose structural motif exhibits the highest strain of them all. Isolated from small-scale cultures of the endophytic fungus CR200 (*Cytospora* sp.), which were collected from a branch of a *Conocarpus erecta* tree in the Guanacaste Conservation area of Costa Rica, cytoskyrin A (**I**) presents a challenging synthetic target by virtue of its cagelike structural motif, as do its siblings whose more (**III**) or less (**II** and **V**) enclosed cages are defined by the number of bonds linking their two

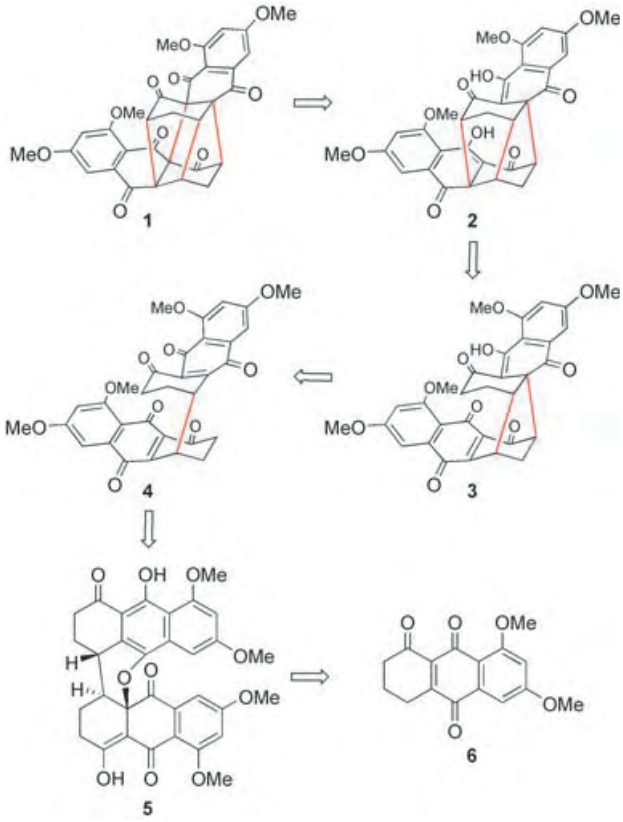
[*] Prof. Dr. K. C. Nicolaou, Dr. C. D. Papageorgiou, Dr. J. L. Piper, Dr. R. K. Chadha
Department of Chemistry and
The Skaggs Institute for Chemical Biology
The Scripps Research Institute
10550 North Torrey Pines Road, La Jolla, CA 92037 (USA)
Fax: (+1) 858-784-2469
E-mail: kcn@scripps.edu
and
Department of Chemistry and Biochemistry
University of California, San Diego
9500 Gilman Drive, La Jolla, CA 92093 (USA)

[**] We thank Prof. Albert Eschenmoser for stimulating discussions and Dr. D. H. Huang and Dr. G. Siuzdak for NMR spectroscopic and mass spectrometric assistance, respectively. Financial support for this work was provided by grants from the National Institutes of Health (USA) and the Skaggs Institute for Chemical Biology, and a postdoctoral fellowship from the George E. Hewitt Foundation (to J.L.P.).

 InterScience © 2005 Wiley-VCH Verlag GmbH & Co. KGaA, Weinheim



Scheme 1. Naturally occurring modified bisanthraquinones.



Scheme 2. Model systems (**1**–**5**) of the bisanthraquinone natural products rugulin, cytoskyrin, deoxyrubroskyrin, skyrin, and their potential precursor anthraquinone monomer.

anthraquinone monomeric units. Herein we report the construction of model systems for all five natural products **I**–**V**, namely compounds **1**–**5**, respectively, from anthraquinone **6** (Scheme 2) through a stepwise or a cascade sequence of reactions, herein coined the "cytoskyrin cascade".

The present investigations were inspired by the novel molecular architectures of the targeted natural products (Scheme 1) and the work of Shibata and co-workers.[2] To scout possible routes to these intriguing structures, the model systems **1**–**5** (Scheme 2) were selected as initial targets. The complexity of these molecules decreases as we move from **1** (whose anthraquinone units are held together by four carbon–carbon bonds) to **4** (which is cojoined by only one single bond). The origins of **4** can be traced retrosynthetically to **6** through a dimerization process that may or may not proceed via dimer **5**, as shown below.[5] Before we reveal our pathway to these model systems, however, a further comment concerning the cagelike core structure of **1**[6] is in order. This novel core structure presented by the parent $C_{12}H_{16}$ hydrocarbon **VI** (Figure 1), named herein "skyrane", is walled by two slightly distorted six-membered rings (forming the top and bottom of a tilted hexagonal capsule) and four uniformly twisted five-membered rings, leading to a considerably strained architecture. As the bonds are removed one by one from this aesthetically appealing capsule, the strain associated with each daughter molecule is expected to decrease. In terms of a synthetic barrier, however, this trend is counterbalanced

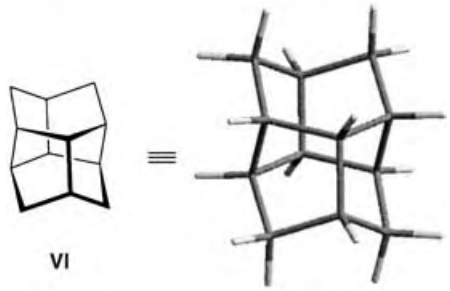
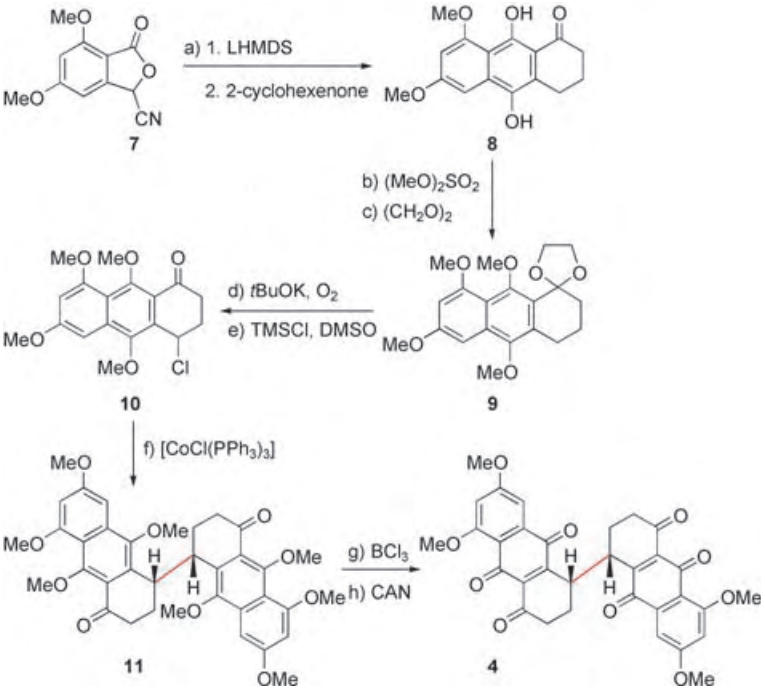


Figure 1. Parent $C_{12}H_{16}$ hydrocarbon, "skyrane".

by entropy: as the cage is being built, proximity should favor the next bond formation.

Scheme 3 summarizes the synthesis of the first model system, bisanthraquinone **4**, through a sequence that features a Hauser annulation[7] to construct the requisite tricyclic system and a radical dimerization to provide the required hexacyclic compound. Thus, treatment of nitrile **7** with LHMDS in THF at −78 °C, followed by addition of 2-cyclohexenone (−78→25 °C) gave crude anthradihydroquinone **8**, which was directly subjected to methylation and dioxolane formation to afford protected compound **9** in 58 % overall yield for the three steps. A subsequent benzylic oxygenation/chlorination sequence then converted **9** into **10** in 57 % overall yield. The anticipated dimerization of **10** was

 © 2005 Wiley-VCH Verlag GmbH & Co. KGaA, Weinheim



Scheme 3. a) **7** (1.1 equiv), THF, LHMDS (1.5 equiv), −78 °C; then 2-cyclohexenone (1.0 equiv) −78→25 °C, 4 h; b) $(MeO)_2SO_2$ (5.0 equiv), K_2CO_3 (5.0 equiv), acetone, reflux, 12 h; c) ethylene glycol (2.0 equiv), benzene, PPTS (0.2 equiv), reflux, 24 h, 58% over three steps; d) *t*BuOK (6.0 equiv), O_2, DMSO, 2 h; e) TMSCl (2.0 equiv), DMSO, 10 min, 57% over two steps; f) $[CoCl(PPh_3)_3]$ (1.2 equiv), benzene, 25 °C, 3 h; g) BCl_3 (2.2 equiv), CH_2Cl_2, −78→25 °C, 12 h; h) CAN (4.0 equiv), CH_3CN/H_2O 1:1, 10 min, 50% over two steps. CAN = cerium ammonium nitrate; DMSO = dimethyl sulfoxide; LHMDS = lithium hexamethyldisilazide; PPTS = pyridinium *p*-toluenesulfonate; TMS = trimethylsilyl.

performed by exposure to $[CoCl(PPh_3)_3]$[8] in benzene at 25 °C, leading, through radical species, to the desired *dl* dimer (**11**) as the major product (55% yield) accompanied by its *meso* isomer (25%). The two isomers were separated by silica-gel flash chromatography and unambiguously identified through X-ray crystallographic analysis of a later intermediate (see below). The two methyl groups residing on the oxygen atoms nearest to the carbonyl moieties were then selectively cleaved from the major isomer **11** by exposure to BCl_3 in CH_2Cl_2 at −78 °C to furnish the corresponding diphenolic compound, whose oxidation with CAN resulted in the formation of the targeted *dl* bisanthraquinone **4** (50% overall yield for the two steps). Compound **4** crystallized in suitable form for X-ray crystallographic analysis (see ORTEP drawing,[9] Figure 2), which confirmed its stereochemical identity and that of its progenitor, compound **11**.

A second pathway to the bisanthraquinone **4** was devised from monoquinone **6**, obtained in quantitative yield by oxidation of hydroquinone **8** with CAN. Thus, exposure of **6** to catalytic amounts of CSA in CH_2Cl_2 at 25 °C for 1 h resulted in the formation of the flavoskyrin model system **5** (94% yield) through dimerization of the enol form **12** of the starting material (Scheme 4). The same transformation (**6**→**5**) could be brought about by a catalytic amount of a mild base (e.g. iPr_2NEt) in 90% yield. This highly efficient dimerization is presumed to proceed either through a Diels–Alder-type[2e,f]

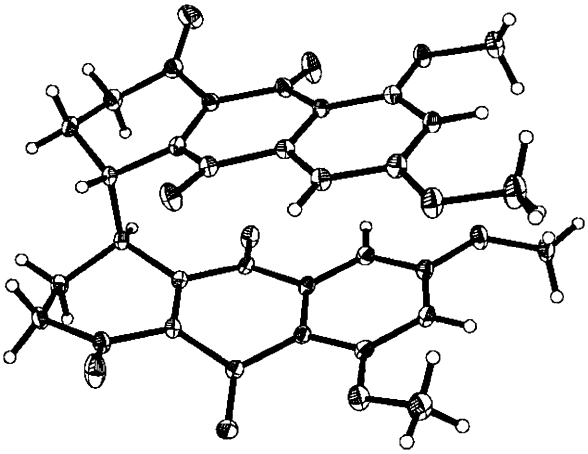
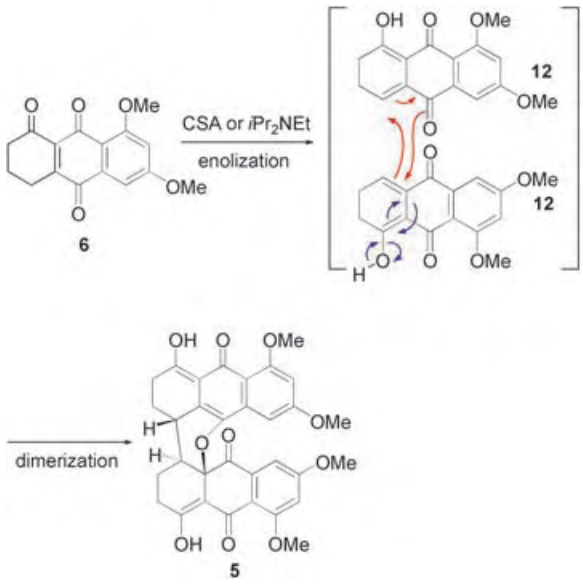


Figure 2. ORTEP drawing of structure **4** (drawn at the 30% probability level).

reaction, or through a double Michael reaction, as shown in Scheme 4. The structure of dimer **5** was confirmed by X-ray crystallographic analysis (see ORTEP drawing,[9] Figure 3). Oxidation of **5** with MnO_2 (presumably through the mechanism shown in Scheme 5, structure **VII**) then furnished the desired *dl* bisanthraquinone **4** in 83% yield (Scheme 6). Remarkably, bisanthraquinone **4** was converted into the deoxyrubroskyrin model system **3** in 65% yield simply by exposure to Et_3N (2.0 equiv) in CH_2Cl_2 at 25 °C for 1 h.[2a,e,f] Even more impressive was the conversion of **3** into the cytoskyrin model structure **2** (95% yield), a process that required longer exposure to Et_3N (5.0 equiv) and slightly higher temperature (16 h, 45 °C). This latter transformation (**3**→**2**) could also be accomplished under acidic conditions, albeit in lower yield (PPTS, 2.0 equiv, toluene, 24 h, 100 °C, 65%). Finally, the cytoskyrin-type



Scheme 4. Postulated mechanism for the dimerization of tricyclic quinone **6**, through enolization and a Diels–Alder or double Michael reaction. CSA = (±)-10-camphorsulfonic acid.

© 2005 Wiley-VCH Verlag GmbH & Co. KGaA, Weinheim

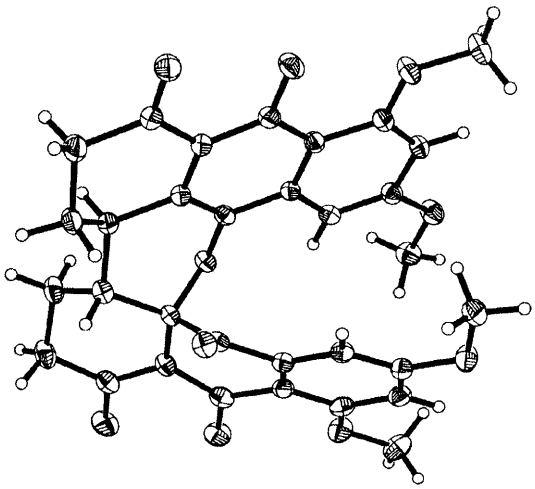
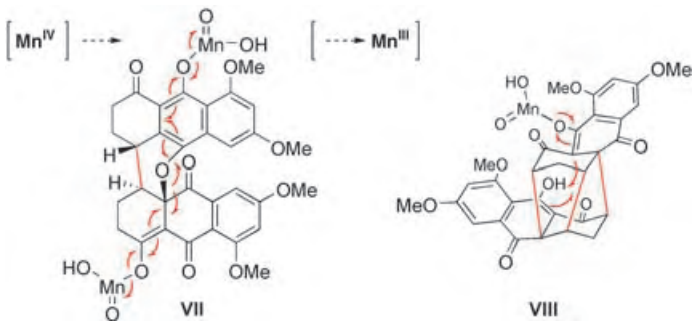


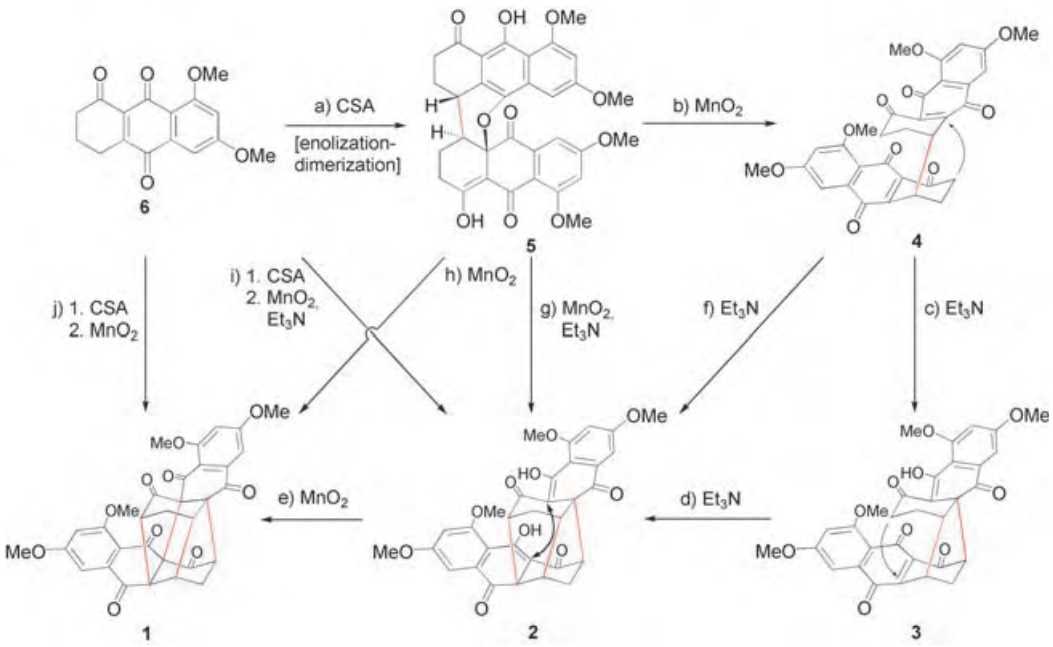
Figure 3. ORTEP drawing of structure **5** (drawn at the 30% probability level).



Scheme 5. Postulated mechanism for the MnO_2 oxidation of compound **5** to **4** (**VII**) and **2** to **1** (**VIII**). This working hypothesis depiction is not based on experimental evidence and is not meant to exclude any other mechanism. The proximity of the Mn=O and enol groups within **VIII** bodes well for an intramolecular interaction between them as part of the mechanism.

compound **2** was transformed into the rugulin-type structure **1** (Table 1) in 95% yield simply by exposure to MnO_2[2a] through an oxidation process that also involved a carbon–carbon bond formation (see Scheme 5, structure **VIII** for a presumed mechanism).

Remarkable as these individual steps may be, they were aesthetically surpassed by the beauty of a number of cascade sequences developed in these studies (Scheme 6). The fact that only a mild base was required to carry out the double Michael reaction leading to **2** (**4**→**3**→**2**; Table 1) and the suspicion that MnO_2 contained such basic species prompted us to attempt this cascade with MnO_2 as the only reagent. Indeed, on exposure to freshly prepared MnO_2 in CH_2Cl_2, compound **5** (Table 1) was transformed into **1** in quantitative yield,[10] through the intermediacy of **4**, then **3**, and finally **2**, all of which were observed by TLC analysis (cascade **5**→**1**; excess MnO_2, 48 h, 45 °C). Interestingly, addition of Et_3N (10.0 equiv) to the starting reaction mixture (**5**, MnO_2) and heating to 45 °C for 20 h resulted in the exclusive formation of **2** (in quantitative yield), with Et_3N apparently inhibiting the last oxidation step (**2**→**1**, presumably through slow deactivation of the MnO_2). Even more impressive was the five-step cascade sequence involving the transformation of the tricyclic monomer **6** into the nonacyclic cytoskyrin model system **2** in 66% yield[10] (cascade **6**→**2**). The latter cascade required treatment of **6** with CSA (0.125 equiv) in CH_2Cl_2 for 1 h at 25 °C, conditions that led to the formation of **5** as indicated by TLC analysis, followed by addition of MnO_2 (excess) and Et_3N (10.0 equiv) and heating to 45 °C with stirring for 36 h, to afford the cytoskyrin model system **2**, through the intermediacy of the fleeting compounds **4** and **3**. This remarkable cascade encompasses an enolization step, followed by a stereoselective dimerization reaction, an oxidation, and finally, an intramolecular double Michael sequence. A similar



Scheme 6. The cytoskyrin cascade: synthesis of flavoskyrin-, skyrin-, deoxyrubroskyrin-, cytoskyrin-, and rugulin-type structures from anthraquinone **6**. All steps can be carried out sequentially in one pot or can be stopped at any stage. Reagents and conditions: a) CSA (0.125 equiv), CH_2Cl_2, 25 °C, 1 h, 94%; b) MnO_2 (10.0 equiv), CH_2Cl_2, 25 °C, 1 h, 83%; c) Et_3N (2.0 equiv), CH_2Cl_2, 1 h, 25 °C, 65%; d) Et_3N (5.0 equiv), CH_2Cl_2, 16 h, 45 °C, 95%; e) MnO_2 (10.0 equiv), CH_2Cl_2, 25 °C, 20 h, 95%; cascade sequences: f) **4**→**2**, Et_3N (5.0 equiv), CH_2Cl_2, 16 h, 45 °C, 95%; g) **5**→**2**, MnO_2 (10.0 equiv), Et_3N (5.0 equiv), CH_2Cl_2, 20 h, 25→45 °C, 100%; h) **5**→**1**, MnO_2 (10.0 equiv), CH_2Cl_2, 48 h, 45 °C, 100%; i) **6**→**2**, CSA (0.125 equiv), CH_2Cl_2, 1 h, 25 °C; then MnO_2 (10.0 equiv), Et_3N (10.0 equiv), 36 h, 45 °C, 66%; j) **6**→**1**, CSA (0.125 equiv), CH_2Cl_2, 1 h, 25 °C; then MnO_2 (10.0 equiv), 88 h, 25 °C, 75%.

© 2005 Wiley-VCH Verlag GmbH & Co. KGaA, Weinheim

experiment in which no Et_3N was added resulted in a six-step cascade transforming **6** to rugulin model system **1** in an impressive 75% yield.

X-ray crystallographic analysis of compound **3**[9] revealed an interesting phenomenon, reminiscent of the classic observation of Ermer with secododecahedrane.[11] As in that case, our initial analysis led to a symmetrical structure (see ORTEP drawing, Figure 4a), an architecture that was contradicted by

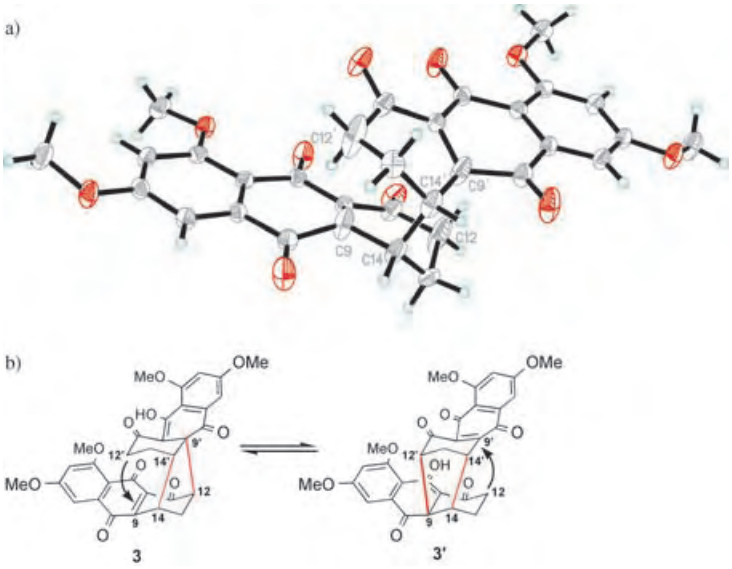


Figure 4. ORTEP drawing of compound **3** (drawn at the 30% probability level) obtained by X-ray crystallographic analysis (using *C*2/*c* space group) at ambient temperature and possible equilibration of **3** and **3′**.

^{1}H NMR spectroscopy, which revealed a nonsymmetrical structure for the molecule.[12] This rare observation may be due to crystal disorder,[13] or dynamic equilibrium involving a two-proton shuttle in which the C12–C9′ bond within **3** breaks as the C12′–C9 bond within **3′** forms (**3**→**3′**, Figure 4b). The structures **3** and **3′** are identical, and X-ray crystallographic analysis reveals an average picture with bond lengths C12–C9′ = C12′–C9 = 2.372 Å and C14–C14′ = 1.56 Å.[14]

The described chemistry provides easy and efficient access to a variety of molecular architectures representing the core structures of numerous natural products, underscoring at the same time the importance of cascade sequences in complex molecule construction. Our experience with the X-ray crystallographic analysis of the deoxyrubroskyrin-type compound **3** should serve as a reminder of the occasional hazards posed by dynamic and/or crystal-disorder phenomena in the solid state and their impact on structure elucidation. While the total synthesis of several members of the bisanthraquinone family of compounds shall now be forthcoming, the gauntlet thrown by skyrane **VI** (Figure 1) is also begging for a solution, a challenge that has not escaped our attention.

Received: June 10, 2005
Published online: August 25, 2005

Table 1: Selected physical properties for **1**–**5**.

1: R_f = 0.53 (CH_2Cl_2/MeOH 10:1); ^{1}H NMR (500 MHz, $CDCl_3$): δ = 6.99 (2H, d, J = 2.0 Hz), 6.80 (2H, d, J = 2.0 Hz), 3.95 (6H, s), 3.91 (6H, s), 3.39 (2H, br), 3.08 (2H, d, J = 8.0 Hz), 2.82 (2H, dd, J = 13.0, 9.0 Hz), 2.28 ppm (2H, d, J = 13.0 Hz); ^{13}C NMR (175 MHz, $CDCl_3$): δ = 201.9, 194.7, 186.9, 164.2, 159.8, 137.8, 122.2, 106.5, 101.4, 74.5, 66.2, 57.0, 56.8, 56.6, 56.0, 39.2 ppm; IR (film): $\tilde{\nu}_{max}$ = 1748, 1684, 1654, 1590, 1560, 1458, 1320, 1236 cm^{-1}; HRMS (ESI TOF) (*m*/*z*): calcd for $C_{32}H_{25}O_{10}^+$: 569.1442 [*M*+H]$^+$; found: 569.1420

2: R_f = 0.80 (CH_2Cl_2/MeOH 10:1); ^{1}H NMR (500 MHz, $CDCl_3$): δ = 15.90 (2H, s), 7.24 (2H, d, J = 2.5 Hz), 6.77 (2H, d, J = 2.5 Hz), 3.95 (6H, s), 3.94 (6H, s), 3.66 (2H, br), 2.89 (2H, d, J = 6.0 Hz), 2.13 (2H, dd, J = 12.0, 6.0 Hz), 1.65 ppm (2H, d, J = 12.0 Hz); ^{13}C NMR (125 MHz, $CDCl_3$): δ = 197.6, 196.5, 173.0, 164.5, 161.8, 135.0, 114.4, 105.6, 104.0, 103.7, 57.8, 57.4, 56.8, 56.0, 48.1, 30.0 ppm; IR (film): $\tilde{\nu}_{max}$ = 2932, 1617, 1574, 1315, 1039, 909, 731 cm^{-1}; HRMS (ESI TOF) (*m*/*z*): calcd for $C_{32}H_{27}O_{10}^+$: 571.1599 [*M*+H]$^+$; found: 571.1585

3: R_f = 0.45 (CH_2Cl_2/MeOH 10:1); ^{1}H NMR (500 MHz, $CDCl_3$): δ = 16.0 (1H, s), 7.21 (1H, d, J = 2.0 Hz), 7.05 (1H, d, J = 2.5 Hz), 6.78 (1H, d, J = 2.5 Hz), 6.76 (1H, d, J = 2.5 Hz), 4.00 (3H, s), 3.98 (1H, d, J = 5.5 Hz), 3.96 (3H, s), 3.93 (3H, s), 3.92 (3H, s), 3.87 (1H, br), 3.18 (1H, d, J = 3.5 Hz), 2.13–2.05 ppm (1H, m), 2.05–1.90 (3H, m), 1.90–1.80 (1H, m), 1.80–1.78 (1H, m); ^{13}C NMR (125 MHz, $CDCl_3$): δ = 196.1, 195.4, 186.1, 186.4, 179.5, 179.3, 164.8, 164.4, 162.6, 161.7, 156.2, 136.6, 134.7, 130.8, 116.1, 115.1, 105.7, 105.4, 104.3, 103.6, 102.6, 60.3, 57.1, 56.9, 56.5, 56.0, 55.9, 39.9, 39.6, 36.1, 27.6, 20.9 ppm; IR (film): $\tilde{\nu}_{max}$ = 1702, 1585, 1558, 1540, 1456, 1340, 1263, 1232 cm^{-1}; HRMS (ESI TOF) (*m*/*z*): calcd for $C_{32}H_{27}O_{10}^+$: 571.1599 [*M*+H]$^+$; found: 571.1593

4: R_f = 0.40 (CH_2Cl_2/MeOH 10:1); ^{1}H NMR (500 MHz, $CDCl_3$): δ = 6.55 (2H, d, J = 2.5 Hz), 6.49 (2H, d, J = 2.5 Hz), 3.88 (6H, s), 3.74 (6H, s), 3.68 (2H, br), 3.08 (2H, ddd, J = 17.5, 7.5, 7.5 Hz), 2.75 (2H, dd, J = 24.0, 4.5 Hz), 2.33–2.25 ppm (4H, m); ^{13}C NMR (125 MHz, $CDCl_3$): δ = 195.3, 187.2, 180.0, 163.9, 160.7, 151.5, 134.9, 134.6, 114.9, 105.2, 101.4, 56.2, 55.8, 34.0, 32.4, 25.2 ppm; IR (film): $\tilde{\nu}_{max}$ = 1780, 1698, 1661, 1590, 1461, 1320, 1255, 1212, 909, 731 cm^{-1}; HRMS (ESI TOF) (*m*/*z*): calcd for $C_{32}H_{27}O_{10}^+$: 571.1599 [*M*+H]$^+$; found: 571.1595

5: R_f = 0.71 (CH_2Cl_2/MeOH 10:1); ^{1}H NMR (500 MHz, $CDCl_3$): δ = 16.28 (1H, s), 15.02 (1H, s), 6.61 (1H, d, J = 2.0 Hz), 6.31 (1H, d, J = 2.0 Hz), 6.19 (1H, d, J = 2.5 Hz), 5.90 (1H, d, J = 2.5 Hz), 3.97 (3H, s), 3.93 (3H, s), 3.56 (3H, s), 3.43 (3H, s), 2.82–2.80 (1H, m), 2.74–2.70 (1H, m), 2.60–2.57 (5H, m), 2.26–2.23 (1H, m), 2.19–2.13 (1H, m), 2.12–2.09 ppm (1H, m); ^{13}C NMR (125 MHz, $CDCl_3$): δ = 202.9, 197.6, 188.1, 184.1, 164.9, 162.0, 161.9, 161.0, 160.7, 139.6, 137.9, 134.6, 125.2, 115.0, 109.8, 108.0, 104.3, 103.8, 102.2, 98.2, 92.0, 82.0, 56.4, 56.2, 55.9, 55.0, 39.6, 38.7, 38.2, 30.4, 29.3, 25.3 ppm; IR (film): $\tilde{\nu}_{max}$ = 1710, 1601, 1558, 1385, 1320, 1207, 1153, 1044 cm^{-1}; HRMS (ESI TOF) (*m*/*z*): calcd for $C_{32}H_{29}O_{10}^+$: 573.1755 [*M*+H]$^+$; found: 573.1742

Keywords: cascade reactions · dimerization · natural products · radicals · synthetic methods

[1] S. F. Brady, M. P. Singh, J. E. Janso, J. Clardy, *Org. Lett.* **2000**, *2*, 4047–4049.

[2] In a series of papers that were intriguing but lacking in details, the Shibata group reported on their investigations in this field, which included both the isolation of and chemical interconversions between some of these natural products and related compounds, see: a) N. Takeda, S. Seo, Y. Ogihara, U. Sankawa, I. Iitaka, I. Kitagawa, S. Shibata, *Tetrahedron* **1973**, *29*, 3703–3719; b) Y. Ogihara, N. Kobayashi, S. Shibata, *Tetrahedron Lett.* **1968**, 1881–1886; c) S. Seo, U. Sankawa, S. Shibata, *Tetrahedron Lett.* **1972**, 731–734; d) S. Shibata, *Pure Appl. Chem.* **1972**, *33*, 109–127; e) S. Seo, U. Sankawa, Y. Ogihara, Y. Iitaka, S. Shibata,

 © 2005 Wiley-VCH Verlag GmbH & Co. KGaA, Weinheim

Tetrahedron **1973**, *29*, 3721 – 3726; f) D.-M. Yang, U. Sankawa, Y. Ebizuka, S. Shibata, *Tetrahedron* **1976**, *32*, 333 – 335.

[3] P. Sedmera, M. Podojil, J. Vokoun, V. Betina, P. Nemec, *Folia Microbiol.* **1978**, *23*, 64 – 67.

[4] B. Franck, R. Chahin, H.-G. Eckert, R. Langenberg, V. Radtke, *Angew. Chem.* **1975**, *87*, 846 – 847; *Angew. Chem. Int. Ed. Engl.* **1975**, *14*, 819 – 820.

[5] Clardy and co-workers speculated on the biosynthetic origins of cytoskyrin A as following a redox path from monomeric 6-methyl-1,3,8-trihydroxyanthraquinone (emodin, see reference [1]). This type of dimerization had been hinted at earlier by the Shibata group (see reference [2e]).

[6] Polysubstituted examples of this cage structure have been described previously: a) J. A. Beisler, J. V. Silverton, A. Penttila, D. H. S. Horn, H. M. Fales, *J. Am. Chem. Soc.* **1971**, *93*, 4850 – 4855; b) K. Hirao, Y. Ohuchi, O. Yonemitsu, *J. Chem. Soc. Chem. Commun.* **1982**, 99 – 100.

[7] F. M. Hauser, S. Chakrapani, W. P. Ellenberger, *J. Org. Chem.* **1991**, *56*, 5248 – 5250.

[8] a) D. Momose, K. Iguchi, T. Sugiyama, Y. Yamada, *Tetrahedron Lett.* **1983**, *24*, 921 – 924; b) S. K. Bagal, R. M. Adlington, R. Marquez, A. R. Cowley, J. E. Baldwin, *Tetrahedron Lett.* **2003**, *44*, 4993 – 4996.

[9] CCDC-274275 (**4**), -274271 (**5**), and -274272 (**3**) contain the supplementary crystallographic data for this paper. These data can be obtained free of charge from the Cambridge Crystallographic Data Centre via www.ccdc.cam.ac.uk/data_request/cif.

[10] The high overall yield for this cascade reflects the higher efficiency by which the final product (**1**) can be purified by chromatography, as opposed to the intermediate compounds (**3** or **2**) whose enolic nature makes their isolation more tedious.

[11] O. Ermer, *Angew. Chem.* **1983**, *95*, 251 – 252; *Angew. Chem. Int. Ed. Engl.* **1983**, *22*, 251 – 252. We thank Professor Scott Rychnovsky for pointing out this reference to us.

[12] The NMR spectroscopic analysis of compound **3** included ^{1}H and ^{13}C NMR data as well as COSY and HMQC correlations, which can be found in the Supporting Information.

[13] a) J. D. Dunitz, G. Filippini, A. Gavezzotti, *Helv. Chim. Acta* **2000**, *83*, 2317 – 2335; b) J. D. Dunitz, J. Bernstein, *Acc. Chem. Res.* **1995**, *28*, 193 – 200, and references therein. We thank Professor Jack Dunitz for pointing out these articles to us and for his stimulating comments.

[14] The X-ray measurements were initially performed at room temperature and the crystal structure was solved and refined in the centrosymmetric space group *C*2/*c* with $Z = 4$, following the general conventions and statistical analysis of data ($|E^2-1| = 0.91$). Accordingly, the molecules of **3** were observed to reside on (average) crystallographic twofold axes. The distance between the carbon atoms C9 and C12′, however, was as short as 2.37 (2) Å, which was far smaller than the expected van der Waals sum of 3.5 Å. Furthermore, the anisotropic temperature factor ellipsoids of both these atoms were distinctly elongated along their line of separation, suggesting that one Michael addition reaction could have taken place, resulting in bond formation between C9 and C12′ and leading to the nonsymmetrical structure **3**, which could exist in dynamic equilibrium with its identical "regioisomer" (**3**′, Figure 4b). Subsequent crystal structure solution and refinement in the lower noncentrosymmetric space group *Cc*,[15] gave a slightly nonsymmetrical molecular structure with C9–C12′ and C9′–C12 distances of 2.24(2) and 2.52(1) Å, respectively. Interestingly, when the same crystal was subjected to low-temperature X-ray measurements (123 K), these bond lengths diverged even further, as revealed by the values of 1.91(2) and 2.81(2) Å, computed by structure solution and refinement in *Cc*. When the *C*2/*c* space group was used the C9–C12′ distance was approximately the same as the room-temperature distance of 2.37 Å (2). These distances were even more drastically different [1.66(2) and 2.95(2) Å, respectively] in *Cc* when the atoms were refined isotropically. Thus, apparently partial dynamic ordering of the crystal structure occurs on cooling. Interestingly, while both the secododecahedrane[11] and the present examples involve carbon atoms at close proximity to each other, in the former case the X-ray analysis revealed a bond, whereas in the latter case it missed a bond.

[15] We thank Professor O. Ermer for suggesting that we revert to this space group (*Cc*) and for critically reviewing our conclusions regarding this anomalous X-ray crystallographic analysis.

 © 2005 Wiley-VCH Verlag GmbH & Co. KGaA, Weinheim

C–H Activation

DOI: 10.1002/anie.200501195

New Iodination Reactions of Saturated Hydrocarbons**

José Barluenga, Esther Campos-Gómez, David Rodríguez, Francisco González-Bobes, and José M. González*

Selective processes that afford functionalized derivatives from the reaction of nonactivated C–H bonds are of current interest.[1] Bromination and chlorination reactions are valuable tools for this purpose with saturated hydrocarbons.[2] However, the related iodination is not so well developed.[3] Herein, we report on new iodination reactions of alkanes under mild thermal conditions. The process relies on the use of the combination of hypervalent iodine, I_2, and trimethylsilyl azide ($TMSN_3$). Furthermore, a related and efficient iodination in water, using H_2O_2 as a convenient source for the oxidant, has also been established.

Hydrocarbons can be iodinated under photochemical conditions by employing $PhI(OAc)_2/I_2/t$BuOH, a process that likely involves the formation of intermediate alkoxyl radicals.[3e] Alternative processes that lead to the development of

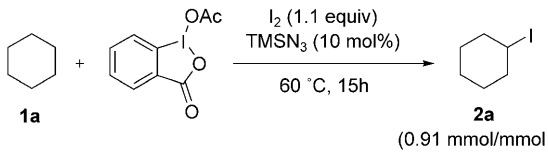
[*] Prof. Dr. J. Barluenga, E. Campos-Gómez, Dr. D. Rodríguez, Dr. F. González-Bobes, Dr. J. M. González
Instituto Universitario de Química Organometálica "Enrique Moles"
Unidad Asociada al C.S.I.C.
Universidad de Oviedo
33071 Oviedo (Spain)
Fax: (+34) 98-510-3450
E-mail: barluenga@uniovi.es

[**] This research was partially supported by the Spanish DGI (MCT-01-BQU-3853). E.C.-G. is grateful to the Spanish M.E.C. for an FPU Fellowship. F.G.-B. thanks the Principado of Asturias for a predoctoral fellowship. Generous support from Merck Sharp & Dohme (UK) is gratefully acknowledged.

Supporting information for this article (^{13}C NMR spectra of compounds **2a–k**) is available on the WWW under http://www.angewandte.org or from the author.

 © 2005 Wiley-VCH Verlag GmbH & Co. KGaA, Weinheim

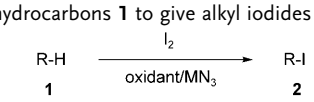
new methodology and involve different types of intermediates as the species responsible for the C–H activation step are of great significance and, overall, might result in new and distinctive synthetic features. Being interested in employing more convenient thermal conditions, we decided to investigate reactions using azide to activate the hypervalent iodine reagent.[4] 1-Acetoxy-1,2-benziodoxole-3(1*H*)-one[5] was chosen as the hypervalent iodine reagent. We expected that a catalytic amount of azide would be able to promote the desired iodination. This assumption was initially validated with cyclohexane (**1a**) as model compound, using $TMSN_3$ as the azide donor (Scheme 1).

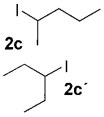
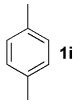
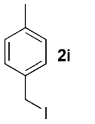
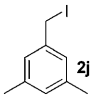
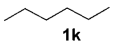
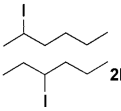


Scheme 1. Synthesis of iodocyclohexane **2a** from the thermal reaction of cyclohexane (**1a**) with I_2 promoted by a cyclic λ^3-iodane and catalytic amounts of $TMSN_3$ (Method A, Table 1).

The concentration of the azide is crucial to accomplish the reported iodination. Routinely, to investigate the scope of the iodination (method A),[6] 4×10^{-3} M of azide was used. The results are summarized in Table 1. This novel iodination can be applied to different alkanes, either cyclic or acyclic. Interestingly, for the latter, an improved selectivity is noted.[3e] Now, only secondary positions are iodinated, without significant evidence for related functionalization of the primary ones. Benzylic positions are equally cleanly iodinated. This new reaction provides useful indicators. It relies on a thermal process; moreover, the use of a catalytic amount of azide and the observed selectivity for the iodination of linear hydrocarbons are also significant. Furthermore, this new process is very convenient with regard to the isolation of **2**, as well as the recovery of the reaction by-product. *o*-Iodobenzoic acid can be easily removed and recycled by simple aqueous extraction at proper pH. For the iodination of xylenes, an additional feature is noted. These are very efficient processes, which give rise to an increase in the incorporation of iodine atoms into the organic structure. Now, under proper conditions, most of the I_2 can be successfully used to functionalize the hydrocarbon.[7] On the basis of the formed products, the well-documented chemistry of azidobenziodoxoles, and taking into consideration the above-mentioned features, we propose that the sequence in Scheme 2 offers a feasible mechanistic rationalization for the reported iodinations.

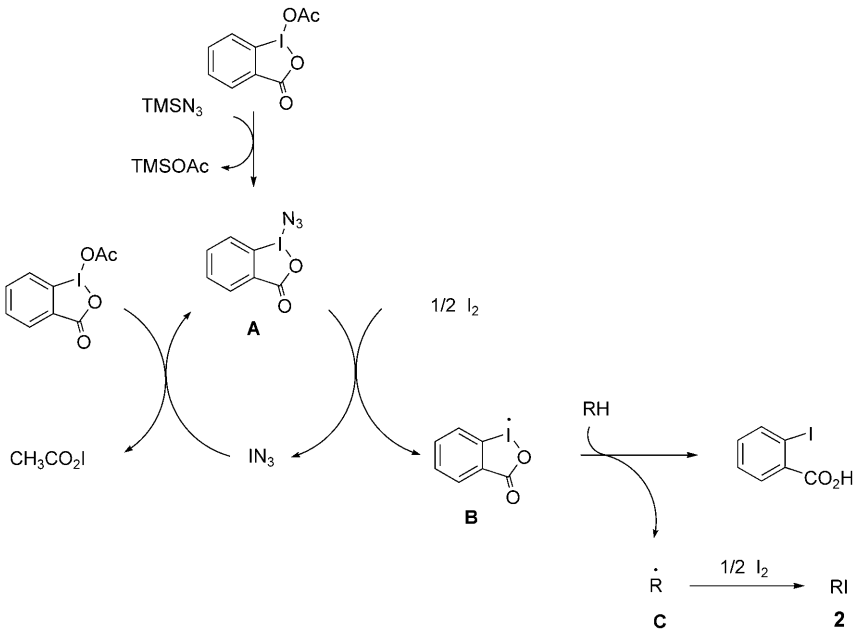
Table 1: Thermal iodination of hydrocarbons **1** to give alkyl iodides **2**.



Entry	1	Method	*t* [h]	2	Yield[a]
1		A[b]	15		0.91
		B[c]	19		1.31 (1.43)[d]
2		A	18		0.89
		B	13		1.88 (1.99)[d]
3		A	18		0.71[e,f]
		B	8		1.03[e] (1.33)[d]
4		A	18		0.38 (0.90)[f]
		B	6		1.33 (1.42)[d]
5		A	30		–[g]
		B	13		1.27
6		A	56		0.58 (0.90)[h]
		B	13		1.08
7		A	18		1.59
		B	19		1.18
8		A	18		1.54
		B	19		1.68
9		A	18		1.58
		B	9		0.57
10		A	17		0.79
		B	20		1.46
11		A	15		0.43[i]
		B	18		–[j]

[a] Given as the ratio between mmol of isolated iodinated compound **2** per mmol of added iodine (mmol of **2** per mmol of I_2). [b] See Scheme 1 and reference [6]. [c] See Scheme 3 and reference [15]. [d] In parentheses, yield obtained by integration from the ^{1}H NMR spectra of the crude reaction mixture (1-phenylethanol or anisole were used as an externally added standard to record the NMR spectra). [e] Ratio **2c**:**2c′** ≈ 2.3:1, by ^{1}H NMR spectroscopy (300 MHz) and GC. [f] Using one equivalent of $TMSN_3$ with respect to the iodane. Iodination of **1c** was not observed when 10 mol% of $TMSN_3$ was used. [g] 0.62 mmol of *trans*-1-acetoxy-1-methyl-2-iodocyclohexane were formed. See reference [3e]. [h] Reaction time 20 h, one equivalent of $TMSN_3$ was used. [i] Ratio **2k**:**2k′** ≈ 1:1.1 by GC. [j] Only traces of iodinated derivatives were detected.

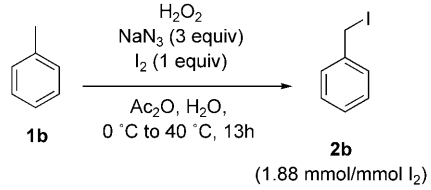
 © 2005 Wiley-VCH Verlag GmbH & Co. KGaA, Weinheim



Scheme 2. Proposed mechanism for the conversion of **1** into **2** (Method A, Table 1).

First, the starting acetoxyiodane leads to the formation of the known[5b,c] azidoiodane **A**. Next, interaction with I_2 should render active species, such as the iodanyl radical **B**,[8] a process in which a fraction of iodine acts as an efficient scavenger of azido radicals. The radical **B** would be responsible for the activation of the alkane[9] giving rise to *o*-iodobenzoic acid and a C-centered radical **C**, which then furnishes **2**[10] by trapping iodine.[11]

In an attempt to perform related reactions using simpler reagents we have explored the reaction of alkanes with iodine, aqueous solutions of NaN_3,[12] and H_2O_2 as oxidant.[13] We found that, in the presence of acetic anhydride, an efficient iodination reaction takes place, as depicted in Scheme 3 for



Scheme 3. Synthesis of α-iodotoluene (**2b**) by a C–H functionalization reaction in water (Method B, Table 1).

the functionalization of the benzylic position of toluene. The addition of small amounts of water adjusts the concentration of H_2O_2 and minimizes the formation of by-products (alcohol, acetate).[14]

This new reaction (see Table 1, method B[15] for data concerning the scope), on average, shows improved efficiency with respect to iodine incorporation into the organic precursor, allows an easy isolation of compounds **2**, and retains the selectivity for the iodination of secondary versus primary positions. Accordingly, linear pentane (**1c**) is nicely iodinated; however, the related *n*-hexane (**1k**) fails to react to appreciable extension. Though yet very preliminary, the previously noted differences for the adsorption of *n*-alkanes on the surface of water might account well for the trend in terms of reactivity in a qualitative sense.[16] This approach offers a convenient method to conduct the iodination of a varied and representative set of hydrocarbons in the presence of water.[17] At the same time, this is a very efficient protocol for directly iodinating alkanes, particularly, considering the high percentage of iodine that is typically incorporated into the structure of the hydrocarbon.

Overall, new reactions and significant experimental advances have been achieved for the iodination of hydrocarbons, which is a notoriously difficult reaction. At the same time, new perspectives for the use of well-established cyclic azidoiodanes have been offered by the present study. The examination of the possible reaction paths followed by using different hypervalent iodine reagents is also of interest with regard to investigating alternative reactive combinations based on simpler reagents. Further studies on the scope and implications of the herein reported chemistry are underway in our laboratories.

Experimental Section

Warning: We have not experienced any explosions while conducting our experiments, either using method A or B (so far, we carried out reactions that lead to about 5 mmol of compounds **2**); however, much care should be taken when working with azides, especially when heating them, as they are potentially explosive compounds.

Method A: All reactions were carried out under a positive pressure of nitrogen. In a typical experiment, I_2 (1.1 mmol, 0.28 g) and $TMSN_3$ (10%, 13 μL) were sequentially added to a suspension of 1-acetoxy-1,2-benziodoxol-3(1*H*)-one (1 mmol, 0.31 g) in cyclohexane (25 mL). The resulting mixture was stirred at 60°C (bath temperature) for 15 h. The mixture was allowed to cool and then quenched with aqueous NaOH (5%, 25 mL). The organic layer was distilled under reduced pressure, and excess cyclohexane was recovered. The distillation residue was diluted with diethyl ether (20 mL) and washed with aqueous $Na_2S_2O_3$ (5%, 30 mL), brine (30 mL), and dried over anhydrous Na_2SO_4. The solvent was removed at reduced pressure and the resulting oil was further purified by column chromatography, by using a mixture of hexanes as eluent, to afford cyclohexyl iodide **2a** (0.21 g, 0.91 mmol) as an irritating colorless oil.

Method B: In a typical experiment, Ac_2O (1.2 mL), H_2O (0.5 mL), and NaN_3 (0.20 g, 3 mmol) were sequentially added to a cooled solution (water/ice bath) of I_2 (0.25 g, 1 mmol) in toluene (5 mL). H_2O_2 (30% in water, 0.3 mL) was added and the mixture was vigorously stirred at 40°C for 13 h. The reaction mixture was poured into a saturated solution of $NaHCO_3$ (20 mL) and washed with aqueous $Na_2S_2O_3$ (5%, 15 mL). The organic layer was dried over anhydrous Na_2SO_4, and the excess toluene was recovered by distillation. The yellowish residue was purified by column chromatography, by using a mixture of hexanes as eluent, to afford benzyl iodide **2b** (0.41 g, 1.88 mmol) as a lachrymatory pale yellow oil.

Received: April 5, 2005
Published online: August 10, 2005

 © 2005 Wiley-VCH Verlag GmbH & Co. KGaA, Weinheim

Keywords: alkanes · azides · C–H activation · hydrogen peroxide · hypervalent iodine

[1] Recent reviews: a) A. A. Fokin, P. R. Schreiner, *Adv. Synth. Catal.* **2003**, *345*, 1035–1052; b) F. Kakiuchi, N. Chatani, *Adv. Synth. Catal.* **2003**, *345*, 1077–1101; recent examples: c) F. Minisci, F. Recupero, C. Gambarotti, C. Punta, R. Paganelli, *Tetrahedron Lett.* **2003**, *44*, 6919–6922; d) M. W. Peters, P. Meinhold, A. Glieder, F. H. Arnold, *J. Am. Chem. Soc.* **2003**, *125*, 13442–13450; e) K. Yamaguchi, S. Shinachi, N. Mizuno, *Chem. Commun.* **2004**, 424–425; f) L. V. Desai, K. L. Hull, M. S. Sanford, *J. Am. Chem. Soc.* **2004**, *126*, 9542–9543; g) B. Sezen, D. Sames, *J. Am. Chem. Soc.* **2004**, *126*, 13244–13246; h) B. C. Bales, P. Brown, A. Dehestani, J. M. Mayer, *J. Am. Chem. Soc.* **2005**, *127*, 2832–2833; recent methane functionalization reactions see, for instance: i) M. Muehlhofer, T. Strassner, W. A. Herrmann, *Angew. Chem.* **2002**, *114*, 1817–1819; *Angew. Chem. Int. Ed.* **2002**, *41*, 1745–1747; j) M. Zerella, S. Mukhopadhyay, A. T. Bell, *Chem. Commun.* **2004**, 1948–1949; k) C. J. Jones, D. Taube, V. R. Ziatdinov, R. A. Periana, R. J. Nielsen, J. Oxgaard, W. A. Goddard III, *Angew. Chem.* **2004**, *116*, 4726–4729; *Angew. Chem. Int. Ed.* **2004**, *43*, 4626–4629.

[2] R. H. Crabtree, A. Habib in *Comprehensive Organic Synthesis, Vol. 7* (Eds.: B. M. Trost, I. Fleming), Pergamon, Oxford, **1991**, chap. 1.1, pp. 1–20.

[3] a) D. D. Tanner, G. C. Gidley, *J. Am. Chem. Soc.* **1968**, *90*, 808–809; b) P. R. Schreiner, O. Lauenstein, E. D. Butova, A. A. Fokin, *Angew. Chem.* **1999**, *111*, 2956–2958; *Angew. Chem. Int. Ed.* **1999**, *38*, 2786–2788; c) A. A. Fokin, O. Lauenstein, P. A. Gunchenko, P. R. Schreiner, *J. Am. Chem. Soc.* **2001**, *123*, 1842–1847; d) P. R. Schreiner, O. Lauenstein, E. D. Butova, P. A. Gunchenko, I. V. Kolomitsin, A. Wittkopp, G. Feder, A. A. Fokin, *Chem. Eur. J.* **2001**, *7*, 4997–5003; e) J. Barluenga, F. González-Bobes, J. M. González, *Angew. Chem.* **2002**, *114*, 2668–2670; *Angew. Chem. Int. Ed.* **2002**, *41*, 2556–2558; f) R. Montoro, T. Wirth, *Org. Lett.* **2003**, *5*, 4729–4731; g) R. Giri, X. Chen, J.-Q. Yu, *Angew. Chem.* **2005**, *117*, 2150–2153; *Angew. Chem. Int. Ed.* **2005**, *44*, 2112–2115.

[4] Recent reviews on hypervalent iodine: a) V. V. Zhdankin, P. J. Stang, *Chem. Rev.* **2002**, *102*, 2523–2584; b) M. Ochiai, *Top. Curr. Chem.* **2003**, *224*, 5–68; c) T. Wirth, *Angew. Chem.* **2005**, *117*, 3722–3731; *Angew. Chem. Int. Ed.* **2005**, *44*, 3656–3665; azidation reaction of unactivated C–H bonds using $PhI(OAc)_2$/$TMSN_3$: d) P. Magnus, J. Lacour, P. A. Evans, M. B. Roe, C. Hulme, *J. Am. Chem. Soc.* **1996**, *118*, 3406–3418, and references therein; e) D.-J. Chen, Z.-C. Chen, *Tetrahedron Lett.* **2000**, *41*, 7361–7363; for related azido-phenylselenylation of alkenes, see: f) M. Tingoli, M. Tiecco, D. Chianelli, R. Balducci, A. Temperini, *J. Org. Chem.* **1991**, *56*, 6809–6813. Azido radicals have been proposed as intermediates for both types of transformations.

[5] Review on benziodoxoles: a) V. V. Zhdankin, *Rev. Heteroat. Chem.* **1997**, *117*, 133–151; preparation of 1-azido-1,2-benziodoxol-3-(1*H*)-3-one: b) V. V. Zhdankin, C. J. Kuehl, A. P. Krasutsky, M. S. Formaneck, J. T. Bolz, *Tetrahedron Lett.* **1994**, *35*, 9677–9680; c) S. Akai, T. Okuno, M. Egi, T. Takada, H. Tohma, Y. Kita, *Heterocycles* **1996**, *42*, 47–51; for synthetic uses: d) V. V. Zhdankin, A. P. Krasutsky, C. J. Kuehl, A. J. Simonsen, J. K. Woodward, B. Mismash, J. T. Bolz, *J. Am. Chem. Soc.* **1996**, *118*, 5192–5197.

[6] Reaction at 60 °C of **1** (25 mL), 1-acetoxy-1,2-benziodoxol-3(1*H*)-one (1 mmol), I_2 (1.1 mmol), and $TMSN_3$ (0.1 mmol, 10 mol % referred to the benziodoxole).

[7] Previously, only one method has been reported incorporating more than one atom of iodine into the alkane for each molecule of the iodine source (CI_4), see reference [3b].

[8] For leading examples on iodine-centered radicals from cyclic hypervalent iodanes: a) M. Ochiai, T. Ito, H. Takahashi, A. Nakanishi, M. Toyonari, T. Sueda, S. Goto, M. Shiro, *J. Am. Chem. Soc.* **1996**, *118*, 7716–7730; b) M. Ochiai, A. Nakanishi, T. Ito, *J. Org. Chem.* **1997**, *62*, 4253–4259; for a recent application: c) K. Iba, S.-i. Fukuyoshi, T. Kusumi, *Chem. Lett.* **2004**, *33*, 716–717.

[9] For studies on the role of cyclic iodanyl radicals in free-radical halogenations of toluene (chlorination and bromination): a) R. L. Amey, J. C. Martin, *J. Am. Chem. Soc.* **1979**, *101*, 3060–3065; for early studies on cyclic iodanyl radicals: b) J. E. Leffler, R. D. Faulkner, C. C. Petropoulos, *J. Org. Chem.* **1958**, *26*, 5435–5437; c) W. Honsberg, J. E. Leffler, *J. Am. Chem. Soc.* **1961**, *82*, 733–735; halogenations with other iodanyl radicals: d) D. D. Tanner, P. B. van Bostelen, *J. Org. Chem.* **1967**, *32*, 1517–1521; e) P. White, R. Breslow, *J. Am. Chem. Soc.* **1990**, *112*, 6842–6847; review on alkane transformations via radicals: f) A. A. Fokin, P. R. Schreiner, *Chem. Rev.* **2002**, *102*, 1551–1593.

[10] In agreement with this hypothesis, the reaction of **1a** (25 mL), I_2 (1 mmol), and **A** (10 mol %, prepared by an independent route), at 60 °C for 24 h, furnished **2a** (99 %, with respect to **A**). No reaction was observed when **1a** and **A** were mixed and heated at 60 °C for 24 h.

[11] For functionalization reactions that incorporate more than 1 mmol of atomic iodine for each mmol of added I_2, the possibility of regenerating cyclic iodanyl radicals upon interaction of *o*-iodobenzoic acid with acetyl hypoiodite cannot be ruled out, at present.

[12] For chemistry on hypervalent iodine compounds that has been conducted by using inorganic sources of iodine see, for instance: a) K. C. Nicolaou, T. Montagnon, P. S. Baran, *Angew. Chem.* **2002**, *114*, 1444–1447; *Angew. Chem. Int. Ed.* **2002**, *41*, 1386–1389; NaN_3/NaI/CAN convert alkenes into azido iodides: b) V. Nair, T. G. George, V. Sheeba, A. Augustine, L. Balagopal, L. G. Nair, *Synlett* **2000**, 1597–1598; Azido radicals are reasonable intermediates for this transformation. For early work on the oxidation of azide anions to azido radicals by reaction with H_2O_2/Fe^{II}: c) F. Minisci, R. Galli, *Tetrahedron Lett.* **1962**, 533–538; d) F. Minisci, R. Galli, *Tetrahedron Lett.* **1963**, 357–360.

[13] Arene iodination with I_2/CH_3CO_3H: a) Y. Ogata, K. Aoki, *J. Am. Chem. Soc.* **1968**, *90*, 6187–6191; for the use of H_2O_2/NaI to functionalize alkenes: b) J. Barluenga, M. Marco-Arias, F. González-Bobes, A. Ballesteros, J. M. González, *Chem. Eur. J.* **2004**, *10*, 1677–1682; for ketone iodinations: c) J. Barluenga, M. Marco-Arias, F. González-Bobes, A. Ballesteros, J. M. González, *Chem. Commun.* **2004**, 2616–2617; sulfonation of methane initiated by H_2O_2/metal chloride: d) S. Mukhopadhyay, A. T. Bell, *Angew. Chem.* **2003**, *115*, 3098–3101; *Angew. Chem. Int. Ed.* **2003**, *42*, 2990–2993.

[14] Very fast stirring is crucial to this iodination reaction. Lowering the speed of stirring employed to mix the reagents may result in a dramatic decrease of the efficiency of the iodination reaction.

[15] Reaction conditions: hydrocarbon **1** (5 mL), Ac_2O (1.2 mL), H_2O (0.5 mL), I_2 (1 mmol), NaN_3 (3 mmol), H_2O_2 (30 % aqueous solution, 0.3 mL). Reagents were mixed at 0 °C and vigorously stirred. Then the reaction mixture was heated at 40 °C.

[16] a) F. Hauxwell, R. H. Ottewill, *J. Colloid Interface Sci.* **1970**, *34*, 473–479; for conformational equilibria of alkanes in aqueous solution, see: b) H. S. Ashbaugh, S. Garde, G. Hummer, E. W. Kaler, M. E. Paulaitis, *Biophys. J.* **1999**, *77*, 645–654, and references therein.

[17] A single observation on the iodination of cyclohexane upon reaction with degassed aqueous solution of Mn^{III}–tetraphenylporphyrin iodide and PhIO as oxidant, is known to date: C. L. Hill, J. A. Smegal, T. J. Henly, *J. Org. Chem.* **1983**, *48*, 3277–3281.

 © 2005 Wiley-VCH Verlag GmbH & Co. KGaA, Weinheim

Nanostructures

DOI: 10.1002/anie.200501282

PbTe Nanorods by Sonoelectrochemistry**

*Xiaofeng Qiu, Yongbing Lou, Anna C. S. Samia, Anando Devadoss, James D. Burgess, Smita Dayal, and Clemens Burda**

Size, shape, and compositional control are at the heart of nanochemistry.[1] Herein, we present a novel method that allows control over all three variables in a simple one-step, wet-chemical procedure. One-dimensional (1D) nanomaterials are of great interest for the construction of high-performance thermoelectric (TE) devices. Theoretical calculations indicate that improvement in TE efficiency can be achieved as the diameter of the 1D structures approaches a few nanometers.[2,3] To date, the most successful synthesis of 1D TE materials has been achieved by electrodeposition within alumina templates. A series of Bi_2Te_3,[4,5] $Bi_{2-x}Sb_xTe_3$,[6] $Bi_2Te_{3-y}Se_y$,[7] and $Bi_{1-x}Sb_x$[8,9] nanowires were prepared by using the template-based method. The advantages of the electrodeposition method include high efficiency, ease of control over composition, highly crystalline products, and room-temperature reaction conditions. However, the diameters of the nanowires synthesized by the template method are well above 10 nm. To get into the sub-10-nm regime, one needs to obtain templates with very narrow channel diameters, which is currently the limiting factor of this technique.

However, advances in combining sonochemistry and electrochemistry have provided a new strategy for the synthesis of nanomaterials.[10–13] The synthesis of quite sophisticated 1D nanomaterials has recently been demonstrated[14] to be possible through careful control of the electrochemistry, sonochemistry, and initial composition of the precursor solutions. As observed, the advantage of the sonoelectrochemical method is that it achieves 1D control without any template, thereby practically overcoming the limitation of generating nanorods with diameters below 10 nm. This diameter is the size regime in which TE properties become enhanced and a controlled synthesis can produce technologically relevant nanomaterials. Herein, we report the first synthesis of monodispersed PbTe nanorods that are sub-10 nm in diameter through a sonoelectrochemical technique.

[*] X. Qiu, Y. Lou, Dr. A. C. S. Samia, S. Dayal, Prof. C. Burda
Center for Chemical Dynamics and Nanomaterials Research
Department of Chemistry
Case Western Reserve University
10900 Euclid Avenue, Cleveland, OH 44106 (USA)
Fax: (+1) 216-368-3006
E-mail: burda@case.edu
A. Devadoss, Prof. J. D. Burgess
Department of Chemistry
Case Western Reserve University
10900 Euclid Avenue, Cleveland, OH 44106 (USA)

[**] C.B. acknowledges support from NSF (CHE-0239688), ACS-PRF (39881-G5M), and the Ohio Board of Regents.

Furthermore, we present the effect of changing the concentration of the coordinating ligand on the resulting composition of the synthesized nanomaterials. Changing the metal/ligand ratio enabled us to tune the composition of the product from pure Te to pure PbTe nanorods.

Lead telluride is the material of choice because of its great potential in high-performance TE devices.[15] Furthermore, it allows the mechanisms that lead to control over the resulting nanorod size and composition to be studied. Basically, the synthesis of PbTe nanorods consists of two steps: First, the electrodeposition of PbTe on the surface of the Ti sonication horn, and second, the dispersion of the PbTe nuclei into solution by pulsed sonication. Control over the electrodeposition process is crucial in obtaining pure and highly crystalline PbTe nanoparticles. Interestingly, we found that the Pb^{2+}/nitrilotriacetic acid (NTA) ratio plays a key role in the synthesis of PbTe nanorods. In contrast to previous studies on the electrodeposition of bulk PbTe,[16] we used a stoichiometric reactant ratio in the synthesis of the nanorods. The introduction of NTA helps to prevent the precipitation of Pb^{2+} ions as $Pb(OH)_2$. Furthermore, electrochemical studies show that NTA acts as more than a coordinating capping agent: it actually determines the final products of the process. The pH value of the solution was monitored during the electrodeposition, and TeO_2 was shown to be sufficiently soluble at $pH < 2$ or $pH > 7$.[16] However, the solubility of NTA was too poor at low pH values to keep the Pb^{2+} ions coordinated and in solution. Therefore, the solution was kept at approximately pH 8 under our experimental conditions, as TeO_2 is dissolved as TeO_3^{2-} ions at this pH value. The overall PbTe reaction equation [Eq. (1)] is (the NTA ligand is omitted for clarity):

$$Pb^{2+} + TeO_3^{2-} + 3\,H_2O + 6\,e^- \rightarrow PbTe + 6\,OH^- \quad (1)$$

Figure 1 shows the cyclic voltammograms of solutions with different NTA concentrations. In this figure, peaks 1, 1′, and 1″ correspond to the reduction of TeO_3^{2-} to Te^{2-} while peaks 2, 2′, and 2″ correspond to the reduction of TeO_3^{2-} to Te^0.[16,17] The potential shifts show that the electrodeposition of PbTe is highly sensitive to the ratio between Pb^{2+} and NTA.

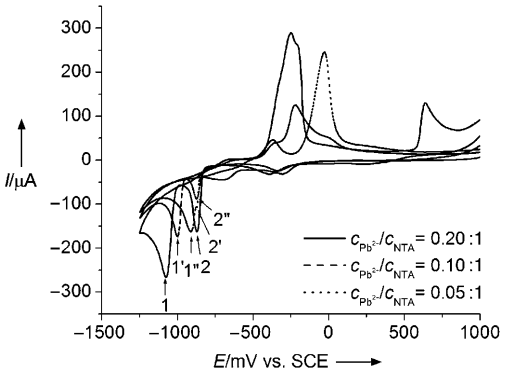


Figure 1. Cyclic voltammogram of the precursor solutions with $c_{Pb^{2+}}/c_{NTA}$ ratios changing from 0.20:1 (solid) to 0.10:1 (dash) then to 0.05:1 (dot). The concentrations of Pb^{2+} and TeO_3^{2-} ions were fixed at 10 mM in all measurements. SCE = saturated calomel electrode.

 © 2005 Wiley-VCH Verlag GmbH & Co. KGaA, Weinheim

At ratios of Pb^{2+}/NTA higher than approximately 0.16:1, the formation of PbTe can be achieved at potentials lower than −1.0 V and only the oxidation peak of PbTe at −0.245 V is observed in the reverse scan. By decreasing the Pb^{2+}/NTA ratio to as low as 0.05:1, peaks 1″ and 2″ almost overlap and the predominant species produced is Te^0, which is proved by the predominant oxidation of Te at −0.029 V during the reverse scan. The precipitation of both PbTe and Te^0 are observed in the intermediate cases in which the Pb^{2+}/NTA ratios are between 0.20:1 and 0.05:1, even when the potential is kept below −1.0 V. Both the oxidation peaks of PbTe at −0.225 V and Te at −0.024 V can be clearly observed in the reverse scan. This tuning of the product outcome was also confirmed by powder X-ray diffraction (XRD) measurements of the isolated nanomaterials. Overall, this observation shows that the Pb^{2+}/NTA ratio controls the nature and concentration of Pb^{2+} ions in solution, which then in turn influences the formation of PbTe.[18] Basically, the PbTe formation predominates when the Pb^{2+}/NTA ratio is high, even at very low concentrations of Te^{2-} ions. However, if the Pb^{2+}/NTA ratio is too low, the thermodynamic solubility constant K_{sp} limits the precipitation of PbTe, which only occurs at relatively high concentrations of Te^{2-} ions. We observed similar phenomena for the synthesis of other semiconductor nanocrystals. These results show that the ratio of metal ion/ligand concentration can be the controlling factor in the redox chemistry involved in the synthesis of semiconductor nanomaterials.

Figure 2 shows the powder XRD pattern of nanorods produced under different Pb^{2+}/NTA ratios. The XRD patterns show that the product exhibits a purely face-centered cubic (fcc) PbTe system ($a = 6.464$ Å; JCPDS card: 78-1905) at a high Pb^{2+}/NTA ratio (a), whereas the product is a purely

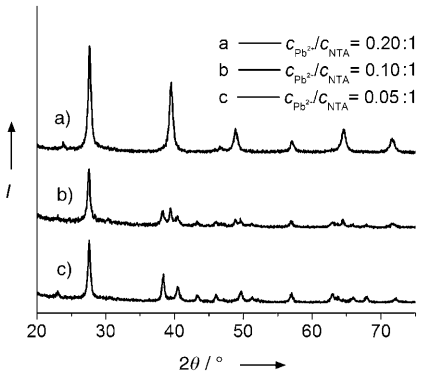


Figure 2. The powder XRD pattern of nanorods synthesized at different Pb^{2+}/NTA ratios. a) Pure PbTe, b) mixture of PbTe and Te, and c) pure Te.

hexagonal tellurium system ($a = 4.457$, $c = 5.927$ Å; JCPDS card: 36-1452) at low Pb^{2+}/NTA ratios of ≤ 0.05:1 (c). The XRD patterns for the products made at intermediate concentration ratios indicate a mixture of PbTe and Te powder. The cyclic voltammetry (CV) and XRD studies together show that the composition of the sample can be controlled by the initial Pb^{2+}/NTA ratio.

Modulation of the morphology is achieved by controlling the current intensity, reagent concentration, reaction time, and ultrasound intensity, as well as the ultrasound pulse on/off ratio. The morphology and crystallinity of the PbTe nanoparticles can be controlled precisely by using the correct sonoelectrochemical conditions.

A transmission electron microscopy (TEM) image of the PbTe nanorods shows a highly uniform nanorod morphology (Figure 3a), in which the nanorods have an average diameter of 7 nm and an aspect ratio of 7. It was found that the reaction time greatly affects the size of the PbTe nanorods and increasing the reaction time yielded larger nanorods with larger aspect ratios. Figure 3c shows the morphology of a PbTe nanorod after reaction for 45 minutes. The resulting nanorod has a diameter of 11.4 nm and a length of 104 nm. Figure 3d shows the nanorod obtained after 1.5 hours, which

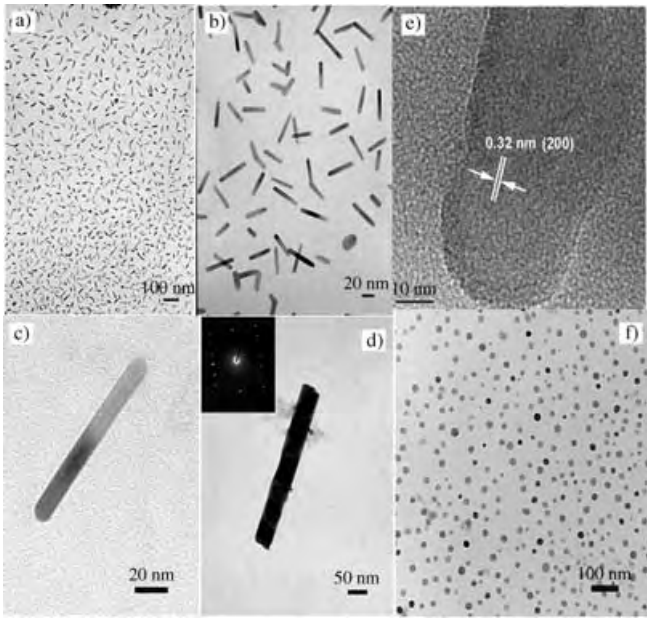


Figure 3. a) TEM image of PbTe nanorods prepared by sonoelectrochemistry at room temperature for 30 minutes. b) Enlarged TEM image of PbTe nanorods prepared under identical conditions. c) TEM image of a nanorod obtained after 45 minutes of reaction. d) TEM image of a nanorod obtained after 1.5 hours of reaction; the inserted selected-area electron-diffraction pattern indicates the single-crystal nature of the shown nanorod. e) HRTEM image of PbTe, a nanorod indicating the (200) lattice plane spacing. f) Spherical PbTe nanoparticles synthesized under a low concentration of Pb^{2+} ions (2 mM).

has a diameter of 43 nm and a length of 370 nm. A high-resolution TEM (HRTEM) study (Figure 3e) shows that the PbTe nanorods are highly crystalline and that the d spacing is 0.32 nm, which indexes to the d(200) planes of the fcc PbTe lattice. This value corresponds exactly to the strongest peak observed in the XRD pattern (Figure 2a). Therefore, the direction of the nanorod growth is perpendicular to the x axis and is along the [001] plane. Figure 3f shows PbTe nanoparticles synthesized under a very low concentration of Pb^{2+} ions (2 mM), and only spherical particles are observed. Increasing the concentration of Pb^{2+} ions causes the spheres to grow and rod-shaped morphologies to be yielded. Such rod growth is likely to occur through Ostwald ripening under the ultrasound cavitation process. Similar growth mechanisms were reported in the thermal synthesis of CdTe nanowires and Ag nanorods.[19,20]

 © 2005 Wiley-VCH Verlag GmbH & Co. KGaA, Weinheim

As the XRD results show, the prepared PbTe nanorods exhibit a cubic lattice structure. The crystalline symmetry of the material also affects the ZT value of the TE materials. Cubic space groups yield maximum degeneracy N_v of the band extrema near the Femi level. The ZT value, which is of merit itself, is proportional to the N_v value.[21] Thus, a further enhancement of the TE power can be reached with cubic PbTe nanorods.

In conclusion, we have successfully achieved the synthesis of PbTe nanorods with a diameter in the sub-10-nm regime that are highly uniform, single-crystalline, and pure through a novel sonoelectrochemical method under ambient conditions. The ratio of metal ion/ligand was used to control the purity of the PbTe nanostructures. These very thin and cubic PbTe nanorods are promising building units for future TE devices. Currently, the sonoelectrochemical synthesis of other nanomaterials is being studied to show the usefulness of this procedure for a broad range of synthetic applications.

Experimental Section

The room-temperature synthesis of the PbTe nanorods is based on constant-current electrodeposition accompanied by applied ultrasonic pulses in an aqueous solution that contains lead nitrate (Aldrich, 99.99%), NTA (Aldrich, 99+%), and TeO_2 (Aldrich, 99+%). A VCX-500 ultrasonic processor from Sonics and Materials Inc. (Ti horn, 0.5 inch in diameter, 20 kHz) worked as the ultrasound source and a Harrison 6102 A DC power supply acted as the current source. The solution was sonicated in the presence of a constant current for 0.5–2 h, and a sonication pulse on/off ratio varying from 1:1 to 1:10 was explored for the nanorod synthesis. Highly crystallized and monodispersed PbTe nanorods were produced with current densities of 10 mA cm^{-2}, ultrasound intensities of approximately 25–45%, and a reaction time of 30 min. After the reaction, the resulting brown–black solution was purified by centrifugation, and the precipitate was washed with distilled water and ethanol and then air dried before analysis.

CV measurements were carried out on a BAS CV 50W with a Pt-disc working electrode, Pt-wire counter electrode, and an SCE reference electrode, and the scan rate was 100 mV s^{-1}. The phase purity of products was characterized by a Scintag X-1 Advanced X-ray diffractometer (XRD, 2.4° min^{-1}, $Cu_{K\alpha}$ radiation). The morphology of the PbTe nanorods was analyzed with a transmission electron microscope, JEOL 1200CX (TEM, accelerating voltage: 80 kV). The HRTEM images were obtained on a FEI Tecnai F30 electron microscope by applying an accelerating voltage of 300 kV.

Received: April 12, 2005
Revised: June 4, 2005
Published online: August 5, 2005

Keywords: electrochemistry · nanorods · PbTe · sonochemistry

[1] C. Burda, X. Chen, R. Narayanan, M. A. El-Sayed, *Chem. Rev.* **2005**, *105*, 1025–1102.
[2] L. D. Hicks, M. S. Dresselhaus, *Phys. Rev. B* **1993**, *47*, 16631–16634.
[3] Y. M. Lin, M. S. Dresselhaus, *Phys. Rev. B* **2003**, *68*, 75304–75314.
[4] S. A. Sapp, B. B. Lakshmi, C. R. Martin, *Adv. Mater.* **1999**, *11*, 402–404.
[5] A. L. Prieto, M. S. Sander, M. S. Martin-Gonzalez, R. Gronsky, T. Sands, A. M. Stacy, *J. Am. Chem. Soc.* **2001**, *123*, 7160–7161.
[6] M. Martin-Gonzalez, A. L. Prieto, R. Gronsky, T. Sands, A. M. Stacy, *Adv. Mater.* **2003**, *15*, 1003–1006.
[7] M. Martin-Gonzalez, G. J. Snyder, A. L. Prieto, R. Gronsky, T. Sands, A. M. Stacy, *Nano Lett.* **2003**, *3*, 973–977.
[8] A. L. Prieto, M. Martin-Gonzalez, J. Keyani, R. Gronsky, T. Sands, A. M. Stacy, *J. Am. Chem. Soc.* **2003**, *125*, 2388–2389.
[9] M. Martin-Gonzalez, A. L. Prieto, M. S. Knox, R. Gronsky, T. Sands, A. M. Stacy, *Chem. Mater.* **2003**, *15*, 1676–1681.
[10] J. Reisse, T. Caulier, C. Deckerkheer, O. Fabre, J. Vandercammen, J. L. Delplancke, R. Winand, *Ultrason. Sonochem.* **1996**, *3*, S147–S151.
[11] J. J. Zhu, S. T. Aruna, Y. Koltypin, A. Gedanken, *Chem. Mater.* **2000**, *12*, 143–147.
[12] Y. Mastai, R. Polsky, Y. Koltypin, A. Gedanken, G. Hodes, *J. Am. Chem. Soc.* **1999**, *121*, 10047–10052.
[13] Y. Mastai, M. Homyonfer, A. Gedanken, G. Hodes, *Adv. Mater.* **1999**, *11*, 1010–1013.
[14] X. F. Qiu, C. Burda, R. L. Fu, L. Pu, H. Y. Chen, J. J. Zhu, *J. Am. Chem. Soc.* **2004**, *126*, 16276–16277.
[15] T. C. Harman, P. J. Taylor, M. P. Walsh, B. E. LaForge, *Science* **2002**, *297*, 2229–2232.
[16] H. Saloniemi, M. Kemell, M. Ritala, M. Leskela, *J. Electroanal. Chem.* **2000**, *482*, 139–148.
[17] H. Saloniemi, T. Kanniainen, M. Ritala, M. Leskela, *Thin Solid Films* **1998**, *326*, 78–82.
[18] G. Riveros, D. Lincot, J. F. Guillemoles, R. Henriquez, R. Schrebler, R. Cordova, H. Gomez, *J. Electroanal. Chem.* **2003**, *558*, 9–17.
[19] Z. Tang, N. A. Kotov, M. Giersig, *Science* **2002**, *297*, 237–240.
[20] B. A. Korgel, D. Fitzmaurice, *Adv. Mater.* **1998**, *10*, 661–665.
[21] F. J. DiSalvo, *Science* **1999**, *285*, 703–706.

 © 2005 Wiley-VCH Verlag GmbH & Co. KGaA, Weinheim

Hypervalent Iodine Reagents

DOI: 10.1002/anie.200501686

Domino Reaction of 2,3-Epoxy-1-alcohols and PIFA in the Presence of H_2O and the Concise Synthesis of (+)-Tanikolide**

Yasuyuki Kita, Satoshi Matsuda, Eri Fujii, Mai Horai, Kayoko Hata, and Hiromichi Fujioka*

The domino reaction can perform several reactions in a single operation and is a very powerful tool to synthesize organic compounds. The development of new and efficient domino

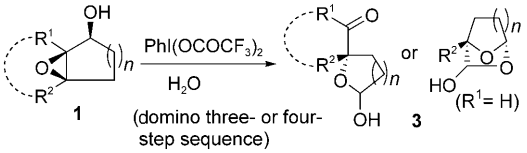
[*] Prof. Dr. Y. Kita, S. Matsuda, E. Fujii, M. Horai, K. Hata, Prof. Dr. H. Fujioka
Graduate School of Pharmaceutical Sciences
Osaka University, 1-6 Yamadaoka,
Suita, Osaka 565-0871 (Japan)
Fax: (+81) 6-6879-8229
E-mail: kita@phs.osaka-u.ac.jp

[**] This work was supported by Grants-in Aid for Scientific Research (S) from the Ministry of Education, Culture, Sports, Science, and Technology (Japan). PIFA = phenyliodine(III) bis(trifluoroacetate).

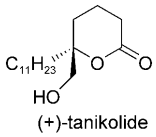
Supporting information for this article is available on the WWW under http://www.angewandte.org or from the author.

© 2005 Wiley-VCH Verlag GmbH & Co. KGaA, Weinheim

reactions is, therefore, a very attractive subject in the field of synthetic organic chemistry.[1] We present herein an efficient domino reaction in which a three- or four-step sequence occurs in a single operation. Thus, the reaction of 2,3-epoxy-1-alcohols[2] with hypervalent iodine(III) reagents[3] in the presence of H_2O allowed the efficient domino three- or four-step sequence to produce lactols **3** in a single operation (Scheme 1). The reaction was applied to the concise synthesis of (+)-tanikolide.



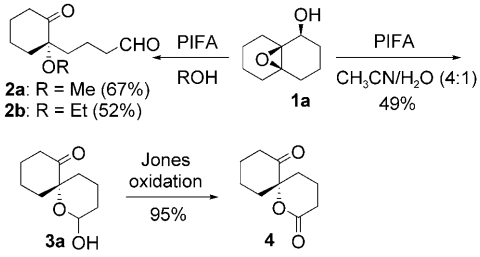
Scheme 1. Domino reaction of 2,3-epoxy-1-alcohols with PIFA in the presence of H_2O.



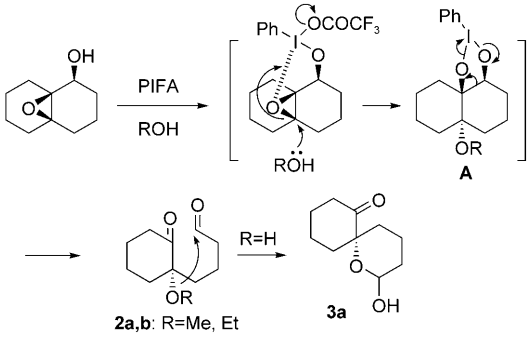
The reaction of bicyclic 2,3-epoxy alcohol **1a** with phenyliodine(III) bis(trifluoroacetate) (PIFA) was examined in the presence of an oxygen-containing nucleophile, an alcohol, or H_2O (when an alcohol was used, it was also employed as the solvent; Scheme 2). A mixture of **1a** (1.0 mmol) in ROH or H_2O/CH_3CN (1:4; 10 mL) was treated with PIFA (1.0 mmol) at 0 °C–RT, with the reaction proceeding smoothly for both nucleophiles. Methoxy keto aldehyde **2a** was obtained in moderate yield from the use of MeOH as the nucleophile, and a similar product **2b** was obtained from EtOH. On the other hand, the lactol **3a** (a mixture of diastereoisomers differing at the acetal position) was obtained from using H_2O. Compound **3a** was converted into the keto lactone **4** by the Jones oxidation.

The formation of **2a**,**b** and **3a** from **1a** is rationalized as follows: first, nucleophilic attack of ROH (R = Me, Et, H) on the oxirane ring gave the alkoxy or hydroxy intermediate **A**, whose C–C bond between the two hydroxy groups was cleaved to give keto aldehyde **2a**,**b** in good yield.[4] When H_2O was used as the nucleophile, a further lactol formation occurred to afford **3a** (Scheme 3).

The generality of the lactol formation was examined next by using various types of epoxy alcohols (Table 1). The bicyclic epoxy alcohols **1a**,**b** gave bicyclic keto lactols **3a**,**b** in fairly good yields (entries 1 and 2). The bicyclic dioxaspiro lactols **3c–i** were obtained in good yields from the monocyclic trisubstituted epoxy alcohols **1c–i**.[5] The formation of **3c–i** is rationalized as a further lactol formation between the hemiacetal hydroxy function and the aldehyde (Scheme 4). No further lactol formation was observed in the keto lactols **3a**,**b**, possibly because access to the ketone moieties is more hindered than to the aldehyde moieties.



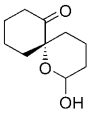
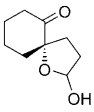
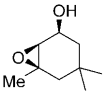
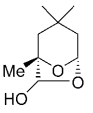
Scheme 2. PIFA treatment of **1a** in the presence of an oxygen-containing nucleophile.



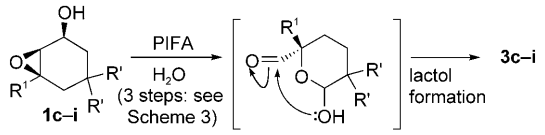
Scheme 3. Plausible reaction mechanism for the formation of **2** and **3**.

The bicyclic keto lactols were converted into the corresponding lactones in two steps. Thus, the reduction of **3e**,**h** with diisobutylaluminum hydride (DIBAH) or the reduction of **3i** of with $NaBH_4$ gave dihydroxy lactols **4e**,**h**,**i**, which were oxidized using Ag_2CO_3/celite[6] to afford the desired lactones **5e**,**h**,**i** in fairly good yields (Scheme 5).

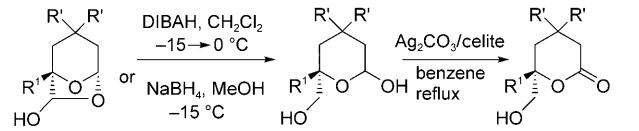
Table 1: Reaction of various 2,3-epoxy alcohols with PIFA in the presence of H_2O.

Entry	Substrate		Product		Yield [%]
1		**1a**		**3a**	49
2		**1b**		**3b**	66
3		**1c** (R^1 = Me)		**3c** (R^1 = Me)	62
4		**1d** (R^1 = Et)		**3d** (R^1 = Et)	74
5		**1e** (R^1 = *n*-$C_{11}H_{23}$)		**3e** (R^1 = *n*-$C_{11}H_{23}$)	72
6		**1f** (R^1 = CH_2CHMe_2)		**3f** (R^1 = CH_2CHMe_2)	67
7		**1g** (R^1 = CH_2Ph)		**3g** (R^1 = CH_2Ph)	72
8		**1h** (R^1 = Ph)		**3h** (R^1 = Ph)	53
9		**1i**		**3i**	65

 © 2005 Wiley-VCH Verlag GmbH & Co. KGaA, Weinheim



Scheme 4. Plausible reaction mechanism for the formation of bicyclic lactols **3c–i**.



3e: $R^1 = n\text{-}C_{11}H_{23}$, R' = H
3h: R^1 = Ph, R' = H
3i: $R^1 = CH_3$, R' = CH_3

4e, **4h**, **4i**

5e (57% over 2 steps)
5h (57% over 2 steps)
5i (98% over 2 steps)

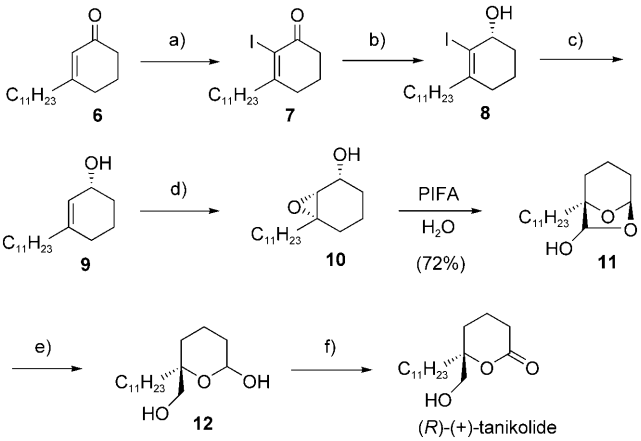
Scheme 5. Conversion of bicyclic lactols into lactones.

With the general transformation of epoxy alcohols to lactols and lactones now available, the application of this method to the concise asymmetric synthesis of (+)-tanikolide was examined next. (+)-Tanikolide is a γ-lactone metabolite of the marine cyanobacterium *Lyngbya majuscula*, which was collected on Tanikeli Island, Madagascar, in 1999 and shows antifungal activity.[7] The enone **6**[8] was converted into the α-iodo enone **7** in 80% yield by using the procedure developed by Sha and Huang.[9] The asymmetric reduction of **7** with the Corey reagent[10] afforded *R*-allyl alcohol **8** in 93% yield with 98% *ee* (optical purity was 98% *ee*, as determined by HPLC analysis of **9** (chiralcel OD and elution with hexane/*i*PrOH (99:1)). The radical reduction[11] of **8** afforded **9** in 84% yield. The stereoselective epoxidation[12] of **9** gave the *cis*-epoxy alcohol **10**. The treatment of **10** with PIFA gave the lactol **11** in 72% yield. Reduction of **11** with DIBAH gave the hydroxy lactol **12**. Chemoselective oxidation of the lactol hydroxy function with Ag_2CO_3/celite[6] afforded (+)-tanikolide in 57% yield over two steps (Scheme 6). ^{1}H NMR spectroscopic analysis (500 MHz) of the corresponding (*R*)-(+)-α-methoxy-α-(trifluoromethyl)phenylacetic acid ester of (+)-tanikolide[13] determined the *ee* value as 98%. Although several synthetic studies of (+)-tanikolide have already been reported,[14] our synthesis provides an alternative approach with few steps and high optical purity.

In conclusion, we have developed a novel transformation of 2,3-epoxy-1-alcohols into lactols in a single operation. The lactone functionality is present in a large variety of biologically active compounds and natural products. As domino reactions can reduce the number of operations in the synthesis of organic compounds, this method opens up a new approach to obtaining optically active lactone compounds and will be very useful in the field of synthetic organic chemistry.

Experimental Section

General procedure for lactol formation (conversion of **10** into **11**): PIFA (281.3 mg, 0.65 mmol) was added to a stirred solution of **10** (175.6 mg, 0.65 mmol) in H_2O/CH_3CN (1:4 (v/v), 6.5 mL) at 0 °C. The reaction mixture was allowed to warm to room temperature and then



Scheme 6. Concise asymmetric synthesis of (*R*)-(+)-tanikolide. a) I_2, trimethylsilyl azide, pyridine, 0 °C→RT (80%); b) (*S*)-5,5-diphenyl-2-methyl-3,4-propan-1,3,2-oxazaborolidine, BH_3Me_2S, THF, 0 °C (93%); c) Et_3B, nBu_3SnH, toluene, 0 °C–RT (84%); d) *t*BuOOH, [VO(acac)$_2$] (acac = acetylacetonate), benzene, 0 °C→RT (96%); e) DIBAH, CH_2Cl_2, −15→0 °C; f) $AgCO_3$/celite, benzene, reflux (57% over 2 steps).

stirred for 12 h. A saturated aqueous $Na_2S_2O_3$ solution was added to a reaction mixture, and the resulting mixture was extracted with EtOAc. The organic layer was dried over Na_2SO_4 and evaporated in vacuo. The residue was purified by column chromatography on SiO_2 using hexane/EtOAc (5:1) as the eluant to give **11** as a single isomer (134.0 mg, 0.47 mmol, 72% yield).

11: colorless crystals; m.p. 45 °C; IR (KBr): $\tilde{\nu} = 3360\ cm^{-1}$; ^{1}H NMR (300 MHz, $CDCl_3$): $\delta = 0.88$ (3H, t, $J = 6.6$ Hz), 1.26 (20H, m), 1.51–1.72 (6H, m), 3.27 (1H, brs), 5.17 (1H, s), 5.67 ppm (1H, s); ^{13}C NMR (75 MHz, $CDCl_3$): $\delta = 14.0$, 15.8, 22.6, 23.8, 29.1, 29.2, 29.3, 29.5 (2C), 29.6 (2C), 30.2, 31.8, 34.0, 83.9, 97.1, 102.2 ppm; $[\alpha]_D^{26} = +54.2$ ($c = 0.54$, $CHCl_3$); elemental analysis (%) for $C_{17}H_{23}O_3$: C 71.79, H 11.34; found: C 71.58, H 11.09.

Received: May 17, 2005
Published online: August 11, 2005

Keywords: domino reactions · epoxy alcohols · hypervalent iodine · natural products · oxygen heterocycles

[1] For examples, see: a) S. F. Mayer, W. Kroutil, K. Faber, *Chem. Soc. Rev.* **2001**, *30*, 332–339; b) P. J. Parsons, C. S. Penkett, A. J. Shell, *Chem. Rev.* **1996**, *96*, 195–206; c) L. F. Tietze, *Chem. Rev.* **1996**, *96*, 115–136; d) R. A. Bunce, *Tetrahedron* **1995**, *51*, 13103–13159; e) L. F. Tietze, U. Beifuss, *Angew. Chem.* **1993**, *105*, 137–170; *Angew. Chem. Int. Ed. Engl.* **1993**, *32*, 131–163.

[2] For our recent examples using 2,3-epoxy-1-alcohol derivatives, see: a) Y. Kita, S. Kitagaki, Y. Yoshida, S. Mihara, D.-F. Fang, M. Kondo, S. Okamoto, R. Imai, S. Akai, H. Fujioka, *J. Org. Chem.* **1997**, *62*, 4991–4997; b) Y. Kita, J. Futamura, Y. Ohba, Y. Sawama, J. K. Ganesh, H. Fujioka, *J. Org. Chem.* **2003**, *68*, 5917–5924; c) H. Fujioka, Y. Yoshida, Y. Kita, *J. Syn. Org. Chem. Jpn.* **2003**, *61*, 133–143; d) Y. Kita, J. Futamura, Y. Ohba, Y. Sawama, J. K. Ganesh, H. Fujioka, *Tetrahedron Lett.* **2003**, *44*, 411–413; e) Y. Kita, S. Matsuda, R. Inoguchi, J. K. Ganesh, H. Fujioka, *Tetrahedron Lett.* **2005**, *46*, 89–91.

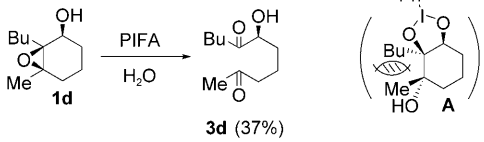
[3] For a recent review on hypervalent iodine chemistry, see: T. Wirth, *Angew. Chem.* **2005**, *117*, 3722–3731; *Angew. Chem. Int. Ed.* **2005**, *44*, 3656–3665; for our reviews on hypervalent iodine(III) reagents, see: a) Y. Kita, H. Tohma, T. Yakura, *Trends Org. Chem.* **1992**, 113–128; b) Y. Kita, T. Takada, H.

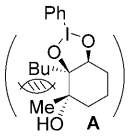
 © 2005 Wiley-VCH Verlag GmbH & Co. KGaA, Weinheim

Tohma, *Pure Appl. Chem.* **1996**, *68*, 627 – 630; c) H. Tohma, Y. Kita, *J. Syn. Org. Chem. Jpn.* **2004**, *62*, 116 – 127; for recent examples of domino reactions using hypervalent iodine reagents, see: S. P. Cook, C. Gaul, S. J. Danishefsky, *Tetrahedron Lett.* **2005**, *46*, 843 – 847; D. Gabrilidis, C. Kalogiros, L. P. Hadjiarapoglou, *Synlett* **2004**, 2566 – 2569.

[4] For oxidative cleavage of 1,2-diols by hypervalent iodine reagents, see: R. Criegee, H. Beucker, *Ann. Chem.* **1939**, *541*, 218 – 238.

[5] Tetrasubstituted *cis*-epoxy alcohol **1d** afforded diketo alcohol **3d** in 37% yield by cleavage of the C2–C3 bond, perhaps as the formation of the five-membered intermediate **A** is unfavorable because of repulsion.





[6] M. Fetizon, M. Golfier, P. Mourgues, *Tetrahedron Lett.* **1972**, 4445 – 4448.

[7] I. P. Singh, K. E. Milligan, W. H. Gerwick, *J. Nat. Prod.* **1999**, *62*, 1333 – 1335.

[8] J.-P. Barnier, V. Morisson, I. Volle, L. Blanco, *Tetrahedron: Asymmetry* **1999**, *10*, 1107 – 1117.

[9] C.-K. Sha, S.-J. Huang, *Tetrahedron Lett.* **1995**, *36*, 6927 – 6928. Asymmetric reduction of the enone **6** to allyl alcohol **9** by the Corey reagent resulted in 77% *ee*; then, asymmetric reduction of iodo enone **7** was attempted: S. Demay, K. Harms, P. Knochel, *Tetrahedron Lett.* **1999**, *40*, 4981 – 4984.

[10] E. J. Corey, R. K. Bakshi, S. Shibata, C.-P. Chen, V. K. Singh, *J. Am. Chem. Soc.* **1987**, *109*, 7925 – 7526. The absolute configuration of the secondary alcohol was deduced by reference to the literature and our previous study (see ref. [2]); this deduction was determined by correlation of the synthesized tanikolide with the natural sample.

[11] a) K. Nozaki, K. Oshima, K. Utimoto, *Bull. Chem. Soc. Jpn.* **1991**, *64*, 403 – 409; b) Y. Yuasa, W. Sato, S. Shibuya, *Synth. Commun.* **1997**, *27*, 573 – 585.

[12] K. B. Sharpless, R. C. Michaelson, *J. Am. Chem. Soc.* **1973**, *95*, 6136 – 6137.

[13] Use of DIBAH in place of $NaBH_4$ increased the yield of (+)-tanikolide.

[14] a) R. M. Kanada, T. Taniguchi, K. Ogasawara, *Synlett* **2000**, 1019 – 1021; b) H. Tanaka, Y. Kozuki, K. Ogasawara, *Tetrahedron Lett.* **2002**, *43*, 4175 – 4178; c) H. Mizutani, M. Watanabe, T. Honda, *Tetrahedron* **2002**, *58*, 8929 – 8936; d) A. E. Koumbis, K. M. Dieti, M. G. Vikentiou, J. K. Gallos, *Tetrahedron Lett.* **2003**, *44*, 2513 – 2516; e) M. Carda, S. Rodríguez, E. Castillo, A. Bellido, S. Díaz-Oltra, J. A. Marco, *Tetrahedron* **2003**, *59*, 857 – 864; f) J. M. Shomaker, B. Borhan, *Org. Biomol. Chem.* **2004**, *2*, 621 – 624; g) T. Ohgiya, S. Nishiyama, *Tetrahedron Lett.* **2004**, *45*, 8273 – 8275; h) H. Arasaka, M. Iwata, M. Makida, Y. Masaki, *Chem. Pharm. Bull.* **2004**, *52*, 848 – 852.

 © 2005 Wiley-VCH Verlag GmbH & Co. KGaA, Weinheim

Diastereoselectivity

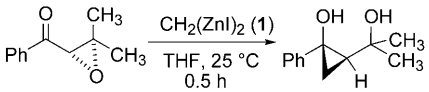
DOI: 10.1002/anie.200501644

Stereospecific and Stereoselective Preparation of 2-(1-Hydroxyalkyl)-1-alkylcyclopropanols from α,β-Epoxy Ketones and Bis(iodozincio)methane**

*Kenichi Nomura, Koichiro Oshima, and Seijiro Matsubara**

The most common method used to prepare cyclopropane compounds involves the reaction of electrophilic Simmons–Smith-type reagents with alkenes.[1] In contrast to this electrophilic [2+1] reaction, a *gem*-organodimetal compound also has the possibility of participating in a nucleophilic [2+1] reaction because it has two nucleophilic sites on one carbon atom.[2,3] In fact, we have already reported the reaction of bis(iodozincio)methane (**1**) with 1,2-diketone to give *cis*-1,2-cyclopropanediol with high diastereoselectivity.[4] In this transformation, **1** acts as a bidentate Lewis acid and fixes the conformation of the 1,2-diketone in the *s-cis* form.[4c] Thus, a substrate which has two Lewis basic sites may interact at two sites with **1**, and may show some characteristic stereochemical performance during subsequent useful molecular transformations.[5] Following this observation, we treated **1** with α,β-epoxy ketone and found that the reaction resulted in the stereospecific formation of 2-(1-hydroxyalkyl)-1-alkylcyclopropanol.[6]

Treatment of 2-benzoyl-1,1-dimethyloxirane (**2a**) with **1** gives (1*R**,2*R**)-2-(1-methyl-1-hydroxyethyl)-1-phenylcyclopropanol (**3a**) as the sole product (Scheme 1). The stereochemistry of the product was determined by single-crystal X-ray analysis (Figure 1).[7] Other examples of reactions conducted that led to formation of a cyclopropane ring are



2a **3a** (67%)

Scheme 1. Reaction of bis(iodozincio)methane (**1**) with α,β-epoxy ketone **2a**.

[*] K. Nomura, Prof. Dr. K. Oshima, Prof. Dr. S. Matsubara
Department of Material Chemistry
Graduate School of Engineering
Kyoto University
Kyoutodaigaku-Katsura, Nishikyo, Kyoto 615-8501 (Japan)
Fax: (+81) 75-383-2438
E-mail: matsubar@orgrxn.mbox.media.kyoto-u.ac.jp

[**] This work was supported financially by the Japanese Ministry of Education, Science, Sports, and Culture. The financial support provided by Chugai Pharmaceutical Co., Ltd. and the Takahashi Industrial and Economical Research Foundation are also acknowledged.

Supporting information for this article is available on the WWW under http://www.angewandte.org or from the author.

© 2005 Wiley-VCH Verlag GmbH & Co. KGaA, Weinheim

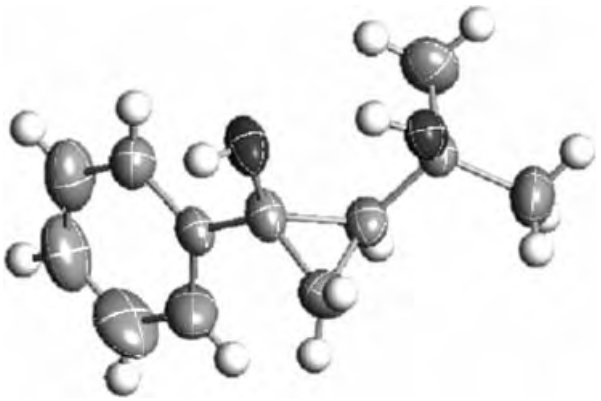
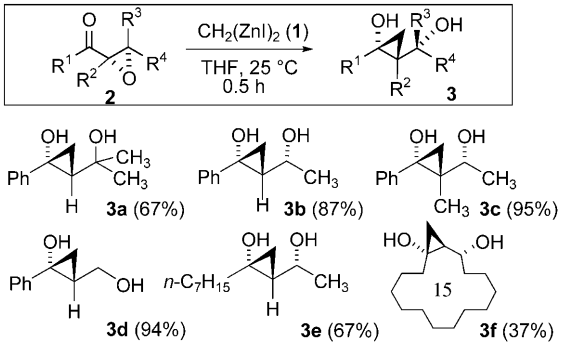


Figure 1. Structure of **3a** as determined by X-ray analysis.



Scheme 2. Preparation of 2-(1-hydroxyalkyl)-1-alkylcyclopropanol **3**.

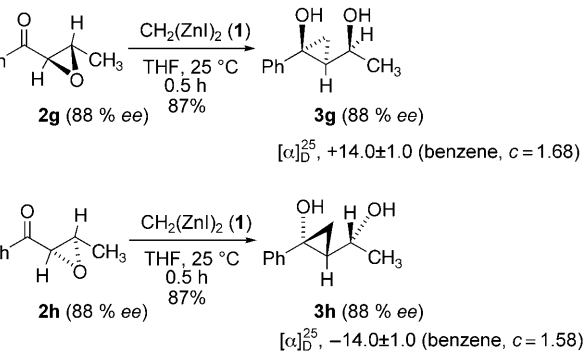
summarized in Scheme 2. In all cases, the reaction yielded a single diastereomer selectively.

An optically active epoxy ketone[8] **2g** was treated with **1** to give (1*S*,2*S*)-2-(*S*-1-hydroxyethyl)-1-phenylcyclopropanol (**3g**) without loss of enantiomeric purity. The reaction involving the enantiomer of **2g** (namely, **2h**) gave the corresponding enantiomer **3h** (Scheme 3).

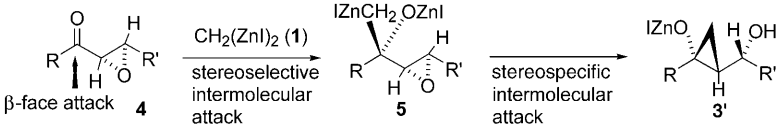
The diastereoselective formation of cyclopropanol **3** can be explained as follows. The reaction starts with the diastereoselective attack of **1** at the carbonyl group as a consequence of the stereogenic center at the α-carbon atom (Scheme 4).[4,9] This step is followed by stereospecific attack on the epoxide.

The explanation shown in Scheme 4 requires diastereoselective attack to the β face of **4**, which needs to be rationalized, since previous reports concerning the diastereoselective metal-mediated nucleophilic attack to an α,β-epoxy ketone occurred from the α face of **4**.[10]

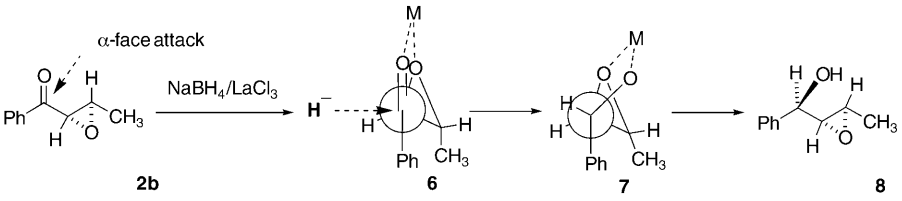
For example, treatment of **2b** with $NaBH_4/LaCl_3$ resulted in the exclusive formation of *erythro*-epoxy alcohol.[11] The diastereoselective reaction was explained by chelation effects to form intermediate **6**, as shown in Scheme 5. Other metal salts, such as $CaCl_2$, $MnCl_2$, and $ZnCl_2$ as well as $LaCl_3$ showed the same effect. Sato et al reported the preparation of 2-(1-hydroxyalkyl)-1-alkylcyclopropanol from an α,β-epoxy ketone and trimethylstannylmethyllithium.[6] Their results did not reveal any diasteromeric selectivity for trisubstituted oxirane substrates such as **3c**. The major isomers were also postulated to be produced by α-face attack of **4** in the case of disubstituted oxirane substrates (namely, **3a**,**b**,**d**–**f**).[6] In the present cyclopropanation reaction, the addition of **1** cannot be explained by a simple chelation intermediate such as **6**,[6,10,11] because the first nucleophilic attack also occurred by β-face attack on **4**. From our ab initio calculations, we propose that coordination of **1** to 2,3-dioxobutane occurs in a face-to-face arrangement, as shown in Figure 2 (**9**: side view; **10**: bottom view).[4c]



Scheme 3. Preparation of optically active 2-(1-hydroxyalkyl)-1-alkylcyclopropanol from optically active α,β-epoxy ketones and bis(iodozincio)methane (**1**).



Scheme 4. Stereochemical requirements for the reaction.



Scheme 5. Diastereoselective reduction of epoxy ketone with $NaBH_4$·$LaCl_3$.

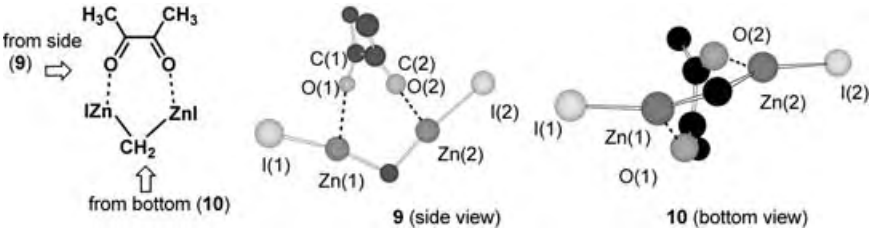


Figure 2. Initial complex formed in the reaction of 2,3-dioxobutane with **1** based on B3LYP/II//B3LYP/I calculations. See ref. [4c].

 © 2005 Wiley-VCH Verlag GmbH & Co. KGaA, Weinheim

Such coordination has two characteristic features: first, the dihedral angle of the diketone part (∢O(1)-C(1)-C(2)-O(2) = 47.7°); and second, the mechanism through which the zinc reagent coordinates to the diketone. A line drawn between the two oxygen atoms of the diketone, and another between the two zinc atoms in the initial complex, cross at almost right angles. In the same way, the nucleophilic attack of **1** on epoxy ketone **2h** can be explained via intermediate **11** (Scheme 6). Attack from the other face via intermediate **13** will be constrained by steric hindrance between **1** and the epoxide ring. Thus, face-to-face coordination will promote attack on the opposite face relative to traditional Cram-chelation intermediates such as **6**.

A cyclic substrate such as **14** or **16** (Scheme 7) will experience some difficulty in differentiating between the intermediate corresponding to **11** and **13** because of steric hindrance of the carbocyclic moiety. Treatment of **14** and **16** with **1**, however, gave the spiro compound with good diastereoselectivity. Figure 3 shows the results of the single-crystal X-ray analysis of the diester obtained from **17a** and 3,5-dinitrobenzoyl chloride.[12]

A derivative of 2-(1-hydroxyalkyl)-1-alkylcyclopropanol is an important intermediate structure of some natural products.[13] In our present method, we report a new diastereofacial selective attack of epoxy ketone by utilizing the Lewis acidity of the dizinc reagent **1**. Bis(iodozincio)-methane (**1**), prepared from diiodomethane and zinc powder, exists as monomeric form without aggregation or a contribution of the Schlenk equilibrium.[14,15] This monomeric structure is crucial when demonstrating its function as an effective bidentate Lewis acid in a stereoselective reaction.

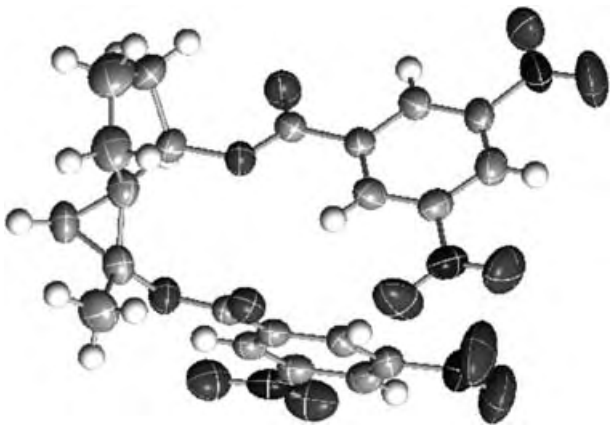
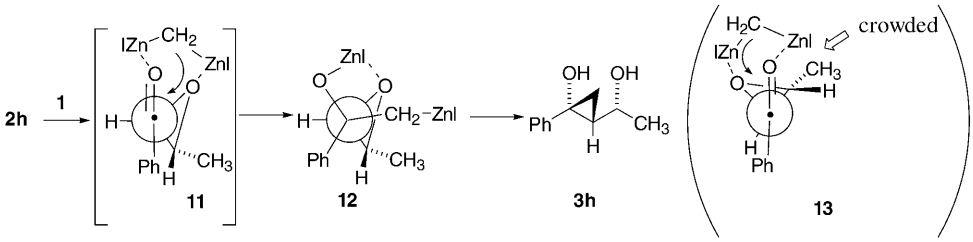
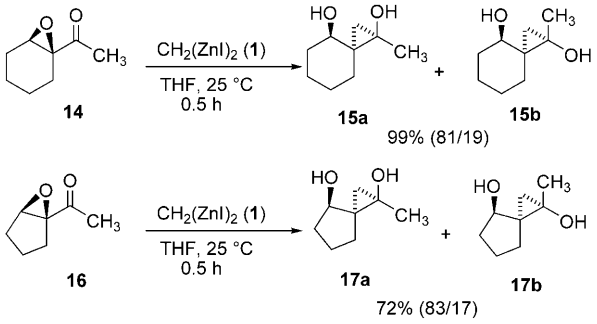


Figure 3. Structure of diester (3,5-dinitrobenzoylester) of **17a** obtained by X-ray analysis.



Scheme 6. Proposal for the stereoselective reaction of **2h** with **1**.



Scheme 7. Formation of spiro derivatives.

Received: May 13, 2005
Published online: August 9, 2005

Keywords: diastereoselectivity · epoxy ketones · small ring systems · zinc

[1] a) H. E. Simmons, R. D. Smith, *J. Am. Chem. Soc.* **1958**, *80*, 5323; b) H. Lebel, J.-F. Marcoux, C. Molinaro, A. B. Charette, *Chem. Rev.* **2003**, *103*, 977; c) A. B. Charette, A. Beauchemin, *Org. React.* **2001**, *58*, 1.

[2] a) S. Matsubara, K. Oshima, K. Utimoto, *J. Organomet. Chem.* **2001**, *617*, 39; S. Matsubara, *J. Org. Synth. Soc. Jpn.* **2000**, *58*, 118; b) P. Knochel, J.-F. Normant, *Tetrahedron Lett.* **1986**, *27*, 4427 and P. Knochel, J.-F. Normant, *Tetrahedron Lett.* **1986**, *27*, 4431; c) I. Marek, J.-F. Normant, *Chem. Rev.* **1996**, *96*, 3241; d) I. Marek, J.-F. Normant in *Organozinc Reagents. A Practical Approach* (Eds.: P. Knochel, P. Jones), Oxford Uninersity Press, Oxford, **1999**, p. 119.

[3] a) D. Beruben, I. Marek, J.-F. Normant, N. Platzer, *J. Org. Chem.* **1995**, *60*, 2488; b) D. Beruben, I. Marek, J.-F. Normant, N. Platzer, *Tetrahedron Lett.* **1993**, *34*, 7575.

[4] a) K. Ukai, K. Oshima, S. Matsubara, *J. Am. Chem. Soc.* **2000**, *122*, 12047; b) K. Nomura, K. Oshima, S. Matsubara, *Tetrahedron Lett.* **2004**, *45*, 5957; c) S. Matsubara, K. Ukai, H. Fushimi, Y. Yokota, H. Yoshino, K. Oshima, K. Omoto, A. Ogawa, Y. Hioki, H. Fujimoto, *Tetrahedron* **2002**, *58*, 8255.

[5] S. Matsubara, H. Yamamoto, K. Oshima, *Angew. Chem.* **2002**, *114*, 2961; *Angew. Chem. Int. Ed.* **2002**, *41*, 2837.

[6] T. Sato, T. Kikuchi, H. Tsujita, A. Kaetsu, N. Sootome, K. Nishida, K. Tachibana, E. Murayama, *Tetrahedron* **1991**, *47*, 3281.

[7] For the X-ray diffraction study, a crystal was mounted on a glass fiber coated with epoxy resin. Measurements were made on a Rigaku Mercury charge-coupled device (CCD) system with graphite monochromated $Mo_{K\alpha}$ radiation. Orthorhombic, $a = 6.1690(7)$, $b = 16.0965(17)$, $c = 22.395(2)$ Å, $\beta = 90.0°$, $V = 2223.8(4)$ Å^3, $Z = 9$, $\rho_{calcd} = 1.148$ Mg m^{-3}, $\lambda(Mo_{K\alpha}) = 0.71073$ Å,

 © 2005 Wiley-VCH Verlag GmbH & Co. KGaA, Weinheim

$T = 296$ K, $2\theta_{max} = 54.1°$, $R = 0.0371$ for 4852 reflections ($I > 2\sigma(I)$).
[8] An optically active epoxy alcohol was oxidized by $(COCl)_2$/DMSO/Et_3N.
[9] K. Ukai, D. Arioka, H. Yoshino, H. Fushimi, K. Oshima, K. Utimoto, S. Matsubara, *Synlett* **2001**, 513.
[10] a) K. Li, L. G. Hamann, M. Koreeda, *Tetrahedron Lett.* **1992**, *33*, 6569; b) T. Nakata, T. Tanaka, T. Oishi, *Tetrahedron Lett.* **1981**, *22*, 7723; c) D. E. Chavez, E. N. Jacobsen, *Angew. Chem.* **2001**, *113*, 3779; *Angew. Chem. Int. Ed.* **2001**, *40*, 3667.
[11] H. Fujii, K. Oshima, K. Utimoto, *Chem. Lett.* **1992**, 967.
[12] Monoclinic, $a = 5.9500(9)$, $b = 22.439(3)$, $c = 22.439(3)$ Å, $\beta = 90.536(3)°$, $V = 2335.9(6)$ Å^3, $Z = 4$, $\rho_{calcd} = 1.508$ Mg m^{-3}, λ-($Mo_{K\alpha}$) = 0.71073 Å, $T = 296$ K, $2\theta_{max} = 54.1°$, $R = 0.0320$ for 5098 reflections ($I > 2\sigma(I)$).
[13] a) R. Tokunoh, H. Tomiyama, M. Sodeoka, M. Shibasaki, *Tetrahedron Lett.* **1996**, *37*, 2449; b) A. Corsaro, U. Chiacchio, R. Adamo, Pistarà, A. Rescifina, R. Romeo, G. Catelani, F. D'Andrea, M. Mariani, E. Attolino, *Tetrahedron* **2004**, *60*, 3787.
[14] S. Matsubara, Y. Yamamoto, K. Utimoto, *Synlett* **1998**, 1471.
[15] S. Matsubara, K. Oshima, H. Matsuoka, K. Matsumoto, K. Ishikawa, E. Matsubara, *Chem. Lett.* **2005**, *34*, 952.

 © 2005 Wiley-VCH Verlag GmbH & Co. KGaA, Weinheim

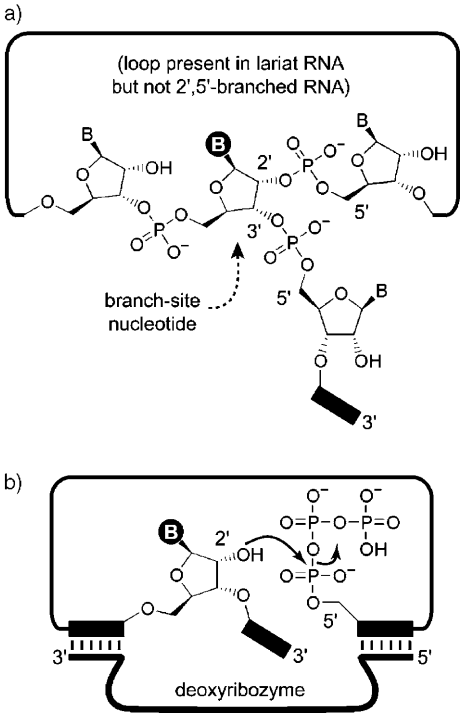


Figure 1. Lariat RNA and its synthesis by a deoxyribozyme (B = A, G, C, or U). a) Connectivity of lariat RNA and 2′,5′-branched RNA. The latter has the same branch-site nucleotide as a lariat but lacks the closed loop. The four illustrated nucleotides constitute the minimal part of a 2′,5′ -branched RNA. b) Deoxyribozyme-catalyzed synthesis of lariat RNA.

DNA Catalysis

DOI: 10.1002/anie.200501643

Efficient One-Step Synthesis of Biologically Related Lariat RNAs by a Deoxyribozyme**

*Yangming Wang and Scott K. Silverman**

Lariat RNAs are intermediates in RNA splicing events catalyzed by group II introns and the spliceosome.[1,2] Lariats have a closed RNA loop with a single 2′–5′ linkage and a single-stranded oligonucleotide attached at the 3′-oxygen atom of the branch-site nucleotide (Figure 1 a). Topologically, lariats are a subclass of 2′,5′-branched RNAs, which do not necessarily have the closed loop that is characteristic of lariats. Owing to their special topology, lariat RNAs are difficult to synthesize by any conventional chemical approach such as solid-phase synthesis,[3] and even the simpler 2′,5′-branched RNA core (without the closed loop of a lariat) is a significant challenge.[4] Recently we reported artificial deoxyribozymes (DNA enzymes)[5] that create branched RNAs in $>90\,\%$ yield by catalyzing the intermolecular reaction of an internal 2′-hydroxy group with a 5′-triphosphate.[6,7] Some of these deoxyribozymes are capable of synthesizing branched RNAs of wide sequence composition.[8,9] Lariat products can result from intramolecular branch formation events (that is, macrocyclizations with single linear RNA substrates), as illustrated in Figure 1 b. Apart from using the frequently impractical biological splicing machinery itself, there is no method present for the synthesis of biologically relevant lariat RNAs, which are often several hundred nucleotides in length and have extensive secondary structure[10] that may interfere with loop formation. Indeed, most of our reported branch-forming deoxyribozymes such as 7S11, which is widely useful for branched RNA synthesis,[8] are not useful with biologically derived RNA sequences as substrates (lariat yield typically $<1\,\%$; data not shown). In contrast to these difficulties, we report herein that the 6BX22 deoxyribozyme can create two common classes of biological lariat RNAs efficiently in one step from readily available RNA substrates.

In previous efforts, we used in vitro selection[11] to identify many deoxyribozymes that synthesize branched RNA.[6–9,12]

[*] Y. Wang, Prof. S. K. Silverman
Department of Chemistry
University of Illinois at Urbana-Champaign
600 South Mathews Avenue, Urbana, IL 61801 (USA)
Fax: (+1) 217-244-8024
E-mail: scott@scs.uiuc.edu

[**] This research was supported by the Burroughs Wellcome Fund (New Investigator Award in the Basic Pharmacological Sciences), the March of Dimes Birth Defects Foundation (Research Grant No. 5-FY02-271), the National Institutes of Health (GM-65966), the American Chemical Society Petroleum Research Fund (38803-G4), and the UIUC Department of Chemistry (all to S.K.S.). S.K.S. is a Fellow of The David and Lucile Packard Foundation. We thank Jonathan Staley (University of Chicago) for the plasmid encoding the ACT1 intron RNA and Scott Stevens (University of Texas at Austin) for the sample of debranching enzyme.

Supporting information for this article is available on the WWW under http://www.angewandte.org or from the author.

 © 2005 Wiley-VCH Verlag GmbH & Co. KGaA, Weinheim

However, our procedure does not select for the particular ability to create lariats. One-step lariat formation is presumably more difficult than simple branch formation because the incipient RNA loop may clash sterically with the DNA structure, thereby inhibiting catalysis. We surveyed many of the branch-forming deoxyribozymes to determine their lariat-formation capabilities. One of these deoxyribozymes, 6BX22,[12] showed promise in this regard and was examined more carefully. The 6BX22 deoxyribozyme has a specific 39-nucleotide DNA enzyme region embedded between Watson–Crick binding arms, as shown schematically in Figure 1b. It was found to require Mn^{2+}; detectable RNA ligation activity was not observed with Mg^{2+}, Ca^{2+}, Zn^{2+}, Fe^{2+}, Co^{2+}, Ni^{2+}, Cd^{2+}, or $[Co(NH_3)_6]^{3+}$ (all as chloride salts at concentrations in the range of 10 μM–10 mM; data not shown). The k_{obs} value for 6BX22-catalyzed branch formation is $\approx 0.07\ min^{-1}$ ($t_{1/2} \approx 10$ min) under standard incubation conditions (Mn^{2+} (20 mM), pH 7.5, 37 °C; see below). The background rate for the analogous DNA-templated reaction (the use of a DNA template that lacks an enzyme region between the DNA binding arms) is much lower; $k_{templated} \approx 4 \times 10^{-7}\ min^{-1}$ [6], which gives a rate enhancement ($k_{obs}/k_{templated}$) of 2×10^5.[13] Therefore, 6BX22 clearly "catalyzes" branch formation. If it merely templated the reaction by increasing the effective substrate concentration, then $k_{obs}/k_{templated}$ would be 1.[5a]

Before studying 6BX22-catalyzed lariat RNA synthesis in detail, we examined the substrate sequence generality of this deoxyribozyme for branch formation. This reaction is simpler than lariat formation because loop closure is not required. The selection procedure in which 6BX22 was identified[12] used RNA substrates that correspond to the conserved branch-site sequences of yeast spliceosomal substrates (Figure 2a), which are common models for understanding RNA splicing.[2] Systematic experiments revealed that sequence changes outside the conserved RNA elements are tolerated well by 6BX22, indicating that this DNA enzyme is general for branch formation with yeast spliceosomal substrates (Figure 2b). Most nucleotide changes within the conserved regions are also tolerated. For example, the branch-site nucleotide itself may be changed from A to C or U with nearly equivalent ligation efficiencies (Figure 2c). A branch-site G is accepted but with diminished yield.

We applied 6BX22 toward the synthesis of three specific representative biological lariat RNAs that are derived from yeast or mammalian spliceosomal substrates, but share no sequence elements outside of the small consensus region. The three RNAs are the 69-nt yeast YBL059W intron with a 51-nt lariat loop,[14] the 130-nt human β-globin IVS1 intron with a 94-nt loop,[15] and the 309-nt yeast actin (ACT1) intron with a 266-nt loop.[16] In each case, a linear 5′-triphosphate substrate was prepared by in vitro transcription with T7 RNA polymerase. By using the linear substrate, the small YBL059W lariat was readily synthesized by 6BX22 in one step and in high yield (Figure 3a). The larger β-globin and ACT1 lariats were also readily prepared (Figure 3b,c). The lariats were formed with k_{obs} values similar to those of the analogous branches, or in the case of β-globin, about sixfold slower (but still with a k_{obs} value that is preparatively useful). Compelling evidence for each lariat structure was provided by several

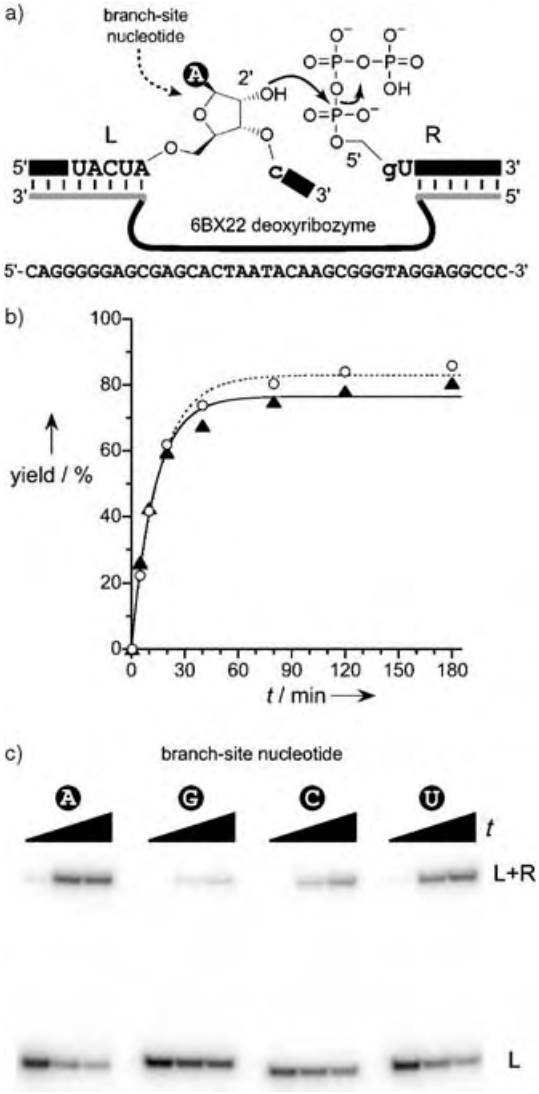


Figure 2. Branched RNA formation by the 6BX22 deoxyribozyme. a) With yeast spliceosomal substrate sequences; the conserved nucleotides are shown explicitly.[2] As demonstrated with the comprehensive experiments shown herein and in the Supporting Information, 6BX22 tolerates nucleotide changes at most of the conserved positions; the sites of tolerance are indicated with uppercase letters. The second nucleotide (U) of the right-hand substrate (R) prefers U, C, or A over G. The sequence of the enzyme region of 6BX22 (the 39 nucleotides not base-paired with the RNA substrates) is given below the structure. The Watson–Crick binding arms of the DNA are shown in light gray. See Experimental Section for full sequences of the left-hand (L) and right-hand (R) substrates. b) Demonstration of the generality of 6BX22 for its RNA substrate sequences; conditions: HEPES (*N*-(2-hydroxyethyl)-piperazine-*N*-(2-ethanesulfonic acid), 50 mM, pH 7.5), NaCl (150 mM), KCl (2 mM), $MnCl_2$ (20 mM), 37 °C. Original RNA sequences that correspond to the core nucleotides of the ACT1 RNA (▲); variant RNA sequences (○, see Experimental Section). For this experiment, $k_{obs} = 0.077 \pm 0.007\ min^{-1}$ (original sequences) and $0.066 \pm 0.004\ min^{-1}$ (variant sequences); errors are standard deviations from exponential curve fits. c) Demonstration of the generality of 6BX22 for branch-site nucleotides ($t = 0$, 0.5, and 1.5 h with 5′-^{32}P-radiolabeled L substrate; 20% PAGE). L+R product yields at $t = 1.5$ h: branch-site A, 71%; G, 5%; C, 33%; U, 64% ($k_{rel} = 1$, 0.085, 0.097, and 0.027, respectively; data not shown). In all cases, partial alkaline hydrolysis of the branched product[6] verified that the site of branching remained unchanged (data not shown).

 © 2005 Wiley-VCH Verlag GmbH & Co. KGaA, Weinheim

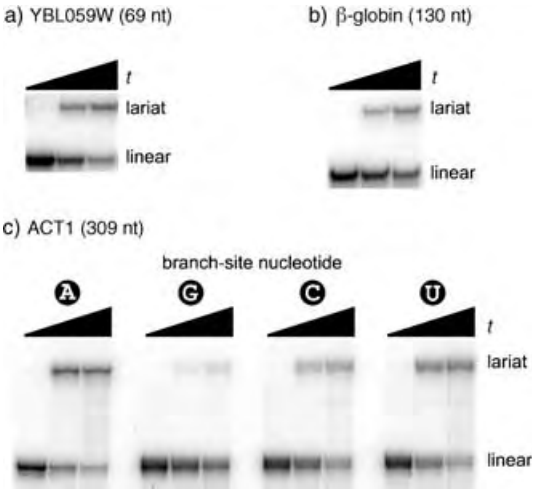


Figure 3. Formation of biologically related lariat RNAs with the 6BX22 deoxyribozyme. a) Synthesis of the 69-nt YBL059W lariat, which has a 51-nt loop (12% PAGE; $t = 0$, 0.5, and 1.5 h). Yield at $t = 1.5$ h: 52%; $k_{obs} = 1.1\ h^{-1}$ (data not shown). b) Synthesis of the 130-nt human β-globin IVS1 lariat, which has a 94-nt loop (8% PAGE; $t = 0$, 2, and 6 h). Yield at $t = 6$ h: 33%; $k_{obs} = 0.17\ h^{-1}$. At $t = 24$ h the yield was ≈50%, but some nonspecific RNA degradation was evident (data not shown). c) Synthesis of the 309-nt ACT1 lariat, which has a 266-nt loop; this was tested with mutants in which the branch-site nucleotide was changed as indicated (6% PAGE; $t = 0$, 0.5, and 1.5 h). Yields at $t = 1.5$ h: branch-site A, 72%; G, 9%; C, 48%; U, 70%. For branch-site A $k_{obs} = 2.8\ h^{-1}$ (data not shown). For the β-globin lariat, disruptor DNA oligonucleotides were required to sequester RNA secondary structure and enable binding of the DNA enzyme to the RNA substrates (Supporting Information). Without disruptors, the β-globin lariat yield was 0.3% at 6 h. A disruptor oligonucleotide was helpful but not absolutely required for ACT1 lariat synthesis, primarily by modestly enhancing the ligation rate (by less than twofold) and by suppressing nonspecific RNA degradation.

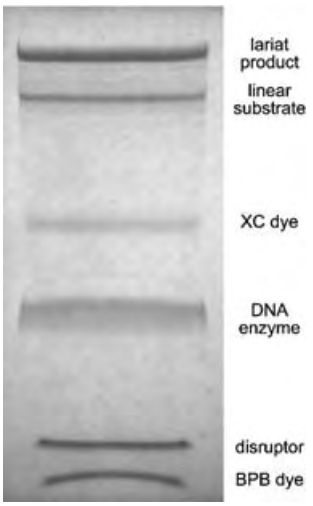


Figure 4. Preparative synthesis of the ACT1 lariat RNA; the image was recorded by UV shadowing of the 6% polyacrylamide gel.

biochemical assays in which the lariat RNA was cleaved with the 10–23 deoxyribozyme[17] and yeast debranching enzyme[18] to generate the predicted pattern of gel bands (Supporting Information). For the β-globin lariat, disruptor DNA oligonucleotides were required to allow the deoxyribozyme to bind productively with its RNA substrates (Supporting Information). For the largest ACT1 lariat, a disruptor helped to prevent RNA degradation, but it was not required for high lariat yield (data not shown).

The yeast ACT1 intron is a particularly common model system for studying spliceosomal RNA processing.[16,19] Artificial synthesis of such lariats without the natural splicing machinery will enable many biochemical experiments, because the sequence requirements of the spliceosome need not be obeyed. For example, the tolerance of 6BX22 toward changes of the branch-site nucleotide during branch formation (Figure 2c) is maintained for lariat synthesis (Figure 3c). Therefore, for the first time, biochemists have access to "real" spliceosomal lariats with mutations at their key branch-site nucleotides. To enable such experiments, preparative-scale (nanomole) synthesis of the ACT1 intron lariat was successfully carried out in high yield (Figure 4).

In summary, we have demonstrated that the 6BX22 deoxyribozyme catalyzes efficient and general one-step lariat synthesis with biological RNAs that are derived from commonly studied yeast and mammalian spliceosomal substrates. The resulting lariats are essentially impossible to synthesize by traditional organic and solid-phase synthesis methods. The only available approach until now has required the use of natural splicing enzymes, which have stringent sequence requirements that impose considerable limitations on the RNA sequences that may be used as substrates. Lariat RNA formation for the YBL059W, β-globin, and ACT1 intron substrates corresponds to the creation of rings with 307, 565, and 1597 atoms, respectively. These DNA-catalyzed macrocyclization reactions succeed without the use of protecting groups despite the presence of hundreds of competitive 2′-hydroxy nucleophiles. This demonstrates an extremely high level of site-selectivity. The reactions also produce very small amounts of side products such as RNA substrate oligomers that are created in large quantity with other deoxyribozymes that synthesize lariat RNAs in low yield.[6] The broadly useful lariat synthesis capacity of 6BX22 is unique in comparison with all of our other deoxyribozymes identified so far, including those such as 7S11, which are quite general for the formation of simpler branched RNAs.[8] The structural basis by which 6BX22—yet none of our other deoxyribozymes—readily tolerates a closed RNA loop in its catalytically active conformation requires further study, as does the mechanism by which 6BX22 achieves its $>10^5$-fold rate enhancement over mere templating. We continue to investigate these fundamental features of catalytic DNA, and we are using synthetic lariats created by 6BX22 to examine key biochemical aspects of RNA splicing.

Experimental Section

Systematic variation of RNA substrate sequences (Figure 2): The original left-hand (L) RNA substrate sequence (which corresponds to that used in the selection procedure[12]) was 5′-GGAAGUCUCAUGUACUAACA-3′. The original right-hand (R) RNA substrate sequence was 5′-GUAUGUUCUAGCGCGGA-3′. Together these

 © 2005 Wiley-VCH Verlag GmbH & Co. KGaA, Weinheim

sequences comprise the "core" of the ACT1 branch. For the experiment shown in Figure 2b, nearly all RNA substrate nucleotides in both L and R were changed by transversions (A↔C and G↔U). In L, changes were made to all nucleotides from the 5′ end through and including UACU. In R, changes were made to all nucleotides after 5′-GU through the 3′ end. In all cases, corresponding transversions were made to the DNA to maintain Watson–Crick complementarity. For the experiment shown in Figure 2c, the L substrate was varied only at the branch-site nucleotide position (UACUAAC). (For experiments with variations at the L substrate UACUA nucleotide and at the R substrate GU nucleotide, see the Supporting Information.) Variation of the 5′-triphosphorylated guanosine (5′-pppG) of the R substrate was not tested. The assays were performed with 5′-^{32}P-radiolabeled L substrate and L/deoxyribozyme/R = 1:3:6, under incubation conditions of HEPES (50 mM, pH 7.5), NaCl (150 mM), KCl (2 mM), and $MnCl_2$ (20 mM) at 37 °C.

Synthesis of the three lariat RNAs (Figure 3): Each linear RNA substrate was prepared by transcription in the presence of α-^{32}P-CTP to give internally ^{32}P-radiolabeled transcript. The assays were carried out under the incubation conditions above and a substrate/deoxyribozyme ratio of 1:2. In all cases, side products (presumably substrate oligomers[6]) were observed in very small amounts: < 3 % yield for YBL059W and β-globin; < 0.1 % yield for ACT1 (data not shown).

Preparative ACT1 lariat synthesis (Figure 4): A sample was prepared that contained 1.0 nmol linear substrate and 1.5 nmol deoxyribozyme plus 2.0 nmol disruptor DNA oligonucleotide (Supporting Information) in HEPES (5 mM, pH 7.5), NaCl (15 mM), and EDTA (ethylenediaminetetraacetic acid, 0.1 mM) in a volume of 150 μL. The sample was annealed by heating at 95 °C for 3 min and then cooling on ice for 5 min. The volume was increased to 200 μL: HEPES (50 mM, pH 7.5), NaCl (150 mM), KCl (2 mM), and $MnCl_2$ (20 mM); Mn^{2+} was added from an aqueous stock solution (1M). The 200-μL solution was incubated at 37 °C for 1.5 h and then mixed with 300 μL low-dye stop solution (80 % formamide, 1 × TBE (tris(hydroxymethyl)aminomethane and boric acid, 89 mM each, pH 8.3), and xylene cyanol and bromophenol blue, 0.0025 % each). The sample was resolved by 6 % PAGE and visualized by UV shadowing; the lariat product was extracted and ethanol-precipitated as described.[7] The isolated yield of lariat RNA product (after gel extraction and ethanol precipitation) was 0.39 nmol starting from 1.0 nmol of linear substrate. This 39 % yield (compared with the 70 % yield observed at the analytical scale without PAGE purification; Figure 3c) reflects losses that are commonly observed during extraction and precipitation of large RNA species from polyacrylamide gels.

Received: May 12, 2005
Published online: August 5, 2005

Keywords: deoxyribozymes · DNA · enzyme catalysis · lariat RNA · macrocycles

[1] C. L. Peebles, P. S. Perlman, K. L. Mecklenburg, M. L. Petrillo, J. H. Tabor, K. A. Jarrell, H. L. Cheng, *Cell* **1986**, *44*, 213.
[2] C. B. Burge, T. Tuschl, P. A. Sharp in *The RNA World*, 2nd ed. (Eds.: R. F. Gesteland, T. R. Cech, J. F. Atkins), Cold Spring Harbor Laboratory Press, Cold Spring Harbor, NY, **1999**, pp. 525 – 560.
[3] a) C. Sund, P. Agback, J. Chattopadhyaya, *Tetrahedron* **1991**, *47*, 9659; b) C. Sund, P. Agback, J. Chattopadhyaya, *Tetrahedron* **1993**, *49*, 649; c) C. B. Reese, Q. Song, *Nucleic Acids Res.* **1999**, *27*, 2672; d) S. Carriero, M. J. Damha, *J. Org. Chem.* **2003**, *68*, 8328.
[4] a) M. J. Damha, K. Ganeshan, R. H. Hudson, S. V. Zabarylo, *Nucleic Acids Res.* **1992**, *20*, 6565; b) B. S. Sproat, B. Beijer, M. Grøtli, U. Ryder, K. L. Morand, A. I. Lamond, *J. Chem. Soc. Perkin Trans. 1* **1994**, 419; c) M. von Büren, G. V. Petersen, K. Rasmussen, G. Brandenburg, J. Wengel, *Tetrahedron* **1995**, *51*, 8491; d) M. Grøtli, R. Eritja, B. Sproat, *Tetrahedron* **1997**, *53*, 11317.
[5] a) S. K. Silverman, *Org. Biomol. Chem.* **2004**, *2*, 2701; b) J. C. Achenbach, W. Chiuman, R. P. Cruz, Y. Li, *Curr. Pharm. Biotechnol.* **2004**, *5*, 321; c) G. M. Emilsson, R. R. Breaker, *Cell. Mol. Life Sci.* **2002**, *59*, 596; d) Y. Lu, *Chem. Eur. J.* **2002**, *8*, 4589.
[6] Y. Wang, S. K. Silverman, *J. Am. Chem. Soc.* **2003**, *125*, 6880.
[7] Y. Wang, S. K. Silverman, *Biochemistry* **2003**, *42*, 15252.
[8] a) R. L. Coppins, S. K. Silverman, *Nat. Struct. Mol. Biol.* **2004**, *11*, 270; b) R. L. Coppins, S. K. Silverman, *J. Am. Chem. Soc.* **2005**, *127*, 2900.
[9] E. D. Pratico, Y. Wang, S. K. Silverman, *Nucleic Acids Res.* **2005**, *33*, 3503.
[10] For example, see the Supporting Information for secondary structures of two of the RNAs studied for the work reported herein.
[11] a) G. F. Joyce, *Annu. Rev. Biochem.* **2004**, *73*, 791; b) D. S. Wilson, J. W. Szostak, *Annu. Rev. Biochem.* **1999**, *68*, 611.
[12] Y. Wang, S. K. Silverman, *Biochemistry* **2005**, *44*, 3017.
[13] If one or more (e.g., 39) random DNA nucleotides are included between the DNA-binding arms in place of the enzyme region, then $k_{templated}$ decreases considerably (data not shown). Therefore, the 6BX22 rate enhancement calculated by using $k_{templated}$ for the DNA template that lacks any enzyme region is a conservative (lower-limit) estimate. Furthermore, as the templated background product is almost certainly linear and not branched RNA[20] (insufficient amounts of this product were available for analysis), the $k_{templated}$ value for the formation of the branched product that 6BX22 actually synthesizes must be lower than the experimentally measured $k_{templated}$ value. This lends further credence to the calculated rate enhancement as a lower-limit estimate.
[14] a) C. A. Davis, L. Grate, M. Spingola, M. Ares, Jr., *Nucleic Acids Res.* **2000**, *28*, 1700; b) L. Grate, M. Ares, Jr., *Methods Enzymol.* **2002**, *350*, 380.
[15] a) R. A. Spritz, P. Jagadeeswaran, P. V. Choudary, P. A. Biro, J. T. Elder, J. K. deRiel, J. L. Manley, M. L. Gefter, B. G. Forget, S. M. Weissman, *Proc. Natl. Acad. Sci. USA* **1981**, *78*, 2455; b) R. Reed, T. Maniatis, *Cell* **1985**, *41*, 95; c) K. B. Hall, M. R. Green, A. G. Redfield, *Proc. Natl. Acad. Sci. USA* **1988**, *85*, 704.
[16] R. Ng, J. Abelson, *Proc. Natl. Acad. Sci. USA* **1980**, *77*, 3912.
[17] S. W. Santoro, G. F. Joyce, *Proc. Natl. Acad. Sci. USA* **1997**, *94*, 4262.
[18] a) S. L. Ooi, C. Dann, 3rd, K. Nam, D. J. Leahy, M. J. Damha, J. D. Boeke, *Methods Enzymol.* **2001**, *342*, 233; b) K. Nam, R. H. Hudson, K. B. Chapman, K. Ganeshan, M. J. Damha, J. D. Boeke, *J. Biol. Chem.* **1994**, *269*, 20613.
[19] J. P. Staley, C. Guthrie, *Mol. Cell* **1999**, *3*, 55.
[20] R. Rohatgi, D. P. Bartel, J. W. Szostak, *J. Am. Chem. Soc.* **1996**, *118*, 3340.

 © 2005 Wiley-VCH Verlag GmbH & Co. KGaA, Weinheim

Annulation

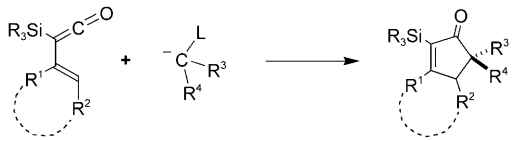
DOI: 10.1002/anie.200501579

Stereoselective Synthesis of Highly Substituted Cyclopentenones through [4+1] Annulations of Trialkylsilyl Vinyl Ketenes with α-Benzotriazolyl Organolithium Compounds**

*Christopher P. Davie and Rick L. Danheiser**

Cyclopentenones serve as valuable synthetic building blocks and are themselves key features in the structure of a number of prostaglandins[1] and other bioactive natural products. Popular strategies for the construction of this important ring system include the intramolecular aldol reaction, the Nazarov cyclization,[2] the Rautenstrauch rearrangement,[3] and the Pauson–Khand reaction.[4,5] Only a few general [4+1] routes to five-membered carbocycles have been reported to date, one example being the method we developed based on anion-accelerated vinylcyclopropane rearrangements.[6,7] Recently, studies by us[8] and others[9] have led to several new [4+1] approaches to the synthesis of the 2-cyclopentenone ring system. Herein, we report a new variant of our stereocontrolled [4+1] annulation strategy that provides especially efficient access to highly substituted and functionalized cyclopentenones.

As outlined in Scheme 1, our [4+1] annulation strategy is based on the reaction of nucleophilic species with leaving groups ("carbenoid reagents") with trialkylsilyl vinyl ketenes

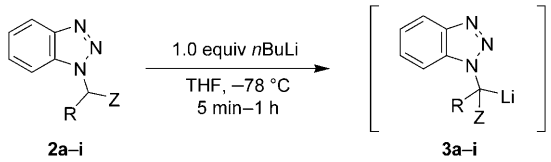


1a: R = *i*Pr, $R^1 = R^2 = CH_3$
1b: R = *i*Pr, $R^1 = R^2 = (CH_2)_4$
1c: R = Et, $R^1 = R^2 = CH_3$

Scheme 1. Strategy for [4+1] annulation. L = leaving group.

("TAS vinyl ketenes").[8] The utility of vinyl ketenes as versatile intermediates in organic synthesis is now well established.[10] However, vinyl ketenes are rarely isolable species and in most applications are generated as transient intermediates which are trapped in situ in [2+2] cycloadditions. Silyl substituents have the ability to suppress the usual propensity of vinyl ketenes to undergo dimerization and [2+2] cycloaddition reactions, thus opening up new opportunities for useful synthetic transformations. For example, TAS vinyl ketenes participate as electron-rich diene components in Diels–Alder and hetero-Diels–Alder reactions leading to cyclohexenones, phenols, and oxygen and nitrogen heterocycles.[11] In the case of reactions with carbenoid reagents, addition initially furnishes dienolate intermediates, which are believed to undergo ionization and subsequent 4π electrocyclization to generate cyclopentenone rings (see below). TAS vinyl ketenes are readily available through several routes, including the photochemical Wolff rearrangement of α′-silyl-α′-diazo-α,β-unsaturated ketones used for the preparation of **1a–c** in this study.[11a]

The goal of the current investigation was to extend the scope of this [4+1] annulation strategy to include the synthesis of cyclopentenones with a much broader range of substituents at the C5 position. A variety of carbenoid reagents were screened with the aim of identifying new classes of molecules that are competent in the desired transformation and are more readily available than the diazo compounds, sulfur ylides, and stable carbenes previously employed.[8] Among the several classes of compounds examined to date, α-benzotriazolyl organolithium compounds of type **3** were best able to meet our requirements (Scheme 2). Extensive research by Katritzky and co-workers over the past two decades has demonstrated the utility of *N*-substituted benzotriazoles as valuable intermediates for organic synthesis.[12] Benzotriazoles of type **2** bearing a wide range of substituents are either commercially available or readily prepared in one or two steps from inexpensive starting materials and undergo metalation with *n*-butyllithium at −78 °C to provide access to α-benzotriazolyl organolithium derivatives of type **3**. The ability of benzotriazole to function as a leaving group is also well documented and has been exploited by Katritzky and co-workers in the context of numerous useful synthetic transformations.[12]



2a–i **3a–i**

a: Z = N(CO$_2$*t*Bu)(Bn), R = H
b: Z = OEt, R = C(H)=CH$_2$
c: Z = OEt, R = C≡CCH$_3$
d: Z = SPh, R = H
e: Z = OMe, R = H
f: Z = 9-carbazolyl, R = H
g: Z = 4-MeOC$_6$H$_4$, R = H
h: Z = OPh, R = CH$_3$
i: Z = SPh, R = CH$_3$

Scheme 2. Preparation of α-benzotriazolyl organolithium compounds. Benzotriazoles **2b** and **2d–f** are commercially available, and the details for the preparation of **2a**, **2c**, and **2g–i** are given in the Supporting Information.

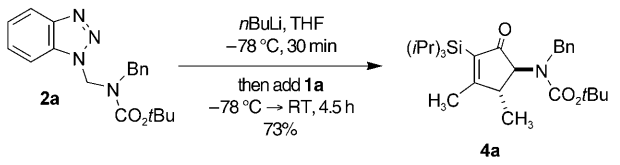
The reaction of the benzotriazolyl carbamate **2a** with TAS vinyl ketene **1a** was examined to investigate the feasibility of the proposed [4+1] annulation (Scheme 3). Benzotriazole **2a**

[*] C. P. Davie, Prof. R. L. Danheiser
Massachusetts Institute of Technology
Department of Chemistry
Cambridge, Massachusetts 02139 (USA)
Fax: (+1) 617-252-1504
E-mail: danheisr@mit.edu

[**] We thank the National Institutes of Health (GM 28273) and Merck Research Laboratories for generous financial support.

Supporting information for this article is available on the WWW under http://www.angewandte.org or from the author.

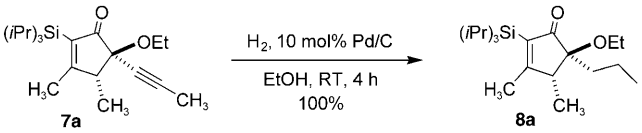
 © 2005 Wiley-VCH Verlag GmbH & Co. KGaA, Weinheim



Scheme 3. Demonstration of the feasibility of the [4+1] annulation. Bn = benzyl.

was prepared in 70% overall yield as previously described by Katritzky and co-workers[13] through protection of benzylamine as its *tert*-butyloxycarbonyl (Boc) derivative and reaction of the crude carbamate with one equivalent of benzotriazole and one equivalent of paraformaldehyde in the presence of catalytic *para*-toluenesulfonic acid (toluene, reflux). Metalation of **2a** with *n*BuLi produced the expected organolithium species, which was found to add smoothly to vinyl ketene **1a** at −78 °C in the desired fashion. Upon warming to room temperature, the resulting dienolate intermediate lost the benzotriazole moiety and cyclopentenone **4a** formed in good yield and with greater than 96% selectivity for the *trans*-substituted isomer.

Tables 1 and 2 delineate the scope of the [4+1] annulation. In some cases, the desired cyclopentenone begins to appear at low temperature during the addition of the organolithium reagent, and formation of the five-membered-ring product is completed simply by warming to room temperature (Table 1). This protocol proved effective for annulations that involve carbenoid reagents with strong electron-donor substituents such as amine derivatives (entries 1 and 2) and the combination of an alkoxy moiety and a vinyl or alkynyl group (entries 3 and 4). Each of these reactions was observed to proceed with a preference for the formation of the cyclopentenone with the heteroatom substituent at C5 *trans* to the substituent at C4. This preference is particularly high with small R^3 groups, such as hydrogen or alkynyl moieties. The latter case is synthetically significant, as the products of such reactions (e.g., **7a**) undergo hydrogenation (Scheme 4) to furnish 5-alkyl-substituted cyclopentenones that cannot be produced directly under such mild conditions or with such high stereoselectivity (see below).

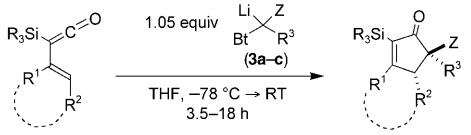


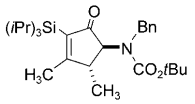
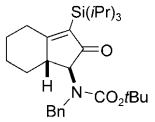
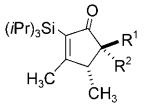
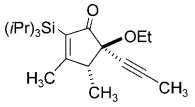
Scheme 4. Preparation of 5-alkyl-substituted cyclopentenones.

Attempted annulation with α-benzotriazolyllithium reagents **3d–i** under similar conditions did not lead to the desired cyclopentenones. Control experiments that employed benzotriazole **3d** confirmed that addition to TAS vinyl ketene **1a** proceeds smoothly at −78 °C in the expected manner, but cyclization of the resulting dienolate intermediate does not then occur. We therefore turned to the use of Lewis acids to promote the crucial ionization of the benzotriazole group required for five-membered-ring formation. Extensive screening studies identified $ZnBr_2$ as particularly effective for the desired transformation.[14] Although no reaction is observed upon addition of one equivalent of $ZnBr_2$ to the dienolate solution, efficient cyclization takes place when two or more equivalents of the Lewis acid are added at −78 °C and the reaction mixture is allowed to warm to room temperature. Under these conditions, the desired [4+1] annulation can be achieved with a variety of carbenoid reagents that bear a single heteroatom substituent such as SPh or OMe (Table 2). Cyclopentenone formation is even observed with the aryl-substituted benzotriazole **3g**, although in this case elevated temperatures are required to complete the cyclization.

A notable feature of these [4+1] annulations is the high level of stereoselectivity observed in most of the reactions. Control experiments established that the stereochemical outcome of these [4+1] annulations is not a consequence of thermodynamic control. Specifically, equilibration experiments yielded mixtures of *trans*- and *cis*-substituted cyclopentenones with ratios significantly different from those obtained in the annulation.[15] Thus, it appears likely that the stereochemical course of the [4+1] annulation reflects a mechanism-based kinetic preference for the observed products.

Table 1: [4+1] Cyclopentenone annulations.[a]

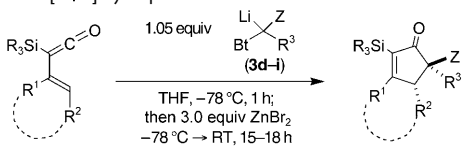


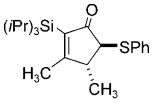
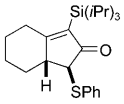
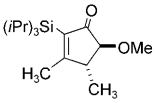
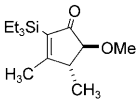
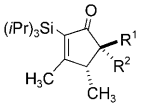
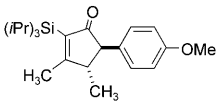
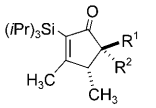
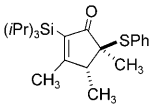
Entry	Ketene	Carbenoid reagent	Product		Yield [%][b] (*trans*/*cis*)[c]
1	**1a**	**3a**		**4a**	73 (≥96:4)
2	**1b**	**3a**		**5a**	67 (≥99:1)
3[d]	**1a**	**3b**		**6a,b**	70 (76:24)
4	**1a**	**3c**		**7a**	54 (97:3)

[a] Only the major diastereomer is shown for cases in which d.r. ≥ 96:4; Bt = benzotriazolyl. [b] Yields of isolated product purified by column chromatography. [c] Ratios determined by ^{1}H NMR spectroscopic analysis. [d] **6a**: R^1 = OEt, R^2 = –CH=CH_2; **6b**: R^1 = –CH=CH_2, R^2 = OEt.

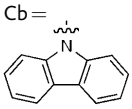
 © 2005 Wiley-VCH Verlag GmbH & Co. KGaA, Weinheim

Table 2: Lewis acid promoted [4+1] cyclopentenone annulations.[a]



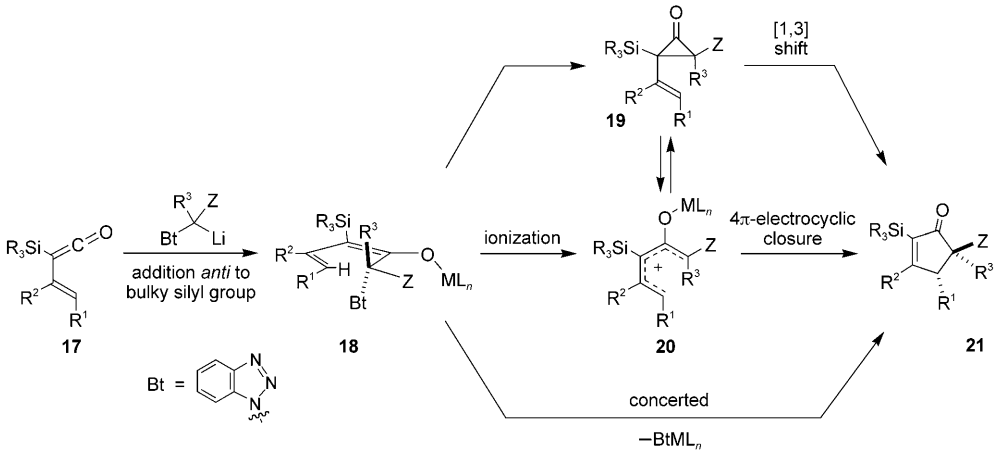
Entry	Ketene	Carbenoid reagent	Product		Yield [%][b] (*trans*/*cis*)[c]
1	**1a**	**3d**		**9a**	69–74 (98:2)
2	**1b**	**3d**		**10a**	75 (98:2)
3	**1a**	**3e**		**11a**	68–82 (≥99:1)
4	**1c**	**3e**		**12a**	67–70 (≥99:1)
5[d]	**1a**	**3f**		**13a,b**	85 (74:26)
6	**1a**	**3g**		**14a**	34[e] (≥99:1)
7[f]	**1a**	**3h**		**15a,b**	65 (77:23)
8	**1a**	**3i**		**16a**	64 (97:3)

[a] Only the major diastereomer is shown for cases in which d.r. ≥ 97:3. [b] Yields of isolated product purified by column chromatography. [c] Ratios determined by ^{1}H NMR spectroscopic analysis. [d] **13a**: R^1 = Cb, R^2 = H; **13b**: R^1 = H, R^2 = Cb. [e] Reaction mixture was allowed to warm to RT over 10 h and then heated at reflux for an additional 4 h. [f] **15a**: R^1 = OPh, R^2 = CH_3; **15b**: R^1 = CH_3, R^2 = OPh. Cb =



Scheme 5 outlines several alternative pathways to account for the mechanism of the [4+1] annulation. Addition of the carbenoid reagent to the vinyl ketene is predicted to be highly stereoselective because of the shielding effect of the bulky trialkylsilyl group and should result in the formation of the *Z*-enolate **18**. Direct formation of the five-membered-ring product could then result from a concerted process in which ring closure is concomitant with leaving-group departure. An alternative pathway involves ionization to produce oxidopentadienylic cation **20**,[16] which should then undergo rapid conrotatory 4π-electrocyclic closure[17] to generate the cyclopentenone product.[18] Finally, the involvement of cyclopropanone intermediates of type **19** cannot be excluded, particularly in view of the finding that simple silyl ketenes react with diazomethane and trimethylsilyldiazomethane to form mono- and bis(silyl)cyclopropanones.[19]

The stereochemical outcome of the [4+1] annulations that we investigated previously[8] is consistent with a mechanism that involves stereospecific conrotatory electrocyclic closure of a 2-oxidopentadienylic cation. In those prior cases, we suggested that ionization of the dienolate intermediate occurs to generate a cation in which the single C1 substituent is *cis* to the oxy anion to minimize nonbonded interactions. A similar mechanism can account for the reactions reported herein, provided that one assumes that ionization leads to the isomer of intermediate **20** shown in Scheme 5 because of an associative interaction between the heteroatom Z and the metal (M = Zn or Li) in **18** and/or **20**. Alternatively, if cyclization of **18** involves a concerted process, then the stereochemical outcome could reflect a preference for the mode of conrotation from **18** that rotates the leaving group *anti*

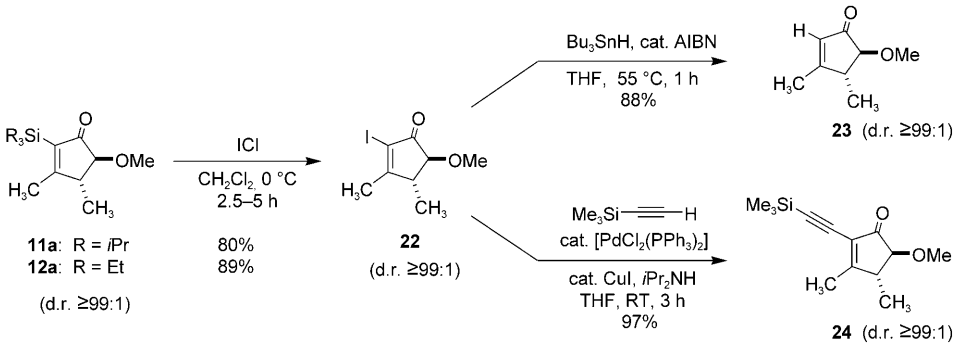


Scheme 5. Possible mechanistic pathways for the [4+1] annulation. M = metal center, L = ligand.

© 2005 Wiley-VCH Verlag GmbH & Co. KGaA, Weinheim

to the incipient σ bond and which proceeds via the transition state in which the donor heteroatom occupies an "outside" position ("torquoselectivity").[20]

The vinyl silane moiety incorporated in the [4+1] annulation products provides a useful handle for further synthetic transformations. Of particular interest to us was their conversion into vinyl halides, as a number of naturally occurring 2-halocyclopentenones have recently been found to exhibit potent antitumor activity.[1] In addition, the utility of 2-haloenones in a variety of transition-metal-catalyzed coupling reactions is well documented. With these ends in mind, we investigated the transformations outlined in Scheme 6 to lay



Scheme 6. Useful synthetic transformations of [4+1] annulation products. AIBN = azobisisobutyronitrile.

the groundwork for future applications of this annulation methodology. Conversion of α-silyl cyclopentenone annulation products **11a** and **12a** into iodoenone **22** proceeded smoothly by using a modification of the method of Alimardanov and Negishi.[21] Reduction of **22** with nBu$_3$SnH then afforded **23**, and Sonogashira coupling proceeded smoothly to furnish **24** with no detectable epimerization or double-bond migration in either case.

Further studies are underway aimed at the development of asymmetric variants of the annulation reaction and its application in the synthesis of natural products.

Received: May 10, 2005
Published online: August 5, 2005

Keywords: annulation · azoles · cyclopentenones · electrocyclic reactions · ketenes

[1] Review: S. M. Roberts, M. G. Santoro, E. S. Sickle, *J. Chem. Soc. Perkin Trans. 1* **2002**, 1735.
[2] a) K. L. Habermas, S. E. Denmark, T. K. Jones, *Org. React.* **1994**, *45*, 1; b) M. A. Tius, *Acc. Chem. Res.* **2003**, *36*, 284.
[3] a) V. Rautenstrauch, *J. Org. Chem.* **1984**, *49*, 950; b) for a recent gold(I)-catalyzed variant, see: X. Shi, D. J. Gorin, F. D. Toste, *J. Am. Chem. Soc.* **2005**, *127*, 5802.
[4] a) N. E. Schore, *Org. React.* **1991**, *40*, 1; b) K. M. Brummond, J. L. Kent, *Tetrahedron* **2000**, *56*, 3263.
[5] For a review of transition-metal-mediated routes to cyclopentenones, see: S. E. Gibson, S. E. Lewis, N. Mainolfi, *J. Organomet. Chem.* **2004**, *689*, 3873.
[6] R. L. Danheiser, J. J. Bronson, K. Okano, *J. Am. Chem. Soc.* **1985**, *107*, 4579, and references therein.
[7] For other recent examples, see: C. Spino, H. Rezaei, K. Dupont-Gaudet, F. Bélanger, *J. Am. Chem. Soc.* **2004**, *126*, 9926, and references therein.
[8] a) J. L. Loebach, D. M. Bennett, R. L. Danheiser, *J. Am. Chem. Soc.* **1998**, *120*, 9690; b) A. M. Dalton, Y. Zhang, C. P. Davie, R. L. Danheiser, *Org. Lett.* **2002**, *4*, 2465; c) for the extension of this strategy to include reactions of nucleophilic carbenes, see: J. H. Rigby, Z. Wang, *Org. Lett.* **2003**, *5*, 263.
[9] For examples, see: a) M. Murakami, K. Itami, Y. Ito, *J. Am. Chem. Soc.* **1999**, *121*, 4130; b) S. V. Gagnier, R. C. Larock, *J. Am. Chem. Soc.* **2003**, *125*, 4804.
[10] G. B. Dudley, K. S. Takaki, D. D. Cha, R. L. Danheiser, *Org. Lett.* **2000**, *2*, 3407, and references therein.
[11] a) J. L. Loebach, D. M. Bennett, R. L. Danheiser, *J. Org. Chem.* **1998**, *63*, 8380; b) D. M. Bennett, I. Okamoto, R. L. Danheiser, *Org. Lett.* **1999**, *1*, 641.
[12] Reviews: a) A. R. Katritzky, X. Lan, J. Z. Yang, O. V. Denisko, *Chem. Rev.* **1998**, *98*, 409; b) A. R. Katritzky, K. Manju, S. K. Singh, N. K. Meher, *Tetrahedron* **2005**, *61*, 2555.
[13] A. R. Katritzky, Z. Luo, Y. Fang, P. J. Steel, *J. Org. Chem.* **2001**, *66*, 2858.
[14] Other Lewis acids that promote the desired reaction in good yield include $BF_3{\cdot}OEt_2$, $AlCl_3$, $Cu(OTf)_2$, $TiCl_4$, and $SnCl_4$.
[15] For example, exposure of **9a** to KO*t*Bu in THF (RT, 19 h) afforded a 91:9 mixture of **9a** and the corresponding *cis* isomer, and similar reaction of **11a** produced a 62:38 mixture of *trans*- and *cis*-substituted cyclopentenones; exposure of **12a** to methanesulfonic acid (MeOH, RT, 32 h) afforded a 70:30 mixture of *trans*/*cis* isomers.
[16] Depending on the reaction conditions, this intermediate may be a free zwitterionic species or could still be associated with the metal center.
[17] Pentadienyl cation electrocyclic ring closures are involved in the mechanism of the Nazarov cyclization; for reviews, see: reference [2a] and S. E. Denmark in *Comprehensive Organic Synthesis*, *Vol. 5* (Eds.: B. M. Trost, I. Fleming), Pergamon, Oxford, **1991**, p. 751.
[18] For the formation of cyclopentenones through the base-induced cyclization of α′-chloro-β′,γ′-unsaturated ketone enolate and enamine derivatives, see: J. Mathew, *J. Org. Chem.* **1991**, *56*, 713. Although it was proposed that these cyclizations proceed by an "intramolecular abnormal S_N2'" mechanism, we believe these reactions more likely involve the cyclization of an oxidopentadienylic cation analogous to **20**. For a related transformation which involves a benzotriazolyl moiety in place of chloride as the leaving group, see: A. R. Katritzky, G. Zhang, J. Jiang, *J. Org. Chem.* **1995**, *60*, 7605.
[19] G. S. Zaitseva, I. F. Lutsenko, A. V. Kisin, Yu. I. Baukov, J. Lorberth, *J. Organomet. Chem.* **1988**, *345*, 253, and references therein.
[20] Theoretical studies predict that electron-donor groups prefer an "outside" position and electron-withdrawing groups an "inside" position in the electrocyclic closure of pentadienylic cations; see: a) E. A. Kallel, K. N. Houk, *J. Org. Chem.* **1989**, *54*, 6006; b) O. N. Faza, C. S. López, R. Álvarez, Á. R. de Lera, *Chem. Eur. J.* **2004**, *10*, 4324.
[21] A. Alimardanov, E.-i. Negishi, *Tetrahedron Lett.* **1999**, *40*, 3839.

 © 2005 Wiley-VCH Verlag GmbH & Co. KGaA, Weinheim

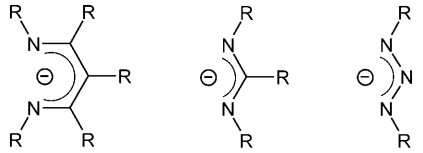
Alkaline-Earth Metal Complexes

DOI: 10.1002/anie.200501494

Stabilization of Aryl–Calcium, –Strontium, and –Barium Compounds by Designed Steric and π-Bonding Encapsulation

*Sven-Oliver Hauber, Falk Lissner, Glen B. Deacon, and Mark Niemeyer**

In the last decade a major theme of organometallic chemistry has been the design and development of alternative ligand systems capable of stabilizing monomeric metal complexes while provoking novel reactivity. Exploration of this field is driven by the potential use of these complexes in catalysis and organic synthesis. Examples of monoanionic chelating N-donor ligands that have received much recent attention (Scheme 1) include the β-diketiminate (**I**)[1] and the amidinate



I **II** **III**

Scheme 1. A comparison of some monoanionic chelating N ligands.

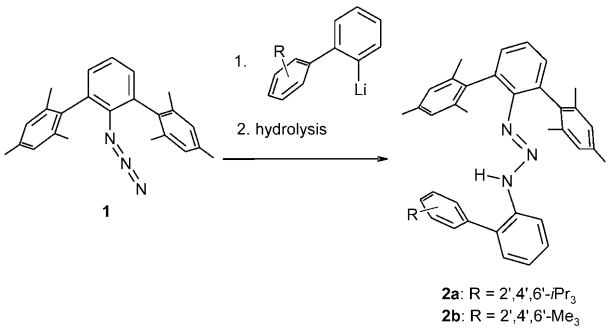
(**II**)[2] ligand systems. Much less attention has been given to the closely related triazenides (**III**).[3,4] This may be attributed to the lack of suitable ligands that are sterically crowded enough to prevent undesirable ligand redistribution reactions and allow better control of the electronic and steric properties at the metal center.

Triazenides are weaker donors than the isoelectronic amidinates and the related β-diketiminates, and should induce greater electrophilicity at a bonded metal atom.[5] This is reflected by the results of an NBO (natural bond orbitals) analysis of the energy-minimized structures[6] of the model anions 1,3-diphenyl-1,3-diketiminate ($\mathbf{I_M}$), 1,3-diphenyl-1,3-diazaallyl ($\mathbf{II_M}$), and 1,3-diphenyltriazenide ($\mathbf{III_M}$) (see Supporting Information), which shows an NPA (natural population analysis) charge for the chelating N atoms of −0.54, −0.60, and −0.38, respectively.

[*] Dipl.-Chem. S.-O. Hauber, Dr. F. Lissner, Priv.-Doz. Dr. M. Niemeyer
Institut für Anorganische Chemie
Universität Stuttgart
Pfaffenwaldring 55, 70569 Stuttgart (Germany)
Fax: (+49) 711-685-4241
E-mail: mn@lanth.de
Prof. Dr. G. B. Deacon
School of Chemistry
Monash University
Clayton 3800 (Australia)

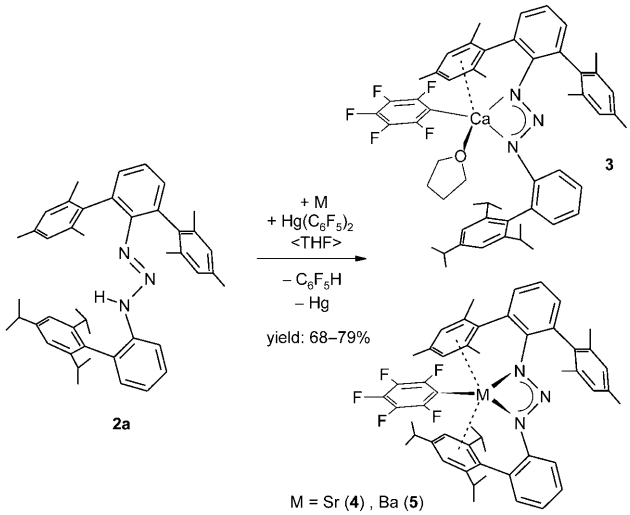
Supporting information for this article is available on the WWW under http://www.angewandte.org or from the author.

We recently succeeded in the preparation of aryl-substituted, sterically crowded triazenes. Ligands of this type may be synthesized in excellent yields by the reaction of different substituted 2-lithiobiphenyls with the *m*-terphenyl azide **1**, followed by hydrolysis (Scheme 2).



Scheme 2. Synthesis of the triazene ligands **2a** and **2b**.

In a first attempt to test their properties, we have used the obtained triazenes to stabilize pentafluorophenyl compounds of the heavier alkaline-earth metals calcium, strontium, and barium. The heteroleptic pentafluorophenyl triazenides are accessible in tetrahydrofuran as solvent by a convenient one-pot transmetalation/deprotonation[7] reaction from the triazene **2a** (HN_3ArAr'), bis(pentafluorophenyl)mercury, and the corresponding alkaline-earth metal (Scheme 3). After crystallization from *n*-heptane, either the THF-free com-



Scheme 3. Synthesis of **3**–**5**.

pounds $[M(C_6F_5)(N_3ArAr')]$ (M = Sr (**4**), Ba (**5**)) or the solvate $[Ca(C_6F_5)(N_3ArAr')(thf)]$ (**3**) were isolated in good yields. It is remarkable that attempts to replace the pentafluorophenyl substituents by a second triazenide ligand have not been successful so far. Apparently, the steric bulk of the latter prevents further substitution or ligand redistribution and therefore formation of the homoleptic complexes.[8]

Solutions of **4** or **5** in aromatic or aliphatic solvents show considerable thermal stability and can be stored at ambient

 © 2005 Wiley-VCH Verlag GmbH & Co. KGaA, Weinheim

temperature for months with only minor decomposition. This may be contrasted with the behavior of some related pentafluorophenyl compounds of the di- and trivalent rare earth metals, which are thermally much more labile.[9] Compared to **4** and **5**, solutions of the calcium complex **3** are more sensitive and decompose within weeks at room temperature or within two days at 70 °C. We have not been able to isolate a well-defined decomposition product so far. However, NMR spectroscopic evidence, in particular a ^{19}F NMR signal at $\delta = -72.3$ ppm, points to the formation of a molecular fluoride, presumably [CaF(N_3ArAr′)(thf)], as one of the main products.

Compounds **3**–**5** were examined by X-ray crystallography.[10] The molecular structures of the Ca and Ba derivatives are shown in Figures 1 and 2, respectively, while important structural parameters for all complexes are summarized in Table 1. Despite the relatively large ionic radii of the M^{2+} ions (Ca: 1.14 Å; Sr: 1.32 Å; Ba: 1.49 Å for coordination number four[11]) the size of the η^2-bonded triazenide ligands enforces the formation of strictly monomeric complexes in which the metal atoms possess apparent low coordination numbers of three (**4**, **5**) and four (**3**). It should be noted that the deviation of the metal atoms from the N_3 plane increases in the order Sr (0.406 Å), Ba (0.706 Å), Ca (0.850 Å), while the bite angles

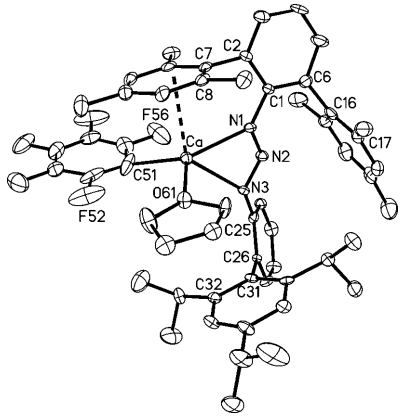


Figure 1. Molecular structure of **3** with thermal ellipsoids set to 30% probability. Hydrogen atoms are omitted for clarity.

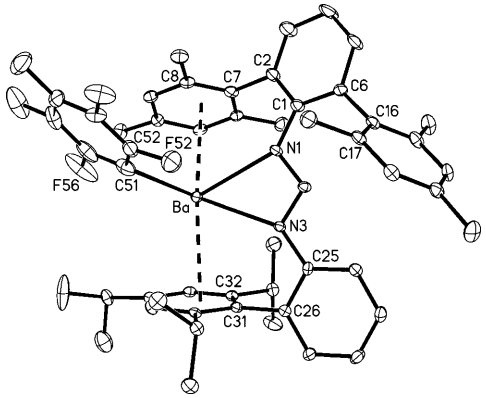


Figure 2. Molecular structure of **5** with thermal ellipsoids set to 50% probability. Hydrogen atoms are omitted for clarity.

Table 1: Important structural parameters [Å, °] for the compounds [(ArAr′N_3)M(C_6F_5)] (**3**–**5**) and the DFT-calculated model complex [(2-MesC_6H_4)(2-TripC_6H_4)N_3SrC_6F_5] (**4_M**).

	M = Ca(thf)	M = Sr	**4_M**	M = Ba
N1–N2	1.338(7)	1.314(7)	1.305	1.309(5)
N2–N3	1.325(6)	1.307(8)	1.307	1.306(4)
Coord. no. (M)	4	3	3	3
M–N1	2.371(5)	2.576(6)	2.591	2.740(3)
M–N3	2.496(6)	2.548(5)	2.596	2.711(3)
N1–M–N3	53.3	48.9	48.7	46.3
M/N_3[a]	0.850	0.406	0.038	0.706
M–C	2.499(11)	2.673(7)	2.638	2.808(5)
M/C_6F_5[b]	0.797	0.712	0.246	1.086
M–O	2.308(5)			
C–M–N2	112.2	114.8	127.0	113.1
η^n/η^n[c]	η^5	η^6/η^5	η^6/η^5	η^5/η^5
M···C(Mes)[d]	3.015–3.132	3.165–3.306	3.310–3.400	3.327–3.430
M···C(Trip)[d]		3.078–3.283	3.277–3.470	3.286–3.406
M···F[e]	3.414	3.076	2.881	3.417

[a] Displacement of M from the N_3 plane. [b] Displacement of M from the C_6F_5 plane. [c] Hapticity of the M···π-arene interaction to the Mes and Trip rings. [d] M···C(arene) distances considered to be bonding. [e] Closest M···F contact.

N1-M-N3 decrease in the order Ca (53.25(18)°), Sr (48.89(17)°), Ba (46.33(10)°).

The average M–N distances to the triazenide ligands (Ca = 2.434, Sr = 2.562, Ba = 2.726 Å) are comparable to those of the amidinates [{PhC($NSiMe_3$)$_2$}$_2$M(thf)$_2$] (M = Ca 2.431 Å,[12a] Sr 2.584 Å[12b]), [{HC(NDip)$_2$}$_2$M(thf)$_n$] (Dip = 2,6-diisopropylphenyl, M = Ca 2.383 Å ($n = 1$), Sr 2.585 Å, Ba 2.728 Å ($n = 2$)),[12d] and [{PhC($NSiMe_3$)$_2$}$_2$Ba(dme)(thf)] (2.779 Å),[12c] which contain five- to seven-coordinate metal atoms, and are longer than those of the four-coordinate homoleptic β-diketiminates [(Dip-nacnac)$_2$M] (Dip-nacnac = (Dip)NC(Me)C(H)C(Me)N(Dip)) (M = Ca 2.379 Å, Sr 2.510 Å, Ba 2.712 Å).[13] Taking into account the apparent lower coordination numbers in the triazenides **3**–**5** the longer M–N bond lengths are most likely a result of the decreased donor ability of the triazenide relative to the amidinate and β-diketiminate ligands and/or a consequence of the additional metal–π-arene interactions (see below). Furthermore, the average Ca–N distance of 2.434 Å in the THF solvate **3** is considerably shorter than the corresponding values found in the eight-coordinate triazenide [Ca{N_3(tol)$_2$}$_2$(dme)$_2$] (av 2.524 Å) (tol = 4-Me-phenyl),[8] which is the only derivative of the heavier alkaline-earth metals currently available for comparison.

Well-defined σ-bonded organometallic compounds of the heavier alkaline-earth metals calcium, strontium, and barium are scarce and are currently restricted to some structurally characterized trimethylsilylmethanides or -benzyls, di- and triphenylmethanides, and acetylides.[14] The heteroleptic pentafluorophenyls **3**–**5** therefore are the first structurally authenticated Ar–Ca, Ar–Sr, and Ar–Ba compounds. The observed M–C distances are toward the short end of the range of M–C bonds reported for other organyls. The Ca–C bond (2.499 Å) is comparable to the value in the four-coordinate alkyl [Ca{CH($SiMe_3$)$_2$}$_2$(dioxane)$_2$] (2.48 Å)[15] but slightly longer than the distance in the two-coordinate compound

 © 2005 Wiley-VCH Verlag GmbH & Co. KGaA, Weinheim

$[Ca\{C(SiMe_3)_3\}_2]$ (2.46 Å).[16] The Sr–C and Ba–C distances of 2.673(7) and 2.808(5) Å, respectively, seem to be the shortest such bonds reported so far. The deviations of the metal atoms from the least-squares plane defined by the carbon atoms of the bonded C_6F_5 ligands also merit comment. They increase in the order Sr (0.712 Å), Ca (0.797 Å), Ba (1.086 Å). These unusually large displacements are explained by the highly ionic, nondirectional character of the metal–carbon bonds,[6] which is further increased by the electronic influence of the fluoro substituents. As a result, relatively weak intra- or intermolecular forces such as steric repulsion or π-stacking may lead to severe distortions (see Figure S5 in the Supporting Information). It is notable that similar, although even larger, displacements in the range 0.75 to 1.50 Å have been observed for the aryl lanthanides $[Ln(Dpp)_2(thf)_2]$ (Dpp = 2,6-$Ph_2C_6H_3$), which also contain highly polar M–C bonds.[17]

Perhaps the most striking features in the solid-state structures of **3**–**5** are the additional metal–π-arene interactions[18] with the pendent arms of the biphenyl and terphenyl groups in the triazenide ligands. These arene rings apparently compete with THF to bind the M^{II} cations, thus allowing the isolation of solvent-free derivatives.[19] The calcium ion in the THF solvate **3** interacts with only one mesityl (Mes) ring in an η^5 fashion,[20] with Ca···C distances in the relatively narrow range 3.015(7)–3.132(7) Å. In the solvent-free compounds **4** and **5** the metal ions show η^6- or η^5-π-arene interactions to one Mes group and also to the triisopropylphenyl (Trip) ring of the triazenide ligand. The resulting, rather distorted pseudo-tetrahedral coordination of the metal cations is reflected in part by the angles N2-M-C51 (Ca: 112.2°; Sr: 114.8°; Ba: 113.1°) and X1-M-X2 (Sr: 129.5°; Ba: 145.0°), where X1 and X2 define the centroids of the coordinated arene rings and the bidentate triazenido ligand occupies only one coordination site. The importance and specificity of the (N_3ArAr') ligand, and in particular its π-bonding capability, is shown by the failure of a reaction analogous to Scheme 3 between Ca, Sr, or Ba, $Hg(C_6F_5)_2$, and the bulky *N*,*N*′-bis(2,6-diisopropylphenyl)formamidine.[12d] Only decomposition products were obtained, plausibly derived from an unstable $[ML(C_6F_5)]$ species.

A relatively short Sr···F52–C52(*ortho*) contact of 3.076 Å is observed in the solid-state crystal structure of the Sr derivative **4**, which is accompanied by different Sr–C51–C52/C56 angles (105.7(5)° and 139.6(6)°). In contrast, the other pentafluoroaryl derivatives show considerably longer M···F contacts of more than 3.41 Å. To clarify if the metal···arene and metal···fluorine interactions also persist in solution, variable-temperature NMR experiments were performed for the most soluble compounds **4** and **5**. At 298 K, the ^{1}H NMR spectra in [D_{14}]methylcyclohexane show only one set of signals for the Mes substituents, which, however, splits at lower temperatures. Upon warming, coalescence is detected at 238 K (**4**) and 258 K (**5**), with corresponding energy barriers of 49.0 and 53.1 kJ mol^{-1}, respectively. This observation can be interpreted in terms of a hindered rotation around the N1–C1 bond and therefore the persistence of the metal–π-arene interactions in solution. A similar behavior, with a rotational barrier of 54.3 kJ mol^{-1}, was recently observed and confirmed by quantum-chemical calculations for the unsolvated ytterbium thiophenolate [Yb(S-2,6-$Trip_2C_6H_3)_2$].[19] In addition, low-temperature ^{19}F NMR experiments for **4** and **5** show coalescence of the signals of the *ortho*-C_6F_5 fluorine atoms at 218 K and 203 K, with corresponding ΔG values of 39.1 and 34.5 kJ mol^{-1}, respectively. Unfortunately, we have not yet been able to determine which intra- or intermolecular processes are responsible for this fluxional behavior. According to preliminary quantum-chemical calculations (see Supporting Information), the binding energy for the Sr···F interaction in the model complex $[H_2N_3SrC_6F_5]$ is estimated to be only 22.1 kJ mol^{-1} at the MP2 level of theory. DFT calculations for the more sophisticated model compound $[\{(1\text{-}MesC_6H_4)(1\text{-}TripC_6H_4)N_3\}Sr(C_6F_5)]$ ($\mathbf{4_M}$), in which the noncoordinating Mes group in **4** has been replaced by a hydrogen atom, reveal a shorter Sr···F contact (2.881 Å for $\mathbf{4_M}$ versus 3.076 Å for **4**) but weaker π-coordination (av M···C 3.363 Å for $\mathbf{4_M}$ versus 3.210 Å for **4**). Since it is known that DFT methods tend to underestimate weak interactions such as π-arene bonding to electropositive metals,[19] it is plausible that in the real systems **3**–**5** these interactions are actually stronger and dominate over any M···F coordination. As a result, decomposition pathways involving *ortho*-fluoride elimination are effectively blocked.

In summary, we have designed and prepared very bulky aryl-substituted triazenide ligands that have permitted the synthesis of the first structurally characterized aryl compounds of the heavier alkaline-earth metals Ca, Sr, and Ba. Kinetic stabilization in the solid-state and in solution through steric and electronic saturation of the metal centers is achieved by additional π-arene interactions to the pendent aryl substituents. These novel, sterically crowded triazenides may find use as ancillary ligands in catalysis and we are currently exploring this field.

Experimental Section

All manipulations were carried out under strictly anaerobic and anhydrous conditions under argon. The starting materials 2-iodo-2′,4′,6′-triisopropylbiphenyl,[21] 2,4,6,2″,4″,6″-hexamethyl-1,1′:3′,1″-terphenyl-2′-azide,[22] and bis(pentafluorophenyl)mercury[23] were prepared by known procedures.

HN_3ArAr' (**2a**): *n*-Butyllithium (44.4 mmol, 2.5 M hexane solution) was added at 0 °C to a solution of 2-iodo-2′,4′,6′-triisopropylbiphenyl (18.1 g, 44.4 mmol) in diethyl ether (250 mL) and stirring was continued for 2 h. The clear solution of the aryl lithium compound thus obtained was then treated with small portions of 2,4,6,2″,4″,6″-hexamethyl-1,1′:3′,1″-terphenyl-2′-azide (15.8 g, 44 mmol). After warming to ambient temperature and stirring for an additional 12 h, the orange solution was quenched with water (400 mL). The aqueous phase was separated and extracted with diethyl ether (3 × 100 mL). The organic phases were combined, repeatedly washed with water, and dried with Na_2SO_4. Filtration followed by solvent removal in vacuo afforded **2a** as a yellow solid. Analytically pure, pale yellow crystals were obtained by recrystallization from hot acetone. Yield: 25.2 g (39.6 mmol, 89 %); m.p. 174–176 °C; ^{1}H NMR (400.1 MHz, [D_6]benzene): δ = 0.87, 1.00, 1.13 (3 × d, $^3J_{H,H}$ = 6.9 Hz, 3 × 6 H; *o* + *p*-$CH(CH_3)_2$), 2.04 (s, 12 H; *o*-CH_3), 2.18 (s, 6 H; *p*-CH_3), 2.54 (sept, $^3J_{H,H}$ = 6.9 Hz, 2 H; *o*-$CH(CH_3)_2$), 2.69 (sept, $^3J_{H,H}$ = 6.9 Hz, 1 H; *p*-$CH(CH_3)_2$), 6.79 (s, 4 H; *m*-Mes), 6.85–7.14 (m, 7 H; various aryl-H), 7.00 (s, 2 H; *m*-Trip), 8.70 ppm (s, 1 H; NH); ^{13}C NMR (62.9 MHz, [D_6]benzene): δ = 20.9 (*o*-CH_3), 21.1 (*p*-CH_3), 23.8, 24.0, 24.5 (*o* + *p*-$CH(CH_3)_2$), 30.7 (*o*-$CH(CH_3)_2$), 34.5 (*p*-$CH(CH_3)_2$), 121.4, 122.2,

 © 2005 Wiley-VCH Verlag GmbH & Co. KGaA, Weinheim

126.8, 128.3, 129.8, 130.8 (aromatic CH), 113.7, 125.6, 134.8, 135.8, 136.1, 137.3, 139.3, 146.2, 147.5, 149.3 ppm (aromatic C). elemental analysis calcd (%) for $C_{45}H_{53}N_3$: C 84.99, H 8.40, N 6.61; found: C 84.88, H 8.41, N 6.64.

[Ba(C_6F_5)(N_3ArAr′)] (**5**): Bis(pentafluorophenyl)mercury (1.07 g, 2.00 mmol) was added at ambient temperature to a stirred mixture of barium ingots (2.5 g, 18.2 mmol) and **2a** (1.27 g, 2.00 mmol) in THF (60 mL). Stirring was continued for 14 h, whereupon the solvent was removed under reduced pressure. The green residue was treated with *n*-heptane, and solid materials were separated by centrifugation. The volume of the resulting deep yellow solution was reduced to incipient crystallization under reduced pressure. Storage in a freezer at −20 °C for several days afforded **5** as a bright yellow, crystalline material. Yield: 1.48 g (1.58 mmol, 79 %); m.p. 144–170 °C (decomp); ^{1}H NMR (250.1 MHz, [D$_6$]benzene): δ = 0.63, 0.78, 1.18 (3 × d, $^3J_{H,H}$ = 6.8 Hz, 3 × 6 H; *o* + *p*-CH(CH_3)$_2$), 2.04 (s, 12 H; *o*-CH_3), 2.19 (s, 6 H; *p*-CH_3), 2.57 (sept, $^3J_{H,H}$ = 6.8 Hz, 2 H; *o*-C*H*(CH$_3$)$_2$), 2.90 (sept, $^3J_{H,H}$ = 6.8 Hz, 1 H; *p*-C*H*(CH$_3$)$_2$), 6.46–7.27 (m, 7 H; various aryl-H), 6.78 (s, 4 H; *m*-Mes), 7.04 ppm (s, 2 H; *m*-Trip); ^{13}C NMR (62.9 MHz, [D$_6$]benzene): δ = 20.8 (*o*-*C*H$_3$), 21.0 0(*p*-*C*H$_3$), 23.1, 24.2, 24.2 (*o* + *p*-CH(*C*H$_3$)$_2$), 30.5 (*o*-*C*H(CH$_3$)$_2$), 33.8 (*p*-*C*H(CH$_3$)$_2$), 116.9, 122.0, 122.0, 123.1, 128.6, 129.0, 129.1, 129.4 (aromatic CH), 128.8, 131.5, 136.6, 137.4, 142.0, 142.4, 148.0, 150.3, 150.6, 152.1 ppm (aromatic C); signals for the C_6F_5 group could not be detected or assigned completely due to signal overlap and their weak appearance; ^{19}F NMR (235.4 MHz, [D$_6$]benzene): δ = −159.0 (m, 2 F; *m*-C_6F_5), −154.2 (tt, $^3J_{F,F}$ = 20.3, $^4J_{F,F}$ = 3.3 Hz, 1 F; *p*-C_6F_5), −113.2 ppm (m, 2 F; *o*-C_6F_5); ^{15}N NMR (40.6 MHz, [D$_6$]benzene): δ = 109.5 (s; -N*N*N-), −69.3, −70.4 ppm (s; -*N*N*N*-); elemental analysis calcd (%) for $C_{51}H_{52}BaF_5N_3$: C 65.21, H 5.58, N 4.47; found: C 64.76, H 5.76, N 4.52.

Details of the preparation and characterization of compounds **2b**, **3**, and **4**, and additional spectroscopic data for **2a** and **5** are given in the Supporting Information.

Received: April 30, 2005

Keywords: barium · calcium · fluorinated ligands · N ligands · strontium

[1] J. Barker, M. Kilner, *Coord. Chem. Rev.* **1994**, *133*, 219.
[2] L. Bourget-Merle, M. F. Lappert, J. R. Severn, *Chem. Rev.* **2002**, *102*, 3031.
[3] D. S. Moore, S. D. Robinson, *Adv. Inorg. Chem. Radiochem.* **1986**, *30*, 1.
[4] K. Vrieze, G. van Koten, in *Comprehensive Coordination Chemistry, Vol. 2* (Ed.: G. Wilkinson), Pergamon, Oxford, **1987**, pp. 189–244.
[5] P. Gantzel, P. J. Walsh, *Inorg. Chem.* **1998**, *37*, 3450.
[6] The Gaussian 03 package (Revision B.01, Gaussian Inc., Pittsburgh PA, 2003) was used for all energy and frequency calculations. The geometries of the molecules were optimized using either density functional theory (DFT) with the functional B3LYP for the model ligands $\mathbf{I_M}$–$\mathbf{III_M}$ (all with implied C_2 symmetry) and the model complex $\mathbf{4_M}$ or second-order Møller–Plesset perturbation theory (MP2) for two conformers of the model compound [$H_2N_3SrC_6F_5$] (C_s symmetry). In each case the GDIIS algorithm with the TIGHT convergence criterion was used. A quasi-relativistic 10-valence-electron pseudopotential was employed for the heavy atom Sr (M. Kaupp, P. von R. Schleyer, H. Stoll, H. Preuss, *J. Chem. Phys.* **1991**, *94*, 1360). The corresponding 6s6p5d valence basis was augmented by one set of f-functions. The basis sets for C, H, N, and F were either 6-311 + G** ($\mathbf{I_M}$–$\mathbf{III_M}$) or 6-31G* ($\mathbf{4_M}$, [$H_2N_3SrC_6F_5$]). All stationary points were characterized by analytical or numerical frequency analyses. The natural bond orbital analysis employed the Gaussian 03 adaptation of the NBO program (E. D. Glendening, A. E. Reed, J. E. Carpenter, F. Weinhold, NBO Version 3.1). For the model complex $\mathbf{4_M}$ the following NPA charges were calculated: +1.728 (Sr), −0.505 (N1), −0.509 (N3), −0.637 (C51).
[7] G. B. Deacon, C. M. Forsyth, S. Nickel, *J. Organomet. Chem.* **2002**, *647*, 50.
[8] Solvated bis- and tris(triazenide) complexes with much less bulky ligands are known for Mg and Ca: S. Westhusin, P. Gantzel, P. J. Walsh, *Inorg. Chem.* **1998**, *37*, 5956.
[9] a) G. B. Deacon, C. M. Forsyth, *Organometallics* **2003**, *22*, 1349; b) L. Maron, E. L. Werkema, L. Perrin, O. Eisenstein, R. A. Andersen, *J. Am. Chem. Soc.* **2005**, *127*, 279; c) M. L. Cole, G. B. Deacon, P. C. Junk, K. Konstas, *Chem. Commun.* **2005**, 1581.
[10] Shock-frozen crystals in Paratone N, programs SHELXTL 5.03 and SHELXL-97, refinement with all data on F^2, non-hydrogen atoms anisotropic, hydrogen atoms at calculated positions. Crystal data for **3**: pale yellow prism (0.20 × 0.20 × 0.10 mm^3) from *n*-heptane at 20 °C, $C_{55}H_{60}CaF_5N_3O$, M_r = 953.92, monoclinic, space group $P2_1/n$, a = 9.380(3), b = 23.159(5), c = 23.142(6) Å, β = 93.93(3)°, V = 5015(3) Å^3, Z = 4, ρ_{calcd} = 1.211 g cm^{-1}, $\mu(Mo_{K\alpha})$ = 0.184 mm^{-1}, Siemens P3 diffractometer, T = 173 K, $2\Theta_{max}$ = 48°, 8420 (R_{int} = 0.106) collected and 7881 unique reflections, 612 parameters, 7 restraints, absorption correction by Ψ-scans, R_1 = 0.117 for 2929 reflections with $I > 2\sigma(I)$, wR_2 = 0.163 (all data), GOF = 1.071. Crystal data for **4**: yellow block (0.15 × 0.08 × 0.06 mm^3) from *n*-heptane at −15 °C, $C_{51}H_{52}F_5N_3Sr$, M_r = 889.58, monoclinic, space group $P2_1/n$, a = 16.051(3), b = 14.970(3), c = 19.128(4) Å, β = 106.79(3)°, V = 4399.9(15) Å^3, Z = 4, ρ_{calcd} = 1.343 g cm^{-1}, $\mu(Mo_{K\alpha})$ = 1.285 mm^{-1}, Nonius Kappa CCD diffractometer, T = 100 K, $2\Theta_{max}$ = 56.6°, 50525 (R_{int} = 0.149) collected and 10346 unique reflections, 571 parameters, 0 restraints, absorption correction from symmetry-related measurements, R_1 = 0.124 for 8127 reflections with $I > 2\sigma(I)$, wR_2 = 0.298 (all data), GOF = 2.33. Crystal data for **5**: yellow block (0.15 × 0.06 × 0.04 mm^3) from *n*-heptane at −20 °C, $C_{51}H_{52}BaF_5N_3$, M_r = 939.30, monoclinic, space group $P2_1/n$, a = 16.4690(4), b = 15.5775(3), c = 18.3051(3) Å, β = 108.2063(11)°, V = 4461.00(16) Å^3, Z = 4, ρ_{calcd} = 1.399 g cm^{-1}, $\mu(Mo_{K\alpha})$ = 0.946 mm^{-1}, Nonius Kappa CCD diffractometer, T = 100 K, $2\Theta_{max}$ = 56.6°, 74322 (R_{int} = 0.175) collected and 10877 unique reflections, 599 parameter, 1 restraint, absorption correction from symmetry-related measurements, R_1 = 0.060 for 7895 reflections with $I > 2\sigma(I)$, wR_2 = 0.114 (all data), GOF = 1.536. CCDC-268134 (**3**),CCDC-268135 (**4**), and CCDC-268136 (**5**) contain the supplementary crystallographic data for this paper. These data can be obtained free of charge from the Cambridge Crystallographic Data Centre via www.ccdc.cam.ac.uk/data_request/cif.
[11] R. D. Shannon, *Acta Crystallogr. Sect. A* **1976**, *32*, 751.
[12] a) M. Westerhausen, W. Schwarz, *Z. Naturforsch. B* **1992**, *47*, 453; b) M. Westerhausen, H. D. Hausen, W. Schwarz, *Z. Anorg. Allg. Chem.* **1992**, *618*, 121; c) M. Westerhausen, W. Schwarz, *Z. Anorg. Allg. Chem.* **1993**, *619*, 1455; d) M. L. Cole, P. C. Junk, *New J. Chem.* **2005**, *29*, 135.
[13] S. Harder, *Organometallics* **2002**, *21*, 3782.
[14] a) T. P. Hanusa, *Coord. Chem. Rev.* **2000**, *210*, 329; b) M. Westerhausen, *Angew. Chem.* **2001**, *113*, 3063; *Angew. Chem. Int. Ed.* **2001**, *40*, 2975; c) J. S. Alexander, K. Ruhlandt-Senge, *Eur. J. Inorg. Chem.* **2002**, 2761.
[15] F. G. N. Cloke, P. B. Hitchcock, M. F. Lappert, G. A. Lawless, B. Royo, *J. Chem. Soc. Chem. Commun.* **1991**, 724.
[16] C. Eaborn, S. A. Hawkes, P. B. Hitchcock, J. D. Smith, *Chem. Commun.* **1997**, 1961.
[17] a) G. Heckmann, M. Niemeyer, *J. Am. Chem. Soc.* **2000**, *122*, 4227; b) M. Niemeyer, *Acta Crystallogr. Sect. E* **2001**, *57*, m578.

 © 2005 Wiley-VCH Verlag GmbH & Co. KGaA, Weinheim

[18] For examples of π-arene interactions to Ca^{2+}, Sr^{2+}, and Ba^{2+}, see: a) M. Westerhausen, M. Krofta, N. Wiberg, J. Knizeh, H. Nöth, A. Pfitzner, *Z. Naturforsch. B* **1998**, *53*, 1489; b) L. Bonomo, E. Solari, R. Scopelliti, C. Floriani, *Chem. Eur. J.* **2001**, *7*, 1322; c) G. Guillemot, E. Solari, C. Rizzoli, C. Floriani, *Chem. Eur. J.* **2002**, *8*, 2072; d) F. Feil, S. Harder, *Eur. J. Inorg. Chem.* **2003**, 3401.
[19] M. Niemeyer, *Eur. J. Inorg. Chem.* **2001**, 1969.
[20] The assignment of the hapticity of the metal–π-arene interactions in compounds **3**–**5** is based on the evaluation of the M–C distances and the angle between the M–centroid vector and the normal of the arene plane (see Supporting Information).
[21] N. Hartmann, M. Niemeyer, *Synth. Commun.* **2001**, *31*, 3839.
[22] J. Gavenonis, T. D. Tilley, *Organometallics* **2002**, *21*, 5549.
[23] G. B. Deacon, J. E. Cosgriff, E. T. Lawrenz, C. M. Forsyth, D. L. Wilkinson, in *Synthetic Methods of Organometallic and Inorganic Chemistry, Vol. 6* (Eds.: W. A. Herrmann, F. T. Edelmann), Thieme, Stuttgart, **1997**, pp. 48–49.

 © 2005 Wiley-VCH Verlag GmbH & Co. KGaA, Weinheim

Synthetic Methods

DOI: 10.1002/anie.200501468

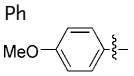
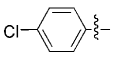
Lithium Benzocyclobuteneoxide as a Precursor of a Vinylogous Enolate: Solvent-Controlled Synthesis of Highly Functionalized Seven-Membered Benzocarbocycles**

José Barluenga, Patricia García-García, Manuel A. Fernández-Rodríguez, Enrique Aguilar, and Isabel Merino*

The role of Fischer carbene complexes (FCCs) as synthetic intermediates in organic chemistry is today perfectly established,[1] although new patterns of reactivity are still amenable. In this context, we have initiated an exploration of the reactivity of FCCs toward *ortho*-quinodimethanes[2] (*o*QDMs) and reported recently that the reaction of symmetric bistrialkylsilyloxy *o*QDMs, readily generated by thermal ring opening of benzocyclobutenes, with alkynyl FCCs follows a tandem [4+2] cycloaddition/cyclopentannulation sequence that leads to benzo[*b*]fluorenes.[3] Choy and Yang have pointed out that the ring opening of metalated benzocyclobuteneoxides takes place at temperatures as low as −25 °C, thus confirming that such a process is favored by the presence of electron-donating groups on the cyclobutene ring.[4] On the other hand, functionalized seven-membered benzocarbocycles are both important synthetic intermediates and key structural elements in various natural products and/or pharmacologically active compounds, such as terpenes, namely, (−)-presphaerene[5] and barbatusol;[6] alkaloids, for example, dragmacidin E;[7] (−)-colchicine, an antitumour agent;[8] nortriptyline and amitriptyline, which have antidepressant activities;[9] and hamigeran C, which is cytotoxic,[10] among others. We describe herein the preliminary results of the reaction of alkynyl FCCs with *o*QDM **1** prepared by Choy and Yang, thus leading to the preparation of highly functionalized seven-membered benzocarbocycles which have not been previously accessed from FCCs.

In our initial experiment (Scheme 1), benzocyclobutenol **2** was deprotonated with *n*BuLi at −78 °C in THF and the reaction mixture was allowed to reach −25 °C to permit the formation of *o*QDM **1**; subsequently, chromium FCC **3** was added, and the reaction was monitored by TLC. However, rather than the expected [4+2] cycloadduct **5** or benzo[*b*]-fluorene **6**, two benzoheptacarbocycles[11] **7a** and **8a** were isolated as a mixture in low yield, among other products (Table 1, entry 1). As far as we know, this reaction is the first example in which oQDM **1** acts as a four-carbon synthon in a formal [4+3] cycloaddition. We switched to the more stable tungsten FCC **4a** to find that the combined yield of the isolated products, [4+3] cycloadducts **7a** and **8a**, was improved to 65 % (entry 2) under similar reaction conditions. Other solvents (hexane, 1,2-dimethoxyethane, toluene, and dioxane) were then examined but produced either low-yielding mixtures of **7a** and **8a** or no identifiable products.

Table 1: Reaction of **1** with alkynyl carbene complexes **3** and **4** in THF.

Entry[a]	FCC	Metal	R	7	Yield [%][b]	8	Yield [%][b]
1	**3**	Cr	Ph	**7a**	8	**8a**	11
2	**4a**	W	Ph	**7a**	49	**8a**	16
3[c]	**4a**	W	Ph	**7a**	–	**8a**	50
4	**4b**	W		**7b**	71	**8b**	14
5	**4c**	W		**7c**	67	**8c**	30
6	**4d**	W		**7d**	52	**8d**	22
7	**4e**	W	*t*Bu	**7e**	50[d]	**8e**	5[d]

[a] All the reactions were carried out on a 0.5-mM scale for the carbene complex (0.033 M) with 1.5 equivalents of benzocyclobutenol (0.05 M). [b] Yields of isolated product based on the starting alkynyl carbene complexes. [c] Reaction performed in diethyl ether. [d] Products could not be separated; yield estimated by ^{1}H NMR (300 MHz) spectroscopic analysis from a fraction enriched in **7e** after flash column chromatography.

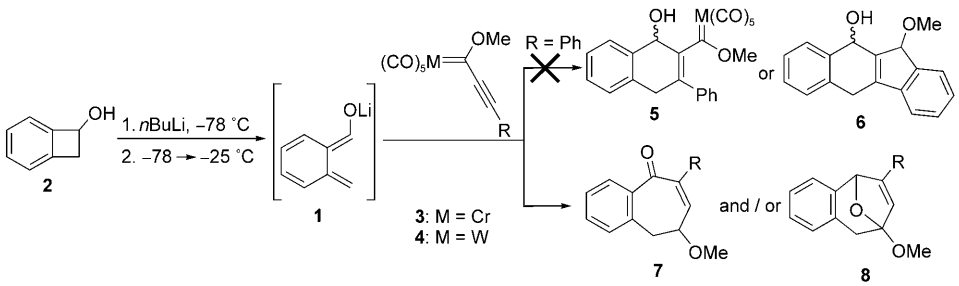
[*] Prof. Dr. J. Barluenga, P. García-García, Dr. M. A. Fernández-Rodríguez, Dr. E. Aguilar, Dr. I. Merino[+] Instituto Universitario de Química Organometálica "Enrique Moles", Unidad Asociada al C.S.I.C. Universidad de Oviedo C/Julián Clavería, 8, 33006 Oviedo (Spain) Fax: (+34) 985-103-450 E-mail: barluenga@uniovi.es

[+] NMR spectroscopic studies.

[**] We thank the Ministerio de Ciencia y Tecnología (Spain; BQU2001-3853), the Consejería de Educación y Cultura del Principado de Asturias (PR-01-GE-11), and the Fundación Ramón Areces for financial support. We also appreciate the generous support given by Merck Sharp and Dohme. P.G.-G. is indebted to the Ministerio de Educación y Ciencia (Spain) for a MEC-FPU predoctoral fellowship.

Supporting information for this article is available on the WWW under http://www.angewandte.org or from the author.

 © 2005 Wiley-VCH Verlag GmbH & Co. KGaA, Weinheim



Scheme 1. Reaction of **1** with alkynyl carbene complexes.

Interestingly, the reaction led exclusively to **8a** when performed in diethyl ether (entry 3). Such a strong solvent effect[12] prompted us to consider the possibility of increasing the yield through additives or by variation of the counterion. However, none of the following approaches led to improved results: the addition of different coordinating reagents (*N*,*N*,*N*′,*N*″,*N*‴-pentamethyldiethylenetriamine (PMDTA), [12]crown-4, *N*,*N*′-dimethyl-*N*,*N*′-propyleneurea (DMPU)), the use of different bases (potassium hexamethyldisilazane (KHMDS), NaHMDS, EtMgBr), and transmetalation strategies (BuLi/$ZnCl_2$) in both diethyl ether or THF.

Considering that at this point we had already created conditions that allowed for the selective formation of two differently functionalized benzoheptacarbocycles, we next tried to expand the scope of such transformations by examining of the nature of the substituents of the carbene complex. Thus, carbene complexes **4b–e** were treated with **1** in THF to obtain moderate to good yields of benzocycloheptenones **7** (Table 1, entries 4–7), which were accompanied by small amounts of benzocycloheptene ketals **8** that could be readily separated by flash column chromatography. The best yields were achieved when the R group was a *para*-substituted aromatic moiety (entries 4 and 5), although the reaction also took place selectively for alkenyl- and alkyl-substituted alkynyl FCCs **4d**, **e** (entries 6 and 7).

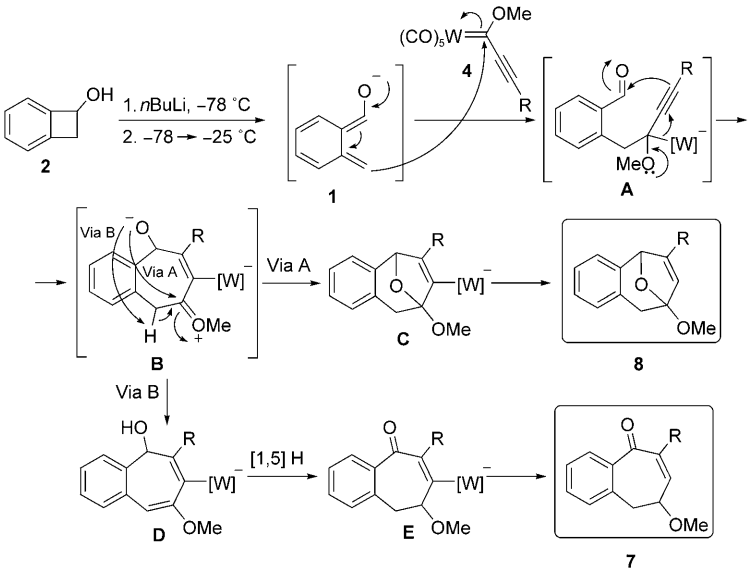
On the other hand, benzocycloheptene ketals **8** were obtained as the unique reaction products, as expected, when carbene complexes **4a–g** were treated with **1** in diethyl ether (Table 2; see also Table 1, entry 3). This reaction was much slower and usually required reaching either room temperature (Table 2, entries 2, 4, and 6) or reflux (entries 5 and 7) to proceed. Again, *para*-substituted alkynylaryl carbene complexes gave the best yields (entries 2 and 3). These reaction conditions tolerate alkenyl (entry 4), alkyl (entries 5 and 6), and silyl (entry 7) groups as substituents in the alkynyl FCC. We also observed that the yield may be improved by performing the reaction at a higher concentration with a higher excess of benzocyclobutenol (Table 2, entry 1 versus Table 1, entry 3).

As a basis for the mechanism, we propose that after the initial deprotonation of benzocyclobutenol **2** at −78 °C, the resulting lithium benzocyclobutenoxide opens to **1** by warming to −25 °C (Scheme 2). Subsequently, *o*QDM **1** would behave as a vinylogous enolate rather than a 1,3-diene, and a nucleophilic attack[13,14] on the carbene carbon of **4** would take place to form intermediate **A**. A 1,2-metal migration,[14] promoted by the methoxy group, would cause simultaneous ring closure to form intermediate **B**. The evolution of **B** could occur by two different routes: In the first (via A), an intramolecular nucleophilic attack would produce the metalated benzocycloheptene ketal **C**, which would account for the formation of **8**, whereas in the second (via B), an intramolecular acid/base reaction would generate the metalated intermediate **D**, thus leading to **E** through a 1,5-hydrogen shift and finally to **7**.

Table 2: Reaction of **1** with tungsten alkynyl carbene complexes **4** in Et_2O.

Entry[a]	FCC	R	8	Yield [%][b]
1[c]	**4a**	Ph	**8a**	70
2	**4b**	MeO	**8b**	56[d]
3	**4c**	Cl	**8c**	86
4	**4d**		**8d**	55[d]
5	**4e**	*t*Bu	**8e**	50[e]
6	**4f**	*n*Bu	**8f**	25[d]
7	**4g**	TMS	**8g**	38[e]

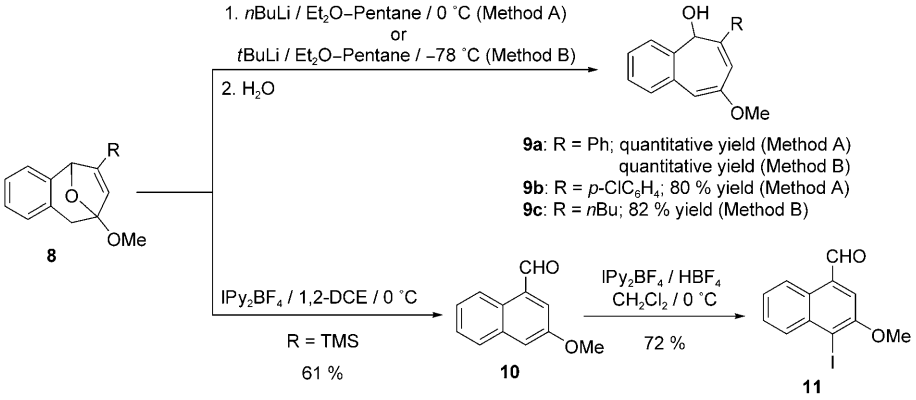
[a] All the reactions were carried out on a 0.5-mM scale for the carbene complex (0.033 M) with 1.5 equivalents of benzocyclobutenol (0.05 M), unless otherwise stated. [b] Yields of isolated product based on the starting alkynyl carbene complexes **4**. [c] Reaction carried out with 5 equivalents of benzocyclobutenol (0.33 M). [d] It was necessary to reach room temperature for the reaction to proceed. [e] It was necessary to reach reflux for the reaction to proceed. TMS = trimethylsilyl.



Scheme 2. Proposed mechanism for the formation of seven-membered benzocarbocycles **7** and **8**.

 © 2005 Wiley-VCH Verlag GmbH & Co. KGaA, Weinheim

Our preliminary results into the reactivity of benzocycloheptene ketals **8** indicate that it is possible to break the heteroatom bridge of **8** by treatment with *n*BuLi or *t*BuLi to form benzocycloheptadienols **9** in good to excellent yields (Scheme 3); therefore, this breakage acts as a direct entry to a



Scheme 3. Chemical transformations of benzocycloheptene ketals **8**. IPy_2BF_4 = bis(pyridine)-iodonium(I) tetrafluoroborate, 1,2-DCE = 1,2-dichloroethene.

third type of functionalized seven-membered benzocarbocycle. On the other hand, we also observed that ring contraction[15] takes place in **8g** (R = TMS) upon treatment with IPy_2BF_4[16] to give **10** in 61% yield. This apparently simple compound has now been prepared for the first time;[17] thus, by using this approach the difficulties that derived from both the electronic nature and the relative position of its substituents have been overcome. Naphthyl aldehyde **10** could be iodinated with IPy_2BF_4 in acidic medium at the C4 position of the naphthalene skeleton to form **11** in 72% yield (Scheme 3), thus expanding the possibilities for further transformations.

In summary, we have established a new and direct route to seven-membered functionalized benzocarbocycles from tungsten alkynyl FCCs. In this transformation, oQDM **1** prepared by Choy and Yang behaves as a vinylogous enolate which acts for the first time as a four-carbon component in a formal [4+3] cycloaddition. The outcome of the reaction is solvent controlled: selective formation of benzocycloheptenones **7** can be achieved in THF, whereas exclusive synthesis of benzocycloheptene ketals **8** occurs in diethyl ether. The latter compounds can be readily transformed in benzocycloheptadienols **9** by a base-promoted opening of the cyclic ketal moiety. Access to the previously unknown 3-methoxy-1-naphthylcarbaldehyde (**10**) is obtained by a ring contraction of cyclic ketal **8g** promoted by IPy_2BF_4. The exploration of transition-metal-catalyzed (Cu, Rh) nucleophilic ring openings[18] of ketals **8** is currently underway and the results will be reported in due course.

Received: April 28, 2005

Keywords: carbene ligands · carbocycles · cycloaddition · enolates · solvent effects

[1] Selected recent reviews: a) J. Barluenga, M. A. Fernández-Rodríguez, E. Aguilar, *J. Organomet. Chem.* **2005**, *690*, 539–587; b) M. Gómez-Gallego, M. J. Mancheño, M. A. Sierra, *Acc. Chem. Res.* **2005**, *38*, 44–53; c) J. Barluenga, J. Santamaría, M. Tomás, *Chem. Rev.* **2004**, *104*, 2259–2283; d) J. W. Herndon, *Coord. Chem. Rev.* **2004**, *248*, 3–79; e) J. Barluenga, J. Flórez, F. J. Fañanás, *J. Organomet. Chem.* **2001**, *624*, 5–17; f) K. H. Dötz, C. Jakel, W. C. Haase, *J. Organomet. Chem.* **2001**, *617–618*, 119–132; g) A. J. Fletcher, S. D. R. Christie, *J. Chem. Soc. Perkin Trans. 1* **2001**, 1–13; h) M. A. Sierra, *Chem. Rev.* **2000**, *100*, 3591–3638; i) A. de Meijere, H. Schirmer, M. Duestsch, *Angew. Chem.* **2000**, *112*, 4124–4162; *Angew. Chem. Int. Ed.* **2000**, *39*, 3964–4002. Books; j) *Metal Carbenes in Organic Synthesis* (Ed.: K. H. Dötz) in *Topics in Organometallic*, *Vol. 13 Chemistry*, Wiley, New York, **2004**; k) *Carbene Chemistry: From Fleeting Intermediates to Powerful Reagents* (Ed.: G. Bertrand), Marcel Dekker, New York, **2002**; l) F. Zaragoza Dörwald in *Metal Carbenes in Organic Synthesis*, Wiley-VCH, Weinheim, **1999**.

[2] a) G. Mehta, S. Cota, *Tetrahedron* **2001**, *57*, 625–659; b) J. L. Segura, N. Martín, *Chem. Rev.* **1999**, *99*, 3199–3246; c) P. Y. Michellys, H. Pellisier, M. Santelli, *Org. Prep. Proced. Int.* **1996**, *28*, 545–608; d) T. Chou, *Rev. Heteroat. Chem.* **1993**, *8*, 65–104; e) N. Martín, C. Seoane, M. Hanack, *Org. Prep. Proced. Int.* **1991**, *23*, 237–272.

[3] J. Barluenga, M. A. Fernández-Rodríguez, E. Aguilar, *Org. Lett.* **2002**, *4*, 3659–3662.

[4] W. Choy, H. Yang, *J. Org. Chem.* **1988**, *53*, 5796–5798.

[5] a) J. Lee, J. Hong, *J. Org. Chem.* **2004**, *69*, 6433–6440; b) F. Cafieri, P. Ciminiello, C. Santacroce, E. Fattorusso, *Phytochemistry* **1983**, *22*, 1824–1825.

[6] a) G. Majetich, Y. Zhang, T. L. Feltman, S. Duncan, Jr., *Tetrahedron Lett.* **1993**, *34*, 445–448; b) E. R. Koft, *Tetrahedron* **1987**, *43*, 5775–5780; c) A. Kelecom, *Tetrahedron* **1983**, *39*, 3603–3608.

[7] R. J. Capon, F. Rooney, L. M. Murray, E. Collins, A. T. R. Sim, J. A. P. Rostas, M. S. Butler, A. R. Carroll, *J. Nat. Prod.* **1998**, *61*, 660–662.

[8] a) H.-G. Capraro, A. Brossi in *The Alkaloids, Vol. 23* (Ed.: A. Brossi), Academic Press, New York, **1984**, pp. 1–70; b) A. Brossi, *J. Med. Chem.* **1990**, *33*, 2311–2319; c) O. Boye, A. Brossi in *The Alkaloids, Vol. 41* (Ed.: A. Brossi, G. A. Cordell), Academic Press, New York, **1992**, pp. 125–176.

[9] M. Williams, E. A. Kovaluk, S. P. Arneric, *J. Med. Chem.* **1999**, *42*, 1481–1500.

[10] a) K. Wellington, R. Cambie, P. Rutledge, P. Bergquist, *J. Nat. Prod.* **2000**, *63*, 79–85; b) R. Cambie, A. Lai, M. Kernan, *J. Nat. Prod.* **1993**, *58*, 940–942.

[11] The identity of all the new compounds was ascertained unequivocally by NMR spectroscopic experiments, including COSY, HMQC, HMBC, and NOESY for selected compounds (see the Supporting Information); an X-Ray structure elucidation for **8a** was also obtained: P. García-García, F. Andina, M. A. Fernández-Rodríguez, E. Aguilar, in preparation.

[12] Solvent-controlled processes that involve FCCs in the synthesis of five-membered carbocycles have been recently highlighted:

 © 2005 Wiley-VCH Verlag GmbH & Co. KGaA, Weinheim

a) F. Zaragoza Dörwald, *Angew. Chem.* **2003**, *115*, 1372 – 1374; *Angew. Chem. Int. Ed.* **2003**, *42*, 1332 – 1334; b) J. Barluenga, S. López, J. Flórez, *Angew. Chem.* **2003**, *115*, 241 – 243; *Angew. Chem. Int. Ed.* **2003**, *42*, 231 – 233.

[13] a) The nucleophilic attack of lithium enolates derived from methyl ketone takes place at the carbene carbon of α,β-unsaturated FCCs: J. Barluenga, J. Alonso, F. J. Fañanás, J. Borge, S. García-Granda, *Angew. Chem.* **2004**, *116*, 5626 – 5629; *Angew. Chem. Int. Ed.* **2004**, *43*, 5510 – 5513, and references cited therein; on the other hand, substituted lithium enolates add to α,β-unsaturated FCCs in the fashion of a Michael addition; see, for example: b) I. Merino, Y. R. S. Laxmi, J. Flórez, J. Barluenga, J. Ezquerra, C. Pedregal, *J. Org. Chem.* **2002**, *67*, 648 – 655.

[14] 1,2-Metal migrations have been invoked in related transformations: a) J. Barluenga, M. Tomás, E. Rubio, J. A. López-Pelegrín, S. García-Granda, P. Pertierra, *J. Am. Chem. Soc.* **1996**, *118*, 695 – 696; this rearrangement could be monitored by NMR spectroscopic analysis: b) J. Barluenga, M. Tomás, A. Ballesteros, J. Santamaría, R. J. Carbajo, F. López-Ortiz, S. García-Granda, P. Pertierra, *Chem. Eur. J.* **1996**, *2*, 88 – 97.

[15] Iodine-promoted ring contractions in seven-membered rings have been previously observed in our group: J. Barluenga, F. González-Bobes, J. M. González, *Angew. Chem.* **2002**, *114*, 2668 – 2670; *Angew. Chem. Int. Ed.* **2002**, *41*, 2556 – 2558.

[16] IPy_2BF_4 (Py = pyridine) is commercially available from either Novabiochem or Aldrich; for recent applications, see: a) J. Barluenga, F. González-Bobes, M. C. Murguía, S. R. Ananthoju, J. M. González, *Chem. Eur. J.* **2004**, *10*, 4206 – 4213; for a brief overall review of early applications, see: b) J. Barluenga, *Pure Appl. Chem.* **1999**, *71*, 431 – 436.

[17] Structurally related compounds, such as 3-hydroxy-1-naphthylcarbaldehyde, have been previously prepared; see: K. Chamontin, V. Lokshin, V. Rossollin, A. Samat, R. Guglielmetti, *Tetrahedron* **1999**, *55*, 5821 – 5830.

[18] a) M. Lautens, K. Fagnou, S. Hiebert, *Acc. Chem. Res.* **2003**, *36*, 48 – 58; b) K. Fagnou, M. Lautens, *Chem. Rev.* **2003**, *103*, 169 – 196; c) P. A. Evans, D. K. Leahy, *J. Am. Chem. Soc.* **2002**, *124*, 7882 – 7883.

 © 2005 Wiley-VCH Verlag GmbH & Co. KGaA, Weinheim

Peptide Helices

DOI: 10.1002/anie.200501247

9/11 Mixed Helices in α/β Peptides Derived from C-Linked Carbo-β-Amino Acid and L-Ala Repeats**

Gangavaram V. M. Sharma, Pendem Nagendar, P. Jayaprakash, Palakodety Radha Krishna, K. V. S. Ramakrishna, and Ajit C. Kunwar**

Oligomers of nonnatural amino acids, which form a variety of secondary structures, have been studied extensively.[1] The impetus for such efforts has invariably been a desire to understand the conformational behavior and to develop these structures into biomolecules with novel properties. The β peptides, a very important class of foldamers, are derived from β-amino acids and exhibit several novel secondary structures.[2–6] The 10/12-mixed helix, unique to β peptides, was discovered by Seebach et al.[4] in β^2/β^3-dipeptide repeats. Theoretical studies by Hofmann and co-workers[7a] and Wu et al.[7b,c] predicted that 10/12 and 12/10 helices are energetically the most favored secondary structures in β peptides in solution. Subsequently, Kessler and co-workers[8] used a cyclic sugar β-amino acid and β-hGly repeats to obtain such mixed helices. In a later study, we demonstrated the presence of robust right-handed 10/12- and 12/10-mixed helices[9] in heterochiral dipeptide repeats from carbo-β^3-amino acid (Caa) residues with "alternating chirality" at the C^β carbon atom. Further studies on peptides with alternating Caa and β-hGly repeats resulted in right- and left-handed 10/12 and 12/10 helices.[10] Although Hofmann and co-workers[11] predicted the existence of mixed helices in homologous α, β, γ, and δ peptides from theoretical studies, the experimental realization of these structures has so far been limited only to β peptides.[4,8–10] From the above studies, it is amply evident that mixed helices invariably resulted from heterodipeptide repeats. However, the α/β-dipeptide repeats reported by Gellman and co-workers[12] showed the coexistence of an

[*] Dr. G. V. M. Sharma, P. Nagendar, P. Jayaprakash, Dr. P. Radha Krishna
D-211, Discovery Laboratory
Organic Chemistry Division III
Indian Institute of Chemical Technology
Hyderabad 500 007 (India)
Fax: (+91) 40-2716-0387/-2719-3108
E-mail: esmvee@iict.res.in

K. V. S. Ramakrishna, Dr. A. C. Kunwar
Centre for Nuclear Magnetic Resonance
Indian Institute of Chemical Technology
Hyderabad 500 007 (India)
Fax: (+91) 40-2719-3108
E-mail: kunwar@iict.res.in

[**] IICT Communication No. 050402. P.N. and P.J. are thankful to CSIR, New Delhi, for financial support.

Supporting information for this article is available on the WWW under http://www.angewandte.org or from the author.

© 2005 Wiley-VCH Verlag GmbH & Co. KGaA, Weinheim

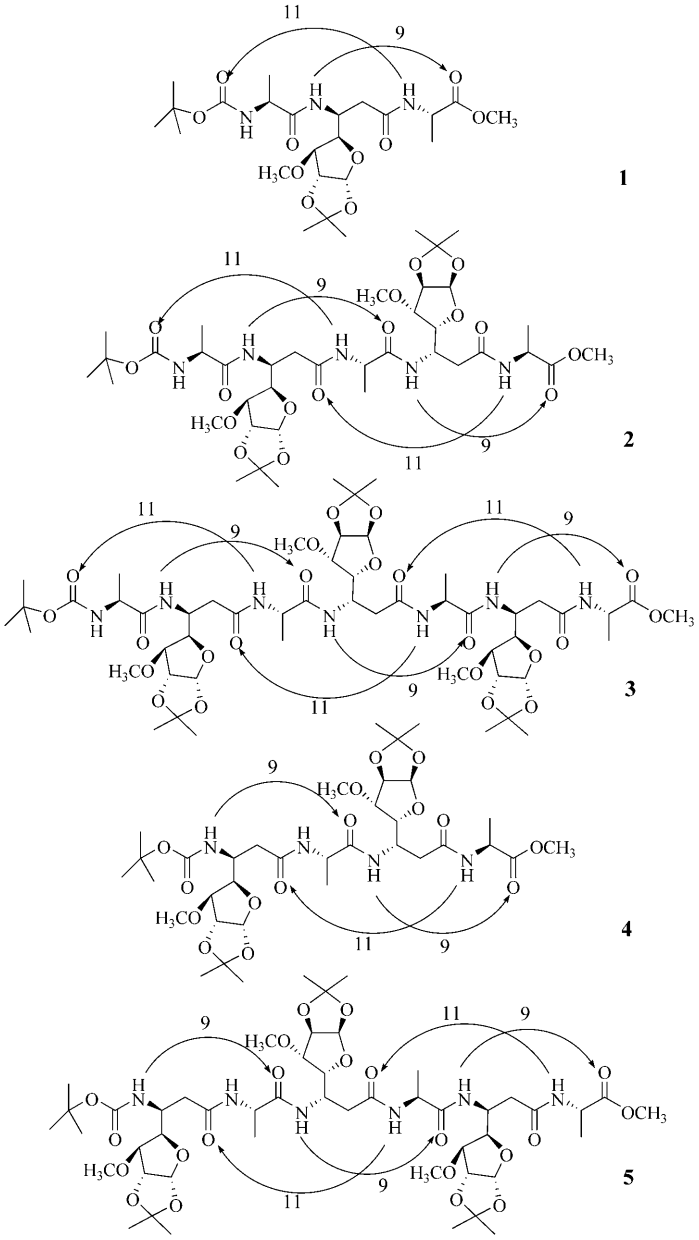
11 helix along with a 14/15 helix, whereas Reiser and coworkers[13] observed a 13 helix in the α/β peptides containing alternate *cis*-β-amino cyclopropane carboxylic acid and L-Ala residues.

Based on the above observations on mixed helices and our own studies on Caa-derived β peptides,[9,10] a hybrid α/β-dipeptide motif was envisaged as a "design control" to identify novel secondary structures. Herein, we report the synthesis of α/β-hybrid peptides from the *S* epimer of Caa[14] and L-Ala, as well as the finding of hitherto unknown and unprecedented 9/11 helices in these peptides by extensive NMR spectroscopy, circular dichroism (CD), and molecular dynamics (MD) studies.

The β peptides **1**–**5** (Scheme 1) were prepared by conventional coupling methods, and structural studies were conducted to analyze their conformational details. All of the peptides (100 μM in methanol) displayed novel CD data with maxima at ≈198 nm along with weaker flat maxima at ≈225 nm; this pattern is distinctly different from the CD profile of a 10/12-mixed helix.

The ^{1}H NMR spectrum of tripeptide **1** displayed downfield shift for two amide protons at δNH = 7.16 and 7.58 ppm, a result that suggests their involvement in hydrogen bonding. Solvent titration studies[15] showed very small chemical-shift changes ($\Delta\delta$NH) of 0.213 and 0.422 ppm for NH(2) and NH(3), respectively, thereby confirming their participation in hydrogen bonding. The observed long-range NOE correlations for C$^\alpha$H(1)/NH(3), C$^\beta$H(2)/NH(3), and NH(2)/NH(3) further support a well-defined structure. Furthermore, the coupling constant values of $^3J_{C^\alpha H/C^\beta H} < 5$ Hz indicate a restricted value of $|\theta| \approx 60°$ for Caa(2). The nondescript $^3J_{NH/C^\alpha H}$ values of 6.8 and 7.5 Hz for Ala(1) and Ala(3), at this stage, prevent us from deducing the structure for **1**. To obtain concrete information for determining the underlying structure in this family, peptides **2** and **3** were investigated.

The ^{1}H NMR spectrum of pentapeptide **2** showed that four of the amide protons (except NH(1)) appear at δNH > 7 ppm, which suggests their participation in hydrogen bonding. The same was further confirmed by solvent titration studies ($\Delta\delta$NH < 0.256 ppm).[15] For Caa(2) and Caa(4), small values of $^3J_{NH/C^\alpha H}$ (< 5.2 Hz) and large values of $^3J_{NH/C^\beta H}$ (9.3 Hz) are consistent with $|\theta| \approx 60°$ and $|\phi| \approx 100°$, respectively. $^3J_{NH/C^\alpha H} = 6.1$ and 5.6 Hz for Ala(1) and Ala(3), respectively, values which correspond to $|\phi| \approx 60°$. To derive the handedness of the structures by NMR spectroscopy, it was crucial to distinguish the resonances of the C$^\alpha$H$_{(pro\text{-}S)}$ and C$^\alpha$H$_{(pro\text{-}R)}$ protons. The NOE correlations for C$^\gamma$H(2)/NH(2), C$^\alpha$H$_{(pro\text{-}S)}$(2)/C$^\delta$H(2), C$^\alpha$H$_{(pro\text{-}R)}$(2)/NH(3), C$^\gamma$H(4)/NH(4), C$^\alpha$H$_{(pro\text{-}S)}$(4)/C$^\delta$H(4), and C$^\alpha$H$_{(pro\text{-}R)}$(4)/NH(5) enabled us to assign these resonances unequivocally and allowed us to deduce a value of about +60° for θ. The distinctive signatures of an 11/9 helix were observed in the ROESY spectrum, in which the NOE correlations for C$^\alpha$H(1)/NH(3) and C$^\alpha$H(3)/NH(5) support an 11-membered hydrogen bond between the CO group of *tert*-butoxycarbonyl (Boc) and NH(3), and between NH(5) and CO(2) (Scheme 1). Similarly, the presence of weak but characteristic NOE correlations for NH(2)/NH(3) and NH(4)/NH(5) are consistent with 9-membered hydrogen bonds between NH(2)–CO(3) and NH(4)–CO(5)



Scheme 1. Structures of α/β-hybrid peptides **1**–**5**; hydrogen-bond interactions are indicated by the arrows.

(Scheme 1). All the distinguishing features discussed above confirm an unprecedented right-handed 11/9/11/9-mixed helix for **2**.

By analogy with the structural information for **2**, the NOE correlations observed in the ROESY spectrum of **1** and the distinct $^3J_{C^\alpha H/C^\beta H}$ and $^3J_{NH/C^\beta H}$ values (for Caa) confirm an 11-membered hydrogen bond between the CO group of Boc and NH(3) and a 9-membered hydrogen bond between NH(2)–CO(3), thereby defining an 11/9 helix. The observation of a helix in a molecule as short as a tripeptide is particularly noteworthy.

Propagation of an exceptionally robust 11/9 helix in heptapeptide **3** was confirmed by NMR spectroscopy, which showed a well-resolved spectrum in the amide region, in

 © 2005 Wiley-VCH Verlag GmbH & Co. KGaA, Weinheim

which NH(2)–NH(6) gave $\delta NH > 7$ ppm and small $\Delta\delta NH$ values of 0.262 ppm in the solvent titration studies,[15] which confirmed hydrogen bonding. The $^3J_{NH/C^\alpha H}$ values of 6.1, 5.6, and 5.1 Hz for Ala(1), Ala(3), and Ala(5), respectively, correspond to $|\phi| \approx 60°$. Similarly, for Caa(2), Caa(4), and Caa(6), values of $^3J_{NH/C^\beta H} > 9.3$ Hz and $^3J_{C^\alpha H/C^\beta H} < 5.6$ Hz imply that $|\phi| \approx 100°$ and $|\theta| \approx 60°$. The assignments of the $C^\alpha H_{(pro\text{-}S)}$ and $C^\alpha H_{(pro\text{-}R)}$ resonances for the Caa residues were obtained similarly to those for **2**. Additionally, NOE correlations for $C^\alpha H(1)/NH(3)$, $C^\alpha H(3)/NH(5)$, $C^\alpha H(5)/NH(7)$, NH(2)/NH(3), NH(4)/NH(5), and NH(6)/NH(7) (Figure 1) as well as the information on hydrogen bonding,

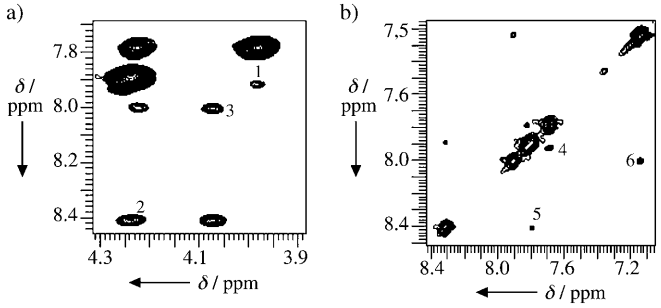


Figure 1. ROESY spectrum of **3**: a) NOE interactions $C^\alpha H(1)/NH(3)$, $C^\alpha H(3)/NH(5)$, and $C^\alpha H(5)/NH(7)$ are marked as 1, 2, and 3, respectively; b) NOE interactions NH(2)/NH(3), NH(4)/NH(5), and NH(6)/NH(7) are marked as 4, 5, and 6, respectively.

confirmed 11-membered hydrogen bonds between NH(3)–CO group of Boc, NH(5)–CO(2), NH(7)–CO(4), and 9-membered hydrogen bonds between NH(2)–CO(3), NH(4)–CO(5), and NH(6)–CO(7) (Scheme 1). The presence of a right-handed 11/9/11/9/11/9 helix and its propagation with the chain length in **3** was evident from all the characteristics described above. The CD profiles of **1**–**3** (Figure 2) showed maxima at around 198 nm and the progressive increase in the molecular ellipticity per residue reflects the enhanced robustness with increasing size of the oligomers.

Similar to our earlier findings with 12/10-mixed helices,[8,9] two possible helical structures (an 11/9 and a 9/11 helix) were

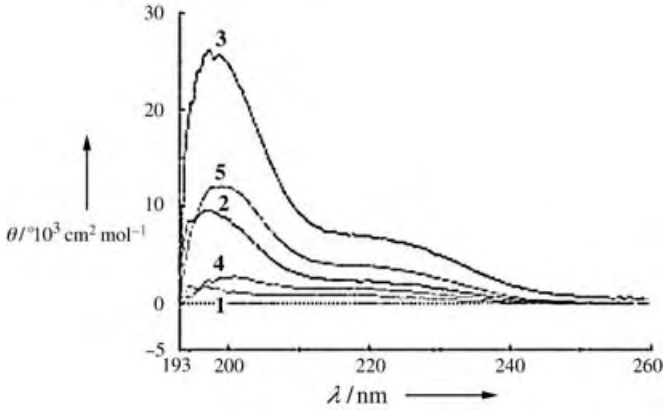


Figure 2. CD profiles of **1**–**5**.

expected in these α/β peptides. Consequently, peptides **4** and **5** were prepared with a Caa monomer at the N terminus to observe the 9/11 helix. The ^{1}H NMR spectrum of **4** showed all the signatures of hydrogen bonding, such as a low-field shift ($\delta NH > 7$ ppm) for two amide protons and small changes of the $\Delta\delta NH$ values in solvent titration studies. Furthermore, the coupling constants and the characteristic long-range NOE correlations for $C^\alpha H(2)/NH(4)$, NH(1)/NH(2), and NH(3)/NH(4) provide compelling evidence for the presence of a unique 9/11/9 helix.

Likewise, a low-field shift ($\delta NH > 7$ ppm) for four amide resonances, and the solvent titration studies ($\Delta\delta H < 0.686$ ppm) confirmed the participation of all the amide groups except NH(2) in hydrogen bonding in **5**. The $^3J_{NH/C^\alpha H}$ coupling constants for Ala(2) and Ala(4) are 4.8 and 5.9 Hz, respectively; these values correspond to $|\phi| \approx 60°$. Furthermore, small $^3J_{C^\alpha H/C^\beta H}$ values for all Caas and distinct NOE correlations for NH(1)/NH(2), NH(3)/NH(4), NH(5)/NH(6), $C^\alpha H(2)/NH(4)$, and $C^\alpha H(4)/NH(6)$ support a propagated right-handed 9/11/9/11/9-mixed helix for **5**. The molecular ellipticity per residue for **5** and the NMR spectroscopic data (larger amide chemical shifts) demonstrate that this helix is more robust than that of **4**.

The $^3J_{C^\beta H/C(4)H}$ values greater than 9 Hz for the Caa residues (except for Caa(1) in **4** and **5**) correspond to $\chi^1(C^\beta H–C^\beta–C(4)–C(4)H) \approx 180°$ in all of the oligomers, as observed in oligomers with 10/12-mixed helices in our earlier study.[9] The $^3J_{C1H/C2H} \approx 4$ Hz, $^3J_{C(2)H/C(3)H} \approx 0$ Hz, and $^3J_{C(3)H/C(4)H} \approx 3$ Hz values for the sugar rings are consistent with a $^3T_2$ sugar pucker, which is similar to that observed earlier. Furthermore, the presence of an envelope conformation for the isopropylidine ring is reflected in the strong $Me_{(pro\text{-}R)}$/C(2)H and $Me_{(pro\text{-}R)}$/C(1)H and the weak $Me_{(pro\text{-}S)}$/C(4)H NOE correlations.

The NOE-restrained MD calculations for **1**–**5** resulted in structures that are in excellent agreement with those obtained above. Volume integrals from the ROESY spectra provided quantitative NOE constraints by using the two-spin approximation. Figures 3 and 4 show a superposition of the 25 lowest-energy structures for **3** and **5**, respectively. For the sake of clarity, the sugar moieties were replaced by methyl groups for the structures in Figures 3 and 4 after the MD calculations. The maximum violations for the NMR-derived constraints for **3** and **5** are 0.25 and 0.33 Å, respectively. The average pairwise heavy-atom and backbone root-mean-square deviations are 0.31 and 0.29 Å for **3**, and 0.58 and 0.47 Å for **5**, respectively. The average dihedral angles of the backbones were derived by excluding the first and last residues. In **3**, the ϕ, θ, and ψ values for Caa are $91 \pm 7°$, $63 \pm 3°$, and $-91 \pm 4°$, respectively, whereas $\phi = -70 \pm 1°$ and $\psi = 135 \pm 2°$ for L-Ala. The corresponding values for **5** are $86 \pm 4°$, $66 \pm 2°$, $-91 \pm 4°$, $-70 \pm 2°$, and $131 \pm 2°$.

In conclusion, our exploratory study on the hybrid α/β-dipeptide repeats resulted in the unprecedented 9/11-mixed helices (9/11 and 11/9). Furthermore, a robust helical structure (11/9) in the shortest α/β tripeptide (L-Ala–Caaβ^3–L-Ala) is a notable feature of the present design. These peptides, in contrast to the reported α/β-mixed peptides derived from cyclic β-amino acids, show a high propensity for

 © 2005 Wiley-VCH Verlag GmbH & Co. KGaA, Weinheim

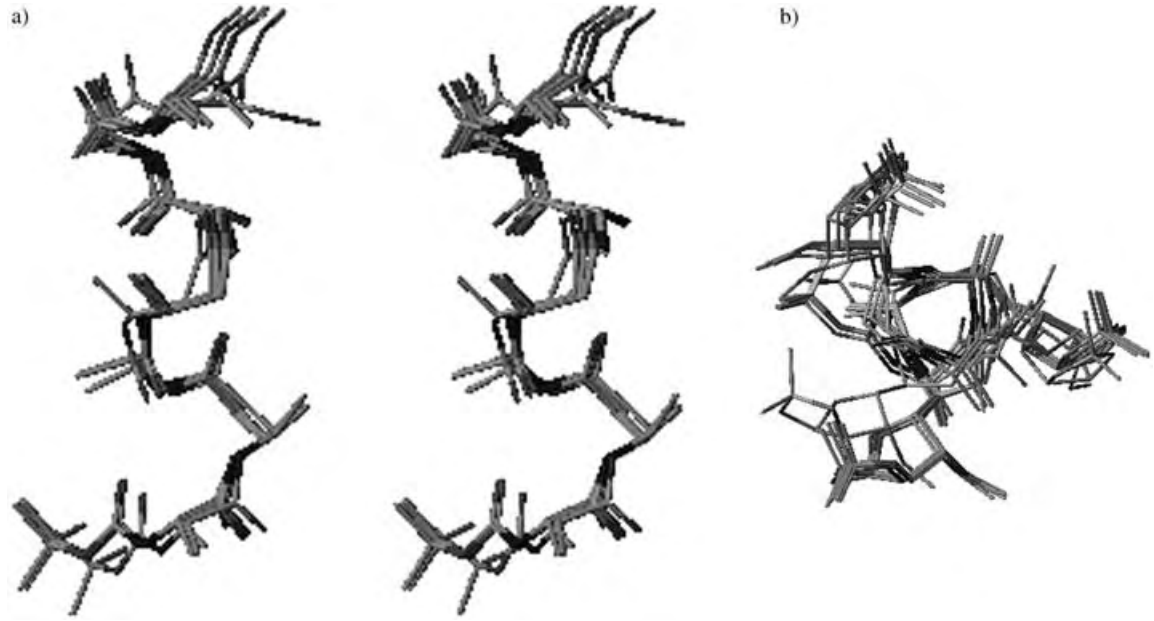


Figure 3. MD structures of **3**: a) stereo view in which sugar moieties were replaced with methyl groups after the calculations for clarity; b) view down the helical axis.

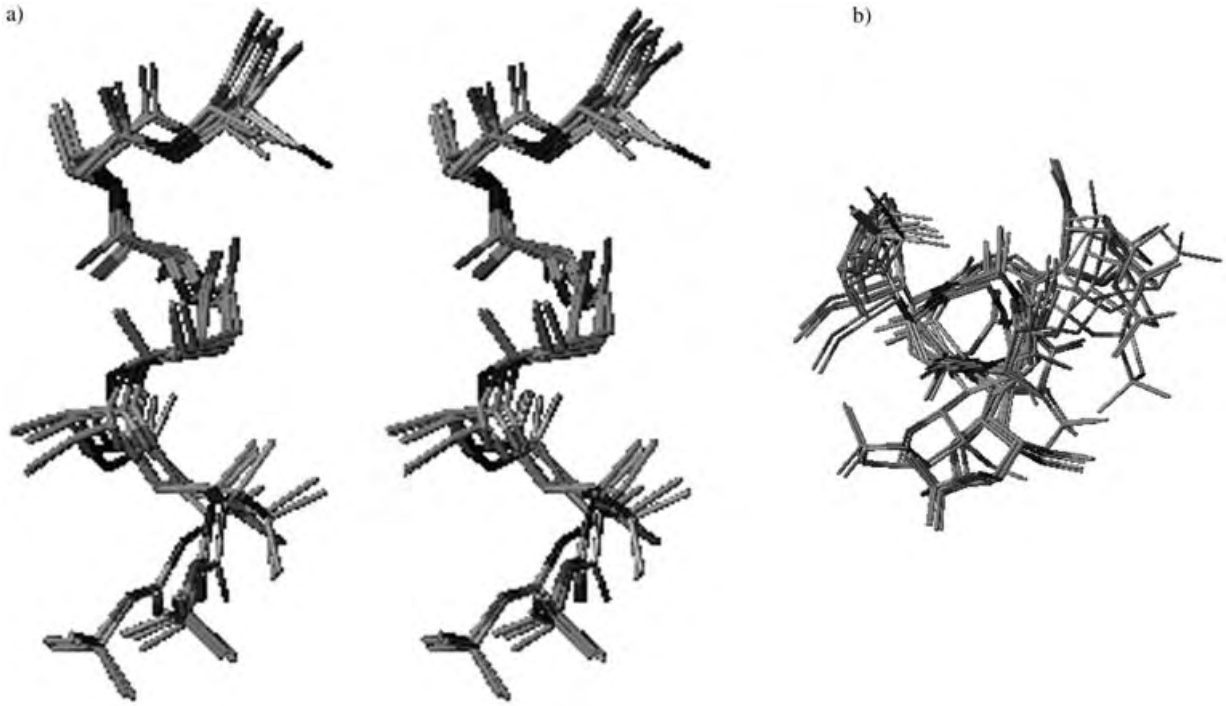


Figure 4. MD structures of **5**: a) stereoview in which sugar moieties were replaced with methyl groups after the calculations for clarity; b) view down the helical axis.

the formation of stable mixed-helical structures. Extrapolation of this study to other α-amino acids will enhance the opportunity of finding not only new secondary structural elements, but also for the introduction of a wide variety of side chains and functionalities to derive desirable properties in this class of peptides.

Received: April 9, 2005
Published online: August 10, 2005

Keywords: amino acids · helical structures · NMR spectroscopy · peptides · structure elucidation

[1] a) D. Seebach, J. L. Matthews, *Chem. Commun.* **1997**, 2015–2022; b) S. H. Gellman, *Acc. Chem. Res.* **1998**, *31*, 173–180; c) K. Gademann, T. Hintermann, J. V. Schreiber, *Curr. Med. Chem.* **1999**, *6*, 905–925; d) W. F. DeGrado, J. P. Schneider, Y. Hamuro, *J. Pept. Res.* **1999**, *54*, 206–217; e) R. P. Cheng, S. H. Gellman, W. F. DeGrado, *Chem. Rev.* **2001**, *101*, 3219–3232;

 © 2005 Wiley-VCH Verlag GmbH & Co. KGaA, Weinheim

f) D. Seebach, A. K. Beck, D. J. Bierbaum, *Chem. Biodiversity* **2004**, *1*, 1111 – 1239.
[2] a) D. Seebach, M. Overhand, F. N. M. Kuhnle, B. Martinoni, L. Oberer, U. Hommel, H. Widmer, *Helv. Chim. Acta* **1996**, *79*, 913 – 941; b) D. H. Appella, L. A. Christianson, I. L. Karle, D. R. Powell, S. H. Gellman, *J. Am. Chem. Soc.* **1996**, *118*, 13071 – 13072.
[3] D. H. Appella, L. A. Christianson, D. A. Klein, D. R. Powell, X. Huang, J. J. Barchi, Jr., S. H. Gellman, *Nature* **1997**, *387*, 381 – 384.
[4] a) D. Seebach, K. Gademann, J. V. Schreiber, J. L. Matthews, T. Hintermann, B. Jaun, *Helv. Chim. Acta* **1997**, *80*, 2033 – 2038; b) D. Seebach, S. Abele, K. Gademann, G. Guichard, T. Hintermann, B. Juan, L. J. Matthews, V. J. Schreiber, L. Oberer, U. Hommel, H. Widmer, *Helv. Chim. Acta* **1998**, *81*, 932 – 982.
[5] S. Abele, D. Seebach, *Helv. Chim. Acta* **1999**, *82*, 1559 – 1571.
[6] a) D. Seebach, S. Abele, T. Sifferien, M. Hanggi, S. Gruner, P. Seiler, *Helv. Chim. Acta* **1998**, *81*, 2218 – 2243; b) T. D. W. Claridge, J. M. Goodman, A. Moreno, D. Angus, S. F. Barker, C. Taillefumier, M. P. Watterson, G. W. J. Fleet, *Tetrahedron Lett.* **2001**, *42*, 4251 – 4255.
[7] a) K. Mohle, R. Gunther, M. Thormann, N. Sewald, H.-J. Hofmann, *Biopolymers* **1999**, *50*, 167 – 184; b) Y.-D. Wu, D.-P. Wang, *J. Am. Chem. Soc.* **1999**, *121*, 9352 – 9362; c) Y.-D. Wu, J.-Q. Lin, Y.-L. Zhao, *Helv. Chim. Acta* **2002**, *85*, 3144 – 3160.
[8] S. A. W. Gruner, V. Truffault, G. Voll, E. Locardi, M. Stockle, H. Kessler, *Chem. Eur. J.* **2002**, *8*, 4366 – 4376.
[9] G. V. M. Sharma, K. Ravinder Reddy, P. Radha Krishna, A. Ravi Sankar, K. Narsimulu, S. Kiran Kumar, P. Jayaprakash, B. Jagannadh, A. C. Kunwar, *J. Am. Chem. Soc.* **2003**, *125*, 13670 – 13671.
[10] G. V. M. Sharma, K. Ravinder Reddy, P. Radha Krishna, A. Ravi Sankar, P. Jayaprakash, B. Jagannadh, A. C. Kunwar, *Angew. Chem.* **2004**, *116*, 4051 – 4055; *Angew. Chem. Int. Ed.* **2004**, *43*, 3961 – 3965.
[11] C. Baldauf, R. Gunther, H.-J. Hofmann, *Angew. Chem.* **2004**, *116*, 1621 – 1624; *Angew. Chem. Int. Ed.* **2004**, *43*, 1594 – 1597.
[12] A. Hayen, M. A. Schmitt, N. Nagassa, K. A. Thomson, S. H. Gellman, *Angew. Chem.* **2004**, *116*, 511 – 516; *Angew. Chem. Int. Ed.* **2004**, *43*, 505 – 510.
[13] S. De Pol, C. Zorn, C. D. Klein, O. Zerbe, O. Reiser, *Angew. Chem.* **2004**, *116*, 517 – 520; *Angew. Chem. Int. Ed.* **2004**, *43*, 511 – 514.
[14] G. V. M. Sharma, V. Goverdhan Reddy, A. Subhash Chander, K. Ravinder Reddy, *Tetrahedron: Asymmetry* **2002**, *13*, 21 – 24.
[15] Solvent titration was carried out by sequentially adding up to 33% of [D_6]DMSO to $CDCl_3$ solutions of the peptides.

 © 2005 Wiley-VCH Verlag GmbH & Co. KGaA, Weinheim

Synthetic Methods

DOI: 10.1002/anie.200501769

Facile Synthesis of Chiral α-Difluoromethyl Amines from *N*-(*tert*-Butylsulfinyl)aldimines**

*Ya Li and Jinbo Hu**

Dedicated to Professor George A. Olah

Fluorinated amines are important synthetic building blocks in the design of antimetabolites and drugs because fluorine causes minimal structural changes and maximal shifts in electron distribution.[1,2] Fluorine lowers the basicity of amines and improves oral absorption, suppresses metabolism, and thus increases the bioavailability of a target drug.[3–5] Among the fluorinated amines, α-difluoromethyl amines are of particular interest as the CF_2H functionality is isosteric to a carbinol (CH_2OH) unit and also, as a lipophilic group, it shares much of the dipolar nature of the latter.[6,7] Therefore, α-difluoromethyl amines can be regarded as more lipophilic bioisosteres of corresponding α-aminocarbinols (or β-amino alcohols), which may feature some significant properties within biologically active molecules.

Despite its importance for applications related to life sciences, the synthesis of α-difluoromethyl amines has not been well explored. The few known methods are mainly based on the use of difluoromethyl carbonyl compounds or their imine derivatives as precursors.[8–12] Pey and Schirlin reported the multistep synthesis of α-difluoromethyl amines from substituted malonate esters with CHF_2Cl followed by a Curtius rearrangement.[13] However, the general and efficient asymmetric synthesis of α-difluoromethyl amines still remains a challenge although it has drawn many synthetic endeavors.[9–12,14] The asymmetric hydrogenation of fluorinated imines are usually difficult, and recently Uneyama and coworkers reported that the palladium-catalyzed asymmetric hydrogenation of difluoromethyl imino esters proceeded with poor enantioselectivity (30% *ee*).[9] Hydride reduction of the C=N bond of chiral difluoromethyl β-sulfinyl-*N*-arylimine only gave 82% diastereomeric excess.[10] Difluoropyruvaldehyde *N*,*S*-ketal was synthesized in three steps from difluoroacetic esters and chiral methyl *p*-tolyl sulfoxide in only 72% enantiomeric excess.[11] Conversion of optically pure β-

[*] Y. Li, Prof. Dr. J. Hu
Key Laboratory of Organofluorine Chemistry
Shanghai Institute of Organic Chemistry
Chinese Academy of Sciences
354 Feng-Lin Rd., Shanghai, 200032 (China)
Fax: (+86) 21-64166128
E-mail: jinbohu@mail.sioc.ac.cn

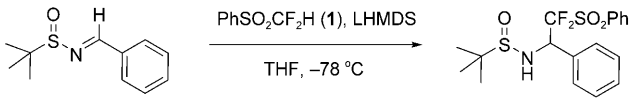
[**] Dedicated to Prof. George A. Olah on the occasion of his receipt of the 2005 Priestley Medal. Support of our work by the "Hundreds Talent Program" from the Chinese Academy of Sciences is gratefully acknowledged.

Supporting information for this article is available on the WWW under http://www.angewandte.org or from the author.

InterScience
© 2005 Wiley-VCH Verlag GmbH & Co. KGaA, Weinheim

bromo-β,β-difluoroalanine derivatives into corresponding β,β-difluoroalanine products led to a decrease in the optical purity (with 80% *ee*).[14] Funabiki et al. attempted L-proline-catalyzed asymmetric Mannich-type reactions with difluoromethyl aldimine, but prolonged reaction times (7 days) were required and the reactions lacked generality.[12] On the other hand, although Prakash et al. elegantly developed the asymmetric synthesis of α-trifluoromethyl amines using $TMSCF_3$ (TMS = trimethylsilyl) and *N*-(*tert*-butylsulfinyl)aldimines,[15] similar asymmetric synthesis of α-difluoromethyl amines using R_3SiCF_2H and *N*-(*tert*-butylsulfinyl)imines proved problematic due to the low reactivity of R_3SiCF_2H reagents.[16] To the best of our knowledge, there is no synthetic method available for the highly stereoselective synthesis of α-difluoromethyl amines using a direct difluoromethylation strategy. Previously, one of us was involved in the development of difluoromethyl phenyl sulfone (**1**) as a versatile reagent for the selective transfer of difluoromethyl, difluoromethylene, and difluoromethylidene building blocks.[17] Herein, we report the first highly stereoselective nucleophilic difluoromethylation reaction using difluoromethyl phenyl sulfone and *N*-(*tert*-butylsulfinyl)aldimines which has enabled us to efficiently synthesize enantiomerically pure α-difluoromethyl amines through a simple and reliable protocol.

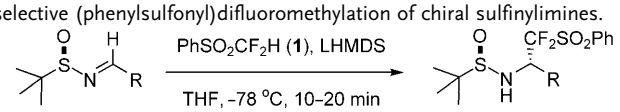
In previous investigations, we found that difluoromethyl phenyl sulfone (**1**) can be used as a convenient difluoromethylating agent for alkyl halides and carbonyl compounds, commonly accomplished through a (phenylsulfonyl)difluoromethylation–reductive desulfonylation strategy.[17d,e] The (phenylsulfonyl)difluoromethyl anion ($PhSO_2CF_2^-$, **2**), generated in situ from **1** and a base such as lithium hexamethyldisilazide (LHMDS) or *t*BuOK, is an excellent nucleophile that can readily undergo addition or substitution reactions with carbonyl compounds, disulfides, and primary alkyl halides.[17] Anion **2**, although difficult to isolate owing to its slow decomposition into difluorocarbene and benzenesulfinate, showed both higher thermal stability and sometimes better nucleophilicity (in the case of alkyl halides) than the trifluoromethyl anion (CF_3^-). Nucleophilic addition reactions between **2** and imines **3** have not been reported, and we envisioned that the reactions would proceed smoothly as a result of the reasonable stability of anion **2** to decomposition and the matched hard-/softness between **2** and imines.[18,19] With these in mind, first we prepared racemic *N*-(*tert*-butylsulfinyl)aldimine **4**[20] as a model compound to test the reaction with difluoromethyl phenyl sulfone (Scheme 1). When LHMDS (2 equiv, dissolved in THF) was added to a solution of aldimine **4** (2 equiv) and $PhSO_2CF_2H$ (1 equiv) in THF at −78 °C, a facile addition reaction occurred and sulfone **1** was quantitatively transformed into product **5** (detected by NMR spectroscopy and TLC) in 15 minutes. More interestingly, analysis of the crude reaction mixture by ^{19}F NMR spectroscopy showed that the reaction proceeded highly diastereoselectively and only



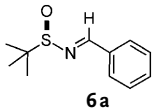
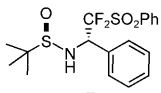
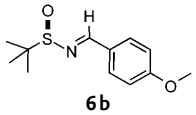
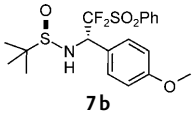
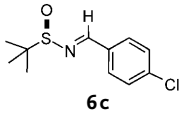
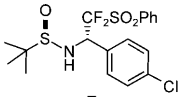
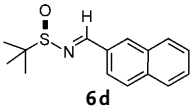
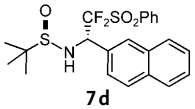
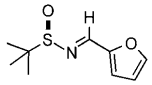
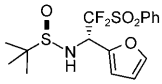
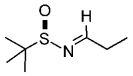
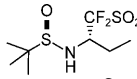
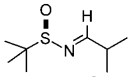
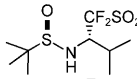
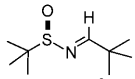
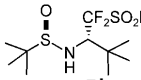
4 **5**

Scheme 1. Nucleophilic (phenylsulfonyl)difluoromethylation of *N*-(*tert*-butylsulfinyl)imine (**4**).

Table 1: Stereoselective (phenylsulfonyl)difluoromethylation of chiral sulfinylimines.



6 **7**

Entry[a]	Sulfinylimine **6**	Product **7**[b]	Yield [%][c]	d.r. [%][d]	$[\alpha]_D^{25}$ [e]
1	 **6a**	 **7a**	95	>99	−27.4 (*c*=0.8)
2	 **6b**	 **7b**	96	>99	−20.7 (*c*=0.7)
3	 **6c**	 **7c**	95	>99	−17.8 (*c*=0.6)
4	 **6d**	 **7d**	98	>99	−5.6 (*c*=1.0)
5	 **6e**	 **7e**	90	>99	−45.5 (*c*=1.0)
6	 **6f**	 **7f**	95	>99	−25.0 (*c*=0.8)
7	 **6g**	 **7g**	94	>99	−54.3 (*c*=0.9)
8	 **6h**	 **7h**	85	>99	−9.7 (*c*=1.0)

[a] In all cases, LHMDS (1.2 equiv) was added to a mixture of **1** (1.0 equiv) and **6** (1.1 equiv) in THF at −78 °C, and the reactions were usually complete in 10–20 min. [b] For entry 1, the configuration was determined by single-crystal X-ray analysis; the others were assigned from transition-state models. [c] Yields of isolated analytically pure material. [d] Diastereomeric ratios were determined by ^{19}F NMR spectroscopy of the crude reaction mixture. [e] Optical rotations were measured in chloroform.

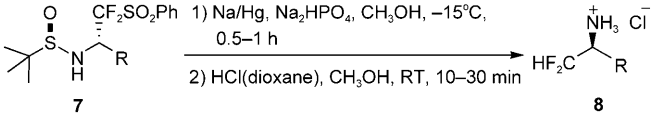
 © 2005 Wiley-VCH Verlag GmbH & Co. KGaA, Weinheim

one single diastereomer (racemic) of **5** was formed. The reactant ratio **4**/**1**/LHMDS was further optimized to 1.1:1.0:1.2, and product **5** was isolated in 95% yield as a single diastereomer (racemic). Potassium *tert*-butoxide was also found to be effective for the reaction, however, slightly lower yields (80–85%) of product were obtained.

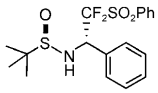
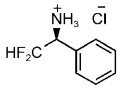
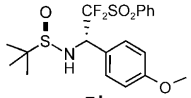
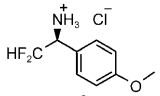
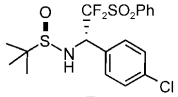
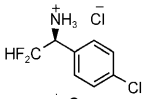
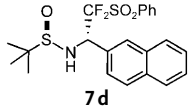
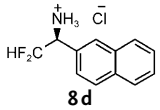
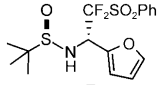
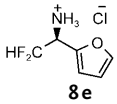
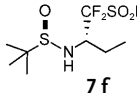
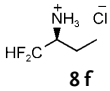
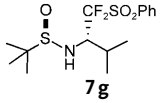
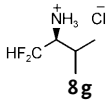
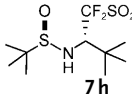
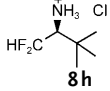
Encouraged by the above results, we predicted that when a homochiral sulfinylimine is subjected to this reaction, enantiomerically pure sulfinamide product could be obtained. The chiral sulfinamide can be further converted into enantiomerically pure α-difluoromethyl amines after deprotection of both *tert*-butylsulfinyl and phenylsulfonyl groups under mild conditions. Therefore, we prepared optically pure (*R*)-(*tert*-butylsulfinyl)aldimines **6**[21] and applied them in this nucleophilic (phenylsulfonyl)difluoromethylation reaction. The optimized reaction conditions as described above were used (**6**/**1**/LHMDS = 1.1:1.0:1.2, −78 °C, 10–20 min), and the results are summarized in Table 1. A variety of structurally diverse (*R*)-(*tert*-butylsulfinyl)aldimines **6** reacted with (phenylsulfonyl)difluoromethyl anion (generated in situ from sulfone **1** and LHMDS) to give the corresponding chiral sulfinamides **7** in excellent yields and with very high diastereoselectivities. Remarkably, the reactions were carried out under basic conditions but were still amenable to sulfinylimines bearing α hydrogen atoms (see entries 6 and 7, Table 1), which is in sharp contrast to their known trifluoromethylation chemistry.[15,18] Prakash et al.[15] and Dolbier and co-workers[18] reported that trifluoromethylation reactions of chiral sulfinylimines (with $TMSCF_3$ or CF_3I/tetrakis(dimethylamino)ethylene) were very sensitive to base (such as CsF), and that sulfinylimines bearing α hydrogen atoms usually gave lower yields. Sterically demanding sulfinylimine **6h** also gave a high yield of product (85%), which is superior to that obtained in the analogous trifluoromethylation reaction.[15,18] In each case as shown in Table 1, the product **7** was obtained as a single diastereomer, as determined by ^{19}F and ^{1}H NMR spectroscopy. Indeed, we observed that the present nucleophilic (phenylsulfonyl)difluoromethylations of sulfinylimines worked even more efficiently than those of carbonyl compounds as previously reported.[17e] The thermal stability, good nucleophilicity, and the softness of the (phenylsulfonyl)difluoromethyl anion generated in situ account for the short reaction times (10–20 min) and excellent chemo- and stereoselectivities. The absolute configuration of sulfinamide **7a** was determined by single-crystal X-ray analysis (see Figure 1a), and the configurations of **7b**–**7h** were assigned by analogy. The sense of diastereoselective induction can be depicted by a nonchelation-controlled addition step to give the Cram products **7** (Figure 1b).[15,18,21b,22]

All of the (phenylsulfonyl)difluoromethylated sulfinamides **7** were selectively deprotected under mild conditions following reported procedures[17,21] to give the corresponding amine salts **8**. Reductive desulfonylation using Na/Hg amalgam followed by acid alcoholysis provided a convenient and facile preparation of **8** from **7**. The results are summarized in Table 2. In all cases, near-quantitative conversions from **7** into **8** (in two continuous deprotection steps) were observed by

Table 2: Preparation of amine salts **8** from **7**.



7 **8**

Entry[a]	Sulfinylimine **7**	Product **8**[b]	Yield [%][c]	$[\alpha]_D^{25}$
1	 **7a**	 **8a**	83	25.4 (c=1.0)[d]
2	 **7b**	 **8b**	96	26.3 (c=0.7)[d]
3	 **7c**	 **8c**	82	24.9 (c=0.5)[d]
4	 **7d**	 **8d**	97	32.9 (c=0.6)[d]
5	 **7e**	 **8e**	88	9.2 (c=0.55)[d]
6	 **7f**	 **8f**	70	−19.7 (c=0.2)[e]
7	 **7g**	 **8g**	72	−26.3 (c=0.3)[e]
8	 **7h**	 **8h**	94	−17.6 (c=0.2)[e]

[a] No purification was necessary between two deprotection steps. [b] The configurations were determined by the fact that no racemerization occurred during the deprotection step. [c] Yields of the isolated analytically pure material. [d] Optical rotations were measured in methanol. [e] Optical rotations were measured in acetone.

 © 2005 Wiley-VCH Verlag GmbH & Co. KGaA, Weinheim

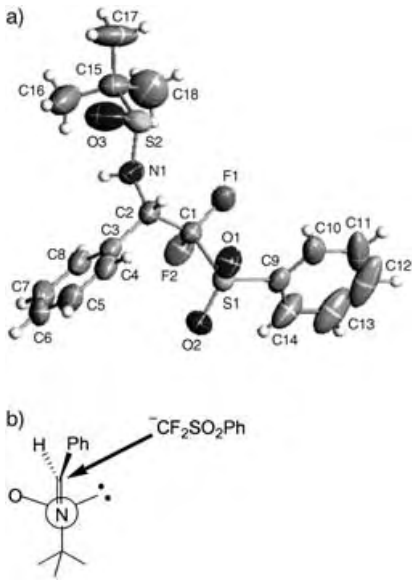
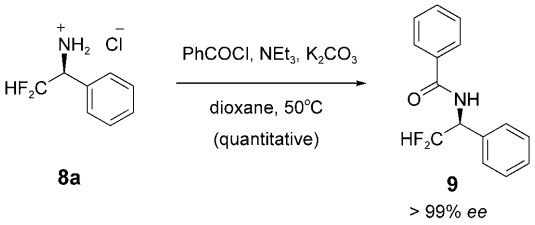


Figure 1. a) X-ray crystal structure of **7a**, and b) depiction of its stereoselective formation.

NMR spectroscopy and the isolated yields of **8** were somewhat affected by the hydroscopicity of the products (see entries 6 and 7, Table 2). To ensure that there was no racemization during the deprotection process, we converted amine salt **8a** into benzamide derivative **9** (Scheme 2). The



Scheme 2. Conversion of amine hydrochloride salt **8a** into chiral benzamide derivative **9**.

high optical purity of **9** (> 99 % *ee*) was determined by chiral HPLC and indicated that the above deprotection procedures are reliable for the preparation of enantiomerically pure α-difluoromethyl amines.

In summary, we have reported the first highly stereoselective and facile synthesis of α-difluoromethyl amines using a nucleophilic difluoromethylation strategy. Nucleophilic (phenylsulfonyl)difluoromethylation of (*R*)-(*N*-*tert*-butylsulfinyl)aldimines with difluoromethyl phenyl sulfone affords the corresponding products in excellent yields and with high diastereoselectivity
(d.r. > 99 %). The facile and convenient deprotection of both *tert*-butylsulfinyl and phenylsulfonyl groups gives the target α-difluoromethyl amines with high enantiomeric purity (*ee* > 99 %). The experimental data reported herein indicate that in a nucleophilic fluoroalkylation reaction, the stability, nucleophilicity, and hard-/softness of a fluorine-bearing carbon nucleophile substantially affect the overall chemical outcome of that reaction. The present synthetic methodology provides a convenient and useful synthetic tool for many applications related to life sciences.

Received: May 23, 2005

Keywords: amines · enantioselectivity · fluorine · sulfonamides · synthetic methods

[1] *Fluorine in Bioorganic Chemistry* (Eds.: J. T. Welch, S. Eswarakrishnan), Wiley, New York, **1991**.
[2] *Biomedical Frontiers of Fluorine Chemistry* (Eds.: I. Ojima, J. R. McCarthy, J. T. Welch), ACS, Washington DC, **1996**.
[3] J. R. McCarthy, *Fluorine in Drug Design: A Tutorial Review*, 17th Winter Fluorine Conference (St Pete Beach, Florida, USA), January 9–14, **2005**.
[4] M. Rowley, D. J. Hallett, S. Goodacre, C. Moyes, J. Crawforth, T. J. Sparey, S. Patel, R. Marwood, S. Patel, S. Thomas, L. Hitzel, D. O'Connor, N. Szeto, J. L. Castro, P. H. Hutson, A. M. MacLeod, *J. Med. Chem.* **2001**, *44*, 1603.
[5] M. B. van Niel, I. Collins, M. S. Beer, H. B. Broughton, S. K. F. Cheng, S. C. Goodacre, A. Heald, K. L. Locker, A. M. MacLeod, D. Morrison, C. R. Moyes, D. O'Connor, A. Pike, M. Rowley, M. G. N. Russell, B. Sohal, J. A. Stanton, S. Thomas, H. Verrier, A. P. Watt, J. L. Castro, *J. Med. Chem.* **1999**, *42*, 2087.
[6] a) P. Kirsch, *Modern Fluoroorganic Chemistry*, Wiley-VCH, Weinheim, **2004**; b) J. A. Erickson, J. I. McLoughlin, *J. Org. Chem.* **1995**, *60*, 1626.
[7] We would like to thank one of the referees for the comment that the difluoromethyl functionality (CF_2H) is isosteric to a carbinol (CH_2OH) rather than a hydroxyl group (OH).
[8] S. Kaneko, T. Yamazaki, T. Kitazume, *J. Org. Chem.* **1993**, *58*, 2302.
[9] H. Abe, H. Amii, K. Uneyama, *Org. Lett.* **2001**, *3*, 313.
[10] S. Fustero, A. Navarro, B. Pina, J. G. Soler, A. Bartolome, A. Asensio, A. Simon, P. Bravo, G. Fronza, A. Volonterio, M. Zanda, *Org. Lett.* **2001**, *3*, 2621.
[11] A. Volonterio, B. Vergani, M. Crucianelli, M. Zanda, *J. Org. Chem.* **1998**, *63*, 7236.
[12] K. Funabiki, M. Nagamori, S. Goushi, M. Matsui, *Chem. Commun.* **2004**, 1928.
[13] P. Pey, D. Schirlin, *Tetrahedron Lett.* **1978**, *19*, 5225.
[14] T. Katagiri, M. Handa, Y. Matsukawa, J. S. D. Kumar, K. Uneyama, *Tetrahedron: Asymmetry* **2001**, *12*, 1303.
[15] a) G. K. S. Prakash, M. Mandal, G. A. Olah, *Angew. Chem.* **2001**, *113*, 609; *Angew. Chem. Int. Ed.* **2001**, *40*, 589; b) G. K. S. Prakash, M. Mandal, *J. Am. Chem. Soc.* **2002**, *124*, 6538.
[16] T. Hagiwara, T. Fuchikami, *Synlett* **1995**, 717.
[17] a) G. K. S. Prakash, J. Hu, G. A. Olah, *J. Org. Chem.* **2003**, *68*, 4457; b) G. K. S. Prakash, J. Hu, T. Mathew, G. A. Olah, *Angew. Chem.* **2003**, *115*, 5374; *Angew. Chem. Int. Ed.* **2003**, *42*, 5216; c) G. K. S. Prakash, J. Hu, Y. Wang, G. A. Olah, *Angew. Chem.* **2004**, *116*, 5315; *Angew. Chem. Int. Ed.* **2004**, *43*, 5203; d) G. K. S. Prakash, J. Hu, Y. Wang, G. A. Olah, *Org. Lett.* **2004**, *6*, 4315; e) G. K. S. Prakash, J. Hu, Y. Wang, G. A. Olah, *Eur. J. Org. Chem.* **2005**, 2218.
[18] Compared with aldehydes and ketones, imines (even activated *N*-*tert*-butanesulfinyl imines) generally display lower reactivity toward nucleophiles. Thus the stability and nucleophilicity of a proper nucleophile are crucial for its reactions with sulfinyl imines. For example, owing to the lower stability of in situ generated CF_3^- ion, the trifluoromethylation reactions of sulfinyl imines are very sensitive to the precursors of the CF_3^- ion and different reaction conditions. See ref. [15], and for a recent report see: W. Xu, W. R. Dolbier, Jr., *J. Org. Chem.* **2005**, *70*, 4741.

 © 2005 Wiley-VCH Verlag GmbH & Co. KGaA, Weinheim

[19] T.-L. Ho, *Hard and Soft Acids and Bases Principle in Organic Chemistry*, Academic, New York, **1977**.
[20] *N*-(*tert*-butylsulfinyl)aldimine was chosen for its higher electrophilicity relative to normal unactivated imines and, more importantly, for its potential as a chiral auxiliary. For details about its preparation, see: a) K. Hovius, J. B. F. N. Engberts, *Tetrahedron Lett.* **1972**, *13*, 181; b) G. Liu, D. A. Cogan, T. D. Owens, T. P. Tang, J. A. Ellman, *J. Org. Chem.* **1999**, *64*, 1278.
[21] a) G. Liu, D. A. Cogan, J. A. Ellman, *J. Am. Chem. Soc.* **1997**, *119*, 9913; b) J. A. Ellman, T. D. Owens, T. P. Tang, *Acc. Chem. Res.* **2002**, *35*, 984.
[22] F. A. Davis, W. McCoull, *J. Org. Chem.* **1999**, *64*, 3396.

 © 2005 Wiley-VCH Verlag GmbH & Co. KGaA, Weinheim

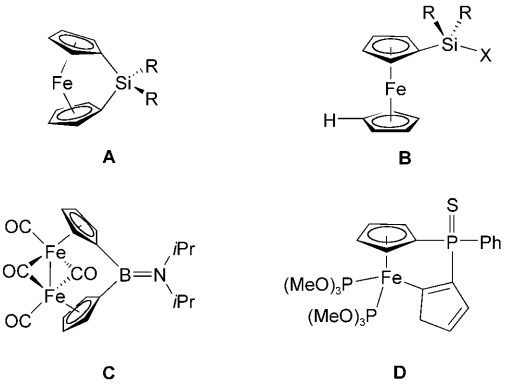
Coordination Modes

DOI: 10.1002/anie.200501155

Reversible, Strain-Controlled Haptotropic Shifts of Cyclopentadienyl Ligands in [1]- and [2]Metallocenophanes**

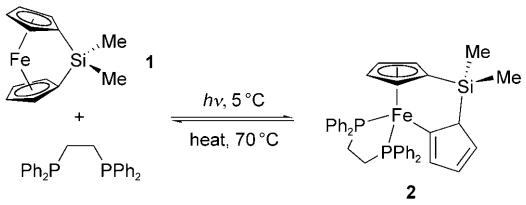
*Makoto Tanabe, Sara C. Bourke, David E. Herbert, Alan J. Lough, and Ian Manners**

Strained rings containing transition-metal elements are of growing interest as a result of their intriguing structures, enhanced reactivity, and ability to function as precursors to high-molecular-weight metallopolymers through ring-opening polymerization.[1–4] Ring-strained metallocenophanes and their analogues have attracted particular attention in this regard and their ring-opened polymeric derivatives exhibit a variety of interesting properties.[3,4] The appreciable ring tilting (α) of the planes of the cyclopentadienyl ligands in ferrocenophanes relative to ferrocene, where the ligands are parallel ($\alpha = 0°$), has been shown to comprise the major contribution to ring strain.[5] Silicon-bridged [1]ferrocenophanes such as **A** ($\alpha \approx 16$–$21°$) have been most well investigated in this area. The moderate ring strain present in **A** has been shown to lead to enhanced reactivity of the bond between the *ipso* cyclopentadienyl (Cp) carbon and the bridging silicon atom. Stoichiometric reactions of **A** with protic regents, for example, lead to facile Si–Cp bond cleavage and to ring-opened species **B**.[6]



In contrast, highly strained, boron-bridged [1]ferrocenophanes ($\alpha \approx 31$–$32°$) have been shown to undergo unexpected ring-opening chemistry involving an Fe–Cp bond on reaction with, for example, $[Fe_2(CO)_9]$ to yield bimetallic species **C**.[7] Very recently, Miyoshi and co-workers have shown that UV-photoirradiation of phosphorus-bridged [1]ferrocenophanes in the presence of a phosphine ligand (e.g., $P(OMe)_3$) leads to a haptotropic shift of a Cp ligand (from η^5 to η^1) to yield the ring-slipped product **D**.[8] Herein, we report some of our initial results from comparative studies of the photolytic reactivity of a range of [1]- and [2]metallocenophanes, which demonstrate that either *reversible* or *irreversible* haptotropic rearrangements from η^5- to η^1-Cp are observed depending on the degree of strain present.

UV-photoirradiation of a slight excess of sila[1]ferrocenophane **1** ($\alpha = 20.8(5)°$)[9] in the presence of 1,2-bis(diphenylphosphanyl)ethane (dppe) in THF at 5 °C led to a haptotropic shift of a Cp ligand from η^5 to η^1 and coordination of the bidentate phosphine ligand to afford [{Fe(η^5-C_5H_4)$SiMe_2$(η^1-C_5H_4)}(dppe)] (**2**) in 90 % yield [Eq. (1)].[10]



(1)

The $^{31}P\{^1H\}$ NMR spectrum of **2** consisted of slightly broad AB doublets at $\delta = 109.4$ and 108.5 ppm[11] with the same coupling constant ($^2J(P,P) = 27.2$ Hz); they were assigned to the diastereotopic phosphine atoms coordinated to the iron center. In the $^{29}Si\{^1H\}$ NMR spectrum, a single broad resonance signal appeared at $\delta = -8.72$ ppm, which is shifted slightly upfield compared to that of **1** ($\delta = -4.6$ ppm).

Figure 1 shows the molecular structure of **2** determined by X-ray crystallography.[12] The photoproduct **2** possesses a

[*] Dr. M. Tanabe,[+] S. C. Bourke, D. E. Herbert, Dr. A. J. Lough, Prof. Dr. I. Manners
Department of Chemistry
University of Toronto
80 St. George Street, Toronto, ON M5S 3H6 (Canada)
Fax: (+1) 416-978-6157
E-mail: imanners@chem.utoronto.ca

[+] Present address:
Chemical Resources Laboratory
Tokyo Institute of Technology
4259 Nagasuta, Midori-ku, Yokohama 226-8503 (Japan)

[**] We thank NSERC and the Canadian Government for a Canadian Research Chair and a Canada Graduate Scholarship (DEH). We also thank Dr. T. Burrow for measuring two-dimensional NMR spectra.

InterScience
© 2005 Wiley-VCH Verlag GmbH & Co. KGaA, Weinheim

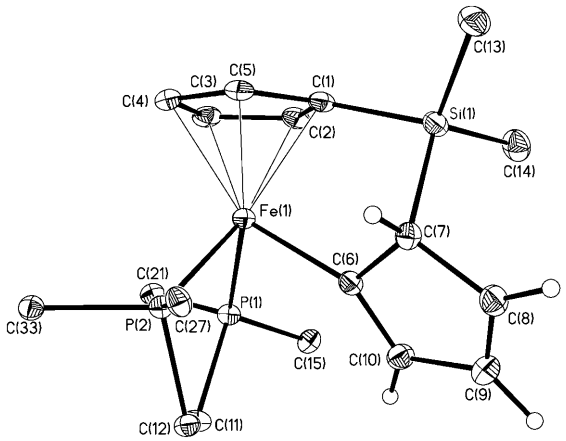


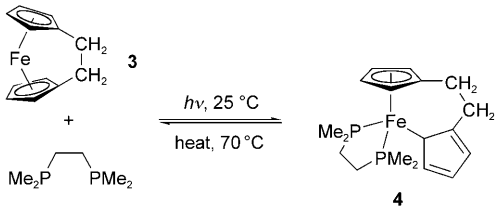
Figure 1. ORTEP drawing of **2** with 30% thermal ellipsoidal plots. Hydrogen atoms are depicted only for the η^1-Cp ring. Phenyl groups of the phosphine ligand are omitted for clarity. Selected bond lengths [Å] and angles [°]: Fe(1)-$Cp_{centroid}$ 1.736(2), Fe(1)-P(1) 2.1543(6), Fe(1)-P(2) 2.1544(6), Fe(1)-C(6) 2.015(2), Si(1)-C(1) 1.862(2), Si(1)-C(7) 1.884(2), C(6)-C(7), 1.524(3), C(6)-C(10) 1.367(3), C(7)-C(8) 1.483(3), C(8)-C(9) 1.343(4), C(9)-C(10) 1.464(3); $Cp_{centroid}$-Fe(1)-C(6) 119.7(9), $Cp_{centroid}$-Fe(1)-P(1) 129.8(9), $Cp_{centroid}$-Fe(1)-P(2) 131.5(9), C(1)-Si(1)-C(7) 99.42(10), Fe(1)-C(6)-C(7) 118.01(16), Si(1)-C(7)-C(6) 100.07(14).

piano-stool geometry around the Fe center. The C(1)-Si(1)-C(7) angle (99.42(10)°) is larger than that of **1** (95.7(4)°),[9] and the angle β (14.0(3)°) of **2**, between the plane of the cyclopentadienyl carbon atoms and the C(1)-Si(1) bond, has decreased significantly (from 37.0(6)° for **1**),[9] indicating that the ring strain is less in **2** than in **1**. The bond lengths for C(6)–C(10) (1.367(3) Å) and C(8)–C(9) (1.343(4) Å) in the σ-bonded Cp ring are shorter than other bond lengths (average 1.490(3) Å), indicating that the double bonds are located in these positions.

All inequivalent proton and carbon signals for the differently coordinated Cp rings were assigned by ^{1}H-^{1}H and ^{1}H-^{13}C COSY NMR spectroscopic methods at −40 °C. Interestingly, one signal in each Cp ring was observed at higher field (δ = 2.82 ppm for η^1-Cp; δ = 3.03 ppm for η^5-Cp). Upon raising the temperature of the solution to 25 °C, all signals in the ^{1}H and ^{31}P{^{1}H} NMR spectra appeared broadened suggesting fluxional behavior around the Fe center.

Remarkably, on heating at 70 °C in [D_6]benzene for 3 h, photoproduct **2** underwent dissociation of the dppe ligand and quantitative retroconversion into **1** [Eq. (1)]. This thermal reaction clearly indicates that, at elevated temperatures, the ring-strained ferrocenophane **1** and dppe are thermodynamically favored compared with the photoproduct **2**. This can be attributed to the greater entropy of the species on the left side of Equation (1) and the enthalpic preference for η^5-Cp coordination. It appears that **2** is metastable at room temperature and that its formation relies on the photoactivation of **1**.

To explore the generality of this surprising reversible reaction, we investigated the analogous chemistry of the ethane-bridged [2]ferrocenophane **3** (α = 21.6(4)°)[13] which has a similar degree of ring strain as **1**. Another ring-slipped Fe complex, [{Fe(η^5-C_5H_4)CH_2CH_2(η^1-C_5H_4)}(dmpe)] (**4**), was obtained from the photolysis of **3** in the presence of 1,2-bis(dimethylphosphanyl)ethane (dmpe) in THF at room temperature [Eq. (2)]. Recrystallization of the crude product from toluene/hexane at −55 °C afforded **4** as dark red crystals in 83% yield.[14] Heating of **4** in [D_8]toluene for 3 h at 70 °C also led to a quantitative reverse haptotropic rearrangement with dissociation of the dmpe ligand.



(2)

Complex **4** was also fully characterized by one- and two-dimensional NMR spectroscopic methods at low temperature and the crystal structure was determined by X-ray diffraction (Figure 2).[12] The piano-stool Fe center, capped by an η^5-Cp

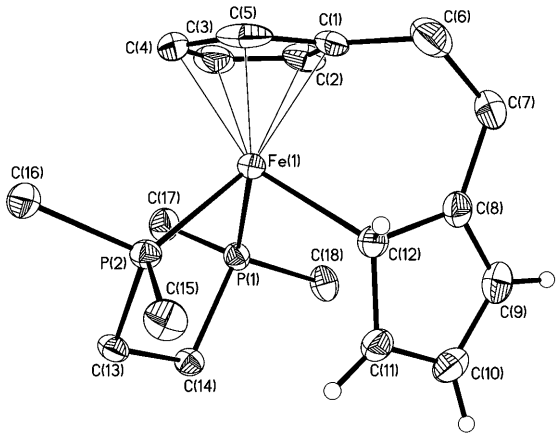


Figure 2. ORTEP drawing of **4** with 30% thermal ellipsoidal plots. Hydrogen atoms are depicted only for the η^1-Cp ring. Selected bond lengths [Å] and angles [°]: Fe(1)-$Cp_{centroid}$ 1.717(5), Fe(1)-P(1) 2.1674(15), Fe(1)-P(2) 2.1776(14), Fe(1)-C(12) 2.201(5), C(1)-C(6) 1.491(8), C(6)-C(7) 1.516(9), C(7)-C(8) 1.512(7), C(8)-C(9) 1.352(8), C(8)-C(12) 1.476(7), C(9)-C(10) 1.428(8), C(10)-C(11) 1.350(8), C(11)-C(12) 1.465(7); $Cp_{centroid}$-Fe(1)-C(12) 120.1(2), $Cp_{centroid}$-Fe(1)-P(1) 125.1(2), $Cp_{centroid}$-Fe(1)-P(2) 128.0(2), C(1)-C(6)-C(7) 111.6(5), C(6)-C(7)-C(8) 113.5(5), C(7)-C(8)-C(12) 124.6(5), Fe(1)-C(12)-C(8) 110.6(3).

ligand, also possesses a chelating dmpe ligand. The C(1)–C(6) bond was found to lie almost in plane with the η^5-Cp ligand (β = 1.9(3)°), indicating that the structure contains no significant ring strain. The two double bonds in the η^1-Cp ring were located at C(8)–C(9) (1.352(8) Å) and C(10)–C(11) (1.350(8) Å), supported by the conformation around C(12) which is not suited to an sp^2 carbon center. Analysis of **4** in the solid state indicated that the η^1-Cp geometry is a tautomer of that in **2**.

The variable-temperature ^{31}P{^{1}H} NMR spectra exhibited two doublets at δ = 81.0 and 78.9 ppm (^2J(P,P) = 39 Hz) at −40 °C that coalesce to give a single signal at 79.0 ppm upon warming to 20 °C. Figure 3 depicts the ^{1}H NMR spectra of **4**

 © 2005 Wiley-VCH Verlag GmbH & Co. KGaA, Weinheim

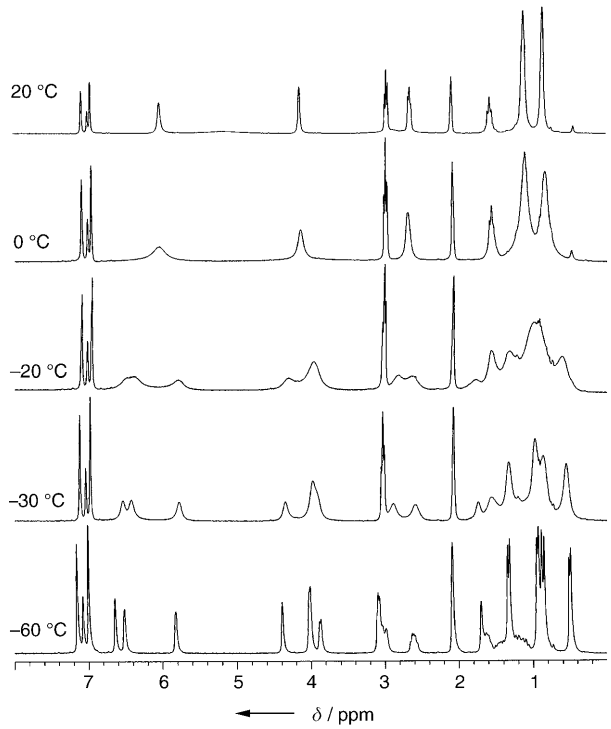
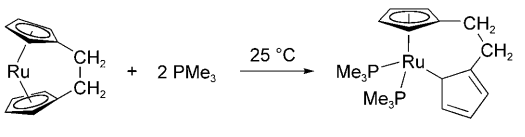


Figure 3. Variable-temperature ^{1}H NMR spectra of **4** between −60 and 20 °C in [D_8]toluene.

between −60 and 20 °C. At −60 °C, eight signals attributed to the two inequivalent Cp rings were observed in the range $\delta =$ 1.70–6.64 ppm. Upon raising the temperature to −20 °C all signals attributable to **4** broadened and coalesced around 0 °C, indicating the same coalescence temperature for both the η^1- and η^5-Cp rings. At 20 °C, two widely broadened signals ($\delta =$ 4.6–5.6 ppm for the η^1-ring; $\delta = 2.8$–3.1 ppm for the η^5-ring; not clearly visible in the spectra) suggest slower fluxional behavior. The fluxional behavior of σ-bonded Cp rings such as that in [Fe(η^1-Cp)(η^5-Cp)(CO)$_2$] has been well studied over the past four decades.[15] The η^1-Cp ring of this species is involved in a fluxional process that consists of successive 1,2-shifts, observable on the NMR time scale, while the η^5-Cp ring signals display no coalescence due to more rapid ring rotation. The dynamic nature of the NMR spectrum of **4** suggests fluxional behavior, which may involve fast successive 1,2-shifts of the η^1-Cp ring and slow coordination mode exchange between the two Cp ligands.

At this point, we investigated the analogous reaction of the more highly ring-strained, ethane-bridged [2]ruthenocenophane **5** which possesses a larger tilt angle of 29.6(5)° by virtue of the larger covalent radius of Ru relative to Fe.[16] When **5** was reacted with excess PMe_3 *without* photoirradiation the new complex [{Ru(η^5-C_5H_4)CH_2CH_2(η^1-C_5H_4)}-(PMe_3)$_2$] (**6**) was formed in a quantitative yield [Eq. (3)].



5 **6** (3)

The solid-state structure of **6** was investigated by single-crystal X-ray crystallography.[12] The molecular structure (Figure 4) and the η^1-Cp ring geometry were similar to that seen for complex **4**. The $Cp_{centroid}$–Ru distance (1.863(3) Å) is longer than the $Cp_{centroid}$–Fe distance in **4** (1.717(5) Å) due to

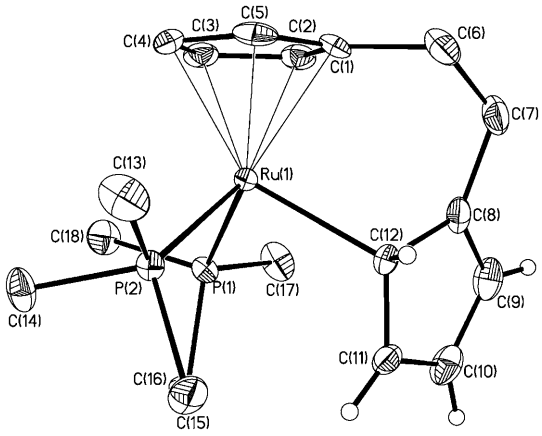


Figure 4. ORTEP drawing of **6** with 30% thermal ellipsoidal plots. Hydrogen atoms are depicted only for the η^1-Cp ring. Selected bond lengths [Å] and angles [°]: Ru(1)-$Cp_{centroid}$ 1.863(3), Ru(1)-P(1) 2.2710(6), Ru(1)-P(2) 2.2719(6), Ru(1)-C(12) 2.275(2), C(1)-C(6) 1.505(4), C(6)-C(7) 1.496(5), C(7)-C(8) 1.508(4), C(8)-C(12) 1.474(3), C(8)-C(9) 1.355(4), C(9)-C(10) 1.425(5), C(10)-C(11) 1.360(4), C(11)-C(12) 1.464(4); $Cp_{centroid}$-Ru(1)-C(12) 117.3(9), $Cp_{centroid}$-Ru(1)-P(1) 124.4(9), $Cp_{centroid}$-Ru(1)-P(2) 123.9(9), C(1)-C(6)-C(7) 112.8(3), C(6)-C(7)-C(8) 114.4(3), C(7)-C(8)-C(12) 126.0(3), Ru(1)-C(12)-C(8) 108.23(16).

the larger size of the ruthenium atom. As expected from the reaction in the absence of UV-photoirradiation, the ring-slipped Ru complex **6** is the thermodynamically stable compound due to the high ring-strain energy of ruthenocenophane **5**. In fact, thermal treatment of **6** in [D_8]toluene (110 °C, 18 h) resulted in no detectable retroconversion to **5**. Similar, irreversible formation of a ring-slipped η^1-Cp complex [{Ru(η^5-Cp)(CH_2CH_2)(η^1-Cp)}(dmpe)] (**7**) was observed with **5** and the chelating diphosphine dmpe.

In summary, ring-strained ferrocenophanes **1** and **3** were found to undergo photochemically and thermally reversible haptotropic shifts (η^5- to η^1-Cp) and the ring-slipped photoproducts **2** and **4** were isolated in the presence of appropriate phosphine ligands. In contrast, the highly ring-strained ruthenocenophane **5** was transformed irreversibly into the analogues **6** and **7** without UV-photoirradiation. We attribute these phenomena to the balance between the release of strain in the [1]- or [2]metallocenophane with the preference for η^5 coordination of the Cp ligand. For **1** and **3**, which possess moderate tilt angles and strain, photoactivation leads to **2** and **4**, which are metastable and retroconvert when heated at 70 °C. In contrast, the highly tilted [2]ruthenocenophane **5** possesses sufficient strain for the more thermodynamically stable species **6** and **7** to be formed irreversibly and without the need for photochemical activation. Currently, we are focusing on the detailed mechanism for the photochemically induced haptotropic rearrangement and the fluxional behavior of ring-slipped Fe and Ru complexes.

 © 2005 Wiley-VCH Verlag GmbH & Co. KGaA, Weinheim

Experimental Section

Basic experimental procedures and analytical equipment used were as noted elsewhere.[4b] The ligands dppe and dmpe were purchased from Aldrich, and trimethylphosphine was obtained from Strem. These phosphine reagents were used as received. The photoirradiation experiments were carried out with Pyrex-glass-filtered emission from a 125-W high-pressure mercury arc lamp (Philips). The emission lines of the mercury lamp were as follows: 578.0, 546.1, 435.8, 404.7, 365.0, 334.1, 313.0, and 302.5 nm.

Preparation of **2**: In the absence of light, dppe (359 mg, 0.9 mmol) was added to a slight excess of sila[1]ferrocenophane **1**[17] (242 mg, 1.0 mmol) dissolved in THF (5 mL). The solution was irradiated for 3 h, with stirring, in a cooling water bath at 5 °C. The reaction mixture was evaporated to dryness. Addition of hexane to the red residue followed by filtration allowed for collection of a red solid which was washed with hexane three times (2 mL), and dried in vacuo (517 mg, 90 % based on dppe). Recrystallization from THF/hexane, by slow evaporation, gave dark red crystals suitable for X-ray crystallography. All signals in the ^{1}H and ^{13}C{^{1}H} NMR spectra at 25 °C and −40 °C were characterized by 2D ^{1}H-^{1}H and ^{1}H-^{13}C NMR experiments. ^{1}H NMR (500 MHz, [D$_8$]toluene, −40 °C): $\delta = 7.88$ (br, 2H, Ph-*ortho*), 7.38 (s, 2H, Ph-*ortho*), 7.13–6.99 (Ph, overlapped with solvent), 6.69 (s, 1H, η^1-C$_5$H$_4$, CH=), 6.61 (s, 1H, η^1-C$_5$H$_4$, CH=), 5.33 (s, 1H, η^1-C$_5$H$_4$, CH=), 5.12 (s, 1H, η^5-C$_5$H$_4$), 4.70 (s, 1H, η^5-C$_5$H$_4$), 4.19 (s, 1H, η^5-C$_5$H$_4$), 3.03 (s, 1H, η^5-C$_5$H$_4$), 2.82 (s, 1H, η^1-C$_5$H$_4$, SiCH), 2.59 (br m, 1H, PCH$_2$), 2.17 (br d, 1H, PCH$_2$, ^2J(H,P) = 34 Hz), 1.87 (br m, 1H, PCH$_2$), 1.69 (br d, 1H, PCH$_2$, ^2J(H,P) = 27 Hz), 0.36 (br, 3H, SiCH$_3$), 0.13 ppm (br, 3H, SiCH$_3$); ^{13}C{^{1}H} NMR (75.4 MHz, [D$_6$]benzene, 25 °C): $\delta = 161.5$ (dd, η^1-C$_5$H$_4$, FeC=, ^2J(C,P) = 26, 38 Hz), 147.1 (Ph-*ipso*), 144.7 (η^1-C$_5$H$_4$, CH=), 141.0 (Ph-*ipso*), 140.7 (Ph-*ipso*), 139.5 (Ph-*ipso*), 135.6 (Ph-*ortho*), 134.0 (η^1-C$_5$H$_4$, CH=), 133.3 (η^1-C$_5$H$_4$, CH=), 131.3 (Ph-*ortho*), 129.8 (Ph), 129.1 (Ph), 103.2 (η^5-C$_5$H$_4$-*ipso*), 87.5 (η^5-C$_5$H$_4$), 84.0 (η^5-C$_5$H$_4$), 80.4 (η^5-C$_5$H$_4$), 74.9 (η^1-C$_5$H$_4$, SiCH), 73.6 (η^5-C$_5$H$_4$), 28.6 (dd, PCH$_2$, J(C,P) = 16, 34 Hz), 25.0 (br t, PCH$_2$), 0.11 (SiCH$_3$), −7.92 ppm (SiCH$_3$); ^{31}P{^{1}H} NMR (121.4 MHz, [D$_6$]benzene, 25 °C): $\delta = 109.4$ (d, J(P,P) = 27.2 Hz), 108.5 ppm (d, J(P,P) = 27.2 Hz); ^{29}Si{^{1}H} NMR (79.4 MHz, [D$_6$]benzene, 25 °C): $\delta = -8.72$ (br); MS analysis was not possible, as the sample decomposed in the spectrometer; elemental analysis: calcd for C$_{38}$H$_{38}$FeP$_2$Si (%): C 71.25, H 5.98; found: C 70.95, H 6.00. A solution of **2** in [D$_6$]benzene, heated at 70 °C for 3 h in the absence of light, turned red in color and underwent a quantitative dissociation of the dppe ligand and reformation of the starting material **1**, as observed by ^{1}H NMR spectroscopy. The UV-photoirradiation of **1** with dmpe in THF at room temperature led to a dark red solution. However, a ^{1}H NMR spectrum of the reaction mixture showed the presence of **1** and free dmpe. In contrast, the photoirradiation of **1** with PMe$_3$ in [D$_6$]benzene at room temperature for 5 h afforded the ring-opened polymer [fcSiMe$_2$]$_n$ in 35 % yield ($M_n = 1.3 \times 10^4$, polydispersity index (PDI) = 1.45).[17a]

Preparation of **4**: The ligand dmpe (333 mg, 2.2 mmol) was added to a solution of ethane-bridged [2]ferrocenophane **3**[13a] (212 mg, 1.0 mmol) in THF (30 mL). The reaction mixture was irradiated for 2 h, with stirring at room temperature. The reaction conversion was estimated at 95 % by ^{1}H NMR spectroscopy. All volatile material in the reaction mixture was removed under high vacuum. The resulting material was dissolved in toluene and filtered through a celite-fritted glass disk. Recrystallization from toluene/hexane (10 mL, 4:1) at −55 °C gave dark red crystals (302 mg, 83 % yield). All signals in the ^{1}H and ^{13}C{^{1}H} NMR spectra at 20 and −60 °C were characterized by 2D ^{1}H-^{1}H and ^{1}H-^{13}C NMR experiments. ^{1}H NMR (300 MHz, [D$_8$]toluene, −60 °C): $\delta = 6.64$ (s, 1H, η^1-C$_5$H$_4$, CH=), 6.51 (s, 1H, η^1-C$_5$H$_4$, CH=), 5.82 (s, 1H, η^1-C$_5$H$_4$, CH=), 4.40 (s, 1H, η^5-C$_5$H$_4$), 4.02 (m, 2H, η^5-C$_5$H$_4$ and η^1-C$_5$H$_4$, overlapped signals), 3.87 (d, 1H, η^5-C$_5$H$_4$, ^3J(H,H) = 6.0 Hz), 3.08 (d, 2H, CpCH$_2$, ^3J(H,H) = 6.3 Hz), 3.02 (d, 1H, CpCH$_2$, ^3J(H,H) = 14 Hz), 2.61 (m, 1H, CpCH$_2$, ^3J(H,H) = 6.0 Hz), 1.70 (s, 1H, η^5-C$_5$H$_4$), 1.05–1.70 (4H, PCH$_2$), 1.33 (d, 3H, PCH$_3$, ^2J(H,P) = 7.5 Hz), 0.94 (d, 3H, PCH$_3$, ^2J(H,P) = 6.6 Hz), 0.87 (d, 3H, PCH$_3$, ^2J(H,P) = 10 Hz), 0.51 ppm (d, 3H, PCH$_3$, ^2J(H,P) = 6.6 Hz); ^{13}C{^{1}H} NMR (100.4 MHz, [D$_8$]toluene, −60 °C): $\delta = 157.4$ (η^1-C$_5$H$_4$-*ipso*, CH$_2$*C*=), 143.9 (η^1-C$_5$H$_4$, CH=), 118.2 (η^1-C$_5$H$_4$, CH=), 117.4 (η^1-C$_5$H$_4$, CH=), 94.4 (η^5-C$_5$H$_4$-*ipso*), 81.0 (η^5-C$_5$H$_4$), 80.1 (η^5-C$_5$H$_4$), 79.4 (η^5-C$_5$H$_4$), 56.3 (η^5-C$_5$H$_4$), 31.9 (dd, PCH$_2$, J(C,P) = 27, 14 Hz), 31.7 (Cp*C*H$_2$), 30.8 (Cp*C*H$_2$), 29.7 (dd, PCH$_2$, J(C,P) = 26, 15 Hz), 23.5 (d, PCH$_3$, J(C,P) = 27 Hz), 22.8 (η^1-C$_5$H$_4$, FeCH), 22.1 (d, PCH$_3$, J(C,P) = 25 Hz), 18.2 (d, PCH$_3$, J(C,P) = 9.5 Hz), 8.93 ppm (dd, PCH$_3$, J(C,P) = 4.5, 12 Hz); ^{31}P{^{1}H} NMR (121.4 MHz, [D$_8$]toluene, −40 °C): $\delta = 81.0$ (d, ^2J(P,P) = 39 Hz), 78.9 ppm (d, ^2J(P,P) = 39 Hz); ^{31}P{^{1}H} NMR (121.4 MHz, [D$_8$]toluene, 20 °C): $\delta = 79.0$ ppm; MS(CI, 70 eV): m/z (%): 362 (2.5) [M^+], 212 (100) [M^+−(PMe$_2$CH$_2$)$_2$], 134 (65) [Fe(C$_5$H$_4$CH$_2$)$^+$], 122 (65) [Fe(C$_5$H$_5$) + H$^+$]; elemental analysis: calcd for C$_{18}$H$_{28}$FeP$_2$ (%): C 59.69, H 7.79; found: C 60.04, H 8.01. A solution of **4** in [D$_6$]benzene, heated at 70 °C for 3 h in the absence of light, was quantitatively converted into a mixture of dmpe and **3**, as observed by ^{1}H NMR spectroscopy. Although UV-photoirradiation of the solution of **3** in THF in the presence of dppe at 5 °C led to a slightly dark red color, the ^{1}H and ^{31}P{^{1}H} NMR spectra did not show any photoproducts. The photoreaction with a threefold excess of PMe$_3$ for 3 h in [D$_6$]benzene at room temperature led to polymerization to yield the yellowish insoluble polymer [fcCH$_2$CH$_2$]$_n$ in 66 % yield.[13b]

Preparation of **6**: A fivefold excess of PMe$_3$ (78 μL, 0.76 mmol) was added to a solution of ethane-bridged [2]ruthenocenophane **5**[16] (39 mg, 0.15 mmol) in [D$_6$]benzene (0.5 mL) at room temperature. The reaction mixture immediately turned from yellow to orange in color without UV-photoirradiation. A ^{1}H NMR spectrum of the reaction mixture showed the quantitative conversion into ring-slipped Ru complex **6**. The volatile material was removed under high vacuum to dryness. Recrystallization from hexane by slow evaporation gave orange crystals suitable for X-ray crystallography. ^{1}H NMR (300 MHz, [D$_6$]benzene, 25 °C): $\delta = 6.54$ (s, 2H, η^1-C$_5$H$_4$), 5.3–5.7 (br, 2H, η^1-C$_5$H$_4$), 4.10 (s, 2H, η^5-C$_5$H$_4$), 3.89 (s, 2H, η^5-C$_5$H$_4$), 3.00 (t, 2H, CpCH$_2$, ^3J(H,H) = 3.2 Hz), 2.43 (t, 2H, CpCH$_2$, ^3J(H,H) = 3.3 Hz), 1.04 ppm (t, 18H, PCH$_3$, ^2J(H,P) = 3.9 Hz); ^{31}P{^{1}H} NMR (121.4 MHz, [D$_6$]benzene, 25 °C): $\delta = 4.65$ ppm; MS(EI, 70 eV): m/z (%): 410 (19) [M^+], 258 (100) [M^+−2PMe$_3$], 180 (36) [Ru-(C$_5$H$_5$CH$_2$)$^+$]. High-resolution MS for C$_{18}$H$_{30}$P$_2$Ru: calcd 410.086, found 410.087. Compound **6** did not show any retroconversion into ruthenocenophane **5** after 18 h at 110 °C in [D$_8$]toluene (^{1}H NMR).

Preparation of **7**: Excess dmpe (70 μL, 0.42 mmol) was added to a [D$_6$]benzene (0.5 mL) solution of ethane-bridged [2]ruthenocenophane **5** (5 mg, 0.019 mmol) at room temperature. The reaction mixture darkened from yellow to orange-yellow without UV-photoirradiation. A ^{1}H NMR spectrum of the reaction mixture showed quantitative conversion of the [2]ruthenocenophane into the ring-slipped Ru complex **7**. ^{1}H NMR (400 MHz, [D$_6$]benzene, 25 °C): δ = 6.32 (s, 2H, η^1-C$_5$H$_4$), 5.40 (br, 2H, η^1-C$_5$H$_4$), 4.56 (s, 2H, η^5-C$_5$H$_4$), 3.94 (s, 2H, η^5-C$_5$H$_4$), 2.96 (t, 2H, CpCH$_2$, ^3J(H,H) = 6.4 Hz), 2.46 (t, 2H, CpCH$_2$, ^3J(H,H) = 6.4 Hz), 1.61 (m, 4H, PCH$_2$), 1.17 ppm (m, 12H, PCH$_3$); ^{31}P{^{1}H} NMR (121.5 MHz, [D$_6$]benzene, 25 °C): δ = 54.2 ppm. ^{1}H NMR analysis of **7** in [D$_6$]benzene at 70 °C showed no evidence of retroconversion into [2]ruthenocenophane **5**. Partial decomposition of a solution of **7** in [D$_8$]toluene was observed at 85 °C but the remaining ring-slipped compound **7** showed no retroconversion into **5** even at 110 °C after 5 h.

Received: April 1, 2005
Published online: August 10, 2005

Keywords: iron · phane ligands · photochemistry · ring strain · ruthenium

 © 2005 Wiley-VCH Verlag GmbH & Co. KGaA, Weinheim

[1] a) C. Laporte, C. Böhler, H. Schönberg, H. Grützmacher, *J. Organomet. Chem.* **2002**, *641*, 227–234; b) C. Laporte, T. Büttner, H. Rüegger, J. Geier, H. Schönberg, H. Grützmacher, *Inorg. Chim. Acta* **2004**, *357*, 1931–1947, and references therein; c) L. Luo, N. Zhu, N.-J. Zhu, E. D. Stevens, S. P. Nolan, P. J. Fagan, *Organometallics* **1994**, *13*, 669–675; d) C. Li, M. E. Cucullu, R. A. McIntyre, E. D. Stevens, S. P. Nolan, *Organometallics* **1994**, *13*, 3621–3627; e) H. K. Sharma, F. Cervantes-Lee, K. H. Pannell, *J. Am. Chem. Soc.* **2004**, *126*, 1326–1327.

[2] a) M. Herberhold, *Angew. Chem.* **1995**, *107*, 1985–1987; *Angew. Chem. Int. Ed. Engl.* **1995**, *34*, 1837–1839; b) H. Urtel, C. Meier, F. Eisenträger, F. Rominger, J. P. Joschek, P. Hofmann, *Angew. Chem.* **2001**, *113*, 803–806; *Angew. Chem. Int. Ed.* **2001**, *40*, 781–784; c) A. Berenbaum, F. Jäkle, A. J. Lough, I. Manners, *Organometallics* **2002**, *21*, 2359–2361; d) H. Braunschweig, F. M. Breitling, E. Gullo, M. Kraft, *J. Organomet. Chem.* **2003**, *680*, 31–42; e) H. Braunschweig, M. Homberger, C. Hu, X. Zheng, E. Gullo, G. Clentsmith, M. Lutz, *Organometallics* **2004**, *23*, 1968–1970; f) F. Schaper, O. Wrobel, R. Schwörer, H.-H. Brintzinger, *Organometallics* **2004**, *23*, 3552–3555; g) A. Berenbaum, I. Manners, *Dalton Trans.* **2004**, 2057–2058; h) U. Vogel, A. J. Lough, I. Manners, *Angew. Chem.* **2004**, *116*, 3383–3387; *Angew. Chem. Int. Ed.* **2004**, *43*, 3321–3325; i) M. Tamm, A. Kunst, T. Bannenberg, E. Herdtweck, P. Sirsch, C. J. Elsevier, J. M. Ernsting, *Angew. Chem.* **2004**, *116*, 5646–5650; *Angew. Chem. Int. Ed.* **2004**, *43*, 5530–5534; j) M. Tamm, A. Kunst, E. Herdtweck, *Chem. Commun.* **2005**, 1729–1731; k) J. A. Schachner, C. L. Lund, J. W. Quail, J. Müller, *Organometallics* **2005**, *24*, 785–787; l) C. Elschenbroich, F. Paganelli, M. Nowotny, B. Neumüller, O. Burghaus, *Z. Anorg. Allg. Chem.* **2004**, *630*, 1599–1606.

[3] a) I. Manners, *Science* **2001**, *294*, 1664–1666; b) I. Manners, *Synthetic Metal-Containing Polymers*, Wiley-VCH, Weinheim, **2004**.

[4] a) I. Manners, *Chem. Commun.* **1999**, 857–865; b) R. Resendes, J. M. Nelson, A. Fischer, F. Jäkle, A. Bartole, A. J. Lough, I. Manners, *J. Am. Chem. Soc.* **2001**, *123*, 2116–2126.

[5] a) R. Rulkens, D. P. Gates, D. Balaishis, J. K. Pudelski, D. F. McIntosh, A. J. Lough, I. Manners, *J. Am. Chem. Soc.* **1997**, *119*, 10976–10986; b) S. Barlow, M. J. Drewitt, T. Dijkstra, J. C. Green, D. O'Hare, C. Whittingham, H. H. Wynn, D. P. Gates, I. Manners, J. M. Nelson, J. K. Pudelski, *Organometallics* **1998**, *17*, 2113–2120.

[6] a) A. B. Fischer, J. B. Kinney, R. H. Staley, M. S. Wrighton, *J. Am. Chem. Soc.* **1979**, *101*, 6501–6506; b) M. J. MacLachlan, M. Ginzburg, J. Zheng, O. Knöll, A. J. Lough, I. Manners, *New J. Chem.* **1998**, *22*, 1409–1415; c) M. J. MacLachlan, S. C. Bourke, A. J. Lough, I. Manners, *J. Am. Chem. Soc.* **2000**, *122*, 2126–2127; d) S. C. Bourke, M. J. MacLachlan, A. J. Lough, I. Manners, *Chem. Eur. J.* **2005**, *11*, 1989–2000.

[7] A. Berenbaum, H. Braunschweig, R. Dirk, U. Englert, J. C. Green, F. Jäkle, A. J. Lough, I. Manners, *J. Am. Chem. Soc.* **2000**, *122*, 5765–5774.

[8] a) T. Mizuta, Y. Imamura, K. Miyoshi, *J. Am. Chem. Soc.* **2003**, *125*, 2068–2069; see also: b) T. Mizuta, M. Onishi, K. Miyoshi, *Organometallics* **2000**, *19*, 5005–5009.

[9] W. Finckh, B.-Z. Tang, D. A. Foucher, D. B. Zamble, R. Ziembinski, A. Lough, I. Manners, *Organometallics* **1993**, *12*, 823–829.

[10] Similar photoirradiation of **1** in the presence of dmpe or PMe_3 was unsuccessful in terms of isolating Cp ring-slipped compounds like **2**; see the Experimental Section.

[11] These chemical shifts are similar to those of the dppe-coordinated Fe complex $[\{(\eta^5\text{-Cp})Fe(dppe)\}_2(\mu\text{-CH=CHCH=CH})]$: M.-C. Chung, X. Gu, B. A. Etzenhouser, A. M. Spuches, P. T. Rye, S. K. Seetharaman, D. J. Rose, J. Zubieta, M. B. Sponsler, *Organometallics* **2003**, *22*, 3485–3494.

[12] Crystallographic data for $C_{38}H_{38}FeP_2Si$ (**2**): $M_r = 640.56$, monoclinic, $P2_1/c$, $a = 8.9389(2)$, $b = 17.1939(2)$, $c = 20.8647(4)$ Å, $\beta = 95.7490(9)°$, $V = 3190.66(10)$ Å^3, $Z = 4$, $\mu = 0.637$ mm^{-1}, $\rho_{calcd} = 1.333$ Mg m^{-3}, 150(1) K, Nonius Kappa-CCD diffractometer using graphite-monochromated $Mo_{K\alpha}$ radiation ($\lambda = 0.71073$ Å), dark red crystal ($0.28 \times 0.18 \times 0.10$ mm^3). Of 28009 reflections collected ($5.1 \le 2\theta \le 55.0°$), 7314 were independent ($R_{int} = 0.0553$). The data frames were integrated and scaled using the Denzo-SMN package.[18] Solution and refinement with SHELXTL-PC V6.12,[19] non-hydrogen atoms were refined with anisotropic parameters, hydrogen atoms were refined on calculated positions using a riding model, $R1 = 0.0401$, $wR2 = 0.1085$ (for all three structure determinations: $R1 = \Sigma(F_o - F_c)/\Sigma F_o$ for $I > 2\sigma(I)$, $wR2 = [\Sigma\{w(F_o^2 - F_c^2)^2\}/\Sigma\{w(F_o^2)^2\}]^{1/2}$) for all data), GOF = 1.035, $\Delta\rho_{max} = 0.370$ e Å^{-3}. Crystallographic data for $C_{18}H_{28}FeP_2$ (**4**): $M_r = 362.19$, monoclinic, $P2_1/c$, $a = 7.9539(4)$, $b = 13.9194(9)$, $c = 16.1807(8)$ Å, $\beta = 102.218(4)°$, $V = 1750.85(17)$ Å^3, $Z = 4$, $\mu = 1.036$ mm^{-1}, $\rho_{calcd} = 1.374$ Mg m^{-3}, 150(1) K, Nonius Kappa-CCD diffractometer using graphite-monochromated $Mo_{K\alpha}$ radiation ($\lambda = 0.71073$ Å), dark red crystal ($0.10 \times 0.08 \times 0.06$ mm^3). Of 14784 reflections collected ($5.1 \le 2\theta \le 55.0°$), 4005 were independent ($R_{int} = 0.0879$). Solution and refinement as for **2**, $R1 = 0.0668$, $wR2 = 0.1702$, GOF = 1.076, $\Delta\rho_{max} = 0.845$ e Å^{-3}. Crystallographic data for $C_{18}H_{30}RuP_2$ (**6**): $M_r = 409.43$, orthorhombic, $P2_12_12_1$, $a = 9.13730(10)$, $b = 13.9938(2)$, $c = 15.1999(2)$ Å, $V = 1943.54(4)$ Å^3, $Z = 4$, $\mu = 0.964$ mm^{-1}, $\rho_{calcd} = 1.399$ Mg m^{-3}, 150(1) K, Nonius Kappa-CCD diffractometer using graphite-monochromated $Mo_{K\alpha}$ radiation ($\lambda = 0.71073$ Å), dark red crystal ($0.16 \times 0.26 \times 0.26$ mm^3). Of 16976 reflections collected ($5.2 \le 2\theta \le 55.0°$), 4440 were independent ($R_{int} = 0.0364$). Solution and refinement as for **2**, $R1 = 0.0234$, $wR2 = 0.0561$, GOF = 1.124, $\Delta\rho_{max} = 0.758$ e Å^{-3}. CCDC-248005 (**2**), CCDC-248004 (**4**), and CCDC-248003 (**6**) contain the supplementary crystallographic data for this paper. These data can be obtained free of charge from the Cambridge Crystallographic Data Centre via www.ccdc.cam.ac.uk/data_request/cif.

[13] a) H. L. Lentzner, W. E. Watts, *Tetrahedron* **1971**, *27*, 4343–4351; b) J. M. Nelson, P. Nguyen, R. Petersen, H. Rengel, P. M. Macdonald, A. J. Lough, I. Manners, N. P. Raju, J. E. Greedan, S. Barlow, D. O'Hare, *Chem. Eur. J.* **1997**, *3*, 573–584.

[14] UV-photoirradiation of **3** with dppe did not lead to a ring-slipped product (^{1}H and ^{31}P{^{1}H} NMR).

[15] a) M. J. Bennett, Jr., F. A. Cotton, A. Davison, J. W. Faller, S. J. Lippard, S. M. Morehouse, *J. Am. Chem. Soc.* **1966**, *88*, 4371–4376; b) F. A. Cotton, *Acc. Chem. Res.* **1968**, *1*, 257–265; c) M. E. Wright, G. O. Nelson, R. S. Glass, *Organometallics* **1985**, *4*, 245–250.

[16] a) J. M. Nelson, A. J. Lough, I. Manners, *Angew. Chem.* **1994**, *106*, 1019–1021; *Angew. Chem. Int. Ed. Engl.* **1994**, *33*, 989–991; b) M. Herberhold, T. Bärtl, *Z. Naturforsch. B* **1995**, *50*, 1692–1698.

[17] a) D. A. Foucher, B.-Z. Tang, I. Manners, *J. Am. Chem. Soc.* **1992**, *114*, 6246–6248; b) Y. Ni, R. Rulkens, I. Manners, *J. Am. Chem. Soc.* **1996**, *118*, 4102–4114.

[18] Z. Otwinowski, W. Minor, *Methods Enzymol.* **1997**, *276*, 307–326.

[19] G. M. Sheldrick, SHELXTL-Windows NT. V6.12, Bruker Analytical X-Ray Systems Inc., Madison, WI, **2001**.

 © 2005 Wiley-VCH Verlag GmbH & Co. KGaA, Weinheim

Redox Chemistry

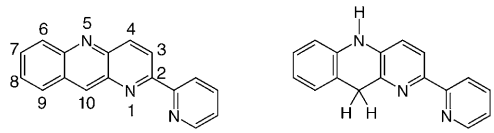
DOI: 10.1002/anie.200500760

Reversible Hydride Generation and Release from the Ligand of $[Ru(pbn)(bpy)_2](PF_6)_2$ Driven by a pbn-Localized Redox Reaction**

*Take-aki Koizumi and Koji Tanaka**

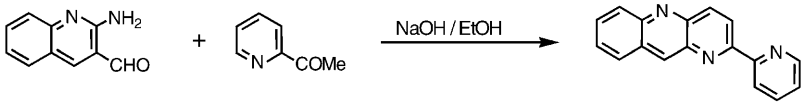
Metal hydrides such as $LiAlH_4$ and $NaBH_4$ have been widely employed in organic synthesis as fundamental reducing agents, and numerous modified forms have been developed for specific purposes. In biological reactions, on the other hand, the NAD^+/NADH redox couple, in which the oxidized form (NAD^+) with a pyridinium structure is reversibly converted into the reduced form (NADH) with two electrons and one proton, plays a key role in reversible hydride transfer reactions. Chemists have focused much attention on the function of NADH as an *organic hydride*. A number of kinetic studies of the hydride transfer,[1] asymmetric reductions of carbonyl compounds,[2] electron and hydrogen-atom transfer[3] with NADH and its model compounds have been carried out. However, as far as we know, all the reactions so far reported using NAD^+/NADH model compounds are stoichiometric.[2,4]

Recently, we revealed that the electrochemical reduction of *cis*-$[Ru(napy\text{-}\kappa N)(CO)(bpy)_2](PF_6)_2$ (napy = 1,8-naphthyridine) at −1.34 V (versus the ferrocene/ferrocenium (Fc/Fc^+) couple) in H_2O results in bond formation between the noncoordinating N atom of napy and the carbonyl carbon atom as well as the subsequent hydrogenation of the napy ring. Reoxidation of the solution at 0.06 V fully regenerated *cis*-$[Ru(napy\text{-}\kappa N)(CO)(bpy)_2]^{2+}$ (Scheme 1).[5] The reversible formation of a C–H bond in a pyridinium ring by two electrons and one proton (Scheme 1) is in good agreement with the NAD^+/NADH redox couple. This observation has driven us to construct a catalytic system that is able to generate and release hydride ions from a ligand of a transition-metal complex, because until now there has been no report of transition-metal complexes operating in the same way as the NAD^+/NADH system. Herein we describe the synthesis and electrochemical behavior of $[Ru(pbn)(bpy)_2](PF_6)_2$ (**1**, pbn = 2-(2-pyridyl)benzo[*b*]-1.5-naphthyridine, bpy = 2,2′-bipyridine; Scheme 2). The electrochemical reduction of **1** under aqueous acidic conditions induces formation of the hydrogenated product $[Ru(pbnH_2)(bpy)_2](PF_6)_2$ (**2**). We also report the electrochemical reduction of acetone by using complex **1** as a precatalyst.



Scheme 2. Ligands used to form a catalytic system.

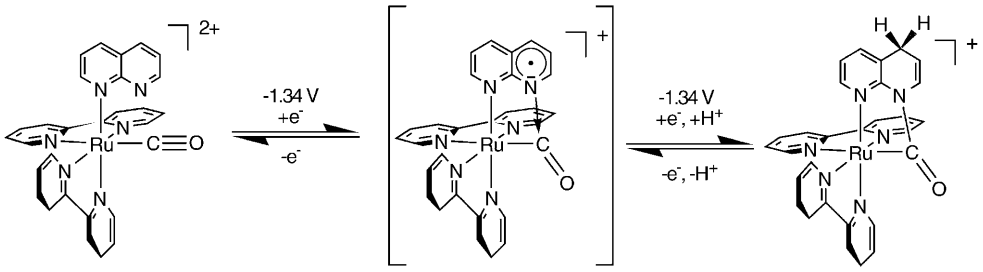
2-(2-Pyridyl)benzo[*b*]-1.5-naphthyridine (pbn) was prepared by coupling 3-aminoquinaldehyde[6] with 2-acetylpyridine in ethanol in the presence of NaOH[7] [Eq. (1)]. $[RuCl_2(bpy)_2]$ was treated with two equivalents of $AgPF_6$ in 2-methoxyethanol, followed by addition of one equivalent of pbn to give $[Ru(pbn)(bpy)_2](PF_6)_2$ (**1**) as a red-purple powder [Eq. (2)]. The structure of complex **1** was determined by X-ray crystallographic analysis (Figure 1)[8] and NMR spectroscopy.



(1)

The addition of hydrochloric acid to a solution of **1** in acetonitrile resulted in a dramatic change from orange-brown to green. The UV/Vis spectra show there is a bathochromic shift of the absorption band of the metal-to-ligand charge transfer (MLCT) based on the pbn ligand from 529 to 604 nm. The extent of the decrease in the energy of the π* orbital of pbn upon protonation of the ligand would be larger than that of the dπ orbital of the Ru(II) atom. As a result, the MLCT band of **1** showed a red-shift as a result of a narrowing of the Ru(dπ)–L(π*) energy gap under acidic conditions. A similar green color has been observed in some ruthenium complexes containing quaternary polypyridine-type ligands.[9]

The cyclic voltammogram of **1** measured in MeCN in the presence of 0.1 M Me_4NBF_4 exhibited one reversible (Ru^{II}/Ru^{III}) redox couple at $E_{1/2} = +1.09$ V (versus Fc/Fc^+) and

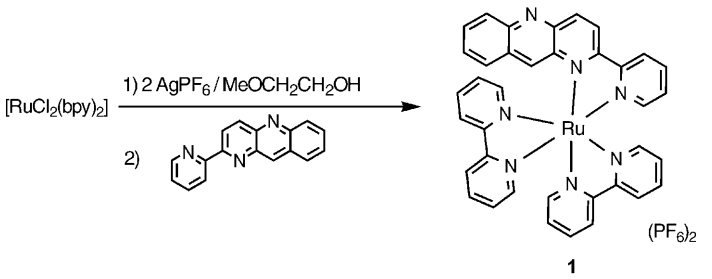


Scheme 1. Electrochemical reduction of *cis*-$[Ru(napy\text{-}\kappa N)(CO)(bpy)_2]^{2+}$.

[*] Dr. T.-a. Koizumi, Prof. K. Tanaka
Institute for Molecular Science and CREST
Japan Science and Technology Agency
5-1 Higashiyama, Myodaiji, Okazaki, Aichi 444-8787 (Japan)
Fax: (+81) 564-59-5582
E-mail: ktanaka@ims.ac.jp

[**] pbn = 2-(2-pyridyl)benzo[*b*]-1,5-naphthyridine, bpy = 2,2′-bipyridine.

 © 2005 Wiley-VCH Verlag GmbH & Co. KGaA, Weinheim



1 (2)

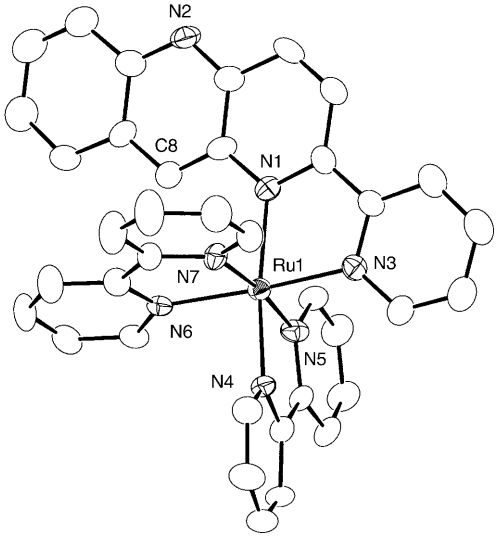


Figure 1. ORTEP drawing of the cationic part of **1** with 50% thermal ellipsoids. Hydrogen atoms are omitted for simplicity. Selected bond length [Å] and angles [°]: Ru1-N1 2.116(5), Ru1-N3 2.051(5), Ru1-N4 2.038(5), Ru1-N5 2.057(6), Ru1-N6 2.082(5), Ru1-N7 2.058(5), N1-Ru1-N3 78.0(2), N1-Ru1-N4 173.1(2); N1-Ru1-N5 98.9(2), N1-Ru1-N6 101.3(2), N1-Ru1-N7 86.4(2), N3-Ru1-N4 95.3(2), N3-Ru1-N5 89.7(2), N3-Ru1-N6 173.9(2), N3-Ru1-N7 95.9(2), N4-Ru1-N5 79.2(2), N4-Ru1-N6 85.5(2), N4-Ru1-N7 96.0(2), N5-Ru1-N6 96.4(2), N5-Ru1-N7 173.0(2), N6-Ru1-N7, 78.0(2).

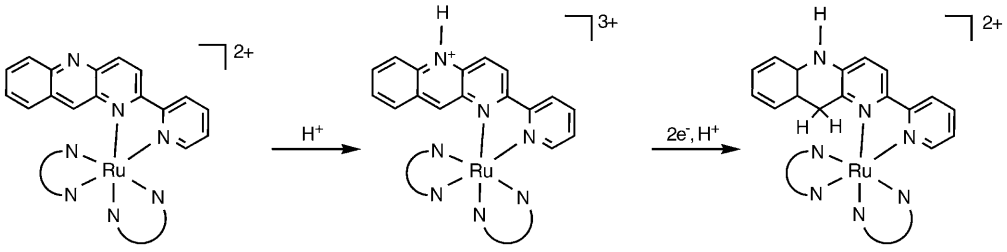
three ligand-based redox processes at $E_{1/2} = -1.03$, -1.65, and -1.92 V. The first of the ligand-based redox processes is assigned to the pbn ligand, and other two waves to bpy redox processes. The first reduction wave appeared at -0.37 V after the addition of 50 equivalents of HCl to the solution. Thus, the protonation of the pbn ligand shifts the redox potentials towards the positive region by approximately 700 mV relative to **1**. The fact that the pbn-based redox reaction takes place reversibly ($\Delta E = 68$ mV) indicates that the radical species generated by the one-electron reduction is stable and does not undergo further reactions, for example, abstraction or dimerization of the H radical by radical coupling.

The potentiostatic electrolysis of **1** in a 1:1 mixture of MeCN and 0.1M AcOH/AcONa buffer solution at -1.14 V (versus Fc/Fc^+) under N_2 consumed electrons corresponding to two electrons per molecule, and then the reaction stopped. The solution turned from red-purple to orange-brown. The ESI-MS spectrum of the resulting solid **2** obtained after drying showed a parent signal at m/z 336.5 with a divalent cation pattern, which is increased by one mass number relative to **1** (m/z 335.5), thus indicating that two hydrogen atoms were added to **1**.

The ^{1}H NMR spectrum of **2** in [D_6]acetone displayed 19 different signals with a total intensity of 27 protons in the aromatic region, which are assigned to two bpy and reduced pbn ligands, including the NH proton. Two characteristic doublets appeared at $\delta = 4.19$ and 3.18 ppm while the singlet peak at $\delta = 8.55$ ppm assigned to the proton on C10 disappeared (Scheme 3).[10]

Dissolving complex **2** in [D_6]acetone resulted in the solution turning from orange-brown to red-orange quite slowly at room temperature. The time-dependent ^{1}H NMR spectrum showed a new signal at $\delta = 3.75$ ppm, which is assigned to the hydrogen atom on the C2 carbon atom of $(CD_3)_2CHOH$. This result indicates that acetone was reduced by **1** to generate 2-propanol, as shown in Scheme 4. Controlled potential electrolysis of **1** (1 mM) was performed in the presence of 0.1M AcOH/AcONa buffer and 0.1M NaCl in an aqueous acetone solution (1:1 v/v, 10 mL) at -1.14 V (versus Fc/Fc^+) with a glassy carbon working electrode. The reaction progressed slowly, and about 20 μmol of 2-propanol formed in 48 h with a current efficiency of approximately 90%. To our knowledge, this is the first example of the electrochemical catalytic reduction of organic molecules by using a NAD^+/NADH model system.

In summary, we have demonstrated the synthesis of a novel ruthenium complex with a ligand that behaves in the same way as the NAD^+/NADH redox couple. We have succeeded in the catalytic reduction of acetone with two electrons and H_2O as a proton source for the first time. The key points of this catalytic system are "hydride" generation and transfer, similar to the function of the NAD^+/NADH redox couple.

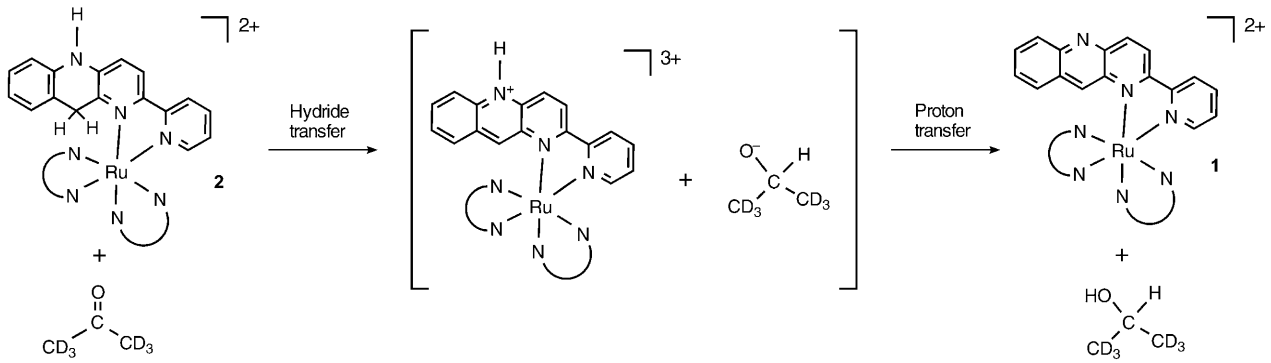


Scheme 3. Electrochemical reduction of $[Ru(pbn)(bpy)_2]^{2+}$.

Experimental Section

1: A solution of $AgPF_6$ (60 mg, 0.24 mmol) in $CH_3OCH_2CH_2OH$ (5 mL) was added to a solution of $[RuCl_2(bpy)_2]$ (53 mg, 0.11 mmol)

 © 2005 Wiley-VCH Verlag GmbH & Co. KGaA, Weinheim



Scheme 4. Mechanism for the reduction of acetone.

in $CH_3OCH_2CH_2OH$ (20 mL) and this mixture was stirred at 70 °C for 2 h. The resulting gray solid was removed by filtration through celite, and then the red-orange filtrate was added to a solution of pbn (28 mg, 0.11 mmol) in $CH_3OCH_2CH_2OH$ (5 mL) and the solution changed immediately from red-orange to red-purple. The reaction mixture was stirred at 70 °C for 12 h. The solution was concentrated to ca. 1 mL and poured into aqueous NH_4PF_6 solution. The reddish purple solid formed was collected and dried in vacuo (92 mg, 88 % yield). Elemental analysis calcd for $C_{37}H_{29}F_{12}N_7OP_2Ru$ (**1**·H_2O): C 45.41, H 2.99, N 10.02; found; C 45.48, H 3.18, N 9.70. ^{1}H NMR (500 MHz, [D_6]acetone): $\delta = 9.15$ (d, J(H,H) = 7.8 Hz, 1 H), 9.09 (d, J(H,H) = 9.3 Hz, 1 H, pbn-H^4), 8.91 (d, J(H,H) = 1.0 Hz, 1 H), 8.90 (d, J(H,H) = 7.8 Hz, 1 H), 8.81 (d, J(H,H) = 9.3 Hz, 1 H, pbn-H^3), 8.71 (d, J(H,H) = 8.3 Hz, 1 H), 8.55 (s, 1 H, pbn-H^{10}), 8.54 (d, J(H,H) = 6.3 Hz, 2 H), 8.47 (d, J(H,H) = 5.4 Hz, 1 H), 8.35 (dt, J(H,H) = 7.8, 1.0 Hz, 1 H), 8.32 (dt, J(H,H) = 7.8, 1.0 Hz, 1 H), 8.27 (dt, J(H,H) = 9.3, 1.0 Hz, 1 H), 8.23 (dt, J(H,H) = 9.3, 1.0 Hz, 1 H), 8.16 (d, J(H,H) = 8.8 Hz, 1 H, pbn-H^6), 8.12 (d, J(H,H) = 4.9 Hz, 1 H), 8.02 (dt, J(H-H) = 7.8, 1.0 Hz, 1 H), 7.99 (d, J(H-H) = 5.4 Hz, 1 H), 7.93 (dt, J(H,H) = 8.3, 1.0 Hz, 1 H, pbn-H^7), 7.85 (dt, J(H,H) = 7.8 1.0 Hz, 1 H), 7.83 (d, J(H,H) = 5.6 Hz, 1 H), 7.67 (dt, J(H,H) = 5.4, 1.0 Hz, 1 H), 7.59 (t, J(H,H) = 7.3 Hz, 1 H, pbn-H^8), 7.56 (dt, J(H,H) = 5.9, 1.0 Hz, 1 H), 7.48 (dt, J(H-H) = 6.3, 1.0 Hz, 1 H), 7.42 (dt, J(H,H) = 7.3, 1.0 Hz, 1 H), 7.33 ppm (d, J(H,H) = 8.3 Hz, 1 H, pbn-H^9). ESI-MS: $m/z = 335.5$ $[M-2PF_6]^{2+}$.

Electrolytic reduction of **1**: Reduction of **1** was performed in a solution of DMF/0.1 M aqueous AcOH/AcONa buffer (1:9, 10 mL) and supporting electrolyte (NaCl, 0.1 M) under controlled potential electrolysis at −1.14 V (versus Fc/Fc$^+$) by using an electrolysis cell consisting of three components: the working (glassy carbon) and counter (platinum plate) electrode compartments were separated by an anion-exchange membrane (AMP). An Ag/Ag$^+$ reference electrode was separated from the working compartment by a luggin capillary. N_2 was bubbled through the solution in the cell for 1 h followed by pre-electrolysis at −1.2 V, then a solution of **1** (19 mg, 20 μmol) in DMF (1 mL) was added. The solution changed from red-purple to orange-brown after about 3 C consumed. After consuming 4.2 C, the solution was transferred to a Schlenk tube, and the solvent was removed by evaporation to give a brown solid. ^{1}H NMR (500 MHz, [D_6]acetone): $\delta = 8.83$ (t, J(H,H) = 7.8 Hz, 2 H), 8.82 (d, J(H,H) = 7.8 Hz, 2 H), 8.68 (s, 1 H, pbnH_2-N*H*), 8.64 (d, J(H,H) = 5.4 Hz, 1 H), 8.52 (d, J(H,H) = 8.3 Hz, 1 H), 8.44 (d, J(H,H) = 8.8 Hz, 1 H, pbnH_2-H^3), 8.17–8.24 (m, 5 H), 8.07 (t, J(H,H) = 7.8 Hz, 1 H), 7.98 (d, J(H,H) = 5.4 Hz, 1 H), 7.84 (d, J(H,H) = 4.9 Hz, 1 H), 7.68 (d, J(H,H) = 5.4 Hz, 1 H), 7.60–7.66 (m, 3 H), 7.52 (t, J(H,H) = 6.8 Hz, 1 H), 7.41 (d, J(H,H) = 8.8 Hz, 1 H, pbnH_2-H^4), 7.33 (t, J(H,H) = 6.3 Hz, 1 H), 7.00 (t, J(H,H) = 7.3 Hz, 1 H, pbnH_2-H^8), 6.71 (d, J(H,H) = 7.8 Hz, 1 H, pbnH_2-H^9), 6.67 (t, J(H,H) = 7.8 Hz, 1 H, pbnH_2-H^7), 6.18 (d, J(H,H) = 7.3 Hz, 1 H, pbnH_2-H^6), 4.19 (d, J(H,H) = 21 Hz, 1 H, pbnH_2-H^{10}), 3.18 ppm (d, J(H,H) = 21 Hz, 1 H, pbnH_2-H^{10}). ESI-MS: $m/z = 336.5$ $[M-2PF_6]^{2+}$.

Electrolytic reduction of acetone: Acetone reduction was performed in a 1:1 solution of acetone/0.1 M aqueous AcOH/AcONa buffer containing **1** (1 mM) and supporting electrolyte (NaCl, 0.1 M) under controlled potential electrolysis at −1.14 V (versus Fc/Fc$^+$) by using an electrolysis cell similar to that used in the reduction of **1**. The analysis of the solution was carried out by sampling 0.1 mL portions from the solution after appropriate intervals of time. Qualitative and quantitative analyses of the product were conducted by using GC-MS and GC, respectively.

Received: March 1, 2005
Published online: August 9, 2005

Keywords: hydrogen transfer · N ligands · redox chemistry · reduction · ruthenium

[1] Recent articles, see: a) B. Zhao, X. Zhu, C.-Z. Xia, J.-P. Cheng, *Tetrahedron Lett.* **2000**, *41*, 257; b) W. M. Schaffer, T. V. Bronnikova, L. F. Olsen, *J. Phys. Chem. B* **2001**, *105*, 5331; c) B. Nidetzky, M. Klimacek, P. Mayr, *Biochemistry* **2001**, *40*, 10371; d) P. Mayr, B. Nidetzky, *Biochem. J.* **2002**, *366*, 889; e) X.-Q. Zhu, L. Cao, Y. Liu, Y. Yang, J.-Y. Lu, J.-S. Wang, J.-P. Cheng, *Chem. Eur. J.* **2003**, *9*, 3937.

[2] Recent articles, see: a) C. Vitry, J. Bédat, Y. Prigent, V. Levacher, G. Dupas, I. Salliot, G. Quéguiner, J. Bourguignon, *Tetrahedron* **2001**, *57*, 9101; b) U. Gran, O. Wennerström, G. Westman, *Tetrahedron* **2001**, *57*, 8897; c) C. Vitry, J.-L. Vasse, G. Dupas, V. Levacher, G. Quéguiner, J. Bourguignon, *Tetrahedron* **2001**, *57*, 3087; d) J.-L. Vasse, G. Dupas, J. Duflos, G. Quéguiner, J. Bourguignon, V. Levacher, *Tetrahedron Lett.* **2001**, *42*, 4613; e) J.-L. Vasse, S. Goumain, V. Levacher, G. Dupas, G. Quéguiner, J. Bourguignon, *Tetrahedron Lett.* **2001**, *42*, 1871; f) Y.-C. Liu, X.-Z. Li, C. Yang, Q.-X. Guo, *Bioorg. Chem.* **2001**, *29*, 14; g) J.-L. Vasse, V. Levacher, J. Bourguignon, G. Dupas, *Tetrahedron: Asymmetry* **2002**, *13*, 227; h) J.-L. Vasse, V. Levacher, J. Bourguignon, G. Dupas, *Tetrahedron* **2003**, *59*, 4911; i) U. Gran, *Tetrahedron* **2003**, 59, 4303; j) D. Zhang, L.-Z. Wu, X. Han, Q.-Z. Yang, L.-P. Zhang, C.-H. Tung, *J. Am. Chem. Soc.* **2004**, *126*, 3440; k) Y. Mikata, S. Aida, S. Yano, *Org. Lett.* **2004**, *6*, 2921.

[3] For recent articles, see: a) X.-Q. Zhu, H.-R. Li, Q. Li, T. Ai, J.-Y. Lu, Y, Yang, J.-P. Cheng, *Chem. Eur. J.* **2003**, *9*, 871; b) Y. Lu, Y. Zhao, K. L. Handoo, V. D. Parker, *Org. Biomol. Chem.* **2003**, *1*, 173; c) C. Selvaraju, P. Ramamurthy, *Chem. Eur. J.* **2004**, *10*, 2253.

[4] For acid-catalyzed hydrogen transfer, see: a) S. Fukuzumi, S. Mochizuki, T. Tanaka, *J. Am. Chem. Soc.* **1989**, *111*, 1497; b) S. Fukuzumi, S. Mochizuki, T. Tanaka, *Inorg. Chem.* **1990**, *29*, 653;

 © 2005 Wiley-VCH Verlag GmbH & Co. KGaA, Weinheim

c) C. J. Murray, T. Webb, *J. Am. Chem. Soc.* **1989**, *111*, 1497; d) S. Fukuzumi, Y. Tokuda, *J. Phys. Chem.* **1993**, *97*, 3737; e) S. Fukuzumi, T. Suenobu, M. Patz, T. Hirasaka, S. Itoh, M. Fujitsuka, O. Ito, *J. Am. Chem. Soc.* **1998**, *120*, 8060; f) S. Fukuzumi, H. Imamori, K. Okamoto, H. Yamada, M. Fujitsuka, O. Ito, D. M. Guldi, *J. Phys. Chem. A* **2002**, *106*, 1903.

[5] T. Tomon, T. Koizumi, K. Tanaka, *Angew. Chem. Int. Ed.* **2005**, *44*, 2229.

[6] A. Godard, G. Quéguiner, *J. Heterocycl. Chem.* **1980**, *17*, 465.

[7] A. Godard, G. Quéguiner, *J. Heterocycl. Chem.* **1982**, *19*, 1289.

[8] Crystallographic data for **1**·acetone: monoclinic, $P2_1/n$ (no. 14), $a = 13.761(10)$, $b = 18.05(1)$, $c = 16.67(1)$ Å, $\beta = 101.558(9)°$, $V = 4056(4)$ Å^3, $Z = 4$, $\rho_{calcd} = 1.668\ g\,cm^{-3}$, $\mu(Mo_{K\alpha}) = 5.65\ cm^{-1}$, $R1(R_w) = 0.098$ (0.234) for 8963 unique data with $I > 2\sigma(I)$ and 568 parameters. A suitable single crystal for the measurement was mounted on a glass fiber. Data were collected at −100 °C on a Rigaku/MSC Mercury CCD diffractometer by using graphite-monochromated $Mo_{K\alpha}$ radiation ($\lambda = 0.71070$ Å). All data were collected and processed using the Crystal Clear program (Rigaku). All the calculations were carried out by using the teXsan software package.[11] All structures were solved by direct methods and expanded using Fourier techniques. Refinements were performed anisotropically for all non-hydrogen atoms by the full-matrix least-squares method. Hydrogen atoms were placed at the calculated positions and were included in the structure calculation without further refinement of the parameters. CCDC-248968 (**1**) contains the supplementary crystallographic data for this paper. These data can be obtained free of charge from the Cambridge Crystallographic Data Centre via www.ccdc.cam.ac.uk/data_request/cif.

[9] a) W. Kaim, W. Matheis, *Chem. Ber.* **1990**, *123*, 1323; b) T. Fujihara, T. Wada, K. Tanaka, *Inorg. Chim. Acta* **2004**, *357*, 1205.

[10] We tried to isolate and recrystallize complex **2**. However, good single crystals of **2** were not obtained, since recrystallization of **2** gave a mixture of **1** and **2**. Complex **2** is unstable in air and in solution under inert atmosphere, and slowly changed into complex **1**. ESI-MS analysis showed **2** at first, but the parent signal of **1** gradually appeared with time. Since the recrystallization has not resulted in purification of **2**, the elemental analysis was not completely satisfactory.

[11] teXane version 1.11, 2000 : Crystal Structure Analysis Package, Molecular Structure Corporation/Rigaku Corporation.

 © 2005 Wiley-VCH Verlag GmbH & Co. KGaA, Weinheim

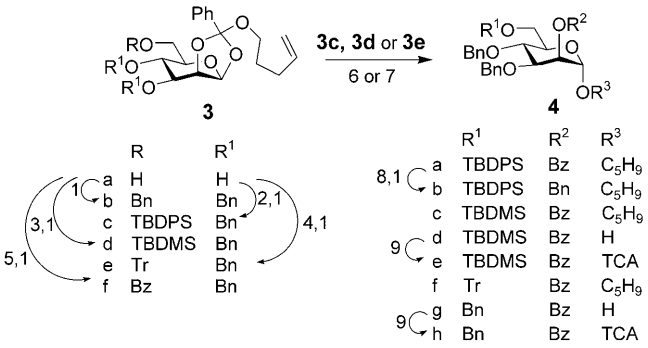
Carbohydrate Synthesis

DOI: 10.1002/anie.200500505

Synthesis of a Lipomannan Component of the Cell-Wall Complex of *Mycobacterium tuberculosis* Is Based on Paulsen's Concept of Donor/Acceptor "Match"**

*K. N. Jayaprakash, Jun Lu, and Bert Fraser-Reid**

The resilience of tuberculosis, evident in the continuing worldwide mortality from this disease,[1] is largely attributable to the dense complex lipoarabinomannan (LAM) capsule that is the major virulence factor of the causative agent *Mycobacterium tuberculosis*.[2] Significant interest stems from recent discoveries showing that LAM exhibits a profound propensity toward immunomodulation,[3] the ability to enhance resistance to various cancers[4,5] and herpes,[6] and a surprising capacity to potentiate HIV antiretroviral drugs.[7] This multifaceted biological profile is matched by its multifaceted architecture,[8] shown as compound **1** by Turnbull



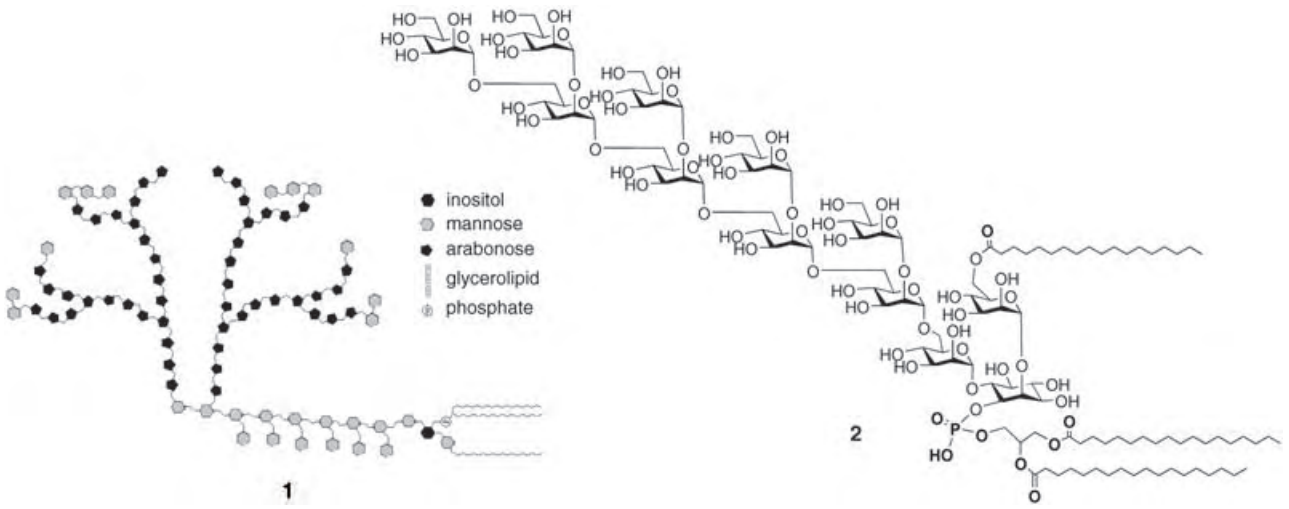
Scheme 1. 1) NaH, BnBr, TBAI, DMF; 2) TBDPSCl, Et_3N, DMAP, CH_2Cl_2; 3) TBDMSCl, imidazole, THF; 4) TrCl, DMAP, Et_3N, py; 5a) TBDMSCl, imidazole, THF, 5b) NaH, BnBr, DMF, 5c) TBAF, THF, 5d) BzCl, DMAP, py; 6) $Yb(OTf)_3$, CH_2Cl_2, O°C; 7) AcOH, H_2O, acetone; 8) NaOMe, CH_2Cl_2, MeOH; 9) CCl_3CN, DBU, CH_2Cl_2. Bn = benzyl, Bz = benzoyl, DMAP = 4-(dimethylamino)pyridine; DMF = *N*,*N*-dimethylformamide; py = pyridine; TBAI = *tert*-butylammonium iodide; TBAF = *tert*-butylammonium fluoride; TBDMS = *tert*-butyldimethylsilyl, TBDPS = *tert*-butyldiphenylsilyl, TCA = trichloroacetyl, Tr = trityl.

[*] Dr. K. N. Jayaprakash, Dr. J. Lu, Prof. Dr. B. Fraser-Reid
Natural Products and Glycotechnology Research Institute, Inc.
595 F Weathersfield Road, Fearrington Post 595 F
Pittsboro, NC 27312 (USA)
Fax: (+1) 919-542-7111
E-mail: dglucose@aol.com

[**] We are grateful to the National Science Foundation (CHE-0243436) for support. We thank Dr. George Dubay, Director of Instrument Operations in the Department of Chemistry, Duke University, for MS and MALDI measurements. A patent has been filed for the compounds and procedures reported in this paper.

Supporting information for this article is available on the WWW under http://www.angewandte.org or from the author.

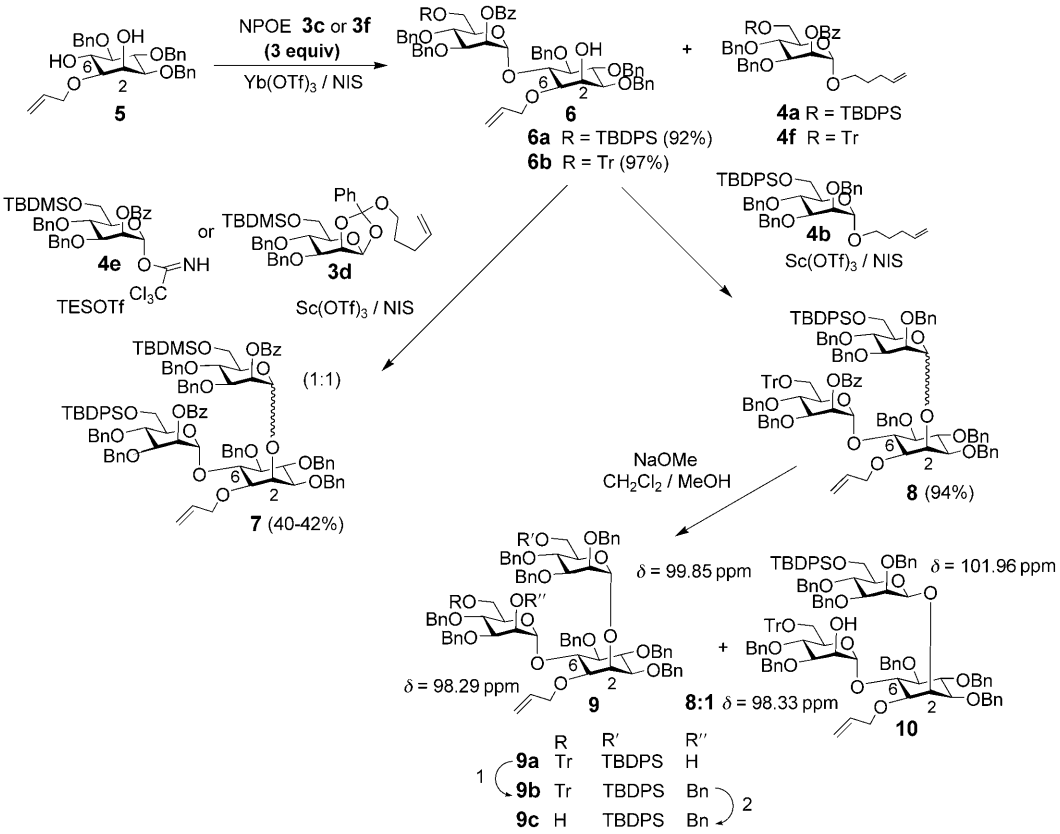
WILEY InterScience DISCOVER SOMETHING GREAT
© 2005 Wiley-VCH Verlag GmbH & Co. KGaA, Weinheim



et al.[9] Subunits of **1**, which reflect the stages in its biosynthesis, are dispersed throughout the cell wall and are of independent interest. For example, the lipomannan (LM) backbone of **1** exhibits "strong proinflammatory and apoptosis-inducing activity".[10] Herein, we outline a novel synthetic strategy for the assembly of the complex lipomannan domain **2**.

The standard approach to compounds such as **2** normally entails skillful deployment of a bewildering variety of protecting groups.[11] However, a less daunting approach relies on an insight into regioselective glycosidation[12] learned, in part, from the seminal concept by Paulsen of a donor/acceptor "match".[13] This insight can be supported by chemoselective donor activation with Lewis acid salts,[14,15] which is preferable to arming and disarming substrate compounds with protecting groups[16] and other strategies of chemical control.[17]

Thus, the *n*-pentenylorthoester (NPOE) **3a** is readily prepared[18] and can be converted into analogues **3b**–**3f** by using standard procedures (Scheme 1, see page 5894). Lanthanide triflates can then be used 1) to rearrange them into disarmed donors (**3c**→**4a**, **3d**→**4c**, and **3e**→**4f**), and 2) to generate iodonium ion (I^+) from *N*-iodosuccinimide (NIS). However, if $Yb(OTf)_3$ is used for the latter purpose, NPOEs are chemoselectively activated[14,15] without affecting disarmed or armed *n*-pentenyl glycosides (NPGs) such as **4a** and **4b**. Alternatively, the hydrolysis of an NPOE gives a protected mannose (for example, **3d**→**4d**), which opens a facile route to popular trichloroacetimidate donors such as **4e**, which can also be activated by $Yb(OTf)_3$.[15,19]



Scheme 2. 1) NaH, BnBr, TBAI, DMF, 2 h, 98%; 2) PTSA, MeOH, CH_2Cl_2, 89%. NPOE = *n*-pentenylorthoester; NIS = *N*-iodosuccinimide; PTSA = *p*-toluenesulfonic acid; TESOTf = triethylsilyl triflate.

 © 2005 Wiley-VCH Verlag GmbH & Co. KGaA, Weinheim

The foregoing salt-based regio- and chemoselectivities are opportune for the formidable challenges presented by compound **2**. The phosphoinositide domain requires the attachment of two mannoside donors, differentiated by O6 protecting groups, to an inositol acceptor diol. Encouraged by the recent success at double differential glycosidation,[15] the known diol **5**[20] was treated with the NPOE **3c** (2 equiv) promoted by $Yb(OTf)_3$/NIS to optimize monoglycosidation, with the confidence that the disarmed NPG **4a** produced by rearrangement would not be activated (Scheme 2).[14] Indeed, **6a** was isolated in 92% yield, and then treated with trichloroacetimidate **4e** (1.5 equiv) by using TESOTf. Compound **7** was obtained in 40% yield, but surprisingly with a selectivity of 1:1 for α/β configurations at the newly formed anomeric center.

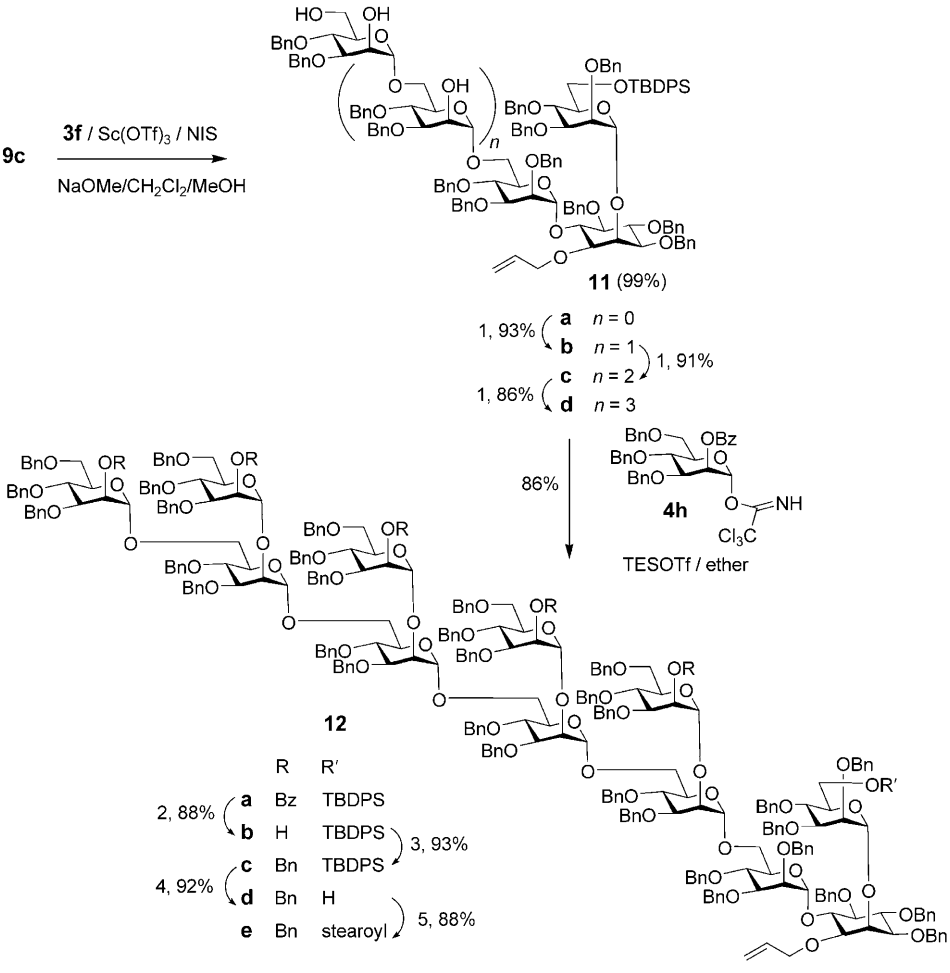
This disappointing stereoselectivity (and modest yield) persisted even if the NPOE **3d** was used together with $Sc(OTf)_3$/NIS. The low yields may be rationalized by donor/acceptor studies, supported by the observations of van Boom and co-workers[21] as well as ours,[22] which indicate that a disarmed donor or NPOE is not a good "match" for inositol-2-OH.

A further problem with **7** was that the TBDMS group could not be selectively removed. This forced us to investigate an alternate route that involved the tritylated analogue **8**. Accordingly, pseudodisaccharide **6b**, prepared in 97% yield from diol **5** and excess NPOE **3f**, was treated with armed NPG **4b** and $Sc(OTf)_3$/NIS. The near quantitative yield (94%) of **8**, supports the "match" between the armed donor **4b** and the inositol-2-OH. The material appeared to be homogeneous by TLC, but debenzoylation led to separable products **9a** and **10** in a ratio of 8:1. The ^{13}C NMR spectroscopic data for the anomeric carbon atoms ($\delta = 99.85$ and 98.29 ppm and $\delta = 101.96$ and 98.33 ppm, as indicated in Scheme 2, see page 5895) identified their configurations as αα and αβ, respectively.

Isolation and benzylation of the αα product led to compound **9b** and thus acceptor **9c**. The latter, upon treatment with the O6-benzoylated NPOE **3f** and activation by $Sc(OTf)_3$/NIS followed by debenzoylation, gave pseudotetrasaccharide **11a** in 93% yield (Scheme 3). Iteration of the last two steps, but with $Yb(OTf)_3$ to ensure regioselective glycosidation at the primary hydroxy group, led to triol **11b**, tetraol **11c**, and pentaol **11d**, with excellent yields maintained throughout. The structure of **11d** was supported by resolved signals in the ^{13}C NMR spectra for six anomeric carbons ($\delta = 100.14$, 100.112, 99.83, 99.72, 99.12, 98.25 ppm).

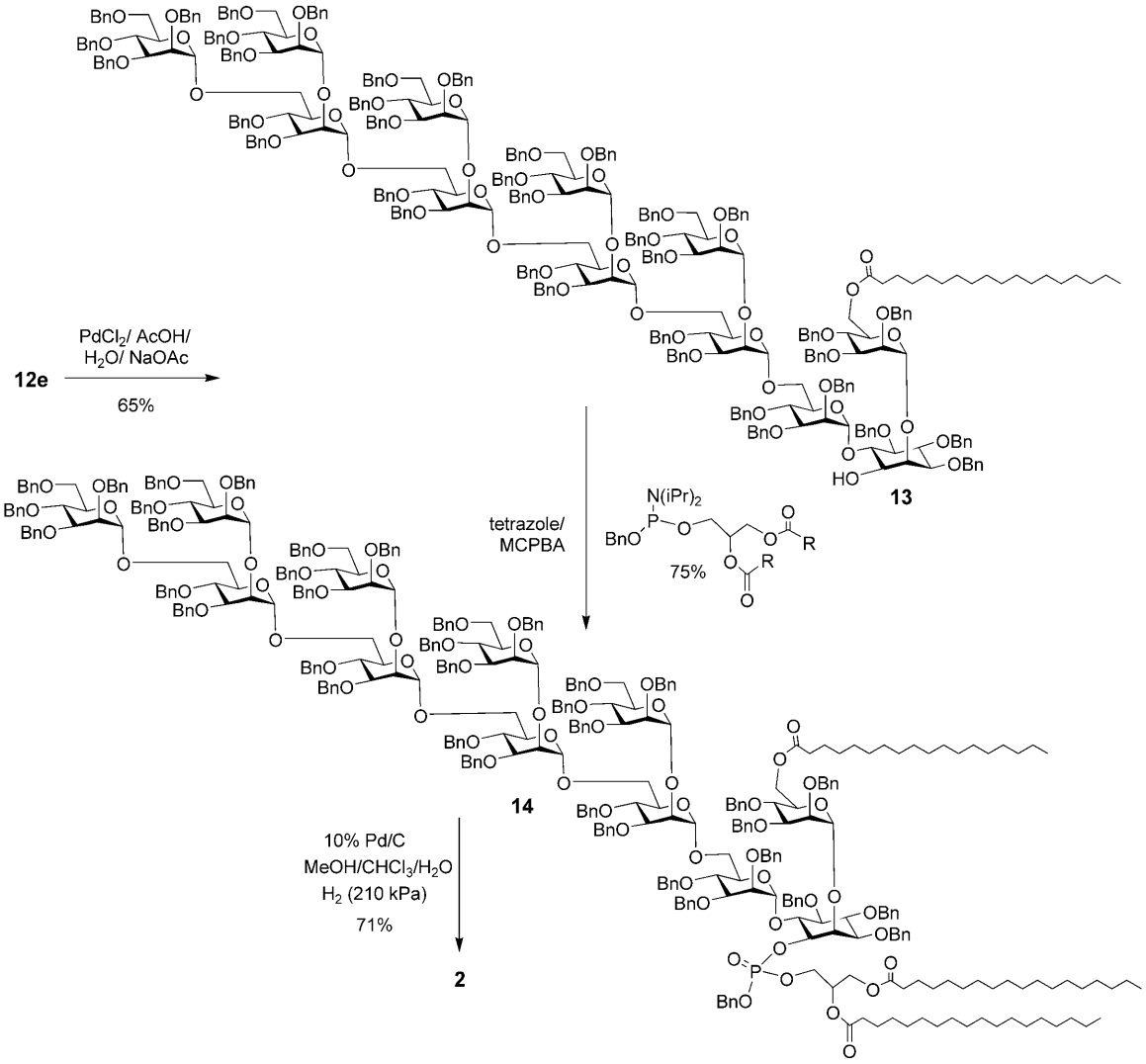
Pentaol **11d** was treated with trichloroacetimidate **4h** (10 equiv) and TESOTf to give the pseudododecasaccharide **12a** in 86% yield. The anomeric signals were merged, but the debenzoylated counterpart, **12b**, displayed seven discrete ($\delta = 102.13$, 101.91, 101.74, 101.29, 101.28, 99.54, 99.32 ppm) and two overlapping sets of two ($\delta = 98.85$, 98.23 ppm) anomeric carbon signals in the ^{13}C NMR spectra, consistent with the 11 pyranoside residues.

Routine high-yielding benzylation and desilylation steps paved the way for installation of the stearoyl ester in **12e** by standard treatment with stearoyl chloride. Palladium-catalyzed deallylation provided **13** (Scheme 4), and the resulting inositol-1-OH cooperated well with our standard phosphoglycero-lipidation protocol[23] involving reaction with the lipidated glyceryl phosphoramidite followed by oxidation with MCPBA.[22a,24] The penultimate product **14** was obtained in 71% yield.



Scheme 3. 1a) **3e**, $Yb(OTf)_3$, NIS, CH_2Cl_2, 1b) NaOMe, MeOH, CH_2Cl_2; 2) NaOMe, MeOH, CH_2Cl_2; 3) NaH, BnBr, TBAI, DMF; 4) TBAF, MS, THF; 5) stearoyl chloride, DMAP, py, CH_2Cl_2.

 © 2005 Wiley-VCH Verlag GmbH & Co. KGaA, Weinheim



Scheme 4. The final steps in the synthesis of **2** from stearoyl ester **12e**. MCPBA = *meta*-chloroperbenzoic acid.

Exhaustive debenzylation of **14** (30 mg) was effected in methanol/chloroform/water solution with palladium (10%) on carbon and hydrogen at 2.1×10^{-5} Pa for 3 h at room temperature. Chromatographic purification (Sephadex column) afforded **2** (10 mg, 71%), which showed eleven anomeric proton signals between $\delta = 4.51$ and 5.02 ppm in the ^{1}H NMR spectra and signals for phosphorus diastereomers at $\delta = 0.61$ and 0.49 ppm in the ^{31}P NMR spectra. Additional confirmation was obtained by MS (for M+2Na: calcd: 2961.4; found: 2961.6). Biological assays on **2** are currently underway and will be reported in due course.

Received: February 10, 2005
Published online: August 3, 2005

Keywords: glycolipids · glycosides · glycosylation · lanthanides · regioselectivity

[1] WHO Global Survillance and Monitoring Project: C. Dye, S. Scheele, P. Dolin, V. Pathania, M. C. Raviglione, *JAMA J. Am. Med. Assoc.* **1999**, *282*, 677–686.

[2] a) M. Riviere, A. Moisand, A. Lopez, G. Puzo, *J. Mol. Biol.* **2004**, *344*, 907–918; b) V. Briken, S. A. Procelli, G. S. Besra, L. Kremer, *Mol. Microbiol.* **2004**, *53*, 391–433; c) P. J. Brennan, *Tuberculosis* **2003**, *1*, 1–7; d) A. Truemann, X. Xidong, L. McDonnell, P. J. Derrick, A. E. Ashcroft, D. Chatterjee, S. W. Homans, *J. Mol. Biol.* **2002**, *316*, 89–100; e) T. L. Lowary in *Glycoscience: Chemistry and Biology*, *Vol. 3* (Eds. B. Fraser-Reid, K. Tatsuta, J. Thiem), Springer, Heildelberg, **2001**, p. 2005; f) D. Chatterjee, *Curr. Opin. Chem. Biol.* **1997**, *1*, 579.

[3] H. Kobatake, T. Buekane, Y. Murakami, S. Niwa, A. Okahira, H. Kushida, *Yakugaku Zasshi* **1981**, *101*, 713–722.

[4] a) Y. Hayashi, T. Ebina, F. Suzuki, N. Ishida, *Microbiol. Immunol.* **1981**, *25*, 305–316; b) H. Sasaki, M. Kobayashi, Yl. Emori, O. Ohya, Y. Hayashi, K. Nomoto, *Biotherapy* **1997**, *10*, 139; c) Y. Emori, H. Sasaki, Y. Hayashi, K. Nomoto, *Biotherapy* **1996**, *9*, 249–272; d) M. Mukai, S. Kibota, S. Morita, A. Akanuma, *Cancer* **1995**, *75*, 2276–2280; e) M. Kobayashi, R. B. Pollard, F. Suzuki, *Anti-Cancer Drugs* **1997**, *8*, 153–156.

[5] a) Y. Luo, X. Chen, T. M. Downs, W. C. DeWold, M. A. O'Donnell, *J. Immunol.* **1999**, *162*, 2399–2405; b) H. Oka, Y.

 © 2005 Wiley-VCH Verlag GmbH & Co. KGaA, Weinheim

Emori, O. Ohya, N. Kobayashi, H. Sasaki, Y. Tanaka, Y. Hayashi, K. Nomoto, *Immunol. Lett.* **1999**, *70*, 109 – 117; c) H. Oka, Y. Shiraishi, H. Sasaki, K. Yoshinaga, Y. Emori, M. Takei, *Biol. Pharm. Bull.* **2003**, *26*, 1336 – 1341; d) H. Oka, Y. Emori, H. Sasaki, Y. Shiraishi, K. Yoshinaga, T. Kurimoto, *Microbiol. Immunol.* **2002**, *46*, 343 – 351; e) H. Oka, H. Sasaki, Y. Shiraishi, Y. Emori, K. Yoshinaga, M. Takei, *Biol. Pharm. Bull.* **2004**, *27*, 82 – 88.

[6] M. Kobayashi, D. N. Herndon, R. B. Pollard, F. Suzuki, *Immunol. Lett.* **1994**, *40*, 199 – 205.

[7] P. Lesprit, A.-M. Zagdanski, A. de la Blanchardiere, M. Rouveau, J.-M. Decazes, J. Frija, P. Lagrange, J. Modai, J.-M. Molina, *Medicine* **1997**, *76*, 423 – 431.

[8] For an excellent survey, see: A. Maureen Rouhi, *Chem. Eng. News* **1999**, *77*(20), 52 – 70.

[9] W. B. Turnbull, K. H. Shimizu, D. Chatterjee, S. W. Homans, A. Truemann, *Angew. Chem.* **2004**, *116*, 4008 – 4012; *Angew. Chem. Int. Ed.* **2004**, *43*, 3918 – 3922.

[10] S. A. Porcelli, G. S. Besra in *Intracellular Pathogens in Membrane Interactions Biogenesis* (Ed.: J. P. Vacuole Gorvel), Kluwer Academic Plenum Publishers, New York, **2004**, pp. 230 – 249.

[11] For example, see: H. Paulsen, *Angew. Chem.* **1982**, *94*, 184 – 201; *Angew. Chem. Int. Ed. Engl.* **1982**, *21*, 155 – 173; a) H. Osborn, T. Khan, *Oligosaccharides: Their Synthesis and Biological Roles*, Oxford University Press, Oxford, UK, **2000**; b) G.-J. Boons, *Tetrahedron* **1996**, *52*, 1095 – 1121.

[12] a) B. Fraser-Reid, J. C. Lopez, A. M. Gomez, C. Uriel, *Eur. J. Org. Chem.* **2004**, 1387 – 1395; b) C. Uriel, A. Gomez, J. Cristobal Lopez, B. Fraser-Reid, *Synlett* **2003**, 2203 – 2207; c) J. C. Lopez, A. M. Gomez, C. Uriel, B. Fraser-Reid, *Tetrahedron Lett.* **2003**, *44*, 1417 – 1420; d) B. Fraser-Reid, J. Cristobal Lopez, K. V. Radhakrishnan, M. Mach, U. Schlueter, A. Gomez, C. Uriel, *J. Am. Chem. Soc.* **2002**, *124*, 3198 – 3199.

[13] H. Paulsen in *Selectivity: a Goal for Synthetic Efficiency* (Eds.: W. Bartmann, B. M. Trost), Verlag Chemie, Basel, **1984**.

[14] K. N. Jayaprakash, B. Fraser-Reid, *Synlett* **2004**, 301 – 305.

[15] K. N. Jayaprakash, B. Fraser-Reid, *Org. Lett.* **2004**, *6*, 4211 – 4214.

[16] a) D. R. Mootoo, P. Konradsson, U. Udodong, B. Fraser-Reid, *J. Am. Chem. Soc.* **1988**, *110*, 5583 – 5584; b) B. Fraser-Reid, Z. Wu, C. W. Andrews, E. Skowronski, J. P. Bowen, *J. Am. Chem. Soc.* **1991**, *113*, 1434 – 1435.

[17] a) G. J. Boons, P. Grice, R. Leslie, S. V. Ley, L. L. Yeung, *Tetrahedron Lett.* **1993**, *34*, 8523; b) G. J. Boons, R. Geurtsen, D. Holmes, *Tetrahedron Lett.* **1995**, *36*, 6325; c) R. W. Friesen, S. J. Danishefsky, *J. Am. Chem. Soc.* **1989**, *111*, 6656; d) R. Roy, F. O. Andersson, M. Letellier, *Tetrahedron Lett.* **1992**, *33*, 6053.

[18] B. Fraser-Reid, J. C. Lopez, K. V. Radhakrishnan, M. Mach, U. Schlueter, A. Gomez, C. Uriel, *Can. J. Chem.* **2002**, *80*, 1075 – 1087.

[19] M. Adinolfi, A. Ladonisi, M. Schiattarella, *Tetrahedron Lett.* **2004**, *45*, 6479.

[20] G. Anilkumar, L. G. Nair, B. Fraser-Reid, *Org. Lett.* **2000**, *2*, 2587 – 2589.

[21] a) C. J. J. Elie, C. E. Verduyn, D. M. Dreff, D. G. A. Brounts, G. A. van der Marel, J. H. van Boom, *Tetrahedron* **1990**, *46*, 8243 – 8254; b) C. J. J. Elie, D. M. Verduyn, D. G. A. Dreff, G. A. Brounts, J. H. van der Marel, J. van Boom, *Carbohydr. Chem.* **1992**, *11*, 715 – 739.

[22] a) G. Anilkumar, M. R. Gilbert, B. Fraser-Reid, *Tetrahedron* **2000**, *56*, 1993 – 1997; b) K. N. Jayaprakash, J. Lu, B. Fraser-Reid, *Bioorg. Med. Chem. Lett.* **2004**, *14*, 3815 – 3819.

[23] K.-L. Yu, B. Fraser-Reid, *Synth. Commun.* **1988**, *18*, 465 – 468.

[24] J. Lu, K. N. Jayaprakash, U. Schlueter, B. Fraser-Reid, *J. Am. Chem. Soc.* **2004**, *126*, 7540 – 7547.

 © 2005 Wiley-VCH Verlag GmbH & Co. KGaA, Weinheim